

# Bibliography of Lewis Research Center Technical Publications Announced in 1989

May 1990



National Aeronautics and  
Space Administration

**Lewis Research Center**  
Cleveland, Ohio 44135





## PREFACE

In 1989, Lewis Research Center's 1314 research authors published 638 technical publications that were announced to and reached the worldwide scientific community. This was our highest number of technical publications in 18 years and an 18.6-percent increase over last year's high production of 538. In addition to this total, 151 contractor-authored research reports were produced at NASA Lewis. It was a record-breaking year: there were 286 symposium/seminar presentations, 102 articles sent directly to journals for publication, and 115 Lewis-hosted conference papers. In each case, the totals were higher than at any other time in Lewis history.

In 1989, Lewis authors published approximately 61 percent of their research contributions in outside publications and the remainder as NASA research reports. Seventy-one percent of Lewis-authored society presentations and journal articles were addressed to members of the following 10 societies—AIAA, ASME, SAE, IEEE, ASEE (American Society of Engineering Education), ACS (American Chemical Society), AIChE, American Nuclear Society, JANNAF (Joint Army-Navy-NASA-Air Force), and ASM (American Society for Metals).

Lewis hosted twelve research conferences and workshops in 1989. Six of these resulted in NASA Conference Publications, including

- International Microgravity Combustion Workshop, January 25–26
- Advanced Propulsion Options Workshop, February 7–8
- Space Electrochemical Research and Technology, April 11–13
- Structural Integrity and Durability of Reusable Space Propulsion Systems, April 18–19
- Conceptual Design for the Space Station Freedom Modular Combustion Facility, May 17–18
- HITEMP Review 1989: Advanced High Temperature Engine Materials Technology Program, October 31–November 2

Three of these conference publications were published at Lewis and made available to the attendees when they registered at the conferences: Space Electrochemical Research and Technology, Structural Integrity and Durability of Reusable Space Propulsion Systems, and HITEMP Review. Other conferences and workshops hosted or sponsored by Lewis in 1989 included

- Transmission Software Workshop, May 9
- Space Power Conference, June 5–7
- Advanced Modulation and Coding Technology Conference, June 21–22
- Unsteady Aerodynamics for Aeroelasticity and Aeroacoustics of Rotating Blades, July 19–20
- The Fifth Thermomechanical Fatigue Workshop, October 10–11
- The Tenth Space Photovoltaic Research and Technology Conference, November 7–9

In 1989, Lewis became the first research and development organization to be designated as a Quality Improvement Prototype by the Office of Management and Budget. One of the factors cited in the selection was "dramatic increases in the number of disclosures of inventions and technical publications." Eighteen patent applications were filed in 1989, and four patents were issued. Several Lewis authors and inventors won awards for these inventions and publications.

Lewis inventor Harold Sliney was chosen as NASA's Inventor of the Year for his composite coating, PS200 (a self-lubricating coating that decreases wear on engine seals and bearings). In addition, several Lewis inventors received R&D 100 Awards from Research & Development magazine. One such award was given for the development of the Varian Associates Model VKP-7990, a multistage depressed collector (MDC) klystron amplifier developed by Peter Ramins and James Dayton (NASA Lewis), Henry Kosmahl (Analex), and Earl McClure (Varian Associates, Palo Alto, California). Another award was given for the development of the Gigabit Monolithic Optical Integrated Receiver, a monolithic optical electronic integrated circuit (OEIC) developed by Kul B. Bhasin (NASA Lewis) and Wayne Walters, Jerry Gustafsen, and Mark Bendett (Honeywell). The final award was given for the development of the Vector Scanning Data Reduction Technique for Pulsed Laser Velocimetry Data, a two-step procedure developed by Mark P. Wernet (NASA Lewis) for recording and analyzing pulsed laser velocimetry photographs.

The 1989 Lewis Distinguished Publication Award was presented to Khairul B.M.Q. Zaman, Daniel J. McKinzie, and Christopher L. Rumsey for their paper entitled "A Natural Low-Frequency Oscillation of the Flow Over an Airfoil Near Stalling Conditions."

A few of the other awards received by Lewis engineers in 1989 follow. David Pofert, Steven Szabo, and Joseph Ziemianski received the Presidential Rank Award for meritorious Executive Service, Christos Chamis was named Engineer of the Year by the Northern Ohio section of the American Institute of Aeronautics and Astronautics (AIAA), and Vincent Lalli was named Engineer of the Year by the Cleveland section of the Institute of Electrical and Electronics Engineers (IEEE).

All of the publications in this collection were announced in the 1989 issues of STAR (Scientific and Technical Aerospace Reports) and IAA (International Aerospace Abstracts). Some 1989 publications will be announced in the 1990 issues of STAR and IAA and will thus appear in the 1990 Lewis Bibliography. However, a few Lewis-authored publications are not included in this compilation because of FEDD (For Early Domestic Dissemination) and ITAR (International Traffic in Arms Regulations) considerations which limit their announcement and distribution.

The arrangement of the material is by NASA subject category, as noted in the Contents. In addition, the various indexes will help locate specific publications by subject, author, corporate source, contract number, and report number.

Richard E. Texler  
Chief, Technical Information Services Division

# TABLE OF CONTENTS

## PREFACE

iii

## AERONAUTICS

Includes aeronautics (general); aerodynamics; air transportation and safety; aircraft communications and navigation; aircraft design, testing and performance; aircraft instrumentation; aircraft propulsion and power; aircraft stability and control; and research and support facilities (air).

For related information see also *Astronautics*.

### 01 AERONAUTICS (GENERAL) 1

### 02 AERODYNAMICS 1

Includes aerodynamics of bodies, combinations, wings, rotors, and control surfaces; and internal flow in ducts and turbomachinery.

For related information see also *34 Fluid Mechanics and Heat Transfer*

### 03 AIR TRANSPORTATION AND SAFETY 16

Includes passenger and cargo air transport operations; and aircraft accidents.

For related information see also *16 Space Transportation* and *85 Urban Technology and Transportation*.

### 04 AIRCRAFT COMMUNICATIONS AND NAVIGATION N.A.

Includes digital and voice communication with aircraft; air navigation systems (satellite and ground based); and air traffic control.

For related information see also *17 Space Communications*, *Spacecraft Communications*, *Command and Tracking* and *32 Communications and Radar*.

### 05 AIRCRAFT DESIGN, TESTING AND PERFORMANCE 17

Includes aircraft simulation technology.

For related information see also *18 Spacecraft Design, Testing and Performance* and *39 Structural Mechanics*. For land transportation vehicles see *85 Urban Technology and Transportation*.

### 06 AIRCRAFT INSTRUMENTATION 19

Includes cockpit and cabin display devices; and flight instruments.

For related information see also *19 Spacecraft Instrumentation* and *35 Instrumentation and Photography*.

### 07 AIRCRAFT PROPULSION AND POWER 19

Includes prime propulsion systems and systems components, e.g., gas turbine engines and compressors; and onboard auxiliary power plants for aircraft.

For related information see also *20 Spacecraft Propulsion and Power*, *28 Propellants and Fuels*, and *44 Energy Production and Conversion*.

### 08 AIRCRAFT STABILITY AND CONTROL 34

Includes aircraft handling qualities; piloting; flight controls; and autopilots.

For related information see also *05 Aircraft Design, Testing and Performance*.

## 09 RESEARCH AND SUPPORT FACILITIES (AIR) 36

Includes airports, hangars and runways; aircraft repair and overhaul facilities; wind tunnels; shock tubes; and aircraft engine test stands.

For related information see also *14 Ground Support Systems and Facilities (Space)*.

## ASTRONAUTICS

Includes astronautics (general); astrodynamics; ground support systems and facilities (space); launch vehicles and space vehicles; space transportation; space communications, spacecraft communications, command and tracking; spacecraft design, testing and performance; spacecraft instrumentation; and spacecraft propulsion and power.

For related information see also *Aeronautics*

### 12 ASTRONAUTICS (GENERAL) 37

For extraterrestrial exploration see *91 Lunar and Planetary Exploration*.

### 13 ASTRODYNAMICS 38

Includes powered and free-flight trajectories; and orbital and launching dynamics.

### 14 GROUND SUPPORT SYSTEMS AND FACILITIES (SPACE) 38

Includes launch complexes, research and production facilities; ground support equipment, e.g., mobile transporters; and simulators.

For related information see also *09 Research and Support Facilities (Air)*.

### 15 LAUNCH VEHICLES AND SPACE VEHICLES 40

Includes boosters; operating problems of launch/space vehicle systems; and reusable vehicles.

For related information see also *20 Spacecraft Propulsion and Power*.

### 16 SPACE TRANSPORTATION 42

Includes passenger and cargo space transportation, e.g., shuttle operations; and space rescue techniques.

For related information see also *03 Air Transportation and Safety* and *18 Spacecraft Design, Testing and Performance*. For space suits see *54 Man/System Technology and Life Support*.

### 17 SPACE COMMUNICATIONS, SPACECRAFT COMMUNICATIONS, COMMAND AND TRACKING 43

Includes telemetry; space communications networks; astronavigation and guidance; and radio blackout.

For related information see also *04 Aircraft Communications and Navigation* and *32 Communications and Radar*.

## **18 SPACECRAFT DESIGN, TESTING AND PERFORMANCE 44**

Includes satellites; space platforms; space stations; spacecraft systems and components such as thermal and environmental controls; and attitude controls.

For life support systems see *54 Man/System Technology and Life Support*. For related information see also *05 Aircraft Design, Testing and Performance*, *39 Structural Mechanics*, and *16 Space Transportation*.

## **19 SPACECRAFT INSTRUMENTATION 47**

For related information see also *06 Aircraft Instrumentation* and *35 Instrumentation and Photography*.

## **20 SPACECRAFT PROPULSION AND POWER 48**

Includes main propulsion systems and components, e.g. rocket engines; and spacecraft auxiliary power sources.

For related information see also *07 Aircraft Propulsion and Power*, *28 Propellants and Fuels*, *44 Energy Production and Conversion*, and *15 Launch Vehicles and Space Vehicles*.

## **CHEMISTRY AND MATERIALS**

Includes chemistry and materials (general); composite materials; inorganic and physical chemistry; metallic materials; nonmetallic materials; propellants and fuels; and materials processing.

## **23 CHEMISTRY AND MATERIALS (GENERAL) 76**

## **24 COMPOSITE MATERIALS 79**

Includes physical, chemical, and mechanical properties of laminates and other composite materials.

For ceramic materials see *27 Nonmetallic Materials*.

## **25 INORGANIC AND PHYSICAL CHEMISTRY 89**

Includes chemical analysis, e.g., chromatography; combustion theory; electrochemistry; and photochemistry.

For related information see also *77 Thermodynamics and Statistical Physics*.

## **26 METALLIC MATERIALS 94**

Includes physical, chemical, and mechanical properties of metals, e.g., corrosion; and metallurgy.

## **27 NONMETALLIC MATERIALS 105**

Includes physical, chemical, and mechanical properties of plastics, elastomers, lubricants, polymers, textiles, adhesives, and ceramic materials.

For composite materials see *24 Composite Materials*.

## **28 PROPELLANTS AND FUELS 116**

Includes rocket propellants, igniters and oxidizers; their storage and handling procedures; and aircraft fuels.

For related information see also *07 Aircraft Propulsion and Power*, *20 Spacecraft Propulsion and Power*, and *44 Energy Production and Conversion*.

## **29 MATERIALS PROCESSING 117**

Includes space-based development of products and processes for commercial application.

For biological materials see *55 Space Biology*.

## **ENGINEERING**

Includes engineering (general); communications and radar; electronics and electrical engineering; fluid mechanics and heat transfer; instrumentation and photography; lasers and masers; mechanical engineering; quality assurance and reliability; and structural mechanics.

For related information see also *Physics*.

## **31 ENGINEERING (GENERAL) 123**

Includes vacuum technology; control engineering; display engineering; cryogenics; and fire prevention.

## **32 COMMUNICATIONS AND RADAR 124**

Includes radar; land and global communications; communications theory; and optical communications.

For related information see also *04 Aircraft Communications and Navigation* and *17 Space Communications, Spacecraft Communications, Command and Tracking*. For search and rescue see *03 Air Transportation and Safety*, and *16 Space Transportation*.

## **33 ELECTRONICS AND ELECTRICAL ENGINEERING 130**

Includes test equipment and maintainability; components, e.g., tunnel diodes and transistors; microminiaturization; and integrated circuitry.

For related information see also *60 Computer Operations and Hardware* and *76 Solid-State Physics*.

## **34 FLUID MECHANICS AND HEAT TRANSFER 140**

Includes boundary layers; hydrodynamics; fluidics; mass transfer and ablation cooling.

For related information see also *02 Aerodynamics* and *77 Thermodynamics and Statistical Physics*.

## **35 INSTRUMENTATION AND PHOTOGRAPHY 168**

Includes remote sensors; measuring instruments and gages; detectors; cameras and photographic supplies; and holography.

For aerial photography see *43 Earth Resources and Remote Sensing*. For related information see also *06 Aircraft Instrumentation* and *19 Spacecraft Instrumentation*.

## **36 LASERS AND MASERS 177**

Includes parametric amplifiers.

For related information see also *76 Solid-State Physics*.

## **37 MECHANICAL ENGINEERING 177**

Includes auxiliary systems (nonpower); machine elements and processes; and mechanical equipment.

## **38 QUALITY ASSURANCE AND RELIABILITY 187**

Includes product sampling procedures and techniques; and quality control.

## **39 STRUCTURAL MECHANICS 190**

Includes structural element design and weight analysis; fatigue; and thermal stress.

For applications see *05 Aircraft Design, Testing and Performance* and *18 Spacecraft Design, Testing and Performance*.

## GEOSCIENCES

Includes geosciences (general); earth resources and remote sensing; energy production and conversion; environment pollution; geophysics; meteorology and climatology; and oceanography.

For related information see also *Space Sciences*.

### 42 GEOSCIENCES (GENERAL) N.A.

### 43 EARTH RESOURCES AND REMOTE SENSING 206

Includes remote sensing of earth resources by aircraft and spacecraft; photogrammetry; and aerial photography.

For instrumentation see *35 Instrumentation and Photography*.

### 44 ENERGY PRODUCTION AND CONVERSION 207

Includes specific energy conversion systems, e.g., fuel cells; global sources of energy; geophysical conversion; and windpower.

For related information see also *07 Aircraft Propulsion and Power*, *20 Spacecraft Propulsion and Power*, and *28 Propellants and Fuels*.

### 45 ENVIRONMENT POLLUTION N.A.

Includes atmospheric, noise, thermal, and water pollution.

### 46 GEOPHYSICS 214

Includes aeronomy; upper and lower atmosphere studies; ionospheric and magnetospheric physics; and geomagnetism.

For space radiation see *93 Space Radiation*.

### 47 METEOROLOGY AND CLIMATOLOGY N.A.

Includes weather forecasting and modification.

### 48 OCEANOGRAPHY N.A.

Includes biological, dynamic, and physical oceanography; and marine resources.

For related information see also *43 Earth Resources and Remote Sensing*.

## LIFE SCIENCES

Includes life sciences (general); aerospace medicine; behavioral sciences; man/system technology and life support; and space biology.

### 51 LIFE SCIENCES (GENERAL) N.A.

### 52 AEROSPACE MEDICINE N.A.

Includes physiological factors; biological effects of radiation; and effects of weightlessness on man and animals.

### 53 BEHAVIORAL SCIENCES N.A.

Includes psychological factors; individual and group behavior; crew training and evaluation; and psychiatric research.

### 54 MAN/SYSTEM TECHNOLOGY AND LIFE SUPPORT 215

Includes human engineering; biotechnology; and space suits and protective clothing.

For related information see also *16 Space Transportation*.

### 55 SPACE BIOLOGY N.A.

Includes exobiology; planetary biology; and extraterrestrial life.

## MATHEMATICAL AND COMPUTER SCIENCES

Includes mathematical and computer sciences (general); computer operations and hardware; computer programming and software; computer systems; cybernetics; numerical analysis; statistics and probability; systems analysis; and theoretical mathematics.

### 59 MATHEMATICAL AND COMPUTER SCIENCES (GENERAL) 216

### 60 COMPUTER OPERATIONS AND HARDWARE 216

Includes hardware for computer graphics, firmware, and data processing.

For components see *33 Electronics and Electrical Engineering*.

### 61 COMPUTER PROGRAMMING AND SOFTWARE 216

Includes computer programs, routines, algorithms, and specific applications, e.g., CAD/CAM.

### 62 COMPUTER SYSTEMS 218

Includes computer networks and special application computer systems.

### 63 CYBERNETICS 219

Includes feedback and control theory, artificial intelligence, robotics and expert systems.

For related information see also *54 Man/System Technology and Life Support*.

### 64 NUMERICAL ANALYSIS 221

Includes iteration, difference equations, and numerical approximation.

### 65 STATISTICS AND PROBABILITY 223

Includes data sampling and smoothing; Monte Carlo method; and stochastic processes.

### 66 SYSTEMS ANALYSIS 223

Includes mathematical modeling; network analysis; and operations research.

### 67 THEORETICAL MATHEMATICS N.A.

Includes topology and number theory.

## PHYSICS

Includes physics (general); acoustics; atomic and molecular physics; nuclear and high-energy physics; optics; plasma physics; solid-state physics; and thermodynamics and statistical physics.

For related information see also *Engineering*.

### 70 PHYSICS (GENERAL) 224

For precision time and time interval (PTTI) see *35 Instrumentation and Photography*; for geophysics, astrophysics or solar physics see *46 Geophysics*, *90 Astrophysics*, or *92 Solar Physics*.

**71 ACOUSTICS** **224**  
Includes sound generation, transmission, and attenuation.  
For noise pollution see *45 Environment Pollution*.

**72 ATOMIC AND MOLECULAR PHYSICS** **229**  
Includes atomic structure, electron properties, and molecular spectra.

**73 NUCLEAR AND HIGH-ENERGY PHYSICS** **230**  
Includes elementary and nuclear particles; and reactor theory.  
For space radiation see *93 Space Radiation*.

**74 OPTICS** **230**  
Includes light phenomena and optical devices.  
For lasers see *36 Lasers and Masers*.

**75 PLASMA PHYSICS** **231**  
Includes magnetohydrodynamics and plasma fusion.  
For ionospheric plasmas see *46 Geophysics*. For space plasmas see *90 Astrophysics*.

**76 SOLID-STATE PHYSICS** **234**  
Includes superconductivity.  
For related information see also *33 Electronics and Electrical Engineering* and *36 Lasers and Masers*.

**77 THERMODYNAMICS AND STATISTICAL PHYSICS** **237**  
Includes quantum mechanics; theoretical physics; and Bose and Fermi statistics.  
For related information see also *25 Inorganic and Physical Chemistry* and *34 Fluid Mechanics and Heat Transfer*.

## **SOCIAL SCIENCES**

Includes social sciences (general); administration and management; documentation and information science; economics and cost analysis; law, political science, and space policy; and urban technology and transportation.

**80 SOCIAL SCIENCES (GENERAL)** **238**  
Includes educational matters.

**81 ADMINISTRATION AND MANAGEMENT** **238**  
Includes management planning and research.

**82 DOCUMENTATION AND INFORMATION SCIENCE** **238**  
Includes information management; information storage and retrieval technology; technical writing; graphic arts; and micrography.  
For computer documentation see *61 Computer Programming and Software*.

**83 ECONOMICS AND COST ANALYSIS** **N.A.**  
Includes cost effectiveness studies.

**84 LAW, POLITICAL SCIENCE AND SPACE POLICY** **N.A.**  
Includes NASA appropriation hearings; aviation law; space law and policy; international law; international cooperation; and patent policy.

**85 URBAN TECHNOLOGY AND TRANSPORTATION** **238**  
Includes applications of space technology to urban problems; technology transfer; technology assessment; and surface and mass transportation.  
For related information see *03 Air Transportation and Safety*, *16 Space Transportation*, and *44 Energy Production and Conversion*.

## **SPACE SCIENCES**

Includes space sciences (general); astronomy; astrophysics; lunar and planetary exploration; solar physics; and space radiation.  
For related information see also *Geosciences*.

**88 SPACE SCIENCES (GENERAL)** **240**

**89 ASTRONOMY** **N.A.**  
Includes radio, gamma-ray, and infrared astronomy; and astrometry.

**90 ASTROPHYSICS** **240**  
Includes cosmology; celestial mechanics; space plasmas; and interstellar and interplanetary gases and dust.  
For related information see also *75 Plasma Physics*.

**91 LUNAR AND PLANETARY EXPLORATION** **241**  
Includes planetology; and manned and unmanned flights.  
For spacecraft design or space stations see *18 Spacecraft Design, Testing and Performance*.

**92 SOLAR PHYSICS** **242**  
Includes solar activity, solar flares, solar radiation and sunspots.  
For related information see *93 Space Radiation*.

**93 SPACE RADIATION** **242**  
Includes cosmic radiation; and inner and outer earth's radiation belts.  
For biological effects of radiation see *52 Aerospace Medicine*. For theory see *73 Nuclear and High-Energy Physics*.

## **GENERAL**

Includes aeronautical, astronautical, and space science related histories, biographies, and pertinent reports too broad for categorization; histories or broad overviews of NASA programs.

**99 GENERAL** **N.A.**

Note: N.A. means that no abstracts were assigned to this category for this issue.

<b>SUBJECT INDEX</b> .....	<b>A-1</b>
<b>PERSONAL AUTHOR INDEX</b> .....	<b>B-1</b>
<b>CORPORATE SOURCE INDEX</b> .....	<b>C-1</b>
<b>CONTRACT NUMBER INDEX</b> .....	<b>D-1</b>
<b>REPORT/ACCESSION NUMBER INDEX</b> .....	<b>E-1</b>

---

# Bibliography of Lewis Research Center Technical Publications Announced in 1989

---

01

## AERONAUTICS (GENERAL)

**N89-22569\*#** National Aeronautics and Space Administration. Lewis Research Center, Cleveland, OH.

**NASA'S PROGRAM ON ICING RESEARCH AND TECHNOLOGY**  
JOHN J. REINMANN, ROBERT J. SHAW, and RICHARD J. RANAUDO 1989 55 p Presented at the Symposium on Flight in Adverse Environmental Conditions, Gol, Norway, 8-12 May 1989; sponsored by AGARD (NASA-TM-101989; E-4692; NAS 1.15:101989) Avail: NTIS HC A04/MF A01 CSCL 01/2

NASA's program in aircraft icing research and technology is reviewed. The program relies heavily on computer codes and modern applied physics technology in seeking icing solutions on a finer scale than those offered in earlier programs. Three major goals of this program are to offer new approaches to ice protection, to improve our ability to model the response of an aircraft to an icing encounter, and to provide improved techniques and facilities for ground and flight testing. This paper reviews the following program elements: (1) new approaches to ice protection; (2) numerical codes for deicer analysis; (3) measurement and prediction of ice accretion and its effect on aircraft and aircraft components; (4) special wind tunnel test techniques for rotorcraft icing; (5) improvements of icing wind tunnels and research aircraft; (6) ground de-icing fluids used in winter operation; (7) fundamental studies in icing; and (8) droplet sizing instruments for icing clouds.

Author

02

## AERODYNAMICS

Includes aerodynamics of bodies, combinations, wings, rotors, and control surfaces; and internal flow in ducts and turbomachinery.

**A89-11110\*#** Cornell Univ., Ithaca, NY.

**DIAGONAL IMPLICIT MULTIGRID ALGORITHM FOR THE EULER EQUATIONS**

DAVID A. CAUGHEY (Cornell University, Ithaca, NY) AIAA Journal (ISSN 0001-1452), vol. 26, July 1988, p. 841-851. Previously cited in issue 08, p. 1037, Accession no. A87-22578. refs (Contract NAG3-645; NAG2-373) Copyright

**A89-12557\*#** Dayton Univ., OH.

**NAVIER-STOKES SOLUTION TO THE FLOWFIELD OVER ICE ACCRETION SHAPES**

J. N. SCOTT, W. L. HANKEY, F. J. GIESSLER, and T. P. GIELDA (Dayton, University, OH) Journal of Aircraft (ISSN 0021-8669), vol. 25, Aug. 1988, p. 710-716. Previously cited in issue 08, p.

1033, Accession no. A87-22414. refs  
(Contract NAG3-665)  
Copyright

**A89-14976\*#** National Aeronautics and Space Administration. Lewis Research Center, Cleveland, OH.

**INVESTIGATION OF OSCILLATING CASCADE AERODYNAMICS BY AN EXPERIMENTAL INFLUENCE COEFFICIENT TECHNIQUE**

DANIEL H. BUFFUM (NASA, Lewis Research Center, Cleveland, OH) and SANFORD FLEETER (Purdue University, West Lafayette, IN) AIAA, ASME, SAE, and ASEE, Joint Propulsion Conference, 24th, Boston, MA, July 11-13, 1988. 12 p. Previously announced in STAR as N88-28041. refs  
(AIAA PAPER 88-2815) Copyright

Fundamental experiments are performed in the NASA Lewis Transonic Oscillating Cascade Facility to investigate the torsion mode unsteady aerodynamics of a biconvex airfoil cascade at realistic values of the reduced frequency for all interblade phase angles at a specified mean flow condition. In particular, an unsteady aerodynamic influence coefficient technique is developed and utilized in which only one airfoil in the cascade is oscillated at a time and the resulting airfoil surface unsteady pressure distribution measured on one dynamically instrumented airfoil. The unsteady aerodynamics of an equivalent cascade with all airfoils oscillating at a specified interblade phase angle are then determined through a vector summation of these data. These influence coefficient determined oscillating cascade data are correlated with data obtained in this cascade with all airfoils oscillating at several interblade phase angle values. The influence coefficients are then utilized to determine the unsteady aerodynamics of the cascade for all interblade phase angles, with these unique data subsequently correlated with predictions from a linearized unsteady cascade model.

Author

**A89-14979\*#** National Aeronautics and Space Administration. Lewis Research Center, Cleveland, OH.

**PNS CALCULATIONS FOR 3-D HYPERSONIC CORNER FLOW WITH TWO TURBULENCE MODELS**

GREGORY E. SMITH, MAY-FUN LIOU (NASA, Lewis Research Center; Sverdrup Technology, Inc., Cleveland, OH), and THOMAS J. BENSON (NASA, Lewis Research Center, Cleveland, OH) AIAA, ASME, SAE, and ASEE, Joint Propulsion Conference, 24th, Boston, MA, July 11-13, 1988. 7 p. refs  
(Contract NAS3-24105)  
(AIAA PAPER 88-2958) Copyright

A three-dimensional parabolized Navier-Stokes code has been used as a testbed to investigate two turbulence models, the McDonald Camarata and Bushnell Beckwith model, in the hypersonic regime. The Bushnell Beckwith form factor correction to the McDonald Camarata mixing length model has been extended to three-dimensional flow by use of an inverse averaging of the resultant length scale contributions from each wall. Two-dimensional calculations are compared with experiment for Mach 18 helium flow over a 4-deg wedge. Corner flow calculations have been performed at Mach 11.8 for a Reynolds number of .67 x 10 to the 6th, based on the duct half-width, and a freestream stagnation temperature of 1750-deg Rankine.

Author

## 02 AERODYNAMICS

**A89-14980\*#** National Aeronautics and Space Administration. Lewis Research Center, Cleveland, OH.

### **HIGH SPEED INLET CALCULATIONS WITH REAL GAS EFFECTS**

WILLIAM J. COIRIER (NASA, Lewis Research Center; Sverdrup Technology, Inc., Cleveland, OH) AIAA, ASME, SAE, and ASEE, Joint Propulsion Conference, 24th, Boston, MA, July 11-13, 1988. 7 p. Previously announced in STAR as N88-26336. refs (Contract NAS3-24105)

(AIAA PAPER 88-3076) Copyright

A 2-D steady-state Navier-Stokes solver has been upgraded to include the effects of frozen and equilibrium air chemistry for applications to high speed flight vehicles. To provide a computationally economical first order approximation to the high temperature physics, variable thermodynamic data is used for the chemically frozen mode to allow for a variation with temperature of the air specific heats and enthalpy. For calculations involving air in chemical equilibrium, a specially modified version of the NASA Lewis Chemical Equilibrium Code, CEC, is used to compute the chemical composition and resultant thermochemical properties. The upgraded solver is demonstrated by comparing results from calorically perfect ( $C_p = \text{constant}$ ), thermally perfect (frozen) and equilibrium air calculations for a variety of geometries, and flight Mach numbers. Author

**A89-14982\*#** National Aeronautics and Space Administration. Lewis Research Center, Cleveland, OH.

### **THREE DIMENSIONAL SIMULATION OF AN UNDEREXPANDED JET INTERACTING WITH A SUPERSONIC CROSS FLOW**

SHENG-TAO YU and JIAN-SHUN SHUEN (NASA, Lewis Research Center; Sverdrup Technology, Inc., Cleveland, OH) AIAA, ASME, SAE, and ASEE, Joint Propulsion Conference, 24th, Boston, MA, July 11-13, 1988. 12 p. refs (AIAA PAPER 88-3181) Copyright

A new three-dimensional computational fluid dynamics (CFD) code has been developed to simulate the flow fields of an underexpanded jet transversely injected into supersonic air stream inside the combustors of ramjets and scramjets. The code employs an implicit finite volume, lower-upper (LU) time marching method to solve the complete three-dimensional Navier-Stokes equations in a fully-coupled and very efficient manner. Results clearly depict the flow characteristics, including the shock structure, separated flow regions around the injector, and the wake flow in the lee of the injector. Author

**A89-15967\*#** National Aeronautics and Space Administration. Lewis Research Center, Cleveland, OH.

### **AUTOMATED DESIGN OF CONTROLLED-DIFFUSION BLADES**

J. M. SANZ (NASA, Lewis Research Center, Cleveland, OH) ASME, Transactions, Journal of Turbomachinery (ISSN 0889-504X), vol. 110, Oct. 1988, p. 540-544. Previously announced in STAR as N88-13304. refs

(ASME PAPER 88-GT-139) Copyright

A numerical automation procedure has been developed to be used in conjunction with an inverse hodograph method for the design of controlled diffusion blades. With this procedure a cascade of airfoils with a prescribed solidity, inlet Mach number, inlet air flow angle, and air flow turning can be produced automatically. The trailing edge thickness of the airfoil, an important quantity in inverse methods, is also prescribed. The automation procedure consists of a multidimensional Newton iteration in which the objective design conditions are achieved by acting on the hodograph input parameters of the underlying inverse code. The method, although more general in scope, is applied in this paper to the design of axial flow compressor blade sections, and a wide range of examples is presented. Author

**A89-16882\*** Arizona Univ., Tucson.

### **EFFECTS OF EXCITATION LEVEL ON THE STABILITY OF AN AXISYMMETRIC MIXING LAYER**

M. M. SAMET and R. A. PETERSEN (Arizona, University, Tucson) Physics of Fluids (ISSN 0031-9171), vol. 31, Nov. 1988, p.

3246-3252. refs

(Contract NAG3-460; NSF MEA-82-10876)

Copyright

The effect of various levels of excitation on the stability and development of an axisymmetric mixing layer was studied experimentally. The flow was excited axisymmetrically by a single speaker placed at the base of the plenum chamber. Measurements of mean and phase-averaged velocity profiles were made using an array of hot-wire probes. The measured profiles were compared to eigenfunctions calculated from linear, viscous stability theory. It is shown that the theoretical predictions, based on measured profiles of mean velocity, compare very well with the phase-averaged measurements, even when the local disturbance reaches levels as high as 24 percent of the jet speed. The cumulative effect of excitation on the mean flow is examined as a function of local Strouhal number as well as excitation level. Author

**A89-17940\*#** National Aeronautics and Space Administration. Lewis Research Center, Cleveland, OH.

### **EULER ANALYSIS OF A SWIRL RECOVERY VANE DESIGN FOR USE WITH AN ADVANCED SINGLE-ROTATION PROPFAN**

CHRISTOPHER J. MILLER (NASA, Lewis Research Center, Cleveland, OH) AIAA, ASME, SAE, and ASEE, Joint Propulsion Conference, 24th, Boston, MA, July 11-13, 1988. 15 p. Previously announced in STAR as N88-29771. refs (AIAA PAPER 88-3152)

Recent work has demonstrated the propulsive efficiency improvement available from single- and counter-rotation propfans as compared with current technology high bypass ratio turbofans. The concept known as swirl recovery vanes (SRV) is examined through the use of a 3-D Euler code. At high speed cruise conditions, the SRV can improve the efficiency level of a single-rotation propfan, but a concern is to have adequate hub choke margin. The SRV was designed with 2-D methods and was predicted to have hub choking at Mach 0.8 cruise. The 3-D Euler analysis properly accounts for sweep effects and 3-D relief, and predicts that at cruise the SRV will recover roughly 5 percent of the 10 percent efficiency loss due to swirl and have a good hub choke margin. Author

**A89-19918\*#** Sverdrup Technology, Inc., Middleburg Heights, OH.

### **HIGH ANGLE-OF-ATTACK HYPERSONIC AERODYNAMICS**

GARY J. HARLOFF (Sverdrup Technology, Inc., Middleburg Heights, OH) Journal of Spacecraft and Rockets (ISSN 0022-4650), vol. 25, Sept.-Oct. 1988, p. 343, 344. Abridged. Previously cited in issue 21, p. 3340, Accession no. A87-49100. (Contract NAS3-24105)

Copyright

**A89-25029\*#** Ohio State Univ., Columbus.

### **STUDIES OF TRANSITION IN BOUNDARY LAYERS**

THORWALD HERBERT and RICHARD J. BODONYI (Ohio State University, Columbus) AIAA, Aerospace Sciences Meeting, 27th, Reno, NV, Jan. 9-12, 1989. 24 p. refs (Contract AF-AFOSR-88-0186; NAG3-743; F49620-88-C-0082) (AIAA PAPER 89-0034) Copyright

Some current studies on transition in boundary layers are briefly reviewed, including work based on the asymptotic transition theory. In particular, attention is given to the appearance of transition, primary instability, transition criterion, nonparallelism and non-linearity, multistructural approach to transition, and two-dimensional nonlinear interactions. The discussion also covers secondary instability, three-dimensional interactions, Floquet theory of secondary instability, breakdown, and boundary-layer receptivity. V.L.

**A89-25180\*#** National Aeronautics and Space Administration. Lewis Research Center, Cleveland, OH.

### **AN UNCONDITIONALLY STABLE RUNGE-KUTTA METHOD FOR UNSTEADY FLOWS**



PHILIP C. E. JORGENSEN and RODRICK V. CHIMA (NASA, Lewis Research Center, Cleveland, OH) AIAA, Aerospace Sciences Meeting, 27th, Reno, NV, Jan. 9-12, 1989. 13 p. Previously announced in STAR as N88-29780. refs (AIAA PAPER 89-0205) Copyright

A quasi-three-dimensional analysis was developed for unsteady rotor-stator interaction in turbomachinery. The analysis solves the unsteady Euler or thin-layer Navier-Stokes equations in a body-fitted coordinate system. It accounts for the effects of rotation, radius change, and stream surface thickness. The Baldwin-Lomax eddy viscosity model is used for turbulent flows. The equations are integrated in time using a four-stage Runge-Kutta scheme with a constant time step. Implicit residual smoothing was employed to accelerate the solution of the time accurate computations. The scheme is described and accuracy analyses are given. Results are shown for a supersonic through-flow fan designed for NASA Lewis. The rotor:stator blade ratio was taken as 1:1. Results are also shown for the first stage of the Space Shuttle Main Engine high pressure fuel turbopump. Here the blade ratio is 2:3. Implicit residual smoothing was used to increase the time step limit of the unsmoothed scheme by a factor of six with negligible differences in the unsteady results. It is felt that the implicitly smoothed Runge-Kutta scheme is easily competitive with implicit schemes for unsteady flows while retaining the simplicity of an explicit scheme. Author

**A89-25454\*#** National Aeronautics and Space Administration. Lewis Research Center, Cleveland, OH.

#### CONTROL OF LAMINAR SEPARATION OVER AIRFOILS BY ACOUSTIC EXCITATION

K. B. M. Q. ZAMAN and D. J. MCKINZIE (NASA, Lewis Research Center, Cleveland, OH) AIAA, Aerospace Sciences Meeting, 27th, Reno, NV, Jan. 9-12, 1989. 13 p. Previously announced in STAR as N89-12552. refs (AIAA PAPER 89-0565) Copyright

The effect of acoustic excitation in reducing laminar separation over two-dimensional airfoils at low angles of attack is investigated experimentally. Airfoils of two different cross sections, each with two different chord lengths, are studied in the chord Reynolds number range of 25,000 is less than  $R_{sub c}$  is less than 100,000. While keeping the amplitude of the excitation induced velocity perturbation a constant, it is found that the most effective frequency scales as  $U$  (sup  $3/2$ ) (sub infinity). The parameter  $St/R$  (sup  $1/2$ )(sub  $c$ ), corresponding to the most effective  $f$  sub  $p$  for all the cases studied, falls in the range of 0.02 to 0.03,  $St$  being the Strouhal number based on the chord. Author

**A89-25485\*#** Georgia Inst. of Tech., Atlanta.

#### EVALUATION OF THREE TURBULENCE MODELS FOR THE PREDICTION OF STEADY AND UNSTEADY AIRLOADS

JIUNN-CHI WU, L. N. SANKAR (Georgia Institute of Technology, Atlanta), and DENNIS L. HUFF (NASA, Lewis Research Center, Cleveland, OH) AIAA, Aerospace Sciences Meeting, 27th, Reno, NV, Jan. 9-12, 1989. 11 p. Research supported by McDonnell Douglas Helicopter Co. Previously announced in STAR as N89-12555. refs (Contract NAG3-768) (AIAA PAPER 89-0609) Copyright

Two dimensional quasi-three dimensional Navier-Stokes solvers were used to predict the static and dynamic airload characteristics of airfoils. The following three turbulence models were used: the Baldwin-Lomax algebraic model, the Johnson-King ODE model for maximum turbulent shear stress, and a two equation k-e model with law-of-the-wall boundary conditions. It was found that in attached flow the three models have good agreement with experimental data. In unsteady separated flows, these models give only a fair correlation with experimental data. Author

**A89-26369\*#** National Aeronautics and Space Administration. Lewis Research Center, Cleveland, OH.

#### EXPERIMENTAL INVESTIGATION OF TRANSONIC OSCILLATING CASCADE AERODYNAMICS

DANIEL H. BUFFUM (NASA, Lewis Research Center, Cleveland,

OH) and SANFORD FLEETER (Purdue University, West Lafayette, IN) AIAA, Aerospace Sciences Meeting, 27th, Reno, NV, Jan. 9-12, 1989. 14 p. refs (AIAA PAPER 89-0321)

Fundamental experiments are performed in the NASA Lewis Transonic Oscillating Cascade Facility to investigate the subsonic and transonic aerodynamics of cascaded airfoils executing torsion mode oscillations at realistic values of reduced frequency. In particular, an unsteady aerodynamic influence coefficient technique is developed and utilized. In this technique, only one airfoil in the cascade is oscillated at a time, with the resulting airfoil surface unsteady pressure distribution measured on one dynamically-instrumented reference airfoil. The unsteady aerodynamics of an equivalent cascade with all airfoils oscillating at any specified interblade phase angle are then determined through a vector summation of these data. Author

**A89-26373\*#** National Aeronautics and Space Administration. Lewis Research Center, Cleveland, OH.

#### LASER VELOCIMETER MEASUREMENTS OF THE FLOWFIELD GENERATED BY AN ADVANCED COUNTERROTATING PROPELLER

GARY G. PODBOY and MARTIN J. KRUPAR (NASA, Lewis Research Center, Cleveland, OH) AIAA, Aerospace Sciences Meeting, 27th, Reno, NV, Jan. 9-12, 1989. 33 p. Previously announced in STAR as N89-13409. refs (AIAA PAPER 89-0434) Copyright

Results are presented of an 0.72 regime, with the advance ratio of each rotor set at 2.80. The measured data indicate only a slight influence of the potential field of each front rotor blade on the flowfield upstream of the rotor. The data measured downstream of the front rotor characterize the tip vortices, vortex sheets and potential field nonuniformities generated by the front rotor. The unsteadiness of the flow in the rotating frame of reference of the aft rotor is also illustrated. Author

**A89-28341\*#** Massachusetts Inst. of Tech., Cambridge.

#### ACTIVE SUPPRESSION OF AERODYNAMIC INSTABILITIES IN TURBOMACHINES

A. H. EPSTEIN, J. E. FLOWCS WILLIAMS, and E. M. GREITZER (MIT, Cambridge, MA) Journal of Propulsion and Power (ISSN 0748-4658), vol. 5, Mar.-Apr. 1989, p. 204-211. Previously cited in issue 22, p. 3219, Accession no. A86-45410. refs (Contract NSG-3208) Copyright

**A89-28405\*#** National Aeronautics and Space Administration. Lewis Research Center, Cleveland, OH.

#### INTERACTION OF AN OBLIQUE SHOCK WAVE WITH TURBULENT HYPERSONIC BLUNT BODY FLOWS

YOUNG J. MOON (NASA, Lewis Research Center; Sverdrup Technology, Inc., Cleveland, OH) and MAURICE HOLT (California, University, Berkeley) AIAA, Aerospace Sciences Meeting, 27th, Reno, NV, Jan. 9-12, 1989. 10 p. refs (Contract NAS3-25266; NCA2-275; NCA2-249) (AIAA PAPER 89-0272)

A shock-on-shock interaction near the cowl lip of an engine inlet is studied numerically by solving the compressible full Navier-Stokes equations. The present study focuses on Edney's type III shock interference pattern in which the turbulent free shear layer impinges on the cowl lip (modeled as a cylinder). Van Leer's flux-vector splitting upwind MUSCL scheme is used in the solver with algebraic turbulence models. Turbulent solutions of surface pressures and heat fluxes along the cowl lip are in reasonably good agreement with experiment except in the local shear layer impingement region. The present study showed some indications that higher order turbulent models may be required to improve the solution near the free shear layer impingement region. Author

**A89-28406\*#** National Aeronautics and Space Administration. Lewis Research Center, Cleveland, OH.

#### UNSTEADY EULER CASCADE ANALYSIS

JONG-SHANG LIU (NASA, Lewis Research Center, Cleveland, OH; Textron Lycoming, Stratford, CT) and PETER M. SOCKOL (NASA, Lewis Research Center, Cleveland, OH) AIAA, Aerospace Sciences Meeting, 27th, Reno, NV, Jan. 9-12, 1989. 8 p. refs (AIAA PAPER 89-0322)

The results of an investigation of the rotor-stator interaction phenomena in turbomachines are presented. Numerical study was carried out by solving the unsteady Euler equations in the blade-to-blade direction for a variety of cascade geometries. The problem of uneven rotor and stator blades is addressed by adopting the tilted time domain technique. Computed solutions are presented and discussed for a NACA 0012 type cascade and the first stage fuel turbopump of the Space Shuttle Main Engine (SSME).

Author

## **A89-28407\*# Case Western Reserve Univ., Cleveland, OH. EXPERIMENTAL AND NUMERICAL INVESTIGATION OF AN OBLIQUE SHOCK WAVE/TURBULENT BOUNDARY LAYER INTERACTION WITH CONTINUOUS SUCTION**

DRISS BENHACHMI, ISAAC GREBER (Case Western Reserve University, Cleveland, OH), and WARREN R. HINGST (NASA, Lewis Research Center, Cleveland, OH) AIAA, Aerospace Sciences Meeting, 27th, Reno, NV, Jan. 9-12, 1989. 14 p. refs (Contract NAG3-61)

(AIAA PAPER 89-0357) Copyright

An numerical and experimental investigation has been conducted into the interaction of an incident oblique shock wave with a turbulent boundary layer, for the cases of a rough plate and a porous plate with suction, at a nominal Mach number of 2.5 and flow deflection angles of 0, 4, 6, and 8 deg. Attention is given to the pitot pressure profiles, wall static pressures, and porous plate local bleed distributions measured for the two plates. Suction is found to increase the strength of the incident shock required to separate the boundary layer; for all shock strengths tested, separation is completely eliminated.

O.C.

**A89-28413\*#** National Aeronautics and Space Administration. Lewis Research Center, Cleveland, OH.

## **NUMERICAL ANALYSIS OF FLOW THROUGH OSCILLATING CASCADE SECTIONS**

DENNIS L. HUFF (NASA, Lewis Research Center, Cleveland, OH) AIAA, Aerospace Sciences Meeting, 27th, Reno, NV, Jan. 9-12, 1989. 24 p. Previously announced in STAR as N89-14220. refs (AIAA PAPER 89-0437)

The design of turbomachinery blades requires the prevention of flutter for all operating conditions. However, flow field predictions used for aeroelastic analysis are not well understood for all flow regimes. The present research focuses on numerical solutions of the Euler and Navier-Stokes equations using an ADI procedure to model two-dimensional, transonic flow through oscillating cascades. The model prescribes harmonic pitching motions for the blade sections for both zero and nonzero interblade phase angles. The code introduces the use of a deforming grid technique for convenient specification of the periodic boundary conditions. Approximate nonreflecting boundary conditions were coded for the inlet and exit boundary conditions. Sample unsteady solutions were performed for an oscillating cascade and compared to experimental data. Also, test cases were run for a flat plate cascade to compare with the unsteady, small-perturbation, subsonic analysis. The predictions for oscillating cascades with nonzero interblade phase angle cases, which were near a resonant condition, differ from the experiment and theory. The zero degree interblade phase angle cases, which were near a resonant condition, differ from the experiment and theory. Studies on reflecting versus nonreflecting inlet and exit boundary conditions show that the treatment of the boundary can have a significant effect on the first harmonic, unsteady pressure distribution for certain flow conditions. Author

**A89-28453\*#** National Aeronautics and Space Administration. Lewis Research Center, Cleveland, OH.

## **AN EXPERIMENTAL INVESTIGATION OF MULTI-ELEMENT AIRFOIL ICE ACCRETION AND RESULTING PERFORMANCE DEGRADATION**

MARK G. POTAPCZUK (NASA, Lewis Research Center, Cleveland, OH) and BRIAN M. BERKOWITZ (NASA, Lewis Research Center; Sverdrup Technology, Inc., Cleveland, OH) AIAA, Aerospace Sciences Meeting, 27th, Reno, NV, Jan. 9-12, 1989. 39 p. Previously announced in STAR as N89-15084. refs (AIAA PAPER 89-0752) Copyright

An investigation of the ice accretion pattern and performance characteristics of a multi-element airfoil was undertaken in the NASA Lewis 6- by 9-Foot Icing Research Tunnel. Several configurations of main airfoil, slat, and flaps were employed to examine the effects of ice accretion and provide further experimental information for code validation purposes. The text matrix consisted of glaze, rime, and mixed icing conditions. Airflow and icing cloud conditions were set to correspond to those typical of the operating environment anticipated for a commercial transport vehicle. Results obtained included ice profile tracings, photographs of the ice accretions, and force balance measurements obtained both during the accretion process and in a post-accretion evaluation over a range of angles of attack. The tracings and photographs indicated significant accretions on the slat leading edge, in gaps between slat or flaps and the main wing, on the flap leading-edge surfaces, and on flap lower surfaces. Force measurements indicate the possibility of severe performance degradation, especially near C sub Lmax, for both light and heavy ice accretion and performance analysis codes presently in use. The LEWICE code was used to evaluate the ice accretion shape developed during one of the rime ice tests. The actual ice shape was then evaluated, using a Navier-Stokes code, for changes in performance characteristics. These predicted results were compared to the measured results and indicate very good agreement.

Author

**A89-29098\*#** Kansas Univ. Center for Research, Inc., Lawrence.

## **LARGE AMPLITUDE ACOUSTIC EXCITATION OF SWIRLING TURBULENT JETS**

R. TAGHAVI (University of Kansas Center for Research, Inc., Lawrence), E. J. RICE (NASA, Lewis Research Center, Cleveland, OH), and S. FAROKHI (Kansas, University, Lawrence) AIAA, Shear Flow Conference, 2nd, Tempe, AZ, Mar. 13-16, 1989. 16 p. Previously announced in STAR as N89-18417. refs (AIAA PAPER 89-0970) Copyright

A swirling jet with a swirl number of  $S = 0.12$  is excited by plane acoustic waves at various Strouhal numbers ( $St = fD/U$  sub alpha). The maximum forcing amplitude of excitation was at 6.88 percent of the time-mean axial velocity at a Strouhal number of  $St = 0.39$ . The maximum time-mean tangential and axial velocities at the nozzle exit were 18 and 84 m/sec respectively. It was observed that the swirling jet was excitable by plane acoustic waves and the preferred Strouhal number based on the nozzle diameter and exit axial velocity of the jet was about 0.39. As a result of excitation at this frequency, the time-mean axial velocity decayed faster along the jet centerline, reaching about 89 percent of its unexcited value at  $x/D = 9$ . Also the half velocity radius and momentum thickness, at 7 nozzle diameters downstream, increased by 13.2 and 5.8 percent respectively, indicating more jet spread and enhanced mixing. To our knowledge, this is the first reported experimental data indicating any mixing enhancement of swirling jets by acoustic excitation.

Author

**A89-29924\*#** National Aeronautics and Space Administration. Lewis Research Center, Cleveland, OH.

## **THREE DIMENSIONAL VISCOUS ANALYSIS OF A HYPERSONIC INLET**

D. R. REDDY, G. E. SMITH, M.-F. LIOU (NASA, Lewis Research Center, Cleveland; Sverdrup Technology, Inc., Middleburg Heights, OH), and T. J. BENSON (NASA, Lewis Research Center, Cleveland, OH) AIAA, Aerospace Sciences Meeting, 27th, Reno, NV, Jan.

9-12, 1989. 8 p. Previously announced in STAR as N89-16759. refs

(AIAA PAPER 89-0004)

The flow fields in supersonic/hypersonic inlets are currently being studied at NASA Lewis Research Center using 2- and 3-D full Navier-Stokes and parabolized Navier-Stokes solvers. These tools have been used to analyze the flow through the McDonnell Douglas Option 2 inlet which has been tested at Calspan in support of the National Aerospace Plane Program. Comparisons between the computational and experimental results are presented. These comparisons lead to better overall understanding of the complex flows present in this class of inlets. The aspects of the flow field emphasized in this work are the 3-D effects, the transition from laminar to turbulent flow, and the strong nonuniformities generated within the inlet. Author

**A89-33735\*#** United Technologies Corp., Windsor Locks, CT.

#### **NEAR WAKES OF ADVANCED TURBOPROPELLERS**

D. B. HANSON (United Technologies Corp., Hamilton Standard Div., Windsor Locks, CT) and W. P. PATRICK (United Technologies Research Center, East Hartford, CT) AIAA, Aeroacoustics Conference, 12th, San Antonio, TX, Apr. 10-12, 1989. 13 p. Research supported by United Technologies Corp. refs (Contract NAS3-23720)

(AIAA PAPER 89-1095) Copyright

The flow in the wake of a model single rotation Prop-Fan rotor operating in a wind tunnel was traversed with a hot-wire anemometer system designed to determine the 3 periodic velocity components. Special data acquisition and data reduction methods were required to deal with the high data frequency, narrow wakes, and large fluctuating air angles in the tip vortex region. The model tip helical Mach number was 1.17, simulating the cruise condition. Although the flow field is complex, flow features such as viscous velocity defects, vortex sheets, tip vortices, and propagating acoustic pulses are clearly identified with the aid of a simple analytical wake theory. Author

**A89-36912\*#** National Aeronautics and Space Administration. Lewis Research Center, Cleveland, OH.

#### **EXPLICIT RUNGE-KUTTA METHOD FOR UNSTEADY ROTOR/STATOR INTERACTION**

PHILIP C. E. JORGENSEN and RODRICK C. CHIMA (NASA, Lewis Research Center, Cleveland, OH) AIAA Journal (ISSN 0001-1452), vol. 27, June 1989, p. 743-749. Previously cited in issue 10, p. 1477, Accession no. A88-27715. refs Copyright

**A89-39189\*#** Flow Research, Inc., Kent, WA.

#### **OPTIMIZING ADVANCED PROPELLER DESIGNS BY SIMULTANEOUSLY UPDATING FLOW VARIABLES AND DESIGN PARAMETERS**

MAGDI H. RIZK (Flow Research, Inc., Kent, WA) Journal of Aircraft (ISSN 0021-8669), vol. 26, June 1989, p. 515-522. Previously cited in issue 16, p. 2593, Accession no. A88-40718. refs (Contract NAS3-24855) Copyright

**A89-40905\*#** California State Univ., Long Beach.

#### **CALCULATION OF FLOW OVER ICED AIRFOILS**

TUNCER CEBECI (California State University, Long Beach) AIAA Journal (ISSN 0001-1452), vol. 27, July 1989, p. 853-861. Previously cited in issue 07, p. 927, Accession no. A88-22078. refs (Contract NAG3-601) Copyright

**A89-41794\*#** Duke Univ., Durham, NC.

#### **ON THE ROLE OF ARTIFICIAL VISCOSITY IN NAVIER-STOKES SOLVERS**

APARAJIT J. MAHAJAN, EARL H. DOWELL, and DONALD B. BLISS (Duke University, Durham, NC) IN: AIAA Computational Fluid Dynamics Conference, 9th, Buffalo, NY, June 13-15, 1989, Technical Papers. Washington, DC, American Institute of

Aeronautics and Astronautics, 1989, p. 197-202. refs (Contract NAG3-724)

(AIAA PAPER 89-1947) Copyright

A method is proposed to determine directly the amount of artificial viscosity needed for stability using an eigenvalue analysis for a finite difference representation of the Navier-Stokes equations. The stability and growth of small perturbations about a steady flow over the airfoils are analyzed for various amounts of artificial viscosity. The eigenvalues were determined for a small perturbation about a steady inviscid flow over a NACA 0012 airfoil at a Mach number of 0.8 and angle of attack of 0 degrees. The movement of the eigenvalue constellation with respect to the amount of artificial viscosity is studied. The stability boundaries as a function of the amount of artificial viscosity from both the eigenvalue analysis and the time marching scheme are also presented. This procedure not only allows for determining the effect of varying amounts of artificial viscosity, but also for the effects of different forms of terms for artificial viscosity. Author

**A89-41814\*#** Toledo Univ., OH.

#### **FLOW OF RAREFIED GASES OVER TWO-DIMENSIONAL BODIES**

DUEN-REN JENG, KENNETH J. DE WITT, THEO G. KEITH, JR. (Toledo, University, OH), and CHAN-HONG CHUNG IN: AIAA Computational Fluid Dynamics Conference, 9th, Buffalo, NY, June 13-15, 1989, Technical Papers. Washington, DC, American Institute of Aeronautics and Astronautics, 1989, p. 389-399. refs (Contract NAG3-577)

(AIAA PAPER 89-1970) Copyright

A kinetic-theory analysis is made of the flow of rarefied gases over two-dimensional bodies of arbitrary curvature. The Boltzmann equation simplified by a model collision integral is written in an arbitrary orthogonal curvilinear coordinate system, and solved by means of finite-difference approximation with the discrete ordinate method. A numerical code is developed which can be applied to any two-dimensional submerged body of arbitrary curvature for the flow regimes from free-molecular to slip at transonic Mach numbers. Predictions are made for the case of a right circular cylinder. Author

**A89-41823\*#** National Aeronautics and Space Administration. Lewis Research Center, Cleveland, OH.

#### **CONSERVATIVE TREATMENT OF BOUNDARY INTERFACES FOR OVERLAID GRIDS AND MULTI-LEVEL GRID ADAPTATIONS**

YOUNG J. MOON (NASA, Lewis Research Center; Sverdrup Technology, Inc., Cleveland, OH) and MENG-SING LIOU (NASA, Lewis Research Center, Cleveland, OH) IN: AIAA Computational Fluid Dynamics Conference, 9th, Buffalo, NY, June 13-15, 1989, Technical Papers. Washington, DC, American Institute of Aeronautics and Astronautics, 1989, p. 480-494. refs (Contract NAS3-25266) (AIAA PAPER 89-1980)

Conservative algorithms for boundary interfaces of overlaid grids are presented. The basic method is zeroth order, and is extended to a higher order method using interpolation and subcell decomposition. The present method, strictly based on a conservative constraint, is tested with overlaid grids for various applications of unsteady and steady supersonic inviscid flows with strong shock waves. The algorithm is also applied to a multi-level grid adaptation in which the next level finer grid is overlaid on the coarse base grid with an arbitrary orientation. Author

**A89-41827\*#** National Aeronautics and Space Administration. Lewis Research Center, Cleveland, OH.

#### **A SIMPLE ALGEBRAIC GRID ADAPTATION SCHEME WITH APPLICATIONS TO TWO- AND THREE-DIMENSIONAL FLOW PROBLEMS**

ANDREW T. HSU (NASA, Lewis Research Center; Sverdrup Technology, Inc., Cleveland, OH) and JOHN K. LYTLE (NASA, Lewis Research Center, Cleveland, OH) IN: AIAA Computational Fluid Dynamics Conference, 9th, Buffalo, NY, June 13-15, 1989, Technical Papers. Washington, DC, American Institute of

## 02 AERODYNAMICS

Aeronautics and Astronautics, 1989, p. 525-532. refs  
(Contract NAS3-25266)  
(AIAA PAPER 89-1984)

An algebraic adaptive grid scheme based on the concept of arc equidistribution is presented which provides high flowfield resolution when applied to two-dimensional and three-dimensional flow problems. The present scheme locally adjusts the grid density using gradients of selected flow variables from either finite difference or finite volume calculations, and it can specify user-prescribed grid stretching such that control of the grid spacing can be maintained in areas of known flowfield behavior. A robust and efficient grid smoothing technique has been incorporated into the adaptive grid routine. R.R.

**A89-41837\*#** National Aeronautics and Space Administration. Lewis Research Center, Cleveland, OH.

### **A TIME ACCURATE FINITE VOLUME HIGH RESOLUTION SCHEME FOR THREE DIMENSIONAL NAVIER-STOKES EQUATIONS**

MENG-SING LIOU (NASA, Lewis Research Center, Cleveland, OH) and ANDREW T. HSU (NASA, Lewis Research Center; Sverdrup Technology, Inc., Cleveland, OH) IN: AIAA Computational Fluid Dynamics Conference, 9th, Buffalo, NY, June 13-15, 1989, Technical Papers. Washington, DC, American Institute of Aeronautics and Astronautics, 1989, p. 622-633. refs  
(AIAA PAPER 89-1994)

A time accurate, three-dimensional, finite volume, high resolution scheme for solving the compressible full Navier-Stokes equations is presented. The present derivation is based on the upwind split formulas, specifically with the application of Roe's (1981) flux difference splitting. A high-order accurate (up to the third order) upwind interpolation formula for the inviscid terms is derived to account for nonuniform meshes. For the viscous terms, discretizations consistent with the finite volume concept are described. A variant of second-order time accurate method is proposed that utilizes identical procedures in both the predictor and corrector steps. Avoiding the definition of midpoint gives a consistent and easy procedure, in the framework of finite volume discretization, for treating viscous transport terms in the curvilinear coordinates. For the boundary cells, a new treatment is introduced that not only avoids the use of 'ghost cells' and the associated problems, but also satisfies the tangency conditions exactly and allows easy definition of viscous transport terms at the first interface next to the boundary cells. Numerical tests of steady and unsteady high speed flows show that the present scheme gives accurate solutions. Author

**A89-42036\*#** Ohio State Univ., Columbus.

### **AN EXPERIMENTAL STUDY OF A REATTACHING SUPERSONIC SHEAR LAYER**

M. SAMIMY (Ohio State University, Columbus) and B. A./K. ABU-HIJLEH AIAA, Fluid Dynamics, Plasma Dynamics and Lasers Conference, 20th, Buffalo, NY, June 12-14, 1989. 6 p. refs  
(Contract NAG3-764; N00014-87-K-0168)  
(AIAA PAPER 89-1801) Copyright

A Mach 1.83 fully developed turbulent boundary layer was separated at a 25.4 mm backward step and formed a free shear layer. The incoming boundary layer thickness, momentum thickness, and Reynolds number were approximately 8 mm, 0.5 mm, and 52x10 to the 6th/m, respectively. A two-component coincident LDV system was used to take velocity measurements of the incoming boundary layer, the free shear layer, and the reattached shear layer. The results confirmed the existence of organized structures in both the free and the reattached shear layer which was reported earlier based on the authors dynamic pressure measurements and Schlieren photographs. Author

### **A89-45428\* Mississippi State Univ., Mississippi State. TRANSONIC FLOW SOLUTIONS ON GENERAL 3D REGIONS USING COMPOSITE-BLOCK GRIDS**

JOE F. THOMPSON and DAVID L. WHITFIELD (Mississippi State University, Mississippi State) IN: International Conference on Numerical Methods in Fluid Dynamics, 11th, Williamsburg, VA, June

27-July 1, 1988, Proceedings. Berlin and New York, Springer-Verlag, 1989, p. 568-572. Research supported by USAF. refs  
(Contract NAG3-767)

Copyright

The construction of computational fluid dynamics (CFD) codes for complicated regions is greatly simplified by a composite-block grid structure since, with the use of a surrounding layer of points on each block, a flow code is then only required basically to operate on rectangular computational regions. The necessary correspondence of points on the surrounding layers (image points) with interior points (object points) is set up by the grid code and made available to the CFD solution code. Author

**A89-45437\*** National Aeronautics and Space Administration. Lewis Research Center, Cleveland, OH.

### **A NATURAL LOW-FREQUENCY OSCILLATION OF THE FLOW OVER AN AIRFOIL NEAR STALLING CONDITIONS**

K. B. M. Q. ZAMAN, D. J. MCKINZIE (NASA, Lewis Research Center, Cleveland, OH), and C. L. RUMSEY (NASA, Langley Research Center, Hampton, VA) Journal of Fluid Mechanics (ISSN 0022-1120), vol. 202, May 1989, p. 403-442. refs  
Copyright

An experimental and computational study of the low-frequency oscillation observed in the flow over an airfoil at the onset of static stall is presented. Wind-tunnel results obtained with two-dimensional airfoil models show that this phenomena takes place only with a transitional state of the separating boundary layer. It is noted that the flowfield does not involve a Karman vortex street. The experimental results agree well with the results of a two-dimensional Navier-Stokes code. The present study demonstrates that the low-frequency oscillations produce intense flow fluctuations which impart much larger unsteady forces to the airfoil than experienced by bluff-body shedding and which may represent the primary aerodynamics of stall flutter of blades and wings. R.R.

**A89-45468\*** National Aeronautics and Space Administration. Lewis Research Center, Cleveland, OH.

### **A NEWTON/UPWIND METHOD AND NUMERICAL STUDY OF SHOCK WAVE/BOUNDARY LAYER INTERACTIONS**

MENG-SING LIOU (NASA, Lewis Research Center, Cleveland, OH) International Journal for Numerical Methods in Fluids (ISSN 0271-2091), vol. 9, July 1989, p. 747-761. refs  
Copyright

The objective of the paper is two-fold. First, an upwind/central differencing method for solving the steady Navier-Stokes equations is described. The symmetric line relation method is used to solve the resulting algebraic system to achieve high computational efficiency. The grid spacings used in the calculations are determined from the triple-deck theory, in terms of Mach and Reynolds numbers and other flow parameters. Thus the accuracy of the numerical solutions is improved by comparing them with experimental, analytical, and other computational results. Secondly, the shock wave/boundary layer interactions are studied numerically, with special attention given to the flow separation. The concept of free interaction is confirmed. Although the separated region varies with Mach and Reynolds numbers, it is found that the transverse velocity component behind the incident shock, which has not been identified heretofore, is also an important parameter. A small change of this quantity is sufficient to eliminate the flow separation entirely. Author

**A89-46769\*#** National Aeronautics and Space Administration. Lewis Research Center, Cleveland, OH.

### **MACH 5 INLET CFD AND EXPERIMENTAL RESULTS**

LOIS J. WEIR (NASA, Lewis Research Center, Cleveland, OH), D. R. REDDY, and GEORGE D. RUPP (NASA, Lewis Research Center; Sverdrup Technology, Inc., Cleveland, OH) AIAA, ASME, SAE, and ASEE, Joint Propulsion Conference, 25th, Monterey, CA, July 10-13, 1989. 15 p. refs  
(AIAA PAPER 89-2355) Copyright

An experimental research program was conducted in the NASA Lewis Research Center 10 ft. by 10 ft. supersonic wind tunnel.

The two-dimensional inlet model was designed to study the Mach 3.0 to 5.0 speed range for an 'over-under' turbojet plus ramjet propulsion system. The model was extensively instrumented to provide both analytical code validation data as well as inlet performance information. Support studies for the program include flow field predictions with both three-dimensional parabolized Navier-Stokes (PNS) and three-dimensional full Navier-Stokes (FNS) analytical codes. Analytical predictions and experimental results are compared. Author

**A89-46771\*** National Aeronautics and Space Administration. Lewis Research Center, Cleveland, OH.

**RECTANGULAR NOZZLE PLUME VELOCITY MODELING FOR USE IN JET NOISE PREDICTION**

U. H. VON GLAHN (NASA, Lewis Research Center, Cleveland, OH) AIAA, ASME, SAE, and ASEE, Joint Propulsion Conference, 25th, Monterey, CA, July 10-13, 1989. 21 p. Previously announced in STAR as N89-22577. refs (AIAA PAPER 89-2357) Copyright

A modeling technique for predicting the axial and transverse velocity characteristics of rectangular nozzle plumes is developed. In this technique, modeling of the plume cross section is initiated at the nozzle exit plane. The technique is demonstrated for the plume issuing from a rectangular nozzle having an aspect ratio of 6.0 and discharging into quiescent air. Application of the present procedures to a nozzle discharging into a moving airstream (flight effect) are then demonstrated. The effects of plume shear layer structure modification on the velocity flowfield are discussed and modeling procedures are illustrated by example. Author

**A89-46847\*** Ohio State Univ., Columbus.

**COMPRESSIBILITY AND SHOCK WAVE INTERACTION EFFECTS ON FREE SHEAR LAYERS**

M. SAMIMY (Ohio State University, Columbus), D. E. ERWIN, and G. S. ELLIOTT AIAA, ASME, SAE, and ASEE, Joint Propulsion Conference, 25th, Monterey, CA, July 10-13, 1989. 13 p. refs (Contract N00014-87-K-0169; NAG3-764) (AIAA PAPER 89-2460) Copyright

Two compressible free shear layers with convective Mach numbers of .51 and .86 were studied as baseline configurations to investigate the effects of compressibility on the turbulence characteristics. These shear layers were then disturbed by the placement of an obstruction in the shear layer in an attempt to enhance the shear layer growth rate. These models produced a curved shock in the supersonic side of the shear layer. The results indicate a significant reduction in turbulence levels with increased compressibility. However, there are not any significant changes due to the bow shock interaction with the shear layer. Author

**A89-47026\*** National Aeronautics and Space Administration. Lewis Research Center, Cleveland, OH.

**LARGE SCALE ADVANCED PROPELLER BLADE PRESSURE DISTRIBUTIONS - PREDICTION AND DATA**

M. NALLASAMY, O. YAMAMOTO, S. WARSJ (NASA, Lewis Research Center; Sverdrup Technology, Inc., Cleveland, OH), and L. J. BOBER (NASA, Lewis Research Center, Cleveland, OH) AIAA, ASME, SAE, and ASEE, Joint Propulsion Conference, 25th, Monterey, CA, July 10-13, 1989. 22 p. refs (AIAA PAPER 89-2696)

Two Euler analysis techniques, finite difference and finite volume, are employed to predict the blade surface pressure distributions of a large scale advanced propeller. The predicted pressure distributions are compared with wind tunnel data. Both techniques produced blade pressure distributions which are in fairly good agreement with the data over the range of test Mach numbers of 0.2 to 0.78. However, the numerical simulations fail to predict correctly the measured pressure distributions for the low Mach number, high power case which seem to have a leading edge vortex. A discussion of the compressibility effects is also presented. Author

**A89-47156\*** Toledo Univ., OH.

**RAREFIED GAS FLOW THROUGH TWO-DIMENSIONAL NOZZLES**

KENNETH J. DE WITT, DUEN-REN JENG, THEO G. KEITH, JR. (Toledo, University, OH), and CHAN-HONG CHUNG AIAA, ASME, SAE, and ASEE, Joint Propulsion Conference, 25th, Monterey, CA, July 10-13, 1989. 12 p. refs (Contract NAG3-577)

(AIAA PAPER 89-2893) Copyright

A kinetic theory analysis is made of the flow of a rarefied gas from one reservoir to another through two-dimensional nozzles with arbitrary curvature. The Boltzmann equation simplified by a model collision integral is solved by means of finite-difference approximations with the discrete ordinate method. The physical space is transformed by a general grid generation technique and the velocity space is transformed to a polar coordinate system. A numerical code is developed which can be applied to any two-dimensional passage of complicated geometry for the flow regimes from free-molecular to slip. Numerical values of flow quantities can be calculated for the entire physical space including both inside the nozzle and in the outside plume. Predictions are made for the case of parallel slots and compared with existing literature data. Also, results for the cases of convergent or divergent slots and two-dimensional nozzles with arbitrary curvature at arbitrary knudsen number are presented. Author

**A89-47187\*** National Aeronautics and Space Administration. Lewis Research Center, Cleveland, OH.

**AVERAGE-PASSAGE SIMULATION OF COUNTER-ROTATING PROPFAN PROPULSION SYSTEMS AS APPLIED TO CRUISE MISSILES**

RICHARD A. MULAC (NASA, Lewis Research Center; Sverdrup Technology, Inc., Cleveland, OH), JON C. SCHNEIDER (McDonnell Douglas Astronautics Co., Saint Louis, MO), and JOHN J. ADAMCZYK (NASA, Lewis Research Center, Cleveland, OH) AIAA, ASME, SAE, and ASEE, Joint Propulsion Conference, 25th, Monterey, CA, July 10-13, 1989. 11 p. Previously announced in STAR as N89-23416. refs (AIAA PAPER 89-2943) Copyright

Counter-rotating propfan (CRP) propulsion technologies are currently being evaluated as cruise missile propulsion systems. The aerodynamic integration concerns associated with this application are being addressed through the computational modeling of the missile body-propfan flowfield interactions. The work described in this paper consists of a detailed analysis of the aerodynamic interactions between the control surfaces and the propfan blades through the solution of the average-passage equation system. Two baseline configurations were studied, the control fins mounted forward of the counter-rotating propeller and the control fins mounted aft of the counter-rotating propeller. In both cases, control fin-propfan separation distance and control fin deflection angle were varied. Author

**A89-48955\*** National Aeronautics and Space Administration. Lewis Research Center, Cleveland, OH.

**NUMERICAL SOLUTION OF PERIODIC VORTICAL FLOWS ABOUT A THIN AIRFOIL**

JAMES R. SCOTT (NASA, Lewis Research Center, Cleveland, OH) and HAFIZ M. ATASSI (Notre Dame, University, IN) AIAA, Thermophysics Conference, 24th, Buffalo, NY, June 12-14, 1989. 11 p. Previously announced in STAR as N89-23413. refs (Contract NAG3-732)

(AIAA PAPER 89-1691) Copyright

A numerical method is developed for computing periodic, three-dimensional, vortical flows around isolated airfoils. The unsteady velocity is split into a vortical component which is a known function of the upstream flow conditions and the Lagrangian coordinates of the mean flow, and an irrotational field whose potential satisfies a nonconstant-coefficient, inhomogeneous, convective wave equation. Solutions for thin airfoils at zero degrees incidence to the mean flow are presented in this paper. Using an elliptic coordinate transformation, the computational domain is transformed into a rectangle. The Sommerfeld radiation condition

## 02 AERODYNAMICS

is applied to the unsteady pressure on the grid line corresponding to the far field boundary. The results are compared with a Possion solver, and it is shown that for maximum accuracy the grid should depend on both the Mach number and reduced frequency. Finally, in order to assess the range of validity of the classical thin airfoil approximation, results for airfoils with zero thickness are compared with results for airfoils with small thickness. Author

**A89-50062\*#** Purdue Univ., West Lafayette, IN.

### **AERODYNAMIC INTERACTION BETWEEN PROPELLERS AND WINGS**

DAVE P. WITKOWSKI, ALEX K. H. LEE, and JOHN P. SULLIVAN (Purdue University, West Lafayette, IN) Journal of Aircraft (ISSN 0021-8669), vol. 26, Sept. 1989, p. 829-836. Previously cited in issue 07, p. 940, Accession no. A88-22495. refs (Contract NSG-3134) Copyright

**A89-50808\*#** National Aeronautics and Space Administration. Lewis Research Center, Cleveland, OH.

### **LOW-SPEED WIND TUNNEL PERFORMANCE OF HIGH-SPEED COUNTERROTATION PROPELLERS AT ANGLE-OF-ATTACK**

CHRISTOPHER E. HUGHES (NASA, Lewis Research Center, Cleveland, OH) and JOHN A. GAZZANIGA (NASA, Lewis Research Center; Sverdrup Technology, Inc., Cleveland, OH) AIAA, ASME, SAE, and ASEE, Joint Propulsion Conference, 25th, Monterey, CA, July 10-12, 1989. 46 p. Previously announced in STAR as N89-25121. refs (AIAA PAPER 89-2583) Copyright

The low-speed aerodynamic performance characteristics of two advanced counterrotation pusher-propeller configurations with cruise design Mach numbers of 0.72 were investigated in the NASA Lewis 9- by 15-Foot Low-Speed Wind Tunnel. The tests were conducted at Mach number 0.20, which is representative of the aircraft take-off/landing flight regime. The investigation determined the effect of nonuniform inflow on the propeller performance characteristics for several blade angle settings and a range of rotational speeds. The inflow was varied by yawing the propeller mode to angle-of-attack by as much as plus or minus 16 degrees and by installing on the counterrotation propeller test rig near the propeller rotors a model simulator of an aircraft engine support pylon and fuselage. The results of the investigation indicated that the low-speed performance of the counterrotation propeller configurations near the take-off target operating points were reasonable and were fairly insensitive to changes in model angle-of-attack without the aircraft pylon/fuselage simulators installed on the propeller test rig. When the aircraft pylon/fuselage simulators were installed, small changes in propeller performance were seen at zero angle-of-attack, but fairly large changes in total power coefficient and very large changes of aft-to-forward-rotor torque ratio were produced when the propeller model was taken to angle-of-attack. The propeller net efficiency, though, was fairly insensitive to any changes in the propeller flowfield conditions near the take-off target operating points. Author

**A89-50810\*#** National Aeronautics and Space Administration. Lewis Research Center, Cleveland, OH.

### **NUMERICAL ANALYSIS OF SUPERSONIC FLOW THROUGH OSCILLATING CASCADE SECTIONS BY USING A DEFORMING GRID**

DENNIS L. HUFF (NASA, Lewis Research Center, Cleveland, OH) and T. S. R. REDDY (Toledo, University, OH) AIAA, ASME, SAE, and ASEE, Joint Propulsion Conference, 25th, Monterey, CA, July 10-12, 1989. 16 p. Previously announced in STAR as N89-25119. refs (AIAA PAPER 89-2805) Copyright

A finite difference code was developed for modeling inviscid, unsteady supersonic flow by solution of the compressible Euler equations. The code uses a deforming grid technique to capture the motion of the airfoils and can model oscillating cascades with any arbitrary interblade phase angle. A flat plate cascade is analyzed, and results are compared with results from a small-perturbation theory. The results show very good agreement

for both the unsteady pressure distributions and the integrated force predictions. The reason for using the numerical Euler code over a small-perturbation theory is the ability to model real airfoils that have thickness and camber. Sample predictions are presented for a section of the rotor on a supersonic throughflow compressor designed at NASA Lewis Research Center. Preliminary results indicate that two-dimensional, flat plate analysis predicts conservative flutter boundaries. Author

### **A89-52498\* Massachusetts Inst. of Tech., Cambridge. CALCULATIONS OF INLET DISTORTION INDUCED COMPRESSOR FLOW FIELD INSTABILITY**

R. CHUE, E. M. GREITZER, C. S. TAN (MIT, Cambridge, MA), T. P. HYNES, and J. P. LONGLEY (Cambridge, University, England) International Journal of Heat and Fluid Flow (ISSN 0142-727X), vol. 10, Sept. 1989, p. 211-223. refs (Contract NSG-3208) Copyright

Calculations of the onset of flow instability are carried out for low-speed multistage axial compressors operating with asymmetric inlet flow. The modeling of the fluid dynamic interaction between the spoiled and unspoiled sectors of the compressor is the most important feature of the calculation procedure. The calculations show that annulus average slope of the compressor pressure rise characteristic equal to zero is a useful approximate stability criterion for situations where the dynamics of the compressor flow field do not couple strongly to the compression system or the structure of the imposed distortion is not similar to that of the eigenmodes of the flow in the compressor annulus. This criterion is employed to investigate the relationship between the present model and the 'parallel compressor' model. Calculations are also presented for cases when compressor and compressor system are closely coupled, and situations in which the compressor is subjected to a rotating distortion. These first-of-a-kind computations, and the accompanying description of the physical mechanisms, show that the stability of the flow in the compressor can be adversely affected if the temporal or spatial structure of the distortion is such that resonant type responses can be evoked either from the compressor or from compressor/compression system interactions. C.E.

**A89-53931\*#** Virginia Polytechnic Inst. and State Univ., Blacksburg.

### **TURBULENCE MODELING IN A HYPERSONIC INLET**

W. F. NG, K. AJMANI, and A. C. TAYLOR, III (Virginia Polytechnic Institute and State University, Blacksburg) AIAA Journal (ISSN 0001-1452), vol. 27, Oct. 1989, p. 1354-1360. Previously cited in issue 18, p. 2995, Accession no. A88-44705. refs (Contract NAG3-676) Copyright

**N89-10025\*#** Pratt and Whitney Aircraft, East Hartford, CT.

### **TURBOFAN FORCED MIXER LOBE FLOW MODELING. PART 3: APPLICATION TO AUGMENT ENGINES Final Report**

T. BARBER, G. C. MOORE, and J. R. BLATT Washington NASA Oct. 1988 32 p (Contract NAS3-23039) (NASA-CR-4147-Pt-3; E-4085; NAS 1.26:4147-Pt-3) Avail: NTIS HC A03/MF A01 CSCL 01A

Military engines frequently need large quantities of thrust for short periods of time. The addition of an augmentor can provide such thrust increases but with a penalty of increased duct length and engine weight. The addition of a forced mixer to the augmentor improves performance and reduces the penalty, as well as providing a method for siting the required flame holders. In this report two augmentor concepts are investigated: a swirl-mixer augmentor and a mixer-flameholder augmentor. Several designs for each concept are included and an experimental assessment of one of the swirl-mixer augmentors is presented. Author



**N89-10844\*#** National Aeronautics and Space Administration. Lewis Research Center, Cleveland, OH.

**THREE COMPONENT LASER ANEMOMETER MEASUREMENTS IN AN ANNULAR CASCADE OF CORE TURBINE VANES WITH CONTOURED END WALL**

LOUIS J. GOLDMAN and RICHARD G. SEASHOLTZ Nov. 1988 44 p

(NASA-TP-2846; E-4183; NAS 1.60:2846) Avail: NTIS HC A03/MF A01 CSCL 20/4

The three mean velocity components were measured in a full-scale annular turbine stator cascade with contoured hub end wall using a newly developed laser anemometer system. The anemometer consists of a standard fringe configuration using fluorescent seed particles to measure the axial and tangential components. The radial component is measured with a scanning confocal Fabry-Perot interferometer. These two configurations are combined in a single optical system that can operate simultaneously in a backscatter mode through a single optical access port. Experimental measurements were obtained both within and downstream of the stator vane row and compared with calculations from a three-dimensional inviscid computer program. In addition, detailed calibration procedures are described that were used, prior to the experiment, to accurately determine the laser beam probe volume location relative to the cascade hardware. Author

**N89-10858\*#** National Aeronautics and Space Administration. Lewis Research Center, Cleveland, OH.

**EXPERIMENTAL INVESTIGATION OF THE PERFORMANCE OF A SUPERSONIC COMPRESSOR CASCADE**

D. L. TWEEDT, H. A. SCHREIBER, and H. STARKEN (Deutsche Forschungs- und Versuchsanstalt fuer Luft- und Raumfahrt, Cologne, West Germany) Jun. 1988 30 p Presented at the 33rd International Gas Turbine and Aeroengine Congress and Exposition, Amsterdam, The Netherlands, 5-9 Jun. 1988; sponsored by ASME

(NASA-TM-100879; E-4113; NAS 1.15:100879) Avail: NTIS HC A03/MF A01 CSCL 01/1

Results are presented from an experimental investigation of a linear, supersonic, compressor cascade tested in the supersonic cascade wind tunnel facility at the DFVLR in Cologne, Federal Republic of Germany. The cascade design was derived from the near-tip section of a high-through-flow axial flow compressor rotor with a design relative inlet Mach number of 1.61. Test data were obtained over a range of inlet Mach numbers from 1.23 to 1.71, and a range of static pressure ratios and axial-velocity-density ratios (AVDR) at the design inlet condition. Flow velocity measurements showing the wave pattern in the cascade entrance region were obtained using a laser transit anemometer. From these measurements, some unique-incidence conditions were determined, thus relating the supersonic inlet Mach number to the inlet flow direction. The influence of static pressure ratio and AVDR on the blade passage flow and the blade-element performance is described, and an empirical correlation is used to show the influence of these two (independent) parameters on the exit flow angle and total-pressure loss for the design inlet condition. Author

**N89-10863\*#** Sverdrup Technology, Inc., Cleveland, OH.

**A DIAGONALLY INVERTED LU IMPLICIT MULTIGRID SCHEME FOR THE 3-D NAVIER-STOKES EQUATIONS AND A TWO EQUATION MODEL OF TURBULENCE Final Report**

JEFFREY W. YOKOTA Oct. 1988 13 p Prepared for presentation at the 27th Aerospace Sciences Meeting, Reno, Nev., 9-12 Jan. 1989; sponsored in part by AIAA

(Contract NAS3-25266)

(NASA-CR-182209; E-4412; AIAA-88-0467; NAS 1.26:182209)

Avail: NTIS HC A03/MF A01 CSCL 01/1

An LU implicit multigrid algorithm is developed to calculate 3-D compressible viscous flows. This scheme solves the full 3-D Reynolds-Averaged Navier-Stokes equation with a two-equation kappa-epsilon model of turbulence. The flow equations are integrated by an efficient, diagonally inverted, LU implicit multigrid scheme while the kappa-epsilon equations are solved, uncoupled

from the flow equations, by a block LU implicit algorithm. The flow equations are solved within the framework of the multigrid method using a four-grid level W-cycle, while the kappa-epsilon equations are iterated only on the finest grid. This treatment of the Reynolds-Averaged Navier-Stokes equations proves to be an efficient method for calculating 3-D compressible viscous flows.

Author

**N89-10865\*#** National Aeronautics and Space Administration. Lewis Research Center, Cleveland, OH.

**EXPERIMENTAL AERODYNAMIC PERFORMANCE OF ADVANCED 40 DEG-SWEPT 10-BLADE PROPELLER MODEL AT MACH 0.6 TO 0.85**

GLENN A. MITCHELL Sep. 1988 43 p

(NASA-TM-88969; E-3437; NAS 1.15:88969) Avail: NTIS HC A03/MF A01 CSCL 01/1

A propeller designated as SR-6, designed with 40 deg of sweep and 10 blades to cruise at Mach 0.8 at an altitude of 10.7 km (35,000 ft), was tested in the NASA Lewis Research Center's 8-by 6-Foot Wind Tunnel. This propeller was one of a series of advanced single rotation propeller models designed and tested as part of the NASA Advanced Turboprop Project. Design-point net efficiency was almost constant to Mach 0.75 but fell above this speed more rapidly than that of any previously tested advanced propeller. Alternative spinners that further reduced the near-hub interblade Mach numbers and relieved the observed hub choking improved performance above Mach 0.75. One spinner attained estimated SR-6 Design-point net deficiencies of 80.6 percent at Mach 0.75 and 79.2 percent at Mach 0.8, higher than the measured performance of any previously tested advanced single-rotation propeller at these speeds. Author

**N89-11717\*#** National Aeronautics and Space Administration. Lewis Research Center, Cleveland, OH.

**INTERACTIVE GRID GENERATION FOR TURBOMACHINERY FLOW FIELD SIMULATIONS**

YUNG K. CHOO, PETER R. EISEMAN (Columbia Univ., New York, N.Y.), and CHARLES RENO 1988 10 p Presented at the 2nd International Conference on Numerical Grid Generation in Computational Fluid Dynamics, Miami Beach, Fla., 5-8 Dec. 1988; sponsored by NASA, AFOSR and Miami Univ.

(NASA-TM-101301; E-4282; NAS 1.15:101301) Avail: NTIS HC A02/MF A01 CSCL 01/1

The control point form of algebraic grid generation presented provides the means that are needed to generate well structured grids for turbomachinery flow simulations. It uses a sparse collection of control points distributed over the flow domain. The shape and position of coordinate curves can be adjusted from these control points while the grid conforms precisely to all boundaries. An interactive program called TURBO, which uses the control point form, is being developed. Basic features of the code are discussed and sample grids are presented. A finite volume LU implicit scheme is used to simulate flow in a turbine cascade on the grid generated by the program. Author

**N89-12552\*#** National Aeronautics and Space Administration. Lewis Research Center, Cleveland, OH.

**CONTROL OF LAMINAR SEPARATION OVER AIRFOILS BY ACOUSTIC EXCITATION**

K. B. M. Q. ZAMAN and D. J. MCKINZIE 1988 19 p Prepared for presentation at the 27th Aerospace Sciences Meeting, Reno, Nev., 9-12 Jan. 1989; sponsored in part by AIAA

(NASA-TM-101379; E-4434; NAS 1.15:101379; AIAA-89-0565)

Avail: NTIS HC A03/MF A01 CSCL 01/1

The effect of acoustic excitation in reducing laminar separation over two-dimensional airfoils at low angles of attack is investigated experimentally. Airfoils of two different cross sections, each with two different chord lengths, are studied in the chord Reynolds number range of 25,000 is less than  $R_{sub c}$  is less than 100,000. While keeping the amplitude of the excitation induced velocity perturbation a constant, it is found that the most effective frequency scales as  $U$  (sup 3/2)/(sub infinity). The parameter  $St/R$  (sup

## 02 AERODYNAMICS

1/2)(sub c), corresponding to the most effective  $f_{sub p}$  for all the cases studied, falls in the range of 0.02 to 0.03,  $St$  being the Strouhal number based on the chord. Author

**N89-12553\*#** Cincinnati Univ., OH. Dept. of Aerospace Engineering and Engineering Mechanics.

### **SIMULATION OF 2-DIMENSIONAL VISCOUS FLOW THROUGH CASCADES USING A SEMI-ELLIPTIC ANALYSIS AND HYBRID C-H GRIDS Final Report**

R. RAMAMURTI, U. GHIA, and K. N. GHIA Washington NASA Oct. 1988 194 p  
(Contract NAG3-194)  
(NASA-CR-4180; REPT-86-9-71; E-4286; NAS 1.26:4180) Avail: NTIS HC A09/MF A01 CSCL 01/1

A semi-elliptic formulation, termed the interacting parabolized Navier-Stokes (IPNS) formulation, is developed for the analysis of a class of subsonic viscous flows for which streamwise diffusion is negligible but which are significantly influenced by upstream interactions. The IPNS equations are obtained from the Navier-Stokes equations by dropping the streamwise viscous-diffusion terms but retaining upstream influence via the streamwise pressure-gradient. A two-step alternating-direction-explicit numerical scheme is developed to solve these equations. The quasi-linearization and discretization of the equations are carefully examined so that no artificial viscosity is added externally to the scheme. Also, solutions to compressible as well as nearly compressible flows are obtained without any modification either in the analysis or in the solution process. The procedure is applied to constricted channels and cascade passages formed by airfoils of various shapes. These geometries are represented using numerically generated curvilinear boundary-oriented coordinates forming an H-grid. A hybrid C-H grid, more appropriate for cascade of airfoils with rounded leading edges, was also developed. Satisfactory results are obtained for flows through cascades of Joukowski airfoils. Author

**N89-12555\*#** National Aeronautics and Space Administration. Lewis Research Center, Cleveland, OH.

### **EVALUATION OF THREE TURBULENCE MODELS FOR THE PREDICTION OF STEADY AND UNSTEADY AIRLOADS**

JIUNN-CHI WU, DENNIS L. HUFF, and L. N. SANKAR (Georgia Inst. of Tech., Atlanta.) 1988 13 p Proposed for presentation at the 27th Aerospace Sciences Meeting, Reno, Nev., 9-12 Jan. 1989; sponsored by AIAA  
(NASA-TM-101413; E-4507; NAS 1.15:101413; AIAA-89-0609)  
Avail: NTIS HC A03/MF A01 CSCL 01/1

Two dimensional quasi-three dimensional Navier-Stokes solvers were used to predict the static and dynamic airload characteristics of airfoils. The following three turbulence models were used: the Baldwin-Lomax algebraic model, the Johnson-King ODE model for maximum turbulent shear stress, and a two equation k- $\epsilon$  model with law-of-the-wall boundary conditions. It was found that in attached flow the three models have good agreement with experimental data. In unsteady separated flows, these models give only a fair correlation with experimental data. Author

**N89-13397\*#** Purdue Univ., West Lafayette, IN.  
**ANALYSIS OF SUPERSONIC PLUG NOZZLE FLOWFIELD AND HEAT TRANSFER**

S. N. B. MURTHY and W. H. SHEU Sep. 1988 180 p  
(Contract NAG3-281)  
(NASA-CR-179554; NAS 1.26:179554) Avail: NTIS HC A09/MF A01 CSCL 01/1

A number of problems pertaining to the flowfield in a plug nozzle, designed as a supersonic thruster nozzle, with provision for cooling the plug with a coolant stream admitted parallel to the plug wall surface, were studied. First, an analysis was performed of the inviscid, nonturbulent, gas dynamic interaction between the primary hot stream and the secondary coolant stream. A numerical prediction code for establishing the resulting flowfield with a dividing surface between the two streams, for various combinations of stagnation and static properties of the two streams, was utilized for illustrating the nature of interactions. Secondly, skin friction

coefficient, heat transfer coefficient and heat flux to the plug wall were analyzed under smooth flow conditions (without shocks or separation) for various coolant flow conditions. A numerical code was suitably modified and utilized for the determination of heat transfer parameters in a number of cases for which data are available. Thirdly, an analysis was initiated for modeling turbulence processes in transonic shock-boundary layer interaction without the appearance of flow separation. Author

**N89-13399\*#** Flow Research, Inc., Kent, WA.

### **USER'S MANUAL FOR AN AERODYNAMIC OPTIMIZATION SCHEME THAT UPDATES FLOW VARIABLES AND DESIGN PARAMETERS SIMULTANEOUSLY Flow Report No. 444**

MAGDI H. RIZK Jul. 1988 33 p  
(Contract NAS3-24855)  
(NASA-CR-182180; NAS 1.26:182180) Avail: NTIS HC A03/MF A01 CSCL 01/1

This user's manual is presented for an aerodynamic optimization program that updates flow variables and design parameters simultaneously. The program was developed for solving constrained optimization problems in which the objective function and the constraint function are dependent on the solution of the nonlinear flow equations. The program was tested by applying it to the problem of optimizing propeller designs. Some reference to this particular application is therefore made in the manual. However, the optimization scheme is suitable for application to general aerodynamic design problems. A description of the approach used in the optimization scheme is first presented, followed by a description of the use of the program. Author

**N89-13409\*#** National Aeronautics and Space Administration. Lewis Research Center, Cleveland, OH.

### **LASER VELOCIMETER MEASUREMENTS OF THE FLOWFIELD GENERATED BY AN ADVANCED COUNTERROTATING PROPELLER**

GARY G. PODBOY and MARTIN J. KRUPAR 1989 33 p  
Prepared for presentation at the 27th Aerospace Sciences Meeting, Reno, Nev., 9-12 Jan. 1989; sponsored by AIAA  
(NASA-TM-101437; E-4525; NAS 1.15:101437; AIAA-89-0434)  
Avail: NTIS HC A03/MF A01 CSCL 01/2

Results are presented of an investigation to measure the flowfield generated by an advanced counterrotating pusher propeller model similar to the full-scale Unducted Fan demonstrator engine. A laser Doppler velocimeter was used to measure the velocity field in several planes normal to the centerline of the model at axial stations upstream and downstream of each rotor. During this investigation, blades of the F4/A4 type were installed on the model which was operating in a freestream Mach 0.72 regime, with the advance ratio of each rotor set at 2.80. The measured data indicate only a slight influence of the potential field of each front rotor blade on the flowfield upstream of the rotor. The data measured downstream of the front rotor characterize the tip vortices, vortex sheets and potential field nonuniformities generated by the front rotor. The unsteadiness of the flow in the rotating frame of reference of the aft rotor is also illustrated. Author

**N89-13412\*#** National Aeronautics and Space Administration. Lewis Research Center, Cleveland, OH.

### **PREDICTIONS OF AIRFOIL AERODYNAMIC PERFORMANCE DEGRADATION DUE TO ICING**

ROBERT J. SHAW, MARK G. POTAPUZUK, and COLIN S. BIDWELL 1988 16 p Presented at the 4th Symposium on Numerical and Physical Aspects of Aerodynamic Flows, Long Beach, Calif., 16-19 Jan. 1989; sponsored by California State Univ.  
(NASA-TM-101434; E-4541; NAS 1.15:101434) Avail: NTIS HC A03/MF A01 CSCL 01/1

An overview of NASA's ongoing efforts to develop an airfoil icing analysis capability is developed. An indication is given to the approaches being followed to calculate the water droplet trajectories past the airfoil, the buildup of ice on the airfoil, and the resultant changes in aerodynamic performance due to the



leading edge ice accretion. Examples are given of current code capabilities/limitations through comparisons of predictions with experimental data gathered in various calibration/validation experiments. A brief discussion of future efforts to extend the analysis to handle three dimensional components is included.

Author

**N89-14220\*#** National Aeronautics and Space Administration. Lewis Research Center, Cleveland, OH.

**NUMERICAL ANALYSIS OF FLOW THROUGH OSCILLATING CASCADE SECTIONS**

DENNIS L. HUFF Jan. 1989 25 p Prepared for presentation at the 27th Aerospace Sciences Meeting, Reno, NV, 9-12 Jan. 1989; sponsored in part by AIAA

(NASA-TM-101417; E-4509; NAS 1.15:101417; AIAA-89-0437)

Avail: NTIS HC A03/MF A01 CSCL 01/1

The design of turbomachinery blades requires the prevention of flutter for all operating conditions. However, flow field predictions used for aeroelastic analysis are not well understood for all flow regimes. The present research focuses on numerical solutions of the Euler and Navier-Stokes equations using an ADI procedure to model two-dimensional, transonic flow through oscillating cascades. The model prescribes harmonic pitching motions for the blade sections for both zero and nonzero interblade phase angles. The code introduces the use of a deforming grid technique for convenient specification of the periodic boundary conditions. Approximate nonreflecting boundary conditions were coded for the inlet and exit boundary conditions. Sample unsteady solutions were performed for an oscillating cascade and compared to experimental data. Also, test cases were run for a flat plate cascade to compare with the unsteady, small-perturbation, subsonic analysis. The predictions for oscillating cascades with nonzero interblade phase angle cases, which were near a resonant condition, differ from the experiment and theory. The zero degree interblade phase angle cases, which were near a resonant condition, differ from the experiment and theory. Studies on reflecting versus nonreflecting inlet and exit boundary conditions show that the treatment of the boundary can have a significant effect on the first harmonic, unsteady pressure distributions for certain flow conditions.

Author

**N89-14221\*#** Pratt and Whitney Aircraft, East Hartford, CT. Engineering Div.

**TURBOFAN FORCED MIXER LOBE FLOW MODELING. 1: EXPERIMENTAL AND ANALYTICAL ASSESSMENT Final Report**

T. BARBER, R. W. PATERSON, and S. A. SKEBE Washington NASA Oct. 1988 155 p

(Contract NAS3-23039)

(NASA-CR-4147-PT-1; E-4083; NAS 1.26:4147-PT-1) Avail: NTIS HC A08/MF A01 CSCL 01/1

A joint analytical and experimental investigation of three-dimensional flowfield development within the lobe region of turbofan forced mixer nozzles is described. The objective was to develop a method for predicting the lobe exit flowfield. In the analytical approach, a linearized inviscid aerodynamical theory was used for representing the axial and secondary flows within the three-dimensional convoluted mixer lobes and three-dimensional boundary layer analysis was applied thereafter to account for viscous effects. The experimental phase of the program employed three planar mixer lobe models having different waveform shapes and lobe heights for which detailed measurements were made of the three-dimensional velocity field and total pressure field at the lobe exit plane. Velocity data was obtained using Laser Doppler Velocimetry (LDV) and total pressure probing and hot wire anemometry were employed to define exit plane total pressure and boundary layer development. Comparison of data and analysis was performed to assess analytical model prediction accuracy. As a result of this study a planar mixed geometry analysis was developed. A principal conclusion is that the global mixer lobe flowfield is inviscid and can be predicted from an inviscid analysis and Kutta condition.

Author

**N89-14222\*#** Pratt and Whitney Aircraft, East Hartford, CT. Engineering Div.

**TURBOFAN FORCED MIXER LOBE FLOW MODELING. 2: THREE-DIMENSIONAL INVISCID MIXER ANALYSIS (FLOMIX) Final Report**

T. BARBER Washington NASA Oct. 1988 75 p

(Contract NAS3-23039)

(NASA-CR-4147-PT-2; E-4084; NAS 1.26:4147-PT-2) Avail: NTIS HC A04/MF A01 CSCL 01/1

A three-dimensional potential analysis (FLOMIX) was formulated and applied to the inviscid flow over a turbofan forced mixer. The method uses a small disturbance formulation to analytically uncouple the circumferential flow from the radial and axial flow problem, thereby reducing the analysis to the solution of a series of axisymmetric problems. These equations are discretized using a flux volume formulation along a Cartesian grid. The method extends earlier applications of the Cartesian method to complex cambered geometries. The effects of power addition are also included within the potential formulation. Good agreement is obtained with an alternate small disturbance analysis for a high penetration symmetric mixer in a planar duct. In addition, calculations showing pressure distributions and induced secondary vorticity fields are presented for practical turbofan mixer configurations, and where possible, comparison was made with available experimental data. A detailed description of the required data input and coordinate definition is presented along with a sample data set for a practical forced mixer configuration. A brief description of the program structure and subroutines is also provided.

Author

**N89-15077\*#** National Aeronautics and Space Administration. Lewis Research Center, Cleveland, OH.

**APPLICATION OF A LOWER-UPPER IMPLICIT SCHEME AND AN INTERACTIVE GRID GENERATION FOR TURBOMACHINERY FLOW FIELD SIMULATIONS**

YUNG K. CHOO, WOO-YUNG SOH, and SEOKKWAN YOON (MCAT Inst., Moffett Field, CA.) 1989 17 p

Proposed for presentation at the 34th International Gas Turbine and Aeroengine Congress and Exposition, Toronto, Ontario, 4-8 Jun. 1989; sponsored by the American Society of Mechanical Engineers

(NASA-TM-101412; E-4374; NAS 1.15:101412) Avail: NTIS HC A03/MF A01 CSCL 01/1

A finite-volume lower-upper (LU) implicit scheme is used to simulate an inviscid flow in a turbine cascade. This approximate factorization scheme requires only the inversion of sparse lower and upper triangular matrices, which can be done efficiently without extensive storage. As an implicit scheme it allows a large time step to reach the steady state. An interactive grid generation program (TURBO), which is being developed, is used to generate grids. This program uses the control point form of algebraic grid generation which uses a sparse collection of control points from which the shape and position of coordinate curves can be adjusted. A distinct advantage of TURBO compared with other grid generation programs is that it allows the easy change of local mesh structure without affecting the grid outside the domain of independence. Sample grids are generated by TURBO for a compressor rotor blade and a turbine cascade. The turbine cascade flow is simulated by using the LU implicit scheme on the grid generated by TURBO.

Author

**N89-15078\*#** National Aeronautics and Space Administration. Lewis Research Center, Cleveland, OH.

**HOT GAS INGESTION TESTING OF AN ADVANCED STOVL CONCEPT IN THE NASA LEWIS 9- BY 15-FOOT LOW SPEED WIND TUNNEL WITH FLOW VISUALIZATION**

ALBERT L. JOHNS, JOSEPH D. FLOOD, THOMAS W. STROCK, and KURT C. AMUEDO (McDonnell-Douglas Corp., St. Louis, MO.) 1988 27 p

Presented at the 24th Joint Propulsion Conference, Boston, MA, 11-13 Jul. 1988; sponsored by AIAA, ASME, SAE and ASEE

(NASA-TM-100952; E-4250; NAS 1.15:100952; AIAA-88-3025)

Avail: NTIS HC A03/MF A01 CSCL 01/1

Advanced Short Takeoff/Vertical Landing (STOVL) aircraft

## 02 AERODYNAMICS

capable of operating from remote sites, damaged runways, and small air capable ships are being pursued for deployment around the turn of the century. To achieve this goal, it is important that the technologies critical to this unique class of aircraft be developed. Recognizing this need, NASA Lewis Research Center, McDonnell Douglas Aircraft, and DARPA defined a cooperative program for testing in the NASA Lewis 9- by 15-Foot Low Speed Wind Tunnel (LSWT) to establish a database for hot gas ingestion, one of the technologies critical to STOVL. Results from a test program are presented along with a discussion of the facility modifications allowing this type of testing at model scale. These modifications to the tunnel include a novel ground plane, an elaborate model support which included 4 degrees of freedom, heated high pressure air for nozzle flow, a suction system exhaust for inlet flow, and tunnel sidewall modifications. Several flow visualization techniques were employed including water mist in the nozzle flows and tufts on the ground plane. Headwind (free-stream) velocity was varied from 8 to 23 knots. Author

**N89-15084\*#** National Aeronautics and Space Administration. Lewis Research Center, Cleveland, OH.

### **AN EXPERIMENTAL INVESTIGATION OF MULTI-ELEMENT AIRFOIL ICE ACCRETION AND RESULTING PERFORMANCE DEGRADATION**

MARK G. POTAPCZUK and BRIAN M. BERKOWITZ (Sverdrup Technology, Inc., Cleveland, OH.) 1989 40 p Presented at the 27th Aerospace Sciences Meeting, Reno, NV, 9-12 Jan. 1989; sponsored by AIAA

(NASA-TM-101441; E-4546; NAS 1.15:101441; AIAA-89-0752)

Avail: NTIS HC A03/MF A01 CSCL 01/1

An investigation of the ice accretion pattern and performance characteristics of a multi-element airfoil was undertaken in the NASA Lewis 6- by 9-Foot Icing Research Tunnel. Several configurations of main airfoil, slat, and flaps were employed to examine the effects of ice accretion and provide further experimental information for code validation purposes. The test matrix consisted of glaze, rime, and mixed icing conditions. Airflow and icing cloud conditions were set to correspond to those typical of the operating environment anticipated for a commercial transport vehicle. Results obtained included ice profile tracings, photographs of the ice accretions, and force balance measurements obtained both during the accretion process and in a post-accretion evaluation over a range of angles of attack. The tracings and photographs indicated significant accretions on the slat leading edge, in gaps between slat or flaps and the main wing, on the flap leading-edge surfaces, and on flap lower surfaces. Force measurements indicate the possibility of severe performance degradation, especially near  $C_{sub} L_{max}$ , for both light and heavy ice accretion and performance analysis codes presently in use. The LEWICE code was used to evaluate the ice accretion shape developed during one of the rime ice tests. The actual ice shape was then evaluated, using a Navier-Stokes code, for changes in performance characteristics. These predicted results were compared to the measured results and indicate very good agreement. Author

**N89-15896\*#** United Technologies Research Center, East Hartford, CT.

### **AN ANALYSIS FOR HIGH SPEED PROPELLER-NACELLE AERODYNAMIC PERFORMANCE PREDICTION. VOLUME 1: THEORY AND APPLICATION Final Report**

T. ALAN EGOLF, OLOF L. ANDERSON, DAVID E. EDWARDS, and ANTON J. LANDGREBE Washington NASA Dec. 1988 261 p

(Contract NAS3-20961; NAS3-22142; NAS3-22257)

(NASA-CR-4199-VOL-1; E-4382; NAS 1.26:4199-VOL-1) Avail:

NTIS HC A12/MF A01 CSCL 01/1

A computer program, the Propeller Nacelle Aerodynamic Performance Prediction Analysis (PANPER), was developed for the prediction and analysis of the performance and airflow of propeller-nacelle configurations operating over a forward speed range inclusive of high speed flight typical of recent propfan designs. A propeller lifting line, wake program was combined with a compressible, viscous center body interaction program, originally

developed for diffusers, to compute the propeller-nacelle flow field, blade loading distribution, propeller performance, and the nacelle forebody pressure and viscous drag distributions. The computer analysis is applicable to single and coaxial counterrotating propellers. The blade geometries can include spanwise variations in sweep, droop, taper, thickness, and airfoil section type. In the coaxial mode of operation the analysis can treat both equal and unequal blade number and rotational speeds on the propeller disks. The nacelle portion of the analysis can treat both free air and tunnel wall configurations including wall bleed. The analysis was applied to many different sets of flight conditions using selected aerodynamic modeling options. The influence of different propeller nacelle-tunnel wall configurations was studied. Comparisons with available test data for both single and coaxial propeller configurations are presented along with a discussion of the results. Author

**N89-15897\*#** United Technologies Research Center, East Hartford, CT.

### **AN ANALYSIS FOR HIGH SPEED PROPELLER-NACELLE AERODYNAMIC PERFORMANCE PREDICTION. VOLUME 2: USER'S MANUAL**

T. ALAN EGOLF, OLOF L. ANDERSON, DAVID E. EDWARDS, and ANTON J. LANDGREBE Washington NASA Dec. 1988 307 p

(Contract NAS3-20961; NAS3-22142; NAS3-22257)

(NASA-CR-4199-VOL-2; E-4399; NAS 1.26:4199-VOL-2) Avail:

NTIS HC A14/MF A01 CSCL 01/1

A user's manual for the computer program developed for the prediction of propeller-nacelle aerodynamic performance reported in, An Analysis for High Speed Propeller-Nacelle Aerodynamic Performance Prediction: Volume 1 -- Theory and Application, is presented. The manual describes the computer program mode of operation requirements, input structure, input data requirements and the program output. In addition, it provides the user with documentation of the internal program structure and the software used in the computer program as it relates to the theory presented in Volume 1. Sample input data setups are provided along with selected printout of the program output for one of the sample setups. Author

**N89-15898\*#** City Coll. of the City Univ. of New York, NY. Dept. of Mechanical Engineering.

### **AN EXPERIMENTAL STUDY OF NEAR WALL FLOW PARAMETERS IN THE BLADE END-WALL CORNER REGION Final Report**

RAKESH K. BHARGAVA and RISHI S. RAJ Washington NASA Jan. 1989 314 p

(Contract NAG3-122)

(NASA-CR-4211; E-4506; NAS 1.26:4211) Avail: NTIS HC

A14/MF A01 CSCL 01/1

The near wall flow parameters in the blade end-wall corner region is investigated. The blade end-wall corner region was simulated by mounting an airfoil section (NACA 65-015 base profile) symmetric blades on both sides of the flat plate with semi-circular leading edge. The initial 7 cm from the leading edge of the flat plate was roughened by gluing No. 4 floor sanding paper to artificially increase the boundary layer thickness on the flat plate. The initial flow conditions of the boundary layer upstream of the corner region are expected to dictate the behavior of flow inside the corner region. Therefore, an experimental investigation was extended to study the combined effect of initial roughness and increased level of free stream turbulence on the development of a 2-D turbulent boundary layer in the absence of the blade. The measurement techniques employed in the present investigation included, the conventional pitot and pitot-static probes, wall taps, the Preston tube, piezoresistive transducer and the normal sensor hot-wire probe. The pitot and pitot-static probes were used to obtain mean velocity profile measurements within the boundary layer. The measurements of mean surface static pressure were obtained with the surface static tube and the conventional wall tap method. The wall shear vector measurements were made with a specially constructed Preston tube. The flush mounted

piezoresistive type pressure transducer were employed to measure the wall pressure fluctuation field. The velocity fluctuation measurements, used in obtaining the wall pressure-velocity correlation data, were made with normal single sensor hot-wire probe. At different streamwise stations, in the blade end-wall corner region, the mean values of surface static pressure varied more on the end-wall surface in the corner region were mainly caused by the changes in the curvature of the streamlines. The magnitude of the wall shear stress in the blade end-wall corner region increased significantly in the close vicinity of the corner line. The maximum value of the wall shear stress and its location from the corner line, on both the surfaces forming the corner region, were observed to change along the corner. These observed changes in the maximum values of the wall shear stress and its location from the corner line could be associated with the stretching and attenuation of the horseshoe vortex. The wall shear stress vectors in the blade end-wall corner region were observed to be more skewed on the end-wall surface as compared to that on the blade surface. The differences in the wall shear stress directions obtained with the Preston tube and flow visualization method were within the range in which the Preston tube was found to be insensitive to the yaw angle.

Author

**N89-16752\*#** National Aeronautics and Space Administration. Lewis Research Center, Cleveland, OH.

#### COMPUTATIONAL METHODS FOR INLET AIRFRAME INTEGRATION

CHARLES E. TOWNE /in VKI, Intake Aerodynamics, Volume 2 43 p 1988

Avail: NTIS HC A14/MF A01

Fundamental equations encountered in computational fluid dynamics (CFD), and analyses used for internal flow are introduced. Irrotational flow; Euler equations; boundary layers; parabolized Navier-Stokes equations; and time averaged Navier-Stokes equations are treated. Assumptions made and solution methods are outlined, with examples. The overall status of CFD in propulsion is indicated.

ESA

**N89-16753\*#** National Aeronautics and Space Administration. Lewis Research Center, Cleveland, OH.

#### CFD APPLICATION TO SUBSONIC INLET AIRFRAME INTEGRATION

BERNHARD H. ANDERSON /in VKI, Intake Aerodynamics, Volume 2 59 p 1988

Avail: NTIS HC A14/MF A01

The fluid dynamics of curved diffuser duct flows of military aircraft is discussed. Three-dimensional parabolized Navier-Stokes analysis, and experiment techniques are reviewed. Flow measurements and pressure distributions are shown. Velocity vectors, and the effects of vortex generators are considered.

ESA

**N89-16754\*#** National Aeronautics and Space Administration. Lewis Research Center, Cleveland, OH.

#### CFD APPLICATION TO SUPERSONIC/HYPERSONIC INLET AIRFRAME INTEGRATION

THOMAS J. BENSON /in VKI, Intake Aerodynamics, Volume 2 62 p 1988

Avail: NTIS HC A14/MF A01

Supersonic external compression inlets are introduced, and the computational fluid dynamics (CFD) codes and tests needed to study flow associated with these inlets are outlined. Normal shock wave turbulent boundary layer interaction is discussed. Boundary layer control is considered. Glancing sidewall shock interaction is treated. The CFD validation of hypersonic inlet configurations is explained. Scramjet inlet modules are shown.

ESA

**N89-16759\*#** National Aeronautics and Space Administration. Lewis Research Center, Cleveland, OH.

#### THREE DIMENSIONAL VISCOUS ANALYSIS OF A HYPERSONIC INLET

D. R. REDDY, G. E. SMITH, M.-F. LIOU, and THOMAS J. BENSON Jan. 1989 9 p Presented at the 27th Aerospace

Sciences Meeting, Reno, NV, 9-12 Jan. 1989; sponsored in part by AIAA Prepared in cooperation with Sverdrup Technology Inc., Cleveland, OH

(NASA-TM-101474; E-4592; NAS 1.15:101474; AIAA-89-0004)

Avail: NTIS HC A02/MF A01 CSCL 01/1

The flow fields in supersonic/hypersonic inlets are currently being studied at NASA Lewis Research Center using 2- and 3-D full Navier-Stokes and Parabolized Navier-Stokes solvers. These tools have been used to analyze the flow through the McDonnell Douglas Option 2 inlet which has been tested at Calspan in support of the National Aerospace Plane Program. Comparisons between the computational and experimental results are presented. These comparisons lead to better overall understanding of the complex flows present in this class of inlets. The aspects of the flow field emphasized in this work are the 3-D effects, the transition from laminar to turbulent flow, and the strong nonuniformities generated within the inlet.

Author

**N89-18417\*#** National Aeronautics and Space Administration. Lewis Research Center, Cleveland, OH.

#### LARGE AMPLITUDE ACOUSTIC EXCITATION OF SWIRLING TURBULENT JETS

R. TAGHAVI, E. J. RICE, and S. FAROKHI (Kansas Univ., Lawrence.) 1989 17 p Presented at the 2nd Shear Flow Conference, Tempe, AZ, 13-16 Mar. 1989; sponsored by AIAA (NASA-TM-101950; E-4643; NAS 1.15:101950; AIAA-89-0970)

Avail: NTIS HC A03/MF A01 CSCL 01/1

A swirling jet with a swirl number of  $S = 0.12$  is exited by plane acoustic waves at various Strouhal numbers ( $St = fD/U$  sub alpha). The maximum forcing amplitude of excitation was at 6.88 percent of the time-mean axial velocity at a Strouhal number of  $St = 0.39$ . The maximum time-mean tangential and axial velocities at the nozzle exit were 18 and 84 m/sec respectively. It was observed that the swirling jet was excitable by plane acoustic waves and the preferred Strouhal number based on the nozzle diameter and exit axial velocity of the jet was about 0.39. As a result of excitation at this frequency, the time-mean axial velocity decayed faster along the jet centerline, reaching about 89 percent of its unexcited value at  $x/D = 9$ . Also the half velocity radius and momentum thickness, at 7 nozzle diameters downstream, increased by 13.2 and 5.8 percent respectively, indicating more jet spread and enhanced mixing. To our knowledge, this is the first reported experimental data indicating any mixing enhancement of swirling jets by acoustic excitation.

Author

**N89-19265\*#** National Aeronautics and Space Administration. Lewis Research Center, Cleveland, OH.

#### WIND-TUNNEL RESULTS OF ADVANCED HIGH-SPEED PROPELLERS AT TAKEOFF, CLIMB, AND LANDING MACH NUMBERS

GEORGE L. STEFKO and ROBERT J. JERACKI Nov. 1985 51 p

(NASA-TM-87030; E-2417; NAS 1.15:87030) Avail: NTIS HC A04/MF A01 CSCL 01/1

Low-speed wind-tunnel performance tests of two advanced propellers have been completed at the NASA Lewis Research Center as part of the NASA Advanced Turboprop Program. The 62.2 cm (24.5 in.) diameter adjustable-pitch models were tested at Mach numbers typical of takeoff, initial climbout, and landing speeds (i.e., from Mach 0.10 to 0.34) at zero angle of attack in the NASA Lewis 10 by 10 Foot Supersonic Wind Tunnel. Both models had eight blades and a cruise-design-point operating condition of Mach 0.80, and 10.668 km (35,000 ft) I.S.A. altitude, a 243.8 m/s (800 ft/sec) tip speed, and a high power loading of 301 kW/sq m (37.5 shp/sq ft). Each model had its own integrally designed area-ruled spinner, but used the same specially contoured nacelle. These features reduced blade-section Mach numbers and relieved blade-root choking at the cruise condition. No adverse or unusual low-speed operating conditions were found during the test with either the straight blade SR-2 or the 45 deg swept SR-3 propeller. Typical efficiencies of the straight and 45 deg swept propellers were 50.2 and 54.9 percent, respectively, at a takeoff

## 02 AERODYNAMICS

condition of Mach 0.20 and 53.7 and 59.1 percent, respectively, at a climb condition of Mach 0.34. Author

**N89-20921\*#** Sandtrap Technology, Inc., Cleveland, OH.  
**COMPARISON OF 3D COMPUTATION AND EXPERIMENT FOR NON-AXISYMMETRIC NOZZLES Final Report**  
H. LAI and E. NELSON Feb. 1989 12 p Presented at the 27th Aerospace Sciences Meeting, Reno, NV, 9-12 Jan. 1989; sponsored in part by AIAA  
(Contract NAS3-24105; NAS3-25266)  
(NASA-CR-182245; E-4574; NAS 1.26:182245; AIAA-89-0007)  
Avail: NTIS HC A03/MF A01 CSCL 01/1

Three dimensional solutions of a single expansion ramp nozzle are computed with the existing PARC computer code by solving the full Navier-Stokes equations. The computations are performed to simulate the non-axisymmetric nozzle flowfield in both the internal/external expansion regions and the exhaust plume in a quiescent ambient environment. Two different configurations of the nozzle at a pressure ratio  $NPR = 10$  are examined. Numerical results of laminar flows are presented, and the wall pressure distributions are compared with the experimental data. Author

**N89-20956\*#** National Aeronautics and Space Administration. Lewis Research Center, Cleveland, OH.  
**AN LDA (LASER-DOPPLER ANEMOMETRY) INVESTIGATION OF THREE-DIMENSIONAL NORMAL SHOCK WAVE BOUNDARY-LAYER INTERACTIONS**  
R. M. CHRISS, W. R. HINGST, A. J. STRAZISAR, and T. G. KEITH, JR. (Toledo Univ., OH.) In NASA, Langley Research Center, Transonic Symposium: Theory, Application, and Experiment, Volume 1, Part 2 p 741-764 Mar. 1989  
Avail: NTIS HC A22/MF A01 CSCL 01/1

Nonintrusive measurements were made of a normal shock wave/boundary layer interaction. Two dimensional measurements were made throughout the interaction region while 3-D measurements were made in the vicinity of the shock wave. The measurements were made in the corner of the test section of a continuous supersonic wind tunnel in which a normal shock wave had been stabilized. Laser Doppler Anemometry, surface pressure measurement and flow visualization techniques were employed for two freestream Mach number test cases: 1.6 and 1.3. The former contained separated flow regions and a system of shock waves. The latter was found to be far less complicated. The results define the flow field structure in detail for each case. Author

**N89-22573\*#** National Aeronautics and Space Administration. Lewis Research Center, Cleveland, OH.  
**SECOND-ORDER ACCURATE NONOSCILLATORY SCHEMES FOR SCALAR CONSERVATION LAWS**  
HUNG T. HUYNH 1989 16 p Proposed for presentation at the 6th International Conference on Numerical Methods in Laminar and Turbulent Flow, Swansea, England, 11-15 Jul. 1989; cosponsored by the Univ. Coll. of Swansea, ONR Branch Office London, Journal for Numerical Methods in Fluids, International Journal for Engineering Computations, and International Journal for Artificial Intelligence  
(NASA-TM-102010; E-4721; NAS 1.15:102010) Avail: NTIS HC A03/MF A01 CSCL 01/1

Explicit finite difference schemes for the computation of weak solutions of nonlinear scalar conservation laws is presented and analyzed. These schemes are uniformly second-order accurate and nonoscillatory in the sense that the number of extrema of the discrete solution is not increasing in time. Author

**N89-22577\*#** National Aeronautics and Space Administration. Lewis Research Center, Cleveland, OH.  
**RECTANGULAR NOZZLE PLUME VELOCITY MODELING FOR USE IN JET NOISE PREDICTION**  
U. H. VONGLAHN 1989 36 p Presented at the 25th Joint Propulsion Conference, Monterey, CA, 10-12 Jul. 1989; sponsored by AIAA, ASME, SAE and ASEE  
(NASA-TM-102047; E-4739; NAS 1.15:102047; AIAA-89-2357)  
Avail: NTIS HC A03/MF A01 CSCL 01/1

A modeling technique for predicting the axial and transverse velocity characteristics of rectangular nozzle plumes is developed. In this technique, modeling of the plume cross section is initiated at the nozzle exit plane. The technique is demonstrated for the plume issuing from a rectangular nozzle having an aspect ratio of 6.0 and discharging into quiescent air. Application of the present procedures to a nozzle discharging into a moving airstream (flight effect) are then demonstrated. The effects of plume shear layer structure modification on the velocity flowfield are discussed and modeling procedures are illustrated by example. Author

**N89-23413\*#** National Aeronautics and Space Administration. Lewis Research Center, Cleveland, OH.  
**NUMERICAL SOLUTION OF PERIODIC VORTICAL FLOWS ABOUT A THIN AIRFOIL**  
JAMES R. SCOTT and HAFIZ M. ATASSI (Notre Dame Univ., IN.) 1989 12 p Presented at the 24th Thermophysics Conference, Buffalo, NY, 12-14 Jun. 1989; sponsored by the AIAA  
(NASA-TM-101998; E-4703; NAS 1.15:101998) Avail: NTIS HC A03/MF A01 CSCL 01/1

A numerical method is developed for computing periodic, three-dimensional, vortical flows around isolated airfoils. The unsteady velocity is split into a vortical component which is a known function of the upstream flow conditions and the Lagrangian coordinates of the mean flow, and an irrotational field whose potential satisfies a nonconstant-coefficient, inhomogeneous, convective wave equation. Solutions for thin airfoils at zero degrees incidence to the mean flow are presented in this paper. Using an elliptic coordinate transformation, the computational domain is transformed into a rectangle. The Sommerfeld radiation condition is applied to the unsteady pressure on the grid line corresponding to the far field boundary. The results are compared with a Possio solver, and it is shown that for maximum accuracy the grid should depend on both the Mach number and reduced frequency. Finally, in order to assess the range of validity of the classical thin airfoil approximation, results for airfoils with zero thickness are compared with results for airfoils with small thickness. Author

**N89-23416\*#** National Aeronautics and Space Administration. Lewis Research Center, Cleveland, OH.  
**AVERAGE-PASSAGE SIMULATION OF COUNTER-ROTATING PROPFAN PROPULSION SYSTEMS AS APPLIED TO CRUISE MISSILES**  
RICHARD A. MULAC, JON C. SCHNEIDER (McDonnell-Douglas Astronautics Co., Saint Louis, MO.), and JOHN J. ADAMCZYK 1989 12 p Prepared for presentation at the 25th Joint Propulsion Conference, Monterey, CA, 10-12 Jul. 1989; sponsored by AIAA, ASME, SAE, and ASEE  
(NASA-TM-102043; E-4791; NAS 1.15:102043; AIAA-89-2943)  
Avail: NTIS HC A03/MF A01 CSCL 01/1

Counter-rotating propfan (CRP) propulsion technologies are currently being evaluated as cruise missile propulsion systems. The aerodynamic integration concerns associated with this application are being addressed through the computational modeling of the missile body-propfan flowfield interactions. The work described in this paper consists of a detailed analysis of the aerodynamic interactions between the control surfaces and the propfan blades through the solution of the average-passage equation system. Two baseline configurations were studied, the control fins mounted forward of the counter-rotating propeller and the control fins mounted aft of the counter-rotating propeller. In both cases, control fin-propfan separation distance and control fin deflection angle were varied. Author

**N89-23417\*#** National Aeronautics and Space Administration. Lewis Research Center, Cleveland, OH.  
**THE LOW FREQUENCY OSCILLATION IN THE FLOW OVER A NACA0012 AIRFOIL WITH AN ICED LEADING EDGE**  
K. B. M. Q. ZAMAN and M. G. POTAPCZUK 1989 16 p Presented at the Conference on Low Reynolds Number Aerodynamics, Notre Dame, IN, 5-7 Jun. 1989; sponsored by Notre Dame Univ.

(NASA-TM-102018; E-4727; NAS 1.15:102018) Avail: NTIS HC A03/MF A01 CSCL 01/1

The unusually low frequency oscillation in the wake of an airfoil is explored experimentally as well as computationally for a NACA0012 airfoil with a glaze ice accretion at the leading edge. Experimentally, flow oscillations were observed at low frequencies that correspond to a Strouhal number of about 0.02. This occurred in the angle of attack range of 8 to 9 deg, near the onset of static stall for this airfoil. With a Navier-Stokes computation, limit-cycle oscillations in the flow and in the aerodynamic forces were also observed at low Strouhal numbers. However, the occurrence of the oscillation is found to depend on the turbulence model in use as well as the Reynolds number. Author

**N89-24269\*** # National Aeronautics and Space Administration. Lewis Research Center, Cleveland, OH.

# **CONSERVATIVE TREATMENT OF BOUNDARY INTERFACES FOR OVERLAID GRIDS AND MULTI-LEVEL GRID ADAPTATIONS**

YOUNG J. MOON (Sverdrup Technology, Inc., Cleveland, OH.) and MENG-SING LIOU 1989 18 p Presented at the 9th Computational Fluid Dynamics Conference, Buffalo, NY, 13-15 Jun. 1989; sponsored by the AIAA (NASA-TM-102080; E-4842; NAS 1.15:102080; AIAA-89-1980) Avail: NTIS HC A03/MF A01 CSCL 01/1

Conservative algorithms for boundary interfaces of overlaid grids are presented. The basic method is zeroth order, and is extended to a higher order method using interpolation and subcell decomposition. The present method, strictly based on a conservative constraint, is tested with overlaid grids for various applications of unsteady and steady supersonic inviscid flows with strong shock waves. The algorithm is also applied to a multi-level grid adaptation in which the next level finer grid is overlaid on the coarse base grid with an arbitrary orientation. Author

**N89-25119\*** # National Aeronautics and Space Administration. Lewis Research Center, Cleveland, OH.

# **NUMERICAL ANALYSIS OF SUPERSONIC FLOW THROUGH OSCILLATING CASCADE SECTIONS BY USING A DEFORMING GRID**

DENNIS L. HUFF and T. S. R. REDDY (Toledo Univ., OH.) 1989 18 p Presented at the 25th Joint Propulsion Conference, Monterey, CA, 10-12 Jul. 1989; cosponsored by the AIAA, ASME, SAE and ASEE (NASA-TM-102053; E-4805; NAS 1.15:102053; AIAA-89-2805) Avail: NTIS HC A03/MF A01 CSCL 01/1

A finite difference code was developed for modeling inviscid, unsteady supersonic flow by solution of the compressible Euler equations. The code uses a deforming grid technique to capture the motion of the airfoils and can model oscillating cascades with any arbitrary interblade phase angle. A flat plate cascade is analyzed, and results are compared with results from a small-perturbation theory. The results show very good agreement for both the unsteady pressure distributions and the integrated force predictions. The reason for using the numerical Euler code over a small-perturbation theory is the ability to model real airfoils that have thickness and camber. Sample predictions are presented for a section of the rotor on a supersonic throughflow compressor designed at NASA Lewis Research Center. Preliminary results indicate that two-dimensional, flat plate analysis predicts conservative flutter boundaries. Author

**N89-25121\*** # National Aeronautics and Space Administration. Lewis Research Center, Cleveland, OH.

# **LOW-SPEED WIND TUNNEL PERFORMANCE OF HIGH-SPEED COUNTERROTATION PROPELLERS AT ANGLE-OF-ATTACK**

CHRISTOPHER E. HUGHES and JOHN A. GAZZANIGA (Sverdrup Technology, Inc., Cleveland, OH.) 1989 47 p Presented at the 25th Joint Propulsion Conference, Monterey, CA, 10-12 Jul. 1989; cosponsored in part by AIAA, ASME, SAE, and ASEE (NASA-TM-102292; E-4883; NAS 1.15:102292; AIAA-89-2583) Avail: NTIS HC A03/MF A01 CSCL 01/1

The low-speed aerodynamic performance characteristics of

two advanced counterrotation pusher-propeller configurations with cruise design Mach numbers of 0.72 were investigated in the NASA Lewis 9- by 15-Foot Low-Speed Wind Tunnel. The tests were conducted at Mach number 0.20, which is representative of the aircraft take-off/landing flight regime. The investigation determined the effect of nonuniform inflow on the propeller performance characteristics for several blade angle settings and a range of rotational speeds. The inflow was varied by yawing the propeller model to angle-of-attack by as much as plus or minus 16 degrees and by installing on the counterrotation propeller test rig near the propeller rotors a model simulator of an aircraft engine support pylon and fuselage. The results of the investigation indicated that the low-speed performance of the counterrotation propeller configurations near the take-off target operating points were reasonable and were fairly insensitive to changes in model angle-of-attack without the aircraft pylon/fuselage simulators installed on the propeller test rig. When the aircraft pylon/fuselage simulators were installed, small changes in propeller performance were seen at zero angle-of-attack, but fairly large changes in total power coefficient and very large changes of aft-to-forward-rotor torque ratio were produced when the propeller model was taken to angle-of-attack. The propeller net efficiency, though, was fairly insensitive to any changes in the propeller flowfield conditions near the take-off target operating points. Author

**N89-25957\*** # National Aeronautics and Space Administration. Lewis Research Center, Cleveland, OH.

# **INFLUENCE OF THICKNESS AND CAMBER ON THE AEROELASTIC STABILITY OF SUPERSONIC THROUGHFLOW FANS: AN ENGINEERING APPROACH**

JOHN K. RAMSEY Jun. 1989 22 p (NASA-TM-101949; E-4642; NAS 1.15:101949) Avail: NTIS HC A03/MF A01 CSCL 01/1

An engineering approach was used to include the nonlinear effects of thickness and camber in an analytical aeroelastic analysis of cascades in supersonic axial flow (supersonic leading-edge locus). A hybrid code using Lighthill's nonlinear piston theory and Lane's linear potential theory was developed to include these nonlinear effects. Lighthill's theory was used to calculate the unsteady pressures on the noninterference surface regions of the airfoils in cascade. Lane's theory was used to calculate the unsteady pressures on the remaining interference surface regions. Two airfoil profiles was investigated (a supersonic throughflow fan design and a NACA 66-206 airfoil with a sharp leading edge). Results show that compared with predictions of Lane's potential theory for flat plates, the inclusion of thickness (with or without camber) may increase or decrease the aeroelastic stability, depending on the airfoil geometry and operating conditions. When thickness effects are included in the aeroelastic analysis, inclusion of camber will influence the predicted stability in proportion to the magnitude of the added camber. The critical interblade phase angle, depending on the airfoil profile and operating conditions, may also be influenced by thickness and camber. Compared with predictions of Lane's linear potential theory, the inclusion of thickness and camber decreased the aerodynamic stiffness and increased the aerodynamic damping at Mach 2 and 2.95 for a cascade of supersonic throughflow fan airfoils oscillating 180 degrees out of phase at a reduced frequency of 0.1. Author

**N89-29323\*** # National Aeronautics and Space Administration. Lewis Research Center, Cleveland, OH.

# **STOL AND STOVL HOT GAS INGESTION AND AIRFRAME HEATING TESTS IN THE NASA LEWIS 9- BY 15-FOOT LOW-SPEED WIND TUNNEL**

ALBERT L. JOHNS Sep. 1989 33 p (NASA-TM-102101; E-4864; NAS 1.15:102101) Avail: NTIS HC A03/MF A01 CSCL 01/1

Short takeoff and landing (STOL) and advanced short takeoff and vertical landing (STOVL) aircraft are being pursued for deployment near the end of this century. These concepts offer unique capabilities not seen in conventional aircraft: for example, shorter takeoff distances and the ability to operate from damaged runways and remote sites. However, special technology is critical

## 02 AERODYNAMICS

to the development of this unique class of aircraft. Some of the real issues that are associated with these concepts are hot gas ingestion and airframe heating while in ground effects. Over the past nine years, NASA Lewis Research Center has been involved in several cooperative programs in the 9- by 15 Foot Low-Speed Wind Tunnel (LSWT) to establish a database for hot gas ingestion and airframe heating. The modifications are presented that were made in the 9- by 15-Foot LSWT, including the evolution of the ground plane, model support system, and tunnel sidewalls; and flow visualization techniques, instrumentation, test procedures, and test results. The 9- by 15-Foot LSWT tests were conducted at full scale exhaust nozzle pressure ratios. The headwind velocities varied from 8 to 120 kn depending on the concept (STOL or STOVL). Typical compressor-face distortions (pressure and temperature), ground plane contours, and model surface temperature profiles are presented. Author

**N89-29329\*#** Kansas Univ. Center for Research, Inc., Lawrence. Flight Research Lab.

### **TURBULENT SWIRLING JETS WITH EXCITATION Interim Report**

RAHMAT TAGHAVI and SAEED FAROKHI Mar. 1988 230 p  
(Contract NCC3-56)  
(NASA-CR-180895; NAS 1.26:180895) Avail: NTIS HC A11/MF A01 CSCL 01/1

An existing cold-jet facility at NASA Lewis Research Center was modified to produce swirling flows with controllable initial tangential velocity distribution. Two extreme swirl profiles, i.e., one with solid-body rotation and the other predominated by a free-vortex distribution, were produced at identical swirl number of 0.48. Mean centerline velocity decay characteristics of the solid-body rotation jet flow exhibited classical decay features of a swirling jet with  $S = 0.48$  reported in the literature. However, the predominantly free-vortex distribution case was on the verge of vortex breakdown, a phenomenon associated with the rotating flows of significantly higher swirl numbers, i.e.,  $S$  sub crit greater than or equal to 0.06. This remarkable result leads to the conclusion that the integrated swirl effect, reflected in the swirl number, is inadequate in describing the mean swirling jet behavior in the near field. The relative size (i.e., diameter) of the vortex core emerging from the nozzle and the corresponding tangential velocity distribution are also controlling factors. Excitability of swirling jets is also investigated by exciting a flow with a swirl number of 0.35 by plane acoustic waves at a constant sound pressure level and at various frequencies. It is observed that the cold swirling jet is excitable by plane waves, and that the instability waves grow about 50 percent less in peak r.m.s. amplitude and saturate further upstream compared to corresponding waves in a jet without swirl having the same axial mass flux. The preferred Strouhal number based on the mass-averaged axial velocity and nozzle exit diameter for both swirling and nonswirling flows is 0.4. Author

## 03

### **AIR TRANSPORTATION AND SAFETY**

Includes passenger and cargo air transport operations; and aircraft accidents.

**A89-27739\*#** Massachusetts Inst. of Tech., Cambridge.  
**INVESTIGATION OF SURFACE WATER BEHAVIOR DURING GLAZE ICE ACCRETION**

R. JOHN HANSMAN, JR. and STEPHEN R. TURNOCK (MIT, Cambridge, MA) Journal of Aircraft (ISSN 0021-8669), vol. 26, Feb. 1989, p. 140-147. Research supported by FAA. Previously cited in issue 07, p. 943, Accession no. A88-22079. refs  
(Contract NAG3-666; NGL-22-009-640)  
Copyright

**A89-28192\*** National Aeronautics and Space Administration. Lewis Research Center, Cleveland, OH.

### **AN OVERVIEW OF THE CURRENT NASA PROGRAM ON AIRCRAFT ICING RESEARCH**

RICHARD J. RANAUDO, ANDREW L. REEHORST, and MARK G. POTAPCZUK (NASA, Lewis Research Center, Cleveland, OH) SAE, Aerospace Technology Conference and Exposition, Anaheim, CA, Oct. 3-6, 1988. 20 p. refs  
(SAE PAPER 881386) Copyright

The NASA Lewis Research Center is presently conducting an aircraft icing research program, the major thrust of which is to advance technologies that improve our ability to model the icing phenomenon and its effect on aircraft. The approach employs three interrelated elements: analysis; wind tunnel experiments; and, considerable flight testing in natural icing clouds. This paper presents a brief overview of this program with emphasis on recent accomplishments. Author

**A89-28451\*#** Massachusetts Inst. of Tech., Cambridge.

### **MODELING OF SURFACE ROUGHNESS EFFECTS ON GLAZE ICE ACCRETION**

R. JOHN HANSMAN, JR., KEIKO YAMAGUCHI (MIT, Cambridge, MA), BRIAN BERKOWITZ (Sverdrup Technology, Inc., Middleburg Heights, OH), and M. POTAPCZUK (NASA, Lewis Research Center, Cleveland, OH) AIAA, Aerospace Sciences Meeting, 27th, Reno, NV, Jan. 9-12, 1989. 9 p. refs  
(Contract NAG3-666; NGL-22-009-640)  
(AIAA PAPER 89-0734) Copyright

The cause and effects of roughness on accreting glaze ice surfaces were studied with microvideo observations. Distinct zones of surface water behavior were observed, including a smooth wet zone in the stagnation region with a uniform water film, a rough zone where surface tension effects caused coalescence of surface water into stationary beads, and a zone where roughness elements grow into horn shapes. In addition, a zone where surface water ran back as rivulets and a dry zone where rime feathers formed were observed. The locations and behaviors of these zones are discussed. A simple multizone modification to the glaze ice accretion model is proposed to include spatial variability in surface roughness. Two test cases using the multizone model showed significant improvements for the prediction of glaze ice shapes. R.B.

**A89-30650\*#** Texas A&M Univ., College Station.  
**ON ICE SHAPE PREDICTION METHODOLOGIES AND COMPARISON WITH EXPERIMENTAL DATA**

K. D. KORKAN and R. K. BRITTON (Texas A & M University, College Station) AIAA, Aerospace Sciences Meeting, 27th, Reno, NV, Jan. 9-12, 1989. 14 p. refs  
(Contract NAG3-626)  
(AIAA PAPER 89-0732) Copyright

Comparisons are made between the analysis of Wilder (1969), Bragg (1982), and the ice shape predictions of LEWICE given a specific airfoil geometry and set of meteorological conditions. Also, comparisons are made between the actual ice shapes as found in flight tests of the NASA Lewis RC Twin Otter and that predicted by the approximate methods noted earlier and LEWICE. Further, an investigation of two important parameters in the analysis of LEWICE has been made. Time stepping and initial surface roughness has been varied to identify any trends in the results. Guidelines have been identified for the correlation of these two parameters with the results in terms of atmospheric conditions. The range of meteorological conditions chosen, such as droplet diameter, free air temperature, and liquid water content has allowed rime, mixed, and glaze ice shapes at the leading edge of an airfoil to be investigated. Author

**A89-54803\*** Massachusetts Inst. of Tech., Cambridge.  
**THE INFLUENCE OF ICE ACCRETION PHYSICS ON THE FORECASTING OF AIRCRAFT ICING CONDITIONS**

R. JOHN HANSMAN, JR. (MIT, Cambridge, MA) IN: International Conference on the Aviation Weather System, 3rd, Anaheim, CA, Jan. 30-Feb. 3, 1989, Preprints. Boston, MA, American



Meteorological Society, 1989, p. 154-158. Research supported by FAA. refs  
(Contract NGL-22-009-640; NAG3-666)  
Copyright

The physics which control aircraft ice accretion are reviewed in the context of identifying and forecasting hazardous icing conditions. The severity of aircraft icing is found to be extremely sensitive to temperature, liquid water content and droplet size distribution particularly near the transition between rime and mixed icing. The difficulty in measurement and the variability of these factors with altitude, position and time coupled with variable aircraft sensitivity make forecasting and identifying icing conditions difficult. Automated Pilot Reports (PIREPS) are suggested as one mechanism for improving the data base necessary to forecast icing conditions. Author

**N89-11725\*#** California State Univ., Long Beach.  
**EFFECTS OF ENVIRONMENTALLY IMPOSED ROUGHNESS ON AIRFOIL PERFORMANCE** Final Contractor Report  
TUNCER CEBECI Jun. 1987 44 p Presented at the Von Karman Inst. for Fluid Dynamics Lecture Series on Influence of Environmental Factors on Aircraft Wing Performance, 16-18 Feb. 1987 Previously announced as N88-15778  
(Contract NAG3-601; NSF MEA-80-18565)  
(NASA-CR-179639; NAS 1.26:179639) Avail: NTIS HC A03/MF A01 CSDL 01/1

The experimental evidence for the effects of rain, insects, and ice on airfoil performance are examined. The extent to which the available information can be incorporated in a calculation method in terms of change of shape and surface roughness is discussed. The methods described are based on the interactive boundary procedure of Cebeci or on the thin layer Navier Stokes procedure developed at NASA. Cases presented show that extensive flow separation occurs on the rough surfaces. Author

**N89-25978\*#** National Aeronautics and Space Administration. Lewis Research Center, Cleveland, OH.  
**INVESTIGATION OF THE FLOW IN THE DIFFUSER SECTION OF THE NASA LEWIS ICING RESEARCH TUNNEL**  
HAROLD E. ADDY, JR. and THEO G. KEITH, JR. (Toledo Univ., OH.) Jan. 1989 13 p Presented at the 27th Aerospace Sciences Meeting, Reno, NV, 9-12 Jan. 1989; sponsored by AIAA Previously announced in IAA as A89-28455  
(NASA-TM-102087; E-4849; NAS 1.15:102087; AIAA-89-0755)  
Avail: NTIS HC A03/MF A01 CSDL 01/3

The flow in the diffuser section of the Icing Research Wind Tunnel at NASA Lewis Research Center is investigated using both tunnel calibration measurements and numerical simulation techniques. Local pressure and temperature measurements are made to establish velocity and temperature profiles in the diffuser of the tunnel. These profiles are compared with similar measurements made prior to renovating the equipment which generates the tunnel's icing cloud. This comparison indicates the manner in which this change affected the flow. The measured data were also compared with a numerical simulation of the flow to help understand how such changes may favorably alter the tunnel flow. Author

## 05

### AIRCRAFT DESIGN, TESTING AND PERFORMANCE

Includes aircraft simulation technology.

**A89-25429\*#** Purdue Univ., West Lafayette, IN.  
**PROPELLER/WING INTERACTION**  
DAVID P. WITKOWSKI, ROBERT T. JOHNSTON, and JOHN P. SULLIVAN (Purdue University, West Lafayette, IN) AIAA, Aerospace Sciences Meeting, 27th, Reno, NV, Jan. 9-12, 1989.

13 p. refs  
(Contract NSG-3134)  
(AIAA PAPER 89-0535) Copyright

The present experimental investigation of the steady-state and unsteady-state effects due to the interaction between a tractor propeller's wake and a wing employs, in the steady case, wind tunnel measurements at low subsonic speed; results are obtained which demonstrate wing performance response to variations in configuration geometry. Other steady-state results involve the propeller-hub lift and side-force due to the wing's influence on the propeller. The unsteady effects of interaction were studied through flow visualization of propeller-tip vortex distortion over a wing, again using a tractor-propeller configuration. O.C.

**A89-25571\*#** Innovative Dynamics, Ithaca, NY.  
**DISTRIBUTED ICE ACCRETION SENSOR FOR SMART AIRCRAFT STRUCTURES**

J. J. GERARDI and G. A. HICKMAN (Innovative Dynamics, Ithaca, NY) AIAA, Aerospace Sciences Meeting, 27th, Reno, NV, Jan. 9-12, 1989. 8 p. refs  
(Contract NAS3-25200)  
(AIAA PAPER 89-0772) Copyright

A distributed ice accretion sensor is presented, based on the concept of smart structures. Ice accretion is determined using spectral techniques to process signals from piezoelectric sensors integral to the airfoil skin. Frequency shifts in the leading edge structural skin modes are correlated to ice thickness. It is suggested that this method may be used to detect ice over large areas with minimal hardware. Results are presented from preliminary tests to measure simulated ice growth. R.B.

**A89-33754\*#** Lockheed Aeronautical Systems Co., Burbank, CA.

**INTERIOR NOISE IN THE UNTREATED GULFSTREAM II PROPFAN TEST ASSESSMENT (PTA) AIRCRAFT**

H. L. KUNTZ and R. A. PRYDZ (Lockheed Aeronautical Systems Co., Kelly Johnson Research and Development Center, Burbank, CA) AIAA, Aeroacoustics Conference, 12th, San Antonio, TX, Apr. 10-12, 1989. 9 p.  
(Contract NAS3-24339)  
(AIAA PAPER 89-1119) Copyright

Interior noise on the Gulfstream II Propfan Test Assessment (PTA) aircraft was measured using 19 wing, 22 fuselage, and 32 cabin-interior microphones to determine the sources of the cabin noise. Results from ground and flight test acoustic and vibration measurements and analyses show that the major source of cabin noise was the airborne propfan blade passage frequency tones. The radiated sound pressure levels and the richness of the harmonic content of the propfan increased with increasing altitude. The acoustic output of the propfan also depended on the shaft power, helical Mach number, and blade passage frequency. I.S.

**A89-39193\*#** Wichita State Univ., KS.  
**ELECTROIMPULSE DEICING - ELECTRODYNAMIC SOLUTION BY DISCRETE ELEMENTS**

W. D. BERNHART and R. L. SCHRAG (Wichita State University, KS) Journal of Aircraft (ISSN 0021-8669), vol. 26, June 1989, p. 547-553. Previously cited in issue 07, p. 945, Accession no. A88-22016. refs  
(Contract NAG3-284)  
Copyright

**A89-39194\*#** Toledo Univ., OH.  
**TWO-DIMENSIONAL SIMULATION OF ELECTROTHERMAL DEICING OF AIRCRAFT COMPONENTS**

W. B. WRIGHT, T. G. KEITH, JR., and K. J. DE WITT (Toledo, University, OH) Journal of Aircraft (ISSN 0021-8669), vol. 26, June 1989, p. 554-562. Previously cited in issue 07, p. 946, Accession no. A88-22208. refs  
(Contract NAG3-72)  
Copyright

## 05 AIRCRAFT DESIGN, TESTING AND PERFORMANCE

**A89-41093\*** Texas A&M Univ., College Station.

### **GENERIC ICING EFFECTS ON FORWARD FLIGHT PERFORMANCE OF A MODEL HELICOPTER ROTOR**

ANA F. TINETTI and KENNETH D. KORKAN (Texas A & M University, College Station) Vertica (ISSN 0360-5450), vol. 13, no. 1, 1989, p. 63-85. refs  
(Contract NAG3-626)  
Copyright

An experimental program using a commercially available model helicopter has been conducted in the TAMU 7 ft x 10 ft Subsonic Wind Tunnel to investigate main rotor performance degradation due to generic ice adhesion. Base and iced performance data were gathered as functions of fuselage incidence, blade collective pitch, main rotor rotational velocity, and freestream velocity. The experimental values have shown that, in general, the presence of generic ice introduces decrements in performance caused by leading edge separation regions and increased surface roughness. In addition to the expected changes in aerodynamic forces caused by variations in test Reynolds number, forward flight data seemed to be influenced by changes in freestream and rotational velocity. The dependence of the data upon such velocity variations was apparently enhanced by increases in blade chord. Author

**A89-50802\*#** National Aeronautics and Space Administration. Lewis Research Center, Cleveland, OH.

### **A SUPERSONIC THROUGH-FLOW FAN ENGINE AIRFRAME INTEGRATION STUDY**

PAUL J. BARNHART (NASA, Lewis Research Center; Sverdrup Technology, Inc., Cleveland, OH) AIAA, AHS, and ASEE, Aircraft Design, Systems and Operations Conference, Seattle, WA, July 31-Aug. 2, 1989. 10 p. refs  
(Contract NAS3-25266)  
(AIAA PAPER 89-2140)

A study is undertaken to investigate the engine airframe integration effects for supersonic through-flow fan engines installed on a Mach 3.20 supersonic cruise vehicle. Six different supersonic through-flow fan engine installations covering the effects of engine size, nacelle contour, nacelle placement, and approximate bypass plume effects are presented. The different supersonic through-flow fan installations are compared with a conventional turbine bypass engine configuration on the same basic airframe. The supersonic through-flow fan engine integrations are shown to be comparable to the turbine bypass engine configuration on the basis of installed nacelle wave drag. The supersonic through-flow fan engine airframe integrated vehicles have superior aerodynamic performance on the basis of maximum lift-to-drag ratio than the turbine bypass engine installation over the entire operating Mach number range from 1.10 to 3.20. When approximate bypass plume modeling is included, the supersonic through-flow fan engine configuration shows even larger improvements over the turbine bypass engine configuration. Author

**N89-13428\*#** Sverdrup Technology, Inc., Cleveland, OH.  
**ANALYTICAL ICE SHAPE PREDICTIONS FOR FLIGHT IN NATURAL ICING CONDITIONS**

BRIAN M. BERKOWITZ and JAMES T. RILEY (Federal Aviation Agency, Atlantic City, N.J.) Dec. 1988 39 p  
(Contract NAS3-24105; DTFA-03-81-A-00209)  
(NASA-CR-182234; E-4547; NAS 1.26:182234; DOT/FAA/CT-88/19) Avail: NTIS HC A03/MF A01 CSDL 01/3

LEWICE is an analytical ice prediction code that has been evaluated against icing tunnel data, but on a more limited basis against flight data. Ice shapes predicted by LEWICE is compared with experimental ice shapes accreted on the NASA Lewis Icing Research Aircraft. The flight data selected for comparison includes liquid water content recorded using a hot wire device and droplet distribution data from a laser spectrometer; the ice shape is recorded using stereo photography. The main findings are as follows: (1) An equivalent sand grain roughness correlation different from that used for LEWICE tunnel comparisons must be employed to obtain satisfactory results for flight; (2) Using this correlation and making no other changes in the code, the comparisons to

ice shapes accreted in flight are in general as good as the comparisons to ice shapes accreted in the tunnel (as in the case of tunnel ice shapes, agreement is least reliable for large glaze ice shapes at high angles of attack); (3) In some cases comparisons can be somewhat improved by utilizing the code so as to take account of the variation of parameters such as liquid water content, which may vary significantly in flight. Author

**N89-15107\*#** Sverdrup Technology, Inc., Cleveland, OH.

### **HASA: HYPERSONIC AEROSPACE SIZING ANALYSIS FOR THE PRELIMINARY DESIGN OF AEROSPACE VEHICLES Final Contractor Report**

GARY J. HARLOFF and BRIAN M. BERKOWITZ Nov. 1988 60 p

(Contract NAS3-24105)

(NASA-CR-182226; E-4496; NAS 1.26:182226) Avail: NTIS HC A04/MF A01 CSDL 01/3

A review of the hypersonic literature indicated that a general weight and sizing analysis was not available for hypersonic orbital, transport, and fighter vehicles. The objective here is to develop such a method for the preliminary design of aerospace vehicles. This report describes the developed methodology and provides examples to illustrate the model, entitled the Hypersonic Aerospace Sizing Analysis (HASA). It can be used to predict the size and weight of hypersonic single-stage and two-stage-to-orbit vehicles and transports, and is also relevant for supersonic transports. HASA is a sizing analysis that determines vehicle length and volume, consistent with body, fuel, structural, and payload weights. The vehicle component weights are obtained from statistical equations for the body, wing, tail, thermal protection system, landing gear, thrust structure, engine, fuel tank, hydraulic system, avionics, electrical system, equipment payload, and propellant. Sample size and weight predictions are given for the Space Shuttle orbiter and other proposed vehicles, including four hypersonic transports, a Mach 6 fighter, a supersonic transport (SST), a single-stage-to-orbit (SSTO) vehicle, a two-stage Space Shuttle with a booster and an orbiter, and two methane-fueled vehicles. Author

**N89-19289\*#** Lockheed-Georgia Co., Marietta. Advanced Design Div.

### **MULTIPLE-PURPOSE SUBSONIC NAVAL AIRCRAFT (MPSNA) MULTIPLE APPLICATION PROPFAN STUDY (MAPS) Final Report**

D. M. WINKELJOHN and C. H. MAYRAND Mar. 1986 88 p  
(Contract NAS3-24528)

(NASA-CR-175096; NAS 1.26:175096; LG86ER0053) Avail: NTIS HC A05/MF A01 CSDL 01/3

A conceptual design study compared a selected propfan-powered aircraft to a turbofan-powered aircraft for multiple Navy carrier-based support missions in the 1995 timeframe. Conventional takeoff and landing (CTOL) propfan and turbofan-powered designs and short takeoff/vertical landing (STOVL) propfan-powered designs are presented. Ten support mission profiles were defined and the aircraft were sized to be able to perform all ten missions. Emphasis was placed on efficient high altitude loiter for Airborne Early Warning (AEW) and low altitude high speed capability for various offensive and tactical support missions. The results of the study show that the propfan-powered designs have lighter gross weights, lower fuel fractions, and equal or greater performance capability than the turbofan-powered designs. Various sensitivities were developed in the study, including the effect of using single-rotation versus counter-rotation propfans and the effect of AEW loiter altitude on vehicle gross weight and empty weight. A propfan technology development plan was presented which illustrates that the development of key components can be achieved without accelerated schedules through the extension of current and planned government and civil propfan programs. Author



**N89-25993\*** Ohio State Univ., Columbus. Dept. of Electrical Engineering.

**ANALYSIS OF MODIFIED SMI METHOD FOR ADAPTIVE ARRAY WEIGHT CONTROL M.S. Thesis**

RONALD LOUIS DILSAVOR 1989 99 p

(Contract NAG3-536)

(NASA-CR-185493; NAS 1.26:185493) Avail: NTIS HC A05/MF A01 CSCL 01/3

An adaptive array is used to receive a desired signal in the presence of weak interference signals which need to be suppressed. A modified sample matrix inversion (SMI) algorithm controls the array weights. The modification leads to increased interference suppression by subtracting a fraction of the noise power from the diagonal elements of the covariance matrix. The modified algorithm maximizes an intuitive power ratio criterion. The expected values and variances of the array weights, output powers, and power ratios as functions of the fraction and the number of snapshots are found and compared to computer simulation and real experimental array performance. Reduced-rank covariance approximations and errors in the estimated covariance are also described.

Author

## 06

## AIRCRAFT INSTRUMENTATION

Includes cockpit and cabin display devices; and flight instruments.

**A89-45107\*** Northwestern Univ., Evanston, IL.

**REVIEW OF FD-TD NUMERICAL MODELING OF ELECTROMAGNETIC WAVE SCATTERING AND RADAR CROSS SECTION**

ALLEN TAFLOVE (Northwestern University, Evanston, IL) and KORADA R. UMASHANKAR (Illinois, University, Chicago) IEEE, Proceedings (ISSN 0018-9219), vol. 77, May 1989, p. 682-699. refs

(Contract F30602-79-C-0039; F19628-82-C-0140; NAG3-635; NSF ECS-85-15777)

Copyright

Applications of the finite-difference time-domain (FD-TD) method for numerical modeling of electromagnetic wave interactions with structures are reviewed, concentrating on scattering and radar cross section (RCS). A number of two- and three-dimensional examples of FD-TD modeling of scattering and penetration are provided. The objects modeled range in nature from simple geometric shapes to extremely complex aerospace and biological systems. Rigorous analytical or experimental validations are provided for the canonical shapes, and it is shown that FD-TD predictive data for near fields and RCS are in excellent agreement with the benchmark data. It is concluded that with continuing advances in FD-TD modeling theory for target features relevant to the RCS problems and in vector and concurrent supercomputer technology, it is likely that FD-TD numerical modeling will occupy an important place in RCS technology in the 1990s and beyond.

I.E.

**N89-13429\*** Toledo Univ., OH. Dept. of Chemical Engineering.

**A COMPARISON OF NUMERICAL METHODS FOR THE PREDICTION OF TWO-DIMENSIONAL HEAT TRANSFER IN AN ELECTROTHERMAL DEICER PAD M.S. Thesis. Final Contractor Report**

WILLIAM B. WRIGHT Washington NASA Dec. 1988 138 p (Contract NAG3-72)

(NASA-CR-4202; E-4380; NAS 1.26:4202) Avail: NTIS HC

A07/MF A01 CSCL 01/4

Transient, numerical simulations of the deicing of composite aircraft components by electrothermal heating have been performed in a 2-D rectangular geometry. Seven numerical schemes and four solution methods were used to find the most

efficient numerical procedure for this problem. The phase change in the ice was simulated using the Enthalpy method along with the Method for Assumed States. Numerical solutions illustrating deicer performance for various conditions are presented. Comparisons are made with previous numerical models and with experimental data. The simulation can also be used to solve a variety of other heat conduction problems involving composite bodies.

Author

**N89-14235\*** Toledo Univ., OH. Dept. of Engineering Science.

**A NUMERICAL SIMULATION OF THE FULL TWO-DIMENSIONAL ELECTROTHERMAL DE-ICER PAD Ph.D. Thesis Final Report**

KONSTANTY C. MASIULANIEC Nov. 1988 206 p

(Contract NAG3-72)

(NASA-CR-4194; E-4381; NAS 1.26:4194) Avail: NTIS HC A10/MF A01 CSCL 01/4

The ability to predict the time-temperature history of electrothermal de-icer pads is important in the subsequent design of improved and more efficient versions. These de-icer pads are installed near the surface of aircraft components, for the specific purpose of removing accreted ice. The proposed numerical model can incorporate the full 2-D geometry through a section of a region (i.e., section of an airfoil), that current 1-D numerical codes are unable to do. Thus, the effects of irregular layers, curvature, etc., can now be accounted for in the thermal transients. Each layer in the actual geometry is mapped via a body-fitted coordinate transformation into uniform, rectangular computational grids. The relevant heat transfer equations are transformed and discretized. To model the phase change that might occur in any accreted ice, in an enthalpy formulation the phase change equations are likewise transformed and discretized. The code developed was tested against numerous classical numerical solutions, as well as against experimental de-icing data on a UH1H rotor blade obtained from the NASA Lewis Research Center. The excellent comparisons obtained show that this code can be a useful tool in predicting the performance of current de-icer models, as well as in the designing of future models.

Author

## 07

## AIRCRAFT PROPULSION AND POWER

Includes prime propulsion systems and systems components, e.g., gas turbine engines and compressors; and onboard auxiliary power plants for aircraft.

**A89-12307\*** Florida Univ., Gainesville.

**CALCULATIONS OF THE UNSTEADY, THREE-DIMENSIONAL FLOW FIELD INSIDE A MOTORED WANKEL ENGINE**

ERLENDUR STEINTHORSSON, TOM I.-P. SHIH (Florida, University, Gainesville), HAROLD J. SCHOCK, JR. (Michigan State University, East Lansing), and JAMES STEGEMAN (NASA, Lewis Research Center, Cleveland, OH) SAE, International Congress and Exposition, Detroit, MI, Feb. 29-Mar. 4, 1988. 31 p. refs (Contract NAG3-363)

(SAE PAPER 880625) Copyright

A computer program (referred to as UF-LRC-3D) was developed for studying the unsteady, three-dimensional flow field inside the combustion chambers of motored Wankel engines as a function of engine design and operating parameters. This paper presents the details of the governing equations and the numerical method used by UF-LRC-3D. Also presented are numerical solutions generated by UF-LRC-3D showing the velocity field inside a motored Wankel engine, the mixing of nonhomogeneous fuel-air mixtures that enter through the intake port, and the mixing that takes place when a gaseous fuel is injected into the combustion chamber during compression.

Author

**A89-12953\*#** National Aeronautics and Space Administration, Washington, DC.

### RETURN OF THE TURBOPROPS

JOHN R. FACEY (NASA, Office of Aeronautics and Space Technology, Washington, DC), JOHN B. WHITLOW, JR., G. KEITH SIEVERS, JOHN GROENEWEG (NASA, Lewis Research Center, Cleveland, OH), KEVIN SHEPHERD, and WILLIAM HENDERSON (NASA, Langley Research Center, Hampton, VA) Aerospace America (ISSN 0740-722X), vol. 26, Oct. 1988, p. 14-18, 20, 22, 23, 35.

Copyright

Recent advances in propfan development for commercial aircraft cruising at high transonic speeds are discussed in a series of brief overviews and illustrated with photographs and diagrams. The efficiency and performance advantages and the problem of noise are examined; the history of turboprop design since the 1950s is recalled; NASA, DOT, FAA, and DOD turboprop projects are described; and the results of wind-tunnel and flight tests on particular propeller models are reviewed. Current trends in aircraft reconfiguration and acoustic redesign to reduce cabin noise levels are also surveyed. T.K.

**A89-13504\*#** National Aeronautics and Space Administration, Lewis Research Center, Cleveland, OH.

### NASA/INDUSTRY ADVANCED TURBOPROP TECHNOLOGY PROGRAM

JOSEPH A. ZIEMIANSKI and JOHN B. WHITLOW, JR. (NASA, Lewis Research Center, Cleveland, OH) IN: ICAS, Congress, 16th, Jerusalem, Israel, Aug. 28-Sept. 2, 1988, Proceedings. Volume 1. Washington, DC, American Institute of Aeronautics and Astronautics, Inc., 1988, p. LIV-LXVII. Previously announced in STAR as N88-24641. refs

Copyright

Experimental and analytical effort shows that use of advanced turboprop (propfan) propulsion instead of conventional turbofans in the older narrow-body airline fleet could reduce fuel consumption for this type of aircraft by up to 50 percent. The NASA Advanced Turboprop (ATP) program was formulated to address the key technologies required for these thin, swept-blade propeller concepts. A NASA, industry, and university team was assembled to develop and validate applicable design codes and prove by ground and flight test the viability of these propeller concepts. Some of the history of the ATP Project, an overview of some of the issues, and a summary of the technology developed to make advanced propellers viable in the high-subsonic cruise speed application are presented. The ATP program was awarded the prestigious Robert J. Collier Trophy for the greatest achievement in aeronautics and astronautics in America in 1987. Author

**A89-13725\*#** National Aeronautics and Space Administration, Lewis Research Center, Cleveland, OH.

### RECENT ADVANCES IN CAPACITANCE TYPE OF BLADE TIP CLEARANCE MEASUREMENTS

JOHN P. BARRANGER (NASA, Lewis Research Center, Cleveland, OH) AIAA, NASA, and AFWAL, Conference on Sensors and Measurements Techniques for Aeronautical Applications, Atlanta, GA, Sept. 7-9, 1988. 9 p. Previously announced in STAR as N88-25460. refs (AIAA PAPER 88-4664)

Two recent electronic advances at NASA-Lewis that meet the blade tip clearance needs of a wide class of fans, compressors, and turbines are described. The first is a frequency modulated (FM) oscillator that requires only a single low cost ultrahigh frequency operational amplifier. Its carrier frequency is 42.8 MHz when used with a 61 cm long hermetically sealed coaxial cable. The oscillator can be calibrated in the static mode and has a negative peak frequency deviation of 400 kHz for a typical rotor blade. High temperature performance tests of the probe and 13 cm of the adjacent cable show good accuracy up to 600 C, the maximum which produces a clearance error of + or - 10 microns at a clearance of 500 microns. In the second advance, a guarded probe configuration allows a longer cable capacitance. The capacitance of the probe is part of a small time constant feedback

in a high speed operational amplifier. The solution of the governing differential equation is applied to a ramp type of input. The results show an amplifier output that contains a term which is proportional to the derivative of the feedback capacitance. The capacitance is obtained by subtracting a balancing reference channel followed by an integration stage. Author

**A89-15080\*** National Aeronautics and Space Administration, Lewis Research Center, Cleveland, OH.

### CRUISE NOISE OF AN ADVANCED COUNTERROTATION TURBOPROP MEASURED FROM AN ADJACENT AIRCRAFT

RICHARD P. WOODWARD, IRVIN J. LOEFFLER, and JAMES H. DITTMAR (NASA, Lewis Research Center, Cleveland, OH) IN: NOISE-CON 88 - Noise control design: Methods and practice; Proceedings of the National Conference on Noise Control Engineering, West Lafayette, IN, June 20-22, 1988. Poughkeepsie, NY, Institute of Noise Control Engineering, 1988, p. 105-110. refs

Copyright

Acoustic test results are presented for a full-scale counterrotation demonstrator engine installed on a Boeing 727 aircraft in place of the right-side turbofan engine. Sideline acoustic data were acquired from a Learjet chase aircraft instrumented with noise and wing-tip flush mount microphones. Data are presented for a 47.2-m sideline at several engine operating conditions and flight Mach numbers of 0.50 and 0.72. B.J.

**A89-16102\*#** Michigan State Univ., East Lansing.

### THERMAL MEASUREMENTS FOR JETS IN DISTURBED AND UNDISTURBED CROSSWIND CONDITIONS

CANDACE E. WARK and JOHN F. FOSS (Michigan State University, East Lansing) AIAA Journal (ISSN 0001-1452), vol. 26, Aug. 1988, p. 901, 902. refs (Contract NAG3-245)

Copyright

A direct comparison is made of the thermal field properties for a low-disturbance and a high-disturbance level condition affecting the low-temperature air jets introduced into gas turbine combustor aft sections in order both to cool the high-temperature gases and quench the combustion reactions. Sixty-four fast-response thermocouples were simultaneously sampled and corrected for their time constant effect at a downstream plane close to the jet exit. Histograms formed from independent samples were sufficiently smooth to approximate a pdf. O.C.

**A89-17941\*#** National Aeronautics and Space Administration, Lewis Research Center, Cleveland, OH.

### EXPERIMENTAL INVESTIGATION OF PROPFAN AEROELASTIC RESPONSE IN OFF-AXIS FLOW WITH MISTUNING

ORAL MEHMED (NASA, Lewis Research Center, Cleveland, OH) and DURBHA V. MURTHY (Toledo University, OH) AIAA, ASME, SAE, and ASEE, Joint Propulsion Conference, 24th, Boston, MA, July 11-13, 1988. 28 p. Previously announced in STAR as N88-28344. refs (AIAA PAPER 88-3153)

Measured vibratory strain amplitudes from off-axis flow are compared for the blades of two, 8-bladed propfan model rotors with mistuning. One rotor had inherent mistuning. The other was intentionally mistuned by replacing every other blade of the first rotor with a blade of same geometry but different frequencies and mode shapes. The data shows that the intentional mistuning had a beneficial effect on the aeroelastic response of the propfan motors for a wide range of off-axis flow angles, blade pitch angles, and rotational speeds. Statistical trends of blade strain amplitudes are compared for both the rotors in terms of the ratio of the maximum to the mean and the coefficient of variation. Author

**A89-17942\*#** National Aeronautics and Space Administration, Lewis Research Center, Cleveland, OH.

### AEROELASTIC RESPONSE OF METALLIC AND COMPOSITE PROPFAN MODELS IN YAWED FLOW

KRISHNA RAO KAZA, ORAL MEHMED, G. V. NARAYANAN

(NASA, Lewis Research Center, Cleveland, OH), and MARC H. WILLIAMS (Purdue University, West Lafayette, IN) AIAA, ASME, SAE, and ASEE, Joint Propulsion Conference, 24th, Boston, MA, July 11-13, 1988. 26 p. Previously announced in STAR as N88-29807. refs  
(AIAA PAPER 88-3154)

An analytical investigation of aeroelastic response of metallic and composite propfan models in yawed flow was performed. The analytical model is based on the normal modes of a rotating blade and the three-dimensional unsteady lifting surface aerodynamic theory including blade mistuning. The calculated blade stresses or strains are compared with published wind tunnel data on two metallic and three composite propfan wind tunnel models. The comparison shows a good agreement between theory and experiment. Additional parametric results indicate that blade response is very sensitive to the blade stiffness and also to blade frequency and mode shape mistuning. From these findings, it is concluded that both frequency and mode shape mistuning should be included in aeroelastic response analysis. Furthermore, both calculated and measured strains show that combined blade frequency and mode shape mistuning has beneficial effects on response due to yawed flow. Author

**A89-17943\*#** National Aeronautics and Space Administration. Lewis Research Center, Cleveland, OH.

**VIBRATION, PERFORMANCE, FLUTTER AND FORCED RESPONSE CHARACTERISTICS OF A LARGE-SCALE PROPFAN AND ITS AEROELASTIC MODEL**

RICHARD AUGUST (NASA, Lewis Research Center; Sverdrup Technology, Inc., Cleveland, OH) and KRISHNA RAO V. KAZA (NASA, Lewis Research Center, Cleveland, OH) AIAA, ASME, SAE, and ASEE, Joint Propulsion Conference, 24th, Boston, MA, July 11-13, 1988. 28 p. Previously announced in STAR as N89-10043. refs  
(AIAA PAPER 88-3155)

An investigation of the vibration, performance, flutter, and forced response of the large-scale propfan, SR7L, and its aeroelastic model, SR7A, has been performed by applying available structural and aeroelastic analytical codes and then correlating measured and calculated results. Finite element models of the blades were used to obtain modal frequencies, displacements, stresses and strains. These values were then used in conjunction with a 3-D, unsteady, lifting surface aerodynamic theory for the subsequent aeroelastic analyses of the blades. The agreement between measured and calculated frequencies and mode shapes for both models is very good. Calculated power coefficients correlate well with those measured for low advance ratios. Flutter results show that both propfans are stable at their respective design points. There is also good agreement between calculated and measured blade vibratory strains due to excitation resulting from yawed flow for the SR7A propfan. The similarity of structural and aeroelastic results show that the SR7A propfan simulates the SR7L characteristics. Author

**A89-20949\*** General Motors Corp., Indianapolis, IN.

**DEVELOPMENT OF AN ANALYTICAL MODEL TO ASSESS FUEL PROPERTY EFFECTS ON COMBUSTOR PERFORMANCE**

R. D. SUTTON, D. L. TROTH, G. A. MILES (General Motors Corp., Allison Gas Turbine Div., Indianapolis, IN), and S. M. RIDDLEBAUGH (NASA, Lewis Research Center, Cleveland, OH) International Journal of Turbo and Jet-Engines (ISSN 0334-0082), vol. 4, no. 3-4, 1987, p. 307-322. refs  
Copyright

A generalized first-order computer model has been developed in order to analytically evaluate the potential effect of alternative fuels' effects on gas turbine combustors. The model assesses the size, configuration, combustion reliability, and durability of the combustors required to meet performance and emission standards while operating on a broad range of fuels. Predictions predicated on combustor flow-field determinations by the model indicate that fuel chemistry, as defined by hydrogen content, exerts a significant influence on flame retardation, liner wall temperature, and smoke emission. O.C.

**A89-20950\*** Yale Univ., New Haven, CT.

**VAPOR DEPOSITION AND CONDENSATE FLOW ON COMBUSTION TURBINE BLADES - THEORETICAL MODEL TO PREDICT/UNDERSTAND SOME CORROSION RATE CONSEQUENCES OF MOLTEN ALKALI SULFATE DEPOSITION IN THE FIELD OR LABORATORY**

DANIEL E. ROSNER and R. NAGARAJAN (Yale University, New Haven, CT) International Journal of Turbo and Jet-Engines (ISSN 0334-0082), vol. 4, no. 3-4, 1987, p. 323-347. refs  
(Contract NAG3-201; NAG3-590)

Copyright

An analysis is undertaken of aerodynamically- and centrifugally-driven liquid condensate layers on nonisothermal combustion turbines' stator vanes and rotor blades. Attention is given to the quantitative consequences of one possible mechanism for the initiation of 'hot corrosion' in the underlying blade material through a 'fluxing' of the protective oxide coating by the molten salt of the Newtonian condensate film. Illustrative calculations are presented for the condensate streamline pattern and the distributions of the steady-state condensate layer thickness, together with the corresponding oxide dissolution rate, for a test turbine blade. O.C.

**A89-22291\*#** National Aeronautics and Space Administration. Lewis Research Center, Cleveland, OH.

**CONTINGENCY POWER FOR SMALL TURBOSHAFT ENGINES**

THOMAS J. BIESIADNY, BRETT BERGER (NASA, Lewis Research Center, Cleveland, OH), GARY A. KLANN, and DAVID A. CLARK (NASA, Lewis Research Center; U.S. Army, Propulsion Directorate, Cleveland, OH) Journal of Propulsion and Power (ISSN 0748-4658), vol. 5, Jan.-Feb. 1989, p. 103-108. Previously cited in issue 20, p. 3156, Accession no. A87-45289. refs  
Copyright

**A89-22927\*** National Aeronautics and Space Administration. Lewis Research Center, Cleveland, OH.

**AIRCRAFT ENGINES. III**

DANIEL C. MIKKELSON (NASA, Lewis Research Center, Cleveland, OH) and GREGORY M. RECK (NASA, Office of Aeronautics and Space Technology, Washington, DC) Exxon Air World, vol. 40, no. 3, 1988, p. 22-26.

Copyright

Prospective powerplant configuration advancements for tilt-rotor subsonic flight, supersonic commercial flight, and hypersonic flight are speculated upon, with a view to possibilities for the exploitation of novel materials and of such advanced fuels as liquid methane and hydrogen. Attention is given to the foldable tilt-rotor concept, which employs a hydraulic torque converter to engage the fan stage of the high-bypass turbofan engine used in forward flight after the tilt-rotor blades have been stowed, and several advanced cycles and turbomechanical configurations for cruise in the high supersonic regime and beyond, through the hypersonic regime, and into orbital velocity. O.C.

**A89-23182\*#** Ohio State Univ., Columbus.

**EXPERIMENTAL STUDY OF ISOTHERMAL SWIRLING FLOWS IN A DUMP COMBUSTOR**

M. SAMIMY (Ohio State University, Columbus) and C. A. LANGENFELD AIAA Journal (ISSN 0001-1452), vol. 26, Dec. 1988, p. 1442-1449. refs  
(Contract F49620-85-C-0013; NAG3-764)

Copyright

Detailed mean and turbulence data were obtained in a dump combustor with and without swirling inlet flow. A two-component LDV was used, and large samples were collected to resolve the second- and third-order correlations of velocity fluctuations with good accuracy. Large-amplitude well-organized oscillations were observed in the swirling flows and discussed. The swirling flows with and without vortex breakdown exhibited significantly different mean flow and turbulence field behavior. Author

**A89-24989\*#** National Aeronautics and Space Administration. Lewis Research Center, Cleveland, OH.

### **NNEPEQ - CHEMICAL EQUILIBRIUM VERSION OF THE NAVY/NASA ENGINE PROGRAM**

L. H. FISHBACH (NASA, Lewis Research Center, Cleveland, OH) and S. GORDON (Sanford Gordon and Associates, Cleveland, OH) ASME, Transactions, Journal of Engineering for Gas Turbines and Power (ISSN 0022-0825), vol. 111, Jan. 1989, p. 114-116. Previously announced in STAR as N88-21161. (ASME PAPER 88-GT-314) Copyright

The Navy NASA Engine Program, NNEP, currently is in use at a large number of government agencies, commercial companies and universities. This computer code has been used extensively to calculate the design and off-design (matched) performance of a broad range of turbine engines, ranging from subsonic turboprops to variable cycle engines for supersonic transports. Recently, there has been increased interest in applications for which NNEP was not capable of simulating, namely, high Mach applications, alternate fuels including cryogenics, and cycles such as the gas generator air-turbo-rocker (ATR). In addition, there is interest in cycles employing ejectors such as for military fighters. New engine component models had to be created for incorporation into NNEP, and it was found necessary to include chemical dissociation effects of high temperature gases. The incorporation of these extended capabilities into NNEP is discussed and some of the effects of these changes are illustrated. Author

**A89-25006\*#** United Technologies Research Center, East Hartford, CT.

### **PERFORMANCE POTENTIAL OF AIR TURBO-RAMJET EMPLOYING SUPERSONIC THROUGH-FLOW FAN**

C. E. KEPLER (United Technologies Research Center, East Hartford, CT) and G. A. CHAMPAGNE (United Technologies Corp., Pratt and Whitney Group, West Palm Beach, FL) AIAA, Aerospace Sciences Meeting, 27th, Reno, NV, Jan. 9-12, 1989. 9 p. refs (Contract NAS3-24843) (AIAA PAPER 89-0010) Copyright

A study was conducted to assess the performance potential of a supersonic through-flow fan in an advanced engine designed to power a Mach-5 cruise vehicle. It included a preliminary evaluation of fan performance requirements and the desirability of supersonic versus subsonic combustion, the design and performance of supersonic fans, and the conceptual design of a single-pass air-turbo-rocket/ramjet engine for a Mach 5 cruise vehicle. The study results showed that such an engine could provide high thrust over the entire speed range from sea-level takeoff to Mach 5 cruise, especially over the transonic speed range, and high fuel specific impulse at the Mach 5 cruise condition, with the fan windmilling. Author

**A89-28403\*#** National Aeronautics and Space Administration. Lewis Research Center, Cleveland, OH.

### **COMPARISON OF 3D COMPUTATION AND EXPERIMENT FOR NON-AXISYMMETRIC NOZZLES**

H. LAI and E. NELSON (NASA, Lewis Research Center, Cleveland; Sverdrup Technology, Inc., Middleburg Heights, OH) AIAA, Aerospace Sciences Meeting, 27th, Reno, NV, Jan. 9-12, 1989. 11 p. refs (Contract NAS3-24105; NAS3-25266) (AIAA PAPER 89-0007)

Three-dimensional solutions of a single expansion ramp nozzle are computed with the existing PARC computer code by solving the full Navier-Stokes equations. The computations are performed to simulate the non-axisymmetric nozzle flowfield in both the internal/external expansion regions and the exhaust plume in a quiescent ambient environment. Two different configurations of the nozzle at a pressure ratio NPR = 10 are examined. Numerical results of laminar flows are presented, and the wall pressure distributions are compared with the experimental data. Author

**A89-28408\*#** National Aeronautics and Space Administration. Lewis Research Center, Cleveland, OH.

### **NUMERICAL INVESTIGATION OF CHEMICALLY REACTING FLOWS IN RAMJET DUMP COMBUSTORS**

KWANG-CHUNG HSIEH (NASA, Lewis Research Center; Sverdrup Technology, Inc., Cleveland, OH) and JONG-SHANG LIU (Textron Lycoming, Stratford, CT) AIAA, Aerospace Sciences Meeting, 27th, Reno, NV, Jan. 9-12, 1989. 15 p. refs (AIAA PAPER 89-0387) Copyright

The time-dependent Navier-Stokes equations, including second-order turbulence model, are numerically integrated by using four-stage Runge-Kutta scheme to predict the steady-state supersonic flow structures in ramjet dump combustors. The formulation is derived for reacting flows with finite-rate chemistry. In the present study, it is firstly attempted to assess the accuracy of existing high-order turbulence model in supersonic flows. The comparison shows reasonable agreement between calculated and measured data in terms of velocity distributions. It is indicated that a modified constant C- $\mu$  for calculating turbulent eddy viscosity is needed in the supersonic flow regime and the adaptive meshing is preferred to capture the recirculation zone. In the reacting flow calculation, the results from a test case of hydrogen and air combustion at premixed condition show that the rearward facing step is able to increase flow residence time and stabilize the flame in supersonic flows. Author

**A89-28462\*#** Purdue Univ., West Lafayette, IN.

### **EFFECT OF HEAVY RAIN ON AVIATION ENGINES**

S. N. B. MURTHY (Purdue University, West Lafayette, IN) AIAA, Aerospace Sciences Meeting, 27th, Reno, NV, Jan. 9-12, 1989. 20 p. refs (Contract NAG3-481; DOT-FA03-83-A-00328) (AIAA PAPER 89-0799) Copyright

High bypass ratio gas turbine engines may ingest water and hail during flight in an environment of thunderstorms, and the performance and the operation-handling characteristics of the engine and its control become affected often substantially and critically. It is, therefore, of interest to establish predictive schemes for determining changes in performance of components and the total system. The current status of development of such predictive schemes is discussed along with illustrative examples. The needs for additional research are discussed, that are essential for improving: (1) the predictive schemes and (2) the methods of simulating in-rain flight conditions on ground. Author

**A89-30745\*#** National Aeronautics and Space Administration. Lewis Research Center, Cleveland, OH.

### **COMPUTATIONAL STRUCTURAL MECHANICS FOR ENGINE STRUCTURES**

CHRISTOS C. CHAMIS (NASA, Lewis Research Center, Cleveland, OH) IN: AIAA, ASME, ASCE, AHS, and ASC, Structures, Structural Dynamics and Materials Conference, 30th, Mobile, AL, Apr. 3-5, 1989, Technical Papers. Part 2. Washington, DC, American Institute of Aeronautics and Astronautics, 1989, p. 868-873. Previously announced in STAR as N88-22399. (AIAA PAPER 89-1260) Copyright

The computational structural mechanics (CSM) program at Lewis encompasses the formulation and solution of structural mechanics problems and the development of integrated software systems to computationally simulate the performance, durability, and life of engine structures. It is structured to supplement, complement, and, whenever possible, replace costly experimental efforts. Specific objectives are to investigate unique advantages of parallel and multiprocessing for reformulating and solving structural mechanics and formulating and solving multidisciplinary mechanics and to develop integrated structural system computational simulators for predicting structural performance, evaluating newly developed methods, and identifying and prioritizing improved or missing methods. Author

**A89-36215\*#** Lockheed Aeronautical Systems Co., Marietta, GA.

# NEAR-FIELD ACOUSTIC CHARACTERISTICS OF A SINGLE-ROTOR PROPFAN

H. W. BARTEL and G. SWIFT (Lockheed Aeronautical Systems Co., Marietta, GA) AIAA, Aerodynamics Conference, 12th, San Antonio, TX, Apr. 10-12, 1989. 13 p. refs (Contract NAS3-24339)

(AIAA PAPER 89-1055) Copyright

The near-field noise characteristics of the SR-7L, an eight-blade, single-rotor, wing-mounted, tractor propfan have been determined. It is found that the noise is dominated by discrete tones, usually at the first order (and occasionally at the second or third order) of the blade-passage frequency. The highest noise levels were noted at conditions of high tip helical speeds and high dynamic pressures.

R.R.

**A89-36397\*** National Aeronautics and Space Administration. Lewis Research Center, Cleveland, OH.

# A REVIEW AND FORECAST OF ENGINE SYSTEM RESEARCH AT THE ARMY PROPULSION DIRECTORATE

GEORGE A. BOBULA (NASA, Lewis Research Center; U.S. Army, Propulsion Directorate, Cleveland, OH) Vertiflite (ISSN 0042-4455), vol. 35, Mar.-Apr. 1989, p. 12-19. Copyright

An account is given of the development status and achievements to date of the U.S. Army Propulsion Directorate's Small Turbine Engine Research (STER) programs, which are experimental investigations of the physics of entire engine systems from the viewpoints of component interactions and/or system dynamics. STER efforts are oriented toward the evaluation of complete turboshaft engine advanced concepts and are conducted at the ECRL-2 indoor, sea-level engine test facility. Attention is given to the results obtained by STER experiments concerned with IR-suppressing engine exhausts, a ceramic turbine-blade shroud, an active shaft-vibration control system, and a ceramic-matrix combustor liner.

O.C.

**A89-47186\*#** National Aeronautics and Space Administration. Lewis Research Center, Cleveland, OH.

# INVESTIGATION OF LOW NOX STAGED COMBUSTOR CONCEPT IN HIGH-SPEED CIVIL TRANSPORT ENGINES

HUNG LEE NGUYEN, DAVID A. BITTKER, and RICHARD W. NIEDZWIECKI (NASA, Lewis Research Center, Cleveland, OH) AIAA, ASME, SAE, and ASEE, Joint Propulsion Conference, 25th, Monterey, CA, July 10-13, 1989. 14 p. Previously announced in STAR as N89-22606. refs

(AIAA PAPER 89-2942) Copyright

Levels of exhaust emissions due to high temperatures in the main combustor of high-speed civil transport (HSCT) engines during supersonic cruise are predicted. These predictions are based on a new combustor design approach: a rich burn/quick quench/lean burn combustor. A two-stage stirred reactor model is used to calculate the combustion efficiency and exhaust emissions of this novel combustor. A propane-air chemical kinetics model is used to simulate the fuel-rich combustion of jet fuel. Predicted engine exhaust emissions are compared with available experimental test data. The effect of HSCT engine operating conditions on the levels of exhaust emissions is also presented. The work described in this paper is a part of the NASA Lewis Research Center High-Speed Civil Transport Low NO(x) Combustor program.

Author

**A89-49688\*#** National Aeronautics and Space Administration. Lewis Research Center, Cleveland, OH.

# TRANSIENT FLOW THRUST PREDICTION FOR AN EJECTOR PROPULSION CONCEPT

C. DRUMMOND (NASA, Lewis Research Center, Cleveland, OH) AIAA, ASME, SAE, and ASEE, Joint Propulsion Conference, 25th, Monterey, CA, July 10-13, 1989. 9 p. Previously announced in STAR as N89-24318. refs

(AIAA PAPER 89-2906) Copyright

A method for predicting transient thrust augmenting ejector characteristics is introduced. The analysis blends classic self-similar

turbulent jet descriptions with a mixing region control volume analysis to predict transient effects in a new way. Details of the theoretical foundation, the solution algorithm, and sample calculations are given.

Author

**A89-52025\*#** National Aeronautics and Space Administration. Lewis Research Center, Cleveland, OH.

# FUEL PROPERTIES EFFECT ON THE PERFORMANCE OF A SMALL HIGH TEMPERATURE RISE COMBUSTOR

WALDO A. ACOSTA (NASA, Lewis Research Center; U.S. Army, Propulsion Directorate, Cleveland, OH) and STEPHEN A. BECKEL (United Technologies Corp., Pratt and Whitney Group, West Palm Beach, FL) AIAA, ASME, SAE, and ASEE, Joint Propulsion Conference, 25th, Monterey, CA, July 10-12, 1989. 11 p. Previously announced in STAR as N89-25238. refs

(Contract N00140-83-C-8899)

(AIAA PAPER 89-2901) Copyright

The performance of an advanced small high temperature rise combustor was experimentally determined at NASA-Lewis. The combustor was designed to meet the requirements of advanced high temperature, high pressure ratio turboshaft engines. The combustor featured an advanced fuel injector and an advanced segmented liner design. The full size combustor was evaluated at power conditions ranging from idle to maximum power. The effect of broad fuel properties was studied by evaluating the combustor with three different fuels. The fuels used were JP-5, a blend of Diesel Fuel Marine/Home Heating Oil, and a blend of Suntec C/Home Heating Oil. The fuel properties effect on the performance of the combustion in terms of pattern factor, liner temperatures, and exhaust emissions are documented.

Author

**A89-53304\*#** National Aeronautics and Space Administration. Lewis Research Center, Cleveland, OH.

# AERONAUTICAL APPLICATIONS OF HIGH-TEMPERATURE SUPERCONDUCTORS

GEORGE E. TURNEY, ROGER W. LUIDENS (NASA, Lewis Research Center, Cleveland, OH), KENNETH UHERKA, and JOHN HULL (Argonne National Laboratory, IL) AIAA, AHS, and ASEE, Aircraft Design, Systems and Operations Conference, Seattle, WA, July 31-Aug. 2, 1989. 14 p. Previously announced in STAR as N89-26008. refs

(AIAA PAPER 89-2142) Copyright

The successful development of high-temperature superconductors (HTS) could have a major impact on future aeronautical propulsion and aeronautical flight vehicle systems. A preliminary examination of the potential application of HTS for aeronautics indicates that significant benefits may be realized through the development and implementation of these newly discovered materials. Applications of high-temperature superconductors (currently substantiated at 95 K) were envisioned for several classes of aeronautical systems, including subsonic and supersonic transports, hypersonic aircraft, V/STOL aircraft, rotorcraft, and solar, microwave and laser powered aircraft. Introduced and described are the particular applications and potential benefits of high-temperature superconductors as related to aeronautics and/or aeronautical systems.

Author

**A89-53956\*** National Aeronautics and Space Administration. Lewis Research Center, Cleveland, OH.

# TURBOFAN ENGINE CONTROL SYSTEM DESIGN USING THE LQG/LTR METHODOLOGY

SANJAY GARG (NASA, Lewis Research Center; Sverdrup Technology, Inc., Cleveland, OH) IN: 1989 American Control Conference, 8th, Pittsburgh, PA, June 21-23, 1989, Proceedings. Volume 1. New York, Institute of Electrical and Electronics Engineers, 1989, p. 134-141. Previously announced in STAR as N89-26004. refs

Copyright

Application of the linear-quadratic-Gaussian with loop-transfer-recovery methodology to design of a control system for a simplified turbofan engine model is considered. The importance of properly scaling the plant to achieve the desired target feedback loop is emphasized. The steps involved in the

## 07 AIRCRAFT PROPULSION AND POWER

application of the methodology are discussed via an example, and evaluation results are presented for a reduced-order compensator. The effect of scaling the plant on the stability robustness evaluation of the closed-loop system is studied in detail. Author

**N89-10043\*** National Aeronautics and Space Administration. Lewis Research Center, Cleveland, OH.

### **VIBRATION, PERFORMANCE, FLUTTER AND FORCED RESPONSE CHARACTERISTICS OF A LARGE-SCALE PROPFAN AND ITS AEROELASTIC MODEL**

RICHARD AUGUST (Sverdrup Technology, Inc., Cleveland, Ohio.) and KRISHNA RAO V. KAZA 1988 28 p Presented at the 24th Joint Propulsion Conference, Boston, Mass., 11-13 Jul. 1988; sponsored by AIAA, ASME, SAE and ASEE (NASA-TM-101322; E-4260; NAS 1.15:101322; AIAA-88-3155) Avail: NTIS HC A03/MF A01 CSCL 21E

An investigation of the vibration, performance, flutter, and forced response of the large-scale propfan, SR7L, and its aeroelastic model, SR7A, has been performed by applying available structural and aeroelastic analytical codes and then correlating measured and calculated results. Finite element models of the blades were used to obtain modal frequencies, displacements, stresses and strains. These values were then used in conjunction with a 3-D, unsteady, lifting surface aerodynamic theory for the subsequent aeroelastic analyses of the blades. The agreement between measured and calculated frequencies and mode shapes for both models is very good. Calculated power coefficients correlate well with those measured for low advance ratios. Flutter results show that both propfans are stable at their respective design points. There is also good agreement between calculated and measured blade vibratory strains due to excitation resulting from yawed flow for the SR7A propfan. The similarity of structural and aeroelastic results show that the SR7A propfan simulates the SR7L characteristics. Author

**N89-11750\*** Flow Research, Inc., Kent, WA.  
**AERODYNAMIC OPTIMIZATION BY SIMULTANEOUSLY UPDATING FLOW VARIABLES AND DESIGN PARAMETERS WITH APPLICATION TO ADVANCED PROPELLER DESIGNS**  
MAGDI H. RIZK Jul. 1988 34 p

(Contract NAS3-24855)  
(NASA-CR-182181; NAS 1.26:182181; FLOW-RR-447) Avail: NTIS HC A03/MF A01 CSCL 21/5

A scheme is developed for solving constrained optimization problems in which the objective function and the constraint function are dependent on the solution of the nonlinear flow equations. The scheme updates the design parameter iterative solutions and the flow variable iterative solutions simultaneously. It is applied to an advanced propeller design problem with the Euler equations used as the flow governing equations. The scheme's accuracy, efficiency and sensitivity to the computational parameters are tested. Author

**N89-11751\*** Sverdrup Technology, Inc., Cleveland, OH.  
**A PRELIMINARY DESIGN STUDY OF SUPERSONIC THROUGH-FLOW FAN INLETS Final Report**

PAUL J. BARNHART Nov. 1988 12 p Previously announced in IAA as A88-53137  
(Contract NAS3-24105)  
(NASA-CR-182224; E-4490; NAS 1.26:182224) Avail: NTIS HC A03/MF A01 CSCL 21/5

From Mach 3.20 cruise propulsion systems, preliminary design studies for two supersonic through-flow fan primary inlets and a single core inlet were undertaken. Method of characteristics and one dimensional performance techniques were applied to assess the potential improvements supersonic through-flow fan technology has over more conventional systems. A fixed geometry supersonic through-flow fan primary inlet was found to have better performance than a conventional inlet design on the basis of total pressure recovery, air flow, aerodynamic drag and size and weight. Author

**N89-12565\*** National Aeronautics and Space Administration. Lewis Research Center, Cleveland, OH.

### **ADVANCED TURBOPROP PROJECT**

ROY D. HAGER and DEBORAH VRABEL (Sverdrup Technology, Inc., Cleveland, Ohio.) 1988 130 p Original contains color illustrations  
(NASA-SP-495; NAS 1.21:495; LC88-1690) Avail: NTIS HC A07/MF A01 CSCL 21/5

At the direction of Congress, a task force headed by NASA was organized in 1975 to identify potential fuel saving concepts for aviation. The result was the Aircraft Energy Efficiency (ACEE) Program implemented in 1976. An important part of the program was the development of advanced turboprop technology for Mach 0.65 to 0.85 applications having the potential fuel saving of 30 to 50 percent relative to existing turbofan engines. A historical perspective is presented of the development and the accomplishments that brought the turboprop to successful flight tests in 1986 and 1987. Author

**N89-12566\*** Sverdrup Technology, Inc., Cleveland, OH.

### **A CONTROL-VOLUME METHOD FOR ANALYSIS OF UNSTEADY THRUST AUGMENTING EJECTOR FLOWS Final Report**

COLIN K. DRUMMOND Nov. 1988 170 p  
(Contract NAS3-25266)

(NASA-CR-182203; E-4461; NAS 1.26:182203) Avail: NTIS HC A08/MF A01 CSCL 21/5

A method for predicting transient thrust augmenting ejector characteristics is presented. The analysis blends classic self-similar turbulent jet descriptions with a control volume mixing region discretization to solicit transient effects in a new way. Division of the ejector into an inlet, diffuser, and mixing region corresponds with the assumption of viscous-dominated phenomenon in the latter. Inlet and diffuser analyses are simplified by a quasi-steady analysis, justified by the assumptions that pressure is the forcing function in those regions. Details of the theoretical foundation, the solution algorithm, and sample calculations are given. Author

**N89-12567\*** Sverdrup Technology, Inc., Cleveland, OH.

### **A REVIEW OF TURBOMACHINERY BLADE-ROW INTERACTION RESEARCH Final Report**

TODD E. SMITH Nov. 1988 38 p  
(Contract NAS3-25266)

(NASA-CR-182211; E-4422; NAS 1.26:182211) Avail: NTIS HC A03/MF A01 CSCL 21/5

Analytical and experimental research in the area of unsteady aerodynamics of turbomachinery has conventionally been applied to blading which oscillates when placed in a uniformly flowing fluid. Comparatively less effort has been offered for the study of blading which is subjected to nonuniformities within the flow field. The fluid dynamic environment of a blade-row embedded within multi-stage turbomachines is dominated by such highly unsteady fluid flow conditions. The production of wakes and circumferential pressure variations from adjacent blade-rows causes large unsteady energy transfers between the fluid and the blades. Determination of the forced response of a blade requires the ability to predict the unsteady loads which are induced by these aerodynamic sources. A review of research publications was done to determine recent investigations of the response of turbomachinery blading subjected to aerodynamic excitations. Such excitations are a direct result of the blade-row aerodynamic interaction which occurs between adjacent cascades of blades. The reports and papers reviewed have been organized into areas emphasizing experimental or analytical efforts. Author

**N89-12568\*** National Aeronautics and Space Administration. Lewis Research Center, Cleveland, OH.

### **DEVELOPMENT OF A THERMAL AND STRUCTURAL ANALYSIS PROCEDURE FOR COOLED RADIAL TURBINES**

GANESH N. KUMAR and RUSSELL G. DEANNA (Army Aviation Research and Development Command, Cleveland, Ohio.) 1988 10 p Presented at the 33rd International Gas Turbine and



Aeroengine Congress and Exposition, Amsterdam, The Netherlands, 6-9 Jun. 1988; sponsored by the American Society of Mechanical Engineers (NASA-TM-101416; E-4515; NAS 1.15:101416; AVSCOM-TR-88-C-037) Avail: NTIS HC A02/MF A01 CSCL 21/5

A procedure for computing the rotor temperature and stress distributions in a cooled radial turbine are considered. Existing codes for modeling the external mainstream flow and the internal cooling flow are used to compute boundary conditions for the heat transfer and stress analysis. The inviscid, quasi three dimensional code computes the external free stream velocity. The external velocity is then used in a boundary layer analysis to compute the external heat transfer coefficients. Coolant temperatures are computed by a viscous three dimensional internal flow code for the momentum and energy equation. These boundary conditions are input to a three dimensional heat conduction code for the calculation of rotor temperatures. The rotor stress distribution may be determined for the given thermal, pressure and centrifugal loading. The procedure is applied to a cooled radial turbine which will be tested at the NASA Lewis Research Center. Representative results are given. Author

**N89-12877\*#** National Aeronautics and Space Administration. Lewis Research Center, Cleveland, OH.

## **TURBINE ENGINE HOT SECTION TECHNOLOGY (HOST) PROJECT**

DANIEL E. SOKOLOWSKI and C. ROBERT ENSIGN *In its* Turbine Engine Hot Section Technology 1986 p 1-6 Oct. 1986 Avail: NTIS HC A21/MF A01 CSCL 20/11

The Hot Section Technology (HOST) Project is a NASA-sponsored endeavor to improve the durability of advanced gas turbine engines for commercial and military aircraft. Through improvements in the analytical models and life prediction systems, designs for future hot section components, the combustor and turbine, will be more accurately analyzed and will incorporate features required for longer life in the more hostile operating environment of high performance engines. E.R.

**N89-12878\*#** National Aeronautics and Space Administration. Lewis Research Center, Cleveland, OH.

## **HOST INSTRUMENTATION R AND D PROGRAM OVERVIEW**

D. R. ENGLUND *In its* Turbine Engine Hot Section Technology 1986 p 7-8 Oct. 1986

Avail: NTIS HC A21/MF A01 CSCL 20/11

The HOST Instrumentation R and D program is focused on two categories of instrumentation. One category is that required to characterize the environment imposed on the hot section components of turbine engines. This category includes instruments for measuring gas flow, gas temperature, and heat flux. The second category is that for measuring the effect of the environment on the hot section components. This category includes strain measuring instruments and an optical system for viewing the interior of an operating combustor to detect cracks, buckling, carbon buildup, etc. E.R.

**N89-12879\*#** National Aeronautics and Space Administration. Lewis Research Center, Cleveland, OH.

## **HOST COMBUSTION R AND T OVERVIEW**

RAYMOND E. GAUGLER *In its* Turbine Engine Hot Section Technology 1986 p 9-11 Oct. 1986

Avail: NTIS HC A21/MF A01 CSCL 21/5

The overall objective of the Turbine Engine Hot Section Technology Combustion Project was to develop and verify improved and more accurate numerical analysis methods for increasing the ability to design with confidence combustion systems for advanced aircraft gas turbine engines. The objective was approached from two directions: computational and experimental. On the computational side, the approach was to first assess and evaluate existing combustor aerothermal analysis models. On the experimental side, three types of experiments are identified; first, fundamental experiments directed toward improved understanding of the flow physics and chemistry; second, experiments run to

provide data for the empirical modeling of complex phenomena; and third, benchmark experiments for computer code validation. E.R.

**N89-12880\*#** National Aeronautics and Space Administration. Lewis Research Center, Cleveland, OH.

## **HOST TURBINE HEAT TRANSFER SUBPROJECT OVERVIEW**

HERBERT J. GLADDEN *In its* Turbine Engine Hot Section Technology 1986 p 13-17 Oct. 1986

Avail: NTIS HC A21/MF A01 CSCL 21/5

The experimental part of the turbine heat transfer subproject consists of six large experiments, which are highlighted in this overview, and three of somewhat more modest scope. One of the initial efforts was the stator airfoil heat transfer program. The non-film cooled and the showerhead film cooled data have already been reported. The gill region film cooling effort is currently underway. The investigation of secondary flows in a 90 deg curved duct, was completed. The first phase examined flows with a relatively thin inlet boundary layer and low free stream turbulence. The second phase studied a thicker inlet boundary layer and higher free stream turbulence. A comparison of analytical and experimental cross flow velocity vectors is shown for the 60 deg plane. Two experiments were also conducted in the high pressure facility. One examined full coverage film cooled vanes, and the other, advanced instrumentation. The other three large experimental efforts were conducted in a rotation reference frame. An experiment to obtain gas path airfoil heat transfer coefficients in the large, low speed turbine was completed. Single-stage data with both high and low-inlet turbulence were taken. The second phase examined a one and one-half stage turbine and focused on the second vane row. Under phase 3 aerodynamic quantities such as interrow time-averaged and rms values of velocity, flow angle, inlet turbulence, and surface pressure distribution were measured. E.R.

**N89-12907\*#** General Electric Co., Fairfield, CT.

## **COMPONENT SPECIFIC MODELING**

R. J. MAFFEO, R. L. MCKNIGHT, M. T. TIPTON, and G. WEBER *In* NASA, Lewis Research Center, Turbine Engine Hot Section Technology 1986 p 269-282 Oct. 1986

(Contract NAS3-23687)

Avail: NTIS HC A21/MF A01 CSCL 21/5

The overall objective of this program is to develop and verify a series of interdisciplinary modeling and analysis techniques that were specialized to address three specific hot section components. These techniques incorporate data as well as theoretical methods from many diverse areas including cycle and performance analysis, heat transfer analysis, linear and nonlinear stress analysis, and mission analysis. Building on the proven techniques already available in these fields, the new methods developed are integrated to provide an accurate, efficient, and unified approach to analyzing combustor burner liners, hollow air-cooled turbine blades, and air-cooled turbine vanes. For these components, the methods developed predict temperature, deformation, stress, and strain histories throughout a complete flight mission. Author

**N89-13432\*#** National Aeronautics and Space Administration. Lewis Research Center, Cleveland, OH.

## **SENSOR FAILURE DETECTION FOR JET ENGINES**

WALTER C. MERRILL Nov. 1988 43 p Submitted for publication

(NASA-TM-101396; E-4402; NAS 1.15:101396) Avail: NTIS HC A03/MF A01 CSCL 21/5

The use of analytical redundancy to improve gas turbine engine control system reliability through sensor failure detection, isolation, and accommodation is surveyed. Both the theoretical and application papers that form the technology base of turbine engine analytical redundancy research are discussed. Also, several important application efforts are reviewed. An assessment of the state-of-the-art in analytical redundancy technology is given. Author

## 07 AIRCRAFT PROPULSION AND POWER

**N89-13433\*#** Garrett Turbine Engine Co., Phoenix, AZ.  
**THERMAL BARRIER COATING LIFE-PREDICTION MODEL DEVELOPMENT Annual Report No. 1**

T. E. STRANGMAN and J. NEUMANN 9 Sep. 1985 62 p  
(Contract NAS3-23945)  
(NASA-CR-175002; NAS 1.26:175002; REPT-21-5477) Avail:  
NTIS HC A04/MF A01 CSCL 21/5

Life predictions are made for two types of strain-tolerant and oxidation-resistant Thermal Barrier Coating (TBC) systems produced by commercial coating suppliers to the gas turbine industry. The plasma-sprayed TBC system, composed of a low-pressure plasma spray (LPPS) applied oxidation-resistant NiCrAlY bond coating and an air-plasma-sprayed yttria (8 percent) partially stabilized zirconia insulative layer, is applied by both Chromalloy and Klock. The second type of TBC is applied by the electron-beam/physical vapor deposition process by Temescal. Thermomechanical and thermochemical testing of the program TBCs is in progress. A number of the former tests has been completed. Fracture mechanics data for the Chromalloy plasma-sprayed TBC system indicate that the cohesive toughness of the zirconia layer is increased by thermal cycling and reduced by high temperature exposure at 1150 C. Eddy current technology feasibility has been established with respect to nondestructively measuring zirconia layer thickness of a TBC system. High pressure turbine blades have been coated with program TBC systems for a piggyback test in a TFE731-5 turbofan factory engine test. Data from this test will be used to validate the TBC life models.

Author

**N89-13436\*#** General Electric Co., Cincinnati, OH. Aircraft Engine Business Group.

**CONSTITUTIVE MODELING FOR ISOTROPIC MATERIALS Annual Report, May 1983 - Apr. 1984**

V. G. RAMASWAMY, R. H. VANSTONE, L. T. DAME, and J. H. LAFFLEN 15 Apr. 1985 86 p  
(Contract NAS3-23927)  
(NASA-CR-174805; NAS 1.26:174805) Avail: NTIS HC A05/MF A01 CSCL 21/5

The first year of progress on a NASA-Lewis contract with the General Electric Co is documented. The purpose of this contract (NAS3-23927) is to develop and evaluate unified constitutive equations for applications to hot-path components of aircraft gas turbine engines such as high pressure turbine blades and vanes. To accomplish this goal, uniaxial, notched, and multiaxial specimens made of conventionally cast Rene 80 are being tested under conditions that simulate engine operating conditions. To reduce the raw data, automated data reduction techniques are being developed that produce computer files containing the information needed to analyze proposed constitutive theories. Described are the analytical methods being developed to determine the parameters for these nonlinear unified theories by using the reduced data files. In another activity, a dedicated finite-element computer code is being developed to use unified theories in the structural analysis of hot-section components. This code was extensively verified for one such theory by successfully predicting the strain histories measured experimentally at the notch root of complex specimens taken from complex laboratory specimens.

Author

**N89-13437\*#** National Aeronautics and Space Administration. Lewis Research Center, Cleveland, OH.

**ISOLATED TESTING OF HIGHLY MANEUVERABLE INLET CONCEPTS**

W. P. NORBY, B. A. HAEFFLE (McDonnell Aircraft Co., St. Louis, Mo.), and R. R. BURLEY Dec. 1986 167 p  
(NASA-CR-179544; NAS 1.26:179544) Avail: NTIS HC A08/MF A01 CSCL 21/5

Ten percent scale models of a Mach 2.2 two dimensional inlet and a Mach 2.0 axisymmetric inlet were tested in the NASA Lewis Research Center 8'x6' Supersonic Wind Tunnel as part of a cooperative effort with the McDonnell Aircraft Company. The objective of this effort was to test methods designed to increase the maneuvering performance of fighter aircraft inlets. Maneuvering improvement concepts were tested up to 40-deg angle of attack

for Mach numbers of 0.6 and 0.9, and up to 25 deg for Mach numbers 1.2 and 1.4. Maneuvering improvement concepts included a rotating cowl lip, auxiliary inlets aft of the inlet throat, and a retracting centerbody for the axisymmetric inlet. Test results show that the rotating cowl design was effective in improving subsonic maneuvering performance for both inlets. Auxiliary inlets did not produce significant performance increases for either model. The retracted centerbody resulted in some performance benefits at high angles of attack. None of the maneuvering improvement concepts were effective at Mach 1.2 and 1.4.

Author

**N89-14237\*#** National Aeronautics and Space Administration. Lewis Research Center, Cleveland, OH.

**ADVANCED CORE TECHNOLOGY: KEY TO SUBSONIC PROPULSION BENEFITS**

ARTHUR J. GLASSMAN, CHRISTOPHER A. SNYDER, and GERALD KNIP, JR. 1989 13 p Prepared for presentation at the 34th International Gas Turbine and Aeroengine Congress and Exposition, Toronto (Ontario), 4-8 Jun. 1989; sponsored in part by ASME  
(NASA-TM-101420; E-4519; NAS 1.15:101420) Avail: NTIS HC A03/MF A01 CSCL 21/5

A study was conducted to identify the potential performance benefits and key technology drivers associated with advanced cores for subsonic high bypass turbofan engines. Investigated first were the individual sensitivities of varying compressor efficiency, pressure ratio and bleed (turbine cooling); combustor pressure recovery; and turbine efficiency and inlet temperature on thermal efficiency and core specific power output. Then, engine cycle and mission performance benefits were determined for systems incorporating all potentially achievable technology advancements. The individual thermodynamic sensitivities are shown over a range of turbine temperatures (at cruise) from 2900 to 3500 R and for both constant (current technology) and optimum (maximum thermal efficiency) overall pressure ratios. It is seen that no single parameter alone will provide a large increase in core thermal efficiency, which is the thermodynamic parameter of most concern for transport propulsion. However, when all potentially achievable advancements are considered, there occurs a synergism that produces significant cycle and mission performance benefits. The nature of these benefits are presented along with the technology challenges.

Author

**N89-14238\*#** National Aeronautics and Space Administration. Lewis Research Center, Cleveland, OH.

**SIMULATION OF 3-D VISCOUS FLOW WITHIN A MULTI-STAGE TURBINE**

JOHN J. ADAMCZYK, MARK L. CELESTINA, TIM A. BEACH, and MARK BARNETT (United Technologies Research Center, East Hartford, Conn.) 1989 14 p Proposed for presentation at the 34th International Gas Turbine and Aeroengine Congress and Exposition, Toronto, Ontario, 4-8 Jun. 1989; sponsored by ASME  
(NASA-TM-101376; E-4430; NAS 1.15:101376) Avail: NTIS HC A03/MF A01 CSCL 21/5

This work outlines a procedure for simulating the flow field within multistage turbomachinery which includes the effects of unsteadiness, compressibility, and viscosity. The associated modeling equations are the average passage equation system which governs the time-averaged flow field within a typical passage of a blade row embedded within a multistage configuration. The results from a simulation of a low aspect ratio stage and a one-half turbine will be presented and compared with experimental measurements. It will be shown that the secondary flow field generated by the rotor causes the aerodynamic performance of the downstream vane to be significantly different from that of an isolated blade row.

Author

**N89-14239\*#** National Aeronautics and Space Administration. Lewis Research Center, Cleveland, OH.

**PLOTTING COMPONENT MAPS IN THE NAVY/NASA ENGINE PROGRAM (NNEP): A METHOD AND ITS USAGE**

ROBERT M. PLENCNER Jan. 1989 20 p



(NASA-TM-101433; E-4539; NAS 1.15:101433) Avail: NTIS HC A03/MF A01 CSCL 21/5

The Navy/NASA Engine Program (NNEP) and the new extended version which handles chemical equilibrium (NNEPEQ) are very general cycle analysis codes that have been used extensively to calculate design and off-design performance of a wide range of turbine engine cycles and configurations. Component maps are used to obtain the off-design engine performance and a matched engine cycle. This paper describes a method of plotting the scaled NNEP compressor and turbine maps as the user runs the NNEP code as well as plotting the operating line defined by all the cases that were computed in that particular NNEP run. Afterwards, an example demonstrates the use of this capability to help analyze an engine cycle model and then make improvements to that cycle.

Author

**N89-15112\*#** National Aeronautics and Space Administration. Lewis Research Center, Cleveland, OH.

## **ANALYSIS OF AN UNSWEPT PROPPAN BLADE WITH A SEMIEMPIRICAL DYNAMIC STALL MODEL**

T. S. R. REDDY (Toledo Univ., OH.) and K. R. V. KAZA Washington, DC Jan. 1989 23 p  
(NASA-TM-4083; E-4196; NAS 1.15:4083) Avail: NTIS HC A03/MF A01 CSCL 21/5

The time history response of a propfan wind tunnel model with dynamic stall is studied analytically. The response obtained from the analysis is compared with available experimental data. The governing equations of motion are formulated in terms of blade normal modes which are calculated using the COSMIC-NASTRAN computer code. The response analysis considered the blade plunging and pitching motions. The lift, drag and moment coefficients for angles of attack below the static stall angle are obtained from a quasi-steady theory. For angles above static stall angles, a semiempirical dynamic stall model based on a correction to angle of attack is used to obtain lift, drag and moment coefficients. Using these coefficients, the aerodynamic forces are calculated at a selected number of strips, and integrated to obtain the total generalized forces. The combined momentum-blade element theory is used to calculate the induced velocity. The semiempirical stall model predicted a limit cycle oscillation near the setting angle at which large vibratory stresses were observed in an experiment. The predicted mode and frequency of oscillation also agreed with those measured in the experiment near the setting angle.

Author

**N89-15114\*#** Calspan-Buffalo Univ. Research Center, NY.

## **DEVELOPMENT OF AN INTEGRATED BEM APPROACH FOR HOT FLUID STRUCTURE INTERACTION Annual Report, Nov. 1987 - Nov. 1988**

GARY F. DARGUSH, PRASANTA K. BANERJEE, and KEITH A. HONKALA (Buffalo Univ., NY.) 20 Dec. 1988 114 p  
(Contract NAG3-712)

(NASA-CR-184587; NAS 1.26:184587) Avail: NTIS HC A06/MF A01 CSCL 21/5

In the present work, the boundary element method (BEM) is chosen as the basic analysis tool, principally because the definition of temperature, flux, displacement and traction are very precise on a boundary-based discretization scheme. One fundamental difficulty is, of course, that a BEM formulation requires a considerable amount of analytical work, which is not needed in the other numerical methods. Progress made toward the development of a boundary element formulation for the study of hot fluid-structure interaction in Earth-to-Orbit engine hot section components is reported. The primary thrust of the program to date has been directed quite naturally toward the examination of fluid flow, since boundary element methods for fluids are at a much less developed state.

Author

**N89-15913\*#** National Aeronautics and Space Administration. Lewis Research Center, Cleveland, OH.

## **NASA ADVANCED PROPELLER RESEARCH**

JOHN F. GROENEWEG and LAWRENCE J. BOBER 30 Sep. 1988 34 p Presented at the Advanced Propellers and Their

Installation on Aircraft, Cranfield, England, 26-27 Sep. 1988; sponsored in part by Royal Aeronautical Society

(NASA-TM-101361; E-4393; NAS 1.15:101361) Avail: NTIS HC A03/MF A01 CSCL 21/5

Acoustic and aerodynamic research at NASA Lewis Research Center on advanced propellers is reviewed including analytical and experimental results on both single and counterrotation. Computational tools used to calculate the detailed flow and acoustic fields are described along with wind tunnel tests to obtain data for code verification. Results from two kinds of experiments are reviewed: (1) performance and near field noise at cruise conditions as measured in the NASA Lewis 8- by 6-foot Wind Tunnel; and (2) far field noise and performance for takeoff/approach conditions as measured in the NASA Lewis 9- by 15-foot Anechoic Wind Tunnel. Detailed measurements of steady blade surface pressures are described along with vortex flow phenomena at off-design conditions. Near field noise at cruise is shown to level out or decrease as tip relative Mach number is increased beyond 1.15. Counterrotation interaction noise is shown to be a dominant source at takeoff but a secondary source at cruise. Effects of unequal rotor diameters and rotor-to-rotor spacing on interaction noise are also illustrated. Comparisons of wind tunnel acoustic measurements to flight results are made. Finally, some future directions in advanced propeller research such as swirl recovery vanes, higher sweep, forward sweep, and ducted propellers are discussed.

Author

**N89-16834\*#** National Aeronautics and Space Administration. Lewis Research Center, Cleveland, OH.

## **THE DESIGN AND DEVELOPMENT OF TRANSONIC MULTISTAGE COMPRESSORS**

C. L. BALL, R. J. STEINKE, and F. A. NEWMAN In Von Karman Institute for Fluid Dynamics, Transonic Compressors, Volume 2 97 p 1988

Avail: NTIS HC A17/MF A01

The development of the transonic multistage compressor is reviewed. Changing trends in design and performance parameters are noted. These changes are related to advances in compressor aerodynamics, computational fluid mechanics and other enabling technologies. The parameters normally given to the designer and those that need to be established during the design process are identified. Criteria and procedures used in the selection of these parameters are presented. The selection of tip speed, aerodynamic loading, flowpath geometry, incidence and deviation angles, blade/vane geometry, blade/vane solidity, stage reaction, aerodynamic blockage, inlet flow per unit annulus area, stage/overall velocity ratio, and aerodynamic losses are considered. Trends in these parameters both spanwise and axially through the machine are highlighted. The effects of flow mixing and methods for accounting for the mixing in the design process are discussed.

ESA

**N89-16837\*#** National Aeronautics and Space Administration. Lewis Research Center, Cleveland, OH.

## **SUPERSONIC THROUGHFLOW FANS**

C. L. BALL and R. D. MOORE In Von Karman Institute for Fluid Dynamics, Transonic Compressors, Volume 2 30 p 1988

Avail: NTIS HC A17/MF A01

Supersonic throughflow fan research, and technology needs are reviewed. The design of a supersonic throughflow fan stage, a facility inlet, and a downstream diffuser is described. The results from the analysis codes used in executing the design are shown. An engine concept intended to permit establishing supersonic throughflow within the fan on the runway and maintaining the supersonic throughflow condition within the fan throughout the flight envelope is presented.

ESA

**N89-16843\*#** United Technologies Research Center, East Hartford, CT.

## **SUPERSONIC THROUGH-FLOW FAN ASSESSMENT**

Contractual Report, Jan. 1986 - Nov. 1988

C. E. KEPLER and G. A. CHAMPAGNE Nov. 1988 166 p

## 07 AIRCRAFT PROPULSION AND POWER

(Contract NAS3-24843)

(NASA-CR-182202; NAS 1.26:182202; UTRC-R88-957367-31)

Avail: NTIS HC A08/MF A01 CSCL 21/5

A study was conducted to assess the performance potential of a supersonic through-flow fan engine for supersonic cruise aircraft. It included a mean-line analysis of fans designed to operate with in-flow velocities ranging from subsonic to high supersonic speeds. The fan performance generated was used to estimate the performance of supersonic fan engines designed for four applications: a Mach 2.3 supersonic transport, a Mach 2.5 fighter, a Mach 3.5 cruise missile, and a Mach 5.0 cruise vehicle. For each application an engine was conceptualized, fan performance and engine performance calculated, weight estimates made, engine installed in a hypothetical vehicle, and mission analysis was conducted. Author

**N89-17599\*#** Adiabatics, Inc., Columbus, IN.

### **ADIABATIC WANKEL TYPE ROTARY ENGINE**

R. KAMO, P. BADGLEY, and D. DOUP Sep. 1988 208 p

(Contract NAS3-24880)

(NASA-CR-182233; NAS 1.26:182233; AI-120) Avail: NTIS HC

A10/MF A01 CSCL 21/5

This SBIR Phase program accomplished the objective of advancing the technology of the Wankel type rotary engine for aircraft applications through the use of adiabatic engine technology. Based on the results of this program, technology is in place to provide a rotor and side and intermediate housings with thermal barrier coatings. A detailed cycle analysis of the NASA 1007R Direct Injection Stratified Charge (DISC) rotary engine was performed which concluded that applying thermal barrier coatings to the rotor should be successful and that it was unlikely that the rotor housing could be successfully run with thermal barrier coatings as the thermal stresses were extensive. Author

**N89-18487\*#** Garrett Turbine Engine Co., Phoenix, AZ.

### **OXIDE-DISPERSION-STRENGTHENED TURBINE BLADES. VOLUME 2**

P. P. MILLAN, JR., J. C. MAYES, and D. R. HUMBERT 1987 51 p

(Contract NAS3-20073)

(NASA-CR-179561-VOL-2; NAS 1.26:179561-VOL-2;

GARRETT-21-5278-2-VOL-2) Avail: NTIS HC A04/MF A01 CSCL 21/5

The overall objective of Project 4 was to develop and test a high-temperature, uncooled gas turbine blade using MA6000 alloy. Production scale up of the MA6000 alloy was achieved with a fair degree of tolerance to non-optimum processing. The blade manufacturing process was also optimized. The mechanical, environmental, and physical property evaluations of MA6000 were conducted. The ultimate tensile strength, to about 704 C (1300 F), is higher than DS MAR-M 247 but with a corresponding lower tensile elongation. Also, above 982 C (1800 F) MA6000 tensile strength does not decrease as rapidly as MAR-M 247 because the ODS mechanism still remains active. Based on oxidation resistance and diffusional stability considerations, NiCrAlY coatings are recommended. CoCrAlY coating should be applied on top of a thin NiCrAlY coating if hot corrosion is expected. Vibration, whirlpit, and high-rotor-rig tests were conducted to ensure successful completion of the engine test of the MA6000 TFE731 high pressure turbine blades. Test results were acceptable. In production quantities, the cost of the Project 4 MA6000 blade is estimated to be twice that of a cast DS MAR-M 247 blade. Author

**N89-19262\*#** National Aeronautics and Space Administration. Lewis Research Center, Cleveland, OH.

### **TURBOMACHINERY AEROELASTICITY AT NASA LEWIS RESEARCH CENTER**

KRISHNA RAO V. KAZA In NASA, Langley Research Center, Transonic Unsteady Aerodynamics and Aeroelasticity 1987, Part 2 p 571-603 Feb. 1989

Avail: NTIS HC A17/MF A01 CSCL 21/5

The turbomachinery aeroelastic effort is focused on unstalled

and stalled flutter, forced response, and whirl flutter of both single rotation and counter rotation propfans. It also includes forced response of the Space Shuttle Main Engine (SSME) turbopump blades. Because of certain unique features of propfans and the SSME turbopump blades, it is not possible to directly use the existing aeroelastic technology of conventional propellers, turbopumps or helicopters. Therefore, reliable aeroelastic stability and response analysis methods for these propulsion systems must be developed. The development of these methods for propfans requires specific basic technology disciplines, such as 2-D and 3-D steady and unsteady aerodynamic theories in subsonic, transonic and supersonic flow regimes; modeling of composite blades; geometric nonlinear effects; and passive and active control of flutter and response. These methods are incorporated in a computer program, ASTROP. The program has flexibility such that new and future models in basic disciplines can be easily implemented. Author

**N89-19299\*#** Hamilton Standard Div., United Aircraft Corp., Windsor Locks, CT.

### **LARGE-SCALE ADVANCED PROP-FAN (LAP) HUB/BLADE RETENTION DESIGN REPORT**

MATTHEW SOULE 31 Jan. 1986 77 p

(Contract NAS3-23051)

(NASA-CR-174786; NAS 1.26:174786; HSER-9247) Avail: NTIS HC A05/MF A01 CSCL 21/5

The Large-scale Advanced Prop-fan (LAP) hub assembly forms a semi-rigid link between the blades, which provide the thrust, and the engine shaft, which provides the torque. The hub and tailshaft is a one piece partially forged part which is carburized, heat treated and machined. A single row ball bearing restrains each of the eight blades in the hub, while the tailshaft secures the propeller to the engine shaft with two cone seats that are preloaded against each other by the Prop-fan retaining nut. The hub also forms the support for the pitch change actuator system, the control and the spinner. The retention transmits the loads from the blades to the hub while allowing the changes in blade pitch. The single row ball bearing retention provides ease of maintenance by allowing individual blade replacement without disassembly of the hub. It has a through hardened inner race which seats against the aluminum blade shank and an outer race which is integral with the barrel. The outer race area is carburized to achieve the hardness necessary to support the ball loads. The balls are kept from contact with each other by a separator. The rotational speed of the propeller keeps the retention submerged in the oil which is contained in the hub by a seal. Stress and strain analysis, material hardness requirements, weight predictions, and stiffness characteristics are discussed. Author

**N89-19300\*#** Douglas Aircraft Co., Inc., Long Beach, CA.

### **MULTIPLE APPLICATION PROPFAN STUDY (MAPS): ADVANCED TACTICAL TRANSPORT Final Report, Aug. 1984 - Apr. 1985**

F. C. NEWTON, R. H. LIEBECK, G. H. MITCHELL, A. MOOIWEER, M. M. PLATTE, T. L. TOOGOOD, and R. A. WRIGHT Mar. 1986 105 p

(Contract NAS3-24348)

(NASA-CR-175003; NAS 1.26:175003) Avail: NTIS HC A06/MF A01 CSCL 21/5

This study was conducted to ascertain potential benefits of a propfan propulsion system application to a blended wing/body military tactical transport. Based on a design cruise Mach no. of 0.75 for the design mission, the results indicate a significant advantage in various figures of merit for the propfan over those of a comparable technology turbopump. Although the propfan has a 1.6 percent greater takeoff gross weight, its life cycle cost is 5.3 percent smaller, partly because of a 27 percent smaller specific fuel consumption. When employed on alternate missions, the propfan configuration offers significantly improved flexibility and capability: an increase in sea level penetration distance of more than 100 percent, or in time-on-station of 24 percent, or in deployment payload of 38 percent. Author

**N89-19305\*#** National Aeronautics and Space Administration. Lewis Research Center, Cleveland, OH.

**ICING RESEARCH TUNNEL TEST OF A MODEL HELICOPTER ROTOR**

THOMAS L. MILLER (Sverdrup Technology, Inc., Cleveland, OH.) and THOMAS H. BOND 1989 14 p Proposed for presentation at the 45th Annual Forum and Technology Display, Boston, MA, 22-24 May 1989; sponsored by the American Helicopter Society (NASA-TM-101978; E-4677; NAS 1.15:101978) Avail: NTIS HC A03/MF A01 CSCL 21/5

An experimental program has been conducted in the NASA Lewis Research Center Icing Research Tunnel (IRT) in which an OH-58 tail rotor assembly was operated in a horizontal plane to simulate the action of a typical main rotor. Ice was accreted on the blades in a variety of rotor and tunnel operating conditions and documentation of the resulting shapes was performed. Rotor torque and vibration are presented as functions of time for several representative test runs, and the effects of various parametric variations on the blade ice shapes are shown. This OH-58 test was the first of its kind in the United States and will encourage additional model rotor icing tunnel testing. Although not a scaled representative of any actual full-scale main rotor system, this rig has produced torque and vibration data which will be useful in assessing the quality of existing rotor icing analyses. Author

**N89-20132\*#** Pratt and Whitney Aircraft, East Hartford, CT. Commercial Engineering Dept.

**STRUCTURAL TAILORING OF ADVANCED TURBOPROPS (STAT) PROGRAMMER'S MANUAL**

K. W. BROWN and P. R. HARVEY Mar. 1989 53 p (Contract NAS3-23941)

(NASA-CR-182164; NAS 1.26:182164; PWA-5967-51) Avail: NTIS HC A04/MF A01 CSCL 21/5

The Structural Tailoring of Advanced Turboprops (STAT) computer program was developed to perform numerical optimizations on highly swept propfan blades. This manual describes the functionality of the STAT system from a programmer's viewpoint. It provides a top-down description of module intent and interaction. The purpose of this manual is to familiarize the programmer with the STAT system should he/she wish to enhance or verify the program's function. Author

**N89-20133\*#** National Aeronautics and Space Administration. Lewis Research Center, Cleveland, OH.

**EXPERIMENTAL INVESTIGATION OF TRANSONIC OSCILLATING CASCADE AERODYNAMICS**

DANIEL H. BUFFUM and SANFORD FLEETER (Purdue Univ., West Lafayette, IN.) Jan. 1989 15 p Presented at the 27th Aerospace Sciences Meeting, Reno, NV, 9-12 Jan. 1989; sponsored in part by AIAA Previously announced in IAA as A89-26369 (Contract NAG3-656)

(NASA-TM-101993; E-4697; NAS 1.15:101993) Avail: NTIS HC A03/MF A01 CSCL 21/5

Fundamental experiments are performed in the NASA Lewis Transonic Oscillating Cascade Facility to investigate the subsonic and transonic aerodynamics of cascaded airfoils executing torsion mode oscillations at realistic values of reduced frequency. In particular, an unsteady aerodynamic influence coefficient technique is developed and utilized. In this technique, only one airfoil in the cascade is oscillated at a time, with the resulting airfoil surface unsteady pressure distribution measured on one dynamically instrumented reference airfoil. The unsteady aerodynamics of an equivalent cascade with all airfoils oscillating at any specified interblade phase angle are then determined through a vector summation of these data. These influence coefficient determined oscillating cascade data were correlated with: (1) data obtained in this cascade with all airfoils oscillating at several interblade phase angle values; and (2) predictions from a classical linearized unsteady cascade model. Author

**N89-20134\*#** Cornell Univ., Ithaca, NY.

**PROPULSION OVER A WIDE MACH NUMBER RANGE Final Report M.S. Thesis**

EDWIN L. RESLER, JR. and BARRY M. GREENBERG Mar. 1989 71 p

(Contract NAG3-803)

(NASA-CR-182267; NAS 1.26:182267) Avail: NTIS HC A04/MF A01 CSCL 21/5

Criteria is presented to assess the relative merits of different propulsion systems. Previous references focus mainly on subsonic or low supersonic flight speeds. The main focus here is on a higher range, from low supersonic to orbital velocities. Air breathing propulsion systems for hypersonic flight present the engine designer with circumstances that differ in important fundamental ways from those encountered in engines designed for operation at subsonic or low supersonic speeds. This analysis highlights the importance of various features of hypersonic engine design. Since the performance of hypersonic engines are energy limited, unlike low speed engines which are stagnation pressure limited, the efficient use of the energy of the fuel used is critical to minimize the take-off fuel mass fraction of the vehicle. Furthermore, since the required energy increase of a vehicle per incremental speed change increases with speed, the engine must be designed to operate efficiently at high speed. An analysis of engine performance in terms of entropy changes of the flow passing through the engine allows comparison of various engine designs as well as a convenient method to determine the effect of individual engine component efficiencies on overall engine performance. Author

**N89-20135\*#** National Aeronautics and Space Administration. Lewis Research Center, Cleveland, OH.

**TOWARD IMPROVED DURABILITY IN ADVANCED AIRCRAFT ENGINE HOT SECTIONS**

DANIEL E. SOKOLOWSKI, ed. Washington Apr. 1989 121 p Proceedings of the 33rd ASME International Gas Turbine and Aeroengine Congress and Exposition, Amsterdam, Netherlands, 5-9 Jun. 1988 Previously announced in IAA as A88-54137 (NASA-TM-4087; E-4468; NAS 1.15:4087) Avail: NTIS HC A06/MF A01 CSCL 21/5

The conference on durability improvement methods for advanced aircraft gas turbine hot-section components discussed NASA's Hot Section Technology (HOST) project, advanced high-temperature instrumentation for hot-section research, the development and application of combustor aerothermal models, and the evaluation of a data base and numerical model for turbine heat transfer. Also discussed are structural analysis methods for gas turbine hot section components, fatigue life-prediction modeling for turbine hot section materials, and the service life modeling of thermal barrier coatings for aircraft gas turbine engines.

**N89-20136\*#** National Aeronautics and Space Administration. Lewis Research Center, Cleveland, OH.

**NASA HOST PROJECT OVERVIEW**

DANIEL E. SOKOLOWSKI In *its* Toward Improved Durability in Advanced Aircraft Engine Hot Sections p 1-4 Apr. 1989 Previously announced in IAA as A88-54138 Avail: NTIS HC A06/MF A01 CSCL 21/5

NASA's Hot Section Technology (HOST) program has developed improved analytical models for the aerothermal environment, thermomechanical loading, material behavior, structural response, and service life of aircraft gas turbine engines' hot section components. These models, in conjunction with sophisticated computer codes, can be used in design analyses of critical combustor and turbine elements. Toward these ends, efforts were undertaken in instrumentation, combustion, turbine heat transfer, structural analysis, fatigue-fracture, and surface protection. Attention is presently given to the organization of HOST activities and their specific subject matter. Author

**N89-20137\*#** National Aeronautics and Space Administration. Lewis Research Center, Cleveland, OH.

**ADVANCED HIGH TEMPERATURE INSTRUMENT FOR HOT SECTION RESEARCH APPLICATIONS**

D. R. ENGLUND and R. G. SEASHOLTZ In *its* Toward Improved Durability in Advanced Aircraft Engine Hot Sections p 5-21 Apr.

## 07 AIRCRAFT PROPULSION AND POWER

1989 Previously announced in IAA as A88-54139  
Avail: NTIS HC A06/MF A01 CSCL 21/5

Programs to develop research instrumentation for use in turbine engine hot sections are described. These programs were initiated to provide improved measurements capability as support for a multidisciplinary effort to establish technology leading to improved hot section durability. Specific measurement systems described here include heat flux sensors, a dynamic gas temperature measuring system, laser anemometry for hot section applications, an optical system for viewing the interior of a combustor during operation, thin film sensors for surface temperature and strain measurements, and high temperature strain measuring systems. The state of development of these sensors and measuring systems is described, and, in some cases, examples of measurements made with these instruments are shown. Work done at the NASA Lewis Research Center and at various contract and grant facilities is covered. Author

**N89-20138\*#** National Aeronautics and Space Administration. Lewis Research Center, Cleveland, OH.

### **ASSESSMENT, DEVELOPMENT, AND APPLICATION OF COMBUSTOR AEROTHERMAL MODELS**

J. D. HOLDEMAN, H. C. MONGIA, and E. J. MULARZ (Army Aviation Systems Command, Cleveland, OH.) *In its* Toward Improved Durability in Advanced Aircraft Engine Hot Sections p 23-37 Apr. 1989 Previously announced in IAA as A88-54140  
Avail: NTIS HC A06/MF A01 CSCL 21/5

The gas turbine combustion system design and development effort is an engineering exercise to obtain an acceptable solution to the conflicting design trade-offs between combustion efficiency, gaseous emissions, smoke, ignition, restart, lean blowout, burner exit temperature quality, structural durability, and life cycle cost. For many years, these combustor design trade-offs have been carried out with the help of fundamental reasoning and extensive component and bench testing, backed by empirical and experience correlations. Recent advances in the capability of computational fluid dynamics codes have led to their application to complex 3-D flows such as those in the gas turbine combustor. A number of U.S. Government and industry sponsored programs have made significant contributions to the formulation, development, and verification of an analytical combustor design methodology which will better define the aerothermal loads in a combustor, and be a valuable tool for design of future combustion systems. The contributions made by NASA Hot Section Technology (HOST) sponsored Aerothermal Modeling and supporting programs are described. Author

**N89-20139\*#** National Aeronautics and Space Administration. Lewis Research Center, Cleveland, OH.

### **REVIEW AND ASSESSMENT OF THE DATABASE AND NUMERICAL MODELING FOR TURBINE HEAT TRANSFER**

H. J. GLADDEN and R. J. SIMONEAU *In its* Toward Improved Durability in Advanced Aircraft Engine Hot Sections p 39-55 Apr. 1989 Previously announced in IAA as A88-54141  
Avail: NTIS HC A06/MF A01 CSCL 21/5

The objectives of the NASA Hot Section Technology (HOST) Turbine Heat Transfer subproject were to obtain a better understanding of the physics of the aerothermodynamic phenomena and to assess and improve the analytical methods used to predict the flow and heat transfer in high-temperature gas turbines. At the time the HOST project was initiated, an across-the-board improvement in turbine design technology was needed. A building-block approach was utilized and the research ranged from the study of fundamental phenomena and modeling to experiments in simulated real engine environments. Experimental research accounted for approximately 75 percent of the funding while the analytical efforts were approximately 25 percent. A healthy government/industry/university partnership, with industry providing almost half of the research, was created to advance the turbine heat transfer design technology base. Author

**N89-20140\*#** National Aeronautics and Space Administration. Lewis Research Center, Cleveland, OH.

### **STRUCTURAL ANALYSIS METHODS DEVELOPMENT FOR TURBINE HOT SECTION COMPONENTS**

R. L. THOMPSON *In its* Toward Improved Durability in Advanced Aircraft Engine Hot Sections p 57-82 Apr. 1989 Previously announced in IAA as A88-54142  
Avail: NTIS HC A06/MF A01 CSCL 21/5

The structural analysis technologies and activities of the NASA Lewis Research Center's gas turbine engine HOT Section Technology (HOST) program are summarized. The technologies synergistically developed and validated include: time-varying thermal/mechanical load models; component-specific automated geometric modeling and solution strategy capabilities; advanced inelastic analysis methods; inelastic constitutive models; high-temperature experimental techniques and experiments; and nonlinear structural analysis codes. Features of the program that incorporate the new technologies and their application to hot section component analysis and design are described. Improved and, in some cases, first-time 3-D nonlinear structural analyses of hot section components of isotropic and anisotropic nickel-base superalloys are presented. Author

**N89-20142\*#** National Aeronautics and Space Administration. Lewis Research Center, Cleveland, OH.

### **FATIGUE LIFE PREDICTION MODELING FOR TURBINE HOT SECTION MATERIALS**

G. R. HALFORD, T. G. MEYER, R. S. NELSON, D. M. NISSLEY, and G. A. SWANSON *In its* Toward Improved Durability in Advanced Aircraft Engine Hot Sections p 97-107 Apr. 1989 Previously announced in IAA as A88-54144 Prepared in cooperation with Pratt and Whitney Aircraft, East Hartford, CT  
Avail: NTIS HC A06/MF A01 CSCL 21/5

A major objective of the fatigue and fracture efforts under the NASA Hot Section Technology (HOST) program was to significantly improve the analytic life prediction tools used by the aeronautical gas turbine engine industry. This was achieved in the areas of high-temperature thermal and mechanical fatigue of bare and coated high-temperature superalloys. The cyclic crack initiation and propagation resistance of nominally isotropic polycrystalline and highly anisotropic single crystal alloys were addressed. Life prediction modeling efforts were devoted to creep-fatigue interaction, oxidation, coatings interactions, multiaxiality of stress-strain states, mean stress effects, cumulative damage, and thermomechanical fatigue. The fatigue crack initiation life models developed to date include the Cyclic Damage Accumulation (CDA) and the Total Strain Version of Strainrange Partitioning (TS-SRP) for nominally isotropic materials, and the Tensile Hysteretic Energy Model for anisotropic superalloys. A fatigue model is being developed based upon the concepts of Path-Independent Integrals (PII) for describing cyclic crack growth under complex nonlinear response at the crack tip due to thermomechanical loading conditions. A micromechanistic oxidation crack extension model was derived. The models are described and discussed. Author

**N89-20143\*#** National Aeronautics and Space Administration. Lewis Research Center, Cleveland, OH.

### **LIFE MODELING OF THERMAL BARRIER COATINGS FOR AIRCRAFT GAS TURBINE ENGINES**

R. A. MILLER *In its* Toward Improved Durability in Advanced Aircraft Engine Hot Sections p 109-115 Apr. 1989 Previously announced in IAA as A88-54145  
Avail: NTIS HC A06/MF A01 CSCL 21/5

Thermal barrier coating life models developed under the NASA Lewis Research Center's Hot Section Technology (HOST) Program are summarized. An initial laboratory model and three design-capable models are discussed. Current understanding of coating failure mechanisms are also summarized. The materials and structural aspects of thermal barrier coatings have been successfully integrated under the HOST program to produce models which may now or in the near future be used in design. Efforts on this program continue at Pratt and Whitney Aircraft where their

model is being extended to the life prediction of physical vapor deposited thermal barrier coatings. Author

**N89-20144\*#** National Aeronautics and Space Administration. Lewis Research Center, Cleveland, OH.

#### VIEWS ON THE IMPACT OF HOST

J. B. ESGAR (Sverdrup Technology, Inc., Cleveland, OH.) and DANIEL E. SOKOLOWSKI *In its* Toward Improved Durability in Advanced Aircraft Engine Hot Sections p 117-123 Apr. 1989 Previously announced in IAA as A88-54146 Avail: NTIS HC A06/MF A01 CSCL 21/5

The Hot Section Technology (HOST) Project, which was initiated by NASA Lewis Research Center in 1980 and concluded in 1987, was aimed at improving advanced aircraft engine hot section durability through better technical understanding and more accurate design analysis capability. The project was a multidisciplinary, multiorganizational, focused research effort that involved 21 organizations and 70 research and technology activities and generated approximately 250 research reports. No major hardware was developed. To evaluate whether HOST had a significant impact on the overall aircraft engine industry in the development of new engines, interviews were conducted with 41 participants in the project to obtain their views. The summarized results of these interviews are presented. Emphasis is placed on results relative to three-dimensional inelastic structural analysis, thermomechanical fatigue testing, constitutive modeling, combustor aerothermal modeling, turbine heat transfer, protective coatings, computer codes, improved engine design capability, reduced engine development costs, and the impacts on technology transfer and the industry-government partnership. Author

**N89-20995\*#** National Aeronautics and Space Administration. Lewis Research Center, Cleveland, OH.

#### A REAL-TIME SIMULATOR OF A TURBOFAN ENGINE

JONATHAN S. LITT (Army Aviation Research and Development Command, Cleveland, OH.), JOHN C. DELAAT, and WALTER C. MERRILL Mar. 1989 32 p (NASA-TM-100869; E-4578; NAS 1.15:100869; AVSCOM-TR-89-C-001; AD-A206830) Avail: NTIS HC A03/MF A01 CSCL 21/5

A real-time digital simulator of a Pratt and Whitney F100 engine has been developed for real-time code verification and for actuator diagnosis during full-scale engine testing. This self-contained unit can operate in an open-loop stand-alone mode or as part of closed-loop control system. It can also be used for control system design and development. Tests conducted in conjunction with the NASA Advanced Detection, Isolation, and Accommodation program show that the simulator is a valuable tool for real-time code verification and as a real-time actuator simulator for actuator fault diagnosis. Although currently a small perturbation model, advances in microprocessor hardware should allow the simulator to evolve into a real-time, full-envelope, full engine simulation. Author

**N89-20996\*#** National Aeronautics and Space Administration. Lewis Research Center, Cleveland, OH.

#### A COMPENDIUM OF CONTROLLED DIFFUSION BLADES GENERATED BY AN AUTOMATED INVERSE DESIGN PROCEDURE

JOSE M. SANZ Mar. 1989 204 p (NASA-TM-101968; E-4665; NAS 1.15:101968) Avail: NTIS HC A10/MF A01 CSCL 21/5

A set of sample cases was produced to test an automated design procedure developed at the NASA Lewis Research Center for the design of controlled diffusion blades. The range of application of the automated design procedure is documented. The results presented include characteristic compressor and turbine blade sections produced with the automated design code as well as various other airfoils produced with the base design method prior to the incorporation of the automated procedure. Author

**N89-21798\*#** National Aeronautics and Space Administration. Lewis Research Center, Cleveland, OH.

#### A PERSPECTIVE ON FUTURE DIRECTIONS IN AEROSPACE PROPULSION SYSTEM SIMULATION

BRENT A. MILLER, JOHN R. SZUCH, RAYMOND E. GAUGLER, and JERRY R. WOOD 1989 9 p Presented at the 4th International Conference, Santa Clara, CA, 30 Apr. - 5 May 1989; sponsored by the International Supercomputing Inst. (NASA-TM-102038; E-4608; NAS 1.15:102038) Avail: NTIS HC A02/MF A01 CSCL 21/5

The design and development of aircraft engines is a lengthy and costly process using today's methodology. This is due, in large measure, to the fact that present methods rely heavily on experimental testing to verify the operability, performance, and structural integrity of components and systems. The potential exists for achieving significant speedups in the propulsion development process through increased use of computational techniques for simulation, analysis, and optimization. This paper outlines the concept and technology requirements for a Numerical Propulsion Simulation System (NPSS) that would provide capabilities to do interactive, multidisciplinary simulations of complete propulsion systems. By combining high performance computing hardware and software with state-of-the-art propulsion system models, the NPSS will permit the rapid calculation, assessment, and optimization of subcomponent, component, and system performance, durability, reliability and weight-before committing to building hardware. Author

**N89-21799\*#** National Aeronautics and Space Administration. Lewis Research Center, Cleveland, OH.

#### AN EXPLICIT RUNGE-KUTTA METHOD FOR TURBULENT REACTING FLOW CALCULATIONS

A. A. BORETTI (Florence Univ., Italy) Apr. 1989 17 p (NASA-TM-101945; E-4635; NAS 1.15:101945) Avail: NTIS HC A03/MF A01 CSCL 21/5

The paper presents a numerical method for the solution of the conservation equations governing steady, reacting, turbulent viscous flow in two-dimensional geometries, in both Cartesian and axisymmetric coordinates. These equations are written in Favre-averaged form and closed with a first order model. A two-equation K-epsilon model, where low Reynolds number and compressibility effects are included, and a modified eddy-break up model are used to simulate fluid mechanics turbulence, chemistry and turbulence-combustion interaction. The solution is obtained by using a pseudo-unsteady method with improved perturbation propagation properties. The equations are discretized in space by using a finite volume formulation. An explicit multi-stage dissipative Runge-Kutta algorithm is then used to advance the flow equations in the pseudo-time. The method is applied to the computation of both diffusion and premixed turbulent reacting flows. The computed temperature distributions compare favorably with experimental data. Author

**N89-22605\*#** National Aeronautics and Space Administration. Lewis Research Center, Cleveland, OH.

#### ACTIVE VIBRATION CONTROL FOR FLEXIBLE ROTOR BY OPTIMAL DIRECT-OUTPUT FEEDBACK CONTROL

KENZOU NONAMI, ELISEO DIRUSSO, and DAVID P. FLEMING 1989 9 p Proposed for presentation at the 12th Biennial Conference on Mechanical Vibration and Noise, Montreal, Quebec, 17-20 Sep. 1989; sponsored by ASME (NASA-TM-101972; E-4672; NAS 1.15:101972) Avail: NTIS HC A02/MF A01 CSCL 21/5

Experimental research tests were performed to actively control the rotor vibrations of a flexible rotor mounted on flexible bearing supports. The active control method used in the tests is called optimal direct-output feedback control. This method uses four electrodynamic actuators to apply control forces directly to the bearing housings in order to achieve effective vibration control of the rotor. The force actuators are controlled by an analog controller that accepts rotor displacement as input. The controller is programmed with experimentally determined feedback coefficients; the output is a control signal to the force actuators. The tests

## 07 AIRCRAFT PROPULSION AND POWER

showed that this active control method reduced the rotor resonance peaks due to unbalance from approximately 250 micrometers down to approximately 25 micrometers (essentially runout level). The tests were conducted over a speed range from 0 to 10,000 rpm; the rotor system had nine critical speeds within this speed range. The method was effective in significantly reducing the rotor vibration for all of the vibration modes and critical speeds. Author

**N89-22606\*** # National Aeronautics and Space Administration. Lewis Research Center, Cleveland, OH.

### **INVESTIGATION OF LOW NOX STAGED COMBUSTOR CONCEPT IN HIGH-SPEED CIVIL TRANSPORT ENGINES**

HUNG LEE NGUYEN, DAVID A. BITTKER, and RICHARD W. NIEDZWIECKI 1989 23 p Presented at the 25th Joint Propulsion Conference, Monterey, CA, 10-12 Jul. 1989; cosponsored by the AIAA, ASME, SAE, and ASCE (NASA-TM-101977; E-4071; NAS 1.15:101977; AIAA-89-2942) Avail: NTIS HC A03/MF A01 CSCL 21/5

Levels of exhaust emissions due to high temperatures in the main combustor of high-speed civil transport (HSCT) engines during supersonic cruise are predicted. These predictions are based on a new combustor design approach: a rich burn/quick quench/lean burn combustor. A two-stage stirred reactor model is used to calculate the combustion efficiency and exhaust emissions of this novel combustor. A propane-air chemical kinetics model is used to simulate the fuel-rich combustion of jet fuel. Predicted engine exhaust emissions are compared with available experimental test data. The effect of HSCT engine operating conditions on the levels of exhaust emissions is also presented. The work described in this paper is a part of the NASA Lewis Research Center High-Speed Civil Transport Low NO(x) Combustor program. Author

**N89-22607\*** # National Aeronautics and Space Administration. Lewis Research Center, Cleveland, OH.

### **TRANSONIC VISCOUS FLOW CALCULATIONS FOR A TURBINE CASCADE WITH A TWO EQUATION TURBULENCE MODEL**

A. A. BORETTI (Florence Univ., Italy) Apr. 1989 16 p (NASA-TM-101944; E-4634; NAS 1.15:101944) Avail: NTIS HC A03/MF A01 CSCL 21/5

A numerical method for the study of steady, transonic, turbulent viscous flow through plane turbine cascades is presented. The governing equations are written in Favre-averaged form and closed with a first order model. The turbulent quantities are expressed according to a two-equation kappa-epsilon model where low Reynolds number and compressibility effects are included. The solution is obtained by using a pseudo-unsteady method with improved perturbation propagation properties. The equations are discretized in space by using a finite volume formulation. An explicit multistage dissipative Runge-Kutta algorithm is then used to advance the flow equations in the pseudo-time. First results of calculations compare fairly well with experimental data. Author

**N89-23465\*** # National Aeronautics and Space Administration. Lewis Research Center, Cleveland, OH.

### **ADVANCES IN COMPUTATIONAL DESIGN AND ANALYSIS OF AIRBREATHING PROPULSION SYSTEMS**

JOHN M. KLINEBERG 1989 19 p Proposed for presentation at the 9th International Symposium on Airbreathing Engines, Athens, Greece, 4-9 Sep. 1989; sponsored by International Society for Air Breathing Engines (NASA-TM-101987; E-4689; NAS 1.15:101987) Avail: NTIS HC A03/MF A01 CSCL 21/5

The development of commercial and military aircraft depends, to a large extent, on engine manufacturers being able to achieve significant increases in propulsion capability through improved component aerodynamics, materials, and structures. The recent history of propulsion has been marked by efforts to develop computational techniques that can speed up the propulsion design process and produce superior designs. The availability of powerful supercomputers, such as the NASA Numerical Aerodynamic Simulator, and the potential for even higher performance offered by parallel computer architectures, have opened the door to the

use of multi-dimensional simulations to study complex physical phenomena in propulsion systems that have previously defied analysis or experimental observation. An overview of several NASA Lewis research efforts is provided that are contributing toward the long-range goal of a numerical test-cell for the integrated, multidisciplinary design, analysis, and optimization of propulsion systems. Specific examples in Internal Computational Fluid Mechanics, Computational Structural Mechanics, Computational Materials Science, and High Performance Computing are cited and described in terms of current capabilities, technical challenges, and future research directions. Author

**N89-24318\*** # National Aeronautics and Space Administration. Lewis Research Center, Cleveland, OH.

### **TRANSIENT FLOW THRUST PREDICTION FOR AN EJECTOR PROPULSION CONCEPT**

COLIN K. DRUMMOND 1989 10 p Presented at the 25th Joint Propulsion Conference, Monterey, CA, 10-14 Jul. 1989; sponsored by AIAA, ASME, SAE and ASCE (NASA-TM-102078; E-4838; NAS 1.15:102078; AIAA-89-2906) Avail: NTIS HC A02/MF A01 CSCL 21/5

A method for predicting transient thrust augmenting ejector characteristics is introduced. The analysis blends classic self-similar turbulent jet descriptions with a mixing region control volume analysis to predict transient effects in a new way. Details of the theoretical foundation, the solution algorithm, and sample calculations are given. Author

**N89-24319\*** # National Aeronautics and Space Administration. Lewis Research Center, Cleveland, OH.

### **A MODEL FOR PREDICTION OF STOVL EJECTOR DYNAMICS**

COLIN K. DRUMMOND 1989 15 p Presented at the 20th Annual Conference on Modeling and Simulation, Pittsburgh, PA, 4-5 May 1989; cosponsored by the Univ. of Pittsburgh, IEEE and ISA (NASA-TM-102098; E-4861; NAS 1.15:102098) Avail: NTIS HC A03/MF A01 CSCL 21/5

A semi-empirical control-volume approach to ejector modeling for transient performance prediction is presented. This new approach is motivated by the need for a predictive real-time ejector sub-system simulation for Short Take-Off Vertical Landing (STOVL) integrated flight and propulsion controls design applications. Emphasis is placed on discussion of the approximate characterization of the mixing process central to thrust augmenting ejector operation. The proposed ejector model suggests transient flow predictions are possible with a model based on steady-flow data. A practical test case is presented to illustrate model calibration. Author

**N89-24320\*** # National Aeronautics and Space Administration. Lewis Research Center, Cleveland, OH.

### **TURBOMACHINERY TECHNOLOGY FOR HIGH-SPEED CIVIL FLIGHT**

NEAL T. SAUNDERS and ARTHUR J. GLASSMAN 1989 26 p Presented at the 34th International Gas Turbine and Aeroengine Congress and Exposition, Toronto, Ontario, 4-8 Jun. 1989; sponsored by the ASME (NASA-TM-102092; E-4746; NAS 1.15:102092) Avail: NTIS HC A03/MF A01 CSCL 21/5

NASA Lewis' research and technology efforts applicable to turbomachinery for high-speed flight are discussed. The potential benefits and cycle requirements for advanced variable cycle engines and the supersonic throughflow fan engine for a high-speed civil transport application are presented. The supersonic throughflow fan technology program is discussed. Technology efforts in the basic discipline areas addressing the severe operating conditions associated with high-speed flight turbomachinery are reviewed. Included are examples of work in internal fluid mechanics, high-temperature materials, structural analysis, instrumentation and controls. Author



**N89-25165\*#** National Aeronautics and Space Administration. Lewis Research Center, Cleveland, OH.

**STRUCTURAL TAILORING OF COUNTER ROTATION PROPFANS**

KENNETH W. BROWN (Pratt and Whitney Aircraft, East Hartford, CT.) and D. A. HOPKINS /in NASA. Langley Research Center, Recent Advances in Multidisciplinary Analysis and Optimization, Part 1 p 389-402 Apr. 1989

(Contract NAS3-23941)

Avail: NTIS HC A23/MF A01 CSCL 21/5

The STAT program was designed for the optimization of single rotation, tractor propfan designs. New propfan designs, however, generally consist of two counter rotating propfan rotors. STAT is constructed to contain two levels of analysis. An interior loop, consisting of accurate, efficient approximate analyses, is used to perform the primary propfan optimization. Once an optimum design has been obtained, a series of refined analyses are conducted. These analyses, while too computer time expensive for the optimization loop, are of sufficient accuracy to validate the optimized design. Should the design prove to be unacceptable, provisions are made for recalibration of the approximate analyses, for subsequent reoptimization. Author

**N89-25238\*#** National Aeronautics and Space Administration. Lewis Research Center, Cleveland, OH.

**FUEL PROPERTIES EFFECT ON THE PERFORMANCE OF A SMALL HIGH TEMPERATURE RISE COMBUSTOR**

WALDO A. ACOSTA and STEPHEN A. BECKEL (Pratt and Whitney Aircraft, West Palm Beach, FL.) Jul. 1989 12 p Presented at the 25th Joint Propulsion Conference, Monterey, CA, 10-12 Jul. 1989; sponsored in part by AIAA, ASME, SAE, and ASEE (Contract N00140-83-C-8899)

(NASA-TM-102096; AVSCOM-TR-89-C-004; E-4857; NAS 1.15:102096; AIAA-89-2901) Avail: NTIS HC A03/MF A01 CSCL 21/5

The performance of an advanced small high temperature rise combustor was experimentally determined at NASA-Lewis. The combustor was designed to meet the requirements of advanced high temperature, high pressure ratio turboshaft engines. The combustor featured an advanced fuel injector and an advanced segmented liner design. The full size combustor was evaluated at power conditions ranging from idle to maximum power. The effect of broad fuel properties was studied by evaluating the combustor with three different fuels. The fuels used were JP-5, a blend of Diesel Fuel Marine/Home Heating Oil, and a blend of Suncor C/Home Heating Oil. The fuel properties effect on the performance of the combustion in terms of pattern factor, liner temperatures, and exhaust emissions are documented. Author

**N89-26003\*#** National Aeronautics and Space Administration. Lewis Research Center, Cleveland, OH.

**ON THE APPLICATIONS OF ALGEBRAIC GRID GENERATION METHODS BASED ON TRANFINITE INTERPOLATION**

HUNG LEE NGUYEN Jun. 1989 25 p (NASA-TM-102095; E-4778; NAS 1.15:102095) Avail: NTIS HC A03/MF A01 CSCL 21/5

Algebraic grid generation methods based on transfinite interpolation called the two-boundary and four-boundary methods are applied for generating grids with highly complex boundaries. These methods yield grid point distributions that allow for accurate application to regions of sharp gradients in the physical domain or time-dependent problems with small length scale phenomena. Algebraic grids are derived using the two-boundary and four-boundary methods for applications in both two- and three-dimensional domains. Grids are developed for distinctly different geometrical problems and the two-boundary and four-boundary methods are demonstrated to be applicable to a wide class of geometries. Author

**N89-26004\*#** Sverdrup Technology, Inc., Cleveland, OH.

**TURBOFAN ENGINE CONTROL SYSTEM DESIGN USING THE LQG/LTR METHODOLOGY Final Report**

SANJAY GARG Jun. 1989 24 p Presented at the American

Control Conference, Pittsburgh, PA, 21-23 Jun. 1989; sponsored by American Automatic Control Council

(Contract NAS3-25266)

(NASA-CR-182303; E-4765; NAS 1.26:182303) Avail: NTIS HC A03/MF A01 CSCL 21/5

Application of the Linear-Quadratic-Gaussian with Loop-Transfer-Recovery methodology to design of a control system for a simplified turbofan engine model is considered. The importance of properly scaling the plant to achieve the desired Target-Feedback-Loop is emphasized. The steps involved in the application of the methodology are discussed via an example, and evaluation results are presented for a reduced-order compensator. The effect of scaling the plant on the stability robustness evaluation of the closed-loop system is studied in detail. Author

**N89-26007\*#** National Aeronautics and Space Administration. Lewis Research Center, Cleveland, OH.

**ENGINEERING STUDY OF THE ROTARY-VEE ENGINE CONCEPT**

EDWARD A. WILLIS, TIMOTHY A. BARTRAND (Sverdrup Technology, Inc., Cleveland, OH.), and JOHN E. BEARD Mar. 1989 38 p Presented at the Annual Congress and Exposition, Detroit, MI, 27 Feb. - 3 Mar. 1989; sponsored by Society of Automotive Engineers

(NASA-TM-101995; E-4698; NAS 1.15:101995; SAE-89-0332)

Avail: NTIS HC A03/MF A01 CSCL 21/5

The applicable thermodynamic cycle and performance considerations when the rotary-vee mechanism is used as an internal combustion (I.C.) heat engine are reviewed. Included is a simplified kinematic analysis and studies of the effects of design parameters on the critical pressures, torques and parasitic losses. A discussion of the principal findings is presented. Author

**N89-26008\*#** National Aeronautics and Space Administration. Lewis Research Center, Cleveland, OH.

**AERONAUTICAL APPLICATIONS OF HIGH-TEMPERATURE SUPERCONDUCTORS**

GEORGE E. TURNEY, ROGER W. LUIDENS, KENNETH UHERKA, and JOHN HULL (Argonne National Lab., IL.) Aug. 1989 15 p Presented at the Aircraft Design, Systems and Operations Conference, Seattle, WA, 31 Jul. - 2 Aug. 1989; sponsored in part by AIAA, AHS, and ASEE

(NASA-TM-102311; E-4951; NAS 1.15:102311) Avail: NTIS HC A03/MF A01 CSCL 21/5

The successful development of high-temperature superconductors (HTS) could have a major impact on future aeronautical propulsion and aeronautical flight vehicle systems. A preliminary examination of the potential application of HTS for aeronautics indicates that significant benefits may be realized through the development and implementation of these newly discovered materials. Applications of high-temperature superconductors (currently substantiated at 95 K) were envisioned for several classes of aeronautical systems, including subsonic and supersonic transports, hypersonic aircraft, V/STOL aircraft, rotorcraft, and solar, microwave and laser powered aircraft. Introduced and described are the particular applications and potential benefits of high-temperature superconductors as related to aeronautics and/or aeronautical systems. Author

**N89-27670\*#** National Aeronautics and Space Administration. Lewis Research Center, Cleveland, OH.

**MACH 5 INLET CFD AND EXPERIMENTAL RESULTS**

LOIS J. WEIR, D. R. REDDY, and GEORGE D. RUPP (Sverdrup Technology, Inc., Cleveland, OH.) Jul. 1989 16 p Presented at the 25th Joint Propulsion Conference, Monterey, CA, 10-12 Jul. 1989; sponsored in part by AIAA, ASME, SAE, and ASEE

(NASA-TM-102317; E-5011; NAS 1.15:102317; AIAA-89-2355) Avail: NTIS HC A03/MF A01 CSCL 21/5

An experimental research program was conducted in the NASA Lewis Research Center 10 x 10 ft supersonic wind tunnel. The 2-D inlet model was designed to study the Mach 3.0 to 5.0 speed range for an over-under turbojet plus ramjet propulsion system.



## 07 AIRCRAFT PROPULSION AND POWER

The model was extensively instrumented to provide both analytical code validation data as well as inlet performance information. Support studies for the program include flow field predictions with both 3-D parabolized Navier-Stokes (PNS) and 3-D full Navier-Stokes (FNS) analytical codes. Analytical predictions and experimental results are compared. Author

**N89-29351\*#** General Electric Co., Cincinnati, OH. Aircraft Engines Dept.

### **REVOLUTIONARY OPPORTUNITIES FOR MATERIALS AND STRUCTURES STUDY, ADDENDUM**

P. D. FEIG 1987 39 p

(Contract NAS3-24622)

(NASA-CR-179642-ADD; NAS 1.26:179642-ADD) Avail: NTIS HC A03/MF A01 CSCL 21/5

This report is an addendum to the Revolutionary Opportunities for Materials and Structures Study (ROMS), modifying the original by the addition of two tasks. The primary purpose of these tasks was to conduct additional aircraft/engine sizing and mission analysis to obtain contributory aircraft performance data such as fuel burns and direct operating costs for both the subsonic and supersonic engines. Author

## 08

### **AIRCRAFT STABILITY AND CONTROL**

Includes aircraft handling qualities; piloting; flight controls; and autopilots.

**A89-16156\*#** National Aeronautics and Space Administration. Lewis Research Center, Cleveland, OH.

### **ADVANCED DETECTION, ISOLATION, AND ACCOMMODATION OF SENSOR FAILURES - REAL-TIME EVALUATION**

WALTER C. MERRILL, JOHN C. DELAAT, and WILLIAM M. BRUTON (NASA, Lewis Research Center, Cleveland, OH) Journal of Guidance, Control, and Dynamics (ISSN 0731-5090), vol. 11, Nov.-Dec. 1988, p. 517-526. Previously announced in STAR as N87-25331. refs Copyright

The objective of the Advanced Detection, Isolation, and Accommodation (ADIA) program is to improve the overall demonstrated reliability of digital electronic control systems for turbine engines by using analytical redundancy to detect sensor failures. The results of a real-time hybrid computer evaluation of the ADIA algorithm are presented. Minimum detectable levels of sensor failures for an F100 engine control system are determined. Also included are details about the microprocessor implementation of the algorithm as well as a description of the algorithm itself. Author

**A89-28454\*#** National Aeronautics and Space Administration. Lewis Research Center, Cleveland, OH.

### **DETERMINATION OF LONGITUDINAL AERODYNAMIC DERIVATIVES USING FLIGHT DATA FROM AN ICING RESEARCH AIRCRAFT**

R. J. RANAUDO, A. L. REEHORST, T. H. BOND (NASA, Lewis Research Center, Cleveland, OH), J. G. BATTERSON (NASA, Langley Research Center, Hampton, VA), and T. M. O'MARA (NASA, Langley Research Center, Hampton, VA; George Washington University, Washington, DC) AIAA, Aerospace Sciences Meeting, 27th, Reno, NV, Jan. 9-12, 1989. 18 p. Previously announced in STAR as N89-15121. refs (AIAA PAPER 89-0754)

A flight test was performed with the NASA Lewis Research Center's DH-6 icing research aircraft. The purpose was to employ a flight test procedure and data analysis method, to determine the accuracy with which the effects of ice on aircraft stability and control could be measured. For simplicity, flight testing was

restricted to the short period longitudinal mode. Two flights were flown in a clean (baseline) configuration, and two flights were flown with simulated horizontal tail ice. Forty-five repeat doublet maneuvers were performed in each of four test configurations, at a given trim speed, to determine the ensemble variation of the estimated stability and control derivatives. Additional maneuvers were also performed in each configuration, to determine the variation in the longitudinal derivative estimates over a wide range of trim speeds. Stability and control derivatives were estimated by a Modified Stepwise Regression (MSR) technique. A measure of the confidence in the derivative estimates was obtained by comparing the standard error for the ensemble of repeat maneuvers, to the average of the estimated standard errors predicted by the MSR program. A multiplicative relationship was determined between the ensemble standard error, and the averaged program standard errors. In addition, a 95 percent confidence interval analysis was performed for the elevator effectiveness estimates,  $C_{sub m sub delta e}$ . This analysis identified the speed range where changes in  $C_{sub m sub delta e}$  could be attributed to icing effects. The magnitude of icing effects on the derivative estimates were strongly dependent on flight speed and aircraft wing flap configuration. With wing flaps up, the estimated derivatives were degraded most at lower speeds corresponding to that configuration. With wing flaps extended to 10 degrees, the estimated derivatives were degraded most at the higher corresponding speeds. The effects of icing on the changes in longitudinal stability and control derivat Author

**A89-30859\*#** Toledo Univ., OH.

### **APPLICATION OF A FULL-POTENTIAL SOLVER TO BENDING-TORSION FLUTTER IN CASCADES**

MILIND A. BAKHLE, THEO G. KEITH, JR. (Toledo, University, OH), and KRISHNA RAO V. KAZA IN: AIAA, ASME, ASCE, AHS, and ASC, Structures, Structural Dynamics and Materials Conference, 30th, Mobile, AL, Apr. 3-5, 1989, Technical Papers. Part 4. Washington, DC, American Institute of Aeronautics and Astronautics, 1989, p. 1982-1990. refs (Contract NSG-3139)

(AIAA PAPER 89-1386) Copyright

A two-dimensional, unsteady, full-potential cascade aerodynamic code has been used for flutter calculations. The code, which uses a time-marching implicit scheme with internal Newton-iterations at each time step, allows oscillatory blade motions with phase lag between adjacent blades to be modeled using a single inter-blade passage. This aerodynamic code has been used with a two-degrees-of-freedom typical section structural model to determine the aeroelastic stability of a bladed disk. The unsteady pressure results calculated from the aerodynamic code have been verified by comparison with results from the linear and linearized potential theories. Flutter results have been presented for two cases. A comparison with linear theory shows identical trends; however, the present calculations show a lower flutter frequency. Author

**A89-47166\*#** National Aeronautics and Space Administration. Lewis Research Center, Cleveland, OH.

### **INTEGRATED FLIGHT/PROPULSION CONTROL STUDY FOR STOVL APPLICATIONS**

JAMES R. MIHALOEWS (NASA, Lewis Research Center, Cleveland, OH) and CARL WEISS (United Technologies Corp., Pratt and Whitney Group, West Palm Beach, FL) AIAA, ASME, SAE, and ASEE, Joint Propulsion Conference, 25th, Monterey, CA, July 10-13, 1989. 7 p.

(AIAA PAPER 89-2908) Copyright

The STOVL Integrated Flight Propulsion Controls (IFPC) Program, initiated by NASA Lewis and NASA Ames to develop the necessary technologies for integrating the flight and propulsion controls of a future STOVL aircraft, is described. A major element of the STOVL IFPC Program is the STOVL Controls Integration Program (SCIP), which focuses on the development of an integrated flight propulsion control for the advanced vectored thrust STOVL concept. The SCIP has progressed to the point of generating top level control requirements. K.K.

**A89-52611\*#** National Aeronautics and Space Administration. Lewis Research Center, Cleveland, OH.

**INTEGRATED FLIGHT/PROPULSION CONTROL SYSTEM DESIGN BASED ON A CENTRALIZED APPROACH**

SANJAY GARG, DUANE L. MATTERN (NASA, Lewis Research Center; Sverdrup Technology, Inc., Cleveland, OH), and RANDY E. BULLARD (NASA, Lewis Research Center, Cleveland, OH) IN: AIAA Guidance, Navigation and Control Conference, Boston, MA, Aug. 14-16, 1989, Technical Papers. Part 1. Washington, DC, American Institute of Aeronautics and Astronautics, 1989, p. 827-839. Previously announced in STAR as N89-26009. refs (AIAA PAPER 89-3520)

An integrated flight/propulsion control system design is presented for the piloted longitudinal landing task with a modern, statically unstable, fighter aircraft. A centralized compensator based on the Linear Quadratic Gaussian/Loop Transfer Recovery methodology is first obtained to satisfy the feedback loop performance and robustness specifications. This high-order centralized compensator is then partitioned into airframe and engine sub-controllers based on modal controllability/observability for the compensator modes. The order of the sub-controllers is then reduced using internally-balanced realization techniques and the sub-controllers are simplified by neglecting the insignificant feedbacks. These sub-controllers have the advantage that they can be implemented as separate controllers on the airframe and the engine while still retaining the important performance and stability characteristics of the full-order centralized compensator. Command prefilters are then designed for the closed-loop system with the simplified sub-controllers to obtain the desired system response to airframe and engine command inputs, and the overall system performance evaluation results are presented. Author

**A89-52628\*#** Mississippi State Univ., Mississippi State. **AN OBSERVER-BASED COMPENSATOR FOR DISTRIBUTED DELAYS IN INTEGRATED CONTROL SYSTEMS**

ROGELIO LUCK (Mississippi State University, Mississippi State) and ASOK RAY (Pennsylvania State University, University Park) IN: AIAA Guidance, Navigation and Control Conference, Boston, MA, Aug. 14-16, 1989, Technical Papers. Part 2. Washington, DC, American Institute of Aeronautics and Astronautics, 1989, p. 988-996. refs

(Contract NAG3-823)

(AIAA PAPER 89-3541) Copyright

This paper presents an algorithm for compensation of delays that are distributed within a control loop. The observer-based algorithm is especially suitable for compensating network-induced delays that are likely to occur in integrated control systems of the future generation aircraft. The robustness of the algorithm relative to uncertainties in the plant model have been examined. Author

**A89-53301\*#** National Aeronautics and Space Administration. Lewis Research Center, Cleveland, OH.

**INTEGRATED FLIGHT/PROPULSION CONTROL SYSTEM DESIGN BASED ON A DECENTRALIZED, HIERARCHICAL APPROACH**

DUANE MATTERN, SANJAY GARG (NASA, Lewis Research Center; Sverdrup Technology, Inc., Cleveland, OH), and RANDY BULLARD (NASA, Lewis Research Center, Cleveland, OH) AIAA, Guidance, Navigation and Control Conference, Boston, MA, Aug. 14-16, 1989. 13 p. refs

(AIAA PAPER 89-3519) Copyright

A sample integrated flight/propulsion control system design is presented for the piloted longitudinal landing task with a modern, statically unstable fighter aircraft. The design procedure is summarized, the vehicle model used in the sample study is described, and the procedure for partitioning the integrated system is presented along with a description of the subsystems. The high-level airframe performance specifications and control design are presented and the control performance is evaluated. The generation of the low-level (engine) subsystem specifications from the airframe requirements are discussed, and the engine performance specifications are presented along with the subsystem control design. A compensator to accommodate the influence of

airframe outputs on the engine subsystem is also considered. Finally, the entire closed loop system performance and stability characteristics are examined. C.D.

**N89-15121\*#** National Aeronautics and Space Administration. Lewis Research Center, Cleveland, OH.

**DETERMINATION OF LONGITUDINAL AERODYNAMIC DERIVATIVES USING FLIGHT DATA FROM AN ICING RESEARCH AIRCRAFT**

R. J. RANAUDO, J. G. BATTERSON, A. L. REEHORST, T. H. BOND, and T. M. OMARA (George Washington Univ., Washington, DC.) 1989 19 p Presented at the 27th Aerospace Sciences Meeting, Reno, NV, 9-12 Jan. 1989; sponsored by AIAA (NASA-TM-101427; E-4528; NAS 1.15:101427; AIAA-89-0754) Avail: NTIS HC A03/MF A01 CSCL 01/3

A flight test was performed with the NASA Lewis Research Center's DH-6 icing research aircraft. The purpose was to employ a flight test procedure and data analysis method, to determine the accuracy with which the effects of ice on aircraft stability and control could be measured. For simplicity, flight testing was restricted to the short period longitudinal mode. Two flights were flown in a clean (baseline) configuration, and two flights were flown with simulated horizontal tail ice. Forty-five repeat doublet maneuvers were performed in each of four test configurations, at a given trim speed, to determine the ensemble variation of the estimated stability and control derivatives. Additional maneuvers were also performed in each configuration, to determine the variation in the longitudinal derivative estimates over a wide range of trim speeds. Stability and control derivatives were estimated by a Modified Stepwise Regression (MSR) technique. A measure of the confidence in the derivative estimates was obtained by comparing the standard error for the ensemble of repeat maneuvers, to the average of the estimated standard errors predicted by the MSR program. A multiplicative relationship was determined between the ensemble standard error, and the averaged program standard errors. In addition, a 95 percent confidence interval analysis was performed for the elevator effectiveness estimates,  $C_{sub m sub delta e}$ . This analysis identified the speed range where changes in  $C_{sub m sub delta e}$  could be attributed to icing effects. The magnitude of icing effects on the derivative estimates were strongly dependent on flight speed and aircraft wing flap configuration. With wing flaps up, the estimated derivatives were degraded most at lower speeds corresponding to that configuration. With wing flaps extended to 10 degrees, the estimated derivatives were degraded most at the higher corresponding speeds. The effects of icing on the changes in longitudinal stability and control derivatives were adequately determined by the flight test procedure and the MSR analysis method discussed herein. Author

**N89-26009\*#** National Aeronautics and Space Administration. Lewis Research Center, Cleveland, OH.

**INTEGRATED FLIGHT/PROPULSION CONTROL SYSTEM DESIGN BASED ON A CENTRALIZED APPROACH**

SANJAY GARG, DUANE L. MATTERN (Sverdrup Technology, Inc., Cleveland, OH.), and RANDY E. BULLARD 1989 41 p Presented at the Guidance, Navigation and Control Conference, Boston, MA, 14-16 Aug. 1989; sponsored by the AIAA (NASA-TM-102137; E-4860; NAS 1.15:102137; AIAA-89-3520) Avail: NTIS HC A03/MF A01 CSCL 01/3

An integrated flight/propulsion control system design is presented for the piloted longitudinal landing task with a modern, statically unstable, fighter aircraft. A centralized compensator based on the Linear Quadratic Gaussian/Loop Transfer Recovery methodology is first obtained to satisfy the feedback loop performance and robustness specifications. This high-order centralized compensator is then partitioned into airframe and engine sub-controllers based on modal controllability/observability for the compensator modes. The order of the sub-controllers is then reduced using internally-balanced realization techniques and the sub-controllers are simplified by neglecting the insignificant feedbacks. These sub-controllers have the advantage that they can be implemented as separate controllers on the airframe and

## 08 AIRCRAFT STABILITY AND CONTROL

the engine while still retaining the important performance and stability characteristics of the full-order centralized compensator. Command prefilterers are then designed for the closed-loop system with the simplified sub-controllers to obtain the desired system response to airframe and engine command inputs, and the overall system performance evaluation results are presented. Author

**N89-27672\*#** Sverdrup Technology, Inc., Cleveland, OH.  
**STABILITY ROBUSTNESS IMPROVEMENT OF DIRECT EIGENSPACE ASSIGNMENT BASED FEEDBACK SYSTEMS USING SINGULAR VALUE SENSITIVITIES Final Report**  
SANJAY GARG Aug. 1989 32 p Presented at the American Control Conference, Pittsburgh, PA, 21-23 Jun. 1989; sponsored in part by American Automatic Control Council  
(Contract NAS3-25266)  
(NASA-CR-182302; E-4853; NAS 1.26:182302) Avail: NTIS HC A03/MF A01 CSCL 01/3

A methodology to improve the stability robustness of feedback control systems designed using direct eigenspace assignment techniques is presented. The method consists of considering the sensitivity of the minimum singular value of the return difference transfer matrix at the plant input to small changes in the desired closed-loop eigenvalues and the specified elements of the desired closed-loop eigenvectors. Closed-form expressions for the gradient of the minimum return difference singular value with respect to desired closed-loop eigenvalue and eigenvector parameters are derived. Closed-form expressions for the gradients of the control feedback gains with respect to the specified eigenspace parameters are obtained as an intermediate step. The use of the gradient information to improve the guaranteed gain and phase margins in eigenspace assignment based designs is demonstrated by application to an advanced fighter aircraft. Author

## 09

### RESEARCH AND SUPPORT FACILITIES (AIR)

Includes airports, hangars and runways; aircraft repair and overhaul facilities; wind tunnels; shock tubes; and aircraft engine test stands.

**A89-28455\*#** National Aeronautics and Space Administration. Lewis Research Center, Cleveland, OH.  
**INVESTIGATION OF THE FLOW IN THE DIFFUSER SECTION OF THE NASA LEWIS ICING RESEARCH TUNNEL**  
HAROLD E. ADDY, JR. (NASA, Lewis Research Center, Cleveland, OH) and THEO G. KEITH, JR. (Toledo, University, OH) AIAA, Aerospace Sciences Meeting, 27th, Reno, NV, Jan. 9-12, 1989. 12 p. refs  
(AIAA PAPER 89-0755) Copyright

The flow in the diffuser section of the Icing Research Wind Tunnel at NASA Lewis Research Center is investigated using both tunnel calibration measurements and numerical simulation techniques. Local pressure and temperature measurements are made to establish velocity and temperature profiles in the diffuser of the tunnel. These profiles are compared with similar measurements made prior to renovating the equipment which generates the tunnel's icing cloud. This comparison indicates the manner in which this change affected the flow. The measured data were also compared with a numerical simulation of the flow to help understand how such changes may favorably alter the tunnel flow. Author

**A89-46905\*#** National Aeronautics and Space Administration. Lewis Research Center, Cleveland, OH.  
**NEW HYPERSONIC FACILITY CAPABILITY AT NASA LEWIS RESEARCH CENTER**  
JEFFREY HAAS, ROGER CHAMBERLIN, and JOHN H. DICUS (NASA, Lewis Research Center, Cleveland, OH) AIAA, ASME, SAE, and ASEE, Joint Propulsion Conference, 25th, Monterey,

CA, July 10-13, 1989. 9 p. Previously announced in STAR as N89-22617.

(AIAA PAPER 89-2534) Copyright

Four facility activities are underway at NASA Lewis Research Center to develop new hypersonic propulsion test capability. Two of these efforts consist of upgrades to existing operational facilities. The other two activities will reactivate facilities that have been in a standby condition for over 15 years. These four activities are discussed and the new test facilities NASA Lewis will have in place to support evolving high speed research programs are described. Author

**N89-16882\*#** Sverdrup Technology, Inc., Cleveland, OH.  
**NASA POWERED LIFT FACILITY INTERNALLY GENERATED NOISE AND ITS TRANSMISSION TO THE ACOUSTIC FAR FIELD Final Report**  
RONALD G. HUFF Nov. 1988 219 p  
(Contract NAS3-25266)  
(NASA-CR-182217; E-4474; NAS 1.26:182217) Avail: NTIS HC A10/MF A01 CSCL 14/2

Noise tests of NASA Lewis Research Center's Powered Lift Facility (PLF) were performed to determine the frequency content of the internally generated noise that reaches the far field. The sources of the internally generated noise are the burner, elbows, valves, and flow turbulence. Tests over a range of nozzle pressure ratios from 1.2 to 3.5 using coherence analysis revealed that low frequency noise below 1200 Hz is transmitted through the nozzle. Broad banded peaks at 240 and 640 Hz were found in the transmitted noise. Aeroacoustic excitation effects are possible in this frequency range. The internal noise creates a noise floor that limits the amount of jet noise suppression that can be measured on the PLF and similar facilities. Author

**N89-21002\*#** National Aeronautics and Space Administration. Lewis Research Center, Cleveland, OH.  
**FLOWFIELD MEASUREMENTS IN THE NASA LEWIS RESEARCH CENTER 9- BY 15-FOOT LOW-SPEED WIND TUNNEL**  
CHRISTOPHER E. HUGHES Mar. 1989 78 p  
(NASA-TM-100883; E-4116; NAS 1.15:100883) Avail: NTIS HC A05/MF A01 CSCL 14/2

An experimental investigation was conducted in the NASA Lewis 9- by 15-Foot Low-Speed Wind Tunnel to determine the flow characteristics in the test section during wind tunnel operation. In the investigation, a 20-probe horizontally-mounted Pitot-static flow survey rake was used to obtain cross-sectional total and static pressure surveys at four axial locations in the test section. At each axial location, the cross-sectional flowfield surveys were made by repositioning the Pitot-static flow survey rake vertically. In addition, a calibration of the new wind tunnel rake instrumentation, used to determine the wind tunnel operating conditions, was performed. Boundary laser surveys were made at three axial locations in the test section. The investigation was conducted at tunnel Mach numbers 0.20, 0.15, 0.10, and 0.05. The test section profile results from the investigation indicate that fairly uniform total pressure profiles (outside the test section boundary layer) and fairly uniform static pressure and Mach number profiles (away from the test section walls and downstream of the test section entrance) exist throughout in the wind tunnel test section. Author

**N89-22617\*#** National Aeronautics and Space Administration. Lewis Research Center, Cleveland, OH.  
**NEW HYPERSONIC FACILITY CAPABILITY AT NASA LEWIS RESEARCH CENTER**  
JEFFREY E. HAAS, ROGER CHAMBERLIN, and JOHN H. DICUS 1989 16 p Presented at the 25th Joint Propulsion Conference, Monterey, CA, 10-12 Jul. 1989; sponsored by AIAA, ASME, SAE and ASEE  
(NASA-TM-102028; E-4760; NAS 1.15:102028; AIAA-89-2534)  
Avail: NTIS HC A03/MF A01 CSCL 14/2

Four facility activities are underway at NASA Lewis Research Center to develop new hypersonic propulsion test capability. Two

of these efforts consist of upgrades to existing operational facilities. The other two activities will reactivate facilities that have been in a standby condition for over 15 years. These four activities are discussed and the new test facilities NASA Lewis will have in place to support evolving high speed research programs are described.

Author

## 12

### ASTRONAUTICS (GENERAL)

**A89-14977\*** National Aeronautics and Space Administration. Lewis Research Center, Cleveland, OH.

#### IN-SITU PROPELLANT ADVANTAGES FOR FAST TRANSFER TO MARS

DIANE L. GALECKI (NASA, Lewis Research Center, Cleveland, OH) AIAA, ASME, SAE, and ASEE, Joint Propulsion Conference, 24th, Boston, MA, July 11-13, 1988. 23 p. refs (AIAA PAPER 88-2901)

The advantages of in situ propellant for a fast transfer to Mars were studied as compared to all earth-based propellants and other options for reduction of total mass in low earth orbit. For a 10-year, 10-mission model and a baseline vehicle taken from the literature, the total reduction in number of earth launches was calculated. The scenario in which the return propellants are transferred to Mars on a slow cargo vehicle provides a 29-percent reduction in ALS launches over the baseline scenario in which all propellants are brought directly from earth. The scenarios in which in situ propellants are used for a successively greater portion of the total mission continue to reduce the number of launches required. With Mars propellant used for the Mars ascent vehicle and the return leg of the mission, a 59-percent reduction in launches is obtained. Finally, if the oxygen, or oxygen and fuel, for the outbound leg of the mission is also obtained by in situ production, from the moon for example, then the total reduction in number of earth launches is more than 80 percent.

Author

**A89-17641\*** National Aeronautics and Space Administration. Lewis Research Center, Cleveland, OH.

#### TECHNOLOGY REQUIREMENTS FOR AN ORBITING FUEL DEPOT - A NECESSARY ELEMENT OF A SPACE INFRASTRUCTURE

R. M. STUBBS, R. R. CORBAN (NASA, Lewis Research Center, Cleveland, OH), and A. J. WILLOUGHBY (Analex Corp., Cleveland, OH) IAF, International Astronautical Congress, 39th, Bangalore, India, Oct. 8-15, 1988. 9 p. Previously announced in STAR as N88-29845. refs

(IAF PAPER 88-035) Copyright

Advanced planning within NASA has identified several bold space exploration initiatives. The successful implementation of these missions will require a supporting space infrastructure which would include a fuel depot, an orbiting facility to store, transfer and process large quantities of cryogenic fluids. In order to adequately plan the technology development programs required to enable the construction and operation of a fuel depot, a multidisciplinary workshop was convened to assess critical technologies and their state of maturity. Since technology requirements depend strongly on the depot design assumptions, several depot concepts are presented with their effect of criticality ratings. Over 70 depot-related technology areas are addressed.

Author

**A89-17861\*** General Dynamics Corp., San Diego, CA.

#### AN ANALYSIS OF POSSIBLE ADVANCED SPACE STRATEGIES FEATURING THE ROLE OF SPACE RESOURCE UTILIZATION

BRUCE CORDELL and OTTO STEINBRONN (General Dynamics Corp., Space Systems Div., San Diego, CA) IAF, International

Astronautical Congress, 39th, Bangalore, India, Oct. 8-15, 1988. 10 p. refs

(Contract NAS3-24564)

(IAF PAPER 88-587) Copyright

Unresolved issues in space planning in the U.S. are examined, focusing on space resource utilization. The role of the Space Station, determining the most profitable space exploration strategies, and space resource use are discussed. Performance modeling suggests that lunar oxygen is useful on the moon and economical in LEO if lunar hydrogen is available. It is found that the use of volatile materials from Phobos and Deimos might be undertaken if lunar hydrogen is unavailable. It is suggested that resource synergisms between operations in the Mars system and in earth-moon space have important commercial possibilities.

R.B.

**A89-40177\*** National Aeronautics and Space Administration. Lewis Research Center, Cleveland, OH.

#### SUMMARY OF THE SECOND INTERNATIONAL CONFERENCE ON TETHERS IN SPACE VENICE, ITALY, OCTOBER 4-8, 1987

JOSEPH C. KOLECKI (NASA, Lewis Research Center, Cleveland, OH) IN: International Conference on Tethers in Space - Toward Flight, 3rd, San Francisco, CA, May 17-19, 1989, Collection of Papers and Abstracts. Washington, DC, American Institute of Aeronautics and Astronautics, Inc., 1989, p. XV-XX. refs (AIAA PAPER 89-1547) Copyright

**A89-45803\*** National Aeronautics and Space Administration. Lewis Research Center, Cleveland, OH.

#### POWER SYSTEMS FOR PRODUCTION, CONSTRUCTION, LIFE SUPPORT, AND OPERATIONS IN SPACE

RONALD J. SOVIE (NASA, Lewis Research Center, Cleveland, OH) IN: Engineering, construction, and operations in space; Proceedings of the Space '88 Conference, Albuquerque, NM, Aug. 29-31, 1988. New York, American Society of Civil Engineers, 1988, p. 928-939. Previously announced in STAR as N88-21254. Copyright

As one looks to man's future in space it becomes obvious that unprecedented amounts of power are required for the exploration, colonization, and exploitation of space. Activities envisioned include interplanetary travel and LEO to GEO transport using electric propulsion, earth and lunar observatories, advance space stations, free-flying manufacturing platforms, communications platforms, and eventually evolutionary lunar and Mars bases. These latter bases would start as camps with modest power requirements (kWes) and evolve to large bases as manufacturing, food production, and life support materials are developed from lunar raw materials. These latter activities require very robust power supplies (MWes). The advanced power system technologies being pursued by NASA to fulfill these future needs are described. Technologies discussed will include nuclear, photovoltaic, and solar dynamic space power systems, including energy storage, power conditioning, power transmission, and thermal management. The state-of-the-art and gains to be made by technology advancements will be discussed. Mission requirements for a variety of applications (LEO, GEO, lunar, and Martian) will be treated, and data for power systems ranging from a few kilowatts to megawatt power systems will be represented. In addition the space power technologies being initiated under NASA's new Civilian Space Technology Initiative (CSTI) and Space Leadership Planning Group Activities will be discussed.

Author

**A89-46735\*** National Aeronautics and Space Administration. Lewis Research Center, Cleveland, OH.

#### NASA'S CHEMICAL TRANSFER PROPULSION PROGRAM FOR PATHFINDER

NED P. HANNUM, FRANK D. BERKOPEC (NASA, Lewis Research Center, Cleveland, OH), and ROBERT L. ZURAWSKI (NASA, Washington, DC) AIAA, ASME, SAE, and ASEE, Joint Propulsion Conference, 25th, Monterey, CA, July 10-13, 1989. 17 p. refs (AIAA PAPER 89-2298) Copyright

Pathfinder is a research and technology project, initiated by NASA in 1989 to support the U.S. civil space program studies for

## 12 ASTRONAUTICS (GENERAL)

the preparation for future space exploration missions. This paper describes the goals and objectives, the management, the technical plan, and technology transfer for the Chemical Transfer Propulsion program, which is a key element of one of the four programmatic thrusts (the Space Transfer) of the Pathfinder. The Chemical Transfer Propulsion will provide the technology for high-performance liquid oxygen/liquid hydrogen expander cycle engines for space-based transfer vehicles as well as for lunar and Mars landers. I.S.

**N89-11768\*#** National Aeronautics and Space Administration. Lewis Research Center, Cleveland, OH.

### **SPACE PROPULSION TECHNOLOGY AND CRYOGENIC FLUID DEPOT**

LARRY A. DIEHL *In* NASA, Washington, Technology for Future NASA Missions: Civil Space Technology Initiative (CSTI) and Pathfinder p 163-177 Sep. 1988  
Avail: NTIS HC A23/MF A01 CSCL 22/1

Information on space propulsion and technology and the cryogenic fluid depot is given in viewgraph form. Information is given on orbit transfer, electric propulsion, spacecraft propulsion, and program objectives. Author

**N89-11770\*#** National Aeronautics and Space Administration. Lewis Research Center, Cleveland, OH.

### **SPACE POWER TECHNOLOGIES**

RONALD J. SOVIE *In* NASA, Washington, Technology for Future NASA Missions: Civil Space Technology Initiative (CSTI) and Pathfinder p 193-218 Sep. 1988  
Avail: NTIS HC A23/MF A01 CSCL 22/1

Information is given in viewgraph form on space power technologies. Energy conversion, the role of nuclear power in space, lunar and Mars bases, and the Pathfinder program are covered. R.J.F.

**N89-22985\*#** National Aeronautics and Space Administration. Lewis Research Center, Cleveland, OH.

### **HUMAN EXPLORATION MISSION STUDIES Abstract Only**

ROBERT L. CATALDO *In* its Space Electrochemical Research and Technology Conference: Abstracts p 4 1989  
Avail: NTIS HC A03/MF A01 CSCL 22/1

The Office of Exploration has established a process whereby all NASA field centers and other NASA Headquarters offices participate in the formulation and analysis of a wide range of mission strategies. These strategies were manifested into specific scenarios or candidate case studies. The case studies provided a systematic approach into analyzing each mission element. First, each case study must address several major themes and rationale including: national pride and international prestige, advancement of scientific knowledge, a catalyst for technology, economic benefits, space enterprise, international cooperation, and education and excellence. Second, the set of candidate case studies are formulated to encompass the technology requirement limits in the life sciences, launch capabilities, space transfer, automation, and robotics in space operations, power, and propulsion. The first set of reference case studies identify three major strategies: human expeditions, science outposts, and evolutionary expansion. During the past year, four case studies were examined to explore these strategies. The expeditionary missions include the Human Expedition to Phobos and Human Expedition to Mars case studies. The Lunar Observatory and Lunar Outpost to Early Mars Evolution case studies examined the later two strategies. This set of case studies established the framework to perform detailed mission analysis and system engineering to define a host of concepts and requirements for various space systems and advanced technologies. The details of each mission are described and, specifically, the results affecting the advanced technologies required to accomplish each mission scenario are presented. Author

**N89-28535\*#** National Aeronautics and Space Administration. Lewis Research Center, Cleveland, OH.

### **COLD-SAT: CRYOGENIC ON-ORBIT LIQUID DEPOT-STORAGE, ACQUISITION AND TRANSFER**

Jul. 1989 14 p Original contains color illustrations  
(NASA-TM-102308; E-4997; NAS 1.15:102308) Avail: NTIS HC A03/MF A01 CSCL 22/1

NASA is entering an era of expanded space activity. Space-based transportation systems will carry cargo and humans from low earth orbit to geosynchronous orbit, to lunar bases, and to the Martian surface. Support of these future missions will require new, long lived, on-orbit systems using subcritical cryogenics for propellants and life support systems. Such on-orbit systems present low gravity fluid management challenges of long term storage and efficient fluid transfer and supply techniques. Development of these cryogenic systems requires on-orbit experimentation to demonstrate the capability of performing these fluid management tasks and to obtain the engineering data base required to correlate analytical tools used for system design. Author

## 13

### **ASTRODYNAMICS**

Includes powered and free-flight trajectories; and orbital and launching dynamics.

**A89-36946\*#** Illinois Univ., Urbana.

### **OPTIMAL TERMINAL MANEUVER FOR A COOPERATIVE IMPULSIVE RENDEZVOUS**

JOHN E. PRUSSING and BRUCE A. CONWAY (Illinois, University, Urbana) Journal of Guidance, Control, and Dynamics (ISSN 0731-5090), vol. 12, May-June 1989, p. 433-435.  
(Contract NAG3-805)

Copyright

An optimal terminal maneuver is presently defined for the cooperative impulsive rendezvous of two spacecraft, in which each vehicle is capable of furnishing all or a part of the velocity change required for the rendezvous. In this maneuver, the final masses of the two vehicles are maximized in a fashion that is equivalent to minimum total propellant consumption. If neither propellant mass fraction constraint is active, one vehicle will supply all of the required velocity change. O.C.

## 14

### **GROUND SUPPORT SYSTEMS AND FACILITIES (SPACE)**

Includes launch complexes, research and production facilities; ground support equipment, e.g., mobile transporters; and simulators.

**A89-15350\*** National Aeronautics and Space Administration. Ames Research Center, Moffett Field, CA.

### **COOPERATING EXPERT SYSTEMS FOR SPACE STATION - POWER/THERMAL SUBSYSTEM TESTBEDS**

CARLA M. WONG (NASA, Ames Research Center, Moffett Field, CA), DAVID J. WEEKS (NASA, Marshall Space Flight Center, Huntsville, AL), GALE R. SUNDBERG (NASA, Lewis Research Center, Cleveland, OH), KATHLEEN L. HEALEY, and JEFFREY S. DOMINICK (NASA, Johnson Space Center, Houston, TX) *In*: 1988 IECEC; Proceedings of the Twenty-third Intersociety Energy Conversion Engineering Conference, Denver, CO, July 31-Aug. 5, 1988. Volume 3. New York, American Society of Mechanical Engineers, 1988, p. 407-414. refs  
Copyright

The Systems Autonomy Demonstration Project (SADP) is a NASA-sponsored series of increasingly complex demonstrations to show the benefits of integrating knowledge-based systems with conventional process control in real-time, real-world problem domains that can facilitate the operations and availability of major Space Station distributed systems. This paper describes the system design, objectives, approaches, and status of each of the testbed knowledge-based systems. Simplified schematics of the systems are shown. C.D.

**A89-15352\*** National Aeronautics and Space Administration. Lewis Research Center, Cleveland, OH.

#### **SIMULATION TEST BEDS FOR THE SPACE STATION ELECTRICAL POWER SYSTEM**

GERALD G. SADLER (NASA, Lewis Research Center, Cleveland, OH) IN: 1988 IECEC; Proceedings of the Twenty-third Intersociety Energy Conversion Engineering Conference, Denver, CO, July 31-Aug. 5, 1988. Volume 3. New York, American Society of Mechanical Engineers, 1988, p. 421-430. Previously announced in STAR as N88-17715.

Copyright

NASA Lewis Research Center and its prime contractor are responsible for developing the electrical power system on the Space Station. The power system will be controlled by a network of distributed processors. Control software will be verified, validated, and tested in hardware and software test beds. Current plans for the software test bed involve using real time and nonreal time simulations of the power system. This paper will discuss the general simulation objectives and configurations, control architecture, interfaces between simulator and controls, types of tests, and facility configurations. Author

**A89-32065\*** Tuskegee Inst., AL.

#### **ARC RESTRIKE IN THE RAIL ACCELERATOR**

PRADOSH K. RAY (Tuskegee University, AL) (Symposium on Electromagnetic Launch Technology, 4th, Austin, TX, Apr. 12-14, 1988) IEEE Transactions on Magnetics (ISSN 0018-9464), vol. 25, Jan. 1989, p. 485-488. refs (Contract NAG3-76)

Copyright

One of the causes of the degradation in rail accelerator performance is the formation of a secondary arc. Experimental evidence of arc restrike and the subsequent growth of this secondary arc is presented. A simple analytical treatment of arc restrike is developed in terms of breakdown of residual vapor atoms. It is found that after the passage of the primary arc, the bore volume contains a large number of residual neutral vapor atoms. If the density of these atoms is in excess of the critical density, then for a certain length of time the condition exists in the bore for the formation of a secondary arc. Evaporation of atoms from the bore surfaces cannot provide a sufficient number of atoms for an arc restrike. A likely source of the high residual atom density is the leakage of a portion of the ablated material that is added to the trailing edge of the primary arc. I.E.

**A89-46530\*** National Aeronautics and Space Administration. Lewis Research Center, Cleveland, OH.

#### **PRELIMINARY ASSESSMENT OF ROVER POWER SYSTEMS FOR THE MARS ROVER SAMPLE RETURN MISSION**

D. J. BENTS (NASA, Lewis Research Center, Cleveland, OH) (IAF, International Conference on Space Power, Cleveland, OH, June 5-7, 1989) Space Power (ISSN 0951-5089), vol. 8, no. 3, 1989, p. 319-332. Previously announced in STAR as N89-23518. refs (IAF PAPER ICOSP89-9-6) Copyright

Four isotope power system concepts were presented and compared on a common basis for application to on-board electrical prime power for an autonomous planetary rover vehicle. A representative design point corresponding to the Mars Rover Sample Return (MRSR) preliminary mission requirements (500 W) was selected for comparison purposes. All systems concepts utilize the General Purpose Heat Source (GPHS) isotope heat source developed by DOE. Two of the concepts employ thermoelectric (TE) conversion: one using the GPHS Radioisotope Thermoelectric

Generator (RTG) used as a reference case, the other using an advanced RTG with improved thermoelectric materials. The other two concepts employed are dynamic isotope power systems (DIPS): one using a closed Brayton cycle (CBC) turboalternator, and the other using a free piston Stirling cycle engine/linear alternator (FPSE) with integrated heat source/heater head. Near-term technology levels have been assumed for concept characterization using component technology figure-of-merit values taken from the published literature. For example, the CBC characterization draws from the historical test database accumulated from space Brayton cycle subsystems and components from the NASA B engine through the mini-Brayton rotating unit. TE system performance is estimated from Voyager/multihundred Watt (MHW)-RTG flight experience through Mod-RTG performance estimates considering recent advances in TE materials under the DOD/DOE/NASA SP-100 and NASA Committee on Scientific and Technological Information programs. The Stirling DIPS system is characterized from scaled-down Space Power Demonstrator Engine (SPDE) data using the GPHS directly incorporated into the heater head. The characterization/comparison results presented here differ from previous comparison of isotope power (made for LEO applications) because of the elevated background temperature on the Martian surface compared to LEO, and the higher sensitivity of dynamic systems to elevated s Author

**A89-47110\*#** National Aeronautics and Space Administration. Lewis Research Center, Cleveland, OH.

#### **DESIGN OF A THRUST STAND FOR HIGH POWER ELECTRIC PROPULSION DEVICES**

THOMAS W. HAAG (NASA, Lewis Research Center, Cleveland, OH) AIAA, ASME, SAE, and ASEE, Joint Propulsion Conference, 25th, Monterey, CA, July 10-13, 1989. 13 p. refs (AIAA PAPER 89-2829) Copyright

A thrust stand for use with high power electric propulsion devices has been designed and tested. The thrust stand was specifically tailored to the needs of a 0.1 to 0.25 MW magnetoplasmadynamic (MPD) thruster program currently in progress at the NASA Lewis Research Center. The thrust stand structure was built as an inverted pendulum arrangement, supported at the base by water-cooled electrical power flexures. Thrust stand tares due to thruster discharge current were demonstrated to be negligible. Tares due to an applied field magnet current, after considerable effort, were reduced to less than 3.0 percent of measured thrust. These tares, however, could be determined independently and subtracted from the indicated thrust measurement. The paper gives a detailed description of the thrust stand design and operation with a 0.1 MW class MPD device. Other thrust stand tares due to vibration and thermal effects are discussed, along with issues of accuracy and repeatability. Author

**A89-47113\*#** National Aeronautics and Space Administration. Lewis Research Center, Cleveland, OH.

#### **PLUME CHARACTERISTICS OF MPD THRUSTERS - A PRELIMINARY EXAMINATION**

R. M. MYERS (NASA, Lewis Research Center; Sverdrup Technology, Inc., Cleveland, OH) AIAA, ASME, SAE, and ASEE, Joint Propulsion Conference, 25th, Monterey, CA, July 10-13, 1989. 20 p. refs

(AIAA PAPER 89-2832) Copyright

A diagnostics facility for MPD thruster plume measurements has been built and is currently undergoing testing. The facility includes electrostatic probes for electron temperature and density measurements, Hall probes for magnetic field and current distribution mapping, and an imaging system to establish the global distribution of plasma species. Preliminary results for MPD thrusters operated at power levels between 30 and 60 kW with solenoidal applied magnetic fields show that the electron density decreases exponentially from  $1 \times 10$  to the 20th/cm to  $2 \times 10$  to the 18th/cm over the first 30 cm of the expansion, while the electron temperature distribution is relatively uniform, decreasing from approximately 2.5 eV to 1.5 eV over the same distance. The radiant intensity of the ArII 4879 A line emission follows similar patterns.



## 14 GROUND SUPPORT SYSTEMS AND FACILITIES (SPACE)

Current distribution measurements indicate that significant fraction of the discharge current is blown into the plume region, and that its distribution depends on the magnitudes of both the discharge current and the applied magnetic field. Author

**N89-13445\*#** Tuskegee Inst., AL. Dept. of Mechanical Engineering.

### **ARC-DRIVEN RAIL ACCELERATOR RESEARCH Final Report**

PRADOSH K. RAY Feb. 1987 50 p

(Contract NAG3-76)

(NASA-CR-179584; NAS 1.26:179584) Avail: NTIS HC A03/MF

A01 CSCL 14/2

Arc-driven rail accelerator research is analyzed by considering wall ablation and viscous drag in the plasma. Plasma characteristics are evaluated through a simple fluid-mechanical analysis considering only wall ablation. By equating the energy dissipated in the plasma with the radiation heat loss, the average properties of the plasma are determined as a function of time and rate of ablation. Locations of two simultaneously accelerating arcs were determined by optical and magnetic probes and from streak camera photographs. All three measurements provide consistent results. Author

**N89-14247\*#** National Aeronautics and Space Administration. Lewis Research Center, Cleveland, OH.

### **POWER SYSTEMS FACILITY**

Jan. 1989 27 p Original contains color illustrations

(NASA-TM-101447; E-4553; NAS 1.15:101447) Avail: NTIS HC

A03/MF A01 CSCL 14/2

In 1984, the President directed NASA to undertake the development of Space Station Freedom, the next step in a broad-based U.S. civil space program to develop space-flight capabilities and to exploit space for scientific, technological, and commercial purposes. Under that direction, NASA awarded contracts in 1985 for concept definition and preliminary design studies. Those studies have been completed and the Space Station Freedom Program is now in the final design and development phase, leading to a permanently manned space station that will be operational in the mid-1990's. Here at the Lewis Research Center, with Rocketdyne, we are developing and building the S.S. Freedom electric power system (EPS) hardware and software. A major portion of the EPS will be tested at Lewis. The Power Systems Facility was specifically designed for testing the EPS and uses the latest in testing equipment. Author

**N89-28545\*#** National Aeronautics and Space Administration. Lewis Research Center, Cleveland, OH.

### **DIGITALLY MODULATED BIT ERROR RATE MEASUREMENT SYSTEM FOR MICROWAVE COMPONENT EVALUATION**

MARY JO W. SHALKHAUSER and JAMES M. BUDINGER Washington Jul. 1989 20 p

(NASA-TP-2912; E-4456; NAS 1.60:2912) Avail: NTIS HC

A03/MF A01 CSCL 14/2

The NASA Lewis Research Center has developed a unique capability for evaluation of the microwave components of a digital communication system. This digitally modulated bit-error-rate (BER) measurement system (DMBERMS) features a continuous data digital BER test set, a data processor, a serial minimum shift keying (SMSK) modem, noise generation, and computer automation. Application of the DMBERMS has provided useful information for the evaluation of existing microwave components and of design goals for future components. The design and applications of this system for digitally modulated BER measurements are discussed. Author

**N89-28549\*#** National Aeronautics and Space Administration. Lewis Research Center, Cleveland, OH.

### **FURNACE FOR TENSILE/FATIGUE TESTING Patent Application**

PAMELA K. BRINDLEY, inventor (to NASA) 21 Jul. 1989 11 p

(NASA-CASE-LEW-14848-1; NAS 1.71:LEW-14848-1;

US-PATENT-APPL-SN-382885) Avail: NTIS HC A03/MF A01

CSCL 14/2

Mechanical properties of short test specimens are tested in tension and fatigue using an improved electrical resistance heating furnace having a short length that mounts between the grips of a typical testing machine. The furnace includes a ceramic inner liner having an oval cross-section to reduce heat loss at the ends. The furnace is divided into a plurality of individually controlled heating zones. Provision is made to supply an inert gas to the volume around the specimen in the center of the furnace. NASA

## 15

## LAUNCH VEHICLES AND SPACE VEHICLES

Includes boosters; operating problems of launch/space vehicle systems; and reusable vehicles.

**A89-17939\*#** National Aeronautics and Space Administration. Lewis Research Center, Cleveland, OH.

### **THE EFFECT OF THE NEAR EARTH MICROMETEOROID ENVIRONMENT ON A HIGHLY REFLECTIVE MIRROR SURFACE**

MICHAEL J. MIRTICH, HERMAN MARK, and WILLIAM R. KERSLAKE (NASA, Lewis Research Center, Cleveland, OH) AIAA, Aerospace Sciences Meeting, 26th, Reno, NE, Jan. 11-14, 1988. 39 p. Previously announced in STAR as N88-29833. refs (AIAA PAPER 88-0026)

A resurgence of interest in placing large solar concentrator solar dynamic systems in space for power generation has brought up again a concern for maintaining the integrity of the optical properties of highly specular reflecting surfaces in the near earth space environment. One of the environmental hazards needing evaluation is the micrometeoroid environment. It has been shown that highly reflective polished metals and thin film coatings degrade when exposed to simulated micrometeoroids in the lab. At NASA-Lewis, a shock tube was used to simulate the phenomenon of micrometeoroid impact by accelerating micron sized particles to hypervelocities. Any changes in the optical properties of surfaces exposed to this impact were then evaluated. The degradation of optical properties of polished metals and thin metallic films after exposure to simulated micrometeoroids was determined as a function of impacting kinetic energy area of the particles. A calibrated sensor was developed to not only detect the micrometeoroid environment, but also to evaluate the degradation of the optical properties of thin aluminum films in space. Results of the simulation are presented and discussed. Author

**A89-50814\*#** National Aeronautics and Space Administration. Lewis Research Center, Cleveland, OH.

### **WEIGHT SAVINGS IN AEROSPACE VEHICLES THROUGH PROPELLANT SCAVENGING**

STEVEN J. SCHNEIDER and BRIAN D. REED (NASA, Lewis Research Center, Cleveland, OH) SAWE, Annual Conference, 47th, Plymouth, MI, May 23-25, 1988. 41 p. Previously announced in STAR as N88-25470. refs (SAWE PAPER 1818) Copyright

Vehicle payload benefits of scavenging hydrogen and oxygen propellants are addressed. The approach used is to select a vehicle and a mission and then select a scavenging system for detailed weight analysis. The Shuttle 2 vehicle on a Space Station rendezvous mission was chosen for study. The propellant scavenging system scavenges liquid hydrogen and liquid oxygen from the launch propulsion tankage during orbital maneuvers and stores them in well insulated liquid accumulators for use in a cryogenic auxiliary propulsion system. The fraction of auxiliary propulsion propellant which may be scavenged for propulsive purposes is estimated to be 45.1 percent. The auxiliary propulsion subsystem dry mass, including the proposed scavenging system, an additional 20 percent for secondary structure, an additional 5 percent for electrical service, a 10 percent weight growth margin, and 15.4 percent propellant reserves and residuals is estimated



to be 6331 kg. This study shows that the fraction of the on-orbit vehicle mass required by the auxiliary propulsion system of this Shuttle 2 vehicle using this technology is estimated to be 12.0 percent compared to 19.9 percent for a vehicle with an earth-storable bipropellant system. This results in a vehicle with the capability of delivering an additional 7820 kg to the Space Station.

Author

**N89-20171\*#** National Aeronautics and Space Administration. Lewis Research Center, Cleveland, OH.

**A DEFINITION STUDY OF THE ON-ORBIT ASSEMBLY OPERATIONS FOR THE OUTBOARD PHOTOVOLTAIC POWER MODULES FOR SPACE STATION FREEDOM M.S. Thesis - Toledo Univ.**

THOMAS J. SOURS Mar. 1989 89 p  
(NASA-TM-102006; E-4712; NAS 1.15:102006) Avail: NTIS HC A05/MF A01 CSCL 22/2

A concept is described for the assembly of the outboard PV modules for Space Station Freedom. Analysis of the on-orbit assembly operations was performed using CADAM design graphics software. A scenario for assembly using the various assembly equipment, as currently defined, is described in words, tables and illustrations. This work is part of ongoing studies in the area of space station assembly. The outboard PV module and the assembly equipment programs are all in definition and preliminary design phases. An input is provided to the design process of assembly equipment programs. It is established that the outboard PV module assembly operations can be performed using the assembly equipment currently planned in the Space Station Freedom Program.

Author

**N89-24409\*#** National Aeronautics and Space Administration. Lewis Research Center, Cleveland, OH.

**THE PATHFINDER CHEMICAL TRANSFER PROPULSION PROGRAM**

NED P. HANNUM, FRANK D. BERKOPEC, and ROBERT L. ZURAWSKI (National Aeronautics and Space Administration, Washington, DC.) May 1989 11 p Presented at the JANNAF Propulsion Meeting, Cleveland, OH, 23-25 May 1989  
(NASA-TM-102084; E-4847; NAS 1.15:102084) Avail: NTIS HC A03/MF A01 CSCL 13/2

Pathfinder is a research and technology initiative by the National Aeronautics and Space Administration (NASA) intended to strengthen the technology base of the United States civil space program in preparation for future space exploration missions. Pathfinder begins in FY-89. One of the four major thrusts of Pathfinder is Space Transfer technology. A key element of this thrust is the Chemical Transfer Propulsion program which will provide the propulsion technology for high performance, liquid oxygen/liquid hydrogen expander cycle engines which are expected to be operated and maintained in space. These advanced engines will enhance or enable a variety of future space exploration missions. This paper describes the goals and objectives, management, technical plan, and technology transfer for the Chemical Transfer Propulsion element of Pathfinder.

Author

**N89-25254\*#** National Aeronautics and Space Administration. Lewis Research Center, Cleveland, OH.

**ADVANCED APS IMPACTS ON VEHICLE PAYLOADS**

STEVEN J. SCHNEIDER and BRIAN D. REED 1989 14 p  
Presented at the JANNAF Propulsion Meeting, Cleveland, OH, 23-25 May 1989  
(NASA-TM-102086; E-4731; NAS 1.15:102086) Avail: NTIS HC A03/MF A01 CSCL 22/2

Advanced auxiliary propulsion system (APS) technology has the potential to both, increase the payload capability of earth-to-orbit (ETO) vehicles by reducing APS propellant mass, and simplify ground operations and logistics by reducing the number of fluids on the vehicle and eliminating toxic, corrosive propellants. The impact of integrated cryogenic APS on vehicle payloads is addressed. In this system, launch propulsion system residuals are scavenged from integral launch propulsion tanks for use in the APS. Sufficient propellant is preloaded into the APS to return to

earth with margin and noncomplete scavenging assumed. No propellant conditioning is required by the APS, but ambient heat soak is accommodated. High temperature rocket materials enable the use of the unconditioned hydrogen/oxygen in the APS and are estimated to give APS rockets specific impulse of up to about 444 sec. The payload benefits are quantified and compared with an uprated monomethylhydrazine/nitrogen tetroxide system in a conservative fashion, by assuming a 25.5 percent weight growth for the hydrogen/oxygen system and a 0 percent weight growth for the uprated system. The combination of scavenging and high performance gives payload impacts which are highly mission specific. A payload benefit of 861 kg (1898 lbm) was estimated for a Space Station Freedom rendezvous mission and 2099 kg (4626 lbm) for a sortie mission, with payload impacts varying with the amount of launch propulsion residual propellants. Missions without liquid propellant scavenging were estimated to have payload penalties, however, operational benefits were still possible.

Author

**N89-26027\*#** Sverdrup Technology, Inc., Cleveland, OH.  
**THE DEVELOPMENT OF POWER SPECIFIC REDLINES FOR SSME SAFETY MONITORING Final Report**

WILLIAM A. MAUL and CLAUDIA M. BOSCH Jun. 1989 36 p  
Presented at the 25th Joint Propulsion Technology Division, Monterey, CA, 10-12 Jul. 1989; cosponsored by the AIAA, ASME, SAE, and ASEE  
(Contract NAS3-25266)  
(NASA-CR-185121; E-4949; NAS 1.26:185121; AIAA-89-2413)  
Avail: NTIS HC A03/MF A01 CSCL 14/2

Over the past several years, there has been an increased awareness in the necessity for rocket engine health monitoring because of the cost and complexity of present and future systems. A current rocket engine system, the Space Shuttle Main Engine (SSME), combines a limited redline system with closed-loop control of the engine's thrust level and mixture ratio. Despite these features, 27 tests of the SSME have resulted in major incidents. A SSME transient model was used to examine the effect of variations in high pressure turbopump performance on various engine parameters. Based on analysis of the responses, several new parameters are proposed for further investigation as power-level specific redlines.

Author

**N89-26876\*#** National Aeronautics and Space Administration. Lewis Research Center, Cleveland, OH.

**NASA'S CHEMICAL TRANSFER PROPULSION PROGRAM FOR PATHFINDER**

NED P. HANNUM, FRANK D. BERKOPEC, and ROBERT L. ZURAWSKI 1989 18 p  
Presented at the 25th Joint Propulsion Conference, Monterey, CA, 10-12 Jul. 1989; cosponsored by the AIAA, ASME, SAE, and ASEE  
(NASA-TM-102298; E-4976; NAS 1.15:102298; AIAA-89-2298)  
Avail: NTIS HC A03/MF A01 CSCL 22/2

Pathfinder is a research and technology project, with specific deliverables, initiated by the National Aeronautics and Space Administration (NASA) which will strengthen the technology base of the United States civil space program in preparation for future space exploration missions. Pathfinder begins in Fiscal Year 1989, and is to advance a collection of critical technologies for these missions and ensure technology readiness for future national decisions regarding exploration of the solar system. The four major thrusts of Pathfinder are: surface exploration, in-space operations, humans-in-space, and space transfer. The space transfer thrust will provide the critical technologies needed for transportation to, and return from, the Moon, Mars, and other planets in the solar system, as well as for reliable and cost-effective Earth-orbit operations. A key element of this thrust is the Chemical Transfer Propulsion program which will provide the propulsion technology for high performance, liquid oxygen/liquid hydrogen expander cycle engines which may be operated and maintained in space. Described here are the program overview including the goals and objectives, management, technical plan, and technology transfer for the Chemical Transfer Propulsion element of Pathfinder.

Author

## SPACE TRANSPORTATION

Includes passenger and cargo space transportation, e.g., shuttle operations; and space rescue techniques.

**A89-17720\*#** National Aeronautics and Space Administration. Lewis Research Center, Cleveland, OH.

**EXPENDABLE LAUNCH VEHICLE TRANSPORTATION FOR THE SPACE STATION**

ROBERT R. CORBAN (NASA, Lewis Research Center, Cleveland, OH) IAF, International Astronautical Congress, 39th, Bangalore, India, Oct. 8-15, 1988. 12 p. refs  
(IAF PAPER 88-198) Copyright

ELVs are presently evaluated as major components of the NASA Space Station's logistics transportation system, augmenting the cargo capacity of the Space Shuttle in support of Station productivity and operational flexibility. The ELVs in question are the Delta II, Atlas II, Titan III, Titan IV, Shuttle-C (unmanned cargo development), European Ariane 5, and Japanese H-II, as well as smaller launch vehicles and OTVs. Early definition of ELV program impacts will preclude the potentially excessive costs of future Space Station modifications. O.C.

**N89-10111\*#** National Aeronautics and Space Administration. Lewis Research Center, Cleveland, OH.

**FIRE BEHAVIOR AND RISK ANALYSIS IN SPACECRAFT**

ROBERT FRIEDMAN and KURT R. SACKSTEDER 1988 14 p  
Prepared for presentation at the Winter Annual Meeting of the American Society of Mechanical Engineers, Chicago, Ill., 28 Nov. - 3 Dec. 1988

(NASA-TM-100944; E-4232; NAS 1.15:100944) Avail: NTIS HC A03/MF A01 CSCL 22B

Practical risk management for present and future spacecraft, including space stations, involves the optimization of residual risks balanced by the spacecraft operational, technological, and economic limitations. Spacecraft fire safety is approached through three strategies, in order of risk: (1) control of fire-causing elements, through exclusion of flammable materials for example; (2) response to incipient fires through detection and alarm; and (3) recovery of normal conditions through extinguishment and cleanup. Present understanding of combustion in low gravity is that, compared to normal gravity behavior, fire hazards may be reduced by the absence of buoyant gas flows yet at the same time increased by ventilation flows and hot particle expulsion. This paper discusses the application of low-gravity combustion knowledge and appropriate aircraft analogies to fire detection, fire fighting, and fire-safety decisions for eventual fire-risk management and optimization in spacecraft. Author

**N89-20179\*#** National Aeronautics and Space Administration. Lewis Research Center, Cleveland, OH.

**EXPENDABLE LAUNCH VEHICLE TRANSPORTATION FOR THE SPACE STATION**

ROBERT R. CORBAN Oct. 1988 13 p Presented at the 39th Congress of the International Astronautical Federation, Bangalore, India, 8-15 Oct. 1988 Previously announced in IAA as A89-17720

(NASA-TM-101947; E-4636; NAS 1.15:101947) Avail: NTIS HC A03/MF A01 CSCL 22/2

Logistics transportation will be a critical element in determining the Space Station Freedom's level of productivity and possible evolutionary options. The current program utilizes the Space Shuttle as the only logistics support vehicle. Augmentation of the total transportation capability by expendable launch vehicles (ELVs) may be required to meet demanding requirements and provide for enhanced manifest flexibility. The total operational concept from ground operations to final return of support hardware or its disposal is required to determine the ELV's benefits and impacts to the Space Station Freedom program. The characteristics of potential

medium and large class ELVs planned to be available in the mid-1990's (both U.S. and international partners' vehicles) indicate a significant range of possible transportation systems with varying degrees of operational support capabilities. The options available for development of a support infrastructure in terms of launch vehicles, logistics carriers, transfer vehicles, and return systems is discussed. Author

**N89-23501\*#** National Inst. of Standards and Technology, Gaithersburg, MD. Center for Fire Research.

**EXPERT SYSTEMS APPLIED TO SPACECRAFT FIRE SAFETY Final Report**

RICHARD L. SMITH and TAKASHI KASHIWAGI Jun. 1989 13 p

(Contract NASA ORDER C-32000-M)

(NASA-CR-182266; E-4812; NAS 1.26:182266) Avail: NTIS HC A03/MF A01 CSCL 22/2

Expert systems are problem-solving programs that combine a knowledge base and a reasoning mechanism to simulate a human expert. The development of an expert system to manage fire safety in spacecraft, in particular the NASA Space Station Freedom, is difficult but clearly advantageous in the long-term. Some needs in low-gravity flammability characteristics, ventilating-flow effects, fire detection, fire extinguishment, and decision models, all necessary to establish the knowledge base for an expert system, are discussed. Author

**N89-24413\*#** National Aeronautics and Space Administration. Lewis Research Center, Cleveland, OH.

**FIRE SAFETY APPLICATIONS FOR SPACECRAFT**

ROBERT FRIEDMAN and SANDRA L. OLSON 1989 29 p  
Presented at the Symposium on Aircraft Fire Safety, Sintra, Portugal, 22-26 May 1989; sponsored by the AGARD/NATO Propulsion Energetics Panel

(NASA-TM-101463; E-4511; NAS 1.15:101463) Avail: NTIS HC A03/MF A01 CSCL 22/2

Fire safety for spacecraft is reviewed by first describing current practices, many of which are adapted directly from aircraft. Then, current analyses and experimental knowledge in low-gravity combustion, with implications for fire safety are discussed. In orbiting spacecraft, the detection and suppression of flames are strongly affected by the large reduction in buoyant flows under low gravity. Generally, combustion intensity is reduced in low gravity. There are some notable exceptions, however, one example being the strong enhancement of flames by low-velocity ventilation flows in space. Finally, the future requirements in fire safety, particularly the needs of long-duration space stations in fire prevention, detection, extinguishment, and atmospheric control are examined. The goal of spacecraft fire-safety investigations is the establishment of trade-offs that promote maximum safety without hampering the useful human and scientific activities in space. Author

**N89-26877\*#** National Aeronautics and Space Administration. Lewis Research Center, Cleveland, OH.

**SATELLITE RELOCATION BY TETHER DEPLOYMENT**

GEOFFREY A. LANDIS and FRANK J. HRACH Apr. 1989 16 p

(NASA-TM-101992; E-4696; NAS 1.15:101992) Avail: NTIS HC A03/MF A01 CSCL 22/2

Several new uses of satellite tethers are discussed, including: (1) using tether extension to reposition a satellite in orbit without fuel expenditure by extending a mass on the end of a tether; (2) using a tether for energy storage to power the satellite during eclipse; and (3) using a tether for eccentricity pumping to correct perturbations in the orbit and as a means of adding energy to the orbit for boosting and orbital transfer. Author

## SPACE COMMUNICATIONS, SPACECRAFT COMMUNICATIONS, COMMAND AND TRACKING

Includes telemetry; space communications networks; astronavigation and guidance; and radio blackout.

**A89-15811\*** National Aeronautics and Space Administration. Lewis Research Center, Cleveland, OH.

**A LASER COMMUNICATION EXPERIMENT UTILIZING THE ACT SATELLITE AND AN AIRBORNE LASER TRANSCEIVER**  
C. PROVENCHER and ROD SPENCE (NASA, Lewis Research Center, Cleveland, OH) IN: Free-space laser communication technologies; Proceedings of the Meeting, Los Angeles, CA, Jan. 11, 12, 1988. Bellingham, WA, Society of Photo-Optical Instrumentation Engineers, 1988, p. 143-152. refs  
Copyright

The Advanced Communications Technology Satellite (ACTS) will carry a laser communications transmitter package in order to attempt the experimental reception of signals transmitted from earth orbit. The ACTS laser package includes both a heterodyne transmitter and a direct-detection transmitter. The laser receiver will be installed in an aircraft that is fitted with the requisite signal window. The anticipated capability of this signal detector is noted.  
O.C.

**A89-38298\*** Motorola, Inc., Chandler, AZ.

### BASEBAND PROCESSOR HARDWARE FOR ADVANCED COMMUNICATION TECHNOLOGY SATELLITE (ACTS)

LARRY BROWN and RICHARD MOAT (Motorola, Inc., Strategic Electronics Div., Chandler, AZ) IN: International Symposium on Space Technology and Science, 16th, Sapporo, Japan, May 22-27, 1988, Proceedings. Volume 2. Tokyo, AGNE Publishing, Inc., 1988, p. 1981-1989. Research supported by TRW, Inc.  
(Contract NAS3-23790)  
Copyright

The ACTS multibeam communication package payload and the baseband processor (BBP) subsystem are described in detail. The BBP provides the flexible message routing capability required to support the ACTS's TDMA burst communications. Advanced technologies employed in the ACTS BBP include coherent serial minimum shift key burst demodulation, a family of high-speed low-power large-scale integrated (LSI) circuits, a maximum-likelihood convolutional decoder on a single LSI chip, and memory architectures using programmable control memories.  
R.R.

**A89-39144\*** Communications Satellite Corp., Clarksburg, MD.  
**INTERSATELLITE LINK APPLICATION TO COMMERCIAL COMMUNICATIONS SATELLITES**

YOUNG S. LEE, ALI E. ATIA (COMSAT, Systems Div., Clarksburg, MD), and DENISE S. PONCHAK (NASA, Lewis Research Center, Cleveland, OH) COMSAT Technical Review (ISSN 0095-9669), vol. 18, Fall 1988, p. 147-189. refs  
(Contract NAS3-24884)  
Copyright

The fundamental characteristics of intersatellite link (ISL) systems, and their application to domestic, regional, and global satellite communications, are described. The quantitative advantages of using ISLs to improve orbit utilization, spectrum occupancy, transmission delay (compared to multi-hop links), coverage, and connectivity, and to reduce the number of earth station antennas, are also presented. Cost-effectiveness and other systems benefits of using ISLs are identified, and the technical and systems planning aspects of ISL systems implementation are addressed.  
Author

**N89-13457\*#** National Aeronautics and Space Administration. Lewis Research Center, Cleveland, OH.

### DESIGN AND IMPLEMENTATION OF A MICROCOMPUTER-BASED USER INTERFACE CONTROLLER FOR BURSTED DATA COMMUNICATIONS SATELLITE GROUND TERMINALS

MARY JO W. SHALKHAUSER Dec. 1988 22 p  
(NASA-TM-101375; E-4428; NAS 1.15:101375) Avail: NTIS HC A03/MF A01 CSCL 09/6

The NASA Lewis Research Center is developing a laboratory-based satellite communications test bed for evaluation of state-of-the-art communications hardware and systems. Most of the digital components of the ground terminals are being constructed in-house at NASA Lewis. One of the ground terminal subsystems, the user interface controller, controls the connection and disconnection of all users to the communication network. The role of the user interface controller in the ground terminal is described and the design and implementation of the micro-computer-based subsystem is discussed.  
Author

**N89-26879\*#** Multipoint Communications Corp., Sunnyvale, CA.  
**PROGRAMMABLE RATE MODEM UTILIZING DIGITAL SIGNAL PROCESSING TECHNIQUES Final Report**

GEORGE K. BUNYA and ROBERT L. WALLACE Jul. 1989 110 p  
(Contract NAS3-25336)  
(NASA-CR-185124; NAS 1.26:185124) Avail: NTIS HC A06/MF A01 CSCL 17/2

The engineering development study to follow was written to address the need for a Programmable Rate Digital Satellite Modem capable of supporting both burst and continuous transmission modes with either binary phase shift keying (BPSK) or quadrature phase shift keying (QPSK) modulation. The preferred implementation technique is an all digital one which utilizes as much digital signal processing (DSP) as possible. Here design tradeoffs in each portion of the modulator and demodulator subsystem are outlined, and viable circuit approaches which are easily repeatable, have low implementation losses and have low production costs are identified. The research involved for this study was divided into nine technical papers, each addressing a significant region of concern in a variable rate modem design. Trivial portions and basic support logic designs surrounding the nine major modem blocks were omitted. In brief, the nine topic areas were: (1) Transmit Data Filtering; (2) Transmit Clock Generation; (3) Carrier Synthesizer; (4) Receive AGC; (5) Receive Data Filtering; (6) RF Oscillator Phase Noise; (7) Receive Carrier Selectivity; (8) Carrier Recovery; and (9) Timing Recovery.  
Author

**N89-26880\*#** Harris Corp., Melbourne, FL.

### ADVANCED MODULATION TECHNOLOGY DEVELOPMENT FOR EARTH STATION DEMODULATOR APPLICATIONS Final Report

R. C. DAVIS, J. V. WERNLUND, J. A. GANN, J. F. ROESCH, T. WRIGHT, and R. D. CROWLEY Jul. 1989 282 p  
(Contract NAS3-24681)  
(NASA-CR-185126; NAS 1.26:185126) Avail: NTIS HC A13/MF A01 CSCL 09/6

The purpose of this contract was to develop a high rate (200 Mbps), bandwidth efficient, modulation format using low cost hardware, in 1990's technology. The modulation format chosen is 16-ary continuous phase frequency shift keying (CPFSK). The implementation of the modulation format uses a unique combination of a limiter/discriminator followed by an accumulator to determine transmitted phase. An important feature of the modulation scheme is the way coding is applied to efficiently gain back the performance lost by the close spacing of the phase points.  
Author

## SPACECRAFT DESIGN, TESTING AND PERFORMANCE

Includes satellites; space platforms; space stations; spacecraft systems and components such as thermal and environmental controls; and attitude controls.

### A89-25405\*# TRW, Inc., Redondo Beach, CA. LARGE STRUCTURE CURRENT COLLECTION IN PLASMA ENVIRONMENTS

N. JOHN STEVENS (TRW Power and Systems Integration Laboratory, Redondo Beach, CA) AIAA, Aerospace Sciences Meeting, 27th, Reno, NV, Jan. 9-12, 1989. 7 p. refs (Contract NAS3-24659) (AIAA PAPER 89-0496) Copyright

The floating potential, relative to the space plasma, of large satellites proposed for future missions is an important factor in the current balance between the plasma particle collection of biased surfaces and exposed conductors. To solve this balance, a knowledge of the plasma current collection processes is required. One of the unknowns in these relationships is the current collection of large areas of conducting surfaces. Only limited experimental data is available on this collection process. Data from one of the few available tests is used herein to verify the applicability of a plasma collection model for large surfaces. The model is then applied to determine the floating potential of the NASA Space Station. Author

### A89-28421\*# National Aeronautics and Space Administration. Lewis Research Center, Cleveland, OH.

#### THE MODULAR COMBUSTION FACILITY FOR THE SPACE STATION LABORATORY - A REQUIREMENTS AND CAPABILITIES STUDY

K. R. SACKSTEDER, R. J. CHUCKSA, and R. C. OEFTERING (NASA, Lewis Research Center, Cleveland, OH) AIAA, Aerospace Sciences Meeting, 27th, Reno, NV, Jan. 9-12, 1989. 6 p. (AIAA PAPER 89-0505)

This paper describes a modular combustion facility for the Space Station, designed to provide facility-level services to interchangeable experiment modules, each of which designed specifically for the needs of a particular combustion experiment. The facility-level services are to include computer devices for the data acquisition, experimental control, and data reduction and analysis; the electrical power conversion and control; video cameras and recordings; the cooling-loop supply; waste management; gas supply; precision gas-mixing; and the combustion diagnostics support. Summarized categories of the data base are provided, which were developed to assimilate and to process the responses from the investigators. I.S.

### A89-28438\*# Teledyne Brown Engineering, Huntsville, AL. THE IMPACT OF AN IVA ROBOT ON THE SPACE STATION MICROGRAVITY ENVIRONMENT

PHILLIP E. HARMAN (Teledyne Brown Engineering, Huntsville, AL) and DOUGLAS A. ROHN (NASA, Lewis Research Center, Cleveland, OH) AIAA, Aerospace Sciences Meeting, 27th, Reno, NV, Jan. 9-12, 1989. 14 p. refs (Contract NAS3-25278) (AIAA PAPER 89-0596) Copyright

In order to maintain a microgravity environment during Space Station operations, it will be necessary to minimize reaction forces. These mechanical forces will typically occur during reboost, docking, equipment operation, intravehicular activities (IVA) robot operation, or crew activity. This paper focuses on those disturbances created by an IVA robot and its impact on the Space Station microgravity environment. The robot dynamic analysis that was used to generate the forcing function as the input into a finite element model of the U.S. Laboratory will be shown. Acceleration levels were determined through analysis and have

shown that a robotic system can sustain reaction forces into the station below 0.0001 g. A comparison between IVA robot effects and crew motion effects on the low-g environment is also described. It is concluded that robot trajectory shaping and motor accelerations feedback can minimize reaction forces. Author

### A89-30737\*# National Aeronautics and Space Administration. Lewis Research Center, Cleveland, OH.

#### FREE-VIBRATION CHARACTERISTICS AND CORRELATION OF A SPACE STATION SPLIT-BLANKET SOLAR ARRAY

KELLY S. CARNEY and FRANCIS J. SHAKER (NASA, Lewis Research Center, Cleveland, OH) IN: AIAA, ASME, ASCE, AHS, and ASC, Structures, Structural Dynamics and Materials Conference, 30th, Mobile, AL, Apr. 3-5, 1989, Technical Papers. Part 2. Washington, DC, American Institute of Aeronautics and Astronautics, 1989, p. 813-819. Previously announced in STAR as N89-15438. refs (AIAA PAPER 89-1252) Copyright

Two methods for studying the free-vibration characteristics of a large split-blanket solar array in a zero-g cantilevered configuration are presented. The zero-g configuration corresponds to an on-orbit configuration of the Space Station solar array. The first method applies the equations of continuum mechanics to determine the natural frequencies of the array; the second uses the finite element method program, MSC/NASTRAN. The stiffness matrix from the NASTRAN solution was found to be erroneously grounded. The results from the two methods are compared. It is concluded that the grounding does not seriously compromise the solution to the elastic modes of the solar array. However, the correct rigid body modes need to be included to obtain the correct dynamic model. Author

### A89-31915\*# Massachusetts Inst. of Tech., Cambridge.

#### INDUCED EMISSION OF RADIATION FROM A LARGE SPACE-STATION-LIKE STRUCTURE IN THE IONOSPHERE

D. E. HASTINGS and J. WANG (MIT, Cambridge, MA) AIAA Journal (ISSN 0001-1452), vol. 27, April 1989, p. 438-445. refs (Contract NAG3-695) Copyright

Large conducting structures in the ionosphere may have currents flowing through them which close in the ionospheric plasma. These currents can arise either from current leakage from an onboard power distribution system or by being induced by the motional electric field. Associated with these currents will be broadband electromagnetic radiation in the Alfvén and lower hybrid bands. The radiation impedance of this electromagnetic radiation is explored for a structure of space-station-like dimensions as a function of the geometry of the structure and the composition of the ionic environment. It is shown that modification of the collecting area of the structure and environment can be used to minimize the radiation impedance. For a space station, the radiated power will at most be of the order of watts, which does not represent a significant power loss. However, the radiation field will give rise to a substantial pollution of the electromagnetic spectrum in the vicinity of the space station. Design choices to minimize this interference are suggested. Author

### A89-35316\* National Aeronautics and Space Administration. Lewis Research Center, Cleveland, OH.

#### OXIDATION AND PROTECTION OF FIBERGLASS-EPOXY COMPOSITE MASTS FOR PHOTOVOLTAIC ARRAYS IN THE LOW EARTH ORBITAL ENVIRONMENT

SHARON K. RUTLEDGE, MICHAEL L. CIANCONE (NASA, Lewis Research Center, Cleveland, OH), PHILLIP E. PAULSEN, and JOYCE A. BRADY (Cleveland State University, OH) IN: Materials stability and environmental degradation; Proceedings of the Symposium, Reno, NV, Apr. 5-7, 1988. Pittsburgh, PA, Materials Research Society, 1988, p. 45-52. refs Copyright

The extent of degradation of fiberglass-epoxy composite masts of the Space Station solar array panel, when these are exposed to atomic oxygen environment of the low-earth orbit, was investigated in ground testing of fiberglass-epoxy composites in

an RF plasma asher. In addition, several methods of protecting the composite structures were evaluated, including an aluminum braid covering, an In-Sn eutectic, and a silicone based paint. It was found that, during exposure, the epoxy at the surface of the composite was oxidized, exposing individual glass fibers which could easily be removed. The results of mass measurements and SEM examination carried out after thermal cycling and flexing of exposed composite samples indicated that coatings such as In-Sn eutectic may provide adequate protection by containing the glass fibers, even though mass loss still occurs. I.S.

**A89-36724\*#** National Aeronautics and Space Administration. Lewis Research Center, Cleveland, OH.

#### **BIG SAVINGS FROM SMALL HOLES**

ALAN WHITE (NASA, Lewis Research Center, Cleveland, OH) Aerospace America (ISSN 0740-722X), vol. 27, May 1989, p. 32-35.

Copyright

The status and results to date of the NASA-Lewis/USAF Astronautics study of technology for large spacecraft heat-dissipation by means of liquid-droplet radiation (LDR) are discussed. The LDR concept uses a droplet generator to create billions of 200-micron droplets of a heatsink fluid which will cool through radiation into deep space as they fly toward a droplet collector. This exposure to the space environment entails the maintenance of vapor pressure as low as 10 to the -7th torr; the fluid must also be very stable chemically. While certain oils are good fluids for LDR use at low temperatures, higher-temperature heatsink fluids include Li, Sn, and Ga liquid metals. O.C.

**A89-51123\*** National Aeronautics and Space Administration. Lewis Research Center, Cleveland, OH.

#### **LOW EARTH ORBITAL ATOMIC OXYGEN SIMULATION FOR MATERIALS DURABILITY EVALUATION**

BRUCE A. BANKS and SHARON K. RUTLEDGE (NASA, Lewis Research Center, Cleveland, OH) IN: European Symposium on Spacecraft Materials in Space Environment, 4th, Toulouse, France, Sept. 6-9, 1988, Proceedings. Toulouse, France, Cepadues Editions, 1989, p. 371-392. refs

Copyright

The erosion yields of numerous materials have been evaluated in low earth orbital space tests. There appears to be three classes of materials: materials of high erosion yield which include most of the hydrocarbon organic materials; materials which either do not react with atomic oxygen or form self-protecting oxides which allow the underlying material to appear durable to atomic oxygen, and materials with low but nonnegligible erosion yields, such as fluoropolymers. A NASA atomic oxygen effects test program has been established to utilize collective data from a multitude of simulation facilities to promote an understanding of mechanism and erosion yield dependencies. Atomic oxygen protective coatings for Kapton polyimide solar array blankets, fiberglass-epoxy composite mast structures, and solar dynamic power system concentrator surfaces have been identified and evaluated under atomic oxygen exposure in RF plasma asher laboratory tests. The control of defect density in protective coatings appears to be the key to the assurance of long-term protection of oxidizable materials in low earth orbit. C.E.

**A89-53327\*#** General Dynamics Corp., San Diego, CA.

#### **COLD-SAT ORBITAL EXPERIMENT CONFIGURED FOR ATLAS LAUNCH**

J. R. SHUSTER, F. O. BENNETT (General Dynamics Corp., Space Systems Div., San Diego, CA), and J. P. WACHTER (Ford Aerospace Corp., Space Systems Div., Palo Alto, CA) CEC, Cryogenic Engineering Conference and International Cryogenic Materials Conference, Los Angeles, CA, July 24-28, 1989, Paper. 11 p.

(Contract NAS3-25062)

The design and requirements for the proposed cryogenic on-orbit liquid depot storage, acquisition, and transfer (COLD-SAT) satellite experiment, which is to be launched by Atlas I, are examined. The COLD-SAT experiments are categorized as class I

and II; class I involves technology related to space transportation missions and class II represents alternative fluid management operations and data. The hardware for the COLD-SAT experiments consists of three hydrogen tanks contained in the experimental module; the experimental module is connected to a three-axis-controlled spacecraft bus, and thrusters are positioned on the forward and aft ends of the spacecraft and on the cylindrical portion of the experimental module. The components and systems of the experiment module and the types of experiments that can be conducted in each tank are described. Diagrams of the spacecraft configuration are provided. I.F.

**A89-54114\*** SDRC, Inc., San Diego, CA.

#### **MODAL REPRESENTATIONS IN CONTROL/STRUCTURE INTERACTION**

PAUL A. BLELLOCH, JEFFREY W. YOUNG (SDRC, Inc., Engineering Services Div., San Diego, CA), and KELLY S. CARNEY (NASA, Lewis Research Center, Cleveland, OH) IN: 1989 American Control Conference, 8th, Pittsburgh, PA, June 21-23, 1989, Proceedings. Volume 3. New York, Institute of Electrical and Electronics Engineers, 1989, p. 2802-2807. refs

Copyright

When control/structure interaction problems are examined, a standard method for representing the structure is to choose a truncated set of normal modes calculated from either a finite-element or a distributed-parameter model. However, the normal modes can neglect important static information about the structure. Using a set of fixed interface modes results in a much more accurate closed-loop model, even when relatively low-bandwidth controllers are used. The fixed interface modes are calculated with control input degrees of freedom held fixed, and standard finite-element software can be used. Illustrative examples include a simple hinged beam and a complex model of the phase-I Space Station configuration. I.E.

**N89-10117\*#** National Aeronautics and Space Administration. Lewis Research Center, Cleveland, OH.

#### **THE SOLAR DYNAMIC RADIATOR WITH A HISTORICAL PERSPECTIVE**

K. L. MCLALLIN, M. L. FLEMING, F. W. HOEHN, and R. L. HOWERTON (Rockwell International Corp., Canoga Park, Calif.) Aug. 1988 12 p Presented at the 23rd Intersociety Energy Conversion Engineering Conference, Denver Colo., 31 Jul. - 5 Aug. 1988; sponsored in part by ASME, AIAA, ANS, SAE, IEEE, ACS, and AIChE (NASA-TM-100972; E-4265; NAS 1.15:100972) Avail: NTIS HC A03/MF A01 CSCL 22B

A historical perspective on pumped-fluid loop space radiators provides a basis for the design of the Space Station Solar Dynamic (SD) power module radiator. SD power modules, capable of generating 25 kW (electrical) each, are planned for growth in Station power requirements. The Brayton cycle SD module configuration incorporates a pumped-fluid loop radiator that must reject up to 99 kW (thermal). The thermal/hydraulic design conditions in combination with required radiator orientation and packaging envelope form a unique set of constraints as compared to previous pumped-fluid loop radiator systems. Nevertheless, past program successes have demonstrated a technology base that can be applied to the SD radiator development program to ensure a low risk, low cost system. Author

**N89-11802\*#** Arinc Research Corp., Annapolis, MD.

#### **SPACE STATION ELECTRICAL POWER SYSTEM AVAILABILITY STUDY Final Contractor Report**

SCOTT R. TURNQUIST and MARK A. TWOMBLY Nov. 1988 192 p

(Contract NASA ORDER C-31003-J)

(NASA-CR-182198; NAS 1.26:182198;

ARINC-RP-5149-11-01-4744) Avail: NTIS HC A09/MF A01 CSCL 22/2

ARINC Research Corporation performed a preliminary reliability, and maintainability (RAM) analysis of the NASA space station Electric Power Station (EPS). The analysis was performed using

## 18 SPACECRAFT DESIGN, TESTING AND PERFORMANCE

the ARINC Research developed UNIRAM RAM assessment methodology and software program. The analysis was performed in two phases: EPS modeling and EPS RAM assessment. The EPS was modeled in four parts: the insolar power generation system, the eclipse power generation system, the power management and distribution system (both ring and radial power distribution control unit (PDCU) architectures), and the power distribution to the inner keel PDCUs. The EPS RAM assessment was conducted in five steps: the use of UNIRAM to perform baseline EPS model analyses and to determine the orbital replacement unit (ORU) criticalities; the determination of EPS sensitivity to on-orbit spared of ORUs and the provision of an indication of which ORUs may need to be spared on-orbit; the determination of EPS sensitivity to changes in ORU reliability; the determination of the expected annual number of ORU failures; and the integration of the power generator system model results with the distribution system model results to assess the full EPS. Conclusions were drawn and recommendations were made.

Author

**N89-11803\*#** Textron Bell Aerospace Co., Buffalo, NY.  
**SPACE STATION AUXILIARY THRUST CHAMBER TECHNOLOGY Final Report**

J. M. SENNEFF Feb. 1987 44 p

(Contract NAS3-24883)

(NASA-CR-179650; NAS 1.26:179650; BELL-REPT-8911-950003)

Avail: NTIS HC A03/MF A01 CSCL 20/8

A program to design, fabricate, and test a 50 lb sub f (222 N) thruster was undertaken to demonstrate the applicability of the reverse flow concept as an item of auxiliary propulsion for the Space Station. The thruster was to operate at a mixture ratio (O/F) of 4, be capable of operating for 2 million lb sub f-seconds (8.896 million N-seconds) impulse with a chamber pressure of 75 psia (52N/sq cm) and a nozzle area ratio of 40. A successful demonstration of an (O/F) of 4 thruster, was followed by the design objective of operating at (O/F) of 8. The demonstration of this thruster resulted in the order of and additional (O/F) of 8 thruster chamber under the present NAS 3-24883 contract. The effort to fabricate and test the second (O/F) of 8 thruster is documented.

Author

**N89-16905\*#** National Aeronautics and Space Administration.  
Lewis Research Center, Cleveland, OH.

**A MODIFIED VAPEPS METHOD FOR PREDICTING VIBROACOUSTIC RESPONSE OF UNREINFORCED MASS LOADED HONEYCOMB PANELS**

MARK E. MCNELIS 1989 12 p Prepared for presentation at the 35th Technical Meeting of the Inst. of Environmental Sciences, Anaheim, CA, 1-5 May 1989

(NASA-TM-101467; E-4579; NAS 1.15:101467) Avail: NTIS HC A03/MF A01 CSCL 22/2

VAPEPS (VibroAcoustic Payload Environment Prediction System) is a computer program used to predict the vibroacoustic response of a structure. An alternate VAPEPS modeling technique, the Modified NASA Lewis Method, is an improvement for modeling unreinforced mass loaded honeycomb panels. The Modified NASA Lewis Method prediction is compared to the standard ASMS VAPEPS prediction, and the acoustic test data for three spacecraft panels. An analytical method of computing variance is presented and used to compute 95 percent confidence levels. These levels are compared to the standard VAPEPS confidence levels and to the envelope of the test data. As a result of using the new methodology suggested in the paper, both the mean prediction and the 95 percent confidence level prediction agree well with the test data in both spectral shape and magnitude. Therefore, the Modified NASA Lewis Method prediction methodology may be used to define more realistic random vibration test levels.

Author

**N89-24418\*#** National Aeronautics and Space Administration.  
Lewis Research Center, Cleveland, OH.

**REVIEW OF THE ENVIRONMENTAL EFFECTS OF THE SPACE STATION FREEDOM PHOTOVOLTAIC POWER MODULE**

HENRY K. NAHRA 1989 8 p Proposed for presentation at the 24th Intersociety Energy Conversion Engineering Conference, Washington, DC, 6-11 Aug. 1989; sponsored by IEEE, AIAA, ANS, ASME, SAE, ACS and AIChE  
(NASA-TM-102076; E-4836; NAS 1.15:102076) Avail: NTIS HC A02/MF A01 CSCL 22/2

An overview is provided of the environment in the low Earth orbit (LEO), the interaction of this environment with the Photovoltaic (PV) Power system of the Space Station Freedom is reviewed, and the environmental programs are described that are designed to investigate the interactions of the LEO environment with the photovoltaic power system. Such programs will support and impact the design of the subsystems of the PV module in order to survive the design lifetime in the LEO natural and induced environment.

Author

**N89-24427\*#** National Aeronautics and Space Administration.  
Lewis Research Center, Cleveland, OH.

**ENERGY STORAGE AND THERMAL CONTROL SYSTEM DESIGN STATUS**

STEPHEN N. SIMONS, BRYAN C. WILLHOITE, and GERT VANOMMERING (Ford Aerospace and Communications Corp., Palo Alto, CA.) 1989 8 p Presented at the 24th Intersociety Energy Conversion Engineering Conference, Washington, DC, 6-11 Aug. 1989; cosponsored by the IEEE, AIAA, ANS, ASME, SAE, ACS and AIChE

(NASA-TM-102136; E-4933; NAS 1.15:102136) Avail: NTIS HC A02/MF A01 CSCL 22/2

The Space Station Freedom electric power system (EPS) will initially rely on photovoltaics for power generation and Ni/H<sub>2</sub> batteries for electrical energy storage. The current design for and the development status of two major subsystems in the PV Power Module is discussed. The energy storage subsystem comprised of high capacity Ni/H<sub>2</sub> batteries and the single-phase thermal control system that rejects the excess heat generated by the batteries and other components associated with power generation and storage is described.

Author

**N89-25267\*#** National Aeronautics and Space Administration.  
Lewis Research Center, Cleveland, OH.

**PROTOFLIGHT PHOTOVOLTAIC POWER MODULE SYSTEM-LEVEL TESTS IN THE SPACE POWER FACILITY**

JUAN C. RIVERA and LUKE A. KIRCH Aug. 1989 21 p Presented at the 24th Intersociety Energy Conversion Engineering Conference, Washington, DC, 6-11 Aug. 1989; sponsored in part by IEEE, AIAA, ANS, ASME, SAE, ACS, and AIChE  
(NASA-TM-102066; E-4823; NAS 1.15:102066) Avail: NTIS HC A03/MF A01 CSCL 22/2

Work Package Four, which includes the NASA-Lewis and Rocketdyne, has selected an approach for the Space Station Freedom Photovoltaic (PV) Power Module flight certification that combines system level qualification and acceptance testing in the thermal vacuum environment: The protoflight vehicle approach. This approach maximizes ground test verification to assure system level performance and to minimize risk of on-orbit failures. The preliminary plans for system level thermal vacuum environmental testing of the protoflight PV Power Module in the NASA-Lewis Space Power Facility (SPF), are addressed. Details of the facility modifications to refurbish SPF, after 13 years of downtime, are briefly discussed. The results of an evaluation of the effectiveness of system level environmental testing in screening out incipient part and workmanship defects and unique failure modes are discussed. Preliminary test objectives, test hardware configurations, test support equipment, and operations are presented.

Author

**N89-26031\*#** Sverdrup Technology, Inc., Cleveland, OH.  
**TWO-TIERED DESIGN ANALYSIS OF A RADIATOR FOR A SOLAR DYNAMIC POWERED STIRLING ENGINE Final Report**  
DONALD C. HAINLEY Jun. 1989 9 p Prepared for presentation at the 24th Intersociety Energy Conversion Engineering Conference, Washington, DC, 6-11 Aug. 1989; sponsored in part by IEEE, AIAA, ANS, ASME, SAE, ACS, and AIChE



(Contract NAS3-25266)

(NASA-CR-182301; E-4851; NAS 1.26:182301) Avail: NTIS HC A02/MF A01 CSCL 22/2

Two separate design approaches for a pumped loop radiator used to transfer heat from the cold end of a solar dynamic powered Stirling engine are described. The first approach uses a standard method to determine radiator requirements to meet specified end of mission conditions. Trade-off studies conducted for the analysis are included. Justification of this concept within the specified parameters of the analysis is provided. The second design approach determines the life performance of the radiator/Stirling system. In this approach, the system performance was altered by reducing the radiator heat transfer area. Performance effects and equilibrium points were determined as radiator segments were removed. This simulates the effect of loss of radiator sections due to micro-meteoroid and space debris penetration. The two designs were compared on the basis of overall system requirements and goals. Author

**N89-26035\*#** National Aeronautics and Space Administration. Lewis Research Center, Cleveland, OH.

**EFFECT OF MICROMETEOROID AND SPACE DEBRIS IMPACTS ON THE SPACE STATION FREEDOM SOLAR ARRAY SURFACES**

HENRY K. NAHRA 1989 12 p Presented at the 1989 Spring Meeting of the Materials Research Society, San Diego, CA, 24-29 Apr. 1989

(NASA-TM-102287; E-4955; NAS 1.15:102287) Avail: NTIS HC A03/MF A01 CSCL 22/2

Both solar and antisolar surfaces of the Space Station Freedom solar arrays are vulnerable to micrometeoroid and space debris impacts. Impacts on the solar surface result in damage to the active area of the solar cell and a corresponding reduction in generated power. Impacts on the antisolar surface could result in damage to the circuit which interconnects the cells which in turn may produce open circuit strings or panels. An evaluation is presented of the power degradation resulting from the impacts of micrometeoroid and space debris on the solar surface of the array blanket. Moreover, given a particle diameter that could damage the circuit interconnecting the cells, the probability of an open circuit panel is computed, along with the probability that the solar array blanket will meet the power requirement over the design lifetime. Author

**N89-26036\*#** National Aeronautics and Space Administration. Lewis Research Center, Cleveland, OH.

**COLD-SAT: A TECHNOLOGY SATELLITE FOR CRYOGENIC EXPERIMENTATION**

H. ARIF and E. W. KROEGER 1989 13 p Presented at the 1989 Cryogenic Engineering Conference and International Cryogenic Materials Conference, Los Angeles, CA, 24-28 Jul. 1989; sponsored by UCLA

(NASA-TM-102286; E-4953; NAS 1.15:102286) Avail: NTIS HC A03/MF A01 CSCL 22/2

NASA-Lewis (LeRC) is involved in the development and validation of analytical models which describe the fluid dynamic and thermodynamic processes associated with the storage, acquisition and transfer of subcritical cryogenic fluids in low gravity. Four concurrent studies, including one in-house at LeRC, are underway to determine the feasibility of performing model validation experiments aboard a free-flying spacecraft (S/C) called Cryogenic On-Orbit Liquid Depot-Storage, Acquisition and Transfer (COLD-SAT), using liquid hydrogen as the cryogen. The technology requirements for the experiments are described along with the initial LeRC concepts for the S/C and an experiment subsystem comprising of cryogenic tankage (a supply dewar and three receiver tanks), gas pressurization bottles (both helium and autogenous hydrogen), their associated plumbing, and instrumentation for data collection. Experiments were categorized into enabling/high priority Class 1 technologies and component/system Class 2 demonstrations. As initially envisioned by LeRC, COLD-SAT would have had a 1997 launch aboard a Delta-2 for a 6 month active lifetime in a 925 km orbit with a pseudo-inertial attitude. Author

**N89-26887\*#** National Aeronautics and Space Administration. Lewis Research Center, Cleveland, OH.

**PHOTOVOLTAIC MODULE ON-ORBIT ASSEMBLY FOR SPACE STATION FREEDOM**

THOMAS SOURS, R. LOVELY, and D. CLARK 1989 10 p Presented at the 24th Intersociety Energy Conversion Engineering Conference, Washington, DC, 6-11 Aug. 1989; cosponsored by the IEEE, AIAA, ANS, ASME, SAE, ACS, and AIChE (NASA-TM-102297; E-4973; NAS 1.15:102297) Avail: NTIS HC A02/MF A01 CSCL 22/2

One of the elements of the Space Station Freedom power system is the Photovoltaic (PV) module. These modules will be assembled on-orbit during the assembly phase of the program. These modules will be assembled either from the shuttle orbiter or from the Mobile Servicing Center (MSC). The different types of assembly operations that will be used to assemble PV Modules are described. Author

**N89-29478\*#** General Electric Co., Cincinnati, OH. Aircraft Engine Business Group.

**REVOLUTIONARY OPPORTUNITIES FOR MATERIALS AND STRUCTURES STUDY, ADDENDUM NO. 1**

F. A. SCHWEIGER Feb. 1987 6 p

(Contract NAS3-24622)

(NASA-CR-179642-ADD-1; NAS 1.26:179642-ADD-1) Avail: NTIS HC A02/MF A01 CSCL 22/2

Four tables (Nos. LIX, LXa, LXb, and LXIV) comprise this Addendum report. They are: LIX - Carbon-carbon development roadmap; LXa - Ceramic matrix composite development roadmap; LXb - Ceramic matrix composite development roadmap; and LXIV - Intermetallic development roadmap. Each table gives a listing of the projected expenditures through the next 10 to 15 years. The tables retain the numbering used in the main report for easy reference. Author

**A89-25341\*#** National Aeronautics and Space Administration. Lewis Research Center, Cleveland, OH.

**HARDWARE DEVELOPMENT FOR THE SURFACE TENSION DRIVEN CONVECTION EXPERIMENT ABOARD THE USML-1 SPACELAB MISSION**

A. D. PLINE, T. P. JACOBSON, J. S. WANHAJINEN, and D. A. PETRARCA (NASA, Lewis Research Center, Cleveland, OH) AIAA, Aerospace Sciences Meeting, 27th, Reno, NV, Jan. 9-12, 1989. 10 p. Previously announced in STAR as N89-11804. refs (AIAA PAPER 89-0406) Copyright

The Surface Tension Driven Convection Experiment is a Space Transportation System flight experiment to study both transient and steady thermocapillary fluid flows aboard the USML-1 Spacelab mission planned for March 1992. Hardware is under development to establish the experimental conditions and perform the specified measurements, for both ground based research and the flight experiment in a Spacelab single rack. Major development areas include an infrared thermal imaging system for surface temperature measurement, a CO<sub>2</sub> laser and control system for surface heating, and for flow visualization, a He-Ne laser and optical system in conjunction with an intensified video camera. For ground based work the components of each system were purchased or designed, and tested individually. The three systems will be interfaced with the balance of the experimental hardware and will constitute a working engineering model. A description of the three systems and examples of the component performance is given along with the plans for the development of flight hardware. Author



## 19 SPACECRAFT INSTRUMENTATION

**A89-36956\*** Rensselaer Polytechnic Inst., Troy, NY.  
**A FACILITY FOR PRECISE TEMPERATURE CONTROL APPLICATIONS IN MICROGRAVITY**

M. E. GLICKSMAN, T. A. LOGRASSO, S. H. TIRMIZI, R. C. HAHN (Rensselaer Polytechnic Institute, Troy, NY), E. WINSA (NASA, Lewis Research Center, Cleveland, OH) et al. (COSPAR, ESA, and International Union of Crystallography, Plenary Meeting, 27th, Symposium on Microgravity, 16th, Espoo, Finland, July 18-29, 1988) *Advances in Space Research* (ISSN 0273-1177), vol. 8, no. 12, 1988, p. 61-68. refs  
(Contract NAG3-333)  
Copyright

The general design, main components, and operation of the isothermal dendritic growth apparatus (IDGA) designed for microgravity experimentation are described. The four major subsystems of the IDGA are a temperature controlled thermostatic bath capable of milli-kelvin stability, a photographic data collection system, a crystal growth chamber, and a growth detection system to initiate data collection. Some of the specific experiments that could utilize the capabilities of the IDGA are dendritic growth in alloys, monotectic systems, life science experiments, and technological applications. V.L.

**N89-11804\*#** National Aeronautics and Space Administration. Lewis Research Center, Cleveland, OH.

**HARDWARE DEVELOPMENT FOR THE SURFACE TENSION DRIVEN CONVECTION EXPERIMENT ABOARD THE USML-1 SPACELAB MISSION**

A. D. PLINE, T. P. JACOBSON, J. S. WANHAJINEN, and D. A. PETRARCA 1988 12 p Prepared for presentation at the 27th Aerospace Sciences Meeting, Reno, Nev., 9-12 Jan. 1989; sponsored in part by AIAA (NASA-TM-101404; E-4488; NAS 1.15:101404; AIAA-89-0406)  
Avail: NTIS HC A03/MF A01 CSCL 22/1

The Surface Tension Driven Convection Experiment is a Space Transportation System flight experiment to study both transient and steady thermocapillary fluid flows aboard the USML-1 Spacelab mission planned for March 1992. Hardware is under development to establish the experimental conditions and perform the specified measurements, for both ground based research and the flight experiment in a Spacelab single rack. Major development areas include an infrared thermal imaging system for surface temperature measurement, a CO<sub>2</sub> laser and control system for surface heating, and for flow visualization, a He-Ne laser and optical system in conjunction with an intensified video camera. For ground based work the components of each system were purchased or designed, and tested individually. The three systems will be interfaced with the balance of the experimental hardware and will constitute a working engineering model. A description of the three systems and examples of the component performance is given along with the plans for the development of flight hardware. Author

## 20

### SPACECRAFT PROPULSION AND POWER

Includes main propulsion systems and components, e.g., rocket engines; and spacecraft auxiliary power sources.

**A89-12305\*** National Aeronautics and Space Administration. Lewis Research Center, Cleveland, OH.

**PROGRESS TOWARD THE EVOLUTION OF A STIRLING SPACE ENGINE**

DONALD L. ALGER (NASA, Lewis Research Center, Cleveland, OH) SAE, International Congress and Exposition, Detroit, MI, Feb. 29-Mar. 4, 1988. 9 p. Previously announced in STAR as N88-14046.

(SAE PAPER 880545) Copyright

Following the successful testing of the 25 kWe Space Power Demonstrator (SPD) engine in 1985, a Stirling Space Engine (SSE)

technology advancement program was initiated. The program's objective was to advance free-piston Stirling engine/linear alternator technology sufficiently so that a Stirling engine system may become a viable candidate for space power applications. Evolution of the SSE technology is planned to occur at three different engine heater temperature levels: 650, 1050, and 1300 K. These temperatures define three phases of technology development with the first phase involving the 650 K SPD engine. Technology development of the 650 K engine and preliminary design of the 1050 K engine will be discussed. Author

**A89-14978\*#** National Aeronautics and Space Administration. Lewis Research Center, Cleveland, OH.

**PERFORMANCE OF 10-KW CLASS XENON ION THRUSTERS**

MICHAEL J. PATTERSON and VINCENT K. RAWLIN (NASA, Lewis Research Center, Cleveland, OH) AIAA, ASME, SAE, and ASEE, Joint Propulsion Conference, 24th, Boston, MA, July 11-13, 1988. 32 p. Previously announced in STAR as N88-28088. refs  
(AIAA PAPER 88-2914)

Presented are performance data for laboratory and engineering model 30 cm-diameter ion thrusters operated with xenon propellant over a range of input power levels from approximately 2 to 20 kW. Also presented are preliminary performance results obtained from laboratory model 50 cm-diameter cusp- and divergent-field ion thrusters operating with both 30 cm- and 50 cm-diameter ion optics up to a 20 kW input power. These data include values of discharge chamber propellant and power efficiencies, as well as values of specific impulse, thruster efficiency, thrust and power. The operation of the 30 cm- and 50 cm-diameter ion optics are also discussed. Author

**A89-14981\*#** National Aeronautics and Space Administration. Lewis Research Center, Cleveland, OH.

**A REUSABLE ROCKET ENGINE INTELLIGENT CONTROL**

WALTER C. MERRILL and CARL F. LORENZO (NASA, Lewis Research Center, Cleveland, OH) AIAA, ASME, SAE, and ASEE, Joint Propulsion Conference, 24th, Boston, MA, July 11-13, 1988. 10 p. Previously announced in STAR as N88-26401.  
(AIAA PAPER 88-3114)

An intelligent control system for reusable space propulsion systems for future launch vehicles is described. The system description includes a framework for the design. The framework consists of an execution level with high-speed control and diagnostics, and a coordination level which marries expert system concepts with traditional control. A comparison is made between air breathing and rocket engine control concepts to assess the relative levels of development and to determine the applicability of air breathing control concepts of future reusable rocket engine systems. Author

**A89-14983\*#** National Aeronautics and Space Administration. Lewis Research Center, Cleveland, OH.

**NAVIER-STOKES CALCULATION OF SOLID-PROPELLANT ROCKET MOTOR INTERNAL FLOWFIELDS**

KWANG-CHUNG HSIEH (NASA, Lewis Research Center; Sverdrup Technology, Inc., Cleveland, OH), VIGOR YANG, and JESSE I. S. TSENG (Pennsylvania State University, University Park) AIAA, ASME, SAE, and ASEE, Joint Propulsion Conference, 24th, Boston, MA, July 11-13, 1988. 11 p. refs  
(Contract F04611-86-K-0082)  
(AIAA PAPER 88-3182) Copyright

A comprehensive numerical analysis has been carried out to study the detailed physical and chemical processes involved in the combustion of homogeneous propellant in a rocket motor. The formulation is based on the time-dependent full Navier-Stokes equations, with special attention devoted to the chemical reactions in both gas and condensed phases. The turbulence closure is achieved using both the Baldwin-Lomax algebraic model and a modified k-epsilon two-equation scheme with a low Reynolds number and near-wall treatment. The effects of variable thermodynamic and transport properties are also included. The system of governing equations are solved using a multi-stage Runge-Kutta scheme with the source terms treated implicitly.

Preliminary results clearly demonstrate the presence of various combustion regimes in the vicinity of propellant surface. The effects of propellant combustion on the motor internal flowfields are investigated in detail. Author

**A89-15187\*** National Aeronautics and Space Administration. Lewis Research Center, Cleveland, OH.

**STATUS OF SEVERAL STIRLING LOSS CHARACTERIZATION EFFORTS AND THEIR SIGNIFICANCE FOR STIRLING SPACE POWER DEVELOPMENT**

ROY C. TEW, JR. (NASA, Lewis Research Center, Cleveland, OH) IN: 1988 IECEC; Proceedings of the Twenty-third Intersociety Energy Conversion Engineering Conference, Denver, CO, July 31-Aug. 5, 1988. Volume 1. New York, American Society of Mechanical Engineers, 1988, p. 113-119. refs  
Copyright

NASA-Lewis and other U.S. Government agencies have supported experimental and analytical programs for the characterization of Stirling cycle engines' thermodynamic losses, with a view to the improvement of Stirling engine design capabilities. The Space Power Demonstrator Engine is noted to have benefited from these efforts; test data and model predictions suggest that even greater performance improvements would be obtainable through additional modifications of engine regenerator and heater hardware. O.C.

**A89-15208\*** National Aeronautics and Space Administration. Lewis Research Center, Cleveland, OH.

**MOVING BELT RADIATOR TECHNOLOGY ISSUES**

K. ALAN WHITE, III (NASA, Lewis Research Center, Cleveland, OH) IN: 1988 IECEC; Proceedings of the Twenty-third Intersociety Energy Conversion Engineering Conference, Denver, CO, July 31-Aug. 5, 1988. Volume 1. New York, American Society of Mechanical Engineers, 1988, p. 365-371. Previously announced in STAR as N88-25477. refs  
Copyright

Development of the Moving Belt Radiator (MBR) as an advanced space radiator concept is discussed. The relative merits of Solid Belt (SBR) Liquid Belt (LBR), and Hybrid Belt (HBR) Radiators are described. Analytical and experimental efforts related to the dynamics of a rotating belt in microgravity are reviewed. The development of methods for transferring heat to the moving belt is discussed, and the results from several experimental investigations are summarized. Limited efforts related to the belt deployment and stowage, and to fabrication of a hybrid belt, are also discussed. Life limiting factors such as seal wear and micrometeoroid resistance are identified. The results from various MBR point design studies for several power levels are compared with advanced Heat Pipe Radiator technology. MBR designs are shown to compare favorably at both 300 and 1000 K temperature levels. However, additional effort will be required to resolve critical technology issues and to demonstrate the advantage of MBR systems. Author

**A89-15209\*** Los Alamos National Lab., NM.

**TRANSIENT PERFORMANCE EVALUATION OF AN INTEGRATED HEAT PIPE-THERMAL STORAGE SYSTEM**

E. KEDDY, J. T. SENA, M. MERRIGAN (Los Alamos National Laboratory, NM), GARY HEIDENREICH (Sundstrand Corp., Rockford, IL), and STEVE JOHNSON (NASA, Lewis Research Center, Cleveland, OH) IN: 1988 IECEC; Proceedings of the Twenty-third Intersociety Energy Conversion Engineering Conference, Denver, CO, July 31-Aug. 5, 1988. Volume 1. New York, American Society of Mechanical Engineers, 1988, p. 373-378.  
Copyright

Transient performance tests of an integrated heat pipe-thermal storage system have been conducted. This system was developed as a part of an Organic Rankine Cycle-Solar Dynamic Power System receiver for future power systems. The integrated system consists of potassium heat pipe elements that incorporate thermal energy storage canisters within the vapor space and an organic fluid (toluene) heater tube used as the condenser region of the heat

pipe. The transient performance tests determined the operating characteristics and power input limits of the integrated heat pipe-thermal storage unit under conditions corresponding to re-acquisition of the sun during emergence from eclipse conditions and to the initial start-up of the solar dynamic power system. The tests demonstrated that the heat pipe-thermal storage element is not limited under conditions corresponding to emergence from eclipse during normal orbital operations and the heat pipe will successfully start-up from the frozen condition with full input power at the onset. Details of the test procedures and results of the tests are presented in this paper. Author

**A89-15224\*** National Aeronautics and Space Administration, Washington, DC.

**NASA AEROSPACE FLIGHT BATTERY SYSTEMS PROGRAM - ISSUES AND ACTIONS**

NORMAN SCHULZE (NASA, Washington, DC) and OLGA D. GONZALEZ-SANABRIA (NASA, Lewis Research Center, Cleveland, OH) IN: 1988 IECEC; Proceedings of the Twenty-third Intersociety Energy Conversion Engineering Conference, Denver, CO, July 31-Aug. 5, 1988. Volume 2. New York, American Society of Mechanical Engineers, 1988, p. 3-5.  
Copyright

The NASA Aerospace Flight Battery Systems Program task status is reviewed. Major tasks incorporated in the program are battery systems, secondary batteries, and primary batteries. B.J.

**A89-15245\*** Sanders Associates, Inc., Nashua, NH.

**AN EXPERIMENTAL ANALYSIS OF A DOPED LITHIUM FLUORIDE DIRECT ABSORPTION SOLAR RECEIVER**

JAMES KESSELI, TOM POLLAK (Sanders Associates, Inc., Nashua, NH), and DOVIE LACY (NASA, Lewis Research Center, Cleveland, OH) IN: 1988 IECEC; Proceedings of the Twenty-third Intersociety Energy Conversion Engineering Conference, Denver, CO, July 31-Aug. 5, 1988. Volume 2. New York, American Society of Mechanical Engineers, 1988, p. 179-185.  
Copyright

An experimental analysis of two key elements of a direct absorption solar receiver for use with Brayton solar dynamic systems was conducted. Experimental data are presented on LiF crystals doped with dysprosium, samarium, and cobalt fluorides. In addition, a simulation of the cavity/window environment was performed and a posttest inspection was conducted to evaluate chemical reactivity, transmissivity, and condensation rate. B.J.

**A89-15267\*** National Aeronautics and Space Administration. Lewis Research Center, Cleveland, OH.

**ENERGY STORAGE CONSIDERATIONS FOR A ROBOTIC MARS SURFACE SAMPLER**

P. M. O'DONNELL, R. L. CATALDO, and O. D. GONZALEZ-SANABRIA (NASA, Lewis Research Center, Cleveland, OH) IN: 1988 IECEC; Proceedings of the Twenty-third Intersociety Energy Conversion Engineering Conference, Denver, CO, July 31-Aug. 5, 1988. Volume 2. New York, American Society of Mechanical Engineers, 1988, p. 385-389. refs  
Copyright

The characteristics of various energy storage systems (including Ni-Cd, Ni-H<sub>2</sub>, Ag-Zn, Li-XS, Na-S, PbSO<sub>4</sub>, and regenerative fuel cell systems) considered for a robotic Mars surface sampler are reviewed. It is concluded that the bipolar nickel-hydrogen battery and the sodium-sulfur battery are both viable candidates as storage systems for the rover's Radioisotope Thermoelectric Generator. For a photovoltaic storage system, the regenerative fuel cell and the bipolar nickel-hydrogen battery are the primary candidates. I.S.

**A89-15278\*** National Aeronautics and Space Administration. Lewis Research Center, Cleveland, OH.

**EFFECT OF LEO CYCLING AT SHALLOW DEPTHS OF DISCHARGE ON MANTECH IPV NICKEL-HYDROGEN CELLS**

JOHN J. SMITHRICK (NASA, Lewis Research Center, Cleveland, OH) IN: 1988 IECEC; Proceedings of the Twenty-third Intersociety Energy Conversion Engineering Conference, Denver, CO, July

## 20 SPACECRAFT PROPULSION AND POWER

31-Aug. 5, 1988. Volume 2. New York, American Society of Mechanical Engineers, 1988, p. 447-451. Previously announced in STAR as N88-25978. refs

Copyright

An individual pressure vessel nickel-hydrogen battery is being considered as an alternate for a nickel-cadmium battery on the Hubble Space Telescope. The space telescope battery will primarily be operating at a shallow depth of discharge (10 percent DOD) with an occasional 40 percent DOD. This shallow DOD raises several issues: (1) What is the cycle life. It is projected to be acceptable; however, there is no reported real time data base for validation. (2) The state of charge of the nickel electrode at the beginning of charge is 90 percent. Will this cause an acceleration of divergence in the battery individual cell voltages. (3) After prolonged cycling at 10 percent DOD, will there be enough capacity remaining to support the 40 percent DOD. (4) Is the state of charge really 90 percent during cycling. There is no reported real time data base at shallow depths of discharge. A data base to address the above issues was initiated. Author

**A89-15279\*** National Aeronautics and Space Administration. Lewis Research Center, Cleveland, OH.

### **EFFECT OF NASA ADVANCED DESIGNS ON THERMAL BEHAVIOR OF NI-H<sub>2</sub> CELLS**

OLGA D. GONZALEZ-SANABRIA (NASA, Lewis Research Center, Cleveland, OH) IN: 1988 IECEC; Proceedings of the Twenty-third Intersociety Energy Conversion Engineering Conference, Denver, CO, July 31-Aug. 5, 1988. Volume 2. New York, American Society of Mechanical Engineers, 1988, p. 453-456. Previously announced in STAR as N88-10132. refs

Copyright

As part of an overall effort to advance the technology of nickel-hydrogen batteries for low earth orbit (LEO) applications, advanced designs for individual pressure vessel (IPV) nickel-hydrogen cells have been conceived. These designs incorporate alternative methods of oxygen recombination which affect the thermal behavior of the cells. The effect of these oxygen recombination methods on the cell temperature profiles will be examined. Author

**A89-15281\*** National Aeronautics and Space Administration. Lewis Research Center, Cleveland, OH.

### **THE EFFECT OF COMPRESSION ON INDIVIDUAL PRESSURE VESSEL NICKEL/HYDROGEN COMPONENTS**

MICHELLE A. MANZO and MARLA E. PEREZ-DAVIS (NASA, Lewis Research Center, Cleveland, OH) IN: 1988 IECEC; Proceedings of the Twenty-third Intersociety Energy Conversion Engineering Conference, Denver, CO, July 31-Aug. 5, 1988. Volume 2. New York, American Society of Mechanical Engineers, 1988, p. 465-469. Previously announced in STAR as N88-28109. refs

Copyright

Compression tests were performed on representative Individual Pressure Vessel (IPV) Nickel/Hydrogen cell components in an effort to better understand the effects of force on component compression and the interactions of components under compression. It appears that the separator is the most easily compressed of all of the stack components. It will typically partially compress before any of the other components begin to compress. The compression characteristics of the cell components in assembly differed considerably from what would be predicted based on individual compression characteristics. Component interactions played a significant role in the stack response to compression. The results of the compression tests were factored into the design and selection of Belleville washers added to the cell stack to accommodate nickel electrode expansion while keeping the pressure on the stack within a reasonable range of the original preset. Author

**A89-15287\*** National Aeronautics and Space Administration. Lewis Research Center, Cleveland, OH.

### **THE APPLICATION OF HIGH TEMPERATURE SUPERCONDUCTORS TO SPACE ELECTRICAL POWER DISTRIBUTION COMPONENTS**

PAUL R. ARON and IRA T. MYERS (NASA, Lewis Research Center, Cleveland, OH) IN: 1988 IECEC; Proceedings of the Twenty-third Intersociety Energy Conversion Engineering Conference, Denver, CO, July 31-Aug. 5, 1988. Volume 2. New York, American Society of Mechanical Engineers, 1988, p. 501-503. Previously announced in STAR as N88-22939. refs

Copyright

Some important space based electrical power distribution systems and components are examined to determine what might be achieved with the introduction of high temperature superconductors (HTS). Components that are compared in a before-and-after fashion include transformers, transmission lines, and capacitors. It is concluded that HTS has its greatest effect on the weight associated with transmission lines, where the weight penalty could be reduced by as much as 130 kg/kW/km of cable. Transformers, because 28 percent of their mass is in the conductor, are reduced in weight by the same factor. Capacitors are helped the least with only negligible savings possible. Finally, because HTS can relax the requirement to use alternating current in order to reduce conductor mass, it will be possible to generate significant savings by eliminating most transformers and capacitors. Author

**A89-15288\*** National Aeronautics and Space Administration. Lewis Research Center, Cleveland, OH.

### **HIGH TEMPERATURE SUPERCONDUCTING MAGNETIC ENERGY STORAGE FOR FUTURE NASA MISSIONS**

KARL A. FAYMON (NASA, Lewis Research Center, Cleveland, OH) and STANLEY J. RUDNICK (Argonne National Laboratory, IL) IN: 1988 IECEC; Proceedings of the Twenty-third Intersociety Energy Conversion Engineering Conference, Denver, CO, July 31-Aug. 5, 1988. Volume 2. New York, American Society of Mechanical Engineers, 1988, p. 511-514. refs

Copyright

Several NASA sponsored studies based on 'conventional' liquid helium temperature level superconductivity technology have concluded that superconducting magnetic energy storage has considerable potential for space applications. The advent of high temperature superconductivity (HTSC) may provide additional benefits over conventional superconductivity technology, making magnetic energy storage even more attractive. The proposed NASA space station is a possible candidate for the application of HTSC energy storage. Alternative energy storage technologies for this and other low Earth orbit missions are compared. Author

**A89-15295\*** National Aeronautics and Space Administration. Lewis Research Center, Cleveland, OH.

### **SPACE STATION POWER SYSTEM REQUIREMENTS**

JOHN W. DUNNING, JR. (NASA, Lewis Research Center, Cleveland, OH) IN: 1988 IECEC; Proceedings of the Twenty-third Intersociety Energy Conversion Engineering Conference, Denver, CO, July 31-Aug. 5, 1988. Volume 3. New York, American Society of Mechanical Engineers, 1988, p. 29-36. Previously announced in STAR as N88-21245.

Copyright

Presented is an overview of the requirements on which the Space Station Electric Power System is based as well as a summary of the design itself. The current design, which is based on silicon photovoltaic arrays, NiH<sub>2</sub> batteries, and 20 kHz distribution technology, meets all of the requirements. Author

**A89-15298\*** Rockwell International Corp., Canoga Park, CA.

### **AN INTEGRATED AND MODULAR DIGITAL MODELING APPROACH FOR THE SPACE STATION ELECTRICAL POWER SYSTEM DEVELOPMENT**

FRANK J. GOMBOS (Rockwell International Corp., Rocketdyne Div., Canoga Park, CA) and NARAYAN DRAVID (NASA, Lewis Research Center, Cleveland, OH) IN: 1988 IECEC; Proceedings of the Twenty-third Intersociety Energy Conversion Engineering Conference, Denver, CO, July 31-Aug. 5, 1988. Volume 3. New York, American Society of Mechanical Engineers, 1988, p. 49-55. Previously announced in STAR as N88-22935. refs

Copyright

An electrical power system for the Space Station was designed,

developed and built. This system provides for electrical power generation, conditioning, storage, and distribution. The initial configuration uses photovoltaic power generation. The power system control is based on a hierarchical architecture to support the requirements of automation. In the preliminary design and technology development phase of the program, various modeling techniques and software tools were evaluated for the purpose of meeting the Space Station power system modeling requirements. Rocketdyne and LeRC jointly selected the EASY5 simulation software, developed by Boeing Computer Services, as a system level modeling tool. The application of the selected analytical modeling approach to represent the entire power system is described. Typical results of model predictions are also summarized. The equipment modeled includes solar arrays, dc to ac converters, resonant inverters, battery storage system, alternator, transmission line, switch gear, and system level microprocessor controls. During the advanced development phase of this program, several models were developed using this approach.

Author

**A89-15304\*** National Aeronautics and Space Administration. Lewis Research Center, Cleveland, OH.

#### TEMPERATURE COEFFICIENTS FOR CONCENTRATOR CELLS AT VARIOUS ELECTRON AND PROTON FLUENCE LEVELS

HENRY B. CURTIS and RUSSELL E. HART, JR. (NASA, Lewis Research Center, Cleveland, OH) IN: 1988 IECEC; Proceedings of the Twenty-third Intersociety Energy Conversion Engineering Conference, Denver, CO, July 31-Aug. 5, 1988. Volume 3. New York, American Society of Mechanical Engineers, 1988, p. 85-89. refs

Copyright

Data are presented on the Isc, Voc and Pmax temperature coefficients for several small concentrator solar cells. The cells are AlGaAs (1.72 eV), GaAs, silicon and InGaAs (1.1 eV) concentrator cells operating at 6.25 and 100 times AM0. The temperature range covered was 25 to 100 C. Cells were irradiated with 1-MeV electrons and 37-MeV protons, and data are presented at different fluence levels.

Author

**A89-15317\*** Jet Propulsion Lab., California Inst. of Tech., Pasadena.

#### NUCLEAR REACTOR POWER AS APPLIED TO A SPACE-BASED RADAR MISSION

L. JAFFE, R. BEATTY, P. BHANDARI, E. CHOW, W. DEININGER, R. EWELL, T. FUJITA, M. GROSSMAN (California Institute of Technology, Jet Propulsion Laboratory, Pasadena), H. BLOOMFIELD, J. HELLER (NASA, Lewis Research Center, Cleveland, OH) et al. IN: 1988 IECEC; Proceedings of the Twenty-third Intersociety Energy Conversion Engineering Conference, Denver, CO, July 31-Aug. 5, 1988. Volume 3. New York, American Society of Mechanical Engineers, 1988, p. 183-190. DOD-DOE-NASA-sponsored research.

Copyright

A space-based radar mission and spacecraft are examined to determine system requirements for a 300 kWe space nuclear reactor power system. The spacecraft configuration and its orbit, launch vehicle, and propulsion are described. Mission profiles are addressed, and storage in assembly orbit is considered. Dynamics and attitude control and the problems of nuclear and thermal radiation are examined.

C.D.

**A89-15327\*** Jet Propulsion Lab., California Inst. of Tech., Pasadena.

#### SYSTEMS ASPECTS OF A SPACE NUCLEAR REACTOR POWER SYSTEM

L. JAFFE, T. FUJITA, R. BEATTY, P. BHANDARI, E. CHOW, W. DEININGER, R. EWELL, M. GROSSMAN (California Institute of Technology, Jet Propulsion Laboratory, Pasadena), H. BLOOMFIELD, J. HELLER (NASA, Lewis Research Center, Cleveland, OH) et al. IN: 1988 IECEC; Proceedings of the Twenty-third Intersociety Energy Conversion Engineering Conference, Denver, CO, July 31-Aug. 5, 1988. Volume 3. New

York, American Society of Mechanical Engineers, 1988, p. 255-261.

Copyright

Various system aspects of a 300-kW nuclear reactor power system for spacecraft have been investigated. Special attention is given to the cases of a reusable OTV and a space-based radar. It is demonstrated that the stowed length of the power system is important to mission design, and that orbital storage for months to years may be needed for missions involving orbital assembly.

R.R.

**A89-15340\*** National Aeronautics and Space Administration. Lewis Research Center, Cleveland, OH.

#### THE SOLAR DYNAMIC RADIATOR WITH A HISTORICAL PERSPECTIVE

K. L. MCLALLIN (NASA, Lewis Research Center, Cleveland, OH), M. L. FLEMING (LTV Corp., Missiles and Electronics Group, Dallas, TX), F. W. HOEHN, and R. HOWERTON (Rockwell International Corp., Rocketdyne Div., Canoga Park, CA) IN: 1988 IECEC; Proceedings of the Twenty-third Intersociety Energy Conversion Engineering Conference, Denver, CO, July 31-Aug. 5, 1988. Volume 3. New York, American Society of Mechanical Engineers, 1988, p. 335-340. refs

Copyright

A historical perspective on pumped loop space radiators provides a basis for the design of the Space Station Solar Dynamic (SD) power module radiator. SD power modules, capable of generating 25 kWe each, are planned for growth Station power requirements. The Brayton (cycle) SD module configuration incorporates a pumped loop radiator that must reject up to 99 kW. The thermal/hydraulic design conditions in combination with required radiator orientation and packaging envelope form a unique set of constraints as compared to previous pumped loop radiator systems. Nevertheless, past program successes have demonstrated a technology base which can be applied to the SD radiator development program to ensure a low risk, low cost system.

Author

**A89-15341\*** National Aeronautics and Space Administration. Lewis Research Center, Cleveland, OH.

#### THERMAL DISTORTION ANALYSIS OF THE SPACE STATION SOLAR DYNAMIC CONCENTRATOR

JEFFERY J. TRUDELL, KENT S. JEFFERIES (NASA, Lewis Research Center, Cleveland, OH), JOSEPH F. BAUMEISTER (NASA, Lewis Research Center; Analox Corp., Cleveland, OH), and VITHAL DALSANIA (NASA, Lewis Research Center; W. L. Tanksley and Associates, Inc., Cleveland, OH) IN: 1988 IECEC; Proceedings of the Twenty-third Intersociety Energy Conversion Engineering Conference, Denver, CO, July 31-Aug. 5, 1988. Volume 3. New York, American Society of Mechanical Engineers, 1988, p. 341-349. Previously announced in STAR as N88-25475. refs

Copyright

A method was developed to evaluate the thermal distortion of the Space Station Solar Dynamic Concentrator and the effects of thermal distortion on concentrator optical performance. The analytical method includes generating temperature distributions with TRASYS and SINDA models, interfacing the SINDA results with the SINDA-NASTRAN Interface Program (SNIP), calculating thermal distortion with a NASTRAN/PATRAN finite element model, and providing flux distribution maps within the receiver with the ray tracing OFFSET program. Temperature distributions, thermally induced slope errors, and flux distribution maps within the receiver are discussed. Results during a typical orbit indicate that temperatures of the hexagonal panels and triangular facets range between -18 and 99 C (-1 to 210 F), facet rotations are less than 0.2 mrad, and a change in facet radius due to thermal flattening is less than 5 percent. The predicted power loss with thermal distortion effects was less than 0.3 percent. The thermal distortion of the Solar Dynamic concentrator has negligible effect on the flux distribution within the receiver cavity.

Author

## 20 SPACECRAFT PROPULSION AND POWER

**A89-15343\*** National Aeronautics and Space Administration. Lewis Research Center, Cleveland, OH.

### **ADVANCED SPACE SOLAR DYNAMIC RECEIVERS**

HAL J. STRUMPF, MURRAY G. COOMBS (Allied-Signal Aerospace Co., AiResearch Los Angeles Div., Torrance, CA), and DOVIE E. LACY (NASA, Lewis Research Center, Cleveland, OH) IN: 1988 IECEC; Proceedings of the Twenty-third Intersociety Energy Conversion Engineering Conference, Denver, CO, July 31-Aug. 5, 1988. Volume 3. New York, American Society of Mechanical Engineers, 1988, p. 357-365.

Copyright

A study has been conducted to generate and evaluate advanced solar heat receiver concepts suitable for orbital application with Brayton and Stirling engine cycles in the 7-kW size range. The generated receiver designs have thermal storage capability (to enable power production during the substantial eclipse period which accompanies typical orbits) and are lighter and smaller than state-of-the-art systems, such as the Brayton solar receiver being designed and developed by AiResearch for the NASA Space Station. Two receiver concepts have been developed in detail: a packed bed receiver and a heat pipe receiver. The packed bed receiver is appropriate for a Brayton engine; the heat pipe receiver is applicable for either a Brayton or Stirling engine. The thermal storage for both concepts is provided by the melting and freezing of a salt. Both receiver concepts offer substantial improvements in size and weight compared to baseline receivers. Author

**A89-15357\*** Purdue Univ., West Lafayette, IN.  
**DYNAMIC CHARACTERISTICS OF A 20 KHZ RESONANT POWER SYSTEM - FAULT IDENTIFICATION AND FAULT RECOVERY**

O. WASYN CZUK (Purdue University, West Lafayette, IN) IN: 1988 IECEC; Proceedings of the Twenty-third Intersociety Energy Conversion Engineering Conference, Denver, CO, July 31-Aug. 5, 1988. Volume 3. New York, American Society of Mechanical Engineers, 1988, p. 451-456.  
(Contract NAG3-848)

Copyright

A detailed simulation of a dc inductor resonant driver and receiver is used to demonstrate the transient characteristics of a 20 kHz resonant power system during fault and overload conditions. The simulated system consists of a dc inductor resonant inverter (driver), a 50-meter transmission cable, and a dc inductor resonant receiver load. Of particular interest are the driver and receiver performance during fault and overload conditions and on the recovery characteristics following removal of the fault. The information gained from these studies sets the stage for further work in fault identification and autonomous power system control.

Author

**A89-15378\*** Ford Aerospace and Communications Corp., Palo Alto, CA.

### **SPACE STATION BATTERY SYSTEM DESIGN AND DEVELOPMENT**

R. J. HAAS, A. K. CHAWATHE, and G. VAN OMMERING (Ford Aerospace Corp., Space Systems Div., Palo Alto, CA) IN: 1988 IECEC; Proceedings of the Twenty-third Intersociety Energy Conversion Engineering Conference, Denver, CO, July 31-Aug. 5, 1988. Volume 3. New York, American Society of Mechanical Engineers, 1988, p. 577-582.

(Contract NAS3-24666)

Copyright

The Space Station Electric Power System will rely on nickel-hydrogen batteries in its photovoltaic power subsystem for energy storage to support eclipse and contingency operations. These 81-Ah batteries will be designed for a 5-year life capability and are configured as orbital replaceable units (ORUs), permitting replacement of worn-out batteries over the anticipated 30-year Station life. This paper describes the baseline design and the development plans for the battery assemblies, the battery ORUs and the battery system. Key elements reviewed are the cells, mechanical and thermal design of the assembly, the ORU approach and interfaces, and the electrical design of the battery system.

The anticipated operational approach is discussed, covering expected performance as well as the processor-controlled charge management and discharge load allocation techniques. Development plans cover verification of materials, cells, assemblies and ORUs, as well as system-level test and analyses. Author

**A89-15392\*** National Aeronautics and Space Administration. Lewis Research Center, Cleveland, OH.

### **EXTENDED SP-100 REACTOR POWER SYSTEMS CAPABILITY**

H. S. BLOOMFIELD, J. M. WINTER, B. I. MCKISSOCK, and R. J. SOVIE (NASA, Lewis Research Center, Cleveland, OH) IN: 1988 IECEC; Proceedings of the Twenty-third Intersociety Energy Conversion Engineering Conference, Denver, CO, July 31-Aug. 5, 1988. Volume 3. New York, American Society of Mechanical Engineers, 1988, p. 671, 672.

Copyright

The SP-100 space nuclear power system development program and the NASA Civil Space Technology Initiative (CSTI) are discussed. The advanced technologies being developed for the CSTI high capacity nuclear reactor power system are outlined. The relationship between the CSTI and the Pathfinder project is considered. R.B.

**A89-15403\*** National Aeronautics and Space Administration. Lewis Research Center, Cleveland, OH.

### **POWER TRANSMISSION STUDIES FOR TETHERED SP-100**

DAVID J. BENTS (NASA, Lewis Research Center, Cleveland, OH) IN: 1988 IECEC; Proceedings of the Twenty-third Intersociety Energy Conversion Engineering Conference, Denver, CO, July 31-Aug. 5, 1988. Volume 3. New York, American Society of Mechanical Engineers, 1988, p. 733-741. Previously announced in STAR as N88-21251. refs

Copyright

The tether and/or transmission line connecting the SP-100 to Space Station presents some unorthodox challenges in high voltage engineering, power transmission, and distribution. The line, which doubles as a structural element of this unusual spacecraft, will convey HVDC from SP-100 to the platform in low Earth orbit, and environment where the local plasma is sufficient to cause breakdown of exposed conductors at potentials of only a few hundred volts. Its anticipated several years operation, and continuously accumulating exposure to meteoroids and debris, raises an increasing likelihood that mechanical damage, including perforation, will be sustained in service. The present concept employs an array of gas insulated solid wall aluminum coaxial tubes; a conceptual design which showed basic feasibility of the SP-100 powered Space Station. Practical considerations of launch, deployment and assembly have led to investigation of reel deployable, dielectric insulated coaxial cables. To be competitive, the dielectric would have to operate reliably in a radiation environment under electrical stresses exceeding 50 kV/cm. The SP-100 transmission line high voltage interfaces are also considered. Author

**A89-15415\*** National Aeronautics and Space Administration. Lewis Research Center, Cleveland, OH.

### **ADVANCED SENSIBLE HEAT SOLAR RECEIVER FOR SPACE POWER**

TIMOTHY J. BENNETT (NASA, Lewis Research Center; Sverdrup Technology, Inc., Cleveland, OH) and DOVIE E. LACY (NASA, Lewis Research Center, Cleveland, OH) IN: 1988 IECEC; Proceedings of the Twenty-third Intersociety Energy Conversion Engineering Conference, Denver, CO, July 31-Aug. 5, 1988. Volume 4. New York, American Society of Mechanical Engineers, 1988, p. 211-216. Previously announced in STAR as N88-21249.

Copyright

NASA Lewis, through in-house efforts, has begun a study to generate a conceptual design of a sensible heat solar receiver and to determine the feasibility of such a system for space power applications. The sensible heat solar receiver generated in this study uses pure lithium as the thermal storage medium and was designed for a 7 kWe Brayton (PCS) operating at 1100 K. The receiver consists of two stages interconnected via temperature

sensing variable conductance sodium heat pipes. The lithium is contained within a niobium vessel and the outer shell of the receiver is constructed of third generation rigid, fibrous ceramic insulation material. Reradiation losses are controlled with niobium and aluminum shields. By nature of design, the sensible heat receiver generated in this study is comparable in both size and mass to a latent heat system of similar thermal capacitance. The heat receiver design and thermal analysis were conducted through the combined use of PATRAN, SINDA, TRASYS, and NASTRAN software packages. Author

**A89-15416\*** National Aeronautics and Space Administration. Lewis Research Center, Cleveland, OH.

**RAY TRACING OPTICAL ANALYSIS OF OFFSET SOLAR COLLECTOR FOR SPACE STATION SOLAR DYNAMIC SYSTEM**

KENT S. JEFFERIES (NASA, Lewis Research Center, Cleveland, OH) IN: 1988 IECEC; Proceedings of the Twenty-third Intersociety Energy Conversion Engineering Conference, Denver, CO, July 31-Aug. 5, 1988. Volume 4. New York, American Society of Mechanical Engineers, 1988, p. 225-232. Previously announced in STAR as N88-22080. Copyright

OFFSET, a detailed ray tracing computer code, was developed at NASA Lewis Research Center to model the offset solar collector for the Space Station solar dynamic electric power system. This model traces rays from 50 points on the face of the sun to 10 points on each of the 456 collector facets. The triangular facets are modeled with spherical, parabolic, or toroidal reflective surface contour and surface slope errors. The rays are then traced through the receiver aperture to the walls of the receiver. Images of the collector and of the sun within the receiver produced by this code provide insight into the collector receiver interface. Flux distribution on the receiver walls, plotted by this code, is improved by a combination of changes to aperture location and receiver tilt angle. Power loss by spillage at the receiver aperture is computed and is considerably reduced by using toroidal facets. Author

**A89-16485\*#** National Aeronautics and Space Administration. Lewis Research Center, Cleveland, OH.

**PERFORMANCE AND LIFETIME ASSESSMENT OF MPD ARC THRUSTER TECHNOLOGY**

JAMES S. SOVEY and MARIS A. MANTENIEKS (NASA, Lewis Research Center, Cleveland, OH) AIAA, ASME, SAE, and ASEE, Joint Propulsion Conference, 24th, Boston, MA, July 11-13, 1988. 35 p. Previously announced in STAR as N88-29860. refs (AIAA PAPER 88-3211) Copyright

A summary of performance and lifetime characteristics of pulsed and steady-state magnetoplasmadynamic (MPD) thrusters is presented. The technical focus is on cargo vehicle propulsion for exploration-class missions to the Moon and Mars. Relatively high MPD thruster efficiencies of 0.43 and 0.69 have been reported at about 5000 s specific impulse using hydrogen and lithium, respectively. Efficiencies of 0.10 to 0.35 in the 1000 to 4500 s specific impulse range have been obtained with other propellants (e.g., Ar, NH<sub>3</sub>, N<sub>2</sub>). Thermal efficiency data in excess of 0.80 at MW power levels using pulsed thrusters indicate the potential of high MPD thruster performance. Extended tests of pulsed and steady-state MPD thrusters yield total impulses at least two to three orders of magnitude below that necessary for cargo vehicle propulsion. Performance tests and diagnostics for life-limiting mechanisms of megawatt-class thrusters will require high fidelity test stands which handle in excess of 10 kA and a vacuum facility whose operational pressure is less than  $3 \times 10^{-4}$  torr. Author

**A89-16486\*#** National Aeronautics and Space Administration. Lewis Research Center, Cleveland, OH.

**IMPACT OF ETO PROPELLANTS ON THE AEROTHERMODYNAMIC ANALYSES OF PROPULSION COMPONENTS**

K. C. CIVINSKAS (NASA, Lewis Research Center; U.S. Army, Propulsion Directorate, Cleveland, OH), R. J. BOYLE (NASA, Lewis

Research Center, Cleveland, OH), and H. V. MCCONNAUGHEY (NASA, Marshall Space Flight Center, Huntsville, AL) AIAA, ASME, SAE, and ASEE, Joint Propulsion Conference, 24th, Boston, MA, July 11-13, 1988. 25 p. Previously announced in STAR as N88-30094. refs (AIAA PAPER 88-3091) Copyright

The operating conditions and the propellant transport properties used in Earth-to-Orbit (ETO) applications affect the aerothermodynamic design of ETO turbomachinery in a number of ways. Some aerodynamic and heat transfer implications of the low molecular weight fluids and high Reynolds number operating conditions on future ETO turbomachinery are discussed. Using the current SSME high pressure fuel turbine as a baseline, the aerothermodynamic comparisons are made for two alternate fuel turbine geometries. The first is a revised first stage rotor blade designed to reduce peak heat transfer. This alternate design resulted in a 23 percent reduction in peak heat transfer. The second design concept was a single stage rotor to yield the same power output as the baseline two stage rotor. Since the rotor tip speed was held constant, the turbine work factor doubled. In this alternate design, the peak heat transfer remained the same as the baseline. While the efficiency of the single stage design was 3.1 points less than the baseline two stage turbine, the design was aerothermodynamically feasible, and may be structurally desirable. Author

**A89-17730\*#** National Aeronautics and Space Administration. Lewis Research Center, Cleveland, OH.

**PHOTOVOLTAICS FOR HIGH CAPACITY SPACE POWER SYSTEMS**

DENNIS J. FLOOD (NASA, Lewis Research Center, Cleveland, OH) IAF, International Astronautical Congress, 39th, Bangalore, India, Oct. 8-15, 1988. 10 p. Previously announced in STAR as N89-10122. refs (IAF PAPER 88-221)

The anticipated energy requirements of future space missions will grow by factors approaching 100 or more, particularly as a permanent manned presence is established in space. The advances that can be expected in solar array performance and lifetime, when coupled with advanced, high energy density storage batteries and/or fuel cells, will continue to make photovoltaic energy conversion a viable power generating option for the large systems of the future. The specific technologies required to satisfy any particular set of power requirements will vary from mission to mission. Nonetheless, in almost all cases the technology push will be toward lighter weight and higher efficiency, whether of solar arrays of storage devices. This paper will describe the content and direction of the current NASA program in space photovoltaic technology. The paper will also discuss projected system level capabilities of photovoltaic power systems in the context of some of the new mission opportunities under study by NASA, such as a manned lunar base, and a manned visit to Mars. Author

**A89-20016\*** National Aeronautics and Space Administration. Lewis Research Center, Cleveland, OH.

**A NEW SPACE STATION POWER SYSTEM**

GEOFFREY A. LANDIS (NASA, Lewis Research Center, Cleveland, OH; Brown University, Providence, RI) Acta Astronautica (ISSN 0094-5765), vol. 17, Sept. 1988, p. 975-977. refs Copyright

A new concept for a Space Station power system is proposed which reduces the drag effect of the solar panels and eliminates eclipsing by the Earth. The solar generator is physically separated from the Space Station, and power transmitted to the station by a microwave beam. The power station can thus be placed high enough that drag is not a significant factor. For a resonant orbit where the ratio of periods s:p is a ratio of odd integers, and the orbital planes nearly perpendicular, an orbit can be chosen such that the line of sight is never blocked if the lower orbit has an altitude greater than calculatable minimum. For the 1:3 resonance, this minimum altitude is 0.5 r(e). Finally, by placing the power station into a sun-synchronous orbit, it can be made to avoid



## 20 SPACECRAFT PROPULSION AND POWER

shadowing by the Earth, thus providing continuous power.

Author

**A89-23281\*** National Aeronautics and Space Administration. Lewis Research Center, Cleveland, OH.

### STATUS OF THE SPACE STATION POWER SYSTEM

COSMO R. BARAONA and DEAN W. SHEIBLEY (NASA, Lewis Research Center, Cleveland, OH) (NASA, Space Electrochemical Research and Technology Conference, Cleveland, OH, Apr. 14-16, 1987) Journal of Power Sources (ISSN 0378-7753), vol. 22, March-Apr. 1988, p. 195-203. Previously announced in STAR as N87-29915.

Copyright

The major requirements and guidelines that affect the manned Space Station configuration and the power systems are explained. The evolution of the Space Station power system from the NASA program development feasibility phase through the current preliminary design phase is described. Several early station concepts are described and linked to the present concept. The recently completed phase B tradeoff study selections of photovoltaic system technologies are described. The present solar dynamic and power management and distribution systems are also summarized for completeness.

Author

**A89-25496\*#** National Aeronautics and Space Administration. Lewis Research Center, Cleveland, OH.

### MODELING OF IMPULSIVE PROPELLANT REORIENTATION

JOHN I. HOCHSTEIN, ALFREDO E. PATAG (Washington University, Saint Louis, MO), and DAVID J. CHATO (NASA, Lewis Research Center, Cleveland, OH) AIAA, Aerospace Sciences Meeting, 27th, Reno, NV, Jan. 9-12, 1989. 24 p. Previously announced in STAR as N89-13495. refs

(Contract NAG3-578)

(AIAA PAPER 89-0628) Copyright

The impulsive propellant reorientation process is modeled using the Energy Calculations for Liquid Propellants in a Space Environment (ECLIPSE) code. A brief description of the process and the computational model is presented. Code validation is documented via comparison to experimentally derived data for small scale tanks. Predictions of reorientation performance are presented for two tanks designed for use in flight experiments and for a proposed full scale OTV tank. A new dimensionless parameter is developed to correlate reorientation performance in geometrically similar tanks. Its success is demonstrated.

Author

**A89-28339\*#** Hughes Research Labs., Malibu, CA.

### MODEL FOR COMPUTING VOLUME-AVERAGED PLASMA PROPERTIES IN ELECTRON-BOMBARDMENT ION THRUSTERS

J. N. MATOSSIAN and J. R. BEATTIE (Hughes Research Laboratories, Malibu, CA) Journal of Propulsion and Power (ISSN 0748-4658), vol. 5, Mar.-Apr. 1989, p. 188-196. Research supported by Hughes Aircraft Co. Previously cited in issue 17, p. 2642, Accession no. A87-41135. refs

(Contract NAS3-23775; NAS3-23860)

Copyright

**A89-28340\*#** National Aeronautics and Space Administration. Lewis Research Center, Cleveland, OH.

### PERFORMANCE CHARACTERIZATIONS OF AN ENGINEERING MODEL MULTIPROPELLANT RESISTOJET

W. EARL MORREN, THOMAS W. HAAG, JAMES S. SOVEY (NASA, Lewis Research Center, Cleveland, OH), and STUART S. HAY Journal of Propulsion and Power (ISSN 0748-4658), vol. 5, Mar.-Apr. 1989, p. 197-203. Previously cited in issue 22, p. 3553, Accession no. A87-50197. refs

**A89-28402\*#** National Aeronautics and Space Administration. Lewis Research Center, Cleveland, OH.

### THE EFFECT OF ADAPTIVE GRID ON HYPERSONIC NOZZLE FLOW CALCULATIONS

ANDREW T. HSU (NASA, Lewis Research Center; Sverdrup

Technology, Inc., Cleveland, OH) AIAA, Aerospace Sciences Meeting, 27th, Reno, NV, Jan. 9-12, 1989. 13 p. refs (AIAA PAPER 89-0006)

Adaptive grid has been applied to the numerical study of generic hypersonic nozzles for the NASP vehicle to evaluate the effect of adaptive grid on solution accuracy. Several cases are calculated with and without adaptive grids; the numerical results are compared with experimental data wherever available, and with numerical results from other researchers. The present work shows that in most situations, especially when free shear layers and shocks exist in the flowfield, adaptive grid is essential in improving solution accuracy.

Author

**A89-29113\*#** Martin Marietta Energy Systems, Inc., Oak Ridge, TN.

### THERMAL ANALYSIS OF HEAT STORAGE CANISTERS FOR A SOLAR DYNAMIC, SPACE POWER SYSTEM

R. P. WICHNER, A. D. SOLOMON, J. B. DRAKE, and P. T. WILLIAMS (Martin Marietta Energy Systems, Inc., Oak Ridge, TN) IN: Solar engineering - 1988; Proceedings of the Tenth Annual ASME Solar Energy Conference, Denver, CO, Apr. 10-14, 1988. New York, American Society of Mechanical Engineers, 1988, p. 319-328. Previously announced in STAR as N88-22075. refs (Contract DE-AC05-84OR-21400; NASA ORDER C-30001-J)

Copyright

A thermal analysis was performed of a thermal energy storage canister of a type suggested for use in a solar receiver for an orbiting Brayton cycle power system. Energy storage for the eclipse portion of the cycle is provided by the latent heat of a eutectic mixture of LiF and CaF<sub>2</sub> contained in the canister. The chief motivation for the study is the prediction of vapor void effects on temperature profiles and the identification of possible differences between ground test data and projected behavior in microgravity. The first phase of this study is based on a two-dimensional, cylindrical coordinates model using an interim procedure for describing void behavior in 1-g and microgravity. The thermal analysis includes the effects of solidification front behavior, conduction in liquid/solid salt and canister materials, void growth and shrinkage, radiant heat transfer across the void, and convection in the melt due to Marangoni-induced flow and, in 1-g, flow due to density gradients. A number of significant differences between 1-g and 0-g behavior were found. This resulted from differences in void location relative to the maximum heat flux and a significantly smaller effective conductance in 0-g due to the absence of gravity-induced convection.

Author

**A89-29116\*#** Garrett Corp., Torrance, CA.

### ADVANCED SOLAR RECEIVERS FOR SPACE POWER

H. J. STRUMPF, M. G. COOMBS (Garrett Corp., Garrett AiResearch Div., Torrance, CA), and D. E. LACY (NASA, Lewis Research Center, Cleveland, OH) IN: Solar engineering - 1988; Proceedings of the Tenth Annual ASME Solar Energy Conference, Denver, CO, Apr. 10-14, 1988. New York, American Society of Mechanical Engineers, 1988, p. 343-352.

Copyright

A study has been conducted to generate and evaluate advanced solar heat receiver concepts suitable for orbital application with Brayton and Stirling engine cycles in the 7-kW size range. The generated receiver designs have thermal storage capability and, when implemented, will be lighter, smaller, and/or more efficient than baseline systems such as the configuration used for the Brayton solar receiver under development by Garrett AiResearch for the NASA Space Station. In addition to the baseline designs, four other receiver concepts were designed and evaluated with respect to Brayton and Stirling engines. These concepts include a higher temperature version of the baseline receiver, a packed bed receiver, a plate-fin receiver, and a heat pipe receiver. The thermal storage for all designs is provided by the melting and freezing of a salt.

Author



**A89-29120\*#** National Aeronautics and Space Administration. Lewis Research Center, Cleveland, OH.

**SPRE 1 FREE-PISTON STIRLING ENGINE TESTING AT NASA LEWIS RESEARCH CENTER**

J. E. CAIRELLI (NASA, Lewis Research Center, Cleveland, OH) IN: Solar engineering - 1988; Proceedings of the Tenth Annual ASME Solar Energy Conference, Denver, CO, Apr. 10-14, 1988. New York, American Society of Mechanical Engineers, 1988, p. 375-382. Previously announced in STAR as N88-11747. Copyright

As part of the NASA funded portion of the SP-100 Advanced Technology Program the Space Power Research Engine (SPRE 1) was designed and built to serve as a research tool for evaluation and development of advanced Stirling engine concepts. The SPRE 1 is designed to produce 12.5 kW electrical power when operated with helium at 15 MPa and with an absolute temperature ratio of two. The engine is now under test in a new test facility which was designed and built at NASA Lewis specifically to test the SPRE 1. The SPRE 1, the NASA facility, the initial SPRE 1 test results, and future SPRE 1 test plans are described. Author

**A89-29122\*#** National Aeronautics and Space Administration. Lewis Research Center, Cleveland, OH.

**PHOTOVOLTAIC POWER MODULES FOR NASA'S MANNED SPACE STATION**

C. A. TATRO (NASA, Lewis Research Center, Cleveland, OH) IN: Solar engineering - 1988; Proceedings of the Tenth Annual ASME Solar Energy Conference, Denver, CO, Apr. 10-14, 1988. New York, American Society of Mechanical Engineers, 1988, p. 489-497. Previously announced in STAR as N88-11745. refs Copyright

The capability and the safety of manned spacecraft are largely dependent upon reliable electric power systems. Two similar space power systems able to survive the low earth orbit environment, are being considered for NASA's Manned Space Station (SS), scheduled to begin operation in the mid 1990's. The Space Station Electric Power System (EPS) is composed of Photovoltaic (PV) Power Modules, Solar Dynamic (SD) Power Modules, and the Power Management and Distribution (PMAD) System. One EPS configuration will deliver 37.5 kW of PV based, utility grade, ac power to SS users. A second 75 kWe PV based EPS option is also being considered for SS deployment. The two EPS options utilize common modules and differ only in the total number of PV Power Modules used. Each PV Power Module supplies 18.75 kWe of ac power and incorporates its own energy storage and thermal control. The general requirements and the current preliminary design configuration of the Space Station PV Power Modules are examined. Author

**A89-29123\*#** National Aeronautics and Space Administration. Lewis Research Center, Cleveland, OH.

**LOW EARTH ORBIT ENVIRONMENTAL EFFECTS ON THE SPACE STATION PHOTOVOLTAIC POWER GENERATION SYSTEMS**

H. K. NAHRA (NASA, Lewis Research Center, Cleveland, OH) IN: Solar engineering - 1988; Proceedings of the Tenth Annual ASME Solar Energy Conference, Denver, CO, Apr. 10-14, 1988. New York, American Society of Mechanical Engineers, 1988, p. 499-507. Previously announced in STAR as N88-12429. refs Copyright

A summary of the low earth orbital environment, its impact on the photovoltaic power systems of the Space Station and the solutions implemented to resolve the environmental concerns or issues are described. Low earth orbital environment (LEO) presents several concerns to the photovoltaic power systems of the Space Station. These concerns include atomic oxygen interaction with the polymeric substrate of the solar arrays, ionized environment effects on the array operating voltage, the effects of the meteoroids and debris impacts and penetration through the different layers of the solar cells and their circuits, and the high energy particle and radiation effects on the overall solar array performance. Potential solutions to some of the degrading environmental interactions that

will provide the photovoltaic power system of the Space Station with the desired life are also summarized. Author

**A89-39031\*#** National Aeronautics and Space Administration. Lewis Research Center, Cleveland, OH.

**LANGMUIR PROBE MEASUREMENTS OF AN ARCJET EXHAUST**

LYNNETTE M. CARNEY (NASA, Lewis Research Center, Cleveland, OH) and THEO G. KEITH (Toledo, University, OH) Journal of Propulsion and Power (ISSN 0748-4658), vol. 5, May-June 1989, p. 287-294. Previously cited in issue 22, p. 3553, Accession no. A87-50193. refs

**A89-40480\*#** National Aeronautics and Space Administration. Lewis Research Center, Cleveland, OH.

**NUCLEAR THERMAL ROCKETS - NEXT STEP TO SPACE**

STANLEY K. BOROWSKI (NASA, Lewis Research Center, Cleveland, OH), EDWARD A. GABRIS, and JOHN MARTINELL (NASA, Washington, DC) Aerospace America (ISSN 0740-722X), vol. 27, June 1989, p. 16-18. Copyright

The prospects for the use of nuclear thermal rockets in manned interplanetary exploration are examined. These rockets offer the possibility for trip times on the order of a year or less in the next two decades. Mission prospects for gas-core concepts are emphasized, showing how such concepts meet the mission requirements. C.D.

**A89-44106\*#** Sverdrup Technology, Inc., Middleburg Heights, OH.

**STRUCTURAL TAILORING OF SPACE SHUTTLE MAIN ENGINE TURBOPUMP BLADES SSME/STAEBL**

ROBERT RUBINSTEIN (Sverdrup Technology, Inc., Middleburg Heights, OH) and CHRISTOS C. CHAMIS (NASA, Lewis Research Center, Cleveland, OH) (Structures, Structural Dynamics and Materials Conference, 27th, San Antonio, TX, May 19-21, 1986, Technical Papers. Part 2, p. 125-130) Journal of Propulsion and Power (ISSN 0748-4658), vol. 5, July-Aug. 1989, p. 421-425. Previously cited in issue 18, p. 2623, Accession no. A86-38895. refs

**A89-44111\*#** Sverdrup Technology, Inc., Cleveland, OH. **EFFECT OF AMBIENT PRESSURE ON THE PERFORMANCE OF A RESISTOJET**

D. H. MANZELLA (Sverdrup Technology, Inc., Cleveland, OH), P. F. PENKO (NASA, Lewis Research Center, Cleveland, OH), K. J. DE WITT, and T. G. KEITH, JR. (Toledo, University, OH) Journal of Propulsion and Power (ISSN 0748-4658), vol. 5, July-Aug. 1989, p. 452-456. Previously cited in issue 18, p. 2824, Accession no. A87-42181. refs (Contract NAG3-577)

**A89-46513\*** National Aeronautics and Space Administration. Lewis Research Center, Cleveland, OH.

**ADVANCES IN THIN-FILM SOLAR CELLS FOR LIGHTWEIGHT SPACE PHOTOVOLTAIC POWER**

GEOFFREY A. LANDIS, SHEILA G. BAILEY, and DENNIS J. FLOOD (NASA, Lewis Research Center, Cleveland, OH) (IAF, International Conference on Space Power, Cleveland, OH, June 5-7, 1989) Space Power (ISSN 0951-5089), vol. 8, no. 1-2, 1989, p. 31-50. refs (IAF PAPER ICOSP89-1-8) Copyright

The development of photovoltaic arrays beyond the next generation is discussed with attention given to the potentials of thin-film polycrystalline and amorphous cells. Of particular importance is the efficiency (the fraction of incident solar energy converted to electricity) and specific power (power to weight ratio). It is found that the radiation tolerance of thin-film materials is far greater than that of single crystal materials. CuInSe<sub>2</sub> shows no degradation when exposed to 1-MeV electrons. K.K.

**A89-46517\*** National Aeronautics and Space Administration. Lewis Research Center, Cleveland, OH.

**SOLAR DYNAMIC POWER FOR SPACE STATION FREEDOM**

THOMAS L. LABUS, RICHARD R. SECUNDE (NASA, Lewis Research Center, Cleveland, OH), and RONALD G. LOVELY (Rockwell International Corp., Rocketdyne Div., Canoga Park, CA) (IAF, International Conference on Space Power, Cleveland, OH, June 5-7, 1989) Space Power (ISSN 0951-5089), vol. 8, no. 1-2, 1989, p. 97-114. Previously announced in STAR as N89-23516. refs

(IAF PAPER ICOSP89-4-1) Copyright

The Space Station Freedom Program is presently planned to consist of two phases. At the completion of Phase 1, Freedom's manned base will consist of a transverse boom with attached manned modules and 75 kW of available electric power supplied by photovoltaic (PV) power sources. In Phase 2, electric power available to the manned base will be increased to 125 kW by the addition of two solar dynamic (SD) power modules, one at each end of the transverse boom. Power for manned base growth beyond Phase 2 will be supplied by additional SD modules. Studies show that SD power for the growth eras will result in life cycle cost savings of \$3 to \$4 billion when compared to PV-supplied power. In the SD power modules for Space Station Freedom, an offset parabolic concentrator collects and focuses solar energy into a heat receiver. To allow full power operation over the entire orbit, the receiver includes integral thermal energy storage by means of the heat of fusion of a salt mixture. Thermal energy is removed from the receiver and converted to electrical energy by a power conversion unit (PCU) which includes a closed brayton cycle (CBC) heat engine and an alternator. The receiver/PCU/radiator combination will be completely assembled and charged with gas and cooling fluid on earth before launch to orbit. The concentrator subassemblies will be pre-aligned and stowed in the orbiter bay before launch. On orbit, the receiver/PCU/radiator assembly will be installed as a unit. The pre-aligned concentrator panels will then be latched together and the total concentrator attached to the receiver/PCU/radiator by the astronauts. After final electric connections are made and checkout is complete, the SD power module will be ready for operation. Author

**A89-46520\*** National Aeronautics and Space Administration. Lewis Research Center, Cleveland, OH.

### FREE-PISTON STIRLING TECHNOLOGY FOR SPACE POWER

JACK G. SLABY (NASA, Lewis Research Center, Cleveland, OH) (IAF, International Conference on Space Power, Cleveland, OH, June 5-7, 1989) Space Power (ISSN 0951-5089), vol. 8, no. 1-2, 1989, p. 137-147. Previously announced in STAR as N89-20194. refs

(IAF PAPER ICOSP89-5-7) Copyright

An overview is presented of the NASA Lewis Research Center free-piston Stirling engine activities directed toward space power. This work is being carried out under NASA's new Civil Space Technology Initiative (CSTI). The overall goal of CSTI's High Capacity Power element is to develop the technology base needed to meet the long duration, high capacity power requirements for future NASA space missions. The Stirling cycle offers an attractive power conversion concept for space power needs. Discussed here is the completion of the Space Power Demonstrator Engine (SPDE) testing-culminating in the generation of 25 kW of engine power from a dynamically-balanced opposed-piston Stirling engine at a temperature ratio of 2.0. Engine efficiency was approximately 22 percent. The SPDE recently has been divided into two separate single-cylinder engines, called Space Power Research Engine (SPRE), that now serve as test beds for the evaluation of key technology disciplines. These disciplines include hydrodynamic gas bearings, high-efficiency linear alternators, space qualified heat pipe heat exchangers, oscillating flow code validation, and engine loss understanding. Author

**A89-46707\*** Electric Propulsion Lab., Inc., Lancaster, CA.

### A DETAILED MODEL OF ELECTROTHERMAL PROPULSION SYSTEMS

GRAEME ASTON and JOHN R. BROPHY (Electric Propulsion Laboratory, Inc., Lancaster, CA) AIAA, ASME, SAE, and ASEE, Joint Propulsion Conference, 25th, Monterey, CA, July 10-13, 1989.

9 p. Research sponsored by SDIO. refs

(Contract NAS3-25464)

(AIAA PAPER 89-2262) Copyright

A semi-empirical model is presented which describes the operating characteristics of resistojet and arcjet engines. Propellants considered include hydrogen, ammonia and hydrazine. Specific engine design and performance correlations are derived from previously published contractor reports, conference and journal papers of the past three decades. Fundamental performance relationships are identified and correlating parameters derived to describe engine operation over a wide range of input powers and propellant mass flow rates. Outputs are presented from a computer program formulated using these modeling relationships. Comparisons are made with present electrothermal engine designs and examples are presented to illustrate the usefulness of the models in predicting engine operation as a function of changes in engine geometry and operating modes. Author

**A89-46712\*** Electric Propulsion Lab., Inc., Lancaster, CA.

### A DETAILED MODEL OF ION PROPULSION SYSTEMS

JOHN R. BROPHY and GRAEME ASTON (Electric Propulsion Laboratory, Inc., Lancaster, CA) AIAA, ASME, SAE, and ASEE, Joint Propulsion Conference, 25th, Monterey, CA, July 10-13, 1989. 15 p. Research sponsored by SDIO. refs

(Contract NAS3-25464)

(AIAA PAPER 89-2268) Copyright

A detailed model for the determination of ion propulsion system masses and performance is presented. The model divides the propulsion system into its component parts and provides mass scaling relationships for each part. In addition, the model is coupled to a detailed ion engine performance model to facilitate investigation of the impact of engine technology assumptions on the overall propulsion system mass and performance. The model is exercised to determine the optimum specific impulse for a selected earth orbit transfer mission. Author

**A89-46736\*** Aerojet TechSystems Co., Sacramento, CA.

### MINIATURE MULTIPLE-FUNCTION PROBE FOR OTV TURBOPUMP HEALTH MONITORING

R. L. BICKFORD and F. N. COLLAMORE (Aerojet TechSystems Co., Sacramento, CA) AIAA, ASME, SAE, and ASEE, Joint Propulsion Conference, 25th, Monterey, CA, July 10-13, 1989. 6 p.

(Contract NAS3-23772)

(AIAA PAPER 89-2303) Copyright

A miniature multifunction rotating machinery shaft displacement sensor designed for a turbopump health monitoring system is described. The sensor probe tip has three independent sensing electrodes running in a groove made in the shaft of the machine. One of these electrodes, situated at the tip of the sensor, measures the radial displacement of the shaft, while the two side electrodes measure the axial displacements of the sides of the groove. The displacement sensor is also used to measure speed, by providing a notch in the side of the groove facing one sensor electrode. Results obtained with experimental sensors demonstrated that multifunction capacitive sensing is practical and reduces instrumentation penetration into rotating machinery housings. I.S.

**A89-46737\*** Aerojet TechSystems Co., Sacramento, CA.

### DESIGN AND TEST OF AN OXYGEN TURBOPUMP FOR A DUAL EXPANDER CYCLE ROCKET ENGINE

P. S. BUCKMANN, N. R. SHIMP, F. VITERI (Aerojet TechSystems Co., Sacramento, CA), and M. PROCTOR (NASA, Lewis Research Center, Cleveland, OH) AIAA, ASME, SAE, and ASEE, Joint Propulsion Conference, 25th, Monterey, CA, July 10-13, 1989. 9 p. refs

(Contract NAS3-23772)

(AIAA PAPER 89-2305) Copyright

A liquid oxygen (LOX) turbopump with an 860 R gaseous oxygen (GOX) turbine drive was designed for a 3750 lb thrust dual expander cycle rocket engine. This turbopump, which requires no interpropellant seals or system purges, features a 156 hp, single

stage, full admission, impulse turbine; an axial flow inducer; a two-stage centrifugal pump with unshrouded impellers; long-life, LOX-lubricated, self-aligning, hydrostatic bearings; and a subcritical rotor design. It is constructed of Monel, a nickel-copper alloy, which has low ignition potential in oxygen. The pump was designed to deliver 34.7 gpm of 4655 psia liquid oxygen at a shaft speed of 75,000 rpm. The dual expander cycle rocket engine and the performance it requires of the LOX turbopump will be discussed as well as the design of the pump, turbine, bearings, and the turbopump rotordynamics. The test program and preliminary test results will also be presented. Author

**A89-46758\*#** National Aeronautics and Space Administration. Lewis Research Center, Cleveland, OH.

### **ANTIPROTON POWERED PROPULSION WITH MAGNETICALLY CONFINED PLASMA ENGINES**

MICHAEL R. LAPOINTE (NASA, Lewis Research Center; Sverdrup Technology, Inc., Cleveland, OH) AIAA, ASME, SAE, and ASEE, Joint Propulsion Conference, 25th, Monterey, CA, July 10-13, 1989. 24 p. refs  
(AIAA PAPER 89-2334)

The reaction of the matter-antimatter annihilation, with its specific energy being over 250 times the specific energy released in nuclear fusion, is considered as an energy source for spacecraft propulsion. A concept of a magnetically confined pulsed plasma engine is described. In this concept, antiproton beams are injected axially into a pulsed magnetic mirror system, where they annihilate with an initially neutral hydrogen gas; the resulting charge annihilation products transfer energy to the hydrogen propellant, which is then exhausted through one end of the pulsed mirror system to provide thrust. Numerical simulations were developed to calculate the annihilation rate of antiprotons in hydrogen and to follow the resulting ion, muon, and electron/positron number density evolutions. I.S.

**A89-46783\*#** Electric Propulsion Lab., Inc., Lancaster, CA.  
**USER INTERACTIVE ELECTRIC PROPULSION SOFTWARE DESIGN**

MARTHA B. ASTON, GRAEME ASTON, and JOHN R. BROPHY (Electric Propulsion Laboratory, Inc., Lancaster, CA) AIAA, ASME, SAE, and ASEE, Joint Propulsion Conference, 25th, Monterey, CA, July 10-13, 1989. 8 p. Research sponsored by SDIO. refs  
(Contract NAS3-25464)  
(AIAA PAPER 89-2376) Copyright

As electric propulsion technology matures from laboratory development to flight application, mission planners and spacecraft designers are increasingly required to determine the benefits and integration issues of using this propulsion capability. A computer software tool for supporting these analyses is presented. This tool combines detailed analytical models describing electric propulsion engine performance and subsystem design, and a software structure that is highly user interactive and adaptable. The software design methodology used to develop this software tool is presented in this paper. Author

**A89-46784\*#** Michigan State Univ., East Lansing.

### **INVESTIGATIONS OF MICROWAVE PLASMAS - APPLICATIONS IN ELECTROTHERMAL THRUSTER SYSTEMS**

SCOTT S. HARABURDA and MARTIN C. HAWLEY (Michigan State University, East Lansing) AIAA, ASME, SAE, and ASEE, Joint Propulsion Conference, 25th, Monterey, CA, July 10-13, 1989. 10 p. refs  
(Contract NSG-3299)  
(AIAA PAPER 89-2378)

Experimental studies which have been conducted to develop understanding of plasma processes used for spacecraft propulsion are reviewed. The techniques discussed are calorimetry and volume measurements using the TM 011 and TM 012 modes in the microwave cavity system. The use of plasmas in electrical propulsion and microwave induction is reviewed. Plasma containment, microwave power production, energy distribution, and the pressure and flow dependence of the energy distribution are

addressed. The plasma dimensions and their dependence on pressure, flow, and power are considered. C.D.

**A89-46855\*#** National Aeronautics and Space Administration. Lewis Research Center, Cleveland, OH.

### **ADVANCED H2/O2 SPACE ENGINE PARAMETRICS**

J. A. SCHNEIDER (Aerojet TechSystems Co., Sacramento, CA) AIAA, ASME, SAE, and ASEE, Joint Propulsion Conference, 25th, Monterey, CA, July 10-13, 1989. 9 p. refs  
(Contract NAS3-23772)  
(AIAA PAPER 89-2300) Copyright

Engine cycle analyses conducted on a 3000-lbf component testing model of an H2/O2-fueled advanced orbit-transfer vehicle engine employing a dual-expander cycle have yielded pressure and temperature trend predictions. On the basis of the results obtained, the dual-expander cycle is projected to be scalable to thrust levels of as much as 50,000 lbf, with chamber pressures of 2000 psi. The high chamber pressure, in conjunction with the use of a gas-gas injector element, facilitates 10:1-range continuously variable throttling. The preferred thrust level for supporting mission studies would be of the order of 20,000 lbf. O.C.

**A89-47035\*#** National Aeronautics and Space Administration. Lewis Research Center, Cleveland, OH.

### **PERFORMANCE OF A 100 KW CLASS APPLIED FIELD MPD THRUSTER**

M. A. MANTENIEKS, J. S. SOVEY, T. W. HAAG, P. RAITANO (NASA, Lewis Research Center, Cleveland, OH), R. M. MYERS, and J. E. PARKES (NASA, Lewis Research Center; Sverdrup Technology, Inc., Cleveland, OH) AIAA, ASME, SAE, and ASEE, Joint Propulsion Conference, 25th, Monterey, CA, July 10-13, 1989. 20 p. refs  
(AIAA PAPER 89-2710)

The performance of a 100 kW class, applied field MPD thruster was evaluated and sensitivities of discharge characteristics to arc current, mass flow rate, and applied magnetic field were investigated. Thermal efficiencies as high as 60 percent, thrust efficiencies up to 21 percent, and specific impulses of up to 1150 s were attained with argon propellant. Thrust levels up to 2.5 N were directly measured with an inverted pendulum thrust stand at discharge input powers up to 57 kW. It was observed that thrust increased monotonically with the product of arc current and magnet current. Author

**A89-47036\*#** Ohio State Univ., Columbus.

### **PLASMA FLOW PROCESSES WITHIN MAGNETIC NOZZLE CONFIGURATIONS**

THOMAS M. YORK, PAVLOS MIKELLIDES (Ohio State University, Columbus), and BARRY A. JACOBY (Lawrence Livermore National Laboratory, Livermore, CA) AIAA, ASME, SAE, and ASEE, Joint Propulsion Conference, 25th, Monterey, CA, July 10-13, 1989. 10 p. refs  
(Contract NAG3-843; DE-AC02-76ET-53018)  
(AIAA PAPER 89-2711) Copyright

An attempt is made to separate the interactive processes occurring in electromagnetic devices and to examine the acceleration of ionized gas within magnetic fields which can guide it through an expansion process. The plasma was generated in a single turn coil 50 cm long with a radius of 5.25 cm which surrounded a quartz tube with an internal radius of 3.81 cm and a length of 100 cm. Choking was found to occur at both sonic and cusp velocities which were coincident in the present experiment. K.K.

**A89-47039\*#** Electric Propulsion Lab., Inc., Lancaster, CA.

### **A 50 CM DIAMETER ANNULAR ION ENGINE**

GRAEME ASTON and JOHN R. BROPHY (Electric Propulsion Laboratory, Inc., Lancaster, CA) AIAA, ASME, SAE, and ASEE, Joint Propulsion Conference, 25th, Monterey, CA, July 10-13, 1989. 8 p. Research sponsored by SDIO. refs  
(Contract NAS3-25623)  
(AIAA PAPER 89-2716) Copyright

An ion engine design is presented which uses an annular

geometry as a means of achieving large engine diameters and hence, high thrust levels. Preliminary results are discussed for discharge-only operation of a 50-cm-diameter annular ion engine. Measured operating parameters presented include discharge current and voltage characteristics, discharge chamber ion current distribution, engine body temperatures, plasma flatness parameter effects and total integrated grid ion current. Author

**A89-47040\*** # National Aeronautics and Space Administration. Lewis Research Center, Cleveland, OH.

**ION OPTICS FOR HIGH POWER 50-CM-DIA ION THRUSTERS**  
VINCENT K. RAWLIN and MARC G. MILLIS (NASA, Lewis Research Center, Cleveland, OH) AIAA, ASME, SAE, and ASEE, Joint Propulsion Conference, 25th, Monterey, CA, July 10-13, 1989. 27 p. refs  
(AIAA PAPER 89-2717)

The process used at the NASA Lewis Research Center to fabricate 30 and 50-cm-diameter ion optics is described. The ion extraction capabilities of the 30 and 50-cm diameter ion optics were evaluated on divergent field and ring-cusp discharge chambers and compared. Perveance was found to be sensitive to the effects of the type and power of the discharge chamber and to the accelerator electrode hole diameter. Levels of up to 0.64 N and 20 kW for thrust and input power, respectively, were demonstrated with the divergent-field discharge chamber. Thruster efficiencies and specific-impulse values up to 79 percent and 5000 seconds, respectively, were achieved with the ring-cusp discharge chamber. I.S.

**A89-47041\*** # Electric Propulsion Lab., Inc., Lancaster, CA.  
**THERMAL MECHANICAL ANALYSES OF LARGE DIAMETER ION ACCELERATOR SYSTEMS**

JOHN R. BROPHY and GRAEME ASTON (Electric Propulsion Laboratory, Inc., Lancaster, CA) AIAA, ASME, SAE, and ASEE, Joint Propulsion Conference, 25th, Monterey, CA, July 10-13, 1989. 8 p. Research sponsored by SDIO. refs  
(Contract NAS3-25623)  
(AIAA PAPER 89-2718) Copyright

Thermal mechanical analyses of large diameter ion accelerator systems are performed using commercially available finite element software executed on a desktop computer. Finite element models of a 30-cm-diameter accelerator system formulated using plate/shell elements give calculated results which agree well with similar published obtained on a mainframe computer. Analyses of a 50-cm-diameter, three-grid accelerator system using measured grid temperatures (corresponding to discharge powers of 653 and 886 watts) indicate that thermally induced grid movements need not be the performance limiting phenomena for accelerator systems of this size. Author

**A89-47042\*** # National Aeronautics and Space Administration. Lewis Research Center, Cleveland, OH.

**STRUCTURAL AND THERMAL RESPONSE OF 30 CM DIAMETER ION THRUSTER OPTICS**

G. MACRAE, R. ZAVESKY, and S. GOODER (NASA, Lewis Research Center, Cleveland, OH) AIAA, ASME, SAE, and ASEE, Joint Propulsion Conference, 25th, Monterey, CA, July 10-13, 1989. 22 p. refs  
(AIAA PAPER 89-2719)

This paper presents tabular and graphical data intended for use in calibrating and validating structural and thermal models of ion thruster optics. A 30-cm-diameter, two electrode, mercury ion thruster was operated using two different electrode assembly designs. With no beam extraction, the transient and steady state temperature profiles and center electrode gaps were measured for three discharge powers. The data showed that the electrode mount design had little effect on the temperatures, but significantly impacted the motion of the electrode center. Equilibrium electrode gaps increased with one design and decreased with the other. Equilibrium displacements in excess of 0.5 mm and gap changes of 0.08 mm were measured at 450 W discharge power. Variations in equilibrium gaps were also found among assemblies of the

same design. The presented data illustrate the necessity for high fidelity ion optics models and development of experimental techniques to allow their validation. Author

**A89-47044\*** # National Aeronautics and Space Administration. Lewis Research Center, Cleveland, OH.

**THE EFFECT OF ELECTRODE CONFIGURATION ON ARCJET PERFORMANCE**

FRANK M. CURRAN (NASA, Lewis Research Center, Cleveland, OH) and DAVID H. MANZELLA (NASA, Lewis Research Center; Sverdrup Technology, Inc., Cleveland, OH) AIAA, ASME, SAE, and ASEE, Joint Propulsion Conference, 25th, Monterey, CA, July 10-13, 1989. 13 p. refs  
(AIAA PAPER 89-2722) Copyright

A segmented anode/nozzle for a low-power (1 kW) arc jet thruster was fabricated to investigate the effect of electrode configuration on the arc jet performance. The five segments of the nozzle, which could be isolated individually or in groups made it possible to observe current distribution from the constrictor through the diverging section of the nozzle; measurements of the potential difference between the cathode and any of the individual segments were possible. Results showed that the discharge initiates in the high pressure region of the nozzle upstream of the diverging section, and then rapidly moves to the diverging section of the nozzle. When the arc was allowed to seat in the diverging section, the anode fall voltage was between 10 to 20 volts. When the current was forced to the high-pressure section of the constrictor, the anode fall voltage increased to more than 40 volts. I.S.

**A89-47116\*** # National Aeronautics and Space Administration. Lewis Research Center, Cleveland, OH.

**THE EFFECT OF TEST-CELL PRESSURE ON RESISTOJET NOZZLE FLOW**

PAUL F. PENKO (NASA, Lewis Research Center, Cleveland, OH), KENNETH J. DE WITT, THEO G. KEITH, JR. (Toledo, University, OH), and CHARLES C. SMITH AIAA, ASME, SAE, and ASEE, Joint Propulsion Conference, 25th, Monterey, CA, July 10-13, 1989. 13 p. refs  
(Contract NAG3-577)  
(AIAA PAPER 89-2838)

Previous experimental work has shown that measured resistojets thrust decreases from that obtained at hard vacuum conditions as the test-cell pressure rises above 0.001 torr. Thrust losses have been observed for both cold and heated flow conditions, and the most significant losses have been experienced using thrusters with low Reynolds number flow and high area ratio nozzles. In order to further investigate nozzle flow characteristics, a pressure probe having four degrees of freedom has been used to obtain stagnation pressure surveys across the nozzle exit planes of four resistojets. The surveys show a change in the ratio of the supersonic core to the viscous boundary layer flow areas as the test-cell pressure increases. The surveys are also used for detecting whether an oblique shock is present in an overexpanded nozzle flow. Thruster temperature measurements and nozzle exit plane pressure surveys indicate that thrust losses are the combined result of convection heat losses and nozzle flow momentum effects. Author

**A89-47117\*** # National Aeronautics and Space Administration. Lewis Research Center, Cleveland, OH.

**INVESTIGATION OF A LIQUID-FED WATER RESISTOJET PLUME**

D. H. MANZELLA (NASA, Lewis Research Center; Sverdrup Technology, Inc., Cleveland, OH) and L. M. CARNEY (NASA, Lewis Research Center, Cleveland, OH) AIAA, ASME, SAE, and ASEE, Joint Propulsion Conference, 25th, Monterey, CA, July 10-13, 1989. 9 p. refs  
(AIAA PAPER 89-2840)

Measurements of mass flux and flow angle were taken throughout the forward flow region of the exhaust of a liquid-fed water resistojets using a quartz crystal microbalance (QCM). The resistojets operated at a mass flow rate of 0.1 g/s with a power input of 330 Watts. Measured values were compared to theoretical

predictions obtained by employing a source flow approximation. Excellent agreement between predicted and measured mass flux values was attained; however, this agreement was highly dependent on knowledge of nozzle flow conditions. Measurements of the temperature at which the exhaust condensed on the QCM were obtained as a function of incident mass flux. Author

**A89-47428\*#** National Aeronautics and Space Administration, Washington, DC.

#### THE NASA ELECTRIC PROPULSION PROGRAM

JAMES R. STONE (NASA, Office of Aeronautics and Space Technology, Washington, DC), DAVID C. BYERS (NASA, Lewis Research Center, Cleveland, OH), and DAVID Q. KING (California Institute of Technology, Jet Propulsion Laboratory, Pasadena) IN: International Electric Propulsion Conference, 20th, Garmisch-Partenkirchen, Federal Republic of Germany, Oct. 3-6, 1988, Proceedings. Bonn, Deutsche Gesellschaft fuer Luft- und Raumfahrt, 1988, p. 17-25. Previously announced in STAR as N88-29859. refs

The NASA OAST Propulsion, Power, and Energy Division supports an electric propulsion program aimed at providing benefits to a broad class of missions. Concepts which have the potential to enable or significantly benefit space exploration and exploitation are identified and advanced toward application in the near and far term. This paper summarizes recent program progress in mission/system analysis; in electrothermal, electrostatic, and electromagnetic propulsion technologies; and in propulsion/spacecraft integration. Author

**A89-47450\*#** National Aeronautics and Space Administration, Lewis Research Center, Cleveland, OH.

#### SUCCESSFUL COMPLETION OF A CYCLIC GROUND TEST OF A MERCURY ION AUXILIARY PROPULSION SYSTEM

DAVID R. FRANCISCO, CHARLES A. LOW, JR., and JOHN L. POWER (NASA, Lewis Research Center, Cleveland, OH) IN: International Electric Propulsion Conference, 20th, Garmisch-Partenkirchen, Federal Republic of Germany, Oct. 3-6, 1988, Proceedings. Bonn, Deutsche Gesellschaft fuer Luft- und Raumfahrt, 1988, p. 208-216. Previously announced in STAR as N88-29873. refs

An engineering model Ion Auxiliary Propulsion System (IAPS) 8-cm thruster (S/N 905) has completed a life test at NASA Lewis Research Center. The mercury ion thruster successfully completed and exceeded the test goals of 2557 on/off cycles and 7057 hr of operation at full thrust. The final 1200 cycles and 3600 hr of the life test were conducted using an engineering model of the IAPS power electronics unit (PEU) and breadboard digital controller and interface unit (DCIU). This portion of the test is described in this paper with a charted history of thruster operating parameters and off-normal events. Performance and operating characteristics were constant throughout the test with only minor variations. The engineering model power electronics unit operated without malfunction; the flight software in the digital controller and interface unit was exercised and verified. Post-test inspection of the thruster revealed facility enhanced accelerator grid erosion but overall the thruster was in good condition. It was concluded that the thruster performance was not drastically degraded by time or cycles. Additional cyclic testing is currently under consideration. Author

**A89-47457\*#** National Aeronautics and Space Administration, Lewis Research Center, Cleveland, OH.

#### DC POWER CONTROL FOR A LIQUID-FED RESISTOJET

ROBERT P. GRUBER (NASA, Lewis Research Center, Cleveland, OH) IN: International Electric Propulsion Conference, 20th, Garmisch-Partenkirchen, Federal Republic of Germany, Oct. 3-6, 1988, Proceedings. Bonn, Deutsche Gesellschaft fuer Luft- und Raumfahrt, 1988, p. 273-282. Previously announced in STAR as N88-29869. refs

A simple breadboard power controller was designed and demonstrated for a new liquid-fed water resistojet. The 1-piece laboratory model thruster has an integrated vaporizer/superheater using a single heating element. Heater temperature was maintained at or near a preset reference value with the closed loop controller

providing pulse width modulated (PWM) dc power into the thruster heater. A combined thruster, temperature readout, PWM transfer function was experimentally determined. This transfer function was used to design a proportional plus integral controller that demonstrated zero steady state error, conservative stability margins and adequate transient response to step changes in propellant flow rate, input voltage and temperature reference. Initial turn-on temperature overshoot from room temperature to a 650 C setpoint was 80 C. In addition, EMI was alleviated by reducing heater  $dI/dt$  and  $dV/dt$  using a simple diode-inductor-capacitor network. Based on limited initial tests, thruster preheat with no propellant flow was necessary to achieve stable system operation during startup. Breadboard power efficiency was 99 percent at 1 kW, and component mass was 0.4 kg excluding the power loss and mass of an input filter required for spacecraft integration. Author

**A89-47487\*#** National Aeronautics and Space Administration, Lewis Research Center, Cleveland, OH.

#### EXPERIMENTAL EVALUATION OF RESISTOJET THRUSTER PLUME SHIELDS

LYNNETTE M. CARNEY (NASA, Lewis Research Center, Cleveland, OH) and ALLAN B. BAILEY (Calspan Corp., Arnold AFB, TN) IN: International Electric Propulsion Conference, 20th, Garmisch-Partenkirchen, Federal Republic of Germany, Oct. 3-6, 1988, Proceedings. Bonn, Deutsche Gesellschaft fuer Luft- und Raumfahrt, 1988, p. 513-526. Previously announced in STAR as N88-29868. refs

(Contract NASA ORDER C-30004-J)

The exhaust of an engineering model resistojet has been investigated using rotary pitot probes and a rotary quartz crystal microbalance. The resistojet operated on CO<sub>2</sub> propellant at a mass flow rate of 0.29 g/sec in both heated and unheated flows. Measurements of local flow angles in the near field of a conical plume shield indicated that the shield was not wholly effective in confining the flow to the region upstream of its exit plane. However, the absolute levels of the measured mass flux into the backflow region were very low, on the order of  $7 \times 10$  to the -7 power g/sq cm/sec or less. The use of a circular disk at the exit plane of the existing conical shield showed some benefit in decreasing the amount of backflow by a factor of two. Lastly, a detached shield placed upstream of the resistojet exit plane demonstrated a small degree of local shielding for the region directly behind it.

Author

#### A89-47494\*# Michigan State Univ., East Lansing. EXPERIMENTS AND ANALYSIS OF A COMPACT ELECTROTHERMAL THRUSTER

JES ASMUSSEN (Michigan State University, East Lansing) and STAN WHITEHAIR (IBM Thomas J. Watson Research Center, Yorktown Heights, NY) IN: International Electric Propulsion Conference, 20th, Garmisch-Partenkirchen, Federal Republic of Germany, Oct. 3-6, 1988, Proceedings. Bonn, Deutsche Gesellschaft fuer Luft- und Raumfahrt, 1988, p. 569-574. refs (Contract NAG3-305)

The description and experimental performance of a compact microwave electrothermal thruster are presented. Experimental tests using N and He propellants with input power levels of 200 W - 1.5 kW are presented. Experimental results produced energy efficiencies of 20-60 percent and specific impulse of 250-450 sec.

Author

**A89-49683\*#** National Aeronautics and Space Administration, Lewis Research Center, Cleveland, OH.

#### A PREMIXED HYDROGEN/OXYGEN CATALYTIC IGNITER

JAMES M. GREEN (NASA, Lewis Research Center; Sverdrup Technology, Inc., Cleveland, OH) AIAA, ASME, SAE, and ASEE, Joint Propulsion Conference, 25th, Monterey, CA, July 10-13, 1989. 9 p. Previously announced in STAR as N89-24445.

(Contract NAS3-25266)

(AIAA PAPER 89-2302) Copyright

The catalytic ignition of hydrogen and oxygen propellants was studied using a premixing hydrogen/oxygen injector. The premixed injector was designed to eliminate problems associated with

## 20 SPACECRAFT PROPULSION AND POWER

catalytic ignition caused by poor propellant mixing in the catalyst bed. Mixture ratio, mass flow rate, and propellant inlet temperature were varied parametrically in testing, and a pulse mode life test of the igniter was conducted. The results of the tests showed that the premixed injector eliminated flame flashback in the reactor and increased the life of the igniter significantly. The results of the experimental program and a comparison with data collected in a previous program are given. Author

**A89-49685\*#** National Aeronautics and Space Administration. Lewis Research Center, Cleveland, OH.

### 5-KW ARCJET POWER ELECTRONICS

R. P. GRUBER, R. W. GOTT, and T. W. HAAG (NASA, Lewis Research Center, Cleveland, OH) AIAA, ASME, SAE, and ASEE, Joint Propulsion Conference, 25th, Monterey, CA, July 10-13, 1989. 25 p. Previously announced in STAR as N89-24446. refs (AIAA PAPER 89-2725) Copyright

The initial design and evaluation of a 5 kW arcjet power electronics breadboard which has been integrated with a modified 1 kW design laboratory arcjet is presented. A single stage, 5 kW full bridge, pulse width modulated (PWM), power converter was developed which was phase shift regulated. The converter used metal oxide semiconductor field effect transistor (MOSFET) power switches and incorporated current mode control and an integral arcjet pulse ignition circuit. The unoptimized power efficiency was 93.5 and 93.9 percent at 5 kW and 50A output at input voltages of 130 and 150V, respectively. Line and load current regulation at 50A output was within one percent. The converter provided up to 6.6 kW to the arcjet with simulated ammonia used as a propellant. Author

**A89-49686\*#** National Aeronautics and Space Administration. Lewis Research Center, Cleveland, OH.

### LIQUID OXYGEN COOLING OF HYDROCARBON FUELED ROCKET THRUST CHAMBERS

ELIZABETH S. ARMSTRONG (NASA, Lewis Research Center, Cleveland, OH) AIAA, ASME, SAE, and ASEE, Joint Propulsion Conference, 25th, Monterey, CA, July 10-13, 1989. 14 p. Previously announced in STAR as N89-24447. refs (AIAA PAPER 89-2739) Copyright

Rocket engines using liquid oxygen (LOX) and hydrocarbon fuel as the propellants are being given serious consideration for future launch vehicle propulsion. Normally, the fuel is used to regeneratively cool the combustion chamber. However, hydrocarbons such as RP-1 are limited in their cooling capability. Another possibility for the coolant is the liquid oxygen. Combustion chambers previously tested with LOX and RP-1 as propellants and LOX as the coolant demonstrated the feasibility of using liquid oxygen as a coolant up to a chamber pressure of 13.8 MPa (2000 psia). However, there was concern as to the effect on the integrity of the chamber liner if oxygen leaks into the combustion zone through fatigue cracks that may develop between the cooling passages and the hot gas side wall. In order to study this effect, chambers were fabricated with slots machined upstream of the throat between the cooling passage wall and the hot gas side wall to simulate cracks. The chambers were tested at a nominal chamber pressure of 8.6 MPa (1247 psia) over a range of mixture ratios from 1.9 to 3.1 using liquid oxygen as the coolant. The results of the testing showed that the leaking LOX did not have a deleterious effect on the chambers in the region of the slots. However, there was unexplained melting in the throat region of both chambers, but not in line with the slots. Author

**A89-49687\*#** National Aeronautics and Space Administration. Lewis Research Center, Cleveland, OH.

### A NUMERICAL STUDY OF CHEMICALLY REACTING FLOW IN NOZZLES

THOMAS J. VANOVERBEKE (NASA, Lewis Research Center, Cleveland, OH) and JIAN-SHUN SHUEN (NASA, Lewis Research Center; Sverdrup Technology, Inc., Cleveland, OH) AIAA, ASME, SAE, and ASEE, Joint Propulsion Conference, 25th, Monterey, CA, July 10-13, 1989. 20 p. Previously announced in STAR as

N89-24444. refs

(AIAA PAPER 89-2793) Copyright

The Space Station uses small rocket motors, called thrusters, for orientation control. Because of the lack of viable design tools for small rockets, the initial thruster design was basically a very small version of a large rocket motor. Thrust measurements of the initial design were lower than predicted. To improve predictions it was decided to develop a version of the RPLUS2D reacting flow code for thruster calculations. RPLUS2D employs an implicit finite volume, lower-upper symmetric successive overrelaxation (LU-SSOR) scheme for solving the complete two-dimensional Navier-Stokes equations and species transport equations in a coupled and very efficient manner. The combustion processes are modeled by a 9-species, 18 step finite-rate chemistry model, and the turbulence is simulated by a Baldwin-Lomax algebraic model. The code is extended to handle multiple subsonic inlet conditions where the total mass flow is governed by conditions calculated at the thruster-throat. Results are shown for a thruster design where the overall mixture ratio is hydrogen rich. A calculation of a large area ratio divergent nozzle is also presented. Author

**A89-50809\*#** National Aeronautics and Space Administration. Lewis Research Center, Cleveland, OH.

### THE EFFECTS OF ARCJET THRUSTER OPERATING CONDITION CONSTRICTOR GEOMETRY ON THE PLASMA PLUME

LYNNETTE M. CARNEY (NASA, Lewis Research Center, Cleveland, OH) and JOHN M. SANKOVIC (Akron, University, OH) AIAA, ASME, SAE, and ASEE, Joint Propulsion Conference, 25th, Monterey, CA, July 10-12, 1989. 28 p. Previously announced in STAR as N89-25281. refs (AIAA PAPER 89-2723) Copyright

Measurements of plasma number density and electron temperature were obtained in the plumes of lab arcjet thrusters using electrostatic probes of both spherical and cylindrical geometry. The two arcjet thrusters used had different constrictor and/or nozzle geometries and operated on mixtures of nitrogen, hydrogen, and ammonia to simulate the decomposition products of hydrazine and ammonia. An increase in the measured electron density was observed for both geometries with increasing arc power at a constant mass flow rate and with increasing mass flow rate at a constant arc current. For a given operating condition, the electron number density decreased exponentially off centerline and followed an inverse distance squared relationship along the thrust axis. Typical measured electron temperatures ranged from 0.1 to 0.2 eV. Author

**A89-50811\*#** National Aeronautics and Space Administration. Lewis Research Center, Cleveland, OH.

### PERFORMANCE CHARACTERIZATION AND TRANSIENT INVESTIGATION OF MULTIPROPELLANT RESISTOJETS

EDWARD P. BRAUNSCHEIDEL (NASA, Lewis Research Center, Cleveland, OH) AIAA, ASME, SAE, and ASEE, Joint Propulsion Conference, 25th, Monterey, CA, July 10-12, 1989. 20 p. Previously announced in STAR as N89-25283. refs (AIAA PAPER 89-2837) Copyright

The multipropellant resistojet thruster design initially was characterized for performance in a vacuum tank using argon, carbon dioxide, nitrogen, and hydrogen, with gas inlet pressures ranging from 13.7 to 310 kPa (2 to 45 psia) over a heat exchanger temperature range of ambient to 1200 C (2200 F). Specific impulse, the measure of performance, had values ranging from 120 to 600 seconds for argon and hydrogen respectively, with a constant heat exchanger temperature of 1200 C (2200 F). When operated under ambient conditions typical specific impulse values obtained for argon and hydrogen ranged from 55 to 290 seconds, respectively. Performance measured with several mixtures of argon and nitrogen showed no significant deviation from predictions obtained by directly weighting the argon and nitrogen individual performance results. Another aspect of the program investigating transient behavior, showed responses depended heavily on the start-up scenario used. Steady state heater temperatures were



achieved in 20 to 75 minutes for argon, and in 10 to 90 minutes for hydrogen. Steady state specific impulses were achieved in 25 to 60, and 20 to 60 minutes, respectively. Author

**A89-53305\*** # National Aeronautics and Space Administration. Lewis Research Center, Cleveland, OH.

### THE DEVELOPMENT OF POWER SPECIFIC REDLINES FOR SSME SAFETY MONITORING

WILLIAM A. MAUL and CLAUDIA M. BOSCH (NASA, Lewis Research Center; Sverdrup Technology, Inc., Cleveland, OH) AIAA, ASME, SAE, and ASEE, Joint Propulsion Conference, 25th, Monterey, CA, July 10-12, 1989. 37 p. Previously announced in STAR as N89-26027. refs (Contract NAS3-25266) (AIAA PAPER 89-2413) Copyright

Over the past several years, there has been an increased awareness in the necessity for rocket engine health monitoring because of the cost and complexity of present and future systems. A current rocket engine system, the Space Shuttle Main Engine (SSME), combines a limited redline system with closed-loop control of the engine's thrust level and mixture ratio. Despite these features, 27 tests of the SSME have resulted in major incidents. An SSME transient model was used to examine the effect of variations in high pressure turbopump performance on various engine parameters. Based on analysis of the responses, several new parameters are proposed for further investigation as power-level specific redlines. Author

**A89-53306\*** # National Aeronautics and Space Administration. Lewis Research Center, Cleveland, OH.

### MODELING OF PULSED PROPELLANT REORIENTATION

A. E. PATAG, J. I. HOCHSTEIN (Washington University, Saint Louis, MO), and D. J. CHATO (NASA, Lewis Research Center, Cleveland, OH) AIAA, ASME, SAE, and ASEE, Joint Propulsion Conference, 25th, Monterey, CA, July 10-12, 1989. 20 p. Previously announced in STAR as N89-26178. refs (AIAA PAPER 89-2727) Copyright

Optimization of the propellant reorientation process can provide increased payload capability and extend the service life of spacecraft. The use of pulsed propellant reorientation to optimize the reorientation process is proposed. The ECLIPSE code was validated for modeling the reorientation process and is used to study pulsed reorientation in small-scale and full-scale propellant tanks. A dimensional analysis of the process is performed and the resulting dimensionless groups are used to present and correlate the computational predictions for reorientation performance. Author

**A89-53354\*** # National Aeronautics and Space Administration. Lewis Research Center, Cleveland, OH.

### ELECTROMAGNETIC EMISSION EXPERIENCES USING ELECTRIC PROPULSION SYSTEMS

JAMES S. SOVEY, LYNNETTE M. CARNEY (NASA, Lewis Research Center, Cleveland, OH), and STEVEN C. KNOWLES (Rocket Research Co., Redmond, WA) Journal of Propulsion and Power (ISSN 0748-4658), vol. 5, Sept.-Oct. 1989, p. 534-547. Previously cited in issue 22, p. 3553, Accession no. A87-50195. refs Copyright

**A89-54068\*** National Aeronautics and Space Administration. Lewis Research Center, Cleveland, OH.

### IDENTIFICATION OF SPACE SHUTTLE MAIN ENGINE DYNAMICS

AHMET DUYAR, TEN-HUEI GUO, and WALTER C. MERRILL (NASA, Lewis Research Center, Cleveland, OH) IN: 1989 American Control Conference, 8th, Pittsburgh, PA, June 21-23, 1989, Proceedings. Volume 3. New York, Institute of Electrical and Electronics Engineers, 1989, p. 2269-2278. Previously announced in STAR as N89-20199. refs Copyright

System identification techniques are used to represent the dynamic behavior of the Space Shuttle Main Engine. The transfer

function matrices of the linearized models of both the closed loop and the open loop system are obtained by using the recursive maximum likelihood method. Author

**N89-10119\*** # Rockwell International Corp., Canoga Park, CA. Rocketdyne Div.

### ORBIT TRANSFER ROCKET ENGINE TECHNOLOGY PROGRAM. PHASE 2: ADVANCED ENGINE STUDY Interim Report

C. ERICKSON, A. MARTINEZ, and B. HINES Feb. 1987 85 p (Contract NAS3-23773) (NASA-CR-179602; NAS 1.26:179602; RI/RD-87-126) Avail: NTIS HC A05/MF A01 CSCL 21H

In Phase 2 of the Advanced Engine Study, the Failure Modes and Effects Analysis (FMEA) maintenance-driven engine design, preliminary maintenance plan, and concept for space operable disconnects generated in Phase 1 were further developed. Based on the results of the vehicle contractors Orbit Transfer Vehicle (OTV) Concept Definition and System Analysis Phase A studies, minor revisions to the engine design were made. Additional refinements in the engine design were identified through further engine concept studies. These included an updated engine balance incorporating experimental heat transfer data from the Enhanced Heat Load Thrust Chamber Study and a Rao optimum nozzle contour. The preliminary maintenance plan of Phase 1 was further developed through additional studies. These included a compilation of critical component lives and life limiters and a review of the Space Shuttle Main Engine (SSME) operations and maintenance manual in order to begin outlining the overall maintenance procedures for the Orbit Transfer Vehicle Engine and identifying technology requirements for streamlining space-based operations. Phase 2 efforts also provided further definition to the advanced fluid coupling devices including the selection and preliminary design of a preferred concept and a preliminary test plan for its further development. Author

**N89-10122\*** # National Aeronautics and Space Administration. Lewis Research Center, Cleveland, OH.

### PHOTOVOLTAICS FOR HIGH CAPACITY SPACE POWER SYSTEMS

DENNIS J. FLOOD Oct. 1988 16 p Presented at the 39th Annual Astronautical Congress of the International Astronautical Federation, Bangalore, India, 8-15 Oct. 1988 (NASA-TM-101341; E-4360; NAS 1.15:101341) Avail: NTIS HC A03/MF A01 CSCL 10B

The anticipated energy requirements of future space missions will grow by factors approaching 100 or more, particularly as a permanent manned presence is established in space. The advances that can be expected in solar array performance and lifetime, when coupled with advanced, high energy density storage batteries and/or fuel cells, will continue to make photovoltaic energy conversion a viable power generating option for the large systems of the future. The specific technologies required to satisfy any particular set of power requirements will vary from mission to mission. Nonetheless, in almost all cases the technology push will be toward lighter weight and higher efficiency, whether of solar arrays or storage devices. This paper will describe the content and direction of the current NASA program in space photovoltaic technology. The paper will also discuss projected system level capabilities of photovoltaic power systems in the context of some of the new mission opportunities under study by NASA, such as a manned lunar base, and a manned visit to Mars. Author

**N89-10123\*** # National Aeronautics and Space Administration. Lewis Research Center, Cleveland, OH.

### TECHNOLOGY ISSUES ASSOCIATED WITH FUELING THE NATIONAL AEROSPACE PLANE WITH SLUSH HYDROGEN

NED P. HANNUM 1988 9 p Prepared for presentation at the 7th Joint Intersociety Cryogenic Conference Symposium, Houston, Tex., 22-26 Jan. 1989; sponsored in part by ASME, AIChE and IIR (NASA-TM-101386; E-4445; NAS 1.15:101386) Avail: NTIS HC A02/MF A01 CSCL 21H



## 20 SPACECRAFT PROPULSION AND POWER

The National Aerospace Plane is a horizontal takeoff and landing, single stage-to-orbit vehicle using hydrogen fuel. The first flights are planned for the mid 1990's. The success of this important national program requires advances in virtually every discipline associated with both airbreathing and space flight. The high heating value, cooling capacity, and combustion properties make hydrogen the fuel of choice, but low density results in a large vehicle. Both fuel cooling capacity and density are increased with the use of slush hydrogen and result in significant reductions in vehicle size. A national program to advance this technology and to find engineering solutions to the many design issues is now under way. The program uses the expertise of the cryogenics production and services industry, the instrumentation industry, universities and governments. The program will be discussed to highlight the major issues and display progress to date. Author

**N89-10943\*** Page (R. J.) Co., Santa Ana, CA.  
**PRELIMINARY DESIGN STUDY OF HYDROGEN AND AMMONIA RESISTOJETS FOR PRIME AND AUXILIARY THRUSTERS Final Report**  
 RUSSELL J. PAGE, WILLIS A. STONER, and LARRY BARKER  
 Oct. 1988 49 p  
 (Contract NAS3-23337)  
 (NASA-CR-182176; NAS 1.26:182176) Avail: NTIS HC A03/MF A01 CSCL 21/8

Designs of high performance resistojets for primary and auxiliary propulsion are described. Thruster power for the primary propulsion application was in the 2 to 3 kW range while auxiliary propulsion power per thruster was 0.15 to 0.25 kW. Propellants considered were hydrogen and ammonia. The report described design techniques used to forecast the temperature and energy flux distributions using mathematical modeling by personal micro-computer. BASIC language is used throughout to give the designer rapid interaction and control. Both designs integrate compact first stage coils with concentric tubular heaters. The hybrid heater design allows better thruster power matching with the spacecraft power bus. Projected specific impulse levels were 760 to 830 s for hydrogen and 380 to 410 s for ammonia. Author

**N89-10944\*** National Aeronautics and Space Administration. Lewis Research Center, Cleveland, OH.  
**NUCLEAR PROPULSION: A VITAL TECHNOLOGY FOR THE EXPLORATION OF MARS AND THE PLANETS BEYOND**  
 STANLEY K. BOROWSKI 1988 47 p Presented at the Case for Mars 3, Boulder, Colo., 18-22 Jul. 1987; sponsored in part by American Astronautical Society, JPL, Los Alamos Lab., NASA Ames Research Center, NASA Johnson Space Center, NASA Marshall Space Flight Center, and Planetary Society  
 (NASA-TM-101354; E-4369; NAS 1.15:101354) Avail: NTIS HC A03/MF A01 CSCL 21/6

The physics and technology issues and performance potential of various direct thrust fission and fusion propulsion concepts are examined. Next to chemical propulsion the solid core fission thermal rocket (SCR) is the only other concept to be experimentally tested at the power (approx 1.5 to 5.0 GW) and thrust levels (approx 0.33 to 1.11 MN) required for manned Mars missions. With a specific impulse of approx 850 s, the SCR can perform various near-Earth, cislunar and interplanetary missions with lower mass and cost requirements than its chemical counterpart. The gas core fission thermal rocket, with a specific power and impulse of approx 50 kW/kg and 5000 s offers the potential for quick courier trips to Mars (of about 80 days) or longer duration exploration cargo missions (lasting about 280 days) with starting masses of about 1000 m tons. Convenient transportation to the outer Solar System will require the development of magnetic and inertial fusion rockets (IFRs). Possessing specific powers and impulses of approx 100 kW/kg and 200-300 kilosecs, IFRs will usher in the era of the true Solar System class spaceship. Even Pluto will be accessible with roundtrip times of less than 2 years and starting masses of about 1500 m tons. Author

**N89-11805\*** Aerojet TechSystems Co., Sacramento, CA.  
**INTEGRATED CONTROL AND HEALTH MANAGEMENT. ORBIT TRANSFER ROCKET ENGINE TECHNOLOGY PROGRAM Final Report**  
 WILFRIED A. HOLZMANN and WARREN R. HAYDEN Oct. 1988 139 p  
 (Contract NAS3-23772)  
 (NASA-CR-182122; NAS 1.26:182122; ATC-2459-42-1) Avail: NTIS HC A07/MF A01 CSCL 21/8

To insure controllability of the baseline design for a 7500 pound thrust, 10:1 throttleable, dual expanded cycle. Hydrogen-Oxygen, orbit transfer rocket engine, an Integrated Controls and Health Monitoring concept was developed. This included: (1) Dynamic engine simulations using a TUTSIM derived computer code; (2) analysis of various control methods; (3) Failure Modes Analysis to identify critical sensors; (4) Survey of applicable sensors technology; and, (5) Study of Health Monitoring philosophies. The engine design was found to be controllable over the full throttling range by using 13 valves, including an oxygen turbine bypass valve to control mixture ratio, and a hydrogen turbine bypass valve, used in conjunction with the oxygen bypass to control thrust. Classic feedback control methods are proposed along with specific requirements for valves, sensors, and the controller. Expanding on the control system, a Health Monitoring system is proposed including suggested computing methods and the following recommended sensors: (1) Fiber optic and silicon bearing deflectionometers; (2) Capacitive shaft displacement sensors; and (3) Hot spot thermocouple arrays. Further work is needed to refine and verify the dynamic simulations and control algorithms, to advance sensor capabilities, and to develop the Health Monitoring computational methods. Author

**N89-11807\*** Arizona State Univ., Tempe. Dept. of Electronics and Computer Technology.  
**IDENTIFICATION OF HIGH PERFORMANCE AND COMPONENT TECHNOLOGY FOR SPACE ELECTRICAL POWER SYSTEMS FOR USE BEYOND THE YEAR 2000 Final Technical Report, 16 May 1986 - 15 Dec. 1988**  
 JAMES E. MAISEL 5 Dec. 1988 227 p  
 (Contract NAG3-714)  
 (NASA-CR-183003; NAS 1.26:183003) Avail: NTIS HC A11/MF A01 CSCL 10/2

Addressed are some of the space electrical power system technologies that should be developed for the U.S. space program to remain competitive in the 21st century. A brief historical overview of some U.S. manned/unmanned spacecraft power systems is discussed to establish the fact that electrical systems are and will continue to become more sophisticated as the power levels approach those on the ground. Adaptive/Expert power systems that can function in an extraterrestrial environment will be required to take an appropriate action during electrical faults so that the impact is minimal. Manhours can be reduced significantly by relinquishing tedious routine system component maintenance to the adaptive/expert system. By cataloging component signatures over time this system can set a flag for a premature component failure and thus possibly avoid a major fault. High frequency operation is important if the electrical power system mass is to be cut significantly. High power semiconductor or vacuum switching components will be required to meet future power demands. System mass tradeoffs have been investigated in terms of operating at high temperature, efficiency, voltage regulation, and system reliability. High temperature semiconductors will be required. Silicon carbide materials will operate at a temperature around 1000 K and the diamond material up to 1300 K. The driver for elevated temperature operation is that radiator mass is reduced significantly because of inverse temperature to the fourth power. Author

**N89-11808\*** Colorado State Univ., Fort Collins. Dept. of Physics.  
**CLOSED-DRIFT THRUSTER INVESTIGATIONS**  
 RAYMOND S. ROBINSON, TERRY D. SCHEMME, and MICHAEL J. PATTERSON Jun. 1986 50 p

(Contract NSG-3011)

(NASA-CR-179497; NAS 1.26:179497) Avail: NTIS HC A03/MF A01 CSCL 21/8

Recent data obtained from a second generation closed-drift thruster design, employing Hall current acceleration is outlined. This type device is emphasized for electric propulsion for geocentric mission applications. Because geocentric mission profiles are best achieved with a specific impulse range of 1000 to 2000 s, closed-drift thrusters are well suited for this application, permitting time payload compromises intermediate of those possible with either electrothermal or electrostatic devices. A discussion is presented of the potential advantages of using a 1000 to 2000 s device for one way orbit raising of nonpower payloads. Because closed-drift thruster operation is not space charge limited, and requires only one power circuit for steady state operation, their application is technically advantageous. Beam, plasma and thrust characteristics are detailed for a range of operating conditions.

Author

**N89-11809\*** Wisconsin Univ., Madison.

**STUDY OF THE GENERATOR/MOTOR OPERATION OF INDUCTION MACHINES IN A HIGH FREQUENCY LINK SPACE POWER SYSTEM Final Report**

THOMAS A. LIPO and PRADEEP K. SOOD Mar. 1987 185 p (Contract NAG3-631)

(NASA-CR-179600; NAS 1.26:179600) Avail: NTIS HC A09/MF A01 CSCL 10/2

Static power conversion systems have traditionally utilized dc current or voltage source links for converting power from one ac or dc form to another since it readily achieves the temporary energy storage required to decouple the input from the output. Such links, however, result in bulky dc capacitors and/or inductors and lead to relatively high losses in the converters due to stresses on the semiconductor switches. The feasibility of utilizing a high frequency sinusoidal voltage link to accomplish the energy storage and decoupling function is examined. In particular, a type of resonant six pulse bridge interface converter is proposed which utilizes zero voltage switching principles to minimize switching losses and uses an easy to implement technique for pulse density modulation to control the amplitude, frequency, and the waveshape of the synthesized low frequency voltage or current. Adaptation of the proposed topology for power conversion to single-phase ac and dc voltage or current outputs is shown to be straight forward. The feasibility of the proposed power circuit and control technique for both active and passive loads are verified by means of simulation and experiment.

Author

**N89-12632\*** National Aeronautics and Space Administration. Lewis Research Center, Cleveland, OH.

**SIMPLIFIED CYCLIC STRUCTURAL ANALYSIS OF SSME TURBINE BLADES**

ALBERT KAUFMAN and J. M. MANDERSCHIED In NASA, Marshall Space Flight Center, Advanced Earth-To-Orbit Propulsion Technology 1986, Volume 2 p 107-124 Oct. 1986 Previously announced as N86-16615

Avail: NTIS HC A99/MF E03 CSCL 21/8

Anisotropic high-temperature alloys are used to meet the safety and durability requirements of turbine blades for high-pressure turbopumps in reusable space propulsion systems. The applicability to anisotropic components of a simplified inelastic structural analysis procedure developed at the NASA Lewis Research Center is assessed. The procedure uses as input the history of the total strain at the critical crack initiation location computed from elastic finite-element analyses. Cyclic heat transfer and structural analyses are performed for the first stage high-pressure fuel turbopump blade of the space shuttle main engine. The blade alloy is directionally solidified MAR-M 246 (nickel base). The analyses are based on a typical test stand engine cycle. Stress-strain histories for the airfoil critical location are computed using both the MARC nonlinear finite-element computer code and the simplified procedure. Additional cases are analyzed in which the material yield strength is arbitrarily reduced to increase the plastic strains and, therefore, the severity of the problem. Good agreement is

shown between the predicted stress-strain solutions from the two methods. The simplified analysis uses about 0.02 percent (5 percent with the required elastic finite-element analyses) of the CPU time used by the nonlinear finite element analysis.

Author

**N89-12649\*** National Aeronautics and Space Administration. Lewis Research Center, Cleveland, OH.

**LIQUID OXYGEN COOLING OF HIGH PRESSURE LOX/HYDROCARBON ROCKET THRUST CHAMBERS**

HAROLD G. PRICE In NASA, Marshall Space Flight Center, Advanced Earth-To-Orbit Propulsion Technology 1986, Volume 2 p 474-528 Oct. 1986

Avail: NTIS HC A99/MF E03 CSCL 21/8

An experimental program using liquid oxygen (LOX) and RP-1 as the propellants and supercritical LOX as the coolant was conducted at 4.14, 8.274, and 13.79 MN/sq m (600, 1200, and 2000 psia) chamber pressure. The objectives of this program were to evaluate the cooling characteristics of LOX with the LOX/RP-1 propellants, the buildup of soot on the hot-gas-side chamber wall and the effect of an internal LOX leak on the structural integrity of the combustor. Five thrust chambers with throat diameters of 6.6 cm (2.6 in) were tested successfully. The first three were tested at 4.14 MN/sq m (600 psia) chamber pressure over a mixture ratio range of 2.25 to 2.92. One of these three was tested over 22 cyclic tests after the first through crack from the coolant channel to the combustion zone was observed with no apparent metal burning or distress. The fourth chamber was tested at 8.274 MN/sq m (1200 psia) chamber pressure over a mixture ratio range of 1.93 to 2.98. The fourth and fifth chambers were tested at 13.79 MN/sq m (2000 psia) chamber pressure over a mixture ratio range of 1.79 to 2.68.

Author

**N89-12665\*** National Aeronautics and Space Administration. Lewis Research Center, Cleveland, OH.

**SP-100 NUCLEAR SPACE POWER SYSTEMS WITH APPLICATION TO SPACE COMMERCIALIZATION**

JOHN M. SMITH 1988 17 p Proposed for presentation at Space Commercialization: Roles of Developing Countries, Nashville, Tenn., 5-10 Mar. 1989; sponsored by AIAA

(NASA-TM-101403; E-4487; NAS 1.15:101403) Avail: NTIS HC A03/MF A01 CSCL 18/9

The purpose of this paper is to familiarize the Space Commercialization Community with the status and characteristics of the SP-100 space nuclear power system. The program is a joint undertaking by the Department of Defense, the Department of Energy and NASA. The goal of the program is to develop, validate, and demonstrate the technology for space nuclear power systems in the range of 10 to 1000 kWe electric for use in the future civilian and military space missions. Also discussed are mission applications which are enhanced and/or enabled by SP-100 technology and how this technology compares to that of more familiar solar power systems. The mission applications include earth orbiting platforms and lunar/Mars surface power.

Author

**N89-13492\*** National Aeronautics and Space Administration. Lewis Research Center, Cleveland, OH.

**POWER CONSIDERATIONS FOR AN EARLY MANNED MARS MISSION UTILIZING THE SPACE STATION**

MARTIN E. VALGORA 1987 15 p Presented at Case for Mars 3, Boulder, Colo., 18-22 Jul. 1987; sponsored by American Aeronautical Society, JPL, Los Alamos National Lab., Ames Research Center, Lyndon B. Johnson Space Center, George C. Marshall Space Flight Center, Planetary Society

(NASA-TM-101436; E-4472; NAS 1.15:101436) Avail: NTIS HC A03/MF A01 CSCL 10/2

Power requirements and candidate electrical power sources were examined for the supporting space infrastructure for an early (2004) manned Mars mission. This two-year mission (60-day stay time) assumed a single six crew piloted vehicle with a Mars lander for four of the crew. The transportation vehicle was assumed to be a hydrogen/oxygen propulsion design with or without large aerobrakes and assembled and checked out on the LEO Space Station. The long transit time necessitated artificial gravity of the

## 20 SPACECRAFT PROPULSION AND POWER

crew by rotating the crew compartments. This rotation complicates power source selection. Candidate power sources were examined for the Lander, Mars Orbiter, supporting Space Station, co-orbiting Propellant Storage Depot, and alternatively, a co-orbiting Propellant Generation (water electrolysis) Depot. Candidates considered were photovoltaics with regenerative fuel cells or batteries, solar dynamics, isotope dynamics, and nuclear power. Author

**N89-13493\*#** Pratt and Whitney Aircraft, West Palm Beach, FL. Government Engine Business.

### **EVALUATION OF COATED COLUMBIUM TEST PANELS HAVING APPLICATION TO A SECONDARY NOZZLE EXTENSION FOR THE RL10 ROCKET ENGINE SYSTEM, PARTS 1 AND 2 Final Report**

KENNETH S. MURPHY and JOAQUIN H. CASTRO Dec. 1988 135 p

(Contract NAS3-25052; NAS3-24238; NAS3-24738)  
(NASA-CR-180809; NAS 1.26:180809) Avail: NTIS HC A07/MF A01 CSCL 21/8

The activity performed on the screening and evaluation of various coatings for application on columbium alloy test panels representative of a radiation-cooled nozzle extension for the RL10 rocket engine is summarized. Vendors and processes of candidate coatings were evaluated. Post engine test evaluations of the two selected coatings are discussed. B.G.

**N89-13495\*#** National Aeronautics and Space Administration. Lewis Research Center, Cleveland, OH.

### **MODELING OF IMPULSIVE PROPELLANT REORIENTATION**

JOHN I. HOCHSTEIN, ALFREDO E. PATAG (Washington Univ., St. Louis, Mo.), and DAVID J. CHATO 1988 24 p Presented at the 27th Aerospace Sciences Meeting, Reno, Nev., 9-12 Jan. 1989; sponsored by AIAA

(Contract NAG3-578)  
(NASA-TM-101440; E-4545; NAS 1.15:101440; AIAA-89-0628)  
Avail: NTIS HC A03/MF A01 CSCL 21/8

The impulsive propellant reorientation process is modeled using the (Energy Calculations for Liquid Propellants in a Space Environment (ECLIPSE) code. A brief description of the process and the computational model is presented. Code validation is documented via comparison to experimentally derived data for small scale tanks. Predictions of reorientation performance are presented for two tanks designed for use in flight experiments and for a proposed full scale OTV tank. A new dimensionless parameter is developed to correlate reorientation performance in geometrically similar tanks. Its success is demonstrated. Author

**N89-14255\*#** National Aeronautics and Space Administration. Lewis Research Center, Cleveland, OH.

### **LEAKAGE PREDICTIONS FOR RAYLEIGH-STEP, HELIUM-PURGE SEALS**

MARGARET P. PROCTOR Dec. 1988 18 p  
(NASA-TM-101352; E-4379; NAS 1.15:101352) Avail: NTIS HC A03/MF A01 CSCL 21/8

Rayleigh-step, helium purge, annular shaft seals, studied for use in liquid oxygen turbopumps, generate a hydrodynamic force that enables the seal to follow shaft perturbations. Hence, smaller clearances can be used to reduce seal leakage. FLOWCAL, a computer code developed by Mechanical Technology Incorporated, predicts gas flow rate through an annular seal with an axial pressure gradient. Analysis of a 50-mm Rayleigh-step, helium-purge, annular seal showed the flow rate increased axial pressure gradient, downstream pressure, and eccentricity ratio. Increased inlet temperature reduced leakage. Predictions made at maximum and minimum clearances (due to centrifugal and thermal growths, machining tolerances and  $\pm$  or  $\pm$  2 percent uncertainty in the clearance measurement) placed wide boundaries on expected flow rates. The widest boundaries were set by thermal growth conditions. Predicted flow rates for a 50-mm Rayleigh-step, helium-purge, annular seal underestimated measured flow rates by three to seven times. However, the analysis did accurately predict flow rates for choked gas flow through annular seals when compared to flow rates measured in two other independent studies. Author

**N89-14256\*#** Aerojet TechSystems Co., Sacramento, CA.

### **ORBIT TRANSFER ROCKET ENGINE TECHNOLOGY**

#### **PROGRAM: OXYGEN MATERIALS COMPATIBILITY TESTING**

##### **Final Report**

LEONARD SCHOENMAN Jan. 1989 224 p

(Contract NAS3-23772)

(NASA-CR-182195; NAS 1.26:182195; REPT-CC0134) Avail: NTIS HC A10/MF A01 CSCL 21/8

Particle impact and frictional heating tests of metals in high pressure oxygen, are conducted in support of the design of an advanced rocket engine oxygen turbopump. Materials having a wide range of thermodynamic properties including heat of combustion and thermal diffusivity were compared in their resistance to ignition and sustained burning. Copper, nickel and their alloys were found superior to iron based and stainless steel alloys. Some materials became more difficult to ignite as oxygen pressure was increased from 7 to 21 MPa (1000 to 3000 psia). Author

**N89-15164\*#** Rockwell International Corp., Canoga Park, CA. Rocketdyne Div.

### **SPACE STATION WP-04 POWER SYSTEM PRELIMINARY ANALYSIS AND DESIGN DOCUMENT, VOLUME 3**

19 Dec. 1986 372 p

(Contract NAS3-24666)

(NASA-CR-179587-VOL-3; NAS 1.26:179587-VOL-3;

RI/RD85-320-2-VOL-3) Avail: NTIS HC A16/MF A01 CSCL 10/2

Rocketdyne plans to generate a system level specification for the Space Station Electric Power System (EPS) in order to facilitate the usage, accountability, and tracking of overall system level requirements. The origins and status of the verification planning effort are traced and an overview of the Space Station program interactions are provided. The work package level interfaces between the EPS and the other Space Station work packages are outlined. A trade study was performed to determine the peaking split between PV and SD, and specifically to compare the inherent total peaking capability with proportionally shared peaking. In order to determine EPS cost drivers for the previous submittal of DRO2, the life cycle cost (LCC) model was run to identify the more significant costs and the factors contributing to them. B.G.

**N89-15170\*#** Ohio State Univ., Columbus. Dept. of Aeronautical and Astronautical Engineering.

### **THE EFFECTS OF MAGNETIC NOZZLE CONFIGURATIONS ON PLASMA THRUSTERS Semiannual Progress Report, 30 Jun. - 31 Dec. 1988**

THOMAS M. YORK 25 Jan. 1989 57 p

(Contract NAG3-843)

(NASA-CR-184678; NAS 1.26:184678; AAE-AARL-P-89-1) Avail: NTIS HC A04/MF A01 CSCL 21/3

Plasma thrusters have been operated at power levels from 10kW to 0.1MW. When these devices have had magnetic fields applied to them which form a nozzle configuration for the expanding plasma, they have shown marked increases in exhaust velocity which is in direct proportion to the magnitude of the applied field. Further, recent results have shown that electrode erosion may be influenced by applied magnetic fields. This research is directed to the experimental and computational study of the effects of applied magnetic field nozzles in the acceleration of plasma flows. Plasma source devices which eliminate the plasma interaction in normal thrusters are studied as most basic. Normal thruster configurations will be studied without applied fields and with applied magnetic nozzle fields. Unique computational studies will utilize existing codes which accurately include transport processes. Unique diagnostic studies will support the experimental studies to generate new data. Both computation and diagnostics will be combined to indicate the physical mechanisms and transport properties that are operative in order to allow scaling and accurate prediction of thruster performance. Author

**N89-15171\*#** National Aeronautics and Space Administration. Lewis Research Center, Cleveland, OH.

# **ISSUES AND OPPORTUNITIES IN SPACE PHOTOVOLTAICS**

ROBERT W. FRANCIS, W. A. SOMERVILLE (Aerospace Corp., El Segundo, CA.), and DENNIS J. FLOOD 1988 14 p Presented at the 20th Photovoltaic Specialists Conference, Las Vegas, NV, 26-30 Sep. 1988; sponsored by the Institute of Electrical and Electronics Engineers

(NASA-TM-101425; E-4526; NAS 1.15:101425) Avail: NTIS HC A03/MF A01 CSCL 10/2

Space power sources are becoming a central focus for determining man's potential and schedule for exploring and utilizing the benefits of space. The ability to search, probe, survey, and communicate throughout the universe will depend on providing adequate power to the instruments to do these jobs. Power requirements for space platforms are increasing and will continue to increase into the 21st century. Photovoltaics have been a dependable power source for space for the last 30 years and have served as the primary source of power on virtually all DOD and NASA satellites. The performance of silicon (Si) solar cells has increased from 10 percent air mass zero (AM0) solar energy conversion efficiency in the early 60's to almost 15 percent on today's spacecraft. Some technologists even think that the potential for solar photovoltaics has reached a plateau. However, present and near-future Air Force and NASA requirements show needs that, if the problems are looked upon as opportunities, can elevate the photovoltaic power source scientist and array structure engineer into the next technological photovoltaic growth curve. Author

**N89-15979\*#** National Aeronautics and Space Administration. Lewis Research Center, Cleveland, OH.

# **HIGH-PRESSURE CALORIMETER CHAMBER TESTS FOR LIQUID OXYGEN/KEROSENE (LOX/RP-1) ROCKET COMBUSTION**

PHILIP A. MASTERS, ELIZABETH S. ARMSTRONG, and HAROLD G. PRICE Dec. 1988 18 p

(NASA-TP-2862; E-2645; NAS 1.60:2862) Avail: NTIS HC A03/MF A01 CSCL 21/8

An experimental program was conducted to investigate the rocket combustion and heat transfer characteristics of liquid oxygen/kerosene (LOX/RP-1) mixtures at high chamber pressures. Two water-cooled calorimeter chambers of different combustion lengths were tested using 37- and 61-element oxidizer-fuel-oxidizer triplet injectors. The tests were conducted at nominal chamber pressures of 4.1, 8.3, and 13.8 MPa abs (600, 1200, and 2000 psia). Heat flux Q/A data were obtained for the entire calorimeter length for oxygen/fuel mixture ratios of 1.8 to 3.3. Test data at 4.1 MPa abs compared favorably with previous test data from another source. Using an injector with a fuel-rich outer zone reduced the throat heat flux by 47 percent with only a 4.5 percent reduction in the characteristic exhaust velocity efficiency  $C^*$  sub eff. The throat heat transfer coefficient was reduced approximately 40 percent because of carbon deposits on the chamber wall. Author

**N89-16917\*#** National Aeronautics and Space Administration. Lewis Research Center, Cleveland, OH.

# **NASA PHOTOVOLTAIC RESEARCH AND TECHNOLOGY**

DENNIS J. FLOOD Dec. 1988 12 p Prepared for the Annual Meeting of the American Institute of Chemical Engineers, Washington, DC, 28 Nov. - 2 Dec. 1988

(NASA-TM-101422; E-4522; NAS 1.15:101422) Avail: NTIS HC A03/MF A01 CSCL 10/2

NASA photovoltaic R and D efforts address future Agency space mission needs through a comprehensive, integrated program. Activities range from fundamental studies of materials and devices to technology demonstrations of prototype hardware. The program aims to develop and apply an improved understanding of photovoltaic energy conversion devices and systems that will increase the performance, reduce the mass, and extend the lifetime of photovoltaic arrays for use in space. To that end, there are efforts aimed at improving cell efficiency, reducing the effects of space particulate radiation damage (primarily electrons and

protons), developing ultralightweight cells, and developing advanced ray component technology for high efficiency concentrator arrays and high performance, ultralightweight arrays. Current goals that have been quantified for the program are to develop cell and array technology capable of achieving 300 watts/kg for future missions for which mass is a critical factor, or 300 watts/sq m for future missions for which array size is a major driver (i.e., Space Station). A third important goal is to develop cell and array technology which will survive the GEO space radiation environment for at least 10 years. Author

**N89-16918\*#** Pratt and Whitney Aircraft, West Palm Beach, FL. Government Engine Business.

# **DESIGN AND ANALYSIS REPORT FOR THE FLIGHT WEIGHT 20-INCH COLUMBIUM SECONDARY NOZZLE FOR THE RL10 ENGINE Final Report**

J. H. CASTRO Feb. 1989 57 p

(Contract NAS3-24238)

(NASA-CR-179612; NAS 1.26:179612) Avail: NTIS HC A04/MF A01 CSCL 21/8

Pratt & Whitney (P and W) is currently under contract to NASA-LeRC for a multi-year program to evaluate the feasibility of the RL10-IIB/IIC engine models and the various improvements which broaden the engine capabilities and range of applications. The features being evaluated include the operation of the RL10 engine at low thrust levels and/or high mixture ratio levels and the addition of a high area ratio (250:1) translating nozzle to the engine to increase its specific impulse while shortening the installed engine length. The translating nozzle for the RL10-IIB/IIC engine is approximately 55 inches long with an exit plane diameter of 71 inches and an inlet plane diameter of 40 inches. This report documents the design and analysis work done investigating a small subscale Columbiu nozzle which could be built and tested to provide findings which then could be incorporated into the high area ratio nozzle final design for the RL10-IIB/IIC engine. This report documents the design and analysis work done investigating a small subscale Columbiu nozzle which could be built and tested to provide findings which then could be incorporated into the high area ratio nozzle final design for the RL10-IIB/IIC engine. The length of the subscale nozzle is 20 in.; its exit diameter is 46 in. With the nozzle in the stowed position, an RL10A-3-3A engine system is 70 inches long (Area Ratio = 61:1); with the nozzle deployed the engine length and area ratio are increased to 90 inches and 83:1 respectively. The increase in area ratio provides a calculated increase of 7 + or - 1 second of specific impulse. Author

**N89-17618\*#** National Aeronautics and Space Administration. Lewis Research Center, Cleveland, OH.

# **UNIQUE MISSION OPTIONS AVAILABLE WITH A MEGAWATT-CLASS NUCLEAR ELECTRIC PROPULSION SYSTEM**

E. P. COOMES, L. A. MCCAULEY (Battelle Columbus Labs., OH.), J. L. CHRISTIAN, M. A. GOMEZ, and W. A. WONG Oct. 1988 10 p Presented at the 24th AIAA/ASME/SAE/ASEE Joint Propulsion Conference, Boston, MA, 11-14 Jul. 1988

(Contract DE-AC06-76RL-01830)

(NASA-TM-101220; NAS 1.15:101220; DE89-001738;

PNL-SA-15519; CONF-880764-5) Avail: NTIS HC A02/MF A01 CSCL 21/3

The advantages of using electric propulsion systems are well-known in the aerospace community with the most common being its high specific impulse, lower propellant requirements, and lower system mass. But these advantages may not be as important as the overall unique mission options electric propulsion makes possible, especially if the system is powered by a megawatt-class nuclear electric power source. Although the lack of suitable electric power systems has been a major drawback to electric propulsion, recent efforts have shown megawatt-class nuclear electric power systems are feasible and could be available by the turn of the century. Coupling this with the resurgence in interest in free-space electromagnetic transmission of energy and technology developments in this area provide a whole new aspect to the

view of electric propulsion. The propulsion system now has a second mission function that may be of more value than the well understood benefits of electric propulsion; that is providing large quantities of prime power in support of a broad spectrum of mission tasks. DOE

**N89-20192\*#** National Aeronautics and Space Administration. Lewis Research Center, Cleveland, OH.

### ADVANCED TECHNOLOGY FOR FUTURE SPACE PROPULSION SYSTEMS

LARRY A. DIEHL Mar. 1989 24 p Presented at a Symposium on Space Commercialization: Roles of Developing Countries, Nashville, TN, 5-10 Mar. 1989; sponsored in part by Tennessee Univ. Space Inst.; AIAA and IAA (NASA-TM-101951; E-4646; NAS 1.15:101951) Avail: NTIS HC A03/MF A01 CSCL 21/8

The NASA Project Pathfinder contains programs to provide technologies for future transfer vehicles including those powered by both advanced chemical and electric propulsion rockets. This paper discusses the Chemical Transfer Propulsion and Cargo Vehicle Propulsion elements of Pathfinder. The program requirements and goals for both elements are discussed, and technical activities which are planned or underway are summarized. Recent progress in programs which support or proceed the Pathfinder activities is detailed. In particular, the NASA Program for Advanced Orbital Transfer Vehicle Propulsion, which acted as the precursor for the Chemical Transfer Propulsion element of Pathfinder is summarized. Author

**N89-20193\*#** National Aeronautics and Space Administration. Lewis Research Center, Cleveland, OH.

### THE EMITTANCE OF SPACE RADIATOR MATERIALS MEASURED AT ELEVATED TEMPERATURES

MICHAEL J. MIRTICH, FRANK DIFILIPPO, JENNIFER BARRY, and MICHAEL KUSSMAUL (Cleveland State Univ., OH.) Apr. 1988 15 p Presented at the 15th International Conference on Metallurgical Coatings, San Diego, CA, 11-15 Apr. 1988; sponsored in part by the American Vacuum Society (NASA-TM-101948; E-4641; NAS 1.15:101948) Avail: NTIS HC A03/MF A01 CSCL 10/2

The spectral emittances of textured space radiator materials between 1.7 and 14.7 micrometer have been evaluated at room temperature and elevated temperature (630 C) in air. Heating in air caused a permanent increase in spectral emittance for all materials tested: HCl/ion beam textured 304 stainless steel, untextured Ti (6 percent Al, 4 percent V), and sandblasted Ti (6 percent Al, 4 percent V). Changes in the surface chemistry and/or surface morphology of these materials were also observed. Elevated temperature spectral emittance was measured in an argon atmosphere and compared to the measurements in air. Similarity between the room temperature and elevated temperature spectral emittance measurements was also investigated, and limited agreement was found. Author

**N89-20194\*#** National Aeronautics and Space Administration. Lewis Research Center, Cleveland, OH.

### FREE-PISTON STIRLING TECHNOLOGY FOR SPACE POWER

JACK G. SLABY 1989 21 p Prepared for presentation at the international Conference on Space Power, Cleveland, OH, 5-7 Jun. 1989; sponsored in part by the International Astronautical Federation (NASA-TM-101956; E-4653; NAS 1.15:101956) Avail: NTIS HC A03/MF A01 CSCL 10/2

An overview is presented of the NASA Lewis Research Center free-piston Stirling engine activities directed toward space power. This work is being carried out under NASA's new Civil Space Technology Initiative (CSTI). The overall goal of CSTI's High Capacity Power element is to develop the technology base needed to meet the long duration, high capacity power requirements for future NASA space missions. The Stirling cycle offers an attractive power conversion concept for space power needs. Discussed here is the completion of the Space Power Demonstrator Engine (SPDE) testing-culminating in the generation of 25 kW of engine power

from a dynamically-balanced opposed-piston Stirling engine at a temperature ratio of 2.0. Engine efficiency was approximately 22 percent. The SPDE recently has been divided into two separate single-cylinder engines, called Space Power Research Engine (SPRE), that now serve as test beds for the evaluation of key technology disciplines. These disciplines include hydrodynamic gas bearings, high-efficiency linear alternators, space qualified heat pipe heat exchangers, oscillating flow code validation, and engine loss understanding. Author

**N89-20199\*#** National Aeronautics and Space Administration. Lewis Research Center, Cleveland, OH.

### IDENTIFICATION OF SPACE SHUTTLE MAIN ENGINE DYNAMICS

AHMET DUYAR, TEN-HUEI GUO (Sverdrup Technology, Inc., Cleveland, OH.), and WALTER C. MERRILL 1989 15 p Proposed for presentation at the American Control Conference, Pittsburgh, PA, 21-23 Jun. 1989; sponsored by AIAA, ASME, AICHE, AISE, ISA and SCS (NASA-TM-101982; E-4680; NAS 1.15:101982) Avail: NTIS HC A03/MF A01 CSCL 21/8

System identification techniques are used to represent the dynamic behavior of the Space Shuttle Main Engine. The transfer function matrices of the linearized models of both the closed loop and the open loop system are obtained by using the recursive maximum likelihood method. Author

**N89-21025\*#** National Aeronautics and Space Administration. Lewis Research Center, Cleveland, OH.

### THREE DIMENSIONAL THERMAL ANALYSIS OF ROCKET THRUST CHAMBERS

M. H. N. NARAGHI (Manhattan Coll., New York.) and E. S. ARMSTRONG Jun. 1988 33 p Presented at the Thermophysics, Plasmadynamics and Lasers Conference, San Antonio, TX, 27-29 Jun. 1988; sponsored in part by AIAA Previously announced in IAA as A88-43721 (NASA-TM-101973; E-4673; NAS 1.15:101973) Avail: NTIS HC A03/MF A01 CSCL 21/8

A numerical model for the three dimensional thermal analysis of rocket thrust chambers and nozzles has been developed. The input to the model consists of the composition of the fuel/oxidant mixture and flow rates, chamber pressure, coolant entrance temperature and pressure, dimensions of the engine, materials and the number of nodes in different parts of the engine. The model allows for temperature variation in three dimensions: axial, radial and circumferential directions and by implementing an iterative scheme, it provides nodal temperature distribution, rates of heat transfer, hot gas and coolant thermal and transport properties. Author

**N89-21834\*#** Hughes Research Labs., Malibu, CA.

### MERCURY ION THRUSTER TECHNOLOGY Final Report, Feb. 1983 - Oct. 1984

J. R. BEATTIE and J. N. MATOSSIAN Mar. 1989 150 p (Contract NAS3-23775) (NASA-CR-174974; NAS 1.26:174974) Avail: NTIS HC A07/MF A01 CSCL 21/8

The Mercury Ion Thruster Technology program was an investigation for improving the understanding of state-of-the-art mercury ion thrusters. Emphasis was placed on optimizing the performance and simplifying the design of the 30 cm diameter ring-cusp discharge chamber. Thruster performance was improved considerably; the baseline beam-ion production cost of the optimized configuration was reduced to Epsilon (sub i) perspective to 130 eV/ion. At a discharge propellant-utilization efficiency of 95 percent, the beam-ion production cost was reduced to about 155 eV/ion, representing a reduction of about 40 eV/ion over the corresponding value for the 30 cm diameter J-series thruster. Comprehensive Langmuir-probe surveys were obtained and compared with similar measurements for a J-series thruster. A successful volume-averaging scheme was developed to correlate thruster performance with the dominant plasma processes that prevail in the two thruster designs. The average Maxwellian electron

temperature in the optimized ring-cusp design is as much as 1 eV higher than it is in the J-series thruster. Advances in ion-extraction electrode fabrication technology were made by improving materials selection criteria, hydroforming and stress-relieving tooling, and fabrications procedures. An ion-extraction performance study was conducted to assess the effect of screen aperture size on ion-optics performance and to verify the effectiveness of a beam-vectoring model for three-grid ion optics. An assessment of the technology readiness of the J-series thruster was completed, and operation of an 8 cm IAPS thruster using a simplified power processor was demonstrated. Author

**N89-22651\*#** National Aeronautics and Space Administration. Lewis Research Center, Cleveland, OH.

**THE NASA SPACE SOLAR CELL ADVANCED RESEARCH PROGRAM**

DENNIS J. FLOOD 1989 9 p Presented at International PVSEC-4, Sydney, Australia, 14-17 Feb. 1989; sponsored by The Institution of Radio and Electronics Engineers of Australia and the Univ. of New South Wales (NASA-TM-102020; E-4747; NAS 1.15:102020) Avail: NTIS HC A02/MF A01 CSCL 10/1

Two major requirements for space solar cells are high efficiency and survivability in the naturally occurring charged particle space radiation environment. Performance limits for silicon space cells are well understood. Advanced cells using GaAs and InP are under development to provide significantly improved capability for the future. Author

**N89-22652\*#** National Aeronautics and Space Administration. Lewis Research Center, Cleveland, OH.

**ANALYSIS OF THE NONVENTED FILL OF A 4.96-CUBIC-METER LIGHTWEIGHT LIQUID HYDROGEN TANK**

DAVID J. CHATO 1989 12 p Proposed for presentation at the 27th National Heat Transfer Conference, Philadelphia, PA, 5-8 Aug. 1989; sponsored by ASME (NASA-TM-102039; E-4750; NAS 1.15:102039) Avail: NTIS HC A03/MF A01 CSCL 21/8

As part of its development of cryogenic fluid management techniques for spacecraft, the NASA Lewis Research Center Cryogenic Fluid Technology Office (CFTO) is planning to perform ground tests of nonvented fill techniques on a 4.96-cubic-meter lightweight liquid hydrogen tank. This tank is similar in size and shape to the tankage planned for CFTO's COLD-SAT liquid hydrogen flight experiment. The analyses used to select two injection systems are presented for nonvented fills of this tank at design flow rates between 220 and 450 kg/hr. The first system uses multiple nozzles spraying from the top of the tank through the ullage space. This system should be capable of liquid fill levels in excess of 95 percent. The second system injects the liquid through a submerged nozzle and should produce fill levels on the order of 80 percent liquid. Author

**N89-22653\*#** National Aeronautics and Space Administration. Lewis Research Center, Cleveland, OH.

**NUMERICAL MODEL OF SOLAR DYNAMIC RADIATOR FOR PARAMETRIC ANALYSIS**

JENNIFER L. RHATIGAN 1989 10 p Prepared for presentation at the 24th Intersociety Energy Conversion Engineering Conference, Washington, DC, 6-11 Aug. 1989; sponsored in part by IEEE, AIAA, ANS, ASME, SAE, and AIChE (NASA-TM-102054; E-4807; NAS 1.15:102054) Avail: NTIS HC A02/MF A01 CSCL 21/8

Growth power requirements for Space Station Freedom will be met through addition of 25 kW solar dynamic (SD) power modules. The SD module rejects waste heat from the power conversion cycle to space through a pumped-loop, multi-panel, deployable radiator. The baseline radiator configuration was defined during the Space Station conceptual design phase and is a function of the state point and heat rejection requirements of the power conversion unit. Requirements determined by the overall station design such as mass, system redundancy, micrometeoroid and space debris impact survivability, launch packaging, costs, and

thermal and structural interaction with other station components have also been design drivers for the radiator configuration. Extensive thermal and power cycle modeling capabilities have been developed which are powerful tools in Station design and analysis, but which prove cumbersome and costly for simple component preliminary design studies. In order to aid in refining the SD radiator to the mature design stage, a simple and flexible numerical model was developed. The model simulates heat transfer and fluid flow performance of the radiator and calculates area mass and impact survivability for many combinations of flow tube and panel configurations, fluid and material properties, and environmental and cycle variations. A brief description and discussion of the numerical model, its capabilities and limitations, and results of the parametric studies performed is presented. Author

**N89-23516\*#** National Aeronautics and Space Administration. Lewis Research Center, Cleveland, OH.

**SOLAR DYNAMIC POWER FOR SPACE STATION FREEDOM**

THOMAS L. LABUS, RICHARD R. SECUNDE, and RONALD G. LOVELY (Rockwell International Corp., Canoga Park, CA.) 1989 24 p Presented at the International Conference on Space Power, Cleveland, OH, 5-7 Jun. 1989; sponsored by the International Astronautical Federation (NASA-TM-102016; E-4730; NAS 1.15:102016) Avail: NTIS HC A03/MF A01 CSCL 22/2

The Space Station Freedom Program is presently planned to consist of two phases. At the completion of Phase 1, Freedom's manned base will consist of a transverse boom with attached manned modules and 75 kW of available electric power supplied by photovoltaic (PV) power sources. In Phase 2, electric power available to the manned base will be increased to 125 kW by the addition of two solar dynamic (SD) power modules, one at each end of the transverse boom. Power for manned base growth beyond Phase 2 will be supplied by additional SD modules. Studies show that SD power for the growth eras will result in life cycle cost savings of \$3 to \$4 billion when compared to PV-supplied power. In the SD power modules for Space Station Freedom, an offset parabolic concentrator collects and focuses solar energy into a heat receiver. To allow full power operation over the entire orbit, the receiver includes integral thermal energy storage by means of the heat of fusion of a salt mixture. Thermal energy is removed from the receiver and converted to electrical energy by a power conversion unit (PCU) which includes a closed brayton cycle (CBC) heat engine and an alternator. The receiver/PCU/radiator combination will be completely assembled and charged with gas and cooling fluid on Earth before launch to orbit. The concentrator subassemblies will be pre-aligned and stowed in the orbiter bay before launch. On orbit, the receiver/PCU/radiator assembly will be installed as a unit. The pre-aligned concentrator panels will then be latched together and the total concentrator attached to the receiver/PCU/radiator by the astronauts. After final electric connections are made and checkout is complete, the SD power module will be ready for operation. Author

**N89-23517\*#** National Aeronautics and Space Administration. Lewis Research Center, Cleveland, OH.

**PHOTOVOLTAIC POWER SYSTEM CONSIDERATIONS FOR FUTURE LUNAR BASES**

DENNIS J. FLOOD and JOSEPH APPELBAUM 1989 8 p Presented at International PVSEC-4, Sydney, Australia, 14-17 Feb. 1989; sponsored by The Institution of Radio and Electronics Engineers of Australia and The University of New South Wales (NASA-TM-102019; E-4744; NAS 1.15:102019) Avail: NTIS HC A02/MF A01 CSCL 10/2

The cost of transportation to the lunar surface places a premium on developing ultralightweight power system technology to support the eventual establishment of a lunar base. The photovoltaic technology issues to be addressed by the Surface Power program element of NASA's Project Pathfinder are described. Author



## 20 SPACECRAFT PROPULSION AND POWER

**N89-23518\*#** National Aeronautics and Space Administration. Lewis Research Center, Cleveland, OH.

### **PRELIMINARY ASSESSMENT OF ROVER POWER SYSTEMS FOR THE MARS ROVER SAMPLE RETURN MISSION**

DAVID J. BENTS 1989 26 p Presented at the International Conference on Space Power, Cleveland, OH, 5-7 Jun. 1989; sponsored by International Astronautical Federation (NASA-TM-102003; E-4707; NAS 1.15:102003) Avail: NTIS HC A03/MF A01 CSCL 10/2

Four isotope power system concepts were presented and compared on a common basis for application to on-board electrical prime power for an autonomous planetary rover vehicle. A representative design point corresponding to the Mars Rover Sample Return (MRSR) preliminary mission requirements (500 W) was selected for comparison purposes. All systems concepts utilize the General Purpose Heat Source (GPHS) isotope heat source developed by DOE. Two of the concepts employ thermoelectric (TE) conversion: one using the GPHS Radioisotope Thermoelectric Generator (RTG) used as a reference case, the other using an advanced RTG with improved thermoelectric materials. The other two concepts employed are dynamic isotope power systems (DIPS): one using a closed Brayton cycle (CBC) turboalternator, and the other using a free piston Stirling cycle engine/linear alternator (FPSE) with integrated heat source/heater head. Near term technology levels have been assumed for concept characterization using component technology figure-of-merit values taken from the published literature. For example, the CBC characterization draws from the historical test database accumulated from space Brayton cycle subsystems and components from the NASA B engine through the mini-Brayton rotating unit. TE system performance is estimated from Voyager/multihundred Watt (MHW)-RTG flight experience through Mod-RTG performance estimates considering recent advances in TE materials under the DOD/DOE/NASA SP-100 and NASA Committee on Scientific and Technological Information programs. The Stirling DIPS system is characterized from scaled-down Space Power Demonstrator Engine (SPDE) data using the GPHS directly incorporated into the heater head. The characterization/comparison results presented here differ from previous comparison of isotope power (made for Low Earth Orbit (LEO) applications) because of the elevated background temperature on the Martian surface compared to LEO, and the higher sensitivity of dynamic systems to elevated sink temperature. The mass advantage of dynamic systems is significantly reduced for this application due to Mars' elevated background temperature. Author

**N89-23519\*#** Pratt and Whitney Aircraft, West Palm Beach, FL. Government Products Div.

### **DESIGN, FABRICATION AND TEST OF THE RL10 DERIVATIVE II CHAMBER/PRIMARY NOZZLE Final Report, Nov. 1984 - Nov. 1986**

R. W. MARABLE Apr. 1989 136 p (Contract NAS3-24738) (NASA-CR-179595; NAS 1.26:179595; FR-19625) Avail: NTIS HC A07/MF A01 CSCL 21/8

The design, fabrication and test of the RL10-II chamber/primary nozzle was accomplished as part of the RL10 Product Improvement Program (PIP). The overall goal of the RL10 PIP was to gain the knowledge and experience necessary to develop new cryogenic upper stage engines to fulfill future NASA requirements. The goal would be reached by producing an RL10 engine designed to be reusable, operate at several thrust levels, and have increased performance. The goals for the chamber/primary nozzle task were: (1) to design a reusable assembly capable of operation at increased mixture ratio and low thrust; (2) to fabricate three assemblies using new or updated techniques where possible; and (3) to test one assembly to verify the design and construction. The design and fabrication phases produced an assembly having improved features such as single piece reinforcing band segments (i.e., Mae West segments) and relocated tube exit braze joints (i.e., hooked tube exit). In addition, a computer program was developed to design the chamber tubes to meet both performance and heat transfer requirements. The test phase showed the specific impulse of the

test bed engine system to be as predicted. These results, along with the heat transfer data obtained, sufficiently proved the overall design of the RL10-II recontoured and shortened chamber/primary nozzle assembly. Author

**N89-23520\*#** National Aeronautics and Space Administration. Lewis Research Center, Cleveland, OH.

### **TEST FACILITY AND PRELIMINARY PERFORMANCE OF A 100 KW CLASS MPD THRUSTER**

JAMES S. SOVEY, MARIS A. MANTENIEKS, THOMAS W. HAAG, PAUL RAITANO, and JAMES E. PARKES (Sverdrup Technology, Inc., Cleveland, OH.) 1989 21 p Presented at the JANNAF Propulsion Meeting, Cleveland, OH, 23-25 May 1989 (NASA-TM-102021; E-4742; NAS 1.15:102021) Avail: NTIS HC A03/MF A01 CSCL 21/3

A 260 kW magnetoplasmadynamic (MPD) thruster test facility was assembled and used to characterize thrusters at power levels up to 130 kW using argon and helium propellants. Sensitivities of discharge characteristics to arc current, mass flow rate, and applied magnetic field were investigated. A thermal efficiency correlation developed by others for low power MPD thrusters defined parametric guidelines to minimize electrode losses in MPD thrusters. Argon and helium results suggest that a parameter defined as the product of arc voltage and the square root of the mass flow rate must exceed .7 V-kg<sup>1/2</sup>-s(-1/2) in order to obtain thermal efficiencies in excess of 60 percent. Author

**N89-23522\*#** National Aeronautics and Space Administration. Lewis Research Center, Cleveland, OH.

### **ARCJET NOZZLE DESIGN IMPACTS**

FRANCIS M. CURRAN, AMY J. SOVIE (Ohio State Univ., Columbus.), and THOMAS W. HAAG May 1989 15 p Prepared for presentation at the 1989 JANNAF Propulsion Meeting, Cleveland OH, 23-25 May 1989 (NASA-TM-102050; E-4802; NAS 1.15:102050) Avail: NTIS HC A03/MF A01 CSCL 21/8

The effect of nozzle configuration on the operating characteristics of a low power dc arcjet thruster was determined. A conical nozzle with a 30 deg converging angle, a 20 deg diverging angle, and an area ratio of 225 served as the baseline case. Variations on the geometry included bell-shaped contours both up and downstream, and a downstream trumpet-shaped contour. The nozzles were operated over a range of specific power near that anticipated for on-orbit operation. Mass flow rate, thrust, current, and voltage were monitored to provide accurate comparisons between nozzles. The upstream contour was found to have minimal effect on arcjet operation. It was determined that the contour of the divergent section of the nozzle, that serves as the anode, was very important in determining the location of arc attachment, and thus had a significant impact on arcjet performance. The conical nozzle was judged to have the optimal current/voltage characteristics and produced the best performance of the nozzles tested. Author

**N89-23527\*#** National Aeronautics and Space Administration. Lewis Research Center, Cleveland, OH.

### **RESULTS FROM BASELINE TESTS OF THE SPRE 1 AND COMPARISON WITH CODE MODEL PREDICTIONS**

JAMES E. CAIRELLI, STEVEN M. GENG, and ROBERT C. SKUPINSKI (Sverdrup Technology, Inc., Cleveland, OH.) 1989 14 p Prepared for presentation at the 24th Intersociety Energy Conversion Engineering Conference, Washington, DC, 6-11 Aug. 1989; sponsored in part by IEEE, AIAA, ANS, ASME, SAE, ACS and AICHE (NASA-TM-102044; E-4792; NAS 1.15:102044) Avail: NTIS HC A03/MF A01 CSCL 10/2

The space power research engine (SPRE), a free piston Stirling engine with linear alternator, is being tested at NASA-Lewis as a candidate for high capacity space power. Results are presented of baseline engine tests at design and off-design operating conditions. The test results are compared with code model prediction. Author



**N89-24436\*#** National Aeronautics and Space Administration. Lewis Research Center, Cleveland, OH.

**PERFORMANCE OF LARGE AREA XENON ION THRUSTERS FOR ORBIT TRANSFER MISSIONS**

VINCENT K. RAWLIN 1989 12 p Presented at the 1989 JANNAF Propulsion Meeting, Cleveland, OH, 23-25 May 1989 (NASA-TM-102049; E-4801; NAS 1.15:102049) Avail: NTIS HC A03/MF A01 CSCL 21/8

Studies have indicated that xenon ion propulsion systems can enable the use of smaller Earth-launch vehicles for satellite placement which results in significant cost savings. These analyses have assumed the availability of advanced, high power ion thrusters operating at about 10 kW or higher. A program was initiated to explore the viability of operating 50 cm diameter ion thrusters at this power level. Operation with several discharge chamber and ion extraction grid set combinations has been demonstrated and data were obtained at power levels to 16 kW. Fifty cm diameter thrusters using state of the art 30 cm diameter grids or advanced technology 50 cm diameter grids allow discharge power and beam current densities commensurate with long life at power levels up to 10 kW. In addition, 50 cm diameter thrusters are shown to have the potential for growth in thrust and power levels beyond 10 kW.

Author

**N89-24438\*#** National Aeronautics and Space Administration. Lewis Research Center, Cleveland, OH.

**CONCENTRATION OF OFF-AXIS RADIATION BY SOLAR CONCENTRATORS FOR SPACE POWER**

KENT S. JEFFERIES 1989 10 p Proposed for presentation at the 24th Intersociety Energy Conversion Engineering Conference, Washington, DC, 6-11 Aug. 1989; sponsored by IEEE, AIAA, ANS, ASME, SAE, ACS and AIChE (NASA-TM-102052; E-4804; NAS 1.15:102052) Avail: NTIS HC A02/MF A01 CSCL 10/1

Off-axis radiation is radiation from any direction not parallel to the axis of the solar concentrator. It will be reflected to regions other than the focus of the parabolic concentrator and possibly concentrated there. Four types of off-axis radiation are discussed. These are: (1) small off-axis angles during walk-off; (2) large off-axis angles; (3) an extended off-axis source such as Earth albedo; and (4) miscellaneous off-axis sources including radio frequency sources and local point sources. A previous analytical study used a computer code named PIXEL to predict concentration of off-axis radiation and a previous experimental study used an 11-m diameter multifaceted dish concentrator to validate the PIXEL analysis. The PIXEL code was limited in that it represented concentration by an ideal parabolic reflector of light from a point source. Another code named OFFSET has been developed to represent the solar concentrator being developed for Space Station Freedom. It is a detailed, ray tracing model which represents 50 ray originating points on the Sun and reflections from 10 points on each of the 456 concentrator facets. Results of this code are generally similar to the PIXEL results although there are small differences due to the more detailed representations of the Sun and concentrator that were used in the OFFSET code.

Author

**N89-24439\*#** National Aeronautics and Space Administration. Lewis Research Center, Cleveland, OH.

**SPACE STATION FREEDOM ELECTRICAL POWER SYSTEM HARDWARE COMMONALITY WITH THE UNITED STATES POLAR PLATFORM**

LORRA L. RIEKER and FRANCIS M. HARABURDA 1989 11 p Presented at the 24th Intersociety Energy Conversion Engineering Conference, Washington, DC, 6-11 Aug. 1989; cosponsored by the IEEE, AIAA, ANS, ASME, SAE, ACS and AIChE (NASA-TM-102074; E-4833; NAS 1.15:102074) Avail: NTIS HC A03/MF A01 CSCL 09/3

The National Aeronautics and Space Administration has adopted the policy to achieve the maximum practical level of commonality for the Space Station Freedom program in order to significantly reduce life cycle costs. Commonality means using identical or similar hardware/software for meeting common sets

of functionally similar requirements. Information on how the concept of commonality is being implemented with respect to electric power system hardware for the Space Station Freedom and the U.S. Polar Platform is presented. Included is a historical account of the candidate common items which have the potential to serve the same power system functions on both Freedom and the Polar Platform.

Author

**N89-24440\*#** National Aeronautics and Space Administration. Lewis Research Center, Cleveland, OH.

**FLIGHT EXPERIMENT OF THERMAL ENERGY STORAGE**

DAVID NAMKOONG 1989 9 p Presented at the 24th Intersociety Energy Conversion Engineering Conference, Washington, DC, 6-11 Aug. 1989; cosponsored by the IEEE, AIAA, ANS, ASME, SAE, ACS and AIChE (NASA-TM-102081; E-4843; NAS 1.15:102081) Avail: NTIS HC A02/MF A01 CSCL 10/3

Thermal energy storage (TES) enables a solar dynamic system to deliver constant electric power through periods of sun and shade. Brayton and Stirling power systems under current considerations for missions in the near future require working fluid temperatures in the 1100 to 1300+ K range. TES materials that meet these requirements fall into the fluoride family of salts. These salts store energy as a heat of fusion, thereby transferring heat to the fluid at constant temperature during shade. The principal feature of fluorides that must be taken into account is the change in volume that occurs with melting and freezing. Salts shrink as they solidify, a change reaching 30 percent for some salts. The location of voids that form as result of the shrinkage is critical when the solar dynamic system reemerges into the sun. Hot spots can develop in the TES container or the container can become distorted if the melting salt cannot expand elsewhere. Analysis of the transient, two-phase phenomenon is being incorporated into a three-dimensional computer code. The code is capable of analysis under microgravity as well as 1 g. The objective of the flight program is to verify the predictions of the code, particularly of the void location and its effect on containment temperature. The four experimental packages comprising the program will be the first tests of melting and freezing conducted under microgravity. Each test package will be installed in a Getaway Special container to be carried by the shuttle. The package will be self-contained and independent of shuttle operations other than the initial opening of the container lid and the final closing of the lid. Upon the return of the test package from flight, the TES container will be radiographed and finally partitioned to examine the exact location and shape of the void. Visual inspection of the void and the temperature data during flight will constitute the bases for code verification.

Author

**N89-24443\*#** National Aeronautics and Space Administration. Lewis Research Center, Cleveland, OH.

**SUMMARY AND EVALUATION OF THE STRATEGIC DEFENSE INITIATIVE SPACE POWER ARCHITECTURE STUDY**

M. EDENBURN, ed. (Sandia National Labs., Albuquerque, NM.) and J. M. SMITH, ed. Mar. 1989 418 p (NASA-TM-102012; E-4724; NAS 1.15:102012) Avail: NTIS HC A18/MF A01 CSCL 10/2

The Space Power Architecture Study (SPAS) identified and evaluated power subsystem options for multimewatt electric (MMWE) space based weapons and surveillance platforms for the Strategic Defense Initiative (SDI) applications. Steady state requirements of less than 1 MMWE are adequately covered by the SP-100 nuclear space power program and hence were not addressed in the SPAS. Four steady state power systems less than 1 MMWE were investigated with little difference between them on a mass basis. The majority of the burst power systems utilized H(2) from the weapons and were either closed (no effluent), open (effluent release) or steady state with storage (no effluent). Closed systems used nuclear or combustion heat source with thermionic, Rankine, turboalternator, fuel cell and battery conversion devices. Open systems included nuclear or combustion heat sources using turboalternator, magnetohydrodynamic, fuel cell or battery power conversion devices. The steady state systems

## 20 SPACECRAFT PROPULSION AND POWER

with storage used the SP-100 or Star-M reactors as energy sources and flywheels, fuel cells or batteries to store energy for burst applications. As with other studies the open systems are by far the lightest, most compact and simplest (most reliable) systems. However, unlike other studies the SPAS studied potential platform operational problems caused by effluents or vibration. Author

**N89-24444\*#** National Aeronautics and Space Administration. Lewis Research Center, Cleveland, OH.

### **A NUMERICAL STUDY OF CHEMICALLY REACTING FLOW IN NOZZLES**

THOMAS J. VANOVERBEKE and JIAN-SHUEN SHUEN (Sverdrup Technology, Inc., Cleveland, OH.) 1989 21 p Presented at the 25th Joint Propulsion Conference, Monterey, CA, 10-12 Jul. 1989; cosponsored by the AIAA, ASME, SAE and ASEE (NASA-TM-102135; E-4932; NAS 1.15:102135; AIAA-89-2793) Avail: NTIS HC A03/MF A01 CSCL 21/8

The space station uses small rocket motors, called thrusters, for orientation control. Because of the lack of viable design tools for small rockets, the initial thruster design was basically a very small version of a large rocket motor. Thrust measurements of the initial design were lower than predicted. To improve predictions it was decided to develop a version of the RPLUS2D reacting flow code for thruster calculations. RPLUS2D employs an implicit finite volume, lower-upper symmetric successive overrelaxation (LU-SSOR) scheme for solving the complete two-dimensional Navier-Stokes equations and species transport equations in a coupled and very efficient manner. The combustion processes are modeled by a 9-species, 18 step finite-rate chemistry model, and the turbulence is simulated by a Baldwin-Lomax algebraic model. The code is extended to handle multiple subsonic inlet conditions where the total mass flow is governed by conditions calculated at the thruster-throat. Results are shown for a thruster design where the overall mixture ratio is hydrogen rich. A calculation of a large area ratio divergent nozzle is also presented. Author

**N89-24445\*#** Sverdrup Technology, Inc., Cleveland, OH.

### **A PREMIXED HYDROGEN/OXYGEN CATALYTIC IGNITER Final Report**

JAMES M. GREEN Jun. 1989 9 p Presented at the 25th Joint Propulsion Conference, Monterey, CA, 10-14, Jul. 1989; cosponsored by the AIAA, ASME, SAE and ASEE (Contract NAS3-25266) (NASA-CR-185113; E-4787; NAS 1.26:185113; AIAA-89-2302) Avail: NTIS HC A02/MF A01 CSCL 21/8

The catalytic ignition of hydrogen and oxygen propellants was studied using a premixing hydrogen/oxygen injector. The premixed injector was designed to eliminate problems associated with catalytic ignition caused by poor propellant mixing in the catalyst bed. Mixture ratio, mass flow rate, and propellant inlet temperature were varied parametrically in testing, and a pulse mode life test of the igniter was conducted. The results of the tests showed that the premixed injector eliminated flame flashback in the reactor and increased the life of the igniter significantly. The results of the experimental program and a comparison with data collected in a previous program are given. Author

**N89-24446\*#** National Aeronautics and Space Administration. Lewis Research Center, Cleveland, OH.

### **THE 5-KW ARCJET POWER ELECTRONICS**

R. P. GRUBER, R. W. GOTT, and T. W. HAAG 1989 26 p Presented at the 25th Joint Propulsion Conference, Monterey, CA, 10-12 Jul. 1989; cosponsored by the AIAA, ASME, SAE and ASEE (NASA-TM-102108; E-4876; NAS 1.15:102108; AIAA-89-2725) Avail: NTIS HC A03/MF A01 CSCL 10/2

The initial design and evaluation of a 5 kW arcjet power electronics breadboard which has been integrated with a modified 1 kW design laboratory arcjet is presented. A single stage, 5 kW full bridge, pulse width modulated (PWM), power converter was developed which was phase shift regulated. The converter used metal oxide semiconductor field effect transistor (MOSFET) power switches and incorporated current mode control and an integral

arcjet pulse ignition circuit. The unoptimized power efficiency was 93.5 and 93.9 percent at 5 kW and 50A output at input voltages of 130 and 150V, respectively. Line and load current regulation at 50A output was within one percent. The converter provided up to 6.6 kW to the arcjet with simulated ammonia used as a propellant. Author

**N89-24447\*#** National Aeronautics and Space Administration. Lewis Research Center, Cleveland, OH.

### **LIQUID OXYGEN COOLING OF HYDROCARBON FUELED ROCKET THRUST CHAMBERS**

ELIZABETH S. ARMSTRONG 1989 15 p Presented at the 25th Joint Propulsion Conference, Monterey, CA, 10-12 Jul. 1989; cosponsored by the AIAA, ASME, SAE and ASEE (NASA-TM-102113; E-4886; NAS 1.15:102113; AIAA-89-2739) Avail: NTIS HC A03/MF A01 CSCL 21/8

Rocket engines using liquid oxygen (LOX) and hydrocarbon fuel as the propellants are being given serious consideration for future launch vehicle propulsion. Normally, the fuel is used to regeneratively cool the combustion chamber. However, hydrocarbons such as RP-1 are limited in their cooling capability. Another possibility for the coolant is the liquid oxygen. Combustion chambers previously tested with LOX and RP-1 as propellants and LOX as the coolant demonstrated the feasibility of using liquid oxygen as a coolant up to a chamber pressure of 13.8 MPa (2000 psia). However, there was concern as to the effect on the integrity of the chamber liner if oxygen leaks into the combustion zone through fatigue cracks that may develop between the cooling passages and the hot gas side wall. In order to study this effect, chambers were fabricated with slots machined upstream of the throat between the cooling passage wall and the hot gas side wall to simulate cracks. The chambers were tested at a nominal chamber pressure of 8.6 MPa (1247 psia) over a range of mixture ratios from 1.9 to 3.1 using liquid oxygen as the coolant. The results of the testing showed that the leaking LOX did not have a deleterious effect on the chambers in the region of the slots. However, there was unexplained melting in the throat region of both chambers, but not in line with the slots. Author

**N89-24448\*#** National Aeronautics and Space Administration. Lewis Research Center, Cleveland, OH.

### **SPACE STATION FREEDOM SOLAR ARRAY DESIGN DEVELOPMENT**

CINDY WINSLOW, KEVIN BILGER (Lockheed Missiles and Space Co., Sunnyvale, CA.), and COSMO R. BARAONA 1989 6 p Presented at the 24th Intersociety Energy Conversion Engineering Conference, Washington, DC, 6-11 Aug. 1989; cosponsored by the IEEE, AIAA, ANS, ASME, SAE, ACS and AIChE (Contract NAS3-25082) (NASA-TM-102105; E-4871; NAS 1.15:102105) Avail: NTIS HC A02/MF A01 CSCL 10/2

The Space Station Freedom Solar Array Program is required to provide a 75 kW power module that uses eight solar array (SA) wings over a four-year period in low Earth orbit (LEO). Each wing will be capable of providing 23.4 kW at the 4-year design point. Lockheed Missiles and Space Company, Inc. (LMSC) is providing the flexible substrate SAs that must survive exposure to the space environment, including atomic oxygen, for an operating life of fifteen years. Trade studies and development testing, important for evolving any design to maturity, are presently underway at LMSC on the flexible solar array. The trade study and development areas being investigated include solar cell module size, solar cell weld pads, panel stiffener frames, materials inherently resistant to atomic oxygen, and weight reduction design alternatives. Author

**N89-25269\*#** National Aeronautics and Space Administration. Lewis Research Center, Cleveland, OH.

### **SOLAR DYNAMIC POWER MODULE DESIGN**

RICHARD R. SECUNDE, THOMAS L. LABUS, and RONALD G. LOVELY (Rockwell International Corp., Canoga Park, CA.) 1989 11 p Presented at the 24th Intersociety Energy Conversion Engineering Conference, Washington, DC, 6-11 Aug. 1989;

cosponsored by the IEEE, AIAA, ANS, ASME, SAE, ACS and AIChE  
(NASA-TM-102055; E-4808; NAS 1.15:102055) Avail: NTIS HC A03/MF A01 CSCL 10/2

Studies have shown that use of solar dynamic (SD) power for the growth eras of the Space Station Freedom program will result in life cycle cost savings when compared to power supplied by photovoltaic sources. In the SD power module, a concentrator collects and focuses solar energy into a heat receiver which has integral thermal energy storage. A power conversion unit (PCU) based on the closed Brayton thermodynamic cycle removes thermal energy from the receiver and converts that energy to electrical energy. Since the closed Brayton cycle is a single phase gas cycle, the conversion hardware (heat exchangers, turbine, compressor, etc.) can be designed for operation in low earth orbit, and tested with confidence in test facilities on earth before launch into space. The concentrator subassemblies will be aligned and the receiver/PCU/radiator combination completely assembled and charged with gas and cooling liquid on earth before launch to, and assembly on orbit. Author

**N89-25271\*#** National Aeronautics and Space Administration. Lewis Research Center, Cleveland, OH.

#### **VARIABLE SPEED INDUCTION MOTOR OPERATION FROM A 20-KHZ POWER BUS**

IRVING G. HANSEN Aug. 1989 8 p Prepared for presentation at the 24th Intersociety Energy Conversion Engineering Conference, Washington, DC, 6-11 Aug. 1989; cosponsored by the IEEE, AIAA, ANS, ASME, SAE, ACS, and AIChE  
(NASA-TM-102061; E-4818; NAS 1.15:102061) Avail: NTIS HC A02/MF A01 CSCL 09/1

Induction motors are recognized for their simple rugged construction. To date, however, their application to variable speed or servo drives was hampered by limitations on their control. Induction motor drives tend to be complex and to display troublesome low speed characteristics due in part to nonsinusoidal driving voltages. A technique was developed which involves direct synthesis of sinusoidal driving voltages from a high frequency power bus and independent control of frequency and voltages. Separation of frequency and voltage allows independent control of rotor and stator flux, full four quadrant operation, and instantaneous torque control. Recent test results, current status of the technology, and proposed aerospace applications will be discussed. Author

**N89-25272\*#** National Aeronautics and Space Administration. Lewis Research Center, Cleveland, OH.

#### **SPACE NUCLEAR REACTOR SHIELDS FOR MANNED AND UNMANNED APPLICATIONS**

BARBARA I. MCKISSOCK and HARVEY S. BLOOMFIELD 1989 16 p Presented at the International Conference on Space Power, Cleveland, OH, 5-7 Jun. 1989; sponsored by the International Astronautical Federation  
(NASA-TM-102064; E-4821; NAS 1.15:102064) Avail: NTIS HC A03/MF A01 CSCL 10/2

Missions which use nuclear reactor power systems require radiation shielding of payload and/or crew areas to predetermined dose rates. Since shielding can become a significant fraction of the total mass of the system, it is of interest to show the effect of various parameters on shield thickness and mass for manned and unmanned applications. Algorithms were developed to give the thicknesses needed if reactor thermal power, separation distances, and dose rates are given as input. The thickness algorithms were combined with models for four different shield geometries to allow tradeoff studies of shield volume and mass for a variety of manned and unmanned missions. Shield design tradeoffs presented in this study include the effects of: higher allowable dose rates; radiation hardened electronics; shorter crew exposure times; shield geometry; distance of the payload and/or crew from the reactor; and changes in the size of the shielded area. Specific NASA missions that were considered in this study include unmanned outer planetary exploration, manned advanced/evolutionary space station, and advanced manned lunar base. Author

**N89-25273\*#** National Aeronautics and Space Administration. Lewis Research Center, Cleveland, OH.

#### **SPACE STATION FREEDOM PHOTOVOLTAIC POWER MODULE DESIGN STATUS**

AMADOR P. JIMENEZ (Rockwell International Corp., Canoga Park, CA.) and MARK A. HOBERECHT 1989 6 p Presented at the 24th Intersociety Energy Conversion Engineering Conference, Washington, DC, 6-11 Aug. 1989; cosponsored by the IEEE, AIAA, ANS, ASME, SAE, ACS and AIChE  
(NASA-TM-102073; E-4832; NAS 1.15:102073) Avail: NTIS HC A02/MF A01 CSCL 10/2

Electric power generation for Space Station Freedom will be provided by four photovoltaic (PV) power modules using silicon solar cells during Phase 1 operation. Each PV power module requires two solar arrays with 32,800 solar cells generating 18.75 kW of dc power for a total of 75 kW. A portion of this power will be stored in nickel-hydrogen batteries for use during eclipse, and the balance will be processed and converted to 20 kHz ac power for distribution to end users through the power management and distribution system. The design incorporates an optimized thermal control system, pointing and tracking provision with the application of gimbals, and the use of orbital replacement units (ORU's) to achieve modularization. Design status of the PV power module, as derived from major trade studies, is discussed at hardware levels ranging from component to system. Details of the design are presented where appropriate. Author

**N89-25274\*#** National Aeronautics and Space Administration. Lewis Research Center, Cleveland, OH.

#### **THE INTRODUCTION OF SPACE TECHNOLOGY POWER SYSTEMS INTO DEVELOPING COUNTRIES**

ALLEN F. ROBERTS (Iowa Univ., Iowa City.) and ANTHONY F. RATAJCZAK Mar. 1989 19 p Presented at the Symposium on Space Commercialization: Roles of Developing Countries, Nashville, TN, 5-10 Mar. 1989; sponsored in part by Tennessee Univ. Space Institute  
(NASA-TM-102042; E-4799; NAS 1.15:102042) Avail: NTIS HC A03/MF A01 CSCL 10/2

Between 1978 and 1984, NASA-Lewis was responsible for the design, fabrication, installation and operational support of 57 photovoltaic power systems in 27 countries. These systems were installed in locations not served by a central power system and ranged in size from 40 W for powering street lights to 29 kW for providing power to a complete village. Several of the system projects had socio/economic studies components that provided for an assessment of how the introduction of both electricity and a novel high technology power system affected the users and their society. Author

**N89-25275\*#** National Aeronautics and Space Administration. Lewis Research Center, Cleveland, OH.

#### **LAUNCH PACKAGING OPTIONS FOR THE PHOTOVOLTAIC POWER MODULE CARGO ELEMENT**

MARK A. HOBERECHT and SCOTT T. VOGT (Rockwell International Corp., Canoga Park, CA.) 1989 7 p Presented at the 24th Intersociety Energy Conversion Engineering Conference, Washington, DC, 6-11 Aug. 1989; cosponsored by the IEEE, AIAA, ANS, ASME, SAE, ACS and AIChE  
(NASA-TM-102072; E-4831; NAS 1.15:102072) Avail: NTIS HC A02/MF A01 CSCL 10/1

The National Aeronautics and Space Administration recently embarked on the Space Station Freedom program, which will utilize the Shuttle Orbiter for transportation to orbit. This task will be accomplished with a number of flights over several years. Each flight is unique in terms of the hardware that is manifested and the method by which it is integrated to form viable cargo elements. Work Package 4 is responsible for the electric power system for Space Station Freedom, and was delegated the authority to develop a photovoltaic (PV) power module cargo element. The PV power module consists of several unique assemblies. The first of these is the combined solar array/beta gimbal assembly. The remaining assemblies form the single combined integrated equipment assembly for each PV power module. These three combined

## 20 SPACECRAFT PROPULSION AND POWER

assemblies are packaged into a launch cradle to form the PV power module cargo element, which is placed in the cargo bay of the Shuttle Orbiter for transportation to orbit. Various constraints determine the packaging options for the three PV power module combined assemblies. The size and shape of the combined assemblies in relation to the Shuttle Orbiter cargo bay dimensions and other manifested hardware are ultimately a factor in determining the acceptable packaging schemes for the PV power module cargo element. Several packaging options for the PV power module cargo element are presented. These options are discussed in terms of their impact on the overall flight hardware manifest as determined by the various constraints. NASA

**N89-25277\*#** National Aeronautics and Space Administration. Lewis Research Center, Cleveland, OH.

### SCALING RESULTS FOR THE LIQUID SHEET RADIATOR (LSR)

DONALD L. CHUBB and FREDERICK D. CALFO 1989 8 p Presented at the 24th Intersociety Energy Conversion Engineering Conference, Washington, DC, 6-11 Aug. 1989; cosponsored by the IEEE, AIAA, ANS, ASME, SAE, ACS, and AIChE (NASA-TM-102100; E-4835; NAS 1.15:102100) Avail: NTIS HC A02/MF A01 CSCL 20/4

Surface tension forces at the edges of a thin liquid (approx. 100 micrometers) sheet flow result in a triangularly shaped sheet. Such a geometry is ideal for an external flow radiator. The experimental investigation of such sheet flows was extended to large sheets (width =  $W = 23.5$  cm, length =  $L$  approx. = 3.5 m). Experimental L/W results are greater than the calculated results. However, more experimental results are necessary for a complete comparison. The calculated emissivity of a sheet of Dow-Corning 705 silicone oil, which is a low temperature (300 to 400K) candidate for a liquid sheet radiator (LSR), is greater than .8 for sheet thicknesses greater than 100 micrometers. Author

**N89-25280\*#** National Aeronautics and Space Administration. Lewis Research Center, Cleveland, OH.

### ESTIMATED PERFORMANCE AND FUTURE POTENTIAL OF SOLAR DYNAMIC AND PHOTOVOLTAIC POWER SYSTEMS FOR SELECTED LEO AND HEO MISSIONS

DAVID J. BENTS and CHENG Y. LU 1989 13 p Presented at the 24th Intersociety Energy Conversion Engineering Conference, Washington, DC, 6-11 Aug. 1989; cosponsored by the IEEE, AIAA, ANS, ASME, SAE, ACS and AIChE (NASA-TM-102083; E-4846; NAS 1.15:102083) Avail: NTIS HC A03/MF A01 CSCL 10/2

Solar Photo Voltaic (PV) and thermal dynamic power systems for application to selected Low Earth Orbit (LEO) and High Eccentric Orbit (Energy) (HEO) missions are characterized in the regime 7 to 35 kWe. Input parameters to the characterization are varied corresponding to anticipated introduction of improved or new technologies. Comparative assessment is made between the two power system types utilizing newly emerging technologies in cells and arrays, energy storage, optical surfaces, heat engines, thermal energy storage, and thermal management. The assessment is made to common ground rules and assumptions. The four missions (space station, sun-synchronous, Van Allen belt and GEO) are representative of the anticipated range of multi-kWe earth orbit missions. System characterizations include all required subsystems, including power conditioning, cabling, structure, to deliver electrical power to the user. Performance is estimated on the basis of three different levels of component technology: (1) state-of-art, (2) near-term, and (3) advanced technologies. These range from planar array silicon/IPV nickel hydrogen batteries and Brayton systems at 1000 K to thin film GaAs with high energy density secondary batteries or regenerative fuel cells and 1300 K Stirling systems with ultra-lightweight concentrators and radiators. The system estimates include design margin for performance degradations from the known environmental mechanisms (micrometeoroids and space debris, atomic oxygen, electron and proton flux) which are modeled and applied depending on the mission. The results give expected performance, mass and drag of multi-kWe earth orbiting solar power

systems and show how overall system figures of merit will improve as new component technologies are incorporated. Author

**N89-25281\*#** National Aeronautics and Space Administration. Lewis Research Center, Cleveland, OH.

### THE EFFECTS OF ARCJET OPERATING CONDITION AND CONSTRICTOR GEOMETRY ON THE PLASMA PLUME

LYNNETTE M. CARNEY and JOHN M. SANKOVIC (Akron Univ., OH.) Jul. 1989 29 p Presented at the 25th Joint Propulsion Conference, Monterey, CA, 10-12 Jul. 1989; sponsored in part by AIAA, ASME, SAE, and ASEE (NASA-TM-102284; E-4877; NAS 1.15:102284; AIAA-89-2723) Avail: NTIS HC A03/MF A01 CSCL 21/8

Measurements of plasma number density and electron temperature were obtained in the plumes of lab arcjet thrusters using electrostatic probes of both spherical and cylindrical geometry. The two arcjet thrusters used had different constrictor and/or nozzle geometries and operated on mixtures of nitrogen, hydrogen, and ammonia to simulate the decomposition products of hydrazine and ammonia. An increase in the measured electron density was observed for both geometries with increasing arc power at a constant mass flow rate and with increasing mass flow rate at a constant arc current. For a given operating condition, the electron number density decreased exponentially off centerline and followed an inverse distance squared relationship along the thrust axis. Typical measured electron temperatures ranged from 0.1 to 0.2 eV. Author

**N89-25282\*#** National Aeronautics and Space Administration. Lewis Research Center, Cleveland, OH.

### CSTI HIGH CAPACITY POWER

JERRY M. WINTER 1989 21 p Presented at the 24th Intersociety Energy Conversion Engineering Conference, Washington, DC, 6-11 Aug. 1989; cosponsored by the IEEE, AIAA, ANS, ASME, SAE, ACS and AIChE (NASA-TM-102059; E-4817; NAS 1.15:102059) Avail: NTIS HC A03/MF A01 CSCL 10/2

The SP-100 program was established in 1983 by DOD, DOE, and NASA as a joint program to develop the technology necessary for space nuclear power systems for military and civil application. During FY-86 and 87, the NASA SP-100 Advanced Technology Program was devised to maintain the momentum of promising technology advancement efforts started during Phase 1 of SP-100 and to strengthen, in key areas, the chances for successful development and growth capability of space nuclear reactor power systems for future space applications. In FY-88, the Advanced Technology Program was incorporated into NASA's new Civil Space Technology Initiative (CSTI). The CSTI Program was established to provide the foundation for technology development in automation and robotics, information, propulsion, and power. The CSTI High Capacity Power Program builds on the technology efforts of the SP-100 program, incorporates the previous NASA SP-100 Advanced Technology project, and provides a bridge to NASA Project Pathfinder. The elements of CSTI High Capacity Power development include Conversion Systems, Thermal Management, Power Management, System Diagnostics, and Environmental Interactions. Technology advancement in all areas, including materials, is required to assure the high reliability and 7 to 10 year lifetime demanded for future space nuclear power systems. The overall program will develop and demonstrate the technology base required to provide a wide range of modular power systems as well as allowing mission independence from solar and orbital attitude requirements. Several recent advancements in CSTI High Capacity power development will be discussed. Author

**N89-25283\*#** National Aeronautics and Space Administration. Lewis Research Center, Cleveland, OH.

### PERFORMANCE CHARACTERIZATION AND TRANSIENT INVESTIGATION OF MULTIPROPELLANT RESISTOJETS

EDWARD P. BRAUNSCHEIDEL Jul. 1989 21 p Presented at the 25th Joint Propulsion Conference, Monterey, CA, 10-12 Jul. 1989; cosponsored by the AIAA, ASME, SAE, and ASEE

(NASA-TM-102118; E-4897; NAS 1.15:102118; AIAA-89-2837)  
 Avail: NTIS HC A03/MF A01 CSCL 21/8

The multipropellant resistojet thruster design initially was characterized for performance in a vacuum tank using argon, carbon dioxide, nitrogen, and hydrogen, with gas inlet pressures ranging from 13.7 to 310 kPa (2 to 45 psia) over a heat exchanger temperature range of ambient to 1200 C (2200 F). Specific impulse, the measure of performance, had values ranging from 120 to 600 seconds for argon and hydrogen respectively, with a constant heat exchanger temperature of 1200 C (2200 F). When operated under ambient conditions typical specific impulse values obtained for argon and hydrogen ranged from 55 to 290 seconds, respectively. Performance measured with several mixtures of argon and nitrogen showed no significant deviation from predictions obtained by directly weighting the argon and nitrogen individual performance results. Another aspect of the program investigating transient behavior, showed responses depended heavily on the start-up scenario used. Steady state heater temperatures were achieved in 20 to 75 minutes for argon, and in 10 to 90 minutes for hydrogen. Steady state specific impulses were achieved in 25 to 60, and 20 to 60 minutes respectively.

Author

**N89-26041\*#** National Aeronautics and Space Administration. Lewis Research Center, Cleveland, OH.

**ADVANCES IN THIN-FILM SOLAR CELLS FOR LIGHTWEIGHT SPACE PHOTOVOLTAIC POWER**

GEOFFREY A. LANDIS, SHEILA G. BAILEY, and DENNIS J. FLOOD 1989 29 p Presented at the International Conference on Space Power, Cleveland, OH, 5-7 Jun. 1989; sponsored by the International Astronautical Federation (NASA-TM-102017; E-4734; NAS 1.15:102017) Avail: NTIS HC A03/MF A01 CSCL 10/1

The present stature and current research directions of photovoltaic arrays as primary power systems for space are reviewed. There have recently been great advances in the technology of thin-film solar cells for terrestrial applications. In a thin-film solar cell the thickness of the active element is only a few microns; transfer of this technology to space arrays could result in ultralow-weight solar arrays with potentially large gains in specific power. Recent advances in thin-film solar cells are reviewed, including polycrystalline copper-indium selenide (CuInSe<sub>2</sub>) and related I-III-VI<sub>2</sub> compounds, polycrystalline cadmium telluride and related II-VI compounds, and amorphous silicon:hydrogen and alloys. The best experimental efficiency on thin-film solar cells to date is 12 percent AMO for CuIn Se<sub>2</sub>. This efficiency is likely to be increased in the next few years. The radiation tolerance of thin-film materials is far greater than that of single-crystal materials. CuIn Se<sub>2</sub> shows no degradation when exposed to 1 MeV electrons. Experimental evidence also suggests that most of all of the radiation damage on thin-films can be removed by a low temperature anneal. The possibility of thin-film multibandgap cascade solar cells is discussed, including the tradeoffs between monolithic and mechanically stacked cells. The best current efficiency for a cascade is 12.5 percent AMO for an amorphous silicon on CuInSe<sub>2</sub> multibandgap combination. Higher efficiencies are expected in the future. For several missions, including solar-electric propulsion, a manned Mars mission, and lunar exploration and manufacturing, thin-film photovoltaic arrays may be a mission-enabling technology.

Author

**N89-26044\*#** National Aeronautics and Space Administration. Lewis Research Center, Cleveland, OH.

**COLD-SAT: AN ORBITAL CRYOGENIC HYDROGEN TECHNOLOGY EXPERIMENT**

J. R. SCHUSTER, JOSEPH P. WACHTER (Ford Aerospace and Communications Corp., Palo Alto, CA.), and ALBERT G. POWERS 1989 14 p Presented at the 40th Congress of the International Astronautical Federation, Malaga, Spain, 8-14 Oct. 1989

(NASA-TM-102303; E-4984; NAS 1.15:102303; IAF-89-057)  
 Avail: NTIS HC A03/MF A01 CSCL 22/1

The COLD-SAT spacecraft will perform subcritical liquid hydrogen storage and transfer experiments under low-gravity

conditions to provide engineering data for future space transportation missions. Consisting of an experiment module mated to a spacecraft bus, COLD-SAT will be placed in an initial 460 km circular orbit by an Atlas I commercial launch vehicle. After deployment, the three-axis-controlled spacecraft bus will provide electric power, experiment control and data management, communications, and attitude control along with propulsive acceleration levels ranging from 10(-6) to 10(-4)g. These accelerations are an important aspect of some of the experiments, as it is desired to know the effects that low gravity levels might have on the heat and mass transfer processes involved. The experiment module will contain the three liquid hydrogen tanks, valves, pressurization equipment, and instrumentation. At launch all the hydrogen will be in the largest tank, which has helium-purged MLI and is loaded and topped off by the hydrogen tanking system used for the Centaur upper stage of the Atlas. The two smaller tanks will be utilized in orbit for performing some of the experiments. The experiments are grouped into two classes on the basis of their priority, and include six regarded as enabling technology and nine regarded as enhancing technology.

Author

**N89-26045\*#** National Aeronautics and Space Administration. Lewis Research Center, Cleveland, OH.

**SPACE STATION FREEDOM POWER MANAGEMENT AND DISTRIBUTION SYSTEM DESIGN**

FRED TERENCE 1989 10 p Prepared for presentation at the 40th Congress of the International Astronautical Federation, Malaga, Spain, 8-14 Oct. 1989

(NASA-TM-102283; E-4950; NAS 1.15:102283) Avail: NTIS HC A02/MF A01 CSCL 21/8

The design is described of the Space Station Freedom Power Management and Distribution (PMAD) System. In addition, the significant trade studies which were conducted are described, which led to the current PMAD system configuration.

Author

**N89-26899\*#** Rockwell International Corp., Canoga Park, CA. Rocketdyne Div.

**OTVE COMBUSTOR WALL CONDITION MONITORING Final Report, Nov. 1986 - Sep. 1988**

BRIAN SZEMENYEI, ROBERT S. NELSON, and S. BARKHOUDARIAN Aug. 1989 38 p Presented at the 24th AIAA/ASME/SAE/ASEE Joint Propulsion Conference on Improved Maintainability of Space-Based Reusable Rocket Engines, Boston, MA, Jul. 1988

(Contract NAS3-23773)

(NASA-CR-182275; NAS 1.26:182275; RI/RD89-212) Avail: NTIS HC A03/MF A01 CSCL 21/8

Conventional ultrasonics, eddy current, and electromagnetic acoustic transduction (EMAT) technologies were evaluated to determine their capability of measuring wall thickness/wear of individual cooling channels in test specimens simulating conditions in the throat region of an OTVE combustion chamber liner. Quantitative results are presented for the eddy current technology, which was shown to measure up to the optimum 20-mil wall thickness with near single channel resolution. Additional results demonstrate the capability of the conventional ultrasonics and EMAT technologies to detect a thinning or cracked wall. Recommendations for additional eddy current and EMAT development tests are presented.

Author

**N89-26903\*#** Cummings (Robert L.), Litchfield, OH.

**PERFORMANCE ESTIMATES FOR THE SPACE STATION POWER SYSTEM BRAYTON CYCLE COMPRESSOR AND TURBINE Final Report**

ROBERT L. CUMMINGS Aug. 1989 35 p

(Contract NASA ORDER C-22187-M)

(NASA-CR-182263; E-4657; NAS 1.26:182263) Avail: NTIS HC A03/MF A01 CSCL 21/8

The methods which have been used by the NASA Lewis Research Center for predicting Brayton Cycle compressor and turbine performance for different gases and flow rates are described. These methods were developed by NASA Lewis during the early days of Brayton cycle component development and they

## 20 SPACECRAFT PROPULSION AND POWER

can now be applied to the task of predicting the performance of the Closed Brayton Cycle (CBC) Space Station Freedom power system. Computer programs are given for performing these calculations and data from previous NASA Lewis Brayton Compressor and Turbine tests is used to make accurate estimates of the compressor and turbine performance for the CBC power system. Results of these calculations are also given. In general, calculations confirm that the CBC Brayton Cycle contractor has made realistic compressor and turbine performance estimates.

Author

**N89-26904\*#** National Aeronautics and Space Administration. Lewis Research Center, Cleveland, OH.

### **DEVELOPMENT OF A HIGH POWER MICROWAVE THRUSTER, WITH A MAGNETIC NOZZLE, FOR SPACE APPLICATIONS**

JOHN L. POWER and RANDALL A. CHAPMAN 1989 26 p  
Presented at the 24th Microwave Power Symposium, Stanford, CT, 21-23 Aug. 1989; sponsored by the International Microwave Power Inst.  
(NASA-TM-102321; E-5017; NAS 1.15:102321) Avail: NTIS HC A03/MF A01 CSCL 21/8

This paper describes the current development of a high-power microwave electrothermal thruster (MET) concept at the NASA Lewis Research Center. Such a thruster would be employed in space for applications such as orbit raising, orbit maneuvering, station change, and possibly trans-lunar or trans-planetary propulsion of spacecraft. The MET concept employs low frequency continuous wave (CW) microwave power to create and continuously pump energy into a flowing propellant gas at relative high pressure via a plasma discharge. The propellant is heated to very high bulk temperatures while passing through the plasma discharge region and then is expanded through a throat-nozzle assembly to produce thrust, as in a conventional rocket engine. Apparatus, which is described, is being assembled at NASA Lewis to test the MET concept to CW power levels of 30 kW at a frequency of 915 MHz. The microwave energy is applied in a resonant cavity applicator and is absorbed by a plasma discharge in the flowing propellant. The ignited plasma acts as a lossy load, and with optimal tuning, energy absorption efficiencies over 95 percent (based on the applied microwave power) are expected. Nitrogen, helium, and hydrogen will be tested as propellants in the MET, at discharge chamber pressures to 10 atm.

Author

**N89-26905\*** Rockwell International Corp., Canoga Park, CA. Rocketdyne Div.

### **SPACE STATION HYDROGEN/OXYGEN THRUSTER TECHNOLOGY Final Report**

G. L. BRILEY and R. S. IACABUCCI Nov. 1988 111 p  
(Contract NAS3-25142)  
(NASA-CR-182280; NAS 1.26:182280; RI/RD88-256) Avail: Issuing Activity CSCL 21/8

The effort expended by the Rocketdyne Division of Rockwell International in fulfilling the requirements of the Space Station Freedom Hydrogen/Oxygen Thruster Technology program is discussed. Included are the basis and the rationale for the design of the thruster, injector, and nozzle; the test results; and the lessons learned, together with conclusions and recommendations for the development of the Space Station Freedom thrusters.

Author

**N89-26906\*#** National Aeronautics and Space Administration. Lewis Research Center, Cleveland, OH.

### **ELECTRIC PROPULSION OPTIONS FOR 10 KW CLASS EARTH SPACE MISSIONS**

M. J. PATTERSON and FRANCIS M. CURRAN May 1989 29 p  
Presented at the JANNAF Propulsion Meeting, Cleveland, OH, 23-25 May 1989  
(NASA-TM-102337; E-5046; NAS 1.15:102337) Avail: NTIS HC A03/MF A01 CSCL 21/3

Five and 10 kW ion and arcjet propulsion system options for a near-term space demonstration experiment have been evaluated. Analyses were conducted to determine first-order propulsion system performance and system component mass estimates. Overall

mission performance of the electric propulsion systems was quantified in terms of the maximum thrusting time, total impulse, and velocity increment capability available when integrated onto a generic spacecraft under fixed mission model assumptions. Maximum available thrusting times for the ion-propelled spacecraft options, launched on a DELTA II 6920 vehicle, range from approximately 8,600 hours for a 4-engine 10 kW system to more than 29,600 hours for a single-engine 5 kW system. Maximum total impulse values and maximum delta-v's range from  $1.2 \times 10^7$  to  $2.1 \times 10^7$  N-s, and 3550 to 6200 m/s, respectively. Maximum available thrusting times for the arcjet propelled spacecraft launched on the DELTA II 6920 vehicle range from approximately 528 hours for the 6-engine 10 kW hydrazine system to 2328 hours for the single-engine 5 kW system. Maximum total impulse values and maximum delta-v's range from  $2.2 \times 10^6$  to  $3.6 \times 10^6$  N-s, and approximately 662 to 1072 m/s, respectively.

Author

**N89-27700\*#** Sverdrup Technology, Inc., Cleveland, OH.

### **ANTI-PROTON POWERED PROPULSION WITH MAGNETICALLY CONFINED PLASMA ENGINES Final Report**

MICHAEL R. LAPOINTE Aug. 1989 26 p  
Presented at the 25th Joint Propulsion Conference, Monterey, CA, 10-12 Jul. 1989; cosponsored by the AIAA, ASME, SAE, and ASEE  
(Contract NAS3-25266)  
(NASA-CR-185131; E-5025; NAS 1.26:185131; AIAA-89-2334) Avail: NTIS HC A03/MF A01 CSCL 21/8

Matter-antimatter annihilation releases more energy per unit mass than any other method of energy production, making it an attractive energy source for spacecraft propulsion. In the magnetically confined plasma engine, antiproton beams are injected axially into a pulsed magnetic mirror system, where they annihilate with an initially neutral hydrogen gas. The resulting charged annihilation products transfer energy to the hydrogen propellant, which is then exhausted through one end of the pulsed mirror system to provide thrust. The calculated energy transfer efficiencies for a low number density ( $10^{14}$ /cu cm) hydrogen propellant are insufficient to warrant operating the engine in this mode. Efficiencies are improved using moderate propellant number densities ( $10^{16}$ /cu cm), but the energy transferred to the plasma in a realistic magnetic mirror system is generally limited to less than 2 percent of the initial proton-antiproton annihilation energy. The energy transfer efficiencies are highest for high number density ( $10^{18}$ /cu cm) propellants, but plasma temperatures are reduced by excessive radiation losses. Low to moderate thrust over a wide range of specific impulse can be generated with moderate propellant number densities, while higher thrust but lower specific impulse may be generated using high propellant number densities. Significant mass will be required to shield the superconducting magnet coils from the high energy gamma radiation emitted by neutral pion decay. The mass of such a radiation shield may dominate the total engine mass, and could severely diminish the performance of antiproton powered engines which utilize magnetic confinement. The problem is compounded in the antiproton powered plasma engine, where lower energy plasma bremsstrahlung radiation may cause shield surface ablation and degradation.

Author

**N89-27701\*#** National Aeronautics and Space Administration. Lewis Research Center, Cleveland, OH.

### **PERFORMANCE OF A 100 KW CLASS APPLIED FIELD MPD THRUSTER**

MARIS A. MANTENIEKS, JAMES S. SOVEY, ROGER M. MYERS, THOMAS W. HAAG, PAUL RAITANO, and JAMES E. PARKES (Sverdrup Technology, Inc., Cleveland, OH.) Jul. 1989 18 p  
Presented at the 25th Joint Propulsion Conference, Monterey, CA, 10-12 Jul. 1989; sponsored in part by AIAA, ASME, SAE, and ASEE  
(NASA-TM-102312; E-5006; NAS 1.15:102312; AIAA-89-2710) Avail: NTIS HC A03/MF A01 CSCL 21/8

Performance of a 100 kW, applied field magnetoplasmadynamic (MPD) thruster was evaluated and sensitivities of discharge characteristics to arc current, mass flow rate, and applied magnetic field were investigated. Thermal efficiencies as high as 60 percent,



thrust efficiencies up to 21 percent, and specific impulses of up to 1150 s were attained with argon propellant. Thrust levels up to 2.5 N were directly measured with an inverted pendulum thrust stand at discharge input powers up to 57 kW. It was observed that thrust increased monotonically with the product of arc current and magnet current. Author

**N89-27702\*#** National Aeronautics and Space Administration. Lewis Research Center, Cleveland, OH.

#### **DEVELOPMENT AND REFINEMENT OF TEST BED SIMULATIONS**

NARAYAN V. DRAVID, DEAN R. MILLER, ALEX G. PATTERSON, and FRANK J. GOMBOS (Rockwell International Corp., Canoga Park, CA.) Aug. 1989 8 p Presented at the 24th Intersociety Energy Conversion Engineering Conference, Washington, DC, 6-11 Aug. 1989; sponsored in part by IEEE, AIAA, ANS, ASME, SAE, ACS, and AIChE  
(NASA-TM-102335; E-5043; NAS 1.15:102335) Avail: NTIS HC A02/MF A01 CSCL 14/2

Lewis Research Center of NASA, with support from Rocketdyne, was engaged in non-real time computer simulation effort for the Space Station Freedom Electric Power System (EPS) EASY5, a simulation package, is used as the primary tool for this activity. Early in the design of the EPS, two test beds were set up at Lewis. The Integrated Test Bed (ITB), that combines and upgrades these test beds, is in the planning stage. The test beds are designed to functionally represent many of the components of the EPS and their interconnections. The simulation effort is primarily directed towards these test beds. Model verification is performed using test bed data. Author

**N89-27703\*#** National Aeronautics and Space Administration. Lewis Research Center, Cleveland, OH.

#### **STRUCTURAL AND THERMAL RESPONSE OF 30 CM DIAMETER ION THRUSTER OPTICS**

G. S. MACRAE, R. J. ZAVESKY, and S. T. GOODER Jul. 1989 29 p Presented at the 25th Joint Propulsion Conference, Monterey, CA, 10-12 Jul. 1989; sponsored in part by AIAA, ASME, SAE, and ASEE  
(NASA-TM-102124; E-4904; NAS 1.15:102124; AIAA-89-2719) Avail: NTIS HC A03/MF A01 CSCL 21/3

Tabular and graphical data are presented which are intended for use in calibrating and validating structural and thermal models of ion thruster optics. A 30 cm diameter, two electrode, mercury ion thruster was operated using two different electrode assembly designs. With no beam extraction, the transient and steady state temperature profiles and center electrode gaps were measured for three discharge powers. The data showed that the electrode mount design had little effect on the temperatures, but significantly impacted the motion of the electrode center. Equilibrium electrode gaps increased with one design and decreased with the other. Equilibrium displacements in excess of 0.5 mm and gap changes of 0.08 mm were measured at 450 W discharge power. Variations in equilibrium gaps were also found among assemblies of the same design. The presented data illustrate the necessity for high fidelity ion optics models and development of experimental techniques to allow their validation. Author

**N89-27704\*#** National Aeronautics and Space Administration. Lewis Research Center, Cleveland, OH.

#### **TOWARD AN ELECTRICAL POWER UTILITY FOR SPACE EXPLORATION**

ROBERT W. BERCAW 1989 6 p Prepared for presentation at the European Space Power Conference, Madrid, Spain, 2-6 Oct. 1989; sponsored in part by ESA  
(NASA-TM-102347; E-5055; NAS 1.15:102347) Avail: NTIS HC A02/MF A01 CSCL 10/2

Plans for space exploration depend on today's technology programs addressing the novel requirements of space-based enterprise. The requirements for electrical power will be formidable: megawatts in magnitude, reliability for multi-year missions and the flexibility to adapt to needs unanticipated at design time. The reasons for considering the power management and distribution

in the various systems from a total mission perspective, rather than simply extrapolating current spacecraft design practice, are discussed. A utility approach to electric power being developed at the Lewis Research Center is described. It integrates requirements from a broad selection of current development programs with studies in which both space and terrestrial technologies are conceptually applied to exploration mission scenarios. Author

**N89-27705\*#** National Aeronautics and Space Administration. Lewis Research Center, Cleveland, OH.

#### **NASA ADVANCED SPACE PHOTOVOLTAIC TECHNOLOGY-STATUS, POTENTIAL AND FUTURE MISSION APPLICATIONS**

DENNIS J. FLOOD, MICHAEL PISZCZOR, JR., PAUL M. STELLA, and GARY L. BENNETT (National Aeronautics and Space Administration, Washington, DC.) 1989 8 p Prepared for presentation at the European Space Power Conference, Madrid, Spain, 2-6 Oct. 1989; sponsored in part by ESA  
(NASA-TM-102093; E-4856; NAS 1.15:102093) Avail: NTIS HC A02/MF A01 CSCL 10/2

The NASA program in space photovoltaic research and development encompasses a wide range of emerging options for future space power systems, and includes both cell and array technology development. The long range goals are to develop technology capable of achieving 300 W/kg for planar arrays, and 300 W/sq m for concentrator arrays. InP and GaAs planar and concentrator cell technologies are under investigation for their potential high efficiency and good radiation resistance. The Advanced Photovoltaic Solar Array (APSA) program is a near term effort aimed at demonstrating 130 W/kg beginning of life specific power using thin (62 micrometer) silicon cells. It is intended to be technology transparent to future high efficiency cells and provides the baseline for development of the 300 W/kg array. Author

**N89-27706\*#** National Aeronautics and Space Administration. Lewis Research Center, Cleveland, OH.

#### **INVESTIGATION OF A LIQUID-FED WATER RESISTOJET PLUME**

D. H. MANZELLA (Sverdrup Technology, Inc., Cleveland, OH.) and L. M. CARNEY Jul. 1989 10 p Presented at the 25th Joint Propulsion Conference, Monterey, CA, 10-12 Jul. 1989; sponsored in part by AIAA, ASME, SAE, and ASEE  
(NASA-TM-102310; E-5005; NAS 1.15:102310; AIAA-89-2840) Avail: NTIS HC A02/MF A01 CSCL 21/8

Measurements of mass flux and flow angle were taken throughout the forward flow region of the exhaust of a liquid-fed water resistojet using a quartz crystal microbalance (QCM). The resistojet operated at a mass flow rate of 0.1 g/s with a power input of 330 Watts. Measured values were compared to theoretical predictions obtained by employing a source flow approximation. Excellent agreement between predicted and measured mass flux values was attained; however, this agreement was highly dependent on knowledge of nozzle flow conditions. Measurements of the temperature at which the exhaust condensed on the QCM were obtained as a function of incident mass flux. Author

**N89-27773\*#** Michigan State Univ., East Lansing. Dept. of Electrical Engineering.

#### **EXPERIMENTS AND ANALYSIS OF A COMPACT ELECTROTHERMAL THRUSTER**

JES ASMUSSEN and STAN WHITEHAIR (IBM Federal Systems Div., Yorktown Heights, NY.) /n DGLR, DGLR/AIAA/JSASS 20th International Electric Propulsion Conference: Proceedings p 569-574 1988  
(Contract NAG3-305) Avail: NTIS HC A99/MF E03 CSCL 21/8

The description and experimental performance of a compact microwave electrothermal thruster (MET) are presented. This thruster uses a coaxial applicator to couple microwave power into a high pressure discharge. Unlike earlier experiments, it uses no fused quartz in the discharge chamber or the nozzle. This allows high temperatures in the discharge chamber without quartz erosion and melting, thereby improving thruster performance and lifetime.



## 20 SPACECRAFT PROPULSION AND POWER

The thruster design is compact, enhancing its potential as a space engine. Experimental tests using nitrogen and helium propellants with input powers levels of 200 W to 1.5 kW are presented. Experimental results, which produce energy efficiencies of 20 to 60 percent and specific impulse of 250 to 450 sec, compare favorably to previous experimental MET performance. ESA

**N89-28570\*#** National Aeronautics and Space Administration. Lewis Research Center, Cleveland, OH.  
**EVOLUTIONARY GROWTH FOR SPACE STATION FREEDOM ELECTRICAL POWER SYSTEM**  
MATTHEW F. MARSHALL, KERRY L. MCLALLIN, and MICHAEL J. ZERNIC 1989 8 p Presented at the 24th Intersociety Energy Conversion Engineering Conference, Washington, DC, 6-11 Aug. 1989; cosponsored by IEEE, AIAA, ANS, ASME, SAE, ACS, and AIChE  
(NASA-TM-102339; E-5047; NAS 1.15:102339) Avail: NTIS HC A02/MF A01 CSCL 22/2

Over an operational lifetime of at least 30 yr, Space Station Freedom will encounter increased space station user requirements and advancing technologies. The space station electrical power system is designed with the flexibility to accommodate these emerging technologies and expert systems and is being designed with the necessary software hooks and hardware scars to accommodate increased growth demand. The electrical power system is planned to grow from the initial 75 kW up to 300 kW. The Phase 1 station will utilize photovoltaic arrays to produce the electrical power; however, for growth to 300 kW, solar dynamic power modules will be utilized. Pairs of 25 kW solar dynamic power modules will be added to the station to reach the power growth level. The addition of solar dynamic power in the growth phase places constraints in the initial space station systems such as guidance navigation and control, external thermal, truss structural stiffness, computational capabilities and storage which must be planned-in in order to facilitate the addition of the solar dynamic modules. Author

**N89-28571\*#** National Aeronautics and Space Administration. Lewis Research Center, Cleveland, OH.  
**ION OPTICS FOR HIGH POWER 50-CM-DIAM ION THRUSTERS**  
VINCENT K. RAWLIN and MARC G. MILLIS Sep. 1989 23 p Presented at the 25th Joint Propulsion Conference, Monterey, CA, 10-12 Jul. 1989; cosponsored by AIAA, ASME, SAE, and ASEE Previously announced in IAA as A89-47040  
(NASA-TM-102143; E-4938; NAS 1.15:102143; AIAA-89-2717) Avail: NTIS HC A03/MF A01 CSCL 21/3

The process used at the NASA-Lewis to fabricate 30 and 50-cm-diameter ion optics is described. The ion extraction capabilities of the 30 and 50-cm diameter ion optics were evaluated on divergent field and ring-cusp discharge chambers and compared. Perveance was found to be sensitive to the effects of the type and power of the discharge chamber and to the accelerator electrode hole diameter. Levels of up to 0.64 N and 20 kW for thrust and input power, respectively, were demonstrated with the divergent-field discharge chamber. Thruster efficiencies and specific impulse values up to 79 percent and 5000 sec., respectively, were achieved with the ring-cusp discharge chamber. E.R.

**N89-29483\*#** Sverdrup Technology, Inc., Cleveland, OH.  
**PLUME CHARACTERISTICS OF MPD THRUSTERS: A PRELIMINARY EXAMINATION Final Report**  
ROGER M. MYERS Sep. 1989 16 p Presented at the 25th Joint Propulsion Conference, Monterey, CA, 10-12 Jul. 1989; cosponsored by AIAA, ASME, SAE, and ASEE  
(Contract NAS3-25266)  
(NASA-CR-185130; E-5018; NAS 1.26:185130; AIAA-89-2832) Avail: NTIS HC A03/MF A01 CSCL 21/8

A diagnostics facility for MPD thruster plume measurements was built and is currently undergoing testing. The facility includes electrostatic probes for electron temperature and density measurements, Hall probes for magnetic field and current distribution mapping, and an imaging system to establish the global

distribution of plasma species. Preliminary results for MPD thruster operated at power levels between 30 and 60 kW with solenoid applied magnetic fields show that the electron density decrease exponentially from  $1 \times 10^{22}$  to  $2 \times 10^{18}$ /cu m over the first 30 cm of the expansion, while the electron temperature distribution is relatively uniform, decreasing from approximately 2.5 eV to 1.5 eV over the same distance. The radiant intensity of the ArII 4879 line emission also decays exponentially. Current distribution measurements indicate that a significant fraction of the discharge current is blown into the plume region, and that its distribution depends on the magnitudes of both the discharge current and the applied magnetic field. Authc

**N89-29484\*#** National Aeronautics and Space Administration. Lewis Research Center, Cleveland, OH.  
**A PROGRAM FOR ADVANCING THE TECHNOLOGY OF SPACE CONCENTRATORS**  
GERALD J. NAUJOKAS (Sverdrup Technology, Inc., Cleveland OH.) and JOSEPH M. SAVINO 1989 8 p Presented at the 24th Intersociety Energy Conversion Engineering Conference Washington, DC, 6-11 Aug. 1989; cosponsored by IEEE, AIAA, ANS, ASME, SAE, ACS, and AIChE  
(NASA-TM-102139; E-4900; NAS 1.15:102139) Avail: NTIS HC A02/MF A01 CSCL 10/1

In 1985, the NASA Lewis Research Center formed a project, the Advanced Solar Dynamics Power Systems Project, for the purpose of advancing the technology of Solar Dynamic Power Systems for space applications beyond 2000. Since then, technology development activities have been initiated for the major components and subsystems such as the concentrator, heat receiver and engine, and radiator. Described here is a program for developing long lived (10 years or more), lighter weight, and more reflective space solar concentrators than is presently possible. The program is progressing along two parallel paths: one is concentrator concept development and the other is the resolution of those critical technology issues that will lead to durable, highly specular, and lightweight reflector elements. Outlined are the specific objectives, long term goals, approach, planned accomplishments for the future, and the present status of the various program elements. Author

## 23

## CHEMISTRY AND MATERIALS (GENERAL)

**A89-12760\*** National Aeronautics and Space Administration. Lewis Research Center, Cleveland, OH.  
**THE PREPARATION OF NEW PERFLUORO ETHER FLUIDS EXHIBITING EXCELLENT THERMAL-OXIDATIVE STABILITIES**  
WILLIAM R. JONES, JR. (NASA, Lewis Research Center, Cleveland, OH), THOMAS R. BIERSCHEK, TIMOTHY J. JUHLKE, HAJIMA KAWA, and RICHARD J. LAGOW (Exfluor Research Corp., Austin, TX) I & EC - Industrial and Engineering Chemistry Research (ISSN 0888-5885), vol. 27, no. 8, 1988, p. 1497-1502. refs Copyright

A series of low molecular weight perfluoroalkyl ethers (PFAEs) were synthesized by direct fluorination. Viscosity-temperature properties and oxidation stabilities were determined. Viscosity-temperature correlations indicated that increases in branching and increases in the size of the branching substituent caused a deterioration in viscometric properties (i.e., an increase in ASTM slope). In addition, increasing the ratio of carbon to oxygen in these compounds also increased the ASTM slope. Preliminary oxidation stability measurements indicated that highly branched PFAE fluids (i.e., those containing quaternary carbons) may be less stable than either those containing a single trifluoromethyl pendant group or those containing no branching at all. Author

**A89-16500\*** Jet Propulsion Lab., California Inst. of Tech., Pasadena.

**HIGH TEMPERATURE THERMAL CONDUCTIVITY MEASUREMENTS ON LANTHANUM SULFIDES USING THE FLASH METHOD**

J. W. VANDERSANDE, C. WOOD, A. ZOLTAN (California Institute of Technology, Jet Propulsion Laboratory, Pasadena), and D. WHITTENBERGER (NASA, Lewis Research Center, Cleveland, OH) IN: Thermal conductivity. Volume 19. New York, Plenum Publishing Corp., 1988, p. 445-452. refs  
Copyright

In the past, high temperature specific heat and hence thermal conductivity measurements, using the flash method have not been very accurate. This is due to the difficulty of exactly determining the amount of heat deposited on the front face of a sample during each flash. This problem has now been solved by sputtering a thin layer of graphite on the standard reference and test samples. Data taken shows that the amount of heat deposited can now be determined to within about 2 percent resulting in more accurate thermal conductivity data. The results of measurements on several lanthanum sulfides with stoichiometries between LaS(1.35) and LaS(1.48) are reported and show a minimum in the lattice thermal conductivity at a composition of around LaS(1.41). This is believed to be due to the scattering of low-frequency phonons by large defects, i.e., second phase material (beta-phase) and pores.

Author

**A89-23028\*** National Aeronautics and Space Administration. Lewis Research Center, Cleveland, OH.

**SPACE 2010**

J. STUART FORDYCE, SALVATORE J. GRISAFFE, and JOSEPH R. STEPHENS (NASA, Lewis Research Center, Cleveland, OH) Advanced Materials and Processes (ISSN 0882-7958), vol. 135, Jan. 1989, p. 69-71.

Copyright

An account is given of the thrust of the NASA-Lewis Research Center's developmental activities in advanced materials for aerospace propulsion and space power systems; these materials must have exceptional strength/weight values, possess high operating temperature capabilities, exhibit long-term property stability, and be affordable within program budgetary constraints. Metal-matrix composites are prominent among emerging materials for space propulsion systems; representative of current interest in this field are the tungsten fiber-reinforced superalloys, which are applicable to liquid rocket propulsion systems' turbomachinery.

O.C.

**A89-33150\*#** Minnesota Mining and Mfg. Co., Saint Paul.  
**DURABLE THIN FILM COATINGS FOR REFLECTORS USED IN LOW EARTH ORBIT**

DONALD J. MCCLURE (3M Corporate Research Process Technologies Laboratory, Saint Paul, MN) Society of Vacuum Coaters, Annual Technical Conference, 32nd, Saint Louis, MO, Apr. 24-28, 1989, Paper. 5 p. refs  
(Contract NAS3-25075)

This paper discusses the properties of thin film coatings used to provide a durable reflective surface for solar concentrators used in the solar dynamic system designed for the Space Station. The material system to be used consists of an adhesion promotion layer, a silver reflective layer, and a protective layer of aluminum oxide and silicon dioxide. The performance characteristics of this system are described and compared to those of several alternative systems which use aluminum as the reflective layer.

I.S.

**A89-41444\*** National Aeronautics and Space Administration. Lewis Research Center, Cleveland, OH.

**DENSITIES OF SOME MOLTEN FLUORIDE SALT MIXTURES SUITABLE FOR HEAT STORAGE IN SPACE POWER APPLICATIONS**

AJAY K. MISRA (NASA, Lewis Research Center, Cleveland, OH) Electrochemical Society, Journal (ISSN 0013-4651), vol. 135, Nov. 1988, p. 2780, 2781. refs  
Copyright

Liquid densities were determined for a number of fluoride salt mixtures suitable for heat storage in space power applications, using a procedure that consisted of measuring the loss of weight of an inert bob in the melt. The density apparatus was calibrated with pure LiF and NaF at different temperatures. Density data for safe binary and ternary fluoride salt eutectics and congruently melting intermediate compounds are presented. In addition, a comparison was made between the volumetric heat storage capacity of different salt mixtures.

I.S.

**A89-53324\*** National Aeronautics and Space Administration. Lewis Research Center, Cleveland, OH.

**THIN FILM COATINGS FOR SPACE ELECTRICAL POWER SYSTEM APPLICATIONS**

DANIEL A. GULINO (NASA, Lewis Research Center, Cleveland, OH) IN: Surface modification technologies II; Proceedings of the Second International Conference, Chicago, IL, Sept. 26-28, 1988. Warrendale, PA, Minerals, Metals and Materials Society, 1989, p. 73-90. Previously announced in STAR as N88-28966. refs  
Copyright

This paper examines some of the ways in which thin film coatings can play a role in aerospace applications. Space systems discussed include photovoltaic and solar dynamic electric power generation systems, including applications in environmental protection, thermal energy storage, and radiator emittance enhancement. Potential applications of diamondlike films to both atmospheric and space based systems are examined. Also, potential uses of thin films of the recently discovered high-temperature superconductive materials are discussed.

Author

**N89-10124\*#** National Aeronautics and Space Administration. Lewis Research Center, Cleveland, OH.

**THE EFFECT OF AL<sub>2</sub>O<sub>3</sub>, CAO, CR<sub>2</sub>O<sub>3</sub> AND MGO ON DEVITRIFICATION OF SILICA**

ISIDOR ZAPLATYNSKY Oct. 1988 14 p  
(NASA-TM-101335; E-4350; NAS 1.15:101335) Avail: NTIS HC A03/MF A01 CSCL 07A

The effect of doping on devitrification of vitreous silica was studied at 1100, 1200, and 1300 C. Dispersion of dopants on a molecular scale was accomplished via a sol-gel technique. All dopants accelerated the devitrification of silica but to different degrees. The most active was CaO followed by MgO, Al<sub>2</sub>O<sub>3</sub>, and Cr<sub>2</sub>O<sub>3</sub>. Pure silica and silica containing Cr<sub>2</sub>O<sub>3</sub> and Al<sub>2</sub>O<sub>3</sub> devitrified to alpha-cristobalite only, whereas silica doped with CaO and MgO produced alpha-quartz and alpha-cristobalite. It appears that prolonged heat treatment would cause alpha-quartz to transform to alpha-cristobalite.

Author

**N89-11815\*#** National Aeronautics and Space Administration. Lewis Research Center, Cleveland, OH.

**MATERIALS TECHNOLOGY ASSESSMENT FOR A 1050 K STIRLING SPACE ENGINE DESIGN**

COULSON M. SCHEUERMANN, ROBERT L. DRESHFIELD, DARRELL J. GAYDOSH, JAMES D. KISER, REBECCA A. MACKAY, DAVID L. MCDANIELS, DONALD W. PETRASEK, RAYMOND D. VANNUCCI, KENNETH J. BOWLES, and GORDON K. WATSON Oct. 1988 35 p  
(NASA-TM-101342; E-4362; NAS 1.15:101342) Avail: NTIS HC A03/MF A01 CSCL 07/1

An assessment of materials technology and proposed materials selection was made for the 1050 K (superalloy) Stirling Space Engine design. The objectives of this assessment were to evaluate previously proposed materials selections, evaluate the current state-of-the-art materials, propose potential alternate materials selections and identify research and development efforts needed to provide materials that can meet the stringent system requirements. This assessment generally reaffirmed the choices made by the contractor. However, in many cases alternative choices were described and suggestions for needed materials and fabrication research and development were made.

Author

## 23 CHEMISTRY AND MATERIALS (GENERAL)

**N89-15981\*#** National Aeronautics and Space Administration. Lewis Research Center, Cleveland, OH.

### **APPLICATIONS OF SURFACE ANALYSIS AND SURFACE THEORY IN TRIBOLOGY**

JOHN FERRANTE 30 Nov. 1988 30 p Presented at the 5th International Conference on Quantitative Surface Analysis, London, England, 15-18 Nov. 1988; sponsored in part by the National Physical Lab.

(NASA-TM-101392; E-4465; NAS 1.15:101392) Avail: NTIS HC A03/MF A01 CSCL 13/9

Tribology, the study of adhesion, friction and wear of materials is a complex field which requires a knowledge of solid state physics, surface physics, chemistry, material science and mechanical engineering. It has been dominated, however, by the more practical need to make equipment work. With the advent of surface analysis and advances in surface and solid state theory, a new dimension has been added to the analysis of interactions at tribological interfaces. In this paper the applications of tribological studies and their limitations are presented. Examples from research at the NASA Lewis Research Center are given. Emphasis is on fundamental studies involving the effects of monolayer coverage and thick films on friction and wear. A summary of the current status of theoretical calculations of defect energetics is presented. In addition, some new theoretical techniques which enable simplified quantitative calculations of adhesion, fracture and friction are discussed. Author

**N89-19371\*#** National Aeronautics and Space Administration. Lewis Research Center, Cleveland, OH.

### **TENSILE AND CREEP RUPTURE BEHAVIOR OF P/M PROCESSED NB-BASE ALLOY, WC-3009**

MOHAN G. HEBSUR (Sverdrup Technology, Inc., Cleveland, OH.) and ROBERT H. TITRAN Sep. 1988 12 p Presented at the TMS-AIME Fall Meeting, Chicago, IL, 25-28 Sep. 1988

(NASA-TM-101954; E-4311; NAS 1.15:101954) Avail: NTIS HC A03/MF A01 CSCL 20/11

Due to its high strength at temperatures up to 1600 K, fabrication of niobium base alloy WC-3009 (Nb30Hf9W) by traditional methods is difficult. Powder metallurgy (P/M) processing offers an attractive fabrication alternative for this high strength alloy. Spherical powders of WC-3009 produced by electron beam atomizing (EBA) process were successfully consolidated into a one inch diameter rod by vacuum hot pressing and swaging techniques. Tensile strength of the fully dense P/M material at 300-1590 K were similar to the arc-melted material. Creep rupture tests in vacuum indicated that WC-3009 exhibits a class 1 solid solution (glide controlled) creep behavior in the 1480 to 1590 K temperature range and stress range of 14 to 70 MPa. The creep behavior was correlated with temperature and stress using a power law relationship. The calculated stress exponent  $n$ , was about 3.2 and the apparent activation energy,  $Q$ , was about 270 kJ/mol. The large creep ductility exhibited by WC-3009 was attributed to its high strain rate sensitivity. Author

**N89-21032\*#** National Aeronautics and Space Administration. Lewis Research Center, Cleveland, OH.

### **CONVECTION AND CHEMISTRY EFFECTS IN CVD: A 3-D ANALYSIS FOR SILICON DEPOSITION**

S. A. GOKOGLU, M. A. KUCZMARSKI, P. TSUI (Sverdrup Technology, Inc., Cleveland, OH.), and A. CHAIT 1989 20 p Prepared for presentation at the Euro CVD 7 Conference, Perpignan, France, 19-23 Jun. 1989; sponsored in part by Institut de Science et de Genie des Matériaux et Precedes

(NASA-TM-102001; E-4702; NAS 1.15:102001) Avail: NTIS HC A03/MF A01 CSCL 07/4

The computational fluid dynamics code FLUENT has been adopted to simulate the entire rectangular-channel-like (3-D) geometry of an experimental CVD reactor designed for Si deposition. The code incorporated the effects of both homogeneous (gas phase) and heterogeneous (surface) chemistry with finite reaction rates of important species existing in silane dissociation. The experiments were designed to elucidate the effects of gravitationally-induced buoyancy-driven convection flows on the

quality of the grown Si films. This goal is accomplished by contrasting the results obtained from a carrier gas mixture of H<sub>2</sub>/Ar with the ones obtained from the same molar mixture ratio of H<sub>2</sub>/He, without any accompanying change in the chemistry. Computationally, these cases are simulated in the terrestrial gravitational field and in the absence of gravity. The numerical results compare favorably with experiments. Powerful computational tools provide invaluable insights into the complex physicochemical phenomena taking place in CVD reactors. Such information is essential for the improved design and optimization of future CVD reactors. Author

**N89-23540\*#** National Aeronautics and Space Administration. Lewis Research Center, Cleveland, OH.

### **ATOMIC OXYGEN EFFECTS ON MATERIALS**

BRUCE A. BANKS, SHARON K. RUTLEDGE, JOYCE A. BRADY, and JAMES E. MERROW (Ohio Univ., Athens.) /in NASA, Langley Research Center, NASA/SDIO Space Environmental Effects on Materials Workshop, Part 1 p 197-239 May 1989

Avail: NTIS HC A16/MF A01 CSCL 11/7

Understanding of the basic processes of atomic oxygen interaction is currently at a very elementary level. However, measurement of erosion yields, surface morphology, and optical properties for low fluences have brought about much progress in the past decade. Understanding the mechanisms and those factors that are important for proper simulation of low Earth orbit is at a much lower level of understanding. The ability to use laboratory simulations with confidence to quantifiably address the functional performance and durability of materials in low Earth orbit will be necessary to assure long-term survivability to the natural space environment. Author

**N89-24451\*#** National Aeronautics and Space Administration. Lewis Research Center, Cleveland, OH.

### **ISOTOPIC STUDY OF OXYGEN DIFFUSION IN OXIDE COATINGS**

DANIEL A. GULINO, LAWRENCE A. KREN, and THERESE M. DEVER (Cleveland State Univ., OH.) 1989 13 p Presented at the 16th International Conference on Metallurgical Coatings, San Diego, CA, 17-21 Apr. 1989; sponsored by the American Vacuum Society

(NASA-TM-102082; E-4764; NAS 1.15:102082) Avail: NTIS HC A03/MF A01 CSCL 11/4

Diffusion of oxygen in thin films of silicon dioxide was studied using oxygen isotopically enriched in oxygen of atomic mass 18 (O-18). This subject is of interest because thin films of dielectrics such as SiO<sub>2</sub> are proposed for use as a protective coatings for solar mirrors in low Earth orbit, which is a strongly oxidizing environment. Films of this material were prepared with a direct current magnetron using reactive sputtering techniques. To produce (O-18)-enriched SiO<sub>2</sub>, a standard 3.5-in.-diameter silicon wafer was reactively sputtered using (O-18)-enriched (95 percent) oxygen as the plasma feed gas. The films were characterized using Rutherford backscattering and Secondary Ion Mass Spectrometer (SIMS) to establish stoichiometry and purity. Subsequently, the films were exposed to an air-derived oxygen plasma in a standard laboratory plasma reactor for durations of up to 10 hr. The concentration ratio of O-16 as a function of depth was determined using SIMS profiling and compared to a baseline, nonplasma exposed sample. A value for the diffusivity of oxygen near the surface of these films was obtained and found to be about 10<sup>-15</sup> cm<sup>2</sup>/sec. Author

**N89-25285\*#** National Aeronautics and Space Administration. Lewis Research Center, Cleveland, OH.

### **CHARACTERIZATION OF CERAMICS AND INTERMETALLICS FABRICATED BY SELF-PROPAGATING HIGH-TEMPERATURE SYNTHESIS**

JANET B. HURST May 1989 21 p (NASA-TM-102004; E-4710; NAS 1.15:102004) Avail: NTIS HC A03/MF A01 CSCL 11/2

Three efforts aimed at investigating the process of self-propagating high temperature synthesis (SHS) for the

fabrication of structural ceramics and intermetallics are summarized. Of special interest was the influence of processing variables such as exothermic dopants, gravity, and green state morphology in materials produced by SHS. In the first effort directed toward the fabrication of SiC, exothermic dopants of yttrium and zirconium were added to SiO<sub>2</sub> or SiO<sub>2</sub> + NiO plus carbon powder mix and processed by SHS. This approach was unsuccessful since it did not produce the desired product of crystalline SiC. In the second effort, the influence of gravity was investigated by examining Ni-Al microstructures which were produced by SHS combustion waves traveling with and opposite the gravity direction. Although final composition and total porosities of the combusted Ni-Al compounds were found to be gravity independent, larger pores were created in those specimens which were combusted opposite to the gravity force direction. Finally, it was found that green microstructure has a significant effect on the appearance of the combusted piece. Severe pressing laminations were observed to arrest the combustion front for TiC samples. Author

## 24

## COMPOSITE MATERIALS

Includes physical, chemical, and mechanical properties of laminates and other composite materials.

**A89-11324\*** Columbia Univ., New York, NY.  
**THE EFFECT OF CO ALLOYING CONTENT ON THE KINETICS OF REACTION ZONE GROWTH IN TUNGSTEN FIBER REINFORCED SUPERALLOY COMPOSITES**

A. RODRIGUEZ, J. K. TIEN (Columbia University, New York), T. CAULFIELD (North American Philips Laboratories, Briarcliff Manor, NY), and D. W. PETRASEK (NASA, Lewis Research Center, Cleveland, OH) Scripta Metallurgica (ISSN 0036-9748), vol. 22, Oct. 1988, p. 1617-1622. (Contract NAG3-410) Copyright

A Co-free modified superalloy similar in composition to Waspaloy is investigated in an effort to understand the effect of Co on reaction zone growth kinetics and verify the chemistry dependence of reaction zone growth in the matrix of tungsten fiber reinforced superalloy composites. The values of the parabolic rate constant, characterizing the kinetics of reaction zone growth, for the Waspaloy matrix and the Co-free alloy as well as five other alloys from a previous study confirm the dependence of reaction zone growth kinetics on cobalt content of the matrix. The Co-free alloy composite exhibits the slowest reaction zone growth among all tungsten fiber reinforced composites studied to date. V.L.

**A89-14099\*** National Aeronautics and Space Administration. Lewis Research Center, Cleveland, OH.  
**THERMO-OXIDATIVE STABILITY STUDIES OF CELION 6000/PMR-15 UNIDIRECTIONAL COMPOSITES, PMR-15, AND CELION 6000 FIBER**

KENNETH J. BOWLES and GREGORY NOWAK (NASA, Lewis Research Center, Cleveland, OH) Journal of Composite Materials (ISSN 0021-9983), vol. 22, Oct. 1988, p. 966-985. refs Copyright

Experimental results on the influence of the thermooxidative resistance characteristics of the fiber and matrix resin on the thermal stability of isothermally aged Celion 6000/PMR-15 matrix resin composites are presented. SEM studies reveal that extreme oxidative erosion of the graphite fiber occurs at elevated temperatures in the presence of the polyimide matrix. The activation energy of oxidation of the composite was shown to be greater than those of the fiber and the matrix resin. R.R.

**A89-14560\*** Case Western Reserve Univ., Cleveland, OH.  
**TRANSMISSION ELECTRON MICROSCOPY OF COMPOSITES**  
 P. PIROUZ, S. C. FARMER, F. ERNST, and J. CHUNG (Case

Western Reserve University, Cleveland, OH) IN: Interfaces in polymer, ceramic, and metal matrix composites; Proceedings of the Second International Conference on Composite Interfaces (ICCI-II), Cleveland, OH, June 13-17, 1988. New York, Elsevier, 1988, p. 141-157. DARPA-supported research. refs (Contract N00014-86-K-0773; NCC3-73; NAG3-758) Copyright

Since interphase-interfaces are often both the structurally weakest and chemically least stable regions of a composite material, they are critical determinants of such macrostructural characteristics as tensile strength and fracture toughness. Attention is presently given to the use of TEM for the study of interfaces between dissimilar materials; electron-diffraction, analytical, and high-resolution forms of TEM are employed, for the cases of both structural and semiconductor composites. The materials studied are SiC/Si, GaP/Si, and SiC fiber- and whisker-reinforced Si<sub>3</sub>N<sub>4</sub>. O.C.

**A89-15727\*** National Aeronautics and Space Administration. Lewis Research Center, Cleveland, OH.

**THERMAL-MECHANICAL FATIGUE TEST APPARATUS FOR METAL MATRIX COMPOSITES AND JOINT ATTACHMENTS**

LEONARD J. WESTFALL and DONALD W. PETRASEK (NASA, Lewis Research Center, Cleveland, OH) IN: Testing technology of metal matrix composites. Philadelphia, PA, American Society for Testing Materials, 1988, p. 3-17. Previously announced in STAR as N86-15378. refs Copyright

Two thermal-mechanical fatigue (TMF) test facilities were designed and developed, one to test tungsten fiber reinforced metal matrix composite specimens at temperature up to 1430C (2600F) and another to test composite/metal attachment bond joints at temperatures up to 760F (1400F). The TMF facility designed for testing tungsten fiber reinforced metal matrix composites permits test specimen temperature excursions from room temperature to 1430C (2600F) with controlled heating and loading rates. A strain-measuring device measures the strain in the test section of the specimen during each heating and cooling cycle with superimposed loads. Data is collected and recorded by a computer. The second facility is designed to test composite/metal attachment bond joints and to permit heating to a maximum temperature of 760C (1400F) within 10 min and cooling to 150C (300F) within 3 min. A computer controls specimen temperature and load cycling. Author

**A89-16283\*** National Aeronautics and Space Administration. Lewis Research Center, Cleveland, OH.

**THE CORRELATION OF LOW-VELOCITY IMPACT RESISTANCE OF GRAPHITE-FIBER-REINFORCED COMPOSITES WITH MATRIX PROPERTIES**

KENNETH J. BOWLES (NASA, Lewis Research Center, Cleveland, OH) IN: Composite materials: Testing and design. Philadelphia, PA, American Society for Testing and Materials, 1988, p. 124-142. Previously announced in STAR as N86-27426. Copyright

Summarized are basic studies that were conducted to correlate the impact resistance of graphite-fiber-reinforced composites with polymer matrix properties. Three crosslinked epoxy resins and a linear polysulfone were selected as composite matrices. As a group, these resins possess a significantly large range of mechanical properties. The mechanical properties of the resins and their respective composites were measured. Neat resin specimens and unidirectional and crossply composite specimens were impact tested with an instrumented dropweight tester. Impact resistances of the specimens were assessed on the basis of loading capability, energy absorption, and extent of damage. Author

**A89-19472\*** Massachusetts Inst. of Tech., Cambridge.  
**FLUID FLOW PHENOMENA IN THE GENERATION OF BORON CARBIDE SUSPENSIONS IN MAGNESIUM MELTS**

O. J. ILEGBUSI and J. SZEKELY (MIT, Cambridge, MA) Ceramic Engineering and Science Proceedings (ISSN 0196-6219), vol. 9,

## 24 COMPOSITE MATERIALS

July-Aug. 1988, p. 1079-1086. refs  
(Contract NAS3-25074)  
Copyright

A mathematical representation is developed for the behavior of moderately concentrated magnesium-boron carbide suspensions when subjected to electromagnetic stirring or mechanical agitation. A power-law relationship is employed for the apparent non-Newtonian viscosity of the suspension. Author

**A89-19486\*** Ohio State Univ., Columbus.  
**CRYSTALLIZATION AND CHARACTERIZATION OF Y2O3-SiO2 GLASSES**

C. H. DRUMMOND, III, W. E. LEE (Ohio State University, Columbus), W. A. SANDERS, and J. D. KISER (NASA, Lewis Research Center, Cleveland, OH) Ceramic Engineering and Science Proceedings (ISSN 0196-6219), vol. 9, Sept.-Oct. 1988, p. 1343-1353. refs  
(Contract NAG3-824)  
Copyright

Glasses in the yttria-silica system with 20-40 mol pct Y2O3 have been subjected to recrystallization studies after melting at 1900-2100 C in W crucibles in 1 and 50 atm N2. The TEM and XRD results obtained indicate the presence of the delta, gamma, gamma-prime, and beta-Y2Si2O7 crystalline phases, depending on melting and quenching conditions. Heat-treatment in air at 1100-1600 C increased the amount of crystallization, and led to the formation of Y2SiO5, cristobalite, and polymorphs of Y2Si2O7. Also investigated were the effects of 5 and 10 wt pct zirconia additions. O.C.

**A89-19487\*** Ohio State Univ., Columbus.  
**MICROSTRUCTURAL EVOLUTION ON CRYSTALLIZING THE GLASSY PHASE IN A 6 WEIGHT PERCENT Y2O3-Si3N4 CERAMIC**

W. E. LEE, C. H. DRUMMOND, III, G. E. HILMAS (Ohio State University, Columbus), J. D. KISER, and W. A. SANDERS (NASA, Lewis Research Center, Cleveland, OH) Ceramic Engineering and Science Proceedings (ISSN 0196-6219), vol. 9, Sept.-Oct. 1988, p. 1355-1365. refs  
Copyright

X-ray diffraction and analytical electron microscopy have been used to study the crystallization of the grain-boundary glass in a 6 wt pct Y2O3-Si3N4 ceramic. Upon crystallization, high densities of dislocations formed in the Si3N4 grains and remained after 5 h at temperature. However, prolonged holds at the crystallization temperature effectively annealed out the dislocations. Other features present in the microstructure are characterized. Author

**A89-20725\*** Akron Univ., OH.  
**A VISCOPLASTIC CONSTITUTIVE THEORY FOR METAL MATRIX COMPOSITES AT HIGH TEMPERATURE**

D. N. ROBINSON, J. R. ELLIS (Akron, University, OH), and S. F. DUFFY (Cleveland State University, OH) IN: Thermal stress, material deformation, and thermo-mechanical fatigue; Proceedings of the 1987 Pressure Vessels and Piping Conference, San Diego, CA, June 28-July 2, 1987. New York, American Society of Mechanical Engineers, 1987, p. 49-56. refs  
(Contract NAG3-379)  
Copyright

A viscoplastic theory is presented for representing the high-temperature deformation behavior of metal matrix composites. The point of view taken is a continuum one where the composite is considered a material in its own right, with its own properties that can be determined for the composite as a whole. It is presumed that a single preferential (fiber) direction is identifiable at each material point (continuum element) admitting the idealization of local transverse isotropy. A key ingredient in this work is the specification of an experimental program for the complete determination of the material functions and parameters for characterizing a particular metal matrix composite. The parameters relating to the strength of anisotropy can be determined through tension/torsion tests on longitudinally and circumferentially reinforced thin-walled tubes. Fundamental aspects of the theory

are explored through a geometric interpretation of some basic features analogous to those of the classical theory of plasticity.

Author

**A89-26291\*** Cleveland State Univ., OH.  
**FINITE ELEMENT SUBSTRUCTURING METHODS FOR COMPOSITE MECHANICS**

P. L. N. MURTHY (Cleveland State University, OH) and C. C. CHAMIS (NASA, Lewis Research Center, Cleveland, OH) IN: Composite materials and structures; Proceedings of the International Conference, Madras, India, Jan. 6-9, 1988. New Delhi, Tata McGraw-Hill Publishing Co., Ltd., 1988, p. 403-414. Previously announced in STAR as N88-17745. refs  
Copyright

Finite element substructuring strategies are presented to obtain numerical solutions for three typical problems of interest to the composites community: (1) impact and toughness characterization of composites using Charpy's impact test specimen; (2) free-edge stress analysis of composite laminates; and (3) fracture toughness predictions of composites for individual and combined fracture of modes I, II, and III. The key issue common to these problems is the presence of singular or near singular stress fields. The regions prone to see steep stress gradients are substructured with progressively refined meshes to study the local response simultaneously with the global response. The results from the select examples indicate that finite element substructuring methods are computationally effective for composite singularity mechanics.

Author

**A89-28344\*#** National Aeronautics and Space Administration.  
Lewis Research Center, Cleveland, OH.

**COMPOSITE MECHANICS FOR ENGINE STRUCTURES**  
CHRISTOS C. CHAMIS (NASA, Lewis Research Center, Cleveland, OH) Journal of Propulsion and Power (ISSN 0748-4658), vol. 5, Mar.-Apr. 1989, p. 228-241. Previously announced in STAR as N88-12552. refs  
Copyright

Recent research activities and accomplishments at Lewis Research Center on composite mechanics for engine structures are summarized. The activities focused mainly on developing procedures for the computational simulation of composite intrinsic and structural behavior. The computational simulation encompasses all aspects of composite mechanics, advanced three-dimensional finite-element methods, damage tolerance, composite structural and dynamic response, and structural tailoring and optimization. Author

**A89-29997\*** National Aeronautics and Space Administration.  
Lewis Research Center, Cleveland, OH.

**A THERMALLY MODIFIED POLYMER MATRIX COMPOSITE MATERIAL WITH STRUCTURAL INTEGRITY TO 371 C**  
KENNETH J. BOWLES (NASA, Lewis Research Center, Cleveland, OH) IN: Materials - Processes: The intercept point; Proceedings of the Twentieth International SAMPE Technical Conference, Minneapolis, MN, Sept. 27-29, 1988. Covina, CA, Society for the Advancement of Material and Process Engineering, 1988, p. 552-561. Previously announced in STAR as N88-25483.  
Copyright

The potential for utilizing surface coatings to inhibit the thermal oxidation of polymer matrix composites was studied. Isothermal, inert gas exposures of graphite/PMR-15 composites indicated that after an initial loss of weight, no significant amounts of thermal degradation products are given off during high temperature exposures in the absence of oxygen. As long as a coating remains effective, the composite material should remain stable. It was also found that the glass transition temperature  $T_{sub g}$  of the matrix resin could be increased to values in excess of 400 C. This resulted in measured short beam shear strengths of 75.9 MPa (11 Ksi), flexural strengths of 1172 MPa (170 Ksi) and flexural moduli of 141 GPa (20.5 Msi) for the material at a test temperature of 371 C. The treatment that was used caused a decrease in the PMR-15 resin density from 1.31 to 1.29 gm/cc. It was concluded that

state-of-the-art composites, protected by oxygen-impervious coatings, can be used as materials of construction with structural integrity to at least 371 C and possibly above. Author

**A89-29998\*** National Aeronautics and Space Administration. Lewis Research Center, Cleveland, OH.

**700 F PROPERTIES OF AUTOCLAVE CURED PMR-II COMPOSITES**

DIANE CIFANI (NASA, Lewis Research Center, Cleveland, OH) IN: Materials - Processes: The intercept point; Proceedings of the Twentieth International SAMPE Technical Conference, Minneapolis, MN, Sept. 27-29, 1988. Covina, CA, Society for the Advancement of Material and Process Engineering, 1988, p. 562-575. Previously announced in STAR as N88-24712. refs Copyright

Studies were conducted to develop autoclave processing parameters for graphite reinforced PMR-2 resin composite materials intended for use in applications at temperatures up to 371 degrees (700 F). The effect of resin composition on autoclaveability was investigated. The effect of various graphite fibers and resin composition on 343 C (650 F) and 371 C (700 F) thermo-oxidative stability and mechanical properties was also investigated. The results of the processing studies show that PMR-2 resin composites can be easily fabricated under autoclave conditions. Autoclaved laminates exposed to 1 atm of air at 343 C (650 F) and 371 C (700 F) exhibited less than 5 percent weight loss after 750 hr exposure to 650 F air and 8 percent weight loss during exposure to 700 F air for 500 hr. After 500 hr exposure, autoclaved laminates exhibited greater than 90 percent retention of initial 650 and 700 F flexural and interlaminar shear strengths. The effect of resin formulated molecular weight and postcure conditions on laminate glass transition temperature is also discussed. Author

**A89-30883\*#** National Aeronautics and Space Administration. Lewis Research Center, Cleveland, OH.

**VIBRATION TESTING OF IMPACT-DAMAGED COMPOSITE LAMINATES**

J. E. GRADY and E. H. MEYN (NASA, Lewis Research Center, Cleveland, OH) IN: AIAA, ASME, ASCE, AHS, and ASC, Structures, Structural Dynamics and Materials Conference, 30th, Mobile, AL, Apr. 3-5, 1989, Technical Papers, Part 4. Washington, DC, American Institute of Aeronautics and Astronautics, 1989, p. 2186-2193. refs

(AIAA PAPER 89-1411) Copyright

A new test is described that can be used to measure changes in vibration properties of impact-damaged composite materials. Impact-induced delamination was observed to significantly affect natural frequencies of vibration and damping properties in cross-ply graphite/epoxy laminates. Natural frequencies are shown to drop by as much as half of their original value and modal damping ratios can increase by a factor of up to eight when large amounts of damage are present. A simple finite element model of the damaged impact specimens was used to predict the effect of delamination on certain vibration properties. Comparison of the finite element calculations with the experimental measurements suggests that delamination was the dominant mechanism of flexural stiffness loss resulting from the transverse impact. Author

**A89-31074\*** Tokyo Univ. (Japan).

**FRACTURE RESISTANCE OF A TiB2 PARTICLE/SiC MATRIX COMPOSITE AT ELEVATED TEMPERATURE**

MICHAEL G. JENKINS (Tokyo, University, Japan), JONATHAN A. SALEM (NASA, Lewis Research Center, Cleveland, OH), and SRINIVASA G. SESHADRI (Standard Oil Engineered Materials Co., Niagara Falls, NY) Journal of Composite Materials (ISSN 0021-9983), vol. 23, Jan. 1989, p. 77-91. Previously announced in STAR as N88-26482. refs

Copyright

The fracture resistance of a commercial TiB2 particle/SiC matrix composite was evaluated at temperatures ranging from 20 to 1400 C. A laser interferometric strain gauge (LiSG) was used to continuously monitor the crack mouth opening displacement (CMOD) of the chevron-notched and straight-notched, three-point

bend specimens used. Crack growth resistance curves (R-curves) were determined from the load versus displacement curves and displacement calibrations. Fracture toughness, work-of-fracture, and R-curve levels were found to decrease with increasing temperature. Microstructure, fracture surface, and oxidation coat were examined to explain the fracture behavior. Author

**A89-31689\*** National Aeronautics and Space Administration. Lewis Research Center, Cleveland, OH.

**ELEVATED TEMPERATURE SLOW PLASTIC DEFORMATION OF NIAL/TiB2 PARTICULATE COMPOSITES**

J. DANIEL WHITTENBERGER (NASA, Lewis Research Center, Cleveland, OH), S. K. MANNAN, B. SPRISLER (Martin Marietta Laboratories, Baltimore, MD), and R. K. VISWANADHAM (Multi-Metals, Louisville, KY) IN: High temperature/high performance composites; Proceedings of the Symposium, Reno, NV, Apr. 5-7, 1988. Pittsburgh, PA, Materials Research Society, 1988, p. 89-94. refs

Copyright

The 'XD' process for production of discontinuously-reinforced metal-matrix composites has been used to enhance the high-temperature strength of NiAl-TiB2 composites with particulate densities of up to 30 vol pct. SEM, TEM, and optical characterizations of the resulting microstructures showed the average TiB2 particle size to be about 1 micron, while the average grain of the NiAl matrix was of the order of 10 microns. Elevated temperature compression tests conducted at 1200 and 1300 K indicated flow strengths to increase with TiB2 content, so that the 20 vol pct TiB2-reinforced composite was three times stronger than the unreinforced NiAl; this is ascribed to the very high density of microstructural tangled dislocations, loops, and subgrain boundaries connecting the particles. O.C.

**A89-32882\*** National Aeronautics and Space Administration. Lewis Research Center, Cleveland, OH.

**TEST METHODS AND DESIGN ALLOWABLES FOR FIBROUS COMPOSITES. VOLUME 2**

CHRISTOS C. CHAMIS, ED. (NASA, Lewis Research Center, Cleveland, OH) Philadelphia, PA, American Society for Testing and Materials, 1989, 301 p. For individual items see A89-32883 to A89-32899.

(ASTM STP-1003) Copyright

Topics discussed include extreme/hostile environment testing, establishing design allowables, and property/behavior specific testing. Papers are presented on environmental effects on the high strain rate properties of graphite/epoxy composite, the low-temperature performance of short-fiber reinforced thermoplastics, the abrasive wear behavior of unidirectional and woven graphite fiber/PEEK, test methods for determining design allowables for fiber reinforced composites, and statistical methods for calculating material allowables for MIL-HDBK-17. Attention is also given to a test method to measure the response of composite materials under reversed cyclic loads, a through-the-thickness strength specimen for composites, the use of torsion tubes to measure in-plane shear properties of filament-wound composites, the influence of test fixture design on the Iosipescu shear test for fiber composite materials, and a method for monitoring in-plane shear modulus in fatigue testing of composites. I.S.

**A89-32885\*** National Aeronautics and Space Administration. Lewis Research Center, Cleveland, OH.

**MECHANICAL PROPERTIES CHARACTERIZATION OF COMPOSITE SANDWICH MATERIALS INTENDED FOR SPACE ANTENNA APPLICATIONS**

KENNETH J. BOWLES and RAYMOND D. VANNUCCI (NASA, Lewis Research Center, Cleveland, OH) IN: Test methods and design allowables for fibrous composites. Volume 2. Philadelphia, PA, American Society for Testing and Materials, 1989, p. 31-44. Previously announced in STAR as N88-10121. refs

Copyright

The composite materials proposed for use in the Advanced Communications Technology Satellite (ACTS) program contains a new, high modulus graphite fiber as the reinforcement. A study



was conducted to measure certain mechanical properties of the new fiber-reinforced material as well as of a composite-faced aluminum honeycomb sandwich structure. Properties were measured at -157, 22, and 121 C. Complete characterization of this material was not intended. Longitudinal tensile, picture-frame shear, short-beam shear, and flexural tests were performed on specimens of the composite face-sheet materials. Unidirectional, cross-plyed, and quasi-isotropic fiber composite ply layup designs were fabricated and tested. These designs had been studied by using NASA's Integrated Composite Analyzer (ICAN) computer program. Flexural tests were conducted on (+/- 60/0 deg) sub s composite-faced sandwich structure material. Resistance strain gages were used to measure strains in the tensile, picture-frame, and sandwich flexural tests. The sandwich flexural strength was limited by the core strength at 157 and 22 c. The adhesive bond strength was the limiting factor at 121 C. Adhesive mechanical properties are reflected in sandwich structure flexural properties when the span-to-depth ratio is great enough to allow a significant shear effect on the load-deflection behavior of the sandwich beam. Most measured properties agreed satisfactorily with the properties predicted by ICAN. Author

**A89-34844\*** National Aeronautics and Space Administration. Lewis Research Center, Cleveland, OH.

**STRENGTH DISTRIBUTION OF REINFORCING FIBERS IN A NICALON FIBER/CHEMICALLY VAPOR INFILTRATED SILICON CARBIDE MATRIX COMPOSITE**

ANDREW J. ECKEL (NASA, Lewis Research Center; Sverdrup Technology, Inc., Cleveland, OH; Washington, University, Seattle) and RICHARD C. BRADT (Washington, University, Seattle) American Ceramic Society, Journal (ISSN 0002-7820), vol. 72, March 1989, p. 455-458. refs (Contract NAGW-199) Copyright

The strength distribution of fibers within a two-dimensional laminate ceramic/ceramic composite consisting of an eight harness satin weave of Nicalon continuous fiber within a chemically vapor infiltrated SiC matrix was determined from analysis of the fracture mirrors of the fibers. Comparison of the fiber strengths and the Weibull moduli with those for Nicalon fibers prior to incorporation into composites suggests that possible fiber damage may occur either during the weaving or during another stage of the composite manufacture. Observations also indicate that it is the higher-strength fibers which experience the greatest extent of fiber pullout and thus make a larger contribution to the overall composite toughness than do the weaker fibers. Author

**A89-35311\*** National Aeronautics and Space Administration. Lewis Research Center, Cleveland, OH.

**AUGER ANALYSIS OF A FIBER/MATRIX INTERFACE IN A CERAMIC MATRIX COMPOSITE**

FRANK S. HONEYC (NASA, Lewis Research Center; Case Western Reserve University, Cleveland, OH) and STEPHEN V. PEPPER (NASA, Lewis Research Center, Cleveland, OH) IN: Adhesion in solids; Proceedings of the Symposium, Reno, NV, Apr. 5-7, 1988. Pittsburgh, PA, Materials Research Society, 1988, p. 303-308. Previously announced in STAR as N88-25487. refs Copyright

Auger electron spectroscopy (AES) depth profiling was used to characterize the fiber/matrix interface of an SiC fiber, reaction bonded Si<sub>3</sub>N<sub>4</sub> matrix composite. Depth profiles of the as received double coated fiber revealed concentration oscillations which disappeared after annealing the fiber in the environment used to fabricate the composite. After the composite was fractured, the Auger depth profiles showed that failure occurred in neither the Beta-SiC fiber body nor in the Si<sub>3</sub>N<sub>4</sub> matrix but, concurrently, at the fiber coating/matrix interface and within the fiber coating itself. Author

**A89-36293\*** National Aeronautics and Space Administration. Lewis Research Center, Cleveland, OH.

**MECHANICS OF COMPOSITE MATERIALS - PAST, PRESENT AND FUTURE**

CHRISTOS C. CHAMIS (NASA, Lewis Research Center, Cleveland, OH) Journal of Composites Technology and Research (ISSN 0885-6804), vol. 11, Spring 1989, p. 3-14. Previously announced in STAR as N88-17744. refs Copyright

Composite mechanics disciplines are presented and described at their various levels of sophistication and attendant scales of application. Correlation with experimental data is used as the prime discriminator between alternative methods and level of sophistication. Major emphasis is placed on: (1) where composite mechanics has been; (2) what it has accomplished; (3) where it is headed, based on present research activities; and (4) at the risk of being presumptuous, where it should be headed. The discussion is developed using selected, but typical examples of each composite mechanics discipline identifying degree of success, with respect to correlation with experimental data, and problems remaining. The discussion is centered about fiber/resin composites drawn mainly from the author's research activities/experience spanning two decades at Lewis. Author

**A89-36310\*** National Aeronautics and Space Administration. Lewis Research Center, Cleveland, OH.

**DYNAMIC DELAMINATION BUCKLING IN COMPOSITE LAMINATES UNDER IMPACT LOADING - COMPUTATIONAL SIMULATION**

JOSEPH E. GRADY, CHRISTOS C. CHAMIS, and ROBERT A. AIELLO (NASA, Lewis Research Center, Cleveland, OH) IN: Composite materials: Fatigue and fracture; Proceedings of the Second Symposium, Cincinnati, OH, Apr. 27, 28, 1987. Volume 2. Philadelphia, PA, American Society for Testing and Materials, 1989, p. 137-149. Previously announced in STAR as N87-28611. refs Copyright

A unique dynamic delamination buckling and delamination propagation analysis capability has been developed and incorporated into a finite element computer program. This capability consists of the following: (1) a modification of the direct time integration solution sequence which provides a new analysis algorithm that can be used to predict delamination buckling in a laminate subjected to dynamic loading, and (2) a new method of modeling the composite laminate using plate bending elements and multipoint constraints. This computer program is used to predict both impact induced buckling in composite laminates with initial delaminations and the strain energy release rate due to extension of the delamination. It is shown that delaminations near the outer surface of a laminate are susceptible to local buckling and buckling-induced delamination propagation when the laminate is subjected to transverse impact loading. The capability now exists to predict the time at which the onset of dynamic delamination buckling occurs, the dynamic buckling mode shape, and the dynamic delamination strain energy release rate. Author

**A89-36320\*** National Aeronautics and Space Administration. Lewis Research Center, Cleveland, OH.

**FIBER COMPOSITE STRUCTURAL DURABILITY AND DAMAGE TOLERANCE - SIMPLIFIED PREDICTIVE METHODS**

CHRISTOS C. CHAMIS and CAROL A. GINTY (NASA, Lewis Research Center, Cleveland, OH) IN: Composite materials: Fatigue and fracture; Proceedings of the Second Symposium, Cincinnati, OH, Apr. 27, 28, 1987. Volume 2. Philadelphia, PA, American Society for Testing and Materials, 1989, p. 338-355. Previously announced in STAR as N88-13409. refs Copyright

Simplified predictive methods and models (theory) to evaluate fiber/polymer-matrix composite material for determining structural durability and damage tolerance are presented and described. This theory includes equations for (1) fatigue and fracture of composites without and with defects, (2) impact resistance and residual strength after impact, (3) thermal fatigue, and (4) combined stress fatigue. Several examples are included to illustrate applications of the theory and to identify significant parameters and sensitivities. Comparisons with limited experimental data are made. Author



**A89-36420\*** Columbia Univ., New York, NY.

**REACTION KINETICS BETWEEN FIBER AND MATRIX**

M. W. KOPP, J. K. TIEN (Columbia University, New York), and D. W. PETRASEK (NASA, Lewis Research Center, Cleveland, OH) IN: Superalloys 1988; Proceedings of the Sixth International Symposium, Champion, PA, Sept. 18-22, 1988. Warrendale, PA, Metallurgical Society, Inc., 1988, p. 193-201. refs (Contract NAG3-410; NAG3-720; AF-AFOSR-86-0312)

Copyright

Interdiffusion and interdiffusion controlled intermediate phase formation in metal matrix composites can be of interest for the prolonged application of these systems at high temperatures. Methods are discussed that address the kinetics of interdiffusion in systems that exhibit solid solution intermixing or the formation of a third intermediate phase at the fiber/matrix interface, or both. The tungsten fiber reinforced niobium and tungsten fiber reinforced superalloy systems are employed as model systems for experimentation and discussion. In an effort to impede interdiffusion, the concept of ion implanted diffusion barriers have been examined. Preliminary results on the feasibility and effectiveness of ion implanted diffusion barriers are presented.

Author

**A89-38637\*** National Aeronautics and Space Administration. Lewis Research Center, Cleveland, OH.

**GRAPHITE/POLYIMIDE COMPOSITES WITH IMPROVED TOUGHNESS**

PETER DELVIGS (NASA, Lewis Research Center, Cleveland, OH) Polymer Composites (ISSN 0272-8397), vol. 10, April 1989, p. 134-139. refs

Copyright

Studies were performed to determine the toughness characteristics of composites prepared from modified addition-type polyimides, using Celion 6000 graphite fiber as the reinforcement. The polyimides were prepared from aromatic diamines containing flexibilizing ether connecting groups. The composite flexural and short beam shear strengths were determined at room temperature and elevated temperatures. Composite toughness was evaluated using 10 deg off axis tensile tests and double cantilever beam fracture tests at room temperature. The effects of the flexibilized resin structure on composite mechanical properties, toughness characteristics, and thermo-oxidative stability are discussed.

Author

**A89-39996\*** State Univ. of New York, Buffalo.

**A PROBABILISTIC FORMULATION FOR FRACTURE ENERGY OF CONTINUOUS FIBRE-MATRIX COMPOSITES**

ROBERT C. WETHERHOLD (New York, State University, Buffalo) Journal of Materials Science Letters (ISSN 0261-8028), vol. 8, May 1989, p. 576, 577.

(Contract NAG3-862)

Copyright

Since the fracture energy is a key design variable in brittle-matrix composites, the calculation of the energy and its probabilistic distribution becomes a prominent issue. A demonstration is presented of the way in which the statistical moments of the fracture-energy random variable may be directly calculated. The case considered is that in which continuous fibers possess periodic points of weakness along their length; the shear strength at the interface caused by the reentry of the fibers into the matrix will produce fiber-debonding.

O.C.

**A89-48957\*** National Aeronautics and Space Administration. Lewis Research Center, Cleveland, OH.

**COMPATIBILITY OF MOLTEN SALTS WITH ADVANCED SOLAR DYNAMIC RECEIVER MATERIALS**

D. A. JAWORSKE (NASA, Lewis Research Center, Cleveland, OH) and W. D. PERRY (Auburn University, AL) AIAA, Thermophysics Conference, 24th, Buffalo, NY, June 12-14, 1989. 7 p. refs (AIAA PAPER 89-1756) Copyright

Metal-coated graphite fibers are being considered as a thermal conductivity enhancement filler material for molten salts in solar dynamic thermal energy storage systems. The successful metal

coating chosen for this application must exhibit acceptable wettability and must be compatible with the molten salt environment. Contact angle values between molten lithium fluoride and several metal, metal fluoride, and metal oxide substrates have been determined at 892 C using a modification of the Wilhelmy plate technique. Reproducible contact angles with repeated exposure to the molten LiF indicated compatibility.

Author

**A89-54258\*** National Aeronautics and Space Administration. Lewis Research Center, Cleveland, OH.

**TRIBOLOGICAL COMPOSITION OPTIMIZATION OF CHROMIUM-CARBIDE-BASED SOLID LUBRICANT COATINGS FOR FOIL GAS BEARINGS AT TEMPERATURES TO 650 C**

CHRISTOPHER DELLACORTE (NASA, Lewis Research Center, Cleveland, OH) IN: Metallurgical coatings 1988; Proceedings of the Fifteenth International Conference, San Diego, CA, Apr. 11-15, 1988. Volume 1. London and New York, Elsevier Applied Science, 1988, p. 87-97. refs

Copyright

The determination of the tribologically optimum composition of chromium-carbide-based solid lubricant coatings using a foil gas bearing test apparatus is described. The coatings contain a wear resistant chromium carbide base stock with the lubricant additives silver and BaF<sub>2</sub>-CaF<sub>2</sub> eutectic. The coating composition is optimized for air-lubricated foil gas bearings at temperatures ranging from 25 to 650 C. The various compositions were prepared by powder blending, then plasma sprayed onto Inconel 718 test journals and diamond ground to the desired coating thickness and surface finish. The journals were operated against preoxidized Ni-Cr alloy foils, and the test bearings were subjected to repeated start-stop cycles under a bearing unit of 14 kPa. Sliding contact between the coated journal and the smooth foil occurs during bearing start-up before lift-off or hydrodynamic lubrication by the air film and during bearing coast-down. The bearings were tested for 9000 start-stop cycles or until specimen reached a predetermined failure level.

C.E.

**A89-54261\*** California Univ., Los Angeles.

**MICROLAMINATE COMPOSITES AS THERMAL BARRIER COATINGS**

M. C. RADHAKRISHNA, H. J. DOERR, C. V. DESHPANDEY, and R. F. BUNSHAH (California, University, Los Angeles) IN: Metallurgical coatings 1988; Proceedings of the Fifteenth International Conference, San Diego, CA, Apr. 11-15, 1988. Volume 1. London and New York, Elsevier Applied Science, 1988, p. 143-150.

(Contract NAG3-701)

Copyright

Thick multiple-layered Ni/NiCoCrAlY and Ti/CoCrAlY microlaminate composites are explored as thermal barrier coatings. The method of fabrication of these laminates and the measurement technique used to determine thermal diffusivity and thermal conductivity of these coatings are discussed. Results indicate that the thermal conductivity of the laminate composite perpendicular to the laminate plane decreases with increasing number of interfaces; the drop in thermal conductivity is likely to be associated with interfaces which act as a barrier to the transfer of heat across them; the variation in thermal conductivity with the number of interfaces is not linear.

C.E.

**N89-10128\*#** Case Western Reserve Univ., Cleveland, OH.

**THERMODYNAMIC ANALYSIS OF COMPATIBILITY OF SEVERAL REINFORCEMENT MATERIALS WITH FEAL ALLOYS**

AJAY K. MISRA Washington NASA Oct. 1988 30 p

(Contract NCC3-43)

(NASA-CR-4172; NAS 1.26:4172) Avail: NTIS HC A03/MF A01 CSCL 11D

Chemical compatibility of several reinforcement materials with FeAl alloys within the concentration range 40 to 50 at pct Al have been analyzed from thermodynamic considerations at 1173 and 1273 K. The reinforcement materials considered in this study include carbides, borides, oxides, nitrides, and silicides. Although

## 24 COMPOSITE MATERIALS

several chemically compatible reinforcement materials are identified, the coefficients of thermal expansion for none of these materials match closely with that of FeAl alloys and this might pose serious problems in the design of composite systems based on FeAl alloys. Author

**N89-10130\*#** National Aeronautics and Space Administration. Lewis Research Center, Cleveland, OH.

### PROPERTIES OF SILICON CARBIDE FIBER-REINFORCED SILICON NITRIDE MATRIX COMPOSITES

RAMAKRISHNA T. BHATT (Army Aviation Systems Command, Cleveland, Ohio.) Jun. 1988 17 p Presented at the International Conference on Whisker- and Fiber-Toughened Ceramics, Oak Ridge, Tenn., 6-9, Jun. 1988; sponsored by American Society for Metals

(NASA-TM-101356; E-4386; NAS 1.15:101356; AVSCOM-TR-88-C-027; AD-A201681) Avail: NTIS HC A03/MF A01 CSCL 11/4

The mechanical properties of NASA Lewis developed SiC/RBSN composites and their thermal and environmental stability have been studied. The composites consist of nearly 30 vol pct of aligned 142 micron diameter chemically vapor-deposited SiC fibers in a relatively porous silicon nitride matrix. In the as-fabricated condition, the unidirectional and 2-D composites exhibited metal-like stress-strain behavior, graceful failure, and showed improved properties when compared with unreinforced matrix of comparable density. Furthermore, the measured room temperature tensile properties were relatively independent of tested volume and were unaffected by artificial notches normal to the loading direction or by thermal shocking from temperatures up to 800 C. The four-point bend strength data measured as a function of temperature to 1400 C in air showed that as-fabricated strength was maintained to 1200 C. At 1400 C, however, nearly 15 pct loss in strength was observed. Measurement of room temperature tensile strength after 100 hr exposure at temperatures to 1400 C in a nitrogen environment indicated no loss from the as-fabricated composite strength. On the other hand, after 100 hr exposure in flowing oxygen at 1200 and 1400 C, the composites showed approximately 40 pct loss from their as-fabricated ultimate tensile strength. Those exposed between 400 to 1200 C showed nearly 60 pct strength loss. Oxidation of the fiber/matrix interface as well as internal oxidation of the porous Si<sub>3</sub>N<sub>4</sub> matrix are likely mechanisms for strength degradation. The excellent strength reproducibility, notch insensitivity, and high temperature strength of the composite makes it an ideal candidate for advanced heat engine applications provided coating or densification methods are developed to avoid internal oxidation attack. Author

**N89-10131\*#** Case Western Reserve Univ., Cleveland, OH. **THERMODYNAMIC ANALYSIS OF COMPATIBILITY OF SEVERAL REINFORCEMENT MATERIALS WITH BETA PHASE NIAL ALLOYS Final Report**

AJAY K. MISRA Washington NASA Nov. 1988 60 p (Contract NCC3-43) (NASA-CR-4171; E-4299; NAS 1.26:4171) Avail: NTIS HC A04/MF A01 CSCL 11/4

Chemical compatibility of several reinforcement materials with beta phase NiAl alloys within the concentration range 40 to 50 at. percent Al have been analyzed from thermodynamic considerations at 1373 and 1573 K. The reinforcement materials considered in this study include carbides, borides, oxides, nitrides, beryllides, and silicides. Thermodynamic data for NiAl alloys have been reviewed and activity of Ni and Al in the beta phase have been derived at 1373 and 1573 K. Criteria for chemical compatibility between the reinforcement material and the matrix have been defined and several chemically compatible reinforcement materials have been defined. Author

**N89-10134\*#** National Aeronautics and Space Administration. Lewis Research Center, Cleveland, OH.

### THERMAL EFFECTS ON THE MECHANICAL PROPERTIES OF SIC FIBER REINFORCED REACTION BONDED SILICON NITRIDE MATRIX (SIC/RBSN) COMPOSITES

R. T. BHATT and R. E. PHILLIPS (Sverdrup Technology, Inc., Cleveland, Ohio.) Oct. 1988 17 p Submitted for publication (NASA-TM-101348; E-4375; NAS 1.15:101348; AVSCOM-TR-88-C-028) Avail: NTIS HC A03/MF A01 CSCL 11/4

The elevated temperature four-point flexural strength and the room temperature tensile and flexural strength properties after thermal shock were measured for ceramic composites consisting of 30 vol pct uniaxially aligned 142 micron diameter SiC fibers in a reaction bonded Si<sub>3</sub>N<sub>4</sub> matrix. The elevated temperature strengths were measured after 15 min of exposure in air at temperatures to 1400 C. Thermal shock treatment was accomplished by heating the composite in air for 15 min at temperatures to 1200 C and then quenching in water at 25 C. The results indicate no significant loss in strength properties either at temperature or after thermal shock when compared with the strength data for composites in the as-fabricated condition. Author

**N89-10952\*#** National Aeronautics and Space Administration. Lewis Research Center, Cleveland, OH.

### LAMINATE BEHAVIOR FOR SIC FIBER-REINFORCED REACTION-BONDED SILICON NITRIDE MATRIX COMPOSITES

R. T. RHATT and R. E. PHILLIPS (Sverdrup Technology, Inc., Cleveland, Ohio.) Oct. 1988 40 p (NASA-TM-101350; E-4377; NAS 1.15:101350; AVSCOM-TR-88-C-30; AD-A201035) Avail: NTIS HC A03/MF A01 CSCL 11/4

The room temperature mechanical properties of SiC fiber reinforced reaction-bonded silicon nitride matrix composite laminates (SiC/RBSN) have been measured. The laminates contained approx 30 volume fraction of aligned 142-micron diameter SiC fiber in a porous RBSN matrix. Three types of laminate studied were unidirectional: (1) (0) sub 8, (2) (10) sub 8, and (3) (45) sub 8, and (90) sub 8; cross plied laminates (0 sub 2/90 sub 2); and angle plied laminates: (+45 sub 2/-45 sub 2). Each laminate contained eight fiber plies. Results of the unidirectionally reinforced composites tested at various angles to the reinforcement direction indicate large anisotropy in in-plane properties. In addition, strength properties of these composites along the fiber direction were independent of specimen gage length and were unaffected by notches normal to the fiber direction. Splitting parallel to the fiber at the notch tip appears to be the dominant crack blunting mechanism responsible for notch insensitive behavior of these composites. In-plane properties of the composites can be improved by 2-D laminate construction. Mechanical property results for (0 sub 2/90 sub 2) sub s and (+45/-45 sub 2) sub s laminates showed that their matrix failure strains were similar to that for (0) sub 8 laminates, but their primary elastic moduli, matrix cracking strengths, and ultimate composite strengths were lower. The elastic properties of unidirectional, cross-ply, and angle-ply composites can be predicted from modified constitutive equations and laminate theory. Further improvements in laminate properties may be achieved by reducing the matrix porosity and by optimizing the bond strength between the SiC fiber and RBSN matrix. Author

**N89-11826\*#** National Aeronautics and Space Administration. Lewis Research Center, Cleveland, OH.

### EFFECT OF LENGTH OF CHOPPED PRISTINE AND INTERCALATED GRAPHITE FIBERS ON THE RESISTIVITY OF FIBER NETWORKS

JAMES R. GAIER and MARK STAHL (Cleveland State Univ., Ohio.) 1988 13 p Presented at the Fall Meeting of the Materials Research Society, Boston, Mass., 28 Nov. - 2 Dec. 1988 (NASA-TM-101395; E-4474; NAS 1.15:101395) Avail: NTIS HC A03/MF A01 CSCL 11/4

Samples of Amoco P-100 fibers were chopped to lengths of 3.14, 2.53, 1.90, 1.27, 0.66 mm, or milled for 2 hours. The two-point resistivity of compacts of these fibers were measured as a function of pressure from 34 kPa to 143 MPa. Samples of each fiber length were intercalated with bromine at room temperature and similarly measured. The low pressure resistivity of the compacts

decreased with increasing fiber length. Intercalation lowered the resistivity of each of the chopped length compacts, but raised the resistivity of the milled fiber compacts. Bulk resistivity of all samples decreased with increasing pressure at similar rates. Even though fiber volumes were as low as 5 percent, all measurements exhibited measurable resistivity. A greater change with pressure in the resistance was observed for shorter fibers than for longer, probably an indication of tighter fiber packing. Intercalation appeared to have no effect on the fiber to fiber contact resistance. Author

**N89-12675\*#** Forest Products Lab., Madison, WI.  
**IMPROVING THE FATIGUE RESISTANCE OF ADHESIVE JOINTS IN LAMINATED WOOD STRUCTURES**

THEODORE L. LAUFENBERG, BRYAN H. RIVER, LIDIJA L. MURMANIS, and ALFRED W. CHRISTIANSEN Aug. 1988 96 p  
 (Contract NASA ORDER C-80015-F; DE-AI01-76ET-20320)  
 (NASA-CR-182165; DOE/NASA/0015-1; NAS 1.26:182165)  
 Avail: NTIS HC A05/MF A01 CSCL 11/4

The premature fatigue failure of a laminated wood/epoxy test beam containing a cross section finger joint was the subject of a multi-disciplinary investigation. The primary objectives were to identify the failure mechanisms which occurred during the finger joint test and to provide avenues for general improvements in the design and fabrication of adhesive joints in laminated wood structures. Author

**N89-12684\*#** National Aeronautics and Space Administration.  
 Lewis Research Center, Cleveland, OH.

**A PROBABILISTIC APPROACH TO COMPOSITE MICROMECHANICS**

T. A. STOCK, P. X. BELLINI, P. L. N. MURTHY (Cleveland State Univ., Ohio.), and C. C. CHAMIS 1988 21 p Presented at the 29th Structures, Structural Dynamics and Materials Conference, Williamsburg, Va., 18-20 Apr. 1988; sponsored by AIAA, ASME, ASCE, AHS and ACS Previously announced in IAA as A88-32312  
 (NASA-TM-101366; E-4405; NAS 1.15:101366) Avail: NTIS HC A03/MF A01 CSCL 11/4

Probabilistic composite micromechanics methods are developed that simulate expected uncertainties in unidirectional fiber composite properties. These methods are in the form of computational procedures using Monte Carlo simulation. A graphite/epoxy unidirectional composite (ply) is studied to demonstrate fiber composite material properties at the micro level. Regression results are presented to show the relative correlation between predicted and response variables in the study. Author

**N89-13521\*#** National Aeronautics and Space Administration.  
 Lewis Research Center, Cleveland, OH.

**FRACTURE TOUGHNESS COMPUTATIONAL SIMULATION OF GENERAL DELAMINATIONS IN FIBER COMPOSITES**

T. E. WILT, P. L. N. MURTHY (Cleveland State Univ., Ohio.), and C. C. CHAMIS 1988 19 p Presented at the 29th Structural Dynamics and Materials Conference, Williamsburg, Va., 18-20 Apr. 1988; sponsored in part by AIAA, ASME, AHS and ASC Previously announced as A88-32219  
 (NASA-TM-101415; E-4513; NAS 1.15:101415) Avail: NTIS HC A03/MF A01 CSCL 11/4

A procedure is described to computationally simulate composite laminate fracture toughness in terms of strain energy release rate. It is also used to evaluate the degradation in laminate structural integrity in terms of displacements, loss in stiffness, loss in vibration frequencies and loss in buckling resistance. Specific laminates are selected for detail studies in order to demonstrate the generality of the procedure. These laminates had center delaminations, off-center delaminations, and pocket delaminations (center and off-center) at the free-edge and center delaminations at the interior. The laminates had two different thicknesses and were made from three different materials. The results obtained are presented in graphical form to illustrate the effects of delamination on the laminate structural integrity and on the laminate strain energy release rate (composite fracture toughness). Author

**N89-13522\*#** National Aeronautics and Space Administration.  
 Lewis Research Center, Cleveland, OH.

**A NASTRAN DMAP ALTER FOR LINEAR BUCKLING ANALYSIS UNDER DYNAMIC LOADING**

ROBERT A. AIELLO and JOSEPH E. GRADY 1988 16 p  
 Proposed for presentation at the 17th NASTRAN User's Colloquium, San Antonio, Tex., 24-28 Apr. 1989; sponsored by the Computer Software Management and Information Center (COSMIC)  
 (NASA-TM-100832; E-4022; NAS 1.15:100832) Avail: NTIS HC A03/MF A01 CSCL 11/4

A unique modification to the NASTRAN solution sequence for transient analysis with direct time integration (COSMIC NASTRAN rigid format 9) was developed and incorporated into a DMAP alter. This DMAP alter calculates the buckling stability of a dynamically loaded structure, and is used to predict the onset of structural buckling under stress wave loading conditions. The modified solution sequence incorporates the linear buckling analysis capability (rigid format 5) of NASTRAN into the existing Transient solution rigid format in such a way as to provide a time dependent eigensolution which is used to assess the buckling stability of the structure as it responds to the impulsive load. As a demonstration of the validity of this modified solution procedure, the dynamic buckling of a prismatic bar subjected to an impulsive longitudinal compression is analyzed and compared to the known theoretical solution. In addition, a dynamic buckling analysis is performed for the analytically less tractable problem of the localized dynamic buckling of an initially flawed composite laminate under transverse impact loading. The addition of this DMAP alter to the transient solution sequence in NASTRAN facilitates the prediction of both time and mode of buckling. Author

**N89-14259\*#** National Aeronautics and Space Administration.  
 Lewis Research Center, Cleveland, OH.

**GRAPHITE FLUORIDE FIBER POLYMER COMPOSITE MATERIAL Patent Application**

CHING-CHEH HUNG, inventor (to NASA) 30 Sep. 1988 10 p  
 (NASA-CASE-LEW-14472-1; NAS 1.71:LEW-14472-1;  
 US-PATENT-APPL-SN-251499) Avail: NTIS HC A02/MF A01 CSCL 11/4

Improved graphite fluoride fibers are produced by contact reaction between highly graphitized fibers and fluorine gas. It is preferable to intercalate the fibers with bromine or fluorine and metal fluoride prior to fluorination. These graphite fluoride fibers are bound by an epoxy. The resulting composites have high thermal conductivity, high electric resistivity, and high emissivity. NASA

**N89-15201\*#** National Aeronautics and Space Administration.  
 Lewis Research Center, Cleveland, OH.

**THE ROLE OF RAPID SOLIDIFICATION PROCESSING IN THE FABRICATION OF FIBER REINFORCED METAL MATRIX COMPOSITES**

IVAN E. LOCCI (Case Western Reserve Univ., Cleveland, OH.) and RONALD D. NOEBE Jan. 1989 45 p  
 (NASA-TM-101450; E-4449; NAS 1.15:101450) Avail: NTIS HC A03/MF A01 CSCL 11/4

Advanced composite processing techniques for fiber reinforced metal matrix composites require the flexibility to meet several widespread objectives. The development of uniquely desired matrix microstructures and uniformly arrayed fiber spacing with sufficient bonding between fiber and matrix to transmit load between them without degradation to the fiber or matrix are the minimum requirements necessary of any fabrication process. For most applications these criteria can be met by fabricating composite monotapes which are then consolidated into composite panels or more complicated components such as fiber reinforced turbine blades. Regardless of the end component, composite monotapes are the building blocks from which near net shape composite structures can be formed. The most common methods for forming composite monotapes are the powder cloth, foil/fiber, plasma spray, and arc spray processes. These practices, however, employ rapid solidification techniques in processing of the composite matrix phase. Consequently, rapid solidification processes play a vital

## 24 COMPOSITE MATERIALS

and yet generally overlooked role in composite fabrication. The future potential of rapid solidification processing is discussed.

Author

**N89-15990\*#** National Aeronautics and Space Administration. Lewis Research Center, Cleveland, OH.

### **FIBER REINFORCED SUPERALLOYS FOR ROCKET ENGINES**

DONALD W. PETRASEK and JOSEPH R. STEPHENS 31 Oct. 1988 21 p Presented at the 72nd Specialists Meeting on Application of Advanced Materials for Turbomachinery and Rocket Propulsion, Bath, England, 3-5 Oct. 1988; sponsored in part by AGARD/NATO Propulsion Energetics Panel (NASA-TM-100880; E-4114; NAS 1.15:100880) Avail: NTIS HC A03/MF A01 CSCL 11/4

High-pressure turbopumps for advanced reusable liquid-propellant rocket engines such as that for the Space Shuttle Main Engine (SSME) require turbine blade materials that operate under extreme conditions of temperature, hydrogen environment, high-cycle fatigue loading, thermal fatigue and thermal shock. Such requirements tax the capabilities of current blade materials. Based on projections of properties for tungsten fiber reinforced superalloy (FRS) composites, it was concluded that FRS turbine blades offer the potential of a several-fold increase in life and over a 200C increase in temperature capability over current SSME blade material. FRS composites were evaluated with respect to mechanical property requirements for SSME blade applications. Compared to the current blade material, the thermal shock resistance of FRS materials is excellent, two to nine times better, and their thermal fatigue resistance is equal to or higher than the current blade material. FRS materials had excellent low and high-cycle fatigue strengths, and thermal shock-induced surface microcracks had no influence on their fatigue strength. The material also exhibited negligible embrittlement when exposed to a hydrogen environment.

Author

**N89-20206\*#** National Aeronautics and Space Administration. Lewis Research Center, Cleveland, OH.

### **FINITE ELEMENT APPLICATIONS TO EXPLORE THE EFFECTS OF PARTIAL BONDING ON METAL MATRIX COMPOSITE PROPERTIES**

J. J. CARUSO, D. TROWBRIDGE, and C. C. CHAMIS Apr. 1989 25 p Presented at the 30th Structures, Structural Dynamics and Materials Conference, Mobile, AL, 3-5 Apr. 1989; sponsored in part by AIAA, ASME, ASCE, AHS, and ACS (NASA-TM-101482; E-4610; NAS 1.15:101482) Avail: NTIS HC A03/MF A01 CSCL 11/4

The mechanics of materials approach (definition of E, G, Nu, and Alpha) and the finite element method are used to explore the effects of partial bonding and fiber fracture on the behavior of high temperature metal matrix composites. Composite ply properties are calculated for various degrees of disbonding to evaluate the sensitivity of these properties to the presence of fiber/matrix disbonding and fiber fracture. The mechanics of materials approach allows for the determination of the basic ply material properties needed for design/analysis of composites. The finite element method provides the necessary structural response (forces and displacements) for the mechanics of materials equations. Results show that disbonding of fractured fibers affect only E sub (111) and alpha sub (111) significantly.

Author

### **N89-21036\*#** Sverdrup Technology, Inc., Cleveland, OH. **THERMODYNAMIC ANALYSIS OF CHEMICAL COMPATIBILITY OF SEVERAL REINFORCEMENT MATERIALS WITH NIOBIUM ALUMINIDES Final Contractor Report**

AJAY K. MISRA Mar. 1989 46 p (Contract NAS3-25266) (NASA-CR-182260; E-4648; NAS 1.26:182260) Avail: NTIS HC A03/MF A01 CSCL 11/4

Chemical compatibility of several reinforcement materials with three niobium aluminides, Nb<sub>3</sub>Al, Nb<sub>2</sub>Al, and NbAl<sub>3</sub>, were examined from thermodynamic considerations. The reinforcement materials considered in this study include carbides, borides, nitrides, oxides, silicides, and Engel-Brewer compounds. Thermodynamics of the

Nb-Al system were reviewed and activities of Nb and Al were derived at desired calculation temperatures. Criteria for chemical compatibility between the reinforcement material and Nb-Al compounds have been defined and several chemically compatible reinforcement materials have been identified.

Author

**N89-22684\*#** National Aeronautics and Space Administration. Lewis Research Center, Cleveland, OH.

### **THE ISOTHERMAL FATIGUE BEHAVIOR OF A UNIDIRECTIONAL SiC/Ti COMPOSITE AND THE Ti ALLOY MATRIX**

JOHN GAYDA, JR., TIMOTHY P. GABB, and ALAN D. FREED Apr. 1989 36 p (NASA-TM-101984; E-4683; NAS 1.15:101984) Avail: NTIS HC A03/MF A01 CSCL 11/4

The high temperature fatigue behavior of a metal matrix composite (MMC) consisting of Ti-15V-3Cr-3Al-3Sn (Ti-15-3) matrix reinforced by 33 vol percent of continuous unidirectional SiC fibers was experimentally and analytically evaluated. Isothermal MMC fatigue tests with constant amplitude loading parallel to the fiber direction were performed at 300 and 550 C. Comparative fatigue tests of the Ti-15-3 matrix alloy were also conducted. Composite fatigue behavior and the in-situ stress state of the fiber and matrix were analyzed with a micromechanical model, the Concentric Cylinder Model (CCM). The cyclic stress-strain response of the composite was stable at 300 C. However, an increase in cyclic mean strain foreshortened MMC fatigue life at high strain ranges at 550 C. Fatigue tests of the matrix alloy and CCM analyses indicated this response was associated with stress relaxation of the matrix in the composite.

Author

**N89-23621\*#** National Aeronautics and Space Administration. Lewis Research Center, Cleveland, OH.

### **COMPOSITE BLADE STRUCTURAL ANALYZER (COBSTRAN) USER'S MANUAL**

ROBERT A. AIELLO Apr. 1989 84 p (NASA-TM-101461; E-4570; NAS 1.15:101461) Avail: NTIS HC A05/MF A01 CSCL 11/4

The installation and use of a computer code, COBSTRAN (Composite Blade STRuctural ANalyzer), developed for the design and analysis of composite turbofan and turboprop blades and also for composite wind turbine blades was described. This code combines composite mechanics and laminate theory with an internal data base of fiber and matrix properties. Inputs to the code are constituent fiber and matrix material properties, factors reflecting the fabrication process, composite geometry and blade geometry. COBSTRAN performs the micromechanics, macromechanics and laminate analyses of these fiber composites. COBSTRAN generates a NASTRAN model with equivalent anisotropic homogeneous material properties. Stress output from NASTRAN is used to calculate individual ply stresses, strains, interply stresses, thru-the-thickness stresses and failure margins. Curved panel structures may be modeled providing the curvature of a cross-section is defined by a single value function. COBSTRAN is written in FORTRAN 77.

Author

### **N89-23622\*#** Sverdrup Technology, Inc., Cleveland, OH. **THEORETICAL ANALYSIS OF COMPATIBILITY OF SEVERAL REINFORCEMENT MATERIALS WITH NIAL AND FEAL MATRICES Final Contractor Report**

AJAY K. MISRA May 1989 21 p Presented at the 13th Annual Conference on Composites and Advanced Ceramics, Cocoa Beach, FL, 18-20 Jan. 1989; sponsored by Advanced Ceramics Association (Contract NAS3-25266) (NASA-CR-182291; E-4796; NAS 1.26:182291) Avail: NTIS HC A03/MF A01 CSCL 11/4

Several potential reinforcement materials were assessed for their chemical, coefficient of thermal expansion (CTE), and mechanical compatibility with the intermetallic matrices based on NiAl and FeAl. Among the ceramic reinforcement materials, Al<sub>2</sub>O<sub>3</sub>, TiC, and TiB<sub>2</sub>, appear to be the optimum choices for NiAl and FeAl matrices. However, the problem of CTE mismatch with the

matrix needs to be solved for these three reinforcement materials. Beryllium-rich intermetallic compounds can be considered as potential reinforcement materials provided suitable reaction barrier coatings can be developed for these. Based on preliminary thermodynamic calculations,  $\text{Sc}_2\text{O}_3$  and  $\text{TiC}$  appear to be suitable as reaction barrier coatings for the beryllides. Several reaction barrier coatings are also suggested for the currently available  $\text{SiC}$  fibers. Author

**N89-23623\*** National Aeronautics and Space Administration. Lewis Research Center, Cleveland, OH.

**LIGHT WEIGHT POLYMER MATRIX COMPOSITE MATERIAL Patent Application**

KENNETH J. BOWLES, inventor (to NASA) and CARL E. LOWELL, inventor (to NASA) 5 Dec. 1988 16 p Sponsored by NASA. Lewis Research Center  
(NASA-CASE-LEW-14734-1; NAS 1.71:LEW-14734-1; US-PATENT-APPL-SN-279624) Avail: NTIS HC A03/MF A01 CSCL 11/4

A graphite fiber reinforced polymer matrix is layed up, cured, and thermally aged at about 750 F in the presence of an inert gas. The heat treatment improves the structural integrity and alters the electrical conductivity of the materials. In the preferred embodiment PMR-15 polyimides and Celion-6000 graphite fibers are used. NASA

**N89-24459\*** National Aeronautics and Space Administration. Lewis Research Center, Cleveland, OH.

**COMPOSITE BLADE STRUCTURAL ANALYZER (COBSTRAN) DEMONSTRATION MANUAL**

ROBERT A. AIELLO Apr. 1989 69 p  
(NASA-TM-101957; E-4735; NAS 1.15:101957) Avail: NTIS HC A04/MF A01 CSCL 11/4

The input deck setup is described for a computer code, composite blade structural analyzer (COBSTRAN) which was developed for the design and analysis of composite turboprop and turboprop blades and also for composite wind turbine blades. This manual is intended for use in conjunction with the COBSTRAN user's manual. Seven demonstration problems are described with pre- and postprocessing input decks. Modeling of blades which are solid thru-the-thickness and also aircraft wing airfoils with internal spars is shown. Corresponding NASTRAN and databank input decks are also shown. Detail descriptions of each line of the pre- and post-processing decks is provided with reference to the Card Groups defined in the user's manual. A dictionary of all program variables and terms used in this manual may be found in Section 6 of the user's manual. Author

**N89-24460\*** National Aeronautics and Space Administration. Lewis Research Center, Cleveland, OH.

**ISOTHERMAL LIFE PREDICTION OF COMPOSITE LAMINA USING A DAMAGE MECHANICS APPROACH**

NADER M. ABUELFOUTOUH, MICHAEL J. VERRILLI, and GARY R. HALFORD Jun. 1989 12 p Presented at the Symposium on High Temperature Composites, Dayton, OH, 13-15 Jun. 1989; sponsored by American Society for Composites Prepared in cooperation with Cairo Univ. (Egypt)  
(NASA-TM-102032; E-4775; NAS 1.15:102032) Avail: NTIS HC A03/MF A01 CSCL 11/4

A method for predicting isothermal plastic fatigue life of a composite lamina is presented in which both fibers and matrix are isotropic materials. In general, the fatigue resistances of the matrix, fibers, and interfacial material must be known in order to predict composite fatigue life. Composite fatigue life is predicted using only the matrix fatigue resistance due to inelasticity micromechanisms. The effect of the fiber orientation on loading direction is accounted for while predicting composite life. The application is currently limited to isothermal cases where the internal thermal stresses that might arise from thermal strain mismatch between fibers and matrix are negligible. The theory is formulated to predict the fatigue life of a composite lamina under either load or strain control. It is applied currently to predict the life of

tungsten-copper composite lamina at 260 C under tension-tension load control. The calculated life of the lamina is in good agreement with available composite low cycle fatigue data. Author

**N89-25290\*** National Aeronautics and Space Administration. Lewis Research Center, Cleveland, OH.

**VIBRATION TESTING OF IMPACT-DAMAGED COMPOSITE LAMINATES**

JOSEPH E. GRADY and ERWIN H. MEYN Jun. 1989 11 p Presented at the 30th Structures, Structural Dynamics and Materials Conference, Mobile, AL, 3-5 Apr. 1989; cosponsored by the AIAA, ASME, ASCE, AHS, and ASC Previously announced in IAA as A89-30883

(NASA-TM-4115; E-4518; NAS 1.15:4115) Avail: NTIS HC A03/MF A01 CSCL 11/4

A new test is described that can be used to measure changes in the vibration properties of impact damaged composite materials. Impact-induced delamination was observed to significantly affect natural frequencies of vibration and damping properties in cross-ply graphite/epoxy laminates. Natural frequencies are shown to drop by as much as half of their original value, and modal damping ratios can increase by a factor of up to eight when large amounts of damage are present. A simple finite element model of the damaged impact specimens was used to predict the effect of delamination on certain vibration properties. A comparison of the finite element calculations with the experimental measurements suggests that delamination was the dominant mechanism of flexural stiffness loss resulting from the transverse impact. Author

**N89-25300\*** National Aeronautics and Space Administration. Lewis Research Center, Cleveland, OH.

**A PREDICTIVE MODEL FOR FAILURE PROPERTIES OF THERMOSET RESINS**

JAMES M. CARUTHERS (Purdue Univ., West Lafayette, IN.) and KENNETH J. BOWLES Jul. 1989 8 p  
(Contract NAG3-599)

(NASA-TM-4128; E-4572; NAS 1.15:4128) Avail: NTIS HC A02/MF A01 CSCL 11/4

A predictive model for the three-dimensional failure behavior of engineering polymers has been developed in a recent NASA-sponsored research program. This model acknowledges the underlying molecular deformation mechanisms and thus accounts for the effects of different chemical compositions, crosslink density, functionality of the curing agent, etc., on the complete nonlinear stress-strain response including yield. The material parameters required by the model can be determined from test-tube quantities of a new resin in only a few days. Thus, we can obtain a first-order prediction of the applicability of a new resin for an advanced aerospace application without synthesizing the large quantities of material needed for failure testing. This technology will effect order-of-magnitude reductions in the time and expense required to develop new engineering polymers. Author

**N89-26048\*** National Aeronautics and Space Administration. Lewis Research Center, Cleveland, OH.

**SIMPLIFIED PROCEDURES FOR DESIGNING ADHESIVELY BONDED COMPOSITE JOINTS**

C. C. CHAMIS and P. L. N. MURTHY Feb. 1989 15 p Presented at the 44th Annual Conference of SPI Composites Inst., Dallas, TX, 6-10 Feb. 1989

(NASA-TM-102120; E-4899; NAS 1.15:102120) Avail: NTIS HC A03/MF A01 CSCL 11/4

Procedures for the preliminary design of composite adhesive joints are described. Typical joints, their respective free body diagrams, and approximate equations for estimating the stresses in each of these typical joints are summarized. Equations are also presented to check the critical conditions of the joint such as minimum length, maximum adhesive shear stress, and peel-off stress. To illustrate the procedure, sample designs are described in step-by-step fashion for a butt joint with single doubler subjected to static loads, cyclic loads, and environmental effects. The results show that unsymmetric adhesive joints are inefficient and should be avoided, and hygrothermal environments and cyclic loads

## 24 COMPOSITE MATERIALS

dramatically reduce the structural integrity of the joint and require several joint lengths compared with those for static load with no environmental effects. Author

**N89-26912\*#** National Aeronautics and Space Administration. Lewis Research Center, Cleveland, OH.

### **TAILORING OF COMPOSITE LINKS FOR OPTIMAL DAMPED ELASTO-DYNAMIC PERFORMANCE**

D. A. SARAVANOS and C. C. CHAMIS 1989 30 p Prepared for presentation at the Design Automation Conference, Montreal, Quebec, 17-20 Sep. 1989; sponsored by ASME (NASA-TM-102094; E-4875; NAS 1.15:102094) Avail: NTIS HC A03/MF A01 CSCL 11/4

A method is developed for the optimal design of composite links based on dynamic performance criteria directly related to structural modal damping and dynamic stiffness. An integrated mechanics theory correlates structural composite damping to the parameters of basic composite material systems, laminate parameters, link shape, and modal deformations. The inclusion of modal properties allows the selective minimization of vibrations associated with specific modes. Ply angles and fiber volumes are tailored to obtain optimal combinations of damping and stiffness. Applications to simple composite links indicate wide margins for trade-offs and illustrate the importance of various design variables to the optimal design. Author

**N89-26919\*#** National Aeronautics and Space Administration. Lewis Research Center, Cleveland, OH.

### **UNIFIED MICROMECHANICS OF DAMPING FOR UNIDIRECTIONAL FIBER REINFORCED COMPOSITES**

D. A. SARAVANOS and C. C. CHAMIS Aug. 1989 28 p Submitted for publication (NASA-TM-102107; E-4874; NAS 1.15:102107) Avail: NTIS HC A03/MF A01 CSCL 11/4

An integrated micromechanics methodology for the prediction of damping capacity in fiber-reinforced polymer matrix unidirectional composites has been developed. Explicit micromechanics equations based on hysteretic damping are presented relating the on-axis damping capacities to the fiber and matrix properties and volume fraction. The damping capacities of unidirectional composites subjected to off-axis loading are synthesized from thermal effect on the damping performance of unidirectional composites due to temperature and moisture variations is also modeled. The damping contributions from interfacial friction between broken fibers and matrix are incorporated. Finally, the temperature rise in continuously vibrating composite plies is estimated. Application examples illustrate the significance of various parameters on the damping performance of unidirectional and off-axis fiber reinforced composites. Author

**N89-26924\*#** National Aeronautics and Space Administration. Lewis Research Center, Cleveland, OH.

### **METAL MATRIX COMPOSITE MICROMECHANICS: IN-SITU BEHAVIOR INFLUENCE ON COMPOSITE PROPERTIES**

P. L. N. MURTHY, D. A. HOPKINS, and C. C. CHAMIS Jul. 1989 21 p Presented at the 3rd Joint Mechanics Conference, San Diego, CA, 9-12 Jul. 1989; sponsored in part by ASCE and ASME (NASA-TM-102302; E-4982; NAS 1.15:102302) Avail: NTIS HC A03/MF A01 CSCL 11/4

Recent efforts in computational mechanics methods for simulating the nonlinear behavior of metal matrix composites have culminated in the implementation of the Metal Matrix Composite Analyzer (METCAN) computer code. In METCAN material nonlinearity is treated at the constituent (fiber, matrix, and interphase) level where the current material model describes a time-temperature-stress dependency of the constituent properties in a material behavior space. The composite properties are synthesized from the constituent instantaneous properties by virtue of composite micromechanics and macromechanics models. The behavior of metal matrix composites depends on fabrication process variables, in situ fiber and matrix properties, bonding between the fiber and matrix, and/or the properties of an interphase

between the fiber and matrix. Specifically, the influence of in situ matrix strength and the interphase degradation on the unidirectional composite stress-strain behavior is examined. These types of studies provide insight into micromechanical behavior that may be helpful in resolving discrepancies between experimentally observed composite behavior and predicted response. Author

**N89-27795\*#** National Aeronautics and Space Administration. Lewis Research Center, Cleveland, OH.

### **COMPUTATIONAL SIMULATION OF HIGH TEMPERATURE METAL MATRIX COMPOSITES CYCLIC BEHAVIOR**

C. C. CHAMIS, P. L. N. MURTHY, and D. A. HOPKINS 8 Nov. 1988 15 p Presented at the ASTM Symposium on Thermal and Mechanical Behavior of Ceramic and Metal Matrix Composites, Atlanta, GA, 7-8 Nov. 1988 (NASA-TM-102115; E-4888; NAS 1.15:102115) Avail: NTIS HC A03/MF A01 CSCL 11/4

A procedure was developed and is described which can be used to computationally simulate the cyclic behavior of high temperature metal matrix composites (HTMMC) and its degradation effects on the structural response. This procedure consists of HTMMC mechanics coupled with a multifactor interaction constituent material relationship and with an incremental iterative nonlinear analysis. The procedure is implemented in a computer code that can be used to computationally simulate the thermomechanical behavior of HTMMC starting from the fabrication process and proceeding through thermomechanical cycling, accounting for the interface/interphase region. Results show that combined thermal/mechanical cycling, the interphase, and in situ matrix properties have significant effects on the structural integrity of HTMMC. Author

**N89-27796\*#** National Aeronautics and Space Administration. Lewis Research Center, Cleveland, OH.

### **TUNGSTEN FIBER REINFORCED COPPER MATRIX COMPOSITES: A REVIEW**

DAVID L. MCDANIELS Sep. 1989 24 p (NASA-TP-2924; E-4318; NAS 1.60:2924) Avail: NTIS HC A03/MF A01 CSCL 11/4

Tungsten fiber reinforced copper matrix (W/Cu) composites have served as an ideal model system with which to analyze the properties of metal matrix composites. A series of research programs were conducted to investigate the stress-strain behavior of W/Cu composites; the effect of fiber content on the strength, modulus, and conductivity of W/Cu composites; and the effect of alloying elements on the behavior of tungsten wire and of W/Cu composites. Later programs investigated the stress-rupture, creep, and impact behavior of these composites at elevated temperatures. Analysis of the results of these programs as allows prediction of the effects of fiber properties, matrix properties, and fiber content on the properties of W/Cu composites. These analyses form the basis for the rule-of-mixtures prediction of composite properties which was universally adopted as the criteria for measuring composite efficiency. In addition, the analyses allows extrapolation of potential properties of other metal matrix composites and are used to select candidate fibers and matrices for development of tungsten fiber reinforced superalloy composite materials for high temperature aircraft and rocket engine turbine applications. The W/Cu composite efforts are summarized, some of the results obtained are described, and an update is provided on more recent work using W/Cu composites as high strength, high thermal conductivity composite materials for high heat flux, elevated temperature applications. Author

**N89-29490\*#** National Aeronautics and Space Administration. Lewis Research Center, Cleveland, OH.

### **INTERMETALLIC AND CERAMIC MATRIX COMPOSITES FOR 815 TO 1370 C (1500 TO 2500 F) GAS TURBINE ENGINE APPLICATIONS**

JOSEPH R. STEPHENS 1989 11 p Proposed for presentation at the Advanced Metal and Ceramic Matrix Composites, Anaheim, CA, 19-22 Feb. 1990; sponsored by The Minerals, Metals and



Materials Society and ASM International  
(NASA-TM-102326; E-5027; NAS 1.15:102326) Avail: NTIS HC  
A03/MF A01 CSCL 11/4

Light weight and potential high temperature capability of intermetallic compounds, such as the aluminides, and structural ceramics, such as the carbides and nitrides, make these materials attractive for gas turbine engine applications. In terms of specific fuel consumption and specific thrust, revolutionary improvements over current technology are being sought by realizing the potential of these materials through their use as matrices combined with high strength, high temperature fibers. The U.S. along with other countries throughout the world have major research and development programs underway to characterize these composites materials; improve their reliability; identify and develop new processing techniques, new matrix compositions, and new fiber compositions; and to predict their life and failure mechanisms under engine operating conditions. The status is summarized of NASA's Advanced High Temperature Engine Materials Technology Program (HITEMP) and the potential benefits are described to be gained in 21st century transport aircraft by utilizing intermetallic and ceramic matrix composite materials. Author

## 25

## INORGANIC AND PHYSICAL CHEMISTRY

Includes chemical analysis, e.g., chromatography; combustion theory; electrochemistry; and photochemistry.

**A89-12330\*** National Aeronautics and Space Administration. Lewis Research Center, Cleveland, OH.

**DEPOSITION OF Na<sub>2</sub>SO<sub>4</sub> FROM SALT-SEEDED COMBUSTION GASES OF A HIGH VELOCITY BURNER RIG**

G. J. SANTORO, F. J. KOHL, C. A. STEARNS (NASA, Lewis Research Center, Cleveland, OH), S. A. GOKOGLU (Analex Corp., Cleveland, OH), and D. A. ROSNER (Yale University, New Haven, CT) IN: High temperature corrosion in energy systems. Warrendale, PA, Metallurgical Society of AIME, 1985, p. 417-434. refs

Copyright

With a view to developing simulation criteria for the laboratory testing of high-temperature materials for gas turbine engines, the deposition rates of sodium sulfate from sodium salt-seeded combustion gases were determined experimentally using a well instrumented high-velocity burner. In the experiments, Na<sub>2</sub>SO<sub>4</sub>, NaCl, NaNO<sub>3</sub>, and simulated sea salt solutions were injected into the combustor of the Mach 0.3 burner rig operating at constant fuel/air ratios. The deposits formed on an inert rotating collector were then weighed and analyzed. The experimental results are compared to Rosner's vapor diffusion theory. Some additional test results, including droplet size distribution of an atomized salt spray, are used in interpreting the deposition rate data. V.L.

**A89-12333\*#** Yale Univ., New Haven, CT.

**TRANSPORT-INDUCED SHIFTS IN CONDENSATE DEW-POINT AND COMPOSITION IN MULTICOMPONENT SYSTEMS WITH CHEMICAL REACTION**

D. E. ROSNER and R. NAGARAJAN (Yale University, New Haven, CT) Chemical Engineering Science (ISSN 0009-2509), vol. 40, no. 2, 1985, p. 177-186. refs  
(Contract NAG3-201; AF-AFOSR-83-0034)

Partial heterogeneous condensation phenomena in multi-component reacting systems are analyzed taking into consideration the chemical element transport phenomena. It is demonstrated that the dew-point surface temperature in chemically reactive systems is not a purely thermodynamic quantity, but is influenced by the multicomponent diffusion and Soret-mass diffusion phenomena. Several distinct dew-points are shown to exist in such systems and, as a result of transport constraints,

the 'sharp' locus between two chemically distinct condensates is systematically moved to a difference mainstream composition.

I.S.

**A89-12334\*** Yale Univ., New Haven, CT.

**OPTICAL METHODS AND RESULTS OF DEW POINT AND DEPOSITION RATE MEASUREMENTS IN SALT/ASH-CONTAINING COMBUSTION GASES - B<sub>2</sub>O<sub>3</sub>(I) DEPOSITION RATES BY INTERFERENCE METHODS AND COMPARISONS WITH THEORY**

K. SESHADRI and D. E. ROSNER (Yale University, New Haven, CT) AIChE Journal (ISSN 0001-1541), vol. 30, March 1984, p. 187-196. refs  
(Contract NSG-3169; NAG3-201; F49620-76-C-0020)  
Copyright

**A89-12335\*** Yale Univ., New Haven, CT.

**LABORATORY STUDIES OF BINARY SALT CVD IN COMBUSTION GAS ENVIRONMENTS**

BAISHEN LIANG and D. E. ROSNER (Yale University, New Haven, CT) AIChE Journal (ISSN 0001-1541), vol. 33, Dec. 1987, p. 1937-1948. refs  
(Contract NAG3-590; DE-AC21-85MC-22075)  
Copyright

A flash-evaporation technique is used to obtain vapor deposition characteristics for the binary alkali sulfates K<sub>2</sub>SO<sub>4</sub> + Na<sub>2</sub>SO<sub>4</sub> at 1 atm above 1100 K. The experimental equipment and techniques are described, and preliminary results are reported which indicate that this experimental technique meets most of the research requirements for studying multicomponent systems of current interest. The various deposition rate effects of introducing additives and the relevant inferences of condensate composition are presented, and the theoretical implications are discussed. It is concluded that alkali sulfate deposition and vaporization in combustion environments are inevitably influenced by chemical reactions such as hydroxide formation, and that solution nonideality is important even for homologous alkali-salt mixtures. C.D.

**A89-12338\*** Yale Univ., New Haven, CT.

**LABORATORY STUDIES OF THE DEPOSITION OF ALKALI SULFATE VAPORS FROM COMBUSTION GASES USING A FLASH-EVAPORATION TECHNIQUE**

DANIEL E. ROSNER and BAISHEN LIANG (Yale University, New Haven, CT) Chemical Engineering Communications (ISSN 0098-6445), vol. 42, no. 1-3, 1986, p. 171-190. refs  
(Contract NSG-3169; AF-AFOSR-84-0034)  
Copyright

A relatively simple experimental technique is proposed and demonstrated for making measurements of absolute dewpoints and relative deposition rates from flowing combustion gases containing condensable inorganic vapors. The method involves first accumulating condensate on a Pt ribbon target maintained below the dewpoint and then flash-evaporating the condensate into the filament wake, where its alkali content is monitored by alkali-atom emission spectroscopy. The advantages of the method over others are demonstrated; in particular, the method can detect liquid condensate inventories which are small enough to be negligibly influenced by surface runoff produced by gas-side shear stress and liquid condensate surface tension gradients. Illustrative Na<sub>2</sub>SO<sub>4</sub> and K<sub>2</sub>SO<sub>4</sub> deposition rate data and corresponding dewpoint data obtained in a series of alkali-seeded propane/air atmospheric flames are presented and discussed. C.D.

**A89-12620\*** National Aeronautics and Space Administration. Lewis Research Center, Cleveland, OH.

**STRUCTURAL CHEMISTRY OF AU(III)-SUBSTITUTED BA<sub>2</sub>YCu<sub>3</sub>O<sub>7-Δ</sub>**

A. F. HEPP, J. R. GAIER, J. J. POUCH (NASA, Lewis Research Center, Cleveland, OH), and P. D. HAMBOURGER (Cleveland State University, OH) Journal of Solid State Chemistry (ISSN 0022-4596), vol. 74, 1988, p. 433-437. refs  
(Contract NCC3-19)  
Copyright



A series of gold-substituted perovskite superconductors  $\text{Ba}_2\text{Y}(\text{Cu}/1-x/\text{Au})\text{3O}(7-\delta)(x = 0-0.1)$  was synthesized. For  $x = 0.1$ , there was no change in the  $a$  and  $b$  lattice parameters ( $a = 3.826 \text{ \AA}$  and  $b = 3.889 \text{ \AA}$ ), but a  $0.06 \text{ \AA}$   $c$ -axis expansion to  $11.75 \text{ \AA}$  was observed. Substituted gold was found to be trivalent by X-ray photoelectron spectroscopy. Replacing  $\text{Cu}(1)$  in the copper oxide chain with a slight reordering of oxygen is consistent with  $c$ -axis expansion. The formal charge of the site remains trivalent, while remaining  $\text{Cu}$  in the chains is reduced to  $\text{Cu}(1)$ , resulting in an oxygen stoichiometry of less than 7. Finally, no large effect on  $T_c$  is observed ( $T_c = 89 \text{ K}$  for  $x = 0.10$ ), in contrast to the effect of a number of other metal ion dopants. These results are discussed relative to the chemistry of  $\text{Au(III)}$  and to the use of the metal in structures containing gold and ceramic superconductors. Author

**A89-12624\*** National Aeronautics and Space Administration. Lewis Research Center, Cleveland, OH.

**A PRELIMINARY REPORT ON THE EFFECTS OF LONG-TERM EXPOSURE OF LIOH ON PURE NICKEL**

J. D. WHITTENBERGER (NASA, Lewis Research Center, Cleveland, OH) *Journal of Materials for Energy Systems* (ISSN 0162-9719), vol. 8, March 1987, p. 385-390. refs Copyright

A 'bread pan' capsule has been designed which allows large numbers of tensile specimens to be simultaneously exposed to molten  $\text{LiOH}$ , its vapor, and vacuum. Capsules and specimens fabricated from the pure nickel alloy  $\text{Ni-200}$  were annealed for 401 hours and 2500 hours at  $775 \text{ K}$ . Examination of the exposed materials revealed that little outward damage in terms of visible attack, weight change, or loss of room temperature tensile properties occurred. In particular, the mechanical behavior of hydroxide-contaminated alloy was essentially identical to that receiving a simple thermal exposure in vacuum. Examination of the microstructures revealed that  $\text{LiOH}$  did produce some nonuniform, shallow intergranular corrosion in  $\text{Ni-200}$ ; however, the extent of the damage was insufficient to produce weakening or embrittlement. Author

**A89-12903\*** Pennsylvania State Univ., University Park. **EFFECT OF ALCOHOL ADDITION ON SHOCK-INITIATED FORMATION OF SOOT FROM BENZENE**

MICHAEL FRENKLACH and TONY YUAN (Pennsylvania State University, University Park) IN: Shock tubes and waves; Proceedings of the Sixteenth International Symposium, Aachen, Federal Republic of Germany, July 26-31, 1987. Weinheim, Federal Republic of Germany, VCH Verlagsgesellschaft mbH, 1988, p. 487-493. refs (Contract NAS3-23542; NAG3-477; NAG3-668) Copyright

Soot formation in benzene-methanol and benzene-ethanol argon-diluted mixtures was studied behind reflected shock waves by monitoring the attenuation of an  $\text{He-Ne}$  laser beam. The experiments were performed at temperatures  $1580-2250 \text{ K}$ , pressures  $2.0-3.0 \text{ bar}$ , and total carbon atom concentrations  $(2.0-2.7) \times 10$  to the 17th atoms/cu cm. The results obtained indicate that the addition of alcohol suppresses the formation of soot from benzene at all temperatures, and that the reduction in soot yields is increased with the amount of alcohol added. The analysis of the results indicates that the suppression effect is probably due to the oxidation of soot and soot precursors by  $\text{OH}$  and the removal of hydrogen atoms by alcohol and water molecules. Author

**A89-14799\*** Yale Univ., New Haven, CT. **OPTICAL EXPERIMENTS ON THERMOPHORETICALLY AUGMENTED SUBMICRON PARTICLE DEPOSITION FROM 'DUSTY' HIGH TEMPERATURE GAS FLOWS**

DANIEL E. ROSNER and SANG-SOO KIM (Yale University, New Haven, CT) *The Chemical Engineering Journal* (ISSN 0300-9467), vol. 29, 1984, p. 147-157. refs (Contract F49620-82-K-0020; NSG-3169) Copyright

A real-time laser reflectivity method and  $\text{Pt}$  ribbon targets are used to obtain experimental data on the initial deposition rate of  $\text{MgO(s)}$  particles of approximately  $700 \text{ nm}$  diameter from otherwise clean combustion products as a function of target temperature (about  $950-1450 \text{ K}$ ) and mainstream gas temperature (about  $1500-1600 \text{ K}$ ). These preliminary data are used to demonstrate the dominant role of thermophoresis (particle drift down a temperature gradient) and to assess the utility of recently developed theoretical methods for predicting and correlating the temperature dependence of thermophoretically augmented convective-diffusion 'dust' deposition rates from flowing hot gases. Author

**A89-16416\*** National Aeronautics and Space Administration. Lewis Research Center, Cleveland, OH.

**THE INTERACTION OF GOLD WITH GALLIUM ARSENIDE**

VICTOR G. WEIZER (NASA, Lewis Research Center, Cleveland, OH) and NAVID S. FATEMI (Sverdrup Technology, Inc., Middleburg Heights, OH) *Journal of Applied Physics* (ISSN 0021-8979), vol. 64, Nov. 1, 1988, p. 4618-4623. refs Copyright

Gold and gold-based alloys, commonly used as solar-cell contact materials, are known to react readily with gallium arsenide. Experiments designed to identify the mechanisms involved in these  $\text{GaAs-metal}$  interactions have yielded several interesting results. It is shown that the reaction of  $\text{GaAs}$  with gold takes place via a dissociative diffusion process. It is shown further that the  $\text{GaAs-metal}$  reaction rate is controlled to a very great extent by the condition of the free surface of the contact metal, an interesting example of which is the previously unexplained increase in the reaction rate that has been observed for samples annealed in a vacuum environment as compared to those annealed in a gaseous ambient. A number of other hard-to-explain observations, such as the low-temperature formation of voids in the gold lattice and crystallite growth on the gold surface, are also explained by invoking this mechanism. Author

**A89-19298\*** Princeton Univ., NJ. **INTERACTIONS BETWEEN GASEOUS ELECTRICAL DISCHARGES AND SINGLE LIQUID DROPLETS**

B. D. SHAW, F. L. DRYER, F. A. WILLIAMS (Princeton University, NJ), and N. GAT (TRW, Inc., Space and Technology Group, Redondo Beach, CA) *Combustion and Flame* (ISSN 0010-2180), vol. 74, Dec. 1988, p. 233-254. refs (Contract NAS3-24640) Copyright

Theoretical estimates and experimental measurements of the effects of sparks on ordered droplet motion are reported for  $1\text{-mm-diameter}$  water and hydrocarbon droplets positioned  $0.5 \text{ mm}$  from the axis of electrodes are reported. The discussion focuses primarily on two-electrode, surge-type spark breakdowns with quasi-steady electric fields applied. Multiple electrode pairs and alternating electric fields and their effects on ordered droplet motion are also briefly discussed. V.L.

**A89-20474\*** Nebraska Univ., Lincoln. **GROWTH OF DIAMOND BY RF PLASMA-ASSISTED CHEMICAL VAPOR DEPOSITION**

DUANE E. MEYER, NATALE J. IANNO, JOHN A. WOOLLAM (Nebraska, University, Lincoln), A. B. SWARTZLANDER, and A. J. NELSON (Solar Energy Research Institute, Golden, CO) *Journal of Materials Research* (ISSN 0884-2914), vol. 3, Nov.-Dec. 1988, p. 1397-1403. refs (Contract NAG3-95) Copyright

A system has been designed and constructed to produce diamond particles by inductively coupled radio-frequency, plasma-assisted chemical vapor deposition. This is a low-pressure, low-temperature process used in an attempt to deposit diamond on substrates of glass, quartz, silicon, nickel, and boron nitride. Several deposition parameters have been varied including substrate temperature, gas concentration, gas pressure, total gas flow rate, RF input power, and deposition time. Analytical methods employed to determine composition and structure of the deposits include

scanning electron microscopy, absorption spectroscopy, scanning Auger microprobe spectroscopy, and Raman spectroscopy. Analysis indicates that particles having a thin graphite surface, as well as diamond particles with no surface coatings, have been deposited. Deposits on quartz have exhibited optical bandgaps as high as 4.5 eV. Scanning electron microscopy analysis shows that particles are deposited on a pedestal which Auger spectroscopy indicates to be graphite. This is a phenomenon that has not been previously reported in the literature. Author

**A89-23146\*** National Aeronautics and Space Administration. Lewis Research Center, Cleveland, OH.

**USE OF PURE NICKEL AND LIOH FOR THERMAL ENERGY STORAGE**

J. D. WHITTENBERGER (NASA, Lewis Research Center, Cleveland, OH) Journal of Materials Engineering (ISSN 0931-7058), vol. 10, Dec. 1988, p. 247-258. refs Copyright

The solid to liquid phase transformation of LiOH has been proposed as an ideal candidate thermal energy storage media for a Rankine Cycle powered electrical generation unit envisioned in Space Station based solar dynamic systems. Due to the corrosive nature of molten hydroxides, long term containment of LiOH is of concern. Pure nickel is thought to be a suitably resistant material, and a program has been instituted to measure the effects of prolonged exposure of liquid and gaseous LiOH on the mechanical properties of pure nickel alloys. Results to date indicate that negligible weight and thickness changes occurred in Ni alloys exposed to LiOH for as long as 2500 hr at 775 K, and essentially no difference in 77-900 K tensile properties could be detected between LiOH exposed and vacuum annealed Ni specimens. Although there was little sign of outward damage, microstructural examination revealed that all hydroxide contaminated tensile test specimens had surface connected intergranular cracks along the gage lengths. Two other potential problems, which have strong implications with respect to a LiOH/Ni energy storage system, were also noted during the corrosion experiments. In particular stress corrosion cracking of weld joints in pressurized vessel and permeation of hydrogen through nickel were observed. Author

**A89-25406\*#** California Univ., La Jolla.

**RADIATIVE STRUCTURES OF LYCOPodium-AIR FLAMES IN LOW GRAVITY**

A. L. BERLAD, V. TANGIRALA (California, University, La Jolla), H. ROSS, and L. FACCA (NASA, Lewis Research Center, Cleveland, OH; California, University, La Jolla) AIAA, Aerospace Sciences Meeting, 27th, Reno, NV, Jan. 9-12, 1989. 9 p. refs (AIAA PAPER 89-0500) Copyright

Initially uniform clouds of fuel particulates in air sustain processes which may lead to particle cloud nonuniformities. In low gravity, flame-induced Kundt's Tube phenomena are observed to form regular patterns of nonuniform particle concentrations. Irregular patterns of particle concentrations also are observed to result from selected nonuniform mixing processes. Low gravity flame propagation for each of these classes of particle cloud flames has been found to depend importantly on the flame-generated infrared radiative fields. The spatial structures of these radiative fields are described. Application is made for the observed classes of lycopodium-air flames. Author

**A89-26406\*** General Motors Research Labs., Warren, MI.  
**CONNECTION BETWEEN ENERGY RELATIONS OF SOLIDS AND MOLECULES**

JOHN R. SMITH (GM Research Laboratories, Warren, MI), HERBERT SCHLOSSER (Cleveland State University, OH), WILLIAM LEAF (Harvard University, Cambridge, MA), JOHN FERRANTE (NASA, Lewis Research Center, Cleveland, OH), and JAMES H. ROSE (DOE, Ames Laboratory, IA) Physical Review A - General Physics, 3rd Series (ISSN 0556-2791), vol. 39, Jan. 15, 1989, p. 514-517. refs (Contract W-7405-ENG-82) Copyright

The universal energy relation, discovered for metallic and

covalent solids as well as nuclear matter, is tested for diatomic molecules. It is found that it applies well to covalent diatomic bonds, but that ionic diatomic bonds are in a distinct class. A simple extension of the universal binding energy relation that includes the effects of ionicity ensues. It yields accurate prediction of spectroscopic data for both ionic and covalent bonds in 150 molecules. The form of the covalent part is given by the universal relation, suggesting an intimate relationship between the energetics of solids and diatomic molecules. Author

**A89-27966\*** Aerodyne Research, Inc., Billerica, MA.  
**SURFACE STUDIES RELEVANT TO SILICON CARBIDE CHEMICAL VAPOR DEPOSITION**

C. D. STINESPRING and J. C. WORMHOUDT (Aerodyne Research Center for Chemical and Environmental Physics, Billerica, MA) Journal of Applied Physics (ISSN 0021-8979), vol. 65, Feb. 15, 1989, p. 1733-1742. refs (Contract NAS3-24531; NAS3-23891) Copyright

Reactions of C<sub>2</sub>H<sub>4</sub>, C<sub>3</sub>H<sub>8</sub>, and CH<sub>4</sub> on the Si(111) surface and C<sub>2</sub>H<sub>4</sub> on the Si(100) surface were investigated for surface temperatures in the range of 1062-1495 K. Results led to the identification of the reaction products, a characterization of the solid-state transport process, a determination of the nucleation mechanism and growth kinetics, and an assessment of orientation effects. Based on these results and on the modeling studies of Stinespring and Wormhoudt (1988) on the associated gas phase chemistry, a physical model for the two-step beta-SiC CVD process is proposed. I.S.

**A89-28084\*** National Aeronautics and Space Administration. Lewis Research Center, Cleveland, OH.

**SODIUM SULFATE - DEPOSITION AND DISSOLUTION OF SILICA**

NATHAN S. JACOBSON (NASA, Lewis Research Center, Cleveland, OH) Oxidation of Metals (ISSN 0030-770X), vol. 31, Feb. 1989, p. 91-103. refs Copyright

The hot-corrosion process for SiO<sub>2</sub>-protected materials involves deposition of Na<sub>2</sub>SO<sub>4</sub> and dissolution of the protective SiO<sub>2</sub> scale. Dew points for Na<sub>2</sub>SO<sub>4</sub> deposition are calculated as a function of pressure, sodium content, and sulfur content. Expected dissolution regimes for SiO<sub>2</sub> are calculated as a function of Na<sub>2</sub>SO<sub>4</sub> basicity. Controlled-condition burner-rig tests on quartz verify some of these predicted dissolution regimes. The basicity of Na<sub>2</sub>SO<sub>4</sub> is not always a simple function of P(SO<sub>3</sub>). Electrochemical measurements of an (Na<sub>2</sub>O) show that carbon creates basic conditions in Na<sub>2</sub>SO<sub>4</sub>, which explains the extensive corrosion of SiO<sub>2</sub>-protected materials containing carbon, such as SiC. Author

**A89-28420\*#** Bradley Univ., Peoria, IL.  
**THE EFFECTS OF RADIATIVE HEAT LOSS ON MICROGRAVITY FLAME SPREAD**

AHMAD FAKHERI (Bradley University, Peoria, IL) and SANDRA L. OLSON (NASA, Lewis Research Center, Cleveland, OH) AIAA, Aerospace Sciences Meeting, 27th, Reno, NV, Jan. 9-12, 1989. 7 p. refs (AIAA PAPER 89-0504) Copyright

The effect of radiative heat loss from the surface of a solid material burning in a zero gravity environment in an opposed flow is studied through the use of a numerical model. Radiative heat loss is found to decrease the flame spread rate, the boundary layer thickness, and pyrolysis lengths. Blowoff extinction is predicted to occur at slower opposed flow velocities than would occur if the radiative loss is not present. The radiative heat fluxes are comparable to the conduction fluxes, indicating the significance of the surface energy loss. Author

**A89-29295\*** National Aeronautics and Space Administration. Lewis Research Center, Cleveland, OH.

**COMPUTER SIMULATION OF CYCLIC OXIDATION**

H. B. PROBST and C. E. LOWELL (NASA, Lewis Research Center,

Cleveland, OH) Journal of Metals (ISSN 0148-6608), vol. 40, Oct. 1988, p. 18-21. refs  
Copyright

A computer program has been developed which simulates the cyclic oxidation behavior of materials. The simulation is based on the assumption that the weight fraction of scale that spalls in any thermal cycle is proportional to the amount of scale present on the surface at the beginning of the cycle. The program provides plots as well as tabular data which describe the cyclic oxidation behavior of a given material. Individual input parameters can be selectively altered and the resulting change in cyclic kinetics determined, allowing the user to quickly survey a wide range of cyclic conditions on the kinetics of a given material. Author

**A89-33369\*#** North Carolina State Univ., Raleigh.  
**THE TURBULENCE CHARACTERISTICS OF A SEPARATED FLOW WITH COMBUSTION**

RICHARD D. GOULD (North Carolina State University, Raleigh), WARREN H. STEVENSON, and H. DOYLE THOMPSON (Purdue University, West Lafayette, IN) IN: International Symposium on Applications of Laser Anemometry to Fluid Mechanics, 4th, Lisbon, Portugal, July 11-14, 1988, Proceedings. Lisbon, Instituto Superior Tecnico, 1988, p. 4.6 (6 p.). refs  
(Contract NAG3-503)

The effects of combustion on the turbulent structure of a flow and vice versa were studied by making simultaneous two-component laser velocimeter measurements in the turbulent flow field following an axisymmetric sudden expansion with and without combustion. Mean axial and radial velocities and Reynolds stresses were measured. In addition, simultaneous time resolved temperature measurements were made in the reacting flow using fast response thermocouples. Velocity-temperature correlations were formed from the velocity and temperature measurements. Author

**A89-35008\*** National Aeronautics and Space Administration. Lewis Research Center, Cleveland, OH.

**OPTICAL MEASUREMENTS OF SOOT AND TEMPERATURE PROFILES IN PREMIXED PROPANE-OXYGEN FLAMES**

V. J. LYONS and P. J. PAGNI (NASA, Lewis Research Center, Cleveland, OH; California, University, Berkeley) IN: Collected papers in heat transfer 1988; Proceedings of the ASME Winter Annual Meeting, Chicago, IL, Nov. 27-Dec. 2, 1988. Volume 2. New York, American Society of Mechanical Engineers, 1988, p. 59-64. Previously announced in STAR as N88-29997. refs  
(Contract NBS-60-NANB5D-0552)  
Copyright

Two laser diagnostic techniques were used to measure soot volume fractions, number densities and soot particle radii in premixed propane/oxygen flat flames. The two techniques used were two wavelength extinction, using 514.5 nm to 632.8 nm and 457.9 nm to 632.8 nm wavelength combinations, and extinction/scattering using 514.5 nm light. The flames were fuel-rich (equivalence ratios from 2.1 to 2.8) and had cold gas velocities varying from 3.4 to 5.5 cm/s. Measurements were made at various heights above the sintered-bronze, water-cooled flat flame burner with the equivalence ratio and cold gas velocity fixed. Also, measurements were made at a fixed height above the burner and fixed cold gas velocity while varying the equivalence ratio. Both laser techniques are based on the same underlying assumptions of particle size distribution and soot optical properties. Full Mie theory was used to determine the extinction coefficients  $K_{sub ext}$  and the scattering efficiencies,  $Q_{sub vv}$ . Temperature measurements in the flames were made using infrared radiometry. Good agreement between the two techniques in terms of soot particle radii, number density and volume fraction was found for intensity ratios ( $I/I_{sub 0}$ ) between 0.1 and 0.8. For intensity ratios higher or lower than this range, the differences in extinction coefficients at the wavelengths chosen for the two-wavelength method are too small to give accurate results for comparing particle radii and number densities. However, when comparing only soot volume fractions, the agreement between the two techniques continued to be good for intensity ratios up to 0.95. Author

**A89-38658\*** Arizona State Univ., Tempe.

**ON THE MODELLING OF SCALAR AND MASS TRANSPORT IN COMBUSTOR FLOWS**

M. NIKJOOY and R. M. C. SO (Arizona State University, Tempe) International Journal for Numerical Methods in Engineering (ISSN 0029-5981), vol. 28, April 1989, p. 861-877. refs  
(Contract NAG3-167; NAG3-260)  
Copyright

Results are presented of a numerical study of swirling and nonswirling combustor flows with and without density variations. Constant-density arguments are used to justify closure assumptions invoked for the transport equations for turbulent momentum and scalar fluxes, which are written in terms of density-weighted variables. Comparisons are carried out with measurements obtained from three different axisymmetric model combustor experiments covering recirculating flow, swirling flow, and variable-density swirling flow inside the model combustors. Results show that the Reynolds stress/flux models do a credible job of predicting constant-density swirling and nonswirling combustor flows with passive scalar transport. However, their improvements over algebraic stress/flux models are marginal. The extension of the constant-density models to variable-density flow calculations shows that the models are equally valid for such flows. S.A.V.

**A89-44002\*** National Aeronautics and Space Administration. Lewis Research Center, Cleveland, OH.

**PERFORMANCE OF LIGHTWEIGHT NICKEL ELECTRODES**

DORIS L. BRITTON (NASA, Lewis Research Center, Cleveland, OH) IN: International Power Sources Symposium, 33rd, Cherry Hill, NJ, June 13-16, 1988, Proceedings. Pennington, NJ, Electrochemical Society, Inc., 1988, p. 467-475. Previously announced in STAR as N88-26430. refs  
Copyright

The NASA Lewis Research Center is currently developing nickel electrodes for nickel-hydrogen (Ni-H<sub>2</sub>) batteries. These electrodes are lighter in weight and have higher energy densities than the heavier state-of-the-art (SOA) sintered nickel electrodes. In the present approach, lightweight materials or plaques are used as conductive supports for the nickel hydroxide active material. These plaques (fiber and felt, nickel plated plastic and graphite) are commercial products that are fabricated into nickel electrodes by electrochemically impregnating them with active material. Evaluation is performed in half cells structured in the bipolar configuration. Initial performance tests include capacity measurements at five discharge levels, C/2, 1.0C, 1.37C, 2.0C and 2.74C. The electrodes that pass the initial tests are life cycle tested in a low earth orbit regime at 80 percent depth of discharge. Different formulations of nickel fiber materials obtained from several manufacturers are currently being tested as possible candidates for nickel electrodes. One particular lightweight fiber mat electrode has accumulated over 3000 cycles to date, with stable capacity and voltage. Life and performance data of this electrode were investigated and presented. Good dimensional stability and active material adherence have been demonstrated in electrodes made from this lightweight plaque. Author

**A89-44536\*** Akron Univ., OH.

**ALKOXYLANE ADSORPTION ON METAL OXIDE SUBSTRATES**

R. D. RAMSIER, G. R. ZHUANG, and P. N. HENRIKSEN (Akron, University, OH) Journal of Vacuum Science and Technology A (ISSN 0734-2101), vol. 7, May-June 1989, pt. 2, p. 1724-1728. Research supported by the University of Akron and U.S. Navy. refs  
(Contract NAG3-813)  
Copyright

Reflection-absorption infrared and inelastic electron tunneling spectroscopies have been used to study adsorption of liquid phase mono-, di-, and trialkoxysilanes on evaporated Al and Cu substrates. Spectral evidence shows that substrate properties influence the chemical and physical nature of trialkoxysilane films and that silane functionality plays a role in molecular orientation. Results show that dialkoxysilane films contain structural gradients, with adsorption

at the monomolecular level influenced by surface morphology, and with organofunctionality and dosing procedure affecting the formation of thicker films. Evidence is presented that monoalkoxysilanes react with alumina surfaces, and a broad, multi-peaked band from 1600 to 1900/cm has been interpreted as characteristic of the silylated  $\text{AlO}(x)\text{Pb}$  interface. Author

**A89-44542\*** Case Western Reserve Univ., Cleveland, OH.  
**PULSED ION BEAM INVESTIGATION OF THE KINETICS OF SURFACE REACTIONS**

C. C. HORTON, T. G. ECK, and R. W. HOFFMAN (Case Western Reserve University, Cleveland, OH) *Journal of Vacuum Science and Technology A* (ISSN 0734-2101), vol. 7, May-June 1989, pt. 2, p. 2143-2146. refs  
 (Contract NAG3-696)  
 Copyright

Pulsed ion beam measurements of the kinetics of surface reactions are discussed for the case where the width of the ion pulse is comparable to the measured reaction time, but short compared to the time between successive pulses. Theoretical expressions are derived for the time dependence of the ion-induced signals for linear surface reactions. Results are presented for CO emission from surface carbon and CF emission from Teflon induced by oxygen ion bombardment. The strengths and limitations of this technique are described. Author

**A89-52202\*** National Aeronautics and Space Administration.  
 Lewis Research Center, Cleveland, OH.

**METAL-SILICON REACTION RATES - THE EFFECTS OF CAPPING**

VICTOR G. WEIZER (NASA, Lewis Research Center, Cleveland, OH) and DAVID S. FATEMI (Sverdrup Technology, Inc., Middleburg Heights, OH) *Journal of Electronic Materials* (ISSN 0361-5235), vol. 18, no. 1, 1989, p. 7-13. refs  
 Copyright

Evidence is presented showing that the presence of the commonly used anti-reflection coating material  $\text{Ta}_2\text{O}_5$  on the free surface of contact metallization can either suppress or enhance, depending on the system, the interaction that takes place at elevated temperatures between the metallization and the underlying Si. The cap layer is shown to suppress both the generation and annihilation of vacancies at the free surface of the metal which are necessary to support metal-Si interactions. Evidence is also presented indicating that the mechanical condition of the free metal surface has a significant effect on the metal-silicon reaction rate. Author

**N89-12589\*#** National Aeronautics and Space Administration.  
 Lewis Research Center, Cleveland, OH.

**THE NASA ATOMIC OXYGEN EFFECTS TEST PROGRAM**

BRUCE A. BANKS, SHARON K. RUTLEDGE, and JOYCE A. BRADY *In* NASA, Goddard Space Flight Center, 15th Space Simulation Conference: Support the Highway to Space Through Testing p 51-65 1988  
 Avail: NTIS HC A21/MF A01 CSCL 07/4

The NASA Atomic Oxygen Effects Test Program was established to compare the low earth orbital simulation characteristics of existing atomic oxygen test facilities and utilize the collective data from a multitude of simulation facilities to promote understanding of mechanisms and erosion yield dependence upon energy, flux, metastables, charge, and environmental species. Four materials chosen for this evaluation include Kapton HN polyimide, FEP Teflon, polyethylene, and graphite single crystals. The conditions and results of atomic oxygen exposure of these materials is reported by the participating organizations and then assembled to identify degrees of dependency of erosion yields that may not be observable from any single atomic oxygen low earth orbital simulation facility. To date, the program includes 30 test facilities. Characteristics of the participating test facilities and results to date are reported. Author

**N89-19402\*#** National Aeronautics and Space Administration.  
 Lewis Research Center, Cleveland, OH.

**ACIDIC ATTACK OF PERFLUORINATED ALKYL ETHER LUBRICANT MOLECULES BY METAL OXIDE SURFACES**

MICHAEL J. ZEHE and OWEN D. FAUT 1989 17 p Proposed for presentation at the Joint Tribology Conference, Fort Lauderdale, FL, 16-19 Oct. 1989; sponsored by STLE and ASME  
 (NASA-TM-101962; E-4660; NAS 1.15:101962) Avail: NTIS HC A03/MF A01 CSCL 07/4

The reactions of linear perfluoropolyalkylether (PFAE) lubricants with  $\alpha\text{-Fe}_2\text{O}_3$  and  $\text{Fe}_2\text{O}_3$ -based solid superacids were studied. The reaction with  $\alpha\text{-Fe}_2\text{O}_3$  proceeds in two stages. The first stage is an initial slow catalytic decomposition of the fluid. This reaction releases reactive gaseous products which attack the metal oxide and convert it to  $\text{FeF}_3$ . The second stage is a more rapid decomposition of the fluid, effected by the surface  $\text{FeF}_3$ . A study of the initial breakdown step was performed using  $\alpha\text{-Fe}_2\text{O}_3$ ,  $\alpha\text{-Fe}_2\text{O}_3$  preconverted to  $\text{FeF}_3$ , and sulfate-promoted  $\alpha\text{-Fe}_2\text{O}_3$  superacids. The results indicate that the breakdown reaction involves acidic attack at fluorine atoms on acetal carbons in the linear PFAE. Possible approaches to combat the problem are outlined. Author

**N89-21051\*#** National Aeronautics and Space Administration.  
 Lewis Research Center, Cleveland, OH.

**FUEL-RICH CATALYTIC COMBUSTION OF JET-A FUEL-EQUIVALENCE RATIOS 5.0 TO 8.0**

THEODORE A. BRABBS and CARMEN M. GRACIA-SALCEDO (Army Aviation Research and Development Command, Cleveland, OH.) May 1989 10 p Prepared for presentation at the Central States Meeting of the Combustion Inst., Dearborn, MI, 30 Apr. - 3 May 1989  
 (NASA-TM-101975; E-4675; AVSCOM-TR-89-C-001; NAS 1.15:101975; AD-A207009) Avail: NTIS HC A02/MF A01 CSCL 21/2

Fuel-rich catalytic combustion (E.R. greater than 5.0) is a unique technique for preheating a hydrocarbon fuel to temperatures much higher than those obtained by conventional heat exchangers. In addition to producing very reactive molecules, the process upgrades the structure of the fuel by the formation of hydrogen and smaller hydrocarbons and produces a cleaner burning fuel by removing some of the fuel carbon from the soot formation chain. With fuel-rich catalytic combustion as the first stage of a two stage combustion system, enhanced fuel properties can be utilized by both high speed engines, where time for ignition and complete combustion is limited, and engines where emission of thermal NO sub x is critical. Two-stage combustion (rich-lean) has been shown to be effective for NO sub x reduction in stationary burners where residence times are long enough to burn-up the soot formed in the first stage. Such residence times are not available in aircraft engines. Thus, the soot-free nature of the present process is critical for high speed engines. The successful application of fuel-rich catalytic combustion to Jet-A, a multicomponent fuel used in gas turbine combustors, is discussed. Author

**N89-22710\*#** National Aeronautics and Space Administration.  
 Lewis Research Center, Cleveland, OH.

**LIGHTWEIGHT FIBROUS NICKEL ELECTRODES FOR NICKEL-HYDROGEN BATTERIES**

DORIS L. BRITTON 1989 10 p Presented at the 4th Annual Battery Conference on Applications and Advances, Long Beach, CA, 17-19 Jan. 1989; sponsored by California State Univ., Long Beach  
 (NASA-TM-101997; E-4701; NAS 1.15:101997) Avail: NTIS HC A02/MF A01 CSCL 10/3

The NASA Lewis Research Center is currently developing nickel electrodes for nickel-hydrogen batteries. These electrodes are lighter in weight and have higher energy densities than the heavier state-of-the-art sintered nickel electrodes. Lightweight fibrous materials or plaques are used as conductive supports for the nickel hydroxide active material. These materials are commercial products that are fabricated into nickel electrodes by electrochemically impregnating them with active material. Evaluation is performed in

half cells structured in the bipolar configuration. Initial performance tests include capacity measurements at five discharge levels, C/2, 1.0C, 1.37C, 2.0C, and 2.74C. The electrodes that pass the initial tests are life cycle-tested in a low Earth orbit regime at 80 percent depth of discharge. Author

## 26

## METALLIC MATERIALS

Includes physical, chemical, and mechanical properties of metals, e.g., corrosion; and metallurgy.

**A89-12326\*** Karlsruhe Univ. (Germany, F.R.).

**MORPHOLOGICAL STUDY OF NEAR THRESHOLD FATIGUE CRACK GROWTH IN A COARSE GRAIN ALUMINUM ALLOY**

GERHARD MAURER (Karlsruhe, Universitaet, Federal Republic of Germany) and H. W. LIU (Syracuse University, New York) IN: Fatigue 84; Proceedings of the Second International Conference on Fatigue and Fatigue Thresholds, University of Birmingham, England, Sept. 3-7, 1984. Warley, England, Engineering Materials Advisory Services, Ltd., 1984, p. 297-306. Research supported by the Stiftung Volkswagenwerk. refs (Contract NAG3-348)

Copyright

Fatigue crack propagation in the near-threshold region has been studied in coarse grain Al 7029 alloy. Over eighty percent of the crack surfaces are planar areas parallel to either 100-oriented or 111-oriented planes. The 100-plane crack surfaces show 'pine tree' morphological features formed by slip on two sets of intersecting planes. The 111-plane crack surfaces were planar and shiny. They were formed primarily by slip on a single dominant 111-oriented slip plane with sparse and very light secondary slip markings. Crack growth rates were measured and correlated with Delta-K. Author

**A89-12625\*** National Aeronautics and Space Administration. Lewis Research Center, Cleveland, OH.

**HIGH TEMPERATURE ISOTHERMAL AND CYCLIC OXIDATION BEHAVIOR OF A SINGLE CRYSTAL NI BASE SUPERALLOY**

M. G. HEBBUR and R. V. MINER (NASA, Lewis Research Center, Cleveland, OH) Journal of Materials for Energy Systems (ISSN 0162-9719), vol. 8, March 1987, p. 363-370. refs

Copyright

High-temperature oxidation behavior of a Ni-base superalloy, PWA1480, developed for use as single-crystal blades and vanes in advanced gas turbines, has been assessed. Isothermal and cyclic oxidation tests up to 200 hours were conducted at 1323, 1410, and 1473 K. The alloy was evaluated as to sample weight change, type of scale formed, type and amount of spall, and microstructural changes. The oxidation attack was more severe in cyclic as compared with isothermal oxidation. Also, enormous growth of the gamma-prime precipitate was observed at 1423 K during cyclic oxidation. Author

**A89-12758\*** Cleveland State Univ., OH.

**MICROSEGREGATION IN DIRECTIONALLY SOLIDIFIED PB-8.4 AT. PCT AU ALLOY**

S. N. TEWARI (Cleveland State University, OH) Metallurgical Transactions A - Physical Metallurgy and Materials Science (ISSN 0360-2133), vol. 19A, May 1988, p. 1351-1364. refs (Contract NCC3-60)

Copyright

The dependence of microsegregation behavior on growth rate and thermal gradient has been examined in a Pb-8.4 at. pct Au alloy material partially directionally solidified and quenched. The composition of the quenched 'liquid' at the dendrite tip (Ct), that of the eutectic-like solid phase freezing from the interdendritic liquid at the base of dendrite (Cse), the volume fraction of this eutectic-like region (fe), and solute profiles in the interdendritic

quenched liquid and ahead of the dendrite have been measured. Two dendritic growth models for solidification of a binary alloy melt in a positive thermal gradient at the liquid-solid interface, one for dendrites with 'minimum undercooled dendrite tip' and the other for an Ivantsov type of dendrite with 'marginally stable tip', have been examined for a quantitative comparison with measured values of Ct, Cse, and fe. Convection in the melt, possibly due to horizontal density gradients, is found to be a serious limitation for theoretical understanding of the observed experimental behavior and meaningful comparison of theories. Author

**A89-13933\*** National Aeronautics and Space Administration. Lewis Research Center, Cleveland, OH.

**THE EFFECT OF SULFUR AND ZIRCONIUM CO-DOPING ON THE OXIDATION OF NICRAL**

JAMES L. SMIALEK (NASA, Lewis Research Center, Cleveland, OH) IN: Symposium on High Temperature Materials Chemistry - IV, Honolulu, HI, Oct. 19-23, 1987, Proceedings. Pennington, NJ, Electrochemical Society, Inc., 1988, p. 241-253. refs

Copyright

The adhesion behavior of Al<sub>2</sub>O<sub>3</sub> scales formed on NiCrAl+Zr alloys was examined as a function of both sulfur and zirconium doping levels. In general, very high levels of zirconium were required to counteract the detrimental effects of sulfur. A sulfur-zirconium adherence map was constructed, as determined from the oxidation and spalling behavior in 1100 C cyclic tests. For low sulfur alloys (less than 500 ppm), the amount of zirconium required for adherence at any given sulfur level can be described by Zr greater than 600 S(0.2) (in ppm). These results underscore the importance of sulfur to adhesion mechanisms and suggest that sulfur gettering is a first order effect of reactive element additions to MCrAl alloys. Author

**A89-15108\*** Case Western Reserve Univ., Cleveland, OH.

**ANALYSIS OF MICROALLOY PRECIPITATE REVERSION IN STEELS**

G. M. MICHAL (Case Western Reserve University, Cleveland, OH) and I. E. LOCCI (NASA, Lewis Research Center, Cleveland, OH) Scripta Metallurgica (ISSN 0036-9748), vol. 22, Nov. 1988, p. 1801-1806. refs

Copyright

The influence of the ferrite to austenite allotropic transformation on the stability of MXn precipitates in an iron matrix is studied. In the MX phase, M is a group IVb or Vb transition metal, such as niobium, titanium, or vanadium. X is carbon or nitrogen and n is in the range of 0.75-1.0. The application of the present model to the case of vanadium carbide reversion in a microalloyed steel is discussed. K.K.

**A89-17115\*#** Idaho Univ., Moscow.

**EFFECTS OF COBALT CONCENTRATION ON THE RELATIVE RESISTANCE TO OCTAHEDRAL AND CUBE SLIP IN NICKLE-BASE SUPERALLOYS**

GENE E. BOBECK (Idaho, University, Moscow) and R. V. MINER (NASA, Lewis Research Center, Cleveland, OH) Metallurgical Transactions A - Physical Metallurgy and Materials Science (ISSN 0360-2133), vol. 19A, Nov. 1988, p. 2733-2739. refs

Compression yielding tests were performed at 760 C on crystals of the Ni base superalloys Rene 150 and a modified MAR-M247, both having two different Co concentrations. For both alloy bases, increasing Co concentration was shown to decrease the critical resolved shear stress for octahedral slip, but to have little effect on that for cube slip. The results suggest that decreasing complex stacking fault energy in the gamma-prime with increasing Co could account for the observed effects. R.R.

**A89-17378\*** Lockheed Missiles and Space Co., Palo Alto, CA.

**MECHANISMS OF ELEVATED-TEMPERATURE DEFORMATION IN THE B2 ALUMINIDES NIAL AND COAL**

D. L. YANEY (Lockheed Missiles and Space Co., Inc., Palo Alto, CA) and W. D. NIX (Stanford University, CA) Journal of Materials Science (ISSN 0022-2461), vol. 23, Sept. 1988, p. 3088-3098.

refs

(Contract NAG3-248)

Copyright

A strain rate change technique, developed previously for distinguishing between pure-metal and alloy-type creep behavior, was used to study the elevated-temperature deformation behavior of the intermetallic compounds NiAl and CoAl. Tests on NiAl were conducted at temperatures between 1100 and 1300 K while tests on CoAl were performed at temperatures ranging from 1200 to 1400 K. NiAl exhibits pure-metal type behavior over the entire temperature range studied. CoAl, however, undergoes a transition from pure-metal to alloy-type deformation behavior as the temperature is decreased from 1400 to 1200 K. Slip appears to be inherently more difficult in CoAl than in NiAl, with lattice friction effects limiting the mobility of dislocations at a much higher temperature in CoAl than in NiAl. The superior strength of CoAl at elevated temperatures may, therefore, be related to a greater lattice friction strengthening effect in CoAl than in NiAl. Author

**A89-17379\*** Connecticut Univ., Storrs.**IRON-BASE SUPERALLOYS - A PHASE ANALYSIS OF THE MULTICOMPONENT SYSTEM (Fe-Mn-Cr-Mo-Nb-Al-Si-C)**

H. GUPTA, H. NOWOTNY (Connecticut, University, Storrs), and F. D. LEMKEY (United Technologies Research Center, East Hartford, CT) *Journal of Materials Science* (ISSN 0022-2461), vol. 23, Sept. 1988, p. 3113-3119. refs (Contract NAG3-271)

Copyright

In the course of studies on the iron-rich multicomponent system Fe-Mn-Cr-Mo-Nb-Al-Si-C, work was concentrated on pertinent quinary and six-component combinations namely Fe-Mn-Al-Si-C, Fe-Cr-Al-Si-C and Fe-Mn-Cr-Al-Si-C which had been elaborated at 65, 72, and 80 wt pct Fe. Manganese acts as a strong stabilizer for the cementite carbide. Chromium seems to stabilize the iron aluminide Fe<sub>2</sub>Al<sub>5</sub> which forms in a considerable amount within an alloy of nominal composition Fe(65)Mn(15)Cr(12)Al(5)Si(2)C(1) (percent by weight). Although the Mn<sub>3</sub>AlC carbide is, like Fe<sub>3</sub>AlC, a perovskite carbide, manganese does not appear to favor the formation of the perovskite carbide. Because of the relatively low sintering temperature (700 C), for a large portion of the samples equilibria conditions are not always reached. Author

**A89-18193\*** Sverdrup Technology, Inc., Middleburg Heights, OH.**MICROSTRUCTURES IN RAPIDLY SOLIDIFIED NIOBIUM ALUMINIDES**

MOHAN G. HEBUR (Sverdrup Technology, Inc., Middleburg Heights, OH) and IVAN E. LOCCI (NASA, Lewis Research Center, Cleveland, OH) IN: *Rapidly solidified materials: Properties and processing; Proceedings of the Second International Conference on Rapidly Solidified Materials*, San Diego, CA, Mar. 7-9, 1988. Metals Park, OH, ASM International, 1988, p. 67-74. Research supported by the U.S. National Research Council. refs Copyright

The microstructures of niobium aluminides produced by chill block melt spinning were compared to those of niobium aluminides produced by conventional casting. The rapidly solidified alloys were rapidly solidified by melt spinning in an argon atmosphere, and the melt-spun ribbons were examined by optical, X-ray, and TEM techniques. Microstructures were found to range from single-phase for Nb-75 at. pct Al (NbAl<sub>3</sub>) to two phase for Nb-46 at. pct Al (NbAl<sub>3</sub> + Nb<sub>2</sub>Al). It was found that the melt spinning of Nb-aluminides produced finer grained microstructures than those produced in induction-melted ingots or in powders produced by the rotating electrode process. Ternary additions such as Cr, Ti, and Si tended to form intermetallic phases along the grain boundaries. I.S.

**A89-18203\*** National Aeronautics and Space Administration. Lewis Research Center, Cleveland, OH.**RAPID SOLIDIFICATION RESEARCH AT THE NASA LEWIS RESEARCH CENTER**

IVAN E. LOCCI (NASA, Lewis Research Center, Cleveland, OH),

THEODORE A. BLOOM (Illinois Institute of Technology, Chicago), and MOHAN G. HEBUR (Sverdrup Technology, Inc., Cleveland, OH) IN: *Rapidly solidified materials: Properties and processing; Proceedings of the Second International Conference on Rapidly Solidified Materials*, San Diego, CA, Mar. 7-9, 1988. Metals Park, OH, ASM International, 1988, p. 207-212.

Copyright

This paper describes the research program initiated at the NASA Lewis Research Center for the study of rapid solidification of high temperature materials, with the major purpose for the development of advanced high-temperature and heat-flux materials for aircraft and aerospace applications. Particular attention is given to the development of three alloys: Ni-aluminides, Nb-alloys, and Cu-alloys. Rapid solidification processing yielded alloys with novel microstructures, very fine grain sizes, reduced chemical segregation, and metastable extended solid solutions. I.S.

**A89-19621\*** National Aeronautics and Space Administration. Lewis Research Center, Cleveland, OH.**MACROSEGREGATION IN UNDERCOOLED Pb-Sn EUTECTIC ALLOYS**

H. C. DE GROH, III (NASA, Lewis Research Center, Cleveland, OH) and V. LAXMANAN (NASA, Lewis Research Center; Case Western Reserve University, Cleveland, OH) IN: *Solidification processing of eutectic alloys; Proceedings of the Symposium*, Cincinnati, OH, Oct. 12-15, 1987. Warrendale, PA, Metallurgical Society, Inc., 1988, p. 229-242. refs

Copyright

A novel technique resulting in large undercoolings in bulk samples (23g) of lead-tin eutectic alloy is described. Samples of eutectic composition were processed with undercoolings ranging from 4 to 20 K and with cooling rates varying between 0.04 to 4 K/sec. The final macrostructure of undercooled samples depends on both the initial undercooling of the melt and the cooling rate. Gravity-driven segregation is found to increase with increasing undercooling. A eutectic Pb-Sn alloy undercooled at 20 K and cooled at 4 K/sec had a composition of about Pb-72 wt pct Sn at the top and 55 pct Sn at the bottom. Macroseggregation in these undercooled lead-tin eutectic alloys is shown to be primarily due to a sink/float mechanism caused by the difference in density of the solid and liquid phases and the undercooling and nucleation behavior of the alloy. Author

**A89-19852\*** National Aeronautics and Space Administration. Lewis Research Center, Cleveland, OH.**CONCEPTS FOR INTERRELATING ULTRASONIC ATTENUATION, MICROSTRUCTURE, AND FRACTURE TOUGHNESS IN POLYCRYSTALLINE SOLIDS**

A. VARY (NASA, Lewis Research Center, Cleveland, OH) *Materials Evaluation* (ISSN 0025-5327), vol. 46, no. 5, 1988, p. 642-649. Previously announced in STAR as N86-25812. refs

Copyright

Conceptual models are advanced for explaining and predicting empirical correlations found between ultrasonic measurements and fracture toughness of polycrystalline solids. The models lead to insights concerning microstructural factors governing fracture processes and associated stress wave interactions. Analysis of the empirical correlations suggested by the models indicate that, in addition to grain size and shape, grain boundary reflections, elastic anisotropy, and dislocation damping are factors that underlie both fracture toughness and ultrasonic attenuation. One outcome is that ultrasonic attenuation can predict the size of crack blunting or process zones that develop in the vicinity of active cracks in metals. This forms a basis for ultrasonic ranking according to variations in fracture toughness. Author

**A89-21395\*** Columbia Univ., New York, NY. **INTERDIFFUSIONAL EFFECTS BETWEEN TiB<sub>2</sub> AND NiAl INTERMETALLICS**

A. J. CARBONE, M. W. KOPP, J. K. TIEN (Columbia University, New York), S. S. LIN, H. L. MARCUS (Texas, University, Austin), and S. L. DRAPER (NASA, Lewis Research Center, Cleveland, OH) *Scripta Metallurgica* (ISSN 0036-9748), vol. 22, Dec. 1988,



p. 1903-1906. refs  
(Contract NAG3-720)  
Copyright

The TiBe12/NiAl composites fabricated by a powder metallurgy technique were examined for the extent of interdiffusion between its components, using scanning Auger microscopy. The results revealed an evidence of a reaction between the two component intermetallics after annealing at 1300 K for 100 h, with a 95-micron reaction zone extending from the TiBe12/NiAl interface. The concentration profile across the reaction zone showed that the Ni, Al, and Be concentrations were in a 1:1:2 ratio, while Ti was present in only very small amounts. I.S.

**A89-22048\*** Syracuse Univ., NY.  
**RESOLVED SHEAR STRESS INTENSITY COEFFICIENT AND FATIGUE CRACK GROWTH IN LARGE CRYSTALS**

Q. CHEN and H. W. LIU (Syracuse University, NY) Theoretical and Applied Fracture Mechanics (ISSN 0167-8442), vol. 10, Oct. 1988, p. 111-122. refs  
(Contract NAG3-348)  
Copyright

Fatigue crack growth tests were carried out on large-grain Al 7029 aluminum alloy and the finite element method was used to calculate the stress field near the tip of a zigzag crack. The resolved shear stresses on all 12 slip systems were computed, and the resolved shear stress intensity coefficient (RSSIC) was defined. The RSSIC was used to analyze the irregular crack path and was correlated with the rate of single-slip-plane shear crack growth. Fatigue crack growth was found to be caused primarily by shear decohesion at a crack tip. When the RSSIC on a single-slip system was much larger than all the others, the crack followed a single-slip plane. When the RSSICs on two conjugate slip systems were comparable, a crack grew in a zigzag manner on these planes and the macrocrack-plane bisected the two active slip planes. The maximum RSSIC on the most active slip system is proposed as a parameter to correlate with the shear fatigue crack growth rate in large crystals. C.D.

**A89-22559\*** Arizona Univ., Tucson.  
**ENTHALPIES OF A BINARY ALLOY DURING SOLIDIFICATION**  
D. R. POIRIER and P. NANDAPURKAR (Arizona, University, Tucson) Metallurgical Transactions A - Physical Metallurgy and Materials Science (ISSN 0360-2133), vol. 19A, Dec. 1988, p. 3057-3061. refs  
(Contract NAG3-723)  
Copyright

The purpose of the paper is to present a method of calculating the enthalpy of a dendritic alloy during solidification. The enthalpies of the dendritic solid and interdendritic liquid of alloys of the Pb-Sn system are evaluated, but the method could be applied to other binaries, as well. The enthalpies are consistent with a recent evaluation of the thermodynamics of Pb-Sn alloys and with the redistribution of solute in the same during dendritic solidification. Because of the heat of mixing in Pb-Sn alloys, the interdendritic liquid of hypoeutectic alloys (Pb-rich) of less than 50 wt pct Sn has enthalpies that increase as temperature decreases during solidification. Author

**A89-22560\*** National Aeronautics and Space Administration.  
Lewis Research Center, Cleveland, OH.  
**DENDRITIC SOLIDIFICATION IN BINARY ALLOYS**  
M. A. CHOPRA (NASA, Lewis Research Center; Cleveland State University, OH), M. E. GLICKSMAN (Rensselaer Polytechnic Institute, Troy, NY), and N. B. SINGH (Westinghouse Research and Development Center, Pittsburgh, PA) Metallurgical Transactions A - Physical Metallurgy and Materials Science (ISSN 0360-2133), vol. 19A, Dec. 1988, p. 3087-3096. refs  
Copyright

Alloys generally solidify dendritically, and associated with that is the microsegregation of impurities. Pure metals also solidify in dendritic form as 'thermal' dendrites, which actually segregate the system's enthalpy. In this investigation, small additions of solute to succinonitrile have been studied and dendritic growth observed

in a supercooled melt. This free dendritic growth-mode is similar to that experienced by equiaxed dendrites found in alloy castings. Observations of these free dendrites include measurement of velocity and tip radius of the dendrites at different supercoolings and solute concentrations. Author

**A89-24358\*** National Aeronautics and Space Administration.  
Lewis Research Center, Cleveland, OH.

**A MONTE CARLO-FINITE ELEMENT MODEL FOR STRAIN ENERGY CONTROLLED MICROSTRUCTURAL EVOLUTION - 'RAFTING' IN SUPERALLOYS**

J. GAYDA (NASA, Lewis Research Center, Cleveland, OH) and D. J. SROLOVITZ (Michigan, University, Ann Arbor) Acta Metallurgica (ISSN 0001-6160), vol. 37, Feb. 1989, p. 641-650. refs  
Copyright

This paper presents a specialized microstructural lattice model, MCFET (Monte Carlo finite element technique), which simulates microstructural evolution in materials in which strain energy has an important role in determining morphology. The model is capable of accounting for externally applied stress, surface tension, misfit, elastic inhomogeneity, elastic anisotropy, and arbitrary temperatures. The MCFET analysis was found to compare well with the results of analytical calculations of the equilibrium morphologies of isolated particles in an infinite matrix. I.S.

**A89-24599\*** National Aeronautics and Space Administration.  
Lewis Research Center, Cleveland, OH.

**EFFECT OF 0.1 AT. PCT ZIRCONIUM ON THE CYCLIC OXIDATION RESISTANCE OF BETA-NIAL**

CHARLES A. BARRETT (NASA, Lewis Research Center, Cleveland, OH) Oxidation of Metals (ISSN 0030-770X), vol. 30, Dec. 1988, p. 361-390. refs  
Copyright

The effect of 0.1 at. pct Zr on the cyclic oxidation of hipped beta-NiAl was studied. Oxidation testing was performed in static air at 1100-1200 C, using 1-hr exposure cycles for test times up to 3000 hr. The weight change versus time data were modeled with the COSP computer program to analyze and predict cyclic-oxidation behavior. Zr additions significantly change the nature of the scale-spalling process during cooling, so that the oxide spalls near the oxide-air interface at a relatively low depth within the scale. Without Zr, the predominantly alpha-Al<sub>2</sub>O<sub>3</sub> scale tends to spall randomly to bare metal at relatively high effective-scale-loss rates, particularly at 1150 C and 1200 C. This leads to higher rates of Al consumption for the Zr-free aluminide and much earlier depletion of Al, leading to eventual breakdown (i.e., failure). Author

**A89-26872\*#** National Aeronautics and Space Administration.  
Lewis Research Center, Cleveland, OH.

**INFLUENCE OF PRECIPITATE MORPHOLOGY ON INTERMEDIATE TEMPERATURE CREEP PROPERTIES OF A NICKEL-BASE SUPERALLOY SINGLE CRYSTAL**

M. V. NATHAL, R. A. MACKAY, and R. V. MINER (NASA, Lewis Research Center, Cleveland, OH) Metallurgical Transactions A - Physical Metallurgy and Materials Science (ISSN 0360-2133), vol. 20A, Jan. 1989, p. 133-141. refs

The relative creep behavior of cuboidal (as-heat treated) and rafted (precipitated at 1000 C) gamma-prime microstructures in the single-crystal Ni-based superalloy NASAIR 100 at 760 C was investigated using SEM and TEM examinations of materials at various stages of creep. It was found that, at high applied stresses, the crystals with cuboidal gamma-prime structure had both lower minimum creep rates and longer rupture lives than the crystals with lamellar gamma-prime. At lower stress levels, the initially cuboidal gamma-prime microstructure maintained a lower creep rate, but exhibited a similar rupture life compared to the prerafted crystals. I.S.



**A89-32803\*** National Aeronautics and Space Administration. Lewis Research Center, Cleveland, OH.

**THE INFLUENCE OF ANNEALING IN THE FERRITE-PLUS-AUSTENITE PHASE FIELD ON THE STABILITY OF VANADIUM CARBIDE PRECIPITATES**

I. E. LOCCI (NASA, Lewis Research Center, Cleveland, OH) and G. M. MICHAL (Case Western Reserve University, Cleveland, OH) Metallurgical Transactions A - Physical Metallurgy and Materials Science (ISSN 0360-2133), vol. 20A, Feb. 1989, p. 237-245. refs

Copyright

The effect of rapid excursions into the ferrite-plus-austenite two-phase field on V4C3 precipitates formed by tempering in the ferrite phases was investigated. Heat treatments were first performed to produce a starting microstructure of fine vanadium carbide particles precipitated in a ferrite matrix, and the microstructure was then subjected to various short-time heat treatment cycles that transformed part of the matrix to austenite. TEM was used to determine the effects of the matrix change on the size, morphology, and distribution of the vanadium carbide particles. R.R.

**A89-32932\*** Aerojet TechSystems Co., Sacramento, CA.

**FRICTION-INDUCED IGNITION OF METALS IN HIGH-PRESSURE OXYGEN**

LEN SCHOENMAN (Aerojet TechSystems Co., Sacramento, CA), JOEL STOLTZFUS (NASA, White Sands Test Facility, Las Cruces, NM), and JOHN KAZAROFF (NASA, Lewis Research Center, Cleveland, OH) IN: Flammability and sensitivity of materials in oxygen-enriched atmospheres; Proceedings of the Symposium, Cambridge, England, Apr. 6-8, 1987. Volume 3. Philadelphia, PA, American Society for Testing and Materials, 1988, p. 105-133. refs

Copyright

Data are presented on friction-induced metal ignition (such as occurring as a result of the possible rubbing of oxygen-pressurized hydrostatic bearings and turbine blade tips) in a high-pressure oxygen environment. Friction heating tests were carried out at oxygen pressures from 1 to 300 atm and surface speeds from 10 to 33 m/sec, using the NASA/White Sands Test Facility. Test results are presented on the rubbing of like material pairs spanning a wide range of burn factors and on that of dissimilar metal pairs having significantly different burn factors, indicating that the burn factor is a suitable index for rank ordering in ignition resistance for the most, but not all, materials. I.S.

**A89-35307\*** National Aeronautics and Space Administration. Lewis Research Center, Cleveland, OH.

**INTERFACIAL ADHESION - THEORY AND EXPERIMENT**

JOHN FERRANTE, AMITAVA BANERJEA (NASA, Lewis Research Center, Cleveland, OH), GUILLERMO H. BOZZOLO (Case Western Reserve University, Cleveland, OH), and CLARENCE W. FINLEY (Pennsylvania State University, New Kensington) IN: Adhesion in solids; Proceedings of the Symposium, Reno, NV, Apr. 5-7, 1988. Pittsburgh, PA, Materials Research Society, 1988, p. 3-16. Previously announced in STAR as N88-20417. refs

Copyright

Adhesion, the binding of different materials at an interface, is of general interest to many branches of technology, e.g., microelectronics, tribology, manufacturing, construction, etc. However, there is a lack of fundamental understanding of such diverse interfaces. In addition, experimental techniques generally have practical objectives, such as the achievement of sufficient strength to sustain mechanical or thermal effects and/or have the proper electronic properties. In addition, the theoretical description of binding at interfaces is quite limited, and a proper data base for such theoretical analysis does not exist. This presentation will review both experimental and theoretical aspects of adhesion in nonpolymer materials. The objective will be to delineate the critical parameters needed, governing adhesion testing along with an outline of testing objectives. A distinction will be made between practical and fundamental objectives. Examples are given where

interfacial bonding may govern experimental consideration. The present status of theory is presented along with recommendations for future progress and needs. Author

**A89-36419\*** National Aeronautics and Space Administration. Lewis Research Center, Cleveland, OH.

**STATUS AND PROGNOSIS FOR ALTERNATIVE ENGINE MATERIALS**

JOSEPH R. STEPHENS and MICHAEL V. NATHAL (NASA, Lewis Research Center, Cleveland, OH) IN: Superalloys 1988; Proceedings of the Sixth International Symposium, Champion, PA, Sept. 18-22, 1988. Warrendale, PA, Metallurgical Society, Inc., 1988, p. 183-192. Previously announced in STAR as N88-24749. refs

Copyright

The current state of research and development of new materials for advanced aircraft engines is reviewed. The advantages and disadvantages of intermetallic compounds and refractory metals as replacements for today's nickel-base alloys are discussed along with some results of research directed at overcoming some of the problems which restrict their application. It is concluded that continuous fiber reinforced intermetallic matrix composites offer one of the best chances for success. However, major technical barriers still exist, especially in the development of suitable fibers. The introduction of these materials into aircraft engines is expected to take in excess of 5 to 10 years. Author

**A89-36427\*** Rockwell International Corp., Canoga Park, CA. **THE INFLUENCE OF HIGH THERMAL GRADIENT CASTING, HOT ISOSTATIC PRESSING AND ALTERNATE HEAT TREATMENT ON THE STRUCTURE AND PROPERTIES OF A SINGLE CRYSTAL NICKEL BASE SUPERALLOY**

L. G. FRITZEMEIER (Rockwell International Corp., Rocketdyne Div., Canoga Park, CA) IN: Superalloys 1988; Proceedings of the Sixth International Symposium, Champion, PA, Sept. 18-22, 1988. Warrendale, PA, Metallurgical Society, Inc., 1988, p. 265-274. Research supported by Rockwell International Corp. refs (Contract NAS3-24646)

Copyright

A development program has been conducted to improve the cyclic properties of the PWA 1480 single-crystal superalloy by reducing or entirely eliminating casting porosity at fatigue-initiation sites, through the use of improved casting process parameters and HIPing; potential mechanical property improvements in a high-pressure hydrogen environment were also sought in alternatives to the standard coating and heat-treatment cycle. High thermal gradient casting was found to yield a reduction in overall casting porosity density and pore sizes. The most dramatic mechanical property improvement resulted from HIPing. O.C.

**A89-36461\*** National Aeronautics and Space Administration. Lewis Research Center, Cleveland, OH.

**ACCELERATED FATIGUE CRACK GROWTH BEHAVIOR OF PWA 1480**

JACK TELESMA and LOUIS J. GHOSN (NASA, Lewis Research Center, Cleveland, OH) IN: Superalloys 1988; Proceedings of the Sixth International Symposium, Champion, PA, Sept. 18-22, 1988. Warrendale, PA, Metallurgical Society, Inc., 1988, p. 615-624. Previously announced in STAR as N88-26436. refs

Copyright

An investigation of the fatigue crack growth (FCG) behavior of PWA 1480 single crystal nickel base superalloy was conducted. Typical Paris region behavior was observed above a delta K of 8 MPa sq rt of m. However, below that stress intensity range, the alloy exhibited highly unusual behavior. This behavior consisted of a region where the crack growth rate became essentially independent of the applied stress intensity. The transition in the FCG behavior was related to a change in the observed crack growth mechanisms. In the Paris region, fatigue failure occurred along (111) facets; however, at the lower stress intensities, (001) fatigue failure was observed. A mechanism was proposed, based on barriers to dislocation motion, to explain the changes in the observed FCG behavior. The FCG data were also evaluated in

terms of a recently proposed stress intensity parameter  $K_{\text{sub}}$ . This parameter, based on the resolved shear stresses on the slip planes, quantified the crack driving force as well as the mode I  $\Delta K$ , and at the same time was also able to predict the microscopic crack path under different stress states. Author

**A89-37899\*** National Aeronautics and Space Administration. Lewis Research Center, Cleveland, OH.

#### TRANSIENT OXIDATION OF SINGLE-CRYSTAL BETA-NIAL

J. DOYCHAK (NASA, Lewis Research Center; Sverdrup Technology, Inc., Middleburg Heights, OH), J. L. SMIALEK (NASA, Lewis Research Center, Cleveland, OH), and T. E. MITCHELL (Los Alamos National Laboratory, NM) Metallurgical Transactions A - Physical Metallurgy and Materials Science (ISSN 0360-2133), vol. 20A, March 1989, p. 499-518. refs

(Contract NAG3-498)

Copyright

The transient oxidation of beta-NiAl in air at 800 C and 1100 C has been studied using electron microscopy. The oxide scale consists predominantly of metastable  $\text{Al}_2\text{O}_3$  phases. Theta- $\text{Al}_2\text{O}_3$  is the major oxide phase within 10.0 hr of oxidation at 800 C and 0.1 hr at 1100 C. The scales form epitaxially on (001) sub beta and (012) sub beta specimens throughout the transient stage, whereas the degree of preferred oxide orientation decreases with oxidation time on (011) sub beta and (111) sub beta specimens. The orientation relationships reflect the small mismatch between parallel close-packed directions in the metal and in the cation sublattice of the oxides. The correlation of distinctive oxide surface morphologies with internal structural defects indicates the strong tendency of the  $\text{Al}_2\text{O}_3$  scale to grow via short-circuit diffusion paths. Author

**A89-38600\*** National Aeronautics and Space Administration. Lewis Research Center, Cleveland, OH.

#### EFFECT OF THE THETA-ALPHA- $\text{Al}_2\text{O}_3$ TRANSFORMATION ON THE OXIDATION BEHAVIOR OF BETA-NIAL+ZR

GEORGE C. RYBICKI and JAMES L. SMIALEK (NASA, Lewis Research Center, Cleveland, OH) Oxidation of Metals (ISSN 0030-770X), vol. 31, April 1989, p. 275-304. refs

Copyright

Isothermal oxidation of NiAl+Zr has been performed over the temperature range of 800-1200 C and studied by TGA, XRD, and SEM. A discontinuous decrease in growth rate of two orders of magnitude was observed at 1000 C due to the formation of alpha- $\text{Al}_2\text{O}_3$  from theta- $\text{Al}_2\text{O}_3$ . This transformation also resulted in a dramatic change in the surface morphology of the scales, as a whisker topography was changed into a weblike network of oxide ridges and radial transformation cracks. It is believed that the ridges are evidence for a short-circuit outward aluminum diffusion growth mechanism that has been documented in a number of O-18 tracer studies. Author

**A89-38859\*** Cincinnati Univ., OH.

#### OXIDE SCALE STRESSES IN POLYCRYSTALLINE NI200

N. JAYARAMAN (Cincinnati, University, OH) and MICHAEL J. VERRILLI (NASA, Lewis Research Center, Cleveland, OH) Journal of Materials Science (ISSN 0022-2461), vol. 24, April 1989, p. 1327-1331. refs

Copyright

An X-ray diffraction method has been successfully used to measure the oxidation stresses at room temperature in annealed and electropolished samples of polycrystalline Ni200 coupons oxidized in the temperature range 760 to 982 C for 4 h. The stresses on the free surface of the oxide were compressive and the average stress through the thickness normal to the oxide layer was found to be tensile. Surface stresses on the oxides formed at temperatures up to 927 C were found to be isotropic and both surface stresses and the average normal stress increased with increasing temperature of oxidation. At 982 C, the surface stresses were lower and this was attributed to the deformation and fracture of oxide layer resulting in stress relaxation. Author

**A89-40116\*** National Aeronautics and Space Administration. Lewis Research Center, Cleveland, OH.

#### PREDICTING MINIMUM AL CONCENTRATIONS FOR PROTECTIVE SCALE FORMATION ON NI-BASE ALLOYS. I - ISOTHERMAL OXIDATION. II - CYCLIC OXIDATION

JAMES A. NESBITT (NASA, Lewis Research Center, Cleveland, OH) Electrochemical Society, Journal (ISSN 0013-4651), vol. 136, May 1989, p. 1511-1527. refs

Copyright

Criteria proposed to predict the minimum bulk Al concentration for the formation of protective  $\text{Al}_2\text{O}_3$  scales on Ni-based alloys during isothermal oxidation (two criteria proposed by Wagner, 1952 and 1959) and cyclic oxidation (the criteria proposed by Wahl, 1983, and Whittle, 1972/Wahl, 1983) were applied to Ni-Al and Ni-Cr-Al(Zr) alloys, respectively. It is shown that the first Wagner (1952) criterion underpredicted, by a factor of 3, the experimentally observed minimum Al concentration for the formation of an external  $\text{Al}_2\text{O}_3$  scale on Ni-Al alloys at 1200 C; the second Wagner criterion predicted a transition from internal oxidation to continuous  $\text{Al}_2\text{O}_3$  formation in good agreement with experimentally observed concentrations. It was also found that the two criteria for an  $\text{Al}_2\text{O}_3$  scale formation during cyclic oxidation of Ni-Cr-Al(Zr) alloys were inadequate to predict the minimum Al concentration necessary for repeated formation of an  $\text{Al}_2\text{O}_3$  scale, regardless of the adherence I.S.

**A89-40162\*** National Aeronautics and Space Administration. Lewis Research Center, Cleveland, OH.

#### OBSERVATIONS OF DIRECTIONAL GAMMA PRIME COARSENING DURING ENGINE OPERATION

S. DRAPER, D. HULL, and R. DRESHFIELD (NASA, Lewis Research Center, Cleveland, OH) Metallurgical Transactions A - Physical Metallurgy and Materials Science (ISSN 0360-2133), vol. 20A, April 1989, p. 683-688. refs

Copyright

Two alloys, NASAIR 100 and a modified NASAIR 100 called Alloy 3, were run as turbine blades in an experimental ground-based Garrett TFE731 engine for up to 200 hours. The stress induced directional coarsening of gamma-prime (rafting) that developed during engine testing was analyzed and compared to previous research from laboratory tests. The blades were found to have formed a lamellar structure, the lamellae being normal to the centrifugal stress axis over much of the span. However, near the surfaces, the blades were found to have formed lamellae parallel to the centrifugal stress axis for certain cycles. Representative photomicrographs of the blades and the effects of stress and temperature on lamellae formation are shown. Author

**A89-43023\*** Marko Materials, Inc., North Billerica, MA.

#### DISPERSOIDS IN RAPIDLY SOLIDIFIED B2 NICKEL ALUMINIDES

S. C. JHA, R. RAY (Marko Materials, Inc., North Billerica, MA), and D. J. GAYDOS (NASA, Lewis Research Center, Cleveland, OH) Scripta Metallurgica (ISSN 0036-9748), vol. 23, May 1989, p. 805-810. refs

(Contract NAS3-25448)

Copyright

Rapid solidification processing has been successfully used to create a uniform distribution of 30-nm TiB<sub>2</sub> and HfC precipitates in a B2-ordered NiAl matrix, in order to enhance the matrix material's high-temperature strength and creep behavior. Attention is drawn to the question of the stability of carbide and boride dispersoids in an NiAl matrix during high-temperature exposures. The present alloys were consolidated at temperatures above 1422 K; the small size of precipitates in materials processed at such high temperatures gives an indication of their thermal stability, and further coarsening of the precipitates at elevated service temperatures is rendered unlikely by their low solubility in the matrix. O.C.

**A89-44568\*** Dartmouth Coll., Hanover, NH.

#### ROOM TEMPERATURE TENSILE DUCTILITY IN POLYCRYSTALLINE B2 NI-30AL-20FE

SUMIT GUHA, PAUL MUNROE, and IAN BAKER (Dartmouth College, Hanover, NH) Scripta Metallurgica (ISSN 0036-9748), vol. 23, June 1989, p. 897-900. refs  
(Contract NAG3-775; NSF DMR-88-01241)  
Copyright

A room-temperature tensile elongation of about 2.5 percent, where the only slip vector observed was the 100, has been determined for a double-extruded B2 Ni-30Al-20Fe alloy consisting of recrystallized equiaxed grains about 25 microns in diameter; these results suggest that 100-slip does not preclude limited ductility in polycrystalline B2 alloys in tension at low temperatures. A suppression of ordering through resort to rapid solidification, in other words, is not necessary for ductility, since the cast and as-extruded alloy presently examined is ordered. O.C.

**A89-45946\*** National Aeronautics and Space Administration. Lewis Research Center, Cleveland, OH.

**FATIGUE CRACK GROWTH BEHAVIOR OF A SINGLE CRYSTAL ALLOY AS OBSERVED THROUGH AN IN SITU FATIGUE LOADING STAGE**

JACK TELESMA and PETER KANTZOS (NASA, Lewis Research Center, Cleveland, OH) IN: Space age metals technology; Proceedings of the Second International SAMPE Metals and Metals Processing Conference, Dayton, OH, Aug. 2-4, 1988. Covina, CA, Society for the Advancement of Material and Process Engineering, 1988, p. 334-344. Previously announced in STAR as N88-22986. refs

Copyright

An in situ fatigue loading stage inside a scanning electron microscope (SEM) was used to determine the fatigue crack growth behavior of a PWA 1480 single-crystal nickel-based superalloy. The loading stage permits real-time viewing of the fatigue damage processes at high magnification. The PWA 1480 single-crystal, single-edge notch specimens were tested with the load axis parallel to the (100) orientation. Two distinct fatigue failure mechanisms were identified. The crack growth rate differed substantially when the failure occurred on a single slip system in comparison to multislip system failure. Two processes by which crack branching is produced were identified and are discussed. Also discussed are the observed crack closure mechanisms. Author

**A89-46506\*** National Aeronautics and Space Administration. Lewis Research Center, Cleveland, OH.

**TEM STUDIES OF OXIDIZED NIAL AND NI3AL CROSS SECTIONS**

J. DOYCHAK (NASA, Lewis Research Center; Sverdrup Technology, Inc., Cleveland, OH) and M. RUHLE (California, University, Santa Barbara) Oxidation of Metals (ISSN 0030-770X), vol. 31, June 1989, p. 431-452. Research supported by NSF, Max-Planck-Institut fuer Metallforschung, and DARPA. refs  
(Contract N00014-86-K-0753)

Copyright

Cross sections of oxide scale/(Ni-Al) intermetallics were prepared by a new method and studied using primarily TEM. The cross sections were prepared by encasing an oxidized metal specimen sandwich in a low-melting-temperature zinc alloy. Observations of oxidized zirconium-doped beta-NiAl cross sections revealed crystallographic voids beneath an adherent Al<sub>2</sub>O<sub>3</sub> scale. The oxide-metal interface was incoherent, but a high dislocation density in the metal near the interface suggested that a large tensile stress was induced by the attached oxide scale. A duplex Al<sub>2</sub>O<sub>3</sub>-NiAl<sub>2</sub>O<sub>4</sub> scale formed on zirconium-doped and zirconium/boron-doped gamma-prime-Ni3Al alloys. Additional results are presented involving oxidation mechanisms and oxide-metal interface structures. Author

**A89-47320\*** Cooper Union, New York, NY.

**KINETICS OF FRACTURE IN FE-3SI STEEL UNDER MODE I LOADING**

MICHAEL H. BESSENDORF (Cooper Union for the Advancement of Science and Art, New York) IN: Nonlinear fracture mechanics. Volume 2. Philadelphia, PA, American Society for Testing and

Materials, 1989, p. 584-593. refs

(Contract NAG3-223)

Copyright

This paper deals with experimental studies of fatigue crack propagation (FCP) in Fe-3Si steel. The FCP experiments were performed on single-edge crack specimens. Results show that an extensive damage zone consisting of slip bands surrounds and precedes the propagating crack. The system of the crack and the damage zone constitutes the crack layer (CL). The results demonstrate that fracture propagates by the translation, expansion, and distortion of the part of CL called the active zone. The contours of the damage distribution show that different loading stresses may cause significantly different shapes of damage. Application of the stability criteria is demonstrated. It was shown that the critical energy release rate depends on the history of loading. Author

**A89-50313\*** Southwest Research Inst., San Antonio, TX.

**INELASTIC DEFORMATION AND DISLOCATION STRUCTURE OF A NICKEL ALLOY - EFFECTS OF DEFORMATION AND THERMAL HISTORIES**

K. S. CHAN and R. A. PAGE (Southwest Research Institute, San Antonio, TX) Metallurgical Transactions A - Physical Metallurgy and Materials Science (ISSN 0360-2133), vol. 19A, Oct. 1988, p. 2477-2486. refs

(Contract NAS3-23925)

Copyright

Inelastic deformation behavior of the cast Ni-base alloy, B1900 + Hf, was investigated using data from step-temperature tensile tests and thermomechanical cyclic tests in the temperature ranges 538-760 C and 760-982 C. The deformation results were correlated with the dislocation structures of deformed specimens, identified by TEM. It was found that, in the 760-982 C temperature range, there are no thermal history effects in the inelastic deformation behavior of B1900 + Hf. In the 538-760 range, anomalous cyclic hardening and, possibly, thermal history effects were observed in thermomechanically deformed alloy, caused by sessile (010) dislocations in the gamma-prime phase. I.S.

**A89-52204\*** National Aeronautics and Space Administration. Lewis Research Center, Cleveland, OH.

**THE LOW CYCLE FATIGUE DEFORMATION RESPONSE OF A SINGLE-CRYSTAL SUPERALLOY AT 650 C**

T. P. GABB, R. V. MINER, J. GAYDA (NASA, Lewis Research Center, Cleveland, OH), and G. WELSCH (Case Western Reserve University, Cleveland, OH) Materials Science and Engineering (ISSN 0921-5093), vol. A108, 1989, p. 189-202. refs

Copyright

The cyclic stress-strain response and the associated deformation structure of the single crystal nickel-base superalloy PWA 1480 were investigated. Specimens of various crystallographic orientations were tested in low-cycle fatigue (LCF) at 650 C, resulting in a significant tension-compression anisotropy in initial yield strength associated with the shearing of gamma-prime precipitates by dislocation pairs, and a LCF cyclic hardening of the crystals associated with dislocation interactions occurring in the gamma phase. In specimens deforming by slip on a single slip system, dislocations of the primary slip system accumulated in the gamma matrix and formed sessile entanglements. In specimens deforming by slip on several slip systems, the dislocations of the different operative slip systems intersected in the gamma matrix and formed sessile arrangements. C.E.

**A89-53497\*** National Aeronautics and Space Administration. Lewis Research Center, Cleveland, OH.

**1200 TO 1400 K SLOW STRAIN RATE COMPRESSIVE BEHAVIOR OF SMALL GRAIN SIZE NIAL/NI2ALTI ALLOYS AND NIAL/NI2ALTI-TIB2 COMPOSITES**

J. DANIEL WHITTENBERGER (NASA, Lewis Research Center, Cleveland, OH), R. K. VISWANADHAM (Multi-Metals, Louisville, KY), S. K. MANNAN, and K. S. KUMAR (Martin Marietta Laboratories, Baltimore, MD) Journal of Materials Research (ISSN

0884-2914), vol. 4, Sept.-Oct. 1989, p. 1164-1171. refs  
Copyright

In order to impart ductility into NiAl-Ni<sub>2</sub>AlTi alloys, small grain size single (Ni-45Al-5Ti) and two (Ni-40Al-10Ti) phase intermetallics are fabricated by a process which yields fine microstructures in NiAl. The results of a study of elevated temperature compressive properties of two small grain size NiAl-Ni<sub>2</sub>AlTi alloys are then described. In addition, the behavior of the Ti-modified nickel aluminides with 20 vol pct TiB<sub>2</sub> particles of approximately 1 micron in diameter is also investigated, since these compositions have the potential for being the matrix material in high temperature particulate-strengthened composites. S.A.V.

**A89-54495\*** General Motors Research Labs., Warren, MI.

#### AVALANCHE IN ADHESION

JOHN R. SMITH (GM Research Laboratories, Warren, MI), GUILLERMO BOZZOLO (Case Western Reserve University, Cleveland, OH), AMITAVA BANERJEA (NASA, Lewis Research Center, Cleveland; Kent State University, OH), and JOHN FERRANTE (NASA, Lewis Research Center, Cleveland, OH) Physical Review Letters (ISSN 0031-9007), vol. 63, Sept. 18, 1989, p. 1269-1272. refs  
Copyright

Consider surfaces being brought into contact. It is proposed that atomic layers can collapse or avalanche together when the interfacial spacing falls below a critical distance. This causes a discontinuous drop in the adhesive binding energy. Avalanche can occur regardless of the stiffness of external supports. A simple understanding of the origin of this phenomenon is provided. A numerical calculation has been carried out for adhesion in Ni. A new wear mechanism due to avalanche is suggested. Author

**N89-10156\*#** National Aeronautics and Space Administration. Lewis Research Center, Cleveland, OH.

#### T55-L-712 TURBINE ENGINE COMPRESSOR HOUSING REFURBISHMENT-PLASMA SPRAY PROJECT

GEORGE W. LEISSLER and JOHN S. YUHAS (Army Aviation Systems Command, Cleveland, Ohio.) Oct. 1988 44 p  
(Contract DA PROJ. 1L1-62209-AH-76)  
(NASA-TM-101310; E-4301; NAS 1.15:101310) Avail: NTIS HC A03/MF A01 CSCL 11/6

A study was conducted to assess the feasibility of reclaiming T55-L-712 turbine engine compressor housings with an 88 wt percent aluminum to 12 wt percent silicon alloy applied by a plasma spray process. Tensile strength testing was conducted on as-sprayed and thermally cycled test specimens which were plasma sprayed with 0.020 to 0.100 in. coating thicknesses. Satisfactory tensile strength values were observed in the as-sprayed tensile specimens. There was essentially no decrease in tensile strength after thermally cycling the tensile specimens. Furthermore, compressor housings were plasma sprayed and thermally cycled in a 150-hr engine test and a 200-hr actual flight test during which the turbine engine was operated at a variety of loads, speeds and torques. The plasma sprayed coating system showed no evidence of degradation or delamination from the compressor housings. As a result of these tests, a procedure was designed and developed for the application of an aluminum-silicon alloy in order to reclaim T55-L-712 turbine engine compressor housings.

Author

**N89-10996\*#** National Aeronautics and Space Administration. Lewis Research Center, Cleveland, OH.

#### INDENTATION PLASTICITY AND FRACTURE IN SILICON

GEORGE C. RYBICKI and P. PIROUZ (Case Western Reserve Univ., Cleveland, Ohio.) Nov. 1988 30 p  
(NASA-TP-2863; E-4184; NAS 1.60:2863) Avail: NTIS HC A03/MF A01 CSCL 11/2

Measurements of the ductile-brittle transition temperature of heavily doped silicon were carried out using indentation techniques. Diamond pyramid hardness tests were performed on the (100) face of heavily doped N-type and P-type and intrinsic silicon single crystals. Tests were performed over the range 200 C to 850 C and loads of 100 to 500 g were used. Samples were subsequently

etched to reveal dislocation rosettes produced by indentation. Intrinsic silicon underwent a ductile-brittle transition at 660 C, P-type at 645 C and N-type at 625 C. Hardness values varied from 1.1 GPa at 700 C to 11.7 GPa at 200 C. Significant effects of hardness on doping were present only at the highest temperatures. Lower loads generally produced higher hardness but load did not affect the Ductile-Brittle Transition Temperature (DBTT). Fracture toughness values ranged from 0.9 MPa m<sup>1/2</sup> at 200 C to 2.75 MPa m<sup>1/2</sup> near the DBTT. Doping did not affect the fracture toughness of silicon. P-type doping increased the size of dislocation rosettes observed after indentation, but N-type did not, in contradiction of the expected results. Results are discussed in terms of the effect of doping on the dislocation mobility in silicon.

Author

**N89-12634\*#** Georgia Inst. of Tech., Atlanta. Fracture and Fatigue Research Lab.

#### CONSTITUTIVE BEHAVIOR OF SINGLE CRYSTAL PWA 1480 AND DIRECTIONALLY SOLIDIFIED MAR-M 246 UNDER MONOTONIC AND CYCLIC LOADS AT HIGH AND LOW TEMPERATURE

WALTER W. MILLIGAN, ERIC S. HURON, and STEPHEN D. ANTOLOVICH /in NASA, Marshall Space Flight Center, Advanced Earth-To-Orbit Propulsion Technology 1986, Volume 2 p 134-171 Oct. 1986

(Contract NAG3-503)

Avail: NTIS HC A99/MF E03 CSCL 21/8

Strain rate, temperature, time, and microstructure had strong effects on the mechanical properties of Directionally Solidified MAR-M 246 + Hf and PWA 1480, and physical damage. This is the first step toward characterizing the constitutive behavior of the alloys from the physical point of view. In the remaining portion of the program, these relationships will be further explored, in hopes of developing constitutive models which will be based on actual microstructural deformation mechanisms in the alloys.

B.G.

**N89-12635\*#** National Aeronautics and Space Administration. Lewis Research Center, Cleveland, OH.

#### HIGH-TEMPERATURE LCF OF NI-201 AND 304L STAINLESS STEEL

GARY R. HALFORD, L. R. JOHNSON, and JAMES A. BROWN (Aerojet TechSystems Co., Sacramento, Calif.) /in NASA, Marshall Space Flight Center, Advanced Earth-To-Orbit Propulsion Technology 1986, Volume 2 p 172-204 Oct. 1986  
Avail: NTIS HC A99/MF E03 CSCL 21/8

The high-temperature, low-cycle fatigue characteristics were investigated for two candidate alloys for use in the nozzle of an advanced design Orbital Maneuverable System (OMS) engine. Strain-controlled, low-cycle, creep-fatigue tests were performed in air on a commercially pure nickel (Ni201) at 483, 594, and 760 C, and on AISI Type 304L stainless steel at 650, 760, and 870 C. Both continuous strain-cycling tests and compressive-strain, hold-time tests were used in the evaluation. Direct comparisons are made between the two materials, and recommendations are presented as to which material offers the greatest potential for use.

Author

**N89-12717\*#** National Aeronautics and Space Administration. Lewis Research Center, Cleveland, OH.

#### INFLUENCE OF ALLOYING ELEMENTS ON THE OXIDATION BEHAVIOR OF NBAL3

M. G. HEB SUR (Sverdrup Technology, Inc., Cleveland, Ohio.), J. R. STEPHENS, J. L. SMIALEK, C. A. BARRETT, and D. S. FOX 30 Sep. 1988 14 p Presented at the Workshop on the Oxidation of High-Temperature Intermetallics, 22-23 Sep. 1988; sponsored in part by NASA-Lewis Research Center, ASM International, Case Western Reserve Univ., The Metallurgical Society of AIME and TMS-AIME, Cleveland  
(NASA-TM-101398; E-4275; NAS 1.15:101398) Avail: NTIS HC A03/MF A01 CSCL 11/6

NbAl<sub>3</sub> is one candidate material for advanced aeropropulsion systems because of its high melting point, low density, and good

oxidation resistance. Although NbAl<sub>3</sub> has the lowest oxidation rate among the binary Nb-Al alloys, it does not form exclusive layers of protective Al<sub>2</sub>O<sub>3</sub> scales. Recently Perkin et al., have shown the feasibility of forming alumina scales on Nb-Al alloys at greatly reduced Al contents. However, the objective was to maintain the high Al content, and hence low density, while achieving the capability of growing protective alumina scales. Alloy development followed approaches similar to those used successfully for superalloys and oxidation resistant MCrAlY coatings. Among the three elements examined (Ti, Si, and Cr) as ternary additions to Nb-Al<sub>3</sub>, Cr was the most effective in favoring the selective oxidation of Al. Nb-41Al-8Cr formed exclusive layers of alumina and had a  $k_{\text{sub p}}$  value of 0.22 mg squared/cm (sup 4)/hr at 1200 C. The addition of 1 wt percent Y to this alloy was also beneficial, resulting in nearly an order of magnitude decrease in  $k_{\text{sub p}}$  at 1200 C. Further improvements were achieved by adding about 1 wt percent Si to the quaternary alloy. The  $k_{\text{sub p}}$  value of 0.012 mg squared/cm (sup 4)/hr for Nb-40Al-8Cr-1Y-1Si at 1200 C was identical to the best NiAl + Zr alloys. These NbAl<sub>3</sub> alloys also exhibited excellent cyclic oxidation resistance for 100 hr at 1200 C, being nearly equivalent to NiAl + Zr. Author

**N89-12720\*#** National Aeronautics and Space Administration. Lewis Research Center, Cleveland, OH.

**EFFECT OF GRAIN SIZE ON THE HIGH TEMPERATURE PROPERTIES OF B2 ALUMINIDES**

J. DANIEL WHITTENBERGER 1987 26 p Presented at the 1987 Northeast Regional Meeting on High Temperature Structural Composites: Synthesis, Characterization and Properties, Hoboken, N.J., 27-29 May 1987; sponsored by the Metallurgy Society of AIME and the Materials Research Society (NASA-TM-101382; E-3557; NAS 1.15:101382) Avail: NTIS HC A03/MF A01 CSCL 11/6

Measurements of the slow plastic flow behavior of cobalt, iron and nickel B2 crystal structure aluminides were conducted on materials fabricated by metallurgical techniques. Due to this processing, the aluminides invariably had small equiaxed grains, ranging in size from about 3 to 60 microns in diameter. Grain size was dependent on the extrusion temperature used for powder consolidation, and it proved to be remarkably stable at elevated temperatures. Mechanical properties of all three aluminides were determined via constant velocity compression testing in air between 1000 and 1400 K at strain rates ranging from approx. 10 to the minus 3 power to 10 to the minus 7 power s (-1). Author

**N89-12911\*#** Cincinnati Univ., OH.

**CONSTITUTIVE MODELING FOR SINGLE CRYSTAL SUPERALLOYS**

D. C. STOFFER, N. JAYARAMAN, M. SHEH, and D. ALDEN /in NASA, Lewis Research Center, Turbine Engine Hot Section Technology 1986 p 327-334 Oct. 1986 (Contract NAG3-511) Avail: NTIS HC A21/MF A01 CSCL 11/6

The inelastic response of single crystal gamma/gamma prime superalloys is quite different from the behavior of polycrystalline nickel base superalloys. Up to a critical temperature the yield stress of single crystal alloys is a function of the material orientation relative to the direction of the applied stress and the material exhibits significant tension/compression asymmetry. This behavior is primarily due to slip on the octahedral slip system. Above the critical temperature there is a sharp drop in the yield stress, cube slip becomes more predominant and the tension/compression asymmetry is reduced. Similar orientation and tension/compression asymmetry is observed in creep and secondary creep above the critical temperature is inferred to occur by octahedral slip. There are two exceptions to this behavior. First, loading near the (111) orientation exhibits cube slip at all temperatures, and; second, loading near the (001) orientation produces only octahedral slip at all temperatures. The constitutive model is based on separating the total global strain into elastic and inelastic components. This model is developed and briefly discussed. Author

**N89-12912\*#** Connecticut Univ., Storrs.

**CONSTITUTIVE MODELLING OF SINGLE CRYSTAL AND DIRECTIONALLY SOLIDIFIED SUPERALLOYS Progress Report**

E. H. JORDAN and K. P. WALKER (Engineering Science Software, Inc., Smithfield, R.I.) /in NASA, Lewis Research Center, Turbine Engine Hot Section Technology 1986 p 335-339 Oct. 1986 (Contract NAG3-512)

Avail: NTIS HC A21/MF A01 CSCL 11/6

The trend towards improved engine efficiency and durability places increasing demands on materials that operate in the hot section of the gas turbine engine. These demands are being met by new coatings and materials such as single crystal and directionally solidified nickel-base superalloys which have greater creep/fatigue resistance at elevated temperatures and reduced susceptibility to grain boundary creep, corrosion and oxidation than conventionally cast alloys. Work carried out as part of a research program aimed at the development of constitutive equations to describe the elevated temperature stress-strain-time behavior of single crystal and directionally solidified turbine blade superalloys is discussed. The program involves both development of suitable constitutive models and their verification through elevated temperature tension-torsion testing of single crystals of PWA 1480. Author

**N89-12918\*#** Syracuse Univ., NY. Dept. of Mechanical and Aerospace Engineering.

**GRAIN BOUNDARY OXIDATION AND ITS EFFECTS ON HIGH TEMPERATURE FATIGUE LIFE**

H. W. LIU and YOSHIKI OSHIDA /in NASA, Lewis Research Center, Turbine Engine Hot Section Technology 1986 p 407-414 Oct. 1986 (Contract NAG3-348)

Avail: NTIS HC A21/MF A01 CSCL 11/6

Fatigue lives at elevated temperatures are often shortened by creep and/or oxidation. Creep causes grain boundary void nucleation and grain boundary cavitation. Grain boundary voids and cavities will accelerate fatigue crack nucleation and propagation, and thereby shorten fatigue life. The functional relationships between the damage rate of fatigue crack nucleation and propagation and the kinetic process of oxygen diffusion depend on the detailed physical processes. The kinetics of grain boundary oxidation penetration was investigated. The statistical distribution of grain boundary penetration depth was analyzed. Its effect on high temperature fatigue life are discussed. A model of intermittent micro-ruptures of grain boundary oxide was proposed for high temperature fatigue crack growth. The details of these studies are reported. Author

**N89-13566\*#** National Aeronautics and Space Administration. Lewis Research Center, Cleveland, OH.

**THE EFFECT OF 0.1 ATOMIC PERCENT ZIRCONIUM ON THE CYCLIC OXIDATION BEHAVIOR OF BETA-NiAl FOR 300 HOURS AT 1200 C**

C. A. BARRETT 1988 19 p Presented at the Workshop on the Oxidation of High-Temperature Intermetallics, Cleveland, Ohio, 22-23 Sep. 1988; sponsored by ASM International, NASA Lewis Research Center, Case Western Reserve Univ, AIME and TMS-AIME (NASA-TM-101408; E-4366; NAS 1.15:101408) Avail: NTIS HC A03/MF A01 CSCL 11/6

The long time effect of 0.1 at percent Zr (0.2 wt percent Zr) on the cyclic oxidation behavior of hipped beta-NiAl was studied. Oxidation testing was performed in static air at 1200 C for up to 3000 one-hour exposure cycles. Specific weight change versus time data was modeled with the COSP computer program to analyze cyclic oxidation behavior. The Zr-free stoichiometric alloy oxidized and spalled randomly to bare metal between cycles at a rate high enough to deplete Al to a low enough level that oxidation breakaway took place as nonprotective NiO replaced the alpha-Al<sub>2</sub>O<sub>3</sub>/NiAl<sub>2</sub>O<sub>4</sub> scale as the controlling oxide. The Zr minimized this severe type of spalling maintaining the protective alpha-Al<sub>2</sub>O<sub>3</sub> scale even out to 3000 hours for the stoichiometric

alloy with no significant Al depletion. A third beta-NiAl alloy containing 0.1 at percent Zr but with 10 percent less Al than the stoichiometric alloy was also tested and showed some depletion of Al, but the protective  $\text{Al}_2\text{O}_3/\text{NiAl}_2\text{O}_4$  was still maintained to close to 2700 hours. Author

**N89-14297\*#** National Aeronautics and Space Administration. Lewis Research Center, Cleveland, OH.

### OXIDATION BEHAVIOR OF $\text{FeAl} + \text{HF, Zr, B}$

JAMES L. SMIALEK and JOSEPH DOYCHAK (Sverdrup Technology, Inc., Cleveland, Ohio.) 1988 15 p Presented at the Workshop on the Oxidation of High-Temperature Intermetallics, Cleveland OH, 22-23 Sep. 1988; sponsored by ASM and TMS AIME Case Western Reserve Univ., AIME and TMS-AIME (NASA-TM-101402; E-4486; NAS 1.15:101402) Avail: NTIS HC A03/MF A01 CSCL 11/6

The oxidation behavior of Fe-40Al-1Hf, Fe-40Al-1Hf-0.4B, and Fe-40Al-0.1Zr-0.4B (at. percent) alloys was characterized after 900, 1000, and 100 C exposures. Isothermal tests revealed parabolic kinetics after a period of transitional theta-alumina scale growth. The parabolic growth rates for the subsequent alpha-alumina scales were about five times higher than those for NiAl+0.1Zr alloys. The isothermally grown scales showed a propensity toward massive scale spallation due to both extensive rumpling from growth stresses and to an inner layer of  $\text{HfO}_2$ . Cyclic oxidation for 200 1-hr cycles produced little degradation at 900 or 1000 C, but caused significant spallation at 1100 C in the form of small segments of the outer scale. The major difference in the cyclic oxidation of the three FeAl alloys was increased initial spallation for FeAl+Zr,B. Although these FeAl alloys showed many similarities to NiAl alloys, they were generally less oxidation resistant. It is believed that this resulted from nonoptimal levels of dopants and larger thermal expansion mismatch stresses. Author

**N89-14303\*** National Aeronautics and Space Administration. Lewis Research Center, Cleveland, OH.

### CASTABLE HOT CORROSION RESISTANT ALLOY Patent

CHARLES A. BARRETT, inventor (to NASA) and WILLIAM H. HOLT, inventor (to NASA) 25 Oct. 1988 6 p Continuation-in-part of US-Patent-Appl-SN-890584, filed 30 Jul. 1986 (NASA-CASE-LEW-14134-2; US-PATENT-4,780,276; US-PATENT-APPL-SN-108331; US-PATENT-CLASS-420-54; US-PATENT-CLASS-420-62; US-PATENT-CLASS-420-79; US-PATENT-CLASS-420-80; US-PATENT-CLASS-420-81) Avail: U.S. Patent and Trademark Office CSCL 11/6

Some 10 wt percent nickel is added to an Fe-base alloy which has a ferrite microstructure to improve the high temperature castability and crack resistance while about 0.2 wt percent zirconium is added for improved high temperature cyclic oxidation and corrosion resistance. The basic material is a high temperature FeCrAl heater alloy, and the addition provides a material suitable for burner rig nozzles.

Official Gazette of the U.S. Patent and Trademark Office

**N89-15218\*#** National Aeronautics and Space Administration. Lewis Research Center, Cleveland, OH.

### HIGH RESOLUTION VIDEO MONITORING OF COATING THICKNESS DURING PLASMA SPRAYING

ROBERT A. MILLER 1988 6 p Presented at the National Thermal Spray Conference, Cincinnati, OH, 23-27 Oct. 1988; sponsored in part by ASM (NASA-TM-101423; E-4523; NAS 1.15:101423) Avail: NTIS HC A02/MF A01 CSCL 11/6

A new approach to monitoring the thickness of plasma sprayed coatings during application is described. The method employs a high resolution video camera and width analyzer to accurately measure the dimensions of samples having simple geometries. This approach is best suited for cylindrical or flat substrates but it may also work for selected locations on more complex geometries. Measurement accuracy is a function of specimen dimensions and extent of magnification. Tolerances of plus or minus 0.5 mil (0.13 mm) on final coating thickness can be achieved. Additionally, the plot of cumulative coating thickness versus the number of passes

has proven to be a useful diagnostic tool. While the ideal plot is linear, strong deviations from linearity - indicating the need for corrective action - may be observed. Author

**N89-15233\*#** National Aeronautics and Space Administration. Lewis Research Center, Cleveland, OH.

### THE OXIDATION OF NI-RICH NI-AL INTERMETALLICS

JOSEPH DOYCHAK (Sverdrup Technology, Inc., Cleveland, OH.), JAMES L. SMIALEK, and CHARLES A. BARRETT Sep. 1988 17 p Presented at the Workshop on the Oxidation of High-Temperature Intermetallics, Cleveland, OH, 22-23 Sep. 1988; sponsored in part by NASA, ASMI, Case Western Reserve Univ., AIME and TMS-AIME (NASA-TM-101455; E-4438; NAS 1.15:101455) Avail: NTIS HC A03/MF A01 CSCL 11/6

The oxidation of Ni-Al intermetallic alloys in the beta-NiAl phase field and in the two phase beta-NiAl/gamma'-Ni<sub>3</sub>Al phase field has been studied between 1000 and 1400 C. The stoichiometric beta-NiAl alloy doped with Zr was superior to other alloy compositions under cyclic and isothermal oxidation. The isothermal growth rates did not increase monotonically as the alloy Al content was decreased. The characteristically ridged alpha- $\text{Al}_2\text{O}_3$  scale morphology, consisting of cells of thin, textured oxide with thick growth ridges at cell boundaries, forms on oxidized beta-NiAl alloys. The correlation of scale features with isothermal growth rates indicates a predominant grain boundary diffusion growth mechanism. The 1200 C cyclic oxidation resistance decreases near the lower end of the beta-NiAl phase field. Author

**N89-16986\*#** National Aeronautics and Space Administration. Lewis Research Center, Cleveland, OH.

### REFRACTORY METAL ALLOYS AND COMPOSITES FOR SPACE NUCLEAR POWER SYSTEMS Final Report

ROBERT H. TITRAN, JOSEPH R. STEPHENS, and DONALD W. PETRASEK Sep. 1988 24 p Presented at the Metallurgical Society Fall Meeting, Chicago, IL, 27-29 Sep. 1988; sponsored in part by the Metallurgical Society of AIME and the American Society for Metals

(Contract DE-AL03-86SF-16310)

(NASA-TM-101364; E-4398; DOE/NASA/16310-8; NAS 1.15:101364) Avail: NTIS HC A03/MF A01 CSCL 11/6

Space power requirements for future NASA and other U.S. missions will range from a few kilowatts to megawatts of electricity. Maximum efficiency is a key goal of any power system in order to minimize weight and size so that the Space Shuttle may be used a minimum number of times to put the power supply into orbit. Nuclear power has been identified as the primary power source to meet these high levels of electrical demand. One method to achieve maximum efficiency is to operate the power supply, energy conservation system, and related components at relatively high temperatures. For systems now in the planning stages, design temperatures range from 1300 K for the immediate future to as high as 1700 K for the advanced systems. NASA Lewis Research Center has undertaken a research program on advanced technology of refractory metal alloys and composites that will provide baseline information for space power systems in the 1990's and the 21st century. Special emphasis is focused on the refractory metal alloys of niobium and on the refractory metal composites which utilize tungsten alloy wires for reinforcement. Basic research on the creep and creep-rupture properties of wires, matrices, and composites are discussed. Author

**N89-17325\*#** Engineering Science Software, Inc., Smithfield, RI.

### CONSTITUTIVE MODELLING OF SINGLE CRYSTAL AND DIRECTIONALLY SOLIDIFIED SUPERALLOYS

KEVIN P. WALKER and ERIC H. JORDAN (Connecticut Univ., Storrs.) In NASA, Lewis Research Center, Turbine Engine Hot Section Technology, 1987 p 299-301 Oct. 1987 (Contract NAG3-512)

Avail: NTIS HC A20/MF A01 CSCL 11/6

Successful attempts were made to model the deformation behavior of nickel base superalloys to be used in gas turbine



engines based on both a macroscopic constitutive model and a micromechanical formulation based on crystallographic slip theory. These models were programmed as FORTRAN subroutines, are currently being used to simulate thermomechanical loading predictions expected at the fatigue critical locations on a single crystal turbine blade. Such analyses form a natural precursor to the application of life prediction methods to gas turbine airfoils.

Author

**N89-17649\*#** National Aeronautics and Space Administration. Lewis Research Center, Cleveland, OH.

**TENSILE BEHAVIOR OF TUNGSTEN AND TUNGSTEN-ALLOY WIRES FROM 1300 TO 1600 K Final Report**

MAN YUN HEE Sep. 1988 18 p Presented at the Metallurgical Society Fall Meeting, Chicago, IL, 27-29 Sep. 1988; sponsored in part by The Metallurgical Society of AIME, and the American Society for Metals

(Contract DE-AI03-86SF-16310)

(NASA-TM-101446; E-4552; NAS 1.15:101446;

DOE/NASA/16310-7) Avail: NTIS HC A03/MF A01 CSCL 11/6

The tensile behavior of a 200-micrometer-diameter tungsten lamp (218CS-W), tungsten + 1.0 atomic percent (a/o) thoria (ST300-W), and tungsten + 0.4 a/o hafnium carbide (WHfC) wires was determined over the temperature range 1300 to 1600 K at strain rates of  $3.3 \times 10^{-2}$  to  $3.3 \times 10^{-5}$  /sec. Although most tests were conducted on as-drawn materials, one series of tests was undertaken on ST300-W wires in four different conditions: as-drawn and vacuum-annealed at 1535 K for 1 hr, with and without electroplating. Whereas heat treatment had no effect on tensile properties, electropolishing significantly increased both the proportional limit and ductility, but not the ultimate tensile strength. Comparison of the behavior of the three alloys indicates that the HfC-dispersed material possesses superior tensile properties. Theoretical calculations indicate that the strength/ductility advantage of WHfC is due to the resistance to recrystallization imparted by the dispersoid.

Author

**N89-17650\*#** National Aeronautics and Space Administration. Lewis Research Center, Cleveland, OH.

**SECONDARY ELECTRON EMISSION CHARACTERISTICS OF UNTREATED AND ION-TEXTURED TITANIUM**

ARTHUR N. CURREN, KENNETH A. JENSEN, and GARY A. BLACKFORD (Case Western Reserve Univ., Cleveland, OH.) Mar. 1989 16 p

(NASA-TP-2902; E-4495; NAS 1.60:2902) Avail: NTIS HC A03/MF A01 CSCL 11/6

Experimentally determined values of true secondary electron emission and relative values of reflected primary electron yield are presented for untreated (simply machined) and ion-textured, high-purity titanium over ranges of primary electron beam energies and beam impingement angles. The purpose of the investigation was to explore the feasibility of using titanium as electrode material in the multistage depressed collectors (MDC's) used in microwave amplifier traveling wave tubes (TWT's) for space communications and aircraft applications. Because of its relatively low density and thermal expansion characteristics and relatively high strength, thermal emissivity, and melting temperature, titanium presents itself as a possible candidate for the MDC electrode application. A detailed description of the method of ion texturing the titanium is included. Although the ion-treated surface considered in this study is not presented as being optimum from the standpoint of secondary electron emission suppression, it nevertheless serves to demonstrate that the surface can be modified by this procedure to significantly reduce these emission characteristics relative to those of the untreated surface. Further studies can reasonably be expected to produce surfaces with even lower secondary emission characteristics. The titanium surface were tested at primary electron beam energies of 200 to 2000 eV and at direct (0 deg) to near-grazing (85 deg) beam impingement angles. True secondary electron emission and relative reflected primary electron yield characteristics of the surfaces were compared with each other and with textured titanium surface exhibited secondary electron

emission characteristics sharply lower than those exhibited by untreated titanium or copper. Clearly, then, in consideration of the secondary electron emission suppression of ion-textured titanium along with its other favorable physical properties, it must be included as a potential candidate for use as MDC electrode material in some applications.

Author

**N89-20227\*#** National Aeronautics and Space Administration. Lewis Research Center, Cleveland, OH.

**FAILURE ANALYSIS OF A STIRLING ENGINE HEAT PIPE**

THOMAS J. MOORE, JAMES E. CAIRELLI, and KAVEH KHALILI (Stirling Thermal Motors, Inc., Ann Arbor, MI.) Mar. 1989 13 p (NASA-TM-101418; E-4516; NAS 1.15:101418) Avail: NTIS HC A03/MF A01 CSCL 11/6

Failure analysis was conducted on a heat pipe from a Stirling Engine test rig which was designed to operate at 1073 K. Premature failure had occurred due to localized overheating at the leading edge of the evaporator fin. It was found that a crack had allowed air to enter the fin and react with the sodium coolant. The origin of the crack was found to be located at the inner surface of the Inconel 600 fin where severe intergranular corrosion had taken place.

Author

**N89-20228\*#** National Aeronautics and Space Administration. Lewis Research Center, Cleveland, OH.

**MECHANICAL PROPERTIES OF MODIFIED LOW COBALT POWDER METALLURGY UDIMET 700 TYPE ALLOYS**

FREDRIC H. HARF Mar. 1989 29 p

(NASA-TM-101481; E-4609; NAS 1.15:101481) Avail: NTIS HC A03/MF A01 CSCL 11/6

Eight superalloys derived from Udimet 700 were prepared by powder metallurgy, hot isostatically pressed, heat treated and their tensile and creep rupture properties determined. Several of these alloys displayed properties superior to those of Udimet 700 similarly prepared, in one case exceeding the creep rupture life tenfold. Filter clogging by extracted gamma prime, its measurement and significance are discussed in an appendix.

Author

**N89-21072\*#** Rockwell International Corp., Canoga Park, CA. Rocketdyne Div.

**ADVANCED SINGLE CRYSTAL FOR SSME TURBOPUMPS**

L. G. FRITZEMEIER Mar. 1989 51 p

(Contract NAS3-24646)

(NASA-CR-182244; NAS 1.26:182244; RI/RD-88-273) Avail: NTIS HC A04/MF A01 CSCL 11/6

The objective of this program was to evaluate the influence of high thermal gradient casting, hot isostatic pressing (HIP) and alternate heat treatments on the microstructure and mechanical properties of a single crystal nickel base superalloy. The alloy chosen for the study was PWA 1480, a well characterized, commercial alloy which had previously been chosen as a candidate for the Space Shuttle Main Engine high pressure turbopump turbine blades. Microstructural characterization evaluated the influence of casting thermal gradient on dendrite arm spacing, casting porosity distribution and alloy homogeneity. Hot isostatic pressing was evaluated as a means of eliminating porosity as a preferred fatigue crack initiation site. The alternate heat treatment was chosen to improve hydrogen environment embrittlement resistance and for potential fatigue life improvement. Mechanical property evaluation was aimed primarily at determining improvements in low cycle and high cycle fatigue life due to the advanced processing methods. Statistically significant numbers of tests were conducted to quantitatively demonstrate life differences. High thermal gradient casting improves as-cast homogeneity, which facilitates solution heat treatment of PWA 1480 and provides a decrease in internal pore size, leading to increases in low cycle and high cycle fatigue lives.

Author

**N89-22673\*#** National Aeronautics and Space Administration. Lewis Research Center, Cleveland, OH.

**FIBER REINFORCED SUPERALLOYS FOR ROCKET ENGINES**

DONALD W. PETRASEK and JOSEPH R. STEPHENS In AGARD, Application of Advanced Material for Turbomachinery and Rocket



## 26 METALLIC MATERIALS

Propulsion 13 p Mar. 1989 Previously announced as N89-15990

Copyright Avail: NTIS HC A13/MF A01 CSCL 11/6

High pressure turbopumps for advanced reusable liquid propellant rocket engines such as that for the Space Shuttle Main Engine (SSME) require turbine blade materials that operate under extreme conditions of temperature, hydrogen environment, high-cycle fatigue loading, thermal fatigue and thermal shock. Such requirements tax the capabilities of current blade materials. Based on projections of properties for tungsten fiber reinforced superalloy (FRS) composites, it was concluded that FRS turbine blades offer the potential of a several fold increase in life and over a 200 C increase in temperature capability over the current SSME blade material. FRS composites were evaluated with respect to mechanical property requirements for SSME blade applications. Compared to the current blade material, the thermal shock resistance of FRS materials is excellent, two to nine times better, and their thermal fatigue resistance is equal to or higher than the current blade material. FRS materials had excellent low and high-cycle fatigue strengths, and thermal shock-induced surface microcracks had no influence on their fatigue strength. The material also exhibited negligible embrittlement when exposed to a hydrogen environment. Author

**N89-23664\*#** National Aeronautics and Space Administration. Lewis Research Center, Cleveland, OH.

### **MACROSEGREGATION AND NUCLEATION IN UNDERCOOLED PB-SN ALLOYS**

HENRY C. DEGROH, III May 1989 36 p  
(NASA-TM-102023; E-4759; NAS 1.15:102023) Avail: NTIS HC A03/MF A01 CSCL 11/6

A technique resulting in large undercoolings in bulk samples (23g) of lead-tin alloys was developed. Samples of Pb-12.5 wt percent Sn, Pb-61 wt percent Sn, and Pb-77 wt percent Sn were processed with undercoolings ranging from 4 to 34 K and with cooling rates varying between 0.04 and 4 K/sec. The nucleation behavior of the Pb-Sn system was found to be nonreciprocal. The solid Sn phase effectively nucleated the Pb phase of the eutectic; however, large undercoolings developed in Sn-rich eutectic liquid in the presence of the solid Pb phase. This phenomenon is believed to be mainly the result of differences in interfacial energies between solid Sn-eutectic liquid, and solid Pb-eutectic liquid rather than lattice misfit between Pb and Sn. Large amounts of segregation developed in the highly undercooled eutectic ingots. This macrosegregation was found to increase as undercooling increases. Macrosegregation in these undercooled eutectic alloys was found to be primarily due to a sink/float mechanism and the nucleation behavior of the alloy. Lead-rich dendrites are the primary phase in the undercooled eutectic system. These dendrites grow rapidly into the undercooled bath and soon break apart due to recalescence and Sn enrichment of the liquid. These fragmented Pb dendrites are then free to settle to the bottom portion of the ingot causing the macrosegregation observed in this study. A eutectic Pb-Sn alloy undercooled 20 K and cooled at 4 K/sec had a composition of about Pb-72 wt percent Sn at the top and 55 percent Sn at the bottom. Author

**N89-26989\*#** National Aeronautics and Space Administration. Lewis Research Center, Cleveland, OH.

### **FATIGUE CRACK GROWTH STUDY OF SCS6/TI-15-3 COMPOSITE**

PETER KANTZOS and JACK TELESMAAN Aug. 1989 20 p  
(NASA-TM-102332; E-5041; NAS 1.15:102332) Avail: NTIS HC A03/MF A01 CSCL 11/6

A study was performed to determine the fatigue crack growth (FCG) behavior and the associated fatigue damage processes in a (0)(8) and (90)(8) oriented SCS6/Ti-15-3 composite. Companion testing (CT) was also done on identically processed Ti-15-3 unreinforced material. The active fatigue crack growth failure processes were very similar for both composite orientations tested. For both orientations, fatigue crack growth was along the fiber direction. It was found that the composite constituent most susceptible to fatigue damage was the interface region and in

particular the carbon coating surrounding the fiber. The failure of the interface region lead to crack initiation and also strongly influenced the FCG behavior in this composite. The failure of the interface region was apparently driven by normal stresses perpendicular to the fiber direction. The FCG rates were considerably higher for the (90)(8) oriented CT specimens in comparison to the unreinforced material. This is consistent with the scenario in which the interface has lower fatigue resistance than the matrix, causing lower composite fatigue resistance. The FCG rates of the (0)(8) composite could not be directly compared to the (90)(8) composite but were shown to increase with an increase in the crack length. Author

**N89-28627\*#** National Aeronautics and Space Administration. Lewis Research Center, Cleveland, OH.

### **THE INTERFACE IN TUNGSTEN FIBER REINFORCED NIOBIUM METAL-MATRIX COMPOSITES Final Report Ph.D.**

**Thesis - Case Western Reserve Univ., Cleveland, OH**  
TONI L. GROBSTEIN Sep. 1989 81 p  
(Contract DE-AI03-86SF-16310)

(NASA-TM-102122; E-4754; DOE/NASA/16310-10; NAS 1.15:102122) Avail: NTIS HC A05/MF A01 CSCL 11/6

The creep resistance of tungsten fiber reinforced niobium metal-matrix composites was evaluated. The interface region between the fiber and matrix was characterized by microhardness and electron probe microanalysis measurements which indicated that its properties were between those of fiber and matrix. However, the measured properties of the composite exceeded those calculated by the rule of mixtures even when the interface zone was assumed to retain all the strength of the fiber. The composite structure appeared to enhance the strengths of both the fibers and the matrix above what they exhibited in stand-alone tests. The effect of fiber orientation and matrix alloy composition on the fiber/matrix interface were also evaluated. Small alloying additions of zirconium and tungsten to the niobium matrix affected the creep resistance of the composites only slightly. A decrease in the creep resistance of the composite with increasing zirconium content in the matrix was ascribed to an increase in the diffusion rate of the fiber/matrix interdiffusion reaction, and a slight increase in the creep resistance of the composite was observed with an addition of 9 w percent tungsten to the matrix. In addition, Kirkendall void formation was observed at the fiber/matrix interface; the void distribution differed depending on the fiber orientation relative to the stress axis. Author

**N89-29522\*#** National Aeronautics and Space Administration. Lewis Research Center, Cleveland, OH.

### **CREEP BEHAVIOR OF TUNGSTEN FIBER REINFORCED NIOBIUM METAL MATRIX COMPOSITES Final Report**

T. L. GROBSTEIN Jan. 1989 21 p Presented at the 6th Symposium on Space Nuclear Power Systems, Albuquerque, NM, 8-12 Jan. 1989; sponsored in part by Inst. for Space Nuclear Power Studies  
(Contract DE-AI03-86SF-16310)

(NASA-TM-102307; E-4995; DOE/NASA/16310-11; NAS 1.15:102307) Avail: NTIS HC A03/MF A01 CSCL 11/6

Tungsten fiber reinforced niobium metal matrix composites were evaluated for use in space nuclear power conversion systems. The composite panels were fabricated using the arc-spray monotape technique at the NASA Lewis Research Center. The creep behavior of W/Nb composite material was determined at 1400 and 1500 K in vacuum over a wide range of applied loads. The time to reach 1 percent strain, the time to rupture, and the minimum creep rate were measured. The W/Nb composites exceeded the properties of monolithic niobium alloys significantly even when compared on a strength to density basis. The effect of fiber orientation on the creep strength also was evaluated. Kirkendall void formation was observed at the fiber/matrix interface; the void distribution differed depending on the fiber orientation relative to the stress axis. A relationship was found between the fiber orientation and the creep strength. Author

## NONMETALLIC MATERIALS

Includes physical, chemical, and mechanical properties of plastics, elastomers, lubricants, polymers, textiles, adhesives, and ceramic materials.

**A89-17097\*** National Aeronautics and Space Administration. Lewis Research Center, Cleveland, OH.

**STRENGTH DISTRIBUTION IN COMMERCIAL SILICON CARBIDE MATERIALS**

SUNIL DUTTA (NASA, Lewis Research Center, Cleveland, OH) American Ceramic Society, Communications (ISSN 0002-7820), vol. 71, Nov. 1988, p. C-474 to C-479. refs  
(Contract DEN3-27)  
Copyright

Four-point flexural strength testing has been conducted in order to establish the baseline strength and reliability of four different commercial SiC types, in conjunction with reliable Weibull modulus values. Average strength of the samples ranged from 380 to 482 MPa at room temperature and 307 to 470 MPa at 1370 C. The strength scatter reflects the effect of flaw variability, which must be minimized to improve reliability in sintered SiC. O.C.

**A89-21442\*** Ohio State Univ., Columbus.

**REACTIONS OF SILICON-BASED CERAMICS IN MIXED OXIDATION CHLORINATION ENVIRONMENTS**

JOHN E. MARRA, ERIC R. KREIDLER (Ohio State University, Columbus), NATHAN S. JACOBSON, and DENNIS S. FOX (NASA, Lewis Research Center, Cleveland, OH) American Ceramic Society, Journal (ISSN 0002-7820), vol. 71, Dec. 1988, p. 1067-1073. Research supported by the Edward Orton Junior Ceramic Foundation. refs  
(Contract DAAG29-82-K-0149)  
Copyright

The reaction of silicon-based ceramics with 2 percent Cl<sub>2</sub>/Ar and 1 percent Cl<sub>2</sub>/1 percent to 20 percent O<sub>2</sub>/Ar at 950 C was studied with thermogravimetric analysis and high-pressure mass spectrometry. Pure Si, SiO<sub>2</sub>, several types of SiC, and Si<sub>3</sub>N<sub>4</sub> were examined. The primary corrosion products were SiCl<sub>4</sub>(g) and SiO<sub>2</sub>(s) with smaller amounts of volatile silicon oxychlorides. The reactions appear to occur by chlorine penetration of the SiO<sub>2</sub> layer, and gas-phase diffusion of the silicon chlorides away from the sample appears to be rate limiting. Pure SiO<sub>2</sub> shows very little reaction with Cl<sub>2</sub>, SiC with excess Si is more reactive than the other materials with Cl<sub>2</sub>, whereas SiC with excess carbon is more reactive than the other materials with Cl<sub>2</sub>/O<sub>2</sub>. Si<sub>3</sub>N<sub>4</sub> shows very little reaction with Cl<sub>2</sub>. These differences are explained on the basis of thermodynamic and microstructural factors. Author

**A89-21444\*** Case Western Reserve Univ., Cleveland, OH.  
**COMPARISON OF THE SURFACE CHARGE BEHAVIOR OF COMMERCIAL SILICON NITRIDE AND SILICON CARBIDE POWDERS**

PAMELA K. WHITMAN and DONALD L. FEKE (Case Western Reserve University, Cleveland, OH) American Ceramic Society, Journal (ISSN 0002-7820), vol. 71, Dec. 1988, p. 1086-1093. refs  
(Contract NAG3-468)  
Copyright

The adsorption and desorption of protons from aqueous solution onto the surfaces of a variety of commercial silicon carbide and silicon nitride powders has been examined using a surface titration methodology. This method provides information on some colloidal characteristics, such as the point of zero charge (pzc) and the variation of proton adsorption with dispersion pH, useful for the prediction of optimal ceramic-processing conditions. Qualitatively, the magnitude of the proton adsorption from solution reveals small differences among all of the materials studied. However, the results show that the pzc for the various silicon nitride powders is affected

by the powder synthesis route. Complementary investigations have shown that milling can also act to shift the pzc exhibited by silicon nitride powder. Also, studies of the role of the electrolyte in the development of surface charge have indicated no evidence of specific adsorption of ammonium ion on either silicon nitride or silicon carbide powders. Author

**A89-26452\*** National Aeronautics and Space Administration. Lewis Research Center, Cleveland, OH.

**CRACK GROWTH RESISTANCE OF TEXTURED ALUMINA**

JONATHAN A. SALEM, JOHN L. SHANNON, JR. (NASA, Lewis Research Center, Cleveland, OH), and RICHARD C. BRADY (Washington, University, Seattle) American Ceramic Society, Journal (ISSN 0002-7820), vol. 72, Jan. 1989, p. 20-27. refs  
Copyright

The crack growth resistance of a textured, extruded alumina body was compared with that of anisotropic, isopressed body of similar grain size, density, and chemistry. R-curve levels reflected the preferred orientation; however, R-curve slopes were the same in all instances, implying a similar crack growth-resistive mechanism. Three orthogonal orientations of crack growth in the two structures exhibited similar forms of K(II) versus Delta-a curves, for which a schematic diagram for polycrystalline ceramics is proposed. Author

**A89-26457\*** Utah Univ., Salt Lake City.

**FRACTURE TOUGHNESS OF POLYCRYSTALLINE CERAMICS IN COMBINED MODE I AND MODE II LOADING**

DILEEP SINGH and DINESH K. SHETTY (Utah, University, Salt Lake City) American Ceramic Society, Journal (ISSN 0002-7820), vol. 72, Jan. 1989, p. 78-84. refs  
(Contract NAG3-789)  
Copyright

The present investigation of the fracture of alumina and zirconia polycrystalline ceramic specimens of precracked-disk type, in diametral compression, evaluated fracture toughness in pure mode I, combined mode I/mode II, and pure mode II, depending on the alignment of the center crack relative to the loading diameter. The mixed-mode fracture-toughness envelope thus obtained exhibits significant deviation to higher fracture toughness in mode II, relative to the predictions of linear elastic fracture mechanics theory. Crack-surface resistance due to grain-interlocking and abrasion are identified as the primary sources of increased fracture resistance in mode II loading of the polycrystalline ceramics. O.C.

**A89-30631** National Aeronautics and Space Administration. Lewis Research Center, Cleveland, OH.

**ON THE ORTHORHOMBIC PHASE IN ZrO<sub>2</sub>-BASED ALLOYS**

A. H. HEUER, V. LANteri, R. CHAIM, R.-R. LEE (Case Western Reserve University, Cleveland, OH), S. C. FARMER (NASA, Lewis Research Center; Case Western Reserve University, Cleveland, OH) et al. Journal of Materials Science (ISSN 0022-2461), vol. 24, Jan. 1989, p. 124-132. refs  
(Contract NSF DMR-82-14128; DE-FG02-84ER-45110)  
Copyright

During TEM observation, a tetragonal (t) to orthorhombic (o) phase transformation often occurs in thin portions of ZrO<sub>2</sub>-containing foils. This transformation is stress-induced and in some senses artifactual, in that the reaction product is actually a high-pressure phase, relative to monoclinic (m) ZrO<sub>2</sub>, that can form from metastable t-ZrO<sub>2</sub> in the TEM because its density is intermediate between t- and m-ZrO<sub>2</sub>. Examples of the formation of o-ZrO<sub>2</sub> in a number of different systems are given. Author

**A89-31502\*** National Aeronautics and Space Administration. Lewis Research Center, Cleveland, OH.

**PRESSURE EFFECTS ON THE THERMAL STABILITY OF SILICON CARBIDE FIBERS**

MARTHA H. JASKOWIAK and JAMES A. DICARLO (NASA, Lewis Research Center, Cleveland, OH) American Ceramic Society, Journal (ISSN 0002-7820), vol. 72, Feb. 1989, p. 192-197.

## 27 NONMETALLIC MATERIALS

Previously announced in STAR as N88-10120. refs  
Copyright

Commercially available polymer derived SiC fibers were treated at temperatures from 1000 to 2200 C in vacuum and argon gas pressure of 1 and 1360 atm. Effects of gas pressure on the thermal stability of the fibers were determined through property comparison between the pressure treated fibers and vacuum treated fibers. Investigation of the thermal stability included studies of the fiber microstructure, weight loss, grain growth, and tensile strength. The 1360 atm argon gas treatment was found to shift the onset of fiber weight loss from 1200 to above 1500 C. Grain growth and tensile strength degradation were correlated with weight loss and were thus also inhibited by high pressure treatments. Additional heat treatment in 1 atm argon of the fibers initially treated at 1360 atm argon caused further weight loss and tensile strength degradation, thus indicating that high pressure inert gas conditions would be effective only in delaying fiber strength degradation. However, if the high gas pressure could be maintained throughout composite fabrication, then the composites could be processed at higher temperatures. Author

**A89-33611\*** National Aeronautics and Space Administration. Lewis Research Center, Cleveland, OH.

### **EFFECTS OF VARIOUS CONSOLIDATION TECHNIQUES ON MICROSTRUCTURE, STRENGTH, AND RELIABILITY OF ALPHA-SiC**

SUNIL DUTTA (NASA, Lewis Research Center, Cleveland, OH) IN: Silicon carbide '87; Proceedings of the Symposium, Columbus, OH, Aug. 2-5, 1987. Westerville, OH, American Ceramic Society, Inc., 1989, p. 201-214. refs  
Copyright

The effects of slurry pressing, HIP, and sinter-HIP on the strength, microstructure, and critical processing flaws in alpha-SiC are examined. Also, the feasibility of glass encapsulation is determined. Baseline strength was improved by about 25 percent by using slurry pressing instead of dry pressing. HIP further improved average strength to as high as 655 MPa. Sinter-HIP did not noticeably improve average strength. Although process-related flaws such as shrinkage cracks and large voids were not seen in HIPed alpha-SiC, surface-related flaws were observed. It is suggested that surface finishing by lapping, polishing, and heat treating might reduce the effect of surface-related flaws, improving the Weibull modulus in HIPed alpha-SiC. R.B.

### **A89-33616\*** Ohio State Univ., Columbus. **THE BEHAVIOR OF SiC AND Si<sub>3</sub>N<sub>4</sub> CERAMICS IN MIXED OXIDATION/CHLORINATION ENVIRONMENTS**

JOHN E. MARRA, ERIC R. KREIDLER (Ohio State University, Columbus), NATHAN S. JACOBSON, and DENNIS S. FOX (NASA, Lewis Research Center, Cleveland, OH) IN: Silicon carbide '87; Proceedings of the Symposium, Columbus, OH, Aug. 2-5, 1987. Westerville, OH, American Ceramic Society, Inc., 1989, p. 275-287. Research supported by the Edward Orton Junior Ceramic Foundation. refs  
(Contract DAAG29-82-K-0149)  
Copyright

The behavior of silicon-based ceramics in mixed oxidation/chlorination environments was studied. High pressure mass spectrometry was used to quantitatively identify the reaction products. The quantitative identification of the corrosion products was coupled with thermogravimetric analysis and thermodynamic equilibrium calculations run under similar conditions in order to deduce the mechanism of corrosion. Variations in the behavior of the different silicon-based materials are discussed. Direct evidence of the existence of silicon oxychloride compounds is presented. Author

### **A89-33619\*** Ford Motor Co., Dearborn, MI. **IMPROVED SILICON CARBIDE FOR ADVANCED HEAT ENGINES. I - PROCESS DEVELOPMENT FOR INJECTION MOLDING**

THOMAS J. WHALEN and WALTER TRELA (Ford Motor Co., Dearborn, MI) IN: Silicon carbide '87; Proceedings of the

Symposium, Columbus, OH, Aug. 2-5, 1987. Westerville, OH, American Ceramic Society, Inc., 1989, p. 343-354. refs  
(Contract NAS3-24384)  
Copyright

Alternate processing methods have been investigated as a means of improving the mechanical properties of injection-molded SiC. Various mixing processes (dry, high-shear, and fluid) were evaluated along with the morphology and particle size of the starting beta-SiC powder. Statistically-designed experiments were used to determine significant effects and interactions of variables in the mixing, injection molding, and binder removal process steps. Improvements in mechanical strength can be correlated with the reduction in flaw size observed in the injection molded green bodies obtained with improved processing methods. Author

### **A89-33620\*** Ford Motor Co., Dearborn, MI. **IMPROVED SILICON CARBIDE FOR ADVANCED HEAT ENGINES. II - PRESSURELESS SINTERING AND MECHANICAL PROPERTIES OF INJECTION MOLDED SILICON CARBIDE**

THOMAS J. WHALEN and J. R. BAER (Ford Motor Co., Dearborn, MI) IN: Silicon carbide '87; Proceedings of the Symposium, Columbus, OH, Aug. 2-5, 1987. Westerville, OH, American Ceramic Society, Inc., 1989, p. 355-366.  
(Contract NAS3-24384)  
Copyright

The influence on density and strength of pressureless sintering in vacuum and argon environments has been evaluated with injection molded SiC materials. Main effects and two factor interactions of sintering (cycle variables temperature, time, heating rate, and atmosphere) were assessed. An improved understanding of the influence of the processing flaws and sintering conditions has been obtained. Strength and density have improved from a baseline level of 299 MPa (43.3 Ksi) and 94 pct of theoretical density to values greater than 483 MPa (70 Ksi) and 97 pct. Author

**A89-34840\*** National Aeronautics and Space Administration. Lewis Research Center, Cleveland, OH.

### **HIGH-FREQUENCY ULTRASONIC CHARACTERIZATION OF SINTERED SILICON CARBIDE**

GEORGE Y. BAAKLINI, EDWARD R. GENERAZIO, and JAMES D. KISER (NASA, Lewis Research Center, Cleveland, OH) American Ceramic Society, Journal (ISSN 0002-7820), vol. 72, March 1989, p. 383-387. Previously announced in STAR as N88-23985. refs  
Copyright

High-frequency 60- to 160-MHz ultrasonic nondestructive evaluation was used to characterize variations in density and microstructural constituents of sintered SiC bars. Ultrasonic characterization methods included longitudinal velocity, reflection coefficient, and precise attenuation measurements. The SiC bars were tailored to provide bulk densities ranging from 90 to 98 percent of theoretical, average grain sizes ranging from 3.0 to 12.0 microns, and average pore sizes ranging from 1.5 to 4.0 microns. Velocity correlated with specimen bulk density irrespective of specimen average grain size, average pore size, and average pore orientation. The attenuation coefficient was found to be sensitive to both density and average pore size variations, but was not affected by large differences in average grain size. Author

### **A89-37670\*** Pennsylvania Univ., Philadelphia. **SYNTHESIS AND STABILITY OF BR<sub>2</sub>, ICL AND IBr INTERCALATED PITCH-BASED GRAPHITE FIBERS**

DOROTHY E. WESSBECHER, WILLIAM C. FORSMAN (Pennsylvania, University, Philadelphia), and JAMES R. GAIER (NASA, Lewis Research Center, Cleveland, OH) Synthetic Metals (ISSN 0379-6779), vol. 26, 1988, p. 185-194. refs  
Copyright

The intercalation of halogens in pitch-based fiber is studied as well as the stability of the resultant intercalation compounds. It is found that IBr intercalates P-100 to yield a high-sigma GIC with

attractive stability properties. During ICI intercalation, the presence of O<sub>2</sub> interferes with the reaction and necessitates a higher threshold pressure for intercalation. K.K.

**A89-41744\*** National Aeronautics and Space Administration. Lewis Research Center, Cleveland, OH.

**HOT ISOSTATIC PRESSING OF SILICON NITRIDE WITH BORON NITRIDE, BORON CARBIDE, AND CARBON ADDITIONS**

DIANE M. MIESKOWSKI and WILLIAM A. SANDERS (NASA, Lewis Research Center, Cleveland, OH) American Ceramic Society, Communications (ISSN 0002-7820), vol. 72, May 1989, p. 840-843. refs

Copyright

Si<sub>3</sub>N<sub>4</sub> test bars containing additions of BN, B<sub>4</sub>C, and C, were hot isostatically pressed in Ta cladding at 1900 and 2050 C to 98.9 percent to 99.5 percent theoretical density. Room-temperature strength data on specimens containing 2 wt pct BN and 0.5 wt pct C were comparable to data obtained for Si<sub>3</sub>N<sub>4</sub> sintered with Y<sub>2</sub>O<sub>3</sub>, Y<sub>2</sub>O<sub>3</sub> and Al<sub>2</sub>O<sub>3</sub>, or ZrO<sub>2</sub>. The 1370 C strengths were less than those obtained for additions of Y<sub>2</sub>O<sub>3</sub> or ZrO<sub>2</sub> but greater than those obtained from a combination of Y<sub>2</sub>O<sub>3</sub> and Al<sub>2</sub>O<sub>3</sub>. SEM fractography indicated that, as with other types of Si<sub>3</sub>N<sub>4</sub>, room-temperature strength was controlled by processing flaws. The decrease in strength at 1370 C was typical of Si<sub>3</sub>N<sub>4</sub> having an amorphous grain-boundary phase. The primary advantage of nonoxide additions appears to be in facilitating specimen removal from the Ta cladding. Author

**A89-48250\*** National Aeronautics and Space Administration. Lewis Research Center, Cleveland, OH.

**ADHESION, FRICTION, AND WEAR OF PLASMA-DEPOSITED THIN SILICON NITRIDE FILMS AT TEMPERATURES TO 700 C**

K. MIYOSHI, J. J. POUCH, S. A. ALTEROVITZ (NASA, Lewis Research Center, Cleveland, OH), D. M. PANTIC, and G. A. JOHNSON (Cincinnati, University, OH) IN: Wear of materials. Volume 2. New York, American Society of Mechanical Engineers, 1989, p. 585-594. Previously announced in STAR as N89-11913. refs

Copyright

The adhesion, friction, and wear behavior of silicon nitride films deposited by low- and high-frequency plasmas (30 kHz and 13.56 MHz) at various temperatures to 700 C in vacuum were examined. The results of the investigation indicated that the Si/N ratios were much greater for the films deposited at 13.56 MHz than for those deposited at 30 kHz. Amorphous silicon was present in both low- and high-frequency plasma-deposited silicon nitride films. However, more amorphous silicon occurred in the films deposited at 13.56 MHz than in those deposited at 30 kHz. Temperature significantly influenced adhesion, friction, and wear of the silicon nitride films. Wear occurred in the contact area at high temperature. The wear correlated with the increase in adhesion and friction for the low- and high-frequency plasma-deposited films above 600 and 500 C, respectively. The low- and high-frequency plasma-deposited thin silicon nitride films exhibited a capability for lubrication (low adhesion and friction) in vacuum at temperatures to 500 and 400 C, respectively. Author

**A89-48892\*** National Aeronautics and Space Administration. Lewis Research Center, Cleveland, OH.

**ULTRASONIC IMAGING OF POROSITY VARIATIONS PRODUCED DURING SINTERING**

EDWARD R. GENERAZIO, DON J. ROTH (NASA, Lewis Research Center, Cleveland, OH), and DAVID B. STANG (NASA, Lewis Research Center; Sverdrup Technology, Inc., Cleveland, OH) American Ceramic Society, Communications (ISSN 0002-7820), vol. 72, July 1989, p. 1282-1285. refs

Copyright

A silicon carbide disk was sintered from 2090 to 2190 C in 25-C steps. After each sintering step, the disk was examined using a precision acoustic scanning system to determine acoustic attenuation and velocity. The bulk density was found to vary nonmonotonically with sintering temperature. The density varied

as much as 10 percent from its value at 2090 C during the sintering process. Local density fluctuations occurred in an organized and history-dependent way. These local density fluctuations varied up to + or - 7 percent of the bulk density and were made visible by acoustic attenuation and velocity mapping. Author

**A89-51258\*** Case Western Reserve Univ., Cleveland, OH.

**TRIBOLOGICAL PROPERTIES OF STRUCTURAL CERAMICS**

DONALD H. BUCKLEY (Case Western Reserve University, Cleveland, OH) and KAZUHISA MIYOSHI (NASA, Lewis Research Center, Cleveland, OH) IN: Structural ceramics. San Diego, CA, Academic Press, Inc., 1989, p. 293-365. Previously announced in STAR as N86-10341. refs

Copyright

The tribological and lubricated behavior of both oxide and nonoxide ceramics are reviewed in this chapter. Ceramics are examined in contact with themselves, other harder materials and metals. Elastic, plastic and fracture behavior of ceramics in solid state contact is discussed. The contact load necessary to initiate fracture in ceramics is shown to be appreciably reduced with tangential motion. Both friction and wear of ceramics are anisotropic and relate to crystal structure as has been observed with metals. Grit size effects in two and three body abrasive wear are observed for ceramics. Both free energy of oxide formation and the d valence bond character of metals are related to the friction and wear characteristics for metals in contact with ceramics. Surface contaminants affect friction and adhesive wear. For example, carbon on silicon carbide and chlorine on aluminum oxide reduce friction while oxygen on metal surfaces in contact with ceramics increases friction. Lubrication increases the critical load necessary to initiate fracture of ceramics both in indentation and with sliding or rubbing. Ceramics compositions both as coatings and in composites are described for the high temperature lubrication of both alloys and ceramics. Author

**A89-54277\*** National Aeronautics and Space Administration. Lewis Research Center, Cleveland, OH.

**ADHESION, FRICTION AND MICROMECHANICAL PROPERTIES OF CERAMICS**

KAZUHISA MIYOSHI (NASA, Lewis Research Center, Cleveland, OH) IN: Metallurgical coatings 1988; Proceedings of the Fifteenth International Conference, San Diego, CA, Apr. 11-15, 1988. Volume 1. London and New York, Elsevier Applied Science, 1988, p. 487-501. Previously announced in STAR as N88-17801. refs

Copyright

The adhesion, friction, and micromechanical properties of ceramics, both in monolithic and coating form, are reviewed. Ceramics are examined in contact with themselves, other harder materials, and metals. For the simplicity of discussion, the tribological properties of concern in the processes are separated into two parts. The first part discusses the pull-off force (adhesion) and the shear force required to break the interfacial junctions between contacting surfaces. The role of chemical bonding in adhesion and friction, and the effects of surface contaminant films and temperature on tribological response with respect to adhesion and friction are discussed. The second part deals with abrasion of ceramics. Elastic, plastic, and fracture behavior of ceramics in solid state contact is discussed. The scratch technique of determining the critical load needed to fracture interfacial adhesive bonds of ceramic deposited on substrates is also addressed. Author

**A89-54982\*** National Aeronautics and Space Administration. Lewis Research Center, Cleveland, OH.

**TRIBOLOGICAL PROPERTIES OF ALUMINA-BORIA-SILICATE FABRIC FROM 25 C TO 850 C**

CHRISTOPHER DELLACORTE (NASA, Lewis Research Center, Cleveland, OH) STLE Tribology Transactions (ISSN 0569-8197), vol. 32, July 1989, p. 325-330. Previously announced in STAR as N88-18726. refs

Copyright

Demanding tribological properties are required of the materials used for the sliding seal between the sidewalls and the lower wall

of the variable area hypersonic engine. Temperatures range from room temperature and below to operating temperatures of 1000 C in an environment of air, hydrogen, and water vapor. Candidate sealing materials for this application are an alumina-boria-silicate, ceramic, fabric rope sliding against the engine walls which may be made from copper- or nickel-based alloys. Using a pin-on-disk tribometer, the friction and wear properties of some of these potential materials and possible lubrication methods are evaluated. The ceramic fabric rope displayed unacceptably high friction coefficients (0.6 to 1.3) and, thus, requires lubrication. Sputtered thin films of gold, silver, and CaF<sub>2</sub> reduced the friction by a factor of two. Sprayed coatings of boride nitride did not effectively lubricate the fabric. Static heat treatment tests at 950 C indicate that the fabric is chemically attacked by large quantities of silver, CaF<sub>2</sub>, and boron nitride. Sputtered films or powder impregnation of the fabric with gold may provide adequate lubrication up to 1000 C without showing any chemical attack. Author

**A89-54985\*** National Aeronautics and Space Administration. Lewis Research Center, Cleveland, OH.

**DEFORMATION AND FRACTURE OF SINGLE-CRYSTAL AND SINTERED POLYCRYSTALLINE SILICON CARBIDE PRODUCED BY CAVITATION**

KAZUHISA MIYOSHI (NASA, Lewis Research Center, Cleveland, OH), SHUJI HATTORI, TSUNENORI OKADA (Fukui University, Japan), and DONALD H. BUCKLEY (Case Western Reserve University, Cleveland, OH) STLE Tribology Transactions (ISSN 0569-8197), vol. 32, July 1989, p. 380-388. Previously announced in STAR as N87-20422. refs Copyright

An investigation was conducted to examine the deformation and fracture behavior of single-crystal and sintered polycrystalline SiC surfaces exposed to cavitation. Cavitation erosion experiments were conducted in distilled water at 25 C by using a magnetostrictive oscillator in close proximity (1 mm) to the surface of SiC. The horn frequency was 20 kHz, and the double amplitude of the vibrating disk was 50 microns. The results of the investigation indicate that the SiC (0001) surface could be deformed in a plastic manner during cavitation. Dislocation etch pits were formed when the surface was chemically etched. The number of defects, including dislocations in SiC (0001) surface, increased with increasing exposure time to cavitation. The presence of intrinsic defects such as voids in the surficial layers of the sintered polycrystalline SiC determined the zones at which fractured grains and fracture pits (pores) were generated. Single-crystal SiC had superior erosion resistance to that of sintered polycrystalline SiC. Author

**N89-10166\*** National Aeronautics and Space Administration. Lewis Research Center, Cleveland, OH.

**A SINTERING MODEL FOR SiC(SUB)W/Si3N4 COMPOSITES**

MARC R. FREEDMAN, JAMES D. KISER, and WILLIAM A. SANDERS 1988 19 p Presented at the 90th Annual Meeting of the American Ceramic Society, Cincinnati, Ohio, 1-5 May 1988 (NASA-TM-101336; E-4354; NAS 1.15:101336) Avail: NTIS HC A03/MF A01 CSCL 11/3

Presented is a model which suggests that it should be possible to pressureless sinter a SiC(sub w)/ Si<sub>3</sub>N<sub>4</sub> composite to theoretical density. Prior failure to achieve complete densification by sintering is attributed to the use of compositions which result in a glass deficit. There is one basic premise for this model. The ratio of glass amount to surface area of nonglass constituents must be the same for both composite and sinterable monolithic Si<sub>3</sub>N<sub>4</sub>. This model suggests that whisker and grain sizes and whisker loading influence the glass amount necessary for successful sintering of composites. According to the model, a large glass amount will be necessary for successful sintering of these composites. However, grain boundary thicknesses in the composite will be less than those in the analogous monolithic materials. This suggests that good high temperature strength may still be attained. A recent report supports the predictions of the model. Author

**N89-11038\*** National Aeronautics and Space Administration. Lewis Research Center, Cleveland, OH.

**PHASE TRANSFORMATIONS IN XEROGELS OF MULLITE COMPOSITION**

MARK J. HYATT and NAROTTAM P. BANSAL (Case Western Reserve Univ., Cleveland, Ohio.) 1988 19 p (NASA-TM-101349; E-4332; NAS 1.15:101349) Avail: NTIS HC A03/MF A01 CSCL 11/3

Monophasic and diphasic xerogels have been prepared as precursors for mullite (3Al<sub>2</sub>O<sub>3</sub>-2SiO<sub>2</sub>). Monophasic xerogel was synthesized from tetraethyl orthosilicate and aluminum nitrate nanohydrate and the diphasic xerogel from colloidal suspension of silica and boehmite. The chemical and structural evolutions, as a function of thermal treatment, in these two types of sol-gel derived mullite precursor powders have been characterized by DTA, TGA, X-ray diffraction, SEM and infrared spectroscopy. Monophasic xerogel transforms to an Al-Si spinel from an amorphous structure at approximately 980 C. The spinel then changes into mullite on further heating. Diphasic xerogel forms mullite at approximately 1360 C. The components of the diphasic powder react independently up to the point of mullite formation. The transformation in the monophasic powder occurs rapidly and yields strongly crystalline mullite with no other phases present. The diphasic powder, however, transforms rather slowly and contains remnants of the starting materials (alpha-Al<sub>2</sub>O<sub>3</sub>, cristobalite) even after heating at high temperatures for long times (1600 C, 6 hr). The diphasic powder could be sintered to high density but not the monophasic powder in spite of its molecular level homogeneity. Author

**N89-11911\*** National Aeronautics and Space Administration. Lewis Research Center, Cleveland, OH.

**TECHNOLOGICAL HURDLES TO THE APPLICATION OF INTERCALATED GRAPHITE FIBERS**

JAMES R. GAIER Dec. 1988 16 p Presented at the Fall Meeting of the Materials Research Society, Boston, Mass., 28 Nov. - 2 Dec. 1988 (NASA-TM-101394; E-4469; NAS 1.15:101394) Avail: NTIS HC A03/MF A01 CSCL 11/3

Before intercalated graphite fibers can be developed as an effective power material, there are several technological hurdles which must be overcome. These include the environmental stability, homogeneity and bulk properties, connection procedures, and costs. Strides were made within the last several years in stability and homogeneity of intercalated graphite fibers. Bulk properties and connection procedures are areas of active research now. Costs are still prohibitive for all but the most demanding applications. None of these problems, however, appear to be unsolvable, and their solution may result in wide spread GOC application. The development of a relatively simple technology application, such as EMI shielding, would stimulate the solution of scale-up problems. Once this technology is developed, then more demanding applications, such as power bus bars, may be possible. Author

**N89-11912\*** National Aeronautics and Space Administration. Lewis Research Center, Cleveland, OH.

**MOLTEN SALT CORROSION OF SiC AND Si3N4**

NATHAN S. JACOBSON, JAMES L. SMIALEK, and DENNIS S. FOX Nov. 1988 68 p (NASA-TM-101346; E-4370; NAS 1.15:101346) Avail: NTIS HC A04/MF A01 CSCL 11/4

Industrial systems such as heat engines and heat exchangers involve harsh environments. The structural materials are subjected to high temperatures as well as corrosive gases and condensed phases. Past experience with metal alloys has shown that these condensed phases can be particularly corrosive and are often the limiting factor in the operation of these systems. In a heat engine the most common condensed corrodent is Na<sub>2</sub>SO<sub>4</sub> whereas in a heat exchanger an oxide slag may be present. The primary emphasis is on Na<sub>2</sub>SO<sub>4</sub> induced corrosion, however, similarities and differences to oxide slag are also discussed. The extensive research on corrosion of metal alloys has led to understanding and controlling corrosion for these materials. Currently silicon based

ceramics are prime candidates for the applications discussed. Therefore it is important to understand the effects of condensed phase deposits on this emerging class of high temperature materials. Both the thermodynamic and strength of the ceramic is also examined. Finally some control strategies for corrosion of silicon based ceramics are explored. Author

**N89-11913\*#** National Aeronautics and Space Administration. Lewis Research Center, Cleveland, OH.

**ADHESION, FRICTION, AND WEAR OF PLASMA-DEPOSITED THIN SILICON NITRIDE FILMS AT TEMPERATURES TO 700 C** K. MIYOSHI, J. J. POUCH, S. A. ALTEROVITZ, D. M. PANTIC, and G. A. JOHNSON 1988 12 p Prepared for presentation at the International Conference on Wear of Materials, Denver, Colo., 9-13 Apr. 1989. Sponsored by ASME Prepared in cooperation with Cincinnati Univ., Ohio (NASA-TM-101377; E-4431; NAS 1.15:101377) Avail: NTIS HC A03/MF A01 CSCL 11/3

The adhesion, friction, and wear behavior of silicon nitride films deposited by low- and high-frequency plasmas (30 kHz and 13.56 MHz) at various temperatures to 700 C in vacuum were examined. The results of the investigation indicated that the Si/N ratios were much greater for the films deposited at 13.56 MHz than for those deposited at 30 kHz. Amorphous silicon was present in both low- and high-frequency plasma-deposited silicon nitride films. However, more amorphous silicon occurred in the films deposited at 13.56 MHz than in those deposited at 30 kHz. Temperature significantly influenced adhesion, friction, and wear of the silicon nitride films. Wear occurred in the contact area at high temperature. The wear correlated with the increase in adhesion and friction for the low- and high-frequency plasma-deposited films above 600 and 500 C, respectively. The low- and high-frequency plasma-deposited thin silicon nitride films exhibited a capability for lubrication (low adhesion and friction) in vacuum at temperatures to 500 and 400 C, respectively. Author

**N89-12746\*#** National Aeronautics and Space Administration. Lewis Research Center, Cleveland, OH.

**SLURRY-PRESSING CONSOLIDATION OF SILICON NITRIDE** WILLIAM A. SANDERS, JAMES D. KISER, and MARC R. FREEDMAN Nov. 1988 19 p (NASA-TM-101365; E-4352; NAS 1.15:101365) Avail: NTIS HC A03/MF A01 CSCL 11/3

A baseline slurry-pressing method for a silicon nitride material is developed. The Si<sub>3</sub>N<sub>4</sub> composition contained 5.8 wt percent SiO<sub>2</sub> and 6.4 wt percent Y<sub>2</sub>O<sub>3</sub>. Slurry-pressing variables included volume percent solids, application of ultrasonic energy, and pH. Twenty vol percent slurry-pressed material was approximately 11 percent stronger than both 30 vol percent slurry-pressed and dry-pressed materials. The Student's t-test showed the difference to be significant at the 99 percent confidence level. Twenty volume percent (300 h) slurry-pressed test bars exhibited strengths as high as 980 MPa. Large, columnar beta-Si<sub>3</sub>N<sub>4</sub> grains caused failure in the highest strength specimens. The improved strength correlated with better structural uniformity as determined by radiography, optical microscopy, and image analysis. Author

**N89-12883\*#** National Aeronautics and Space Administration. Lewis Research Center, Cleveland, OH.

**HOST SURFACE PROTECTION R AND T OVERVIEW** ROBERT A. MILLER *In its* Turbine Engine Hot Section Technology 1986 p 45-50 Oct. 1986 Avail: NTIS HC A21/MF A01 CSCL 11/3

Most of the efforts in the HOST Surface Protection Subproject were focused on thermal barrier coating (TBC) life prediction. Also, a small effort, consisting primarily of wrapping up and reporting the work of previous years, remained on the airfoil deposition modeling. The work performed under the airfoil deposition modeling program element was concerned with modeling the deposition of corrodants onto turbine airfoils. Accomplishments included verification of the chemically frozen boundary (CFBL) theory. Encouraging results were also achieved with the recently developed local thermochemical equilibrium (LTCE) theory. The surface

protection subprogram was devoted to thermal-barrier-coating life modeling. This modeling is an essential step in the development of TBC's. E.R.

**N89-12919\*#** National Aeronautics and Space Administration. Lewis Research Center, Cleveland, OH.

**A STUDY ON THERMAL BARRIER COATINGS INCLUDING THERMAL EXPANSION MISMATCH AND BOND COAT OXIDATION**

GEORGE C. CHANG, WORAPHAT PHUCHAROEN (Cleveland State Univ., Ohio.), and ROBERT A. MILLER *In its* Turbine Engine Hot Section Technology 1986 p 415-434 Oct. 1986 (Contract NCC3-27)

Avail: NTIS HC A21/MF A01 CSCL 11/3

The present investigation deals with a plasma-sprayed thermal barrier coating (TBC) intended for high temperature applications to advanced gas turbine blades. Typically, this type of coating system consists of a zirconia-yttria ceramic layer with a nickel-chromium-aluminum bond coat on a superalloy substrate. The problem on hand is a complex one due to the fact that bond coat oxidation and thermal mismatch occur in the TBC. Cracking in the TBC has also been experimentally illustrated. A clearer understanding of the mechanical behavior of the TBC is investigated. The stress states in a model thermal barrier coating as it cools down in air is studied. The powerful finite element method was utilized to model a coating cylindrical specimen. Four successively refined finite element models were developed. Some results obtained using the first two models have been reported previously. The major accomplishment is the successful development of an elastic TBC finite element model known as TBCG with interface geometry between the ceramic layer and the bond coat. An equally important milestone is the near-completion of the new elastic-plastic TBC finite element model called TBCGEP which yielded initial results. Representative results are presented. Author

**N89-12920\*#** Garrett Turbine Engine Co., Phoenix, AZ. **THERMAL BARRIER COATING LIFE PREDICTION MODEL DEVELOPMENT**

T. E. STRANGMAN, J. F. NEUMANN, and A. LIU *In* NASA, Lewis Research Center, Turbine Engine Hot Section Technology 1986 p 435-445 Oct. 1986 (Contract NAS3-23945)

Avail: NTIS HC A21/MF A01 CSCL 11/3

Thermal barrier coatings (TBCs) for turbine airfoils in high-performance engines represent an advanced materials technology with both performance and durability benefits. The foremost TBC benefit is the reduction of heat transferred into air-cooled components, which yields performance and durability benefits. This program focuses on predicting the lives of two types of strain-tolerant and oxidation-resistant TBC systems that are produced by commercial coating suppliers to the gas turbine industry. The plasma-sprayed TBC system, composed of a low-pressure plasma-spray (LPPS) or an argon shrouded plasma-spray (ASPS) applied oxidation resistant NiCrAlY (or CoNiCrAlY) bond coating and an air-plasma-sprayed yttria (8 percent) partially stabilized zirconia insulative layer, is applied by Chromalloy, Klock, and Union Carbide. The second type of TBC is applied by the electron beam-physical vapor deposition (EB-PVD) process by Temescal. Author

**N89-12921\*#** General Electric Co., Fairfield, CT. Aircraft Engine Business Group.

**THERMAL BARRIER COATING LIFE PREDICTION MODEL**

B. H. PILSNER, R. V. HILLERY, R. L. MCKNIGHT, T. S. COOK, K. S. KIM, and E. C. DUDERSTADT *In* NASA, Lewis Research Center, Turbine Engine Hot Section Technology 1986 p 447-467 Oct. 1986

(Contract NAS3-23943)

Avail: NTIS HC A21/MF A01 CSCL 11/3

The objectives of this program are to determine the predominant modes of degradation of a plasma sprayed thermal barrier coating system, and then to develop and verify life prediction models



## 27 NONMETALLIC MATERIALS

accounting for these degradation modes. The program is divided into two phases, each consisting of several tasks. The work in Phase 1 is aimed at identifying the relative importance of the various failure modes, and developing and verifying life prediction model(s) for the predominant model for a thermal barrier coating system. Two possible predominant failure mechanisms being evaluated are bond coat oxidation and bond coat creep. The work in Phase 2 will develop design-capable, causal, life prediction models for thermomechanical and thermochemical failure modes, and for the exceptional conditions of foreign object damage and erosion. Author

**N89-12922\*# Pratt and Whitney Aircraft, East Hartford, CT.  
THERMAL BARRIER COATING LIFE PREDICTION MODEL  
DEVELOPMENT**

J. T. DEMASI and K. D. SHEFFLER In NASA, Lewis Research Center, Turbine Engine Hot Section Technology 1986 p 469-483 Oct. 1986

(Contract NAS3-23944)

Avail: NTIS HC A21/MF A01 CSCL 11/3

The objective of this program is to establish a methodology to predict Thermal Barrier Coating (TBC) life on gas turbine engine components. The approach involves experimental life measurement coupled with analytical modeling of relevant degradation modes. The coating being studied is a flight qualified two layer system, designated PWA 264, consisting of a nominal ten mil layer of seven percent yttria partially stabilized zirconia plasma deposited over a nominal five mil layer of low pressure plasma deposited NiCoCrAlY. Thermal barrier coating degradation modes being investigated include: thermomechanical fatigue, oxidation, erosion, hot corrosion, and foreign object damage. Author

**N89-13621\*# General Electric Co., Cincinnati, OH. Aircraft Engine Business Group.**

**THERMAL BARRIER COATING LIFE PREDICTION MODEL  
DEVELOPMENT Final Report**

R. V. HILLERY, B. H. PILSNER, R. L. MCKNIGHT, T. S. COOK, and M. S. HARTLE Nov. 1988 150 p

(Contract NAS3-23493)

(NASA-CR-180807; NAS 1.26:180807; R87-AEB586) Avail: NTIS HC A07/MF A01 CSCL 11/3

This report describes work performed to determine the predominant modes of degradation of a plasma sprayed thermal barrier coating system and to develop and verify life prediction models accounting for these degradation modes. The primary TBC system consisted of a low pressure plasma sprayed NiCrAlY bond coat, an air plasma sprayed ZrO<sub>2</sub>-Y<sub>2</sub>O<sub>3</sub> top coat, and a Rene' 80 substrate. The work was divided into 3 technical tasks. The primary failure mode to be addressed was loss of the zirconia layer through spalling. Experiments showed that oxidation of the bond coat is a significant contributor to coating failure. It was evident from the test results that the species of oxide scale initially formed on the bond coat plays a role in coating degradation and failure. It was also shown that elevated temperature creep of the bond coat plays a role in coating failure. An empirical model was developed for predicting the test life of specimens with selected coating, specimen, and test condition variations. In the second task, a coating life prediction model was developed based on the data from Task 1 experiments, results from thermomechanical experiments performed as part of Task 2, and finite element analyses of the TBC system during thermal cycles. The third and final task attempted to verify the validity of the model developed in Task 2. This was done by using the model to predict the test lives of several coating variations and specimen geometries, then comparing these predicted lives to experimentally determined test lives. It was found that the model correctly predicts trends, but that additional refinement is needed to accurately predict coating life. Author

**N89-13642\*# National Aeronautics and Space Administration.  
Lewis Research Center, Cleveland, OH.**

**THERMAL BARRIER COATINGS. ABSTRACTS AND FIGURES  
1985 220 p Workshop held in Cleveland, Ohio, 21-22 May**

1985

(NASA-CP-10019; E-4425; NAS 1.55:10019) Avail: NTIS HC A10/MF A01 CSCL 11/3

The Thermal Barrier Coatings Workshop was held May 21 and 22, 1985, at the NASA Lewis Research Center in Cleveland, Ohio. Six sessions covered Failure Mechanisms and Life Modeling, Effects of Oxidation and Creep, Phase Stability and Microstructural Aspects, Nondestructive and Analytical Assessment, Coating Development, and Alternative Applications.

**N89-13646\*# National Aeronautics and Space Administration.  
Lewis Research Center, Cleveland, OH.**

**THE EFFECT OF OXIDATION ON THE HIGH HEAT FLUX  
BEHAVIOR OF A THERMAL BARRIER COATING**

ROBERT A. MILLER In *its* Thermal Barrier Coatings. Abstracts and Figures p 33-42 1985

Avail: NTIS HC A10/MF A01 CSCL 11/3

The effect of oxidation on the high heat flux behavior of a thermal barrier coating was evaluated by cyclically exposing preoxidized specimens to a 3000 C nitrogen plasma. The thermal barrier coatings consisted of a 0.025 cm layer of air-plasma-sprayed ZrO<sub>2</sub>-7 percent Y<sub>2</sub>O<sub>3</sub> and a 0.012 cm layer of low pressure-plasma-sprayed NiCoCrAlY applied over 0.13 cm diameter B1900+Hf cylindrical substrates. A gradient of 800 C is produced across the ceramic layer in each 0.5 second exposure. This is much more severe than the gradient encountered on a gas turbine engine. Prior to exposure, the specimens were preoxidized at 1200 C for time from 0 to 20 hours. These coatings were found to be tolerant to the high heat flux plasma flame for all but the most severe preoxidations. However, life degraded rapidly for preoxidation times in excess of 15 hours at 1200 C. A log-log plot of cycles-to-failure vs estimated oxidative weight gain yield a straight or nearly straight line, and this line could be rationalized using an oxidation-based model that was developed previously for low heat flux applications. Author

**N89-13648\*# National Aeronautics and Space Administration.  
Lewis Research Center, Cleveland, OH.**

**AN INVESTIGATION OF ENVIRONMENTAL INFLUENCE ON  
THE CREEP BEHAVIOR OF A LOW PRESSURE PLASMA  
SPRAYED NICOCHRALY ALLOY**

M. G. HEBBURN and R. V. MINER In *its* Thermal Barrier Coatings. Abstracts and Figures p 53-58 1985

Avail: NTIS HC A10/MF A01 CSCL 11/3

Low pressure sprayed MCrAlY overlay coatings are currently being used on advanced single crystal superalloy blades for gas turbine engines. Many studies were made on the influence of coatings on the mechanical properties of superalloys in oxidizing or hot-corroding environments, but very few on the properties of the bulk coating alloy itself. The creep behavior of a typical NiCoCrAlY alloy (PWA 276) was studied in air and vacuum. The as-received low pressure plasma sprayed NiCoCrAlY plates were heat treated for 4 h at 1080 C followed by 32 h at 870 C, the heat treatment applied to coated superalloy parts. Standard creep specimens 12.7 mm long and 3.2 mm in diameter were then machined. Constant load creep-rupture tests were performed in air and vacuum at 650, 850, and 1050 C and various initial stresses. In addition, some specimens were preoxidized at 1050 C for 100 h prior to testing. Results are briefly discussed. Author

**N89-13654\*# Cleveland State Univ., OH.**

**EXAMINATION OF COATING FAILURE BY ACOUSTIC  
EMISSION**

CHRISTOPHER C. BERNDT In NASA, Lewis Research Center, Thermal Barrier Coatings. Abstracts and Figures p 127-137 1985

(Contract NCC3-27)

Avail: NTIS HC A10/MF A01 CSCL 11/3

Coatings of NiCrAlY bond coat with a zirconia - 12 wt percent yttria overlay were applied to disc-shaped specimens of U-700 alloy. A waveguide of 1 mm diameter platinum was TIG welded to the specimen and allowed it to be suspended in a tubular furnace. The specimen was thermally cycled to 1150 C, and the acoustic



emission (AE) monitored. The weight gain per thermal cycle was also measured. A computer system based on the IBM-XT microcomputer was used extensively to acquire the AE data with respect to temperature. This system also controlled the temperature by using a PD software loop. Several different types of AE analyses were performed. A major feature of these tests, not addressed by previous work in this area, was that the coatings covered 100 percent of the specimen and also that the AE was amplified at two different levels. It is believed that this latter feature allows a qualitative appraisal of the relative number of cracks per AE event. The difference in AE counts between the two channels is proportional to the number of cracks per AE event, and this parameter may be thought of as the crack density. The ratio of the AE count difference to the AE count magnitude of one channel is inversely proportional to the crack growth. Both of these parameters allow the crack distribution and crack growth within each specimen to be qualitatively followed during the thermal cycling operation. Recent results which used these principles will be presented.

Author

**N89-13662\*#** National Aeronautics and Space Administration. Lewis Research Center, Cleveland, OH.

**CYCLIC STRESS ANALYSIS OF CERAMIC COATED GAS TURBINE SEALS**

JOE PADOVAN, DAN DOUGHERTY (General Tire and Rubber Co., Akron, Ohio.), and BOB HENDRICKS *In its Thermal Barrier Coatings. Abstracts and Figures p 203-209* 1985 (Contract NAG3-265)

Avail: NTIS HC A10/MF A01 CSCL 11/3

Through the use of the Finite Element Method, the cyclic thermomechanical response of ceramic coated gas turbine parts is considered. The analysis includes temperature dependent elastic-plastic-creep material properties and cyclic thermal loads. To demonstrate the cyclic thermomechanical response, a ceramic coated outer gas path seal is studied. The analysis will estimate the significant residual stress field created by the cyclic thermal loads.

Author

**N89-13666\*#** National Aeronautics and Space Administration. Lewis Research Center, Cleveland, OH.

**HIGH-STRENGTH SILICON CARBIDES BY HOT ISOSTATIC PRESSING**

SUNIL DUTTA 1988 19 p Presented at the 3rd International Symposium on Ceramic Materials and Components for Engines, Las Vegas, Nev., 27-30 Nov. 1988; sponsored by the American Ceramic Society

(NASA-TM-101400; E-4484; NAS 1.15:101400) Avail: NTIS HC A03/MF A01 CSCL 11/3

Silicon carbide has strong potential for heat engine hardware and other high-temperature applications because of its low density, good strength, high oxidation resistance, and good high-temperature creep resistance. Hot isostatic pressing (HIP) was used for producing alpha and beta silicon carbide (SiC) bodies with near-theoretical density, ultrafine grain size, and high strength at processing temperatures of 1900 to 2000 C. The HIPed materials exhibited ultrafine grain size. Furthermore, no phase transformation from beta to alpha was observed in HIPed beta-SiC. Both materials exhibited very high average flexural strength. It was also shown that alpha-SiC bodies without any sintering aids, when HIPed to high final density, can exhibit very high strength. Fracture toughness  $K_{IC}$  values were determined to be 3.6 to 4.0 MPa m (sup 1/2) for HIPed alpha-SiC and 3.7 to 4.1 MPa m (sup 1/2) for HIPed beta-SiC. In the HIPed specimens strength-controlling flaws were typically surface related. In spite of improvements in material properties such as strength and fracture toughness by elimination of the larger strength-limiting flaws and by grain size refinement, HIPing has no effect on the Weibull modulus.

Author

**N89-14310\*#** National Aeronautics and Space Administration. Lewis Research Center, Cleveland, OH.

**STABILITY OF BULK BA2YCU3O(7-X) IN A VARIETY OF ENVIRONMENTS**

JAMES R. GAIER, ALOYSIUS F. HEPP, HENRY B. CURTIS,

DONALD A. SCHUPP, PAUL D. HAMBOURGER, and JAMES W. BLUE (Cleveland Clinic Foundation, OH.) Dec. 1988 13 p Presented at the Fall Meeting of the Materials Research Society, Boston, MA, 28 Nov. - 2 Dec. 1988 (NASA-TM-101401; E-4485; NAS 1.15:101401) Avail: NTIS HC A03/MF A01 CSCL 11/3

Small bars of ceramic  $Ba_2YCu_3O(7-x)$  were fabricated and subjected to environments similar to those that might be encountered during some NASA missions. These conditions include ambient conditions, high humidity, vacuum, and high fluences of electrons and protons. The normal state resistivity or critical current density ( $J_{sc}$ ) were monitored during these tests to assess the stability of the material. When normal state resistivity is used as a criterion, the ambient stability of these samples was relatively good, exhibiting only a 2 percent degradation over a 3 month period. The humidity stability was shown to be very poor, and to be a steep function of temperature. Samples stored at 50 C for 40 min increased in normal state resistivity by four orders of magnitude. Kinetic analysis indicates that the degradation reaction is second order with water vapor concentration. It is suspected that humidity degradation also accounts for the ambient instability. The samples were stable to vacuum over a period of at least 3 months. Degradation of  $J_{sc}$  in a 1 MeV electron fluence of  $9.7 \times 10$  to the 14th e-/sq cm was determined to be no more than about 2 percent. Degradation of  $J_{sc}$  in a  $8.7 \times 10$  to the 14th p(+)/sq cm of 42 MeV protons was found to be grain size dependent. Samples with smaller grain size and initial  $J_{sc}$  of about 240 A/sq cm showed no degradation, while that with larger grain size and an initial  $J_{sc}$  of about 30 A/sq cm degraded to 37 percent of its original value.

Author

**N89-14311\*#** State Univ. of New York, Buffalo. Dept. of Civil Engineering.

**DEVELOPMENT OF BEM FOR CERAMIC COMPOSITES Interim Status Report, Mar. - Dec. 1988**

P. K. BANERJEE, G. F. DARGUSH, and D. P. HENRY 9 Dec. 1988 76 p Prepared for Calspan-Buffalo Univ. Research Center, NY

(Contract NAG3-888)

(NASA-CR-183313; NAS 1.26:183313) Avail: NTIS HC A05/MF A01 CSCL 11/3

Progress is summarized in the development of a boundary element code BEST3D, designed for the micromechanical studies of advanced ceramic composites. Additional effort was made in generalizing the implementation to allow the program to be applicable to real problems in the aerospace industry.

B.G.

**N89-14338\*#** National Aeronautics and Space Administration. Lewis Research Center, Cleveland, OH.

**SOME COMPOSITE BEARING AND SEAL MATERIALS FOR GAS TURBINE APPLICATIONS: A REVIEW**

HAROLD E. SLINEY 1989 15 p Prepared for presentation at the 34th International Gas Turbine and Aeroengine Congress and Exposition, Toronto, Ontario, 4-8 Jun. 1989; sponsored by ASME (NASA-TM-101451; E-4561; NAS 1.15:101451) Avail: NTIS HC A03/MF A01 CSCL 11/1

A review is made of the selection and tribological testing of materials for high-temperature bearings and seals. The goal is to achieve good tribological properties over a wide range of temperatures because bearings and seals must be functional from low temperature start-up conditions on up to the maximum temperatures encountered during engine operation. Plasma sprayed composite coatings with favorable tribological properties from 25 to 900 C are discussed. The performance of these coatings in simple tribological bench tests is described. Examples are also given of their performance in high-speed sliding contact seals and as Stirling cylinder liner materials, and as back up lubricants for compliant foil gas bearings.

Author

## 27 NONMETALLIC MATERIALS

**N89-15235\*#** National Aeronautics and Space Administration. Lewis Research Center, Cleveland, OH.

### **ADDITION POLYMERS FROM 1,4,5,8-TETRAHYDRO-1,4:5,8-DIEPOXYANTHRACENE AND BIS-DIENES. 2: EVIDENCE FOR THERMAL DEHYDRATION OCCURRING IN THE CURE PROCESS**

MARY ANN B. MEADOR, MICHAEL A. OLSHAVSKY, MICHAEL A. MEADOR, and MYONG-KU AHN (Indiana State Univ., Terre Haute.) 1988 8 p Proposed for presentation at the 197th National Meeting of the American Chemical Society, Dallas, TX, 9-14 Apr. 1989  
(NASA-TM-101385; E-4442; NAS 1.15:101385) Avail: NTIS HC A02/MF A01 CSCL 11/3

Diels-Alder cycloaddition copolymers from 1,4,5,8-tetrahydro-1,4:5,8-diepoxyanthracene and anthracene end-capped polyimide oligomers appear, by thermogravimetric analysis (TGA), to undergo dehydration at elevated temperatures. This would produce thermally stable pentyptycene units along the polymer backbone, and render the polymers incapable of unzipping through a retro-Diels-Alder pathway. High resolution solid  $^{13}\text{C}$  nuclear magnetic resonance (NMR) of one formulation of the polymer system before and after heating at elevated temperatures, shows this to indeed be the case. NMR spectra of solid samples of the polymer before and after heating correlated well with those of the parent pentyptycene model compound before and after acid-catalyzed dehydration. Isothermal gravimetric analyses and viscosities of the polymer before and after heat treatment support dehydration as a mechanism for the cure reaction. Author

**N89-15251\*#** Ford Motor Co., Dearborn, MI. Scientific Lab.  
**IMPROVED SILICON CARBIDE FOR ADVANCED HEAT ENGINES Annual Report**

T. J. WHALEN and W. L. WINTERBOTTOM Sep. 1986 103 p  
(Contract NAS3-24384)  
(NASA-CR-179477; NAS 1.26:179477) Avail: NTIS HC A06/MF A01 CSCL 11/3

Work performed to develop silicon carbide materials of high strength and to form components of complex shape and high reliability is described. A beta-SiC powder and binder system was adapted to the injection molding process and procedures and process parameters developed capable of providing a sintered silicon carbide material with improved properties. The initial effort has been to characterize the baseline precursor materials (beta silicon carbide powder and boron and carbon sintering aids), develop mixing and injection molding procedures for fabricating test bars, and characterize the properties of the sintered materials. Parallel studies of various mixing, dewaxing, and sintering procedures have been carried out in order to distinguish process routes for improving material properties. A total of 276 MOR bars of the baseline material have been molded, and 122 bars have been fully processed to a sinter density of approximately 95 percent. The material has a mean MOR room temperature strength of 43.31 ksi (299 MPa), a Weibull characteristic strength of 45.8 ksi (315 MPa), and a Weibull modulus of 8.0. Mean values of the MOR strengths at 1000, 1200, and 1400 C are 41.4, 43.2, and 47.2 ksi, respectively. Strength controlling flaws in this material were found to consist of regions of high porosity and were attributed to agglomerates originating in the initial mixing procedures. The mean stress rupture life at 1400 C of five samples tested at 172 MPa (25 ksi) stress was 62 hours and at 207 MPa (30 ksi) stress was 14 hours. New fluid mixing techniques have been developed which significantly reduce flaw size and improve the strength of the material. Initial MOR tests indicate the strength of the fluid-mixed material exceeds the baseline property by more than 33 percent. Author

**N89-15257\*#** National Aeronautics and Space Administration. Lewis Research Center, Cleveland, OH.

### **STRENGTH OF HOT ISOSTATICALLY PRESSED AND SINTERED REACTION BONDED SILICON NITRIDES CONTAINING Y<sub>2</sub>O<sub>3</sub>**

WILLIAM A. SANDERS and DIANE M. MIESKOWSKI Jan. 1989

10 p  
(NASA-TM-101443; E-4429; NAS 1.15:101443) Avail: NTIS HC A02/MF A01 CSCL 11/2

The hot isostatic pressing of reaction bonded Si<sub>3</sub>N<sub>4</sub> containing Y<sub>2</sub>O<sub>3</sub> produced specimens with greater room temperature strengths than those by high pressure nitrogen sintering of the same material. Average room temperature bend strengths for hot isostatically pressed reaction bonded silicon nitride and high pressure nitrogen sintered reaction bonded silicon nitride were 767 and 670 MPa, respectively. Values of 472 and 495 MPa were observed at 1370 C. For specimens of similar but lower Y<sub>2</sub>O<sub>3</sub> content produced from Si<sub>3</sub>N<sub>4</sub> powder using the same high pressure nitrogen sintering conditions, the room temperature strength was 664 MPa and the 1370 C strength was 402 MPa. The greater strengths of the reaction bonded silicon nitride materials in comparison to the sintered silicon nitride powder material are attributed to the combined effect of processing method and higher Y<sub>2</sub>O<sub>3</sub> content. Author

**N89-16065\*#** National Aeronautics and Space Administration. Lewis Research Center, Cleveland, OH.

### **HOT CORROSION OF CERAMIC ENGINE MATERIALS Final Report**

DENNIS S. FOX, NATHAN S. JACOBSON, and JAMES L. SMIALEK 1988 19 p Presented at the 26th Automotive Technology Development Contractors Coordination Meeting, Dearborn, MI, 24-27 Oct. 1988; sponsored in part by DOE (Contract DE-AL01-85CE-50111)  
(NASA-TM-101439; E-4544; NAS 1.15:101439; DOE/NASA/50111-2) Avail: NTIS HC A03/MF A01 CSCL 11/2

A number of commercially available SiC and Si<sub>3</sub>N<sub>4</sub> materials were exposed to 1000 C in a high velocity, pressurized burner rig as a simulation of a turbine engine environment. Sodium impurities added to the burner flame resulted in molten Na<sub>2</sub>SO<sub>4</sub> deposition, attack of the SiC and Si<sub>3</sub>N<sub>4</sub> and formation of substantial Na<sub>2</sub>O-x(SiO<sub>2</sub>) corrosion product. Room temperature strength of the materials decreased. This was a result of the formation of corrosion pits in SiC, and grain boundary dissolution and pitting in Si<sub>3</sub>N<sub>4</sub>. Corrosion regimes for such Si-based ceramics have been predicted using thermodynamics and verified in rig tests of SiO<sub>2</sub> coupons. Protective mullite coatings are being investigated as a solution to the corrosion problem for SiC and Si<sub>3</sub>N<sub>4</sub>. Limited corrosion occurred to cordierite (Mg<sub>2</sub>Al<sub>4</sub>Si<sub>5</sub>O<sub>18</sub>) but some cracking of the substrate occurred. Author

### **N89-17334\*#** Pratt and Whitney Aircraft, East Hartford, CT. **HIGH TEMPERATURE CONSTITUTIVE AND CRACK INITIATION MODELING OF COATED SINGLE CRYSTAL SUPERALLOYS**

THOMAS G. MEYER, DAVID M. NISSLEY, and GUSTAV A. SWANSON In NASA, Lewis Research Center, Turbine Engine Hot Section Technology, 1987 p 401-412 Oct. 1987  
(Contract NAS3-23939)  
Avail: NTIS HC A20/MF A01 CSCL 11/2

The purpose of this program is to develop life prediction models for anisotropic materials used in gas turbine airfoils. In the base portion of the program, two coated single crystal alloys are being tested. They are PWA 286 overlay coated and PWA 273 aluminide coated PWA 1480 and PWA 286 overlay coated Alloy 185. Viscoplastic constitutive models for these materials are also being developed to predict the cyclic stress-strain histories required for life prediction of the lab specimens and actual airfoil designs. Author

**N89-17668\*#** National Aeronautics and Space Administration. Lewis Research Center, Cleveland, OH.

### **DYNAMIC POROSITY VARIATIONS IN CERAMICS**

EDWARD R. GENERAZIO, DAVID B. STANG (Sverdrup Technology, Inc., Cleveland, OH.), and DON J. ROTH Dec. 1988 7 p  
(NASA-TM-101340; E-4358; NAS 1.15:101340) Avail: NTIS HC A02/MF A01 CSCL 11/2

A silicon carbide disk was sintered from 2090 to 2190 C in 25 C steps. After each sintering step the disk was examined using a precision acoustic scanning system to determine acoustic attenuation and velocity. The bulk density was found to vary nonmonotonically with sintering temperature. During the sintering process, the density varied as much as 10 pct from its value at 2090 C. Local density fluctuations were observed to occur in an organized and history-dependent way. These local density fluctuations varied up to + or - 7 pct of the bulk density and were made visible by acoustic attenuation and velocity mapping.

Author

**N89-18550\*#** Pratt and Whitney Aircraft, East Hartford, CT. Engineering Div.

**MATE PROGRAM: EROSION RESISTANT COMPRESSOR AIRFOIL COATING, VOLUME 2 Final Report**

MELVIN FRELING Mar. 1987 22 p

(Contract NAS3-20072)

(NASA-CR-179645; NAS 1.26:179645; PW-5574-212-VOL-2)

Avail: NTIS HC A03/MF A01 CSCL 11/2

The performance of candidate erosion resistant airfoil coatings installed in ground tested experimental JT8D and JT9D engines and subjected to cyclic endurance at idle, takeoff and intermediate power conditions has been evaluated. Engine tests were terminated prior to the scheduled 1000 cycles of endurance test due to high cycle fatigue fracture of the Gator-Gard plasma sprayed 88WC-12Co coating on titanium alloy airfoils. Coated steel (AMS5616) and nickel base alloy (Incoloy 901) performed well in both engine tests. Post test airfoil analyses consisted of binocular, scanning electron microscope and metallographic examinations.

Author

**N89-19421\*#** AiResearch Casting Co., Torrance, CA.

**IMPROVED SILICON NITRIDE FOR ADVANCED HEAT ENGINES Annual Contractor Report**

HUN C. YEH and HO T. FANG (Garrett Turbine Engine Co., Phoenix, AZ.) Feb. 1987 113 p

(Contract NAS3-24385)

(NASA-CR-179525; NAS 1.26:179525; AIRESEARCH-86-60365)

Avail: NTIS HC A06/MF A01 CSCL 11/2

The technology base required to fabricate silicon nitride components with the strength, reliability, and reproducibility necessary for actual heat engine applications is presented. Task 2 was set up to develop test bars with high Weibull slope and greater high temperature strength, and to conduct an initial net shape component fabrication evaluation. Screening experiments were performed in Task 7 on advanced materials and processing for input to Task 2. The technical efforts performed in the second year of a 5-yr program are covered. The first iteration of Task 2 was completed as planned. Two half-replicated, fractional factorial (2 sup 5), statistically designed matrix experiments were conducted. These experiments have identified Denka 9FW Si3N4 as an alternate raw material to GTE SN502 Si3N4 for subsequent process evaluation. A detailed statistical analysis was conducted to correlate processing conditions with as-processed test bar properties. One processing condition produced a material with a 97 ksi average room temperature MOR (100 percent of goal) with 13.2 Weibull slope (83 percent of goal); another condition produced 86 ksi (6 percent over baseline) room temperature strength with a Weibull slope of 20 (125 percent of goal).

Author

**N89-19435\*#** National Aeronautics and Space Administration. Lewis Research Center, Cleveland, OH.

**ADHESION IN CERAMICS AND MAGNETIC MEDIA**

KAZUHISA MIYOSHI Mar. 1989 19 p Prepared for presentation at the 5th International Congress on Tribology, Helsinki, Finland, 12-15 Jun. 1989

(NASA-TM-101476; E-4596; NAS 1.15:101476) Avail: NTIS HC A03/MF A01 CSCL 11/2

When a ceramic is brought into contact with a metal or a polymeric material such as a magnetic medium, strong bonds form between the materials. For ceramic-to-metal contacts, adhesion and friction are strongly dependent on the ductility of the metals.

Hardness of metals plays a much more important role in adhesion and friction than does the surface energy of metals. Adhesion, friction, surface energy, and hardness of a metal are all related to its Young's modulus and shear modulus, which have a marked dependence on the electron configuration of the metal. An increase in shear modulus results in a decrease in area of contact that is greater than the corresponding increase in surface energy (the bond energy) with shear modulus. Consequently, the adhesion and friction decrease with increasing shear modulus. For ceramics in contact with polymeric magnetic tapes, environment is extremely important. For example, a nitrogen environment reduces adhesion and friction when ferrite contacts polymeric tape, whereas a vacuum environment strengthens the ferrite-to-tape adhesion and increases friction. Adhesion and friction are strongly dependent on the particle loading of the tape. An increase in magnetic particle concentration increases the complex modulus of the tape, and a lower real area of contact and lower friction result.

Author

**N89-20252\*#** National Aeronautics and Space Administration. Lewis Research Center, Cleveland, OH.

**CRYSTALLIZATION KINETICS OF BAO-AL2O3-SIO2 GLASSES**

NAROTTAM P. BANSAL (Case Western Reserve Univ., Cleveland, OH.) and MARK J. HYATT May 1988 22 p Presented at the 90th Annual Meeting of the American Ceramic Society, Cincinnati, OH, 1-5 May 1988

(NASA-TM-101964; E-4662; NAS 1.15:101964) Avail: NTIS HC A03/MF A01 CSCL 11/3

Barium aluminosilicate glasses are being investigated as matrix materials in high-temperature ceramic composites for structural applications. Kinetics of crystallization of two refractory glass compositions in the barium aluminosilicate system were studied by differential thermal analysis (DTA), X-ray diffraction (XRD), and scanning electron microscopy (SEM). From variable heating rate DTA, the crystallization activation energies for glass compositions (wt percent) 10BaO-38Al2O3-51SiO2-1MoO3 (glass A) and 39BaO-25Al2O3-35SiO2-1MoO3 (glass B) were determined to be 553 and 558 kJ/mol, respectively. On thermal treatment, the crystalline phases in glasses A and B were identified as mullite (3Al2O3-2SiO2) and hexacelsian (BaO-Al2O3-2SiO2), respectively. Hexacelsian is a high-temperature polymorph which is metastable below 1590 C. It undergoes structural transformation into the orthorhombic form at approximately 300 C accompanied by a large volume change which is undesirable for structural applications. A process needs to be developed where stable monoclinic celsian, rather than hexacelsian, precipitates out as the crystal phase in glass B.

Author

**N89-20253\*#** National Aeronautics and Space Administration. Lewis Research Center, Cleveland, OH.

**DESIGN, DEVELOPMENT AND APPLICATIONS OF NOVEL TECHNIQUES FOR STUDYING SURFACE MECHANICAL PROPERTIES**

KAZUHISA MIYOSHI 1989 12 p Presented at the Spring Meeting of the Materials Research Society, San Diego, CA, 24-28 Apr. 1989

(NASA-TM-101959; E-4654; NAS 1.15:101959) Avail: NTIS HC A03/MF A01 CSCL 11/3

Research is reviewed for the adhesion, friction, and micromechanical properties of materials and examples of the results presented. The ceramic and metallic materials studied include silicon carbide, aluminum oxide, and iron-base amorphous alloys. The design and operation of a torsion balance adapted for study of adhesion from the Cavendish balance are discussed first. The pull-off force (adhesion) and shear force (friction) required to break the interfacial junctions between contacting surfaces of the materials were examined at various temperatures in a vacuum. The surface chemistry of the materials was analyzed by X-ray photoelectron spectroscopy. Properties and environmental conditions of the surface regions which affect adhesion and friction-such as surface segregation, composition, crystal structure, surface chemistry, and temperature were also studied.

Author

## 27 NONMETALLIC MATERIALS

**N89-21100\*#** National Aeronautics and Space Administration. Lewis Research Center, Cleveland, OH.

**EVALUATION OF ATOMIC OXYGEN RESISTANT PROTECTIVE COATINGS FOR FIBERGLASS-EPOXY COMPOSITES IN LEO**  
SHARON K. RUTLEDGE, PHILLIP E. PAULSEN, and JOYCE A. BRADY (Sverdrup Technology, Inc., Cleveland, OH.) 1989 13 p Presented at the 34th SAMPE Technical Conference, Reno, NV, 8-11 May 1989  
(NASA-TM-101955; E-4649; NAS 1.15:101955) Avail: NTIS HC A03/MF A01 CSCL 11/2

Fiberglass-epoxy composite masts are the prime structural members for the Space Station Freedom solar array. At the altitude where Space Station Freedom will operate, atomic oxygen atoms are the most predominant species. Atomic oxygen is highly reactive and has been shown to oxidize organic and some metallic materials. Tests with random and directed atomic oxygen exposure have shown that the epoxy is removed from the composite exposing brittle glass fibers which could be easily removed from the surface where they could contaminate Space Station Freedom Systems. Protection or fiber containment systems; inorganic based paints, aluminum braid, and a metal coating; were evaluated for resistance to atomic oxygen, vacuum ultraviolet radiation, thermal cycling, and mechanical flexing. All appeared to protect well against atomic oxygen and provide fiber containment except for the single aluminum braid covering. UV radiation resistance was acceptable and in general, thermal cycling and flexure had little to no effect on the mass loss rate for most coatings. Author

**N89-21103\*#** National Aeronautics and Space Administration. Lewis Research Center, Cleveland, OH.

**DEGRADATION AND CROSSLINKING OF PERFLUOROALKYL POLYETHERS UNDER X-RAY IRRADIATION IN ULTRAHIGH VACUUM**

SHIGEYUKI MORI (National Academy of Sciences - National Research Council, Washington, DC.) and WILFREDO MORALES Mori. 1989 15 p Prepared in cooperation with Iwate Univ., Morioka (Japan)  
(NASA-TP-2910; E-4500; NAS 1.60:2910) Avail: NTIS HC A03/MF A01 CSCL 11/2

Degradation of three types of commercially available perfluoroalkyl polyethers (PFPE)-Demnum S200, Fomblin Z25, and Krytox 16256-by X-ray irradiation was studied by using X-ray photoemission spectroscopy (XPS) and a mass spectrometer under ultra-high-vacuum conditions. The carbons in the polymers were characterized by chemical shifts of C1s binding energies. Gaseous products containing COF<sub>2</sub> and low-molecular-weight fluorocarbons were formed. From Fomblin Z25, which has acetal linkages (-OCF<sub>2</sub>O-), a large quantity of COF<sub>2</sub> gas was evolved. Liquid products became tacky after a long irradiation time, and some did not dissolve in Freon. High-pressure liquid chromatography (HPLC) showed that molecular weight distribution became broader and that higher molecular weight polymers were formed from Demnum and Krytox. We concluded from these results that degradation and cross-linking took place simultaneously. Demnum crosslinked more easily than the other fluids. The time dependence of both XPS spectra of C1s and mass spectra showed that C-O-bonded carbons in PFPE'S were removed faster than other carbons. There was no substrate effect on the degradation reaction because the first-order rate constants calculated from the change of gaseous products were similar when stainless steel (440C) and gold-coated surfaces were used. Metal fluorides were formed on stainless steel during the reaction. A mechanism for the degradation of PFPE'S is discussed on the basis of their molecular structures. Author

**N89-21104\*#** National Aeronautics and Space Administration. Lewis Research Center, Cleveland, OH.

**SIMULATION OF THE LOW EARTH ORBITAL ATOMIC OXYGEN INTERACTION WITH MATERIALS BY MEANS OF AN OXYGEN ION BEAM**

BRUCE A. BANKS, SHARON K. RUTLEDGE, PHILLIP E. PAULSEN, and THOMAS J. STEUBER (Sverdrup Technology, Inc., Cleveland, OH.) 1989 32 p Presented at the 18th Annual Symposium on Applied Vacuum Science and Technology,

Clearwater Beach, FL, 6-8 Feb. 1989; sponsored by American Vacuum Society  
(NASA-TM-101971; E-4671; NAS 1.15:101971) Avail: NTIS HC A03/MF A01 CSCL 11/3

Atomic oxygen is the predominant species in low-Earth orbit between the altitudes of 180 and 650 km. These highly reactive atoms are a result of photodissociation of diatomic oxygen molecules from solar photons having a wavelength less than or equal to 2430 Å. Spacecraft in low-Earth orbit collide with atomic oxygen in the 3P ground state at impact energies of approximately 4.2 to 4.5 eV. As a consequence, organic materials previously used for high altitude geosynchronous spacecraft are severely oxidized in the low-Earth orbital environment. The evaluation of materials durability to atomic oxygen requires ground simulation of this environment to cost effectively screen materials for durability. Directed broad beam oxygen sources are necessary to evaluate potential spacecraft materials performance before and after exposure to the simulated low-Earth orbital environment. This paper presents a description of a low energy, broad oxygen ion beam source used to simulate the low-Earth orbital atomic oxygen environment. The results of materials interaction with this beam and comparison with actual in-space tests of the same materials will be discussed. Resulting surface morphologies appear to closely replicate those observed in space tests. Author

**N89-21105\*#** TRW Space Technology Labs., Redondo Beach, CA.

**IMPROVED HIGH-TEMPERATURE RESISTANT MATRIX RESINS**

H. E. GREEN, G. E. CHANG, W. F. WRIGHT, K. UEDA, and M. K. ORELL Apr. 1989 84 p  
(Contract NAS3-23933)  
(NASA-CR-180826; NAS 1.26:180826) Avail: NTIS HC A05/MF A01 CSCL 11/3

A study was performed with the objective of developing matrix resins that exhibit improved thermo-oxidative stability over state-of-the-art high temperature resins for use at temperatures up to 644 K (700 F) and air pressures up to 0.7 MPa (100 psia). The work was based upon a TRW discovered family of polyimides currently licensed to and marketed by Ethyl Corporation as EYMYD(R) resins. The approach investigated to provide improved thermo-oxidative properties was to use halogenated derivatives of the diamine, 2, 2-bis (4-(4-aminophenoxy)phenyl) hexa-fluoropropane (4-BDAF). Polyimide neat resins and Celion(R) 12,000 composites prepared from fluorine substituted 4-BDAF demonstrated unexpectedly lower glass transition temperatures (T<sub>g</sub>) and thermo-oxidative stabilities than the baseline 4-BDAF/PMDA polymer. Author

**N89-21894\*#** National Aeronautics and Space Administration. Lewis Research Center, Cleveland, OH.

**INFLUENCE OF SEVERAL METAL IONS ON THE GELATION ACTIVATION ENERGY OF SILICON TETRAETHOXIDE**

NAROTTAM P. BANSAL 1988 18 p Presented at the 90th Annual Meeting of the American Ceramic Society, Cincinnati, OH, 1-5 May 1988  
(NASA-TM-101380; E-4390; NAS 1.15:101380) Avail: NTIS HC A03/MF A01 CSCL 11/3

The effects of nine metal cations (Li(+), Na(+), Mg(2+), Ca(2+), Sr(2+), Cu(2+), Al(3+), La(3+), and Y(3+)) on silica gel formation has been investigated by studying the hydrolysis and polycondensation of silicon tetraethoxide (TEOS) in the presence of metal nitrates. The influence of water: TEOS mole ratio, metal ion concentration, and the reaction temperature has been investigated. The overall activation energy for gel formation has been determined from the temperature dependence of the time of gelation for each system. The activation energy for -Si-O-Si- network formation is found to be 54.5 kJ/mol. The gel formation time as well as the activation energy sharply increase in the presence of Cu(2+), Al(3+), La(3+) and Y(3+). In contrast, the presence of Li(+), Na(+), Mg(2+), Ca(2+), or, Sr(2+) lowers the gelation time, but has no appreciable effect on the activation energy. This difference may be attributed to the participation or

nonparticipation of the metal ions in the formation of the three-dimensional polymeric network during the polycondensation step. The concentration of metal ion ( $Mg(2+)$ ,  $Ca(2+)$ ,  $Y(3+)$  or the water: TEOS mole ratio had no appreciable effect on the gelation activation energy. A simple test has been proposed to determine whether a metal ion would act as a network intermediate or modifier in silica and other glassy networks. Author

**N89-21895\*#** National Aeronautics and Space Administration. Lewis Research Center, Cleveland, OH.

**EFFECT OF PROCESSING ON FRACTURE TOUGHNESS OF SILICON CARBIDE AS DETERMINED BY VICKERS INDENTATIONS**

CHRISTINE M. DANNELS (Case Western Reserve Univ., Cleveland, OH.) and SUNIL DUTTA May 1989 18 p (NASA-TM-101456; E-4565; NAS 1.15:101456) Avail: NTIS HC A03/MF A01 CSCL 11/3

Several alpha-SiC materials were processed by hot isostatic pressing (HIPing) and by sintering an alpha-SiC powder containing boron and carbon. Several beta-SiC materials were processed by HIPing a beta-SiC powder with boron and carbon additions. The fracture toughnesses  $K_{(sub\ 1c)}$  of these beta- and alpha-SiC materials were estimated from measurements of Vickers indentations. The three formulas used to estimate  $K_{(sub\ 1c)}$  from the indentation fracture patterns resulted in three ranges of  $K_{(sub\ 1c)}$  estimates. Furthermore, each formula measured the effects of processing differently. All three estimates indicated that fine-grained HIPed alpha-SiC has a higher  $K_{(sub\ 1c)}$  than coarsened-grained sintered alpha-SiC. Hot isostatically pressed beta-SiC, which had an ultrafine grain structure, exhibited a  $K_{(sub\ 1c)}$  comparable to that of HIPed alpha-SiC. Author

**N89-22671\*#** National Aeronautics and Space Administration. Lewis Research Center, Cleveland, OH.

**THRUST CHAMBER THERMAL BARRIER COATING TECHNIQUES**

RICHARD J. QUENTMEYER In AGARD, Application of Advanced Material for Turbomachinery and Rocket Propulsion 10 p Mar. 1989 Previously announced as N88-24690 Copyright Avail: NTIS HC A13/MF A01 CSCL 11/3

Methods for applying thermal barrier coatings to the hot-gas side wall of rocket thrust chambers in order to significantly reduce the heat transfer in high heat flux regions has been the focus of technology efforts for many years. A successful technique developed by NASA-Lewis that starts with the coating on a mandrel and then builds the thrust chamber around it by electroforming appropriate materials is described. This results in a smooth coating with exceptional adherence, as was demonstrated in hot fire rig tests. The low cycle fatigue life of chambers with coatings applied in this manner was increased dramatically compared to uncoated chambers. Author

**N89-23678\*#** Alfred Univ., NY.

**PREPARATION AND EVALUATION OF SILICON NITRIDE MATRICES FOR SILICON NITRIDE-SIC FIBER COMPOSITES M.S. Thesis Final Technical Report**

SCOTT R. AXELSON Feb. 1988 63 p (Contract NCC3-59)

(NASA-CR-184798; NAS 1.26:184798) Avail: NTIS HC A04/MF A01 CSCL 11/3

Continuous silicon carbide (SiC) fiber was added to three types of silicon nitride ( $Si_3N_4$ ) matrices. Efforts were aimed at producing a dense  $Si_3N_4$  matrix from reaction-bonded silicon nitride (RBSN) by hot-isostatic-pressing (HIP) and pressureless sintering, and from  $Si_3N_4$  powder by hot-pressing. The sintering additives utilized were chosen to allow for densification, while not causing severe degradation of the fiber. The ceramic microstructures were evaluated using scanning optical microscopy. Vickers indentation was used to determine the microhardness and fracture toughness values of the matrices. The RBSN matrices in this study did not reach more than 80 percent of theoretical density after sintering at various temperatures, pressures, and additive levels. Hot-pressing  $Si_3N_4$  powder produced the highest density matrices;

hardness and toughness values were within an order of magnitude of the best literature values. The best sintering aid composition chosen included  $Y_2O_3$ ,  $SiO_2$ , and  $Al_2O_3$  or AlN. Photomicrographs demonstrate a significant reduction of fiber attack by this additive composition. Author

**N89-23691\*#** National Aeronautics and Space Administration. Lewis Research Center, Cleveland, OH.

**UNDERCUTTING OF DEFECTS IN THIN FILM PROTECTIVE COATINGS ON POLYMER SURFACES EXPOSED TO ATOMIC OXYGEN**

SHARON K. RUTLEDGE and JUDITH A. MIHELIC (Cleveland State Univ., OH.) 1989 10 p Presented at the 16th International Conference on Metallurgical Coatings, San Diego, CA, 17-21 Apr. 1989; sponsored by American Vacuum Society (NASA-TM-101986; E-4686; NAS 1.15:101986) Avail: NTIS HC A02/MF A01 CSCL 11/3

Protection for polymeric surfaces is needed to make them durable in the low Earth orbital environment, where oxidation by atomic oxygen is the predominant failure mechanism. Thin film coatings of oxides such as silicon dioxide are viable candidates to provide this protection, but concern has been voiced over the ability of these coatings to protect when defects are present in the coating due to surface anomalies occurring during the deposition process, handling, or micrometeoroid and debris bombardment in low Earth orbit. When a defected coating protecting a polymer substrate is exposed to atomic oxygen, the defect provides a pathway to the underlying polymer allowing oxidation and subsequent undercutting to occur. Defect undercutting was studied for sputter deposited coatings of silicon dioxide on polyimide Kapton. Preliminary results indicate that undercutting may be limited as long as the coating remains intact with the substrate. Therefore, coatings may not need to be defect free to give protection to the underlying surface. Author

**N89-24487\*#** National Aeronautics and Space Administration. Lewis Research Center, Cleveland, OH.

**TIME DEPENDENT RELIABILITY MODEL INCORPORATING CONTINUUM DAMAGE MECHANICS FOR HIGH-TEMPERATURE CERAMICS**

STEPHEN F. DUFFY (Cleveland State Univ., OH.) and JOHN P. GYKENYESI May 1989 20 p (Contract NCC3-99)

(NASA-TM-102046; E-4794; NAS 1.15:102046) Avail: NTIS HC A03/MF A01 CSCL 11/3

Presently there are many opportunities for the application of ceramic materials at elevated temperatures. In the near future ceramic materials are expected to supplant high temperature metal alloys in a number of applications. It thus becomes essential to develop a capability to predict the time-dependent response of these materials. The creep rupture phenomenon is discussed, and a time-dependent reliability model is outlined that integrates continuum damage mechanics principles and Weibull analysis. Several features of the model are presented in a qualitative fashion, including predictions of both reliability and hazard rate. In addition, a comparison of the continuum and the microstructural kinetic equations highlights a strong resemblance in the two approaches. Author

**N89-26091\*#** National Aeronautics and Space Administration. Lewis Research Center, Cleveland, OH.

**REACTION OF PERFLUOROALKYLPOLYETHERS (PFPE) WITH 440C STEEL IN VACUUM UNDER SLIDING CONDITIONS AT ROOM TEMPERATURE**

SHIGEYUKI MORI (Iwate Univ., Morioka, Japan) and WILFREDO MORALES Jan. 1989 12 p (NASA-TP-2883; E-4209; NAS 1.60:2883) Avail: NTIS HC A03/MF A01 CSCL 07/4

Reactions of perfluoroalkylpolyethers (PFPE: Fomblin, Demnum and Krytox) were studied during the sliding contact of stainless steel specimens under ultrahigh vacuum conditions. All three fluids reacted with the steel specimens during sliding. Fomblin, which has acetal linkages, decomposed under the sliding conditions

## 27 NONMETALLIC MATERIALS

generating gaseous products, (COF<sub>2</sub> and fluorinated carbons) which were detected by a quadrupole mass spectrometer. Gaseous products were not detected for the Demnum and Krytox fluids. The amount of gaseous products from Fomblin increased with increasing sliding speed. At the end of the sliding experiments, the wear scar and deposits on the specimens were examined by small spot size XPS. The oxide layer on the specimen surface was removed during sliding, and metal fluorides were formed on the worn surface. The surface of the wear scar and deposits were covered with adsorbed PFPE. Based on these results, it was concluded that the decomposition reaction on Fomblin was initiated by contacting the fluid with a fresh metal surface which was formed during sliding. Author

**N89-26095\*#** National Aeronautics and Space Administration. Lewis Research Center, Cleveland, OH.

### **DETERMINATION OF THE THERMAL STABILITY OF PERFLUOROALKYLETHERS BY TENSIMETRY: INSTRUMENTATION AND PROCEDURE**

LARRY S. HELMICK (Cedarville Coll., OH.) and WILLIAM R. JONES, JR. 1989 31 p Presented at the STLE-ASME Tribology Conference, Fort Lauderdale, FL, 16-19 Oct. 1989 (NASA-TM-102116; E-4891; NAS 1.15:102116) Avail: NTIS HC A03/MF A01 CSCL 11/3

A computerized tensimeter and experimental procedure for determination of the thermal decomposition temperature (T<sub>sub d</sub>) of perfluoro alkylethers were developed and tested. Both the apparatus and the procedure are described in detail. Results of testing with bis(2-ethylhexyl) phthalate and trimethylolpropane triheptanoate demonstrate that the reciprocal of the decomposition temperature is a linear function of the logarithm of the gas volume/heated liquid volume ratio. The T<sub>sub d</sub> obtained for each compound at a gas volume/heated liquid volume ratio of one was similar to the value previously reported using an isotenoscope technique. Results of testing with a polymer of hexafluoropropylene oxide demonstrate that this instrument and procedure can be used to determine the T<sub>sub d</sub> of perfluoroalkylethers. Author

**N89-27836\*#** National Aeronautics and Space Administration. Lewis Research Center, Cleveland, OH.

### **ION BEAM AND PLASMA METHODS OF PRODUCING DIAMONDLIKE CARBON FILMS**

DIANE M. SWEC, MICHAEL J. MIRTICH, and BRUCE A. BANKS Aug. 1988 17 p Presented at the 32nd Annual International Technical Symposium on Optical and Optoelectronic Applied Science and Engineering, San Diego, CA, 14-19 Aug. 1988; sponsored in part by Society of Photo-Optical Instrumentation Engineers (NASA-TM-102301; E-4980; NAS 1.15:102301) Avail: NTIS HC A03/MF A01 CSCL 11/7

A variety of plasma and ion beam techniques was employed to generate diamondlike carbon films. These methods included the use of RF sputtering, dc glow discharge, vacuum arc, plasma gun, ion beam sputtering, and both single and dual ion beam deposition. Since films were generated using a wide variety of techniques, the physico-chemical properties of these films varied considerably. In general, these films had characteristics that were desirable in a number of applications. For example, the films generated using both single and dual ion beam systems were evaluated for applications including power electronics as insulated gates and protective coatings on transmitting windows. These films were impervious to reagents which dissolve graphitic and polymeric carbon structures. Nuclear reaction and combustion analysis indicated hydrogen to carbon ratios to be 1.00, which allowed the films to have good transmittance not only in the infrared, but also in the visible. Other evaluated properties of these films include band gap, resistivity, adherence, density, microhardness, and intrinsic stress. The results of these studies and those of the other techniques for depositing diamondlike carbon films are presented. Author

**N89-28651\*#** National Aeronautics and Space Administration. Lewis Research Center, Cleveland, OH.

### **ARC-TEXTURED HIGH EMITTANCE RADIATOR SURFACES Patent Application**

BRUCE A. BANKS, inventor (to NASA) 18 Jul. 1989 11 p (NASA-CASE-LEW-14679-1; NAS 1.71:LEW-14679-1; US-PATENT-APPL-SN-381240) Avail: NTIS HC A03/MF A01 CSCL 11/3

High emittance radiator surfaces are produced by arc-texturing. This process produces such a surface on a metal by scanning it with a low voltage electric arc from a carbon electrode in an inert environment. NASA

**N89-29538\*** National Aeronautics and Space Administration. Lewis Research Center, Cleveland, OH.

### **FIBER REINFORCED CERAMIC MATERIAL Patent**

RAMAKRISHNA T. BHATT, inventor (to NASA) 1 Nov. 1988 7 p Filed 15 Apr. 1987 Supersedes N87-27810 (25 - 22, p 2985) Division of US-Patent-Appl-SN-886149, filed 16 Jul. 1986 (NASA-CASE-LEW-14392-2; US-PATENT-4,781,993; US-PATENT-APPL-SN-038560; US-PATENT-APPL-SN-886149; US-PATENT-CLASS-428-698; US-PATENT-CLASS-428-288; US-PATENT-CLASS-428-367; US-PATENT-CLASS-428-375; US-PATENT-CLASS-428-390; US-PATENT-CLASS-428-408) Avail: U.S. Patent and Trademark Office CSCL 11/2

A strong and tough SiC/RBSN composite material is comprised of silicon fibers and a reaction bonded silicon nitride (RBSN) matrix. This composite material may be used at elevated temperatures up to at least 1400 C.

Official Gazette of the U.S. Patent and Trademark Office

## 28

## PROPELLANTS AND FUELS

Includes rocket propellants, igniters, and oxidizers; their storage and handling procedures; and aircraft fuels.

**A89-22277\*#** Drexel Univ., Philadelphia, PA.

### **DEGRADATION MECHANISMS OF N-DODECANE WITH SULFUR AND NITROGEN DOPANTS DURING THERMAL STRESSING**

K. T. REDDY, N. P. CERNANSKY (Drexel University, Philadelphia, PA), and R. S. COHEN (Temple University, Philadelphia, PA) Journal of Propulsion and Power (ISSN 0748-4658), vol. 5, Jan.-Feb. 1989, p. 6-13. Research supported by Drexel University. Previously cited in issue 20, p. 3192, Accession no. A87-45372. refs (Contract NAG3-183) Copyright

**A89-42695\*** Drexel Univ., Philadelphia, PA.

### **NOX FORMATION FROM THE COMBUSTION OF MONODISPERSE N-HEPTANE SPRAYS DOPED WITH FUEL-NITROGEN ADDITIVES**

HAMID SARV and NICHOLAS P. CERNANSKY (Drexel University, Philadelphia) Combustion and Flame (ISSN 0010-2180), vol. 76, June 1989, p. 265-283. refs (Contract NAG3-382) Copyright

A series of experiments with simulated synthetic fuels were conducted in order to investigate the effect of droplet size on the conversion of fuel-nitrogen to NO<sub>x</sub>. Pyridine and pyrrole were added to n-heptane as nitrogen-containing additives and burned as monodisperse fuel droplets under various operating conditions in a spray combustion facility. The experimental results indicate that under stoichiometric and fuel-rich conditions, reducing the droplet size increases the efficiency of fuel-N conversion to NO<sub>x</sub>. This observation is associated with improved oxidation of the pyrolysis fragments of the additive by better oxygen penetration through



## MATERIALS PROCESSING

the droplet flame zone. The dominant reactions by which fuel-N is transformed to NO<sub>x</sub> were also considered analytically by a premixed laminar flame code. The calculations are compared to the small droplet size results. Author

**A89-47148\*#** National Aeronautics and Space Administration. Lewis Research Center, Cleveland, OH.

### IGNITION AND COMBUSTION OF METALLIZED PROPELLANTS

DIANE L. GALECKI (NASA, Lewis Research Center, Cleveland, OH) AIAA, ASME, SAE, and ASEE, Joint Propulsion Conference, 25th, Monterey, CA, July 10-13, 1989. 10 p. refs (AIAA PAPER 89-2883)

An experimental program was conducted to investigate the ignition and combustion properties of a gelled, metallized fuel, A1/JP20, burned with gaseous oxygen, and to compare the results to the ignition and combustion properties of neat RP1. Both a Cstar efficiency and a specific impulse efficiency were calculated by comparing experimental values with those from a one-dimensional chemical equilibrium computer code. For most operating conditions, the efficiencies of the A1/JP10 were only 2 to 6 percent less than those of the neat RP1. Author

**A89-51339\*#** National Aeronautics and Space Administration. Lewis Research Center, Cleveland, OH.

### FUELING THE NATIONAL AERO-SPACE PLANE WITH SLUSH HYDROGEN

NED P. HANNUM and FRANK D. BERKOPEC (NASA, Lewis Research Center, Cleveland, OH) AIAA, National Aerospace Plane Conference, 1st, Dayton, OH, July 20, 21, 1989. 12 p. (AIAA PAPER 89-5014) Copyright

The National Aerospace Plane is a horizontal take off and landing, single stage-to-orbit vehicle using hydrogen as the fuel. The first flights are planned for the mid 1990s. The high heating value, cooling capacity, and combustion properties make hydrogen the fuel of choice, but the low density results in a large vehicle. Both the fuel cooling capacity and density are increased with the use of slush hydrogen and result in significant reductions in size of the vehicle. A national program to advance this technology and to find engineering solutions to the many design issues is now underway. Author

**N89-17017\*#** National Aeronautics and Space Administration. Lewis Research Center, Cleveland, OH.

### EXPERIMENTAL VERIFICATION OF THE THERMODYNAMIC PROPERTIES FOR A JET-A FUEL

CARMEN M. GRACIASALCEDO, THEODORE A. BRABBS, and BONNIE J. MCBRIDE Sep. 1988 10 p Presented at the 196th National Meeting of the American Chemical Society, Los Angeles, CA, 25-30 Sep. 1988 Prepared in cooperation with Army Aviation Systems Command, Cleveland, OH; and Sverdrup Technology, Inc., Cleveland, OH (NASA-TM-101475; E-4593; NAS 1.15:101475) Avail: NTIS HC A02/MF A01 CSDL 21/4

Thermodynamic properties for a Jet-A fuel were determined by Shell Development Company in 1970 under a contract for NASA Lewis Research Center. The polynomial fit necessary to include Jet-A fuel (liquid and gaseous phases) in the library of thermodynamic properties of the NASA Lewis Chemical Equilibrium Program is calculated. To verify the thermodynamic data, the temperatures of mixtures of liquid Jet-A injected into a hot nitrogen stream were experimentally measured and compared to those calculated by the program. Iso-octane, a fuel for which the thermodynamic properties are well known, was used as a standard to calibrate the apparatus. The measured temperatures for the iso-octane/nitrogen mixtures reproduced the calculated temperatures except for a small loss due to the non-adiabatic behavior of the apparatus. The measurements for Jet-A were corrected for this heat loss and showed excellent agreement with the calculated temperatures. These experiments show that this process can be adequately described by the thermodynamic properties fitted for the Chemical Equilibrium Program. Author

Includes space-based development of products and processes for commercial applications.

**A89-17106\*#** National Aeronautics and Space Administration. Lewis Research Center, Cleveland, OH.

### BULK UNDERCOOLING, NUCLEATION, AND MACROSEGREGATION OF PB-SN ALLOYS

H. C. DEGROH, III (NASA, Lewis Research Center, Cleveland, OH) and V. LAXMANAN (Case Western Reserve University, Cleveland, OH) Metallurgical Transactions A - Physical Metallurgy and Materials Science (ISSN 0360-2133), vol. 19A, Nov. 1988, p. 2651-2658. refs

Preliminary ground-based studies on the undercooling behavior of large samples (23 g) of lead-tin alloys are presented. Evidence of gravity-related segregation effects is found, and a possible area for future microgravity experimentation is thus identified. Detailed descriptions of the experimental procedure used to achieve bulk undercoolings of between 0.5 and 34 K, depending on composition, are given. The bulk undercoolings obtained in this study are comparable with those found in small droplets. The large size of the present samples enabled the observation of sedimentation and other macrosegregation processes. Author

**A89-17112\*** Case Western Reserve Univ., Cleveland, OH.

### GRAVITATIONAL MACROSEGREGATION IN UNIDIRECTIONALLY SOLIDIFIED LEAD-TIN ALLOY

L. WANG, V. LAXMANAN, and J. F. WALLACE (Case Western Reserve University, Cleveland, OH) Metallurgical Transactions A - Physical Metallurgy and Materials Science (ISSN 0360-2133), vol. 19A, Nov. 1988, p. 2687-2694. refs (Contract NAG3-417)

Copyright

Nine small samples of binary lead-tin alloys were solidified unidirectionally upward, with both cooling rate and thermal gradient being closely controlled. Results presented include thermal measurements, chemical composition measurements, and microstructural characterization. In the six Pb-15 wt pct Sn ingots, normal macrosegregation was observed, with Sn content being highest at the top of the ingot. No significant macrosegregation was noted in the three ingots of nominal composition Sn-15 wt pct Sn. R.R.

**A89-17784\*#** National Aeronautics and Space Administration. Lewis Research Center, Cleveland, OH.

### FACILITIES FOR MICROGRAVITY COMBUSTION RESEARCH

K. R. SACKSTEDER (NASA, Lewis Research Center, Cleveland, OH) IAF, International Astronautical Congress, 39th, Bangalore, India, Oct. 8-15, 1988. 10 p. refs (IAF PAPER 88-355)

The microgravity test facilities at NASA Lewis Research Center are discussed. Low gravity combustion test apparatus and experiments are examined including the study of solid surface combustion and droplet combustion. Plans for the Space Station capability and the Modular Combustion Facility are described. R.B.

**A89-22747\*#** National Aeronautics and Space Administration. Lewis Research Center, Cleveland, OH.

### THERMOCAPILLARY MIGRATION OF A LARGE GAS SLUG IN A TUBE

M. M. HASAN and R. BALASUBRAMANIAM (NASA, Lewis Research Center, Cleveland, OH) Journal of Thermophysics and Heat Transfer (ISSN 0887-8722), vol. 3, Jan. 1989, p. 87-89. Copyright

The steady-state motion exhibited by a large gas slug that is contained in a liquid-filled tube and subjected to a linear temperature variation is analyzed, taking the thermally-induced



## 29 MATERIALS PROCESSING

gradient of the gas-liquid surface tension into account. An expression which characterizes the terminal velocity of the gas slug has been derived. O.C.

**A89-25060\*#** National Aeronautics and Space Administration. Lewis Research Center, Cleveland, OH.

### **CONVECTIVE FLOWS IN ENCLOSURES WITH VERTICAL TEMPERATURE OR CONCENTRATION GRADIENTS**

L. W. WANG, A. T. CHAI (NASA, Lewis Research Center, Cleveland, OH), and D. J. SUN (National Cheng Kung University, Tainan, Republic of China) AIAA, Aerospace Sciences Meeting, 27th, Reno, NV, Jan. 9-12, 1989. 11 p. Research supported by the National Research Council of the Republic of China. Previously announced in STAR as N89-12753. refs (AIAA PAPER 89-0069) Copyright

The transport process in the fluid phase during the growth of a crystal has a profound influence on the structure and quality of the solid phase. In vertical growth techniques the fluid phase is often subjected to vertical temperature and concentration gradients. The main objective is to obtain more experimental data on convective flows in enclosures with vertical temperature or concentration gradients. Among actual crystal systems the parameters vary widely. The parametric ranges studied for mass transfer are mainly dictated by the electrochemical system employed to impose concentration gradients. Temperature or concentration difference are maintained between two horizontal end walls. The other walls are kept insulated. Experimental measurements and observations were made of the heat transfer or mass transfer, flow patterns, and the mean and fluctuating temperature distribution. The method used to visualize the flow pattern in the thermal cases is an electrochemical pH-indicator method. Laser shadowgraphs are employed to visualize flow patterns in the solutal cases. Author

**A89-25197\*#** Westinghouse Research and Development Center, Pittsburgh, PA.

### **EVALUATION OF TRANSPORT CONDITIONS DURING PHYSICAL VAPOR TRANSPORT GROWTH OF OPTO-ELECTRONIC CRYSTALS**

N. B. SINGH, R. MAZELSKY, and M. E. GLICKSMAN (Westinghouse Research and Development Center, Pittsburgh, PA) AIAA, Aerospace Sciences Meeting, 27th, Reno, NV, Jan. 9-12, 1989. 4 p. refs (Contract NAS3-25274) (AIAA PAPER 89-0229) Copyright

Transport conditions were evaluated during the vapor phase growth of mercurous chloride crystals in a closed tube. Experimentally observed growth rates were much smaller than those calculated by the Hertz-Knudsen (H-K) equation. The Arrhenius behavior of growth rate with the temperature was used to derive the sticking coefficient. A one-dimensional diffusion model was used to calculate the total mass flux and was compared with the condensing flux. It was predicted that growth occurred in the convecto-diffusive range. Author

**A89-25201\*#** National Aeronautics and Space Administration. Lewis Research Center, Cleveland, OH.

### **MICROGRAVITY RESEARCH IN NASA GROUND-BASED FACILITIES**

JACK LEKAN (NASA, Lewis Research Center, Cleveland, OH) AIAA, Aerospace Sciences Meeting, 27th, Reno, NV, Jan. 9-12, 1989. 14 p. Previously announced in STAR as N89-15047. refs (AIAA PAPER 89-0236) Copyright

An overview of reduced gravity research performed in NASA ground-based facilities sponsored by Microgravity Science and Applications Program of the NASA Office of Space Science and Applications is presented. A brief description and summary of the operations and capabilities of each of these facilities along with an overview of the historical usage of them is included. The goals and program elements of the Microgravity Science and Applications programs are described and the specific programs that utilize the low gravity facilities are identified. Results from two particular

investigations in combustion (flame spread over solid fuels) and fluid physics (gas-liquid flows at microgravity conditions) are presented. Author

**A89-25261\*#** National Aeronautics and Space Administration. Lewis Research Center, Cleveland, OH.

### **EFFECTS OF CRUCIBLE WETTING DURING SOLIDIFICATION OF IMMISCIBLE PB-ZN ALLOYS**

H. C. DE GROH, III and H. B. PROBST (NASA, Lewis Research Center, Cleveland, OH) AIAA, Aerospace Sciences Meeting, 27th, Reno, NV, Jan. 9-12, 1989. 7 p. Previously announced in STAR as N89-14341. refs (AIAA PAPER 89-0304) Copyright

Many industrial uses for liquid phase miscibility gap alloys are proposed. However, the commercial production of these alloys into useful ingots with a reasonable amount of homogeneity is arduous because of their immiscibility in the liquid state. In the low-g environment of space gravitational settling forces are abated, thus solidification of an immiscible alloy with a uniform distribution of phases becomes feasible. Elimination of gravitational settling and coalescence processes in low-g also makes possible the study of other separation and coarsening mechanisms. Even with gravitational separation forces reduced, many low-g experiments have resulted in severely segregated structures. The segregation in many cases was due to preferential wetting of the crucible by one of the immiscible liquids. The objective was to analyze the wetting behavior of Pb-Zn alloys on various crucible materials in an effort to identify a crucible in which the fluid flow induced by preferential wetting is minimized. It is proposed that by choosing the crucible for a particular alloy so that the difference in surface energy between the solid and two liquid phases is minimized, the effects of preferential wetting can be diminished and possibly avoided. Qualitative experiments were conducted and have shown the competitive wetting behavior of the immiscible Pb-Zn system and 13 different crucible materials. Author

**A89-25495\*#** Arizona Univ., Tucson.

### **THERMOSOLUTAL CONVECTION DURING DENDRITIC SOLIDIFICATION**

J. C. HEINRICH, P. NANDAPURKAR, D. R. POIRIER (Arizona, University, Tucson), and S. FELICELLI AIAA, Aerospace Sciences Meeting, 27th, Reno, NV, Jan. 9-12, 1989. 9 p. refs (Contract NAG3-723) (AIAA PAPER 89-0626) Copyright

This paper presents a mathematical model for directional solidification of a binary alloy including a dendritic region underlying an all-liquid region. It is assumed initially that there exists a nonconvecting state with planar isotherms and isoconcentrates solidifying at a constant velocity. The stability of this system has been analyzed and nonlinear calculations are performed that show the effect of convection in the solidification process when the system is unstable. Results of calculations for various cases defined by the initial temperature gradient at the dendrite tips and varying strength of the gravitational field are presented for systems involving lead-tin alloys. The results show that the systems are stable for a gravitational constant of 0.0001 g(0) and that convection can be suppressed by appropriate choice of the container's size for higher values of the gravitational constant. It is also concluded that for the lead-tin systems considered, convection in the mushy zone is not significant below the upper 20 percent of the dendritic zone, if at all. Author

**A89-25627\*#** National Aeronautics and Space Administration. Lewis Research Center, Cleveland, OH.

### **FLIGHT HARDWARE AND TELE-OPERATIONS SUPPORTING THE ISOTHERMAL DENDRITIC GROWTH EXPERIMENT ABOARD THE SPACE SHUTTLE**

E. WINSA, G. KRAFT (NASA, Lewis Research Center, Cleveland, OH), M. GLICKSMAN (Rensselaer Polytechnic Institute, Troy, NY), D. MILLER, and R. ABRAMCZYK (Sverdrup Technology, Inc., Cleveland, OH) AIAA, Aerospace Sciences Meeting, 27th, Reno, NV, Jan. 9-12, 1989. 11 p. (AIAA PAPER 89-0863) Copyright

The Isothermal Dendritic Growth Experiment, which is expected to fly on the Space Shuttle to study dendritic solidification of molten metals such as iron and aluminum, is examined. Succinonitrile and pivalic acid are substituted for metals to permit visualization of dendritic growth. The technical features of the apparatus are described, including temperature control, the photographic system, and slow scan television. The teleoperations techniques for the experiment are discussed in detail. R.B.

**A89-28418\*#** National Aeronautics and Space Administration. Lewis Research Center, Cleveland, OH.

**DROPLET COMBUSTION DROP TOWER TESTS USING MODELS OF THE SPACE FLIGHT APPARATUS**

J. B. HAGGARD, M. H. BRACE (NASA, Lewis Research Center, Cleveland, OH), J. L. KROPP (TRW, Inc., TRW Space and Technology Group, Redondo Beach, CA), and F. L. DRYER (Princeton University, NJ) AIAA, Aerospace Sciences Meeting, 27th, Reno, NV, Jan. 9-12, 1989. 8 p. (AIAA PAPER 89-0501)

An engineering model built for droplet combustion drop tower tests is described. The model was built using a design with mechanical and electrical assemblies of the same level of complexity as they will have in flight. The model was tested for functional operation and integrated into a 5-sec drop tower. Test data obtained to date are presented together with model and test cell diagrams. I.S.

**A89-28419\*#** National Aeronautics and Space Administration. Lewis Research Center, Cleveland, OH.

**THE SOLID SURFACE COMBUSTION SPACE SHUTTLE EXPERIMENT HARDWARE DESCRIPTION AND GROUND-BASED TEST RESULTS**

D. M. VENTO, R. J. ZAVESKY, K. R. SACKSTEDER (NASA, Lewis Research Center, Cleveland, OH), and R. A. ALTENKIRCH (Mississippi State University, Mississippi State) AIAA, Aerospace Sciences Meeting, 27th, Reno, NV, Jan. 9-12, 1989. 8 p. (AIAA PAPER 89-0503) Copyright

The Lewis Research Center is developing a series of microgravity combustion experiments for the Space Shuttle. The Solid Surface Combustion Experiment (SSCE) is the first to be completed. SSCE will study flame spreading over thermally thin fuels (ashless filter paper) under microgravity conditions. The flight hardware consists of a combustion chamber containing the sample and a computer which takes the data and controls the experiment. Experimental data will include gas-phase and solid-phase temperature measurements and motion pictures of the combustion process. Flame spread rates will be determined from the motion pictures. Author

**A89-28439\*#** National Aeronautics and Space Administration. Lewis Research Center, Cleveland, OH.

**GROUND-BASED SIMULATION OF TELEPRESENCE FOR MATERIALS SCIENCE EXPERIMENTS**

JAMES C. JOHNSTON, BRUCE N. ROSENTHAL, MARY JO BONNER (NASA, Lewis Research Center, Cleveland, OH), RICHARD C. HAHN, and BRUCE HERBACH (Rensselaer Polytechnic Institute, Troy, NY) AIAA, Aerospace Sciences Meeting, 27th, Reno, NV, Jan. 9-12, 1989. 8 p. (AIAA PAPER 89-0597) Copyright

A series of ground-based telepresence experiments have been performed to determine the minimum video frame rate and resolution required for the successive performance of materials science experiments in space. The approach used is to simulate transmission between earth and space station with transmission between laboratories on earth. The experiments include isothermal dendrite growth, physical vapor transport, and glass melting. Modifications of existing apparatus, software developed, and the establishment of an inhouse network are reviewed. A.A.F.

**A89-30450\*#** National Aeronautics and Space Administration. Lewis Research Center, Cleveland, OH.

**INTERACTION OF SURFACE RADIATION WITH CONVECTION IN CRYSTAL GROWTH BY PHYSICAL VAPOR TRANSPORT**

MOHAMMAD KASSEMI and WALTER M. B. DUVAL (NASA, Lewis Research Center, Cleveland, OH) AIAA, Aerospace Sciences Meeting, 27th, Reno, NV, Jan. 9-12, 1989. 11 p. Research supported by the National Research Council. refs (AIAA PAPER 89-0228) Copyright

Growth of single crystals from vapor in closed ampoules is governed by an intricate interplay between mass, momentum and heat transfer processes. The objective of this study is to examine and isolate the effects of surface radiation heat transfer on the vapor transport process using a mathematical model. The model consists of a set of coupled nonlinear partial differential equations for conservation of mass, momentum, energy and species, and the integrodifferential equations which represent radiative exchange. It depends on five important physical parameters. These are Grashof number, Prandtl number, Schmidt number, aspect ratio and the radiation-conduction number. The effects of these dimensionless groupings are systematically investigated. From the cases examined, it is concluded that surface radiation can change the flow structure appreciably. This is especially true in microgravity environment where radiation competes primarily with conduction in modifying the thermal profiles. The numerical results also show that in the presence of radiation, the top heating configuration (source on top) is no longer stable and that near the growing crystal, radiation-induced vortices can introduce significant nonuniformities in the growth flux. Author

**A89-35015\*** Michigan Univ., Ann Arbor.

**COMBINED ROLES OF BUOYANCY AND ORIENTATION IN NUCLEATE POOL BOILING**

H. MERTE, JR. (Michigan, University, Ann Arbor) IN: Collected papers in heat transfer 1988; Proceedings of the ASME Winter Annual Meeting, Chicago, IL, Nov. 27-Dec. 2, 1988. Volume 2. New York, American Society of Mechanical Engineers, 1988, p. 179-186. refs (Contract NAG3-663) Copyright

The paper presents results obtained during pool boiling from flat surfaces over body force levels of  $a/g = -1$  to 0 to 20 for LN2 and R-113 under steady and transient conditions. Pyrex and metal surfaces are used. Particular attention is given to the case where the effective gravity is perpendicular to the heating surface. At the lower levels of heat flux with nucleate boiling, the heater surface superheat first increases and then decreases as the body force increases above  $a/g = 1$ . This is due to the greater contribution of nonboiling convection. K.K.

**A89-40897\*** Akron Univ., OH.

**STEADY-STATE THERMAL-SOLUTAL DIFFUSION IN A FLOAT ZONE**

G. W. YOUNG (Akron, University, OH) and A. CHAIT (NASA, Lewis Research Center, Cleveland, OH) Journal of Crystal Growth (ISSN 0022-0248), vol. 96, no. 1, May 1989, p. 65-95. refs (Contract NSF DMS-86-04047) Copyright

A model for a float zone in a thin vertical sheet is used to study the formation of the zone configuration for both pure and binary systems of Si and GeGa. Equations describing the steady two-dimensional diffusion of solute in the melt and diffusion of heat in the feed material and the product crystal are presented. The material properties, asymptotic solutions for the temperature and concentration profiles, and melting, solidifying, and melt/gas interfacial shapes are determined in the small aspect ratio limit. R.R.

**A89-53278\*#** Kentucky Univ., Lexington.

**EFFECTS OF FURNACE TEMPERATURE PROFILE ON THE INTERFACE SHAPE DURING BRIDGMAN CRYSTAL GROWTH**

K. TAGHAVI (Kentucky, University, Lexington) and W. M. B. DUVAL (NASA, Lewis Research Center, Cleveland, OH) IN: ASME 1988 National Heat Transfer Conference, Houston, TX, July 24-27, 1988, Proceedings. Volume 2. New York, American Society of Mechanical Engineers, 1988, p. 435-444. refs Copyright

## 29 MATERIALS PROCESSING

The effects of asymmetry in furnace temperature profile and pulling velocity on the crystal interface shape are demonstrated while neglecting the latent heat of solidification. It is concluded that the furnace temperature profile may be varied in order to influence the interface shape of the crystal. An exact thermal analysis is performed on the Bridgman technique by including the latent heat of solidification as a source term. The exact temperature field is obtained for the case of a flat melt-crystal interface. The earlier observation regarding the influence of furnace temperature profile on the crystal interface shape is confirmed and a criterion for a flat crystal interface is obtained. Various furnace temperature profiles are selected and their corresponding results are presented. Author

**N89-11920\*#** Tennessee Univ., Knoxville. Dept. of Mechanical and Aerospace Engineering.

**AN EXPERIMENTAL AND ANALYTICAL INVESTIGATION OF THERMOACOUSTIC CONVECTION HEAT TRANSFER IN GRAVITY AND ZERO-GRAVITY ENVIRONMENTS**

MASOOD PARANG Apr. 1986 185 p

(Contract NAG3-239)

(NASA-CR-179575; NAS 1.26:179575) Avail: NTIS HC A09/MF A01 CSCL 12/1

An experimental and analytical study of Thermoacoustic Convection heat transfer in gravity and zero-gravity environments is presented. The experimental apparatus consisted of a cylinder containing air as a fluid. The side wall of the cylinder was insulated while the bottom wall was allowed to remain at the ambient temperature. The enclosed air was rapidly heated by the top surface which consisted of a thin stainless steel foil connected to a battery pack as the power source. Thermocouples were used to measure the transient temperature of the air on the axis of the cylinder. The output of the thermocouples was displayed on digital thermometers and the temperature displays were recorded on film using a high-speed movie camera. Temperature measurements were obtained in the zero-gravity environment by dropping the apparatus in the 2-Seconds Zero-Gravity Drop Tower Facilities of NASA Lewis Research Center. In addition, experiments were also performed in the gravity environment and the results are compared in detail with those obtained under zero-gravity conditions. Author

**N89-12753\*#** National Aeronautics and Space Administration. Lewis Research Center, Cleveland, OH.

**CONVECTIVE FLOWS IN ENCLOSURES WITH VERTICAL TEMPERATURE OR CONCENTRATION GRADIENTS**

L. W. WANG, A. T. CHAI, and D. J. SUN (National Cheng Kung Univ., Tainan, Taiwan) 1988 18 p Presented at the 27th Aerospace Sciences Meeting, Reno, Nev., 9-12 Jan. 1989; sponsored by the American Institute of Aeronautics and Astronautics

(NASA-TM-101373; E-4421; NAS 1.15:101373; AIAA-89-0069)

Avail: NTIS HC A03/MF A01 CSCL 22/1

The transport process in the fluid phase during the growth of a crystal has a profound influence on the structure and quality of the solid phase. In vertical growth techniques the fluid phase is often subjected to vertical temperature and concentration gradients. The main objective is to obtain more experimental data on convective flows in enclosures with vertical temperature or concentration gradients. Among actual crystal systems the parameters vary widely. The parametric ranges studied for mass transfer are mainly dictated by the electrochemical system employed to impose concentration gradients. Temperature or concentration difference are maintained between two horizontal end walls. The other walls are kept insulated. Experimental measurements and observations were made of the heat transfer or mass transfer, flow patterns, and the mean and fluctuating temperature distribution. The method used to visualize the flow pattern in the thermal cases is an electrochemical pH-indicator method. Laser shadowgraphs are employed to visualize flow patterns in the solutal cases. Author

**N89-14341\*#** National Aeronautics and Space Administration. Lewis Research Center, Cleveland, OH.

**EFFECTS OF CRUCIBLE WETTING DURING SOLIDIFICATION OF IMMISCIBLE PB-ZN**

HENRY C. DEGROH, III and HUBERT B. PROBST Dec. 1988 8 p Presented at the 27th Aerospace Sciences Meeting, Reno, NV, 9-12 Jan. 1989

(NASA-TM-101372; E-4419; NAS 1.15:101372) Avail: NTIS HC A02/MF A01 CSCL 22/1

Many industrial uses for liquid phase miscibility gap alloys are proposed. However, the commercial production of these alloys into useful ingots with a reasonable amount of homogeneity is arduous because of their immiscibility in the liquid state. In the low-g environment of space gravitational settling forces are abated, thus solidification of an immiscible alloys with a uniform distribution of phases becomes feasible. Elimination of gravitational settling and coalescence processes in low-g also makes possible the study of other separation and coarsening mechanisms. Even with gravitational separation forces reduced, many low-g experiments have resulted in severely segregated structures. The segregation in many cases was due to preferential wetting of the crucible by one of the immiscible liquids. The objective was to analyze the wetting behavior of Pb-Zn alloys on various crucible materials in an effort to identify a crucible in which the fluid flow induced by preferential wetting is minimized. It is proposed that by choosing the crucible for a particular alloy so that the difference in surface energy between the solid and two liquid phases is minimized, the effects of preferential wetting can be diminished and possibly avoided. Qualitative experiments were conducted and have shown the competitive wetting behavior of the immiscible Pb-Zn system and 13 different crucible materials. Author

**N89-17046\*#** National Aeronautics and Space Administration. Lewis Research Center, Cleveland, OH.

**BEHAVIOR IN NORMAL AND REDUCED GRAVITY OF AN ENCLOSED LIQUID/GAS SYSTEM WITH NONUNIFORM HEATING FROM ABOVE**

H. D. ROSS, D. N. SCHILLER, P. DISIMILE, and W. A. SIRIGNANO Jan. 1989 12 p Presented at the 27th Aerospace Sciences Meeting, Reno, NV, 9-12 Jan. 1989; sponsored in part by AIAA Prepared in cooperation with California Univ., Irvine; and Cincinnati Univ., OH •

(NASA-TM-101471; E-4585; NAS 1.15:101471) Avail: NTIS HC A03/MF A01 CSCL 12/1

The temperature and velocity fields have been investigated for a single-phase gas system and a two-layer gas-and-liquid system enclosed in a circular cylinder being heated suddenly and nonuniformly from above. The transient response of the gas, liquid, and container walls was modelled numerically in normal and reduced gravity (10 to the -5 g). Verification of the model was accomplished via flow visualization experiments in 10 cm high by 10 cm diameter plexiglass cylinders. Author

**N89-17682\*#** National Aeronautics and Space Administration. Lewis Research Center, Cleveland, OH.

**MICROGRAVITY COMBUSTION DIAGNOSTICS WORKSHOP**

GILBERT J. SANTORO, ed., PAUL S. GREENBERG, ed., and NANCY D. PILTCH, ed. 1988 47 p Workshop held in Cleveland, OH, 28-29 Jul. 1987

(NASA-CP-10017; E-4213; NAS 1.55:10017) Avail: NTIS HC A03/MF A01 CSCL 22/1

Through the Microgravity Science and Applications Division (MSAD) of the Office of Space Science and Applications (OSSA) at NASA Headquarters, a program entitled, Advanced Technology Development (ATD) was promulgated with the objective of providing advanced technologies that will enable the development of future microgravity science and applications experimental flight hardware. Among the ATD projects one, Microgravity Combustion Diagnostics (MCD), has the objective of developing advanced diagnostic techniques and technologies to provide nonperturbing measurements of combustion characteristics and parameters that will enhance the scientific integrity and quality of microgravity combustion experiments. As part of the approach to this project,

a workshop was held on July 28 and 29, 1987, at the NASA Lewis Research Center. A small group of laser combustion diagnosticians met with a group of microgravity combustion experimenters to discuss the science requirements, the state-of-the-art of laser diagnostic technology, and plan the direction for near-, intermediate-, and long-term programs. This publication describes the proceedings of that workshop. Author

**N89-19442\*#** California Univ., Irvine.

**EXPERIMENT PLANS TO STUDY PREIGNITION PROCESSES OF A POOL FIRE IN LOW GRAVITY M.S. Thesis - 1988 Final Report**

DAVID N. SCHILLER Mar. 1989 128 p

(Contract NAG3-627)

(NASA-CR-182256; NAS 1.26:182256) Avail: NTIS HC A07/MF A01 CSCL 22/1

Science requirements are specified to guide experimental studies of transient heat transfer and fluid flow in an enclosure containing a two-layer gas-and-liquid system heated unevenly from above. Specifications are provided for experiments in three separate settings: (1) a normal gravity laboratory, (2) the NASA-LeRC Drop towers, and (3) a space-based laboratory (e.g., Shuttle, Space Station). A rationale is developed for both minimum and desired requirement levels. The principal objective of the experimental effort is to validate a computational model of the enclosed liquid fuel pool during the preignition phase and to determine via measurement the role of gravity on the behavior of the system. Preliminary results of single-phase normal gravity experiments and simulations are also presented. Author

**N89-20295\*#** GTE Labs., Inc., Waltham, MA.

**A COMPARATIVE STUDY OF THE INFLUENCE OF BUOYANCY DRIVEN FLUID FLOW ON GAAS CRYSTAL GROWTH**

J. A. KAFALAS and A. H. BELLOWES In NASA, Washington, Microgravity Science and Applications Flight Programs, January - March 1987, Selected Papers, Volume 1 p 337-347 Oct. 1988 (Contract NAS3-24644)

Avail: NTIS HC A21/MF A01 CSCL 22/1

A systematic investigation of the effect of gravity driven fluid flow on GaAs crystal growth was performed. It includes GaAs crystal growth in the microgravity environment aboard the Space Shuttle. The program involves a controlled comparative study of crystal growth under a variety of earth based conditions with variable orientation and applied magnetic field in addition to the microgravity growth. Earth based growth will be performed under stabilizing as well as destabilizing temperature gradients. The boules grown in space and on earth will be fully characterized to correlate the degree of convection with the distribution of impurities. Both macro- and micro-segregation will be determined. The space growth experiment will be flown in a self-contained payload container through NASA's Get Away Special program. Author

**N89-20299\*#** National Aeronautics and Space Administration, Lewis Research Center, Cleveland, OH.

**ISOTHERMAL DENDRITIC GROWTH: A LOW GRAVITY EXPERIMENT**

M. E. GLICKSMAN, R. C. HAHN, T. A. LOGRASSO, E. R. RUBINSTEIN, M. E. SELLECK (Rensselaer Polytechnic Inst., Troy, NY.), and E. WINSA In NASA, Washington, Microgravity Science and Applications Flight Programs, January - March 1987, Selected Papers, Volume 1 p 411-425 Oct. 1988

Avail: NTIS HC A21/MF A01 CSCL 22/1

The Isothermal Dendritic Growth Experiment is an active crystal growth experiment designed to test dendritic growth theory at low undercoolings where convection prohibits such studies at 1 g. The experiment will be essentially autonomous, though limited in-flight interaction through a computer interface is planned. One of the key components of the apparatus will be a crystal growth chamber capable of achieving oriented single crystal dendritic growth. Recent work indicates that seeding the chamber with a crystal of the proper orientation will not, in and of itself, be sufficient to meet this requirement. Additional flight hardware and software

required for the STS flight experiment are currently being developed at NASA Lewis Research Center and at Rensselaer Polytechnic Institute. Author

**N89-20300\*#** National Aeronautics and Space Administration, Lewis Research Center, Cleveland, OH.

**ISOTHERMAL SOLIDIFICATION IN A BINARY ALLOY MELT**

V. LAXMANAN (Case Western Reserve Univ., Cleveland, OH.) In NASA, Washington, Microgravity Science and Applications Flight Programs, January - March 1987, Selected Papers, Volume 1 p 427-457 Oct. 1988

Avail: NTIS HC A21/MF A01 CSCL 22/1

A space shuttle experiment employing the General Purpose (Rocket) Furnace (GPF) in its isothermal mode of operation is manifested on MSL-3, circa 1989. The central aim of this experiment is to investigate the effect of reduced gravity levels on the segregation behavior in a slowly, and isothermally, cooled sample of a binary Pb-15 wt percent Sn alloy. This experiment would thus be able to simulate, in a small laboratory sample, about 20 mm dia 60 mm high and weighing about 150 grams, some aspects of the segregation phenomena occurring in large industrial ingots. Ground-based experiments conducted in the single-cavity simulator of the GPF, located at Marshall Space Flight Center (MSFC), in support of the microgravity experiment are described in detail. The results of the MSFC experiments are compared with other related experiments conducted at Case Western Reserve University (CWRU), wherein the isothermal constraints were relaxed. Author

**N89-20320\*#** Maryland Univ., College Park. Inst. for Physical Science and Technology.

**CRITICAL FLUID LIGHT SCATTERING**

ROBERT W. GAMMON In NASA, Washington, Microgravity Science and Applications Flight Programs, January - March 1987, Selected Papers, Volume 2 p 805-830 Oct. 1988 (Contract NAG3-727)

Avail: NTIS HC A13/MF A01 CSCL 22/1

The objective is to measure the decay rates of critical density fluctuations in a simple fluid (xenon) very near its liquid-vapor critical point using laser light scattering and photon correlation spectroscopy. Such experiments were severely limited on Earth by the presence of gravity which causes large density gradients in the sample when the compressibility diverges approaching the critical point. The goal is to measure fluctuation decay rates at least two decades closer to the critical point than is possible on earth, with a resolution of 3 microK. This will require loading the sample to 0.1 percent of the critical density and taking data as close as 100 microK to the critical temperature. The minimum mission time of 100 hours will allow a complete range of temperature points to be covered, limited by the thermal response of the sample. Other technical problems have to be addressed such as multiple scattering and the effect of wetting layers. The experiment entails measurement of the scattering intensity fluctuation decay rate at two angles for each temperature and simultaneously recording the scattering intensities and sample turbidity (from the transmission). The analyzed intensity and turbidity data gives the correlation length at each temperature and locates the critical temperature. The fluctuation decay rate data from these measurements will provide a severe test of the generalized hydrodynamic theories of transport coefficients in the critical regions. When compared to equivalent data from binary liquid critical mixtures they will test the universality of critical dynamics. Author

**N89-20321\*#** National Aeronautics and Space Administration, Lewis Research Center, Cleveland, OH.

**PARTICLE CLOUD MIXING IN MICROGRAVITY**

H. ROSS, L. FACCA, V. TANGIRALA, and A. L. BERLAD (California Univ., San Diego, La Jolla.) Jan. 1989 14 p Presented at the 26th Aerospace Sciences Meeting, Reno, NV, 11-14 Jan. 1988; sponsored in part by AIAA

(NASA-TM-101484; E-4618; NAS 1.15:101484; AIAA-88-0453)

Avail: NTIS HC A03/MF A01 CSCL 22/1

## 29 MATERIALS PROCESSING

Quasi-steady flame propagation through clouds of combustible particles requires quasi-steady transport properties and quasi-steady particle number density. Microgravity conditions may be employed to help achieve the conditions of quiescent, uniform clouds needed for such combustion studies. Joint experimental and theoretical NASA-UCSD studies were concerned with the use of acoustic, electrostatic, and other methods of dispersion of fuel particulates. Results of these studies are presented for particle clouds in long cylindrical tubes. Author

**N89-21134\*** Arizona Univ., Tucson. Dept. of Materials Science and Engineering.

### COMPUTER SIMULATION OF MACROSEGREGATION IN DIRECTIONALLY SOLIDIFIED CIRCULAR INGOTS

K. S. YEUM and D. R. POIRIER 7 Jan. 1988 65 p

(Contract NAG3-723)

(NASA-CR-182838; NAS 1.26:182838) Avail: NTIS HC A04/MF A01 CSCL 22/1

The formulation and employment of a computer code designed to simulate the directional solidification of lead-rich Pb-Sn alloys in the form of an ingot with a uniform and circular cross-section are described. The formulation is for steady-state solidification in which convection in the all-liquid zone is ignored. Particular attention was given to designing a code to simulate the effect of a subtle variation of temperature in the radial direction. This is important because a very small temperature difference between the center and the surface of the ingot (e.g., less than 0.5 C) is enough to cause substantial convection within the mushy-zone when the solidification rate is approximately 0.001 to 0.0001 cm/s. Author

**N89-25353\*** Naval Research Lab., Washington, DC. Computational Physics and Fluid Dynamics Lab.

### TIME-DEPENDENT COMPUTATIONAL STUDIES OF FLAMES IN MICROGRAVITY Final Report, 1985 Dec. - 1988 Dec.

ELAINE S. ORAN and K. KAILASANATH Jun. 1989 111 p

(Contract NASA ORDER C-80001-G)

(NASA-CR-182298; NAS 1.26:182298) Avail: NTIS HC A06/MF A01 CSCL 22/1

The research performed at the Center for Reactive Flow and Dynamical Systems in the Laboratory for Computational Physics and Fluid Dynamics, at the Naval Research Laboratory, in support of the NASA Microgravity Science and Applications Program is described. The primary focus was on investigating fundamental questions concerning the propagation and extinction of premixed flames in Earth gravity and in microgravity environments. The approach was to use detailed time-dependent, multispecies, numerical models as tools to simulate flames in different gravity environments. The models include a detailed chemical kinetics mechanism consisting of elementary reactions among the eight reactive species involved in hydrogen combustion, coupled to algorithms for convection, thermal conduction, viscosity, molecular and thermal diffusion, and external forces. The external force, gravity, can be put in any direction relative to flame propagation and can have a range of values. A combination of one-dimensional and two-dimensional simulations was used to investigate the effects of curvature and dilution on ignition and propagation of flames, to help resolve fundamental questions on the existence of flammability limits when there are no external losses or buoyancy forces in the system, to understand the mechanism leading to cellular instability, and to study the effects of gravity on the transition to cellular structure. A flame in a microgravity environment can be extinguished without external losses, and the mechanism leading to cellular structure is not preferential diffusion but a thermo-diffusive instability. The simulations have also led to a better understanding of the interactions between buoyancy forces and the processes leading to thermo-diffusive instability. Author

**N89-26114\*** National Aeronautics and Space Administration. Lewis Research Center, Cleveland, OH.

### FEASIBILITY OF REDUCED GRAVITY EXPERIMENTS INVOLVING QUIESCENT, UNIFORM PARTICLE CLOUD COMBUSTION

HOWARD D. ROSS, LILY T. FACCA, ABRAHAM L. BERLAD, and

VENKAT TANGIRALA (California Univ., San Diego.) Mar. 1989 40 p  
(NASA-TM-101371; E-4417; NAS 1.15:101371) Avail: NTIS HC A03/MF A01 CSCL 22/1

The study of combustible particle clouds is of fundamental scientific interest as well as a practical concern. The principal scientific interests are the characteristic combustion properties, especially flame structure, propagation rates, stability limits, and the effects of stoichiometry, particle type, transport phenomena, and nonadiabatic processes on these properties. The feasibility tests for the particle cloud combustion experiment (PCCE) were performed in reduced gravity in the following stages: (1) fuel particles were mixed into cloud form inside a flammability tube; (2) when the concentration of particles in the cloud was sufficiently uniform, the particle motion was allowed to decay toward quiescence; (3) an igniter was energized which both opened one end of the tube and ignited the suspended particle cloud; and (4) the flame proceeded down the tube length, with its position and characteristic features being photographed by high-speed cameras. Gravitational settling and buoyancy effects were minimized because of the reduced gravity environment in the NASA Lewis drop towers and aircraft. Feasibility was shown as quasi-steady flame propagation which was observed for fuel-rich mixtures. Of greatest scientific interest is the finding that for near-stoichiometric mixtures, a new mode of flame propagation was observed, now called a chattering flame. These flames did not propagate steadily through the tube. Chattering modes of flame propagation are not expected to display extinction limits that are the same as those for acoustically undisturbed, uniform, quiescent clouds. A low concentration of fuel particles, uniformly distributed in a volume, may not be flammable but may be made flammable, as was observed, through induced segregation processes. A theory was developed which showed that chattering flame propagation was controlled by radiation from combustion products which heated the successive discrete laminae sufficiently to cause autoignition. Author

**N89-28665\*** National Aeronautics and Space Administration. Lewis Research Center, Cleveland, OH.

### MICROGRAVITY COMBUSTION SCIENCE: A PROGRAM OVERVIEW

Jan. 1989 20 p

(NASA-TM-101424; E-4524; NAS 1.15:101424) Avail: NTIS HC A03/MF A01 CSCL 12/1

The promise of microgravity combustion research is introduced by way of a brief survey of results, the available set of reduced gravity facilities, and plans for experimental capabilities in the Space Station era. The study of fundamental combustion processes in a microgravity environment is a relatively new scientific endeavor. A few simple, precursor experiments were conducted in the early 1970's. Today the advent of the U.S. space shuttle and the anticipation of the Space Station Freedom provide for scientists and engineers a special opportunity, in the form of long duration microgravity laboratories, and need, in the form of spacecraft fire safety and a variety of terrestrial applications, to pursue fresh insight into the basic physics of combustion. The microgravity environment enables a new range of experiments to be performed since buoyancy-induced flows are nearly eliminated, normally obscured forces and flows may be isolated, gravitational settling or sedimentation is nearly eliminated, and larger time or length scales in experiments become permissible. The range of experiments completed to date was not broad, but is growing. Unexpected phenomena have been observed often in microgravity combustion experiments, raising questions about the degree of accuracy and completion of our classical understanding and our ability to estimate spacecraft fire hazards. Because of the field's relative immaturity, instrumentation has been restricted primarily to high-speed photography. To better explain these findings, more sophisticated diagnostic instrumentation, similar to that evolving in terrestrial laboratories, is being developed for use on Space Station Freedom and, along the way, in existing microgravity facilities. Author

**N89-28666\*#** National Aeronautics and Space Administration. Lewis Research Center, Cleveland, OH.

**NUMERICAL STUDIES OF CONVECTIVE HEAT TRANSFER IN AN INCLINED SEMIANNULAR ENCLOSURE**

LIN-WEN WANG, CHAIN-NAN YUNG, AN-TI CHAI, and NASSER RASHIDNIA (Sverdrup Technology, Inc., Cleveland, OH.) Aug. 1989 9 p Presented at the National Heat Transfer Conference, Philadelphia, PA, 6-9 Aug. 1989; sponsored in part by ASME (NASA-TM-102011; E-4723; NAS 1.15:102011) Avail: NTIS HC A02/MF A01 CSCL 22/1

Natural convection heat transfer in a two-dimensional differentially heated semiannular enclosure is studied. The enclosure is isothermally heated and cooled at the inner and outer walls, respectively. A commercial software based on the SIMPLER algorithm was used to simulate the velocity and temperature profiles. Various parameters that affect the momentum and heat transfer processes were examined. These parameters include the Rayleigh number, Prandtl number, radius ratio, and the angle of inclination. A flow regime extending from conduction-dominated to convection-dominated flow was examined. The computed results of heat transfer are presented as a function of flow parameter and geometric factors. It is found that the heat transfer rate attains a minimum when the enclosure is tilted about +50 deg with respect to the gravitational direction. Author

## 31

## ENGINEERING (GENERAL)

Includes vacuum technology; control engineering; display engineering; cryogenics; and fire prevention.

**A89-15388\*** National Aeronautics and Space Administration. Lewis Research Center, Cleveland, OH.

**MULTI-HUNDRED KILOWATT ROLL RING ASSEMBLY EVALUATION RESULTS**

DAVID D. RENZ (NASA, Lewis Research Center, Cleveland, OH) IN: 1988 IECEC; Proceedings of the Twenty-third Intersociety Energy Conversion Engineering Conference, Denver, CO, July 31-Aug. 5, 1988. Volume 3. New York, American Society of Mechanical Engineers, 1988, p. 643-648. Previously announced in STAR as N88-21375. Copyright

NASA Lewis Research Center has been evaluating low loss multi-hundred-kilowatt Roll Ring assemblies (an 8 circuit and a 4 circuit) for use on Space Station as the rotating joint power transfer device. In this device ac or dc power is transferred across the rotating joint through compressed rotating flexures. Results and conclusions of the evaluation program are presented. Author

**N89-14348\*#** National Aeronautics and Space Administration. Lewis Research Center, Cleveland, OH.

**LIQUID SHEET RADIATOR APPARATUS Patent Application**

DONALD L. CHUBB, inventor (to NASA) 15 Sep. 1988 14 p (NASA-CASE-LEW-14295-1; NAS 1.71:LEW-14295-1; US-PATENT-APPL-SN-244377) Avail: NTIS HC A03/MF A01 CSCL 13/2

An external flow, liquid sheet radiator apparatus adapted for space applications has as its radiating surface a thin stable liquid sheet formed by fluid flow through a very narrow slit affixed to the sheet generator. NASA

**N89-19446\*#** National Aeronautics and Space Administration. Lewis Research Center, Cleveland, OH.

**THE SOLID SURFACE COMBUSTION SPACE SHUTTLE EXPERIMENT HARDWARE DESCRIPTION AND GROUND-BASED TEST RESULTS**

D. M. VENTO, R. J. ZAVESKY, K. R. SACKSTEDER, and R. A. ALTENKIRCH (Mississippi State Univ., Mississippi State.) Jan. 1989 9 p Presented at the 27th Aerospace Sciences Meeting,

Reno, NV, 8-12 Jan. 1989; sponsored by AIAA Previously announced in IAA as A89-28419

(NASA-TM-101963; E-4661; NAS 1.15:101963) Avail: NTIS HC A02/MF A01 CSCL 22/2

The Lewis Research Center is developing a series of microgravity combustion experiments for the Space Shuttle. The Solid Surface Combustion Experiment (SSCE) is the first to be completed. SSCE will study flame spreading over thermally thin fuels (ashless filter paper) under microgravity conditions. The flight hardware consists of a combustion chamber containing the sample and a computer which takes the data and controls the experiment. Experimental data will include gas-phase and solid-phase temperature measurements and motion pictures of the combustion process. Flame spread rates will be determined from the motion pictures. Author

**N89-20324\*#** National Aeronautics and Space Administration. Lewis Research Center, Cleveland, OH.

**LOW FREQUENCY VIBRATION ISOLATION TECHNOLOGY FOR MICROGRAVITY SPACE EXPERIMENTS**

CARLOS M. GRODSINSKY and GERALD V. BROWN 1989 10 p Proposed for presentation at the 12th Biennial Conference on Mechanical Vibration and Noise, Montreal, Quebec, 17-20 Sep. 1989; sponsored by ASME (NASA-TM-101448; E-4557; NAS 1.15:101448) Avail: NTIS HC A02/MF A01 CSCL 13/2

The dynamic acceleration environment observed on Space Shuttle flights to date and predicted for the Space Station has complicated the analysis of prior microgravity experiments and prompted concern for the viability of proposed space experiments requiring long-term, low-g environments. Isolation systems capable of providing significant improvements in this environment exist, but have not been demonstrated in flight configurations. This paper presents a summary of the theoretical evaluation for two one degree-of-freedom (DOF) active magnetic isolators and their predicted response to both direct and base excitations, that can be used to isolate acceleration sensitive microgravity space experiments. Author

**N89-27038\*#** National Aeronautics and Space Administration. Lewis Research Center, Cleveland, OH.

**MEASUREMENTS OF COMPLEX PERMITTIVITY OF MICROWAVE SUBSTRATES IN THE 20 TO 300 K TEMPERATURE RANGE FROM 26.5 TO 40.0 GHZ**

FELIX A. MIRANDA, WILLIAM L. GORDON (Case Western Reserve Univ., Cleveland, OH.), VERNON O. HEINEN, BEN T. EBIHARA, and KUL B. BHASIN Jul. 1989 10 p Presented at the Cryogenic Engineering Conference, Los Angeles, CA, 24-28 Jul. 1989; sponsored in part by California Univ., Los Angeles (NASA-TM-102123; E-4903; NAS 1.15:102123) Avail: NTIS HC A02/MF A01 CSCL 13/2

A knowledge of the dielectric properties of microwave substrates at low temperatures is useful in the design of superconducting microwave circuits. Results are reported for a study of the complex permittivity of sapphire (Al<sub>2</sub>O<sub>3</sub>), magnesium oxide (MgO), silicon oxide (SiO<sub>2</sub>), lanthanum aluminate (LaAlO<sub>3</sub>), and zirconium oxide (ZrO<sub>2</sub>), in the 20 to 300 Kelvin temperature range, at frequencies from 26.5 to 40.0 GHz. The values of the real and imaginary parts of the complex permittivity were obtained from the scattering parameters, which were measured using a HP-8510 automatic network analyzer. For these measurements, the samples were mounted on the cold head of a helium gas closed cycle refrigerator, in a specially designed vacuum chamber. An arrangement of wave guides, with mica windows, was used to connect the cooling system to the network analyzer. A decrease in the value of the real part of the complex permittivity of these substrates, with decreasing temperature, was observed. For MgO and Al<sub>2</sub>O<sub>3</sub>, the decrease from room temperature to 20 K was of 7 and 15 percent, respectively. For LaAlO<sub>3</sub>, it decreased by 14 percent, for ZrO<sub>2</sub> by 15 percent, and for SiO<sub>2</sub> by 2 percent, in the above mentioned temperature range. Author



## 31 ENGINEERING (GENERAL)

**N89-27868\*** National Aeronautics and Space Administration. Lewis Research Center, Cleveland, OH.

### **INDIUM PHOSPHIDE SOLAR CELL RESEARCH IN THE US: COMPARISON WITH NONPHOTOVOLTAIC SOURCES**

I. WEINBERG, C. K. SWARTZ, and R. E. HART, JR. 1989 13 p Prepared for presentation at the European Space Power Conference, Madrid, Spain, 2-6 Oct. 1989; sponsored in part by ESA

(NASA-TM-102103; E-4869; NAS 1.15:102103) Avail: NTIS HC A03/MF A01 CSCL 10/1

Highlights of the InP solar cell research program are presented. Homojunction cells with AMO efficiencies approaching 19 percent were demonstrated while 17 percent was achieved for indium tin oxide (ITO)/InP cells. The superior radiation resistance of these latter two cell configurations over both Si and GaAs were demonstrated. InP cells on board the LIPS III satellite show no degradation after more than a year in orbit. Computer modeling calculations were directed toward radiation damage predictions and the specification of concentrator cell parameters. Computed array specific powers, for a specific orbit, are used to compare the performance of an InP solar cell array to solar dynamic and nuclear systems. Author

## 32

### **COMMUNICATIONS AND RADAR**

Includes radar; land and global communications; communications theory; and optical communications.

**A89-15152\*** Illinois Univ., Urbana.

### **RAY-TUBE INTEGRATION IN SHOOTING AND BOUNCING RAY METHOD**

S. W. LEE (Illinois, University, Urbana), H. LING (Texas, University, Austin), and R. CHOU (Ohio State University, Columbus) Microwave and Optical Technology Letters (ISSN 0895-2477), vol. 1, Oct. 1988, p. 286-289. Research supported by the University of Illinois. refs

(Contract NAG3-745; NCA2-322; NSF ECS-86-57524)

Copyright

Based on three formulations of the Huygen's principle, explicit expressions is given for the far field contribution from a small ray tube. This expression is useful in shooting and bouncing rays for solving complex scattering problems. Author

**A89-15819\*** National Aeronautics and Space Administration. Lewis Research Center, Cleveland, OH.

### **OPTOELECTRONIC SIGNAL PROCESSING FOR PHASED-ARRAY ANTENNAS; PROCEEDINGS OF THE MEETING, LOS ANGELES, CA, JAN. 12, 13, 1988**

KUL B. BHASIN, ED. (NASA, Lewis Research Center, Cleveland, OH) and BRIAN M. HENDRICKSON, ED. (USAF, Rome Air Development Center, Griffiss AFB, NY) Meeting sponsored by SPIE, Bellingham, WA, Society of Photo-Optical Instrumentation Engineers (SPIE Proceedings. Volume 886), 1988, 265 p. For individual items see A89-15820 to A89-15846. (SPIE-886) Copyright

Papers are presented on fiber optic links for airborne satellite applications, optoelectronic techniques for broadband switching, and GaAs circuits for a monolithic optical controller. Other topics include the optical processing of covariance matrices for adaptive processors, an optical linear heterodyne matrix-vector processor, and an EHF fiber optic-based array. An adaptive optical signal processing architecture using a signed-digit number system is considered along with microwave fiber optic links for phased arrays. R.R.

**A89-21222\*** Northwestern Univ., Evanston, IL.  
**AN APPLICATION OF THE WKBJ TECHNIQUE TO THE ON-SURFACE RADIATION CONDITION**

THOMAS G. MOORE, GREGORY A. KRIEGSMANN, and ALLEN TAFLOVE (Northwestern University, Evanston, IL) IEEE Transactions on Antennas and Propagation (ISSN 0018-926X), vol. 36, Sept. 1988, p. 1329-1331.

(Contract NAG3-635; NSF MCS-83-00578; NSF DMS-87-00794)

Copyright

The on-surface radiation-condition method and the WKBJ method for approximating solutions to differential equations are used to derive an analytic formula for the surface currents on a two-dimensional perfectly conducting convex target. The currents are induced by an incident TE-polarized plane wave. The case of a circular cylinder is used to demonstrate the usefulness of the combined methods. It is shown that a two-term expansion yields good results for the surface currents and excellent results for the ensuing bistatic radar cross section. I.E.

**A89-22455\*** Ohio State Univ., Columbus.

### **AN EXPERIMENTAL ADAPTIVE ARRAY TO SUPPRESS WEAK INTERFERING SIGNALS**

ERIC K. WALTON, INDER J. GUPTA, AHARON A. KSIENSKI (Ohio State University, Columbus), and JAMES WARD IEEE Transactions on Antennas and Propagation (ISSN 0018-926X), vol. 36, Nov. 1988, p. 1551-1559. Research supported by the Ohio State University Research Foundation. refs

(Contract NAG3-536)

Copyright

An experimental adaptive antenna system to suppress weak interfering signals is described. It is a sidelobe canceller with two auxiliary elements. Modified feedback loops are used to control the array weights. The received signals are simulated in hardware for parameter control. Digital processing is used for algorithm implementation and performance evaluation. The experimental results are presented. They show that interfering signals as much as 10 dB below the thermal noise level in the main channel are suppressed by 20-30 dB. Such a system has potential application in suppressing the interference encountered in direct broadcast satellite communication systems. I.E.

**A89-26769\*** Toledo Univ., OH.

### **CODED MULTIPLE CHIRP SPREAD SPECTRUM SYSTEM AND OVERLAY SERVICE**

JUNGHWAN KIM (Toledo, University, OH), TIMOTHY PRATT (Virginia Polytechnic Institute and State University, Blacksburg), and TRI T. HA (U.S. Naval Postgraduate School, Monterey, CA) IN: GLOBECOM '88 - IEEE Global Telecommunications Conference and Exhibition, Hollywood, FL, Nov. 28-Dec. 1, 1988, Conference Record. Volume 1. New York, Institute of Electrical and Electronics Engineers, Inc., 1988, p. 561-565. refs

(Contract NAS3-24887)

Copyright

An asynchronous spread-spectrum system called coded multiple chirp is proposed, and the possible spread-spectrum overlay over an analog FM-TV signal is investigated by computer simulation. Multiple single-sloped up and down chirps are encoded by a pseudonoise code and decoded by dechirpers (pulse-compression filters) followed by a digital code correlator. The performance of the proposed system, expressed in terms of in probability of bit error and code miss probability, is similar to that of FSK (frequency shift keying) using codewords if sufficient compression gain is used. When chirp is used to overlay an FM-TV channel, two chirp signals with data rate up to 25 kb/s could be overlaid in a 36-MHz satellite transponder without significant mutual interference. Performance estimates for a VSAT (very small aperture terminal) earth station operating at C-band show that a 2.4-m antenna and 300-mW transmitter could send a 2.4-kb/s signal to a large central earth station over an occupied channel. I.E.

**A89-34242\*** Texas Univ., Austin.

### **SHOOTING AND BOUNCING RAYS - CALCULATING THE RCS OF AN ARBITRARILY SHAPED CAVITY**

HAO LING (Texas, University, Austin), RI-CHEE CHOU (Ohio State University, Columbus), and SHUNG-WU LEE (Illinois, University, Urbana) IEEE Transactions on Antennas and Propagation (ISSN



0018-926X), vol. 37, Feb. 1989, p. 194-205. Research supported by the University of Texas and Cray Research, Inc. refs (Contract NAG3-475)

Copyright

A ray-shooting approach is presented for calculating the interior radar cross section (RCS) from a partially open cavity. In the problem considered, a dense grid of rays is launched into the cavity through the opening. The rays bounce from the cavity walls based on the laws of geometrical optics and eventually exit the cavity via the aperture. The ray-bouncing method is based on tracking a large number of rays launched into the cavity through the opening and determining the geometrical optics field associated with each ray by taking into consideration (1) the geometrical divergence factor, (2) polarization, and (3) material loading of the cavity walls. A physical optics scheme is then applied to compute the backscattered field from the exit rays. This method is so simple in concept that there is virtually no restriction on the shape or material loading of the cavity. Numerical results obtained by this method are compared with those for the modal analysis for a circular cylinder terminated by a PEC plate. RCS results for an S-bend circular cylinder generated on the Cray X-MP supercomputer show significant RCS reduction. Some of the limitations and possible extensions of this technique are discussed.

I.E.

**A89-39594\*** Ohio State Univ., Columbus.

**MODAL, RAY, AND BEAM TECHNIQUES FOR ANALYZING THE EM SCATTERING BY OPEN-ENDED WAVEGUIDE CAVITIES**

PRABHAKAR H. PATHAK and ROBERT J. BURKHOLDER (Ohio State University, Columbus) IEEE Transactions on Antennas and Propagation (ISSN 0018-926X), vol. 37, May 1989, p. 635-647. refs

(Contract NAG3-476; N00014-88-K-0004; N60530-85-C-0249; F33615-84-K-1550)

Copyright

The problem of high-frequency electromagnetic (EM) scattering by open-ended waveguide cavities with an interior termination is analyzed via three different approaches. When cavities can be adequately modeled by joining together piecewise separable waveguide sections, a hybrid combination of asymptotic high-frequency and modal techniques is employed. In the case of more arbitrarily shaped waveguide cavities for which modes cannot even be defined in the conventional sense, the geometrical optics ray approach proves to be highly useful. However, at sufficiently high frequencies, both of these approaches tend to become inefficient. Hence, a paraxial Gaussian beam technique, which retains much of the simplicity of the ray approximation but is potentially more efficient, is investigated. Typical numerical results based on the different approaches are discussed.

I.E.

**A89-39595\*** Texas Univ., Austin.

**HIGH-FREQUENCY RCS OF OPEN CAVITIES WITH RECTANGULAR AND CIRCULAR CROSS SECTIONS**

HAO LING (Texas, University, Austin), SHUNG-WU LEE (Illinois, University, Urbana), and RI-CHEE CHOU (Ohio State University, Columbus) IEEE Transactions on Antennas and Propagation (ISSN 0018-926X), vol. 37, May 1989, p. 648-654. refs

(Contract NSF ECS-86-57524; NAG3-475)

Copyright

The radar cross-section (RCS) analysis of open-ended cavities with rectangular and circular cross sections is carried out using the waveguide modal approach and the shooting-and-bouncing ray (SBR) approach. For a cavity opening on the order of ten wavelengths or larger, the comparison between the two approaches is excellent. It is also observed that at lower frequencies the SBR results deviate from the more accurate modal results. On the other hand, the SBR approach allows for greater flexibility in geometrical modeling, and can be applied to problems where waveguide modes cannot be easily found. SBR results for an offset rectangular cavity and a circular cavity with rounded endplate are presented.

I.E.

**A89-42758\*** Hughes Aircraft Co., El Segundo, CA.

**A METHOD FOR PRODUCING A SHAPED CONTOUR RADIATION PATTERN USING A SINGLE SHAPED REFLECTOR AND A SINGLE FEED**

ALAN R. CHERRETTE (Hughes Aircraft Co., Space and Communication Group, El Segundo, CA), SHUNG-WU LEE (Illinois, University, Urbana), and ROBERTO J. ACOSTA (NASA, Lewis Research Center, Cleveland, OH) IEEE Transactions on Antennas and Propagation (ISSN 0018-926X), vol. 37, June 1989, p. 698-706. Previously announced in STAR as N89-10275. refs

(Contract NAG3-419)

Copyright

Eliminating the corporate feed network in shaped contour beam antennas will reduce the expense, weight, and RF loss of the antenna system. One way of producing a shaped contour beam without using a feed network is to use a single shaped reflector with a single feed element. For a prescribed contour beam and feed, an optimization method for designing the reflector shape is given. As a design example, a shaped reflector is designed to produce a continental U.S. coverage (CONUS) beam. The RF performance of the shaped reflector is then verified by physical optics.

Author

**A89-42768\*** Clemson Univ., SC.

**MUTUAL COUPLING IN A FINITE PLANAR ARRAY WITH INTERELEMENT HOLES PRESENT**

JOHN W. SILVESTRO (Clemson University, SC) IEEE Transactions on Antennas and Propagation (ISSN 0018-926X), vol. 37, June 1989, p. 791-794. refs

(Contract NAG3-291)

Copyright

The mutual coupling in a finite planar array with interelement holes present was considered. A computer program designed to study mutual coupling between rectangular waveguides was modified to include coupling between elements of different sizes. This modified program was used to study the problem of widely spaced rectangular waveguides that form smaller rectangular holes in the ground plane. Comparisons with experimental data confirmed the validity of the model. Tests run at various hole sizes showed that holes that are much smaller than their cutoff size have little effect on the coupling. For the rectangular-hole case, hole widths of less than half the cutoff width of the dominant mode had little effect.

I.E.

**A89-43543\*** Clemson Univ., SC.

**APERTURE IMPEDANCE OF FLARED HORNS**

J. W. SILVESTRO (Clemson University, SC) and R. E. COLLIN (Case Western Reserve University, Cleveland, OH) IEEE Proceedings, Part H - Microwaves, Antennas and Propagation (ISSN 0950-107X), vol. 136, pt. H, no. 3, June 1989, p. 235-240. refs

(Contract NAG3-291)

Copyright

The method of moments is often used when solving for the mutual coupling in arrays of aperture antennas. For elements that are waveguides or gradually flared horns the aperture fields can be approximated by a finite sum of waveguide modal functions. To solve for the flared horn case an approximation for the aperture impedances of the modes in the horn is needed. The WKB approach can be used to find these impedances, but this technique has an important limitation. It is known to fail in the vicinity of its turning points. The turning point is the cutoff point of the mode being considered. To overcome this limitation a different technique, the spherical mode approach, is discussed. This approach has no cutoff problems and works well for conical and pyramidal horns. Comparisons between the impedances and the resulting dominant mode reflection coefficient found using the two techniques are presented to illustrate this point.

Author

**A89-53134\*** Minnesota Univ., Minneapolis.

**RIGOROUS ANALYSIS OF A CIRCULAR PATCH ANTENNA EXCITED BY A MICROSTRIP TRANSMISSION LINE**

MARAT DAVIDOVITZ (Minnesota, University, Minneapolis) and

YUEN TZE LO (Illinois, University, Urbana) IEEE Transactions on Antennas and Propagation (ISSN 0018-926X), vol. 37, Aug. 1989, p. 949-958. refs  
(Contract NAG3-418; F19628-85-C-0052)  
Copyright

Boundary conditions are enforced on a portion of the microstrip feed line as well as the patch antenna. The integral equation for the unknown currents on the antenna and feed is solved by applying the Galerkin method of moments in the Fourier transform domain. The validity of the solution is tested by comparison of computed results with experimental data. The theoretical treatment proves to be applicable to the most common feeding arrangements, namely, the direct edge-feed and proximity coupling excitation. In the latter case, two-layer substrates having distinct dielectric constants are studied. The purpose of the study is to deduce, for a given overall substrate thickness, the smallest line-ground plane separation for which a match of the radiator to the feed line is still possible. The advantages of such a configuration are discussed. I.E.

**A89-53136\*** Hughes Aircraft Co., El Segundo, CA.  
**COMPENSATION OF REFLECTOR ANTENNA SURFACE DISTORTION USING AN ARRAY FEED**

ALAN R. CHERRETTE (Hughes Aircraft Co., Space and Communication Div., El Segundo, CA), ROBERTO J. ACOSTA (NASA, Lewis Research Center, Cleveland, OH), PETER T. LAM (Deskin Research Group, Santa Clara, CA), and SHUNG-WU LEE (Illinois, University, Urbana) IEEE Transactions on Antennas and Propagation (ISSN 0018-926X), vol. 37, Aug. 1989, p. 966-978. Previously announced in STAR as N88-18805. refs  
(Contract NAG3-419)  
Copyright

The dimensional stability of the surface of a large reflector antenna is important when high gain or low sidelobe performance is desired. If the surface is distorted due to thermal or structural reasons, antenna performance can be improved through the use of an array feed. The design of the array feed and its relation to the surface distortion are examined. The sensitivity of antenna performance to changing surface parameters for fixed feed array geometries is also studied. This allows determination of the limits of usefulness for feed array compensation. Author

**N89-10213\*#** Ohio State Univ., Columbus. ElectroScience Lab.  
**CALCULATION OF THE EFFECTS OF ICE ON THE BACKSCATTER OF A GROUND PLANE**

K. M. LAMBERT and L. PETERS, JR. Sep. 1988 55 p  
(Contract NAG3-913)  
(NASA-CR-183303; NAS 1.26:183303; ESL-TR-720964-1) Avail: NTIS HC A04/MF A01 CSCL 20/14

Described is a technique for examining the effect of a rough ice layer on the backscatter of a ground plane. The technique is applied to the special case of a rough ice layer that is periodic in space. By assuming that the roughness is periodic, the backscatter of the ground plane can be found from the backscatter of a single period. Backscatter calculations are presented for a single period in which the thickness of the ice layer has a Gaussian shape. Author

**N89-10215\*#** National Aeronautics and Space Administration. Lewis Research Center, Cleveland, OH.

**A METHOD FOR PRODUCING A SHAPED CONTOUR RADIATION PATTERN USING A SINGLE SHAPED REFLECTOR AND A SINGLE FEED**

A. R. CHERRETTE, S. W. LEE (Illinois Univ., Urbana.), and R. J. ACOSTA Oct. 1988 45 p  
(Contract NAG3-419)  
(NASA-TM-101369; E-4408; NAS 1.15:101369) Avail: NTIS HC A03/MF A01 CSCL 20/14

Eliminating the corporate feed network in shaped contour beam antennas will reduce the expense, weight, and RF loss of the antenna system. One way of producing a shaped contour beam without using a feed network is to use a single shaped reflector with a single feed element. For a prescribed contour beam and

feed, an optimization method for designing the reflector shape is given. As a design example, a shaped reflector is designed to produce a continental U.S. coverage (CONUS) beam. The RF performance of the shaped reflector is then verified by physical optics. Author

**N89-10223\*#** Ohio State Univ., Columbus. ElectroScience Lab.  
**MEASUREMENT OF THE PROPERTIES OF LOSSY MATERIALS INSIDE A FINITE CONDUCTING CYLINDER Final Report**

R. CALDECOTT, A. DOMINEK, and A. PARK Oct. 1988 30 p  
(Contract NAG3-784)  
(NASA-CR-182500; NAS 1.26:182500; FR-719300-4) Avail: NTIS HC A03/MF A01 CSCL 20/14

A computer code was developed to automatically perform swept frequency reflection and transmission measurements using a HP5510B Network Analyzer and computer. This software is used in conjunction with a modified high temperature test rig to obtain reflection measurements from a flat material sample. The software allows data processing to eliminate measurement errors and to obtain a reflection coefficient in the frequency or time domain. A description of the program is presented. Author

**N89-10225\*#** Ohio State Univ., Columbus. ElectroScience Lab.  
**MATERIAL PARAMETER DETERMINATION FROM SCATTERING MEASUREMENTS**

A. DOMINEK, A. PARK, and L. PETERS, JR. Sep. 1988 43 p  
(Contract NAG3-784)  
(NASA-CR-183312; NAS 1.26:183312; ESL-TR-719300-3) Avail: NTIS HC A03/MF A01 CSCL 20/14

The electrical, macroscopic performance of isotropic material can generally be described through their constitutive scalar parameters, permittivity and permeability which are symbolically represented by epsilon and mu, respectively. These parameters relate the electric and magnetic flux densities to the electric and magnetic fields through the following relationships: (1)  $D = \epsilon E$ ; and (2)  $B = \mu H$ . It is through these parameters that the interaction of electromagnetic waves with material can be quantized in terms of reflection and transmission coefficients, and propagation and attenuation factors. Author

**N89-14369\*#** Communications Satellite Corp., Clarksburg, MD.  
**ASSESSMENT OF SATELLITE COMMUNICATIONS QUALITY STUDY. ADDENDUM 1: IMPACT OF PROPAGATION DELAY ON DATA TRANSMISSION Final Report**

S. J. CAMPANELLA and D. M. CHITRE Nov. 1988 100 p  
(Contract NAS3-23790)  
(NASA-CR-182229; NAS 1.26:182229) Avail: NTIS HC A05/MF A01 CSCL 17/2

The single factor that irrevocably distinguishes geostationary satellite telephony transmission from terrestrial transmission is the greater propagation delay over satellite links. This difference has always provoked vigorous debate over the impact of delay on the subscribers using services incorporating satellite links. The issue is addressed from a variety of directions including human factors studies, laboratory subjective tests that evaluate delay with and without echo, and field tests that obtain data on the opinion of subscribers regarding the quality of service of operational circuits in both national U.S. domestic and international trans-Atlantic network. The tests involved the use of both echo suppressors and echo cancellers. Author

**N89-17078\*#** Ford Aerospace and Communications Corp., Palo Alto, CA.

**THE POTENTIAL IMPACT OF MMICS ON FUTURE SATELLITE COMMUNICATIONS Final Report, 1 Apr. 1987 - 31 Aug. 1988**

VERNON E. DUNN Sep. 1988 133 p  
(Contract NAS3-25077)  
(NASA-CR-182227; NAS 1.26:182227) Avail: NTIS HC A07/MF A01 CSCL 17/2

This is the Final Report representing the results of a 17-month study on the future trends and requirements of Monolithic Microwave Integrated Circuits (MMIC) for space communication

applications. Specifically this report identifies potential space communication applications of MMICs, assesses the impact of MMIC on the classes of systems that were identified, determines the present status and probable 10-year growth in capability of required MMIC and competing technologies, identifies the applications most likely to benefit from further MMIC development and presents recommendations for NASA development activities to address the needs of these applications. Author

**N89-17079\*#** Ford Aerospace and Communications Corp., Palo Alto, CA. Space Systems Div.

**THE POTENTIAL IMPACT OF MMICS ON FUTURE SATELLITE COMMUNICATIONS: EXECUTIVE SUMMARY Final Report, 1 Apr. 1987 - 31 Aug. 1988**

VERNON E. DUNN Sep. 1988 38 p

(Contract NAS3-25077)

(NASA-CR-182227-EXEC-SUMM; NAS 1.26:182227-EXEC-SUMM) Avail: NTIS HC A03/MF A01 CSCL 17/2

This Executive Summary presents the results of a 17-month study on the future trends and requirements for Monolithic Microwave Integrated circuits (MMIC) for space communication application. Specifically this report identifies potential space communication applications of MMICs, assesses the impact of MMIC on the classes of systems that were identified, determines the present status and probable 10-year growth in capability of required MMIC and competing technologies, identifies the applications most likely to benefit from further MMIC development, and presents recommendations for NASA development activities to address the needs of these applications. Author

**N89-17756\*#** National Aeronautics and Space Administration. Lewis Research Center, Cleveland, OH.

**ADAPTIVE FEED ARRAY COMPENSATION SYSTEM FOR REFLECTOR ANTENNA SURFACE DISTORTION**

ROBERTO J. ACOSTA and A. ZAMAN 1989 7 p Proposed for presentation at the 1989 IEEE AP-S International Symposium and URSI Radio Science Meeting, San Jose, CA, 26-30 Jun. 1989

(NASA-TM-101458; E-4568; NAS 1.15:101458) Avail: NTIS HC A02/MF A01 CSCL 20/14

The feasibility of a closed loop adaptive feed array system for compensating reflector surface deformations has been investigated. The performance characteristics (gain, sidelobe level, pointing, etc.) of large communication antenna systems degrade as the reflector surface distorts mainly due to thermal effects from a varying solar flux. The compensating systems described in this report can be used to maintain the design performance characteristics independent of thermal effects on the reflector surface. The proposed compensating system employs the concept of conjugate field matching to adjust the feed array complex excitation coefficients. Author

**N89-17767\*#** National Aeronautics and Space Administration. Lewis Research Center, Cleveland, OH.

**UNIVERSAL TEST FIXTURE FOR MONOLITHIC MM-WAVE INTEGRATED CIRCUITS CALIBRATED WITH AN AUGMENTED TRD ALGORITHM**

ROBERT R. ROMANOFISKY and KURT A. SHALKHAUSER Mar. 1989 42 p Presented at the 13th International Conference on Infrared and mm-Waves, Honolulu, Hawaii, 5-9 Dec. 1988 (NASA-TP-2875; E-3983; NAS 1.60:2875) Avail: NTIS HC A03/MF A01 CSCL 09/3

The design and evaluation of a novel fixturing technique for characterizing millimeter wave solid state devices is presented. The technique utilizes a cosine-tapered ridge guide fixture and a one-tier de-embedding procedure to produce accurate and repeatable device level data. Advanced features of this technique include nondestructive testing, full waveguide bandwidth operation, universality of application, and rapid, yet repeatable, chip-level characterization. In addition, only one set of calibration standards is required regardless of the device geometry. Author

**N89-19449\*#** Harris Corp., Melbourne, FL. Government Communication Systems Div.

**A 20 GHZ LOW NOISE, LOW COST RECEIVER FOR DIGITAL SATELLITE COMMUNICATION SYSTEM, GROUND TERMINAL APPLICATIONS Final Report**

GLEN ALLEN 15 Dec. 1988 244 p

(Contract NAS3-24244)

(NASA-CR-182243; NAS 1.26:182243) Avail: NTIS HC A11/MF A01 CSCL 17/2

A 45 month effort for the development of a 20 GHz, low-noise, low-cost receiver for digital, satellite communication system, ground terminal applications is discussed. Six proof-of-concept receivers were built in two lots of three each. Performance was generally consistent between the two lots. Except for overall noise figure, parameters were within or very close to specification. While noise figure was specified as 3.5 dB, typical performance was measured at 3.0 to 5.5 dB, over the full temperature range of minus 30 C to plus 75 C. NASA

**N89-20355\*#** Ohio State Univ., Columbus. ElectroScience Lab. **ELECTROMAGNETIC PROPERTIES OF ICE COATED SURFACES Semiannual Report**

A. DOMINEK, E. WALTON, N. WANG, and L. BEARD Feb. 1989 19 p

(Contract NAG3-913)

(NASA-CR-184780; NAS 1.26:184780; ESL-720964-2) Avail: NTIS HC A03/MF A01 CSCL 20/14

The electromagnetic scattering from ice coated structures is examined. The influence of ice is shown from a measurement standpoint and related to a simple analytical model. A hardware system for the realistic measurement of ice coated structures is also being developed to use in an existing NASA Lewis icing tunnel. Presently, initial measurements have been performed with a simulated tunnel to aid in the development. Author

**N89-20364\*#** Ohio State Univ., Columbus. ElectroScience Lab. **ANALYSIS OF MODIFIED SMI METHOD FOR ADAPTIVE ARRAY WEIGHT CONTROL**

R. L. DILSAVOR and R. L. MOSES Feb. 1989 88 p

(Contract NAG3-536)

(NASA-CR-184904; NAS 1.26:184904; ELS-TR-716111-6) Avail: NTIS HC A05/MF A01 CSCL 09/3

An adaptive array is applied to the problem of receiving a desired signal in the presence of weak interference signals which need to be suppressed. A modification, suggested by Gupta, of the sample matrix inversion (SMI) algorithm controls the array weights. In the modified SMI algorithm, interference suppression is increased by subtracting a fraction F of the noise power from the diagonal elements of the estimated covariance matrix. Given the true covariance matrix and the desired signal direction, the modified algorithm is shown to maximize a well-defined, intuitive output power ratio criterion. Expressions are derived for the expected value and variance of the array weights and output powers as a function of the fraction F and the number of snapshots used in the covariance matrix estimate. These expressions are compared with computer simulation and good agreement is found. A trade-off is found to exist between the desired level of interference suppression and the number of snapshots required in order to achieve that level with some certainty. The removal of noise eigenvectors from the covariance matrix inverse is also discussed with respect to this application. Finally, the type and severity of errors which occur in the covariance matrix estimate are characterized through simulation. Author

**N89-21138\*#** Illinois Univ., Urbana-Champaign.

**A COMPARISON OF REFLECTOR ANTENNA DESIGNS FOR WIDE-ANGLE SCANNING**

M. ZIMMERMAN, S. W. LEE, B. HOUSHMAND, Y. RAHMAT-SAMII, and R. ACOSTA Feb. 1989 30 p Presented at the NASA Technology Workshop for Earth Science Geostationary Platforms, 21-22 Sep. 1988, Hampton, VA Prepared in cooperation with Jet Propulsion Lab., California Inst. of Tech., Pasadena, and NASA,

Lewis Research Center, Cleveland, OH  
(NASA-TM-101459; E-4569; NAS 1.15:101459) Avail: NTIS HC A03/MF A01 CSCL 20/14

Conventional reflector antennas are typically designed for up to + or - 20 beamwidths scan. An attempt was made to stretch this scan range to some + or - 300 beamwidths. Six single and dual reflector antennas were compared. It is found that a symmetrical parabolic reflector with  $f/D = 2$  and a single circular waveguide feed has the minimum scan loss (only 0.6 dB at Theta sub 0 = 8 deg, or a 114 beamwidths scan). The scan is achieved by tilting the parabolic reflector by an angle equal to the half-scan angle. The  $f/D$  may be shortened if a cluster 7 to 19 elements instead of one element is used for the feed. The cluster excitation is adjusted for each new beam scan direction to compensate for the imperfect field distribution over the reflector aperture. The antenna can be folded into a Cassegrain configuration except that, due to spillover and blockage considerations, the amount of folding achievable is small. Author

**N89-21142\*#** National Aeronautics and Space Administration. Lewis Research Center, Cleveland, OH.  
**EXTERNAL ELECTRO-OPTIC PROBING OF MILLIMETER-WAVE INTEGRATED CIRCUITS**  
J. F. WHITAKER, J. A. VALDMANIS, T. A. JACKSON, K. B. BHASIN, ROBERT R. ROMANOFSKY, and G. A. MOUROU (Michigan Univ., Ann Arbor.) 1989 6 p Prepared for presentation at the IEEE MTT-S International Microwave Symposium, Long Beach, CA, 13-15 Jun. 1989  
(NASA-TM-101990; E-4693; NAS 1.15:101990) Avail: NTIS HC A02/MF A01 CSCL 20/14

An external, noncontact electro-optic measurement system, designed to operate at the wafer level with conventional wafer probing equipment and without any special circuit preparation, has been developed. Measurements have demonstrated the system's ability to probe continuous and pulsed signals on microwave integrated circuits on arbitrary substrates with excellent spatial resolution. Experimental measurements on a variety of digital and analog circuits, including a GaAs selectively-doped heterostructure transistor prescaler, an NMOS silicon multiplexer, and a GaAs power amplifier MMIC are reported. Author

**N89-23753\*#** National Aeronautics and Space Administration. Lewis Research Center, Cleveland, OH.  
**A SEGMENTED MIRROR ANTENNA FOR RADIOMETERS**  
S. W. LEE, B. HOUSHMAND, M. ZIMMERMAN (Illinois Univ., Urbana.), and R. ACOSTA May 1989 40 p  
(Contract NAG3-419)  
(NASA-TM-102045; E-4793; NAS 1.15:102045) Avail: NTIS HC A03/MF A01 CSCL 20/14

An antenna is designed for the radiometer application of the planned NASA Earth Science Geostationary Platforms in the 1990's. The antenna consists of two parts: a regular parabolic dish of 5 meters in diameter which converts the radiation from feeds into a collimated beam, and a movable mirror that redirects the beam to a prescribed scan direction. The mirror is composed of 28 segmented planar conducting plates, mostly one square meter in size. The secondary pattern of the antenna was analyzed based on a physical optics analysis. For frequencies between 50 and 230 GHz, and for a scan range of + or - 8 deg (270 beamwidths scan at 230 GHz), the worst calculated beam efficiency is 95 percent. To cover such a wide frequency and scan range, each of the 28 plates is individually controlled for a tilting less than 4 deg, and for a sliding less than 0.5 cm. The sliding is done at discrete steps. At 230 GHz, a step size of 2 mil is sufficient. The plate positions must be reset for each frequency and for each scan direction. Once the position is set, the frequency bandwidth of the antenna is very narrow. Author

**N89-23756\*#** Virginia Polytechnic Inst. and State Univ., Blacksburg. Dept. of Electrical Engineering.  
**STUDY OF SPREAD SPECTRUM MULTIPLE ACCESS SYSTEMS FOR SATELLITE COMMUNICATIONS WITH OVERLAY ON CURRENT SERVICES: EXECUTIVE SUMMARY**

TRI T. HA and TIMOTHY PRATT Dec. 1987 21 p  
(Contract NAS3-24887)  
(NASA-CR-180827-EXEC-SUMM; NAS 1.26:180827-EXEC-SUMM)  
Avail: NTIS HC A03/MF A01 CSCL 17/2

Two different methods of generating spread spectrum signals for an overlay service are discussed, and the data rate and efficiency which can be achieved while maintaining low interference with existing traffic are examined. B.G.

**N89-23757\*#** Virginia Polytechnic Inst. and State Univ., Blacksburg. Dept. of Electrical Engineering.  
**STUDY OF SPREAD SPECTRUM MULTIPLE ACCESS SYSTEMS FOR SATELLITE COMMUNICATIONS WITH OVERLAY ON CURRENT SERVICES**  
TRI T. HA and TIMOTHY PRATT 1989 255 p  
(Contract NAS3-24887)  
(NASA-CR-180827; NAS 1.26:180827) Avail: NTIS HC A12/MF A01 CSCL 17/2

The feasibility of using spread spectrum techniques to provide a low-cost multiple access system for a very large number of low data terminals was investigated. Two applications of spread spectrum technology to very small aperture terminal (VSAT) satellite communication networks are presented. Two spread spectrum multiple access systems which use a form of noncoherent M-ary FSK (MFSK) as the primary modulation are described and the throughput analyzed. The analysis considers such factors as satellite power constraints and adjacent satellite interference. Also considered is the effect of on-board processing on the multiple access efficiency and the feasibility of overlaying low data rate spread spectrum signals on existing satellite traffic as a form of frequency reuse is investigated. The use of chirp is examined for spread spectrum communications. In a chirp communication system, each data bit is converted into one or more up or down sweeps of frequency, which spread the RF energy across a broad range of frequencies. Several different forms of chirp communication systems are considered, and a multiple-chirp coded system is proposed for overlay service. The mutual interference problem is examined in detail and a performance analysis undertaken for the case of a chirp data channel overlaid on a video channel. Author

**N89-24518\*#** Ohio State Univ., Columbus. ElectroScience Lab.  
**ANALYSIS OF THE EM SCATTERING FROM ARBITRARY OPEN-ENDED WAVEGUIDE CAVITIES USING AXIAL GAUSSIAN BEAM TRACKING Final Report**  
R. J. BURKHOLDER and P. H. PATHAK Dec. 1988 80 p  
(Contract NAG3-476)  
(NASA-CR-185054; NAS 1.26:185054; REPT-719630-1) Avail: NTIS HC A05/MF A01 CSCL 20/14

The electromagnetic (EM) scattering from a planar termination located inside relatively arbitrarily shaped open-ended waveguide cavities with smoothly curved interior walls is analyzed using a Gaussian Beam (GB) expansion of the incident plane wave fields in the open end. The cavities under consideration may contain perfectly-conducting interior walls with or without a thin layer of material coating, or the walls may be characterized by an impedance boundary condition. In the present approach, the GB's are tracked only to the termination of the waveguide cavity via beam reflections from interior waveguide cavity walls. The Gaussian beams are tracked approximately only along their beam axes; this approximation which remains valid for relatively well focussed beams assumes that an incident GB gives rise to a reflected GB with parameters related to the incident beam and the radius of curvature of the wall. It is found that this approximation breaks down for GB's which come close to grazing a convex surface and when the width of the incident beam is comparable to the radius of curvature of the surface. The expansion of the fields at the open end depend on the incidence angle only through the expansion coefficients, so the GB's need to be tracked through the waveguide cavity only once for a wide range of incidence angles. At the termination, the sum of all the GB's are integrated using a result developed from a generalized reciprocity principle, to give the fields scattered from the interior of the cavity. The rim

edge at the open end of the cavity is assumed to be sharp and the external scattering from the rim is added separately using Geometrical Theory of Diffraction. The results based on the present approach are compared with solutions based on the hybrid asymptotic modal method. The agreement is found to be very good for cavities made up of planar surfaces, and also for cavities with curved surfaces which are not too long with respect to their width. Author

**N89-24519\*#** Ohio State Univ., Columbus. ElectroScience Lab.  
**A HYBRID ASYMPTOTIC-MODAL ANALYSIS OF THE EM SCATTERING BY AN OPEN-ENDED S-SHAPED RECTANGULAR WAVEGUIDE CAVITY**

P. H. LAW, R. J. BURKHOLDER, and P. H. PATHAK Dec. 1988 53 p  
 (Contract NAG3-476)  
 (NASA-CR-185053; NAS 1.26:185053; REPT-719630-2) Avail: NTIS HC A04/MF A01 CSCL 20/14

The electromagnetic fields (EM) backscatter from a 3-dimensional perfectly conducting S-shaped open-ended cavity with a planar interior termination is analyzed when it is illuminated by an external plane wave. The analysis is based on a self-consistent multiple scattering method which accounts for the multiple wave interactions between the open end and the interior termination. The scattering matrices which described the reflection and transmission coefficients of the waveguide modes reflected and transmitted at each junction between the different waveguide sections, as well as the scattering from the edges at the open end are found via asymptotic high frequency methods such as the geometrical and physical theories of diffraction used in conjunction with the equivalent current method. The numerical results for an S-shaped inlet cavity are compared with the backscatter from a straight inlet cavity; the backscattered patterns are different because the curvature of an S-shaped inlet cavity redistributes the energy reflected from the interior termination in a way that is different from a straight inlet cavity. Author

**N89-24520\*#** National Aeronautics and Space Administration. Lewis Research Center, Cleveland, OH.

**MICROWAVE CHARACTERISTICS OF GAAS MMIC INTEGRATABLE OPTICAL DETECTORS**

PAUL C. CLASPY, SCOTT M. HILL (Case Western Reserve Univ., Cleveland, OH.), and KUL B. BHASIN Jun. 1989 6 p Presented at the IEEE MTT-S International Microwave Symposium, Long Beach, CA, 13-15 Jun. 1989  
 (NASA-TM-101485; E-4621; NAS 1.15:101485) Avail: NTIS HC A02/MF A01 CSCL 20/14

Interdigitated photoconductive detectors were fabricated on microwave device structures, making them easily integratable with Monolithic Microwave Integrated Circuits (MMIC). Detector responsivity as high as 2.5 A/W and an external quantum efficiency of 3.81 were measured. Response speed was nearly independent of electrode geometry, and all detectors had usable response at frequencies to 6 GHz. A small signal model of the detectors based on microwave measurements was also developed. Author

**N89-25365\*#** National Aeronautics and Space Administration. Lewis Research Center, Cleveland, OH.

**PERFORMANCE OF FIVE 30 GHZ SATELLITE RECEIVERS**

ROBERT J. KERCZEWSKI, GEORGE E. PONCHAK, and ROBERT R. ROMANOFKY 1989 7 p Presented at the 1989 IEEE MTT-S International Microwave Symposium, Long Beach, CA, 13-15 Jun. 1989  
 (NASA-TM-101960; E-4620; NAS 1.15:101960) Avail: NTIS HC A02/MF A01 CSCL 17/2

Technology development contracts funded by NASA have resulted in five 30 GHz satellite receivers of various design. The results of tests performed at NASA-Lewis to determine the operating characteristics of the receivers and their ability to perform in a digital satellite link are presented and discussed. Author

**N89-26126\*#** Ohio State Univ., Columbus. Dept. of Electrical Engineering.

**ADAPTIVE ARRAY FOR WEAK INTERFERING SIGNALS: GEOSTATIONARY SATELLITE EXPERIMENTS M.S. Thesis**

KARL STEADMAN 1989 148 p  
 (Contract NAG3-536)  
 (NASA-CR-185450; NAS 1.26:185450) Avail: NTIS HC A07/MF A01 CSCL 20/14

The performance of an experimental adaptive array is evaluated using signals from an existing geostationary satellite interference environment. To do this, an earth station antenna was built to receive signals from various geostationary satellites. In these experiments the received signals have a frequency of approximately 4 GHz (C-band) and have a bandwidth of over 35 MHz. These signals are downconverted to a 69 MHz intermediate frequency in the experimental system. Using the downconverted signals, the performance of the experimental system for various signal scenarios is evaluated. In this situation, due to the inherent thermal noise, qualitative instead of quantitative test results are presented. It is shown that the experimental system can null up to two interfering signals well below the noise level. However, to avoid the cancellation of the desired signal, the use of a steering vector is needed. Various methods to obtain an estimate of the steering vector are proposed. K.C.D.

**N89-27923\*#** National Aeronautics and Space Administration. Lewis Research Center, Cleveland, OH.

**PARAMETRIC STUDY OF ELECTROMAGNETIC WAVES PROPAGATING IN ABSORBING CURVED S DUCTS**

KENNETH J. BAUMEISTER Jul. 1989 25 p  
 (NASA-TM-102024; E-4761; NAS 1.15:102024) Avail: NTIS HC A03/MF A01 CSCL 20/14

A finite-element Galerkin formulation has been developed to study attenuation of transverse magnetic (TM) waves propagating in two-dimensional S-curved ducts with absorbing walls. In the frequency range where the duct diameter and electromagnetic wave length are nearly equal, the effect of duct length, curvature (duct offset), and absorber wall thickness was examined. For a given offset in the curved duct, the length of the S-duct was found to significantly affect both the absorptive and reflective characteristics of the duct. For a straight and a curved duct with perfect electric conductor terminations, power attenuation contours were examined to determine electromagnetic wall properties associated with maximum input signal absorption. Offset of the S-duct was found to significantly affect the value of the wall permittivity associated with the optimal attenuation of the incident electromagnetic wave. Author

**N89-27927\*#** National Aeronautics and Space Administration. Lewis Research Center, Cleveland, OH.

**DIGITAL CODEC FOR REAL-TIME PROCESSING OF BROADCAST QUALITY VIDEO SIGNALS AT 1.8 BITS/PIXEL**

MARY JO SHALKHAUSER and WAYNE A. WHYTE, JR. 1989 10 p Prepared for presentation at the Global Telecommunications Conference, Dallas, TX, 27-30 Nov. 1989; sponsored in part by IEEE  
 (NASA-TM-102325; E-5026; NAS 1.15:102325) Avail: NTIS HC A02/MF A01 CSCL 17/2

Advances in very large-scale integration and recent work in the field of bandwidth efficient digital modulation techniques have combined to make digital video processing technically feasible and potentially cost competitive for broadcast quality television transmission. A hardware implementation was developed for a DPCM-based digital television bandwidth compression algorithm which processes standard NTSC composite color television signals and produces broadcast quality video in real time at an average of 1.8 bits/pixel. The data compression algorithm and the hardware implementation of the CODEC are described, and performance results are provided. Author

## ELECTRONICS AND ELECTRICAL ENGINEERING

Includes test equipment and maintainability; components, e.g., tunnel diodes and transistors; microminiaturization; and integrated circuitry.

**A89-10342\*** Massachusetts Inst. of Tech., Lexington.  
**DESIGN OF A GaAs TRAVELLING WAVE MACH-ZEHNDER ELECTRO-OPTIC MODULATOR**

DAVID M. MATERNA (MIT, Lexington, MA), ALTAN M. FERENDECI (Case Western Reserve University, Cleveland, OH), and KUL B. BHASIN (NASA, Lewis Research Center, Cleveland, OH) IN: Optoelectronic materials, devices, packaging, and interconnects; Proceedings of the Meeting, San Diego, CA, Aug. 19-21, 1987. Bellingham, WA, Society of Photo-Optical Instrumentation Engineers, 1988, p. 195-198. refs

Copyright

The analysis and design of a GaAlAs Mach-Zehnder electrooptic modulator operating at 820 nm is presented. Optical modulation is achieved through coplanar 50-ohm traveling-wave microwave electrodes with a resulting 3-dB bandwidth-length product of 11.95 GHz cm. Author

**A89-10343\*** Cincinnati Univ., OH.  
**CHARACTERIZATION OF GaAlAs OPTICAL WAVEGUIDE HETEROSTRUCTURES GROWN BY MOLECULAR BEAM EPITAXY**

C. J. RADENS, H. E. JACKSON, J. T. BOYD (Cincinnati, University, OH), K. B. BHASIN, J. J. POUCH (NASA, Lewis Research Center, Cleveland, OH) et al. IN: Optoelectronic materials, devices, packaging, and interconnects; Proceedings of the Meeting, San Diego, CA, Aug. 19-21, 1987. Bellingham, WA, Society of Photo-Optical Instrumentation Engineers, 1988, p. 199-202. USAF-supported research. refs

Copyright

Multiple-layer GaAlAs optical waveguide heterostructures have been grown by MBE. These samples were designed to operate at 840 nm with negligible coupling of guided light to the absorbing GaAs substrate. The Al concentration was 13 percent for the guiding layer and was 16 percent for the cladding layers. The process for growing waveguide layers was calibrated primarily by high-energy electron diffraction, with the optical quality confirmed by photoluminescence measurements. Channel waveguide structures having widths of 5 microns were etched in a low-pressure magnetically confined multipolar plasma reactor. The resulting waveguide structures were characterized by Raman spectroscopy, ellipsometry, AES, and optical-waveguide loss measurements.

Author

**A89-15308\*** National Aeronautics and Space Administration.  
 Lewis Research Center, Cleveland, OH.

**PROGRESS IN INP SOLAR CELL RESEARCH**

I. WEINBERG and D. J. BRINKER (NASA, Lewis Research Center, Cleveland, OH) IN: 1988 IECEC; Proceedings of the Twenty-third Intersociety Energy Conversion Engineering Conference, Denver, CO, July 31-Aug. 5, 1988. Volume 3. New York, American Society of Mechanical Engineers, 1988, p. 121-126. Previously announced in STAR as N88-24870. refs

Copyright

Progress, in the past year, in InP solar cell research is reviewed. Small area cells with AMO, total area efficiencies of 18.8 percent were produced by OMCVD and Ion Implantation. Larger area cells (2 and 4 sq cm) were processed on a production basis. One thousand of the 2 sq cm cells will be used to supply power to a small piggyback lunar orbiter scheduled for launch in February 1990. Laboratory tests of ITO/InP cells, under 10 MeV proton irradiation, indicate radiation resistance comparable to InP n/P homojunction cells. Computer modeling studies indicate that, for identical geometries and dopant concentrations, InP solar cells

are significantly more radiation resistant than GaAs under 1 MeV electron irradiation. Additional computer modeling calculations were used to produce rectangular and circular InP concentrator cell designs for both the low concentration SLATS and higher concentration Cassegrainian Concentrators. Author

**A89-15367\*** Toledo Univ., OH.

**A FOURIER ANALYSIS FOR A FAST SIMULATION ALGORITHM**

ROGER J. KING (Toledo, University, OH) IN: 1988 IECEC; Proceedings of the Twenty-third Intersociety Energy Conversion Engineering Conference, Denver, CO, July 31-Aug. 5, 1988. Volume 3. New York, American Society of Mechanical Engineers, 1988, p. 509-516. refs

(Contract NAG3-708)

Copyright

This paper presents a derivation of compact expressions for the Fourier series analysis of the steady-state solution of a typical switching converter. The modeling procedure for the simulation and the steady-state solution is described, and some desirable traits for its matrix exponential subroutine are discussed. The Fourier analysis algorithm was tested on a phase-controlled parallel-loaded resonant converter, providing an experimental confirmation. I.S.

**A89-15387\*** National Aeronautics and Space Administration.  
 Lewis Research Center, Cleveland, OH.

**POWER COMPONENTS FOR THE SPACE STATION 20-KHZ POWER DISTRIBUTION SYSTEM**

DAVID D. RENZ (NASA, Lewis Research Center, Cleveland, OH) IN: 1988 IECEC; Proceedings of the Twenty-third Intersociety Energy Conversion Engineering Conference, Denver, CO, July 31-Aug. 5, 1988. Volume 3. New York, American Society of Mechanical Engineers, 1988, p. 637-641. Previously announced in STAR as N88-21374. refs

Copyright

Since 1984, NASA Lewis Research Center was developing high power, high frequency space power components as part of The Space Station Advanced Development program. The purpose of the Advanced Development program was to accelerate existing component programs to ensure their availability for use on the Space Station. These components include a rotary power transfer device, remote power controllers, remote bus isolators, high power semiconductor, a high power semiconductor package, high frequency-high power cable, high frequency-high power connectors, and high frequency-high power transformers. All the components were developed to the prototype level and will be installed in the Lewis Research Center Space Station power system test bed.

Author

**A89-15391\*** Purdue Univ., West Lafayette, IN.

**SIMULATION AND CONTROL OF A 20 KHZ SPACECRAFT POWER SYSTEM**

O. WASYNZUK and P. C. KRAUSE (Purdue University, West Lafayette, IN) IN: 1988 IECEC; Proceedings of the Twenty-third Intersociety Energy Conversion Engineering Conference, Denver, CO, July 31-Aug. 5, 1988. Volume 3. New York, American Society of Mechanical Engineers, 1988, p. 663-669.

(Contract NAS3-25119)

Copyright

A detailed computer representation of four Mapham inverters connected in a series, parallel arrangement has been implemented. System performance is illustrated by computer traces for the four Mapham inverters connected to a Litz cable with parallel resistance and dc receiver loads at the receiving end of the transmission cable. Methods of voltage control and load sharing between the inverters are demonstrated. Also, the detailed computer representation is used to design and to demonstrate the advantages of a feed-forward voltage control strategy. It is illustrated that with a computer simulation of this type, the performance and control of spacecraft power systems may be investigated with relative ease and facility. Author



**A89-15824\*** Case Western Reserve Univ., Cleveland, OH.  
**MICROWAVE RESPONSE OF AN HEMT PHOTOCONDUCTOR**  
 P. C. CLASPY (Case Western Reserve University, Cleveland, OH) and K. B. BHASIN (NASA, Lewis Research Center, Cleveland, OH) IN: Optoelectronic signal processing for phased-array antennas; Proceedings of the Meeting, Los Angeles, CA, Jan. 12, 13, 1988. Bellingham, WA, Society of Photo-Optical Instrumentation Engineers, 1988, p. 46-51. Previously announced in STAR as N88-18835. refs  
 Copyright

Interdigitated photodetectors of various geometries have been fabricated on GaAlAs/GaAs heterostructure material. Optical response characteristics of these devices have been examined at both dc and microwave frequencies. The microwave response, at frequencies to 8 GHz, was studied by illuminating the devices with the output of an internally modulated GaAlGa diode laser. Results of these measurements are presented and compared with that of GaAs photoconductors. Author

**A89-15825\*** GTE Labs., Inc., Waltham, MA.  
**OPTOELECTRONIC TECHNIQUES FOR BROADBAND SWITCHING**

S. F. SU, L. JOU, and J. LENART (GTE Laboratories, Inc., Waltham, MA) IN: Optoelectronic signal processing for phased-array antennas; Proceedings of the Meeting, Los Angeles, CA, Jan. 12, 13, 1988. Bellingham, WA, Society of Photo-Optical Instrumentation Engineers, 1988, p. 52-59. refs  
 (Contract NAS3-24673)  
 Copyright

Optoelectronic switching employs a hybrid optical/electronic principle to perform the switching function and is applicable for either analog broadband or high-bit rate digital switching. The major advantages of optoelectronic switching include high isolation, low crosstalk, small physical size, light weight, and low power consumption. These advantages make optoelectronic switching an excellent candidate for on-board satellite switching. This paper describes a number of optoelectronic switching architectures. System components required for implementing these switching architectures are discussed. Performance of these architectures are evaluated by calculating their crosstalk, isolation, insertion loss, matrix size, drive power, throughput, and switching speed. Technologies needed for monolithic optoelectronic switching are also identified. Author

**A89-15827\*** National Aeronautics and Space Administration. Lewis Research Center, Cleveland, OH.  
**GAAS MMIC ELEMENTS IN PHASED-ARRAY ANTENNAS**  
 REGIS F. LEONARD (NASA, Lewis Research Center, Cleveland, OH) IN: Optoelectronic signal processing for phased-array antennas; Proceedings of the Meeting, Los Angeles, CA, Jan. 12, 13, 1988. Bellingham, WA, Society of Photo-Optical Instrumentation Engineers, 1988, p. 72-79. refs  
 Copyright

Over the last six years NASA Lewis Research Center has carried out a program aimed at the development of advanced monolithic microwave integrated circuit technology, principally for use in phased-array antenna applications. Arising out of the Advanced Communications Technology Satellite (ACTS) program, the initial targets of the program were chips which operated at 30 and 20 GHz. Included in this group of activities were monolithic power modules with an output of 2 watts at GHz, variable phase shifters at both 20 and 30 GHz, low noise technology at 30 GHz, and a fully integrated (phase shifter, variable gain amplifier, power amplifier) transmit module at 20 GHz. Subsequent developments are centered on NASA mission requirements, particularly Space Station communications systems and deep space data communications. Author

**A89-15828\*** Honeywell, Inc., Bloomington, MN.  
**GAAS CIRCUITS FOR MONOLITHIC OPTICAL CONTROLLER**  
 G. GUSTAFSON, M. BENDETT, J. CARNEY, R. MACTAGGART, S. PALMQUIST (Honeywell Sensors and Signal Processing Laboratories, Bloomington, MN) et al. IN: Optoelectronic signal

processing for phased-array antennas; Proceedings of the Meeting, Los Angeles, CA, Jan. 12, 13, 1988. Bellingham, WA, Society of Photo-Optical Instrumentation Engineers, 1988, p. 80-87.  
 (Contract NAS3-24745)  
 Copyright

GaAs circuits for use in a fully monolithic 1 Gb/s optical controller have been developed and tested. The circuits include photodetectors, transimpedance amplifiers and 1:16 demultiplexers that can directly control the phase of MMIC phase shifters. The entire chip contains approximately 300 self-aligned gate E/D-mode MESFETs. The MESFETs have one micron-wide gate and the E-mode FETs typically have transconductance of 200 ms/mm. Results of simulations and tests are reported. Also, the design and layout of the fully monolithic chip is discussed. Author

**A89-15845\*** National Aeronautics and Space Administration. Lewis Research Center, Cleveland, OH.

**OPTICALLY CONTROLLED PHASED-ARRAY TECHNOLOGY FOR SPACE COMMUNICATION SYSTEMS**

RICHARD R. KUNATH and KUL B. BHASIN (NASA, Lewis Research Center, Cleveland, OH) IN: Optoelectronic signal processing for phased-array antennas; Proceedings of the Meeting, Los Angeles, CA, Jan. 12, 13, 1988. Bellingham, WA, Society of Photo-Optical Instrumentation Engineers, 1988, p. 234-238. Previously announced in STAR as N88-18809. refs  
 Copyright

Using MMICs in phased-array applications above 20 GHz requires complex RF and control signal distribution systems. Conventional waveguide, coaxial cable, and microstrip methods are undesirable due to their high weight, high loss, limited mechanical flexibility and large volume. An attractive alternative to these transmission media, for RF and control signal distribution in MMIC phased-array antennas, is optical fiber. Presented are potential system architectures and their associated characteristics. The status of high frequency opto-electronic components needed to realize the potential system architectures is also discussed. It is concluded that an optical fiber network will reduce weight and complexity, and increase reliability and performance, but may require higher power. Author

**A89-21200\*** Emerson Electric Co., Saint Louis, MO.  
**A VERSATILE POWER CONVERTER FOR HIGH-FREQUENCY LINK SYSTEMS**

PRADEEP K. SOOD (Emerson Electric Co., Saint Louis, MO), THOMAS A. LIPO (Wisconsin, University, Madison), and IRVING G. HANSEN (NASA, Lewis Research Center, Cleveland, OH) (IEEE, Applied Power Electronics Conference, San Diego, CA, Mar. 2-6, 1987) IEEE Transactions on Power Electronics (ISSN 0885-8993), vol. 3, Oct. 1988, p. 383-390. refs  
 (Contract NAG3-361)  
 Copyright

A single-phase HF link appears to be an attractive alternative to the dc link commonly used in power conversion systems. Here, a power converter suitable for one-step conversion of the single-phase HF link voltage to the three-phase LF voltages typically required for interfacing with system sources and loads is proposed. The converter utilizes zero-voltage switching principles to minimize switching losses and an easy-to-implement technique of pulse-density modulation for the control of the amplitude, frequency, and waveshape of the synthesized LF signals. Adaptation of the proposed topology for power conversion to single-phase ac and dc voltage or current outputs is shown to be straightforward. The feasibility of the proposed power circuit and the control technique has been experimentally verified. I.E.

**A89-24139\*** National Aeronautics and Space Administration. Lewis Research Center, Cleveland, OH.

**MODELING OF SOME COPLANAR WAVEGUIDE DISCONTINUITIES**

RAINEE N. SIMONS and GEORGE E. PONCHAK (NASA, Lewis Research Center, Cleveland, OH) (IEEE, International Microwave Symposium, 25th, New York, NY, May 25-27, 1988) IEEE Transactions on Microwave Theory and Techniques (ISSN



0018-9480), vol. 36, Dec. 1988, p. 1796-1803. Previously announced in STAR as N88-17880. refs  
Copyright

Presented are lumped equivalent circuit models for several coplanar waveguide discontinuities such as an open circuit, a series gap, and a symmetric step, and their element values as a function of the discontinuity physical dimensions. The model element values are de-embedded from measured S parameters. The frequency dependence of the effective dielectric constant is measured and compared to computed values. Author

**A89-26862\*** Analatom, Inc., Westlake, OH.

**ELECTRONIC STRUCTURE OF BAO/W CATHODE SURFACES**  
WOLFGANG MULLER (Analatom, Inc., Westlake, OH) IEEE Transactions on Electron Devices (ISSN 0018-9383), vol. 36, Jan. 1989, pt. 2, p. 180-187. refs  
(Contract NAS3-24744; NAS3-25085)  
Copyright

The local electronic structure of the emissive layer of barium dispenser thermionic cathodes is investigated theoretically using the relativistic scattered-wave approach. The interaction of Ba and O with W, Os, and W-Os alloy surfaces is studied with atomic clusters modeling different absorption environments representative of B- and M-type cathodes. Ba is found to be strongly oxidized, while O and the metal substrate are in a reduced chemical state. The presence of O enhances the surface dipole and Ba binding energy relative to Ba on W. Model results for W-Os alloy substrates show only relatively small changes in Ba and O for identical geometries, but very large charge redistributions inside the substrate, which are attributed to the electronegativity difference between Os and W. If Os is present in the surface layer, the charge transfer from Ba to the substrate and the Ba binding energy increase relative to W. Explanations are offered for the improved electron emission from alloy surfaces and the different emission enhancement for different alloy substrates. I.E.

**A89-30443\*** Sverdrup Technology, Inc., Cleveland, OH.  
**THE EFFECT OF METAL SURFACE PASSIVATION ON THE AU-INP INTERACTION**

NAVID S. FATEMI (Sverdrup Technology, Inc., Cleveland, OH) and VICTOR G. WEIZER (NASA, Lewis Research Center, Cleveland, OH) Journal of Applied Physics (ISSN 0021-8979), vol. 65, March 1, 1989, p. 2111-2115. refs  
Copyright

The effect of SiO<sub>2</sub> encapsulation on reaction rates in the Au-InP system was studied. Scanning electron microscopy and x-ray photoelectron spectroscopy were used to investigate surface and/or interface morphologies and in-depth compositional profiles. It was found that the rate of dissolution of InP into Au and subsequent phase transformations are largely dependent on the condition of the free surface of the metalization. SiO<sub>2</sub> capping of Au is reported for the first time to suppress the Au-InP reaction rate. The Au-InP interaction is shown to be quite similar to the Au-GaAs interaction despite differences in behavior of the group-V elements. Author

**A89-31987\*#** National Aeronautics and Space Administration. Lewis Research Center, Cleveland, OH.

**COMPUTATIONALLY GENERATED VELOCITY TAPER FOR EFFICIENCY ENHANCEMENT IN A COUPLED-CAVITY TRAVELING-WAVE TUBE**

JEFFREY D. WILSON (NASA, Lewis Research Center, Cleveland, OH) IEEE Transactions on Electron Devices (ISSN 0018-9383), vol. 36, Apr. 1989, pt. 2, p. 811-816. refs

A computational routine has been created to generate velocity tapers for efficiency enhancement in coupled-cavity TWTs. Programmed into the NASA multidimensional large-signal coupled-cavity TWT computer code, the routine generates the gradually decreasing cavity periods required to maintain a prescribed relationship between the circuit phase velocity and the electron-bunch velocity. Computational results for several computer-generated tapers are compared to those for an existing coupled-cavity TWT with a three-step taper. Guidelines are

developed for prescribing the bunch-phase profile to produce a taper for efficiency. The resulting taper provides a calculated RF efficiency 45 percent higher than the step taper at center frequency and at least 37 percent higher over the bandwidth. I.E.

**A89-31988\*#** National Aeronautics and Space Administration. Lewis Research Center, Cleveland, OH.

**ISOTROPIC GRAPHITE MULTISTAGE DEPRESSED COLLECTORS - A PROGRESS REPORT**

PETER RAMINS and BEN T. EBIHARA (NASA, Lewis Research Center, Cleveland, OH) IEEE Transactions on Electron Devices (ISSN 0018-9383), vol. 36, Apr. 1989, pt. 2, p. 817-824. refs

A small isotropic-graphite-electrode multistage depressed collector (MDC) was designed, fabricated, and evaluated in conjunction with a 500-W CW 4.8-9.6-GHz TWT. The carbon electrode surfaces were used to improve the TWT overall efficiency by minimizing the secondary-electron emission losses in the MDC. The design and fabrication of the brazed graphite MDC assembly are described. The TWT and graphite-electrode MDC bakeout and processing (outgassing) characteristics were evaluated and found to be comparable to those for TWTs equipped with copper-electrode MDCs. The TWT and MDC performance was optimized for broadband CW operation at saturation. The average RF, overall, and MDC efficiencies were 14.9, 46.4, and 83.6 percent, respectively, across the octave operating band. A 1500-h CW test showed no gas buildup and excellent stability of the electrode surfaces. I.E.

**A89-32857\*** University of Eastern Kentucky, Richmond.

**STUDY OF OPTICAL OUTPUT COUPLERS FOR SUBMILLIMETER WAVELENGTH BACKWARD-WAVE OSCILLATORS (BWO'S)**

JERRY D. COOK (Eastern Kentucky University, Richmond, KY), NORBERT STANKIEWICZ (NASA, Lewis Research Center, Cleveland, OH), and MARK PODANY (NASA, Lewis Research Center; Analox Corp., Cleveland, OH) International Journal of Infrared and Millimeter Waves (ISSN 0195-9271), vol. 10, Jan. 1989, p. 161-177. refs  
Copyright

Several scaled experiments of optical output couplers for submillimeter backward-wave oscillators (BWOs). Various designs of planar antennas (Vivaldi horns) lens-feed systems (hyper-hemispherical lens) were constructed and tested between 20 and 100 GHz using a spectrum analyzer. The lens system was also tested at 337 GHz using a CO<sub>2</sub> pumped FIR laser. It is found that Vivaldi horns have unsatisfactory resonances, perhaps because the horns studied were relatively short. Several techniques to maximize and flatten the frequency response of these horns are presented. The results suggest that alternate coupling schemes are superior to Vivaldi horns. R.B.

**A89-33625\*** National Aeronautics and Space Administration. Lewis Research Center, Cleveland, OH.

**CRYSTAL GROWTH OF SiC FOR ELECTRONIC APPLICATIONS**

LAWRENCE G. MATUS and J. ANTHONY POWELL (NASA, Lewis Research Center, Cleveland, OH) IN: Silicon carbide '87; Proceedings of the Symposium, Columbus, OH, Aug. 2-5, 1987. Westerville, OH, American Ceramic Society, Inc., 1989, p. 447-455. refs  
Copyright

The development of SiC as a high temperature semiconductor material is discussed, focusing on the epitaxial growth of single crystal SiC films on inexpensive single crystal silicon wafers. Progress in the improvement of film morphology and the elimination of antiphase disorder is examined. Potential candidate materials for high temperature semiconductor devices are compared and SiC films are evaluated. R.B.

**A89-33696\*** National Aeronautics and Space Administration. Lewis Research Center, Cleveland, OH.

**OPTICALLY INTERCONNECTED PHASED ARRAYS**

KUL B. BHASIN and RICHARD R. KUNATH (NASA, Lewis

Research Center, Cleveland, OH) IN: Interconnection of high speed and high frequency devices and systems; Proceedings of the Meeting, Newport Beach, CA, Mar. 15, 17, 1988. Bellingham, WA, Society of Photo-Optical Instrumentation Engineers, 1988, p. 36-43. Previously announced in STAR as N88-21400. refs  
Copyright

Phased-array antennas are required for many future NASA missions. They will provide agile electronic beam forming for communications and tracking in the range of 1 to 100 GHz. Such phased arrays are expected to use several hundred GaAs monolithic integrated circuits (MMICs) as transmitting and receiving elements. However, the interconnections of these elements by conventional coaxial cables and waveguides add weight, reduce flexibility, and increase electrical interference. Alternative interconnections based on optical fibers, optical processing, and holography are under evaluation as possible solutions. In this paper, the current status of these techniques is described. Since high-frequency optical components such as photodetectors, lasers, and modulators are key elements in these interconnections, their performance and limitations are discussed. Author

**A89-37824\*** National Aeronautics and Space Administration. Lewis Research Center, Cleveland, OH.

**DOPING DIRECTED AT THE OXYGEN SITES IN Y1BA2CU3O(7-DELTA) - THE EFFECT OF SULFUR, FLUORINE, AND CHLORINE**

N. P. BANSAL (NASA, Lewis Research Center, Cleveland, OH), D. BOYNE, and D. E. FARRELL (Case Western Reserve University, Cleveland, OH) Journal of Superconductivity (ISSN 0896-1107), vol. 1, Dec. 1988, p. 417-425. refs

(Contract NAG3-814)

Copyright

The effect of three dopants directed at the oxygen sites in Y1Ba2Cu3O(7-delta) have been investigated: sulfur, fluorine, and chlorine. Single-phase material has been obtained up to a (nominal) replacement of about 1 percent of the oxygen. Although the lattice parameters are unchanged, all dopants raise Tc (very slightly), sharpen the resistive transition, reduce the normal state resistivity, and very substantially increase the (magnetically determined) fraction of the material that is superconducting. All of these results differ qualitatively from those obtained with dopants directed at other locations in the 123 structure, and it is suggested that small additions of sulfur, fluorine, or chlorine may help to stabilize the ideal 123 stoichiometry. Author

**A89-42742\*** Case Western Reserve Univ., Cleveland, OH.

**DEEP-LEVEL TRANSIENT SPECTROSCOPY OF AL(X)GA(1-X)AS/GAAS USING NONDESTRUCTIVE ACOUSTO-ELECTRIC VOLTAGE MEASUREMENT**

MASSOOD TABIB-AZAR and FARES HAJJAR (Case Western Reserve University, Cleveland, OH) IEEE Transactions on Electron Devices (ISSN 0018-9383), vol. 36, June 1989, p. 1189-1195. refs

(Contract NAG3-816)

Copyright

The amplitude and the transient time constant of the acoustoelectric voltage were measured as a function of temperature to determine the activation energy of deep levels in Al(x)Ga(1-x)As/GaAs grown by molecular-beam epitaxy. In comparison to other methods based on monitoring the capacitance transient, deep-level transient spectroscopy has several advantages. The technique is nondestructive and highly sensitive, and, because of the dependence of the polarity of the acoustoelectric voltage on the carrier type, it yields information about the charge of the transient carriers and the type of deep traps involved in the release or trapping of these carriers. I.E.

**A89-43469\*** Cincinnati Univ., OH.

**SUBMICRON NICKEL-OXIDE-GOLD TUNNEL DIODE DETECTORS FOR RECTENNAS**

A. B. HOOFRING, V. J. KAPOOR (Cincinnati, University, OH), and W. KRAWCZONEK (NASA, Lewis Research Center, Cleveland,

OH) Journal of Applied Physics (ISSN 0021-8979), vol. 66, July 1, 1989, p. 430-437. refs

Copyright

The characteristics of a metal-oxide-metal (MOM) tunnel diode made of nickel, nickel-oxide, and gold, designed and fabricated by standard integrated circuit technology for use in FIR rectennas, are presented. The MOM tunnel diode was formed by overlapping a 0.8-micron-wide layer of 1000-A of nickel, which was oxidized to form a thin layer of nickel oxide, with a 1500 A-thick layer of gold. The dc current-voltage characteristics of the MOM diode showed that the current dependence on voltage was linear about zero bias up to a bias of about 70 mV. The maximum detection of a low-level signal (10-mV ac) was determined to be at a dc voltage of 70 mV across the MOM diode. The rectified output signal due to a chopped 10.6-micron CO2 laser incident upon the rectenna device was found to increase with dc bias, with a maximum value of 1000 nV for a junction bias of 100 mV at room temperature. I.S.

**A89-44518\*** Midwest Research Inst., Golden, CO.

**HIGH-EFFICIENCY SOLAR CELLS FABRICATED FROM DIRECT-CURRENT MAGNETRON SPUTTERED N-INDIUM TIN OXIDE ONTO P-INP GROWN BY ATMOSPHERIC PRESSURE METALORGANIC VAPOR PHASE EPITAXY**

X. LI, M. W. WANLASS, T. A. GESSERT, K. A. EMERY, and T. J. COUTTS (Solar Energy Research Institute, Golden, CO) Journal of Vacuum Science and Technology A (ISSN 0734-2101), vol. 7, May-June 1989, pt. 1, p. 827-832. refs

(Contract DE-AC02-83CH-10093; NASA ORDER C-30005-K)

Copyright

An attempt is made to improve device efficiencies by depositing indium tin oxide onto epitaxially grown p-InP on p(+)-InP substrates. This leads to a reduction in the device series resistance, high-quality reproducible surfaces, and an improvement in the transport properties of the base layer. Moreover, many of the facets associated with badly characterized bulk liquid encapsulated Czochralski substrates used in previous investigations are removed in this way. K.K.

**A89-45266\*#** Michigan Univ., Ann Arbor.

**EXTERNAL ELECTRO-OPTIC PROBING OF MILLIMETER-WAVE INTEGRATED CIRCUITS**

J. F. WHITAKER, J. A. VALDMANIS (Michigan, University, Ann Arbor), T. A. JACKSON (Rochester, University, NY), K. B. BHASIN, R. ROMANOFKY (NASA, Lewis Research Center, Cleveland, OH) et al. IEEE, International Microwave Symposium and Workshops, Long Beach, CA, June 14-16, 1989, Paper. 4 p. Research sponsored by the Empire State Electric Energy Research Corp., New York State Energy Research and Development Authority, Ontario-Hydro, and University of Rochester. refs

(Contract NCC3-130; F49620-87-C-0016)

An external, noncontact electro-optic measurement system, designed to operate at the wafer level with conventional wafer probing equipment and without any special circuit preparation, has been developed. Measurements have demonstrated the system's ability to probe continuous and pulsed signals on microwave integrated circuits on arbitrary substrates with excellent spatial resolution. Experimental measurements on a variety of digital and analog circuits, including a GaAs selectively-doped heterostructure transistor prescaler, an NMOS silicon multiplexer, and a GaAs power amplifier MMIC are reported. Author

**A89-49998\*** Air Force Wright Aeronautical Labs., Wright-Patterson AFB, OH.

**CHARACTERIZATION OF MULTILAYER GAAS/ALGAAS TRANSISTOR STRUCTURES BY VARIABLE ANGLE SPECTROSCOPIC ELLIPSOMETRY**

KENNETH G. MERKEL (USAF, Electronics Technology Laboratory, Wright-Patterson AFB, OH), PAUL G. SNYDER, JOHN A. WOOLLAM (Nebraska, University, Lincoln), SAMUEL ALTEROVITZ (NASA, Lewis Research Center, Cleveland, OH), and A. K. RAI (Universal Energy Systems, Inc., Dayton OH) Japanese Journal of Applied Physics, Part 1 (ISSN 0021-4922), vol. 28, June 1989,

p. 1118-1123. refs  
(Contract NAG3-154)  
Copyright

Variable angle of incidence spectroscopic ellipsometry (VASE) has been implemented as a means of determining layer thickness, alloy composition, and growth quality of GaAs/AlGaAs samples composed of relatively thick layers as well as superlattices. The structures studied in this work contained GaAs/AlGaAs multilayers with a superlattice 'barrier' and were grown for later formation of modulation-doped field effect transistors (MODFETs). Sample modeling was performed by treating the superlattice as a bulk AlGaAs layer of unknown composition. Extremely good data fits were realized when five layer thicknesses and two alloy ratios were allowed to vary in a regression analysis. Room temperature excitonic effects associated with the e-hh(1), e-lh(1) and e-hh(2) transitions were observed in the VASE data. Author

**A89-50472\*** Toledo Univ., OH.

## A DESIGN PROCEDURE FOR THE PHASE-CONTROLLED PARALLEL-LOADED RESONANT INVERTER

ROGER J. KING (Toledo, University, OH) IEEE Transactions on Aerospace and Electronic Systems (ISSN 0018-9251), vol. 25, July 1989, p. 497-507. refs  
(Contract NAG3-708)  
Copyright

High-frequency-link power conversion and distribution based on a resonant inverter (RI) has been recently proposed. The design of several topologies is reviewed, and a simple approximate design procedure is developed for the phase-controlled parallel-loaded RI. This design procedure seeks to ensure the benefits of resonant conversion and is verified by data from a laboratory 2.5 kVA, 20-kHz converter. A simple phasor analysis is introduced as a useful approximation for design purposes. The load is considered to be a linear impedance (or an ac current sink). The design procedure is verified using a 2.5-kVA 20-kHz RI. Also obtained are predictable worst-case ratings for each component of the resonant tank circuit and the inverter switches. For a given load VA requirement, below-resonance operation is found to result in a significantly lower tank VA requirement. Under transient conditions such as load short-circuit, a reversal of the expected commutation sequence is possible. I.E.

**A89-54417\*** Illinois Univ., Urbana.

## CALCULATION OF THE ELECTRON WAVE FUNCTION IN A GRADED-CHANNEL DOUBLE-HETEROJUNCTION MODULATION-DOPED FIELD-EFFECT TRANSISTOR

D. S. L. MUI, M. B. PATIL, and H. MORKOC (Illinois, University, Urbana) Applied Physics Letters (ISSN 0003-6951), vol. 55, Sept. 18, 1989, p. 1223-1225. Research supported by DOE. refs  
(Contract NAG3-613; AF-AFOSR-89-0239)  
Copyright

Three double-heterojunction modulation-doped field-effect transistor structures with different channel composition are investigated theoretically. All of these transistors have an  $\text{In}(x)\text{Ga}(1-x)\text{As}$  channel sandwiched between two doped  $\text{Al}(0.3)\text{Ga}(0.7)\text{As}$  barriers with undoped spacer layers. In one of the structures,  $x$  varies from 0 from either heterojunction to 0.15 at the center of the channel quadratically; in the other two, constant values of  $x$  of 0 and 0.15 are used. The Poisson and Schroedinger equations are solved self-consistently for the electron wave function in all three cases. The results showed that the two-dimensional electron gas (2DEG) concentration in the channel of the quadratically graded structure is higher than the  $x = 0$  one and slightly lower than the  $x = 0.15$  one, and the mean distance of the 2DEG is closer to the center of the channel for this transistor than the other two. These two effects have important implications on the electron mobility in the channel. Author

**A89-54963\*** Texas Univ., Arlington.

## COMPUTER ANALYSIS OF THE NEGATIVE DIFFERENTIAL RESISTANCE SWITCHING PHENOMENON OF DOUBLE-INJECTION DEVICES

TSAY-JIU SHIEH (Texas, University, Arlington) IEEE Transactions

on Electron Devices (ISSN 0018-9383), vol. 36, Sept. 1989, pt. 1, p. 1787-1792. refs  
(Contract NSG-3022)  
Copyright

By directly solving the semiconductor differential equations for the double-injection (DI) devices involving two interacting deep levels, the authors studied the negative differential resistance switching characteristic and its relationship with the device dimension, doping level, and dependence on the deep impurity profile. Computer simulation showed that although one can increase the threshold voltage by increasing the device length, the excessive holding voltage that would follow would put this device in a very limited application such as pulse power source. The excessive leakage current in the low conductance state also jeopardizes the attempt to use the device for any practical purpose. Unless there are new materials and deep impurities found that have a great differential hole and electron capture cross sections and a reasonable energy bandgap for low intrinsic carrier concentration, no big improvement in the fate of DI devices is expected in the near future. I.E.

**N89-10235\*#** National Aeronautics and Space Administration. Lewis Research Center, Cleveland, OH.

## SEQUENTIALLY EVAPORATED THIN Y-BA-CU-O SUPERCONDUCTOR FILMS: COMPOSITION AND PROCESSING EFFECTS

GEORGE J. VALCO, NORMAN J. ROHRER (Ohio State Univ., Columbus.), JOSEPH D. WARNER, and KUL B. BHASIN Oct. 1988 10 p Presented at the 35th National Vacuum Symposium, Atlanta, Ga., 3-7 Oct. 1988; sponsored by the American Vacuum Society  
(NASA-TM-101388; E-4448; NAS 1.15:101388) Avail: NTIS HC A02/MF A01 CSCL 09/1

Thin films of  $\text{YBa}_2\text{Cu}_3\text{O}(7\text{-}\beta)$  have been grown by sequential evaporation of Cu, Y, and  $\text{BaF}_2$  on  $\text{SrTiO}_3$  and  $\text{MgO}$  substrates. The onset temperatures were as high as 93 K while  $T_{\text{sub c}}$  was 85 K. The Ba/Y ratio was varied from 1.9 to 4.0. The Cu/Y ratio was varied from 2.8 to 3.4. The films were then annealed at various times and temperatures. The times ranged from 15 min to 3 hr, while the annealing temperatures used ranged from 850 C to 900 C. A good correlation was found between transition temperature ( $T_{\text{sub c}}$ ) and the annealing conditions; the films annealed at 900 C on  $\text{SrTiO}_3$  had the best  $T_{\text{sub c}}$ 's. There was a weaker correlation between composition and  $T_{\text{sub c}}$ . Barium poor films exhibited semiconducting normal state resistance behavior while barium rich films were metallic. The films were analyzed by resistance versus temperature measurements and scanning electron microscopy. The analysis of the films and the correlations are reported. Author

**N89-11128\*#** National Aeronautics and Space Administration. Lewis Research Center, Cleveland, OH.

## STUDY OF OPTICAL OUTPUT COUPLERS FOR SUBMILLIMETER WAVELENGTH BACKWARD-WAVE OSCILLATORS (BWO'S)

JERRY D. COOK, NORBERT STANKIEWICZ, and MARK PODANY (Analex Corp., Cleveland, Ohio.) 1988 19 p Prepared for presentation at the 13th International Conference on Infrared and Millimeter Waves, Honolulu, Hawaii, 5-9 Dec. 1988; sponsored in part by Society of Photo-Optical and Instrumentation Engineers  
(NASA-TM-101360; E-4335; NAS 1.15:101360) Avail: NTIS HC A03/MF A01 CSCL 09/3

The machining of slow wave structures for high frequency backward-wave oscillators (BWO) is extremely difficult beyond 1 THz. Recently a microfabrication technique using photolithography and ion-beam assisted etching has been used to construct a prototype BWO operating at 200 to 265 GHz. The output coupler for such tubes remains a problem. Waveguides do not exist or are very lossy at the frequencies of interest (300 to 2000 GHz). This paper discusses several scaled experiments of optical output couplers for submillimeter BWOs. Various designs of planar antennas (Vivaldi horns) and lens-feed systems (Hyper-hemispherical lens) were constructed and tested between

20 and 100 GHz using a spectrum analyzer. The lens system was also tested at 337 GHz using a CO<sub>2</sub> pumped FIR laser.

Author

**N89-11129\*#** National Aeronautics and Space Administration. Lewis Research Center, Cleveland, OH.

#### DEPOSITION AND CHARACTERIZATION OF ZNS/SI

#### HETEROJUNCTIONS PRODUCED BY VACUUM EVAPORATION

GEOFFREY A. LANDIS, JOSEPH J. LOFERSKI, and ROLAND BEAULIEU (Brown Univ., Providence, R. I.) 1988 18 p  
Presented at the 5th North Coast American Vacuum Society Symposium, Cleveland, Ohio, 2 Jun. 1988

(NASA-TM-101359; E-4389; NAS 1.15:101359) Avail: NTIS HC A03/MF A01 CSCL 09/3

Isotype heterojunctions of ZnS (lattice constant 5.41 Å) were grown on silicon (lattice constant 5.43 Å) p-n junctions to form a minority-carrier mirror. The deposition process was vacuum evaporation from a ZnS powder source onto a heated (450 °C) substrate. Both planar (100) and textured (111) surfaces were used. A reduction of the minority-carrier recombination at the surface was seen from increased short-wavelength quantum response and increased illuminated open-circuit voltage. The minority-carrier diffusion length was not degraded by the process.

Author

**N89-12819\*#** National Aeronautics and Space Administration. Lewis Research Center, Cleveland, OH.

#### RADIATION RESISTANCE AND COMPARATIVE

#### PERFORMANCE OF ITO/INP AND N/P INP HOMOJUNCTION SOLAR CELLS

I. WEINBERG, C. K. SWARTZ, R. E. HART, JR., and T. J. COUTTS (Midwest Research Inst., Golden, Colo.) 30 Sep. 1988 11 p  
Presented at the 20th Photovoltaic Specialists Conference, Las Vegas, Nev., 26-30 Sep. 1988; sponsored in part by IEEE

(NASA-TM-101387; E-4447; NAS 1.15:101387) Avail: NTIS HC A03/MF A01 CSCL 09/1

The radiation resistance of ITO/InP cells processed by DC magnetron sputtering is compared to that of standard n/p InP and GaAs homojunction cells. After 20 MeV proton irradiations, it is found that the radiation resistance of the present ITO/InP cell is comparable to that of the n/p homojunction InP cell and that both InP cell types have radiation resistance significantly greater than GaAs. The relatively lower radiation resistance, observed at higher fluence, for the InP cell with the deepest junction depth, is attributed to losses in the cells emitter region. Diode parameters obtained from  $I_{sub} - V_{sub}$  plots, data from surface Raman spectroscopy, and determinations of surface conductivity types are used to investigate the configuration of the ITO/InP cells. It is concluded that these latter cells are n/p homojunctions, the n-region consisting of a disordered layer at the oxide semiconductor.

Author

**N89-12820\*#** Case Western Reserve Univ., Cleveland, OH. Dept. of Electrical Engineering and Applied Physics.

#### MICROWAVE CHARACTERISTICS OF INTERDIGITATED PHOTOCONDUCTORS ON A HEMT STRUCTURE M.S. Thesis. Final Contractor Report

SCOTT M. HILL and PAUL C. CLASPY Nov. 1988 90 p  
(Contract NCC3-99)

(NASA-CR-182197; NAS 1.26:182197) Avail: NTIS HC A05/MF A01 CSCL 09/1

Interdigitated photoconductive detectors of various geometries were fabricated on AlGaAs/GaAs heterostructure material. The processes used in the fabrication of these devices are described, and the results of a study of their optical and electrical characteristics are presented.

Author

**N89-13706\*#** GTE Labs., Inc., Waltham, MA.

#### STUDY OF OPTOELECTRONIC SWITCH FOR SATELLITE-SWITCHED TIME-DIVISION MULTIPLE ACCESS

SHING-FONG SU, LIZ JOU, and JOE LENART 24 Jun. 1987 73 p

(Contract NAS3-24673)

(NASA-CR-179630; NAS 1.26:179630) Avail: NTIS HC A04/MF A01 CSCL 09/1

The use of optoelectronic switching for satellite switched time division multiple access will improve the isolation and reduce the crosstalk of an IF switch matrix. The results are presented of a study on optoelectronic switching. Tasks include literature search, system requirements study, candidate switching architecture analysis, and switch model optimization. The results show that the power divided and crossbar switching architectures are good candidates for an IF switch matrix.

Author

**N89-13722\*#** National Aeronautics and Space Administration. Lewis Research Center, Cleveland, OH.

#### CHARACTERIZATION OF ZRO2 BUFFER LAYERS FOR SEQUENTIALLY EVAPORATED Y-Ba-CuO ON SI AND AL2O3 SUBSTRATES

GEORGE J. VALCO, NORMAN J. ROHRER (Ohio State Univ., Columbus.), JOHN J. POUCH, JOSEPH D. WARNER, and KUL B. BHASIN Nov. 1988 12 p  
Presented at the Conference on Science and Technology of Thin Film Superconductors, Colorado Springs, Colo., 14-18 Nov. 1988; sponsored in part by DOE, SERI, NBS, NRL, and LBL

(NASA-TM-101432; E-4536; NAS 1.15:101432) Avail: NTIS HC A03/MF A01 CSCL 09/1

Thin film high temperature superconductors have the potential to change the microwave technology for space communications systems. For such applications it is desirable that the films be formed on substrates such as Al<sub>2</sub>O<sub>3</sub> which have good microwave properties. The use of ZrO<sub>2</sub> buffer layers between Y-Ba-Cu-O and the substrate has been investigated. These superconducting films have been formed by multilayer sequential electron beam evaporation of Cu, BaF<sub>2</sub> and Y with subsequent annealing. The three layer sequence of Y/BaF<sub>2</sub>/Cu is repeated four times for a total of twelve layers. Such a multilayer film, approximately 1 micron thick, deposited directly on SrTiO<sub>3</sub> and annealed at 900 °C for 45 min produces a film with a superconducting onset of 93 K and critical temperature of 85 K. Auger electron spectroscopy in conjunction with argon ion sputtering was used to obtain the distribution of each element as a function of depth for an unannealed film, the annealed film on SrTiO<sub>3</sub> and annealed films on ZrO<sub>2</sub> buffer layers. The individual layers were apparent. After annealing, the bulk of the film on SrTiO<sub>3</sub> is observed to be fairly uniform while films on the substrates with buffer layers are less uniform. The Y-Ba-Cu-O/ZrO<sub>2</sub> interface is broad with a long Ba tail into the ZrO<sub>2</sub>, suggesting interaction between the film and the buffer layer. The underlying ZrO<sub>2</sub>/Si interface is sharper. The detailed Auger results are presented and compared with samples annealed at different temperatures and durations.

Author

**N89-15335\*#** Sperry Corp., Phoenix, AZ. Aerospace and Marine Group.

#### MULTI-HUNDRED KILOWATT ROLL RING ASSEMBLY Final Report

PETER E. JACOBSON 1 Apr. 1985 122 p

(Contract NAS3-24264)

(NASA-CR-174832; NAS 1.26:174832; S71-5240-1/2-0) Avail: NTIS HC A06/MF A01 CSCL 09/3

A program was completed to develop an evaluation unit of a high power rotary transfer device for potential application in a space environment. This device was configured around a Roll Ring concept which performs the same function as a slip ring/brush assembly with a rolling instead of sliding interface. An eight circuit Evaluation Unit (EU) and a portable Test Fixture (TF) were designed and fabricated. The EU was designed to transfer currents to 200 amperes at a potential of as high as 500 volts for an ultimate 100 kW/circuit transfer capability. The EU was evaluated in vacuum at dc transfer currents of 50 to 200 amperes at voltages to 10 volts and at 500 volts at 2 amperes. Power transfer to levels of 2 kW through each of the eight circuits was completed. Power transfer in vacuum at levels and efficiencies not previously achieved was demonstrated. The terminal-to-terminal resistance was measured to be greater than 0.42 milliohms which translates to an efficiency

### 33 ELECTRONICS AND ELECTRICAL ENGINEERING

at 100 kW of 99.98 percent. The EU and TF have been delivered to the Lewis Research Center and are being prepared for testing at increased power levels and for life testing, which will include both dc and ac power. Author

**N89-15336\*#** Varian Associates, Palo Alto, CA. Microwave Tube Div.

#### **DEVELOPMENT OF A 39.5 GHZ KARP TRAVELING WAVE TUBE FOR USE IN SPACE Final Report, Jan. 1981 - Jul. 1984**

A. JACQUEZ and D. WILSON Oct. 1988 72 p  
(Contract NAS3-23259)  
(NASA-CR-182182; NAS 1.26:182182) Avail: NTIS HC A04/MF A01 CSCL 09/1

A millimeter-wave TWT was developed using a dispersive, high-impedance forward wave interaction structure based on a ladder, with non-space-harmonic interaction, for a tube with high gain per inch and high efficiency. The 'Tunneladder' interaction structure combines ladder properties modified to accommodate Pierce gun beam optics on a radially magnetized PM focusing structure. The development involved the fabrication of chemically milled, shaped ladders diffusion brazed to each ridge of a double ridged waveguide. Cold-test data are presented, representing the omega-Beta and impedance characteristics of the modified ladder circuit. These results were used in small and large-signal computer programs to predict TWT gain and efficiency. A laboratory model tube was designed and fabricated, including all major subassemblies. Author

**N89-15337\*#** National Aeronautics and Space Administration. Lewis Research Center, Cleveland, OH.

#### **PERFORMANCE OF A MULTISTAGE DEPRESSED COLLECTOR WITH MACHINED TITANIUM ELECTRODES**

PETER RAMINS and BEN T. EBIHARA Jan. 1989 10 p  
(NASA-TP-2891; E-4400; NAS 1.60:2891) Avail: NTIS HC A02/MF A01 CSCL 09/1

The performance of a multistage depressed collector (MDC) with machined titanium electrodes was evaluated in conjunction with an 800-W, 8- to 18-GHz travelling-wave tube (TWT) and was compared with the performances of geometrically identical copper and isotropic graphite electrode MDC's operated with the same TWT. The titanium electrode MDC produced a modest (about 3 percent) improvement in the MDC and the TWT overall efficiencies as compared with the copper electrode MDC, but its performance was substantially lower than that of the isotropic graphite electrode MDC. Author

**N89-15338\*#** National Aeronautics and Space Administration. Lewis Research Center, Cleveland, OH.

#### **COMMON SOURCE-MULTIPLE LOAD VS. SEPARATE SOURCE-INDIVIDUAL LOAD PHOTOVOLTAIC SYSTEM**

JOSEPH APPELBAUM 1989 8 p Prepared for presentation at the 4th International Photovoltaic Science and Engineering Conference, Sydney, Australia, 14-17 Feb. 1989; sponsored in part by Inst. of Radio and Electronics Engineers, and New South Wales Univ., Sydney, Australia Prepared in cooperation with Tel-Aviv Univ. (Israel)  
(NASA-TM-101465; E-4521; NAS 1.15:101465) Avail: NTIS HC A02/MF A01 CSCL 10/2

A comparison of system performance is made for two possible system setups: (1) individual loads powered by separate solar cell sources; and (2) multiple loads powered by a common solar cell source. A proof for resistive loads is given that shows the advantage of a common source over a separate source photovoltaic system for a large range of loads. For identical loads, both systems perform the same. Author

**N89-19493\*#** National Aeronautics and Space Administration. Lewis Research Center, Cleveland, OH.

#### **STARTING CHARACTERISTICS OF DIRECT CURRENT MOTORS POWERED BY SOLAR CELLS**

S. SINGER and J. APPELBAUM Mar. 1989 20 p Prepared in cooperation with Tel-Aviv Univ. (Israel)

(NASA-TM-101981; E-4550-1; NAS 1.15:101981) Avail: NTIS HC A03/MF A01 CSCL 09/1

Direct current motors are used in photovoltaic systems. Important characteristics of electric motors are the starting to rated current and torque ratios. These ratios are dictated by the size of the solar cell array and are different for the various dc motor types. Discussed here is the calculation of the starting to rated current ratio and starting to rated torque ratio of the permanent magnet, and series and shunt excited motors when powered by solar cells for two cases: with and without a maximum-power-point-tracker (MPPT) included in the system. Comparing these two cases, one gets a torque magnification of about 3 for the permanent magnet motor and about 7 for other motor types. The calculation of the torques may assist the PV system designer to determine whether or not to include an MPPT in the system. Author

**N89-20385\*#** National Aeronautics and Space Administration. Lewis Research Center, Cleveland, OH.

#### **THE MARS CLIMATE FOR A PHOTOVOLTAIC SYSTEM OPERATION**

JOSEPH APPELBAUM and DENNIS J. FLOOD 1989 21 p Prepared for presentation at the International Conference on Space Power, Cleveland, OH, 5-7 Jun. 1989; sponsored in part by International Astronautical Federation Prepared in cooperation with Tel-Aviv Univ. (Israel).  
(NASA-TM-101994; E-4645; NAS 1.15:101994) Avail: NTIS HC A03/MF A01 CSCL 10/2

Detailed information on the climatic conditions on Mars are very desirable for the design of photovoltaic systems for establishing outposts on the Martian surface. The distribution of solar insolation (global, direct and diffuse) and ambient temperature is addressed. This data are given at the Viking lander's locations and can also be used, to a first approximation, for other latitudes. The insolation data is based on measured optical depth of the Martian atmosphere derived from images taken of the sun with a special diode on the Viking cameras; and computation based on multiple wavelength and multiple scattering of the solar radiation. The ambient temperature (diurnal and yearly distribution) is based on direct measurements with a thermocouple at 1.6 m above the ground at the Viking lander locations. The insolation and ambient temperature information are short term data. New information about Mars may be forthcoming in the future from new analysis of previously collected data or from future flight missions. The Mars climate data for photovoltaic system operation will thus be updated accordingly. Author

**N89-21169\*#** National Aeronautics and Space Administration. Lewis Research Center, Cleveland, OH.

#### **ANALYTICAL AND EXPERIMENTAL PROCEDURES FOR DETERMINING PROPAGATION CHARACTERISTICS OF MILLIMETER-WAVE GALLIUM ARSENIDE MICROSTRIP LINES**

ROBERT R. ROMANOFSKY Mar. 1989 21 p  
(NASA-TP-2899; E-4273; NAS 1.60:2899) Avail: NTIS HC A03/MF A01 CSCL 20/14

In this report, a thorough analytical procedure is developed for evaluating the frequency-dependent loss characteristics and effective permittivity of microstrip lines. The technique is based on the measured reflection coefficient of microstrip resonator pairs. Experimental data, including quality factor Q, effective relative permittivity, and fringing for 50-ohm lines on gallium arsenide (GaAs) from 26.5 to 40.0 GHz are presented. The effects of an imperfect open circuit, coupling losses, and loading of the resonant frequency are considered. A cosine-tapered ridge-guide test fixture is described. It was found to be well suited to the device characterization. Author

**N89-21171\*#** National Aeronautics and Space Administration. Lewis Research Center, Cleveland, OH.

#### **DESIGN, FABRICATION, AND PERFORMANCE OF BRAZED, GRAPHITE ELECTRODE, MULTISTAGE DEPRESSED COLLECTORS WITH 500-W, CONTINUOUS WAVE, 4.8- TO 9.6-GHZ TRAVELING-WAVE TUBES**

PETER RAMINS and BEN EBIHARA Mar. 1989 18 p  
(NASA-TP-2904; E-4361; NAS 1.60:2904) Avail: NTIS HC  
A03/MF A01 CSCL 09/1

A small, isotropic graphite electrode, multistage depressed collector (MDC) was designed, fabricated, and evaluated in conjunction with a 500-W, continuous wave (CW), 4.8- to 9.6-GHz traveling-wave tube (TWT). The carbon electrode surfaces were used to improve the TWT overall efficiency by minimizing the secondary electron emission losses in the MDC. The design and fabrication of the brazed graphite MDC assembly are described. The brazing technique, which used copper braze filler metal, is compatible with both vacuum and the more commonly available hydrogen atmosphere brazing furnaces. The TWT and graphite electrode MCC bakeout, processing, and outgassing characteristics were evaluated and found to be comparable to TWT's equipped with copper electrode MDC's. The TWT and MDC performance was optimized for broadband CW operation at saturation. The average radiofrequency (RF), overall, and MDC efficiencies were 14.9, 46.4, and 83.6 percent, respectively, across the octave operating band. A 1500-hr CW test, conducted without the use of an appendage ion pump, showed no gas buildup and excellent stability of the electrode surfaces. Author

**N89-21172\*#** National Aeronautics and Space Administration. Lewis Research Center, Cleveland, OH.

**CHANNELIZED COPLANAR WAVEGUIDE: DISCONTINUITIES, JUNCTIONS, AND PROPAGATION CHARACTERISTICS**

RAINEE N. SIMONS (Case Western Reserve Univ., Cleveland, OH.), GEORGE E. PONCHAK, KONSTANTINOS S. MARTZAKLIS, and ROBERT R. ROMANOFKY 1989 7 p Proposed for presentation at the 1989 IEEE MTT-S International Microwave Symposium, Long Beach, CA, 13-15 Jun. 1989  
(NASA-TM-101483; E-4616; NAS 1.15:101483) Avail: NTIS HC  
A02/MF A01 CSCL 09/1

A new variant of CPW which has been termed channelized CPW, CCPW, is presented. Measured and computed propagation characteristics are presented. Lumped equivalent circuit element values for a CCPW open circuit and right angle bend have been obtained. CCPW power divider junctions and a coax-to-CCPW in-phase, radial power divider are also presented. Author

**N89-21173\*#** Honeywell, Inc., Bloomington, MN. Sensors and Signal Processing Lab.

**DEVELOPMENT OF GALLIUM ARSENIDE HIGH-SPEED, LOW-POWER SERIAL PARALLEL INTERFACE MODULES: EXECUTIVE SUMMARY Final Report**

31 May 1988 38 p  
(Contract NAS3-24676)  
(NASA-CR-182272; NAS 1.26:182272) Avail: NTIS HC A03/MF  
A01 CSCL 09/1

Final report to NASA LeRC on the development of gallium arsenide (GaAs) high-speed, low power serial/parallel interface modules. The report discusses the development and test of a family of 16, 32 and 64 bit parallel to serial and serial to parallel integrated circuits using a self aligned gate MESFET technology developed at the Honeywell Sensors and Signal Processing Laboratory. Lab testing demonstrated 1.3 GHz clock rates at a power of 300 mW. This work was accomplished under contract number NAS3-24676. Author

**N89-21174\*#** National Aeronautics and Space Administration. Lewis Research Center, Cleveland, OH.

**RESTRICTIVE LOADS POWERED BY SEPARATE OR BY COMMON ELECTRICAL SOURCES**

J. APPELBAUM Mar. 1989 20 p  
(NASA-TM-102008; E-4594; NAS 1.15:102008) Avail: NTIS HC  
A03/MF A01 CSCL 09/3

In designing a multiple load electrical system, the designer may wish to compare the performance of two setups: a common electrical source powering all loads, or separate electrical sources powering individual loads. Three types of electrical sources: an ideal voltage source, an ideal current source, and solar cell source powering resistive loads were analyzed for their performances in

separate and common source systems. A mathematical proof is given, for each case, indicating the merit of the separate or common source system. The main conclusions are: (1) identical resistive loads powered by ideal voltage sources perform the same in both system setups, (2) nonidentical resistive loads powered by ideal voltage sources perform the same in both system setups, (3) nonidentical resistive loads powered by ideal current sources have higher performance in separate source systems, and (4) nonidentical resistive loads powered by solar cells have higher performance in a common source system for a wide range of load resistances. Author

**N89-22020\*#** National Aeronautics and Space Administration. Lewis Research Center, Cleveland, OH.

**OPTICAL DETECTORS FOR GAAS MMIC INTEGRATION: TECHNOLOGY ASSESSMENT**

P. C. CLASPY (National Academy of Sciences - National Research Council, Washington, DC.) and K. B. BHASIN 1989 10 p  
Presented at the 1989 Technical Symposium on Aerospace Sensing, Orlando, FL, 27-31 Mar. 1989; sponsored by the Society of Photo-Optical Instrumentation Engineers  
(NASA-TM-102025; E-4767; NAS 1.15:102025) Avail: NTIS HC  
A02/MF A01 CSCL 09/1

Fiber optic links are being considered to transmit digital and analog signals in phased array antenna feed networks in space communications systems. The radiating elements in these arrays will be GaAs monolithic microwave integrated circuits (MMIC's) in numbers ranging from a few hundred to several thousand. If such optical interconnects are to be practical it appears essential that the associated components, including detectors, be monolithically integrated on the same chip as the microwave circuitry. The general issue of monolithic integration of microwave and optoelectronic components is addressed from the point of view of fabrication technology and compatibility. Particular attention is given to the fabrication technology of various types of GaAs optical detectors that are designed to operate at a wavelength of 830 nm. Author

**N89-23002\*#** National Aeronautics and Space Administration. Lewis Research Center, Cleveland, OH.

**IMPEDANCE STUDIES OF NI/CD AND NI/H CELLS USING THE CELL CASE AS REFERENCE ELECTRODE Abstract Only**

MARGARET A. REID *In its* Space Electrochemical Research and Technology Conference: Abstracts p 29 1989  
Avail: NTIS HC A03/MF A01 CSCL 09/3

Many impedance studies were carried out on Ni electrodes and Ni/Cd and Ni/H batteries. In order for impedance to become a diagnostic tool, accurate and reproducible measurements must be made, and some way of separating the contributions of the individual electrodes must be found. Using the PAR and the Solartron impedance equipment, studies have found that consistent measurements can be made if the cells or electrodes are equilibrated at the voltage of interest. In the charged state, equilibration times required are short, on the order of a few hours or less, but the equilibration time required becomes progressively longer as the voltage is lowered. The cell case can be used as a reference electrode during impedance measurements. The voltage of the case with respect to the electrodes is unimportant provided that it does not change appreciably during the course of the measurement. Measurements were made with several uncycled Ni/Cd cells, one from a lot which was known to have faulty Cd electrodes and another from a lot which showed excellent cycle life and presumably had good Cd electrodes. The impedances of the Ni electrodes vs. the case were similar, while the impedance of the poor Cd electrodes vs. the case. A 50 AH Ni/H cell was also investigated. After subtraction of the ohmic resistances, the sums of the impedances of the individual electrodes were very close to the impedance of the total cell. This indicates that the method is valid for examining the characteristics of the individual electrodes in situ. Author



**N89-23007\*#** National Aeronautics and Space Administration. Lewis Research Center, Cleveland, OH.

## **NICKEL-HYDROGEN CAPACITY LOSS ON STORAGE Abstract Only**

MICHELLE A. MANZO *In its* Space Electrochemical Research and Technology Conference: Abstracts p 34 1989  
 Avail: NTIS HC A03/MF A01 CSCL 09/3

Nickel-hydrogen batteries are rapidly becoming accepted for use in low-earth-orbit and geosynchronous orbit applications. With their increased use it has become evident that the storage procedures commonly used for nickel-cadmium cells are not adequate for the nickel-hydrogen system. The capacity loss exhibited by nickel electrodes from various manufacturers when exposed to different storage conditions was determined. A comprehensive test matrix was developed to evaluate capacity loss in nickel electrodes from four different manufacturers. Two types of tests were run; individual electrode tests, which involved flooded capacity and impedance measurements before and after storage under varied conditions of temperature, hydrogen pressure, and electrolyte concentration; and cell tests which primarily evaluated the effects of state-of-charge on storage. The cell tests evaluated capacity loss on cells stored open circuit, shorted and trickle charged at C/100 following a full charge. The results indicate that capacity loss varies with the specific electrode manufacturing process, storage temperature and hydrogen pressure. In general, electrodes stored at low temperatures or low hydrogen pressures exhibited a smaller loss in capacity over the twenty-eight day storage period than those stored at high pressure and high temperature. The capacity loss appears to correlate with the level of cobalt in the nickel electrode, with the most significant loss of capacity occurring in electrodes with higher cobalt levels. Impedance measurements appear to correlate well with the capacity loss observed for a given type of electrode but do not correlate well with the capacity loss between electrodes fabricated by different manufacturers. There was a definite correlation between the electrode potential measured immediately following storage and the measured capacity loss. Author

**N89-23791\*#** National Aeronautics and Space Administration. Lewis Research Center, Cleveland, OH.

## **SEQUENTIALLY EVAPORATED THIN Y-Ba-CO-O SUPERCONDUCTING FILMS ON MICROWAVE SUBSTRATES**

G. J. VALCO, N. J. ROHRER (Ohio State Univ., Columbus.), J. D. WARNER, and K. B. BHASIN 1989 9 p Presented at the Workshop on High Temperature Superconductivity, Huntsville, AL, 23-25 May 1989; cosponsored by the US Army Missile Command, the US Army Strategic Defense Command and the ARO (Contract NCC3-105)  
 (NASA-TM-102068; E-4825; NAS 1.15:102068) Avail: NTIS HC A02/MF A01 CSCL 20/12

The development of high T sub c superconducting thin films on various microwave substrates is of major interest in space electronic systems. Thin films of YBa<sub>2</sub>Cu<sub>3</sub>O<sub>7</sub>( $\Delta$ ) were formed on SrTiO<sub>3</sub>, MgO, ZrO<sub>2</sub> coated Al<sub>2</sub>O<sub>3</sub>, and LaAlO<sub>3</sub> substrates by multi-layer sequential evaporation and subsequent annealing in oxygen. The technique allows controlled deposition of Cu, BaF<sub>2</sub> and Y layers, as well as the ZrO buffer layers, to achieve reproducibility for microwave circuit fabrication. The three layer structure of Cu/BaF<sub>2</sub>/Y is repeated a minimum of four times. The films were annealed in an ambient of oxygen bubbled through water at temperatures between 850 C and 900 C followed by slow cooling (-2 C/minute) to 450 C, a low temperature anneal, and slow cooling to room temperature. Annealing times ranged from 15 minutes to 5 hrs. at high temperature and 0 to 6 hr. at 450 C. Silver contacts for four probe electrical measurements were formed by evaporation followed with an anneal at 500 C. The films were characterized by resistance-temperature measurements, energy dispersive X-ray spectroscopy, X-ray diffraction, and scanning electron microscopy. Critical transition temperatures ranged from 30 K to 87 K as a function of the substrate, composition of the film, thicknesses of the layers, and annealing conditions. Microwave ring resonator circuits were also patterned on these MgO and LaAlO<sub>3</sub> substrates. Author

**N89-23792\*#** National Aeronautics and Space Administration. Lewis Research Center, Cleveland, OH.

## **MAGNIFICATION OF STARTING TORQUES OF DC MOTORS BY MAXIMUM POWER POINT TRACKERS IN PHOTOVOLTAIC SYSTEMS**

JOSEPH APPELBAUM and S. SINGER (Colorado Univ., Colorado Springs.) 1989 8 p Proposed for presentation at the 24th Intersociety Energy Conversion Engineering Conference, Washington, DC, 6-11 Aug. 1989; sponsored by IEEE, AIAA, ANS, ASME, SAE, ACS and AIChE  
 (NASA-TM-102040; E-4741; NAS 1.15:102040) Avail: NTIS HC A02/MF A01 CSCL 09/3

Direct current (dc) motors are used in terrestrial photovoltaic (PV) systems such as in water-pumping systems for irrigation and water supply. Direct current motors may also be used for space applications. Simple and low weight systems including dc motors may be of special interest in space where the motors are directly coupled to the solar cell array (with no storage). The system will operate only during times when sufficient insolation is available. An important performance characteristic of electric motors is the starting to rated torque ratio. Different types of dc motors have different starting torque ratios. These ratios are dictated by the size of solar cell array, and the developed motor torque may not be sufficient to overcome the load starting torque. By including a maximum power point tracker (MPPT) in the PV system, the starting to rated torque ratio will increase, the amount of which depends on the motor type. The starting torque ratio is calculated for the permanent magnet, series and shunt excited dc motors when powered by solar cell arrays for two cases: with and without MPPT's. Defining a motor torque magnification by the ratio of the motor torque with an MPPT to the motor torque without an MPPT, a magnification of 3 was obtained for the permanent magnet motor and a magnification of 7 for both the series and shunt motors. The effect of the variation of solar insolation on the motor starting torque was covered. All motor types are less sensitive to insolation variation in systems including MPPT's as compared to systems with MPPT's. The analysis of this paper will assist the PV system designer to determine whether or not to include an MPPT in the system for a specific motor type. Author

**N89-24529\*#** National Aeronautics and Space Administration. Lewis Research Center, Cleveland, OH.

## **PHOTOVOLTAIC POWER SYSTEM OPERATION IN THE MARS ENVIRONMENT**

JOSEPH APPELBAUM (Tel-Aviv Univ., Israel ) and DENNIS J. FLOOD 1989 13 p Presented at the 24th Intersociety Energy Conversion Engineering Conference, Washington, DC, 6-11 Aug. 1989; cosponsored by the IEEE, AIAA, ANS, ASME, SAE, ACS and AIChE  
 (NASA-TM-102075; E-4740; NAS 1.15:102075) Avail: NTIS HC A03/MF A01 CSCL 10/1

Detailed information on the environmental conditions on Mars are very desirable for the design of photovoltaic systems for establishing outposts on the Martian surface. The variation of solar insolation (global, direct, and diffuse) at the Viking lander's locations is addressed. It can be used, to a first approximation, for other latitudes. The radiation data is based on measured optical depth of the Martian atmosphere derived from images taken of the sun with a special diode on the Viking cameras; and computation based on multiple wavelength and multiple scattering of the solar radiation. The data are used to make estimates of photovoltaic system power, area and mass for a surface power system using regenerative fuel cells for storage and nighttime operation. Author

**N89-24530\*#** Hughes Aircraft Co., Torrance, CA. Electron Dynamics Div.

## **DEVELOPMENT OF A 75-WATT 60-GHZ TRAVELING-WAVE TUBE FOR INTERSATELLITE COMMUNICATIONS**

A. L. ROUSSEAU, I. TAMMARU, and J. P. VASZARI Sep. 1988 129 p  
 (Contract NAS3-23351)  
 (NASA-CR-182135; W-10301; NAS 1.26:182135) Avail: NTIS HC A07/MF A01 CSCL 09/1



This program covers the initial design and development of a 75 watt, 60 GHz traveling-wave tube for intersatellite communications. The objective frequency band was 59 to 64 GHz, with a minimum tube gain of 35 dB. The objective overall efficiency at saturation was 40 percent. The tube, designated the 961H, used a coupled-cavity interaction circuit with periodic permanent magnet beam focusing to minimize the weight. For efficiency enhancement, it incorporated a four-stage depressed collector capable of radiation cooling in space. The electron gun had a low-temperature (type-M) cathode and an isolated anode. Two tubes were built and tested; one feasibility model with a single-stage collector and one experimental model that incorporated the multistage collector. Author

**N89-24532\*#** Analox Corp., Cleveland, OH.  
**COMPUTED PERFORMANCE OF THE HALF-SCALE  
 ACCURATE ANTENNA REFLECTOR Final Report**

KEVIN M. LAMBERT May 1989 33 p  
 (Contract NAS3-24564)  
 (NASA-CR-182284; E-4748; NAS 1.26:182284) Avail: NTIS HC  
 A03/MF A01 CSCL 09/3

The performance of the half-scale, accurate antenna reflector was studied. The antenna is evaluated for use as a compact range reflector. The reflector is studied for use with three separate feed antennas. Author

**N89-25403\*#** National Aeronautics and Space Administration.  
 Lewis Research Center, Cleveland, OH.

**DEVELOPMENT AND TESTING OF A 20-KHZ COMPONENT  
 TEST BED**

ROBERT M. BUTTON, ANDREW S. BRUSH, and RICHARD C. SUNDBERG (General Dynamics Corp., San Diego, CA.) Aug. 1989 8 p Presented at the 24th Intersociety Energy Conversion Engineering Conference, Washington, DC, 6-11 Aug. 1989; sponsored in part by IEEE, AIAA, ANS, ASME, SAE, ACS, and AICHE  
 (Contract NAS3-25266)  
 (NASA-TM-102141; E-4940; NAS 1.15:102141) Avail: NTIS HC  
 A02/MF A01 CSCL 09/3

A history of the General Dynamics Space Systems Division 20 kHz Breadboard is presented including its current configuration and its role in the Space Station Freedom (SSF) program. Highlights and results are presented on a series of tests conducted on the 20 kHz Breadboard. The first test presented is the 20 kHz Breadboard Acceptance test. This test verified the operation of the delivered Breadboard and also characterized the main components of the system. Next, an indepth efficiency testing effort is presented. The tests attempted to apportion all the power losses in the 20 kHz Breadboard Main Invert Units. Distortion test data is presented showing the distortion characteristics of a Mapham inverter. Lastly, current work on the 20 kHz Breadboard is presented including Main Inverter Unit paralleling tests. Conclusions are summarized and references given. Author

**N89-26143\*#** Michigan Univ., Ann Arbor. Solid-State Electronics Lab.

**MICROWAVE AND MILLIMETER-WAVE POWER GENERATION  
 IN SILICON CARBIDE (SiC) IMPATT DEVICES Final Report, 1  
 Nov. 1984 - 26 Jun. 1988**

I. MEHDI, GEORGE I. HADDAD, and R. K. MAINS Jun. 1989  
 28 p  
 (Contract NAG3-168)  
 (NASA-CR-185050; E-4910; NAS 1.26:185050) Avail: NTIS HC A03/MF  
 A01 CSCL 09/3

There are two points that should be noted. First, in the thermal resistance calculations it is assumed that the device is operating at 773 K while the results of the room temperature simulations are used. This was done because there is not enough information to correctly predict the material parameters at 773 K. Since, in general, device performance degrades with increasing temperature, the cw results are perhaps a bit optimistic. Second, the electric field in these structures gets extremely high and there might be

some possibility of tunneling. This was not incorporated into the simulation. Again, this could result in different device operating conditions. Author

**N89-26148\*#** National Aeronautics and Space Administration.  
 Lewis Research Center, Cleveland, OH.

**DISTORTION AND REGULATION CHARACTERIZATION OF A  
 MAPHAM INVERTER**

RICHARD C. SUNDBERG, ANDREW S. BRUSH, ROBERT M. BUTTON, and ALEXANDER G. PATTERSON (Analox Corp., Cleveland, OH.) Aug. 1989 10 p Presented at the 24th Intersociety Energy Conversion Engineering Conference, Washington, DC, 6-11 Aug. 1989; sponsored in part by IEEE, AIAA, ANS, ASME, SAE, ACS, and AICHE  
 (NASA-TM-102089; E-4854; NAS 1.15:102089) Avail: NTIS HC  
 A02/MF A01 CSCL 09/3

Output voltage Total Harmonic Distortion (THD) of a 20kHz, 6kVA Mapham resonant inverter is characterized as a function of its switching-to-resonant frequency ratio,  $f_{sub s}/f_{sub r}$ , using the EASY5 engineering analysis system. EASY5 circuit simulation results are compared with hardware test results to verify the accuracy of the simulations. The effects of load on the THD versus  $f_{sub s}/f_{sub r}$  ratio is investigated for resistive, leading, and lagging power factor load impedances. The effect of the series output capacitor on the Mapham inverter output voltage distortion and inherent load regulation is characterized under loads of various power factors and magnitudes. An optimum series capacitor value which improves the inherent load regulation to better than 3 percent is identified. The optimum series capacitor value is different than the value predicted from a modeled frequency domain analysis. An explanation is proposed which takes into account the conduction overlap in the inductor pairs during steady-state inverter operation, which decreases the effective inductance of a Mapham inverter. A fault protection and current limit method is discussed which allows the Mapham inverter to operate into a short circuit, even when the inverter resonant circuit becomes overdamped. Author

**N89-26149\*#** National Aeronautics and Space Administration.  
 Lewis Research Center, Cleveland, OH.

**FREQUENCY DOMAIN MODEL FOR ANALYSIS OF  
 PARALLELED, SERIES-OUTPUT-CONNECTED MAPHAM  
 INVERTERS**

ANDREW S. BRUSH, RICHARD C. SUNDBERG (General Dynamics Corp., San Diego, CA.), and ROBERT M. BUTTON Aug. 1989 8 p Presented at the 24th Intersociety Energy Conversion Engineering Conference, Washington, DC, 6-11 Aug. 1989; sponsored in part by IEEE, AIAA, ANS, ASME, SAE, ACS, and AICHE  
 (Contract NAS3-25266)  
 (NASA-TM-102140; E-4939; NAS 1.15:102140) Avail: NTIS HC  
 A02/MF A01 CSCL 09/1

The Mapham resonant inverter is characterized as a two-port network driven by a selected periodic voltage. The two-port model is then used to model a pair of Mapham inverters connected in series and employing phasor voltage regulation. It is shown that the model is useful for predicting power output in paralleled inverter units, and for predicting harmonic current output of inverter pairs, using standard power flow techniques. Some examples are compared to data obtained from testing hardware inverters. Author

**N89-26150\*#** Sverdrup Technology, Inc., Cleveland, OH.  
**PARALLELING POWER MOSFETS IN THEIR ACTIVE REGION:  
 EXTENDED RANGE OF PASSIVELY FORCED CURRENT  
 SHARING Final Report**

JANIS M. NIEDRA Jul. 1989 14 p  
 (Contract NAS3-24105; NAS3-25266)  
 (NASA-CR-180902; E-4910; NAS 1.26:180902) Avail: NTIS HC  
 A03/MF A01 CSCL 09/1

A simple passive circuit that improves current balance in paralleled power MOSFETs that are not precisely matched and that are operated in their active region from a common gate drive are exhibited. A nonlinear circuit consisting of diodes and resistors

## 34 FLUID MECHANICS AND HEAT TRANSFER

generates the differential gate potential required to correct for unbalance while maintaining low losses over a range of current. Also application of a thin tape wound magnetic core to effect dynamic current balance is reviewed, and a simple theory is presented showing that for operation in the active region the branch currents tend to revert to their normal unbalanced values even if the core is not driven into saturation. Results of several comparative experiments are given. Author

### 34

## FLUID MECHANICS AND HEAT TRANSFER

Includes boundary layers; hydrodynamics; fluidics; mass transfer; and ablation cooling.

**A89-10176\*** Houston Univ., TX.

### PASSIVE AND ACTIVE CONTROL OF JET TURBULENCE

A. K. M. FAZLE HUSSAIN and H. S. HUSAIN (Houston, University, TX) IN: Turbulence management and relaminarisation; Proceedings of the IUTAM Symposium, Bangalore, India, Jan. 13-23, 1987. Berlin and New York, Springer-Verlag, 1988, p. 445-457. refs

(Contract N00014-85-K-0126; NAG3-408)

Copyright

Techniques for controlling the generation, growth, and interactions of large coherent structures in turbulent flows are discussed, reviewing the results of recent experimental investigations. The fundamental principles of active and passive coherent-structure manipulation are outlined; the effects of geometric modification are examined for the case of an elliptic jet; and particular attention is given to passive control via self-excitation, turbulence and noise suppression, control of pairing interaction via two-frequency excitation, and unsteady boundary-layer separation in wall jets. Diagrams and graphs of typical results are provided. T.K.

**A89-11107\*#** Stanford Univ., CA.

### EXPERIMENTAL STUDY OF THE DEVELOPMENT OF LONGITUDINAL VORTEX PAIRS EMBEDDED IN A TURBULENT BOUNDARY LAYER

WAYNE R. PAULEY and JOHN K. EATON (Stanford University, CA) AIAA Journal (ISSN 0001-1452), vol. 26, July 1988, p. 816-823. Previously cited in issue 18, p. 2853, Accession no. A87-42376. refs

(Contract DE-FG03-86ER-13608; NAG3-522)

Copyright

**A89-11567\*** Arizona Univ., Tucson.

### ON THE PREFERRED MODE OF JET INSTABILITY

R. A. PETERSEN and M. M. SAMET (Arizona, University, Tucson) Journal of Fluid Mechanics (ISSN 0022-1120), vol. 194, Sept. 1988, p. 153-173. refs

(Contract NAG3-460; NSF MEA-82-10876)

Copyright

The preferred mode of instability was investigated in an axisymmetric air jet of moderate Reynolds number. Natural instabilities are shown to scale with local shear-layer thickness and the preferred mode is shown to be a shear-layer instability. The spatial evolution of the preferred mode was examined by exciting the flow acoustically and then mapping the phase-locked velocity fluctuations. Throughout the potential core region the phase-locked profiles are shown to agree with the eigensolutions of the Orr-Sommerfeld stability equations provided the calculations are based on measured, mean velocity profiles. The excitation intensity was varied from low levels, where the flow was merely tagged, to high levels where the mean flow was substantially distorted, and over that range of excitation there was no apparent deterioration in the agreement with stability predictions. Author

**A89-12327\*** Yale Univ., New Haven, CT.

### RATIONAL ENGINEERING CORRELATIONS OF DIFFUSIONAL AND INERTIAL PARTICLE DEPOSITION BEHAVIOR IN NON-ISOTHERMAL FORCED CONVECTION ENVIRONMENTS

D. E. ROSNER, S. A. GOKOGLU, and R. ISRAEL (Yale University, New Haven, CT) IN: Fouling of heat exchanger surfaces; Proceedings of the Engineering Foundation Conference, White Haven, PA, Oct. 31-Nov. 5, 1982. New York, Engineering Foundation, 1982, p. 235-256. refs

(Contract F49620-82-K-0020; NAG3-201)

Copyright

A multiparameter correlation approach to the study of particle deposition rates in engineering applications is discussed with reference to two specific examples, one dealing with thermophoretically augmented small particle convective diffusion and the other involving larger particle inertial impaction. The validity of the correlations proposed here is demonstrated through rigorous computations including all relevant phenomena and interactions. Such representations are shown to minimize apparent differences between various geometric, flow, and physicochemical parameters, allowing many apparently different physicochemical situations to be described in a unified way. V.L.

**A89-12331\*** National Aeronautics and Space Administration. Lewis Research Center, Cleveland, OH.

### DISCUSSION OF MILLS ET AL. ON 'THE EFFECT OF WALL SUCTION AND THERMOPHORESIS ON AEROSOL PARTICLE DEPOSITION FROM A LAMINAR BOUNDARY LAYER ON A FLAT PLATE'

S. A. GOKOGLU (NASA, Lewis Research Center, Cleveland, OH) International Journal of Heat and Mass Transfer (ISSN 0017-9310), vol. 30, no. 7, 1987, p. 1559, 1560; Reply, p. 1560, 1561. refs

Copyright

**A89-12336\*** Yale Univ., New Haven, CT.

### USE OF A GENERALIZED STOKES NUMBER TO DETERMINE THE AERODYNAMIC CAPTURE EFFICIENCY OF NON-STOKESIAN PARTICLES FROM A COMPRESSIBLE GAS FLOW

R. ISRAEL and D. E. ROSNER (Yale University, New Haven, CT) Aerosol Science and Technology (ISSN 0278-6826), vol. 2, no. 1, 1983, p. 45-51. refs

(Contract F49620-82-K-0020; NAG3-201)

Copyright

The aerodynamic capture efficiency of small but nondiffusing particles suspended in a high-speed stream flowing past a target is known to be influenced by parameters governing small particle inertia, departures from the Stokes drag law, and carrier fluid compressibility. By defining an effective Stokes number in terms of the actual (prevailing) particle stopping distance, local fluid viscosity, and inviscid fluid velocity gradient at the target nose, it is shown that these effects are well correlated in terms of a 'standard' (cylindrical collector, Stokes drag, incompressible flow,  $\text{sq rt Re}$  much greater than 1) capture efficiency curve. Thus, a correlation follows that simplifies aerosol capture calculations in the parameter range already included in previous numerical solutions, allows rational engineering predictions of deposition in situations not previously specifically calculated, and should facilitate the presentation of performance data for gas cleaning equipment and aerosol instruments. Author

**A89-12337\*** Yale Univ., New Haven, CT.

### AERODYNAMICALLY-DRIVEN CONDENSATE LAYER THICKNESS DISTRIBUTIONS ON ISOTHERMAL CYLINDRICAL SURFACES

D. E. ROSNER, D. GUNES (Yale University, New Haven, CT), and N. NAZIH-ANOUS Chemical Engineering Communications (ISSN 0098-6445), vol. 24, 1983, p. 275-287. refs

(Contract NAG3-201)

Copyright

A simple yet rather general mathematical model is presented for predicting the distribution of condensate layer thickness when aerodynamic shear is the dominant mechanism of liquid flow along

the surface. The Newtonian condensate film is treated using well-known thin-layer (lubrication theory) approximations, and condensate supply is taken to be the result of either convective diffusion or inertial impaction. Illustrative calculations for a circular cylinder in a crossflow at  $Re = 100,000$  reveal the consequences of alternate condensate arrival mechanisms and the existence of thicker reverse-flow films behind the position of gas boundary-layer separation. The present formulation is readily generalized to include transient liquid layer flows on noncircular objects of variable surface temperature, as encountered in turbine-blade materials testing or operation. Author

**A89-12339\*** National Aeronautics and Space Administration. Lewis Research Center, Cleveland, OH.

## WINDWARD FRACTION OF THE TOTAL MASS OR HEAT TRANSPORT FOR FLOW PAST A CIRCULAR CYLINDER

S. GOKOGLU (NASA, Lewis Research Center, Cleveland, OH) and D. E. ROSNER (Yale University, New Haven, CT) *Aerosol Science and Technology* (ISSN 0278-6826), vol. 2, no. 4, 1983, p. 543, 544. refs

(Contract NAG3-201)

Copyright

The windward fraction of the total mass or heat transport for flow past a cylindrical aerodynamic object was estimated using the available experimental data for the angular distribution of the Nusselt transfer coefficient,  $Nu(\theta, Re)$ . The  $Re$  dependence of the windward surface fraction was calculated for the values of  $Re$  between 2 and 400,000. The results obtained from polar integrations of data from eight sources indicate that, for Reynolds numbers up to about 2000, more than 70 percent of the total transfer occurs on the windward surface. For the  $Re$  values above 100,000, the windward percentage is less than 50 percent. I.S.

**A89-12340\*** Yale Univ., New Haven, CT.

## THERMOPHORETICALLY ENHANCED MASS TRANSPORT RATES TO SOLID AND TRANSPIRATION-COOLED WALLS ACROSS TURBULENT (LAW-OF-THE-WALL) BOUNDARY LAYERS

SULEYMAN A. GOKOGLU and DANIEL E. ROSNER (Yale University, New Haven, CT) *I & EC - Industrial and Engineering Chemistry, Fundamentals* (ISSN 0196-4313), vol. 24, May 1985, p. 208-214. refs

(Contract F49620-82-K-0020; NAG3-201)

Copyright

Convective-diffusion mass transfer rate predictions are made for both solid wall and transpiration-cooled 'law-of-the-wall' nonisothermal turbulent boundary layers (TBLs), including the mechanism of thermophoresis, i.e., small particle mass transport 'down a temperature gradient'. The present calculations are confined to low mass-loading situations but span the entire particle size range from vapor molecules to particles near the onset of inertial ('eddy') impaction. It is shown that, when  $Sc$  is much greater than 1, thermophoresis greatly increases particle deposition rates to internally cooled solid walls, but only partially offsets the appreciable reduction in deposition rates associated with dust-free gas-transpiration-cooled surfaces. Thus, efficient particle sampling from hot dusty gases can be carried out using transpiration 'shielded' probe surfaces. Author

## A89-12752\*# Detroit Diesel Allison, Indianapolis, IN. MEASUREMENTS OF HEAT TRANSFER DISTRIBUTION OVER THE SURFACES OF HIGHLY LOADED TURBINE NOZZLE GUIDE VANES

D. A. NEALY, M. S. MIHELIC, L. D. HYLTON (General Motors Corp., Detroit Diesel Allison Div., Indianapolis, IN), and H. J. GLADDEN (NASA, Lewis Research Center, Cleveland, OH) *ASME, Transactions, Journal of Engineering for Gas Turbines and Power* (ISSN 0022-0825), vol. 106, Jan. 1984, p. 149-158. Previously cited in issue 23, p. 3394, Accession no. A83-47910. refs

(Contract NAS3-22761)

Copyright

**A89-12753\*#** National Aeronautics and Space Administration. Lewis Research Center, Cleveland, OH.

## DETERMINATION OF CONVECTIVE DIFFUSION HEAT/MASS TRANSFER RATES TO BURNER RIG TEST TARGETS COMPARABLE IN SIZE TO CROSS-STREAM JET DIAMETER

S. A. GOKOGLU and G. J. SANTORO (NASA, Lewis Research Center, Cleveland, OH) *ASME, Transactions, Journal of Heat Transfer* (ISSN 0022-1481), vol. 110, May 1988, p. 449-455. Previously cited in issue 23, p. 3449, Accession no. A86-48140. refs

Copyright

**A89-14599\*** National Aeronautics and Space Administration. Lewis Research Center, Cleveland, OH.

## EFFECT OF PARTICULATE THERMOPHORESIS IN REDUCING THE FOULING RATE ADVANTAGES OF EFFUSION-COOLING

S. A. GOKOGLU (NASA, Lewis Research Center, Cleveland, OH; Yale University, New Haven, CT) and D. E. ROSNER (Yale University, New Haven, CT) *International Journal of Heat and Fluid Flow* (ISSN 0142-727X), vol. 5, March 1984, p. 37-41. refs (Contract F49620-82-K-0020; NAG3-201)

Copyright

To predict small-particle diffusional mass transfer (deposition), including particle thermophoresis, transpiration cooling, and variable properties, the coupled ordinary differential equations governing self-similar laminar boundary layers are solved numerically. Under typical combustion turbine conditions, although diffusional deposition rates can be dramatically reduced by transpiration cooling (e.g., by some 5-decades for mainstream submicron particles corresponding to a Schmidt number of about 100 and a wall transpiration-cooled to  $T_w/T_e = 0.8$ ), actual deposition rate reductions will be smaller than previously expected (by about 1 decade for particles with  $Sc$  of about 100), owing to thermophoretic particle drift caused by the colder wall. Such microdroplets, small enough to behave like heavy molecules in combustion systems, are often important because they can cause adherence of the much larger ash particles which inertially impact on the same surface. Author

**A89-14600\*** National Aeronautics and Space Administration. Lewis Research Center, Cleveland, OH.

## VISCOUS DISSIPATION EFFECTS ON THERMOPHORETICALLY AUGMENTED AEROSOL PARTICLE TRANSPORT ACROSS LAMINAR BOUNDARY LAYERS

S. A. GOKOGLU (NASA, Lewis Research Center, Cleveland, OH) and D. E. ROSNER (Yale University, New Haven, CT) *International Journal of Heat and Fluid Flow* (ISSN 0142-727X), vol. 6, Dec. 1985, p. 293-297. refs

(Contract NAG3-201; AF-AFOSR-84-0034)

Copyright

The effect of viscous dissipation on mass transport across nonisothermal low-mass-loading laminar boundary layers of dusty gas is investigated theoretically by means of numerical simulations. The derivation of the model is outlined, and numerical results are presented in extensive graphs and characterized in detail. The dissipation effects are found to be significant, increasing total particle-deposition rates; the intensity of the effects depends on the ratio of wall temperature to mainstream static temperature. T.K.

**A89-15143\*** National Aeronautics and Space Administration. Lewis Research Center, Cleveland, OH.

## UNSTEADY SOLUTION OF INCOMPRESSIBLE NAVIER-STOKES EQUATIONS

W. Y. SOH (NASA, Lewis Research Center; Sverdrup Technology, Inc., Cleveland, OH) and JOHN W. GOODRICH (NASA, Lewis Research Center, Cleveland, OH) *Journal of Computational Physics* (ISSN 0021-9991), vol. 79, Nov. 1988, p. 113-134. refs

Copyright

The numerical scheme used by the present time-accurate FEM numerical method for incompressible Navier-Stokes equations, using primitive variables as the unknowns, is a Crank-Nicholson implicit treatment of all equation terms with central differencing

## 34 FLUID MECHANICS AND HEAT TRANSFER

for space derivatives. The introduction of a continuous auxiliary system in pseudo-time, with artificial compressibility, yields the incompressible solution at the advanced time level; time-accurate solutions are thereby obtained for two-dimensional fluid flows in a square cavity, in the cases of both an impulsively starting lid and an oscillating lid. O.C.

**A89-15188\*** National Aeronautics and Space Administration. Lewis Research Center, Cleveland, OH.

### **DESCRIPTION OF AN OSCILLATING FLOW PRESSURE DROP TEST RIG**

J. GARY WOOD (NASA, Lewis Research Center, Cleveland, OH), ERIC L. MILLER (Sverdrup Technology, Inc., Cleveland, OH), DAVID R. GEDEON (Gedeon Associates, Athens, OH), and GARY E. KOESTER (Sunpower, Inc., Athens, OH) IN: 1988 IECEC; Proceedings of the Twenty-third Intersociety Energy Conversion Engineering Conference, Denver, CO, July 31-Aug. 5, 1988. Volume 1. New York, American Society of Mechanical Engineers, 1988, p. 121-126. Previously announced in STAR as N88-22933.

Copyright

A test rig designed to generate heat exchanger pressure drop information under oscillating flow conditions is described. This oscillating flow rig is based on a variable stroke and variable frequency linear drive motor. A frequency capability of 120 hertz and a mean test pressure up to 15 mPA (2200 psi) allows for testing at flow conditions found in modern high specific power Stirling engines. An important design feature of this rig is that it utilizes a single close coupled dynamic pressure transducer to measure the pressure drop across the test sample. This eliminates instrumentation difficulties associated with the pressure sensing lines common to differential pressure transducers. Another feature of the rig is that it utilizes a single displacement piston. This allows for testing of different sample lengths and configurations without hardware modifications. All data acquisition and reduction for the rig is performed with a dedicated personal computer. Thus the overall system design efficiently integrates the testing and data reduction procedures. The design methodology and details of the test rig are described. Author

**A89-15189\*** Minnesota Univ., Minneapolis.

### **EFFECT OF TRANSITION ON OSCILLATION FLOW LOSSES IN STIRLING ENGINE COOLERS AND HEATERS**

J. R. SEUME and T. W. SIMON (Minnesota, University, Minneapolis) IN: 1988 IECEC; Proceedings of the Twenty-third Intersociety Energy Conversion Engineering Conference, Denver, CO, July 31-Aug. 5, 1988. Volume 1. New York, American Society of Mechanical Engineers, 1988, p. 127-132. Research supported by AMOCO Foundation. refs

(Contract NAG3-598)

Copyright

To improve the prediction of Stirling engine performance, a more realistic model of oscillating flow losses in tubular heat exchangers is necessary. An experimental investigation has therefore been initiated to determine the effects of flow oscillation on fluid mechanics and heat transfer in ducts. This paper presents the first velocity measurements taken in this investigation.

Author

**A89-15190\*** National Aeronautics and Space Administration. Lewis Research Center, Cleveland, OH.

### **THE DESIGN AND FABRICATION OF A STIRLING ENGINE HEAT EXCHANGER MODULE WITH AN INTEGRAL HEAT PIPE**

JEFFREY G. SCHREIBER (NASA, Lewis Research Center, Cleveland, OH) IN: 1988 IECEC; Proceedings of the Twenty-third Intersociety Energy Conversion Engineering Conference, Denver, CO, July 31-Aug. 5, 1988. Volume 1. New York, American Society of Mechanical Engineers, 1988, p. 133-140. Previously announced in STAR as N88-26732. refs

Copyright

The conceptual design of a free-piston Stirling Space Engine (SSE) intended for space power applications has been generated. The engine was designed to produce 25 kW of electric power with heat supplied by a nuclear reactor. A novel heat exchanger

module was designed to reduce the number of critical joints in the heat exchanger assembly while also incorporating a heat pipe as the link between the engine and the heat source. Two inexpensive verification tests are proposed. The SSE heat exchanger module is described and the operating conditions for the module are outlined. The design process of the heat exchanger modules, including the sodium heat pipe, is briefly described. Similarities between the proposed SSE heat exchanger modules and the LeRC test modules for two test engines are presented. The benefits and weaknesses of using a sodium heat pipe to transport heat to a Stirling engine are discussed. Similarly, the problems encountered when using a true heat pipe, as opposed to a more simple reflux boiler, are described. The instruments incorporated into the modules and the test program are also outlined. Author

**A89-16451\*#** National Aeronautics and Space Administration. Lewis Research Center, Cleveland, OH.

### **NUMERICAL STUDY OF THE INTERACTIONS BETWEEN DROPLETS AT INTERMEDIATE REYNOLDS NUMBERS**

JIAN-SHUN SHUEN (NASA, Lewis Research Center, Cleveland, OH) Journal of Propulsion and Power (ISSN 0748-4658), vol. 4, Nov.-Dec. 1988, p. 481-489. Previously cited in issue 09, p. 1247, Accession no. A87-24926. refs

Copyright

**A89-16458\*#** Calspan-Buffalo Univ. Research Center, NY.

### **TURBINE-STAGE HEAT TRANSFER - COMPARISON OF SHORT-DURATION MEASUREMENTS WITH STATE-OF-THE-ART PREDICTIONS**

WILLIAM J. RAE, DALE B. TAULBEE, MICHAEL G. DUNN (Calspan-Buffalo University Research Center, NY), and KESTUTIS C. CIVINSKAS (NASA, Lewis Research Center, Cleveland, OH) Journal of Propulsion and Power (ISSN 0748-4658), vol. 4, Nov.-Dec. 1988, p. 541-548. Previously cited in issue 20, p. 2961, Accession no. A86-42656. refs

(Contract NAG3-469; NAG3-581)

Copyright

**A89-16884\*** National Aeronautics and Space Administration. Lewis Research Center, Cleveland, OH.

### **OBSERVATIONS OF THE FREQUENCIES IN A SPHERE WAKE AND OF DRAG INCREASE BY ACOUSTIC EXCITATION**

H. J. KIM and P. A. DURBIN (NASA, Lewis Research Center, Cleveland, OH) Physics of Fluids (ISSN 0031-9171), vol. 31, Nov. 1988, p. 3260-3265. refs

Copyright

Vortex shedding and instability wave frequencies have been measured in the wakes of spheres in the Reynolds number range 500 less than Re less than 60,000. The effect of acoustic excitation was examined and an interaction between the two frequency modes was found at the lower Reynolds numbers; through this interaction, external forcing at the instability frequency could change the vortex shedding frequency. The development of the mean wake was manipulated by forcing near to the dominant shear layer instability frequency. With this forcing, the separated shear layer moved closer to the surface of the sphere and the reversed flow region of the wake was shortened. Concomitantly, the base pressure decreased and drag increased. Author

**A89-16957\*** National Aeronautics and Space Administration. Lewis Research Center, Cleveland, OH.

### **APPLICATION OF ADVANCED COMPUTATIONAL TECHNOLOGY TO PROPULSION CFD**

JOHN R. SZUCH (NASA, Lewis Research Center, Cleveland, OH) (George Washington University and NASA, Symposium on Advances and Trends in Computational Structural Mechanics and Fluid Dynamics, Washington, DC, Oct. 17-19, 1988) Computers and Structures (ISSN 0045-7949), vol. 30, no. 1-2, 1988, p. 375-384. Previously announced in STAR as N88-19102. refs

Copyright

The Internal Fluid Mechanics Division of the NASA Lewis Research Center is combining the key elements of computational

fluid dynamics, aerothermodynamic experiments, and advanced computational technology to bring internal computational fluid dynamics (ICFM) to a state of practical application for aerospace propulsion system design. This paper presents an overview of efforts underway at NASA Lewis to advance and apply computational technology to ICFM. These efforts include the use of modern, software engineering principles for code development, the development of an AI-based user-interface for large codes, the establishment of a high-performance, data communications network to link ICFM researchers and facilities, and the application of parallel processing to speed up computationally intensive and/or time-critical ICFM problems. A multistage compressor flow physics program is cited as an example of efforts to use advanced computational technology to enhance a current NASA Lewis ICFM research program.

Author

**A89-17459\*** National Aeronautics and Space Administration. Lewis Research Center, Cleveland, OH.  
**SIMPLE HIGH-ACCURACY RESOLUTION PROGRAM FOR CONVECTIVE MODELLING OF DISCONTINUITIES**  
 B. P. LEONARD (NASA, Lewis Research Center, Cleveland; Akron, University, OH) International Journal for Numerical Methods in Fluids (ISSN 0271-2091), vol. 8, Oct. 1988, p. 1291-1318. Previously announced in STAR as N88-13931. refs  
 Copyright

For steady multidimensional convection, the Quadratic Upstream Interpolation for Convective Kinematics (QUICK) scheme has several attractive properties. However, for highly convective simulation of step profiles, QUICK produces unphysical overshoots and a few oscillations, and this may cause serious problems in nonlinear flows. Fortunately, it is possible to modify the convective flux by writing the normalized convected control-volume face value as a function of the normalized adjacent upstream node value, developing criteria for monotonic resolution without sacrificing formal accuracy. This results in a nonlinear functional relationship between the normalized variables, whereas standard methods are all linear in this sense. The resulting Simple High Accuracy Resolution Program (SHARP) can be applied to steady multidimensional flows containing thin shear or mixing layers, shock waves, and other frontal phenomena. This represents a significant advance in modeling highly convective flows of engineering and geophysical importance. SHARP is based on an explicit, conservative, control-volume flux formation, equally applicable to one, two, or three dimensional elliptic, parabolic, hyperbolic, or mixed-flow regimes. Results are given for the bench-mark purely convective first-order results and the nonmonotonic predictions of second- and third-order upwinding.

Author

**A89-19123\*#** Yale Univ., New Haven, CT.  
**BOUNDARY LAYER EFFECTS ON PARTICLE IMPACTION AND CAPTURE**  
 D. E. ROSNER and J. FERNANDEZ DE LA MORA (Yale University, New Haven, CT) ASME, Transactions, Journal of Fluids Engineering (ISSN 0098-2202), vol. 106, March 1984, p. 113, 114; Author's Closure, p. 114, 115. refs  
 (Contract F49620-82-K-0020; NAG3-201)  
 Copyright

The inertial impaction and deposition of small particles on larger bodies with viscous boundary layers are considered theoretically, in a detailed comment on a paper by Menguturk et al. (1983). Topics addressed include cushion effects, the dimensionless groups corresponding to the diameter range (3-6 microns) examined by Menguturk et al. in a numerical example, analogous effects of particle-gas energy and mass exchange in boundary layers, and the combined effects of particle inertia and diffusion. It is argued that the inertial effects can be characterized in terms of a body, boundary-layer, or sublayer Stokes number. In a reply by Menguturk et al., the focus is on the application of the theoretical model to the erosion of blade surfaces in large gas turbines; the Stokes number is found to be of limited practical value in these cases, because the particle motion is not primarily normal to the blade surfaces.

T.K.

**A89-19906\*#** National Aeronautics and Space Administration. Lewis Research Center, Cleveland, OH.

**LU IMPLICIT MULTIGRID ALGORITHM FOR THE THREE-DIMENSIONAL EULER EQUATIONS**  
 JEFFREY W. YOKOTA (NASA, Lewis Research Center, Cleveland, OH) and D. A. CAUGHEY (Cornell University, Ithaca, NY) AIAA Journal (ISSN 0001-1452), vol. 26, Sept. 1988, p. 1061-1069. NSERC-supported research. Previously cited in issue 08, p. 1102. Accession no. A87-22645. refs  
 (Contract NAG3-645)  
 Copyright

**A89-20223\*** National Aeronautics and Space Administration. Lewis Research Center, Cleveland, OH.

**ACCURATE BOUNDARY CONDITIONS FOR EXTERIOR PROBLEMS IN GAS DYNAMICS**  
 THOMAS HAGSTROM (NASA, Lewis Research Center, Cleveland, OH; New York, State University, Stony Brook) and S. I. HARIHARAN (Akron, University, OH) Mathematics of Computation (ISSN 0025-5718), vol. 51, Oct. 1988, p. 581-597. Previously announced in STAR as N88-19182. refs  
 (Contract NSF DMS-86-04047)  
 Copyright

The numerical solution of exterior problems is typically accomplished by introducing an artificial, far-field boundary and solving the equations on a truncated domain. For hyperbolic systems, boundary conditions at this boundary are often derived by imposing a principle of no reflection. However, waves with spherical symmetry in gas dynamics satisfy equations where incoming and outgoing Riemann variables are coupled. This suggests that natural reflections may be important. A reflecting boundary condition is proposed based on an asymptotic solution of the far-field equations. Nonlinear energy estimates are obtained for the truncated problem and numerical experiments presented to validate the theory.

Author

**A89-20425\*** Yale Univ., New Haven, CT.  
**MASS TRANSFER ACROSS COMBUSTION GAS THERMAL BOUNDARY LAYERS - POWER PRODUCTION AND MATERIALS PROCESSING IMPLICATIONS**  
 D. E. ROSNER (Yale University, New Haven, CT) IN: Heat transfer in fire and combustion systems. New York, American Society of Mechanical Engineers, 1985, p. 3-8. refs  
 (Contract AF-AFOSR-84-0034; NAG3-201; DE-AC21-85MC-22075)  
 Copyright

The effects of Soret diffusion (for vapors) and thermophoresis (for particles) are illustrated using recent optical experiments and boundary layer computations. Mass transfer rate augmentations of up to a factor of 1000 were observed and predicted for submicron-particle capture by cooled solid surfaces, while mass transfer suppressions of more than 10 to the -10th-fold were predicted for 'overheated' surfaces. It is noted that the results obtained are of interest in connection with such technological applications as fly-ash capture in power generation equipment and glass droplet deposition in optical-waveguide manufacture.

B.J.

**A89-21296\*** Arizona Univ., Tucson.  
**HEAT OF MIXING AND MORPHOLOGICAL STABILITY**  
 P. NANDAPURKAR and D. R. POIRIER (Arizona, University, Tucson) Journal of Crystal Growth (ISSN 0022-0248), vol. 92, no. 1-2, Oct. 1988, p. 88-96. refs  
 (Contract NAG3-723)  
 Copyright

A mathematical model, which incorporates heat of mixing in the energy balance, has been developed to analyze the morphological stability of a planar solid-liquid interface during the directional solidification of a binary alloy. It is observed that the stability behavior is almost that predicted by the analysis of Mullins and Sekerka (1963) at low growth velocities, while deviations in the critical concentration of about 20-25 percent are observed under rapid solidification conditions for certain systems. The calculations indicate that a positive heat of mixing makes the

planar interface more unstable, whereas a negative heat of mixing makes it more stable, in terms of the critical concentration.

Author

**A89-22736\*#** Clemson Univ., SC.  
**DEVELOPMENT OF A SPECIAL-PURPOSE TEST SURFACE  
 GUIDED BY UNCERTAINTY ANALYSIS**

T. WANG (Clemson University, SC) and T. W. SIMON (Minnesota, University, Minneapolis) Journal of Thermophysics and Heat Transfer (ISSN 0887-8722), vol. 3, Jan. 1989, p. 19-26. Research supported by the University of Minnesota and South Carolina Energy Research and Development Center. Previously cited in issue 07, p. 955, Accession no. A88-22121. refs  
 (Contract NAG3-286)  
 Copyright

**A89-22811\*#** National Aeronautics and Space Administration.  
 Lewis Research Center, Cleveland, OH.  
**EFFICIENT NUMERICAL SIMULATION OF A  
 ONE-DIMENSIONAL ELECTROTHERMAL DEICER PAD**

R. J. ROELKE (NASA, Lewis Research Center, Cleveland, OH), T. G. KEITH, JR., K. J. DE WITT, and W. B. WRIGHT (Toledo, University, OH) Journal of Aircraft (ISSN 0021-8669), vol. 25, Dec. 1988, p. 1097-1105. Previously cited in issue 13, p. 1983, Accession no. A87-32190. refs  
 (Contract NAG3-72)  
 Copyright

**A89-22819\*#** National Aeronautics and Space Administration.  
 Lewis Research Center, Cleveland, OH.  
**ON THE WIND FORCE NEEDED TO DISLodge A DROP  
 ADHERED TO A SURFACE**

PAUL A. DURBIN (NASA, Lewis Research Center, Cleveland, OH) Journal of Fluid Mechanics (ISSN 0022-1120), vol. 196, Nov. 1988, p. 205-222. refs  
 Copyright

The dislodging by dynamic pressure forces of a drop adhered by surface tension to a plane is considered. The method involves the numerical solution of the integrodifferential equation describing the drop shape and the obtaining of the critical Weber number as a function of contact angle hysteresis. The study assumes high-Reynolds-number free-streamline separation from the drop.

R.R.

**A89-22822\*#** National Aeronautics and Space Administration.  
 Lewis Research Center, Cleveland, OH.  
**INVESTIGATION OF THE FLOW BETWEEN A PAIR OF  
 CIRCULAR CYLINDERS IN THE FLOPPING REGIME**

H. J. KIM and P. A. DURBIN (NASA, Lewis Research Center, Cleveland, OH) Journal of Fluid Mechanics (ISSN 0022-1120), vol. 196, Nov. 1988, p. 431-448. refs  
 Copyright

The wakes of a pair of circular cylinders are grossly unsteady when the cylinders are separated in a direction normal to the approaching flow by less than one cylinder diameter. The wakes flop randomly between two asymmetric states. The time-scale for the flopping is several orders of magnitude longer than the timescale of vortex shedding, and also several orders of magnitude longer than the timescale for instability of the separating shear layers. When a splitter plate is positioned suitably on the centerline of the cylinders, the flopping can be stopped and the flow made to assume either of the asymmetric states, or a symmetric steady state. For a range of plate positions a new, periodic oscillation occurs. Acoustic excitation can also destroy the flopping mean flow, replacing it by a symmetric flow.

Author

**A89-22823\*#** National Aeronautics and Space Administration.  
 Lewis Research Center, Cleveland, OH.  
**INSTABILITIES CAUSED BY OSCILLATING ACCELERATIONS  
 NORMAL TO A VISCOUS FLUID-FLUID INTERFACE**

DAVID JACQMIN and WALTER M. B. DUVAL (NASA, Lewis Research Center, Cleveland, OH) Journal of Fluid Mechanics

(ISSN 0022-1120), vol. 196, Nov. 1988, p. 495-511. refs  
 Copyright

The case of two incompressible viscous fluids (with different densities) which meet at a planar interface and are subject to an externally imposed oscillating acceleration directed normal to the interface is studied. The linear evolution of perturbations to the basic-state flow is investigated. It is found that the critical Stokes-Reynolds number and the most unstable perturbation wavelengths are insensitive to the degree of density and viscosity differences between the two fluids.

R.R.

**A89-23238\*#** National Aeronautics and Space Administration.  
 Lewis Research Center, Cleveland, OH.  
**CONSIDERATIONS ON THE MOVING CONTACT-LINE  
 SINGULARITY, WITH APPLICATION TO FRICTIONAL DRAG  
 ON A SLENDER DROP**

P. A. DURBIN (NASA, Lewis Research Center, Cleveland, OH) Journal of Fluid Mechanics (ISSN 0022-1120), vol. 197, Dec. 1988, p. 157-169. refs  
 Copyright

It has previously been shown that the no-slip boundary conditions leads to a singularity at a moving contact line and that this presumes some form of slip. Present considerations on the energetics of slip due to shear stress lead to a yield stress boundary condition. A model for the distortion of the liquid state near solid boundaries gives a physical basis for this boundary condition. The yield stress condition is illustrated by an analysis of a slender drop rolling down an incline. That analysis provides a formula for the frictional drag resisting the drop movement. With the present boundary condition, the length of the slip region becomes a property of the fluid flow.

Author

**A89-23242\*#** National Aeronautics and Space Administration.  
 Lewis Research Center, Cleveland, OH.  
**NONLINEAR SPATIAL EVOLUTION OF AN EXTERNALLY  
 EXCITED INSTABILITY WAVE IN A FREE SHEAR LAYER**

M. E. GOLDSTEIN and LENNART S. HULTGREN (NASA, Lewis Research Center, Cleveland, OH) Journal of Fluid Mechanics (ISSN 0022-1120), vol. 197, Dec. 1988, p. 295-330. refs  
 Copyright

This paper considers a disturbance evolving from a strictly linear finite-growth-rate instability wave, with nonlinear effects first becoming important in the critical layer. By incorporating viscous effects into the nonlinear critical-layer analysis of Goldstein and Leib (1988), it was possible to demonstrate how an initially linear instability wave evolves as it propagates downstream and how the viscous effects eventually become important, even when the viscosity is very small, due to continually decreasing scales generated by the nonlinear effects.

I.S.

**A89-24603\*#** Princeton Univ., NJ.  
**AN ASYMPTOTIC DESCRIPTION OF TRANSIENT SETTLING  
 AND ULTRAFILTRATION OF COLLOIDAL DISPERSIONS**

K. E. DAVIS and W. B. RUSSEL (Princeton University, NJ) Physics of Fluids A (ISSN 0899-8213), vol. 1, Jan. 1989, p. 82-100. refs  
 (Contract NAG3-584; DE-FG02-85ER-45210)  
 Copyright

The present model for the sedimentation of colloidal systems includes a diffusion term in the governing equation which, in the regions above the sediment, acts as small perturbation to the Kynch (1952) theory. Within the sediment, diffusion is comparable to convection due to the high solid volume fraction. An application of the method of matched asymptotic expansions to the conservation equation allows a complete description of the settling process to be formulated, with specific attention to volume-fraction evolution in the sediment.

O.C.

**A89-25001\*#** Virginia Polytechnic Inst. and State Univ., Blacksburg.

**VISCOUS ANALYSIS OF HIGH SPEED FLOWS USING AN  
 UPWIND FINITE VOLUME TECHNIQUE**

W. F. NG, C. R. MITCHELL, K. AJMANI, A. C. TAYLOR, III, and J. S. BROCK (Virginia Polytechnic Institute and State University,



Blacksburg) AIAA, Aerospace Sciences Meeting, 27th, Reno, NV, Jan. 9-12, 1989. 9 p. refs  
(Contract NAG3-870)

(AIAA PAPER 89-0001) Copyright

A numerical study using an upwind finite volume technique to analyze high speed viscous flows is described. Two test cases were considered: a Mach 4.0 shock wave/laminar-boundary-layer interaction, and Mach 14.1 compression corners (15-deg and 24-deg ramp angle). PNS, TLNS, and NS equation results were obtained on each test case. As expected, PNS solutions are not adequate to resolve the flow physics. For the grids used in this study, there is no noticeable difference between the TLNS and full NS solutions. Both the TLNS and full NS solutions compared favorably with experimental data.

Author

**A89-25047\*#** National Aeronautics and Space Administration. Lewis Research Center, Cleveland, OH.

#### **FUEL SPRAY SIMULATION WITH TWO-FLUID NOZZLES**

ROBERT D. INGEBO (NASA, Lewis Research Center, Cleveland, OH) AIAA, Aerospace Sciences Meeting, 27th, Reno, NV, Jan. 9-12, 1989. 9 p. Previously announced in STAR as N89-12028. refs

(AIAA PAPER 89-0053) Copyright

Two-phase interacting flow inside a two-fluid fuel atomizer was investigated and a correction of aerodynamic and liquid-surface forces with characteristic drop diameter was obtained for liquid-jet breakup in Mach 1 gas flow. Nitrogen gas mass-flux was varied from 6 to 50 g/sq cm sec by using four differently sized two-fluid atomizers with nozzle diameters varying from 0.32 to 0.56 cm. The correlation was derived by using the acoustic gas velocity,  $V_{sub}$ , as a basic parameter in defining and evaluating the dimensionless product of the Weber (We) and Reynolds (Re) numbers. By using the definition of WeRe, it was found that the ratio of orifice diameter to Sauter mean drop diameter could be correlated with the dimensionless ratio WeRe and the gas to liquid density ratio.

Author

**A89-25061\*#** National Aeronautics and Space Administration. Lewis Research Center, Cleveland, OH.

#### **BEHAVIOR IN NORMAL AND REDUCED GRAVITY OF AN ENCLOSED LIQUID/GAS SYSTEM WITH NONUNIFORM HEATING FROM ABOVE**

H. D. ROSS (NASA, Lewis Research Center, Cleveland, OH), D. N. SCHILLER, W. A. SIRIGNANO (California, University, Irvine), and P. DISIMILE (Cincinnati, University, OH) AIAA, Aerospace Sciences Meeting, 27th, Reno, NV, Jan. 9-12, 1989. 11 p. Previously announced in STAR as N89-17046. refs  
(Contract NAG3-627)

(AIAA PAPER 89-0070)

The temperature and velocity fields have been investigated for a single-phase gas system and a two-layer gas-and-liquid system enclosed in a circular cylinder being heated suddenly and nonuniformly from above. The transient response of the gas, liquid, and container walls was modeled numerically in normal and reduced gravity (0.00001 g). Verification of the model was accomplished via flow visualization experiments in 10-cm-high by 10-cm-diameter plexiglass cylinders.

Author

#### **A89-25091\*#** Flow Research, Inc., Kent, WA. **SHOCK-WAVE-INDUCED MIXING ENHANCEMENT IN SCRAMJET COMBUSTORS**

S. MENON (Flow Research, Inc., Kent, WA) AIAA, Aerospace Sciences Meeting, 27th, Reno, NV, Jan. 9-12, 1989. 16 p. refs  
(Contract NAS3-25332)

(AIAA PAPER 89-0104) Copyright

An experimental study of the interaction between a weak shock wave and a supersonic shear layer was carried out to determine the possibility of shock-induced mixing enhancement. A supersonic (Mach 2.5) stream of nitrogen was mixed with a sonic helium jet downstream of a rearward-facing step to simulate the mixing region in the vicinity of a SCRAMJET flameholder. A small wedge was used to generate an oblique shock wave that impinges on the mixing layer. Schlieren flow visualization and Rayleigh scattering

concentration measurements were carried out. The results indicate that significant spreading of the shear layer may occur downstream of the shock/shear layer interaction region. Further study is required to determine the mechanism of the observed spreading and the extent of the increase in mixing efficiency. Since there are shock-induced losses, an optimum mixing enhancement configuration will have to be determined before the method can be validated and successfully implemented in a SCRAMJET combustor.

Author

**A89-25148\*#** National Aeronautics and Space Administration. Lewis Research Center, Cleveland, OH.

#### **AXISYMMETRIC CONFINED TURBULENT JET DIRECTED TOWARDS THE LIQUID SURFACE FROM BELOW**

MOHAMMAD M. HASAN (NASA, Lewis Research Center, Cleveland, OH) and CHIN-SHUN LIN (NASA, Lewis Research Center; Analox Corp., Cleveland, OH) AIAA, Aerospace Sciences Meeting, 27th, Reno, NV, Jan. 9-12, 1989. 11 p. Previously announced in STAR as N89-13749. refs

(AIAA PAPER 89-0172) Copyright

A numerical simulation is presented of an axisymmetric turbulent jet discharging axially from below into a cylindrical tank and directed towards the liquid vapor interface. The liquid vapor interface is assumed to be flat and shear free. The k-epsilon turbulence model is used to calculate the eddy viscosity. The turbulence intensity distribution and the length scale associated with the k-epsilon model are calculated as functions of jet flow rates and systems parameters. Numerical results are compared with appropriate experimental data. The problems associated with the free surface boundary conditions for the turbulent quantities are discussed.

Author

#### **A89-25303\*#** Rockwell International Corp., Canoga Park, CA. **PRELIMINARY STUDY OF THE INTERACTIONS CAUSED BY CROSSING SHOCK WAVES AND A TURBULENT BOUNDARY LAYER**

A. C. KETCHUM (Rockwell International Corp., Rocketdyne Div., Canoga Park, CA), S. M. BOGDONOFF (Princeton University, NJ), E. M. FERNANDO (Flow Research, Inc., Kent, WA), and P. F. BATCHO AIAA, Aerospace Sciences Meeting, 27th, Reno, NV, Jan. 9-12, 1989. 12 p. refs

(Contract F49620-86-C-0094; AF-AFOSR-89-0033; NAG3-926)

(AIAA PAPER 89-0359) Copyright

The subject research, the first phase of an extended study of the interaction of crossing shock waves with a turbulent boundary layer, has revealed the complexity of the resulting flow. Detailed surface visualization and mean wall static pressure distributions show little resemblance to the inviscid flow approximation, and the exploratory high frequency measurements show that the flow downstream of the theoretical inviscid shock crossing position has a significant unsteady characteristic. Further developments of the (unsteady) high frequency measurements are required to fully characterize the unsteadiness and the requirements to include this component in flowfield modeling.

Author

**A89-25382\*#** National Aeronautics and Space Administration. Lewis Research Center, Cleveland, OH.

#### **A DIAGONALLY INVERTED LU IMPLICIT MULTIGRID SCHEME FOR THE 3-D NAVIER-STOKES EQUATIONS AND A TWO EQUATION MODEL OF TURBULENCE**

JEFFREY W. YOKOTA (NASA, Lewis Research Center; Sverdrup Technology, Inc., Cleveland, OH) AIAA, Aerospace Sciences Meeting, 27th, Reno, NV, Jan. 9-12, 1989. 11 p. Previously announced in STAR as N89-10863. refs

(AIAA PAPER 89-0467) Copyright

An LU implicit multigrid algorithm is developed to calculate 3-D compressible viscous flows. This scheme solves the full 3-D Reynolds-Averaged Navier-Stokes equation with a two-equation kappa-epsilon model of turbulence. The flow equations are integrated by an efficient, diagonally inverted, LU implicit multigrid scheme while the kappa-epsilon equations are solved, uncoupled from the flow equations, by a block LU implicit algorithm. The flow equations are solved within the framework of the multigrid

method using a four-grid level W-cycle, while the kappa-epsilon equations are iterated only on the finest grid. This treatment of the Reynolds-Averaged Navier-Stokes equations proves to be an efficient method for calculating 3-D compressible viscous flows.

Author

**A89-25543\*#** General Motors Corp., Indianapolis, IN.  
**SOLUTION OF THREE-DIMENSIONAL FLOW PROBLEMS USING A FLUX-SPLINE METHOD**

K. KARKI, H. MONGIA (General Motors Corp., Allison Gas Turbine Div., Indianapolis, IN), and S. PATANKAR (Minnesota, University, Minneapolis) AIAA, Aerospace Sciences Meeting, 27th, Reno, NV, Jan. 9-12, 1989. 9 p. refs  
 (Contract NAS3-24350)  
 (AIAA PAPER 89-0687) Copyright

This paper reports the application of a flux-spline scheme to three-dimensional fluid flow problems. The performance of this scheme is contrasted with that of the power-law differencing scheme. The numerical results are compared with reference solutions available in the literature. For the problems considered in this study, the flux-spline scheme is significantly more accurate than the power-law scheme.

Author

**A89-25554\*#** Dayton Univ., OH.  
**A NUMERICAL INVESTIGATION OF THE INFLUENCE OF SURFACE ROUGHNESS ON HEAT TRANSFER IN ICE ACCRETION**

J. N. SCOTT and W. L. HANKEY (Dayton, University, OH) AIAA, Aerospace Sciences Meeting, 27th, Reno, NV, Jan. 9-12, 1989. 10 p. refs  
 (Contract NAG3-665)  
 (AIAA PAPER 89-0737) Copyright

The flowfield and resulting heat transfer rate over a series of ice accretion shapes is obtained by solving the Navier-Stokes equations. The influence of surface roughness on surface heat transfer is examined by including blockage, form drag, and stagnation heating effects as source terms in the governing equations. The results indicate increases of a factor of three in cooling rates due to distributed roughness compared to smooth surfaces. In addition, droplet impingement efficiencies are studied for the same series of ice accretion shapes using a time-dependent solution procedure.

R.B.

**A89-27693\*#** General Motors Corp., Indianapolis, IN.  
**EVOLUTION OF PARTICLE-LADEN JET FLOWS - A THEORETICAL AND EXPERIMENTAL STUDY**

A. A. MOSTAFA, H. C. MONGIA (General Motors Corp., Allison Gas Turbine Div., Indianapolis, IN), V. G. MCDONELL, and G. S. SAMUELSEN (California, University, Irvine) AIAA Journal (ISSN 0001-1452), vol. 27, Feb. 1989, p. 167-183. Previously cited in issue 20, p. 3220, Accession no. A87-45457. refs  
 (Contract NAS3-24350)  
 Copyright

**A89-28401\*#** National Aeronautics and Space Administration.  
 Lewis Research Center, Cleveland, OH.  
**THREE DIMENSIONAL PNS SOLUTIONS OF HYPERSONIC INTERNAL FLOWS WITH EQUILIBRIUM CHEMISTRY**

MAY-FUN LIQU (NASA, Lewis Research Center; Sverdrup Technology, Inc., Cleveland, OH) AIAA, Aerospace Sciences Meeting, 27th, Reno, NV, Jan. 9-12, 1989. 25 p. refs  
 (Contract NAS3-24105)  
 (AIAA PAPER 89-0002)

An implicit procedure for solving parabolized Navier-Stokes equations under the assumption of a general equation of state for a gas in chemical equilibrium is given. A general and consistent approach for the evaluation of Jacobian matrices in the implicit operator avoids the use of unnecessary auxiliary quantities and approximations, and leads to a simple expression. Applications to two- and three-dimensional flow problems show efficiency in computer time and economy in storage.

Author

**A89-28409\*#** National Aeronautics and Space Administration.  
 Lewis Research Center, Cleveland, OH.

**FLUX SPLITTING ALGORITHMS FOR TWO-DIMENSIONAL VISCOUS FLOWS WITH FINITE-RATE CHEMISTRY**

JIAN-SHUN SHUEN (NASA, Lewis Research Center; Sverdrup Technology, Inc., Cleveland, OH) and MENG-SING LIQU (NASA, Lewis Research Center, Cleveland, OH) AIAA, Aerospace Sciences Meeting, 27th, Reno, NV, Jan. 9-12, 1989. 32 p. refs  
 (AIAA PAPER 89-0388)

The Roe flux-difference splitting method has been extended to treat two-dimensional viscous flows with nonequilibrium chemistry. The derivations have avoided unnecessary assumptions or approximations. For spatial discretization, the second-order Roe upwind differencing is used for the convective terms and central differencing for the viscous terms. An upwind-based TVD scheme is applied to eliminate oscillations and obtain a sharp representation of discontinuities. A two-stage Runge-Kutta method is used to time integrate the discretized Navier-Stokes and species transport equations for the asymptotic steady solutions. The present method is then applied to two types of flows: the shock wave/boundary layer interaction problems and the jet in cross flows.

Author

**A89-28410\*#** National Aeronautics and Space Administration.  
 Lewis Research Center, Cleveland, OH.

**THREE-DIMENSIONAL CALCULATION OF SUPERSONIC REACTING FLOWS USING AN LU SCHEME**

SHENG-TAO YU, Y.-L. PETER TSAI, ED., and JIAN-SHUN SHUEN (NASA, Lewis Research Center; Sverdrup Technology, Inc., Cleveland, OH) AIAA, Aerospace Sciences Meeting, 27th, Reno, NV, Jan. 9-12, 1989. 12 p. refs  
 (AIAA PAPER 89-0391) Copyright

A new three-dimensional numerical program incorporated with comprehensive real gas property models has been developed to simulate supersonic reacting flows. The code employs an implicit finite volume, Lower-Upper (LU) time-marching method to solve the complete Navier-Stokes and species equations in a fully-coupled and very efficient manner. A chemistry model with nine species and eighteen reaction steps are adopted in the program to represent the chemical reaction of H<sub>2</sub> and air. To demonstrate the capability of the program, flow fields of underexpanded hydrogen jets transversely injected into supersonic air stream inside the combustors of scramjets are calculated. Results clearly depict the flow characteristics, including the shock structure, separated flow regions around the injector, and the distribution of the combustion products.

Author

**A89-28958\*#** National Aeronautics and Space Administration.  
 Lewis Research Center, Cleveland, OH.

**TRANSIENT RADIATIVE COOLING OF AN ABSORBING AND SCATTERING CYLINDER**

R. SIEGEL (NASA, Lewis Research Center, Cleveland, OH) ASME, Transactions, Journal of Heat Transfer (ISSN 0022-1481), vol. 111, Feb. 1989, p. 199-203. refs  
 Copyright

The transient cooling of an absorbing, emitting, and scattering cylinder is studied by using the forward integration of energy transfer equations. The analysis presented here provides cooling curves for a cylindrical region, initially at uniform temperature and then suddenly exposed to a much cooler environment. Results are presented for several optical radii and different values of the scattering albedo.

V.L.

**A89-28996\*** National Aeronautics and Space Administration.  
 Lewis Research Center, Cleveland, OH.

**BOUNDARY-LAYER RECEPTIVITY TO LONG-WAVE FREE-STREAM DISTURBANCES**

M. E. GOLDSTEIN and LENNART S. HULTGREN (NASA, Lewis Research Center, Cleveland, OH) IN: Annual review of fluid mechanics. Volume 21. Palo Alto, CA, Annual Reviews, Inc., 1989, p. 137-166. refs  
 Copyright

The present treatment of the early stages of boundary layer-transition phenomena, where the unsteady motion is of small

amplitude and can be accordingly treated as a small perturbation of an appropriate mean flow, elaborates the Heinrich et al. (1988) discussion of the role played by this 'receptivity' stage: in which the unsteady flow exhibits the same harmonic time-dependence as the externally-imposed forcing. Freestream disturbance wavelengths are noted to often be much longer than the Tollmien-Schlichting wavelength. Attention is given to the variety of wavelength-reduction mechanisms able to couple the long-wavelength, freestream disturbances to the comparatively short Tollmien-Schlichting waves. O.C.

**A89-28999\*** Imperial Coll. of Science and Technology, London (England).

## COHERENT STRUCTURES IN TRANSITIONAL AND TURBULENT FREE SHEAR FLOWS

J. T. C. LIU (Imperial College of Science and Technology, London, England; Brown University, Providence, RI) IN: Annual review of fluid mechanics. Volume 21. Palo Alto, CA, Annual Reviews, Inc., 1989, p. 285-315. Research supported by DARPA. refs (Contract NSF MSM-83-20307; NAG3-673) Copyright

The development of a quantitative understanding of large-scale coherent structures in shear flows has led to the recognition of their evolutionary features and 'rules' of nonlinear interaction among each other. These determinations, in conjunction with the study of fine-grained turbulence and mean motion, constitute a general view of hydrodynamical instabilities that has resulted in useful concepts for the achievement of shear-flow control. The dynamical role of longitudinal structures in free shear flows is presently exemplified by the axisymmetric and helical modes in a round jet, which resemble the two-dimensional and spanwise-periodic three-dimensional modes in a two-dimensional mean flow. O.C.

**A89-30482\*#** National Aeronautics and Space Administration. Lewis Research Center, Cleveland, OH.

## EFFECTS OF CORE TURBULENCE ON JET EXCITABILITY

REDA R. MANKBADI, EDWARD J. RICE (NASA, Lewis Research Center, Cleveland, OH), and GANESH RAMAN (NASA, Lewis Research Center; Sverdrup Technology, Inc., Cleveland, OH) AIAA, Shear Flow Conference, 2nd, Tempe, AZ, Mar. 13-16, 1989. 8 p. Previously announced in STAR as N89-14403. refs (AIAA PAPER 89-0966) Copyright

The effects of varying freestream core turbulence on the evolution of a circular jet with and without tonal excitation are examined. Measurements are made on an 8.8 cm diameter jet at a Mach number of 0.3. The jet is excited by plane waves at Strouhal number 0.5. For the excited and unexcited cases the turbulence level is varied by screens and grids placed upstream of the nozzle exit. The experiment results are compared with a theoretical model which incorporates a variable core turbulence and considers the energy interactions between the mean flow, the turbulence and the forced component. Both data and theory indicate that increasing the freestream turbulence diminishes the excitability of the jet and reduces the effect of excitation on the spreading rate of the jet. Author

**A89-30483\*#** National Aeronautics and Space Administration. Lewis Research Center, Cleveland, OH.

## MULTIPLE COHERENT MODE INTERACTION IN A DEVELOPING ROUND JET

S. S. LEE (NASA, Lewis Research Center, Cleveland, OH; Brown University, Providence, RI) and J. T. C. LIU (Brown University, Providence, RI) AIAA, Shear Flow Conference, 2nd, Tempe, AZ, Mar. 13-16, 1989. 11 p. Research supported by DARPA. refs (Contract NSF MSM-83-20307; NAG3-673; NAG3-1016) (AIAA PAPER 89-0967) Copyright

The integral energy method has been used in order to study the nonlinear interactions of the large-scale coherent structure in a spatially developing round jet. The streamwise development of a jet is obtained in terms of the mean flow shear layer momentum thickness, the wave mode kinetic energy and the wave mode phase angle. It is shown that the nonlinear interaction between wave modes is dependent on the wave mode phase angles. The

initial wave mode phase angles as well as the initial energy densities play a significant role in the streamwise evolution of the large-scale coherent wave modes and the mean flow. Author

**A89-30908\*** Houston Univ., TX.

## TURBULENCE MANAGEMENT IN FREE SHEAR FLOWS BY CONTROL OF COHERENT STRUCTURES

HYDER S. HUSAIN, JAMES E. BRIDGES, and FAZLE HUSSAIN (Houston, University, TX) IN: Transport phenomena in turbulent flows: Theory, experiment, and numerical simulation; Proceedings of the Second International Symposium, Tokyo, Japan, Oct. 1987. New York, Hemisphere Publishing Corp., 1988, p. 111-130. refs (Contract N00014-85-K-0126; NAG3-408) Copyright

The possibility of controlling turbulence by manipulating coherent structures is discussed. The processes of the generation, evolution, and interaction of coherent structures are described together with measurements necessary to analyze such coherent-structure properties as coherent vorticity, incoherent turbulence intensities, coherent and incoherent Reynolds stresses, and coherent turbulence production. Experimental findings are presented, in which the modified coherent structures were shown to result in favorable effects on the turbulence field. I.S.

**A89-31844\*** Utah Univ., Salt Lake City.

## EFFECTS OF HEAT RELEASE ON THE LARGE-SCALE STRUCTURE IN TURBULENT MIXING LAYERS

P. A. MCMURTRY (Utah, University, Salt Lake City), J. J. RILEY (Washington, University, Seattle), and R. W. METCALFE (Houston, University, TX) Journal of Fluid Mechanics (ISSN 0022-1120), vol. 199, Feb. 1989, p. 297-332. refs (Contract NAS3-24229; N00014-87-K-0174) Copyright

The effects of chemical heat release on the large-scale structure in a chemically reacting turbulent mixing layer have been studied using three-dimensional time-dependent simulations. Moderate heat release is found to slow the development of the large-scale structures and to shift their wavelengths to larger scales. The results suggest that previously unexplained anomalies observed in the mean velocity profiles of reacting jets and mixing layers may be the result of vorticity generation by baroclinic torques. R.R.

**A89-33779\*** National Aeronautics and Space Administration. Lewis Research Center, Cleveland, OH.

## NONLINEAR INTERACTION BETWEEN THE SINUSOIDAL AND VARICOSE INSTABILITY MODES IN A PLANE WAKE

S. J. LEIB (NASA, Lewis Research Center; Sverdrup Technology, Inc., Cleveland, OH) and M. E. GOLDSTEIN (NASA, Lewis Research Center, Cleveland, OH) Physics of Fluids A (ISSN 0899-8213), vol. 1, March 1989, p. 513-521. refs Copyright

The nonlinear interaction between sinusoidal and varicose instability modes in a plane wake is examined in the nonlinear-nonequilibrium critical layer regime. Equations governing the evolution of the instability wave amplitudes and critical layer vorticity distributions are derived. Numerical solutions for these equations are obtained for a number of wake defects and initial amplitude ratios. The results show that the primary effects of the nonlinear interaction are the suppression of the varicose mode and the downstream shift of the peak of the sinusoidal mode. Author

**A89-34426\*** National Aeronautics and Space Administration. Lewis Research Center, Cleveland, OH.

## DIRECT NUMERICAL SIMULATIONS OF A TEMPORALLY EVOLVING MIXING LAYER SUBJECT TO FORCING

R. W. CLAUS (NASA, Lewis Research Center, Cleveland, OH) Computers and Fluids (ISSN 0045-7930), vol. 17, no. 2, 1989, p. 301-312. Previously announced in STAR as N87-23933. refs Copyright

The vortical evolution of mixing layers subject to various types of forcing is numerically simulated using pseudospectral methods. The effect of harmonic forcing and random noise in the initial

conditions is examined with some results compared to experimental data. Spanwise forcing is found to enhance streamwise vorticity in a nonlinear process leading to a slow, secondary growth of the shear layer. The effect of forcing on a chemical reaction is favorably compared with experimental data at low Reynolds numbers. Combining harmonic and subharmonic forcing is shown to both augment and later destroy streamwise vorticity. Author

**A89-34795\*#** National Aeronautics and Space Administration. Lewis Research Center, Cleveland, OH.  
**THE SOLUTION OF THE ELROD ALGORITHM FOR A DYNAMICALLY LOADED JOURNAL BEARING USING MULTIGRID TECHNIQUES**

C. M. WOODS (NASA, Lewis Research Center, Cleveland, OH) and D. E. BREWE (NASA, Lewis Research Center; U.S. Army, Propulsion Directorate, Cleveland, OH) ASME, Transactions, Journal of Tribology (ISSN 0742-4787), vol. 111, April 1989, p. 302-308. Previously announced in STAR as N88-25854. refs (ASME PAPER 88-TRIB-23) Copyright

A numerical solution to a theoretical model of vapor cavitation in a dynamically loaded journal bearing is developed utilizing a multigrid iteration technique. The method is compared with a noniterative approach in terms of computational time and accuracy. The computational model is based on the Elrod algorithm, a control volume approach to the Reynolds equation which mimics the Jakobsson-Floberg and Olsson cavitation theory. Besides accounting for a moving cavitation boundary and conservation of mass at the boundary, it also conserves mass within the cavitated region via a smeared mass or striated flow extending to both surfaces in the film gap. The mixed nature of the equations (parabolic in the full film zone and hyperbolic in the cavitated zone) coupled with the dynamic aspects of the problem create interesting difficulties for the present solution approach. Emphasis is placed on the methods found to eliminate solution instabilities. Excellent results are obtained for both accuracy and reduction of computational time. Author

**A89-34912\*** Scientific Research Associates, Inc., Glastonbury, CT.  
**BIPOLAR COORDINATES FOR COMPUTATION OF TRANSITION DUCT FLOWS**

R. K. MADABHUSHI and R. LEVY (Scientific Research Associates, Inc., Glastonbury, CT) IN: Recent developments in computational fluid dynamics; Proceedings of the Symposium, ASME Winter Annual Meeting, Chicago, IL, Nov. 27-Dec. 2, 1988. New York, American Society of Mechanical Engineers, 1988, p. 185-192. refs

(Contract NAS3-24224)

Copyright

Numerical simulation techniques for flows in jet-engine transition ducts with changing cross sections are developed and demonstrated. The boundary-conforming grids required are generated using bipolar coordinates, and the singularities arising at the no-slip boundaries are treated as described by de Vahl Davis (1979) and Tsai and Levy (1987). Grids for several typical configurations are employed in computations with the three-dimensional laminar/turbulent viscous-flow solver of Levy et al. (1983), and the results are presented graphically. The scheme used to deal with singularities is shown to be robust, suggesting that the bipolar grids may be applicable to Navier-Stokes computations. T.K.

**A89-34926\*** General Electric Co., Fairfield, CT.  
**HEAT TRANSFER IN GAS TURBINE ENGINES AND THREE-DIMENSIONAL FLOWS; PROCEEDINGS OF THE SYMPOSIUM, ASME WINTER ANNUAL MEETING, CHICAGO, IL, NOV. 27-DEC. 2, 1988**

E. ELOVIC, ED. (General Electric Co., Fairfield, CT), J. E. O'BRIEN, ED. (NASA, Lewis Research Center, Cleveland, OH), and D. W. PEPPER, ED. (Marquardt Co., Van Nuys, CA) Meeting sponsored by ASME, Heat Transfer Division. New York, American Society of Mechanical Engineers, 1988, 127 p. For individual items see

A89-34927 to A89-34935.

Copyright

The present conference on heat transfer characteristics of gas turbines and three-dimensional flows discusses velocity-temperature fluctuation correlations at the flow stagnation flow of a circular cylinder in turbulent flow, heat transfer across turbulent boundary layers with pressure gradients, the effect of jet grid turbulence on boundary layer heat transfer, and heat transfer characteristics predictions for discrete-hole film cooling. Also discussed are local heat transfer in internally cooled turbine airfoil leading edges, secondary flows in vane cascades and curved ducts, three-dimensional numerical modeling in gas turbine coal combustor design, numerical and experimental results for tube-fin heat exchanger airflow and heating characteristics, and the computation of external hypersonic three-dimensional flow field and heat transfer characteristics. O.C.

**A89-34927\*** National Aeronautics and Space Administration. Lewis Research Center, Cleveland, OH.

**CORRELATIONS OF VELOCITY AND TEMPERATURE FLUCTUATIONS IN THE STAGNATION-POINT FLOW OF CIRCULAR CYLINDER IN TURBULENT FLOW**

C. R. WANG (NASA, Lewis Research Center, Cleveland, OH) IN: Heat transfer in gas turbine engines and three-dimensional flows; Proceedings of the Symposium, ASME Winter Annual Meeting, Chicago, IL, Nov. 27-Dec. 2, 1988. New York, American Society of Mechanical Engineers, 1988, p. 1-16. refs

Copyright

The present analyses of boundary layer flow and turbulence transport attempt to characterize the influence of freestream turbulence on the surface heat-transfer rate and stagnation point region skin friction of a circular cross-section cylinder in turbulent flow. The Reynolds stress-transport equations and k-epsilon two-equation turbulence modeling are used, yielding time-averaged turbulence double-correlations, mean-flow properties, surface heat-transfer rate, and skin-friction with freestream isotropic turbulence. A comparison of analytical results with experimental data indicates that large Reynolds normal stresses are induced at the boundary layer edge by the kinetic energy of the turbulence. O.C.

**A89-34928\*** National Aeronautics and Space Administration. Lewis Research Center, Cleveland, OH.

**EFFECTS OF WAKE PASSING ON STAGNATION REGION HEAT TRANSFER**

J. E. O'BRIEN (NASA, Lewis Research Center, Cleveland, OH) IN: Heat transfer in gas turbine engines and three-dimensional flows; Proceedings of the Symposium, ASME Winter Annual Meeting, Chicago, IL, Nov. 27-Dec. 2, 1988. New York, American Society of Mechanical Engineers, 1988, p. 17-28. refs

Copyright

In the present experimental study, an annular-flow wind tunnel fitted with a spoked-wheel wake generator was used to ascertain both time-averaged and time-resolved effects of wake passing in a cylinder stagnation region; the cylindrical spokes generated wakes simulating those of a turbine inlet guide vanes. The time-averaged heat transfer results obtained indicate an asymmetric heat-transfer coefficient distribution about the stagnation line, with higher heat-transfer coefficients on the side corresponding to the suction side of the turbine blade. Spectra of the hot-film records indicate that vortex-shedding is a major contributor to the unsteady buffeting of the test-cylinder boundary layer at circumferential stations located at both + and -60 deg from the stagnation line, despite making only a minor contribution to the stagnation line itself. O.C.

**A89-35002\*** National Aeronautics and Space Administration. Lewis Research Center, Cleveland, OH.

**A HIGH HEAT FLUX EXPERIMENT FOR VERIFICATION OF THERMOSTRUCTURAL ANALYSIS**

H. J. GLADDEN and M. E. MELIS (NASA, Lewis Research Center, Cleveland, OH) IN: Collected papers in heat transfer 1988; Proceedings of the ASME Winter Annual Meeting, Chicago, IL,

Nov. 27-Dec. 2, 1988. Volume 2. New York, American Society of Mechanical Engineers, 1988, p. 1-11. Previously announced in STAR as N89-12026. refs  
Copyright

A major concern in advancing the state of the art technologies for hypersonic vehicles is the development of an aeropropulsion system capable of handling the high heat fluxes during flight. The leading edges of such systems must not only tolerate the maximum heating rates, but must also minimize distortions to the flow field due to excessive blunting and/or thermal warping of the compression surface to achieve the high inlet performance required. A combined analytical and experimental effort to study the aerothermodynamic loads on actively cooled structures for hypersonic applications was established. A hydrogen/oxygen rocket engine was modified to establish a high enthalpy high heat flux environment. The facility provides heat flux levels from about 200 up to 10000 Btu/sq ft/sec. Cross flow and parallel flow regeneratively cooled model can be tested and analyzed by using cooling fluids of water and hydrogen. Results are presented of the experiment and the characteristics of the Hot Gas Test Facility. The predicted temperature results of the cross flow model are compared with the experimental data on the first monolithic specimens and are found to be in good agreement. Thermal stress analysis results are also presented. Author

**A89-36906\*#** Kansas Univ., Lawrence.  
**EFFECT OF INITIAL SWIRL DISTRIBUTION ON THE EVOLUTION OF A TURBULENT JET**

S. FAROKHI, R. TAGHAVI (Kansas, University, Lawrence), and E. J. RICE (NASA, Lewis Research Center, Cleveland, OH) AIAA Journal (ISSN 0001-1452), vol. 27, June 1989, p. 700-706. Previously cited in issue 20, p. 3344, Accession no. A88-48893. refs  
(Contract NCC3-56)  
Copyright

**A89-36908\*#** Lockheed Aeronautical Systems Co., Marietta, GA.

**EFFECTS OF NOZZLE EXIT BOUNDARY-LAYER CONDITIONS ON EXCITABILITY OF HEATED FREE JETS**

J. LEPICOVSKY and W. H. BROWN (Lockheed Aeronautical Systems Co., Marietta, GA) AIAA Journal (ISSN 0001-1452), vol. 27, June 1989, p. 712-718. Previously cited in issue 06, p. 806, Accession no. A88-20182. refs  
(Contract NAS3-23708)  
Copyright

**A89-36916\*#** United Technologies Research Center, East Hartford, CT.

**CALCULATION OF UNSTEADY FLOWS IN TURBOMACHINERY USING THE LINEARIZED EULER EQUATIONS**

KENNETH C. HALL (United Technologies Research Center, East Hartford, CT) and EDWARD F. CRAWLEY (MIT, Cambridge, MA) AIAA Journal (ISSN 0001-1452), vol. 27, June 1989, p. 777-787. Research supported by the General Electric Co., General Motors Corp., and Fannie and John Hertz Foundation. Previously announced in STAR as N87-22948. refs  
(Contract NSG-3079)  
Copyright

A method for calculating unsteady flows in cascades is presented. The model, which is based on the linearized unsteady Euler equations, accounts for blade loading shock motion, wake motion, and blade geometry. The mean flow through the cascade is determined by solving the full nonlinear Euler equations. Assuming the unsteadiness in the flow is small, then the Euler equations are linearized about the mean flow to obtain a set of linear variable coefficient equations which describe the small amplitude, harmonic motion of the flow. These equations are discretized on a computational grid via a finite volume operator and solved directly subject to an appropriate set of linearized boundary conditions. The steady flow, which is calculated prior to the unsteady flow, is found via a Newton iteration procedure. An important feature of the analysis is the use of shock fitting to

model steady and unsteady shocks. Use of the Euler equations with the unsteady Rankine-Hugoniot shock jump conditions correctly models the generation of steady and unsteady entropy and vorticity at shocks. In particular, the low frequency shock displacement is correctly predicted. Results of this method are presented for a variety of test cases. Predicted unsteady transonic flows in channels are compared to full nonlinear Euler solutions obtained using time-accurate, time-marching methods. The agreement between the two methods is excellent for small to moderate levels of flow unsteadiness. The method is also used to predict unsteady flows in cascades due to blade motion (flutter problem) and incoming disturbances (gust response problem).

Author

**A89-37825\*#** National Aeronautics and Space Administration. Lewis Research Center, Cleveland, OH.

**SUBHARMONIC AND FUNDAMENTAL HIGH AMPLITUDE EXCITATION OF AN AXISYMMETRIC JET**

GANESH RAMAN (NASA, Lewis Research Center; Sverdrup Technology, Inc., Cleveland, OH) and EDWARD J. RICE (NASA, Lewis Research Center, Cleveland, OH) AIAA, Shear Flow Conference, 2nd, Tempe, AZ, Mar. 13-16, 1989. 27 p. refs  
(AIAA PAPER 89-0993) Copyright

The effect of simultaneous excitation at the fundamental and subharmonic frequencies on the behavior of a circular jet shear layer is studied. Attention is given to the effect of the initial phase difference, the Strouhal number pair, and amplitudes of the fundamental and subharmonic tones. High-amplitude excitation devices which can provide a wide range of forcing conditions when used in conjunction with equipment that produces complex waveforms are used. K.K.

**A89-37931\*** National Aeronautics and Space Administration. Lewis Research Center, Cleveland, OH.

**THE SECONDARY FLOW AND ITS STABILITY FOR NATURAL CONVECTION IN A TALL VERTICAL ENCLOSURE**

ARNON CHAIT (NASA, Lewis Research Center, Cleveland, OH) and SEPPO A. KORPELA (Ohio State University, Columbus) Journal of Fluid Mechanics (ISSN 0022-1120), vol. 200, March 1989, p. 189-216. refs  
(Contract NSF CBT-85-12042; NSF ECS-85-15056)  
Copyright

The multicellular flow between two vertical parallel plates is numerically simulated using a time-splitting pseudospectral method. The steady flow of air and the time-periodic flow of oil are investigated, and descriptions of these flows using both physical and spectral approaches are presented. The time dependence of the flow and temperature fields of oil are shown, and the dynamics of the process is discussed. The spectral transfer of energy among the axial modes comprising the flow is explored. The three-dimensional linear stability of the multicellular air flow is parametrically studied. The domain of stable two-dimensional cellular motion is found to be constrained by the Eckhaus instability and by two types of monotone instability. The two-dimensional multicellular flow is unstable above a Grashof number of about 8550. S.A.V.

**A89-38619\*** Arizona Univ., Tucson.

**THREE-DIMENSIONAL WAVE PACKETS AND INSTABILITY WAVES IN FREE SHEAR LAYERS AND THEIR RECEPTIVITY**

THOMAS F. Balsa (Arizona, University, Tucson) Journal of Fluid Mechanics (ISSN 0022-1120), vol. 201, April 1989, p. 77-97. refs  
(Contract NAG3-485)  
Copyright

A study is made of the evolution of strongly three-dimensional disturbances which are generated by a point force in a parallel mixing layer. When the input force is a pulse, a wave packet develops whose wavefronts are approximately parallel to the spanwise direction. This is in sharp contrast to a wave packet in a wall boundary layer for which the wavefronts are strongly curved. On the other hand, when the input disturbance is oscillating harmonically in time, a spatially growing instability wave develops

in a downstream wedge of  $(x, z)$ -space. The size of this wedge, as a function of excitation frequency and velocity ratio, is determined. The receptivity of the shear layer to pulse-type and harmonic excitation is also studied. It is found that the shear layer is especially sensitive to relatively high-frequency forcing on its centreline. Author

**A89-40400\*** National Aeronautics and Space Administration. Lewis Research Center, Cleveland, OH.

## RESPONSE OF A CHEMICALLY REACTING SHEAR LAYER TO STREAMWISE VORTICITY

R. W. CLAUS (NASA, Lewis Research Center, Cleveland, OH) AIAA, Shear Flow Conference, 2nd, Tempe, AZ, Mar. 13-16, 1989. 14 p. refs

(AIAA PAPER 89-0978) Copyright

A series of Direct Numerical Simulations are performed of a temporally evolving shear layer subject to both harmonic (2D) and streamwise (3D) forcing. The interaction and coupling of these various 2D and 3D modes is shown to significantly alter the development of the flow. The scale of the 3D modes is quite important to the coupling process with greatly enhanced mixing and product formation resulting from 3D modes that are rapidly amplified by the spanwise vorticity. In general, the longer wavelength 3D modes are found to be highly efficient at increasing the momentum transport while the shorter wavelengths increase mass transport. Author

**A89-41803\*** National Aeronautics and Space Administration. Lewis Research Center, Cleveland, OH.

## ASSESSMENT OF NUMERICAL TECHNIQUES FOR UNSTEADY FLOW CALCULATIONS

KWANG-CHUNG HSIEH (NASA, Lewis Research Center; Sverdrup Technology, Inc., Cleveland, OH) IN: AIAA Computational Fluid Dynamics Conference, 9th, Buffalo, NY, June 13-15, 1989, Technical Papers. Washington, DC, American Institute of Aeronautics and Astronautics, 1989, p. 280-291. refs

(AIAA PAPER 89-1956) Copyright

The characteristics of unsteady flow motions have long been a serious concern in the study of various fluid dynamic and combustion problems. With the advancement of computer resources, numerical approaches to these problems appear to be feasible. The objective of this paper is to assess the accuracy of several numerical schemes for unsteady flow calculations. In the present study, Fourier error analysis is performed for various numerical schemes based on a two-dimensional wave equation. Four methods sieved from the error analysis are then adopted for further assessment. Model problems include unsteady quasi-one-dimensional inviscid flows, two-dimensional wave propagations, and unsteady two-dimensional inviscid flows. According to the comparison between numerical and exact solutions, although second-order upwind scheme captures the unsteady flow and wave motions quite well, it is relatively more dissipative than sixth-order central difference scheme. Among various numerical approaches tested in this paper, the best performed one is Runge-Kutta method for time integration and six-order central difference for spatial discretization. Author

**A89-42090\*** Lehigh Univ., Bethlehem, PA.

## ASYMPTOTIC STRUCTURE AND SIMILARITY SOLUTIONS FOR THREE-DIMENSIONAL TURBULENT BOUNDARY LAYERS

A. T. DEGANI and J. D. A. WALKER (Lehigh University, Bethlehem, PA) AIAA, Fluid Dynamics, Plasma Dynamics and Lasers Conference, 20th, Buffalo, NY, June 12-14, 1989. 15 p. refs

(Contract NAG3-771)

(AIAA PAPER 89-1863) Copyright

The asymptotic structure of the three-dimensional turbulent boundary layer is investigated in the limit of large Reynolds numbers. A self-consistent, but relatively complex, two-layer structure exists and the simplest situation, corresponding to a plane of symmetry, is considered in this paper as a first step. The adjustment of the streamwise velocity to relative rest, through an outer defect layer and then an inner wall layer, is similar to that in two-dimensional flow. The adjustment of the cross-streamwise

velocity is more complicated and it is shown that two terms in the expansion are required to obtain useful results, and in particular to obtain the velocity skew angle at the wall near the symmetry plane. The conditions under which self-similarity is achieved near a plane of symmetry are investigated. A set of ordinary differential equations is developed which describe the streamwise and cross-streamwise velocities near a plane of symmetry in a self-similar flow through two orders of magnitude. Calculated numerical solutions of these equations yield trends which are consistent with experimental observations. Author

**A89-43210\*** State Univ. of New York, Buffalo.

## PREDICTION OF UNSTEADY ROTOR-SURFACE HEAT TRANSFER FROM WAKE PASSINGS

DALE B. TAULBEE and LE TRAN (New York, State University, Buffalo) AIAA, Thermophysics Conference, 24th, Buffalo, NY, June 12-14, 1989. 11 p. refs

(Contract NAG3-581)

(AIAA PAPER 89-1692) Copyright

Predictions using boundary-layer theory with a low-Reynolds number kinetic-energy/dissipation turbulence model are reported for the unsteady heat-flux distributions on the rotor blade surfaces. With an assumed sinusoidal variation for the unsteady surface pressure depicting the effects of convected wake segments, unsteady inviscid-freestream velocity and total enthalpy distributions are determined. Unsteady variations in freestream turbulence due to the wake passings are also considered. The unsteady boundary-layer equations, subject to these freestream conditions, are solved numerically. It was found that most of the unsteady variations in surface heat transfer are due to unsteady pressure changes and not variations in the freestream turbulence. Calculations are made for the Garrett TFE 731-2 HP turbine and the magnitudes of the heat-transfer variations are compared with the measurements of Dunn and Seymour. Author

**A89-43235\*** Manhattan Coll., New York.

## RADIATIVE HEAT TRANSFER IN ROCKET THRUST CHAMBERS AND NOZZLES

K. J. HAMMAD and M. H. N. NARAGHI (Manhattan College, Riverdale, NY) AIAA, Thermophysics Conference, 24th, Buffalo, NY, June 12-14, 1989. 10 p. refs

(Contract NAG3-892)

(AIAA PAPER 89-1720) Copyright

Numerical models based on the discrete exchange factor (DEF) and the zonal methods for radiative analysis of rocket engines containing a radiatively participating medium have been developed. These models implement a new technique for calculating the direct exchange factors to account for possible blockage by the nozzle throat. Given the gas and surface temperature distributions, engine geometry, and radiative properties, the models compute the wall radiative heat fluxes at different axial positions. The results of sample calculations for a typical rocket engine (engine 700 at NASA), which uses RP-1 (a kerosene-type propellant), are presented for a wide range of surface and gas properties. It is found that the heat transfer by radiation can reach up to 50 percent of that due to convection. The maximum radiative heat flux is at the inner side of the engine, where the gas temperature is the highest. While the results of both models are in excellent agreement, the computation time of the DEF method is found to be much smaller. Author

**A89-45397\*** National Aeronautics and Space Administration. Lewis Research Center, Cleveland, OH.

## CALCULATION OF SHOCKED FLOWS BY MATHEMATICAL PROGRAMMING

JOHN E. LAVERY (NASA, Lewis Research Center, Cleveland, OH) IN: International Conference on Numerical Methods in Fluid Dynamics, 11th, Williamsburg, VA, June 27-July 1, 1988, Proceedings. Berlin and New York, Springer-Verlag, 1989, p. 360-363. refs

Copyright

A framework for using mathematical programming to solve Burgers' equation is presented. The steady-state inviscid Burgers'



equation with given boundary conditions is considered, and the physically relevant solution is discretized using a four-point difference scheme for the viscous term and a two-point difference scheme for the inviscid term. The framework is then used to solve the Euler equations for quasi-one-dimensional flows on grids with variable spacing. C.D.

**A89-45398\*** National Aeronautics and Space Administration. Lewis Research Center, Cleveland, OH.

## UNIVERSAL LIMITER FOR HIGH ORDER EXPLICIT CONSERVATIVE ADVECTION SCHEMES

B. P. LEONARD (NASA, Lewis Research Center, Cleveland, OH) and H. S. NIKNAFS (Akron, University, OH) IN: International Conference on Numerical Methods in Fluid Dynamics, 11th, Williamsburg, VA, June 27-July 1, 1988, Proceedings. Berlin and New York, Springer-Verlag, 1989, p. 364-368. Copyright

A simple method for construction of nonoscillatory, explicit, conservative advection schemes of arbitrarily high accuracy is described. Four test profiles are considered: an isolated sine-squared wave, a unit step function, a semiellipse, and a narrow Gaussian. A universal limiter guarantees monotonic resolution of the step. Sharpness increases uniformly with the order of the base scheme. C.D.

**A89-45424\*** National Aeronautics and Space Administration. Lewis Research Center, Cleveland, OH.

## A DETAILED ANALYSIS OF INVISCID FLUX SPLITTING ALGORITHMS FOR REAL GASES WITH EQUILIBRIUM OR FINITE-RATE CHEMISTRY

JIAN-SHUN SHUEN (NASA, Lewis Research Center; Sverdrup Technology, Inc., Cleveland, OH), MENG-SING LIOU (NASA, Lewis Research Center, Cleveland, OH), and BRAM VAN LEER (Michigan, University, Ann Arbor) IN: International Conference on Numerical Methods in Fluid Dynamics, 11th, Williamsburg, VA, June 27-July 1, 1988, Proceedings. Berlin and New York, Springer-Verlag, 1989, p. 543-547. refs Copyright

The extension of the known flux-vector and flux-difference splittings to real gases via rigorous mathematical procedures is demonstrated. Formulations of both equilibrium and finite-rate chemistry for real-gas flows are described, with emphasis on derivations of finite-rate chemistry. Split-flux formulas from other authors are examined. A second-order upwind-based TVD scheme is adopted to eliminate oscillations and to obtain a sharp representation of discontinuities. C.D.

**A89-46749\*#** National Aeronautics and Space Administration. Lewis Research Center, Cleveland, OH.

## GAS DENSITY EFFECT ON DROPSIZE OF SIMULATED FUEL SPRAYS

ROBERT D. INGEBO (NASA, Lewis Research Center, Cleveland, OH) AIAA, ASME, SAE, and ASEE, Joint Propulsion Conference, 25th, Monterey, CA, July 10-13, 1989. 9 p. Previously announced in STAR as N89-22053. refs (AIAA PAPER 89-2322) Copyright

Two-phase flow in pneumatic two-fluid fuel nozzles was investigated experimentally to determine the effect of atomizing-gas density and gas mass-flux on liquid-jet breakup in sonic-velocity gas-flow. Dropsizes data were obtained for the following atomizing-gases: nitrogen; argon; carbon dioxide; and helium. They were selected to cover a gas molecular-weight range of 4 to 44. Atomizing-gas mass-flux ranged from 6 to 50 g/sq cm-sec and four differently sized two-fluid fuel nozzles were used having orifice diameters that varied from 0.32 to 0.56 cm. The ratio of liquid-jet diameter to SMD,  $D_{sub} / o/D_{sub} 32$ , was correlated with aerodynamic and liquid-surface forces based on the product of the Weber and Reynolds number, and gas-to-liquid density ratio,  $\rho_{sub} g / \rho_{sub} 1$ . To correlate spray dropsizes with breakup forces produced by using different atomizing-gases, a new molecular-scale dimensionless group was derived. The derived dimensionless group was used to obtain an expression for the ratio of liquid-jet diameter to SMD,  $D_{sub} / o/D_{sub} 32$ . The

mathematical expression of this phenomenon incorporates the product of the Weber and Reynolds number, liquid viscosity, surface tension, acoustic gas velocity, the RMS velocity of gas molecules, the acceleration of gas molecules due to gravity, and gas viscosity. The mathematical expression encompassing these parameters agrees well with the atomization theory for liquid-jet breakup in high velocity gas flow. Also, it was found that at the same gas mass-flux, helium was considerably more effective than nitrogen in producing small droplet sprays with SMD's in the order of 5 micrometers. Author

**A89-46934\*#** National Aeronautics and Space Administration. Lewis Research Center, Cleveland, OH.

## A GENERALIZED ONE DIMENSIONAL COMPUTER CODE FOR TURBOMACHINERY COOLING PASSAGE FLOW CALCULATIONS

GANESH N. KUMAR (NASA, Lewis Research Center; Sverdrup Technology, Inc., Cleveland, OH), RICHARD J. ROELKE (NASA, Lewis Research Center, Cleveland, OH), and PETER L. MEITNER (NASA, Lewis Research Center; U.S. Army, Propulsion Directorate, Cleveland, OH) AIAA, ASME, SAE, and ASEE, Joint Propulsion Conference, 25th, Monterey, CA, July 10-13, 1989. 13 p. Previously announced in STAR as N89-22862. refs (AIAA PAPER 89-2574)

A generalized one-dimensional computer code for analyzing the flow and heat transfer in the turbomachinery cooling passages was developed. This code is capable of handling rotating cooling passages with turbulators, 180 degree turns, pin fins, finned passages, by-pass flows, tip cap impingement flows, and flow branching. The code is an extension of a one-dimensional code developed by P. Meitner. In the subject code, correlations for both heat transfer coefficient and pressure loss computations were developed to model each of the above mentioned type of coolant passages. The code has the capability of independently computing the friction factor and heat transfer coefficient on each side of a rectangular passage. Either the mass flow at the inlet to the channel or the exit plane pressure can be specified. For a specified inlet total temperature, inlet total pressure, and exit static pressure, the code computes the flow rates through the main branch and the subbranches, flow through tip cap for impingement cooling, in addition to computing the coolant pressure, temperature, and heat transfer coefficient distribution in each coolant flow branch. Predictions from the subject code for both nonrotating and rotating passages agree well with experimental data. The code was used to analyze the cooling passage of a research cooled radial rotor. Author

**A89-47122\*#** Massachusetts Inst. of Tech., Cambridge.

## VAPOR CONDENSATION AT A TURBULENT LIQUID SURFACE IN SYSTEMS WITH POSSIBLE SPACED-BASED APPLICATIONS

J. S. BROWN, M. R. HELMICK, and A. A. SONIN (MIT, Cambridge, MA) AIAA, ASME, SAE, and ASEE, Joint Propulsion Conference, 25th, Monterey, CA, July 10-13, 1989. 13 p. refs (Contract NAG3-731) (AIAA PAPER 89-2846) Copyright

Brown and Sonin's (1989) correlation is used to predict the condensation rate in three different systems and the results are compared with experimental data. These systems are: (1) a cylindrical system with turbulent mixing provided by an axial submerged jet, (2) a channel flow with grid-induced turbulence, and (3) a swirling film flow in a cylinder. The first and third system are of interest for space applications. While all the present data are from ground-based laboratory tests, the comparisons are restricted to conditions of low Richardson number, where the local condensation rate per unit area at the liquid surface is not affected by buoyancy effects. K.K.

## A89-47161\*# General Motors Corp., Indianapolis, IN. A NUMERICAL AND EXPERIMENTAL STUDY OF CONFINED SWIRLING JETS

M. NIKJOOY, H. C. MONGIA (General Motors Corp., Allison Gas Turbine Div., Indianapolis, IN), G. S. SAMUELSEN, and V. G.

## 34 FLUID MECHANICS AND HEAT TRANSFER

MCDONELL (California, University, Irvine) AIAA, ASME, SAE, and ASEE, Joint Propulsion Conference, 25th, Monterey, CA, July 10-13, 1989. 14 p. refs  
(Contract NAS3-2450)  
(AIAA PAPER 89-2898) Copyright

A numerical and experimental study of a confined strong swirling flow is presented. Detailed velocity measurements are made using a two-component laser Doppler velocimeter (LDV) technique. Computations are performed using a differential second-moment (DSM) closure. The effect of inlet dissipation rate on calculated mean and turbulence fields is investigated. Various model constants are employed in the pressure-strain model to demonstrate their influences on the predicted results. Finally, comparison of the DSM calculations with the algebraic second-moment (ASM) closure results shows that the DSM is better suited for complex swirling flow analysis. Author

**A89-48958\*** # National Aeronautics and Space Administration. Lewis Research Center, Cleveland, OH.

### NUMERICAL STUDIES OF THE EFFECTS OF JET-INDUCED MIXING ON LIQUID-VAPOR INTERFACE CONDENSATION

CHIN-SHUN LIN (NASA, Lewis Research Center; Analox Corp., Cleveland, OH) AIAA, Thermophysics Conference, 24th, Buffalo, NY, June 12-14, 1989. 21 p. Previously announced in STAR as N89-23818. refs  
(Contract NAS3-24564)  
(AIAA PAPER 89-1744) Copyright

Numerical solutions of jet-induced mixing in a partially full cryogenic tank are presented. An axisymmetric laminar jet is discharged from the central part of the tank bottom toward the liquid-vapor interface. Liquid is withdrawn at the same volume flow rate from the outer part of the tank. The jet is at a temperature lower than the interface, which is maintained at a certain saturation temperature. The interface is assumed to be flat and shear-free and the condensation-induced velocity is assumed to be negligibly small compared with radial interface velocity. Finite-difference method is used to solve the nondimensional form of steady state continuity, momentum, and energy equations. Calculations are conducted for jet Reynolds numbers ranging from 150 to 600 and Prandtl numbers ranging from 0.85 to 2.65. The effects of above stated parameters on the condensation Nusselt and Stanton numbers which characterize the steady-state interface condensation process are investigated. Detailed analysis to gain a better understanding of the fundamentals of fluid mixing and interface condensation is performed. Author

**A89-50071\*** # National Aeronautics and Space Administration. Lewis Research Center, Cleveland, OH.

### TRANSITION LIMITS FOR WATER-DROPLET CRYSTALLIZATION WITH THE NASA LEWIS ICING NOZZLE

C. JOHN MAREK (NASA, Lewis Research Center, Cleveland, OH) Journal of Aircraft (ISSN 0021-8669), vol. 26, Sept. 1989, p. 887, 888. Previously cited in issue 07, p. 1004, Accession no. A88-22209.  
Copyright

**A89-50147\*** Minnesota Univ., Minneapolis.

### A BLOCK-CORRECTED SUBDOMAIN SOLUTION PROCEDURE FOR RECIRCULATING FLOW CALCULATIONS

M. E. BRAATEN and S. V. PATANKAR (Minnesota, University, Minneapolis) Numerical Heat Transfer (ISSN 1040-7790), vol. 15, no. 1, 1989, p. 1-20. refs  
(Contract NAG3-596)  
Copyright

This paper describes a robust and efficient subdomain solution procedure for two-dimensional recirculating flows. The solution domain is divided into a number of overlapping subdomains, and a direct fully coupled solution is obtained for each subdomain using a sparse matrix form of LU decomposition. An effective parabolic block correction procedure, which calculates global corrections to the tentative solution by a marching technique similar to that used for boundary layer flows, is used to accelerate the convergence of the basic procedure. The use of effective block

correction is found to be essential for the success of the subdomain approach on strongly recirculating flows. In a number of laminar two-dimensional flows, the new block-corrected method performed extremely well, rivaling the best direct methods in execution time, while requiring substantially less computer storage. The new method proved to be from two to ten times faster than conventional iterative methods, while requiring only a moderate increase in storage. Author

**A89-51873\*** Washington Univ., Seattle.

### THE USE OF DIRECT NUMERICAL SIMULATION IN THE STUDY OF TURBULENT, CHEMICALLY-REACTING FLOWS

J. J. RILEY (Washington, University, Seattle) and P. A. MCMURTRY (Sandia National Laboratories, Livermore, CA) IN: Turbulent reactive flows. New York, Springer-Verlag, 1989, p. 486-514. Research supported by DOE. refs  
(Contract NAS3-24229; N00014-87-K-0174)  
Copyright

Full turbulence simulations are used here to study the effects of chemical heat release on the large-scale structures in turbulent mixing layers. In agreement with laboratory results, it is found that the heat release lowers the rate at which the mixing layer grows and reduces the rate at which chemical products are formed. The baroclinic torque and thermal expansion in the mixing layer produce changes in the flame vortex structure that act to produce more diffuse vortices than in the constant density case, resulting in lower rotation rates of the large-scale structures. Previously unexplained anomalies observed in the mean velocity profiles of reacting jets and mixing layer are shown to result from vorticity generation by baroclinic torques. Calculations of the energy in the various wavenumbers shows that the heat release has a stabilizing effect on the growth rate of individual modes. This methodology can be applied for Reynolds numbers less than several hundred and for Damkohler numbers less than about ten. C.D.

**A89-51880\*** California Univ., Davis.

### PDF - TRANSPORT EQUATIONS FOR CHEMICALLY REACTING FLOWS

W. KOLLMANN (California, University, Davis) (CNRS and NSF, U.S.A.-France Joint Workshop on Turbulent Reactive Flows, Rouen, France, July 6-10, 1987) IN: Turbulent reactive flows. New York, Springer-Verlag, 1989, p. 715-730. refs  
(Contract NAG3-667)  
Copyright

The closure problem for the transport equations for pdf and the characteristic functions of turbulent, chemically reacting flows is addressed. The properties of the linear and closed equations for the characteristic functional for Eulerian and Lagrangian variables are established, and the closure problem for the finite-dimensional case is discussed for pdf and characteristic functions. It is shown that the closure for the scalar dissipation term in the pdf equation developed by Dopazo (1979) and Kollmann et al. (1982) results in a single integral, in contrast to the pdf, where double integration is required. Some recent results using pdf methods obtained for turbulent flows with combustion, including effects of chemical nonequilibrium, are discussed. C.D.

**A89-51883\*** Michigan Univ., Ann Arbor.

### TURBULENT MULTIPHASE FLOWS

G. M. FAETH (Michigan, University, Ann Arbor) IN: Turbulent reactive flows. New York, Springer-Verlag, 1989, p. 784-814. refs  
(Contract AF-AFOSR-85-0244; DAAL03-86-K-0154; NAG3-190; N00014-85-C-0148)  
Copyright

Measurements and predictions of the structure of several multiphase flows are considered. The properties of dense sprays near the exits of pressure-atomizing injectors and of noncombusting and combusting dilute dispersed flows in round-jet configurations are addressed. It is found that the properties of dense sprays exhibit structure and mixing properties similar to variable-density single-phase flows at high Reynolds numbers within the atomization regime. The degree of development and turbulence levels at the

injector exit have a surprisingly large effect on the structure and mixing properties of pressure-atomized sprays, particularly when the phase densities are large. Contemporary stochastic analysis of dilute multiphase flows provides encouraging predictions of turbulent dispersion for a wide variety of jetlike flows, particle-laden jets in gases and liquids, noncondensing and condensing bubbly jets, and nonevaporating, evaporating, and combusting sprays.

C.D.

**A89-52500\*** General Motors Corp., Indianapolis, IN.  
**A NUMERICAL AND EXPERIMENTAL STUDY OF COAXIAL JETS**

M. NIKJOOY, K. C. KARKI, H. C. MONGIA (General Motors Corp., Allison Gas Turbine Div., Indianapolis, IN), V. G. MCDONELL, and G. S. SAMUELSEN (California, University, Irvine) *International Journal of Heat and Fluid Flow* (ISSN 0142-727X), vol. 10, Sept. 1989, p. 253-261. refs

(Contract NAS3-24350)

Copyright

An algebraic stress model and the standard k-epsilon model is applied to predict the mean and turbulence quantities for axisymmetric, nonswirling coaxial jets without confinement. To investigate the effects of numerical (false) diffusion on the predicted results, three different discretization schemes, namely, hybrid, power-law, and the flux-spline, are employed. In addition, an experimental study is conducted to provide data of good quality, especially near the inlet, for model assessment. The results show that the use of the algebraic stress model leads to better agreement between the numerical results and experimental data. Author

**A89-53172\*** National Aeronautics and Space Administration.  
 Lewis Research Center, Cleveland, OH.

**APPLICATION OF MULTI-GRID METHODS FOR SOLVING THE NAVIER-STOKES EQUATIONS**

A. O. DEMUREN (NASA, Lewis Research Center, Cleveland, OH; Lagos, University, Nigeria) *Institution of Mechanical Engineers, Proceedings, Part C - Journal of Mechanical Engineering Science* (ISSN 0954-4062), vol. 203, no. C4, 1989, p. 255-265. Research supported by DFG. refs

Copyright

This paper presents the application of a class of multi-grid methods to the solution of the Navier-Stokes equations for two-dimensional laminar flow problems. The methods consists of combining the full approximation scheme-full multi-grid technique (FAS-FMG) with point-, line- or plane-relaxation routines for solving the Navier-Stokes equations in primitive variables. The performance of the multi-grid methods is compared to those of several single-grid methods. The results show that much faster convergence can be procured through the use of the multi-grid approach than through the various suggestions for improving single-grid methods. The importance of the choice of relaxation scheme for the multi-grid method is illustrated. Author

**A89-53262\*#** Manhattan Coll., New York.  
**RADIATIVE TRANSFER IN RECTANGULAR ENCLOSURES - A DISCRETIZED EXCHANGE FACTOR SOLUTION**

M. H. N. NARAGHI (Manhattan College, Riverdale, NY) and M. KASSEMI (NASA, Lewis Research Center, Cleveland, OH) IN: *ASME 1988 National Heat Transfer Conference, Houston, TX, July 24-27, 1988, Proceedings. Volume 1.* New York, American Society of Mechanical Engineers, 1988, p. 259-267. refs

Copyright

The discretized exchange factor method is used to analyze radiative exchange in a rectangular enclosure. The results compare excellently with those of other methods, especially the zonal method. Since the direct exchange factors are between nodal points no integration is necessary for evaluation of these factors. It is found that the present approach provides accurate results even when a small number of nodes is used. Author

**A89-53282\*#** National Aeronautics and Space Administration.  
 Lewis Research Center, Cleveland, OH.  
**HEAT TRANSFER IN AEROSPACE PROPULSION**

R. J. SIMONEAU, R. C. HENDRICKS, and H. J. GLADDEN (NASA, Lewis Research Center, Cleveland, OH) IN: *ASME 1988 National Heat Transfer Conference, Houston, TX, July 24-27, 1988, Proceedings. Volume 3.* New York, American Society of Mechanical Engineers, 1988, p. 1-22. Previously announced in STAR as N88-23957. refs

Copyright

Presented is an overview of heat transfer related research in support of aerospace propulsion, particularly as seen from the perspective of the NASA Lewis Research Center. Aerospace propulsion is defined to cover the full spectrum from conventional aircraft power plants through the Aerospace Plane to space propulsion. The conventional subsonic/supersonic aircraft arena, whether commercial or military, relies on the turbine engine. A key characteristic of turbine engines is that they involve fundamentally unsteady flows which must be properly treated. Space propulsion is characterized by very demanding performance requirements which frequently push systems to their limits and demand tailored designs. The hypersonic flight propulsion systems are subject to severe heat loads and the engine and airframe are truly one entity. The impact of the special demands of each of these aerospace propulsion systems on heat transfer is explored.

Author

**A89-53286\*#** National Aeronautics and Space Administration.  
 Lewis Research Center, Cleveland, OH.

**UNSTEADY HEAT TRANSFER IN TURBINE BLADE DUCTS - FOCUS ON COMBUSTOR SOURCES**

K. J. BAUMEISTER (NASA, Lewis Research Center, Cleveland, OH) and R. HUFF (Huff and Associates, Cleveland, OH) IN: *ASME 1988 National Heat Transfer Conference, Houston, TX, July 24-27, 1988, Proceedings. Volume 3.* New York, American Society of Mechanical Engineers, 1988, p. 319-328. Previously announced in STAR as N88-18870. refs

Copyright

Thermal waves generated by either turbine rotor blades cutting through nonuniform combustor temperature fields or unsteady burning could lead to thermal fatigue cracking in the blades. To determine the magnitude of the thermal oscillation in blades with complex shapes and material compositions, a finite element Galerkin formulation has been developed to study combustor generated thermal wave propagation in a model two-dimensional duct with a uniform plug flow profile. The reflection and transmission of the thermal waves at the entrance and exit boundaries are determined by coupling the finite element solutions at the entrance and exit to the eigenfunctions of an infinitely long adiabatic duct. Example solutions are presented. In general, thermal wave propagation from an air passage into a metallic blade wall is small and not a problem. However, if a thermal barrier coating is applied to a metallic surface under conditions of a high heat transfer, a good impedance match is obtained and a significant portion of the thermal wave can pass into the blade material. Author

**A89-53288\*#** National Aeronautics and Space Administration.  
 Lewis Research Center, Cleveland, OH.

**THERMOSOLUTAL CONVECTION IN HIGH-ASPECT-RATIO ENCLOSURES**

L. W. WANG (NASA, Lewis Research Center, Cleveland, OH) and C. T. CHEN (National Cheng Kung University, Tainan, Republic of China) IN: *ASME 1988 National Heat Transfer Conference, Houston, TX, July 24-27, 1988, Proceedings. Volume 3.* New York, American Society of Mechanical Engineers, 1988, p. 403-408. Previously announced in STAR as N88-18871. refs

Copyright

Convection in high-aspect-ratio rectangular enclosures with combined horizontal temperature and concentration gradients is studied experimentally. An electrochemical system is employed to impose the concentration gradients. The solutal buoyancy force either opposes or augments the thermal buoyancy force. Due to a large difference between the thermal and solutal diffusion rates the flow possesses double-diffusive characteristics. Various complex flow patterns are observed with different experimental conditions. Author

## 34 FLUID MECHANICS AND HEAT TRANSFER

**A89-53307\*** # National Aeronautics and Space Administration. Lewis Research Center, Cleveland, OH.

**CFD IN THE CONTEXT OF IHPTET - THE INTEGRATED HIGH PERFORMANCE TURBINE ENGINE TECHNOLOGY PROGRAM**  
ROBERT J. SIMONEAU (NASA, Lewis Research Center, Cleveland, OH) and DALE A. HUDSON (USAF, Wright Research and Development Center, Wright-Patterson AFB, OH) AIAA, ASME, SAE, and ASEE, Joint Propulsion Conference, 25th, Monterey, CA, July 10-12, 1989. 20 p. Previously announced in STAR as N89-26174. refs

(AIAA PAPER 89-2904) Copyright

The Integrated High Performance Turbine Engine Technology (IHPTET) Program is an integrated DOD/NASA technology program designed to double the performance capability of today's most advanced military turbine engines as we enter the twenty-first century. Computational Fluid Dynamics (CFD) is expected to play an important role in the design/analysis of specific configurations within this complex machine. In order to do this, a plan is being developed to ensure the timely impact of CFD on IHPTET. The developing philosophy of CFD in the context of IHPTET is discussed. The key elements in the developing plan and specific examples of state-of-the-art CFD efforts which are IHPTET turbine engine relevant are discussed. Author

**A89-54424\*** # National Aeronautics and Space Administration. Lewis Research Center, Cleveland, OH.

**HIGH SPEED CORNER AND GAP-SEAL COMPUTATIONS USING AN LU-SGS SCHEME**

WILLIAM J. COIRIER (NASA, Lewis Research Center, Cleveland, OH) AIAA, ASME, SAE, and ASEE, Joint Propulsion Conference, 25th, Monterey, CA, July 10-12, 1989. 15 p. Previously announced in STAR as N89-27103. refs

(AIAA PAPER 89-2669) Copyright

The hybrid Lower-Upper Symmetric Gauss-Seidel (LU-SGS) algorithm was added to a widely used series of 2D/3D Euler/Navier-Stokes solvers and was demonstrated for a particular class of high-speed flows. A limited study was conducted to compare the hybrid LU-SGS for approximate Newton iteration and diagonalized Beam-Warming (DBW) schemes on a work and convergence history basis. The hybrid LU-SGS algorithm is more efficient and easier to implement than the DBW scheme originally present in the code for the cases considered. The code was validated for the hypersonic flow through two mutually perpendicular flat plates and then used to investigate the flow field in and around a simplified scramjet module gap seal configuration. Due to the similarities, the gap seal flow was compared to hypersonic corner flow at the same freestream conditions and Reynolds number. Author

**A89-54766\*** State Univ. of New York, Buffalo.

**ADVANCED DEVELOPMENT OF THE BOUNDARY ELEMENT METHOD FOR STEADY-STATE HEAT CONDUCTION**

G. F. DARGUSH and PRASANTA K. BANERJEE (New York, State University, Buffalo) International Journal for Numerical Methods in Engineering (ISSN 0029-5981), vol. 28, Sept. 1989, p. 2123-2142. Research supported by General Motors Corp. refs

(Contract NAS3-23697)

Copyright

Considerable progress has been made in recent years toward advancing the state-of-the-art in solid mechanics boundary element technology. In the present work, much of this new technology is applied in the development of a general-purpose boundary element method (BEM) for steady-state heat conduction. In particular, the BEM implementation involves the use of higher-order conforming elements, self-adaptive integration and multi-region capability. Two- and three-dimensional, as well as axisymmetric analysis, are incorporated within a unified framework. In addition, techniques are introduced for the calculation of boundary flux, and for the inclusion of thermal resistance across interfaces. As a final extension, an efficient formulation is developed for the analysis of solid three-dimensional bodies with embedded holes. For this last class of problems, the new BEM formulation is particularly attractive, since use of the alternatives (i.e. finite element or finite

difference methods) is not practical. A number of detailed examples illustrate the suitability and robustness of the present approach for steady-state heat conduction. Author

**N89-10242\*** # National Aeronautics and Space Administration. Lewis Research Center, Cleveland, OH.

**DISCRETIZATION FORMULAS FOR UNSTRUCTURED GRIDS**

KENNETH J. BAUMEISTER 1988 12 p Proposed for presentation at the 2nd International Conference on Numerical Grid Generation in Computational Fluid Dynamics, Miami Beach, Fla., 5-8 Dec. 1988; sponsored by NASA, AFOSR and Miami Univ.

(NASA-TM-101298; E-4094; NAS 1.15:101298) Avail: NTIS HC A03/MF A01 CSCL 20/4

The Galerkin weighted residual technique using linear triangular weight functions is employed to develop finite difference formula in cartesian coordinates for the Laplacian operator, first derivative operators and the function for unstructured triangular grids. The weighted residual coefficients associated with the weak formulation of the Laplacian operator are shown to agree with the Taylor series approach on a global average. In addition, a simple algorithm is presented to determine the Voronoi (finite difference) area of an unstructured grid. Author

**N89-10246\*** # National Aeronautics and Space Administration. Lewis Research Center, Cleveland, OH.

**HIGH-RESOLUTION HEAT-TRANSFER-COEFFICIENT MAPS APPLICABLE TO COMPOUND-CURVE SURFACES USING LIQUID CRYSTALS IN A TRANSIENT WIND TUNNEL**

TERRY V. JONES (Oxford Univ., England) and STEVEN A. HIPPENSTEELE Aug. 1988 12 p Presented at the ASME National Heat Transfer Conference, Pittsburgh, Pa., 9-12 Aug. 1987

(NASA-TM-89855; E-3269; NAS 1.15:89855) Avail: NTIS HC A03/MF A01 CSCL 20/4

Tests were performed in a transient heat transfer tunnel in which the model under test was preheated prior to allowing room temperature air to be suddenly drawn over the model. The resulting movement of isothermal contours on the model is revealed using a surface coating of thermochromic liquid crystals that display distinctive colors at particular temperatures. A video record is obtained of a temperature and time data pair for all points on the model during a single test. Experiments on a duct model are reported in which the model was preheated using a hot air stream. A manner in which initial model temperature nonuniformities could be taken into account was investigated. The duct model was also tested with a steady-state measurement technique and results were compared with the transient measurements, but recognizing that differences existed between the upstream thermal boundary conditions. The steady-state and transient measurements were shown to be consistent with predicted values. The main advantage of this transient heat transfer technique using liquid crystals is that since the test model need not be actively heated, high-resolution measurements on surfaces with complex shapes may be obtained. Author

**N89-12010\*** # Detroit Diesel Allison, Indianapolis, IN.

**IMPROVED NUMERICAL METHODS FOR TURBULENT VISCOUS FLOWS AEROTHERMAL MODELING PROGRAM, PHASE 2 Final Report**

K. C. KARKI, S. V. PATANKAR, A. K. RUNCHAL, and H. C. MONGIA Jun. 1988 93 p

(Contract NAS3-24350)  
(NASA-CR-182169; EDR-13519; NAS 1.26:182169) Avail: NTIS HC A05/MF A01 CSCL 20/4

The details of a study to develop accurate and efficient numerical schemes to predict complex flows are described. In this program, several discretization schemes were evaluated using simple test cases. This assessment led to the selection of three schemes for an in-depth evaluation based on two-dimensional flows. The scheme with the superior overall performance was incorporated in a computer program for three-dimensional flows. To improve the computational efficiency, the selected discretization

scheme was combined with a direct solution approach in which the fluid flow equations are solved simultaneously rather than sequentially. Author

**N89-12026\*#** National Aeronautics and Space Administration. Lewis Research Center, Cleveland, OH.

**A HIGH HEAT FLUX EXPERIMENT FOR VERIFICATION OF THERMOSTRUCTURAL ANALYSIS**

HERBERT J. GLADDEN and MATTHEW E. MELIS Dec. 1988 17 p Presented at the Winter Annual Meeting of the ASME, Chicago, Ill., 28 Nov. - 2 Dec. 1988 Original document contains color illustrations (NASA-TM-100931; E-4202; NAS 1.15:100931) Avail: NTIS HC A03/MF A01 CSCL 20/4

A major concern in advancing the state of the art technologies for hypersonic vehicles is the development of an aeropropulsion system capable of handling the high heat fluxes during flight. The leading edges of such systems must not only tolerate the maximum heating rates, but must also minimize distortions to the flow field due to excessive blunting and/or thermal warping of the compression surface to achieve the high inlet performance required. A combined analytical and experimental effort to study the aerothermodynamic loads on actively cooled structures for hypersonic applications was established. A hydrogen/oxygen rocket engine was modified to establish a high enthalpy high heat flux environment. The facility provides heat flux levels from about 200 up to 10000 Btu/sq ft/sec. Cross flow and parallel flow regeneratively cooled model can be tested and analyzed by using cooling fluids of water and hydrogen. Results are presented of the experiment and the characteristics of the Hot Gas Test Facility. The predicted temperature results of the cross flow model are compared with the experimental data on the first monolithic specimens and are found to be in good agreement. Thermal stress analysis results are also presented. Author

**N89-12028\*#** National Aeronautics and Space Administration. Lewis Research Center, Cleveland, OH.

**FLUID SPRAY SIMULATION WITH TWO-FLUID NOZZLES**

ROBERT D. INGEBO 1988 14 p Proposed for presentation at the 27th Aerospace Sciences Meeting, Reno, Nev., 9-12 Jan. 1989; sponsored by AIAA (NASA-TM-101367; E-4406; NAS 1.15:101367; AIAA-89-0053) Avail: NTIS HC A03/MF A01 CSCL 20/4

Two-phase interacting flow inside a two-fluid fuel atomizer was investigated and a correction of aerodynamic and liquid-surface forces with characteristic drop diameter was obtained for liquid-jet breakup in Mach 1 gas flow. Nitrogen gas mass-flux was varied from 6 to 50 g/sq cm sec by using four differently sized two-fluid atomizers with nozzle diameters varying from 0.32 to 0.56 cm. The correlation was derived by using the acoustic gas velocity,  $V_{sub}$ , as a basic parameter in defining and evaluating the dimensionless product of the Weber (We) and Reynolds (Re) numbers. By using the definition of WeRe, it was found that the ratio of orifice diameter to Sauter mean drop diameter could be correlated with the dimensionless ratio WeRe and the gas to liquid density ratio. Author

**N89-12835\*#** Naval Postgraduate School, Monterey, CA. Dept. of Aeronautics.

**A NUMERICAL METHOD FOR COMPUTING UNSTEADY 2-D BOUNDARY LAYER FLOWS Interim Contractor Report**

ANDREAS KRAINER Washington NASA Dec. 1988 62 p (Contract NASA ORDER C-80017-F) (NASA-CR-4198; E-4394; NAS 1.26:4198) Avail: NTIS HC A04/MF A01 CSCL 20/4

A numerical method for computing unsteady two-dimensional boundary layers in incompressible laminar and turbulent flows is described and applied to a single airfoil changing its incidence angle in time. The solution procedure adopts a first order panel method with a simple wake model to solve for the inviscid part of the flow, and an implicit finite difference method for the viscous part of the flow. Both procedures integrate in time in a step-by-step fashion, in the course of which each step involves the solution of

the elliptic Laplace equation and the solution of the parabolic boundary layer equations. The Reynolds shear stress term of the boundary layer equations is modeled by an algebraic eddy viscosity closure. The location of transition is predicted by an empirical data correlation originating from Michel. Since transition and turbulence modeling are key factors in the prediction of viscous flows, their accuracy will be of dominant influence to the overall results. Author

**N89-12836\*#** Science Applications International Corp., Sunnyvale, CA.

**MASS FLOW METER USING THE TRIBOELECTRIC EFFECT FOR MEASUREMENT IN CRYOGENICS Final Report**

HENRY BERNATOWICZ, JOCK CUNNINGHAM, and STEVE WOLFF Apr. 1987 76 p (Contract NAS3-24648) (NASA-CR-179572; NAS 1.26:179572; SAIC-87/1612) Avail: NTIS HC A05/MF A01 CSCL 20/4

The use of triboelectric charge to measure the mass flow rate of cryogens for the Space Shuttle Main Engine was investigated. Cross correlation of the triboelectric charge signals was used to determine the transit time of the cryogen between two sensor locations in a .75-in tube. The ring electrode sensors were mounted in a removable spool piece. Three spool pieces were constructed for delivery, each with a different design. One set of electronics for implementation of the cross correlation and flow calculation was constructed for delivery. Tests were made using a laboratory flow loop using liquid freon and transformer oil. The measured flow precision was 1 percent and the response was linear. The natural frequency distribution of the triboelectric signal was approximately  $1/f$ . The sensor electrodes should have an axial length less than approximately one-tenth pipe diameter. The electrode spacing should be less than approximately one pipe diameter. Tests using liquid nitrogen demonstrated poor tribo-signal to noise ratio. Most of the noise was microphonic and common to both electrode systems. The common noise rejection facility of the correlator was successful in compensating for this noise but the signal was too small to enable reliable demonstration of the technique in liquid nitrogen. Author

**N89-12837\*#** Auburn International, Inc., Danvers, MA.

**MASS FLOW MEASUREMENT OF LIQUID CRYOGENS USING THE TRIBOELECTRIC EFFECT Final Report**

RONALD L. DECHENE 12 Aug. 1986 65 p (Contract NAS3-24873) (NASA-CR-179519; NAS 1.26:179519) Avail: NTIS HC A04/MF A01 CSCL 20/4

A cross correlator technique using triboelectric technology has been shown to be a feasible method to measure liquid flow rate for liquid nitrogen and JP4 jet fuel. This technology, invented and pioneered by Auburn International, Inc., is also expected to be suitable for use with all other insulating liquids and cryogenics. The technology described is particularly well suited for cryogenic use, since the sensor is non-contacting and non-intrusive, and therefore, causes no additional pressure drop within the flow stream. Further development of the in-line sensor is required to produce a prototypical version for the test purposes under SSME fuel flow conditions. However, with the knowledge gained from this feasibility study, it is very likely that an acceptable sensor design for a full test bed evaluation could be produced. Author

**N89-12838\*#** Tennessee Univ. Space Inst., Tullahoma.

**INFLUENCE OF BULK TURBULENCE AND ENTRANCE BOUNDARY LAYER THICKNESS ON THE CURVED DUCT FLOW FIELD Final Contractor Report**

R. A. CRAWFORD Nov. 1988 88 p (Contract NAG3-617) (NASA-CR-4188; E-4458; NAS 1.26:4188; UTSI/88-07) Avail: NTIS HC A05/MF A01 CSCL 20/4

The influence of bulk turbulence and boundary layer thickness on the secondary flow development in a square, 90 degree turning duct was investigated. A three-dimensional laser velocimetry system was utilized to measure the mean and fluctuating

components of velocity at six cross-planes in the duct. The results from this investigation, with entrance boundary layer thickness of 20 percent, were compared with the thin boundary layer results documented in NASA CR-174811. The axial velocity profiles, cross-flow velocities, and turbulence intensities were compared and evaluated with regard to the influence of bulk turbulence intensity and boundary layer thickness, and the influence was significant. The results of this investigation expand the 90 degree curved duct experimental data base to higher turbulence levels and thicker entrance boundary layers. The experimental results provide a challenging benchmark data base for computational fluid dynamics code development and validation. The variation of inlet bulk turbulence intensity provides additional information to aid in turbulence model evaluation. Author

**N89-12890\*#** General Motors Corp., Detroit, MI. Gas Turbine Engine Div.

#### **AEROTHERMAL MODELING PROGRAM, PHASE 2**

K. C. KARKI, H. C. MONGIA, SUHAS V. PATANKAR, and A. K. RUNCHAL /in NASA, Lewis Research Center, Turbine Engine Hot Section Technology 1986 p 105-113 Oct. 1986 (Contract NAS3-24350)

Avail: NTIS HC A21/MF A01 CSCL 20/4

The main objective of the NASA sponsored Aerothermal Modeling Program, Phase 2-Element A, is to develop an improved numerical scheme for predicting combustor flow fields. This effort consists of the following three technical tasks. Task 1 involves the selection and evaluation of various candidate numerical techniques. Task 2 involves an in-depth evaluation of the selected numerical schemes. Task 3 involves the convection-diffusion scheme and the direct solver that will be incorporated in the NASA 3-D elliptic code (COM3S). E.R.

**N89-12891\*#** General Motors Corp., Detroit, MI. Gas Turbine Engine Div.

#### **AEROTHERMAL MODELING PROGRAM, PHASE 2. ELEMENT B: FLOW INTERACTION EXPERIMENT**

M. NIKJOOY, H. C. MONGIA, S. N. B. MURTHY, and J. P. SULLIVAN /in NASA, Lewis Research Center, Turbine Engine Hot Section Technology 1986 p 115-124 Oct. 1986 (Contract NAS3-24350)

Avail: NTIS HC A21/MF A01 CSCL 20/4

The design process was improved and the efficiency, life, and maintenance costs of the turbine engine hot section was enhanced. Recently, there has been much emphasis on the need for improved numerical codes for the design of efficient combustors. For the development of improved computational codes, there is a need for an experimentally obtained data base to be used at test cases for the accuracy of the computations. The purpose of Element-B is to establish a benchmark quality velocity and scalar measurements of the flow interaction of circular jets with swirling flow typical of that in the dome region of annular combustor. In addition to the detailed experimental effort, extensive computations of the swirling flows are to be compared with the measurements for the purpose of assessing the accuracy of current and advanced turbulence and scalar transport models. Author

**N89-12892\*#** General Motors Corp., Detroit, MI. Gas Turbine Engine Div.

#### **AEROTHERMAL MODELING PROGRAM, PHASE 2. ELEMENT C: FUEL INJECTOR-AIR SWIRL CHARACTERIZATION**

A. A. MOSTAFA, H. C. MONGIA, V. G. MCDONNELL, and G. S. SAMUELSEN /in NASA, Lewis Research Center, Turbine Engine Hot Section Technology 1986 p 125-131 Oct. 1986 (Contract NAS3-24350)

Avail: NTIS HC A21/MF A01 CSCL 20/4

The main objectives of the NASA-sponsored Aerothermal Modeling Program, Phase 2-Element C, are experimental evaluation of the air swirler interaction with a fuel injector in a simulated combustor chamber, assessment of the current two-phase models, and verification of the improved spray evaporation/dispersion models. This experimental and numerical

program consists of five major tasks. Brief descriptions of the five tasks are given. Author

**N89-12894\*#** Minnesota Univ., Minneapolis. Dept. of Mechanical Engineering.

#### **EFFICIENT NUMERICAL TECHNIQUES FOR COMPLEX FLUID FLOWS**

SUHAS V. PATANKAR /in NASA, Lewis Research Center, Turbine Engine Hot Section Technology 1986 p 141-143 Oct. 1986 (Contract NAG3-596)

Avail: NTIS HC A21/MF A01 CSCL 20/4

The central feature in any flow prediction method is the treatment of the coupling between the momentum and continuity equations. In natural-convection flows, the energy equation also becomes strongly coupled with the momentum equations. Because of the nonlinear nature of the coupling, these equations are solved iteratively. Iterative methods are often prone to slow convergence, divergence, and extreme sensitivity to underrelaxation factors. The aim of the present research is to develop more efficient and reliable solution schemes for the coupled flow equations. Such schemes will significantly reduce the expense of computing complex flows encountered in combustion chambers, gas turbines, heat exchangers, and other practical equipment. In the work completed so far, a technique employing norm reduction in conjunction with the successive-substitution and Newton-Raphson techniques was developed. Also, a block-correction procedure for the flow equations is currently being formulated and tested. Author

**N89-12895\*#** Avco-Everett Research Lab., MA.

#### **IMPROVED NUMERICAL METHODS FOR TURBULENT VISCOUS RECIRCULATING FLOWS**

J. P. VANDOORMAAL, A. TURAN, and G. D. RAITHY /in NASA, Lewis Research Center, Turbine Engine Hot Section Technology 1986 p 145-150 Oct. 1986 (Contract NAS3-24351)

Avail: NTIS HC A21/MF A01 CSCL 20/4

The objective of the present study is to improve both the accuracy and computational efficiency of existing numerical techniques used to predict viscous recirculating flows in combustors. A review of the status of the study is presented along with some illustrative results. The effort to improve the numerical techniques consists of the following technical tasks: (1) selection of numerical techniques to be evaluated; (2) two dimensional evaluation of selected techniques; and (3) three dimensional evaluation of technique(s) recommended in Task 2. Author

**N89-12896\*#** Tennessee Univ. Space Inst., Tullahoma.

#### **INFLUENCE OF BULK TURBULENCE AND ENTRANCE BOUNDARY LAYER THICKNESS ON THE CURVED DUCT FLOW FIELD**

ROGER A. CRAWFORD and CARROLL E. PETERS /in NASA, Lewis Research Center, Turbine Engine Hot Section Technology 1986 p 151-157 Oct. 1986 (Contract NAG3-617)

Avail: NTIS HC A21/MF A01 CSCL 20/4

The objective of this investigation was the experimental evaluation of bulk turbulence and boundary thickness influence on the secondary flow development in a square, 90 deg turning duct. A three dimensional laser velocimetry system was utilized to measure the mean and fluctuating components of velocity in the large curved duct facility. The three dimensional development of the viscous shear layers in the curved duct has a strong influence on the complete flow field. Since ducted three dimensional flows are found in many engineering applications, including gas turbine engines, and contain high turbulence levels and high wall heat transfer rates, they present a difficult challenge to computational fluid mechanics codes. Turbulence modeling remains one of constraints to CFD advance due to inadequate physical understanding and experimental definition of turbulent shear flows. The results of this investigation expand the curved duct data base to higher turbulence levels and thicker entrance boundary layers. The experimental results provide a challenging benchmark data



base for computational fluid dynamics code development and validation. The variation of inlet bulk turbulence intensity provides additional information to aid in turbulence model evaluation.

Author

**N89-12897\*#** United Technologies Research Center, East Hartford, CT.

**MEASUREMENT OF AIRFOIL HEAT TRANSFER COEFFICIENTS ON A TURBINE STAGE**

ROBERT P. DRING, MICHAEL F. BLAIR, and H. DAVID JOSLYN  
In NASA, Lewis Research Center, Turbine Engine Hot Section Technology 1986 p 159-176 Oct. 1986  
(Contract NAS3-2317)

Avail: NTIS HC A21/MF A01 CSCL 20/4

The Primary basis for heat transfer analysis of turbine airfoils is experimental data obtained in linear cascades. These data were very valuable in identifying the major heat transfer and fluid flow features of a turbine airfoil. The first program objective is to obtain a detailed set of heat transfer coefficients along the midspan of a stator and a rotor in a rotating turbine stage. The data are to be compared to some standard analysis of blade boundary layer heat transfer which is in use today. A second program objective is to obtain a detailed set of heat transfer coefficients along the midspan of a stator located in the wake of an upstream turbine stage.

E.R.

**N89-12898\*#** Arizona State Univ., Tempe. Dept. of Mechanical and Aerospace Engineering.

**HEAT TRANSFER IN THE TIP REGION OF A ROTOR BLADE SIMULATOR**

M. K. CHYU, H. K. MOON, and D. E. METZGER In NASA, Lewis Research Center, Turbine Engine Hot Section Technology 1986 p 177-192 Oct. 1986  
(Contract NAG3-623)

Avail: NTIS HC A21/MF A01 CSCL 20/4

In gas turbines, the blades of axial turbine stages rotate in close proximity to a stationary peripheral wall. Differential expansion of the turbine wheel, blades, and the shroud causes variations in the size of the clearance gap between blade tip and stationary shroud. The necessity to tolerate this differential thermal expansion dictates that the clearance gap cannot be eliminated altogether, despite accurate engine machining. Pressure differences between the pressure and suction sides of a blade drives a flow through the clearance gap. This flow, the tip leakage flow, is detrimental to engine performance. The primary detrimental effect of tip leakage flow is the reduction of turbine stage efficiency, and a second is the convective heat transfer associated with the flow. The surface area at the blade tip in contact with the hot working gas represents an additional thermal loading on the blade which, together with heat transfer to the suction and pressure side surface area, must be removed by the blade internal cooling flows. Experimental results concerned with the local heat transfer characteristics on all surfaces of shrouded, rectangular cavities are reported. A brief discussion of the mass transfer system used is given.

Author

**N89-12899\*#** Pratt and Whitney Aircraft, East Hartford, CT.

**COOLANT PASSAGE HEAT TRANSFER WITH ROTATION**

T. J. HAJEK, J. WAGNER, and B. V. JOHNSON In NASA, Lewis Research Center, Turbine Engine Hot Section Technology 1986 p 193-206 Oct. 1986  
(Contract NAS3-23691)

Avail: NTIS HC A21/MF A01 CSCL 20/4

In current and advanced gas turbine engines, increased speeds, pressures and temperatures are used to reduce specific fuel consumption and increase thrust/weight ratios. Hence, the turbine airfoils are subjected to increased heat loads escalating the cooling requirements to satisfy life goals. The efficient use of cooling air requires that the details of local geometry and flow conditions be adequately modeled to predict local heat loads and the corresponding heat transfer coefficients. The objective of this program is to develop a heat transfer and pressure drop data base, computational fluid dynamic techniques and correlations for multi-pass rotating coolant passages with and without flow

turbulators. The experimental effort is focused on the simulation of configurations and conditions expected in the blades of advanced aircraft high pressure turbines. With the use of this data base, the effects of Coriolis and buoyancy forces on the coolant side flow can be included in the design of turbine blades.

Author

**N89-12900\*#** Stanford Univ., CA. Dept. of Mechanical Engineering.

**HEAT TRANSFER WITH VERY HIGH FREE-STREAM TURBULENCE AND STREAMWISE VORTICES**

ROBERT J. MOFFAT, PAUL MACIEJEWSKI, JOHN K. EATON, and WAYNE PAULEY In NASA, Lewis Research Center, Turbine Engine Hot Section Technology 1986 p 207-217 Oct. 1986  
(Contract NAG3-522)

Avail: NTIS HC A21/MF A01 CSCL 20/4

Results are presented for two experimental programs related to augmentation of heat transfer by complex flow characteristics. In one program, high free stream turbulence (up to 63 percent) was shown to increase the Stanton number by more than a factor of 5, compared with the normally expected value based on x-Reynolds number. These experiments are being conducted in a free-jet facility, near the margins of the jet. To a limited extent, the mean velocity, turbulence intensity, and integral length scale can be separately varied. The results show that scale is a very important factor in determining the augmentation. Detailed studies of the turbulence structure are being carried out using an orthogonal triple hot-wire anemometer equipped with a fourth wire for measuring temperature. The  $v'$  component of turbulence appears to be distributed differently from  $u'$  or  $w'$ . In the second program, the velocity distributions and boundary layer thicknesses associated with a pair of counter-rotating, streamwise vortices were measured. There is a region of considerably thinned boundary layer between the two vortices when they are of approximately the same strength. If one vortex is much stronger than the other, the weaker vortex may be lifted off the surface and absorbed into the stronger.

Author

**N89-12901\*#** Minnesota Univ., Minneapolis. Dept. of Mechanical Engineering.

**DEVELOPMENT OF LOW REYNOLDS NUMBER TWO EQUATION TURBULENCE MODELS FOR PREDICTING EXTERNAL HEAT TRANSFER ON TURBINE BLADES**

SUHAS V. PATANKAR and RODNEY C. SCHMIDT In NASA, Lewis Research Center, Turbine Engine Hot Section Technology 1986 p 219-232 Oct. 1986  
(Contract NAG3-579)

Avail: NTIS HC A21/MF A01 CSCL 20/4

A research effort was underway to study the use of two equation low Reynolds number turbulence models in predicting gas side heat transfer on turbine blades. The major objectives of this work are basically threefold: study the predictive capabilities of two equation low Reynolds number turbulence models under the conditions characteristic of modern gas turbine blades; explore potential improvements to the models themselves as well as to the specification of initial conditions; and provide a comparison of the predictions of these models with the experimental data from a broad range of recently available turbine cascade experiments. The problems associated with predicting the boundary layer transition from laminar to turbulent flow are emphasized, as this may be the most serious deficiency of current modeling techniques. The results and conclusions of the first two phases are briefly described.

Author

**N89-12902\*#** National Aeronautics and Space Administration. Lewis Research Center, Cleveland, OH.

**TURBINE STATOR FLOW FIELD SIMULATIONS**

R. C. BUGGELN, W. R. BRILEY, S. J. SHAMROTH, and H. MCDONALD In NASA, Lewis Research Center, Turbine Engine Hot Section Technology 1986 p 233-235 Oct. 1986  
(Contract NAS3-24358)

Avail: NTIS HC A21/MF A01 CSCL 20/4

The increased capability and accessibility of modern computers, coupled with increasingly sophisticated and accurate numerical

and physical modeling, has led to a marked impact of numerical simulations upon current turbine design and research problems. The turbine section represents a considerable challenge as it contains significant regions of complex three-dimensional flow, including both aerodynamic and heat transfer phenomena. The focus of the present effort is the development of an efficient and accurate three-dimensional Navier-Stokes calculation procedure for application to the turbine stator and rotor problems. In particular, an effective procedure is sought which: (1) adequately represents the flow physics, (2) allows for sufficient resolution in regions of small length scale, and (3) has sufficiently good convergence properties so as to allow use on a regular basis. Author

**N89-12903\*#** General Motors Corp., Detroit, MI. Gas Turbine Div.

## **TURBINE AIRFOIL FILM COOLING**

LARRY D. HYLTON In NASA, Lewis Research Center, Turbine Engine Hot Section Technology 1986 p 237-241 Oct. 1986 (Contract NAS3-24619)

Avail: NTIS HC A21/MF A01 CSCL 20/4

Emphasis is placed on developing more accurate analytical models for predicting turbine airfoil external heat transfer rates. Performance goals of new engines require highly refined, accurate design tools to meet durability requirements. In order to obtain improvements in analytical capabilities, programs are required which focus on enhancing analytical techniques through verification of new models by comparison with relevant experimental data. The objectives of the current program are to develop an analytical approach, based on boundary layer theory, for predicting the effects of airfoil film cooling on downstream heat transfer rates and to verify the resulting analytical method by comparison of predictions with hot cascade data obtained under this program. Author

**N89-13731\*#** Grumman Aerospace Corp., Bethpage, NY. Space Systems Div.

## **SOLAR DYNAMIC HEAT REJECTION TECHNOLOGY. TASK 1: SYSTEM CONCEPT DEVELOPMENT Final Report**

ERIC GUSTAFSON and ALBERT W. CARLSON Jun. 1987 120 p

(Contract NAS3-24665)

(NASA-CR-179618; NAS 1.26:179618) Avail: NTIS HC A06/MF A01 CSCL 20/4

The results are presented of a concept development study of heat rejection systems for Space Station solar dynamic power systems. The heat rejection concepts are based on recent developments in high thermal transport capacity heat pipe radiators. The thermal performance and weights of each of the heat rejection subsystems is addressed in detail, and critical technologies which require development tests and evaluation for successful demonstration are assessed and identified. Baseline and several alternate heat rejection system configurations and optimum designs are developed for both Brayton and Rankine cycles. The thermal performance, mass properties, assembly requirements, reliability, maintenance requirements and life cycle cost are determined for each configuration. A specific design was then selected for each configuration which represents an optimum design for that configuration. The final recommendations of heat rejection system configuration for either the Brayton or Rankine cycles depend on the priorities established for the evaluation criteria. Author

**N89-13741\*#** National Aeronautics and Space Administration. Lewis Research Center, Cleveland, OH.

## **A NEAR-WALL TURBULENCE MODEL AND ITS APPLICATION TO FULLY DEVELOPED TURBULENT CHANNEL AND PIPE FLOWS**

S.-W. KIM Nov. 1988 31 p

(Contract NASA ORDER C-99066-G)

(NASA-TM-101399; ICOMP-88-20; E-4483; NAS 1.15:101399)

Avail: NTIS HC A03/MF A01 CSCL 20/4

A near wall turbulence model and its incorporation into a multiple-time-scale turbulence model are presented. In the method, the conservation of mass, momentum, and the turbulent kinetic energy equations are integrated up to the wall; and the energy

transfer rate and the dissipation rate inside the near wall layer are obtained from algebraic equations. The algebraic equations for the energy transfer rate and the dissipation rate inside the near wall layer were obtained from a k-equation turbulence model and the near wall analysis. A fully developed turbulent channel flow and fully developed turbulent pipe flows were solved using a finite element method to test the predictive capability of the turbulence model. The computational results compared favorably with experimental data. It is also shown that the present turbulence model could resolve the over shoot phenomena of the turbulent kinetic energy and the dissipation rate in the region very close to the wall. Author

**N89-13749\*#** National Aeronautics and Space Administration. Lewis Research Center, Cleveland, OH.

## **AXISYMMETRIC CONFINED TURBULENT JET DIRECTED TOWARDS THE LIQUID SURFACE FROM BELOW**

MOHAMMAD M. HASAN and CHIN-SHUN LIN (Analex Corp., Cleveland, Ohio.) 1988 11 p Presented at the 27th Aerospace Sciences Meeting, Reno, Nev., 9-12 Jan. 1989; sponsored by AIAA

(NASA-TM-101409; E-4499; NAS 1.15:101409; AIAA-89-0172)

Avail: NTIS HC A03/MF A01 CSCL 20/4

A numerical simulation is presented of an axisymmetric turbulent jet discharging axially from below into a cylindrical tank and directed towards the liquid vapor interface. The liquid vapor interface is assumed to be flat and shear free. The k-epsilon turbulence model is used to calculate the eddy viscosity. The turbulence intensity distribution and the length scale associated with the k-epsilon model are calculated as functions of jet flow rates and systems parameters. Numerical results are compared with appropriate experimental data. The problems associated with the free surface boundary conditions for the turbulent quantities are discussed. Author

**N89-13754\*#** General Motors Corp., Indianapolis, IN. Allison Gas Turbine Div.

## **THE EFFECTS OF LEADING EDGE AND DOWNSTREAM FILM COOLING ON TURBINE VANE HEAT TRANSFER Final Report**

L. D. HYLTON, V. NIRMALAN, B. K. SULTANIAN, and R. M. KAUFMAN Nov. 1988 175 p

(Contract NAS3-24619)

(NASA-CR-182133; NAS 1.26:182133; ALLISON-EDR-13481)

Avail: NTIS HC A08/MF A01 CSCL 20/4

The progress under contract NAS3-24619 toward the goal of establishing a relevant data base for use in improving the predictive design capabilities for external heat transfer to turbine vanes, including the effect of downstream film cooling with and without leading edge showerhead film cooling. Experimental measurements were made in a two-dimensional cascade previously used to obtain vane surface heat transfer distributions on nonfilm cooled airfoils under contract NAS3-22761 and leading edge showerhead film cooled airfoils under contract NAS3-23695. The principal independent parameters (Mach number, Reynolds number, turbulence, wall-to-gas temperature ratio, coolant-to-gas temperature ratio, and coolant-to-gas pressure ratio) were maintained over ranges consistent with actual engine conditions and the test matrix was structured to provide an assessment of the independent influence of parameters of interest, namely, exit Mach number, exit Reynolds number, coolant-to-gas temperature ratio, and coolant-to-gas pressure ratio. Data provide a data base for downstream film cooled turbine vanes and extends the data bases generated in the two previous studies. The vane external heat transfer obtained indicate that considerable cooling benefits can be achieved by utilizing downstream film cooling. The data obtained and presented illustrate the interaction of the variables and should provide the airfoil designer and computational analyst the information required to improve heat transfer design capabilities for film cooled turbine airfoils. Author

**N89-13755\*#** Purdue Univ., West Lafayette, IN. School of Aeronautics and Astronautics.

**LDV MEASUREMENTS IN AN ANNULAR COMBUSTOR MODEL**  
**M.S. Thesis**

DEAN A. BARRON Aug. 1986 161 p

(Contract NAS3-24350)

(NASA-CR-182207; NAS 1.26:182207; PURDUE-MS-34971)

Avail: NTIS HC A08/MF A01 CSCL 20/4

The design and setup of a Laser Doppler Velocimeter (LDV) system used to take velocity measurements in an annular combustor model are covered. The annular combustor model is of contemporary design using 60 degree flat vane swirlers, producing a strong recirculation zone. Detailed measurements are taken of the swirler inlet air flow and of the downstream enclosed swirling flow. The laser system used is a two color, two component system set up in forward scatter. Detailed are some of the special considerations needed for LDV use in the confined turbulent flow of the combustor model. The LDV measurements in a single swirler rig indicated that the flow changes radically in the first duct height. After this, a flow profile is set up and remains constant in shape. The magnitude of the velocities gradually decays due to viscous damping.

Author

**N89-13756\*#** United Technologies Research Center, East Hartford, CT.

**THE EFFECTS OF INLET TURBULENCE AND ROTOR/STATOR INTERACTIONS ON THE AERODYNAMICS AND HEAT TRANSFER OF A LARGE-SCALE ROTATING TURBINE MODEL, VOLUME 1 Final Report**

R. P. DRING, M. F. BLAIR, H. D. JOSLYN, G. D. POWER, and J. M. VERDON Washington, D.C. Jul. 1987 173 p

(Contract NAS3-23717)

(NASA-CR-4079; E-3536; NAS 1.26:4079;

UTRC-R86-956480-VOL-1) Avail: NTIS HC A08/MF A01 CSCL 20/4

A combined experimental and analytical program was conducted to examine the effects of inlet turbulence on airfoil heat transfer. Heat transfer measurements were obtained using low conductivity airfoils with miniature thermocouples welded to a thin, electrically heated surface skin. Heat transfer data were acquired for various combinations of low or high inlet turbulence intensity, flow coefficient (incidence), first-stator/rotor axial spacing, Reynolds number, and relative circumferential position of the first and second stators. Aerodynamic measurements include distributions of the mean and fluctuating velocities at the turbine inlet and, for each airfoil row, midspan airfoil surface pressures and circumferential distributions of the downstream steady state pressures and fluctuating velocities. Analytical results include airfoil heat transfer predictions and an examination of solutions of the unsteady boundary layer equipment.

Author

**N89-13757\*#** National Aeronautics and Space Administration. Lewis Research Center, Cleveland, OH.

**THREE-DIMENSIONAL MARGINAL SEPARATION**

PETER W. DUCK Dec. 1988 33 p

(Contract SAA-C99066G)

(NASA-TM-101411; E-4503; NAS 1.15:101411; ICOMP-88-22)

Avail: NTIS HC A03/MF A01 CSCL 20/4

The three dimensional marginal separation of a boundary layer along a line of symmetry is considered. The key equation governing the displacement function is derived, and found to be a nonlinear integral equation in two space variables. This is solved iteratively using a pseudo-spectral approach, based partly in double Fourier space, and partly in physical space. Qualitatively, the results are similar to previously reported two dimensional results (which are also computed to test the accuracy of the numerical scheme); however quantitatively the three dimensional results are much different.

Author

**N89-14386\*#** National Aeronautics and Space Administration. Lewis Research Center, Cleveland, OH.

**EXPERIMENTAL RESULTS FOR A TWO-DIMENSIONAL SUPERSONIC INLET USED AS A THRUST DEFLECTING NOZZLE**

ALBERT L. JOHNS and PAUL L. BURSTADT 1984 14 p

Presented at the 19th Joint Propulsion Conference, Seattle, WA, 27-29 Jun. 1983; cosponsored by AIAA, SAE and ASME Sponsored by NASA, Washington, D.C. Original contains color illustrations

(NASA-TM-83439; E-1737; NAS 1.15:83439) Avail: NTIS HC A03/MF A01 CSCL 20/4

Nearly all supersonic V/STOL aircraft concepts are dependent on the thrust deflecting capability of a nozzle. In one unique concept, referred to as the reverse flow dual fan, not only is there a thrust deflecting nozzle for the fan and core engine exit flow, but because of the way the propulsion system operates during vertical takeoff and landing, the supersonic inlet is also used as a thrust deflecting nozzle. This paper presents results of an experimental study to evaluate the performance of a supersonic inlet used as a thrust deflecting nozzle for this reverse flow dual fan concept. Results are presented in terms of nozzle thrust coefficient and thrust vector angle for a number of inlet/nozzle configurations. Flow visualization and nozzle exit flow survey results are also shown.

Author

**N89-14403\*#** National Aeronautics and Space Administration. Lewis Research Center, Cleveland, OH.

**EFFECTS OF CORE TURBULENCE ON JET EXCITABILITY**

REDA R. MANKBADI, GANESH RAMAN (Sverdrup Technology, Inc., Cleveland, Ohio.), and EDWARD J. RICE 1989 11 p

Prepared for presentation at the 2nd Shear Flow Control Conference, Tempe, AZ, 13-16 Mar. 1989; sponsored by AIAA Prepared in cooperation with Cairo Univ. (Egypt)

(Contract SAA-C99066G)

(NASA-TM-101405; ICOMP-88-21; E-4497; NAS 1.15:101405;

AIAA-89-0966) Avail: NTIS HC A03/MF A01 CSCL 20/4

The effects of varying freestream core turbulence on the evolution of a circular jet with and without tonal excitation are examined. Measurements are made on an 8.8 cm diameter jet at a Mach number of 0.3. The jet is excited by plane waves at Strouhal number 0.5. For the excited and unexcited cases the turbulence level is varied by screens and grids placed upstream of the nozzle exit. The experiment results are compared with a theoretical model which incorporates a variable core turbulence and considers the energy interactions between the mean flow, the turbulence and the forced component. Both data and theory indicate that increasing the freestream turbulence diminishes the excitability of the jet and reduces the effect of excitation on the spreading rate of the jet.

Author

**N89-15366\*#** National Aeronautics and Space Administration. Lewis Research Center, Cleveland, OH.

**EXPERIMENTAL DETERMINATION OF STATOR ENDWALL HEAT TRANSFER**

ROBERT J. BOYLE and LOUIS M. RUSSELL 1989 21 p

Proposed for presentation at the 34th International Gas Turbine and Aeroengine Congress and Exposition, Toronto, Ontario, 4-8 Jun. 1989; sponsored by ASME

(NASA-TM-101419; E-4517; NAS 1.15:101419) Avail: NTIS HC A03/MF A01 CSCL 20/4

Local Stanton numbers were experimentally determined for the endwall surface of a turbine vane passage. A six vane linear cascade having vanes with an axial chord of 13.81 cm was used. Results were obtained for Reynolds numbers based on inlet velocity and axial chord between 73,000 and 495,000. The test section was connected to a low pressure exhaust system. Ambient air was drawn into the test section, inlet velocity was controlled up to a maximum of 59.4 m/sec. The effect of the inlet boundary layer thickness on the endwall heat transfer was determined for a range of test section flow rates. The liquid crystal measurement technique was used to measure heat transfer. Endwall heat transfer was determined by applying electrical power to a foil heater

## 34 FLUID MECHANICS AND HEAT TRANSFER

attached to the cascade endwall. The temperature at which the liquid crystal exhibited a specific color was known from a calibration test. Lines showing this specific color were isotherms, and because of uniform heat generation they were also lines of nearly constant heat transfer. Endwall static pressures were measured, along with surveys of total pressure and flow angles at the inlet and exit of the cascade. Author

**N89-16132\*** Virginia Polytechnic Inst. and State Univ., Blacksburg. Dept. of Mechanical Engineering.  
**A PREDICTION OF 3-D VISCOUS FLOW AND PERFORMANCE OF THE NASA LOW-SPEED CENTRIFUGAL COMPRESSOR**  
JOHN MOORE and JOAN G. MOORE Jan. 1989 67 p  
(Contract NAG3-919)  
(NASA-CR-184765; NAS 1.26:184765; TRG-JM/89-1) Avail:  
NTIS HC A04/MF A01 CSCL 20/4

A prediction of the 3-D turbulent flow in the NASA Low-Speed Centrifugal Compressor Impeller has been made. The calculation was made for the compressor design conditions with the specified uniform tip clearance gap. The predicted performance is significantly worse than that predicted in the NASA design study. This is explained by the high tip leakage flow in the present calculation and by the different model adopted for tip leakage flow mixing. The calculation gives an accumulation for high losses in the shroud/pressure-side quadrant near the exit of the impeller. It also predicts a region of meridional backflow near the shroud wall. Both of these flow features should be extensive enough in the NASA impeller to allow detailed flow measurements, leading to improved flow modelling. Recommendations are made for future flow studies in the NASA impeller. Author

**N89-17304\*** General Motors Corp., Indianapolis, IN. Gas Turbine Div.  
**AEROTHERMAL MODELING PROGRAM. PHASE 2, ELEMENT B: FLOW INTERACTION EXPERIMENT**  
M. NIKJOOY, H. C. MONGIA, S. N. B. MURTHY, and J. P. SULLIVAN (Purdue Univ., West Lafayette, IN.) In NASA, Lewis Research Center, Turbine Engine Hot Section Technology, 1987 p 91-99 Oct. 1987  
(Contract NAS3-24350)  
Avail: NTIS HC A20/MF A01 CSCL 20/4

NASA has instituted an extensive effort to improve the design process and data base for the hot section components of gas turbine engines. The purpose of element B is to establish a benchmark quality data set that consists of measurements of the interaction of circular jets with swirling flow. Such flows are typical of those that occur in the primary zone of modern annular combustion liners. Extensive computations of the swirling flows are to be compared with the measurements for the purpose of assessing the accuracy of current physical models used to predict such flows. Author

**N89-17306\*** United Technologies Research Center, East Hartford, CT.  
**APPLICATION OF ADVANCED DIAGNOSTICS TO AIRBLAST INJECTOR FLOWS**  
JOHN B. MCVEY, JAN B. KENNEDY, and SID RUSSELL In NASA, Lewis Research Center, Turbine Engine Hot Section Technology, 1987 p 111-118 Oct. 1987  
(Contract NAS3-24352)  
Avail: NTIS HC A20/MF A01 CSCL 20/4

This effort is concerned with the application of both conventional laser velocimetry and phase Doppler anemometry to the flow produced by an airblast nozzle. The emphasis is placed on the acquisition of data using actual engine injector/swirler components at (noncombusting) conditions simulating those encountered in the engine. The objective of the effort was to test the applicability of the instrumentation to real injector flows, to develop information on the behavior of injectors at high flow, and to provide data useful in the development of physical models of injector flows. Author

**N89-17309\*** Stanford Univ., CA.

### **HEAT TRANSFER WITH VERY HIGH FREE-STREAM TURBULENCE AND HEAT TRANSFER WITH STREAMWISE VORTICES**

ROBERT J. MOFFAT, PAUL MACIEJEWSKI, JOHN K. EATON, and WAYNE PAULEY In NASA, Lewis Research Center, Turbine Engine Hot Section Technology, 1987 p 131-154 Oct. 1987  
(Contract NAG3-522)  
Avail: NTIS HC A20/MF A01 CSCL 20/4

Two experimental programs related to augmentation of heat transfer by complex flow characteristics are reviewed. The first program deals with very high turbulence (up to 63 percent) which was shown to result in Stanton numbers as much as five times the expected values. Results from a number of trials show that fixing the free stream velocity, x-Reynolds number, turbulence intensity and integral length scale does not fix the Stanton number. Two such cases were found in which the Stanton number of one was 40 percent larger than the other. Mean velocity and mean temperature profiles are presented, as well as profiles of turbulence intensity within the boundary layer. The second program deals with vortices originating at bluff bodies and traveling downstream embedded in the wall boundary layer. Velocity vector maps from the boundary layers and distributions of Stanton number on the wall are presented for three types of bodies: square, cylindrical and teardrop. The heat transfer and velocity maps do not show evidence of the expected horseshoe vortices but, instead, show a strong common flow up vortex pair. The fluid mechanic mechanism responsible for this secondary flow field has not yet been identified. Author

**N89-17310\*** Minnesota Univ., Minneapolis.

### **A LOW-REYNOLDS-NUMBER TWO-EQUATION TURBULENCE MODEL FOR PREDICTING HEAT TRANSFER ON TURBINE BLADES**

SUHAS V. PATANKAR and RODNEY C. SCHMIDT In NASA, Lewis Research Center, Turbine Engine Hot Section Technology, 1987 p 155-167 Oct. 1987  
(Contract NAG3-579)  
Avail: NTIS HC A20/MF A01 CSCL 20/4

A modified form of the Lam-Bremhorst low-Reynolds number kappa-epsilon turbulence model was developed for predicting transitional boundary layer flows under conditions characteristic of gas turbine blades. The application of the model to flows with pressure gradients is described. Tests against a number of turbine blade cascade data sets are included. Some additional refinements of the model that were made in recent months are explained. Author

**N89-17311\*** United Technologies Research Center, East Hartford, CT.

### **MEASUREMENT OF AIRFOIL HEAT TRANSFER COEFFICIENTS ON A TURBINE STAGE**

ROBERT P. DRING, MICHAEL F. BLAIR, and H. DAVID JOSLYN In NASA, Lewis Research Center, Turbine Engine Hot Section Technology, 1987 p 169-179 Oct. 1987  
(Contract NAS3-23717)  
Avail: NTIS HC A20/MF A01 CSCL 20/4

A combined experimental and analytical program was conducted to examine the impact of a number of variables on the midspan heat transfer coefficients of the three airfoil rows in a one and one-half stage large scale turbine model. Variables included stator/rotor axial spacing, Reynolds number, turbine inlet turbulence, flow coefficient, relevant stator 1/stator 2 circumferential position, and rotation. Heat transfer data were acquired on the suction and pressure surfaces of the three airfoils. High density data were also acquired in the leading edge stagnation regions. Extensive documentation of the steady and unsteady aerodynamics was acquired. Finally, heat transfer data were compared with both a steady and an unsteady boundary layer analysis. Author

**N89-17312\*#** Arizona State Univ., Tempe.

## HEAT TRANSFER IN THE TIP REGION OF A ROTOR BLADE SIMULATOR

M. K. CHYU and D. E. METZGER /in NASA, Lewis Research Center, Turbine Engine Hot Section Technology, 1987 p 181-197 Oct. 1987

(Contract NAG3-623)

Avail: NTIS HC A20/MF A01 CSDL 20/4

The measurement of mass transfer from cavities is discussed with emphasis on the effect of cavity orientations relative to the main flow direction. A finite difference computation for turbulent air flow and heat transfer over a two-dimensional shrouded rectangular cavity is discussed. Author

**N89-17313\*#** Scientific Research Associates, Inc., Glastonbury, CT.

## TWO- AND THREE-DIMENSIONAL TURBINE BLADE ROW FLOW FIELD SIMULATIONS

R. C. BUGGELN, W. R. BRILEY, H. MCDONALD, S. J. SHAMROTH, and B. C. WEINBERG /in NASA, Lewis Research Center, Turbine Engine Hot Section Technology, 1987 p 199-209 Oct. 1987 Prepared in cooperation with General Motors Corp., Indianapolis, IN

(Contract NAS3-24358; NAS3-23695)

Avail: NTIS HC A20/MF A01 CSDL 20/4

Work performed in the numerical simulation of turbine passage flows via a Navier-Stokes approach is discussed. Both laminar and turbulent simulations in both two and three dimensions are discussed. An outline of the approach, background, and an overview of the results are given. Author

**N89-17314\*#** Pratt and Whitney Aircraft, East Hartford, CT.

## COOLANT PASSAGE HEAT TRANSFER WITH ROTATION

T. J. HAJEK, J. H. WAGNER, and B. V. JOHNSON (United Technologies Research Center, East Hartford, CT.) /in NASA, Lewis Research Center, Turbine Engine Hot Section Technology, 1987 p 211-223 Oct. 1987

(Contract NAS3-23691)

Avail: NTIS HC A20/MF A01 CSDL 20/4

The objective is to develop a heat transfer and pressure drop data base, computational fluid dynamic techniques and heat transfer correlations for rotating multipass coolant passages, with and without flow tabulators. The experimental effort is focused on the simulation of configurations and conditions expected in the blades of advanced aircraft high pressure turbines. With the use of this data base, the effects of Coriolis and buoyancy forces on the coolant side flow can be included in the design of turbine blades. Author

**N89-17315\*#** General Motors Corp., Indianapolis, IN. Gas Turbine Div.

## TURBINE AIRFOIL FILM COOLING

L. D. HYLTON, V. NIRMALAN, B. K. SULTANIAN, and R. M. KAUFMAN /in NASA, Lewis Research Center, Turbine Engine Hot Section Technology, 1987 p 225-238 Oct. 1987

(Contract NAS3-24619)

Avail: NTIS HC A20/MF A01 CSDL 20/4

The experimental data obtained in this program gives insight into the physical phenomena that occur on a film cooled airfoil, and should provide a relevant data base for verification of new design tools. Results indicate that the downstream film cooling process is a complex function of the thermal dilution and turbulence augmentation parameters with trends actually reversing as blowing strength and coolant-to-gas temperature ratio varied. The pressure surface of the airfoil is shown to exhibit a considerably higher degree of sensitivity to changes in the film cooling parameters and, consequently, should prove to be more of a challenge than the suction surface in accurately predicting heat transfer levels with downstream film cooling. Author

**N89-18635\*#** National Aeronautics and Space Administration, Lewis Research Center, Cleveland, OH.

## CFD VALIDATION EXPERIMENTS FOR INTERNAL FLOWS

LOUIS A. POVINELLI /in AGARD, Validation of Computational Fluid Dynamics. Volume 1: Symposium Papers and Round Table Discussion 13 p Dec. 1988 Previously announced as N88-16679

Copyright Avail: NTIS HC A25/MF A01 CSDL 20/4

Computational Fluid Dynamics (CFD) validation experiments at NASA Lewis are described. The material presented summarized the research in 3 areas: Inlets, ducts and nozzles; Turbomachinery; and Chemically reacting flows. The specific validation activities are concerned with shock boundary layer interactions, vortex generator effects, large low speed centrifugal compressor measurements, transonic fan shock structure, rotor/stator kinetic energy distributions, stator wake shedding characteristics, boundary layer transition, multiphase flow and reacting shear layers. These experiments are intended to provide CFD validation data for the internal flow fields within aerospace propulsion system components. Author

**N89-18664\*#** National Aeronautics and Space Administration, Lewis Research Center, Cleveland, OH.

## HIGH-RESOLUTION LIQUID-CRYSTAL HEAT-TRANSFER MEASUREMENTS ON THE END WALL OF A TURBINE PASSAGE WITH VARIATIONS IN REYNOLDS NUMBER

STEVEN A. HIPPENSTEELE and LOUIS M. RUSSELL 1988 15 p Presented at the 25th National Heat Transfer Conference, Houston, TX, 24-27 Jul. 1988; sponsored by ASME

(NASA-TM-100827; E-4004; NAS 1.15:100827) Avail: NTIS HC A03/MF A01 CSDL 20/4

Local heat-transfer coefficients were experimentally mapped on the end-wall surface of a three-times turbine vane passage in a static, single-row cascade operated with room-temperature inlet air over a range of Reynolds numbers. The test surface was a composite of commercially available materials: a Mylar sheet with a layer of cholesteric liquid crystals, which change color with temperature, and a heater made of a polyester sheet coated with vapor-deposited gold, which produces uniform heat flux. After the initial selection and calibration of the composite sheet, accurate, quantitative, and continuous heat-transfer coefficients were mapped over the end-wall surface. The local heat-transfer coefficients (expressed as nondimensional Stanton number) are presented for inlet Reynolds numbers (based on vane axial chord) from 0.83 x 10(5) to 3.97 x 10(5). Author

**N89-19503\*#** Purdue Univ., West Lafayette, IN. Thermal Sciences and Propulsion Center.

## THE EFFECT OF PREWHIRL ON THE INTERNAL AERODYNAMICS AND PERFORMANCE OF A MIXED FLOW RESEARCH CENTRIFUGAL COMPRESSOR

WILLIAM B. BRYAN and SANFORD FLEETER Dec. 1987 159 p

(Contract NSG-3285)

(NASA-CR-184756; NAS 1.26:184756; AVSCOM-TR-87-C-35; ME-TSPC-TR-87-13) Avail: NTIS HC A08/MF A01 CSDL 20/4

The internal three-dimensional steady and time-varying flow through the diffusing elements of a centrifugal impeller were investigated using a moderate scale, subsonic, mixed flow research compressor facility. The characteristics of the test facility which permit the measurement of internal flow conditions throughout the entire research compressor and radial diffuser for various operating conditions are described. Results are presented in the form of graphs and charts to cover a range of mass flow rates with inlet guide vane settings varying from minus 15 degrees to plus 45 degrees. The static pressure distributions in the compressor inlet section and on the impeller and exit diffuser vanes, as well as the overall pressure and temperature rise and mass flow rate, were measured and analyzed at each operating point to determine the overall performance as well as the detailed aerodynamics throughout the compressor. NASA

**N89-20407\*#** National Aeronautics and Space Administration, Lewis Research Center, Cleveland, OH.

## CONTROL-VOLUME BASED NAVIER-STOKES EQUATION SOLVER VALID AT ALL FLOW VELOCITIES

S.-W. KIM Feb. 1989 40 p  
(NASA-TM-101488; E-4629; ICOMP-89-5; NAS 1.15:101488)  
Avail: NTIS HC A03/MF A01 CSCL 20/4

A control-volume based finite difference method to solve the Reynolds averaged Navier-Stokes equations is presented. A pressure correction equation valid at all flow velocities and a pressure staggered grid layout are used in the method. Example problems presented herein include: a developing laminar channel flow, developing laminar pipe flow, a lid-driven square cavity flow, a laminar flow through a 90-degree bent channel, a laminar polar cavity flow, and a turbulent supersonic flow over a compression ramp. A k-epsilon turbulence model supplemented with a near-wall turbulence model was used to solve the turbulent flow. It is shown that the method yields accurate computational results even when highly skewed, unequally spaced, curved grids are used. It is also shown that the method is strongly convergent for high Reynolds number flows. Author

**N89-21192\*#** National Aeronautics and Space Administration. Lewis Research Center, Cleveland, OH.  
**NUMERICAL COMPUTATION OF SHOCK WAVE-TURBULENT BOUNDARY LAYER INTERACTION IN TRANSONIC FLOW OVER AN AXISYMMETRIC CURVED HILL**

S.-W. KIM Feb. 1989 31 p  
(Contract NASA ORDER C-99066-G)  
(NASA-TM-101473; E-4589; ICOMP-89-3; NAS 1.15:101473)  
Avail: NTIS HC A03/MF A01 CSCL 20/4

A control-volume based finite difference computation of a turbulent transonic flow over an axisymmetric curved hill is presented. The numerical method is based on the SIMPLE algorithm, and hence the conservation of mass equation is replaced by a pressure correction equation for compressible flows. The turbulence is described by a k-epsilon turbulence model supplemented by a near-wall turbulence model. In the method, the dissipation rate in the region very close to the wall is obtained from an algebraic equation and that for the rest of the flow domain is obtained by solving a partial differential equation for the dissipation rate. The other flow equations are integrated up to the wall. It is shown that the present turbulence model yields the correct location of the compression shock. The other computational results are also in good agreement with experimental data. Author

**N89-21196\*#** National Aeronautics and Space Administration. Lewis Research Center, Cleveland, OH.  
**ON THE CONDITIONS FOR RESONANCE INTERACTIONS OF INSTABILITY WAVES IN THE AXISYMMETRIC JET**  
REDA R. MANKBADI, GANESH RAMAN, and EDWARD J. RICE (Sverdrup Technology, Inc., Cleveland, OH.) Mar. 1989 13 p  
Prepared in cooperation with Cairo Univ. (Egypt)  
(Contract NASA ORDER C-99066-G)  
(NASA-TM-101477; E-4598; ICOMP-89-4; NAS 1.15:101477)  
Avail: NTIS HC A03/MF A01 CSCL 20/4

The conditions for resonance interaction between two instability waves in an axisymmetric jet were investigated. Considerations of the energy equation of the wave resulting from the interaction indicate that the phase angle between the wave-induced stresses and the wave-induced strains plays a crucial role in the resonance interaction. This fact is demonstrated experimentally by exciting a jet at fundamental and subharmonic frequencies. The phase angle between the waves stresses and strains was varied by varying the initial phase-difference between the two excitation waves. The subharmonic resonance was found to be highly dependent on this angle. Favorable agreement was found between the phase angles predicted by a nonlinear theory and the measured ones. The theory is used to explain the subharmonic's resonance in terms of the phase-angles. Author

**N89-21197\*#** National Aeronautics and Space Administration. Lewis Research Center, Cleveland, OH.  
**THE RESPONSE OF A LAMINAR BOUNDARY LAYER IN SUPERSONIC FLOW TO SMALL AMPLITUDE PROGRESSIVE WAVES**

PETER W. DUCK Mar. 1989 39 p  
(Contract NASA ORDER C-99066-G)  
(NASA-TM-101965; E-4663; NAS 1.15:101965; ICOMP-89-6)  
Avail: NTIS HC A03/MF A01 CSCL 20/4

The effect of a small amplitude progressive wave on the laminar boundary layer on a semi-infinite flat plate, due to a uniform supersonic freestream flow, is considered. The perturbation to the flow divides into two streamwise zones. In the first, relatively close to the leading edge of the plate, on a transverse scale comparable to the boundary layer thickness, the perturbation flow is described by a form of the unsteady linearized compressible boundary layer equations. In the freestream, this component of flow is governed by the wave equation, the solution of which provides the outer velocity conditions for the boundary layer. This system is solved numerically, and also the asymptotic structure in the far downstream limit is studied. This reveals a breakdown and a subsequent second streamwise zone, where the flow disturbance is predominantly inviscid. The two zones are shown to match in a proper asymptotic sense. Author

**N89-22053\*#** National Aeronautics and Space Administration. Lewis Research Center, Cleveland, OH.  
**GAS DENSITY EFFECT ON DROPSIZE OF SIMULATED FUEL SPRAYS**

ROBERT D. INGEBO 1989 14 p Presented at the 25th Joint Propulsion Conference, Monterey, CA, 10-12 Jul. 1989; cosponsored by the AIAA, ASME, SAE, and ASSE  
(NASA-TM-102013; E-4725; NAS 1.15:102013) Avail: NTIS HC A03/MF A01 CSCL 20/4

Two-phase flow in pneumatic two-fluid fuel nozzles was investigated experimentally to determine the effect of atomizing-gas density and gas mass-flux on liquid-jet breakup in sonic-velocity gas-flow. Dropsizes data were obtained for the following atomizing-gases: nitrogen; argon; carbon dioxide; and helium. They were selected to cover a gas molecular-weight range of 4 to 44. Atomizing-gas mass-flux ranged from 6 to 50 g/sq cm-sec and four differently sized two-fluid fuel nozzles were used having orifice diameters that varied from 0.32 to 0.56 cm. The ratio of liquid-jet diameter to SMD,  $D_{sub} o/D_{sub} 32$ , was correlated with aerodynamic and liquid-surface forces based on the product of the Weber and Reynolds number,  $We*Re$ , and gas-to-liquid density ratio,  $\rho_{sub} g/\rho_{sub} l$ . To correlate spray dropsizes with breakup forces produced by using different atomizing-gases, a new molecular-scale dimensionless group was derived. The derived dimensionless group was used to obtain an expression for the ratio of liquid-jet diameter to SMD,  $D_{sub} o/D_{sub} 32$ . The mathematical expression of this phenomenon incorporates the product of the Weber and Reynolds number, liquid viscosity, surface tension, acoustic gas velocity, the RMS velocity of gas molecules, the acceleration of gas molecules due to gravity, and gas viscosity. The mathematical expression encompassing these parameters agrees well with the atomization theory for liquid-jet breakup in high velocity gas flow. Also, it was found that at the same gas mass-flux, helium was considerably more effective than nitrogen in producing small droplet sprays with SMD's in the order of 5 micrometers. Author

**N89-22054\*#** National Aeronautics and Space Administration. Lewis Research Center, Cleveland, OH.  
**UNSTEADY THERMOCAPILLARY MIGRATION OF BUBBLES**  
LOREN H. DILL and R. BALASUBRAMANIAM (Case Western Reserve Univ., Cleveland, OH.) 1988 13 p Presented at the 3rd International Colloquium on Drops and Bubbles, Monterey, CA, 18-21 Sep. 1988; sponsored by JPL  
(NASA-TM-101338; E-4357; NAS 1.15:101338) Avail: NTIS HC A03/MF A01 CSCL 20/4

Upon the introduction of a gas bubble into a liquid possessing a uniform thermal gradient, an unsteady thermo-capillary flow begins. Ultimately, the bubble attains a constant velocity. This theoretical analysis focuses upon the transient period for a bubble in a microgravity environment and is restricted to situations wherein the flow is sufficiently slow such that inertial terms in the Navier-Stokes equation and convective terms in the energy



equation may be safely neglected (i.e., both Reynolds and Marangoni numbers are small). The resulting linear equations were solved analytically in the Laplace domain with the Prandtl number of the liquid as a parameter; inversion was accomplished numerically using a standard IMSL routine. In the asymptotic long-time limit, the theory agrees with the steady-state theory of Young, Goldstein, and Block. The theory predicts that more than 90 percent of the terminal steady velocity is achieved when the smallest dimensionless time, i.e., the one based upon the largest time scale-viscous or thermal-equals unity. Author

**N89-22861\*#** National Aeronautics and Space Administration. Lewis Research Center, Cleveland, OH.

**ON THE LAGRANGIAN DESCRIPTION OF UNSTEADY BOUNDARY LAYER SEPARATION. PART 2: THE SPINNING SPHERE**

LEON L. VANDOMMELEN May 1989 26 p  
(NASA-TM-102027; E-4771; NAS 1.15:102027) Avail: NTIS HC A03/MF A01 CSCL 20/4

A theory to explain the initial stages of unsteady separation was proposed by Van Dommelen and Cowley (1989). This theory is verified for the separation process that occurs at the equatorial plane of a sphere or a spheroid which is impulsively spun around an axis of symmetry. A Lagrangian numerical scheme is developed which gives results in good agreement with Eulerian computations, but which is significantly more accurate. This increased accuracy, and a simpler structure to the solution, also allows verification of the Eulerian structure, including the presence of logarithmic terms. Further, while the Eulerian computations broke down at the first occurrence of separation, it is found that the Lagrangian computation can be continued. It is argued that this separated solution does provide useful insight into the further evolution of the separated flow. A remarkable conclusion is that an unseparated vorticity layer at the wall, a familiar feature in unsteady separation processes, disappears in finite time. Author

**N89-22862\*#** National Aeronautics and Space Administration. Lewis Research Center, Cleveland, OH.

**A GENERALIZED ONE-DIMENSIONAL COMPUTER CODE FOR TURBOMACHINERY COOLING PASSAGE FLOW CALCULATIONS**

GANESH N. KUMAR, RICHARD J. ROELKE, and PETER L. MEITNER (Army Aviation Systems Command, Cleveland, OH.) 1989 14 p Prepared for presentation at the 25th Joint Propulsion Conference, Monterey, CA, 10-12 Jul. 1989; sponsored in part by AIAA, ASME, SAE, and ASEE  
(Contract DA PROJ. 1L1-61102-AH-45)  
(NASA-TM-102079; E-4839; NAS 1.15:102079; AVSCOM-TR-89-C-013) Avail: NTIS HC A03/MF A01 CSCL 20/4

A generalized one-dimensional computer code for analyzing the flow and heat transfer in the turbomachinery cooling passages was developed. This code is capable of handling rotating cooling passages with turbulators, 180 degree turns, pin fins, finned passages, by-pass flows, tip cap impingement flows, and flow branching. The code is an extension of a one-dimensional code developed by P. Meitner. In the subject code, correlations for both heat transfer coefficient and pressure loss computations were developed to model each of the above mentioned type of coolant passages. The code has the capability of independently computing the friction factor and heat transfer coefficient on each side of a rectangular passage. Either the mass flow at the inlet to the channel or the exit plane pressure can be specified. For a specified inlet total temperature, inlet total pressure, and exit static pressure, the code computes the flow rates through the main branch and the subbranches, flow through tip cap for impingement cooling, in addition to computing the coolant pressure, temperature, and heat transfer coefficient distribution in each coolant flow branch. Predictions from the subject code for both nonrotating and rotating passages agree well with experimental data. The code was used to analyze the cooling passage of a research cooled radial rotor. Author

**N89-23809\*#** National Aeronautics and Space Administration. Lewis Research Center, Cleveland, OH.

**ADVANCED COMPUTATIONAL TECHNIQUES FOR HYPERSONIC PROPULSION**

LOUIS A. POVINELLI 1989 24 p Proposed for presentation at the 9th International Symposium on Air Breathing Engines, Athens, Greece, 4-9 Sep. 1989; sponsored by AIAA and International Society for Air Breathing Engines  
(NASA-TM-102005; E-4711; NAS 1.15:102005) Avail: NTIS HC A03/MF A01 CSCL 20/4

Computational Fluid Dynamics (CFD) has played a major role in the resurgence of hypersonic flight, on the premise that numerical methods will allow performance of simulations at conditions for which no ground test capability exists. Validation of CFD methods is being established using the experimental data base available, which is below Mach 8. It is important, however, to realize the limitations involved in the extrapolation process as well as the deficiencies that exist in numerical methods at the present time. Current features of CFD codes are examined for application to propulsion system components. The shortcomings in simulation and modeling are identified and discussed. Author

**N89-23813\*#** National Aeronautics and Space Administration. Lewis Research Center, Cleveland, OH.

**ON THE NATURE OF NAVIER-STOKES TURBULENCE Ph.D. Thesis - Case Western Reserve Univ.**

ROBERT G. DEISSLER (Case Western Reserve Univ., Cleveland, OH.) May 1989 102 p  
(NASA-TM-101983; E-4682; NAS 1.15:101983) Avail: NTIS HC A06/MF A01 CSCL 20/4

Several turbulent and nonturbulent solutions of the Navier-Stokes equations are obtained. The unaveraged equations are used numerically in conjunction with tools and concepts from nonlinear dynamics, including time series, phase portraits, Poincare sections, largest Liapunov exponents, power spectra, and strange attractors. Initially neighboring solutions for a low-Reynolds-number fully developed turbulence are compared. The solutions, separate exponentially with time, having a positive Liapunov exponent. Thus the turbulence is characterized as chaotic. In a search for solutions which contrast with the turbulent ones, the Reynolds number is reduced. Several qualitatively different flows are noted. These are, fully chaotic, complex period, weakly chaotic, simple periodic, and fixed-point. Of these, only the fully chaotic flows are classified as turbulent. Those flows have both a positive Liapunov exponent and Poincare sections without pattern. By contrast, the weakly chaotic flows have some pattern in their Poincare sections. The fixed-point and periodic flows are nonturbulent, since turbulence, is both time-dependent and aperiodic. Turbulent solutions are obtained in which energy cascades from large to small-scale motions. In general, the spectral energy transfer takes place between wavenumber bands that are considerably separated. The special transfer can occur either as a result of nonlinear turbulence self-interaction or by interaction of turbulence with mean gradients. Turbulent systems are compared with those studied in kinetic theory. The two types of systems are fundamentally different (continuous and dissipative as opposed to discrete and conservative), but there are similarities. For instance, both are nonlinear and show sensitive dependence on initial conditions. Also, the turbulent and molecular stress tensors are identical if the macroscopic velocities for the turbulent stress are replaced by molecular velocities. Author

**N89-23818\*#** Analox Corp., Cleveland, OH.  
**NUMERICAL STUDIES OF THE EFFECTS OF JET-INDUCED MIXING ON LIQUID-VAPOR INTERFACE CONDENSATION Final Report**

CHIN-SHUN LIN Apr. 1989 22 p Presented at the 24th Thermophysics Conference, Buffalo, NY, 12-14 Jun. 1989; sponsored by AIAA  
(Contract NAS3-24564)  
(NASA-CR-182285; E-4749; NAS 1.26:182285; AIAA-89-1744) Avail: NTIS HC A03/MF A01 CSCL 20/4

Numerical solutions of jet-induced mixing in a partially full

cryogenic tank are presented. An axisymmetric laminar jet is discharged from the central part of the tank bottom toward the liquid-vapor interface. Liquid is withdrawn at the same volume flow rate from the outer part of the tank. The jet is at a temperature lower than the interface, which is maintained at a certain saturation temperature. The interface is assumed to be flat and shear-free and the condensation-induced velocity is assumed to be negligibly small compared with radial interface velocity. Finite-difference method is used to solve the nondimensional form of steady state continuity, momentum, and energy equations. Calculations are conducted for jet Reynolds numbers ranging from 150 to 600 and Prandtl numbers ranging from 0.85 to 2.65. The effects of above stated parameters on the condensation Nusselt and Stanton numbers which characterize the steady-state interface condensation process are investigated. Detailed analysis to gain a better understanding of the fundamentals of fluid mixing and interface condensation is performed. Author

**N89-23821\*#** National Aeronautics and Space Administration. Lewis Research Center, Cleveland, OH.

## ON THE LAGRANGIAN DESCRIPTION OF UNSTEADY BOUNDARY LAYER SEPARATION. PART 1: GENERAL THEORY

LEON L. VANDOMMELEN and STEPHEN J. COWLEY (Imperial Coll. of Science and Technology, London, England ) May 1989 50 p

(Contract NASA-SAA-C-99066-G)

(NASA-TM-102026; E-4770; ICOMP-89-8; NAS 1.15:102026)

Avail: NTIS HC A03/MF A01 CSCL 20/4

Although unsteady, high-Reynolds number, laminar boundary layers have conventionally been studied in terms of Eulerian coordinates, a Lagrangian approach may have significant analytical and computational advantages. In Lagrangian coordinates the classical boundary layer equations decouple into a momentum equation for the motion parallel to the boundary, and a hyperbolic continuity equation (essentially a conserved Jacobian) for the motion normal to the boundary. The momentum equations, plus the energy equation if the flow is compressible, can be solved independently of the continuity equation. Unsteady separation occurs when the continuity equation becomes singular as a result of touching characteristics, the condition for which can be expressed in terms of the solution of the momentum equations. The solutions to the momentum and energy equations remain regular. Asymptotic structures for a number of unsteady 3-D separating flows follow and depend on the symmetry properties of the flow. In the absence of any symmetry, the singularity structure just prior to separation is found to be quasi 2-D with a displacement thickness in the form of a crescent shaped ridge. Physically the singularities can be understood in terms of the behavior of a fluid element inside the boundary layer which contracts in a direction parallel to the boundary and expands normal to it, thus forcing the fluid above it to be ejected from the boundary layer. Author

**N89-23823\*#** National Aeronautics and Space Administration. Lewis Research Center, Cleveland, OH.

## TWO-DIMENSIONAL NUMERICAL SIMULATION OF A STIRLING ENGINE HEAT EXCHANGER

MOUNIR B. IBRAHIM (Cleveland State Univ., OH.), ROY C. TEW, and JAMES E. DUDENHOEFER 1989 13 p Prepared for presentation at the 24th Intersociety Energy Conversion Engineering Conference, Washington, DC, 6-11 Aug. 1989; sponsored by IEEE, AIAA, ANS, ASME, SAE, ACS, and AIChE (NASA-TM-102057; E-4815; NAS 1.15:102057) Avail: NTIS HC A03/MF A01 CSCL 20/4

The first phase of an effort to develop multidimensional models of Stirling engine components is described; the ultimate goal is to model an entire engine working space. More specifically, parallel plate and tubular heat exchanger models with emphasis on the central part of the channel (i.e., ignoring hydrodynamic and thermal end effects) are described. The model assumes: laminar, incompressible flow with constant thermophysical properties. In addition, a constant axial temperature gradient is imposed. The governing equations, describing the model, were solved using

Crank-Nicolson finite-difference scheme. Model predictions were compared with analytical solutions for oscillating/reversing flow and heat transfer in order to check numerical accuracy. Excellent agreement was obtained for the model predictions with analytical solutions available for both flow in circular tubes and between parallel plates. Also the heat transfer computational results are in good agreement with the heat transfer analytical results for parallel plates. Author

**N89-24575\*#** National Aeronautics and Space Administration. Lewis Research Center, Cleveland, OH.

## NONLINEAR EVOLUTION OF INTERACTING OBLIQUE WAVES ON TWO-DIMENSIONAL SHEAR LAYERS

M. E. GOLDSTEIN and S.-W. CHOI Jun. 1989 33 p

(Contract NASA ORDER C-99066-G)

(NASA-TM-102030; E-4404-1; NAS 1.15:102030; ICOMP-89-10)

Avail: NTIS HC A03/MF A01 CSCL 20/4

The effects of critical layer nonlinearity are considered on spatially growing oblique instability waves on nominally two-dimensional shear layers between parallel streams. The analysis shows that three-dimensional effects cause nonlinearity to occur at much smaller amplitudes than it does in two-dimensional flows. The nonlinear instability wave amplitude is determined by an integro-differential equation with cubic type nonlinearity. The numerical solutions to this equation are worked out and discussed in some detail. The numerical solutions always end in a singularity at a finite downstream distance. Author

**N89-24577\*#** National Aeronautics and Space Administration. Lewis Research Center, Cleveland, OH.

## SOME CHARACTERISTICS OF BYPASS TRANSITION IN A HEATED BOUNDARY LAYER

K. H. SOHN, J. E. OBRIEN, and E. RESHOTKO (Case Western Reserve Univ., Cleveland, OH.) 1989 8 p Presented at the 7th Symposium on Turbulent Shear Flows, Stanford, CA, 21-23 Aug. 1989; sponsored by the Turbulent Shear Flow Committee (NASA-TM-102126; E-4912; NAS 1.15:102126) Avail: NTIS HC A02/MF A01 CSCL 20/4

Experimental measurements of both mean and conditionally sampled characteristics of laminar, transitional and low Reynolds number turbulent boundary layers on a heated flat plate are presented. Measurements were obtained in air over a range of freestream turbulence intensities from 0.3 percent to 6 percent with a freestream velocity of 30.5 m/s and zero pressure gradient. Conditional sampling performed in the transitional boundary layers indicate the existence of a near-wall drop in intermittency, especially pronounced at low intermittencies. Nonturbulent intervals were observed to possess large levels of low-frequency unsteadiness, and turbulent intervals had peak intensities as much as 50 percent higher than were measured at fully turbulent stations. Heat transfer results were consistent with results of previous researchers and Reynolds analogy factors were found to be well predicted by laminar and turbulent correlations which accounted for unheated starting length. A small dependence of the turbulent Reynolds analogy factors on freestream turbulence level was observed. Laminar boundary layer spectra indicated selective amplification of unstable frequencies. These instabilities appear to play a dominant role in the transition process only for the lowest freestream turbulence level studied, however. Author

**N89-25409\*#** National Aeronautics and Space Administration. Lewis Research Center, Cleveland, OH.

## DETERMINATION OF COMBUSTION GAS TEMPERATURES BY INFRARED RADIOMETRY IN SOOTING AND NONSOOTING FLAMES

VALERIE J. LYONS and CARMEN M. GRACIA-SALCEDO (Army Aviation Systems Command, Cleveland, OH.) Feb. 1989 13 p (Contract DA PROJ. 1L1-61102-AH-45)

(NASA-TP-2900; E-4446; NAS 1.60:2900; AVSCOM-TR-88-C-008; AD-A205373) Avail: NTIS HC A03/MF A01 CSCL 21/2

Flame temperatures in nonsooting and sooting environments were successfully measured by radiometry for pre-mixed propane-oxygen laminar flames stabilized on a water-cooled,

porous sintered-bronze burner. The measured temperatures in the nonsooting flames were compared with fine-wire thermocouple measurements. The results show excellent agreement below 1700 K, and when the thermocouple measurements were corrected for radiation effects, the agreement was good for even higher temperatures. The benefits of radiometry are: (1) the flow is not disturbed by an intruding probe, (2) calibration is easily done using a blackbody source, and (3) measurements can be made even with soot present. The theory involved in the radiometry measurements and the energy balance calculations used to correct the thermocouple temperature measurements are discussed.

Author

**N89-26172\*#** Cornell Univ., Ithaca, NY. School of Mechanical and Aerospace Engineering.

**MULTIGRID CALCULATION OF THREE-DIMENSIONAL TURBOMACHINERY FLOWS Final Report, 1 Sep. 1985 - 30 Jan. 1989**

DAVID A. CAUGHEY Jun. 1989 28 p Sponsored by NSF; IBM and Corporate Research Inst. (Contract NAG3-645) (NASA-CR-185332; NAS 1.26:185332; FDA-89-07) Avail: NTIS HC A03/MF A01 CSCL 20/4

Research was performed in the general area of computational aerodynamics, with particular emphasis on the development of efficient techniques for the solution of the Euler and Navier-Stokes equations for transonic flows through the complex blade passages associated with turbomachines. In particular, multigrid methods were developed, using both explicit and implicit time-stepping schemes as smoothing algorithms. The specific accomplishments of the research have included: (1) the development of an explicit multigrid method to solve the Euler equations for three-dimensional turbomachinery flows based upon the multigrid implementation of Jameson's explicit Runge-Kutta scheme (Jameson 1983); (2) the development of an implicit multigrid scheme for the three-dimensional Euler equations based upon lower-upper factorization; (3) the development of a multigrid scheme using a diagonalized alternating direction implicit (ADI) algorithm; (4) the extension of the diagonalized ADI multigrid method to solve the Euler equations of inviscid flow for three-dimensional turbomachinery flows; and also (5) the extension of the diagonalized ADI multigrid scheme to solve the Reynolds-averaged Navier-Stokes equations for two-dimensional turbomachinery flows. K.C.D.

**N89-26174\*#** National Aeronautics and Space Administration. Lewis Research Center, Cleveland, OH.

**CFD IN THE CONTEXT OF IHPTET: THE INTEGRATED HIGH PERFORMANCE TURBINE TECHNOLOGY PROGRAM**

ROBERT J. SIMONEAU and DALE A. HUDSON (Air Force Wright Research and Development Center, Wright-Patterson AFB, OH.) 1989 17 p Presented at the 25th Joint Propulsion Conference, Monterey, CA, 10-12 Jul. 1989; cosponsored by the AIAA, ASME, SAE, and ASEE (NASA-TM-102132; E-4868; NAS 1.15:102132; AIAA-89-2904) Avail: NTIS HC A03/MF A01 CSCL 20/4

The Integrated High Performance Turbine Engine Technology (IHPTET) Program is an integrated DOD/NASA technology program designed to double the performance capability of today's most advanced military turbine engines as we enter the twenty-first century. Computational Fluid Dynamics (CFD) is expected to play an important role in the design/analysis of specific configurations within this complex machine. In order to do this, a plan is being developed to ensure the timely impact of CFD on IHPTET. The developing philosophy of CFD in the context of IHPTET is discussed. The key elements in the developing plan and specific examples of state-of-the-art CFD efforts which are IHPTET turbine engine relevant are discussed.

Author

**N89-26175\*#** National Aeronautics and Space Administration. Lewis Research Center, Cleveland, OH.

**FAR FIELD EXPANSION FOR ANISOTROPIC WAVE EQUATIONS**

S. I. HARIHARAN and THOMAS HAGSTROM (State Univ. of New York, Stony Brook.) Jun. 1989 12 p (NASA-TM-102112; E-4882; ICOMP-89-14; NAS 1.15:102112) Avail: NTIS HC A03/MF A01 CSCL 20/4

A necessary ingredient for the numerical simulation of many time dependent phenomena in acoustics and aerodynamics is the imposition of accurate radiation conditions at artificial boundaries. The asymptotic analysis of propagating waves provides a rational approach to the development of such conditions. A far field asymptotic expansion of solutions of anisotropic wave equations is derived. This generalizes the well known Friedlander expansion for the standard wave operator. The expansion is used to derive a hierarchy of radiation conditions of increasing accuracy. Two numerical experiments are given to illustrate the utility of this approach. The first application is the study of unsteady vortical disturbances impinging on a flat plate; the second is the simulation of inviscid flow past an impulsively started cylinder.

Author

**N89-26177\*#** National Aeronautics and Space Administration. Lewis Research Center, Cleveland, OH.

**COMPARATIVE THERMAL ANALYSIS OF THE SPACE STATION FREEDOM PHOTOVOLTAIC DEPLOYABLE BOOM STRUCTURE USING TRASYS, NEVADA, AND SINDA PROGRAMS**

JOSEPH F. BAUMEISTER (Analex Corp., Cleveland, OH.), DUANE E. BEACH, and SASAN C. ARMAND Jul. 1989 10 p Presented at the 19th Intersociety Conference on Environmental Systems, San Diego, CA, 24-26 Jul. 1989; sponsored in part by the Society of Automotive Engineers (NASA-TM-102062; E-4819; NAS 1.15:102062) Avail: NTIS HC A02/MF A01 CSCL 20/4

The proposed Space Station Photovoltaic Deployable Boom was analyzed for operating temperatures. The boom glass/epoxy structure design needs protective shielding from environmental degradation. The protective shielding optical properties (solar absorptivity and emissivity) dictate the operating temperatures of the boom components. The Space Station Boom protective shielding must also withstand the effects of the extendible/retractable coiling action within the mast canister. A thermal analysis method was developed for the Space Station Deployable Boom to predict transient temperatures for a variety of surface properties. The modeling procedures used to evaluate temperatures within the boom structure incorporated the TRASYS, NEVADA, and SINDA thermal analysis programs. Use of these programs led to a comparison between TRASYS and NEVADA analysis methods. Comparing TRASYS and NEVADA results exposed differences in the environmental solar flux predictions.

Author

**N89-26178\*#** National Aeronautics and Space Administration. Lewis Research Center, Cleveland, OH.

**MODELING OF PULSED PROPELLANT REORIENTATION**

A. E. PATAG, J. I. HOCHSTEIN (Washington Univ., Saint Louis, MO.), and D. J. CHATO Jul. 1989 19 p Presented at the 25th Joint Propulsion Conference, Monterey, CA, 10-12 Jul. 1989; sponsored in part by AIAA, ASME, SAE, and ASEE (Contract NAG3-578) (NASA-TM-102117; AIAA-89-2727; E-4892; NAS 1.15:102117) Avail: NTIS HC A03/MF A01 CSCL 20/4

Optimization of the propellant reorientation process can provide increased payload capability and extend the service life of spacecraft. The use of pulsed propellant reorientation to optimize the reorientation process is proposed. The ECLIPSE code was validated for modeling the reorientation process and is used to study pulsed reorientation in small-scale and full-scale propellant tanks. A dimensional analysis of the process is performed and the resulting dimensionless groups are used to present and correlate the computational predictions for reorientation performance.

Author

**N89-26179\*#** Yale Univ., New Haven, CT.  
**THEORETICAL STUDIES IN SUPPORT OF THE 3M-VAPOR TRANSPORT (PVTOS-) EXPERIMENTS Final Report**

### 34 FLUID MECHANICS AND HEAT TRANSFER

DANIEL E. ROSNER and DAVID E. KEYES Jul. 1989 54 p  
(Contract NAG3-898)  
(NASA-CR-185122; NAS 1.26:185122) Avail: NTIS HC A04/MF  
A01 CSCL 20/4

Results are reported for a preliminary theoretical study of the coupled mass-, momentum-, and heat-transfer conditions expected within small ampoules used to grow oriented organic solid (OS-) films, by physical vapor transport (PVT) in microgravity environments. It is shown that previous studies made restrictive assumptions (e.g., smallness of  $\Delta T/T$ , equality of molecular diffusivities) not valid under PVTOS conditions, whereas the important phenomena of sidewall gas creep, Soret transport of the organic vapor, and large vapor phase supersaturations associated with the large prevailing temperature gradients were not previously considered. Rational estimates are made of the molecular transport properties relevant to copper-phthalocyanine monomeric vapor in a gas mixture containing  $H_2(g)$  and  $Xe(g)$ . Efficient numerical methods have been developed and are outlined/illustrated here to making steady axisymmetric gas flow calculations within such ampoules, allowing for realistic realistic  $\Delta T/T$  (sub)-w-values, and even corrections to Navier-Stokes-Fourier 'closure' for the governing continuum differential equations. High priority follow-on studies are outlined based on these new results. Author

**N89-26180\*#** National Aeronautics and Space Administration. Lewis Research Center, Cleveland, OH.  
**MESH REFINEMENT IN A TWO-DIMENSIONAL LARGE EDDY SIMULATION OF A FORCED SHEAR LAYER**  
R. W. CLAUS, P. G. HUANG, and J. M. MACINNES (Princeton Univ., NJ.) Jun. 1989 20 p  
(NASA-TM-102129; E-4844; NAS 1.15:102129) Avail: NTIS HC A03/MF A01 CSCL 20/4

A series of large eddy simulations are made of a forced shear layer and compared with experimental data. Several mesh densities were examined to separate the effect of numerical inaccuracy from modeling deficiencies. The turbulence model that was used to represent small scale, 3-D motions correctly predicted some gross features of the flow field, but appears to be structurally incorrect. The main effect of mesh refinement was to act as a filter on the scale of vortices that developed from the inflow boundary conditions. Author

**N89-26182\*#** University of Southern California, Los Angeles. Dept. of Aerospace Engineering.  
**LIQUID DROPLET GENERATION Final Report**  
E. P. MUNTZ, MELISSA ORME, TONY FARNHAM, G. PHAM VANDIEP, and P. HUERRE Jun. 1989 72 p  
(Contract NAS3-25068)  
(NASA-CR-182246; NAS 1.26:182246) Avail: NTIS HC A04/MF A01 CSCL 20/4

A pre-prototype segment of a droplet sheet generator for a liquid droplet radiator was designed, constructed and tested. The ability to achieve a uniform, non-diverging droplet sheet is limited by manufacturing tolerances on nozzle parallelism. For an array of 100, 100 micrometer diameters nozzles spaced 5 stream diameters apart, typical standard deviations in stream alignment were plus or minus 10 mrad. The drop to drop fractional speed variations of the drops in typical streams were similar and independent of position in the array. The absolute value of the speed dispersion depended on the amplitude of the disturbance applied to the stream. A second generation preliminary design of a 5200 stream segment of a droplet sheet generator was completed. The design is based on information developed during testing of the pre-prototype segment, along with the results of an acoustical analysis for the stagnation cavity pressure fluctuations used to break-up the streams into droplets. Author

**N89-27103\*#** National Aeronautics and Space Administration. Lewis Research Center, Cleveland, OH.  
**HIGH SPEED CORNER AND GAP-SEAL COMPUTATIONS USING AN LU-SGS SCHEME**  
WILLIAM J. COIRIER 1989 16 p Presented at the 25th Joint

Propulsion Conference, Monterey, CA, 10-12 Jul. 1989; cosponsored by the AIAA, ASME, SAE, and ASEE  
(NASA-TM-102138; E-4936; NAS 1.15:102138; AIAA-89-2669)  
Avail: NTIS HC A03/MF A01 CSCL 20/4

The hybrid Lower-Upper Symmetric Gauss-Seidel (LU-SGS) algorithm was added to a widely used series of 2D/3D Euler/Navier-Stokes solvers and was demonstrated for a particular class of high-speed flows. A limited study was conducted to compare the hybrid LU-SGS for approximate Newton iteration and diagonalized Beam-Warming (DBW) schemes on a work and convergence history basis. The hybrid LU-SGS algorithm is more efficient and easier to implement than the DBW scheme originally present in the code for the cases considered. The code was validated for the hypersonic flow through two mutually perpendicular flat plates and then used to investigate the flow field in and around a simplified scramjet module gap seal configuration. Due to the similarities, the gap seal flow was compared to hypersonic corner flow at the same freestream conditions and Reynolds number. Author

**N89-27114\*#** National Aeronautics and Space Administration. Lewis Research Center, Cleveland, OH.  
**STABILITY OF A RIGID ROTOR SUPPORTED ON OIL-FILM JOURNAL BEARINGS UNDER DYNAMIC LOAD**  
B. C. MAJUMDAR and D. E. BREWE (Army Aviation Systems Command, Cleveland, OH.) 1987 13 p Presented at the National Seminar on Bearings, Madras, India, 17-18 Sep. 1987  
(NASA-TM-102309; E-3727; NAS 1.15:102309; AVSCOM-TR-87-C-26; AD-A212958) Avail: NTIS HC A03/MF A01 CSCL 20/4

Most published work relating to dynamically loaded journal bearings are directed to determining the minimum film thickness from the predicted journal trajectories. These do not give any information about the subsynchronous whirl stability of journal bearing systems since they do not consider the equations of motion. It is, however, necessary to know whether the bearing system operation is stable or not under such an operating condition. The stability characteristics of the system are analyzed. A linearized perturbation theory about the equilibrium point can predict the threshold of stability; however it does not indicate postwhirl orbit detail. The linearized method may indicate that a bearing is unstable for a given operating condition whereas the nonlinear analysis may indicate that it forms a stable limit cycle. For this reason, a nonlinear transient analysis of a rigid rotor supported on oil journal bearings under: (1) a unidirectional constant load, (2) a unidirectional periodic load, and (3) variable rotating load are performed. The hydrodynamic forces are calculated after solving the time-dependent Reynolds equation by a finite difference method with a successive overrelaxation scheme. Using these forces, equations of motion are solved by the fourth-order Runge-Kutta method to predict the transient behavior of the rotor. With the aid of a high-speed digital computer and graphics, the journal trajectories are obtained for several different operating conditions. Author

**N89-27115\*#** National Aeronautics and Space Administration. Lewis Research Center, Cleveland, OH.  
**CALCULATION OF TURBULENCE-DRIVEN SECONDARY MOTION IN DUCTS WITH ARBITRARY CROSS SECTION**  
A. O. DEMUREN (Lagos Univ., Nigeria) Jul. 1989 23 p  
(Contract NASA ORDER C-99066-G)  
(NASA-TM-102142; ICOMP-89-16; E-4941; NAS 1.15:102142)  
Avail: NTIS HC A03/MF A01 CSCL 20/4

Calculation methods for turbulent duct flows are generalized for ducts with arbitrary cross-sections. The irregular physical geometry is transformed into a regular one in computational space, and the flow equations are solved with a finite-volume numerical procedure. The turbulent stresses are calculated with an algebraic stress model derived by simplifying model transport equations for the individual Reynolds stresses. Two variants of such a model are considered. These procedures enable the prediction of both the turbulence-driven secondary flow and the anisotropy of the Reynolds stresses, in contrast to some of the earlier calculation

methods. Model predictions are compared to experimental data for developed flow in triangular duct, trapezoidal duct and a rod-bundle geometry. The correct trends are predicted, and the quantitative agreement is mostly fair. The simpler variant of the algebraic stress model procured better agreement with the measured data.

GRA

**N89-27118\*** # Ohio State Univ., Columbus. Dept. of Aeronautical and Astronautical Engineering.

**INTERACTION BETWEEN TOLLMIE-SCHLICHTING WAVES AND FREE-STREAM DISTURBANCES IN BOUNDARY-LAYER FLOWS**

R. J. BODONYI Aug. 1989 53 p

(Contract NAG3-743)

(NASA-CR-185847; NAS 1.26:185847) Avail: NTIS HC A04/MF A01 CSCL 20/4

A numerical study of the generation of Tollmien-Schlichting (T-S) waves due to the interaction between a small freestream disturbance and a small localized variation of the surface geometry has been carried out using finite difference methods. The nonlinear steady flow is of the viscous-inviscid interactive type while the unsteady disturbed flow is assumed to be governed by the Navier-Stokes equations linearized about this flow. Numerical solutions illustrate the growth or decay of the T-S waves generated by the interaction between the freestream disturbance and the surface distortion, depending on the value of the scaled Strouhal number. An important result of this receptivity problem is the numerical determination of the amplitude of the Tollmien-Schlichting waves.

Author

**N89-27121\*** # National Aeronautics and Space Administration. Lewis Research Center, Cleveland, OH.

**ARCJET CATHODE PHENOMENA**

FRANCIS M. CURRAN, THOMAS W. HAAG, and JOHN F. RAQUET (Air Force Academy, CO.) May 1989 17 p Presented at the JANNAF Propulsion Meeting, Cleveland, OH, 23-25 May 1989 (NASA-TM-102099; E-4841; NAS 1.15:102099) Avail: NTIS HC A03/MF A01 CSCL 20/4

Cathode tips made from a number of different materials were tested in a modular arcjet thruster in order to examine cathode phenomena. Periodic disassembly and examination, along with the data collected during testing, indicated that all of the tungsten-based materials behaved similarly despite the fact that in one of these samples the percentage of thorium oxide was doubled and another was 25 percent rhenium. The mass loss rate from a 2 percent thoriated rhenium cathode was found to be an order of magnitude greater than that observed using 2 percent thoriated tungsten. Detailed analysis of one of these cathode tips showed that the molten crater contained pure tungsten to a depth of about 150 microns. Problems with thermal stress cracking were encountered in the testing of a hafnium carbide tip. Post test analysis showed that the active area of the tip had chemically reacted with the propellant. A 100 hour continuous test was run at about 1 kW. Post test analysis revealed no dendrite formation, such as observed in a 30 kW arcjet lifetest, near the cathode crater. The cathodes from both this test and a previously run 1000 hour cycled test displayed nearly identical arc craters. Data and calculations indicate that the mass losses observed in testing can be explained by evaporation.

Author

**N89-27980\*** # National Aeronautics and Space Administration. Lewis Research Center, Cleveland, OH.

**EXPERIENCE WITH ADVANCED INSTRUMENTATION IN A HOT SECTION CASCADE**

FREDERICK C. YEH and HERBERT J. GLADDEN 1989 14 p Prepared for presentation at the Winter Annual Meeting of the American Society of Mechanical Engineers, San Francisco, CA, 10-15 Dec. 1989

(NASA-TM-102294; E-4962; NAS 1.15:102294) Avail: NTIS HC A03/MF A01 CSCL 20/4

The Lewis Research Center gas turbine Hot Section Test Facility was developed to provide a real engine environment with known boundary conditions for the aerothermal performance

evaluation and verification of computer design codes. This verification process requires experimental measurements in a hostile environment. The research instruments used in this facility are presented, and their characteristics and how they perform in this environment are discussed. The research instrumentation consisted of conventional pressure and temperature sensors, as well as thin-film thermocouples and heat flux gages. The hot gas temperature was measured by an aspirated temperature probe and by a dual-element, fast-response temperature probe. The data acquisition mode was both steady state and time dependent. These experiments were conducted over a wide range of gas Reynolds numbers, exit gas Mach numbers, and heat flux levels. This facility was capable of testing at temperatures up to 1600 K, and at pressures up to 18 atm. These corresponded to an airfoil exit Reynolds number range of  $0.5 \times 10(6)$  to  $2.5 \times 10(6)$  based on the airfoil chord of 5.55 cm. The results characterize the performance capability and the durability of the instrumentation. The challenge of making measurements in hostile environments is also discussed. The instruments exhibited more than adequate durability to achieve the measurement profile. About 70 percent of the thin-film thermocouples and the dual-element temperature probe survived several hundred thermal cycles and more than 35 hr at gas temperatures up to 1600 K. Within the experimental uncertainty, the steady-state and transient heat flux measurements were comparable and consistent over the range of Reynolds numbers tested.

Author

**N89-28737\*** # Pennsylvania State Univ., University Park. Dept. of Mechanical Engineering.

**SKIN-FRICTION MEASUREMENTS BY LASER INTERFEROMETRY (Computer Diskette Supplement)**

K.-S. KIM and G. S. SETTLES /n AGARD, A Survey of Measurements and Measuring Techniques in Rapidly Distorted Compressible Turbulent Boundary Layers 8 p May 1989 Computer diskette supplement (data file): IBM compatible DS HD 5.25-inch formatted 1.2 MB using MS DOS 3.20 (Contract NAG3-527)

Copyright Avail: NTIS HC A11/MF A01; set of 5 computer diskettes available from NASA Scientific and Technical Information Facility, BWI Airport, MD at \$13.00/set CSCL 20/4

The measurement of skin friction in rapidly distorted compressible flows is difficult, and very few reliable techniques are available. A recent development, the laser interferometer skin friction (LISF) meter, promises to be useful for this purpose. This technique interferometrically measures the time rate of thinning of an oil film applied to an aerodynamic surface. Under the proper conditions the wall shear stress may thus be found directly, without reference to flow properties. The applicability of the LISF meter to supersonic boundary layers is examined experimentally. Its accuracy and repeatability are assessed, and conditions required for its successful application are considered.

Author

**N89-28748\*** # National Aeronautics and Space Administration. Lewis Research Center, Cleveland, OH.

**THE UPPER-BRANCH STABILITY OF COMPRESSIBLE BOUNDARY LAYER FLOWS**

J. S. B. GAJJAR and J. W. COLE (Iowa State Univ. of Science and Technology, Ames.) Aug. 1989 36 p Prepared in cooperation with Exeter Univ. (England) (NASA-TM-102128; ICOMP-89-15; E-4916; NAS 1.15:102128) Avail: NTIS HC A03/MF A01 CSCL 20/4

The upper-branch linear and nonlinear stability of compressible boundary layer flows is studied using the approach of Smith and Bodonyi (1982) for a similar incompressible problem. Both pressure gradient boundary layers and Blasius flow are considered with and without heat transfer, and the neutral eigenrelations incorporating compressibility effects are obtained explicitly. The compressible nonlinear viscous critical layer equations are derived and solved numerically and the results indicate some solutions with positive phase shift across the critical layer. Various limiting cases are investigated including the case of much larger disturbance amplitudes and this indicates the structure for the strongly nonlinear critical layer of the Benney-Bergeon (1969) type.

### 34 FLUID MECHANICS AND HEAT TRANSFER

It is also shown how a match with the inviscid neutral inflexional modes arising from the generalized inflexion point criterion, is achieved. Author

**N89-28749\*#** National Aeronautics and Space Administration. Lewis Research Center, Cleveland, OH.

#### **CALCULATION OF REATTACHING SHEAR LAYERS IN DIVERGENT CHANNEL WITH A MULTIPLE-TIME-SCALE TURBULENCE MODEL**

S.-W. KIM Aug. 1989 27 p  
(Contract NASA ORDER C-99066-G)  
(NASA-TM-102293; ICOMP-89-18; E-4965; NAS 1.15:102293)  
Avail: NTIS HC A03/MF A01 CSCL 20/4

Numerical calculations of turbulent reattaching shear layers in a divergent channel are presented. The turbulence is described by a multiple-time-scale turbulence model. The turbulent flow equations are solved by a control-volume based finite difference method. The computational results are compared with those obtained using k-epsilon turbulence models and algebraic Reynolds stress turbulence models. It is shown that the multiple-time-scale turbulence model yields significantly improved computational results than the other turbulence models in the region where the turbulence is in a strongly inequilibrium state. Author

**N89-29714\*#** National Aeronautics and Space Administration. Lewis Research Center, Cleveland, OH.

#### **MULTIWAVE INTERACTIONS IN TURBULENT JETS**

REDA R. MANKBADI Sep. 1989 46 p  
(Contract NASA ORDER C-99066-G)  
(NASA-TM-101985; E-4685; ICOMP-89-12; NAS 1.15:101985)  
Avail: NTIS HC A03/MF A01 CSCL 20/4

Nonlinear wave-wave interactions in turbulent jets were investigated based on the integrated energy of each scale of motion in a cross section of the jet. The analysis indicates that two frequency components in the axisymmetric mode can interact with other background frequencies in the axisymmetric mode, thereby amplifying an enormous number of other frequencies. Two frequency components in a single helical mode cannot, by themselves, amplify other frequency components. But combinations of frequency components of helical and axisymmetric modes can amplify other frequencies in other helical modes. The present computations produce several features consistent with experimental observations such as: (1) dependency of the interactions on the initial phase differences, (2) enhancement of the momentum thickness under multifrequency forcing, and (3) the increase in background turbulence under forcing. In a multifrequency-excited jet, mixing enhancement was found to be a result of the turbulence enhancement rather than simply the amplification of forced wave components. The excitation waves pump energy from the mean flow to the turbulence, thus enhancing the latter. The high frequency waves enhance the turbulence close to the jet exit, but, the low frequency waves are most effective further downstream. Author

**N89-29725\*#** National Aeronautics and Space Administration. Lewis Research Center, Cleveland, OH.

#### **NUMERICAL INVESTIGATION OF AN INTERNAL LAYER IN TURBULENT FLOW OVER A CURVED HILL**

S.-W. KIM Oct. 1989 44 p  
(Contract C99066G)  
(NASA-TM-102230; E-5035; ICOMP-89-20; NAS 1.15:102230)  
Avail: NTIS HC A03/MF A01 CSCL 20/4

The development of an internal layer in a turbulent boundary layer flow over a curved hill is investigated numerically. The turbulence field of the boundary layer flow over the curved hill is compared with that of a turbulent flow over a symmetric airfoil (which has the same geometry as the curved hill except that the leading and trailing edge plates were removed) to study the influence of the strongly curved surface on the turbulence field. The turbulent flow equations are solved by a control-volume based finite difference method. The turbulence is described by a multiple-time-scale turbulence model supplemented with a near-wall turbulence model. Computational results for the mean flow field

(pressure distributions on the walls, wall shearing stresses and mean velocity profiles), the turbulence structure (Reynolds stress and turbulent kinetic energy profiles), and the integral parameters (displacement and momentum thicknesses) compared favorably with the measured data. Computational results show that the internal layer is a strong turbulence field which is developed beneath the external boundary layer and is located very close to the wall. Development of the internal layer was more obviously observed in the Reynolds stress profiles and in the turbulent kinetic energy profiles than in the mean velocity profiles. In this regard, the internal layers is significantly different from wall-bounded simple shear layers in which the mean velocity profile characterizes the boundary layer most distinguishably. Development of such an internal layer, characterized by an intense turbulence field, is attributed to the enormous mean flow strain rate caused by the streamline curvature and the strong pressure gradient. In the turbulent flow over the curved hill, the internal layer begin to form near the forward corner of the hill, merges with the external boundary layer, and develops into a new fully turbulent boundary layer as the fluid flows in the downstream direction. For the flow over the symmetric airfoil, the boundary layer began to form from almost the same location as that of the curved hill, grew in its strength, and formed a fully turbulent boundary layer from mid-part of the airfoil and in the downstream region. Computational results also show that the detailed turbulence structure in the region very close to the wall of the curved hill is almost the same as that of the airfoil in most of the curved regions except near the leading edge. Thus the internal layer of the curved hill and the boundary layer of the airfoil were also almost the same. Development of the wall shearing stress and separation of the boundary layer at the rear end of the curved hill mostly depends on the internal layer and is only slightly influenced by the external boundary layer flow. Author

**N89-29726\*#** National Aeronautics and Space Administration. Lewis Research Center, Cleveland, OH.

#### **TIME DOMAIN NUMERICAL CALCULATIONS OF UNSTEADY VORTICAL FLOWS ABOUT A FLAT PLATE AIRFOIL**

S. I. HARIHARAN, PING YU (Akron Univ., OH.), and J. R. SCOTT Sep. 1989 24 p  
(Contract C99066G)  
(NASA-TM-102318; E-5014; ICOMP-89-19; NAS 1.15:102318)  
Avail: NTIS HC A03/MF A01 CSCL 20/4

A time domain numerical scheme is developed to solve for the unsteady flow about a flat plate airfoil due to imposed upstream, small amplitude, transverse velocity perturbations. The governing equation for the resulting unsteady potential is a homogeneous, constant coefficient, convective wave equation. Accurate solution of the problem requires the development of approximate boundary conditions which correctly model the physics of the unsteady flow in the far field. A uniformly valid far field boundary condition is developed, and numerical results are presented using this condition. The stability of the scheme is discussed, and the stability restriction for the scheme is established as a function of the Mach number. Finally, comparisons are made with the frequency domain calculation by Scott and Atassi, and the relative strengths and weaknesses of each approach are assessed. Author

### 35

#### **INSTRUMENTATION AND PHOTOGRAPHY**

Includes remote sensors; measuring instruments and gages; detectors; cameras and photographic supplies; and holography.

**A89-10366\*** National Aeronautics and Space Administration. Lewis Research Center, Cleveland, OH.

#### **FIBER-OPTIC TEMPERATURE SENSOR USING A SPECTRUM-MODULATING SEMICONDUCTOR ETALON**

GLENN BEHEIM (NASA, Lewis Research Center, Cleveland, OH),



KLAUS FRITSCH (John Carroll University, Cleveland, OH), and DONALD J. ANTHAN (Cleveland State University, OH) IN: Fiber optic and laser sensors V; Proceedings of the Meeting, San Diego, CA, Aug. 17-19, 1987. Bellingham, WA, Society of Photo-Optical Instrumentation Engineers, 1988, p. 238-246. Previously announced in STAR as N87-25329. refs  
Copyright

Described is a fiber-optic temperature sensor that uses a spectrum modulating SiC etalon. The spectral output of this type of sensor may be analyzed to obtain a temperature measurement which is largely independent of the transmission properties of the sensor's fiber-optic link. A highly precise laboratory spectrometer is described in detail, and this instrument is used to study the properties of this type of sensor. Also described are a number of different spectrum analyzers that are more suitable for use in a practical thermometer. Author

**A89-10368\*** National Aeronautics and Space Administration. Lewis Research Center, Cleveland, OH.

**AMPLITUDE SPECTRUM MODULATION TECHNIQUE FOR ANALOG DATA PROCESSING IN FIBER OPTIC SENSING SYSTEM WITH TEMPORAL SEPARATION OF CHANNELS**

GRIGORY ADAMOVSKY (NASA, Lewis Research Center, Cleveland, OH) IN: Fiber optic and laser sensors V; Proceedings of the Meeting, San Diego, CA, Aug. 17-19, 1987. Bellingham, WA, Society of Photo-Optical Instrumentation Engineers, 1988, p. 264-270. Previously announced in STAR as N87-25562.  
Copyright

A novel technique to analyze analog data in fiber optic sensing systems with temporal separation of channels is proposed. A theoretical explanation of the process is presented and an experimental setup that was used to obtain data is described. Author

**A89-12276\*** National Aeronautics and Space Administration. Lewis Research Center, Cleveland, OH.

**THE DUAL ELEMENT METHOD OF STRAIN GAUGE TEMPERATURE COMPENSATION**

DAVID R. ENGLUND (NASA, Lewis Research Center, Cleveland, OH) IN: SEM, Annual Hostile Environments and High Temperature Measurements Conference, 4th, Windsor Locks, CT, Mar. 24, 25, 1987, Proceedings. Bethel, CT, Society for Experimental Mechanics, Inc., 1987, p. 40-42.  
Copyright

The use of a known temperature compensation technique is suggested to reduce the overall temperature sensitivity of a PdCr strain gauge system being developed for turbine engine research. The temperature compensation technique proposed for this application uses a resistance thermometer in an adjacent leg of the strain gauge bridge circuit to cancel the thermally generated resistance change of the strain gauge. Equations for calculating the required compensation resistor values and the sensitivity of the resulting strain gauge bridge to both temperature and strain are presented. V.L.

**A89-14985\*#** National Aeronautics and Space Administration. Lewis Research Center, Cleveland, OH.

**APPLICATION OF OPTICAL CORRELATION TECHNIQUES TO PARTICLE IMAGING**

MARK P. WERNET (NASA, Lewis Research Center, Cleveland, OH) and ROBERT V. EDWARDS (Case Western Reserve University, Cleveland, OH) AIAA, NASA, and AFWAL, Conference on Sensors and Measurements Techniques for Aeronautical Applications, Atlanta, GA, Sept. 7-9, 1988. 18 p. Previously announced in STAR as N88-29152. refs  
(AIAA PAPER 88-4661) Copyright

Pulsed laser sheet velocimetry yields nonintrusive measurements of velocity vectors across an extended 2-dimensional region of the flow field. The application of optical correlation techniques to the analysis of multiple exposure laser light sheet photographs can reduce and/or simplify the data reduction time and hardware. Here, Matched Spatial Filters (MSF) are used in a pattern recognition system. Usually MSFs are used

to identify the assembly line parts. In this application, the MSFs are used to identify the iso-velocity vector contours in the flow. The patterns to be recognized are the recorded particle images in a pulsed laser light sheet photograph. Measurement of the direction of the particle image displacements between exposures yields the velocity vector. The particle image exposure sequence is designed such that the velocity vector direction is determined unambiguously. A global analysis technique is used in comparison to the more common particle tracking algorithms and Young's fringe analysis technique. Author

**A89-17347\*** National Aeronautics and Space Administration. Lewis Research Center, Cleveland, OH.

**SURFACE TEMPERATURE DETERMINATION IN SURFACE ANALYTIC SYSTEMS BY INFRARED OPTICAL PYROMETRY**

DONALD R. WHEELER, WILLIAM R. JONES, JR., and STEPHEN V. PEPPER (NASA, Lewis Research Center, Cleveland, OH) Journal of Vacuum Science and Technology A (ISSN 0734-2101), vol. 6, Nov.-Dec. 1988, p. 3166-3168.  
Copyright

An IR pyrometric technique for measuring the surface temperatures of metal specimens in an ultrahigh-vacuum analytic chamber is described and demonstrated. The experimental setup comprises a commercial IR microscope with a long-working-distance right-angle objective (focal spot diameter 1 mm at 53 cm), a metal-coated glass vacuum chamber with a Ta-mesh-covered quartz viewport, an Mo specimen stub with an internal heating element, and a Ta disk test specimen with a flat side coated with a high-emissivity graphite film. The results of an initial calibration test are presented graphically and briefly characterized. The measurement error at 450 C is found to be less than 10 C. T.K.

**A89-22279\*#** Ohio State Univ., Columbus.

**PERFORMANCE OF LASER DOPPLER VELOCIMETER WITH POLYDISPERSE SEED PARTICLES IN HIGH-SPEED FLOWS**

M. SAMIMY (Ohio State University, Columbus) and B. A. K. ABU-HIJLEH Journal of Propulsion and Power (ISSN 0748-4658), vol. 5, Jan.-Feb. 1989, p. 21-25. refs  
(Contract NAG3-764)  
Copyright

The flowfield behind an oblique shock wave, where the LDV measured velocities are seed-particle-size dependent, was used to investigate the effects of LDV system parameters on the range of detectable polydisperse seed particles. The parameters included frequency shifting, laser power, scattered signal amplification level, and number of required fringe crossings. The results showed that with polydisperse seed particles ranging from 0.1 to 4.0 microns available in the flow, the average diameter of the detected particles could change from 0.2 to 3.0 microns by changing different LDV system parameters. The effects of this shift in the range of detectable particles on the frequency response of LDV are discussed. Author

**A89-25570\*#** National Aeronautics and Space Administration. Lewis Research Center, Cleveland, OH.

**PERFORMANCE OF THE FORWARD SCATTERING SPECTROMETER PROBE IN NASA'S ICING RESEARCH TUNNEL**

EDWARD A. HOVENAC (NASA, Lewis Research Center; Sverdrup Technology, Inc., Cleveland, OH) and ROBERT F. IDE (NASA, Lewis Research Center; U.S. Army, Propulsion Directorate, Cleveland, OH) AIAA, Aerospace Sciences Meeting, 27th, Reno, NV, Jan. 9-12, 1989. 9 p. Previously announced in STAR as N89-12845.  
(AIAA PAPER 89-0769) Copyright

Two Forward Scattering Spectrometer Probes were used to measure droplet distributions in the NASA Lewis Icing Research Tunnel. The instruments showed good agreement when the median volume diameter (MVD) was approximately 16 micrometers. Coincidence events affected much of the data and caused the measured MVD to be about 2 to 3 micrometers larger than

expected. Coincidence events were reduced by shutting down half of the spray bars in the tunnel during certain tests. Author

## **A89-27663\*# Rensselaer Polytechnic Inst., Troy, NY. DEVELOPMENT AND APPLICATIONS OF OPTICAL INTERFEROMETRIC MICROMETROLOGY IN THE ANGSTROM AND SUBANGSTROM RANGE**

JAMES L. LAUER (Rensselaer Polytechnic Institute, Troy, NY) and PHILLIP B. ABEL (NASA, Lewis Research Center, Cleveland, OH) IN: International Instrumentation Symposium, 34th, Albuquerque, NM, May 2-6, 1988, Proceedings. Research Triangle Park, NC, Instrument Society of America, 1988, p. 243-253. refs

The characteristics of the scanning tunneling microscope and atomic force microscope (AFM) are briefly reviewed, and optical methods, mainly interferometry, of sufficient resolution to measure AFM deflections are discussed. The methods include optical resonators, laser interferometry, multiple-beam interferometry, and evanescent wave detection. Experimental results using AFM are reviewed. C.D.

## **A89-33379\*# Arizona State Univ., Tempe. CALIBRATION OF SINGLE PARTICLE SIZING VELOCIMETERS USING PHOTOMASK RETICLES**

E. D. HIRLEMAN (Arizona State University, Tempe), D. J. HOLVE (Insitex, Inc., San Ramon, CA), and E. A. HOVENAC (NASA, Lewis Research Center, Cleveland, OH) IN: International Symposium on Applications of Laser Anemometry to Fluid Mechanics, 4th, Lisbon, Portugal, July 11-14, 1988, Proceedings. Lisbon, Instituto Superior Tecnico, 1988, p. 6.10 (5 p.). Research supported by FAA. refs

The development of photomask reticle calibration standards for single particle instruments is discussed. The calibration method studied involves the use of photomask reticles where the particle artifacts are actually disks of chrome thin film in the clear field reticles produced by photolithography and etching processes. Consideration is given to various aspects of theory, design, and performance. K.K.

## **A89-37298\* Simon Fraser Univ., Burnaby (British Columbia). DESIGN AND SIMULATED PERFORMANCE OF A CARS SPECTROMETER FOR DYNAMIC TEMPERATURE MEASUREMENTS USING ELECTRONIC HETERODYNING**

M. JAMAL DEEN (Simon Fraser University, Burnaby, Canada) and E. D. THOMPSON (Lehigh University, Bethlehem, PA) Applied Optics (ISSN 0003-6935), vol. 28, April 1, 1989, p. 1409-1416. Research supported by Lehigh University and Case Western Reserve University. refs  
(Contract NAG3-432)  
Copyright

A new design for generating CARS signals and for the detection and processing of these signals is presented and evaluated. The design is based on electronic heterodyning of the CARS spectrum of nitrogen at two selected narrowband frequencies, ratioing the resulting signal strengths, and comparing this ratio with a theoretically derived temperature scale. A reference cell is incorporated into the design for system calibration and for accurate temperature measurements. The spectrometer is found capable of measuring temperature in the submillisecond time scale with an accuracy of 10 percent in the 1000-2000 K temperature range. A typical result using the Hg(x)Cd(1-x)Te photomixer for  $T = 1500$  K,  $\Delta T = 50$  K is a SNR of 21 dB and a data collection rate of 300 Hz. Author

## **A89-39302\* National Aeronautics and Space Administration. Lewis Research Center, Cleveland, OH. INTENSITY-BASED FIBRE-OPTIC SENSING SYSTEM USING CONTRAST MODULATION OF SUBCARRIER INTERFERENCE PATTERN**

G. ADAMOVSKY, T. N. SHERER (NASA, Lewis Research Center, Cleveland, OH), and D. J. MAITLAND (Cleveland State University, OH) Electronics Letters (ISSN 0013-5194), vol. 25, March 2, 1989, p. 325, 326.

(Contract NCC3-58)

Copyright

A novel technique to compensate for unwanted intensity losses in a fiber-optic sensing system is described. The technique involves a continuous sinusoidal modulation of the light source intensity at radio frequencies and an intensity sensor placed in an unbalanced interferometer. The system shows high sensitivity and stability. C.D.

## **A89-43532\* Illinois Univ., Urbana.**

### **HIGH PRESSURE MULTIAXIAL EXTENSOMETRY**

PETER KURATH (Illinois University, Urbana) IN: Annual Hostile Environments and High Temperature Measurements Conference, 4th, Windsor Locks, CT, Mar. 24, 25, 1987, Proceedings. Bethel, CT, Society for Experimental Mechanics, Inc., 1987, p. 74-81. refs

(Contract NAG3-465)

Copyright

The development of a multiple degree-of-freedom extensometer to measure axial, torsional, and diametrical strains on a tubular laboratory fatigue specimen is described. It is found that the overall accuracy of the extensometer is limited by cross talk due to torsional displacements in an ambient environment. If only axial and diametrical deformation occur, error induced by cross talk is less than + or - 0.5 percent. K.K.

## **A89-43842\* National Aeronautics and Space Administration. Lewis Research Center, Cleveland, OH.**

### **HIGH TEMPERATURE OPTICAL STRAIN MEASUREMENT SYSTEM**

CHRISTIAN T. LANT (NASA, Lewis Research Center; Sverdrup Technology, Inc., Cleveland, OH) IN: Annual Hostile Environments and High Temperature Measurements Conference, 5th, Costa Mesa, CA, Mar. 22, 23, 1988, Proceedings. Bethel, CT, Society for Experimental Mechanics, Inc., 1988, p. 8-11.  
Copyright

A high temperature strain measurement system being developed at the NASA Lewis Research Center utilizes laser speckle shift relations to measure strain components on the surface of a hot specimen in near real time. Features of this system include a totally noncontacting measurement capability and a rotatable gauge axis, allowing an optical rosette to be implemented and principal strains to be determined. Preliminary results and background work are presented. Author

## **A89-44122\* Cleveland State Univ., OH.**

### **AN IMPROVED CORRECTION ALGORITHM FOR NUMBER DENSITY MEASUREMENTS MADE WITH THE FORWARD SCATTERING SPECTROMETER PROBE**

JAMES A. LOCK (Cleveland State University, OH) and EDWARD A. HOVENAC (NASA, Lewis Research Center; Sverdrup Technology, Inc., Cleveland, OH) Review of Scientific Instruments (ISSN 0034-6748), vol. 60, June 1989, p. 1143-1153. refs  
Copyright

A correction factor to the number density measured by the Forward Scattering Spectrometer Probe (FSSP) which compensates for dead time and coincidence errors was determined by calculating the probabilities of, and the average number of particles in, the six possible types of dead time and coincidence events. These probabilities and averages were calculated by means of a probabilistic model based on Poisson statistics. A Monte Carlo computer simulation of the FSSP operation was also carried out and the number density correction factor was compared with the Monte Carlo data. For an actual number density of 2000/cu cm, it was found that the measured number density was of the order of 300/cu cm. Author

## **A89-44123\* Cleveland State Univ., OH.**

### **A CORRECTION ALGORITHM FOR PARTICLE SIZE DISTRIBUTION MEASUREMENTS MADE WITH THE FORWARD-SCATTERING SPECTROMETER PROBE**

JAMES A. LOCK (Cleveland State University, OH) and EDWARD A. HOVENAC (NASA, Lewis Research Center; Sverdrup

Technology, Inc., Cleveland, OH) Review of Scientific Instruments (ISSN 0034-6748), vol. 60, June 1989, p. 1154-1160. refs  
Copyright

A correction algorithm for evaluating the particle size distribution measurements of atmospheric aerosols obtained with a forward-scattering spectrometer probe (FSSP) is examined. A model based on Poisson statistics is employed to calculate the average diameter and rms width of the particle size distribution. The dead time and coincidence errors in the measured number density are estimated. The model generated data are compared with a Monte Carlo simulation of the FSSP operation. It is observed that the correlation between the actual and measured size distribution is nonlinear. It is noted that the algorithm permits more accurate calculation of the average diameter and rms width of the distribution compared to uncorrected measured quantities.

I.F.

**A89-45909\*** Naval Postgraduate School, Monterey, CA.  
**SPATIAL RESOLUTION AND DOWNWASH VELOCITY CORRECTIONS FOR MULTIPLE-HOLE PRESSURE PROBES IN COMPLEX FLOWS**

P. M. LIGRANI, L. R. BAUN (U.S. Naval Postgraduate School, Monterey, CA), and B. A. SINGER (High Technology Corp., Hampton, VA) Experiments in Fluids (ISSN 0723-4864), vol. 7, no. 6, June 1989, p. 424-426. Research sponsored by the U.S. Army. refs

(Contract NASA ORDER C-80019-F)

Copyright

Correction schemes for finite spatial resolution and induced downwash velocity are presented which have application to the measurement of complex three-dimensional flow fields using five-hole angle-type pressure probes. In the study, induced downwash velocity is assumed to be proportional to the transverse gradients of streamwise velocity. The present correction schemes are validated by application to flows including vortices embedded within turbulent boundary layers and flows in a curved channel with 1.27-cm width, a 40-to-1 aspect ratio, and 59.7 cm of convex surface curvature.

R.R.

**A89-46980\*** Cleveland State Univ., OH.  
**A SELF DIAGNOSTIC SYSTEM FOR PIEZOELECTRIC SENSORS**

WILLIAM J. ATHERTON and PATRICK M. FLANAGAN (Cleveland State University, OH) AIAA, ASME, SAE, and ASEE, Joint Propulsion Conference, 25th, Monterey, CA, July 10-13, 1989, 6 p.

(Contract NAG3-889)

(AIAA PAPER 89-2638) Copyright

A technique for determining the mounting conditions of a piezoelectric accelerometer is presented. This technique electrically stimulates the piezoelectric element in the 'diagnostic' frequency band measuring the electrical frequency response characteristics across a capacitive load impedance. The diagnostic frequency band is typically much higher than the operating bandwidth of the accelerometer. The resonant frequencies of the accelerometer are included in the diagnostic band. By monitoring the shift in these resonant frequencies, via electrical stimulation techniques, certain diagnostic conditions including mounting conditions can be determined. Experimental data from a compression mode accelerometer is used to demonstrate this technique.

Author

**A89-47378\*** North Carolina State Univ., Raleigh.  
**PARAMETRIC STUDY OF STATISTICAL BIAS IN LASER DOPPLER VELOCIMETRY**

RICHARD D. GOULD (North Carolina State University, Raleigh), WARREN H. STEVENSON, and H. DOYLE THOMPSON (Purdue University, West Lafayette, IN) AIAA Journal (ISSN 0001-1452), vol. 27, Aug. 1989, p. 1140-1142. refs  
(Contract NAG3-503)

Copyright

Analytical studies have often assumed that LDV velocity bias depends on turbulence intensity in conjunction with one or more characteristic time scales, such as the time between validated

signals, the time between data samples, and the integral turbulence time-scale. These parameters are presently varied independently, in an effort to quantify the biasing effect. Neither of the post facto correction methods employed is entirely accurate. The mean velocity bias error is found to be nearly independent of data validation rate.

O.C.

**A89-47717\*** Texas A&M Univ., College Station.  
**PIEZOELECTRIC PUSHERS FOR ACTIVE VIBRATION CONTROL OF ROTATING MACHINERY**

A. B. PALAZZOLO, R. R. LIN, R. M. ALEXANDER (Texas A & M University, College Station), A. F. KASCAK (NASA, Lewis Research Center; U.S. Army, Cleveland, OH), and J. MONTAGUE (Sverdrup Technology, Inc., Middleburg Heights, OH) ASME, Transactions, Journal of Vibration, Acoustics, Stress, and Reliability in Design (ISSN 0739-3717), vol. 111, July 1989, p. 298-305. Research supported by the Texas A & M Turbomachinery Research Consortium. Previously announced in STAR as N88-23229. refs  
(Contract NAG3-763)

Copyright

The active control of rotordynamic vibrations and stability by magnetic bearings and electromagnetic shakers have been discussed extensively in the literature. These devices, though effective, are usually large in volume and add significant weight to the stator. The use of piezoelectric pushers may provide similar degrees of effectiveness in light, compact packages. Tests are currently being conducted with piezoelectric pusher-based active vibration control. Results from tests performed on NASA test rigs as preliminary verification of the related theory are presented.

Author

**A89-54278\*** Swiss Center for Electronics and Microtechnology, Inc., Neuchatel.

**THE SCRATCH TEST - DIFFERENT CRITICAL LOAD DETERMINATION TECHNIQUES**

J. SEKLER, H. E. HINTERMANN (Swiss Centre for Electronics and Microtechnology, Inc., Neuchatel, Switzerland), and P. A. STEINMANN (NASA, Lewis Research Center, Cleveland, OH; Swiss Centre for Electronics and Microtechnology, Inc., Neuchatel, Switzerland) IN: Metallurgical coatings 1988; Proceedings of the Fifteenth International Conference, San Diego, CA, Apr. 11-15, 1988. Volume 1. London and New York, Elsevier Applied Science, 1988, p. 519-529. refs

Copyright

Different critical load determination techniques such as microscopy, acoustic emission, normal, tangential, and lateral forces used for scratch test evaluation of complex or multilayer coatings are investigated. The applicability of the scratch test to newly developed coating techniques, systems, and applications is discussed. Among the methods based on the use of a physical measurement, acoustic emission detection is the most effective. The dynamics ratio between the signals below and above the critical load for the acoustic emission (much greater than 100) is well above that obtained with the normal, tangential, and lateral forces. The present commercial instruments are limited in load application performance. A scratch tester able to apply accurate loads as low as 0.01 N would probably overcome most of the actual limitations and would be expected to extend the scratch testing technique to different application fields such as optics and microelectronics.

C.E.

**A89-54281\*** Technical Research Centre of Finland, Espoo.  
**ADHESION SCRATCH TESTING - A ROUND-ROBIN EXPERIMENT**

A. J. PERRY (GTE Valenite Corp., Troy, MI), J. VALLI (Technical Research Centre of Finland, Espoo), and P. A. STEINMANN (NASA, Lewis Research Center, Cleveland, OH; Swiss Centre for Electronics and Microtechnology, Inc., Neuchatel, Switzerland) IN: Metallurgical coatings 1988; Proceedings of the Fifteenth International Conference, San Diego, CA, Apr. 11-15, 1988. Volume 1. London and New York, Elsevier Applied Science, 1988, p. 559-575. refs

Copyright

### 35 INSTRUMENTATION AND PHOTOGRAPHY

Six sets of samples, TiN coated by chemical or physical vapor deposition methods (CVD or PVD) onto cemented carbide or high-speed steel (HSS), and TiC coated by CVD onto cemented carbide have been scratch tested using three types of commercially available scratch adhesion tester. With exception of one cemented carbide set, the reproducibility of the critical loads for any given set with a given stylus is excellent, about + or - 5 percent, and is about + or - 20 percent for different styli. Any differences in critical loads recorded for any given sample set can be attributed to the condition of the stylus (clean, new, etc.), the instrument used, the stylus itself (friction coefficient, etc.), and the sample set itself. One CVD set showed remarkably large differences in critical loads for different styli, which is thought to be related to a mechanical interaction between stylus and coating which is enhanced by a plastic deformability in the film related to the coating microstructure. The critical load for TiN on HSS increases with coating thickness, and differences in frictional conditions led to a systematic variation in the critical loads depending on the stylus used. C.E.

**N89-10269\*#** National Aeronautics and Space Administration. Lewis Research Center, Cleveland, OH.

#### **PERFORMANCE OF MULTIMIRROR QUARTZLINE LAMPS IN A HIGH-PRESSURE, UNDERWATER ENVIRONMENT**

HOWARD A. SLATER 1988 8 p Presented at the 32nd Annual International Symposium on Optical and Optoelectronic Applied Science and Engineering, San Diego, Calif., 14-19 Aug. 1988; sponsored by the Society of Photo-Optical Instrumentation Engineers (NASA-TM-101374; E-4427; NAS 1.15:101374) Avail: NTIS HC A02/MF A01 CSCL 14/2

Multimirror Quartzline Lamps are extremely versatile and effective for nonconventional imaging requirements such as high-speed photo and video instrumentation and high-magnification imaging. The lamps' versatility though, is not limited to conventional environments. Many research experiments and projects require a high pressure environment. Continuous photographic data acquisition in a high-pressure vessel requires wall penetrations and creates design problems as well as potential failure sites. Underwater photography adds the extra consideration of a liquid. This report expands upon the basic research presented in, Performance of Multimirror Quartzline Lamps in High-Pressure Environments, (NASA-TM-83793, Ernie Walker and Howard Slater, 1984). The report provides information to professional industrial, scientific, and technical photographers as well as research personnel on the survivability of lighting a multimirror quartzline lamp in a nonconventional high-pressure underwater environment. Test results of lighted ELH 300 W multimirror quartzline lamps under high-pressure conditions are documented and general information on the lamps' intensity (footcandle output), cone of light coverage, approximate color temperature is provided. Continuous lighting considerations in liquids are also discussed. Author

**N89-11192\*#** General Electric Co., Cincinnati, OH. Advanced Technology Operation.

#### **SENSORS FOR CERAMIC COMPONENTS IN ADVANCED PROPULSION SYSTEMS: SUMMARY OF LITERATURE SURVEY AND CONCEPT ANALYSIS, TASK 3 REPORT**

W. H. BENNETHUM and L. T. SHERWOOD Aug. 1988 108 p (Contract NAS3-25140) (NASA-CR-180900; NAS 1.26:180900) Avail: NTIS HC A06/MF A01 CSCL 14/2

The results of a literature survey and concept analysis related to sensing techniques for measuring of surface temperature, strain, and heat flux for (non-specific) ceramic materials exposed to elevated temperatures (to 2200 K) are summarized. Concepts capable of functioning in a gas turbine hot section environment are favored but others are reviewed also. Recommendation are made for sensor development in each of the three areas. Author

**N89-11198\*#** National Aeronautics and Space Administration. Lewis Research Center, Cleveland, OH.

#### **PARTICLE SIZING BY WEIGHTED MEASUREMENTS OF SCATTERED LIGHT**

DONALD R. BUCHELE Oct. 1988 40 p (NASA-TM-100968; E-4396; NAS 1.15:100968) Avail: NTIS HC A03/MF A01 CSCL 14/2

A description is given of a measurement method, applicable to a poly-dispersion of particles, in which the intensity of scattered light at any angle is weighted by a factor proportional to that angle. Determination is then made of four angles at which the weighted intensity is four fractions of the maximum intensity. These yield four characteristic diameters, i.e., the diameters of the volume/area mean ( $D_{32}$  the Sauter mean) and the volume/diameter mean ( $D_{31}$ ); the diameters at cumulative volume fractions of 0.5 ( $D_{v0.5}$  the volume median) and 0.75 ( $D_{v0.75}$ ). They also yield the volume dispersion of diameters. Mie scattering computations show that an average diameter less than three micrometers cannot be accurately measured. The results are relatively insensitive to extraneous background light and to the nature of the diameter distribution. Also described is an experimental method of verifying the conclusions by using two microscopic slides coated with polystyrene microspheres to simulate the particles and the background. Author

**N89-12048\*** National Aeronautics and Space Administration. Lewis Research Center, Cleveland, OH.

#### **GAS PARTICLE RADIATOR Patent**

DONALD L. CHUBB, inventor (to NASA) 13 Sep. 1988 5 p Filed 9 Oct. 1986 Supersedes N87-15452 (25 - 07, p 905) (NASA-CASE-LEW-14297-1; US-PATENT-4,770,232; US-PATENT-APPL-SN-917125; US-PATENT-CLASS-165-41; US-PATENT-CLASS-165-904; US-PATENT-CLASS-126-443; US-PATENT-CLASS-126-901) Avail: US Patent and Trademark Office CSCL 14/2

A gas particle radiator adapted to operate in a microgravity space environment having a transparent boundary which transmits energy in the infrared spectrum, and a gas particle mixture that yields high absorption and emittances are described.

Official Gazette of the U.S. Patent and Trademark Office

**N89-12845\*#** National Aeronautics and Space Administration. Lewis Research Center, Cleveland, OH.

#### **PERFORMANCE OF THE FORWARD SCATTERING SPECTROMETER PROBE IN NASA'S ICING RESEARCH TUNNEL**

EDWARD A. HOVENAC and ROBERT F. IDE (Army Aviation Research and Development Command, Cleveland, Ohio.) 1988 11 p Proposed for presentation at the 27th Aerospace Sciences Meeting, Reno, Nev., 9-12 Jan. 1989; sponsored by AIAA (NASA-TM-101381; E-4435; NAS 1.15:101381; AVSCOM-TR-88-C-036; AIAA-89-0769; AD-A205577) Avail: NTIS HC A03/MF A01 CSCL 14/2

Two Forward Scattering Spectrometer Probes were used to measure droplet distributions in the NASA Lewis Icing Research Tunnel. The instruments showed good agreement when the median volume diameter (MVD) was approximately 16 micrometers. Coincidence events affect much of the data and caused the measured MVD to be about 2 to 3 micrometers larger than expected. Coincidence events were reduced by shutting down half of the spray bars in the tunnel during certain tests. Author

**N89-12884\*#** Pratt and Whitney Aircraft, East Hartford, CT. Engineering Div.

#### **FURTHER DEVELOPMENT OF THE DYNAMIC GAS TEMPERATURE MEASUREMENT SYSTEM**

D. L. ELMORE, W. W. ROBINSON, and W. B. WATKINS In NASA, Lewis Research Center, Turbine Engine Hot Section Technology 1986 p 51-60 Oct. 1986 (Contract NAS3-24228)

Avail: NTIS HC A21/MF A01 CSCL 14/2

The objective of this effort was to experimentally verify a dynamic gas temperature measurement system in laboratory

experiments. The dynamic gas temperature measurement system verification program is described. A brief description of the sensor geometry and construction is followed by a discussion of the probe heat transfer analysis and subsequent compensation method. The laboratory experiments are described and experimental results are discussed. Finally, directions for further investigation are given.

E.R.

**N89-12886\*#** Northwestern Univ., Evanston, IL.

**ELEVATED TEMPERATURE STRAIN GAGES**

J. O. BRITTAIN, D. GESLIN, and J. F. LEI /in NASA, Lewis Research Center, Turbine Engine Hot Section Technology 1986 p 69-84 Oct. 1986

(Contract NAG3-501)

Avail: NTIS HC A21/MF A01 CSCL 14/2

One of the goals of the HOST Program is the development of electrical resistance strain gages for static strain measurements at temperatures equal to or greater than 1273 K. Strain gage materials must have a reproducible or predictable response to temperature, time and strain. It is the objective of this research to investigate criteria for the selection of materials for such applications through electrical properties studies. The results of the investigation of two groups of materials, refractory compounds and binary alloy solid solutions are presented.

Author

**N89-12887\*#** National Aeronautics and Space Administration, Lewis Research Center, Cleveland, OH.

**DEVELOPMENT OF A HIGH TEMPERATURE STATIC STRAIN SENSOR**

CHARLES O. HULSE, RICHARD S. BAILEY, and HOWARD P. GRANT /in NASA, Lewis Research Center, Turbine Engine Hot Section Technology 1986 p 85-90 Oct. 1986

(Contract NAS3-23722)

Avail: NTIS HC A21/MF A01 CSCL 14/2

The goal of this program is to develop an electrical resistance strain gage system which will accurately measure the static strains of superalloy blades and vanes in gas turbine engines running on a test stand. Accurate knowledge of these strains is essential to reaching the goals of the HOST program in the selection and experimental verification of the various theoretical models developed to understand and improve the performance of these engines. The specific objective is to develop a complete system capable of making strain measurements of up to + or - 10 percent of full scale during a 50 hour period at temperatures as high as 1250 K. In addition to survival and stability, attaining a low temperature coefficient of resistance, of the order of 20 ppm/K or less, was a major goal. This requirement arises from the presently unavoidable uncertainties in measurement of the exact temperatures inside gas turbines for use in making corrections for apparent strain due to temperature.

Author

**N89-12888\*#** National Aeronautics and Space Administration, Lewis Research Center, Cleveland, OH.

**THE NASA LEWIS STRAIN GAUGE LABORATORY: AN UPDATE**

H. F. HOBART /in its Turbine Engine Hot Section Technology 1986 p 91-96 Oct. 1986

Avail: NTIS HC A21/MF A01 CSCL 14/2

Efforts continue in the development and evaluation of electrical resistance strain gauges of the thin film and small diameter wire type. Results obtained early in 1986 on some Chinese gauges and Kanthal A-1 gauges mounted on a Hastelloy-X substrate are presented. More recent efforts include: (1) the determination of the uncertainty in the ability to establish gauge factor, (2) the evaluation of sputtered gauges that were fabricated at Lewis, (3) an investigation of the efficacy of dual element temperature compensated gauges when using strain gauge alloys having large thermal coefficients of resistance, and (4) an evaluation of the practical methods of stabilizing gauges whose apparent strain is dependent on cooling rate (e.g., FeCrAl gauges).

Author

**N89-13771\*#** Pratt and Whitney Aircraft, West Palm Beach, FL, Government Products Div.

**FURTHER DEVELOPMENT OF THE DYNAMIC GAS TEMPERATURE MEASUREMENT SYSTEM. VOLUME 2: COMPUTER PROGRAM USER'S MANUAL Final Report**

DANA R. STOCKS Aug. 1986 141 p

(Contract NAS3-24228)

(NASA-CR-179513-VOL-2; NAS 1.26:179513-VOL-2;

P/W/GPD-FR-19381-VOL-2) Avail: NTIS HC A07/MF A01

CSCL 14/2

The Dynamic Gas Temperature Measurement System compensation software accepts digitized data from two different diameter thermocouples and computes a compensated frequency response spectrum for one of the thermocouples. Detailed discussions of the physical system, analytical model, and computer software are presented in this volume and in Volume 1 of this report under Task 3. Computer program software restrictions and test cases are also presented. Compensated and uncompensated data may be presented in either the time or frequency domain. Time domain data are presented as instantaneous temperature vs time. Frequency domain data may be presented in several forms such as power spectral density vs frequency.

Author

**N89-14416\*#** National Aeronautics and Space Administration, Lewis Research Center, Cleveland, OH.

**AUTOMATED DATA ACQUISITION AND PROCESSING FOR A HOHLRAUM REFLECTOMETER**

FRANK DIFILIPPO (Case Western Reserve Univ., Cleveland, OH.) and MICHAEL J. MIRTICH Dec. 1988 8 p

(NASA-TM-101393; E-4466; NAS 1.15:101393) Avail: NTIS HC A02/MF A01 CSCL 14/2

A computer and data acquisition board were used to automate a Perkin-Elmer Model 13 spectrophotometer with a Hohlraum reflectivity attachment. Additional electronic circuitry was necessary for amplification, filtering, and debouncing. The computer was programmed to calculate spectral emittance from 1.7 to 14.7 micrometers and also total emittance versus temperature. Automation of the Hohlraum reflectometer reduced the time required to determine total emittance versus temperature from about three hours to about 40 minutes.

Author

**N89-14418\*#** National Aeronautics and Space Administration, Lewis Research Center, Cleveland, OH.

**HEAT FLUX MEASUREMENTS**

CURT H. LIEBERT and DONALD H. WEIKLE 1989 14 p Proposed for presentation at the 34th International Gas Turbine and Aeroengine Congress and Exposition, Toronto, Ontario, 4-8 Jun. 1989; sponsored by ASME

(NASA-TM-101428; E-4530; NAS 1.15:101428) Avail: NTIS HC A03/MF A01 CSCL 14/2

A new automated, computer controlled heat flux measurement facility is described. Continuous transient and steady-state surface heat flux values varying from about 0.3 to 6 MW/sq m over a temperature range of 100 to 1200 K can be obtained in the facility. An application of this facility is the development of heat flux gauges for continuous fast transient surface heat flux measurement on turbine blades operating in space shuttle main engine turbopumps. The facility is useful for durability testing at fast temperature transients.

Author

**N89-15380\*#** National Aeronautics and Space Administration, Lewis Research Center, Cleveland, OH.

**TECHNIQUE FOR TEMPERATURE COMPENSATION OF EDDY-CURRENT PROXIMITY PROBES**

ROBERT M. MASTERS Jan. 1989 10 p

(NASA-TP-2880; E-4316; NAS 1.60:2880) Avail: NTIS HC A02/MF A01 CSCL 14/2

Eddy-current proximity probes are used in turbomachinery evaluation testing and operation to measure distances, primarily vibration, deflection, or displacement of shafts, bearings and seals. Measurements of steady-state conditions made with standard eddy-current proximity probes are susceptible to error caused by temperature variations during normal operation of the component

## 35 INSTRUMENTATION AND PHOTOGRAPHY

under investigation. Errors resulting from temperature effects for the specific probes used in this study were approximately 1.016 x 10 to the -3 mm/deg C over the temperature range of -252 to 100 C. This report examines temperature caused changes on the eddy-current proximity probe measurement system, establishes their origin, and discusses what may be done to minimize their effect on the output signal. In addition, recommendations are made for the installation and operation of the electronic components associated with an eddy-current proximity probe. Several techniques are described that provide active on-line error compensation for over 95 percent of the temperature effects.

Author

**N89-16139\*#** National Aeronautics and Space Administration. Lewis Research Center, Cleveland, OH.

### **RAMAN INTENSITY AS A PROBE OF CONCENTRATION NEAR A CRYSTAL GROWING IN SOLUTION**

R. ALLEN WILKINSON Feb. 1989 12 p  
(NASA-TP-2865; E-4397; NAS 1.60:2865) Avail: NTIS HC A03/MF A01 CSCL 14/2

The feasibility of using Raman spectral scattering signals for measurements of concentration profiles near a crystal interface during growth or dissolution is discussed. With KH<sub>2</sub>PO<sub>4</sub> (KDF) as a test material, optical multichannel analyzer (OMA) detection of a solute Raman vibrational band provided direct quantification of solute concentration with band intensity. The intersection of incident laser and Raman collection optics provided 3-D selective point measurements of the solution concentration field. Unlike many other techniques, the Raman band intensity is not sensitive to the typical temperature variations. Precision calibration of Raman intensity versus KDP concentration with less than 1 pct standard deviation error levels was demonstrated. A fiber optic, which sampled incident laser intensity and coupled it to the OMA, provided a fully synchronized monitor of fluctuations in laser power to correlate with observed Raman signals. With 1 W of laser power at the sample, good data statistics required eight repeated data collections at approximately 2.5 min collection. The accumulated time represents the concentration measurement time at one spatial location. Photomicroscopy documented a 30 micrometer diameter by 200 micrometer of laser Raman scattering region in the solution near the crystal surface. The laser beam was able to approach up to 25 micrometer from the crystal surface. However, a crystal surface reflected intensity contribution was weakly detectable. Nucleated microcrystals were seen in the crystal-growing solution. These microcrystals convect right up to the crystal surface and indicate no quiet diffusion region under normal gravity conditions. Translation of the solution cell with respect to the optics caused systematic intensity errors.

Author

**N89-17211\*#** National Aeronautics and Space Administration. Lewis Research Center, Cleveland, OH.

### **DEVELOPMENT OF AN INFRARED IMAGING SYSTEM FOR THE SURFACE TENSION DRIVEN CONVECTION EXPERIMENT**

ALEXANDER D. PLINE Jan. 1989 12 p Presented at the Non-Contact Temperature Measurement Workshop, Pasadena, CA, 17-19 Jan. 1989; sponsored by JPL  
(NASA-TM-101479; E-4605; NAS 1.15:101479) Avail: NTIS HC A03/MF A01 CSCL 14/2

An infrared imaging system is used to quantify the imposed surface temperature distribution along a liquid/gas free surface in support of the Surface Tension Driven Convection Experiment, a planned Space Transportation System flight experiment. For ground-based work a commercially available instrument was used to determine the feasibility of using the type of imaging system for this experiment. The ground-based work was used as a baseline for compiling specifications for a flight qualified imager to be designed, fabricated, tested and qualified for flight. The requirements and specifications for the flight model are given along with the reasons for departures from the ground-based equipment. The flight qualification requirements discussed are a representative sample of the necessary procedures which must be followed to flight qualify diagnostic equipment for use aboard the STS. The

potential problems and concerns associated with operating an imaging system in orbit are also discussed.

Author

**N89-17299\*#** United Technologies Research Center, East Hartford, CT.

### **DEVELOPMENT OF A HIGH TEMPERATURE THIN FILM STATIC STRAIN GAGE**

CHARLES O. HULSE, RICHARD S. BAILEY, HOWARD P. GRANT, and JOHN S. PRZYBYSZEWSKI (Pratt and Whitney Aircraft, East Hartford, CT.) In NASA, Lewis Research Center, Turbine Engine Hot Section Technology, 1987 p 43-51 Oct. 1987  
(Contract NAS3-23722)

Avail: NTIS HC A20/MF A01 CSCL 14/2

The objective is to develop a new thin film resistance strain gage system which will be suitable for use inside gas turbine engines on blades or vanes at temperatures up to 1250 K. These gages are to be capable of making strain measurements to plus or minus 2000 microstrain with total errors of no more than plus or minus 10 percent during a 50 hour period. In addition to survival and stability in this hostile environment, attaining a low temperature coefficient of resistance, of the order of 20 ppm/K or less, is an important goal. This requirement arises from the presently unavoidable uncertainties in the measurement of exact temperatures inside gas turbine engines for use in making corrections for apparent strain.

Author

**N89-17301\*#** National Aeronautics and Space Administration. Lewis Research Center, Cleveland, OH.

### **PROGRESS ON A PDCR WIRE STRAIN GAGE**

DAVID R. ENGLUND In its Turbine Engine Hot Section Technology, 1987 p 77-79 Oct. 1987

Avail: NTIS HC A20/MF A01 CSCL 14/2

The principal activity under the HOST effort to improve the state of the art in high temperature static strain measurement has been a contract under which a palladium-chromium (PdCr) alloy was developed. The contract effort is continuing with the goal of developing a thin film high temperature static strain gage system. In addition to this effort, researchers contracted with Battelle-Columbus Laboratories to draw the PdCr alloy into wire while researchers at Lewis worked to gain experience with this alloy as a wire strain gage.

Author

**N89-17302\*#** National Aeronautics and Space Administration. Lewis Research Center, Cleveland, OH.

### **A COMPARISON OF TURBULENCE MEASUREMENT METHODS**

GUSTAVE C. FRALICK In its Turbine Engine Hot Section Technology, 1987 p 81-84 Oct. 1987

Avail: NTIS HC A20/MF A01 CSCL 14/2

An experiment is described in which temperature (density) and velocity are measured separately but simultaneously as functions of time so that it is possible to determine the relationships among velocity, density, and the product of density and velocity. Temperatures were measured with a dual-wire thermocouple probe. Velocity data were supplied by a fringe laser-Doppler anemometer. Signals from thermocouples and the laser were recorded on FM magnetic tape for later processing.

Author

**N89-18671\*#** National Aeronautics and Space Administration. Lewis Research Center, Cleveland, OH.

### **AMPLITUDE SPECTRUM MODULATION TECHNIQUE FOR ANALOG DATA PROCESSING IN FIBER OPTIC SENSING SYSTEM WITH TEMPORAL SEPARATION OF CHANNELS**

GRIGORY ADAMOVSKY 1987 9 p Presented at O-E Fibers '87, a Symposium on Fiber Optics and Integrated Optoelectronics, San Diego, CA, 16-21 Aug. 1987; sponsored by SPIE, International Society for Optical Engineering Previously announced in IAA as A89-10368

(NASA-TM-100152; E-3714; NAS 1.15:100152) Avail: NTIS HC A02/MF A01 CSCL 14/2

A novel technique to analyze data in fiber optic sensing systems with temporal separation of channels is proposed. A theoretical



explanation of the process is presented and an experimental setup that was used to obtain the data is described. NASA

**N89-21224\*#** National Aeronautics and Space Administration. Lewis Research Center, Cleveland, OH.

**INFRARED SURFACE TEMPERATURE MEASUREMENTS FOR THE SURFACE TENSION DRIVEN CONVECTION EXPERIMENT**  
M.S. Thesis - Case Western Reserve Univ., Aug. 1988

ALEXANDER D. PLINE Mar. 1989 29 p  
(NASA-TM-101353; E-4383; NAS 1.15:101353) Avail: NTIS HC A03/MF A01 CSCL 14/2

In support of the Surface Tension Driven Convection Experiment (STDCE), a planned space transportation system (STS) flight experiment, a commercially available infrared thermal imaging system is used to quantify the imposed thermal signature along the free surface. The system was tested and calibrated for the STDCE with ground-based equivalents of the STDCE hardware. Before using the system, consideration was given to the radiation characteristics of the target (silicone oil). Absorption coefficients were calculated to understand the surface depth as seen by the imager and the penetration depth of the surface heater (CO<sub>2</sub> laser). The performance and operational specifications for the imager and image processing system are described in detail to provide an understanding of the equipment. Measurements made with the system were compared to thermocouple measurements and a calculated surface temperature distribution. This comparison showed that in certain regions the IR imager measurements were within 5 percent of the overall temperature difference across the free surface. In other regions the measurements were within + or - 10 percent of the overall temperature gradient across the free surface. The effective emissivity of silicone oil for these experimental conditions was also determined. Measurement errors and their possible solutions are discussed. Author

**N89-23850\*#** National Aeronautics and Space Administration. Lewis Research Center, Cleveland, OH.

**A VECTOR SCANNING PROCESSING TECHNIQUE FOR PULSED LASER VELOCIMETRY**

MARK P. WERNET and ROBERT V. EDWARDS (Case Western Reserve Univ., Cleveland, OH.) 1989 19 p Prepared for presentation at the 13th International Congress on Instrumentation in Aerospace Simulation Facilities, Goettingen (Federal Rep. of Germany), 18-21 Sep. 1989; sponsored by IEEE  
(NASA-TM-102048; E-4798; NAS 1.15:102048) Avail: NTIS HC A03/MF A01 CSCL 14/2

Pulsed laser sheet velocimetry yields nonintrusive measurements of two-dimensional velocity vectors across an extended planar region of a flow. Current processing techniques offer high precision (1 pct) velocity estimates, but can require several hours of processing time on specialized array processors. Under some circumstances, a simple, fast, less accurate (approx. 5 pct), data reduction technique which also gives unambiguous velocity vector information is acceptable. A direct space domain processing technique was examined. The direct space domain processing technique was found to be far superior to any other techniques known, in achieving the objectives listed above. It employs a new data coding and reduction technique, where the particle time history information is used directly. Further, it has no 180 deg directional ambiguity. A complex convection vortex flow was recorded and completely processed in under 2 minutes on an 80386 based PC, producing a 2-D velocity vector map of the flow field. Hence, using this new space domain vector scanning (VS) technique, pulsed laser velocimetry data can be reduced quickly and reasonably accurately, without specialized array processing hardware. Author

**N89-23851\*#** Physical Sciences, Inc., Andover, MA.  
**HIGH-TEMPERATURE LDV SEED PARTICLE DEVELOPMENT**  
Final Report

MICHAEL B. FRISH and VICKY G. PIERCE May 1989 33 p  
(Contract NAS3-25284)  
(NASA-CR-182265; NAS 1.26:182265; PSI-2062/TR-890) Avail: NTIS HC A03/MF A01 CSCL 14/2

The feasibility of developing a method for making monodisperse, unagglomerated spherical particles greater than 50 nm in diameter was demonstrated. Carbonaceous particles were made by pyrolyzing ethylene with a pulsed CO<sub>2</sub> laser, thereby creating a non-equilibrium mixture of carbon, hydrogen, hydrocarbon vapors, and unpyrolyzed ethylene. Via a complex series of reactions, the carbon and hydrocarbon vapors quickly condensed into the spherical particles. By cooling and dispersing them in a supersonic expansion immediately after their creation, the hot newly-formed spheres were prevented from colliding and coalescing, thus preventing the problem of agglomeration which as plagued other investigators studying laser-simulated particle formation. The cold particles could be left suspended in the residual gases indefinitely without agglomerating. Their uniform sizes and unagglomerated nature were visualized by collecting the particles on filters that were subsequently examined using electron microscopy. It was found the mean particle size can be coarsely controlled by varying the initial ethylene pressure, and can be finely controlled by varying the fluence (energy/unit area) with which the laser irradiates the gas. The motivating application for this research was to manufacture particles that could be used as laser Doppler velocimetry (LDV) seeds in high-temperature high-speed flows. Though the particles made in this program will not evaporate until heated to about 3000 K, and thus could serve as LDV seeds in some applications, they are not ideal when the hot atmosphere is also oxidizing. In that situation, ceramic materials would be preferable. Research performed elsewhere has demonstrated that selected ceramic materials can be manufactured by laser pyrolysis of appropriate supply gases. It is anticipated that, when the same gases are used in conjunction with the rapid cooling technique, unagglomerated spherical ceramic particles can be made with little difficulty. Such particles would also be valuable to manufacturers of ceramic or abrasive products, and this technique may find its greatest commercial potential in those areas. Author

**N89-24591\*#** National Aeronautics and Space Administration. Lewis Research Center, Cleveland, OH.

**HOLOGRAPHIC INTERFEROMETRY WITH AN INJECTION SEEDED ND:YAG LASER AND TWO REFERENCE BEAMS**

ARTHUR J. DECKER May 1989 23 p  
(NASA-TM-102056; E-4809; NAS 1.15:102056) Avail: NTIS HC A03/MF A01 CSCL 20/6

The performance of twin injection seeded Nd:YAG lasers is compared with the performance of an argon-ion laser for recording dual-reference-beam holograms in AGFA 8E56 emulsion. Optical heterodyning is used to measure interference, and the results are expressed in terms of heterodyning signal level and intensity signal-to-noise. The Nd:YAG laser system is to be used for optical inspections of structures for cracks, defects, gas leaks, and structural changes. Author

**N89-24593\*#** National Aeronautics and Space Administration. Lewis Research Center, Cleveland, OH.

**ON THE DYNAMIC RESPONSE OF PRESSURE TRANSMISSION LINES IN THE RESEARCH OF HELIUM-CHARGED FREE PISTON STIRLING ENGINES**

ERIC L. MILLER (Sverdrup Technology, Inc., Cleveland, OH.) and JAMES E. DUDENHOEFER 1989 8 p Prepared for presentation at the 24th Intersociety Energy Conversion Engineering Conference, Washington, DC, 6-11 Aug. 1989; sponsored in part by IEEE, AIAA, ANS, ASME, SAE, ACS, and AIChE  
(NASA-TM-102121; E-4902; NAS 1.15:102121) Avail: NTIS HC A02/MF A01 CSCL 14/2

In free piston Stirling engine research the integrity of both amplitude and phase of the dynamic pressure measurements is critical to the characterization of cycle dynamics and thermodynamics. It is therefore necessary to appreciate all possible sources of signal distortion when designing pressure measurement systems for this type of research. The signal distortion inherent to pressure transmission lines is discussed. Based on results from classical analysis, guidelines are formulated to describe the dynamic response properties of a volume-terminated transmission

## 35 INSTRUMENTATION AND PHOTOGRAPHY

tube for applications involving helium-charged free piston Stirling engines. The scope and limitations of the dynamic response analysis are considered. Author

**N89-25432\*#** Connecticut Univ., Storrs. Dept. of Mechanical Engineering and Physics.

**X-RAY BASED EXTENSOMETRY Final Report, 15 Dec. 1987 - 15 Dec. 1988**

E. H. JORDAN and D. M. PEASE Dec. 1988 26 p  
(Contract NAG3-854)  
(NASA-CR-185058; NAS 1.26:185058) Avail: NTIS HC A03/MF A01 CSCL 14/2

A totally new method of extensometry using an X-ray beam was proposed. The intent of the method is to provide a non-contacting technique that is immune to problems associated with density variations in gaseous environments that plague optical methods. X-rays are virtually unrefractable even by solids. The new method utilizes X-ray induced X-ray fluorescence or X-ray induced optical fluorescence of targets that have melting temperatures of over 3000 F. Many different variations of the basic approaches are possible. In the year completed, preliminary experiments were completed which strongly suggest that the method is feasible. The X-ray induced optical fluorescence method appears to be limited to temperatures below roughly 1600 F because of the overwhelming thermal optical radiation. The X-ray induced X-ray fluorescence scheme appears feasible up to very high temperatures. In this system there will be an unknown tradeoff between frequency response, cost, and accuracy. The exact tradeoff can only be estimated. It appears that for thermomechanical tests with cycle times on the order of minutes a very reasonable system may be feasible. The intended applications involve very high temperatures in both materials testing and monitoring component testing. Gas turbine engines, rocket engines, and hypersonic vehicles (NASP) all involve measurement needs that could partially be met by the proposed technology. Author

**N89-26208\*#** Aerojet TechSystems Co., Sacramento, CA.  
**INTEGRATED CONTROL AND HEALTH MONITORING CAPACITIVE DISPLACEMENT SENSOR DEVELOPMENT TASK. ORBIT TRANSFER ROCKET ENGINE TECHNOLOGY PROGRAM Final Report**

FRANK N. COLLAMORE Jul. 1989 110 p  
(Contract NAS3-23772)  
(NASA-CR-182279; NAS 1.26:182279) Avail: NTIS HC A06/MF A01 CSCL 14/2

The development of a miniature multifunction turbomachinery shaft displacement sensor using state-of-the-art non-contract capacitive sensing technology is described. Axial displacement, radial displacement, and speed are sensed using a single probe within the envelope normally required for a single function. A survey of displacement sensing technology is summarized including inductive, capacitive, optical and ultrasonic techniques. The design and operation of an experimental triple function sensor is described. Test results are included showing calibration tests and simultaneous dynamic testing of multiple functions. Recommendations for design changes are made to improve low temperature performance, reliability, and for design of a flight type signal conditioning unit. Author

**N89-26218\*#** Sverdrup Technology, Inc., Cleveland, OH.  
**TWO-DIMENSIONAL HIGH TEMPERATURE OPTICAL STRAIN MEASUREMENT SYSTEM, PHASE 2 Final Report**

CHRISTIAN T. LANT Jul. 1989 22 p  
(Contract NAS3-25266)  
(NASA-CR-185116; E-4923; NAS 1.26:185116) Avail: NTIS HC A03/MF A01 CSCL 14/2

A laser speckle strain measurement system with two-dimensional measurement capabilities has been built and tested for high temperature applications. The 1st and 2nd principle strains at a point on a specimen are calculated from three components of one-dimensional strain. Strain components are detected by cross-correlating reference and shifted speckle

patterns recorded before and after straining the specimen. Speckle patterns are recorded by a linear photodiode array camera. Accurate strains have been measured at temperatures up to 650 C. Stable speckle correlations and linear stress-strain relations have been demonstrated up to 750 C. The resolution of the system is 15 microstrains, with a gauge length less than 1 mm. Author

**N89-27152\*#** Miletus Associates, Inc., Albuquerque, NM.  
**FILM ANNOTATION SYSTEM FOR A SPACE EXPERIMENT**

W. R. BROWNE and S. S. JOHNSON Jul. 1989 124 p  
(Contract NAS3-25055)  
(NASA-CR-185114; NAS 1.26:185114) Avail: NTIS HC A06/MF A01 CSCL 14/5

This microprocessor system was designed to control and annotate a Nikon 35 mm camera for the purpose of obtaining photographs and data at predefined time intervals. The single STD BUSS interface card was designed in such a way as to allow it to be used in either a stand alone application with minimum features or installed in a STD BUSS computer allowing for maximum features. This control system also allows the exposure of twenty eight alpha/numeric characters across the bottom of each photograph. The data contains such information as camera identification, frame count, user defined text, and time to .01 second. Author

**N89-27998\*#** National Aeronautics and Space Administration. Lewis Research Center, Cleveland, OH.

**COMPENSATION FOR EFFECTS OF AMBIENT TEMPERATURE ON RARE-EARTH DOPED FIBER OPTIC THERMOMETER**

G. ADAMOVSKY, J. L. SOTOMAYOR, M. J. KRASOWSKI, and J. G. EUSTACE (John Carroll Univ., Cleveland, OH.) 1989 14 p  
Presented at the Fiber Optic and Laser Sensors 7, Boston, MA, 5-8 Sep. 1989; sponsored by the Society of Photo-Optical Instrumentation Engineers  
(Contract NAG3-984)  
(NASA-TM-102282; E-4946; NAS 1.15:102282) Avail: NTIS HC A03/MF A01 CSCL 14/2

Variations in ambient temperature have a negative effect on the performance of any fiber optic sensing system. A change in ambient temperature may alter the design parameters of fiber optic cables, connectors, sources, detectors, and other fiber optic components and eventually the performance of the entire system. The thermal stability of components is especially important in a system which employs intensity modulated sensors. Several referencing schemes have been developed to account for the variable losses that occur within the system. However, none of these conventional compensating techniques can be used to stabilize the thermal drift of the light source in a system based on the spectral properties of the sensor material. The compensation for changes in ambient temperature becomes especially important in fiber optic thermometers doped with rare earths. Different approaches to solving this problem are searched and analyzed. Author

**N89-27999\*#** National Aeronautics and Space Administration. Lewis Research Center, Cleveland, OH.

**SPECKLE INTERFEROMETRY USING FIBER OPTIC PHASE STEPPING**

CAROLYN R. MERCER and GLENN BEHEIM Aug. 1989 9 p  
Presented at the Symposium on Optical and Optoelectronic Applied Science and Engineering, San Diego, CA, 6-11 Aug. 1989; sponsored in part by Society of Photo-Optical Instrumentation Engineers  
(NASA-TM-102331; E-5040; NAS 1.15:102331) Avail: NTIS HC A02/MF A01 CSCL 14/2

A system employing closed-loop phase-stepping is used to measure the out-of-plane deformation of a diffusely reflecting object. Optical fibers are used to provide reference and object beam illumination for a standard two-beam speckle interferometer, providing set-up flexibility and ease of alignment. Piezoelectric fiber-stretchers and a phase-measurement/servo system are used to provide highly accurate phase steps. Intensity data is captured with a charge-injection-device camera, and is converted into a

phase map using a desktop computer. The closed-loop phase-stepping system provides 90 deg phase steps which are accurate to 0.02 deg, greatly improving this system relative to open-loop interferometers. The system is demonstrated on a speckle interferometer, measuring the rigid-body translation of a diffusely reflecting object with an accuracy  $\pm$  or  $\pm$  10 deg, or roughly  $\pm$  or  $\pm$  15 nanometers. This accuracy is achieved without the use of a pneumatically mounted optics table. Author

**N89-28806\*** National Aeronautics and Space Administration. Lewis Research Center, Cleveland, OH.

**FATIGUE TESTING APPARATUS Patent Application**

ROBERT J. BUZZARD, inventor (to NASA) 21 Aug. 1989 14 p  
(NASA-CASE-LEW-14124-1; NAS 1.71:LEW-14124-1;  
US-PATENT-APPL-SN-396263) Avail: NTIS HC A03/MF A01  
CSCL 14/2

An apparatus is provided for obtaining a single crack in fatigue loading which emanates from a predetermined starting notch in a test specimen. This crack propagates in a direction in line with that of the applied Mode 2 load. The loading may be performed either monotonically or in a cyclic fatigue. NASA

## 36

## LASERS AND MASERS

Includes parametric amplifiers.

**A89-17507\*** Tennessee Univ., Tullahoma.

**RECOVERY OF EXCITATION INTENSITY DEPENDENCE IN PULSED, FOCUSED BEAMS - NONSATURATED CASE**

WILHELMUS M. RUYTEN and J. W. L. LEWIS (Tennessee, University, Tullahoma) Optical Society of America, Journal, B: Optical Physics (ISSN 0740-3224), vol. 5, Nov. 1988, p. 2368-2373. refs  
(Contract NAG3-682)  
Copyright

It is shown how the dependence of a nonsaturated excitation process on local, instantaneous intensity can be obtained from temporally and spatially unresolved data by inversion, even for a nonuniform intensity distribution in the probe volume. This treatment is in contrast with the usual approach in which effects of nonuniform excitation are either disregarded or simulated. For exponential intensity profiles, the solution is obtained in the form of an Abel inversion. The ill-conditioned nature of the problem is demonstrated, and extension to the study of intensity-dependent line shapes is made. Author

**A89-36457\*** National Aeronautics and Space Administration. Lewis Research Center, Cleveland, OH.

**ISOTHERMAL AND 'BITHERMAL' THERMOMECHANICAL FATIGUE BEHAVIOR OF A NICOCRALY-COATED SINGLE CRYSTAL SUPERALLOY**

J. GAYDA, T. P. GABB, and R. V. MINER (NASA, Lewis Research Center, Cleveland, OH) IN: Superalloys 1988; Proceedings of the Sixth International Symposium, Champion, PA, Sept. 18-22, 1988. Warrendale, PA, Metallurgical Society, Inc., 1988, p. 575-584. Previously announced in STAR as N88-24766. refs  
Copyright

Specimens of single crystal PWA 1480 with group of zone axes (100) orientation, bare, or with NiCoCrAlY coating PWA 276, were tested in low cycle fatigue (LCF) at 650, 870, and 1050 C, and in simplified bithermal thermomechanical fatigue (TMF) tests between these temperatures. These tests were examined as a bridge between isothermal LCF and general TMF. In the bithermal test, and inelastic strain is applied at one temperature,  $T_{sub\ max}$ , and reversed at  $T_{sub\ min}$ . The out-of-phase (OP) test type imposing tension at  $T_{sub\ min}$  and compression at  $T_{sub\ max}$  received most study, since it was more damaging than the in-phase

type. Specifically investigated were the effects of: inelastic strain range, the coating,  $\Delta T$ ,  $T_{sub\ max}$ ,  $T_{sub\ min}$ , and the environment. Author

**N89-12885\*** National Aeronautics and Space Administration. Lewis Research Center, Cleveland, OH.

**LASER ANEMOMETRY: A STATUS REPORT**

MARK P. WERNET, RICHARD G. SEASHOLTZ, DONALD H. WEIKLE, and LAWRENCE G. OBERLE *In its Turbine Engine Hot Section Technology* 1986 p 61-68 Oct. 1986  
Avail: NTIS HC A21/MF A01 CSCL 20/5

A laser anemometer system is being developed for the warm turbine facility as part of the HOST program. The system will be built using results obtained from the analytical and experimental research program. The status report of the laser anemometry applications research effort is presented. The designs for the turbine casing, the windows, and the positioning system were completed. A block diagram of the laser anemometer system, signal processing scheme, and computer system is given. Author

**N89-12889\*** National Aeronautics and Space Administration. Lewis Research Center, Cleveland, OH.

**SUMMARY OF LASER SPECKLE PHOTOGRAMMETRY FOR HOST**

FRANK G. POLLACK *In its Turbine Engine Hot Section Technology* 1986 p 97-103 Oct. 1986  
Avail: NTIS HC A21/MF A01 CSCL 20/5

High temperature static strain measurement capability is important for the success of the HOST program. As part of the NASA Lewis effort to develop the technology for improved hot-section durability, the HOST instrumentation program has, as a major goal, the development of methods for measuring strain at high temperature. Development work includes both improvements in resistance strain-gauge technology and, as an alternative approach, the development of optical techniques for high temperature strain measurement. Author

## 37

## MECHANICAL ENGINEERING

Includes auxiliary systems (nonpower); machine elements and processes; and mechanical equipment.

**A89-12301\*** Mechanical Technology, Inc., Latham, NY.

**MOD II STIRLING ENGINE OVERVIEWS**

ROGER A. FARRELL (Mechanical Technology, Inc., Latham, NY) SAE, International Congress and Exposition, Detroit, MI, Feb. 29-Mar. 4, 1988. 14 p. DOE-sponsored research. refs  
(Contract DEN3-32)  
(SAE PAPER 880539) Copyright

The Mod II engine is a second-generation automotive Stirling engine (ASE) optimized for part-power operation. It has been designed specifically to meet the fuel economy and exhaust emissions objectives of the ASE development program. The design, test experience, performance, and comparison of data to analytical performance estimates of the Mod II engine to date are reviewed. Estimates of Mod II performance in its final configuration are also given. Author

**A89-12303\*** Mechanical Technology, Inc., Latham, NY.

**ALTERNATIVE FUEL CAPABILITIES OF THE MOD II STIRLING VEHICLE**

ALBERT W. GRANDIN and WILLIAM D. ERNST (Mechanical Technology, Inc., Latham, NY) SAE, International Congress and Exposition, Detroit, MI, Feb. 29-Mar. 4, 1988. 8 p.  
(Contract DEN3-32)

(SAE PAPER 880543) Copyright

The Stirling engine's characteristics make it a prime candidate

for both multifuel and alternative fuel uses. In this paper, the relevant engine characteristics of the Mod II Stirling engine are examined, including the external heat system and basic operation. Adaptation of the Stirling to multifuel operation is addressed, and its experience with alternative fuels in automotive applications is summarized. The results of the U.S. Air Force review of the Stirling's multifuel capability are described, and the Stirling's advantages with liquid, gaseous, and solid fuels are discussed. C.D.

**A89-12304\*** National Aeronautics and Space Administration. Lewis Research Center, Cleveland, OH.

## **HOT PISTON RING/CYLINDER LINER MATERIALS - SELECTION AND EVALUATION**

HAROLD E. SLINEY (NASA, Lewis Research Center, Cleveland, OH) SAE, International Congress and Exposition, Detroit, MI, Feb. 29-Mar. 4, 1988. 12 p. refs (SAE PAPER 880544) Copyright

A materials testing program to determine whether automotive Stirling engine efficiency can be improved by locating 'hot piston rings' near the top of the pistons is described. Candidate materials were screened theoretically and experimentally by friction and wear tests. Based on the test results, a cobalt-based alloy, Stellite 6B, was chosen for the piston rings and PS200, which consists of a metal-bonded chromium carbide matrix with dispersed solid lubricants, was chosen as the cylinder coating. Tests of a modified engine and a baseline engine showed that the hot ring did reduce specific fuel consumption by up to 7 percent for some operating conditions and averaged about three percent for all conditions evaluated. Related applications of high-temperature coatings for shaft seals and as backup lubricants for gas bearings are also described. C.D.

**A89-12308\*** National Aeronautics and Space Administration. Lewis Research Center, Cleveland, OH.

## **REGRESSED RELATIONS FOR FORCED CONVECTION HEAT TRANSFER IN A DIRECT INJECTION STRATIFIED CHARGE ROTARY ENGINE**

CHI M. LEE (NASA, Lewis Research Center, Cleveland, OH) and HAROLD J. SCHOCK (Michigan State University, East Lansing) SAE, International Congress and Exposition, Detroit, MI, Feb. 29-Mar. 4, 1988. 12 p. Previously announced in STAR as N88-13345. refs (SAE PAPER 880626) Copyright

Currently, the heat transfer equation used in the rotary combustion engine (RCE) simulation model is taken from piston engine studies. These relations have been empirically developed by the experimental input coming from piston engines whose geometry differs considerably from that of the RCE. The objective of this work was to derive equations to estimate heat transfer coefficients in the combustion chamber of an RCE. This was accomplished by making detailed temperature and pressure measurements in a direct injection stratified charge (DISC) RCE under a range of conditions. For each specific measurement point, the local gas velocity was assumed equal to the local rotor tip speed. Local physical properties of the fluids were then calculated. Two types of correlation equations were derived and are described in this paper. The first correlation expresses the Nusselt number as a function of the Prandtl number, Reynolds number, and characteristic temperature ratio; the second correlation expresses the forced convection heat transfer coefficient as a function of fluid temperature, pressure and velocity. Author

**A89-12751\*#** National Aeronautics and Space Administration. Lewis Research Center, Cleveland, OH.

## **ACOUSTIC EMISSION EVALUATION OF PLASMA-SPRAYED THERMAL BARRIER COATINGS**

C. C. BERNDT (NASA, Lewis Research Center, Cleveland, OH) ASME, Transactions, Journal of Engineering for Gas Turbines and Power (ISSN 0022-0825), vol. 107, Jan. 1985, p. 142-146. Previously cited in issue 23, p. 3403, Accession no. A84-47046. refs (Contract NAG3-164; NCC3-27) Copyright

**A89-18906\*** National Aeronautics and Space Administration. Lewis Research Center, Cleveland, OH.

## **ADVANCED TRANSMISSION STUDIES**

JOHN J. COY (NASA, Lewis Research Center, Cleveland, OH) and ROBERT C. BILL (NASA, Lewis Research Center; U.S. Army, Propulsion Directorate, Cleveland, OH) IN: AHS, Annual Forum, 44th, Washington, DC, June 16-18, 1988, Proceedings. Alexandria, VA, American Helicopter Society, 1988, p. 651-662. Previously announced in STAR as N88-21454. refs Copyright

The NASA Lewis Research Center and the U.S. Army Aviation Systems Command share an interest in advancing the technology for helicopter propulsion systems. In particular, this paper presents highlights from that portion of the program in drive train technology and the related mechanical components. The major goals of the program are to increase the life, reliability, and maintainability; reduce the weight, noise, and vibration; and maintain the relatively high mechanical efficiency of the gear train. The current activity emphasizes noise reduction technology and analytical code development followed by experimental verification. Selected significant advances in technology for transmissions are reviewed, including advance configurations and new analytical tools. Finally, the plan for future transmission research is presented. Author

**A89-19834\*#** Bolt, Beranek, and Newman, Inc., Cambridge, MA.

## **EFFECTS OF BEARING OFFSET AND FLEXIBILITY ON THE MESH FORCE DISTRIBUTION OF SPIRAL BEVEL GEARS**

W. D. MARK (BBN Laboratories, Inc., Cambridge, MA) ASME, Transactions, Journal of Mechanisms, Transmission, and Automation in Design (ISSN 0738-0666), vol. 110, June 1988, p. 203-210. refs (Contract NAS3-23703) Copyright

For straight or spiral bevel gears of nominal spherical involute design, the resultant total force vector transmitted by the gear mesh, in the absence of friction, lies in the plane of tooth contact. This force vector can be characterized by three scalar components, two orthogonal force components lying in the plane of contact and the resultant moment taken about the nominal center of the zone of contact. Equations for these three generalized force components are derived. The equations are expressed in terms of tooth pair/gear body stiffnesses, bearing/bearing support flexibility influence coefficients, the shaft input torque, deviations of the tooth running surfaces from perfect spherical involute surfaces, and bearing centerline offsets from the positions occupied by the base cone axes of the perfect involute bevel gear counterparts to the actual gears under consideration. Inertial forces arising from transverse and axial vibrations of the gear bodies are assumed to be negligible in comparison with the bearing support reaction forces. Author

**A89-19835\*#** Bolt, Beranek, and Newman, Inc., Cambridge, MA.

## **AN EXTREMUM PRINCIPLE FOR COMPUTATION OF THE ZONE OF TOOTH CONTACT AND GENERALIZED TRANSMISSION ERROR OF SPIRAL BEVEL GEARS**

W. D. MARK (BBN Laboratories, Inc., Cambridge, MA) ASME, Transactions, Journal of Mechanisms, Transmission, and Automation in Design (ISSN 0738-0666), vol. 110, June 1988, p. 211-220. refs (Contract NAS3-23703) Copyright

For a given set of forces transmitted by the gears, each of the three components of the generalized transmission error of spiral bevel gears is shown to be stationary with respect to small independent variations in the positions of the endpoints of the lines of tooth contact about their true values. The tangential generalized transmission error component is shown to take on a minimum value at the true endpoint positions. A computational procedure based on the method of steepest descent is described for computing the true line of contact endpoint positions and the three components of the generalized transmission error. A method

for computing the Fourier series coefficients of the tooth meshing harmonics of the three generalized transmission error components also is provided.

Author

**A89-21000\*** Illinois Univ., Chicago.

**TRANSMISSION ERRORS AND BEARING CONTACT OF SPUR, HELICAL AND SPIRAL BEVEL GEARS**

F. L. LITVIN, J. ZHANG, H.-T. LEE (Illinois, University, Chicago), and R. F. HANDSCHUH (NASA, Lewis Research Center; U.S. Army, Aviation Research and Development Command, Cleveland, OH) SAE, International Off-Highway and Powerplant Congress and Exposition, Milwaukee, WI, Sept. 12-15, 1988. 13 p. refs (SAE PAPER 881294) Copyright

An investigation of transmission errors and bearing contact of spur, helical and spiral bevel gears was performed. Modified tooth surfaces for these gears have been proposed in order to absorb linear transmission errors caused by gear misalignment and localize the bearing contact. Numerical examples for spur, helical, and spiral bevel gears are presented to illustrate the behavior of the modified gear surfaces to misalignment and errors of assembly. The numerical results indicate that the modified surfaces will perform with a low level of transmission error in nonideal operating environment.

Author

**A89-22290\*** General Motors Corp., Indianapolis, IN.

**DESIGN AND TEST OF A PROPPAN GEAR SYSTEM**

N. E. ANDERSON, L. NIGHTINGALE, and D. A. WAGNER (General Motors Corp., Allison Gas Turbine Div., Indianapolis, IN) Journal of Propulsion and Power (ISSN 0748-4658), vol. 5, Jan.-Feb. 1989, p. 95-102. Previously cited in issue 20, p. 3240, Accession no. A87-45374. refs (Contract NAS3-24341) Copyright

**A89-24992\*** Rockwell International Corp., Canoga Park, CA.

**EXPERIMENTAL RESULTS FOR LABYRINTH GAS SEALS WITH HONEYCOMB STATORS - COMPARISONS TO SMOOTH-STATOR SEALS AND THEORETICAL PREDICTIONS**

LARRY HAWKINS (Rockwell International Corp., Rocketdyne Div., Canoga Park, CA), DARA CHILDS, and KEITH HALE (Texas A & M University, College Station) ASME, Transactions, Journal of Tribology (ISSN 0742-4787), vol. 111, Jan. 1989, p. 161-168. refs

(Contract NAG3-181; F49620-82-K-0033)

(ASME PAPER 88-TRIB-40) Copyright

Experimental measurements are presented for the rotordynamic stiffness and damping coefficients of a teeth-on-rotor labyrinth seal with a honeycomb stator. Inlet circumferential velocity, inlet pressure, rotor speed, and seal clearance are primary variables. Results are compared to data for teeth-on-rotor labyrinth seals with smooth stators and to analytical predictions from a two-control-volume compressible flow model. The experimental results show that the honeycomb-stator configuration is more stable than the smooth-stator configuration at low rotor speeds. At high rotor speeds, the stator surface does not affect stability. The theoretical model predicts the cross-coupled stiffness of the honeycomb-stator seal correctly within 25 percent of measured values. The model provides accurate predictions of direct damping for large clearance seals; however, the model predictions and test results diverge with increasing running speed. Overall, the model does not perform as well for low clearance seals as for high clearance seals.

Author

**A89-25181\*** Mississippi State Univ., Mississippi State.

**A SIMPLE TIME-ACCURATE TURBOMACHINERY ALGORITHM WITH NUMERICAL SOLUTIONS OF AN UNEVEN BLADE COUNT CONFIGURATION**

J. MARK JANUS and DAVID L. WHITFIELD (Mississippi State University, Mississippi State) AIAA, Aerospace Sciences Meeting, 27th, Reno, NV, Jan. 9-12, 1989. 20 p. refs (Contract NAG3-767; NAG3-869)

(AIAA PAPER 89-0206) Copyright

The present computer algorithm for the time-accurate flow

analysis of rotating turbomachines is based on the finite-volume method and employs a high-resolution approximate Riemann solver for interface flux definitions and an implicit numerical scheme that possesses apparent unconditional stability. Block-block interfaces, including dynamic ones, are treated in such a way as to mimic interior block communication. The turbomachine configurations treated by way of illustration are 8-8-bladed and 11-9-bladed versions of a contrarotating unducted fan engine.

O.C.

**A89-29306\*** Illinois Univ., Chicago.

**CROWNED SPUR GEARS - METHODS FOR GENERATION AND TOOTH CONTACT ANALYSIS. I - BASIC CONCEPTS, GENERATION OF THE PINION TOOTH SURFACE BY A PLANE**

F. L. LITVIN (Illinois, University, Chicago), R. F. HANDSCHUH (NASA, Lewis Research Center, Cleveland, OH), and J. ZHANG ASME, Transactions, Journal of Mechanisms, Transmission, and Automation in Design (ISSN 0738-0666), vol. 110, Sept. 1988, p. 337-342.

Copyright

A topology of crowned spur pinion tooth surface that reduces the level of transmission errors due to misalignment is proposed. The geometry of the deviated pinion tooth surface and regular gear tooth surface, along with tooth contact analysis is discussed. Generation of the deviated pinion tooth surface by a plane whose motion is controlled by a five-degree-of-freedom system is proposed. Numerical results are included and indicate that transmission errors remain low as the gears are misaligned.

Author

**A89-34794\*** Texas A&M Univ., College Station.

**ANNULAR HONEYCOMB SEALS: TEST RESULTS FOR LEAKAGE AND ROTORDYNAMIC COEFFICIENTS - COMPARISONS TO LABYRINTH AND SMOOTH CONFIGURATIONS**

D. CHILDS, D. ELROD, and K. HALE (Texas A & M University, College Station) ASME, Transactions, Journal of Tribology (ISSN 0742-4787), vol. 111, April 1989, p. 293-300; Discussion, p. 300, 301. refs

(Contract NAG3-181; F49620-82-K-0033)

(ASME PAPER 88-TRIB-35) Copyright

Test results are presented for leakage and rotordynamic coefficients for seven honeycomb seals. All seals have the same radius, length, and clearance; however, the cell depths and diameters are varied. Rotordynamic data, which are presented, consist of the direct and cross-coupled stiffness coefficients and the direct damping coefficients. The rotordynamic-coefficient data show a considerable sensitivity to changes in cell dimensions; however, no clear trends are identifiable. Comparisons of test data for the honeycomb seals with labyrinth and smooth annular seals shows the honeycomb seal had the best sealing (minimum leakage) performance, followed in order by the labyrinth and smooth seals. For prerotated fluids entering the seal, in the direction of shaft rotation, the honeycomb seal has the best rotordynamic stability followed in order by the labyrinth and smooth. For no prerotation, or fluid prerotation against shaft rotation, the labyrinth seal has the best rotordynamic stability followed in order by the smooth and honeycomb seals.

Author

**A89-34798\*** Texas A&M Univ., College Station.

**AN ENTRANCE REGION FRICTION FACTOR MODEL APPLIED TO ANNULAR SEAL ANALYSIS - THEORY VERSUS EXPERIMENT FOR SMOOTH AND HONEYCOMB SEALS**

D. ELROD, C. NELSON, and D. CHILDS (Texas A & M University, College Station) ASME, Transactions, Journal of Tribology (ISSN 0742-4787), vol. 111, April 1989, p. 337-343. refs (Contract NAG3-181)

(ASME PAPER 88-TRIB-41) Copyright

A friction factor model is developed for the entrance-region of a duct. The model is used in an annular gas seal analysis similar to Nelson's (1984). Predictions of the analysis are compared to experimental results for a smooth-stator/smooth-rotor seal and three honeycomb-stator/smooth-rotor seals. The model predicts a

leakage and direct damping well. The model overpredicts the dependence of cross-coupled stiffness on fluid prerotation. The model predicts direct stiffness poorly. Author

**A89-37665\*** # Illinois Univ., Chicago.

**CROWNED SPUR GEARS - METHODS FOR GENERATION AND TOOTH CONTACT ANALYSIS. II - GENERATION OF THE PINION TOOTH SURFACE BY A SURFACE OF REVOLUTION**  
F. L. LITVIN (Illinois, University, Chicago), R. F. HANDSCHUH (NASA, Lewis Research Center, Cleveland, OH), and J. ZHANG ASME, Transactions, Journal of Mechanisms, Transmission, and Automation in Design (ISSN 0738-0666), vol. 110, Sept. 1988, p. 343-347.

Copyright

A method for generation of crowned pinion tooth surfaces using a surface of revolution is developed. The crowned pinion meshes with a regular involute gear and has a prescribed parabolic type of transmission errors when the gears operate in the aligned mode. When the gears are misaligned the transmission error remains parabolic with the maximum level still remaining very small (less than 0.34 arc second for the numerical examples). Tooth Contact Analysis (TCA) is used to simulate the conditions of meshing, determine the transmission error, and the bearing contact.

Author

**A89-46697\*** # National Aeronautics and Space Administration. Lewis Research Center, Cleveland, OH.

**CERAMIC BEARINGS FOR USE IN GAS TURBINE ENGINES**  
E. V. ZARETSKY (NASA, Lewis Research Center, Cleveland, OH) ASME, Transactions, Journal of Engineering for Gas Turbines and Power (ISSN 0022-0825), vol. 111, Jan. 1989, p. 146-154; Discussion, p. 154, 155; Author's Closure, p. 156, 157. Previously announced in STAR as N88-18007. refs

Copyright

Three decades of research by U.S. industry and government laboratories have produced a vast body of data related to the use of ceramic rolling element bearings and bearing components for aircraft gas turbine engines. Materials such as alumina, silicon carbide, titanium carbide, silicon nitride, and a crystallized glass ceramic have been investigated. Rolling-element endurance tests and analysis of full-complement bearings have been performed. Materials and bearing design methods have continuously improved over the years. This paper reviews a wide range of data and analyses with emphasis on how early NASA contributions as well as more recent data can enable the engineer or metallurgist to determine just where ceramic bearings are most applicable for gas turbines.

Author

**A89-47105\*** # National Aeronautics and Space Administration. Lewis Research Center, Cleveland, OH.

**SURFACE FATIGUE LIFE OF CARBURIZED AND HARDENED M50NiL AND AISI 9310 SPUR GEARS AND ROLLING-CONTACT TEST BARS**

DENNIS P. TOWNSEND (NASA, Lewis Research Center, Cleveland, OH) and ERIC N. BAMBERGER (General Electric Co., Cincinnati, OH) AIAA, ASME, SAE, and ASCE, Joint Propulsion Conference, 25th, Monterey, CA, July 10-13, 1989. 10 p. Previously announced in STAR as N89-22111. refs

(AIAA PAPER 89-2819) Copyright

Spur gear endurance tests and rolling-element surface tests were conducted to investigate vacuum-induction-melted, vacuum-arc-melted (VIM-VAR) M50NiL steel for use as a gear steel in advanced aircraft applications, to determine its endurance characteristics, and to compare the results with those for standard VAR and VIM-VAR AISI 9310 gear material. Tests were conducted with spur gears and rolling-contact bars manufactured from VIM-VAR M50NiL and VAR and VIM-VAR AISI 9310. The gear pitch diameter was 8.9 cm (3.5 in.). Gear test conditions were an inlet oil temperature of 320 K (116 F), and outlet oil temperature of 350 K (170 F), a maximum Hertz stress of 1.71 GPa (248 ksi), and a speed of 10,000 rpm. Bench rolling-element fatigue tests were conducted at ambient temperatures with a bar speed of 12,500 rpm and a maximum Hertz stress of 4.83 GPa (700 ksi).

The VIM-VAR M50NiL gears had a surface fatigue life that was 4.5 and 11.5 times that for VIM-VAR and VAR AISI 9310 gears, respectively. The surface fatigue life of the VIM-VAR M50NiL rolling-contact bars was 13.2 and 21.6 times that for the VIM-VAR and VAR AISI 9310, respectively. The VIM-VAR M50NiL material was shown to have good resistance to fracture through a fatigue spall and to have fatigue life far superior to that of both VIM-VAR and VAR AISI 9310 gears and rolling-contact bars. Author

**A89-47173\*** # Akron Univ., OH.

**TRANSMISSION OVERHAUL AND REPLACEMENT PREDICTIONS USING WEIBULL AND RENEWAL THEORY**

M. SAVAGE (Akron, University, OH) and D. G. LEWICKI (NASA, Lewis Research Center; U.S. Army, Propulsion Directorate, Cleveland, OH) AIAA, ASME, SAE, and ASCE, Joint Propulsion Conference, 25th, Monterey, CA, July 10-13, 1989. 9 p. Previously announced in STAR as N89-22925. refs

(AIAA PAPER 89-2919)

A method to estimate the frequency of transmission overhauls is presented. This method is based on the two-parameter Weibull statistical distribution for component life. A second method is presented to estimate the number of replacement components needed to support the transmission overhaul pattern. The second method is based on renewal theory. Confidence statistics are applied with both methods to improve the statistical estimate of sample behavior. A transmission example is also presented to illustrate the use of the methods. Transmission overhaul frequency and component replacement calculations are included in the example. Author

**A89-47250\*** National Aeronautics and Space Administration. Lewis Research Center, Cleveland, OH.

**SELECTION OF ROLLING-ELEMENT BEARING STEELS FOR LONG-LIFE APPLICATIONS**

ERWIN V. ZARETSKY (NASA, Lewis Research Center, Cleveland, OH) IN: ASTM International Symposium on the Effect of Steel Manufacturing Processes on the Quality of Bearing Steels, Phoenix, AZ, Nov. 4-6, 1986, Proceedings. Philadelphia, PA, American Society for Testing and Materials, 1989, p. 5-43. Previously announced in STAR as N87-11993. refs

Copyright

Nearly four decades of research in bearing steel metallurgy and processing have resulted in improvements in bearing life by a factor of 100 over that obtained in the early 1940s. For critical applications such as aircraft, these improvements have resulted in longer lived, more reliable commercial aircraft engines. Material factors such as hardness, retained austenite, grain size and carbide size, number, and area can influence rolling-element fatigue life. Bearing steel processing such as double vacuum melting can have a greater effect on bearing life than material chemistry. The selection and specification of a bearing steel is dependent on the integration of all these considerations into the bearing design and application. The paper reviews rolling-element fatigue data and analysis which can enable the engineer or metallurgist to select a rolling-element bearing steel for critical applications where long life is required. Author

**A89-47719\*** # National Aeronautics and Space Administration. Lewis Research Center, Cleveland, OH.

**EFFECT OF DESIGN VARIABLES, TEMPERATURE GRADIENTS, AND SPEED ON LIFE AND RELIABILITY OF A ROTATING DISK**

E. V. ZARETSKY (NASA, Lewis Research Center, Cleveland, OH), T. E. SMITH, and R. AUGUST (NASA, Lewis Research Center; Sverdrup Technology, Inc., Cleveland, OH) ASME, Transactions, Journal of Vibration, Acoustics, Stress, and Reliability in Design (ISSN 0739-3717), vol. 111, July 1989, p. 311-316. Previously announced in STAR as N87-13755. refs

Copyright

A generalized methodology to predict the fatigue life and reliability of a rotating disk such as used for aircraft engine turbines and compressors is advanced. The approach incorporates the computed life of elemental stress volumes to predict system life



and reliability. Disk speed and thermal gradients as well as design variables such as disk diameter and thickness and bolt hole size, number and location are considered. Author

**A89-51477\*** Michigan State Univ., East Lansing.  
**STRATIFIED CHARGE ROTARY ENGINE - INTERNAL FLOW STUDIES AT THE MSU ENGINE RESEARCH LABORATORY**  
 F. HAMADY, J. KOSTERMAN, E. CHOUINARD, C. SOMERTON, H. SCHOCK (Michigan State University, East Lansing), K. CHUN, and Y. HICKS (NASA, Lewis Research Center, Cleveland, OH) SAE, International Congress and Exposition, Detroit, MI, Feb. 27-Mar. 3, 1989. 18 p. Research supported by Michigan State University. refs  
 (SAE PAPER 890331) Copyright

High-speed visualization and laser Doppler velocimetry (LDV) systems consisting of a 40-watt copper vapor laser, mirrors, cylindrical lenses, a high speed camera, a synchronization timing system, and a particle generator were developed for the study of the fuel spray-air mixing flow characteristics within the combustion chamber of a motored rotary engine. The laser beam is focused down to a sheet approximately 1 mm thick, passing through the combustion chamber and illuminates smoke particles entrained in the intake air. The light scattered off the particles is recorded by a high speed rotating prism camera. Movies are made showing the air flow within the combustion chamber. The results of a movie showing the development of a high-speed (100 Hz) high-pressure (68.94 MPa, 10,000 psi) fuel jet are also discussed. The visualization system is synchronized so that a pulse generated by the camera triggers the laser's thyatron. C.E.

**A89-51492\*** National Aeronautics and Space Administration. Lewis Research Center, Cleveland, OH.  
**ENGINEERING STUDY ON THE ROTARY-VEE ENGINE CONCEPT**

EDWARD A. WILLIS (NASA, Lewis Research Center, Cleveland, OH), TIMOTHY A. BARTLAND (NASA, Lewis Research Center; Sverdrup Technology, Inc., Cleveland, OH), and JOHN E. BEARD (Louisiana State University, Baton Rouge) IN: Rotary engine design: Analysis and developments; Proceedings of the International Congress and Exposition, Detroit, MI, Feb. 27-Mar. 3, 1989. Warrendale, PA, Society of Automotive Engineers, Inc., 1989, p. 77-94. refs  
 (SAE PAPER 890332) Copyright

This paper provides a review of the applicable thermodynamic cycle and performance considerations when the rotary-vee mechanism is used as an internal combustion (IC) heat engine. Included is a simplified kinematic analysis and studies of the effects of design parameters on the critical pressures, torques and parasitic losses. A discussion of the principal findings is presented.

Author

**A89-51493\*** National Aeronautics and Space Administration. Lewis Research Center, Cleveland, OH.

**STRAIN MEASUREMENTS IN A ROTARY ENGINE HOUSING**  
 C. M. LEE, T. H. BOND, H. E. ADDY, K. S. CHUN (NASA, Lewis Research Center, Cleveland, OH), and C. Y. LU (Cleveland State University, OH) IN: Rotary engine design: Analysis and developments; Proceedings of the International Congress and Exposition, Detroit, MI, Feb. 27-Mar. 3, 1989. Warrendale, PA, Society of Automotive Engineers, Inc., 1989, p. 95-116. refs  
 (SAE PAPER 890333) Copyright

The development of structural design tools for Rotary Combustion Engines (RCE) using Finite Element Modeling (FEM) requires knowledge about the response of engine materials to various service conditions. This paper describes experimental work that studied housing deformation as a result of thermal, pressure and mechanical loads. The measurement of thermal loads, clamping pressure, and deformation was accomplished by use of high-temperature strain gauges, thermocouples, and a high speed data acquisition system. FEM models for heat transfer stress analysis of the rotor housing will be verified and refined based on these experimental results. Author

**A89-53364\*#** Akron Univ., OH.  
**COMPUTERIZED LIFE AND RELIABILITY MODELING FOR TURBOPROP TRANSMISSIONS**  
 M. SAVAGE (Akron, University, OH), K. C. RADIL, D. G. LEWICKI (U.S. Army, Aviation Research and Technology Activity, Cleveland, OH), and J. J. COY (NASA, Lewis Research Center, Cleveland, OH) Journal of Propulsion and Power (ISSN 0748-4658), vol. 5, Sept.-Oct. 1989, p. 610-614. Previously cited in issue 20, p. 3364, Accession no. A88-48031. refs  
 Copyright

**A89-54977\*** Pittsburgh Univ., PA.  
**ON THE PERFORMANCE OF FINITE JOURNAL BEARINGS LUBRICATED WITH MICROPOLAR FLUIDS**

M. M. KHONSARI (Pittsburgh, University, PA) and D. E. BREWE (NASA, Lewis Research Center, Cleveland, OH) STLE Tribology Transactions (ISSN 0569-8197), vol. 32, April 1989, p. 155-160. Previously announced in STAR as N88-15983. refs  
 Copyright

A study of the performance parameters for a journal bearing of finite length lubricated with micropolar fluids is undertaken. Results indicate that a significantly higher load carrying capacity than the Newtonian fluids may result depending on the size of material characteristics length and the coupling number. It is also shown that although the frictional force associated with micropolar fluid is, in general, higher than that of a Newtonian fluid, the friction coefficient of micropolar fluids tends to be lower than that of the Newtonian. Author

**N89-10282\*#** National Aeronautics and Space Administration. Lewis Research Center, Cleveland, OH.

**GENERATION OF A CROWNED PINION TOOTH SURFACE BY A SURFACE OF REVOLUTION**

F. L. LITVIN, J. ZHANG, and R. F. HANDSCHUH (Army Aviation Systems Command, Cleveland, Ohio.) Sep. 1988 15 p  
 (Contract NAG3-655)  
 (NASA-TM-100260; E-3888; NAS 1.15:100260; AVSCOM-TR-87-C-34; AD-A201037) Avail: NTIS HC A03/MF A01 CSCL 13/9

A method of generating crowned pinion tooth surfaces using a surface of revolution is developed. The crowned pinion meshes with a regular involute gear and has a prescribed parabolic type of transmission errors when the gears operate in the aligned mode. When the gears are misaligned the transmission error remains parabolic with the maximum level still remaining very small (less than 0.34 arc sec for the numerical examples). Tooth contact analysis (TCA) is used to simulate the conditions of meshing, determine the transmission error, and determine the bearing contact. Author

**N89-10283\*#** National Aeronautics and Space Administration. Lewis Research Center, Cleveland, OH.

**GENERATION OF A CROWNED PINION TOOTH SURFACE BY A PLANE**

F. L. LITVIN, J. ZHANG, and R. F. HANDSCHUH (Army Aviation Systems Command, Cleveland, Ohio.) Sep. 1988 15 p  
 (Contract NAG3-655)  
 (NASA-TM-100259; E-3887; NAS 1.15:100259; AVSCOM-TR-87-C-33; AD-A201036) Avail: NTIS HC A03/MF A01 CSCL 13/9

The topology of a crowned spur pinion tooth surface that reduces the level of transmission errors due to misalignment is described. The geometry of the modified pinion tooth surface and of the regular involute gear tooth surface is discussed. The tooth contact analysis between the meshing surfaces is also described. Generating a modified pinion tooth surface by a plane whose motion is controlled by a 5-degree-of-freedom system is investigated. The numerical results included indicate that the transmission error remains low as the gears are misaligned. Author

## 37 MECHANICAL ENGINEERING

**N89-12870\*#** Carnegie-Mellon Univ., Pittsburgh, PA. Dept. of Mechanical Engineering.

### **DYNAMICS OF FACE AND ANNULAR SEALS WITH**

**TWO-PHASE FLOW Final Report, 15 Mar. 1981 - 18 Nov. 1988**  
WILLIAM F. HUGHES, PRITHWISH BASU, PAUL A. BEATTY,  
RICHARD M. BEELER, and STEPHEN LAU Nov. 1988 270 p  
(Contract NAG3-166)  
(NASA-CR-183352; NAS 1.26:183352) Avail: NTIS HC A12/MF  
A01 CSCL 11/1

A detailed study was made of face and annular seals under conditions where boiling, i.e., phase change of the leaking fluid, occurs within the seal. Many seals operate in this mode because of flashing due to pressure drop and/or heat input from frictional heating. Some of the distinctive behavior characteristics of two phase seals are discussed, particularly their axial stability. The main conclusions are that seals with two phase flow may be unstable if improperly balanced. Detailed theoretical analyses of low (laminar) and high (turbulent) leakage seals are presented along with computer codes, parametric studies, and in particular a simplified PC based code that allows for rapid performance prediction: calculations of stiffness coefficients, temperature and pressure distributions, and leakage rates for parallel and coned face seals. A simplified combined computer code for the performance prediction over the laminar and turbulent ranges of a two phase flow is described and documented. The analyses, results, and computer codes are summarized. Author

**N89-13788\*#** Carnegie-Mellon Univ., Pittsburgh, PA. Dept. of Mechanical Engineering.

### **THERMAL EFFECTS IN TWO-PHASE FLOW THROUGH FACE SEALS Ph.D. Thesis**

PRITHWISH BASU May 1988 166 p  
(Contract NAG3-166)  
(NASA-CR-185968; NAS 1.26:185968) Avail: NTIS HC A08/MF  
A01 CSCL 11/1

When liquid is sealed at high temperature, it flashes inside the seal due to pressure drop and/or viscous heat dissipation. Two-phase seals generally exhibit more erratic behavior than their single phase counterparts. Thermal effects, which are often neglected in single phase seal analyses, play an important role in determining seal behavior under two-phase operation. It is necessary to consider the heat generation due to viscous shear, conduction into the seal rings and convection with the leakage flow. Analytical models developed work reasonably well at the two extremes - for low leakage rates when convection is neglected and for higher leakage rates when conduction is neglected. A preliminary model, known as the Film Coefficient Model, is presented which considers conduction and convection both, and allows continuous boiling over an extended region unlike the previous low-leakage rate model which neglects convection and always forces a discrete boiling interface. Another simplified, semi-analytical model, based on the assumption of isothermal conditions along the seal interface, has been developed for low leakage rates. The Film Coefficient Model may be used for more accurate and realistic description. Author

**N89-13793\*#** California Univ., Santa Barbara. Dept. of Mechanical Engineering.

### **GEAR OPTIMIZATION Final Contractor Report**

G. N. VANDERPLAATS, XIANG CHEN, and NING-TIAN ZHANG  
Washington NASA Dec. 1988 65 p  
(Contract NAG3-683)  
(NASA-CR-4201; E-4459; NAS 1.26:4201) Avail: NTIS HC  
A04/MF A01 CSCL 13/9

The use of formal numerical optimization methods for the design of gears is investigated. To achieve this, computer codes were developed for the analysis of spur gears and spiral bevel gears. These codes calculate the life, dynamic load, bending strength, surface durability, gear weight and size, and various geometric parameters. It is necessary to calculate all such important responses because they all represent competing requirements in the design process. The codes developed here were written in subroutine form and coupled to the COPES/ADS general purpose

optimization program. This code allows the user to define the optimization problem at the time of program execution. Typical design variables include face width, number of teeth and diametral pitch. The user is free to choose any calculated response as the design objective to minimize or maximize and may impose lower and upper bounds on any calculated responses. Typical examples include life maximization with limits on dynamic load, stress, weight, etc. or minimization of weight subject to limits on life, dynamic load, etc. The research codes were written in modular form for easy expansion and so that they could be combined to create a multiple reduction optimization capability in future. Author

**N89-13794\*#** National Aeronautics and Space Administration. Lewis Research Center, Cleveland, OH.

### **EFFECT OF ADVANCED COMPONENT TECHNOLOGY ON HELICOPTER TRANSMISSIONS**

DAVID G. LEWICKI and DENNIS P. TOWNSEND 1989 18 p  
Prepared for presentation at the International Power Transmission and Gearing Conference, Chicago, Ill., 25-27 Apr. 1989; sponsored by ASME Prepared in cooperation with Army Aviation Systems Command, Cleveland, Ohio  
(NASA-TM-101431; E-4531; NAS 1.15:101431;  
AVSCOM-TR-87-C-38) Avail: NTIS HC A03/MF A01 CSCL  
01/3

Experimental tests were performed on the NASA/Bell Helicopter Textron (BHT) 500 hp advanced technology transmission (ATT) at the NASA Lewis Research Center. The ATT was a retrofit of the OH-58C helicopter 236 kW (317 hp) main rotor transmission, upgraded to 373 kW (500 hp), with a design goal of retaining long life with a minimum increase in cost, weight, and size. Vibration, strain, efficiency, deflection, and temperature experiments were performed and the results were compared to previous experiments on the OH-58A, OH-58C, and UH-60A transmissions. The high-contact-ratio gears and the cantilevered-mounted, flexible ring gear of the ATT reduced vibration compared to that of the OH-58C. The ATT flexible ring gear improved planetary load sharing compared to that of the rigid ring gear of the UH-60A transmission. The ATT mechanical efficiency was lower than that of the OH-58A transmission, probably due to the high-contact-ratio planetary gears. Author

**N89-14450\*#** National Aeronautics and Space Administration. Lewis Research Center, Cleveland, OH.

### **IMPROVEMENT IN FINITE ELEMENT MESHES: HEAT TRANSFER IN AN INFINITE CYLINDER**

MADAN G. KITTUR, RONALD L. HUSTON (Cincinnati Univ., OH.), and FRED B. OSWALD Dec. 1988 15 p Prepared in cooperation with Army Aviation Research and Development Command, Cleveland, Ohio  
(Contract NSG-3188; DA-1L1-62209-A-47-A)  
(NASA-TM-101410; E-4226; NAS 1.15:101410;  
AVSCOM-TR-88-C-021) Avail: NTIS HC A03/MF A01 CSCL  
20/13

An extension of a structural finite element mesh improvement technique to heat conduction analysis is presented. The mesh improvement concept was originally presented by Prager in studying tapered, axially loaded bars. It was further shown that an improved mesh can be obtained by minimizing the trace of the stiffness matrix. These procedures are extended and applied to the analysis of heat conduction in an infinitely long hollow circular cylinder. Author

**N89-14452\*#** National Aeronautics and Space Administration. Lewis Research Center, Cleveland, OH.

### **THE ROLE OF THERMAL AND LUBRICANT BOUNDARY LAYERS IN THE TRANSIENT THERMAL ANALYSIS OF SPUR GEARS**

L. E. EL-BAYOUMY, L. S. AKIN, D. P. TOWNSEND, and F. C. CHOY (Akron Univ., OH.) 1989 17 p Proposed for presentation at the 5th International Power Transmission and Gearing Conference, Chicago, IL, 25-27 Apr. 1989; sponsored by ASME Prepared in cooperation with Army Aviation Research and Development Command, Cleveland, OH

(Contract DA PROJ. 1L1-62209-A-47-A)  
(NASA-TM-101435; E-4413; NAS 1.15:101435;  
AVSCOM-TR-88-C-032; AD-A205574) Avail: NTIS HC A03/MF  
A01 CSCL 13/9

An improved convection heat-transfer model has been developed for the prediction of the transient tooth surface temperature of spur gears. The dissipative quality of the lubricating fluid is shown to be limited to the capacity extent of the thermal boundary layer. This phenomenon can be of significance in the determination of the thermal limit of gears accelerating to the point where gear scoring occurs. Steady-state temperature prediction is improved considerably through the use of a variable integration time step that substantially reduces computer time. Computer-generated plots of temperature contours enable the user to animate the propagation of the thermal wave as the gears come into and out of contact, thus contributing to better understanding of this complex problem. This model has a much better capability at predicting gear-tooth temperatures than previous models.

Author

**N89-14453\*** # National Aeronautics and Space Administration. Lewis Research Center, Cleveland, OH.

**TOOTH CONTACT SHIFT IN LOADED SPIRAL BEVEL GEARS**  
**O, IL, 25-27 APR. 1989; SPONSORED BY ASME**

M. SAVAGE, P. C. ALTIDIS, D. G. LEWICKI, J. J. COY, and F. L. LITVIN (Illinois Univ., Chicago.) 1989 12 p Prepared for presentation at the 5th International Power Transmission and Gearing Conference, Chicago, IL, 25-27 Apr. 1989; sponsored by ASME

(Contract NAG3-55; DA PROJ. 1L1-61102-AH-45)  
(NASA-TM-101438; E-4542; NAS 1.15:101438;  
AVSCOM-TR-87-C-36) Avail: NTIS HC A03/MF A01 CSCL  
13/9

An analytical method is presented to predict the shifts of the contact ellipses of spiral bevel gear teeth under load. The contact ellipse shift is the motion of the tooth contact position from the ideal pitch point to its location under load. The shifts are due to the elastic motions of the gear and pinion supporting shafts and bearings. The calculations include the elastic deflections of the gear shafts and the deflections of the four shaft bearings. The method assumes that the surface curvature of each tooth is constant near the unloaded pitch point. Results from these calculations will help designers reduce transmission weight without seriously reducing transmission performance.

Author

**N89-15413\*** # National Aeronautics and Space Administration. Lewis Research Center, Cleveland, OH.

**DYNAMIC LOADING OF SPUR GEARS WITH LINEAR OR PARABOLIC TOOTH PROFILE MODIFICATION**

HSIANG HSI LIN (Memphis State Univ., TN.), FRED B. OSWALD, and DENNIS P. TOWNSEND 1989 19 p Prepared for presentation at the 5th International Power Transmission and Gearing Conference, Chicago, IL, 25-27 Apr. 1989; sponsored by ASME Sponsored in part by Army

(Contract DA PROJ. 1L1-62209-AH-76)  
(NASA-TM-101444; E-4225; NAS 1.15:101444;  
AVSCOM-TR-88-C-003; AD-A206258) Avail: NTIS HC A03/MF  
A01 CSCL 13/9

A computer simulation was conducted to investigate the effects of both linear and parabolic tooth profile modification on the dynamic response of low-contact-ratio spur gears. The effect of the total amount of modification and the length of the modification zone were studied at various loads and speeds to find the optimal profile modification for minimal dynamic loading. Design charts consisting of normalized maximum dynamic load curves were generated for gear systems operated at various loads and with different tooth profile modification. An optimum profile modification can be determined from these design charts to minimize the dynamic loads of spur gear systems.

Author

**N89-15414\*** # National Aeronautics and Space Administration. Lewis Research Center, Cleveland, OH.

**WEAR CONSIDERATION IN GEAR DESIGN FOR SPACE APPLICATIONS**

LEE S. AKIN (California State Univ., Long Beach.) and DENNIS P. TOWNSEND 1989 8 p Prepared for presentation at the 5th International Power Transmission and Gearing Conference, Chicago, IL, 25-27 Apr. 1989; sponsored by ASME  
(Contract NAG3-20; DA PROJ. 1L1-62209-A-47-A)  
(NASA-TM-101457; E-4532; NAS 1.15:101457;  
AVSCOM-TR-88-C-033; AD-A205575) Avail: NTIS HC A02/MF  
A01 CSCL 13/9

A procedure is described that was developed for evaluating the wear in a set of gears in mesh under high load and low rotational speed. The method can be used for any low-speed gear application, with nearly negligible oil film thickness, and is especially useful in space stepping mechanism applications where determination of pointing error due to wear is important, such as in long life sensor antenna drives. A method is developed for total wear depth at the ends of the line of action using a very simple formula with the slide to roll ratio  $V_{\text{sub}} s/V_{\text{sub}} r$ . A method is also developed that uses the wear results to calculate the transmission error also known as pointing error of a gear mesh.

Author

**N89-15415\*** # National Aeronautics and Space Administration. Lewis Research Center, Cleveland, OH.

**LUBRICANT JET FLOW PHENOMENA IN SPUR AND HELICAL GEARS WITH MODIFIED ADDENDUMS; FOR RADIALLY DIRECTED INDIVIDUAL JETS**

LEE S. AKIN (California State Univ., Long Beach.) and DENNIS P. TOWNSEND 1989 13 p Prepared for presentation at the 5th International Power Transmission and Gearing Conference, Chicago, IL, 25-27 Apr. 1989; sponsored by ASME  
(Contract NAG3-20; DA PROJ. 1L1-62209-A-47-A)  
(NASA-TM-101460; E-4533; NAS 1.15:101460;  
AVSCOM-TR-88-C-034; AD-A205576) Avail: NTIS HC A03/MF  
A01 CSCL 13/9

This paper develops the mathematical relations for the Virtual Kinetic Model as an improvement over the vectorial model developed earlier. The model solution described provides the most energy efficient means of cooling gears, i.e., it requires the least pressure or pumping power to distribute the coolant onto the tooth surface. Further, this nozzle orientation allows impingement to the root of the tooth if needed and provides the most cooling control when compared to into-mesh and out-of-mesh cooling.

Author

**N89-17248\*** # National Aeronautics and Space Administration. Lewis Research Center, Cleveland, OH.

**COMPUTER-AIDED DESIGN OF BEVEL GEAR TOOTH SURFACES**

HUNG CHANG SHUO, RONALD L. HUSTON (Cincinnati Univ., OH.), and JOHN J. COY 1989 19 p Prepared for presentation at the 5th International Power Transmission and Gearing Conference, Chicago, IL, 25-27 Apr. 1989; sponsored in part by ASME Prepared in cooperation with Army Aviation Systems Command, Cleveland, OH

(Contract NAG3-188; DA PROJ. 1L1-62209-A-47-A)  
(NASA-TM-101449; E-4558; NAS 1.15:101449;  
AVSCOM-TR-88-C-005) Avail: NTIS HC A03/MF A01 CSCL  
13/9

This paper presents a computer-aided design procedure for generating bevel gears. The development is based on examining a perfectly plastic, cone-shaped gear blank rolling over a cutting tooth on a plane crown rack. The resulting impression on the plastic gear blank is the envelope of the cutting tooth. This impression and envelope thus form a conjugate tooth surface. Equations are presented for the locus of points on the tooth surface. The same procedures are then extended to simulate the generation of a spiral bevel gear. The corresponding governing equations are presented.

Author

**N89-18685\*#** National Aeronautics and Space Administration. Lewis Research Center, Cleveland, OH.

## **VIBRATION SIGNATURE ANALYSIS OF MULTISTAGE GEAR TRANSMISSION**

F. K. CHOY, Y. K. TU, M. SAVAGE (Akron Univ., OH.), and D. P. TOWNSEND 1989 14 p Prepared for presentation at the 5th International Power Transmission and Gearing Conference, Chicago, IL, 25-27 Apr. 1989; sponsored by ASME (Contract DA PROJ. 1L1-62209-A-47-A) (NASA-TM-101442; E-4534; NAS 1.15:101442; AVSCOM-TR-88-C-040) Avail: NTIS HC A03/MF A01 CSCL 13/9

An analysis is presented for multistage multimesh gear transmission systems. The analysis predicts the overall system dynamics and the transmissibility to the gear box or the enclosed structure. The modal synthesis approach of the analysis treats the uncoupled lateral/torsional model characteristics of each stage or component independently. The vibration signature analysis evaluates the global dynamics coupling in the system. The method synthesizes the interaction of each modal component or stage with the nonlinear gear mesh dynamics and the modal support geometry characteristics. The analysis simulates transient and steady state vibration events to determine the resulting torque variations, speeds, changes, rotor imbalances, and support gear box motion excitations. A vibration signature analysis examines the overall dynamic characteristics of the system, and the individual model component responses. The gear box vibration analysis also examines the spectral characteristics of the support system.

Author

## **N89-20472\*#** Mechanical Technology, Inc., Latham, NY. **HIGH SPEED BALANCING APPLIED TO THE T700 ENGINE Final Report**

J. WALTON, C. LEE, and M. MARTIN Mar. 1989 110 p Prepared in cooperation with Army Aviation Systems Command, Cleveland, OH (Contract NAS3-23929; NAS3-24633; DA PROJ. 1L1-62209-AH-76) (NASA-CR-180899; NAS 1.26:180899; MTI-87TR56; AVSCOM-TR-88-C-007) Avail: NTIS HC A06/MF A01 CSCL 13/9

The work performed under Contracts NAS3-23929 and NAS3-24633 is presented. MTI evaluated the feasibility of high-speed balancing for both the T700 power turbine rotor and the compressor rotor. Modifications were designed for the existing Corpus Christi Army Depot (CCAD) T53/T55 high-speed balancing system for balancing T700 power turbine rotors. Tests conducted under these contracts included a high-speed balancing evaluation for T700 power turbines in the Army/NASA drivetrain facility at MTI. The high-speed balancing tests demonstrated the reduction of vibration amplitudes at operating speed for both low-speed balanced and non-low-speed balanced T700 power turbines. In addition, vibration data from acceptance tests of T53, T55, and T700 engines were analyzed and a vibration diagnostic procedure developed.

Author

## **N89-21239\*#** Mechanical Technology, Inc., Latham, NY. **ADVANCED HELIUM PURGE SEALS FOR LIQUID OXYGEN (LOX) TURBOPUMPS Final Report, Sep. 1985 - Aug. 1987**

WILBUR SHAPIRO and CHESTER C. LEE Mar. 1989 175 p (Contract NAS3-24645) (NASA-CR-182105; NAS 1.26:182105; MTI-87TR72) Avail: NTIS HC A08/MF A01 CSCL 13/9

Program objectives were to determine three advanced configurations of helium buffer seals capable of providing improved performance in a space shuttle main engine (SSME), high-pressure liquid oxygen (LOX) turbopump environment, and to provide NASA with the analytical tools to determine performance of a variety of seal configurations. The three seal designs included solid-ring fluid-film seals often referred to as floating ring seals, back-to-back fluid-film face seals, and a circumferential sector seal that incorporated inherent clearance adjustment capabilities. Of the three seals designed, the sector seal is favored because the

self-adjusting clearance features accommodate the variations in clearance that will occur because of thermal and centrifugal distortions without compromising performance. Moreover, leakage can be contained well below the maximum target values; minimizing leakage is important on the SSME since helium is provided by an external tank. A reduction in tank size translates to an increase in payload that can be carried on board the shuttle. The computer codes supplied under this program included a code for analyzing a variety of gas-lubricated, floating ring, and sector seals; a code for analyzing gas-lubricated face seals; a code for optimizing and analyzing gas-lubricated spiral-groove face seals; and a code for determining fluid-film face seal response to runner excitations in as many as five degrees of freedom. These codes proved invaluable for optimizing designs and estimating final performance of the seals described.

Author

**N89-21243\*#** National Aeronautics and Space Administration. Lewis Research Center, Cleveland, OH.

## **COMPARISON STUDY OF GEAR DYNAMIC COMPUTER PROGRAMS AT NASA LEWIS RESEARCH CENTER**

JAMES J. ZAKRAJESEK Mar. 1989 31 p Prepared in cooperation with Army Aviation Research and Development Command, Cleveland, OH (Contract DA PROJ. 1L1-62209-AH-76) (NASA-TP-2901; E-4144; NAS 1.60:2901; AVSCOM-TR-88-C-010) Avail: NTIS HC A03/MF A01 CSCL 13/9

A comparison study was performed on four gear dynamic analysis computer programs developed under NASA/Army sponsorship. These programs are GRDYNMULT (a multimesh program applicable to a number of epicyclic systems), TELSGE (a single mesh program), PGT (a multimesh program applicable to a planetary system with three planets), and DANST (a single mesh program). The capabilities and features, input and output options, and technical aspects of the programs were reviewed and compared. Results are presented in a concise tabular form. Parametric studies of the program models were performed to investigate the predicted results of the programs as input parameters such as speed, torque, and mesh damping were varied. In general, the program models predicted similar dynamic load and stress levels as operating conditions were varied. Flash temperature predictions from programs GRDYNMULT and TELSGE indicated similar trends; however, actual values were not in close agreement. The program GRDYNMULT was found to be the most versatile in system size, type, and analysis capabilities. The programs DANST, TELSGE, and PGT are more specialized for specific systems; however, in specific areas they provide a more detailed treatment than GRDYNMULT.

Author

**N89-21244\*#** National Aeronautics and Space Administration. Lewis Research Center, Cleveland, OH.

## **MODAL ANALYSIS OF GEAR HOUSING AND MOUNTS**

TEIK C. LIM, RAJ. SINGH (Ohio State Univ., Columbus.), and JAMES J. ZAKRAJESEK Feb. 1989 14 p Presented at the 7th International Modal Analysis Conference, Las Vegas, NV, 30 Jan. - 2 Feb. 1989; sponsored in part by Union College and the Society for Experimental Mechanics, Inc. Prepared in cooperation with Army Aviation Systems Command, Cleveland, OH (Contract DA PROJ. 1L1-62209-A-47-A) (NASA-TM-101445; E-4551; NAS 1.15:101445; AVSCOM-TR-88-C-041; AD-A206969) Avail: NTIS HC A03/MF A01 CSCL 13/9

Dynamic finite element analysis of a real gear housing is presented. The analysis was conducted for the housing without the rotating components (gears, shafts, and bearings). Both rigid and flexible mounting conditions for the gear housing are considered in this analysis. The flexible support simulates the realistic mounting condition on a rotorcraft, and the rigid one is analyzed for comparison purposes. The effect of gear housing stiffeners is also evaluated. The results indicate that the first six natural modes of the flexibly mounted gear housing in the 0 to 200 Hz range correspond to the translational and rotational rigid body vibration modes of the housing. Above this range, the housing plate elastic modes begin to occur. In the case of the rigid mount,

only the housing plate elastic modes are observed which are verified by modal analysis experiments. Parametric studies show that the housing plate stiffeners and rigid mounts tend to increase most of the natural frequencies, the lower ones being affected the most. Author

**N89-21245\*#** National Aeronautics and Space Administration. Lewis Research Center, Cleveland, OH.

**INVESTIGATION OF WEIBULL STATISTICS IN FRACTURE ANALYSIS OF CAST ALUMINUM**

FREDERIC A. HOLLAND, JR. and ERWIN V. ZARETSKY 1989 18 p Prepared for presentation at the Failure Prevention and Reliability Conference, Montreal, Quebec, 17-20 Sep. 1989 (NASA-TM-102000; E-4452; NAS 1.15:102000) Avail: NTIS HC A03/MF A01 CSCL 20/11

The fracture strengths of two large batches of A357-T6 cast aluminum coupon specimens were compared by using two-parameter Weibull analysis. The minimum number of these specimens necessary to find the fracture strength of the material was determined. The applicability of three-parameter Weibull analysis was also investigated. A design methodology based on the combination of elementary stress analysis and Weibull statistical analysis is advanced and applied to the design of a spherical pressure vessel shell. The results from this design methodology are compared with results from the applicable ASME pressure vessel code. Author

**N89-22108\*#** Teledyne Brown Engineering, Huntsville, AL. Space Program Div.

**USER NEEDS, BENEFITS AND INTEGRATION OF ROBOTIC SYSTEMS IN A SPACE STATION LABORATORY Interim Report, Oct. 1987 - Jan. 1989**

K. E. FARNELL, J. A. RICHARD, E. PLOGE, M. B. BADGLEY, C. R. KONKEL, and W. R. DODD Jan. 1989 175 p (Contract NAS3-25278) (NASA-CR-182261; NAS 1.26:182261; TBE-SSD-P601-89-40) Avail: NTIS HC A08/MF A01 CSCL 13/9

The methodology, results and conclusions of the User Needs, Benefits, and Integration Study (UNBIS) of Robotic Systems in the Space Station Microgravity and Materials Processing Facility are summarized. Study goals include the determination of user requirements for robotics within the Space Station, United States Laboratory. Three experiments were selected to determine user needs and to allow detailed investigation of microgravity requirements. A NASTRAN analysis of Space Station response to robotic disturbances, and acceleration measurement of a standard industrial robot (Intellex Model 660) resulted in selection of two ranges of low gravity manipulation: Level 1 (10<sup>-3</sup> to 10<sup>-5</sup> G at greater than 1 Hz.) and Level 2 (less than = 10<sup>-6</sup> G at 0.1 Hz). This included an evaluation of microstepping methods for controlling stepper motors and concluded that an industrial robot actuator can perform milli-G motion without modification. Relative merits of end-effectors and manipulators were studied in order to determine their ability to perform a range of tasks related to the three low gravity experiments. An Effectivity Rating was established for evaluating these robotic system capabilities. Preliminary interface requirements were determined such that definition of requirements for an orbital flight demonstration experiment may be established. Author

**N89-22111\*#** National Aeronautics and Space Administration. Lewis Research Center, Cleveland, OH.

**SURFACE FATIGUE LIFE OF CARBURIZED AND HARDENED M50NiL AND AISI 9310 SPUR GEARS AND ROLLING-CONTACT TEST BARS**

DENNIS P. TOWNSEND and ERIC N. BAMBERGER (General Electric Co., Cincinnati, OH.) 1989 18 p Presented at the 25th Joint Propulsion Conference, Monterey, CA, 10-12 Jul. 1989; cosponsored by the AIAA, ASME, SAE, and ASEE (Contract DA PROJ. 1L1-62209-A-47A) (NASA-TM-101979; E-4678; NAS 1.15:101979; AVSCOM-TR-89-C-011) Avail: NTIS HC A03/MF A01 CSCL 13/9

Spur gear endurance tests and rolling-element surface tests were conducted to investigate vacuum-induction-melted, vacuum-arc-melted (VIM-VAR) M50NiL steel for use as a gear steel in advanced aircraft applications, to determine its endurance characteristics, and to compare the results with those for standard VAR and VIM-VAR AISI 9310 gear material. Tests were conducted with spur gears and rolling-contact bars manufactured from VIM-VAR M50NiL and VAR and VIM-VAR AISI 9310. The gear pitch diameter was 8.9 cm (3.5 in.). Gear test conditions were an inlet oil temperature of 320 K (116 F), and outlet oil temperature of 350 K (170 F), a maximum Hertz stress of 1.71 GPa (248 ksi), and a speed of 10,000 rpm. Bench rolling-element fatigue tests were conducted at ambient temperatures with a bar speed of 12,500 rpm and a maximum Hertz stress of 4.83 GPa (700 ksi). The VIM-VAR M50NiL gears had a surface fatigue life that was 4.5 and 11.5 times that for VIM-VAR and VAR AISI 9310 gears, respectively. The surface fatigue life of the VIM-VAR M50NiL rolling-contact bars was 13.2 and 21.6 times that for the VIM-VAR and VAR AISI 9310, respectively. The VIM-VAR M50NiL material was shown to have good resistance to fracture through a fatigue spall and to have fatigue life far superior to that of both VIM-VAR and VAR AISI 9310 gears and rolling-contact bars. Author

**N89-22891\*#** National Aeronautics and Space Administration. Lewis Research Center, Cleveland, OH.

**ROTORDYNAMIC INSTABILITY PROBLEMS IN HIGH-PERFORMANCE TURBOMACHINERY, 1988**

Washington, DC Feb. 1989 454 p Workshop held in College Station, TX, 16-18 May 1988; sponsored by NASA, Lewis Research Center, Cleveland, OH, Texas A and M Univ., College Station, ARO, Durham, NC, and Aeropropulsion Lab., Wright-Patterson AFB, OH (NASA-CP-3026; E-4227; NAS 1.55:3026) Avail: NTIS HC A20/MF A01 CSCL 13/9

The continuing trend toward a unified view is supported with several developments in the design and manufacture of turbomachines with enhanced stability characteristics along with data and associated numerical/theoretical results. The intent is to provide a continuing impetus for an understanding and resolution of these problems. Topics addressed include: field experience, dampers, seals, impeller forces, bearings, and compressor and rotor modeling.

**N89-22899\*#** Texas A&M Univ., College Station. **ANNULAR HONEYCOMB SEALS: TEST RESULTS FOR LEAKAGE AND ROTORDYNAMIC COEFFICIENTS; COMPARISONS TO LABYRINTH AND SMOOTH CONFIGURATIONS**

DARA W. CHILDS, DAVID ELROD, and KEITH HALE In NASA, Lewis Research Center, Rotordynamic Instability Problems in High-Performance Turbomachinery, 1988 p 143-159 Feb. 1989 Previously announced in X89-10207 (Contract NAG3-181; F49620-82-K-0033) Avail: NTIS HC A20/MF A01 CSCL 11/1

Test results are presented for leakage and rotordynamic coefficients for seven honeycomb seals. All seals have the same radius, length, and clearance; however, the cell depths and diameters are varied. Rotordynamic data, which are presented, consist of the direct and cross-coupled stiffness coefficients and the direct damping coefficients. The rotordynamic-coefficient data show a considerable sensitivity to changes in cell dimensions; however, no clear trends are identifiable. Comparisons of test data for the honeycomb seals with labyrinth and smooth annular seals show the honeycomb seal had the best sealing (minimum leakage) performance, followed in order by the labyrinth and smooth seals. For prerotated fluid entering the seal, in the direction of shaft rotation, the honeycomb seal has the best rotordynamic stability followed in order by the labyrinth and smooth. For no prerotation, or fluid prerotation against shaft rotation, the labyrinth seal has the best rotordynamic stability followed in order by the smooth and honeycomb seals. Author

### 37 MECHANICAL ENGINEERING

**N89-22919\*#** National Aeronautics and Space Administration. Lewis Research Center, Cleveland, OH.

#### **EFFECTS OF LUBRICATION ON THE PERFORMANCE OF HIGH SPEED SPUR GEARS**

HACHIRO MIZUTANI, YUICHI ISIKAWA (Mechanical Engineering Lab., Tsukuba, Japan), and DENNIS P. TOWNSEND Apr. 1989 10 p Presented at the 5th International Power Transmission and Gearing Conference, Chicago, IL, 24-27 Apr. 1989; sponsored in part by ASME (NASA-TM-101969; E-4666; NAS 1.15:101969) Avail: NTIS HC A02/MF A01 CSCL 13/9

An experimental analysis was conducted to determine power loss and gear noise of high speed spur gears with long addendum under various conditions of load, speed, and oil jet pressure for into mesh lubrication. Power losses were calculated from temperature measurements of lubricating oil, gears, gear box, and oil flow rate. Furthermore, power loss was divided into windage loss, friction loss and churning loss. The results show that windage loss and churning loss were the main components of gear power loss of high gear speed. In addition, lubricating conditions had some influences on gear noise especially under low oil temperature or high viscosity. Author

**N89-22920\*#** Illinois Univ., Chicago. Dept. of Mechanical Engineering.

#### **TOPOLOGY OF MODIFIED HELICAL GEARS AND TOOTH CONTACT ANALYSIS (TCA) PROGRAM Final Report**

FAYDOR L. LITVIN and JIAO ZHANG Washington NASA Apr. 1989 159 p (Contract NAG3-655; DA PROJ. 1L1-62209-A-47-A) (NASA-CR-4224; E-4626; NAS 1.26:4224; AVSCOM-TR-89-C-002; AD-A213170) Avail: NTIS HC A08/MF A01 CSCL 13/9

The contents of this report covers: (1) development of optimal geometries for crowned helical gears; (2) a method for their generation; (3) tooth contact analysis (TCA) computer programs for the analysis of meshing and bearing contact of the crowned helical gears; and (4) modelling and simulation of gear shaft deflection. The developed method for synthesis was used to determine the optimal geometry for a crowned helical pinion surface and was directed to localize the bearing contact and guarantee favorable shape and a low level of transmission errors. Two new methods for generation of the crowned helical pinion surface are proposed. One is based on the application of a tool with a surface of revolution that slightly deviates from a regular cone surface. The tool can be used as a grinding wheel or as a shaver. The other is based on a crowning pinion tooth surface with predesigned transmission errors. The pinion tooth surface can be generated by a computer-controlled automatic grinding machine. The TCA program simulates the meshing and bearing contact of the misaligned gears. The transmission errors are also determined. The gear shaft deformation was modelled and investigated. It was found that the deflection of gear shafts has the same effect as gear misalignment. Author

**N89-22925\*#** National Aeronautics and Space Administration. Lewis Research Center, Cleveland, OH.

#### **TRANSMISSION OVERHAUL AND REPLACEMENT PREDICTIONS USING WEIBULL AND RENEWEL THEORY**

M. SAVAGE and D. G. LEWICKI (Army Aviation Systems Command, Cleveland, OH.) 1989 12 p Presented at the 25th Joint Propulsion Conference, Monterey, CA, 10-12 Jul. 1989; cosponsored by the AIAA, ASME, SAE and ASEE (Contract DA PROJ. 1L1-62209-A-47-A) (NASA-TM-102022; E-4756; NAS 1.15:102022; AVSCOM-TR-89-C-007; AIAA-89-2919) Avail: NTIS HC A03/MF A01 CSCL 13/9

A method to estimate the frequency of transmission overhauls is presented. This method is based on the two-parameter Weibull statistical distribution for component life. A second method is presented to estimate the number of replacement components needed to support the transmission overhaul pattern. The second method is based on renewal theory. Confidence statistics are applied with both methods to improve the statistical estimate of

sample behavior. A transmission example is also presented to illustrate the use of the methods. Transmission overhaul frequency and component replacement calculations are included in the example. Author

**N89-23876\*#** Texas A&M Univ., College Station. Turbomachinery Lab.

#### **FRICTION FACTOR DATA FOR FLAT PLATE TESTS OF SMOOTH AND HONEYCOMB SURFACES M.S. Thesis**

TAE WOONG HA May 1989 100 p (Contract NAG3-181) (NASA-CR-184977; NAS 1.26:184977; TL-SEAL-1-89) Avail: NTIS HC A05/MF A01 CSCL 20/3

Friction factors for honeycomb surfaces were measured with a flat plate tester. The flat plate test apparatus was described and a method was discussed for determining the friction factor experimentally. The friction factor model was developed for the flat plate test based on the Fanno Line Flow. The comparisons of the friction factor were plotted for smooth surfaces and six-honeycomb surfaces with three-clearances, 6.9 bar to 17.9 bar range of inlet pressures, and 5,000 to 100,000 range of the Reynolds number. The optimum geometries for the maximum friction factor were found as a function of cell width to cell depth and cell width to clearance ratios. Author

**N89-24607\*#** National Aeronautics and Space Administration. Lewis Research Center, Cleveland, OH.

#### **COMPARISON OF PREDICTED AND MEASURED TEMPERATURES OF UH-60A HELICOPTER TRANSMISSION**

HAROLD H. COE Washington Apr. 1989 15 p (NASA-TP-2911; NAS 1.60:2911; E-4588; AVSCOM-TR-89-C-010) Avail: NTIS HC A03/MF A01 CSCL 13/9

The 2109-kW (2828-hp) UH-60A Black Hawk helicopter transmission was one of the transmissions used to obtain an experimental data base. Component improvements or new transmission concepts can thus be evaluated by comparison with the established data. Results of efficiency and vibration tests of the UH-60A have been reported previously. In this investigation the transmission was instrumented internally and tested over a range of operating conditions. The speed was varied from 50 to 100 percent of the full rated value, and the torque was varied from 10 to 100 percent of the full rated value. Temperatures of internal bearings and gears were measured. The computer program Planetsys was used to simulate the thermal performance of this transmission. The calculated temperatures were then compared with the corresponding measured values. The highest measured temperature was 405 K (270 F) on the outer race of the high-speed input shaft roller bearing, at the 100-percent power condition. In general, the predicted temperatures compared very well with the measured values, most of them being within 5 kelvin (9 F). Specifically, the temperatures predicted for the single-row spherical roller planetary bearing averaged only about 4 kelvin (8 F) lower than the highest measured value. Author

**N89-26246\*#** Detroit Diesel Allison, Indianapolis, IN. Gas Turbine Div.

#### **AGT (ADVANCED GAS TURBINE) TECHNOLOGY PROJECT Final Report**

Aug. 1988 203 p (Contract DEN3-168) (NASA-CR-182127; DOE/NASA/0168-11; EDR-13295; NAS 1.26:182127) Avail: NTIS HC A10/MF A01 CSCL 20/5

An overall summary documentation is provided for the Advanced Gas Turbine Technology Project conducted by the Allison Gas Turbine Division of General Motors. This advanced, high risk work was initiated in October 1979 under charter from the U.S. Congress to promote an engine for transportation that would provide an alternate to reciprocating spark ignition (SI) engines for the U.S. automotive industry and simultaneously establish the feasibility of advanced ceramic materials for hot section components to be used in an automotive gas turbine. As this program evolved, dictates of available funding, Government charter, and technical developments caused program emphases



to focus on the development and demonstration of the ceramic turbine hot section and away from the development of engine and powertrain technologies and subsequent vehicular demonstrations. Program technical performance concluded in June 1987. The AGT 100 program successfully achieved project objectives with significant technology advances. Specific AGT 100 program achievements are: (1) Ceramic component feasibility for use in gas turbine engines has been demonstrated; (2) A new, 100 hp engine was designed, fabricated, and tested for 572 hour at operating temperatures to 2200 F, uncooled; (3) Statistical design methodology has been applied and correlated to experimental data acquired from over 5500 hour of rig and engine testing; (4) Ceramic component processing capability has progressed from a rudimentary level able to fabricate simple parts to a sophisticated level able to provide complex geometries such as rotors and scrolls; (5) Required improvements for monolithic and composite ceramic gas turbine components to meet automotive reliability, performance, and cost goals have been identified; (6) The combustor design demonstrated lower emissions than 1986 Federal Standards on methanol, JP-5, and diesel fuel. Thus, the potential for meeting emission standards and multifuel capability has been initiated; (7) Small turbine engine aerodynamic and mechanical design capability has been initiated; and (8) An infrastructure of manpower, facilities, materials, and fabrication capabilities has been established which is available for continued development of ceramic component technology in gas turbine and other heat engines. Author

**N89-28015\*** National Aeronautics and Space Administration. Lewis Research Center, Cleveland, OH.

## TOPOLOGY OF MODIFIED HELICAL GEARS

F. L. LITVIN, J. ZHANG, R. F. HANDSCHUH (Army Aviation Systems Command, Cleveland, OH.), and J. J. COY 1989 21 p Presented at the 5th International Power Transmission and Gearing Conference, Chicago, IL, 24-27 Apr. 1989; sponsored by the ASME

(Contract DA PROJ. 1L1-62209-A-47-A)

(NASA-TM-102134; E-4054; NAS 1.15:102134;

AVSCOM-TR-89-C-004) Avail: NTIS HC A03/MF A01 CSCI 13/9

The topology of several types of modified surfaces of helical gears is proposed. The modified surfaces allow absorption of a linear or almost linear function of transmission errors. These errors are caused by gear misalignment and an improvement of the contact of gear tooth surfaces. Principles and corresponding programs for computer aided simulation of meshing and contact of gears have been developed. The results of this investigation are illustrated with numerical examples. Author

**N89-28830\*** National Aeronautics and Space Administration. Lewis Research Center, Cleveland, OH.

## HIGH TEMPERATURE FLEXIBLE SEAL Patent Application

BRUCE M. STEINETZ, inventor (to NASA) and PAUL J. SIROCKY, inventor (to NASA) 30 Dec. 1988 14 p

(NASA-CASE-LEW-14695-1; NAS 1.71:LEW-14695-1;

US-PATENT-APPL-SN-292146) Avail: NTIS HC A03/MF A01 CSCI 11/1

This device is concerned with sealing the sliding interfaces between structural panels that are roughly perpendicular to each other or whose edges are butted against one another. The gap which the seal element must seal in not uniform along the seal length requiring significant seal flexibility. The seal is mounted in a rectangular groove in a moveable structural panel. The seal comprises a plurality of rectangular shaped wafers stacked next to one another and preloaded in the axial direction to minimize leakage between wafers. The wafers are laterally preloaded to maintain sealing contact along the wafer faces which engage the adjacent wall of a sidewall using one of several approaches, such as the pressurized linear bellows. The seal accommodates distortions in the adjacent panel by relative sliding between adjacent wafers. Leakage between wafers is further minimized with good wafer surface finishes. Leakage between the seal nose and the adjacent structural panel is minimized when sealing against a distorted sidewall with relatively thin wafers and suitable seal

preload apparatus. Leakage behind the seal is minimized with good groove tolerances and good sealing contact between the preload system and the back of the peripheral edge of the wafers.

NASA

## 38

# QUALITY ASSURANCE AND RELIABILITY

Includes product sampling procedures and techniques; and quality control.

**A89-14700\*** Cleveland State Univ., OH.

## RADIOGRAPHIC AND ULTRASONIC CHARACTERIZATION OF SINTERED SILICON CARBIDE

G. Y. BAAKLINI (Cleveland State University, OH) and P. B. ABEL (NASA, Lewis Research Center, Cleveland, OH) Materials Evaluation (ISSN 0025-5327), vol. 46, Oct. 1988, p. 1477-1483. Previously announced in STAR as N88-12106. refs Copyright

The capabilities were investigated of projection microfocus X-radiography, ultrasonic velocity and attenuation, and reflection scanning acoustic microscopy for characterizing silicon carbide specimens. Silicon carbide batches covered a range of densities and different microstructural characteristics. Room temperature, four point flexural strength tests were conducted. Fractography was used to identify types, sizes, and locations of fracture origins. Fracture toughness values were calculated from fracture strength and flaw characterization data. Detection capabilities of radiography and acoustic microscopy for fracture-causing flaws were evaluated. Applicability of ultrasonics for verifying material strength and toughness was examined. Author

**A89-23936\*** National Aeronautics and Space Administration. Lewis Research Center, Cleveland, OH.

## ULTRASONIC ATTENUATION MEASUREMENTS DETERMINE ONSET, DEGREE, AND COMPLETION OF RECRYSTALLIZATION

E. R. GENERAZIO (NASA, Lewis Research Center, Cleveland, OH) Materials Evaluation (ISSN 0025-5327), vol. 46, Aug. 1988, p. 1198-1203. Previously announced in STAR as N87-10399. refs

Copyright

Ultrasonic attenuation was measured for cold worked Nickel 200 samples annealed at increasing temperatures. Localized dislocation density variations, crystalline order and volume percent of recrystallized phase were determined over the anneal temperature range using transmission electron microscopy, X-ray diffraction, and metallurgy. The exponent of the frequency dependence of the attenuation was found to be a key variable relating ultrasonic attenuation to the thermal kinetics of the recrystallization process. Identification of this key variable allows for the ultrasonic determination of onset, degree, and completion of recrystallization. Author

**A89-25852\*** Northwestern Univ., Evanston, IL.

## KUHN-TUCKER OPTIMIZATION BASED RELIABILITY ANALYSIS FOR PROBABILISTIC FINITE ELEMENTS

W. K. LIU, G. BESTERFIELD, M. LAWRENCE, and T. BELYTSCHKO (Northwestern University, Evanston, IL) IN: Computational probabilistic methods; Proceedings of the Joint ASME/SES Applied Mechanics and Engineering Sciences Conference, Berkeley, CA, June 20-22, 1988. New York, American Society of Mechanical Engineers, 1988, p. 135-149. refs (Contract NAG3-822)

Copyright

The fusion of probability finite element method (PFEM) and reliability analysis for fracture mechanics is considered. Reliability analysis with specific application to fracture mechanics is presented, and computational procedures are discussed. Explicit

### 38 QUALITY ASSURANCE AND RELIABILITY

expressions for the optimization procedure with regard to fracture mechanics are given. The results show the PFEM is a very powerful tool in determining the second-moment statistics. The method can determine the probability of failure or fracture subject to randomness in load, material properties and crack length, orientation, and location. C.D.

**A89-32305\*** National Aeronautics and Space Administration. Lewis Research Center, Cleveland, OH.

#### THE ACOUSTO-ULTRASONIC APPROACH

ALEX VARY (NASA, Lewis Research Center, Cleveland, OH) IN: Acousto-ultrasonics: Theory and application; Proceedings of the Conference, Blacksburg, VA, July 12-15, 1987. New York, Plenum Publishing Corp., 1988, p. 1-21. Previously announced in STAR as N87-20562. refs  
Copyright

The nature and underlying rationale of the acousto-ultrasonic approach is reviewed, needed advanced signal analysis and evaluation methods suggested, and application potentials discussed. Acousto-ultrasonics is an NDE technique combining aspects of acoustic emission methodology with ultrasonic simulation of stress waves. This approach uses analysis of simulated stress waves for detecting and mapping variations of mechanical properties. Unlike most NDE, acousto-ultrasonics is less concerned with flaw detection than with the assessment of the collective effects of various flaws and material anomalies. Acousto-ultrasonics has been applied chiefly to laminated and filament-wound fiber reinforced composites. It has been used to assess the significant strength and toughness reducing effects that can be wrought by combinations of essentially minor flaws and diffuse flaw populations. Acousto-ultrasonics assesses integrated defect states and the resultant variations in properties such as tensile, shear, and flexural strengths and fracture resistance. Matrix cure state, porosity, fiber orientation, fiber volume fraction, fiber-matrix bonding, and interlaminar bond quality are underlying factors. Author

**A89-36571\*** Illinois Univ., Urbana.

#### NONDESTRUCTIVE EVALUATION/CHARACTERIZATION OF COMPOSITE MATERIALS AND STRUCTURES USING THE ACOUSTO-ULTRASONIC TECHNIQUES

H. L. M. DOS REIS (Illinois, University, Urbana) and A. VARY (NASA, Lewis Research Center, Cleveland, OH) IN: SEM Fall Conference, Indianapolis, IN, Nov. 7, 8, 1988, Proceedings. Bethel, CT, Society for Experimental Mechanics, Inc., 1988, p. 25-32. refs  
Copyright

This paper introduces the nature and the underlying rationale of the acousto-ultrasonic stress wave factor technique and some of its applications to composite materials and structures. Furthermore, two examples of successful application of the acousto-ultrasonic technique are presented in detail. In the first example, the acousto-ultrasonic technique is used to evaluate the adhesive bond strength between rubber layers and steel plates, and in the second example the technique is used to monitor progressive damage in wire rope. Author

**A89-42864\*** National Aeronautics and Space Administration. Lewis Research Center, Cleveland, OH.

#### ACOUSTO-ULTRASONICS - AN UPDATE

ALEX VARY (NASA, Lewis Research Center, Cleveland, OH) Journal of Acoustic Emission (ISSN 0730-0050), vol. 8, Jan.-June 1989, p. S175-S178. refs  
Copyright

The application possibilities and limitations of acousto-ultrasonics are reviewed. One of the most useful aspects of acousto-ultrasonics is its ability to assess degradation and damage states in composites. The sensitivity of the acousto-ultrasonic approach for detecting and measuring subtle but significant material property variations in composites has been demonstrated. K.K.

#### N89-12914\*# Pratt and Whitney Aircraft, East Hartford, CT. CREEP FATIGUE LIFE PREDICTION FOR ENGINE HOT SECTION MATERIALS (ISOTROPIC): FOURTH YEAR PROGRESS REVIEW

RICHARD S. NELSON and JOHN F. SCHOENDORF IN NASA, Lewis Research Center, Turbine Engine Hot Section Technology 1986 p 359-370 Oct. 1986  
(Contract NAS3-23288)

Avail: NTIS HC A21/MF A01 CSCL 14/4

As gas turbine technology continues to advance, the need for advanced life prediction methods for hot section components is becoming more and more evident. The complex local strain and temperature histories at critical locations must be accurately interpreted to account for the effects of various damage mechanisms (such as fatigue, creep, and oxidation) and their possible interactions. As part of the overall NASA HOST effort, this program is designed to investigate these fundamental damage processes, identify modeling strategies, and develop practical models which can be used to guide the early design and development of new engines and to increase the durability of existing engines. Author

#### N89-12916\*# Pratt and Whitney Aircraft, East Hartford, CT. LIFE PREDICTION AND CONSTITUTIVE MODELS FOR ENGINE HOT SECTION

G. A. SWANSON, T. G. MEYER, and D. M. NISSLEY IN NASA, Lewis Research Center, Turbine Engine Hot Section Technology 1986 p 385-397 Oct. 1986  
(Contract NAS3-23939)

Avail: NTIS HC A21/MF A01 CSCL 14/4

The purpose of this program is to develop life prediction models for coated anisotropic materials used in gas turbine airfoils. In the program, two single crystal alloys and two coatings are being tested. These include PWA 1480, Alloy 185, overlay coating (PWA 286), and aluminide coating (PWA 273). Constitutive models are also being developed for these materials to predict the time independent (plastic) and time dependent (creep) strain histories of the materials in the lab tests and for actual design conditions. This nonlinear material behavior is particularly important for high temperature gas turbine applications and is basic to any life prediction system. Some of the accomplishments of the program are highlighted. Author

**N89-18694\*#** Massachusetts Inst. of Tech., Cambridge. Dept. of Mechanical Engineering.

#### ENERGY IN ELASTIC FIBER EMBEDDED IN ELASTIC MATRIX CONTAINING INCIDENT SH WAVE Final Report

JAMES H. WILLIAMS, JR. and RAYMOND J. NAGEM Washington NASA Jan. 1989 16 p  
(Contract NAG3-328)

(NASA-CR-4205; E-4489; NAS 1.26:4205) Avail: NTIS HC A03/MF A01 CSCL 14/4

A single elastic fiber embedded in an infinite elastic matrix is considered. An incident plane SH wave is assumed in the infinite matrix, and an expression is derived for the total energy in the fiber due to the incident SH wave. A nondimensional form of the fiber energy is plotted as a function of the nondimensional wavenumber of the SH wave. It is shown that the fiber energy attains maximum values at specific values of the wavenumber of the incident wave. The results obtained here are interpreted in the context of phenomena observed in acousto-ultrasonic experiments on fiber reinforced composite materials. Author

**N89-19578\*#** National Aeronautics and Space Administration. Lewis Research Center, Cleveland, OH.

#### INTERFACING LABORATORY INSTRUMENTS TO MULTIUSER, VIRTUAL MEMORY COMPUTERS

EDWARD R. GENERAZIO, DAVID B. STANG (Sverdrup Technology, Inc., Cleveland, OH.), and DON J. ROTH Washington Mar. 1989 29 p  
(NASA-TM-4106; E-4510; NAS 1.15:4106) Avail: NTIS HC A03/MF A01 CSCL 14/4

Incentives, problems and solutions associated with interfacing

laboratory equipment with multiuser, virtual memory computers are presented. The major difficulty concerns how to utilize these computers effectively in a medium sized research group. This entails optimization of hardware interconnections and software to facilitate multiple instrument control, data acquisition and processing. The architecture of the system that was devised, and associated programming and subroutines are described. An example program involving computer controlled hardware for ultrasonic scan imaging is provided to illustrate the operational features. Author

**N89-20489\*#** Cleveland State Univ., OH.

**RELIABILITY-BASED FAILURE ANALYSIS OF BRITTLE MATERIALS**

LYNN M. POWERS and LOUIS J. GHOSN Feb. 1989 128 p  
(Contract NCC3-46)  
(NASA-CR-184799; NAS 1.26:184799) Avail: NTIS HC A07/MF A01 CSCL 09/4

The reliability of brittle materials under a generalized state of stress is analyzed using the Batdorf model. The model is modified to include the reduction in shear due to the effect of the compressive stress on the microscopic crack faces. The combined effect of both surface and volume flaws is included. Due to the nature of fracture of brittle materials under compressive loading, the component is modeled as a series system in order to establish bounds on the probability of failure. A computer program was written to determine the probability of failure employing data from a finite element analysis. The analysis showed that for tensile loading a single crack will be the cause of total failure but under compressive loading a series of microscopic cracks must join together to form a dominant crack. Author

**N89-20490\*#** National Aeronautics and Space Administration. Lewis Research Center, Cleveland, OH.

**NONDESTRUCTIVE EVALUATION OF ADVANCED CERAMICS**

STANLEY J. KLIMA and HAROLD E. KAUTZ 1988 11 p  
Presented at the 26th Automotive Technology Development Contractor's Coordination Meeting, Dearborn, MI, 24-27 Oct. 1988; sponsored by DOE  
(NASA-TM-101489; E-4632; NAS 1.15:101489) Avail: NTIS HC A03/MF A01 CSCL 14/4

A review is presented of Lewis Research Center efforts to develop nondestructive evaluation techniques for characterizing advanced ceramic materials. Various approaches involved the use of analytical ultrasonics to characterize monolithic ceramic microstructures, acousto-ultrasonics for characterizing ceramic matrix composites, damage monitoring in impact specimens by microfocus X-ray radiography and scanning ultrasonics, and high resolution computed X-ray tomography to identify structural features in fiber reinforced ceramics. Author

**N89-21256\*#** Virginia Polytechnic Inst. and State Univ., Blacksburg. Dept. of Engineering Science and Mechanics.

**A STUDY OF THE STRESS WAVE FACTOR TECHNIQUE FOR EVALUATION OF COMPOSITE MATERIALS Final Report**

J. C. DUKE, JR., E. G. HENNEKE, II, M. T. KIERNAN, and P. P. GROSSKOPF Washington NASA Jan. 1989 61 p  
(Contract NAG3-172)  
(NASA-CR-4195; E-4385; NAS 1.26:4195) Avail: NTIS HC A04/MF A01 CSCL 14/4

The acousto-ultrasonic approach for nondestructive evaluation provides a measurement procedure for quantifying the integrated effect of globally distributed damage characteristic of fiber reinforced composite materials. The evaluation procedure provides a stress wave factor that correlates closely with several material performance parameters. The procedure was investigated for a variety of materials including advanced composites, hybrid structure bonds, adhesive bonds, wood products, and wire rope. The research program focused primarily on development of fundamental understanding and applications advancements of acousto-ultrasonics for materials characterization. This involves characterization of materials for which detection, location, and identification of imperfections cannot at present be analyzed

satisfactorily with mechanical performance prediction models. In addition to presenting definitive studies on application potentials, the understanding of the acousto-ultrasonic method as applied to advanced composites is reviewed. Author

**N89-27204\*#** Rockwell International Corp., Canoga Park, CA. Rocketdyne Div.

**OTVE TURBOPUMP CONDITION MONITORING, TASK E.5**

**Final Report, Oct. 1988 - Sep. 1989**

PAUL T. COLEMAN and J. J. COLLINS Aug. 1989 27 p  
(Contract NAS3-23773)  
(NASA-CR-182274; NAS 1.26:182274; RI/RD89-214-TASK-E.5)  
Avail: NTIS HC A03/MF A01 CSCL 14/4

Recent work has been carried out on development of isotope wear analysis and optical and eddy current technologies to provide bearing wear measurements and real time monitoring of shaft speed, shaft axial displacement and shaft orbit of the Orbit Transfer Vehicle hydrostatic bearing tester. Results show shaft axial displacement can be optically measured (at the same time as shaft orbital motion and speed) to within 0.3 mils by two fiberoptic deflectometers. Evaluation of eddy current probes showed that, in addition to measuring shaft orbital motion, they can be used to measure shaft speed without having to machine grooves on the shaft surface as is the usual practice for turbomachinery. The interim results of this condition monitoring effort are presented. Author

**N89-28851\*#** National Aeronautics and Space Administration. Lewis Research Center, Cleveland, OH.

**NON-UNIFORM TRANSITION CONDUCTIVITY OF SUPERCONDUCTING CERAMIC**

EDWARD R. GENERAZIO, DON J. ROTH, and ALOYSIUS F. HEPP Jul. 1989 9 p  
Presented at the 16th Annual Review of Progress in Quantitative Nondestructive Evaluation, Brunswick, ME, 23-28 Jul. 1989; sponsored in part by DOE, AFWAL, ONR and ASNT  
(NASA-TM-102133; E-4928; NAS 1.15:102133) Avail: NTIS HC A02/MF A01 CSCL 14/4

The effects of microstructural variations on the superconducting properties of  $\text{SmBa}_2\text{Cu}_3\text{O}_x$  are investigated. A scanning eddy current probe revealed the onset and growth of a normal conducting region. Resistance versus temperature measurements taken at different regions of the sample support the concept of a physically mixed state system. Regional variations in porosity and grain size distributions affect the observed superconducting transition. Author

**N89-28853\*#** National Aeronautics and Space Administration. Lewis Research Center, Cleveland, OH.

**ULTRASONIC IMAGING OF TEXTURED ALUMINA**

DAVID B. STANG (Sverdrup Technology, Inc., Cleveland, OH.), JONATHAN A. SALEM, and EDWARD R. GENERAZIO May 1989 11 p  
(NASA-TM-101478; E-4600; NAS 1.15:101478) Avail: NTIS HC A03/MF A01 CSCL 14/4

Ultrasonic images representing the bulk attenuation and velocity of a set of alumina samples were obtained by a pulse-echo contact scanning technique. The samples were taken from larger bodies that were chemically similar but were processed by extrusion or isostatic processing. The crack growth resistance and fracture toughness of the larger bodies were found to vary with processing method and test orientation. The results presented here demonstrate that differences in texture that contribute to variations in structural performance can be revealed by analytic ultrasonic techniques. Author

## STRUCTURAL MECHANICS

Includes structural element design and weight analysis; fatigue; and thermal stress.

**A89-11246\*** National Aeronautics and Space Administration. Lewis Research Center, Cleveland, OH.

**FIBER COMPOSITE SANDWICH THERMOSTRUCTURAL BEHAVIOR - COMPUTATIONAL SIMULATION**

CHRISTOS C. CHAMIS, ROBERT A. AIELLO (NASA, Lewis Research Center, Cleveland, OH), and POPPU L. N. MURTHY (NASA, Lewis Research Center, Cleveland; Cleveland State University, OH) *Journal of Composites Technology and Research* (ISSN 0885-6804), vol. 10, Fall 1988, p. 93-99. refs

Copyright

Four computational simulation methods with different levels of sophistication were used to simulate thermal behavior and structural changes of composite sandwich panels with a honeycomb core subjected to a variety of environmental effects. The models on which these methods are based include three-dimensional finite-element modeling, three-dimensional finite-element modeling assuming a homogeneous core, laminate theory, and simple equations for predicting the equivalent properties of the honeycomb core. A procedure was developed and embedded in a composite mechanics computer code, which made it possible to conduct parametric studies to determine 'optimum' composite sandwich configurations for specific applications. The procedure was applied for the evaluation of composite sandwich behavior at the global, local, laminate, ply, and micromechanics levels when the composite sandwich is subjected to hygral, thermal, and mechanical loading environments. I.S.

**A89-15734\*** National Aeronautics and Space Administration. Lewis Research Center, Cleveland, OH.

**A UNIQUE SET OF MICROMECHANICS EQUATIONS FOR HIGH-TEMPERATURE METAL MATRIX COMPOSITES**

DALE A. HOPKINS and CHRISTOS C. CHAMIS (NASA, Lewis Research Center, Cleveland, OH) IN: *Testing technology of metal matrix composites*. Philadelphia, PA, American Society for Testing Materials, 1988, p. 159-175; Discussion, p. 176. Previously announced in STAR as N86-24757. refs

Copyright

A unique set of micromechanics equations is presented for high-temperature metal matrix composites. The set includes expressions to predict mechanical properties, thermal properties and constituent microstresses for the unidirectional fiber reinforced ply. The equations are derived based on a mechanics of materials formulation assuming a square array unit cell model of a single fiber, surrounding matrix and an interphase to account for the chemical reaction which commonly occurs between fiber and matrix. A three-dimensional finite element analysis was used to perform a preliminary validation of the equations. Excellent agreement between properties predicted using the micromechanics equations and properties simulated by the finite element analyses are demonstrated. Implementation of the micromechanics equations as part of an integrated computational capability for nonlinear structural analysis of high temperature multilayered fiber composites is illustrated. Author

**A89-15735\*** National Aeronautics and Space Administration. Lewis Research Center, Cleveland, OH.

**THERMOVISCOPLASTIC NONLINEAR CONSTITUTIVE RELATIONSHIPS FOR STRUCTURAL ANALYSIS OF HIGH-TEMPERATURE METAL MATRIX COMPOSITES**

CHRISTOS C. CHAMIS and DALE A. HOPKINS (NASA, Lewis Research Center, Cleveland, OH) IN: *Testing technology of metal matrix composites*. Philadelphia, PA, American Society for Testing Materials, 1988, p. 177-196.

Copyright

A set of thermoviscoplastic nonlinear constitutive relationships (TVP-NCR) developed for application to high-temperature metal matrix composites (HT-MMC) is described. The structural response of a turbine blade, made from fiber-reinforced superalloy HT-MMC and subject to representative loading conditions, is evaluated. Results indicate that this set of TVP-NCR is computationally effective. K.K.

**A89-16278\*** Cleveland State Univ., OH.

**COMPOSITE INTERLAMINAR FRACTURE TOUGHNESS - THREE-DIMENSIONAL FINITE-ELEMENT MODELING FOR MIXED MODE I, II, AND FRACTURE**

PAPPU L. N. MURTHY (Cleveland State University, OH) and CHRISTOS C. CHAMIS (NASA, Lewis Research Center, Cleveland, OH) IN: *Composite materials: Testing and design*. Philadelphia, PA, American Society for Testing and Materials, 1988, p. 23-40. Previously announced in STAR as N87-13491.

Copyright

A computational method/procedure is described which can be used to simulate individual and mixed mode interlaminar fracture progression in fiber composite laminates. Different combinations of Modes 1, 2, and 3 fracture are simulated by varying the crack location through the specimen thickness and by selecting appropriate unsymmetric laminate configurations. The contribution of each fracture mode to strain energy release rate is determined by the local crack closure methods while the mixed mode is determined by global variables. The strain energy release rates are plotted versus extending crack length, where slow crack growth, stable crack growth, and rapid crack growth regions are easily identified. Graphical results are presented to illustrate the effectiveness and versatility of the computational simulation for: (1) evaluating mixed-mode interlaminar fracture, (2) for identifying respective dominant parameters, and (3) for selecting possible simple test methods. Author

**A89-16279\*** National Aeronautics and Space Administration. Lewis Research Center, Cleveland, OH.

**SUBLAMINATE- OR PLY-LEVEL ANALYSIS OF COMPOSITES AND STRAIN ENERGY RELEASE RATES OF END-NOTCH AND MIXED-MODE FRACTURE SPECIMENS**

RAO R. VALISETTY and CHRISTOS C. CHAMIS (NASA, Lewis Research Center, Cleveland, OH) IN: *Composite materials: Testing and design*. Philadelphia, PA, American Society for Testing and Materials, 1988, p. 41-56. refs

Copyright

The sublaminate or ply-level analysis of composite structures is presently undertaken by a computational procedure yielding the stresses in regions affected by delaminations, transverse cracks, and discontinuities that are related to material properties, geometries, and loads. Attention is given to layers or groups of layers that are immediately affected by flaws; these are analyzed as if they were homogeneous bodies in equilibrium, in isolation from the rest of the laminate. Computed stresses agree with those from a three-dimensional FEM analysis. O.C.

**A89-16939\*** Southwest Research Inst., San Antonio, TX.

**PROBABILISTIC STRUCTURAL ANALYSIS METHODS AND APPLICATIONS**

T. A. CRUSE, Y.-T. WU (Southwest Research Institute, San Antonio, TX), B. DIAS (Stanford University, CA), and K. R. RAJAGOPAL (Rockwell International Corp., Rocketdyne Div., Canoga Park, CA) (George Washington University and NASA, Symposium on Advances and Trends in Computational Structural Mechanics and Fluid Dynamics, Washington, DC, Oct. 17-19, 1988) *Computers and Structures* (ISSN 0045-7949), vol. 30, no. 1-2, 1988, p. 163-170. refs

(Contract NAS3-24389)

Copyright

An advanced algorithm for simulating the probabilistic distribution of structural responses due to statistical uncertainties in loads, geometry, material properties, and boundary conditions is reported. The method effectively combines an advanced algorithm for calculating probability levels for multivariate problems

(fast probability integration) together with a general-purpose finite-element code for stress, vibration, and buckling analysis. Application is made to a space propulsion system turbine blade for which the geometry and material properties are treated as random variables.

Author

**A89-17396\*** Southwest Research Inst., San Antonio, TX.  
**THE CONSTITUTIVE REPRESENTATION OF  
 HIGH-TEMPERATURE CREEP DAMAGE**

K. S. CHAN (Southwest Research Institute, San Antonio, TX) International Journal of Plasticity (ISSN 0749-6419), vol. 4, no. 4, 1988, p. 355-370. Research supported by Southwest Research Institute. refs  
 (Contract NAS3-23925)  
 Copyright

The elastic-viscoplastic constitutive equations of Bodner-Partom were applied to modeling creep damage in a high temperature Ni-alloy, B1900 + Hf. Both tertiary creep in bulk materials and creep crack growth in flawed materials were considered. In the latter case, the energy rate line integral was used for characterizing the crack driving force, and the rate of crack extension was computed using a local damage formulation that assumed fracture was controlled by cavitation occurring within the crack-tip process zone. The results of this investigation were used to assess the evolution equation for isotropic damage utilized in the Bodner-Partom constitutive equations.

Author

**A89-17432\*** National Aeronautics and Space Administration.  
 Lewis Research Center, Cleveland, OH.

**INFLUENCE OF FATIGUE CRACK WAKE LENGTH AND  
 STATE OF STRESS ON CRACK CLOSURE**

JACK TELESMA and DOUGLAS M. FISHER (NASA, Lewis Research Center, Cleveland, OH) IN: Mechanics of fatigue crack closure. Philadelphia, PA, American Society for Testing and Materials, 1988, p. 568-582. Previously announced in STAR as N86-22686. refs

Copyright

The location of crack closure with respect to crack wake and specimen thickness under different loading conditions was determined. The rate of increase of  $K_{sub CL}$  in the crack wake was found to be significantly higher for plasticity induced closure in comparison to roughness induced closure. Roughness induced closure was uniform throughout the thickness of the specimen while plasticity induced closure levels were 50 percent higher in the near surface region than in the midthickness. The influence of state of stress on low-high load interaction effects was also examined. Load interaction effects differed depending upon the state of stress and were explained in terms of  $\Delta K_{sub eff}$ .

Author

**A89-19914\*** Georgia Inst. of Tech., Atlanta.  
**SOLUTION METHODS FOR ONE-DIMENSIONAL  
 VISCOELASTIC PROBLEMS**

JOHN M. STUBSTAD and GEORGE J. SIMITSES (Georgia Institute of Technology, Atlanta) (Structures, Structural Dynamics and Materials Conference, 28th, Monterey, CA, Apr. 6-8, 1987, Technical Papers. Part 1, p. 458-465) AIAA Journal (ISSN 0001-1452), vol. 26, Sept. 1988, p. 1127-1134. Previously cited in issue 14, p. 2167, Accession no. A87-33604. refs  
 (Contract NAG3-534)  
 Copyright

**A89-21133\*** Lockheed Missiles and Space Co., Palo Alto, CA.  
**A 20-DOF HYBRID STRESS GENERAL SHELL ELEMENT**

DAVID S. KANG (Lockheed Research Laboratories, Palo Alto, CA) and THEODORE H. H. PIAN (MIT, Cambridge, MA) (Chinese Society of Theoretical and Applied Mechanics, International Conference on Computational Engineering Mechanics, Beijing, People's Republic of China, June 21-25, 1987) Computers and Structures (ISSN 0045-7949), vol. 30, no. 4, 1988, p. 789-794. refs

(Contract NAG3-33)

Copyright

A hybrid-stress general shell element is developed based on the Hellinger-Reissner principle modified for relaxed element compatibility conditions. The element is based on a thin-shell theory with Love-Kirchhoff hypothesis. It is of quadrilateral shape with only four corner nodes and five degrees of freedom per node. The geometry of the element is approximated through a cubic polynomial surface patch. Numerical examples consisting of torsion-loaded slit cylinder and pinched cylinders with open ends and rigid diaphragmed ends demonstrate excellent performance of the present element.

Author

**A89-25849\*#** Stanford Univ., CA.  
**AN APPROACH TO PROBABILISTIC FINITE ELEMENT  
 ANALYSIS USING A MIXED-ITERATIVE FORMULATION**

J. B. DIAS (Stanford University, CA) and S. NAKAZAWA (MARC Analysis Research Corp., Palo Alto, CA) IN: Computational probabilistic methods; Proceedings of the Joint ASME/SES Applied Mechanics and Engineering Sciences Conference, Berkeley, CA, June 20-22, 1988. New York, American Society of Mechanical Engineers, 1988, p. 75-86. refs  
 (Contract NAS3-24389)  
 Copyright

An efficient algorithm for computing the response sensitivity of finite element problems based on a mixed-iterative formulation is proposed. This method does not involve explicit differentiation of the tangent stiffness array and can be used with formulations for which a consistent tangent stiffness is not readily available. The method has been successfully applied to probabilistic finite element analysis of problems using the proposed mixed formulation, and this exercise has provided valuable insights regarding the extension of the method to a more general class of problems to include material and geometric nonlinearities.

Author

**A89-27744\*#** National Central Univ., Chung-Li (Taiwan).  
**TECHNIQUE FOR THE PREDICTION OF AIRFOIL FLUTTER  
 CHARACTERISTICS IN SEPARATED FLOW**

JIUNN-CHI WU (National Central University, Chung-Li, Republic of China), L. N. SANKAR (Georgia Institute of Technology, Atlanta), and K. R. V. KAZA (Structures, Structural Dynamics and Materials Conference, 28th, Monterey, CA, Apr. 6-8, 1987 and AIAA Dynamics Specialists Conference, Monterey, CA, Apr. 9, 10, 1987, Technical Papers. Part 2B, p. 664-673) Journal of Aircraft (ISSN 0021-8669), vol. 26, Feb. 1989, p. 168-177. Previously cited in issue 14, p. 2173, Accession no. A87-33719. refs  
 (Contract NAG3-730)  
 Copyright

**A89-28070\*** National Aeronautics and Space Administration.  
 Lewis Research Center, Cleveland, OH.

**A COMPUTATIONAL PROCEDURE FOR AUTOMATED  
 FLUTTER ANALYSIS**

DURBHA V. MURTHY (NASA, Lewis Research Center, Cleveland; Toledo, University, OH) and KRISHNA RAO V. KAZA (NASA, Lewis Research Center, Cleveland, OH) Communications in Applied Numerical Methods (ISSN 0748-8025), vol. 5, Jan. 1989, p. 29-37. refs

Copyright

A direct solution procedure for computing the flutter Mach number and the flutter frequency is applied to the aeroelastic analysis of propfans using a finite element structural model and an unsteady aerodynamic model based on a three-dimensional subsonic compressible lifting surface theory. An approximation to the Jacobian matrix that improves the efficiency of the iterative process is presented. The Jacobian matrix is indirectly approximated from approximate derivatives of the flutter matrix, which are updated only in the direction of the last move. Examples are used to illustrate the convergence properties. The direct solution procedure facilitates the automated flutter analysis in addition to contributing to the efficient use of computer time as well as the analyst's time.

Author

## **A89-29600\*** Case Western Reserve Univ., Cleveland, OH. **EXPOSURE TIME CONSIDERATIONS IN HIGH TEMPERATURE LOW CYCLE FATIGUE**

S. KALLURI, S. S. MANSON (Case Western Reserve University, Cleveland, OH), and G. R. HALFORD (NASA, Lewis Research Center, Cleveland, OH) IN: Mechanical behaviour of materials - V; Proceedings of the Fifth International Conference, Beijing, People's Republic of China, June 3-6, 1987. Volume 2. Oxford and New York, Pergamon Press, 1988, p. 1029-1036. Previously announced in STAR as N87-28944. refs  
(Contract NAG3-553; NAG3-337)  
Copyright

The Conventional Strainrange Partitioning (CSR) method for High-Temperature, Low-Cycle Fatigue (HTLCF) life prediction has its origins in the modeling of first-order, creep-fatigue waveform effects while treating as second-order effects, the influence of metallurgical or environmental time dependencies. Procedures are proposed to include the latter explicitly in the inelastic strainrange-life relations. For brevity, only the CP life relation will be presented in detail. The exposure-time effect within the CP inelastic strainrange (tensile creep reversed by compressive plasticity) was determined by tensile stresshold-time experiments for 316 SS at 816 C. Reductions in CP cyclic life of a factor of about two were observed with an increase in exposure time or a corresponding decrease in creep rate by a factor of about 100. The CP life relation has been modified to be expressed in terms of either Steady State Creep Rate (SSCR) or Exposure Time (ET). The applicability and accuracy of the time-dependent CP life relations is demonstrated by conducting verification experiments involving complex hysteresis loops. Metallographic examination revealed time-dependent degradation attributable to oxide formation and precipitation of carbides along grain boundaries. Author

## **A89-30666\*** National Aeronautics and Space Administration. Lewis Research Center, Cleveland, OH. **FINITE ELEMENT APPLICATIONS TO EXPLORE THE EFFECTS OF PARTIAL BONDING ON METAL MATRIX COMPOSITE PROPERTIES**

J. J. CARUSO, C. C. CHAMIS (NASA, Lewis Research Center, Cleveland, OH), and D. TROWBRIDGE (Akron, University, OH) IN: AIAA, ASME, ASCE, AHS, and ASC, Structures, Structural Dynamics and Materials Conference, 30th, Mobile, AL, Apr. 3-5, 1989, Technical Papers. Part 1. Washington, DC, American Institute of Aeronautics and Astronautics, 1989, p. 140-154.  
(AIAA PAPER 89-1175) Copyright

The mechanics of materials approach (definition of E, G, nu, and alpha) and the finite element method are used to explore the effects of partial bonding and fiber fracture on the behavior of high temperature metal matrix composites. Composite ply properties are calculated for various degrees of debonding to evaluate the sensitivity of these properties to the presence of fiber/matrix debonding and fiber fracture. The mechanics of materials approach allows for the determination of the basic ply material properties needed for design/analysis of composites. The finite element method provides the necessary structural response (forces and displacements) for the mechanics of materials equations. Results show that debonding of fractured fibers affect only E-(11) and alpha-(11) significantly. Author

## **A89-30681\*** National Aeronautics and Space Administration. Lewis Research Center, Cleveland, OH. **MECHANICS OF DAMPING FOR FIBER COMPOSITE LAMINATES INCLUDING HYGRO-THERMAL EFFECTS**

D. A. SARAVANOS and C. C. CHAMIS (NASA, Lewis Research Center, Cleveland, OH) IN: AIAA, ASME, ASCE, AHS, and ASC, Structures, Structural Dynamics and Materials Conference, 30th, Mobile, AL, Apr. 3-5, 1989, Technical Papers. Part 1. Washington, DC, American Institute of Aeronautics and Astronautics, 1989, p. 296-303. refs  
(AIAA PAPER 89-1191) Copyright

An integrated mechanics theory has been developed for the modeling of composite damping from the micromechanics to the laminate level. Simplified, design oriented equations based on

hysteretic damping are presented for on-axis plies, off-axis plies, and laminates including the effect of temperature, moisture, and interply hysteretic damping. The temperature rise within vibrating composite laminates resulting from strain energy dissipation is also modeled, and their coupled hygro-thermo-mechanical response is predicted. The method correlates well with reported damping measurements. Application examples illustrate the effect of various ply, laminate, and hygro-thermal parameters on the overall damping performance of composite laminates. Author

## **A89-30754\*** Clarkson Univ., Potsdam, NY. **STRUCTURAL BEHAVIOR OF COMPOSITES WITH PROGRESSIVE FRACTURE**

L. MINNETYAN (Clarkson University, Potsdam, NY), P. L. N. MURTHY (Cleveland State University, OH), and C. C. CHAMIS (NASA, Lewis Research Center, Cleveland, OH) IN: AIAA, ASME, ASCE, AHS, and ASC, Structures, Structural Dynamics and Materials Conference, 30th, Mobile, AL, Apr. 3-5, 1989, Technical Papers. Part 2. Washington, DC, American Institute of Aeronautics and Astronautics, 1989, p. 968-978. refs  
(AIAA PAPER 89-1271) Copyright

The objective of the study is to unify several computational tools developed for the prediction of progressive damage and fracture with efforts for the prediction of the overall response of damaged composite structures. In particular, a computational finite element model for the damaged structure is developed using a computer program as a byproduct of the analysis of progressive damage and fracture. Thus, a single computational investigation can predict progressive fracture and the resulting variation in structural properties of angleplied composites. V.L.

## **A89-30842\*** National Aeronautics and Space Administration. Lewis Research Center, Cleveland, OH. **STRUCTURAL TAILORING OF LAMINATE PROPERTIES**

P. B. THANEDAR and C. C. CHAMIS (NASA, Lewis Research Center, Cleveland, OH) IN: AIAA, ASME, ASCE, AHS, and ASC, Structures, Structural Dynamics and Materials Conference, 30th, Mobile, AL, Apr. 3-5, 1989, Technical Papers. Part 4. Washington, DC, American Institute of Aeronautics and Astronautics, 1989, p. 1828-1831. refs  
(AIAA PAPER 89-1367)

In this study, structural synthesis techniques have been applied to tailor the composite laminate properties from the micromechanics to the laminate level for a desirable structural response. It is also demonstrated how to establish upper and lower bounds on design variables based on reliability considerations. The question of reliability arises in fiber composite analysis and design because of the inherent scatter that is observed in the constituent material properties in the experimental data. The symmetric composite laminates subject to mechanical loading are considered and no hygrothermal effects are taken into account in the present research. Application examples illustrate the effects of various ply and laminate parameters on the overall properties and structural response of composite laminates. Author

## **A89-30843\*** Texas Univ., San Antonio. **PROBABILISTIC CONSTITUTIVE RELATIONSHIPS FOR MATERIAL STRENGTH DEGRADATION MODELS**

L. BOYCE (Texas, University, San Antonio) and C. C. CHAMIS (NASA, Lewis Research Center, Cleveland, OH) IN: AIAA, ASME, ASCE, AHS, and ASC, Structures, Structural Dynamics and Materials Conference, 30th, Mobile, AL, Apr. 3-5, 1989, Technical Papers. Part 4. Washington, DC, American Institute of Aeronautics and Astronautics, 1989, p. 1832-1839. Research supported by the Case Institute of Computational Mechanics in Propulsion. refs  
(AIAA PAPER 89-1368) Copyright

In the present probabilistic methodology for the strength of aerospace propulsion system structural components subjected to such environmentally-induced primitive variables as loading stresses, high temperature, chemical corrosion, and radiation, time is encompassed as an interacting element, allowing the projection of creep and fatigue effects. A probabilistic constitutive equation is postulated to account for the degradation of strength due to



these primitive variables which may be calibrated by an appropriately curve-fitted least-squares multiple regression of experimental data. The resulting probabilistic constitutive equation is embodied in the PROMISS code for aerospace propulsion component random strength determination. O.C.

**A89-30844\*# Southwest Research Inst., San Antonio, TX.  
AN APPROXIMATE METHODS APPROACH TO  
PROBABILISTIC STRUCTURAL ANALYSIS**

R. C. MCCLUNG, H. R. MILLWATER, Y.-T. WU, B. H. THACKER, and O. H. BURNSIDE (Southwest Research Institute, San Antonio, TX) IN: AIAA, ASME, ASCE, AHS, and ASC, Structures, Structural Dynamics and Materials Conference, 30th, Mobile, AL, Apr. 3-5, 1989, Technical Papers. Part 4. Washington, DC, American Institute of Aeronautics and Astronautics, 1989, p. 1840-1845. refs (Contract NAS3-24389) Copyright (AIAA PAPER 89-1369)

A probabilistic structural analysis method (PSAM) is described which makes an approximate calculation of the structural response of a system, including the associated probabilistic distributions, with minimal computation time and cost, based on a simplified representation of the geometry, loads, and material. The method employs the fast probability integration (FPI) algorithm of Wu and Wirsching. Typical solution strategies are illustrated by formulations for a representative critical component chosen from the Space Shuttle Main Engine (SSME) as part of a major NASA-sponsored program on PSAM. Typical results are presented to demonstrate the role of the methodology in engineering design and analysis. Author

**A89-30846\*# Southwest Research Inst., San Antonio, TX.  
AN ADVANCED PROBABILISTIC STRUCTURAL ANALYSIS  
METHOD FOR IMPLICIT PERFORMANCE FUNCTIONS**

Y.-T. WU, H. R. MILLWATER, and T. A. CRUSE (Southwest Research Institute, San Antonio, TX) IN: AIAA, ASME, ASCE, AHS, and ASC, Structures, Structural Dynamics and Materials Conference, 30th, Mobile, AL, Apr. 3-5, 1989, Technical Papers. Part 4. Washington, DC, American Institute of Aeronautics and Astronautics, 1989, p. 1852-1859. refs (Contract NAS3-24389) Copyright (AIAA PAPER 89-1371)

In probabilistic structural analysis, the performance or response functions usually are implicitly defined and must be solved by numerical analysis methods such as finite element methods. In such cases, the most commonly used probabilistic analysis tool is the mean-based, second-moment method which provides only the first two statistical moments. This paper presents a generalized advanced mean value (AMV) method which is capable of establishing the distributions to provide additional information for reliability design. The method requires slightly more computations than the second-moment method but is highly efficient relative to the other alternative methods. In particular, the examples show that the AMV method can be used to solve problems involving non-monotonic functions that result in truncated distributions. Author

**A89-34849\* National Aeronautics and Space Administration.  
Lewis Research Center, Cleveland, OH.  
WEIBULL CRACK DENSITY COEFFICIENT FOR  
POLYDIMENSIONAL STRESS STATES**

BERNARD GROSS and JOHN P. GYEKENYESI (NASA, Lewis Research Center, Cleveland, OH) American Ceramic Society, Communications (ISSN 0002-7820), vol. 72, March 1989, p. 506, 507. refs Copyright

A structural ceramic analysis and reliability evaluation code has recently been developed encompassing volume and surface flaw induced fracture, modeled by the two-parameter Weibull probability density function. A segment of the software involves computing the Weibull polydimensional stress state crack density coefficient from uniaxial stress experimental fracture data. The relationship of the polydimensional stress coefficient to the uniaxial

stress coefficient is derived for a shear-insensitive material with a random surface flaw population. Author

**A89-36177\*# Case Western Reserve Univ., Cleveland, OH.  
IDENTIFICATION OF STRUCTURAL INTERFACE  
CHARACTERISTICS USING COMPONENT MODE SYNTHESIS**

A. A. HUCKELBRIDGE (Case Western Reserve University, Cleveland, OH) and C. LAWRENCE (NASA, Lewis Research Center, Cleveland, OH) ASME, Transactions, Journal of Vibration, Acoustics, Stress, and Reliability in Design (ISSN 0739-3717), vol. 111, April 1989, p. 140-147. Previously announced in STAR as N87-24006. refs Copyright

The inability to adequately model connections has limited the ability to predict overall system dynamic response. Connections between structural components are often mechanically complex and difficult to accurately model analytically. Improved analytical models for connections are needed to improve system dynamic predictions. This study explores combining Component Mode synthesis methods for coupling structural components with Parameter Identification procedures for improving the analytical modeling of the connections. Improvements in the connection properties are computed in terms of physical parameters so the physical characteristics of the connections can be better understood, in addition to providing improved input for the system model. Two sample problems, one utilizing simulated data, the other using experimental data from a rotor dynamic test rig, are presented. Author

**A89-36185\*# National Aeronautics and Space Administration.  
Lewis Research Center, Cleveland, OH.**

**CREEP LIFE PREDICTION BASED ON STOCHASTIC MODEL  
OF MICROSTRUCTURALLY SHORT CRACK GROWTH**

TAKAYUKI KITAMURA (NASA, Lewis Research Center, Cleveland, OH) and RYUICHI OHTANI (Kyoto University, Japan) ASME, Transactions, Journal of Engineering Materials and Technology (ISSN 0094-4289), vol. 111, April 1989, p. 169-175. Previously announced in STAR as N88-12825. refs Copyright

A nondimensional model of microstructurally short crack growth in creep is developed based on a detailed observation of the creep fracture process of 304 stainless steel. In order to deal with the scatter of small crack growth rate data caused by microstructural inhomogeneity, a random variable technique is used in the model. A cumulative probability of the crack length at an arbitrary time,  $G(\bar{a}, \bar{t})$ , and that of the time when a crack reaches an arbitrary length,  $F(\bar{t}, \bar{a})$ , are obtained numerically by means of a Monte Carlo method.  $G(\bar{a}, \bar{t})$ , and  $F(\bar{t}, \bar{a})$  are the probabilities for a single crack. However, multiple cracks generally initiate on the surface of a smooth specimen from the early stage of creep life to the final stage. Taking into account the multiple crack initiations, the actual crack length distribution observed on the surface of a specimen is predicted by the combination of probabilities for a single crack. The prediction shows a fairly good agreement with the experimental result for creep of 304 stainless steel at 923 K. The probability of creep life is obtained from an assumption that creep fracture takes place when the longest crack reaches a critical length. The observed and predicted scatter of the life is fairly small for the specimens tested. Author

**A89-36294\* Cleveland State Univ., OH.  
FREE-EDGE DELAMINATION - LAMINATE WIDTH AND  
LOADING CONDITIONS EFFECTS**

PAPPU L. N. MURTHY (Cleveland State University, OH) and CHRISTOS C. CHAMIS (NASA, Lewis Research Center, Cleveland, OH) Journal of Composites Technology and Research (ISSN 0885-6804), vol. 11, Spring 1989, p. 15-22. Previously announced in STAR as N88-12551. refs Copyright

The width and loading conditions effects on free-edge stress fields in composite laminates are investigated using a three-dimensional finite element analysis. This analysis includes a

## 39 STRUCTURAL MECHANICS

special free-edge region refinement or superelement with progressive substructuring (mesh refinement) and finite thickness interply layers. The different loading conditions include in-plane and out-of-plane bending, combined axial tension and in-plane shear, twisting, uniform temperature and uniform moisture. Results obtained indicate that: axial tension causes the smallest magnitude of interlaminar free edge stress compared to other loading conditions; free-edge delamination data obtained from laboratory specimens cannot be scaled to structural components; and composite structural components are not likely to delaminate.

Author

**A89-36920\*** Sverdrup Technology, Inc., Middleburg Heights, OH.

### **PROBABILISTIC STRUCTURAL ANALYSIS TO QUANTIFY UNCERTAINTIES ASSOCIATED WITH TURBOPUMP BLADES**

VINOD K. NAGPAL, ROBERT RUBINSTEIN (Sverdrup Technology, Inc., Middleburg Heights, OH), and CHRISTOS C. CHAMIS (NASA, Lewis Research Center, Cleveland, OH) (Structures, Structural Dynamics and Materials Conference, 28th, Monterey, CA, Apr. 6-8, 1987, Technical Papers. Part 1, p. 268-274) AIAA Journal (ISSN 0001-1452), vol. 27, June 1989, p. 809-813. Previously cited in issue 14, p. 2166, Accession no. A87-33581. refs  
Copyright

**A89-42339\*** Cincinnati Univ., OH.

### **FINITE-ELEMENT GRID IMPROVEMENT BY MINIMIZATION OF STIFFNESS MATRIX TRACE**

MADAN G. KITTUR, RONALD L. HUSTON (Cincinnati, University, OH), and FRED B. OSWALD (NASA, Lewis Research Center, Cleveland, OH) Computers and Structures (ISSN 0045-7949), vol. 31, no. 6, 1989, p. 891-896. Previously announced in STAR as N88-13604. refs  
Copyright

A new and simple method of finite-element grid improvement is presented. The objective is to improve the accuracy of the analysis. The procedure is based on a minimization of the trace of the stiffness matrix. For a broad class of problems this minimization is seen to be equivalent to minimizing the potential energy. The method is illustrated with the classical tapered bar problem examined earlier by Prager and Masur. Identical results are obtained.

Author

**A89-42984\*** Illinois Univ., Chicago.

### **DAMAGE ANALYSIS OF A CRACK LAYER**

J. BOTSIS (Illinois, University, Chicago) Journal of Materials Science (ISSN 0022-2461), vol. 24, June 1989, p. 2018-2024. refs  
(Contract NAG3-754)  
Copyright

Damage analysis of a crack layer in polystyrene is carried out by employing optical microscopy and principles of quantitative stereology. The results show that, within the quasistatic phase of crack layer propagation, the average crazing density, along the trailing edge of the active zone, is constant. This is consistent with a self-similarity hypothesis of damage evolution employed by the crack layer theory. The average crazing densities within the active zone and along its trailing edge are found to be practically equal. A layer of constant crazing density, adjacent to the crack planes, accompanies the crack during its quasi-static growth. This suggests that: (1) a certain level of crazing density should be reached, around the crack tip, prior to crack advance; (2) the specific energy, associated with this 'core' of damage, could be considered as a Griffith's type energy. The results are in favor of certain hypothesis adopted by the crack layer theory.

Author

**A89-43527\*** Connecticut Univ., Storrs.

### **BIAXIAL THERMO-MECHANICAL FATIGUE**

ERIC H. JORDAN (Connecticut, University, Storrs) IN: Annual Hostile Environments and High Temperature Measurements Conference, 4th, Windsor Locks, CT, Mar. 24, 25, 1987, Proceedings. Bethel, CT, Society for Experimental Mechanics, Inc.,

1987, p. 1-6.

(Contract NAG3-512)

Copyright

Stress-strain and durability information is often desirable for situations in which strain and temperature are changing simultaneously. To obtain such information, strain controlled uniaxial push-pull tests have typically been done. In order to control the mechanical strain, it is necessary in such tests to compute the mechanical strain from the total measured strain using measured temperature and the thermal expansion properties of the specimen. A system for conducting torsional thermomechanical tests is described which has the great advantage that the torsional strain is unaffected by the changing temperature and thus real time computations of quantities is not required for control of the test and the mechanical strain need not be determined from the subtraction of two measured quantities as is the case in the uniaxial test. In addition to describing torsional thermomechanical tests, guidelines for software to be used in running biaxial thermomechanical tests will also be presented.

Author

**A89-43528\*** National Aeronautics and Space Administration. Lewis Research Center, Cleveland, OH.

### **THE NASA LEWIS RESEARCH CENTER HIGH TEMPERATURE FATIGUE AND STRUCTURES LABORATORY**

M. A. MCGAW and P. A. BARTOLOTTA (NASA, Lewis Research Center, Cleveland, OH) IN: Annual Hostile Environments and High Temperature Measurements Conference, 4th, Windsor Locks, CT, Mar. 24, 25, 1987, Proceedings. Bethel, CT, Society for Experimental Mechanics, Inc., 1987, p. 12-29.  
Copyright

The physical organization of the NASA Lewis Research Center High Temperature Fatigue and Structures Laboratory is described. Particular attention is given to uniaxial test systems, high cycle/low cycle testing systems, axial torsional test systems, computer system capabilities, and a laboratory addition. The proposed addition will double the floor area of the present laboratory and will be equipped with its own control room.

K.K.

**A89-47025\*** Toledo Univ., OH.

### **AEROELASTIC ANALYSIS OF PROP FAN BLADES WITH A SEMIEMPIRICAL DYNAMIC STALL MODEL**

T. S. R. REDDY (Toledo, University, OH) and ORAL MEHMED (NASA, Lewis Research Center, Cleveland, OH) AIAA, ASME, SAE, and ASEE, Joint Propulsion Conference, 25th, Monterey, CA, July 10-13, 1989, 20 p. refs  
(AIAA PAPER 89-2695)

The time-history response of a propfan wind-tunnel model with dynamic stall was studied analytically. The response obtained from the analysis was compared with available experimental data. The governing equations of motion were formulated in terms of blade normal modes calculated using the COSMIC-NASTRAN computer code. The response analysis considered the blade plunging and pitching motions. The lift, drag, and moment coefficients for angles of attack below the static stall angle were obtained from a quasi-steady theory. For angles above static stall angles, a semiempirical dynamic stall model based on a correction to the angle of attack was used to obtain lift, drag, and moment coefficients. Using these coefficients, the aerodynamic forces were calculated at a selected number of strips, and integrated to obtain the total generalized forces. The combined momentum-blade element theory was used to calculate the induced velocity. The semiempirical stall model predicted a limit cycle oscillation near the setting angle at which large vibratory stresses were observed in an experiment. The predicted mode and frequency of oscillation also agreed with those measured in the experiment near this setting angle. The results also correlated well with the other published data that used a semiempirical dynamic stall model based on a synthesized procedure.

Author

**A89-47370\*** Georgia Inst. of Tech., Atlanta.

### **NONISOTHERMAL ELASTOVISCOPLASTIC SNAP-THROUGH AND CREEP BUCKLING OF SHALLOW ARCHES**

R. RIFF (Georgia Institute of Technology, Atlanta) (Structures,

Structural Dynamics and Materials Conference, 28th, Monterey, CA, Apr. 6-8, 1987, Technical Papers. Part 1, p. 466-472) AIAA Journal (ISSN 0001-1452), vol. 27, Aug. 1989, p. 1110-1115. Previously cited in issue 14, p. 2167, Accession no. A87-33605. refs  
(Contract NAG3-534)  
Copyright

**A89-47705\*#** Connecticut Univ., Storrs.  
**FRACTURE MECHANICS APPLIED TO ELEVATED TEMPERATURE CRACK GROWTH**

E. H. JORDAN (Connecticut, University, Storrs; United Technologies Corp., Pratt and Whitney Aircraft Group, East Hartford) and G. J. MEYERS (MOOG, Inc., East Aurora, NY) ASME, Transactions, Journal of Engineering Materials and Technology (ISSN 0094-4289), vol. 111, July 1989, p. 306-313. refs  
(Contract NAS3-22550)  
Copyright

Twenty-six isothermal crack growth tests were performed on Hastelloy-X tubular specimens at a variety of temperatures and strain ranges. Conditions were selected to include nominally elastic and nominally plastic conditions. A number of parameters including the stress intensity factor, strain intensity factor, J-integral, Crack Opening Displacement, and Tompkins model were examined for their ability to correlate the data. Test conditions were selected such that growth rates at a single value of the parameter were obtained at radially different crack lengths, thus exploring the geometry independence of the correlating parameter. None of the parameters were fully satisfactory. However, COD calculated from J-integral appeared to be the most successful. Author

**A89-48663\*#** National Aeronautics and Space Administration. Lewis Research Center, Cleveland, OH.

**ANALYTICAL FLUTTER INVESTIGATION OF A COMPOSITE PROPPAN MODEL**

K. R. V. KAZA, O. MEHMED (NASA, Lewis Research Center, Cleveland, OH), G. V. NARAYANAN (Sverdrup Technology, Inc., Cleveland, OH), and D. V. MURTHY (Toledo, University, OH) (Structures, Structural Dynamics and Materials Conference, 28th, Monterey, CA, Apr. 6-8, 1987 and AIAA Dynamics Specialists Conference, Monterey, CA, Apr. 9, 10, 1987, Technical Papers. Part 2A, p. 84-97) Journal of Aircraft (ISSN 0021-8669), vol. 26, Aug. 1989, p. 772-780. Previously cited in issue 17, p. 2695, Accession no. A87-40497. refs  
Copyright

**A89-48674\*** National Aeronautics and Space Administration. Lewis Research Center, Cleveland, OH.

**DESIGN PROCEDURES FOR FIBER COMPOSITE BOX BEAMS**  
CRISTOS C. CHAMIS (NASA, Lewis Research Center, Cleveland, OH) and PAPPU L. N. MURTHY (Cleveland State University, OH) Journal of Reinforced Plastics and Composites (ISSN 0731-6844), vol. 8, July 1989, p. 370-397.  
Copyright

Step-by-step procedures are described which can be used for the preliminary design of fiber composite box beams subjected to combined loadings. These procedures include a collection of approximate closed-form equations so that all the required calculations can be performed using pocket calculators. Included is an illustrative example of a tapered cantilever box beam subjected to combined loads. The box beam is designed to satisfy strength, displacement, buckling, and frequency requirements. Author

**N89-12876\*#** National Aeronautics and Space Administration. Lewis Research Center, Cleveland, OH.

**TURBINE ENGINE HOT SECTION TECHNOLOGY 1986**  
Oct. 1986 488 p Workshop held in Cleveland, Ohio, 21-22 Oct. 1986  
(NASA-CP-2444; E-3205; NAS 1.55:2444) Avail: NTIS HC A21/MF A01 CSCL 20/11

The Turbine Engine Hot Section Technology (HOST) Project of the NASA Lewis Research Center sponsored a workshop to

discuss current research pertinent to turbine engine durability problems. Presentations were made concerning the hot section environment and the behavior of combustion liners, turbine blades, and turbine vanes. The presentations were divided into six sessions: Instrumentation, Combustion, Turbine Heat Transfer, Structural Analysis, Fatigue and Fracture, and Surface Protection. Topics discussed included modeling of thermal and fluid-flow phenomena, structural analysis, fatigue and fracture, surface protective coatings, constitutive behavior of materials, stress-strain response, and life-prediction methods. Researchers from industry, academia, and government presented results of their work sponsored by the HOST project.

**N89-12881\*#** National Aeronautics and Space Administration. Lewis Research Center, Cleveland, OH.

**HOST STRUCTURAL ANALYSIS PROGRAM OVERVIEW**

ROBERT L. THOMPSON *In its* Turbine Engine Hot Section Technology 1986 p 19-31 Oct. 1986  
Avail: NTIS HC A21/MF A01 CSCL 20/11

Hot-section components of aircraft gas turbine engines are subjected to severe thermal structural loading conditions, especially during the startup and takeoff portions of the engine cycle. The most severe and damaging stresses and strains are those induced by the steep thermal gradients induced during the startup transient. These transient stresses and strains are also the most difficult to predict, in part because the temperature gradients and distributions are not well known or readily predictable and, in part, because the cyclic elastic-viscoplastic behavior of the materials at these extremes of temperature and strain are not well known or readily predictable. A broad spectrum of structures related technology programs is underway to address these deficiencies at the basic as well as the applied level. The three key program elements in the HOST structural analysis program are computations, constitutive modeling, and experiments for each research activity. Also shown are tables summarizing each of the activities. E.R.

**N89-12882\*#** National Aeronautics and Space Administration. Lewis Research Center, Cleveland, OH.

**FATIGUE AND FRACTURE OVERVIEW**

GARY R. HALFORD *In its* Turbine Engine Hot Section Technology 1986 p 33-43 Oct. 1986  
Avail: NTIS HC A21/MF A01 CSCL 20/11

The accomplishments achieved under the isotropic creep-fatigue crack initiation life prediction program are summarized. A sizeable creep-fatigue crack initiation data base was generated on the nickel-base superalloy, B-1900. Companion constitutive modeling programs have also generated extensive data bases on the same heat of material. The crack initiation results have formed the basis of a new approach to creep-fatigue life prediction. The term Cyclic Damage Accumulation (CDA) was coined for the method, which was evaluated under isothermal, uniaxial conditions. Stringent laboratory verification experiments were used to test the accuracy of the method. Considering the quite limited material property data needed to evaluate the constants in the approach, the prediction accuracy is acceptable. At the expense of the larger data base required, Lewis developed total strain-strainrange partitioning method (TS-SRP) is capable of a higher degree of accuracy. E.R.

**N89-12904\*#** Southwest Research Inst., San Antonio, TX.

**CONSTITUTIVE MODELING FOR ISOTROPIC MATERIALS**

ULRIC S. LINDHOLM and KWAI S. CHAN *In* NASA, Lewis Research Center, Turbine Engine Hot Section Technology 1986 p 243-253 Oct. 1986  
(Contract NAS3-23925)

Avail: NTIS HC A21/MF A01 CSCL 20/11

The objective of the program is to evaluate and develop existing constitutive models for use in finite-element structural analysis of turbine engine hot section components. The class of constitutive equation studied is considered unified in that all inelastic deformation including plasticity, creep, and stress relaxation are treated in a single term rather than a classical separation of plasticity (time independent) and creep (time dependent) behavior.

The unified theories employed also do not utilize the classical yield surface or plastic potential concept. The models are constructed from an appropriate flow law, a scalar kinetic relation between strain rate, temperature and stress, and evolutionary equations for internal variables describing strain or work hardening, both isotropic and directional (kinematic). This and other studies have shown that the unified approach is particularly suited for determining the cyclic behavior of superalloy type blade and vane materials and is entirely compatible with three-dimensional inelastic finite-element formulations. The behavior was examined of a second nickel-base alloy, MAR-M247, and compared it with the Bodner-Partom model, further examined procedures for determining the material-specific constants in the models, and exercised the MARC code for a turbine blade under simulated flight spectrum loading. Results are summarized. Author

**N89-12906\*#** General Electric Co., Fairfield, CT.  
**ON 3D INELASTIC ANALYSIS METHODS FOR HOT SECTION COMPONENTS**

R. L. MCKNIGHT, P. C. CHEN, L. T. DAME, R. V. HOLT, H. HUANG, M. HARTLE, S. GELLIN, D. H. ALLEN, and W. E. HAISLER /in NASA, Lewis Research Center, Turbine Engine Hot Section Technology 1986 p 257-268 Oct. 1986  
 (Contract NAS3-23698)

Avail: NTIS HC A21/MF A01 CSCL 20/11

Accomplishments are described for the 2-year program, to develop advanced 3-D inelastic structural stress analysis methods and solution strategies for more accurate and cost effective analysis of combustors, turbine blades and vanes. The approach was to develop a matrix of formulation elements and constitutive models. Three constitutive models were developed in conjunction with optimized iterating techniques, accelerators, and convergence criteria within a framework of dynamic time incrementing. Three formulations models were developed; an eight-noded mid-surface shell element, a nine-noded mid-surface shell element and a twenty-noded isoparametric solid element. A separate computer program was developed for each combination of constitutive model-formulation model. Each program provides a functional stand alone capability for performing cyclic nonlinear structural analysis. In addition, the analysis capabilities incorporated into each program can be abstracted in subroutine form for incorporation into other codes or to form new combinations. Author

**N89-12908\*#** Akron Univ., OH.  
**A MULTIAXIAL THEORY OF VISCOPLASTICITY FOR ISOTROPIC MATERIALS**

D. N. ROBINSON and J. R. ELLIS /in NASA, Lewis Research Center, Turbine Engine Hot Section Technology 1986 p 283-291 Oct. 1986  
 (Contract NAG3-379)

Avail: NTIS HC A21/MF A01 CSCL 20/11

Many viscoplastic constitutive models for high temperature structural alloys are based exclusively on uniaxial test data. Generalization to multiaxial states of stress is made by assuming the stress dependence to be on the second principal invariant ( $J_2$ ) of the deviatoric stress, frequently called the effective stress. If such a  $J_2$  theory, based on uniaxial testing, is called upon to predict behavior under conditions other than uniaxial, e.g., pure shear, and it does so poorly, nothing is left to adjust in the theory. For a fully isotropic material whose inelastic deformation behavior is relatively independent of hydrostatic stress, the most general stress dependence is on the two (non-zero) principal invariants of the deviatoric stress,  $J_2$  and  $J_3$ . These invariants constitute what is known as an integrity basis for the material. A time dependent constitutive theory with stress dependence on  $J_2$  and  $J_3$  is presented, that reduces to a known  $J_2$  theory as a special case. Author

**N89-12909\*#** National Aeronautics and Space Administration, Lewis Research Center, Cleveland, OH.  
**THERMOMECHANICAL CHARACTERIZATION OF HASTELLOY-X UNDER UNIAXIAL CYCLIC LOADING**  
 J. R. ELLIS, P. A. BARTOLOTTA, G. P. ALLEN, and D. N.

ROBINSON (Akron Univ., Ohio.) /in its Turbine Engine Hot Section Technology 1986 p 293-305 Oct. 1986  
 Avail: NTIS HC A21/MF A01 CSCL 20/11

In most high-temperature engineering applications, components are subjected to complex combinations of thermal and mechanical loading during service. A number of viscoplastic constitutive models were proposed which potentially can provide mathematical descriptions of material response under such conditions. Implementation of these models into large finite element codes such as MARC has already resulted in much improved inelastic analysis capability for hot-section aircraft engine components. However, a number of questions remain regarding the validity of methods adopted in characterizing these constitutive models for particular high-temperature materials. One area of concern is that the majority of experimental data available for this purpose are determined under isothermal conditions. This is in contrast to service conditions which, as noted above, almost always involve some form of thermal cycling. The obvious question arises as to whether a constitutive model characterized using an isothermal data base can adequately predict material response under thermomechanical conditions. An experimental program was initiated within the HOST program to address this particular concern. The results of the most recent isothermal and thermomechanical experiments are described. Author

**N89-12913\*#** National Aeronautics and Space Administration, Lewis Research Center, Cleveland, OH.

**HIGH TEMPERATURE STRESS-STRAIN ANALYSIS**

ROBERT L. THOMPSON and PAUL E. MOORHEAD /in its Turbine Engine Hot Section Technology 1986 p 341-357 Oct. 1986  
 Avail: NTIS HC A21/MF A01 CSCL 20/11

The objectives of the high-temperature structures program are threefold: to assist in the development of analytical tools needed to improve design analyses and procedures for the efficient and accurate prediction of the nonlinear structural response of hot-section components; to aid in the calibration, validation, and evaluation of the analytical tools by comparing predictions with experimental data; and to evaluate existing as well as advanced temperature and strain measurement instrumentation. As the analytical tools, test methods, tests, instrumentations, as well as data acquisition, management, and analysis methods are developed and evaluated, a proven, integrated analysis and experiment method will result in a more accurate prediction of the cyclic life of hot section components. Author

**N89-12915\*#** General Electric Co., Fairfield, CT.  
**ELEVATED TEMPERATURE CRACK GROWTH**

S. N. MALIK, R. H. VANSTONE, K. S. KIM, and J. H. LAFFEN /in NASA, Lewis Research Center, Turbine Engine Hot Section Technology 1986 p 371-383 Oct. 1986  
 (Contract NAS3-23940)

Avail: NTIS HC A21/MF A01 CSCL 20/11

It is necessary to relate the processes that control crack growth in the immediate vicinity of the crack tip to parameters that can be calculated from remote quantities, such as forces, stresses, or displacements. The most likely parameters appear to be certain path-independent (PI) integrals, several of which have already been proposed for application to high temperature inelastic problems. The ability of currently available PI-integrals to correlate fatigue crack propagation under conditions that simulate the engine combustor liner environment was determined. The utility of advanced fracture mechanics measurements will also be evaluated and determined during the course of the program. E.R.

**N89-12930\*#** National Aeronautics and Space Administration, Lewis Research Center, Cleveland, OH.

**CALCULATION OF WEIBULL STRENGTH PARAMETERS AND BATDORF FLOW-DENSITY CONSTANTS FOR VOLUME- AND SURFACE-FLAW-INDUCED FRACTURE IN CERAMICS**

SHANTARAM S. PAI and JOHN P. GYKENYESI Oct. 1988  
 32 p Presented at the 3rd International Symposium on Ceramic Materials and Components for Engines, Las Vegas, Nev., 27-30

Nov. 1988; sponsored in part by the American Ceramic Society (NASA-TM-100890; E-4128; NAS 1.15:100890) Avail: NTIS HC A03/MF A01 CSCL 20/11

The calculation of shape and scale parameters of the two-parameter Weibull distribution is described using the least-squares analysis and maximum likelihood methods for volume- and surface-flaw-induced fracture in ceramics with complete and censored samples. Detailed procedures are given for evaluating 90 percent confidence intervals for maximum likelihood estimates of shape and scale parameters, the unbiased estimates of the shape parameters, and the Weibull mean values and corresponding standard deviations. Furthermore, the necessary steps are described for detecting outliers and for calculating the Kolmogorov-Smirnov and the Anderson-Darling goodness-of-fit statistics and 90 percent confidence bands about the Weibull distribution. It also shows how to calculate the Batdorf flaw-density constants by using the Weibull distribution statistical parameters. The techniques described were verified with several example problems, from the open literature, and were coded. The techniques described were verified with several example problems from the open literature, and were coded in the Structural Ceramics Analysis and Reliability Evaluation (SCARE) design program. Author

**N89-12931\*** # Georgia Inst. of Tech., Atlanta. Dept. of Aerospace Engineering.

**NON-ISOTHERMAL BUCKLING BEHAVIOR OF VISCOPLASTIC SHELL STRUCTURES**

RICHARD RIFF and G. J. SIMITSES 1988 6 p

(Contract NAG3-534)

(NASA-CR-183013; NAS 1.26:183013) Avail: NTIS HC A02/MF A01 CSCL 20/11

Described are the mathematical model and solution methodologies for analyzing the structural response of thin, metallic elasto-viscoplastic shell structures under large thermomechanical loads and their non-isothermal buckling behavior. Among the system responses associated with these loads and conditions are snap-through, buckling, thermal buckling, and creep buckling. This geometric and material nonlinearities (of high order) can be anticipated and are considered in the model and the numerical treatment. Author

**N89-12932\*** # Georgia Inst. of Tech., Atlanta. School of Aerospace Engineering.

**CONSIDERATIONS IN DEVELOPMENT AND IMPLEMENTATION OF ELASTO-VISCOPLASTIC CONSTITUTIVE MODEL FOR HIGH TEMPERATURE APPLICATIONS**

RICHARD RIFF 1988 2 p

(Contract NAG3-534)

(NASA-CR-183403; NAS 1.26:183403) Avail: NTIS HC A02/MF A01 CSCL 20/11

The prediction of inelastic behavior of metallic materials at elevated temperatures has increased in importance in recent years. The operating conditions within the hot section of a rocket motor or a modern gas turbine engine present an extremely harsh thermomechanical environment. Large thermal transients are induced each time the engine is started or shut down. Additional thermal transients from an elevated ambient occur whenever the engine power level is adjusted to meet flight requirements. The structural elements employed in such hot sections, as well as any engine components located therein, must be capable of withstanding such extreme conditions. Failure of a component would, due to the critical nature of the hot section, lead to an immediate and catastrophic loss in power. Consequently, assuring satisfactory long term performance for such components is a major concern. Nonisothermal loading of structures often causes excursion of stress well into the inelastic range. Moreover, the influence of geometry changes on the response is also significant in most cases. Therefore, both material and geometric nonlinear effects are considered. Author

**N89-13819\*** # Toledo Univ., OH.

**SOLUTION AND SENSITIVITY ANALYSIS OF A COMPLEX TRANSCENDENTAL EIGENPROBLEM WITH PAIRS OF REAL EIGENVALUES Final Report**

DURBHA V. MURTHY Jan. 1989 25 p

(Contract NAG3-742)

(NASA-CR-182241; E-4560; NAS 1.26:182241) Avail: NTIS HC A03/MF A01 CSCL 20/11

This paper considers complex transcendental eigenvalue problems where one is interested in pairs of eigenvalues that are restricted to take real values only. Such eigenvalue problems arise in dynamic stability analysis of nonconservative physical systems, i.e., flutter analysis of aeroelastic systems. Some available solution methods are discussed and a new method is presented. Two computational approaches are described for analytical evaluation of the sensitivities of these eigenvalues when they are dependent on other parameters. The algorithms presented are illustrated through examples. Author

**N89-13820\*** # Case Western Reserve Univ., Cleveland, OH. Dept. of Civil Engineering.

**LOCAL-GLOBAL ANALYSIS OF CRACK GROWTH IN CONTINUOUSLY REINFORCED CERAMIC MATRIX COMPOSITES Final Report**

ROBERTO BALLARINI and SHAMIN AHMED Dec. 1988 26 p

Proposed for presentation at the 34th International Gas Turbine and Aeroengine Congress and Exposition, Toronto, Ontario, 4-8 Jun. 1989

(Contract NAG3-856)

(NASA-CR-182231; E-4537; NAS 1.26:182231) Avail: NTIS HC A03/MF A01 CSCL 20/11

The development is described of a mathematical model for predicting the strength and micromechanical failure characteristics of continuously reinforced ceramic matrix composites. The local-globe analysis models the vicinity of a propagating crack tip as a local heterogeneous region (LHR) consisting of spring like representation of the matrix, fibers and interfaces. This region is embedded in an anisotropic continuum (representing the bulk composite) which is modeled by conventional finite elements. Parametric studies are conducted to investigate the effects of LHR size, component properties, interface conditions, etc. on the strength and sequence of the failure processes in the unidirectional composite system. The results are compared with those predicted by the models developed by Marshall et al. (1985) and by Budiansky et al. (1986). Author

**N89-14457\*** # Georgia Inst. of Tech., Atlanta. School of Aerospace Engineering.

**ANALYSIS OF SHELL-TYPE STRUCTURES SUBJECTED TO TIME-DEPENDENT MECHANICAL AND THERMAL LOADING Semiannual Status Report**

G. J. SIMITSES and R. RIFF Oct. 1988 48 p

(Contract NAG3-534)

(NASA-CR-183005; NAS 1.26:183005) Avail: NTIS HC A03/MF A01 CSCL 20/11

The objective of this research is to develop a general mathematical model and solution methodologies for analyzing structural response of thin, metallic shell-type structures under large transient, cyclic or static thermomechanical loads. Among the system responses, which are associated with these load conditions, are thermal buckling, creep buckling and ratcheting. Thus, geometric as well as material-type nonlinearities (of high order) can be anticipated and must be considered in the development of the mathematical model. Furthermore, this must also be accommodated in the solution procedures. Author

**N89-14465\*** # National Aeronautics and Space Administration. Lewis Research Center, Cleveland, OH.

**PARAMETRIC STUDIES OF ADVANCED TURBOPROPS**

J. G. MASER, D. G. FERTIS (Akron Univ., OH.), C. C. CHAMIS, and R. A. AIELLO 1988 16 p Presented at the 29th Structures, Structural Dynamics and Materials Conference, Williamsburg, VA, 18-20 Apr. 1988; sponsored by AIAA, ASME, ASCE, AHS and

## 39 STRUCTURAL MECHANICS

ACS

(NASA-TM-101389; E-4451; NAS 1.15:101389) Avail: NTIS HC A03/MF A01 CSCL 20/11

The effects of geometric variables (sweep and twist) on the structural performance of advanced turboprops are investigated. The investigation is limited to aerodynamically efficient turboprops using an acceptable design configuration as a baseline. The baseline configuration is modified using a seven by seven array of independently varying sweep and twist parameters while maintaining acceptable aerodynamic efficiency. The turboprop structural performance is evaluated in terms of critical speeds, tip displacements, and vibration frequencies where geometric nonlinearities are included. The results obtained are presented in such a manner as to highlight the effects of sweep and twist on the structural performance of aerodynamically efficient turboprop configurations.

Author

**N89-14470\*#** National Aeronautics and Space Administration. Lewis Research Center, Cleveland, OH.

### **A REVIEW OF FAILURE MODELS FOR UNIDIRECTIONAL CERAMIC MATRIX COMPOSITES UNDER MONOTONIC LOADS**

DAVID E. TRIPP, JOHN H. HEMANN (Cleveland State Univ., OH.), and JOHN P. GYKENYESI 1989 19 p Proposed for presentation at the 34th International Gas Turbine and Aeroengine Congress and Exposition, Toronto, Ontario, 4-8 Jun. 1989; sponsored by the American Society of Mechanical Engineers (NASA-TM-101421; E-4520; NAS 1.15:101421) Avail: NTIS HC A03/MF A01 CSCL 20/11

Ceramic matrix composites offer significant potential for improving the performance of turbine engines. In order to achieve their potential, however, improvements in design methodology are needed. In the past most components using structural ceramic matrix composites were designed by trial and error since the emphasis of feasibility demonstration minimized the development of mathematical models. To understand the key parameters controlling response and the mechanics of failure, the development of structural failure models is required. A review of short term failure models with potential for ceramic matrix composite laminates under monotonic loads is presented. Phenomenological, semi-empirical, shear-lag, fracture mechanics, damage mechanics, and statistical models for the fast fracture analysis of continuous fiber unidirectional ceramic matrix composites under monotonic loads are surveyed.

Author

**N89-15434\*#** Texas Univ., San Antonio. Div. of Engineering. **PROBABILISTIC ANALYSIS FOR FATIGUE STRENGTH DEGRADATION OF MATERIALS Annual Report**

LOLA ROYCE Jan. 1989 133 p

(Contract NAG3-867)

(NASA-CR-182844; NAS 1.26:182844) Avail: NTIS HC A07/MF A01 CSCL 20/11

This report presents the results of the first year of a research program conducted for NASA-LeRC by the University of Texas at San Antonio. The research included development of methodology that provides a probabilistic treatment of lifetime prediction of structural components of aerospace propulsion systems subjected to fatigue. Material strength degradation models, based on primitive variables, include both a fatigue strength reduction model and a fatigue crack growth model. Linear elastic fracture mechanics is utilized in the latter model. Probabilistic analysis is based on simulation, and both maximum entropy and maximum penalized likelihood methods are used for the generation of probability density functions. The resulting constitutive relationships are included in several computer programs, RANDOM2, RANDOM3, and RANDOM4. These programs determine the random lifetime of an engine component, in mechanical load cycles, to reach a critical fatigue strength or crack size. The material considered was a cast nickel base superalloy, one typical of those used in the Space Shuttle Main Engine.

Author

**N89-15437\*#** National Aeronautics and Space Administration. Lewis Research Center, Cleveland, OH.

### **NONINTERACTIVE MACROSCOPIC RELIABILITY MODEL FOR CERAMIC MATRIX COMPOSITES WITH ORTHOTROPIC MATERIAL SYMMETRY**

STEPHEN F. DUFFY (Cleveland State Univ., OH.) and JANE M. MANDERSCHIED 1989 9 p Prepared for presentation at the 34th International Gas Turbine and Aeroengine Congress and Exposition, Toronto, Ontario, 4-8 Jun. 1989; sponsored by ASME (NASA-TM-101414; E-4512; NAS 1.15:101414) Avail: NTIS HC A02/MF A01 CSCL 20/11

A macroscopic noninteractive reliability model for ceramic matrix composites is presented. The model is multiaxial and applicable to composites that can be characterized as orthotropic. Tensorial invariant theory is used to create an integrity basis with invariants that correspond to physical mechanisms related to fracture. This integrity basis is then used to construct a failure function per unit volume (or area) of material. It is assumed that the overall strength of the composite is governed by weakest link theory. This leads to a Weibull type model similar in nature to the principle of independent action (PIA) model for isotropic monolithic ceramics. An experimental program to obtain model parameters is briefly discussed. In addition, qualitative features of the model are illustrated by presenting reliability surfaces for various model parameters.

Author

**N89-15438\*#** National Aeronautics and Space Administration. Lewis Research Center, Cleveland, OH.

### **FREE-VIBRATION CHARACTERISTICS AND CORRELATION OF A SPACE STATION SPLIT-BLANKET SOLAR ARRAY**

KELLY S. CARNEY and FRANCIS J. SHAKER 1989 15 p Prepared for presentation at the 30th Structures, Structural Dynamics and Materials Conference, Mobile, AL, 3-5 Apr. 1989; sponsored in part by AIAA, ASME, ASCE, AHS and ACS (NASA-TM-101452; E-4563; NAS 1.15:101452) Avail: NTIS HC A03/MF A01 CSCL 20/11

Two methods for studying the free-vibration characteristics of a large split-blanket solar array in a zero-g cantilevered configuration are presented. The zero-g configuration corresponds to an on-orbit configuration of the Space Station solar array. The first method applies the equations of continuum mechanics to determine the natural frequencies of the array; the second uses the finite element method program, MSC/NASTRAN. The stiffness matrix from the NASTRAN solution was found to be erroneously grounded. The results from the two methods are compared. It is concluded that the grounding does not seriously compromise the solution to the elastic modes of the solar array. However, the correct rigid body modes need to be included to obtain the correct dynamic model.

Author

**N89-16183\*#** National Aeronautics and Space Administration. Lewis Research Center, Cleveland, OH.

### **THERMOVISCOPLASTIC MODEL WITH APPLICATION TO COPPER**

ALAN D. FREED Dec. 1988 18 p

(NASA-TP-2845; E-4280; NAS 1.60:2845) Avail: NTIS HC A03/MF A01 CSCL 20/11

A viscoplastic model is developed which is applicable to anisothermal, cyclic, and multiaxial loading conditions. Three internal state variables are used in the model; one to account for kinematic effects, and the other two to account for isotropic effects. One of the isotropic variables is a measure of yield strength, while the other is a measure of limit strength. Each internal state variable evolves through a process of competition between strain hardening and recovery. There is no explicit coupling between dynamic and thermal recovery in any evolutionary equation, which is a useful simplification in the development of the model. The thermodynamic condition of intrinsic dissipation constrains the thermal recovery function of the model. Application of the model is made to copper, and cyclic experiments under isothermal, thermomechanical, and nonproportional loading conditions are considered. Correlations and predictions of the model are representative of observed material behavior.

Author



**N89-16193\*** # Ohio State Univ., Columbus. Dept. of Aeronautical and Astronautical Engineering.

**A NOVEL APPROACH IN FORMULATION OF SPECIAL TRANSITION ELEMENTS: MESH INTERFACE ELEMENTS**  
Status Report

NESRIN SARIGUL Jan. 1989 67 p  
(Contract NAG3-790; RF PROJ. 765939/719301)  
(NASA-CR-184768; NAS 1.26:184768) Avail: NTIS HC A04/MF A01 CSCL 20/11

The objective of this research is to develop more accurate and efficient advanced methods for solution of singular problems encountered in various branches of mechanics. The research program includes the formulation of new class elements called Mesh Interface Elements (MIE) to connect meshes of traditional elements either in three dimensions or in three and two dimensions. The finite element formulations are based on the boolean sum and blending operators. In today's advanced aircraft and space structure applications, steep temperature and/or stress gradients are commonly encountered. The analysis methods need to incorporate these steep gradients into the solution efficiently and accurately. Mesh Interface Elements are formulated and tested to account for the steep gradient effects. At present, the heat transfer and structural analysis problems are formulated from uncoupled theory point of view. The status report, first, summarizes the general formulation for heat transfer and structural analysis by including the newly introduced varying material properties at material nodal points of the elements concept. The the formulation of mesh interface elements is detailed. On the computational efficiency side, a hidden-symbolic computation concept developed by the author is given. Verification examples are included from the heat transfer and structural analysis problems. The appendix includes listings of the computer modules developed for this purpose.

Author

**N89-17286\*** # National Aeronautics and Space Administration. Lewis Research Center, Cleveland, OH.

**STOCHASTIC MODELING OF CRACK INITIATION AND SHORT-CRACK GROWTH UNDER CREEP AND CREEP-FATIGUE CONDITIONS**

TAKAYUKI KITAMURA, LOUIS J. GHOSN, and RYUICHI OHTANI Jan. 1989 20 p Prepared in cooperation with Cleveland State Univ., OH and Kyoto Univ. (Japan) •  
(NASA-TM-101358; E-4386; NAS 1.15:101358) Avail: NTIS HC A03/MF A01 CSCL 20/11

A simplified stochastic model is proposed for crack initiation and short-crack growth under creep and creep-fatigue conditions. Material inhomogeneity provides the random nature of crack initiation and early growth. In the model, the influence of microstructure is introduced by the variability of: (1) damage accumulation along grain boundaries, (2) critical damage required for crack initiation or growth, and (3) the grain-boundary length. The probabilities of crack initiation and growth are derived by using convolution integrals. The model is calibrated and used to predict the crack density and crack-growth rate of short cracks of 304 stainless steel under creep and creep-fatigue conditions. The mean-crack initiation lives are predicted to be within an average deviation of about 10 percent from the experimental results. The predicted cumulative distributions of crack-growth rate follow the experimental data closely. The applicability of the simplified stochastic model is discussed and the future research direction is outlined.

Author

**N89-17298\*** # National Aeronautics and Space Administration. Lewis Research Center, Cleveland, OH.

**TURBINE ENGINE HOT SECTION TECHNOLOGY, 1987**

Oct. 1987 464 p Workshop held in Cleveland, OH, 20-21 Oct. 1987  
(NASA-CP-2493; E-3745; NAS 1.55:2493) Avail: NTIS HC A20/MF A01 CSCL 20/11

Presentations were made concerning the development of design analysis tools for combustor liners, turbine vanes, and turbine blades. Presentations were divided into six sections: instrumentation, combustion, turbine heat transfer, structural

analysis, fatigue and fracture, surface protective coatings, constitutive behavior of materials, stress-strain response and life prediction methods. For individuals titles, see N89-17299 through N89-17337.

**N89-17316\*** # Pratt and Whitney Aircraft, East Hartford, CT.  
**THREE-DIMENSIONAL INELASTIC ANALYSIS METHODS FOR HOT SECTION COMPONENTS**

E. S. TODD In NASA, Lewis Research Center, Turbine Engine Hot Section Technology, 1987 p 239-240 Oct. 1987  
(Contract NAS3-23697)  
Avail: NTIS HC A20/MF A01 CSCL 20/11

The objective of this program is to produce a series of new computer codes that permit more accurate and efficient three-dimensional inelastic structural analysis of combustor liners, turbine blades, and turbine vanes. Each code embodies a progression of mathematical models for increasingly comprehensive representation of the geometrical features, loading conditions, and forms of nonlinear material response that distinguish these three groups of hot section components.

Author

**N89-17317\*** # Pratt and Whitney Aircraft, East Hartford, CT.

**THREE-DIMENSIONAL INELASTIC ANALYSIS FOR HOT SECTION COMPONENTS, BEST 3D CODE**

RAYMOND B. WILSON and PRASANTA K. BANERJEE (State Univ. of New York, Buffalo.) In NASA, Lewis Research Center, Turbine Engine Hot Section Technology, 1987 p 241-248 Oct. 1987  
(Contract NAS3-23697)

Avail: NTIS HC A20/MF A01 CSCL 20/11

The goal is the development of an alternative stress analysis tool, distinct from the finite element method, applicable to the engineering analysis of gas turbine engine structures. The boundary element method was selected for this development effort on the basis of its already demonstrated applicability to a variety of geometries and problem types characteristic of gas turbine engine components. Major features of the BEST3D computer program are described, and some of the significant developments carried out as part of the Inelastic Methods Contract are outlined.

Author

**N89-17319\*** # National Aeronautics and Space Administration. Lewis Research Center, Cleveland, OH.

**MECHANICS OF MATERIALS MODEL**

JEFFREY P. MEISTER In its Turbine Engine Hot Section Technology, 1987 p 255-257 Oct. 1987  
Avail: NTIS HC A20/MF A01 CSCL 20/11

The Mechanics of Materials Model (MOMM) is a three-dimensional inelastic structural analysis code for use as an early design stage tool for hot section components. MOMM is a stiffness method finite element code that uses a network of beams to characterize component behavior. The MOMM contains three material models to account for inelastic material behavior. These include the simplified material model, which assumes a bilinear stress-strain response; the state-of-the-art model, which utilizes the classical elastic-plastic-creep strain decomposition; and Walker's viscoplastic model, which accounts for the interaction between creep and plasticity that occurs under cyclic loading conditions.

Author

**N89-17321\*** # National Aeronautics and Space Administration. Lewis Research Center, Cleveland, OH.

**THREE-DIMENSIONAL INELASTIC ANALYSIS METHODS FOR HOT SECTION COMPONENTS**

JOSEPH LACKNEY (Sverdrup Technology, Inc., Cleveland, OH.) and C. C. CHAMIS In its Turbine Engine Hot Section Technology, 1987 p 267-271 Oct. 1987  
(Contract NAS3-23698)

Avail: NTIS HC A20/MF A01 CSCL 20/11

The objective was to develop analytical methods capable of evaluating the cyclic time dependent inelasticity which occurs in hot section engine components. Because of the large excursions

in temperature associated with hot section engine components, the techniques developed must be able to accommodate large variations in material behavior including plasticity and creep. To meet this objective, a matrix consisting of three constitutive mode-element formulations was developed. A separate program for each combination of constitutive mode-element model was written. The source codes of the nine programs range in size from 7300 lines for the Bodner/twenty code to 19,000 lines for the Haisler and Allen/nine code. All the codes were given a stand alone capability of performing cyclic nonlinear analysis. Author

**N89-17326\*#** National Aeronautics and Space Administration. Lewis Research Center, Cleveland, OH.

## USE OF INELASTIC STRAIN AS A BASIS FOR ANALYZING THERMOMECHANICAL TEST DATA

P. A. BARTOLOTTA and J. R. ELLIS *In its* Turbine Engine Hot Section Technology, 1987 p 303-315 Oct. 1987  
 Avail: NTIS HC A20/MF A01 CSCL 20/11

It was shown that the proposed data analysis method, based on inelastic strain-time response, can be used effectively to represent cyclic response at elevated temperatures for Hastelloy-X. A high level of confidence in this method was built by making comparisons of the experimental and fitted data in two forms. Because of this level of confidence, the analysis was taken one step further and inelastic strain rates were calculated from the derivatives of the fit equations. Author

**N89-17327\*#** National Aeronautics and Space Administration. Lewis Research Center, Cleveland, OH.

## PRELIMINARY STUDY OF CREEP THRESHOLDS AND THERMOMECHANICAL RESPONSE IN HAYNES 188 AT TEMPERATURES IN THE RANGE 649 TO 871 C

J. R. ELLIS, P. A. BARTOLOTTA, and S. W. MLADSI *In its* Turbine Engine Hot Section Technology, 1987 p 317-334 Oct. 1987  
 Avail: NTIS HC A20/MF A01 CSCL 20/11

The following conclusions were drawn from this study of creep thresholds and thermomechanical response: (1) creep threshold can be determined using the latest electrohydraulic test equipment, providing that test durations are short and relatively large accumulations of creep strain are used in defining the threshold; (2) significant creep strains were measured under monotonic loading as stress levels as low as 4 ksi at temperatures predicted for solar receiver service; and (3) the material exhibited creep ratchetting during simulated service cycles, a result not predicted by analysis using current constitutive models for Haynes 188. Author

**N89-17328\*#** National Aeronautics and Space Administration. Lewis Research Center, Cleveland, OH.

## FINITE ELEMENT IMPLEMENTATION OF VISCOPLASTIC MODELS

V. K. ARYA *In its* Turbine Engine Hot Section Technology, 1987 p 335-348 Oct. 1987  
 Avail: NTIS HC A20/MF A01 CSCL 20/11

A brief description of the implementation in MARK, the general purpose finite element structural analysis code, of two viscoplastic models developed by Robinson is given. One model is for isotropic materials and the other is for metal matrix composites. Also presented are analytical results obtained for hot section components using these models. Author

**N89-17329\*#** National Aeronautics and Space Administration. Lewis Research Center, Cleveland, OH.

## STRUCTURAL RESPONSE OF AN ADVANCED COMBUSTOR LINER: TEST AND ANALYSIS

PAUL E. MOORHEAD, ROBERT L. THOMPSON, M. TONG, and M. HIGGINS (Sverdrup Technology, Inc., Cleveland, OH.) *In its* Turbine Engine Hot Section Technology, 1987 p 349-356 Oct. 1987  
 Avail: NTIS HC A20/MF A01 CSCL 20/11

An advanced (segmented) combustor liner supplied by Pratt and Whitney Aircraft was tested in the structural component test

rig at Lewis Research Center. It was found that the segmented liner operated at much lower temperatures than the conventional liner (about 400 F lower) for the same heat flux. At the lower temperatures and low thermal gradients, little distortion to the segments was observed. The operating conditions were not severe enough to distort or damage the segmented liner. Author

**N89-17330\*#** National Aeronautics and Space Administration. Lewis Research Center, Cleveland, OH.

## THERMAL EXPANSION MISMATCH AND PLASTICITY IN THERMAL BARRIER COATING

GEORGE C. CHANG, WORAPHAT PHUCHAROEN (Cleveland State Univ., OH.), and ROBERT A. MILLER *In its* Turbine Engine Hot Section Technology, 1987 p 357-368 Oct. 1987  
 Avail: NTIS HC A20/MF A01 CSCL 20/11

The basic objective of this investigation is the quantitative determination of stress states in a model thermal barrier coating (TBC) as it cools in the air to 600 C from an assumed stress-free state at 700 C. This model is intended to represent a thin plasma-sprayed zirconia-yttria ceramic layer with a nickel chromium-aluminum-yttrium bond coat on a cylindrical substrate made of nickel-based superalloys typically found in gas turbines. Author

**N89-17331\*#** Garrett Turbine Engine Co., Phoenix, AZ.

## THERMAL BARRIER COATING LIFE-PREDICTION MODEL DEVELOPMENT

T. E. STRANGMAN, J. F. NEUMANN, and A. LIU *In* NASA, Lewis Research Center, Turbine Engine Hot Section Technology, 1987 p 369-375 Oct. 1987  
 (Contract NAS3-23945)

Avail: NTIS HC A20/MF A01 CSCL 20/11  
 The primary objective of this program was to develop an operative thermal barrier coating (TBC) design model for life prediction. The objective was successfully accomplished with the development, calibration, and demonstration of a mechanistic thermochemical model which rapidly predicts TBC life as a function of engine, mission, and materials system parameters. This thermochemical design model accounts for the three operative TBC damage modes (bond coating oxidation, zirconia toughness reduction, and molten salt film damage), which all contribute to spalling of the insulating zirconia layer. Author

**N89-17333\*#** Pratt and Whitney Aircraft, East Hartford, CT.

## THERMAL BARRIER COATING LIFE PREDICTION MODEL DEVELOPMENT

J. T. DEMASI, S. L. MANNING, M. ORTIZ, and K. D. SHEFFLER *In* NASA, Lewis Research Center, Turbine Engine Hot Section Technology, 1987 p 385-399 Oct. 1987  
 (Contract NAS3-23944)

Avail: NTIS HC A20/MF A01 CSCL 20/11  
 The objectives of this program are to increase understanding of thermal barrier coating (TBC) degradation and failure modes, to generate quantitative ceramic failure life data under cyclic thermal conditions which simulate those encountered in gas turbine engine service, and to develop an analytical methodology for prediction of coating life in the engine. Observations of degradation and failure modes in plasma deposited ceramic indicate that spallation failure results from progressive cracking of the ceramic parallel to and adjacent to, but not coincident with the metal-ceramic interface. Author

**N89-17335\*#** General Electric Co., Cincinnati, OH. Aircraft Engines.

## ELEVATED TEMPERATURE CRACK GROWTH

K. S. KIM, R. H. VANSTONE, S. N. MALIK, and J. H. LAFLEN *In* NASA, Lewis Research Center, Turbine Engine Hot Section Technology, 1987 p 413-422 Oct. 1987  
 (Contract NAS3-23940)

Avail: NTIS HC A20/MF A01 CSCL 20/11  
 The purpose is to determine the ability of currently available P-I integrals to correlate fatigue crack propagation under conditions that simulate the turbojet engine combustor liner environment. The

utility of advanced fracture mechanics measurements will also be evaluated. Research showed that the experimentally measured displacements and loads can be accurately predicted by finite element analyses that consider the growth of the fatigue crack. These results are being used to evaluate nonlinear fracture mechanics parameters for correlating the observed fatigue crack growth rates for different strain ranges. Author

**N89-17336\*#** Pratt and Whitney Aircraft, East Hartford, CT.  
**CREEP FATIGUE LIFE PREDICTION FOR ENGINE HOT SECTION MATERIALS (ISOTROPIC) FIFTH YEAR PROGRESS REVIEW**

RICHARD S. NELSON and PETER R. HARVEY *In* NASA, Lewis Research Center, Turbine Engine Hot Section Technology, 1987 p 423-434 Oct. 1987  
 (Contract NAS3-23288)

Avail: NTIS HC A20/MF A01 CSCL 20/11

The need for advanced life prediction methods for hot section components for gas turbine engines is becoming more and more evident. The complex local strain and temperature histories at critical locations must be accurately interpreted to account for the effects of various damage mechanisms and their possible interactions. This program is designed to investigate these fundamental damage processes, identify modeling strategies, and develop practical models which can be used to guide the early design and development of new engines and to increase the durability of existing engines. Author

**N89-17337\*#** National Aeronautics and Space Administration, Lewis Research Center, Cleveland, OH.

**TOTAL STRAIN VERSION OF STRAINRANGE PARTITIONING FOR THERMOMECHANICAL FATIGUE AT LOW STRAINS**

G. R. HALFORD and J. F. SALTSMAN *In its* Turbine Engine Hot Section Technology, 1987 p 435-458 Oct. 1987  
 Avail: NTIS HC A20/MF A01 CSCL 20/11

A new method is proposed for characterizing and predicting the thermal fatigue behavior of materials. The method is based on three innovations in characterizing high temperature material behavior: (1) the bithermal concept of fatigue testing; (2) advanced, nonlinear, cyclic constitutive models; and (3) the total strain version of traditional strainrange partitioning. Author

**N89-18696\*#** Aerostructures, Inc., Arlington, VA.  
**MODAL FORCED VIBRATION ANALYSIS OF AERODYNAMICALLY EXCITED TURBOSYSTEMS Final Report**

V. ELCHURI Jul. 1985 133 p  
 (Contract NAS3-24387)  
 (NASA-CR-174966; NAS 1.26:174966) Avail: NTIS HC A07/MF A01 CSCL 20/11

Theoretical aspects of a new capability to determine the vibratory response of turbosystems subjected to aerodynamic excitation are presented. Turbosystems such as advanced turbopropellers with highly swept blades, and axial-flow compressors and turbines can be analyzed using this capability. The capability has been developed and implemented in the April 1984 release of the general purpose finite element program NASTRAN. The dynamic response problem is addressed in terms of the normal modal coordinates of these tuned rotating cyclic structures. Both rigid and flexible hubs/disks are considered. Coriolis and centripetal accelerations, as well as differential stiffness effects are included. Generally non-uniform steady inflow fields and uniform flow fields arbitrarily inclined at small angles with respect to the axis of rotation of the turbosystem are considered sources of aerodynamic excitation. The spatial non-uniformities are considered to be small deviations from a principally uniform inflow. Subsonic and supersonic relative inflows are addressed, with provision for linearly interpolating transonic airloads. Author

**N89-19581\*#** Texas Univ., San Antonio. Div. of Engineering.  
**FATIGUE CRACK GROWTH MODEL RANDOM2 USER MANUAL. APPENDIX 1: DEVELOPMENT OF ADVANCED METHODOLOGIES FOR PROBABILISTIC CONSTITUTIVE RELATIONSHIPS OF MATERIAL STRENGTH MODELS Annual Report**

LOLA BOYCE and THOMAS B. LOVELACE Jan. 1989 37 p  
 (Contract NAG3-867)  
 (NASA-CR-184775-APP-1; NAS 1.26:184775-APP-1) Avail: NTIS HC A03/MF A01 CSCL 20/11

FORTTRAN program RANDOM2 is presented in the form of a user's manual. RANDOM2 is based on fracture mechanics using a probabilistic fatigue crack growth model. It predicts the random lifetime of an engine component to reach a given crack size. Details of the theoretical background, input data instructions, and a sample problem illustrating the use of the program are included. NASA

**N89-19582\*#** Texas Univ., San Antonio. Div. of Engineering.  
**FATIGUE STRENGTH REDUCTION MODEL: RANDOM3 AND RANDOM4 USER MANUAL. APPENDIX 2: DEVELOPMENT OF ADVANCED METHODOLOGIES FOR PROBABILISTIC CONSTITUTIVE RELATIONSHIPS OF MATERIAL STRENGTH MODELS Annual Report**

LOLA BOYCE and THOMAS B. LOVELACE Jan. 1989 80 p  
 (Contract NAG3-867)  
 (NASA-CR-184796-APP-2; NAS 1.26:184796-APP-2) Avail: NTIS HC A05/MF A01 CSCL 20/11

FORTTRAN programs RANDOM3 and RANDOM4 are documented in the form of a user's manual. Both programs are based on fatigue strength reduction, using a probabilistic constitutive model. The programs predict the random lifetime of an engine component to reach a given fatigue strength. The theoretical backgrounds, input data instructions, and sample problems illustrating the use of the programs are included. NASA

**N89-19583\*#** Aerostructures, Inc., Arlington, VA.  
**NASTRAN SUPPLEMENTAL DOCUMENTATION FOR MODAL FORCED VIBRATION ANALYSIS OF AERODYNAMICALLY EXCITED TURBOSYSTEMS Final Report**

V. ELCHURI and P. R. PAMIDI (RPK Corp., Columbia, MD.) Jul. 1985 133 p  
 (Contract NAS3-24387)  
 (NASA-CR-174967; NAS 1.26:174967) Avail: NTIS HC A07/MF A01 CSCL 20/11

This report is a supplemental NASTRAN document for a new capability to determine the vibratory response of turbosystems subjected to aerodynamic excitation. Supplements of NASTRAN Theoretical, User's, Programmer's, and Demonstration Manuals are included. Turbosystems such as advanced turbopropellers with highly swept blades, and axial-flow compressors and turbines can be analyzed using this capability, which has been developed and implemented in the April 1984 release of the general purpose finite element program NASTRAN. The dynamic response problem is addressed in terms of the normal modal coordinates of these tuned rotating cyclic structures. Both rigid and flexible hubs/disks are considered. Coriolis and centripetal accelerations, as well as differential stiffness effects are included. Generally nonuniform steady inflow fields and uniform flow fields arbitrarily inclined at small angles with respect to the axis of rotation of the turbosystem are considered as the sources of aerodynamic excitation. The spatial nonuniformities are considered to be small deviations from a principally uniform inflow. Subsonic relative inflows are addressed, with provision for linearly interpolating transonic airloads. Author

**N89-20514\*#** National Aeronautics and Space Administration, Lewis Research Center, Cleveland, OH.

**RESULTS OF INPHASE AXIAL-TORSIONAL FATIGUE EXPERIMENTS ON 304 STAINLESS STEEL**

PETER J. BONACUSE and SREERAMESH KALLURI (Sverdrup Technology, Inc., Cleveland, OH.) Mar. 1989 22 p Prepared in cooperation with Army Aviation Research and Development

Command, Cleveland, OH  
(NASA-TM-101464; E-4576; NAS 1.15:101464;  
AVSCOM-TR-88-C-022) Avail: NTIS HC A03/MF A01 CSCL  
20/11

A series of axial-torsional, inphase, strain-controlled, low-cycle fatigue tests were performed at room temperature on tubular specimens of 304 stainless steel. The program was conducted in cooperation with the task group on multiaxial fatigue research of ASTM committee E-09. The objective was to quantify the variability in multiaxial test results among several laboratories. Only included is data which was generated at the NASA Lewis Research Center's High Temperature Fatigue and Structures Laboratory. The experimental equipment and procedures used are described. The tubular specimens were polished on the outer surface to aid in the use of a cellulose film surface replication technique for crack detection. However, cracking initiated predominantly on the internal surface for all specimens. Honing of the bore of the tubular specimens lessened but did not entirely eliminate this problem. The observed fatigue lives are compared with lives calculated from three multiaxial life models. Constants for the life prediction models were obtained from uniaxial and torsional tests performed on the same heat of material. The observed fatigue lives agreed with calculated lives to within a factor of two for all but one of the life prediction models. Author

**N89-21258\*#** Georgia Inst. of Tech., Atlanta. School of Materials Engineering.

**DEFORMATION MODELING AND CONSTITUTIVE MODELING FOR ANISOTROPIC SUPERALLOYS Final Contractor Report**  
WALTER W. MILLIGAN and STEPHEN D. ANTOLOVICH  
Washington NASA Feb. 1989 294 p  
(Contract NAG3-503)  
(NASA-CR-4215; E-4543; NAS 1.26:4215) Avail: NTIS HC  
A13/MF A01 CSCL 20/11

A study of deformation mechanisms in the single crystal superalloy PWA 1480 was conducted. Monotonic and cyclic tests were conducted from 20 to 1093 C. Both (001) and near-(123) crystals were tested, at strain rates of 0.5 and 50 percent/minute. The deformation behavior could be grouped into two temperature regimes: low temperatures, below 760 C; and high temperatures, above 820 to 950 C depending on the strain rate. At low temperatures, the mechanical behavior was very anisotropic. An orientation dependent CRSS, a tension-compression asymmetry, and anisotropic strain hardening were all observed. The material was deformed by planar octahedral slip. The anisotropic properties were correlated with the ease of cube cross-slip, as well as the number of active slip systems. At high temperatures, the material was isotropic, and deformed by homogeneous gamma by-pass. It was found that the temperature dependence of the formation of superlattice-intrinsic stacking faults was responsible for the local minimum in the CRSS of this alloy at 400 C. It was proposed that the cube cross-slip process must be reversible. This was used to explain the reversible tension-compression asymmetry, and was used to study models of cross-slip. As a result, the cross-slip model proposed by Paidar, Pope and Vitek was found to be consistent with the proposed slip reversibility. The results were related to anisotropic viscoplastic constitutive models. The model proposed by Walter and Jordan was found to be capable of modeling all aspects of the material anisotropy. Temperature and strain rate boundaries for the model were proposed, and guidelines for numerical experiments were proposed. Author

**N89-21265\*#** Case Western Reserve Univ., Cleveland, OH. Dept. of Civil Engineering.

**ANALYSIS OF INTERFACE CRACK BRANCHING**  
R. BALLARINI, D. J. MUKAI, and G. R. MILLER (Washington Univ., Seattle.) Mar. 1989 23 p  
(Contract NAG3-856)  
(NASA-CR-182273; NAS 1.26:182273) Avail: NTIS HC A03/MF  
A01 CSCL 20/11

A solution is presented for the problem of a finite length crack branching off the interface between two bonded dissimilar isotropic materials. Results are presented in terms of the ratio of the energy

release rate of a branched interface crack to the energy release rate of a straight interface crack with the same total length. It is found that this ratio reaches a maximum when the interface crack branches into the softer material. Longer branches tend to have smaller maximum energy release rate ratio angles indicating that all else being equal, a branch crack will tend to turn back parallel to the interface as it grows. Author

**N89-21266\*#** National Aeronautics and Space Administration. Lewis Research Center, Cleveland, OH.

**CHARACTERIZATION OF STRUCTURAL CONNECTIONS USING FREE AND FORCED RESPONSE TEST DATA**  
CHARLES LAWRENCE and ARTHUR A. HUCKELBRIDGE (Case Western Reserve Univ., Cleveland, OH.) 1989 14 p Proposed for presentation at the 12th Biennial Conference on Mechanical Vibration and Noise, Montreal, Quebec, 17-20 Sep. 1989; sponsored by ASME  
(NASA-TM-101991; E-4695; NAS 1.15:101991) Avail: NTIS HC  
A03/MF A01 CSCL 20/11

The accurate prediction of system dynamic response often has been limited by deficiencies in existing capabilities to characterize connections adequately. Connections between structural components often are complex mechanically, and difficult to accurately model analytically. Improved analytical models for connections are needed to improve system dynamic predictions. A procedure for identifying physical connection properties from free and forced response test data is developed, then verified utilizing a system having both a linear and nonlinear connection. Connection properties are computed in terms of physical parameters so that the physical characteristics of the connections can better be understood, in addition to providing improved input for the system model. The identification procedure is applicable to multi-degree of freedom systems, and does not require that the test data be measured directly at the connection locations. Author

**N89-22939\*#** National Aeronautics and Space Administration. Lewis Research Center, Cleveland, OH.

**STRUCTURAL DYNAMICS BRANCH RESEARCH AND ACCOMPLISHMENTS FOR FY 1988**  
Apr. 1989 48 p  
(NASA-TM-101406; E-4498; NAS 1.15:101406) Avail: NTIS HC  
A03/MF A01 CSCL 20/11

Fiscal year 1988 research highlights from the Structural Dynamics Branch at NASA Lewis Research Center are described. Highlights from the branch's major work areas -- aeroelasticity, vibration control, dynamic systems, and computational structural methods -- are included as well as a complete listing of the FY 88 branch publications. Author

**N89-22948\*#** National Aeronautics and Space Administration. Lewis Research Center, Cleveland, OH.

**A NASTRAN DMAP ALTER FOR LINEAR BUCKLING ANALYSIS UNDER DYNAMIC LOADING**  
ROBERT A. AIELLO and JOSEPH E. GRADY In Computer Software Management and Information Center Seventeenth NASTRAN (R) Users' Colloquium p 187-200 Mar. 1989  
Previously announced as N89-13522  
Avail: NTIS HC A17/MF A01; also available from COSMIC, Athens, GA 30602 CSCL 20/11

A modification to the NASTRAN solution sequence for transient analysis with direct time integration (COSMIC NASTRAN rigid format 9) was developed and incorporated into a DMAP alter. This DMAP alter calculates the buckling stability of a dynamically loaded structure, and is used to predict the onset of structural buckling under stress-wave loading conditions. The modified solution sequence incorporates the linear buckling analysis capability (rigid format 5) of NASTRAN into the existing Transient solution rigid format in such a way as to provide a time dependent eigensolution which is used to assess the buckling stability of the structure as it responds to the impulsive load. As a demonstration of the validity of this modified solution procedure, the dynamic buckling of a prismatic bar subjected to an impulsive longitudinal compression is analyzed and compared to the known theoretical

solution. In addition, a dynamic buckling analysis is performed for the analytically less tractable problem of the localized dynamic buckling of an initially flawed composite laminate under transverse impact loading. The addition of this DMAP alter to the transient solution sequence in NASTRAN facilitates the computational prediction of both the time at which the onset of dynamic buckling occurs in an impulsively loaded structure, and the dynamic buckling mode shapes of that structure. Author

**N89-23890\*#** Texas Univ., San Antonio. Div. of Engineering.  
**FATIGUE CRACK GROWTH MODEL RANDOM2 USER MANUAL, APPENDIX 1 Annual Report**  
LOLA BOYCE and THOMAS B. LOVELACE Jan. 1989 37 p  
(Contract NAG3-867)  
(NASA-CR-184939; NAS 1.26:184939) Avail: NTIS HC A03/MF A01 CSCL 20/11

The FORTRAN program RANDOM2 is documented. RANDOM2 is based on fracture mechanics using a probabilistic fatigue crack growth model. It predicts the random lifetime of an engine component to reach a given crack size. Included in this user manual are details regarding the theoretical background of RANDOM2, input data, instructions and a sample problem illustrating the use of RANDOM2. Appendix A gives information on the physical quantities, their symbols, FORTRAN names, and both SI and U.S. Customary units. Appendix B includes photocopies of the actual computer printout corresponding to the sample problem. Appendices C and D detail the IMSL, Ver. 10(1), subroutines and functions called by RANDOM2 and a SAS/GRAPH(2) program that can be used to plot both the probability density function (p.d.f.) and the cumulative distribution function (c.d.f.). Author

**N89-23891\*#** Texas Univ., San Antonio. Div. of Engineering.  
**FATIGUE STRENGTH REDUCTION MODEL: RANDOM3 AND RANDOM4 USER MANUAL, APPENDIX 2 Annual Report**  
LOLA BOYCE and THOMAS B. LOVELACE Jan. 1989 80 p  
(Contract NAG3-867)  
(NASA-CR-184940; NAS 1.26:184940) Avail: NTIS HC A05/MF A01 CSCL 20/11

The FORTRAN programs RANDOM3 and RANDOM4 are documented. They are based on fatigue strength reduction, using a probabilistic constitutive model. They predict the random lifetime of an engine component to reach a given fatigue strength. Included in this user manual are details regarding the theoretical backgrounds of RANDOM3 and RANDOM4. Appendix A gives information on the physical quantities, their symbols, FORTRAN names, and both SI and U.S. Customary units. Appendix B and C include photocopies of the actual computer printout corresponding to the sample problems. Appendices D and E detail the IMSL, Version 10(1), subroutines and functions called by RANDOM3 and RANDOM4 and SAS/GRAPH(2) programs that can be used to plot both the probability density functions (p.d.f.) and the cumulative distribution functions (c.d.f.). A.D.

**N89-23918\*#** Case Western Reserve Univ., Cleveland, OH. Dept. of Civil Engineering.  
**FINITE ELEMENT MODELING OF FRICTIONALLY RESTRAINED COMPOSITE INTERFACES Final Report**  
ROBERTO BALLARINI and SHAMIM AHMED Apr. 1989 23 p  
(Contract NAG3-856)  
(NASA-CR-182281; NAS 1.26:182281) Avail: NTIS HC A03/MF A01 CSCL 20/11

The use of special interface finite elements to model frictional restraint in composite interfaces is described. These elements simulate Coulomb friction at the interface, and are incorporated into a standard finite element analysis of a two-dimensional isolated fiber pullout test. Various interfacial characteristics, such as the distribution of stresses at the interface, the extent of slip and delamination, load diffusion from fiber to matrix, and the amount of fiber extraction or depression are studied for different friction coefficients. The results are compared to those obtained analytically using a singular integral equation approach, and those obtained

by assuming a constant interface shear strength. The usefulness of these elements in micromechanical modeling of fiber-reinforced composite materials is highlighted. Author

**N89-24635\*#** National Aeronautics and Space Administration. Lewis Research Center, Cleveland, OH.

**TRIBOLOGY: THE STORY OF LUBRICATION AND WEAR**

DONALD H. BUCKLEY, WILLIAM R. JONES, JR., HAROLD E. SLINEY, ERWIN V. ZARETSKY, DENNIS P. TOWNSEND, and STUART H. LOEWENTHAL 1985 145 p Seminar F-107 held in Cleveland, OH, 18 Oct. 1985  
(NASA-TM-101430; E-4535; NAS 1.15:101430) Avail: NTIS HC A07/MF A01 CSCL 20/11

Topics addressed include: lubrication and design of high speed rolling element bearings, high speed gears, and traction drives.

**N89-24636\*#** National Aeronautics and Space Administration. Lewis Research Center, Cleveland, OH.

**SOLID LUBRICANT MATERIALS FOR HIGH TEMPERATURES: A REVIEW**

HAROLD E. SLINEY *In its Tribology: The Story of Lubrication and Wear* p 55-81 1985 Submitted for publication  
Avail: NTIS HC A07/MF A01 CSCL 20/11

Solid lubricants that can be used above 300 C in air are discussed, including coatings and self-lubricating composite bearing materials. The lubricants considered are representative dichalcogenides, graphite, graphite fluoride, polyimides, soft oxides, oxidatively stable fluorides, and hard coating materials. A few general design considerations relevant to solid lubrication are interspersed. Author

**N89-24669\*#** Georgia Inst. of Tech., Atlanta. School of Aerospace Engineering.

**ANALYSIS OF SHELL-TYPE STRUCTURES SUBJECTED TO TIME-DEPENDENT MECHANICAL AND THERMAL LOADING Semiannual Status Report**

G. J. SIMITSES May 1989 9 p  
(Contract NAG3-534)

(NASA-CR-184989; NAS 1.26:184989) Avail: NTIS HC A02/MF A01 CSCL 20/11

The objective is to develop a general mathematical model and solution methodologies for analyzing structural response of thin, metallic shell-type structures under large transient, cyclic, or static thermomechanical loads. Among the system responses, which are associated with these load conditions, are thermal buckling, creep buckling, and ratcheting. Thus, geometric as well as material-type nonlinearities (of high order) can be anticipated and must be considered in the development of the mathematical model. Furthermore, this must also be accommodated in the solution procedures. Author

**N89-25485\*#** National Aeronautics and Space Administration. Lewis Research Center, Cleveland, OH.

**PROCEDURES FOR CHARACTERIZING AN ALLOY AND PREDICTING CYCLIC LIFE WITH THE TOTAL STRAIN VERSION OF STRAINRANGE PARTITIONING**

JAMES F. SALTSMAN and GARY R. HALFORD Washington Jun. 1989 24 p  
(NASA-TM-4102; E-4457; NAS 1.15:4102) Avail: NTIS HC A03/MF A01 CSCL 20/11

Procedures are presented for characterizing an alloy and predicting cyclic life for isothermal and thermomechanical fatigue conditions by using the total strain version of strainrange partitioning (TS-SRP). Numerical examples are given. Two independent alloy characteristics are deemed important: failure behavior, as reflected by the inelastic strainrange versus cyclic life relations; and flow behavior, as indicated by the cyclic stress-strain-time response (i.e., the constitutive behavior). Failure behavior is characterized by conducting creep-fatigue tests in the strain regime, wherein the testing times are reasonably short and the inelastic strains are large enough to be determined accurately. At large strainranges, stress-hold, strain-limited tests are preferred because a high rate of creep damage per cycle is inherent in this type of test. At

## 39 STRUCTURAL MECHANICS

small strain ranges, strain-hold cycles are more appropriate. Flow behavior is characterized by conducting tests wherein the specimen is usually cycled far short of failure and the wave shape is appropriate for the duty cycle of interest. In characterizing an alloy pure fatigue, or PP, failure tests are conducted first. Then depending on the needs of the analyst a series of creep-fatigue tests are conducted. As many of the three generic SRP cycles are featured as are required to characterize the influence of creep on fatigue life (i.e., CP, PC, and CC cycles, respectively, for tensile creep only, compressive creep only, and both tensile and compressive creep). Any mean stress effects on life also must be determined and accounted for when determining the SRP inelastic strain range versus life relations for cycles featuring creep. This is particularly true for small strain ranges. The life relations thus are established for a theoretical zero mean stress condition. Author

**N89-25490\*#** National Aeronautics and Space Administration. Lewis Research Center, Cleveland, OH.

### **ADVANCED METHODS FOR 3-D INELASTIC STRUCTURAL ANALYSIS FOR HOT ENGINE STRUCTURES**

C. C. CHAMIS Jul. 1989 12 p Presented at the 2nd National Congress on Mechanics, Athens, Greece, 29 Jun. - 1 Jul. 1989; sponsored by the Hellenic Society for Theoretical and Applied Mechanics

(NASA-TM-102106; E-4873; NAS 1.15:102106) Avail: NTIS HC A03/MF A01 CSCL 20/11

Three-dimensional Inelastic Analysis Methods are described. These methods were incorporated into a series of new computer codes embodying a progression of mathematical models (mechanics of materials, specially finite element, boundary element) for streamlined analysis of hot engine structures such as: (1) combustor liners, (2) turbine blades, and (3) turbine vanes. These models address the effects of high temperatures and thermal/mechanical loadings on the local (stress/strain) and global (displacements, frequencies, amplitudes, buckling) structural behavior of the three respective components. The methods and the three computer codes, referred to as MOMM (Mechanics Of Materials Model), MHOST (MARC-Hot Section Technology), and BEST3D (Boundary Element Stress Technology), have been developed and are briefly described. Author

**N89-26259\*#** National Aeronautics and Space Administration. Lewis Research Center, Cleveland, OH.

### **COMPUTATIONAL STRUCTURAL MECHANICS FOR ENGINE STRUCTURES**

C. C. CHAMIS 1989 12 p Presented at the 30th Structures, Structural Dynamics and Materials (SDM) Conference, Mobile, AL, 3-5 Apr. 1989; cosponsored by the AIAA, ASME, ASCE, AHS, and ACS

(NASA-TM-102119; E-4898; NAS 1.15:102119) Avail: NTIS HC A03/MF A01 CSCL 20/11

The computational structural mechanics (CSM) program at Lewis encompasses: (1) fundamental aspects for formulating and solving structural mechanics problems, and (2) development of integrated software systems to computationally simulate the performance/durability/life of engine structures. It is structured to mainly supplement, complement, and whenever possible replace, costly experimental efforts which are unavoidable during engineering research and development programs. Specific objectives include: investigate unique advantages of parallel and multiprocesses for: reformulating/solving structural mechanics and formulating/solving multidisciplinary mechanics and develop integrated structural system computational simulators for: predicting structural performances, evaluating newly developed methods, and for identifying and prioritizing improved/missing methods needed. Herein the CSM program is summarized with emphasis on the Engine Structures Computational Simulator (ESCS). Typical results obtained using ESCS are described to illustrate its versatility. Author

**N89-26260\*#** National Aeronautics and Space Administration. Lewis Research Center, Cleveland, OH.

### **NONLINEAR MESOMECHANICS OF COMPOSITES WITH PERIODIC MICROSTRUCTURE Rept. No. 1**

KEVIN P. WALKER, ERIC H. JORDAN (Connecticut Univ., Storrs.), and ALAN D. FREED Jun. 1989 82 p (Contract NAG3-882)

(NASA-TM-102051; E-4670; NAS 1.15:102051) Avail: NTIS HC A05/MF A01 CSCL 20/11

This work is concerned with modeling the mechanical deformation or constitutive behavior of composites comprised of a periodic microstructure under small displacement conditions at elevated temperature. A mesomechanics approach is adopted which relates the micromechanical behavior of the heterogeneous composite with its in-service macroscopic behavior. Two different methods, one based on a Fourier series approach and the other on a Green's function approach, are used in modeling the micromechanical behavior of the composite material. Although the constitutive formulations are based on a micromechanical approach, it should be stressed that the resulting equations are volume averaged to produce overall effective constitutive relations which relate the bulk, volume averaged, stress increment to the bulk, volume averaged, strain increment. As such, they are macromodels which can be used directly in nonlinear finite element programs such as MARC, ANSYS and ABAQUS or in boundary element programs such as BEST3D. In developing the volume averaged or effective macromodels from the micromechanical models, both approaches will require the evaluation of volume integrals containing the spatially varying strain distributions throughout the composite material. By assuming that the strain distributions are spatially constant within each constituent phase or within a given subvolume within each constituent phase of the composite material, the volume integrals can be obtained in closed form. This simplified micromodel can then be volume averaged to obtain an effective macromodel suitable for use in the MARC, ANSYS and ABAQUS nonlinear finite element programs via user constitutive subroutines such as HYPELA and CMUSER. This effective macromodel can be used in a nonlinear finite element structural analysis to obtain the strain-temperature history at those points in the structure where thermomechanical cracking and damage are expected to occur, the so called damage critical points of the structure. Author

### **N89-26261\*# Akron Univ., OH. Dept. of Civil Engineering. ON FINITE ELEMENT IMPLEMENTATION AND COMPUTATIONAL TECHNIQUES FOR CONSTITUTIVE MODELING OF HIGH TEMPERATURE COMPOSITES Final Report**

A. F. SALEEB, T. Y. P. CHANG, T. WILT, and I. ISKOVITZ Jul. 1989 157 p

(Contract NAG3-901)

(NASA-CR-185120; NAS 1.26:185120) Avail: NTIS HC A08/MF A01 CSCL 20/11

The research work performed during the past year on finite element implementation and computational techniques pertaining to high temperature composites is outlined. In the present research, two main issues are addressed: efficient geometric modeling of composite structures and expedient numerical integration techniques dealing with constitutive rate equations. In the first issue, mixed finite elements for modeling laminated plates and shells were examined in terms of numerical accuracy, locking property and computational efficiency. Element applications include (currently available) linearly elastic analysis and future extension to material nonlinearity for damage predictions and large deformations. On the material level, various integration methods to integrate nonlinear constitutive rate equations for finite element implementation were studied. These include explicit, implicit and automatic subincrementing schemes. In all cases, examples are included to illustrate the numerical characteristics of various methods that were considered. Author



**N89-27223\*#** National Aeronautics and Space Administration. Lewis Research Center, Cleveland, OH.

**OPTIMUM INTERFACE PROPERTIES FOR METAL MATRIX COMPOSITES**

LOUIS J. GHOSN (Sverdrup Technology, Inc., Cleveland, OH.) and BRADLEY A. LERCH Aug. 1989 21 p (NASA-TM-102295; E-4964; NAS 1.15:102295) Avail: NTIS HC A03/MF A01 CSCL 20/11

Due to the thermal expansion coefficient mismatch (CTE) between the fiber and the matrix, high residual stresses exist in metal matrix composite systems upon cool down from processing temperature to room temperature. An interface material can be placed between the fiber and the matrix to reduce the high tensile residual stresses in the matrix. A computer program was written to minimize the residual stress in the matrix subject to the interface material properties. The decision variables are the interface modulus, thickness and thermal expansion coefficient. The properties of the interface material are optimized such that the average distortion energy in the matrix and the interface is minimized. As a result, the only active variable is the thermal expansion coefficient. The optimum modulus of the interface is always the minimum allowable value and the interface thickness is always the maximum allowable value, independent of the fiber/matrix system. The optimum interface thermal expansion coefficient is always between the values of the fiber and the matrix. Using this analysis, a survey of materials was conducted for use as fiber coatings in some specific composite systems. Author

**N89-28029\*#** National Aeronautics and Space Administration. Lewis Research Center, Cleveland, OH.

**A DATA ACQUISITION AND CONTROL PROGRAM FOR AXIAL-TORSIONAL FATIGUE TESTING**

SREERAMESH KALLURI and PETER J. BONACUSE (Army Aviation Systems Command, Cleveland, OH.) May 1989 23 p Presented at the Symposium on the Applications of Automation Technology to Fatigue and Fracture Testing, Kansas City, MO, 22-23 May 1989; sponsored in part by the American Society for Testing and Materials Prepared in cooperation with Army Aviation Systems Command, Cleveland, OH (NASA-TM-102041; E-4790; NAS 1.15:102041; AVSCOM-TR-89-C-002) Avail: NTIS HC A03/MF A01 CSCL 20/11

A computer program was developed for data acquisition and control of axial-torsional fatigue experiments. The multitasked, interrupt-driven program was written in Pascal and Assembly. This program is capable of dual-channel control and six-channel data acquisition. It can be utilized to perform inphase and out-of-phase axial-torsional isothermal fatigue or deformation experiments. The program was successfully used to conduct inphase axial-torsional fatigue experiments on 304 stainless steel at room temperature and on Hastelloy X at 800 C. The details of the software and some of the results generated to date are presented. Author

**N89-28030\*#** National Aeronautics and Space Administration. Lewis Research Center, Cleveland, OH.

**PROBABILISTIC STRUCTURAL ANALYSIS METHODS OF HOT ENGINE STRUCTURES**

C. C. CHAMIS and D. A. HOPKINS Jun. 1989 17 p Presented at the 34th International Gas Turbine and Aeroengine Congress and Exposition, Toronto, Ontario, 4-8 Jun. 1989; sponsored in part by ASME (NASA-TM-102091; E-4855; NAS 1.15:102091) Avail: NTIS HC A03/MF A01 CSCL 20/11

Development of probabilistic structural analysis methods for hot engine structures at Lewis Research Center is presented. Three elements of the research program are: (1) composite load spectra methodology; (2) probabilistic structural analysis methodology; and (3) probabilistic structural analysis application. Recent progress includes: (1) quantification of the effects of uncertainties for several variables on high pressure fuel turbopump (HPFT) turbine blade temperature, pressure, and torque of the space shuttle main engine (SSME); (2) the evaluation of the cumulative distribution function for various structural response variables based on assumed

uncertainties in primitive structural variables; and (3) evaluation of the failure probability. Collectively, the results demonstrate that the structural durability of hot engine structural components can be effectively evaluated in a formal probabilistic/reliability framework. Author

**N89-28036\*#** National Aeronautics and Space Administration. Lewis Research Center, Cleveland, OH.

**REFINEMENTS IN A VISCOPLASTIC MODEL**

A. D. FREED and K. P. WALKER (Engineering Science Software, Inc., Smithfield, RI.) 1989 18 p Prepared for presentation at the Winter Annual Meeting of the American Society of Mechanical Engineers, San Francisco, CA, 10-15 Dec. 1989 (NASA-TM-102338; E-4988; NAS 1.15:102338) Avail: NTIS HC A03/MF A01 CSCL 20/11

A thermodynamically admissible theory of viscoplasticity with two internal variables (a back stress and a drag strength) is presented. Six material functions characterize a specific viscoplastic model. In the pursuit of compromise between accuracy and simplicity, a model is developed that is a hybrid of two existing viscoplastic models. A limited number of applications of the model to Al, Cu, and Ni are presented. A novel implicit integration method is also discussed. Applications are made to obtain solutions using this viscoplastic model. Author

**N89-29776\*#** National Aeronautics and Space Administration. Lewis Research Center, Cleveland, OH.

**COMPUTATIONAL STRUCTURAL METHODS AT NASA LEWIS**

L. J. KIRALY /in NASA. Langley Research Center, NASA Workshop on Computational Structural Mechanics 1987, Part 1 p 61-74 Feb. 1989 Avail: NTIS HC A17/MF A01 CSCL 20/11

Viewgraphs on computational structural methods at the Lewis Research Center are given. Program objectives, work elements, resources, parallel-processing, FY-87 accomplishments, FY-88 plans, and a summary of current and planned activities are illustrated. Author

**TRANSPUTER PARALLEL PROCESSING AT NASA LEWIS RESEARCH CENTER**

GRAHAM K. ELLIS /in NASA. Langley Research Center, NASA Workshop on Computational Structural Mechanics 1987, Part 1 p 107-136 Feb. 1989 Avail: NTIS HC A17/MF A01 CSCL 20/11

The transputer parallel processing lab at NASA Lewis Research Center (LeRC) consists of 69 processors (transputers) that can be connected into various networks for use in general purpose concurrent processing applications. The main goal of the lab is to develop concurrent scientific and engineering application programs that will take advantage of the computational speed increases available on a parallel processor over the traditional sequential processor. Current research involves the development of basic programming tools. These tools will help standardize program interfaces to specific hardware by providing a set of common libraries for applications programmers. The thrust of the current effort is in developing a set of tools for graphics rendering/animation. The applications programmer currently has two options for on-screen plotting. One option can be used for static graphics displays and the other can be used for animated motion. The option for static display involves the use of 2-D graphics primitives that can be called from within an application program. These routines perform the standard 2-D geometric graphics operations in real-coordinate space as well as allowing multiple windows on a single screen. Author

**N89-29792\*#** National Aeronautics and Space Administration. Lewis Research Center, Cleveland, OH.

**COMPUTATIONAL STRUCTURAL MECHANICS ENGINE STRUCTURES COMPUTATIONAL SIMULATOR**

C. C. CHAMIS /in NASA, Langley Research Center, NASA

## 39 STRUCTURAL MECHANICS

Workshop on Computational Structural Mechanics 1987, Part 2 p 459-485 Feb. 1989

Avail: NTIS HC A16/MF A01 CSCL 20/11

The Computational Structural Mechanics (CSM) program at Lewis encompasses: (1) fundamental aspects for formulating and solving structural mechanics problems, and (2) development of integrated software systems to computationally simulate the performance/durability/life of engine structures. Author

**N89-29803\*** # Northwestern Univ., Evanston, IL.

### **PROBABILISTIC FINITE ELEMENTS (PFEM) STRUCTURAL DYNAMICS AND FRACTURE MECHANICS**

WING-KAM LIU, TED BELYTSCHKO, A. MANI, and G. BESTERFIELD /in NASA. Langley Research Center, NASA Workshop on Computational Structural Mechanics 1987, Part 3 p 903-941 Feb. 1989

(Contract NAG3-535)

Avail: NTIS HC A18/MF A01 CSCL 20/11

The purpose of this work is to develop computationally efficient methodologies for assessing the effects of randomness in loads, material properties, and other aspects of a problem by a finite element analysis. The resulting group of methods is called probabilistic finite elements (PFEM). The overall objective of this work is to develop methodologies whereby the lifetime of a component can be predicted, accounting for the variability in the material and geometry of the component, the loads, and other aspects of the environment; and the range of response expected in a particular scenario can be presented to the analyst in addition to the response itself. Emphasis has been placed on methods which are not statistical in character; that is, they do not involve Monte Carlo simulations. The reason for this choice of direction is that Monte Carlo simulations of complex nonlinear response require a tremendous amount of computation. The focus of efforts so far has been on nonlinear structural dynamics. However, in the continuation of this project, emphasis will be shifted to probabilistic fracture mechanics so that the effect of randomness in crack geometry and material properties can be studied interactively with the effect of random load and environment. Author

**N89-29804\*** # National Aeronautics and Space Administration. Lewis Research Center, Cleveland, OH.

### **THE 3-D INELASTIC ANALYSES FOR COMPUTATIONAL STRUCTURAL MECHANICS**

D. A. HOPKINS and C. C. CHAMIS /in NASA. Langley Research Center, NASA Workshop on Computational Structural Mechanics 1987, Part 3 p 943-979 Feb. 1989

Avail: NTIS HC A18/MF A01 CSCL 20/11

The 3-D inelastic analysis method is a focused program with the objective to develop computationally effective analysis methods and attendant computer codes for three-dimensional, nonlinear time and temperature dependent problems present in the hot section of turbojet engine structures. Development of these methods was a major part of the Hot Section Technology (HOST) program over the past five years at Lewis Research Center. Author

**N89-29805\*** # Ohio State Univ., Columbus. Dept. of Aeronautical and Astronautical Engineering.

### **SPECIALTY FUNCTIONS SINGULARITY MECHANICS PROBLEMS**

NESRIN SARIGUL /in NASA. Langley Research Center, NASA Workshop on Computational Structural Mechanics 1987, Part 3 p 981-1012 Feb. 1989

(Contract NAG3-790)

Avail: NTIS HC A18/MF A01 CSCL 20/11

The focus is in the development of more accurate and efficient advanced methods for solution of singular problems encountered in mechanics. At present, finite element methods in conjunction with special functions, boolean sum and blending interpolations are being considered. In dealing with systems which contain a singularity, special finite elements are being formulated to be used in singular regions. Further, special transition elements are being formulated to couple the special element to the mesh that models

the rest of the system, and to be used in conjunction with 1-D, 2-D and 3-D elements within the same mesh. Computational simulation with a least squares fit is being utilized to construct special elements, if there is an unknown singularity in the system. A novel approach is taken in formulation of the elements in that: (1) the material properties are modified to include time, temperature, coordinate and stress dependant behavior within the element; (2) material properties vary at nodal points of the elements; (3) a hidden-symbolic computation scheme is developed and utilized in formulating the elements; and (4) special functions and boolean sum are utilized in order to interpolate the field variables and their derivatives along the boundary of the elements. It may be noted that the proposed methods are also applicable to fluids and coupled problems. Author

**N89-29810\*** # National Aeronautics and Space Administration. Lewis Research Center, Cleveland, OH.

### **MULTI-GRID FOR STRUCTURES ANALYSIS**

ALBERT F. KASCAK /in NASA. Langley Research Center, NASA Workshop on Computational Structural Mechanics 1987, Part 3 p 1133-1182 Feb. 1989

Avail: NTIS HC A18/MF A01 CSCL 20/11

In structural analysis the amount of computational time necessary for a solution is proportional to the number of degrees of freedom times the bandwidth squared. In implicit time analysis, this must be done at each discrete point in time. If, in addition, the problem is nonlinear, then this solution must be iterated at each point in time. If the bandwidth is large, the size of the problem that can be analyzed is severely limited. The multi-grid method is a possible algorithm which can make this solution much more computationally efficient. This method has been used for years in computational fluid mechanics. It works on the fact that relaxation is very efficient on the high frequency components of the solution (nearest neighbor interactions) and not very good on low frequency components of the solution (far interactions). The multi-grid method is then to relax the solution on a particular model until the residual stops changing. This indicates that the solution contains the higher frequency components. A coarse model is then generated for the lower frequency components to the solution. The model is then relaxed for the lower frequency components of the solution. These lower frequency components are then interpolated to the fine model. In computational fluid mechanics the equations are usually expressed as finite differences. Author

## 43

## **EARTH RESOURCES AND REMOTE SENSING**

Includes remote sensing of earth resources by aircraft and spacecraft; photogrammetry; and aerial photography.

**N89-10403\*** # National Aeronautics and Space Administration. Lewis Research Center, Cleveland, OH.

### **DATA REPORT FOR THE SIPLE COAST (ANTARCTICA) PROJECT**

R. A. BINDSCHADLER, S. N. STEPHENSON, E. P. ROBERTS, D. R. MACAYEAL, and D. R. LINDSTROM (Chicago Univ., Ill.) Oct. 1988 108 p

(NASA-TM-100708; NAS 1.15:100708; REPT-88B-0214) Avail: NTIS HC A06/MF A01 CSCL 08/2

This report presents data collected during three field seasons of glaciological studies in the Antarctica and describes the methods employed. The region investigated covers the mouths of Ice Streams B and C (the Siple Coast) and Crary Ice Rise on the Ross Ice Shelf. Measurements included in the report are as follows: surface velocity and deformation from repeated satellite geociever positions; surface topography from optical levelling; radar sounding of ice thickness; accumulation rates; near-surface densities and temperature profiles; and mapping from aerial photography. Author

## ENERGY PRODUCTION AND CONVERSION

Includes specific energy conversion systems, e.g., fuel cells; global sources of energy; geophysical conversion; and windpower.

**A89-15250\*** Westinghouse Electric Corp., Pittsburgh, PA.  
**EFFECTS OF OPERATING PARAMETERS ON PAFC STACK PERFORMANCE**

M. T. LE, R. R. HOLMAN, and W. L. LIAO (Westinghouse Electric Corp., Advanced Energy Systems Div., Pittsburgh, PA) IN: 1988 IECEC; Proceedings of the Twenty-third Intersociety Energy Conversion Engineering Conference, Denver, CO, July 31-Aug. 5, 1988. Volume 2. New York, American Society of Mechanical Engineers, 1988, p. 251-255. DOE-supported research. (Contract DEN3-290)

Copyright

This work was performed to assess actual relationships of phosphoric acid fuel cell voltage responses obtained from subscale cells with air-cooled and full size cells in stacks as a function of operating parameters. Key relationships were verified and found to be in agreement with the Nerst equation. An empirical equation was developed to predict cell voltages as a function of the measureable parameters.

Author

**A89-15258\*** International Fuel Cells Corp., South Windsor, CT.  
**ALKALINE FUEL CELL PERFORMANCE INVESTIGATION**

R. E. MARTIN (International Fuel Cells Corp., South Windsor, CT) and M. A. MANZO (NASA, Lewis Research Center, Cleveland, OH) IN: 1988 IECEC; Proceedings of the Twenty-third Intersociety Energy Conversion Engineering Conference, Denver, CO, July 31-Aug. 5, 1988. Volume 2. New York, American Society of Mechanical Engineers, 1988, p. 301-304. Previously announced in STAR as N88-27267. refs

(Contract NAS3-22234)

Copyright

An exploratory experimental fuel cell test program was conducted to investigate the performance characteristics of alkaline laboratory research electrodes. The objective of this work was to establish the effect of temperature, pressure, and concentration upon performance and evaluate candidate cathode configurations having the potential for improved performance. The performance characterization tests provided data to empirically establish the effect of temperature, pressure, and concentration upon performance for cell temperatures up to 300 F and reactant pressures up to 200 psia. Evaluation of five gold alloy cathode catalysts revealed that three doped gold alloys had more than two times the surface areas of reference cathodes and therefore offered the best potential for improved performance.

Author

**A89-15280\*** Hughes Aircraft Co., Malibu, CA.  
**THE EFFECT OF DIFFERENT ALKALI METAL HYDROXIDES ON NICKEL ELECTRODE LIFE**

H. S. LIM, S. A. VERZWYVELT, and S. K. CLEMENT (Hughes Aircraft Co., Malibu, CA) IN: 1988 IECEC; Proceedings of the Twenty-third Intersociety Energy Conversion Engineering Conference, Denver, CO, July 31-Aug. 5, 1988. Volume 2. New York, American Society of Mechanical Engineers, 1988, p. 457-463. refs

(Contract NAS3-22238)

Copyright

An accelerated cycle-life test (100-percent depth of discharge) of a sintered-type Ni electrode has been carried out in a flooded cell containing different alkali metal hydroxide electrolytes such as LiOH, NaOH, KOH, RbOH, and CsOH. Decrease in Ni electrode capacity with cycling was reduced as the radius of the alkali metal ions, with possible exception of CsOH.

Author

**A89-23280\*** National Aeronautics and Space Administration. Lewis Research Center, Cleveland, OH.

**SPACE ELECTROCHEMICAL RESEARCH AND TECHNOLOGY CONFERENCE, CLEVELAND, OH, APR. 14-16, 1987, PROCEEDINGS**

LAWRENCE H. THALLER, ED. (NASA, Lewis Research Center, Cleveland, OH) Conference sponsored by NASA. Journal of Power Sources (ISSN 0378-7753), vol. 22, March-Apr. 1988, 259 p. Previously announced in STAR as N87-29914.

Copyright

The conference provided a forum to assess critical needs and technologies for the NASA electrochemical energy conversion and storage program. It was aimed at providing guidance to NASA on the appropriate direction and emphasis of that program. A series of related overviews were presented in the areas of NASA advanced mission models (space stations, low and geosynchronous Earth orbit missions, planetary missions, and space transportation). Papers were presented and workshops conducted in a variety of technical areas, including advanced rechargeables, advanced concepts, critical physical electrochemical issues, and modeling.

Author

**A89-23283\*** Hughes Research Labs., Malibu, CA.  
**KOH CONCENTRATION EFFECT ON CYCLE LIFE OF NICKEL-HYDROGEN CELLS. III - CYCLE LIFE TEST**

H. S. LIM and S. A. VERZWYVELT (Hughes Research Laboratories, Malibu, CA) (NASA, Space Electrochemical Research and Technology Conference, Cleveland, OH, Apr. 14-16, 1987) Journal of Power Sources (ISSN 0378-7753), vol. 22, March-Apr. 1988, p. 213-220. Previously announced in STAR as N87-29920. refs

(Contract NAS3-22238)

Copyright

A cycle life test of Ni/H<sub>2</sub> cells containing electrolytes of various KOH concentrations and a sintered type nickel electrode was carried out at 23 C using a 45 min accelerated low earth orbit (LEO) cycle regime at 80 percent depth of discharge. One of three cells containing 26 percent KOH has achieved over 28,000 cycles, and the other two 19,000 cycles, without a sign of failure. Two other cells containing 31 percent KOH electrolyte, which is the concentration presently used in aerospace cells, failed after 2,979 and 3,620 cycles. This result indicates that the cycle life of the present type of Ni/H<sub>2</sub> cells may be extended by a factor of 5 to 10 simply by lowering the KOH concentration. Long cycle life of a Ni/H<sub>2</sub> battery at high depth-of-discharge operation is desired, particularly for an LEO spacecraft application. Typically, battery life of about 30,000 cycles is required for a five year mission in an LEO. Such a cycle life with presently available cells can be assured only at a very low depth-of-discharge operation. Results of testing already show that the cycle life of an Ni/H<sub>2</sub> cell is tremendously improved by simply using an electrolyte of low KOH concentration.

Author

**A89-23290\*** Case Western Reserve Univ., Cleveland, OH.  
**THEORETICAL PERFORMANCE OF HYDROGEN-BROMINE RECHARGEABLE SPE FUEL CELL**

R. F. SAVINELL and S. D. FRITTS (Case Western Reserve University, Cleveland, OH) (NASA, Space Electrochemical Research and Technology Conference, Cleveland, OH, Apr. 14-16, 1987) Journal of Power Sources (ISSN 0378-7753), vol. 22, March-Apr. 1988, p. 423-440. Previously announced in STAR as N87-29945. refs

(Contract NAG3-500; NSF CBT-86-96073)

Copyright

A mathematical model was formulated to describe the performance of a hydrogen-bromine fuel cell. Porous electrode theory was applied to the carbon felt flow-by electrode and was coupled to theory describing the solid polymer electrolyte (SPE) system. Parametric studies using the numerical solution to this model were performed to determine the effect of kinetic, mass transfer, and design parameters on the performance of the fuel cell. The results indicate that the cell performance is most sensitive to the transport properties of the SPE membrane. The model was also shown to be a useful tool for scale-up studies.

Author

## 44 ENERGY PRODUCTION AND CONVERSION

**A89-29114\*#** University of South Florida, Tampa.  
**EVALUATION OF ALTERNATIVE PHASE CHANGE MATERIALS FOR ENERGY STORAGE IN SOLAR DYNAMIC APPLICATIONS**

R. A. CRANE (South Florida, University, Tampa, FL) and M. O. DUSTIN (NASA, Lewis Research Center, Cleveland, OH) IN: Solar engineering - 1988; Proceedings of the Tenth Annual ASME Solar Energy Conference, Denver, CO, Apr. 10-14, 1988. New York, American Society of Mechanical Engineers, 1988, p. 329-334. refs  
Copyright

The performance of fluoride salt and metallic thermal energy storage materials are compared in terms of basic performance as applied to solar dynamic power generation. Specific performance considerations include uniformity of cycle inlet temperature, peak cavity temperature, TES utilization, and system weights. Also investigated were means of enhancing the thermal conductivity of the salts and its effect on the system performance. Author

**A89-44005\*** National Aeronautics and Space Administration. Lewis Research Center, Cleveland, OH.  
**SMALL SCALE BIPOLAR NICKEL-HYDROGEN TESTING**

MICHELLE A. MANZO (NASA, Lewis Research Center, Cleveland, OH) IN: International Power Sources Symposium, 33rd, Cherry Hill, NJ, June 13-16, 1988, Proceedings. Pennington, NJ, Electrochemical Society, Inc., 1988, p. 494-502. Previously announced in STAR as N88-25059.  
Copyright

Bipolar nickel-hydrogen batteries, ranging in capacity from 6 to 40 A-hr, have been tested at the NASA Lewis Research Center over the past six years. Small scale tests of 1 A-hr nickel-hydrogen stacks have been initiated as a means of screening design and component variations for bipolar nickel-hydrogen cells and batteries. Four small-scale batteries have been built and tested. Characterization and limited cycle testing were performed to establish the validity of test results in the scaled down hardware. The results show characterization test results to be valid. LEO test results in the small scale hardware have limited value. Author

**A89-44883\*** Midwest Research Inst., Golden, CO.  
**HIGH-EFFICIENCY INDIUM TIN OXIDE/INDIUM PHOSPHIDE SOLAR CELLS**

X. LI, M. W. WANLASS, T. A. GESSERT, K. A. EMERY, and T. J. COUTTS (Solar Energy Research Institute, Golden, CO) Applied Physics Letters (ISSN 0003-6951), vol. 54, June 26, 1989, p. 2674-2676. refs  
(Contract DE-AC02-83CH-10093; NASA ORDER C-30005-K)  
Copyright

Improvements in the performance of indium tin oxide (ITO)/indium phosphide solar cells have been realized by the dc magnetron sputter deposition of n-ITO onto an epitaxial p/(+) structure grown on commercial p/(+) bulk substrates. The highest efficiency cells were achieved when the surface of the epilayer was exposed to an Ar/H<sub>2</sub> plasma before depositing the bulk of the ITO in a more typical Ar/O<sub>2</sub> plasma. With H<sub>2</sub> processing, global efficiencies of 18.9 percent were achieved. It is suggested that the excellent performance of these solar cells results from the optimization of the doping, thickness, transport, and surface properties of the p-type base, as well as from better control over the ITO deposition procedure. R.R.

**A89-52203\*** National Aeronautics and Space Administration. Lewis Research Center, Cleveland, OH.  
**SPACE SOLAR CELL RESEARCH**

DENNIS J. FLOOD (NASA, Lewis Research Center, Cleveland, OH) Chemical Engineering Progress (ISSN 0360-7275), April 1989, p. 62-67.  
Copyright

A brief overview is given of the scope of the NASA space solar cell research and development program. Silicon cells, gallium arsenide cells, indium phosphide cells, and superlattice solar cells are addressed, indicating the state of the art of each type in

outer space and their advantages and drawbacks for use in outer space. Contrasts between efficiency in space and on earth are pointed out. C.D.

**N89-10405\*#** National Aeronautics and Space Administration. Lewis Research Center, Cleveland, OH.  
**HYDROGEN-BROMINE FUEL CELL ADVANCE COMPONENT DEVELOPMENT**

JOANN CHARLESTON and JAMES REED (Atlanta Univ., Ga.) 1988 16 p Presented at the National Technical Association Conference, Chicago, Ill., 13-16 Jul. 1988  
(NASA-TM-101345; E-4368; NAS 1.15:101345) Avail: NTIS HC A03/MF A01 CSCL 10/2

Advanced cell component development is performed by NASA Lewis to achieve improved performance and longer life for the hydrogen-bromine fuel cells system. The state-of-the-art hydrogen-bromine system utilizes the solid polymer electrolyte (SPE) technology, similar to the SPE technology developed for the hydrogen-oxygen fuel cell system. These studies are directed at exploring the potential for this system by assessing and evaluating various types of materials for cell parts and electrode materials for Bromine-hydrogen bromine environment and fabricating experimental membrane/electrode-catalysts by chemical deposition. Author

**N89-10409\*#** National Aeronautics and Space Administration. Lewis Research Center, Cleveland, OH.  
**OXYGEN ELECTRODE BIFUNCTIONAL ELECTROCATALYST NICO<sub>2</sub>O<sub>4</sub> SPINEL**

WILLIAM L. FIELDER and JOSEPH SINGER Sep. 1988 22 p  
(NASA-TM-100947; E-4238; NAS 1.15:100947) Avail: NTIS HC A03/MF A01 CSCL 10/1

A significant increase in energy density may be possible if a two-unit alkaline regenerative H<sub>2</sub>-O<sub>2</sub> fuel cell is replaced with a single-unit system that uses passive means for H<sub>2</sub>O transfer and thermal control. For this single-unit system, new electrocatalysts for the O<sub>2</sub> electrode will be required which are not only bifunctionally active but also chemically and electrochemically stable between the voltage range of about 0.7 and 1.5 V. NiCo<sub>2</sub>O<sub>4</sub> spinel is reported to have certain characteristics that make it useful for a study of electrode fabrication techniques. High surface area NiCo<sub>2</sub>O<sub>4</sub> powder was fabricated into unsupported, bifunctional, PTFE-bonded, porous gas fuel cell electrodes by commercial sources using varying PTFE contents and sintering temperatures. The object of this study is to measure the bifunctional activities of these electrodes and to observe what performance differences might result from different commercial electrode fabricators. O<sub>2</sub> evolution and O<sub>2</sub> reduction data were obtained at 80 C (31 percent KOH). An irreversible reaction (i.e., aging) occurred during O<sub>2</sub> evolution at potentials greater than about 1.5 V. Anodic Tafel slopes of 0.06 and 0.12 V/decade were obtained for the aged electrodes. Within the range of 15 to 25 percent, the PTFE content was not a critical parameter for optimizing the electrode for O<sub>2</sub> evolution activity. Sintering temperatures between 300 and 340 C may be adequate but heating at 275 C may not be sufficient to properly sinter the PTFE-NiCo<sub>2</sub>O<sub>4</sub> mixture. Electrode disintegration was observed during O<sub>2</sub> reduction. Transport of O<sub>2</sub> to the NiCo<sub>2</sub>O<sub>4</sub> surface became prohibitive at greater than about -0.02 A/sq cm. Cathodic Tafel slopes of -0.6 and -0.12 V/decade were assumed for the O<sub>2</sub> reduction process. A PTFE content of 25 percent (or greater) appears to be preferable for sintering the PTFE-NiCo<sub>2</sub>O<sub>4</sub> mixture. Author

**N89-11315\*#** Lockheed Missiles and Space Co., Sunnyvale, CA.  
**PV MODULES FOR GROUND TESTING Final Report**

10 Sep. 1986 132 p  
(Contract NAS3-24657)  
(NASA-CR-179476; NAS 1.26:179476; LMSC/D973480) Avail: NTIS HC A07/MF A01 CSCL 10/1

The main objective was to design and build a minimum of three photovoltaic test panels for plasma interaction experiments. These experiments are intended to provide data on the interactions

between high-voltage solar arrays and the space plasma environment. Data gathered will significantly contribute to the development of design criteria for the space station solar arrays. Electrical isolation between the solar cell strings and the module mounting plate is required for high-voltage bias. Author

**N89-12122\*#** Cleveland State Univ., OH. Dept. of Chemical Engineering.

**MATHEMATICAL MODELING OF SOLID OXIDE FUEL CELLS  
Final Contractor Report**

CHENG-YI LU and THOMAS M. MALONEY Aug. 1988 10 p  
(Contract NCC3-17; DE-AI21-80ET-17088)  
(NASA-CR-182188; E-4319; DOE/NASA/0017-5; NAS  
1.26:182188) Avail: NTIS HC A02/MF A01 CSCL 10/2

Development of predictive techniques, with regard to cell behavior, under various operating conditions is needed to improve cell performance, increase energy density, reduce manufacturing cost, and to broaden utilization of various fuels. Such technology would be especially beneficial for the solid oxide fuel cells (SOFC) at its early demonstration stage. The development of computer models to calculate the temperature, CD, reactant distributions in the tubular and monolithic SOFCs. Results indicate that problems of nonuniform heat generation and fuel gas depletion in the tubular cell module, and of size limitations in the monolithic (MOD 0) design may be encountered during FC operation. Author

**N89-12123\*#** National Aeronautics and Space Administration. Lewis Research Center, Cleveland, OH.

**INP HOMOJUNCTION SOLAR CELL PERFORMANCE ON THE  
LIPS 3 FLIGHT EXPERIMENT**

DAVID J. BRINKER, RUSSELL E. HART, JR., IRVING WEINBERG, and BRIAN S. SMITH 1988 11 p Presented at the 20th Photovoltaic Specialists Conference, Las Vegas, Nev., 26-30 Sep. 1988; sponsored by IEEE  
(NASA-TM-101390; E-4454; NAS 1.15:101390) Avail: NTIS HC A03/MF A01 CSCL 10/1

Performance data for the NASA Lewis Research Center indium phosphide n+p homojunction solar cell module on the LIPS 3 Flight Experiment is presented. The objective of the experiment is to measure the performance of InP cells in the natural radiation environment of the 1100 km altitude, 60+ deg inclination orbit. Analysis of flight data indicates that the performance of the four cells throughout the first year is near expected values. No degradation in short-circuit current was seen, as was expected from radiation tolerance studies of similar cells. Details of the cell structure and flight module design are discussed. The results of the temperature dependency and radiation tolerance studies necessary for normalization and analysis of the data are included. Author

**N89-13103\*#** Cleveland State Univ., OH. Dept. of Chemical Engineering.

**ASSESSMENT AND COMPARISON OF 100-MW COAL  
GASIFICATION PHOSPHORIC ACID FUEL CELL POWER  
PLANTS**

CHENG-YI LU Aug. 1988 9 p Presented at the 1988 Fuel Cell Seminar, Long Beach, Calif., 23-26 Oct. 1988; sponsored by the National Fuel Cell Coordinating Group  
(Contract NCC3-17; DE-AI21-80ET-17088)  
(NASA-CR-182189; E-4320; DOE/NASA/0017-7; NAS  
1.26:182189) Avail: NTIS HC A02/MF A01 CSCL 10/1

One of the advantages of fuel cell (FC) power plants is fuel versatility. With changes only in the fuel processor, the power plant will be able to accept a variety of fuels. This study was performed to design process diagrams, evaluate performance, and to estimate cost of 100 MW coal gasifier (CG)/phosphoric acid fuel cell (PAFC) power plant systems utilizing coal, which is the largest single potential source of alternate hydrocarbon liquids and gases in the United States, as the fuel. Results of this study will identify the most promising integrated CG/PAFC design and its near-optimal operating conditions. The comparison is based on the performance and cost of electricity which is calculated under consistent financial assumptions. Author

**N89-16224\*#** Sanders Associates, Inc., Nashua, NH.

**ADVANCED HEAT RECEIVER CONCEPTUAL DESIGN STUDY  
Final Report, May 1986 - Jul. 1988**

JAMES KESSELL, ROGER SAUNDERS, and GARY BATCHELDER Oct. 1988 238 p  
(Contract NAS3-24858)  
(NASA-CR-182177; NAS 1.26:182177) Avail: NTIS HC A11/MF A01 CSCL 10/1

Solar Dynamic space power systems are candidate electrical power generating systems for future NASA missions. One of the key components of the solar dynamic power system is the solar receiver/thermal energy storage (TES) subsystem. Receiver development was conducted by NASA in the late 1960's and since then a very limited amount of work has been done in this area. Consequently the state of the art (SOA) receivers designed for the IOC space station are large and massive. The objective of the Advanced Heat Receiver Conceptual Design Study is to conceive and analyze advanced high temperature solar dynamic Brayton and Stirling receivers. The goal is to generate innovative receiver concepts that are half of the mass, smaller, and more efficient than the SOA. It is also necessary that these innovative receivers offer ease of manufacturing, less structural complexity and fewer thermal stress problems. Advanced Brayton and Stirling receiver storage units are proposed and analyzed in this study which can potentially meet these goals. Author

**N89-17356\*#** National Aeronautics and Space Administration. Lewis Research Center, Cleveland, OH.

**THE EFFECT OF DIFFERENT MODULE CONFIGURATIONS ON  
THE RADIATION TOLERANCE OF MULTI-JUNCTION SOLAR  
CELLS**

JAMES M. GEE and HENRY B. CURTIS 1988 20 p Prepared in cooperation with Sandia National Labs., Albuquerque, NM Sponsored by NASA  
(Contract DE-AC04-76DP-00789)  
(NASA-TM-101251; NAS 1.15:101251; DE89-000304;  
SAND-88-0628C; CONF-880965-2) Avail: NTIS HC A03/MF A01 CSCL 10/1

The effect of different module configurations on the performance of multijunction (MJ) solar cells in a radiation environment was investigated. Module configuration refers to the electrical circuit in which the subcells of the multijunction cell are wired. Experimental data for AlGaAs, GaAs, InGaAs, and silicon single-junction concentrator cells subjected to 1 MeV electron irradiation was used to calculate the expected performance of AlGaAs/InGaAs, AlGa/silicon, GaAs/InGaAs, and GaAs/silicon MJ concentrator cells. These calculations included independent, series, and voltage-matched configurations. The module configuration was found to have a significant impact on the radiation tolerance characteristic of the MJ cells. DOE

**N89-17941\*#** Space Power, Inc., San Jose, CA.

**MEGAWATT CLASS NUCLEAR SPACE POWER SYSTEMS  
(MCNPS) CONCEPTUAL DESIGN AND EVALUATION  
REPORT. VOLUME 1: OBJECTIVES, SUMMARY RESULTS  
AND INTRODUCTION Final Report**

J. R. WETCH et al. Sep. 1988 40 p Sponsored in part by DOD, Washington, DC and DOE, Washington, DC  
(Contract NAS3-23867)  
(NASA-CR-179614-VOL-1; NAS 1.26:179614-VOL-1; SPI-25-1)  
Avail: NTIS HC A03/MF A01 CSCL 10/2

The objective was to determine which reactor, conversion, and radiator technologies would best fulfill future Megawatt Class Nuclear Space Power System Requirements. Specifically, the requirement was 10 megawatts for 5 years of full power operation and 10 years systems life on orbit. A variety of liquid metal and gas cooled reactors, static and dynamic conversion systems, and passive and dynamic radiators were considered. Four concepts were selected for more detailed study. The concepts are: a gas cooled reactor with closed cycle Brayton turbine-alternator conversion with heat pipe and pumped tube-fin heat rejection; a lithium cooled reactor with a free piston Stirling engine-linear alternator and a pumped tube-fin radiator; a lithium cooled reactor

## 44 ENERGY PRODUCTION AND CONVERSION

with potassium Rankine turbine-alternator and heat pipe radiator; and a lithium cooled incore thermionic static conversion reactor with a heat pipe radiator. The systems recommended for further development to meet a 10 megawatt long life requirement are the lithium cooled reactor with the K-Rankine conversion and heat pipe radiator, and the lithium cooled incore thermionic reactor with heat pipe radiator. Author

**N89-18967\*#** Space Power, Inc., San Jose, CA.  
**MEGAWATT CLASS NUCLEAR SPACE POWER SYSTEMS (MCNSPS) CONCEPTUAL DESIGN AND EVALUATION REPORT. VOLUME 4: CONCEPTS SELECTION, CONCEPTUAL DESIGNS, RECOMMENDATIONS**

J. R. WETCH et al. Sep. 1988 111 p  
(Contract NAS3-23867)

(NASA-CR-179614-VOL-4; NAS 1.26:179614-VOL-4; SPI-25-1-VOL-4) Avail: NTIS HC A06/MF A01 CSCL 10/2

A study was conducted by NASA Lewis Research Center for the Triagency SP-100 program office. The objective was to determine which reactor, conversion and radiator technologies would best fulfill future Megawatt Class Nuclear Space Power System Requirements. The requirement was 10 megawatts for 5 years of full power operation and 10 years system life on orbit. A variety of liquid metal and gas cooled reactors, static and dynamic conversion systems, and passive and dynamic radiators were considered. Four concepts were selected for more detailed study: (1) a gas cooled reactor with closed cycle Brayton turbine-alternator conversion with heatpipe and pumped tube fin rejection, (2) a Lithium cooled reactor with a free piston Stirling engine-linear alternator and a pumped tube-fin radiator, (3) a Lithium cooled reactor with a Potassium Rankine turbine-alternator and heat pipe radiator, and (4) a Lithium cooled incore thermionic static conversion reactor with a heat pipe radiator. The systems recommended for further development to meet a 10 megawatt long life requirement are the Lithium cooled reactor with the K-Rankine conversion and heat pipe radiator, and the Lithium cooled incore thermionic reactor with heat pipe radiator. Author

**N89-19737\*#** National Aeronautics and Space Administration. Lewis Research Center, Cleveland, OH.

**RE-1000 FREE-PISTON STIRLING ENGINE SENSITIVITY TEST RESULTS Final Report**

JEFFREY G. SCHREIBER, STEVEN M. GENG, and GARY V. LORENZ Oct. 1986 130 p  
(Contract DE-AI05-82OR-1005)

(NASA-TM-88846; DOE/NASA/1005-11; E-3277; NAS 1.15:88846) Avail: NTIS HC A07/MF A01 CSCL 10/2

The NASA Lewis Research Center has been testing a 1 kW (1.33 hp) free-piston Stirling engine. The tests performed over the past several years have been on a single cylinder machine known as the RE-1000. The data recorded were to aid in the investigation of the dynamics and thermo-dynamics of the free-piston Stirling engine. The data are intended to be used primarily for computer code validation. NASA reports TM-82999, TM-83407, and TM-87126 give initial results of the engine tests. The tests were designed to investigate the sensitivity of the engine performance to variations on the mean pressure of the working space, the working fluid used, heater and cooler temperatures, regenerator porosity, power piston mass and displacer dynamics. These tests have now been completed. Some of the data collected in the sensitivity tests are presented. In all, 781 data points were recorded. A completed description of the engine and test facility is given. Many of the data can be found in tabular form, and a microfiche containing all of the data points can be requested from the NASA Lewis. Author

**N89-20545\*#** National Aeronautics and Space Administration. Lewis Research Center, Cleveland, OH.

**MARS MANNED TRANSPORTATION VEHICLE**

MARLA E. PEREZ-DAVIS and KARL A. FAYMON Jul. 1987 12 p Presented at the Case for Mars III, Boulder, CO, 18-22 Jul. 1987; sponsored in part by American Astronautical Society; Jet Propulsion Lab.; NASA, Ames Res. Ctr.; NASA, Johnson Space

Ctr; NASA, Marshall Space Flight Ctr.; and The Planetary Society (NASA-TM-101487; E-4627; NAS 1.15:101487) Avail: NTIS HC A03/MF A01 CSCL 13/6

A viable power system technology for a surface transportation vehicle to explore the planet Mars is presented. A number of power traction systems were investigated, and it was found that a regenerative hydrogen-oxygen fuel cell appears to be attractive for a manned Mars rover application. Mission requirements were obtained from the Manned Mars Mission Working Group. Power systems weights, power, and reactants requirements were determined as a function of vehicle weights for vehicles weighing from 6,000 to 16,000 lb (2,722 to 7,257 kg), (Earth weight). The vehicle performance requirements were: velocity, 10 km/hr; range, 100 km; slope climbing capability, 30 deg uphill for 50 km; mission duration, 5 days; and crew, 5. Power requirements for the operation of scientific equipment and support system capabilities were also specified and included in this study. The concept developed here would also be applicable to a Lunar based vehicle for Lunar exploration. The reduced gravity on the Lunar surface, (over that on the Martian surface), would result in an increased range or capability over that of the Mars vehicle since many of the power and energy requirements for the vehicle are gravity dependent. Author

**N89-21417\*#** National Aeronautics and Space Administration. Lewis Research Center, Cleveland, OH.

**GAS TURBINE ALTERNATIVE FUELS COMBUSTION CHARACTERISTICS Final Report**

R. JAMES ROLLBUHLER Feb. 1989 27 p  
(Contract DE-AI01-85CE-50111)

(NASA-TM-101470; E-4584; DOE/NASA/50111-3; NAS 1.15:101470) Avail: NTIS HC A03/MF A01 CSCL 21/4

An experimental investigation was conducted to obtain combustion performance and exhaust pollutant concentrations for specific synthetic hydrocarbon fuels. Baseline comparison fuels used were gasoline and diesel fuel number two. Testing was done over a range of fuel to air mass ratios, total mass flow rates, and input combustion air temperatures in a flame-tube-type gas turbine combustor. Test results were obtained in terms of released heat and combustion gas emission values. The results were comparable to those obtained with the base fuels with variations being obtained with changing operating conditions. The release of carbon particles during the tests was minimal. Author

**N89-21419\*#** National Aeronautics and Space Administration. Lewis Research Center, Cleveland, OH.

**CRYOGENIC REACTANT STORAGE FOR LUNAR BASE REGENERATIVE FUEL CELLS**

LISA L. KOHOUT 1989 30 p Presented at the International Conference on Space Power, Cleveland, OH, 5-7 Jun. 1989; sponsored by the International Astronautical Federation (NASA-TM-101980; E-4679; NAS 1.15:101980) Avail: NTIS HC A03/MF A01 CSCL 10/2

There are major advantages to be gained by integrating a cryogenic reactant storage system with a hydrogen-oxygen regenerative fuel cell (RFC) to provide on-site electrical power during the lunar night. Although applicable to any power system using hydrogen-oxygen RFC's for energy storage, cryogenic reactant storage offers a significant benefit whenever the sun/shade cycle and energy storage period approach hundreds of hours. For solar power installations on the moon, cryogenic reactant storage reduces overall specific mass and meteoroid vulnerability of the system. In addition, it offers synergistic benefits to on-site users, such as availability of primary fuel cell reactants for surface rover vehicles and cryogenic propellants for OTV's. The integration involves processing and storing the RFC reactant streams as cryogenic liquids rather than pressurized gases, so that reactant containment (tankage per unit mass of reactants) can be greatly reduced. Hydrogen-oxygen alkaline RFC's, GaAs photovoltaic (PV) arrays, and space cryogenic processing/refrigeration technologies are assumed to be available for the conceptual system design. Advantages are demonstrated by comparing the characteristics of two power system concepts:



a conventional lunar surface PV/RFC power system using pressurized gas storage in SOA filament wound pressure vessels and, that same system with gas liquefaction and storage replacing the pressurized storage. Comparisons are made at 20 and 250 kWe. Although cryogenic storage adds a processing plant (drying and liquefaction) to the system plus 30 percent more solar array to provide processing power, the approximate order of magnitude reduction in tankage mass, confirmed by this analysis, results in a reduction in overall total system mass of approximately 50 percent. Author

**N89-22177\*#** National Aeronautics and Space Administration. Lewis Research Center, Cleveland, OH.

**A V-GROOVED GAAS SOLAR CELL**

S. G. BAILEY, N. S. FATEMI, G. A. LANDIS (National Academy of Sciences - National Research Council, Washington, DC.), D. M. WILT, R. D. THOMAS, and A. ARRISON 1988 9 p Presented at the 20th Photovoltaic Specialists Conference, Las Vegas, NV, 26-30 Sep. 1988; sponsored by the IEEE (NASA-TM-101970; E-4668; NAS 1.15:101970) Avail: NTIS HC A02/MF A01 CSCL 10/1

V-grooved GaAs solar cells promise the benefits of improved optical coupling, higher short-circuit current, and increased tolerance to particle radiation compared to planar cells. A GaAs homojunction cell was fabricated by etching a V-groove pattern into an n epilayer (2.1 x 10 to the 17th power per cu cm) grown by metalorganic chemical vapor deposition (MOCVD) on an n+ substrate (2.8 x 10 to the 18th power per cu cm) and then depositing and MOCVD p epilayer (4.2 x 10 to the 18th power per cu cm). Reflectivity measurements on cells with and without an antireflective coating confirm the expected decrease in reluctance of the microgrooved cell compared to the planar structure. The short circuit current of the V-grooved solar cell was 13 percent higher than that of the planar control. Author

**N89-22980\*#** Space Power, Inc., San Jose, CA.  
**MEGAWATT CLASS NUCLEAR SPACE POWER SYSTEMS (MCNSPS) CONCEPTUAL DESIGN AND EVALUATION REPORT. VOLUME 3, TECHNOLOGIES 2: POWER CONVERSION Final Report**

J. R. WETCH et al. Sep. 1988 136 p (Contract NAS3-23867) (NASA-CR-179614-VOL-3; NAS 1.26:179614-VOL-3; SPI-25-1-VOL-3) Avail: NTIS HC A07/MF A01 CSCL 10/2

The major power conversion concepts considered for the Megawatt Class Nuclear Space Power System (MCNSPS) are discussed. These concepts include: (1) Rankine alkali-metal-vapor turbine alternators; (2) in-core thermionic conversion; (3) Brayton gas turbine alternators; and (4) free piston Stirling engine linear alternators. Considerations important to the coupling of these four conversion alternatives to an appropriate nuclear reactor heat source are examined along with the comparative performance characteristics of the combined systems meeting MCNSPS requirements. M.G.

**N89-22981\*#** Space Power, Inc., San Jose, CA.  
**MEGAWATT CLASS NUCLEAR SPACE POWER SYSTEMS (MCNSPS) CONCEPTUAL DESIGN AND EVALUATION REPORT. VOLUME 2, TECHNOLOGIES 1: REACTORS, HEAT TRANSPORT, INTEGRATION ISSUES Final Report**

J. R. WETCH et al. Sep. 1988 143 p (Contract NAS3-23867) (NASA-CR-179614-VOL-2; NAS 1.26:179614-VOL-2; SPI-25-1-VOL-2) Avail: NTIS HC A07/MF A01 CSCL 10/2

The objectives of the Megawatt Class Nuclear Space Power System (MCNSPS) study are summarized and candidate systems and subsystems are described. Particular emphasis is given to the heat rejection system and the space reactor subsystem. Author

**N89-22982\*#** National Aeronautics and Space Administration. Lewis Research Center, Cleveland, OH.

**SPACE ELECTROCHEMICAL RESEARCH AND TECHNOLOGY CONFERENCE: ABSTRACTS Abstracts Only**

Washington 1989 49 p Conference held in Cleveland, OH, 11-13 Apr. 1989 (NASA-CP-10029; E-4708; NAS 1.55:10029) Avail: NTIS HC A03/MF A01 CSCL 10/1

The objectives of the conference were to examine current technologies, research efforts, and advanced ideas, and to identify technical barriers which affect the advancement of electrochemical energy storage systems for space applications. Papers were presented and workshops were conducted in four technical areas: advanced concepts, hydrogen-oxygen fuel cells and electrolyzers, the nickel electrode, and advanced rechargeable batteries.

**N89-22996\*#** National Aeronautics and Space Administration. Lewis Research Center, Cleveland, OH.

**HYDROGEN-OXYGEN PROTON-EXCHANGE MEMBRANE FUEL CELLS AND ELECTROLYZERS Abstract Only**

R. BALDWIN, M. PHAM, A. LEONIDA, J. MCELROY, and T. NALETTE (Hamilton Standard, Windsor Locks, CT.) In its Space Electrochemical Research and Technology Conference: Abstracts p 19-20 1989 Avail: NTIS HC A03/MF A01 CSCL 10/1

Hydrogen-oxygen SPE fuel cells and SPE electrolyzers (products of Hamilton Standard) both use a Proton-Exchange Membrane (PEM) as the sole electrolyte. The SPE cells have demonstrated a ten year life capability under load conditions. Ultimate life of PEM fuel cells and electrolyzers is primarily related to the chemical stability of the membrane. For perfluorocarbon proton-exchange membranes an accurate measure of the membrane stability is the fluoride loss rate. Millions of cell hours have contributed to establishing a relationship between fluoride loss rates and average expected ultimate cell life. Several features were introduced into SPE fuel cells and SPE electrolyzers such that applications requiring greater than or equal to 100,000 hours of life can be considered. Equally important as the ultimate life is the voltage stability of hydrogen-oxygen fuel cells and electrolyzers. Here again the features of SPE fuel cells and SPE electrolyzers have shown a cell voltage stability in the order of 1 microvolt per hour. That level of stability were demonstrated for tens of thousands of hours in SPE fuel cells at up to 500 amps per square foot (ASF) current density. The SPE electrolyzers have demonstrated the same at 1000 ASF. Many future extraterrestrial applications for fuel cells require that they be self recharged. To translate the proven SPE cell life and stability into a highly reliable extraterrestrial electrical energy storage system, a simplification of supporting equipment is required. Static phase separation, static fluid transport and static thermal control will be most useful in producing required system reliability. Although some 200,000 SPE fuel cell hours were recorded in earth orbit with static fluid phase separation, no SPE electrolyzer has, as yet, operated in space. Author

**N89-22998\*#** Giner, Inc., Waltham, MA.  
**OXYGEN ELECTRODES FOR RECHARGEABLE ALKALINE FUEL CELLS Abstract Only**

L. SWETTE and N. KACKLEY In NASA, Lewis Research Center, Space Electrochemical Research and Technology Conference: Abstracts p 23-24 1989 (Contract NAS3-24635) Avail: NTIS HC A03/MF A01 CSCL 10/1

Electrocatalysts and supports for the positive electrode of moderate temperature single-unit rechargeable alkaline fuel cells are being investigated and developed. Candidate support materials were drawn from transition metal carbides, borides, nitrides and oxides which have high conductivity (greater than 1 ohm/cm). Candidate catalyst materials were selected largely from metal oxides of the form ABO sub x (where A = Pb, Cd, Mn, Ti, Zr, La, Sr, Na, and B = Pt, Pd, Ir, Ru, Ni (Co) which were investigated and/or developed for one function only, O2 reduction or O2 evolution. The electrical conductivity requirement for catalysts may be lower, especially if integrated with a higher conductivity support.

## 44 ENERGY PRODUCTION AND CONVERSION

All candidate materials of acceptable conductivity are subjected to corrosion testing. Materials that survive chemical testing are examined for electrochemical corrosion activity. For more stringent corrosion testing, and for further evaluation of electrocatalysts (which generally show significant O<sub>2</sub> evolution at 1.4 V), samples are held at 1.6 V or 0.6 V for about 100 hours. The surviving materials are then physically and chemically analyzed for signs of degradation. To evaluate the bifunctional oxygen activity of candidate catalysts, Teflon-bonded electrodes are fabricated and tested in a floating electrode configuration. Many of the experimental materials being studied have required development of a customized electrode fabrication procedure. In advanced development, the goal is to reduce the polarization to about 300 to 350 mV. Approximately six support materials and five catalyst materials were identified to date for further development. The test results will be described. Author

**N89-23000\*#** National Aeronautics and Space Administration. Lewis Research Center, Cleveland, OH.

**CORROSION TESTING OF CANDIDATES FOR THE ALKALINE FUEL CELL CATHODE Abstract Only**  
JOSEPH SINGER and WILLIAM L. FIELDER *In its* Space Electrochemical Research and Technology Conference: Abstracts p 27 1989  
(Contract NAS3-25119)  
Avail: NTIS HC A03/MF A01 CSCL 10/1

It is desirable to employ a corrosion screening test for catalyst or support candidates for the fuel cell cathode before entering upon optimization of the candidate or of the catalytic electrode. To this end, corrosion test electrodes, intended for complete immersion and maximum wetting, have been made with 30 to 40 vol. pct Teflon; with perovskites this is about 10 to 15 pct. The candidates were synthesized by methods intended for single-phase product without special emphasis on high surface area, although the substances tested were no coarser than 2 m squared/g. A typical loading was 25 mg/cm sq of the pure substance, usually on gold screen, a few mm squared of which were left bare for contacting. Contact to the gold lead wire was made by welding with a micro-torch or a spot-welder. Corrosion testing consisted of obtaining current-voltage data under flowing inert gas in the potential region for reduction of O<sub>2</sub>. The electrode was immersed in 30 pct KOH. Observations were made at 20 C and 80 C, and the results compared with data from gold standards. Results with some perovskites, pyrochlores, spinels, and interstitial compounds will be discussed. Author

**N89-23025\*#** National Aeronautics and Space Administration. Lewis Research Center, Cleveland, OH.

**INP (INDIUM PHOSPHIDE): INTO THE FUTURE**  
HENRY W. BRANDHORST, JR. Mar. 1989 10 p Presented at the 1st International Conference on Indium Phosphide, Norman OK, 20-22 Mar. 1989; sponsored by the Society of Photo-Optical Instrumentation Engineers  
(NASA-TM-102058; E-4816; NAS 1.15:102058) Avail: NTIS HC A02/MF A01 CSCL 10/1

Major industry is beginning to be devoted to indium phosphide and its potential applications. Key to these applications are high speed and radiation tolerance; however the high cost of indium phosphide may be an inhibitor to progress. The broad applicability of indium phosphide to many devices will be discussed with an emphasis on photovoltaics. Major attention is devoted to radiation tolerance and means of reducing cost of devices. Some of the approaches applicable to solar cells may also be relevant to other devices. The intent is to display the impact of visionary leadership in the field and enable the directions and broad applicability of indium phosphide. Author

**N89-24704\*#** National Aeronautics and Space Administration. Lewis Research Center, Cleveland, OH.

**SPACE PHOTOVOLTAIC RESEARCH AND TECHNOLOGY, 1988. HIGH EFFICIENCY, SPACE ENVIRONMENT, AND ARRAY TECHNOLOGY**  
Washington Apr. 1989 362 p Conference held in Cleveland,

OH, 19-21 Apr. 1988

(NASA-CP-3030; E-4587; NAS 1.55:3030) Avail: NTIS HC A16/MF A01 CSCL 10/1

The 9th Space Photovoltaic Research and Technology conference was held at the NASA Lewis Research Center from April 19 to 21, 1988. The papers and workshop summaries report remarkable progress on a wide variety of approaches in space photovoltaics, for both near and far term applications. Among the former is the recently developed high efficiency GaAs/Ge cell, which formed the focus of a workshop discussion on heteroepitaxial cells. Still aimed at the long term, but with a significant payoff in a new mission capability, are InP cells, with their potentially dramatic improvement in radiation resistance. Approaches to near term, array specific powers exceeding 130 W/kg are also reported, and advanced concentrator panel technology with the potential to achieve over 250 W/sq m is beginning to take shape.

**N89-24707\*#** National Aeronautics and Space Administration. Lewis Research Center, Cleveland, OH.

**PROGRESS IN INDIUM PHOSPHIDE SOLAR CELL RESEARCH**  
IRVING WEINBERG, CLIFFORD K. SWARTZ, and R. E. HART, JR. *In its* Space Photovoltaic Research and Technology, 1988. High Efficiency, Space Environment, and Array Technology p 19-27 Apr. 1989  
Avail: NTIS HC A16/MF A01 CSCL 10/1

Progress, dating from the start of the Lewis program, is reviewed emphasizing processing techniques which have achieved the highest efficiencies in a given year. To date, the most significant achievement has been attainment of AM0 total area efficiencies approaching 19 percent. Although closed tube diffusion is not considered to be an optimum process, reasonably efficient 2cm x 2cm and 1cm x 2cm InP cells have been produced in quantity by this method with a satellite to be launched in 1990 using these cells. Proton irradiation of these relatively large area cells indicates radiation resistance comparable to that previously reported for smaller InP cells. A similar result is found for the initial proton irradiations of ITO/InP cells processed by D. C. sputtering. With respect to computer modelling, a comparison of n/p homojunction InP and GaAs cells of identical geometries and dopant concentrations has confirmed the superior radiation resistance of InP cells under 1 MeV electron irradiations. Author

**N89-24711\*#** National Aeronautics and Space Administration. Lewis Research Center, Cleveland, OH.

**PREDICTED PERFORMANCE OF INP SOLAR CELLS IN CASSEGRAINIAN AND SLATS SPACE CONCENTRATOR ARRAYS AT 20 TO 100 AM0, 80 TO 100 C**  
CHANDRA GORADIA, WILLIAM THESLING, MANJU GHALLA GORADIA (Cleveland State Univ., OH.), IRVING WEINBERG, and CLIFFORD K. SWARTZ *In its* Space Photovoltaic Research and Technology, 1988. High Efficiency, Space Environment, and Array Technology p 66-78 Apr. 1989  
Avail: NTIS HC A16/MF A01 CSCL 10/1

Researchers have calculated the expected performance dependence of near-optimally designed shallow homojunction n+pp-InP solar cells on incident intensities up to 200 AM0 and temperatures up to 100 C (373K). Both circular and rectangular cells have been considered, the former for use in a Cassegrainian concentrator array at 100 AM0, 80 to 100 C and the latter for use in a Slats type concentrator array at 20 AM0 80 to 100 C. Calculation of the temperature dependence of the performance parameters I sub sc, V sub oc, FF and eta was done by first verifying that the use of the measured temperature variation of I sub sc, of the best published value of the temperature dependence of the bandgap of InP, and of the temperature dependences of the lifetimes and mobilities of electrons and holes the same as in equivalently doped GaAs, gave calculated results that closely matched measured data on the temperature variation of I sub sc, V sub oc, and FF of four existing InP cells at 1 AM0. It was then assumed that the same temperature dependences of I sub sc, the bandgap and lifetimes and mobilities would hold in the near-optimally designed cells at the higher concentrations. Author

**N89-24719\*#** National Aeronautics and Space Administration. Lewis Research Center, Cleveland, OH.

## ULTRA-THIN, LIGHT-TRAPPING SILICON SOLAR CELLS

GEOFFREY A. LANDIS *In its* Space Photovoltaic Research and Technology, 1988. High Efficiency, Space Environment, and Array Technology p 151-161 Apr. 1989

Avail: NTIS HC A16/MF A01 CSCL 10/1

Design concepts for ultra-thin (2 to 10 microns) high efficiency single-crystal silicon cells are discussed. Light trapping allows more light to be absorbed at a given thickness, or allows thinner cells of a given Jsc. Extremely thin cells require low surface recombination velocity at both surfaces, including the ohmic contacts. Reduction of surface recombination by growth of heterojunctions of ZnS and GaP on Si has been demonstrated. The effects of these improvements on AM0 efficiency is shown. The peak efficiency increases, and the optimum thickness decreases. Cells under 10 microns thickness can retain almost optimum power. The increase of absorptance due to light trapping is considered. This is not a problem if the light-trapping cells are sufficiently thin. Ultra-thin cells have high radiation tolerance. A 2 microns thick light-trapping cell remains over 18 percent efficient after the equivalent of 20 years in geosynchronous orbit. Including a 50 microns thick coverglass, the thin cells had specific power after irradiation over ten times higher than the baseline design.

Author

**N89-24721\*#** National Aeronautics and Space Administration. Lewis Research Center, Cleveland, OH.

## HIGH EFFICIENCY GAAS-GE TANDEM SOLAR CELLS GROWN BY MOCVD

S. M. VERNON, S. P. TOBIN, C. BAJGAR, VICTOR E. HAVEN, L. M. GEOFFROY, D. R. LILLINGTON (Spectrolab, Inc., Sylmar, CA.), and R. E. HART, JR. *In its* Space Photovoltaic Research and Technology, 1988. High Efficiency, Space Environment, and Array Technology p 167-176 Apr. 1989

Avail: NTIS HC A16/MF A01 CSCL 10/1

High conversion efficiency and low weight are obviously desirable for solar cells intended for space applications. One promising structure is GaAs on Ge. The advantages of using Ge wafers as substrates include the following: they offer high efficiency by forming a two-junction tandem cell; low weight combined with superior strength allows usage of thin (3 mil) wafers; and they are a good substrate for GaAs, being lattice matched, thermal expansion matched, and available as large-area wafers.

Author

**N89-24725\*#** Delaware Univ., Newark. Dept. of Electrical Engineering.

## A NEW STRUCTURE FOR COMPARING SURFACE PASSIVATION MATERIALS OF GAAS SOLAR CELLS

GREGORY C. DESALVO and ALLEN M. BARNETT *In* NASA, Lewis Research Center, Space Photovoltaic Research and Technology, 1988. High Efficiency, Space Environment, and Array Technology p 221-228 Apr. 1989

(Contract NAG3-422)

Avail: NTIS HC A16/MF A01 CSCL 10/1

The surface recombination velocity ( $S_{sub\ rec}$ ) for bare GaAs is typically as high as 10 to the 6th power to 10 to the 7th power cm/sec, which dramatically lowers the efficiency of GaAs solar cells. Early attempts to circumvent this problem by making an ultra thin junction ( $x_j$  less than .1 micron) proved unsuccessful when compared to lowering  $S_{sub\ rec}$  by surface passivation. Present day GaAs solar cells use an GaAlAs window layer to passivate the top surface. The advantages of GaAlAs in surface passivation are its high bandgap energy and lattice matching to GaAs. Although GaAlAs is successful in reducing the surface recombination velocity, it has other inherent problems of chemical instability (Al readily oxidizes) and ohmic contact formation. The search for new, more stable window layer materials requires a means to compare their surface passivation ability. Therefore, a device structure is needed to easily test the performance of different passivating candidates. Such a test device is described.

Author

**N89-24728\*#** National Aeronautics and Space Administration. Lewis Research Center, Cleveland, OH.

## CHEMICAL ETCHING AND ORGANOMETALLIC CHEMICAL VAPOR DEPOSITION ON VARIED GEOMETRIES OF GAAS

SHEILA G. BAILEY, GEOFFREY A. LANDIS, and DAVID M. WILT *In its* Space Photovoltaic Research and Technology, 1988. High Efficiency, Space Environment, and Array Technology p 250-263 Apr. 1989

Avail: NTIS HC A16/MF A01 CSCL 10/1

Results of micron-spaced geometries produced by wet chemical etching and subsequent OMCVD growth on various GaAs surfaces are presented. The polar lattice increases the complexity of the process. The slow-etch planes defined by anisotropic etching are not always the same as the growth facets produced during MOCVD deposition, especially for deposition on higher-order planes produced by the hex groove etching.

Author

**N89-24732\*#** National Aeronautics and Space Administration. Lewis Research Center, Cleveland, OH.

## DOMED FRESNEL LENS CONCENTRATOR TECHNOLOGY FOR SPACE APPLICATION

MICHAEL F. PISZCZOR, JR. and MARK J. ONEILL (ENTECH Corp., Dallas-Fort Worth Airport, TX.) *In its* Space Photovoltaic Research and Technology, 1988. High Efficiency, Space Environment, and Array Technology p 286-291 Apr. 1989

Avail: NTIS HC A16/MF A01 CSCL 10/1

Over the past three years, NASA Lewis and Entech, Inc. have been investigating the use of high efficiency refractive photovoltaic concentrators for use in space. The design currently under investigation uses a square domed Fresnel lens to focus light on a GaAs concentrator cell. A prismatic cell cover, which directs light away from the front contacts and thus eliminates metalization losses, is applied to the top of the GaAs cell to further enhance array efficiency. The latest experimental results based on testing the GaAs cell/prism cover assembly at standard and operating conditions are presented.

Author

**N89-24737\*#** National Aeronautics and Space Administration. Lewis Research Center, Cleveland, OH.

## A COMPARISON OF THE RADIATION TOLERANCE CHARACTERISTICS OF MULTI-JUNCTION SOLAR CELLS WITH SERIES AND VOLTAGE-MATCHED CONFIGURATIONS

JAMES M. GEE (Sandia National Labs., Albuquerque, NM.) and HENRY B. CURTIS *In its* Space Photovoltaic Research and Technology, 1988. High Efficiency, Space Environment, and Array Technology p 332-338 Apr. 1989 Previously announced as N86-24017

(Contract DE-AC04-76DP-00789)

Avail: NTIS HC A16/MF A01 CSCL 10/1

The effect of series and voltage-matched configurations on the performance of multijunction solar cells in a radiation environment was investigated. It was found that the configuration of the multijunction solar cell can have a significant impact on its radiation tolerance characteristics.

Author

**N89-24738\*#** Wayne State Univ., Detroit, MI.

## RADIATION RESISTANCE STUDIES OF AMORPHOUS SILICON FILMS

JAMES R. WOODYARD and J. SCOTT PAYSON *In* NASA, Lewis Research Center, Space Photovoltaic Research and Technology, 1988. High Efficiency, Space Environment, and Array Technology p 339-347 Apr. 1989

(Contract NAG3-833)

Avail: NTIS HC A16/MF A01 CSCL 10/1

Hydrogenated amorphous silicon thin films were irradiated with 2.00 MeV helium ions using fluences ranging from  $1E11$  to  $1E15$  cm<sup>-2</sup>. The films were characterized using photothermal deflection spectroscopy and photoconductivity measurements. The investigations show that the radiation introduces sub-band-gap states 1.35 eV below the conduction band and the states increase supralinearly with fluence. Photoconductivity measurements suggest the density of states above the Fermi energy is not changing drastically with fluence.

Author

## 44 ENERGY PRODUCTION AND CONVERSION

**N89-24741\*#** Sverdrup Technology, Inc., Cleveland, OH.  
**NASA LEWIS STIRLING ENGINE COMPUTER CODE EVALUATION Final Report**

TIMOTHY J. SULLIVAN Jan. 1989 43 p  
(Contract NAS3-24105; DE-AI01-85CE-50112)  
(NASA-CR-182248; DOE/NASA/4105-4; E-4580; NAS 1.26:182248) Avail: NTIS HC A03/MF A01

In support of the U.S. Department of Energy's Stirling Engine Highway Vehicle Systems program, the NASA Lewis Stirling engine performance code was evaluated by comparing code predictions without engine-specific calibration factors to GPU-3, P-40, and RE-1000 Stirling engine test data. The error in predicting power output was -11 percent for the P-40 and 12 percent for the RE-1000 at design conditions and 16 percent for the GPU-3 at near-design conditions (2000 rpm engine speed versus 3000 rpm at design). The efficiency and heat input predictions showed better agreement with engine test data than did the power predictions. Concerning all data points, the error in predicting the GPU-3 brake power was significantly larger than for the other engines and was mainly a result of inaccuracy in predicting the pressure phase angle. Analysis into this pressure phase angle prediction error suggested that improvements to the cylinder hysteresis loss model could have a significant effect on overall Stirling engine performance predictions. Author

**N89-25506\*#** National Aeronautics and Space Administration.  
Lewis Research Center, Cleveland, OH.

**CHALLENGES FOR FUTURE SPACE POWER SYSTEMS**

HENRY W. BRANDHORST, JR. 1989 6 p Presented at the European Space Power Conference, Madrid, Spain, 2-6 Oct. 1989; sponsored by the ESA  
(NASA-TM-102063; E-4820; NAS 1.15:102063) Avail: NTIS HC A02/MF A01 CSCL 10/2

The future appears rich in missions that will extend the frontiers of knowledge, human presence in space, and opportunities for profitable commerce. The key to success of these ventures is the availability of plentiful, cost effective electric power and assured, low cost access to space. While forecasts of space power needs are problematic, an assessment of future needs based on terrestrial experience was made. These needs fall into three broad categories-survival, self sufficiency and industrialization. The cost of delivering payloads to orbital locations from low earth orbit (LEO) to Mars was determined and future launch cost reductions projected. From these factors, then, projections of the performance necessary for future solar and nuclear space power options were made. These goals are largely dependent upon orbital location and energy storage needs. Author

**N89-26291\*#** National Aeronautics and Space Administration.  
Lewis Research Center, Cleveland, OH.

**THE GAAS SOLAR CELLS WITH V-GROOVED EMITTERS**

SHEILA G. BAILEY, N. FATEMI (Sverdrup Technology, Inc., Cleveland, OH.), D. M. WILT, GEOFFREY A. LANDIS, and R. D. THOMAS 1989 6 p Presented at the European Space Power Conference, Madrid, Spain, 2-6 Oct. 1989; sponsored by the ESA  
(NASA-TM-102104; E-4870; NAS 1.15:102104) Avail: NTIS HC A02/MF A01 CSCL 10/1

Geometrically structured surfaces have become increasingly important to solar cell efficiency improvements and radiation tolerance. Gallium arsenide solar cells with a V-grooved front surface which demonstrate improved optical coupling and higher short-circuit current compared to planar cells were fabricated. GaAs homojunction cells were fabricated by organometallic chemical vapor deposition (OMCVD) on an n+ substrate. The V-grooves were formed on the surface with an anisotropic etch, and an n-type buffer and p-type emitter were grown by OMCVD, followed by ohmic contacts. Reflectivity measurements show significantly lower reflectance for the microgrooved cell compared to the planar structure. The short circuit current of the V-grooved solar cell is consistently higher than that of the planar controls. Author

**N89-26292\*#** National Aeronautics and Space Administration.  
Lewis Research Center, Cleveland, OH.

**ON-ORBIT RESULTS OF THE LIPS 3/INP HOMOJUNCTION SOLAR CELL EXPERIMENT**

DAVID J. BRINKER 1989 7 p Presented at the European Space Power Conference, Madrid, Spain, 2-6 Oct. 1989; sponsored by the ESA  
(NASA-TM-102131; E-4921; NAS 1.15:102131) Avail: NTIS HC A02/MF A01 CSCL 10/1

The flight performance of NASA Lewis Research Center's indium phosphide homojunction solar cell module on the LIPS 3 satellite is presented. A module of four n+p cells was fabricated and has been on-orbit on the LIPS 3 spacecraft since 1987. The experimental objective is the measurement of InP cell performance in the natural radiation environment of the 1100 kilometer altitude, 60 deg inclination, circular orbit. Flight data from the first year is near expected values, with no degradation in short-circuit current. The temperature dependence of current-voltage parameters is included along with the laboratory radiation tolerance studies necessary for normalization and analysis of the data. Details of the cell structure and flight module design are also discussed. Author

**N89-27256\*#** University of South Florida, Tampa.

**THERMAL EVALUATION OF ADVANCED SOLAR DYNAMIC HEAT RECEIVER PERFORMANCE Final Report, Jan - Dec. 1988**

ROGER A. CRANE Mar. 1989 131 p  
(Contract NAG3-851)  
(NASA-CR-185117; NAS 1.26:185117) Avail: NTIS HC A07/MF A01 CSCL 10/1

The thermal performance of a variety of concepts for thermal energy storage as applied to solar dynamic applications is discussed. It is recognized that designs providing large thermal gradients or large temperature swings during orbit are susceptible to early mechanical failure. Concepts incorporating heat pipe technology may encounter operational limitations over sufficiently large ranges. By reviewing the thermal performance of basic designs, the relative merits of the basic concepts are compared. In addition the effect of thermal enhancement and metal utilization as applied to each design provides a partial characterization of the performance improvements to be achieved by developing these technologies. Author

46

## GEOPHYSICS

Includes aeronomy; upper and lower atmosphere studies; ionospheric and magnetospheric physics; and geomagnetism.

**A89-34791\*#** Massachusetts Inst. of Tech., Cambridge.  
**BOUNDS ON CURRENT COLLECTION FROM THE FAR FIELD BY PLASMA CLOUDS IN THE IONOSPHERE**

D. E. HASTINGS and J. BLANDINO (MIT, Cambridge, MA) Journal of Geophysical Research (ISSN 0148-0227), vol. 94, March 1, 1989, p. 2737-2744. refs  
(Contract NAG3-681)  
Copyright

Plasma clouds can enhance the collection of current to a charged body in the ionosphere in two ways. The first is by providing a large collection area for ionospheric electrons to be collected. The second is by ionization of neutral gas in the vicinity of the plasma cloud. The collection of electrons across a magnetic field is examined, and it is shown that the effective collection area is limited to the region of the cloud where the magnetic field effects are overwhelmed by the electric field effects from the charged body. Upper and lower bounds are obtained for the radius of the core region where the electric field influence dominates. From

these, upper and lower bounds are obtained for the current collection.  
Author

**A89-43680\*** Jet Propulsion Lab., California Inst. of Tech., Pasadena.

#### THE PLASMA WAKE OF THE SHUTTLE ORBITER

G. B. MURPHY (California Institute of Technology, Jet Propulsion Laboratory, Pasadena; Iowa, University, Iowa City), D. L. REASONER (NASA, Marshall Space Flight Center, Huntsville, AL; Iowa, University, Iowa City), A. TRIBBLE, N. D'ANGELO, J. S. PICKETT (Iowa, University, Iowa City) et al. Journal of Geophysical Research (ISSN 0148-0227), vol. 94, June 1, 1989, p. 6866-6872. refs

(Contract NAS8-32807; NAG3-449)

Copyright

One of the objectives of the Plasma Diagnostics Package (PDP) instrumentation on Spacelab 2 was to obtain information about the plasma wake of the Shuttle Orbiter. Plasma density and electron temperature data are presented, which were obtained while the PDP was attached to the Shuttle remote manipulator system, and while the PDP was a free-flying satellite. Wake crossings by the PDP from about 40 m to about 240 m behind the Orbiter provide information about the structure of the mid and far wake of the Orbiter. As expected, the wake is characterized by density depressions, relative to the ambient ionospheric plasma, and by enhancements of the electron temperature, particularly in the near and mid wake. The observed electron temperature enhancements appear to be in line with previous spacecraft observations.

Author

**A89-43698\*** Iowa Univ., Iowa City.

#### ELECTRON VELOCITY DISTRIBUTIONS AND PLASMA WAVES ASSOCIATED WITH THE INJECTION OF AN ELECTRON BEAM INTO THE IONOSPHERE

L. A. FRANK, W. R. PATERSON, W. S. KURTH (Iowa, University, Iowa City), M. ASHOUR-ABDALLA (California, University, Los Angeles), D. SCHRIEVER (Max-Planck-Institut fuer extraterrestrische Physik, Garching, Federal Republic of Germany) et al. Journal of Geophysical Research (ISSN 0148-0227), vol. 94, June 1, 1989, p. 6995-7001. refs

(Contract NAS8-32807; F19628-88-K-0011; F19628-88-K-0022; NAS8-36011; NAG3-449; NGL-16-001-002; NAGW-235)

Copyright

An electron beam was injected into earth's ionosphere on August 1, 1985, during the flight of the Space Shuttle Challenger as part of the objectives of the Spacelab 2 mission. In the wake of the Space Shuttle a magnetically aligned sheet of electrons returning from the direction of propagation of the beam was detected with the free-flying Plasma Diagnostics Package. The thickness of this sheet of returning electrons was about 20 m. Large intensifications of broadband electrostatic noise were also observed within this sheet of electrons. A numerical simulation of the interaction of the electron beam with the ambient ionospheric plasmas is employed to show that the electron beam excites electron plasma oscillations and that it is possible for the ion acoustic instability to provide a returning flux of hot electrons by means of quasi-linear diffusion.

Author

## 54

### MAN/SYSTEM TECHNOLOGY AND LIFE SUPPORT

Includes human engineering; biotechnology; and space suits and protective clothing.

**A89-11682\*** Case Western Reserve Univ., Cleveland, OH.  
**ROBOTS FOR MANIPULATION IN A MICRO-GRAVITY ENVIRONMENT**

R. D. QUINN (Case Western Reserve University, Cleveland, OH)

and C. LAWRENCE (NASA, Lewis Research Center, Cleveland, OH) IN: Dynamics and control of large structures; Proceedings of the Sixth VPI&SU/AIAA Symposium, Blacksburg, VA, June 29-July 1, 1987. Blacksburg, VA, Virginia Polytechnic Institute and State University, 1988, p. 515-528. refs

This paper is concerned with the development of control strategies and mechanisms for robots operating in the micro-gravity environment of Space Station. These robots must be capable of conducting experiments and manufacturing processes without disturbing the micro-gravity environment through base reactions/motions. Approaches discussed for controlling the robot base reactions/motions include strategies making use of manipulators with redundant degrees of freedom, actuators at the robot base, and a redundant (balancing) arm. Two degree-of-freedom, traction-drive joints are discussed as well as the conceptual design for a traction-driven manipulator.

Author

**A89-36933\*** National Aeronautics and Space Administration, Lewis Research Center, Cleveland, OH.

#### MODEL-BASED ANALYSIS OF CONTROL/DISPLAY INTERACTION IN THE HOVER TASK

SANJAY GARG (NASA, Lewis Research Center; Sverdrup Technology, Inc., Cleveland, OH) and DAVID K. SCHMIDT (Purdue University, West Lafayette, IN) Journal of Guidance, Control, and Dynamics (ISSN 0731-5090), vol. 12, May-June 1989, p. 342-350. Previously cited in issue 22, p. 3633, Accession no. A87-49580. refs

(Contract NAG4-1)

Copyright

**A89-52647\*** Case Western Reserve Univ., Cleveland, OH.

#### NEW RESULTS CONCERNING THE USE OF KINEMATICALLY REDUNDANT MANIPULATORS IN MICROGRAVITY ENVIRONMENTS

R. D. QUINN and N. J. LIN (Case Western Reserve University, Cleveland, OH) IN: AIAA Guidance, Navigation and Control Conference, Boston, MA, Aug. 14-16, 1989, Technical Papers. Part 2. Washington, DC, American Institute of Aeronautics and Astronautics, 1989, p. 1150-1157. refs

(Contract NAG3-761)

(AIAA PAPER 89-3562) Copyright

This paper is concerned with the development of control strategies for kinematically redundant manipulators to be used in Space Station laboratories. These robots must be able to conduct experiments and manufacturing processes without disturbing the microgravity environment, and thus their dynamic base reactions/motions must be nearly eliminated. Redundant degrees of freedom permit the inverse kinematics problem to be solved in conjunction with the minimization of a cost function defined as a weighted sum of the base reactions. It is shown that the weights in the cost function should be used as an additional set of parameters in the minimization problem. The actual performance of the local optimal trajectory approach is demonstrated to be not as good as was previously reported.

Author

**N89-21479\*** Pittsburgh Univ., PA. Dept. of Electrical Engineering.

#### COMPUTER SIMULATION OF A PILOT IN V/STOL AIRCRAFT CONTROL LOOPS Final Report

WILLIAM G. VOGT, MARLIN H. MICKLE, MARK E. ZIPF, and SENOL KUCUK 31 Jan. 1989 447 p

(Contract NAG3-729)

(NASA-CR-184815; NAS 1.26:184815) Avail: NTIS HC A19/MF A01 CSCL 05/8

The objective was to develop a computerized adaptive pilot model for the computer model of the research aircraft, the Harrier II AV-8B V/STOL with special emphasis on propulsion control. In fact, two versions of the adaptive pilot are given. The first, simply called the Adaptive Control Model (ACM) of a pilot includes a parameter estimation algorithm for the parameters of the aircraft and an adaption scheme based on the root locus of the poles of the pilot controlled aircraft. The second, called the Optimal Control Model of the pilot (OCM), includes an adaption algorithm and an

## 59 MATHEMATICAL AND COMPUTER SCIENCES (GENERAL)

optimal control algorithm. These computer simulations were developed as a part of the ongoing research program in pilot model simulation supported by NASA Lewis from April 1, 1985 to August 30, 1986 under NASA Grant NAG 3-606 and from September 1, 1986 through November 30, 1988 under NASA Grant NAG 3-729. Once installed, these pilot models permitted the computer simulation of the pilot model to close all of the control loops normally closed by a pilot actually manipulating the control variables. The current version of this has permitted a baseline comparison of various qualitative and quantitative performance indices for propulsion control, the control loops and the work load on the pilot. Actual data for an aircraft flown by a human pilot furnished by NASA was compared to the outputs furnished by the computerized pilot and found to be favorable. Author

59

### MATHEMATICAL AND COMPUTER SCIENCES (GENERAL)

**A89-34964\*** Akron Univ., OH.

#### **SYMBOLIC DERIVATION OF MATERIAL PROPERTY MATRICES IN FINITE ELEMENT ANALYSIS**

H. Q. TAN (Akron, University, OH) IN: Symbolic computation in fluid mechanics and heat transfer; Proceedings of the Symposium, ASME Winter Annual Meeting, Chicago, IL, Nov. 27-Dec. 2, 1988. New York, American Society of Mechanical Engineers, 1988, p. 111-116. refs

(Contract NSF EET-87-14628; NAG3-872)

Copyright

The principles and operation of MMAX, a symbolic-computation program which automates the process of generating property matrices for structural materials, are briefly described and illustrated with sample analyses of a rubberlike material and an elastoplastic material. MMAX is written in LISP under the symbolic finite-element generator FINGER and the general symbolic manipulator MACSYMA; it first derives the formulas required by mathematical manipulation, and then translates the formulas into FORTRAN code, adapted to the particular type of machine to be used for the numerical calculations. This approach is shown to combine efficiently the advantages of symbolic and numerical computation for engineering applications. T.K.

**N89-18045\*#** National Aeronautics and Space Administration. Ames Research Center, Moffett Field, CA.

#### **SYSTEMS AUTONOMY TECHNOLOGY: EXECUTIVE SUMMARY AND PROGRAM PLAN**

JOHN S BULL, ed. Dec. 1987 167 p Prepared in cooperation with NASA. Goddard Space Flight Center, Greenbelt, MD; JPL, Calif., Inst. of Tech., Pasadena; Johnson Space Center; Kennedy Space Center; Langley Research Center; Lewis Research Center and Marshall Space Flight Center (NASA-TM-100999; A-88174; NAS 1.15:100999) Avail: NTIS HC A08/MF A01 CSCL 09/2

The National Space Strategy approved by the President and Congress in 1984 sets for NASA a major goal of conducting effective and productive space applications and technology programs which contribute materially toward United States leadership and security. To contribute to this goal, OAST supports the Nation's civil and defense space programs and overall economic growth. OAST objectives are to ensure timely provision of new concepts and advanced technologies, to support both the development of NASA missions in space and the space activities of industry and other organizations, to utilize the strengths of universities in conducting the NASA space research and technology program, and to maintain the NASA centers in positions of strength in critical space technology areas. In line with these objectives, NASA has established a new program in space automation and

robotics that will result in the development and transfer and automation technology to increase the capabilities, productivity, and safety of NASA space programs including the Space Station, automated space platforms, lunar bases, Mars missions, and other deep space ventures. The NASA/OAST Automation and Robotics program is divided into two parts. Ames Research Center has the lead role in developing and demonstrating System Autonomy capabilities for space systems that need to make their own decisions and do their own planning. The Jet Propulsion Laboratory has the lead role for Telerobotics (that portion of the program that has a strong human operator component in the control loop and some remote handling requirement in space). This program is intended to be a working document for NASA Headquarters, Program Offices, and implementing Project Management. Author

60

### COMPUTER OPERATIONS AND HARDWARE

Includes hardware for computer graphics, firmware, and data processing.

**N89-29032\*#** National Aeronautics and Space Administration. Lewis Research Center, Cleveland, OH.

#### **A REAL TIME MICROCOMPUTER IMPLEMENTATION OF SENSOR FAILURE DETECTION FOR TURBOFAN ENGINES**

JOHN C. DELAAT and WALTER C. MERRILL Aug. 1989 27 p (NASA-TM-102327; E-5029; NAS 1.15:102327) Avail: NTIS HC A03/MF A01 CSCL 09/2

An algorithm was developed which detects, isolates, and accommodates sensor failures using analytical redundancy. The performance of this algorithm was demonstrated on a full-scale F100 turbofan engine. The algorithm was implemented in real-time on a microprocessor-based controls computer which includes parallel processing and high order language programming. Parallel processing was used to achieve the required computational power for the real-time implementation. High order language programming was used in order to reduce the programming and maintenance costs of the algorithm implementation software. The sensor failure algorithm was combined with an existing multivariable control algorithm to give a complete control implementation with sensor analytical redundancy. The real-time microprocessor implementation of the algorithm which resulted in the successful completion of the algorithm engine demonstration, is described. Author

61

### COMPUTER PROGRAMMING AND SOFTWARE

Includes computer programs, routines, and algorithms, and specific applications, e.g., CAD/CAM.

**A89-16963\*** National Aeronautics and Space Administration. Lewis Research Center, Cleveland, OH.

#### **THE DEVELOPMENT OF AN INTELLIGENT INTERFACE TO A COMPUTATIONAL FLUID DYNAMICS FLOW-SOLVER CODE**

ANTHONY D. WILLIAMS (NASA, Lewis Research Center, Cleveland, OH) (George Washington University and NASA, Symposium on Advances and Trends in Computational Structural Mechanics and Fluid Dynamics, Washington, DC, Oct. 17-19, 1988) Computers and Structures (ISSN 0045-7949), vol. 30, no. 1-2, 1988, p. 431-438. Previously announced in STAR as N88-26127. refs

Copyright

Researchers at NASA Lewis are currently developing an 'intelligent' interface to aid in the development and use of large,



computational fluid dynamics flow-solver codes for studying the internal fluid behavior of aerospace propulsion systems. This paper discusses the requirements, design, and implementation of an intelligent interface to Proteus, a general purpose, three-dimensional, Navier-Stokes flow solver. The interface is called PROTAIS to denote its introduction of artificial intelligence (AI) concepts to the Proteus code. Author

**A89-38846\*** RE/SPEC, Inc., Albuquerque, NM.  
**GRAPHICAL POSTPROCESSING FOR 3-D MESH QUALITY EVALUATION**

M. J. PANTHAKI (RE/SPEC, Inc., Albuquerque, NM), J. F. ABEL, and P. A. WAWRZYNEK (Cornell University, Ithaca, NY) Engineering Computations (ISSN 0264-4401), vol. 6, March 1989, p. 25-34. Research supported by the State University of New York and Cornell University. refs (Contract NAG3-395) Copyright

An important objective of three-dimensional graphical finite-element postprocessing is to indicate to the engineer the accuracy of analysis results. The inclusion of mesh quality sensors permits a subjective evaluation of the adequacy of a single analysis being interpreted. For graphical approaches, both strain-energy-density gradients and discontinuities of unsmoothed responses and their gradients have proved to be effective sensors. Interactive graphical tools which can display discontinuity information effectively are described; these are essentially different from the ordinary methods used for the viewing of smoothed results. Author

**N89-12917\*** National Aeronautics and Space Administration. Lewis Research Center, Cleveland, OH.

**AUTOMATION SOFTWARE FOR A MATERIALS TESTING LABORATORY**

MICHAEL A. MCGAW and PETER J. BONACUSE *In its* Turbine Engine Hot Section Technology 1986 p 399-406 Oct. 1986 Avail: NTIS HC A21/MF A01 CSCL 09/2

A comprehensive software system for automating much of the experimental process has recently been completed at the Lewis Research Center's high-temperature fatigue and structures laboratory. The system was designed to support experiment definition and conduct, results analysis and archiving, and report generation activities. This was accomplished through the design and construction of several software systems, as well as through the use of several commercially available software products, all operating on a local, distributed minicomputer system. Experimental capabilities currently supported in an automated fashion include both isothermal and thermomechanical fatigue and deformation testing capabilities. The future growth and expansion of this system will be directed toward providing multiaxial test control, enhanced thermomechanical test control, and higher test frequency (hundreds of hertz). Author

**N89-13993\*** Ohio State Univ., Columbus. ElectroScience Lab.  
**ENGINEERING CALCULATIONS FOR SOLVING THE ORBITAL ALLOTMENT PROBLEM**

C. REILLY, E. K. WALTON, C. MOUNT-CAMPBELL, R. CALDECOTT, E. AEBKER, and F. MATA Aug. 1988 36 p (Contract NAG3-159) (NASA-CR-184607; NAS 1.26:184607; ESL-718688-7) Avail: NTIS HC A03/MF A01 CSCL 09/2

Four approaches for calculating downlink interferences for shaped-beam antennas are described. An investigation of alternative mixed-integer programming models for satellite synthesis is summarized. Plans for coordinating the various programs developed under this grant are outlined. Two procedures for ordering satellites to initialize the k-permutation algorithm are proposed. Results are presented for the k-permutation algorithms. Feasible solutions are found for 5 of the 6 problems considered. Finally, it is demonstrated that the k-permutation algorithm can be used to solve arc allotment problems. Author

**N89-13996\*** MARC Analysis Research Corp., Palo Alto, CA.

**MHOST VERSION 4.2. VOLUME 1: USERS' MANUAL**

SHOHEI NAKAZAWA 1989 135 p (Contract NAS3-23697) (NASA-CR-182235-VOL-1; NAS 1.26:182235-VOL-1) Avail: NTIS HC A07/MF A01 CSCL 09/2

This manual describes the user options available for running the MHOST finite element analysis package. MHOST is a solid and structural analysis program based on mixed finite element technology, and is specifically designed for three-dimensional inelastic analysis. A family of two- and three-dimensional continuum elements along with beam and shell structural elements can be utilized. Many options are available in the constitutive equation library, the solution algorithms and the analysis capabilities. An overview of the algorithms, a general description of the input data formats, and a discussion of input data for selecting solution algorithms are given. Author

**N89-15623\*** Oak Ridge National Lab., TN.

**MODELING CYCLIC MELTING AND REFREEZING IN A HOLLOW METAL CANISTER**

D. G. WILSON and R. E. FLANERY Sep. 1988 44 p (Contract NASA ORDER C-30001-J; DE-AC05-84OR-21400) (NASA-CR-184630; NAS 1.26:184630; DE89-001325; ORNL-6497) Avail: NTIS HC A03/MF A01 CSCL 09/2

This report documents the mathematical model and computational algorithms used in a pair of computer programs that do energy redistribution calculations as part of a comprehensive simulation for thermal and structural analyses of one component of a thermal energy storage system for the manned space station. The complete problem includes cyclic melting and refreezing, fluid flow, and void formation and movement, as well as conductive and convective heat transfer in a three dimensional setting. The problem is posed in a hollow, metal canister filled with a high temperature phase change material. The heat transfer equations discussed here consist of a pair of partial differential equations for energy transfer (one linear the other mildly nonlinear), coupled with a constitutive relation for energy and temperature. This constitutes a weak, enthalpy formulation of the phase change problem. The partial differential equations are approximated by a system of coupled Crank Nicholson-type finite difference equations. These nonlinear, implicit equations are solved for enthalpy (energy content) and temperature fields simultaneously. A successive overrelaxation iteration scheme with red/black ordering is used to solve the nonlinear difference equations. The algorithms have been vectorized for rapid execution on the Cray X-MP supercomputer and techniques used to do this are discussed. DOE

**N89-20641\*** National Aeronautics and Space Administration. Lewis Research Center, Cleveland, OH.

**AUTOMATING THE MULTIPROCESSING ENVIRONMENT**

DALE J. ARPASI Mar. 1989 10 p (NASA-TM-4103; E-4426; NAS 1.15:4103) Avail: NTIS HC A02/MF A01 CSCL 09/2

An approach to automate the programming and operation of tree-structured networks of multiprocessor systems is discussed. A conceptual, knowledge-based operating environment is presented, and requirements for two major technology elements are identified as follows: (1) An intelligent information translator is proposed for implementing information transfer between dissimilar hardware and software, thereby enabling independent and modular development of future systems and promoting a language-independence of codes and information; (2) A resident system activity manager, which recognizes the systems capabilities and monitors the status of all systems within the environment, is proposed for integrating dissimilar systems into effective parallel processing resources to optimally meet user needs. Finally, key computational capabilities which must be provided before the environment can be realized are identified. Author

## 61 COMPUTER PROGRAMMING AND SOFTWARE

**N89-24055\*** National Aeronautics and Space Administration. Lewis Research Center, Cleveland, OH.

**LABORATORY PROCESS CONTROL USING NATURAL LANGUAGE COMMANDS FROM A PERSONAL COMPUTER**  
HERBERT A. WILL and MICHAEL A. MACKIN Apr. 1989 14 p  
(NASA-TM-101988; E-4690; NAS 1.15:101988) Avail: NTIS HC A03/MF A01 CSCL 09/2

PC software is described which provides flexible natural language process control capability with an IBM PC or compatible machine. Hardware requirements include the PC, and suitable hardware interfaces to all controlled devices. Software required includes the Microsoft Disk Operating System (MS-DOS) operating system, a PC-based FORTRAN-77 compiler, and user-written device drivers. Instructions for use of the software are given as well as a description of an application of the system. Author

## 62

### COMPUTER SYSTEMS

Includes computer networks and special application computer systems.

**A89-50100\*** Akron Univ., OH.

**HIERARCHICAL POLY TREE COMPUTER ARCHITECTURES DEFINED BY COMPUTATIONAL MULTIDISCIPLINARY MECHANICS**

JOE PADOVAN, DOUG GUTE, and KEITH JOHNSON (Akron, University, OH) Computers and Structures (ISSN 0045-7949), vol. 32, no. 5, 1989, p. 1133-1163. refs  
(Contract NAG3-664)  
Copyright

This paper will develop an alternative computer architecture called the Poly Tree. Based on the requirements of computational mechanics and the concept of hierarchical substructuring, the paper will explore the development of problem-dependent parallel networks of processors which will enable significant, often superlinear, speed enhancements; provide a logical/efficient framework for linear/nonlinear and transient structural mechanics problems; and provide a logical framework from which to apply model reduction procedures. In addition, the paper will explore optimal processor arrangements which define the overall system granularity. Consideration will also be given to system I/O requirements. Author

**N89-17422\*** National Aeronautics and Space Administration. Lewis Research Center, Cleveland, OH.

**PARALLEL GAUSSIAN ELIMINATION OF A BLOCK TRIDIAGONAL MATRIX USING MULTIPLE MICROCOMPUTERS**

RICHARD A. BLECH Washington, DC Feb. 1989 35 p  
(NASA-TP-2892; E-4199; NAS 1.60:2892) Avail: NTIS HC A03/MF A01 CSCL 09/2

The solution of a block tridiagonal matrix using parallel processing is demonstrated. The multiprocessor system on which results were obtained and the software environment used to program that system are described. Theoretical partitioning and resource allocation for the Gaussian elimination method used to solve the matrix are discussed. The results obtained from running 1, 2 and 3 processor versions of the block tridiagonal solver are presented. The PASCAL source code for these solvers is given in the appendix, and may be transportable to other shared memory parallel processors provided that the synchronization outlines are reproduced on the target system. Author

**N89-17424\*** National Aeronautics and Space Administration. Lewis Research Center, Cleveland, OH.

**A DATA ACQUISITION AND STORAGE SYSTEM FOR THE ION AUXILIARY PROPULSION SYSTEM CYCLIC THRUSTER TEST**

JOHN A. HAMLEY Feb. 1989 15 p  
(NASA-TM-101469; E-4583; NAS 1.15:101469) Avail: NTIS HC A03/MF A01 CSCL 09/2

A nine-track tape drive interfaced to a standard personal computer was used to transport data from a remote test site to the NASA Lewis mainframe computer for analysis. The Cyclic Ground Test of the Ion Auxiliary Propulsion System (IAPS), which successfully achieved its goal of 2557 cycles and 7057 hr of thrusting beam on time generated several megabytes of test data over many months of continuous testing. A flight-like controller and power supply were used to control the thruster and acquire data. Thruster data was converted to RS232 format and transmitted to a personal computer, which stored the raw digital data on the nine-track tape. The tape format was such that with minor modifications, mainframe flight data analysis software could be used to analyze the Cyclic Ground Test data. The personal computer also converted the digital data to engineering units and displayed real time thruster parameters. Hardcopy data was printed at a rate dependent on thruster operating conditions. The tape drive provided a convenient means to transport the data to the mainframe for analysis, and avoided a development effort for new data analysis software for the Cyclic test. This paper describes the data system, interfacing and software requirements. Author

**N89-20684\*** National Aeronautics and Space Administration. Lewis Research Center, Cleveland, OH.

**A MESSAGE PASSING KERNEL FOR THE HYPERCLUSTER PARALLEL PROCESSING TEST BED**

RICHARD A. BLECH, ANGELA QUEALY (Sverdrup Technology, Inc., Cleveland, OH.), and GARY L. COLE 1989 10 p Presented at the 4th Conference on Hypercubes, Concurrent Computers and Applications, Monterey, CA, 6-8 Mar. 1989; sponsored by DOE, Strategic Defense Initiative Organization, Dept. of the Air Force, AFOSR and NASA, Ames Research Center  
(NASA-TM-101952; E-4652; NAS 1.15:101952) Avail: NTIS HC A02/MF A01 CSCL 09/2

A Message-Passing Kernel (MPK) for the Hypercluster parallel-processing test bed is described. The Hypercluster is being developed at the NASA Lewis Research Center to support investigations of parallel algorithms and architectures for computational fluid and structural mechanics applications. The Hypercluster resembles the hypercube architecture except that each node consists of multiple processors communicating through shared memory. The MPK efficiently routes information through the Hypercluster, using a message-passing protocol when necessary and faster shared-memory communication whenever possible. The MPK also interfaces all of the processors with the Hypercluster operating system (HYCLOPS), which runs on a Front-End Processor (FEP). This approach distributes many of the I/O tasks to the Hypercluster processors and eliminates the need for a separate I/O support program on the FEP. Author

**N89-20685\*** National Aeronautics and Space Administration. Lewis Research Center, Cleveland, OH.

**INITIAL OPERATING CAPABILITY FOR THE HYPERCLUSTER PARALLEL-PROCESSING TEST BED**

GARY L. COLE, RICHARD A. BLECH, and ANGELA QUEALY (Sverdrup Technology, Inc., Cleveland, OH.) Mar. 1989 10 p Presented at the 4th Conference on Hypercubes, Concurrent Computers, and Applications, Monterey, CA, 6-8 Mar. 1989; sponsored in part by DOE, Strategic Defense Initiative Organization, USAF, and NASA, Ames Research Center  
(NASA-TM-101953; E-4647; NAS 1.15:101953) Avail: NTIS HC A02/MF A01 CSCL 09/2

The NASA Lewis Research Center is investigating the benefits of parallel processing to applications in computational fluid and structural mechanics. To aid this investigation, NASA Lewis is developing the Hypercluster, a multi-architecture, parallel-processing test bed. The initial operating capability (IOC) being developed for the Hypercluster is described. The IOC will provide a user with a programming/operating environment that is interactive, responsive, and easy to use. The IOC effort includes the development of the Hypercluster Operating System

(HYCLOPS). HYCLOPS runs in conjunction with a vendor-supplied disk operating system on a Front-End Processor (FEP) to provide interactive, run-time operations such as program loading, execution, memory editing, and data retrieval. Run-time libraries, that augment the FEP FORTRAN libraries, are being developed to support parallel and vector processing on the Hypercluster. Special utilities are being provided to enable passage of information about application programs and their mapping to the operating system. Communications between the FEP and the Hypercluster are being handled by dedicated processors, each running a Message-Passing Kernel, (MPK). A shared-memory interface allows rapid data exchange between HYCLOPS and the communications processors. Input/output handlers are built into the HYCLOPS-MPK interface, eliminating the need for the user to supply separate I/O support programs on the FEP. Author

## 63

## CYBERNETICS

Includes feedback and control theory, artificial intelligence, robotics and expert systems.

**A89-10798\*** National Aeronautics and Space Administration. Lewis Research Center, Cleveland, OH.

**IECON '87: INDUSTRIAL APPLICATIONS OF CONTROL AND SIMULATION; PROCEEDINGS OF THE 1987 INTERNATIONAL CONFERENCE ON INDUSTRIAL ELECTRONICS, CONTROL, AND INSTRUMENTATION, CAMBRIDGE, MA, NOV. 3, 4, 1987** TOM T. HARTLEY, ED. (NASA, Lewis Research Center, Cleveland; Akron, University, OH) Conference sponsored by IEEE and SPIE. Bellingham, WA, Society of Photo-Optical Instrumentation Engineers (SPIE Proceedings. Volume 853), 1987. 189 p. No individual items are abstracted in this volume. (SPIE-853) Copyright

Recent advances in control-system design and simulation are discussed in reviews and reports. Among the topics considered are fast algorithms for generating near-optimal binary decision programs, trajectory control of robot manipulators with compensation of load effects via a six-axis force sensor, matrix integrators for real-time simulation, a high-level control language for an autonomous land vehicle, and a practical engineering design method for stable model-reference adaptive systems. Also addressed are the identification and control of flexible-limb robots with unknown loads, adaptive control and robust adaptive control for manipulators with feedforward compensation, adaptive pole-placement controllers with predictive action, variable-structure strategies for motion control, and digital signal-processor-based variable-structure controls. T.K.

**A89-17965\*** Systems Control Technology, Inc., Palo Alto, CA. **EFFECT OF MODEL UNCERTAINTY ON FAILURE DETECTION - THE THRESHOLD SELECTOR** ABBAS EMAMI-NAEINI, MUHAMMAD M. AKHTER, and STEPHEN M. ROCK (Systems Control Technology, Inc., Palo Alto, CA) IEEE Transactions on Automatic Control (ISSN 0018-9286), vol. 33, Dec. 1988, p. 1106-1115. refs (Contract NAS3-24079) Copyright

The performance of all failure detection, isolation, and accommodation (DIA) algorithms is influenced by the presence of model uncertainty. A unique framework is presented to incorporate a knowledge of modeling error in the analysis and design of failure detection systems. The tools being used are very similar to those in robust control theory. A concept is introduced called the threshold selector, which is a nonlinear inequality whose solution defines the set of detectable sensor failure signals. The threshold selector represents an innovative tool for analysis and synthesis of DIA algorithms. It identifies the optimal threshold to be used in innovations-based DIA algorithms. The optimal threshold is shown

to be a function of the bound on modeling errors, the noise properties, the speed of DIA filters, and the classes of reference and failure signals. The size of the smallest detectable failure is also determined. The results are applied to a multivariable turbofan jet engine example, which demonstrates improvements compared to previous studies. I.E.

**A89-22499\*#** Pennsylvania State Univ., University Park. **INTEGRATED COMMUNICATION AND CONTROL SYSTEMS. I - ANALYSIS**

YORAM HALEVI and ASOK RAY (Pennsylvania State University, University Park) ASME, Transactions, Journal of Dynamic Systems, Measurement and Control (ISSN 0022-0434), vol. 110, Dec. 1988, p. 367-373. Research supported by the Allied-Signal Aerospace Co. refs (Contract NSF DMC-87-07648; NAG3-823) (ASME PAPER 88-WA/DSC-1) Copyright

The paper presents the results of an ICCS analysis focusing on discrete-time control systems subject to time-varying delays. The present analytical technique is applicable to integrated dynamic systems such as those encountered in advanced aircraft, spacecraft, and the real-time control of robots and machine tools via a high-speed network within an autonomous manufacturing environment. The significance of data latency and missynchronization between individual system components in ICCS networks is discussed in view of the time-varying delays. K.K.

**A89-22500\*#** Pennsylvania State Univ., University Park. **INTEGRATED COMMUNICATION AND CONTROL SYSTEMS. II - DESIGN CONSIDERATIONS**

ASOK RAY and YORAM HALEVI (Pennsylvania State University, University Park) ASME, Transactions, Journal of Dynamic Systems, Measurement and Control (ISSN 0022-0434), vol. 110, Dec. 1988, p. 374-381. Research supported by the Allied-Signal Aerospace Co. refs (Contract NSF DMC-87-07648; NAG3-823) (ASME PAPER 88-WA/DSC-2) Copyright

The ICCS design issues for nonperiodic and stochastic delays are addressed and the framework for alternative design procedures is outlined. The impact of network-induced delays on system stability is investigated and their physical significance is demonstrated using a simulation. The negative effects of vacant sampling and message rejection at the controller are demonstrated. K.K.

**A89-28605\*#** National Aeronautics and Space Administration. Lewis Research Center, Cleveland, OH.

**A PARAMETRIC LQ APPROACH TO MULTIOBJECTIVE CONTROL SYSTEM DESIGN**

DOUG KYR (NASA, Lewis Research Center, Cleveland, OH) and MARC BUCHNER (Case Western Reserve University, Cleveland, OH) IN: IEEE Conference on Decision and Control, 27th, Austin, TX, Dec. 7-9, 1988, Proceedings. Volume 2. New York, Institute of Electrical and Electronics Engineers, Inc., 1988, p. 1278-1284. Previously announced in STAR as N89-12283. refs (Contract NAG3-659)

The synthesis of a constant parameter output feedback control law of constrained structure is set in a multiple-objective linear quadratic regulator (MOLQR) framework. The use of intuitive objective functions such as model-following ability and closed-loop trajectory sensitivity allows multiple-objective decision-making techniques, such as the surrogate worth tradeoff method, to be applied. For the continuous-time deterministic problem with an infinite time horizon, dynamic compensators as well as static output feedback controllers can be synthesized using a descent Anderson-Moore algorithm modified to impose linear equality constraints on the feedback gains by moving in feasible directions. Results of three different examples are presented, including a unique reformulation of the sensitivity reduction problem. Author

**A89-31087\*#** Cincinnati Univ., OH. **VISION SENSING TECHNIQUES IN AERONAUTICS AND ASTRONAUTICS**

E. L. HALL (Cincinnati, University, OH) IN: Machine intelligence and autonomy for aerospace systems. Washington, DC, American Institute of Aeronautics and Astronautics, Inc., 1988, p. 249-269. refs

(Contract NSF ECS-84-05258; NAG3-717)

Copyright

The close relationship between sensing and other tasks in orbital space, and the integral role of vision sensing in practical aerospace applications, are illustrated. Typical space mission-vision tasks encompass the docking of space vehicles, the detection of unexpected objects, the diagnosis of spacecraft damage, and the inspection of critical spacecraft components. Attention is presently given to image functions, the 'windowing' of a view, the number of cameras required for inspection tasks, the choice of incoherent or coherent (laser) illumination, three-dimensional-to-two-dimensional model-matching, edge- and region-segmentation techniques, and motion analysis for tracking. O.C.

**A89-35044\*#** Pennsylvania State Univ., University Park.  
**OBSERVER DESIGN FOR COMPENSATION OF  
 NETWORK-INDUCED DELAYS IN INTEGRATED  
 COMMUNICATION AND CONTROL SYSTEMS**

R. LUCK and A. RAY (Pennsylvania State University, University Park) IN: Recent advances in control of nonlinear and distributed parameter systems, robust control, and aerospace control applications; Proceedings of the Symposium, ASME Winter Annual Meeting, Chicago, IL, Nov. 27-Dec. 2, 1988. New York, American Society of Mechanical Engineers, 1988, p. 175-182. refs

(Contract NAG3-823; NSF DMC-87-07648)

Copyright

A method for compensating the effects of network-induced delays in integrated communication and control systems (ICCS) is proposed, and a finite-dimensional time-invariant ICCS model is developed. The problem of analyzing systems with time-varying and stochastic delays is circumvented by the application of a deterministic observer. For the case of controller-to-actuator delays, the observed design must rely on an extended model which represents the delays as additional states. R.R.

**A89-52603\*#** Mississippi State Univ., Mississippi State.  
**EXTENDED OBSERVABILITY OF LINEAR TIME-INVARIANT  
 SYSTEMS UNDER RECURRENT LOSS OF OUTPUT DATA**

ROGELIO LUCK (Mississippi State University, Mississippi State), ASOK RAY (Pennsylvania State University, University Park), and YORAM HALEVI (Technion - Israel Institute of Technology, Haifa) IN: AIAA Guidance, Navigation and Control Conference, Boston, MA, Aug. 14-16, 1989, Technical Papers. Part 1. Washington, DC, American Institute of Aeronautics and Astronautics, 1989, p. 741-748. refs

(Contract NAG3-823; NSF DMC-87-07648)

(AIAA PAPER 89-3510) Copyright

Recurrent loss of sensor data in integrated control systems of an advanced aircraft may occur under different operating conditions that include detected frame errors and queue saturation in computer networks, and bad data suppression in signal processing. This paper presents an extension of the concept of observability based on a set of randomly selected nonconsecutive outputs in finite-dimensional, linear, time-invariant systems. Conditions for testing extended observability have been established. Author

**A89-53958\*** National Aeronautics and Space Administration.  
 Lewis Research Center, Cleveland, OH.

**STABILITY ROBUSTNESS IMPROVEMENT OF DIRECT  
 EIGENSPACE ASSIGNMENT BASED FEEDBACK SYSTEMS  
 USING SINGULAR VALUE SENSITIVITIES**

SANJAY GARG (NASA, Lewis Research Center; Sverdrup Technology, Inc., Cleveland, OH) IN: 1989 American Control Conference, 8th, Pittsburgh, PA, June 21-23, 1989, Proceedings. Volume 1. New York, Institute of Electrical and Electronics Engineers, 1989, p. 148-158. refs

Copyright

A methodology to improve the stability robustness of feedback

control systems designed using direct eigenspace assignment techniques is presented. The method consists of considering the sensitivity of the minimum singular value of the return difference transfer matrix at the plant input to small changes in the desired closed-loop eigenvalues and the specified elements of the desired closed-loop eigenvectors. Closed-form expressions for the gradient of the minimum return difference singular value with respect to desired closed-loop eigenvalue and eigenvector parameters are derived. Closed-form expressions for the gradients of the control feedback gains with respect to the specified eigenspace parameters are obtained as an intermediate step. The use of the gradient information to improve the guaranteed gain and phase margins in eigenspace assignment based designs is demonstrated by application to an advanced fighter aircraft. I.E.

**A89-53984\*** Akron Univ., OH.

**COMPUTATIONAL FLUID DYNAMIC CONTROL**

TOM T. HARTLEY and ALEX DEABREU-GARCIA (Akron, University, OH) IN: 1989 American Control Conference, 8th, Pittsburgh, PA, June 21-23, 1989, Proceedings. Volume 1. New York, Institute of Electrical and Electronics Engineers, 1989, p. 692, 693.

(Contract NAG3-904)

Copyright

A general technique is presented for modeling fluid, or gas, dynamic systems specifically for the development of control systems. The numerical methods which are generally used in computational fluid dynamics are borrowed to create either continuous-time or discrete-time models of the particular fluid system. The resulting equations can be either left in a nonlinear form, or easily linearized about an operating point. As there are typically very many states in these systems, the usual linear model reduction methods can be used on them to allow a low-order controller to be designed. A simple example is given which typifies many internal flow control problems. The resulting control is termed computational fluid dynamic control. I.E.

**N89-12283\*#** National Aeronautics and Space Administration.  
 Lewis Research Center, Cleveland, OH.

**A PARAMETRIC LQ APPROACH TO MULTIOBJECTIVE  
 CONTROL SYSTEM DESIGN**

DOUGLAS E. KYR and MARC BUCHNER (Case Western Reserve Univ., Cleveland, Ohio.) 1988 13 p Proposed for presentation at the 27th Conference on Decision and Control, Austin, Tex., 7-9 Dec. 1988; sponsored by IEEE

(Contract NAG3-659)

(NASA-TM-101316; E-4312; NAS 1.15:101316) Avail: NTIS HC A03/MF A01 CSCL 09/2

The synthesis of a constant parameter output feedback control law of constrained structure is set in a multiple objective linear quadratic regulator (MOLQR) framework. The use of intuitive objective functions such as model-following ability and closed-loop trajectory sensitivity, allow multiple objective decision making techniques, such as the surrogate worth tradeoff method, to be applied. For the continuous-time deterministic problem with an infinite time horizon, dynamic compensators as well as static output feedback controllers can be synthesized using a descent Anderson-Moore algorithm modified to impose linear equality constraints on the feedback gains by moving in feasible directions. Results of three different examples are presented, including a unique reformulation of the sensitivity reduction problem. Author

**N89-12309\*#** National Aeronautics and Space Administration.  
 Lewis Research Center, Cleveland, OH.

**AN EXPERT SYSTEM FOR RESTRUCTURABLE CONTROL**

JONATHAN LITT 1988 9 p Prepared in cooperation with Army Aviation Research and Development Command, Cleveland, Ohio

(NASA-TM-101378; E-4433; NAS 1.15:101378;

AVSCOM-TR-88-C-023; AD-A201038) Avail: NTIS HC A02/MF A01 CSCL 09/2

Work in progress on an expert system which restructures and tunes control systems on-line is presented. The expert system

coordinates the different methods for redesigning and implementing the control strategies due to system changes. The research is directed toward aircraft and jet engine applications. The implementation is written in LISP and is currently running on a special purpose LISP machine. Author

**N89-24856\*** National Aeronautics and Space Administration. Lewis Research Center, Cleveland, OH.

**NEUROMORPHIC LEARNING OF CONTINUOUS-VALUED MAPPINGS IN THE PRESENCE OF NOISE: APPLICATION TO REAL-TIME ADAPTIVE CONTROL**

TERRY TROUDET (Sverdrup Technology, Inc., Cleveland, OH.) and WALTER C. MERRILL 1989 14 p Presented at the International Conference on Neural Networks, Washington, DC, 18-22 Jun. 1989; sponsored by the IEEE (NASA-TM-101999; E-4706; NAS 1.15:101999) Avail: NTIS HC A03/MF A01 CSCL 09/2

The ability of feed-forward neural net architectures to learn continuous-valued mappings in the presence of noise is demonstrated in relation to parameter identification and real-time adaptive control applications. Factors and parameters influencing the learning performance of such nets in the presence of noise are identified. Their effects are discussed through a computer simulation of the Back-Error-Propagation algorithm by taking the example of the cart-pole system controlled by a nonlinear control law. Adequate sampling of the state space is found to be essential for canceling the effect of the statistical fluctuations and allowing learning to take place. Author

## 64

### NUMERICAL ANALYSIS

Includes iteration, difference equations, and numerical approximation.

**A89-14397\*** National Aeronautics and Space Administration. Lewis Research Center, Cleveland, OH.

**RECURSIVE ALGORITHMS FOR VECTOR EXTRAPOLATION METHODS**

WILLIAM F. FORD (NASA, Lewis Research Center, Cleveland, OH) and AVRAM SIDI (Technion - Israel Institute of Technology, Haifa) Applied Numerical Mathematics (ISSN 0168-9274), vol. 4, Nov. 1988, p. 477-489. refs Copyright

Three classes of recursion relations are devised for implementing some extrapolation methods for vector sequences. One class of recursion relations can be used to implement methods like the modified minimal polynomial extrapolation and the topological epsilon algorithm; another allows implementation of methods like minimal polynomial and reduced rank extrapolation; while the remaining class can be employed in the implementation of the vector E-algorithm. Operation counts and storage requirements for these methods are also discussed, and some related techniques for special applications are also presented. Included are methods for the rapid evaluations of the vector E-algorithm. Author

**A89-22756\*** National Aeronautics and Space Administration. Lewis Research Center, Cleveland, OH.

**NONOSCILLATORY SOLUTION OF THE STEADY-STATE INVISCID BURGERS' EQUATION BY MATHEMATICAL PROGRAMMING**

JOHN E. LAVERY (NASA, Lewis Research Center, Cleveland, OH) Journal of Computational Physics (ISSN 0021-9991), vol. 79, Dec. 1988, p. 436-448. refs Copyright

In order to obtain the physically relevant discontinuous numerical solution, the steady-state inviscid Burgers' equation is singularly perturbed through the addition of a small amount of viscosity. A

'cell-centered' finite-difference scheme is proposed which employs two points for the inviscid part and four points for the viscous one. While difficulties are experienced in the capture of interior layers centered at node points, computational results for interior layers centered between node points, and for boundary layers, exhibit accurate nonoscillatory solutions whose discontinuities are captured in one cell on both coarse and fine grids. O.C.

**A89-28030\*** Textron Bell Aerospace Co., Buffalo, NY.

**NONLINEAR ANALYSIS USING TEMPORAL FINITE ELEMENTS**

SLADE GELLIN (Bell Aerospace Textron, Buffalo, NY) and JAMES M. PITARRESI (New York, State University, Binghamton) Engineering Analysis (ISSN 0264-682X), vol. 5, Sept. 1988, p. 126-132. refs

(Contract NAS3-23279)

Copyright

A formulation method, based on Hamilton's law of varying action, for finite elements in space and time incorporating nonlinear geometric and material behavior is presented. Case studies using elastic-plastic axial rod elements are carried out to demonstrate the accuracy, convergence and generality of the method. Author

**A89-34963\*** Akron Univ., OH.

**SYMBOLIC GENERATION OF CONSTITUTIVE EQUATIONS**

H. Q. TAN, X. DONG (Akron, University, OH), and S. M. ARNOLD (NASA, Lewis Research Center, Cleveland, OH) IN: Symbolic computation in fluid mechanics and heat transfer; Proceedings of the Symposium, ASME Winter Annual Meeting, Chicago, IL, Nov. 27-Dec. 2, 1988. New York, American Society of Mechanical Engineers, 1988, p. 103-109. refs

(Contract NAG3-872)

Copyright

The use of the symbolic manipulation program MACSYMA for the automatic generation of constitutive equations describing the thermomechanical behavior of complex materials such as metal-matrix composites is demonstrated. Problem-specific algorithms are developed; e.g., for partial differentiation by the chain rule, automatic generation of tree structures, special tensor analysis, and the simplification of expressions. The resulting subprogram package, SDICE, is shown to be fully applicable to both isotropic and anisotropic materials; its potential usefulness as a basis for FEM analyses is indicated. T.K.

**A89-37746\*** National Aeronautics and Space Administration. Lewis Research Center, Cleveland, OH.

**GLOBAL PROPERTIES OF PSEUDOSPECTRAL METHODS**

A. SOLOMONOFF (NASA, Lewis Research Center, Cleveland, OH) and E. TURKEL (NASA, Lewis Research Center, Cleveland, OH; Tel Aviv University, Israel) Journal of Computational Physics (ISSN 0021-9991), vol. 81, April 1989, p. 239-276. refs (Contract NAS1-17070; NAS1-18107)

Copyright

The present application of polynomial interpolation methods to function-approximation and numerical solutions for hyperbolic and elliptic PDEs allows the explicit construction of the derivative matrix for a general sequence of collocation points. An evaluation of the effect of several factors on the performance of these methods indicates an inability to interpret global methods in terms of local ones; the accuracy of the approximation will differ when the function's large gradients occur near the center of the region or near the boundary, irrespective of the boundary vicinity's collocation-point density. O.C.

**N89-10575\*** National Aeronautics and Space Administration. Lewis Research Center, Cleveland, OH.

**AN ALGORITHM FOR UNSTEADY FLOWS WITH STRONG CONVECTION**

VALLORIE PERIDIER and J. DAVID A. WALKER Oct. 1988 15 p

(Contract C99066G; F49620-85-C-0033)

(NASA-TM-100828; E-4016; NAS 1.15:100828; ICOMP-88-5)

Avail: NTIS HC A03/MF A01 CSCL 12/1

An implicit ADI numerical method for the calculation of 2-D unsteady flows with strong convection effects is described. The method is based on the conventional Crank-Nicholson approach for parabolic equations but an upwind-downwind differencing is used for the first order spatial derivatives associated with convection. The differencing is carried out in the current and previous time plane in such a way that the algorithm is second order accurate in both space and time. The difference equations are factored into sequential operators, one in each independent spatial variable; the solution at each time step may then be computed as a sequence of tridiagonal matrix problems. The method may be used in a noniterative manner although iteration at each time step is recommended in situations where the effects of convection are strong. Author

**N89-11469\*** # National Aeronautics and Space Administration. Lewis Research Center, Cleveland, OH.

**A NUMERICAL STUDY OF ENO AND TVD SCHEMES FOR SHOCK CAPTURING**

SHIH-HUNG CHANG (Cleveland State Univ., Ohio.) and MENG-SING LIOU Sep. 1988 24 p  
(NASA-TM-101355; E-4384; ICOMP-88-18; NAS 1.15:101355)  
Avail: NTIS HC A03/MF A01 CSCL 12/1

The numerical performance of a second-order upwind-based total variation diminishing (TVD) scheme and that of a uniform second-order essentially non-oscillatory (ENO) scheme for shock capturing are compared. The TVD scheme used is a modified version of Liou, using the flux-difference splitting (FDS) of Roe and his superbee function as the limiter. The construction of the basic ENO scheme is based on Harten, Engquist, Osher, and Chakravarthy, and the 2-D extensions are obtained by using a Strang-type of fractional-step time-splitting method. Numerical results presented include both steady and unsteady, 1-D and 2-D calculations. All the chosen test problems have exact solutions so that numerical performance can be measured by comparing the computer results to them. For 1-D calculations, the standard shock-tube problems of Sod and Lax are chosen. A very strong shock-tube problem, with the initial density ratio of 400 to 1 and pressure ratio of 500 to 1, is also used to study the behavior of the two schemes. For 2-D calculations, the shock wave reflection problems are adopted for testing. The cases presented in this report include flows with Mach numbers of 2.9, 5.0, and 10.0. Author

**N89-12337\*** # National Aeronautics and Space Administration. Lewis Research Center, Cleveland, OH.

**ON THE ACCURACY OF SOLVING TRIANGULAR SYSTEMS IN PARALLEL**

NAI-KUAN TSAO (Wayne State Univ., Detroit, Mich.) Nov. 1988 27 p  
(Contract NASA ORDER C-99066-G)  
(NASA-TM-101384; E-4439; ICOMP-88-19; NAS 1.15:101384)  
Avail: NTIS HC A03/MF A01 CSCL 12/1

An error complexity analysis of two algorithms for solving a unit-diagonal triangular system is given. The results show that the unusual sequential algorithm is optimal in terms of having the minimal maximum and cumulative error complexity measures. The parallel algorithm described by Sameh and Brent is shown to be essentially equivalent to the optimal sequential one. Some numerical experiments are also taught. Author

**N89-14794\*** # National Aeronautics and Space Administration. Lewis Research Center, Cleveland, OH.

**UNIVERSAL LIMITER FOR TRANSIENT INTERPOLATION MODELING OF THE ADVECTIVE TRANSPORT EQUATIONS: THE ULTIMATE CONSERVATIVE DIFFERENCE SCHEME**

B. P. LEONARD Sep. 1988 117 p  
(Contract NASA ORDER C-99066-G)  
(NASA-TM-100916; ICOMP-88-11; E-4169; NAS 1.15:100916)  
Avail: NTIS HC A06/MF A01 CSCL 12/1

A fresh approach is taken to the embarrassingly difficult problem of adequately modeling simple pure advection. An explicit conservative control-volume formation makes use of a universal

limiter for transient interpolation modeling of the advective transport equations. This ULTIMATE conservative difference scheme is applied to unsteady, one-dimensional scalar pure advection at constant velocity, using three critical test profiles: an isolated sine-squared wave, a discontinuous step, and a semi-ellipse. The goal, of course, is to devise a single robust scheme which achieves sharp monotonic resolution of the step without corrupting the other profiles. The semi-ellipse is particularly challenging because of its combination of sudden and gradual changes in gradient. The ULTIMATE strategy can be applied to explicit conservation schemes of any order of accuracy. Second-order schemes are unsatisfactory, showing steepening and clipping typical of currently popular so-called high resolution shock-capturing of TVD schemes. The ULTIMATE third-order upwind scheme is highly satisfactory for most flows of practical importance. Higher order methods give predictably better step resolution, although even-order schemes generate a (monotonic) waviness in the difficult semi-ellipse simulation. Little is to be gained above ULTIMATE fifth-order upwinding which gives results close to the ultimate for which one might hope. Author

**N89-20710\*** # National Aeronautics and Space Administration. Lewis Research Center, Cleveland, OH.

**ON THE EQUIVALENCE OF GAUSSIAN ELIMINATION AND GAUSS-JORDAN REDUCTION IN SOLVING LINEAR EQUATIONS**

NAI-KUAN TSAO Feb. 1989 22 p Prepared in cooperation with Wayne State Univ., Detroit, MI  
(Contract NASA ORDER C-99066-G)  
(NASA-TM-101466; ICOMP-89-2; E-4577; NAS 1.15:101466)  
Avail: NTIS HC A03/MF A01 CSCL 12/1

A novel general approach to round-off error analysis using the error complexity concepts is described. This is applied to the analysis of the Gaussian Elimination and Gauss-Jordan scheme for solving linear equations. The results show that the two algorithms are equivalent in terms of our error complexity measures. Thus the inherently parallel Gauss-Jordan scheme can be implemented with confidence if parallel computers are available. Author

**N89-21595\*** # National Aeronautics and Space Administration. Lewis Research Center, Cleveland, OH.

**INSTITUTE FOR COMPUTATIONAL MECHANICS IN PROPULSION (ICOMP) Annual Report No. 3, 1988**

Mar. 1989 62 p  
(Contract NASA ORDER C-99066-G)  
(NASA-TM-101961; E-4656; NAS 1.15:101961; ICOMP-89-1)  
Avail: NTIS HC A04/MF A01 CSCL 12/1

The Institute for Computational Mechanics in Propulsion (ICOMP) is operated jointly by Case Western Reserve University and the NASA Lewis Research Center in Cleveland, Ohio. The purpose of ICOMP is to develop techniques to improve problem-solving capabilities in all aspects of computational mechanics related to propulsion. This report describes the activities at ICOMP during 1988. Author

**N89-22392\*** # National Aeronautics and Space Administration. Lewis Research Center, Cleveland, OH.

**LEAST-SQUARES FINITE ELEMENTS FOR STOKES PROBLEM**

BO-NAN JIANG and C. L. CHANG (Cleveland State Univ., OH.) Dec. 1988 17 p  
(Contract NASA ORDER C-99066-G)  
(NASA-TM-101308; E-4298; ICOMP-88-16; NAS 1.15:101308)  
Avail: NTIS HC A03/MF A01 CSCL 12/1

A least-squares method based on the first-order velocity-pressure-vorticity formulation for the Stokes problem is proposed. This method leads to a minimization problem rather than to a saddle-point problem. The choice of the combinations of elements is thus not subject to the Ladyzhenskaya-Babuska-Brezzi (LBB) condition. Numerical results are given for the optimal rate of convergence for equal-order interpolations. Author



**N89-22397\*#** National Aeronautics and Space Administration. Lewis Research Center, Cleveland, OH.

**ABSORBING BOUNDARY CONDITIONS FOR SECOND-ORDER HYPERBOLIC EQUATIONS**

HONG JIANG and YAU SHU WONG (Alberta Univ., Edmonton.) Apr. 1989 33 p Sponsored by Izaak Walton Killam Memorial Scholarship and Natural Sciences and Engineering Research Council of Canada

(Contract NASA ORDER C-99066-G)

(NASA-TM-102009; ICOMP-89-7; E-4719; NAS 1.15:102009)

Avail: NTIS HC A03/MF A01 CSCL 12/1

A uniform approach to construct absorbing artificial boundary conditions for second-order linear hyperbolic equations is proposed. The nonlocal boundary condition is given by a pseudodifferential operator that annihilates travelling waves. It is obtained through the dispersion relation of the differential equation by requiring that the initial-boundary value problem admits the wave solutions travelling in one direction only. Local approximation of this global boundary condition yields an  $n$ th-order differential operator. It is shown that the best approximations must be in the canonical forms which can be factorized into first-order operators. These boundary conditions are perfectly absorbing for wave packets propagating at certain group velocities. A hierarchy of absorbing boundary conditions is derived for transonic small perturbation equations of unsteady flows. These examples illustrate that the absorbing boundary conditions are easy to derive, and the effectiveness is demonstrated by the numerical experiments.

Author

**N89-24865\*#** National Aeronautics and Space Administration. Lewis Research Center, Cleveland, OH.

**ON THE EQUIVALENCE OF A CLASS OF INVERSE DECOMPOSITION ALGORITHMS FOR SOLVING SYSTEMS OF LINEAR EQUATIONS**

NAI-KUAN TSAO (Wayne State Univ., Detroit, MI.) May 1989 28 p

(Contract NASA ORDER C-99066-G)

(NASA-TM-102036; ICOMP-89-11; E-4785; NAS 1.15:102036)

Avail: NTIS HC A03/MF A01 CSCL 12/1

A class of direct inverse decomposition algorithms for solving systems of linear equations is presented. Their behavior in the presence of round-off errors is analyzed. It is shown that under some mild restrictions on their implementation, the class of direct inverse decomposition algorithms presented are equivalent in terms of the error complexity measures.

Author

**N89-24872\*#** Michigan Univ., Ann Arbor.

**A GENUINELY MULTI-DIMENSIONAL UPWIND CELL-VERTEX SCHEME FOR THE EULER EQUATIONS**

KENNETH G. POWELL and BRAM VANLEER (National Aeronautics and Space Administration. Lewis Research Center, Cleveland, OH.) May 1989 22 p Presented at the 27th Aerospace Sciences Meeting, Reno, NV, 9-12 Jan. 1989; sponsored by AIAA Previously announced in IAA as A89-25084 (Contract NASA ORDER C-99066-G)

(NASA-TM-102029; E-4772; NAS 1.15:102029; ICOMP-89-13;

AIAA-89-0095) Avail: NTIS HC A03/MF A01 CSCL 12/1

The solution of the two-dimensional Euler equations is based on the two-dimensional linear convection equation and the Euler-equation decomposition developed by Hirsch et al. The scheme is genuinely two-dimensional. At each iteration, the data are locally decomposed into four variables, allowing convection in appropriate directions. This is done via a cell-vertex scheme with a downwind-weighted distribution step. The scheme is conservative, and third-order accurate in space. The derivation and stability analysis of the scheme for the convection equation, and the derivation of the extension to the Euler equations are given. Preconditioning techniques based on local values of the convection speeds are discussed. The scheme for the Euler equations is applied to two channel-flow problems. It is shown to converge rapidly to a solution that agrees well with that of a third-order upwind solver.

Author

**N89-30008\*#** National Aeronautics and Space Administration. Lewis Research Center, Cleveland, OH.

**LEAST-SQUARES FINITE ELEMENT METHOD FOR FLUID DYNAMICS**

BO-NAN JIANG and LOUIS A. POVINELLI Aug. 1989 37 p

(Contract NASA ORDER C-99066-G)

(NASA-TM-102352; E-5061; ICOMP-89-23; NAS 1.15:102352)

Avail: NTIS HC A03/MF A01 CSCL 12/1

An overview is given of new developments of the least squares finite element method (LSFEM) in fluid dynamics. Special emphasis is placed on the universality of LSFEM; the symmetry and positiveness of the algebraic systems obtained from LSFEM; the accommodation of LSFEM to equal order interpolations for incompressible viscous flows; and the natural numerical dissipation of LSFEM for convective transport problems and high speed compressible flows. The performance of LSFEM is illustrated by numerical examples.

Author

## 65

### STATISTICS AND PROBABILITY

Includes data sampling and smoothing; Monte Carlo method; and stochastic processes.

**A89-25843\*#** Southwest Research Inst., San Antonio, TX.

**PROBABILISTIC METHODS FOR STRUCTURAL RESPONSE ANALYSIS**

Y.-T. WU, O. H. BURNSIDE, and T. A. CRUSE (Southwest Research Institute, San Antonio, TX) IN: Computational probabilistic methods; Proceedings of the Joint ASME/SES Applied Mechanics and Engineering Sciences Conference, Berkeley, CA, June 20-22, 1988. New York, American Society of Mechanical Engineers, 1988, p. 1-14. refs

(Contract NAS3-24389)

Copyright

This paper addresses current work to develop probabilistic structural analysis methods for integration with a specially developed probabilistic finite element code. The goal is to establish distribution functions for the structural responses of stochastic structures under uncertain loadings. Several probabilistic analysis methods are proposed covering efficient structural probabilistic analysis methods, correlated random variables, and response of linear system under stationary random loading.

Author

## 66

### SYSTEMS ANALYSIS

Includes mathematical modeling; network analysis; and operations research.

**N89-17453\*#** National Aeronautics and Space Administration. Lewis Research Center, Cleveland, OH.

**PARALLEL PROCESSING OF A ROTATING SHAFT SIMULATION**

DALE J. ARPASI Feb. 1989 68 p

(NASA-TM-101462; E-4290; NAS 1.15:101462) Avail: NTIS HC A04/MF A01 CSCL 12/2

A FORTRAN program describing the vibration modes of a rotor-bearing system is analyzed for parallelism in this simulation using a Pascal-like structured language. Potential vector operations are also identified. A critical path through the simulation is identified and used in conjunction with somewhat fictitious processor characteristics to determine the time to calculate the problem on a parallel processing system having those characteristics. A parallel processing overhead time is included as a parameter for proper

## 70 PHYSICS (GENERAL)

evaluation of the gain over serial calculation. The serial calculation time is determined for the same fictitious system. An improvement of up to 640 percent is possible depending on the value of the overhead time. Based on the analysis, certain conclusions are drawn pertaining to the development needs of parallel processing technology, and to the specification of parallel processing systems to meet computational needs. Author

## 70

### PHYSICS (GENERAL)

**A89-24191\*** Northwestern Univ., Evanston, IL.  
**THEORY AND APPLICATION OF RADIATION BOUNDARY OPERATORS**

THOMAS G. MOORE, GREGORY A. KRIEGSMANN, ALLEN TAFLOVE (Northwestern University, Evanston, IL), and JEFFREY G. BLASCHAK (MIT, Lexington, MA) IEEE Transactions on Antennas and Propagation (ISSN 0018-926X), vol. 36, Dec. 1988, p. 1797-1812. refs  
(Contract NAG3-635; NSF MCS-83-00578)  
Copyright

A succinct unified review is provided of the theory of radiation boundary operators. With the recent introduction of the on-surface radiation condition (OSRC) method and the continued growth of finite-difference and finite-element techniques for modeling electromagnetic wave scattering problems, the understanding and use of radiation boundary operators has become increasingly important. Results are presented to illustrate the application of radiation boundary operators in both these areas. Recent OSRC results include analysis of the scattering behavior of both electrically small and large cylinders, a reactively loaded acoustic sphere, and a simple reentrant duct. Radiation boundary operator results include the demonstration of the effectiveness of higher-order operators in truncating finite-difference time-domain grids. I.E.

**A89-41722\*** Carnegie-Mellon Univ., Pittsburgh, PA.

**A HEAT-DRIVEN MONOCHROMATIC LIGHT SOURCE**

FRANCIS STEFANI (Carnegie-Mellon University, Pittsburgh, PA) and JOHN L. LAWLESS (Space Power, Inc., San Jose, CA) IEEE Transactions on Plasma Science (ISSN 0093-3813), vol. 17, April 1989, p. 295-302. refs  
(Contract NAG3-437)  
Copyright

The efficiency with which heat may be converted into resonance radiation in a cesium thermionic diode is investigated theoretically. An analytical model of a thermionic converter is used which combines the coupled effects of line radiation transport, excited-state kinetics, and plasma diffusion. Operating regimes are established for various degrees of optical density in the plasma. The results indicate that monochromatic radiation can be produced with efficiencies on the order of 30 percent, provided that there is an adequate voltage drop across the plasma. A drop of 1 V was used since it can be maintained without any electrical power input to the device. It is found that high efficiencies are due to the higher interelectrode distances which the solutions accommodate, and that radiation can be generated efficiently, even with optically dense gases. I.E.

**N89-19965\*#** National Aeronautics and Space Administration.  
Lewis Research Center, Cleveland, OH.

**ACOUSTIC WAVE PROPAGATION IN HETEROGENEOUS STRUCTURES INCLUDING EXPERIMENTAL VALIDATION**

KENNETH J. BAUMEISTER and MILO D. DAHL Apr. 1989 19 p Prepared for presentation at the 12th Aeroacoustics Conference, San Antonio, TX, 10-12 Apr. 1989; sponsored by AIAA

(NASA-TM-101486; E-4622; NAS 1.15:101486) Avail: NTIS HC A03/MF A01 CSCL 20/3

A finite element model was developed to solve for the acoustic pressure and energy fields in a heterogeneous suppressor. The derivations from the governing equations assumed that the material properties could vary with position resulting in a heterogeneous variable property two-dimensional wave equation. This eliminated the necessity of finding the boundary conditions between different materials. For a two media region consisting of part air and part bulk absorber, a model was used to describe the bulk absorber properties in two directions. Complex metallic structures inside the air duct are simulated by simply changing element properties from air to the structural material in a pattern to describe the desired shapes. To verify the numerical theory, experiments were conducted without flow in a rectangular duct with a single folded cavity mounted above the duct and absorbing material mounted inside a cavity. Changes in a nearly plane wave sound field were measured on the wall opposite the absorbing cavity. Fairly good agreement was found in the standing wave pattern upstream of the absorber and in the decay of pressure level opposite the absorber, as a function of distance along the duct. The finite element model provides a convenient method for evaluating the acoustic properties of bulk absorbers. Author

**N89-25670\*#** National Aeronautics and Space Administration.  
Lewis Research Center, Cleveland, OH.

**ACOUSTIC PROPAGATION IN CURVED DUCTS WITH EXTENDED REACTING WALL TREATMENT**

KENNETH J. BAUMEISTER 1989 21 p Prepared for presentation at the Winter Annual Meeting of the American Society of Mechanical Engineers, San Francisco, CA, 10-15 Dec. 1989 (NASA-TM-102110; E-4880; NAS 1.15:102110) Avail: NTIS HC A03/MF A01 CSCL 20/3

A finite-element Galerkin formulation was employed to study the attenuation of acoustic waves propagating in two-dimensional S-curved ducts with absorbing walls without a mean flow. The reflection and transmission at the entrance and the exit of a curved duct were determined by coupling the finite-element solutions in the curved duct to the eigenfunctions of an infinite, uniform, hard wall duct. In the frequency range where the duct height and acoustic wave length are nearly equal, the effects of duct length, curvature (duct offset) and absorber thickness were examined. For a given offset in the curved duct, the length of the S-duct was found to significantly affect both the absorptive and reflective characteristics of the duct. A means of reducing the number of elements in the absorber region was also presented. In addition, for a curved duct, power attenuation contours were examined to determine conditions for maximum acoustic power absorption. Again, wall curvature was found to significantly effect the optimization process. Author

## 71

### ACOUSTICS

Includes sound generation, transmission, and attenuation.

**A89-10112\*#** United Technologies Corp., Windsor Locks, CT.

**RESULTS OF ACOUSTIC TESTS OF A PROP-FAN MODEL**

F. B. METZGER and P. C. BROWN (United Technologies Corp., Windsor Locks, CT) Journal of Aircraft (ISSN 0021-8669), vol. 25, July 1988, p. 653-658. Previously cited in issue 20, p. 3285, Accession no. A87-45282.  
(Contract NAS3-24222)  
Copyright

**A89-12561\*#** National Aeronautics and Space Administration.  
Lewis Research Center, Cleveland, OH.

**CRUISE NOISE OF THE 2/9 SCALE MODEL SR-7A PROPELLER**

JAMES H. DITTMAR (NASA, Lewis Research Center, Cleveland, OH) and DAVID B. STANG (Sverdrup Technology, Inc., Cleveland, OH) *Journal of Aircraft* (ISSN 0021-8669), vol. 25, Aug. 1988, p. 740-746. Previously cited in issue 04, p. 570, Accession no. A88-16565. refs  
Copyright

**A89-15083\*** National Aeronautics and Space Administration. Lewis Research Center, Cleveland, OH.

**EFFECT OF AERODYNAMIC DETUNING ON SUPERSONIC ROTOR DISCRETE FREQUENCY NOISE GENERATION**

D. HOYNIK and SANFORD FLEETER (NASA, Lewis Research Center, Cleveland, OH) IN: NOISE-CON 88 - Noise control design: Methods and practice; Proceedings of the National Conference on Noise Control Engineering, West Lafayette, IN, June 20-22, 1988. Poughkeepsie, NY, Institute of Noise Control Engineering, 1988, p. 149-154.

Copyright

A mathematical model was developed to predict the effect of alternate blade circumferential aerodynamic detuning on the discrete frequency noise generation of a supersonic rotor. Aerodynamic detuning was shown to have a small beneficial effect on the noise generation for reduced frequencies less than 3. For reduced frequencies greater than 3, however, the aerodynamic detuning either increased or decreased the noise generated, depending on the value of the reduced frequency. B.J.

**A89-22285\*#** National Aeronautics and Space Administration. Lewis Research Center, Cleveland, OH.

**EFFECTS OF WIND-TUNNEL WALL ABSORPTION ON ACOUSTIC RADIATION OF PROPELLERS**

KENNETH J. BAUMEISTER (NASA, Lewis Research Center, Cleveland, OH) and WALTER EVERSMAN (Missouri-Rolla, University, Rolla) *Journal of Propulsion and Power* (ISSN 0748-4658), vol. 5, Jan.-Feb. 1989, p. 56-63. Previously cited in issue 05, p. 672, Accession no. A87-17991. refs

Copyright

**A89-33724\*#** United Technologies Corp., Windsor Locks, CT.  
**SOUND POWER SPECTRUM AND WAVE DRAG OF A PROPELLER IN FLIGHT**

D. B. HANSON (United Technologies Corp., Hamilton Standard Div., Windsor Locks, CT) AIAA, Aeroacoustics Conference, 12th, San Antonio, TX, Apr. 10-12, 1989. 17 p. Research supported by United Technologies Corp. refs

(Contract NAS3-23720)

(AIAA PAPER 89-1081) Copyright

Theory is presented for the sound power and sound power spectrum of a single rotation propeller in forward flight. Calculations are based on the linear wave equation with sources distributed over helicoidal surfaces to represent effects of blade thickness and steady loading. Sound power is distributed continuously over frequency, as would be expected from Doppler effects, rather than in discrete harmonics. The theory is applied to study effects of sweep and Mach number in propfans. An acoustic efficiency is defined as the ratio of radiated sound power to shaft input power. This value is the linear estimate of the effect of wave drag due to the supersonic blade section speeds. It is shown that the acoustic efficiency is somewhat less than 1 percent for a well designed propfan. Author

**A89-33725\*#** Arizona Univ., Tucson.

**INFLUENCE OF AIRFOIL THICKNESS ON CONVECTED GUST INTERACTION NOISE**

E. J. KERSCHEN and C. T. TSAI (Arizona, University, Tucson) AIAA, Aeroacoustics Conference, 12th, San Antonio, TX, Apr. 10-12, 1989. 10 p. refs

(Contract NAG3-357)

(AIAA PAPER 89-1082) Copyright

The case of a symmetric airfoil at zero angle of attack is considered in order to determine the influence of airfoil thickness on sound generated by interaction with convected gusts. The analysis is based on a linearization of the Euler equations about

the subsonic mean flow past the airfoil. Primary sound generation is found to occur in a local region surrounding the leading edge, with the size of the local region scaling on the gust wavelength. For a parabolic leading edge, moderate leading edge thickness is shown to decrease the noise level in the low Mach number limit.

V.L.

**A89-33767\*#** McDonnell-Douglas Research Labs., Saint Louis, MO.

**NEAR-FIELD ACOUSTIC ENVIRONMENT OF A SUPERSONIC PLUME ADJACENT TO A WALL**

R. W. WLEZIEN (McDonnell Douglas Research Laboratories, Saint Louis, MO) AIAA, Aeroacoustics Conference, 12th, San Antonio, TX, Apr. 10-12, 1989. 11 p. refs

(Contract NAS3-24621)

(AIAA PAPER 89-1137) Copyright

The interaction of a supersonic plume with an adjacent plane surface has been studied using phase-conditioned schlieren flow visualization and near-field microphone measurements. As a consequence of interaction with the wall, the round and 3:1 rectangular/divergent nozzle configurations generated the most intense screech at about one throat diameter from the wall. It is found that the low-aspect-ratio rectangular nozzle has a screech oscillation parallel to the wall which is enhanced by proximity to the wall. R.R.

**A89-36214\*#** National Aeronautics and Space Administration. Lewis Research Center, Cleveland, OH.

**ACOUSTIC WAVE PROPAGATION IN HETEROGENEOUS STRUCTURES INCLUDING EXPERIMENTAL VALIDATION**

KENNETH J. BAUMEISTER and MILO D. DAHL (NASA, Lewis Research Center, Cleveland, OH) AIAA, Aeroacoustics Conference, 12th, San Antonio, TX, Apr. 10-12, 1989. 12 p. Previously announced in STAR as N89-19965. refs

(AIAA PAPER 89-1044)

A finite element model was developed to solve for the acoustic pressure and energy fields in a heterogeneous suppressor. The derivations from the governing equations assumed that the material properties could vary with position resulting in a heterogeneous variable property two-dimensional wave equation. This eliminated the necessity of finding the boundary conditions between different materials. For a two-media region consisting of part air and part bulk absorber, a model was used to describe the bulk absorber properties in two directions. Complex metallic structures inside the air duct are simulated by simply changing element properties from air to the structural material in a pattern to describe the desired shapes. To verify the numerical theory, experiments were conducted without flow in a rectangular duct with a single folded cavity mounted above the duct and absorbing material mounted inside a cavity. Changes in a nearly plane wave sound field were measured on the wall opposite the absorbing cavity. Fairly good agreement was found in the standing wave pattern upstream of the absorber and in the decay of pressure level opposite the absorber, as a function of distance along the duct. The finite element model provides a convenient method for evaluating the acoustic properties of bulk absorbers. Author

**A89-36216\*#** Lockheed Aeronautical Systems Co., Marietta, GA.

**INSTALLED PROPFAN (SR-7L) FAR-FIELD NOISE CHARACTERISTICS**

N. N. REDDY, H. W. BARTEL, and M. SALIKUDDIN (Lockheed Aeronautical Systems Co., Marietta, GA) AIAA, Aeroacoustics Conference, 12th, San Antonio, TX, Apr. 10-12, 1989. 7 p.

(Contract NAS3-24339)

(AIAA PAPER 89-1056) Copyright

Far-field noise characteristics of the SR-7L single-rotor propfan were obtained from the Propfan Test Assessment (PTA) aircraft flight tests. The aircraft was flown at low altitudes (about 310m) above the ground at a constant speed of about 92 m/sec. The acoustic data were acquired with an array of ground-flush microphones positioned on both sides of the flight path. Propfan-generated noise levels were extracted from the total

aircraft noise, and these data were then used to study the far-field noise characteristics. The directivities at the polar and azimuthal planes, and the variations of the blade-order tone levels with propfan power and blade tip Mach number were derived. The effect of inflow angle was studied by changing the nacelle tilt angle. The levels and the directivity were very sensitive to the nacelle tilt angle (i.e., inflow angle). The noise levels in the aft quadrant were found to be higher than in the forward quadrant. Also, the noise levels on the starboard side of the aircraft were found to be higher than on the port side. The noise levels increase with propfan power and rotational speed. Author

**A89-36217\*** Lockheed Aeronautical Systems Co., Marietta, GA.

## **LATERAL NOISE ATTENUATION OF THE ADVANCED PROPELLER OF THE PROPFAN TEST ASSESSMENT AIRCRAFT**

F. W. CHAMBERS, N. N. REDDY, and H. W. BARTEL (Lockheed Aeronautical Systems Co., Marietta, GA) AIAA, Aeroacoustics Conference, 12th, San Antonio, TX, Apr. 10-12, 1989. 9 p. refs (Contract NAS3-24339) (AIAA PAPER 89-1057) Copyright

Lateral noise attenuation characteristics of the advanced propeller are determined using the flight test results of the testbed aircraft, Propfan Test Assessment (PTA), with a single, large-scale propfan. The acoustic data were obtained with an array of ground-mounted microphones positioned at distances up to 2.47 km (8100 feet) to the side of the flight path. The aircraft was flown at a Mach number of 0.31 for a variety of operating conditions. The lateral noise attenuation in a frequency range containing the blade passage frequency of the propeller was found to have positive magnitudes on the propfan side and negative magnitudes on the opposite side. The measured attenuation exhibits a strong dependence upon the elevation angle. The results also display a clear dependence upon the angle at which the propeller and nacelle are mounted on the wing (inflow angle). Author

**A89-36218\*** Lockheed Aeronautical Systems Co., Marietta, GA.

## **FLUCTUATING PRESSURES ON WING SURFACES IN THE SLIPSTREAM OF A SINGLE-ROTOR PROPFAN**

G. SWIFT and H. W. BARTEL (Lockheed Aeronautical Systems Co., Marietta, GA) AIAA, Aeroacoustics Conference, 12th, San Antonio, TX, Apr. 10-12, 1989. 12 p. (Contract NAS3-24339) (AIAA PAPER 89-1058) Copyright

Measurements of the fluctuating pressure levels (FPLs) induced on a Propfan Test Assessment wing by the SR-7L propfan slipstream within the airplane flight envelope were obtained as a function of propfan operating conditions. It is shown that FPLs were high over most of the flight envelope, and that the spectra were dominated by the propfan first-order blade passage frequency tone. The highest FPLs were found at the lowest aircraft test altitudes and Mach numbers and for propfan conditions of lowest rotational tip speed and highest power. R.R.

**A89-39195\*** Sverdrup Technology, Inc., Cleveland, OH. **HIGH-SPEED PROPELLER PERFORMANCE AND NOISE PREDICTIONS AT TAKEOFF/LANDING CONDITIONS**

M. NALLASAMY (Sverdrup Technology, Inc., Cleveland, OH), R. P. WOODWARD, and J. F. GROENEWEG (NASA, Lewis Research Center, Cleveland, OH) Journal of Aircraft (ISSN 0021-8669), vol. 26, June 1989, p. 563-569. Previously cited in issue 07, p. 1088, Accession no. A88-22193. refs Copyright

**A89-40175\*** National Aeronautics and Space Administration. Lewis Research Center, Cleveland, OH.

## **UNSTEADY BLADE PRESSURE MEASUREMENTS ON A MODEL COUNTERROTATION PROPELLER**

LAURENCE J. HEIDELBERG and RICHARD P. WOODWARD (NASA, Lewis Research Center, Cleveland, OH) AIAA,

Aeroacoustics Conference, 12th, San Antonio, TX, Apr. 10-12, 1989. 21 p. Previously announced in STAR as N89-20779. (AIAA PAPER 89-1144) Copyright

In an exploratory effort an advanced counterrotation propeller instrumented with blade-mounted pressure transducers was tested in the NASA Lewis 9- by 15-Foot Anechoic Wind Tunnel at a simulated takeoff and landing speed of Mach 0.20. The propeller's aft diameter was reduced to investigate possible noise reductions resulting from reduced blade row interaction with the tip vortex. The propeller was tested at three blade row spacings at fixed blade setting angles, at the maximum blade row spacing at higher blade setting angles and at propeller axis angles attack to the flow up to + or - 16 deg. A limited number of unsteady blade surface pressure measurements were made on both rotors of the model counterrotation propeller. Emphasis was placed on determining the effects of rotor-rotor interactions on the blade surface pressures. A unique method of processing the pressure signals was developed that enables even weak interaction waveforms and spectra to be separated from the total signal. The interaction on the aft rotor was many times stronger than that on the forward rotor. The fundamental rotor interaction tone exhibited complicated behavior but generally increased with rotational speed and blade setting angle and decreased with rotor spacing. With the propeller axis at an angle to the flow, the phase response of the aft rotor appeared to be significantly affected by the presence of the forward rotor. Author

**A89-40469\*** Texas A&M Univ., College Station. **DETERMINATION OF NEAR AND FAR FIELD ACOUSTICS FOR ADVANCED PROPELLER CONFIGURATIONS**

K. D. KORKAN, S. M. JAEGER, and J. H. KIM (Texas A & M University, College Station) AIAA, Aeroacoustics Conference, 12th, San Antonio, TX, Apr. 10-12, 1989. 14 p. refs (Contract NAG3-354) (AIAA PAPER 89-1040) Copyright

A method has been studied for predicting the acoustic field of the SR-3 transonic propfan using flow data generated by two versions of the NASPROP-E computer code. Since the flow fields calculated by the solvers include the shock-wave system of the propeller, the nonlinear quadrupole noise source term is included along with the monopole and dipole noise sources in the calculation of the acoustic near field. Acoustic time histories in the near field are determined by transforming the azimuthal coordinate in the rotating, blade-fixed coordinate system to the time coordinate in a nonrotating coordinate system. Fourier analysis of the pressure time histories is used to obtain the frequency spectra of the near-field noise. Author

**A89-40472\*** National Aeronautics and Space Administration. Lewis Research Center, Cleveland, OH.

## **COMPARISON OF PROPELLER CRUISE NOISE DATA TAKEN IN THE NASA LEWIS 8- BY 6-FOOT WIND TUNNEL WITH OTHER TUNNEL AND FLIGHT DATA**

JAMES DITTMAR (NASA, Lewis Research Center, Cleveland, OH) AIAA, Aeroacoustics Conference, 12th, San Antonio, TX, Apr. 10-12, 1989. 22 p. Previously announced in STAR as N89-21628. refs (AIAA PAPER 89-1059) Copyright

The noise of advanced high speed propeller models measured in the NASA 8- by 6-foot wind tunnel has been compared with model propeller noise measured in another tunnel and with full-scale propeller noise measured in flight. Good agreement was obtained for the noise of a model counterrotation propeller tested in the 8- by 6-foot wind tunnel and in the acoustically treated test section of the Boeing Transonic Wind Tunnel. This good agreement indicates the relative validity of taking cruise noise data on a plate in the 8- by 6-foot wind tunnel compared with the free-field method in the Boeing tunnel. Good agreement was also obtained for both single rotation and counter-rotation model noise comparisons with full-scale propeller noise in flight. The good scale model to full-scale comparisons indicate both the validity of the 8- by 6-foot wind tunnel data and the ability to scale to full size. Boundary layer refraction on the plate provides a limitation to the

measurement of forward arc noise in the 8- by 6-foot wind tunnel at the higher harmonics of the blade passing tone. The use of a validated boundary layer refraction model to adjust the data could remove this limitation. Author

**A89-40473\*** # National Aeronautics and Space Administration. Lewis Research Center, Cleveland, OH.

**PREDICTION OF UNSTEADY BLADE SURFACE PRESSURES ON AN ADVANCED PROPELLER AT AN ANGLE OF ATTACK**

M. NALLASAMY (NASA, Lewis Research Center; Sverdrup Technology, Inc., Cleveland, OH) and J. F. GROENEWEG (NASA, Lewis Research Center, Cleveland, OH) AIAA, Aerodynamics Conference, 12th, San Antonio, TX, Apr. 10-12, 1989. 20 p. refs (Contract NAS3-25266) (AIAA PAPER 89-1060)

The paper considers the numerical solution of the unsteady, three-dimensional, Euler equations to obtain the blade surface pressures of an advanced propeller at an angle of attack. The specific configuration considered is the SR7L propeller at cruise conditions with a 4.6 deg inflow angle corresponding to the +2 deg nacelle tilt of the Propeller Test Assessment (PTA) flight test condition. The results indicate nearly sinusoidal response of the blade loading, with angle of attack. For the first time, detailed variations of the chordwise loading as a function of azimuthal angle are presented. It is observed that the blade is lightly loaded for part of the revolution and shocks appear from hub to about 80 percent radial station for the highly loaded portion of the revolution. Author

**A89-40478\*** # Texas A&M Univ., College Station. **AN ACOUSTIC EXPERIMENTAL AND THEORETICAL INVESTIGATION OF SINGLE DISC PROPELLERS**

ELIZABETH A. BUMANN and KENNETH D. KORKAN (Texas A & M University, College Station) AIAA, Aerodynamics Conference, 12th, San Antonio, TX, Apr. 10-12, 1989. 17 p. refs (Contract NAG3-354) (AIAA PAPER 89-1146) Copyright

An experimental study of the acoustic field associated with two, three, and four blade propeller configurations with a blade root angle of 50 deg was performed in the Texas A&M University 5 ft. x 6 ft. acoustically-insulated subsonic wind tunnel. A waveform analysis package was utilized to obtain experimental acoustic time histories, frequency spectra, and overall sound pressure level (OASPL) and served as a basis for comparison to the theoretical acoustic compact source theory of Succi (1979). Valid for subsonic tip speeds, the acoustic analysis replaced each blade by an array of spiraling point sources which exhibited a unique force vector and volume. The computer analysis of Succi was modified to include a propeller performance strip analysis which used a NACA 4-digit series airfoil data bank to calculate lift and drag for each blade segment given the geometry and motion of the propeller. Theoretical OASPL predictions were found to moderately overpredict experimental values for all operating conditions and propeller configurations studied. Author

**A89-46772\*** # National Aeronautics and Space Administration. Langley Research Center, Hampton, VA.

**SUPERSONIC JET NOISE AND THE HIGH SPEED CIVIL TRANSPORT**

JOHN M. SEINER (NASA, Langley Research Center, Hampton, VA) and EUGENE A. KREJSA (NASA, Lewis Research Center, Cleveland, OH) AIAA, ASME, SAE, and ASCE, Joint Propulsion Conference, 25th, Monterey, CA, July 10-13, 1989. 24 p. refs (AIAA PAPER 89-2358)

An evaluation is made of the comparative advantages of prospective SST engine noise-suppression systems, with a view to their effectiveness in meeting the federally-mandated community noise standards of FAR 36 Stage III. A noise-suppression system must be capable of removing at least 4 EPNdB of noise percent thrust loss at takeoff. While none of the suppressors presently discussed is capable of meeting this goal, the inverted velocity profile/annular convergent-divergent plug/acoustically-treated ejector suppressor combination of configurational elements appears

to represent the most efficient noise-control apparatus. Noncircular cross-section nozzle geometries also furnish a general noise reduction advantage over circular ones. O.C.

**A89-48953\*** # National Aeronautics and Space Administration. Lewis Research Center, Cleveland, OH.

**NOISE OF A MODEL COUNTERROTATION PROPELLER WITH SIMULATED FUSELAGE AND SUPPORT PYLON AT TAKEOFF/APPROACH CONDITIONS**

RICHARD P. WOODWARD and CHRISTOPHER E. HUGHES (NASA, Lewis Research Center, Cleveland, OH) AIAA, Aerodynamics Conference, 12th, San Antonio, TX, Apr. 10-12, 1989. 25 p. Previously announced in STAR as N89-24138. refs (AIAA PAPER 89-1143) Copyright

Two modern high-speed advanced counterrotation propellers, F7/A7 and F7/A3 were tested in the NASA Lewis Research Center's 9- by 15-foot Anechoic Wind Tunnel at simulated takeoff/approach conditions of 0.2 Mach number. Both rotors were of similar diameter on the F7/A7 propeller, while the aft rotor diameter of the F7/A3 propeller was 85 percent of the forward propeller to reduce tip vortex-aft rotor interaction. The two propellers were designed for similar performance. The propellers were tested in both the clean configuration, and installed configuration consisting of a simulated upstream nacelle support pylon and fuselage section. Acoustic measurements were made with an axially translating microphone probe, and with a polar microphone probe which was fixed to the propeller nacelle and could make both sideline and circumferential acoustic surveys. Aerodynamic measurements were also made to establish propeller operating conditions. The propellers were run at blade setting angles (front angle/rear angle) of 41.1/39.4 deg for the F7/A7 propeller, and 41.1/46.4 deg for the F7/A3 propeller. The forward rotors were tested over a range of tip speeds from 165 to 259 m/sec (540 to 850 ft/sec), and both propellers were tested at the maximum rotor-rotor spacing, based on pitch change axis separation, of 14.99 cm (5.90 in.). The data presented in this paper are for 0 deg propeller axis angle of attack. Results are presented for the baseline, pylon-alone, and strut + fuselage configurations. The presence of the simulated fuselage resulted in higher rotor-alone tone levels in a direction normal to the advancing propeller blade near the fuselage. A corresponding rotor-alone tone reduction was often observed 180 deg circumferentially from this region of increased noise. A significant rotor-alone increase for both rotors was observed diametrically opposite the fuselage. In some cases, interaction tone levels were likewise affected by the simulated installation. Author

**N89-10603\*** # National Aeronautics and Space Administration. Lewis Research Center, Cleveland, OH.

**THE EFFECT OF FRONT-TO-REAR PROPELLER SPACING ON THE INTERACTION NOISE AT CRUISE CONDITIONS OF A MODEL COUNTERROTATION PROPELLER HAVING A REDUCED DIAMETER AFT PROPELLER**

JAMES H. DITTMAR, ELIOTT B. GORDON (Sverdrup Technology, Inc., Cleveland, Ohio.), and ROBERT J. JERACKI Oct. 1988 30 p (NASA-TM-101329; E-4340; NAS 1.15:101329) Avail: NTIS HC A03/MF A01 CSCL 20/1

The effect of forward-to-aft propeller spacing on the interaction noise of a counterrotation propeller with reduced aft diameter was measured at cruise conditions. In general, the tones at 100 percent speed decreased from close to nominal spacing as expected from a wake decay model. However, when the spacing was further increased to the far position, the noise did not decrease as expected and in some cases increased. The behavior at the far spacing was attributed to changing forward propeller performance, which produced larger wakes. The results of this experiment indicate that simple wake decay model is sufficient to describe the behavior of the interaction noise only if the aerodynamic coupling of the two propellers does not change with spacing. If significant coupling occurs such that the loading of the forward propeller is altered, the interaction noise does not necessarily decrease with larger forward-to-aft propeller spacing. Author

**N89-15685\*#** National Aeronautics and Space Administration. Lewis Research Center, Cleveland, OH.

**ACOUSTIC EVALUATION OF THE HELMHOLTZ RESONATOR TREATMENT IN THE NASA LEWIS 8- BY 6-FOOT SUPERSONIC WIND TUNNEL**

LAURENCE J. HEIDELBERG and ELLIOT B. GORDON (Sverdrup Technology, Inc., Cleveland, OH.) Jan. 1989 12 p (NASA-TM-101407; E-4147; NAS 1.15:101407) Avail: NTIS HC A03/MF A01 CSCL 20/1

The acoustic consequences of sealing the Helmholtz resonators of the NASA Lewis 8- by 6-Foot Supersonic Wind Tunnel (8x6 SWT) were experimentally evaluated. This resonator sealing was proposed in order to avoid entrapment of hydrogen during tests of advanced hydrogen-fueled engines. The resonators were designed to absorb energy in the 4- to 20-Hz range; thus, this investigation is primarily concerned with infrasound. Limited internal and external noise measurements were made at tunnel Mach numbers ranging from 0.5 to 2.0. Although the resonators were part of the acoustic treatment installed because of a community noise problem their sealing did not seem to indicate a reoccurrence of the problem would result. Two factors were key to this conclusion: (1) A large bulk treatment muffler downstream of the resonators was able to make up for much of the attenuation originally provided by the resonators, and (2) there was no noise source in the tunnel test section. The previous community noise problem occurred when a large ramjet was tested in an open-loop tunnel configuration. If a propulsion system producing high noise levels at frequencies of less than 10 Hz were tested, the conclusion on community noise would have to be reevaluated. Author

**N89-15686\*#** National Aeronautics and Space Administration. Lewis Research Center, Cleveland, OH.

**MEASURED FAR-FIELD FLIGHT NOISE OF A COUNTERROTATION TURBOPROP AT CRUISE CONDITIONS**

RICHARD P. WOODWARD, IRVIN J. LOEFFLER, and JAMES H. DITTMAR Jan. 1989 20 p (NASA-TM-101383; E-4437; NAS 1.15:101383) Avail: NTIS HC A03/MF A01 CSCL 20/1

Modern high speed propeller (advanced turboprop) aircraft are expected to operate on 50 to 60 percent less fuel than the 1980 vintage turbofan fleet while at the same time matching the flight speed and performance of those aircraft. Counterrotation turboprop engines offer additional fuel savings by means of upstream propeller swirl recovery. This paper presents acoustic sideline results for a full-scale counterrotation turboprop engine at cruise conditions. The engine was installed on a Boeing 727 aircraft in place of the right-side turbofan engine. Acoustic data were taken from an instrumented Learjet chase plane. Sideline acoustic results are presented for 0.50 and 0.72 Mach cruise conditions. A scale model of the engine propeller was tested in a wind tunnel at 0.72 Mach cruise conditions. The model data were adjusted to flight acquisition conditions and were in general agreement with the flight results. Author

**N89-20776\*#** Sverdrup Technology, Inc., Cleveland, OH.  
**NOISE GENERATED BY A FLIGHT WEIGHT, AIR FLOW CONTROL VALVE IN A VERTICAL TAKEOFF AND LANDING AIRCRAFT THRUST VECTORING SYSTEM Final Report**

RONALD G. HUFF Feb. 1989 55 p Prepared in cooperation with Huff (Ronald G.) and Associates, North Olmsted, OH (Contract NAS3-25266) (NASA-CR-182232; E-4556; NAS 1.16:182232) Avail: NTIS HC A04/MF A01 CSCL 20/1

Tests were conducted in the NASA Lewis Research Center's Powered Lift Facility to experimentally evaluate the noise generated by a flight weight, 12 in. butterfly valve installed in a proposed vertical takeoff and landing thrust vectoring system. Fluctuating pressure measurements were made in the circular duct upstream and downstream of the valve. This data report presents the results of these tests. The maximum overall sound pressure level is generated in the duct downstream of the valve and reached a value of 180 dB at a valve pressure ratio of 2.8. At the higher

valve pressure ratios the spectra downstream of the valve is broad banded with its maximum at 1000 Hz. Author

**N89-20779\*#** National Aeronautics and Space Administration. Lewis Research Center, Cleveland, OH.

**UNSTEADY BLADE PRESSURE MEASUREMENTS ON A MODEL COUNTERROTATION PROPELLER**

LAURENCE J. HEIDELBERG and RICHARD P. WOODWARD Apr. 1989 22 p Presented at the 12th Aeroacoustics Conference, San Antonio, TX, 10-12 Apr. 1989; sponsored in part by AIAA (NASA-TM-102002; E-4684; NAS 1.15:102002; AIAA-89-1144) Avail: NTIS HC A03/MF A01 CSCL 20/1

In an exploratory effort an advanced counterrotation propeller instrumented with blade-mounted pressure transducers was tested in the NASA Lewis 9- by 15-Foot Anechoic Wind Tunnel at a simulated takeoff and landing speed of Mach 0.20. The propeller's aft diameter was reduced to investigate possible noise reductions resulting from reduced blade row interaction with the tip vortex. The propeller was tested at three blade row spacings at fixed blade setting angles, at the maximum blade row spacing at higher blade setting angles and at propeller axis angles attack to the flow up to + or - 16 deg. A limited number of unsteady blade surface pressure measurements were made on both rotors of the model counterrotation propeller. Emphasis was placed on determining the effects of rotor-rotor interactions on the blade surface pressures. A unique method of processing the pressure signals was developed that enables even weak interaction waveforms and spectra to be separated from the total signal. The interaction on the aft rotor was many times stronger than that on the forward rotor. The fundamental rotor interaction tone exhibited complicated behavior but generally increased with rotational speed and blade setting angle and decreased with rotor spacing. With the propeller axis at an angle to the flow, the phase response of the aft rotor appeared to be significantly affected by the presence of the forward rotor. Author

**N89-21628\*#** National Aeronautics and Space Administration. Lewis Research Center, Cleveland, OH.

**COMPARISON OF PROPELLER CRUISE NOISE DATA TAKEN IN THE NASA LEWIS 8- BY 6-FOOT WIND TUNNEL WITH OTHER TUNNEL AND FLIGHT DATA**

JAMES H. DITTMAR Apr. 1989 23 p Presented at the 12th Aeroacoustics Conference, San Antonio, TX, 10-12 Apr. 1989; sponsored in part by AIAA (NASA-TM-101976; E-4676; NAS 1.15:101976; AIAA-89-1059) Avail: NTIS HC A03/MF A01 CSCL 20/1

The noise of advanced high speed propeller models measured in the NASA 8- by 6-foot wind tunnel has been compared with model propeller noise measured in another tunnel and with full-scale propeller noise measured in flight. Good agreement was obtained for the noise of a model counterrotation propeller tested in the 8- by 6-foot wind tunnel and in the acoustically treated test section of the Boeing Transonic Wind Tunnel. This good agreement indicates the relative validity of taking cruise noise data on a plate in the 8- by 6-foot wind tunnel compared with the free-field method in the Boeing tunnel. Good agreement was also obtained for both single rotation and counter-rotation model noise comparisons with full-scale propeller noise in flight. The good scale model to full-scale comparisons indicate both the validity of the 8- by 6-foot wind tunnel data and the ability to scale to full size. Boundary layer refraction on the plate provides a limitation to the measurement of forward arc noise in the 8- by 6-foot wind tunnel at the higher harmonics of the blade passing tone. The use of a validated boundary layer refraction model to adjust the data could remove this limitation. Author

**N89-24138\*#** National Aeronautics and Space Administration. Lewis Research Center, Cleveland, OH.

**NOISE OF A MODEL COUNTERROTATION PROPELLER WITH SIMULATED FUSELAGE AND SUPPORT PYLON AT TAKEOFF/APPROACH CONDITIONS**

RICHARD P. WOODWARD and CHRISTOPHER E. HUGHES Apr. 1989 26 p Presented at the 12th Aeroacoustics Conference,



San Antonio, TX, 10-12 Apr. 1989; sponsored by AIAA  
(NASA-TM-101996; E-4700; NAS 1.15:101996; AIAA-89-1143)  
Copyright Avail: NTIS HC A03/MF A01 CSCL 20/1

Two modern high-speed advanced counterrotation propellers, F7/A7 and F7/A3 were tested in the NASA Lewis Research Centers's 9- by 15-foot Anechoic Wind Tunnel at simulated takeoff/approach conditions of 0.2 Mach number. Both rotors were of similar diameter on the F7/A7 propeller, while the aft rotor diameter of the F7/A3 propeller was 85 percent of the forward propeller to reduce tip vortex-aft rotor interaction. The two propellers were designed for similar performance. The propellers were tested in both the clean configuration, and installed configuration consisting of a simulated upstream nacelle support pylon and fuselage section. Acoustic measurements were made with an axially translating microphone probe, and with a polar microphone probe which was fixed to the propeller nacelle and could make both sideline and circumferential acoustic surveys. Aerodynamic measurements were also made to establish propeller operating conditions. The propellers were run at blade setting angles (front angle/rear angle) of 41.1/39.4 deg for the F7/A7 propeller, and 41.1/46.4 deg for the F7/A3 propeller. The forward rotors were tested over a range of tip speeds from 165 to 259 m/sec (540 to 850 ft/sec), and both propellers were tested at the maximum rotor-rotor spacing, based on pitch change axis separation, of 14.99 cm (5.90 in.). The data presented in this paper are for 0 deg propeller axis angle of attack. Results are presented for the baseline, pylon-alone, and strut + fuselage configurations. The presence of the simulated fuselage resulted in higher rotor-alone tone levels in a direction normal to the advancing propeller blade near the fuselage. A corresponding rotor-alone tone reduction was often observed 180 deg circumferentially from this region of increased noise. A significant rotor-alone increase for both rotors was observed diametrically opposite the fuselage. In some cases, interaction tone levels were likewise affected by the simulated installation. Author

**N89-24139\*#** General Electric Co., Cincinnati, OH. Advanced Engineering Technologies Dept.  
**HIGH SPEED TURBOPROP AEROACOUSTIC STUDY (SINGLE ROTATION). VOLUME 1: MODEL DEVELOPMENT Final Report**  
C. E. WHITFIELD, P. R. GLIEBE, R. MANI, and P. MUNGUR  
May 1989 185 p  
(Contract NAS3-23721)  
(NASA-CR-182257-VOL-1; NAS 1.26:182257-VOL-1) Avail: NTIS HC A09/MF A01 CSCL 20/1

A frequency-domain noncompact-source theory for the steady loading and volume-displacement (thickness) noise of high speed propellers has been developed and programmed. Both near field and far field effects have been considered. The code utilizes blade surface pressure distributions obtained from three-dimensional nonlinear aerodynamic flow field analysis programs as input for evaluating the steady loading noise. Simplified mathematical models of the velocity fields induced at the propeller disk by nearby wing and fuselage surfaces and by angle-of-attack operation have been developed to provide estimates of the unsteady loading imposed on the propeller by these potential field type interactions. These unsteady blade loadings have been coupled to a chordwise compact propeller unsteady loading noise model to provide predictions of unsteady loading noise caused by these installation effects. Finally, an analysis to estimate the corrections to be applied to the free-field noise predictions in order to arrive at the measurable fuselage sound pressure levels has been formulated and programmed. This analysis considers the effects of fuselage surface reflection and diffraction together with surface boundary layer refraction. The steady loading and thickness model and the unsteady loading model have been verified using NASA-supplied data for the SR-2 and SR-3 model propfans. In addition, the steady loading and thickness model has been compared with data from the SR-6 model propfan. These theoretical models have been employed in the evaluation of the SR-7 powered Gulfstream aircraft in terms of noise characteristics at representative takeoff, cruise, and approach operating conditions. In all cases, agreement between theory and experiment is encouraging. Author

**N89-24886\*#** National Aeronautics and Space Administration. Lewis Research Center, Cleveland, OH.

**CRUISE NOISE OF THE SR-2 PROPELLER MODEL IN A WIND TUNNEL**

JAMES H. DITTMAR Apr. 1989 29 p  
(NASA-TM-101480; E-4606; NAS 1.15:101480) Avail: NTIS HC A03/MF A01 CSCL 20/1

Noise data on the SR-2 model propeller were taken in the NASA Lewis Research Center 8- by 6-Foot Wind Tunnel. The maximum blade passing tone rises with increasing helical tip Mach number to a peak level at a helical tip Mach number of about 1.05; then it remains the same or decreases at higher helical tip Mach numbers. This behavior, which has been observed with other propeller models, points to the possibility of using higher propeller tip speeds to limit airplane cabin noise while maintaining high flight speed and efficiency. Noise comparisons of the straight-blade SR-2 propeller and the swept-blade SR-7A propeller showed that the tailored sweep of the SR-7A appears to be the cause of both lower peak noise levels and a slower noise increase with increasing helical tip Mach number. Author

**N89-25675\*#** National Aeronautics and Space Administration. Lewis Research Center, Cleveland, OH.

**IN-FLIGHT MEASUREMENT OF PROPELLER NOISE ON THE FUSELAGE OF AN AIRPLANE**

FREDERIC G. PLA (Sverdrup Technology, Inc., Cleveland, OH.), RICHARD RANAUDO, and RICHARD P. WOODWARD Jul. 1989 58 p  
(Contract NAS3-24105)  
(NASA-TM-102285; E-4952; NAS 1.15:102285) Avail: NTIS HC A04/MF A01 CSCL 20/1

In-flight measurements of propeller noise on the fuselage of an OV-10A aircraft were obtained using a horizontal and a vertical microphone array. A wide range of flight conditions were tested including changes in angle of attack, sideslip angle, power coefficient, helical tip Mach number and advance ratio, and propeller direction of rotation. Results show a dependence of the level and directivity of the tones on the angle of attack and on the sideslip angle with the propeller direction of rotation, which is similar to results obtained in wind tunnel tests with advanced propeller designs. The level of the tones at each microphone increases with increasing angle of attack for inboard-down propeller rotation and decreases for inboard-up rotation. The level also increases with increasing sideslip angle for both propeller directions of rotation. Increasing the power coefficient results in a slight increase in the level of the tones. A strong shock wave is generated by the propeller blades even at relatively low helical tip Mach numbers resulting in high harmonic levels. As the helical tip Mach number and the advance ratio are increased, the level of the higher harmonics increases much faster than the level of the blade passage frequency. Author

## 72

### ATOMIC AND MOLECULAR PHYSICS

Includes atomic structure, electron properties, and molecular spectra.

**N89-19973\*#** Colorado State Univ., Fort Collins. Dept. of Mechanical Engineering.

**THE DIVERGENCE CHARACTERISTICS OF CONSTRAINED-SHEATH OPTICS SYSTEMS FOR USE WITH 5-EV ATOMIC OXYGEN SOURCES Final Report, Apr. 1987 - Sep. 1988**

JOHN R. ANDERSON and PAUL J. WILBUR Jan. 1989 58 p  
(Contract NAG3-791)  
(NASA-CR-182238; NAS 1.26:182238) Avail: NTIS HC A04/MF A01 CSCL 20/8

The potential usefulness of the constrained sheath optics

## 73 NUCLEAR AND HIGH-ENERGY PHYSICS

concept as a means of controlling the divergence of low energy, high current density ion beams is examined numerically and experimentally. Numerical results demonstrate that some control of the divergence of typical ion beamlets can be achieved at perveance levels of interest by contouring the surface of the constrained sheath properly. Experimental results demonstrate that a sheath can be constrained by a wire mesh attached to the screen plate of the ion optics system. The numerically predicted beamlet divergence characteristics are shown to depart from those measured experimentally, and additional numerical analysis is used to demonstrate that this departure is probably due to distortions of the sheath caused by the fact that it attempts to conform to the individual wires that make up the sheath constraining mesh. The concept is considered potentially useful in controlling the divergence of ion beamlets in applications where low divergence, low energy, high current density beamlets are being sought, but more work is required to demonstrate this for net beam ion energies as low as 5 eV. Author

73

## NUCLEAR AND HIGH-ENERGY PHYSICS

Includes elementary and nuclear particles; and reactor theory.

**N89-13227\*#** Oregon State Univ., Corvallis.  
**SPACE REACTOR ASSESSMENT AND VALIDATION STUDY**  
**Abstract Only**

STEPHEN GEDEON and DENNIS MOREY In New Mexico Univ.,  
Nuclear Technology for the Year 2000 p 24 1987  
(Contract NAG3-752)  
Avail: NTIS HC A06/MF A01

The present difficulties experienced by the United States in launching payloads into space has suggested a number of problems which are associated with the handling of hazardous materials in spacecraft. The question has arisen as to the safety of launching highly radioactive material such as plutonium-238, related to the possibility of its dispersion into the atmosphere during a launch vehicle explosion. An alternative is the use of a small nuclear reactor which is not started until it is in space and contains little or no radioactivity at launch. A first order assessment of six small reactor concepts with power levels up to 100 MWe was performed. Both the nuclear feasibility of these concepts to operate at their rated power levels between 7 and 10 years and the capability of these concepts to remain subcritical both before and during launch and also in the case of water immersion during a potential launch failure or abort were investigated. Author

**N89-14831\*#** National Aeronautics and Space Administration.  
Lewis Research Center, Cleveland, OH.

### NUCLEAR REACTOR POWER AS APPLIED TO A SPACE-BASED RADAR MISSION

L. JAFFE, T. FUJITA, R. BEATTY, P. BHANDARI, E. CHOW, W. DEININGER, R. EWELL, M. GROSSMAN, T. KIA, B. NESMITH (Jet Propulsion Lab., California Inst. of Tech., Pasadena.) et al. 1988 17 p Presented at the 23rd Intersociety Energy Conversion Engineering Conference, Denver, CO, 31 Jul. 1988 Prepared in cooperation with Los Alamos National Lab., NM (Contract W-7405-ENG-36) (NASA-TM-101200; NAS 1.15:101200; DE89-000341; LA-UR-88-3253; CONF-880702-23) Avail: NTIS HC A03/MF A01 CSCL 18/5

The SP-100 Project was established to develop and demonstrate feasibility of a space reactor power system (SRPS) at power levels of 10's of kilowatts to a megawatt. To help determine systems requirements for the SRPS, a mission and spacecraft were examined which utilize this power system for a space-based radar to observe moving objects. Aspects of the mission and spacecraft bearing on the power system were the

primary objectives of this study; performance of the radar itself was not within the scope. The study was carried out by the Systems Design Audit Team of the SP-100 Project. DOE

74

## OPTICS

Includes light phenomena; and optical devices.

**A89-12236\*** Rensselaer Polytechnic Inst., Troy, NY.

### CRYSTALLIZATION OF BAF<sub>2</sub>-ZNF<sub>2</sub>-YBF<sub>3</sub>-THF<sub>4</sub> GLASS

ROBERTO GARCIA, ROBERT H. DOREMUS, SEN-HOU KO, TRACEY MARGRAF (Rensselaer Polytechnic Institute, Troy, NY), and NAROTTAM P. BANSAL (NASA, Lewis Research Center, Cleveland, OH; Rensselaer Polytechnic Institute, Troy, NY) Journal of Materials Research (ISSN 0884-2914), vol. 3, Sept.-Oct. 1988, p. 989-995. refs (Contract N00014-83-K-0278) Copyright

The phases and the rates of crystallization in a Ba-Zn-Yb-Th fluoride glass were studied using differential scanning calorimetry, XRD, and observational and chemical SEM analyses. The crystallizing phases that were identified included a BaYbTh fluoride, ZnF<sub>2</sub>, and YbF<sub>3</sub>. The BaYbTh fluoride crystallized first at about 450 C, and ZnF<sub>2</sub>, which was excluded from this phase, crystallized at its surfaces. At higher temperatures, the BaYbTh fluoride phase decomposed partially to BaThF<sub>6</sub> and YbF<sub>3</sub> phases. I.S.

**A89-41530\*** National Aeronautics and Space Administration.  
Lewis Research Center, Cleveland, OH.

### COMPARISON OF THE BIDIRECTIONAL REFLECTANCE DISTRIBUTION FUNCTION OF VARIOUS SURFACES

RENE FERNANDEZ, RICHARD G. SEASHOLTZ, LAWRENCE G. OBERLE (NASA, Lewis Research Center, Cleveland, OH), and JAIKRISHNAN R. KADAMBI (Case Western Reserve University, Cleveland, OH) IN: Stray light and contamination in optical systems; Proceedings of the Meeting, San Diego, CA, Aug. 17-19, 1988. Bellingham, WA, Society of Photo-Optical Instrumentation Engineers, 1989, p. 292-305. refs Copyright

This paper describes the development and use of a system to measure the bidirectional reflectance distribution function (BRDF) of various surfaces. The BRDF measurements are to be used in the analysis and design of optical measurement systems such as laser anemometers. An Ar-ion laser (514 nm) was the light source. Preliminary results are presented for eight samples: two glossy black paints, two flat black paints, black glass, sand-blasted Al, unworked Al, and a white paint. A BaSO<sub>4</sub> white reflectance standard was used as the reference sample throughout the tests. Author

**A89-46812\*#** Rockwell International Corp., Canoga Park, CA.  
**FIBEROPTICS FOR LIQUID PROPELLANT ROCKET ENGINE ENVIRONMENTS**

R. DELCHER, A. DERGEVORKIAN, and S. BARKHOUDARIAN (Rockwell International Corp., Rocketdyne Div., Canoga Park, CA) AIAA, ASME, SAE, and ASCE, Joint Propulsion Conference, 25th, Monterey, CA, July 10-13, 1989. 5 p. (Contract NAS3-25346) (AIAA PAPER 89-2416) Copyright

Interest is increasing in the use of fiber optics on liquid-fueled rocket engines in recognition of their immunity to lightning and EMI, light weight, high-frequency response, and the possibility offered by optical technologies to measure additional important engine parameters for which present measurement methods are impractical. This paper discusses the requirements to be placed on fiber optics applied to liquid-fueled rocket engines; identifies manufacturers of fibers that appear to have promise for the harsh

rocket engine applications; and summarizes information on the characteristics of these fibers obtained from the manufacturers, program testing, and the general literature. Author

**A89-48249\*** National Aeronautics and Space Administration. Lewis Research Center, Cleveland, OH.

#### **FRESNEL DIFFRACTION BY SPHERICAL OBSTACLES**

EDWARD A. HOVENAC (NASA, Lewis Research Center; Sverdrup Technology, Inc., Cleveland, OH) American Journal of Physics (ISSN 0002-9505), vol. 57, Jan. 1989, p. 79-84. refs  
Copyright

Lommel functions were used to solve the Fresnel-Kirchhoff diffraction integral for the case of a spherical obstacle. Comparisons were made between Fresnel diffraction theory and Mie scattering theory. Fresnel theory is then compared to experimental data. Experiment and theory typically deviated from one another by less than 10 percent. A unique experimental setup using mercury spheres suspended in a viscous fluid significantly reduced optical noise. The major source of error was due to the Gaussian-shaped laser beam. Author

**N89-13256\*#** General Electric Co., Cincinnati, OH. Aircraft Engine Business Group.

#### **FIBER OPTIC CONTROL SYSTEM INTEGRATION Final Report**

G. L. POPPEL, W. M. GLASHEEN, and J. C. RUSSELL Feb. 1987 72 p

(Contract NAS3-24624)

(NASA-CR-179568; NAS 1.26:179568; R87AEB111) Avail: NTIS HC A04/MF A01 CSCL 20/6

A total fiber optic, integrated propulsion/flight control system concept for advanced fighter aircraft is presented. Fiber optic technology pertaining to this system is identified and evaluated for application readiness. A fiber optic sensor vendor survey was completed, and the results are reported. The advantages of centralized/direct architecture are reviewed, and the concept of the protocol branch is explained. Preliminary protocol branch selections are made based on the F-18/F404 application. Concepts for new optical tools are described. Development plans for the optical technology and the described system are included. Author

**N89-27506\*#** National Aeronautics and Space Administration. Lewis Research Center, Cleveland, OH.

#### **DIAMONDLIKE CARBON PROTECTIVE COATINGS FOR OPTICAL WINDOWS**

DIANE M. SWEC and MICHAEL J. MIRTICH 1989 16 p  
Presented at the 1989 Technical Symposia on Aerospace Sensing, Orlando, FL, 27-31 Mar. 1989; sponsored by The International Society for Optical Engineering  
(NASA-TM-102111; E-4881; NAS 1.15:102111) Avail: NTIS HC A03/MF A01 CSCL 20/6

Diamonddike carbon (DLC) films were deposited on infrared transmitting optical windows and were evaluated as protective coatings for these windows exposed to particle and rain erosion. The DLC films were deposited on zinc selenide (ZnSe) and zinc sulfide (ZnS) by three different ion beam methods: (1) sputter deposition from a carbon target using an 8-cm argon ion source; (2) direct deposition by a 30-cm hollow cathode ion source with hydrocarbon gas in argon; and (3) dual beam direct deposition by the 30-cm hollow cathode ion source and an 8-cm argon ion source. In an attempt to improve the adherence of the DLC films on ZnS and ZnSe, ion beam cleaning, ion implantation with helium and neon ions, or sputter deposition of a thin, ion beam intermediate coating was employed prior to deposition of the DLC film. The protection that the DLC films afforded the windows from particle and rain erosion was evaluated, along with the hydrogen content, adherence, intrinsic stress, and infrared transmittance of the films. Because of the elevated stress levels in the ion beam sputtered DLC films and in those ion beam deposited with butane, films thicker than 0.1 micron and with good adherence on ZnS and ZnSe could not be generated. An intermediate coating of germanium successfully allowed the DLC films to remain adherent

to the optical windows and caused only negligible reduction in the specular transmittance of the ZnS and ZnSe at 10 microns. Author

## 75

### PLASMA PHYSICS

Includes magnetohydrodynamics and plasma fusion.

**A89-16409\*** Illinois Univ., Champaign.

#### **TOWNSEND COEFFICIENTS FOR ELECTRON SCATTERING OVER DIELECTRIC SURFACES**

TIMOTHY L. PECK and MARK J. KUSHNER (Illinois, University, Champaign) Journal of Applied Physics (ISSN 0021-8979), vol. 64, Nov. 1, 1988, p. 4404-4409. refs  
(Contract NAG3-741)

Copyright

A method for describing the probability of initiating flashover discharges across dielectric surfaces is presented in which a transport coefficient for electron multiplication similar to the Townsend coefficient used for gas discharges is defined. The coefficient is a function of the scaling parameter (charge released from the cathode)/(cathode-anode separation) and is also a measure of the growth of the sheath on the dielectric surface resulting from electron scattering. Results are discussed as to when the source of seed electrons does not necessarily depend upon field emission at the cathode-vacuum-dielectric triple point. For these conditions, there is a different functional dependence of flashover probability on voltage and geometry than when field emission provides the seed electrons. As a result, criteria previously used to predict flashover discharges may not apply. Author

**A89-24292\*** Iowa Univ., Iowa City.

#### **COHERENT CERENKOV RADIATION FROM THE SPACELAB 2 ELECTRON BEAM**

W. M. FARRELL, D. A. GURNETT, and C. K. GOERTZ (Iowa, University, Iowa City) Journal of Geophysical Research (ISSN 0148-0227), vol. 94, Jan. 1, 1989, p. 443-452. refs

(Contract NAS8-32807; NAG3-449; NSG-7632; NGL-16-001-002; NGL-16-001-043; NAGW-235)

Copyright

The plasma environment of the Spacelab 2 mission was investigated through the deployment of the Plasma Diagnostics Package (PDP) by the Space Shuttle Orbiter and the Orbiter's ejection of a continuous 1-keV/50-mA electron beam along a field line. As the PDP flew by the beam, its plasma-wave instrument detected intense whistler-mode radiation originating from the beam. A detailed model has been developed of the coherent Cerenkov emission process, using a one-dimensional computer simulation of the beam to model the expected phase space structure of the electrons. The power calculated for the modeled 200-m beam segment can easily account for the measured whistler mode wave power. O.C.

**A89-25537\*#** Colorado State Univ., Fort Collins.

#### **PLASMA CONTACTING - AN ENABLING TECHNOLOGY**

JOHN D. WILLIAMS and PAUL J. WILBUR (Colorado State University, Fort Collins) AIAA, Aerospace Sciences Meeting, 27th, Reno, NV, Jan. 9-12, 1989. 12 p. refs  
(Contract NAG3-776)

(AIAA PAPER 89-0677) Copyright

An experimental study of plasma contacting with an emphasis on the electron collection mode of this process is described. Results illustrating variations in plasma property profiles and potential differences that develop at hollow cathode plasma contactors are presented. A model of the electron collection plasma contacting process that is consistent with experimentally measured results is reviewed. The shortcomings of laboratory results as direct

predictors of contactor performance in space and their usefulness in validating numerical models of the contacting process, that can be used to predict such performance, are discussed. Author

**A89-39391\*** National Aeronautics and Space Administration. Lewis Research Center, Cleveland, OH.

**THE STABILITY ANALYSIS OF MAGNETOHYDRODYNAMIC EQUILIBRIA - COMPARING THE THERMODYNAMIC APPROACH WITH THE ENERGY PRINCIPLE**

R. P. BRINKMANN (NASA/Fermilab Astrophysics Center, Batavia; Chicago, University, IL; Bochum, Ruhr-Universitaet, Federal Republic of Germany) Physics of Fluids B (ISSN 0899-8221), vol. 1, May 1989, p. 987-995. Research supported by DOE. refs Copyright

This paper is a contribution to the stability analysis of current-carrying plasmas, i.e., plasma systems that are forced by external mechanisms to carry a nonrelaxing electrical current. Under restriction to translationally invariant configurations, the thermodynamic stability criterion for a multicomponent plasma is rederived within the framework of nonideal MHD. The chosen dynamics neglects scalar resistivity, but allows for other types of dissipation effects both in Ohm's law and in the equation of motion. In the second section of the paper, the thermodynamic stability criterion is compared with the ideal MHD based energy principle of Bernstein et al. With the help of Schwarz's inequality, it is shown that the former criterion is always more 'pessimistic' than the latter, i.e., that thermodynamic stability implies stability according to the MHD principle, but not vice versa. This result confirms the physical plausible idea that dissipational effects tend to weaken the stability properties of current-carrying plasma equilibria by breaking the constraints of ideal MHD and allowing for possibly destabilizing effects such as magnetic field line reconfiguration. Author

**A89-39395\*** Massachusetts Inst. of Tech., Cambridge.  
**THE PHYSICS OF POSITIVELY BIASED CONDUCTORS SURROUNDED BY DIELECTRICS IN CONTACT WITH A PLASMA**

DANIEL E. HASTINGS and PATRICK CHANG (MIT, Cambridge, MA) Physics of Fluids B (ISSN 0899-8221), vol. 1, May 1989, p. 1123-1132. refs  
(Contract AF-AFOSR-87-0340; NAG3-695) Copyright

The physics of a positively biased conductor surrounded by dielectrics in contact with plasma is investigated. It is shown that because of the presence of secondary emission from the surrounding dielectrics, the voltage of the surfaces near the conductor has three solutions. The high- and low-voltage solutions are stable, while the intermediate-voltage solution is unstable. This theory is applied to explain the snapover effect observed on high-voltage solar arrays that involve the use of highly biased surfaces in contact with the space environment. Author

**A89-40188\*#** Colorado State Univ., Fort Collins.  
**GROUND-BASED TESTS OF HOLLOW CATHODE PLASMA CONTACTORS**

JOHN D. WILLIAMS and PAUL J. WILBUR (Colorado State University, Fort Collins) IN: International Conference on Tethers in Space - Toward Flight, 3rd, San Francisco, CA, May 17-19, 1989, Collection of Papers and Abstracts. Washington, DC, American Institute of Aeronautics and Astronautics, Inc., 1989, p. 77-87. refs  
(Contract NAG3-776)  
(AIAA PAPER 89-1558) Copyright

Experimental results are presented which describe operation of and the plasma environment associated with a hollow cathode-based plasma contactor collecting electrons from an ambient, low density Maxwellian plasma when the boundary between the contactor and the ambient plasma is nearly hemispherical. Basic physical features of the process of electron collection identified on the basis of these results include a double-sheath across which a substantial potential difference can develop and substantial ionization of neutral gas coming from the

cathode by the electrons being collected. Experimental results obtained when the diameter of the anode is too small to yield a hemispherical double-sheath are shown to induce distortion of this sheath but it is argued that the same basic phenomena are still active in this case. Data obtained in these experiments should serve to validate numerical models of this process that are being developed to predict plasma contactor performance in space. Preliminary performance and plasma property results measured on a contactor emitting electrons are examined and some physical elements of this process are identified. Author

**A89-40190\*#** Maxwell Labs., Inc., La Jolla, CA.  
**A MODEL OF ELECTRON COLLECTING PLASMA CONTRACTORS**

V. A. DAVIS, I. KATZ, M. J. MANDELL, and D. E. PARKS (Maxwell Laboratories, Inc., S-Cubed Div., La Jolla, CA) IN: International Conference on Tethers in Space - Toward Flight, 3rd, San Francisco, CA, May 17-19, 1989, Collection of Papers and Abstracts. Washington, DC, American Institute of Aeronautics and Astronautics, Inc., 1989, p. 94-99. refs  
(Contract NAS3-23881)  
(AIAA PAPER 89-1560) Copyright

A model of plasma contractors is being developed, which can be used to describe electron collection in a laboratory test tank and in the space environment. To validate the model development, laboratory experiments are conducted in which the source plasma is separated from the background plasma by a double layer. Model calculations show that an increase in ionization rate with potential produces a steep rise in collected current with increasing potential. R.B.

**A89-43356\*** Systems Science and Software, San Diego, CA.  
**ON THE NEED FOR SPACE TESTS OF PLASMA CONTACTORS AS ELECTRON COLLECTORS**

IRA KATZ and VICTORIA ANN DAVIS (Systems Science and Software, San Diego, CA) IN: Space tethers for science in the space station era; Proceedings of the Second International Conference, Venice, Italy, Oct. 4-8, 1987. Bologna, Societa Italiana di Fisica, 1988, p. 241-244. refs  
(Contract NAS3-23881) Copyright

An analysis is presented of laboratory experiments that have shown that hollow plasma sources can provide low-impedance contact with a background plasma. In particular, some experiments show an report an 'ignited mode' of electron collection using plasma sources where almost an ampere was collected at a potential of 100 volts. The experimental results are compared with theoretical and computational models of plasma layers. Preliminary results indicate that the measured potential profiles and collected currents during the 'ignited mode' correspond to an increase in the background plasma thermal current of more than an order of magnitude. The results imply that the 'ignited mode' results are substantially impacted by the laboratory electron source and the tank size. Only experiments performed in space will be able to provide the correct boundary conditions for reliably testing high electron collection by plasma contactors. C.D.

**A89-43357\*** Colorado State Univ., Fort Collins.  
**EXPERIMENTAL VALIDATION OF A PHENOMENOLOGICAL MODEL OF THE PLASMA CONTACTING PROCESS**

JOHN D. WILLIAMS, PAUL J. WILBUR, and JEFF M. MONHEISER (Colorado State University, Fort Collins) IN: Space tethers for science in the space station era; Proceedings of the Second International Conference, Venice, Italy, Oct. 4-8, 1987. Bologna, Societa Italiana di Fisica, 1988, p. 245-253. refs  
(Contract NAG9-120; NAG3-776) Copyright

A preliminary model of the plasma coupling process is presented which describes the phenomena observed in ground-based experiments using a hollow cathode plasma contactor to collect electrons from a dilute ambient plasma under conditions where magnetic field effects can be neglected. The locations of the double-sheath region boundaries are estimated and correlated with

experimental results. Ion production mechanisms in the plasma plume caused by discharge electrons from the contactor cathode and by electrons streaming into the plasma plume through the double-sheath from the ambient plasma are also discussed.

C.D.

**A89-43359\*** National Aeronautics and Space Administration. Lewis Research Center, Cleveland, OH.

**GROUND-BASED PLASMA CONTACTOR CHARACTERIZATION**

MICHAEL J. PATTERSON (NASA, Lewis Research Center, Cleveland, OH) and RANDALL S. AADLAND IN: Space tethers for science in the space station era; Proceedings of the Second International Conference, Venice, Italy, Oct. 4-8, 1987. Bologna, Societa Italiana di Fisica, 1988, p. 261-268. refs

Copyright

This paper presents recent NASA Lewis Research Center plasma contactor experimental results, as well as a description of the plasma contactor test facility. The operation of a 24-cm-diameter plasma source with hollow cathode was investigated in the 'ignited-mode' regime of electron current collection from 0.1 to 7.0 A. These results are compared to those obtained with a 12-cm plasma source. Full two-dimensional plasma potential profiles were constructed from emissive probe traces of the contactor plume. The experimentally measured dimensions of the plume sheaths were then compared to those theoretically predicted, using a model of a spherical double sheath. Results are consistent for currents up to approximately 1.0 A. For currents above 1.0 A, substantial deviations from theory occur. These deviations are due to sheath asphericity, and, possibly, volume ionization in the double-sheath region.

Author

**A89-45631\*** Utah State Univ., Logan.

**A NUMERICAL MODEL OF ELECTRODYNAMICS OF PLASMA WITHIN THE CONTAMINANT GAS CLOUD OF THE SPACE SHUTTLE ORBITER AT LOW EARTH ORBIT**

J. VINCENT ECCLES, W. JOHN RAITT (Utah State University, Logan), and PETER M. BANKS (Stanford University, CA) Journal of Geophysical Research (ISSN 0148-0227), vol. 94, July 1, 1989, p. 9049-9063. refs

(Contract NAG3-792; NAGW-235)

Copyright

A two-dimensional cloud was used to study the plasma dynamics within the outgas cloud associated with the Orbiter. It is shown that the polarization field is not symmetric about the direction of motion of the outgas cloud. It rotates in a way that can be predicted in simple cases by the ratio of the Hall and Pederson currents within the outgas cloud. The polarization field magnitude produced in the model was not large.

K.K.

**A89-45632\*** Jet Propulsion Lab., California Inst. of Tech., Pasadena.

**THE POLAR CODE WAKE MODEL - COMPARISON WITH IN SITU OBSERVATIONS**

G. MURPHY (California Institute of Technology, Jet Propulsion Laboratory, Pasadena) and I. KATZ (Systems Science and Software, La Jolla, CA) Journal of Geophysical Research (ISSN 0148-0227), vol. 94, July 1, 1989, p. 9065-9070. refs

(Contract NAS8-32807; F19628-86-C-0056; NAG3-449)

Copyright

Measurements made by the plasma diagnostics package during Spacelab 2 are discussed and compared with predictions made with the Air Force Geophysics Laboratory POLAR wake code. This code uses a complex geometric model of the orbiter and the self-similar solution of the expansion of a plasma into a vacuum as its model basis. Excellent qualitative and quantitative agreement is found at distances greater than about 30 m. At least to the first order, the model's approximations are justified.

K.K.

**A89-53209\*** Iowa Univ., Iowa City.

**PLASMA DENSITY, TEMPERATURE AND TURBULENCE IN THE WAKE OF THE SHUTTLE ORBITER**

A. C. TRIBBLE, J. S. PICKETT, N. D'ANGELO (Iowa, University,

Iowa City), and G. B. MURPHY (California Institute of Technology, Jet Propulsion Laboratory, Pasadena; Iowa, University, Iowa City) Planetary and Space Science (ISSN 0032-0633), vol. 37, Aug. 1989, p. 1001-1010. refs

(Contract NAG3-449; NAS8-32807)

Copyright

In situ observations of the plasma density, temperature, and turbulence in the near wake, midwake, and far wake of the Shuttle Orbiter are presented. The results show that the plasma disturbances produced by the passage of the Orbiter extend downstream for a distance of several hundred meters behind the Orbiter. It is found that the electron density profile exhibits nonmonotonic behavior, and that most of the 6-40-Hz turbulence in the wake is confined to a region about 20 m downstream of the Orbiter. The saturation  $\Delta N(e)/N(e)$  spectra rapidly decline in the 10,000-100,000-Hz decade, both in the ambient ionosphere and in the wake.

R.R.

**A89-54759\*** Iowa Univ., Iowa City.

**PLASMA DENSITY FLUCTUATIONS OBSERVED DURING SPACE SHUTTLE ORBITER WATER RELEASES**

J. S. PICKETT, N. D'ANGELO, and W. S. KURTH (Iowa, University, Iowa City) Journal of Geophysical Research (ISSN 0148-0227), vol. 94, Sept. 1, 1989, p. 12081-12086. refs

(Contract NAG3-449)

Copyright

Observations by the Langmuir probe on the Plasma Diagnostics Package flown as part of the Spacelab 2 mission in the summer of 1985 show a strong increase in the level of turbulence near the Shuttle Orbiter during operations in which liquid water is released. The spectrum of the plasma density fluctuations peaks at the lowest frequencies measured (a few Hz) and extends up to a few kHz, near the lower hybrid frequency. Two potential mechanisms for generating the plasma turbulence are suggested which are both based on the production of water ions as a result of charge exchange with the ambient oxygen ions in the ionosphere. The first mechanism proposed is the ion-plasma instability which arises from the drift of the contaminant with respect to the ambient oxygen ions. The other mechanism proposed is the Ott-Farley instability, which is a result of the ring distribution formed by the 'pick-up' water ions.

Author

**N89-14842\*#** National Aeronautics and Space Administration. Lewis Research Center, Cleveland, OH.

**LUNAR HELIUM-3 AND FUSION POWER**

Washington, DC Sep. 1988 234 p Workshop held in Cleveland, Ohio, 25-26 Apr. 1988

(NASA-CP-10018; E-4254; NAS 1.55:10018) Avail: NTIS HC A11/MF A01 CSCL 20/9

The NASA Office of Exploration sponsored the NASA Lunar Helium-3 and Fusion Power Workshop. The meeting was held to understand the potential of using He-3 from the moon for terrestrial fusion power production. It provided an overview, two parallel working sessions, a review of sessions, and discussions. The lunar mining session concluded that mining, beneficiation, separation, and return of He-3 from the moon would be possible but that a large scale operation and improved technology is required. The fusion power session concluded that: (1) that He-3 offers significant, possibly compelling, advantages over fusion of tritium, principally increased reactor life, reduced radioactive wastes, and high efficiency conversion, (2) that detailed assessment of the potential of the D/He-3 fuel cycle requires more information, and (3) D/He-3 fusion may be best for commercial purposes, although D/T fusion is more near term.

**N89-21658\*#** Colorado State Univ., Fort Collins. Dept. of Mechanical Engineering.

**SPACE PLASMA CONTRACTOR RESEARCH, 1988 Annual Report, 1 Jan. 1988 - 1 Jan. 1989**

JOHN D. WILLIAMS and PAUL J. WILBUR Feb. 1989 61 p

(Contract NAG3-776)

(NASA-CR-182283; NAS 1.26:182283) Avail: NTIS HC A04/MF A01 CSCL 20/9

## 75 PLASMA PHYSICS

Results of experiments conducted on hollow cathode-based plasma contractors are reported. Specific tests in which attempts were made to vary plasma conditions in the simulated ionospheric plasma are described. Experimental results showing the effects of contractor flowrate and ion collecting surface size on contractor performance and contractor plasma plume geometry are presented. In addition to this work, one-dimensional solutions to spherical and cylindrical space-charge limited double-sheath problems are developed. A technique is proposed that can be used to apply these solutions to the problem of current flow through elongated double-sheaths that separate two cold plasmas. Two conference papers which describe the essential features of the plasma contacting process and present data that should facilitate calibration of comprehensive numerical models of the plasma contacting process are also included. Author

**N89-23555\*** National Aeronautics and Space Administration. Lewis Research Center, Cleveland, OH.

### **SURFACE PHENOMENA IN PLASMA ENVIRONMENTS**

C. K. PURVIS and D. C. FERGUSON / In NASA, Langley Research Center, NASA/SDIO Space Environmental Effects on Materials Workshop, Part 2 p 511-534 May 1989  
Avail: NTIS HC A12/MF A01 CSCL 20/9

Plasma interactions and their effects on materials depend on a number of factors, including the pre-existing environment, the properties of surface materials and the characteristics of the system. An additional dimension is the question of mission: some payloads may be much more sensitive to plasma interactions than others. As an example, a payload whose objective is to measure the ambient environment will be more sensitive to any effects than will a power system. Material specific effects include charging and its associated effects, which can result in short- and long-term damage. Selection of materials for a particular application requires consideration of all factors and assessment of effects due to all causes. Proper selection and suitability determination requires analysis to identify the actual environment combined with testing under exposure to single and combined environment factors. Author

## 76

## SOLID-STATE PHYSICS

Includes superconductivity.

### **A89-13945\*** Nebraska Univ., Lincoln. **THIN-FILM HERMETICITY - A QUANTITATIVE ANALYSIS OF DIAMONDLIKE CARBON USING VARIABLE ANGLE SPECTROSCOPIC ELLIPSOMETRY**

S. ORZESZKO, BHOLA N. DE, JOHN A. WOOLLAM (Nebraska, University, Lincoln), JOHN J. POUCH, SAMUEL A. ALTEROVITZ (NASA, Lewis Research Center, Cleveland, OH) et al. Journal of Applied Physics (ISSN 0021-8979), vol. 64, Oct. 15, 1988, p. 4175-4180. Research supported by Control Data Corp. refs (Contract NAG3-154; DAAL04-86-C-0030)  
Copyright

This paper reports on the successful application of variable-angle spectroscopic ellipsometry to quantitative thin-film hermeticity evaluation. It is shown that, under a variety of film preparations and moisture introduction conditions, water penetrates only a very thin diamondlike carbon (DLC) top surface-roughness region. Thus, DLC is an excellent candidate for use as protective coatings in adverse chemical and aqueous environments. Author

**A89-20037\*** Arkansas Univ., Fayetteville.  
**TRANSPORT CRITICAL CURRENT AND MAGNETIZATION MEASUREMENTS OF MELT-PROCESSED YBA<sub>2</sub>CU<sub>3</sub>O<sub>7</sub>(7-X)**  
A. H. HERMANN, Z. Z. SHENG, W. KIEHL, D. MARSH, A. EL ALI (Arkansas, University, Fayetteville) et al. Journal of Applied Physics (ISSN 0021-8979), vol. 64, Nov. 15, 1988, pt. 1, p. 5050-5055.

refs  
(Contract NCC3-19; NAG3-873)  
Copyright

This paper reports on the magnetic field dependence of the transport critical current and dc magnetic susceptibility measurements on YBa<sub>2</sub>Cu<sub>3</sub>O<sub>7-x</sub> superconductors formed by melt-solid reactions at 950 C between Ba-Cu-O (or Tb-Ba-cu-O) and solid nonstoichiometric Y-Ba-Cu oxide. Four-probe dc critical current measurements at 77, 64, and 4.2 K show strong depression of the critical current density with increasing magnetic field, in agreement with a model of weakly linked superconducting regions. Diamagnetic shielding and Meissner flux expulsion measurements in the temperature range 10-300 K show about one-third volume fraction of perfect superconductivity. Both shielding and flux expulsion were observed to be approximately temperature independent below 60 K, indicating strong coupling between the grains throughout the entire volume below this temperature. Author

**A89-20467\*** National Aeronautics and Space Administration. Lewis Research Center, Cleveland, OH.

### **EFFECT OF PROCESSING PARAMETERS ON THE CHARACTERISTICS OF HIGH-TC SUPERCONDUCTOR YBA<sub>2</sub>CU<sub>3</sub>O<sub>Y</sub>**

NAROTTAM P. BANSAL (NASA, Lewis Research Center, Cleveland, OH) Journal of Materials Research (ISSN 0884-2914), vol. 3, Nov.-Dec. 1988, p. 1304-1310. refs  
Copyright

SEM, thermogravimetric analysis, powder X-ray diffraction, and measurements of electrical resistivity and magnetic susceptibility, are presently used to characterize the influence of sintering temperature, sintering and annealing atmospheres, and quench-rate on the properties of the YBa<sub>2</sub>Cu<sub>3</sub>O<sub>y</sub> superconducting oxide. It is established that annealing in oxygen, together with slow cooling rates, are required for preparation of high-T<sub>c</sub> superconductors with sharp transitions; rapid quenching from high temperature does not yield good superconductors, due to low oxygen content. O.C.

### **A89-21473\*** Case Western Reserve Univ., Cleveland, OH. **EXPERIMENTAL EVIDENCE FOR A TRANSVERSE MAGNETIZATION OF THE ABRIKOSOV LATTICE IN ANISOTROPIC SUPERCONDUCTORS**

D. E. FARREL (Case Western Reserve University, Cleveland, OH), C. M. WILLIAMS, S. A. WOLF (U.S. Navy, Naval Research Laboratory, Washington, DC), N. P. BANSAL (NASA, Lewis Research Center, Cleveland, OH), and V. G. KOGAN (Iowa State University of Science and Technology, Ames) Physical Review Letters (ISSN 0031-9007), vol. 61, Dec. 12, 1988, p. 2805-2808. refs  
(Contract NAG3-814)  
Copyright

The torque on a superconductor in a magnetic field H has been thought to be dominated by trapped flux or sample shape effects, but it has recently been suggested that an anisotropic type-II material should experience an intrinsic torque for H(c1) much less than H, which in turn is less than H(c2). The predicted phenomenon results from transverse magnetization of the Abrikosov lattice. Measurements are presented on copper-oxide superconductors which delineate the experimental regime in which extrinsic effects are negligible and confirm the existence of the predicted intrinsic torque. Author

### **A89-21871\*** Pittsburgh Univ., PA. **RAMAN DETERMINATION OF LAYER STRESSES AND STRAINS FOR HETEROSTRUCTURES AND ITS APPLICATION TO THE CUBIC SiC/Si SYSTEM**

Z. C. FENG (Pittsburgh, University, PA), W. J. CHOYKE (Pittsburgh, University; Westinghouse Research and Development Center, PA), and J. A. POWELL (NASA, Lewis Research Center, Cleveland, OH) Journal of Applied Physics (ISSN 0021-8979), vol. 64, Dec. 15, 1988, p. 6827-6835. refs  
(Contract NAG3-603; NSF DMR-84-03596)  
Copyright



A set of formulas for a generalized axial stress in diamond and zinc-blende semiconductors under axial stress is derived to calculate stress-related Raman shifts. By analyzing known Raman data on cubic SiC under hydrostatic pressures, one of the Raman-stress coefficients was obtained, and the existing elastic stiffness constants of cubic SiC were optimized. A method for calculating the stress and strain in SiC films on (100) Si is proposed. It is suggested that the stress and strain expressions and the method of the stress and strain determinations in heterostructures are quite general and may be used for other systems. I.S.

**A89-22886\*** National Aeronautics and Space Administration. Lewis Research Center, Cleveland, OH.

**INTERACTION OF AU, AG, AND BI IONS WITH  $\text{Ba}_2\text{YCu}_3\text{O}_{7-y}$  - IMPLICATIONS FOR SUPERCONDUCTOR APPLICATIONS**

A. F. HEPP, J. R. GAIER, J. J. POUCH (NASA, Lewis Research Center, Cleveland, OH), and P. D. HAMBOURGER (Cleveland State University, OH) IN: Processing and applications of high  $T_c$  superconductors. Warrendale, PA, Metallurgical Society, 1988, p. 213-221. refs  
(Contract NCC3-19)  
Copyright

Results are presented on the reactions of Au, Ag, and Bi ions with  $\text{Ba}_2\text{YCu}_3\text{O}_{7-y}$  oxides and on the properties of the resultant materials. The results indicate that  $\text{Au}(3+)$  structural chemistry makes gold an excellent candidate for multiphase structures of the  $\text{Ba}_2\text{Y}(\text{Cu}/1-x/\text{Au}/x)\text{O}_{7-y}$ -type substituted superconductors. Silver is structurally and chemically compatible with the perovskite structure, but when it forms a second phase, it does so without the destruction of the superconducting phase, making silver a useful metal for metal/ceramic applications. On the other hand, bismuth was shown to degrade  $T_c$  phase or to form other phases, indicating that it may not be useful in applications with rare-earth-based superconductors. I.S.

**A89-22887\*** National Aeronautics and Space Administration. Lewis Research Center, Cleveland, OH.

**IMPROVED SYNTHESIS OF CERAMIC SUPERCONDUCTORS WITH ALKALINE EARTH PEROXIDES - SYNTHESIS AND PROCESSING OF  $\text{Ba}_2\text{YCu}_3\text{O}_{7-x}$**

A. F. HEPP, J. R. GAIER, W. H. PHILIPP, J. D. WARNER, P. R. ARON, J. J. POUCH (NASA, Lewis Research Center, Cleveland, OH) et al. IN: Processing and applications of high  $T_c$  superconductors. Warrendale, PA, Metallurgical Society, 1988, p. 177-191. refs  
(Contract NCC3-19)  
Copyright

Synthesis processes for the preparation of ceramic conductors  $\text{Ba}_2\text{YCu}_3\text{O}_{7-x}$  from  $\text{BaO}_2$  or  $\text{BaCO}_3$  in flowing  $\text{O}_2$  or  $\text{N}_2$  are described, and the characteristics of the materials produced in these processes are compared. Results of EDAX, XRD, SEM, and dc resistivity analyses demonstrated that superconducting materials made from  $\text{BaO}_2$  were more homogeneous, denser, and more metallic than materials produced from  $\text{BaCO}_3$ , because of the higher reactivity of  $\text{BaO}_2$ . Potential applications of this processes are discussed. I.S.

**A89-23482\*** Michigan Technological Univ., Houghton.  
**THE SURFACE MORPHOLOGY OF CRYSTALS MELTING UNDER SOLUTIONS OF DIFFERENT DENSITIES**

DACHENG FANG and A. HELLAWELL (Michigan Technological University, Houghton) Journal of Crystal Growth (ISSN 0022-0248), vol. 92, no. 3-4, Oct. 1988, p. 364-370. refs  
(Contract NAG3-560)  
Copyright

Examples of solids melting beneath liquids are described for cases where the bulk liquid volume is stabilized against convection by a positive vertical temperature gradient, either with, or without local density inversion at the melting interface. The examples include ice melting beneath brine or methanol solutions and tin or lead melting under molten Sn-20 wt pct Pb or Pb-20 wt pct Sn, respectively. Without density inversion the melting is slow, purely

diffusion controlled and the interfaces are smooth; with convection assisted melting the rate increases by some two orders of magnitude and the interfaces develop a rough profile - in the case of ice both irregular and quasi-steady state features are observed. The observations are discussed in terms of prevailing temperature and concentration gradients. Author

**A89-27794\*** Cincinnati Univ., OH.

**PLASMA DEPOSITED SILICON NITRIDE FOR INDIUM PHOSPHIDE ENCAPSULATION**

G. J. VALCO, V. J. KAPOOR, M. D. BIEDENBENDER (Cincinnati, University, OH), and W. D. WILLIAMS (NASA, Lewis Research Center, Cleveland, OH) Electrochemical Society, Journal (ISSN 0013-4651), vol. 136, Jan. 1989, p. 175-182. refs  
Copyright

The composition and the annealing characteristics of plasma-deposited silicon-nitride encapsulating films on the ion-implanted InP substrates were investigated, using two different substrate-cleaning procedures (organic solvents and HF or  $\text{HIO}_3$  solutions) prior to encapsulation. The effect of plasma deposition of silicon nitride on the InP substrates was assessed through the current-voltage characteristics of Schottky diodes. Results of XPS analyses showed that the cleaning procedure that employed HF solution left less oxygen on the InP surface than the procedure involving  $\text{HIO}_3$ . No chemical interaction between the film and the substrate was observed before or after annealing. I.S.

**A89-29299\*** State Univ. of New York, Plattsburgh.

**SHUBNIKOV-DE HAAS MEASUREMENTS OF THE 2-D ELECTRON GAS IN PSEUDOMORPHIC  $\text{In}_{0.1}\text{Ga}_{0.9}\text{As}$  GROWN ON GaAs**

P. P. SZYDLIC (New York, State University, Plattsburgh), S. A. ALTEROVITZ, E. J. HAUGLAND (NASA, Lewis Research Center, Cleveland, OH), B. SEGALL (Case Western Reserve University, Cleveland, OH), T. S. HENDERSON (Illinois, University, Urbana) et al. Superlattices and Microstructures (ISSN 0749-6036), vol. 4, no. 4-5, 1988, p. 619-621. refs  
(Contract NCC3-25; NAG3-613)  
Copyright

Shubnikov-de Haas (SdH) measurements performed on a 200 Å layer of pseudomorphic  $\text{In}_{0.1}\text{Ga}_{0.9}\text{As}$  grown by MBE on undoped GaAs with an overlayer of  $\text{Al}_{0.15}\text{Ga}_{0.85}\text{As}$  are presented. These measurements were performed in magnetic fields up to 1.4 tesla at  $T$  in the range of 1.4-10 K. It was found that only one subband was populated with a density of  $5.8 \times 10^{10}$  the  $11/\text{cm}^2$ -squared and an effective mass at the Fermi level  $m(\text{asterisk}) = (0.060 \pm \text{or} - 0.001)m(0)$ . K.K.

**A89-30335\*** Iowa State Univ. of Science and Technology, Ames.

**CRITICAL CURRENTS OF ALIGNED GRAINS OF TL-Ba-Ca-Cu-O COMPOUNDS**

M. M. FANG, D. K. FINNEMORE (Iowa State University of Science and Technology, Ames), D. E. FARRELL (Case Western Reserve University, Cleveland, OH), and N. R. BANSAL (NASA, Lewis Research Center, Cleveland, OH) (DOE and Electric Power Research Institute, International Conference on Critical Currents in High-Temperature Superconductors, Snowmass Village, CO, Aug. 16-19, 1988) Cryogenics, Supplement (ISSN 0011-2275), vol. 29, March 1989, p. 347-349. refs  
(Contract W-7405-ENG-82)  
Copyright

A study of irreversibility in the magnetization curves of  $\text{Ti}_2\text{Ba}_2\text{Ca}_2\text{Cu}_3\text{O}_{10}$  and  $\text{Ti}_2\text{Ba}_2\text{Ca}_1\text{Cu}_2\text{O}_8$  was undertaken to determine the intragranular critical currents and the effects of flux-creep in grain-aligned samples of these materials. For fields of greater than 0.3 T, and  $H$  parallel to  $c$  axis, the critical supercurrent falls approximately exponentially with both magnetic field and temperature. Flux-creep is found to be linear in the logarithm of time at low fields over a wide temperature range. Author

**A89-30421\*** Nebraska Univ., Lincoln.

**HIGHLY ORIENTED TL2BA2CA2CU3O10 THIN FILMS BY PULSED LASER EVAPORATION**

S. H. LIOU, K. D. AYLESWORTH, N. J. IANNO, B. JOHS, D. THOMPSON (Nebraska, University, Lincoln) et al. Applied Physics Letters (ISSN 0003-6951), vol. 54, Feb. 20, 1989, p. 760-762. refs

(Contract NAG3-866)

Copyright

Superconducting thin films on MgO (100) substrates with nearly pure  $Tl_2Ba_2Ca_2Cu_3O_{10}$  (2:2:2:3) phase using pulsed laser evaporation and postannealing have been fabricated. The films had c axes perpendicular to the substrates. Superconducting films with onset temperatures of 125 K and zero resistance at 110 K were obtained. X-ray microprobe fluorescence measurements indicate that a typical composition of films is  $Tl(0.66)Ba(1.77)Ca(1.46)Cu_3O(x)$  which is low in Tl compared to that expected for the 2:2:2:3 phase. A typical grain size is greater than 10 microns revealed by scanning electron microscopy. Author

**A89-38608\*** Nebraska Univ., Lincoln.

**PREPARATION OF HIGH T(C) TL-BA-CA-CU-O THIN FILMS BY PULSED LASER EVAPORATION AND TL2O3 VAPOR PROCESSING**

B. JOHS, D. THOMPSON, N. J. IANNO, JOHN A. WOOLLAM, S. H. LIOU (Nebraska, University, Lincoln) et al. Applied Physics Letters (ISSN 0003-6951), vol. 54, May 1, 1989, p. 1810, 1811. Research supported by the International Society for Hybrid Microelectronics. refs

(Contract NAG3-866)

Copyright

Tl-Ba-Ca-Cu-O superconducting thin films with zero-resistance temperatures up to 115 K have been prepared using a  $Tl_2O_3$  vapor process on Ba-Ca-Cu-O precursor thin films. The Ba-Ca-Cu-O thin films were made by laser deposition on Y-stabilized  $ZrO_2$  substrates. This technique minimizes problems caused by the toxicity of  $Tl_2O_3$ , and its subsequent decomposition to the volatile and toxic  $Tl_2O$  upon heating. Therefore, it may have practical application in the fabrication of high T(c) Tl-Ba-Ca-Cu-O superconducting thin-film devices. Author

**A89-43928\*** Ames Lab., IA.

**FREE ENERGY SURFACES IN THE SUPERCONDUCTING MIXED STATE**

D. K. FINNEMORE, M. M. FANG (DOE, Ames Laboratory, IA), N. P. BANSAL (NASA, Lewis Research Center, Cleveland, OH), and D. E. FARRELL (Case Western Reserve University, Cleveland, OH) IN: Advances in superconductivity; Proceedings of the First International Symposium on Superconductivity (ISS '88), Nagoya, Japan, Aug. 28-31, 1988. Tokyo and New York, Springer-Verlag, 1989, p. 389-392. refs

Copyright

The free energy surface for  $Tl_2Ba_2Ca_2Cu_3O_{10}$  has been measured as a function of temperature and magnetic field to determine the fundamental thermodynamic properties of the mixed state. The change in free energy,  $G(H)-G(O)$ , is found to be linear in temperature over a wide range indicating that the specific heat is independent of field. Author

**A89-44527\*** Illinois Univ., Urbana.

**EFFECTS OF MICROSTRUCTURE AND NONSTOICHIOMETRY ON ELECTRICAL PROPERTIES OF VANADIUM DIOXIDE FILMS**

EIJI KUSANO and JEREMY A. THEIL (Illinois, University, Urbana) Journal of Vacuum Science and Technology A (ISSN 0734-2101), vol. 7, May-June 1989, pt. 1, p. 1314-1317. refs

(Contract NAG3-591)

Copyright

Voided growth structures of sputter-deposited films affect strongly their optical and electrical properties. Vanadium dioxide is an interesting material to study effects of film microstructure and nonstoichiometry on electrical properties because its phase

transition makes it possible to investigate electrical behavior both in a semiconducting phase and in a metallic phase. Vanadium oxide films were deposited with different vanadium oxygen ratios for substrate temperatures between 250 and 550 C by dc reactive magnetron sputtering. The resistivity ratios between a semiconducting phase and a metallic phase are limited to 1000 order by voided boundaries and oxygen vacancies. The voided boundaries are defined by columnar structure and agglomerated grain growth. The results emphasize the necessity of a combination of post deposition to obtain the film with a favorable structure and postdeposition annealing to control the film stoichiometry.

Author

**A89-44552\*** Nebraska Univ., Lincoln.

**RADIO-FREQUENCY PLASMA CHEMICAL VAPOR DEPOSITION GROWTH OF DIAMOND**

DUANE E. MEYER, RODNEY O. DILLON, and JOHN A. WOOLLAM (Nebraska, University, Lincoln) Journal of Vacuum Science and Technology A (ISSN 0734-2101), vol. 7, May-June 1989, pt. 2, p. 2325-2327. Research supported by the Center for Microelectronics and Optical Materials Research of Nebraska and Applied Sciences Corp. refs

(Contract NAG3-95)

Copyright

Plasma chemical vapor deposition (CVD) at 13.56 MHz has been used to produce diamond particles in two different inductively coupled systems with a mixture of methane and hydrogen. The effect of a diamondlike carbon (DLC) overcoating on silicon, niobium, and stainless-steel substrates has been investigated and in the case of silicon has been found to enhance particle formation as compared to uncoated polished silicon. In addition the use of carbon monoxide in hydrogen has been found to produce well-defined individual faceted particles as well as polycrystalline films on quartz and DLC coated silicon substrates. Plasma CVD is a competitive approach to production of diamond films. It has the advantage over microwave systems of being easily scaled to large volume and high power. Author

**N89-11553\*#** National Aeronautics and Space Administration. Lewis Research Center, Cleveland, OH.

**USE OF HIGH TEMPERATURE SUPERCONDUCTORS IN MAGNETOPLASMA DYNAMIC SYSTEMS**

C. B. REED (Argonne National Lab., Ill.) and J. S. SOVEY 1988 7 p Presented at the Conference on Superconductivity and Applications, Buffalo, N.Y., 18 Apr. 1988 Prepared in cooperation with National Aeronautics and Space Administration, Cleveland, Ohio

(Contract W-31-109-ENG-38)

(NASA-TM-101219; NAS 1.15:101219; DE88-011954;

CONF-880466-5) Avail: NTIS HC A02/MF A01 CSCL 20/12

The use of Tesla-class high-temperature superconducting magnets may have an extremely large impact on critical development issues (erosion, heat transfer, and performance) related to magnetoplasma dynamic (MPD) thrusters and also may provide significant benefits in reducing the mass of magnetics used in the power processing system. These potential performance improvements, coupled with additional benefits of high-temperature superconductivity, provide a very strong motivation to develop high-temperature superconductivity (HTS) applied-field MPD thruster propulsion systems. The application of HTS to MPD thruster propulsion systems may produce an enabling technology for these electric propulsion systems. This paper summarizes the impact that HTS may have upon MPD propulsion systems. DOE

**N89-26739\*#** Michigan Univ., Ann Arbor. Solid State Electronics Lab.

**MOLECULAR BEAM EPITAXIAL GROWTH OF HIGH-QUALITY INSB ON INP AND GAAS SUBSTRATES**

J. E. OH, P. K. BHATTACHARYA, Y. C. CHEN, and S. TSUKAMOTO 1989 17 p

(Contract NAG3-988; NSF ECSE-88-00659)

(NASA-CR-185440; NAS 1.26:185440) Avail: NTIS HC A03/MF A01 CSCL 20/12

## THERMODYNAMICS AND STATISTICAL PHYSICS

Includes quantum mechanics; theoretical physics; and Bose and Fermi statistics.

Epitaxial layers of InSb were grown on InP and GaAs substrates by molecular beam epitaxy. The dependence of the epilayer quality on flux ratio,  $J_{\text{sub Sb4}}/J_{\text{sub In}}$ , was studied. Deviation from an optimum value of  $J_{\text{sub Sb4}}/J_{\text{sub In}}$  (approx. 2) during growth led to deterioration in the surface morphology and the electrical and crystalline qualities of the films. Room temperature electron mobilities as high as 70,000 and 53,000 sq cm/V-s were measured in InSb layers grown on InP and GaAs substrates, respectively. Unlike the previous results, the conductivity in these films is n-type even at  $T = 13$  K, and no degradation of the electron mobility due to the high density of dislocations was observed. The measured electron mobilities (and carrier concentrations) at 77 K in InSb layers grown on InP and GaAs substrates are 110,000 sq cm/V-s ( $3 \times 10^{15}$  cm<sup>-3</sup>) and 55,000 sq cm/V-s ( $4.95 \times 10^{15}$  cm<sup>-3</sup>), respectively, suggesting their application to electronic devices at cryogenic temperatures. Author

**N89-26740\*** # Michigan Univ., Ann Arbor. Solid State Electronics Lab.

**SURFACE MORPHOLOGIES AND ELECTRICAL PROPERTIES OF MOLECULAR BEAM EPITAXIAL INSB AND INAS(X)SB(1-X) GROWN ON GAAS AND INP SUBSTRATES**

J. E. OH, Y. C. CHEN, P. K. BHATTACHARYA, and S. TSUKAMOTO 1989 19 p Sponsored by NSF and NASA, Langley Research Center, Hampton, VA (Contract NAG3-988) (NASA-CR-185439; NAS 1.26:185439) Avail: NTIS HC A03/MF A01 CSCL 20/12

Surface morphologies and electrical properties of molecular beam epitaxial InSb and InAs(x)Sb(1-x) grown on GaAs and InP substrates are discussed. The crystals are all n-type at 300 K and lower temperatures. The surface morphology and electrical characteristics are strongly dependent on Sb(4)/In flux ratio and substrate temperature. The highest mobilities in InSb on InP are 70,000 at 300 K and 110,000 cm<sup>2</sup>/V.s ( $n=3 \times 10^{15}$  cm<sup>-3</sup>) at 77 K. The mobilities in the alloys also increase monotonically with lowering of temperature. Good quality InAs(x)Sb(1-x) was grown directly on InP substrates by molecular beam epitaxy. K.C.D.

**N89-30088\*** # National Aeronautics and Space Administration. Lewis Research Center, Cleveland, OH.

**MILLIMETER WAVE TRANSMISSION STUDIES OF YBA2CU3O7-DELTA THIN FILMS IN THE 26.5 TO 40.0 GHZ FREQUENCY RANGE**

F. A. MIRANDA, W. L. GORDON, K. B. BHASIN, V. O. HEINEN, J. D. WARNER, and G. J. VALCO (Ohio State Univ., Columbus.) 1989 13 p Presented at the 3rd Annual Conference on Superconductivity and Applications, Buffalo, NY, 19-21 Sep. 1989; sponsored by The New York State Inst. of Superconductivity (NASA-TM-102345; E-5053; NAS 1.15:102345) Avail: NTIS HC A03/MF A01 CSCL 20/12

Millimeter wave transmission measurements through YBa<sub>2</sub>Cu<sub>3</sub>O<sub>7-δ</sub> thin films on MgO, ZrO<sub>2</sub> and LaAlO<sub>3</sub> substrates, are reported. The films (approx. 1 micron) were deposited by sequential evaporation and laser ablation techniques. Transition temperatures  $T_{\text{sub c}}$ , ranging from 89.7 K for the Laser Ablated film on LaAlO<sub>3</sub> to approximately 72 K for the sequentially evaporated film on MgO, were obtained. The values of the real and imaginary parts of the complex conductivity,  $\sigma_1$  and  $\sigma_2$ , are obtained from the transmission data, assuming a two fluid model. The BCS approach is used to calculate values for an effective energy gap from the obtained values of  $\sigma_1$ . A range of gap values from 2 DELTA o/K  $T_{\text{sub c}}$  = 4.19 to 4.35 was obtained. The magnetic penetration depth is evaluated from the deduced values of  $\sigma_2$ . These results are discussed together with the frequency dependence of the normalized transmission amplitude,  $P/P_{\text{sub c}}$ , below and above  $T_{\text{sub c}}$ . Author

**A89-23488\*** National Aeronautics and Space Administration. Lewis Research Center, Cleveland, OH.

**MEASUREMENT OF THE DIFFUSION COEFFICIENT OF ACETONE IN SUCCINONITRILE AT ITS MELTING POINT**

M. A. CHOPRA (NASA, Lewis Research Center, Cleveland, OH), M. E. GLICKSMAN (Rensselaer Polytechnic Institute, Troy, NY), and N. B. SINGH (Westinghouse Research and Development Center, Pittsburgh, PA) Journal of Crystal Growth (ISSN 0022-0248), vol. 92, no. 3-4, Oct. 1988, p. 543-546. refs Copyright

The diffusion coefficient of acetone in liquid succinonitrile at 331.1 K was determined using the method of McBain and Dawson (1935). Only dilute mixtures of SCN-acetone were studied. The interdiffusion constant was determined to be 0.0000127 sq cm/s and was essentially independent of the acetone concentration over the range investigated (0.5 to 18 mol pct acetone). Author

**A89-28347\*** # Idaho National Engineering Lab., Idaho Falls.

**KINETIC ENERGY EQUATIONS FOR THE AVERAGE-PASSAGE EQUATION SYSTEM**

RICHARD W. JOHNSON (EG&G Idaho, Inc., Idaho Falls) and JOHN J. ADAMCZYK (NASA, Lewis Research Center, Cleveland, OH) Journal of Propulsion and Power (ISSN 0748-4658), vol. 5, Mar.-Apr. 1989, p. 252-254. refs (Contract DE-AC07-76ID-01570) Copyright

Important kinetic energy equations derived from the average-passage equation sets are documented, with a view to their interrelationships. These kinetic equations may be used for closing the average-passage equations. The turbulent kinetic energy transport equation used is formed by subtracting the mean kinetic energy equation from the averaged total instantaneous kinetic energy equation. The aperiodic kinetic energy equation, averaged steady kinetic energy equation, averaged unsteady kinetic energy equation, and periodic kinetic energy equation, are also treated. O.C.

**A89-41259\*** Kansas Univ., Lawrence.

**A MODEL FOR INCLUDING THERMAL CONDUCTION IN MOLECULAR DYNAMICS SIMULATIONS**

YUE WU and ROBERT J. FRIAUF (Kansas, University, Lawrence) Journal of Applied Physics (ISSN 0021-8979), vol. 65, June 15, 1989, p. 4714-4718. refs (Contract NSG-3290) Copyright

A technique is introduced for including thermal conduction in molecular dynamics simulations for solids. A model is developed to allow energy flow between the computational cell and the bulk of the solid when periodic boundary conditions cannot be used. Thermal conduction is achieved by scaling the velocities of atoms in a transitional boundary layer. The scaling factor is obtained from the thermal diffusivity, and the results show good agreement with the solution for a continuous medium at long times. The effects of different temperature and size of the system, and of variations in strength parameter, atomic mass, and thermal diffusivity were investigated. In all cases, no significant change in simulation results has been found. Author

**A89-48960\*** Ecole Centrale de Lyon (France).

**UNIVERSAL FEATURES OF THE EQUATION OF STATE OF SOLIDS**

PASCAL VINET (Lyon, Ecole Centrale, Ecully, France), JAMES H. ROSE (Iowa State University of Science and Technology, Ames), JOHN FERRANTE (NASA, Lewis Research Center, Cleveland, OH), and JOHN R. SMITH (GM Research Laboratories, Warren, MI)

## 80 SOCIAL SCIENCES (GENERAL)

Journal of Physics: Condensed Matter (ISSN 0953-8984), vol. 1, 1989, p. 1941-1963. Research supported by the Ministère des Relations Extérieures. refs  
(Contract W-7405-ENG-82)  
Copyright

A study of the energetics of solids leads to the conclusion that the equation of state for all classes of solids in compression can be expressed in terms of a universal function. The form of this universal function is determined by scaling experimental compression data for measured isotherms of a wide variety of solids. The equation of state is thus known (in the absence of phase transitions), if zero-pressure volume and isothermal compression and its pressure derivative are known. The discovery described in this paper has two immediate consequences: first, despite the well known differences in the microscopic energetics of the various classes of solids, there is a single equation of state for all classes in compression; and second, a new method is provided for analyzing measured isotherms and extrapolating high-pressure data from low-pressure (e.g. acoustic) data.

Author

80

## SOCIAL SCIENCES (GENERAL)

Includes educational matters.

**N89-23911\*#** National Aeronautics and Space Administration. Lewis Research Center, Cleveland, OH.

### **AGE DISTRIBUTION AMONG NASA SCIENTISTS AND ENGINEERS**

MICHAEL L. CIANCONE /in NASA, Marshall Space Flight Center, The 23rd Aerospace Mechanisms Symposium p 279-287 Mar. 1989

Avail: NTIS HC A15/MF A01 CSCL 20/11

The loss of technical expertise through attrition in NASA and the aerospace industry is discussed. This report documents historical age-related information for scientific and engineering personnel in general and the NASA Lewis Research Center in particular, for 1968 through 1987. Recommendations are made to promote discussion and to establish the groundwork for action.

Author

81

## ADMINISTRATION AND MANAGEMENT

Includes management planning and research.

**N89-24216\*#** National Aeronautics and Space Administration. Lewis Research Center, Cleveland, OH.

### **COMPREHENSIVE REPORT OF AEROPROPULSION, SPACE PROPULSION, SPACE POWER, AND SPACE SCIENCE APPLICATIONS OF THE LEWIS RESEARCH CENTER Annual Report, 1988**

1988 167 p Original contains color illustrations  
(NASA-TM-100925; NAS 1.15:100925) Avail: NTIS HC A08/MF A01 CSCL 05/1

The research activities of the Lewis Research Center for 1988 are summarized. The projects included are within basic and applied technical disciplines essential to aeropropulsion, space propulsion, space power, and space science/applications. These disciplines are materials science and technology, structural mechanics, life prediction, internal computational fluid mechanics, heat transfer, instruments and controls, and space electronics. A.D.

238

82

## DOCUMENTATION AND INFORMATION SCIENCE

Includes information management; information storage and retrieval technology; technical writing; graphic arts; and micrography.

**N89-18259\*#** National Aeronautics and Space Administration. Lewis Research Center, Cleveland, OH.

### **BIBLIOGRAPHY OF LEWIS RESEARCH CENTER TECHNICAL PUBLICATIONS ANNOUNCED IN 1986**

May 1987 349 p  
(NASA-TM-89887; E-3574; NAS 1.15:89887) Avail: NTIS HC A15/MF A01 CSCL 05/2

This compilation of abstracts describes and indexes the technical reporting that resulted from the scientific and engineering work performed and managed by the Lewis Research Center in 1986. All the publications were announced in the 1986 issues of Scientific and Technical Aerospace Reports (STAR) and/or International Aerospace Abstracts (IAA). Included are research reports, journal articles, conference presentations, patents and patent applications, and theses.

Author

85

## URBAN TECHNOLOGY AND TRANSPORTATION

Includes applications of space technology to urban problems; technology transfer; technology assessment; and surface and mass transportation.

**N89-11637\*#** National Aeronautics and Space Administration. Lewis Research Center, Cleveland, OH.

### **A PERSPECTIVE ON SPACE EXPLORATION TECHNOLOGY CATALYSIS: A RATIONALE FOR INITIATING 21ST CENTURY EXPANSION OF HUMAN CIVILIZATION INTO OUTER SPACE**

GARY A. P. HORSHAM Oct. 1988 10 p  
(NASA-TM-101362; E-4395; NAS 1.15:101362) Avail: NTIS HC A02/MF A01 CSCL 12/1

The rationale for human exploration of space is examined. Observations of the technocatalytic potential are presented. Transferability to the terrestrial environment of 21st Century Earth is discussed. The many threats to future survival of this planet's sensitive ecosystem are also discussed in relation to the technoeological harmony that might be achievable due to the extreme demands that are naturally imposed on the development of (civilian/human) space technology. The human attempt to inhabit the inner solar system (the Moon, Mars, etc.) is proposed as the ultimate and most appropriate technology driver for the myriad of socioeconomic, ecological, and technological needs that will accompany 21st Century Earth societies.

Author

**N89-12504\*#** Mechanical Technology, Inc., Latham, NY.  
**CONCEPTUAL DESIGN OF AN ADVANCED STIRLING CONVERSION SYSTEM FOR TERRESTRIAL POWER GENERATION Final Report**

Jan. 1988 378 p Prepared in cooperation with Sanders Associates, Inc., Nashua, N.H., Thermacore, Inc., Lancaster, Pa. and Pioneer Engineering and Manufacturing Co., Madison Heights, Mich.

(Contract DEN3-372; DE-AT04-85AL-33408)  
(NASA-CR-180890; DOE/NASA/0372-1; NAS 1.26:180890; MTI-87TR57) Avail: NTIS HC A17/MF A01 CSCL 10/2

A free piston Stirling engine coupled to an electric generator or alternator with a nominal kWe power output absorbing thermal energy from a nominal 100 square meter parabolic solar collector and supplying electric power to a utility grid was identified. The results of the conceptual design study of an Advanced Stirling

Conversion System (ASCS) were documented. The objectives are as follows: define the ASCS configuration; provide a manufacturability and cost evaluation; predict ASCS performance over the range of solar input required to produce power; estimate system and major component weights; define engine and electrical power conditioning control requirements; and define key technology needs not ready by the late 1980s in meeting efficiency, life, cost, and with goals for the ASCS. B.G.

**N89-14182\*#** Stirling Technology Co., Richland, WA.  
**THE 25 KWE SOLAR THERMAL STIRLING HYDRAULIC ENGINE SYSTEM: CONCEPTUAL DESIGN Final Report**  
 MAURICE WHITE, GRANT EMIGH, JACK NOBLE, PETER RIGGLE, and TORVALD SORENSON Jan. 1988 242 p  
 (Contract DEN3-371; DE-AT04-85AL-33408)  
 (NASA-CR-180889; DOE/NASA/0371-1; NAS 1.26:180889; REPT-8803) Avail: NTIS HC A11/MF A01 CSCL 10/2

The conceptual design and analysis of a solar thermal free-piston Stirling hydraulic engine system designed to deliver 25 kWe when coupled to a 11 meter test bed concentrator is documented. A manufacturing cost assessment for 10,000 units per year was made. The design meets all program objectives including a 60,000 hr design life, dynamic balancing, fully automated control, more than 33.3 percent overall system efficiency, properly conditioned power, maximum utilization of annualized insolation, and projected production costs. The system incorporates a simple, rugged, reliable pool boiler reflux heat pipe to transfer heat from the solar receiver to the Stirling engine. The free-piston engine produces high pressure hydraulic flow which powers a commercial hydraulic motor that, in turn, drives a commercial rotary induction generator. The Stirling hydraulic engine uses hermetic bellows seals to separate helium working gas from hydraulic fluid which provides hydrodynamic lubrication to all moving parts. Maximum utilization of highly refined, field proven commercial components for electric power generation minimizes development cost and risk. Author

**N89-17548\*#** Southwest Research Inst., San Antonio, TX.  
**THE EFFECT OF INSULATED COMBUSTION CHAMBER SURFACES ON DIRECT-INJECTED DIESEL ENGINE PERFORMANCE, EMISSIONS, AND COMBUSTION**  
 DANIEL W. DICKEY, SHANNON VINYARD, and RIFAT KERIBAR (Integral Technologies, Inc., Westmont, IL.) Sep. 1988 176 p  
 (Contract DEN3-330)  
 (NASA-CR-182204; NAS 1.26:182204; DOE/NASA/0330-3; SWRI-8966) Avail: NTIS HC A09/MF A01 CSCL 13/2

The combustion chamber of a single-cylinder, direct-injected diesel engine was insulated with ceramic coatings to determine the effect of low heat rejection (LHR) operation on engine performance, emissions, and combustion. In comparison to the baseline cooled engine, the LHR engine had lower thermal efficiency, with higher smoke, particulate, and full load carbon monoxide emissions. The unburned hydrocarbon emissions were reduced across the load range. The nitrous oxide emissions increased at some part-load conditions and were reduced slightly at full loads. The poor LHR engine performance was attributed to degraded combustion characterized by less premixed burning, lower heat release rates, and longer combustion duration compared to the baseline cooled engine. Author

**N89-23382\*#** Ricardo-ITI, Westmont, IL.  
**METHODS FOR HEAT TRANSFER AND TEMPERATURE FIELD ANALYSIS OF THE INSULATED DIESEL, PHASE 3 Final Report**  
 THOMAS MOREL, SYED WAHIDUZZAMAN, EDWARD F. FORT, RIFAT KERIBAR, and PAUL N. BLUMBERG Dec. 1988 171 p  
 (Contract DEN3-342; DE-AI01-86CE-50162)  
 (NASA-CR-182237; DOE/NASA/0342-3; NAS 1.26:182237) Avail: NTIS HC A08/MF A01 CSCL 20/4

Work during Phase 3 of a program aimed at developing a comprehensive heat transfer and thermal analysis methodology for design analysis of insulated diesel engines is described. The overall program addresses all the key heat transfer issues: (1) spatially and time-resolved convective and radiative in-cylinder heat

transfer, (2) steady-state conduction in the overall structure, and (3) cyclical and load/speed temperature transients in the engine structure. These are all accounted for in a coupled way together with cycle thermodynamics. This methodology was developed during Phases 1 and 2. During Phase 3, an experimental program was carried out to obtain data on heat transfer under cooled and insulated engine conditions and also to generate a database to validate the developed methodology. A single cylinder Cummins diesel engine was instrumented for instantaneous total heat flux and heat radiation measurements. Data were acquired over a wide range of operating conditions in two engine configurations. One was a cooled baseline. The other included ceramic coated components (0.050 inches plasma sprayed zirconia)-piston, head and valves. The experiments showed that the insulated engine has a smaller heat flux than the cooled one. The model predictions were found to be in very good agreement with the data. Author

**N89-25078\*#** National Aeronautics and Space Administration. Lewis Research Center, Cleveland, OH.  
**INITIAL CHARACTERIZATION OF A MODULAR HEAT EXCHANGER WITH AN INTEGRAL HEAT PIPE**  
 JEFFREY G. SCHREIBER 1989 8 p Presented at the 24th Intersociety Energy Conversion Engineering Conference, Washington, DC, 6-11 Aug. 1989; cosponsored by the IEEE, AIAA, ANS, ASME, SAE, ACS and AIChE  
 (NASA-TM-102097; E-4859; NAS 1.15:102097) Avail: NTIS HC A02/MF A01 CSCL 05/1

As part of the Civil Space Technology Initiative (CSTI) Advanced Technology program, a conceptual design of the Stirling space engine (SSE) was generated. The overall goal of the CSTI high capacity power element is to develop the technology base needed to meet the long duration, high capacity power requirements for future NASA space missions. The free-piston Stirling engine (FPSE) was chosen as the growth option in the CSTI program. A major goal during the conceptual design of the SSE was to reduce the number of critical joints. One area of concern was the heat exchanger assemblies that typically have the majority of critical joints. The solution proposed in the SSE conceptual design used 40 modular heat exchangers. Each module has its own integral heat pipe to transport heat from the heat source to the engine. A demonstration of the modular concept was undertaken before committing to the detailed design of the SSE heat exchangers. An existing FPSE was modified as a test bed for modular heat exchanger evaluation. The engine incorporated three heat exchanger modules, each having a sodium filled heat pipe. The thermal loading of these modules was intended to be similar to the conditions projected for the SSE modules. The engine was assembled and tests are underway. The design and fabrication of the heat exchanger modules and the engine used for these tests were described. Evaluation of the individual heat pipes before installation in the engine is described. The initial test results with the modules in operation on the engine were presented. Future tests involving the engine were outlined. Author

**N89-26781\*#** National Aeronautics and Space Administration. Lewis Research Center, Cleveland, OH.  
**COMPARISON OF CONCEPTUAL DESIGNS FOR 25 KWE ADVANCED STIRLING CONVERSION SYSTEMS FOR DISH ELECTRIC APPLICATION Final Report**  
 RICHARD K. SHALTENS and JEFFREY G. SCHREIBER 1989 16 p Prepared for presentation at the 24th Intersociety Energy Conversion Engineering Conference, Washington, DC, 6-11 Aug. 1989; sponsored in part by IEEE, AIAA, ANS, ASME, SAE, ACS, and AIChE  
 (Contract DE-AT04-85AL-33408)  
 (NASA-TM-102085; E-4806; DOE/NASA/33408-3; NAS 1.15:102085) Avail: NTIS HC A03/MF A01 CSCL 10/2

The Advanced Stirling Conversion System (ASCS) Project is managed by NASA Lewis Research Center through a cooperative interagency agreement with DOE. Conceptual designs for the ASCS's were completed under parallel contracts in 1987 by Mechanical Technology Inc. (MTI) of Latham, NY, and Stirling Technology Company (STC) of Richland, WA. Each design features

## 88 SPACE SCIENCES (GENERAL)

a free-piston Stirling engine, a liquid metal heat pipe receiver, and a means to provide about 25 kW of electric power to a utility grid while meeting DOE's long term performance and cost goals. An independent assessment showed that both designs are manufacturable and have the potential to easily meet DOE's long term cost goals. Author

88

## SPACE SCIENCES (GENERAL)

**N89-15047\*** National Aeronautics and Space Administration. Lewis Research Center, Cleveland, OH.

### **MICROGRAVITY RESEARCH IN NASA GROUND-BASED FACILITIES**

JACK LEKAN 1989 17 p Presented at the 27th Aerospace Sciences Meeting, Reno, NV, 9-12 Jan. 1989; sponsored by AIAA (NASA-TM-101397; E-4477; NAS 1.15:101397; AIAA-89-0236) Avail: NTIS HC A03/MF A01 CSCL 22/1

An overview of reduced gravity research performed in NASA ground-based facilities sponsored by the Microgravity Science and Applications Program of the NASA Office of Space Science and Applications is presented. A brief description and summary of the operations and capabilities of each of these facilities along with an overview of the historical usage of them is included. The goals and program elements of the Microgravity Science and Applications programs are described and the specific programs that utilize the low gravity facilities are identified. Results from two particular investigations in combustion (flame spread over solid fuels) and fluid physics (gas-liquid flows at microgravity conditions) are presented. Author

**N89-23529\*** National Aeronautics and Space Administration. Lewis Research Center, Cleveland, OH.

### **OVERVIEW OF ENVIRONMENTAL FACTORS**

C. K. PURVIS In NASA, Langley Research Center, NASA/SDIO Space Environmental Effects on Materials Workshop, Part 1 p 5-24 May 1989 Avail: NTIS HC A16/MF A01 CSCL 11/7

The orbital environment is complex, dynamic, and comprised of both natural and system-induced components. Several environment factors are important for materials. Materials selection/suitability determination requires consideration of each and all factors, including synergisms among them. Understanding and evaluating these effects will require ground testing, modeling, and focused flight experimentation. Author

90

## ASTROPHYSICS

Includes cosmology; celestial mechanics; space plasmas; and interstellar and interplanetary gases and dust.

**A89-14618\*** Institut d'Astrophysique, Paris (France).

### **PATTERNS OF THE COSMIC MICROWAVE BACKGROUND FROM EVOLVING STRING NETWORKS**

FRANCOIS R. BOUCHET (CNRS, Institut d'Astrophysique, Paris, France; California, University, Berkeley; Ecole Polytechnique, Palaiseau, France; Lawrence Livermore National Laboratory, Livermore, CA), DAVID P. BENNETT (Chicago, University, IL; NASA/Fermilab Astrophysics Center, Batavia, IL), and ALBERT STEBBINS (NASA/Fermilab Astrophysics Center, Batavia, IL) Nature (ISSN 0028-0836), vol. 335, Sept. 29, 1988, p. 410-414.

NSF-DOE-supported research. refs

Copyright

A network of cosmic strings generated in the early universe may still exist today. As the strings move across the sky, they produce, by gravitational lensing, a characteristic pattern of anisotropies in the temperature of the cosmic microwave background. The observed absence of such anisotropies places constraints on theories in which galaxy formation is seeded by strings, but it is anticipated that the next generation of experiments will detect them. Author

**A89-15426** National Aeronautics and Space Administration. Lewis Research Center, Cleveland, OH.

### **THE LARGE-SCALE MICROWAVE BACKGROUND ANISOTROPY IN DECAYING PARTICLE COSMOLOGY**

MIROSLAW PANEK (NASA/Fermilab Astrophysics Center, Batavia, IL) Astrophysical Journal, Part 1 (ISSN 0004-637X), vol. 334, Nov. 1, 1988, p. 1-5. NASA-DOE-supported research. refs Copyright

The quadrupole anisotropy of the microwave background radiation in cosmological models with decaying particles is investigated. A conservative upper limit on value of the quadrupole moment combined with other constraints gives an upper limit on the redshift of the decay  $z(d)$  of less than 3-6. Author

**A89-19604\*** National Aeronautics and Space Administration. Lewis Research Center, Cleveland, OH.

### **COSMIC STRINGS AND THE LARGE-SCALE STRUCTURE**

ALBERT STEBBINS (NASA/Fermilab Astrophysics Center, Batavia, IL) IN: The post-recombination universe; Proceedings of the NATO Advanced Study Institute, Cambridge, England, July 27-Aug. 7, 1987. Dordrecht, Kluwer Academic Publishers, 1988, p. 285-287. refs Copyright

A possible problem for cosmic string models of galaxy formation is presented. If very large voids are common and if loop fragmentation is not much more efficient than presently believed, then it may be impossible for string scenarios to produce the observed large-scale structure with  $\Omega_0 = 1$  and without strong environmental biasing. Author

**A89-19610\*** National Aeronautics and Space Administration. Lewis Research Center, Cleveland, OH.

### **COSMIC STRINGS - A PROBLEM OR A SOLUTION?**

DAVID P. BENNETT (NASA/Fermilab Astrophysics Center, Batavia; Chicago, University, IL) and FRANCOIS R. BOUCHET (Lawrence Livermore National Laboratory, Livermore, CA) IN: The post-recombination universe; Proceedings of the NATO Advanced Study Institute, Cambridge, England, July 27-Aug. 7, 1987. Dordrecht, Kluwer Academic Publishers, 1988, p. 351-354. Previously announced in STAR as N88-18535. refs Copyright

The most fundamental issue in the theory of cosmic strings is addressed by means of Numerical Simulations: the existence of a scaling solution. The resolution of this question will determine whether cosmic strings can form the basis of an attractive theory of galaxy formation or prove to be a cosmological disaster like magnetic monopoles or domain walls. After a brief discussion of our numerical technique, results are presented which, though still preliminary, offer the best support to date of this scaling hypothesis. Author

**A89-20377\*** Chicago Univ., IL.

### **SUPERHEAVY MAGNETIC MONOPOLES AND MAIN-SEQUENCE STARS**

JOSHUA A. FRIEMAN, KATHERINE FREESE (Chicago, University, IL), and MICHAEL S. TURNER (NASA/Fermi National Accelerator Laboratory, Batavia; Chicago, University, IL) Astrophysical Journal, Part 1 (ISSN 0004-637X), vol. 335, Dec. 15, 1988, p. 844-861. refs

(Contract DE-AC02-80ER-10773; DE-AC03-76SF-00515)

Copyright

The interactions of superheavy monopoles with stars of mass



0.6-25 solar masses are studied. It is shown that captured monopoles cluster near the stellar center, and that their contribution to the total stellar luminosity and their effects on the structure of stars will be unobservable as long as the flux is significantly below the Parker (1970, 1971) bound. It is suggested that all but the strongly magnetic stars will retain a substantial fraction of the monopoles they capture. R.R.

**A89-36278\*** California Univ., Santa Barbara.

#### IS THE GREAT ATTRACTOR REALLY A GREAT WALL?

ALBERT STEBBINS (California, University, Santa Barbara; Toronto, University, Canada) and MICHAEL S. TURNER (NASA/Fermi National Accelerator Laboratory, Batavia; California, University, Santa Barbara; Chicago, University, IL) *Astrophysical Journal*, Part 2 - Letters (ISSN 0004-637X), vol. 339, April 1, 1989, p. L13-L16. Research supported by NSF, DOE, NSERC, and Canadian Institute for Advanced Research. refs  
Copyright

Some of the cosmological consequences of a late-time phase transition which produces light domain walls are discussed. The observed peculiar velocity field of the universe and the observed isotropy of the microwave background radiation severely constrain the wall surface density in such a scenario:  $G(\omega)$  less than about  $0.0001 H_0$  ( $H_0$  is the present value of the Hubble parameter). The most interesting consequence of such a phase transition is the possibility that the local, coherent streaming motion of about 600 km/s reported by Dressler et al (1987) could be explained by the repulsive effect of a relic domain wall within the Hubble volume provided that  $G(\omega)/H_0 = 0.0001$ . Author

**A89-41385\*** Pennsylvania State Univ., University Park.

#### FORMATION OF POLYCYCLIC AROMATIC HYDROCARBONS IN CIRCUMSTELLAR ENVELOPES

MICHAEL FRENKLACH and ERIC D. FEIGELSON (Pennsylvania State University, University Park) *Astrophysical Journal*, Part 1 (ISSN 0004-637X), vol. 341, June 1, 1989, p. 372-384. refs  
(Contract NAG3-668; NSF AST-83-51447)  
Copyright

Production of polycyclic aromatic hydrocarbons in carbon-rich circumstellar envelopes was investigated using a kinetic approach. A detailed chemical reaction mechanism of gas-phase PAH formation and growth, containing approximately 100 reactions of 40 species, was numerically solved under the physical conditions expected in cool stellar winds. The chemistry is based on studies of soot production in hydrocarbon pyrolysis and combustion. Several first-ring and second-ring cyclization processes were considered. A linear lumping algorithm was used to describe PAH growth beyond the second aromatic ring. PAH production using this mechanism was examined with respect to a grid of idealized constant velocity stellar winds as well as several published astrophysical models. The basic result is that the onset of PAH production in the interstellar envelopes is predicted to occur within the temperature interval of 1100 to 900 K. The absolute amounts of the PAHs formed, however, are very sensitive to a number of parameters, both chemical and astrophysical, whose values are not accurately known. Astrophysically meaningful quantities of PAHs require particularly dense and slow stellar winds and high initial acetylene abundance. It is suggested that most of the PAHs may be produced in a relatively small fraction of carbon-rich red giants. Author

**A89-46577\*** Ben Gurion Univ. of the Negev, Beersheva (Israel).  
**NUCLEOSYNTHESIS, NEUTRINO BURSTS AND GAMMA-RAYS FROM COALESCING NEUTRON STARS**

DAVID EICHLER (Negev, University, Beersheba, Israel; Maryland, University, College Park), MARIO LIVIO (Technion - Israel Institute of Technology, Haifa), TSVI PIRAN (Jerusalem, Hebrew University, Israel; Princeton University Observatory, NJ), and DAVID N. SCHRAMM (NASA/Fermilab Astrophysics Center, Batavia; Chicago, University, IL) *Nature* (ISSN 0028-0836), vol. 340, July 13, 1989, p. 126-128. Research supported by NSF and U.S.-Israel Binational Science Foundation. refs  
Copyright

It is pointed out here that neutron-star collisions should synthesize neutron-rich heavy elements, thought to be formed by rapid neutron capture (the r-process). Furthermore, these collisions should produce neutrino bursts and resultant bursts of gamma rays; the latter should comprise a subclass of observable gamma-ray bursts. It is argued that observed r-process abundances and gamma-ray burst rates predict rates for these collisions that are both significant and consistent with other estimates. C.D.

**A89-53833\*** National Aeronautics and Space Administration. Lewis Research Center, Cleveland, OH.

#### A COASTING COSMOLOGY

EDWARD W. KOLB (NASA/Fermi National Accelerator Laboratory, Batavia, IL) *Astrophysical Journal*, Part 1 (ISSN 0004-637X), vol. 344, Sept. 15, 1989, p. 543-550. Research supported by DOE. refs  
(Contract NAGW-1340)  
Copyright

A Friedmann-Robertson-Walker cosmology with energy density decreasing in expansion as  $1/R$ -squared, where  $R$  is the Robertson-Walker scale factor, is studied. In such a model the universe expands with constant velocity; hence the term coasting cosmology. Observational consequences of such a model include the age of the universe, the luminosity distance-redshift relation (the Hubble diagram), the angular diameter distance-redshift relation, and the galaxy number count as a function of redshift. These observations are used to limit the parameters of the model. Among the interesting consequences of the model are the possibility of an ever-expanding closed universe, a model universe with multiple images at different redshifts of the same object, a universe with  $\Omega - 1$  not equal to 0 stable in expansion, and a closed universe with radius smaller than  $1/H_0$ . Author

## 91

### LUNAR AND PLANETARY EXPLORATION

Includes planetology; and manned and unmanned flights.

**A89-46529\*** National Aeronautics and Space Administration. Lewis Research Center, Cleveland, OH.

#### THE MARS CLIMATE FOR A PHOTOVOLTAIC SYSTEM OPERATION

JOSEPH APPELBAUM and DENNIS J. FLOOD (NASA, Lewis Research Center, Cleveland, OH) (IAF, International Conference on Space Power, Cleveland, OH, June 5-7, 1989) *Space Power* (ISSN 0951-5089), vol. 8, no. 3, 1989, p. 307-317. Previously announced in STAR as N89-20385. refs  
(IAF PAPER ICOSP89-9-5) Copyright

Detailed information on the climatic conditions on Mars are very desirable for the design of photovoltaic systems for establishing outposts on the Martian surface. The distribution of solar insolation (global, direct and diffuse) and ambient temperature is addressed. This data are given at the Viking lander's locations and can also be used, to a first approximation, for other latitudes. The insolation data is based on measured optical depth of the Martian atmosphere derived from images taken of the sun with a special diode on the Viking cameras; and computation based on multiple wavelength and multiple scattering of the solar radiation. The ambient temperature (diurnal and yearly distribution) is based on direct measurements with a thermocouple at 1.6 m above the ground at the Viking lander locations. The insolation and ambient temperature information are short term data. New information about Mars may be forthcoming in the future from new analysis of previously collected data or from future flight missions. The Mars climate data for photovoltaic system operation will thus be updated accordingly. Author

## 91 LUNAR AND PLANETARY EXPLORATION

**N89-14853\*#** National Aeronautics and Space Administration. Lewis Research Center, Cleveland, OH.

### **ASSESSMENT OF LUNAR SOURCES OF HE-3 FOR USE ON EARTH**

ROBERT E. ENGLISH *In its Lunar Helium-3 and Fusion Power* p 227-231 Sep. 1988

Avail: NTIS HC A11/MF A01 CSCL 03/2

As a gross measure of the economics of mining lunar sources of He-3, the energy densities (GJ/ton) of lunar soils were compared with the energy densities of various existing and future terrestrial sources of energy. On this basis, only the very richest lunar ores appear competitive with coal. Future lunar exploration might emphasize identification of lunar soils having higher concentrations of He-3. Author

**N89-23397\*#** National Aeronautics and Space Administration. Lewis Research Center, Cleveland, OH.

### **COMPARISON OF SOLAR PHOTOVOLTAIC AND NUCLEAR REACTOR POWER SYSTEMS FOR A HUMAN-TENDED LUNAR OBSERVATORY**

J. M. HICKMAN and H. S. BLOOMFIELD 1989 7 p Proposed for presentation at the 24th Intersociety Energy Conversion Engineering Conference, Washington, DC, 6-11 Aug. 1989; sponsored by IEEE, AIAA, ANS, ASME, SAE, ACS and AIChE (NASA-TM-102015; E-4729; NAS 1.15:102015) Avail: NTIS HC A02/MF A01 CSCL 03/2

Photovoltaic and nuclear surface power systems were examined at the 20 to 100 kW power level range for use at a human-tended lunar astronomical observatory, and estimates of the power system masses were made. One system, consisting of an SP-100 thermoelectric nuclear power supply integrated with a lunar lander, is recommended for further study due to its low system mass, potential for modular growth, and applicability to other surface power missions, particularly in the Martian system. Author

**N89-26799\*#** National Aeronautics and Space Administration. Lewis Research Center, Cleveland, OH.

### **SOLAR POWER FOR THE LUNAR NIGHT**

GEOFFREY A. LANDIS May 1989 19 p Presented at the 9th Biennial SSI/Princeton Conference on Space Manufacturing, Princeton, NJ, 10-13 May 1989; sponsored by Space Studies Inst. (NASA-TM-102127; E-4913; NAS 1.15:102127) Avail: NTIS HC A03/MF A01 CSCL 03/2

Providing power over the 354 hour lunar night provides a considerable challenge to solar power concepts for a moonbase. Concepts are reviewed for providing night power for a solar powered moonbase. The categories of solutions considered are electrical storage, physical storage, transmitted power, and innovative concepts. Electrical storage is the most well-developed option. Less developed electrical storage options are capacitors and superconducting inductors. Physical storage options include storage of potential energy and storage of energy in flywheels. Thermal storage has potentially high energy/weight, but problems of conduction and radiation losses during the night need to be addressed. Transmitted power considers use of microwave or laser beams to transmit power either from orbit or directly from the Earth. Finally, innovative concepts proposed include reflecting light from orbital mirrors, locating the moonbase at a lunar pole, converting reflected Earthlight, or moving the moonbase to follow the sun. Author

**N89-27619\*#** National Aeronautics and Space Administration. Lewis Research Center, Cleveland, OH.

### **LUNAR PRODUCTION OF SOLAR CELLS**

GEOFFREY A. LANDIS and MARIA ANTONIETTA PERINO (Aeritalia S.p.A., Turin, Italy) May 1989 18 p Presented at the 9th Biennial SSI/Princeton Conference on Space Manufacturing, Princeton, NJ, 10-13 May 1989; sponsored by the Space Studies Inst. (NASA-TM-102102; E-4866; NAS 1.15:102102) Avail: NTIS HC A03/MF A01 CSCL 03/2

The feasibility of manufacturing of solar cells on the moon for spacecraft applications is examined. Because of the much lower

escape velocity, there is a great advantage in lunar manufacture of solar cells compared to Earth manufacture. Silicon is abundant on the moon, and new refining methods allow it to be reduced and purified without extensive reliance on materials unavailable on the moon. Silicon and amorphous silicon solar cells could be manufactured on the moon for use in space. Concepts for the production of a baseline amorphous silicon cell are discussed, and specific power levels are calculated for cells designed for both lunar and Earth manufacture. Author

## 92

### **SOLAR PHYSICS**

Includes solar activity, solar flares, solar radiation and sunspots.

**N89-27623\*#** National Aeronautics and Space Administration. Lewis Research Center, Cleveland, OH.

### **SOLAR RADIATION ON MARS**

JOSEPH APPELBAUM and DENNIS J. FLOOD Aug. 1989 33 p Prepared in cooperation with Tel-Aviv Univ. (Israel) (NASA-TM-102299; E-4865; NAS 1.15:102299) Avail: NTIS HC A03/MF A01 CSCL 03/2

Detailed information on solar radiation characteristics on Mars are necessary for effective design of future planned solar energy systems operating on the surface of Mars. Presented here is a procedure and solar radiation related data from which the diurnally, hourly and daily variation of the global, direct beam and diffuse insolation on Mars are calculated. The radiation data are based on measured optical depth of the Martian atmosphere derived from images taken of the sun with a special diode on the Viking cameras; and computation based on multiple wavelength and multiple scattering of the solar radiation. Author

## 93

### **SPACE RADIATION**

Includes cosmic radiation; and inner and outer earth's radiation belts.

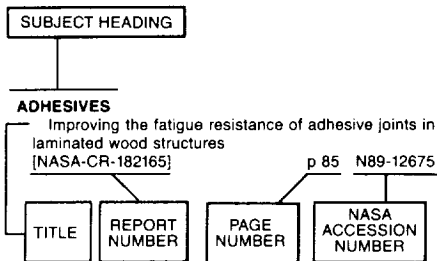
**A89-26985\*** National Aeronautics and Space Administration. Lewis Research Center, Cleveland, OH.

### **LIMITS TO THE RADIATIVE DECAYS OF NEUTRINOS AND AXIONS FROM GAMMA-RAY OBSERVATIONS OF SN 1987A**

EDWARD W. KOLB and MICHAEL S. TURNER (NASA/Fermilab Astrophysics Center, Batavia; Chicago, University, IL) Physical Review Letters (ISSN 0031-9007), vol. 62, Jan. 30, 1989, p. 509-512. Research supported by DOE and Alfred P. Sloan Foundation. refs Copyright

Gamma-ray observations obtained by the SMM gamma-ray spectrometer in the energy range 4.1-6.4 MeV are used to provide limits on the possible radiative decay of neutrinos and axions emitted by SN 1987A. For branching ratio values for the radiative decay modes of less than about 0.0001, the present limits are more stringent than those based upon the photon flux from decaying relic neutrinos. The data are also used to set an axion mass limit. R.R.

## Typical Subject Index Listing



The subject heading is a key to the subject content of the document. Titles, report numbers, and accession numbers of pertinent documents are provided under each subject heading. When the title is insufficiently descriptive of document content, a title extension is added, separated from the title by three hyphens. The report number helps to indicate the type of document cited (e.g., NASA report, NASA translation, NASA contractor report). The NASA accession number is the number by which the document abstracts are arranged in this journal and by which the document is sold or requested. The titles, with title extensions if present, are arranged under each subject heading in ascending accession number order. The subject headings have been selected from the latest revision of the *NASA Thesaurus* (NASA SP-7064).

## A

- ABLATION**  
Arc-driven rail accelerator research [NASA-CR-179584] p 40 N89-13445
- ABSORBERS (MATERIALS)**  
Parametric study of electromagnetic waves propagating in absorbing curved S ducts [NASA-TM-102024] p 129 N89-27923
- ABSORPTIVITY**  
A V-grooved GaAs solar cell [NASA-TM-101970] p 211 N89-22177
- ABSTRACTS**  
Bibliography of Lewis Research Center technical publications announced in 1986 [NASA-TM-89887] p 238 N89-18259
- ACCELERATED LIFE TESTS**  
KOH concentration effect on cycle life of nickel-hydrogen cells. III - Cycle life test p 207 A89-23283
- ACCELERATION (PHYSICS)**  
Instabilities caused by oscillating accelerations normal to a viscous fluid-fluid interface p 144 A89-22823  
The effects of magnetic nozzle configurations on plasma thrusters [NASA-CR-184678] p 64 N89-15170
- ACCELEROMETERS**  
A self diagnostic system for piezoelectric sensors [AIAA PAPER 89-2638] p 171 A89-46980
- ACCUMULATORS**  
Isotropic graphite multistage depressed collectors - A progress report --- carbon electrode performance p 132 A89-31988  
Performance of a multistage depressed collector with machined titanium electrodes [NASA-TP-2891] p 136 N89-15337
- ACETONE**  
Measurement of the diffusion coefficient of acetone in succinonitrile at its melting point p 237 A89-23488

## ACOUSTIC ATTENUATION

- Lateral noise attenuation of the advanced propeller of the propan test assessment aircraft [AIAA PAPER 89-1057] p 226 A89-36217

## ACOUSTIC DUCTS

- Acoustic wave propagation in heterogeneous structures including experimental validation [AIAA PAPER 89-1044] p 225 A89-36214  
Acoustic wave propagation in heterogeneous structures including experimental validation [NASA-TM-101486] p 224 N89-19965

## ACOUSTIC EMISSION

- Acoustic emission evaluation of plasma-sprayed thermal barrier coatings p 178 A89-12751  
Nondestructive evaluation/characterization of composite materials and structures using the acousto-ultrasonic techniques p 188 A89-36571  
Acousto-ultrasonics - An update p 188 A89-42864  
The scratch test - Different critical load determination techniques --- adhesive strength of thin hard coatings p 171 A89-54278

## ACOUSTIC EXCITATION

- Observations of the frequencies in a sphere wake and of drag increase by acoustic excitation p 142 A89-16884  
Control of laminar separation over airfoils by acoustic excitation [AIAA PAPER 89-0565] p 3 A89-25454  
Large amplitude acoustic excitation of swirling turbulent jets [AIAA PAPER 89-0970] p 4 A89-29098  
Subharmonic and fundamental high amplitude excitation of an axisymmetric jet [AIAA PAPER 89-0993] p 149 A89-37825  
Control of laminar separation over airfoils by acoustic excitation [NASA-TM-101379] p 9 N89-12552  
Large amplitude acoustic excitation of swirling turbulent jets [NASA-TM-101950] p 13 N89-18417

## ACOUSTIC MEASUREMENT

- Deep-level transient spectroscopy of Al(x)Ga(1-x)As/GaAs using nondestructive acousto-electric voltage measurement p 133 A89-42742  
Acoustic evaluation of the Helmholtz resonator treatment in the NASA Lewis 8- by 6-foot supersonic wind tunnel [NASA-TM-101407] p 228 N89-15685

## ACOUSTIC PROPAGATION

- Lateral noise attenuation of the advanced propeller of the propan test assessment aircraft [AIAA PAPER 89-1057] p 226 A89-36217  
Energy in elastic fiber embedded in elastic matrix containing incident SH wave [NASA-CR-4205] p 188 N89-18694  
Acoustic propagation in curved ducts with extended reacting wall treatment [NASA-TM-102110] p 224 N89-25670

## ACOUSTIC PROPERTIES

- Determination of near and far field acoustics for advanced propeller configurations [AIAA PAPER 89-1040] p 226 A89-40469

## ACOUSTICS

- Effects of wind-tunnel wall absorption on acoustic radiation of propellers p 225 A89-22285  
The acousto-ultrasonic approach --- for NDE p 188 A89-32305  
Comparison of propeller cruise noise data taken in the NASA Lewis 8- by 6-foot wind tunnel with other tunnel and flight data [AIAA PAPER 89-1059] p 226 A89-40472  
An experimental and analytical investigation of thermoacoustic convection heat transfer in gravity and zero-gravity environments [NASA-CR-179575] p 120 N89-11920  
NASA powered lift facility internally generated noise and its transmission to the acoustic far field [NASA-CR-182217] p 36 N89-16882

- A modified VAPEPS method for predicting vibroacoustic response of unreinforced mass loaded honeycomb panels [NASA-TM-101467] p 46 N89-16905

- Acoustic wave propagation in heterogeneous structures including experimental validation [NASA-TM-101486] p 224 N89-19965

- Comparison of propeller cruise noise data taken in the NASA Lewis 8- by 6-foot wind tunnel with other tunnel and flight data [NASA-TM-101976] p 228 N89-21628

- In-flight measurement of propeller noise on the fuselage of an airplane [NASA-TM-102285] p 229 N89-25675

- Liquid droplet generation [NASA-CR-182246] p 166 N89-26182

## ACTIVATION ENERGY

- Thermo-oxidative stability studies of Celion 6000/PMR-15 unidirectional composites, PMR-15, and Celion 6000 fiber p 79 A89-14099

## ACTIVE CONTROL

- Passive and active control of jet turbulence p 140 A89-10176  
Active vibration control for flexible rotor by optimal direct-output feedback control [NASA-TM-101972] p 31 N89-22605

## ACTS

- A laser communication experiment utilizing the ACT satellite and an airborne laser transceiver p 43 A89-15811  
Baseband processor hardware for Advanced Communication Technology Satellite (ACTS) p 43 A89-38298

## ACTUATORS

- Variable speed induction motor operation from a 20-kHz power bus [NASA-TM-102061] p 71 N89-25271

## ADAPTIVE CONTROL

- IECON '87: Industrial applications of control and simulation; Proceedings of the 1987 International Conference on Industrial Electronics, Control, and Instrumentation, Cambridge, MA, Nov. 3, 4, 1987 [SPIE-853] p 219 A89-10798  
Identification of high performance and component technology for space electrical power systems for use beyond the year 2000 [NASA-CR-183003] p 62 N89-11807  
Adaptive feed array compensation system for reflector antenna surface distortion [NASA-TM-101458] p 127 N89-17756  
Low frequency vibration isolation technology for microgravity space experiments [NASA-TM-101448] p 123 N89-20324  
Computer simulation of a pilot in V/STOL aircraft control loops [NASA-CR-184815] p 215 N89-21479  
Neuromorphic learning of continuous-valued mappings in the presence of noise: Application to real-time adaptive control [NASA-TM-101999] p 221 N89-24856  
Analysis of modified SMI method for adaptive array weight control [NASA-CR-185493] p 19 N89-25993

## ADAPTIVE FILTERS

- A simple algebraic grid adaptation scheme with applications to two- and three-dimensional flow problems [AIAA PAPER 89-1984] p 5 A89-41827

## ADDITIVES

- Doping directed at the oxygen sites in Y1Ba2Cu3O(7-delta) - The effect of sulfur, fluorine, and chlorine p 133 A89-37824  
The effect of Al2O3, CaO, Cr2O3 and MgO on devitrification of silica [NASA-TM-101335] p 77 N89-10124  
Strength of hot isostatically pressed and sintered reaction bonded silicon nitrides containing Y2O3 [NASA-TM-101443] p 112 N89-15257

## ADHESION

- Interfacial adhesion - Theory and experiment p 97 A89-35307

- Adhesion, friction, and wear of plasma-deposited thin silicon nitride films at temperatures to 700 C p 107 A89-48250
- Tribological properties of structural ceramics p 107 A89-51258
- Adhesion, friction and micromechanical properties of ceramics p 107 A89-54277
- Avalanche in adhesion --- interfacial separation between two Ni crystals p 100 A89-54495
- Adhesion, friction, and wear of plasma-deposited thin silicon nitride films at temperatures to 700 C [NASA-TM-101377] p 109 N89-11913
- Applications of surface analysis and surface theory in tribology [NASA-TM-101392] p 78 N89-15981
- Adhesion in ceramics and magnetic media [NASA-TM-101476] p 113 N89-19435
- Design, development and applications of novel techniques for studying surface mechanical properties [NASA-TM-101959] p 113 N89-20253
- ADHESION TESTS**
- The scratch test - Different critical load determination techniques --- adhesive strength of thin hard coatings p 171 A89-54278
- Adhesion scratch testing - A round-robin experiment p 171 A89-54281
- Simplified procedures for designing adhesively bonded composite joints [NASA-TM-102120] p 87 N89-26048
- ADHESIVE BONDING**
- On the wind force needed to dislodge a drop adhered to a surface p 144 A89-22819
- Nondestructive evaluation/characterization of composite materials and structures using the acousto-ultrasonic techniques p 188 A89-36571
- Improving the fatigue resistance of adhesive joints in laminated wood structures [NASA-CR-182165] p 85 N89-12675
- Adhesion in ceramics and magnetic media [NASA-TM-101476] p 113 N89-19435
- Simplified procedures for designing adhesively bonded composite joints [NASA-TM-102120] p 87 N89-26048
- ADHESIVES**
- Improving the fatigue resistance of adhesive joints in laminated wood structures [NASA-CR-182165] p 85 N89-12675
- ADIABATIC FLOW**
- Adiabatic Wankel type rotary engine [NASA-CR-182233] p 28 N89-17599
- ADSORPTION**
- Comparison of the surface charge behavior of commercial silicon nitride and silicon carbide powders p 105 A89-21444
- ADVECTION**
- Universal limiter for high order explicit conservative advection schemes p 151 A89-45398
- Universal limiter for transient interpolation modeling of the advective transport equations: The ULTIMATE conservative difference scheme [NASA-TM-100916] p 222 N89-14794
- AEROACOUSTICS**
- Results of acoustic tests of a prop-fan model p 224 A89-10112
- Sound power spectrum and wave drag of a propeller in flight [AIAA PAPER 89-1081] p 225 A89-33724
- Influence of airfoil thickness on convected gust interaction noise [AIAA PAPER 89-1082] p 225 A89-33725
- Near wakes of advanced turbopropellers [AIAA PAPER 89-1095] p 5 A89-33735
- Near-field acoustic environment of a supersonic plume adjacent to a wall [AIAA PAPER 89-1137] p 225 A89-33767
- Installed propfan (SR-7L) far-field noise characteristics [AIAA PAPER 89-1056] p 225 A89-36216
- Fluctuating pressures on wing surfaces in the slipstream of a single-rotor propfan [AIAA PAPER 89-1058] p 226 A89-36218
- An acoustic experimental and theoretical investigation of single disc propellers [AIAA PAPER 89-1146] p 227 A89-40478
- AEROACOUSTIC CHARACTERISTICS**
- Measurements of heat transfer distribution over the surfaces of highly loaded turbine nozzle guide vanes p 141 A89-12752
- Effects of excitation level on the stability of an axisymmetric mixing layer p 2 A89-16882
- Calculation of flow over iced airfoils p 5 A89-40905
- User's manual for an aerodynamic optimization scheme that updates flow variables and design parameters simultaneously [NASA-CR-182180] p 10 N89-13399

- Multiple Application Propfan Study (MAPS): Advanced tactical transport [NASA-CR-175003] p 28 N89-19300
- AERODYNAMIC COEFFICIENTS**
- Experimental aerodynamic performance of advanced 40 deg-swept 10-blade propeller model at Mach 0.6 to 0.85 [NASA-TM-88969] p 9 N89-10865
- An analysis for high speed propeller-nacelle aerodynamic performance prediction. Volume 1: Theory and application [NASA-CR-4199-VOL-1] p 12 N89-15896
- Time domain numerical calculations of unsteady vortical flows about a flat plate airfoil [NASA-TM-102318] p 168 N89-29726
- AERODYNAMIC CONFIGURATIONS**
- Aerodynamic optimization by simultaneously updating flow variables and design parameters with application to advanced propeller designs [NASA-CR-182181] p 24 N89-11750
- Revolutionary opportunities for materials and structures study, addendum [NASA-CR-179642-ADD] p 34 N89-29351
- AERODYNAMIC DRAG**
- Use of a generalized Stokes number to determine the aerodynamic capture efficiency of non-Stokesian particles from a compressible gas flow p 140 A89-12336
- A preliminary design study of supersonic through-flow fan inlets [NASA-CR-182224] p 24 N89-11751
- AERODYNAMIC FORCES**
- Modal forced vibration analysis of aerodynamically excited turbosystems [NASA-CR-174966] p 201 N89-18696
- AERODYNAMIC HEAT TRANSFER**
- Navier-Stokes solution to the flowfield over ice accretion shapes p 1 A89-12557
- Measurements of heat transfer distribution over the surfaces of highly loaded turbine nozzle guide vanes p 141 A89-12752
- AERODYNAMIC INTERFERENCE**
- A review of turbomachinery blade-row interaction research [NASA-CR-182211] p 24 N89-12567
- AERODYNAMIC LOADS**
- Propeller/wing interaction [AIAA PAPER 89-0535] p 17 A89-25429
- Evaluation of three turbulence models for the prediction of steady and unsteady airloads [AIAA PAPER 89-0609] p 3 A89-25485
- Evaluation of three turbulence models for the prediction of steady and unsteady airloads [NASA-TM-101413] p 10 N89-12555
- NASTRAN supplemental documentation for modal forced vibration analysis of aerodynamically excited turbosystems [NASA-CR-174967] p 201 N89-19583
- High speed turboprop aeroacoustic study (single rotation). Volume 1: Model development [NASA-CR-182257-VOL-1] p 229 N89-24139
- AERODYNAMIC NOISE**
- Cruise noise of the 2/9 scale model SR-7A propeller p 224 A89-12561
- High speed turboprop aeroacoustic study (single rotation). Volume 1: Model development [NASA-CR-182257-VOL-1] p 229 N89-24139
- Cruise noise of the SR-2 propeller model in a wind tunnel [NASA-TM-101480] p 229 N89-24886
- AERODYNAMIC STABILITY**
- Turbomachinery aeroelasticity at NASA Lewis Research Center p 28 N89-19262
- AERODYNAMIC STALLING**
- A natural low-frequency oscillation of the flow over an airfoil near stalling conditions p 6 A89-45437
- Analysis of an unswept propfan blade with a semiempirical dynamic stall model [NASA-TM-4083] p 27 N89-15112
- AEROELASTICITY**
- Aerodynamically-driven condensate layer thickness distributions on isothermal cylindrical surfaces p 140 A89-12337
- AEROELASTICITY**
- Experimental investigation of propfan aeroelastic response in off-axis flow with mistuning [AIAA PAPER 88-3153] p 20 A89-17941
- Aeroelastic response of metallic and composite propfan models in yawed flow [AIAA PAPER 88-3154] p 20 A89-17942
- Vibration, performance, flutter and forced response characteristics of a large-scale propfan and its aeroelastic model [AIAA PAPER 88-3155] p 21 A89-17943
- Technique for the prediction of airfoil flutter characteristics in separated flow p 191 A89-27744
- A computational procedure for automated flutter analysis p 191 A89-28070

- Application of a full-potential solver to bending-torsion flutter in cascades [AIAA PAPER 89-1386] p 34 A89-30859
- Aeroelastic analysis of prop fan blades with a semiempirical dynamic stall model [AIAA PAPER 89-2695] p 194 A89-47025
- Analytical flutter investigation of a composite propfan model p 195 A89-48663
- Vibration, performance, flutter and forced response characteristics of a large-scale propfan and its aeroelastic model [NASA-TM-101322] p 24 N89-10043
- Turbomachinery aeroelasticity at NASA Lewis Research Center p 28 N89-19262
- Structural dynamics branch research and accomplishments for FY 1988 [NASA-TM-101406] p 202 N89-22939
- Influence of thickness and camber on the aeroelastic stability of supersonic throughflow fans: An engineering approach [NASA-TM-101949] p 15 N89-25957
- AERONAUTICS**
- Vision sensing techniques in aeronautics and astronautics p 219 A89-31087
- AEROSOLS**
- Discussion of Mills et al. on 'The effect of wall suction and thermophoresis on aerosol particle deposition from a laminar boundary layer on a flat plate' p 140 A89-12331
- Viscous dissipation effects on thermophoretically augmented aerosol particle transport across laminar boundary layers p 141 A89-14600
- An improved correction algorithm for number density measurements made with the forward scattering spectrometer probe p 170 A89-44122
- AEROSPACE ENGINEERING**
- Interactions between gaseous electrical discharges and single liquid droplets p 90 A89-19298
- Comprehensive report of aeropropulsion, space propulsion, space power, and space science applications of the Lewis Research Center [NASA-TM-100925] p 238 N89-24216
- AEROSPACE ENVIRONMENTS**
- Low earth orbit environmental effects on the Space Station photovoltaic power generation systems p 55 A89-29123
- Gas particle radiator [NASA-CASE-LEW-14297-1] p 172 N89-12048
- Wear consideration in gear design for space applications [NASA-TM-101457] p 183 N89-15414
- AEROSPACE PLANES**
- Fueling the National Aero-Space Plane with slush hydrogen [AIAA PAPER 89-5014] p 117 A89-51339
- Heat transfer in aerospace propulsion p 153 A89-53282
- Technology issues associated with fueling the national aerospace plane with slush hydrogen [NASA-TM-101386] p 61 N89-10123
- AEROSPACE SAFETY**
- The development of power specific redlines for SSME safety monitoring [AIAA PAPER 89-2413] p 61 A89-53305
- Expert systems applied to spacecraft fire safety [NASA-CR-182266] p 42 N89-23501
- The development of power specific redlines for SSME safety monitoring [NASA-CR-185121] p 41 N89-26027
- AEROSPACE SYSTEMS**
- Vision sensing techniques in aeronautics and astronautics p 219 A89-31087
- Space Electrochemical Research and Technology Conference: Abstracts [NASA-CP-10029] p 211 N89-22982
- AEROTHERMODYNAMICS**
- Turbine-stage heat transfer - Comparison of short-duration measurements with state-of-the-art predictions p 142 A89-16458
- Impact of ETO propellants on the aerothermodynamic analyses of propulsion components --- Earth To Orbit [AIAA PAPER 88-3091] p 53 A89-16486
- High angle-of-attack hypersonic aerodynamics p 2 A89-19918
- Flux splitting algorithms for two-dimensional viscous flows with finite-rate chemistry [AIAA PAPER 89-0388] p 146 A89-28409
- A high heat flux experiment for verification of thermostructural analysis p 148 A89-35002
- Improved numerical methods for turbulent viscous flows aerothermal modeling program, phase 2 [NASA-CR-182169] p 154 N89-12010
- A high heat flux experiment for verification of thermostructural analysis [NASA-TM-100931] p 155 N89-12026

- Aerothermal modeling program, phase 2  
p 156 N89-12890
- Aerothermal modeling program, phase 2, Element B:  
Flow interaction experiment p 156 N89-12891
- Aerothermal modeling program, phase 2, Element C:  
Fuel injector-air swirl characterization p 156 N89-12892
- Aerothermal modeling program, Phase 2, element B:  
Flow interaction experiment p 160 N89-17304
- Measurement of airfoil heat transfer coefficients on a turbine stage p 160 N89-17311
- Two- and three-dimensional turbine blade row flow field simulations p 161 N89-17313
- Toward improved durability in advanced aircraft engine hot sections  
[NASA-TM-4087] p 29 N89-20135
- NASA HOST project overview p 29 N89-20136
- Assessment, development, and application of combustor aerothermal models p 30 N89-20138
- Review and assessment of the database and numerical modeling for turbine heat transfer p 30 N89-20139
- Views on the impact of HOST p 31 N89-20144
- AGING (BIOLOGY)**  
Age distribution among NASA scientists and engineers p 238 N89-23911
- AIR DUCTS**  
Acoustic wave propagation in heterogeneous structures including experimental validation  
[AIAA PAPER 89-1044] p 225 A89-36214
- Acoustic wave propagation in heterogeneous structures including experimental validation  
[NASA-TM-101486] p 224 N89-19965
- AIR FLOW**  
Radiative structures of lycopodium-air flames in low gravity  
[AIAA PAPER 89-0500] p 91 A89-25406
- The secondary flow and its stability for natural convection in a tall vertical enclosure p 149 A89-37931
- Stratified charge rotary engine - Internal flow studies at the MSU engine research laboratory  
[SAE PAPER 890331] p 181 A89-51477
- Friction factor data for flat plate tests of smooth and honeycomb surfaces  
[NASA-CR-184977] p 186 N89-23876
- Time domain numerical calculations of unsteady vortical flows about a flat plate airfoil  
[NASA-TM-102318] p 168 N89-29726
- AIR JETS**  
On the preferred mode of jet instability p 140 A89-11567
- Three dimensional simulation of an underexpanded jet interacting with a supersonic cross flow  
[AIAA PAPER 88-3181] p 2 A89-14982
- AIR POLLUTION**  
A numerical model of electrodynamics of plasma within the contaminant gas cloud of the Space Shuttle Orbiter at low earth orbit p 233 A89-45631
- AIRBORNE LASERS**  
A laser communication experiment utilizing the ACT satellite and an airborne laser transceiver p 43 A89-15811
- AIRCRAFT COMPARTMENTS**  
Interior noise in the untreated Gulfstream II Propfan Test Assessment (PTA) aircraft  
[AIAA PAPER 89-1119] p 17 A89-33754
- AIRCRAFT CONSTRUCTION MATERIALS**  
Revolutionary opportunities for materials and structures study, addendum  
[NASA-CR-179642-ADD] p 34 N89-29351
- Revolutionary opportunities for materials and structures study, addendum no. 1  
[NASA-CR-179642-ADD-1] p 47 N89-29478
- AIRCRAFT CONTROL**  
Determination of longitudinal aerodynamic derivatives using flight data from an icing research aircraft  
[AIAA PAPER 89-0754] p 34 A89-28454
- Model-based analysis of control/display interaction in the hover task p 215 A89-36933
- Integrated flight/propulsion control study for STOVL applications  
[AIAA PAPER 89-2908] p 34 A89-47166
- Extended observability of linear time-invariant systems under recurrent loss of output data  
[AIAA PAPER 89-3510] p 220 A89-52603
- An observer-based compensator for distributed delays in integrated control systems  
[AIAA PAPER 89-3541] p 35 A89-52628
- Determination of longitudinal aerodynamic derivatives using flight data from an icing research aircraft  
[NASA-TM-101427] p 35 N89-15121
- AIRCRAFT DESIGN**  
Aircraft engines, III p 21 A89-22927
- Aeronautical applications of high-temperature superconductors  
[AIAA PAPER 89-2142] p 23 A89-53304
- Structural tailoring of counter rotation propfans  
p 33 N89-25165
- Aeronautical applications of high-temperature superconductors  
[NASA-TM-102311] p 33 N89-26008
- AIRCRAFT ENGINES**  
Return of the turboprops p 20 A89-12953
- Effect of aerodynamic detuning on supersonic rotor discrete frequency noise generation p 225 A89-15083
- Aircraft engines, III p 21 A89-22927
- Performance potential of air turbo-ramjet employing supersonic through-flow fan  
[AIAA PAPER 89-0010] p 22 A89-25006
- Effect of heavy rain on aviation engines  
[AIAA PAPER 89-0799] p 22 A89-28462
- Probabilistic constitutive relationships for material strength degradation models  
[AIAA PAPER 89-1368] p 192 A89-30843
- Ceramic bearings for use in gas turbine engines p 180 A89-46697
- HOST combustion R and T overview p 25 N89-12879
- HOST structural analysis program overview p 195 N89-12881
- Turbine Engine Hot Section Technology, 1987  
[NASA-CP-2493] p 199 N89-17298
- Toward improved durability in advanced aircraft engine hot sections  
[NASA-TM-4087] p 29 N89-20135
- NASA HOST project overview p 29 N89-20136
- Review and assessment of the database and numerical modeling for turbine heat transfer p 30 N89-20139
- Life modeling of thermal barrier coatings for aircraft gas turbine engines p 30 N89-20143
- Views on the impact of HOST p 31 N89-20144
- Comprehensive report of aeropropulsion, space propulsion, space power, and space science applications of the Lewis Research Center  
[NASA-TM-100925] p 238 N89-24216
- AIRCRAFT EQUIPMENT**  
Electroimpulse deicing - Electrodynamical solution by discrete elements p 17 A89-39193
- AIRCRAFT FUELS**  
Degradation mechanisms of n-dodecane with sulfur and nitrogen dopants during thermal stressing p 116 A89-22277
- AIRCRAFT HAZARDS**  
Distributed ice accretion sensor for smart aircraft structures  
[AIAA PAPER 89-0772] p 17 A89-25571
- NASA's program on icing research and technology  
[NASA-TM-101989] p 1 N89-22569
- AIRCRAFT INSTRUMENTS**  
Distributed ice accretion sensor for smart aircraft structures  
[AIAA PAPER 89-0772] p 17 A89-25571
- AIRCRAFT LANDING**  
Integrated flight/propulsion control system design based on a centralized approach  
[AIAA PAPER 89-3520] p 35 A89-52611
- Integrated flight/propulsion control system design based on a decentralized, hierarchical approach  
[AIAA PAPER 89-3519] p 35 A89-53301
- Integrated flight/propulsion control system design based on a centralized approach  
[NASA-TM-102137] p 35 N89-26009
- AIRCRAFT MODELS**  
Icing research tunnel test of a model helicopter rotor  
[NASA-TM-101978] p 29 N89-19305
- AIRCRAFT NOISE**  
Cruise noise of the 2/9 scale model SR-7A propeller p 224 A89-12561
- Interior noise in the untreated Gulfstream II Propfan Test Assessment (PTA) aircraft  
[AIAA PAPER 89-1119] p 17 A89-33754
- Near-field acoustic characteristics of a single-rotor propfan  
[AIAA PAPER 89-1055] p 23 A89-36215
- Installed propfan (SR-7L) far-field noise characteristics  
[AIAA PAPER 89-1056] p 225 A89-36216
- Lateral noise attenuation of the advanced propeller of the propfan test assessment aircraft  
[AIAA PAPER 89-1057] p 226 A89-36217
- The effect of front-to-rear propeller spacing on the interaction noise at cruise conditions of a model counterrotation propeller having a reduced diameter aft propeller  
[NASA-TM-101329] p 227 N89-10603
- Measured far-field flight noise of a counterrotation turboprop at cruise conditions  
[NASA-TM-101383] p 228 N89-15686
- Noise generated by a flight weight, air flow control valve in a vertical takeoff and landing aircraft thrust vectoring system  
[NASA-CR-182232] p 228 N89-20776
- High speed turboprop aeroacoustic study (single rotation). Volume 1: Model development  
[NASA-CR-182257-VOL-1] p 229 N89-24139
- Cruise noise of the SR-2 propeller model in a wind tunnel  
[NASA-TM-101480] p 229 N89-24886
- AIRCRAFT PARTS**  
Two-dimensional simulation of electrothermal deicing of aircraft components p 17 A89-39194
- AIRCRAFT PERFORMANCE**  
Return of the turboprops p 20 A89-12953
- An overview of the current NASA program on aircraft icing research  
[SAE PAPER 881386] p 16 A89-28192
- Effects of environmentally imposed roughness on airfoil performance  
[NASA-CR-179639] p 17 N89-11725
- Multiple Application Propfan Study (MAPS): Advanced tactical transport  
[NASA-CR-175003] p 28 N89-19300
- Revolutionary opportunities for materials and structures study, addendum  
[NASA-CR-179642-ADD] p 34 N89-29351
- AIRCRAFT STABILITY**  
Active suppression of aerodynamic instabilities in turbomachines p 3 A89-28341
- Determination of longitudinal aerodynamic derivatives using flight data from an icing research aircraft  
[AIAA PAPER 89-0754] p 34 A89-28454
- Determination of longitudinal aerodynamic derivatives using flight data from an icing research aircraft  
[NASA-TM-101427] p 35 N89-15121
- AIRCRAFT STRUCTURES**  
Distributed ice accretion sensor for smart aircraft structures  
[AIAA PAPER 89-0772] p 17 A89-25571
- A comparison of numerical methods for the prediction of two-dimensional heat transfer in an electrothermal deicer pad  
[NASA-CR-4202] p 19 N89-13429
- Improved silicon carbide for advanced heat engines  
[NASA-CR-179477] p 112 N89-15251
- Electromagnetic properties of ice coated surfaces  
[NASA-CR-184780] p 127 N89-20355
- Revolutionary opportunities for materials and structures study, addendum  
[NASA-CR-179642-ADD] p 34 N89-29351
- AIRCRAFT WAKES**  
The low frequency oscillation in the flow over a NACA0012 airfoil with an iced leading edge  
[NASA-TM-102018] p 14 N89-23417
- AIRFOIL OSCILLATIONS**  
Experimental investigation of transonic oscillating cascade aerodynamics  
[AIAA PAPER 89-0321] p 3 A89-26369
- Technique for the prediction of airfoil flutter characteristics in separated flow p 191 A89-27744
- A natural low-frequency oscillation of the flow over an airfoil near stalling conditions p 6 A89-45437
- Experimental investigation of transonic oscillating cascade aerodynamics  
[NASA-TM-101993] p 29 N89-20133
- The low frequency oscillation in the flow over a NACA0012 airfoil with an iced leading edge  
[NASA-TM-102018] p 14 N89-23417
- AIRFOIL PROFILES**  
On ice shape prediction methodologies and comparison with experimental data  
[AIAA PAPER 89-0732] p 16 A89-30650
- Numerical solution of periodic vortical flows about a thin airfoil  
[AIAA PAPER 89-1691] p 7 A89-48955
- Numerical solution of periodic vortical flows about a thin airfoil  
[NASA-TM-101998] p 14 N89-23413
- The low frequency oscillation in the flow over a NACA0012 airfoil with an iced leading edge  
[NASA-TM-102018] p 14 N89-23417
- AIRFOILS**  
Control of laminar separation over airfoils by acoustic excitation  
[AIAA PAPER 89-0565] p 3 A89-25454
- Investigation of surface water behavior during glaze ice accretion p 16 A89-27739
- An experimental investigation of multi-element airfoil ice accretion and resulting performance degradation  
[AIAA PAPER 89-0752] p 4 A89-28453
- Calculation of flow over iced airfoils p 5 A89-40905
- Numerical analysis of supersonic flow through oscillating cascade sections by using a deforming grid  
[AIAA PAPER 89-2805] p 8 A89-50810
- Effects of environmentally imposed roughness on airfoil performance  
[NASA-CR-179639] p 17 N89-11725

## AIRFRAMES

- Control of laminar separation over airfoils by acoustic excitation  
[NASA-TM-101379] p 9 N89-12552
- Simulation of 2-dimensional viscous flow through cascades using a semi-elliptic analysis and hybrid C-H grids  
[NASA-CR-4180] p 10 N89-12553
- HOST turbine heat transfer subproject overview  
p 25 N89-12880
- Measurement of airfoil heat transfer coefficients on a turbine stage  
p 157 N89-12897
- Turbine airfoil film cooling  
p 158 N89-12903
- Life prediction and constitutive models for engine hot section  
p 188 N89-12916
- Thermal barrier coating life prediction model development  
p 109 N89-12920
- Predictions of airfoil aerodynamic performance degradation due to icing  
[NASA-TM-101434] p 10 N89-13412
- The effects of inlet turbulence and rotor/stator interactions on the aerodynamics and heat transfer of a large-scale rotating turbine model, volume 1  
[NASA-CR-4079] p 159 N89-13756
- An experimental investigation of multi-element airfoil ice accretion and resulting performance degradation  
[NASA-TM-101441] p 12 N89-15084
- Measurement of airfoil heat transfer coefficients on a turbine stage  
p 160 N89-17311
- Turbine airfoil film cooling  
p 161 N89-17315
- Thermal barrier coating life-prediction model development  
p 200 N89-17331
- High temperature constitutive and crack initiation modeling of coated single crystal superalloys  
p 112 N89-17334
- MATE program: Erosion resistant compressor airfoil coating, volume 2  
[NASA-CR-179645] p 113 N89-18550
- Numerical analysis of supersonic flow through oscillating cascade sections by using a deforming grid  
[NASA-TM-102053] p 15 N89-25119
- Influence of thickness and camber on the aeroelastic stability of supersonic throughflow fans: An engineering approach  
[NASA-TM-101949] p 15 N89-25957
- AIRFRAMES**
- STOL and STOVL hot gas ingestion and airframe heating tests in the NASA Lewis 9- by 15-foot low-speed wind tunnel  
[NASA-TM-102101] p 15 N89-29323
- ALCOHOLS**
- Effect of alcohol addition on shock-initiated formation of soot from benzene  
p 90 A89-12903
- ALGORITHMS**
- The solution of the Elrod algorithm for a dynamically loaded journal bearing using multigrid techniques  
[ASME PAPER 88-TRIB-23] p 148 A89-34795
- High speed corner and gap-seal computations using an LU-SGS scheme  
[AIAA PAPER 89-2669] p 154 A89-54424
- An algorithm for unsteady flows with strong convection  
[NASA-TM-100828] p 221 N89-10575
- On the accuracy of solving triangular systems in parallel  
[NASA-TM-101384] p 222 N89-12337
- Universal test fixture for monolithic mm-wave integrated circuits calibrated with an augmented TRD algorithm  
[NASA-TP-2875] p 127 N89-17767
- Analysis of modified SMI method for adaptive array weight control  
[NASA-CR-184904] p 127 N89-20364
- A message passing kernel for the hypercluster parallel processing test bed  
[NASA-TM-101952] p 218 N89-20684
- Conservative treatment of boundary interfaces for overlaid grids and multi-level grid adaptations  
[NASA-TM-102080] p 15 N89-24269
- On the equivalence of a class of inverse decomposition algorithms for solving systems of linear equations  
[NASA-TM-102036] p 223 N89-24865
- Space nuclear reactor shields for manned and unmanned applications  
[NASA-TM-102064] p 71 N89-25272
- Time-dependent computational studies of flames in microgravity  
[NASA-CR-182298] p 122 N89-25353
- Analysis of modified SMI method for adaptive array weight control  
[NASA-CR-185493] p 19 N89-25993
- High speed corner and gap-seal computations using an LU-SGS scheme  
[NASA-TM-102138] p 166 N89-27103
- Multi-grid for structures analysis  
p 206 N89-29810
- ALIGNMENT**
- Topology of modified helical gears  
[NASA-TM-102134] p 187 N89-28015

## ALKALI METALS

- The effect of different alkali metal hydroxides on nickel electrode life  
p 207 A89-15280
- ALKALINE BATTERIES**
- Alkaline fuel cell performance investigation  
p 207 A89-15258
- Oxygen electrodes for rechargeable alkaline fuel cells  
p 211 N89-22998
- Corrosion testing of candidates for the alkaline fuel cell cathode  
p 212 N89-23000
- ALKYL COMPOUNDS**
- Reaction of perfluoroalkylpolyethers (PFPE) with 440C steel in vacuum under sliding conditions at room temperature  
[NASA-TP-2883] p 115 N89-26091
- ALKYLATES**
- Determination of the thermal stability of perfluoroalkylethers by tensimetry: Instrumentation and Procedure  
[NASA-TM-102116] p 116 N89-26095
- ALLOYING**
- Analysis of microalloy precipitate reversion in steels  
p 94 A89-15108
- ALLOYS**
- Castable hot corrosion resistant alloy  
[NASA-CASE-LEW-14134-2] p 102 N89-14303
- Refractory metal alloys and composites for space nuclear power systems  
[NASA-TM-101364] p 102 N89-16986
- Progress on a PdCr wire strain gage  
p 174 N89-17301
- Oxide-dispersion-strengthened turbine blades. Volume 2  
[NASA-CR-179561-VOL-2] p 28 N89-18487
- Procedures for characterizing an alloy and predicting cyclic life with the total strain version of Strainrange Partitioning  
[NASA-TM-4102] p 203 N89-25485
- ALTERNATING DIRECTION IMPLICIT METHODS**
- Diagonal implicit multigrid algorithm for the Euler equations  
p 1 A89-11110
- Multigrid calculation of three-dimensional turbomachinery flows  
[NASA-CR-185332] p 165 N89-26172
- ALUMINIDES**
- Mechanisms of elevated-temperature deformation in the B2 aluminides NiAl and CoAl  
p 94 A89-17378
- Elevated temperature slow plastic deformation of NiAl/TiB2 particulate composites  
p 81 A89-31689
- Dispersoids in rapidly solidified B2 nickel aluminides  
p 98 A89-43023
- TEM studies of oxidized NiAl and Ni3Al cross sections  
p 99 A89-46506
- Thermodynamic analysis of compatibility of several reinforcement materials with beta phase NiAl alloys  
[NASA-CR-4171] p 84 N89-10131
- Effect of grain size on the high temperature properties of B2 aluminides  
[NASA-TM-101382] p 101 N89-12720
- The effect of 0.1 atomic percent zirconium on the cyclic oxidation behavior of beta-NiAl for 300 hours at 1200 C  
[NASA-TM-101408] p 101 N89-13566
- Thermodynamic analysis of chemical compatibility of several reinforcement materials with niobium aluminides  
[NASA-CR-182260] p 86 N89-21036
- Theoretical analysis of compatibility of several reinforcement materials with NiAl and FeAl matrices  
[NASA-CR-182291] p 86 N89-23622
- Characterization of ceramics and intermetallics fabricated by self-propagating high-temperature synthesis  
[NASA-TM-102004] p 78 N89-25285
- ALUMINUM**
- Oxidation behavior of FeAl+Hf,Zr,B  
[NASA-TM-101402] p 102 N89-14297
- The oxidation of Ni-rich Ni-Al intermetallics  
[NASA-TM-101455] p 102 N89-15233
- Investigation of Weibull statistics in fracture analysis of cast aluminum  
[NASA-TM-102000] p 185 N89-21245
- ALUMINUM ALLOYS**
- Morphological study of near threshold fatigue crack growth in a coarse grain aluminum alloy  
p 94 A89-12326
- The effect of sulfur and zirconium co-doping on the oxidation of NiCrAl  
p 94 A89-13933
- Resolved shear stress intensity coefficient and fatigue crack growth in large crystals  
p 96 A89-22048
- Effect of 0.1 at. pct Zirconium on the cyclic oxidation resistance of beta-NiAl  
p 96 A89-24599
- Effect of the theta-alpha-Al2O3 transformation on the oxidation behavior of beta-NiAl + Zr  
p 98 A89-38600
- Predicting minimum Al concentrations for protective scale formation on Ni-base alloys. I - Isothermal oxidation.  
II - Cyclic oxidation  
p 98 A89-40116

- Room temperature tensile ductility in polycrystalline B2 Ni-30Al-20Fe  
p 98 A89-44568
- Thermodynamic analysis of compatibility of several reinforcement materials with FeAl alloys  
[NASA-CR-4172] p 83 N89-10128
- Influence of alloying elements on the oxidation behavior of NbAl3  
[NASA-TM-101398] p 100 N89-12717
- Thermodynamic analysis of chemical compatibility of several reinforcement materials with niobium aluminides  
[NASA-CR-182260] p 86 N89-21036
- ALUMINUM BORON COMPOSITES**
- Mechanisms of elevated-temperature deformation in the B2 aluminides NiAl and CoAl  
p 94 A89-17378
- ALUMINUM GALLIUM ARSENIDES**
- Design of a GaAlAs travelling wave Mach-Zehnder electro-optic modulator  
p 130 A89-10342
- Characterization of GaAlAs optical waveguide heterostructures grown by molecular beam epitaxy  
p 130 A89-10343
- Deep-level transient spectroscopy of Al(x)Ga(1-x)As/GaAs using nondestructive acousto-electric voltage measurement  
p 133 A89-42742
- Characterization of multilayer GaAs/AlGaAs transistor structures by variable angle spectroscopic ellipsometry  
p 133 A89-49998
- Microwave characteristics of interdigitated photoconductors on a HEMT structure  
[NASA-CR-182197] p 135 N89-12820
- ALUMINUM OXIDES**
- Crack growth resistance of textured alumina  
p 105 A89-26452
- Fracture toughness of polycrystalline ceramics in combined mode I and mode II loading  
p 105 A89-26457
- Effect of the theta-alpha-Al2O3 transformation on the oxidation behavior of beta-NiAl + Zr  
p 98 A89-38600
- Ultrasonic imaging of textured alumina  
[NASA-TM-101478] p 189 N89-28853
- ALUMINUM SILICATES**
- Phase transformations in xerogels of mullite composition  
[NASA-TM-101349] p 108 N89-11038
- AMBIENT TEMPERATURE**
- The Mars climate for a photovoltaic system operation [IAF PAPER ICOSP89-9-5] p 241 A89-46529
- The Mars climate for a photovoltaic system operation  
[NASA-TM-101994] p 136 N89-20385
- Compensation for effects of ambient temperature on rare-earth doped fiber optic thermometer  
[NASA-TM-102282] p 176 N89-27998
- AMMONIA**
- Preliminary design study of hydrogen and ammonia resistojets for prime and auxiliary thrusters  
[NASA-CR-182176] p 62 N89-10943
- AMPLITUDE MODULATION**
- Amplitude spectrum modulation technique for analog data processing in fiber optic sensing system with temporal separation of channels  
p 169 A89-10368
- ANALOG DATA**
- Amplitude spectrum modulation technique for analog data processing in fiber optic sensing system with temporal separation of channels  
p 169 A89-10368
- Coded multiple chirp spread spectrum system and overlay service  
p 124 A89-26769
- ANEMOMETERS**
- Calibration of single particle sizing velocimeters using photomask reticles  
p 170 A89-33379
- ANGLE OF ATTACK**
- Prediction of unsteady blade surface pressures on an advanced propeller at an angle of attack  
[AIAA PAPER 89-1060] p 227 A89-40473
- Low-speed wind tunnel performance of high-speed counterrotation propellers at angle-of-attack  
[AIAA PAPER 89-2583] p 8 A89-50808
- Low-speed wind tunnel performance of high-speed counterrotation propellers at angle-of-attack  
[NASA-TM-102292] p 15 N89-25121
- ANISOTROPIC MEDIA**
- Life prediction and constitutive models for engine hot section  
p 188 N89-12916
- ANISOTROPY**
- Deformation modeling and constitutive modeling for anisotropic superalloys  
[NASA-CR-4215] p 202 N89-21258
- ANNEALING**
- Interdiffusional effects between TiBe12 and NiAl intermetallics  
p 95 A89-21395
- Plasma deposited silicon nitride for indium phosphide encapsulation  
p 235 A89-27794
- The influence of annealing in the ferrite-plus-austenite phase field on the stability of vanadium carbide precipitates  
p 97 A89-32803



- Sequentially evaporated thin Y-Ba-Co-O  
superconducting films on microwave substrates  
[NASA-TM-102068] p 138 N89-23791
- ANNIHILATION REACTIONS**  
Antiproton powered propulsion with magnetically  
confined plasma engines  
[AIAA PAPER 89-2334] p 57 A89-46758  
Antiproton powered propulsion with magnetically  
confined plasma engines  
[NASA-CR-185131] p 74 N89-27700
- ANNULAR DUCTS**  
Annular honeycomb seals: Test results for leakage and  
rotordynamic coefficients; comparisons to labyrinth and  
smooth configurations p 185 N89-22899
- ANNULAR FLOW**  
Three component laser anemometer measurements in  
an annular cascade of core turbine vanes with contoured  
end wall  
[NASA-TP-2846] p 9 N89-10844  
LDV measurements in an annular combustor model  
[NASA-CR-182207] p 159 N89-13755  
Numerical studies of convective heat transfer in an  
inclined semiannular enclosure  
[NASA-TM-102011] p 123 N89-28666
- ANNULI**  
An entrance region friction factor model applied to  
annular seal analysis - Theory versus experiment for  
smooth and honeycomb seals  
[ASME PAPER 88-TRIB-41] p 179 A89-34798
- ANTARCTIC REGIONS**  
Data report for the Siple Coast (Antarctica) project  
[NASA-TM-100708] p 206 N89-10403
- ANTENNA ARRAYS**  
Optoelectronic signal processing for phased-array  
antennas; Proceedings of the Meeting, Los Angeles, CA,  
Jan. 12, 13, 1988  
[SPIE-886] p 124 A89-15819  
GaAs MMIC elements in phased-array antennas  
p 131 A89-15827  
An experimental adaptive array to suppress weak  
interfering signals p 124 A89-22455  
Mutual coupling in a finite planar array with interelement  
holes present p 125 A89-42768  
Aperture impedance of flared horns  
p 125 A89-43543  
Compensation of reflector antenna surface distortion  
using an array feed p 126 A89-53136  
Adaptive feed array compensation system for reflector  
antenna surface distortion p 127 N89-17756  
Analysis of modified SMI method for adaptive array  
weight control p 127 N89-20364  
Analysis of modified SMI method for adaptive array  
weight control p 19 N89-25993  
Adaptive array for weak interfering signals:  
Geostationary satellite experiments  
[NASA-CR-185450] p 129 N89-26126
- ANTENNA DESIGN**  
Mechanical properties characterization of composite  
sandwich materials intended for space antenna  
applications p 81 A89-32885  
Optically interconnected phased arrays  
p 132 A89-33696  
A comparison of reflector antenna designs for  
wide-angle scanning  
[NASA-TM-101459] p 127 N89-21138
- ANTENNA FEEDS**  
An experimental adaptive array to suppress weak  
interfering signals p 124 A89-22455  
Compensation of reflector antenna surface distortion  
using an array feed p 126 A89-53136  
Adaptive feed array compensation system for reflector  
antenna surface distortion p 127 N89-17756  
[NASA-TM-101458] p 127 N89-21138  
A comparison of reflector antenna designs for  
wide-angle scanning  
[NASA-TM-101459] p 127 N89-21138  
Computed performance of the half-scale accurate  
antenna reflector  
[NASA-CR-182284] p 139 N89-24532
- ANTENNA RADIATION PATTERNS**  
A method for producing a shaped contour radiation  
pattern using a single shaped reflector and a single feed  
p 125 A89-42758  
A method for producing a shaped contour radiation  
pattern using a single shaped reflector and a single feed  
[NASA-TM-101369] p 126 N89-10215  
Analysis of modified SMI method for adaptive array  
weight control p 127 N89-20364  
[NASA-CR-184904] p 127 N89-20364
- ANTENNAS**  
Optically controlled phased-array technology for space  
communication systems p 131 A89-15845
- Optically interconnected phased arrays  
p 132 A89-33696
- ANTHRACENE**  
Addition polymers from  
1,4,5,8-tetrahydro-1,4,5,8-diepoxyanthracene and  
Bis-dienes. 2: Evidence for thermal dehydration occurring  
in the cure process  
[NASA-TM-101385] p 112 N89-15235
- ANTIFRICTION BEARINGS**  
Selection of rolling-element bearing steels for long-life  
applications p 180 A89-47250
- ANTIMATTER**  
Antiproton powered propulsion with magnetically  
confined plasma engines  
[AIAA PAPER 89-2334] p 57 A89-46758
- ANTIPROTONS**  
Antiproton powered propulsion with magnetically  
confined plasma engines  
[AIAA PAPER 89-2334] p 57 A89-46758  
Antiproton powered propulsion with magnetically  
confined plasma engines  
[NASA-CR-185131] p 74 N89-27700
- ANTIREFLECTION COATINGS**  
Metal-silicon reaction rates - The effects of capping  
p 93 A89-52202  
The GaAs solar cells with V-grooved emitters  
[NASA-TM-102104] p 214 N89-26291
- APERTURES**  
Aperture impedance of flared horns  
p 125 A89-43543
- APPLICATIONS PROGRAMS (COMPUTERS)**  
Fatigue crack growth model RANDOM2 user manual,  
appendix 1 p 203 N89-23890  
[NASA-CR-184939] p 203 N89-23890  
Fatigue strength reduction model: RANDOM3 and  
RANDOM4 user manual, appendix 2 p 203 N89-23891  
[NASA-CR-184940] p 203 N89-23891  
Flight experiment of thermal energy storage  
[NASA-TM-102081] p 69 N89-24440  
A data acquisition and control program for axial-torsional  
fatigue testing  
[NASA-TM-102041] p 205 N89-28029
- APPROACH**  
Noise of a model counterrotation propeller with  
simulated fuselage and support pylon at takeoff/approach  
conditions p 227 A89-48953  
[AIAA PAPER 89-1143] p 227 A89-48953  
Noise of a model counterrotation propeller with  
simulated fuselage and support pylon at takeoff/approach  
conditions p 228 N89-24138  
[NASA-TM-101996] p 228 N89-24138
- APPROXIMATION**  
An application of the WKB technique to the on-surface  
radiation condition p 124 A89-21222  
Absorbing boundary conditions for second-order  
hyperbolic equations  
[NASA-TM-102009] p 223 N89-22397
- ARC DISCHARGES**  
Arc restrike in the rail accelerator p 39 A89-32065  
Performance of a 100 kW class applied field MPD  
thruster  
[NASA-TM-102312] p 74 N89-27701
- ARC GENERATORS**  
Arc-driven rail accelerator research  
[NASA-CR-179584] p 40 N89-13445
- ARC JET ENGINES**  
Performance and lifetime assessment of MPD arc  
thruster technology  
[AIAA PAPER 88-3211] p 53 A89-16485  
Langmuir probe measurements of an arcjet exhaust  
p 55 A89-39031  
A detailed model of electrothermal propulsion systems  
[AIAA PAPER 89-2262] p 56 A89-46707  
Performance of a 100 kW class applied field MPD  
thruster  
[AIAA PAPER 89-2710] p 57 A89-47035  
The effect of electrode configuration on arcjet  
performance p 58 A89-47044  
[AIAA PAPER 89-2722] p 58 A89-47044  
5-kW arcjet power electronics p 60 A89-49685  
[AIAA PAPER 89-2725] p 60 A89-49685  
The effects of arcjet thruster operating condition  
constrictor geometry on the plasma plume  
[AIAA PAPER 89-2723] p 60 A89-50809  
Test facility and preliminary performance of a 100 kW  
class MPD thruster  
[NASA-TM-102021] p 68 N89-23520  
Arcjet nozzle design impacts  
[NASA-TM-102050] p 68 N89-23522  
The 5-kW arcjet power electronics  
[NASA-TM-102108] p 70 N89-24446  
The effects of arcjet operating condition and constrictor  
geometry on the plasma plume  
[NASA-TM-102284] p 72 N89-25281
- Electric propulsion options for 10 kW class earth space  
missions  
[NASA-TM-102337] p 74 N89-26906  
Arcjet cathode phenomena  
[NASA-TM-102099] p 167 N89-27121  
Experiments and analysis of a compact electrothermal  
thruster p 75 N89-27773
- ARCHES**  
Nonisothermal elastoviscoplastic snap-through and  
creep buckling of shallow arches p 194 A89-47370
- ARCHITECTURE (COMPUTERS)**  
Hierarchical Poly Tree computer architectures defined  
by computational multidisciplinary mechanics  
p 218 A89-50100  
Initial operating capability for the hypercluster  
parallel-processing test bed  
[NASA-TM-101953] p 218 N89-20685
- ARGON PLASMA**  
Performance of a 100 kW class applied field MPD  
thruster  
[NASA-TM-102312] p 74 N89-27701
- ARIANE LAUNCH VEHICLE**  
Expandable launch vehicle transportation for the space  
station  
[NASA-TM-101947] p 42 N89-20179
- ARRAYS**  
Common source-multiple load vs. separate  
source-individual load photovoltaic system  
[NASA-TM-101465] p 136 N89-15338
- ARTIFICIAL INTELLIGENCE**  
The development of an intelligent interface to a  
computational fluid dynamics flow-solver code  
p 216 A89-16963  
User needs, benefits and integration of robotic systems  
in a space station laboratory  
[NASA-CR-182261] p 185 N89-22108
- ARTIFICIAL SATELLITES**  
COLD-SAT: Cryogenic On-Orbit Liquid Depot-Storage,  
Acquisition and Transfer  
[NASA-TM-102308] p 38 N89-28535
- ASHES**  
Optical methods and results of dew point and deposition  
rate measurements in salt/ash-containing combustion  
gases - B2O3(l) deposition rates by interference methods  
and comparisons with theory p 89 A89-12334
- ASTRONAUTICS**  
Vision sensing techniques in aeronautics and  
astronautics p 219 A89-31087
- ASTRONOMICAL MODELS**  
The large-scale microwave background anisotropy in  
decaying particle cosmology p 240 A89-15426  
A coasting cosmology p 241 A89-53833
- ASTRONOMICAL OBSERVATORIES**  
Comparison of solar photovoltaic and nuclear reactor  
power systems for a human-tended lunar observatory  
[NASA-TM-102015] p 242 N89-23397
- ASTROPHYSICS**  
A coasting cosmology p 241 A89-53833
- ASYMPTOTIC METHODS**  
A hybrid asymptotic-modal analysis of the EM scattering  
by an open-ended S-shaped rectangular waveguide  
cavity  
[NASA-CR-185053] p 129 N89-24519
- ASYMPTOTIC PROPERTIES**  
Asymptotic structure and similarity solutions for  
three-dimensional turbulent boundary layers  
[AIAA PAPER 89-1863] p 150 A89-42090
- ASYMPTOTIC SERIES**  
Far field expansion for anisotropic wave equations  
[NASA-TM-102112] p 165 N89-26175
- ATLAS LAUNCH VEHICLES**  
COLD-SAT orbital experiment configured for Atlas  
launch p 45 A89-53327
- ATMOSPHERIC PRESSURE**  
On the orthorhombic phase in ZrO<sub>2</sub>-based alloys  
p 105 A89-30631
- ATOMIC STRUCTURE**  
Electronic structure of BaO/W cathode surfaces  
p 132 A89-26862
- ATOMIZING**  
Gas density effect on droplet size of simulated fuel  
sprays  
[AIAA PAPER 89-2322] p 151 A89-46749  
Application of advanced diagnostics to airblast injector  
flows p 160 N89-17306  
Gas density effect on droplet size of simulated fuel  
sprays  
[NASA-TM-102013] p 162 N89-22053
- AUGMENTATION**  
Turbofan forced mixer lobe flow modeling. Part 3:  
Application to augment engines  
[NASA-CR-4147-Pt-3] p 8 N89-10025
- AUSTENITIC STAINLESS STEELS**  
High-temperature LCF of Ni-201 and 304L stainless  
steel p 100 N89-12635

**AUTOCLAVES**

700 F Properties of autoclave cured PMR-II composites p 81 A89-29998

**AUTOMATIC CONTROL**

Automated design of controlled-diffusion blades [ASME PAPER 88-GT-139] p 2 A89-15967  
Automation software for a materials testing laboratory p 217 N89-12917  
Automated data acquisition and processing for a Hohraum reflectometer [NASA-TM-101393] p 173 N89-14416  
Automating the multiprocessing environment [NASA-TM-4103] p 217 N89-20641

**AUTOMOBILE ENGINES**

Mod II Stirling engine overviews [SAE PAPER 880539] p 177 A89-12301

**AUXILIARY POWER SOURCES**

Materials technology assessment for a 1050 K Stirling space engine design [NASA-TM-101342] p 77 N89-11815

**AUXILIARY PROPULSION**

Performance characterizations of an engineering model multipropellant resistojet p 54 A89-28340  
Successful completion of a cyclic ground test of a mercury ion Auxiliary Propulsion System p 59 A89-47450  
A data acquisition and storage system for the ion auxiliary propulsion system cyclic thruster test [NASA-TM-101469] p 218 N89-17424  
Advanced APS impacts on vehicle payloads [NASA-TM-102086] p 41 N89-25254

**AVALANCHE DIODES**

Microwave and millimeter-wave power generation in silicon carbide (SiC) IMPATT devices [NASA-CR-185050] p 139 N89-26143

**AVIATION METEOROLOGY**

An overview of the current NASA program on aircraft icing research [SAE PAPER 881386] p 16 A89-28192  
On ice shape prediction methodologies and comparison with experimental data [AIAA PAPER 89-0732] p 16 A89-30650  
The influence of ice accretion physics on the forecasting of aircraft icing conditions p 16 A89-54803

**AXIAL FLOW**

Experimental investigation of propfan aeroelastic response in off-axis flow with mistuning [AIAA PAPER 88-3153] p 20 A89-17941  
Experimental investigation of the performance of a supersonic compressor cascade [NASA-TM-100879] p 9 N89-10858

**AXIAL FLOW TURBINES**

Heat transfer in the tip region of a rotor blade simulator p 161 N89-17312

**AXIAL LOADS**

Thermomechanical characterization of Hastelloy-X under uniaxial cyclic loading p 196 N89-12909  
A NASTRAN DMAP alter for linear buckling analysis under dynamic loading p 85 N89-13522  
A NASTRAN DMAP alter for linear buckling analysis under dynamic loading p 202 N89-22948

**AXIAL STRAIN**

A data acquisition and control program for axial-torsional fatigue testing [NASA-TM-102041] p 205 N89-28029

**AXIAL STRESS**

Weibull crack density coefficient for polydimensional stress states p 193 A89-34849  
Biaxial thermo-mechanical fatigue p 194 A89-43527  
High pressure multiaxial extensometry p 170 A89-43532  
Creep fatigue life prediction for engine hot section materials (isotropic): Fourth year progress review p 188 N89-12914  
Results of inphase axial-torsional fatigue experiments on 304 stainless steel [NASA-TM-101464] p 201 N89-20514

**AXISYMMETRIC FLOW**

Effects of excitation level on the stability of an axisymmetric mixing layer p 2 A89-16882  
Subharmonic and fundamental high amplitude excitation of an axisymmetric jet [AIAA PAPER 89-0993] p 149 A89-37825  
Numerical studies of the effects of jet-induced mixing on liquid-vapor interface condensation [AIAA PAPER 89-1744] p 152 A89-48958  
Comparison of 3D computation and experiment for non-axisymmetric nozzles [NASA-CR-182245] p 14 N89-20921  
Numerical studies of the effects of jet-induced mixing on liquid-vapor interface condensation [NASA-CR-182285] p 163 N89-23818

**B**

**BACKGROUND RADIATION**

Is the great attractor really a great wall? --- late-time cosmological phase transition producing coherent velocity caused by relic domain wall repulsive effect p 241 A89-36278

**BACKSCATTERING**

Calculation of the effects of ice on the backscatter of a ground plane [NASA-CR-183303] p 126 N89-10213  
A hybrid asymptotic-modal analysis of the EM scattering by an open-ended S-shaped rectangular waveguide cavity [NASA-CR-185053] p 129 N89-24519

**BACKWARD WAVES**

Study of optical output couplers for submillimeter wavelength backward-wave oscillators (BWO's) p 132 A89-32857  
Study of optical output couplers for submillimeter wavelength backward-wave oscillators (BWO's) [NASA-TM-101360] p 134 N89-11128

**BALANCING**

High speed balancing applied to the T700 engine [NASA-CR-180899] p 184 N89-20472

**BAND STRUCTURE OF SOLIDS**

Universal features of the equation of state of solids p 237 A89-48960

**BARIUM FLUORIDES**

Crystallization of BaF<sub>2</sub>-ZnF<sub>2</sub>-YbF<sub>3</sub>-ThF<sub>4</sub> glass p 230 A89-12236

**BARIUM OXIDES**

Improved synthesis of ceramic superconductors with alkaline earth peroxides - Synthesis and processing of Ba<sub>2</sub>YCuo<sub>3</sub>O(7-x) p 235 A89-22887  
Electronic structure of BaO/W cathode surfaces p 132 A89-26862  
Non-uniform transition conductivity of superconducting ceramic [NASA-TM-102133] p 189 N89-28851

**BARRIER LAYERS**

Thermal Barrier Coatings. Abstracts and figures [NASA-CP-10019] p 110 N89-13642  
The effect of oxidation on the high heat flux behavior of a thermal barrier coating p 110 N89-13646

**BEAM INJECTION**

Electron velocity distributions and plasma waves associated with the injection of an electron beam into the ionosphere p 215 A89-43698

**BEAM WAVEGUIDES**

A segmented mirror antenna for radiometers [NASA-TM-102045] p 128 N89-23753

**BEAMS (RADIATION)**

Analysis of the EM scattering from arbitrary open-ended waveguide cavities using axial Gaussian Beam tracking [NASA-CR-185054] p 128 N89-24518

**BEAMS (SUPPORTS)**

Multi-grid for structures analysis p 206 N89-29810

**BEARING ALLOYS**

Selection of rolling-element bearing steels for long-life applications p 180 A89-47250

**BEARINGS**

Transmission errors and bearing contact of spur, helical and spiral bevel gears [SAE PAPER 881294] p 179 A89-21000  
Some composite bearing and seal materials for gas turbine applications: A review [NASA-TM-101451] p 111 N89-14338  
Tooth contact shift in loaded spiral bevel gears o, IL, 25-27 Apr. 1989; sponsored by ASME [NASA-TM-101438] p 183 N89-14453  
Rotordynamic Instability Problems in High-Performance Turbomachinery, 1988 [NASA-CP-3026] p 185 N89-22891  
Solid lubricant materials for high temperatures: A review p 203 N89-24636  
OTVE turbopump condition monitoring, task E.5 [NASA-CR-182274] p 189 N89-27204

**BIBLIOGRAPHIES**

Bibliography of Lewis Research Center technical publications announced in 1986 [NASA-TM-89887] p 238 N89-18259

**BIDIRECTIONAL REFLECTANCE**

Comparison of the bidirectional reflectance distribution function of various surfaces p 230 A89-41530

**BINARY ALLOYS**

Heat of mixing and morphological stability p 143 A89-21296  
Enthalpies of a binary alloy during solidification p 96 A89-22559  
Dendritic solidification in binary alloys p 96 A89-22560  
Thermosolutal convection during dendritic solidification [AIAA PAPER 89-0626] p 118 A89-25495  
Elevated temperature strain gages p 173 N89-12886

Isothermal solidification in a binary alloy melt p 121 N89-20300

**BINDING**

Thermal-mechanical fatigue test apparatus for metal matrix composites and joint attachments p 79 A89-15727

**BIPOLARITY**

Small scale bipolar nickel-hydrogen testing p 208 A89-44005

**BIT ERROR RATE**

Coded multiple chirp spread spectrum system and overlay service p 124 A89-26769  
Advanced modulation technology development for earth station demodulator applications [NASA-CR-185126] p 43 N89-26880  
Digitally modulated bit error rate measurement system for microwave component evaluation [NASA-TP-2912] p 40 N89-28545

**BLADE SLAP NOISE**

Near-field acoustic characteristics of a single-rotor propfan [AIAA PAPER 89-1055] p 23 A89-36215

**BLADE TIPS**

Recent advances in capacitance type of blade tip clearance measurements [AIAA PAPER 88-4664] p 20 A89-13725  
Heat transfer in the tip region of a rotor blade simulator p 157 N89-12898  
Heat transfer in the tip region of a rotor blade simulator p 161 N89-17312

**BLASIUS FLOW**

The upper-branch stability of compressible boundary layer flows [NASA-TM-102128] p 167 N89-28748

**BLUFF BODIES**

Windward fraction of the total mass or heat transport for flow past a circular cylinder p 141 A89-12339  
Heat transfer with very high free-stream turbulence and heat transfer with streamwise vortices p 160 N89-17309

**BLUNT BODIES**

Interaction of an oblique shock wave with turbulent hypersonic blunt body flows [AIAA PAPER 89-0272] p 3 A89-28405

**BODY-WING AND TAIL CONFIGURATIONS**

Multiple Application Propfan Study (MAPS): Advanced tactical transport [NASA-CR-175003] p 28 N89-19300

**BOILING**

Dynamics of face and annular seals with two-phase flow [NASA-CR-183352] p 182 N89-12870

**BONDING**

Interfacial adhesion - Theory and experiment p 97 A89-35307  
Finite element applications to explore the effects of partial bonding on metal matrix composite properties [NASA-TM-101482] p 86 N89-20206

**BOOMS (EQUIPMENT)**

Comparative thermal analysis of the space station Freedom photovoltaic deployable boom structure using TRASYS, NEVADA, and SINDA programs [NASA-TM-102062] p 165 N89-26177

**BORON**

Oxidation behavior of FeAl + Hf, Zr, B [NASA-TM-101402] p 102 N89-14297

**BORON CARBIDES**

Fluid flow phenomena in the generation of boron carbide suspensions in magnesium melts p 79 A89-19472  
Hot isostatic pressing of silicon nitride with boron nitride, boron carbide, and carbon additions p 107 A89-41744

**BORON NITRIDES**

Hot isostatic pressing of silicon nitride with boron nitride, boron carbide, and carbon additions p 107 A89-41744

**BORON OXIDES**

Optical methods and results of dew point and deposition rate measurements in salt/ash-containing combustion gases - B2O3(l) deposition rates by interference methods and comparisons with theory p 89 A89-12334

**BOUNDARY ELEMENT METHOD**

Advanced development of the boundary element method for steady-state heat conduction p 154 A89-54766

Development of BEM for ceramic composites [NASA-CR-183313] p 111 N89-14311  
Development of an integrated BEM approach for hot fluid structure interaction [NASA-CR-184587] p 27 N89-15114  
Three-dimensional inelastic analysis for hot section components, BEST 3D code p 199 N89-17317

**BOUNDARY LAYER EQUATIONS**

Prediction of unsteady rotor-surface heat transfer from wake passages [AIAA PAPER 89-1692] p 150 A89-43210

On the Lagrangian description of unsteady boundary layer separation. Part 2: The spinning sphere [NASA-TM-102027] p 163 N89-22861

On the Lagrangian description of unsteady boundary layer separation. Part 1: General theory [NASA-TM-102026] p 164 N89-23821

**BOUNDARY LAYER FLOW**

Boundary layer effects on particle impaction and capture p 143 A89-19123

Preliminary study of the interactions caused by crossing shock waves and a turbulent boundary layer [AIAA PAPER 89-0359] p 145 A89-25303

Correlations of velocity and temperature fluctuations in the stagnation-point flow of circular cylinder in turbulent flow p 148 A89-34927

Influence of bulk turbulence and entrance boundary layer thickness on the curved duct flow field p 156 N89-12896

Turbine airfoil film cooling p 158 N89-12903

Analysis of supersonic plug nozzle flowfield and heat transfer [NASA-CR-179554] p 10 N89-13397

A low-Reynolds-number two-equation turbulence model for predicting heat transfer on turbine blades p 160 N89-17310

On the Lagrangian description of unsteady boundary layer separation. Part 1: General theory [NASA-TM-102026] p 164 N89-23821

Interaction between Tollmien-Schlichting waves and free-stream disturbances in boundary-layer flows [NASA-CR-185847] p 167 N89-27118

The upper-branch stability of compressible boundary layer flows [NASA-TM-102128] p 167 N89-28748

Numerical investigation of an internal layer in turbulent flow over a curved hill [NASA-TM-102230] p 168 N89-29725

**BOUNDARY LAYER SEPARATION**

Investigation of the flow between a pair of circular cylinders in the flopping regime p 144 A89-22822

Three-dimensional marginal separation [NASA-TM-101411] p 159 N89-13757

An LDA (Laser-Doppler Anemometry) investigation of three-dimensional normal shock wave boundary-layer interactions p 14 N89-20956

Interaction between Tollmien-Schlichting waves and free-stream disturbances in boundary-layer flows [NASA-CR-185847] p 167 N89-27118

**BOUNDARY LAYER STABILITY**

Boundary-layer receptivity to long-wave free-stream disturbances p 146 A89-28996

**BOUNDARY LAYER TRANSITION**

Development of a special-purpose test surface guided by uncertainty analysis p 144 A89-22736

Studies of transition in boundary layers [AIAA PAPER 89-0034] p 2 A89-25029

Development of low Reynolds number two equation turbulence models for predicting external heat transfer on turbine blades p 157 N89-12901

CFD validation experiments for internal flows p 161 N89-18635

Some characteristics of bypass transition in a heated boundary layer [NASA-TM-102126] p 164 N89-24577

**BOUNDARY LAYERS**

Direct numerical simulations of a temporally evolving mixing layer subject to forcing p 147 A89-34426

Development of a thermal and structural analysis procedure for cooled radial turbines [NASA-TM-101416] p 24 N89-12568

Heat transfer with very high free-stream turbulence and heat transfer with streamwise vortices p 160 N89-17309

On the Lagrangian description of unsteady boundary layer separation. Part 2: The spinning sphere [NASA-TM-102027] p 163 N89-22861

**BOUNDARY LUBRICATION**

Tribology: The Story of Lubrication and Wear [NASA-TM-101430] p 203 N89-24635

**BOUNDARY VALUE PROBLEMS**

Accurate boundary conditions for exterior problems in gas dynamics p 143 A89-20223

Numerical analysis of flow through oscillating cascade sections [AIAA PAPER 89-0437] p 4 A89-28413

Effects of nozzle exit boundary-layer conditions on excitability of heated free jets p 149 A89-36908

Conservative treatment of boundary interfaces for overlaid grids and multi-level grid adaptations [AIAA PAPER 89-1980] p 5 A89-41823

Numerical solution of periodic vortical flows about a thin airfoil [AIAA PAPER 89-1691] p 7 A89-48955

Numerical analysis of flow through oscillating cascade sections [NASA-TM-101417] p 11 N89-14220

Absorbing boundary conditions for second-order hyperbolic equations [NASA-TM-102009] p 223 N89-22397

On the Lagrangian description of unsteady boundary layer separation. Part 2: The spinning sphere [NASA-TM-102027] p 163 N89-22861

Numerical solution of periodic vortical flows about a thin airfoil [NASA-TM-101998] p 14 N89-23413

On the applications of algebraic grid generation methods based on transfinite interpolation [NASA-TM-102095] p 33 N89-26003

Far field expansion for anisotropic wave equations [NASA-TM-102112] p 165 N89-26175

Theoretical studies in support of the 3M-vapor transport (PVTOS-) experiments [NASA-CR-185122] p 165 N89-26179

**BOW WAVES**

Compressibility and shock wave interaction effects on free shear layers [AIAA PAPER 89-2460] p 7 A89-46847

**BOX BEAMS**

Design procedures for fiber composite box beams p 195 A89-48674

**BRAYTON CYCLE**

Solar dynamic heat rejection technology. Task 1: System concept development [NASA-CR-179618] p 158 N89-13731

Megawatt Class Nuclear Space Power Systems (MCNSPS) conceptual design and evaluation report. Volume 4: Concepts selection, conceptual designs, recommendations [NASA-CR-179614-VOL-4] p 210 N89-18967

Megawatt Class Nuclear Space Power Systems (MCNSPS) conceptual design and evaluation report. Volume 3, technologies 2: Power conversion [NASA-CR-179614-VOL-3] p 211 N89-22980

Solar dynamic power module design [NASA-TM-102055] p 70 N89-25269

Performance estimates for the Space Station power system Brayton Cycle compressor and turbine [NASA-CR-182263] p 73 N89-26903

Thermal evaluation of advanced solar dynamic heat receiver performance [NASA-CR-185117] p 214 N89-27256

**BRAZING**

Design, fabrication, and performance of brazed, graphite electrode, multistage depressed collectors with 500-W, continuous wave, 4.8- to 9.6-GHz traveling-wave tubes [NASA-TP-2904] p 136 N89-21171

**BREADBOARD MODELS**

dc power control for a liquid-fed resistojet p 59 A89-47457

5-kW arcjet power electronics [AIAA PAPER 89-2725] p 60 A89-49685

The 5-kW arcjet power electronics [NASA-TM-102108] p 70 N89-24446

Development and testing of a 20-kHz component test bed [NASA-TM-102141] p 139 N89-25403

**BRIDGMAN METHOD**

Effects of furnace temperature profile on the interface shape during Bridgman crystal growth p 119 A89-53278

**BRITTLE MATERIALS**

A probabilistic formulation for fracture energy of continuous fibre-matrix composites p 83 A89-39996

Reliability-based failure analysis of brittle materials [NASA-CR-184799] p 189 N89-20489

**BROADBAND**

Optoelectronic techniques for broadband switching p 131 A89-15825

**BROADCASTING**

Digital CODEC for real-time processing of broadcast quality video signals at 1.8 bits/pixel [NASA-TM-102325] p 129 N89-27927

**BROMIDES**

Hydrogen-bromine fuel cell advance component development [NASA-TM-101345] p 208 N89-10405

**BROMINE**

Hydrogen-bromine fuel cell advance component development [NASA-TM-101345] p 208 N89-10405

**BUBBLES**

Unsteady thermocapillary migration of bubbles [NASA-TM-101338] p 162 N89-22054

**BUCKLING**

Dynamic delamination buckling in composite laminates under impact loading - Computational simulation p 82 A89-36310

A NASTRAN DMAP alter for linear buckling analysis under dynamic loading [NASA-TM-100832] p 85 N89-13522

A NASTRAN DMAP alter for linear buckling analysis under dynamic loading p 202 N89-22948

**BUOYANCY**

Combined roles of buoyancy and orientation in nucleate pool boiling p 119 A89-35015

A comparative study of the influence of buoyancy driven fluid flow on GaAs crystal growth p 121 N89-20295

**BURGER EQUATION**

Nonoscillatory solution of the steady-state inviscid Burgers' equation by mathematical programming p 221 A89-22756

Calculation of shocked flows by mathematical programming p 150 A89-45397

**BURNERS**

Determination of convective diffusion heat/mass transfer rates to burner rig test targets comparable in size to cross-stream jet diameter p 141 A89-12753

**BUTT JOINTS**

Simplified procedures for designing adhesively bonded composite joints [NASA-TM-102120] p 87 N89-26048

**BUTTERFLY VALVES**

Noise generated by a flight weight, air flow control valve in a vertical takeoff and landing aircraft thrust vectoring system [NASA-CR-182232] p 228 N89-20776

**BYPASS RATIO**

Some characteristics of bypass transition in a heated boundary layer [NASA-TM-102126] p 164 N89-24577

**C**

**CALIBRATING**

Calibration of single particle sizing velocimeters using photomask reticles p 170 A89-33379

Universal test fixture for monolithic mm-wave integrated circuits calibrated with an augmented TRD algorithm [NASA-TP-2875] p 127 N89-17767

**CALORIMETERS**

High-pressure calorimeter chamber tests for liquid oxygen/kerosene (LOX/RP-1) rocket combustion [NASA-TP-2862] p 65 N89-15979

**CAMBER**

Influence of thickness and camber on the aeroelastic stability of supersonic throughflow fans: An engineering approach [NASA-TM-101949] p 15 N89-25957

**CANS**

Modeling cyclic melting and refreezing in a hollow metal canister [NASA-CR-184630] p 217 N89-15623

**CANTILEVER BEAMS**

Solution methods for one-dimensional viscoelastic problems p 191 A89-19914

Design procedures for fiber composite box beams p 195 A89-48674

**CAPACITANCE**

Recent advances in capacitance type of blade tip clearance measurements [AIAA PAPER 88-4664] p 20 A89-13725

Nickel-hydrogen capacity loss on storage p 138 N89-23007

**CAPACITORS**

The application of high temperature superconductors to space electrical power distribution components p 50 A89-15287

**CAPILLARY FLOW**

Thermocapillary migration of a large gas slug in a tube p 117 A89-22747

Hardware development for the Surface Tension Driven Convection Experiment aboard the USML-1 Spacelab mission [AIAA PAPER 89-0406] p 47 A89-25341

Hardware development for the surface tension driven convection experiment aboard the USML-1 spacelab mission [NASA-TM-101404] p 48 N89-11804

Infrared surface temperature measurements for the surface tension driven convection experiment [NASA-TM-101353] p 175 N89-21224

Unsteady thermocapillary migration of bubbles [NASA-TM-101338] p 162 N89-22054

**CARBON**

Thin-film hermeticity - A quantitative analysis of diamondlike carbon using variable angle spectroscopic ellipsometry p 234 A89-13945

High-temperature LDV seed particle development [NASA-CR-182265] p 175 N89-23851

Diamondlike carbon protective coatings for optical windows [NASA-TM-102111] p 231 N89-27506

Ion beam and plasma methods of producing diamondlike carbon films [NASA-TM-102301] p 116 N89-27836

## CARBON DIOXIDE LASERS

- A vector scanning processing technique for pulsed laser velocimetry  
[NASA-TM-102048] p 175 N89-23850  
High-temperature LDV seed particle development  
[NASA-CR-182265] p 175 N89-23851

## CARBON FIBER REINFORCED PLASTICS

- Thermo-oxidative stability studies of Celion 6000/PMR-15 unidirectional composites, PMR-15, and Celion 6000 fiber p 79 A89-14099  
Synthesis and stability of Br<sub>2</sub>, ICl and IBr intercalated pitch-based graphite fibers p 106 A89-37670  
Graphite/polyimide composites with improved toughness p 83 A89-38637  
The role of rapid solidification processing in the fabrication of fiber reinforced metal matrix composites [NASA-TM-101450] p 85 N89-15201

## CARBONATES

- Improved synthesis of ceramic superconductors with alkaline earth peroxides - Synthesis and processing of Ba<sub>2</sub>YCu<sub>3</sub>O(7-x) p 235 A89-22887

## CARGO

- Space propulsion technology and cryogenic fluid depot p 38 N89-11768

## CARRIER INJECTION

- Computer analysis of the negative differential resistance switching phenomenon of double-injection devices p 134 A89-54963

## CARRIER MOBILITY

- Surface morphologies and electrical properties of molecular beam epitaxial InSb and InAs(x)Sb(1-x) grown on GaAs and InP substrates [NASA-CR-185439] p 237 N89-26740

## CASCADE FLOW

- Investigation of oscillating cascade aerodynamics by an experimental influence coefficient technique [AIAA PAPER 88-2815] p 1 A89-14976  
LU implicit multigrid algorithm for the three-dimensional Euler equations p 143 A89-19906  
A simple time-accurate turbomachinery algorithm with numerical solutions of an uneven blade count configuration [AIAA PAPER 89-0206] p 179 A89-25181  
Experimental investigation of transonic oscillating cascade aerodynamics [AIAA PAPER 89-0321] p 3 A89-28369  
Unsteady Euler cascade analysis [AIAA PAPER 89-0322] p 3 A89-28406  
Numerical analysis of flow through oscillating cascade sections [AIAA PAPER 89-0437] p 4 A89-28413  
Application of a full-potential solver to bending-torsion flutter in cascades [AIAA PAPER 89-1386] p 34 A89-30859  
Calculation of unsteady flows in turbomachinery using the linearized Euler equations p 149 A89-36916  
Numerical analysis of supersonic flow through oscillating cascade sections by using a deforming grid [AIAA PAPER 89-2805] p 8 A89-50810  
Three component laser anemometer measurements in an annular cascade of core turbine vanes with contoured end wall [NASA-TP-2846] p 9 N89-10844  
Experimental investigation of the performance of a supersonic compressor cascade [NASA-TM-100879] p 9 N89-10858  
Simulation of 2-dimensional viscous flow through cascades using a semi-elliptic analysis and hybrid C-H grids [NASA-CR-4180] p 10 N89-12553  
Numerical analysis of flow through oscillating cascade sections [NASA-TM-101417] p 11 N89-14220  
Experimental investigation of transonic oscillating cascade aerodynamics [NASA-TM-101993] p 29 N89-20133  
Transonic viscous flow calculations for a turbine cascade with a two equation turbulence model [NASA-TM-101944] p 32 N89-22607  
Numerical analysis of supersonic flow through oscillating cascade sections by using a deforming grid [NASA-TM-102053] p 15 N89-25119  
Influence of thickness and camber on the aeroelastic stability of supersonic throughflow fans: An engineering approach [NASA-TM-101949] p 15 N89-25957
- CAST ALLOYS**  
The influence of high thermal gradient casting, hot isostatic pressing and alternate heat treatment on the structure and properties of a single crystal nickel base superalloy p 97 A89-36427
- CASTING**  
Castable hot corrosion resistant alloy [NASA-CASE-LEW-14134-2] p 102 N89-14303  
Advanced single crystal for SSME turbopumps [NASA-CR-182244] p 103 N89-21072

- Investigation of Weibull statistics in fracture analysis of cast aluminum [NASA-TM-102000] p 185 N89-21245

## CATALYSTS

- Alkaline fuel cell performance investigation p 207 A89-15258  
A premixed hydrogen/oxygen catalytic igniter [AIAA PAPER 89-2302] p 59 A89-49683  
A premixed hydrogen/oxygen catalytic igniter [NASA-CR-185113] p 70 N89-24445

## CATALYTIC ACTIVITY

- Fuel-rich catalytic combustion of Jet-A fuel-equivalence ratios 5.0 to 8.0 [NASA-TM-101975] p 93 N89-21051

## CATHODES

- Alkaline fuel cell performance investigation p 207 A89-15258  
Oxygen electrodes for rechargeable alkaline fuel cells p 211 N89-22998  
Arcjet cathode phenomena [NASA-TM-102099] p 167 N89-27121

## CATIONS

- Influence of several metal ions on the gelation activation energy of silicon tetraethoxide [NASA-TM-101380] p 114 N89-21894

## CAVITATION CORROSION

- Deformation and fracture of single-crystal and sintered polycrystalline silicon carbide produced by cavitation p 108 A89-54985

## CAVITATION FLOW

- Thermocapillary migration of a large gas slug in a tube p 117 A89-22747  
Control-volume based Navier-Stokes equation solver valid at all flow velocities [NASA-TM-101488] p 161 N89-20407

## CAVITIES

- Heat transfer in the tip region of a rotor blade simulator p 161 N89-17312  
Analysis of the EM scattering from arbitrary open-ended waveguide cavities using axial Gaussian Beam tracking [NASA-CR-185054] p 128 N89-24518  
Liquid droplet generation [NASA-CR-182246] p 166 N89-26182

## CAVITY RESONATORS

- Shooting and bouncing rays - Calculating the RCS of an arbitrarily shaped cavity p 124 A89-34242  
Acoustic wave propagation in heterogeneous structures including experimental validation [AIAA PAPER 89-1044] p 225 A89-36214  
Acoustic wave propagation in heterogeneous structures including experimental validation [NASA-TM-101486] p 224 N89-19965  
Development of a 75-watt 60-GHz traveling-wave tube for intersatellite communications [NASA-CR-182135] p 138 N89-24530

## CELL CATHODES

- Corrosion testing of candidates for the alkaline fuel cell cathode p 212 N89-23000

## CENTRIFUGAL COMPRESSORS

- The effect of prewhirl on the internal aerodynamics and performance of a mixed flow research centrifugal compressor [NASA-CR-184756] p 161 N89-19503

## CERAMIC BONDING

- A study on thermal barrier coatings including thermal expansion mismatch and bond coat oxidation p 109 N89-12919

## CERAMIC COATINGS

- The scratch test - Different critical load determination techniques --- adhesive strength of thin hard coatings p 171 A89-54278  
Thermal expansion mismatch and plasticity in thermal barrier coating p 200 N89-17330

## CERAMIC FIBERS

- Auger analysis of a fiber/matrix interface in a ceramic matrix composite p 82 A89-35311  
Properties of silicon carbide fiber-reinforced silicon nitride matrix composites [NASA-TM-101356] p 84 N89-10130  
A study of the stress wave factor technique for evaluation of composite materials p 189 N89-21256  
[NASA-CR-4195] p 171 A89-54278  
The isothermal fatigue behavior of a unidirectional SiC/Ti composite and the Ti alloy matrix [NASA-TM-101984] p 86 N89-22684  
Theoretical analysis of compatibility of several reinforcement materials with NiAl and FeAl matrices [NASA-CR-182291] p 86 N89-23622  
Preparation and evaluation of silicon nitride matrices for silicon nitride-SiC fiber composites [NASA-CR-184798] p 115 N89-23678

## CERAMIC MATRIX COMPOSITES

- Reactions of silicon-based ceramics in mixed oxidation chlorination environments p 105 A89-21442

- Strength distribution of reinforcing fibers in a Nicalon fiber/chemically vapor infiltrated silicon carbide matrix composite p 82 A89-34844  
Auger analysis of a fiber/matrix interface in a ceramic matrix composite p 82 A89-35311  
Thermal effects on the mechanical properties of SiC fiber reinforced reaction bonded silicon nitride matrix (SiC/RBSN) composites p 84 N89-10134  
Laminate behavior for SiC fiber-reinforced reaction-bonded silicon nitride matrix composites [NASA-TM-101350] p 84 N89-10952  
Local-global analysis of crack growth in continuously reinforced ceramic matrix composites [NASA-CR-182231] p 197 N89-13820  
Development of BEM for ceramic composites [NASA-CR-183313] p 111 N89-14311  
A review of failure models for unidirectional ceramic matrix composites under monotonic loads [NASA-TM-101421] p 198 N89-14470  
Noninteractive macroscopic reliability model for ceramic matrix composites with orthotropic material symmetry [NASA-TM-101414] p 198 N89-15437  
Nondestructive evaluation of advanced ceramics [NASA-TM-101489] p 189 N89-20490  
A study of the stress wave factor technique for evaluation of composite materials p 189 N89-21256  
[NASA-CR-4195] p 189 N89-21256  
Preparation and evaluation of silicon nitride matrices for silicon nitride-SiC fiber composites [NASA-CR-184798] p 115 N89-23678  
Time dependent reliability model incorporating continuum damage mechanics for high-temperature ceramics [NASA-TM-102046] p 115 N89-24487  
Intermetallic and ceramic matrix composites for 815 to 1370 C (1500 to 2500 F) gas turbine engine applications [NASA-TM-102326] p 88 N89-29490  
Fiber reinforced ceramic material [NASA-CASE-LEW-14392-2] p 116 N89-29538
- CERAMICS**  
Crack growth resistance of textured alumina p 105 A89-26452  
Fracture toughness of polycrystalline ceramics in combined mode I and mode II loading p 105 A89-26457  
On the orthorhombic phase in ZrO<sub>2</sub>-based alloys p 105 A89-30631  
Fracture resistance of a TiB<sub>2</sub> particle/SiC matrix composite at elevated temperature p 81 A89-31074  
The behavior of SiC and Si<sub>3</sub>N<sub>4</sub> ceramics in mixed oxidation/chlorination environments p 106 A89-33616  
Weibull crack density coefficient for polydimensional stress states p 193 A89-34849  
Ceramic bearings for use in gas turbine engines p 180 A89-46697  
Tribological properties of structural ceramics p 107 A89-51258  
Adhesion, friction and micromechanical properties of ceramics p 107 A89-54277  
Tribological properties of alumina-boria-silicate fabric from 25 C to 850 C p 107 A89-54982  
A sintering model for SiC(sub)w/Si<sub>3</sub>N<sub>4</sub> composites [NASA-TM-101336] p 108 N89-10166  
Phase transformations in xerogels of mullite composition [NASA-TM-101349] p 108 N89-11038  
Sensors for ceramic components in advanced propulsion systems: Summary of literature survey and concept analysis, task 3 report [NASA-CR-180900] p 172 N89-11192  
Molten salt corrosion of SiC and Si<sub>3</sub>N<sub>4</sub> [NASA-TM-101346] p 108 N89-11912  
Slurry-pressing consolidation of silicon nitride [NASA-TM-101365] p 109 N89-12746  
Calculation of Weibull strength parameters and Batdorf flow-density constants for volume- and surface-flaw-induced fracture in ceramics [NASA-TM-100890] p 196 N89-12930  
Cyclic stress analysis of ceramic coated gas turbine seals p 111 N89-13662  
Hot corrosion of ceramic engine materials [NASA-TM-101439] p 112 N89-16065  
Thermal barrier coating life prediction model development p 200 N89-17333  
The effect of insulated combustion chamber surfaces on direct-injected diesel engine performance, emissions, and combustion [NASA-CR-182204] p 239 N89-17548  
Dynamic porosity variations in ceramics [NASA-TM-101340] p 112 N89-17668  
Improved silicon nitride for advanced heat engines [NASA-CR-179525] p 113 N89-19421  
Adhesion in ceramics and magnetic media [NASA-TM-101476] p 113 N89-19435

- Life modeling of thermal barrier coatings for aircraft gas turbine engines p 30 N89-20143
- Design, development and applications of novel techniques for studying surface mechanical properties [NASA-TM-101959] p 113 N89-20253
- Nondestructive evaluation of advanced ceramics [NASA-TM-101489] p 189 N89-20490
- Characterization of ceramics and intermetallics fabricated by self-propagating high-temperature synthesis [NASA-TM-102004] p 78 N89-25285
- Non-uniform transition conductivity of superconducting ceramic [NASA-TM-102133] p 189 N89-28851
- Fiber reinforced ceramic material [NASA-CASE-LEW-14392-2] p 116 N89-29538
- CERENKOV RADIATION**
- Coherent Cerenkov radiation from the Spacelab 2 electron beam p 231 A89-24292
- CERMETS**
- Micro laminate composites as thermal barrier coatings p 83 A89-54261
- CHALLENGER (ORBITER)**
- Electron velocity distributions and plasma waves associated with the injection of an electron beam into the ionosphere p 215 A89-43698
- CHANNEL FLOW**
- A near-wall turbulence model and its application to fully developed turbulent channel and pipe flows [NASA-TM-101399] p 158 N89-13741
- A genuinely multi-dimensional upwind cell-vertex scheme for the Euler equations [NASA-TM-102029] p 223 N89-24872
- Calculation of reattaching shear layers in divergent channel with a multiple-time-scale turbulence model [NASA-TM-102293] p 168 N89-28749
- CHARACTERISTICS**
- The divergence characteristics of constrained-sheath optics systems for use with 5-eV atomic oxygen sources [NASA-CR-182238] p 229 N89-19973
- CHARACTERIZATION**
- Mechanical properties characterization of composite sandwich materials intended for space antenna applications p 81 A89-32885
- High-frequency ultrasonic characterization of sintered silicon carbide p 106 A89-34840
- Deposition and characterization of ZnS/Si heterojunctions produced by vacuum evaporation [NASA-TM-101359] p 135 N89-11129
- CHARGE TRANSFER**
- Connection between energy relations of solids and molecules p 91 A89-26406
- CHEMICAL ATTACK**
- A preliminary report on the effects of long-term exposure of LiOH on pure nickel p 90 A89-12624
- CHEMICAL BONDS**
- Connection between energy relations of solids and molecules p 91 A89-26406
- CHEMICAL COMPOSITION**
- Predicting minimum Al concentrations for protective scale formation on Ni-base alloys. I - Isothermal oxidation. II - Cyclic oxidation p 98 A89-40116
- Sequentially evaporated thin Y-Ba-Cu-O superconductor films: Composition and processing effects [NASA-TM-101388] p 134 N89-10235
- Phase transformations in xerogels of mullite composition [NASA-TM-101349] p 108 N89-11038
- CHEMICAL EQUILIBRIUM**
- NNEPQ - Chemical equilibrium version of the Navy/NASA Engine Program [ASME PAPER 88-GT-314] p 22 A89-24989
- Three dimensional PNS solutions of hypersonic internal flows with equilibrium chemistry [AIAA PAPER 89-0002] p 146 A89-28401
- A detailed analysis of inviscid flux splitting algorithms for real gases with equilibrium or finite-rate chemistry p 151 A89-45424
- Experimental verification of the thermodynamic properties for a jet-A fuel [NASA-TM-101475] p 117 N89-17017
- CHEMICAL PROPULSION**
- NASA's Chemical Transfer Propulsion Program for Pathfinder [AIAA PAPER 89-2298] p 37 A89-46735
- NASA's Chemical Transfer Propulsion Program for Pathfinder [NASA-TM-102298] p 41 N89-26876
- CHEMICAL REACTION CONTROL**
- Acidic attack of perfluorinated alkyl ether lubricant molecules by metal oxide surfaces [NASA-TM-101962] p 93 N89-19402
- CHEMICAL REACTIONS**
- Transport-induced shifts in condensate dew-point and composition in multicomponent systems with chemical reaction p 89 A89-12333
- Flux splitting algorithms for two-dimensional viscous flows with finite-rate chemistry [AIAA PAPER 89-0388] p 146 A89-28409
- The effect of metal surface passivation on the Au-InP interaction p 132 A89-30443
- Response of a chemically reacting shear layer to streamwise vorticity [AIAA PAPER 89-0978] p 150 A89-40400
- Influence of several metal ions on the gelation activation energy of silicon tetraethoxide [NASA-TM-101380] p 114 N89-21894
- CHIRP**
- Coded multiple chirp spread spectrum system and overlay service p 124 A89-26769
- CHIRP SIGNALS**
- Study of spread spectrum multiple access systems for satellite communications with overlay on current services: Executive summary [NASA-CR-180827-EXEC-SUMM] p 128 N89-23756
- Study of spread spectrum multiple access systems for satellite communications with overlay on current services [NASA-CR-180827] p 128 N89-23757
- CHLORINATION**
- Reactions of silicon-based ceramics in mixed oxidation chlorination environments p 105 A89-21442
- CHROMIUM ALLOYS**
- The effect of sulfur and zirconium co-doping on the oxidation of NiCrAl p 94 A89-13933
- CHROMIUM CARBIDES**
- Tribological composition optimization of chromium-carbide-based solid lubricant coatings for foil gas bearings at temperatures to 650 C p 83 A89-54258
- CIRCULAR CYLINDERS**
- Aerodynamically-driven condensate layer thickness distributions on isothermal cylindrical surfaces p 140 A89-12337
- Windward fraction of the total mass or heat transport for flow past a circular cylinder p 141 A89-12339
- An application of the WKBJ technique to the on-surface radiation condition p 124 A89-21222
- Investigation of the flow between a pair of circular cylinders in the flopping regime p 144 A89-22822
- Theory and application of radiation boundary operators p 224 A89-24191
- Transient radiative cooling of an absorbing and scattering cylinder p 146 A89-28958
- Correlations of velocity and temperature fluctuations in the stagnation-point flow of circular cylinder in turbulent flow p 148 A89-34927
- Review of FD-TD numerical modeling of electromagnetic wave scattering and radar cross section p 19 A89-45107
- CIRCULAR WAVEGUIDES**
- High-frequency RCS of open cavities with rectangular and circular cross sections p 125 A89-39595
- CIVIL AVIATION**
- Supersonic jet noise and the high speed civil transport [AIAA PAPER 89-2358] p 227 A89-46772
- CLASSICAL MECHANICS**
- Composite mechanics for engine structures p 80 A89-28344
- CLEARANCES**
- Recent advances in capacitance type of blade tip clearance measurements [AIAA PAPER 88-4664] p 20 A89-13725
- CLIMATE**
- The Mars climate for a photovoltaic system operation [IAF PAPER ICOSP89-9.5] p 241 A89-46529
- The Mars climate for a photovoltaic system operation [NASA-TM-101994] p 136 N89-20385
- CLINICAL MEDICINE**
- Integrated control and health management. Orbit transfer rocket engine technology program [NASA-CR-182122] p 62 N89-11805
- CLOSED CYCLES**
- Behavior in normal and reduced gravity of an enclosed liquid/gas system with nonuniform heating from above [AIAA PAPER 89-0070] p 145 A89-25061
- Behavior in normal and reduced gravity of an enclosed liquid/gas system with nonuniform heating from above [NASA-TM-101471] p 120 N89-17046
- CLOSURE LAW**
- Theoretical studies in support of the 3M-vapor transport (PVTOS-) experiments [NASA-CR-185122] p 165 N89-26179
- CLOUDS**
- Particle cloud mixing in microgravity [NASA-TM-101484] p 121 N89-20321
- CLOUDS (METEOROLOGY)**
- An overview of the current NASA program on aircraft icing research [SAE PAPER 881386] p 16 A89-28192
- COAL GASIFICATION**
- Assessment and comparison of 100-MW coal gasification phosphoric acid fuel cell power plants [NASA-CR-182189] p 209 N89-13103
- COARSENESS**
- Observations of directional gamma prime coarsening during engine operation p 98 A89-40162
- COATINGS**
- Thin film coatings for space electrical power system applications p 77 A89-53324
- Evaluation of coated columbium test panels having application to a secondary nozzle extension for the RL10 rocket engine system, parts 1 and 2 [NASA-CR-180809] p 64 N89-13493
- Examination of coating failure by acoustic emission p 110 N89-13654
- Optimum interface properties for metal matrix composites [NASA-TM-102295] p 205 N89-27223
- COAXIAL CABLES**
- Power transmission studies for tethered SP-100 p 52 A89-15403
- COAXIAL FLOW**
- A numerical and experimental study of coaxial jets p 153 A89-52500
- COBALT**
- Mechanisms of elevated-temperature deformation in the B2 aluminides NiAl and CoAl p 94 A89-17378
- Oxygen electrode bifunctional electrocatalyst NiCo<sub>2</sub>O<sub>4</sub> spinel [NASA-TM-100947] p 208 N89-10409
- COBALT ALLOYS**
- The effect of Co alloying content on the kinetics of reaction zone growth in tungsten fiber reinforced superalloy composites p 79 A89-11324
- Effects of cobalt concentration on the relative resistance to octahedral and cube slip in nickel-base superalloys p 94 A89-17115
- Preliminary study of creep thresholds and thermomechanical response in Haynes 188 at temperatures in the range 649 to 871 C p 200 N89-17327
- CODING**
- The development of an intelligent interface to a computational fluid dynamics flow-solver code p 216 A89-16963
- Advanced modulation technology development for earth station demodulator applications [NASA-CR-185126] p 43 N89-26880
- COEFFICIENT OF FRICTION**
- Adhesion scratch testing - A round-robin experiment p 171 A89-54281
- Tribological properties of alumina-borax-silicate fabric from 25 C to 850 C p 107 A89-54982
- Finite element modeling of frictionally restrained composite interfaces [NASA-CR-182281] p 203 N89-23918
- COHERENT ELECTROMAGNETIC RADIATION**
- Coherent Cerenkov radiation from the Spacelab 2 electron beam p 231 A89-24292
- COLD WORKING**
- Ultrasonic attenuation measurements determine onset, degree, and completion of recrystallization p 187 A89-23936
- COLLOIDS**
- An asymptotic description of transient settling and ultrafiltration of colloidal dispersions p 144 A89-24603
- COMBINED STRESS**
- Biaxial thermo-mechanical fatigue p 194 A89-43527
- COMBUSTIBLE FLOW**
- Numerical investigation of chemically reacting flows in ramjet dump combustors [AIAA PAPER 89-0387] p 22 A89-28408
- Three-dimensional calculation of supersonic reacting flows using an LU scheme [AIAA PAPER 89-0391] p 146 A89-28410
- Effects of heat release on the large-scale structure in turbulent mixing layers p 147 A89-31844
- On the modelling of scalar and mass transport in combustor flows p 92 A89-38658
- Response of a chemically reacting shear layer to streamwise vorticity [AIAA PAPER 89-0978] p 150 A89-40400
- The use of direct numerical simulation in the study of turbulent, chemically-reacting flows p 152 A89-51873
- Pdf - Transport equations for chemically reacting flows p 152 A89-51880
- Turbulent multiphase flows p 152 A89-51883
- Particle cloud mixing in microgravity [NASA-TM-101484] p 121 N89-20321
- An explicit Runge-Kutta method for turbulent reacting flow calculations [NASA-TM-101945] p 31 N89-21799
- COMBUSTION**
- Facilities for microgravity combustion research [IAF PAPER 88-355] p 117 A89-17784

## COMBUSTION CHAMBERS

- Optical measurements of soot and temperature profiles in premixed propane-oxygen flames p 92 A89-35008
- Turbine Engine Hot Section Technology, 1987 [NASA-CP-2493] p 189 N89-17298
- The solid surface combustion space shuttle experiment hardware description and ground-based test results [NASA-TM-101963] p 123 N89-19446
- COMBUSTION CHAMBERS**
- Calculations of the unsteady, three-dimensional flow field inside a motored Wankel engine [SAE PAPER 880625] p 19 A89-12307
- Thermal measurements for jets in disturbed and undisturbed crosswind conditions p 20 A89-16102
- Development of an analytical model to assess fuel property effects on combustor performance p 21 A89-20949
- Shock-wave-induced mixing enhancement in scramjet combustors [AIAA PAPER 89-0104] p 145 A89-25091
- On the modelling of scalar and mass transport in combustor flows p 92 A89-38658
- Investigation of low NOx staged combustor concept in high-speed civil transport engines [AIAA PAPER 89-2942] p 23 A89-47186
- Liquid oxygen cooling of hydrocarbon fueled rocket thrust chambers [AIAA PAPER 89-2739] p 60 A89-49686
- Fuel properties effect on the performance of a small high temperature rise combustor [AIAA PAPER 89-2901] p 23 A89-52025
- Unsteady heat transfer in turbine blade ducts - Focus on combustor sources p 153 A89-53286
- Turbobfan forced mixer lobe flow modeling. Part 3: Application to augment engines [NASA-CR-4147-Pt-3] p 8 N89-10025
- Turbine Engine Hot Section Technology (HOST) Project p 25 N89-12877
- HOST structural analysis program overview p 195 N89-12881
- Further development of the dynamic gas temperature measurement system p 172 N89-12884
- Aerothrmal modeling program, phase 2 p 156 N89-12890
- Aerothrmal modeling program, phase 2. Element B: Flow interaction experiment p 156 N89-12891
- Aerothrmal modeling program, phase 2. Element C: Fuel injector-air swirl characterization p 156 N89-12892
- Efficient numerical techniques for complex fluid flows p 156 N89-12894
- On 3D inelastic analysis methods for hot section components p 196 N89-12906
- Component specific modeling p 25 N89-12907
- Elevated temperature crack growth p 196 N89-12915
- LDV measurements in an annular combustor model [NASA-CR-182207] p 159 N89-13755
- High-pressure calorimeter chamber tests for liquid oxygen/kerosene (LOX/RP-1) rocket combustion [NASA-TP-2862] p 65 N89-15979
- Application of advanced diagnostics to airblast injector flows p 180 N89-17306
- Three-dimensional inelastic analysis methods for hot section components p 199 N89-17316
- Structural response of an advanced combustor liner: Test and analysis p 200 N89-17329
- Elevated temperature crack growth p 200 N89-17335
- The effect of insulated combustion chamber surfaces on direct-injected diesel engine performance, emissions, and combustion [NASA-CR-182204] p 239 N89-17548
- Assessment, development, and application of combustor aerothermal models p 30 N89-20138
- Mercury ion thruster technology [NASA-CR-174974] p 66 N89-21834
- Investigation of low NOx staged combustor concept in high-speed civil transport engines [NASA-TM-101977] p 32 N89-22606
- Design, fabrication and test of the RL10 derivative II chamber/primary nozzle [NASA-CR-179595] p 68 N89-23519
- Liquid oxygen cooling of hydrocarbon fueled rocket thrust chambers [NASA-TM-102113] p 70 N89-24447
- Fuel properties effect on the performance of a small high temperature rise combustor [NASA-TM-102096] p 33 N89-25238
- Advanced methods for 3-D inelastic structural analysis for hot engine structures [NASA-TM-102106] p 204 N89-25490
- OTVE combustor wall condition monitoring [NASA-CR-182275] p 73 N89-26899

## COMBUSTION CHEMISTRY

- Navier-Stokes calculation of solid-propellant rocket motor internal flowfields [AIAA PAPER 88-3182] p 48 A89-14983
- Characterization of ceramics and intermetallics fabricated by self-propagating high-temperature synthesis [NASA-TM-102004] p 78 N89-25285

## COMBUSTION EFFICIENCY

- Development of an analytical model to assess fuel property effects on combustor performance p 21 A89-20949
- Investigation of low NOx staged combustor concept in high-speed civil transport engines [AIAA PAPER 89-2942] p 23 A89-47186
- Aerothrmal modeling program, phase 2. Element B: Flow interaction experiment p 156 N89-12891
- Assessment, development, and application of combustor aerothermal models p 30 N89-20138
- Investigation of low NOx staged combustor concept in high-speed civil transport engines [NASA-TM-101977] p 32 N89-22606

## COMBUSTION PHYSICS

- Determination of convective diffusion heat/mass transfer rates to burner rig test targets comparable in size to cross-stream jet diameter p 141 A89-12753
- Numerical study of the interactions between droplets at intermediate Reynolds numbers p 142 A89-16451
- Mass transfer across combustion gas thermal boundary layers - Power production and materials processing implications p 143 A89-20425
- Radiative structures of lycopodium-air flames in low gravity [AIAA PAPER 89-0500] p 91 A89-25406
- Droplet combustion drop tower tests using models of the space flight apparatus [AIAA PAPER 89-0501] p 119 A89-28418
- The modular combustion facility for the Space Station laboratory - A requirements and capabilities study [AIAA PAPER 89-0505] p 44 A89-28421
- Microgravity Combustion Diagnostics Workshop [NASA-CP-10017] p 120 N89-17682
- Microgravity combustion science: A program overview [NASA-TM-101424] p 122 N89-28665

## COMBUSTION PRODUCTS

- Deposition of Na2SO4 from salt-seeded combustion gases of a high velocity burner rig p 89 A89-12330
- Optical methods and results of dew point and deposition rate measurements in salt/ash-containing combustion gases - B2O3(l) deposition rates by interference methods and comparisons with theory p 89 A89-12334
- Laboratory studies of binary salt CVD in combustion gas environments p 89 A89-12335
- Laboratory studies of the deposition of alkali sulfate vapors from combustion gases using a flash-evaporation technique p 89 A89-12338
- Effect of alcohol addition on shock-initiated formation of soot from benzene p 90 A89-12903
- NOx formation from the combustion of monodisperse n-heptane sprays doped with fuel-nitrogen additives p 116 A89-42695
- The effect of insulated combustion chamber surfaces on direct-injected diesel engine performance, emissions, and combustion [NASA-CR-182204] p 239 N89-17548

## COMBUSTION STABILITY

- Feasibility of reduced gravity experiments involving quiescent, uniform particle cloud combustion [NASA-TM-101371] p 122 N89-26114

## COMBUSTION TEMPERATURE

- Fuel properties effect on the performance of a small high temperature rise combustor [AIAA PAPER 89-2901] p 23 A89-52025
- Gas turbine alternative fuels combustion characteristics [NASA-TM-101470] p 210 N89-21417
- Fuel properties effect on the performance of a small high temperature rise combustor [NASA-TM-102096] p 33 N89-25238
- Determination of combustion gas temperatures by infrared radiometry in sooting and nonsooting flames [NASA-TP-2900] p 164 N89-25409

## COMMERCIAL AIRCRAFT

- Supersonic jet noise and the high speed civil transport [AIAA PAPER 89-2358] p 227 A89-46772

## COMMERCIAL SPACECRAFT

- Intersatellite link application to commercial communications satellites p 43 A89-39144

## COMMONALITY

- Space Station Freedom electrical power system hardware commonality with the United States Polar Platform [NASA-TM-102074] p 69 N89-24439

## COMMUNICATION NETWORKS

- Integrated communication and control systems. I - Analysis [ASME PAPER 88-WA/DSC-1] p 219 A89-22499
- Integrated communication and control systems. II - Design considerations [ASME PAPER 88-WA/DSC-2] p 219 A89-22500

## COMMUNICATION SATELLITES

- Intersatellite link application to commercial communications satellites p 43 A89-39144
- Digitally modulated bit error rate measurement system for microwave component evaluation [NASA-TP-2912] p 40 N89-28545

## COMMUNICATIONS TECHNOLOGY SATELLITE

- Baseband processor hardware for Advanced Communication Technology Satellite (ACTS) p 43 A89-38298

## COMMUTER AIRCRAFT

- Aircraft engines. III p 21 A89-22927

## COMPARISON

- Comparison of propeller cruise noise data taken in the NASA Lewis 8- by 6-foot wind tunnel with other tunnel and flight data [AIAA PAPER 89-1059] p 226 A89-40472
- Comparison of propeller cruise noise data taken in the NASA Lewis 8- by 6-foot wind tunnel with other tunnel and flight data [NASA-TM-101976] p 228 N89-21628

## COMPATIBILITY

- Thermodynamic analysis of compatibility of several reinforcement materials with FeAl alloys [NASA-CR-4172] p 83 N89-10128
- Thermodynamic analysis of compatibility of several reinforcement materials with beta phase NiAl alloys [NASA-CR-4171] p 84 N89-10131
- Orbit transfer rocket engine technology program: Oxygen materials compatibility testing [NASA-CR-182195] p 64 N89-14256

## COMPENSATION

- Adaptive feed array compensation system for reflector antenna surface distortion [NASA-TM-101458] p 127 N89-17756

## COMPLEX VARIABLES

- Solution and sensitivity analysis of a complex transcendental eigenproblem with pairs of real eigenvalues [NASA-CR-182241] p 197 N89-13819

## COMPONENT RELIABILITY

- Power components for the Space Station 20-kHz power distribution system p 130 A89-15387
- Probabilistic structural analysis to quantify uncertainties associated with turbopump blades p 194 A89-36920
- Small scale bipolar nickel-hydrogen testing p 208 A89-44005
- Transmission overhaul and replacement predictions using Weibull and renewal theory [AIAA PAPER 89-2919] p 180 A89-47173
- Space station electrical power system availability study [NASA-CR-182198] p 45 N89-11802
- Design and implementation of a microcomputer-based user interface controller for burst data communications satellite ground terminals [NASA-TM-101375] p 43 N89-13457
- Transmission overhaul and replacement predictions using Weibull and renewal theory [NASA-TM-102022] p 186 N89-22925
- Fatigue crack growth model RANDOM2 user manual, appendix 1 [NASA-CR-184939] p 203 N89-23890
- Fatigue strength reduction model: RANDOM3 and RANDOM4 user manual, appendix 2 [NASA-CR-184940] p 203 N89-23891
- CSTI High Capacity Power [NASA-TM-102059] p 72 N89-25282

## COMPOSITE MATERIALS

- Transmission electron microscopy of composites p 79 A89-14560
- Composite interlaminar fracture toughness - Three-dimensional finite-element modeling for mixed mode I, II, and fracture p 190 A89-16278
- Composite mechanics for engine structures p 80 A89-28344
- 700 F properties of autoclave cured PMR-II composites p 81 A89-29998
- Mechanical properties characterization of composite sandwich materials intended for space antenna applications p 81 A89-32885
- Dynamic delamination buckling in composite laminates under impact loading - Computational simulation p 82 A89-36310
- Status and prognosis for alternative engine materials p 97 A89-36419
- Nondestructive evaluation/characterization of composite materials and structures using the acousto-ultrasonic techniques p 188 A89-36571



A sintering model for SiC(sub)w/Si3N4 composites [NASA-TM-101336] p 108 N89-10166

A NASTRAN DMAP alter for linear buckling analysis under dynamic loading [NASA-TM-100832] p 85 N89-13522

Graphite fluoride fiber polymer composite material [NASA-CASE-LEW-14472-1] p 85 N89-14259

Some composite bearing and seal materials for gas turbine applications: A review [NASA-TM-101451] p 111 N89-14338

Improved silicon carbide for advanced heat engines [NASA-CR-179477] p 112 N89-15251

Refractory metal alloys and composites for space nuclear power systems [NASA-TM-101364] p 102 N89-16986

Thermodynamic analysis of chemical compatibility of several reinforcement materials with niobium aluminides [NASA-CR-182260] p 86 N89-21036

A NASTRAN DMAP alter for linear buckling analysis under dynamic loading p 202 N89-22948

Fatigue crack growth study of SCS6/Ti-15-3 composite [NASA-TM-102332] p 104 N89-26989

**COMPOSITE STRUCTURES**

Fiber composite sandwich thermostructural behavior - Computational simulation p 190 A89-11246

Transmission electron microscopy of composites p 79 A89-14560

Sublaminar- or ply-level analysis of composites and strain energy release rates of end-notch and mixed-mode fracture specimens p 190 A89-16279

Composite mechanics for engine structures p 80 A89-28344

Finite element applications to explore the effects of partial bonding on metal matrix composite properties [AIAA PAPER 89-1175] p 192 A89-30666

Vibration testing of impact-damaged composite laminates [AIAA PAPER 89-1411] p 81 A89-30883

Oxidation and protection of fiberglass-epoxy composite masts for photovoltaic arrays in the low earth orbital environment p 44 A89-35316

Nondestructive evaluation/characterization of composite materials and structures using the acousto-ultrasonic techniques p 188 A89-36571

A comparison of numerical methods for the prediction of two-dimensional heat transfer in an electrothermal deicer pad [NASA-CR-4202] p 19 N89-13429

Vibration testing of impact-damaged composite laminates [NASA-TM-4115] p 87 N89-25290

On finite element implementation and computational techniques for constitutive modeling of high temperature composites [NASA-CR-185120] p 204 N89-26261

**COMPRESSIBILITY EFFECTS**

Compressibility and shock wave interaction effects on free shear layers [AIAA PAPER 89-2460] p 7 A89-46847

**COMPRESSIBLE FLOW**

Use of a generalized Stokes number to determine the aerodynamic capture efficiency of non-Stokesian particles from a compressible gas flow p 140 A89-12336

A diagonally inverted LU implicit multigrid scheme for the 3-D Navier-Stokes equations and a two equation model of turbulence [AIAA PAPER 89-0467] p 145 A89-25382

A time accurate finite volume high resolution scheme for three dimensional Navier-Stokes equations [AIAA PAPER 89-1994] p 6 A89-41837

Numerical analysis of supersonic flow through oscillating cascade sections by using a deforming grid [AIAA PAPER 89-2805] p 8 A89-50810

A diagonally inverted LU implicit multigrid scheme for the 3-D Navier-Stokes equations and a two equation model of turbulence [NASA-CR-182209] p 9 N89-10863

Development of an integrated BEM approach for hot fluid structure interaction [NASA-CR-184587] p 27 N89-15114

On the Lagrangian description of unsteady boundary layer separation. Part 1: General theory [NASA-TM-102026] p 164 N89-23821

Numerical analysis of supersonic flow through oscillating cascade sections by using a deforming grid [NASA-TM-102053] p 15 N89-25119

Skin-friction measurements by laser interferometry p 167 N89-28737

The upper-branch stability of compressible boundary layer flows [NASA-TM-102128] p 167 N89-28748

**COMPRESSION LOADS**

The effect of compression on Individual Pressure Vessel Nickel/Hydrogen components --- for energy storage in low earth orbits p 50 A89-15281

Tooth contact shift in loaded spiral bevel gears o, IL, 25-27 Apr. 1989; sponsored by ASME [NASA-TM-101438] p 183 N89-14453

Reliability-based failure analysis of brittle materials [NASA-CR-184799] p 189 N89-20489

**COMPRESSION TESTS**

The effect of compression on Individual Pressure Vessel Nickel/Hydrogen components --- for energy storage in low earth orbits p 50 A89-15281

1200 to 1400 K slow strain rate compressive behavior of small grain size NiAl/Ni2AlTi alloys and NiAl/Ni2AlTi-TiB2 composites p 99 A89-53497

**COMPRESSIVE STRENGTH**

Reliability-based failure analysis of brittle materials [NASA-CR-184799] p 189 N89-20489

**COMPRESSOR BLADES**

Automated design of controlled-diffusion blades [ASME PAPER 88-GT-139] p 2 A89-15967

MATE program: Erosion resistant compressor airfoil coating, volume 2 [NASA-CR-179645] p 113 N89-18550

**COMPRESSOR EFFICIENCY**

Advanced core technology: Key to subsonic propulsion benefits [NASA-TM-101420] p 26 N89-14237

**COMPRESSOR ROTORS**

The effect of prewhirl on the internal aerodynamics and performance of a mixed flow research centrifugal compressor [NASA-CR-184756] p 161 N89-19503

**COMPRESSORS**

T55-L-712 turbine engine compressor housing refurbishment-plasma spray project [NASA-TM-101310] p 100 N89-10156

A prediction of 3-D viscous flow and performance of the NASA low-speed centrifugal compressor [NASA-CR-184765] p 160 N89-16132

Rotordynamic Instability Problems in High-Performance Turbomachinery, 1988 [NASA-CP-3026] p 185 N89-22891

Performance estimates for the Space Station power system Brayton Cycle compressor and turbine [NASA-CR-182263] p 73 N89-26903

**COMPUTATION**

High speed inlet calculations with real gas effects [AIAA PAPER 89-3076] p 2 A89-14980

**COMPUTATIONAL ASTROPHYSICS**

Patterns of the cosmic microwave background from evolving string networks p 240 A89-14618

**COMPUTATIONAL FLUID DYNAMICS**

Diagonal implicit multigrid algorithm for the Euler equations p 1 A89-11110

On the preferred mode of jet instability p 140 A89-11567

Navier-Stokes solution to the flowfield over ice accretion shapes p 1 A89-12557

Application of advanced computational technology to propulsion CFD p 142 A89-16957

The development of an intelligent interface to a computational fluid dynamics flow-solver code p 216 A89-16963

Simple high-accuracy resolution program for convective modelling of discontinuities p 143 A89-17459

Studies of transition in boundary layers [AIAA PAPER 89-0034] p 2 A89-25029

A simple time-accurate turbomachinery algorithm with numerical solutions of an uneven blade count configuration [AIAA PAPER 89-0206] p 179 A89-25181

A diagonally inverted LU implicit multigrid scheme for the 3-D Navier-Stokes equations and a two equation model of turbulence [AIAA PAPER 89-0467] p 145 A89-25382

Three dimensional PNS solutions of hypersonic internal flows with equilibrium chemistry [AIAA PAPER 89-0002] p 146 A89-28401

The effect of adaptive grid on hypersonic nozzle flow calculations [AIAA PAPER 89-0006] p 54 A89-28402

Unsteady Euler cascade analysis [AIAA PAPER 89-0322] p 3 A89-28406

Three-dimensional calculation of supersonic reacting flows using an LU scheme [AIAA PAPER 89-0391] p 146 A89-28410

Numerical analysis of flow through oscillating cascade sections [AIAA PAPER 89-0437] p 4 A89-28413

Nonlinear interaction between the sinuous and varicose instability modes in a plane wake p 147 A89-33779

Bipolar coordinates for computation of transition duct flows p 148 A89-34912

Calculation of unsteady flows in turbomachinery using the linearized Euler equations p 149 A89-36916

Three-dimensional wave packets and instability waves in free shear layers and their receptivity p 149 A89-38619

Optimizing advanced propeller designs by simultaneously updating flow variables and design parameters p 5 A89-39189

Calculation of flow over iced airfoils p 5 A89-40905

On the role of artificial viscosity in Navier-Stokes solvers [AIAA PAPER 89-1947] p 5 A89-41794

Assessment of numerical techniques for unsteady flow calculations [AIAA PAPER 89-1956] p 150 A89-41803

Conservative treatment of boundary interfaces for overlaid grids and multi-level grid adaptations [AIAA PAPER 89-1980] p 5 A89-41823

Radiative heat transfer in rocket thrust chambers and nozzles [AIAA PAPER 89-1720] p 150 A89-43235

Calculation of shocked flows by mathematical programming p 150 A89-45397

Universal limiter for high order explicit conservative advection schemes p 151 A89-45398

Transonic flow solutions on general 3D regions using composite-block grids p 6 A89-45428

A natural low-frequency oscillation of the flow over an airfoil near stalling conditions p 6 A89-45437

A Newton/upwind method and numerical study of shock wave/boundary layer interactions p 6 A89-45468

Mach 5 inlet CFD and experimental results [AIAA PAPER 89-2355] p 6 A89-46769

Large scale advanced propeller blade pressure distributions - Prediction and data [AIAA PAPER 89-2696] p 7 A89-47026

Rarefied gas flow through two-dimensional nozzles [AIAA PAPER 89-2893] p 7 A89-47156

A numerical and experimental study of confined swirling jets [AIAA PAPER 89-2898] p 151 A89-47161

Numerical solution of periodic vortical flows about a thin airfoil [AIAA PAPER 89-1691] p 7 A89-48955

A block-corrected subdomain solution procedure for recirculating flow calculations p 152 A89-50147

Numerical analysis of supersonic flow through oscillating cascade sections by using a deforming grid [AIAA PAPER 89-2805] p 8 A89-50810

Pdf - Transport equations for chemically reacting flows p 152 A89-51880

A numerical and experimental study of coaxial jets p 153 A89-52500

CFD in the context of IHPTET - The Integrated High Performance Turbine Engine Technology Program [AIAA PAPER 89-2904] p 154 A89-53307

Computational fluid dynamic control p 220 A89-53984

A diagonally inverted LU implicit multigrid scheme for the 3-D Navier-Stokes equations and a two equation model of turbulence [NASA-CR-182209] p 9 N89-10863

Effects of environmentally imposed roughness on airfoil performance [NASA-CR-179639] p 17 N89-11725

Improved numerical methods for turbulent viscous flows aerothermal modeling program, phase 2 [NASA-CR-182169] p 154 N89-12010

Simulation of 2-dimensional viscous flow through cascades using a semi-elliptic analysis and hybrid C-H grids [NASA-CR-4180] p 10 N89-12553

A control-volume method for analysis of unsteady thrust augmenting ejector flows [NASA-CR-182203] p 24 N89-12566

A numerical method for computing unsteady 2-D boundary layer flows [NASA-CR-4198] p 155 N89-12835

Influence of bulk turbulence and entrance boundary layer thickness on the curved duct flow field [NASA-CR-4188] p 155 N89-12838

Improved numerical methods for turbulent viscous recirculating flows p 156 N89-12895

LDV measurements in an annular combustor model [NASA-CR-182207] p 159 N89-13755

Numerical analysis of flow through oscillating cascade sections [NASA-TM-101417] p 11 N89-14220

Turbofan forced mixer lobe flow modeling. 1: Experimental and analytical assessment [NASA-CR-4147-PT-1] p 11 N89-14221

Turbofan forced mixer lobe flow modeling. 2: Three-dimensional inviscid mixer analysis (FLOMIX) [NASA-CR-4147-PT-2] p 11 N89-14222

Universal limiter for transient interpolation modeling of the advective transport equations: The ULTIMATE conservative difference scheme [NASA-TM-100916] p 222 N89-14794

Development of an integrated BEM approach for hot fluid structure interaction [NASA-CR-184587] p 27 N89-15114

- Computational methods for inlet airframe integration p 13 N89-16752
- CFD application to subsonic inlet airframe integration --- computational fluid dynamics (CFD) p 13 N89-16753
- CFD application to supersonic/hypersonic inlet airframe integration --- computational fluid dynamics (CFD) p 13 N89-16754
- The design and development of transonic multistage compressors p 27 N89-16834
- CFD validation experiments for internal flows p 161 N89-18635
- Assessment, development, and application of combustor aerothermal models p 30 N89-20138
- Comparison of 3D computation and experiment for non-axisymmetric nozzles p 14 N89-20921
- [NASA-CR-182245] p 14 N89-20921
- Convection and chemistry effects in CVD: A 3-D analysis for silicon deposition p 78 N89-21032
- [NASA-TM-102001] p 78 N89-21032
- An explicit Runge-Kutta method for turbulent reacting flow calculations p 31 N89-21799
- [NASA-TM-101945] p 31 N89-21799
- Transonic viscous flow calculations for a turbine cascade with a two equation turbulence model p 32 N89-22607
- [NASA-TM-101944] p 32 N89-22607
- Numerical solution of periodic vortical flows about a thin airfoil p 14 N89-23413
- [NASA-TM-101998] p 14 N89-23413
- Advances in computational design and analysis of airbreathing propulsion systems p 32 N89-23465
- [NASA-TM-101987] p 32 N89-23465
- Advanced computational techniques for hypersonic propulsion p 163 N89-23809
- [NASA-TM-102005] p 163 N89-23809
- Nonlinear evolution of interacting oblique waves on two-dimensional shear layers p 164 N89-24575
- [NASA-TM-102030] p 164 N89-24575
- On the dynamic response of pressure transmission lines in the research of helium-charged free piston Stirling engines p 175 N89-24593
- [NASA-TM-102121] p 175 N89-24593
- A genuinely multi-dimensional upwind cell-vertex scheme for the Euler equations p 223 N89-24872
- [NASA-TM-102029] p 223 N89-24872
- Numerical analysis of supersonic flow through oscillating cascade sections by using a deforming grid p 15 N89-25119
- [NASA-TM-102053] p 15 N89-25119
- Multigrid calculation of three-dimensional turbomachinery flows p 165 N89-26172
- [NASA-CR-185332] p 165 N89-26172
- CFD in the context of IHPTET: The Integrated High Performance Turbine Technology Program p 165 N89-26174
- [NASA-TM-102132] p 165 N89-26174
- Far field expansion for anisotropic wave equations p 165 N89-26175
- [NASA-TM-102112] p 165 N89-26175
- Stability of a rigid rotor supported on oil-film journal bearings under dynamic load p 166 N89-27114
- [NASA-TM-102309] p 166 N89-27114
- Calculation of turbulence-driven secondary motion in ducts with arbitrary cross section p 166 N89-27115
- [NASA-TM-102142] p 166 N89-27115
- Mach 5 inlet CFD and experimental results p 33 N89-27670
- [NASA-TM-102317] p 33 N89-27670
- Least-squares finite element method for fluid dynamics p 223 N89-30008
- [NASA-TM-102352] p 223 N89-30008
- COMPUTATIONAL GEOMETRY**
- On the applications of algebraic grid generation methods based on transfinite interpolation p 33 N89-26003
- [NASA-TM-102095] p 33 N89-26003
- COMPUTATIONAL GRIDS**
- Diagonal implicit multigrid algorithm for the Euler equations p 1 A89-11110
- LU implicit multigrid algorithm for the three-dimensional Euler equations p 143 A89-19906
- Solution of three-dimensional flow problems using a flux-spline method p 146 A89-25543
- [AIAA PAPER 89-0687] p 146 A89-25543
- The effect of adaptive grid on hypersonic nozzle flow calculations p 54 A89-28402
- [AIAA PAPER 89-0006] p 54 A89-28402
- The solution of the Eirod algorithm for a dynamically loaded journal bearing using multigrid techniques p 148 A89-34795
- [ASME PAPER 88-TRIB-23] p 148 A89-34795
- Graphical postprocessing for 3-D mesh quality evaluation p 217 A89-38846
- Finite-element grid improvement by minimization of stiffness matrix trace p 194 A89-42339
- Transonic flow solutions on general 3D regions using composite-block grids p 6 A89-45428
- Numerical analysis of supersonic flow through oscillating cascade sections by using a deforming grid p 8 A89-50810
- [AIAA PAPER 89-2805] p 8 A89-50810
- Discretization formulas for unstructured grids p 154 N89-10242
- [NASA-TM-101298] p 154 N89-10242
- Interactive grid generation for turbomachinery flow field simulations p 9 N89-11717
- [NASA-TM-101301] p 9 N89-11717
- Simulation of 2-dimensional viscous flow through cascades using a semi-elliptic analysis and hybrid C-H grids p 10 N89-12553
- [NASA-CR-4180] p 10 N89-12553
- A novel approach in formulation of special transition elements: Mesh interface elements p 199 N89-16193
- [NASA-CR-184768] p 199 N89-16193
- Conservative treatment of boundary interfaces for overlaid grids and multi-level grid adaptations p 15 N89-24269
- [NASA-TM-102080] p 15 N89-24269
- Numerical analysis of supersonic flow through oscillating cascade sections by using a deforming grid p 15 N89-25119
- [NASA-TM-102053] p 15 N89-25119
- On the applications of algebraic grid generation methods based on transfinite interpolation p 33 N89-26003
- [NASA-TM-102095] p 33 N89-26003
- Multigrid calculation of three-dimensional turbomachinery flows p 165 N89-26172
- [NASA-CR-185332] p 165 N89-26172
- Mesh refinement in a two-dimensional large eddy simulation of a forced shear layer p 166 N89-26180
- [NASA-TM-102129] p 166 N89-26180
- Multi-grid for structures analysis p 206 N89-29810
- COMPUTER AIDED DESIGN**
- Structural tailoring of Space Shuttle Main Engine turbopump blades SSME/STAEBL p 55 A89-44106
- User interactive electric propulsion software design [AIAA PAPER 89-2376] p 57 A89-46783
- Computer-aided design of bevel gear tooth surfaces [NASA-TM-101449] p 183 N89-17248
- A compendium of controlled diffusion blades generated by an automated inverse design procedure p 31 N89-20996
- [NASA-TM-101968] p 31 N89-20996
- Comparison study of gear dynamic computer programs at NASA Lewis Research Center p 184 N89-21243
- [NASA-TP-2901] p 184 N89-21243
- A perspective on future directions in aerospace propulsion system simulation p 31 N89-21798
- [NASA-TM-102038] p 31 N89-21798
- Advances in computational design and analysis of airbreathing propulsion systems p 32 N89-23465
- [NASA-TM-101987] p 32 N89-23465
- Structural tailoring of counter rotation propfans p 33 N89-25165
- Tailoring of composite links for optimal damped elasto-dynamic performance p 88 N89-26912
- [NASA-TM-102094] p 88 N89-26912
- COMPUTER GRAPHICS**
- Graphical postprocessing for 3-D mesh quality evaluation p 217 A89-38846
- Interactive grid generation for turbomachinery flow field simulations p 9 N89-11717
- [NASA-TM-101301] p 9 N89-11717
- Advances in computational design and analysis of airbreathing propulsion systems p 32 N89-23465
- [NASA-TM-101987] p 32 N89-23465
- Transputer parallel processing at NASA Lewis Research Center p 205 N89-29778
- COMPUTER NETWORKS**
- Integrated communication and control systems. I - Analysis p 219 A89-22499
- [ASME PAPER 88-WA/DSC-1] p 219 A89-22499
- Extended observability of linear time-invariant systems under recurrent loss of output data p 220 A89-52603
- [AIAA PAPER 89-3510] p 220 A89-52603
- Interfacing laboratory instruments to multiuser, virtual memory computers p 188 N89-19578
- [NASA-TM-4106] p 188 N89-19578
- Automating the multiprocessing environment p 217 N89-20641
- [NASA-TM-4103] p 217 N89-20641
- Transputer parallel processing at NASA Lewis Research Center p 205 N89-29778
- COMPUTER PROGRAMMING**
- A generalized one dimensional computer code for turbomachinery cooling passage flow calculations p 151 A89-46934
- [AIAA PAPER 89-2574] p 151 A89-46934
- Automating the multiprocessing environment p 217 N89-20641
- [NASA-TM-4103] p 217 N89-20641
- Initial operating capability for the hypercluster parallel-processing test bed p 218 N89-20685
- [NASA-TM-101953] p 218 N89-20685
- Institute for Computational Mechanics in Propulsion (ICOMP) p 222 N89-21595
- [NASA-TM-101961] p 222 N89-21595
- A generalized one-dimensional computer code for turbomachinery cooling passage flow calculations p 163 N89-22862
- [NASA-TM-102079] p 163 N89-22862
- COMPUTER PROGRAMS**
- High speed inlet calculations with real gas effects p 2 A89-14980
- [AIAA PAPER 88-3076] p 2 A89-14980
- Thermal-mechanical fatigue test apparatus for metal matrix composites and joint attachments p 79 A89-15727
- The development of an intelligent interface to a computational fluid dynamics flow-solver code p 216 A89-16963
- NNEPEQ - Chemical equilibrium version of the Navy/NASA Engine Program p 22 A89-24989
- [ASME PAPER 88-GT-314] p 22 A89-24989
- Evaluation of three turbulence models for the prediction of steady and unsteady airloads p 3 A89-25485
- [AIAA PAPER 89-0609] p 3 A89-25485
- Modeling of impulsive propellant reorientation [AIAA PAPER 89-0628] p 54 A89-25496
- Computer simulation of cyclic oxidation p 91 A89-29295
- Computational structural mechanics for engine structures p 22 A89-30745
- [AIAA PAPER 89-1260] p 22 A89-30745
- Mutual coupling in a finite planar array with interelement holes present p 125 A89-42768
- A generalized one dimensional computer code for turbomachinery cooling passage flow calculations p 151 A89-46934
- [AIAA PAPER 89-2574] p 151 A89-46934
- Analytical flutter investigation of a composite propfan model p 195 A89-48663
- A numerical study of chemically reacting flow in nozzles p 60 A89-49687
- [AIAA PAPER 89-2793] p 60 A89-49687
- Computerized life and reliability modeling for turboprop transmissions p 181 A89-53364
- Measurement of the properties of lossy materials inside a finite conducting cylinder p 126 N89-10223
- [NASA-CR-182500] p 126 N89-10223
- Evaluation of three turbulence models for the prediction of steady and unsteady airloads p 10 N89-12555
- [NASA-TM-101413] p 10 N89-12555
- Influence of bulk turbulence and entrance boundary layer thickness on the curved duct flow field p 156 N89-12896
- Automation software for a materials testing laboratory p 217 N89-12917
- Predictions of airfoil aerodynamic performance degradation due to icing p 10 N89-13412
- [NASA-TM-101434] p 10 N89-13412
- Constitutive modeling for isotropic materials p 26 N89-13436
- [NASA-CR-174805] p 26 N89-13436
- Modeling of impulsive propellant reorientation p 64 N89-13495
- [NASA-TM-101440] p 64 N89-13495
- Examination of coating failure by acoustic emission p 110 N89-13654
- LDV measurements in an annular combustor model p 159 N89-13755
- [NASA-CR-182207] p 159 N89-13755
- Gear optimization p 182 N89-13793
- [NASA-CR-4201] p 182 N89-13793
- MHOST version 4.2. Volume 1: Users' manual p 217 N89-13996
- [NASA-CR-182235-VOL-1] p 217 N89-13996
- Plotting component maps in the Navy/NASA Engine Program (NNEP): A method and its usage p 26 N89-14239
- [NASA-TM-101433] p 26 N89-14239
- Development of BEM for ceramic composites p 111 N89-14311
- [NASA-CR-183313] p 111 N89-14311
- Development of an integrated BEM approach for hot fluid structure interaction p 27 N89-15114
- [NASA-CR-184587] p 27 N89-15114
- An analysis for high speed propeller-nacelle aerodynamic performance prediction. Volume 1: Theory and application p 12 N89-15896
- [NASA-CR-4199-VOL-1] p 12 N89-15896
- Three-dimensional inelastic analysis for hot section components, BEST 3D code p 199 N89-17317
- Three-dimensional inelastic analysis methods for hot section components p 199 N89-17321
- CFD validation experiments for internal flows p 161 N89-18635
- Interfacing laboratory instruments to multiuser, virtual memory computers p 188 N89-19578
- [NASA-TM-4106] p 188 N89-19578
- Fatigue crack growth model RANDOM2 user manual. Appendix 1: Development of advanced methodologies for probabilistic constitutive relationships of material strength models p 201 N89-19581
- [NASA-CR-184775-APP-1] p 201 N89-19581
- Fatigue strength reduction model: RANDOM3 and RANDOM4 user manual. Appendix 2: Development of advanced methodologies for probabilistic constitutive relationships of material strength models p 201 N89-19582
- [NASA-CR-184796-APP-2] p 201 N89-19582
- A message passing kernel for the hypercluster parallel processing test bed p 218 N89-20684
- [NASA-TM-101952] p 218 N89-20684
- Convection and chemistry effects in CVD: A 3-D analysis for silicon deposition p 78 N89-21032
- [NASA-TM-102001] p 78 N89-21032
- Computer simulation of macrosegregation in directionally solidified circular ingots p 122 N89-21134
- [NASA-CR-182838] p 122 N89-21134

- Advanced helium purge seals for Liquid Oxygen (LOX) turbopumps  
[NASA-CR-182105] p 184 N89-21239
- Comparison study of gear dynamic computer programs at NASA Lewis Research Center  
[NASA-TP-2901] p 184 N89-21243
- A generalized one-dimensional computer code for turbomachinery cooling passage flow calculations  
[NASA-TM-102079] p 163 N89-22862
- Composite blade structural analyzer (COBSTRAN) user's manual  
[NASA-TM-101461] p 86 N89-23621
- A numerical study of chemically reacting flow in nozzles  
[NASA-TM-102135] p 70 N89-24444
- Advanced methods for 3-D inelastic structural analysis for hot engine structures  
[NASA-TM-102106] p 204 N89-25490
- Comparative thermal analysis of the space station Freedom photovoltaic deployable boom structure using TRASYS, NEVADA, and SINDA programs  
[NASA-TM-102062] p 165 N89-26177
- Computational structural mechanics for engine structures  
[NASA-TM-102119] p 204 N89-26259
- Nonlinear mesomechanics of composites with periodic microstructure  
[NASA-TM-102051] p 204 N89-26260
- Metal matrix composite micromechanics: In-situ behavior influence on composite properties  
[NASA-TM-102302] p 88 N89-26924
- Film annotation system for a space experiment  
[NASA-CR-185114] p 176 N89-27152
- Numerical studies of convective heat transfer in an inclined semiannular enclosure  
[NASA-TM-102011] p 123 N89-28666
- The 3-D inelastic analyses for computational structural mechanics  
p 206 N89-29804
- COMPUTER SYSTEMS PERFORMANCE**
- A perspective on future directions in aerospace propulsion system simulation  
[NASA-TM-102038] p 31 N89-21798
- COMPUTER TECHNIQUES**
- Hierarchical Poly Tree computer architectures defined by computational multidisciplinary mechanics  
p 218 A89-50100
- Institute for Computational Mechanics in Propulsion (ICOMP)  
[NASA-TM-101961] p 222 N89-21595
- COMPUTER VISION**
- Vision sensing techniques in aeronautics and astronautics  
p 219 A89-31087
- COMPUTERIZED SIMULATION**
- Fiber composite sandwich thermostructural behavior - Computational simulation  
p 190 A89-11246
- An integrated and modular digital modeling approach for the Space Station electrical power system development  
p 50 A89-15298
- Simulation test beds for the Space Station electrical power system  
p 39 A89-15352
- Dynamic characteristics of a 20 kHz resonant power system - Fault identification and fault recovery  
p 52 A89-15357
- Cosmic strings - A problem or a solution?  
p 240 A89-19610
- Computer simulation of cyclic oxidation  
p 91 A89-29295
- Computationally generated velocity taper for efficiency enhancement in a coupled-cavity traveling-wave tube  
p 132 A89-31987
- Bipolar coordinates for computation of transition duct flows  
p 148 A89-34912
- Dynamic delamination buckling in composite laminates under impact loading - Computational simulation  
p 82 A89-36310
- Two-dimensional simulation of electrothermal deicing of aircraft components  
p 17 A89-39194
- A correction algorithm for particle size distribution measurements made with the forward-scattering spectrometer probe  
p 170 A89-44123
- Interactive grid generation for turbomachinery flow field simulations  
[NASA-TM-101301] p 9 N89-11717
- Effects of environmentally imposed roughness on airfoil performance  
[NASA-CR-179639] p 17 N89-11725
- Mathematical modeling of solid oxide fuel cells  
[NASA-CR-182188] p 209 N89-12122
- A control-volume method for analysis of unsteady thrust augmenting ejector flows  
[NASA-CR-182203] p 24 N89-12566
- A probabilistic approach to composite micromechanics  
[NASA-TM-101366] p 85 N89-12684
- HOST combustion R and T overview  
p 25 N89-12879
- Turbine stator flow field simulations  
p 157 N89-12902
- Predictions of airfoil aerodynamic performance degradation due to icing  
[NASA-TM-101434] p 10 N89-13412
- Parallel processing of a rotating shaft simulation  
[NASA-TM-101462] p 223 N89-17453
- A definition study of the on-orbit assembly operations for the outboard photovoltaic power modules for Space Station Freedom  
[NASA-TM-102006] p 41 N89-20171
- Computer simulation of macrosegregation in directionally solidified circular ingots  
[NASA-CR-182838] p 122 N89-21134
- Computer simulation of a pilot in V/STOL aircraft control loops  
[NASA-CR-184815] p 215 N89-21479
- A perspective on future directions in aerospace propulsion system simulation  
[NASA-TM-102038] p 31 N89-21798
- The isothermal fatigue behavior of a unidirectional SiC/Ti composite and the Ti alloy matrix  
[NASA-TM-101984] p 86 N89-22684
- Topology of modified helical gears and Tooth Contact Analysis (TCA) program  
[NASA-CR-4224] p 186 N89-22920
- Advances in computational design and analysis of airbreathing propulsion systems  
[NASA-TM-101987] p 32 N89-23465
- Advanced computational techniques for hypersonic propulsion  
[NASA-TM-102005] p 163 N89-23809
- Two-dimensional numerical simulation of a Stirling engine heat exchanger  
[NASA-TM-102057] p 164 N89-23823
- A model for prediction of STOVL ejector dynamics  
[NASA-TM-102098] p 32 N89-24319
- Comparison of predicted and measured temperatures of UH-60A helicopter transmission  
[NASA-TP-2911] p 186 N89-24607
- NASA Lewis Stirling engine computer code evaluation  
[NASA-CR-182248] p 214 N89-24741
- Mesh refinement in a two-dimensional large eddy simulation of a forced shear layer  
[NASA-TM-102129] p 166 N89-26180
- On finite element implementation and computational techniques for constitutive modeling of high temperature composites  
[NASA-CR-185120] p 204 N89-26261
- Development and refinement of test bed simulations  
[NASA-TM-102335] p 75 N89-27702
- Computational simulation of high temperature metal matrix composites cyclic behavior  
[NASA-TM-102115] p 88 N89-27795
- Indium phosphide solar cell research in the US: Comparison with nonphotovoltaic sources  
[NASA-TM-102103] p 124 N89-27868
- Computational structural mechanics engine structures computational simulator  
p 205 N89-29792
- CONCENTRATORS**
- Temperature coefficients for concentrator cells at various electron and proton fluence levels  
p 51 A89-15304
- Thermal distortion analysis of the Space Station solar dynamic concentrator  
p 51 A89-15341
- Predicted performance of InP solar cells in Cassegrainian and slats space concentrator arrays at 20 to 100 AMO, 80 to 100 C  
p 212 N89-24711
- Domed Fresnel lens concentrator technology for space application  
p 213 N89-24732
- Thermal evaluation of advanced solar dynamic heat receiver performance  
[NASA-CR-185117] p 214 N89-27256
- A program for advancing the technology of space concentrators  
[NASA-TM-102139] p 76 N89-29484
- CONDENSATES**
- Aerodynamically-driven condensate layer thickness distributions on isothermal cylindrical surfaces  
p 140 A89-12337
- Vapor deposition and condensate flow on combustion turbine blades - Theoretical model to predict/understand some corrosion rate consequences of molten alkali sulfate deposition in the field or laboratory  
p 21 A89-20950
- CONDENSATION**
- Transport-induced shifts in condensate dew-point and composition in multicomponent systems with chemical reaction  
p 89 A89-12333
- CONDENSING**
- Vapor condensation at a turbulent liquid surface in systems with possible spaced-based applications  
[AIAA PAPER 89-2846] p 151 A89-47122
- Numerical studies of the effects of jet-induced mixing on liquid-vapor interface condensation  
[AIAA PAPER 89-1744] p 152 A89-48958
- Numerical studies of the effects of jet-induced mixing on liquid-vapor interface condensation  
[NASA-CR-182285] p 163 N89-23818
- CONDUCTION**
- Measurement of the properties of lossy materials inside a finite conducting cylinder  
[NASA-CR-182500] p 126 N89-10223
- CONDUCTIVE HEAT TRANSFER**
- Advanced development of the boundary element method for steady-state heat conduction  
p 154 A89-54766
- CONFERENCES**
- IECON '87: Industrial applications of control and simulation; Proceedings of the 1987 International Conference on Industrial Electronics, Control, and Instrumentation, Cambridge, MA, Nov. 3, 4, 1987  
[SPIE-853] p 219 A89-10798
- Optoelectronic signal processing for phased-array antennas; Proceedings of the Meeting, Los Angeles, CA, Jan. 12, 13, 1988  
[SPIE-886] p 124 A89-15819
- Test methods and design allowables for fibrous composites. Volume 2  
[ASTM STP-1003] p 81 A89-32882
- Heat transfer in gas turbine engines and three-dimensional flows; Proceedings of the Symposium, ASME Winter Annual Meeting, Chicago, IL, Nov. 27-Dec. 2, 1988  
p 148 A89-34926
- The NASA Electric Propulsion Program  
p 59 A89-47428
- Turbine Engine Hot Section Technology 1986  
[NASA-CP-2444] p 195 N89-12876
- Thermal Barrier Coatings. Abstracts and figures  
[NASA-CP-10019] p 110 N89-13642
- Turbine Engine Hot Section Technology, 1987  
[NASA-CP-2493] p 199 N89-17298
- Microgravity Combustion Diagnostics Workshop  
[NASA-CP-10017] p 120 N89-17682
- Toward improved durability in advanced aircraft engine hot sections  
[NASA-TM-4087] p 29 N89-20135
- Rotordynamic Instability Problems in High-Performance Turbomachinery, 1988  
[NASA-CP-3026] p 185 N89-22891
- Space Electrochemical Research and Technology Conference: Abstracts  
[NASA-CP-10029] p 211 N89-22962
- Tribology: The Story of Lubrication and Wear  
[NASA-TM-101430] p 203 N89-24635
- Space Photovoltaic Research and Technology, 1988. High Efficiency, Space Environment, and Array Technology  
[NASA-CP-3030] p 212 N89-24704
- CONFORMAL MAPPING**
- Conservative treatment of boundary interfaces for overlaid grids and multi-level grid adaptations  
[AIAA PAPER 89-1980] p 5 A89-41823
- A simple algebraic grid adaptation scheme with applications to two- and three-dimensional flow problems  
[AIAA PAPER 89-1984] p 5 A89-41827
- CONICAL NOZZLES**
- Arcjet nozzle design impacts  
[NASA-TM-102050] p 68 N89-23522
- CONNECTORS**
- Characterization of structural connections using free and forced response test data  
[NASA-TM-101991] p 202 N89-21266
- CONSERVATION EQUATIONS**
- An explicit Runge-Kutta method for turbulent reacting flow calculations  
[NASA-TM-101945] p 31 N89-21799
- CONSERVATION LAWS**
- Nonoscillatory solution of the steady-state inviscid Burgers' equation by mathematical programming  
p 221 A89-22756
- Second-order accurate nonoscillatory schemes for scalar conservation laws  
[NASA-TM-102010] p 14 N89-22573
- CONSOLIDATION**
- Slurry-pressing consolidation of silicon nitride  
[NASA-TM-101365] p 109 N89-12746
- CONSTITUTIVE EQUATIONS**
- The constitutive representation of high-temperature creep damage  
p 191 A89-17396
- A viscoplastic constitutive theory for metal matrix composites at high temperature  
p 80 A89-20725
- Symbolic generation of constitutive equations  
p 221 A89-34963
- Material parameter determination from scattering measurements  
[NASA-CR-183312] p 126 N89-10225
- Constitutive modeling for isotropic materials  
p 195 N89-12904
- A multiaxial theory of viscoplasticity for isotropic materials  
p 196 N89-12908

- Constitutive modeling for single crystal superalloys  
p 101 N89-12911
- Constitutive modelling of single crystal and directionally solidified superalloys  
p 101 N89-12912
- Life prediction and constitutive models for engine hot section  
p 188 N89-12916
- Deformation modeling and constitutive modeling for anisotropic superalloys  
[NASA-CR-4215]  
p 202 N89-21258
- CONTACT LOADS**  
Crowned spur gears - Methods for generation and tooth contact analysis. I - Basic concepts, generation of the pinion tooth surface by a plane  
p 179 A89-29306
- Tooth contact shift in loaded spiral bevel gears o, IL, 25-27 Apr. 1989, sponsored by ASME  
[NASA-TM-101438]  
p 183 N89-14453
- CONTACTORS**  
Ground-based plasma contactor characterization  
p 233 A89-43359
- CONTAMINATION**  
Experimental evaluation of resistojet thruster plume shields  
p 59 A89-47487
- CONTINUOUS RADIATION**  
Design, fabrication, and performance of brazed, graphite electrode, multistage depressed collectors with 500-W, continuous wave, 4.8- to 9.6-GHz traveling-wave tubes  
[NASA-TP-2904]  
p 136 N89-21171
- CONTINUUM MECHANICS**  
Mechanics of damping for fiber composite laminates including hygro-thermal effects  
[AIAA PAPER 89-1191]  
p 192 A89-30681
- Time dependent reliability model incorporating continuum damage mechanics for high-temperature ceramics  
[NASA-TM-102046]  
p 115 N89-24487
- CONTOURS**  
A method for producing a shaped contour radiation pattern using a single shaped reflector and a single feed  
p 125 A89-42758
- A method for producing a shaped contour radiation pattern using a single shaped reflector and a single feed  
[NASA-TM-101369]  
p 126 N89-10215
- COUNTERROTATING PROPELLERS**  
Unsteady blade pressure measurements on a model counterrotation propeller  
[AIAA PAPER 89-1144]  
p 226 A89-40175
- Average-passage simulation of counter-rotating propfan propulsion systems as applied to cruise missiles  
[AIAA PAPER 89-2943]  
p 7 A89-47187
- Noise of a model counterrotation propeller with simulated fuselage and support pylon at takeoff/approach conditions  
[AIAA PAPER 89-1143]  
p 227 A89-48953
- Low-speed wind tunnel performance of high-speed counterrotation propellers at angle-of-attack  
[AIAA PAPER 89-2583]  
p 8 A89-50808
- Unsteady blade pressure measurements on a model counterrotation propeller  
[NASA-TM-102002]  
p 228 N89-20779
- Average-passage simulation of counter-rotating propfan propulsion systems as applied to cruise missiles  
[NASA-TM-102043]  
p 14 N89-23416
- Noise of a model counterrotation propeller with simulated fuselage and support pylon at takeoff/approach conditions  
[NASA-TM-101996]  
p 228 N89-24138
- Low-speed wind tunnel performance of high-speed counterrotation propellers at angle-of-attack  
[NASA-TM-102292]  
p 15 N89-25121
- CONTROL EQUIPMENT**  
Simulation and control of a 20 kHz spacecraft power system  
p 130 A89-15391
- CONTROL SIMULATION**  
IECON '87: Industrial applications of control and simulation; Proceedings of the 1987 International Conference on Industrial Electronics, Control, and Instrumentation, Cambridge, MA, Nov. 3, 4, 1987  
[SPIE-853]  
p 219 A89-10798
- CONTROL STABILITY**  
Stability robustness improvement of direct eigenspace assignment based feedback systems using singular value sensitivities  
p 220 A89-53958
- Stability robustness improvement of direct eigenspace assignment based feedback systems using singular value sensitivities  
[NASA-CR-182302]  
p 36 N89-27672
- CONTROL SYSTEMS DESIGN**  
IECON '87: Industrial applications of control and simulation; Proceedings of the 1987 International Conference on Industrial Electronics, Control, and Instrumentation, Cambridge, MA, Nov. 3, 4, 1987  
[SPIE-853]  
p 219 A89-10798
- A reusable rocket engine intelligent control  
[AIAA PAPER 88-3114]  
p 48 A89-14981
- Optically controlled phased-array technology for space communication systems  
p 131 A89-15845

- Effect of model uncertainty on failure detection - The threshold selector  
p 219 A89-17965
- Integrated communication and control systems. I - Analysis  
[ASME PAPER 88-WA/DSC-1]  
p 219 A89-22499
- Integrated communication and control systems. II - Design considerations  
[ASME PAPER 88-WA/DSC-2]  
p 219 A89-22500
- A parametric LQ approach to multiobjective control system design  
p 219 A89-28605
- Observer design for compensation of network-induced delays in integrated communication and control systems  
p 220 A89-35044
- Integrated flight/propulsion control study for STOV applications  
[AIAA PAPER 89-2908]  
p 34 A89-47166
- Integrated flight/propulsion control system design based on a centralized approach  
[AIAA PAPER 89-3520]  
p 35 A89-52611
- An observer-based compensator for distributed delays in integrated control systems  
[AIAA PAPER 89-3541]  
p 35 A89-52628
- Integrated flight/propulsion control system design based on a decentralized, hierarchical approach  
[AIAA PAPER 89-3519]  
p 35 A89-53301
- Turbofan engine control system design using the LQG/LTR methodology  
p 23 A89-53956
- Stability robustness improvement of direct eigenspace assignment based feedback systems using singular value sensitivities  
p 220 A89-53958
- Computational fluid dynamic control  
p 220 A89-53984
- Identification of Space Shuttle Main Engine dynamics  
p 61 A89-54068
- Modal representations in control/structure interaction  
p 45 A89-54114
- Space station electrical power system availability study  
[NASA-CR-182198]  
p 45 N89-11802
- Integrated control and health management. Orbit transfer rocket engine technology program  
[NASA-CR-182122]  
p 62 N89-11805
- A parametric LQ approach to multiobjective control system design  
[NASA-TM-101316]  
p 220 N89-12283
- An expert system for restructurable control  
[NASA-TM-101378]  
p 220 N89-12309
- Design and implementation of a microcomputer-based user interface controller for bursted data communications satellite ground terminals  
[NASA-TM-101375]  
p 43 N89-13457
- Identification of space shuttle main engine dynamics  
[NASA-TM-101982]  
p 66 N89-20199
- Advances in computational design and analysis of airbreathing propulsion systems  
[NASA-TM-101987]  
p 32 N89-23465
- Turbofan engine control system design using the LQG/LTR methodology  
[NASA-CR-182303]  
p 33 N89-26004
- Integrated flight/propulsion control system design based on a centralized approach  
[NASA-TM-102137]  
p 35 N89-26009
- Stability robustness improvement of direct eigenspace assignment based feedback systems using singular value sensitivities  
[NASA-CR-182302]  
p 36 N89-27672
- CONTROL THEORY**  
New results concerning the use of kinematically redundant manipulators in microgravity environments  
[AIAA PAPER 89-3562]  
p 215 A89-52647
- CONTROLLERS**  
GaAs circuits for monolithic optical controller  
p 131 A89-15828
- Fiber optic control system integration  
[NASA-CR-179568]  
p 231 N89-13256
- Integrated control and health monitoring capacitive displacement sensor development task. Orbit transfer rocket engine technology program  
[NASA-CR-182279]  
p 176 N89-26208
- CONVECTION**  
Determination of convective diffusion heat/mass transfer rates to burner rig test targets comparable in size to cross-stream jet diameter  
p 141 A89-12753
- Interaction of surface radiation with convection in crystal growth by physical vapor transport  
[AIAA PAPER 89-0228]  
p 119 A89-30450
- An algorithm for unsteady flows with strong convection  
[NASA-TM-100828]  
p 221 N89-10575
- Development of an infrared imaging system for the surface tension driven convection experiment  
[NASA-TM-101479]  
p 174 N89-17211
- Infrared surface temperature measurements for the surface tension driven convection experiment  
[NASA-TM-101353]  
p 175 N89-21224

**CONVECTIVE FLOW**

- Simple high-accuracy resolution program for convective modelling of discontinuities  
p 143 A89-17459
- Convective flows in enclosures with vertical temperature or concentration gradients  
[AIAA PAPER 89-0069]  
p 118 A89-25060
- Convective flows in enclosures with vertical temperature or concentration gradients  
[NASA-TM-101373]  
p 120 N89-12753
- A genuinely multi-dimensional upwind cell-vertex scheme for the Euler equations  
[NASA-TM-102029]  
p 223 N89-24872
- CONVECTIVE HEAT TRANSFER**  
Impact of ETO propellants on the aerothermodynamic analyses of propulsion components --- Earth To Orbit  
[AIAA PAPER 88-3091]  
p 53 A89-16486
- Development of a special-purpose test surface guided by uncertainty analysis  
p 144 A89-22736
- Thermosolutal convection during dendritic solidification  
[AIAA PAPER 89-0626]  
p 118 A89-25495
- An experimental and analytical investigation of thermoacoustic convection heat transfer in gravity and zero-gravity environments  
[NASA-CR-179575]  
p 120 N89-11920
- Heat transfer in the tip region of a rotor blade simulator  
p 157 N89-12898
- Development of an integrated BEM approach for hot fluid structure interaction  
[NASA-CR-184587]  
p 27 N89-15114
- Numerical studies of convective heat transfer in an inclined semiannular enclosure  
[NASA-TM-102011]  
p 123 N89-28666
- CONVERGENT-DIVERGENT NOZZLES**  
Comparison of 3D computation and experiment for non-axisymmetric nozzles  
[AIAA PAPER 89-0007]  
p 22 A89-28403
- A numerical study of chemically reacting flow in nozzles  
[AIAA PAPER 89-2793]  
p 60 A89-49687
- A numerical study of chemically reacting flow in nozzles  
[NASA-TM-102135]  
p 70 N89-24444
- COOLANTS**  
Development of a thermal and structural analysis procedure for cooled radial turbines  
[NASA-TM-101416]  
p 24 N89-12568
- Coolant passage heat transfer with rotation  
p 161 N89-17314
- COOLING**  
Liquid oxygen cooling of high pressure LOX/hydrocarbon rocket thrust chambers  
p 63 N89-12649
- Lubricant jet flow phenomena in spur and helical gears with modified addendums; for radially directed individual jets  
[NASA-TM-101460]  
p 183 N89-15415
- Thermal expansion mismatch and plasticity in thermal barrier coating  
p 200 N89-17330
- Macrosegregation and nucleation in undercooled Pb-Sn alloys  
[NASA-TM-102023]  
p 104 N89-23664
- Optimum interface properties for metal matrix composites  
[NASA-TM-102295]  
p 205 N89-27223
- COOLING SYSTEMS**  
Big savings from small holes --- Liquid Droplet Radiator project for space vehicles  
p 45 A89-36724
- Numerical model of solar dynamic radiator for parametric analysis  
[NASA-TM-102054]  
p 67 N89-22653
- Scaling results for the Liquid Sheet Radiator (LSR)  
[NASA-TM-102100]  
p 72 N89-25277
- COORDINATES**  
Specialty functions singularity mechanics problems  
p 206 N89-29805
- COPLANARITY**  
Modeling of some coplanar waveguide discontinuities  
p 131 A89-24139
- COPOLYMERS**  
Addition polymers from 1,4,5,8-tetrahydro-1,4,5,8-diepoxyanthracene and Bis-dienes. 2: Evidence for thermal dehydration occurring in the cure process  
[NASA-TM-101385]  
p 112 N89-15235
- COPPER**  
Thermoviscoplastic model with application to copper  
[NASA-TP-2845]  
p 198 N89-16183
- Tungsten fiber reinforced copper matrix composites: A review  
[NASA-TP-2924]  
p 88 N89-27796
- COPPER OXIDES**  
Transport critical current and magnetization measurements of melt-processed YBa<sub>2</sub>Cu<sub>3</sub>O<sub>7-x</sub>  
p 234 A89-20037

- Non-uniform transition conductivity of superconducting ceramic  
[NASA-TM-102133] p 189 N89-28851
- CORE FLOW**  
Effects of core turbulence on jet excitability  
[AIAA PAPER 89-0966] p 147 A89-30482  
Effects of core turbulence on jet excitability  
[NASA-TM-101405] p 159 N89-14403
- CORNER FLOW**  
PNS calculations for 3-D hypersonic corner flow with two turbulence models  
[AIAA PAPER 88-2958] p 1 A89-14979  
An experimental study of near wall flow parameters in the blade end-wall corner region  
[NASA-CR-4211] p 12 N89-15898
- CORRECTION**  
Spatial resolution and downwash velocity corrections for multiple-hole pressure probes in complex flows  
p 171 A89-45909
- CORRELATION**  
Application of optical correlation techniques to particle imaging  
[AIAA PAPER 88-4661] p 169 A89-14985  
A comparison of turbulence measurement methods  
p 174 N89-17302
- CORROSION**  
Molten salt corrosion of SiC and Si<sub>3</sub>N<sub>4</sub>  
[NASA-TM-101346] p 108 N89-11912
- CORROSION RESISTANCE**  
Sodium sulfate - Deposition and dissolution of silica  
p 91 A89-28084  
The behavior of SiC and Si<sub>3</sub>N<sub>4</sub> ceramics in mixed oxidation/chlorination environments p 106 A89-33616  
Castable hot corrosion resistant alloy  
[NASA-CASE-LEW-14134-2] p 102 N89-14303  
MATE program: Erosion resistant compressor airfoil coating, volume 2  
[NASA-CR-179645] p 113 N89-18550
- CORROSION TESTS**  
Corrosion testing of candidates for the alkaline fuel cell cathode  
p 212 N89-23000
- COSMOLOGY**  
Patterns of the cosmic microwave background from evolving string networks  
p 240 A89-14618  
Cosmic strings and the large-scale structure  
p 240 A89-19604  
Cosmic strings - A problem or a solution?  
p 240 A89-19610  
Is the great attractor really a great wall? --- late-time cosmological phase transition producing coherent velocity caused by relic domain wall repulsive effect  
p 241 A89-36278  
A coasting cosmology  
p 241 A89-53833
- COUNTER ROTATION**  
Cruise noise of an advanced counterrotation turboprop measured from an adjacent aircraft  
p 20 A89-15080  
Laser velocimeter measurements of the flowfield generated by an advanced counterrotating propeller  
[AIAA PAPER 89-0434] p 3 A89-26373  
Comparison of propeller cruise noise data taken in the NASA Lewis 8- by 6-foot wind tunnel with other tunnel and flight data  
[AIAA PAPER 89-1059] p 226 A89-40472  
The effect of front-to-rear propeller spacing on the interaction noise at cruise conditions of a model counterrotation propeller having a reduced diameter aft propeller  
[NASA-TM-101329] p 227 N89-10603  
Laser velocimeter measurements of the flowfield generated by an advanced counterrotating propeller  
[NASA-TM-101437] p 10 N89-13409  
Measured far-field flight noise of a counterrotation turboprop at cruise conditions  
[NASA-TM-101383] p 228 N89-15686  
Comparison of propeller cruise noise data taken in the NASA Lewis 8- by 6-foot wind tunnel with other tunnel and flight data  
[NASA-TM-101976] p 228 N89-21628  
Structural tailoring of counter rotation propfans  
p 33 N89-25165
- COUPLED MODES**  
Computationally generated velocity taper for efficiency enhancement in a coupled-cavity traveling-wave tube  
p 132 A89-31987  
Mutual coupling in a finite planar array with interelement holes present  
p 125 A89-42768  
Aperture impedance of flared horns  
p 125 A89-43543
- COUPLERS**  
Study of optical output couplers for submillimeter wavelength backward-wave oscillators (BWO's)  
[NASA-TM-101360] p 134 N89-11128
- COVALENT BONDS**  
Connection between energy relations of solids and molecules  
p 91 A89-26406
- COVARIANCE**  
Analysis of modified SMI method for adaptive array weight control  
[NASA-CR-184904] p 127 N89-20364  
Analysis of modified SMI method for adaptive array weight control  
[NASA-CR-185493] p 19 N89-25993
- CRACK CLOSURE**  
Influence of fatigue crack wake length and state of stress on crack closure  
p 191 A89-17432  
Elevated temperature crack growth  
p 200 N89-17335
- CRACK GEOMETRY**  
Probabilistic Finite Elements (PFEM) structural dynamics and fracture mechanics  
p 206 N89-29803
- CRACK INITIATION**  
Radiographic and ultrasonic characterization of sintered silicon carbide  
p 187 A89-14700  
Creep life prediction based on stochastic model of microstructurally short crack growth  
p 193 A89-36185  
Simplified cyclic structural analysis of SSME turbine blades  
p 63 N89-12632  
Fatigue and fracture overview  
p 195 N89-12882  
Stochastic modeling of crack initiation and short-crack growth under creep and creep-fatigue conditions  
[NASA-TM-101358] p 199 N89-17286  
High temperature constitutive and crack initiation modeling of coated single crystal superalloys  
p 112 N89-17334  
Fatigue life prediction modeling for turbine hot section materials  
p 30 N89-20142  
Analysis of interface crack branching  
[NASA-CR-182273] p 202 N89-21265
- CRACK OPENING DISPLACEMENT**  
Fracture mechanics applied to elevated temperature crack growth  
p 195 A89-47705
- CRACK PROPAGATION**  
Morphological study of near threshold fatigue crack growth in a coarse grain aluminum alloy  
p 94 A89-12326  
Resolved shear stress intensity coefficient and fatigue crack growth in large crystals  
p 96 A89-22048  
Crack growth resistance of textured alumina  
p 105 A89-26452  
Creep life prediction based on stochastic model of microstructurally short crack growth  
p 193 A89-36185  
Accelerated fatigue crack growth behavior of PWA 1480  
p 97 A89-36461  
Fatigue crack growth behavior of a single crystal alloy as observed through an in situ fatigue loading stage  
p 99 A89-45946  
Kinetics of fracture in Fe-3Si steel under mode I loading  
p 99 A89-47320  
Fracture mechanics applied to elevated temperature crack growth  
p 195 A89-47705  
Avalanche in adhesion --- interfacial separation between two Ni crystals  
p 100 A89-54495  
Elevated temperature crack growth  
p 196 N89-12915  
Grain boundary oxidation and its effects on high temperature fatigue life  
p 101 N89-12918  
Examination of coating failure by acoustic emission  
p 110 N89-13654  
Local-global analysis of crack growth in continuously reinforced ceramic matrix composites  
[NASA-CR-182231] p 197 N89-13820  
Stochastic modeling of crack initiation and short-crack growth under creep and creep-fatigue conditions  
[NASA-TM-101358] p 199 N89-17286  
Elevated temperature crack growth  
p 200 N89-17335
- Fatigue crack growth model RANDOM2 user manual, appendix 1  
[NASA-CR-184939] p 203 N89-23890
- CRACKS**  
Total strain version of strainrange partitioning for thermomechanical fatigue at low strains  
p 201 N89-17337  
Arcjet cathode phenomena  
[NASA-TM-102099] p 167 N89-27121
- CREEP ANALYSIS**  
Stochastic modeling of crack initiation and short-crack growth under creep and creep-fatigue conditions  
[NASA-TM-101358] p 199 N89-17286
- CREEP BUCKLING**  
Nonisothermal elastoviscoplastic snap-through and creep buckling of shallow arches  
p 194 A89-47370  
Non-isothermal buckling behavior of viscoplastic shell structures  
[NASA-CR-183013] p 197 N89-12931
- CREEP PROPERTIES**  
Influence of precipitate morphology on intermediate temperature creep properties of a nickel-base superalloy single crystal  
p 96 A89-26872  
Creep life prediction based on stochastic model of microstructurally short crack growth  
p 193 A89-36185  
High-temperature LCF of Ni-201 and 304L stainless steel  
p 100 N89-12635  
Fatigue and fracture overview  
p 195 N89-12882  
Creep fatigue life prediction for engine hot section materials (isotropic): Fourth year progress review  
p 188 N89-12914  
Grain boundary oxidation and its effects on high temperature fatigue life  
p 101 N89-12918  
An investigation of environmental influence on the creep behavior of a low pressure plasma sprayed NiCoCrAlY alloy  
p 110 N89-13648  
Preliminary study of creep thresholds and thermomechanical response in Haynes 188 at temperatures in the range 649 to 871 C  
p 200 N89-17327  
Total strain version of strainrange partitioning for thermomechanical fatigue at low strains  
p 201 N89-17337  
Procedures for characterizing an alloy and predicting cyclic life with the total strain version of Strainrange Partitioning  
[NASA-TM-4102] p 203 N89-25485  
The interface in tungsten fiber reinforced niobium metal-matrix composites  
[NASA-TM-102122] p 104 N89-28627  
Creep behavior of tungsten fiber reinforced niobium metal matrix composites  
[NASA-TM-102307] p 104 N89-29522
- CREEP RUPTURE STRENGTH**  
Tensile and creep rupture behavior of P/M processed Nb-base alloy, WC-3009  
[NASA-TM-101954] p 78 N89-19371  
Creep behavior of tungsten fiber reinforced niobium metal matrix composites  
[NASA-TM-102307] p 104 N89-29522
- CREEP STRENGTH**  
Exposure time considerations in high temperature low cycle fatigue  
p 192 A89-29600  
Stochastic modeling of crack initiation and short-crack growth under creep and creep-fatigue conditions  
[NASA-TM-101358] p 199 N89-17286  
Creep behavior of tungsten fiber reinforced niobium metal matrix composites  
[NASA-TM-102307] p 104 N89-29522
- CREEP TESTS**  
The constitutive representation of high-temperature creep damage  
p 191 A89-17396  
Preliminary study of creep thresholds and thermomechanical response in Haynes 188 at temperatures in the range 649 to 871 C  
p 200 N89-17327  
Procedures for characterizing an alloy and predicting cyclic life with the total strain version of Strainrange Partitioning  
[NASA-TM-4102] p 203 N89-25485
- CREW WORKSTATIONS**  
Space nuclear reactor shields for manned and unmanned applications  
[NASA-TM-102064] p 71 N89-25272
- CRITICAL FLOW**  
Nonlinear spatial evolution of an externally excited instability wave in a free shear layer  
p 144 A89-23242  
The upper-branch stability of compressible boundary layer flows  
[NASA-TM-102128] p 167 N89-28748
- CRITICAL LOADING**  
The scratch test - Different critical load determination techniques --- adhesive strength of thin hard coatings  
p 171 A89-54278  
Adhesion scratch testing - A round-robin experiment  
p 171 A89-54281

## CRITICAL POINT

Critical fluid light scattering p 121 N89-20320

## CROSS FLOW

Three dimensional simulation of an underexpanded jet interacting with a supersonic cross flow  
[AIAA PAPER 88-3181] p 2 A89-14982  
Thermal measurements for jets in disturbed and undisturbed crosswind conditions p 20 A89-16102  
Three-dimensional marginal separation  
[NASA-TM-101411] p 159 N89-13757

## CROSSLINKING

The correlation of low-velocity impact resistance of graphite-fiber-reinforced composites with matrix properties p 79 A89-16283  
Degradation and crosslinking of perfluoroalkyl polyethers under X-ray irradiation in ultrahigh vacuum  
[NASA-TP-2910] p 114 N89-21103

## CRUCIBLES

Effects of crucible wetting during solidification of immiscible Pb-Zn alloys  
[AIAA PAPER 89-0304] p 118 A89-25261  
Effects of crucible wetting during solidification of immiscible Pb-Zn  
[NASA-TM-101372] p 120 N89-14341

## CRUISE MISSILES

Average-passage simulation of counter-rotating propfan propulsion systems as applied to cruise missiles  
[AIAA PAPER 89-2943] p 7 A89-47187  
Average-passage simulation of counter-rotating propfan propulsion systems as applied to cruise missiles  
[NASA-TM-102043] p 14 N89-23416

## CRUISING FLIGHT

Cruise noise of an advanced counterrotation turboprop measured from an adjacent aircraft p 20 A89-15080  
Performance potential of air turbo-ramjet employing supersonic through-flow fan  
[AIAA PAPER 89-0010] p 22 A89-25006  
A supersonic through-flow fan engine airframe integration study  
[AIAA PAPER 89-2140] p 18 A89-50802  
The effect of front-to-rear propeller spacing on the interaction noise at cruise conditions of a model counterrotation propeller having a reduced diameter aft propeller  
[NASA-TM-101329] p 227 N89-10603  
Measured far-field flight noise of a counterrotation turboprop at cruise conditions  
[NASA-TM-101383] p 228 N89-15686  
Supersonic through-flow fan assessment  
[NASA-CR-182202] p 27 N89-16843

## CRYOGENIC EQUIPMENT

Analysis of the nonvented fill of a 4.96-cubic-meter lightweight liquid hydrogen tank  
[NASA-TM-102039] p 67 N89-22652

## CRYOGENIC FLUID STORAGE

Technology requirements for an orbiting fuel depot - A necessary element of a space infrastructure  
[IAF PAPER 88-035] p 37 A89-17641  
COLD-SAT: A technology satellite for cryogenic experimentation  
[NASA-TM-102286] p 47 N89-26036  
COLD-SAT: An orbital cryogenic hydrogen technology experiment  
[NASA-TM-102303] p 73 N89-26044  
COLD-SAT: Cryogenic On-Orbit Liquid Depot-Storage, Acquisition and Transfer  
[NASA-TM-102308] p 38 N89-28535

## CRYOGENIC FLUIDS

Mass flow meter using the triboelectric effect for measurement in cryogenics  
[NASA-CR-179572] p 155 N89-12836  
Mass flow measurement of liquid cryogenics using the triboelectric effect  
[NASA-CR-179519] p 155 N89-12837  
Analysis of the nonvented fill of a 4.96-cubic-meter lightweight liquid hydrogen tank  
[NASA-TM-102039] p 67 N89-22652

## CRYOGENIC ROCKET PROPELLANTS

Technology issues associated with fueling the national aerospace plane with slush hydrogen  
[NASA-TM-101386] p 61 N89-10123  
Advanced APS impacts on vehicle payloads  
[NASA-TM-102086] p 41 N89-25254  
COLD-SAT: Cryogenic On-Orbit Liquid Depot-Storage, Acquisition and Transfer  
[NASA-TM-102308] p 38 N89-28535

## CRYOGENICS

Space propulsion technology and cryogenic fluid depot p 38 N89-11768  
Cryogenic reactant storage for lunar base regenerative fuel cells  
[NASA-TM-101980] p 210 N89-21419

## CRYOPUMPING

Design and test of an oxygen turbopump for a dual expander cycle rocket engine  
[AIAA PAPER 89-2305] p 56 A89-46737

## CRYSTAL DEFECTS

High temperature constitutive and crack initiation modeling of coated single crystal superalloys p 112 N89-17334

## CRYSTAL DISLOCATIONS

Indentation plasticity and fracture in silicon  
[NASA-TP-2863] p 100 N89-10996  
Molecular beam epitaxial growth of high-quality InSb on InP and GaAs substrates  
[NASA-CR-185440] p 236 N89-26739

## CRYSTAL GROWTH

Dendritic solidification in binary alloys p 96 A89-22560  
Convective flows in enclosures with vertical temperature or concentration gradients  
[AIAA PAPER 89-0069] p 118 A89-25060  
Evaluation of transport conditions during physical vapor transport growth of opto-electronic crystals  
[AIAA PAPER 89-0229] p 118 A89-25197  
Flight hardware and tele-operations supporting the Isothermal Dendritic Growth Experiment aboard the Space Shuttle  
[AIAA PAPER 89-0863] p 118 A89-25627  
Interaction of surface radiation with convection in crystal growth by physical vapor transport  
[AIAA PAPER 89-0228] p 119 A89-30450  
Crystal growth of SiC for electronic applications p 132 A89-33625  
A facility for precise temperature control applications in microgravity p 48 A89-36956  
Characterization of multilayer GaAs/AlGaAs transistor structures by variable angle spectroscopic ellipsometry p 133 A89-49998  
Effects of furnace temperature profile on the interface shape during Bridgman crystal growth p 119 A89-53278  
Convective flows in enclosures with vertical temperature or concentration gradients  
[NASA-TM-101373] p 120 N89-12753  
Raman intensity as a probe of concentration near a crystal growing in solution  
[NASA-TP-2865] p 174 N89-16139  
Isothermal dendritic growth: A low gravity experiment p 121 N89-20299  
A V-grooved GaAs solar cell  
[NASA-TM-101970] p 211 N89-22177

## CRYSTAL STRUCTURE

Structural chemistry of Au(III)-substituted Ba<sub>2</sub>YCu<sub>3</sub>O<sub>7</sub>( $\delta$ ) p 89 A89-12620  
Effect of processing parameters on the characteristics of high-Tc superconductor YBa<sub>2</sub>Cu<sub>3</sub>O<sub>y</sub> p 234 A89-20467  
Growth of diamond by RF plasma-assisted chemical vapor deposition p 90 A89-20474  
Avalanche in adhesion --- interfacial separation between two Ni crystals p 100 A89-54495  
Design, development and applications of novel techniques for studying surface mechanical properties  
[NASA-TM-101959] p 113 N89-20253

## CRYSTAL SURFACES

The surface morphology of crystals melting under solutions of different densities p 235 A89-23482

## CRYSTALLIZATION

Crystallization of BaF<sub>2</sub>-ZnF<sub>2</sub>-YbF<sub>3</sub>-ThF<sub>4</sub> glass p 230 A89-12236  
Crystallization and characterization of Y<sub>2</sub>O<sub>3</sub>-SiO<sub>2</sub> glasses p 80 A89-19486  
Microstructural evolution on crystallizing the glassy phase in a 6 weight percent Y<sub>2</sub>O<sub>3</sub>-Si<sub>3</sub>N<sub>4</sub> ceramic p 80 A89-19487  
Transition limits for water-droplet crystallization with the NASA Lewis icing nozzle p 152 A89-50071  
The effect of Al<sub>2</sub>O<sub>3</sub>, CaO, Cr<sub>2</sub>O<sub>3</sub> and MgO on devitrification of silica  
[NASA-TM-101335] p 77 N89-10124  
Crystallization kinetics of BaO-Al<sub>2</sub>O<sub>3</sub>-SiO<sub>2</sub> glasses  
[NASA-TM-101964] p 113 N89-20252

## CRYSTALLOGRAPHY

Constitutive modelling of single crystal and directionally solidified superalloys p 102 N89-17325

## CURING

700 F properties of autoclave cured PMR-II composites p 81 A89-29998  
Addition polymers from 1,4,5,8-tetrahydro-1,4,5,8-diepoxyanthracene and Bis-dienes. 2: Evidence for thermal dehydration occurring in the cure process  
[NASA-TM-101385] p 112 N89-15235

## CURRENT DENSITY

Critical currents of aligned grains of Ti-Ba-Ca-Cu-O compounds p 235 A89-30335  
Experimental validation of a phenomenological model of the plasma contacting process p 232 A89-43357  
A V-grooved GaAs solar cell  
[NASA-TM-101970] p 211 N89-22177

## CURRENT DISTRIBUTION

Transport critical current and magnetization measurements of melt-processed YBa<sub>2</sub>Cu<sub>3</sub>O<sub>7</sub>(x) p 234 A89-20037  
Paralleling power MOSFETs in their active region: Extended range of passively forced current sharing  
[NASA-CR-180902] p 139 N89-26150

## CURRENT REGULATORS

Distortion and regulation characterization of a Mapham inverter  
[NASA-TM-102089] p 139 N89-26148

## CURRENT SHEETS

A vector scanning processing technique for pulsed laser velocimetry  
[NASA-TM-102048] p 175 N89-23850

## CURVATURE

Acoustic propagation in curved ducts with extended reacting wall treatment  
[NASA-TM-102110] p 224 N89-25670

## CYANO COMPOUNDS

Measurement of the diffusion coefficient of acetone in succinonitrile at its melting point p 237 A89-23488

## CYCLES

Modeling cyclic melting and refreezing in a hollow metal canister  
[NASA-CR-184630] p 217 N89-15623

## CYCLIC HYDROCARBONS

Formation of polycyclic aromatic hydrocarbons in circumstellar envelopes p 241 A89-41385

## CYCLIC LOADS

High temperature isothermal and cyclic oxidation behavior of a single crystal Ni base superalloy p 94 A89-12625  
Exposure time considerations in high temperature low cycle fatigue p 192 A89-29600  
Constitutive behavior of single crystal PWA 1480 and directionally solidified MAR-M 246 under monotonic and cyclic loads at high and low temperature p 100 N89-12634

Thermomechanical characterization of Hastelloy-X under uniaxial cyclic loading p 196 N89-12909  
Analysis of shell-type structures subjected to time-dependent mechanical and thermal loading  
[NASA-CR-183005] p 197 N89-14457  
Procedures for characterizing an alloy and predicting cyclic life with the total strain version of Strainrange Partitioning  
[NASA-TM-4102] p 203 N89-25485

Simplified procedures for designing adhesively bonded composite joints  
[NASA-TM-102120] p 87 N89-26048

## CYLINDERS

Measurement of the properties of lossy materials inside a finite conducting cylinder  
[NASA-CR-182500] p 126 N89-10223

## CYLINDRICAL BODIES

Improvement in finite element meshes: Heat transfer in an infinite cylinder p 182 N89-14450  
Heat transfer with very high free-stream turbulence and heat transfer with streamwise vortices p 160 N89-17309

## CZOCHRALSKI METHOD

A comparative study of the influence of buoyancy driven fluid flow on GaAs crystal growth p 121 N89-20295

## D

## DAMAGE

Fiber composite structural durability and damage tolerance - Simplified predictive methods p 82 A89-36320  
The NASA atomic oxygen effects test program p 93 N89-12589

## DAMAGE ASSESSMENT

The constitutive representation of high-temperature creep damage p 191 A89-17396  
Structural behavior of composites with progressive fracture  
[AIAA PAPER 89-1271] p 192 A89-30754  
Acousto-ultrasonics - An update p 188 A89-42864  
Damage analysis of a crack layer p 194 A89-42984  
Fatigue and fracture overview p 195 N89-12882  
Thermal barrier coating life prediction model development p 110 N89-12922

## DAMPERS

Rotordynamic Instability Problems in High-Performance Turbomachinery, 1988  
[NASA-CP-3026] p 185 N89-22891

## DATA ACQUISITION

Automated data acquisition and processing for a Hohlraum reflectometer  
[NASA-TM-101393] p 173 N89-14416



- A data acquisition and storage system for the ion auxiliary propulsion system cyclic thruster test  
[NASA-TM-101469] p 218 N89-17424
- A data acquisition and control program for axial-torsional fatigue testing  
[NASA-TM-102041] p 205 N89-28029
- DATA BASES**
- Coolant passage heat transfer with rotation  
p 161 N89-17314
- Review and assessment of the database and numerical modeling for turbine heat transfer p 30 N89-20139
- DATA COMPRESSION**
- Digital CODEC for real-time processing of broadcast quality video signals at 1.8 bits/pixel  
[NASA-TM-102325] p 129 N89-27927
- DATA LINKS**
- Intersatellite link application to commercial communications satellites p 43 A89-39144
- DATA PROCESSING**
- Amplitude spectrum modulation technique for analog data processing in fiber optic sensing system with temporal separation of channels p 169 A89-10368
- Automation software for a materials testing laboratory p 217 N89-12917
- Automated data acquisition and processing for a Hohlraum reflectometer  
[NASA-TM-101393] p 173 N89-14416
- Amplitude spectrum modulation technique for analog data processing in fiber optic sensing system with temporal separation of channels  
[NASA-TM-100152] p 174 N89-18671
- DATA PROCESSING EQUIPMENT**
- Baseband processor hardware for Advanced Communication Technology Satellite (ACTS)  
p 43 A89-38298
- DATA REDUCTION**
- Amplitude spectrum modulation technique for analog data processing in fiber optic sensing system with temporal separation of channels  
[NASA-TM-100152] p 174 N89-18671
- DATA STORAGE**
- A data acquisition and storage system for the ion auxiliary propulsion system cyclic thruster test  
[NASA-TM-101469] p 218 N89-17424
- DATA TRANSMISSION**
- Digitally modulated bit error rate measurement system for microwave component evaluation  
[NASA-TP-2912] p 40 N89-28545
- DECAY RATES**
- Critical fluid light scattering p 121 N89-20320
- DEFECTS**
- Calculation of Weibull strength parameters and Batdorf flow-density constants for volume- and surface-flaw-induced fracture in ceramics  
[NASA-TM-100890] p 196 N89-12930
- Arjet cathode phenomena  
[NASA-TM-102099] p 167 N89-27121
- DEFLECTION**
- Tooth contact shift in loaded spiral bevel gears o, IL, 25-27 Apr. 1989; sponsored by ASME  
[NASA-TM-101438] p 183 N89-14453
- DEFORMATION**
- Accelerated fatigue crack growth behavior of PWA 1480 p 97 A89-36461
- Deformation and fracture of single-crystal and sintered polycrystalline silicon carbide produced by cavitation  
p 108 A89-54985
- Deformation modeling and constitutive modeling for anisotropic superalloys  
[NASA-CR-4215] p 202 N89-21258
- Nonlinear mesomechanics of composites with periodic microstructure  
[NASA-TM-102051] p 204 N89-26260
- Speckle interferometry using fiber optic phase stepping  
[NASA-TM-102331] p 176 N89-27999
- DEGRADATION**
- An experimental investigation of multi-element airfoil ice accretion and resulting performance degradation  
[AIAA PAPER 89-0752] p 4 A89-28453
- Predictions of airfoil aerodynamic performance degradation due to icing  
[NASA-TM-101434] p 10 N89-13412
- An experimental investigation of multi-element airfoil ice accretion and resulting performance degradation  
[NASA-TM-101441] p 12 N89-15084
- Probabilistic analysis for fatigue strength degradation of materials  
[NASA-CR-182844] p 198 N89-15434
- A comparison of the radiation tolerance characteristics of multijunction solar cells with series and voltage-matched configurations p 213 N89-24737
- Probabilistic structural analysis methods of hot engine structures  
[NASA-TM-102091] p 205 N89-28030
- DEHYDRATION**
- Addition of polymers from 1,4,5,8-tetrahydro-1,4,5,8-diepoxyanthracene and Bis-dienes. 2: Evidence for thermal dehydration occurring in the cure process  
[NASA-TM-101385] p 112 N89-15235
- DEICERS**
- Efficient numerical simulation of a one-dimensional electrothermal deicer pad p 144 A89-22811
- A comparison of numerical methods for the prediction of two-dimensional heat transfer in an electrothermal deicer pad  
[NASA-CR-4202] p 19 N89-13429
- A numerical simulation of the full two-dimensional electrothermal de-icer pad  
[NASA-CR-4194] p 19 N89-14235
- DEICING**
- Electroimpulse deicing - Electrodynamical solution by discrete elements p 17 A89-39193
- Two-dimensional simulation of electrothermal deicing of aircraft components p 17 A89-39194
- NASA's program on icing research and technology  
[NASA-TM-101989] p 1 N89-22569
- DELAMINATING**
- Free-edge delamination - Laminate width and loading conditions effects p 193 A89-36294
- Dynamic delamination buckling in composite laminates under impact loading - Computational simulation p 82 A89-36310
- Fracture toughness computational simulation of general delaminations in fiber composites  
[NASA-TM-101415] p 85 N89-13521
- Finite element modeling of frictionally restrained composite interfaces  
[NASA-CR-182281] p 203 N89-23918
- Vibration testing of impact-damaged composite laminates  
[NASA-TM-4115] p 87 N89-25290
- DEMULATION**
- Programmable rate modem utilizing digital signal processing techniques  
[NASA-CR-185124] p 43 N89-26879
- DEMODULATORS**
- Advanced modulation technology development for earth station demodulator applications  
[NASA-CR-185126] p 43 N89-26880
- DENDRITIC CRYSTALS**
- Enthalpies of a binary alloy during solidification p 96 A89-22559
- Dendritic solidification in binary alloys p 96 A89-22560
- Thermosolutal convection during dendritic solidification  
[AIAA PAPER 89-0626] p 118 A89-25495
- Flight hardware and tele-operations supporting the Isothermal Dendritic Growth Experiment aboard the Space Shuttle  
[AIAA PAPER 89-0863] p 118 A89-25627
- A facility for precise temperature control applications in microgravity p 48 A89-36956
- Isothermal dendritic growth: A low gravity experiment p 121 N89-20299
- DENSIFICATION**
- Preparation and evaluation of silicon nitride matrices for silicon nitride-SiC fiber composites  
[NASA-CR-184798] p 115 N89-23678
- DENSITY MEASUREMENT**
- An improved correction algorithm for number density measurements made with the forward scattering spectrometer probe p 170 A89-44122
- Critical fluid light scattering p 121 N89-20320
- X-ray based extensometry  
[NASA-CR-185058] p 176 N89-25432
- DEPLOYMENT**
- Satellite relocation by tether deployment  
[NASA-TM-101992] p 42 N89-26877
- DEPOSITION**
- Rational engineering correlations of diffusional and inertial particle deposition behavior in non-isothermal forced convection environments p 140 A89-12327
- Optical methods and results of dew point and deposition rate measurements in salt/ash-containing combustion gases - B<sub>2</sub>O<sub>3</sub>(l) deposition rates by interference methods and comparisons with theory p 89 A89-12334
- Optical experiments on thermophoretically augmented submicron particle deposition from 'dusty' high temperature gas flows p 90 A89-14799
- Sodium sulfate - Deposition and dissolution of silica p 91 A89-28084
- Adhesion, friction, and wear of plasma-deposited thin silicon nitride films at temperatures to 700 C p 107 A89-48250
- Adhesion, friction, and wear of plasma-deposited thin silicon nitride films at temperatures to 700 C  
[NASA-TM-101377] p 109 N89-11913
- Diamondlike carbon protective coatings for optical windows  
[NASA-TM-102111] p 231 N89-27506
- Ion beam and plasma methods of producing diamondlike carbon films  
[NASA-TM-102301] p 116 N89-27836
- DESIGN ANALYSIS**
- Application of advanced computational technology to propulsion CFD p 142 A89-16957
- Euler analysis of a swirl recovery vane design for use with an advanced single-rotation propfan  
[AIAA PAPER 88-3152] p 2 A89-17940
- Advanced transmission studies p 178 A89-18906
- Optimizing advanced propeller designs by simultaneously updating flow variables and design parameters p 5 A89-39189
- High-speed propeller performance and noise predictions at takeoff/landing conditions p 226 A89-39195
- Effect of design variables, temperature gradients, and speed on life and reliability of a rotating disk p 180 A89-47719
- Engineering study on the rotary-vee engine concept  
[SAE PAPER 890332] p 181 A89-51492
- PV modules for ground testing  
[NASA-CR-179476] p 208 N89-11315
- Aerodynamic optimization by simultaneously updating flow variables and design parameters with application to advanced propeller designs  
[NASA-CR-182181] p 24 N89-11750
- User's manual for an aerodynamic optimization scheme that updates flow variables and design parameters simultaneously  
[NASA-CR-182180] p 10 N89-13399
- Wear consideration in gear design for space applications  
[NASA-TM-101457] p 183 N89-15414
- The design and development of transonic multistage compressors p 27 N89-16834
- Computer-aided design of bevel gear tooth surfaces  
[NASA-TM-101449] p 183 N89-17248
- Mercury ion thruster technology  
[NASA-CR-174974] p 66 N89-21834
- Advances in computational design and analysis of airbreathing propulsion systems  
[NASA-TM-101987] p 32 N89-23465
- Review of the environmental effects of the Space Station Freedom photovoltaic power module  
[NASA-TM-102076] p 46 N89-24418
- Composite Blade Structural Analyzer (COBSTRAN) demonstration manual  
[NASA-TM-101957] p 87 N89-24459
- Space Station Freedom power management and distribution system design  
[NASA-TM-102283] p 73 N89-26045
- Thermal evaluation of advanced solar dynamic heat receiver performance  
[NASA-CR-185117] p 214 N89-27256
- DESORPTION**
- Comparison of the surface charge behavior of commercial silicon nitride and silicon carbide powders p 105 A89-21444
- DETECTORS**
- Microwave characteristics of interdigitated photoconductors on a HEMT structure  
[NASA-CR-182197] p 135 N89-12820
- DEW POINT**
- Transport-induced shifts in condensate dew-point and composition in multicomponent systems with chemical reaction p 89 A89-12333
- Optical methods and results of dew point and deposition rate measurements in salt/ash-containing combustion gases - B<sub>2</sub>O<sub>3</sub>(l) deposition rates by interference methods and comparisons with theory p 89 A89-12334
- Laboratory studies of binary salt CVD in combustion gas environments p 89 A89-12335
- Laboratory studies of the deposition of alkali sulfate vapors from combustion gases using a flash-evaporation technique p 89 A89-12338
- DIAGNOSIS**
- Optical measurements of soot and temperature profiles in premixed propane-oxygen flames p 92 A89-35008
- Microgravity Combustion Diagnostics Workshop  
[NASA-CP-10017] p 120 N89-17682
- DIAMONDS**
- Growth of diamond by RF plasma-assisted chemical vapor deposition p 90 A89-20474
- Radio-frequency plasma chemical vapor deposition growth of diamond p 236 A89-44552
- Ion beam and plasma methods of producing diamondlike carbon films  
[NASA-TM-102301] p 116 N89-27836
- DIATOMIC GASES**
- The NASA atomic oxygen effects test program p 93 N89-12589

## DIATOMIC MOLECULES

Connection between energy relations of solids and molecules p 91 A89-26406

## DIELECTRICS

Townsend coefficients for electron scattering over dielectric surfaces p 231 A89-16409  
The physics of positively biased conductors surrounded by dielectrics in contact with a plasma p 232 A89-39395

Measurements of complex permittivity of microwave substrates in the 20 to 300 K temperature range from 26.5 to 40.0 GHz [NASA-TM-102123] p 123 N89-27038

## DIESEL ENGINES

The effect of insulated combustion chamber surfaces on direct-injected diesel engine performance, emissions, and combustion [NASA-CR-182204] p 239 N89-17548

Methods for heat transfer and temperature field analysis of the insulated diesel, phase 3 [NASA-CR-182237] p 239 N89-23382

## DIFFERENCE EQUATIONS

Universal limiter for transient interpolation modeling of the advective transport equations: The ULTIMATE conservative difference scheme [NASA-TM-100916] p 222 N89-14794

## DIFFUSERS

Investigation of the flow in the diffuser section of the NASA Lewis Icing Research Tunnel [AIAA PAPER 89-0755] p 36 A89-28455  
Investigation of the flow in the diffuser section of the NASA Lewis icing research tunnel [NASA-TM-102087] p 17 N89-25978

## DIFFUSION

Determination of convective diffusion heat/mass transfer rates to burner rig test targets comparable in size to cross-stream jet diameter p 141 A89-12753  
Automated design of controlled-diffusion blades [ASME PAPER 88-GT-139] p 2 A89-15967  
A compendium of controlled diffusion blades generated by an automated inverse design procedure [NASA-TM-101968] p 31 N89-20996

## DIFFUSION COEFFICIENT

Measurement of the diffusion coefficient of acetone in succinonitrile at its melting point p 237 A89-23488

## DIGITAL DATA

Performance of five 30 GHz satellite receivers [NASA-TM-101960] p 129 N89-25365  
Digitally modulated bit error rate measurement system for microwave component evaluation [NASA-TP-2912] p 40 N89-28545

## DIGITAL ELECTRONICS

A real time microcomputer implementation of sensor failure detection for turbofan engines [NASA-TM-102327] p 216 N89-29032

## DIGITAL SIMULATION

Response of a chemically reacting shear layer to streamwise vorticity [AIAA PAPER 89-0978] p 150 A89-40400  
The use of direct numerical simulation in the study of turbulent, chemically-reacting flows p 152 A89-51873  
A real-time simulator of a turbofan engine [NASA-TM-100869] p 31 N89-20995

## DIGITAL TECHNIQUES

Programmable rate modem utilizing digital signal processing techniques [NASA-CR-185124] p 43 N89-26879

## DIMENSIONAL STABILITY

Dynamics of face and annular seals with two-phase flow [NASA-CR-183352] p 182 N89-12870

## DIRECT BROADCAST SATELLITES

An experimental adaptive array to suppress weak interfering signals p 124 A89-22455

## DIRECT CURRENT

Dynamic characteristics of a 20 kHz resonant power system - Fault identification and fault recovery p 52 A89-15357  
dc power control for a liquid-fed resistor p 59 A89-47457

Magnification of starting torques of dc motors by maximum power point trackers in photovoltaic systems [NASA-TM-102040] p 138 N89-23792

## DIRECTIONAL SOLIDIFICATION (CRYSTALS)

Microsegregation in directionally solidified Pb-8.4 at. pct Au alloy p 94 A89-12758  
Bulk undercooling, nucleation, and macrosegregation of Pb-Sn alloys p 117 A89-17106  
Gravitational macrosegregation in unidirectionally solidified lead-tin alloy p 117 A89-17112  
Heat of mixing and morphological stability p 143 A89-21296  
Dendritic solidification in binary alloys p 96 A89-22560

Thermosolutal convection during dendritic solidification [AIAA PAPER 89-0626] p 118 A89-25495

Constitutive modelling of single crystal and directionally solidified superalloys p 101 N89-12912

Isothermal solidification in a binary alloy melt p 121 N89-20300

Computer simulation of macrosegregation in directionally solidified circular ingots [NASA-CR-182838] p 122 N89-21134

## DISCONTINUITY

Simple high-accuracy resolution program for convective modelling of discontinuities p 143 A89-17459

## DISCRETE FUNCTIONS

Discretization formulas for unstructured grids [NASA-TM-101298] p 154 N89-10242

## DISK OPERATING SYSTEM (DOS)

Laboratory process control using natural language commands from a personal computer [NASA-TM-101988] p 218 N89-24055

## DISKS (SHAPES)

An acoustic experimental and theoretical investigation of single disc propellers [AIAA PAPER 89-1146] p 227 A89-40478

## DISPLACEMENT

Integrated control and health monitoring capacitive displacement sensor development task. Orbit transfer rocket engine technology program [NASA-CR-182279] p 176 N89-26208  
OTVE turbopump condition monitoring, task E.5 [NASA-CR-182274] p 189 N89-27204

## DISPLAY DEVICES

Model-based analysis of control/display interaction in the hover task p 215 A89-36933

## DISSOCIATION

NNEPEQ - Chemical equilibrium version of the Navy/NASA Engine Program [ASME PAPER 88-GT-314] p 22 A89-24989

## DISTORTION

Distortion and regulation characterization of a Mapham inverter [NASA-TM-102089] p 139 N89-26148

## DISTRIBUTED PARAMETER SYSTEMS

Modal representations in control/structure interaction p 45 A89-54114

## DISTRIBUTION (PROPERTY)

Strength distribution in commercial silicon carbide materials p 105 A89-17097

## DISTRIBUTION FUNCTIONS

Comparison of the bidirectional reflectance distribution function of various surfaces p 230 A89-41530

## DIVERGENCE

The divergence characteristics of constrained-sheath optics systems for use with 5-eV atomic oxygen sources [NASA-CR-182238] p 229 N89-19973

## DOCUMENTATION

Bibliography of Lewis Research Center technical publications announced in 1986 [NASA-TM-89887] p 238 N89-18259

## DOMAIN WALL

Is the great attractor really a great wall? --- late-time cosmological phase transition producing coherent velocity caused by relic domain wall repulsive effect p 241 A89-36278

## DOPED CRYSTALS

The effect of sulfur and zirconium co-doping on the oxidation of NiCrAl p 94 A89-13933

Doping directed at the oxygen sites in Y1Ba2Cu3O(7-delta) - The effect of sulfur, fluorine, and chlorine p 133 A89-37824

Calculation of the electron wave function in a graded-channel double-heterojunction modulation-doped field-effect transistor p 134 A89-54417

Indentation plasticity and fracture in silicon [NASA-TP-2863] p 100 N89-10996

## DOUBLE BASE ROCKET PROPELLANTS

Ignition and combustion of metallized propellants [AIAA PAPER 89-2883] p 117 A89-47148

## DOWNWASH

Spatial resolution and downwash velocity corrections for multiple-hole pressure probes in complex flows p 171 A89-45909

## DROP SIZE

On the wind force needed to dislodge a drop adhered to a surface p 144 A89-22819

Gas density effect on droplet size of simulated fuel sprays [AIAA PAPER 89-2322] p 151 A89-46749

Transition limits for water-droplet crystallization with the NASA Lewis icing nozzle p 152 A89-50071

Particle sizing by weighted measurements of scattered light [NASA-TM-100968] p 172 N89-11198

Gas density effect on droplet size of simulated fuel sprays [NASA-TM-102013] p 162 N89-22053

## DROP TOWERS

Droplet combustion drop tower tests using models of the space flight apparatus [AIAA PAPER 89-0501] p 119 A89-28418

## DROPS (LIQUIDS)

Numerical study of the interactions between droplets at intermediate Reynolds numbers p 142 A89-16451  
Interactions between gaseous electrical discharges and single liquid droplets p 90 A89-19298

Considerations on the moving contact-line singularity, with application to frictional drag on a slender drop p 144 A89-23238

Transition limits for water-droplet crystallization with the NASA Lewis icing nozzle p 152 A89-50071

Liquid droplet generation [NASA-CR-182246] p 166 N89-26182

## DUAL THRUST NOZZLES

Experimental results for a two-dimensional supersonic inlet used as a thrust deflecting nozzle [NASA-TM-83439] p 159 N89-14386

## DUCT GEOMETRY

Bipolar coordinates for computation of transition duct flows p 148 A89-34912

## DUCTED FLOW

Bipolar coordinates for computation of transition duct flows p 148 A89-34912  
CFD application to subsonic inlet airframe integration --- computational fluid dynamics (CFD) p 13 N89-16753

## DUCTILITY

Room temperature tensile ductility in polycrystalline B2 Ni-30Al-20Fe p 98 A89-44568

## DUCTS

Unsteady heat transfer in turbine blade ducts - Focus on combustor sources p 153 A89-53286

Influence of bulk turbulence and entrance boundary layer thickness on the curved duct flow field [NASA-CR-4188] p 155 N89-12838

Acoustic propagation in curved ducts with extended reacting wall treatment [NASA-TM-102110] p 224 N89-25670

Calculation of turbulence-driven secondary motion in ducts with arbitrary cross section [NASA-TM-102142] p 166 N89-27115

Parametric study of electromagnetic waves propagating in absorbing curved S ducts [NASA-TM-102024] p 129 N89-27923

## DUMP COMBUSTORS

Experimental study of isothermal swirling flows in a dump combustor p 21 A89-23182

Numerical investigation of chemically reacting flows in ramjet dump combustors [AIAA PAPER 89-0387] p 22 A89-28408

## DURABILITY

Computational structural mechanics for engine structures [AIAA PAPER 89-1260] p 22 A89-30745

The NASA atomic oxygen effects test program p 93 N89-12589

## DYNAMIC CHARACTERISTICS

Dynamic characteristics of a 20 kHz resonant power system - Fault identification and fault recovery p 52 A89-15357

## DYNAMIC LOADS

The solution of the Elrod algorithm for a dynamically loaded journal bearing using multigrig techniques [ASME PAPER 88-TRIB-23] p 148 A89-34795

Free-edge delamination - Laminate width and loading conditions effects p 193 A89-36294

Dynamic delamination buckling in composite laminates under impact loading - Computational simulation p 82 A89-36310

Dynamic loading of spur gears with linear or parabolic tooth profile modification [NASA-TM-101444] p 183 N89-15413

Stability of a rigid rotor supported on oil-film journal bearings under dynamic load [NASA-TM-102309] p 166 N89-27114

## DYNAMIC MODELS

Identification of Space Shuttle Main Engine dynamics p 61 A89-54068

Identification of space shuttle main engine dynamics [NASA-TM-101982] p 66 N89-20199

## DYNAMIC PRESSURE

On the wind force needed to dislodge a drop adhered to a surface p 144 A89-22819

## DYNAMIC RESPONSE

Microwave response of an HEMT photoconductor p 131 A89-15824

Experimental investigation of propan aeroelastic response in off-axis flow with mistuning [AIAA PAPER 88-3153] p 20 A89-17941

Vibration, performance, flutter and forced response characteristics of a large-scale propan and its aeroelastic model [AIAA PAPER 88-3155] p 21 A89-17943

- Probabilistic methods for structural response analysis  
p 223 A89-25843
- Vibration, performance, flutter and forced response characteristics of a large-scale propfan and its aeroelastic model  
[NASA-TM-101322] p 24 N89-10043
- Turbomachinery aeroelasticity at NASA Lewis Research Center  
p 28 N89-19262
- Structural dynamics branch research and accomplishments for FY 1988  
[NASA-TM-101406] p 202 N89-22939
- On the dynamic response of pressure transmission lines in the research of helium-charged free piston Stirling engines  
[NASA-TM-102121] p 175 N89-24593
- Tailoring of composite links for optimal damped elasto-dynamic performance  
[NASA-TM-102094] p 88 N89-26912
- DYNAMIC STABILITY**  
Rotordynamic Instability Problems in High-Performance Turbomachinery, 1988  
[NASA-CP-3026] p 185 N89-22891
- DYNAMIC STRUCTURAL ANALYSIS**  
A computational procedure for automated flutter analysis  
p 191 A89-28070
- Free-vibration characteristics and correlation of a Space Station split-blanket solar array  
[AIAA PAPER 89-1252] p 44 A89-30737
- Structural behavior of composites with progressive fracture  
[AIAA PAPER 89-1271] p 192 A89-30754
- Identification of structural interface characteristics using component mode synthesis  
p 193 A89-36177
- Non-isothermal buckling behavior of viscoplastic shell structures  
[NASA-CR-183013] p 197 N89-12931
- Free-vibration characteristics and correlation of a space station split-blanket solar array  
[NASA-TM-101452] p 198 N89-15438
- Characterization of structural connections using free and forced response test data  
[NASA-TM-101991] p 202 N89-21266
- Structural dynamics branch research and accomplishments for FY 1988  
[NASA-TM-101406] p 202 N89-22939
- Computational structural mechanics for engine structures  
[NASA-TM-102119] p 204 N89-26259
- DYNAMIC TESTS**  
Dynamic porosity variations in ceramics  
[NASA-TM-101340] p 112 N89-17668
- DYNAMICAL SYSTEMS**  
Further development of the dynamic gas temperature measurement system. Volume 2: Computer program user's manual  
[NASA-CR-179513-VOL-2] p 173 N89-13771

## E

- EARTH GRAVITATION**  
Time-dependent computational studies of flames in microgravity  
[NASA-CR-182298] p 122 N89-25353
- EARTH IONOSPHERE**  
Electron velocity distributions and plasma waves associated with the injection of an electron beam into the ionosphere  
p 215 A89-43698
- Space plasma contractor research, 1988  
[NASA-CR-182283] p 233 N89-21658
- EARTH OBSERVATIONS (FROM SPACE)**  
Space 2010 --- Space Station Freedom future explorations  
p 77 A89-23028
- EARTH ORBITAL ENVIRONMENTS**  
In-situ propellant advantages for fast transfer to Mars  
[AIAA PAPER 88-2901] p 37 A89-14977
- Effect of NASA advanced designs on thermal behavior of Ni-H<sub>2</sub> cells  
p 50 A89-15279
- High temperature superconducting magnetic energy storage for future NASA missions  
p 50 A89-15288
- Expendable launch vehicle transportation for the Space Station  
[IAF PAPER 88-198] p 42 A89-17720
- Durable thin film coatings for reflectors used in low earth orbit  
p 77 A89-33150
- Oxidation and protection of fiberglass-epoxy composite masts for photovoltaic arrays in the low earth orbital environment  
p 44 A89-35316
- A numerical model of electrodynamics of plasma within the contaminant gas cloud of the Space Shuttle Orbiter at low earth orbit  
p 233 A89-45631
- The POLAR code wake model - Comparison with in situ observations --- Shuttle Orbiter plasma wake ion and electron density simulation  
p 233 A89-45632
- Low earth orbital atomic oxygen simulation for materials durability evaluation  
p 45 A89-51123

- COLD-SAT orbital experiment configured for Atlas launch  
p 45 A89-53327
- Simulation of the low earth orbital atomic oxygen interaction with materials by means of an oxygen ion beam  
[NASA-TM-101971] p 114 N89-21104
- Overview of environmental factors  
p 240 N89-23529
- Atomic oxygen effects on materials  
p 78 N89-23540
- Undercutting of defects in thin film protective coatings on polymer surfaces exposed to atomic oxygen  
[NASA-TM-101986] p 115 N89-23691
- Review of the environmental effects of the Space Station Freedom photovoltaic power module  
[NASA-TM-102076] p 46 N89-24418
- EARTH ORBITS**  
Extended SP-100 reactor power systems capability  
p 52 A89-15392
- Low earth orbit environmental effects on the Space Station photovoltaic power generation systems  
p 55 A89-29123
- ECCENTRIC ORBITS**  
Estimated performance and future potential of solar dynamic and photovoltaic power systems for selected LEO and HEO missions  
[NASA-TM-102083] p 72 N89-25280
- EDDY CURRENTS**  
Technique for temperature compensation of eddy-current proximity probes  
[NASA-TP-2880] p 173 N89-15380
- EDDY VISCOSITY**  
Mesh refinement in a two-dimensional large eddy simulation of a forced shear layer  
[NASA-TM-102129] p 166 N89-26180
- EDGES**  
Free-edge delamination - Laminate width and loading conditions effects  
p 193 A89-36294
- EFFICIENCY**  
Experimental aerodynamic performance of advanced 40 deg-swept 10-blade propeller model at Mach 0.6 to 0.85  
[NASA-TM-88969] p 9 N89-10865
- Wind-tunnel results of advanced high-speed propellers at takeoff, climb, and landing Mach numbers  
[NASA-TM-87030] p 13 N89-19265
- EIGENVALUES**  
Stability robustness improvement of direct eigenspace assignment based feedback systems using singular value sensitivities  
p 220 A89-53958
- Solution and sensitivity analysis of a complex transcendental eigenproblem with pairs of real eigenvalues  
[NASA-CR-182241] p 197 N89-13819
- Stability robustness improvement of direct eigenspace assignment based feedback systems using singular value sensitivities  
[NASA-CR-182302] p 36 N89-27672
- EIGENVECTORS**  
Stability robustness improvement of direct eigenspace assignment based feedback systems using singular value sensitivities  
p 220 A89-53958
- Stability robustness improvement of direct eigenspace assignment based feedback systems using singular value sensitivities  
[NASA-CR-182302] p 36 N89-27672
- EJECTORS**  
Transient flow thrust prediction for an ejector propulsion concept  
[AIAA PAPER 89-2906] p 23 A89-49688
- A control-volume method for analysis of unsteady thrust augmenting ejector flows  
[NASA-CR-182203] p 24 N89-12566
- Transient flow thrust prediction for an ejector propulsion concept  
[NASA-TM-102078] p 32 N89-24318
- A model for prediction of STOV<sub>L</sub> ejector dynamics  
[NASA-TM-102098] p 32 N89-24319
- ELASTIC DEFORMATION**  
Inelastic deformation and dislocation structure of a nickel alloy - Effects of deformation and thermal histories  
p 99 A89-50313
- ELASTIC PROPERTIES**  
Simplified cyclic structural analysis of SSME turbine blades  
p 63 N89-12632
- ELASTODYNAMICS**  
Tailoring of composite links for optimal damped elasto-dynamic performance  
[NASA-TM-102094] p 88 N89-26912
- ELASTOPLASTICITY**  
Nonlinear analysis using temporal finite elements  
p 221 A89-28030
- Nonisothermal elastoviscoplastic snap-through and creep buckling of shallow arches  
p 194 A89-47370
- A study on thermal barrier coatings including thermal expansion mismatch and bond coat oxidation  
p 109 N89-12919

- ELECTRIC BATTERIES**  
NASA Aerospace Flight Battery Systems Program - Issues and actions  
p 49 A89-15224
- Space Electrochemical Research and Technology Conference, Cleveland, OH, Apr. 14-16, 1987, Proceedings  
p 207 A89-23280
- ELECTRIC BRIDGES**  
The dual element method of strain gauge temperature compensation  
p 169 A89-12276
- 5-kW arcjet power electronics  
[AIAA PAPER 89-2725] p 60 A89-49685
- The 5-kW arcjet power electronics  
[NASA-TM-102108] p 70 N89-24446
- ELECTRIC CHARGE**  
Mass flow meter using the triboelectric effect for measurement in cryogenics  
[NASA-CR-179572] p 155 N89-12836
- Nickel-hydrogen capacity loss on storage  
p 138 N89-23007
- ELECTRIC CONTACTS**  
Plasma contacting - An enabling technology  
[AIAA PAPER 89-0677] p 231 A89-25537
- Ground-based tests of hollow cathode plasma contactors  
[AIAA PAPER 89-1558] p 232 A89-40188
- A model of electron collecting plasma contactors  
[AIAA PAPER 89-1560] p 232 A89-40190
- ELECTRIC CURRENT**  
An application of the WKB technique to the on-surface radiation condition  
p 124 A89-21222
- The stability analysis of magnetohydrodynamic equilibria - Comparing the thermodynamic approach with the energy principle  
p 232 A89-39391
- Restrictive loads powered by separate or by common electrical sources  
[NASA-TM-102008] p 137 N89-21174
- ELECTRIC DISCHARGES**  
Interactions between gaseous electrical discharges and single liquid droplets  
p 90 A89-19298
- Lightweight fibrous nickel electrodes for nickel-hydrogen batteries  
[NASA-TM-101997] p 93 N89-22710
- ELECTRIC ENERGY STORAGE**  
Nickel-hydrogen capacity loss on storage  
p 138 N89-23007
- ELECTRIC GENERATORS**  
Comparison of solar photovoltaic and nuclear reactor power systems for a human-tended lunar observatory  
[NASA-TM-102015] p 242 N89-23397
- ELECTRIC MOTORS**  
Starting characteristics of direct current motors powered by solar cells  
[NASA-TM-101981] p 136 N89-19493
- ELECTRIC POTENTIAL**  
Restrictive loads powered by separate or by common electrical sources  
[NASA-TM-102008] p 137 N89-21174
- ELECTRIC POWER SUPPLIES**  
Extended SP-100 reactor power systems capability  
p 52 A89-15392
- Solar dynamic power for Space Station Freedom  
[IAF PAPER ICOSP89-4-1] p 55 A89-46517
- Solar dynamic power for space station freedom  
[NASA-TM-102016] p 67 N89-23516
- Space Station Freedom electrical power system hardware commonality with the United States Polar Platform  
[NASA-TM-102074] p 69 N89-24439
- Microwave and millimeter-wave power generation in silicon carbide (SiC) IMPATT devices  
[NASA-CR-185050] p 139 N89-26143
- Photovoltaic module on-orbit assembly for Space Station Freedom  
[NASA-TM-102297] p 47 N89-26887
- Development and refinement of test bed simulations  
[NASA-TM-102335] p 75 N89-27702
- ELECTRIC POWER TRANSMISSION**  
Power transmission studies for tethered SP-100  
p 52 A89-15403
- ELECTRIC PROPULSION**  
Performance and lifetime assessment of MPD arc thruster technology  
[AIAA PAPER 88-3211] p 53 A89-16485
- A detailed model of electrothermal propulsion systems  
[AIAA PAPER 89-2262] p 56 A89-46707
- User interactive electric propulsion software design  
[AIAA PAPER 89-2376] p 57 A89-46783
- Investigations of microwave plasmas - Applications in electrothermal thruster systems  
[AIAA PAPER 89-2378] p 57 A89-46784
- Design of a thrust stand for high power electric propulsion devices  
[AIAA PAPER 89-2829] p 39 A89-47110
- The NASA Electric Propulsion Program  
p 59 A89-47428

## ELECTRIC ROCKET ENGINES

- Successful completion of a cyclic ground test of a mercury ion Auxiliary Propulsion System p 59 A89-47450
- dc power control for a liquid-fed resistor p 59 A89-47457
- Experiments and analysis of a compact electrothermal thruster p 59 A89-47494
- The effects of arcjet thruster operating condition constrictor geometry on the plasma plume [AIAA PAPER 89-2723] p 60 A89-50809
- Electromagnetic emission experiences using electric propulsion systems p 61 A89-53354
- Space propulsion technology and cryogenic fluid depot p 38 A89-11768
- Advanced technology for future space propulsion systems [NASA-TM-101951] p 66 A89-20192
- Mercury ion thruster technology [NASA-CR-174974] p 66 A89-21834
- The effects of arcjet operating condition and constrictor geometry on the plasma plume [NASA-TM-102284] p 72 A89-25281
- Electric propulsion options for 10 kW class earth space missions [NASA-TM-102337] p 74 A89-26906
- Experiments and analysis of a compact electrothermal thruster p 75 A89-27773
- ELECTRIC ROCKET ENGINES**
- Use of high temperature superconductors in magnetoplasmadynamic systems [NASA-TM-101219] p 236 A89-11553
- ELECTRIC SPARKS**
- Interactions between gaseous electrical discharges and single liquid droplets p 90 A89-19298
- ELECTRIC SWITCHES**
- Study of optoelectronic switch for satellite-switched time-division multiple access [NASA-CR-179630] p 135 A89-13706
- ELECTRICAL FAULTS**
- Paralleling power MOSFETs in their active region: Extended range of passively forced current sharing [NASA-CR-180902] p 139 A89-26150
- ELECTRICAL IMPEDANCE**
- Aperture impedance of flared horns p 125 A89-43543
- Rigorous analysis of a circular patch antenna excited by a microstrip transmission line p 125 A89-53134
- ELECTRICAL INSULATION**
- Power transmission studies for tethered SP-100 p 52 A89-15403
- ELECTRICAL MEASUREMENT**
- Recent advances in capacitance type of blade tip clearance measurements [AIAA PAPER 88-4664] p 20 A89-13725
- Deep-level transient spectroscopy of Al(x)Ga(1-x)As/GaAs using nondestructive acousto-electric voltage measurement p 133 A89-42742
- ELECTRICAL PROPERTIES**
- Effects of microstructure and nonstoichiometry on electrical properties of vanadium dioxide films p 236 A89-44527
- Microwave characteristics of interdigitated photoconductors on a HEMT structure [NASA-CR-182197] p 135 A89-12820
- ELECTRICAL RESISTANCE**
- Effect of processing parameters on the characteristics of high-Tc superconductor YBa<sub>2</sub>Cu<sub>3</sub>O<sub>7</sub> p 234 A89-20467
- The NASA Lewis Strain Gauge Laboratory: An update p 173 A89-12888
- Development of a high temperature thin film static strain gage p 174 A89-17299
- Restrictive loads powered by separate or by common electrical sources [NASA-TM-102008] p 137 A89-21174
- ELECTRICAL RESISTIVITY**
- Effect of length of chopped pristine and intercalated graphite fibers on the resistivity of fiber networks [NASA-TM-101395] p 84 A89-11826
- Stability of bulk Ba<sub>2</sub>YCu<sub>3</sub>O<sub>7-x</sub> in a variety of environments [NASA-TM-101401] p 111 A89-14310
- Oxygen electrodes for rechargeable alkaline fuel cells p 211 A89-22998
- Light weight polymer matrix composite material [NASA-CASE-LEW-14734-1] p 87 A89-23623
- ELECTRO-OPTICS**
- Design of a GaAlAs travelling wave Mach-Zehnder electro-optic modulator p 130 A89-10342
- Optoelectronic signal processing for phased-array antennas: Proceedings of the Meeting, Los Angeles, CA, Jan. 12, 13, 1988 [SPIE-886] p 124 A89-15819
- External electro-optic probing of millimeter-wave integrated circuits p 133 A89-45266

- External electro-optic probing of millimeter-wave integrated circuits [NASA-TM-101990] p 128 A89-21142
- ELECTROCATALYSTS**
- Space Electrochemical Research and Technology Conference, Cleveland, OH, Apr. 14-16, 1987, Proceedings p 207 A89-23280
- Oxygen electrode bifunctional electrocatalyst NiCo<sub>2</sub>O<sub>4</sub> spinel [NASA-TM-100947] p 208 A89-10409
- Space Electrochemical Research and Technology Conference: Abstracts [NASA-CP-10029] p 211 A89-22982
- Oxygen electrodes for rechargeable alkaline fuel cells p 211 A89-22998
- ELECTROCHEMICAL CELLS**
- Effect of NASA advanced designs on thermal behavior of Ni-H<sub>2</sub> cells p 50 A89-15279
- ELECTROCHEMISTRY**
- Space Electrochemical Research and Technology Conference, Cleveland, OH, Apr. 14-16, 1987, Proceedings p 207 A89-23280
- Convective flows in enclosures with vertical temperature or concentration gradients [AIAA PAPER 89-0069] p 118 A89-25060
- Convective flows in enclosures with vertical temperature or concentration gradients [NASA-TM-101373] p 120 A89-12753
- Lightweight fibrous nickel electrodes for nickel-hydrogen batteries [NASA-TM-101997] p 93 A89-22710
- Space Electrochemical Research and Technology Conference: Abstracts [NASA-CP-10029] p 211 A89-22982
- ELECTRODE MATERIALS**
- Isotropic graphite multistage depressed collectors - A progress report --- carbon electrode performance p 132 A89-31988
- Design, fabrication, and performance of brazed, graphite electrode, multistage depressed collectors with 500-W, continuous wave, 4.8- to 9.6-GHz traveling-wave tubes [NASA-TP-2904] p 136 A89-21171
- Oxygen electrodes for rechargeable alkaline fuel cells p 211 A89-22998
- ELECTRODES**
- The effect of different alkali metal hydroxides on nickel electrode life p 207 A89-15280
- Performance of lightweight nickel electrodes p 92 A89-44002
- Structural and thermal response of 30 cm diameter ion thruster optics [AIAA PAPER 89-2719] p 58 A89-47042
- Oxygen electrode bifunctional electrocatalyst NiCo<sub>2</sub>O<sub>4</sub> spinel [NASA-TM-100947] p 208 A89-10409
- Performance of a multistage depressed collector with machined titanium electrodes [NASA-TP-2891] p 136 A89-15337
- Lightweight fibrous nickel electrodes for nickel-hydrogen batteries [NASA-TM-101997] p 93 A89-22710
- Space Electrochemical Research and Technology Conference: Abstracts [NASA-CP-10029] p 211 A89-22982
- Corrosion testing of candidates for the alkaline fuel cell cathode p 212 A89-23000
- Impedance studies of Ni/Cd and Ni/H cells using the cell case as reference electrode p 137 A89-23002
- Nickel-hydrogen capacity loss on storage p 138 A89-23007
- ELECTRODYNAMICS**
- Electroimpulse deicing - Electrodynamical solution by discrete elements p 17 A89-39193
- A numerical model of electrodynamics of plasma within the contaminant gas cloud of the Space Shuttle Orbiter at low earth orbit p 233 A89-45631
- ELECTROFORMING**
- Thrust chamber thermal barrier coating techniques p 115 A89-22671
- ELECTROKINETICS**
- Comparison of the surface charge behavior of commercial silicon nitride and silicon carbide powders p 105 A89-21444
- ELECTROLYTES**
- Hydrogen-oxygen proton-exchange membrane fuel cells and electrolyzers p 211 A89-22996
- ELECTROLYTIC CELLS**
- The effect of different alkali metal hydroxides on nickel electrode life p 207 A89-15280
- ELECTROMAGNETIC ABSORPTION**
- The GaAs solar cells with V-grooved emitters [NASA-TM-102104] p 214 A89-26291
- Parametric study of electromagnetic waves propagating in absorbing curved S ducts [NASA-TM-102024] p 129 A89-27923

- ELECTROMAGNETIC NOISE**
- Analysis of modified SMI method for adaptive array weight control [NASA-CR-184904] p 127 A89-20364
- ELECTROMAGNETIC PROPULSION**
- Experiments and analysis of a compact electrothermal thruster p 59 A89-47494
- ELECTROMAGNETIC PULSES**
- Shooting and bouncing rays - Calculating the RCS of an arbitrarily shaped cavity p 124 A89-34242
- ELECTROMAGNETIC RADIATION**
- Induced emission of radiation from a large space-station-like structure in the ionosphere p 44 A89-31915
- Electromagnetic emission experiences using electric propulsion systems p 61 A89-53354
- Analytical and experimental procedures for determining propagation characteristics of millimeter-wave gallium arsenide microstrip lines [NASA-TP-2899] p 136 A89-21169
- Parametric study of electromagnetic waves propagating in absorbing curved S ducts [NASA-TM-102024] p 129 A89-27923
- ELECTROMAGNETIC SCATTERING**
- Ray-tube integration in shooting and bouncing ray method p 124 A89-15152
- Modal, ray, and beam techniques for analyzing the EM scattering by open-ended waveguide cavities p 125 A89-39594
- Review of FD-TD numerical modeling of electromagnetic wave scattering and radar cross section p 19 A89-45107
- Material parameter determination from scattering measurements [NASA-CR-183312] p 126 A89-10225
- Analysis of the EM scattering from arbitrary open-ended waveguide cavities using axial Gaussian Beam tracking [NASA-CR-185054] p 128 A89-24518
- A hybrid asymptotic-modal analysis of the EM scattering by an open-ended S-shaped rectangular waveguide cavity [NASA-CR-185053] p 129 A89-24519
- ELECTROMAGNETIC WAVE TRANSMISSION**
- A hybrid asymptotic-modal analysis of the EM scattering by an open-ended S-shaped rectangular waveguide cavity [NASA-CR-185053] p 129 A89-24519
- Parametric study of electromagnetic waves propagating in absorbing curved S ducts [NASA-TM-102024] p 129 A89-27923
- ELECTRON BEAMS**
- Coherent Cerenkov radiation from the Spacelab 2 electron beam p 231 A89-24292
- Electron velocity distributions and plasma waves associated with the injection of an electron beam into the ionosphere p 215 A89-43698
- ELECTRON BOMBARDMENT**
- Model for computing volume-averaged plasma properties in electron-bombardment ion thrusters p 54 A89-28339
- ELECTRON DENSITY (CONCENTRATION)**
- Model for computing volume-averaged plasma properties in electron-bombardment ion thrusters p 54 A89-28339
- ELECTRON DIFFRACTION**
- Characterization of GaAlAs optical waveguide heterostructures grown by molecular beam epitaxy p 130 A89-10343
- ELECTRON EMISSION**
- Secondary electron emission characteristics of untreated and ion-textured titanium [NASA-TP-2902] p 103 A89-17650
- Design, fabrication, and performance of brazed, graphite electrode, multistage depressed collectors with 500-W, continuous wave, 4.8- to 9.6-GHz traveling-wave tubes [NASA-TP-2904] p 136 A89-21171
- ELECTRON GAS**
- Shubnikov-de Haas measurements of the 2-D electron gas in pseudomorphic In(0.1)Ga(0.9)As grown on GaAs p 235 A89-29299
- ELECTRON MICROSCOPY**
- Transmission electron microscopy of composites p 79 A89-14560
- TEM studies of oxidized NiAl and Ni<sub>3</sub>Al cross sections p 99 A89-46506
- ELECTRON MOBILITY**
- Calculation of the electron wave function in a graded-channel double-heterojunction modulation-doped field-effect transistor p 134 A89-54417
- ELECTRON ORBITALS**
- Electronic structure of BaO/W cathode surfaces p 132 A89-26862
- ELECTRON PLASMA**
- Experimental validation of a phenomenological model of the plasma contacting process p 232 A89-43357

- ELECTRON SCATTERING**  
Townsend coefficients for electron scattering over dielectric surfaces p 231 A89-16409
- ELECTRON SPECTROSCOPY**  
Alkoxysilane adsorption on metal oxide substrates p 92 A89-44536
- ELECTRON TUNNELING**  
Alkoxysilane adsorption on metal oxide substrates p 92 A89-44536
- ELECTRONIC CONTROL**  
IECON '87: Industrial applications of control and simulation; Proceedings of the 1987 International Conference on Industrial Electronics, Control, and Instrumentation, Cambridge, MA, Nov. 3, 4, 1987 [SPIE-853] p 219 A89-10798  
A real time microcomputer implementation of sensor failure detection for turbofan engines [NASA-TM-102327] p 216 N89-29032
- ELECTRONS**  
Plasma contacting - An enabling technology [AIAA PAPER 89-0677] p 231 A89-25537  
A model of electron collecting plasma contractors [AIAA PAPER 89-1560] p 232 A89-40190
- ELECTROSTATIC PROBES**  
Langmuir probe measurements of an arcjet exhaust p 55 A89-39031
- ELECTROTHERMAL ENGINES**  
Investigations of microwave plasmas - Applications in electrothermal thruster systems [AIAA PAPER 89-2378] p 57 A89-46784
- ELEMENTARY PARTICLES**  
The large-scale microwave background anisotropy in decaying particle cosmology p 240 A89-15426
- ELLIPSOIDAL**  
Thin-film hermeticity - A quantitative analysis of diamondlike carbon using variable angle spectroscopic ellipsometry p 234 A89-13945  
Characterization of multilayer GaAs/AlGaAs transistor structures by variable angle spectroscopic ellipsometry p 133 A89-49998
- ELLIPTIC DIFFERENTIAL EQUATIONS**  
Global properties of pseudospectral methods p 221 A89-37746
- EMISSION SPECTRA**  
The emittance of space radiator materials measured at elevated temperatures [NASA-TM-101948] p 66 N89-20193
- EMITTERS**  
The GaAs solar cells with V-grooved emitters [NASA-TM-102104] p 214 A89-26291
- EMULSIONS**  
Holographic interferometry with an injection seeded Nd:YAG laser and two reference beams [NASA-TM-102056] p 175 N89-24591
- ENCAPSULATING**  
Plasma deposited silicon nitride for indium phosphide encapsulation p 235 A89-27794
- ENCLOSURES**  
Thermosolutal convection in high-aspect-ratio enclosures p 153 A89-53288
- END PLATES**  
Experimental determination of stator endwall heat transfer [NASA-TM-101419] p 159 N89-15366  
An experimental study of near wall flow parameters in the blade end-wall corner region [NASA-CR-4211] p 12 N89-15898
- ENERGY CONSERVATION**  
NASA/industry advanced turboprop technology program p 20 A89-13504  
Advanced turboprop project [NASA-SP-495] p 24 N89-12565  
Wind-tunnel results of advanced high-speed propellers at takeoff, climb, and landing Mach numbers [NASA-TM-87030] p 13 N89-19265
- ENERGY CONVERSION**  
Multi-hundred kilowatt roll ring assembly evaluation results --- for Space Station power transmission p 123 A89-15388  
Megawatt Class Nuclear Space Power Systems (MCNPS) conceptual design and evaluation report. Volume 4: Concepts selection, conceptual designs, recommendations [NASA-CR-179614-VOL-4] p 210 N89-18967  
Megawatt Class Nuclear Space Power Systems (MCNPS) conceptual design and evaluation report. Volume 3, technologies 2: Power conversion [NASA-CR-179614-VOL-3] p 211 N89-22980  
Comparison of solar photovoltaic and nuclear reactor power systems for a human-tended lunar observatory [NASA-TM-102015] p 242 N89-23397
- ENERGY CONVERSION EFFICIENCY**  
Status of several Stirling loss characterization efforts and their significance for Stirling space power development p 49 A89-15187
- Progress in InP solar cell research p 130 A89-15308  
High-efficiency indium tin oxide/indium phosphide solar cells p 208 A89-44883  
Advances in thin-film solar cells for lightweight space photovoltaic power [IAF PAPER ICOSP89-1-8] p 55 A89-46513  
The NASA Space Solar Cell Advanced Research Program [NASA-TM-102020] p 67 N89-22651  
Energy storage and thermal control system design status [NASA-TM-102136] p 46 N89-24427  
Progress in indium phosphide solar cell research p 212 N89-24707  
Ultra-thin, light-trapping silicon solar cells p 213 N89-24719  
Effect of micrometeoroid and space debris impacts on the Space Station Freedom solar array surfaces [NASA-TM-102287] p 47 N89-26035
- ENERGY REQUIREMENTS**  
Power systems for production, construction, life support, and operations in space p 37 A89-45803  
Challenges for future space power systems [NASA-TM-102063] p 214 N89-25506
- ENERGY STORAGE**  
Energy storage considerations for a robotic Mars surface sampler p 49 A89-15267  
Effect of LEO cycling at shallow depths of discharge on MANTECH IPV nickel-hydrogen cells p 49 A89-15278  
Advanced space solar dynamic receivers p 52 A89-15343  
Theoretical performance of hydrogen-bromine rechargeable SPE fuel cell --- Solid Polymer Electrolyte p 207 A89-23290  
Evaluation of alternative phase change materials for energy storage in solar dynamic applications p 208 A89-29114  
Power systems for production, construction, life support, and operations in space p 37 A89-45803  
Compatibility of molten salts with advanced solar dynamic receiver materials [AIAA PAPER 89-1756] p 83 A89-48957  
Study of the generator/motor operation of induction machines in a high frequency link space power system [NASA-CR-179600] p 63 N89-11809  
Cryogenic reactant storage for lunar base regenerative fuel cells [NASA-TM-101980] p 210 N89-21419  
Space Electrochemical Research and Technology Conference: Abstracts [NASA-CP-10029] p 211 N89-22982  
Photovoltaic power system operation in the Mars environment [NASA-TM-102075] p 138 N89-24529  
Solar power for the lunar night [NASA-TM-102127] p 242 N89-26799
- ENERGY TECHNOLOGY**  
Space solar cell research p 208 A89-52203  
The introduction of space technology power systems into developing countries [NASA-TM-102042] p 71 N89-25274
- ENERGY TRANSFER**  
Gas particle radiator [NASA-CASE-LEW-14297-1] p 172 N89-12048  
Energy in elastic fiber embedded in elastic matrix containing incident SH wave [NASA-CR-4205] p 188 N89-18694  
On the nature of Navier-Stokes turbulence [NASA-TM-101983] p 163 N89-23813
- ENGINE AIRFRAME INTEGRATION**  
Integrated flight/propulsion control study for STOVL applications [AIAA PAPER 89-2908] p 34 A89-47166  
Average-passage simulation of counter-rotating propfan propulsion systems as applied to cruise missiles [AIAA PAPER 89-2943] p 7 A89-47187  
A supersonic through-flow fan engine airframe integration study [AIAA PAPER 89-2140] p 18 A89-50802  
Computational methods for inlet airframe integration p 13 N89-16752  
CFD application to subsonic inlet airframe integration --- computational fluid dynamics (CFD) p 13 N89-16753  
CFD application to supersonic/hypersonic inlet airframe integration --- computational fluid dynamics (CFD) p 13 N89-16754  
Average-passage simulation of counter-rotating propfan propulsion systems as applied to cruise missiles [NASA-TM-102043] p 14 N89-23416
- ENGINE CONTROL**  
Advanced detection, isolation, and accommodation of sensor failures - Real-time evaluation p 34 A89-16156
- Effect of model uncertainty on failure detection - The threshold selector p 219 A89-17965  
Integrated flight/propulsion control system design based on a decentralized, hierarchical approach [AIAA PAPER 89-3519] p 35 A89-53301  
Sensor failure detection for jet engines [NASA-TM-101396] p 25 N89-13432  
NASA Lewis Stirling engine computer code evaluation [NASA-CR-182248] p 214 N89-24741
- ENGINE COOLANTS**  
Contingency power for small turboshaft engines p 21 A89-22291  
Liquid oxygen cooling of hydrocarbon fueled rocket thrust chambers [AIAA PAPER 89-2739] p 60 A89-49686  
Coolant passage heat transfer with rotation p 157 N89-12899  
Liquid oxygen cooling of hydrocarbon fueled rocket thrust chambers [NASA-TM-102113] p 70 N89-24447
- ENGINE DESIGN**  
Mod II Stirling engine overviews [SAE PAPER 880539] p 177 A89-12301  
Calculations of the unsteady, three-dimensional flow field inside a motored Wankel engine [SAE PAPER 880625] p 19 A89-12307  
The design and fabrication of a Stirling engine heat exchanger module with an integral heat pipe p 142 A89-15190  
Automated design of controlled-diffusion blades [ASME PAPER 88-GT-139] p 2 A89-15967  
Impact of ETO propellants on the aerothermodynamic analyses of propulsion components --- Earth To Orbit [AIAA PAPER 88-3091] p 53 A89-16486  
Design and test of a propfan gear system p 179 A89-22290  
Aircraft engines. III p 21 A89-22927  
Status and prognosis for alternative engine materials p 97 A89-36419  
Free-piston Stirling technology for space power [IAF PAPER ICOSP89-5-7] p 56 A89-46520  
Advanced H<sub>2</sub>/O<sub>2</sub> space engine parametrics [AIAA PAPER 89-2300] p 57 A89-46855  
Engineering study on the rotary-vee engine concept [SAE PAPER 890332] p 181 A89-51492  
CFD in the context of IHPTET - The Integrated High Performance Turbine Engine Technology Program [AIAA PAPER 89-2904] p 154 A89-53307  
A preliminary design study of supersonic through-flow fan inlets [NASA-CR-182224] p 24 N89-11751  
Closed-drift thruster investigations [NASA-CR-179497] p 62 N89-11808  
HOST combustion R and T overview p 25 N89-12879  
The 25 kWe solar thermal Stirling hydraulic engine system: Conceptual design [NASA-CR-180889] p 239 N89-14182  
Parametric studies of advanced turboprops [NASA-TM-101389] p 197 N89-14465  
A review of failure models for unidirectional ceramic matrix composites under monotonic loads [NASA-TM-101421] p 198 N89-14470  
The design and development of transonic multistage compressors p 27 N89-16834  
Supersonic throughflow fans p 27 N89-16837  
Large-scale Advanced Prop-fan (LAP) hub/blade retention design report [NASA-CR-174786] p 28 N89-19299  
Propulsion over a wide Mach number range [NASA-CR-182267] p 29 N89-20134  
Assessment, development, and application of combustor aerothermal models p 30 N89-20138  
Review and assessment of the database and numerical modeling for turbine heat transfer p 30 N89-20139  
Structural analysis methods development for turbine hot section components p 30 N89-20140  
Views on the impact of HOST p 31 N89-20144  
Free-piston Stirling technology for space power [NASA-TM-101956] p 66 N89-20194  
A perspective on future directions in aerospace propulsion system simulation [NASA-TM-102038] p 31 N89-21798  
Results from baseline tests of the SPRE 1 and comparison with code model predictions [NASA-TM-102044] p 68 N89-23527  
Advanced methods for 3-D inelastic structural analysis for hot engine structures [NASA-TM-102106] p 204 N89-25490  
Engineering study of the rotary-vee engine concept [NASA-TM-101995] p 33 N89-26007  
Two-tiered design analysis of a radiator for a solar dynamic powered Stirling engine [NASA-CR-182301] p 46 N89-26031

## ENGINE FAILURE

- CFD in the context of IHPTET: The Integrated High Performance Turbine Technology Program  
[NASA-TM-102132] p 165 N89-26174
- AGT (Advanced Gas Turbine) technology project  
[NASA-CR-182127] p 186 N89-26246
- Computational structural mechanics for engine structures  
[NASA-TM-102119] p 204 N89-26259
- Comparison of conceptual designs for 25 kWe advanced Stirling conversion systems for dish electric application  
[NASA-TM-102085] p 239 N89-26781
- Computational structural mechanics engine structures computational simulator p 205 N89-29792
- ENGINE FAILURE**
- Advanced detection, isolation, and accommodation of sensor failures - Real-time evaluation p 34 N89-16156
- Active suppression of aerodynamic instabilities in turbo-machines p 3 N89-28341
- Sensor failure detection for jet engines  
[NASA-TM-101396] p 25 N89-13432
- ENGINE INLETS**
- Experimental study of isothermal swirling flows in a dump combustor p 21 N89-23182
- HOST turbine heat transfer subproject overview p 25 N89-12880
- Influence of bulk turbulence and entrance boundary layer thickness on the curved duct flow field p 156 N89-12896
- CFD application to subsonic inlet airframe integration --- computational fluid dynamics (CFD) p 13 N89-16753
- CFD application to supersonic/hypersonic inlet airframe integration --- computational fluid dynamics (CFD) p 13 N89-16754
- Mach 5 inlet CFD and experimental results  
[NASA-TM-102317] p 33 N89-27670
- ENGINE MONITORING INSTRUMENTS**
- Miniature multiple-function probe for OTV turbopump health monitoring p 56 N89-46736
- Fiberoptics for liquid propellant rocket engine environments  
[AIAA PAPER 89-2416] p 230 N89-46812
- ENGINE NOISE**
- Cruise noise of an advanced counterrotation turboprop measured from an adjacent aircraft p 20 N89-15080
- Effect of aerodynamic detuning on supersonic rotor discrete frequency noise generation p 225 N89-15083
- NASA powered lift facility internally generated noise and its transmission to the acoustic far field  
[NASA-CR-182217] p 36 N89-16882
- ENGINE PARTS**
- Composite mechanics for engine structures p 80 N89-28344
- Computational structural mechanics for engine structures  
[AIAA PAPER 89-1260] p 22 N89-30745
- Improved silicon carbide for advanced heat engines. I - Process development for injection molding p 106 N89-33619
- Improved silicon carbide for advanced heat engines. II - Pressureless sintering and mechanical properties of injection molded silicon carbide p 106 N89-33620
- Status and prognosis for alternative engine materials p 97 N89-36419
- Ceramic bearings for use in gas turbine engines p 180 N89-46697
- Turbine Engine Hot Section Technology (HOST) Project p 25 N89-12877
- A review of failure models for unidirectional ceramic matrix composites under monotonic loads  
[NASA-TM-101421] p 198 N89-14470
- Development of an integrated BEM approach for hot fluid structure interaction p 27 N89-15114
- Improved silicon carbide for advanced heat engines  
[NASA-CR-179477] p 112 N89-15251
- Probabilistic analysis for fatigue strength degradation of materials p 198 N89-15434
- Hot corrosion of ceramic engine materials  
[NASA-TM-101439] p 112 N89-16065
- Finite element implementation of viscoplastic models p 200 N89-17328
- Improved silicon nitride for advanced heat engines  
[NASA-CR-179525] p 113 N89-19421
- Fatigue strength reduction model: RANDOM3 and RANDOM4 user manual. Appendix 2: Development of advanced methodologies for probabilistic constitutive relationships of material strength models  
[NASA-CR-184796-APP-2] p 201 N89-19582
- Structural analysis methods development for turbine hot section components p 30 N89-20140
- Fatigue crack growth model RANDOM2 user manual, appendix 1  
[NASA-CR-184939] p 203 N89-23890

- Fatigue strength reduction model: RANDOM3 and RANDOM4 user manual, appendix 2 p 203 N89-23891
- [NASA-CR-184940] p 203 N89-23891
- AGT (Advanced Gas Turbine) technology project  
[NASA-CR-182127] p 186 N89-26246
- Computational structural mechanics for engine structures  
[NASA-TM-102119] p 204 N89-26259
- Computational structural mechanics engine structures computational simulator p 205 N89-29792
- The 3-D inelastic analyses for computational structural mechanics p 206 N89-29804
- ENGINE TESTING LABORATORIES**
- Test facility and preliminary performance of a 100 kW class MPD thruster  
[NASA-TM-102021] p 68 N89-23520
- ENGINE TESTS**
- Results of acoustic tests of a prop-fan model p 224 N89-10112
- Description of an oscillating flow pressure drop test rig p 142 N89-15188
- Contingency power for small turboshaft engines p 21 N89-22291
- NNEPEQ - Chemical equilibrium version of the Navy/NASA Engine Program  
[ASME PAPER 88-GT-314] p 22 N89-24989
- SPRE 1 free-piston Stirling engine testing at NASA Lewis Research Center p 55 N89-29120
- A review and forecast of engine system research at the Army Propulsion Directorate p 23 N89-36397
- Observations of directional gamma prime coarsening during engine operation p 98 N89-40162
- Effect of ambient pressure on the performance of a resistojet p 55 N89-44111
- The effect of electrode configuration on arcjet performance  
[AIAA PAPER 89-2722] p 58 N89-47044
- Strain measurements in a rotary engine housing  
[SAE PAPER 890333] p 181 N89-51493
- Supersonic through-flow fan assessment  
[NASA-CR-182202] p 27 N89-16843
- A data acquisition and storage system for the ion auxiliary propulsion system cyclic thruster test  
[NASA-TM-101469] p 218 N89-17424
- Oxide-dispersion-strengthened turbine blades. Volume 2  
[NASA-CR-179561-VOL-2] p 28 N89-18487
- RE-1000 free-piston Stirling engine sensitivity test results  
[NASA-TM-88846] p 210 N89-19737
- Advanced high temperature instrument for hot section research applications p 29 N89-20137
- A real-time simulator of a turbofan engine  
[NASA-TM-100869] p 31 N89-20995
- Design, fabrication and test of the RL10 derivative II chamber/primary nozzle  
[NASA-CR-179595] p 68 N89-23519
- Test facility and preliminary performance of a 100 kW class MPD thruster  
[NASA-TM-102021] p 68 N89-23520
- Results from baseline tests of the SPRE 1 and comparison with code model predictions p 68 N89-23527
- Performance of large area xenon ion thrusters for orbit transfer missions  
[NASA-TM-102049] p 69 N89-24436
- Initial characterization of a modular heat exchanger with an integral heat pipe p 239 N89-25078
- [NASA-TM-102097] p 239 N89-25078
- A real time microcomputer implementation of sensor failure detection for turbofan engines  
[NASA-TM-102327] p 216 N89-29032
- ENGINEERING MANAGEMENT**
- Performance characterizations of an engineering model multipropellant resistojet p 54 N89-28340
- Engineering calculations for solving the orbital allotment problem  
[NASA-CR-184607] p 217 N89-13993
- ENTHALPY**
- Heat of mixing and morphological stability p 143 N89-21296
- Enthalpies of a binary alloy during solidification p 96 N89-22559
- Efficient numerical simulation of a one-dimensional electrothermal deicer pad p 144 N89-22811
- ENVIRONMENT EFFECTS**
- Alternative fuel capabilities of the Mod II Stirling vehicle  
[SAE PAPER 880543] p 177 N89-12303
- ENVIRONMENT MODELS**
- Effects of environmentally imposed roughness on airfoil performance  
[NASA-CR-179639] p 17 N89-11725

## ENVIRONMENTAL TESTS

- Test methods and design allowables for fibrous composites. Volume 2 p 81 N89-32882
- [ASTM STP-1003] p 81 N89-32882
- The NASA Lewis Research Center High Temperature Fatigue and Structures Laboratory p 194 N89-43528
- Simulation of the low earth orbital atomic oxygen interaction with materials by means of an oxygen ion beam p 114 N89-21104
- [NASA-TM-101971] p 114 N89-21104
- Undercutting of defects in thin film protective coatings on polymer surfaces exposed to atomic oxygen  
[NASA-TM-101986] p 115 N89-23691
- ENVIRONMENTS**
- Performance of multimirror quartzline lamps in a high-pressure, underwater environment  
[NASA-TM-101374] p 172 N89-10269
- EPITAXY**
- Crystal growth of SiC for electronic applications p 132 N89-33625
- EPOXY MATRIX COMPOSITES**
- The correlation of low-velocity impact resistance of graphite-fiber-reinforced composites with matrix properties p 79 N89-16283
- Evaluation of atomic oxygen resistant protective coatings for fiberglass-epoxy composites in LEO  
[NASA-TM-101955] p 114 N89-21100
- EPOXY RESINS**
- The correlation of low-velocity impact resistance of graphite-fiber-reinforced composites with matrix properties p 79 N89-16283
- Oxidation and protection of fiberglass-epoxy composite masts for photovoltaic arrays in the low earth orbital environment p 44 N89-35316
- EQUATIONS OF STATE**
- Universal features of the equation of state of solids p 237 N89-48960
- EQUIPMENT SPECIFICATIONS**
- The effects of leading edge and downstream film cooling on turbine vane heat transfer  
[NASA-CR-182133] p 158 N89-13754
- Space station WP-04 power system preliminary analysis and design document, volume 3 p 64 N89-15164
- [NASA-CR-179587-VOL-3] p 64 N89-15164
- Isothermal dendritic growth: A low gravity experiment p 121 N89-20299
- Film annotation system for a space experiment  
[NASA-CR-185114] p 176 N89-27152
- EROSION**
- The NASA atomic oxygen effects test program p 93 N89-12589
- MATE program: Erosion resistant compressor airfoil coating, volume 2  
[NASA-CR-179645] p 113 N89-18550
- Diamondlike carbon protective coatings for optical windows  
[NASA-TM-102111] p 231 N89-27506
- EROSIVE BURNING**
- Boundary layer effects on particle impaction and capture p 143 N89-19123
- ERROR ANALYSIS**
- On the accuracy of solving triangular systems in parallel  
[NASA-TM-101384] p 222 N89-12337
- On the equivalence of Gaussian elimination and Gauss-Jordan reduction in solving linear equations  
[NASA-TM-101466] p 222 N89-20710
- On the equivalence of a class of inverse decomposition algorithms for solving systems of linear equations  
[NASA-TM-102036] p 223 N89-24865
- ERRORS**
- On the accuracy of solving triangular systems in parallel  
[NASA-TM-101384] p 222 N89-12337
- ESTIMATES**
- Performance estimates for the Space Station power system Brayton Cycle compressor and turbine  
[NASA-CR-182263] p 73 N89-26903
- ETALONS**
- Fiber-optic temperature sensor using a spectrum-modulating semiconductor etalon p 168 N89-10366
- ETCHING**
- A V-grooved GaAs solar cell p 211 N89-22177
- [NASA-TM-101970] p 211 N89-22177
- Chemical etching and organometallic chemical vapor deposition on varied geometries of GaAs p 213 N89-24728
- ETHERS**
- The preparation of new perfluoro ether fluids exhibiting excellent thermal-oxidative stabilities p 76 N89-12760
- EULER EQUATIONS OF MOTION**
- Diagonal implicit multigrid algorithm for the Euler equations p 1 N89-11110
- Simple high-accuracy resolution program for convective modelling of discontinuities p 143 N89-17459



- Euler analysis of a swirl recovery vane design for use with an advanced single-rotation propfan  
[AIAA PAPER 88-3152] p 2 A89-17940
- LU implicit multigrid algorithm for the three-dimensional Euler equations p 143 A89-19906
- Unsteady Euler cascade analysis  
[AIAA PAPER 89-0322] p 3 A89-28406
- Numerical analysis of flow through oscillating cascade sections  
[AIAA PAPER 89-0437] p 4 A89-28413
- Calculation of unsteady flows in turbomachinery using the linearized Euler equations p 149 A89-36916
- High speed corner and gap-seal computations using an LU-SGS scheme  
[AIAA PAPER 89-2669] p 154 A89-54424
- Numerical analysis of flow through oscillating cascade sections  
[NASA-TM-101417] p 11 N89-14220
- A genuinely multi-dimensional upwind cell-vertex scheme for the Euler equations  
[NASA-TM-102029] p 223 N89-24872
- Multigrid calculation of three-dimensional turbomachinery flows  
[NASA-CR-185332] p 165 N89-26172
- High speed corner and gap-seal computations using an LU-SGS scheme  
[NASA-TM-102138] p 166 N89-27103
- EULER-LAGRANGE EQUATION**  
On the Lagrangian description of unsteady boundary layer separation. Part 1: General theory  
[NASA-TM-102026] p 164 N89-23821
- EUTECTIC ALLOYS**  
Microsegregation in directionally solidified Pb-8.4 at. pct Au alloy p 94 A89-12758
- Macroscopic segregation in undercooled Pb-Sn eutectic alloys p 95 A89-19621
- Macroscopic segregation and nucleation in undercooled Pb-Sn alloys  
[NASA-TM-102023] p 104 N89-23664
- EVALUATION**  
Multi-hundred kilowatt roll ring assembly evaluation results --- for Space Station power transmission  
p 123 A89-15388
- The acousto-ultrasonic approach --- for NDE  
p 188 A89-32305
- Technique for temperature compensation of eddy-current proximity probes  
[NASA-TP-2880] p 173 N89-15380
- Acoustic evaluation of the Helmholtz resonator treatment in the NASA Lewis 8- by 6-foot supersonic wind tunnel  
[NASA-TM-101407] p 228 N89-15685
- EVAPORATION**  
Highly oriented Ti2Ba2Ca2Cu3O10 thin films by pulsed laser evaporation p 236 A89-30421
- Sequentially evaporated thin Y-Ba-Cu-O superconductor films: Composition and processing effects  
[NASA-TM-101388] p 134 N89-10235
- Deposition and characterization of ZnS/Si heterojunctions produced by vacuum evaporation  
[NASA-TM-101359] p 135 N89-11129
- Sequentially evaporated thin Y-Ba-Co-O superconducting films on microwave substrates  
[NASA-TM-102068] p 138 N89-23791
- EXCITATION**  
Recovery of excitation intensity dependence in pulsed, focused beams - Nonsaturated case p 177 A89-17507
- Effects of core turbulence on jet excitability  
[AIAA PAPER 89-0966] p 147 A89-30482
- Effects of core turbulence on jet excitability  
[NASA-TM-101405] p 159 N89-14403
- NASTRAN supplemental documentation for model forced vibration analysis of aerodynamically excited turbosystems  
[NASA-CR-174967] p 201 N89-19583
- EXHAUST EMISSION**  
Langmuir probe measurements of an arcjet exhaust p 55 A89-39031
- Investigation of low NOx staged combustor concept in high-speed civil transport engines  
[AIAA PAPER 89-2942] p 23 A89-47186
- Fuel properties effect on the performance of a small high temperature rise combustor  
[AIAA PAPER 89-2901] p 23 A89-52025
- Gas turbine alternative fuels combustion characteristics  
[NASA-TM-101470] p 210 N89-21417
- Investigation of low NOx staged combustor concept in high-speed civil transport engines  
[NASA-TM-101977] p 32 N89-22606
- Fuel properties effect on the performance of a small high temperature rise combustor  
[NASA-TM-102096] p 33 N89-25238
- EXHAUST FLOW SIMULATION**  
Comparison of 3D computation and experiment for non-axisymmetric nozzles  
[AIAA PAPER 89-0007] p 22 A89-28403
- EXHAUST GASES**  
Effects of nozzle exit boundary-layer conditions on excitability of heated free jets p 149 A89-36908
- Hot gas ingestion testing of an advanced STOVL concept in the NASA Lewis 9- by 15-foot low speed wind tunnel with flow visualization  
[NASA-TM-100952] p 11 N89-15078
- EXHAUST NOZZLES**  
Rectangular nozzle plume velocity modeling for use in jet noise prediction  
[AIAA PAPER 89-2357] p 7 A89-46771
- Rectangular nozzle plume velocity modeling for use in jet noise prediction  
[NASA-TM-102047] p 14 N89-22577
- EXHAUST VELOCITY**  
Rectangular nozzle plume velocity modeling for use in jet noise prediction  
[AIAA PAPER 89-2357] p 7 A89-46771
- The effects of magnetic nozzle configurations on plasma thrusters  
[NASA-CR-184678] p 64 N89-15170
- Rectangular nozzle plume velocity modeling for use in jet noise prediction  
[NASA-TM-102047] p 14 N89-22577
- EXOTHERMIC REACTIONS**  
Effects of heat release on the large-scale structure in turbulent mixing layers p 147 A89-31844
- Characterization of ceramics and intermetallics fabricated by self-propagating high-temperature synthesis  
[NASA-TM-102004] p 78 N89-25285
- EXPENDABLE STAGES (SPACECRAFT)**  
Expendable launch vehicle transportation for the Space Station  
[IAF PAPER 88-198] p 42 A89-17720
- EXPERIMENT DESIGN**  
Hardware development for the Surface Tension Driven Convection Experiment aboard the USML-1 Spacelab mission  
[AIAA PAPER 89-0406] p 47 A89-25341
- Interfacial adhesion - Theory and experiment  
p 97 A89-35307
- Hardware development for the surface tension driven convection experiment aboard the USML-1 spacelab mission  
[NASA-TM-101404] p 48 N89-11804
- Automation software for a materials testing laboratory  
p 217 N89-12917
- Isothermal dendritic growth: A low gravity experiment  
p 121 N89-20299
- Microgravity combustion science: A program overview  
[NASA-TM-101424] p 122 N89-28665
- EXPERIMENTATION**  
Experiment plans to study preignition processes of a pool fire in low gravity  
[NASA-CR-182256] p 121 N89-19442
- EXPERT SYSTEMS**  
A reusable rocket engine intelligent control  
[AIAA PAPER 88-3114] p 48 A89-14981
- Cooperating expert systems for Space Station - Power/thermal subsystem testbeds p 38 A89-15350
- Identification of high performance and component technology for space electrical power systems for use beyond the year 2000  
[NASA-CR-183003] p 62 N89-11807
- An expert system for restructurable control  
[NASA-TM-101378] p 220 N89-12309
- Expert systems applied to spacecraft fire safety  
[NASA-CR-182266] p 42 N89-23501
- Evolutionary growth for Space Station Freedom electrical power system  
[NASA-TM-102339] p 76 N89-28570
- Computational structural mechanics engine structures computational simulator p 205 N89-29792
- EXPLOSIONS**  
Space reactor assessment and validation study p 230 N89-13227
- EXPOSURE**  
Exposure time considerations in high temperature low cycle fatigue p 192 A89-29600
- EXTENSOMETERS**  
High pressure multiaxial extensometry p 170 A89-43532
- X-ray based extensometry  
[NASA-CR-185058] p 176 N89-25432
- EXTINGUISHING**  
Time-dependent computational studies of flames in microgravity  
[NASA-CR-182298] p 122 N89-25353
- EXTRAPOLATION**  
Recursive algorithms for vector extrapolation methods p 221 A89-14397
- EXTRATERRESTRIAL RADIATION**  
The NASA Space Solar Cell Advanced Research Program  
[NASA-TM-102020] p 67 N89-22651
- EXTRATERRESTRIAL RESOURCES**  
An analysis of possible advanced space strategies featuring the role of space resource utilization  
[IAF PAPER 88-587] p 37 A89-17861
- EXTREMELY HIGH FREQUENCIES**  
Development of a 75-watt 60-GHz traveling-wave tube for intersatellite communications  
[NASA-CR-182135] p 138 N89-24530

## F

## FABRICATION

- Hydrogen-bromine fuel cell advance component development  
[NASA-TM-101345] p 208 N89-10405
- Space station auxiliary thrust chamber technology  
[NASA-CR-179650] p 46 N89-11803
- The role of rapid solidification processing in the fabrication of fiber reinforced metal matrix composites  
[NASA-TM-101450] p 85 N89-15201
- Tensile and creep rupture behavior of P/M processed Nb-base alloy, WC-3009  
[NASA-TM-101954] p 78 N89-19371
- Improved silicon nitride for advanced heat engines  
[NASA-CR-179525] p 113 N89-19421
- Optical detectors for GaAs MMIC integration: Technology assessment  
[NASA-TM-102025] p 137 N89-22020
- A V-grooved GaAs solar cell  
[NASA-TM-101970] p 211 N89-22177
- Design, fabrication and test of the RL10 derivative II chamber/primary nozzle  
[NASA-CR-179595] p 68 N89-23519
- High efficiency GaAs-Ge tandem solar cells grown by MOCVD p 213 N89-24721

## FABRICS

- Tribological properties of alumina-boria-silicate fabric from 25 C to 850 C p 107 A89-54982

## FABRY-PEROT INTERFEROMETERS

- Three component laser anemometer measurements in an annular cascade of core turbine vanes with contoured end wall  
[NASA-TP-2846] p 9 N89-10844

## FACE CENTERED CUBIC LATTICES

- Effects of cobalt concentration on the relative resistance to octahedral and cube slip in nickel-base superalloys  
p 94 A89-17115

## FAILURE

- A predictive model for failure properties of thermoset resins  
[NASA-TM-4128] p 87 N89-25300

## FAILURE ANALYSIS

- Effect of model uncertainty on failure detection - The threshold selector p 219 A89-17965
- Structural behavior of composites with progressive fracture  
[AIAA PAPER 89-1271] p 192 A89-30754
- Thermal barrier coating life prediction model  
p 109 N89-12921
- Thermal barrier coating life prediction model development p 110 N89-12922
- Sensor failure detection for jet engines  
[NASA-TM-101396] p 25 N89-13432
- Thermal Barrier Coatings. Abstracts and figures  
[NASA-CP-10019] p 110 N89-13642
- Examination of coating failure by acoustic emission  
p 110 N89-13654
- Failure analysis of a Stirling engine heat pipe  
[NASA-TM-101418] p 103 N89-20227
- Fatigue crack growth model RANDOM2 user manual, appendix 1  
[NASA-CR-184939] p 203 N89-23890
- Procedures for characterizing an alloy and predicting cyclic life with the total strain version of Strainrange Partitioning  
[NASA-TM-4102] p 203 N89-25485
- Probabilistic structural analysis methods of hot engine structures  
[NASA-TM-102091] p 205 N89-28030
- A real time microcomputer implementation of sensor failure detection for turbofan engines  
[NASA-TM-102327] p 216 N89-29032
- FAILURE MODES**  
The correlation of low-velocity impact resistance of graphite-fiber-reinforced composites with matrix properties p 79 A89-16283
- Fracture toughness of polycrystalline ceramics in combined mode I and mode II loading  
p 105 A89-26457

## FANS

- Improving the fatigue resistance of adhesive joints in laminated wood structures  
[NASA-CR-182185] p 85 N89-12675
- A review of failure models for unidirectional ceramic matrix composites under monotonic loads  
[NASA-TM-101421] p 198 N89-14470
- Failure analysis of a Stirling engine heat pipe  
[NASA-TM-101418] p 103 N89-20227
- Fatigue testing apparatus  
[NASA-CASE-LEW-14124-1] p 177 N89-28806

## FANS

- Influence of thickness and camber on the aeroelastic stability of supersonic throughflow fans: An engineering approach  
[NASA-TM-101949] p 15 N89-25957

## FAR FIELDS

- Bounds on current collection from the far field by plasma clouds in the ionosphere p 214 A89-34791
- Installed propfan (SR-71) far-field noise characteristics  
[AIAA PAPER 89-1056] p 225 A89-36216
- Determination of near and far field acoustics for advanced propeller configurations  
[AIAA PAPER 89-1040] p 226 A89-40469
- Measured far-field flight noise of a counterrotation turboprop at cruise conditions  
[NASA-TM-101383] p 228 N89-15686
- A comparison of reflector antenna designs for wide-angle scanning  
[NASA-TM-101459] p 127 N89-21138
- Computed performance of the half-scale accurate antenna reflector  
[NASA-CR-182284] p 139 N89-24532
- Far field expansion for anisotropic wave equations  
[NASA-TM-102112] p 165 N89-26175

## FATIGUE (MATERIALS)

- Influence of fatigue crack wake length and state of stress on crack closure p 181 A89-17432
- Fatigue crack growth behavior of a single crystal alloy as observed through an in situ fatigue loading stage  
p 99 A89-45946
- Constitutive behavior of single crystal PWA 1480 and directionally solidified MAR-M 246 under monotonic and cyclic loads at high and low temperature  
p 100 N89-12634
- Improving the fatigue resistance of adhesive joints in laminated wood structures  
[NASA-CR-182185] p 85 N89-12675
- Turbine Engine Hot Section Technology 1986  
[NASA-CP-2444] p 195 N89-12876
- Elevated temperature crack growth  
p 196 N89-12915
- Automation software for a materials testing laboratory  
p 217 N89-12917
- Fatigue crack growth study of SCS6/Ti-15-3 composite  
[NASA-TM-102332] p 104 N89-26989

## FATIGUE LIFE

- Exposure time considerations in high temperature low cycle fatigue p 192 A89-29600
- Computational structural mechanics for engine structures  
[AIAA PAPER 89-1260] p 22 A89-30745
- Accelerated fatigue crack growth behavior of PWA 1480  
p 97 A89-36461
- Surface fatigue life of carburized and hardened M50NiL and AISI 9310 spur gears and rolling-contact test bars  
[AIAA PAPER 89-2819] p 180 A89-47105
- Transmission overhaul and replacement predictions using Weibull and renewal theory  
[AIAA PAPER 89-2919] p 180 A89-47173
- Computerized life and reliability modeling for turboprop transmissions  
p 181 A89-53364
- Fatigue and fracture overview  
p 195 N89-12882
- Creep fatigue life prediction for engine hot section materials (isotropic): Fourth year progress review  
p 188 N89-12914
- Grain boundary oxidation and its effects on high temperature fatigue life  
p 101 N89-12918
- Probabilistic analysis for fatigue strength degradation of materials  
[NASA-CR-182844] p 198 N89-15434
- Stochastic modeling of crack initiation and short-crack growth under creep and creep-fatigue conditions  
[NASA-TM-101358] p 199 N89-17286
- Fatigue life prediction modeling for turbine hot section materials  
p 30 N89-20142
- Results of inphase axial-torsional fatigue experiments on 304 stainless steel  
[NASA-TM-101464] p 201 N89-20514
- Surface fatigue life of carburized and hardened M50NiL and AISI 9310 spur gears and rolling-contact test bars  
[NASA-TM-101979] p 185 N89-22111
- Thrust chamber thermal barrier coating techniques  
p 115 N89-22671
- Fiber reinforced superalloys for rocket engines  
p 103 N89-22673

- The isothermal fatigue behavior of a unidirectional SiC/Ti composite and the Ti alloy matrix  
[NASA-TM-101984] p 86 N89-22684
- Transmission overhaul and replacement predictions using Weibull and renewal theory  
[NASA-TM-102022] p 186 N89-22925
- Fatigue crack growth model RANDOM2 user manual, appendix 1  
[NASA-CR-184939] p 203 N89-23890
- Fatigue strength reduction model: RANDOM3 and RANDOM4 user manual, appendix 2  
[NASA-CR-184940] p 203 N89-23891
- Isothermal life prediction of composite lamina using a damage mechanics approach  
[NASA-TM-102032] p 87 N89-24460
- Procedures for characterizing an alloy and predicting cyclic life with the total strain version of Strainrange Partitioning  
[NASA-TM-4102] p 203 N89-25485
- Probabilistic structural analysis methods of hot engine structures  
[NASA-TM-102091] p 205 N89-28030

## FATIGUE TESTS

- Thermal-mechanical fatigue test apparatus for metal matrix composites and joint attachments  
p 79 A89-15727
- High pressure multiaxial extensometry  
p 170 A89-43532
- The low cycle fatigue deformation response of a single-crystal superalloy at 650 C  
p 99 A89-52204
- Fatigue crack growth model RANDOM2 user manual. Appendix 1: Development of advanced methodologies for probabilistic constitutive relationships of material strength models  
[NASA-CR-184775-APP-1] p 201 N89-19581
- Fatigue strength reduction model: RANDOM3 and RANDOM4 user manual. Appendix 2: Development of advanced methodologies for probabilistic constitutive relationships of material strength models  
[NASA-CR-184796-APP-2] p 201 N89-19582
- Surface fatigue life of carburized and hardened M50NiL and AISI 9310 spur gears and rolling-contact test bars  
[NASA-TM-101979] p 185 N89-22111
- Procedures for characterizing an alloy and predicting cyclic life with the total strain version of Strainrange Partitioning  
[NASA-TM-4102] p 203 N89-25485
- A data acquisition and control program for axial-torsional fatigue testing  
[NASA-TM-102041] p 205 N89-28029
- Furnace for tensile/fatigue testing  
[NASA-CASE-LEW-14848-1] p 40 N89-28549
- Fatigue testing apparatus  
[NASA-CASE-LEW-14124-1] p 177 N89-28806
- FAULT TOLERANCE**
- Dynamic characteristics of a 20 kHz resonant power system - Fault identification and fault recovery  
p 52 A89-15357
- Advanced detection, isolation, and accommodation of sensor failures - Real-time evaluation  
p 34 A89-16156
- Effect of model uncertainty on failure detection - The threshold selector  
p 219 A89-17965

## FEASIBILITY ANALYSIS

- Oxide-dispersion-strengthened turbine blades. Volume 2  
[NASA-CR-179561-VOL-2] p 28 N89-18487

## FEEDBACK CONTROL

- Integrated communication and control systems. II - Design considerations  
[ASME PAPER 88-WA/DSC-2] p 219 A89-22500
- Turboprop engine control system design using the LQG/LTR methodology  
p 23 A89-53956
- Stability robustness improvement of direct eigenspace assignment based feedback systems using singular value sensitivities  
p 220 A89-53958
- Identification of Space Shuttle Main Engine dynamics  
p 61 A89-54068
- Identification of space shuttle main engine dynamics  
[NASA-TM-101982] p 66 N89-20199
- Active vibration control for flexible rotor by optimal direct-output feedback control  
[NASA-TM-101972] p 31 N89-22605
- Turboprop engine control system design using the LQG/LTR methodology  
[NASA-CR-182303] p 33 N89-26004
- Stability robustness improvement of direct eigenspace assignment based feedback systems using singular value sensitivities  
[NASA-CR-182302] p 36 N89-27672

## FEEDFORWARD CONTROL

- Neuromorphic learning of continuous-valued mappings in the presence of noise: Application to real-time adaptive control  
[NASA-TM-101999] p 221 N89-24856

## FIBER COMPOSITES

- Fiber composite sandwich thermostructural behavior - Computational simulation  
p 190 A89-11246
- A unique set of micromechanics equations for high-temperature metal matrix composites  
p 190 A89-15734
- The correlation of low-velocity impact resistance of graphite-fiber-reinforced composites with matrix properties  
p 79 A89-16283
- Finite element substructuring methods for composite mechanics  
p 80 A89-26291
- Finite element applications to explore the effects of partial bonding on metal matrix composite properties  
[AIAA PAPER 89-1175] p 192 A89-30666
- Mechanics of damping for fiber composite laminates including hygro-thermal effects  
[AIAA PAPER 89-1191] p 192 A89-30681
- Structural behavior of composites with progressive fracture  
[AIAA PAPER 89-1271] p 192 A89-30754
- Structural tailoring of laminate properties  
[AIAA PAPER 89-1367] p 192 A89-30842
- Pressure effects on the thermal stability of silicon carbide fibers  
p 105 A89-31502
- Test methods and design allowables for fibrous composites. Volume 2  
[ASTM STP-1003] p 81 A89-32882
- Strength distribution of reinforcing fibers in a Nicalon fiber/chemically vapor infiltrated silicon carbide matrix composite  
p 82 A89-34844
- Mechanics of composite materials - Past, present and future  
p 82 A89-36293
- Fiber composite structural durability and damage tolerance - Simplified predictive methods  
p 82 A89-36320
- Reaction kinetics between fiber and matrix  
p 83 A89-36420
- A probabilistic formulation for fracture energy of continuous fibre-matrix composites  
p 83 A89-39996
- Design procedures for fiber composite box beams  
p 195 A89-48674
- Thermodynamic analysis of compatibility of several reinforcement materials with FeAl alloys  
[NASA-CR-4172] p 83 N89-10128
- Properties of silicon carbide fiber-reinforced silicon nitride matrix composites  
[NASA-TM-101356] p 84 N89-10130
- Laminate behavior for SiC fiber-reinforced reaction-bonded silicon nitride matrix composites  
[NASA-TM-101350] p 84 N89-10952
- Fracture toughness computational simulation of general delaminations in fiber composites  
[NASA-TM-101415] p 85 N89-13521
- Local-global analysis of crack growth in continuously reinforced ceramic matrix composites  
[NASA-CR-182231] p 197 N89-13820
- Energy in elastic fiber embedded in elastic matrix containing incident SH wave  
p 188 N89-18694
- [NASA-CR-4205] p 188 N89-18694
- A study of the stress wave factor technique for evaluation of composite materials  
[NASA-CR-4195] p 189 N89-21256
- Fiber reinforced superalloys for rocket engines  
p 103 N89-22673
- Composite blade structural analyzer (COBSTRAN) user's manual  
[NASA-TM-101461] p 86 N89-23621
- Light weight polymer matrix composite material  
[NASA-CASE-LEW-14734-1] p 87 N89-23623
- Preparation and evaluation of silicon nitride matrices for silicon nitride-SiC fiber composites  
[NASA-CR-184798] p 115 N89-23678
- Finite element modeling of frictionally restrained composite interfaces  
[NASA-CR-182281] p 203 N89-23918
- Isothermal life prediction of composite lamina using a damage mechanics approach  
[NASA-TM-102032] p 87 N89-24460
- Simplified procedures for designing adhesively bonded composite joints  
[NASA-TM-102120] p 87 N89-26048
- Tailoring of composite links for optimal damped elasto-dynamic performance  
[NASA-TM-102094] p 88 N89-26912
- Unified micromechanics of damping for unidirectional fiber reinforced composites  
[NASA-TM-102107] p 88 N89-26919
- Tungsten fiber reinforced copper matrix composites: A review  
[NASA-TP-2924] p 88 N89-27796
- The interface in tungsten fiber reinforced niobium metal-matrix composites  
[NASA-TM-102122] p 104 N89-28627
- Intermetallic and ceramic matrix composites for 815 to 1370 C (1500 to 2500 F) gas turbine engine applications  
[NASA-TM-102326] p 88 N89-29490

- Creep behavior of tungsten fiber reinforced niobium metal matrix composites [NASA-TM-102307] p 104 N89-29522
- Fiber reinforced ceramic material [NASA-CASE-LEW-14392-2] p 116 N89-29538
- FIBER OPTICS**
- Fiber-optic temperature sensor using a spectrum-modulating semiconductor etalon p 168 A89-10366
- Amplitude spectrum modulation technique for analog data processing in fiber optic sensing system with temporal separation of channels p 169 A89-10368
- Intensity-based fibre-optic sensing system using contrast modulation of subcarrier interference pattern p 170 A89-39302
- Fiber optics for liquid propellant rocket engine environments [AIAA PAPER 89-2416] p 230 A89-46812
- Fiber optic control system integration [NASA-CR-179568] p 231 N89-13256
- Amplitude spectrum modulation technique for analog data processing in fiber optic sensing system with temporal separation of channels [NASA-TM-100152] p 174 N89-18671
- Optical detectors for GaAs MMIC integration: Technology assessment [NASA-TM-102025] p 137 N89-22020
- Compensation for effects of ambient temperature on rare-earth doped fiber optic thermometer [NASA-TM-102282] p 176 N89-27998
- Speckle interferometry using fiber optic phase stepping [NASA-TM-102331] p 176 N89-27999
- FIBER STRENGTH**
- Pressure effects on the thermal stability of silicon carbide fibers p 105 A89-31502
- Strength distribution of reinforcing fibers in a Nicalon fiber/chemically vapor infiltrated silicon carbide matrix composite p 82 A89-34844
- Synthesis and stability of Br<sub>2</sub>, ICl and IBr intercalated pitch-based graphite fibers p 106 A89-37670
- FIBERS**
- Thermodynamic analysis of compatibility of several reinforcement materials with beta phase NiAl alloys [NASA-CR-4171] p 84 N89-10131
- Thermal effects on the mechanical properties of SiC fiber reinforced reaction bonded silicon nitride matrix (SiC/RBSN) composites [NASA-TM-101348] p 84 N89-10134
- Effect of length of chopped pristine and intercalated graphite fibers on the resistivity of fiber networks [NASA-TM-101395] p 84 N89-11826
- Technological hurdles to the application of intercalated graphite fibers [NASA-TM-101394] p 108 N89-11911
- Graphite fluoride fiber polymer composite material [NASA-CASE-LEW-14472-1] p 85 N89-14259
- Metal matrix composite micromechanics: In-situ behavior influence on composite properties [NASA-TM-102302] p 88 N89-26924
- Optimum interface properties for metal matrix composites [NASA-TM-102295] p 205 N89-27223
- FIELD EFFECT TRANSISTORS**
- Optoelectronic techniques for broadband switching p 131 A89-15825
- Characterization of multilayer GaAs/AlGaAs transistor structures by variable angle spectroscopic ellipsometry p 133 A89-49998
- Calculation of the electron wave function in a graded-channel double-heterojunction modulation-doped field-effect transistor p 134 A89-54417
- Development of gallium arsenide high-speed, low-power serial parallel interface modules: Executive summary [NASA-CR-182272] p 137 N89-21173
- Paralleling power MOSFETs in their active region: Extended range of passively forced current sharing [NASA-CR-180902] p 139 N89-26150
- FIGHTER AIRCRAFT**
- Integrated flight/propulsion control system design based on a decentralized, hierarchical approach [AIAA PAPER 89-3519] p 35 A89-53301
- FILM COOLING**
- Turbine airfoil film cooling p 158 N89-12903
- The effects of leading edge and downstream film cooling on turbine vane heat transfer [NASA-CR-182133] p 158 N89-13754
- Turbine airfoil film cooling p 161 N89-17315
- Scaling results for the Liquid Sheet Radiator (LSR) [NASA-TM-102100] p 72 N89-25277
- FILTRATION**
- An asymptotic description of transient settling and ultrafiltration of colloidal dispersions p 144 A89-24603
- FINITE DIFFERENCE THEORY**
- Navier-Stokes solution to the flowfield over ice accretion shapes p 1 A89-12557
- Accurate boundary conditions for exterior problems in gas dynamics p 143 A89-20223
- Nonoscillatory solution of the steady-state inviscid Burgers' equation by mathematical programming p 221 A89-22756
- Efficient numerical simulation of a one-dimensional electrothermal deicer pad p 144 A89-22811
- Review of FD-TD numerical modeling of electromagnetic wave scattering and radar cross section p 19 A89-45107
- A numerical model of electrodynamics of plasma within the contaminant gas cloud of the Space Shuttle Orbiter at low earth orbit p 233 A89-45631
- Numerical analysis of supersonic flow through oscillating cascade sections by using a deforming grid [AIAA PAPER 89-2805] p 8 A89-50810
- A numerical method for computing unsteady 2-D boundary layer flows [NASA-CR-4198] p 155 N89-12835
- Heat transfer in the tip region of a rotor blade simulator p 161 N89-17312
- Numerical computation of shock wave-turbulent boundary layer interaction in transonic flow over an axisymmetric curved hill [NASA-TM-101473] p 162 N89-21192
- Numerical analysis of supersonic flow through oscillating cascade sections by using a deforming grid [NASA-TM-102053] p 15 N89-25119
- Interaction between Tollmien-Schlichting waves and free-stream disturbances in boundary-layer flows [NASA-CR-185847] p 167 N89-27118
- FINITE ELEMENT METHOD**
- A unique set of micromechanics equations for high-temperature metal matrix composites p 190 A89-15734
- Composite interlaminar fracture toughness - Three-dimensional finite-element modeling for mixed mode I, II, and fracture p 190 A89-16278
- Sublimate- or ply-level analysis of composites and strain energy release rates of end-notch and mixed-mode fracture specimens p 190 A89-16279
- Probabilistic structural analysis methods and applications p 190 A89-16939
- A 20-DOF hybrid stress general shell element p 191 A89-21133
- Effects of wind-tunnel wall absorption on acoustic radiation of propellers p 225 A89-22285
- A Monte Carlo-finite element model for strain energy controlled microstructural evolution - 'Rafting' in superalloys p 96 A89-24358
- Probabilistic methods for structural response analysis p 223 A89-25843
- An approach to probabilistic finite element analysis using a mixed-iterative formulation p 191 A89-25849
- Kuhn-Tucker optimization based reliability analysis for probabilistic finite elements p 187 A89-25852
- Finite element substructuring methods for composite mechanics p 80 A89-26291
- Nonlinear analysis using temporal finite elements p 221 A89-28030
- A computational procedure for automated flutter analysis p 191 A89-28070
- Finite element applications to explore the effects of partial bonding on metal matrix composite properties [AIAA PAPER 89-1175] p 192 A89-30666
- Free-vibration characteristics and correlation of a Space Station split-blanket solar array [AIAA PAPER 89-1252] p 44 A89-30737
- Symbolic derivation of material property matrices in finite element analysis p 216 A89-34964
- Acoustic wave propagation in heterogeneous structures including experimental validation [AIAA PAPER 89-1044] p 225 A89-36214
- Graphical postprocessing for 3-D mesh quality evaluation p 217 A89-38846
- Finite element grid improvement by minimization of stiffness matrix trace p 194 A89-42339
- Radiative transfer in rectangular enclosures - A discretized exchange factor solution p 153 A89-53262
- HOST surface protection R and T overview p 109 N89-12883
- Constitutive modeling for isotropic materials p 195 N89-12904
- Constitutive modeling for isotropic materials [NASA-CR-174805] p 26 N89-13436
- Cyclic stress analysis of ceramic coated gas turbine seals p 111 N89-13662
- MHOST version 4.2. Volume 1: Users' manual [NASA-CR-182235-VOL-1] p 217 N89-13996
- Improvement in finite element meshes: Heat transfer in an infinite cylinder [NASA-TM-101410] p 182 N89-14450
- Parametric studies of advanced turboprops [NASA-TM-101389] p 197 N89-14465
- Free-vibration characteristics and correlation of a space station split-blanket solar array [NASA-TM-101452] p 198 N89-15438
- Turbine Engine Hot Section Technology, 1987 [NASA-CP-2493] p 199 N89-17298
- Mechanics of materials model p 199 N89-17319
- Three-dimensional inelastic analysis methods for hot section components p 199 N89-17321
- Finite element implementation of viscoplastic models p 200 N89-17328
- Structural response of an advanced combustor liner: Test and analysis p 200 N89-17329
- Thermal expansion mismatch and plasticity in thermal barrier coating p 200 N89-17330
- High temperature constitutive and crack initiation modeling of coated single crystal superalloys p 112 N89-17334
- Elevated temperature crack growth p 200 N89-17335
- Acoustic wave propagation in heterogeneous structures including experimental validation [NASA-TM-101486] p 224 N89-19965
- Structural Tailoring of Advanced Turboprops (STAT) programmer's manual [NASA-CR-182164] p 29 N89-20132
- Finite element applications to explore the effects of partial bonding on metal matrix composite properties [NASA-TM-101482] p 86 N89-20206
- Modal analysis of gear housing and mounts [NASA-TM-101445] p 184 N89-21244
- Least-squares finite elements for Stokes problem [NASA-TM-101308] p 222 N89-22392
- Finite element modeling of frictionally restrained composite interfaces [NASA-CR-182281] p 203 N89-23918
- Acoustic propagation in curved ducts with extended reacting wall treatment [NASA-TM-102110] p 224 N89-25670
- Nonlinear mesomechanics of composites with periodic microstructure [NASA-TM-102051] p 204 N89-26260
- On finite element implementation and computational techniques for constitutive modeling of high temperature composites [NASA-CR-185120] p 204 N89-26261
- Structural and thermal response of 30 cm diameter ion thruster optics [NASA-TM-102124] p 75 N89-27703
- Probabilistic Finite Elements (PFEM) structural dynamics and fracture mechanics p 206 N89-29803
- The 3-D inelastic analyses for computational structural mechanics p 206 N89-29804
- Specialty functions singularity mechanics problems p 206 N89-29805
- Least-squares finite element method for fluid dynamics [NASA-TM-102352] p 223 N89-30008
- FINITE VOLUME METHOD**
- Diagonal implicit multigrid algorithm for the Euler equations p 1 A89-11110
- Viscous analysis of high speed flows using an upwind finite volume technique [AIAA PAPER 89-0001] p 144 A89-25001
- Three-dimensional calculation of supersonic reacting flows using an LU scheme [AIAA PAPER 89-0391] p 146 A89-28410
- A time accurate finite volume high resolution scheme for three dimensional Navier-Stokes equations [AIAA PAPER 89-1994] p 6 A89-41837
- A control-volume method for analysis of unsteady thrust augmenting ejector flows [NASA-CR-182203] p 24 N89-12566
- Calculation of turbulence-driven secondary motion in ducts with arbitrary cross section [NASA-TM-102142] p 166 N89-27115
- FIRE EXTINGUISHERS**
- Fire safety applications for spacecraft [NASA-TM-101463] p 42 N89-24413
- FIRE PREVENTION**
- Fire behavior and risk analysis in spacecraft [NASA-TM-100944] p 42 N89-10111
- Expert systems applied to spacecraft fire safety [NASA-CR-182266] p 42 N89-23501
- Fire safety applications for spacecraft [NASA-TM-101463] p 42 N89-24413
- FIRES**
- Experiment plans to study preignition processes of a pool fire in low gravity [NASA-CR-182256] p 121 N89-19442
- Expert systems applied to spacecraft fire safety [NASA-CR-182266] p 42 N89-23501
- FLAME PROPAGATION**
- Radiative structures of lycopodium-air flames in low gravity [AIAA PAPER 89-0500] p 91 A89-25406

## FLAME TEMPERATURE

The solid surface combustion Space Shuttle experiment hardware description and ground-based test results  
[AIAA PAPER 89-0503] p 119 A89-28419  
The effects of radiative heat loss on microgravity flame spread

[AIAA PAPER 89-0504] p 91 A89-28420

Experiment plans to study preignition processes of a pool fire in low gravity  
[NASA-CR-182256] p 121 N89-19442

The solid surface combustion space shuttle experiment hardware description and ground-based test results  
[NASA-TM-101963] p 123 N89-19446

Particle cloud mixing in microgravity  
[NASA-TM-101484] p 121 N89-20321

Time-dependent computational studies of flames in microgravity  
[NASA-CR-182298] p 122 N89-25353

Feasibility of reduced gravity experiments involving quiescent, uniform particle cloud combustion  
[NASA-TM-101371] p 122 N89-26114

## FLAME TEMPERATURE

Determination of combustion gas temperatures by infrared radiometry in sooting and nonsooting flames  
[NASA-TP-2900] p 164 N89-25409

## FLAMMABILITY

Friction-induced ignition of metals in high-pressure oxygen  
p 97 A89-32932

Microgravity combustion science: A program overview  
[NASA-TM-101424] p 122 N89-28665

## FLARED BODIES

Aperture impedance of flared horns  
p 125 A89-43543

## FLASH LAMPS

High temperature thermal conductivity measurements on lanthanum sulfides using the flash method  
p 77 A89-16500

## FLAT PLATES

The response of a laminar boundary layer in supersonic flow to small amplitude progressive waves  
[NASA-TM-101965] p 162 N89-21197

A segmented mirror antenna for radiometers  
[NASA-TM-102045] p 128 N89-23753

Some characteristics of bypass transition in a heated boundary layer  
[NASA-TM-102126] p 164 N89-24577

Time domain numerical calculations of unsteady vortical flows about a flat plate airfoil  
[NASA-TM-102318] p 168 N89-29726

## FLAT SURFACES

Combined roles of buoyancy and orientation in nucleate pool boiling  
p 119 A89-35015

## FLEXIBILITY

Tooth contact shift in loaded spiral bevel gears o, IL, 25-27 Apr. 1989; sponsored by ASME  
[NASA-TM-101438] p 183 N89-14453

High temperature flexible seal  
[NASA-CASE-LEW-14695-1] p 187 N89-28830

## FLEXIBLE SPACECRAFT

Modal representations in control/structure interaction  
p 45 A89-54114

## FLIGHT CONDITIONS

Effect of heavy rain on aviation engines  
[AIAA PAPER 89-0799] p 22 A89-28462

## FLIGHT CONTROL

Integrated flight/propulsion control study for STOVL applications  
[AIAA PAPER 89-2908] p 34 A89-47166

Integrated flight/propulsion control system design based on a centralized approach  
[AIAA PAPER 89-3520] p 35 A89-52611

Integrated flight/propulsion control system design based on a decentralized, hierarchical approach  
[AIAA PAPER 89-3519] p 35 A89-53301

Fiber optic control system integration  
[NASA-CR-179568] p 231 N89-13256

Computer simulation of a pilot in V/STOL aircraft control loops  
[NASA-CR-184815] p 215 N89-21479

Integrated flight/propulsion control system design based on a centralized approach  
[NASA-TM-102137] p 35 N89-26009

## FLIGHT HAZARDS

A numerical investigation of the influence of surface roughness on heat transfer in ice accretion  
[AIAA PAPER 89-0737] p 146 A89-25554

Effect of heavy rain on aviation engines  
[AIAA PAPER 89-0799] p 22 A89-28462

On ice shape prediction methodologies and comparison with experimental data  
[AIAA PAPER 89-0732] p 16 A89-30650

The influence of ice accretion physics on the forecasting of aircraft icing conditions  
p 16 A89-54803

## FLIGHT TESTS

Cruise noise of an advanced counterrotation turboprop measured from an adjacent aircraft  
p 20 A89-15080

Determination of longitudinal aerodynamic derivatives using flight data from an icing research aircraft  
[AIAA PAPER 89-0754] p 34 A89-28454

On ice shape prediction methodologies and comparison with experimental data  
[AIAA PAPER 89-0732] p 16 A89-30650

Comparison of propeller cruise noise data taken in the NASA Lewis 8- by 6-foot wind tunnel with other tunnel and flight data  
[AIAA PAPER 89-1059] p 226 A89-40472

InP homojunction solar cell performance on the LIPS 3 flight experiment  
[NASA-TM-101390] p 209 N89-12123

Determination of longitudinal aerodynamic derivatives using flight data from an icing research aircraft  
[NASA-TM-101427] p 35 N89-15121

Measured far-field flight noise of a counterrotation turboprop at cruise conditions  
[NASA-TM-101383] p 228 N89-15686

Comparison of propeller cruise noise data taken in the NASA Lewis 8- by 6-foot wind tunnel with other tunnel and flight data  
[NASA-TM-101976] p 228 N89-21628

NASA's program on icing research and technology  
[NASA-TM-101989] p 1 N89-22569

## FLOAT ZONES

Steady-state thermal-solutal diffusion in a float zone  
p 119 A89-40897

## FLOATING POINT ARITHMETIC

On the accuracy of solving triangular systems in parallel  
[NASA-TM-101384] p 222 N89-12337

## FLOW CHARACTERISTICS

The effect of prewhirl on the internal aerodynamics and performance of a mixed flow research centrifugal compressor  
[NASA-CR-184756] p 161 N89-19503

On the conditions for resonance interactions of instability waves in the axisymmetric jet  
[NASA-TM-101477] p 162 N89-21196

On the nature of Navier-Stokes turbulence  
[NASA-TM-101983] p 163 N89-23813

Turbulent swirling jets with excitation  
[NASA-CR-180895] p 16 N89-29329

Numerical investigation of an internal layer in turbulent flow over a curved hill  
[NASA-TM-102230] p 168 N89-29725

## FLOW DISTORTION

Calculations of inlet distortion induced compressor flow field instability  
p 8 A89-52498

## FLOW DISTRIBUTION

Calculations of the unsteady, three-dimensional flow field inside a motored Wankel engine  
[SAE PAPER 880625] p 19 A89-12307

Aerodynamically-driven condensate layer thickness distributions on isothermal cylindrical surfaces  
p 140 A89-12337

Application of optical correlation techniques to particle imaging  
[AIAA PAPER 88-4661] p 169 A89-14985

Description of an oscillating flow pressure drop test rig  
p 142 A89-15188

Turbine-stage heat transfer - Comparison of short-duration measurements with state-of-the-art predictions  
p 142 A89-16458

Experimental study of isothermal swirling flows in a dump combustor  
p 21 A89-23182

Evaluation of three turbulence models for the prediction of steady and unsteady airloads  
[AIAA PAPER 89-0609] p 3 A89-25485

Laser velocimeter measurements of the flowfield generated by an advanced counterrotating propeller  
[AIAA PAPER 89-0434] p 3 A89-26373

Comparison of 3D computation and experiment for non-axisymmetric nozzles  
[AIAA PAPER 89-0007] p 22 A89-28403

Investigation of the flow in the diffuser section of the NASA Lewis Icing Research Tunnel  
[AIAA PAPER 89-0755] p 36 A89-28455

Calculation of flow over iced airfoils  
p 5 A89-40905

A generalized one dimensional computer code for turbomachinery cooling passage flow calculations  
[AIAA PAPER 89-2574] p 151 A89-46934

Average-passage simulation of counter-rotating propfan propulsion systems as applied to cruise missiles  
[AIAA PAPER 89-2943] p 7 A89-47187

Numerical solution of periodic vortical flows about a thin airfoil  
[AIAA PAPER 89-1691] p 7 A89-48955

A numerical study of chemically reacting flow in nozzles  
[AIAA PAPER 89-2793] p 60 A89-49687

Interactive grid generation for turbomachinery flow field simulations  
[NASA-TM-101301] p 9 N89-11717

Evaluation of three turbulence models for the prediction of steady and unsteady airloads  
[NASA-TM-101413] p 10 N89-12555

Influence of bulk turbulence and entrance boundary layer thickness on the curved duct flow field  
[NASA-CR-4188] p 155 N89-12838

Aerothelmal modeling program, phase 2  
p 156 N89-12890

Aerothelmal modeling program, phase 2. Element B: Flow interaction experiment  
p 156 N89-12891

Influence of bulk turbulence and entrance boundary layer thickness on the curved duct flow field  
p 156 N89-12896

Measurement of airfoil heat transfer coefficients on a turbine stage  
p 157 N89-12897

Turbine stator flow field simulations  
p 157 N89-12902

Analysis of supersonic plug nozzle flowfield and heat transfer  
[NASA-CR-179554] p 10 N89-13397

User's manual for an aerodynamic optimization scheme that updates flow variables and design parameters simultaneously  
[NASA-CR-182180] p 10 N89-13399

Laser velocimeter measurements of the flowfield generated by an advanced counterrotating propeller  
[NASA-TM-101437] p 10 N89-13409

Turbofan forced mixer lobe flow modeling. 1: Experimental and analytical assessment  
[NASA-CR-4147-PT-1] p 11 N89-14221

Application of a lower-upper implicit scheme and an interactive grid generation for turbomachinery flow field simulations  
[NASA-TM-101412] p 11 N89-15077

Application of advanced diagnostics to airblast injector flows  
p 160 N89-17306

Measurement of airfoil heat transfer coefficients on a turbine stage  
p 160 N89-17311

Two- and three-dimensional turbine blade row flow field simulations  
p 161 N89-17313

CFD validation experiments for internal flows  
p 161 N89-18635

Flowfield measurements in the NASA Lewis Research Center 9- by 15-foot low-speed wind tunnel  
[NASA-TM-100883] p 36 N89-21002

A generalized one-dimensional computer code for turbomachinery cooling passage flow calculations  
[NASA-TM-102079] p 163 N89-22862

Numerical solution of periodic vortical flows about a thin airfoil  
[NASA-TM-101998] p 14 N89-23413

Average-passage simulation of counter-rotating propfan propulsion systems as applied to cruise missiles  
[NASA-TM-102043] p 14 N89-23416

The low frequency oscillation in the flow over a NACA0012 airfoil with an iced leading edge  
[NASA-TM-102018] p 14 N89-23417

High speed turboprop aeroacoustic study (single rotation). Volume 1: Model development  
[NASA-CR-182257-VOL-1] p 229 N89-24139

A numerical study of chemically reacting flow in nozzles  
[NASA-TM-102135] p 70 N89-24444

Investigation of the flow in the diffuser section of the NASA Lewis icing research tunnel  
[NASA-TM-102087] p 17 N89-25978

Mesh refinement in a two-dimensional large eddy simulation of a forced shear layer  
[NASA-TM-102129] p 166 N89-26180

Mach 5 inlet CFD and experimental results  
[NASA-TM-102317] p 33 N89-27670

Least-squares finite element method for fluid dynamics  
[NASA-TM-102352] p 223 N89-30008

## FLOW EQUATIONS

Kinetic energy equations for the average-passage equation system  
p 237 A89-28347

Asymptotic structure and similarity solutions for three-dimensional turbulent boundary layers  
[AIAA PAPER 89-1863] p 150 A89-42090

Efficient numerical techniques for complex fluid flows  
p 156 N89-12894

Computational methods for inlet airframe integration  
p 13 N89-16752

An explicit Runge-Kutta method for turbulent reacting flow calculations  
[NASA-TM-101945] p 31 N89-21799

Second-order accurate nonoscillatory schemes for scalar conservation laws  
p 14 N89-22573

The upper-branch stability of compressible boundary layer flows  
[NASA-TM-102128] p 167 N89-28748

Numerical investigation of an internal layer in turbulent flow over a curved hill  
[NASA-TM-102230] p 168 N89-29725

**FLOW MEASUREMENT**

- Three component laser anemometer measurements in an annular cascade of core turbine vanes with contoured end wall  
[NASA-TP-2846] p 9 N89-10844
- Effect of grain size on the high temperature properties of B2 aluminides  
[NASA-TM-101382] p 101 N89-12720
- Mass flow meter using the triboelectric effect for measurement in cryogenics  
[NASA-CR-179572] p 155 N89-12836
- Mass flow measurement of liquid cryogens using the triboelectric effect  
[NASA-CR-179519] p 155 N89-12837
- The effect of prewhirl on the internal aerodynamics and performance of a mixed flow research centrifugal compressor  
[NASA-CR-184756] p 161 N89-19503
- Control-volume based Navier-Stokes equation solver valid at all flow velocities  
[NASA-TM-101488] p 161 N89-20407
- Turbulent swirling jets with excitation  
[NASA-CR-180895] p 16 N89-29329

**FLOW STABILITY**

- On the preferred mode of jet instability  
p 140 A89-11567
- Effects of excitation level on the stability of an axisymmetric mixing layer  
p 2 A89-16882
- Nonlinear spatial evolution of an externally excited instability wave in a free shear layer  
p 144 A89-23242
- Studies of transition in boundary layers  
[AIAA PAPER 89-0034] p 2 A89-25029
- Nonlinear interaction between the sinuous and varicose instability modes in a plane wake  
p 147 A89-33779
- The secondary flow and its stability for natural convection in a tall vertical enclosure  
p 149 A89-37931
- Calculations of inlet distortion induced compressor flow field instability  
p 8 A89-52498
- Scaling results for the Liquid Sheet Radiator (LSR)  
[NASA-TM-102100] p 72 N89-25277
- Influence of thickness and camber on the aeroelastic stability of supersonic throughflow fans: An engineering approach  
[NASA-TM-101949] p 15 N89-25957
- The upper-branch stability of compressible boundary layer flows  
[NASA-TM-102128] p 167 N89-28748

**FLOW THEORY**

- Evolution of particle-laden jet flows - A theoretical and experimental study  
p 146 A89-27693
- Heat transfer with very high free-stream turbulence and heat transfer with streamwise vortices  
p 160 N89-17309

**FLOW VELOCITY**

- Performance of laser Doppler velocimeter with polydisperse seed particles in high-speed flows  
p 169 A89-22279
- Spatial resolution and downwash velocity corrections for multiple-hole pressure probes in complex flows  
p 171 A89-45909
- Numerical solution of periodic vortical flows about a thin airfoil  
[AIAA PAPER 89-1691] p 7 A89-48955
- Development of a thermal and structural analysis procedure for cooled radial turbines  
[NASA-TM-101416] p 24 N89-12568
- Influence of bulk turbulence and entrance boundary layer thickness on the curved duct flow field  
[NASA-CR-4188] p 155 N89-12838
- Laser anemometry: A status report  
p 177 N89-12885
- Heat transfer with very high free-stream turbulence and streamwise vortices  
p 157 N89-12900
- Supersonic through-flow fan assessment  
[NASA-CR-182202] p 27 N89-16843
- A comparison of turbulence measurement methods  
p 174 N89-17302
- Numerical solution of periodic vortical flows about a thin airfoil  
[NASA-TM-101998] p 14 N89-23413
- A vector scanning processing technique for pulsed laser velocimetry  
[NASA-TM-102048] p 175 N89-23850
- Scaling results for the Liquid Sheet Radiator (LSR)  
[NASA-TM-102100] p 72 N89-25277

**FLOW VISUALIZATION**

- Compressibility and shock wave interaction effects on free shear layers  
[AIAA PAPER 89-2460] p 7 A89-46847
- Hot gas ingestion testing of an advanced STOVL concept in the NASA Lewis 9-by-15-foot low speed wind tunnel with flow visualization  
[NASA-TM-100952] p 11 N89-15078

**FLUENCE**

- Atomic oxygen effects on materials  
p 78 N89-23540

- Radiation resistance studies of amorphous silicon films  
p 213 N89-24738

**FLUID DYNAMICS**

- Evaluation of three turbulence models for the prediction of steady and unsteady airloads  
[AIAA PAPER 89-0609] p 3 A89-25485
- Evaluation of three turbulence models for the prediction of steady and unsteady airloads  
[NASA-TM-101413] p 10 N89-12555
- Heat transfer with very high free-stream turbulence and heat transfer with streamwise vortices  
p 160 N89-17309
- COLD-SAT: A technology satellite for cryogenic experimentation  
[NASA-TM-102286] p 47 N89-26036
- Interaction between Tollmien-Schlichting waves and free-stream disturbances in boundary-layer flows  
[NASA-CR-185847] p 167 N89-27118

**FLUID FLOW**

- Turboflow forced mixer lobe flow modeling. Part 3: Application to augment engines  
[NASA-CR-4147-Pt-3] p 8 N89-10025
- Aerodynamic optimization by simultaneously updating flow variables and design parameters with application to advanced propeller designs  
[NASA-CR-182181] p 24 N89-11750
- Measurement of airfoil heat transfer coefficients on a turbine stage  
p 157 N89-12897
- Liquid sheet radiator apparatus  
[NASA-CASE-LEW-14295-1] p 123 N89-14348
- Coolant passage heat transfer with rotation  
p 161 N89-17314
- Experiment plans to study preignition processes of a pool fire in low gravity  
[NASA-CR-182256] p 121 N89-19442
- A comparative study of the influence of buoyancy driven fluid flow on GaAs crystal growth  
p 121 N89-20295

**FLUID MANAGEMENT**

- Modeling of impulsive propellant reorientation  
[AIAA PAPER 89-0628] p 54 A89-25496
- Modeling of pulsed propellant reorientation  
[AIAA PAPER 89-2727] p 61 A89-53306
- Modeling of impulsive propellant reorientation  
[NASA-TM-101440] p 64 N89-13495
- Analysis of the nonvented fill of a 4.96-cubic-meter lightweight liquid hydrogen tank  
[NASA-TM-102039] p 67 N89-22652
- Modeling of pulsed propellant reorientation  
[NASA-TM-102117] p 165 N89-26178
- COLD-SAT: Cryogenic On-Orbit Liquid Depot-Storage, Acquisition and Transfer  
[NASA-TM-102308] p 38 N89-28535

**FLUIDS**

- Critical fluid light scattering  
p 121 N89-20320

**FLUORIDES**

- Graphite fluoride fiber polymer composite material  
[NASA-CASE-LEW-14472-1] p 85 N89-14259
- Flight experiment of thermal energy storage  
[NASA-TM-102081] p 69 N89-24440

**FLUTTER**

- Analytical flutter investigation of a composite propfan model  
p 195 A89-48663

**FLUTTER ANALYSIS**

- Vibration, performance, flutter and forced response characteristics of a large-scale propfan and its aeroelastic model  
[AIAA PAPER 88-3155] p 21 A89-17943
- Technique for the prediction of airfoil flutter characteristics in separated flow  
p 191 A89-27744
- A computational procedure for automated flutter analysis  
p 191 A89-28070
- Application of a full-potential solver to bending-torsion flutter in cascades  
[AIAA PAPER 89-1386] p 34 A89-30859
- Aeroelastic analysis of prop fan blades with a semiempirical dynamic stall model  
[AIAA PAPER 89-2695] p 194 A89-47025
- Vibration, performance, flutter and forced response characteristics of a large-scale propfan and its aeroelastic model  
[NASA-TM-101322] p 24 N89-10043
- Analysis of an unswept propfan blade with a semiempirical dynamic stall model  
[NASA-TM-4083] p 27 N89-15112
- Turbomachinery aeroelasticity at NASA Lewis Research Center  
p 28 N89-19262

**FLUX DENSITY**

- Lightweight fibrous nickel electrodes for nickel-hydrogen batteries  
[NASA-TM-101997] p 93 N89-22710

**FLUX VECTOR SPLITTING**

- Flux splitting algorithms for two-dimensional viscous flows with finite-rate chemistry  
[AIAA PAPER 89-0388] p 146 A89-28409

- A detailed analysis of inviscid flux splitting algorithms for real gases with equilibrium or finite-rate chemistry  
p 151 A89-45424

**FLYWHEELS**

- Solar power for the lunar night  
[NASA-TM-102127] p 242 N89-26799

**FORCE DISTRIBUTION**

- Effects of bearing offset and flexibility on the mesh force distribution of spiral bevel gears  
p 178 A89-19834

**FORCED CONVECTION**

- Regressed relations for forced convection heat transfer in a direct injection stratified charge rotary engine  
[SAE PAPER 880626] p 178 A89-12308
- Rational engineering correlations of diffusional and inertial particle deposition behavior in non-isothermal forced convection environments  
p 140 A89-12327
- Impact of ETO propellants on the aerothermodynamic analyses of propulsion components --- Earth To Orbit  
[AIAA PAPER 88-0091] p 53 A89-16486

**FORCED VIBRATION**

- Vibration, performance, flutter and forced response characteristics of a large-scale propfan and its aeroelastic model  
[AIAA PAPER 88-3155] p 21 A89-17943
- Vibration, performance, flutter and forced response characteristics of a large-scale propfan and its aeroelastic model  
[NASA-TM-101322] p 24 N89-10043
- Modal forced vibration analysis of aerodynamically excited turbosystems  
[NASA-CR-174966] p 201 N89-18696
- NASTRAN supplemental documentation for modal forced vibration analysis of aerodynamically excited turbosystems  
[NASA-CR-174967] p 201 N89-19583

**FORWARD SCATTERING**

- Performance of the forward scattering spectrometer probe in NASA's Icing Research Tunnel  
[AIAA PAPER 89-0769] p 169 A89-25570
- An improved correction algorithm for number density measurements made with the forward scattering spectrometer probe  
p 170 A89-44122
- A correction algorithm for particle size distribution measurements made with the forward-scattering spectrometer probe  
p 170 A89-44123
- Performance of the forward scattering spectrometer probe in NASA's icing research tunnel  
[NASA-TM-101381] p 172 N89-12845

**FOURIER ANALYSIS**

- A Fourier analysis for a fast simulation algorithm --- for switching converters  
p 130 A89-15367

**FRACTOGRAPHY**

- Strength distribution of reinforcing fibers in a Nicalon fiber/chemically vapor infiltrated silicon carbide matrix composite  
p 82 A89-34844

**FRACTURE MECHANICS**

- Kuhn-Tucker optimization based reliability analysis for probabilistic finite elements  
p 187 A89-25852
- Structural behavior of composites with progressive fracture  
[AIAA PAPER 89-1271] p 192 A89-30754
- Isothermal and "bithermal" thermomechanical fatigue behavior of a NiCoCrAlY-coated single crystal superalloy  
p 177 A89-36457
- Fracture mechanics applied to elevated temperature crack growth  
p 195 A89-47705
- Turbine Engine Hot Section Technology 1986  
[NASA-CP-2444] p 195 N89-12876
- Fatigue and fracture overview  
p 195 N89-12882
- Calculation of Weibull strength parameters and Batdorf flow-density constants for volume- and surface-flaw-induced fracture in ceramics  
[NASA-TM-100890] p 196 N89-12930
- An investigation of environmental influence on the creep behavior of a low pressure plasma sprayed NiCoCrAlY alloy  
p 110 N89-13648
- Local-global analysis of crack growth in continuously reinforced ceramic matrix composites  
[NASA-CR-182231] p 197 N89-13820
- Turbine Engine Hot Section Technology, 1987  
[NASA-CP-2493] p 199 N89-17298
- Fatigue crack growth model RANDOM2 user manual. Appendix 1: Development of advanced methodologies for probabilistic constitutive relationships of material strength models  
[NASA-CR-184775-APP-1] p 201 N89-19581
- Fatigue life prediction modeling for turbine hot section materials  
p 30 N89-20142
- Finite element applications to explore the effects of partial bonding on metal matrix composite properties  
[NASA-TM-101482] p 86 N89-20206
- Investigation of Weibull statistics in fracture analysis of cast aluminum  
[NASA-TM-102000] p 185 N89-21245
- Analysis of interface crack branching  
[NASA-CR-182273] p 202 N89-21265

- Unified micromechanics of damping for unidirectional fiber reinforced composites  
[NASA-TM-102107] p 88 N89-26919
- Fatigue crack growth study of SC56/Ti-15-3 composite  
[NASA-TM-102332] p 104 N89-26989
- Probabilistic structural analysis methods of hot engine structures  
[NASA-TM-102091] p 205 N89-28030
- Probabilistic Finite Elements (PFEM) structural dynamics and fracture mechanics p 206 N89-29803
- FRACTURE STRENGTH**
- Transmission electron microscopy of composites p 79 A89-14560
- Composite interlaminar fracture toughness - Three-dimensional finite-element modeling for mixed mode I, II, and fracture p 190 A89-16278
- Sublaminar- or ply-level analysis of composites and strain energy release rates of end-notch and mixed-mode fracture specimens p 190 A89-16279
- Strength distribution in commercial silicon carbide materials p 105 A89-17097
- Concepts for interrelating ultrasonic attenuation, microstructure, and fracture toughness in polycrystalline solids p 95 A89-19852
- Finite element substructuring methods for composite mechanics p 80 A89-26291
- Crack growth resistance of textured alumina p 105 A89-26452
- Fracture toughness of polycrystalline ceramics in combined mode I and mode II loading p 105 A89-26457
- Probabilistic constitutive relationships for material strength degradation models  
[AIAA PAPER 89-1368] p 192 A89-30843
- Fracture resistance of a TiB<sub>2</sub> particle/SiC matrix composite at elevated temperature p 81 A89-31074
- A probabilistic formulation for fracture energy of continuous fibre-matrix composites p 83 A89-39996
- Indentation plasticity and fracture in silicon  
[NASA-TP-2863] p 100 N89-10996
- Fracture toughness computational simulation of general delaminations in fiber composites  
[NASA-TM-101415] p 85 N89-13521
- High-strength silicon carbides by hot isostatic pressing  
[NASA-TM-101400] p 111 N89-13666
- Investigation of Weibull statistics in fracture analysis of cast aluminum p 185 N89-21245
- Effect of processing on fracture toughness of silicon carbide as determined by Vickers indentations  
[NASA-TM-101456] p 115 N89-21895
- Preparation and evaluation of silicon nitride matrices for silicon nitride-SiC fiber composites  
[NASA-CR-184798] p 115 N89-23678
- Fatigue strength reduction model: RANDOM3 and RANDOM4 user manual, appendix 2 p 203 N89-23891
- Ultrasonic imaging of textured alumina  
[NASA-TM-101478] p 189 N89-28853
- FRACTURING**
- Deformation and fracture of single-crystal and sintered polycrystalline silicon carbide produced by cavitation p 108 A89-54985
- FREE BOUNDARIES**
- Nonlinear spatial evolution of an externally excited instability wave in a free shear layer p 144 A89-23242
- FREE CONVECTION**
- Hardware development for the Surface Tension Driven Convection Experiment aboard the USML-1 Spacelab mission  
[AIAA PAPER 89-0406] p 47 A89-25341
- The secondary flow and its stability for natural convection in a tall vertical enclosure p 149 A89-37931
- Thermosolutal convection in high-aspect-ratio enclosures p 153 A89-53288
- Hardware development for the surface tension driven convection experiment aboard the USML-1 spacelab mission  
[NASA-TM-101404] p 48 N89-11804
- FREE FLOW**
- Boundary-layer receptivity to long-wave free-stream disturbances p 146 A89-28996
- Coherent structures in transitional and turbulent free shear flows p 147 A89-28999
- Turbulence management in free shear flows by control of coherent structures p 147 A89-30908
- Heat transfer with very high free-stream turbulence and streamwise vortices p 157 N89-12900
- Heat transfer with very high free-stream turbulence and heat transfer with streamwise vortices p 160 N89-17309
- The response of a laminar boundary layer in supersonic flow to small amplitude progressive waves  
[NASA-TM-101965] p 162 N89-21197

- Interaction between Tollmien-Schlichting waves and free-stream disturbances in boundary-layer flows  
[NASA-CR-185847] p 167 N89-27118
- FREE JETS**
- Effect of initial swirl distribution on the evolution of a turbulent jet p 149 A89-36906
- Effects of nozzle exit boundary-layer conditions on excitability of heated free jets p 149 A89-36908
- FREE VIBRATION**
- Free-vibration characteristics and correlation of a Space Station split-blanket solar array  
[AIAA PAPER 89-1252] p 44 A89-30737
- Free-vibration characteristics and correlation of a space station split-blanket solar array  
[NASA-TM-101452] p 198 N89-15438
- FREE-PISTON ENGINES**
- Description of an oscillating flow pressure drop test rig p 142 A89-15188
- SPRE 1 free-piston Stirling engine testing at NASA Lewis Research Center p 55 A89-29120
- Conceptual design of an advanced Stirling conversion system for terrestrial power generation  
[NASA-CR-180890] p 238 N89-12504
- The 25 kW solar thermal Stirling hydraulic engine system: Conceptual design  
[NASA-CR-180889] p 239 N89-14182
- Results from baseline tests of the SPRE 1 and comparison with code model predictions  
[NASA-TM-102044] p 68 N89-23527
- On the dynamic response of pressure transmission lines in the research of helium-charged free piston Stirling engines  
[NASA-TM-102121] p 175 N89-24593
- Comparison of conceptual designs for 25 kW advanced Stirling conversion systems for dish electric application  
[NASA-TM-102085] p 239 N89-26781
- FREZZING**
- Analytical ice shape predictions for flight in natural icing conditions  
[NASA-CR-182234] p 18 N89-13428
- Flight experiment of thermal energy storage  
[NASA-TM-102081] p 69 N89-24440
- FREQUENCY ASSIGNMENT**
- Engineering calculations for solving the orbital allotment problem  
[NASA-CR-184607] p 217 N89-13993
- FREQUENCY CONTROL**
- Variable speed induction motor operation from a 20-kHz power bus  
[NASA-TM-102061] p 71 N89-25271
- FREQUENCY MODULATION**
- Coded multiple chirp spread spectrum system and overlay service p 124 A89-26769
- FRESNEL DIFFRACTION**
- Fresnel diffraction by spherical obstacles p 231 A89-48249
- FRESNEL LENSES**
- Domed Fresnel lens concentrator technology for space application p 213 N89-24732
- FRICTION**
- Friction-induced ignition of metals in high-pressure oxygen p 97 A89-32932
- Adhesion, friction, and wear of plasma-deposited thin silicon nitride films at temperatures to 700 C p 107 A89-48250
- Tribological properties of structural ceramics p 107 A89-51258
- Adhesion, friction, and micromechanical properties of ceramics p 107 A89-54277
- Adhesion, friction, and wear of plasma-deposited thin silicon nitride films at temperatures to 700 C  
[NASA-TM-101377] p 109 N89-11913
- Applications of surface analysis and surface theory in tribology  
[NASA-TM-101392] p 78 N89-15981
- Adhesion in ceramics and magnetic media  
[NASA-TM-101476] p 113 N89-19435
- Design, development and applications of novel techniques for studying surface mechanical properties  
[NASA-TM-101859] p 113 N89-20253
- Effects of lubrication on the performance of high speed spur gears  
[NASA-TM-101969] p 186 N89-22919
- FRICTION DRAG**
- Considerations on the moving contact-line singularity, with application to frictional drag on a slender drop p 144 A89-23238
- FRICTION FACTOR**
- An entrance region friction factor model applied to annular seal analysis - Theory versus experiment for smooth and honeycomb seals  
[ASME PAPER 88-TRIB-41] p 179 A89-34798
- Friction factor data for flat plate tests of smooth and honeycomb surfaces  
[NASA-CR-184977] p 186 N89-23876

**FRICTION MEASUREMENT**

- Skin-friction measurements by laser interferometry p 167 N89-28737
- FUEL CELL POWER PLANTS**
- Assessment and comparison of 100-MW coal gasification phosphoric acid fuel cell power plants  
[NASA-CR-182189] p 209 N89-13103
- FUEL CELLS**
- Space power technologies p 38 N89-11770
- Mathematical modeling of solid oxide fuel cells  
[NASA-CR-182188] p 209 N89-12122
- Corrosion testing of candidates for the alkaline fuel cell cathode p 212 N89-23000
- FUEL COMBUSTION**
- Optical methods and results of dew point and deposition rate measurements in salt/ash-containing combustion gases - B2O3(l) deposition rates by interference methods and comparisons with theory p 89 A89-12334
- The solid surface combustion Space Shuttle experiment hardware description and ground-based test results  
[AIAA PAPER 89-0503] p 119 A89-28419
- The turbulence characteristics of a separated flow with combustion p 92 A89-33369
- Fuel-rich catalytic combustion of Jet-A fuel-equivalence ratios 5.0 to 8.0  
[NASA-TM-101975] p 93 N89-21051
- Gas turbine alternative fuels combustion characteristics  
[NASA-TM-101470] p 210 N89-21417
- Feasibility of reduced gravity experiments involving quiescent, uniform particle cloud combustion  
[NASA-TM-101371] p 122 N89-26114
- FUEL CONSUMPTION**
- Alternative fuel capabilities of the Mod II Stirling vehicle  
[SAE PAPER 880543] p 177 A89-12303
- NASA/industry advanced turboprop technology program p 20 A89-13504
- Advanced turboprop project  
[NASA-SP-495] p 24 N89-12565
- Methods for heat transfer and temperature field analysis of the insulated diesel, phase 3  
[NASA-CR-182237] p 239 N89-23382
- FUEL CONTROL**
- Modeling of impulsive propellant reorientation  
[AIAA PAPER 89-0628] p 54 A89-25496
- Modeling of pulsed propellant reorientation  
[AIAA PAPER 89-2727] p 61 A89-53306
- Modeling of impulsive propellant reorientation  
[NASA-TM-101440] p 64 N89-13495
- Modeling of pulsed propellant reorientation  
[NASA-TM-102117] p 165 N89-26178
- FUEL FLOW**
- Stratified charge rotary engine - Internal flow studies at the MSU engine research laboratory  
[SAE PAPER 890331] p 181 A89-51477
- FUEL INJECTION**
- Regressed relations for forced convection heat transfer in a direct injection stratified charge rotary engine  
[SAE PAPER 880626] p 178 A89-12308
- dc power control for a liquid-fed resistor p 59 A89-47457
- Fuel properties effect on the performance of a small high temperature rise combustor  
[AIAA PAPER 89-2901] p 23 A89-52025
- Turbofan forced mixer lobe flow modeling. Part 3: Application to augment engines  
[NASA-CR-4147-Pt-3] p 8 N89-10025
- Aerothermal modeling program, phase 2. Element C: Fuel injector-air swirl characterization p 156 N89-12892
- Application of advanced diagnostics to airblast injector flows p 160 N89-17306
- Fuel properties effect on the performance of a small high temperature rise combustor  
[NASA-TM-102096] p 33 N89-25238
- FUEL SPRAYS**
- Numerical study of the interactions between droplets at intermediate Reynolds numbers p 142 A89-16451
- Fuel spray simulation with two-fluid nozzles  
[AIAA PAPER 89-0053] p 145 A89-25047
- Radiative structures of lycopodium-air flames in low gravity  
[AIAA PAPER 89-0500] p 91 A89-25406
- Evolution of particle-laden jet flows - A theoretical and experimental study p 146 A89-27693
- NOx formation from the combustion of monodisperse n-heptane sprays doped with fuel-nitrogen additives p 116 A89-42695
- Gas density effect on droplet size of simulated fuel sprays  
[AIAA PAPER 89-2322] p 151 A89-46749
- Turbulent multiphase flows p 152 A89-51883
- Fluid spray simulation with two-fluid nozzles  
[NASA-TM-101367] p 155 N89-12028



- Application of advanced diagnostics to airblast injector flows p 160 N89-17308
- Gas density effect on droplet size of simulated fuel sprays [NASA-TM-102013] p 162 N89-22053
- FUEL TESTS**
- Degradation mechanisms of n-dodecane with sulfur and nitrogen dopants during thermal stressing p 116 A89-22277
- FURNACES**
- Effects of furnace temperature profile on the interface shape during Bridgman crystal growth p 119 A89-53278
- Furnace for tensile/fatigue testing [NASA-CASE-LEW-14848-1] p 40 N89-28549
- FUSELAGES**
- In-flight measurement of propeller noise on the fuselage of an airplane [NASA-TM-102285] p 229 N89-25675
- G**
- GALACTIC EVOLUTION**
- Cosmic strings and the large-scale structure p 240 A89-19604
- GALERKIN METHOD**
- Discretization formulas for unstructured grids [NASA-TM-101298] p 154 N89-10242
- Acoustic propagation in curved ducts with extended reacting wall treatment [NASA-TM-102110] p 224 N89-25670
- GALLIUM ARSENIDES**
- GaAs MMIC elements in phased-array antennas p 131 A89-15827
- GaAs circuits for monolithic optical controller p 131 A89-15828
- The interaction of gold with gallium arsenide p 90 A89-16416
- Shubnikov-de Haas measurements of the 2-D electron gas in pseudomorphic In(0.1)Ga(0.9)As grown on GaAs p 235 A89-29299
- A comparative study of the influence of buoyancy driven fluid flow on GaAs crystal growth p 121 N89-20295
- Development of gallium arsenide high-speed, low-power serial parallel interface modules: Executive summary [NASA-CR-182272] p 137 N89-21173
- Optical detectors for GaAs MMIC integration: Technology assessment [NASA-TM-102025] p 137 N89-22020
- A V-grooved GaAs solar cell [NASA-TM-101970] p 211 N89-22177
- The NASA Space Solar Cell Advanced Research Program [NASA-TM-102020] p 67 N89-22651
- Microwave characteristics of GaAs MMIC integratable optical detectors [NASA-TM-101485] p 129 N89-24520
- High efficiency GaAs-Ge tandem solar cells grown by MOCVD p 213 N89-24721
- A new structure for comparing surface passivation materials of GaAs solar cells p 213 N89-24725
- Chemical etching and organometallic chemical vapor deposition on varied geometries of GaAs p 213 N89-24728
- Domed Fresnel lens concentrator technology for space application p 213 N89-24732
- The GaAs solar cells with V-grooved emitters [NASA-TM-102104] p 214 N89-26291
- Molecular beam epitaxial growth of high-quality InSb on InP and GaAs substrates [NASA-CR-185440] p 236 N89-26739
- GAMMA RAY BURSTS**
- Nucleosynthesis, neutrino bursts and gamma-rays from coalescing neutron stars p 241 A89-46577
- GAMMA RAY SPECTROMETERS**
- Limits to the radiative decays of neutrinos and axions from gamma-ray observations of SN 1987A p 242 A89-26985
- GAS BEARINGS**
- Tribological composition optimization of chromium-carbide-based solid lubricant coatings for foil gas bearings at temperatures to 650 C p 83 A89-54258
- GAS DENSITY**
- Gas density effect on droplet size of simulated fuel sprays [AIAA PAPER 89-2322] p 151 A89-46749
- Gas density effect on droplet size of simulated fuel sprays [NASA-TM-102013] p 162 N89-22053
- GAS DISCHARGES**
- Interactions between gaseous electrical discharges and single liquid droplets p 90 A89-19298

- GAS DYNAMICS**
- Accurate boundary conditions for exterior problems in gas dynamics p 143 A89-20223
- Effects of heat release on the large-scale structure in turbulent mixing layers p 147 A89-31844
- Computational fluid dynamic control p 220 A89-53984
- Aerothermal modeling program, phase 2. Element C: Fuel injector-air swirl characterization p 156 N89-12892
- Further development of the dynamic gas temperature measurement system. Volume 2: Computer program user's manual [NASA-CR-179513-VOL-2] p 173 N89-13771
- GAS EVOLUTION**
- Pulsed ion beam investigation of the kinetics of surface reactions p 93 A89-44542
- GAS FLOW**
- Flow of rarefied gases over two-dimensional bodies [AIAA PAPER 89-1970] p 5 A89-41814
- Rarefied gas flow through two-dimensional nozzles [AIAA PAPER 89-2893] p 7 A89-47156
- GAS STREAMS**
- Use of a generalized Stokes number to determine the aerodynamic capture efficiency of non-Stokesian particles from a compressible gas flow p 140 A89-12336
- GAS TEMPERATURE**
- Further development of the dynamic gas temperature measurement system p 172 N89-12884
- A comparison of turbulence measurement methods p 174 N89-17302
- Determination of combustion gas temperatures by infrared radiometry in sooting and nonsooting flames [NASA-TP-2900] p 164 N89-25409
- Experience with advanced instrumentation in a hot section cascade [NASA-TM-102294] p 167 N89-27980
- GAS TURBINE ENGINES**
- Measurements of heat transfer distribution over the surfaces of highly loaded turbine nozzle guide vanes p 141 A89-12752
- Thermal measurements for jets in disturbed and undisturbed crosswind conditions p 20 A89-16102
- Development of an analytical model to assess fuel property effects on combustor performance p 21 A89-20949
- Composite mechanics for engine structures p 80 A89-28344
- Effect of heavy rain on aviation engines [AIAA PAPER 89-0799] p 22 A89-28462
- Heat transfer in gas turbine engines and three-dimensional flows; Proceedings of the Symposium, ASME Winter Annual Meeting, Chicago, IL, Nov. 27-Dec. 2, 1988 p 148 A89-34926
- Effects of wake passing on stagnation region heat transfer p 148 A89-34928
- Ceramic bearings for use in gas turbine engines p 180 A89-46697
- Fuel properties effect on the performance of a small high temperature rise combustor [AIAA PAPER 89-2901] p 23 A89-52025
- Development of a thermal and structural analysis procedure for cooled radial turbines [NASA-TM-101416] p 24 N89-12568
- Turbine Engine Hot Section Technology 1986 [NASA-CP-2444] p 195 N89-12876
- Turbine Engine Hot Section Technology (HOST) Project p 25 N89-12877
- HOST instrumentation R and D program overview p 25 N89-12878
- HOST combustion R and T overview p 25 N89-12879
- HOST turbine heat transfer subproject overview p 25 N89-12880
- HOST structural analysis program overview p 195 N89-12881
- Fatigue and fracture overview p 195 N89-12882
- HOST surface protection R and T overview p 109 N89-12883
- Further development of the dynamic gas temperature measurement system p 172 N89-12884
- Laser anemometry: A status report p 177 N89-12885
- Aerothermal modeling program, phase 2. Element B: Flow interaction experiment p 156 N89-12891
- Efficient numerical techniques for complex fluid flows p 156 N89-12894
- Heat transfer in the tip region of a rotor blade simulator p 157 N89-12898
- Coolant passage heat transfer with rotation p 157 N89-12899
- Turbine stator flow field simulations p 157 N89-12902
- Constitutive modeling for isotropic materials p 195 N89-12904

- Creep fatigue life prediction for engine hot section materials (isotropic): Fourth year progress review p 188 N89-12914
- Turbine Engine Hot Section Technology, 1987 [NASA-CP-2493] p 199 N89-17298
- Development of a high temperature thin film static strain gage p 174 N89-17299
- Aerothermal modeling program, Phase 2, element B: Flow interaction experiment p 160 N89-17304
- Application of advanced diagnostics to airblast injector flows p 160 N89-17306
- A low-Reynolds-number two-equation turbulence model for predicting heat transfer on turbine blades p 160 N89-17310
- Measurement of airfoil heat transfer coefficients on a turbine stage p 160 N89-17311
- Two- and three-dimensional turbine blade row flow field simulations p 161 N89-17313
- Coolant passage heat transfer with rotation p 161 N89-17314
- Turbine airfoil film cooling p 161 N89-17315
- Three-dimensional inelastic analysis methods for hot section components p 199 N89-17316
- Three-dimensional inelastic analysis for hot section components, BEST 3D code p 199 N89-17317
- Mechanics of materials model p 199 N89-17319
- Three-dimensional inelastic analysis methods for hot section components p 199 N89-17321
- Constitutive modelling of single crystal and directionally solidified superalloys p 102 N89-17325
- Finite element implementation of viscoplastic models p 200 N89-17328
- Structural response of an advanced combustor liner: Test and analysis p 200 N89-17329
- Thermal expansion mismatch and plasticity in thermal barrier coating p 200 N89-17330
- Thermal barrier coating life-prediction model development p 200 N89-17331
- Thermal barrier coating life prediction model development p 200 N89-17333
- High temperature constitutive and crack initiation modeling of coated single crystal superalloys p 112 N89-17334
- Creep fatigue life prediction for engine hot section materials (ISOTROPIC) fifth year progress review p 201 N89-17336
- High-resolution liquid-crystal heat-transfer measurements on the end wall of a turbine passage with variations in Reynolds number p 161 N89-18664
- Toward improved durability in advanced aircraft engine hot sections [NASA-TM-100827] p 29 N89-20135
- NASA HOST project overview p 29 N89-20136
- Assessment, development, and application of combustor aerothermal models p 30 N89-20138
- Review and assessment of the database and numerical modeling for turbine heat transfer p 30 N89-20139
- Structural analysis methods development for turbine hot section components p 30 N89-20140
- Fatigue life prediction modeling for turbine hot section materials p 30 N89-20142
- Life modeling of thermal barrier coatings for aircraft gas turbine engines p 30 N89-20143
- Views on the impact of HOST p 31 N89-20144
- High speed balancing applied to the T700 engine [NASA-CR-180899] p 184 N89-20472
- Fuel-rich catalytic combustion of Jet-A fuel-equivalence ratios 5.0 to 8.0 [NASA-TM-101975] p 93 N89-21051
- Gas turbine alternative fuels combustion characteristics [NASA-TM-101470] p 210 N89-21417
- Fuel properties effect on the performance of a small high temperature rise combustor [NASA-TM-102096] p 33 N89-25238
- Intermetallic and ceramic matrix composites for 815 to 1370 C (1500 to 2500 F) gas turbine engine applications [NASA-TM-102326] p 88 N89-29490
- GAS TURBINES**
- Experimental investigation of the performance of a supersonic compressor cascade [NASA-TM-100879] p 9 N89-10858
- Constitutive behavior of single crystal PWA 1480 and directionally solidified MAR-M 246 under monotonic and cyclic loads at high and low temperature p 100 N89-12634
- HOST structural analysis program overview p 195 N89-12881
- Considerations in development and implementation of elasto-viscoplastic constitutive model for high temperature applications [NASA-CR-183403] p 197 N89-12932
- Constitutive modeling for isotropic materials [NASA-CR-174805] p 26 N89-13436

- Thermal Barrier Coatings. Abstracts and figures  
[NASA-CP-10019] p 110 N89-13642
- The effect of oxidation on the high heat flux behavior of a thermal barrier coating p 110 N89-13646
- Cyclic stress analysis of ceramic coated gas turbine seals p 111 N89-13662
- Plotting component maps in the Navy/NASA Engine Program (NNEP): A method and its usage  
[NASA-TM-101433] p 26 N89-14239
- Some composite bearing and seal materials for gas turbine applications: A review  
[NASA-TM-101451] p 111 N89-14338
- Heat flux measurements  
[NASA-TM-101428] p 173 N89-14418
- Oxide-dispersion-strengthened turbine blades. Volume 2  
[NASA-CR-179561-VOL-2] p 28 N89-18487
- AGT (Advanced Gas Turbine) technology project  
[NASA-CR-182127] p 186 N89-26246
- GASEOUS DIFFUSION**
- Windward fraction of the total mass or heat transport for flow past a circular cylinder p 141 A89-12339
- Isotopic study of oxygen diffusion in oxide coatings  
[NASA-TM-102082] p 78 N89-24451
- GASES**
- Behavior in normal and reduced gravity of an enclosed liquid/gas system with nonuniform heating from above  
[AIAA PAPER 89-0070] p 145 A89-25061
- Behavior in normal and reduced gravity of an enclosed liquid/gas system with nonuniform heating from above  
[NASA-TM-101471] p 120 N89-17046
- GASOL (FUEL)**
- Alternative fuel capabilities of the Mod II Stirling vehicle  
[SAE PAPER 880543] p 177 A89-12303
- GAUSS EQUATION**
- High speed corner and gap-seal computations using an LU-SGS scheme  
[AIAA PAPER 89-2669] p 154 A89-54424
- High speed corner and gap-seal computations using an LU-SGS scheme  
[NASA-TM-102138] p 166 N89-27103
- GAUSSIAN ELIMINATION**
- Parallel Gaussian elimination of a block tridiagonal matrix using multiple microcomputers  
[NASA-TP-2892] p 218 N89-17422
- On the equivalence of Gaussian elimination and Gauss-Jordan reduction in solving linear equations  
[NASA-TM-101466] p 222 N89-20710
- On the equivalence of a class of inverse decomposition algorithms for solving systems of linear equations  
[NASA-TM-102036] p 223 N89-24865
- GEAR TEETH**
- Effects of bearing offset and flexibility on the mesh force distribution of spiral bevel gears p 178 A89-19834
- An extremum principle for computation of the zone of tooth contact and generalized transmission error of spiral bevel gears p 178 A89-19835
- Transmission errors and bearing contact of spur, helical and spiral bevel gears  
[SAE PAPER 881294] p 179 A89-21000
- Crowned spur gears - Methods for generation and tooth contact analysis. I - Basic concepts, generation of the pinion tooth surface by a plane p 179 A89-29306
- Crowned spur gears - Methods for generation and Tooth Contact Analysis. II - Generation of the pinion tooth surface by a surface of revolution p 180 A89-37665
- Generation of a crowned pinion tooth surface by a surface of revolution  
[NASA-TM-100260] p 181 N89-10282
- Gear optimization  
[NASA-CR-4201] p 182 N89-13793
- The role of thermal and lubricant boundary layers in the transient thermal analysis of spur gears  
[NASA-TM-101435] p 182 N89-14452
- Tooth contact shift in loaded spiral bevel gears o, IL, 25-27 Apr. 1989; sponsored by ASME  
[NASA-TM-101438] p 183 N89-14453
- Lubricant jet flow phenomena in spur and helical gears with modified addendums; for radially directed individual jets  
[NASA-TM-101460] p 183 N89-15415
- Computer-aided design of bevel gear tooth surfaces  
[NASA-TM-101449] p 183 N89-17248
- Effects of lubrication on the performance of high speed spur gears  
[NASA-TM-101969] p 186 N89-22919
- Topology of modified helical gears and Tooth Contact Analysis (TCA) program  
[NASA-CR-4224] p 186 N89-22920
- Topology of modified helical gears  
[NASA-TM-102134] p 187 N89-28015
- GEARS**
- Advanced transmission studies p 178 A89-18906
- Design and test of a propfan gear system p 179 A89-22290
- Surface fatigue life of carburized and hardened M50NiL and AISI 9310 spur gears and rolling-contact test bars  
[AIAA PAPER 89-2819] p 180 A89-47105
- Generation of a crowned pinion tooth surface by a plane  
[NASA-TM-100259] p 181 N89-10283
- Gear optimization  
[NASA-CR-4201] p 182 N89-13793
- Dynamic loading of spur gears with linear or parabolic tooth profile modification  
[NASA-TM-101444] p 183 N89-15413
- Wear consideration in gear design for space applications  
[NASA-TM-101457] p 183 N89-15414
- Computer-aided design of bevel gear tooth surfaces  
[NASA-TM-101449] p 183 N89-17248
- Vibration signature analysis of multistage gear transmission  
[NASA-TM-101442] p 184 N89-18685
- Comparison study of gear dynamic computer programs at NASA Lewis Research Center  
[NASA-TP-2901] p 184 N89-21243
- Modal analysis of gear housing and mounts  
[NASA-TM-101445] p 184 N89-21244
- Surface fatigue life of carburized and hardened M50NiL and AISI 9310 spur gears and rolling-contact test bars  
[NASA-TM-101979] p 185 N89-22111
- Topology of modified helical gears and Tooth Contact Analysis (TCA) program  
[NASA-CR-4224] p 186 N89-22920
- Tribology: The Story of Lubrication and Wear  
[NASA-TM-101430] p 203 N89-24635
- Topology of modified helical gears  
[NASA-TM-102134] p 187 N89-28015
- GELATION**
- Influence of several metal ions on the gelation activation energy of silicon tetraethoxide  
[NASA-TM-101380] p 114 N89-21894
- GELLED ROCKET PROPELLANTS**
- Ignition and combustion of metallized propellants  
[AIAA PAPER 89-2883] p 117 A89-47148
- GEOMAGNETISM**
- Surface phenomena in plasma environments p 234 N89-23555
- GEOMETRICAL OPTICS**
- Ray-tube integration in shooting and bouncing ray method p 124 A89-15152
- Shooting and bouncing rays - Calculating the RCS of an arbitrarily shaped cavity p 124 A89-34242
- Modal, ray, and beam techniques for analyzing the EM scattering by open-ended waveguide cavities p 125 A89-39594
- High-frequency RCS of open cavities with rectangular and circular cross sections p 125 A89-39595
- GERMANIUM**
- High efficiency GaAs-Ge tandem solar cells grown by MOCVD p 213 N89-24721
- GET AWAY SPECIALS (STS)**
- Flight experiment of thermal energy storage  
[NASA-TM-102081] p 69 N89-24440
- GIBBS FREE ENERGY**
- Free energy surfaces in the superconducting mixed state p 236 A89-43928
- GLACIOLOGY**
- Data report for the Siple Coast (Antarctica) project  
[NASA-TM-100708] p 206 N89-10403
- GLASS**
- Crystallization of BaF<sub>2</sub>-ZnF<sub>2</sub>-YbF<sub>3</sub>-ThF<sub>4</sub> glass p 230 A89-12236
- Crystallization kinetics of BaO-Al<sub>2</sub>O<sub>3</sub>-SiO<sub>2</sub> glasses  
[NASA-TM-101964] p 113 N89-20252
- GLASS FIBER REINFORCED PLASTICS**
- Evaluation of atomic oxygen resistant protective coatings for fiberglass-epoxy composites in LEO  
[NASA-TM-101955] p 114 N89-21100
- GLAZES**
- Modeling of surface roughness effects on glaze ice accretion  
[AIAA PAPER 89-0734] p 16 A89-28451
- GOLD**
- Structural chemistry of Au(III)-substituted Ba<sub>2</sub>YCu<sub>3</sub>O<sub>7</sub>( $\delta$ ) p 89 A89-12620
- The effect of metal surface passivation on the Au-InP interaction p 132 A89-30443
- Submicron nickel-oxide-gold tunnel diode detectors for rectennas p 133 A89-43469
- GOLD ALLOYS**
- The interaction of gold with gallium arsenide p 90 A89-16416
- GRAIN BOUNDARIES**
- Grain boundary oxidation and its effects on high temperature fatigue life p 101 N89-12918
- GRAIN SIZE**
- Morphological study of near threshold fatigue crack growth in a coarse grain aluminum alloy p 94 A89-12326
- Observations of directional gamma prime coarsening during engine operation p 98 A89-40162
- Effect of grain size on the high temperature properties of B2 aluminides  
[NASA-TM-101382] p 101 N89-12720
- High-temperature LDV seed particle development  
[NASA-CR-182265] p 175 N89-23851
- GRAPHITE**
- The correlation of low-velocity impact resistance of graphite-fiber-reinforced composites with matrix properties p 79 A89-16283
- Isotropic graphite multistage depressed collectors - A progress report - carbon electrode performance p 132 A89-31988
- Graphite/polyimide composites with improved toughness p 83 A89-38637
- Compatibility of molten salts with advanced solar dynamic receiver materials p 83 A89-48957
- Effect of length of chopped pristine and intercalated graphite fibers on the resistivity of fiber networks  
[NASA-TM-101395] p 84 N89-11826
- Light weight polymer matrix composite material  
[NASA-CASE-LEW-14734-1] p 87 N89-23623
- GRAPHITE-EPOXY COMPOSITES**
- Design procedures for fiber composite box beams p 195 A89-48674
- Technological hurdles to the application of intercalated graphite fibers  
[NASA-TM-101394] p 108 N89-11911
- A probabilistic approach to composite micromechanics  
[NASA-TM-101366] p 85 N89-12684
- Vibration testing of impact-damaged composite laminates  
[NASA-TM-4115] p 87 N89-25290
- GRAPHITE-POLYIMIDE COMPOSITES**
- A thermally modified polymer matrix composite material with structural integrity to 371 C p 80 A89-29997
- 700 F properties of autoclave cured PMR-II composites p 81 A89-29998
- GRAPHITIZATION**
- Graphite fluoride fiber polymer composite material  
[NASA-CASE-LEW-14472-1] p 85 N89-14259
- GRAVITATIONAL EFFECTS**
- An experimental and analytical investigation of thermoacoustic convection heat transfer in gravity and zero-gravity environments  
[NASA-CR-179575] p 120 N89-11920
- A comparative study of the influence of buoyancy driven fluid flow on GaAs crystal growth p 121 N89-20295
- GRAVITATIONAL FIELDS**
- Behavior in normal and reduced gravity of an enclosed liquid/gas system with nonuniform heating from above  
[AIAA PAPER 89-0070] p 145 A89-25061
- Behavior in normal and reduced gravity of an enclosed liquid/gas system with nonuniform heating from above  
[NASA-TM-101471] p 120 N89-17046
- GRID GENERATION (MATHEMATICS)**
- A diagonally inverted LU implicit multigrid scheme for the 3-D Navier-Stokes equations and a two equation model of turbulence  
[AIAA PAPER 89-0467] p 145 A89-25382
- Conservative treatment of boundary interfaces for overlaid grids and multi-level grid adaptations  
[AIAA PAPER 89-1980] p 5 A89-41823
- A simple algebraic grid adaptation scheme with applications to two- and three-dimensional flow problems  
[AIAA PAPER 89-1984] p 5 A89-41827
- A diagonally inverted LU implicit multigrid scheme for the 3-D Navier-Stokes equations and a two equation model of turbulence  
[NASA-CR-182209] p 9 N89-10863
- Interactive grid generation for turbomachinery flow field simulations  
[NASA-TM-101301] p 9 N89-11717
- Improvement in finite element meshes: Heat transfer in an infinite cylinder  
[NASA-TM-101410] p 182 N89-14450
- Application of a lower-upper implicit scheme and an interactive grid generation for turbomachinery flow field simulations  
[NASA-TM-101412] p 11 N89-15077
- On the applications of algebraic grid generation methods based on transfinite interpolation  
[NASA-TM-102095] p 33 N89-26003
- GROUND SUPPORT EQUIPMENT**
- Design and implementation of a microcomputer-based user interface controller for bursted data communications satellite ground terminals  
[NASA-TM-101375] p 43 N89-13457
- GROUND SUPPORT SYSTEMS**
- Cooperating expert systems for Space Station - Power/thermal subsystem testbeds p 38 A89-15350
- Microgravity research in NASA ground-based facilities  
[AIAA PAPER 89-0236] p 118 A89-25201

- Microgravity research in NASA ground-based facilities  
[NASA-TM-101397] p 240 N89-15047
- GROUND TESTS**
- Ground-based tests of hollow cathode plasma  
contactors [AIAA PAPER 89-1558] p 232 A89-40188
- Experimental validation of a phenomenological model  
of the plasma contacting process p 232 A89-43357
- Successful completion of a cyclic ground test of a  
mercury ion Auxiliary Propulsion System p 59 A89-47450
- PV modules for ground testing  
[NASA-CR-179476] p 208 N89-11315
- NASA's program on icing research and technology  
[NASA-TM-101989] p 1 N89-22569
- GUIDE VANES**
- Measurements of heat transfer distribution over the  
surfaces of highly loaded turbine nozzle guide vanes  
p 141 A89-12752
- Effects of wake passing on stagnation region heat  
transfer p 148 A89-34928
- Average-passage simulation of counter-rotating propan  
propulsion systems as applied to cruise missiles  
[AIAA PAPER 89-2943] p 7 A89-47187
- Average-passage simulation of counter-rotating propan  
propulsion systems as applied to cruise missiles  
[NASA-TM-102043] p 14 N89-23416
- GUSTS**
- Influence of airfoil thickness on convected gust  
interaction noise [AIAA PAPER 89-1082] p 225 A89-33725
- H**
- HAFNIUM**
- Oxidation behavior of FeAl + Hf, Zr, B  
[NASA-TM-101402] p 102 N89-14297
- HAFNIUM ALLOYS**
- Inelastic deformation and dislocation structure of a nickel  
alloy - Effects of deformation and thermal histories  
p 99 A89-50313
- HALL EFFECT**
- Closed-drift thruster investigations  
[NASA-CR-179497] p 62 N89-11808
- HAMILTONIAN FUNCTIONS**
- Nonlinear analysis using temporal finite elements  
p 221 A89-28030
- HARDNESS**
- Indentation plasticity and fracture in silicon  
[NASA-TP-2863] p 100 N89-10996
- HARMONICS**
- Distortion and regulation characterization of a Mapham  
inverter [NASA-TM-102089] p 139 N89-26148
- HARRIER AIRCRAFT**
- Computer simulation of a pilot in V/STOL aircraft control  
loops [NASA-CR-184815] p 215 N89-21479
- HASTELLOY (TRADEMARK)**
- Fracture mechanics applied to elevated temperature  
crack growth p 195 A89-47705
- Thermomechanical characterization of Hastelloy-X  
under uniaxial cyclic loading p 196 N89-12909
- Use of inelastic strain as a basis for analyzing  
thermomechanical test data p 200 N89-17326
- HEALTH**
- Integrated control and health management. Orbit  
transfer rocket engine technology program  
[NASA-CR-182122] p 62 N89-11805
- HEAT EXCHANGERS**
- Effect of transition on oscillation flow losses in Stirling  
engine coolers and heaters p 142 A89-15189
- The design and fabrication of a Stirling engine heat  
exchanger module with an integral heat pipe p 142 A89-15190
- Moving Belt Radiator technology issues  
p 49 A89-15208
- Radiative transfer in rectangular enclosures - A  
discretized exchange factor solution p 153 A89-53262
- Molten salt corrosion of SiC and Si3N4  
[NASA-TM-101346] p 108 N89-11912
- HEAT FLUX**
- Effect of NASA advanced designs on thermal behavior  
of Ni-H2 cells p 50 A89-15279
- Correlations of velocity and temperature fluctuations in  
the stagnation-point flow of circular cylinder in turbulent  
flow p 148 A89-34927
- A high heat flux experiment for verification of  
thermostructural analysis p 148 A89-35002
- Radiative heat transfer in rocket thrust chambers and  
nozzles [AIAA PAPER 89-1720] p 150 A89-43235

- Sensors for ceramic components in advanced  
propulsion systems: Summary of literature survey and  
concept analysis, task 3 report [NASA-CR-180900] p 172 N89-11192
- A high heat flux experiment for verification of  
thermostructural analysis [NASA-TM-100931] p 155 N89-12026
- HOST instrumentation R and D program overview  
p 25 N89-12878
- The effect of oxidation on the high heat flux behavior  
of a thermal barrier coating p 110 N89-13646
- Heat flux measurements  
[NASA-TM-101428] p 173 N89-14418
- Structural response of an advanced combustor liner:  
Test and analysis p 200 N89-17329
- Experience with advanced instrumentation in a hot  
section cascade [NASA-TM-102294] p 167 N89-27980
- HEAT PIPES**
- The design and fabrication of a Stirling engine heat  
exchanger module with an integral heat pipe p 142 A89-15190
- Moving Belt Radiator technology issues  
p 49 A89-15208
- Transient performance evaluation of an integrated heat  
pipe-thermal storage system p 49 A89-15209
- Advanced space solar dynamic receivers  
p 52 A89-15343
- Solar dynamic heat rejection technology. Task 1: System  
concept development [NASA-CR-179618] p 158 N89-13731
- Megawatt Class Nuclear Space Power Systems  
(MCNSPS) conceptual design and evaluation report.  
Volume 4: Concepts selection, conceptual designs,  
recommendations [NASA-CR-179614-VOL-4] p 210 N89-18967
- Failure analysis of a Stirling engine heat pipe  
[NASA-TM-101418] p 103 N89-20227
- Megawatt Class Nuclear Space Power Systems  
(MCNSPS) conceptual design and evaluation report.  
Volume 2, technologies 1: Reactors, heat transport,  
integration issues [NASA-CR-179614-VOL-2] p 211 N89-22981
- Initial characterization of a modular heat exchanger with  
an integral heat pipe [NASA-TM-102097] p 239 N89-25078
- Comparison of conceptual designs for 25 kW advanced  
Stirling conversion systems for dish electric application  
[NASA-TM-102085] p 239 N89-26781
- Thermal evaluation of advanced solar dynamic heat  
receiver performance [NASA-CR-185117] p 214 N89-27256
- HEAT RADIATORS**
- The solar dynamic radiator with a historical  
perspective [NASA-TM-100972] p 45 N89-10117
- Solar dynamic heat rejection technology. Task 1: System  
concept development [NASA-CR-179618] p 158 N89-13731
- Megawatt Class Nuclear Space Power Systems  
(MCNSPS) conceptual design and evaluation report.  
Volume 4: Concepts selection, conceptual designs,  
recommendations [NASA-CR-179614-VOL-4] p 210 N89-18967
- Megawatt Class Nuclear Space Power Systems  
(MCNSPS) conceptual design and evaluation report.  
Volume 2, technologies 1: Reactors, heat transport,  
integration issues [NASA-CR-179614-VOL-2] p 211 N89-22981
- Scaling results for the Liquid Sheet Radiator (LSR)  
[NASA-TM-102100] p 72 N89-25277
- Two-tiered design analysis of a radiator for a solar  
dynamic powered Stirling engine [NASA-CR-182301] p 46 N89-26031
- Arc-textured high emittance radiator surfaces  
[NASA-CASE-LEW-14679-1] p 116 N89-28651
- HEAT RESISTANT ALLOYS**
- The effect of Co alloying content on the kinetics of  
reaction zone growth in tungsten fiber reinforced superalloy  
composites p 79 A89-11324
- High temperature isothermal and cyclic oxidation  
behavior of a single crystal Ni base superalloy p 94 A89-12625
- Effects of cobalt concentration on the relative resistance  
to octahedral and cube slip in nickel-base superalloys  
p 94 A89-17115
- Iron-base superalloys - A phase analysis of the  
multicomponent system (Fe-Mn-Cr-Mo-Nb-Al-Si-C)  
p 95 A89-13739
- The constitutive representation of high-temperature  
creep damage p 191 A89-17396
- Rapid solidification research at the NASA Lewis  
Research Center p 95 A89-18203
- A Monte Carlo-finite element model for strain energy  
controlled microstructural evolution - 'Rafting' in  
superalloys p 96 A89-24358

- Influence of precipitate morphology on intermediate  
temperature creep properties of a nickel-base superalloy  
single crystal p 96 A89-26872
- The influence of high thermal gradient casting, hot  
isostatic pressing and alternate heat treatment on the  
structure and properties of a single crystal nickel base  
superalloy p 97 A89-36427
- Isothermal and 'bithermal' thermomechanical fatigue  
behavior of a NiCoCrAlY-coated single crystal superalloy  
p 177 A89-36457
- Accelerated fatigue crack growth behavior of PWA  
1480 p 97 A89-36461
- Transient oxidation of single-crystal beta-NiAl  
p 98 A89-37899
- Fatigue crack growth behavior of a single crystal alloy  
as observed through an in situ fatigue loading stage  
p 99 A89-45946
- The low cycle fatigue deformation response of a  
single-crystal superalloy at 650 C p 99 A89-52204
- Simplified cyclic structural analysis of SSME turbine  
blades p 63 N89-12632
- Constitutive behavior of single crystal PWA 1480 and  
directionally solidified MAR-M 246 under monotonic and  
cyclic loads at high and low temperature p 100 N89-12634
- A multiaxial theory of viscoplasticity for isotropic  
materials p 196 N89-12908
- Constitutive modeling for single crystal superalloys  
p 101 N89-12911
- Constitutive modelling of single crystal and directionally  
solidified superalloys p 101 N89-12912
- An investigation of environmental influence on the creep  
behavior of a low pressure plasma sprayed NiCoCrAlY  
alloy p 110 N89-13648
- Fiber reinforced superalloys for rocket engines  
[NASA-TM-100880] p 86 N89-15990
- Constitutive modelling of single crystal and directionally  
solidified superalloys p 102 N89-17325
- High temperature constitutive and crack initiation  
modelling of coated single crystal superalloys p 112 N89-17334
- Structural analysis methods development for turbine hot  
section components p 30 N89-20140
- Fatigue life prediction modeling for turbine hot section  
materials p 30 N89-20142
- Advanced single crystal for SSME turbopumps  
[NASA-CR-182244] p 103 N89-21072
- Deformation modeling and constitutive modeling for  
anisotropic superalloys [NASA-CR-4215] p 202 N89-21258
- Fiber reinforced superalloys for rocket engines  
p 103 N89-22673
- Time dependent reliability model incorporating  
continuum damage mechanics for high-temperature  
ceramics [NASA-TM-102046] p 115 N89-24487
- Computational simulation of high temperature metal  
matrix composites cyclic behavior [NASA-TM-102115] p 88 N89-27795
- HEAT STORAGE**
- Transient performance evaluation of an integrated heat  
pipe-thermal storage system p 49 A89-15209
- Use of pure nickel and LiOH for thermal energy  
storage p 91 A89-23146
- Thermal analysis of heat storage canisters for a solar  
dynamic, space power system p 54 A89-29113
- Advanced solar receivers for space power  
p 54 A89-29116
- Densities of some molten fluoride salt mixtures suitable  
for heat storage in space power applications p 77 A89-41444
- Flight experiment of thermal energy storage  
[NASA-TM-102081] p 69 N89-24440
- HEAT TRANSFER**
- Determination of convective diffusion heat/mass  
transfer rates to burner rig test targets comparable in size  
to cross-stream jet diameter p 141 A89-12753
- Effect of transition on oscillation flow losses in Stirling  
engine coolers and heaters p 142 A89-15189
- Turbine-stage heat transfer - Comparison of  
short-duration measurements with state-of-the-art  
predictions p 142 A89-16458
- Mass transfer across combustion gas thermal boundary  
layers - Power production and materials processing  
implications p 143 A89-20425
- Efficient numerical simulation of a one-dimensional  
electrothermal deicer pad p 144 A89-22811
- A numerical investigation of the influence of surface  
roughness on heat transfer in ice accretion  
[AIAA PAPER 89-0737] p 146 A89-25554
- Heat transfer in gas turbine engines and  
three-dimensional flows; Proceedings of the Symposium,  
ASME Winter Annual Meeting, Chicago, IL, Nov. 27-Dec.  
2, 1988 p 148 A89-34926
- Effects of wake passing on stagnation region heat  
transfer p 148 A89-34928

Prediction of unsteady rotor-surface heat transfer from wake passings  
[AIAA PAPER 89-1692] p 150 A89-43210

A generalized one dimensional computer code for turbomachinery cooling passage flow calculations  
[AIAA PAPER 89-2574] p 151 A89-46934

Heat transfer in aerospace propulsion  
p 153 A89-53282

Unsteady heat transfer in turbine blade ducts - Focus on combustor sources  
p 153 A89-53286

Thermosolutal convection in high-aspect-ratio enclosures  
p 153 A89-53288

Development of a thermal and structural analysis procedure for cooled radial turbines  
[NASA-TM-101416] p 24 N89-12568

Turbine Engine Hot Section Technology 1986  
[NASA-CP-2444] p 195 N89-12876

HOST turbine heat transfer subproject overview  
p 25 N89-12880

Aerothermal modeling program, phase 2  
p 156 N89-12890

Heat transfer with very high free-stream turbulence and streamwise vortices  
p 157 N89-12900

Development of low Reynolds number two equation turbulence models for predicting external heat transfer on turbine blades  
p 157 N89-12901

Analysis of supersonic plug nozzle flowfield and heat transfer  
[NASA-CR-179554] p 10 N89-13397

Analytical ice shape predictions for flight in natural icing conditions  
[NASA-CR-182234] p 18 N89-13428

A comparison of numerical methods for the prediction of two-dimensional heat transfer in an electrothermal deicer pad  
[NASA-CR-4202] p 19 N89-13429

The effects of leading edge and downstream film cooling on turbine vane heat transfer  
[NASA-CR-182133] p 158 N89-13754

The effects of inlet turbulence and rotor/stator interactions on the aerodynamics and heat transfer of a large-scale rotating turbine model, volume 1  
[NASA-CR-4079] p 159 N89-13756

Improvement in finite element meshes: Heat transfer in an infinite cylinder  
[NASA-TM-101410] p 182 N89-14450

Experimental determination of stator endwall heat transfer  
[NASA-TM-101419] p 159 N89-15366

Turbine Engine Hot Section Technology, 1987  
[NASA-CP-2493] p 199 N89-17298

Heat transfer with very high free-stream turbulence and heat transfer with streamwise vortices  
p 160 N89-17309

A low-Reynolds-number two-equation turbulence model for predicting heat transfer on turbine blades  
p 160 N89-17310

Measurement of airfoil heat transfer coefficients on a turbine stage  
p 160 N89-17311

Heat transfer in the tip region of a rotor blade simulator  
p 161 N89-17312

Two- and three-dimensional turbine blade row flow field simulations  
p 161 N89-17313

Coolant passage heat transfer with rotation  
p 161 N89-17314

Turbine airfoil film cooling  
p 161 N89-17315

High-resolution liquid-crystal heat-transfer measurements on the end wall of a turbine passage with variations in Reynolds number  
[NASA-TM-100827] p 161 N89-18664

Experiment plans to study preignition processes of a pool fire in low gravity  
[NASA-CR-182256] p 121 N89-19442

Review and assessment of the database and numerical modeling for turbine heat transfer  
p 30 N89-20139

Three dimensional thermal analysis of rocket thrust chambers  
[NASA-TM-101973] p 66 N89-21025

A generalized one-dimensional computer code for turbomachinery cooling passage flow calculations  
[NASA-TM-102079] p 163 N89-22862

Methods for heat transfer and temperature field analysis of the insulated diesel, phase 3  
[NASA-CR-182237] p 239 N89-23382

Two-dimensional numerical simulation of a Stirling engine heat exchanger  
[NASA-TM-102057] p 164 N89-23823

Some characteristics of bypass transition in a heated boundary layer  
[NASA-TM-102126] p 164 N89-24577

Experience with advanced instrumentation in a hot section cascade  
[NASA-TM-102294] p 167 N89-27980

## HEAT TRANSFER COEFFICIENTS

Regressed relations for forced convection heat transfer in a direct injection stratified charge rotary engine  
[SAE PAPER 880626] p 178 A89-12308

Windward fraction of the total mass or heat transport for flow past a circular cylinder  
p 141 A89-12339

High-resolution heat-transfer-coefficient maps applicable to compound-curve surfaces using liquid crystals in a transient wind tunnel  
[NASA-TM-89855] p 154 N89-10246

Measurement of airfoil heat transfer coefficients on a turbine stage  
p 157 N89-12897

Coolant passage heat transfer with rotation  
p 157 N89-12899

Turbine airfoil film cooling  
p 158 N89-12903

Measurement of airfoil heat transfer coefficients on a turbine stage  
p 160 N89-17311

Coolant passage heat transfer with rotation  
p 161 N89-17314

## HEAT TREATMENT

The influence of high thermal gradient casting, hot isostatic pressing and alternate heat treatment on the structure and properties of a single crystal nickel base superalloy  
p 97 A89-36427

Mechanical properties of modified low cobalt powder metallurgy Udimet 700 type alloys  
[NASA-TM-101481] p 103 N89-20228

## HEATING

Behavior in normal and reduced gravity of an enclosed liquid/gas system with nonuniform heating from above  
[AIAA PAPER 89-0070] p 145 A89-25061

Behavior in normal and reduced gravity of an enclosed liquid/gas system with nonuniform heating from above  
[NASA-TM-101471] p 120 N89-17046

Furnace for tensile/fatigue testing  
[NASA-CASE-LEW-14848-1] p 40 N89-28549

## HEATING EQUIPMENT

Two-dimensional simulation of electrothermal deicing of aircraft components  
p 17 A89-39194

## HELICOPTER ENGINES

A review and forecast of engine system research at the Army Propulsion Directorate  
p 23 A89-36397

## HELICOPTER PERFORMANCE

Generic icing effects on forward flight performance of a model helicopter rotor  
p 18 A89-41093

## HELICOPTER PROPELLER DRIVE

Comparison of predicted and measured temperatures of UH-60A helicopter transmission  
[NASA-TP-2911] p 186 N89-24607

## HELICOPTER TAIL ROTORS

Icing research tunnel test of a model helicopter rotor  
[NASA-TM-101978] p 29 N89-19305

## HELICOPTERS

Advanced transmission studies  
p 178 A89-18906

Effect of advanced component technology on helicopter transmissions  
[NASA-TM-101431] p 182 N89-13794

## HELIUM

Leakage predictions for Rayleigh-step, helium-purge seals  
[NASA-TM-101352] p 64 N89-14255

Advanced helium purge seals for Liquid Oxygen (LOX) turbopumps  
[NASA-CR-182105] p 184 N89-21239

## HELIUM ISOTOPIES

Lunar Helium-3 and Fusion Power  
[NASA-CP-10018] p 233 N89-14842

Assessment of lunar sources of He-3 for use on earth  
p 242 N89-14853

## HELMHOLTZ RESONATORS

Acoustic wave propagation in heterogeneous structures including experimental validation  
[AIAA PAPER 89-1044] p 225 A89-36214

Acoustic evaluation of the Helmholtz resonator treatment in the NASA Lewis 8- by 6-foot supersonic wind tunnel  
[NASA-TM-101407] p 228 N89-15685

Acoustic wave propagation in heterogeneous structures including experimental validation  
[NASA-TM-101486] p 224 N89-19965

## HEPTANES

NOx formation from the combustion of monodisperse n-heptane sprays doped with fuel-nitrogen additives  
p 116 A89-42695

## HETEROJUNCTION DEVICES

Development of gallium arsenide high-speed, low-power serial parallel interface modules: Executive summary  
[NASA-CR-182272] p 137 N89-21173

## HETEROJUNCTIONS

Characterization of GaAlAs optical waveguide heterostructures grown by molecular beam epitaxy  
p 130 A89-10343

Calculation of the electron wave function in a graded-channel double-heterojunction modulation-doped field-effect transistor  
p 134 A89-54417

Deposition and characterization of ZnS/Si heterojunctions produced by vacuum evaporation  
[NASA-TM-101359] p 135 N89-11129

Ultra-thin, light-trapping silicon solar cells  
p 213 N89-24719

## HEURISTIC METHODS

Graphical postprocessing for 3-D mesh quality evaluation  
p 217 A89-38846

## HIERARCHIES

Hierarchical Poly Tree computer architectures defined by computational multidisciplinary mechanics  
p 218 A89-50100

## HIGH ASPECT RATIO

Thermosolutal convection in high-aspect-ratio enclosures  
p 153 A89-53288

## HIGH CURRENT

Multi-hundred kilowatt roll ring assembly  
[NASA-CR-174832] p 135 N89-15335

## HIGH ELECTRON MOBILITY TRANSISTORS

Microwave response of an HEMT photoconductor  
p 131 A89-15824

Microwave characteristics of GaAs MMIC integratable optical detectors  
[NASA-TM-101485] p 129 N89-24520

## HIGH FREQUENCIES

A versatile power converter for high-frequency link systems  
p 131 A89-21200

High-frequency ultrasonic characterization of sintered silicon carbide  
p 106 A89-34840

## HIGH PRESSURE

High pressure multiaxial extensometry  
p 170 A89-43532

Performance of multimirror quartzline lamps in a high-pressure, underwater environment  
[NASA-TM-101374] p 172 N89-10269

High-pressure calorimeter chamber tests for liquid oxygen/kerosene (LOX/RP-1) rocket combustion  
[NASA-TP-2862] p 65 N89-15979

## HIGH PRESSURE OXYGEN

Friction-induced ignition of metals in high-pressure oxygen  
p 97 A89-32932

## HIGH RESOLUTION

High-resolution heat-transfer-coefficient maps applicable to compound-curve surfaces using liquid crystals in a transient wind tunnel  
[NASA-TM-89855] p 154 N89-10246

## HIGH SPEED

High speed inlet calculations with real gas effects  
[AIAA PAPER 88-3076] p 2 A89-14980

Performance of laser Doppler velocimeter with polydisperse seed particles in high-speed flows  
p 169 A89-22279

Viscous analysis of high speed flows using an upwind finite volume technique  
[AIAA PAPER 89-0001] p 144 A89-25001

An analysis for high speed propeller-nacelle aerodynamic performance prediction. Volume 1: Theory and application  
[NASA-CR-4199-VOL-1] p 12 N89-15896

An analysis for high speed propeller-nacelle aerodynamic performance prediction. Volume 2: User's manual  
[NASA-CR-4199-VOL-2] p 12 N89-15897

High speed balancing applied to the T700 engine  
[NASA-CR-180899] p 184 N89-20472

## HIGH SPEED CAMERAS

Feasibility of reduced gravity experiments involving quiescent, uniform particle cloud combustion  
[NASA-TM-101371] p 122 N89-26114

## HIGH SPEED PHOTOGRAPHY

Stratified charge rotary engine - Internal flow studies at the MSU engine research laboratory  
[SAE PAPER 890331] p 181 A89-51477

## HIGH STRENGTH

Improved silicon carbide for advanced heat engines  
[NASA-CR-179477] p 112 N89-15251

## HIGH TEMPERATURE

High temperature thermal conductivity measurements on lanthanum sulfides using the flash method  
p 77 A89-16500

A viscoplastic constitutive theory for metal matrix composites at high temperature  
p 80 A89-20725

Exposure time considerations in high temperature low cycle fatigue  
p 192 A89-29600

A thermally modified polymer matrix composite material with structural integrity to 371 C  
p 80 A89-29997

Fracture resistance of a TiB2 particle/SiC matrix composite at elevated temperature  
p 81 A89-31074

Effect of grain size on the high temperature properties of B2 aluminides  
[NASA-TM-101382] p 101 N89-12720

Turbine Engine Hot Section Technology (HOST) Project  
p 25 N89-12877

Elevated temperature strain gages  
p 173 N89-12886

- Development of a high temperature static strain sensor p 173 N89-12887
- The NASA Lewis Strain Gauge Laboratory: An update [NASA-TM-101432] p 173 N89-12888
- High temperature stress-strain analysis p 196 N89-12913
- Characterization of ZrO<sub>2</sub> buffer layers for sequentially evaporated Y-Ba-CuO on Si and Al<sub>2</sub>O<sub>3</sub> substrates [NASA-TM-101432] p 135 N89-13722
- Improved silicon carbide for advanced heat engines [NASA-CR-179477] p 112 N89-15251
- Oxide-dispersion-strengthened turbine blades. Volume 2 [NASA-CR-179561-VOL-2] p 28 N89-18487
- The emittance of space radiator materials measured at elevated temperatures [NASA-TM-101948] p 66 N89-20193
- Improved high-temperature resistant matrix resins [NASA-CR-180826] p 114 N89-21105
- High-temperature LDV seed particle development [NASA-CR-182265] p 175 N89-23851
- Solid lubricant materials for high temperatures: A review p 203 N89-24636
- X-ray based extensometry [NASA-CR-185058] p 176 N89-25432
- On finite element implementation and computational techniques for constitutive modeling of high temperature composites [NASA-CR-185120] p 204 N89-26261
- High temperature flexible seal [NASA-CASE-LEW-14695-1] p 187 N89-28830
- HIGH TEMPERATURE ENVIRONMENTS**
- High speed inlet calculations with real gas effects [AIAA PAPER 88-3076] p 2 N89-14980
- High temperature optical strain measurement system p 170 N89-43842
- Considerations in development and implementation of elasto-viscoplastic constitutive model for high temperature applications [NASA-CR-183403] p 197 N89-12932
- Development of a high temperature thin film static strain gage p 174 N89-17299
- Thermal barrier coating life prediction model development p 200 N89-17333
- High temperature constitutive and crack initiation modeling of coated single crystal superalloys p 112 N89-17334
- Elevated temperature crack growth p 200 N89-17335
- Total strain version of strainrange partitioning for thermomechanical fatigue at low strains p 201 N89-17337
- Views on the impact of HOST p 31 N89-20144
- Experience with advanced instrumentation in a hot section cascade [NASA-TM-102294] p 167 N89-27980
- HIGH TEMPERATURE FLUIDS**
- Fuel-rich catalytic combustion of Jet-A fuel-equivalence ratios 5.0 to 8.0 [NASA-TM-101975] p 93 N89-21051
- HIGH TEMPERATURE GASES**
- Deposition of Na<sub>2</sub>SO<sub>4</sub> from salt-seeded combustion gases of a high velocity burner rig p 89 N89-12330
- Determination of convective diffusion heat/mass transfer rates to burner rig test targets comparable in size to cross-stream jet diameter p 141 N89-12753
- Optical experiments on thermophoretically augmented submicron particle deposition from 'dusty' high temperature gas flows p 90 N89-14799
- Hot gas ingestion testing of an advanced STOVL concept in the NASA Lewis 9- by 15-foot low speed wind tunnel with flow visualization [NASA-TM-100952] p 11 N89-15078
- HIGH TEMPERATURE RESEARCH**
- Toward improved durability in advanced aircraft engine hot sections [NASA-TM-4087] p 29 N89-20135
- Advanced high temperature instrument for hot section research applications p 29 N89-20137
- Structural analysis methods development for turbine hot section components p 30 N89-20140
- HIGH TEMPERATURE SUPERCONDUCTORS**
- Structural chemistry of Au(III)-substituted Ba<sub>2</sub>YCu<sub>3</sub>O<sub>7</sub>( $\delta$ ) p 89 N89-12620
- The application of high temperature superconductors to space electrical power distribution components p 50 N89-15287
- High temperature superconducting magnetic energy storage for future NASA missions p 50 N89-15288
- Transport critical current and magnetization measurements of melt-processed YBa<sub>2</sub>Cu<sub>3</sub>O<sub>7</sub>( $\delta$ ) p 234 N89-20037
- Effect of processing parameters on the characteristics of high-T<sub>c</sub> superconductor YBa<sub>2</sub>Cu<sub>3</sub>O<sub>7</sub> p 234 N89-20467
- Interaction of Au, Ag, and Bi ions with Ba<sub>2</sub>YCu<sub>3</sub>O<sub>7</sub>( $\delta$ ) - Implications for superconductor applications p 235 N89-22886
- Improved synthesis of ceramic superconductors with alkaline earth peroxides - Synthesis and processing of Ba<sub>2</sub>YCu<sub>3</sub>O<sub>7</sub>( $\delta$ ) p 235 N89-22887
- Critical currents of aligned grains of Ti-Ba-Ca-Cu-O compounds p 235 N89-30335
- Highly oriented Ti<sub>2</sub>Ba<sub>2</sub>Ca<sub>2</sub>Cu<sub>3</sub>O<sub>10</sub> thin films by pulsed laser evaporation p 236 N89-30421
- Doping directed at the oxygen sites in YBa<sub>2</sub>Cu<sub>3</sub>O<sub>7</sub>( $\delta$ ) - The effect of sulfur, fluorine, and chlorine p 133 N89-37824
- Preparation of high T<sub>c</sub> Ti-Ba-Ca-Cu-O thin films by pulsed laser evaporation and TiO<sub>2</sub> vapor processing p 236 N89-38608
- Free energy surfaces in the superconducting mixed state p 236 N89-43928
- Aeronautical applications of high-temperature superconductors [AIAA PAPER 89-2142] p 23 N89-53304
- Use of high temperature superconductors in magnetoplasma dynamic systems [NASA-TM-101219] p 236 N89-11553
- Stability of bulk Ba<sub>2</sub>YCu<sub>3</sub>O<sub>7</sub>( $\delta$ ) in a variety of environments [NASA-TM-101401] p 111 N89-14310
- Aeronautical applications of high-temperature superconductors [NASA-TM-102311] p 33 N89-26008
- Measurements of complex permittivity of microwave substrates in the 20 to 300 K temperature range from 26.5 to 40.0 GHz [NASA-TM-102123] p 123 N89-27038
- Non-uniform transition conductivity of superconducting ceramic [NASA-TM-102133] p 189 N89-28851
- Millimeter wave transmission studies of YBa<sub>2</sub>Cu<sub>3</sub>O<sub>7</sub>( $\delta$ ) thin films in the 26.5 to 40.0 GHz frequency range [NASA-TM-102345] p 237 N89-30088
- HIGH TEMPERATURE TESTS**
- The dual element method of strain gauge temperature compensation p 169 N89-12276
- High temperature isothermal and cyclic oxidation behavior of a single crystal Ni base superalloy p 94 N89-12625
- The constitutive representation of high-temperature creep damage p 191 N89-17396
- Finite element applications to explore the effects of partial bonding on metal matrix composite properties [AIAA PAPER 89-1175] p 192 N89-30666
- Fracture mechanics applied to elevated temperature crack growth p 195 N89-47705
- The low cycle fatigue deformation response of a single-crystal superalloy at 650 C p 99 N89-52204
- Tribological composition optimization of chromium-carbide-based solid lubricant coatings for foil gas bearings at temperatures to 650 C p 83 N89-54258
- Elevated temperature crack growth p 196 N89-12915
- HISTORIES**
- The Solar Dynamic radiator with a historical perspective p 51 N89-15340
- HOHLRAUMS**
- Automated data acquisition and processing for a Hohlraum reflectometer [NASA-TM-101393] p 173 N89-14416
- HOLLOW CATHODES**
- Ground-based tests of hollow cathode plasma contactors [AIAA PAPER 89-1558] p 232 N89-40188
- On the need for space tests of plasma contactors as electron collectors p 232 N89-43356
- Experimental validation of a phenomenological model of the plasma contacting process p 232 N89-43357
- Ground-based plasma contactor characterization p 233 N89-43359
- Space plasma contactor research, 1988 [NASA-CR-182283] p 233 N89-21658
- HOLOGRAPHIC INTERFEROMETRY**
- Holographic interferometry with an injection seeded Nd:YAG laser and two reference beams [NASA-TM-102056] p 175 N89-24591
- HOLOGRAPHY**
- Optoelectronic techniques for broadband switching p 131 N89-15825
- HOMOJUNCTIONS**
- InP homojunction solar cell performance on the LIPS 3 flight experiment [NASA-TM-101390] p 209 N89-12123
- Predicted performance of InP solar cells in Cassagrainian and slats space concentrator arrays at 20 to 100 AMO, 80 to 100 C p 212 N89-24711
- The GaAs solar cells with V-grooved emitters [NASA-TM-102104] p 214 N89-26291
- On-orbit results of the LIPS 3/InP homojunction solar cell experiment [NASA-TM-102131] p 214 N89-26292
- HOONEYCOMB CORES**
- Fiber composite sandwich thermostructural behavior - Computational simulation p 190 N89-11246
- HOONEYCOMB STRUCTURES**
- Experimental results for labyrinth gas seals with honeycomb stators - Comparisons to smooth-stator seals and theoretical predictions [ASME PAPER 88-TRIB-40] p 179 N89-24992
- Annular honeycomb seals: Test results for leakage and rotordynamic coefficients - Comparisons to labyrinth and smooth configurations [ASME PAPER 88-TRIB-35] p 179 N89-34794
- A modified VAPEPS method for predicting vibroacoustic response of unreinforced mass loaded honeycomb panels [NASA-TM-101467] p 46 N89-16905
- Annular honeycomb seals: Test results for leakage and rotordynamic coefficients; comparisons to labyrinth and smooth configurations p 185 N89-22899
- Friction factor data for flat plate tests of smooth and honeycomb surfaces [NASA-CR-184977] p 186 N89-23876
- HORIZONTAL FLIGHT**
- Generic icing effects on forward flight performance of a model helicopter rotor p 18 N89-41093
- HORN ANTENNAS**
- Aperture impedance of flared horns p 125 N89-43543
- HOT CORROSION**
- Deposition of Na<sub>2</sub>SO<sub>4</sub> from salt-seeded combustion gases of a high velocity burner rig p 89 N89-12330
- Vapor deposition and condensate flow on combustion turbine blades - Theoretical model to predict/understand some corrosion rate consequences of molten alkali sulfate deposition in the field or laboratory p 21 N89-20950
- Sodium sulfate - Deposition and dissolution of silica p 91 N89-28084
- Transient oxidation of single-crystal beta-NiAl p 98 N89-37899
- Castable hot corrosion resistant alloy [NASA-CASE-LEW-14134-2] p 102 N89-14303
- Hot corrosion of ceramic engine materials [NASA-TM-101439] p 112 N89-16065
- HOT ISOSTATIC PRESSING**
- The influence of high thermal gradient casting, hot isostatic pressing and alternate heat treatment on the structure and properties of a single crystal nickel base superalloy p 97 N89-36427
- Hot isostatic pressing of silicon nitride with boron nitride, boron carbide, and carbon additions p 107 N89-41744
- High-strength silicon carbides by hot isostatic pressing [NASA-TM-101400] p 111 N89-13666
- Strength of hot isostatically pressed and sintered reaction bonded silicon nitrides containing Y<sub>2</sub>O<sub>3</sub> [NASA-TM-101443] p 112 N89-15257
- Effect of processing on fracture toughness of silicon carbide as determined by Vickers indentations [NASA-TM-101456] p 115 N89-21895
- Preparation and evaluation of silicon nitride matrices for silicon nitride-SiC fiber composites [NASA-CR-184798] p 115 N89-23678
- HOT SURFACES**
- Structural analysis methods development for turbine hot section components p 30 N89-20140
- HOUSINGS**
- Strain measurements in a rotary engine housing [SAE PAPER 890333] p 181 N89-51493
- T55-L-712 turbine engine compressor housing refurbishment-plasma spray project [NASA-TM-101310] p 100 N89-10156
- HOVERING**
- Model-based analysis of control/display interaction in the hover task p 215 N89-36933
- HUBS**
- Large-scale Advanced Prop-fan (LAP) hub/blade retention design report [NASA-CR-174786] p 28 N89-19299
- HUMAN PERFORMANCE**
- Age distribution among NASA scientists and engineers p 238 N89-23911
- HUYGENS PRINCIPLE**
- Ray-tube integration in shooting and bouncing ray method p 124 N89-15152
- HYDRAULIC EQUIPMENT**
- The 25 kW solar thermal Stirling hydraulic engine system: Conceptual design [NASA-CR-180889] p 239 N89-14182

## HYDROBROMIDES

## HYDROBROMIDES

Theoretical performance of hydrogen-bromine rechargeable SPE fuel cell — Solid Polymer Electrolyte p 207 A89-23290

## HYDROCARBON COMBUSTION

Effect of alcohol addition on shock-initiated formation of soot from benzene p 90 A89-12903  
NOx formation from the combustion of monodisperse n-heptane sprays doped with fuel-nitrogen additives p 116 A89-42695

## HYDROCARBON FUELS

Liquid oxygen cooling of hydrocarbon fueled rocket thrust chambers [AIAA PAPER 89-2739] p 60 A89-49686  
Liquid oxygen cooling of hydrocarbon fueled rocket thrust chambers [NASA-TM-102113] p 70 N89-24447

## HYDROCARBONS

Surface studies relevant to silicon carbide chemical vapor deposition p 91 A89-27966  
Gas turbine alternative fuels combustion characteristics [NASA-TM-101470] p 210 N89-21417

## HYDRODYNAMIC EQUATIONS

Considerations on the moving contact-line singularity, with application to frictional drag on a slender drop p 144 A89-23238

## HYDROGEN

Preliminary design study of hydrogen and ammonia resistojets for prime and auxiliary thrusters [NASA-CR-182176] p 82 N89-10943  
Space station hydrogen/oxygen thruster technology [NASA-CR-182280] p 74 N89-26905

## HYDROGEN ENGINES

Fueling the National Aero-Space Plane with slush hydrogen [AIAA PAPER 89-5014] p 117 A89-51339  
Advanced technology for future space propulsion systems [NASA-TM-101951] p 66 N89-20192

## HYDROGEN FUELS

Fueling the National Aero-Space Plane with slush hydrogen [AIAA PAPER 89-5014] p 117 A89-51339  
Technology issues associated with fueling the national aerospace plane with slush hydrogen [NASA-TM-101386] p 61 N89-10123  
Antiproton powered propulsion with magnetically confined plasma engines [NASA-CR-185131] p 74 N89-27700

## HYDROGEN OXYGEN ENGINES

Advanced H<sub>2</sub>/O<sub>2</sub> space engine parametrics [AIAA PAPER 89-2300] p 57 A89-46855  
A premixed hydrogen/oxygen catalytic igniter [AIAA PAPER 89-2302] p 59 A89-49683  
Orbit transfer rocket engine technology program. Phase 2: Advanced engine study [NASA-CR-179602] p 61 N89-10119  
Design, fabrication and test of the RL10 derivative II chamber/primary nozzle [NASA-CR-179595] p 68 N89-23519  
The Pathfinder Chemical Transfer Propulsion program [NASA-TM-102084] p 41 N89-24409  
A premixed hydrogen/oxygen catalytic igniter [NASA-CR-185113] p 70 N89-24445  
Advanced APS impacts on vehicle payloads [NASA-TM-102086] p 41 N89-25254

## HYDROGEN OXYGEN FUEL CELLS

Hydrogen-bromine fuel cell advance component development [NASA-TM-101345] p 208 N89-10405

Oxygen electrode bifunctional electrocatalyst NiCo<sub>2</sub>O<sub>4</sub> spinel [NASA-TM-100947] p 208 N89-10409

Mars manned transportation vehicle [NASA-TM-101487] p 210 N89-20545

Cryogenic reactant storage for lunar base regenerative fuel cells [NASA-TM-101980] p 210 N89-21419

Space Electrochemical Research and Technology Conference: Abstracts [NASA-CP-10029] p 211 N89-22982

Hydrogen-oxygen proton-exchange membrane fuel cells and electrolyzers p 211 N89-22996

Summary and evaluation of the Strategic Defense Initiative Space Power Architecture Study [NASA-TM-102012] p 69 N89-24443

## HYDROGEN PLASMA

Antiproton powered propulsion with magnetically confined plasma engines [NASA-CR-185131] p 74 N89-27700

## HYDROXIDES

The effect of different alkali metal hydroxides on nickel electrode life p 207 A89-15280

## HYGRAL PROPERTIES

Mechanics of damping for fiber composite laminates including hygro-thermal effects [AIAA PAPER 89-1191] p 192 A89-30681

## HYPERBOLIC DIFFERENTIAL EQUATIONS

Accurate boundary conditions for exterior problems in gas dynamics p 143 A89-20223  
Global properties of pseudospectral methods p 221 A89-37746

Absorbing boundary conditions for second-order hyperbolic equations [NASA-TM-102009] p 223 N89-22397

## HYPERBOLIC FUNCTIONS

Far field expansion for anisotropic wave equations [AIAA PAPER 102112] p 165 N89-26175

## HYPERCUBE MULTIPROCESSORS

A message passing kernel for the hypercluster parallel processing test bed [NASA-TM-101952] p 218 N89-20684

Initial operating capability for the hypercluster parallel-processing test bed [NASA-TM-101953] p 218 N89-20685

## HYPERSONIC AIRCRAFT

Mach 5 inlet CFD and experimental results [AIAA PAPER 89-2355] p 6 A89-46769

## HYPERSONIC COMBUSTION

Advanced computational techniques for hypersonic propulsion [NASA-TM-102005] p 163 N89-23809

## HYPERSONIC FLIGHT

New hypersonic facility capability at NASA Lewis Research Center [AIAA PAPER 89-2534] p 36 A89-46905

Propulsion over a wide Mach number range [NASA-CR-182267] p 29 N89-20134

New hypersonic facility capability at NASA Lewis Research Center [NASA-TM-102028] p 36 N89-22617

Advanced computational techniques for hypersonic propulsion [NASA-TM-102005] p 163 N89-23809

## HYPERSONIC FLOW

PNS calculations for 3-D hypersonic corner flow with two turbulence models [AIAA PAPER 88-2958] p 1 A89-14979

Three dimensional PNS solutions of hypersonic internal flows with equilibrium chemistry [AIAA PAPER 89-0002] p 146 A89-28401

Interaction of an oblique shock wave with turbulent hypersonic blunt body flows [AIAA PAPER 89-0272] p 3 A89-28405

Three dimensional viscous analysis of a hypersonic inlet [AIAA PAPER 89-0004] p 4 A89-29924

Turbulence modeling in a hypersonic inlet p 8 A89-53931

High speed corner and gap-seal computations using an LU-SGS scheme [AIAA PAPER 89-2669] p 154 A89-54424

Three dimensional viscous analysis of a hypersonic inlet [NASA-TM-101474] p 13 N89-16759

High speed corner and gap-seal computations using an LU-SGS scheme [NASA-TM-102136] p 166 N89-27103

## HYPERSONIC INLETS

Mach 5 inlet CFD and experimental results [AIAA PAPER 89-2355] p 6 A89-46769

Turbulence modeling in a hypersonic inlet p 8 A89-53931

CFD application to supersonic/hypersonic inlet airframe integration — computational fluid dynamics (CFD) p 13 N89-16754

## HYPERSONIC NOZZLES

The effect of adaptive grid on hypersonic nozzle flow calculations [AIAA PAPER 89-0006] p 54 A89-28402

## HYPERSONIC VEHICLES

High angle-of-attack hypersonic aerodynamics p 2 A89-19918

A high heat flux experiment for verification of thermostructural analysis p 148 A89-35002

New hypersonic facility capability at NASA Lewis Research Center [AIAA PAPER 89-2534] p 36 A89-46905

A high heat flux experiment for verification of thermostructural analysis [NASA-TM-100931] p 155 N89-12026

HASA: Hypersonic Aerospace Sizing Analysis for the preliminary design of aerospace vehicles [NASA-CR-182226] p 18 N89-15107

New hypersonic facility capability at NASA Lewis Research Center [NASA-TM-102028] p 36 N89-22617

## HYPERSONIC WIND TUNNELS

New hypersonic facility capability at NASA Lewis Research Center [AIAA PAPER 89-2534] p 36 A89-46905

New hypersonic facility capability at NASA Lewis Research Center [NASA-TM-102028] p 36 N89-22617

## HYPERVELOCITY IMPACT

The effect of the near earth micrometeoroid environment on a highly reflective mirror surface [AIAA PAPER 88-0026] p 40 A89-17939

## HYSTERESIS

NASA Lewis Stirling engine computer code evaluation [NASA-CR-182248] p 214 N89-24741

A data acquisition and control program for axial-torsional fatigue testing [NASA-TM-102041] p 205 N89-28029

## ICE

Calculation of the effects of ice on the backscatter of a ground plane [NASA-CR-183303] p 126 N89-10213

## ICE FORMATION

Navier-Stokes solution to the flowfield over ice accretion shapes p 1 A89-12557

A numerical investigation of the influence of surface roughness on heat transfer in ice accretion [AIAA PAPER 89-0737] p 146 A89-25554

Performance of the forward scattering spectrometer probe in NASA's Icing Research Tunnel [AIAA PAPER 89-0769] p 169 A89-25570

Distributed ice accretion sensor for smart aircraft structures [AIAA PAPER 89-0772] p 17 A89-25571

Investigation of surface water behavior during glaze ice accretion p 16 A89-27739

An overview of the current NASA program on aircraft icing research [SAE PAPER 881386] p 16 A89-28192

Modeling of surface roughness effects on glaze ice accretion [AIAA PAPER 89-0734] p 16 A89-28451

An experimental investigation of multi-element airfoil ice accretion and resulting performance degradation [AIAA PAPER 89-0752] p 4 A89-28453

Determination of longitudinal aerodynamic derivatives using flight data from an icing research aircraft [AIAA PAPER 89-0754] p 34 A89-28454

Investigation of the flow in the diffuser section of the NASA Lewis Icing Research Tunnel [AIAA PAPER 89-0755] p 36 A89-28455

On ice shape prediction methodologies and comparison with experimental data [AIAA PAPER 89-0732] p 16 A89-30850

Calculation of flow over iced airfoils p 5 A89-40905

Generic icing effects on forward flight performance of a model helicopter rotor p 18 A89-41093

Transition limits for water-droplet crystallization with the NASA Lewis icing nozzle p 152 A89-50071

The influence of ice accretion physics on the forecasting of aircraft icing conditions p 16 A89-54803

Performance of the forward scattering spectrometer probe in NASA's icing research tunnel [NASA-TM-101381] p 172 N89-12845

Predictions of airfoil aerodynamic performance degradation due to icing [NASA-TM-101434] p 10 N89-13412

Analytical ice shape predictions for flight in natural icing conditions [NASA-CR-182234] p 18 N89-13428

A numerical simulation of the full two-dimensional electrothermal de-icer pad [NASA-CR-4194] p 19 N89-14235

An experimental investigation of multi-element airfoil ice accretion and resulting performance degradation [NASA-TM-101441] p 12 N89-15084

Determination of longitudinal aerodynamic derivatives using flight data from an icing research aircraft [NASA-TM-101427] p 35 N89-15121

Icing research tunnel test of a model helicopter rotor [NASA-TM-101978] p 29 N89-19305

Electromagnetic properties of ice coated surfaces [NASA-CR-184780] p 127 N89-20355

NASA's program on icing research and technology [NASA-TM-101989] p 1 N89-22569

The low frequency oscillation in the flow over a NACA0012 airfoil with an iced leading edge [NASA-TM-102018] p 14 N89-23417

Investigation of the flow in the diffuser section of the NASA Lewis icing research tunnel [NASA-TM-102087] p 17 N89-25978



## ICE PREVENTION

- A numerical simulation of the full two-dimensional electrothermal de-icer pad  
[NASA-CR-4194] p 19 N89-14235
- NASA's program on icing research and technology  
[NASA-TM-101989] p 1 N89-22569

## IGNITERS

- A premixed hydrogen/oxygen catalytic igniter  
[AIAA PAPER 89-2302] p 59 A89-49683
- A premixed hydrogen/oxygen catalytic igniter  
[NASA-CR-185113] p 70 N89-24445

## IGNITION

- Friction-induced ignition of metals in high-pressure oxygen p 97 A89-32932
- Experiment plans to study preignition processes of a pool fire in low gravity  
[NASA-CR-182256] p 121 N89-19442

## IMPACT DAMAGE

- Vibration testing of impact-damaged composite laminates  
[AIAA PAPER 89-1411] p 81 A89-30883
- Vibration testing of impact-damaged composite laminates  
[NASA-TM-4115] p 87 N89-25290
- Effect of micrometeoroid and space debris impacts on the Space Station Freedom solar array surfaces  
[NASA-TM-102287] p 47 N89-26035

## IMPACT LOADS

- Dynamic delamination buckling in composite laminates under impact loading - Computational simulation p 82 A89-36310

## IMPACT RESISTANCE

- The correlation of low-velocity impact resistance of graphite-fiber-reinforced composites with matrix properties p 79 A89-16283

## IMPEDANCE

- Impedance studies of Ni/Cd and Ni/H cells using the cell case as reference electrode p 137 N89-23002
- Distortion and regulation characterization of a Mapham inverter  
[NASA-TM-102089] p 139 N89-26148

## IMPEDANCE MEASUREMENT

- Impedance studies of Ni/Cd and Ni/H cells using the cell case as reference electrode p 137 N89-23002

## IMPELLERS

- A prediction of 3-D viscous flow and performance of the NASA low-speed centrifugal compressor  
[NASA-CR-184765] p 160 N89-16132
- Rotordynamic Instability Problems in High-Performance Turbomachinery, 1988  
[NASA-CP-3026] p 185 N89-22891

## IMPULSES

- Modeling of pulsed propellant reorientation  
[AIAA PAPER 89-2727] p 61 A89-53306
- Modeling of pulsed propellant reorientation  
[NASA-TM-102117] p 165 N89-26178

## IN-FLIGHT MONITORING

- In-flight measurement of propeller noise on the fuselage of an airplane  
[NASA-TM-102285] p 229 N89-25675

## INCIDENT RADIATION

- Theory and application of radiation boundary operators p 224 A89-24191
- Concentration of off-axis radiation by solar concentrators for space power  
[NASA-TM-102052] p 69 N89-24438

## INCOMPRESSIBLE BOUNDARY LAYER

- An experimental study of a reattaching supersonic shear layer  
[AIAA PAPER 89-1801] p 6 A89-42036

## INCOMPRESSIBLE FLOW

- Unsteady solution of incompressible Navier-Stokes equations p 141 A89-15143
- Development of an integrated BEM approach for hot fluid structure interaction  
[NASA-CR-184587] p 27 N89-15114
- Least-squares finite element method for fluid dynamics  
[NASA-TM-102352] p 223 N89-30008

## INCOMPRESSIBLE FLUIDS

- Instabilities caused by oscillating accelerations normal to a viscous fluid-fluid interface p 144 A89-22823

## INDEXES (DOCUMENTATION)

- Bibliography of Lewis Research Center technical publications announced in 1986  
[NASA-TM-89887] p 238 N89-18259

## INDIUM ANTIMONIDES

- Molecular beam epitaxial growth of high-quality InSb on InP and GaAs substrates  
[NASA-CR-185440] p 236 N89-26739
- Surface morphologies and electrical properties of molecular beam epitaxial InSb and InAs(x)Sb(1-x) grown on GaAs and InP substrates  
[NASA-CR-185439] p 237 N89-26740

## INDIUM ARSENIDES

- Shubnikov-de Haas measurements of the 2-D electron gas in pseudomorphic In(0.1)Ga(0.9)As grown on GaAs  
[NASA-CR-185439] p 235 A89-29299
- Surface morphologies and electrical properties of molecular beam epitaxial InSb and InAs(x)Sb(1-x) grown on GaAs and InP substrates  
[NASA-CR-185439] p 237 N89-26740

## INDIUM PHOSPHIDES

- Progress in InP solar cell research p 130 A89-15306
- Plasma deposited silicon nitride for indium phosphide encapsulation p 235 A89-27794
- The effect of metal surface passivation on the Au-InP interaction p 132 A89-30443
- High-efficiency solar cells fabricated from direct-current magnetron sputtered n-indium tin oxide onto p-InP grown by atmospheric pressure metalorganic vapor phase epitaxy p 133 A89-44518
- High-efficiency indium tin oxide/indium phosphide solar cells p 208 A89-44883
- InP homojunction solar cell performance on the LIPS 3 flight experiment  
[NASA-TM-101390] p 209 N89-12123
- Radiation resistance and comparative performance of ITO/InP and n/p InP homojunction solar cells  
[NASA-TM-101387] p 135 N89-12819
- The NASA Space Solar Cell Advanced Research Program  
[NASA-TM-102020] p 67 N89-22651
- InP (Indium Phosphide): Into the future  
[NASA-TM-102058] p 212 N89-23025
- Progress in indium phosphide solar cell research p 212 N89-24707
- Predicted performance of InP solar cells in Cassagrainian and slats space concentrator arrays at 20 to 100 AMO, 80 to 100 C p 212 N89-24711
- On-orbit results of the LIPS 3/InP homojunction solar cell experiment  
[NASA-TM-102131] p 214 N89-26292
- Molecular beam epitaxial growth of high-quality InSb on InP and GaAs substrates  
[NASA-CR-185440] p 236 N89-26739
- Indium phosphide solar cell research in the US: Comparison with nonphotovoltaic sources  
[NASA-TM-102103] p 124 N89-27868

## INDUCTION MOTORS

- Variable speed induction motor operation from a 20-kHz power bus  
[NASA-TM-102061] p 71 N89-25271

## INELASTIC STRESS

- On 3D inelastic analysis methods for hot section components p 196 N89-12906
- Considerations in development and implementation of elasto-viscoplastic constitutive model for high temperature applications  
[NASA-CR-183403] p 197 N89-12932
- Use of inelastic strain as a basis for analyzing thermomechanical test data p 200 N89-17326
- Procedures for characterizing an alloy and predicting cyclic life with the total strain version of Strainrange Partitioning  
[NASA-TM-4102] p 203 N89-25485

## INFLUENCE COEFFICIENT

- Investigation of oscillating cascade aerodynamics by an experimental influence coefficient technique  
[AIAA PAPER 88-2815] p 1 A89-14976

## INFRARED ABSORPTION

- Alkoxysilane adsorption on metal oxide substrates p 92 A89-44536

## INFRARED IMAGERY

- Development of an infrared imaging system for the surface tension driven convection experiment  
[NASA-TM-101479] p 174 N89-17211
- Infrared surface temperature measurements for the surface tension driven convection experiment  
[NASA-TM-101353] p 175 N89-21224

## INFRARED INSTRUMENTS

- Surface temperature determination in surface analytic systems by infrared optical pyrometry p 169 A89-17347

## INFRARED RADIOMETERS

- Determination of combustion gas temperatures by infrared radiometry in sooting and nonsooting flames  
[NASA-TP-2900] p 164 N89-25409

## INFRARED REFLECTION

- Alkoxysilane adsorption on metal oxide substrates p 92 A89-44536

## INFRARED SPECTRA

- Gas particle radiator  
[NASA-CASE-LEW-14297-1] p 172 N89-12048

## INGESTION (ENGINES)

- STOL and STOVL hot gas ingestion and airframe heating tests in the NASA Lewis 9- by 15-foot low-speed wind tunnel  
[NASA-TM-102101] p 15 N89-29323

## INGOTS

- Computer simulation of macrosegregation in directionally solidified circular ingots  
[NASA-CR-182838] p 122 N89-21134

## INJECTION MOLDING

- Improved silicon carbide for advanced heat engines. I - Process development for injection molding p 106 A89-33619
- Improved silicon carbide for advanced heat engines  
[NASA-CR-179477] p 112 N89-15251

## INJECTORS

- A premixed hydrogen/oxygen catalytic igniter  
[AIAA PAPER 89-2302] p 59 A89-49683
- Application of advanced diagnostics to airblast injector flows p 160 N89-17306
- A premixed hydrogen/oxygen catalytic igniter  
[NASA-CR-185113] p 70 N89-24445

## INLET AIRFRAME CONFIGURATIONS

- Computational methods for inlet airframe integration p 13 N89-16752
- CFD application to subsonic inlet airframe integration --- computational fluid dynamics (CFD) p 13 N89-16753
- CFD application to supersonic/hypersonic inlet airframe integration --- computational fluid dynamics (CFD) p 13 N89-16754

## INLET FLOW

- High speed inlet calculations with real gas effects  
[AIAA PAPER 88-3076] p 2 A89-14980
- Turbine-stage heat transfer - Comparison of short-duration measurements with state-of-the-art predictions p 142 A89-16458
- Three dimensional viscous analysis of a hypersonic inlet  
[AIAA PAPER 89-0004] p 4 A89-29924
- Calculations of inlet distortion induced compressor flow field instability p 8 A89-52498
- A preliminary design study of supersonic through-flow fan inlets  
[NASA-CR-182224] p 24 N89-11751
- Influence of bulk turbulence and entrance boundary layer thickness on the curved duct flow field p 156 N89-12896

- Isolated testing of highly maneuverable inlet concepts  
[NASA-CR-179544] p 26 N89-13437
- The effects of inlet turbulence and rotor/stator interactions on the aerodynamics and heat transfer of a large-scale rotating turbine model, volume 1  
[NASA-CR-4079] p 159 N89-13756
- Experimental results for a two-dimensional supersonic inlet used as a thrust deflecting nozzle  
[NASA-TM-83439] p 159 N89-14386
- Measurement of airfoil heat transfer coefficients on a turbine stage p 180 N89-17311
- Advanced computational techniques for hypersonic propulsion  
[NASA-TM-102005] p 163 N89-23809

## INLET PRESSURE

- Friction factor data for flat plate tests of smooth and honeycomb surfaces  
[NASA-CR-184977] p 186 N89-23876

## INORGANIC CHEMISTRY

- Structural chemistry of Au(III)-substituted Ba<sub>2</sub>YCu<sub>3</sub>O(7- $\delta$ ) p 89 A89-12620

## INORGANIC SULFIDES

- High temperature thermal conductivity measurements on lanthanum sulfides using the flash method p 77 A89-16500

## INSOLATION

- The Mars climate for a photovoltaic system operation  
[IAF PAPER ICOSP89-9-5] p 241 A89-46529
- The Mars climate for a photovoltaic system operation  
[NASA-TM-101994] p 136 N89-20385
- Solar radiation on Mars  
[NASA-TM-102299] p 242 N89-27623

## INSTRUMENT ERRORS

- An improved correction algorithm for number density measurements made with the forward scattering spectrometer probe p 170 A89-44122
- A correction algorithm for particle size distribution measurements made with the forward-scattering spectrometer probe p 170 A89-44123
- Parametric study of statistical bias in laser Doppler velocimetry p 171 A89-47378

## INSTRUMENT PACKAGES

- HOST instrumentation R and D program overview p 25 N89-12878

## INSULATION

- The effect of insulated combustion chamber surfaces on direct-injected diesel engine performance, emissions, and combustion  
[NASA-CR-182204] p 239 N89-17548

## INTAKE SYSTEMS

- Three dimensional viscous analysis of a hypersonic inlet  
[AIAA PAPER 89-0004] p 4 A89-29924

# INTEGRAL EQUATIONS

- Isolated testing of highly maneuverable inlet concepts [NASA-CR-179544] p 26 N89-13437
- Hot gas ingestion testing of an advanced STOV concept in the NASA Lewis 9- by 15-foot low speed wind tunnel with flow visualization [NASA-TM-100952] p 11 N89-15078
- Three dimensional viscous analysis of a hypersonic inlet [NASA-TM-101474] p 13 N89-16759
- INTEGRAL EQUATIONS**
- Three-dimensional marginal separation [NASA-TM-101411] p 159 N89-13757
- INTEGRALS**
- Elevated temperature crack growth p 200 N89-17335
- INTEGRATED CIRCUITS**
- GaAs MMIC elements in phased-array antennas p 131 A89-15827
- GaAs circuits for monolithic optical controller p 131 A89-15828
- External electro-optic probing of millimeter-wave integrated circuits p 133 A89-45266
- The potential impact of MMICs on future satellite communications [NASA-CR-182227] p 126 N89-17078
- The potential impact of MMICs on future satellite communications: Executive summary [NASA-CR-182227-EXEC-SUMM] p 127 N89-17079
- Universal test fixture for monolithic mm-wave integrated circuits calibrated with an augmented TRD algorithm [NASA-TP-2875] p 127 N89-17767
- External electro-optic probing of millimeter-wave integrated circuits [NASA-TM-101990] p 128 N89-21142
- Optical detectors for GaAs MMIC integration: Technology assessment [NASA-TM-102025] p 137 N89-22020
- Microwave characteristics of GaAs MMIC integratable optical detectors [NASA-TM-101485] p 129 N89-24520
- INTEGRATED OPTICS**
- Optical detectors for GaAs MMIC integration: Technology assessment [NASA-TM-102025] p 137 N89-22020
- INTERACTIONAL AERODYNAMICS**
- Three dimensional simulation of an underexpanded jet interacting with a supersonic cross flow [AIAA PAPER 88-3181] p 2 A89-14982
- Propeller/wing interaction [AIAA PAPER 89-0535] p 17 A89-25429
- Interaction of an oblique shock wave with turbulent hypersonic blunt body flows [AIAA PAPER 89-0272] p 3 A89-28405
- Experimental and numerical investigation of an oblique shock wave/turbulent boundary layer interaction with continuous suction [AIAA PAPER 89-0357] p 4 A89-28407
- Fluctuating pressures on wing surfaces in the slipstream of a single-rotor propfan [AIAA PAPER 89-1058] p 226 A89-36218
- Explicit Runge-Kutta method for unsteady rotor/stator interaction p 5 A89-36912
- Average-passage simulation of counter-rotating propfan propulsion systems as applied to cruise missiles [AIAA PAPER 89-2943] p 7 A89-47187
- Aerodynamic interaction between propellers and wings p 8 A89-50062
- An LDA (Laser-Doppler Anemometry) investigation of three-dimensional normal shock wave boundary-layer interactions p 14 N89-20956
- Average-passage simulation of counter-rotating propfan propulsion systems as applied to cruise missiles [NASA-TM-102043] p 14 N89-23416
- High speed turboprop aeroacoustic study (single rotation). Volume 1: Model development [NASA-CR-182257-VOL-1] p 229 N89-24139
- INTERACTIVE CONTROL**
- Application of a lower-upper implicit scheme and an interactive grid generation for turbomachinery flow field simulations [NASA-TM-101412] p 11 N89-15077
- INTERATOMIC FORCES**
- Connection between energy relations of solids and molecules p 91 A89-26406
- INTERCALATION**
- Synthesis and stability of Br<sub>2</sub>, ICl and IBr intercalated pitch-based graphite fibers p 106 A89-37670
- Effect of length of chopped pristine and intercalated graphite fibers on the resistivity of fiber networks [NASA-TM-101395] p 84 N89-11826
- Technological hurdles to the application of intercalated graphite fibers [NASA-TM-101394] p 108 N89-11911
- INTERFACE STABILITY**
- Heat of mixing and morphological stability p 143 A89-21296

# INTERFACES

- The development of an intelligent interface to a computational fluid dynamics flow-solver code p 216 A89-16963
- Interfacial adhesion - Theory and experiment p 97 A89-35307
- Auger analysis of a fiber/matrix interface in a ceramic matrix composite p 82 A89-35311
- Identification of structural interface characteristics using component mode synthesis p 193 A89-36177
- A novel approach in formulation of special transition elements: Mesh interface elements [NASA-CR-184768] p 199 N89-16193
- Interfacing laboratory instruments to multiuser, virtual memory computers [NASA-TM-4106] p 188 N89-19578
- Optimum interface properties for metal matrix composites [NASA-TM-102295] p 205 N89-27223
- INTERFACIAL TENSION**
- On the wind force needed to dislodge a drop adhered to a surface p 144 A89-22819
- Hardware development for the Surface Tension Driven Convection Experiment aboard the USML-1 Spacelab mission [AIAA PAPER 89-0406] p 47 A89-25341
- Hardware development for the surface tension driven convection experiment aboard the USML-1 spacelab mission [NASA-TM-101404] p 48 N89-11804
- Development of an infrared imaging system for the surface tension driven convection experiment [NASA-TM-101479] p 174 N89-17211
- Infrared surface temperature measurements for the surface tension driven convection experiment [NASA-TM-101353] p 175 N89-21224
- Finite element modeling of frictionally restrained composite interfaces [NASA-CR-182281] p 203 N89-23918
- INTERFERENCE IMMUNITY**
- An experimental adaptive array to suppress weak interfering signals p 124 A89-22455
- INTERGRANULAR CORROSION**
- A preliminary report on the effects of long-term exposure of LiOH on pure nickel p 90 A89-12624
- Failure analysis of a Stirling engine heat pipe [NASA-TM-101418] p 103 N89-20227
- INTERMETALLICS**
- Mechanisms of elevated-temperature deformation in the B2 aluminides NiAl and CoAl p 94 A89-17378
- Microstructures in rapidly solidified niobium aluminides p 95 A89-18193
- Interdiffusional effects between TiBe12 and NiAl intermetallics p 95 A89-21395
- Transient oxidation of single-crystal beta-NiAl p 98 A89-37899
- TEM studies of oxidized NiAl and Ni3Al cross sections p 99 A89-46506
- The oxidation of Ni-rich Ni-Al intermetallics [NASA-TM-101455] p 102 N89-15233
- Theoretical analysis of compatibility of several reinforcement materials with NiAl and FeAl matrices [NASA-CR-182291] p 86 N89-23622
- Characterization of ceramics and intermetallics fabricated by self-propagating high-temperature synthesis [NASA-TM-102004] p 78 N89-25285
- Intermetallic and ceramic matrix composites for 815 to 1370 C (1500 to 2500 F) gas turbine engine applications [NASA-TM-102326] p 88 N89-29490
- INTERNAL COMBUSTION ENGINES**
- Engineering study of the rotary-vee engine concept [NASA-TM-101995] p 33 N89-26007
- INTERNAL WAVES**
- Numerical investigation of an internal layer in turbulent flow over a curved hill [NASA-TM-102230] p 168 N89-29725
- INTERPLANETARY FLIGHT**
- Nuclear thermal rockets - Next step to space p 55 A89-40480
- Nuclear propulsion: A vital technology for the exploration of Mars and the planets beyond [NASA-TM-101354] p 62 N89-10944
- INTERPOLATION**
- Universal limiter for transient interpolation modeling of the advective transport equations: The ULTIMATE conservative difference scheme [NASA-TM-100916] p 222 N89-14794
- On the applications of algebraic grid generation methods based on transfinite interpolation [NASA-TM-102095] p 33 N89-26003
- Specialty functions singularity mechanics problems p 206 N89-29805
- Multi-grid for structures analysis p 206 N89-29810

# INTERPROCESSOR COMMUNICATION

- Observer design for compensation of network-induced delays in integrated communication and control systems p 220 A89-35044
- INTERSTELLAR CHEMISTRY**
- Formation of polycyclic aromatic hydrocarbons in circumstellar envelopes p 241 A89-41385
- INTRAVEHICULAR ACTIVITY**
- The impact of an IVA robot on the Space Station microgravity environment [AIAA PAPER 89-0596] p 44 A89-28438
- INVERTED CONVERTERS (DC TO AC)**
- Simulation and control of a 20 kHz spacecraft power system p 130 A89-15391
- A design procedure for the phase-controlled parallel-loaded resonant inverter p 134 A89-50472
- INVERTERS**
- Distortion and regulation characterization of a Mapham inverter [NASA-TM-102089] p 139 N89-26148
- Frequency domain model for analysis of paralleled, series-output-connected Mapham inverters [NASA-TM-102140] p 139 N89-26149
- INVISID FLOW**
- Boundary layer effects on particle impaction and capture p 143 A89-19123
- A detailed analysis of inviscid flux splitting algorithms for real gases with equilibrium or finite-rate chemistry p 151 A89-45424
- Numerical analysis of supersonic flow through oscillating cascade sections by using a deforming grid [AIAA PAPER 89-2805] p 8 A89-50810
- A numerical method for computing unsteady 2-D boundary layer flows [NASA-CR-4198] p 155 N89-12835
- Turbofan forced mixer lobe flow modeling. 2: Three-dimensional inviscid mixer analysis (FLOMIX) [NASA-CR-4147-PT-2] p 11 N89-14222
- Conservative treatment of boundary interfaces for overlaid grids and multi-level grid adaptations [NASA-TM-102080] p 15 N89-24269
- Numerical analysis of supersonic flow through oscillating cascade sections by using a deforming grid [NASA-TM-102053] p 15 N89-25119
- Multigrid calculation of three-dimensional turbomachinery flows [NASA-CR-185332] p 165 N89-26172
- ION ACCELERATORS**
- Thermal mechanical analyses of large diameter ion accelerator systems [AIAA PAPER 89-2718] p 58 A89-47041
- ION BEAMS**
- Pulsed ion beam investigation of the kinetics of surface reactions p 93 A89-44542
- The divergence characteristics of constrained-sheath optics systems for use with 5-eV atomic oxygen sources [NASA-CR-185332] p 229 N89-19973
- Simulation of the low earth orbital atomic oxygen interaction with materials by means of an oxygen ion beam [NASA-TM-101971] p 114 N89-21104
- ION ENGINES**
- Performance of 10-kW class xenon ion thrusters [AIAA PAPER 89-2914] p 48 A89-14978
- A detailed model of ion propulsion systems [AIAA PAPER 89-2268] p 56 A89-46712
- A 50 cm diameter annular ion engine [AIAA PAPER 89-2716] p 57 A89-47039
- Ion optics for high power 50-cm-dia ion thrusters [AIAA PAPER 89-2717] p 58 A89-47040
- Thermal mechanical analyses of large diameter ion accelerator systems [AIAA PAPER 89-2718] p 58 A89-47041
- The NASA Electric Propulsion Program p 59 A89-47428
- Closed-drift thruster investigations [NASA-CR-179497] p 62 N89-11808
- Mercury ion thruster technology [NASA-CR-174974] p 66 N89-21834
- Performance of large area xenon ion thrusters for orbit transfer missions [NASA-TM-102049] p 69 N89-24436
- Structural and thermal response of 30 cm diameter ion thruster optics [NASA-TM-102124] p 75 N89-27703
- Ion optics for high power 50-cm-dia ion thrusters [NASA-TM-102143] p 76 N89-28571
- ION EXCHANGE MEMBRANE ELECTROLYTES**
- Hydrogen-oxygen proton-exchange membrane fuel cells and electrolyzers p 211 N89-22996
- ION IMPLANTATION**
- Plasma deposited silicon nitride for indium phosphide encapsulation p 235 A89-27794

# ION PLATING

Secondary electron emission characteristics of untreated and ion-textured titanium [NASA-TP-2902] p 103 N89-17650

# ION PROPULSION

A detailed model of ion propulsion systems [AIAA PAPER 89-2268] p 56 A89-46712  
Ion optics for high power 50-cm-dia ion thrusters [AIAA PAPER 89-2717] p 58 A89-47040

Closed-drift thruster investigations [NASA-CR-179497] p 62 N89-11808

A data acquisition and storage system for the ion auxiliary propulsion system cyclic thruster test [NASA-TM-101469] p 218 N89-17424

Advanced technology for future space propulsion systems [NASA-TM-101951] p 66 N89-20192

Mercury ion thruster technology [NASA-CR-174974] p 66 N89-21834

Performance of large area xenon ion thrusters for orbit transfer missions [NASA-TM-102049] p 69 N89-24436

Ion optics for high power 50-cm-dia ion thrusters [NASA-TM-102143] p 76 N89-28571

# IONOSPHERIC CURRENTS

Bounds on current collection from the far field by plasma clouds in the ionosphere p 214 A89-34791

# IONOSPHERIC ELECTRON DENSITY

The POLAR code wake model - Comparison with in situ observations --- Shuttle Orbiter plasma wake ion and electron density simulation p 233 A89-45632

Plasma density, temperature and turbulence in the wake of the Shuttle Orbiter p 233 A89-53209

# IONOSPHERIC ION DENSITY

Induced emission of radiation from a large space-station-like structure in the ionosphere p 44 A89-31915

The POLAR code wake model - Comparison with in situ observations --- Shuttle Orbiter plasma wake ion and electron density simulation p 233 A89-45632

# IRON

Thermodynamic analysis of compatibility of several reinforcement materials with FeAl alloys [NASA-CR-4172] p 83 N89-10128

# IRON ALLOYS

Iron-base superalloys - A phase analysis of the multicomponent system (Fe-Mn-Cr-Mo-Nb-Al-Si-C) p 95 A89-17379

The influence of annealing in the ferrite-plus-austenite phase field on the stability of vanadium carbide precipitates p 97 A89-32803

Kinetics of fracture in Fe-3Si steel under mode I loading p 99 A89-47320

Oxidation behavior of FeAl + Hf,Zr,B [NASA-TM-101402] p 102 N89-14297

Theoretical analysis of compatibility of several reinforcement materials with NiAl and FeAl matrices [NASA-CR-182291] p 86 N89-23622

# IRRADIATION

Stability of bulk Ba<sub>2</sub>YCu<sub>3</sub>O(7-x) in a variety of environments [NASA-TM-101401] p 111 N89-14310

Radiation resistance studies of amorphous silicon films p 213 N89-24738

# ISOTHERMAL FLOW

Experimental study of isothermal swirling flows in a dump combustor p 21 A89-23182

# ISOTHERMAL PROCESSES

Aerodynamically-driven condensate layer thickness distributions on isothermal cylindrical surfaces p 140 A89-12337

Isothermal and 'bithermal' thermomechanical fatigue behavior of a NiCoCrAlY-coated single crystal superalloy p 177 A89-36457

Thermomechanical characterization of Hastelloy-X under uniaxial cyclic loading p 196 N89-12909

Non-isothermal buckling behavior of viscoplastic shell structures [NASA-CR-183013] p 197 N89-12931

Use of inelastic strain as a basis for analyzing thermomechanical test data p 200 N89-17326

Isothermal dendritic growth: A low gravity experiment p 121 N89-20299

Isothermal solidification in a binary alloy melt p 121 N89-20300

# ISOTROPIC MEDIA

Material parameter determination from scattering measurements [NASA-CR-183312] p 126 N89-10225

Constitutive modeling for isotropic materials p 195 N89-12904

A multi-axial theory of viscoplasticity for isotropic materials p 196 N89-12908

# ISOTROPY

Creep fatigue life prediction for engine hot section materials (ISOTROPIC) fifth year progress review p 201 N89-17336

# ITERATION

Three-dimensional marginal separation [NASA-TM-101411] p 159 N89-13757

# ITERATIVE SOLUTION

An approach to probabilistic finite element analysis using a mixed-iterative formulation p 191 A89-25849

# ITO (SEMICONDUCTORS)

High-efficiency indium tin oxide/indium phosphide solar cells p 208 A89-44883

# J

# J INTEGRAL

Kinetics of fracture in Fe-3Si steel under mode I loading p 99 A89-47320

Fracture mechanics applied to elevated temperature crack growth p 195 A89-47705

# JAMMING

Analysis of modified SMI method for adaptive array weight control [NASA-CR-184904] p 127 N89-20364

# JET AIRCRAFT

Fiber optic control system integration [NASA-CR-179568] p 231 N89-13256

# JET AIRCRAFT NOISE

Rectangular nozzle plume velocity modeling for use in jet noise prediction [AIAA PAPER 89-2357] p 7 A89-46771

Supersonic jet noise and the high speed civil transport [AIAA PAPER 89-2358] p 227 A89-46772

Rectangular nozzle plume velocity modeling for use in jet noise prediction [NASA-TM-102047] p 14 N89-22577

# JET ENGINE FUELS

Experimental verification of the thermodynamic properties for a jet-A fuel [NASA-TM-101475] p 117 N89-17017

Fuel-rich catalytic combustion of Jet-A fuel-equivalence ratios 5.0 to 8.0 [NASA-TM-101975] p 93 N89-21051

# JET ENGINES

Advanced H<sub>2</sub>/O<sub>2</sub> space engine parametrics [AIAA PAPER 89-2300] p 57 A89-46855

Sensor failure detection for jet engines [NASA-TM-101396] p 25 N89-13432

Computational structural mechanics engine structures computational simulator p 205 N89-29792

# JET FLOW

Thermal measurements for jets in disturbed and undisturbed crosswind conditions p 20 A89-16102

Large amplitude acoustic excitation of swirling turbulent jets [AIAA PAPER 89-0970] p 4 A89-29098

Effects of core turbulence on jet excitability [AIAA PAPER 89-0966] p 147 A89-30482

Multiple coherent mode interaction in a developing round jet [AIAA PAPER 89-0967] p 147 A89-30483

Subharmonic and fundamental high amplitude excitation of an axisymmetric jet [AIAA PAPER 89-0993] p 149 A89-37825

A numerical and experimental study of confined swirling jets [AIAA PAPER 89-2898] p 151 A89-47161

Effects of core turbulence on jet excitability [NASA-TM-101405] p 159 N89-14403

Lubricant jet flow phenomena in spur and helical gears with modified addendums; for radially directed individual jets [NASA-TM-101460] p 183 N89-15415

Aerothermal modeling program. Phase 2, element B: Flow interaction experiment p 160 N89-17304

Large amplitude acoustic excitation of swirling turbulent jets [NASA-TM-101950] p 13 N89-18417

On the conditions for resonance interactions of instability waves in the axisymmetric jet [NASA-TM-101477] p 162 N89-21196

Turbulent swirling jets with excitation [NASA-CR-180895] p 16 N89-29329

# JET MIXING FLOW

Shock-wave-induced mixing enhancement in scramjet combustors [AIAA PAPER 89-0104] p 145 A89-25091

Effect of initial swirl distribution on the evolution of a turbulent jet p 149 A89-36906

Effects of nozzle exit boundary-layer conditions on excitability of heated free jets p 149 A89-36908

Numerical studies of the effects of jet-induced mixing on liquid-vapor interface condensation [AIAA PAPER 89-1744] p 152 A89-48958

Aerothermal modeling program, phase 2. Element C: Fuel injector-air swirl characterization p 156 N89-12892

Numerical studies of the effects of jet-induced mixing on liquid-vapor interface condensation [NASA-CR-182285] p 163 N89-23818

# JET NOZZLES

The effect of electrode configuration on arcjet performance [AIAA PAPER 89-2722] p 58 A89-47044

# JET PROPULSION

Advanced core technology: Key to subsonic propulsion benefits [NASA-TM-101420] p 26 N89-14237

# JOINING

Optically interconnected phased arrays p 132 A89-33696

# JOINTS (JUNCTIONS)

Thermal-mechanical fatigue test apparatus for metal matrix composites and joint attachments p 79 A89-15727

Identification of structural interface characteristics using component mode synthesis p 193 A89-36177

Improving the fatigue resistance of adhesive joints in laminated wood structures [NASA-CR-182165] p 85 N89-12675

# JOURNAL BEARINGS

The solution of the Elrod algorithm for a dynamically loaded journal bearing using multigrid techniques [ASME PAPER 88-TRIB-23] p 148 A89-34795

On the performance of finite journal bearings lubricated with micropolar fluids p 181 A89-54977

Stability of a rigid rotor supported on oil-film journal bearings under dynamic load [NASA-TM-102309] p 166 N89-27114

# K

# K-EPSILON TURBULENCE MODEL

Axisymmetric confined turbulent jet directed towards the liquid surface from below [AIAA PAPER 89-0172] p 145 A89-25148

A diagonally inverted LU implicit multigrid scheme for the 3-D Navier-Stokes equations and a two equation model of turbulence [AIAA PAPER 89-0467] p 145 A89-25382

A numerical and experimental study of coaxial jets p 153 A89-52500

A diagonally inverted LU implicit multigrid scheme for the 3-D Navier-Stokes equations and a two equation model of turbulence [NASA-CR-182209] p 9 N89-10863

A near-wall turbulence model and its application to fully developed turbulent channel and pipe flows [NASA-TM-101399] p 158 N89-13741

Axisymmetric confined turbulent jet directed towards the liquid surface from below [NASA-TM-101409] p 158 N89-13749

Transonic viscous flow calculations for a turbine cascade with a two equation turbulence model [NASA-TM-101944] p 32 N89-22607

# KAPTON (TRADEMARK)

Undercutting of defects in thin film protective coatings on polymer surfaces exposed to atomic oxygen [NASA-TM-101986] p 115 N89-23691

# KEROSENE

High-pressure calorimeter chamber tests for liquid oxygen/kerosene (LOX/RP-1) rocket combustion [NASA-TP-2862] p 65 N89-15979

# KINEMATICS

Simple high-accuracy resolution program for convective modelling of discontinuities p 143 A89-17459

Engineering study of the rotary-vee engine concept [NASA-TM-101995] p 33 N89-26007

# KINETIC ENERGY

Kinetic energy equations for the average-passage equation system p 237 A89-28347

# KINETIC EQUATIONS

Kinetic energy equations for the average-passage equation system p 237 A89-28347

# KINETIC THEORY

Flow of rarefied gases over two-dimensional bodies [AIAA PAPER 89-1970] p 5 A89-41814

# KNOWLEDGE BASES (ARTIFICIAL INTELLIGENCE)

Expert systems applied to spacecraft fire safety [NASA-CR-182266] p 42 N89-23501

# L

# LABYRINTH SEALS

Experimental results for labyrinth gas seals with honeycomb stators - Comparisons to smooth-stator seals and theoretical predictions [ASME PAPER 88-TRIB-40] p 179 A89-24992

Annular honeycomb seals: Test results for leakage and rotordynamic coefficients; comparisons to labyrinth and smooth configurations p 185 N89-22899

**LAMINAR BOUNDARY LAYER**

Discussion of Mills et al. on 'The effect of wall suction and thermophoresis on aerosol particle deposition from a laminar boundary layer on a flat plate'

p 140 A89-12331  
Effect of particulate thermophoresis in reducing the fouling rate advantages of effusion-cooling p 141 A89-14599

Viscous dissipation effects on thermophoretically augmented aerosol particle transport across laminar boundary layers p 141 A89-14600

Viscous analysis of high speed flows using an upwind finite volume technique p 144 A89-25001 [AIAA PAPER 89-0001]

Boundary-layer receptivity to long-wave free-stream disturbances p 146 A89-28996

A Newton/upwind method and numerical study of shock wave/boundary layer interactions p 6 A89-45468

The response of a laminar boundary layer in supersonic flow to small amplitude progressive waves [NASA-TM-101965] p 162 N89-21197

On the Lagrangian description of unsteady boundary layer separation. Part 1: General theory p 164 N89-23821 [NASA-TM-102026]

Some characteristics of bypass transition in a heated boundary layer p 164 N89-24577 [NASA-TM-102126]

**LAMINAR FLOW**

Studies of transition in boundary layers [AIAA PAPER 89-0034] p 2 A89-25029

Control of laminar separation over airfoils by acoustic excitation [AIAA PAPER 89-0565] p 3 A89-25454

Application of multi-grid methods for solving the Navier-Stokes equations p 153 A89-53172

Control of laminar separation over airfoils by acoustic excitation [NASA-TM-101379] p 9 N89-12552

Two- and three-dimensional turbine blade row flow field simulations p 161 N89-17313

Control-volume based Navier-Stokes equation solver valid at all flow velocities [NASA-TM-101488] p 161 N89-20407

**LAMINAR MIXING**

Effects of excitation level on the stability of an axisymmetric mixing layer p 2 A89-16882

**LAMINATES**

Composite interlaminar fracture toughness - Three-dimensional finite-element modeling for mixed mode I, II, and fracture p 190 A89-16278

Mechanics of damping for fiber composite laminates including hygro-thermal effects [AIAA PAPER 89-1191] p 192 A89-30681

Structural behavior of composites with progressive fracture [AIAA PAPER 89-1271] p 192 A89-30754

Structural tailoring of laminate properties [AIAA PAPER 89-1367] p 192 A89-30842

Vibration testing of impact-damaged composite laminates [AIAA PAPER 89-1411] p 81 A89-30883

Microlaminate composites as thermal barrier coatings p 83 A89-54261

Laminate behavior for SiC fiber-reinforced reaction-bonded silicon nitride matrix composites [NASA-TM-101350] p 84 N89-10952

Improving the fatigue resistance of adhesive joints in laminated wood structures [NASA-CR-182165] p 85 N89-12675

Vibration testing of impact-damaged composite laminates [NASA-TM-4115] p 87 N89-25290

Tailoring of composite links for optimal damped elastodynamic performance [NASA-TM-102094] p 88 N89-26912

**LAND ICE**

Data report for the Siple Coast (Antarctica) project [NASA-TM-100708] p 206 N89-10403

**LANDING**

High-speed propeller performance and noise predictions at takeoff/landing conditions p 226 A89-39195

**LANDING MODULES**

NASA's Chemical Transfer Propulsion Program for Pathfinder [NASA-TM-102298] p 41 N89-26876

**LANTHANUM COMPOUNDS**

High temperature thermal conductivity measurements on lanthanum sulfides using the flash method p 77 A89-16500

**LARGE SPACE STRUCTURES**

Large structure current collection in plasma environments [AIAA PAPER 89-0496] p 44 A89-25405

Induced emission of radiation from a large space-station-like structure in the ionosphere p 44 A89-31915

Big savings from small holes --- Liquid Droplet Radiator project for space vehicles p 45 A89-36724

**LASER ANEMOMETERS**

Comparison of the bidirectional reflectance distribution function of various surfaces p 230 A89-41530

Three component laser anemometer measurements in an annular cascade of core turbine vanes with contoured end wall [NASA-TP-2846] p 9 N89-10844

Laser anemometry: A status report p 177 N89-12885

Advanced high temperature instrument for hot section research applications p 29 N89-20137

An LDA (Laser-Doppler Anemometry) investigation of three-dimensional normal shock wave boundary-layer interactions p 14 N89-20956

A vector scanning processing technique for pulsed laser velocimetry [NASA-TM-102048] p 175 N89-23850

**LASER APPLICATIONS**

Optical experiments on thermophoretically augmented submicron particle deposition from 'dusty' high temperature gas flows p 90 A89-14799

Optical measurements of soot and temperature profiles in premixed propane-oxygen flames p 92 A89-35008

High temperature optical strain measurement system p 170 A89-43842

**LASER BEAMS**

Application of optical correlation techniques to particle imaging [AIAA PAPER 88-4661] p 169 A89-14985

High-temperature LDV seed particle development [NASA-CR-182265] p 175 N89-23851

**LASER DOPPLER VELOCIMETERS**

Performance of laser Doppler velocimeter with polydisperse seed particles in high-speed flows p 169 A89-22279

Laser velocimeter measurements of the flowfield generated by an advanced counterrotating propeller [AIAA PAPER 89-0434] p 3 A89-26373

The turbulence characteristics of a separated flow with combustion p 92 A89-33369

A numerical and experimental study of confined swirling jets [AIAA PAPER 89-2898] p 151 A89-47161

Parametric study of statistical bias in laser Doppler velocimetry p 171 A89-47378

Stratified charge rotary engine - Internal flow studies at the MSU engine research laboratory [SAE PAPER 890331] p 181 A89-51477

Laser velocimeter measurements of the flowfield generated by an advanced counterrotating propeller [NASA-TM-101437] p 10 N89-13409

LDV measurements in an annular combustor model [NASA-CR-182207] p 159 N89-13755

A comparison of turbulence measurement methods p 174 N89-17302

An LDA (Laser-Doppler Anemometry) investigation of three-dimensional normal shock wave boundary-layer interactions p 14 N89-20956

High-temperature LDV seed particle development [NASA-CR-182265] p 175 N89-23851

**LASER HEATING**

Hardware development for the Surface Tension Driven Convection Experiment aboard the USML-1 Spacelab mission [AIAA PAPER 89-0406] p 47 A89-25341

Preparation of high T(c) Ti-Ba-Ca-Cu-O thin films by pulsed laser evaporation and TiO<sub>2</sub> vapor processing p 236 A89-38608

Hardware development for the surface tension driven convection experiment aboard the USML-1 spacelab mission [NASA-TM-101404] p 48 N89-11804

**LASER INTERFEROMETRY**

Development and applications of optical interferometric micrometry in the Angstrom and subangstrom range p 170 A89-27663

Skin-friction measurements by laser interferometry p 167 N89-28737

**LASER OUTPUTS**

Summary of laser speckle photogrammetry for HOST p 177 N89-12889

Two-dimensional high temperature optical strain measurement system, phase 2 [NASA-CR-185116] p 176 N89-26218

**LATTICE PARAMETERS**

Experimental evidence for a transverse magnetization of the Abrikosov lattice in anisotropic superconductors p 234 A89-21473

**LEAD (METAL)**

Effects of crucible wetting during solidification of immiscible Pb-Zn alloys [AIAA PAPER 89-0304] p 118 A89-25261

Effects of crucible wetting during solidification of immiscible Pb-Zn [NASA-TM-101372] p 120 N89-14341

**LEAD ALLOYS**

Microsegregation in directionally solidified Pb-8.4 at. pct Au alloy p 94 A89-12758

Bulk undercooling, nucleation, and macrosegregation of Pb-Sn alloys p 117 A89-17106

Gravitational macrosegregation in unidirectionally solidified lead-tin alloy p 117 A89-17112

Macrosegregation in undercooled Pb-Sn eutectic alloys p 95 A89-19621

The surface morphology of crystals melting under solutions of different densities p 235 A89-23482

Macrosegregation and nucleation in undercooled Pb-Sn alloys [NASA-TM-102023] p 104 N89-23664

**LEADING EDGES**

Electroimpulse deicing - Electrodynamic solution by discrete elements p 17 A89-39193

The effects of leading edge and downstream film cooling on turbine vane heat transfer [NASA-CR-182133] p 158 N89-13754

The low frequency oscillation in the flow over a NACA0012 airfoil with an iced leading edge [NASA-TM-102018] p 14 N89-23417

**LEAKAGE**

Annular honeycomb seals: Test results for leakage and rotordynamic coefficients - Comparisons to labyrinth and smooth configurations [ASME PAPER 88-TRIB-35] p 179 A89-34794

An entrance region friction factor model applied to annular seal analysis - Theory versus experiment for smooth and honeycomb seals [ASME PAPER 88-TRIB-41] p 179 A89-34798

Dynamics of face and annular seals with two-phase flow [NASA-CR-183352] p 182 N89-12870

Leakage predictions for Rayleigh-step, helium-purge seals [NASA-TM-101352] p 64 N89-14255

Annular honeycomb seals: Test results for leakage and rotordynamic coefficients; comparisons to labyrinth and smooth configurations p 185 N89-22899

High temperature flexible seal [NASA-CASE-LEW-14695-1] p 187 N89-28830

**LEAST SQUARES METHOD**

Nonoscillatory solution of the steady-state inviscid Burgers' equation by mathematical programming p 221 A89-22756

Least-squares finite elements for Stokes problem [NASA-TM-101308] p 222 N89-22392

Specialty functions singularity mechanics problems p 206 N89-29805

Least-squares finite element method for fluid dynamics [NASA-TM-102352] p 223 N89-30006

**LENGTH**

Effect of length of chopped pristine and intercalated graphite fibers on the resistivity of fiber networks [NASA-TM-101395] p 84 N89-11826

**LIFE (DURABILITY)**

Performance and lifetime assessment of MPD arc thruster technology [AIAA PAPER 88-3211] p 53 A89-16485

Mechanics of composite materials - Past, present and future p 82 A89-36293

Fiber composite structural durability and damage tolerance - Simplified predictive methods p 82 A89-36320

Selection of rolling-element bearing steels for long-life applications p 180 A89-47250

Successful completion of a cyclic ground test of a mercury ion Auxiliary Propulsion System p 59 A89-47450

Effect of design variables, temperature gradients, and speed on life and reliability of a rotating disk p 180 A89-47719

Low earth orbital atomic oxygen simulation for materials durability evaluation p 45 A89-51123

Thermal barrier coating life-prediction model development [NASA-CR-175002] p 26 N89-13433

Thermal barrier coating life prediction model development [NASA-CR-180807] p 110 N89-13621

Thermal Barrier Coatings. Abstracts and figures [NASA-CP-10019] p 110 N89-13642

Probabilistic analysis for fatigue strength degradation of materials [NASA-CR-182844] p 198 N89-15434

- Thermal barrier coating life-prediction model development p 200 N89-17331
- Thermal barrier coating life prediction model development p 200 N89-17333
- High temperature constitutive and crack initiation modeling of coated single crystal superalloys p 112 N89-17334
- Creep fatigue life prediction for engine hot section materials (ISOTROPIC) fifth year progress review p 201 N89-17336
- Toward improved durability in advanced aircraft engine hot sections [NASA-TM-4087] p 29 N89-20135
- Life modeling of thermal barrier coatings for aircraft gas turbine engines p 30 N89-20143
- Lightweight fibrous nickel electrodes for nickel-hydrogen batteries [NASA-TM-101997] p 93 N89-22710
- Review of the environmental effects of the Space Station Freedom photovoltaic power module [NASA-TM-102076] p 46 N89-24418
- Time dependent reliability model incorporating continuum damage mechanics for high-temperature ceramics [NASA-TM-102046] p 115 N89-24487
- Experience with advanced instrumentation in a hot section cascade [NASA-TM-102294] p 167 N89-27980
- Arc-textured high emittance radiator surfaces [NASA-CASE-LEW-14679-1] p 116 N89-28651
- Probabilistic Finite Elements (PFEM) structural dynamics and fracture mechanics p 206 N89-29803
- LIFE CYCLE COSTS**
- Space Station Freedom electrical power system hardware commonality with the United States Polar Platform [NASA-TM-102074] p 69 N89-24439
- LIGHT BEAMS**
- Recovery of excitation intensity dependence in pulsed, focused beams - Nonsaturated case p 177 A89-17507
- LIGHT EMISSION**
- Study of optical output couplers for submillimeter wavelength backward-wave oscillators (BWO's) [NASA-TM-101360] p 134 N89-11128
- LIGHT EMITTING DIODES**
- Compensation for effects of ambient temperature on rare-earth doped fiber optic thermometer [NASA-TM-102282] p 176 N89-27998
- LIGHT MODULATION**
- Intensity-based fibre-optic sensing system using contrast modulation of subcarrier interference pattern p 170 A89-39302
- LIGHT SCATTERING**
- Particle sizing by weighted measurements of scattered light [NASA-TM-100968] p 172 N89-11198
- Critical fluid light scattering p 121 N89-20320
- LIGHT SOURCES**
- A heat-driven monochromatic light source p 224 A89-41722
- LINEAR EQUATIONS**
- On the equivalence of Gaussian elimination and Gauss-Jordan reduction in solving linear equations [NASA-TM-101466] p 222 N89-20710
- On the equivalence of a class of inverse decomposition algorithms for solving systems of linear equations [NASA-TM-102036] p 223 N89-24865
- LINEAR OPERATORS**
- Solution methods for one-dimensional viscoelastic problems p 191 A89-19914
- LINEAR QUADRATIC GAUSSIAN CONTROL**
- Integrated flight/propulsion control system design based on a centralized approach [AIAA PAPER 89-3520] p 35 A89-52611
- Turbofan engine control system design using the LQG/LTR methodology p 23 A89-53956
- Turbofan engine control system design using the LQG/LTR methodology [NASA-CR-182303] p 33 N89-26004
- Integrated flight/propulsion control system design based on a centralized approach [NASA-TM-102137] p 35 N89-26009
- LINEAR QUADRATIC REGULATOR**
- A parametric LQ approach to multiobjective control system design p 219 A89-28605
- A parametric LQ approach to multiobjective control system design [NASA-TM-101316] p 220 N89-12283
- LINEAR SYSTEMS**
- Extended observability of linear time-invariant systems under recurrent loss of output data [AIAA PAPER 89-3510] p 220 A89-52603

**LINEARITY**

- Dynamic loading of spur gears with linear or parabolic tooth profile modification [NASA-TM-101444] p 183 N89-15413

**LINEARIZATION**

- Calculation of unsteady flows in turbomachinery using the linearized Euler equations p 149 A89-36916

**LININGS**

- Hot piston ring/cylinder liner materials - Selection and evaluation [SAE PAPER 880544] p 178 A89-12304
- Fuel properties effect on the performance of a small high temperature rise combustor [AIAA PAPER 89-2901] p 23 A89-52025
- Component specific modeling p 25 N89-12907
- Three-dimensional inelastic analysis methods for hot section components p 199 N89-17316
- Structural response of an advanced combustor liner: Test and analysis p 200 N89-17329
- Elevated temperature crack growth p 200 N89-17335

- Fuel properties effect on the performance of a small high temperature rise combustor [NASA-TM-102096] p 33 N89-25238

**LINKAGES**

- Tailoring of composite links for optimal damped elasto-dynamic performance [NASA-TM-102094] p 88 N89-26912

**LIQUEFIED NATURAL GAS**

- Alternative fuel capabilities of the Mod II Stirling vehicle [SAE PAPER 880543] p 177 A89-12303

**LIQUID ALLOYS**

- The surface morphology of crystals melting under solutions of different densities p 235 A89-23482

**LIQUID ATOMIZATION**

- Transition limits for water-droplet crystallization with the NASA Lewis icing nozzle p 152 A89-50071

**LIQUID CRYSTALS**

- High-resolution heat-transfer-coefficient maps applicable to compound-curve surfaces using liquid crystals in a transient wind tunnel [NASA-TM-89855] p 154 N89-10246
- High-resolution liquid-crystal heat-transfer measurements on the end wall of a turbine passage with variations in Reynolds number [NASA-TM-100827] p 161 N89-18664

**LIQUID FLOW**

- Scaling results for the Liquid Sheet Radiator (LSR) [NASA-TM-102100] p 72 N89-25277

**LIQUID FUELS**

- Experiment plans to study preignition processes of a pool fire in low gravity [NASA-CR-182256] p 121 N89-19442

**LIQUID HYDROGEN**

- Fueling the National Aero-Space Plane with slush hydrogen [AIAA PAPER 89-5014] p 117 A89-51339
- COLD-SAT orbital experiment configured for Atlas launch p 45 A89-53327
- Analysis of the nonvented fill of a 4.96-cubic-meter lightweight liquid hydrogen tank [NASA-TM-102039] p 67 N89-22652
- COLD-SAT: A technology satellite for cryogenic experimentation [NASA-TM-102286] p 47 N89-26036
- COLD-SAT: An orbital cryogenic hydrogen technology experiment [NASA-TM-102303] p 73 N89-26044

**LIQUID INJECTION**

- Analysis of the nonvented fill of a 4.96-cubic-meter lightweight liquid hydrogen tank [NASA-TM-102039] p 67 N89-22652

**LIQUID OXYGEN**

- Liquid oxygen cooling of hydrocarbon fueled rocket thrust chambers [AIAA PAPER 89-2739] p 60 A89-49686
- Liquid oxygen cooling of high pressure LOX/hydrocarbon rocket thrust chambers p 63 N89-12649
- High-pressure calorimeter chamber tests for liquid oxygen/kerosene (LOX/RP-1) rocket combustion [NASA-TP-2862] p 65 N89-15979
- Liquid oxygen cooling of hydrocarbon fueled rocket thrust chambers [NASA-TM-102113] p 70 N89-24447
- LIQUID PHASES**
- Convective flows in enclosures with vertical temperature or concentration gradients [AIAA PAPER 89-0069] p 118 A89-25060
- Convective flows in enclosures with vertical temperature or concentration gradients [NASA-TM-101373] p 120 N89-12753

**LIQUID PROPELLANT ROCKET ENGINES**

- Fiberoptics for liquid propellant rocket engine environments [AIAA PAPER 89-2416] p 230 A89-46812
- Liquid oxygen cooling of hydrocarbon fueled rocket thrust chambers [AIAA PAPER 89-2739] p 60 A89-49686
- Liquid oxygen cooling of high pressure LOX/hydrocarbon rocket thrust chambers p 63 N89-12649
- Liquid oxygen cooling of hydrocarbon fueled rocket thrust chambers [NASA-TM-102113] p 70 N89-24447
- NASA's Chemical Transfer Propulsion Program for Pathfinder [NASA-TM-102298] p 41 N89-26876
- LIQUID SURFACES**
- Vapor condensation at a turbulent liquid surface in systems with possible spaced-based applications [AIAA PAPER 89-2846] p 151 A89-47122

**LIQUID-LIQUID INTERFACES**

- Instabilities caused by oscillating accelerations normal to a viscous fluid-fluid interface p 144 A89-22823

**LIQUID-SOLID INTERFACES**

- Macroscopic segregation in undercooled Pb-Sn eutectic alloys p 95 A89-19621
- Heat of mixing and morphological stability p 143 A89-21296
- Dendritic solidification in binary alloys p 96 A89-22560
- Considerations on the moving contact-line singularity, with application to frictional drag on a slender drop p 144 A89-23238
- Fuel spray simulation with two-fluid nozzles [AIAA PAPER 89-0053] p 145 A89-25047
- Effects of crucible wetting during solidification of immiscible Pb-Zn alloys [AIAA PAPER 89-0304] p 118 A89-25261
- Effects of furnace temperature profile on the interface shape during Bridgman crystal growth p 119 A89-53278
- Fluid spray simulation with two-fluid nozzles [NASA-TM-101367] p 155 N89-12028
- Effects of crucible wetting during solidification of immiscible Pb-Zn [NASA-TM-101372] p 120 N89-14341

**LIQUID-VAPOR EQUILIBRIUM**

- Vapor condensation at a turbulent liquid surface in systems with possible spaced-based applications [AIAA PAPER 89-2846] p 151 A89-47122

**LIQUID-VAPOR INTERFACES**

- A preliminary report on the effects of long-term exposure of LiOH on pure nickel p 90 A89-12624
- Axisymmetric confined turbulent jet directed towards the liquid surface from below [AIAA PAPER 89-0172] p 145 A89-25148
- Numerical studies of the effects of jet-induced mixing on liquid-vapor interface condensation [AIAA PAPER 89-1744] p 152 A89-48958
- Axisymmetric confined turbulent jet directed towards the liquid surface from below [NASA-TM-101409] p 158 N89-13749
- Numerical studies of the effects of jet-induced mixing on liquid-vapor interface condensation [NASA-CR-182285] p 163 N89-23818

**LIQUIDS**

- Behavior in normal and reduced gravity of an enclosed liquid/gas system with nonuniform heating from above [AIAA PAPER 89-0070] p 145 A89-25061
- dc power control for a liquid-fed resistojel p 59 A89-47457
- Mass flow measurement of liquid cryogenics using the triboelectric effect [NASA-CR-179519] p 155 N89-12837
- Behavior in normal and reduced gravity of an enclosed liquid/gas system with nonuniform heating from above [NASA-TM-101471] p 120 N89-17046

**LITERATURE**

- A review of turbomachinery blade-row interaction research [NASA-CR-182211] p 24 N89-12567

**LITHIUM COMPOUNDS**

- Megawatt Class Nuclear Space Power Systems (MCNPS) conceptual design and evaluation report. Volume 4: Concepts selection, conceptual designs, recommendations [NASA-CR-179614-VOL-4] p 210 N89-18967

**LITHIUM FLUORIDES**

- An experimental analysis of a doped lithium fluoride direct absorption solar receiver p 49 A89-15245
- Densities of some molten fluoride salt mixtures suitable for heat storage in space power applications p 77 A89-41444

**LITHIUM HYDROXIDES**

- A preliminary report on the effects of long-term exposure of LiOH on pure nickel p 90 A89-12624

- Use of pure nickel and LiOH for thermal energy storage p 91 A89-23146
- LOAD DISTRIBUTION (FORCES)**
- Design procedures for fiber composite box beams p 195 A89-48674
- Finite element modeling of frictionally restrained composite interfaces [NASA-CR-182281] p 203 N89-23918
- LOAD TESTS**
- A data acquisition and control program for axial-torsional fatigue testing [NASA-TM-102041] p 205 N89-28029
- LOADS (FORCES)**
- Fatigue crack growth behavior of a single crystal alloy as observed through an in situ fatigue loading stage p 99 A89-45946
- Analysis of shell-type structures subjected to time-dependent mechanical and thermal loading [NASA-CR-183005] p 197 N89-14457
- A modified VAPEPS method for predicting vibroacoustic response of unreinforced mass loaded honeycomb panels [NASA-TM-101467] p 46 N89-16905
- Distortion and regulation characterization of a Mapham inverter [NASA-TM-102089] p 139 N89-26148
- Fatigue testing apparatus [NASA-CASE-LEW-14124-1] p 177 N89-28806
- LOGISTICS**
- Space propulsion technology and cryogenic fluid depot p 38 N89-11768
- LONG TERM EFFECTS**
- A preliminary report on the effects of long-term exposure of LiOH on pure nickel p 90 A89-12624
- LOSSY MEDIA**
- Measurement of the properties of lossy materials inside a finite conducting cylinder [NASA-CR-182500] p 126 N89-10223
- LOW FREQUENCIES**
- The low frequency oscillation in the flow over a NACA0012 airfoil with an iced leading edge [NASA-TM-102018] p 14 N89-23417
- LOW REYNOLDS NUMBER**
- Development of low Reynolds number two equation turbulence models for predicting external heat transfer on turbine blades p 157 N89-12901
- LOW SPEED**
- A prediction of 3-D viscous flow and performance of the NASA low-speed centrifugal compressor [NASA-CR-184765] p 160 N89-16132
- LOW SPEED WIND TUNNELS**
- Flowfield measurements in the NASA Lewis Research Center 9- by 15-foot low-speed wind tunnel [NASA-TM-100883] p 36 N89-21002
- STOL and STOLV hot gas ingestion and airframe heating tests in the NASA Lewis 9- by 15-foot low-speed wind tunnel [NASA-TM-102101] p 15 N89-29323
- LOW TEMPERATURE TESTS**
- Icing research tunnel test of a model helicopter rotor [NASA-TM-101978] p 29 N89-19305
- LUBRICANTS**
- On the performance of finite journal bearings lubricated with micropolar fluids p 181 A89-54977
- Tribological properties of alumina-boria-silicate fabric from 25 C to 850 C p 107 A89-54982
- The role of thermal and lubricant boundary layers in the transient thermal analysis of spur gears [NASA-TM-101435] p 182 N89-14452
- LUBRICATING OILS**
- Effects of lubrication on the performance of high speed spur gears [NASA-TM-101969] p 186 N89-22919
- LUBRICATION**
- Lubricant jet flow phenomena in spur and helical gears with modified addendums; for radially directed individual jets [NASA-TM-101460] p 183 N89-15415
- LUBRICATION SYSTEMS**
- Acidic attack of perfluorinated alkyl ether lubricant molecules by metal oxide surfaces [NASA-TM-101962] p 93 N89-19402
- LUNAR BASES**
- A perspective on space exploration technology catalysis: A rationale for initiating 21st Century expansion of human civilization into outer space [NASA-TM-101362] p 238 N89-11637
- Space power technologies p 38 N89-11770
- Comparison of solar photovoltaic and nuclear reactor power systems for a human-tended lunar observatory [NASA-TM-102015] p 242 N89-23397
- Photovoltaic power system considerations for future lunar bases [NASA-TM-102019] p 67 N89-23517
- Solar power for the lunar night [NASA-TM-102127] p 242 N89-26799

- Lunar production of solar cells [NASA-TM-102102] p 242 N89-27619
- LUNAR EXPLORATION**
- Human exploration mission studies p 38 N89-22965
- LUNAR OBSERVATORIES**
- Comparison of solar photovoltaic and nuclear reactor power systems for a human-tended lunar observatory [NASA-TM-102015] p 242 N89-23397
- LUNAR SOIL**
- Lunar Helium-3 and Fusion Power [NASA-CP-10018] p 233 N89-14842
- Assessment of lunar sources of He-3 for use on earth p 242 N89-14853
- LUNAR SURFACE**
- An analysis of possible advanced space strategies featuring the role of space resource utilization [IAF PAPER 88-587] p 37 A89-17861

## M

- MACH NUMBER**
- A supersonic through-flow fan engine airframe integration study [AIAA PAPER 89-2140] p 18 A89-50802
- Experimental aerodynamic performance of advanced 40 deg-swept 10-blade propeller model at Mach 0.6 to 0.85 [NASA-TM-88969] p 9 N89-10865
- A preliminary design study of supersonic through-flow fan inlets [NASA-CR-182224] p 24 N89-11751
- Mach 5 inlet CFD and experimental results [NASA-TM-102317] p 33 N89-27670
- MACH-ZEHNDER INTERFEROMETERS**
- Design of a GaAlAs travelling wave Mach-Zehnder electro-optic modulator p 130 A89-10342
- MACHINE LEARNING**
- Neuromorphic learning of continuous-valued mappings in the presence of noise: Application to real-time adaptive control [NASA-TM-101999] p 221 N89-24856
- MACHINING**
- Generation of a crowned pinion tooth surface by a surface of revolution [NASA-TM-100260] p 181 N89-10282
- Generation of a crowned pinion tooth surface by a plane [NASA-TM-100259] p 181 N89-10283
- Performance of a multistage depressed collector with machined titanium electrodes [NASA-TP-2891] p 136 N89-15337
- Secondary electron emission characteristics of untreated and ion-textured titanium [NASA-TP-2902] p 103 N89-17650
- MAGNESIUM**
- Fluid flow phenomena in the generation of boron carbide suspensions in magnesium melts p 79 A89-19472
- MAGNESIUM OXIDES**
- Optical experiments on thermophoretically augmented submicron particle deposition from 'dusty' high temperature gas flows p 90 A89-14799
- MAGNETIC CHARGE DENSITY**
- Material parameter determination from scattering measurements [NASA-CR-183312] p 126 N89-10225
- MAGNETIC COMPRESSION**
- Antiproton powered propulsion with magnetically confined plasma engines [AIAA PAPER 89-2334] p 57 A89-46758
- MAGNETIC CORES**
- Paralleling power MOSFETs in their active region: Extended range of passively forced current sharing [NASA-CR-180902] p 139 N89-26150
- MAGNETIC ENERGY STORAGE**
- High temperature superconducting magnetic energy storage for future NASA missions p 50 A89-15288
- MAGNETIC FIELDS**
- Plasma flow processes within magnetic nozzle configurations [AIAA PAPER 89-2711] p 57 A89-47036
- The effects of magnetic nozzle configurations on plasma thrusters [NASA-CR-184678] p 64 N89-15170
- Plume characteristics of MPD thrusters: A preliminary examination [NASA-CR-185130] p 76 N89-29483
- MAGNETIC MONOPOLES**
- Superheavy magnetic monopoles and main-sequence stars p 240 A89-20377
- MAGNETIC PERMEABILITY**
- Transport critical current and magnetization measurements of melt-processed YBa<sub>2</sub>Cu<sub>3</sub>O<sub>7-x</sub> p 234 A89-20037
- MAGNETIC TAPES**
- Adhesion in ceramics and magnetic media [NASA-TM-101476] p 113 N89-19435

## MAGNETIZATION

- Experimental evidence for a transverse magnetization of the Abrikosov lattice in anisotropic superconductors p 234 A89-21473
- MAGNETOHYDRODYNAMIC FLOW**
- Plasma flow processes within magnetic nozzle configurations [AIAA PAPER 89-2711] p 57 A89-47036
- The effects of magnetic nozzle configurations on plasma thrusters [NASA-CR-184678] p 64 N89-15170
- MAGNETOHYDRODYNAMIC STABILITY**
- The stability analysis of magnetohydrodynamic equilibria - Comparing the thermodynamic approach with the energy principle p 232 A89-39391
- MAGNETOHYDRODYNAMIC TURBULENCE**
- Plasma density fluctuations observed during Space Shuttle Orbiter water releases p 233 A89-54759
- MAGNETOPLASMA DYNAMICS**
- Performance and lifetime assessment of MPD arc thruster technology [AIAA PAPER 88-3211] p 53 A89-16485
- Performance of a 100 kW class applied field MPD thruster [AIAA PAPER 89-2710] p 57 A89-47035
- Design of a thrust stand for high power electric propulsion devices [AIAA PAPER 89-2829] p 39 A89-47110
- Plume characteristics of MPD thrusters - A preliminary examination [AIAA PAPER 89-2832] p 39 A89-47113
- Use of high temperature superconductors in magnetoplasma dynamic systems [NASA-TM-101219] p 236 N89-11553
- Performance of a 100 kW class applied field MPD thruster [NASA-TM-102312] p 74 N89-27701
- MAGNETRON SPUTTERING**
- High-efficiency solar cells fabricated from direct-current magnetron sputtered n-indium tin oxide onto p-InP grown by atmospheric pressure metalorganic vapor phase epitaxy p 133 A89-44518
- Isotopic study of oxygen diffusion in oxide coatings [NASA-TM-102082] p 78 N89-24451
- MAIN SEQUENCE STARS**
- Superheavy magnetic monopoles and main-sequence stars p 240 A89-20377
- MAINTAINABILITY**
- Space station electrical power system availability study [NASA-CR-182198] p 45 N89-11802
- MAINTENANCE**
- Transmission overhaul and replacement predictions using Weibull and renewal theory [AIAA PAPER 89-2919] p 180 A89-47173
- Transmission overhaul and replacement predictions using Weibull and renewal theory [NASA-TM-102022] p 186 N89-22925
- MAN MACHINE SYSTEMS**
- Model-based analysis of control/display interaction in the hover task p 215 A89-36933
- MANAGEMENT METHODS**
- Weight savings in aerospace vehicles through propellant scavenging [SAWE PAPER 1818] p 40 A89-50814
- MANAGEMENT PLANNING**
- Systems autonomy technology: Executive summary and program plan [NASA-TM-100999] p 216 N89-18045
- MANEUVERS**
- Isolated testing of highly maneuverable inlet concepts [NASA-CR-179544] p 26 N89-13437
- MANIPULATORS**
- Robots for manipulation in a micro-gravity environment p 215 A89-11682
- New results concerning the use of kinematically redundant manipulators in microgravity environments [AIAA PAPER 89-3562] p 215 A89-52647
- MANNED MARS MISSIONS**
- Power considerations for an early manned Mars mission utilizing the space station [NASA-TM-101436] p 63 N89-13492
- Human exploration mission studies p 38 N89-22985
- MANNED SPACE FLIGHT**
- In-situ propellant advantages for fast transfer to Mars [AIAA PAPER 88-2901] p 37 A89-14977
- Nuclear thermal rockets - Next step to space p 55 A89-40480
- A perspective on space exploration technology catalysis: A rationale for initiating 21st Century expansion of human civilization into outer space [NASA-TM-101362] p 238 N89-11637
- MANNED SPACECRAFT**
- NASA's Chemical Transfer Propulsion Program for Pathfinder [NASA-TM-102298] p 41 N89-26876



**MANUFACTURING**

Computer-aided design of bevel gear tooth surfaces  
[NASA-TM-101449] p 183 N89-17248

**MAPPING**

Plotting component maps in the Navy/NASA Engine Program (NNEP): A method and its usage  
[NASA-TM-101433] p 26 N89-14239  
Plume characteristics of MPD thrusters: A preliminary examination  
[NASA-CR-185130] p 76 N89-29483

**MARANGONI CONVECTION**

Thermocapillary migration of a large gas slug in a tube  
p 117 A89-22747

**MARS (PLANET)**

In-situ propellant advantages for fast transfer to Mars  
[AIAA PAPER 88-2901] p 37 A89-14977  
Solar radiation on Mars  
[NASA-TM-102299] p 242 N89-27623

**MARS ATMOSPHERE**

The Mars climate for a photovoltaic system operation  
[IAF PAPER ICOSP89-9-5] p 241 A89-46529  
The Mars climate for a photovoltaic system operation  
[NASA-TM-101994] p 136 N89-20385  
Photovoltaic power system operation in the Mars environment  
[NASA-TM-102075] p 138 N89-24529  
Solar radiation on Mars  
[NASA-TM-102299] p 242 N89-27623

**MARS LANDING**

Energy storage considerations for a robotic Mars surface sampler  
p 49 A89-15267

**MARS PROBES**

Energy storage considerations for a robotic Mars surface sampler  
p 49 A89-15267

**MARS SAMPLE RETURN MISSIONS**

Preliminary assessment of rover power systems for the Mars Rover Sample Return Mission  
[IAF PAPER ICOSP89-9-6] p 39 A89-46530  
Preliminary assessment of rover power systems for the Mars Rover Sample Return Mission  
[NASA-TM-102003] p 68 N89-23518

**MARS SURFACE**

Nuclear propulsion: A vital technology for the exploration of Mars and the planets beyond  
[NASA-TM-101354] p 62 N89-10944  
A perspective on space exploration technology catalysis: A rationale for initiating 21st Century expansion of human civilization into outer space  
[NASA-TM-101362] p 238 N89-11637  
Mars manned transportation vehicle  
[NASA-TM-101487] p 210 N89-20545  
Solar radiation on Mars  
[NASA-TM-102299] p 242 N89-27623

**MASS DISTRIBUTION**

A modified VAPEPS method for predicting vibroacoustic response of unreinforced mass loaded honeycomb panels  
[NASA-TM-101467] p 46 N89-16905

**MASS FLOW**

Optical experiments on thermophoretically augmented submicron particle deposition from 'dusty' high temperature gas flows  
p 90 A89-14799  
Mass flow meter using the triboelectric effect for measurement in cryogenics  
[NASA-CR-179572] p 155 N89-12836  
Mass flow measurement of liquid cryogenics using the triboelectric effect  
[NASA-CR-179519] p 155 N89-12837  
Investigation of a liquid-fed water resistojet plume  
[NASA-TM-102310] p 75 N89-27706

**MASS FLOW RATE**

Effect of particulate thermophoresis in reducing the fouling rate advantages of effusion-cooling  
p 141 A89-14599  
Viscous dissipation effects on thermophoretically augmented aerosol particle transport across laminar boundary layers  
p 141 A89-14600

**MASS TRANSFER**

Laboratory studies of the deposition of alkali sulfate vapors from combustion gases using a flash-evaporation technique  
p 89 A89-12338  
Windward fraction of the total mass or heat transport for flow past a circular cylinder  
p 141 A89-12339  
Thermophoretically enhanced mass transport rates to solid and transpiration-cooled walls across turbulent (law-of-the-wall) boundary layers  
p 141 A89-12340  
Mass transfer across combustion gas thermal boundary layers - Power production and materials processing implications  
p 143 A89-20425  
On the modelling of scalar and mass transport in combustor flows  
p 92 A89-38658

**MATERIALS SCIENCE**

Hot piston ring/cylinder liner materials - Selection and evaluation  
[SAE PAPER 880544] p 178 A89-12304

**MATERIALS TESTS**

Test methods and design allowances for fibrous composites. Volume 2  
[ASTM STP-1003] p 81 A89-32882  
The NASA Lewis Research Center High Temperature Fatigue and Structures Laboratory  
p 194 A89-43528

**MATHEMATICAL MODELS**

A unique set of micromechanics equations for high-temperature metal matrix composites  
p 190 A89-15734  
Simple high-accuracy resolution program for convective modelling of discontinuities  
p 143 A89-17459  
Concepts for interrelating ultrasonic attenuation, microstructure, and fracture toughness in polycrystalline solids  
p 95 A89-19852  
Enthalpies of a binary alloy during solidification  
p 96 A89-22559

Space Electrochemical Research and Technology Conference, Cleveland, OH, Apr. 14-16, 1987, Proceedings  
p 207 A89-23280

Theoretical performance of hydrogen-bromine rechargeable SPE fuel cell --- Solid Polymer Electrolyte  
p 207 A89-23290

Modeling of impulsive propellant reorientation  
[AIAA PAPER 89-0628] p 54 A89-25496  
Creep life prediction based on stochastic model of microstructurally short crack growth  
p 193 A89-36185  
Gas density effect on droplet size of simulated fuel sprays  
[AIAA PAPER 89-2322] p 151 A89-46749

Rectangular nozzle plume velocity modeling for use in jet noise prediction  
[AIAA PAPER 89-2357] p 7 A89-46771  
Analytical flutter investigation of a composite propfan model  
p 195 A89-48663

Numerical studies of the effects of jet-induced mixing on liquid-vapor interface condensation  
[AIAA PAPER 89-1744] p 152 A89-48958  
Transient flow thrust prediction for an ejector propulsion concept  
[AIAA PAPER 89-2906] p 23 A89-49688

Modeling of pulsed propellant reorientation  
[AIAA PAPER 89-2727] p 61 A89-53306

Identification of Space Shuttle Main Engine dynamics  
p 61 A89-54068

Space station electrical power system availability study  
[NASA-CR-182198] p 45 N89-11802  
Improved numerical methods for turbulent viscous flows  
aerothermal modeling program, phase 2  
[NASA-CR-182169] p 154 N89-12010

Mathematical modeling of solid oxide fuel cells  
[NASA-CR-182188] p 209 N89-12122

A control-volume method for analysis of unsteady thrust augmenting ejector flows  
[NASA-CR-182203] p 24 N89-12566  
Development of a thermal and structural analysis procedure for cooled radial turbines  
[NASA-TM-101416] p 24 N89-12568

Aerothermal modeling program, phase 2  
p 156 N89-12890

Constitutive modeling for isotropic materials  
p 195 N89-12904

Component specific modeling  
p 25 N89-12907  
Thermomechanical characterization of Hastelloy-X under uniaxial cyclic loading  
p 196 N89-12909

Constitutive modeling for single crystal superalloys  
p 101 N89-12911

Constitutive modelling of single crystal and directionally solidified superalloys  
p 101 N89-12912

Life prediction and constitutive models for engine hot section  
p 188 N89-12916

Thermal barrier coating life prediction model development  
p 109 N89-12920

Thermal barrier coating life prediction model  
p 109 N89-12921

Thermal barrier coating life prediction model development  
p 110 N89-12922

Analytical ice shape predictions for flight in natural icing conditions  
[NASA-CR-182234] p 18 N89-13428

Constitutive modeling for isotropic materials  
[NASA-CR-174805] p 26 N89-13436

Modeling of impulsive propellant reorientation  
[NASA-TM-101440] p 64 N89-13495

Thermal Barrier Coatings. Abstracts and figures  
[NASA-CP-10019] p 110 N89-13642

Local-global analysis of crack growth in continuously reinforced ceramic matrix composites  
[NASA-CR-182231] p 197 N89-13820

Turbofan forced mixer lobe flow modeling. 1: Experimental and analytical assessment  
[NASA-CR-4147-PT-1] p 11 N89-14221

Turbofan forced mixer lobe flow modeling. 2: Three-dimensional inviscid mixer analysis (FLOMIX)  
[NASA-CR-4147-PT-2] p 11 N89-14222

Parametric studies of advanced turboprops

[NASA-TM-101389] p 197 N89-14465

Universal limiter for transient interpolation modeling of the advective transport equations: The ULTIMATE conservative difference scheme  
[NASA-TM-100916] p 222 N89-14794

Analysis of an unswept propfan blade with a semiempirical dynamic stall model  
[NASA-TM-4083] p 27 N89-15112

Modeling cyclic melting and refreezing in a hollow metal canister  
[NASA-CR-184630] p 217 N89-15623

Mechanics of materials model  
p 199 N89-17319

Thermal barrier coating life-prediction model development  
p 200 N89-17331

Vibration signature analysis of multistage gear transmission  
[NASA-TM-101442] p 184 N89-18685

The divergence characteristics of constrained-sheath optics systems for use with 5-eV atomic oxygen sources  
[NASA-CR-182238] p 229 N89-19973

Review and assessment of the database and numerical modeling for turbine heat transfer  
p 30 N89-20139

Fatigue life prediction modeling for turbine hot section materials  
p 30 N89-20142

Identification of space shuttle main engine dynamics  
[NASA-TM-101982] p 66 N89-20199

Results of inphase axial-torsional fatigue experiments on 304 stainless steel  
[NASA-TM-101464] p 201 N89-20514

Computer simulation of macrosegregation in directionally solidified circular ingots  
[NASA-CR-182838] p 122 N89-21134

Deformation modeling and constitutive modeling for anisotropic superalloys  
[NASA-CR-4215] p 202 N89-21258

Characterization of structural connections using free and forced response test data  
[NASA-TM-101991] p 202 N89-21266

Gas density effect on droplet size of simulated fuel sprays  
[NASA-TM-102013] p 162 N89-22053

Unsteady thermocapillary migration of bubbles  
[NASA-TM-101338] p 162 N89-22054

Rectangular nozzle plume velocity modeling for use in jet noise prediction  
[NASA-TM-102047] p 14 N89-22577

Numerical model of solar dynamic radiator for parametric analysis  
[NASA-TM-102054] p 67 N89-22653

Rotordynamic Instability Problems in High-Performance Turbomachinery, 1988  
[NASA-CP-3026] p 185 N89-22891

Numerical studies of the effects of jet-induced mixing on liquid-vapor interface condensation  
[NASA-CR-182285] p 163 N89-23818

Two-dimensional numerical simulation of a Stirling engine heat exchanger  
[NASA-TM-102057] p 164 N89-23823

Finite element modeling of frictionally restrained composite interfaces  
[NASA-CR-182281] p 203 N89-23918

High speed turboprop aeroacoustic study (single rotation). Volume 1: Model development  
[NASA-CR-182257-VOL-1] p 229 N89-24139

Transient flow thrust prediction for an ejector propulsion concept  
[NASA-TM-102078] p 32 N89-24318

Time dependent reliability model incorporating continuum damage mechanics for high-temperature ceramics  
[NASA-TM-102046] p 115 N89-24487

Analysis of shell-type structures subjected to time-dependent mechanical and thermal loading  
[NASA-CR-184989] p 203 N89-24669

A predictive model for failure properties of thermoset resins  
[NASA-TM-4128] p 87 N89-25300

Time-dependent computational studies of flames in microgravity  
[NASA-CR-182298] p 122 N89-25353

Advanced methods for 3-D inelastic structural analysis for hot engine structures  
[NASA-TM-102106] p 204 N89-25490

Acoustic propagation in curved ducts with extended reacting wall treatment  
[NASA-TM-102110] p 224 N89-25670

Modeling of pulsed propellant reorientation  
[NASA-TM-102117] p 165 N89-26178

Theoretical studies in support of the 3M-vapor transport (PVTOS-) experiments  
[NASA-CR-185122] p 165 N89-26179

Nonlinear mesomechanics of composites with periodic microstructure  
[NASA-TM-102051] p 204 N89-26260

- Structural and thermal response of 30 cm diameter ion thruster optics  
[NASA-TM-102124] p 75 N89-27703  
Investigation of a liquid-fed water resistojet plume  
[NASA-TM-102310] p 75 N89-27706  
Refinements in a viscoplastic model  
[NASA-TM-102338] p 205 N89-28036  
Multiwave interactions in turbulent jets  
[NASA-TM-101985] p 168 N89-29714

**MATHEMATICAL PROGRAMMING**

- Nonoscillatory solution of the steady-state inviscid Burgers' equation by mathematical programming  
p 221 A89-22756  
Calculation of shocked flows by mathematical programming  
p 150 A89-45397

**MATRICES (MATHEMATICS)**

- Parallel Gaussian elimination of a block tridiagonal matrix using multiple microcomputers  
[NASA-TP-2892] p 218 N89-17422

**MATRIX MATERIALS**

- Analysis of microalloy precipitate reversion in steels  
p 94 A89-15108  
A probabilistic formulation for fracture energy of continuous fibre-matrix composites  
p 83 A89-39996  
Crystallization kinetics of BaO-Al<sub>2</sub>O<sub>3</sub>-SiO<sub>2</sub> glasses  
[NASA-TM-101964] p 113 N89-20252  
Theoretical analysis of compatibility of several reinforcement materials with NiAl and FeAl matrices  
[NASA-CR-182291] p 86 N89-23622  
Preparation and evaluation of silicon nitride matrices for silicon nitride-SiC fiber composites  
[NASA-CR-184798] p 115 N89-23678  
Tailoring of composite links for optimal damped elastodynamic performance  
[NASA-TM-102094] p 88 N89-26912  
Metal matrix composite micromechanics: In-situ behavior influence on composite properties  
[NASA-TM-102302] p 88 N89-26924  
Fatigue crack growth study of SCS6/Ti-15-3 composite  
[NASA-TM-102332] p 104 N89-26989  
Optimum interface properties for metal matrix composites  
[NASA-TM-102295] p 205 N89-27223  
The interface in tungsten fiber reinforced niobium metal-matrix composites  
[NASA-TM-102122] p 104 N89-28627

**MATRIX METHODS**

- Symbolic derivation of material property matrices in finite element analysis  
p 216 A89-34964

**MATTER-ANTIMATTER PROPULSION**

- Antiproton powered propulsion with magnetically confined plasma engines  
[AIAA PAPER 89-2334] p 57 A89-46758  
Antiproton powered propulsion with magnetically confined plasma engines  
[NASA-CR-185131] p 74 N89-27700

**MEASURING INSTRUMENTS**

- Turbine Engine Hot Section Technology 1986  
[NASA-CP-2444] p 195 N89-12876  
High resolution video monitoring of coating thickness during plasma spraying  
[NASA-TM-101423] p 102 N89-15218

**MECHANICAL DRIVES**

- Advanced transmission studies  
p 178 A89-18906  
Comparison study of gear dynamic computer programs at NASA Lewis Research Center  
[NASA-TP-2901] p 184 N89-21243  
Modal analysis of gear housing and mounts  
[NASA-TM-101445] p 184 N89-21244  
Tribology: The Story of Lubrication and Wear  
[NASA-TM-101430] p 203 N89-24635

**MECHANICAL ENGINEERING**

- The design and development of transonic multistage compressors  
p 27 N89-18834

**MECHANICAL PROPERTIES**

- Microsegregation in directionally solidified Pb-8.4 at. pct Au alloy  
p 94 A89-12758  
The correlation of low-velocity impact resistance of graphite-fiber-reinforced composites with matrix properties  
p 79 A89-16283  
Crystallization and characterization of Y<sub>2</sub>O<sub>3</sub>-SiO<sub>2</sub> glasses  
p 80 A89-19486  
Mechanical properties characterization of composite sandwich materials intended for space antenna applications  
p 81 A89-32885  
Effects of various consolidation techniques on microstructure, strength, and reliability of alpha-SiC  
p 106 A89-33611  
Improved silicon carbide for advanced heat engines. I - Process development for injection molding  
p 106 A89-33619  
Improved silicon carbide for advanced heat engines. II - Pressureless sintering and mechanical properties of injection molded silicon carbide  
p 106 A89-33620

- Symbolic derivation of material property matrices in finite element analysis  
p 216 A89-34964

- Mechanics of composite materials - Past, present and future  
p 82 A89-36293

- Acousto-ultrasonics - An update  
p 188 A89-42864

- Adhesion, friction and micromechanical properties of ceramics  
p 107 A89-54277

- Properties of silicon carbide fiber-reinforced silicon nitride matrix composites  
[NASA-TM-101356] p 84 N89-10130

- Thermal effects on the mechanical properties of SiC fiber reinforced reaction bonded silicon nitride matrix (SiC/RBSN) composites  
[NASA-TM-101348] p 84 N89-10134

- Constitutive behavior of single crystal PWA 1480 and directionally solidified MAR-M 246 under monotonic and cyclic loads at high and low temperature  
p 100 N89-12634

- Mechanical properties of modified low cobalt powder metallurgy Udimet 700 type alloys  
[NASA-TM-101481] p 103 N89-20228

- Crystallization kinetics of BaO-Al<sub>2</sub>O<sub>3</sub>-SiO<sub>2</sub> glasses  
[NASA-TM-101964] p 113 N89-20252

- Design, development and applications of novel techniques for studying surface mechanical properties  
[NASA-TM-101959] p 113 N89-20253

- Deformation modeling and constitutive modeling for anisotropic superalloys  
[NASA-CR-4215] p 202 N89-21258

- Metal matrix composite micromechanics: In-situ behavior influence on composite properties  
[NASA-TM-102302] p 88 N89-26924

- Furnace for tensile/fatigue testing  
[NASA-CASE-LEW-14848-1] p 40 N89-28549

- Specialty functions singularity mechanics problems  
p 206 N89-29805

**MELT SPINNING**

- Microstructures in rapidly solidified niobium aluminides  
p 95 A89-18193

- Rapid solidification research at the NASA Lewis Research Center  
p 95 A89-18203

**MELTING**

- The surface morphology of crystals melting under solutions of different densities  
p 235 A89-23482

- Modeling cyclic melting and refreezing in a hollow metal canister  
[NASA-CR-184630] p 217 N89-15623

- Flight experiment of thermal energy storage  
[NASA-TM-102081] p 69 N89-24440

**MELTING POINTS**

- Measurement of the diffusion coefficient of acetone in succinonitrile at its melting point  
p 237 A89-23488

**MELTS (CRYSTAL GROWTH)**

- Fluid flow phenomena in the generation of boron carbide suspensions in magnesium melts  
p 79 A89-19472

- The influence of annealing in the ferrite-plus-austenite phase field on the stability of vanadium carbide precipitates  
p 97 A89-32803

- Steady-state thermal-solutal diffusion in a float zone  
p 119 A89-40897

- Isothermal solidification in a binary alloy melt  
p 121 N89-20300

**MERCURY (METAL)**

- Mercury ion thruster technology  
[NASA-CR-174974] p 66 N89-21834

**MERCURY COMPOUNDS**

- Evaluation of transport conditions during physical vapor transport growth of opto-electronic crystals  
[AIAA PAPER 89-0229] p 118 A89-25197

**MERCURY ION ENGINES**

- Model for computing volume-averaged plasma properties in electron-bombardment ion thrusters  
p 54 A89-28339

- Structural and thermal response of 30 cm diameter ion thruster optics  
[AIAA PAPER 89-2719] p 58 A89-47042

- Successful completion of a cyclic ground test of a mercury ion Auxiliary Propulsion System  
p 59 A89-47450

**MESH**

- Improvement in finite element meshes: Heat transfer in an infinite cylinder  
[NASA-TM-101410] p 182 N89-14450

**MESSAGE PROCESSING**

- A message passing kernel for the hypercluster parallel processing test bed  
[NASA-TM-101952] p 218 N89-20684

- Initial operating capability for the hypercluster parallel-processing test bed  
[NASA-TM-101953] p 218 N89-20685

**METAL COMBUSTION**

- Friction-induced ignition of metals in high-pressure oxygen  
p 97 A89-32932

- Ignition and combustion of metallized propellants  
[AIAA PAPER 89-2883] p 117 A89-47148

**METAL CRYSTALS**

- Effects of cobalt concentration on the relative resistance to octahedral and cube slip in nickel-base superalloys  
p 94 A89-17115

- Thermosolutal convection during dendritic solidification  
[AIAA PAPER 89-0626] p 118 A89-25495

**METAL FATIGUE**

- Morphological study of near threshold fatigue crack growth in a coarse grain aluminum alloy  
p 94 A89-12326

- Resolved shear stress intensity coefficient and fatigue crack growth in large crystals  
p 96 A89-22048

- Isothermal and 'bithermal' thermomechanical fatigue behavior of a NiCoCrAlY-coated single crystal superalloy  
p 177 A89-36457

- Surface fatigue life of carburized and hardened M50NiL and AISI 9310 spur gears and rolling-contact test bars  
[AIAA PAPER 89-2819] p 180 A89-47105

- Kinetics of fracture in Fe-3Si steel under mode I loading  
p 99 A89-47320

- The low cycle fatigue deformation response of a single-crystal superalloy at 650 C  
p 99 A89-52204

- High-temperature LCF of Ni-201 and 304L stainless steel  
p 100 N89-12635

- Constitutive modelling of single crystal and directionally solidified superalloys  
p 102 N89-17325

- Fatigue life prediction modeling for turbine hot section materials  
p 30 N89-20142

- Results of inphase axial-torsional fatigue experiments on 304 stainless steel  
[NASA-TM-101464] p 201 N89-20514

- Surface fatigue life of carburized and hardened M50NiL and AISI 9310 spur gears and rolling-contact test bars  
[NASA-TM-101979] p 185 N89-22111

- Fatigue crack growth model RANDOM2 user manual, appendix 1  
[NASA-CR-184939] p 203 N89-23890

- Fatigue strength reduction model: RANDOM3 and RANDOM4 user manual, appendix 2  
[NASA-CR-184940] p 203 N89-23891

**METAL FIBERS**

- The effect of Co alloying content on the kinetics of reaction zone growth in tungsten fiber reinforced superalloy composites  
p 79 A89-11324

- Thermal-mechanical fatigue test apparatus for metal matrix composites and joint attachments  
p 79 A89-15727

- Reaction kinetics between fiber and matrix  
p 83 A89-36420

- Fiber reinforced superalloys for rocket engines  
[NASA-TM-100880] p 86 N89-15990

- Fiber reinforced superalloys for rocket engines  
p 103 N89-22673

**METAL HALIDES**

- Evaluation of transport conditions during physical vapor transport growth of opto-electronic crystals  
[AIAA PAPER 89-0229] p 118 A89-25197

**METAL IONS**

- Interaction of Au, Ag, and Bi ions with Ba<sub>2</sub>YCu<sub>3</sub>O(7-y) - Implications for superconductor applications  
p 235 A89-22886

- Influence of several metal ions on the gelation activation energy of silicon tetraethoxide  
[NASA-TM-101380] p 114 N89-21894

**METAL MATRIX COMPOSITES**

- The effect of Co alloying content on the kinetics of reaction zone growth in tungsten fiber reinforced superalloy composites  
p 79 A89-11324

- Thermal-mechanical fatigue test apparatus for metal matrix composites and joint attachments  
p 79 A89-15727

- A unique set of micromechanics equations for high-temperature metal matrix composites  
p 190 A89-15734

- Thermoviscoplastic nonlinear constitutive relationships for structural analysis of high-temperature metal matrix composites  
p 190 A89-15735

- Fluid flow phenomena in the generation of boron carbide suspensions in magnesium melts  
p 79 A89-19472

- A viscoplastic constitutive theory for metal matrix composites at high temperature  
p 80 A89-20725

- Interdiffusion effects between TiBe<sub>12</sub> and NiAl intermetallics  
p 95 A89-21395

- Finite element applications to explore the effects of partial bonding on metal matrix composite properties  
[AIAA PAPER 89-1175] p 192 A89-30666

- Fracture resistance of a TiB<sub>2</sub> particle/SiC matrix composite at elevated temperature  
p 81 A89-31074

- Elevated temperature slow plastic deformation of NiAl/TiB<sub>2</sub> particulate composites  
p 81 A89-31689

- Symbolic generation of constitutive equations  
p 221 A89-34963

- Reaction kinetics between fiber and matrix  
p 83 A89-36420

C4

- 1200 to 1400 K slow strain rate compressive behavior of small grain size NiAl/Ni<sub>2</sub>AlTi alloys and NiAl/Ni<sub>2</sub>AlTi-TiB<sub>2</sub> composites p 99 A89-53497
- The role of rapid solidification processing in the fabrication of fiber reinforced metal matrix composites [NASA-TM-101450] p 85 N89-15201
- Finite element implementation of viscoplastic models p 200 N89-17328
- Finite element applications to explore the effects of partial bonding on metal matrix composite properties [NASA-TM-101482] p 86 N89-20206
- The isothermal fatigue behavior of a unidirectional SiC/Ti composite and the Ti alloy matrix [NASA-TM-101984] p 86 N89-22684
- Theoretical analysis of compatibility of several reinforcement materials with NiAl and FeAl matrices [NASA-CR-182291] p 86 N89-23622
- Isothermal life prediction of composite lamina using a damage mechanics approach [NASA-TM-102032] p 87 N89-24460
- On finite element implementation and computational techniques for constitutive modeling of high temperature composites [NASA-CR-185120] p 204 N89-26261
- Metal matrix composite micromechanics: In-situ behavior influence on composite properties [NASA-TM-102302] p 88 N89-26924
- Optimum interface properties for metal matrix composites [NASA-TM-102295] p 205 N89-27223
- Computational simulation of high temperature metal matrix composites cyclic behavior [NASA-TM-102115] p 88 N89-27795
- Tungsten fiber reinforced copper matrix composites: A review [NASA-TP-2924] p 88 N89-27796
- The interface in tungsten fiber reinforced niobium metal-matrix composites [NASA-TM-102122] p 104 N89-28627
- Revolutionary opportunities for materials and structures study, addendum no. 1 [NASA-CR-179642-ADD-1] p 47 N89-29478
- Creep behavior of tungsten fiber reinforced niobium metal matrix composites [NASA-TM-102307] p 104 N89-29522
- METAL OXIDES**
- Oxide scale stresses in polycrystalline Ni200 p 98 A89-38859
- Alkoxysilane adsorption on metal oxide substrates p 92 A89-44536
- Acidic attack of perfluorinated alkyl ether lubricant molecules by metal oxide surfaces [NASA-TM-101962] p 93 N89-19402
- METAL POWDER**
- Effect of grain size on the high temperature properties of B2 aluminides [NASA-TM-101382] p 101 N89-12720
- METAL SURFACES**
- The interaction of gold with gallium arsenide p 90 A89-16416
- The effect of metal surface passivation on the Au-InP interaction p 132 A89-30443
- Combined roles of buoyancy and orientation in nucleate pool boiling p 119 A89-35015
- Metal-silicon reaction rates - The effects of capping p 93 A89-52202
- Arc-textured high emittance radiator surfaces [NASA-CASE-LEW-14679-1] p 116 N89-28651
- METAL VAPORS**
- Theoretical studies in support of the 3M-vapor transport (PVTOS-) experiments [NASA-CR-185122] p 165 N89-26179
- METALLOGRAPHY**
- Use of pure nickel and LiOH for thermal energy storage p 91 A89-23146
- METALS**
- Computer simulation of cyclic oxidation p 91 A89-29295
- Adhesion in ceramics and magnetic media [NASA-TM-101476] p 113 N89-19435
- Design, development and applications of novel techniques for studying surface mechanical properties [NASA-TM-101959] p 113 N89-20253
- METEORITES**
- Overview of environmental factors p 240 N89-23529
- METEORITIC DAMAGE**
- The effect of the near earth micrometeoroid environment on a highly reflective mirror surface [AIAA PAPER 88-0026] p 40 A89-17939
- METHODOLOGY**
- A review of failure models for unidirectional ceramic matrix composites under monotonic loads [NASA-TM-101421] p 198 N89-14470
- MICROCOMPUTERS**
- Design and implementation of a microcomputer-based user interface controller for burst data communications satellite ground terminals [NASA-TM-101375] p 43 N89-13457
- Parallel Gaussian elimination of a block tridiagonal matrix using multiple microcomputers [NASA-TP-2892] p 218 N89-17422
- A real time microcomputer implementation of sensor failure detection for turbofan engines [NASA-TM-102327] p 216 N89-29032
- MICROCRACKS**
- Examination of coating failure by acoustic emission p 110 N89-13654
- MICROGRAVITY APPLICATIONS**
- Robots for manipulation in a micro-gravity environment p 215 A89-11682
- Gravitational macrosegregation in unidirectionally solidified lead-tin alloy p 117 A89-17112
- Facilities for microgravity combustion research [IAF PAPER 88-355] p 117 A89-17784
- A facility for precise temperature control applications in microgravity p 48 A89-36956
- Vapor condensation at a turbulent liquid surface in systems with possible spaced-based applications [AIAA PAPER 89-2846] p 151 A89-47122
- Microgravity combustion science: A program overview [NASA-TM-101424] p 122 N89-28665
- MICROHARDNESS**
- Preparation and evaluation of silicon nitride matrices for silicon nitride-SiC fiber composites [NASA-CR-184798] p 115 N89-23678
- MICROINSTRUMENTATION**
- Development and applications of optical interferometric micrometrology in the Angstrom and subangstrom range p 170 A89-27663
- MICROMECHANICS**
- A unique set of micromechanics equations for high-temperature metal matrix composites p 190 A89-15734
- Structural tailoring of laminate properties [AIAA PAPER 89-1367] p 192 A89-30842
- Mechanics of composite materials - Past, present and future p 82 A89-36293
- Adhesion, friction and micromechanical properties of ceramics p 107 A89-54277
- A probabilistic approach to composite micromechanics [NASA-TM-101366] p 85 N89-12684
- Nonlinear mesomechanics of composites with periodic microstructure [NASA-TM-102051] p 204 N89-26260
- Tailoring of composite links for optimal damped elasto-dynamic performance [NASA-TM-102094] p 88 N89-26912
- Metal matrix composite micromechanics: In-situ behavior influence on composite properties [NASA-TM-102302] p 88 N89-26924
- MICROMETEORIODS**
- The effect of the near earth micrometeoroid environment on a highly reflective mirror surface [AIAA PAPER 88-0026] p 40 A89-17939
- Effect of micrometeoroid and space debris impacts on the Space Station Freedom solar array surfaces [NASA-TM-102287] p 47 N89-26035
- MICROPOLAR FLUIDS**
- On the performance of finite journal bearings lubricated with micropolar fluids p 181 A89-54977
- MICROPROCESSORS**
- Film annotation system for a space experiment [NASA-CR-185114] p 176 N89-27152
- MICROSTRIP ANTENNAS**
- Rigorous analysis of a circular patch antenna excited by a microstrip transmission line p 125 A89-53134
- MICROSTRIP TRANSMISSION LINES**
- Rigorous analysis of a circular patch antenna excited by a microstrip transmission line p 125 A89-53134
- Analytical and experimental procedures for determining propagation characteristics of millimeter-wave gallium arsenide microstrip lines [NASA-TP-2899] p 136 N89-21169
- MICROSTRUCTURE**
- Transmission electron microscopy of composites p 79 A89-14560
- Radiographic and ultrasonic characterization of sintered silicon carbide p 187 A89-14700
- Gravitational macrosegregation in unidirectionally solidified lead-tin alloy p 117 A89-17112
- Microstructures in rapidly solidified niobium aluminides p 95 A89-18193
- Microstructural evolution on crystallizing the glassy phase in a 6 weight percent Y<sub>2</sub>O<sub>3</sub>-Si<sub>3</sub>N<sub>4</sub> ceramic p 80 A89-19487
- Concepts for interrelating ultrasonic attenuation, microstructure, and fracture toughness in polycrystalline solids p 95 A89-19852
- A Monte Carlo-finite element model for strain energy controlled microstructural evolution - 'Rafting' in superalloys p 96 A89-24358
- Effects of various consolidation techniques on microstructure, strength, and reliability of alpha-SiC p 106 A89-33611
- High-strength silicon carbides by hot isostatic pressing [NASA-TM-101400] p 111 N89-13666
- Design, development and applications of novel techniques for studying surface mechanical properties [NASA-TM-101959] p 113 N89-20253
- Deformation modeling and constitutive modeling for anisotropic superalloys [NASA-CR-4215] p 202 N89-21258
- Preparation and evaluation of silicon nitride matrices for silicon nitride-SiC fiber composites [NASA-CR-184798] p 115 N89-23678
- Characterization of ceramics and intermetallics fabricated by self-propagating high-temperature synthesis [NASA-TM-102004] p 78 N89-25285
- Nonlinear mesomechanics of composites with periodic microstructure [NASA-TM-102051] p 204 N89-26260
- Non-uniform transition conductivity of superconducting ceramic [NASA-TM-102133] p 189 N89-28851
- MICROWAVE CIRCUITS**
- GaAs MMIC elements in phased-array antennas p 131 A89-15827
- GaAs circuits for monolithic optical controller p 131 A89-15828
- The potential impact of MMICs on future satellite communications [NASA-CR-182227] p 126 N89-17078
- The potential impact of MMICs on future satellite communications: Executive summary [NASA-CR-182227-EXEC-SUMM] p 127 N89-17079
- Universal test fixture for monolithic mm-wave integrated circuits calibrated with an augmented TRD algorithm [NASA-TP-2875] p 127 N89-17767
- Optical detectors for GaAs MMIC integration: Technology assessment [NASA-TM-102025] p 137 N89-22020
- Microwave characteristics of GaAs MMIC integratable optical detectors [NASA-TM-101485] p 129 N89-24520
- Performance of five 30 GHz satellite receivers [NASA-TM-101960] p 129 N89-25365
- MICROWAVE EQUIPMENT**
- Digitally modulated bit error rate measurement system for microwave component evaluation [NASA-TP-2912] p 40 N89-28545
- MICROWAVE FREQUENCIES**
- Microwave response of an HEMT photoconductor p 131 A89-15824
- Experiments and analysis of a compact electrothermal thruster p 59 A89-47494
- MICROWAVE OSCILLATORS**
- Study of optical output couplers for submillimeter wavelength backward-wave oscillators (BWO's) p 132 A89-32857
- MICROWAVE PHOTOGRAPHY**
- Investigation of surface water behavior during glaze ice accretion p 16 A89-27739
- MICROWAVE TRANSMISSION**
- Analytical and experimental procedures for determining propagation characteristics of millimeter-wave gallium arsenide microstrip lines [NASA-TP-2899] p 136 N89-21169
- Channelized coplanar waveguide: Discontinuities, junctions, and propagation characteristics [NASA-TM-101483] p 137 N89-21172
- Performance of five 30 GHz satellite receivers [NASA-TM-101960] p 129 N89-25365
- MICROWAVES**
- Microwave characteristics of GaAs MMIC integratable optical detectors [NASA-TM-101485] p 129 N89-24520
- Microwave and millimeter-wave power generation in silicon carbide (SiC) IMPATT devices [NASA-CR-185050] p 139 N89-26143
- Development of a high power microwave thruster, with a magnetic nozzle, for space applications [NASA-TM-102321] p 74 N89-26904
- Measurements of complex permittivity of microwave substrates in the 20 to 300 K temperature range from 26.5 to 40.0 GHz [NASA-TM-102123] p 123 N89-27038
- MILITARY AIRCRAFT**
- Multiple-Purpose Subsonic Naval Aircraft (MPSNA) Multiple Application Propfan Study (MAPS) [NASA-CR-175096] p 18 N89-19289
- Multiple Application Propfan Study (MAPS): Advanced tactical transport [NASA-CR-175003] p 28 N89-19300

## MILITARY HELICOPTERS

## MILITARY HELICOPTERS

A review and forecast of engine system research at the Army Propulsion Directorate p 23 A89-36397

## MILITARY OPERATIONS

SP-100 nuclear space power systems with application to space commercialization p 63 N89-12665 [NASA-TM-101403]

## MILLIMETER WAVES

External electro-optic probing of millimeter-wave integrated circuits p 133 A89-45266  
Development of a 39.5 GHz Karp traveling wave tube for use in space p 136 N89-15336 [NASA-CR-182182]  
Universal test fixture for monolithic mm-wave integrated circuits calibrated with an augmented TRD algorithm [NASA-TP-2875] p 127 N89-17767  
External electro-optic probing of millimeter-wave integrated circuits p 128 N89-21142 [NASA-TM-101990]  
Development of a 75-watt 60-GHz traveling-wave tube for intersatellite communications p 138 N89-24530 [NASA-CR-182135]  
Microwave and millimeter-wave power generation in silicon carbide (SiC) IMPATT devices p 139 N89-26143 [NASA-CR-185050]  
Millimeter wave transmission studies of YBa<sub>2</sub>Cu<sub>3</sub>O<sub>7- $\delta$</sub>  thin films in the 26.5 to 40.0 GHz frequency range p 237 N89-30088 [NASA-TM-102345]

## MINING

Lunar Helium-3 and Fusion Power p 233 N89-14842 [NASA-CP-10018]  
Assessment of lunar sources of He-3 for use on earth p 242 N89-14853

## MIRRORS

The effect of the near earth micrometeoroid environment on a highly reflective mirror surface p 40 A89-17939 [AIAA PAPER 88-0026]  
Performance of multimirror quartzline lamps in a high-pressure, underwater environment p 172 N89-10269 [NASA-TM-101374]  
A segmented mirror antenna for radiometers p 128 N89-23753 [NASA-TM-102045]

## MIS (SEMICONDUCTORS)

Metal-silicon reaction rates - The effects of capping p 93 A89-52202

## MISALIGNMENT

Topology of modified helical gears and Tooth Contact Analysis (TCA) program p 186 N89-22920 [NASA-CR-4224]  
Topology of modified helical gears p 187 N89-28015 [NASA-TM-102134]

## MISSILE CONFIGURATIONS

Average-passage simulation of counter-rotating propfan propulsion systems as applied to cruise missiles [AIAA PAPER 89-2943] p 7 A89-47187  
Average-passage simulation of counter-rotating propfan propulsion systems as applied to cruise missiles p 14 N89-23416 [NASA-TM-102043]

## MISSILES

High angle-of-attack hypersonic aerodynamics p 2 A89-19918

## MISSION PLANNING

In-situ propellant advantages for fast transfer to Mars [AIAA PAPER 88-2901] p 37 A89-14977  
Nuclear reactor power as applied to a space-based radar mission p 51 A89-15317  
SP-100 nuclear space power systems with application to space commercialization p 63 N89-12665 [NASA-TM-101403]  
Unique mission options available with a megawatt-class nuclear electric propulsion system p 65 N89-17618 [NASA-TM-101220]  
Human exploration mission studies p 38 N89-22985  
Toward an electrical power utility for space exploration [NASA-TM-102347] p 75 N89-27704  
NASA advanced space photovoltaic technology-status, potential and future mission applications p 75 N89-27705 [NASA-TM-102093]

## MIXED OXIDES

Structural chemistry of Au(III)-substituted Ba<sub>2</sub>YCu<sub>3</sub>O<sub>7- $\delta$</sub>  p 89 A89-12620  
Transport critical current and magnetization measurements of melt-processed YBa<sub>2</sub>Cu<sub>3</sub>O<sub>7- $\delta$</sub>  p 234 A89-20037  
Effect of processing parameters on the characteristics of high-T<sub>c</sub> superconductor YBa<sub>2</sub>Cu<sub>3</sub>O<sub>y</sub> p 234 A89-20467  
Interaction of Au, Ag, and Bi ions with Ba<sub>2</sub>YCu<sub>3</sub>O<sub>7- $\delta$</sub>  - Implications for superconductor applications p 235 A89-22886  
Improved synthesis of ceramic superconductors with alkaline earth peroxides - Synthesis and processing of Ba<sub>2</sub>YCu<sub>3</sub>O<sub>7- $\delta$</sub>  p 235 A89-22887  
Critical currents of aligned grains of Ti-Ba-Ca-Cu-O compounds p 235 A89-30335

Highly oriented Ti<sub>2</sub>Ba<sub>2</sub>Ca<sub>2</sub>Cu<sub>3</sub>O<sub>10</sub> thin films by pulsed laser evaporation p 236 A89-30421  
Doping directed at the oxygen sites in Y<sub>1</sub>Ba<sub>2</sub>Cu<sub>3</sub>O<sub>7- $\delta$</sub>  - The effect of sulfur, fluorine, and chlorine p 133 A89-37824  
Preparation of high T<sub>c</sub> Ti-Ba-Ca-Cu-O thin films by pulsed laser evaporation and Ti<sub>2</sub>O<sub>3</sub> vapor processing p 236 A89-38608  
Free energy surfaces in the superconducting mixed state p 236 A89-43928

## MIXING

Direct numerical simulations of a temporally evolving mixing layer subject to forcing p 147 A89-34426  
Turbofan forced mixer lobe flow modeling. Part 3: Application to augment engines p 8 N89-10025 [NASA-CR-4147-PT-3]

## MIXING LAYERS (FLUIDS)

Effects of excitation level on the stability of an axisymmetric mixing layer p 2 A89-16882  
Turbulence management in free shear flows by control of coherent structures p 147 A89-30908  
Effects of heat release on the large-scale structure in turbulent mixing layers p 147 A89-31844  
Nonlinear interaction between the sinuous and varicose instability modes in a plane wake p 147 A89-33779  
Direct numerical simulations of a temporally evolving mixing layer subject to forcing p 147 A89-34426  
Three-dimensional wave packets and instability waves in free shear layers and their receptivity p 149 A89-38619

The use of direct numerical simulation in the study of turbulent, chemically-reacting flows p 152 A89-51873  
Turbofan forced mixer lobe flow modeling. 1: Experimental and analytical assessment p 11 N89-14221 [NASA-CR-4147-PT-1]  
Turbofan forced mixer lobe flow modeling. 2: Three-dimensional inviscid mixer analysis (FLOMIX) p 11 N89-14222 [NASA-CR-4147-PT-2]

## MODAL RESPONSE

Modal, ray, and beam techniques for analyzing the EM scattering by open-ended waveguide cavities p 125 A89-39594  
Modal representations in control/structure interaction p 45 A89-54114  
Tailoring of composite links for optimal damped elasto-dynamic performance [NASA-TM-102094] p 88 N89-26912

## MODELS

Vibration, performance, flutter and forced response characteristics of a large-scale propfan and its aeroelastic model p 21 A89-17943 [AIAA PAPER 88-3155]  
Modeling of some coplanar waveguide discontinuities p 131 A89-24139  
Performance characterizations of an engineering model multipropellant resistojet p 54 A89-28340  
Computerized life and reliability modeling for turboprop transmissions p 181 A89-53364  
Vibration, performance, flutter and forced response characteristics of a large-scale propfan and its aeroelastic model p 24 N89-10043 [NASA-TM-101322]  
A sintering model for SiC(sub)/Si<sub>3</sub>N<sub>4</sub> composites p 108 N89-10166 [NASA-TM-101336]  
Noninteractive macroscopic reliability model for ceramic matrix composites with orthotropic material symmetry [NASA-TM-101414] p 198 N89-15437  
Thermoviscoplastic model with application to copper [NASA-TP-2845] p 198 N89-16183  
Stochastic modeling of crack initiation and short-crack growth under creep and creep-fatigue conditions [NASA-TM-101358] p 199 N89-17286  
Frequency domain model for analysis of paralleled, series-output-connected Mapham inverters p 139 N89-26149 [NASA-TM-102140]

## MODEMS

Programmable rate modem utilizing digital signal processing techniques [NASA-CR-185124] p 43 N89-26879

## MODULATION

Fiber-optic temperature sensor using a spectrum-modulating semiconductor etalon p 168 A89-10366  
Advanced modulation technology development for earth station demodulator applications [NASA-CR-185126] p 43 N89-26880  
Digitally modulated bit error rate measurement system for microwave component evaluation [NASA-TP-2912] p 40 N89-28545

## MODULATORS

Design of a GaAlAs travelling wave Mach-Zehnder electro-optic modulator p 130 A89-10342

## MODULES

A definition study of the on-orbit assembly operations for the outboard photovoltaic power modules for Space Station Freedom [NASA-TM-102006] p 41 N89-20171  
Photovoltaic module on-orbit assembly for Space Station Freedom [NASA-TM-102297] p 47 N89-26887

## MODULUS OF ELASTICITY

Theoretical analysis of compatibility of several reinforcement materials with NiAl and FeAl matrices [NASA-CR-182291] p 86 N89-23622

## MOLECULAR BEAM EPITAXY

Characterization of GaAlAs optical waveguide heterostructures grown by molecular beam epitaxy p 130 A89-10343  
Shubnikov-de Haas measurements of the 2-D electron gas in pseudomorphic In<sub>0.1</sub>Ga<sub>0.9</sub>As grown on GaAs p 235 A89-29299  
Deep-level transient spectroscopy of Al(x)Ga(1-x)As/GaAs using nondestructive acousto-electric voltage measurement p 133 A89-42742

Molecular beam epitaxial growth of high-quality InSb on InP and GaAs substrates p 236 N89-26739 [NASA-CR-185440]  
Surface morphologies and electrical properties of molecular beam epitaxial InSb and InAs(x)Sb(1-x) grown on GaAs and InP substrates p 237 N89-26740 [NASA-CR-185439]

## MOLECULAR BEAMS

Pulsed ion beam investigation of the kinetics of surface reactions p 93 A89-44542

## MOLECULAR PHYSICS

A model for including thermal conduction in molecular dynamics simulations p 237 A89-41259

## MOLECULAR SPECTRA

Connection between energy relations of solids and molecules p 91 A89-26406

## MOLECULAR STRUCTURE

Light weight polymer matrix composite material [NASA-CASE-LEW-14734-1] p 87 N89-23623

## MOLTEN SALTS

Densities of some molten fluoride salt mixtures suitable for heat storage in space power applications p 77 A89-41444  
Compatibility of molten salts with advanced solar dynamic receiver materials [AIAA PAPER 89-1756] p 83 A89-48957  
Molten salt corrosion of SiC and Si<sub>3</sub>N<sub>4</sub> [NASA-TM-101346] p 108 N89-11912

## MOM (SEMICONDUCTORS)

Submicron nickel-oxide-gold tunnel diode detectors for rectennas p 133 A89-43469

## MOMENTUM TRANSFER

Numerical studies of convective heat transfer in an inclined semiannular enclosure [NASA-TM-102011] p 123 N89-28666

## MONITORS

High resolution video monitoring of coating thickness during plasma spraying [NASA-TM-101423] p 102 N89-15218  
Integrated control and health monitoring capacitive displacement sensor development task. Orbit transfer rocket engine technology program [NASA-CR-182279] p 176 N89-26208  
OTVE turbopump condition monitoring, task E.5 [NASA-CR-182274] p 189 N89-27204

## MONOCHROMATIC RADIATION

A heat-driven monochromatic light source p 224 A89-41722

## MONOTONE FUNCTIONS

Second-order accurate nonoscillatory schemes for scalar conservation laws [NASA-TM-102010] p 14 N89-22573

## MONTE CARLO METHOD

A Monte Carlo-finite element model for strain energy controlled microstructural evolution - 'Ratting' in superalloys p 96 A89-24358  
Creep life prediction based on stochastic model of microstructurally short crack growth p 193 A89-36185  
An improved correction algorithm for number density measurements made with the forward scattering spectrometer probe p 170 A89-44122  
A correction algorithm for particle size distribution measurements made with the forward-scattering spectrometer probe p 170 A89-44123

## MORPHOLOGY

Crystallization kinetics of BaO-Al<sub>2</sub>O<sub>3</sub>-SiO<sub>2</sub> glasses [NASA-TM-101964] p 113 N89-20252  
Surface morphologies and electrical properties of molecular beam epitaxial InSb and InAs(x)Sb(1-x) grown on GaAs and InP substrates p 237 N89-26740 [NASA-CR-185439]

**MOTORS**

Magnification of starting torques of dc motors by maximum power point trackers in photovoltaic systems [NASA-TM-102040] p 138 N89-23792

**MULLITES**

Phase transformations in xerogels of mullite composition [NASA-TM-101349] p 108 N89-11038

**MULTIGRID METHODS**

Application of multi-grid methods for solving the Navier-Stokes equations p 153 A89-53172

**MULTIPHASE FLOW**

Turbulent multiphase flows p 152 A89-51883

**MULTIPLE ACCESS**

Study of spread spectrum multiple access systems for satellite communications with overlay on current services: Executive summary [NASA-CR-180827-EXEC-SUMM] p 128 N89-23756  
Study of spread spectrum multiple access systems for satellite communications with overlay on current services [NASA-CR-180827] p 128 N89-23757

**MULTIPROCESSING (COMPUTERS)**

Parallel Gaussian elimination of a block tridiagonal matrix using multiple microcomputers [NASA-TP-2892] p 218 N89-17422  
Interfacing laboratory instruments to multiuser, virtual memory computers [NASA-TM-4106] p 188 N89-19578  
Automating the multiprocessing environment [NASA-TM-4103] p 217 N89-20641

**MULTIVARIATE STATISTICAL ANALYSIS**

Probabilistic structural analysis methods and applications p 190 A89-16939

**MUSHY ZONES**

Computer simulation of macrosegregation in directionally solidified circular ingots [NASA-CR-182838] p 122 N89-21134

**N****NACELLES**

An analysis for high speed propeller-nacelle aerodynamic performance prediction. Volume 1: Theory and application [NASA-CR-4199-VOL-1] p 12 N89-15896

An analysis for high speed propeller-nacelle aerodynamic performance prediction. Volume 2: User's manual [NASA-CR-4199-VOL-2] p 12 N89-15897

**NASA PROGRAMS**

An experimental analysis of a doped lithium fluoride direct absorption solar receiver p 49 A89-15245

High temperature superconducting magnetic energy storage for future NASA missions p 50 A89-15288

Microgravity research in NASA ground-based facilities [AIAA PAPER 89-0236] p 118 A89-25201

An overview of the current NASA program on aircraft icing research [SAE PAPER 881386] p 16 A89-28192

The solid surface combustion Space Shuttle experiment hardware description and ground-based test results [AIAA PAPER 89-0503] p 119 A89-28419

The NASA Lewis Research Center High Temperature Fatigue and Structures Laboratory p 194 A89-43528

NASA's Chemical Transfer Propulsion Program for Pathfinder [AIAA PAPER 89-2298] p 37 A89-46735

Microgravity research in NASA ground-based facilities [NASA-TM-101397] p 240 N89-15047

NASA advanced propeller research [NASA-TM-101361] p 27 N89-15913

NASA HOST project overview p 29 N89-20136

Views on the impact of HOST p 31 N89-20144

Comparison of conceptual designs for 25 kW advanced Stirling conversion systems for dish electric application [NASA-TM-102085] p 239 N89-26781

NASA's Chemical Transfer Propulsion Program for Pathfinder [NASA-TM-102298] p 41 N89-26876

**NASA SPACE PROGRAMS**

Baseband processor hardware for Advanced Communication Technology Satellite (ACTS) p 43 A89-38298

NASA photovoltaic research and technology [NASA-TM-101422] p 65 N89-16917

Systems autonomy technology: Executive summary and program plan [NASA-TM-100999] p 216 N89-18045

Human exploration mission studies p 38 N89-22985

The Pathfinder Chemical Transfer Propulsion program [NASA-TM-102084] p 41 N89-24409

**NASTRAN**

A NASTRAN DMAP alter for linear buckling analysis under dynamic loading [NASA-TM-100832] p 85 N89-13522

Modal forced vibration analysis of aerodynamically excited turbosystems [NASA-CR-174966] p 201 N89-18696

NASTRAN supplemental documentation for modal forced vibration analysis of aerodynamically excited turbosystems [NASA-CR-174967] p 201 N89-19583

A NASTRAN DMAP alter for linear buckling analysis under dynamic loading p 202 N89-22948

**NATURAL LANGUAGE (COMPUTERS)**

Laboratory process control using natural language commands from a personal computer [NASA-TM-101988] p 218 N89-24055

**NAVIER-STOKES EQUATION**

Navier-Stokes solution to the flowfield over ice accretion shapes p 1 A89-12557

PNS calculations for 3-D hypersonic corner flow with two turbulence models [AIAA PAPER 88-2958] p 1 A89-14979

Navier-Stokes calculation of solid-propellant rocket motor internal flowfields [AIAA PAPER 88-3182] p 48 A89-14983

Unsteady solution of incompressible Navier-Stokes equations p 141 A89-15143

A diagonally inverted LU implicit multigrid scheme for the 3-D Navier-Stokes equations and a two equation model of turbulence [AIAA PAPER 89-0467] p 145 A89-25382

Evaluation of three turbulence models for the prediction of steady and unsteady airloads [AIAA PAPER 89-0609] p 3 A89-25485

Three dimensional PNS solutions of hypersonic internal flows with equilibrium chemistry [AIAA PAPER 89-0002] p 146 A89-28401

Numerical analysis of flow through oscillating cascade sections [AIAA PAPER 89-0437] p 4 A89-28413

On the role of artificial viscosity in Navier-Stokes solvers [AIAA PAPER 89-1947] p 5 A89-41794

A time accurate finite volume high resolution scheme for three dimensional Navier-Stokes equations [AIAA PAPER 89-1994] p 6 A89-41837

A Newton/upwind method and numerical study of shock wave/boundary layer interactions p 6 A89-45468

Application of multi-grid methods for solving the Navier-Stokes equations p 153 A89-53172

High speed corner and gap-seal computations using an LU-SGS scheme [AIAA PAPER 89-2669] p 154 A89-54424

A diagonally inverted LU implicit multigrid scheme for the 3-D Navier-Stokes equations and a two equation model of turbulence [NASA-CR-182209] p 9 N89-10863

Simulation of 2-dimensional viscous flow through cascades using a semi-elliptic analysis and hybrid C-H grids [NASA-CR-4180] p 10 N89-12553

Evaluation of three turbulence models for the prediction of steady and unsteady airloads [NASA-TM-101413] p 10 N89-12555

Turbine stator flow field simulations p 157 N89-12902

Numerical analysis of flow through oscillating cascade sections [NASA-TM-101417] p 11 N89-14220

Control-volume based Navier-Stokes equation solver valid at all flow velocities [NASA-TM-101488] p 161 N89-20407

Comparison of 3D computation and experiment for non-axisymmetric nozzles [NASA-CR-182245] p 14 N89-20921

On the nature of Navier-Stokes turbulence [NASA-TM-101983] p 163 N89-23813

Multigrid calculation of three-dimensional turbomachinery flows [NASA-CR-185332] p 165 N89-26172

High speed corner and gap-seal computations using an LU-SGS scheme [NASA-TM-102138] p 166 N89-27103

Interaction between Tollmien-Schlichting waves and free-stream disturbances in boundary-layer flows [NASA-CR-185847] p 167 N89-27118

Mach 5 inlet CFD and experimental results [NASA-TM-102317] p 33 N89-27670

**NEAR FIELDS**

Near-field acoustic environment of a supersonic plume adjacent to a wall [AIAA PAPER 89-1137] p 225 A89-33767

Near-field acoustic characteristics of a single-rotor propan [AIAA PAPER 89-1055] p 23 A89-36215

Determination of near and far field acoustics for advanced propeller configurations [AIAA PAPER 89-1040] p 226 A89-40469

Computed performance of the half-scale accurate antenna reflector [NASA-CR-182284] p 139 N89-24532

**NEAR WAKES**

Near wakes of advanced turbopropellers [AIAA PAPER 89-1095] p 5 A89-33735

The plasma wake of the Shuttle Orbiter p 215 A89-43680

**NEGATIVE RESISTANCE CIRCUITS**

Computer analysis of the negative differential resistance switching phenomenon of double-injection devices p 134 A89-54963

**NEODYMIUM LASERS**

Holographic interferometry with an injection seeded Nd:YAG laser and two reference beams [NASA-TM-102056] p 175 N89-24591

**NETWORK CONTROL**

Integrated communication and control systems. I - Analysis [ASME PAPER 88-WA/DSC-1] p 219 A89-22499

Integrated communication and control systems. II - Design considerations [ASME PAPER 88-WA/DSC-2] p 219 A89-22500

**NEURAL NETS**

Neuromorphic learning of continuous-valued mappings in the presence of noise: Application to real-time adaptive control [NASA-TM-101999] p 221 N89-24856

**NEUTRINOS**

Limits to the radiative decays of neutrinos and axions from gamma-ray observations of SN 1987A p 242 A89-26985

Nucleosynthesis, neutrino bursts and gamma-rays from coalescing neutron stars p 241 A89-46577

**NEUTRON STARS**

Nucleosynthesis, neutrino bursts and gamma-rays from coalescing neutron stars p 241 A89-46577

**NEWTON METHODS**

A Newton/upwind method and numerical study of shock wave/boundary layer interactions p 6 A89-45468

**NICKEL**

Mechanisms of elevated-temperature deformation in the B2 aluminides NiAl and CoAl p 94 A89-17378

Use of pure nickel and LiOH for thermal energy storage p 91 A89-23146

Performance of lightweight nickel electrodes p 92 A89-44002

Avalanche in adhesion --- interfacial separation between two Ni crystals p 100 A89-54495

Oxygen electrode bifunctional electrocatalyst NiCo2O4 spinel [NASA-TM-100947] p 208 N89-10409

High-temperature LCF of Ni-201 and 304L stainless steel p 100 N89-12635

**NICKEL ALLOYS**

A preliminary report on the effects of long-term exposure of LiOH on pure nickel p 90 A89-12624

High temperature isothermal and cyclic oxidation behavior of a single crystal Ni base superalloy p 94 A89-12625

The effect of sulfur and zirconium co-doping on the oxidation of NiCrAl p 94 A89-13933

Effects of cobalt concentration on the relative resistance to octahedral and cube slip in nickel-base superalloys p 94 A89-17115

Interdiffusional effects between TiBe12 and NiAl intermetallics p 95 A89-21395

Ultrasonic attenuation measurements determine onset, degree, and completion of recrystallization p 187 A89-23936

Effect of 0.1 at. pct Zirconium on the cyclic oxidation resistance of beta-NiAl p 96 A89-24599

Influence of precipitate morphology on intermediate temperature creep properties of a nickel-base superalloy single crystal p 96 A89-26872

Elevated temperature slow plastic deformation of NiAl/TiB2 particulate composites p 81 A89-31689

The influence of high thermal gradient casting, hot isostatic pressing and alternate heat treatment on the structure and properties of a single crystal nickel base superalloy p 97 A89-36427

Transient oxidation of single-crystal beta-NiAl p 98 A89-37899

Effect of the theta-alpha-Al2O3 transformation on the oxidation behavior of beta-NiAl + Zr p 98 A89-38600

Oxide scale stresses in polycrystalline Ni200 p 98 A89-38859

Predicting minimum Al concentrations for protective scale formation on Ni-base alloys. I - Isothermal oxidation. II - Cyclic oxidation p 98 A89-40116

Observations of directional gamma prime coarsening during engine operation p 98 A89-40162

- Dispersoids in rapidly solidified B2 nickel aluminides p 98 A89-43023
- Room temperature tensile ductility in polycrystalline B2 Ni-30Al-20Fe p 98 A89-44568
- TEM studies of oxidized NiAl and NiAl cross sections p 99 A89-46506
- Inelastic deformation and dislocation structure of a nickel alloy - Effects of deformation and thermal histories p 99 A89-50313
- The low cycle fatigue deformation response of a single-crystal superalloy at 650 C p 99 A89-52204
- 1200 to 1400 K slow strain rate compressive behavior of small grain size NiAl/Ni<sub>2</sub>AlTi alloys and NiAl/Ni<sub>2</sub>AlTi-TiB<sub>2</sub> composites p 99 A89-53497
- Thermodynamic analysis of compatibility of several reinforcement materials with beta phase NiAl alloys [NASA-CR-4171] p 84 A89-10131
- Simplified cyclic structural analysis of SSME turbine blades p 63 A89-12632
- Constitutive behavior of single crystal PWA 1480 and directionally solidified MAR-M 246 under monotonic and cyclic loads at high and low temperature p 100 A89-12634
- Constitutive modeling for isotropic materials p 195 A89-12904
- The effect of 0.1 atomic percent zirconium on the cyclic oxidation behavior of beta-NiAl for 300 hours at 1200 C [NASA-TM-101408] p 101 A89-13566
- The oxidation of Ni-rich Ni-Al intermetallics [NASA-TM-101455] p 102 A89-15233
- Constitutive modelling of single crystal and directionally solidified superalloys p 102 A89-17325
- Advanced single crystal for SSME turbopumps [NASA-CR-182244] p 103 A89-21072
- Theoretical analysis of compatibility of several reinforcement materials with NiAl and FeAl matrices [NASA-CR-182291] p 86 A89-23622
- Characterization of ceramics and intermetallics fabricated by self-propagating high-temperature synthesis [NASA-TM-102004] p 78 A89-25285
- NICKEL CADMIUM BATTERIES**
- Impedance studies of Ni/Cd and Ni/H cells using the cell case as reference electrode p 137 A89-23002
- NICKEL HYDROGEN BATTERIES**
- Effect of LEO cycling at shallow depths of discharge on MANTECH IPV nickel-hydrogen cells p 49 A89-15278
- Effect of NASA advanced designs on thermal behavior of Ni-H<sub>2</sub> cells p 50 A89-15279
- The effect of compression on Individual Pressure Vessel Nickel/Hydrogen components --- for energy storage in low earth orbits p 50 A89-15281
- KOH concentration effect on cycle life of nickel-hydrogen cells. III - Cycle life test p 207 A89-23283
- Performance of lightweight nickel electrodes p 92 A89-44002
- Small scale bipolar nickel-hydrogen testing p 208 A89-44005
- Lightweight fibrous nickel electrodes for nickel-hydrogen batteries [NASA-TM-101997] p 93 A89-22710
- Impedance studies of Ni/Cd and Ni/H cells using the cell case as reference electrode p 137 A89-23002
- Nickel-hydrogen capacity loss on storage p 138 A89-23007
- Energy storage and thermal control system design status [NASA-TM-102136] p 46 A89-24427
- NICKEL OXIDES**
- Submicron nickel-oxide-gold tunnel diode detectors for rectennas p 133 A89-43469
- NICKEL PLATE**
- The effect of different alkali metal hydroxides on nickel electrode life p 207 A89-15280
- NIObIUM**
- Reaction kinetics between fiber and matrix p 83 A89-36420
- Design and analysis report for the flight weight 20-inch Columbian secondary nozzle for the RL10 engine [NASA-CR-179612] p 65 A89-16918
- NIObIUM ALLOYS**
- Microstructures in rapidly solidified niobium aluminides p 95 A89-18193
- Influence of alloying elements on the oxidation behavior of NbAl<sub>3</sub> [NASA-TM-101398] p 100 A89-12717
- Evaluation of coated columbium test panels having application to a secondary nozzle extension for the RL10 rocket engine system, parts 1 and 2 [NASA-CR-180809] p 64 A89-13493
- Tensile and creep rupture behavior of P/M processed Nb-base alloy, WC-3009 [NASA-TM-101954] p 78 A89-19371
- Thermodynamic analysis of chemical compatibility of several reinforcement materials with niobium aluminides [NASA-CR-182260] p 86 A89-21036
- Creep behavior of tungsten fiber reinforced niobium metal matrix composites [NASA-TM-102307] p 104 A89-29522
- NITROGEN**
- Adhesion in ceramics and magnetic media [NASA-TM-101476] p 113 A89-19435
- NITROGEN COMPOUNDS**
- Degradation mechanisms of n-dodecane with sulfur and nitrogen dopants during thermal stressing p 116 A89-22277
- NITROGEN OXIDES**
- NO<sub>x</sub> formation from the combustion of monodisperse n-heptane sprays doped with fuel-nitrogen additives p 116 A89-42695
- Investigation of low NO<sub>x</sub> staged combustor concept in high-speed civil transport engines [AIAA PAPER 89-2942] p 23 A89-47186
- Investigation of low NO<sub>x</sub> staged combustor concept in high-speed civil transport engines [NASA-TM-101977] p 32 A89-22606
- NOISE**
- Neuromorphic learning of continuous-valued mappings in the presence of noise: Application to real-time adaptive control [NASA-TM-101999] p 221 A89-24856
- NOISE (SOUND)**
- Comparison of propeller cruise noise data taken in the NASA Lewis 8- by 6-foot wind tunnel with other tunnel and flight data [AIAA PAPER 89-1059] p 226 A89-40472
- Comparison of propeller cruise noise data taken in the NASA Lewis 8- by 6-foot wind tunnel with other tunnel and flight data [NASA-TM-101976] p 228 A89-21628
- NOISE GENERATORS**
- Effect of aerodynamic detuning on supersonic rotor discrete frequency noise generation p 225 A89-15083
- Influence of airfoil thickness on convected gust interaction noise [AIAA PAPER 89-1082] p 225 A89-33725
- Noise of a model counterrotation propeller with simulated fuselage and support pylon at takeoff/approach conditions [AIAA PAPER 89-1143] p 227 A89-48953
- Noise of a model counterrotation propeller with simulated fuselage and support pylon at takeoff/approach conditions [NASA-TM-101996] p 228 A89-24138
- NOISE INTENSITY**
- Noise of a model counterrotation propeller with simulated fuselage and support pylon at takeoff/approach conditions [AIAA PAPER 89-1143] p 227 A89-48953
- Effects of lubrication on the performance of high speed spur gears [NASA-TM-101969] p 186 A89-22919
- Noise of a model counterrotation propeller with simulated fuselage and support pylon at takeoff/approach conditions [NASA-TM-101996] p 228 A89-24138
- NOISE MEASUREMENT**
- Interior noise in the untreated Gulfstream II Propfan Test Assessment (PTA) aircraft [AIAA PAPER 89-1119] p 17 A89-33754
- NOISE POLLUTION**
- Supersonic jet noise and the high speed civil transport [AIAA PAPER 89-2358] p 227 A89-46772
- NOISE PREDICTION**
- High-speed propeller performance and noise predictions at takeoff/landing conditions p 226 A89-39195
- NOISE PREDICTION (AIRCRAFT)**
- Influence of airfoil thickness on convected gust interaction noise [AIAA PAPER 89-1082] p 225 A89-33725
- Near-field acoustic characteristics of a single-rotor propan [AIAA PAPER 89-1055] p 23 A89-36215
- Installed propan (SR-7L) far-field noise characteristics [AIAA PAPER 89-1056] p 225 A89-36216
- Lateral noise attenuation of the advanced propeller of the propan test assessment aircraft [AIAA PAPER 89-1057] p 226 A89-36217
- Fluctuating pressures on wing surfaces in the slipstream of a single-rotor propan [AIAA PAPER 89-1058] p 226 A89-36218
- An acoustic experimental and theoretical investigation of single disc propellers [AIAA PAPER 89-1146] p 227 A89-40478
- Rectangular nozzle plume velocity modeling for use in jet noise prediction [AIAA PAPER 89-2357] p 7 A89-46771
- Rectangular nozzle plume velocity modeling for use in jet noise prediction [NASA-TM-102047] p 14 A89-22577
- High speed turboprop aeroacoustic study (single rotation). Volume 1: Model development [NASA-CR-182257-VOL-1] p 229 A89-24139
- NOISE PROPAGATION**
- High speed turboprop aeroacoustic study (single rotation). Volume 1: Model development [NASA-CR-182257-VOL-1] p 229 A89-24139
- NOISE REDUCTION**
- Acoustic wave propagation in heterogeneous structures including experimental validation [AIAA PAPER 89-1044] p 225 A89-36214
- Supersonic jet noise and the high speed civil transport [AIAA PAPER 89-2358] p 227 A89-46772
- Effect of advanced component technology on helicopter transmissions [NASA-TM-101431] p 182 A89-13794
- NASA powered lift facility internally generated noise and its transmission to the acoustic far field [NASA-CR-182217] p 36 A89-16882
- Acoustic wave propagation in heterogeneous structures including experimental validation [NASA-TM-101486] p 224 A89-19965
- Analysis of modified SMI method for adaptive array weight control [NASA-CR-185493] p 19 A89-25993
- NONDESTRUCTIVE TESTS**
- Radiographic and ultrasonic characterization of sintered silicon carbide p 187 A89-14700
- Concepts for interrelating ultrasonic attenuation, microstructure, and fracture toughness in polycrystalline solids p 95 A89-19852
- Ultrasonic attenuation measurements determine onset, degree, and completion of recrystallization p 187 A89-23936
- The acousto-ultrasonic approach --- for NDE p 188 A89-32305
- Nondestructive evaluation/characterization of composite materials and structures using the acousto-ultrasonic techniques p 188 A89-36571
- Deep-level transient spectroscopy of Al(x)Ga(1-x)As/GaAs using nondestructive acousto-electric voltage measurement p 133 A89-42742
- Thermal Barrier Coatings. Abstracts and figures [NASA-CP-10019] p 110 A89-13642
- Energy in elastic fiber embedded in elastic matrix containing incident SH wave [NASA-CR-4205] p 188 A89-18694
- Nondestructive evaluation of advanced ceramics [NASA-TM-101489] p 189 A89-20490
- A study of the stress wave factor technique for evaluation of composite materials [NASA-CR-4195] p 189 A89-21256
- A new structure for comparing surface passivation materials of GaAs solar cells p 213 A89-24725
- OTVE combustor wall condition monitoring [NASA-CR-182275] p 73 A89-26899
- Ultrasonic imaging of textured alumina [NASA-TM-101478] p 189 A89-28853
- NONISOTHERMAL PROCESSES**
- Unsteady thermocapillary migration of bubbles [NASA-TM-101338] p 162 A89-22054
- NONLINEAR EVOLUTION EQUATIONS**
- Nonlinear spatial evolution of an externally excited instability wave in a free shear layer p 144 A89-23242
- Nonlinear evolution of interacting oblique waves on two-dimensional shear layers [NASA-TM-102030] p 164 A89-24575
- NONLINEAR OPTICS**
- Recovery of excitation intensity dependence in pulsed, focused beams - Nonsaturated case p 177 A89-17507
- Design and simulated performance of a CARS spectrometer for dynamic temperature measurements using electronic heterodyning p 170 A89-37298
- NONLINEARITY**
- Simplified cyclic structural analysis of SSME turbine blades p 63 A89-12632
- MHOST version 4.2. Volume 1: Users' manual [NASA-CR-182235-VOL-1] p 217 A89-13996
- Nonlinear evolution of interacting oblique waves on two-dimensional shear layers [NASA-TM-102030] p 164 A89-24575
- Paralleling power MOSFETs in their active region: Extended range of passively forced current sharing [NASA-CR-180902] p 139 A89-26150
- Metal matrix composite micromechanics: In-situ behavior influence on composite properties [NASA-TM-102302] p 88 A89-26924
- The 3-D inelastic analyses for computational structural mechanics p 206 A89-29804
- Multi-grid for structures analysis p 206 A89-29810



**NONOSCILLATORY ACTION**

- A numerical study of ENO and TVD schemes for shock capturing  
[NASA-TM-101355] p 222 N89-11469
- Second-order accurate nonoscillatory schemes for scalar conservation laws  
[NASA-TM-102010] p 14 N89-22573

**NONUNIFORMITY**

- Behavior in normal and reduced gravity of an enclosed liquid/gas system with nonuniform heating from above  
[AIAA PAPER 89-0070] p 145 A89-25061
- Behavior in normal and reduced gravity of an enclosed liquid/gas system with nonuniform heating from above  
[NASA-TM-101471] p 120 N89-17046

**NORMAL SHOCK WAVES**

- An LDA (Laser-Doppler Anemometry) investigation of three-dimensional normal shock wave boundary-layer interactions  
p 14 N89-20956

**NOTCH TESTS**

- Sublimate- or ply-level analysis of composites and strain energy release rates of end-notch and mixed-mode fracture specimens  
p 190 A89-16279
- Kinetics of fracture in Fe-3Si steel under mode I loading  
p 99 A89-47320

**NOZZLE DESIGN**

- Comparison of 3D computation and experiment for non-axisymmetric nozzles  
[NASA-CR-182245] p 14 N89-20921
- Design, fabrication and test of the RL10 derivative II chamber/primary nozzle  
[NASA-CR-179595] p 68 N89-23519
- Arcjet nozzle design impacts  
[NASA-TM-102050] p 68 N89-23522
- Advanced computational techniques for hypersonic propulsion  
[NASA-TM-102005] p 163 N89-23809
- Space station hydrogen/oxygen thruster technology  
[NASA-CR-182280] p 74 N89-26905

**NOZZLE FLOW**

- Fuel spray simulation with two-fluid nozzles  
[AIAA PAPER 89-0053] p 145 A89-25047
- The effect of adaptive grid on hypersonic nozzle flow calculations  
[AIAA PAPER 89-0006] p 54 A89-28402
- Comparison of 3D computation and experiment for non-axisymmetric nozzles  
[AIAA PAPER 89-0007] p 22 A89-28403
- Near-field acoustic environment of a supersonic plume adjacent to a wall  
[AIAA PAPER 89-1137] p 225 A89-33767
- Effects of nozzle exit boundary-layer conditions on excitability of heated free jets  
p 149 A89-36908
- Rectangular nozzle plume velocity modeling for use in jet noise prediction  
[AIAA PAPER 89-2357] p 7 A89-46771
- The effect of test-cell pressure on resistojet nozzle flow  
[AIAA PAPER 89-2838] p 58 A89-47116
- Rarefied gas flow through two-dimensional nozzles  
[AIAA PAPER 89-2893] p 7 A89-47156
- Fluid spray simulation with two-fluid nozzles  
[NASA-TM-101367] p 155 N89-12028
- Turbofan forced mixer lobe flow modeling. 1: Experimental and analytical assessment  
[NASA-CR-4147-PT-1] p 11 N89-14221
- Turbofan forced mixer lobe flow modeling. 2: Three-dimensional inviscid mixer analysis (FLOMIX)  
[NASA-CR-4147-PT-2] p 11 N89-14222
- Rectangular nozzle plume velocity modeling for use in jet noise prediction  
[NASA-TM-102047] p 14 N89-22577
- Advanced computational techniques for hypersonic propulsion  
[NASA-TM-102005] p 163 N89-23809
- Turbulent swirling jets with excitation  
[NASA-CR-180895] p 16 N89-29329

**NOZZLE GEOMETRY**

- Plasma flow processes within magnetic nozzle configurations  
[AIAA PAPER 89-2711] p 57 A89-47036
- The effects of arcjet thruster operating condition constrictor geometry on the plasma plume  
[AIAA PAPER 89-2723] p 60 A89-50809
- High-temperature LCF of Ni-201 and 304L stainless steel  
p 100 N89-12635
- The effects of magnetic nozzle configurations on plasma thrusters  
[NASA-CR-184678] p 64 N89-15170
- The effects of arcjet operating condition and constrictor geometry on the plasma plume  
[NASA-TM-102284] p 72 N89-25281

**NOZZLES**

- Design and analysis report for the flight weight 20-inch Columbian secondary nozzle for the RL10 engine  
[NASA-CR-179612] p 65 N89-16918

**NUCLEAR ASTROPHYSICS**

- Superheavy magnetic monopoles and main-sequence stars  
p 240 A89-20377

**NUCLEAR ELECTRIC PROPULSION**

- Unique mission options available with a megawatt-class nuclear electric propulsion system  
[NASA-TM-101220] p 65 N89-17618

**NUCLEAR ENERGY**

- Power systems for production, construction, life support, and operations in space  
p 37 A89-45803

**NUCLEAR ENGINE FOR ROCKET VEHICLES**

- Nuclear thermal rockets - Next step to space  
p 55 A89-40480
- Nuclear propulsion: A vital technology for the exploration of Mars and the planets beyond  
[NASA-TM-101354] p 62 N89-10944

**NUCLEAR FUSION**

- Nucleosynthesis, neutrino bursts and gamma-rays from coalescing neutron stars  
p 241 A89-46577
- Lunar Helium-3 and Fusion Power  
[NASA-CP-10018] p 233 N89-14842

**NUCLEAR MAGNETIC RESONANCE**

- Addition of polymers from 1,4,5,8-tetrahydro-1,4,5,8-diepoxyanthracene and Bis-dienes. 2: Evidence for thermal dehydration occurring in the cure process  
[NASA-TM-101385] p 112 N89-15235

**NUCLEAR POWER REACTORS**

- Space nuclear reactor shields for manned and unmanned applications  
[NASA-TM-102064] p 71 N89-25272
- CSTI High Capacity Power  
[NASA-TM-102059] p 72 N89-25282

**NUCLEAR PROPULSION**

- Nuclear propulsion: A vital technology for the exploration of Mars and the planets beyond  
[NASA-TM-101354] p 62 N89-10944

**NUCLEAR REACTORS**

- Systems aspects of a space nuclear reactor power system  
p 51 A89-15327
- Extended SP-100 reactor power systems capability  
p 52 A89-15392
- Nuclear reactor power as applied to a space-based radar mission  
[NASA-TM-101200] p 230 N89-14831

**NUCLEATE BOILING**

- Combined roles of buoyancy and orientation in nucleate pool boiling  
p 119 A89-35015

**NUCLEATION**

- Bulk undercooling, nucleation, and macrosegregation of Pb-Sn alloys  
p 117 A89-17106
- Macrosegregation and nucleation in undercooled Pb-Sn alloys  
[NASA-TM-102023] p 104 N89-23664

**NUMERICAL ANALYSIS**

- Numerical analysis of flow through oscillating cascade sections  
[AIAA PAPER 89-0437] p 4 A89-28413
- Direct numerical simulations of a temporally evolving mixing layer subject to forcing  
p 147 A89-34426
- An algorithm for unsteady flows with strong convection  
[NASA-TM-100828] p 221 N89-10575
- A numerical study of ENO and TVD schemes for shock capturing  
[NASA-TM-101355] p 222 N89-11469
- HOST combustion R and T overview  
p 25 N89-12879

- A comparison of numerical methods for the prediction of two-dimensional heat transfer in an electrothermal deicer pad  
[NASA-CR-4202] p 19 N89-13429

- Numerical analysis of flow through oscillating cascade sections  
[NASA-TM-101417] p 11 N89-14220

- A numerical simulation of the full two-dimensional electrothermal de-icer pad  
[NASA-CR-4194] p 19 N89-14235

**NUMERICAL CONTROL**

- Comparison of the bidirectional reflectance distribution function of various surfaces  
p 230 A89-41530
- Design and implementation of a microcomputer-based user interface controller for burst data communications satellite ground terminals  
[NASA-TM-101375] p 43 N89-13457

**NUMERICAL FLOW VISUALIZATION**

- Bipolar coordinates for computation of transition duct flows  
p 148 A89-34912

**NUMERICAL INTEGRATION**

- Global properties of pseudospectral methods  
p 221 A89-37746

**OBLIQUE SHOCK WAVES**

- Performance of laser Doppler velocimeter with polydisperse seed particles in high-speed flows  
p 169 A89-22279

- Interaction of an oblique shock wave with turbulent hypersonic blunt body flows  
[AIAA PAPER 89-0272] p 3 A89-28405

- Nonlinear evolution of interacting oblique waves on two-dimensional shear layers  
[NASA-TM-102030] p 164 N89-24575

**OBSERVABILITY (SYSTEMS)**

- Observer design for compensation of network-induced delays in integrated communication and control systems  
p 220 A89-35044

- Extended observability of linear time-invariant systems under recurrent loss of output data  
[AIAA PAPER 89-3510] p 220 A89-52603

- An observer-based compensator for distributed delays in integrated control systems  
[AIAA PAPER 89-3541] p 35 A89-52628

**ON-LINE SYSTEMS**

- An expert system for restructurable control  
[NASA-TM-101378] p 220 N89-12309

**ONE DIMENSIONAL FLOW**

- Calculation of shocked flows by mathematical programming  
p 150 A89-45397

**OPERATING SYSTEMS (COMPUTERS)**

- Initial operating capability for the hypercluster parallel-processing test bed  
[NASA-TM-101953] p 218 N89-20685

**OPERATING TEMPERATURE**

- Turbine Engine Hot Section Technology (HOST) Project  
p 25 N89-12877
- Comparison of predicted and measured temperatures of UH-60A helicopter transmission  
[NASA-TP-2911] p 186 N89-24607

**OPTICAL COMMUNICATION**

- A laser communication experiment utilizing the ACT satellite and an airborne laser transceiver  
p 43 A89-15811

**OPTICAL COUPLING**

- Study of optical output couplers for submillimeter wavelength backward-wave oscillators (BWO's)  
p 132 A89-32857

- The GaAs solar cells with V-grooved emitters  
[NASA-TM-102104] p 214 A89-26291

**OPTICAL EQUIPMENT**

- GaAs circuits for monolithic optical controller  
p 131 A89-15828
- Diamondlike carbon protective coatings for optical windows  
[NASA-TM-102111] p 231 N89-27506

**OPTICAL FIBERS**

- Optically controlled phased-array technology for space communication systems  
p 131 A89-15845
- Intensity-based fibre-optic sensing system using contrast modulation of subcarrier interference pattern  
p 170 A89-39302

- Compensation for effects of ambient temperature on rare-earth doped fiber optic thermometer  
[NASA-TM-102282] p 176 N89-27998

**OPTICAL HETERODYNING**

- Design and simulated performance of a CARS spectrometer for dynamic temperature measurements using electronic heterodyning  
p 170 A89-37298
- Holographic interferometry with an injection seeded Nd:YAG laser and two reference beams  
[NASA-TM-102056] p 175 N89-24591

**OPTICAL MEASUREMENT**

- Ray tracing optical analysis of offset solar collector for Space Station solar dynamic system  
p 53 A89-15416
- Development and applications of optical interferometric micrometrology in the Angstrom and subangstrom range  
p 170 A89-27663

- Fiber optics for liquid propellant rocket engine environments  
[AIAA PAPER 89-2416] p 230 A89-46812

**OPTICAL MEASURING INSTRUMENTS**

- Calibration of single particle sizing velocimeters using photomask reticles  
p 170 A89-33379
- Intensity-based fibre-optic sensing system using contrast modulation of subcarrier interference pattern  
p 170 A89-39302

- Comparison of the bidirectional reflectance distribution function of various surfaces  
p 230 A89-41530

- High temperature optical strain measurement system  
p 170 A89-43842

- Two-dimensional high temperature optical strain measurement system, phase 2  
[NASA-CR-185116] p 176 N89-26218

- Compensation for effects of ambient temperature on rare-earth doped fiber optic thermometer  
[NASA-TM-102282] p 176 N89-27998

## OPTICAL PROPERTIES

- Fresnel diffraction by spherical obstacles  
p 231 A89-48249
- Microwave characteristics of interdigitated photoconductors on a HEMT structure  
[NASA-CR-182197] p 135 N89-12820

## OPTICAL SWITCHING

- Optoelectronic techniques for broadband switching  
p 131 A89-15825
- Study of optoelectronic switch for satellite-switched time-division multiple access  
[NASA-CR-179630] p 135 N89-13706

## OPTICAL THICKNESS

- The Mars climate for a photovoltaic system operation  
[IAF PAPER ICOSP89-9.5] p 241 A89-46529
- The Mars climate for a photovoltaic system operation  
[NASA-TM-101994] p 136 N89-20385
- Photovoltaic power system operation in the Mars environment  
[NASA-TM-102075] p 138 N89-24529

## OPTICAL TRANSFER FUNCTION

- Amplitude spectrum modulation technique for analog data processing in fiber optic sensing system with temporal separation of channels  
[NASA-TM-100152] p 174 N89-18671

## OPTICAL WAVEGUIDES

- Design of a GaAlAs travelling wave Mach-Zehnder electro-optic modulator  
p 130 A89-10342
- Characterization of GaAlAs optical waveguide heterostructures grown by molecular beam epitaxy  
p 130 A89-10343

## OPTICS

- Optically interconnected phased arrays  
p 132 A89-33696

## OPTIMAL CONTROL

- Model-based analysis of control/display interaction in the hover task  
p 215 A89-36933
- Optimal terminal maneuver for a cooperative impulsive rendezvous  
p 38 A89-36946
- New results concerning the use of kinematically redundant manipulators in microgravity environments  
[AIAA PAPER 89-3562] p 215 A89-52647
- Computer simulation of a pilot in V/STOL aircraft control loops  
[NASA-CR-184815] p 215 N89-21479
- Active vibration control for flexible rotor by optimal direct-output feedback control  
[NASA-TM-101972] p 31 N89-22605

## OPTIMIZATION

- Optimizing advanced propeller designs by simultaneously updating flow variables and design parameters  
p 5 A89-39189
- Finite-element grid improvement by minimization of stiffness matrix trace  
p 194 A89-42339
- Structural tailoring of Space Shuttle Main Engine turbopump blades SSME/STAEBL  
p 55 A89-44106
- Aerodynamic optimization by simultaneously updating flow variables and design parameters with application to advanced propeller designs  
[NASA-CR-182181] p 24 N89-11750
- User's manual for an aerodynamic optimization scheme that updates flow variables and design parameters simultaneously  
[NASA-CR-182180] p 10 N89-13399
- Gear optimization  
[NASA-CR-4201] p 182 N89-13793
- Improved silicon nitride for advanced heat engines  
[NASA-CR-179525] p 113 N89-19421
- Structural tailoring of counter rotation propfans  
p 33 N89-25165
- Tailoring of composite links for optimal damped elasto-dynamic performance  
[NASA-TM-102094] p 88 N89-26912

## OPTIONS

- Expendable launch vehicle transportation for the space station  
[NASA-TM-101947] p 42 N89-20179

## OPTOELECTRONIC DEVICES

- Optoelectronic signal processing for phased-array antennas; Proceedings of the Meeting, Los Angeles, CA, Jan. 12, 13, 1988  
[SPIE-886] p 124 A89-15819
- Optoelectronic techniques for broadband switching  
p 131 A89-15825
- Study of optoelectronic switch for satellite-switched time-division multiple access  
[NASA-CR-179630] p 135 N89-13706
- Amplitude spectrum modulation technique for analog data processing in fiber optic sensing system with temporal separation of channels  
[NASA-TM-100152] p 174 N89-18671
- Optical detectors for GaAs MMIC integration: Technology assessment  
[NASA-TM-102025] p 137 N89-22020

## ORBIT MANEUVERING ENGINE (SPACE SHUTTLE)

- High-temperature LCF of Ni-201 and 304L stainless steel  
p 100 N89-12635

## ORBIT TRANSFER VEHICLES

- Systems aspects of a space nuclear reactor power system  
p 51 A89-15327
- Miniature multiple-function probe for OTV turbopump health monitoring  
[AIAA PAPER 89-2303] p 56 A89-46736
- Advanced H<sub>2</sub>/O<sub>2</sub> space engine parametrics  
[AIAA PAPER 89-2300] p 57 A89-46855
- Ion optics for high power 50-cm-dia ion thrusters  
[AIAA PAPER 89-2717] p 58 A89-47040
- Orbit transfer rocket engine technology program. Phase 2: Advanced engine study  
[NASA-CR-179602] p 61 N89-10119
- Integrated control and health management. Orbit transfer rocket engine technology program  
[NASA-CR-182122] p 62 N89-11805
- Orbit transfer rocket engine technology program: Oxygen materials compatibility testing  
[NASA-CR-182195] p 64 N89-14256
- Advanced technology for future space propulsion systems  
[NASA-TM-101951] p 66 N89-20192
- Launch packaging options for the photovoltaic power module cargo element  
[NASA-TM-102072] p 71 N89-25275
- Integrated control and health monitoring capacitive displacement sensor development task. Orbit transfer rocket engine technology program  
[NASA-CR-182279] p 176 N89-26208
- NASA's Chemical Transfer Propulsion Program for Pathfinder  
[NASA-TM-102298] p 41 N89-26876
- OTV turbopump condition monitoring, task E.5  
[NASA-CR-182274] p 189 N89-27204
- Ion optics for high power 50-cm-dia ion thrusters  
[NASA-TM-102143] p 76 N89-28571

## ORBITAL ASSEMBLY

- Power considerations for an early manned Mars mission utilizing the space station  
[NASA-TM-101436] p 63 N89-13492
- A definition study of the on-orbit assembly operations for the outboard photovoltaic power modules for Space Station Freedom  
[NASA-TM-102006] p 41 N89-20171
- Photovoltaic module on-orbit assembly for Space Station Freedom  
[NASA-TM-102297] p 47 N89-26887

## ORBITAL MANEUVERS

- Orbit transfer rocket engine technology program. Phase 2: Advanced engine study  
[NASA-CR-179602] p 61 N89-10119

## ORBITAL SERVICING

- Technology requirements for an orbiting fuel depot - A necessary element of a space infrastructure  
[IAF PAPER 88-035] p 37 A89-17641
- Orbit transfer rocket engine technology program. Phase 2: Advanced engine study  
[NASA-CR-179602] p 61 N89-10119

## ORBITAL SPACE TESTS

- On-orbit results of the LIPS 3/InP homojunction solar cell experiment  
[NASA-TM-102131] p 214 N89-26292

## ORBITAL VELOCITY

- Technology issues associated with fueling the national aerospace plane with slush hydrogen  
[NASA-TM-101386] p 61 N89-10123

## ORGANOMETALLIC COMPOUNDS

- Chemical etching and organometallic chemical vapor deposition on varied geometries of GaAs  
p 213 N89-24728

## ORTHOTROPISM

- Noninteractive macroscopic reliability model for ceramic matrix composites with orthotropic material symmetry  
[NASA-TM-101414] p 198 N89-15437

## OSCILLATING FLOW

- Description of an oscillating flow pressure drop test rig  
p 142 A89-15188
- Effect of transition on oscillation flow losses in Stirling engine coolers and heaters  
p 142 A89-15189
- Investigation of the flow between a pair of circular cylinders in the flopping regime  
p 144 A89-22822
- Instabilities caused by oscillating accelerations normal to a viscous fluid-fluid interface  
p 144 A89-22823
- Experimental investigation of transonic oscillating cascade aerodynamics  
[AIAA PAPER 89-0321] p 3 A89-26369
- A natural low-frequency oscillation of the flow over an airfoil near stalling conditions  
p 6 A89-45437
- Numerical analysis of supersonic flow through oscillating cascade sections by using a deforming grid  
[AIAA PAPER 89-2805] p 8 A89-50810

- Experimental investigation of transonic oscillating cascade aerodynamics  
[NASA-TM-101993] p 29 N89-20133

- Numerical analysis of supersonic flow through oscillating cascade sections by using a deforming grid  
[NASA-TM-102053] p 15 N89-25119

## OSCILLATION DAMPERS

- Low frequency vibration isolation technology for microgravity space experiments  
[NASA-TM-101448] p 123 N89-20324

## OSCILLATIONS

- Investigation of oscillating cascade aerodynamics by an experimental influence coefficient technique  
[AIAA PAPER 88-2815] p 1 A89-14976
- A review of turbomachinery blade-row interaction research  
[NASA-CR-182211] p 24 N89-12567

## OSCILLATORS

- Study of optical output couplers for submillimeter wavelength backward-wave oscillators (BWO's)  
[NASA-TM-101360] p 134 N89-11128

## OUTPUT

- Study of optical output couplers for submillimeter wavelength backward-wave oscillators (BWO's)  
[NASA-TM-101360] p 134 N89-11128

## OXIDATION

- Reactions of silicon-based ceramics in mixed oxidation chlorination environments  
p 105 A89-21442
- Computer simulation of cyclic oxidation  
p 91 A89-29295
- TEM studies of oxidized NiAl and Ni<sub>3</sub>Al cross sections  
p 99 A89-46506
- Grain boundary oxidation and its effects on high temperature fatigue life  
p 101 N89-12918
- A study on thermal barrier coatings including thermal expansion mismatch and bond coat oxidation  
p 109 N89-12919
- The effect of 0.1 atomic percent zirconium on the cyclic oxidation behavior of beta-NiAl for 300 hours at 1200 C  
[NASA-TM-101408] p 101 N89-13566
- The effect of oxidation on the high heat flux behavior of a thermal barrier coating  
p 110 N89-13646
- The oxidation of Ni-rich Ni-Al intermetallics  
[NASA-TM-101455] p 102 N89-15233

## OXIDATION RESISTANCE

- High temperature isothermal and cyclic oxidation behavior of a single crystal Ni base superalloy  
p 94 A89-12625
- The effect of sulfur and zirconium co-doping on the oxidation of NiCrAl  
p 94 A89-13933
- Thermo-oxidative stability studies of Celion 6000/PMR-15 unidirectional composites, PMR-15, and Celion 6000 fiber  
p 79 A89-14099
- Effect of 0.1 at. pct Zirconium on the cyclic oxidation resistance of beta-NiAl  
p 96 A89-24599
- A thermally modified polymer matrix composite material with structural integrity to 371 C  
p 80 A89-29997
- The behavior of SiC and Si<sub>3</sub>N<sub>4</sub> ceramics in mixed oxidation/chlorination environments  
p 106 A89-33616
- Effect of the theta-alpha-Al<sub>2</sub>O<sub>3</sub> transformation on the oxidation behavior of beta-NiAl + Zr  
p 98 A89-38600
- Influence of alloying elements on the oxidation behavior of NbAl<sub>3</sub>  
[NASA-TM-101398] p 100 N89-12717
- Oxidation behavior of FeAl + Hf, Zr, B  
[NASA-TM-101402] p 102 N89-14297
- Evaluation of atomic oxygen resistant protective coatings for fiberglass-epoxy composites in LEO  
[NASA-TM-101955] p 114 N89-21100
- Undercutting of defects in thin film protective coatings on polymer surfaces exposed to atomic oxygen  
[NASA-TM-101986] p 115 N89-23691

## OXIDE FILMS

- Preparation of high T(c) Ti-Ba-Ca-Cu-O thin films by pulsed laser evaporation and TiO<sub>3</sub> vapor processing  
p 236 A89-38608
- Oxide scale stresses in polycrystalline Ni200  
p 98 A89-38859
- Predicting minimum Al concentrations for protective scale formation on Ni-base alloys. I - Isothermal oxidation. II - Cyclic oxidation  
p 98 A89-40116
- Effects of microstructure and nonstoichiometry on electrical properties of vanadium dioxide films  
p 236 A89-44527
- Isotopic study of oxygen diffusion in oxide coatings  
[NASA-TM-102082] p 78 N89-24451

## OXYGEN

- Oxygen electrode bifunctional electrocatalyst NiCo<sub>2</sub>O<sub>4</sub> spinel  
[NASA-TM-100947] p 208 N89-10409
- The NASA atomic oxygen effects test program  
p 93 N89-12589
- Orbit transfer rocket engine technology program: Oxygen materials compatibility testing  
[NASA-CR-182195] p 64 N89-14256

- The divergence characteristics of constrained-sheath optics systems for use with 5-eV atomic oxygen sources [NASA-CR-182238] p 229 N89-19973
- Space station hydrogen/oxygen thruster technology [NASA-CR-182280] p 74 N89-26905
- OXYGEN ATOMS**
- Low earth orbital atomic oxygen simulation for materials durability evaluation p 45 A89-51123
- Evaluation of atomic oxygen resistant protective coatings for fiberglass-epoxy composites in LEO [NASA-TM-101955] p 114 N89-21100
- Atomic oxygen effects on materials p 78 N89-23540
- Undercutting of defects in thin film protective coatings on polymer surfaces exposed to atomic oxygen [NASA-TM-101986] p 115 N89-23691
- OXYGEN IONS**
- Pulsed ion beam investigation of the kinetics of surface reactions p 93 A89-44542
- Simulation of the low earth orbital atomic oxygen interaction with materials by means of an oxygen ion beam [NASA-TM-101971] p 114 N89-21104
- OXYGEN ISOTOPES**
- Isotopic study of oxygen diffusion in oxide coatings [NASA-TM-102082] p 78 N89-24451
- OXYGEN RECOMBINATION**
- Space Station Freedom Solar Array design development [NASA-TM-102105] p 70 N89-24448
- OXYGEN-HYDROCARBON ROCKET ENGINES**
- Liquid oxygen cooling of hydrocarbon fueled rocket thrust chambers [AIAA PAPER 89-2739] p 60 A89-49686
- Liquid oxygen cooling of high pressure LOX/hydrocarbon rocket thrust chambers p 63 N89-12649
- High-pressure calorimeter chamber tests for liquid oxygen/kerosene (LOX/RP-1) rocket combustion [NASA-TP-2862] p 65 N89-15979
- Liquid oxygen cooling of hydrocarbon fueled rocket thrust chambers [NASA-TM-102113] p 70 N89-24447
- P**
- P-I-N JUNCTIONS**
- Computer analysis of the negative differential resistance switching phenomenon of double-injection devices p 134 A89-54963
- P-TYPE SEMICONDUCTORS**
- High-efficiency solar cells fabricated from direct-current magnetron sputtered n-indium tin oxide onto p-InP grown by atmospheric pressure metalorganic vapor phase epitaxy p 133 A89-44518
- PANEL METHOD (FLUID DYNAMICS)**
- A numerical method for computing unsteady 2-D boundary layer flows [NASA-CR-4198] p 155 N89-12835
- PANELS**
- A modified VAPEPS method for predicting vibroacoustic response of unreinforced mass loaded honeycomb panels [NASA-TM-101467] p 46 N89-16905
- High temperature flexible seal [NASA-CASE-LEW-14695-1] p 187 N89-28830
- PARABOLAS**
- Dynamic loading of spur gears with linear or parabolic tooth profile modification [NASA-TM-101444] p 183 N89-15413
- PARABOLIC REFLECTORS**
- Concentration of off-axis radiation by solar concentrators for space power [NASA-TM-102052] p 69 N89-24438
- Adaptive array for weak interfering signals: Geostationary satellite experiments [NASA-CR-185450] p 129 N89-26126
- Comparison of conceptual designs for 25 kWe advanced Stirling conversion systems for dish electric application [NASA-TM-102085] p 239 N89-26781
- PARALLEL FLOW**
- Development of an integrated BEM approach for hot fluid structure interaction [NASA-CR-184587] p 27 N89-15114
- PARALLEL PLATES**
- The secondary flow and its stability for natural convection in a tall vertical enclosure p 149 A89-37931
- Two-dimensional numerical simulation of a Stirling engine heat exchanger [NASA-TM-102057] p 164 N89-23823
- PARALLEL PROCESSING (COMPUTERS)**
- Parallel processing of a rotating shaft simulation [NASA-TM-101462] p 223 N89-17453
- Automating the multiprocessing environment [NASA-TM-4103] p 217 N89-20641
- A message passing kernel for the hypercluster parallel processing test bed [NASA-TM-101952] p 218 N89-20684
- Initial operating capability for the hypercluster parallel-processing test bed [NASA-TM-101953] p 218 N89-20685
- On the equivalence of Gaussian elimination and Gauss-Jordan reduction in solving linear equations [NASA-TM-101466] p 222 N89-20710
- Advances in computational design and analysis of airbreathing propulsion systems [NASA-TM-101987] p 32 N89-23465
- Computational structural methods at NASA Lewis p 205 N89-29776
- Transputer parallel processing at NASA Lewis Research Center p 205 N89-29778
- Computational structural mechanics engine structures computational simulator p 205 N89-29792
- PARALLEL PROGRAMMING**
- Parallel Gaussian elimination of a block tridiagonal matrix using multiple microcomputers [NASA-TP-2892] p 218 N89-17422
- PARAMETER IDENTIFICATION**
- Characterization of structural connections using free and forced response test data [NASA-TM-101991] p 202 N89-21266
- Neuromorphic learning of continuous-valued mappings in the presence of noise: Application to real-time adaptive control [NASA-TM-101999] p 221 N89-24856
- PARAMETERIZATION**
- A parametric LQ approach to multiobjective control system design p 219 A89-28605
- A parametric LQ approach to multiobjective control system design [NASA-TM-101316] p 220 N89-12283
- PARTICLE ACCELERATION**
- Arc restriking in the rail accelerator p 39 A89-32065
- PARTICLE DIFFUSION**
- The interaction of gold with gallium arsenide p 90 A89-16416
- Interdiffusional effects between TiBe12 and NiAl intermetallics p 95 A89-21395
- PARTICLE INTERACTIONS**
- Numerical study of the interactions between droplets at intermediate Reynolds numbers p 142 A89-16451
- Interaction of Au, Ag, and Bi ions with Ba2YCu3O(7-y) - Implications for superconductor applications p 235 A89-22886
- PARTICLE LADEN JETS**
- Boundary layer effects on particle impaction and capture p 143 A89-19123
- Evolution of particle-laden jet flows - A theoretical and experimental study p 146 A89-27693
- PARTICLE MOTION**
- Rational engineering correlations of diffusional and inertial particle deposition behavior in non-isothermal forced convection environments p 140 A89-12327
- Use of a generalized Stokes number to determine the aerodynamic capture efficiency of non-Stokesian particles from a compressible gas flow p 140 A89-12336
- Viscous dissipation effects on thermophoretically augmented aerosol particle transport across laminar boundary layers p 141 A89-14600
- Application of optical correlation techniques to particle imaging [AIAA PAPER 88-4661] p 169 A89-14985
- PARTICLE SIZE DISTRIBUTION**
- Performance of laser Doppler velocimeter with polydisperse seed particles in high-speed flows p 169 A89-22279
- Performance of the forward scattering spectrometer probe in NASA's Icing Research Tunnel [AIAA PAPER 89-0769] p 169 A89-25570
- Optical measurements of soot and temperature profiles in premixed propane-oxygen flames p 92 A89-35008
- A correction algorithm for particle size distribution measurements made with the forward-scattering spectrometer probe p 170 A89-44123
- Particle sizing by weighted measurements of scattered light [NASA-TM-100968] p 172 N89-11198
- Performance of the forward scattering spectrometer probe in NASA's icing research tunnel [NASA-TM-101381] p 172 N89-12845
- PARTICLE TRACKS**
- Application of optical correlation techniques to particle imaging [AIAA PAPER 88-4661] p 169 A89-14985
- PASSIVITY**
- The effect of metal surface passivation on the Au-InP interaction p 132 A89-30443
- A new structure for comparing surface passivation materials of GaAs solar cells p 213 N89-24725
- PAYLOAD CONTROL**
- Space nuclear reactor shields for manned and unmanned applications [NASA-TM-102064] p 71 N89-25272
- PAYLOAD DELIVERY (STS)**
- Advanced APS impacts on vehicle payloads [NASA-TM-102086] p 41 N89-25254
- PERFLUORO COMPOUNDS**
- The preparation of new perfluoro ether fluids exhibiting excellent thermal-oxidative stabilities p 76 A89-12760
- Reaction of perfluoroalkylpolyethers (PFPE) with 440C steel in vacuum under sliding conditions at room temperature [NASA-TP-2883] p 115 N89-26091
- Determination of the thermal stability of perfluoroalkylethers by tensimetry: Instrumentation and Procedure [NASA-TM-102116] p 116 N89-26095
- PERFORMANCE PREDICTION**
- Return of the turboprops p 20 A89-12953
- Effects of operating parameters on PAFC stack performance p 207 A89-15250
- Two-dimensional simulation of electrothermal deicing of aircraft components p 17 A89-39194
- Transient flow thrust prediction for an ejector propulsion concept [AIAA PAPER 89-2906] p 23 A89-49688
- Conceptual design of an advanced Stirling conversion system for terrestrial power generation [NASA-CR-180890] p 238 N89-12504
- HOST surface protection R and T overview p 109 N89-12883
- Predictions of airfoil aerodynamic performance degradation due to icing [NASA-TM-101434] p 10 N89-13412
- An analysis for high speed propeller-nacelle aerodynamic performance prediction. Volume 1: Theory and application [NASA-CR-4199-VOL-1] p 12 N89-15896
- An analysis for high speed propeller-nacelle aerodynamic performance prediction. Volume 2: User's manual [NASA-CR-4199-VOL-2] p 12 N89-15897
- Views on the impact of HOST p 31 N89-20144
- Results of inphase axial-torsional fatigue experiments on 304 stainless steel [NASA-TM-101464] p 201 N89-20514
- Transonic viscous flow calculations for a turbine cascade with a two equation turbulence model [NASA-TM-101944] p 32 N89-22607
- Transient flow thrust prediction for an ejector propulsion concept [NASA-TM-102078] p 32 N89-24318
- A model for prediction of STOVL ejector dynamics [NASA-TM-102098] p 32 N89-24319
- Isothermal life prediction of composite lamina using a damage mechanics approach [NASA-TM-102032] p 87 N89-24460
- Computed performance of the half-scale accurate antenna reflector [NASA-CR-182284] p 139 N89-24532
- NASA Lewis Stirling engine computer code evaluation [NASA-CR-182248] p 214 N89-24741
- Estimated performance and future potential of solar dynamic and photovoltaic power systems for selected LEO and HEO missions [NASA-TM-102083] p 72 N89-25280
- Frequency domain model for analysis of paralleled, series-output-connected Mapham inverters [NASA-TM-102140] p 139 N89-26149
- PERFORMANCE TESTS**
- Acoustic emission evaluation of plasma-sprayed thermal barrier coatings p 178 A89-12751
- Performance of 10-kW class xenon ion thrusters [AIAA PAPER 88-2914] p 48 A89-14978
- Transient performance evaluation of an integrated heat pipe-thermal storage system p 49 A89-15209
- Alkaline fuel cell performance investigation p 207 A89-15258
- Simulation test beds for the Space Station electrical power system p 39 A89-15352
- Performance and lifetime assessment of MPD arc thruster technology [AIAA PAPER 88-3211] p 53 A89-16485
- Vibration, performance, flutter and forced response characteristics of a large-scale propfan and its aeroelastic model [AIAA PAPER 88-3155] p 21 A89-17943
- Performance of the forward scattering spectrometer probe in NASA's Icing Research Tunnel [AIAA PAPER 89-0769] p 169 A89-25570
- Performance characterizations of an engineering model multipropellant resistojel p 54 A89-28340
- An experimental investigation of multi-element airfoil ice accretion and resulting performance degradation [AIAA PAPER 89-0752] p 4 A89-28453

- High-speed propeller performance and noise predictions at takeoff/landing conditions p 226 A89-39195  
Small scale bipolar nickel-hydrogen testing p 208 A89-44005  
Effect of ambient pressure on the performance of a resistor p 55 A89-44111  
Free-piston Stirling technology for space power [IAF PAPER ICOSP89-5-7] p 56 A89-46520  
Vibration, performance, flutter and forced response characteristics of a large-scale propfan and its aeroelastic model p 24 N89-10043  
Space station auxiliary thrust chamber technology [NASA-TM-101322] p 46 N89-11803  
Radiation resistance and comparative performance of ITO/InP and n/p InP homojunction solar cells [NASA-TM-101387] p 135 N89-12819  
Performance of the forward scattering spectrometer probe in NASA's icing research tunnel [NASA-TM-101381] p 172 N89-12845  
Evaluation of coated columbium test panels having application to a secondary nozzle extension for the RL10 rocket engine system, parts 1 and 2 [NASA-CR-180809] p 64 N89-13493  
Effect of advanced component technology on helicopter transmissions [NASA-TM-101431] p 182 N89-13794  
An experimental investigation of multi-element airfoil ice accretion and resulting performance degradation [NASA-TM-101441] p 12 N89-15084  
Performance of a multistage depressed collector with machined titanium electrodes [NASA-TP-2891] p 136 N89-15337  
Technique for temperature compensation of eddy-current proximity probes [NASA-TP-2880] p 173 N89-15380  
The effect of different module configurations on the radiation tolerance of multijunction solar cells [NASA-TM-101251] p 209 N89-17356  
Icing research tunnel test of a model helicopter rotor [NASA-TM-101978] p 29 N89-19305  
RE-1000 free-piston Stirling engine sensitivity test results [NASA-TM-88846] p 210 N89-19737  
Free-piston Stirling technology for space power [NASA-TM-101956] p 66 N89-20194  
A comparison of reflector antenna designs for wide-angle scanning [NASA-TM-101459] p 127 N89-21138  
Design, fabrication and test of the RL10 derivative II chamber/primary nozzle [NASA-CR-179595] p 68 N89-23519  
Computed performance of the half-scale accurate antenna reflector [NASA-CR-182284] p 139 N89-24532  
Comparison of predicted and measured temperatures of UH-60A helicopter transmission [NASA-TP-2911] p 186 N89-24607  
Protoflight photovoltaic power module system-level tests in the space power facility [NASA-TM-102066] p 46 N89-25267  
Performance of five 30 GHz satellite receivers [NASA-TM-101960] p 129 N89-25365  
Development and testing of a 20-kHz component test bed [NASA-TM-102141] p 139 N89-25403  
Indium phosphide solar cell research in the US: Comparison with nonphotovoltaic sources [NASA-TM-102103] p 124 N89-27868
- PERMANENT MAGNETS**  
Starting characteristics of direct current motors powered by solar cells [NASA-TM-101981] p 136 N89-19493
- PERMITTIVITY**  
Measurements of complex permittivity of microwave substrates in the 20 to 300 K temperature range from 26.5 to 40.0 GHz [NASA-TM-102123] p 123 N89-27038
- PEROXIDES**  
Improved synthesis of ceramic superconductors with alkaline earth peroxides - Synthesis and processing of Ba<sub>2</sub>YCu<sub>3</sub>O(7-x) p 235 A89-22887
- PERSONAL COMPUTERS**  
Laboratory process control using natural language commands from a personal computer [NASA-TM-101988] p 218 N89-24055
- PERTURBATION**  
The response of a laminar boundary layer in supersonic flow to small amplitude progressive waves [NASA-TM-101965] p 162 N89-21197
- PHASE CHANGE MATERIALS**  
Evaluation of alternative phase change materials for energy storage in solar dynamic applications p 208 A89-29114  
Advanced solar receivers for space power p 54 A89-29116
- Preliminary study of creep thresholds and thermomechanical response in Haynes 188 at temperatures in the range 649 to 871 C p 200 N89-17327
- PHASE COHERENCE**  
Multiple coherent mode interaction in a developing round jet [AIAA PAPER 89-0967] p 147 A89-30483
- PHASE CONTROL**  
A versatile power converter for high-frequency link systems p 131 A89-21200  
A design procedure for the phase-controlled parallel-loaded resonant inverter p 134 A89-50472
- PHASE DIAGRAMS**  
Measurement of the diffusion coefficient of acetone in succinonitrile at its melting point p 237 A89-23488
- PHASE SEPARATION (MATERIALS)**  
Macroscopic segregation in undercooled Pb-Sn eutectic alloys p 95 A89-19621
- PHASE SHIFT**  
Speckle interferometry using fiber optic phase stepping [NASA-TM-102331] p 176 N89-27999
- PHASE SHIFT CIRCUITS**  
GaAs circuits for monolithic optical controller p 131 A89-15828
- PHASE SHIFT KEYING**  
Programmable rate modem utilizing digital signal processing techniques [NASA-CR-185124] p 43 N89-26879
- PHASE TRANSFORMATIONS**  
Analysis of microalloy precipitate reversion in steels p 94 A89-15108  
Iron-base superalloys - A phase analysis of the multicomponent system (Fe-Mn-Cr-Mo-Nb-Al-Si-C) p 95 A89-17379  
Thermal analysis of heat storage canisters for a solar dynamic, space power system p 54 A89-29113  
On the orthorhombic phase in ZrO<sub>2</sub>-based alloys p 105 A89-30631  
The influence of annealing in the ferrite-plus-austenite phase field on the stability of vanadium carbide precipitates p 97 A89-32803  
Effect of the theta-alpha-Al<sub>2</sub>O<sub>3</sub> transformation on the oxidation behavior of beta-NiAl + Zr p 98 A89-38600  
Phase transformations in xerogels of mullite composition [NASA-TM-101349] p 108 N89-11038  
High-strength silicon carbides by hot isostatic pressing [NASA-TM-101400] p 111 N89-13666  
Modeling cyclic melting and refreezing in a hollow metal canister [NASA-CR-184630] p 217 N89-15623
- PHASED ARRAYS**  
Optoelectronic signal processing for phased-array antennas; Proceedings of the Meeting, Los Angeles, CA, Jan. 12, 13, 1988 [SPIE-886] p 124 A89-15819  
GaAs MMIC elements in phased-array antennas p 131 A89-15827  
Optically controlled phased-array technology for space communication systems p 131 A89-15845  
Optically interconnected phased arrays p 132 A89-33696
- PHOSPHORIC ACID**  
Assessment and comparison of 100-MW coal gasification phosphoric acid fuel cell power plants [NASA-CR-182189] p 209 N89-13103
- PHOSPHORIC ACID FUEL CELLS**  
Effects of operating parameters on PAFC stack performance p 207 A89-15250
- PHOTOCONDUCTORS**  
Microwave response of an HEMT photoconductor p 131 A89-15824  
Microwave characteristics of interdigitated photoconductors on a HEMT structure [NASA-CR-182197] p 135 N89-12820  
Microwave characteristics of GaAs MMIC integratable optical detectors [NASA-TM-101485] p 129 N89-24520
- PHOTODISSOCIATION**  
The NASA atomic oxygen effects test program p 93 N89-12589
- PHOTOELECTRON SPECTROSCOPY**  
Degradation and crosslinking of perfluoroalkyl polyethers under X-ray irradiation in ultrahigh vacuum [NASA-TP-2910] p 114 N89-21103
- PHOTOGRAMMETRY**  
Summary of laser speckle photogrammetry for HOST p 177 N89-12889
- PHOTOGRAPHY**  
Film annotation system for a space experiment [NASA-CR-185114] p 176 N89-27152
- PHOTOMASKS**  
Calibration of single particle sizing velocimeters using photomask reticles p 170 A89-33379
- PHOTOMETERS**  
Optoelectronic techniques for broadband switching p 131 A89-15825
- PHOTOVOLTAIC CELLS**  
An integrated and modular digital modeling approach for the Space Station electrical power system development p 50 A89-15298  
Temperature coefficients for concentrator cells at various electron and proton fluence levels p 51 A89-15304  
Status of the Space Station power system p 54 A89-23281  
Photovoltaic power modules for NASA's manned Space Station p 55 A89-29122  
Low earth orbit environmental effects on the Space Station photovoltaic power generation systems p 55 A89-29123  
Oxidation and protection of fiberglass-epoxy composite masts for photovoltaic arrays in the low earth orbital environment p 44 A89-35316  
Power systems for production, construction, life support, and operations in space p 37 A89-45803  
Solar dynamic power for Space Station Freedom [IAF PAPER ICOSP89-4-1] p 55 A89-46517  
The Mars climate for a photovoltaic system operation [IAF PAPER ICOSP89-9-5] p 241 A89-46529  
PV modules for ground testing [NASA-CR-179476] p 208 N89-11315  
Issues and opportunities in space photovoltaics [NASA-TM-101425] p 65 N89-15171  
Common source-multiple load vs. separate source-individual load photovoltaic system [NASA-TM-101465] p 136 N89-15338  
NASA photovoltaic research and technology [NASA-TM-101422] p 65 N89-16917  
A definition study of the on-orbit assembly operations for the outboard photovoltaic power modules for Space Station Freedom [NASA-TM-102006] p 41 N89-20171  
The Mars climate for a photovoltaic system operation [NASA-TM-101994] p 136 N89-20385  
Solar dynamic power for space station freedom [NASA-TM-102016] p 67 N89-23516  
Photovoltaic power system considerations for future lunar bases [NASA-TM-102019] p 67 N89-23517  
Magnification of starting torques of dc motors by maximum power point trackers in photovoltaic systems [NASA-TM-102040] p 138 N89-23792  
Review of the environmental effects of the Space Station Freedom photovoltaic power module [NASA-TM-102076] p 46 N89-24418  
Protoflight photovoltaic power module system-level tests in the space power facility [NASA-TM-102066] p 46 N89-25267  
The introduction of space technology power systems into developing countries [NASA-TM-102042] p 71 N89-25274  
Advances in thin-film solar cells for lightweight space photovoltaic power [NASA-TM-102017] p 73 N89-26041  
Comparative thermal analysis of the space station Freedom photovoltaic deployable boom structure using TRASYS, NEVADA, and SINDA programs [NASA-TM-102062] p 165 N89-26177  
Solar power for the lunar night [NASA-TM-102127] p 242 N89-26799  
NASA advanced space photovoltaic technology-status, potential and future mission applications [NASA-TM-102093] p 75 N89-27705  
Evolutionary growth for Space Station Freedom electrical power system [NASA-TM-102339] p 76 N89-28570
- PHOTOVOLTAIC CONVERSION**  
The NASA Space Solar Cell Advanced Research Program [NASA-TM-102020] p 67 N89-22651  
InP (Indium Phosphide): Into the future [NASA-TM-102058] p 212 N89-23025  
Space Station Freedom Solar Array design development [NASA-TM-102105] p 70 N89-24448  
Space Station Freedom photovoltaic power module design status [NASA-TM-102073] p 71 N89-25273  
Launch packaging options for the photovoltaic power module cargo element [NASA-TM-102072] p 71 N89-25275  
Estimated performance and future potential of solar dynamic and photovoltaic power systems for selected LEO and HEO missions [NASA-TM-102083] p 72 N89-25280
- PHOTOVOLTAIC EFFECT**  
Photovoltaics for high capacity space power systems [IAF PAPER 88-221] p 53 A89-17730

Photovoltaics for high capacity space power systems  
[NASA-TM-101341] p 61 N89-10122

Starting characteristics of direct current motors powered by solar cells  
[NASA-TM-101981] p 136 N89-19493

Space Photovoltaic Research and Technology, 1988. High Efficiency, Space Environment, and Array Technology  
[NASA-CP-3030] p 212 N89-24704

Photovoltaic module on-orbit assembly for Space Station Freedom  
[NASA-TM-102297] p 47 N89-26887

**PHYSICAL OPTICS**

Shooting and bouncing rays - Calculating the RCS of an arbitrarily shaped cavity p 124 A89-34242

**PIEZOELECTRIC CRYSTALS**

Development and applications of optical interferometric micrometry in the Angstrom and subangstrom range p 170 A89-27663

**PIEZOELECTRIC TRANSDUCERS**

Distributed ice accretion sensor for smart aircraft structures  
[AIAA PAPER 89-0772] p 17 A89-25571

**PIEZOELECTRICITY**

A self diagnostic system for piezoelectric sensors  
[AIAA PAPER 89-2638] p 171 A89-46980

Piezoelectric pushers for active vibration control of rotating machinery p 171 A89-47717

**PILOT PERFORMANCE**

Computer simulation of a pilot in V/STOL aircraft control loops  
[NASA-CR-184815] p 215 N89-21479

**PIPE FLOW**

Thermocapillary migration of a large gas slug in a tube p 117 A89-22747

A near-wall turbulence model and its application to fully developed turbulent channel and pipe flows  
[NASA-TM-101399] p 158 N89-13741

Control-volume based Navier-Stokes equation solver valid at all flow velocities  
[NASA-TM-101488] p 161 N89-20407

**PISTON ENGINES**

Hot piston ring/cylinder liner materials - Selection and evaluation  
[SAE PAPER 880544] p 178 A89-12304

Engineering study on the rotary-vee engine concept  
[SAE PAPER 890332] p 181 A89-51492

**PITCH (MATERIAL)**

Synthesis and stability of Br<sub>2</sub>, ICl and IBr intercalated pitch-based graphite fibers p 106 A89-37670

**PIXELS**

Digital CODEC for real-time processing of broadcast quality video signals at 1.8 bits/pixel  
[NASA-TM-102325] p 129 N89-27927

**PLANE WAVES**

Recovery of excitation intensity dependence in pulsed, focused beams - Nonsaturated case p 177 A89-17507

Theory and application of radiation boundary operators p 224 A89-24191

**PLASMA ACCELERATION**

Plasma flow processes within magnetic nozzle configurations  
[AIAA PAPER 89-2711] p 57 A89-47036

Arc-driven rail accelerator research  
[NASA-CR-179584] p 40 N89-13445

**PLASMA CLOUDS**

Bounds on current collection from the far field by plasma clouds in the ionosphere p 214 A89-34791

**PLASMA CONDUCTIVITY**

Arc restrike in the rail accelerator p 39 A89-32065

**PLASMA CONTROL**

Antiproton powered propulsion with magnetically confined plasma engines  
[NASA-CR-185131] p 74 N89-27700

**PLASMA CURRENTS**

The stability analysis of magnetohydrodynamic equilibria - Comparing the thermodynamic approach with the energy principle p 232 A89-39391

**PLASMA DENSITY**

The POLAR code wake model - Comparison with in situ observations --- Shuttle Orbiter plasma wake ion and electron density simulation p 233 A89-45632

The effects of arcjet thruster operating condition constrictor geometry on the plasma plume  
[AIAA PAPER 89-2723] p 60 A89-50809

Plasma density fluctuations observed during Space Shuttle Orbiter water releases p 233 A89-54759

The effects of arcjet operating condition and constrictor geometry on the plasma plume  
[NASA-TM-102284] p 72 N89-25281

**PLASMA DIAGNOSTICS**

Coherent Cerenkov radiation from the Spacelab 2 electron beam p 231 A89-24292

The plasma wake of the Shuttle Orbiter p 215 A89-43680

The POLAR code wake model - Comparison with in situ observations --- Shuttle Orbiter plasma wake ion and electron density simulation p 233 A89-45632

Plume characteristics of MPD thrusters - A preliminary examination  
[AIAA PAPER 89-2832] p 39 A89-47113

The effects of arcjet thruster operating condition constrictor geometry on the plasma plume  
[AIAA PAPER 89-2723] p 60 A89-50809

Plasma density, temperature and turbulence in the wake of the Shuttle Orbiter p 233 A89-53209

Plasma density fluctuations observed during Space Shuttle Orbiter water releases p 233 A89-54759

The effects of arcjet operating condition and constrictor geometry on the plasma plume  
[NASA-TM-102284] p 72 N89-25281

Plume characteristics of MPD thrusters: A preliminary examination  
[NASA-CR-185130] p 76 N89-29483

**PLASMA DIFFUSION**

A heat-driven monochromatic light source p 224 A89-41722

**PLASMA DIODES**

A heat-driven monochromatic light source p 224 A89-41722

**PLASMA ELECTRODES**

On the need for space tests of plasma contactors as electron collectors p 232 A89-43356

**PLASMA ENGINES**

Antiproton powered propulsion with magnetically confined plasma engines  
[AIAA PAPER 89-2334] p 57 A89-46758

Design of a thrust stand for high power electric propulsion devices  
[AIAA PAPER 89-2829] p 39 A89-47110

Plume characteristics of MPD thrusters - A preliminary examination  
[AIAA PAPER 89-2832] p 39 A89-47113

Closed-drift thruster investigations  
[NASA-CR-179497] p 62 N89-11808

Test facility and preliminary performance of a 100 kW class MPD thruster  
[NASA-TM-102021] p 68 N89-23520

Antiproton powered propulsion with magnetically confined plasma engines  
[NASA-CR-185131] p 74 N89-27700

**PLASMA FREQUENCIES**

Model for computing volume-averaged plasma properties in electron-bombardment ion thrusters p 54 A89-28339

**PLASMA GENERATORS**

Ground-based plasma contactor characterization p 233 A89-43359

**PLASMA HEATING**

Growth of diamond by RF plasma-assisted chemical vapor deposition p 90 A89-20474

**PLASMA INTERACTIONS**

The physics of positively biased conductors surrounded by dielectrics in contact with a plasma p 232 A89-39395

Plasma density, temperature and turbulence in the wake of the Shuttle Orbiter p 233 A89-53209

Surface phenomena in plasma environments p 234 A89-23555

**PLASMA PHYSICS**

Space plasma contactor research, 1988  
[NASA-CR-182283] p 233 N89-21658

**PLASMA POTENTIALS**

Ground-based plasma contactor characterization p 233 A89-43359

**PLASMA PROPULSION**

Performance and lifetime assessment of MPD arc thruster technology  
[AIAA PAPER 88-3211] p 53 A89-16485

Investigations of microwave plasmas - Applications in electrothermal thruster systems  
[AIAA PAPER 89-2378] p 57 A89-46784

Performance of a 100 kW class applied field MPD thruster  
[AIAA PAPER 89-2710] p 57 A89-47035

The effects of magnetic nozzle configurations on plasma thrusters  
[NASA-CR-184678] p 64 N89-15170

Test facility and preliminary performance of a 100 kW class MPD thruster  
[NASA-TM-102021] p 68 N89-23520

Antiproton powered propulsion with magnetically confined plasma engines  
[NASA-CR-185131] p 74 N89-27700

Performance of a 100 kW class applied field MPD thruster  
[NASA-TM-102312] p 74 N89-27701

**PLASMA SHEATHS**

Experimental validation of a phenomenological model of the plasma contacting process p 232 A89-43357

## PLASMA SPRAYING

Acoustic emission evaluation of plasma-sprayed thermal barrier coatings p 178 A89-12751

Plasma deposited silicon nitride for indium phosphide encapsulation p 235 A89-27794

Radio-frequency plasma chemical vapor deposition growth of diamond p 236 A89-44552

Microlaminate composites as thermal barrier coatings p 83 A89-54261

Thermal Barrier Coatings. Abstracts and figures  
[NASA-CP-10019] p 110 N89-13642

An investigation of environmental influence on the creep behavior of a low pressure plasma sprayed NiCoCrAlY alloy p 110 N89-13648

High resolution video monitoring of coating thickness during plasma spraying  
[NASA-TM-101423] p 102 N89-15218

Thermal barrier coating life-prediction model development p 200 N89-17331

Thermal barrier coating life prediction model development p 200 N89-17333

**PLASMA TEMPERATURE**

Plasma density, temperature and turbulence in the wake of the Shuttle Orbiter p 233 A89-53209

**PLASMA TURBULENCE**

Plasma density, temperature and turbulence in the wake of the Shuttle Orbiter p 233 A89-53209

**PLASMA WAVES**

Electron velocity distributions and plasma waves associated with the injection of an electron beam into the ionosphere p 215 A89-43698

**PLASMA-ELECTROMAGNETIC INTERACTION**

A numerical model of electrodynamics of plasma within the contaminant gas cloud of the Space Shuttle Orbiter at low earth orbit p 233 A89-45631

**PLASMA-PARTICLE INTERACTIONS**

Coherent Cerenkov radiation from the Spacelab 2 electron beam p 231 A89-24292

**PLASMAS (PHYSICS)**

Development of a high power microwave thruster, with a magnetic nozzle, for space applications  
[NASA-TM-102321] p 74 N89-26904

**PLASTIC DEFORMATION**

Elevated temperature slow plastic deformation of NiAl/TiB<sub>2</sub> particulate composites p 81 A89-31689

Constitutive modeling for single crystal superalloys p 101 N89-12911

**PLASTIC FLOW**

Effect of grain size on the high temperature properties of B2 aluminides  
[NASA-TM-102382] p 101 N89-12720

**PLASTIC PROPERTIES**

Indentation plasticity and fracture in silicon  
[NASA-TP-2863] p 100 N89-10996

Three-dimensional inelastic analysis methods for hot section components p 199 N89-17321

Thermal expansion mismatch and plasticity in thermal barrier coating p 200 N89-17330

Isothermal life prediction of composite lamina using a damage mechanics approach  
[NASA-TM-102032] p 87 N89-24460

**PLATES (STRUCTURAL MEMBERS)**

Multi-grid for structures analysis p 206 N89-29810

**PLOTTING**

Plotting component maps in the Navy/NASA Engine Program (NNEP): A method and its usage  
[NASA-TM-101433] p 26 N89-14239

**PLUG NOZZLES**

Analysis of supersonic plug nozzle flowfield and heat transfer  
[NASA-CR-179554] p 10 N89-13397

**PLUMES**

Near-field acoustic environment of a supersonic plume adjacent to a wall  
[AIAA PAPER 89-1137] p 225 A89-33767

Rectangular nozzle plume velocity modeling for use in jet noise prediction  
[AIAA PAPER 89-2357] p 7 A89-46771

Investigation of a liquid-fed water resistojet plume  
[AIAA PAPER 89-2840] p 58 A89-47117

Experimental evaluation of resistojet thruster plume shields p 59 A89-47487

The effects of arcjet thruster operating condition constrictor geometry on the plasma plume  
[AIAA PAPER 89-2723] p 60 A89-50809

Rectangular nozzle plume velocity modeling for use in jet noise prediction  
[NASA-TM-102047] p 14 N89-22577

The effects of arcjet operating condition and constrictor geometry on the plasma plume  
[NASA-TM-102284] p 72 N89-25281

Investigation of a liquid-fed water resistojet plume  
[NASA-TM-102310] p 75 N89-27706

Plume characteristics of MPD thrusters: A preliminary examination  
[NASA-CR-185130] p 76 N89-29483

## PLY ORIENTATION

## PLY ORIENTATION

Local-global analysis of crack growth in continuously reinforced ceramic matrix composites  
[NASA-CR-182231] p 197 N89-13820

## POLARIZATION (CHARGE SEPARATION)

Oxygen electrodes for rechargeable alkaline fuel cells  
p 211 N89-22998

## POLARIZATION (WAVES)

An application of the WKBJ technique to the on-surface radiation condition p 124 A89-21222  
Review of FD-TD numerical modeling of electromagnetic wave scattering and radar cross section  
p 19 A89-45107

## POLYCRYSTALS

Surface temperature determination in surface analytic systems by infrared optical pyrometry  
p 169 A89-17347

Concepts for interrelating ultrasonic attenuation, microstructure, and fracture toughness in polycrystalline solids p 95 A89-19852  
Fracture toughness of polycrystalline ceramics in combined mode I and mode II loading  
p 105 A89-26457

Oxide scale stresses in polycrystalline Ni200  
p 98 A89-38859

Room temperature tensile ductility in polycrystalline B2 Ni-30Al-20Fe p 98 A89-44568  
Deformation and fracture of single-crystal and sintered polycrystalline silicon carbide produced by cavitation  
p 108 A89-54985

## POLYETHER RESINS

Degradation and crosslinking of perfluoroalkyl polyethers under X-ray irradiation in ultrahigh vacuum  
[NASA-TP-2910] p 114 N89-21103

Reaction of perfluoroalkylpolyethers (PFPE) with 440C steel in vacuum under sliding conditions at room temperature  
[NASA-TP-2883] p 115 N89-26091

## POLYIMIDE RESINS

Thermo-oxidative stability studies of Celion 6000/PMR-15 unidirectional composites, PMR-15, and Celion 6000 fiber p 79 A89-14099  
Graphite/polyimide composites with improved toughness p 83 A89-38637

## POLYIMIDES

Undercutting of defects in thin film protective coatings on polymer surfaces exposed to atomic oxygen  
[NASA-TM-101986] p 115 N89-23691

## POLYMER MATRIX COMPOSITES

Thermo-oxidative stability studies of Celion 6000/PMR-15 unidirectional composites, PMR-15, and Celion 6000 fiber p 79 A89-14099

A thermally modified polymer matrix composite material with structural integrity to 371 C p 80 A89-29997  
Graphite/polyimide composites with improved toughness p 83 A89-38637

Light weight polymer matrix composite material  
[NASA-CASE-LEW-14734-1] p 87 N89-23623

Tailoring of composite links for optimal damped elasto-dynamic performance  
[NASA-TM-102094] p 88 N89-26912

## POLYMERIC FILMS

Adhesion in ceramics and magnetic media  
[NASA-TM-101476] p 113 N89-19435

## POLYMERIZATION

Graphite fluoride fiber polymer composite material  
[NASA-CASE-LEW-14472-1] p 85 N89-14259

## POLYSTYRENE

Damage analysis of a crack layer p 194 A89-42984

## POROSITY

Dynamic porosity variations in ceramics  
[NASA-TM-101340] p 112 N89-17668

## POROUS BOUNDARY LAYER CONTROL

Experimental and numerical investigation of an oblique shock wave/turbulent boundary layer interaction with continuous suction  
[AIAA PAPER 89-0357] p 4 A89-28407

## POROUS MATERIALS

Ultrasonic imaging of porosity variations produced during sintering p 107 A89-48892

## POTASSIUM COMPOUNDS

Laboratory studies of binary salt CVD in combustion gas environments p 89 A89-12335  
Laboratory studies of the deposition of alkali sulfate vapors from combustion gases using a flash-evaporation technique p 89 A89-12338

## POTASSIUM HYDROXIDES

KOH concentration effect on cycle life of nickel-hydrogen cells. III - Cycle life test p 207 A89-23283

## POWDER (PARTICLES)

Improved silicon carbide for advanced heat engines  
[NASA-CR-179477] p 112 N89-15251

## POWDER METALLURGY

Effect of grain size on the high temperature properties of B2 aluminides  
[NASA-TM-101382] p 101 N89-12720

Tensile and creep rupture behavior of P/M processed

Nb-base alloy, WC-3009  
[NASA-TM-101954] p 78 N89-19371

Mechanical properties of modified low cobalt powder metallurgy Udmet 700 type alloys  
[NASA-TM-101481] p 103 N89-20228

Effect of processing on fracture toughness of silicon carbide as determined by Vickers indentations  
[NASA-TM-101456] p 115 N89-21895

## POWER CONDITIONING

Power systems for production, construction, life support, and operations in space p 37 A89-45803  
dc power control for a liquid-fed resistojet  
p 59 A89-47457

5-kW arcjet power electronics

[AIAA PAPER 89-2725] p 60 A89-49685

The 5-kW arcjet power electronics  
[NASA-TM-102108] p 70 N89-24446

## POWER CONVERTERS

A versatile power converter for high-frequency link systems p 131 A89-21200

5-kW arcjet power electronics  
[AIAA PAPER 89-2725] p 60 A89-49685

A design procedure for the phase-controlled parallel-loaded resonant inverter p 134 A89-50472

Study of the generator/motor operation of induction machines in a high frequency link space power system  
[NASA-CR-179600] p 63 N89-11809

Numerical model of solar dynamic radiator for parametric analysis

[NASA-TM-102054] p 67 N89-22653

The 5-kW arcjet power electronics  
[NASA-TM-102108] p 70 N89-24446

## POWER EFFICIENCY

Ion optics for high power 50-cm-dia ion thrusters  
[AIAA PAPER 89-2717] p 58 A89-47040

The effect of electrode configuration on arcjet performance  
[AIAA PAPER 89-2722] p 58 A89-47044

Effects of lubrication on the performance of high speed spur gears  
[NASA-TM-101969] p 186 N89-22919

Estimated performance and future potential of solar dynamic and photovoltaic power systems for selected LEO and HEO missions  
[NASA-TM-102083] p 72 N89-25280

Ion optics for high power 50-cm-diam ion thrusters  
[NASA-TM-102143] p 76 N89-28571

## POWER LIMITERS

Channelized coplanar waveguide: Discontinuities, junctions, and propagation characteristics  
[NASA-TM-101483] p 137 N89-21172

## POWER MODULES (STS)

Photovoltaic power modules for NASA's manned Space Station p 55 A89-29122

Protoflight photovoltaic power module system-level tests in the space power facility  
[NASA-TM-102066] p 46 N89-25267

## POWER SPECTRA

Sound power spectrum and wave drag of a propeller in flight  
[AIAA PAPER 89-1081] p 225 A89-33724

## POWER SUPPLY CIRCUITS

Cooperating expert systems for Space Station - Power/thermal subsystem testbeds p 38 A89-15350

Multi-hundred kilowatt roll ring assembly evaluation results -- for Space Station power transmission  
p 123 A89-15388

Multi-hundred kilowatt roll ring assembly  
[NASA-CR-174832] p 135 N89-15335

## POWER TRANSMISSION

Power components for the Space Station 20-kHz power distribution system p 130 A89-15387

Power systems for production, construction, life support, and operations in space p 37 A89-45803

Solar power for the lunar night  
[NASA-TM-102127] p 242 N89-26799

## POWERED LIFT AIRCRAFT

NASA powered lift facility internally generated noise and its transmission to the acoustic far field  
[NASA-CR-182217] p 36 N89-16882

## PRECIPITATES

Analysis of microalloy precipitate reversion in steels  
p 94 A89-15108

## PRECIPITATION HARDENING

Influence of precipitate morphology on intermediate temperature creep properties of a nickel-base superalloy single crystal p 96 A89-26872

The influence of annealing in the ferrite-plus-austenite phase field on the stability of vanadium carbide precipitates p 97 A89-32803

Dispersoids in rapidly solidified B2 nickel aluminides  
p 98 A89-43023

## PREDICTION ANALYSIS TECHNIQUES

Creep life prediction based on stochastic model of microstructurally short crack growth p 193 A89-36185

Prediction of unsteady rotor-surface heat transfer from wake passages  
[AIAA PAPER 89-1692] p 150 A89-43210

Mathematical modeling of solid oxide fuel cells  
[NASA-CR-182188] p 209 N89-12122

Aerothermal modeling program, phase 2  
p 156 N89-12890

Efficient numerical techniques for complex fluid flows  
p 156 N89-12894

Improved numerical methods for turbulent viscous recirculating flows p 156 N89-12895

Development of low Reynolds number two equation turbulence models for predicting external heat transfer on turbine blades p 157 N89-12901

Turbine airfoil film cooling p 158 N89-12903

Creep fatigue life prediction for engine hot section materials (isotropic): Fourth year progress review  
p 188 N89-12914

Life prediction and constitutive models for engine hot section p 188 N89-12916

Thermal barrier coating life prediction model development p 109 N89-12920

Thermal barrier coating life prediction model  
p 109 N89-12921

Thermal barrier coating life prediction model development p 110 N89-12922

Analytical ice shape predictions for flight in natural icing conditions  
[NASA-CR-182234] p 18 N89-13428

Vibration signature analysis of multistage gear transmission  
[NASA-TM-101442] p 184 N89-18685

Fatigue life prediction modeling for turbine hot section materials p 30 N89-20142

Fatigue crack growth model RANDOM2 user manual, appendix 1  
[NASA-CR-184939] p 203 N89-23890

Fatigue strength reduction model: RANDOM3 and RANDOM4 user manual, appendix 2  
[NASA-CR-184940] p 203 N89-23891

## PREDICTIONS

Fiber composite structural durability and damage tolerance - Simplified predictive methods  
p 82 A89-36320

A numerical method for computing unsteady 2-D boundary layer flows  
[NASA-CR-4198] p 155 N89-12835

Thermal barrier coating life-prediction model development  
[NASA-CR-175002] p 26 N89-13433

Thermal barrier coating life prediction model development  
[NASA-CR-180807] p 110 N89-13621

Leakage predictions for Rayleigh-step, helium-purge seals  
[NASA-TM-101352] p 64 N89-14255

The role of thermal and lubricant boundary layers in the transient thermal analysis of spur gears  
[NASA-TM-101435] p 182 N89-14452

A prediction of 3-D viscous flow and performance of the NASA low-speed centrifugal compressor  
[NASA-CR-184765] p 160 N89-16132

A modified VAPEPS method for predicting vibroacoustic response of unreinforced mass loaded honeycomb panels  
[NASA-TM-101467] p 46 N89-16905

Thermal barrier coating life-prediction model development p 200 N89-17331

Thermal barrier coating life prediction model development p 200 N89-17333

A predictive model for failure properties of thermoset resins  
[NASA-TM-4128] p 87 N89-25300

## PREMIXED FLAMES

Optical measurements of soot and temperature profiles in premixed propane-oxygen flames p 92 A89-35008

Time-dependent computational studies of flames in microgravity  
[NASA-CR-182298] p 122 N89-25353

Determination of combustion gas temperatures by infrared radiometry in sooting and nonsooting flames  
[NASA-TP-2900] p 164 N89-25409

## PREMIXING

A premixed hydrogen/oxygen catalytic igniter  
[AIAA PAPER 89-2302] p 59 A89-49683

A premixed hydrogen/oxygen catalytic igniter  
[NASA-CR-185113] p 70 N89-24445

## PRESSING

Slurry-pressing consolidation of silicon nitride  
[NASA-TM-101385] p 109 N89-12746

## PRESSURE DEPENDENCE

NASA Lewis Stirling engine computer code evaluation  
[NASA-CR-182248] p 214 N89-24741



- PRESSURE DISTRIBUTION**  
 Prediction of unsteady blade surface pressures on an advanced propeller at an angle of attack  
 [AIAA PAPER 89-1060] p 227 A89-40473  
 Large scale advanced propeller blade pressure distributions - Prediction and data  
 [AIAA PAPER 89-2696] p 7 A89-47026
- PRESSURE EFFECTS**  
 Pressure effects on the thermal stability of silicon carbide fibers  
 p 105 A89-31502  
 Effect of ambient pressure on the performance of a resistojet  
 p 55 A89-44111  
 Effect of length of chopped pristine and intercalated graphite fibers on the resistivity of fiber networks  
 [NASA-TM-101395] p 84 N89-11826  
 COLD-SAT: An orbital cryogenic hydrogen technology experiment  
 [NASA-TM-102303] p 73 N89-26044
- PRESSURE GRADIENTS**  
 Determination of the thermal stability of perfluoroalkylethers by tensimetry: Instrumentation and Procedure  
 [NASA-TM-102116] p 116 N89-26095
- PRESSURE MEASUREMENT**  
 Unsteady blade pressure measurements on a model counterrotation propeller  
 [AIAA PAPER 89-1144] p 226 A89-40175  
 The effect of prewhirl on the internal aerodynamics and performance of a mixed flow research centrifugal compressor  
 [NASA-CR-184756] p 161 N89-19503  
 Unsteady blade pressure measurements on a model counterrotation propeller  
 [NASA-TM-102002] p 228 N89-20779  
 On the dynamic response of pressure transmission lines in the research of helium-charged free piston Stirling engines  
 [NASA-TM-102121] p 175 N89-24593
- PRESSURE OSCILLATIONS**  
 Fluctuating pressures on wing surfaces in the slipstream of a single-rotor propfan  
 [AIAA PAPER 89-1058] p 226 A89-36218
- PRESSURE RATIO**  
 Advanced core technology: Key to subsonic propulsion benefits  
 [NASA-TM-101420] p 26 N89-14237
- PRESSURE REDUCTION**  
 Coolant passage heat transfer with rotation  
 p 161 N89-17314
- PRESSURE SENSORS**  
 Unsteady blade pressure measurements on a model counterrotation propeller  
 [AIAA PAPER 89-1144] p 226 A89-40175  
 Unsteady blade pressure measurements on a model counterrotation propeller  
 [NASA-TM-102002] p 228 N89-20779
- PRESSURE VESSELS**  
 The effect of compression on Individual Pressure Vessel Nickel/Hydrogen components --- for energy storage in low earth orbits  
 p 50 A89-15281  
 Total strain version of strainrange partitioning for thermomechanical fatigue at low strains  
 p 201 N89-17337  
 Investigation of Weibull statistics in fracture analysis of cast aluminum  
 [NASA-TM-102000] p 185 N89-21245
- PRISMS**  
 Domed Fresnel lens concentrator technology for space application  
 p 213 N89-24732
- PROBABILITY DENSITY FUNCTIONS**  
 Pdf - Transport equations for chemically reacting flows  
 p 152 A89-51880
- PROBABILITY DISTRIBUTION FUNCTIONS**  
 Probabilistic structural analysis methods of hot engine structures  
 [NASA-TM-102091] p 205 N89-28030
- PROBABILITY THEORY**  
 Probabilistic structural analysis methods and applications  
 p 190 A89-16939  
 Probabilistic methods for structural response analysis  
 p 223 A89-25843  
 An approach to probabilistic finite element analysis using a mixed-iterative formulation  
 p 191 A89-25849  
 Kuhn-Tucker optimization based reliability analysis for probabilistic finite elements  
 p 187 A89-25852  
 Probabilistic constitutive relationships for material strength degradation models  
 [AIAA PAPER 89-1368] p 192 A89-30843  
 An approximate methods approach to probabilistic structural analysis  
 [AIAA PAPER 89-1369] p 193 A89-30844  
 An advanced probabilistic structural analysis method for implicit performance functions  
 [AIAA PAPER 89-1371] p 193 A89-30846  
 Probabilistic structural analysis to quantify uncertainties associated with turbopump blades  
 p 194 A89-36920
- A probabilistic approach to composite micromechanics  
 [NASA-TM-101366] p 85 N89-12684  
 Probabilistic analysis for fatigue strength degradation of materials  
 [NASA-CR-182844] p 198 N89-15434
- PROBES**  
 Technique for temperature compensation of eddy-current proximity probes  
 [NASA-TP-2880] p 173 N89-15380
- PROBLEM SOLVING**  
 Composite Blade Structural Analyzer (COBSTRAN) demonstration manual  
 [NASA-TM-101957] p 87 N89-24459  
 On the applications of algebraic grid generation methods based on transfinite interpolation  
 [NASA-TM-102095] p 33 N89-26003
- PROCESS CONTROL (INDUSTRY)**  
 IECON '87: Industrial applications of control and simulation; Proceedings of the 1987 International Conference on Industrial Electronics, Control, and Instrumentation, Cambridge, MA, Nov. 3, 4, 1987  
 [SPIE-853] p 219 A89-10798  
 The role of rapid solidification processing in the fabrication of fiber reinforced metal matrix composites  
 [NASA-TM-101450] p 85 N89-15201  
 Optimum interface properties for metal matrix composites  
 [NASA-TM-102295] p 205 N89-27223
- PRODUCT DEVELOPMENT**  
 The design and development of transonic multistage compressors  
 p 27 N89-16834  
 Assessment, development, and application of combustor aerothermal models  
 p 30 N89-20138
- PROFILES**  
 Dynamic loading of spur gears with linear or parabolic tooth profile modification  
 [NASA-TM-101444] p 183 N89-15413
- PROGRAM VERIFICATION (COMPUTERS)**  
 CFD validation experiments for internal flows  
 p 161 N89-18635
- PROJECT MANAGEMENT**  
 Institute for Computational Mechanics in Propulsion (ICOMP)  
 [NASA-TM-101961] p 222 N89-21595  
 Age distribution among NASA scientists and engineers  
 p 238 N89-23911  
 NASA's Chemical Transfer Propulsion Program for Pathfinder  
 [NASA-TM-102298] p 41 N89-26876
- PROJECT PLANNING**  
 Human exploration mission studies  
 p 38 N89-22985  
 A program for advancing the technology of space concentrators  
 [NASA-TM-102139] p 76 N89-29484
- PROJECTILES**  
 Arc restrike in the rail accelerator  
 p 39 A89-32065  
 Arc-driven rail accelerator research  
 [NASA-CR-179584] p 40 N89-13445
- PROP-FAN TECHNOLOGY**  
 Results of acoustic tests of a prop-fan model  
 p 224 A89-10112  
 Return of the turboprops  
 p 20 A89-12953  
 Euler analysis of a swirl recovery vane design for use with an advanced single-rotation propfan  
 [AIAA PAPER 88-3152] p 2 A89-17940  
 Experimental investigation of propfan aeroelastic response in off-axis flow with mistuning  
 [AIAA PAPER 88-3153] p 20 A89-17941  
 Design and test of a propfan gear system  
 p 179 A89-22290  
 Sound power spectrum and wave drag of a propeller in flight  
 [AIAA PAPER 89-1081] p 225 A89-33724  
 Near wakes of advanced turbopropellers  
 [AIAA PAPER 89-1095] p 5 A89-33735  
 Interior noise in the untreated Gulfstream II Propfan Test Assessment (PTA) aircraft  
 [AIAA PAPER 89-1119] p 17 A89-33754  
 Near-field acoustic characteristics of a single-rotor propfan  
 [AIAA PAPER 89-1055] p 23 A89-36215  
 Installed propfan (SR-7L) far-field noise characteristics  
 [AIAA PAPER 89-1056] p 225 A89-36216  
 Lateral noise attenuation of the advanced propeller of the propfan test assessment aircraft  
 [AIAA PAPER 89-1057] p 226 A89-36217  
 Fluctuating pressures on wing surfaces in the slipstream of a single-rotor propfan  
 [AIAA PAPER 89-1058] p 226 A89-36218  
 Aeroelastic analysis of prop fan blades with a semiempirical dynamic stall model  
 [AIAA PAPER 89-2695] p 194 A89-47025  
 Large scale advanced propeller blade pressure distributions - Prediction and data  
 [AIAA PAPER 89-2696] p 7 A89-47026
- PROPELLER BLADES**  
 Average-passage simulation of counter-rotating propfan propulsion systems as applied to cruise missiles  
 [AIAA PAPER 89-2943] p 7 A89-47187  
 Analytical flutter investigation of a composite propfan model  
 p 195 A89-48663  
 Advanced turboprop project  
 [NASA-SP-495] p 24 N89-12565  
 Analysis of an unswept propfan blade with a semiempirical dynamic stall model  
 [NASA-TM-4083] p 27 N89-15112  
 Wind-tunnel results of advanced high-speed propellers at takeoff, climb, and landing Mach numbers  
 [NASA-TM-87030] p 13 N89-19265  
 Multiple-Purpose Subsonic Naval Aircraft (MPSNA) Multiple Application Propfan Study (MAPS)  
 [NASA-CR-175096] p 18 N89-19289  
 Large-scale Advanced Prop-fan (LAP) hub/blade retention design report  
 [NASA-CR-174786] p 28 N89-19299  
 Average-passage simulation of counter-rotating propfan propulsion systems as applied to cruise missiles  
 [NASA-TM-102043] p 14 N89-23416  
 Structural tailoring of counter rotation propfans  
 p 33 N89-25165
- PROPAGATION MODES**  
 Multiple coherent mode interaction in a developing round jet  
 [AIAA PAPER 89-0967] p 147 A89-30483
- PROPELLANT COMBUSTION**  
 Langmuir probe measurements of an arcjet exhaust  
 p 55 A89-39031  
 A premixed hydrogen/oxygen catalytic igniter  
 [AIAA PAPER 89-2302] p 59 A89-49683  
 Turbine Engine Hot Section Technology 1986  
 [NASA-CP-2444] p 195 N89-12876  
 A premixed hydrogen/oxygen catalytic igniter  
 [NASA-CR-185113] p 70 N89-24445
- PROPELLANT STORAGE**  
 In-situ propellant advantages for fast transfer to Mars  
 [AIAA PAPER 88-2901] p 37 A89-14977  
 Weight savings in aerospace vehicles through propellant scavenging  
 [SAWE PAPER 1818] p 40 A89-50814  
 COLD-SAT orbital experiment configured for Atlas launch  
 p 45 A89-53327
- PROPELLANT TANKS**  
 Analysis of the nonvented fill of a 4.96-cubic-meter lightweight liquid hydrogen tank  
 [NASA-TM-102039] p 67 N89-22652
- PROPELLANT TRANSFER**  
 Modeling of pulsed propellant reorientation  
 [AIAA PAPER 89-2727] p 61 A89-53306  
 Analysis of the nonvented fill of a 4.96-cubic-meter lightweight liquid hydrogen tank  
 [NASA-TM-102039] p 67 N89-22652  
 COLD-SAT: An orbital cryogenic hydrogen technology experiment  
 [NASA-TM-102303] p 73 N89-26044  
 Modeling of pulsed propellant reorientation  
 [NASA-TM-102117] p 165 N89-26178  
 COLD-SAT: Cryogenic On-Orbit Liquid Depot-Storage, Acquisition and Transfer  
 [NASA-TM-102308] p 38 N89-28535
- PROPELLANTS**  
 Preliminary design study of hydrogen and ammonia resistojets for prime and auxiliary thrusters  
 [NASA-CR-182176] p 62 N89-10943  
 Development of a high power microwave thruster, with a magnetic nozzle, for space applications  
 [NASA-TM-102321] p 74 N89-26904
- PROPELLER BLADES**  
 Vibration, performance, flutter and forced response characteristics of a large-scale propfan and its aeroelastic model  
 [AIAA PAPER 88-3155] p 21 A89-17943  
 Optimizing advanced propeller designs by simultaneously updating flow variables and design parameters  
 p 5 A89-39189  
 High-speed propeller performance and noise predictions at takeoff/landing conditions  
 p 226 A89-39195  
 Unsteady blade pressure measurements on a model counterrotation propeller  
 [AIAA PAPER 89-1144] p 226 A89-40175  
 Prediction of unsteady blade surface pressures on an advanced propeller at an angle of attack  
 [AIAA PAPER 89-1060] p 227 A89-40473  
 An acoustic experimental and theoretical investigation of single disc propellers  
 [AIAA PAPER 89-1146] p 227 A89-40478  
 Large scale advanced propeller blade pressure distributions - Prediction and data  
 [AIAA PAPER 89-2696] p 7 A89-47026  
 Low-speed wind tunnel performance of high-speed counterrotation propellers at angle-of-attack  
 [AIAA PAPER 89-2583] p 8 A89-50808

## PROPELLER EFFICIENCY

- Vibration, performance, flutter and forced response characteristics of a large-scale propfan and its aeroelastic model  
[NASA-TM-101322] p 24 N89-10043
- Analysis of an unswept propfan blade with a semiempirical dynamic stall model  
[NASA-TM-4083] p 27 N89-15112
- Large-scale Advanced Prop-fan (LAP) hub/blade retention design report  
[NASA-CR-174786] p 28 N89-19299
- Structural Tailoring of Advanced Turboprops (STAT) programmer's manual  
[NASA-CR-182164] p 29 N89-20132
- Unsteady blade pressure measurements on a model counterrotation propeller  
[NASA-TM-102002] p 228 N89-20779
- High speed turboprop aeroacoustic study (single rotation). Volume 1: Model development  
[NASA-CR-182257-VOL-1] p 229 N89-24139
- Low-speed wind tunnel performance of high-speed counterrotation propellers at angle-of-attack  
[NASA-TM-102292] p 15 N89-25121
- PROPELLER EFFICIENCY**
- Return of the turboprops p 20 A89-12953
- Sound power spectrum and wave drag of a propeller in flight p 225 A89-33724
- Determination of near and far field acoustics for advanced propeller configurations  
[AIAA PAPER 89-1081] p 226 A89-40469
- Aerodynamic interaction between propellers and wings  
[AIAA PAPER 89-1040] p 8 A89-50062
- Low-speed wind tunnel performance of high-speed counterrotation propellers at angle-of-attack  
[AIAA PAPER 89-2583] p 8 A89-50808
- Structural Tailoring of Advanced Turboprops (STAT) programmer's manual  
[NASA-CR-182164] p 29 N89-20132
- Low-speed wind tunnel performance of high-speed counterrotation propellers at angle-of-attack  
[NASA-TM-102292] p 15 N89-25121
- PROPELLER FANS**
- Cruise noise of the 2/9 scale model SR-7A propeller  
[AIAA PAPER 88-3154] p 224 A89-12561
- Aeroelastic response of metallic and composite propfan models in yawed flow  
[AIAA PAPER 88-3154] p 20 A89-17942
- A computational procedure for automated flutter analysis  
[AIAA PAPER 89-2695] p 194 A89-47025
- Aeroelastic analysis of prop fan blades with a semiempirical dynamic stall model  
[AIAA PAPER 89-2695] p 194 A89-47025
- Average-passage simulation of counter-rotating propfan propulsion systems as applied to cruise missiles  
[AIAA PAPER 89-2943] p 7 A89-47187
- Average-passage simulation of counter-rotating propfan propulsion systems as applied to cruise missiles  
[NASA-TM-102043] p 14 N89-23416
- PROPELLER NOISE**
- In-flight measurement of propeller noise on the fuselage of an airplane  
[NASA-TM-102285] p 229 N89-25675
- PROPELLER SLIPSTREAMS**
- Aerodynamic interaction between propellers and wings  
[AIAA PAPER 88-3152] p 8 A89-50062
- PROPELLERS**
- NASA/industry advanced turboprop technology program  
[AIAA PAPER 88-3152] p 2 A89-17940
- Euler analysis of a swirl recovery vane design for use with an advanced single-rotation propfan  
[AIAA PAPER 89-0535] p 17 A89-25429
- Propeller/wing interaction  
[AIAA PAPER 89-0535] p 17 A89-25429
- Laser velocimeter measurements of the flowfield generated by an advanced counterrotating propeller  
[AIAA PAPER 89-0434] p 3 A89-26373
- Comparison of propeller cruise noise data taken in the NASA Lewis 8- by 6-foot wind tunnel with other tunnel and flight data  
[AIAA PAPER 89-1059] p 226 A89-40472
- The effect of front-to-rear propeller spacing on the interaction noise at cruise conditions of a model counterrotation propeller having a reduced diameter aft propeller  
[NASA-TM-101329] p 227 N89-10603
- Experimental aerodynamic performance of advanced 40 deg-swept 10-blade propeller model at Mach 0.6 to 0.85  
[NASA-TM-88969] p 9 N89-10865
- Aerodynamic optimization by simultaneously updating flow variables and design parameters with application to advanced propeller designs  
[NASA-CR-182181] p 24 N89-11750
- Laser velocimeter measurements of the flowfield generated by an advanced counterrotating propeller  
[NASA-TM-101437] p 10 N89-13409

- Parametric studies of advanced turboprops  
[NASA-TM-101389] p 197 N89-14465
- Measured far-field flight noise of a counterrotation turboprop at cruise conditions  
[NASA-TM-101383] p 228 N89-15686
- An analysis for high speed propeller-nacelle aerodynamic performance prediction. Volume 1: Theory and application  
[NASA-CR-4199-VOL-1] p 12 N89-15896
- An analysis for high speed propeller-nacelle aerodynamic performance prediction. Volume 2: User's manual  
[NASA-CR-4199-VOL-2] p 12 N89-15897
- NASA advanced propeller research  
[NASA-TM-101361] p 27 N89-15913
- Comparison of propeller cruise noise data taken in the NASA Lewis 8- by 6-foot wind tunnel with other tunnel and flight data  
[NASA-TM-101976] p 228 N89-21628
- High speed turboprop aeroacoustic study (single rotation). Volume 1: Model development  
[NASA-CR-182257-VOL-1] p 229 N89-24139
- Cruise noise of the SR-2 propeller model in a wind tunnel  
[NASA-TM-101480] p 229 N89-24886
- PROPULSION**
- Fiber optic control system integration  
[NASA-CR-179568] p 231 N89-13256
- Advanced computational techniques for hypersonic propulsion  
[NASA-TM-102005] p 163 N89-23809
- PROPULSION SYSTEM CONFIGURATIONS**
- A reusable rocket engine intelligent control  
[AIAA PAPER 88-3114] p 48 A89-14981
- Application of advanced computational technology to propulsion CFD  
[AIAA PAPER 89-2908] p 142 A89-16957
- Advanced transmission studies p 178 A89-18906
- Integrated flight/propulsion control study for STOVL applications  
[AIAA PAPER 89-2908] p 34 A89-47166
- Average-passage simulation of counter-rotating propfan propulsion systems as applied to cruise missiles  
[AIAA PAPER 89-2943] p 7 A89-47187
- The NASA Electric Propulsion Program p 59 A89-47428
- Heat transfer in aerospace propulsion  
[AIAA PAPER 89-2142] p 153 A89-53282
- Aeronautical applications of high-temperature superconductors  
[AIAA PAPER 89-2142] p 23 A89-53304
- Liquid oxygen cooling of high pressure LOX/hydrocarbon rocket thrust chambers  
[AIAA PAPER 89-2142] p 63 N89-12649
- Probabilistic analysis for fatigue strength degradation of materials  
[NASA-CR-182844] p 198 N89-15434
- Design and analysis report for the flight weight 20-inch Columbium secondary nozzle for the RL10 engine  
[NASA-CR-179612] p 65 N89-16918
- Unique mission options available with a megawatt-class nuclear electric propulsion system  
[NASA-TM-101220] p 65 N89-17618
- CFD validation experiments for internal flows  
[AIAA PAPER 89-2943] p 161 N89-18635
- Institute for Computational Mechanics in Propulsion (ICOMP) p 222 N89-21595
- Average-passage simulation of counter-rotating propfan propulsion systems as applied to cruise missiles  
[NASA-TM-102043] p 14 N89-23416
- Advances in computational design and analysis of airbreathing propulsion systems  
[NASA-TM-101987] p 32 N89-23465
- Turbomachinery technology for high-speed civil flight  
[NASA-TM-102092] p 32 N89-24320
- Aeronautical applications of high-temperature superconductors  
[NASA-TM-102311] p 33 N89-26008
- Revolutionary opportunities for materials and structures study, addendum  
[NASA-CR-179642-ADD] p 34 N89-29351
- PROPULSION SYSTEM PERFORMANCE**
- A detailed model of electrothermal propulsion systems  
[AIAA PAPER 89-2262] p 56 A89-46707
- A detailed model of ion propulsion systems  
[AIAA PAPER 89-2268] p 56 A89-46712
- New hypersonic facility capability at NASA Lewis Research Center  
[AIAA PAPER 89-2534] p 36 A89-46905
- Performance of a 100 kW class applied field MPD thruster  
[AIAA PAPER 89-2710] p 57 A89-47035
- Experiments and analysis of a compact electrothermal thruster p 59 A89-47494

- Performance characterization and transient investigation of multipropellant resistojets  
[AIAA PAPER 89-2837] p 60 A89-50811
- Integrated flight/propulsion control system design based on a centralized approach  
[AIAA PAPER 89-3520] p 35 A89-52611
- The development of power specific redlines for SSME safety monitoring  
[AIAA PAPER 89-2413] p 61 A89-53305
- Supersonic throughflow fans p 27 N89-16837
- Turbomachinery aeroelasticity at NASA Lewis Research Center p 28 N89-19262
- Propulsion over a wide Mach number range  
[NASA-CR-182267] p 29 N89-20134
- A perspective on future directions in aerospace propulsion system simulation  
[NASA-TM-102038] p 31 N89-21798
- New hypersonic facility capability at NASA Lewis Research Center p 36 N89-22617
- [NASA-TM-102028] p 36 N89-22617
- Design, fabrication and test of the RL10 derivative II chamber/primary nozzle  
[NASA-CR-179595] p 68 N89-23519
- Test facility and preliminary performance of a 100 kW class MPD thruster  
[NASA-TM-102021] p 68 N89-23520
- Performance of large area xenon ion thrusters for orbit transfer missions  
[NASA-TM-102049] p 69 N89-24436
- Advanced APS impacts on vehicle payloads  
[NASA-TM-102086] p 41 N89-25254
- Performance characterization and transient investigation of multipropellant resistojets  
[NASA-TM-102118] p 72 N89-25283
- Integrated flight/propulsion control system design based on a centralized approach  
[NASA-TM-102137] p 35 N89-26009
- The development of power specific redlines for SSME safety monitoring  
[NASA-CR-185121] p 41 N89-26027
- Electric propulsion options for 10 kW class earth space missions  
[NASA-TM-102337] p 74 N89-26906
- Performance of a 100 kW class applied field MPD thruster  
[NASA-TM-102312] p 74 N89-27701
- PROPULSIVE EFFICIENCY**
- The development of power specific redlines for SSME safety monitoring  
[AIAA PAPER 89-2413] p 61 A89-53305
- Propulsion over a wide Mach number range  
[NASA-CR-182267] p 29 N89-20134
- A perspective on future directions in aerospace propulsion system simulation  
[NASA-TM-102038] p 31 N89-21798
- Advanced APS impacts on vehicle payloads  
[NASA-TM-102086] p 41 N89-25254
- The development of power specific redlines for SSME safety monitoring  
[NASA-CR-185121] p 41 N89-26027
- Antiproton powered propulsion with magnetically confined plasma engines  
[NASA-CR-185131] p 74 N89-27700
- Performance of a 100 kW class applied field MPD thruster  
[NASA-TM-102312] p 74 N89-27701
- PROTECTIVE COATINGS**
- A thermally modified polymer matrix composite material with structural integrity to 371 C  
[AIAA PAPER 89-2997] p 80 A89-29997
- Durable thin film coatings for reflectors used in low earth orbit  
[AIAA PAPER 89-3150] p 77 A89-33150
- Oxidation and protection of fiberglass-epoxy composite masts for photovoltaic arrays in the low earth orbital environment  
[AIAA PAPER 89-35316] p 44 A89-35316
- Isothermal and 'bithermal' thermomechanical fatigue behavior of a NiCoCrAlY-coated single crystal superalloy  
[AIAA PAPER 89-36457] p 177 A89-36457
- Predicting minimum Al concentrations for protective scale formation on Ni-base alloys. I - Isothermal oxidation. II - Cyclic oxidation  
[AIAA PAPER 89-40116] p 98 A89-40116
- Tribological composition optimization of chromium-carbide-based solid lubricant coatings for foil gas bearings at temperatures to 650 C  
[AIAA PAPER 89-54258] p 83 A89-54258
- Micro laminate composites as thermal barrier coatings  
[AIAA PAPER 89-54261] p 83 A89-54261
- Thermal barrier coating life-prediction model development  
[NASA-CR-175002] p 26 N89-13433
- The effect of insulated combustion chamber surfaces on direct-injected diesel engine performance, emissions, and combustion  
[NASA-CR-182204] p 239 N89-17548
- MATE program: Erosion resistant compressor airfoil coating, volume 2  
[NASA-CR-179645] p 113 N89-18550

## R

- Evaluation of atomic oxygen resistant protective coatings for fiberglass-epoxy composites in LEO [NASA-TM-101955] p 114 N89-21100
- Undercutting of defects in thin film protective coatings on polymer surfaces exposed to atomic oxygen [NASA-TM-101986] p 115 N89-23691
- Isotopic study of oxygen diffusion in oxide coatings [NASA-TM-102082] p 78 N89-24451
- Diamondlike carbon protective coatings for optical windows [NASA-TM-102111] p 231 N89-27506
- Ion beam and plasma methods of producing diamondlike carbon films [NASA-TM-102301] p 116 N89-27836
- PROVING**
- Simulation test beds for the Space Station electrical power system p 39 A89-15352
- Experimental verification of the thermodynamic properties for a jet-A fuel [NASA-TM-101475] p 117 N89-17017
- PROXIMITY**
- Technique for temperature compensation of eddy-current proximity probes [NASA-TP-2880] p 173 N89-15380
- PULSE COMMUNICATION**
- A 20 GHz low noise, low cost receiver for digital satellite communication system, ground terminal applications [NASA-CR-182243] p 127 N89-19449
- PULSE DURATION MODULATION**
- A versatile power converter for high-frequency link systems p 131 A89-21200
- 5-kW arcjet power electronics [AIAA PAPER 89-2725] p 60 A89-49685
- The 5-kW arcjet power electronics [NASA-TM-102108] p 70 N89-24446
- PULSE MODULATION**
- Study of the generator/motor operation of induction machines in a high frequency link space power system [NASA-CR-179600] p 63 N89-11809
- PULSED JET ENGINES**
- Antiproton powered propulsion with magnetically confined plasma engines [NASA-CR-185131] p 74 N89-27700
- PULSED LASERS**
- Highly oriented Ti2Ba2Ca2Cu3O10 thin films by pulsed laser evaporation p 236 A89-30421
- A vector scanning processing technique for pulsed laser velocimetry [NASA-TM-102048] p 175 N89-23850
- PULSED RADIATION**
- Recovery of excitation intensity dependence in pulsed, focused beams - Nonsaturated case p 177 A89-17507
- PUMP SEALS**
- Advanced helium purge seals for Liquid Oxygen (LOX) turbopumps [NASA-CR-182105] p 184 N89-21239
- PURGING**
- Leakage predictions for Rayleigh-step, helium-purge seals [NASA-TM-101352] p 64 N89-14255
- PYLONS**
- Noise of a model counterrotation propeller with simulated fuselage and support pylon at takeoff/approach conditions [AIAA PAPER 89-1143] p 227 A89-48953
- Noise of a model counterrotation propeller with simulated fuselage and support pylon at takeoff/approach conditions [NASA-TM-101996] p 228 N89-24138
- PYROLYSIS**
- High-temperature LDV seed particle development [NASA-CR-182265] p 175 N89-23851
- Q**
- QUALITY CONTROL**
- Molecular beam epitaxial growth of high-quality InSb on InP and GaAs substrates [NASA-CR-185440] p 236 N89-26739
- QUANTITATIVE ANALYSIS**
- Thin-film hermeticity - A quantitative analysis of diamondlike carbon using variable angle spectroscopic ellipsometry p 234 A89-13945
- QUANTUM EFFICIENCY**
- The GaAs solar cells with V-grooved emitters [NASA-TM-102104] p 214 N89-26291
- QUARTZ LAMPS**
- Performance of multimirror quartzline lamps in a high-pressure, underwater environment [NASA-TM-101374] p 172 N89-10269
- QUATERNARY ALLOYS**
- Influence of alloying elements on the oxidation behavior of NbAl3 [NASA-TM-101398] p 100 N89-12717

## RADAR CROSS SECTIONS

- Ray-tube integration in shooting and bouncing ray method p 124 A89-15152
- An application of the WKBJ technique to the on-surface radiation condition p 124 A89-21222
- Shooting and bouncing rays - Calculating the RCS of an arbitrarily shaped cavity p 124 A89-34242
- High-frequency RCS of open cavities with rectangular and circular cross sections p 125 A89-39595
- Review of FD-TD numerical modeling of electromagnetic wave scattering and radar cross section p 19 A89-45107
- Electromagnetic properties of ice coated surfaces [NASA-CR-184780] p 127 N89-20355
- RADAR DETECTION**
- Electromagnetic properties of ice coated surfaces [NASA-CR-184780] p 127 N89-20355
- RADAR ECHOES**
- Electromagnetic properties of ice coated surfaces [NASA-CR-184780] p 127 N89-20355
- RADIAL FLOW**
- The effect of prewhirl on the internal aerodynamics and performance of a mixed flow research centrifugal compressor [NASA-CR-184756] p 161 N89-19503
- RADIAL VELOCITY**
- The turbulence characteristics of a separated flow with combustion p 92 A89-33369
- RADIANT COOLING**
- Transient radiative cooling of an absorbing and scattering cylinder p 146 A89-28958
- Liquid sheet radiator apparatus [NASA-CASE-LEW-14295-1] p 123 N89-14348
- RADIATION ABSORPTION**
- Effects of wind-tunnel wall absorption on acoustic radiation of propellers p 225 A89-22265
- RADIATION DAMAGE**
- InP (Indium Phosphide): Into the future [NASA-TM-102058] p 212 N89-23025
- Radiation resistance studies of amorphous silicon films p 213 N89-24738
- RADIATION DISTRIBUTION**
- Patterns of the cosmic microwave background from evolving string networks p 240 A89-14618
- Theory and application of radiation boundary operators p 224 A89-24191
- RADIATION EFFECTS**
- Low earth orbit environmental effects on the Space Station photovoltaic power generation systems p 55 A89-29123
- The NASA atomic oxygen effects test program p 93 N89-12589
- Radiation resistance and comparative performance of ITO/InP and n/p InP homojunction solar cells [NASA-TM-101387] p 135 N89-12819
- Stability of bulk Ba2YCu3O(7-x) in a variety of environments [NASA-TM-101401] p 111 N89-14310
- The effect of different module configurations on the radiation tolerance of multijunction solar cells [NASA-TM-101251] p 209 N89-17356
- Evaluation of atomic oxygen resistant protective coatings for fiberglass-epoxy composites in LEO [NASA-TM-101955] p 114 N89-21100
- Degradation and crosslinking of perfluoroalkyl polyethers under X-ray irradiation in ultrahigh vacuum [NASA-TP-2910] p 114 N89-21103
- InP (Indium Phosphide): Into the future [NASA-TM-102058] p 212 N89-23025
- Overview of environmental factors p 240 N89-23529
- Atomic oxygen effects on materials p 78 N89-23540
- Photovoltaic power system operation in the Mars environment [NASA-TM-102075] p 138 N89-24529
- A comparison of the radiation tolerance characteristics of multijunction solar cells with series and voltage-matched configurations p 213 N89-24737
- Advances in thin-film solar cells for lightweight space photovoltaic power [NASA-TM-102017] p 73 N89-26041
- On-orbit results of the LIPS 3/InP homojunction solar cell experiment [NASA-TM-102131] p 214 N89-26292
- Indium phosphide solar cell research in the US: Comparison with nonphotovoltaic sources [NASA-TM-102103] p 124 N89-27868
- RADIATION HAZARDS**
- Space reactor assessment and validation study p 230 N89-13227
- RADIATION MEASUREMENT**
- Solar radiation on Mars [NASA-TM-102299] p 242 N89-27623

## RADIATION PYROMETERS

- Determination of combustion gas temperatures by infrared radiometry in sooting and nonsooting flames [NASA-TP-2900] p 164 N89-25409

## RADIATION SHIELDING

- Space nuclear reactor shields for manned and unmanned applications [NASA-TM-102064] p 71 N89-25272

## RADIATION TOLERANCE

- Progress in indium phosphide solar cell research p 212 N89-24707
- A comparison of the radiation tolerance characteristics of multijunction solar cells with series and voltage-matched configurations p 213 N89-24737
- Radiation resistance studies of amorphous silicon films p 213 N89-24738

## RADIATIVE HEAT TRANSFER

- Moving Belt Radiator technology issues p 49 A89-15208
- The effects of radiative heat loss on microgravity flame spread [AIAA PAPER 89-0504] p 91 A89-28420
- Transient radiative cooling of an absorbing and scattering cylinder p 146 A89-28958
- Interaction of surface radiation with convection in crystal growth by physical vapor transport [AIAA PAPER 89-0228] p 119 A89-30450
- Radiative heat transfer in rocket thrust chambers and nozzles [AIAA PAPER 89-1720] p 150 A89-43235
- Radiative transfer in rectangular enclosures - A discretized exchange factor solution p 153 A89-53262

## RADIATIVE LIFETIME

- Limits to the radiative decays of neutrinos and axions from gamma-ray observations of SN 1987A p 242 A89-26985

## RADIO COMMUNICATION

- A 20 GHz low noise, low cost receiver for digital satellite communication system, ground terminal applications [NASA-CR-182243] p 127 N89-19449

## RADIO FREQUENCY DISCHARGE

- Radio-frequency plasma chemical vapor deposition growth of diamond p 236 A89-44552

## RADIO FREQUENCY HEATING

- Growth of diamond by RF plasma-assisted chemical vapor deposition p 90 A89-20474

## RADIO FREQUENCY INTERFERENCE

- Electromagnetic emission experiences using electric propulsion systems p 61 A89-53354
- Analysis of modified SMI method for adaptive array weight control [NASA-CR-185493] p 19 N89-25993
- Adaptive array for weak interfering signals: Geostationary satellite experiments [NASA-CR-185450] p 129 N89-26126

## RADIO RECEIVERS

- A 20 GHz low noise, low cost receiver for digital satellite communication system, ground terminal applications [NASA-CR-182243] p 127 N89-19449

## RADIOACTIVE DECAY

- The large-scale microwave background anisotropy in decaying particle cosmology p 240 A89-15426

## RADIOGRAPHY

- Radiographic and ultrasonic characterization of sintered silicon carbide p 187 A89-14700

## RADIOISOTOPE BATTERIES

- Preliminary assessment of rover power systems for the Mars Rover Sample Return Mission [IAF PAPER ICOSP89-9-6] p 39 A89-46530
- Preliminary assessment of rover power systems for the Mars Rover Sample Return Mission [NASA-TM-102003] p 68 N89-23518

## RADIOMETERS

- A segmented mirror antenna for radiometers [NASA-TM-102045] p 128 N89-23753

## RAILGUN ACCELERATORS

- Arc restrike in the rail accelerator p 39 A89-32065
- Arc-driven rail accelerator research [NASA-CR-179584] p 40 N89-13445

## RAIN

- Effect of heavy rain on aviation engines [AIAA PAPER 89-0799] p 22 A89-28462

## RAMAN SPECTRA

- Raman determination of layer stresses and strains for heterostructures and its application to the cubic SiC/Si system p 234 A89-21871
- Raman intensity as a probe of concentration near a crystal growing in solution [NASA-TP-2865] p 174 N89-16139

## RAMAN SPECTROSCOPY

- Characterization of GaAlAs optical waveguide heterostructures grown by molecular beam epitaxy p 130 A89-10343

Design and simulated performance of a CARS spectrometer for dynamic temperature measurements using electronic heterodyning p 170 A89-37298  
Raman intensity as a probe of concentration near a crystal growing in solution [NASA-TP-2865] p 174 N89-16139

**RANKINE CYCLE**

Solar dynamic heat rejection technology. Task 1: System concept development [NASA-CR-179618] p 158 N89-13731  
Megawatt Class Nuclear Space Power Systems (MCNSPS) conceptual design and evaluation report. Volume 4: Concepts selection, conceptual designs, recommendations [NASA-CR-179614-VOL-4] p 210 N89-18967  
Megawatt Class Nuclear Space Power Systems (MCNSPS) conceptual design and evaluation report. Volume 3, technologies 2: Power conversion [NASA-CR-179614-VOL-3] p 211 N89-22980

**RAPID QUENCHING (METALLURGY)**

Microstructures in rapidly solidified niobium aluminides p 95 A89-18193  
Rapid solidification research at the NASA Lewis Research Center p 95 A89-18203  
Dispersoids in rapidly solidified B2 nickel aluminides p 98 A89-43023

**RAPID TRANSIT SYSTEMS**

Turbomachinery technology for high-speed civil flight [NASA-TM-102092] p 32 N89-24320

**RAREFIED GAS DYNAMICS**

Flow of rarefied gases over two-dimensional bodies [AIAA PAPER 89-1970] p 5 A89-41814  
Rarefied gas flow through two-dimensional nozzles [AIAA PAPER 89-2893] p 7 A89-47156

**RAY TRACING**

Ray-tube integration in shooting and bouncing ray method p 124 A89-15152  
Ray tracing optical analysis of offset solar collector for Space Station solar dynamic system p 53 A89-15416  
Shooting and bouncing rays - Calculating the RCS of an arbitrarily shaped cavity p 124 A89-34242

**RAYLEIGH DISTRIBUTION**

Leakage predictions for Rayleigh-step, helium-purge seals [NASA-TM-101352] p 64 N89-14255

**REACTION BONDING**

Thermal effects on the mechanical properties of SiC fiber reinforced reaction bonded silicon nitride matrix (SiC/RBSN) composites [NASA-TM-101348] p 84 N89-10134  
Laminate behavior for SiC fiber-reinforced reaction-bonded silicon nitride matrix composites [NASA-TM-101350] p 84 N89-10952  
Strength of hot isostatically pressed and sintered reaction bonded silicon nitrides containing Y2O3 [NASA-TM-101443] p 112 N89-15257  
Preparation and evaluation of silicon nitride matrices for silicon nitride-SiC fiber composites [NASA-CR-184798] p 115 N89-23678  
Fiber reinforced ceramic material [NASA-CASE-LEW-14392-2] p 116 N89-29538

**REACTION KINETICS**

Reactions of silicon-based ceramics in mixed oxidation chlorination environments p 105 A89-21442  
Reaction kinetics between fiber and matrix p 83 A89-36420  
Pulsed ion beam investigation of the kinetics of surface reactions p 93 A89-44542  
A numerical study of chemically reacting flow in nozzles [AIAA PAPER 89-2793] p 60 A89-49687  
Crystallization kinetics of BaO-Al2O3-SiO2 glasses [NASA-TM-101964] p 113 N89-20252  
A numerical study of chemically reacting flow in nozzles [NASA-TM-102135] p 70 N89-24444

**REACTOR DESIGN**

Megawatt Class Nuclear Space Power Systems (MCNSPS) conceptual design and evaluation report. Volume 4: Concepts selection, conceptual designs, recommendations [NASA-CR-179614-VOL-4] p 210 N89-18967  
Megawatt Class Nuclear Space Power Systems (MCNSPS) conceptual design and evaluation report. Volume 3, technologies 2: Power conversion [NASA-CR-179614-VOL-3] p 211 N89-22980  
Megawatt Class Nuclear Space Power Systems (MCNSPS) conceptual design and evaluation report. Volume 2, technologies 1: Reactors, heat transport, integration issues [NASA-CR-179614-VOL-2] p 211 N89-22981

**REACTOR TECHNOLOGY**

Megawatt Class Nuclear Space Power Systems (MCNSPS) conceptual design and evaluation report. Volume 1: Objectives, summary results and introduction [NASA-CR-179614-VOL-1] p 209 N89-17941

**REAL GASES**

High speed inlet calculations with real gas effects [AIAA PAPER 88-3076] p 2 A89-14980  
A detailed analysis of inviscid flux splitting algorithms for real gases with equilibrium or finite-rate chemistry p 151 A89-45424

**REAL TIME OPERATION**

Neuromorphic learning of continuous-valued mappings in the presence of noise: Application to real-time adaptive control [NASA-TM-101999] p 221 N89-24856  
Digital CODEC for real-time processing of broadcast quality video signals at 1.8 bits/pixel [NASA-TM-102325] p 129 N89-27927  
A real time microcomputer implementation of sensor failure detection for turbofan engines [NASA-TM-102327] p 216 N89-29032

**REATTACHED FLOW**

An experimental study of a reattaching supersonic shear layer [AIAA PAPER 89-1801] p 6 A89-42036  
Calculation of reattaching shear layers in divergent channel with a multiple-time-scale turbulence model [NASA-TM-102293] p 168 N89-28749

**RECEIVERS**

Transient flow thrust prediction for an ejector propulsion concept [AIAA PAPER 89-2906] p 23 A89-49688  
Advanced heat receiver conceptual design study [NASA-CR-182177] p 209 N89-16224  
Transient flow thrust prediction for an ejector propulsion concept [NASA-TM-102078] p 32 N89-24318  
Performance of five 30 GHz satellite receivers [NASA-TM-101960] p 129 N89-25365

**RECHARGING**

Theoretical performance of hydrogen-bromine rechargeable SPE fuel cell --- Solid Polymer Electrolyte p 207 A89-23290  
Oxygen electrodes for rechargeable alkaline fuel cells p 211 N89-22998

**RECIRCULATIVE FLUID FLOW**

Solution of three-dimensional flow problems using a flux-spline method [AIAA PAPER 89-0687] p 146 A89-25543  
A block-corrected subdomain solution procedure for recirculating flow calculations p 152 A89-50147  
Efficient numerical techniques for complex fluid flows p 156 N89-12894  
Improved numerical methods for turbulent viscous recirculating flows p 156 N89-12895

**RECLAMATION**

T55-L-712 turbine engine compressor housing refurbishment-plasma spray project [NASA-TM-101310] p 100 N89-10156

**RECOMBINATION REACTIONS**

A new structure for comparing surface passivation materials of GaAs solar cells p 213 N89-24725

**RECRYSTALLIZATION**

Ultrasonic attenuation measurements determine onset, degree, and completion of recrystallization p 187 A89-23936

**RECTANGLES**

Thermosolutal convection in high-aspect-ratio enclosures p 153 A89-53288

**RECTANGULAR WAVEGUIDES**

High-frequency RCS of open cavities with rectangular and circular cross sections p 125 A89-39595  
Mutual coupling in a finite planar array with interelement holes present p 125 A89-42768  
A hybrid asymptotic-modal analysis of the EM scattering by an open-ended S-shaped rectangular waveguide cavity [NASA-CR-185053] p 129 N89-24519

**RECTENNAS**

Submicron nickel-oxide-gold tunnel diode detectors for rectennas p 133 A89-43469

**RECURSIVE FUNCTIONS**

Recursive algorithms for vector extrapolation methods p 221 A89-14397

**REDUCED GRAVITY**

Moving Belt Radiator technology issues p 49 A89-15208  
Bulk undercooling, nucleation, and macrosegregation of Pb-Sn alloys p 117 A89-17106  
Facilities for microgravity combustion research [IAF PAPER 88-355] p 117 A89-17784  
Thermocapillary migration of a large gas slug in a tube p 117 A89-22747  
Behavior in normal and reduced gravity of an enclosed liquid/gas system with nonuniform heating from above [AIAA PAPER 89-0070] p 145 A89-25061  
Microgravity research in NASA ground-based facilities [AIAA PAPER 89-0236] p 118 A89-25201

Effects of crucible wetting during solidification of immiscible Pb-Zn alloys [AIAA PAPER 89-0304] p 118 A89-25261  
Radiative structures of lycopodium-air flames in low gravity [AIAA PAPER 89-0500] p 91 A89-25406  
Modeling of impulsive propellant reorientation [AIAA PAPER 89-0628] p 54 A89-25496  
The solid surface combustion Space Shuttle experiment hardware description and ground-based test results [AIAA PAPER 89-0503] p 119 A89-28419  
The effects of radiative heat loss on microgravity flame spread [AIAA PAPER 89-0504] p 91 A89-28420  
The impact of an IVA robot on the Space Station microgravity environment [AIAA PAPER 89-0596] p 44 A89-28438  
Free-vibration characteristics and correlation of a Space Station split-blanket solar array [AIAA PAPER 89-1252] p 44 A89-30737  
Combined roles of buoyancy and orientation in nucleate pool boiling p 119 A89-35015  
Modeling of pulsed propellant reorientation [AIAA PAPER 89-2727] p 61 A89-53306  
Gas particle radiator [NASA-CASE-LEW-14297-1] p 172 N89-12048  
Modeling of impulsive propellant reorientation [NASA-TM-101440] p 64 N89-13495  
Effects of crucible wetting during solidification of immiscible Pb-Zn [NASA-TM-101372] p 120 N89-14341  
Microgravity research in NASA ground-based facilities [NASA-TM-101397] p 240 N89-15047  
Free-vibration characteristics and correlation of a space station split-blanket solar array [NASA-TM-101452] p 198 N89-15438  
Behavior in normal and reduced gravity of an enclosed liquid/gas system with nonuniform heating from above [NASA-TM-101471] p 120 N89-17046  
Microgravity Combustion Diagnostics Workshop [NASA-CP-10017] p 120 N89-17682  
Experiment plans to study preignition processes of a pool fire in low gravity [NASA-CR-182256] p 121 N89-19442  
The solid surface combustion space shuttle experiment hardware description and ground-based test results [NASA-TM-101963] p 123 N89-19446  
A comparative study of the influence of buoyancy driven fluid flow on GaAs crystal growth p 121 N89-20295  
Isothermal dendritic growth: A low gravity experiment p 121 N89-20299  
Critical fluid light scattering p 121 N89-20320  
Particle cloud mixing in microgravity [NASA-TM-101484] p 121 N89-20321  
Low frequency vibration isolation technology for microgravity space experiments [NASA-TM-101448] p 123 N89-20324  
Convection and chemistry effects in CVD: A 3-D analysis for silicon deposition [NASA-TM-102001] p 78 N89-21032  
Fire safety applications for spacecraft [NASA-TM-101463] p 42 N89-24413  
Time-dependent computational studies of flames in microgravity [NASA-CR-182298] p 122 N89-25353  
Feasibility of reduced gravity experiments involving quiescent, uniform particle cloud combustion [NASA-TM-101371] p 122 N89-26114  
Modeling of pulsed propellant reorientation [NASA-TM-102117] p 165 N89-26178  
Theoretical studies in support of the 3M-vapor transport (PVTOS-) experiments [NASA-CR-185122] p 165 N89-26179  
COLD-SAT: Cryogenic On-Orbit Liquid Depot-Storage, Acquisition and Transfer [NASA-TM-102308] p 38 N89-28535

**REDUNDANCY**  
New results concerning the use of kinematically redundant manipulators in microgravity environments [AIAA PAPER 89-3562] p 215 A89-52647  
Sensor failure detection for jet engines [NASA-TM-101396] p 25 N89-13432

**REDUNDANCY ENCODING**  
Advanced detection, isolation, and accommodation of sensor failures - Real-time evaluation p 34 A89-16156

**REFLECTANCE**  
The effect of the near earth micrometeoroid environment on a highly reflective mirror surface [AIAA PAPER 88-0026] p 40 A89-17939  
Analytical and experimental procedures for determining propagation characteristics of millimeter-wave gallium arsenide microstrip lines [NASA-TP-28991] p 136 N89-21169  
A V-grooved GaAs solar cell [NASA-TM-101970] p 211 N89-22177

- The GaAs solar cells with V-grooved emitters  
[NASA-TM-102104] p 214 N89-26291
- REFLECTED WAVES**  
Concentration of off-axis radiation by solar concentrators for space power  
[NASA-TM-102052] p 69 N89-24438
- REFLECTION**  
Accurate boundary conditions for exterior problems in gas dynamics p 143 A89-20223
- REFLECTOMETERS**  
Automated data acquisition and processing for a Hohraum reflectometer  
[NASA-TM-101393] p 173 N89-14416
- REFLECTOR ANTENNAS**  
Compensation of reflector antenna surface distortion using an array feed p 126 A89-53136  
A comparison of reflector antenna designs for wide-angle scanning  
[NASA-TM-101459] p 127 N89-21138  
A segmented mirror antenna for radiometers  
[NASA-TM-102045] p 128 N89-23753  
Adaptive array for weak interfering signals: Geostationary satellite experiments  
[NASA-CR-185450] p 129 N89-26126
- REFLECTORS**  
A method for producing a shaped contour radiation pattern using a single shaped reflector and a single feed p 125 A89-42758  
A method for producing a shaped contour radiation pattern using a single shaped reflector and a single feed  
[NASA-TM-101369] p 126 N89-10215  
Adaptive feed array compensation system for reflector antenna surface distortion  
[NASA-TM-101458] p 127 N89-17756  
Computed performance of the half-scale accurate antenna reflector  
[NASA-CR-182284] p 139 N89-24532
- REFRACTORY COATINGS**  
Life modeling of thermal barrier coatings for aircraft gas turbine engines p 30 N89-20143
- REFRACTORY MATERIALS**  
Thermoviscoplastic nonlinear constitutive relationships for structural analysis of high-temperature metal matrix composites p 190 A89-15735  
Elevated temperature strain gages p 173 N89-12886  
Theoretical analysis of compatibility of several reinforcement materials with NiAl and FeAl matrices  
[NASA-CR-182291] p 86 N89-23622  
Isothermal life prediction of composite lamina using a damage mechanics approach  
[NASA-TM-102032] p 87 N89-24460  
Time dependent reliability model incorporating continuum damage mechanics for high-temperature ceramics  
[NASA-TM-102046] p 115 N89-24487
- REFRACTORY METAL ALLOYS**  
The effect of Co alloying content on the kinetics of reaction zone growth in tungsten fiber reinforced superalloy composites p 79 A89-11324
- REFRACTORY METALS**  
Refractory metal alloys and composites for space nuclear power systems  
[NASA-TM-101364] p 102 N89-16986
- REFUELING**  
Technology requirements for an orbiting fuel depot - A necessary element of a space infrastructure  
[IAF PAPER 88-035] p 37 A89-17641
- REGENERATIVE FUEL CELLS**  
Space Electrochemical Research and Technology Conference, Cleveland, OH, Apr. 14-16, 1987, Proceedings p 207 A89-23280  
Theoretical performance of hydrogen-bromine rechargeable SPE fuel cell --- Solid Polymer Electrolyte p 207 A89-23290  
Cryogenic reactant storage for lunar base regenerative fuel cells  
[NASA-TM-101980] p 210 N89-21419  
Hydrogen-oxygen proton-exchange membrane fuel cells and electrolyzers p 211 N89-22996  
Photovoltaic power system considerations for future lunar bases  
[NASA-TM-102019] p 67 N89-23517
- REGOLITH**  
Lunar Helium-3 and Fusion Power  
[NASA-CP-10018] p 233 N89-14842
- REGRESSION ANALYSIS**  
Regressed relations for forced convection heat transfer in a direct injection stratified charge rotary engine  
[SAE PAPER 880626] p 178 A89-12308
- REINFORCING FIBERS**  
Thermal-mechanical fatigue test apparatus for metal matrix composites and joint attachments p 79 A89-15727  
Pressure effects on the thermal stability of silicon carbide fibers p 105 A89-31502
- Strength distribution of reinforcing fibers in a Nicalon fiber/chemically vapor infiltrated silicon carbide matrix composite p 82 A89-34844  
Synthesis and stability of Br<sub>2</sub>, ICl and IBr intercalated pitch-based graphite fibers p 106 A89-37670  
Fiber reinforced superalloys for rocket engines  
[NASA-TM-100880] p 86 N89-15990  
Energy in elastic fiber embedded in elastic matrix containing incident SH wave  
[NASA-CR-4205] p 188 N89-18694  
Theoretical analysis of compatibility of several reinforcement materials with NiAl and FeAl matrices  
[NASA-CR-182291] p 86 N89-23622  
Finite element modeling of frictionally restrained composite interfaces  
[NASA-CR-182281] p 203 N89-23918  
Unified micromechanics of damping for unidirectional fiber reinforced composites  
[NASA-TM-102107] p 88 N89-26919  
Revolutionary opportunities for materials and structures study, addendum no. 1  
[NASA-CR-179642-ADD-1] p 47 N89-29478
- REINFORCING MATERIALS**  
Theoretical analysis of compatibility of several reinforcement materials with NiAl and FeAl matrices  
[NASA-CR-182291] p 86 N89-23622
- RELAXATION (MECHANICS)**  
A 20-DOF hybrid stress general shell element p 191 A89-21133
- RELIABILITY**  
NASA Aerospace Flight Battery Systems Program - Issues and actions p 49 A89-15224  
Effect of design variables, temperature gradients, and speed on life and reliability of a rotating disk p 180 A89-47719  
Noninteractive macroscopic reliability model for ceramic matrix composites with orthotropic material symmetry  
[NASA-TM-101414] p 198 N89-15437
- RELIABILITY ANALYSIS**  
Kuhn-Tucker optimization based reliability analysis for probabilistic finite elements p 187 A89-25852  
An advanced probabilistic structural analysis method for implicit performance functions p 193 A89-30846  
Transmission overhaul and replacement predictions using Weibull and renewal theory  
[AIAA PAPER 89-1371] p 180 A89-47173  
Computerized life and reliability modeling for turboprop transmissions p 181 A89-53364  
Transmission overhaul and replacement predictions using Weibull and renewal theory  
[NASA-TM-102022] p 186 N89-22925
- RELIABILITY ENGINEERING**  
Fatigue strength reduction model: RANDOM3 and RANDOM4 user manual. Appendix 2: Development of advanced methodologies for probabilistic constitutive relationships of material strength models  
[NASA-CR-184796-APP-2] p 201 N89-19582  
Toward improved durability in advanced aircraft engine hot sections  
[NASA-TM-4087] p 29 N89-20135
- RELIC RADIATION**  
Patterns of the cosmic microwave background from evolving string networks p 240 A89-14618  
The large-scale microwave background anisotropy in decaying particle cosmology p 240 A89-15426
- RELOCATION**  
Satellite relocation by tether deployment  
[NASA-TM-101992] p 42 N89-26877
- REMOTE CONTROL**  
Ground-based simulation of telepresence for materials science experiments --- remote viewing and control of processes aboard Space Station  
[AIAA PAPER 89-0597] p 119 A89-28439
- REMOTE MANIPULATOR SYSTEM**  
Photovoltaic module on-orbit assembly for Space Station Freedom  
[NASA-TM-102297] p 47 N89-26887
- REMOTE SENSING**  
Ground-based simulation of telepresence for materials science experiments --- remote viewing and control of processes aboard Space Station  
[AIAA PAPER 89-0597] p 119 A89-28439  
Sensors for ceramic components in advanced propulsion systems: Summary of literature survey and concept analysis, task 3 report  
[NASA-CR-180900] p 172 N89-11192
- REMOTE SENSORS**  
Advanced detection, isolation, and accommodation of sensor failures - Real-time evaluation p 34 A89-16156
- RENDEZVOUS GUIDANCE**  
Optimal terminal maneuver for a cooperative impulsive rendezvous p 38 A89-36946
- REQUIREMENTS**  
Space Station power system requirements p 50 A89-15295
- PV modules for ground testing  
[NASA-CR-179476] p 208 N89-11315  
Study of the generator/motor operation of induction machines in a high frequency link space power system  
[NASA-CR-179600] p 63 N89-11809  
Space station WP-04 power system preliminary analysis and design document, volume 3  
[NASA-CR-179587-VOL-3] p 64 N89-15164  
Megawatt Class Nuclear Space Power Systems (MCNPS) conceptual design and evaluation report. Volume 1: Objectives, summary results and introduction  
[NASA-CR-179614-VOL-1] p 209 N89-17941
- RESEARCH AIRCRAFT**  
Determination of longitudinal aerodynamic derivatives using flight data from an icing research aircraft  
[AIAA PAPER 89-0754] p 34 A89-28454  
Determination of longitudinal aerodynamic derivatives using flight data from an icing research aircraft  
[NASA-TM-101427] p 35 N89-15121
- RESEARCH AND DEVELOPMENT**  
Space solar cell research p 208 A89-52203  
HOST instrumentation R and D program overview p 25 N89-12878  
NASA photovoltaic research and technology  
[NASA-TM-101422] p 65 N89-16917  
Bibliography of Lewis Research Center technical publications announced in 1986  
[NASA-TM-89887] p 238 N89-18259
- RESEARCH FACILITIES**  
Microgravity research in NASA ground-based facilities  
[AIAA PAPER 89-0236] p 118 A89-25201  
Power systems facility  
[NASA-TM-101447] p 40 N89-14247  
Microgravity research in NASA ground-based facilities  
[NASA-TM-101397] p 240 N89-15047  
NASA powered lift facility internally generated noise and its transmission to the acoustic far field  
[NASA-CR-182217] p 36 N89-16882  
Institute for Computational Mechanics in Propulsion (ICOMP) p 222 N89-21595
- RESEARCH MANAGEMENT**  
The Pathfinder Chemical Transfer Propulsion program  
[NASA-TM-102084] p 41 N89-24409
- RESEARCH PROJECTS**  
A review and forecast of engine system research at the Army Propulsion Directorate p 23 A89-36397
- RESIDUAL STRENGTH**  
Fiber composite structural durability and damage tolerance - Simplified predictive methods p 82 A89-36320
- RESIDUAL STRESS**  
Optimum interface properties for metal matrix composites  
[NASA-TM-102295] p 205 N89-27223
- RESIN MATRIX COMPOSITES**  
700 F properties of autoclave cured PMR-II composites p 81 A89-29998  
Mechanics of composite materials - Past, present and future p 82 A89-36293  
Synthesis and stability of Br<sub>2</sub>, ICl and IBr intercalated pitch-based graphite fibers p 106 A89-37670  
Improved high-temperature resistant matrix resins  
[NASA-CR-180826] p 114 N89-21105
- RESISTOJET ENGINES**  
Performance characterizations of an engineering model multipropellant resistojets p 54 A89-28340  
Effect of ambient pressure on the performance of a resistojets p 55 A89-44111  
A detailed model of electrothermal propulsion systems  
[AIAA PAPER 89-2262] p 56 A89-46707  
The effect of test-cell pressure on resistojets nozzle flow  
[AIAA PAPER 89-2838] p 58 A89-47116  
Investigation of a liquid-fed water resistojets plume  
[AIAA PAPER 89-2840] p 58 A89-47117  
dc power control for a liquid-fed resistojets p 59 A89-47457  
Experimental evaluation of resistojets thruster plume shields p 59 A89-47487  
Performance characterization and transient investigation of multipropellant resistojets p 60 A89-50811  
Preliminary design study of hydrogen and ammonia resistojets for prime and auxiliary thrusters  
[NASA-CR-182176] p 62 N89-10943  
Performance characterization and transient investigation of multipropellant resistojets p 72 N89-25283  
Investigation of a liquid-fed water resistojets plume  
[NASA-TM-102310] p 75 N89-27706
- RESONANCE FLUORESCENCE**  
A heat-driven monochromatic light source p 224 A89-41722

# **RESONANT FREQUENCIES**

## **RESONANT FREQUENCIES**

- A natural low-frequency oscillation of the flow over an airfoil near stalling conditions p 6 A89-45437  
 A design procedure for the phase-controlled parallel-loaded resonant inverter p 134 A89-50472  
 On the conditions for resonance interactions of instability waves in the axisymmetric jet  
 [NASA-TM-101477] p 162 N89-21196  
 Distortion and regulation characterization of a Mapam inverter  
 [NASA-TM-102089] p 139 N89-26148

## **RETICLES**

- Calibration of single particle sizing velocimeters using photomask reticles p 170 A89-33379

## **REUSABLE ROCKET ENGINES**

- A reusable rocket engine intelligent control  
 [AIAA PAPER 88-3114] p 48 A89-14981  
 Design, fabrication and test of the RL10 derivative II chamber/primary nozzle  
 [NASA-CR-179595] p 68 N89-23519  
 The Pathfinder Chemical Transfer Propulsion program  
 [NASA-TM-102084] p 41 N89-24409

## **REVISIONS**

- Dynamic loading of spur gears with linear or parabolic tooth profile modification  
 [NASA-TM-101444] p 183 N89-15413

## **REVOLVING**

- Crowned spur gears - Methods for generation and Tooth Contact Analysis. II - Generation of the pinion tooth surface by a surface of revolution p 180 A89-37665  
 Generation of a crowned pinion tooth surface by a surface of revolution p 181 N89-10282

## **REYNOLDS NUMBER**

- Regressed relations for forced convection heat transfer in a direct injection stratified charge rotary engine  
 [SAE PAPER 880626] p 178 A89-12308  
 Windward fraction of the total mass or heat transport for flow past a circular cylinder p 141 A89-12339  
 Numerical study of the interactions between droplets at intermediate Reynolds numbers p 142 A89-16451  
 A low-Reynolds-number two-equation turbulence model for predicting heat transfer on turbine blades p 160 N89-17310

- High-resolution liquid-crystal heat-transfer measurements on the end wall of a turbine passage with variations in Reynolds number  
 [NASA-TM-100827] p 161 N89-18664

## **REYNOLDS STRESS**

- The turbulence characteristics of a separated flow with combustion p 92 A89-33369  
 Asymptotic structure and similarity solutions for three-dimensional turbulent boundary layers  
 [AIAA PAPER 89-1863] p 150 A89-42090  
 Calculation of turbulence-driven secondary motion in ducts with arbitrary cross section  
 [NASA-TM-102142] p 166 N89-27115

## **RIEMANN WAVES**

- Far field expansion for anisotropic wave equations  
 [NASA-TM-102112] p 165 N89-26175

## **RIGID STRUCTURES**

- Stability of a rigid rotor supported on oil-film journal bearings under dynamic load  
 [NASA-TM-102309] p 166 N89-27114

## **RING STRUCTURES**

- Multi-hundred kilowatt roll ring assembly  
 [NASA-CR-174832] p 135 N89-15335

## **RINGS**

- Multi-hundred kilowatt roll ring assembly evaluation results --- for Space Station power transmission p 123 A89-15388

## **RISK**

- Fire behavior and risk analysis in spacecraft  
 [NASA-TM-100944] p 42 N89-10111

## **RL-10 ENGINES**

- Design, fabrication and test of the RL10 derivative II chamber/primary nozzle  
 [NASA-CR-179595] p 68 N89-23519

## **ROBOTICS**

- New results concerning the use of kinematically redundant manipulators in microgravity environments  
 [AIAA PAPER 89-3562] p 215 A89-52647  
 Systems autonomy technology: Executive summary and program plan  
 [NASA-TM-100999] p 216 N89-18045  
 User needs, benefits and integration of robotic systems in a space station laboratory  
 [NASA-CR-182261] p 185 N89-22108  
 Structural dynamics branch research and accomplishments for FY 1988  
 [NASA-TM-101406] p 202 N89-22939

## **ROBOTS**

- Robots for manipulation in a micro-gravity environment p 215 A89-11682  
 Energy storage considerations for a robotic Mars surface sampler p 49 A89-15267

- The impact of an IVA robot on the Space Station microgravity environment  
 [AIAA PAPER 89-0596] p 44 A89-28438

## **ROBUSTNESS (MATHEMATICS)**

- Stability robustness improvement of direct eigenspace assignment based feedback systems using singular value sensitivities  
 [NASA-CR-182302] p 36 N89-27672

## **ROCKET ENGINE CASES**

- Three dimensional thermal analysis of rocket thrust chambers  
 [NASA-TM-101973] p 66 N89-21025

## **ROCKET ENGINE DESIGN**

- A detailed model of electrothermal propulsion systems  
 [AIAA PAPER 89-2262] p 56 A89-46707  
 A detailed model of ion propulsion systems  
 [AIAA PAPER 89-2268] p 56 A89-46712  
 Design and test of an oxygen turbopump for a dual expander cycle rocket engine  
 [AIAA PAPER 89-2305] p 56 A89-46737  
 A 50 cm diameter annular ion engine  
 [AIAA PAPER 89-2716] p 57 A89-47039  
 The effect of test-cell pressure on resistojel nozzle flow  
 [AIAA PAPER 89-2838] p 58 A89-47116  
 Design, fabrication and test of the RL10 derivative II chamber/primary nozzle  
 [NASA-CR-179595] p 68 N89-23519  
 The Pathfinder Chemical Transfer Propulsion program  
 [NASA-TM-102084] p 41 N89-24409  
 NASA's Chemical Transfer Propulsion Program for Pathfinder  
 [NASA-TM-102298] p 41 N89-26876

## **ROCKET ENGINES**

- Miniature multiple-function probe for OTV turbopump health monitoring  
 [AIAA PAPER 89-2303] p 56 A89-46736  
 A numerical study of chemically reacting flow in nozzles  
 [AIAA PAPER 89-2793] p 60 A89-49687  
 Integrated control and health management. Orbit transfer rocket engine technology program  
 [NASA-CR-182122] p 62 N89-11805  
 Considerations in development and implementation of elasto-viscoplastic constitutive model for high temperature applications  
 [NASA-CR-183403] p 197 N89-12932  
 Evaluation of coated columbium test panels having application to a secondary nozzle extension for the RL10 rocket engine system, parts 1 and 2  
 [NASA-CR-180809] p 64 N89-13493  
 Orbit transfer rocket engine technology program: Oxygen materials compatibility testing  
 [NASA-CR-182195] p 64 N89-14256  
 Thrust chamber thermal barrier coating techniques p 115 N89-22671  
 Fiber reinforced superalloys for rocket engines p 103 N89-22673  
 A numerical study of chemically reacting flow in nozzles  
 [NASA-TM-102135] p 70 N89-24444  
 Development of a high power microwave thruster, with a magnetic nozzle, for space applications p 74 N89-26904  
 Space station hydrogen/oxygen thruster technology  
 [NASA-CR-182280] p 74 N89-26905  
 Performance of a 100 kW class applied field MPD thruster  
 [NASA-TM-102312] p 74 N89-27701

## **ROCKET EXHAUST**

- Plume characteristics of MPD thrusters - A preliminary examination  
 [AIAA PAPER 89-2832] p 39 A89-47113  
 Investigation of a liquid-fed water resistojel plume  
 [AIAA PAPER 89-2840] p 58 A89-47117

## **ROCKET FIRING**

- A premixed hydrogen/oxygen catalytic igniter  
 [AIAA PAPER 89-2302] p 59 A89-49683  
 A premixed hydrogen/oxygen catalytic igniter  
 [NASA-CR-185113] p 70 N89-24445

## **ROCKET NOZZLES**

- Radiative heat transfer in rocket thrust chambers and nozzles  
 [AIAA PAPER 89-1720] p 150 A89-43235  
 Design, fabrication and test of the RL10 derivative II chamber/primary nozzle  
 [NASA-CR-179595] p 68 N89-23519  
 Development of a high power microwave thruster, with a magnetic nozzle, for space applications p 74 N89-26904  
 Space station hydrogen/oxygen thruster technology  
 [NASA-CR-182280] p 74 N89-26905

## **ROCKET PROPELLANTS**

- Performance characterizations of an engineering model multipropellant resistojel p 54 A89-28340

## **ROCKET TEST FACILITIES**

- Plume characteristics of MPD thrusters - A preliminary examination  
 [AIAA PAPER 89-2832] p 39 A89-47113

## **ROLL**

- Multi-hundred kilowatt roll ring assembly evaluation results --- for Space Station power transmission p 123 A89-15388

## **ROLLER BEARINGS**

- Ceramic bearings for use in gas turbine engines p 180 A89-46697  
 Selection of rolling-element bearing steels for long-life applications p 180 A89-47250  
 Comparison of predicted and measured temperatures of UH-60A helicopter transmission  
 [NASA-TP-2911] p 186 N89-24607  
 Tribology: The Story of Lubrication and Wear  
 [NASA-TM-101430] p 203 N89-24635

## **ROLLING CONTACT LOADS**

- Surface fatigue life of carburized and hardened M50NiL and AISI 9310 spur gears and rolling-contact test bars  
 [AIAA PAPER 89-2819] p 180 A89-47105  
 Surface fatigue life of carburized and hardened M50NiL and AISI 9310 spur gears and rolling-contact test bars  
 [NASA-TM-101979] p 185 N89-22111

## **ROTARY ENGINES**

- Regressed relations for forced convection heat transfer in a direct injection stratified charge rotary engine  
 [SAE PAPER 880626] p 178 A89-12308  
 Stratified charge rotary engine - Internal flow studies at the MSU engine research laboratory  
 [SAE PAPER 890331] p 181 A89-51477  
 Engineering study on the rotary-vee engine concept  
 [SAE PAPER 890332] p 181 A89-51492  
 Strain measurements in a rotary engine housing  
 [SAE PAPER 890333] p 181 A89-51493  
 Adiabatic Wankel type rotary engine  
 [NASA-CR-182233] p 28 N89-17599

## **ROTARY STABILITY**

- Active suppression of aerodynamic instabilities in turbomachines p 3 A89-28341

## **ROTARY WING AIRCRAFT**

- Contingency power for small turboshaft engines p 21 A89-22291  
 NASA's program on icing research and technology  
 [NASA-TM-101989] p 1 N89-22569

## **ROTARY WINGS**

- Two-dimensional simulation of electrothermal deicing of aircraft components p 17 A89-39194  
 Icing research tunnel test of a model helicopter rotor  
 [NASA-TM-101978] p 29 N89-19305

## **ROTATING CYLINDERS**

- Moving Belt Radiator technology issues p 49 A89-15208  
 Engineering study on the rotary-vee engine concept  
 [SAE PAPER 890332] p 181 A89-51492

## **ROTATING DISKS**

- Effect of design variables, temperature gradients, and speed on life and reliability of a rotating disk p 180 A89-47719

## **ROTATING SHAFTS**

- Parallel processing of a rotating shaft simulation  
 [NASA-TM-101462] p 223 N89-17453  
 OTVE turbopump condition monitoring, task E.5  
 [NASA-CR-182274] p 189 N89-27204

## **ROTATING STALLS**

- Aeroelastic analysis of prop fan blades with a semiempirical dynamic stall model  
 [AIAA PAPER 89-2695] p 194 A89-47025

## **ROTATION**

- Multi-hundred kilowatt roll ring assembly  
 [NASA-CR-174832] p 135 N89-15335  
 In-flight measurement of propeller noise on the fuselage of an airplane  
 [NASA-TM-102285] p 229 N89-25675

## **ROTOR AERODYNAMICS**

- Results of acoustic tests of a prop-fan model p 224 A89-10112  
 A simple time-accurate turbomachinery algorithm with numerical solutions of an uneven blade count configuration  
 [AIAA PAPER 89-0206] p 179 A89-25181  
 Unsteady blade pressure measurements on a model counterrotation propeller  
 [AIAA PAPER 89-1144] p 226 A89-40175  
 Prediction of unsteady blade surface pressures on an advanced propeller at an angle of attack  
 [AIAA PAPER 89-1060] p 227 A89-40473  
 Piezoelectric pushers for active vibration control of rotating machinery p 171 A89-47717  
 Unsteady blade pressure measurements on a model counterrotation propeller p 228 N89-20779  
 [NASA-TM-102002]  
 Rotordynamic Instability Problems in High-Performance Turbomachinery, 1988  
 [NASA-CP-3026] p 185 N89-22891



- Annular honeycomb seals: Test results for leakage and rotordynamic coefficients; comparisons to labyrinth and smooth configurations p 185 N89-22899
- ROTOR BLADES**
- Effect of aerodynamic detuning on supersonic rotor discrete frequency noise generation p 225 A89-15083
- Generic icing effects on forward flight performance of a model helicopter rotor p 18 A89-41093
- Prediction of unsteady rotor-surface heat transfer from wake passages [AIAA PAPER 89-1692] p 150 A89-43210
- ROTOR BLADES (TURBOMACHINERY)**
- Explicit Runge-Kutta method for unsteady rotor/stator interaction p 5 A89-36912
- Numerical analysis of supersonic flow through oscillating cascade sections by using a deforming grid [AIAA PAPER 89-2805] p 8 A89-50810
- Measurement of airfoil heat transfer coefficients on a turbine stage p 157 N89-12897
- Heat transfer in the tip region of a rotor blade simulator p 157 N89-12898
- High speed balancing applied to the T700 engine [NASA-CR-180899] p 184 A89-20472
- Composite blade structural analyzer (COBSTRAN) user's manual [NASA-TM-101461] p 86 N89-23621
- Composite Blade Structural Analyzer (COBSTRAN) demonstration manual [NASA-TM-101957] p 87 N89-24459
- Numerical analysis of supersonic flow through oscillating cascade sections by using a deforming grid [NASA-TM-102053] p 15 N89-25119
- Multigrid calculation of three-dimensional turbomachinery flows [NASA-CR-185332] p 165 N89-26172
- ROTOR BODY INTERACTIONS**
- Noise of a model counterrotation propeller with simulated fuselage and support pylon at takeoff/approach conditions [AIAA PAPER 89-1143] p 227 A89-48953
- Aerodynamic interaction between propellers and wings p 8 A89-50062
- Noise of a model counterrotation propeller with simulated fuselage and support pylon at takeoff/approach conditions [NASA-TM-101996] p 228 N89-24138
- ROTOR SPEED**
- Experimental results for labyrinth gas seals with honeycomb stators - Comparisons to smooth-stator seals and theoretical predictions [ASME PAPER 88-TRIB-40] p 179 A89-24992
- ROTORS**
- An unconditionally stable Runge-Kutta method for unsteady flows [AIAA PAPER 89-0205] p 2 A89-25180
- Annular honeycomb seals: Test results for leakage and rotordynamic coefficients - Comparisons to labyrinth and smooth configurations [ASME PAPER 88-TRIB-35] p 179 A89-34794
- An entrance region friction factor model applied to annular seal analysis - Theory versus experiment for smooth and honeycomb seals [ASME PAPER 88-TRIB-41] p 179 A89-34798
- Development of a thermal and structural analysis procedure for cooled radial turbines [NASA-TM-101416] p 24 N89-12568
- The effects of inlet turbulence and rotor/stator interactions on the aerodynamics and heat transfer of a large-scale rotating turbine model, volume 1 [NASA-CR-4079] p 159 N89-13756
- Active vibration control for flexible rotor by optimal direct-output feedback control [NASA-TM-101972] p 31 N89-22605
- ROVING VEHICLES**
- Preliminary assessment of rover power systems for the Mars Rover Sample Return Mission [IAF PAPER ICOSP89-9-6] p 39 A89-46530
- Mars manned transportation vehicle [NASA-TM-101487] p 210 N89-20545
- Preliminary assessment of rover power systems for the Mars Rover Sample Return Mission [NASA-TM-102003] p 68 N89-23518
- RP-1 ROCKET PROPELLANTS**
- Liquid oxygen cooling of high pressure LOX/hydrocarbon rocket thrust chambers p 63 N89-12649
- High-pressure calorimeter chamber tests for liquid oxygen/kerosene (LOX/RP-1) rocket combustion [NASA-TP-2862] p 65 N89-15979
- RUN TIME (COMPUTERS)**
- Multi-grid for structures analysis p 206 N89-29810
- RUNGE-KUTTA METHOD**
- An unconditionally stable Runge-Kutta method for unsteady flows [AIAA PAPER 89-0205] p 2 A89-25180
- Explicit Runge-Kutta method for unsteady rotor/stator interaction p 5 A89-36912
- An explicit Runge-Kutta method for turbulent reacting flow calculations [NASA-TM-101945] p 31 N89-21799
- RURAL AREAS**
- The introduction of space technology power systems into developing countries [NASA-TM-102042] p 71 N89-25274
- S**
- SAFETY MANAGEMENT**
- Fire behavior and risk analysis in spacecraft [NASA-TM-100944] p 42 N89-10111
- Fire safety applications for spacecraft [NASA-TM-101463] p 42 N89-24413
- SAMARIUM COMPOUNDS**
- Non-uniform transition conductivity of superconducting ceramic [NASA-TM-102133] p 189 N89-28851
- SANDWICH STRUCTURES**
- Fiber composite sandwich thermostructural behavior - Computational simulation p 190 A89-11246
- Mechanical properties characterization of composite sandwich materials intended for space antenna applications p 81 A89-32885
- SATELLITE COMMUNICATION**
- Assessment of satellite communications quality study. Addendum 1: Impact of propagation delay on data transmission [NASA-CR-182229] p 126 N89-14369
- The potential impact of MMICs on future satellite communications [NASA-CR-182227] p 126 N89-17078
- The potential impact of MMICs on future satellite communications: Executive summary [NASA-CR-182227-EXEC-SUMM] p 127 N89-17079
- A 20 GHz low noise, low cost receiver for digital satellite communication system, ground terminal applications [NASA-CR-182243] p 127 N89-19449
- Analysis of modified SMI method for adaptive array weight control [NASA-CR-184904] p 127 N89-20364
- Study of spread spectrum multiple access systems for satellite communications with overlay on current services: Executive summary [NASA-CR-180827-EXEC-SUMM] p 128 N89-23756
- Study of spread spectrum multiple access systems for satellite communications with overlay on current services [NASA-CR-180827] p 128 N89-23757
- Development of a 75-watt 60-GHz traveling-wave tube for satellite communications [NASA-CR-182135] p 138 N89-24530
- Performance of five 30 GHz satellite receivers [NASA-TM-101960] p 129 N89-25365
- Programmable rate modem utilizing digital signal processing techniques [NASA-CR-185124] p 43 N89-26879
- SATELLITE GROUND SUPPORT**
- A 20 GHz low noise, low cost receiver for digital satellite communication system, ground terminal applications [NASA-CR-182243] p 127 N89-19449
- SATELLITE LIFETIME**
- Arcjet nozzle design impacts [NASA-TM-102050] p 68 N89-23522
- SATELLITE ORBITS**
- Satellite relocation by tether deployment [NASA-TM-101992] p 42 N89-26877
- SATELLITE PERTURBATION**
- Satellite relocation by tether deployment [NASA-TM-101992] p 42 N89-26877
- SATELLITE POWER TRANSMISSION**
- Study of spread spectrum multiple access systems for satellite communications with overlay on current services: Executive summary [NASA-CR-180827-EXEC-SUMM] p 128 N89-23756
- SATELLITE TRANSMISSION**
- Intersatellite link application to commercial communications satellites p 43 A89-39144
- Assessment of satellite communications quality study. Addendum 1: Impact of propagation delay on data transmission [NASA-CR-182229] p 126 N89-14369
- SATELLITE-BORNE INSTRUMENTS**
- Baseband processor hardware for Advanced Communication Technology Satellite (ACTS) p 43 A89-38298
- SCALARS**
- On the modelling of scalar and mass transport in combustor flows p 92 A89-38658
- SCALE (CORROSION)**
- Transient oxidation of single-crystal beta-NiAl p 98 A89-37899
- TEM studies of oxidized NiAl and Ni3Al cross sections p 99 A89-46506
- SCALE MODELS**
- Cruise noise of the 2/9 scale model SR-7A propeller p 224 A89-12561
- SCALING**
- Scaling results for the Liquid Sheet Radiator (LSR) [NASA-TM-102100] p 72 N89-25277
- SCANNING**
- A vector scanning processing technique for pulsed laser velocimetry [NASA-TM-102048] p 175 N89-23850
- SCANNING TUNNELING MICROSCOPY**
- Development and applications of optical interferometric micrometrology in the Angstrom and subangstrom range p 170 A89-27663
- SCATTERING COEFFICIENTS**
- Transient radiative cooling of an absorbing and scattering cylinder p 146 A89-28958
- SCAVENGING**
- Weight savings in aerospace vehicles through propellant scavenging [SAWE PAPER 1818] p 40 A89-50814
- SCIENTISTS**
- Age distribution among NASA scientists and engineers p 238 N89-23911
- SEA ICE**
- Data report for the Siple Coast (Antarctica) project [NASA-TM-100708] p 206 N89-10403
- SEALING**
- Advanced helium purge seals for Liquid Oxygen (LOX) turbopumps [NASA-CR-182105] p 184 N89-21239
- Friction factor data for flat plate tests of smooth and honeycomb surfaces [NASA-CR-184977] p 186 N89-23876
- High temperature flexible seal [NASA-CASE-LEW-14695-1] p 187 N89-28830
- SEALS (STOPPERS)**
- Annular honeycomb seals: Test results for leakage and rotordynamic coefficients - Comparisons to labyrinth and smooth configurations [ASME PAPER 88-TRIB-35] p 179 A89-34794
- An entrance region friction factor model applied to annular seal analysis - Theory versus experiment for smooth and honeycomb seals [ASME PAPER 88-TRIB-41] p 179 A89-34798
- Tribological properties of alumina-boria-silicate fabric from 25 C to 850 C p 107 A89-54982
- Dynamics of face and annular seals with two-phase flow [NASA-CR-183352] p 182 N89-12870
- Cyclic stress analysis of ceramic coated gas turbine seals p 111 N89-13662
- Thermal effects in two-phase flow through face seals [NASA-CR-185968] p 182 N89-13788
- Leakage predictions for Rayleigh-step, helium-purge seals [NASA-TM-101352] p 64 N89-14255
- Some composite bearing and seal materials for gas turbine applications: A review [NASA-TM-101451] p 111 N89-14338
- Rotordynamic Instability Problems in High-Performance Turbomachinery, 1988 [NASA-CP-3026] p 185 N89-22891
- Annular honeycomb seals: Test results for leakage and rotordynamic coefficients; comparisons to labyrinth and smooth configurations p 185 N89-22899
- High temperature flexible seal [NASA-CASE-LEW-14695-1] p 187 N89-28830
- SECONDARY EMISSION**
- The physics of positively biased conductors surrounded by dielectrics in contact with a plasma p 232 A89-39395
- Secondary electron emission characteristics of untreated and ion-textured titanium [NASA-TP-2902] p 103 N89-17650
- SECONDARY FLOW**
- The secondary flow and its stability for natural convection in a tall vertical enclosure p 149 A89-37931
- Influence of bulk turbulence and entrance boundary layer thickness on the curved duct flow field p 156 N89-12896
- SECONDARY INJECTION**
- Design and analysis report for the flight weight 20-inch Columbia secondary nozzle for the RL10 engine [NASA-CR-179612] p 65 N89-16918
- SEGMENTS**
- Structural response of an advanced combustor liner: Test and analysis p 200 N89-17329
- SELECTION**
- Selection of rolling-element bearing steels for long-life applications p 180 A89-47250

**SELF EXCITATION**

- Modal forced vibration analysis of aerodynamically excited turbosystems  
[NASA-CR-174966] p 201 N89-18696

**SELF LUBRICATION**

- Tribology: The Story of Lubrication and Wear  
[NASA-TM-101430] p 203 N89-24635  
Solid lubricant materials for high temperatures: A review p 203 N89-24636

**SEMICONDUCTING FILMS**

- Raman determination of layer stresses and strains for heterostructures and its application to the cubic SiC/Si system p 234 A89-21871

**SEMICONDUCTORS (MATERIALS)**

- Fiber-optic temperature sensor using a spectrum-modulating semiconductor etalon p 168 A89-10366  
Crystal growth of SiC for electronic applications p 132 A89-33625  
Metal-silicon reaction rates - The effects of capping p 93 A89-52202  
Space solar cell research p 208 A89-52203  
Microwave and millimeter-wave power generation in silicon carbide (SiC) IMPATT devices p 139 N89-26143  
The GaAs solar cells with V-grooved emitters [NASA-TM-102104] p 214 N89-26291  
Surface morphologies and electrical properties of molecular beam epitaxial InSb and InAs(x)Sb(1-x) grown on GaAs and InP substrates [NASA-CR-185439] p 237 N89-26740

**SEMIEMPIRICAL EQUATIONS**

- Aeroelastic analysis of prop fan blades with a semiempirical dynamic stall model [AIAA PAPER 89-2695] p 194 A89-47025

**SENSITIVITY**

- Solution and sensitivity analysis of a complex transcendental eigenproblem with pairs of real eigenvalues [NASA-CR-182241] p 197 N89-13819  
RE-1000 free-piston Stirling engine sensitivity test results [NASA-TM-88846] p 210 N89-19737

**SENSORS**

- Intensity-based fibre-optic sensing system using contrast modulation of subcarrier interference pattern p 170 A89-39302  
A self diagnostic system for piezoelectric sensors [AIAA PAPER 89-2638] p 171 A89-46980  
Integrated control and health monitoring capacitive displacement sensor development task. Orbit transfer rocket engine technology program [NASA-CR-182279] p 176 N89-26208

**SEPARATED FLOW**

- Control of laminar separation over airfoils by acoustic excitation [AIAA PAPER 89-0565] p 3 A89-25454  
Evaluation of three turbulence models for the prediction of steady and unsteady airloads [AIAA PAPER 89-0609] p 3 A89-25485  
Technique for the prediction of airfoil flutter characteristics in separated flow p 191 A89-27744  
The turbulence characteristics of a separated flow with combustion p 92 A89-33369  
Control of laminar separation over airfoils by acoustic excitation [NASA-TM-101379] p 9 N89-12552  
Evaluation of three turbulence models for the prediction of steady and unsteady airloads [NASA-TM-101413] p 10 N89-12555  
On the Lagrangian description of unsteady boundary layer separation. Part 2: The spinning sphere [NASA-TM-102027] p 163 N89-22861

**SEPARATION**

- Bulk undercooling, nucleation, and macrosegregation of Pb-Sn alloys p 117 A89-17106  
Gravitational macrosegregation in unidirectionally solidified lead-tin alloy p 117 A89-17112

**SEQUENCING**

- Laboratory process control using natural language commands from a personal computer [NASA-TM-101988] p 218 N89-24055

**SERIES EXPANSION**

- Far field expansion for anisotropic wave equations [NASA-TM-102112] p 165 N89-26175

**SERVICE LIFE**

- Effect of LEO cycling at shallow depths of discharge on MANTECH IPV nickel-hydrogen cells p 49 A89-15278  
The effect of different alkali metal hydroxides on nickel electrode life p 207 A89-15280  
Space 2010 --- Space Station Freedom future explorations p 77 A89-23028  
KOH concentration effect on cycle life of nickel-hydrogen cells. III - Cycle life test p 207 A89-23283

- Transmission overhaul and replacement predictions using Weibull and renewal theory [AIAA PAPER 89-2919] p 180 A89-47173  
Life prediction and constitutive models for engine hot section p 188 N89-12916  
Thermal barrier coating life prediction model development p 109 N89-12920  
Thermal barrier coating life prediction model p 109 N89-12921  
Thermal barrier coating life prediction model development p 110 N89-12922  
Fatigue strength reduction model: RANDOM3 and RANDOM4 user manual. Appendix 2: Development of advanced methodologies for probabilistic constitutive relationships of material strength models [NASA-CR-184796-APP-2] p 201 N89-19582  
Transmission overhaul and replacement predictions using Weibull and renewal theory [NASA-TM-102022] p 186 N89-22925  
Fatigue crack growth model RANDOM2 user manual, appendix 1 [NASA-CR-184939] p 203 N89-23890  
Fatigue strength reduction model: RANDOM3 and RANDOM4 user manual, appendix 2 [NASA-CR-184940] p 203 N89-23891  
Refinements in a viscoplastic model [NASA-TM-102338] p 205 N89-28036  
Intermetallic and ceramic matrix composites for 815 to 1370 C (1500 to 2500 F) gas turbine engine applications [NASA-TM-102326] p 88 N89-29490

**SETTLING**

- An asymptotic description of transient settling and ultrafiltration of colloidal dispersions p 144 A89-24603

**SH WAVES**

- Energy in elastic fiber embedded in elastic matrix containing incident SH wave [NASA-CR-4205] p 188 N89-18694

**SHAFTS (MACHINE ELEMENTS)**

- Modal analysis of gear housing and mounts [NASA-TM-101445] p 184 N89-21244

**SHAPE CONTROL**

- A method for producing a shaped contour radiation pattern using a single shaped reflector and a single feed p 125 A89-42758  
A method for producing a shaped contour radiation pattern using a single shaped reflector and a single feed [NASA-TM-101369] p 126 N89-10215

**SHEAR FLOW**

- Passive and active control of jet turbulence p 140 A89-10176  
Coherent structures in transitional and turbulent free shear flows p 147 A89-28999  
Turbulence management in free shear flows by control of coherent structures p 147 A89-30908

**SHEAR LAYERS**

- On the preferred mode of jet instability p 140 A89-11567  
Investigation of the flow between a pair of circular cylinders in the flopping regime p 144 A89-22822  
Nonlinear spatial evolution of an externally excited instability wave in a free shear layer p 144 A89-23242  
Shock-wave-induced mixing enhancement in scramjet combustors [AIAA PAPER 89-0104] p 145 A89-25091  
Subharmonic and fundamental high amplitude excitation of an axisymmetric jet [AIAA PAPER 89-0993] p 149 A89-37825  
Three-dimensional wave packets and instability waves in free shear layers and their receptivity p 149 A89-38619  
Response of a chemically reacting shear layer to streamwise vorticity [AIAA PAPER 89-0978] p 150 A89-40400  
An experimental study of a reattaching supersonic shear layer [AIAA PAPER 89-1801] p 6 A89-42036  
Compressibility and shock wave interaction effects on free shear layers [AIAA PAPER 89-2460] p 7 A89-46847  
Nonlinear evolution of interacting oblique waves on two-dimensional shear layers [NASA-TM-102030] p 164 N89-24575  
Mesh refinement in a two-dimensional large eddy simulation of a forced shear layer [NASA-TM-102129] p 166 N89-26180  
Calculation of reattaching shear layers in divergent channel with a multiple-time-scale turbulence model [NASA-TM-102293] p 168 N89-28749  
Multiwave interactions in turbulent jets [NASA-TM-101985] p 168 N89-29714

**SHEAR STRESS**

- Resolved shear stress intensity coefficient and fatigue crack growth in large crystals p 96 A89-22048  
Free-edge delamination - Laminar width and loading conditions effects p 193 A89-36294  
On finite element implementation and computational techniques for constitutive modeling of high temperature composites [NASA-CR-185120] p 204 N89-26261  
Skin-friction measurements by laser interferometry p 167 N89-28737  
Numerical investigation of an internal layer in turbulent flow over a curved hill [NASA-TM-102230] p 168 N89-29725

**SHELL THEORY**

- A 20-DOF hybrid stress general shell element p 191 A89-21133  
Analysis of shell-type structures subjected to time-dependent mechanical and thermal loading [NASA-CR-184989] p 203 N89-24669

**SHELLS (STRUCTURAL FORMS)**

- Non-isothermal buckling behavior of viscoplastic shell structures [NASA-CR-183013] p 197 N89-12931  
Analysis of shell-type structures subjected to time-dependent mechanical and thermal loading [NASA-CR-184989] p 203 N89-24669

**SHIELDING**

- Experimental evaluation of resistojet thruster plume shields p 59 A89-47487

**SHOCK WAVE INTERACTION**

- Effect of alcohol addition on shock-initiated formation of soot from benzene p 90 A89-12903  
Viscous analysis of high speed flows using an upwind finite volume technique [AIAA PAPER 89-0001] p 144 A89-25001  
Shock-wave-induced mixing enhancement in scramjet combustors [AIAA PAPER 89-0104] p 145 A89-25091  
Preliminary study of the interactions caused by crossing shock waves and a turbulent boundary layer [AIAA PAPER 89-0359] p 145 A89-25303  
Interaction of an oblique shock wave with turbulent hypersonic blunt body flows [AIAA PAPER 89-0272] p 3 A89-28405  
Experimental and numerical investigation of an oblique shock wave/turbulent boundary layer interaction with continuous suction [AIAA PAPER 89-0357] p 4 A89-28407  
A Newton/upwind method and numerical study of shock wave/boundary layer interactions p 6 A89-45468  
Compressibility and shock wave interaction effects on free shear layers [AIAA PAPER 89-2460] p 7 A89-46847  
An LDA (Laser-Doppler Anemometry) investigation of three-dimensional normal shock wave boundary-layer interactions p 14 N89-20956

**SHOCK WAVE PROPAGATION**

- Calculation of shocked flows by mathematical programming p 150 A89-45397

**SHOCK WAVES**

- Calculation of unsteady flows in turbomachinery using the linearized Euler equations p 149 A89-36916  
A numerical study of ENO and TVD schemes for shock capturing [NASA-TM-101355] p 222 N89-11469  
Numerical computation of shock wave-turbulent boundary layer interaction in transonic flow over an axisymmetric curved hill [NASA-TM-101473] p 162 N89-21192  
Conservative treatment of boundary interfaces for overlaid grids and multi-level grid adaptations [NASA-TM-102080] p 15 N89-24269

**SHORT CIRCUIT CURRENTS**

- A V-grooved GaAs solar cell [NASA-TM-101970] p 211 N89-22177  
The GaAs solar cells with V-grooved emitters [NASA-TM-102104] p 214 N89-26291

**SHORT CRACKS**

- Fatigue crack growth model RANDOM2 user manual. Appendix 1: Development of advanced methodologies for probabilistic constitutive relationships of material strength models [NASA-CR-184775-APP-1] p 201 N89-19581

**SHORT TAKEOFF AIRCRAFT**

- A model for prediction of STOVL ejector dynamics [NASA-TM-102098] p 32 N89-24319

**SIDLOBE REDUCTION**

- An experimental adaptive array to suppress weak interfering signals p 124 A89-22455

**SIDLOBES**

- Compensation of reflector antenna surface distortion using an array feed p 126 A89-53136

**SIGNAL ANALYSIS**

- Amplitude spectrum modulation technique for analog data processing in fiber optic sensing system with temporal separation of channels [NASA-TM-100152] p 174 N89-18671  
External electro-optic probing of millimeter-wave integrated circuits [NASA-TM-101990] p 128 N89-21142

**SIGNAL DISTORTION**

On the dynamic response of pressure transmission lines in the research of helium-charged free piston Stirling engines

[NASA-TM-102121] p 175 N89-24593

**SIGNAL PROCESSING**

Optoelectronic signal processing for phased-array antennas; Proceedings of the Meeting, Los Angeles, CA, Jan. 12, 13, 1988

[SPIE-886] p 124 A89-15819

Analysis of modified SMI method for adaptive array weight control

[NASA-CR-184904] p 127 N89-20364

Study of spread spectrum multiple access systems for satellite communications with overlay on current services

[NASA-CR-180827] p 128 N89-23757

Analysis of modified SMI method for adaptive array weight control

[NASA-CR-185493] p 19 N89-25993

Adaptive array for weak interfering signals: Geostationary satellite experiments

[NASA-CR-185450] p 129 N89-26126

Programmable rate modem utilizing digital signal processing techniques

[NASA-CR-185124] p 43 N89-26879

**SIGNAL RECEPTION**

Analysis of modified SMI method for adaptive array weight control

[NASA-CR-184904] p 127 N89-20364

Analysis of modified SMI method for adaptive array weight control

[NASA-CR-185493] p 19 N89-25993

Adaptive array for weak interfering signals: Geostationary satellite experiments

[NASA-CR-185450] p 129 N89-26126

**SIGNATURE ANALYSIS**

Vibration signature analysis of multistage gear transmission

[NASA-TM-101442] p 184 N89-18685

**SILANES**

Alkoxysilane adsorption on metal oxide substrates

p 92 A89-44536

**SILICA GEL**

Influence of several metal ions on the gelation activation energy of silicon tetraethoxide

[NASA-TM-101380] p 114 N89-21894

**SILICA GLASS**

Crystallization and characterization of Y<sub>2</sub>O<sub>3</sub>-SiO<sub>2</sub> glasses

p 80 A89-19486

**SILICON**

Metal-silicon reaction rates - The effects of capping

p 93 A89-52202

Indentation plasticity and fracture in silicon

[NASA-TP-2863] p 100 N89-10996

Deposition and characterization of ZnS/Si heterojunctions produced by vacuum evaporation

[NASA-TM-101359] p 135 N89-11129

Ultra-thin, light-trapping silicon solar cells

p 213 N89-24719

**SILICON ALLOYS**

Kinetics of fracture in Fe-3Si steel under mode I loading

p 99 A89-47320

Radiation resistance studies of amorphous silicon films

p 213 N89-24738

**SILICON CARBIDES**

Radiographic and ultrasonic characterization of sintered silicon carbide

p 187 A89-14700

Strength distribution in commercial silicon carbide materials

p 105 A89-17097

Comparison of the surface charge behavior of commercial silicon nitride and silicon carbide powders

p 105 A89-21444

Raman determination of layer stresses and strains for heterostructures and its application to the cubic SiC/Si system

p 234 A89-21871

Surface studies relevant to silicon carbide chemical vapor deposition

p 91 A89-27966

Pressure effects on the thermal stability of silicon carbide fibers

p 105 A89-31502

Effects of various consolidation techniques on microstructure, strength, and reliability of alpha-SiC

p 106 A89-33611

The behavior of SiC and Si<sub>3</sub>N<sub>4</sub> ceramics in mixed oxidation/chlorination environments

p 106 A89-33616

Improved silicon carbide for advanced heat engines. I - Process development for injection molding

p 106 A89-33619

Improved silicon carbide for advanced heat engines. II - Pressureless sintering and mechanical properties of injection molded silicon carbide

p 106 A89-33620

Crystal growth of SiC for electronic applications

p 132 A89-33625

High-frequency ultrasonic characterization of sintered silicon carbide

p 106 A89-34840

Strength distribution of reinforcing fibers in a Nicalon fiber/chemically vapor infiltrated silicon carbide matrix composite

p 82 A89-34844

Auger analysis of a fiber/matrix interface in a ceramic matrix composite

p 82 A89-35311

Ultrasonic imaging of porosity variations produced during sintering

p 107 A89-48892

Deformation and fracture of single-crystal and sintered polycrystalline silicon carbide produced by cavitation

p 108 A89-54985

Properties of silicon carbide fiber-reinforced silicon nitride matrix composites

[NASA-TM-101356] p 84 N89-10130

Thermal effects on the mechanical properties of SiC fiber reinforced reaction bonded silicon nitride matrix (SiC/RBSN) composites

[NASA-TM-101348] p 84 N89-10134

A sintering model for SiC(sub)w/Si<sub>3</sub>N<sub>4</sub> composites

[NASA-TM-101336] p 108 N89-10166

High-strength silicon carbides by hot isostatic pressing

[NASA-TM-101400] p 111 N89-13666

Improved silicon carbide for advanced heat engines

[NASA-CR-179477] p 112 N89-15251

Effect of processing on fracture toughness of silicon carbide as determined by Vickers indentations

[NASA-TM-101456] p 115 N89-21895

The isothermal fatigue behavior of a unidirectional SiC/Ti composite and the Ti alloy matrix

[NASA-TM-101984] p 86 N89-22684

Preparation and evaluation of silicon nitride matrices for silicon nitride-SiC fiber composites

[NASA-CR-184798] p 115 N89-23678

Characterization of ceramics and intermetallics fabricated by self-propagating high-temperature synthesis

[NASA-TM-102004] p 78 N89-25285

Microwave and millimeter-wave power generation in silicon carbide (SiC) IMPATT devices

[NASA-CR-185050] p 139 N89-26143

Fatigue crack growth study of SCS8/Ti-15-3 composite

[NASA-TM-102332] p 104 N89-26989

**SILICON CONTROLLED RECTIFIERS**

Computer analysis of the negative differential resistance switching phenomenon of double-injection devices

p 134 A89-54963

**SILICON DIOXIDE**

Sodium sulfate - Deposition and dissolution of silica

p 91 A89-28084

The effect of Al<sub>2</sub>O<sub>3</sub>, CaO, Cr<sub>2</sub>O<sub>3</sub> and MgO on devitrification of silica

[NASA-TM-101335] p 77 N89-10124

Undercutting of defects in thin film protective coatings on polymer surfaces exposed to atomic oxygen

[NASA-TM-101986] p 115 N89-23691

Isotopic study of oxygen diffusion in oxide coatings

[NASA-TM-102082] p 78 N89-24451

**SILICON FILMS**

Convection and chemistry effects in CVD: A 3-D analysis for silicon deposition

[NASA-TM-102001] p 78 N89-21032

**SILICON NITRIDES**

Microstructural evolution on crystallizing the glassy phase in a 6 weight percent Y<sub>2</sub>O<sub>3</sub>-Si<sub>3</sub>N<sub>4</sub> ceramic

p 80 A89-19487

Comparison of the surface charge behavior of commercial silicon nitride and silicon carbide powders

p 105 A89-21444

Plasma deposited silicon nitride for indium phosphide encapsulation

p 235 A89-27794

The behavior of SiC and Si<sub>3</sub>N<sub>4</sub> ceramics in mixed oxidation/chlorination environments

p 106 A89-33616

Auger analysis of a fiber/matrix interface in a ceramic matrix composite

p 82 A89-35311

Hot isostatic pressing of silicon nitride with boron nitride, boron carbide, and carbon additions

p 107 A89-41744

Adhesion, friction, and wear of plasma-deposited thin silicon nitride films at temperatures to 700 C

p 107 A89-48250

Properties of silicon carbide fiber-reinforced silicon nitride matrix composites

[NASA-TM-101356] p 84 N89-10130

A sintering model for SiC(sub)w/Si<sub>3</sub>N<sub>4</sub> composites

[NASA-TM-101336] p 108 N89-10166

Laminate behavior for SiC fiber-reinforced reaction-bonded silicon nitride matrix composites

[NASA-TM-101350] p 84 N89-10952

Adhesion, friction, and wear of plasma-deposited thin silicon nitride films at temperatures to 700 C

[NASA-TM-101377] p 109 N89-11913

Slurry-pressing consolidation of silicon nitride

[NASA-TM-101365] p 109 N89-12746

Strength of hot isostatically pressed and sintered reaction bonded silicon nitrides containing Y<sub>2</sub>O<sub>3</sub>

[NASA-TM-101443] p 112 N89-15257

Improved silicon nitride for advanced heat engines

[NASA-CR-179525] p 113 N89-19421

Preparation and evaluation of silicon nitride matrices for silicon nitride-SiC fiber composites

[NASA-CR-184798] p 115 N89-23678

**SIMULATION**

A Fourier analysis for a fast simulation algorithm --- for switching converters

p 130 A89-15367

Townsend coefficients for electron scattering over dielectric surfaces

p 231 A89-16409

Direct numerical simulations of a temporally evolving mixing layer subject to forcing

p 147 A89-34426

A numerical simulation of the full two-dimensional electrothermal de-icer pad

[NASA-CR-4194] p 19 N89-14235

Simulation of 3-D viscous flow within a multi-stage turbine

[NASA-TM-101376] p 26 N89-14238

Application of a lower-upper implicit scheme and an interactive grid generation for turbomachinery flow field simulations

[NASA-TM-101412] p 11 N89-15077

**SIMULATORS**

Heat transfer in the tip region of a rotor blade simulator

p 161 N89-17312

A real-time simulator of a turbofan engine

[NASA-TM-100869] p 31 N89-20995

Computational structural mechanics engine structures computational simulator

p 205 N89-29792

**SINE WAVES**

Universal limiter for high order explicit conservative advection schemes

p 151 A89-45398

**SINGLE CRYSTALS**

Surface temperature determination in surface analytic systems by infrared optical pyrometry

p 169 A89-17347

Reactions of silicon-based ceramics in mixed oxidation chlorination environments

p 105 A89-21442

Influence of precipitate morphology on intermediate temperature creep properties of a nickel-base superalloy single crystal

p 96 A89-26872

The influence of high thermal gradient casting, hot isostatic pressing and alternate heat treatment on the structure and properties of a single crystal nickel base superalloy

p 97 A89-36427

Isothermal and 'bithermal' thermomechanical fatigue behavior of a NiCoCrAlY-coated single crystal superalloy

p 177 A89-36457

Accelerated fatigue crack growth behavior of PWA 1480

p 97 A89-36461

Transient oxidation of single-crystal beta-NiAl

p 98 A89-37899

Observations of directional gamma prime coarsening during engine operation

p 98 A89-40162

Fatigue crack growth behavior of a single crystal alloy as observed through an in situ fatigue loading stage

p 99 A89-45946

The low cycle fatigue deformation response of a single-crystal superalloy at 650 C

p 99 A89-52204

Deformation and fracture of single-crystal and sintered polycrystalline silicon carbide produced by cavitation

p 108 A89-54985

Indentation plasticity and fracture in silicon

[NASA-TP-2863] p 100 N89-10996

Constitutive behavior of single crystal PWA 1480 and directionally solidified MAR-M 246 under monotonic and cyclic loads at high and low temperature

p 100 N89-12634

Constitutive modeling for single crystal superalloys

p 101 N89-12911

Constitutive modelling of single crystal and directionally solidified superalloys

p 101 N89-12912

Constitutive modelling of single crystal and directionally solidified superalloys

p 102 N89-17325

High temperature constitutive and crack initiation modeling of coated single crystal superalloys

p 112 N89-17334

Advanced single crystal for SSME turbopumps

[NASA-CR-182244] p 103 N89-21072

**SINGULARITY (MATHEMATICS)**

Considerations on the moving contact-line singularity, with application to frictional drag on a slender drop

p 144 A89-23238

Specialty functions singularity mechanics problems

p 206 N89-29805

**SINTERING**

Effect of processing parameters on the characteristics of high-Tc superconductor YBa<sub>2</sub>Cu<sub>3</sub>O<sub>y</sub>

p 234 A89-20467

Reactions of silicon-based ceramics in mixed oxidation chlorination environments

p 105 A89-21442

Improved silicon carbide for advanced heat engines. II - Pressureless sintering and mechanical properties of injection molded silicon carbide

p 106 A89-33620

High-frequency ultrasonic characterization of sintered silicon carbide

p 106 A89-34840

- Ultrasonic imaging of porosity variations produced during sintering p 107 A89-48892
- Deformation and fracture of single-crystal and sintered polycrystalline silicon carbide produced by cavitation p 108 A89-54985
- A sintering model for SiC(sub)w/Si3N4 composites [NASA-TM-101336] p 108 A89-10166
- Strength of hot isostatically pressed and sintered reaction bonded silicon nitrides containing Y2O3 [NASA-TM-101443] p 112 A89-15257
- Preparation and evaluation of silicon nitride matrices for silicon nitride-SiC fiber composites [NASA-CR-184798] p 115 A89-23678
- SISO (CONTROL SYSTEMS)**
- Stability robustness improvement of direct eigenspace assignment based feedback systems using singular value sensitivities [NASA-CR-182302] p 36 A89-27672
- SIZE DETERMINATION**
- Calibration of single particle sizing velocimeters using photomask reticles p 170 A89-33379
- SIZING**
- HASA: Hypersonic Aerospace Sizing Analysis for the preliminary design of aerospace vehicles [NASA-CR-182226] p 18 A89-15107
- SKIN FRICTION**
- Correlations of velocity and temperature fluctuations in the stagnation-point flow of circular cylinder in turbulent flow p 148 A89-34927
- Skin-friction measurements by laser interferometry p 167 A89-28737
- SLIDING CONTACT**
- Avalanche in adhesion --- interfacial separation between two Ni crystals p 100 A89-54495
- SLIDING FRICTION**
- Reaction of perfluoroalkylpolyethers (PFPE) with 440C steel in vacuum under sliding conditions at room temperature [NASA-TP-2883] p 115 A89-26091
- SLIPSTREAMS**
- Fluctuating pressures on wing surfaces in the slipstream of a single-rotor propfan [AIAA PAPER 89-1058] p 226 A89-36218
- SLURRIES**
- Slurry-pressing consolidation of silicon nitride [NASA-TM-101365] p 109 A89-12746
- SLUSH**
- Fueling the National Aero-Space Plane with slush hydrogen [AIAA PAPER 89-5014] p 117 A89-51339
- SMALL PERTURBATION FLOW**
- Absorbing boundary conditions for second-order hyperbolic equations [NASA-TM-102009] p 223 A89-22397
- SMOKE DETECTORS**
- Fire safety applications for spacecraft [NASA-TM-101463] p 42 A89-24413
- SODIUM SULFATES**
- Deposition of Na2SO4 from salt-seeded combustion gases of a high velocity burner rig p 89 A89-12330
- Laboratory studies of binary salt CVD in combustion gas environments p 89 A89-12335
- Laboratory studies of the deposition of alkali sulfate vapors from combustion gases using a flash-evaporation technique p 89 A89-12338
- Sodium sulfate - Deposition and dissolution of silica p 91 A89-28084
- SOFTWARE ENGINEERING**
- Automation software for a materials testing laboratory p 217 A89-12917
- Laboratory process control using natural language commands from a personal computer [NASA-TM-101988] p 218 A89-24055
- SOFTWARE TOOLS**
- An integrated and modular digital modeling approach for the Space Station electrical power system development p 50 A89-15298
- User interactive electric propulsion software design [AIAA PAPER 89-2376] p 57 A89-46783
- Measurement of the properties of lossy materials inside a finite conducting cylinder p 126 A89-10223
- [NASA-CR-182500]
- Transputer parallel processing at NASA Lewis Research Center p 205 A89-29778
- SOL-GEL PROCESSES**
- Influence of several metal ions on the gelation activation energy of silicon tetraethoxide [NASA-TM-101380] p 114 A89-21894
- SOLAR ARRAYS**
- Photovoltaics for high capacity space power systems [IAF PAPER 88-221] p 53 A89-17730
- Free-vibration characteristics and correlation of a Space Station split-blanket solar array [AIAA PAPER 89-1252] p 44 A89-30737
- Photovoltaics for high capacity space power systems [NASA-TM-101341] p 61 A89-10122
- PV modules for ground testing [NASA-CR-179476] p 208 A89-11315
- Free-vibration characteristics and correlation of a space station split-blanket solar array [NASA-TM-101452] p 198 A89-15438
- Photovoltaic power system considerations for future lunar bases [NASA-TM-102019] p 67 A89-23517
- Space Station Freedom Solar Array design development [NASA-TM-102105] p 70 A89-24448
- Space Photovoltaic Research and Technology, 1988. High Efficiency, Space Environment, and Array Technology [NASA-CP-3030] p 212 A89-24704
- Predicted performance of InP solar cells in Cassegrainian and slats space concentrator arrays at 20 to 100 AMO, 80 to 100 C p 212 A89-24711
- Space Station Freedom photovoltaic power module design status [NASA-TM-102073] p 71 A89-25273
- Launch packaging options for the photovoltaic power module cargo element [NASA-TM-102072] p 71 A89-25275
- Effect of micrometeoroid and space debris impacts on the Space Station Freedom solar array surfaces [NASA-TM-102287] p 47 A89-26035
- Advances in thin-film solar cells for lightweight space photovoltaic power [NASA-TM-102017] p 73 A89-26041
- Photovoltaic module on-orbit assembly for Space Station Freedom [NASA-TM-102297] p 47 A89-26887
- NASA advanced space photovoltaic technology-status, potential and future mission applications [NASA-TM-102093] p 75 A89-27705
- SOLAR CELLS**
- Temperature coefficients for concentrator cells at various electron and proton fluence levels p 51 A89-15304
- Progress in InP solar cell research p 130 A89-15308
- Thermal analysis of heat storage canisters for a solar dynamic, space power system p 54 A89-29113
- High-efficiency solar cells fabricated from direct-current magnetron sputtered n-indium tin oxide onto p-InP grown by atmospheric pressure metalorganic vapor phase epitaxy p 133 A89-44518
- High-efficiency indium tin oxide/indium phosphide solar cells p 208 A89-44883
- Advances in thin-film solar cells for lightweight space photovoltaic power [IAF PAPER ICOSP89-1-8] p 55 A89-46513
- Metal-silicon reaction rates - The effects of capping p 93 A89-52202
- Space solar cell research p 208 A89-52203
- InP homojunction solar cell performance on the LIPS 3 flight experiment [NASA-TM-101390] p 209 A89-12123
- Radiation resistance and comparative performance of ITO/InP and n/p InP homojunction solar cells [NASA-TM-101387] p 135 A89-12819
- Issues and opportunities in space photovoltaics [NASA-TM-101425] p 65 A89-15171
- Common source-multiple load vs. separate source-individual load photovoltaic system [NASA-TM-101465] p 136 A89-15338
- The effect of different module configurations on the radiation tolerance of multijunction solar cells [NASA-TM-101251] p 209 A89-17356
- Starting characteristics of direct current motors powered by solar cells [NASA-TM-101981] p 136 A89-19493
- Restrictive loads powered by separate or by common electrical sources [NASA-TM-102008] p 137 A89-21174
- A V-grooved GaAs solar cell [NASA-TM-101970] p 211 A89-22177
- The NASA Space Solar Cell Advanced Research Program [NASA-TM-102020] p 67 A89-22651
- Comparison of solar photovoltaic and nuclear reactor power systems for a human-tended lunar observatory [NASA-TM-102015] p 242 A89-23397
- Energy storage and thermal control system design status [NASA-TM-102138] p 46 A89-24427
- Space Station Freedom Solar Array design development [NASA-TM-102105] p 70 A89-24448
- Photovoltaic power system operation in the Mars environment [NASA-TM-102075] p 138 A89-24529
- Space Photovoltaic Research and Technology, 1988. High Efficiency, Space Environment, and Array Technology [NASA-CP-3030] p 212 A89-24704
- Progress in indium phosphide solar cell research p 212 A89-24707
- Ultra-thin, light-trapping silicon solar cells p 213 A89-24719
- High efficiency GaAs-Ge tandem solar cells grown by MOVCD p 213 A89-24721
- A new structure for comparing surface passivation materials of GaAs solar cells p 213 A89-24725
- Chemical etching and organometallic chemical vapor deposition on varied geometries of GaAs p 213 A89-24728
- Domed Fresnel lens concentrator technology for space application p 213 A89-24732
- A comparison of the radiation tolerance characteristics of multijunction solar cells with series and voltage-matched configurations p 213 A89-24737
- Radiation resistance studies of amorphous silicon films p 213 A89-24738
- Estimated performance and future potential of solar dynamic and photovoltaic power systems for selected LEO and HEO missions [NASA-TM-102083] p 72 A89-25280
- The GaAs solar cells with V-grooved emitters [NASA-TM-102104] p 214 A89-26291
- On-orbit results of the LIPS 3/InP homojunction solar cell experiment [NASA-TM-102131] p 214 A89-26292
- Solar power for the lunar night [NASA-TM-102127] p 242 A89-26799
- Lunar production of solar cells [NASA-TM-102102] p 242 A89-27619
- NASA advanced space photovoltaic technology-status, potential and future mission applications [NASA-TM-102093] p 75 A89-27705
- Indium phosphide solar cell research in the US: Comparison with nonphotovoltaic sources [NASA-TM-102103] p 124 A89-27868
- SOLAR COLLECTORS**
- An experimental analysis of a doped lithium fluoride direct absorption solar receiver p 49 A89-15245
- Progress in InP solar cell research p 130 A89-15308
- Thermal distortion analysis of the Space Station solar dynamic concentrator p 51 A89-15341
- Advanced sensible heat solar receiver for space power p 52 A89-15415
- Ray tracing optical analysis of offset solar collector for Space Station solar dynamic system p 53 A89-15416
- The effect of the near earth micrometeoroid environment on a highly reflective mirror surface [AIAA PAPER 88-0026] p 40 A89-17939
- Advanced solar receivers for space power p 54 A89-29116
- Advanced heat receiver conceptual design study [NASA-CR-182177] p 209 A89-16224
- Preliminary study of creep thresholds and thermomechanical response in Haynes 188 at temperatures in the range 649 to 871 C p 200 A89-17327
- The effect of different module configurations on the radiation tolerance of multijunction solar cells [NASA-TM-101251] p 209 A89-17356
- Solar dynamic power module design [NASA-TM-102055] p 70 A89-25269
- A program for advancing the technology of space concentrators [NASA-TM-102139] p 76 A89-29484
- SOLAR DYNAMIC POWER SYSTEMS**
- Transient performance evaluation of an integrated heat pipe-thermal storage system p 49 A89-15209
- An experimental analysis of a doped lithium fluoride direct absorption solar receiver p 49 A89-15245
- Space Station power system requirements p 50 A89-15295
- The Solar Dynamic radiator with a historical perspective p 51 A89-15340
- Thermal distortion analysis of the Space Station solar dynamic concentrator p 51 A89-15341
- Advanced space solar dynamic receivers p 52 A89-15343
- Space Station battery system design and development p 52 A89-15378
- Advanced sensible heat solar receiver for space power p 52 A89-15415
- Ray tracing optical analysis of offset solar collector for Space Station solar dynamic system p 53 A89-15416
- Photovoltaics for high capacity space power systems [IAF PAPER 88-221] p 53 A89-17730
- Status of the Space Station power system p 54 A89-23281

- Evaluation of alternative phase change materials for energy storage in solar dynamic applications p 208 A89-29114
- Photovoltaic power modules for NASA's manned Space Station p 55 A89-29122
- Durable thin film coatings for reflectors used in low earth orbit p 77 A89-33150
- Densities of some molten fluoride salt mixtures suitable for heat storage in space power applications p 77 A89-41444
- Power systems for production, construction, life support, and operations in space p 37 A89-45803
- Solar dynamic power for Space Station Freedom [IAF PAPER ICOSP89-4-1] p 55 A89-46517
- Compatibility of molten salts with advanced solar dynamic receiver materials [AIAA PAPER 89-1756] p 83 A89-48957
- The solar dynamic radiator with a historical perspective [NASA-TM-100972] p 45 A89-10117
- Photovoltaics for high capacity space power systems [NASA-TM-101341] p 61 A89-10122
- Solar dynamic heat rejection technology. Task 1: System concept development [NASA-CR-179618] p 158 A89-13731
- The 25 kW solar thermal Stirling hydraulic engine system: Conceptual design [NASA-CR-180889] p 239 A89-14182
- Power systems facility [NASA-TM-101447] p 40 A89-14247
- Advanced heat receiver conceptual design study [NASA-CR-182177] p 209 A89-16224
- Numerical model of solar dynamic radiator for parametric analysis [NASA-TM-102054] p 67 A89-22653
- Solar dynamic power for space station freedom [NASA-TM-102016] p 67 A89-23516
- Concentration of off-axis radiation by solar concentrators for space power [NASA-TM-102052] p 69 A89-24438
- Flight experiment of thermal energy storage [NASA-TM-102081] p 69 A89-24440
- Solar dynamic power module design [NASA-TM-102055] p 70 A89-25269
- Estimated performance and future potential of solar dynamic and photovoltaic power systems for selected LEO and HEO missions [NASA-TM-102083] p 72 A89-25280
- Comparison of conceptual designs for 25 kW advanced Stirling conversion systems for dish electric application [NASA-TM-102085] p 239 A89-26781
- Performance estimates for the Space Station power system Brayton Cycle compressor and turbine [NASA-CR-182263] p 73 A89-26903
- Thermal evaluation of advanced solar dynamic heat receiver performance [NASA-CR-185117] p 214 A89-27256
- A program for advancing the technology of space concentrators [NASA-TM-102139] p 76 A89-29484
- SOLAR ENERGY**
- The introduction of space technology power systems into developing countries [NASA-TM-102042] p 71 A89-25274
- Thermal evaluation of advanced solar dynamic heat receiver performance [NASA-CR-185117] p 214 A89-27256
- Solar radiation on Mars [NASA-TM-102299] p 242 A89-27623
- SOLAR ENERGY CONVERSION**
- Solar dynamic power module design [NASA-TM-102055] p 70 A89-25269
- Comparison of conceptual designs for 25 kW advanced Stirling conversion systems for dish electric application [NASA-TM-102085] p 239 A89-26781
- A program for advancing the technology of space concentrators [NASA-TM-102139] p 76 A89-29484
- SOLAR GENERATORS**
- A new Space Station power system p 53 A89-20016
- Thermal analysis of heat storage canisters for a solar dynamic, space power system p 54 A89-29113
- SOLAR MAXIMUM MISSION**
- Limits to the radiative decays of neutrinos and axions from gamma-ray observations of SN 1987A p 242 A89-26985
- SOLAR POWER SATELLITES**
- A new Space Station power system p 53 A89-20016
- SOLAR RADIATION**
- The NASA atomic oxygen effects test program p 93 A89-12589
- Photovoltaic power system operation in the Mars environment [NASA-TM-102075] p 138 A89-24529
- Solar radiation on Mars [NASA-TM-102299] p 242 A89-27623
- SOLAR REFLECTORS**
- Durable thin film coatings for reflectors used in low earth orbit p 77 A89-33150
- SOLID ELECTRODES**
- The effect of electrode configuration on arcjet performance [AIAA PAPER 89-2722] p 58 A89-47044
- Design, fabrication, and performance of brazed, graphite electrode, multistage depressed collectors with 500-W, continuous wave, 4.8- to 9.6-GHz traveling-wave tubes [NASA-TP-2904] p 136 A89-21171
- Hydrogen-oxygen proton-exchange membrane fuel cells and electrolyzers p 211 A89-22996
- SOLID LUBRICANTS**
- Tribological composition optimization of chromium-carbide-based solid lubricant coatings for foil gas bearings at temperatures to 650 C p 83 A89-54258
- Tribological properties of alumina-boria-silicate fabric from 25 C to 850 C p 107 A89-54982
- Solid lubricant materials for high temperatures: A review p 203 A89-24636
- SOLID PROPELLANT COMBUSTION**
- Navier-Stokes calculation of solid-propellant rocket motor internal flowfields [AIAA PAPER 88-3182] p 48 A89-14983
- Ignition and combustion of metallized propellants [AIAA PAPER 89-2883] p 117 A89-47148
- SOLID PROPELLANT IGNITION**
- Ignition and combustion of metallized propellants [AIAA PAPER 89-2883] p 117 A89-47148
- SOLID STATE DEVICES**
- Universal test fixture for monolithic mm-wave integrated circuits calibrated with an augmented TRD algorithm [NASA-TP-2875] p 127 A89-17767
- Development of gallium arsenide high-speed, low-power serial parallel interface modules: Executive summary [NASA-CR-182272] p 137 A89-21173
- SOLID SURFACES**
- The solid surface combustion space shuttle experiment hardware description and ground-based test results [NASA-TM-101963] p 123 A89-19446
- SOLID SUSPENSIONS**
- Fluid flow phenomena in the generation of boron carbide suspensions in magnesium melts p 79 A89-19472
- An asymptotic description of transient settling and ultrafiltration of colloidal dispersions p 144 A89-24603
- SOLID-SOLID INTERFACES**
- Transmission electron microscopy of composites p 79 A89-14560
- Analysis of microalloy precipitate reversion in steels p 94 A89-15108
- The interaction of gold with gallium arsenide p 90 A89-16416
- Finite element modeling of frictionally restrained composite interfaces [NASA-CR-182281] p 203 A89-23918
- SOLIDIFICATION**
- Microstructures in rapidly solidified niobium aluminides p 95 A89-18193
- Rapid solidification research at the NASA Lewis Research Center p 95 A89-18203
- Enthalpies of a binary alloy during solidification p 96 A89-22559
- Effects of crucible wetting during solidification of immiscible Pb-Zn alloys [AIAA PAPER 89-0304] p 118 A89-25261
- Effects of crucible wetting during solidification of immiscible Pb-Zn [NASA-TM-101372] p 120 A89-14341
- The role of rapid solidification processing in the fabrication of fiber reinforced metal matrix composites [NASA-TM-101450] p 85 A89-15201
- SOLIDS**
- A model for including thermal conduction in molecular dynamics simulations p 237 A89-41259
- Universal features of the equation of state of solids p 237 A89-48960
- SOLUTIONS**
- Thermosolutal convection in high-aspect-ratio enclosures p 153 A89-53288
- SOLUTIONS**
- Solution and sensitivity analysis of a complex transcendental eigenproblem with pairs of real eigenvalues [NASA-CR-182241] p 197 A89-13819
- Raman intensity as a probe of concentration near a crystal growing in solution [NASA-TP-2865] p 174 A89-16139
- SOOT**
- Effect of alcohol addition on shock-initiated formation of soot from benzene p 90 A89-12903
- Optical measurements of soot and temperature profiles in premixed propane-oxygen flames p 92 A89-35008
- Determination of combustion gas temperatures by infrared radiometry in sooting and nonsooting flames [NASA-TP-2900] p 164 A89-25409
- SOUND PROPAGATION**
- Acoustic wave propagation in heterogeneous structures including experimental validation [AIAA PAPER 89-1044] p 225 A89-36214
- SOUND WAVES**
- Effects of wind-tunnel wall absorption on acoustic radiation of propellers p 225 A89-22285
- Acoustic wave propagation in heterogeneous structures including experimental validation [AIAA PAPER 89-1044] p 225 A89-36214
- An acoustic experimental and theoretical investigation of single disc propellers [AIAA PAPER 89-1146] p 227 A89-40478
- Acoustic wave propagation in heterogeneous structures including experimental validation [NASA-TM-101486] p 224 A89-19965
- SOUND-SOUND INTERACTIONS**
- The effect of front-to-rear propeller spacing on the interaction noise at cruise conditions of a model counterrotation propeller having a reduced diameter aft propeller [NASA-TM-101329] p 227 A89-10603
- SPACE BASED RADAR**
- Nuclear reactor power as applied to a space-based radar mission p 51 A89-15317
- Systems aspects of a space nuclear reactor power system p 51 A89-15327
- Nuclear reactor power as applied to a space-based radar mission [NASA-TM-101200] p 230 A89-14831
- SPACE CHARGE**
- Space plasma contractor research, 1988 [NASA-CR-182283] p 233 A89-21658
- SPACE COLONIES**
- A perspective on space exploration technology catalysis: A rationale for initiating 21st Century expansion of human civilization into outer space [NASA-TM-101362] p 238 A89-11637
- SPACE COMMERCIALIZATION**
- SP-100 nuclear space power systems with application to space commercialization [NASA-TM-101403] p 63 A89-12665
- SPACE COMMUNICATION**
- Optically controlled phased-array technology for space communication systems p 131 A89-15845
- Engineering calculations for solving the orbital allotment problem [NASA-CR-184607] p 217 A89-13993
- SPACE DEBRIS**
- Overview of environmental factors p 240 A89-23529
- Effect of micrometeoroid and space debris impacts on the Space Station Freedom solar array surfaces [NASA-TM-102287] p 47 A89-26035
- SPACE ELECTRIC ROCKET TESTS**
- Performance of large area xenon ion thrusters for orbit transfer missions [NASA-TM-102049] p 69 A89-24436
- SPACE ENVIRONMENT SIMULATION**
- Droplet combustion drop tower tests using models of the space flight apparatus [AIAA PAPER 89-0501] p 119 A89-28418
- SPACE EXPLORATION**
- An analysis of possible advanced space strategies featuring the role of space resource utilization [IAF PAPER 88-587] p 37 A89-17861
- Space 2010 --- Space Station Freedom future explorations p 77 A89-23028
- The NASA Electric Propulsion Program p 59 A89-47428
- A perspective on space exploration technology catalysis: A rationale for initiating 21st Century expansion of human civilization into outer space [NASA-TM-101362] p 238 A89-11637
- SP-100 nuclear space power systems with application to space commercialization [NASA-TM-101403] p 63 A89-12665
- Issues and opportunities in space photovoltaics [NASA-TM-101425] p 65 A89-15171
- Systems autonomy technology: Executive summary and program plan [NASA-TM-100999] p 216 A89-18045
- Human exploration mission studies p 38 A89-22985
- NASA's Chemical Transfer Propulsion Program for Pathfinder [NASA-TM-102298] p 41 A89-26876
- Toward an electrical power utility for space exploration [NASA-TM-102347] p 75 A89-27704
- SPACE FLIGHT**
- Summary of the Second International Conference on Tethers in Space Venice, Italy, October 4-8, 1987 [AIAA PAPER 89-1547] p 37 A89-40177

# SPACE INDUSTRIALIZATION

- Use of high temperature superconductors in magnetoplasma dynamic systems [NASA-TM-101219] p 236 N89-11553
- SPACE INDUSTRIALIZATION**
- Human exploration mission studies p 38 N89-22985
- SPACE LOGISTICS**
- Expendable launch vehicle transportation for the Space Station [IAF PAPER 88-198] p 42 A89-17720
- SPACE MANUFACTURING**
- Lunar production of solar cells [NASA-TM-102102] p 242 N89-27619
- SPACE MISSIONS**
- High temperature superconducting magnetic energy storage for future NASA missions p 50 A89-15288
- Space nuclear reactor shields for manned and unmanned applications [NASA-TM-102064] p 71 N89-25272
- SPACE PLASMAS**
- Large structure current collection in plasma environments [AIAA PAPER 89-0496] p 44 A89-25405
- Plasma contacting - An enabling technology [AIAA PAPER 89-0677] p 231 A89-25537
- Induced emission of radiation from a large space-station-like structure in the ionosphere p 44 A89-31915
- Ground-based tests of hollow cathode plasma contactors [AIAA PAPER 89-1558] p 232 A89-40188
- A model of electron collecting plasma contactors [AIAA PAPER 89-1560] p 232 A89-40190
- On the need for space tests of plasma contactors as electron collectors p 232 A89-43356
- Experimental validation of a phenomenological model of the plasma contacting process p 232 A89-43357
- The plasma wake of the Shuttle Orbiter p 215 A89-43680
- The POLAR code wake model - Comparison with in situ observations --- Shuttle Orbiter plasma wake ion and electron density simulation p 233 A89-45632
- PV modules for ground testing [NASA-CR-179476] p 208 N89-11315
- Space plasma contractor research, 1988 [NASA-CR-182283] p 233 N89-21658
- Overview of environmental factors p 240 N89-23529
- Surface phenomena in plasma environments p 234 N89-23555
- SPACE PLATFORMS**
- Technology requirements for an orbiting fuel depot - A necessary element of a space infrastructure [IAF PAPER 88-035] p 37 A89-17641
- SPACE POWER REACTORS**
- Nuclear reactor power as applied to a space-based radar mission p 51 A89-15317
- Systems aspects of a space nuclear reactor power system p 51 A89-15327
- Extended SP-100 reactor power systems capability p 52 A89-15392
- Power transmission studies for tethered SP-100 p 52 A89-15403
- Space power technologies p 38 N89-11770
- SP-100 nuclear space power systems with application to space commercialization p 63 N89-12665
- [NASA-TM-101403]
- Nuclear reactor power as applied to a space-based radar mission p 230 N89-14831
- [NASA-TM-101200]
- Refractory metal alloys and composites for space nuclear power systems p 102 N89-16986
- [NASA-TM-101364]
- Megawatt Class Nuclear Space Power Systems (MCNSPS) conceptual design and evaluation report. Volume 1: Objectives, summary results and introduction [NASA-CR-179614-VOL-1] p 209 N89-17941
- Megawatt Class Nuclear Space Power Systems (MCNSPS) conceptual design and evaluation report. Volume 4: Concepts selection, conceptual designs, recommendations [NASA-CR-179614-VOL-4] p 210 N89-18967
- Megawatt Class Nuclear Space Power Systems (MCNSPS) conceptual design and evaluation report. Volume 3, technologies 2: Power conversion [NASA-CR-179614-VOL-3] p 211 N89-22980
- Megawatt Class Nuclear Space Power Systems (MCNSPS) conceptual design and evaluation report. Volume 2, technologies 1: Reactors, heat transport, integration issues [NASA-CR-179614-VOL-2] p 211 N89-22981
- Comparison of solar photovoltaic and nuclear reactor power systems for a human-tended lunar observatory [NASA-TM-102015] p 242 N89-23397
- Summary and evaluation of the Strategic Defense Initiative Space Power Architecture Study [NASA-TM-102012] p 69 N89-24443

## SPACE POWER UNIT REACTORS

- CSTI High Capacity Power [NASA-TM-102059] p 72 N89-25282
- SPACE PROCESSING**
- Effects of crucible wetting during solidification of immiscible Pb-Zn alloys [AIAA PAPER 89-0304] p 118 A89-25261
- Thermosolutal convection during dendritic solidification [AIAA PAPER 89-0626] p 118 A89-25495
- Flight hardware and tele-operations supporting the Isothermal Dendritic Growth Experiment aboard the Space Shuttle [AIAA PAPER 89-0863] p 118 A89-25627
- Ground-based simulation of telepresence for materials science experiments --- remote viewing and control of processes aboard Space Station [AIAA PAPER 89-0597] p 119 A89-28439
- Vapor condensation at a turbulent liquid surface in systems with possible space-based applications [AIAA PAPER 89-2846] p 151 A89-47122
- Effects of crucible wetting during solidification of immiscible Pb-Zn [NASA-TM-101372] p 120 N89-14341
- SPACE PROGRAMS**
- NASA's Chemical Transfer Propulsion Program for Pathfinder [NASA-TM-102298] p 41 N89-26876
- SPACE SHUTTLE MAIN ENGINE**
- An approximate methods approach to probabilistic structural analysis [AIAA PAPER 89-1369] p 193 A89-30844
- Structural tailoring of Space Shuttle Main Engine turbopump blades SSME/STAEBL p 55 A89-44106
- The development of power specific redlines for SSME safety monitoring [AIAA PAPER 89-2413] p 61 A89-53305
- Identification of Space Shuttle Main Engine dynamics p 61 A89-54068
- Simplified cyclic structural analysis of SSME turbine blades p 63 N89-12632
- Constitutive behavior of single crystal PWA 1480 and directionally solidified MAR-M 246 under monotonic and cyclic loads at high and low temperature p 100 N89-12634
- Mass flow meter using the triboelectric effect for measurement in cryogenics [NASA-CR-179572] p 155 N89-12836
- Heat flux measurements [NASA-TM-101428] p 173 N89-14418
- Fiber reinforced superalloys for rocket engines [NASA-TM-100880] p 86 N89-15990
- Identification of space shuttle main engine dynamics [NASA-TM-101982] p 66 N89-20199
- Advanced single crystal for SSME turbopumps [NASA-CR-182244] p 103 N89-21072
- The development of power specific redlines for SSME safety monitoring [NASA-CR-185121] p 41 N89-26027
- Probabilistic structural analysis methods of hot engine structures [NASA-TM-102091] p 205 N89-28030
- SPACE SHUTTLE ORBITERS**
- High angle-of-attack hypersonic aerodynamics p 2 A89-19918
- The plasma wake of the Shuttle Orbiter p 215 A89-43680
- A numerical model of electrodynamics of plasma within the contaminant gas cloud of the Space Shuttle Orbiter at low earth orbit p 233 A89-45631
- Plasma density, temperature and turbulence in the wake of the Shuttle Orbiter p 233 A89-53209
- Plasma density fluctuations observed during Space Shuttle Orbiter water releases p 233 A89-54759
- SPACE SHUTTLE PAYLOADS**
- Flight hardware and tele-operations supporting the Isothermal Dendritic Growth Experiment aboard the Space Shuttle [AIAA PAPER 89-0863] p 118 A89-25627
- Development of an infrared imaging system for the surface tension driven convection experiment [NASA-TM-101479] p 174 N89-17211
- The solid surface combustion space shuttle experiment hardware description and ground-based test results [NASA-TM-101963] p 123 N89-19446
- SPACE SHUTTLES**
- Expendable launch vehicle transportation for the space station [NASA-TM-101947] p 42 N89-20179
- Low frequency vibration isolation technology for microgravity space experiments [NASA-TM-101448] p 123 N89-20324
- SPACE STATION PAYLOADS**
- The modular combustion facility for the Space Station laboratory - A requirements and capabilities study [AIAA PAPER 89-0505] p 44 A89-28421

- Ground-based simulation of telepresence for materials science experiments --- remote viewing and control of processes aboard Space Station [AIAA PAPER 89-0597] p 119 A89-28439
- SPACE STATION POLAR PLATFORMS**
- Space Station Freedom electrical power system hardware commonality with the United States Polar Platform [NASA-TM-102074] p 69 N89-24439
- SPACE STATION POWER SUPPLIES**
- The Solar Dynamic radiator with a historical perspective p 51 A89-15340
- Cooperating expert systems for Space Station - Power/thermal subsystem testbeds p 38 A89-15350
- Space Station battery system design and development p 52 A89-15378
- Power components for the Space Station 20-kHz power distribution system p 130 A89-15387
- A new Space Station power system p 53 A89-20016
- Status of the Space Station power system p 54 A89-23281
- Densities of some molten fluoride salt mixtures suitable for heat storage in space power applications p 77 A89-41444
- Solar dynamic power for Space Station Freedom [IAF PAPER ICOSP89-4-1] p 55 A89-46517
- Space station electrical power system availability study [NASA-CR-182198] p 45 N89-11802
- Study of the generator/motor operation of induction machines in a high frequency link space power system [NASA-CR-179600] p 63 N89-11809
- Space station WP-04 power system preliminary analysis and design document, volume 3 [NASA-CR-179587-VOL-3] p 64 N89-15164
- A definition study of the on-orbit assembly operations for the outboard photovoltaic power modules for Space Station Freedom [NASA-TM-102006] p 41 N89-20171
- Numerical model of solar dynamic radiator for parametric analysis [NASA-TM-102054] p 67 N89-22653
- Solar dynamic power for space station freedom [NASA-TM-102016] p 67 N89-23516
- Comprehensive report of aeropropulsion, space propulsion, space power, and space science applications of the Lewis Research Center [NASA-TM-100925] p 238 N89-24216
- Review of the environmental effects of the Space Station Freedom photovoltaic power module [NASA-TM-102076] p 46 N89-24418
- Energy storage and thermal control system design status [NASA-TM-102136] p 46 N89-24427
- Concentration of off-axis radiation by solar concentrators for space power [NASA-TM-102052] p 69 N89-24438
- Space Station Freedom Solar Array design development [NASA-TM-102105] p 70 N89-24448
- Solar dynamic power module design [NASA-TM-102055] p 70 N89-25269
- Space Station Freedom photovoltaic power module design status [NASA-TM-102073] p 71 N89-25273
- Challenges for future space power systems [NASA-TM-102063] p 214 N89-25506
- Space Station Freedom power management and distribution system design [NASA-TM-102283] p 73 N89-26045
- Performance estimates for the Space Station power system Brayton Cycle compressor and turbine [NASA-CR-182263] p 73 N89-26903
- Development and refinement of test bed simulations [NASA-TM-102335] p 75 N89-27702
- Evolutionary growth for Space Station Freedom electrical power system [NASA-TM-102339] p 76 N89-28570
- SPACE STATION PROPULSION**
- Space station auxiliary thrust chamber technology [NASA-CR-179650] p 46 N89-11803
- SPACE STATION STRUCTURES**
- Induced emission of radiation from a large space-station-like structure in the ionosphere p 44 A89-31915
- Oxidation and protection of fiberglass-epoxy composite masts for photovoltaic arrays in the low earth orbital environment p 44 A89-35316
- Space station WP-04 power system preliminary analysis and design document, volume 3 [NASA-CR-179587-VOL-3] p 64 N89-15164
- A definition study of the on-orbit assembly operations for the outboard photovoltaic power modules for Space Station Freedom [NASA-TM-102006] p 41 N89-20171



Solar dynamic power module design  
[NASA-TM-102055] p 70 N89-25269

Space Station Freedom photovoltaic power module design status  
[NASA-TM-102073] p 71 N89-25273

**SPACE STATIONS**

Robots for manipulation in a micro-gravity environment p 215 A89-11682

Space Station power system requirements p 50 A89-15295

An integrated and modular digital modeling approach for the Space Station electrical power system development p 50 A89-15298

Simulation test beds for the Space Station electrical power system p 39 A89-15352

Multi-hundred kilowatt roll ring assembly evaluation results --- for Space Station power transmission p 123 A89-15388

Ray tracing optical analysis of offset solar collector for Space Station solar dynamic system p 53 A89-15416

GaAs MMIC elements in phased-array antennas p 131 A89-15827

Expendable launch vehicle transportation for the Space Station

[IAF PAPER 88-198] p 42 A89-17720

An analysis of possible advanced space strategies featuring the role of space resource utilization

[IAF PAPER 88-587] p 37 A89-17861

Performance characterizations of an engineering model multipropellant resistojel p 54 A89-28340

The impact of an IVA robot on the Space Station microgravity environment

[AIAA PAPER 89-0596] p 44 A89-28438

Photovoltaic power modules for NASA's manned Space Station p 55 A89-29122

Free-vibration characteristics and correlation of a Space Station split-blanket solar array

[AIAA PAPER 89-1252] p 44 A89-30737

Low earth orbital atomic oxygen simulation for materials durability evaluation p 45 A89-51123

The solar dynamic radiator with a historical perspective

[NASA-TM-100972] p 45 N89-10117

Power considerations for an early manned Mars mission utilizing the space station

[NASA-TM-101436] p 63 N89-13492

Solar dynamic heat rejection technology. Task 1: System concept development

[NASA-CR-179618] p 158 N89-13731

Power systems facility

[NASA-TM-101447] p 40 N89-14247

Free-vibration characteristics and correlation of a space station split-blanket solar array

[NASA-TM-101452] p 198 N89-15438

Expendable launch vehicle transportation for the space station

[NASA-TM-101947] p 42 N89-20179

User needs, benefits and integration of robotic systems in a space station laboratory

[NASA-CR-182261] p 185 N89-22108

Expert systems applied to spacecraft fire safety

[NASA-CR-182266] p 42 N89-23501

Energy storage and thermal control system design status

[NASA-TM-102136] p 46 N89-24427

Space Station Freedom electrical power system hardware commonality with the United States Polar Platform

[NASA-TM-102074] p 69 N89-24439

Launch packaging options for the photovoltaic power module cargo element

[NASA-TM-102072] p 71 N89-25275

Development and testing of a 20-kHz component test bed

[NASA-TM-102141] p 139 N89-25403

Space Station Freedom power management and distribution system design

[NASA-TM-102283] p 73 N89-26045

Comparative thermal analysis of the space station Freedom photovoltaic deployable boom structure using TRASYS, NEVADA, and SINDA programs

[NASA-TM-102062] p 165 N89-26177

Photovoltaic module on-orbit assembly for Space Station Freedom

[NASA-TM-102297] p 47 N89-26887

Space station hydrogen/oxygen thruster technology

[NASA-CR-182280] p 74 N89-26905

Evolutionary growth for Space Station Freedom electrical power system

[NASA-TM-102339] p 76 N89-28570

**SPACE TRANSPORTATION**

Extended SP-100 reactor power systems capability p 52 A89-15392

Expendable launch vehicle transportation for the Space Station

[IAF PAPER 88-198] p 42 A89-17720

NASA's Chemical Transfer Propulsion Program for Pathfinder

[AIAA PAPER 89-2298] p 37 A89-46735

Advanced technology for future space propulsion systems

[NASA-TM-101951] p 66 N89-20192

**SPACE TRANSPORTATION SYSTEM**

Launch packaging options for the photovoltaic power module cargo element

[NASA-TM-102072] p 71 N89-25275

**SPACEBORNE EXPERIMENTS**

Coherent Cerenkov radiation from the Spacelab 2 electron beam p 231 A89-24292

Flight hardware and tele-operations supporting the Isothermal Dendritic Growth Experiment aboard the Space Shuttle

[AIAA PAPER 89-0863] p 118 A89-25627

Droplet combustion drop tower tests using models of the space flight apparatus

[AIAA PAPER 89-0501] p 119 A89-28418

The solid surface combustion Space Shuttle experiment hardware description and ground-based test results

[AIAA PAPER 89-0503] p 119 A89-28419

Ground-based simulation of telepresence for materials science experiments --- remote viewing and control of processes aboard Space Station

[AIAA PAPER 89-0597] p 119 A89-28439

A facility for precise temperature control applications in microgravity p 48 A89-36956

COLD-SAT orbital experiment configured for Atlas launch p 45 A89-53327

Plasma density fluctuations observed during Space Shuttle Orbiter water releases p 233 A89-54759

Development of an infrared imaging system for the surface tension driven convection experiment

[NASA-TM-101479] p 174 N89-17211

The solid surface combustion space shuttle experiment hardware description and ground-based test results

[NASA-TM-101963] p 123 N89-19446

Infrared surface temperature measurements for the surface tension driven convection experiment

[NASA-TM-101353] p 175 N89-21224

Flight experiment of thermal energy storage

[NASA-TM-102081] p 69 N89-24440

COLD-SAT: A technology satellite for cryogenic experimentation

[NASA-TM-102286] p 47 N89-26036

COLD-SAT: An orbital cryogenic hydrogen technology experiment

[NASA-TM-102303] p 73 N89-26044

**SPACEBORNE LASERS**

A laser communication experiment utilizing the ACT satellite and an airborne laser transceiver

[NASA-TM-101581] p 43 A89-15811

**SPACECRAFT ANTENNAS**

Mechanical properties characterization of composite sandwich materials intended for space antenna applications p 81 A89-32885

**SPACECRAFT CHARGING**

Large structure current collection in plasma environments

[AIAA PAPER 89-0496] p 44 A89-25405

Plasma contacting - An enabling technology

[AIAA PAPER 89-0677] p 231 A89-25537

Induced emission of radiation from a large space-station-like structure in the ionosphere

[NASA-TM-101915] p 44 A89-31915

On the need for space tests of plasma contactors as electron collectors p 232 A89-43356

Surface phenomena in plasma environments p 234 N89-23555

**SPACECRAFT COMPONENTS**

Identification of structural interface characteristics using component mode synthesis p 193 A89-36177

The NASA atomic oxygen effects test program p 93 N89-12589

**SPACECRAFT CONFIGURATIONS**

Nuclear reactor power as applied to a space-based radar mission p 51 A89-15317

Status of the Space Station power system p 54 A89-23281

**SPACECRAFT CONSTRUCTION MATERIALS**

Low earth orbital atomic oxygen simulation for materials durability evaluation p 45 A89-51123

Aeronautical applications of high-temperature superconductors

[AIAA PAPER 89-2142] p 23 A89-53304

The NASA atomic oxygen effects test program p 93 N89-12589

Stability of bulk Ba<sub>2</sub>YCu<sub>3</sub>O<sub>7-x</sub> in a variety of environments

[NASA-TM-101401] p 111 N89-14310

Overview of environmental factors p 240 N89-23529

Atomic oxygen effects on materials p 78 N89-23540

Aeronautical applications of high-temperature superconductors

[NASA-TM-102311] p 33 N89-26008

Fatigue crack growth study of SCS6/Ti-15-3 composite

[NASA-TM-102332] p 104 N89-26989

**SPACECRAFT CONTROL**

Modal representations in control/structure interaction p 45 A89-54114

**SPACECRAFT DESIGN**

Status of the Space Station power system p 54 A89-23281

Weight savings in aerospace vehicles through propellant scavenging

[SAWE PAPER 1818] p 40 A89-50814

Aeronautical applications of high-temperature superconductors

[AIAA PAPER 89-2142] p 23 A89-53304

HASA: Hypersonic Aerospace Sizing Analysis for the preliminary design of aerospace vehicles

[NASA-CR-182226] p 18 N89-15107

Numerical model of solar dynamic radiator for parametric analysis

[NASA-TM-102054] p 67 N89-22653

Solar dynamic power module design

[NASA-TM-102055] p 70 N89-25269

Aeronautical applications of high-temperature superconductors

[NASA-TM-102311] p 33 N89-26008

Evolutionary growth for Space Station Freedom electrical power system

[NASA-TM-102339] p 76 N89-28570

**SPACECRAFT ENVIRONMENTS**

The NASA atomic oxygen effects test program p 93 N89-12589

**SPACECRAFT EQUIPMENT**

Development of a 39.5 GHz Karp traveling wave tube for use in space

[NASA-CR-182182] p 136 N89-15336

Development of a 75-watt 60-GHz traveling-wave tube for intersatellite communications

[NASA-CR-182135] p 138 N89-24530

**SPACECRAFT GUIDANCE**

Optimal terminal maneuver for a cooperative impulsive rendezvous p 38 A89-36946

**SPACECRAFT LAUNCHING**

Space reactor assessment and validation study p 230 N89-13227

**SPACECRAFT MODULES**

The modular combustion facility for the Space Station laboratory - A requirements and capabilities study

[AIAA PAPER 89-0505] p 44 A89-28421

**SPACECRAFT POWER SUPPLIES**

Progress toward the evolution of a Stirling Space Engine

[SAE PAPER 880545] p 48 A89-12305

Status of several Stirling loss characterization efforts and their significance for Stirling space power development p 49 A89-15187

The design and fabrication of a Stirling engine heat exchanger module with an integral heat pipe p 142 A89-15190

NASA Aerospace Flight Battery Systems Program - Issues and actions p 49 A89-15224

Energy storage considerations for a robotic Mars surface sampler p 49 A89-15267

Effect of LEO cycling at shallow depths of discharge on MANTECH IPV nickel-hydrogen cells p 49 A89-15278

The application of high temperature superconductors to space electrical power distribution components p 50 A89-15287

An integrated and modular digital modeling approach for the Space Station electrical power system development p 50 A89-15298

Nuclear reactor power as applied to a space-based radar mission p 51 A89-15317

Systems aspects of a space nuclear reactor power system p 51 A89-15327

Advanced space solar dynamic receivers p 52 A89-15343

Simulation test beds for the Space Station electrical power system p 39 A89-15352

Simulation and control of a 20 kHz spacecraft power system p 130 A89-15391

Advanced sensible heat solar receiver for space power p 52 A89-15415

Photovoltaics for high capacity space power systems

[IAF PAPER 88-221] p 53 A89-17730

KOH concentration effect on cycle life of nickel-hydrogen cells. III - Cycle life test p 207 A89-23283

Theoretical performance of hydrogen-bromine rechargeable SPE fuel cell --- Solid Polymer Electrolyte p 207 A89-23290

Thermal analysis of heat storage canisters for a solar dynamic, space power system p 54 A89-29113

## SPACECRAFT PROPULSION

Evaluation of alternative phase change materials for energy storage in solar dynamic applications p 208 A89-29114

Advanced solar receivers for space power p 54 A89-29116

SPRE 1 free-piston Stirling engine testing at NASA Lewis Research Center p 55 A89-29120

Photovoltaic power modules for NASA's manned Space Station p 55 A89-29122

Low earth orbit environmental effects on the Space Station photovoltaic power generation systems p 55 A89-29123

Power systems for production, construction, life support, and operations in space p 37 A89-45803

Advances in thin-film solar cells for lightweight space photovoltaic power [IAF PAPER ICOSP89-1-8] p 55 A89-46513

Free-piston Stirling technology for space power [IAF PAPER ICOSP89-5-7] p 56 A89-46520

Preliminary assessment of rover power systems for the Mars Rover Sample Return Mission [IAF PAPER ICOSP89-9-6] p 39 A89-46530

Space solar cell research p 208 A89-52203

Thin film coatings for space electrical power system applications p 77 A89-53324

Photovoltaics for high capacity space power systems [NASA-TM-101341] p 61 A89-10122

Identification of high performance and component technology for space electrical power systems for use beyond the year 2000 p 62 A89-11807

InP homojunction solar cell performance on the LIPS 3 flight experiment [NASA-TM-101390] p 209 A89-12123

Space reactor assessment and validation study p 230 A89-13227

Power considerations for an early manned Mars mission utilizing the space station [NASA-TM-101436] p 63 A89-13492

Power systems facility [NASA-TM-101447] p 40 A89-14247

Issues and opportunities in space photovoltaics [NASA-TM-101425] p 65 A89-15171

Advanced heat receiver conceptual design study [NASA-CR-182177] p 209 A89-16224

NASA photovoltaic research and technology [NASA-TM-101422] p 65 A89-16917

Free-piston Stirling technology for space power [NASA-TM-101956] p 66 A89-20194

Megawatt Class Nuclear Space Power Systems (MCNSPS) conceptual design and evaluation report. Volume 3, technologies 2: Power conversion [NASA-CR-179614-VOL-3] p 211 A89-22980

Megawatt Class Nuclear Space Power Systems (MCNSPS) conceptual design and evaluation report. Volume 2, technologies 1: Reactors, heat transport, integration issues [NASA-CR-179614-VOL-2] p 211 A89-22981

Preliminary assessment of rover power systems for the Mars Rover Sample Return Mission [NASA-TM-102003] p 68 A89-23518

Results from baseline tests of the SPRE 1 and comparison with code model predictions p 68 A89-23527

[NASA-TM-102044] p 68 A89-23527

Comprehensive report of aeropropulsion, space propulsion, space power, and space science applications of the Lewis Research Center [NASA-TM-100925] p 238 A89-24216

Summary and evaluation of the Strategic Defense Initiative Space Power Architecture Study [NASA-TM-102012] p 69 A89-24443

Space Photovoltaic Research and Technology, 1988. High Efficiency, Space Environment, and Array Technology [NASA-CP-3030] p 212 A89-24704

Progress in indium phosphide solar cell research p 212 A89-24707

Ultra-thin, light-trapping silicon solar cells p 213 A89-24719

Domed Fresnel lens concentrator technology for space application p 213 A89-24732

Launch packaging options for the photovoltaic power module cargo element [NASA-TM-102072] p 71 A89-25275

Development and testing of a 20-kHz component test bed [NASA-TM-102141] p 139 A89-25403

Challenges for future space power systems [NASA-TM-102063] p 214 A89-25506

Frequency domain model for analysis of paralleled, series-output-connected Mapham inverters [NASA-TM-102140] p 139 A89-26149

Liquid droplet generation [NASA-CR-182246] p 166 A89-26182

Comparison of conceptual designs for 25 kWe advanced Stirling conversion systems for dish electric application [NASA-TM-102085] p 239 A89-26781

Toward an electrical power utility for space exploration [NASA-TM-102347] p 75 A89-27704

NASA advanced space photovoltaic technology-status, potential and future mission applications [NASA-TM-102093] p 75 A89-27705

A program for advancing the technology of space concentrators [NASA-TM-102139] p 76 A89-29484

### SPACECRAFT PROPULSION

Performance of 10-kW class xenon ion thrusters [AIAA PAPER 88-2914] p 48 A89-14978

Nuclear reactor power as applied to a space-based radar mission p 51 A89-15317

Space 2010 --- Space Station Freedom future explorations p 77 A89-23028

Model for computing volume-averaged plasma properties in electron-bombardment ion thrusters p 54 A89-28339

Probabilistic constitutive relationships for material strength degradation models [AIAA PAPER 89-1368] p 192 A89-30843

NASA's Chemical Transfer Propulsion Program for Pathfinder p 37 A89-46735

[AIAA PAPER 89-2298] p 37 A89-46735

Miniature multiple-function probe for OTV turbopump health monitoring [AIAA PAPER 89-2303] p 56 A89-46736

User interactive electric propulsion software design [AIAA PAPER 89-2376] p 57 A89-46783

Advanced H<sub>2</sub>/O<sub>2</sub> space engine parametrics [AIAA PAPER 89-2300] p 57 A89-46855

Performance of a 100 kW class applied field MPD thruster [AIAA PAPER 89-2710] p 57 A89-47035

Plasma flow processes within magnetic nozzle configurations [AIAA PAPER 89-2711] p 57 A89-47036

A 50 cm diameter annular ion engine [AIAA PAPER 89-2716] p 57 A89-47039

Ion optics for high power 50-cm-dia ion thrusters [AIAA PAPER 89-2717] p 58 A89-47040

Thermal mechanical analyses of large diameter ion accelerator systems [AIAA PAPER 89-2718] p 58 A89-47041

The effect of electrode configuration on arcjet performance [AIAA PAPER 89-2722] p 58 A89-47044

Design of a thrust stand for high power electric propulsion devices [AIAA PAPER 89-2829] p 39 A89-47110

Investigation of a liquid-fed water resistojel plume [AIAA PAPER 89-2840] p 58 A89-47117

Experiments and analysis of a compact electrothermal thruster p 59 A89-47494

Heat transfer in aerospace propulsion p 153 A89-53282

Preliminary design study of hydrogen and ammonia resistojets for prime and auxiliary thrusters [NASA-CR-182176] p 62 A89-10943

Space propulsion technology and cryogenic fluid depot p 38 A89-11768

Advanced technology for future space propulsion systems [NASA-TM-101951] p 66 A89-20192

Comprehensive report of aeropropulsion, space propulsion, space power, and space science applications of the Lewis Research Center [NASA-TM-100925] p 238 A89-24216

The Pathfinder Chemical Transfer Propulsion program [NASA-TM-102084] p 41 A89-24409

Performance of large area xenon ion thrusters for orbit transfer missions [NASA-TM-102049] p 69 A89-24436

Advanced APS impacts on vehicle payloads [NASA-TM-102086] p 41 A89-25254

NASA's Chemical Transfer Propulsion Program for Pathfinder [NASA-TM-102298] p 41 A89-26876

Development of a high power microwave thruster, with a magnetic nozzle, for space applications [NASA-TM-102321] p 74 A89-26904

Space station hydrogen/oxygen thruster technology [NASA-CR-182280] p 74 A89-26905

Electric propulsion options for 10 kW class earth space missions [NASA-TM-102337] p 74 A89-26906

Experiments and analysis of a compact electrothermal thruster p 75 A89-27773

Ion optics for high power 50-cm-dia ion thrusters [NASA-TM-102143] p 76 A89-28571

### SPACECRAFT RADIATORS

Moving Belt Radiator technology issues p 49 A89-15208

The Solar Dynamic radiator with a historical perspective p 51 A89-15340

Big savings from small holes --- Liquid Droplet Radiator project for space vehicles p 45 A89-36724

Gas particle radiator [NASA-CASE-LEW-14297-1] p 172 A89-12048

Liquid sheet radiator apparatus [NASA-CASE-LEW-14295-1] p 123 A89-14348

The emittance of space radiator materials measured at elevated temperatures p 66 A89-20193

[NASA-TM-101948] p 66 A89-20193

Numerical model of solar dynamic radiator for parametric analysis p 67 A89-22653

[NASA-TM-102054] p 67 A89-22653

Scaling results for the Liquid Sheet Radiator (LSR) [NASA-TM-102100] p 72 A89-25277

Two-tiered design analysis of a radiator for a solar dynamic powered Stirling engine [NASA-CR-182301] p 46 A89-26031

Liquid droplet generation [NASA-CR-182246] p 166 A89-26182

### SPACECRAFT STRUCTURES

Simulation of the low earth orbital atomic oxygen interaction with materials by means of an oxygen ion beam [NASA-TM-101971] p 114 A89-21104

### SPACECRAFT SURVIVABILITY

Fire behavior and risk analysis in spacecraft [NASA-TM-100944] p 42 A89-10111

### SPACECRAFT TEMPERATURE

Big savings from small holes --- Liquid Droplet Radiator project for space vehicles p 45 A89-36724

### SPACELAB PAYLOADS

The plasma wake of the Shuttle Orbiter p 215 A89-43680

Plasma density fluctuations observed during Space Shuttle Orbiter water releases p 233 A89-54759

### SPALLING

The effect of 0.1 atomic percent zirconium on the cyclic oxidation behavior of beta-NiAl for 300 hours at 1200 C [NASA-TM-101408] p 101 A89-13566

### SPATIAL RESOLUTION

Spatial resolution and downwash velocity corrections for multiple-hole pressure probes in complex flows p 171 A89-45909

External electro-optic probing of millimeter-wave integrated circuits [NASA-TM-101990] p 128 A89-21142

### SPECIFIC IMPULSE

Performance characterization and transient investigation of multipropellant resistojets [AIAA PAPER 89-2837] p 60 A89-50811

Design, fabrication and test of the RL10 derivative II chamber/primary nozzle [NASA-CR-179595] p 68 A89-23519

Performance characterization and transient investigation of multipropellant resistojets [NASA-TM-102118] p 72 A89-25283

### SPECKLE INTERFEROMETRY

Summary of laser speckle photogrammetry for HOST p 177 A89-12889

Speckle interferometry using fiber optic phase stepping [NASA-TM-102331] p 176 A89-27999

### SPECKLE PATTERNS

Summary of laser speckle photogrammetry for HOST p 177 A89-12889

Two-dimensional high temperature optical strain measurement system, phase 2 [NASA-CR-185116] p 176 A89-26218

### SPECTRAL METHODS

Global properties of pseudospectral methods p 221 A89-37746

### SPECTROMETERS

Performance of the forward scattering spectrometer probe in NASA's Icing Research Tunnel [AIAA PAPER 89-0769] p 169 A89-25570

An improved correction algorithm for number density measurements made with the forward scattering spectrometer probe p 170 A89-44122

A correction algorithm for particle size distribution measurements made with the forward-scattering spectrometer probe p 170 A89-44123

Performance of the forward scattering spectrometer probe in NASA's icing research tunnel [NASA-TM-101381] p 172 A89-12845

### SPECTROSCOPIC ANALYSIS

Thin-film hermeticity - A quantitative analysis of diamondlike carbon using variable angle spectroscopic ellipsometry p 234 A89-13945

### SPECTROSCOPY

Deep-level transient spectroscopy of Al(x)Ga(1-x)As/GaAs using nondestructive acousto-electric voltage measurement p 133 A89-42742

## SPECTRUM ANALYSIS

Fiber-optic temperature sensor using a spectrum-modulating semiconductor etalon p 168 A89-10366

## SPHERES

Observations of the frequencies in a sphere wake and of drag increase by acoustic excitation p 142 A89-16884

Fresnel diffraction by spherical obstacles p 231 A89-48249

High-temperature LDV seed particle development [NASA-CR-182265] p 175 N89-23851

## SPINEL

Oxygen electrode bifunctional electrocatalyst NiCo<sub>2</sub>O<sub>4</sub> spinel [NASA-TM-100947] p 208 N89-10409

## SPLINE FUNCTIONS

Efficient numerical simulation of a one-dimensional electrothermal deicer pad p 144 A89-22811

Solution of three-dimensional flow problems using a flux-spline method [AIAA PAPER 89-0687] p 146 A89-25543

## SPRAYED COATINGS

Acoustic emission evaluation of plasma-sprayed thermal barrier coatings p 178 A89-12751

High resolution video monitoring of coating thickness during plasma spraying [NASA-TM-101423] p 102 N89-15218

Thermal barrier coating life-prediction model development p 200 N89-17331

Thermal barrier coating life prediction model development p 200 N89-17333

## SPREAD SPECTRUM TRANSMISSION

Coded multiple chirp spread spectrum system and overlay service p 124 A89-26769

Study of spread spectrum multiple access systems for satellite communications with overlay on current services: Executive summary [NASA-CR-180827-EXEC-SUMM] p 128 N89-23756

Study of spread spectrum multiple access systems for satellite communications with overlay on current services [NASA-CR-180827] p 128 N89-23757

## SPUTTERING

Ion beam and plasma methods of producing diamondlike carbon films [NASA-TM-102301] p 116 N89-27836

## SQUARE WAVES

Universal limiter for high order explicit conservative advection schemes p 151 A89-45398

## STABILITY

Stability of a rigid rotor supported on oil-film journal bearings under dynamic load [NASA-TM-102309] p 166 N89-27114

## STAGNATION FLOW

Correlations of velocity and temperature fluctuations in the stagnation-point flow of circular cylinder in turbulent flow p 148 A89-34927

Effects of wake passing on stagnation region heat transfer p 148 A89-34928

## STAINLESS STEELS

Creep life prediction based on stochastic model of microstructurally short crack growth p 193 A89-36185

Results of inphase axial-torsional fatigue experiments on 304 stainless steel [NASA-TM-101464] p 201 N89-20514

Reaction of perfluoroalkylpolyethers (PFPE) with 440C steel in vacuum under sliding conditions at room temperature [NASA-TP-2883] p 115 N89-26091

## STANDARDS

High speed balancing applied to the T700 engine [NASA-CR-180899] p 184 N89-20472

## STARTING

Starting characteristics of direct current motors powered by solar cells [NASA-TM-101981] p 136 N89-19493

## STATIC LOADS

Simplified procedures for designing adhesively bonded composite joints [NASA-TM-102120] p 87 N89-26048

## STATIC PRESSURE

Flowfield measurements in the NASA Lewis Research Center 9- by 15-foot low-speed wind tunnel [NASA-TM-100883] p 36 N89-21002

## STATOR BLADES

Explicit Runge-Kutta method for unsteady rotor/stator interaction p 5 A89-36912

Three component laser anemometer measurements in an annular cascade of core turbine vanes with contoured end wall [NASA-TP-2846] p 9 N89-10844

## STATORS

Experimental results for labyrinth gas seals with honeycomb stators - Comparisons to smooth-stator seals and theoretical predictions [ASME PAPER 88-TRIB-40] p 179 A89-24992

An unconditionally stable Runge-Kutta method for unsteady flows [AIAA PAPER 89-0205] p 2 A89-25180

Piezoelectric pushers for active vibration control of rotating machinery p 171 A89-47717

HOST turbine heat transfer subproject overview p 25 N89-12880

Turbine stator flow field simulations p 157 N89-12902

The effects of inlet turbulence and rotor/stator interactions on the aerodynamics and heat transfer of a large-scale rotating turbine model, volume 1 [NASA-CR-4079] p 159 N89-13756

Experimental determination of stator endwall heat transfer [NASA-TM-101419] p 159 N89-15366

## STEADY FLOW

Status of several Stirling loss characterization efforts and their significance for Stirling space power development p 49 A89-15187

Simple high-accuracy resolution program for convective modelling of discontinuities p 143 A89-17459

Advanced development of the boundary element method for steady-state heat conduction p 154 A89-54766

Conservative treatment of boundary interfaces for overlaid grids and multi-level grid adaptations [NASA-TM-102080] p 15 N89-24269

A model for prediction of STOVLE ejector dynamics [NASA-TM-102098] p 32 N89-24319

## STEADY STATE

Steady-state thermal-solutal diffusion in a float zone p 119 A89-40897

Summary and evaluation of the Strategic Defense Initiative Space Power Architecture Study [NASA-TM-102012] p 69 N89-24443

## STEELS

Analysis of microalloy precipitate reversion in steels p 94 A89-15108

Surface fatigue life of carburized and hardened M50NiL and AISI 9310 spur gears and rolling-contact test bars [AIAA PAPER 89-2819] p 180 A89-47105

Selection of rolling-element bearing steels for long-life applications p 180 A89-47250

Surface fatigue life of carburized and hardened M50NiL and AISI 9310 spur gears and rolling-contact test bars [NASA-TM-101979] p 185 N89-22111

## STELLAR ENVELOPES

Formation of polycyclic aromatic hydrocarbons in circumstellar envelopes p 241 A89-41385

## STELLAR EVOLUTION

Superheavy magnetic monopoles and main-sequence stars p 240 A89-20377

## STELLAR INTERIORS

Superheavy magnetic monopoles and main-sequence stars p 240 A89-20377

## STIFFNESS

Tailoring of composite links for optimal damped elasto-dynamic performance [NASA-TM-102094] p 88 N89-26912

## STIRLING CYCLE

Hot piston ring/cylinder liner materials - Selection and evaluation [SAE PAPER 880544] p 178 A89-12304

Free-piston Stirling technology for space power [IAF PAPER ICOSP89-5-7] p 56 A89-46520

RE-1000 free-piston Stirling engine sensitivity test results [NASA-TM-88846] p 210 N89-19737

Free-piston Stirling technology for space power [NASA-TM-101956] p 66 N89-20194

Initial characterization of a modular heat exchanger with an integral heat pipe [NASA-TM-102097] p 239 N89-25078

Comparison of conceptual designs for 25 kW advanced Stirling conversion systems for dish electric application [NASA-TM-102085] p 239 N89-26781

Thermal evaluation of advanced solar dynamic heat receiver performance [NASA-CR-185117] p 214 N89-27256

## STIRLING ENGINES

Mod II Stirling engine overviews [SAE PAPER 880539] p 177 A89-12301

Alternative fuel capabilities of the Mod II Stirling vehicle [SAE PAPER 880543] p 177 A89-12303

Progress toward the evolution of a Stirling Space Engine [SAE PAPER 880545] p 48 A89-12305

Status of several Stirling loss characterization efforts and their significance for Stirling space power development p 49 A89-15187

Description of an oscillating flow pressure drop test rig p 142 A89-15188

Effect of transition on oscillation flow losses in Stirling engine coolers and heaters p 142 A89-15189

The design and fabrication of a Stirling engine heat exchanger module with an integral heat pipe p 142 A89-15190

SPRE 1 free-piston Stirling engine testing at NASA Lewis Research Center p 55 A89-29120

Free-piston Stirling technology for space power [IAF PAPER ICOSP89-5-7] p 56 A89-46520

Materials technology assessment for a 1050 K Stirling space engine design [NASA-TM-101342] p 77 N89-11815

Conceptual design of an advanced Stirling conversion system for terrestrial power generation [NASA-CR-180890] p 238 N89-12504

The 25 kW solar thermal Stirling hydraulic engine system: Conceptual design [NASA-CR-180889] p 239 N89-14182

Megawatt Class Nuclear Space Power Systems (MCNPS) conceptual design and evaluation report. Volume 4: Concepts selection, conceptual designs, recommendations [NASA-CR-179614-VOL-4] p 210 N89-18967

RE-1000 free-piston Stirling engine sensitivity test results [NASA-TM-88846] p 210 N89-19737

Free-piston Stirling technology for space power [NASA-TM-101956] p 66 N89-20194

Failure analysis of a Stirling engine heat pipe [NASA-TM-101418] p 103 N89-20227

Megawatt Class Nuclear Space Power Systems (MCNPS) conceptual design and evaluation report. Volume 3: technologies 2: Power conversion [NASA-CR-179614-VOL-3] p 211 N89-22980

Results from baseline tests of the SPRE 1 and comparison with code model predictions [NASA-TM-102044] p 68 N89-23527

Two-dimensional numerical simulation of a Stirling engine heat exchanger [NASA-TM-102057] p 164 N89-23823

On the dynamic response of pressure transmission lines in the research of helium-charged free piston Stirling engines [NASA-TM-102121] p 175 N89-24593

NASA Lewis Stirling engine computer code evaluation [NASA-CR-182248] p 214 N89-24741

Initial characterization of a modular heat exchanger with an integral heat pipe [NASA-TM-102097] p 239 N89-25078

CSTI High Capacity Power [NASA-TM-102059] p 72 N89-25282

Two-tiered design analysis of a radiator for a solar dynamic powered Stirling engine [NASA-CR-182301] p 46 N89-26031

Comparison of conceptual designs for 25 kW advanced Stirling conversion systems for dish electric application [NASA-TM-102085] p 239 N89-26781

STOCHASTIC PROCESSES

Observer design for compensation of network-induced delays in integrated communication and control systems p 220 A89-35044

Stochastic modeling of crack initiation and short-crack growth under creep and creep-fatigue conditions [NASA-TM-101358] p 199 N89-17286

## STOKES FLOW

Use of a generalized Stokes number to determine the aerodynamic capture efficiency of non-Stokesian particles from a compressible gas flow p 140 A89-12336

Least-squares finite elements for Stokes problem [NASA-TM-101308] p 222 N89-22392

STOKES THEOREM (VECTOR CALCULUS)

Least-squares finite elements for Stokes problem [NASA-TM-101308] p 222 N89-22392

## STORAGE BATTERIES

Space Station battery system design and development p 52 A89-15378

Small scale bipolar nickel-hydrogen testing p 208 A89-44005

Cryogenic reactant storage for lunar base regenerative fuel cells [NASA-TM-101980] p 210 N89-21419

Space Electrochemical Research and Technology Conference: Abstracts [NASA-CP-10029] p 211 N89-22982

## STORAGE STABILITY

Nickel-hydrogen capacity loss on storage p 138 N89-23007

## STRAIN ENERGY METHODS

A Monte Carlo-finite element model for strain energy controlled microstructural evolution - 'Rafting' in superalloys p 96 A89-24358

- Graphical postprocessing for 3-D mesh quality evaluation p 217 A89-38846
- STRAIN ENERGY RELEASE RATE**
- Sublimate- or ply-level analysis of composites and strain energy release rates of end-notch and mixed-mode fracture specimens p 190 A89-16279
- Fracture toughness computational simulation of general delaminations in fiber composites [NASA-TM-101415] p 85 N89-13521
- Analysis of interface crack branching [NASA-CR-182273] p 202 N89-21265
- STRAIN GAGES**
- The dual element method of strain gauge temperature compensation p 169 A89-12276
- High temperature optical strain measurement system p 170 A89-43842
- Elevated temperature strain gages p 173 N89-12886
- Development of a high temperature static strain sensor p 173 N89-12887
- The NASA Lewis Strain Gauge Laboratory: An update p 173 N89-12888
- Development of a high temperature thin film static strain gage p 174 N89-17299
- Progress on a PdCr wire strain gage p 174 N89-17301
- Advanced high temperature instrument for hot section research applications p 29 N89-20137
- Two-dimensional high temperature optical strain measurement system, phase 2 [NASA-CR-185116] p 176 N89-26218
- STRAIN MEASUREMENT**
- The dual element method of strain gauge temperature compensation p 169 A89-12276
- Biaxial thermo-mechanical fatigue p 194 A89-43527
- High pressure multiaxial extensometry p 170 A89-43532
- High temperature optical strain measurement system p 170 A89-43842
- Strain measurements in a rotary engine housing [SAE PAPER 890333] p 181 A89-51493
- Sensors for ceramic components in advanced propulsion systems: Summary of literature survey and concept analysis, task 3 report [NASA-CR-180900] p 172 N89-11192
- Elevated temperature strain gages p 173 N89-12886
- Development of a high temperature static strain sensor p 173 N89-12887
- The NASA Lewis Strain Gauge Laboratory: An update p 173 N89-12888
- High temperature stress-strain analysis p 196 N89-12913
- Progress on a PdCr wire strain gage p 174 N89-17301
- Advanced high temperature instrument for hot section research applications p 29 N89-20137
- Two-dimensional high temperature optical strain measurement system, phase 2 [NASA-CR-185116] p 176 N89-26218
- STRAIN RATE**
- 1200 to 1400 K slow strain rate compressive behavior of small grain size NiAl/Ni<sub>2</sub>AlTi alloys and NiAl/Ni<sub>2</sub>AlTi-TiB<sub>2</sub> composites p 99 A89-53497
- Use of inelastic strain as a basis for analyzing thermomechanical test data p 200 N89-17326
- Procedures for characterizing an alloy and predicting cyclic life with the total strain version of Strainrange Partitioning [NASA-TM-4102] p 203 N89-25485
- Refinements in a viscoplastic model [NASA-TM-102338] p 205 N89-28036
- STRATIFIED FLOW**
- Regressed relations for forced convection heat transfer in a direct injection stratified charge rotary engine [SAE PAPER 880626] p 178 A89-12308
- STRESS ANALYSIS**
- Aeroelastic response of metallic and composite propfan models in yawed flow [AIAA PAPER 88-3154] p 20 A89-17942
- Finite element substructuring methods for composite mechanics p 80 A89-26291
- Weibull crack density coefficient for polydimensional stress states p 193 A89-34849
- A high heat flux experiment for verification of thermostructural analysis p 148 A89-35002
- A high heat flux experiment for verification of thermostructural analysis [NASA-TM-100931] p 155 N89-12026
- On 3D inelastic analysis methods for hot section components p 196 N89-12906
- Component specific modeling p 25 N89-12907
- A multiaxial theory of viscoplasticity for isotropic materials p 196 N89-12908
- Constitutive modeling for single crystal superalloys p 101 N89-12911
- High temperature stress-strain analysis p 196 N89-12913
- An investigation of environmental influence on the creep behavior of a low pressure plasma sprayed NiCoCrAlY alloy p 110 N89-13648
- Cyclic stress analysis of ceramic coated gas turbine seals p 111 N89-13662
- Three-dimensional inelastic analysis for hot section components, BEST 3D code p 199 N89-17317
- Reliability-based failure analysis of brittle materials [NASA-CR-184799] p 189 N89-20489
- Modal analysis of gear housing and mounts [NASA-TM-101445] p 184 N89-21244
- Investigation of Weibull statistics in fracture analysis of cast aluminum [NASA-TM-102000] p 185 N89-21245
- The isothermal fatigue behavior of a unidirectional SiC/Ti composite and the Ti alloy matrix [NASA-TM-101984] p 86 N89-22684
- Composite blade structural analyzer (COBSTRAN) user's manual [NASA-TM-101461] p 86 N89-23621
- X-ray based extensometry [NASA-CR-185058] p 176 N89-25432
- Computational structural mechanics for engine structures [NASA-TM-102119] p 204 N89-26259
- STRESS CYCLES**
- HOST surface protection R and T overview p 109 N89-12883
- Fatigue strength reduction model: RANDOM3 and RANDOM4 user manual, appendix 2 [NASA-CR-184940] p 203 N89-23891
- Procedures for characterizing an alloy and predicting cyclic life with the total strain version of Strainrange Partitioning [NASA-TM-4102] p 203 N89-25485
- STRESS DISTRIBUTION**
- A unique set of micromechanics equations for high-temperature metal matrix composites p 190 A89-15734
- Free-edge delamination - Laminate width and loading conditions effects p 193 A89-36294
- Analysis of interface crack branching [NASA-CR-182273] p 202 N89-21265
- Finite element modeling of frictionally restrained composite interfaces [NASA-CR-182281] p 203 N89-23918
- STRESS INTENSITY FACTORS**
- Influence of fatigue crack wake length and state of stress on crack closure p 191 A89-17432
- Resolved shear stress intensity coefficient and fatigue crack growth in large crystals p 96 A89-22048
- STRESS MEASUREMENT**
- High temperature stress-strain analysis p 196 N89-12913
- STRESS RELAXATION**
- Oxide scale stresses in polycrystalline Ni200 p 98 A89-38859
- STRESS WAVES**
- Acousto-ultrasonics - An update p 188 A89-42864
- A study of the stress wave factor technique for evaluation of composite materials [NASA-CR-4195] p 189 N89-21256
- STRESS-STRAIN DIAGRAMS**
- 1200 to 1400 K slow strain rate compressive behavior of small grain size NiAl/Ni<sub>2</sub>AlTi alloys and NiAl/Ni<sub>2</sub>AlTi-TiB<sub>2</sub> composites p 99 A89-53497
- Simplified cyclic structural analysis of SSME turbine blades p 63 N89-12632
- STRESS-STRAIN RELATIONSHIPS**
- Raman determination of layer stresses and strains for heterostructures and its application to the cubic SiC/Si system p 234 A89-21871
- Nonlinear analysis using temporal finite elements p 221 A89-28030
- Constitutive modelling of single crystal and directionally solidified superalloys p 101 N89-12912
- High temperature stress-strain analysis p 196 N89-12913
- Constitutive modeling for isotropic materials [NASA-CR-174805] p 26 N89-13436
- Total strain version of strainrange partitioning for thermomechanical fatigue at low strains p 201 N89-17337
- The isothermal fatigue behavior of a unidirectional SiC/Ti composite and the Ti alloy matrix [NASA-TM-101984] p 86 N89-22684
- Two-dimensional high temperature optical strain measurement system, phase 2 [NASA-CR-185116] p 176 N89-26218
- Metal matrix composite micromechanics: In-situ behavior influence on composite properties [NASA-TM-102302] p 88 N89-26924
- Tungsten fiber reinforced copper matrix composites: A review [NASA-TP-2924] p 88 N89-27796
- Refinements in a viscoplastic model [NASA-TM-102338] p 205 N89-28036
- STRESS-STRAIN-TIME RELATIONS**
- Procedures for characterizing an alloy and predicting cyclic life with the total strain version of Strainrange Partitioning [NASA-TM-4102] p 203 N89-25485
- STRING THEORY**
- Patterns of the cosmic microwave background from evolving string networks p 240 A89-14618
- Cosmic strings and the large-scale structure p 240 A89-19604
- Cosmic strings - A problem or a solution? p 240 A89-19610
- STRUCTURAL ANALYSIS**
- Thermoviscoplastic nonlinear constitutive relationships for structural analysis of high-temperature metal matrix composites p 190 A89-15735
- Probabilistic structural analysis methods and applications p 190 A89-16939
- Solution methods for one-dimensional viscoelastic problems p 191 A89-19914
- Probabilistic methods for structural response analysis p 223 A89-25843
- Nonlinear analysis using temporal finite elements p 221 A89-28030
- Computational structural mechanics for engine structures [AIAA PAPER 89-1260] p 22 A89-30745
- An approximate methods approach to probabilistic structural analysis [AIAA PAPER 89-1369] p 193 A89-30844
- An advanced probabilistic structural analysis method for implicit performance functions [AIAA PAPER 89-1371] p 193 A89-30846
- Fiber composite structural durability and damage tolerance - Simplified predictive methods p 82 A89-36320
- Thermal mechanical analyses of large diameter ion accelerator systems [AIAA PAPER 89-2718] p 58 A89-47041
- Structural and thermal response of 30 cm diameter ion thruster optics [AIAA PAPER 89-2719] p 58 A89-47042
- Development of a thermal and structural analysis procedure for cooled radial turbines [NASA-TM-101416] p 24 N89-12568
- Simplified cyclic structural analysis of SSME turbine blades p 63 N89-12632
- Turbine Engine Hot Section Technology 1986 [NASA-CP-2444] p 195 N89-12876
- On 3D inelastic analysis methods for hot section components p 196 N89-12906
- Component specific modeling p 25 N89-12907
- Constitutive modeling for isotropic materials [NASA-CR-174805] p 26 N89-13436
- A NASTRAN DMAP alter for linear buckling analysis under dynamic loading [NASA-TM-100832] p 85 N89-13522
- MHOST version 4.2. Volume 1: Users' manual [NASA-CR-182235-VOL-1] p 217 N89-13996
- Parametric studies of advanced turboprops [NASA-TM-101389] p 197 N89-14465
- Turbine Engine Hot Section Technology, 1987 [NASA-CP-2493] p 199 N89-17298
- Three-dimensional inelastic analysis methods for hot section components p 199 N89-17316
- Three-dimensional inelastic analysis for hot section components, BEST 3D code p 199 N89-17317
- Mechanics of materials model p 199 N89-17319
- Three-dimensional inelastic analysis methods for hot section components p 199 N89-17321
- Use of inelastic strain as a basis for analyzing thermomechanical test data p 200 N89-17326
- Structural response of an advanced combustor liner: Test and analysis p 200 N89-17329
- Structural analysis methods development for turbine hot section components p 30 N89-20140
- Views on the impact of HOST p 31 N89-20144
- A NASTRAN DMAP alter for linear buckling analysis under dynamic loading p 202 N89-22948
- Composite blade structural analyzer (COBSTRAN) user's manual [NASA-TM-101461] p 86 N89-23621
- Composite Blade Structural Analyzer (COBSTRAN) demonstration manual [NASA-TM-101957] p 87 N89-24459
- Advanced methods for 3-D inelastic structural analysis for hot engine structures [NASA-TM-102106] p 204 N89-25490
- Structural and thermal response of 30 cm diameter ion thruster optics [NASA-TM-102124] p 75 N89-27703

- Probabilistic structural analysis methods of hot engine structures [NASA-TM-102091] p 205 N89-28030
- Computational structural methods at NASA Lewis p 205 N89-29776
- Probabilistic Finite Elements (PFEM) structural dynamics and fracture mechanics p 206 N89-29803
- The 3-D inelastic analyses for computational structural mechanics p 206 N89-29804
- Specialty functions singularity mechanics problems p 206 N89-29805
- Multi-grid for structures analysis p 206 N89-29810
- STRUCTURAL DESIGN**
- Structural tailoring of laminate properties [AIAA PAPER 89-1367] p 192 A89-30842
- Probabilistic constitutive relationships for material strength degradation models [AIAA PAPER 89-1368] p 192 A89-30843
- Probabilistic structural analysis to quantify uncertainties associated with turbopump blades p 194 A89-36920
- Structural tailoring of Space Shuttle Main Engine turbopump blades SSME/STAEBL p 55 A89-44106
- Design procedures for fiber composite box beams p 195 A89-48674
- PV modules for ground testing [NASA-CR-179476] p 208 N89-11315
- Space station auxiliary thrust chamber technology [NASA-CR-179650] p 46 N89-11803
- Conceptual design of an advanced Stirling conversion system for terrestrial power generation [NASA-CR-180890] p 238 N89-12504
- High-temperature LCF of Ni-201 and 304L stainless steel p 100 N89-12635
- Liquid oxygen cooling of high pressure LOX/hydrocarbon rocket thrust chambers p 63 N89-12649
- The effects of leading edge and downstream film cooling on turbine vane heat transfer [NASA-CR-182133] p 158 N89-13754
- LDV measurements in an annular combustor model [NASA-CR-182207] p 159 N89-13755
- Summary and evaluation of the Strategic Defense Initiative Space Power Architecture Study [NASA-TM-102012] p 69 N89-24443
- Solid lubricant materials for high temperatures: A review p 203 N89-24636
- Structural tailoring of counter rotation propfans p 33 N89-25165
- Space Station Freedom photovoltaic power module design status [NASA-TM-102073] p 71 N89-25273
- Two-tiered design analysis of a radiator for a solar dynamic powered Stirling engine [NASA-CR-182301] p 46 N89-26031
- AGT (Advanced Gas Turbine) technology project [NASA-CR-182127] p 186 N89-26246
- STRUCTURAL DESIGN CRITERIA**
- Test methods and design allowables for fibrous composites. Volume 2 [ASTM STP-1003] p 81 A89-32882
- Symbolic derivation of material property matrices in finite element analysis p 216 A89-34964
- STRUCTURAL ENGINEERING**
- Computational structural methods at NASA Lewis p 205 N89-29776
- Computational structural mechanics engine structures computational simulator p 205 N89-29792
- STRUCTURAL MEMBERS**
- Identification of structural interface characteristics using component mode synthesis p 193 A89-36177
- STRUCTURAL RELIABILITY**
- An advanced probabilistic structural analysis method for implicit performance functions [AIAA PAPER 89-1371] p 193 A89-30846
- Time dependent reliability model incorporating continuum damage mechanics for high-temperature ceramics [NASA-TM-102046] p 115 N89-24487
- STRUCTURAL STABILITY**
- A thermally modified polymer matrix composite material with structural integrity to 371 C p 80 A89-29997
- Application of a full-potential solver to bending-torsion flutter in cascades [AIAA PAPER 89-1386] p 34 A89-30859
- A NASTRAN DMAP alter for linear buckling analysis under dynamic loading [NASA-TM-100832] p 85 N89-13522
- A NASTRAN DMAP alter for linear buckling analysis under dynamic loading p 202 N89-22948
- STRUCTURAL VIBRATION**
- Piezoelectric pushers for active vibration control of rotating machinery p 171 A89-47717
- Structural dynamics branch research and accomplishments for FY 1988 [NASA-TM-101406] p 202 N89-22939
- Unified micromechanics of damping for unidirectional fiber reinforced composites [NASA-TM-102107] p 88 N89-26919
- SUBMILLIMETER WAVES**
- Study of optical output couplers for submillimeter wavelength backward-wave oscillators (BWO's) p 132 A89-32857
- Study of optical output couplers for submillimeter wavelength backward-wave oscillators (BWO's) [NASA-TM-101360] p 134 N89-11128
- SUBSONIC FLOW**
- A computational procedure for automated flutter analysis p 191 A89-28070
- CFD application to subsonic inlet airframe integration --- computational fluid dynamics (CFD) p 13 N89-16753
- SUBSONIC SPEED**
- Advanced core technology: Key to subsonic propulsion benefits [NASA-TM-101420] p 26 N89-14237
- Turbulent swirling jets with excitation [NASA-CR-180895] p 16 N89-29329
- SUBSTRATES**
- Deposition and characterization of ZnS/Si heterojunctions produced by vacuum evaporation [NASA-TM-101359] p 135 N89-11129
- Characterization of ZrO<sub>2</sub> buffer layers for sequentially evaporated Y-Ba-CuO on Si and Al<sub>2</sub>O<sub>3</sub> substrates [NASA-TM-101432] p 135 N89-13722
- Sequentially evaporated thin Y-Ba-Co-O superconducting films on microwave substrates [NASA-TM-102068] p 138 N89-23791
- Measurements of complex permittivity of microwave substrates in the 20 to 300 K temperature range from 26.5 to 40.0 GHz [NASA-TM-102123] p 123 N89-27038
- SUBSTRUCTURES**
- Finite element substructuring methods for composite mechanics p 80 A89-26291
- SUCTION**
- Discussion of Mills et al. on 'The effect of wall suction and thermophoresis on aerosol particle deposition from a laminar boundary layer on a flat plate' p 140 A89-12331
- Experimental and numerical investigation of an oblique shock wave/turbulent boundary layer interaction with continuous suction [AIAA PAPER 89-0357] p 4 A89-28407
- SULFATES**
- Vapor deposition and condensate flow on combustion turbine blades - Theoretical model to predict/understand some corrosion rate consequences of molten alkali sulfate deposition in the field or laboratory p 21 A89-20950
- SULFUR**
- The effect of sulfur and zirconium co-doping on the oxidation of NiCrAl p 94 A89-13933
- SULFUR COMPOUNDS**
- Degradation mechanisms of n-dodecane with sulfur and nitrogen dopants during thermal stressing p 116 A89-22277
- SUPERCONDUCTING FILMS**
- Highly oriented Ti<sub>2</sub>Ba<sub>2</sub>Ca<sub>2</sub>Cu<sub>3</sub>O<sub>10</sub> thin films by pulsed laser evaporation p 236 A89-30421
- Sequentially evaporated thin Y-Ba-Cu-O superconductor films: Composition and processing effects [NASA-TM-101388] p 134 N89-10235
- Measurements of complex permittivity of microwave substrates in the 20 to 300 K temperature range from 26.5 to 40.0 GHz [NASA-TM-102123] p 123 N89-27038
- Millimeter wave transmission studies of YBa<sub>2</sub>Cu<sub>3</sub>O<sub>7</sub>-delta thin films in the 26.5 to 40.0 GHz frequency range [NASA-TM-102345] p 237 N89-30088
- SUPERCONDUCTING MAGNETS**
- Development of a high power microwave thruster, with a magnetic nozzle, for space applications [NASA-TM-102321] p 74 N89-26904
- SUPERCONDUCTIVITY**
- Sequentially evaporated thin Y-Ba-Co-O superconducting films on microwave substrates [NASA-TM-102068] p 138 N89-23791
- Non-uniform transition conductivity of superconducting ceramic [NASA-TM-102133] p 189 N89-28851
- SUPERCONDUCTORS**
- Experimental evidence for a transverse magnetization of the Abrikosov lattice in anisotropic superconductors p 234 A89-21473
- Sequentially evaporated thin Y-Ba-Cu-O superconductor films: Composition and processing effects [NASA-TM-101388] p 134 N89-10235
- Characterization of ZrO<sub>2</sub> buffer layers for sequentially evaporated Y-Ba-CuO on Si and Al<sub>2</sub>O<sub>3</sub> substrates [NASA-TM-101432] p 135 N89-13722
- SUPERCOOLING**
- Macroscopic segregation in undercooled Pb-Sn eutectic alloys p 95 A89-19621
- SUPERLATTICES**
- Characterization of multilayer GaAs/AlGaAs transistor structures by variable angle spectroscopic ellipsometry p 133 A89-49998
- SUPERNOVA 1987A**
- Limits to the radiative decays of neutrinos and axions from gamma-ray observations of SN 1987A p 242 A89-26985
- SUPERSONIC AIRCRAFT**
- Effect of aerodynamic detuning on supersonic rotor discrete frequency noise generation p 225 A89-15083
- Supersonic through-flow fan assessment [NASA-CR-182202] p 27 N89-16843
- SUPERSONIC BOUNDARY LAYERS**
- An experimental study of a reattaching supersonic shear layer [AIAA PAPER 89-1801] p 6 A89-42036
- Skin-friction measurements by laser interferometry p 167 N89-28737
- SUPERSONIC COMBUSTION RAMJET ENGINES**
- Performance potential of air turbo-ramjet employing supersonic through-flow fan [AIAA PAPER 89-0010] p 22 A89-25006
- Shock-wave-induced mixing enhancement in scramjet combustors [AIAA PAPER 89-0104] p 145 A89-25091
- Numerical investigation of chemically reacting flows in ramjet dump combustors [AIAA PAPER 89-0387] p 22 A89-28408
- Three-dimensional calculation of supersonic reacting flows using an LU scheme [AIAA PAPER 89-0391] p 146 A89-28410
- SUPERSONIC COMPRESSORS**
- Supersonic throughflow fans p 27 N89-16837
- SUPERSONIC FLIGHT**
- Supersonic throughflow fans p 27 N89-16837
- SUPERSONIC FLOW**
- Three dimensional simulation of an underexpanded jet interacting with a supersonic cross flow [AIAA PAPER 88-3181] p 2 A89-14982
- Near-field acoustic environment of a supersonic plume adjacent to a wall [AIAA PAPER 89-1137] p 225 A89-33767
- Flow of rarefied gases over two-dimensional bodies [AIAA PAPER 89-1970] p 5 A89-41814
- Conservative treatment of boundary interfaces for overlaid grids and multi-level grid adaptations [AIAA PAPER 89-1980] p 5 A89-41823
- A supersonic through-flow fan engine airframe integration study [AIAA PAPER 89-2140] p 18 A89-50802
- Numerical analysis of supersonic flow through oscillating cascade sections by using a deforming grid [AIAA PAPER 89-2805] p 8 A89-50810
- Experimental investigation of the performance of a supersonic compressor cascade [NASA-TM-100879] p 9 N89-10858
- A preliminary design study of supersonic through-flow fan inlets [NASA-CR-182224] p 24 N89-11751
- Control-volume based Navier-Stokes equation solver valid at all flow velocities [NASA-TM-101488] p 161 N89-20407
- Comparison of 3D computation and experiment for non-axisymmetric nozzles [NASA-CR-182245] p 14 N89-20921
- The response of a laminar boundary layer in supersonic flow to small amplitude progressive waves [NASA-TM-101965] p 162 N89-21197
- Conservative treatment of boundary interfaces for overlaid grids and multi-level grid adaptations [NASA-TM-102080] p 15 N89-24269
- Numerical analysis of supersonic flow through oscillating cascade sections by using a deforming grid [NASA-TM-102053] p 15 N89-25119
- Influence of thickness and camber on the aeroelastic stability of supersonic throughflow fans: An engineering approach [NASA-TM-101949] p 15 N89-25957
- SUPERSONIC INLETS**
- CFD application to supersonic/hypersonic inlet airframe integration --- computational fluid dynamics (CFD) p 13 N89-16754
- SUPERSONIC NOZZLES**
- Comparison of 3D computation and experiment for non-axisymmetric nozzles [AIAA PAPER 89-0007] p 22 A89-28403
- Analysis of supersonic plug nozzle flowfield and heat transfer [NASA-CR-179554] p 10 N89-13397

# SUPERSONIC SPEED

## SUPERSONIC SPEED

- Investigation of low NOx staged combustor concept in high-speed civil transport engines [AIAA PAPER 89-2942] p 23 A89-47186
- Investigation of low NOx staged combustor concept in high-speed civil transport engines [NASA-TM-101977] p 32 N89-22606

## SUPERSONIC TRANSPORTS

- Supersonic jet noise and the high speed civil transport [AIAA PAPER 89-2358] p 227 A89-46772
- HASA: Hypersonic Aerospace Sizing Analysis for the preliminary design of aerospace vehicles [NASA-CR-182226] p 18 N89-15107
- Revolutionary opportunities for materials and structures study, addendum [NASA-CR-179642-ADD] p 34 N89-29351

## SUPERSONIC WIND TUNNELS

- New hypersonic facility capability at NASA Lewis Research Center [AIAA PAPER 89-2534] p 36 A89-46905
- Acoustic evaluation of the Helmholtz resonator treatment in the NASA Lewis 8- by 6-foot supersonic wind tunnel [NASA-TM-101407] p 228 N89-15685
- Wind-tunnel results of advanced high-speed propellers at takeoff, climb, and landing Mach numbers [NASA-TM-87030] p 13 N89-19265
- New hypersonic facility capability at NASA Lewis Research Center [NASA-TM-102028] p 36 N89-22617

## SUPPLYING

- Space propulsion technology and cryogenic fluid depot p 38 N89-11768

## SURFACE COOLING

- Analysis of supersonic plug nozzle flowfield and heat transfer [NASA-CR-179554] p 10 N89-13397

## SURFACE CRACKS

- Damage analysis of a crack layer p 194 A89-42984

## SURFACE DEFECTS

- Weibull crack density coefficient for polydimensional stress states p 193 A89-34849
- Undercutting of defects in thin film protective coatings on polymer surfaces exposed to atomic oxygen [NASA-TM-101986] p 115 N89-23691

## SURFACE DISTORTION

- Thermal distortion analysis of the Space Station solar dynamic concentrator p 51 A89-15341
- Compensation of reflector antenna surface distortion using an array feed p 126 A89-53136
- Adaptive feed array compensation system for reflector antenna surface distortion [NASA-TM-101458] p 127 N89-17756

## SURFACE FINISHING

- Secondary electron emission characteristics of untreated and ion-textured titanium [NASA-TP-2902] p 103 N89-17650
- Undercutting of defects in thin film protective coatings on polymer surfaces exposed to atomic oxygen [NASA-TM-101986] p 115 N89-23691

## SURFACE GEOMETRY

- Development of a special-purpose test surface guided by uncertainty analysis p 144 A89-22736
- Crowned spur gears - Methods for generation and tooth contact analysis. I - Basic concepts, generation of the pinion tooth surface by a plane p 179 A89-29306
- Crowned spur gears - Methods for generation and Tooth Contact Analysis. II - Generation of the pinion tooth surface by a surface of revolution p 180 A89-37665
- Generation of a crowned pinion tooth surface by a surface of revolution [NASA-TM-100260] p 181 N89-10282

## SURFACE LAYERS

- Aerodynamically-driven condensate layer thickness distributions on isothermal cylindrical surfaces p 140 A89-12337

## SURFACE PROPERTIES

- Comparison of the surface charge behavior of commercial silicon nitride and silicon carbide powders p 105 A89-21444
- Hardware development for the Surface Tension Driven Convection Experiment aboard the USML-1 Spacelab mission [AIAA PAPER 89-0406] p 47 A89-25341
- Interaction of surface radiation with convection in crystal growth by physical vapor transport p 119 A89-30450
- Hardware development for the surface tension driven convection experiment aboard the USML-1 spacelab mission [NASA-TM-101404] p 48 N89-11804
- Summary of laser speckle photogrammetry for HOST p 177 N89-12889
- Applications of surface analysis and surface theory in tribology [NASA-TM-101392] p 78 N89-15981

- Friction factor data for flat plate tests of smooth and honeycomb surfaces [NASA-CR-184977] p 186 N89-23876

- Surface morphologies and electrical properties of molecular beam epitaxial InSb and InAs(x)Sb(1-x) grown on GaAs and InP substrates [NASA-CR-185439] p 237 N89-26740
- Arcjet cathode phenomena [NASA-TM-102099] p 167 N89-27121

## SURFACE REACTIONS

- Surface studies relevant to silicon carbide chemical vapor deposition p 91 A89-27966
- Pulsed ion beam investigation of the kinetics of surface reactions p 93 A89-44542
- Design, development and applications of novel techniques for studying surface mechanical properties [NASA-TM-101959] p 113 N89-20253
- Atomic oxygen effects on materials p 78 N89-23540

- Surface phenomena in plasma environments p 234 N89-23555
- Arc-textured high emittance radiator surfaces [NASA-CASE-LEW-14679-1] p 116 N89-28651

## SURFACE ROUGHNESS

- Townsend coefficients for electron scattering over dielectric surfaces p 231 A89-16409
- Investigation of surface water behavior during glaze ice accretion p 16 A89-27739
- On ice shape prediction methodologies and comparison with experimental data [AIAA PAPER 89-0732] p 16 A89-30650
- Calculation of the effects of ice on the backscatter of a ground plane [NASA-CR-183303] p 126 N89-10213

## SURFACE ROUGHNESS EFFECTS

- A numerical investigation of the influence of surface roughness on heat transfer in ice accretion [AIAA PAPER 89-0737] p 146 A89-25554
- Modeling of surface roughness effects on glaze ice accretion p 16 A89-28451
- Effects of environmentally imposed roughness on airfoil performance [NASA-CR-179639] p 17 N89-11725

## SURFACE TEMPERATURE

- Surface temperature determination in surface analytic systems by infrared optical pyrometry p 169 A89-17347
- Surface studies relevant to silicon carbide chemical vapor deposition p 91 A89-27966
- Sensors for ceramic components in advanced propulsion systems: Summary of literature survey and concept analysis, task 3 report [NASA-CR-180900] p 172 N89-11192
- Advanced high temperature instrument for hot section research applications p 29 N89-20137
- Infrared surface temperature measurements for the surface tension driven convection experiment [NASA-TM-101353] p 175 N89-21224

## SURGES

- Active suppression of aerodynamic instabilities in turbomachines p 3 A89-28341

## SURVEYS

- Views on the impact of HOST p 31 N89-20144

## SWEAT COOLING

- Effect of particulate thermophoresis in reducing the fouling rate advantages of effusion-cooling p 141 A89-14599

## SWIRLING

- Euler analysis of a swirl recovery vane design for use with an advanced single-rotation propan [AIAA PAPER 88-3152] p 2 A89-17940
- Experimental study of isothermal swirling flows in a dump combustor p 21 A89-23182
- Large amplitude acoustic excitation of swirling turbulent jets [AIAA PAPER 89-0970] p 4 A89-29098
- Effect of initial swirl distribution on the evolution of a turbulent jet p 149 A89-36906
- A numerical and experimental study of confined swirling jets [AIAA PAPER 89-2898] p 151 A89-47161
- Aerothermal modeling program, Phase 2, element B: Flow interaction experiment p 160 N89-17304
- Large amplitude acoustic excitation of swirling turbulent jets [NASA-TM-101950] p 13 N89-18417

## SWITCHING CIRCUITS

- A Fourier analysis for a fast simulation algorithm --- for switching converters p 130 A89-15367
- Computer analysis of the negative differential resistance switching phenomenon of double-injection devices p 134 A89-54963

## SYMBOLIC PROGRAMMING

- Symbolic generation of constitutive equations p 221 A89-34963

- Symbolic derivation of material property matrices in finite element analysis p 216 A89-34964

## SYNCHRONOUS PLATFORMS

- A segmented mirror antenna for radiometers [NASA-TM-102045] p 128 N89-23753

## SYNCHRONOUS SATELLITES

- Adaptive array for weak interfering signals: Geostationary satellite experiments [NASA-CR-185450] p 129 N89-26126

## SYNTHESIS (CHEMISTRY)

- Improved synthesis of ceramic superconductors with alkaline earth peroxides - Synthesis and processing of Ba<sub>2</sub>YCu<sub>3</sub>O(7-x) p 235 A89-22887
- Characterization of ceramics and intermetallics fabricated by self-propagating high-temperature synthesis [NASA-TM-102004] p 78 N89-25285

## SYNTHETIC FUELS

- Alternative fuel capabilities of the Mod II Stirling vehicle [SAE PAPER 880543] p 177 A89-12303
- Gas turbine alternative fuels combustion characteristics [NASA-TM-101470] p 210 N89-21417

## SYSTEM FAILURES

- Effect of model uncertainty on failure detection - The threshold selector p 219 A89-17965
- Extended observability of linear time-invariant systems under recurrent loss of output data [AIAA PAPER 89-3510] p 220 A89-52603

## SYSTEMS ANALYSIS

- An expert system for restructurable control [NASA-TM-101378] p 220 N89-12309
- Systems autonomy technology: Executive summary and program plan [NASA-TM-100999] p 216 N89-18045

## SYSTEMS ENGINEERING

- Materials technology assessment for a 1050 K Stirling space engine design [NASA-TM-101342] p 77 N89-11815
- Cryogenic reactant storage for lunar base regenerative fuel cells [NASA-TM-101980] p 210 N89-21419

## SYSTEMS INTEGRATION

- Integrated communication and control systems. I - Analysis [ASME PAPER 88-WA/DSC-1] p 219 A89-22499
- Integrated communication and control systems. II - Design considerations [ASME PAPER 88-WA/DSC-2] p 219 A89-22500
- Integrated flight/propulsion control system design based on a centralized approach [AIAA PAPER 89-3520] p 35 A89-52611
- An observer-based compensator for distributed delays in integrated control systems [AIAA PAPER 89-3541] p 35 A89-52628
- Integrated flight/propulsion control system design based on a decentralized, hierarchical approach [AIAA PAPER 89-3519] p 35 A89-53301
- Fiber optic control system integration [NASA-CR-179568] p 231 N89-13256
- Space station WP-04 power system preliminary analysis and design document, volume 3 [NASA-CR-179587-VOL-3] p 64 N89-15164
- User needs, benefits and integration of robotic systems in a space station laboratory [NASA-CR-182261] p 185 N89-22108
- Integrated flight/propulsion control system design based on a centralized approach [NASA-TM-102137] p 35 N89-26009
- Investigation of a liquid-fed water resistojet plume [NASA-TM-102310] p 75 N89-27706

## SYSTEMS MANAGEMENT

- Space Station Freedom power management and distribution system design [NASA-TM-102283] p 73 N89-26045

# T

## TAKEOFF

- High-speed propeller performance and noise predictions at takeoff/landing conditions p 226 A89-39195
- Noise of a model counterrotation propeller with simulated fuselage and support pylon at takeoff/approach conditions [AIAA PAPER 89-1143] p 227 A89-48953
- Noise of a model counterrotation propeller with simulated fuselage and support pylon at takeoff/approach conditions [NASA-TM-101996] p 228 N89-24138

## TANTALUM OXIDES

- Metal-silicon reaction rates - The effects of capping p 93 A89-52202



- TAPERING**  
Computationally generated velocity taper for efficiency enhancement in a coupled-cavity traveling-wave tube p 132 A89-31987
- TEAMS**  
Age distribution among NASA scientists and engineers p 238 N89-23911
- TECHNOLOGICAL FORECASTING**  
Aircraft engines. III p 21 A89-22927  
Challenges for future space power systems [NASA-TM-102063] p 214 N89-25506
- TECHNOLOGY ASSESSMENT**  
Progress toward the evolution of a Stirling Space Engine [SAE PAPER 880545] p 48 A89-12305  
Power systems for production, construction, life support, and operations in space p 37 A89-45803  
A perspective on space exploration technology catalysis: A rationale for initiating 21st Century expansion of human civilization into outer space [NASA-TM-101362] p 238 N89-11637  
Space station electrical power system availability study [NASA-CR-182198] p 45 N89-11802  
Integrated control and health management. Orbit transfer rocket engine technology program [NASA-CR-182122] p 62 N89-11805  
Materials technology assessment for a 1050 K Stirling space engine design [NASA-TM-101342] p 77 N89-11815  
Assessment and comparison of 100-MW coal gasification phosphoric acid fuel cell power plants [NASA-CR-182189] p 209 N89-13103  
Assessment of satellite communications quality study. Addendum 1: Impact of propagation delay on data transmission [NASA-CR-182229] p 126 N89-14369  
Issues and opportunities in space photovoltaics [NASA-TM-101425] p 65 N89-15171  
NASA photovoltaic research and technology [NASA-TM-101422] p 65 N89-16917  
The potential impact of MMICs on future satellite communications: Executive summary [NASA-CR-182227-EXEC-SUMM] p 127 N89-17079  
Assessment, development, and application of combustor aerothermal models p 30 N89-20138  
Review and assessment of the database and numerical modeling for turbine heat transfer p 30 N89-20139  
NASA advanced space photovoltaic technology-status, potential and future mission applications [NASA-TM-102093] p 75 N89-27705
- TELEOPERATORS**  
Flight hardware and tele-operations supporting the Isothermal Dendritic Growth Experiment aboard the Space Shuttle [AIAA PAPER 89-0863] p 118 A89-25627  
User needs, benefits and integration of robotic systems in a space station laboratory [NASA-CR-182261] p 185 N89-22108
- TELEPHONY**  
Assessment of satellite communications quality study. Addendum 1: Impact of propagation delay on data transmission [NASA-CR-182229] p 126 N89-14369
- TELEVISION TRANSMISSION**  
Coded multiple chirp spread spectrum system and overlay service p 124 A89-26769
- TEMPERATURE COMPENSATION**  
The dual element method of strain gauge temperature compensation p 169 A89-12276  
Technique for temperature compensation of eddy-current proximity probes [NASA-TP-2880] p 173 N89-15380  
Compensation for effects of ambient temperature on rare-earth doped fiber optic thermometer [NASA-TM-102282] p 176 N89-27998
- TEMPERATURE CONTROL**  
Cooperating expert systems for Space Station - Power/thermal subsystem testbeds p 38 A89-15350  
A facility for precise temperature control applications in microgravity p 48 A89-36956
- TEMPERATURE DEPENDENCE**  
Surface morphologies and electrical properties of molecular beam epitaxial InSb and InAs(x)Sb(1-x) grown on GaAs and InP substrates [NASA-CR-185439] p 237 N89-26740
- TEMPERATURE DISTRIBUTION**  
Thermal distortion analysis of the Space Station solar dynamic concentrator p 51 A89-15341  
Efficient numerical simulation of a one-dimensional electrothermal diode pad p 144 A89-22811  
High-resolution liquid-crystal heat-transfer measurements on the end wall of a turbine passage with variations in Reynolds number [NASA-TM-100827] p 161 N89-18664
- Methods for heat transfer and temperature field analysis of the insulated diesel, phase 3 [NASA-CR-182237] p 239 N89-23382
- TEMPERATURE EFFECTS**  
Thermal distortion analysis of the Space Station solar dynamic concentrator p 51 A89-15341  
A unique set of micromechanics equations for high-temperature metal matrix composites p 190 A89-15734  
A viscoplastic constitutive theory for metal matrix composites at high temperature p 80 A89-20725  
Adhesion, friction, and wear of plasma-deposited thin silicon nitride films at temperatures to 700 C p 107 A89-48250  
Transition limits for water-droplet crystallization with the NASA Lewis icing nozzle p 152 A89-50071  
Thermal effects on the mechanical properties of SiC fiber reinforced reaction bonded silicon nitride matrix (SiC/RBSN) composites [NASA-TM-101348] p 84 N89-10134  
Adhesion, friction, and wear of plasma-deposited thin silicon nitride films at temperatures to 700 C [NASA-TM-101377] p 109 N89-11913  
Effect of grain size on the high temperature properties of B2 aluminides [NASA-TM-101382] p 101 N89-12720  
Coolant passage heat transfer with rotation p 157 N89-12899  
Component specific modeling p 25 N89-12907  
Addition of polymers from 1,4,5,8-tetrahydro-1,4,5,8-diepoxyanthracene and Bis-dienes. 2: Evidence for thermal dehydration occurring in the cure process [NASA-TM-101385] p 112 N89-15235  
Atomic oxygen effects on materials p 78 N89-23540
- TEMPERATURE GRADIENTS**  
Convective flows in enclosures with vertical temperature or concentration gradients [AIAA PAPER 89-0069] p 118 A89-25060  
A high heat flux experiment for verification of thermostructural analysis p 148 A89-35002  
Effect of design variables, temperature gradients, and speed on life and reliability of a rotating disk p 180 A89-47719  
A high heat flux experiment for verification of thermostructural analysis [NASA-TM-100931] p 155 N89-12026  
Convective flows in enclosures with vertical temperature or concentration gradients [NASA-TM-101373] p 120 N89-12753  
Unsteady thermocapillary migration of bubbles [NASA-TM-101338] p 162 N89-22054  
Determination of the thermal stability of perfluoroalkylethers by tensimetry: Instrumentation and Procedure [NASA-TM-102116] p 116 N89-26095
- TEMPERATURE MEASUREMENT**  
Surface temperature determination in surface analytic systems by infrared optical pyrometry p 169 A89-17347  
Design and simulated performance of a CARS spectrometer for dynamic temperature measurements using electronic heterodyning p 170 A89-37298  
Sensors for ceramic components in advanced propulsion systems: Summary of literature survey and concept analysis, task 3 report [NASA-CR-180900] p 172 N89-11192  
Further development of the dynamic gas temperature measurement system p 172 N89-12884  
Further development of the dynamic gas temperature measurement system. Volume 2: Computer program user's manual [NASA-CR-179513-VOL-2] p 173 N89-13771  
Heat flux measurements [NASA-TM-101428] p 173 N89-14418  
Technique for temperature compensation of eddy-current proximity probes [NASA-TP-2880] p 173 N89-15380  
Development of a high temperature thin film static strain gage p 174 N89-17299  
High-resolution liquid-crystal heat-transfer measurements on the end wall of a turbine passage with variations in Reynolds number [NASA-TM-100827] p 161 N89-18664  
Advanced high temperature instrument for hot section research applications p 29 N89-20137  
The emittance of space radiator materials measured at elevated temperatures [NASA-TM-101948] p 66 N89-20193  
Infrared surface temperature measurements for the surface tension driven convection experiment [NASA-TM-101353] p 175 N89-21224  
Determination of combustion gas temperatures by infrared radiometry in sooting and nonsooting flames [NASA-TP-2900] p 164 N89-25409
- Experience with advanced instrumentation in a hot section cascade [NASA-TM-102294] p 167 N89-27980
- TEMPERATURE MEASURING INSTRUMENTS**  
HOST instrumentation R and D program overview p 25 N89-12878
- TEMPERATURE PROBES**  
Further development of the dynamic gas temperature measurement system p 172 N89-12884  
Experience with advanced instrumentation in a hot section cascade [NASA-TM-102294] p 167 N89-27980
- TEMPERATURE PROFILES**  
Effect of NASA advanced designs on thermal behavior of Ni-H2 cells p 50 A89-15279
- TEMPERATURE SENSORS**  
Fiber-optic temperature sensor using a spectrum-modulating semiconductor etalon p 168 A89-10366
- TENSILE PROPERTIES**  
Influence of fatigue crack wake length and state of stress on crack closure p 191 A89-17432  
Tensile and creep rupture behavior of P/M processed Nb-base alloy, WC-3009 [NASA-TM-101954] p 78 N89-19371  
The isothermal fatigue behavior of a unidirectional SiC/Ti composite and the Ti alloy matrix [NASA-TM-101984] p 86 N89-22684
- TENSILE STRENGTH**  
Room temperature tensile ductility in polycrystalline B2 Ni-30Al-20Fe p 98 A89-44568  
Tensile behavior of tungsten and tungsten-alloy wires from 1300 to 1600 K [NASA-TM-101446] p 103 N89-17649
- TENSILE TESTS**  
Inelastic deformation and dislocation structure of a nickel alloy - Effects of deformation and thermal histories p 99 A89-50313  
Furnace for tensile/fatigue testing [NASA-CASE-LEW-14848-1] p 40 N89-28549
- TERMINAL GUIDANCE**  
Optimal terminal maneuver for a cooperative impulsive rendezvous p 38 A89-36946
- TEST EQUIPMENT**  
Simulation test beds for the Space Station electrical power system p 39 A89-15352
- TEST FACILITIES**  
Facilities for microgravity combustion research [IAF PAPER 88-355] p 117 A89-17784  
A facility for precise temperature control applications in microgravity p 48 A89-36956  
Design of a thrust stand for high power electric propulsion devices [AIAA PAPER 89-2829] p 39 A89-47110  
Icing research tunnel test of a model helicopter rotor [NASA-TM-101978] p 29 N89-19305  
The effect of prewhirl on the internal aerodynamics and performance of a mixed flow research centrifugal compressor [NASA-CR-184756] p 161 N89-19503  
A real-time simulator of a turbofan engine [NASA-TM-100869] p 31 N89-20995  
Protoflight photovoltaic power module system-level tests in the space power facility [NASA-TM-102066] p 46 N89-25267  
Plume characteristics of MPD thrusters: A preliminary examination [NASA-CR-185130] p 76 N89-29483
- TEST STANDS**  
Description of an oscillating flow pressure drop test rig p 142 A89-15188  
Test facility and preliminary performance of a 100 kW class MPD thruster [NASA-TM-102021] p 68 N89-23520
- TESTS**  
The design and fabrication of a Stirling engine heat exchanger module with an integral heat pipe p 142 A89-15190
- TETHERING**  
Summary of the Second International Conference on Tethers in Space Venice, Italy, October 4-8, 1987 [AIAA PAPER 89-1547] p 37 A89-40177
- TETHERLINES**  
Power transmission studies for tethered SP-100 p 52 A89-15403  
Summary of the Second International Conference on Tethers in Space Venice, Italy, October 4-8, 1987 [AIAA PAPER 89-1547] p 37 A89-40177  
A model of electron collecting plasma contractors [AIAA PAPER 89-1560] p 232 A89-40190  
On the need for space tests of plasma contractors as electron collectors p 232 A89-43356  
Satellite relocation by tether deployment [NASA-TM-101992] p 42 N89-26877

# TEXTURES

## TEXTURES

Crack growth resistance of textured alumina p 105 A89-26452  
The emittance of space radiator materials measured at elevated temperatures [NASA-TM-101948] p 66 N89-20193

## THALLIUM COMPOUNDS

Critical currents of aligned grains of Ti-Ba-Ca-Cu-O compounds p 235 A89-30335  
Highly oriented Ti2Ba2Ca2Cu3O10 thin films by pulsed laser evaporation p 236 A89-30421  
Preparation of high T(c) Ti-Ba-Ca-Cu-O thin films by pulsed laser evaporation and TiO3 vapor processing p 236 A89-38608

## THERMAL ABSORPTION

Transient radiative cooling of an absorbing and scattering cylinder p 146 A89-28958

## THERMAL ANALYSIS

Thermal measurements for jets in disturbed and undisturbed crosswind conditions p 20 A89-16102  
Thermal analysis of heat storage canisters for a solar dynamic, space power system p 54 A89-29113  
A high heat flux experiment for verification of thermostructural analysis p 148 A89-35002  
Thermal mechanical analyses of large diameter ion accelerator systems p 58 A89-47041 [AIAA PAPER 89-2718]  
Structural and thermal response of 30 cm diameter ion thruster optics p 58 A89-47042 [AIAA PAPER 89-2719]  
Effects of furnace temperature profile on the interface shape during Bridgman crystal growth p 119 A89-53278

An experimental and analytical investigation of thermocoustic convection heat transfer in gravity and zero-gravity environments p 120 N89-11920 [NASA-CR-179575]  
A high heat flux experiment for verification of thermostructural analysis p 155 N89-12026 [NASA-TM-100931]  
Development of a thermal and structural analysis procedure for cooled radial turbines p 24 N89-12568 [NASA-TM-101416]  
Thermal effects in two-phase flow through face seals p 182 N89-13788 [NASA-CR-185968]  
The role of thermal and lubricant boundary layers in the transient thermal analysis of spur gears p 182 N89-14452 [NASA-TM-101435]  
Modeling cyclic melting and refreezing in a hollow metal canister p 217 N89-15623 [NASA-CR-184630]  
Structural analysis methods development for turbine hot section components p 30 N89-20140  
Three dimensional thermal analysis of rocket thrust chambers p 66 N89-21025 [NASA-TM-101973]  
Methods for heat transfer and temperature field analysis of the insulated diesel, phase 3 p 239 N89-23382 [NASA-CR-182237]  
Comparison of predicted and measured temperatures of UH-60A helicopter transmission p 186 N89-24607 [NASA-TP-2911]  
Comparative thermal analysis of the space station Freedom photovoltaic deployable boom structure using TRASYS, NEVADA, and SINDA programs p 165 N89-26177 [NASA-TM-102062]  
Thermal evaluation of advanced solar dynamic heat receiver performance p 214 N89-27256 [NASA-CR-185117]  
Structural and thermal response of 30 cm diameter ion thruster optics p 75 N89-27703 [NASA-TM-102124]

Thrust chamber thermal barrier coating techniques p 115 N89-22671

## THERMAL BOUNDARY LAYER

Mass transfer across combustion gas thermal boundary layers - Power production and materials processing implications p 143 A89-20425  
The role of thermal and lubricant boundary layers in the transient thermal analysis of spur gears p 182 N89-14452 [NASA-TM-101435]

## THERMAL BUCKLING

Non-isothermal buckling behavior of viscoplastic shell structures p 197 N89-12931 [NASA-CR-183013]

## THERMAL CONDUCTIVITY

High temperature thermal conductivity measurements on lanthanum sulfides using the flash method p 77 A89-16500  
A model for including thermal conduction in molecular dynamics simulations p 237 A89-41259

## THERMAL CONTROL COATINGS

Acoustic emission evaluation of plasma-sprayed thermal barrier coatings p 178 A89-12751

Low earth orbit environmental effects on the Space Station photovoltaic power generation systems p 55 A89-29123

Turbine Engine Hot Section Technology 1986 [NASA-CP-2444] p 195 N89-12876  
HOST surface protection R and T overview p 109 N89-12883

A study on thermal barrier coatings including thermal expansion mismatch and bond coat oxidation p 109 N89-12919

Thermal barrier coating life prediction model development p 109 N89-12920

Thermal barrier coating life prediction model p 109 N89-12921

Thermal barrier coating life prediction model development p 110 N89-12922

Thermal barrier coating life prediction model development [NASA-CR-180807] p 110 N89-13621

Thermal Barrier Coatings. Abstracts and figures [NASA-CP-10019] p 110 N89-13642

The effect of oxidation on the high heat flux behavior of a thermal barrier coating p 110 N89-13646

Turbine Engine Hot Section Technology, 1987 [NASA-CP-2493] p 199 N89-17298

Thermal expansion mismatch and plasticity in thermal barrier coating p 200 N89-17330

Thermal barrier coating life-prediction model development p 200 N89-17331

Thermal barrier coating life prediction model development p 200 N89-17333

High temperature constitutive and crack initiation modeling of coated single crystal superalloys p 112 N89-17334

Energy storage and thermal control system design status [NASA-TM-102136] p 46 N89-24427

## THERMAL CYCLING TESTS

Thermal-mechanical fatigue test apparatus for metal matrix composites and joint attachments p 79 A89-15727

Effect of 0.1 at. pct Zirconium on the cyclic oxidation resistance of beta-NiAl p 96 A89-24599

Analysis of shell-type structures subjected to time-dependent mechanical and thermal loading p 197 N89-14457 [NASA-CR-183005]

Structural response of an advanced combustor liner: Test and analysis p 200 N89-17329

Creep fatigue life prediction for engine hot section materials (ISOTROPIC) fifth year progress review p 201 N89-17336

Thrust chamber thermal barrier coating techniques p 115 N89-22671

Computational simulation of high temperature metal matrix composites cyclic behavior [NASA-TM-102115] p 88 N89-27795

## THERMAL DECOMPOSITION

Determination of the thermal stability of perfluoroalkylethers by tensimetry: Instrumentation and Procedure p 116 N89-26095 [NASA-TM-102116]

## THERMAL DEGRADATION

Degradation mechanisms of n-dodecane with sulfur and nitrogen dopants during thermal stressing p 116 N89-22277

Arcjet cathode phenomena [NASA-TM-102099] p 167 N89-27121

Computational simulation of high temperature metal matrix composites cyclic behavior [NASA-TM-102115] p 88 N89-27795

## THERMAL DIFFUSION

Steady-state thermal-solutal diffusion in a float zone p 119 A89-40897

## THERMAL EMISSION

Unsteady heat transfer in turbine blade ducts - Focus on combustor sources p 153 A89-53286

Arc-textured high emittance radiator surfaces [NASA-CASE-LEW-14679-1] p 116 N89-28651

## THERMAL ENERGY

Transient performance evaluation of an integrated heat pipe-thermal storage system p 49 A89-15209

Flight experiment of thermal energy storage [NASA-TM-102081] p 69 N89-24440

## THERMAL EXPANSION

Heat transfer in the tip region of a rotor blade simulator p 157 N89-12898

A study on thermal barrier coatings including thermal expansion mismatch and bond coat oxidation p 109 N89-12919

Thermal expansion mismatch and plasticity in thermal barrier coating p 200 N89-17330

Theoretical analysis of compatibility of several reinforcement materials with NiAl and FeAl matrices [NASA-CR-182291] p 86 N89-23622

Optimum interface properties for metal matrix composites [NASA-TM-102295] p 205 N89-27223

## THERMAL FATIGUE

Biaxial thermo-mechanical fatigue p 194 A89-43527

The NASA Lewis Research Center High Temperature Fatigue and Structures Laboratory p 194 A89-43528

High-temperature LCF of Ni-201 and 304L stainless steel p 100 N89-12635

Turbine Engine Hot Section Technology, 1987 [NASA-CP-2493] p 199 N89-17298

Elevated temperature crack growth p 200 N89-17335

Creep fatigue life prediction for engine hot section materials (ISOTROPIC) fifth year progress review p 201 N89-17336

Total strain version of strainrange partitioning for thermomechanical fatigue at low strains p 201 N89-17337

Fatigue life prediction modeling for turbine hot section materials p 30 N89-20142

The isothermal fatigue behavior of a unidirectional SiC/Ti composite and the Ti alloy matrix [NASA-TM-101984] p 86 N89-22684

## THERMAL INSULATION

Life modeling of thermal barrier coatings for aircraft gas turbine engines p 30 N89-20143

Methods for heat transfer and temperature field analysis of the insulated diesel, phase 3 [NASA-CR-182237] p 239 N89-23382

## THERMAL NOISE

An experimental adaptive array to suppress weak interfering signals p 124 A89-22455

## THERMAL PROTECTION

Acoustic emission evaluation of plasma-sprayed thermal barrier coatings p 178 A89-12751

Microlaminate composites as thermal barrier coatings p 83 A89-54261

Thermal barrier coating life-prediction model development [NASA-CR-175002] p 26 N89-13433

Life modeling of thermal barrier coatings for aircraft gas turbine engines p 30 N89-20143

Thrust chamber thermal barrier coating techniques p 115 N89-22671

Comparative thermal analysis of the space station Freedom photovoltaic deployable boom structure using TRASYS, NEVADA, and SINDA programs [NASA-TM-102062] p 165 N89-26177

## THERMAL STABILITY

The preparation of new perfluoro ether fluids exhibiting excellent thermal-oxidative stabilities p 76 A89-12760

Thermo-oxidative stability studies of Celion 6000/PMR-15 unidirectional composites, PMR-15, and Celion 6000 fiber p 79 A89-14099

Degradation mechanisms of n-dodecane with sulfur and nitrogen dopants during thermal stressing p 116 A89-22277

A thermally modified polymer matrix composite material with structural integrity to 371 C p 80 A89-29997

Mechanics of damping for fiber composite laminates including hygro-thermal effects [AIAA PAPER 89-1191] p 192 A89-30681

Pressure effects on the thermal stability of silicon carbide fibers p 105 A89-31502

Elevated temperature slow plastic deformation of NiAl/TiB2 particulate composites p 81 A89-31689

Dispersoids in rapidly solidified B2 nickel aluminides p 98 A89-43023

Acidic attack of perfluorinated alkyl ether lubricant molecules by metal oxide surfaces p 93 N89-19402 [NASA-TM-101962]

Determination of the thermal stability of perfluoroalkylethers by tensimetry: Instrumentation and Procedure p 116 N89-26095 [NASA-TM-102116]

## THERMAL STRESSES

Mechanisms of elevated-temperature deformation in the B2 aluminides NiAl and CoAl p 94 A89-17378

Thermal analysis of heat storage canisters for a solar dynamic, space power system p 54 A89-29113

HOST structural analysis program overview p 195 N89-12881

Coolant passage heat transfer with rotation p 157 N89-12899

Thermal expansion mismatch and plasticity in thermal barrier coating p 200 N89-17330

Total strain version of strainrange partitioning for thermomechanical fatigue at low strains p 201 N89-17337

Isothermal life prediction of composite lamina using a damage mechanics approach [NASA-TM-102032] p 87 N89-24460

Analysis of shell-type structures subjected to time-dependent mechanical and thermal loading [NASA-CR-184989] p 203 N89-24669

- THERMAL VACUUM TESTS**  
Protoflight photovoltaic power module system-level tests in the space power facility [NASA-TM-102066] p 46 N89-25267
- THERMIONIC CATHODES**  
Electronic structure of BaO/W cathode surfaces p 132 A89-26862
- THERMIONIC CONVERTERS**  
Megawatt Class Nuclear Space Power Systems (MCNSPS) conceptual design and evaluation report. Volume 3, technologies 2: Power conversion [NASA-CR-179614-VOL-3] p 211 N89-22980
- THERMIONIC DIODES**  
A heat-driven monochromatic light source p 224 A89-41722
- THERMOCOUPLES**  
Experience with advanced instrumentation in a hot section cascade [NASA-TM-102294] p 167 N89-27980
- THERMODYNAMIC CYCLES**  
Improved silicon carbide for advanced heat engines. I - Process development for injection molding p 106 A89-33619  
Flight experiment of thermal energy storage [NASA-TM-102081] p 69 N89-24440  
On the dynamic response of pressure transmission lines in the research of helium-charged free piston Stirling engines [NASA-TM-102121] p 175 N89-24593
- THERMODYNAMIC EQUILIBRIUM**  
The stability analysis of magnetohydrodynamic equilibria - Comparing the thermodynamic approach with the energy principle p 232 A89-39391
- THERMODYNAMIC PROPERTIES**  
Laboratory studies of binary salt CVD in combustion gas environments p 89 A89-12335  
Status of several Stirling loss characterization efforts and their significance for Stirling space power development p 49 A89-15187  
Free energy surfaces in the superconducting mixed state p 236 A89-43928  
Thermodynamic analysis of compatibility of several reinforcement materials with beta phase NiAl alloys [NASA-CR-4171] p 84 N89-10131  
Advanced core technology: Key to subsonic propulsion benefits [NASA-TM-101420] p 26 N89-14237  
Experimental verification of the thermodynamic properties for a jet-A fuel [NASA-TM-101475] p 117 N89-17017  
Preliminary study of creep thresholds and thermomechanical response in Haynes 188 at temperatures in the range 649 to 871 C p 200 N89-17327  
Thermodynamic analysis of chemical compatibility of several reinforcement materials with niobium aluminides [NASA-CR-182260] p 86 N89-21036  
Improved high-temperature resistant matrix resins [NASA-CR-180826] p 114 N89-21105  
Engineering study of the rotary-vee engine concept [NASA-TM-101995] p 33 N89-26007  
COLD-SAT: A technology satellite for cryogenic experimentation [NASA-TM-102286] p 47 N89-26036  
Refinements in a viscoplastic model [NASA-TM-102338] p 205 N89-28036
- THERMODYNAMICS**  
Thermal-mechanical fatigue test apparatus for metal matrix composites and joint attachments p 79 A89-15727  
Isothermal and 'bithermal' thermomechanical fatigue behavior of a NiCoCrAlY-coated single crystal superalloy p 177 A89-36457  
Thermodynamic analysis of compatibility of several reinforcement materials with FeAl alloys [NASA-CR-4172] p 83 N89-10128  
Molten salt corrosion of SiC and Si3N4 [NASA-TM-101346] p 108 N89-11912  
Experiment plans to study preignition processes of a pool fire in low gravity [NASA-CR-182256] p 121 N89-19442  
Optimum interface properties for metal matrix composites [NASA-TM-102295] p 205 N89-27223  
Computational structural mechanics engine structures computational simulator p 205 N89-29792
- THERMOELECTRIC GENERATORS**  
Preliminary assessment of rover power systems for the Mars Rover Sample Return Mission [IAF PAPER ICOSP89-9-6] p 39 A89-46530  
Preliminary assessment of rover power systems for the Mars Rover Sample Return Mission [NASA-TM-102003] p 68 N89-23518
- THERMOELECTRIC POWER GENERATION**  
Investigations of microwave plasmas - Applications in electrothermal thruster systems [AIAA PAPER 89-2378] p 57 A89-46784  
Comparison of solar photovoltaic and nuclear reactor power systems for a human-tended lunar observatory [NASA-TM-102015] p 242 N89-23397
- THERMOELECTRICITY**  
CSTI High Capacity Power [NASA-TM-102059] p 72 N89-25282
- THERMOMECHANICAL TREATMENT**  
Inelastic deformation and dislocation structure of a nickel alloy - Effects of deformation and thermal histories p 99 A89-50313  
Thermomechanical characterization of Hastelloy-X under uniaxial cyclic loading p 196 N89-12909
- THERMOMETERS**  
The dual element method of strain gauge temperature compensation p 169 A89-12276  
Compensation for effects of ambient temperature on rare-earth doped fiber optic thermometer [NASA-TM-102282] p 176 N89-27998
- THERMOMIGRATION**  
Unsteady thermocapillary migration of bubbles [NASA-TM-101338] p 162 N89-22054
- THERMONUCLEAR POWER GENERATION**  
Comparison of solar photovoltaic and nuclear reactor power systems for a human-tended lunar observatory [NASA-TM-102015] p 242 N89-23397
- THERMOPHORESIS**  
Discussion of Mills et al. on 'The effect of wall suction and thermophoresis on aerosol particle deposition from a laminar boundary layer on a flat plate' p 140 A89-12331  
Thermophoretically enhanced mass transport rates to solid and transpiration-cooled walls across turbulent (law-of-the-wall) boundary layers p 141 A89-12340  
Effect of particulate thermophoresis in reducing the fouling rate advantages of effusion-cooling p 141 A89-14599  
Viscous dissipation effects on thermophoretically augmented aerosol particle transport across laminar boundary layers p 141 A89-14600  
Optical experiments on thermophoretically augmented submicron particle deposition from 'dusty' high temperature gas flows p 90 A89-14799  
Mass transfer across combustion gas thermal boundary layers - Power production and materials processing implications p 143 A89-20425
- THERMOPHYSICAL PROPERTIES**  
Revolutionary opportunities for materials and structures study, addendum no. 1 [NASA-CR-179642-ADD-1] p 47 N89-29478
- THERMOPLASTIC RESINS**  
The correlation of low-velocity impact resistance of graphite-fiber-reinforced composites with matrix properties p 79 A89-16283
- THERMOSETTING RESINS**  
A predictive model for failure properties of thermoset resins [NASA-TM-4128] p 87 N89-25300
- THERMOVISCOELASTICITY**  
Thermoviscoplastic nonlinear constitutive relationships for structural analysis of high-temperature metal matrix composites p 190 A89-15735  
Nonisothermal elastoviscoplastic snap-through and creep buckling of shallow arches p 194 A89-47370  
Thermoviscoplastic model with application to copper [NASA-TP-2845] p 198 N89-16183
- THICKNESS**  
High resolution video monitoring of coating thickness during plasma spraying [NASA-TM-101423] p 102 N89-15218  
Influence of thickness and camber on the aeroelastic stability of supersonic throughflow fans: An engineering approach [NASA-TM-101949] p 15 N89-25957  
OTVE combustor wall condition monitoring [NASA-CR-182275] p 73 N89-26899
- THIN AIRFOILS**  
Influence of airfoil thickness on convected gust interaction noise [AIAA PAPER 89-1082] p 225 A89-33725  
Numerical solution of periodic vortical flows about a thin airfoil [AIAA PAPER 89-1691] p 7 A89-48955  
Numerical solution of periodic vortical flows about a thin airfoil [NASA-TM-101998] p 14 N89-23413
- THIN FILMS**  
Thin-film hermeticity - A quantitative analysis of diamondlike carbon using variable angle spectroscopic ellipsometry p 234 A89-13945  
Highly oriented Ti2Ba2Ca2Cu3O10 thin films by pulsed laser evaporation p 236 A89-30421
- Durable thin film coatings for reflectors used in low earth orbit p 77 A89-33150  
Preparation of high T(c) Ti-Ba-Ca-Cu-O thin films by pulsed laser evaporation and Ti2O3 vapor processing p 236 A89-38608  
Advances in thin-film solar cells for lightweight space photovoltaic power [IAF PAPER ICOSP89-1-8] p 55 A89-46513  
Adhesion, friction, and wear of plasma-deposited thin silicon nitride films at temperatures to 700 C p 107 A89-48250  
Thin film coatings for space electrical power system applications p 77 A89-53324  
The scratch test - Different critical load determination techniques --- adhesive strength of thin hard coatings p 171 A89-54278  
Sequentially evaporated thin Y-Ba-Cu-O superconductor films: Composition and processing effects [NASA-TM-101388] p 134 N89-10235  
Adhesion, friction, and wear of plasma-deposited thin silicon nitride films at temperatures to 700 C [NASA-TM-101377] p 109 N89-11913  
Characterization of ZrO2 buffer layers for sequentially evaporated Y-Ba-CuO on Si and Al2O3 substrates [NASA-TM-101432] p 135 N89-13722  
Liquid sheet radiator apparatus [NASA-CASE-LEW-14295-1] p 123 N89-14348  
Development of a high temperature thin film static strain gage p 174 N89-17299  
Progress on a PdCr wire strain gage p 174 N89-17301  
Sequentially evaporated thin Y-Ba-Co-O superconducting films on microwave substrates [NASA-TM-102068] p 138 N89-23791  
Radiation resistance studies of amorphous silicon films p 213 N89-24738  
Advances in thin-film solar cells for lightweight space photovoltaic power [NASA-TM-102017] p 73 N89-26041  
Diamondlike carbon protective coatings for optical windows [NASA-TM-102111] p 231 N89-27506  
Ion beam and plasma methods of producing diamondlike carbon films [NASA-TM-102301] p 116 N89-27836
- THIN WALLED SHELLS**  
A 20-DOF hybrid stress general shell element p 191 A89-21133  
Analysis of shell-type structures subjected to time-dependent mechanical and thermal loading [NASA-CR-183005] p 197 N89-14457
- THREE DIMENSIONAL BODIES**  
Composite interlaminar fracture toughness - Three-dimensional finite-element modeling for mixed mode I, II, and fracture p 190 A89-16278
- THREE DIMENSIONAL BOUNDARY LAYER**  
Asymptotic structure and similarity solutions for three-dimensional turbulent boundary layers [AIAA PAPER 89-1863] p 150 A89-42090  
Influence of bulk turbulence and entrance boundary layer thickness on the curved duct flow field [NASA-CR-4188] p 155 N89-12838
- THREE DIMENSIONAL FLOW**  
Calculations of the unsteady, three-dimensional flow field inside a motored Wankel engine [SAE PAPER 880625] p 19 A89-12307  
Three dimensional simulation of an underexpanded jet interacting with a supersonic cross flow [AIAA PAPER 88-3181] p 2 A89-14982  
LU implicit multigrid algorithm for the three-dimensional Euler equations p 143 A89-19906  
A diagonally inverted LU implicit multigrid scheme for the 3-D Navier-Stokes equations and a two equation model of turbulence [AIAA PAPER 89-0467] p 145 A89-25382  
Solution of three-dimensional flow problems using a flux-spline method [AIAA PAPER 89-0687] p 146 A89-25543  
Kinetic energy equations for the average-passage equation system p 237 A89-28347  
Three dimensional PNS solutions of hypersonic internal flows with equilibrium chemistry [AIAA PAPER 89-0002] p 146 A89-28401  
Three-dimensional calculation of supersonic reacting flows using an LU scheme [AIAA PAPER 89-0391] p 146 A89-28410  
Three dimensional viscous analysis of a hypersonic inlet [AIAA PAPER 89-0004] p 4 A89-29924  
Heat transfer in gas turbine engines and three-dimensional flows; Proceedings of the Symposium, ASME Winter Annual Meeting, Chicago, IL, Nov. 27-Dec. 2, 1988 p 148 A89-34926

## THREE DIMENSIONAL MODELS

- A simple algebraic grid adaptation scheme with applications to two- and three-dimensional flow problems  
[AIAA PAPER 89-1984] p 5 A89-41827
- A time accurate finite volume high resolution scheme for three dimensional Navier-Stokes equations  
[AIAA PAPER 89-1994] p 6 A89-41837
- Transonic flow solutions on general 3D regions using composite-block grids p 6 A89-45428
- Spatial resolution and downwash velocity corrections for multiple-hole pressure probes in complex flows p 171 A89-45909
- A diagonally inverted LU implicit multigrid scheme for the 3-D Navier-Stokes equations and a two equation model of turbulence  
[NASA-CR-182209] p 9 N89-10863
- Turbine stator flow field simulations p 157 N89-12902
- Turbofan forced mixer lobe flow modeling. 1: Experimental and analytical assessment  
[NASA-CR-4147-PT-1] p 11 N89-14221
- Turbofan forced mixer lobe flow modeling. 2: Three-dimensional inviscid mixer analysis (FLOMIX)  
[NASA-CR-4147-PT-2] p 11 N89-14222
- Simulation of 3-D viscous flow within a multi-stage turbine p 26 N89-14238
- [NASA-TM-101376] p 26 N89-14238
- A prediction of 3-D viscous flow and performance of the NASA low-speed centrifugal compressor  
[NASA-CR-184765] p 160 N89-16132
- Three dimensional viscous analysis of a hypersonic inlet  
[NASA-TM-101474] p 13 N89-16759
- Two- and three-dimensional turbine blade row flow field simulations p 161 N89-17313
- Multigrid calculation of three-dimensional turbomachinery flows  
[NASA-CR-185332] p 165 N89-26172
- THREE DIMENSIONAL MODELS**
- Response of a chemically reacting shear layer to streamwise vorticity  
[AIAA PAPER 89-0978] p 150 A89-40400
- Comparison of 3D computation and experiment for non-axisymmetric nozzles p 14 N89-20921
- [NASA-CR-182245] p 14 N89-20921
- A hybrid asymptotic-modal analysis of the EM scattering by an open-ended S-shaped rectangular waveguide cavity  
[NASA-CR-185053] p 129 N89-24519
- THRESHOLDS**
- Effect of model uncertainty on failure detection - The threshold selector p 219 A89-17965
- THRUST**
- The effect of test-cell pressure on resistojel nozzle flow  
[AIAA PAPER 89-2838] p 58 A89-47116
- Performance characterization and transient investigation of multipropellant resistojets p 60 A89-50811
- [AIAA PAPER 89-2837] p 60 A89-50811
- Turbofan forced mixer lobe flow modeling. Part 3: Application to augment engines p 8 N89-10025
- [NASA-CR-4147-PT-3] p 8 N89-10025
- Performance characterization and transient investigation of multipropellant resistojets p 72 N89-25283
- [NASA-TM-102118] p 72 N89-25283
- THRUST AUGMENTATION**
- A control-volume method for analysis of unsteady thrust augmenting ejector flows  
[NASA-CR-182203] p 24 N89-12566
- A model for prediction of STOVL ejector dynamics  
[NASA-TM-102098] p 32 N89-24319
- THRUST CHAMBERS**
- Radiative heat transfer in rocket thrust chambers and nozzles p 150 A89-43235
- [AIAA PAPER 89-1720] p 150 A89-43235
- Space station auxiliary thrust chamber technology  
[NASA-CR-179650] p 46 N89-11803
- Liquid oxygen cooling of high pressure LOX/hydrocarbon rocket thrust chambers p 63 N89-12649
- Three dimensional thermal analysis of rocket thrust chambers p 66 N89-21025
- [NASA-TM-101973] p 66 N89-21025
- Thrust chamber thermal barrier coating techniques p 115 N89-22671
- THRUST CONTROL**
- Performance characterization and transient investigation of multipropellant resistojets p 60 A89-50811
- [AIAA PAPER 89-2837] p 60 A89-50811
- The effects of magnetic nozzle configurations on plasma thrusters p 64 N89-15170
- [NASA-CR-184678] p 64 N89-15170
- Performance characterization and transient investigation of multipropellant resistojets p 72 N89-25283
- [NASA-TM-102118] p 72 N89-25283

## THRUST MEASUREMENT

- A numerical study of chemically reacting flow in nozzles p 60 A89-49687
- [AIAA PAPER 89-2793] p 60 A89-49687
- A data acquisition and storage system for the ion auxiliary propulsion system cyclic thruster test  
[NASA-TM-101469] p 218 N89-17424
- Arjet nozzle design impacts p 68 N89-23522
- [NASA-TM-102050] p 68 N89-23522
- A numerical study of chemically reacting flow in nozzles p 70 N89-24444
- [NASA-TM-102135] p 70 N89-24444
- THRUST VECTOR CONTROL**
- Noise generated by a flight weight, air flow control valve in a vertical takeoff and landing aircraft thrust vectoring system p 228 N89-20776
- [NASA-CR-182232] p 228 N89-20776
- TIME DEPENDENCE**
- Analysis of shell-type structures subjected to time-dependent mechanical and thermal loading p 197 N89-14457
- [NASA-CR-183005] p 197 N89-14457
- Time dependent reliability model incorporating continuum damage mechanics for high-temperature ceramics p 115 N89-24487
- [NASA-TM-102046] p 115 N89-24487
- Analysis of shell-type structures subjected to time-dependent mechanical and thermal loading p 203 N89-24669
- [NASA-CR-184989] p 203 N89-24669
- Time-dependent computational studies of flames in microgravity p 122 N89-25353
- [NASA-CR-182298] p 122 N89-25353
- TIME DIVISION MULTIPLE ACCESS**
- Study of optoelectronic switch for satellite-switched time-division multiple access p 135 N89-13706
- [NASA-CR-179630] p 135 N89-13706
- Digitally modulated bit error rate measurement system for microwave component evaluation p 40 N89-28545
- [NASA-TP-2912] p 40 N89-28545
- TIME DIVISION MULTIPLEXING**
- Observer design for compensation of network-induced delays in integrated communication and control systems p 220 A89-35044
- TIME LAG**
- Observer design for compensation of network-induced delays in integrated communication and control systems p 220 A89-35044
- TIME MARCHING**
- Nonlinear analysis using temporal finite elements p 221 A89-28030
- TIN ALLOYS**
- Bulk undercooling, nucleation, and macrosegregation of Pb-Sn alloys p 117 A89-17106
- Gravitational macrosegregation in unidirectionally solidified lead-tin alloy p 117 A89-17112
- Macrosegregation in undercooled Pb-Sn eutectic alloys p 95 A89-19621
- The surface morphology of crystals melting under solutions of different densities p 235 A89-23482
- Macrosegregation and nucleation in undercooled Pb-Sn alloys p 104 N89-23664
- [NASA-TM-102023] p 104 N89-23664
- TIN OXIDES**
- High-efficiency solar cells fabricated from direct-current magnetron sputtered n-indium tin oxide onto p-InP grown by atmospheric pressure metalorganic vapor phase epitaxy p 133 A89-44518
- TIP SPEED**
- Cruise noise of the 2/9 scale model SR-7A propeller p 224 A89-12561
- TITAN LAUNCH VEHICLES**
- Expendable launch vehicle transportation for the space station p 42 N89-20179
- [NASA-TM-101947] p 42 N89-20179
- TITANIUM**
- Performance of a multistage depressed collector with machined titanium electrodes p 136 N89-15337
- [NASA-TP-2891] p 136 N89-15337
- Secondary electron emission characteristics of untreated and ion-textured titanium p 103 N89-17650
- [NASA-TP-2902] p 103 N89-17650
- Fatigue crack growth study of SCS6/Ti-15-3 composite p 104 N89-26989
- [NASA-TM-102332] p 104 N89-26989
- TITANIUM ALLOYS**
- Interdiffusional effects between TiBe12 and NiAl intermetallics p 95 A89-21395
- The isothermal fatigue behavior of a unidirectional SiC/Ti composite and the Ti alloy matrix p 86 N89-22684
- [NASA-TM-101984] p 86 N89-22684
- TITANIUM BORIDES**
- Elevated temperature slow plastic deformation of NiAl/TiB2 particulate composites p 81 A89-31689
- Dispersoids in rapidly solidified B2 nickel aluminides p 98 A89-43023

## TITANIUM CARBIDES

- Characterization of ceramics and intermetallics fabricated by self-propagating high-temperature synthesis p 78 N89-25285
- [NASA-TM-102004] p 78 N89-25285
- TITANIUM NITRIDES**
- Adhesion scratch testing - A round-robin experiment p 171 A89-54281
- TOLLMIE-SCHLICHTING WAVES**
- Interaction between Tollmien-Schlichting waves and free-stream disturbances in boundary-layer flows p 167 N89-27118
- [NASA-CR-185847] p 167 N89-27118
- TOPOLOGY**
- Topology of modified helical gears p 187 N89-28015
- [NASA-TM-102134] p 187 N89-28015
- TORQUE**
- Magnification of starting torques of dc motors by maximum power point trackers in photovoltaic systems p 138 N89-23792
- [NASA-TM-102040] p 138 N89-23792
- Variable speed induction motor operation from a 20-kHz power bus p 71 N89-25271
- [NASA-TM-102061] p 71 N89-25271
- TORSION**
- A data acquisition and control program for axial-torsional fatigue testing p 205 N89-28029
- [NASA-TM-102041] p 205 N89-28029
- TORSIONAL STRESS**
- A 20-DOF hybrid stress general shell element p 191 A89-21133
- Results of inphase axial-torsional fatigue experiments on 304 stainless steel p 201 N89-20514
- [NASA-TM-101464] p 201 N89-20514
- TOUGHNESS**
- The correlation of low-velocity impact resistance of graphite-fiber-reinforced composites with matrix properties p 79 A89-16283
- Finite element substructuring methods for composite mechanics p 80 A89-26291
- Graphite/polyimide composites with improved toughness p 83 A89-38637
- TOWNSEND DISCHARGE**
- Townsend coefficients for electron scattering over dielectric surfaces p 231 A89-18409
- TRACKING (POSITION)**
- Magnification of starting torques of dc motors by maximum power point trackers in photovoltaic systems p 138 N89-23792
- [NASA-TM-102040] p 138 N89-23792
- TRAJECTORY CONTROL**
- New results concerning the use of kinematically redundant manipulators in microgravity environments p 215 A89-52647
- [AIAA PAPER 89-3562] p 215 A89-52647
- TRANSCENDENTAL FUNCTIONS**
- Solution and sensitivity analysis of a complex transcendental eigenproblem with pairs of real eigenvalues p 197 N89-13819
- [NASA-CR-182241] p 197 N89-13819
- TRANSDUCERS**
- Mass flow measurement of liquid cryogenics using the triboelectric effect p 155 N89-12837
- [NASA-CR-179519] p 155 N89-12837
- TRANSFER ORBITS**
- Impact of ETO propellants on the aerothermodynamic analyses of propulsion components - Earth To Orbit p 53 A89-16486
- [AIAA PAPER 88-3091] p 53 A89-16486
- TRANSFORMERS**
- The application of high temperature superconductors to space electrical power distribution components p 50 A89-15287
- TRANSIENT HEATING**
- Efficient numerical simulation of a one-dimensional electrothermal deicer pad p 144 A89-22811
- Transient radiative cooling of an absorbing and scattering cylinder p 146 A89-28958
- High-resolution heat-transfer-coefficient maps applicable to compound-curve surfaces using liquid crystals in a transient wind tunnel p 154 N89-10246
- [NASA-TM-89855] p 154 N89-10246
- The role of thermal and lubricant boundary layers in the transient thermal analysis of spur gears p 182 N89-14452
- [NASA-TM-101435] p 182 N89-14452
- TRANSIENT RESPONSE**
- Transient performance evaluation of an integrated heat pipe-thermal storage system p 49 A89-15209
- Transient flow thrust prediction for an ejector propulsion concept p 23 A89-49688
- [AIAA PAPER 89-2906] p 23 A89-49688
- Performance characterization and transient investigation of multipropellant resistojets p 60 A89-50811
- [AIAA PAPER 89-2837] p 60 A89-50811
- Characterization of structural connections using free and forced response test data p 202 N89-21266
- [NASA-TM-101991] p 202 N89-21266
- Transient flow thrust prediction for an ejector propulsion concept p 32 N89-24318
- [NASA-TM-102078] p 32 N89-24318

- Performance characterization and transient investigation of multipropellant resistojets  
[NASA-TM-102118] p 72 N89-25283
- TRANSITION FLOW**  
Effect of transition on oscillation flow losses in Stirling engine coolers and heaters p 142 A89-15189  
Coherent structures in transitional and turbulent free shear flows p 147 A89-28999  
Bipolar coordinates for computation of transition duct flows p 148 A89-34912
- TRANSITION LAYERS**  
Boundary-layer receptivity to long-wave free-stream disturbances p 146 A89-28996
- TRANSITION POINTS**  
A novel approach in formulation of special transition elements: Mesh interface elements  
[NASA-CR-184768] p 199 N89-16193
- TRANSITION TEMPERATURE**  
Effect of processing parameters on the characteristics of high-Tc superconductor YBa<sub>2</sub>Cu<sub>3</sub>O<sub>y</sub>  
p 234 A89-20467  
Indentation plasticity and fracture in silicon  
[NASA-TP-2863] p 100 N89-10996  
Millimeter wave transmission studies of YBa<sub>2</sub>Cu<sub>3</sub>O<sub>7</sub>-delta thin films in the 26.5 to 40.0 GHz frequency range  
[NASA-TM-102345] p 237 N89-30088
- TRANSMISSION EFFICIENCY**  
Computationally generated velocity taper for efficiency enhancement in a coupled-cavity traveling-wave tube p 132 A89-31987
- TRANSMISSION LINES**  
The application of high temperature superconductors to space electrical power distribution components p 50 A89-15287  
Channelized coplanar waveguide: Discontinuities, junctions, and propagation characteristics  
[NASA-TM-101483] p 137 N89-21172  
On the dynamic response of pressure transmission lines in the research of helium-charged free piston Stirling engines  
[NASA-TM-102121] p 175 N89-24593
- TRANSMISSIONS (MACHINE ELEMENTS)**  
Advanced transmission studies p 178 A89-18906  
Effects of bearing offset and flexibility on the mesh force distribution of spiral bevel gears p 178 A89-19834  
An extremum principle for computation of the zone of tooth contact and generalized transmission error of spiral bevel gears p 178 A89-19835  
Transmission errors and bearing contact of spur, helical and spiral bevel gears  
[SAE PAPER 881294] p 179 A89-21000  
Crowned spur gears - Methods for generation and Tooth Contact Analysis. II - Generation of the pinion tooth surface by a surface of revolution p 180 A89-37665  
Transmission overhaul and replacement predictions using Weibull and renewal theory  
[AIAA PAPER 89-2919] p 180 A89-47173  
Computerized life and reliability modeling for turboprop transmissions p 181 A89-53364  
Generation of a crowned pinion tooth surface by a plane p 181 N89-10283  
Effect of advanced component technology on helicopter transmissions  
[NASA-TM-101431] p 182 N89-13794  
Vibration signature analysis of multistage gear transmission p 184 N89-18685  
Transmission overhaul and replacement predictions using Weibull and renewal theory  
[NASA-TM-102022] p 186 N89-22925  
Comparison of predicted and measured temperatures of UH-60A helicopter transmission  
[NASA-TP-29111] p 186 N89-24607  
Topology of modified helical gears  
[NASA-TM-102134] p 187 N89-28015
- TRANSONIC COMPRESSORS**  
The design and development of transonic multistage compressors p 27 N89-16834
- TRANSONIC FLOW**  
Diagonal implicit multigrid algorithm for the Euler equations p 1 A89-11110  
LU implicit multigrid algorithm for the three-dimensional Euler equations p 143 A89-19906  
Experimental investigation of transonic oscillating cascade aerodynamics  
[AIAA PAPER 89-0321] p 3 A89-26369  
Determination of near and far field acoustics for advanced propeller configurations  
[AIAA PAPER 89-1040] p 226 A89-40469  
Transonic flow solutions on general 3D regions using composite-block grids p 6 A89-45428  
Experimental investigation of transonic oscillating cascade aerodynamics  
[NASA-TM-101993] p 29 N89-20133
- Numerical computation of shock wave-turbulent boundary layer interaction in transonic flow over an axisymmetric curved hill  
[NASA-TM-101473] p 162 N89-21192  
Absorbing boundary conditions for second-order hyperbolic equations  
[NASA-TM-102009] p 223 N89-22397  
Multigrid calculation of three-dimensional turbomachinery flows  
[NASA-CR-185332] p 165 N89-26172
- TRANSONIC FLUTTER**  
Technique for the prediction of airfoil flutter characteristics in separated flow p 191 A89-27744
- TRANSPIRATION**  
Thermophoretically enhanced mass transport rates to solid and transpiration-cooled walls across turbulent (law-of-the-wall) boundary layers p 141 A89-12340
- TRANSPORT AIRCRAFT**  
Investigation of low NOx staged combustor concept in high-speed civil transport engines  
[AIAA PAPER 89-2942] p 23 A89-47186  
Multiple Application Propfan Study (MAPS): Advanced tactical transport  
[NASA-CR-175003] p 28 N89-19300  
Investigation of low NOx staged combustor concept in high-speed civil transport engines  
[NASA-TM-101977] p 32 N89-22606
- TRANSPORT PROPERTIES**  
Surface studies relevant to silicon carbide chemical vapor deposition p 91 A89-27966  
Pdf - Transport equations for chemically reacting flows p 152 A89-51880
- TRANSPORT THEORY**  
Universal limiter for transient interpolation modeling of the advective transport equations: The ULTIMATE conservative difference scheme  
[NASA-TM-100916] p 222 N89-14794
- TRANSPUTERS**  
Transputer parallel processing at NASA Lewis Research Center p 205 N89-29778
- TRANSVERSE WAVES**  
Parametric study of electromagnetic waves propagating in absorbing curved S ducts  
[NASA-TM-102024] p 129 N89-27923
- TRAVELING WAVE TUBES**  
Computationally generated velocity taper for efficiency enhancement in a coupled-cavity traveling-wave tube p 132 A89-31987  
Isotropic graphite multistage depressed collectors - A progress report --- carbon electrode performance p 132 A89-31988  
Development of a 39.5 GHz Karp traveling wave tube for use in space  
[NASA-CR-182182] p 136 N89-15336  
Design, fabrication, and performance of brazed, graphite electrode, multistage depressed collectors with 500-W, continuous wave, 4.8- to 9.6-GHz traveling-wave tubes  
[NASA-TP-2904] p 136 N89-21171  
Development of a 75-watt 60-GHz traveling-wave tube for intersatellite communications  
[NASA-CR-182135] p 138 N89-24530
- TRAVELING WAVES**  
Design of a GaAlAs travelling wave Mach-Zehnder electro-optic modulator p 130 A89-10342
- TREES (MATHEMATICS)**  
Hierarchical Poly Tree computer architectures defined by computational multidisciplinary mechanics p 218 A89-50100
- TRIBOLOGY**  
Tribological properties of structural ceramics p 107 A89-51258  
Tribological composition optimization of chromium-carbide-based solid lubricant coatings for foil gas bearings at temperatures to 650 C p 83 A89-54258  
Adhesion, friction and micromechanical properties of ceramics p 107 A89-54277  
Tribological properties of alumina-boria-silicate fabric from 25 C to 850 C p 107 A89-54982  
Mass flow meter using the triboelectric effect for measurement in cryogenics  
[NASA-CR-179572] p 155 N89-12836  
Applications of surface analysis and surface theory in tribology  
[NASA-TM-101392] p 78 N89-15981  
Acidic attack of perfluorinated alkyl ether lubricant molecules by metal oxide surfaces  
[NASA-TM-101962] p 93 N89-19402  
Tribology: The Story of Lubrication and Wear  
[NASA-TM-101430] p 203 N89-24635  
Solid lubricant materials for high temperatures: A review p 203 N89-24636
- TRUSSES**  
Three-dimensional marginal separation  
[NASA-TM-101411] p 159 N89-13757
- TUBE HEAT EXCHANGERS**  
Two-dimensional numerical simulation of a Stirling engine heat exchanger  
[NASA-TM-102057] p 164 N89-23823  
Initial characterization of a modular heat exchanger with an integral heat pipe  
[NASA-TM-102097] p 239 N89-25078
- TUNGSTEN**  
Thermal-mechanical fatigue test apparatus for metal matrix composites and joint attachments p 79 A89-15727  
Electronic structure of BaO/W cathode surfaces p 132 A89-26862  
Reaction kinetics between fiber and matrix p 83 A89-36420  
Tungsten fiber reinforced copper matrix composites: A review  
[NASA-TP-2924] p 88 N89-27796
- TUNGSTEN ALLOYS**  
Fiber reinforced superalloys for rocket engines  
[NASA-TM-100880] p 86 N89-15990  
Tensile behavior of tungsten and tungsten-alloy wires from 1300 to 1600 K  
[NASA-TM-101446] p 103 N89-17649  
Creep behavior of tungsten fiber reinforced niobium metal matrix composites  
[NASA-TM-102307] p 104 N89-29522
- TUNGSTEN CARBIDES**  
Tensile behavior of tungsten and tungsten-alloy wires from 1300 to 1600 K  
[NASA-TM-101446] p 103 N89-17649
- TUNING**  
Experimental investigation of propfan aeroelastic response in off-axis flow with mistuning  
[AIAA PAPER 88-3153] p 20 A89-17941
- TUNNEL DIODES**  
Submicron nickel-oxide-gold tunnel diode detectors for rectennas p 133 A89-43469
- TURBINE BLADES**  
Deposition of Na<sub>2</sub>SO<sub>4</sub> from salt-seeded combustion gases of a high velocity burner rig p 89 A89-12330  
High temperature isothermal and cyclic oxidation behavior of a single crystal Ni base superalloy p 94 A89-12625  
Recent advances in capacitance type of blade tip clearance measurements  
[AIAA PAPER 88-4664] p 20 A89-13725  
Impact of ETO propellants on the aerothermodynamic analyses of propulsion components --- Earth To Orbit  
[AIAA PAPER 88-3091] p 53 A89-16486  
Vapor deposition and condensate flow on combustion turbine blades - Theoretical model to predict/understand some corrosion rate consequences of molten alkali sulfate deposition in the field or laboratory p 21 A89-20950  
Calculation of unsteady flows in turbomachinery using the linearized Euler equations p 149 A89-36916  
Probabilistic structural analysis to quantify uncertainties associated with turbopump blades p 194 A89-36920  
Observations of directional gamma prime coarsening during engine operation p 98 A89-40162  
Structural tailoring of Space Shuttle Main Engine turbopump blades SSME/STAEBL p 55 A89-44106  
Unsteady heat transfer in turbine blade ducts - Focus on combustor sources p 153 A89-53286  
Simplified cyclic structural analysis of SSME turbine blades p 63 A89-12632  
Constitutive behavior of single crystal PWA 1480 and directionally solidified MAR-M 246 under monotonic and cyclic loads at high and low temperature p 100 N89-12634  
Development of a high temperature static strain sensor p 173 N89-12887  
Development of low Reynolds number two equation turbulence models for predicting external heat transfer on turbine blades p 157 N89-12901  
On 3D inelastic analysis methods for hot section components p 196 N89-12906  
Component specific modeling p 25 N89-12907  
Constitutive modelling of single crystal and directionally solidified superalloys p 101 N89-12912  
Elevated temperature crack growth p 196 N89-12915  
Heat flux measurements  
[NASA-TM-101428] p 173 N89-14418  
An experimental study of near wall flow parameters in the blade end-wall corner region  
[NASA-CR-4211] p 12 N89-15898  
Fiber reinforced superalloys for rocket engines  
[NASA-TM-100880] p 86 N89-15990  
Turbine Engine Hot Section Technology, 1987  
[NASA-CP-2493] p 199 N89-17298  
Development of a high temperature thin film static strain gage p 174 N89-17299  
A low-Reynolds-number two-equation turbulence model for predicting heat transfer on turbine blades p 160 N89-17310

## TURBINE ENGINES

- Measurement of airfoil heat transfer coefficients on a turbine stage p 160 N89-17311
- Heat transfer in the tip region of a rotor blade simulator p 161 N89-17312
- Two- and three-dimensional turbine blade row flow field simulations p 161 N89-17313
- Coolant passage heat transfer with rotation p 161 N89-17314
- Three-dimensional inelastic analysis methods for hot section components p 199 N89-17316
- Constitutive modelling of single crystal and directionally solidified superalloys p 102 N89-17325
- Oxide-dispersion-strengthened turbine blades. Volume 2 p 28 N89-18487
- [NASA-CR-179561-VOL-2] p 28 N89-18487
- Life modeling of thermal barrier coatings for aircraft gas turbine engines p 30 N89-20143
- A compendium of controlled diffusion blades generated by an automated inverse design procedure [NASA-TM-101968] p 31 N89-20996
- Fiber reinforced superalloys for rocket engines p 103 N89-22673
- Composite blade structural analyzer (COBSTRAN) user's manual [NASA-TM-101461] p 86 N89-23621
- Turbomachinery technology for high-speed civil flight [NASA-TM-102092] p 32 N89-24320
- Composite Blade Structural Analyzer (COBSTRAN) demonstration manual [NASA-TM-101957] p 87 N89-24459
- TURBINE ENGINES**
- Advanced detection, isolation, and accommodation of sensor failures - Real-time evaluation p 34 A89-16156
- NNEPEQ - Chemical equilibrium version of the Navy/NASA Engine Program [ASME PAPER 88-GT-314] p 22 A89-24989
- A review and forecast of engine system research at the Army Propulsion Directorate p 23 A89-36397
- T55-L-712 turbine engine compressor housing refurbishment-plasma spray project [NASA-TM-101310] p 100 N89-10156
- The effects of inlet turbulence and rotor/stator interactions on the aerodynamics and heat transfer of a large-scale rotating turbine model, volume 1 [NASA-CR-4079] p 159 N89-13756
- MHOST version 4.2. Volume 1: Users' manual [NASA-CR-182235-VOL-1] p 217 N89-13996
- Plotting component maps in the Navy/NASA Engine Program (NNEP): A method and its usage [NASA-TM-101433] p 26 N89-14239
- A review of failure models for unidirectional ceramic matrix composites under monotonic loads [NASA-TM-101421] p 198 N89-14470
- Development of an integrated BEM approach for hot fluid structure interaction [NASA-CR-184587] p 27 N89-15114
- Advanced high temperature instrument for hot section research applications p 29 N89-20137
- Transonic viscous flow calculations for a turbine cascade with a two equation turbulence model [NASA-TM-101944] p 32 N89-22607
- TURBINE PUMPS**
- Structural tailoring of Space Shuttle Main Engine turbopump blades SSME/STAEBL p 55 A89-44106
- Miniature multiple-function probe for OTV turbopump health monitoring [AIAA PAPER 89-2303] p 56 A89-46736
- Design and test of an oxygen turbopump for a dual expander cycle rocket engine [AIAA PAPER 89-2305] p 56 A89-46737
- The development of power specific redlines for SSME safety monitoring [AIAA PAPER 89-2413] p 61 A89-53305
- Heat flux measurements [NASA-TM-101428] p 173 N89-14418
- Advanced single crystal for SSME turbopumps [NASA-CR-182244] p 103 N89-21072
- Advanced helium purge seals for Liquid Oxygen (LOX) turbopumps [NASA-CR-182105] p 184 N89-21239
- The development of power specific redlines for SSME safety monitoring [NASA-CR-185121] p 41 N89-26027
- OTVE turbopump condition monitoring, task E.5 [NASA-CR-182274] p 189 N89-27204
- Probabilistic structural analysis methods of hot engine structures [NASA-TM-102091] p 205 N89-28030
- TURBINE WHEELS**
- Turbine-stage heat transfer - Comparison of short-duration measurements with state-of-the-art predictions p 142 A89-16458
- TURBOCOMPRESSORS**
- Automated design of controlled-diffusion blades [ASME PAPER 88-GT-139] p 2 A89-15967

- Active suppression of aerodynamic instabilities in turbomachines p 3 A89-28341
- Calculations of inlet distortion induced compressor flow field instability p 8 A89-52498
- Experimental investigation of the performance of a supersonic compressor cascade [NASA-TM-100879] p 9 N89-10858
- Simulation of 3-D viscous flow within a multi-stage turbine [NASA-TM-101376] p 26 N89-14238
- Performance estimates for the Space Station power system Brayton Cycle compressor and turbine [NASA-CR-182263] p 73 N89-26903
- TURBOFAN AIRCRAFT**
- Multiple-Purpose Subsonic Naval Aircraft (MPSNA) Multiple Application Propfan Study (MAPS) [NASA-CR-175096] p 18 N89-19289
- Multiple Application Propfan Study (MAPS): Advanced tactical transport [NASA-CR-175003] p 28 N89-19300
- TURBOFAN ENGINES**
- Cruise noise of an advanced counterrotation turboprop measured from an adjacent aircraft p 20 A89-15080
- Euler analysis of a swirl recovery vane design for use with an advanced single-rotation propfan [AIAA PAPER 88-3152] p 2 A89-17940
- Performance potential of air turbo-ramjet employing supersonic through-flow fan [AIAA PAPER 89-0010] p 22 A89-25006
- A supersonic through-flow fan engine airframe integration study [AIAA PAPER 89-2140] p 18 A89-50802
- CFD in the context of IHPTET - The Integrated High Performance Turbine Engine Technology Program [AIAA PAPER 89-2904] p 154 A89-53307
- Turbofan engine control system design using the LQG/LTR methodology p 23 A89-53956
- Turbofan forced mixer lobe flow modeling, Part 3: Application to augment engines p 8 N89-10025
- [NASA-CR-4147-PT-3] p 8 N89-10025
- A preliminary design study of supersonic through-flow fan inlets [NASA-CR-182224] p 24 N89-11751
- Advanced core technology: Key to subsonic propulsion benefits [NASA-TM-101420] p 26 N89-14237
- Supersonic through-flow fan assessment [NASA-CR-182202] p 27 N89-16843
- A real-time simulator of a turbofan engine [NASA-TM-100869] p 31 N89-20995
- Turbofan engine control system design using the LQG/LTR methodology [NASA-CR-182303] p 33 N89-26004
- CFD in the context of IHPTET: The Integrated High Performance Turbine Technology Program [NASA-TM-102132] p 165 N89-26174
- A real time microcomputer implementation of sensor failure detection for turbofan engines [NASA-TM-102327] p 216 N89-29032
- TURBOFANS**
- Effects of wind-tunnel wall absorption on acoustic radiation of propellers p 225 A89-22285
- Turbofan forced mixer lobe flow modeling, 2: Three-dimensional inviscid mixer analysis (FLOMIX) [NASA-CR-4147-PT-2] p 11 N89-14222
- Supersonic throughflow fans p 27 N89-16837
- Turbomachinery technology for high-speed civil flight [NASA-TM-102092] p 32 N89-24320
- TURBOGENERATORS**
- Megawatt Class Nuclear Space Power Systems (MCNSPS) conceptual design and evaluation report. Volume 3, technologies 2: Power conversion [NASA-CR-179614-VOL-3] p 211 N89-22980
- TURBOJET ENGINE CONTROL**
- Turbofan engine control system design using the LQG/LTR methodology p 23 A89-53956
- Turbofan engine control system design using the LQG/LTR methodology p 33 N89-26004
- [NASA-CR-182303] p 33 N89-26004
- A real time microcomputer implementation of sensor failure detection for turbofan engines [NASA-TM-102327] p 216 N89-29032
- TURBOJET ENGINES**
- Elevated temperature crack growth p 200 N89-17335
- The 3-D inelastic analyses for computational structural mechanics p 206 N89-29804
- TURBOMACHINE BLADES**
- A review of turbomachinery blade-row interaction research [NASA-CR-182211] p 24 N89-12567
- Turbine airfoil film cooling p 158 N89-12903
- Multigrad calculation of three-dimensional turbomachinery flows [NASA-CR-185332] p 165 N89-26172

- Probabilistic structural analysis methods of hot engine structures [NASA-TM-102091] p 205 N89-28030
- TURBOMACHINERY**
- Effect of particulate thermophoresis in reducing the fouling rate advantages of effusion-cooling p 141 A89-14599
- An unconditionally stable Runge-Kutta method for unsteady flows p 2 A89-25180
- [AIAA PAPER 89-0205] p 2 A89-25180
- A simple time-accurate turbomachinery algorithm with numerical solutions of an uneven blade count configuration p 179 A89-25181
- [AIAA PAPER 89-0206] p 179 A89-25181
- Kinetic energy equations for the average-passage equation system p 237 A89-28347
- Calculation of unsteady flows in turbomachinery using the linearized Euler equations p 149 A89-36916
- A generalized one dimensional computer code for turbomachinery cooling passage flow calculations [AIAA PAPER 89-2574] p 151 A89-46934
- Interactive grid generation for turbomachinery flow field simulations [NASA-TM-101301] p 9 N89-11717
- Simulation of 3-D viscous flow within a multi-stage turbine [NASA-TM-101376] p 26 N89-14238
- Application of a lower-upper implicit scheme and an interactive grid generation for turbomachinery flow field simulations [NASA-TM-101412] p 11 N89-15077
- Experimental determination of stator endwall heat transfer [NASA-TM-101419] p 159 N89-15366
- Technique for temperature compensation of eddy-current proximity probes [NASA-TP-2880] p 173 N89-15380
- Modal forced vibration analysis of aerodynamically excited turbosystems p 201 N89-18696
- [NASA-CR-174966] p 201 N89-18696
- Turbomachinery aeroelasticity at NASA Lewis Research Center p 28 N89-19262
- NASTRAN supplemental documentation for modal forced vibration analysis of aerodynamically excited turbosystems [NASA-CR-174967] p 201 N89-19583
- A generalized one-dimensional computer code for turbomachinery cooling passage flow calculations [NASA-TM-102079] p 163 N89-22862
- Rotordynamic Instability Problems in High-Performance Turbomachinery, 1988 [NASA-CP-3026] p 185 N89-22891
- Structural dynamics branch research and accomplishments for FY 1988 [NASA-TM-101406] p 202 N89-22939
- Turbomachinery technology for high-speed civil flight [NASA-TM-102092] p 32 N89-24320
- Multigrad calculation of three-dimensional turbomachinery flows [NASA-CR-185332] p 165 N89-26172
- TURBOPROP AIRCRAFT**
- Return of the turboprops p 20 A89-12953
- NASA/industry advanced turboprop technology program p 20 A89-13504
- Cruise noise of an advanced counterrotation turboprop measured from an adjacent aircraft p 20 A89-15080
- Advanced turboprop project [NASA-SP-495] p 24 N89-12565
- High speed turboprop aeroacoustic study (single rotation). Volume 1: Model development [NASA-CR-182257-VOL-1] p 229 N89-24139
- Cruise noise of the SR-2 propeller model in a wind tunnel [NASA-TM-101480] p 229 N89-24886
- TURBOPROP ENGINES**
- Near wakes of advanced turbopropellers [AIAA PAPER 89-1095] p 5 A89-33735
- Computerized life and reliability modeling for turboprop transmissions p 181 A89-53364
- Experimental aerodynamic performance of advanced 40 deg-swept 10-blade propeller model at Mach 0.6 to 0.85 [NASA-TM-88969] p 9 N89-10865
- Parametric studies of advanced turboprops [NASA-TM-101389] p 197 N89-14465
- Measured far-field flight noise of a counterrotation turboprop at cruise conditions [NASA-TM-101383] p 228 N89-15686
- NASA advanced propeller research [NASA-TM-101361] p 27 N89-15913
- Wind-tunnel results of advanced high-speed propellers at takeoff, climb, and landing Mach numbers [NASA-TM-87030] p 13 N89-19265
- Structural Tailoring of Advanced Turboprops (STAT) programmer's manual [NASA-CR-182164] p 29 N89-20132



## SUBJECT INDEX

High speed turboprop aeroacoustic study (single rotation). Volume 1: Model development [NASA-CR-182257-VOL-1] p 229 N89-24139

**TURBOSHAPTS**  
Contingency power for small turboshaft engines p 21 A89-22291  
Integrated control and health monitoring capacitive displacement sensor development task. Orbit transfer rocket engine technology program [NASA-CR-182279] p 176 N89-26208

**TURBULENCE**  
Effects of core turbulence on jet excitability [AIAA PAPER 89-0966] p 147 A89-30482  
Direct numerical simulations of a temporally evolving mixing layer subject to forcing p 147 A89-34426  
Effects of core turbulence on jet excitability [NASA-TM-101405] p 159 N89-14403  
Heat transfer with very high free-stream turbulence and heat transfer with streamwise vortices p 160 N89-17309  
On the nature of Navier-Stokes turbulence [NASA-TM-101983] p 163 N89-23813

**TURBULENCE METERS**  
Turbulence management in free shear flows by control of coherent structures p 147 A89-30908

**TURBULENCE MODELS**  
PNS calculations for 3-D hypersonic corner flow with two turbulence models p 1 A89-14979  
Turbulence modeling in a hypersonic inlet p 8 A89-53931  
Evaluation of three turbulence models for the prediction of steady and unsteady airloads [NASA-TM-101413] p 10 N89-12555  
Influence of bulk turbulence and entrance boundary layer thickness on the curved duct flow field [NASA-CR-4188] p 155 N89-12838  
Development of low Reynolds number two equation turbulence models for predicting external heat transfer on turbine blades p 157 N89-12901  
A low-Reynolds-number two-equation turbulence model for predicting heat transfer on turbine blades p 160 N89-17310  
A model for prediction of STOVU ejector dynamics [NASA-TM-102098] p 32 N89-24319  
Mesh refinement in a two-dimensional large eddy simulation of a forced shear layer [NASA-TM-102129] p 166 N89-26180  
Calculation of turbulence-driven secondary motion in ducts with arbitrary cross section [NASA-TM-102142] p 166 N89-27115  
Calculation of reattaching shear layers in divergent channel with a multiple-time-scale turbulence model [NASA-TM-102293] p 168 N89-28749

**TURBULENT BOUNDARY LAYER**  
Experimental study of the development of longitudinal vortex pairs embedded in a turbulent boundary layer p 140 A89-11107  
Thermophoretically enhanced mass transport rates to solid and transpiration-cooled walls across turbulent (law-of-the-wall) boundary layers p 141 A89-12340  
Axisymmetric confined turbulent jet directed towards the liquid surface from below p 145 A89-25148  
Preliminary study of the interactions caused by crossing shock waves and a turbulent boundary layer [AIAA PAPER 89-0359] p 145 A89-25303  
Experimental and numerical investigation of an oblique shock wave/turbulent boundary layer interaction with continuous suction p 4 A89-28407  
Effects of nozzle exit boundary-layer conditions on excitability of heated free jets p 149 A89-36908  
An experimental study of a reattaching supersonic shear layer p 6 A89-42036  
Asymptotic structure and similarity solutions for three-dimensional turbulent boundary layers [AIAA PAPER 89-1863] p 150 A89-42090  
Axisymmetric confined turbulent jet directed towards the liquid surface from below p 158 N89-13749  
Some characteristics of bypass transition in a heated boundary layer [NASA-TM-102126] p 164 N89-24577

**TURBULENT FLOW**  
Experimental study of isothermal swirling flows in a dump combustor p 21 A89-23182  
Studies of transition in boundary layers [AIAA PAPER 89-0034] p 2 A89-25029  
Evaluation of three turbulence models for the prediction of steady and unsteady airloads [AIAA PAPER 89-0609] p 3 A89-25485  
Interaction of an oblique shock wave with turbulent hypersonic blunt body flows p 3 A89-28405 [AIAA PAPER 89-0272]

Numerical investigation of chemically reacting flows in ramjet dump combustors p 22 A89-28408 [AIAA PAPER 89-0387]  
Coherent structures in transitional and turbulent free shear flows p 147 A89-28999  
Turbulence management in free shear flows by control of coherent structures p 147 A89-30908  
Effects of heat release on the large-scale structure in turbulent mixing layers p 147 A89-31844  
The turbulence characteristics of a separated flow with combustion p 92 A89-33369  
Correlations of velocity and temperature fluctuations in the stagnation-point flow of circular cylinder in turbulent flow p 148 A89-34927  
The use of direct numerical simulation in the study of turbulent, chemically-reacting flows p 152 A89-51873  
Turbulent multiphase flows p 152 A89-51883  
Turbulence modeling in a hypersonic inlet p 8 A89-53931  
Improved numerical methods for turbulent viscous flows aerothermal modeling program, phase 2 [NASA-CR-182169] p 154 N89-12010  
Evaluation of three turbulence models for the prediction of steady and unsteady airloads [NASA-TM-101413] p 10 N89-12555  
Influence of bulk turbulence and entrance boundary layer thickness on the curved duct flow field [NASA-CR-4188] p 155 N89-12838  
Improved numerical methods for turbulent viscous recirculating flows p 156 N89-12895  
Heat transfer with very high free-stream turbulence and streamwise vortices p 157 N89-12900  
A near-wall turbulence model and its application to fully developed turbulent channel and pipe flows [NASA-TM-101399] p 158 N89-13741  
The effects of inlet turbulence and rotor/stator interactions on the aerodynamics and heat transfer of a large-scale rotating turbine model, volume 1 [NASA-CR-4079] p 159 N89-13756  
A prediction of 3-D viscous flow and performance of the NASA low-speed centrifugal compressor [NASA-CR-184765] p 160 N89-16132  
A comparison of turbulence measurement methods p 174 N89-17302  
Aerothermal modeling program. Phase 2, element B: Flow interaction experiment p 160 N89-17304  
A low-Reynolds-number two-equation turbulence model for predicting heat transfer on turbine blades p 160 N89-17310  
Measurement of airfoil heat transfer coefficients on a turbine stage p 160 N89-17311  
Control-volume based Navier-Stokes equation solver valid at all flow velocities [NASA-TM-101488] p 161 N89-20407  
Numerical computation of shock wave-turbulent boundary layer interaction in transonic flow over an axisymmetric curved hill [NASA-TM-101473] p 162 N89-21192  
On the conditions for resonance interactions of instability waves in the axisymmetric jet [NASA-TM-101477] p 162 N89-21196  
An explicit Runge-Kutta method for turbulent reacting flow calculations [NASA-TM-101945] p 31 N89-21799  
Calculation of turbulence-driven secondary motion in ducts with arbitrary cross section [NASA-TM-102142] p 166 N89-27115  
Calculation of reattaching shear layers in divergent channel with a multiple-time-scale turbulence model [NASA-TM-102293] p 168 N89-28749  
Turbulent swirling jets with excitation [NASA-CR-180895] p 16 N89-29329  
Numerical investigation of an internal layer in turbulent flow over a curved hill [NASA-TM-102230] p 168 N89-29725

**TURBULENT JETS**  
Passive and active control of jet turbulence p 140 A89-10176  
Axisymmetric confined turbulent jet directed towards the liquid surface from below p 145 A89-25148 [AIAA PAPER 89-0172]  
Large amplitude acoustic excitation of swirling turbulent jets [AIAA PAPER 89-0970] p 4 A89-29098  
Effect of initial swirl distribution on the evolution of a turbulent jet p 149 A89-36906  
Vapor condensation at a turbulent liquid surface in systems with possible spaced-based applications [AIAA PAPER 89-2846] p 151 A89-47122  
Transient flow thrust prediction for an ejector propulsion concept [AIAA PAPER 89-2906] p 23 A89-49688  
A numerical and experimental study of coaxial jets p 153 A89-52500

## TWO PHASE FLOW

A control-volume method for analysis of unsteady thrust augmenting ejector flows p 24 N89-12566 [NASA-CR-182203]  
Axisymmetric confined turbulent jet directed towards the liquid surface from below p 158 N89-13749 [NASA-TM-101409]  
Large amplitude acoustic excitation of swirling turbulent jets p 13 N89-18417 [NASA-TM-101950]  
Transient flow thrust prediction for an ejector propulsion concept p 32 N89-24318 [NASA-TM-102078]  
Multiwave interactions in turbulent jets [NASA-TM-101985] p 168 N89-29714

**TURBULENT MIXING**  
Particle cloud mixing in microgravity [NASA-TM-101484] p 121 N89-20321

**TURBULENT WAKES**  
Prediction of unsteady rotor-surface heat transfer from wake passages [AIAA PAPER 89-1692] p 150 A89-43210

**TVD SCHEMES**  
A numerical study of ENO and TVD schemes for shock capturing [NASA-TM-101355] p 222 N89-11469

**TWO DIMENSIONAL BODIES**  
Flow of rarefied gases over two-dimensional bodies [AIAA PAPER 89-1970] p 5 A89-41814  
A comparison of numerical methods for the prediction of two-dimensional heat transfer in an electrothermal deicer pad [NASA-CR-4202] p 19 N89-13429

**TWO DIMENSIONAL BOUNDARY LAYER**  
A numerical method for computing unsteady 2-D boundary layer flows [NASA-CR-4198] p 155 N89-12835

**TWO DIMENSIONAL FLOW**  
Flux splitting algorithms for two-dimensional viscous flows with finite-rate chemistry [AIAA PAPER 89-0388] p 146 A89-28409  
A simple algebraic grid adaptation scheme with applications to two- and three-dimensional flow problems [AIAA PAPER 89-1984] p 5 A89-41827  
A block-corrected subdomain solution procedure for recirculating flow calculations p 152 A89-50147  
Application of multi-grid methods for solving the Navier-Stokes equations p 153 A89-53172  
Experimental results for a two-dimensional supersonic inlet used as a thrust deflecting nozzle [NASA-TM-83439] p 159 N89-14386  
Two- and three-dimensional turbine blade row flow field simulations p 161 N89-17313  
Nonlinear evolution of interacting oblique waves on two-dimensional shear layers [NASA-TM-102030] p 164 N89-24575  
A genuinely multi-dimensional upwind cell-vertex scheme for the Euler equations p 223 N89-24872 [NASA-TM-102029]  
Multigrid calculation of three-dimensional turbomachinery flows [NASA-CR-185332] p 165 N89-26172

**TWO DIMENSIONAL MODELS**  
Rarefied gas flow through two-dimensional nozzles [AIAA PAPER 89-2893] p 7 A89-47156  
A numerical study of chemically reacting flow in nozzles [AIAA PAPER 89-2793] p 60 A89-49687  
A numerical simulation of the full two-dimensional electrothermal de-icer pad [NASA-CR-4194] p 19 N89-14235  
A numerical study of chemically reacting flow in nozzles [NASA-TM-102135] p 70 N89-24444

**TWO FLUID MODELS**  
Gas density effect on droplets of simulated fuel sprays [AIAA PAPER 89-2322] p 151 A89-46749  
Gas density effect on droplets of simulated fuel sprays [NASA-TM-102013] p 162 N89-22053  
Millimeter wave transmission studies of YBa<sub>2</sub>Cu<sub>3</sub>O<sub>7</sub>-delta thin films in the 26.5 to 40.0 GHz frequency range [NASA-TM-102345] p 237 N89-30088

**TWO PHASE FLOW**  
Rational engineering correlations of diffusional and inertial particle deposition behavior in non-isothermal forced convection environments p 140 A89-12327  
Navier-Stokes solution to the flowfield over ice accretion shapes p 1 A89-12557  
Fuel spray simulation with two-fluid nozzles [AIAA PAPER 89-0053] p 145 A89-25047  
Gas density effect on droplets of simulated fuel sprays [AIAA PAPER 89-2322] p 151 A89-46749

## UDIMET ALLOYS

- Fluid spray simulation with two-fluid nozzles  
[NASA-TM-101367] p 155 N89-12028  
Dynamics of face and annular seals with two-phase flow  
[NASA-CR-183352] p 182 N89-12870  
Thermal effects in two-phase flow through face seals  
[NASA-CR-185968] p 182 N89-13788  
Gas density effect on droplet size of simulated fuel sprays  
[NASA-TM-102013] p 162 N89-22053

## U

### UDIMET ALLOYS

- Mechanical properties of modified low cobalt powder metallurgy Udimet 700 type alloys  
[NASA-TM-101481] p 103 N89-20228

### UH-60A HELICOPTER

- Comparison of predicted and measured temperatures of UH-60A helicopter transmission  
[NASA-TP-2911] p 186 N89-24607

### ULTRASONIC FLAW DETECTION

- Ultrasonic attenuation measurements determine onset, degree, and completion of recrystallization  
p 187 A89-23936

### ULTRASONIC RADIATION

- Ultrasonic attenuation measurements determine onset, degree, and completion of recrystallization  
p 188 A89-42864

### ULTRASONIC SCANNERS

- Ultrasonic imaging of porosity variations produced during sintering  
p 107 A89-48892

### ULTRASONIC TESTS

- Radiographic and ultrasonic characterization of sintered silicon carbide  
p 187 A89-14700  
High-frequency ultrasonic characterization of sintered silicon carbide  
p 106 A89-34840

- Nondestructive evaluation/characterization of composite materials and structures using the acousto-ultrasonic techniques  
p 188 A89-36571  
Energy in elastic fiber embedded in elastic matrix containing incident SH wave  
p 188 N89-18694

- Nondestructive evaluation of advanced ceramics  
[NASA-TM-101489] p 189 N89-20490  
A study of the stress wave factor technique for evaluation of composite materials  
p 189 N89-21256

### ULTRASONICS

- Concepts for interrelating ultrasonic attenuation, microstructure, and fracture toughness in polycrystalline solids  
p 95 A89-19852

- The acousto-ultrasonic approach --- for NDE  
p 188 A89-32305

- Ultrasonic imaging of textured alumina  
[NASA-TM-101478] p 189 N89-28853

### ULTRAVIOLET RADIATION

- Townsend coefficients for electron scattering over dielectric surfaces  
p 231 A89-16409

### ULTRAVIOLET SPECTRA

- The NASA atomic oxygen effects test program  
p 93 N89-12589

### UNIVERSE

- Cosmic strings and the large-scale structure  
p 240 A89-19604

### UNSTEADY AERODYNAMICS

- Investigation of oscillating cascade aerodynamics by an experimental influence coefficient technique  
[AIAA PAPER 88-2815] p 1 A89-14976

- Effect of aerodynamic detuning on supersonic rotor discrete frequency noise generation  
p 225 A89-15083  
Aeroelastic response of metallic and composite propfan models in yawed flow  
p 20 A89-17942

- Instabilities caused by oscillating accelerations normal to a viscous fluid-fluid interface  
p 144 A89-22823  
Experimental investigation of transonic oscillating cascade aerodynamics  
[AIAA PAPER 89-0321] p 3 A89-26369

- Numerical analysis of flow through oscillating cascade sections  
[AIAA PAPER 89-0437] p 4 A89-28413

- On the role of artificial viscosity in Navier-Stokes solvers  
[AIAA PAPER 89-1947] p 5 A89-41794

- Prediction of unsteady rotor-surface heat transfer from wake passages  
[AIAA PAPER 89-1692] p 150 A89-43210

- A review of turbomachinery blade-row interaction research  
[NASA-CR-182211] p 24 N89-12567

- Numerical analysis of flow through oscillating cascade sections  
[NASA-TM-101417] p 11 N89-14220

- Experimental investigation of transonic oscillating cascade aerodynamics  
[NASA-TM-101993] p 29 N89-20133

- On the Lagrangian description of unsteady boundary layer separation. Part 2: The spinning sphere  
[NASA-TM-102027] p 163 N89-22861

- Influence of thickness and camber on the aeroelastic stability of supersonic throughflow fans: An engineering approach  
[NASA-TM-101949] p 15 N89-25957

### UNSTEADY FLOW

- Calculations of the unsteady, three-dimensional flow field inside a motored Wankel engine  
[SAE PAPER 880625] p 19 A89-12307

- Unsteady solution of incompressible Navier-Stokes equations  
p 141 A89-15143

- Status of several Stirling loss characterization efforts and their significance for Stirling space power development  
p 49 A89-15187

- Effect of transition on oscillation flow losses in Stirling engine coolers and heaters  
p 142 A89-15189

- An unconditionally stable Runge-Kutta method for unsteady flows  
[AIAA PAPER 89-0205] p 2 A89-25180

- Kinetic energy equations for the average-passage equation system  
p 237 A89-28347

- Unsteady Euler cascade analysis  
[AIAA PAPER 89-0322] p 3 A89-28406

- Explicit Runge-Kutta method for unsteady rotor/stator interaction  
p 5 A89-36912

- Calculation of unsteady flows in turbomachinery using the linearized Euler equations  
p 149 A89-36916

- Assessment of numerical techniques for unsteady flow calculations  
[AIAA PAPER 89-1956] p 150 A89-41803

- Transient flow thrust prediction for an ejector propulsion concept  
[AIAA PAPER 89-2906] p 23 A89-49688

- Numerical analysis of supersonic flow through oscillating cascade sections by using a deforming grid  
[AIAA PAPER 89-2805] p 8 A89-50810

- Unsteady heat transfer in turbine blade ducts - Focus on combustor sources  
p 153 A89-53286

- An algorithm for unsteady flows with strong convection  
[NASA-TM-100828] p 221 N89-10575

- A control-volume method for analysis of unsteady thrust augmenting ejector flows  
[NASA-CR-182203] p 24 N89-12566

- A numerical method for computing unsteady 2-D boundary layer flows  
[NASA-CR-4198] p 155 N89-12835

- Absorbing boundary conditions for second-order hyperbolic equations  
[NASA-TM-102009] p 223 N89-22397

- On the Lagrangian description of unsteady boundary layer separation. Part 1: General theory  
[NASA-TM-102026] p 164 N89-23821

- Conservative treatment of boundary interfaces for overlaid grids and multi-level grid adaptations  
[NASA-TM-102080] p 15 N89-24269

- Transient flow thrust prediction for an ejector propulsion concept  
[NASA-TM-102078] p 32 N89-24318

- Numerical analysis of supersonic flow through oscillating cascade sections by using a deforming grid  
[NASA-TM-102053] p 15 N89-25119

- Time domain numerical calculations of unsteady vortical flows about a flat plate airfoil  
[NASA-TM-102318] p 168 N89-29726

- Further development of the dynamic gas temperature measurement system. Volume 2: Computer program user's manual  
[NASA-CR-182180] p 10 N89-13399

- [NASA-CR-179513-VOL-2] p 173 N89-13771

- MHOST version 4.2. Volume 1: Users' manual  
[NASA-CR-182235-VOL-1] p 217 N89-13996

- An analysis for high speed propeller-nacelle aerodynamic performance prediction. Volume 2: User's manual  
[NASA-CR-4199-VOL-2] p 12 N89-15897

- NASTRAN supplemental documentation for modal forced vibration analysis of aerodynamically excited turbosystems  
[NASA-CR-174967] p 201 N89-19583

- Composite blade structural analyzer (COBSTRAN) user's manual  
[NASA-TM-101461] p 86 N89-23621

- Fatigue crack growth model RANDOM2 user manual, appendix 1  
[NASA-CR-184939] p 203 N89-23890

- Effects of leading edge and downstream film cooling on turbine vane heat transfer  
[NASA-CR-182133] p 158 N89-13754

- Experimental determination of stator endwall heat transfer  
[NASA-TM-101419] p 159 N89-15366

- Three-dimensional inelastic analysis methods for hot section components  
p 199 N89-17316

- Deposition of Na<sub>2</sub>SO<sub>4</sub> from salt-seeded combustion gases of a high velocity burner rig  
p 89 A89-12330

- Laboratory studies of binary salt CVD in combustion gas environments  
p 89 A89-12335

- Laboratory studies of the deposition of alkali sulfate vapors from combustion gases using a flash-evaporation technique  
p 89 A89-12338

- Growth of diamond by RF plasma-assisted chemical vapor deposition  
p 90 A89-20474

- Vapor deposition and condensate flow on combustion turbine blades - Theoretical model to predict/understand some corrosion rate consequences of molten alkali sulfate deposition in the field or laboratory  
p 21 A89-20950

## SUBJECT INDEX

- Fatigue strength reduction model: RANDOM3 and RANDOM4 user manual, appendix 2  
[NASA-CR-184940] p 203 N89-23891

- Composite Blade Structural Analyzer (COBSTRAN) demonstration manual  
[NASA-TM-101957] p 87 N89-24459

### USER REQUIREMENTS

- Conceptual design of an advanced Stirling conversion system for terrestrial power generation  
[NASA-CR-180890] p 238 N89-12504

- Mars manned transportation vehicle  
[NASA-TM-101487] p 210 N89-20545

- User needs, benefits and integration of robotic systems in a space station laboratory  
[NASA-CR-182261] p 185 N89-22108

## V

### V GROOVES

- A V-grooved GaAs solar cell  
[NASA-TM-101970] p 211 N89-22177

- The GaAs solar cells with V-grooved emitters  
[NASA-TM-102104] p 214 N89-26291

### V/STOL AIRCRAFT

- Model-based analysis of control/display interaction in the hover task  
p 215 A89-36933

- Integrated flight/propulsion control study for STOVL applications  
[AIAA PAPER 89-2908] p 34 A89-47166

- Experimental results for a two-dimensional supersonic inlet used as a thrust deflecting nozzle  
[NASA-TM-83439] p 159 N89-14386

- Hot gas ingestion testing of an advanced STOVL concept in the NASA Lewis 9- by 15-foot low speed wind tunnel with flow visualization  
[NASA-TM-100952] p 11 N89-15078

- Multiple-Purpose Subsonic Naval Aircraft (MPSNA) Multiple Application Propan Study (MAPS)  
[NASA-CR-175096] p 18 N89-19289

- STOL and STOVL hot gas ingestion and airframe heating tests in the NASA Lewis 9- by 15-foot low-speed wind tunnel  
[NASA-TM-102101] p 15 N89-29323

- Deposition and characterization of ZnS/Si heterojunctions produced by vacuum evaporation  
[NASA-TM-101359] p 135 N89-11129

- Reaction of perfluoroalkylpolyethers (PFPE) with 440C steel in vacuum under sliding conditions at room temperature  
[NASA-TP-2883] p 115 N89-26091

- The influence of annealing in the ferrite-plus-austenite phase field on the stability of vanadium carbide precipitates  
p 97 A89-32803

- Effects of microstructure and nonstoichiometry on electrical properties of vanadium dioxide films  
p 236 A89-44527

- Euler analysis of a swirl recovery vane design for use with an advanced single-rotation propan  
[AIAA PAPER 88-3152] p 2 A89-17940

- Development of a high temperature static strain sensor  
p 173 N89-12887

- On 3D inelastic analysis methods for hot section components  
p 196 N89-12906

- Component specific modeling  
p 25 N89-12907

- Elevated temperature crack growth  
p 196 N89-12915

- The effects of leading edge and downstream film cooling on turbine vane heat transfer  
[NASA-CR-182133] p 158 N89-13754

- Experimental determination of stator endwall heat transfer  
[NASA-TM-101419] p 159 N89-15366

- Three-dimensional inelastic analysis methods for hot section components  
p 199 N89-17316

- Deposition of Na<sub>2</sub>SO<sub>4</sub> from salt-seeded combustion gases of a high velocity burner rig  
p 89 A89-12330

- Laboratory studies of binary salt CVD in combustion gas environments  
p 89 A89-12335

- Laboratory studies of the deposition of alkali sulfate vapors from combustion gases using a flash-evaporation technique  
p 89 A89-12338

- Growth of diamond by RF plasma-assisted chemical vapor deposition  
p 90 A89-20474

- Vapor deposition and condensate flow on combustion turbine blades - Theoretical model to predict/understand some corrosion rate consequences of molten alkali sulfate deposition in the field or laboratory  
p 21 A89-20950

- Raman determination of layer stresses and strains for heterostructures and its application to the cubic SiC/Si system p 234 A89-21871
- Evaluation of transport conditions during physical vapor transport growth of opto-electronic crystals [AIAA PAPER 89-0229] p 118 A89-25197
- Surface studies relevant to silicon carbide chemical vapor deposition p 91 A89-27966
- Interaction of surface radiation with convection in crystal growth by physical vapor transport [AIAA PAPER 89-0228] p 119 A89-30450
- Strength distribution of reinforcing fibers in a Nicalon fiber/chemically vapor infiltrated silicon carbide matrix composite p 82 A89-34844
- Radio-frequency plasma chemical vapor deposition growth of diamond p 236 A89-44552
- Adhesion scratch testing - A round-robin experiment p 171 A89-54281
- Thermal barrier coating life prediction model development p 200 N89-17333
- Convection and chemistry effects in CVD: A 3-D analysis for silicon deposition [NASA-TM-102001] p 78 N89-21032
- A V-grooved GaAs solar cell [NASA-TM-101970] p 211 N89-22177
- High efficiency GaAs-Ge tandem solar cells grown by MOCVD p 213 N89-24721
- Chemical etching and organometallic chemical vapor deposition on varied geometries of GaAs p 213 N89-24728
- Theoretical studies in support of the 3M-vapor transport (PVTOS-) experiments [NASA-CR-185122] p 165 N89-26179
- VAPOR PHASE EPITAXY**
- Crystal growth of SiC for electronic applications p 132 A89-33625
- High-efficiency solar cells fabricated from direct-current magnetron sputtered n-indium tin oxide onto p-InP grown by atmospheric pressure metalorganic vapor phase epitaxy p 133 A89-44518
- VARIABILITY**
- Aerodynamic optimization by simultaneously updating flow variables and design parameters with application to advanced propeller designs [NASA-CR-182181] p 24 N89-11750
- Dynamic porosity variations in ceramics [NASA-TM-101340] p 112 N89-17668
- VARIABLE CYCLE ENGINES**
- Turbomachinery technology for high-speed civil flight [NASA-TM-102092] p 32 N89-24320
- VARIABLE PITCH PROPELLERS**
- Wind-tunnel results of advanced high-speed propellers at takeoff, climb, and landing Mach numbers [NASA-TM-87030] p 13 N89-19265
- VARIATIONS**
- A numerical study of ENO and TVD schemes for shock capturing [NASA-TM-101355] p 222 N89-11469
- VECTOR ANALYSIS**
- A vector scanning processing technique for pulsed laser velocimetry [NASA-TM-102048] p 175 N89-23850
- VECTORS (MATHEMATICS)**
- Recursive algorithms for vector extrapolation methods p 221 A89-14397
- VELOCITY DISTRIBUTION**
- Effect of initial swirl distribution on the evolution of a turbulent jet p 149 A89-36906
- Time domain numerical calculations of unsteady vortical flows about a flat plate airfoil [NASA-TM-102318] p 168 N89-29726
- VELOCITY MEASUREMENT**
- Application of optical correlation techniques to particle imaging [AIAA PAPER 88-4661] p 169 A89-14985
- A numerical and experimental study of confined swirling jets [AIAA PAPER 89-2898] p 151 A89-47161
- Three component laser anemometer measurements in an annular cascade of core turbine vanes with contoured end wall [NASA-TM-2846] p 9 N89-10844
- LDV measurements in an annular combustor model [NASA-CR-182207] p 159 N89-13755
- A comparison of turbulence measurement methods p 174 N89-17302
- VENTILATION**
- Fire safety applications for spacecraft [NASA-TM-101463] p 42 N89-24413
- VERTICAL LANDING**
- Noise generated by a flight weight, air flow control valve in a vertical takeoff and landing aircraft thrust vectoring system [NASA-CR-182232] p 228 N89-20776
- VERTICAL TAKEOFF**
- Noise generated by a flight weight, air flow control valve in a vertical takeoff and landing aircraft thrust vectoring system [NASA-CR-182232] p 228 N89-20776
- VIBRATION**
- Vibration signature analysis of multistage gear transmission [NASA-TM-101442] p 184 N89-18685
- VIBRATION DAMPING**
- Experimental results for labyrinth gas seals with honeycomb stators - Comparisons to smooth-stator seals and theoretical predictions [ASME PAPER 88-TRIB-40] p 179 A89-24992
- Piezoelectric pushers for active vibration control of rotating machinery p 171 A89-47717
- Active vibration control for flexible rotor by optimal direct-output feedback control [NASA-TM-101972] p 31 N89-22605
- Structural dynamics branch research and accomplishments for FY 1988 [NASA-TM-101406] p 202 N89-22939
- Tailoring of composite links for optimal damped elasto-dynamic performance [NASA-TM-102094] p 88 N89-26912
- Unified micromechanics of damping for unidirectional fiber reinforced composites [NASA-TM-102107] p 88 N89-26919
- VIBRATION ISOLATORS**
- Low frequency vibration isolation technology for microgravity space experiments [NASA-TM-101448] p 123 N89-20324
- VIBRATION TESTS**
- Vibration testing of impact-damaged composite laminates [AIAA PAPER 89-1411] p 81 A89-30883
- A modified VAPEPS method for predicting vibroacoustic response of unreinforced mass loaded honeycomb panels [NASA-TM-101467] p 46 N89-16905
- Modal forced vibration analysis of aerodynamically excited turbosystems [NASA-CR-174966] p 201 N89-18696
- Structural Tailoring of Advanced Turboprops (STAT) programmer's manual [NASA-CR-182164] p 29 N89-20132
- Vibration testing of impact-damaged composite laminates [NASA-TM-4115] p 87 N89-25290
- VIBRATIONAL SPECTRA**
- Design and simulated performance of a CARS spectrometer for dynamic temperature measurements using electronic heterodyning p 170 A89-37298
- VIDEO EQUIPMENT**
- High resolution video monitoring of coating thickness during plasma spraying [NASA-TM-101423] p 102 N89-15218
- VIDEO SIGNALS**
- Digital CODEC for real-time processing of broadcast quality video signals at 1.8 bits/pixel [NASA-TM-102325] p 129 N89-27927
- VIRTUAL MEMORY SYSTEMS**
- Interfacing laboratory instruments to multiuser, virtual memory computers [NASA-TM-4106] p 188 N89-19578
- VISCOELASTICITY**
- Solution methods for one-dimensional viscoelastic problems p 191 A89-19914
- VISCOPLASTICITY**
- A viscoplastic constitutive theory for metal matrix composites at high temperature p 80 A89-20725
- Nonisothermal elastoviscoplastic snap-through and creep buckling of shallow arches p 194 A89-47370
- A multiaxial theory of viscoplasticity for isotropic materials p 196 N89-12908
- Non-isothermal buckling behavior of viscoplastic shell structures [NASA-CR-183013] p 197 N89-12931
- Considerations in development and implementation of elasto-viscoplastic constitutive model for high temperature applications [NASA-CR-183403] p 197 N89-12932
- MHOST version 4.2. Volume 1: Users' manual [NASA-CR-182235-VOL-1] p 217 N89-13996
- Thermoviscoplastic model with application to copper [NASA-TM-2845] p 198 N89-16183
- Finite element implementation of viscoplastic models p 200 N89-17328
- Refinements in a viscoplastic model [NASA-TM-102338] p 205 N89-28036
- VISCOSITY**
- On the role of artificial viscosity in Navier-Stokes solvers [AIAA PAPER 89-1947] p 5 A89-41794
- VISCOUS FLOW**
- Viscous analysis of high speed flows using an upwind finite volume technique [AIAA PAPER 89-0001] p 144 A89-25001
- A diagonally inverted LU implicit multigrid scheme for the 3-D Navier-Stokes equations and a two equation model of turbulence [AIAA PAPER 89-0467] p 145 A89-25382
- Flux splitting algorithms for two-dimensional viscous flows with finite-rate chemistry [AIAA PAPER 89-0388] p 146 A89-28409
- Three dimensional viscous analysis of a hypersonic inlet [AIAA PAPER 89-0004] p 4 A89-29924
- A diagonally inverted LU implicit multigrid scheme for the 3-D Navier-Stokes equations and a two equation model of turbulence [NASA-CR-182209] p 9 N89-10863
- Improved numerical methods for turbulent viscous flows aerothermal modeling program, phase 2 [NASA-CR-182169] p 154 N89-12010
- Simulation of 2-dimensional viscous flow through cascades using a semi-elliptic analysis and hybrid C-H grids [NASA-CR-4180] p 10 N89-12553
- Improved numerical methods for turbulent viscous recirculating flows p 156 N89-12895
- Three-dimensional marginal separation [NASA-TM-101411] p 159 N89-13757
- Simulation of 3-D viscous flow within a multi-stage turbine [NASA-TM-101376] p 26 N89-14238
- Development of an integrated BEM approach for hot fluid structure interaction [NASA-CR-184587] p 27 N89-15114
- Three dimensional viscous analysis of a hypersonic inlet [NASA-TM-101474] p 13 N89-16759
- An explicit Runge-Kutta method for turbulent reacting flow calculations [NASA-TM-101945] p 31 N89-21799
- Transonic viscous flow calculations for a turbine cascade with a two equation turbulence model [NASA-TM-101944] p 32 N89-22607
- Least-squares finite element method for fluid dynamics [NASA-TM-102352] p 223 N89-30008
- VISCOUS FLUIDS**
- Instabilities caused by oscillating accelerations normal to a viscous fluid-fluid interface p 144 A89-22823
- VITREOUS MATERIALS**
- Crystallization and characterization of Y<sub>2</sub>O<sub>3</sub>-SiO<sub>2</sub> glasses p 80 A89-19486
- Microstructural evolution on crystallizing the glassy phase in a 6 weight percent Y<sub>2</sub>O<sub>3</sub>-Si<sub>3</sub>N<sub>4</sub> ceramic p 80 A89-19487
- VOIDS**
- Arjet cathode phenomena [NASA-TM-102099] p 167 N89-27121
- VOLT-AMPERE CHARACTERISTICS**
- Effects of operating parameters on PAFC stack performance p 207 A89-15250
- Temperature coefficients for concentrator cells at various electron and proton fluence levels p 51 A89-15304
- Computer analysis of the negative differential resistance switching phenomenon of double-injection devices p 134 A89-54963
- VOLTAGE CONVERTERS (AC TO AC)**
- A Fourier analysis for a fast simulation algorithm --- for switching converters p 130 A89-15367
- VOLTAGE REGULATORS**
- Distortion and regulation characterization of a Mapham inverter [NASA-TM-102089] p 139 N89-26148
- VORTEX BREAKDOWN**
- Turbulent swirling jets with excitation [NASA-CR-180895] p 16 N89-29329
- VORTEX GENERATORS**
- The use of direct numerical simulation in the study of turbulent, chemically-reacting flows p 152 A89-51873
- VORTEX SHEDDING**
- Observations of the frequencies in a sphere wake and of drag increase by acoustic excitation p 142 A89-16884
- Investigation of the flow between a pair of circular cylinders in the flopping regime p 144 A89-22822
- VORTICES**
- Experimental study of the development of longitudinal vortex pairs embedded in a turbulent boundary layer p 140 A89-11107
- Nonlinear interaction between the sinuous and varicose instability modes in a plane wake p 147 A89-33779
- Numerical solution of periodic vortical flows about a thin airfoil [AIAA PAPER 89-1691] p 7 A89-48955

## VORTICITY

Heat transfer with very high free-stream turbulence and streamwise vortices p 157 N89-12900  
Heat transfer with very high free-stream turbulence and heat transfer with streamwise vortices p 160 N89-17309

A low-Reynolds-number two-equation turbulence model for predicting heat transfer on turbine blades p 160 N89-17310

Numerical solution of periodic vortical flows about a thin airfoil [NASA-TM-101998] p 14 N89-23413

Time domain numerical calculations of unsteady vortical flows about a flat plate airfoil [NASA-TM-102318] p 168 N89-29726

## VORTICITY

Response of a chemically reacting shear layer to streamwise vorticity [AIAA PAPER 89-0978] p 150 A89-40400

## W

## WAFERS

External electro-optic probing of millimeter-wave integrated circuits p 133 A89-45266

## WAKES

Observations of the frequencies in a sphere wake and of drag increase by acoustic excitation p 142 A89-16884

Nonlinear interaction between the sinuous and varicose instability modes in a plane wake p 147 A89-33779

Effects of wake passing on stagnation region heat transfer p 148 A89-34928

## WALL FLOW

Discussion of Mills et al. on 'The effect of wall suction and thermophoresis on aerosol particle deposition from a laminar boundary layer on a flat plate' p 140 A89-12331

Arc-driven rail accelerator research [NASA-CR-179584] p 40 N89-13445

A near-wall turbulence model and its application to fully developed turbulent channel and pipe flows [NASA-TM-101399] p 158 N89-13741

An experimental study of near wall flow parameters in the blade end-wall corner region [NASA-CR-4211] p 12 N89-15898

## WALL JETS

Turbulence management in free shear flows by control of coherent structures p 147 A89-30908

## WALLS

Acoustic wave propagation in heterogeneous structures including experimental validation [AIAA PAPER 89-1044] p 225 A89-36214

Heat transfer with very high free-stream turbulence and heat transfer with streamwise vortices p 160 N89-17309

Acoustic wave propagation in heterogeneous structures including experimental validation [NASA-TM-101486] p 224 N89-19965

Acoustic propagation in curved ducts with extended reacting wall treatment [NASA-TM-102110] p 224 N89-25670

OTVE combustor wall condition monitoring [NASA-CR-182275] p 73 N89-26899

## WANKEL ENGINES

Calculations of the unsteady, three-dimensional flow field inside a motored Wankel engine [SAE PAPER 880625] p 19 A89-12307

Adiabatic Wankel type rotary engine [NASA-CR-182233] p 28 N89-17599

## WATER

Investigation of a liquid-fed water resistojet plume [AIAA PAPER 89-2840] p 58 A89-47117

Investigation of a liquid-fed water resistojet plume [NASA-TM-102310] p 75 N89-27706

## WATER INJECTION

Contingency power for small turboshaft engines p 21 A89-22291

## WAVE AMPLIFICATION

Multiwave interactions in turbulent jets [NASA-TM-101985] p 168 N89-29714

## WAVE ATTENUATION

Ultrasonic attenuation measurements determine onset, degree, and completion of recrystallization p 187 A89-23936

Parametric study of electromagnetic waves propagating in absorbing curved S ducts [NASA-TM-102024] p 129 N89-27923

## WAVE DRAG

Sound power spectrum and wave drag of a propeller in flight [AIAA PAPER 89-1081] p 225 A89-33724

## WAVE EXCITATION

Nonlinear spatial evolution of an externally excited instability wave in a free shear layer p 144 A89-23242

## WAVE FRONTS

Three-dimensional wave packets and instability waves in free shear layers and their receptivity p 149 A89-38619

## WAVE FUNCTIONS

Calculation of the electron wave function in a graded-channel double-heterojunction modulation-doped field-effect transistor p 134 A89-54417

## WAVE INTERACTION

Multiple coherent mode interaction in a developing round jet [AIAA PAPER 89-0967] p 147 A89-30483

On the conditions for resonance interactions of instability waves in the axisymmetric jet [NASA-TM-101477] p 162 N89-21196

Interaction between Tollmien-Schlichting waves and free-stream disturbances in boundary-layer flows [NASA-CR-185847] p 167 N89-27118

Multiwave interactions in turbulent jets [NASA-TM-101985] p 168 N89-29714

## WAVE PACKETS

Three-dimensional wave packets and instability waves in free shear layers and their receptivity p 149 A89-38619

## WAVE PROPAGATION

Acoustic wave propagation in heterogeneous structures including experimental validation [AIAA PAPER 89-1044] p 225 A89-36214

Unsteady heat transfer in turbine blade ducts - Focus on combustor sources p 153 A89-53286

Acoustic wave propagation in heterogeneous structures including experimental validation [NASA-TM-101486] p 224 N89-19965

On the conditions for resonance interactions of instability waves in the axisymmetric jet [NASA-TM-101477] p 162 N89-21196

Absorbing boundary conditions for second-order hyperbolic equations [NASA-TM-102009] p 223 N89-22397

Far field expansion for anisotropic wave equations [NASA-TM-102112] p 165 N89-26175

Parametric study of electromagnetic waves propagating in absorbing curved S ducts [NASA-TM-102024] p 129 N89-27923

Millimeter wave transmission studies of YBa<sub>2</sub>Cu<sub>3</sub>O<sub>7- $\delta$</sub>  thin films in the 26.5 to 40.0 GHz frequency range [NASA-TM-102345] p 237 N89-30088

## WAVE REFLECTION

Theory and application of radiation boundary operators p 224 A89-24191

## WAVE SCATTERING

An application of the WKBJ technique to the on-surface radiation condition p 124 A89-21222

Theory and application of radiation boundary operators p 224 A89-24191

Electronic structure of BaO/W cathode surfaces p 132 A89-26862

Review of FD-TD numerical modeling of electromagnetic wave scattering and radar cross section p 19 A89-45107

## WAVEGUIDE WINDOWS

Modeling of some coplanar waveguide discontinuities p 131 A89-24139

## WAVEGUIDES

Modal, ray, and beam techniques for analyzing the EM scattering by open-ended waveguide cavities p 125 A89-39594

Channelized coplanar waveguide: Discontinuities, junctions, and propagation characteristics [NASA-TM-101483] p 137 N89-21172

Analysis of the EM scattering from arbitrary open-ended waveguide cavities using axial Gaussian Beam tracking [NASA-CR-185054] p 128 N89-24518

## WEAPON SYSTEMS

Summary and evaluation of the Strategic Defense Initiative Space Power Architecture Study [NASA-TM-102012] p 69 N89-24443

## WEAR

Adhesion, friction, and wear of plasma-deposited thin silicon nitride films at temperatures to 700 C p 107 A89-48250

Tribological properties of structural ceramics p 107 A89-51258

Avalanche in adhesion --- interfacial separation between two Ni crystals p 100 A89-54495

Adhesion, friction, and wear of plasma-deposited thin silicon nitride films at temperatures to 700 C [NASA-TM-101377] p 109 N89-11913

Wear consideration in gear design for space applications [NASA-TM-101457] p 183 N89-15414

Applications of surface analysis and surface theory in tribology [NASA-TM-101392] p 78 N89-15981

Tribology: The Story of Lubrication and Wear [NASA-TM-101430] p 203 N89-24635

OTVE combustor wall condition monitoring [NASA-CR-182275] p 73 N89-26899

OTVE turbopump condition monitoring, task E.5 [NASA-CR-182274] p 189 N89-27204

## WEAR TESTS

Some composite bearing and seal materials for gas turbine applications: A review [NASA-TM-101451] p 111 N89-14338

Effects of lubrication on the performance of high speed spur gears [NASA-TM-101969] p 186 N89-22919

## WEATHER FORECASTING

The influence of ice accretion physics on the forecasting of aircraft icing conditions p 16 A89-54803

## WEIBULL DENSITY FUNCTIONS

Weibull crack density coefficient for polydimensional stress states p 193 A89-34849

Transmission overhaul and replacement predictions using Weibull and renewal theory [AIAA PAPER 89-2919] p 180 A89-47173

Calculation of Weibull strength parameters and Batdori flow-density constants for volume- and surface-flaw-induced fracture in ceramics [NASA-TM-100890] p 196 N89-12930

Investigation of Weibull statistics in fracture analysis of cast aluminum [NASA-TM-102000] p 185 N89-21245

Transmission overhaul and replacement predictions using Weibull and renewal theory [NASA-TM-102022] p 186 N89-22925

## WEIGHT REDUCTION

The application of high temperature superconductors to space electrical power distribution components p 50 A89-15287

Performance of lightweight nickel electrodes p 92 A89-44002

Weight savings in aerospace vehicles through propellant scavenging [SAWE PAPER 1818] p 40 A89-50814

Effect of advanced component technology on helicopter transmissions [NASA-TM-101431] p 182 N89-13794

Lightweight fibrous nickel electrodes for nickel-hydrogen batteries [NASA-TM-101997] p 93 N89-22710

Photovoltaic power system considerations for future lunar bases [NASA-TM-102019] p 67 N89-23517

Space Station Freedom Solar Array design development [NASA-TM-102105] p 70 N89-24448

Advances in thin-film solar cells for lightweight space photovoltaic power [NASA-TM-102017] p 73 N89-26041

A program for advancing the technology of space concentrators [NASA-TM-102139] p 76 N89-29484

## WEIGHTING FUNCTIONS

Discretization formulas for unstructured grids [NASA-TM-101298] p 154 N89-10242

Particle sizing by weighted measurements of scattered light [NASA-TM-100968] p 172 N89-11198

Analysis of modified SMI method for adaptive array weight control [NASA-CR-185493] p 19 N89-25993

## WEIGHTLESSNESS

An experimental and analytical investigation of thermoacoustic convection heat transfer in gravity and zero-gravity environments [NASA-CR-179575] p 120 N89-11920

## WETTABILITY

Effects of crucible wetting during solidification of immiscible Pb-Zn alloys [AIAA PAPER 89-0304] p 118 A89-25261

Effects of crucible wetting during solidification of immiscible Pb-Zn [NASA-TM-101372] p 120 N89-14341

## WIND DIRECTION

Thermal measurements for jets in disturbed and undisturbed crosswind conditions p 20 A89-18102

## WIND PRESSURE

On the wind force needed to dislodge a drop adhered to a surface p 144 A89-22819

## WIND TUNNEL CALIBRATION

Investigation of the flow in the diffuser section of the NASA Lewis Icing Research Tunnel [AIAA PAPER 89-0755] p 36 A89-28455

Flowfield measurements in the NASA Lewis Research Center 9- by 15-foot low-speed wind tunnel [NASA-TM-100883] p 36 N89-21002

Investigation of the flow in the diffuser section of the NASA Lewis icing research tunnel [NASA-TM-102087] p 17 N89-25978

**WIND TUNNEL MODELS**

- Aeroelastic analysis of prop fan blades with a semiempirical dynamic stall model  
[AIAA PAPER 89-2695] p 194 A89-47025
- Isolated testing of highly maneuverable inlet con cepts [NASA-CR-179544] p 26 N89-13437
- Analysis of an unswept propfan blade with a semiempirical dynamic stall model  
[NASA-TM-4083] p 27 N89-15112

**WIND TUNNEL TESTS**

- Cruise noise of the 2/9 scale model SR-7A propeller p 224 A89-12561
- Observations of the frequencies in a sphere wake and of drag increase by acoustic excitation p 142 A89-16884
- Investigation of surface water behavior during glaze ice accretion p 16 A89-27739
- Modeling of surface roughness effects on glaze ice accretion p 16 A89-28451
- An experimental investigation of multi-element airfoil ice accretion and resulting performance degradation [AIAA PAPER 89-0752] p 4 A89-28453
- Investigation of the flow in the diffuser section of the NASA Lewis Icing Research Tunnel [AIAA PAPER 89-0755] p 36 A89-28455
- Near wakes of advanced turbopropellers [AIAA PAPER 89-1095] p 5 A89-33735
- Unsteady blade pressure measurements on a model counterrotation propeller [AIAA PAPER 89-1144] p 226 A89-40175
- Comparison of propeller cruise noise data taken in the NASA Lewis 8- by 6-foot wind tunnel with other tunnel and flight data [AIAA PAPER 89-1059] p 226 A89-40472
- A natural low-frequency oscillation of the flow over an airfoil near stalling conditions p 6 A89-45437
- Mach 5 inlet CFD and experimental results [AIAA PAPER 89-2355] p 6 A89-46769
- Compressibility and shock wave interaction effects on free shear layers [AIAA PAPER 89-2460] p 7 A89-46847
- Low-speed wind tunnel performance of high-speed counterrotation propellers at angle-of-attack [AIAA PAPER 89-2583] p 8 A89-50808
- High-resolution heat-transfer-coefficient maps applicable to compound-curve surfaces using liquid crystals in a transient wind tunnel [NASA-TM-89855] p 154 N89-10246
- Hot gas ingestion testing of an advanced STOVL concept in the NASA Lewis 9- by 15-foot low speed wind tunnel with flow visualization [NASA-TM-100952] p 11 N89-15078
- An experimental investigation of multi-element airfoil ice accretion and resulting performance degradation [NASA-TM-101441] p 12 N89-15084
- Wind-tunnel results of advanced high-speed propellers at takeoff, climb, and landing Mach numbers [NASA-TM-87030] p 13 N89-19265
- Unsteady blade pressure measurements on a model counterrotation propeller [NASA-TM-102002] p 228 N89-20779
- An LDA (Laser-Doppler Anemometry) investigation of three-dimensional normal shock wave boundary-layer interactions p 14 N89-20956
- Flowfield measurements in the NASA Lewis Research Center 9- by 15-foot low-speed wind tunnel [NASA-TM-100883] p 36 N89-21002
- Comparison of propeller cruise noise data taken in the NASA Lewis 8- by 6-foot wind tunnel with other tunnel and flight data [NASA-TM-101976] p 228 N89-21628
- NASA's program on icing research and technology [NASA-TM-101989] p 1 N89-22569
- Cruise noise of the SR-2 propeller model in a wind tunnel [NASA-TM-101480] p 229 N89-24886
- Low-speed wind tunnel performance of high-speed counterrotation propellers at angle-of-attack [NASA-TM-102292] p 15 N89-25121
- Investigation of the flow in the diffuser section of the NASA Lewis icing research tunnel [NASA-TM-102087] p 17 N89-25978
- Mach 5 inlet CFD and experimental results [NASA-TM-102317] p 33 N89-27670
- STOL and STOVL hot gas ingestion and airframe heating tests in the NASA Lewis 9- by 15-foot low-speed wind tunnel [NASA-TM-102101] p 15 N89-29323

**WIND TUNNEL WALLS**

- Effects of wind-tunnel wall absorption on acoustic radiation of propellers p 225 A89-22285

**WIND TUNNELS**

- Performance of the forward scattering spectrometer probe in NASA's Icing Research Tunnel [AIAA PAPER 89-0769] p 169 A89-25570

- Performance of the forward scattering spectrometer probe in NASA's icing research tunnel [NASA-TM-101381] p 172 N89-12845

**WINDOWS (APERTURES)**

- A new structure for comparing surface passivation materials of GaAs solar cells p 213 N89-24725
- Diamondlike carbon protective coatings for optical windows [NASA-TM-102111] p 231 N89-27506

**WING LOADING**

- Propeller/wing interaction [AIAA PAPER 89-0535] p 17 A89-25429

**WINGS**

- Propeller/wing interaction [AIAA PAPER 89-0535] p 17 A89-25429
- A numerical investigation of the influence of surface roughness on heat transfer in ice accretion [AIAA PAPER 89-0737] p 146 A89-25554
- Aerodynamic interaction between propellers and wings p 8 A89-50062

**WIRE**

- Progress on a PdCr wire strain gage p 174 N89-17301
- Tensile behavior of tungsten and tungsten-alloy wires from 1300 to 1600 K [NASA-TM-101446] p 103 N89-17649

**WOOD**

- Improving the fatigue resistance of adhesive joints in laminated wood structures [NASA-CR-182165] p 85 N89-12675

**WORKING FLUIDS**

- Advanced space solar dynamic receivers p 52 A89-15343
- Flight experiment of thermal energy storage [NASA-TM-102081] p 69 N89-24440

**X**

**X RAY ANALYSIS**

- Radiographic and ultrasonic characterization of sintered silicon carbide p 187 A89-14700

**X RAY FLUORESCENCE**

- X-ray based extensometry [NASA-CR-185058] p 176 N89-25432

**XENON**

- Performance of 10-kW class xenon ion thrusters [AIAA PAPER 88-2914] p 48 A89-14978
- Ion optics for high power 50-cm-dia ion thrusters [AIAA PAPER 89-2717] p 58 A89-47040
- Performance of large area xenon ion thrusters for orbit transfer missions [NASA-TM-102049] p 69 N89-24436
- Ion optics for high power 50-cm-diam ion thrusters [NASA-TM-102143] p 76 N89-28571

**Y**

**YAG LASERS**

- Holographic interferometry with an injection seeded Nd:YAG laser and two reference beams [NASA-TM-102056] p 175 N89-24591

**YAW**

- Aeroelastic response of metallic and composite propfan models in yawed flow [AIAA PAPER 88-3154] p 20 A89-17942

**YIELD POINT**

- Fiber composite structural durability and damage tolerance - Simplified predictive methods p 82 A89-36320

**YIELD STRENGTH**

- Simplified cyclic structural analysis of SSME turbine blades p 63 N89-12632

**YTTRIUM OXIDES**

- Crystallization and characterization of Y<sub>2</sub>O<sub>3</sub>-SiO<sub>2</sub> glasses p 80 A89-19486
- Microstructural evolution on crystallizing the glassy phase in a 6 weight percent Y<sub>2</sub>O<sub>3</sub>-Si<sub>3</sub>N<sub>4</sub> ceramic p 80 A89-19487
- On the orthorhombic phase in ZrO<sub>2</sub>-based alloys p 105 A89-30631
- Strength of hot isostatically pressed and sintered reaction bonded silicon nitrides containing Y<sub>2</sub>O<sub>3</sub> [NASA-TM-101443] p 112 N89-15257

**Z**

**ZINC**

- Effects of crucible wetting during solidification of immiscible Pb-Zn alloys [AIAA PAPER 89-0304] p 118 A89-25261
- Effects of crucible wetting during solidification of immiscible Pb-Zn [NASA-TM-101372] p 120 N89-14341

**ZINC FLUORIDES**

- Crystallization of BaF<sub>2</sub>-ZnF<sub>2</sub>-YbF<sub>3</sub>-ThF<sub>4</sub> glass p 230 A89-12236

**ZINC SELENIDES**

- Diamondlike carbon protective coatings for optical windows [NASA-TM-102111] p 231 N89-27506

**ZINC SULFIDES**

- Deposition and characterization of ZnS/Si heterojunctions produced by vacuum evaporation [NASA-TM-101359] p 135 N89-11129
- Diamondlike carbon protective coatings for optical windows [NASA-TM-102111] p 231 N89-27506

**ZIRCONIUM**

- The effect of sulfur and zirconium co-doping on the oxidation of NiCrAl p 94 A89-13933
- The effect of 0.1 atomic percent zirconium on the cyclic oxidation behavior of beta-NiAl for 300 hours at 1200 C [NASA-TM-101408] p 101 N89-13566
- Oxidation behavior of FeAl + Hf, Zr, B [NASA-TM-101402] p 102 N89-14297

**ZIRCONIUM ALLOYS**

- Effect of 0.1 at. pct Zirconium on the cyclic oxidation resistance of beta-NiAl p 96 A89-24599
- Effect of the theta-alpha-Al<sub>2</sub>O<sub>3</sub> transformation on the oxidation behavior of beta-NiAl + Zr p 98 A89-38600

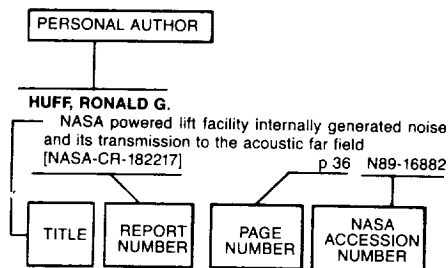
**ZIRCONIUM OXIDES**

- Fracture toughness of polycrystalline ceramics in combined mode I and mode II loading p 105 A89-26457
- On the orthorhombic phase in ZrO<sub>2</sub>-based alloys p 105 A89-30631
- Micro laminate composites as thermal barrier coatings p 83 A89-54261





## Typical Personal Author Index Listing



Listings in this index are arranged alphabetically by personal author. The NASA accession number denotes the number by which the citation is identified.

## A

- AADLAND, RANDALL S.**  
Ground-based plasma contactor characterization  
p 233 A89-43359
- ABEL, J. F.**  
Graphical postprocessing for 3-D mesh quality evaluation  
p 217 A89-38846
- ABEL, P. B.**  
Radiographic and ultrasonic characterization of sintered silicon carbide  
p 187 A89-14700
- ABEL, PHILLIP B.**  
Development and applications of optical interferometric micrometry in the Angstrom and subangstrom range  
p 170 A89-27663
- ABRAMCZYK, R.**  
Flight hardware and tele-operations supporting the Isothermal Dendritic Growth Experiment aboard the Space Shuttle  
[AIAA PAPER 89-0863] p 118 A89-25627
- ABU-HIJLEH, B. A. K.**  
Performance of laser Doppler velocimeter with polydisperse seed particles in high-speed flows  
p 169 A89-22279
- ABU-HIJLEH, B. A. K.**  
An experimental study of a reattaching supersonic shear layer  
[AIAA PAPER 89-1801] p 6 A89-42036
- ABUELFOUOH, NADER M.**  
Isothermal life prediction of composite lamina using a damage mechanics approach  
[NASA-TM-102032] p 87 A89-24460
- ACOSTA, R.**  
A comparison of reflector antenna designs for wide-angle scanning  
[NASA-TM-101459] p 127 A89-21138
- ACOSTA, R.**  
A segmented mirror antenna for radiometers  
[NASA-TM-102045] p 128 A89-23753
- ACOSTA, R. J.**  
A method for producing a shaped contour radiation pattern using a single shaped reflector and a single feed  
[NASA-TM-101369] p 126 A89-10215
- ACOSTA, ROBERTO J.**  
A method for producing a shaped contour radiation pattern using a single shaped reflector and a single feed  
p 125 A89-42758
- Compensation of reflector antenna surface distortion using an array feed** p 126 A89-53136
- Adaptive feed array compensation system for reflector antenna surface distortion** p 127 A89-17756
- [NASA-TM-101458]**
- ACOSTA, WALDO A.**  
Fuel properties effect on the performance of a small high temperature rise combustor  
[AIAA PAPER 89-2901] p 23 A89-52025
- Fuel properties effect on the performance of a small high temperature rise combustor** p 33 A89-25238
- [NASA-TM-102096]**
- ADAMCZYK, JOHN J.**  
Kinetic energy equations for the average-passage equation system p 237 A89-28347
- Average-passage simulation of counter-rotating propfan propulsion systems as applied to cruise missiles** p 7 A89-47187
- [AIAA PAPER 89-2943]**
- Simulation of 3-D viscous flow within a multi-stage turbine** p 26 A89-14238
- [NASA-TM-101376]**
- Average-passage simulation of counter-rotating propfan propulsion systems as applied to cruise missiles** p 14 A89-23416
- [NASA-TM-102043]**
- ADAMOVSKEY, G.**  
Intensity-based fibre-optic sensing system using contrast modulation of subcarrier interference pattern  
p 170 A89-39302
- Compensation for effects of ambient temperature on rare-earth doped fiber optic thermometer** p 176 A89-27996
- [NASA-TM-102282]**
- ADAMOVSKEY, GRIGORY**  
Amplitude spectrum modulation technique for analog data processing in fiber optic sensing system with temporal separation of channels p 169 A89-10368
- Amplitude spectrum modulation technique for analog data processing in fiber optic sensing system with temporal separation of channels** p 174 A89-18671
- [NASA-TM-100152]**
- ADDY, H. E.**  
Strain measurements in a rotary engine housing  
[SAE PAPER 890333] p 181 A89-51493
- ADDY, HAROLD E., JR.**  
Investigation of the flow in the diffuser section of the NASA Lewis icing Research Tunnel  
[AIAA PAPER 89-0755] p 36 A89-28455
- Investigation of the flow in the diffuser section of the NASA Lewis icing research tunnel** p 17 A89-25978
- [NASA-TM-102087]**
- AEBKER, E.**  
Engineering calculations for solving the orbital allotment problem  
[NASA-CR-184607] p 217 A89-13993
- AHMED, SHAMIM**  
Finite element modeling of frictionally restrained composite interfaces  
[NASA-CR-182281] p 203 A89-23918
- AHMED, SHAMIN**  
Local-global analysis of crack growth in continuously reinforced ceramic matrix composites  
[NASA-CR-182231] p 197 A89-13820
- AHN, MYONG-KU**  
Addition polymers from 1,4,5,8-tetrahydro-1,4,5,8-diepoxyanthracene and Bis-dienes. 2: Evidence for thermal dehydration occurring in the cure process  
[NASA-TM-101385] p 112 A89-15235
- AIELLO, R. A.**  
Parametric studies of advanced turboprops  
[NASA-TM-101389] p 197 A89-14465
- AIELLO, ROBERT A.**  
Fiber composite sandwich thermostructural behavior - Computational simulation p 190 A89-11246
- Dynamic delamination buckling in composite laminates under impact loading - Computational simulation** p 82 A89-36310
- A NASTRAN DMAP alter for linear buckling analysis under dynamic loading** p 85 A89-13522
- [NASA-TM-100832]**
- A NASTRAN DMAP alter for linear buckling analysis under dynamic loading** p 202 A89-22948
- Composite blade structural analyzer (COBSTRAN) user's manual** p 86 A89-23621
- [NASA-TM-101461]**
- Composite Blade Structural Analyzer (COBSTRAN) demonstration manual** p 87 A89-24459
- [NASA-TM-101957]**
- AJMANI, K.**  
Viscous analysis of high speed flows using an upwind finite volume technique  
[AIAA PAPER 89-0001] p 144 A89-25001
- Turbulence modeling in a hypersonic inlet** p 8 A89-53931
- AKHTER, MUHAMMAD M.**  
Effect of model uncertainty on failure detection - The threshold selector p 219 A89-17965
- AKIN, L. S.**  
The role of thermal and lubricant boundary layers in the transient thermal analysis of spur gears  
[NASA-TM-101435] p 182 A89-14452
- AKIN, LEE S.**  
Wear consideration in gear design for space applications  
[NASA-TM-101457] p 183 A89-15414
- Lubricant jet flow phenomena in spur and helical gears with modified addendums; for radially directed individual jets** p 183 A89-15415
- [NASA-TM-101460]**
- ALDEN, D.**  
Constitutive modeling for single crystal superalloys p 101 A89-12911
- ALEXANDER, R. M.**  
Piezoelectric pushers for active vibration control of rotating machinery p 171 A89-47717
- ALGER, DONALD L.**  
Progress toward the evolution of a Stirling Space Engine  
[SAE PAPER 880545] p 48 A89-12305
- ALLEN, D. H.**  
On 3D inelastic analysis methods for hot section components p 196 A89-12906
- ALLEN, G. P.**  
Thermomechanical characterization of Hastelloy-X under uniaxial cyclic loading p 196 A89-12909
- ALLEN, GLEN**  
A 20 GHz low noise, low cost receiver for digital satellite communication system, ground terminal applications  
[NASA-CR-182243] p 127 A89-19449
- ALTENKIRCH, R. A.**  
The solid surface combustion Space Shuttle experiment hardware description and ground-based test results  
[AIAA PAPER 89-0503] p 119 A89-28419
- The solid surface combustion space shuttle experiment hardware description and ground-based test results** p 123 A89-19446
- [NASA-TM-101963]**
- ALTEROVITZ, S. A.**  
Shubnikov-de Haas measurements of the 2-D electron gas in pseudomorphic In(0.1)Ga(0.9)As grown on GaAs p 235 A89-29299
- Adhesion, friction, and wear of plasma-deposited thin silicon nitride films at temperatures to 700 C** p 107 A89-48250
- Adhesion, friction, and wear of plasma-deposited thin silicon nitride films at temperatures to 700 C** p 109 A89-11913
- [NASA-TM-101377]**
- ALTEROVITZ, SAMUEL**  
Characterization of multilayer GaAs/AlGaAs transistor structures by variable angle spectroscopic ellipsometry p 133 A89-49998
- ALTEROVITZ, SAMUEL A.**  
Thin-film hermeticity - A quantitative analysis of diamondlike carbon using variable angle spectroscopic ellipsometry p 234 A89-13945
- ALTIDIS, P. C.**  
Tooth contact shift in loaded spiral bevel gears o, IL, 25-27 Apr. 1989; sponsored by ASME  
[NASA-TM-101438] p 183 A89-14453
- AMUEDO, KURT C.**  
Hot gas ingestion testing of an advanced STOVL concept in the NASA Lewis 9- by 15-foot low speed wind tunnel with flow visualization  
[NASA-TM-100952] p 11 A89-15078

## ANDERSON, BERNHARD H.

## ANDERSON, BERNHARD H.

CFD application to subsonic inlet airframe integration  
p 13 N89-16753

## ANDERSON, JOHN R.

The divergence characteristics of constrained-sheath optics systems for use with 5-eV atomic oxygen sources  
[NASA-CR-182238] p 229 N89-19973

## ANDERSON, N. E.

Design and test of a propan gear system  
p 179 A89-22290

## ANDERSON, OLOF L.

An analysis for high speed propeller-nacelle aerodynamic performance prediction. Volume 1: Theory and application  
[NASA-CR-4199-VOL-1] p 12 N89-15896

An analysis for high speed propeller-nacelle aerodynamic performance prediction. Volume 2: User's manual  
[NASA-CR-4199-VOL-2] p 12 N89-15897

## ANTHAN, DONALD J.

Fiber-optic temperature sensor using a spectrum-modulating semiconductor etalon  
p 168 A89-10366

## ANTOLOVICH, STEPHEN D.

Constitutive behavior of single crystal PWA 1480 and directionally solidified MAR-M 246 under monotonic and cyclic loads at high and low temperature  
p 100 N89-12634

Deformation modeling and constitutive modeling for anisotropic superalloys  
[NASA-CR-4215] p 202 N89-21258

## APPELBAUM, J.

Starting characteristics of direct current motors powered by solar cells  
[NASA-TM-101981] p 136 N89-19493

Restrictive loads powered by separate or by common electrical sources  
[NASA-TM-102008] p 137 N89-21174

## APPELBAUM, JOSEPH

The Mars climate for a photovoltaic system operation  
[IAF PAPER ICOSP89-9-5] p 241 A89-46529

Common source-multiple load vs. separate source-individual load photovoltaic system  
[NASA-TM-101465] p 136 N89-15338

The Mars climate for a photovoltaic system operation  
[NASA-TM-101994] p 136 N89-20385

Photovoltaic power system considerations for future lunar bases  
[NASA-TM-102019] p 67 N89-23517

Magnification of starting torques of dc motors by maximum power point trackers in photovoltaic systems  
[NASA-TM-102040] p 138 N89-23792

Photovoltaic power system operation in the Mars environment  
[NASA-TM-102075] p 138 N89-24529

Solar radiation on Mars  
[NASA-TM-102299] p 242 N89-27623

## ARIF, H.

COLD-SAT: A technology satellite for cryogenic experimentation  
[NASA-TM-102286] p 47 N89-26036

## ARMAND, SASAN C.

Comparative thermal analysis of the space station Freedom photovoltaic deployable boom structure using TRASYS, NEVADA, and SINDA programs  
[NASA-TM-102062] p 165 N89-26177

## ARMSTRONG, E. S.

Three dimensional thermal analysis of rocket thrust chambers  
[NASA-TM-101973] p 66 N89-21025

## ARMSTRONG, ELIZABETH S.

Liquid oxygen cooling of hydrocarbon fueled rocket thrust chambers  
[AIAA PAPER 89-2739] p 60 A89-49686

High-pressure calorimeter chamber tests for liquid oxygen/kerosene (LOX/RP-1) rocket combustion  
[NASA-TP-2862] p 65 N89-15979

Liquid oxygen cooling of hydrocarbon fueled rocket thrust chambers  
[NASA-TM-102113] p 70 N89-24447

## ARNOLD, S. M.

Symbolic generation of constitutive equations  
p 221 A89-34963

## ARON, P. R.

Improved synthesis of ceramic superconductors with alkaline earth peroxides - Synthesis and processing of Ba<sub>2</sub>YCu<sub>3</sub>O<sub>7-x</sub>  
p 235 A89-22887

## ARON, PAUL R.

The application of high temperature superconductors to space electrical power distribution components  
p 50 A89-15287

## ARPASI, DALE J.

Parallel processing of a rotating shaft simulation  
[NASA-TM-101462] p 223 N89-17453

Automating the multiprocessing environment  
[NASA-TM-4103] p 217 N89-20641

## ARRISON, A.

A V-grooved GaAs solar cell  
[NASA-TM-101970] p 211 N89-22177

## ARYA, V. K.

Finite element implementation of viscoplastic models  
p 200 N89-17328

## ASHOUR-ABDALLA, M.

Electron velocity distributions and plasma waves associated with the injection of an electron beam into the ionosphere  
p 215 A89-43698

## ASMUSSEN, JES

Experiments and analysis of a compact electrothermal thruster  
p 59 A89-47494

Experiments and analysis of a compact electrothermal thruster  
p 75 N89-27773

## ASTON, GRAEME

A detailed model of electrothermal propulsion systems  
[AIAA PAPER 89-2262] p 56 A89-46707

A detailed model of ion propulsion systems  
[AIAA PAPER 89-2268] p 56 A89-46712

User interactive electric propulsion software design  
[AIAA PAPER 89-2376] p 57 A89-46783

A 50 cm diameter annular ion engine  
[AIAA PAPER 89-2716] p 57 A89-47039

Thermal mechanical analyses of large diameter ion accelerator systems  
[AIAA PAPER 89-2718] p 58 A89-47041

## ASTON, MARTHA B.

User interactive electric propulsion software design  
[AIAA PAPER 89-2376] p 57 A89-46783

## ATASSI, HAFIZ M.

Numerical solution of periodic vortical flows about a thin airfoil  
[AIAA PAPER 89-1691] p 7 A89-48955

Numerical solution of periodic vortical flows about a thin airfoil  
[NASA-TM-101998] p 14 N89-23413

## ATHERTON, WILLIAM J.

A self diagnostic system for piezoelectric sensors  
[AIAA PAPER 89-2638] p 171 A89-46980

## ATIA, ALI E.

Intersatellite link application to commercial communications satellites  
p 43 A89-39144

## AUGUST, R.

Effect of design variables, temperature gradients, and speed on life and reliability of a rotating disk  
p 180 A89-47719

## AUGUST, RICHARD

Vibration, performance, flutter and forced response characteristics of a large-scale propfan and its aeroelastic model  
[AIAA PAPER 88-3155] p 21 A89-17943

Vibration, performance, flutter and forced response characteristics of a large-scale propfan and its aeroelastic model  
[NASA-TM-101322] p 24 N89-10043

## AXELSON, SCOTT R.

Preparation and evaluation of silicon nitride matrices for silicon nitride-SiC fiber composites  
[NASA-CR-184798] p 115 N89-23678

## AYLESWORTH, K. D.

Highly oriented Ti<sub>2</sub>Ba<sub>2</sub>Ca<sub>2</sub>Cu<sub>3</sub>O<sub>10</sub> thin films by pulsed laser evaporation  
p 236 A89-30421

## B

## BAKLINI, G. Y.

Radiographic and ultrasonic characterization of sintered silicon carbide  
p 187 A89-14700

## BAKLINI, GEORGE Y.

High-frequency ultrasonic characterization of sintered silicon carbide  
p 106 A89-34840

## BADGLEY, M. B.

User needs, benefits and integration of robotic systems in a space station laboratory  
[NASA-CR-182261] p 185 N89-22108

## BADGLEY, P.

Adiabatic Wankel type rotary engine  
[NASA-CR-182233] p 28 N89-17599

## BAER, J. R.

Improved silicon carbide for advanced heat engines. II - Pressureless sintering and mechanical properties of injection molded silicon carbide  
p 106 A89-33620

## BAILEY, ALLAN B.

Experimental evaluation of resistojet thruster plume shields  
p 59 A89-47487

## BAILEY, RICHARD S.

Development of a high temperature static strain sensor  
p 173 N89-12887

Development of a high temperature thin film static strain gage  
p 174 N89-17299

## BAILEY, S. G.

A V-grooved GaAs solar cell  
[NASA-TM-101970] p 211 N89-22177

## BAILEY, SHEILA G.

Advances in thin-film solar cells for lightweight space photovoltaic power  
[IAF PAPER ICOSP89-1-8] p 55 A89-46513

Chemical etching and organometallic chemical vapor deposition on varied geometries of GaAs  
p 213 N89-24728

Advances in thin-film solar cells for lightweight space photovoltaic power  
[NASA-TM-102017] p 73 N89-26041

The GaAs solar cells with V-grooved emitters  
[NASA-TM-102104] p 214 N89-26291

## BAJGAR, C.

High efficiency GaAs-Ge tandem solar cells grown by MOCVD  
p 213 N89-24721

## BAKER, IAN

Room temperature tensile ductility in polycrystalline B2 Ni-30Al-20Fe  
p 98 A89-44568

## BAKHLE, MILIND A.

Application of a full-potential solver to bending-torsion flutter in cascades  
[AIAA PAPER 89-1386] p 34 A89-30859

## BALASUBRAMANIAM, R.

Thermocapillary migration of a large gas slug in a tube  
p 117 A89-22747

Unsteady thermocapillary migration of bubbles  
[NASA-TM-101338] p 162 N89-22054

## BALDWIN, R.

Hydrogen-oxygen proton-exchange membrane fuel cells and electrolyzers  
p 211 N89-22996

## BALL, C. L.

The design and development of transonic multistage compressors  
p 27 N89-16834

Supersonic throughflow fans  
p 27 N89-16837

## BALLARINI, R.

Analysis of interface crack branching  
[NASA-CR-182273] p 202 N89-21265

## BALLARINI, ROBERTO

Local-global analysis of crack growth in continuously reinforced ceramic matrix composites  
[NASA-CR-182231] p 197 N89-13820

Finite element modeling of frictionally restrained composite interfaces  
[NASA-CR-182281] p 203 N89-23918

## BALSA, THOMAS F.

Three-dimensional wave packets and instability waves in free shear layers and their receptivity  
p 149 A89-38619

## BAMBERGER, ERIC N.

Surface fatigue life of carburized and hardened M50NiL and AISI 9310 spur gears and rolling-contact test bars  
[AIAA PAPER 89-2819] p 180 A89-47105

Surface fatigue life of carburized and hardened M50NiL and AISI 9310 spur gears and rolling-contact test bars  
[NASA-TM-101979] p 185 N89-22111

## BANERJEE, AMITAVA

Interfacial adhesion - Theory and experiment  
p 97 A89-35307

Avalanche in adhesion  
p 100 A89-54495

## BANERJEE, P. K.

Development of BEM for ceramic composites  
[NASA-CR-183313] p 111 N89-14311

## BANERJEE, PRASANTA K.

Advanced development of the boundary element method for steady-state heat conduction  
p 154 A89-54766

Development of an integrated BEM approach for hot fluid structure interaction  
[NASA-CR-184587] p 27 N89-15114

Three-dimensional inelastic analysis for hot section components, BEST 3D code  
p 199 N89-17317

## BANKS, BRUCE A.

Low earth orbital atomic oxygen simulation for materials durability evaluation  
p 45 A89-51123

The NASA atomic oxygen effects test program  
p 93 N89-12589

Simulation of the low earth orbital atomic oxygen interaction with materials by means of an oxygen ion beam  
[NASA-TM-101971] p 114 N89-21104

Atomic oxygen effects on materials  
p 78 N89-23540

Ion beam and plasma methods of producing diamondlike carbon films  
[NASA-TM-102301] p 116 N89-27836

Arc-textured high emittance radiator surfaces  
[NASA-CASE-LEW-14679-1] p 116 N89-28651

## BANKS, PETER M.

A numerical model of electrodynamics of plasma within the contaminant gas cloud of the Space Shuttle Orbiter at low earth orbit  
p 233 A89-45631

## BANSAL, N. P.

Experimental evidence for a transverse magnetization of the Abrikosov lattice in anisotropic superconductors  
p 234 A89-21473

- Doping directed at the oxygen sites in  $\text{YBa}_2\text{Cu}_3\text{O}_{7-\delta}$  - The effect of sulfur, fluorine, and chlorine p 133 A89-37824
- Free energy surfaces in the superconducting mixed state p 236 A89-43928
- BANSAL, N. R.**  
Critical currents of aligned grains of Ti-Ba-Ca-Cu-O compounds p 235 A89-30335
- BANSAL, NAROTTAM P.**  
Crystallization of  $\text{BaF}_2\text{-ZnF}_2\text{-YbF}_3\text{-ThF}_4$  glass p 230 A89-12236  
Effect of processing parameters on the characteristics of high-Tc superconductor  $\text{YBa}_2\text{Cu}_3\text{O}_y$  p 234 A89-20467  
Phase transformations in xerogels of mullite composition p 108 N89-11038  
Crystallization kinetics of  $\text{BaO-Al}_2\text{O}_3\text{-SiO}_2$  glasses [NASA-TM-101964] p 113 N89-20252  
Influence of several metal ions on the gelation activation energy of silicon tetraethoxide [NASA-TM-101380] p 114 N89-21894
- BARAONA, COSMO R.**  
Status of the Space Station power system p 54 A89-23281  
Space Station Freedom Solar Array design development [NASA-TM-102105] p 70 N89-24448
- BARBER, T.**  
Turbofan forced mixer lobe flow modeling. Part 3: Application to augment engines [NASA-CR-4147-PT-3] p 8 N89-10025  
Turbofan forced mixer lobe flow modeling. 1: Experimental and analytical assessment [NASA-CR-4147-PT-1] p 11 N89-14221  
Turbofan forced mixer lobe flow modeling. 2: Three-dimensional inviscid mixer analysis (FLOMIX) [NASA-CR-4147-PT-2] p 11 N89-14222
- BARKER, LARRY**  
Preliminary design study of hydrogen and ammonia resistojets for prime and auxiliary thrusters [NASA-CR-182176] p 62 N89-10943
- BARKHOUDARIAN, S.**  
Fiberoptics for liquid propellant rocket engine environments [AIAA PAPER 89-2416] p 230 A89-46812  
OTVE combustor wall condition monitoring [NASA-CR-182275] p 73 N89-26899
- BARNETT, ALLEN M.**  
A new structure for comparing surface passivation materials of GaAs solar cells p 213 N89-24725
- BARNETT, MARK**  
Simulation of 3-D viscous flow within a multi-stage turbine [NASA-TM-101376] p 26 N89-14238
- BARNHART, PAUL J.**  
A supersonic through-flow fan engine airframe integration study [AIAA PAPER 89-2140] p 18 A89-50802  
A preliminary design study of supersonic through-flow fan inlets [NASA-CR-182224] p 24 N89-11751
- BARRANGER, JOHN P.**  
Recent advances in capacitance type of blade tip clearance measurements [AIAA PAPER 88-4664] p 20 A89-13725
- BARRETT, C. A.**  
Influence of alloying elements on the oxidation behavior of NbAl<sub>3</sub> [NASA-TM-101398] p 100 N89-12717  
The effect of 0.1 atomic percent zirconium on the cyclic oxidation behavior of beta-NiAl for 300 hours at 1200 C [NASA-TM-101408] p 101 N89-13566
- BARRETT, CHARLES A.**  
Effect of 0.1 at. pct Zirconium on the cyclic oxidation resistance of beta-NiAl p 96 A89-24599  
Castable hot corrosion resistant alloy [NASA-CASE-LEW-14134-2] p 102 N89-14303  
The oxidation of Ni-rich Ni-Al intermetallics [NASA-TM-101455] p 102 N89-15233
- BARRON, DEAN A.**  
LDV measurements in an annular combustor model [NASA-CR-182207] p 159 N89-13755
- BARRY, JENNIFER**  
The emittance of space radiator materials measured at elevated temperatures [NASA-TM-101948] p 66 N89-20193
- BARTEL, H. W.**  
Near-field acoustic characteristics of a single-rotor propfan [AIAA PAPER 89-1055] p 23 A89-36215  
Installed propfan (SR-7L) far-field noise characteristics [AIAA PAPER 89-1056] p 225 A89-36216  
Lateral noise attenuation of the advanced propeller of the propfan test assessment aircraft [AIAA PAPER 89-1057] p 226 A89-36217
- Fluctuating pressures on wing surfaces in the slipstream of a single-rotor propfan [AIAA PAPER 89-1058] p 226 A89-36218
- BARTLAND, TIMOTHY A.**  
Engineering study on the rotary-vee engine concept [SAE PAPER 890332] p 181 A89-51492
- BARTOLOTTA, P. A.**  
The NASA Lewis Research Center High Temperature Fatigue and Structures Laboratory p 194 A89-43528  
Thermomechanical characterization of Hastelloy-X under uniaxial cyclic loading p 196 N89-12909  
Use of inelastic strain as a basis for analyzing thermomechanical test data p 200 N89-17326  
Preliminary study of creep thresholds and thermomechanical response in Haynes 188 at temperatures in the range 649 to 871 C p 200 N89-17327
- BARTRAND, TIMOTHY A.**  
Engineering study of the rotary-vee engine concept [NASA-TM-101995] p 33 N89-26007
- BASU, PRITHWISH**  
Dynamics of face and annular seals with two-phase flow [NASA-CR-183352] p 182 N89-12870  
Thermal effects in two-phase flow through face seals [NASA-CR-185968] p 182 N89-13788
- BATCHELDER, GARY**  
Advanced heat receiver conceptual design study [NASA-CR-182177] p 209 N89-16224
- BATCHO, P. F.**  
Preliminary study of the interactions caused by crossing shock waves and a turbulent boundary layer [AIAA PAPER 89-0359] p 145 A89-25303
- BATTERSON, J. G.**  
Determination of longitudinal aerodynamic derivatives using flight data from an icing research aircraft [AIAA PAPER 89-0754] p 34 A89-28454  
Determination of longitudinal aerodynamic derivatives using flight data from an icing research aircraft [NASA-TM-101427] p 35 N89-15121
- BAUMEISTER, JOSEPH F.**  
Thermal distortion analysis of the Space Station solar dynamic concentrator p 51 A89-15341  
Comparative thermal analysis of the space station Freedom photovoltaic deployable boom structure using TRASYS, NEVADA, and SINDA programs [NASA-TM-102062] p 165 N89-26177
- BAUMEISTER, K. J.**  
Unsteady heat transfer in turbine blade ducts - Focus on combustor sources p 153 A89-53286
- BAUMEISTER, KENNETH J.**  
Effects of wind-tunnel wall absorption on acoustic radiation of propellers p 225 A89-22285  
Acoustic wave propagation in heterogeneous structures including experimental validation [AIAA PAPER 89-1044] p 225 A89-36214  
Discretization formulas for unstructured grids [NASA-TM-101298] p 154 N89-10242  
Acoustic wave propagation in heterogeneous structures including experimental validation [NASA-TM-101486] p 224 N89-19965  
Acoustic propagation in curved ducts with extended reacting wall treatment [NASA-TM-102110] p 224 N89-25670  
Parametric study of electromagnetic waves propagating in absorbing curved S ducts [NASA-TM-102024] p 129 N89-27923
- BAUN, L. R.**  
Spatial resolution and downwash velocity corrections for multiple-hole pressure probes in complex flows p 171 A89-45909
- BEACH, DUANE E.**  
Comparative thermal analysis of the space station Freedom photovoltaic deployable boom structure using TRASYS, NEVADA, and SINDA programs [NASA-TM-102062] p 165 N89-26177
- BEACH, TIM A.**  
Simulation of 3-D viscous flow within a multi-stage turbine [NASA-TM-101376] p 26 N89-14238
- BEARD, JOHN E.**  
Engineering study on the rotary-vee engine concept [SAE PAPER 890332] p 181 A89-51492  
Engineering study of the rotary-vee engine concept [NASA-TM-101995] p 33 N89-26007
- BEARD, L.**  
Electromagnetic properties of ice coated surfaces [NASA-CR-184780] p 127 N89-20355
- BEATTIE, J. R.**  
Model for computing volume-averaged plasma properties in electron-bombardment ion thrusters p 54 A89-28339  
Mercury ion thruster technology [NASA-CR-174974] p 66 N89-21834
- BEATTY, PAUL A.**  
Dynamics of face and annular seals with two-phase flow [NASA-CR-183352] p 182 N89-12870
- BEATTY, R.**  
Nuclear reactor power as applied to a space-based radar mission p 51 A89-15317  
Systems aspects of a space nuclear reactor power system p 51 A89-15327  
Nuclear reactor power as applied to a space-based radar mission [NASA-TM-101200] p 230 N89-14831
- BEAULIEU, ROLAND**  
Deposition and characterization of ZnS/Si heterojunctions produced by vacuum evaporation [NASA-TM-101359] p 135 N89-11129
- BECKEL, STEPHEN A.**  
Fuel properties effect on the performance of a small high temperature rise combustor [AIAA PAPER 89-2901] p 23 A89-52025  
Fuel properties effect on the performance of a small high temperature rise combustor [NASA-TM-102096] p 33 N89-25238
- BEELER, RICHARD M.**  
Dynamics of face and annular seals with two-phase flow [NASA-CR-183352] p 182 N89-12870
- BEHEIM, GLENN**  
Fiber-optic temperature sensor using a spectrum-modulating semiconductor etalon p 168 A89-10366  
Speckle interferometry using fiber optic phase stepping [NASA-TM-102331] p 176 N89-27999
- BELLINI, P. X.**  
A probabilistic approach to composite micromechanics [NASA-TM-101366] p 85 N89-12684
- BELLOWS, A. H.**  
A comparative study of the influence of buoyancy driven fluid flow on GaAs crystal growth p 121 N89-20295
- BELYTSCHKO, T.**  
Kuhn-Tucker optimization based reliability analysis for probabilistic finite elements p 187 A89-25852
- BELYTSCHKO, TED**  
Probabilistic Finite Elements (PFEM) structural dynamics and fracture mechanics p 206 N89-29803
- BENDETT, M.**  
GaAs circuits for monolithic optical controller p 131 A89-15828
- BENHACHMI, DRISS**  
Experimental and numerical investigation of an oblique shock wave/turbulent boundary layer interaction with continuous suction [AIAA PAPER 89-0357] p 4 A89-28407
- BENNETHUM, W. H.**  
Sensors for ceramic components in advanced propulsion systems: Summary of literature survey and concept analysis, task 3 report [NASA-CR-180900] p 172 N89-11192
- BENNETT, DAVID P.**  
Patterns of the cosmic microwave background from evolving string networks p 240 A89-14618  
Cosmic strings - A problem or a solution? p 240 A89-19610
- BENNETT, F. O.**  
COLD-SAT orbital experiment configured for Atlas launch p 45 A89-53327
- BENNETT, GARY L.**  
NASA advanced space photovoltaic technology-status, potential and future mission applications [NASA-TM-102093] p 75 N89-27705
- BENNETT, TIMOTHY J.**  
Advanced sensible heat solar receiver for space power p 52 A89-15415
- BENSON, T. J.**  
Three dimensional viscous analysis of a hypersonic inlet [AIAA PAPER 89-0004] p 4 A89-29924
- BENSON, THOMAS J.**  
PNS calculations for 3-D hypersonic corner flow with two turbulence models [AIAA PAPER 88-2958] p 1 A89-14979  
CFD application to supersonic/hypersonic inlet airframe integration p 13 N89-16754  
Three dimensional viscous analysis of a hypersonic inlet [NASA-TM-101474] p 13 N89-16759
- BENTS, D. J.**  
Preliminary assessment of rover power systems for the Mars Rover Sample Return Mission [IAF PAPER ICOSP89-9-6] p 39 A89-46530
- BENTS, DAVID J.**  
Power transmission studies for tethered SP-100 p 52 A89-15403

- Preliminary assessment of rover power systems for the Mars Rover Sample Return Mission  
[NASA-TM-102003] p 68 N89-23518
- Estimated performance and future potential of solar dynamic and photovoltaic power systems for selected LEO and HEO missions  
[NASA-TM-102083] p 72 N89-25280
- BERCAW, ROBERT W.**  
Toward an electrical power utility for space exploration  
[NASA-TM-102347] p 75 N89-27704
- BERGER, BRETT**  
Contingency power for small turboshaft engines  
p 21 A89-22291
- BERKOPEC, FRANK D.**  
NASA's Chemical Transfer Propulsion Program for Pathfinder  
[AIAA PAPER 89-2298] p 37 A89-46735
- Fueling the National Aero-Space Plane with slush hydrogen  
[AIAA PAPER 89-5014] p 117 A89-51339
- The Pathfinder Chemical Transfer Propulsion program  
[NASA-TM-102084] p 41 N89-24409
- NASA's Chemical Transfer Propulsion Program for Pathfinder  
[NASA-TM-102298] p 41 N89-26876
- BERKOWITZ, BRIAN**  
Modeling of surface roughness effects on glaze ice accretion  
[AIAA PAPER 89-0734] p 16 A89-28451
- BERKOWITZ, BRIAN M.**  
An experimental investigation of multi-element airfoil ice accretion and resulting performance degradation  
[AIAA PAPER 89-0752] p 4 A89-28453
- Analytical ice shape predictions for flight in natural icing conditions  
[NASA-CR-182234] p 18 N89-13428
- An experimental investigation of multi-element airfoil ice accretion and resulting performance degradation  
[NASA-TM-101441] p 12 N89-15084
- HASA: Hypersonic Aerospace Sizing Analysis for the preliminary design of aerospace vehicles  
[NASA-CR-182226] p 18 N89-15107
- BERLAD, A. L.**  
Radiative structures of lycopodium-air flames in low gravity  
[AIAA PAPER 89-0500] p 91 A89-25406
- Particle cloud mixing in microgravity  
[NASA-TM-101484] p 121 N89-20321
- BERLAD, ABRAHAM L.**  
Feasibility of reduced gravity experiments involving quiescent, uniform particle cloud combustion  
[NASA-TM-101371] p 122 N89-26114
- BERNATOWICZ, HENRY**  
Mass flow meter using the triboelectric effect for measurement in cryogenics  
[NASA-CR-179572] p 155 N89-12836
- BERNDT, C. C.**  
Acoustic emission evaluation of plasma-sprayed thermal barrier coatings  
p 178 A89-12751
- BERNDT, CHRISTOPHER C.**  
Examination of coating failure by acoustic emission  
p 110 N89-13654
- BERNHART, W. D.**  
Electroimpulse deicing - Electrodynamic solution by discrete elements  
p 17 A89-39193
- BESSENDORF, MICHAEL H.**  
Kinetics of fracture in Fe-3Si steel under mode I loading  
p 99 A89-47320
- BESTERFIELD, G.**  
Kuhn-Tucker optimization based reliability analysis for probabilistic finite elements  
p 187 A89-25852
- Probabilistic Finite Elements (PFEM) structural dynamics and fracture mechanics  
p 206 N89-29803
- BHANDARI, P.**  
Nuclear reactor power as applied to a space-based radar mission  
p 51 A89-15317
- Systems aspects of a space nuclear reactor power system  
p 51 A89-15327
- Nuclear reactor power as applied to a space-based radar mission  
[NASA-TM-101200] p 230 N89-14831
- BHARGAVA, RAKESH K.**  
An experimental study of near wall flow parameters in the blade end-wall corner region  
[NASA-CR-4211] p 12 N89-15898
- BHASIN, K. B.**  
Characterization of GaAlAs optical waveguide heterostructures grown by molecular beam epitaxy  
p 130 A89-10343
- Microwave response of an HEMT photoconductor  
p 131 A89-15824
- External electro-optic probing of millimeter-wave integrated circuits  
p 133 A89-45266
- External electro-optic probing of millimeter-wave integrated circuits  
[NASA-TM-101990] p 128 N89-21142
- Optical detectors for GaAs MMIC integration: Technology assessment  
[NASA-TM-102025] p 137 N89-22020
- Sequentially evaporated thin Y-Ba-Co-O superconducting films on microwave substrates  
[NASA-TM-102068] p 138 N89-23791
- Millimeter wave transmission studies of YBa<sub>2</sub>Cu<sub>3</sub>O<sub>7</sub>-delta thin films in the 26.5 to 40.0 GHz frequency range  
[NASA-TM-102345] p 237 N89-30088
- BHASIN, KUL B.**  
Design of a GaAlAs travelling wave Mach-Zehnder electro-optic modulator  
p 130 A89-10342
- Optoelectronic signal processing for phased-array antennas; Proceedings of the Meeting, Los Angeles, CA, Jan. 12, 13, 1988  
[SPIE-886] p 124 A89-15819
- Optically controlled phased-array technology for space communication systems  
p 131 A89-15845
- Optically interconnected phased arrays  
p 132 A89-33696
- Sequentially evaporated thin Y-Ba-Cu-O superconductor films: Composition and processing effects  
[NASA-TM-101388] p 134 N89-10235
- Characterization of ZrO<sub>2</sub> buffer layers for sequentially evaporated Y-Ba-CuO on Si and Al<sub>2</sub>O<sub>3</sub> substrates  
[NASA-TM-101432] p 135 N89-13722
- Microwave characteristics of GaAs MMIC integratable optical detectors  
[NASA-TM-101485] p 129 N89-24520
- Measurements of complex permittivity of microwave substrates in the 20 to 300 K temperature range from 26.5 to 40.0 GHz  
[NASA-TM-102123] p 123 N89-27038
- BHATT, R. T.**  
Thermal effects on the mechanical properties of SiC fiber reinforced reaction bonded silicon nitride matrix (SiC/RBSN) composites  
[NASA-TM-101348] p 84 N89-10134
- BHATT, RAMAKRISHNA T.**  
Properties of silicon carbide fiber-reinforced silicon nitride matrix composites  
[NASA-TM-101356] p 84 N89-10130
- Fiber reinforced ceramic material  
[NASA-CASE-LEW-14392-2] p 116 N89-29538
- BHATTACHARYA, P. K.**  
Molecular beam epitaxial growth of high-quality InSb on InP and GaAs substrates  
[NASA-CR-185440] p 236 N89-26739
- Surface morphologies and electrical properties of molecular beam epitaxial InSb and InAs(x)Sb(1-x) grown on GaAs and InP substrates  
[NASA-CR-185439] p 237 N89-26740
- BICKFORD, R. L.**  
Miniature multiple-function probe for OTV turbopump health monitoring  
[AIAA PAPER 89-2303] p 56 A89-46736
- BIDWELL, COLIN S.**  
Predictions of airfoil aerodynamic performance degradation due to icing  
[NASA-TM-101434] p 10 N89-13412
- BIEDENBENDER, M. D.**  
Plasma deposited silicon nitride for indium phosphide encapsulation  
p 235 A89-27794
- BIERSCHENK, THOMAS R.**  
The preparation of new perfluoro ether fluids exhibiting excellent thermal-oxidative stabilities  
p 76 A89-12760
- BIESIADNY, THOMAS J.**  
Contingency power for small turboshaft engines  
p 21 A89-22291
- BILGER, KEVIN**  
Space Station Freedom Solar Array design development  
[NASA-TM-102105] p 70 N89-24448
- BILL, ROBERT C.**  
Advanced transmission studies  
p 178 A89-18906
- BINDSCHADLER, R. A.**  
Data report for the Siple Coast (Antarctica) project  
[NASA-TM-100708] p 206 N89-10403
- BITTKER, DAVID A.**  
Investigation of low NO<sub>x</sub> staged combustor concept in high-speed civil transport engines  
[AIAA PAPER 89-2942] p 23 A89-47186
- Investigation of low NO<sub>x</sub> staged combustor concept in high-speed civil transport engines  
[NASA-TM-101977] p 32 N89-22606
- BLACKFORD, GARY A.**  
Secondary electron emission characteristics of untreated and ion-textured titanium  
[NASA-TP-2902] p 103 N89-17650
- BLAIR, M. F.**  
The effects of inlet turbulence and rotor/stator interactions on the aerodynamics and heat transfer of a large-scale rotating turbine model, volume 1  
[NASA-CR-4079] p 159 N89-13756
- BLAIR, MICHAEL F.**  
Measurement of airfoil heat transfer coefficients on a turbine stage  
p 157 N89-12897
- Measurement of airfoil heat transfer coefficients on a turbine stage  
p 160 N89-17311
- BLANDINO, J.**  
Bounds on current collection from the far field by plasma clouds in the ionosphere  
p 214 A89-34791
- BLASCHAK, JEFFREY G.**  
Theory and application of radiation boundary operators  
p 224 A89-24191
- BLATT, J. R.**  
Turbofan forced mixer lobe flow modeling. Part 3: Application to augment engines  
[NASA-CR-4147-Pt-3] p 8 N89-10025
- BLECH, RICHARD A.**  
Parallel Gaussian elimination of a block tridiagonal matrix using multiple microcomputers  
[NASA-TP-2692] p 218 N89-17422
- A message passing kernel for the hypercluster parallel processing test bed  
[NASA-TM-101952] p 218 N89-20684
- Initial operating capability for the hypercluster parallel-processing test bed  
[NASA-TM-101953] p 218 N89-20685
- BLELLOCH, PAUL A.**  
Modal representations in control/structure interaction  
p 45 A89-54114
- BLISS, DONALD B.**  
On the role of artificial viscosity in Navier-Stokes solvers  
[AIAA PAPER 89-1947] p 5 A89-41794
- BLOOM, THEODORE A.**  
Rapid solidification research at the NASA Lewis Research Center  
p 95 A89-18203
- BLOOMFIELD, H.**  
Nuclear reactor power as applied to a space-based radar mission  
p 51 A89-15317
- Systems aspects of a space nuclear reactor power system  
p 51 A89-15327
- BLOOMFIELD, H. S.**  
Extended SP-100 reactor power systems capability  
p 52 A89-15392
- Comparison of solar photovoltaic and nuclear reactor power systems for a human-tended lunar observatory  
[NASA-TM-102015] p 242 N89-23397
- BLOOMFIELD, HARVEY S.**  
Space nuclear reactor shields for manned and unmanned applications  
[NASA-TM-102064] p 71 N89-25272
- BLUE, JAMES W.**  
Stability of bulk Ba<sub>2</sub>YCu<sub>3</sub>O<sub>7-x</sub> in a variety of environments  
[NASA-TM-101401] p 111 N89-14310
- BLUMBERG, PAUL N.**  
Methods for heat transfer and temperature field analysis of the insulated diesel, phase 3  
[NASA-CR-182237] p 239 N89-23382
- BOBECK, GENE E.**  
Effects of cobalt concentration on the relative resistance to octahedral and cube slip in nickle-base superalloys  
p 94 A89-17115
- BOBER, L. J.**  
Large scale advanced propeller blade pressure distributions - Prediction and data  
[AIAA PAPER 89-2696] p 7 A89-47026
- BOBER, LAWRENCE J.**  
NASA advanced propeller research  
[NASA-TM-101361] p 27 N89-15913
- BOBULA, GEORGE A.**  
A review and forecast of engine system research at the Army Propulsion Directorate  
p 23 A89-36397
- BODONYI, R. J.**  
Interaction between Tollmien-Schlichting waves and free-stream disturbances in boundary-layer flows  
[NASA-CR-185847] p 167 N89-27118
- BODONYI, RICHARD J.**  
Studies of transition in boundary layers  
[AIAA PAPER 89-0034] p 2 A89-25029
- BOGDONOFF, S. M.**  
Preliminary study of the interactions caused by crossing shock waves and a turbulent boundary layer  
[AIAA PAPER 89-0359] p 145 A89-25303
- BONACUSE, PETER J.**  
Automation software for a materials testing laboratory  
p 217 N89-12917
- Results of inphase axial-torsional fatigue experiments on 304 stainless steel  
[NASA-TM-101464] p 201 N89-20514
- A data acquisition and control program for axial-torsional fatigue testing  
[NASA-TM-102041] p 205 N89-28029
- BOND, T. H.**  
Determination of longitudinal aerodynamic derivatives using flight data from an icing research aircraft  
[AIAA PAPER 89-0754] p 34 A89-28454

- Strain measurements in a rotary engine housing  
[SAE PAPER 890333] p 181 A89-51493
- Determination of longitudinal aerodynamic derivatives using flight data from an icing research aircraft  
[NASA-TM-101427] p 35 N89-15121
- BOND, THOMAS H.**  
Icing research tunnel test of a model helicopter rotor  
[NASA-TM-101978] p 29 N89-19305
- BONNER, MARY JO**  
Ground-based simulation of telepresence for materials science experiments  
[AIAA PAPER 89-0597] p 119 A89-28439
- BORETTI, A. A.**  
An explicit Runge-Kutta method for turbulent reacting flow calculations  
[NASA-TM-101945] p 31 N89-21799
- Transonic viscous flow calculations for a turbine cascade with a two equation turbulence model  
[NASA-TM-101944] p 32 N89-22607
- BOROWSKI, STANLEY K.**  
Nuclear thermal rockets - Next step to space  
p 55 A89-40480
- Nuclear propulsion: A vital technology for the exploration of Mars and the planets beyond  
[NASA-TM-101354] p 62 N89-10944
- BOSCH, CLAUDIA M.**  
The development of power specific redlines for SSME safety monitoring  
[AIAA PAPER 89-2413] p 61 A89-53305
- The development of power specific redlines for SSME safety monitoring  
[NASA-CR-185121] p 41 N89-26027
- BOTSIS, J.**  
Damage analysis of a crack layer p 194 A89-42984
- BOUCHET, FRANCOIS R.**  
Patterns of the cosmic microwave background from evolving string networks p 240 A89-14618
- Cosmic strings - A problem or a solution? p 240 A89-19610
- BOWLES, KENNETH J.**  
Thermo-oxidative stability studies of Celion 6000/PMR-15 unidirectional composites, PMR-15, and Celion 6000 fiber p 79 A89-14099
- The correlation of low-velocity impact resistance of graphite-fiber-reinforced composites with matrix properties p 79 A89-16283
- A thermally modified polymer matrix composite material with structural integrity to 371 C p 80 A89-29997
- Mechanical properties characterization of composite sandwich materials intended for space antenna applications p 81 A89-32685
- Materials technology assessment for a 1050 K Stirling space engine design  
[NASA-TM-101342] p 77 N89-11815
- Light weight polymer matrix composite material  
[NASA-CASE-LEW-14734-1] p 87 N89-23623
- A predictive model for failure properties of thermoset resins  
[NASA-TM-4128] p 87 N89-25300
- BOYCE, L.**  
Probabilistic constitutive relationships for material strength degradation models  
[AIAA PAPER 89-1368] p 192 A89-30843
- BOYCE, LOLA**  
Fatigue crack growth model RANDOM2 user manual. Appendix 1: Development of advanced methodologies for probabilistic constitutive relationships of material strength models  
[NASA-CR-184775-APP-1] p 201 N89-19581
- Fatigue strength reduction model: RANDOM3 and RANDOM4 user manual. Appendix 2: Development of advanced methodologies for probabilistic constitutive relationships of material strength models  
[NASA-CR-184796-APP-2] p 201 N89-19582
- Fatigue crack growth model RANDOM2 user manual, appendix 1  
[NASA-CR-184939] p 203 N89-23890
- Fatigue strength reduction model: RANDOM3 and RANDOM4 user manual, appendix 2  
[NASA-CR-184940] p 203 N89-23891
- BOYD, J. T.**  
Characterization of GaAlAs optical waveguide heterostructures grown by molecular beam epitaxy  
p 130 A89-10343
- BOYLE, R. J.**  
Impact of ETO propellants on the aerothermodynamic analyses of propulsion components  
[AIAA PAPER 88-3091] p 53 A89-16486
- BOYLE, ROBERT J.**  
Experimental determination of stator endwall heat transfer  
[NASA-TM-101419] p 159 N89-15366
- BOYNE, D.**  
Doping directed at the oxygen sites in Y1Ba2Cu3O(7-delta) - The effect of sulfur, fluorine, and chlorine p 133 A89-37824
- BOZZOLO, GUILLERMO**  
Avalanche in adhesion p 100 A89-54495
- BOZZOLO, GUILLERMO H.**  
Interfacial adhesion - Theory and experiment p 97 A89-35307
- BRAATEN, M. E.**  
A block-corrected subdomain solution procedure for recirculating flow calculations p 152 A89-50147
- BRAUBS, THEODORE A.**  
Experimental verification of the thermodynamic properties for a jet-A fuel  
[NASA-TM-101475] p 117 N89-17017
- Fuel-rich catalytic combustion of Jet-A fuel-equivalence ratios 5.0 to 8.0  
[NASA-TM-101975] p 93 N89-21051
- BRACE, M. H.**  
Droplet combustion drop tower tests using models of the space flight apparatus  
[AIAA PAPER 89-0501] p 119 A89-28418
- BRADY, RICHARD C.**  
Crack growth resistance of textured alumina p 105 A89-26452
- Strength distribution of reinforcing fibers in a Nicalon fiber/chemically vapor infiltrated silicon carbide matrix composite p 82 A89-34844
- BRADY, JOYCE A.**  
Oxidation and protection of fiberglass-epoxy composite masts for photovoltaic arrays in the low earth orbital environment p 44 A89-35316
- The NASA atomic oxygen effects test program p 93 N89-12589
- Evaluation of atomic oxygen resistant protective coatings for fiberglass-epoxy composites in LEO  
[NASA-TM-101955] p 114 N89-21100
- Atomic oxygen effects on materials p 78 N89-23540
- BRANDHORST, HENRY W., JR.**  
InP (Indium Phosphide): into the future  
[NASA-TM-102058] p 212 N89-23025
- Challenges for future space power systems  
[NASA-TM-102063] p 214 N89-25506
- BRAUNSCHEIDEL, EDWARD P.**  
Performance characterization and transient investigation of multipropellant resistojets  
[AIAA PAPER 89-2837] p 60 A89-50811
- Performance characterization and transient investigation of multipropellant resistojets  
[NASA-TM-102118] p 72 N89-25283
- BREWE, D. E.**  
The solution of the Eirod algorithm for a dynamically loaded journal bearing using multigrid techniques  
[ASME PAPER 88-TRIB-23] p 148 A89-34795
- On the performance of finite journal bearings lubricated with micropolar fluids p 181 A89-54977
- Stability of a rigid rotor supported on oil-film journal bearings under dynamic load  
[NASA-TM-102309] p 166 N89-27114
- BRIDGES, JAMES E.**  
Turbulence management in free shear flows by control of coherent structures p 147 A89-30908
- BRILEY, G. L.**  
Space station hydrogen/oxygen thruster technology  
[NASA-CR-182280] p 74 N89-26905
- BRILEY, W. R.**  
Turbine stator flow field simulations p 157 N89-12902
- Two- and three-dimensional turbine blade row flow field simulations p 161 N89-17313
- BRINDLEY, PAMELA K.**  
Furnace for tensile/fatigue testing  
[NASA-CASE-LEW-14848-1] p 40 N89-28549
- BRINKER, D. J.**  
Progress in InP solar cell research p 130 A89-15308
- BRINKER, DAVID J.**  
InP homojunction solar cell performance on the LIPS 3 flight experiment  
[NASA-TM-101390] p 209 N89-12123
- On-orbit results of the LIPS 3/InP homojunction solar cell experiment  
[NASA-TM-102131] p 214 N89-26292
- BRINKMANN, R. P.**  
The stability analysis of magnetohydrodynamic equilibria - Comparing the thermodynamic approach with the energy principle p 232 A89-39391
- BRITTAIN, J. O.**  
Elevated temperature strain gages p 173 N89-12886
- BRITTON, DORIS L.**  
Performance of lightweight nickel electrodes p 92 A89-44002
- Lightweight fibrous nickel electrodes for nickel-hydrogen batteries  
[NASA-TM-101997] p 93 N89-22710
- BRITTON, R. K.**  
On ice shape prediction methodologies and comparison with experimental data  
[AIAA PAPER 89-0732] p 16 A89-30650
- BROCK, J. S.**  
Viscous analysis of high speed flows using an upwind finite volume technique  
[AIAA PAPER 89-0001] p 144 A89-25001
- BROPHY, JOHN R.**  
A detailed model of electrothermal propulsion systems  
[AIAA PAPER 89-2262] p 56 A89-46707
- A detailed model of ion propulsion systems  
[AIAA PAPER 89-2268] p 56 A89-46712
- User interactive electric propulsion software design  
[AIAA PAPER 89-2376] p 57 A89-46783
- A 50 cm diameter annular ion engine  
[AIAA PAPER 89-2716] p 57 A89-47039
- Thermal mechanical analyses of large diameter ion accelerator systems  
[AIAA PAPER 89-2718] p 58 A89-47041
- BROWN, GERALD V.**  
Low frequency vibration isolation technology for microgravity space experiments  
[NASA-TM-101448] p 123 N89-20324
- BROWN, J. S.**  
Vapor condensation at a turbulent liquid surface in systems with possible spaced-based applications  
[AIAA PAPER 89-2846] p 151 A89-47122
- BROWN, JAMES A.**  
High-temperature LCF of Ni-201 and 304L stainless steel p 100 N89-12635
- BROWN, K. W.**  
Structural Tailoring of Advanced Turboprops (STAT) programmer's manual  
[NASA-CR-182164] p 29 N89-20132
- BROWN, KENNETH W.**  
Structural tailoring of counter rotation propfans p 33 N89-25165
- BROWN, LARRY**  
Baseband processor hardware for Advanced Communication Technology Satellite (ACTS) p 43 A89-38298
- BROWN, P. C.**  
Results of acoustic tests of a prop-fan model p 224 A89-10112
- BROWN, W. H.**  
Effects of nozzle exit boundary-layer conditions on excitability of heated free jets p 149 A89-36908
- BROWNE, W. R.**  
Film annotation system for a space experiment  
[NASA-CR-185114] p 176 N89-27152
- BRUSH, ANDREW S.**  
Development and testing of a 20-kHz component test bed  
[NASA-TM-102141] p 139 N89-25403
- Distortion and regulation characterization of a Mapham inverter  
[NASA-TM-102089] p 139 N89-26148
- Frequency domain model for analysis of paralleled, series-output-connected Mapham inverters  
[NASA-TM-102140] p 139 N89-26149
- BRUTON, WILLIAM M.**  
Advanced detection, isolation, and accommodation of sensor failures - Real-time evaluation p 34 A89-16156
- BRYAN, WILLIAM B.**  
The effect of prewhirl on the internal aerodynamics and performance of a mixed flow research centrifugal compressor  
[NASA-CR-184756] p 161 N89-19503
- BUCHHELE, DONALD R.**  
Particle sizing by weighted measurements of scattered light  
[NASA-TM-100968] p 172 N89-11198
- BUCHNER, MARC**  
A parametric LQ approach to multiobjective control system design p 219 A89-28605
- A parametric LQ approach to multiobjective control system design  
[NASA-TM-101316] p 220 N89-12283
- BUCKLEY, DONALD H.**  
Tribological properties of structural ceramics p 107 A89-51258
- Deformation and fracture of single-crystal and sintered polycrystalline silicon carbide produced by cavitation p 108 A89-54985
- Tribology: The Story of Lubrication and Wear  
[NASA-TM-101430] p 203 N89-24635
- BUCKMANN, P. S.**  
Design and test of an oxygen turbopump for a dual expander cycle rocket engine  
[AIAA PAPER 89-2305] p 56 A89-46737
- BUDINGER, JAMES M.**  
Digitally modulated bit error rate measurement system for microwave component evaluation  
[NASA-TP-2912] p 40 N89-28545

## BUFFUM, DANIEL H.

## BUFFUM, DANIEL H.

- Investigation of oscillating cascade aerodynamics by an experimental influence coefficient technique  
[AIAA PAPER 88-2815] p 1 A89-14976
- Experimental investigation of transonic oscillating cascade aerodynamics  
[AIAA PAPER 89-0321] p 3 A89-26369
- Experimental investigation of transonic oscillating cascade aerodynamics  
[NASA-TM-101993] p 29 N89-20133

## BUGGELN, R. C.

- Turbine stator flow field simulations  
p 157 N89-12902
- Two- and three-dimensional turbine blade row flow field simulations  
p 161 N89-17313

## BULL, JOHN S.

- Systems autonomy technology: Executive summary and program plan  
[NASA-TM-100999] p 216 N89-18045

## BULLARD, RANDY

- Integrated flight/propulsion control system design based on a decentralized, hierarchical approach  
[AIAA PAPER 89-3519] p 35 A89-53301

## BULLARD, RANDY E.

- Integrated flight/propulsion control system design based on a centralized approach  
[AIAA PAPER 89-3520] p 35 A89-52611
- Integrated flight/propulsion control system design based on a centralized approach  
[NASA-TM-102137] p 35 N89-26009

## BUMANN, ELIZABETH A.

- An acoustic experimental and theoretical investigation of single disc propellers  
[AIAA PAPER 89-1146] p 227 A89-40478

## BUNSHAH, R. F.

- Micro laminate composites as thermal barrier coatings  
p 83 A89-54261

## BUNYA, GEORGE K.

- Programmable rate modem utilizing digital signal processing techniques  
[NASA-CR-185124] p 43 N89-26879

## BURKHOLDER, R. J.

- Analysis of the EM scattering from arbitrary open-ended waveguide cavities using axial Gaussian Beam tracking  
[NASA-CR-185054] p 128 N89-24518

- A hybrid asymptotic-modal analysis of the EM scattering by an open-ended S-shaped rectangular waveguide cavity  
[NASA-CR-185053] p 129 N89-24519

## BURKHOLDER, ROBERT J.

- Modal, ray, and beam techniques for analyzing the EM scattering by open-ended waveguide cavities  
p 125 A89-39594

## BURLEY, R. R.

- Isolated testing of highly maneuverable inlet concepts  
[NASA-CR-179544] p 26 N89-13437

## BURNSIDE, O. H.

- Probabilistic methods for structural response analysis  
p 223 A89-25843
- An approximate methods approach to probabilistic structural analysis  
[AIAA PAPER 89-1369] p 193 A89-30844

## BURSTADT, PAUL L.

- Experimental results for a two-dimensional supersonic inlet used as a thrust deflecting nozzle  
[NASA-TM-83439] p 159 N89-14386

## BUTTON, ROBERT M.

- Development and testing of a 20-kHz component test bed  
[NASA-TM-102141] p 139 N89-25403

- Distortion and regulation characterization of a Mapham inverter  
[NASA-TM-102089] p 139 N89-26148

- Frequency domain model for analysis of paralleled, series-output-connected Mapham inverters  
[NASA-TM-102140] p 139 N89-26149

## BUZZARD, ROBERT J.

- Fatigue testing apparatus  
[NASA-CASE-LEW-14124-1] p 177 N89-28806

## BYERS, DAVID C.

- The NASA Electric Propulsion Program  
p 59 A89-47428

## C

## CAIRELLI, J. E.

- SPRE 1 free-piston Stirling engine testing at NASA Lewis Research Center  
p 55 A89-29120

## CAIRELLI, JAMES E.

- Failure analysis of a Stirling engine heat pipe  
[NASA-TM-101418] p 103 N89-20227
- Results from baseline tests of the SPRE 1 and comparison with code model predictions  
[NASA-TM-102044] p 68 N89-23527

## CALDECOTT, R.

- Measurement of the properties of lossy materials inside a finite conducting cylinder  
[NASA-CR-182500] p 126 N89-10223

- Engineering calculations for solving the orbital allotment problem  
[NASA-CR-184607] p 217 N89-13993

## CALFO, FREDERICK D.

- Scaling results for the Liquid Sheet Radiator (LSR)  
[NASA-TM-102100] p 72 N89-25277

## CAMPANELLA, S. J.

- Assessment of satellite communications quality study. Addendum 1: Impact of propagation delay on data transmission  
[NASA-CR-182229] p 126 N89-14369

## CARBONE, A. J.

- Interdiffusional effects between TiBe12 and NiAl intermetallics  
p 95 A89-21395

## CARLSON, ALBERT W.

- Solar dynamic heat rejection technology. Task 1: System concept development  
[NASA-CR-179618] p 158 N89-13731

## CARNEY, J.

- GaAs circuits for monolithic optical controller  
p 131 A89-15828

## CARNEY, KELLY S.

- Free-vibration characteristics and correlation of a Space Station split-blanket solar array  
[AIAA PAPER 89-1252] p 44 A89-30737
- Modal representations in control/structure interaction  
p 45 A89-54114

- Free-vibration characteristics and correlation of a space station split-blanket solar array  
[NASA-TM-101452] p 198 N89-15438

## CARNEY, L. M.

- Investigation of a liquid-fed water resistojet plume  
[AIAA PAPER 89-2840] p 58 A89-47117

- Investigation of a liquid-fed water resistojet plume  
[NASA-TM-102310] p 75 N89-27706

## CARNEY, LYNNETTE M.

- Langmuir probe measurements of an arcjet exhaust  
p 55 A89-39031

- Experimental evaluation of resistojet thruster plume shields  
p 59 A89-47487

- The effects of arcjet thruster operating condition constrictor geometry on the plasma plume  
[AIAA PAPER 89-2723] p 60 A89-50809

- Electromagnetic emission experiences using electric propulsion systems  
p 61 A89-53354

- The effects of arcjet operating condition and constrictor geometry on the plasma plume  
[NASA-TM-102284] p 72 N89-25281

## CARUSO, J. J.

- Finite element applications to explore the effects of partial bonding on metal matrix composite properties  
[AIAA PAPER 89-1175] p 192 A89-30666

- Finite element applications to explore the effects of partial bonding on metal matrix composite properties  
[NASA-TM-101482] p 86 N89-20206

## CARUTHERS, JAMES M.

- A predictive model for failure properties of thermoset resins  
[NASA-TM-4128] p 87 N89-25300

## CASTRO, J. H.

- Design and analysis report for the flight weight 20-inch Columbia secondary nozzle for the RL10 engine  
[NASA-CR-179612] p 65 N89-16918

## CASTRO, JOAQUIN H.

- Evaluation of coated columbium test panels having application to a secondary nozzle extension for the RL10 rocket engine system, parts 1 and 2  
[NASA-CR-180809] p 64 N89-13493

## CATALDO, R. L.

- Energy storage considerations for a robotic Mars surface sampler  
p 49 A89-15267

## CATALDO, ROBERT L.

- Human exploration mission studies  
p 38 N89-22985

## CAUGHEY, D. A.

- LU implicit multigrid algorithm for the three-dimensional Euler equations  
p 143 A89-19906

## CAUGHEY, DAVID A.

- Diagonal implicit multigrid algorithm for the Euler equations  
p 1 A89-11110

- Multigrid calculation of three-dimensional turbomachinery flows  
[NASA-CR-185332] p 165 N89-26172

## CAULFIELD, T.

- The effect of Co alloying content on the kinetics of reaction zone growth in tungsten fiber reinforced superalloy composites  
p 79 A89-11324

## CEBECI, TUNCER

- Calculation of flow over iced airfoils  
p 5 A89-40905

- Effects of environmentally imposed roughness on airfoil performance  
[NASA-CR-179639] p 17 N89-11725

## CELESTINA, MARK L.

- Simulation of 3-D viscous flow within a multi-stage turbine  
[NASA-TM-101376] p 26 N89-14238

## CERNANSKY, N. P.

- Degradation mechanisms of n-dodecane with sulfur and nitrogen dopants during thermal stressing  
p 116 A89-22277

## CERNANSKY, NICHOLAS P.

- NOx formation from the combustion of monodisperse n-heptane sprays doped with fuel-nitrogen additives  
p 116 A89-42695

## CHAI, A. T.

- Convective flows in enclosures with vertical temperature or concentration gradients  
[AIAA PAPER 89-0069] p 118 A89-25060

- Convective flows in enclosures with vertical temperature or concentration gradients  
[NASA-TM-101373] p 120 N89-12753

## CHAI, AN-TI

- Numerical studies of convective heat transfer in an inclined semiannular enclosure  
[NASA-TM-102011] p 123 N89-28666

## CHAIM, R.

- On the orthorhombic phase in ZrO<sub>2</sub>-based alloys  
p 105 A89-30631

## CHAIT, A.

- Steady-state thermal-solutal diffusion in a float zone  
p 119 A89-40897

- Convection and chemistry effects in CVD: A 3-D analysis for silicon deposition  
[NASA-TM-102001] p 78 N89-21032

## CHAIT, ARNON

- The secondary flow and its stability for natural convection in a tall vertical enclosure  
p 149 A89-37931

## CHAMBERLIN, ROGER

- New hypersonic facility capability at NASA Lewis Research Center  
[AIAA PAPER 89-2534] p 36 A89-46905

- New hypersonic facility capability at NASA Lewis Research Center  
[NASA-TM-102028] p 36 N89-22617

## CHAMBERS, F. W.

- Lateral noise attenuation of the advanced propeller of the propan test assessment aircraft  
[AIAA PAPER 89-1057] p 226 A89-36217

## CHAMIS, C. C.

- Finite element substructuring methods for composite mechanics  
p 80 A89-26291

- Finite element applications to explore the effects of partial bonding on metal matrix composite properties  
[AIAA PAPER 89-1175] p 192 A89-30666

- Mechanics of damping for fiber composite laminates including hygro-thermal effects  
[AIAA PAPER 89-1191] p 192 A89-30681

- Structural behavior of composites with progressive fracture  
[AIAA PAPER 89-1271] p 192 A89-30754

- Structural tailoring of laminate properties  
[AIAA PAPER 89-1367] p 192 A89-30842

- Probabilistic constitutive relationships for material strength degradation models  
[AIAA PAPER 89-1368] p 192 A89-30843

- A probabilistic approach to composite micromechanics  
[NASA-TM-101366] p 85 N89-12684

- Fracture toughness computational simulation of general delaminations in fiber composites  
[NASA-TM-101415] p 85 N89-13521

- Parametric studies of advanced turboprops  
[NASA-TM-101389] p 197 N89-14465

- Three-dimensional inelastic analysis methods for hot section components  
p 199 N89-17321

- Finite element applications to explore the effects of partial bonding on metal matrix composite properties  
[NASA-TM-101482] p 86 N89-20206

- Advanced methods for 3-D inelastic structural analysis for hot engine structures  
[NASA-TM-102106] p 204 N89-25490

- Simplified procedures for designing adhesively bonded composite joints  
[NASA-TM-102120] p 87 N89-26048

- Computational structural mechanics for engine structures  
[NASA-TM-102119] p 204 N89-26259

- Tailoring of composite links for optimal damped elasto-dynamic performance  
[NASA-TM-102094] p 88 N89-26912

- Unified micromechanics of damping for unidirectional fiber reinforced composites  
[NASA-TM-102107] p 88 N89-26919

- Metal matrix composite micromechanics: In-situ behavior influence on composite properties  
[NASA-TM-102302] p 88 N89-26924

- Computational simulation of high temperature metal matrix composites cyclic behavior  
[NASA-TM-102115] p 88 N89-27795



- Probabilistic structural analysis methods of hot engine structures  
[NASA-TM-102091] p 205 N89-28030
- Computational structural mechanics engine structures computational simulation p 205 N89-29792
- The 3-D inelastic analyses for computational structural mechanics p 206 N89-29804
- CHAMIS, CHRISTOS C.**
- Fiber composite sandwich thermostructural behavior - Computational simulation p 190 A89-11246
- A unique set of micromechanics equations for high-temperature metal matrix composites p 190 A89-15734
- Thermoviscoplastic nonlinear constitutive relationships for structural analysis of high-temperature metal matrix composites p 190 A89-15735
- Composite interlaminar fracture toughness - Three-dimensional finite-element modeling for mixed mode I, II, and fracture p 190 A89-16278
- Sublaminar or ply-level analysis of composites and strain energy release rates of end-notch and mixed-mode fracture specimens p 190 A89-16279
- Composite mechanics for engine structures p 80 A89-28344
- Computational structural mechanics for engine structures [AIAA PAPER 89-1260] p 22 A89-30745
- Test methods and design allowables for fibrous composites. Volume 2 [ASTM STP-1003] p 81 A89-32882
- Mechanics of composite materials - Past, present and future p 82 A89-36293
- Free-edge delamination - Laminar width and loading conditions effects p 193 A89-36294
- Dynamic delamination buckling in composite laminates under impact loading - Computational simulation p 82 A89-36310
- Fiber composite structural durability and damage tolerance - Simplified predictive methods p 82 A89-36320
- Probabilistic structural analysis to quantify uncertainties associated with turbopump blades p 194 A89-36920
- Structural tailoring of Space Shuttle Main Engine turbopump blades SSME/STAEIL p 55 A89-44106
- CHAMIS, CRISTOS C.**
- Design procedures for fiber composite box beams p 195 A89-48674
- CHAMPAGNE, G. A.**
- Performance potential of air turbo-ramjet employing supersonic through-flow fan [AIAA PAPER 89-0010] p 22 A89-25006
- Supersonic through-flow fan assessment [NASA-CR-182202] p 27 N89-16843
- CHAN, K. S.**
- The constitutive representation of high-temperature creep damage p 191 A89-17396
- Inelastic deformation and dislocation structure of a nickel alloy - Effects of deformation and thermal histories p 99 A89-50313
- CHAN, KWAI S.**
- Constitutive modeling for isotropic materials p 195 N89-12904
- CHANG, C. L.**
- Least-squares finite elements for Stokes problem [NASA-TM-101308] p 222 N89-22392
- CHANG, G. E.**
- Improved high-temperature resistant matrix resins [NASA-CR-180826] p 114 N89-21105
- CHANG, GEORGE C.**
- A study on thermal barrier coatings including thermal expansion mismatch and bond coat oxidation p 109 N89-12919
- Thermal expansion mismatch and plasticity in thermal barrier coating p 200 N89-17330
- CHANG, PATRICK**
- The physics of positively biased conductors surrounded by dielectrics in contact with a plasma p 232 A89-39395
- CHANG, SHIH-HUNG**
- A numerical study of ENO and TVD schemes for shock capturing [NASA-TM-101355] p 222 N89-11469
- CHANG, T. Y. P.**
- On finite element implementation and computational techniques for constitutive modeling of high temperature composites [NASA-CR-185120] p 204 N89-26261
- CHAPMAN, RANDALL A.**
- Development of a high power microwave thruster, with a magnetic nozzle, for space applications [NASA-TM-102321] p 74 N89-26904
- CHARLESTON, JOANN**
- Hydrogen-bromine fuel cell advance component development [NASA-TM-101345] p 208 N89-10405
- CHATO, D. J.**
- Modeling of pulsed propellant reorientation [AIAA PAPER 89-2727] p 61 A89-53306
- Modeling of pulsed propellant reorientation [NASA-TM-102117] p 165 N89-26178
- CHATO, DAVID J.**
- Modeling of impulsive propellant reorientation [AIAA PAPER 89-0628] p 54 A89-25496
- Modeling of impulsive propellant reorientation [NASA-TM-101440] p 64 N89-13495
- Analysis of the nonvented fill of a 4.96-cubic-meter lightweight liquid hydrogen tank [NASA-TM-102039] p 67 N89-22652
- CHAWATHE, A. K.**
- Space Station battery system design and development p 52 A89-15378
- CHEN, C. T.**
- Thermosolutal convection in high-aspect-ratio enclosures p 153 A89-53288
- CHEN, P. C.**
- On 3D inelastic analysis methods for hot section components p 196 N89-12906
- CHEN, Q.**
- Resolved shear stress intensity coefficient and fatigue crack growth in large crystals p 96 A89-22048
- CHEN, XIANG**
- Gear optimization [NASA-CR-4201] p 182 N89-13793
- CHEN, Y. C.**
- Molecular beam epitaxial growth of high-quality InSb on InP and GaAs substrates [NASA-CR-185440] p 236 N89-26739
- Surface morphologies and electrical properties of molecular beam epitaxial InSb and InAs(x)Sb(1-x) grown on GaAs and InP substrates [NASA-CR-185439] p 237 N89-26740
- CHERRETTE, A. R.**
- A method for producing a shaped contour radiation pattern using a single shaped reflector and a single feed [NASA-TM-101369] p 126 N89-10215
- CHERRETTE, ALAN R.**
- A method for producing a shaped contour radiation pattern using a single shaped reflector and a single feed p 125 A89-42758
- Compensation of reflector antenna surface distortion using an array feed p 126 A89-53136
- CHILDS, D.**
- Annular honeycomb seals: Test results for leakage and rotordynamic coefficients - Comparisons to labyrinth and smooth configurations [ASME PAPER 88-TRIB-35] p 179 A89-34794
- An entrance region friction factor model applied to annular seal analysis - Theory versus experiment for smooth and honeycomb seals [ASME PAPER 88-TRIB-41] p 179 A89-34798
- CHILDS, DARA**
- Experimental results for labyrinth gas seals with honeycomb stators - Comparisons to smooth-stator seals and theoretical predictions [ASME PAPER 88-TRIB-40] p 179 A89-24992
- CHILDS, DARA W.**
- Annular honeycomb seals: Test results for leakage and rotordynamic coefficients; comparisons to labyrinth and smooth configurations p 185 N89-22899
- CHIMA, RODRICK C.**
- Explicit Runge-Kutta method for unsteady rotor/stator interaction p 5\_ A89-36912
- CHIMA, RODRICK V.**
- An unconditionally stable Runge-Kutta method for unsteady flows [AIAA PAPER 89-0205] p 2 A89-25180
- CHITRE, D. M.**
- Assessment of satellite communications quality study. Addendum 1: Impact of propagation delay on data transmission [NASA-CR-182229] p 126 N89-14369
- CHOI, S.-W.**
- Nonlinear evolution of interacting oblique waves on two-dimensional shear layers [NASA-TM-102030] p 164 N89-24575
- CHOO, YUNG K.**
- Interactive grid generation for turbomachinery flow field simulations [NASA-TM-101301] p 9 N89-11717
- Application of a lower-upper implicit scheme and an interactive grid generation for turbomachinery flow field simulations [NASA-TM-101412] p 11 N89-15077
- CHOPRA, M. A.**
- Dendritic solidification in binary alloys p 96 A89-22560
- Measurement of the diffusion coefficient of acetone in succinonitrile at its melting point p 237 A89-23488
- CHOU, R.**
- Ray-tube integration in shooting and bouncing ray method p 124 A89-15152
- CHOU, RI-CHIEE**
- Shooting and bouncing rays - Calculating the RCS of an arbitrarily shaped cavity p 124 A89-34242
- High-frequency RCS of open cavities with rectangular and circular cross sections p 125 A89-39595
- CHOUMARD, E.**
- Stratified charge rotary engine - Internal flow studies at the MSU engine research laboratory [SAE PAPER 890331] p 181 A89-51477
- CHOW, E.**
- Nuclear reactor power as applied to a space-based radar mission p 51 A89-15317
- Systems aspects of a space nuclear reactor power system p 51 A89-15327
- Nuclear reactor power as applied to a space-based radar mission [NASA-TM-101200] p 230 N89-14831
- CHOY, F. C.**
- The role of thermal and lubricant boundary layers in the transient thermal analysis of spur gears [NASA-TM-101435] p 182 N89-14452
- CHOY, F. K.**
- Vibration signature analysis of multistage gear transmission [NASA-TM-101442] p 184 N89-18685
- CHOYKE, W. J.**
- Raman determination of layer stresses and strains for heterostructures and its application to the cubic SiC/Si system p 234 A89-21871
- CHRISS, R. M.**
- An LDA (Laser-Doppler Anemometry) investigation of three-dimensional normal shock wave boundary-layer interactions p 14 N89-20956
- CHRISTIAN, J. L.**
- Unique mission options available with a megawatt-class nuclear electric propulsion system [NASA-TM-101220] p 65 N89-17618
- CHRISTIANSEN, ALFRED W.**
- Improving the fatigue resistance of adhesive joints in laminated wood structures [NASA-CR-182165] p 85 N89-12675
- CHUBB, DONALD L.**
- Gas particle radiator [NASA-CASE-LEW-14297-1] p 172 N89-12048
- Liquid sheet radiator apparatus [NASA-CASE-LEW-14295-1] p 123 N89-14348
- Scaling results for the Liquid Sheet Radiator (LSR) [NASA-TM-102100] p 72 N89-25277
- CHUCKSA, R. J.**
- The modular combustion facility for the Space Station laboratory - A requirements and capabilities study [AIAA PAPER 89-0505] p 44 A89-28421
- CHUE, R.**
- Calculations of inlet distortion induced compressor flow field instability p 8 A89-52498
- CHUN, K.**
- Stratified charge rotary engine - Internal flow studies at the MSU engine research laboratory [SAE PAPER 890331] p 181 A89-51477
- CHUN, K. S.**
- Strain measurements in a rotary engine housing [SAE PAPER 890333] p 181 A89-51493
- CHUNG, CHAN-HONG**
- Flow of rarefied gases over two-dimensional bodies [AIAA PAPER 89-1970] p 5 A89-41814
- Rarefied gas flow through two-dimensional nozzles [AIAA PAPER 89-2893] p 7 A89-47156
- CHUNG, J.**
- Transmission electron microscopy of composites p 79 A89-14560
- CHYU, M. K.**
- Heat transfer in the tip region of a rotor blade simulator p 157 N89-12898
- Heat transfer in the tip region of a rotor blade simulator p 161 N89-17312
- CIANCONE, MICHAEL L.**
- Oxidation and protection of fiberglass-epoxy composite masts for photovoltaic arrays in the low earth orbital environment p 44 A89-35316
- Age distribution among NASA scientists and engineers p 238 N89-23911
- CIFANI, DIANE**
- 700 F properties of autoclave cured PMR-II composites p 81 A89-29998
- CIVINSKAS, K. C.**
- Impact of ETO propellants on the aerothermodynamic analyses of propulsion components [AIAA PAPER 88-3091] p 53 A89-16486
- CIVINSKAS, KESTUTIS C.**
- Turbine-stage heat transfer - Comparison of short-duration measurements with state-of-the-art predictions p 142 A89-16458
- CLARK, D.**
- Photovoltaic module on-orbit assembly for Space Station Freedom [NASA-TM-102297] p 47 N89-26887

## CLARK, DAVID A.

- CLARK, DAVID A.**  
Contingency power for small turboshaft engines  
p 21 A89-22291
- CLASPY, P. C.**  
Microwave response of an HEMT photoconductor  
p 131 A89-15824  
Optical detectors for GaAs MMIC integration:  
Technology assessment  
[NASA-TM-102025] p 137 N89-22020
- CLASPY, PAUL C.**  
Microwave characteristics of interdigitated  
photoconductors on a HEMT structure  
[NASA-CR-182197] p 135 N89-12820  
Microwave characteristics of GaAs MMIC integratable  
optical detectors  
[NASA-TM-101485] p 129 N89-24520
- CLAUS, R. W.**  
Direct numerical simulations of a temporally evolving  
mixing layer subject to forcing p 147 A89-34426  
Response of a chemically reacting shear layer to  
streamwise vorticity  
[AIAA PAPER 89-0978] p 150 A89-40400  
Mesh refinement in a two-dimensional large eddy  
simulation of a forced shear layer  
[NASA-TM-102129] p 166 N89-26180
- CLEMENT, S. K.**  
The effect of different alkali metal hydroxides on nickel  
electrode life p 207 A89-15280
- COE, HAROLD H.**  
Comparison of predicted and measured temperatures  
of UH-60A helicopter transmission  
[NASA-TP-2911] p 186 N89-24607
- COHEN, R. S.**  
Degradation mechanisms of n-dodecane with sulfur and  
nitrogen dopants during thermal stressing p 116 A89-22277
- COIRIER, WILLIAM J.**  
High speed inlet calculations with real gas effects  
[AIAA PAPER 88-3076] p 2 A89-14980  
High speed corner and gap-seal computations using an  
LU-SGS scheme p 154 A89-54424  
High speed corner and gap-seal computations using an  
LU-SGS scheme  
[NASA-TM-102138] p 166 N89-27103
- COLE, GARY L.**  
A message passing kernel for the hypercluster parallel  
processing test bed  
[NASA-TM-101952] p 218 N89-20684  
Initial operating capability for the hypercluster  
parallel-processing test bed  
[NASA-TM-101953] p 218 N89-20685
- COLE, J. W.**  
The upper-branch stability of compressible boundary  
layer flows  
[NASA-TM-102128] p 167 N89-28748
- COLEMAN, PAUL T.**  
OTVE turbopump condition monitoring, task E.5  
[NASA-CR-182274] p 189 N89-27204
- COLLAMORE, F. N.**  
Miniature multiple-function probe for OTV turbopump  
health monitoring  
[AIAA PAPER 89-2303] p 56 A89-46736
- COLLAMORE, FRANK N.**  
Integrated control and health monitoring capacitive  
displacement sensor development task. Orbit transfer  
rocket engine technology program  
[NASA-CR-182279] p 176 N89-26208
- COLLIN, R. E.**  
Aperture impedance of flared horns p 125 A89-43543
- COLLINS, J. J.**  
OTVE turbopump condition monitoring, task E.5  
[NASA-CR-182274] p 189 N89-27204
- CONWAY, BRUCE A.**  
Optimal terminal maneuver for a cooperative impulsive  
rendezvous p 38 A89-36946
- COOK, JERRY D.**  
Study of optical output couplers for submillimeter  
wavelength backward-wave oscillators (BWO's)  
p 132 A89-32857  
Study of optical output couplers for submillimeter  
wavelength backward-wave oscillators (BWO's)  
[NASA-TM-101360] p 134 N89-11128
- COOK, T. S.**  
Thermal barrier coating life prediction model  
p 109 N89-12921  
Thermal barrier coating life prediction model  
development  
[NASA-CR-180807] p 110 N89-13621
- COOMBS, M. G.**  
Advanced solar receivers for space power  
p 54 A89-29116
- COOMBS, MURRAY G.**  
Advanced space solar dynamic receivers  
p 52 A89-15343

- COOMES, E. P.**  
Unique mission options available with a megawatt-class  
nuclear electric propulsion system  
[NASA-TM-101220] p 65 N89-17618
- CORBAN, R. R.**  
Technology requirements for an orbiting fuel depot - A  
necessary element of a space infrastructure  
[IAF PAPER 88-035] p 37 A89-17641
- CORBAN, ROBERT R.**  
Expendable launch vehicle transportation for the Space  
Station  
[IAF PAPER 88-198] p 42 A89-17720  
Expendable launch vehicle transportation for the space  
station  
[NASA-TM-101947] p 42 N89-20179
- CORDELL, BRUCE**  
An analysis of possible advanced space strategies  
featuring the role of space resource utilization  
[IAF PAPER 88-587] p 37 A89-17861
- COUTTS, T. J.**  
High-efficiency solar cells fabricated from direct-current  
magnetron sputtered n-indium tin oxide onto p-InP grown  
by atmospheric pressure metalorganic vapor phase  
epitaxy p 133 A89-44518  
High-efficiency indium tin oxide/indium phosphide solar  
cells p 208 A89-44883  
Radiation resistance and comparative performance of  
ITO/InP and n/p InP homojunction solar cells  
[NASA-TM-101387] p 135 N89-12819
- COWLEY, STEPHEN J.**  
On the Lagrangian description of unsteady boundary  
layer separation. Part 1: General theory  
[NASA-TM-102026] p 164 N89-23821
- COY, J. J.**  
Computerized life and reliability modeling for turboprop  
transmissions p 181 A89-53364  
Tooth contact shift in loaded spiral bevel gears o, IL,  
25-27 Apr. 1989; sponsored by ASME  
[NASA-TM-101438] p 183 N89-14453  
Topology of modified helical gears  
[NASA-TM-102134] p 187 N89-28015
- COY, JOHN J.**  
Advanced transmission studies p 178 A89-18906  
Computer-aided design of bevel gear tooth surfaces  
[NASA-TM-101449] p 183 N89-17248
- CRANE, R. A.**  
Evaluation of alternative phase change materials for  
energy storage in solar dynamic applications p 208 A89-29114
- CRANE, ROGER A.**  
Thermal evaluation of advanced solar dynamic heat  
receiver performance  
[NASA-CR-185117] p 214 N89-27256
- CRAWFORD, R. A.**  
Influence of bulk turbulence and entrance boundary layer  
thickness on the curved duct flow field  
[NASA-CR-4188] p 155 N89-12838
- CRAWFORD, ROGER A.**  
Influence of bulk turbulence and entrance boundary layer  
thickness on the curved duct flow field p 156 N89-12896
- CRAWLEY, EDWARD F.**  
Calculation of unsteady flows in turbomachinery using  
the linearized Euler equations p 149 A89-36916
- CROWLEY, R. D.**  
Advanced modulation technology development for earth  
station demodulator applications  
[NASA-CR-185126] p 43 N89-26880
- CRUSE, T. A.**  
Probabilistic structural analysis methods and  
applications p 190 A89-16939  
Probabilistic methods for structural response analysis  
p 223 A89-25843  
An advanced probabilistic structural analysis method for  
implicit performance functions  
[AIAA PAPER 89-1371] p 193 A89-30846
- CUMMINGS, ROBERT L.**  
Performance estimates for the Space Station power  
system Brayton Cycle compressor and turbine  
[NASA-CR-182263] p 73 N89-26903
- CUNNINGHAM, JOCK**  
Mass flow meter using the triboelectric effect for  
measurement in cryogenics  
[NASA-CR-179572] p 155 N89-12836
- CURRAN, FRANCIS M.**  
Arcjet nozzle design impacts  
[NASA-TM-102050] p 68 N89-23522  
Electric propulsion options for 10 kW class earth space  
missions  
[NASA-TM-102337] p 74 N89-26906  
Arcjet cathode phenomena  
[NASA-TM-102099] p 167 N89-27121
- CURRAN, FRANK M.**  
The effect of electrode configuration on arcjet  
performance  
[AIAA PAPER 89-2722] p 58 A89-47044

- CURREN, ARTHUR N.**  
Secondary electron emission characteristics of  
untreated and ion-textured titanium  
[NASA-TP-2902] p 103 N89-17650
- CURTIS, HENRY B.**  
Temperature coefficients for concentrator cells at  
various electron and proton fluence levels  
p 51 A89-15304  
Stability of bulk Ba<sub>2</sub>YCu<sub>3</sub>O(7-x) in a variety of  
environments p 111 N89-14310  
The effect of different module configurations on the  
radiation tolerance of multijunction solar cells  
[NASA-TM-101251] p 209 N89-17356  
A comparison of the radiation tolerance characteristics  
of multijunction solar cells with series and voltage-matched  
configurations p 213 N89-24737

## D

- D'ANGELO, N.**  
The plasma wake of the Shuttle Orbiter  
p 215 A89-43680  
Plasma density, temperature and turbulence in the wake  
of the Shuttle Orbiter p 233 A89-53209  
Plasma density fluctuations observed during Space  
Shuttle Orbiter water releases p 233 A89-54759
- DAHL, MILO D.**  
Acoustic wave propagation in heterogeneous structures  
including experimental validation  
[AIAA PAPER 89-1044] p 225 A89-36214  
Acoustic wave propagation in heterogeneous structures  
including experimental validation  
[NASA-TM-101486] p 224 N89-19965
- DALSANIA, VITHAL**  
Thermal distortion analysis of the Space Station solar  
dynamic concentrator p 51 A89-15341
- DAME, L. T.**  
On 3D inelastic analysis methods for hot section  
components p 196 N89-12906  
Constitutive modeling for isotropic materials  
[NASA-CR-174805] p 26 N89-13436
- DANNELS, CHRISTINE M.**  
Effect of processing on fracture toughness of silicon  
carbide as determined by Vickers indentations  
[NASA-TM-101456] p 115 N89-21895
- DARGUSH, G. F.**  
Advanced development of the boundary element  
method for steady-state heat conduction p 154 A89-54766  
Development of BEM for ceramic composites  
[NASA-CR-183313] p 111 N89-14311
- DARGUSH, GARY F.**  
Development of an integrated BEM approach for hot  
fluid structure interaction  
[NASA-CR-184587] p 27 N89-15114
- DAVIDOVITZ, MARAT**  
Rigorous analysis of a circular patch antenna excited  
by a microstrip transmission line p 125 A89-53134
- DAVIS, K. E.**  
An asymptotic description of transient settling and  
ultrafiltration of colloidal dispersions p 144 A89-24603
- DAVIS, R. C.**  
Advanced modulation technology development for earth  
station demodulator applications  
[NASA-CR-185126] p 43 N89-26880
- DAVIS, V. A.**  
A model of electron collecting plasma contractors  
[AIAA PAPER 89-1560] p 232 A89-40190
- DAVIS, VICTORIA ANN**  
On the need for space tests of plasma contractors as  
electron collectors p 232 A89-43356
- DE GROH, H. C., III**  
Macroscopic segregation in undercooled Pb-Sn eutectic  
alloys p 95 A89-19621  
Effects of crucible wetting during solidification of  
immiscible Pb-Zn alloys  
[AIAA PAPER 89-0304] p 118 A89-25261
- DE WITT, K. J.**  
Efficient numerical simulation of a one-dimensional  
electrothermal deicer pad p 144 A89-22811  
Two-dimensional simulation of electrothermal deicing of  
aircraft components p 17 A89-39194  
Effect of ambient pressure on the performance of a  
resistojet p 55 A89-44111
- DE WITT, KENNETH J.**  
Flow of rarefied gases over two-dimensional bodies  
[AIAA PAPER 89-1970] p 5 A89-41814  
The effect of test-cell pressure on resistojet nozzle  
flow  
[AIAA PAPER 89-2838] p 58 A89-47116  
Rarefied gas flow through two-dimensional nozzles  
[AIAA PAPER 89-2893] p 7 A89-47156

- DE, BHOLA N.**  
Thin-film hermeticity - A quantitative analysis of diamondlike carbon using variable angle spectroscopic ellipsometry p 234 A89-13945
- DEABREU-GARCIA, ALEX**  
Computational fluid dynamic control p 220 A89-53984
- DEANNA, RUSSELL G.**  
Development of a thermal and structural analysis procedure for cooled radial turbines [NASA-TM-101416] p 24 N89-12568
- DECHENE, RONALD L.**  
Mass flow measurement of liquid cryogenics using the triboelectric effect [NASA-CR-179519] p 155 N89-12837
- DECKER, ARTHUR J.**  
Holographic interferometry with an injection seeded Nd:YAG laser and two reference beams [NASA-TM-102056] p 175 N89-24591
- DEEN, M. JAMAL**  
Design and simulated performance of a CARS spectrometer for dynamic temperature measurements using electronic heterodyning p 170 A89-37298
- DEGANI, A. T.**  
Asymptotic structure and similarity solutions for three-dimensional turbulent boundary layers [AIAA PAPER 89-1863] p 150 A89-42090
- DEGROH, H. C., III**  
Bulk undercooling, nucleation, and macrosegregation of Pb-Sn alloys p 117 A89-17106
- DEGROH, HENRY C., III**  
Effects of crucible wetting during solidification of immiscible Pb-Zn [NASA-TM-101372] p 120 N89-14341  
Macrosegregation and nucleation in undercooled Pb-Sn alloys [NASA-TM-102023] p 104 N89-23664
- DEININGER, W.**  
Nuclear reactor power as applied to a space-based radar mission p 51 A89-15317  
Systems aspects of a space nuclear reactor power system p 51 A89-15327  
Nuclear reactor power as applied to a space-based radar mission [NASA-TM-101200] p 230 N89-14831
- DEISSLER, ROBERT G.**  
On the nature of Navier-Stokes turbulence [NASA-TM-101983] p 163 N89-23813
- DELAAT, JOHN C.**  
Advanced detection, isolation, and accommodation of sensor failures - Real-time evaluation p 34 A89-16156  
A real-time simulator of a turbofan engine [NASA-TM-100869] p 31 N89-20995  
A real time microcomputer implementation of sensor failure detection for turbofan engines [NASA-TM-102327] p 216 N89-29032
- DELCHER, R.**  
Fiber optics for liquid propellant rocket engine environments [AIAA PAPER 89-2416] p 230 A89-46812
- DELLACORTE, CHRISTOPHER**  
Tribological composition optimization of chromium-carbide-based solid lubricant coatings for foil gas bearings at temperatures to 650 C p 83 A89-54258  
Tribological properties of alumina-boria-silicate fabric from 25 C to 850 C p 107 A89-54982
- DELVIGS, PETER**  
Graphite/polyimide composites with improved toughness p 83 A89-38637
- DEMASI, J. T.**  
Thermal barrier coating life prediction model development p 110 N89-12922  
Thermal barrier coating life prediction model development p 200 N89-17333
- DEMUREN, A. O.**  
Application of multi-grid methods for solving the Navier-Stokes equations p 153 A89-53172  
Calculation of turbulence-driven secondary motion in ducts with arbitrary cross section [NASA-TM-102142] p 166 N89-27115
- DERGEVORKIAN, A.**  
Fiber optics for liquid propellant rocket engine environments [AIAA PAPER 89-2416] p 230 A89-46812
- DESALVO, GREGORY C.**  
A new structure for comparing surface passivation materials of GaAs solar cells p 213 N89-24725
- DESHANDEY, C. V.**  
Microlaminate composites as thermal barrier coatings p 83 A89-54261
- DEVER, THERESE M.**  
Isotopic study of oxygen diffusion in oxide coatings [NASA-TM-102082] p 78 N89-24451
- DIAS, B.**  
Probabilistic structural analysis methods and applications p 190 A89-16939
- DIAS, J. B.**  
An approach to probabilistic finite element analysis using a mixed-iterative formulation p 191 A89-25849
- DICARLO, JAMES A.**  
Pressure effects on the thermal stability of silicon carbide fibers p 105 A89-31502
- DICKEY, DANIEL W.**  
The effect of insulated combustion chamber surfaces on direct-injected diesel engine performance, emissions, and combustion [NASA-CR-182204] p 239 N89-17548
- DICUS, JOHN H.**  
New hypersonic facility capability at NASA Lewis Research Center [AIAA PAPER 89-2534] p 36 A89-46905  
New hypersonic facility capability at NASA Lewis Research Center [NASA-TM-102028] p 36 N89-22617
- DIEHL, LARRY A.**  
Space propulsion technology and cryogenic fluid depot p 38 N89-11768  
Advanced technology for future space propulsion systems [NASA-TM-101951] p 66 N89-20192
- DIFILIPPO, FRANK**  
Automated data acquisition and processing for a Hohlraum reflectometer [NASA-TM-101393] p 173 N89-14416  
The emittance of space radiator materials measured at elevated temperatures [NASA-TM-101948] p 66 N89-20193
- DILL, LOREN H.**  
Unsteady thermocapillary migration of bubbles [NASA-TM-101338] p 162 N89-22054
- DILLON, RODNEY O.**  
Radio-frequency plasma chemical vapor deposition growth of diamond p 236 A89-44552
- DILSAVOR, R. L.**  
Analysis of modified SMI method for adaptive array weight control [NASA-CR-184904] p 127 N89-20364
- DILSAVOR, RONALD LOUIS**  
Analysis of modified SMI method for adaptive array weight control [NASA-CR-185493] p 19 N89-25993
- DIRUSSO, ELISEO**  
Active vibration control for flexible rotor by optimal direct-output feedback control [NASA-TM-101972] p 31 N89-22605
- DISIMILE, P.**  
Behavior in normal and reduced gravity of an enclosed liquid/gas system with nonuniform heating from above [AIAA PAPER 89-0070] p 145 A89-25061  
Behavior in normal and reduced gravity of an enclosed liquid/gas system with nonuniform heating from above [NASA-TM-101471] p 120 N89-17046
- DITTMAR, JAMES**  
Comparison of propeller cruise noise data taken in the NASA Lewis 8- by 6-foot wind tunnel with other tunnel and flight data [AIAA PAPER 89-1059] p 226 A89-40472
- DITTMAR, JAMES H.**  
Cruise noise of the 2/9 scale model SR-7A propeller p 224 A89-12561  
Cruise noise of an advanced counterrotation turboprop measured from an adjacent aircraft p 20 A89-15080  
The effect of front-to-rear propeller spacing on the interaction noise at cruise conditions of a model counterrotation propeller having a reduced diameter aft propeller [NASA-TM-101329] p 227 N89-10603  
Measured far-field flight noise of a counterrotation turboprop at cruise conditions [NASA-TM-101383] p 228 N89-15686  
Comparison of propeller cruise noise data taken in the NASA Lewis 8- by 6-foot wind tunnel with other tunnel and flight data [NASA-TM-101976] p 228 N89-21628  
Cruise noise of the SR-2 propeller model in a wind tunnel [NASA-TM-101480] p 229 N89-24886
- DODD, W. R.**  
User needs, benefits and integration of robotic systems in a space station laboratory [NASA-CR-182261] p 185 N89-22108
- DOERR, H. J.**  
Microlaminate composites as thermal barrier coatings p 83 A89-54261
- DOMINEK, A.**  
Measurement of the properties of lossy materials inside a finite conducting cylinder [NASA-CR-182500] p 126 N89-10223
- Material parameter determination from scattering measurements [NASA-CR-183312] p 126 N89-10225  
Electromagnetic properties of ice coated surfaces [NASA-CR-184780] p 127 N89-20355
- DOMINICK, JEFFREY S.**  
Cooperating expert systems for Space Station - Power/thermal subsystem testbeds p 38 A89-15350
- DONG, X.**  
Symbolic generation of constitutive equations p 221 A89-34963
- DOREMUS, ROBERT H.**  
Crystallization of BaF<sub>2</sub>-ZnF<sub>2</sub>-YbF<sub>3</sub>-ThF<sub>4</sub> glass p 230 A89-12236
- DOS REIS, H. L. M.**  
Nondestructive evaluation/characterization of composite materials and structures using the acousto-ultrasonic techniques p 188 A89-36571
- DOUGHERTY, DAN**  
Cyclic stress analysis of ceramic coated gas turbine seals p 111 N89-13662
- DOUP, D.**  
Adiabatic Wankel type rotary engine [NASA-CR-182233] p 28 N89-17599
- DOWELL, EARL H.**  
On the role of artificial viscosity in Navier-Stokes solvers [AIAA PAPER 89-1947] p 5 A89-41794
- DOYCHAK, J.**  
Transient oxidation of single-crystal beta-NiAl p 98 A89-37899  
TEM studies of oxidized NiAl and Ni<sub>3</sub>Al cross sections p 99 A89-46506
- DOYCHAK, JOSEPH**  
Oxidation behavior of FeAl + Hf, Zr, B [NASA-TM-101402] p 102 N89-14297  
The oxidation of Ni-rich Ni-Al intermetallics [NASA-TM-101455] p 102 N89-15233
- DRAKE, J. B.**  
Thermal analysis of heat storage canisters for a solar dynamic, space power system p 54 A89-29113
- DRAPER, S.**  
Observations of directional gamma prime coarsening during engine operation p 98 A89-40162
- DRAPER, S. L.**  
Interdiffusional effects between TiBe<sub>12</sub> and NiAl intermetallics p 95 A89-21395
- DRAVID, NARAYAN**  
An integrated and modular digital modeling approach for the Space Station electrical power system development p 50 A89-15298
- DRAVID, NARAYAN V.**  
Development and refinement of test bed simulations [NASA-TM-102335] p 75 N89-27702
- DRESHFIELD, R.**  
Observations of directional gamma prime coarsening during engine operation p 98 A89-40162
- DRESHFIELD, ROBERT L.**  
Materials technology assessment for a 1050 K Stirling space engine design [NASA-TM-101342] p 77 N89-11815
- DRING, R. P.**  
The effects of inlet turbulence and rotor/stator interactions on the aerodynamics and heat transfer of a large-scale rotating turbine model, volume 1 [NASA-CR-4079] p 159 N89-13756
- DRING, ROBERT P.**  
Measurement of airfoil heat transfer coefficients on a turbine stage p 157 N89-12897  
Measurement of airfoil heat transfer coefficients on a turbine stage p 160 N89-17311
- DRUMMOND, C.**  
Transient flow thrust prediction for an ejector propulsion concept [AIAA PAPER 89-2906] p 23 A89-49688
- DRUMMOND, C. H., III**  
Crystallization and characterization of Y<sub>2</sub>O<sub>3</sub>-SiO<sub>2</sub> glasses p 80 A89-19486  
Microstructural evolution on crystallizing the glassy phase in a 6 weight percent Y<sub>2</sub>O<sub>3</sub>-Si<sub>3</sub>N<sub>4</sub> ceramic p 80 A89-19487
- DRUMMOND, COLIN K.**  
A control-volume method for analysis of unsteady thrust augmenting ejector flows [NASA-CR-182203] p 24 N89-12566  
Transient flow thrust prediction for an ejector propulsion concept [NASA-TM-102078] p 32 N89-24318  
A model for prediction of STOLV ejector dynamics [NASA-TM-102098] p 32 N89-24319
- DRYER, F. L.**  
Interactions between gaseous electrical discharges and single liquid droplets p 90 A89-19298  
Droplet combustion drop tower tests using models of the space flight apparatus [AIAA PAPER 89-0501] p 119 A89-28418

**DUCK, PETER W.**

- Three-dimensional marginal separation  
[NASA-TM-101411] p 159 N89-13757  
The response of a laminar boundary layer in supersonic flow to small amplitude progressive waves  
[NASA-TM-101965] p 162 N89-21197

**DUDEHOFER, JAMES E.**

- Two-dimensional numerical simulation of a Stirling engine heat exchanger  
[NASA-TM-102057] p 164 N89-23823  
On the dynamic response of pressure transmission lines in the research of helium-charged free piston Stirling engines  
[NASA-TM-102121] p 175 N89-24593

**DUDESTADT, E. C.**

- Thermal barrier coating life prediction model  
p 109 N89-12921

**DUFFY, S. F.**

- A viscoplastic constitutive theory for metal matrix composites at high temperature p 80 A89-20725

**DUFFY, STEPHEN F.**

- Noninteractive macroscopic reliability model for ceramic matrix composites with orthotropic material symmetry  
[NASA-TM-101414] p 198 N89-15437  
Time dependent reliability model incorporating continuum damage mechanics for high-temperature ceramics  
[NASA-TM-102046] p 115 N89-24487

**DUKE, J. C., JR.**

- A study of the stress wave factor technique for evaluation of composite materials  
[NASA-CR-4195] p 189 N89-21256

**DUNN, MICHAEL G.**

- Turbine-stage heat transfer - Comparison of short-duration measurements with state-of-the-art predictions p 142 A89-16458

**DUNN, VERNON E.**

- The potential impact of MMICs on future satellite communications  
[NASA-CR-182227] p 126 N89-17078  
The potential impact of MMICs on future satellite communications: Executive summary  
[NASA-CR-182227-EXEC-SUMM] p 127 N89-17079

**DUNNING, JOHN W., JR.**

- Space Station power system requirements  
p 50 A89-15295

**DURBIN, P. A.**

- Observations of the frequencies in a sphere wake and of drag increase by acoustic excitation p 142 A89-16884  
Investigation of the flow between a pair of circular cylinders in the flopping regime p 144 A89-22822  
Considerations on the moving contact-line singularity, with application to frictional drag on a slender drop p 144 A89-23238

**DURBIN, PAUL A.**

- On the wind force needed to dislodge a drop adhered to a surface p 144 A89-22819

**DUSTIN, M. O.**

- Evaluation of alternative phase change materials for energy storage in solar dynamic applications p 208 A89-29114

**DUTTA, SUNIL**

- Strength distribution in commercial silicon carbide materials p 105 A89-17097  
Effects of various consolidation techniques on microstructure, strength, and reliability of alpha-SiC p 106 A89-33611  
High-strength silicon carbides by hot isostatic pressing  
[NASA-TM-101400] p 111 N89-13666  
Effect of processing on fracture toughness of silicon carbide as determined by Vickers indentations  
[NASA-TM-101458] p 115 N89-21895

**DUVAL, W. M. B.**

- Effects of furnace temperature profile on the interface shape during Bridgman crystal growth p 119 A89-53278

**DUVAL, WALTER M. B.**

- Instabilities caused by oscillating accelerations normal to a viscous fluid-fluid interface p 144 A89-22823  
Interaction of surface radiation with convection in crystal growth by physical vapor transport  
[AIAA PAPER 89-0228] p 119 A89-30450

**DUYAR, AHMET**

- Identification of Space Shuttle Main Engine dynamics p 61 A89-54068  
Identification of space shuttle main engine dynamics  
[NASA-TM-101982] p 66 N89-20199

**E****EATON, JOHN K.**

- Experimental study of the development of longitudinal vortex pairs embedded in a turbulent boundary layer p 140 A89-11107

- Heat transfer with very high free-stream turbulence and streamwise vortices p 157 N89-12900  
Heat transfer with very high free-stream turbulence and heat transfer with streamwise vortices p 160 N89-17309

**EBIHARA, BEN**

- Design, fabrication, and performance of brazed, graphite electrode, multistage depressed collectors with 500-W, continuous wave, 4.8- to 9.6-GHz traveling-wave tubes  
[NASA-TP-2904] p 136 N89-21171

**EBIHARA, BEN T.**

- Isotropic graphite multistage depressed collectors - A progress report p 132 A89-31988  
Performance of a multistage depressed collector with machined titanium electrodes  
[NASA-TP-2891] p 136 N89-15337  
Measurements of complex permittivity of microwave substrates in the 20 to 300 K temperature range from 26.5 to 40.0 GHz  
[NASA-TM-102123] p 123 N89-27038

**ECCLES, J. VINCENT**

- A numerical model of electrodynamics of plasma within the contaminant gas cloud of the Space Shuttle Orbiter at low earth orbit p 233 A89-45631

**ECK, T. G.**

- Pulsed ion beam investigation of the kinetics of surface reactions p 93 A89-44542

**ECKEL, ANDREW J.**

- Strength distribution of reinforcing fibers in a Nicalon fiber/chemically vapor infiltrated silicon carbide matrix composite p 82 A89-34844

**EDENBURN, M.**

- Summary and evaluation of the Strategic Defense Initiative Space Power Architecture Study  
[NASA-TM-102012] p 69 N89-24443

**EDWARDS, DAVID E.**

- An analysis for high speed propeller-nacelle aerodynamic performance prediction. Volume 1: Theory and application  
[NASA-CR-4199-VOL-1] p 12 N89-15896  
An analysis for high speed propeller-nacelle aerodynamic performance prediction. Volume 2: User's manual  
[NASA-CR-4199-VOL-2] p 12 N89-15897

**EDWARDS, ROBERT V.**

- Application of optical correlation techniques to particle imaging  
[AIAA PAPER 88-4661] p 169 A89-14985  
A vector scanning processing technique for pulsed laser velocimetry  
[NASA-TM-102048] p 175 N89-23850

**EGOLF, T. ALAN**

- An analysis for high speed propeller-nacelle aerodynamic performance prediction. Volume 1: Theory and application  
[NASA-CR-4199-VOL-1] p 12 N89-15896  
An analysis for high speed propeller-nacelle aerodynamic performance prediction. Volume 2: User's manual  
[NASA-CR-4199-VOL-2] p 12 N89-15897

**EICHLER, DAVID**

- Nucleosynthesis, neutrino bursts and gamma-rays from coalescing neutron stars p 241 A89-46577

**EISEMAN, PETER R.**

- Interactive grid generation for turbomachinery flow field simulations  
[NASA-TM-101301] p 9 N89-11717

**EL ALI, A.**

- Transport critical current and magnetization measurements of melt-processed YBa<sub>2</sub>Cu<sub>3</sub>O(7-x)  
p 234 A89-20037

**EL-BAYOUMY, L. E.**

- The role of thermal and lubricant boundary layers in the transient thermal analysis of spur gears  
[NASA-TM-101435] p 182 N89-14452

**ELCHURI, V.**

- Modal forced vibration analysis of aerodynamically excited turbosystems  
[NASA-CR-174966] p 201 N89-18696  
NASTRAN supplemental documentation for modal forced vibration analysis of aerodynamically excited turbosystems  
[NASA-CR-174967] p 201 N89-19583

**ELLIOTT, G. S.**

- Compressibility and shock wave interaction effects on free shear layers  
[AIAA PAPER 89-2460] p 7 A89-46847

**ELLIS, GRAHAM K.**

- Transputer parallel processing at NASA Lewis Research Center p 205 N89-29778

**ELLIS, J. R.**

- A viscoplastic constitutive theory for metal matrix composites at high temperature p 80 A89-20725  
A multiaxial theory of viscoplasticity for isotropic materials p 196 N89-12908

- Thermomechanical characterization of Hastelloy-X under uniaxial cyclic loading p 196 N89-12909  
Use of inelastic strain as a basis for analyzing thermomechanical test data p 200 N89-17326  
Preliminary study of creep thresholds and thermomechanical response in Haynes 188 at temperatures in the range 649 to 871 C p 200 N89-17327

**ELMORE, D. L.**

- Further development of the dynamic gas temperature measurement system p 172 N89-12884

**ELOVIC, E.**

- Heat transfer in gas turbine engines and three-dimensional flows; Proceedings of the Symposium, ASME Winter Annual Meeting, Chicago, IL, Nov. 27-Dec. 2, 1988 p 148 A89-34926

**ELROD, D.**

- Annular honeycomb seals: Test results for leakage and rotordynamic coefficients - Comparisons to labyrinth and smooth configurations  
[ASME PAPER 88-TRIB-35] p 179 A89-34794  
An entrance region friction factor model applied to annular seal analysis - Theory versus experiment for smooth and honeycomb seals  
[ASME PAPER 88-TRIB-41] p 179 A89-34798

**ELROD, DAVID**

- Annular honeycomb seals: Test results for leakage and rotordynamic coefficients; comparisons to labyrinth and smooth configurations p 185 N89-22899

**EMAMI-NAEINI, ABBAS**

- Effect of model uncertainty on failure detection - The threshold selector p 219 A89-17965

**EMERY, K. A.**

- High-efficiency solar cells fabricated from direct-current magnetron sputtered n-indium tin oxide onto p-InP grown by atmospheric pressure metalorganic vapor phase epitaxy p 133 A89-44518  
High-efficiency indium tin oxide/indium phosphide solar cells p 208 A89-44883

**EMIGH, GRANT**

- The 25 kW solar thermal Stirling hydraulic engine system: Conceptual design  
[NASA-CR-180889] p 239 N89-14182

**ENGLISH, ROBERT E.**

- Assessment of lunar sources of He-3 for use on earth p 242 N89-14853

**ENGLUND, D. R.**

- HOST instrumentation R and D program overview p 25 N89-12878  
Advanced high temperature instrument for hot section research applications p 29 N89-20137

**ENGLUND, DAVID R.**

- The dual element method of strain gauge temperature compensation p 169 A89-12276  
Progress on a PdCr wire strain gage p 174 N89-17301

**ENSIGN, C. ROBERT**

- Turbine Engine Hot Section Technology (HOST) Project p 25 N89-12877

**EPSTEIN, A. H.**

- Active suppression of aerodynamic instabilities in turbomachines p 3 A89-28341

**ERICKSON, C.**

- Orbit transfer rocket engine technology program. Phase 2: Advanced engine study  
[NASA-CR-179602] p 61 N89-10119

**ERNST, F.**

- Transmission electron microscopy of composites p 79 A89-14560

**ERNST, WILLIAM D.**

- Alternative fuel capabilities of the Mod II Stirling vehicle  
[SAE PAPER 880543] p 177 A89-12303

**ERWIN, D. E.**

- Compressibility and shock wave interaction effects on free shear layers  
[AIAA PAPER 89-2460] p 7 A89-46847

**ESGAR, J. B.**

- Views on the impact of HOST p 31 N89-20144

**EUSTACE, J. G.**

- Compensation for effects of ambient temperature on rare-earth doped fiber optic thermometer  
[NASA-TM-102282] p 176 N89-27998

**EVERSMAN, WALTER**

- Effects of wind-tunnel wall absorption on acoustic radiation of propellers p 225 A89-22285

**EWELL, R.**

- Nuclear reactor power as applied to a space-based radar mission p 51 A89-15317  
Systems aspects of a space nuclear reactor power system p 51 A89-15327  
Nuclear reactor power as applied to a space-based radar mission  
[NASA-TM-101200] p 230 N89-14831

## F

- FACCA, L.**  
Radiative structures of lycopodium-air flames in low gravity  
[AIAA PAPER 89-0500] p 91 A89-25406  
Particle cloud mixing in microgravity  
[NASA-TM-101484] p 121 N89-20321
- FACCA, LILY T.**  
Feasibility of reduced gravity experiments involving quiescent, uniform particle cloud combustion  
[NASA-TM-101371] p 122 N89-26114
- FACEY, JOHN R.**  
Return of the turboprops p 20 A89-12953
- FAETH, G. M.**  
Turbulent multiphase flows p 152 A89-51883
- FAKHERI, AHMAD**  
The effects of radiative heat loss on microgravity flame spread  
[AIAA PAPER 89-0504] p 91 A89-28420
- FANG, DACHENG**  
The surface morphology of crystals melting under solutions of different densities p 235 A89-23482
- FANG, HO T.**  
Improved silicon nitride for advanced heat engines  
[NASA-CR-179525] p 113 N89-19421
- FANG, M. M.**  
Critical currents of aligned grains of Ti-Ba-Ca-Cu-O compounds p 235 A89-30335  
Free energy surfaces in the superconducting mixed state p 236 A89-43928
- FARMER, S. C.**  
Transmission electron microscopy of composites p 79 A89-14560  
On the orthorhombic phase in ZrO<sub>2</sub>-based alloys p 105 A89-30631
- FARNELL, K. E.**  
User needs, benefits and integration of robotic systems in a space station laboratory  
[NASA-CR-182261] p 185 N89-22108
- FARNHAM, TONY**  
Liquid droplet generation  
[NASA-CR-182246] p 166 N89-26182
- FAROKHI, S.**  
Large amplitude acoustic excitation of swirling turbulent jets  
[AIAA PAPER 89-0970] p 4 A89-29098  
Effect of initial swirl distribution on the evolution of a turbulent jet p 149 A89-36906  
Large amplitude acoustic excitation of swirling turbulent jets  
[NASA-TM-101950] p 13 N89-18417
- FAROKHI, SAEED**  
Turbulent swirling jets with excitation  
[NASA-CR-180895] p 16 N89-29329
- FARREL, D. E.**  
Experimental evidence for a transverse magnetization of the Abrikosov lattice in anisotropic superconductors p 234 A89-21473
- FARRELL, D. E.**  
Critical currents of aligned grains of Ti-Ba-Ca-Cu-O compounds p 235 A89-30335  
Doping directed at the oxygen sites in YBa<sub>2</sub>Cu<sub>3</sub>O<sub>7</sub>( $\delta$ ) - The effect of sulfur, fluorine, and chlorine p 133 A89-37824  
Free energy surfaces in the superconducting mixed state p 236 A89-43928
- FARRELL, ROGER A.**  
Mod II Stirling engine overviews  
[SAE PAPER 880539] p 177 A89-12301
- FARRELL, W. M.**  
Coherent Cerenkov radiation from the Spacelab 2 electron beam p 231 A89-24292
- FATEMI, N.**  
The GaAs solar cells with V-grooved emitters  
[NASA-TM-102104] p 214 N89-26291
- FATEMI, N. S.**  
A V-grooved GaAs solar cell  
[NASA-TM-101970] p 211 N89-22177
- FATEMI, NAVID S.**  
The interaction of gold with gallium arsenide p 90 A89-16416  
The effect of metal surface passivation on the Au-InP interaction p 132 A89-30443  
Metal-silicon reaction rates - The effects of capping p 93 A89-52202
- FAUT, OWEN D.**  
Acidic attack of perfluorinated alkyl ether lubricant molecules by metal oxide surfaces  
[NASA-TM-101962] p 93 N89-19402
- FAYMON, KARL A.**  
High temperature superconducting magnetic energy storage for future NASA missions p 50 A89-15288  
Mars manned transportation vehicle  
[NASA-TM-101487] p 210 N89-20545
- FAZLE HUSSAIN, A. K. M.**  
Passive and active control of jet turbulence p 140 A89-10176
- FEIG, P. D.**  
Revolutionary opportunities for materials and structures study, addendum  
[NASA-CR-179642-ADD] p 34 N89-29351
- FEIGELSON, ERIC D.**  
Formation of polycyclic aromatic hydrocarbons in circumstellar envelopes p 241 A89-41385
- FEKE, DONALD L.**  
Comparison of the surface charge behavior of commercial silicon nitride and silicon carbide powders p 105 A89-21444
- FELICELLI, S.**  
Thermosolutal convection during dendritic solidification  
[AIAA PAPER 89-0626] p 118 A89-25495
- FENG, Z. C.**  
Raman determination of layer stresses and strains for heterostructures and its application to the cubic SiC/Si system p 234 A89-21871
- FERENDECI, ALTAN M.**  
Design of a GaAlAs travelling wave Mach-Zehnder electro-optic modulator p 130 A89-10342
- FERGUSON, D. C.**  
Surface phenomena in plasma environments p 234 N89-23555
- FERNANDEZ DE LA MORA, J.**  
Boundary layer effects on particle impaction and capture p 143 A89-19123
- FERNANDEZ, RENE**  
Comparison of the bidirectional reflectance distribution function of various surfaces p 230 A89-41530
- FERNANDO, E. M.**  
Preliminary study of the interactions caused by crossing shock waves and a turbulent boundary layer  
[AIAA PAPER 89-0359] p 145 A89-25303
- FERRANTE, JOHN**  
Connection between energy relations of solids and molecules p 91 A89-26406  
Interfacial adhesion - Theory and experiment p 97 A89-35307  
Universal features of the equation of state of solids p 237 A89-48960  
Avalanche in adhesion p 100 A89-54495  
Applications of surface analysis and surface theory in tribology  
[NASA-TM-101392] p 78 N89-15981
- FERTIS, D. G.**  
Parametric studies of advanced turboprops  
[NASA-TM-101389] p 197 N89-14465
- FFOWCS WILLIAMS, J. E.**  
Active suppression of aerodynamic instabilities in turbomachines p 3 A89-28341
- FIELDER, WILLIAM L.**  
Oxygen electrode bifunctional electrocatalyst NiCo<sub>2</sub>O<sub>4</sub> spinel  
[NASA-TM-100947] p 208 N89-10409  
Corrosion testing of candidates for the alkaline fuel cell cathode p 212 N89-23000
- FINLEY, CLARENCE W.**  
Interfacial adhesion - Theory and experiment p 97 A89-35307
- FINNEMORE, D. K.**  
Critical currents of aligned grains of Ti-Ba-Ca-Cu-O compounds p 235 A89-30335  
Free energy surfaces in the superconducting mixed state p 236 A89-43928
- FISHBACH, L. H.**  
NNEPEQ - Chemical equilibrium version of the Navy/NASA Engine Program  
[ASME PAPER 88-GT-314] p 22 A89-24989
- FISHER, DOUGLAS M.**  
Influence of fatigue crack wake length and state of stress on crack closure p 191 A89-17432
- FLANAGAN, PATRICK M.**  
A self diagnostic system for piezoelectric sensors  
[AIAA PAPER 89-2638] p 171 A89-46980
- FLANERY, R. E.**  
Modeling cyclic melting and refreezing in a hollow metal canister  
[NASA-CR-184630] p 217 N89-15623
- FLEETER, SANFORD**  
Investigation of oscillating cascade aerodynamics by an experimental influence coefficient technique  
[AIAA PAPER 88-2815] p 1 A89-14976  
Effect of aerodynamic detuning on supersonic rotor discrete frequency noise generation p 225 A89-15083  
Experimental investigation of transonic oscillating cascade aerodynamics  
[AIAA PAPER 89-0321] p 3 A89-26369  
The effect of prewhirl on the internal aerodynamics and performance of a mixed flow research centrifugal compressor  
[NASA-CR-184756] p 161 N89-19503
- Experimental investigation of transonic oscillating cascade aerodynamics  
[NASA-TM-101993] p 29 N89-20133
- FLEMING, DAVID P.**  
Active vibration control for flexible rotor by optimal direct-output feedback control  
[NASA-TM-101972] p 31 N89-22605
- FLEMING, M. L.**  
The Solar Dynamic radiator with a historical perspective p 51 A89-15340  
The solar dynamic radiator with a historical perspective  
[NASA-TM-100972] p 45 N89-10117
- FLOOD, DENNIS J.**  
Photovoltaics for high capacity space power systems  
[IAF PAPER 88-221] p 53 A89-17730  
Advances in thin-film solar cells for lightweight space photovoltaic power  
[IAF PAPER ICOSP89-1-8] p 55 A89-46513  
The Mars climate for a photovoltaic system operation  
[IAF PAPER ICOSP89-9-5] p 241 A89-46529  
Space solar cell research p 208 A89-52203  
Photovoltaics for high capacity space power systems  
[NASA-TM-101341] p 61 N89-10122  
Issues and opportunities in space photovoltaics  
[NASA-TM-101425] p 65 N89-15171  
NASA photovoltaic research and technology  
[NASA-TM-101422] p 65 N89-16917  
The Mars climate for a photovoltaic system operation  
[NASA-TM-101994] p 136 N89-20385  
The NASA Space Solar Cell Advanced Research Program  
[NASA-TM-102020] p 67 N89-22651  
Photovoltaic power system considerations for future lunar bases  
[NASA-TM-102019] p 67 N89-23517  
Photovoltaic power system operation in the Mars environment  
[NASA-TM-102075] p 138 N89-24529  
Advances in thin-film solar cells for lightweight space photovoltaic power  
[NASA-TM-102017] p 73 N89-26041  
Solar radiation on Mars  
[NASA-TM-102299] p 242 N89-27623  
NASA advanced space photovoltaic technology-status, potential and future mission applications  
[NASA-TM-102093] p 75 N89-27705
- FLOOD, JOSEPH D.**  
Hot gas ingestion testing of an advanced STOVL concept in the NASA Lewis 9- by 15-foot low speed wind tunnel with flow visualization  
[NASA-TM-100952] p 11 N89-15078
- FORD, WILLIAM F.**  
Recursive algorithms for vector extrapolation methods p 221 A89-14397
- FORDYCE, J. STUART**  
Space 2010 p 77 A89-23028
- FORSMAN, WILLIAM C.**  
Synthesis and stability of Br<sub>2</sub>, ICl and IBr intercalated pitch-based graphite fibers p 106 A89-37670
- FORT, EDWARD F.**  
Methods for heat transfer and temperature field analysis of the insulated diesel, phase 3  
[NASA-CR-182237] p 239 N89-23382
- FOSS, JOHN F.**  
Thermal measurements for jets in disturbed and undisturbed crosswind conditions p 20 A89-16102
- FOX, D. S.**  
Influence of alloying elements on the oxidation behavior of NbAl<sub>3</sub>  
[NASA-TM-101398] p 100 N89-12717
- FOX, DENNIS S.**  
Reactions of silicon-based ceramics in mixed oxidation chlorination environments p 105 A89-21442  
The behavior of SiC and Si<sub>3</sub>N<sub>4</sub> ceramics in mixed oxidation/chlorination environments p 106 A89-33616  
Molten salt corrosion of SiC and Si<sub>3</sub>N<sub>4</sub>  
[NASA-TM-101346] p 108 N89-11912  
Hot corrosion of ceramic engine materials  
[NASA-TM-101439] p 112 N89-16065
- FRALICK, GUSTAVE C.**  
A comparison of turbulence measurement methods p 174 N89-17302
- FRANCIS, ROBERT W.**  
Issues and opportunities in space photovoltaics  
[NASA-TM-101425] p 65 N89-15171
- FRANCISCO, DAVID R.**  
Successful completion of a cyclic ground test of a mercury ion Auxiliary Propulsion System p 59 A89-47450
- FRANK, L. A.**  
Electron velocity distributions and plasma waves associated with the injection of an electron beam into the ionosphere p 215 A89-43698

## FREED, A. D.

## FREED, A. D.

Refinements in a viscoplastic model  
[NASA-TM-102338] p 205 N89-28036

## FREED, ALAN D.

Thermoviscoplastic model with application to copper  
[NASA-TP-2845] p 198 N89-16183

The isothermal fatigue behavior of a unidirectional SiC/Ti  
composite and the Ti alloy matrix

[NASA-TM-101984] p 86 N89-22684

Nonlinear mesomechanics of composites with periodic  
microstructure

[NASA-TM-102051] p 204 N89-26260

## FREEDMAN, MARC R.

A sintering model for SiC(sub)w/Si3N4 composites  
[NASA-TM-101336] p 108 N89-10166

Slurry-pressing consolidation of silicon nitride  
[NASA-TM-101365] p 109 N89-12746

## FREESE, KATHERINE

Superheavy magnetic monopoles and main-sequence  
stars p 240 A89-20377

## FRELING, MELVIN

MATE program: Erosion resistant compressor airfoil  
coating, volume 2

[NASA-CR-179645] p 113 N89-18550

## FRENKLACH, MICHAEL

Effect of alcohol addition on shock-initiated formation  
of soot from benzene p 90 A89-12903

Formation of polycyclic aromatic hydrocarbons in  
circumstellar envelopes p 241 A89-41385

## FRIAUF, ROBERT J.

A model for including thermal conduction in molecular  
dynamics simulations p 237 A89-41259

## FRIEDMAN, ROBERT

Fire behavior and risk analysis in spacecraft  
[NASA-TM-100944] p 42 N89-10111

Fire safety applications for spacecraft  
[NASA-TM-101463] p 42 N89-24413

## FRIEMAN, JOSHUA A.

Superheavy magnetic monopoles and main-sequence  
stars p 240 A89-20377

## FRISH, MICHAEL B.

High-temperature LDV seed particle development  
[NASA-CR-182265] p 175 N89-23851

## FRITSCH, KLAUS

Fiber-optic temperature sensor using a  
spectrum-modulating semiconductor etalon

p 168 A89-10366

## FRITTS, S. D.

Theoretical performance of hydrogen-bromine  
rechargeable SPE fuel cell p 207 A89-23290

## FRITZMEIER, L. G.

The influence of high thermal gradient casting, hot  
isostatic pressing and alternate heat treatment on the  
structure and properties of a single crystal nickel base  
superalloy p 97 A89-36427

Advanced single crystal for SSME turbopumps  
[NASA-CR-182244] p 103 N89-21072

## FUJITA, T.

Nuclear reactor power as applied to a space-based radar  
mission p 51 A89-15317

Systems aspects of a space nuclear reactor power  
system p 51 A89-15327

Nuclear reactor power as applied to a space-based radar  
mission

[NASA-TM-101200] p 230 N89-14831

## G

## GABB, T. P.

Isothermal and 'bithermal' thermomechanical fatigue  
behavior of a NiCoCrAlY-coated single crystal superalloy  
p 177 A89-36457

The low cycle fatigue deformation response of a  
single-crystal superalloy at 650 C p 99 A89-52204

## GABB, TIMOTHY P.

The isothermal fatigue behavior of a unidirectional SiC/Ti  
composite and the Ti alloy matrix

[NASA-TM-101984] p 86 N89-22684

## GABRIS, EDWARD A.

Nuclear thermal rockets - Next step to space  
p 55 A89-40480

## GAIER, J. R.

Structural chemistry of Au(III)-substituted  
Ba2YCu3O(7-delta) p 89 A89-12620

Interaction of Au, Ag, and Bi ions with Ba2YCu3O(7-y)  
- Implications for superconductor applications

p 235 A89-22886

Improved synthesis of ceramic superconductors with  
alkaline earth peroxides - Synthesis and processing of  
Ba2YCu3O(7-x) p 235 A89-22887

## GAIER, JAMES R.

Synthesis and stability of Br2, ICl and IBr intercalated  
pitch-based graphite fibers p 106 A89-37670

Effect of length of chopped pristine and intercalated  
graphite fibers on the resistivity of fiber networks

[NASA-TM-101395] p 84 N89-11826

Technological hurdles to the application of intercalated  
graphite fibers

[NASA-TM-101394] p 108 N89-11911

Stability of bulk Ba2YCu3O(7-x) in a variety of  
environments

[NASA-TM-101401] p 111 N89-14310

## GAJJAR, J. S. B.

The upper-branch stability of compressible boundary  
layer flows

[NASA-TM-102128] p 167 N89-28748

## GALECKI, DIANE L.

In-situ propellant advantages for fast transfer to Mars  
[AIAA PAPER 88-2901] p 37 A89-14977

Ignition and combustion of metallized propellants  
[AIAA PAPER 89-2883] p 117 A89-47148

## GAMMON, ROBERT W.

Critical fluid light scattering p 121 N89-20320

## GANN, J. A.

Advanced modulation technology development for earth  
station demodulator applications

[NASA-CR-185126] p 43 N89-26880

## GARCIA, ROBERTO

Crystallization of BaF2-ZnF2-YbF3-ThF4 glass  
p 230 A89-12236

## GARG, SANJAY

Model-based analysis of control/display interaction in  
the hover task p 215 A89-36933

Integrated flight/propulsion control system design based  
on a centralized approach

[AIAA PAPER 89-3520] p 35 A89-52611

Integrated flight/propulsion control system design based  
on a decentralized, hierarchical approach

[AIAA PAPER 89-3519] p 35 A89-53301

Turbofan engine control system design using the  
LQG/LTR methodology p 23 A89-53956

Stability robustness improvement of direct eigenspace  
assignment based feedback systems using singular value  
sensitivities p 220 A89-53958

Turbofan engine control system design using the  
LQG/LTR methodology

[NASA-CR-182303] p 33 N89-26004

Integrated flight/propulsion control system design based  
on a centralized approach

[NASA-TM-102137] p 35 N89-26009

Stability robustness improvement of direct eigenspace  
assignment based feedback systems using singular value  
sensitivities

[NASA-CR-182302] p 36 N89-27672

## GAT, N.

Interactions between gaseous electrical discharges and  
single liquid droplets p 90 A89-19298

## GAUGLER, RAYMOND E.

HOST combustion R and T overview p 25 N89-12879

A perspective on future directions in aerospace  
propulsion system simulation

[NASA-TM-102038] p 31 N89-21798

## GAYDA, J.

A Monte Carlo-finite element model for strain energy  
controlled microstructural evolution - 'Rafting' in  
superalloys p 96 A89-23458

Isothermal and 'bithermal' thermomechanical fatigue  
behavior of a NiCoCrAlY-coated single crystal superalloy

p 177 A89-36457

The low cycle fatigue deformation response of a  
single-crystal superalloy at 650 C p 99 A89-52204

GAYDA, JOHN, JR.

The isothermal fatigue behavior of a unidirectional SiC/Ti  
composite and the Ti alloy matrix

[NASA-TM-101984] p 86 N89-22684

## GAYDOSH, D. J.

Dispersoids in rapidly solidified B2 nickel aluminides  
p 98 A89-43023

## GAYDOSH, DARRELL J.

Materials technology assessment for a 1050 K Stirling  
space engine design

[NASA-TM-101342] p 77 N89-11815

## GAZZANIGA, JOHN A.

Low-speed wind tunnel performance of high-speed  
counterrotation propellers at angle-of-attack

[AIAA PAPER 89-2583] p 8 A89-50808

Low-speed wind tunnel performance of high-speed  
counterrotation propellers at angle-of-attack

[NASA-TM-102292] p 15 N89-25121

## GEDEON, DAVID R.

Description of an oscillating flow pressure drop test rig  
p 142 A89-15188

## GEDEON, STEPHEN

Space reactor assessment and validation study  
p 230 N89-13227

## GEE, JAMES M.

The effect of different module configurations on the  
radiation tolerance of multijunction solar cells

[NASA-TM-101251] p 209 N89-17356

A comparison of the radiation tolerance characteristics  
of multijunction solar cells with series and voltage-matched  
configurations p 213 N89-24737

## GELLIN, S.

On 3D inelastic analysis methods for hot section  
components p 196 N89-12906

## GELLIN, SLADE

Nonlinear analysis using temporal finite elements  
p 221 A89-28030

## GENERAZIO, E. R.

Ultrasonic attenuation measurements determine onset,  
degree, and completion of recrystallization

p 187 A89-23936

## GENERAZIO, EDWARD R.

High-frequency ultrasonic characterization of sintered  
silicon carbide p 106 A89-34840

Ultrasonic imaging of porosity variations produced during  
sintering p 107 A89-48892

Dynamic porosity variations in ceramics

[NASA-TM-101340] p 112 N89-17668

Interfacing laboratory instruments to multiuser, virtual  
memory computers

[NASA-TM-101406] p 188 N89-19578

Non-uniform transition conductivity of superconducting  
ceramic

[NASA-TM-102133] p 189 N89-28851

Ultrasonic imaging of textured alumina

[NASA-TM-101478] p 189 N89-28853

## GENG, STEVEN M.

RE-1000 free-piston Stirling engine sensitivity test  
results

[NASA-TM-88846] p 210 N89-19737

Results from baseline tests of the SPRE 1 and  
comparison with code model predictions

[NASA-TM-102044] p 68 N89-23527

## GEOFFROY, L. M.

High efficiency GaAs-Ge tandem solar cells grown by  
MOCVD p 213 N89-24721

## GERARDI, J. J.

Distributed ice accretion sensor for smart aircraft  
structures

[AIAA PAPER 89-0772] p 17 A89-25571

## GESLIN, D.

Elevated temperature strain gages p 173 N89-12886

## GESSERT, T. A.

High-efficiency solar cells fabricated from direct-current  
magnetron sputtered n-indium tin oxide onto p-InP grown  
by atmospheric pressure metalorganic vapor phase  
epitaxy p 133 A89-44518

High-efficiency indium tin oxide/indium phosphide solar  
cells p 208 A89-44883

## GHIA, K. N.

Simulation of 2-dimensional viscous flow through  
cascades using a semi-elliptic analysis and hybrid C-H  
grids

[NASA-CR-4180] p 10 N89-12553

## GHIA, U.

Simulation of 2-dimensional viscous flow through  
cascades using a semi-elliptic analysis and hybrid C-H  
grids

[NASA-CR-4180] p 10 N89-12553

## GHOSH, LOUIS J.

Accelerated fatigue crack growth behavior of PWA  
1480 p 97 A89-36461

Stochastic modeling of crack initiation and short-crack  
growth under creep and creep-fatigue conditions

[NASA-TM-101358] p 199 N89-17286

Reliability-based failure analysis of brittle materials  
[NASA-CR-184799] p 189 N89-20489

Optimum interface properties for metal matrix  
composites

[NASA-TM-102295] p 205 N89-27223

## GIELDA, T. P.

Navier-Stokes solution to the flowfield over ice accretion  
shapes p 1 A89-12557

## GIESLER, F. J.

Navier-Stokes solution to the flowfield over ice accretion  
shapes p 1 A89-12557

## GINTY, CAROL A.

Fiber composite structural durability and damage  
tolerance - Simplified predictive methods

p 82 A89-36320

## GLADDEN, H. J.

Measurements of heat transfer distribution over the  
surfaces of highly loaded turbine nozzle guide vanes

p 141 A89-12752

A high heat flux experiment for verification of  
thermostructural analysis p 148 A89-35002

Heat transfer in aerospace propulsion p 153 A89-53282



- Review and assessment of the database and numerical modeling for turbine heat transfer p 30 N89-20139
- GLADDEN, HERBERT J.**  
A high heat flux experiment for verification of thermostructural analysis  
[NASA-TM-100931] p 155 N89-12026  
HOST turbine heat transfer subproject overview p 25 N89-12880
- Experience with advanced instrumentation in a hot section cascade  
[NASA-TM-102294] p 167 N89-27980
- GLASHEEN, W. M.**  
Fiber optic control system integration  
[NASA-CR-179568] p 231 N89-13256
- GLASSMAN, ARTHUR J.**  
Advanced core technology: Key to subsonic propulsion benefits  
[NASA-TM-101420] p 26 N89-14237  
Turbomachinery technology for high-speed civil flight  
[NASA-TM-102092] p 32 N89-24320
- GLICKSMAN, M.**  
Flight hardware and tele-operations supporting the Isothermal Dendritic Growth Experiment aboard the Space Shuttle  
[AIAA PAPER 89-0863] p 118 N89-25627
- GLICKSMAN, M. E.**  
Dendritic solidification in binary alloys p 96 N89-22560  
Measurement of the diffusion coefficient of acetone in succinonitrile at its melting point p 237 N89-23488  
Evaluation of transport conditions during physical vapor transport growth of opto-electronic crystals  
[AIAA PAPER 89-0229] p 118 N89-25197  
A facility for precise temperature control applications in microgravity p 48 N89-36956  
Isothermal dendritic growth: A low gravity experiment p 121 N89-20299
- GLIEBE, P. R.**  
High speed turboprop aeroacoustic study (single rotation). Volume 1: Model development  
[NASA-CR-182257-VOL-1] p 229 N89-24139
- GOERTZ, C. K.**  
Coherent Cerenkov radiation from the Spacelab 2 electron beam p 231 N89-24292
- GOKOGLU, S.**  
Windward fraction of the total mass or heat transport for flow past a circular cylinder p 141 N89-12339
- GOKOGLU, S. A.**  
Rational engineering correlations of diffusional and inertial particle deposition behavior in non-isothermal forced convection environments p 140 N89-12327  
Deposition of Na<sub>2</sub>SO<sub>4</sub> from salt-seeded combustion gases of a high velocity burner rig p 89 N89-12330  
Discussion of Mills et al. on 'The effect of wall suction and thermophoresis on aerosol particle deposition from a laminar boundary layer on a flat plate' p 140 N89-12331  
Determination of convective diffusion heat/mass transfer rates to burner rig test targets comparable in size to cross-stream jet diameter p 141 N89-12753  
Effect of particulate thermophoresis in reducing the fouling rate advantages of effusion-cooling p 141 N89-14599  
Viscous dissipation effects on thermophoretically augmented aerosol particle transport across laminar boundary layers p 141 N89-14600  
Convection and chemistry effects in CVD: A 3-D analysis for silicon deposition  
[NASA-TM-102001] p 78 N89-21032
- GOKOGLU, SULEYMAN A.**  
Thermophoretically enhanced mass transport rates to solid and transpiration-cooled walls across turbulent (law-of-the-wall) boundary layers p 141 N89-12340
- GOLDMAN, LOUIS J.**  
Three component laser anemometer measurements in an annular cascade of core turbine vanes with contoured end wall  
[NASA-TP-2846] p 9 N89-10844
- GOLDSTEIN, M. E.**  
Nonlinear spatial evolution of an externally excited instability wave in a free shear layer p 144 N89-23242  
Boundary-layer receptivity to long-wave free-stream disturbances p 146 N89-28996  
Nonlinear interaction between the sinusoidal and varicose instability modes in a plane wake p 147 N89-33779  
Nonlinear evolution of interacting oblique waves on two-dimensional shear layers  
[NASA-TM-102030] p 164 N89-24575
- GOMBOS, FRANK J.**  
An integrated and modular digital modeling approach for the Space Station electrical power system development p 50 N89-15298  
Development and refinement of test bed simulations  
[NASA-TM-102335] p 75 N89-27702
- GOMEZ, M. A.**  
Unique mission options available with a megawatt-class nuclear electric propulsion system  
[NASA-TM-101220] p 65 N89-17618
- GONZALEZ-SANABRIA, O. D.**  
Energy storage considerations for a robotic Mars surface sampler p 49 N89-15267
- GONZALEZ-SANABRIA, OLGA D.**  
NASA Aerospace Flight Battery Systems Program - Issues and actions p 49 N89-15224  
Effect of NASA advanced designs on thermal behavior of Ni-H<sub>2</sub> cells p 50 N89-15279
- GOODER, S.**  
Structural and thermal response of 30 cm diameter ion thruster optics  
[AIAA PAPER 89-2719] p 58 N89-47042
- GOODER, S. T.**  
Structural and thermal response of 30 cm diameter ion thruster optics  
[NASA-TM-102124] p 75 N89-27703
- GOODRICH, JOHN W.**  
Unsteady solution of incompressible Navier-Stokes equations p 141 N89-15143
- GORADIA, CHANDRA**  
Predicted performance of InP solar cells in Cassegrainian and slats space concentrator arrays at 20 to 100 AMO, 80 to 100 C p 212 N89-24711
- GORADIA, MANJU GHALLA**  
Predicted performance of InP solar cells in Cassegrainian and slats space concentrator arrays at 20 to 100 AMO, 80 to 100 C p 212 N89-24711
- GORDON, ELIOTT B.**  
The effect of front-to-rear propeller spacing on the interaction noise at cruise conditions of a model counterrotation propeller having a reduced diameter aft propeller  
[NASA-TM-101329] p 227 N89-10603
- GORDON, ELLIOT B.**  
Acoustic evaluation of the Helmholtz resonator treatment in the NASA Lewis 8- by 6-foot supersonic wind tunnel  
[NASA-TM-101407] p 228 N89-15685
- GORDON, S.**  
NNEPEQ - Chemical equilibrium version of the Navy/NASA Engine Program  
[ASME PAPER 88-GT-314] p 22 N89-24989
- GORDON, W. L.**  
Millimeter wave transmission studies of YBa<sub>2</sub>Cu<sub>3</sub>O<sub>7</sub>-delta thin films in the 26.5 to 40.0 GHz frequency range  
[NASA-TM-102345] p 237 N89-30088
- GORDON, WILLIAM L.**  
Measurements of complex permittivity of microwave substrates in the 20 to 300 K temperature range from 26.5 to 40.0 GHz  
[NASA-TM-102123] p 123 N89-27038
- GOTT, R. W.**  
5-kW arcjet power electronics  
[AIAA PAPER 89-2725] p 60 N89-49685  
The 5-kW arcjet power electronics  
[NASA-TM-102108] p 70 N89-24446
- GOULD, RICHARD D.**  
The turbulence characteristics of a separated flow with combustion p 92 N89-33369  
Parametric study of statistical bias in laser Doppler velocimetry p 171 N89-47378
- GRACIASALCEDO, CARMEN M.**  
Fuel-rich catalytic combustion of Jet-A fuel-equivalence ratios 5.0 to 8.0  
[NASA-TM-101975] p 93 N89-21051  
Determination of combustion gas temperatures by infrared radiometry in sooting and nonsooting flames  
[NASA-TP-2900] p 164 N89-25409
- GRACIASALCEDO, CARMEN M.**  
Experimental verification of the thermodynamic properties for a jet-A fuel  
[NASA-TM-101475] p 117 N89-17017
- GRADY, J. E.**  
Vibration testing of impact-damaged composite laminates  
[AIAA PAPER 89-1411] p 81 N89-30883
- GRADY, JOSEPH E.**  
Dynamic delamination buckling in composite laminates under impact loading - Computational simulation p 82 N89-36310  
A NASTRAN DMAP alter for linear buckling analysis under dynamic loading  
[NASA-TM-100832] p 85 N89-13522  
A NASTRAN DMAP alter for linear buckling analysis under dynamic loading p 202 N89-22948  
Vibration testing of impact-damaged composite laminates  
[NASA-TM-4115] p 87 N89-25290
- GRANDIN, ALBERT W.**  
Alternative fuel capabilities of the Mod II Stirling engine vehicle  
[SAE PAPER 880543] p 177 N89-12303
- GRANT, HOWARD P.**  
Development of a high temperature static strain sensor p 173 N89-12887  
Development of a high temperature thin film static strain gage p 174 N89-17299
- GREBER, ISAAC**  
Experimental and numerical investigation of an oblique shock wave/turbulent boundary layer interaction with continuous suction  
[AIAA PAPER 89-0357] p 4 N89-28407
- GREEN, H. E.**  
Improved high-temperature resistant matrix resins  
[NASA-CR-180826] p 114 N89-21105
- GREEN, JAMES M.**  
A premixed hydrogen/oxygen catalytic igniter  
[AIAA PAPER 89-2302] p 59 N89-49683  
A premixed hydrogen/oxygen catalytic igniter  
[NASA-CR-185113] p 70 N89-24445
- GREENBERG, BARRY M.**  
Propulsion over a wide Mach number range  
[NASA-CR-182267] p 29 N89-20134
- GREENBERG, PAUL S.**  
Microgravity Combustion Diagnostics Workshop  
[NASA-CP-10017] p 120 N89-17682
- GREITZER, E. M.**  
Active suppression of aerodynamic instabilities in turbomachines p 3 N89-28341  
Calculations of inlet distortion induced compressor flow field instability p 8 N89-52498
- GRISAFFE, SALVATORE J.**  
Space 2010 p 77 N89-23028
- GROBSTEIN, T. L.**  
Creep behavior of tungsten fiber reinforced niobium metal matrix composites  
[NASA-TM-102307] p 104 N89-29522
- GROBSTEIN, TONI L.**  
The interface in tungsten fiber reinforced niobium metal-matrix composites  
[NASA-TM-102122] p 104 N89-28627
- GRODSINSKY, CARLOS M.**  
Low frequency vibration isolation technology for microgravity space experiments  
[NASA-TM-101448] p 123 N89-20324
- GROENEWEG, J. F.**  
High-speed propeller performance and noise predictions at takeoff/landing conditions p 226 N89-39195  
Prediction of unsteady blade surface pressures on an advanced propeller at an angle of attack  
[AIAA PAPER 89-1060] p 227 N89-40473
- GROENEWEG, JOHN**  
Return of the turboprops p 20 N89-12953
- GROENEWEG, JOHN F.**  
NASA advanced propeller research  
[NASA-TM-101361] p 27 N89-15913
- GROSS, BERNARD**  
Weibull crack density coefficient for polydimensional stress states p 193 N89-34849
- GROSSKOPF, P. P.**  
A study of the stress wave factor technique for evaluation of composite materials  
[NASA-CR-4195] p 189 N89-21256
- GROSSMAN, M.**  
Nuclear reactor power as applied to a space-based radar mission p 51 N89-15317  
Systems aspects of a space nuclear reactor power system p 51 N89-15327  
Nuclear reactor power as applied to a space-based radar mission  
[NASA-TM-101200] p 230 N89-14831
- GRUBER, R. P.**  
5-kW arcjet power electronics  
[AIAA PAPER 89-2725] p 60 N89-49685  
The 5-kW arcjet power electronics  
[NASA-TM-102108] p 70 N89-24446
- GRUBER, ROBERT P.**  
dc power control for a liquid-fed resistojet p 59 N89-47457
- GUHA, SUMIT**  
Room temperature tensile ductility in polycrystalline B2 Ni-30Al-20Fe p 98 N89-44568
- GULINO, DANIEL A.**  
Thin film coatings for space electrical power system applications p 77 N89-53324  
Isotopic study of oxygen diffusion in oxide coatings  
[NASA-TM-102082] p 78 N89-24451
- GUNES, D.**  
Aerodynamically-driven condensate layer thickness distributions on isothermal cylindrical surfaces p 140 N89-12337
- GUO, TEN-HUEI**  
Identification of Space Shuttle Main Engine dynamics p 61 N89-54068

## GUPTA, H.

Identification of space shuttle main engine dynamics  
[NASA-TM-101982] p 66 N89-20199

## GUPTA, H.

Iron-base superalloys - A phase analysis of the  
multicomponent system (Fe-Mn-Cr-Mo-Nb-Al-Si-C)  
p 95 A89-17379

## GUPTA, INDER J.

An experimental adaptive array to suppress weak  
interfering signals p 124 A89-22455

## GURNETT, D. A.

Coherent Cerenkov radiation from the Spacelab 2  
electron beam p 231 A89-24292

## GUSTAFSON, ERIC

Solar dynamic heat rejection technology. Task 1: System  
concept development  
[NASA-CR-179618] p 158 N89-13731

## GUSTAFSON, G.

GaAs circuits for monolithic optical controller  
p 131 A89-15828

## GUTE, DOUG

Hierarchical Poly Tree computer architectures defined  
by computational multidisciplinary mechanics  
p 218 A89-50100

## GYEKENYESI, JOHN P.

Weibull crack density coefficient for polydimensional  
stress states p 193 A89-34849  
Calculation of Weibull strength parameters and Batdorf  
flow-density constants for volume- and  
surface-flaw-induced fracture in ceramics  
[NASA-TM-100890] p 196 N89-12930  
A review of failure models for unidirectional ceramic  
matrix composites under monotonic loads  
[NASA-TM-101421] p 198 N89-14470  
Time dependent reliability model incorporating  
continuum damage mechanics for high-temperature  
ceramics  
[NASA-TM-102046] p 115 N89-24487

## H

## HA, TAE WOONG

Friction factor data for flat plate tests of smooth and  
honeycomb surfaces  
[NASA-CR-184977] p 186 N89-23876

## HA, TRI T.

Coded multiple chirp spread spectrum system and  
overlay service p 124 A89-26769  
Study of spread spectrum multiple access systems for  
satellite communications with overlay on current services:  
Executive summary  
[NASA-CR-180827-EXEC-SUMM] p 128 N89-23756  
Study of spread spectrum multiple access systems for  
satellite communications with overlay on current  
services  
[NASA-CR-180827] p 128 N89-23757

## HAAG, T. W.

Performance of a 100 kW class applied field MPD  
thruster  
[AIAA PAPER 89-2710] p 57 A89-47035  
5-kW arcjet power electronics  
[AIAA PAPER 89-2725] p 60 A89-49685  
The 5-kW arcjet power electronics  
[NASA-TM-102108] p 70 N89-24446

## HAAG, THOMAS W.

Performance characterizations of an engineering model  
multipropellant resistojet p 54 A89-28340  
Design of a thrust stand for high power electric  
propulsion devices  
[AIAA PAPER 89-2829] p 39 A89-47110  
Test facility and preliminary performance of a 100 kW  
class MPD thruster  
[NASA-TM-102021] p 68 N89-23520  
Arcjet nozzle design impacts  
[NASA-TM-102050] p 68 N89-23522  
Arcjet cathode phenomena  
[NASA-TM-102099] p 167 N89-27121  
Performance of a 100 kW class applied field MPD  
thruster  
[NASA-TM-102312] p 74 N89-27701

## HAAS, JEFFREY

New hypersonic facility capability at NASA Lewis  
Research Center  
[AIAA PAPER 89-2534] p 36 A89-46905

## HAAS, JEFFREY E.

New hypersonic facility capability at NASA Lewis  
Research Center  
[NASA-TM-102028] p 36 N89-22617

## HAAS, R. J.

Space Station battery system design and development  
p 52 A89-15378

## HADDAD, GEORGE I.

Microwave and millimeter-wave power generation in  
silicon carbide (SiC) IMPATT devices  
[NASA-CR-185050] p 139 N89-26143

## HAEFFELE, B. A.

Isolated testing of highly maneuverable inlet concepts  
[NASA-CR-179544] p 26 N89-13437

## HAGER, ROY D.

Advanced turboprop project  
[NASA-SP-495] p 24 N89-12565

## HAGGARD, J. B.

Droplet combustion drop tower tests using models of  
the space flight apparatus  
[AIAA PAPER 89-0501] p 119 A89-28418

## HAGSTROM, THOMAS

Accurate boundary conditions for exterior problems in  
gas dynamics p 143 A89-20223  
Far field expansion for anisotropic wave equations  
[NASA-TM-102112] p 165 N89-26175

## HAHN, R. C.

A facility for precise temperature control applications  
in microgravity p 48 A89-36956  
Isothermal dendritic growth: A low gravity experiment  
p 121 N89-20299

## HAHN, RICHARD C.

Ground-based simulation of telepresence for materials  
science experiments  
[AIAA PAPER 89-0597] p 119 A89-28439

## HAINLEY, DONALD C.

Two-tiered design analysis of a radiator for a solar  
dynamic powered Stirling engine  
[NASA-CR-182301] p 46 N89-26031

## HAISLER, W. E.

On 3D inelastic analysis methods for hot section  
components p 196 N89-12906

## HAJEK, T. J.

Coolant passage heat transfer with rotation  
p 157 N89-12899  
Coolant passage heat transfer with rotation  
p 161 N89-17314

## HAJJAR, FARES

Deep-level transient spectroscopy of  
Al(x)Ga(1-x)As/GaAs using nondestructive  
acousto-electric voltage measurement  
p 133 A89-42742

## HALE, K.

Annular honeycomb seals: Test results for leakage and  
rotordynamic coefficients - Comparisons to labyrinth and  
smooth configurations  
[ASME PAPER 88-TRIB-35] p 179 A89-34794

## HALE, KEITH

Experimental results for labyrinth gas seals with  
honeycomb stators - Comparisons to smooth-stator seals  
and theoretical predictions  
[ASME PAPER 88-TRIB-40] p 179 A89-24992  
Annular honeycomb seals: Test results for leakage and  
rotordynamic coefficients; comparisons to labyrinth and  
smooth configurations p 185 N89-22899

## HALEVI, YORAM

Integrated communication and control systems. I -  
Analysis  
[ASME PAPER 88-WA/DSC-1] p 219 A89-22499  
Integrated communication and control systems. II -  
Design considerations  
[ASME PAPER 88-WA/DSC-2] p 219 A89-22500  
Extended observability of linear time-invariant systems  
under recurrent loss of output data  
[AIAA PAPER 89-3510] p 220 A89-52603

## HALFORD, G. R.

Exposure time considerations in high temperature low  
cycle fatigue p 192 A89-29600  
Total strain version of strainrange partitioning for  
thermomechanical fatigue at low strains  
p 201 N89-17337  
Fatigue life prediction modeling for turbine hot section  
materials p 30 N89-20142

## HALFORD, GARY R.

High-temperature LCF of Ni-201 and 304L stainless  
steel p 100 N89-12635  
Fatigue and fracture overview p 195 N89-12882  
Isothermal life prediction of composite lamina using a  
damage mechanics approach  
[NASA-TM-102032] p 87 N89-24460  
Procedures for characterizing an alloy and predicting  
cyclic life with the total strain version of Strainrange  
Partitioning  
[NASA-TM-4102] p 203 N89-25485

## HALL, E. L.

Vision sensing techniques in aeronautics and  
astronautics p 219 A89-31087

## HALL, KENNETH C.

Calculation of unsteady flows in turbomachinery using  
the linearized Euler equations p 149 A89-36916

## HAMADY, F.

Stratified charge rotary engine - Internal flow studies  
at the MSU engine research laboratory  
[SAE PAPER 890331] p 181 A89-51477

## HAMBOURGER, P. D.

Structural chemistry of Au(III)-substituted  
Ba<sub>2</sub>YCu<sub>3</sub>O(7- $\delta$ ) p 89 A89-12620

Interaction of Au, Ag, and Bi ions with Ba<sub>2</sub>YCu<sub>3</sub>O(7- $\gamma$ )  
- Implications for superconductor applications  
p 235 A89-22886

## HAMBOURGER, PAUL D.

Stability of bulk Ba<sub>2</sub>YCu<sub>3</sub>O(7- $\gamma$ ) in a variety of  
environments p 111 N89-14310

## HAMLEY, JOHN A.

A data acquisition and storage system for the ion auxiliary  
propulsion system cyclic thruster test  
[NASA-TM-101469] p 218 N89-17424

## HAMMAD, K. J.

Radiative heat transfer in rocket thrust chambers and  
nozzles  
[AIAA PAPER 89-1720] p 150 A89-43235

## HANDSCHUH, R. F.

Transmission errors and bearing contact of spur, helical  
and spiral bevel gears  
[SAE PAPER 881294] p 179 A89-21000

Crowned spur gears - Methods for generation and tooth  
contact analysis. I - Basic concepts, generation of the  
pinion tooth surface by a plane p 179 A89-29306

Crowned spur gears - Methods for generation and Tooth  
Contact Analysis. II - Generation of the pinion tooth surface  
by a surface of revolution p 180 A89-37665

Generation of a crowned pinion tooth surface by a  
surface of revolution p 181 N89-10282  
[NASA-TM-100260]

Generation of a crowned pinion tooth surface by a  
plane p 181 N89-10283

Topology of modified helical gears  
[NASA-TM-102134] p 187 N89-28015

## HANKEY, W. L.

Navier-Stokes solution to the flowfield over ice accretion  
shapes p 1 A89-12557

A numerical investigation of the influence of surface  
roughness on heat transfer in ice accretion  
[AIAA PAPER 89-0737] p 146 A89-25554

## HANNUM, NED P.

NASA's Chemical Transfer Propulsion Program for  
Pathfinder p 37 A89-46735  
[AIAA PAPER 89-2298]

Fueling the National Aero-Space Plane with slush  
hydrogen p 117 A89-51339  
[AIAA PAPER 89-5014]

Technology issues associated with fueling the national  
aerospace plane with slush hydrogen  
[NASA-TM-101386] p 61 N89-10123

The Pathfinder Chemical Transfer Propulsion program  
[NASA-TM-102084] p 41 N89-24409

NASA's Chemical Transfer Propulsion Program for  
Pathfinder p 41 N89-26876  
[NASA-TM-102298]

## HANSEN, IRVING G.

A versatile power converter for high-frequency link  
systems p 131 A89-21200  
Variable speed induction motor operation from a 20-kHz  
power bus  
[NASA-TM-102061] p 71 N89-25271

## HANSMAN, R. JOHN, JR.

Investigation of surface water behavior during glaze ice  
accretion p 16 A89-27739

Modeling of surface roughness effects on glaze ice  
accretion p 16 A89-28451  
[AIAA PAPER 89-0734]

The influence of ice accretion physics on the forecasting  
of aircraft icing conditions p 16 A89-54803

## HANSON, D. B.

Sound power spectrum and wave drag of a propeller  
in flight p 225 A89-33724  
[AIAA PAPER 89-1081]

Near wakes of advanced turbopropellers  
[AIAA PAPER 89-1095] p 5 A89-33735

## HARABURDA, FRANCIS M.

Space Station Freedom electrical power system  
hardware commonality with the United States Polar  
Platform p 69 N89-24439  
[NASA-TM-102074]

## HARABURDA, SCOTT S.

Investigations of microwave plasmas - Applications in  
electrothermal thruster systems  
[AIAA PAPER 89-2378] p 57 A89-46784

## HARF, FREDRIC H.

Mechanical properties of modified low cobalt powder  
metallurgy Udimet 700 type alloys  
[NASA-TM-101481] p 103 N89-20228

## HARIHARAN, S. I.

Accurate boundary conditions for exterior problems in  
gas dynamics p 143 A89-20223  
Far field expansion for anisotropic wave equations  
[NASA-TM-102112] p 165 N89-26175

Time domain numerical calculations of unsteady vortical  
flows about a flat plate airfoil  
[NASA-TM-102318] p 168 N89-29726

- HARLOFF, GARY J.**  
High angle-of-attack hypersonic aerodynamics  
p 2 A89-19918  
HASA: Hypersonic Aerospace Sizing Analysis for the preliminary design of aerospace vehicles  
[NASA-CR-182226] p 18 N89-15107
- HARMAN, PHILLIP E.**  
The impact of an IVA robot on the Space Station microgravity environment  
[AIAA PAPER 89-0596] p 44 A89-28438
- HART, R. E., JR.**  
Radiation resistance and comparative performance of ITO/InP and n/p InP homojunction solar cells  
[NASA-TM-101387] p 135 N89-12819  
Progress in indium phosphide solar cell research  
p 212 N89-24707  
High efficiency GaAs-Ge tandem solar cells grown by MOCVD  
p 213 N89-24721  
Indium phosphide solar cell research in the US: Comparison with nonphotovoltaic sources  
[NASA-TM-102103] p 124 N89-27868
- HART, RUSSELL E., JR.**  
Temperature coefficients for concentrator cells at various electron and proton fluence levels  
p 51 A89-15304  
InP homojunction solar cell performance on the LIPS 3 flight experiment  
[NASA-TM-101390] p 209 N89-12123
- HARTLE, M.**  
On 3D inelastic analysis methods for hot section components  
p 196 N89-12906
- HARTLE, M. S.**  
Thermal barrier coating life prediction model development  
[NASA-CR-180807] p 110 N89-13621
- HARTLEY, TOM T.**  
IECON '87: Industrial applications of control and simulation; Proceedings of the 1987 International Conference on Industrial Electronics, Control, and Instrumentation, Cambridge, MA, Nov. 3, 4, 1987  
[SPIE-853] p 219 A89-10798  
Computational fluid dynamic control  
p 220 A89-53984
- HARVEY, P. R.**  
Structural Tailoring of Advanced Turboprops (STAT) programmer's manual  
[NASA-CR-182164] p 29 N89-20132
- HARVEY, PETER R.**  
Creep fatigue life prediction for engine hot section materials (ISOTROPIC) fifth year progress review  
p 201 N89-17336
- HASAN, M. M.**  
Thermocapillary migration of a large gas slug in a tube  
p 117 A89-22747
- HASAN, MOHAMMAD M.**  
Axisymmetric confined turbulent jet directed towards the liquid surface from below  
[AIAA PAPER 89-0172] p 145 A89-25148  
Axisymmetric confined turbulent jet directed towards the liquid surface from below  
[NASA-TM-101409] p 158 N89-13749
- HASTINGS, D. E.**  
Induced emission of radiation from a large space-station-like structure in the ionosphere  
p 44 A89-31915  
Bounds on current collection from the far field by plasma clouds in the ionosphere  
p 214 A89-34791
- HASTINGS, DANIEL E.**  
The physics of positively biased conductors surrounded by dielectrics in contact with a plasma  
p 232 A89-39395
- HATTORI, SHUJI**  
Deformation and fracture of single-crystal and sintered polycrystalline silicon carbide produced by cavitation  
p 108 A89-54985
- HAUGLAND, E. J.**  
Shubnikov-de Haas measurements of the 2-D electron gas in pseudomorphic In(0.1)Ga(0.9)As grown on GaAs  
p 235 A89-29299
- HAVEN, VICTOR E.**  
High efficiency GaAs-Ge tandem solar cells grown by MOCVD  
p 213 N89-24721
- HAWKINS, LARRY**  
Experimental results for labyrinth gas seals with honeycomb stators - Comparisons to smooth-stator seals and theoretical predictions  
[ASME PAPER 88-TRIB-40] p 179 A89-24992
- HAWLEY, MARTIN C.**  
Investigations of microwave plasmas - Applications in electrothermal thruster systems  
[AIAA PAPER 89-2378] p 57 A89-46784
- HAY, STUART S.**  
Performance characterizations of an engineering model multipropellant resistojet  
p 54 A89-28340
- HAYDEN, WARREN R.**  
Integrated control and health management. Orbit transfer rocket engine technology program  
[NASA-CR-182122] p 62 N89-11805
- HEALEY, KATHLEEN L.**  
Cooperating expert systems for Space Station - Power/thermal subsystem testbeds  
p 38 A89-15350
- HEBSUR, M. G.**  
High temperature isothermal and cyclic oxidation behavior of a single crystal Ni base superalloy  
p 94 A89-12625  
Influence of alloying elements on the oxidation behavior of NbAl3  
[NASA-TM-101398] p 100 N89-12717  
An investigation of environmental influence on the creep behavior of a low pressure plasma sprayed NiCoCrAlY alloy  
p 110 N89-13648
- HEBSUR, MOHAN G.**  
Microstructures in rapidly solidified niobium aluminides  
p 95 A89-18193  
Rapid solidification research at the NASA Lewis Research Center  
p 95 A89-18203  
Tensile and creep rupture behavior of P/M processed Nb-base alloy, WC-3009  
[NASA-TM-101954] p 78 N89-19371
- HEE, MAN YUN**  
Tensile behavior of tungsten and tungsten-alloy wires from 1300 to 1600 K  
[NASA-TM-101446] p 103 N89-17649
- HEIDELBERG, LAURENCE J.**  
Unsteady blade pressure measurements on a model counterrotation propeller  
[AIAA PAPER 89-1144] p 226 A89-40175  
Acoustic evaluation of the Helmholtz resonator treatment in the NASA Lewis 8- by 6-foot supersonic wind tunnel  
[NASA-TM-101407] p 228 N89-15685  
Unsteady blade pressure measurements on a model counterrotation propeller  
[NASA-TM-102002] p 228 N89-20779
- HEIDENREICH, GARY**  
Transient performance evaluation of an integrated heat pipe-thermal storage system  
p 49 A89-15209
- HEINEN, V. O.**  
Millimeter wave transmission studies of YBa2Cu3O7-delta thin films in the 26.5 to 40.0 GHz frequency range  
[NASA-TM-102345] p 237 N89-30088
- HEINEN, VERNON O.**  
Measurements of complex permittivity of microwave substrates in the 20 to 300 K temperature range from 26.5 to 40.0 GHz  
[NASA-TM-102123] p 123 N89-27038
- HEINRICH, J. C.**  
Thermosolutal convection during dendritic solidification  
[AIAA PAPER 89-0626] p 118 A89-25495
- HELLAWELL, A.**  
The surface morphology of crystals melting under solutions of different densities  
p 235 A89-23482
- HELLER, J.**  
Nuclear reactor power as applied to a space-based radar mission  
p 51 A89-15317  
Systems aspects of a space nuclear reactor power system  
p 51 A89-15327
- HELMICK, LARRY S.**  
Determination of the thermal stability of perfluoroalkylethers by tensimetry: Instrumentation and Procedure  
[NASA-TM-102116] p 116 N89-26095
- HELMICK, M. R.**  
Vapor condensation at a turbulent liquid surface in systems with possible spaced-based applications  
[AIAA PAPER 89-2846] p 151 A89-47122
- HEMANN, JOHN H.**  
A review of failure models for unidirectional ceramic matrix composites under monotonic loads  
[NASA-TM-101421] p 198 N89-14470
- HENDERSON, T. S.**  
Shubnikov-de Haas measurements of the 2-D electron gas in pseudomorphic In(0.1)Ga(0.9)As grown on GaAs  
p 235 A89-29299
- HENDERSON, WILLIAM**  
Return of the turboprops  
p 20 A89-12953
- HENDRICKS, BOB**  
Cyclic stress analysis of ceramic coated gas turbine seals  
p 111 N89-13662
- HENDRICKS, R. C.**  
Heat transfer in aerospace propulsion  
p 153 A89-53282
- HENDRICKSON, BRIAN M.**  
Optoelectronic signal processing for phased-array antennas; Proceedings of the Meeting, Los Angeles, CA, Jan. 12, 13, 1988  
[SPIE-886] p 124 A89-15819
- HENNEKE, E. G., II**  
A study of the stress wave factor technique for evaluation of composite materials  
[NASA-CR-4195] p 189 N89-21256
- HENRIKSEN, P. N.**  
Alkoxysilane adsorption on metal oxide substrates  
p 92 A89-44536
- HENRY, D. P.**  
Development of BEM for ceramic composites  
[NASA-CR-183313] p 111 N89-14311
- HEPP, A. F.**  
Structural chemistry of Au(III)-substituted Ba2YCu3O(7-delta)  
p 89 A89-12620  
Interaction of Au, Ag, and Bi ions with Ba2YCu3O(7-y)  
- Implications for superconductor applications  
p 235 A89-22886  
Improved synthesis of ceramic superconductors with alkaline earth peroxides - Synthesis and processing of Ba2YCu3O(7-x)  
p 235 A89-22887
- HEPP, ALOYSIUS F.**  
Stability of bulk Ba2YCu3O(7-x) in a variety of environments  
[NASA-TM-101401] p 111 N89-14310  
Non-uniform transition conductivity of superconducting ceramic  
[NASA-TM-102133] p 189 N89-28851
- HERBACH, BRUCE**  
Ground-based simulation of telepresence for materials science experiments  
[AIAA PAPER 89-0597] p 119 A89-28439
- HERBERT, THORWALD**  
Studies of transition in boundary layers  
[AIAA PAPER 89-0034] p 2 A89-25029
- HERMANN, A. H.**  
Transport critical current and magnetization measurements of melt-processed YBa2Cu3O(7-x)  
p 234 A89-20037
- HEUER, A. H.**  
On the orthorhombic phase in ZrO2-based alloys  
p 105 A89-30631
- HICKMAN, G. A.**  
Distributed ice accretion sensor for smart aircraft structures  
[AIAA PAPER 89-0772] p 17 A89-25571
- HICKMAN, J. M.**  
Comparison of solar photovoltaic and nuclear reactor power systems for a human-tended lunar observatory  
[NASA-TM-102015] p 242 N89-23397
- HICKS, Y.**  
Stratified charge rotary engine - Internal flow studies at the MSU engine research laboratory  
[SAE PAPER 890331] p 181 A89-51477
- HIGGINS, M.**  
Structural response of an advanced combustor liner: Test and analysis  
p 200 N89-17329
- HILL, SCOTT M.**  
Microwave characteristics of interdigitated photoconductors on a HEMT structure  
[NASA-CR-182197] p 135 N89-12820  
Microwave characteristics of GaAs MMIC integratable optical detectors  
[NASA-TM-101485] p 129 N89-24520
- HILLERY, R. V.**  
Thermal barrier coating life prediction model  
p 109 N89-12921  
Thermal barrier coating life prediction model development  
[NASA-CR-180807] p 110 N89-13621
- HILMAS, G. E.**  
Microstructural evolution on crystallizing the glassy phase in a 6 weight percent Y2O3-Si3N4 ceramic  
p 80 A89-19487
- HINES, B.**  
Orbit transfer rocket engine technology program. Phase 2: Advanced engine study  
[NASA-CR-179602] p 61 N89-10119
- HINGST, W. R.**  
An LDA (Laser-Doppler Anemometry) investigation of three-dimensional normal shock wave boundary-layer interactions  
p 14 N89-20956
- HINGST, WARREN R.**  
Experimental and numerical investigation of an oblique shock wave/turbulent boundary layer interaction with continuous suction  
[AIAA PAPER 89-0357] p 4 A89-28407
- HINTERMANN, H. E.**  
The scratch test - Different critical load determination techniques  
p 171 A89-54278
- HIPPENSTEELE, STEVEN A.**  
High-resolution heat-transfer-coefficient maps applicable to compound-curve surfaces using liquid crystals in a transient wind tunnel  
[NASA-TM-89855] p 154 N89-10246

- High-resolution liquid-crystal heat-transfer measurements on the end wall of a turbine passage with variations in Reynolds number [NASA-TM-100827] p 161 N89-18664
- HIRLEMAN, E. D.**  
Calibration of single particle sizing velocimeters using photomask reticles p 170 A89-33379
- HOBART, H. F.**  
The NASA Lewis Strain Gauge Laboratory: An update p 173 N89-12888
- HOBERECHT, MARK A.**  
Space Station Freedom photovoltaic power module design status [NASA-TM-102073] p 71 N89-25273  
Launch packaging options for the photovoltaic power module cargo element [NASA-TM-102072] p 71 N89-25275
- HOCHSTEIN, J. I.**  
Modeling of pulsed propellant reorientation [AIAA PAPER 89-2727] p 61 A89-53306  
Modeling of pulsed propellant reorientation [NASA-TM-102117] p 165 N89-26178
- HOCHSTEIN, JOHN I.**  
Modeling of impulsive propellant reorientation [AIAA PAPER 89-0628] p 54 A89-25496  
Modeling of impulsive propellant reorientation [NASA-TM-101440] p 64 N89-13495
- HOEHN, F. W.**  
The Solar Dynamic radiator with a historical perspective p 51 A89-15340  
The solar dynamic radiator with a historical perspective [NASA-TM-100972] p 45 N89-10117
- HOFFMAN, R. W.**  
Pulsed ion beam investigation of the kinetics of surface reactions p 93 A89-44542
- HOLDMAN, J. D.**  
Assessment, development, and application of combustor aerothermal models p 30 N89-20138
- HOLLAND, FREDERIC A., JR.**  
Investigation of Weibull statistics in fracture analysis of cast aluminum [NASA-TM-102000] p 185 N89-21245
- HOLMAN, R. R.**  
Effects of operating parameters on PAFC stack performance p 207 A89-15250
- HOLT, MAURICE**  
Interaction of an oblique shock wave with turbulent hypersonic blunt body flows [AIAA PAPER 89-0272] p 3 A89-28405
- HOLT, R. V.**  
On 3D inelastic analysis methods for hot section components p 196 N89-12906
- HOLT, WILLIAM H.**  
Castable hot corrosion resistant alloy [NASA-CASE-LEW-14134-2] p 102 N89-14303
- HOLVE, D. J.**  
Calibration of single particle sizing velocimeters using photomask reticles p 170 A89-33379
- HOLZMANN, WILFRIED A.**  
Integrated control and health management. Orbit transfer rocket engine technology program [NASA-CR-182122] p 62 N89-11805
- HONEY, FRANK S.**  
Auger analysis of a fiber/matrix interface in a ceramic matrix composite p 82 A89-35311
- HONKALA, KEITH A.**  
Development of an integrated BEM approach for hot fluid structure interaction [NASA-CR-184587] p 27 N89-15114
- HOOFRING, A. B.**  
Submicron nickel-oxide-gold tunnel diode detectors for rectennas p 133 A89-43469
- HOPKINS, D. A.**  
Structural tailoring of counter rotation propfans p 33 N89-25165  
Metal matrix composite micromechanics: In-situ behavior influence on composite properties [NASA-TM-102302] p 88 N89-26924  
Computational simulation of high temperature metal matrix composites cyclic behavior [NASA-TM-102115] p 88 N89-27795  
Probabilistic structural analysis methods of hot engine structures [NASA-TM-102091] p 205 N89-28030  
The 3-D inelastic analyses for computational structural mechanics p 206 N89-29804
- HOPKINS, DALE A.**  
A unique set of micromechanics equations for high-temperature metal matrix composites p 190 A89-15734  
Thermoviscoplastic nonlinear constitutive relationships for structural analysis of high-temperature metal matrix composites p 190 A89-15735
- HORSHAM, GARY A. P.**  
A perspective on space exploration technology catalysis: A rationale for initiating 21st Century expansion of human civilization into outer space [NASA-TM-101362] p 238 N89-11637
- HORTON, C. C.**  
Pulsed ion beam investigation of the kinetics of surface reactions p 93 A89-44542
- HOUSHMAND, B.**  
A comparison of reflector antenna designs for wide-angle scanning [NASA-TM-101459] p 127 N89-21138  
A segmented mirror antenna for radiometers [NASA-TM-102045] p 128 N89-23753
- HOVENAC, E. A.**  
Calibration of single particle sizing velocimeters using photomask reticles p 170 A89-33379
- HOVENAC, EDWARD A.**  
Performance of the forward scattering spectrometer probe in NASA's Icing Research Tunnel [AIAA PAPER 89-0769] p 169 A89-25570  
An improved correction algorithm for number density measurements made with the forward scattering spectrometer probe p 170 A89-44122  
A correction algorithm for particle size distribution measurements made with the forward-scattering spectrometer probe p 170 A89-44123  
Fresnel diffraction by spherical obstacles p 231 A89-48249  
Performance of the forward scattering spectrometer probe in NASA's icing research tunnel [NASA-TM-101381] p 172 N89-12845
- HOWERTON, R.**  
The Solar Dynamic radiator with a historical perspective p 51 A89-15340
- HOWERTON, R. L.**  
The solar dynamic radiator with a historical perspective [NASA-TM-100972] p 45 N89-10117
- HOYNAK, D.**  
Effect of aerodynamic detuning on supersonic rotor discrete frequency noise generation p 225 A89-15083
- HRACH, FRANK J.**  
Satellite relocation by tether deployment [NASA-TM-101992] p 42 N89-26877
- HSIEH, KWANG-CHUNG**  
Navier-Stokes calculation of solid-propellant rocket motor internal flowfields [AIAA PAPER 88-3182] p 48 A89-14983  
Numerical investigation of chemically reacting flows in ramjet dump combustors [AIAA PAPER 89-0387] p 22 A89-28408  
Assessment of numerical techniques for unsteady flow calculations [AIAA PAPER 89-1956] p 150 A89-41803
- HSU, ANDREW T.**  
The effect of adaptive grid on hypersonic nozzle flow calculations [AIAA PAPER 89-0006] p 54 A89-28402  
A simple algebraic grid adaptation scheme with applications to two- and three-dimensional flow problems [AIAA PAPER 89-1984] p 5 A89-41827  
A time accurate finite volume high resolution scheme for three dimensional Navier-Stokes equations [AIAA PAPER 89-1994] p 6 A89-41837
- HUANG, H.**  
On 3D inelastic analysis methods for hot section components p 196 N89-12906
- HUANG, P. G.**  
Mesh refinement in a two-dimensional large eddy simulation of a forced shear layer [NASA-TM-102129] p 166 N89-26180
- HUCKELBRIDGE, A. A.**  
Identification of structural interface characteristics using component mode synthesis p 193 A89-36177
- HUCKELBRIDGE, ARTHUR A.**  
Characterization of structural connections using free and forced response test data [NASA-TM-101991] p 202 N89-21266
- HUDSON, DALE A.**  
CFD in the context of IHPTET - The Integrated High Performance Turbine Engine Technology Program [AIAA PAPER 89-2904] p 154 A89-53307  
CFD in the context of IHPTET: The Integrated High Performance Turbine Technology Program [NASA-TM-102132] p 165 N89-26174
- HUERRE, P.**  
Liquid droplet generation [NASA-CR-182246] p 166 N89-26182
- HUFF, DENNIS L.**  
Evaluation of three turbulence models for the prediction of steady and unsteady airloads [AIAA PAPER 89-0609] p 3 A89-25485
- Numerical analysis of flow through oscillating cascade sections [AIAA PAPER 89-0437] p 4 A89-28413  
Numerical analysis of supersonic flow through oscillating cascade sections by using a deforming grid [AIAA PAPER 89-2805] p 8 A89-50810  
Evaluation of three turbulence models for the prediction of steady and unsteady airloads [NASA-TM-101413] p 10 N89-12555  
Numerical analysis of flow through oscillating cascade sections [NASA-TM-101417] p 11 N89-14220  
Numerical analysis of supersonic flow through oscillating cascade sections by using a deforming grid [NASA-TM-102053] p 15 N89-25119
- HUFF, R.**  
Unsteady heat transfer in turbine blade ducts - Focus on combustor sources p 153 A89-53286
- HUFF, RONALD G.**  
NASA powered lift facility internally generated noise and its transmission to the acoustic far field [NASA-CR-182217] p 36 N89-16882  
Noise generated by a flight weight, air flow control valve in a vertical takeoff and landing aircraft thrust vectoring system [NASA-CR-182232] p 228 N89-20776
- HUGHES, CHRISTOPHER E.**  
Noise of a model counterrotation propeller with simulated fuselage and support pylon at takeoff/approach conditions [AIAA PAPER 89-1143] p 227 A89-48953  
Low-speed wind tunnel performance of high-speed counterrotation propellers at angle-of-attack [AIAA PAPER 89-2583] p 8 A89-50808  
Flowfield measurements in the NASA Lewis Research Center 9- by 15-foot low-speed wind tunnel [NASA-TM-100883] p 36 N89-21002  
Noise of a model counterrotation propeller with simulated fuselage and support pylon at takeoff/approach conditions [NASA-TM-101996] p 228 N89-24138  
Low-speed wind tunnel performance of high-speed counterrotation propellers at angle-of-attack [NASA-TM-102292] p 15 N89-25121
- HUGHES, WILLIAM F.**  
Dynamics of face and annular seals with two-phase flow [NASA-CR-183352] p 182 N89-12870
- HULL, D.**  
Observations of directional gamma prime coarsening during engine operation p 98 A89-40162
- HULL, JOHN**  
Aeronautical applications of high-temperature superconductors [AIAA PAPER 89-2142] p 23 A89-53304  
Aeronautical applications of high-temperature superconductors [NASA-TM-102311] p 33 N89-26008
- HULSE, CHARLES O.**  
Development of a high temperature static strain sensor p 173 N89-12887  
Development of a high temperature thin film static strain gage p 174 N89-17299
- HULTGREN, LENNART S.**  
Nonlinear spatial evolution of an externally excited instability wave in a free shear layer p 144 A89-23242  
Boundary-layer receptivity to long-wave free-stream disturbances p 146 A89-28996
- HUMBERT, D. R.**  
Oxide-dispersion-strengthened turbine blades. Volume 2 [NASA-CR-179561-VOL-2] p 28 N89-18487
- HUNG, CHING-CHEH**  
Graphite fluoride fiber polymer composite material [NASA-CASE-LEW-14472-1] p 85 N89-14259
- HURON, ERIC S.**  
Constitutive behavior of single crystal PWA 1480 and directionally solidified MAR-M 246 under monotonic and cyclic loads at high and low temperature p 100 N89-12634
- HURST, JANET B.**  
Characterization of ceramics and intermetallics fabricated by self-propagating high-temperature synthesis [NASA-TM-102004] p 78 N89-25285
- HUSAIN, H. S.**  
Passive and active control of jet turbulence p 140 A89-10176
- HUSAIN, HYDER S.**  
Turbulence management in free shear flows by control of coherent structures p 147 A89-30908
- HUSSAIN, FAZLE**  
Turbulence management in free shear flows by control of coherent structures p 147 A89-30908

- HUSTON, RONALD L.**  
Finite-element grid improvement by minimization of stiffness matrix trace p 194 A89-42339  
Improvement in finite element meshes: Heat transfer in an infinite cylinder [NASA-TM-101410] p 182 N89-14450  
Computer-aided design of bevel gear tooth surfaces [NASA-TM-101449] p 183 N89-17248
- HUYNH, HUNG T.**  
Second-order accurate nonoscillatory schemes for scalar conservation laws [NASA-TM-102010] p 14 N89-22573
- HYATT, MARK J.**  
Phase transformations in xerogels of mullite composition [NASA-TM-101349] p 108 N89-11038  
Crystallization kinetics of BaO-Al<sub>2</sub>O<sub>3</sub>-SiO<sub>2</sub> glasses [NASA-TM-101964] p 113 N89-20252
- HYLTON, L. D.**  
Measurements of heat transfer distribution over the surfaces of highly loaded turbine nozzle guide vanes The effects of leading edge and downstream film cooling on turbine vane heat transfer [NASA-CR-182133] p 158 N89-13754  
Turbine airfoil film cooling p 161 N89-17315
- HYLTON, LARRY D.**  
Turbine airfoil film cooling p 158 N89-12903
- HYNES, T. P.**  
Calculations of inlet distortion induced compressor flow field instability p 8 A89-52498
- IACABUCCI, R. S.**  
Space station hydrogen/oxygen thruster technology [NASA-CR-182280] p 74 N89-26905
- IANNO, N. J.**  
Highly oriented Ti<sub>2</sub>Ba<sub>2</sub>Ca<sub>2</sub>Cu<sub>3</sub>O<sub>10</sub> thin films by pulsed laser evaporation p 236 A89-30421  
Preparation of high T(c) Ti-Ba-Ca-Cu-O thin films by pulsed laser evaporation and TiO<sub>3</sub> vapor processing p 236 A89-38608
- IANNO, NATALE J.**  
Growth of diamond by RF plasma-assisted chemical vapor deposition p 90 A89-20474
- IBRAHIM, MOUNIR B.**  
Two-dimensional numerical simulation of a Stirling engine heat exchanger [NASA-TM-102057] p 164 N89-23823
- IDE, ROBERT F.**  
Performance of the forward scattering spectrometer probe in NASA's Icing Research Tunnel [AIAA PAPER 89-0769] p 169 A89-25570  
Performance of the forward scattering spectrometer probe in NASA's icing research tunnel [NASA-TM-101381] p 172 N89-12845
- ILEGBUSI, O. J.**  
Fluid flow phenomena in the generation of boron carbide suspensions in magnesium melts p 79 A89-19472
- INGEBO, ROBERT D.**  
Fuel spray simulation with two-fluid nozzles [AIAA PAPER 89-0053] p 145 A89-25047  
Gas density effect on droplet size of simulated fuel sprays [AIAA PAPER 89-2322] p 151 A89-46749  
Fluid spray simulation with two-fluid nozzles [NASA-TM-101367] p 155 N89-12028  
Gas density effect on droplet size of simulated fuel sprays [NASA-TM-102013] p 162 N89-22053
- ISIKAWA, YUICHI**  
Effects of lubrication on the performance of high speed spur gears [NASA-TM-101969] p 186 N89-22919
- ISKOVITZ, I.**  
On finite element implementation and computational techniques for constitutive modeling of high temperature composites [NASA-CR-185120] p 204 N89-26261
- ISRAEL, R.**  
Rational engineering correlations of diffusional and inertial particle deposition behavior in non-isothermal forced convection environments p 140 A89-12327  
Use of a generalized Stokes number to determine the aerodynamic capture efficiency of non-Stokesian particles from a compressible gas flow p 140 A89-12336
- JACKSON, H. E.**  
Characterization of GaAlAs optical waveguide heterostructures grown by molecular beam epitaxy [NASA-CR-185120] p 130 A89-10343
- JACKSON, T. A.**  
External electro-optic probing of millimeter-wave integrated circuits p 133 A89-45266  
External electro-optic probing of millimeter-wave integrated circuits [NASA-TM-101990] p 128 N89-21142
- JACOBSON, NATHAN S.**  
Reactions of silicon-based ceramics in mixed oxidation chlorination environments p 105 A89-21442  
Sodium sulfate - Deposition and dissolution of silica p 91 A89-28084  
The behavior of SiC and Si<sub>3</sub>N<sub>4</sub> ceramics in mixed oxidation/chlorination environments p 106 A89-33616  
Molten salt corrosion of SiC and Si<sub>3</sub>N<sub>4</sub> [NASA-TM-101346] p 108 N89-11912  
Hot corrosion of ceramic engine materials [NASA-TM-101439] p 112 N89-16065
- JACOBSON, PETER E.**  
Multi-hundred kilowatt roll ring assembly [NASA-CR-174832] p 135 N89-15335
- JACOBSON, T. P.**  
Hardware development for the Surface Tension Driven Convection Experiment aboard the USML-1 Spacelab mission [AIAA PAPER 89-0406] p 47 A89-25341  
Hardware development for the surface tension driven convection experiment aboard the USML-1 spacelab mission [NASA-TM-101404] p 48 N89-11804
- JACOBY, BARRY A.**  
Plasma flow processes within magnetic nozzle configurations [AIAA PAPER 89-2711] p 57 A89-47036
- JACQMIN, DAVID**  
Instabilities caused by oscillating accelerations normal to a viscous fluid-fluid interface p 144 A89-22823
- JACQUEZ, A.**  
Development of a 39.5 GHz Karp traveling wave tube for use in space [NASA-CR-182182] p 136 N89-15336
- JAEGGER, S. M.**  
Determination of near and far field acoustics for advanced propeller configurations [AIAA PAPER 89-1040] p 226 A89-40469
- JAFFE, L.**  
Nuclear reactor power as applied to a space-based radar mission p 51 A89-15317  
Systems aspects of a space nuclear reactor power system p 51 A89-15327  
Nuclear reactor power as applied to a space-based radar mission [NASA-TM-101200] p 230 N89-14831
- JANUS, J. MARK**  
A simple time-accurate turbomachinery algorithm with numerical solutions of an uneven blade count configuration [AIAA PAPER 89-0206] p 179 A89-25181
- JASKOWIAK, MARTHA H.**  
Pressure effects on the thermal stability of silicon carbide fibers p 105 A89-31502
- JAWORSKE, D. A.**  
Compatibility of molten salts with advanced solar dynamic receiver materials [AIAA PAPER 89-1756] p 83 A89-48957
- JAYARAMAN, N.**  
Oxide scale stresses in polycrystalline Ni<sub>200</sub> p 98 A89-38859  
Constitutive modeling for single crystal superalloys p 101 N89-12911
- JEFFERIES, KENT S.**  
Thermal distortion analysis of the Space Station solar dynamic concentrator p 51 A89-15341  
Ray tracing optical analysis of offset solar collector for Space Station solar dynamic system p 53 A89-15416  
Concentration of off-axis radiation by solar concentrators for space power [NASA-TM-102052] p 69 N89-24438
- JENG, DUEN-REN**  
Flow of rarefied gases over two-dimensional bodies [AIAA PAPER 89-1970] p 5 A89-41814  
Rarefied gas flow through two-dimensional nozzles [AIAA PAPER 89-2893] p 7 A89-47156
- JENKINS, MICHAEL G.**  
Fracture resistance of a TiB<sub>2</sub> particle/SiC matrix composite at elevated temperature p 81 A89-31074
- JENSEN, KENNETH A.**  
Secondary electron emission characteristics of untreated and ion-textured titanium [NASA-TP-2902] p 103 N89-17650
- JERACKI, ROBERT J.**  
The effect of front-to-rear propeller spacing on the interaction noise at cruise conditions of a model counterrotation propeller having a reduced diameter aft propeller [NASA-TM-101329] p 227 N89-10603
- Wind-tunnel results of advanced high-speed propellers at takeoff, climb, and landing Mach numbers [NASA-TM-87030] p 13 N89-19265
- JHA, S. C.**  
Dispersoids in rapidly solidified B2 nickel aluminides p 98 A89-43023
- JIANG, BO-NAN**  
Least-squares finite elements for Stokes problem [NASA-TM-101308] p 222 N89-22392  
Least-squares finite element method for fluid dynamics [NASA-TM-102352] p 223 N89-30008
- JIANG, HONG**  
Absorbing boundary conditions for second-order hyperbolic equations [NASA-TM-102009] p 223 N89-22397
- JIMENEZ, AMADOR P.**  
Space Station Freedom photovoltaic power module design status [NASA-TM-102073] p 71 N89-25273
- JOHNS, ALBERT L.**  
Experimental results for a two-dimensional supersonic inlet used as a thrust deflecting nozzle [NASA-TM-83439] p 159 N89-14386  
Hot gas ingestion testing of an advanced STOVL concept in the NASA Lewis 9- by 15-foot low speed wind tunnel with flow visualization [NASA-TM-100952] p 11 N89-15078  
STOL and STOVL hot gas ingestion and airframe heating tests in the NASA Lewis 9- by 15-foot low-speed wind tunnel [NASA-TM-102101] p 15 N89-29323
- JOHNSON, B. V.**  
Coolant passage heat transfer with rotation p 157 N89-12899  
Coolant passage heat transfer with rotation p 161 N89-17314
- JOHNSON, G. A.**  
Adhesion, friction, and wear of plasma-deposited thin silicon nitride films at temperatures to 700 C p 107 A89-48250  
Adhesion, friction, and wear of plasma-deposited thin silicon nitride films at temperatures to 700 C [NASA-TM-101377] p 109 N89-11913
- JOHNSON, KEITH**  
Hierarchical Poly Tree computer architectures defined by computational multidisciplinary mechanics p 218 A89-50100
- JOHNSON, L. R.**  
High-temperature LCF of Ni-201 and 304L stainless steel p 100 N89-12635
- JOHNSON, RICHARD W.**  
Kinetic energy equations for the average-passage equation system p 237 A89-28347
- JOHNSON, S. S.**  
Film annotation system for a space experiment [NASA-CR-185114] p 176 N89-27152
- JOHNSON, STEVE**  
Transient performance evaluation of an integrated heat pipe-thermal storage system p 49 A89-15209
- JOHNSTON, JAMES C.**  
Ground-based simulation of telepresence for materials science experiments [AIAA PAPER 89-0597] p 119 A89-28439
- JOHNSTON, ROBERT T.**  
Propeller/wing interaction [AIAA PAPER 89-0535] p 17 A89-25429
- JOHS, B.**  
Highly oriented Ti<sub>2</sub>Ba<sub>2</sub>Ca<sub>2</sub>Cu<sub>3</sub>O<sub>10</sub> thin films by pulsed laser evaporation p 236 A89-30421  
Preparation of high T(c) Ti-Ba-Ca-Cu-O thin films by pulsed laser evaporation and TiO<sub>3</sub> vapor processing p 236 A89-38608
- JONES, TERRY V.**  
High-resolution heat-transfer-coefficient maps applicable to compound-curve surfaces using liquid crystals in a transient wind tunnel [NASA-TM-89855] p 154 N89-10246
- JONES, WILLIAM R., JR.**  
The preparation of new perfluoro ether fluids exhibiting excellent thermal-oxidative stabilities p 76 A89-12760  
Surface temperature determination in surface analytic systems by infrared optical pyrometry p 169 A89-17347  
Tribology: The Story of Lubrication and Wear [NASA-TM-101430] p 203 N89-24635  
Determination of the thermal stability of perfluoroalkylethers by tensimetry: Instrumentation and Procedure [NASA-TM-102116] p 116 N89-26095
- JORDAN, E. H.**  
Fracture mechanics applied to elevated temperature crack growth p 195 A89-47705  
Constitutive modelling of single crystal and directionally solidified superalloys p 101 N89-12912

## JORDAN, ERIC H.

- X-ray based extensometry  
[NASA-CR-185058] p 176 N89-25432
- JORDAN, ERIC H.**  
Biaxial thermo-mechanical fatigue p 194 A89-43527  
Constitutive modelling of single crystal and directionally solidified superalloys p 102 N89-17325  
Nonlinear mesomechanics of composites with periodic microstructure  
[NASA-TM-102051] p 204 N89-26260
- JORGENSEN, PHILIP C. E.**  
An unconditionally stable Runge-Kutta method for unsteady flows p 2 A89-25180  
[AIAA PAPER 89-0205]  
Explicit Runge-Kutta method for unsteady rotor/stator interaction p 5 A89-36912
- JOSLYN, H. D.**  
The effects of inlet turbulence and rotor/stator interactions on the aerodynamics and heat transfer of a large-scale rotating turbine model, volume 1  
[NASA-CR-4079] p 159 N89-13756
- JOSLYN, H. DAVID**  
Measurement of airfoil heat transfer coefficients on a turbine stage p 157 N89-12897  
Measurement of airfoil heat transfer coefficients on a turbine stage p 160 N89-17311
- JOU, L.**  
Optoelectronic techniques for broadband switching p 131 A89-15825
- JOU, LIZ**  
Study of optoelectronic switch for satellite-switched time-division multiple access  
[NASA-CR-179630] p 135 N89-13706
- JUHLKE, TIMOTHY J.**  
The preparation of new perfluoro ether fluids exhibiting excellent thermal-oxidative stabilities p 76 A89-12760

## K

- KACKLEY, N.**  
Oxygen electrodes for rechargeable alkaline fuel cells p 211 N89-22998
- KADAMBI, JAIRISHNAN R.**  
Comparison of the bidirectional reflectance distribution function of various surfaces p 230 A89-41530
- KAFALAS, J. A.**  
A comparative study of the influence of buoyancy driven fluid flow on GaAs crystal growth p 121 N89-20295
- KAILASANATH, K.**  
Time-dependent computational studies of flames in microgravity  
[NASA-CR-182298] p 122 N89-25353
- KALLURI, S.**  
Exposure time considerations in high temperature low cycle fatigue p 192 A89-29600
- KALLURI, SREERAMESH**  
Results of inphase axial-torsional fatigue experiments on 304 stainless steel  
[NASA-TM-101464] p 201 N89-20514  
A data acquisition and control program for axial-torsional fatigue testing  
[NASA-TM-102041] p 205 N89-28029
- KAMO, R.**  
Adiabatic Wankel type rotary engine  
[NASA-CR-182233] p 28 N89-17599
- KANG, DAVID S.**  
A 20-DOF hybrid stress general shell element p 191 A89-21133
- KANTZOS, PETER**  
Fatigue crack growth behavior of a single crystal alloy as observed through an in situ fatigue loading stage p 99 A89-45946  
Fatigue crack growth study of SCS6/Ti-15-3 composite  
[NASA-TM-102332] p 104 N89-26989
- KAPOOR, V. J.**  
Plasma deposited silicon nitride for indium phosphide encapsulation p 235 A89-27794  
Submicron nickel-oxide-gold tunnel diode detectors for rectennas p 133 A89-43469
- KARKI, K.**  
Solution of three-dimensional flow problems using a flux-spline method  
[AIAA PAPER 89-0687] p 146 A89-25543
- KARKI, K. C.**  
A numerical and experimental study of coaxial jets p 153 A89-52500  
Improved numerical methods for turbulent viscous flows aerothermal modeling program, phase 2  
[NASA-CR-182169] p 154 N89-12010  
Aerothermal modeling program, phase 2 p 156 N89-12890
- KASCAK, A. F.**  
Piezoelectric pushers for active vibration control of rotating machinery p 171 A89-47717
- KASCAK, ALBERT F.**  
Multi-grid for structures analysis p 206 N89-29810
- KASHIWAGI, TAKASHI**  
Expert systems applied to spacecraft fire safety  
[NASA-CR-182266] p 42 N89-23501
- KASSEMI, M.**  
Radiative transfer in rectangular enclosures - A discretized exchange factor solution p 153 A89-53262
- KASSEMI, MOHAMMAD**  
Interaction of surface radiation with convection in crystal growth by physical vapor transport  
[AIAA PAPER 89-0228] p 119 A89-30450
- KATZ, I.**  
A model of electron collecting plasma contractors  
[AIAA PAPER 89-1560] p 232 A89-40190  
The POLAR code wake model - Comparison with in situ observations p 233 A89-45632
- KATZ, IRA**  
On the need for space tests of plasma contractors as electron collectors p 232 A89-43356
- KAUFMAN, ALBERT**  
Simplified cyclic structural analysis of SSME turbine blades p 63 N89-12632
- KAUFMAN, R. M.**  
The effects of leading edge and downstream film cooling on turbine vane heat transfer  
[NASA-CR-182133] p 158 N89-13754  
Turbine airfoil film cooling p 161 N89-17315
- KAUTZ, HAROLD E.**  
Nondestructive evaluation of advanced ceramics  
[NASA-TM-101489] p 189 N89-20490
- KAWA, HAJIMA**  
The preparation of new perfluoro ether fluids exhibiting excellent thermal-oxidative stabilities p 76 A89-12760
- KAZA, K. R. V.**  
Technique for the prediction of airfoil flutter characteristics in separated flow p 191 A89-27744  
Analytical flutter investigation of a composite propfan model p 195 A89-48663  
Analysis of an unswept propfan blade with a semiempirical dynamic stall model  
[NASA-TM-4083] p 27 N89-15112
- KAZA, KRISHNA RAO**  
Aeroelastic response of metallic and composite propfan models in yawed flow  
[AIAA PAPER 88-3154] p 20 A89-17942
- KAZA, KRISHNA RAO V.**  
Vibration, performance, flutter and forced response characteristics of a large-scale propfan and its aeroelastic model  
[AIAA PAPER 88-3155] p 21 A89-17943  
A computational procedure for automated flutter analysis p 191 A89-28070  
Application of a full-potential solver to bending-torsion flutter in cascades  
[AIAA PAPER 89-1386] p 34 A89-30859  
Vibration, performance, flutter and forced response characteristics of a large-scale propfan and its aeroelastic model  
[NASA-TM-101322] p 24 N89-10043  
Turbomachinery aeroelasticity at NASA Lewis Research Center p 28 N89-19262
- KAZAROFF, JOHN**  
Friction-induced ignition of metals in high-pressure oxygen p 97 A89-32932
- KEDDY, E.**  
Transient performance evaluation of an integrated heat pipe-thermal storage system p 49 A89-15209
- KEITH, T. G., JR.**  
Efficient numerical simulation of a one-dimensional electrothermal deicer pad p 144 A89-22811  
Two-dimensional simulation of electrothermal deicing of aircraft components p 17 A89-39194  
Effect of ambient pressure on the performance of a resistojet p 55 A89-44111  
An LDA (Laser-Doppler Anemometry) investigation of three-dimensional normal shock wave boundary-layer interactions p 14 N89-20956
- KEITH, THEO G.**  
Langmuir probe measurements of an arcjet exhaust p 55 A89-39031
- KEITH, THEO G., JR.**  
Investigation of the flow in the diffuser section of the NASA Lewis Icing Research Tunnel p 36 A89-28455  
[AIAA PAPER 89-0755]  
Application of a full-potential solver to bending-torsion flutter in cascades p 34 A89-30859  
Flow of rarefied gases over two-dimensional bodies  
[AIAA PAPER 89-1970] p 5 A89-41814  
The effect of test-cell pressure on resistojet nozzle flow  
[AIAA PAPER 89-2838] p 58 A89-47116  
Rarefied gas flow through two-dimensional nozzles  
[AIAA PAPER 89-2893] p 7 A89-47156
- Investigation of the flow in the diffuser section of the NASA Lewis icing research tunnel  
[NASA-TM-102087] p 17 N89-25978
- KENNEDY, JAN B.**  
Application of advanced diagnostics to airblast injector flows p 160 N89-17306
- KEPLER, C. E.**  
Performance potential of air turbo-ramjet employing supersonic through-flow fan  
[AIAA PAPER 89-0010] p 22 A89-25006  
Supersonic through-flow fan assessment  
[NASA-CR-182202] p 27 N89-16843
- KERCZEWSKI, ROBERT J.**  
Performance of five 30 GHz satellite receivers  
[NASA-TM-101960] p 129 N89-25365
- KERIBAR, RIFAT**  
The effect of insulated combustion chamber surfaces on direct-injected diesel engine performance, emissions, and combustion  
[NASA-CR-182204] p 239 N89-17548  
Methods for heat transfer and temperature field analysis of the insulated diesel, phase 3  
[NASA-CR-182237] p 239 N89-23382
- KERSCHEN, E. J.**  
Influence of airfoil thickness on convected gust interaction noise  
[AIAA PAPER 89-1082] p 225 A89-33725
- KERSLAKE, WILLIAM R.**  
The effect of the near earth micrometeoroid environment on a highly reflective mirror surface  
[AIAA PAPER 88-0026] p 40 A89-17939
- KESSELI, JAMES**  
An experimental analysis of a doped lithium fluoride direct absorption solar receiver p 49 A89-15245  
Advanced heat receiver conceptual design study  
[NASA-CR-182177] p 209 N89-16224
- KETCHUM, A. C.**  
Preliminary study of the interactions caused by crossing shock waves and a turbulent boundary layer  
[AIAA PAPER 89-0359] p 145 A89-25303
- KEYES, DAVID E.**  
Theoretical studies in support of the 3M-vapor transport (PVTOS-) experiments  
[NASA-CR-185122] p 165 N89-26179
- KHALILI, KAVEH**  
Failure analysis of a Stirling engine heat pipe  
[NASA-TM-101418] p 103 N89-20227
- KHONSARI, M. M.**  
On the performance of finite journal bearings lubricated with micropolar fluids p 181 A89-54977
- KIA, T.**  
Nuclear reactor power as applied to a space-based radar mission  
[NASA-TM-101200] p 230 N89-14831
- KIEHL, W.**  
Transport critical current and magnetization measurements of melt-processed YBa<sub>2</sub>Cu<sub>3</sub>O<sub>7-x</sub> p 234 A89-20037
- KIERNAN, M. T.**  
A study of the stress wave factor technique for evaluation of composite materials  
[NASA-CR-4195] p 189 N89-21256
- KIM, H. J.**  
Observations of the frequencies in a sphere wake and of drag increase by acoustic excitation p 142 A89-16884  
Investigation of the flow between a pair of circular cylinders in the flopping regime p 144 A89-22822
- KIM, J. H.**  
Determination of near and far field acoustics for advanced propeller configurations  
[AIAA PAPER 89-1040] p 226 A89-40469
- KIM, JUNGHWAN**  
Coded multiple chirp spread spectrum system and overlay service p 124 A89-26769
- KIM, K. S.**  
Elevated temperature crack growth p 196 N89-12915  
Thermal barrier coating life prediction model p 109 N89-12921  
Elevated temperature crack growth p 200 N89-17335
- KIM, K.-S.**  
Skin-friction measurements by laser interferometry p 167 N89-28737
- KIM, S.-W.**  
A near-wall turbulence model and its application to fully developed turbulent channel and pipe flows  
[NASA-TM-101399] p 158 N89-13741  
Control-volume based Navier-Stokes equation solver valid at all flow velocities  
[NASA-TM-101488] p 161 N89-20407  
Numerical computation of shock wave-turbulent boundary layer interaction in transonic flow over an axisymmetric curved hill  
[NASA-TM-101473] p 162 N89-21192



- Calculation of reattaching shear layers in divergent channel with a multiple-time-scale turbulence model [NASA-TM-102293] p 168 N89-28749
- KIM, S.-W.**  
Numerical investigation of an internal layer in turbulent flow over a curved hill [NASA-TM-102230] p 168 N89-29725
- KIM, SANG-SOO**  
Optical experiments on thermophoretically augmented submicron particle deposition from 'dusty' high temperature gas flows p 90 A89-14799
- KING, DAVID Q.**  
The NASA Electric Propulsion Program p 59 A89-47428
- KING, ROGER J.**  
A Fourier analysis for a fast simulation algorithm p 130 A89-15367  
A design procedure for the phase-controlled parallel-loaded resonant inverter p 134 A89-50472
- KIRALY, L. J.**  
Computational structural methods at NASA Lewis p 205 N89-29776
- KIRCH, LUKE A.**  
Protoflight photovoltaic power module system-level tests in the space power facility [NASA-TM-102066] p 46 N89-25267
- KISER, J. D.**  
Crystallization and characterization of Y<sub>2</sub>O<sub>3</sub>-SiO<sub>2</sub> glasses p 80 A89-19486  
Microstructural evolution on crystallizing the glassy phase in a 6 weight percent Y<sub>2</sub>O<sub>3</sub>-Si<sub>3</sub>N<sub>4</sub> ceramic p 80 A89-19487
- KISER, JAMES D.**  
High-frequency ultrasonic characterization of sintered silicon carbide p 106 A89-34840  
A sintering model for SiC(sub)w/Si<sub>3</sub>N<sub>4</sub> composites [NASA-TM-101336] p 108 N89-10166  
Materials technology assessment for a 1050 K Stirling space engine design [NASA-TM-101342] p 77 N89-11815  
Slurry-pressing consolidation of silicon nitride [NASA-TM-101365] p 109 N89-12746
- KITAMURA, TAKAYUKI**  
Creep life prediction based on stochastic model of microstructurally short crack growth p 193 A89-36185  
Stochastic modeling of crack initiation and short-crack growth under creep and creep-fatigue conditions [NASA-TM-101358] p 199 N89-17286
- KITTUR, MADAN G.**  
Finite-element grid improvement by minimization of stiffness matrix trace p 194 A89-42339  
Improvement in finite element meshes: Heat transfer in an infinite cylinder [NASA-TM-101410] p 182 N89-14450
- KLANN, GARY A.**  
Contingency power for small turboshaft engines p 21 A89-22291
- KLIMA, STANLEY J.**  
Nondestructive evaluation of advanced ceramics [NASA-TM-101489] p 189 N89-20490
- KLINEBERG, JOHN M.**  
Advances in computational design and analysis of airbreathing propulsion systems [NASA-TM-101987] p 32 N89-23465
- KNIP, GERALD, JR.**  
Advanced core technology: Key to subsonic propulsion benefits [NASA-TM-101420] p 26 N89-14237
- KNOWLES, STEVEN C.**  
Electromagnetic emission experiences using electric propulsion systems p 61 A89-53354
- KO, SEN-HOU**  
Crystallization of BaF<sub>2</sub>-ZnF<sub>2</sub>-YbF<sub>3</sub>-ThF<sub>4</sub> glass p 230 A89-12236
- KOESTER, GARY E.**  
Description of an oscillating flow pressure drop test rig p 142 A89-15188
- KOGAN, V. G.**  
Experimental evidence for a transverse magnetization of the Abrikosov lattice in anisotropic superconductors p 234 A89-21473
- KOHL, F. J.**  
Deposition of Na<sub>2</sub>SO<sub>4</sub> from salt-seeded combustion gases of a high velocity burner rig p 89 A89-12330
- KOHOUT, LISA L.**  
Cryogenic reactant storage for lunar base regenerative fuel cells [NASA-TM-101980] p 210 N89-21419
- KOLB, EDWARD W.**  
Limits to the radiative decays of neutrinos and axions from gamma-ray observations of SN 1987A p 242 A89-26985  
A coasting cosmology p 241 A89-53833
- KOLECKI, JOSEPH C.**  
Summary of the Second International Conference on Tethers in Space Venice, Italy, October 4-8, 1987 [AIAA PAPER 89-1547] p 37 A89-40177
- KOLLMANN, W.**  
Pdf - Transport equations for chemically reacting flows p 152 A89-51880
- KONKEL, C. R.**  
User needs, benefits and integration of robotic systems in a space station laboratory [NASA-CR-182261] p 185 N89-22108
- KOPP, M. W.**  
Interdiffusional effects between TiBe<sub>12</sub> and NiAl intermetallics p 95 A89-21395  
Reaction kinetics between fiber and matrix p 83 A89-36420
- KORKAN, K. D.**  
On ice shape prediction methodologies and comparison with experimental data [AIAA PAPER 89-0732] p 16 A89-30650  
Determination of near and far field acoustics for advanced propeller configurations [AIAA PAPER 89-1040] p 226 A89-40469
- KORKAN, KENNETH D.**  
An acoustic experimental and theoretical investigation of single disc propellers [AIAA PAPER 89-1146] p 227 A89-40478  
Generic icing effects on forward flight performance of a model helicopter rotor p 18 A89-41093
- KORPELA, SEPPO A.**  
The secondary flow and its stability for natural convection in a tall vertical enclosure p 149 A89-37931
- KOSTERMAN, J.**  
Stratified charge rotary engine - Internal flow studies at the MSU engine research laboratory [SAE PAPER 890331] p 181 A89-51477
- KRAFT, G.**  
Flight hardware and tele-operations supporting the Isothermal Dendritic Growth Experiment aboard the Space Shuttle [AIAA PAPER 89-0863] p 118 A89-25627
- KRAINER, ANDREAS**  
A numerical method for computing unsteady 2-D boundary layer flows [NASA-CR-4198] p 155 N89-12835
- KRASOWSKI, M. J.**  
Compensation for effects of ambient temperature on rare-earth doped fiber optic thermometer [NASA-TM-102282] p 176 N89-27998
- KRAUSE, P. C.**  
Simulation and control of a 20 kHz spacecraft power system p 130 A89-15391
- KRAWCZONEK, W.**  
Submicron nickel-oxide-gold tunnel diode detectors for rectennas p 133 A89-43469
- KREIDLER, ERIC R.**  
Reactions of silicon-based ceramics in mixed oxidation chlorination environments p 105 A89-21442  
The behavior of SiC and Si<sub>3</sub>N<sub>4</sub> ceramics in mixed oxidation/chlorination environments p 106 A89-33616
- KREJSA, EUGENE A.**  
Supersonic jet noise and the high speed civil transport [AIAA PAPER 89-2358] p 227 A89-46772
- KREN, LAWRENCE A.**  
Isotopic study of oxygen diffusion in oxide coatings [NASA-TM-102082] p 78 N89-24451
- KRIEGSMANN, GREGORY A.**  
An application of the WKB technique to the on-surface radiation condition p 124 A89-21222  
Theory and application of radiation boundary operators p 224 A89-24191
- KROEGER, E. W.**  
COLD-SAT: A technology satellite for cryogenic experimentation [NASA-TM-102286] p 47 N89-26036
- KROPP, J. L.**  
Droplet combustion drop tower tests using models of the space flight apparatus [AIAA PAPER 89-0501] p 119 A89-28418
- KRUPAR, MARTIN J.**  
Laser velocimeter measurements of the flowfield generated by an advanced counterrotating propeller [AIAA PAPER 89-0434] p 3 A89-26373  
Laser velocimeter measurements of the flowfield generated by an advanced counterrotating propeller [NASA-TM-101437] p 10 N89-13409
- KSIENSKI, AHARON A.**  
An experimental adaptive array to suppress weak interfering signals p 124 A89-22455
- KUCUK, SENOL**  
Computer simulation of a pilot in V/STOL aircraft control loops [NASA-CR-184815] p 215 N89-21479
- KUCZMARSKI, M. A.**  
Convection and chemistry effects in CVD: A 3-D analysis for silicon deposition [NASA-TM-102001] p 78 N89-21032
- KUMAR, GANESH N.**  
A generalized one dimensional computer code for turbomachinery cooling passage flow calculations [AIAA PAPER 89-2574] p 151 A89-46934  
Development of a thermal and structural analysis procedure for cooled radial turbines [NASA-TM-101416] p 24 N89-12568  
A generalized one-dimensional computer code for turbomachinery cooling passage flow calculations [NASA-TM-102079] p 163 N89-22862
- KUMAR, K. S.**  
1200 to 1400 K slow strain rate compressive behavior of small grain size NiAl/Ni<sub>2</sub>AlTi alloys and NiAl/Ni<sub>2</sub>AlTi-TiB<sub>2</sub> composites p 99 A89-53497
- KUNATH, RICHARD R.**  
Optically controlled phased-array technology for space communication systems p 131 A89-15845  
Optically interconnected phased arrays p 132 A89-33696
- KUNTZ, H. L.**  
Interior noise in the untreated Gulfstream II Propfan Test Assessment (PTA) aircraft [AIAA PAPER 89-1119] p 17 A89-33754
- KURATH, PETER**  
High pressure multiaxial extensometry p 170 A89-43532
- KURTH, W. S.**  
Electron velocity distributions and plasma waves associated with the injection of an electron beam into the ionosphere p 215 A89-43698  
Plasma density fluctuations observed during Space Shuttle Orbiter water releases p 233 A89-54759
- KUSANO, EIJI**  
Effects of microstructure and nonstoichiometry on electrical properties of vanadium dioxide films p 236 A89-44527
- KUSHNER, MARK J.**  
Townsend coefficients for electron scattering over dielectric surfaces p 231 A89-16409
- KUSSMAUL, MICHAEL**  
The emittance of space radiator materials measured at elevated temperatures [NASA-TM-101948] p 66 N89-20193
- KYR, DOUG**  
A parametric LQ approach to multiobjective control system design p 219 A89-28605
- KYR, DOUGLAS E.**  
A parametric LQ approach to multiobjective control system design [NASA-TM-101316] p 220 N89-12283

## L

- LABUS, THOMAS L.**  
Solar dynamic power for Space Station Freedom [IAF PAPER ICOSP89-4.1] p 55 A89-46517  
Solar dynamic power for space station freedom [NASA-TM-102016] p 67 N89-23516  
Solar dynamic power module design [NASA-TM-102055] p 70 N89-25269
- LACKNEY, JOSEPH**  
Three-dimensional inelastic analysis methods for hot section components p 199 N89-17321
- LACY, D. E.**  
Advanced solar receivers for space power p 54 A89-29116
- LACY, DOVIE**  
An experimental analysis of a doped lithium fluoride direct absorption solar receiver p 49 A89-15245
- LACY, DOVIE E.**  
Advanced space solar dynamic receivers p 52 A89-15343  
Advanced sensible heat solar receiver for space power p 52 A89-15415
- LAFLEN, J. H.**  
Elevated temperature crack growth p 196 N89-12915  
Constitutive modeling for isotropic materials [NASA-CR-174805] p 26 N89-13436  
Elevated temperature crack growth p 200 N89-17335
- LAGOW, RICHARD J.**  
The preparation of new perfluoro ether fluids exhibiting excellent thermal-oxidative stabilities p 76 A89-12760
- LAI, H.**  
Comparison of 3D computation and experiment for non-axisymmetric nozzles [AIAA PAPER 89-0007] p 22 A89-28403  
Comparison of 3D computation and experiment for non-axisymmetric nozzles [NASA-CR-182245] p 14 N89-20921

## LAM, PETER T.

- LAM, PETER T.**  
Compensation of reflector antenna surface distortion using an array feed p 126 A89-53136
- LAMBERT, K. M.**  
Calculation of the effects of ice on the backscatter of a ground plane [NASA-CR-183303] p 126 N89-10213
- LAMBERT, KEVIN M.**  
Computed performance of the half-scale accurate antenna reflector [NASA-CR-182284] p 139 N89-24532
- LANDGREBE, ANTON J.**  
An analysis for high speed propeller-nacelle aerodynamic performance prediction. Volume 1: Theory and application [NASA-CR-4199-VOL-1] p 12 N89-15896  
An analysis for high speed propeller-nacelle aerodynamic performance prediction. Volume 2: User's manual [NASA-CR-4199-VOL-2] p 12 N89-15897
- LANDIS, G. A.**  
A V-grooved GaAs solar cell [NASA-TM-101970] p 211 N89-22177
- LANDIS, GEOFFREY A.**  
A new Space Station power system p 53 A89-20016  
Advances in thin-film solar cells for lightweight space photovoltaic power [IAF PAPER ICOSP89-1-8] p 55 A89-46513  
Deposition and characterization of ZnS/Si heterojunctions produced by vacuum evaporation [NASA-TM-101359] p 135 N89-11129  
Ultra-thin, light-trapping silicon solar cells p 213 N89-24719  
Chemical etching and organometallic chemical vapor deposition on varied geometries of GaAs p 213 N89-24728  
Advances in thin-film solar cells for lightweight space photovoltaic power [NASA-TM-102017] p 73 N89-26041  
The GaAs solar cells with V-grooved emitters [NASA-TM-102104] p 214 N89-26291  
Solar power for the lunar night [NASA-TM-102127] p 242 N89-26799  
Satellite relocation by tether deployment [NASA-TM-101992] p 42 N89-26877  
Lunar production of solar cells [NASA-TM-102102] p 242 N89-27619
- LANGENFELD, C. A.**  
Experimental study of isothermal swirling flows in a dump combustor p 21 A89-23182
- LANT, CHRISTIAN T.**  
High temperature optical strain measurement system p 170 A89-43842
- LANTIERI, V.**  
Two-dimensional high temperature optical strain measurement system, phase 2 [NASA-CR-185116] p 176 N89-26218
- LANTERI, V.**  
On the orthorhombic phase in ZrO<sub>2</sub>-based alloys p 105 A89-30631
- LAPOINTE, MICHAEL R.**  
Antiproton powered propulsion with magnetically confined plasma engines [AIAA PAPER 89-2334] p 57 A89-46758  
Antiproton powered propulsion with magnetically confined plasma engines [NASA-CR-185131] p 74 N89-27700
- LAU, STEPHEN**  
Dynamics of face and annular seals with two-phase flow [NASA-CR-183352] p 182 N89-12870
- LAUER, JAMES L.**  
Development and applications of optical interferometric micrometrology in the Angstrom and subangstrom range p 170 A89-27663
- LAUFENBERG, THEODORE L.**  
Improving the fatigue resistance of adhesive joints in laminated wood structures [NASA-CR-182165] p 85 N89-12675
- LAVERY, JOHN E.**  
Nonoscillatory solution of the steady-state inviscid Burgers' equation by mathematical programming p 221 A89-22756  
Calculation of shocked flows by mathematical programming p 150 A89-45397
- LAW, P. H.**  
A hybrid asymptotic-modal analysis of the EM scattering by an open-ended S-shaped rectangular waveguide cavity [NASA-CR-185053] p 129 N89-24519
- LAWLESS, JOHN L.**  
A heat-driven monochromatic light source p 224 A89-41722
- LAWRENCE, C.**  
Robots for manipulation in a micro-gravity environment p 215 A89-11682

- Identification of structural interface characteristics using component mode synthesis p 193 A89-36177
- LAWRENCE, CHARLES**  
Characterization of structural connections using free and forced response test data [NASA-TM-101991] p 202 N89-21266
- LAWRENCE, M.**  
Kuhn-Tucker optimization based reliability analysis for probabilistic finite elements p 187 A89-25852
- LAXMANAN, V.**  
Bulk undercooling, nucleation, and macrosegregation of Pb-Sn alloys p 117 A89-17106  
Gravitational macrosegregation in unidirectionally solidified lead-tin alloy p 117 A89-17112  
Macrosegregation in undercooled Pb-Sn eutectic alloys p 95 A89-19621  
Isothermal solidification in a binary alloy melt p 121 N89-20300
- LE, M. T.**  
Effects of operating parameters on PAFC stack performance p 207 A89-15250
- LEAF, WILLIAM**  
Connection between energy relations of solids and molecules p 91 A89-26406
- LEE, ALEX K. H.**  
Aerodynamic interaction between propellers and wings p 8 A89-50062
- LEE, C.**  
High speed balancing applied to the T700 engine [NASA-CR-180899] p 184 N89-20472
- LEE, C. M.**  
Strain measurements in a rotary engine housing [SAE PAPER 890333] p 181 A89-51493
- LEE, CHESTER C.**  
Advanced helium purge seals for Liquid Oxygen (LOX) turbopumps [NASA-CR-182105] p 184 N89-21239
- LEE, CHI M.**  
Regressed relations for forced convection heat transfer in a direct injection stratified charge rotary engine [SAE PAPER 880626] p 178 A89-12308
- LEE, H.-T.**  
Transmission errors and bearing contact of spur, helical and spiral bevel gears [SAE PAPER 881294] p 179 A89-21000
- LEE, R.-R.**  
On the orthorhombic phase in ZrO<sub>2</sub>-based alloys p 105 A89-30631
- LEE, S. S.**  
Multiple coherent mode interaction in a developing round jet [AIAA PAPER 89-0967] p 147 A89-30483
- LEE, S. W.**  
Ray-tube integration in shooting and bouncing ray method p 124 A89-15152  
A method for producing a shaped contour radiation pattern using a single shaped reflector and a single feed [NASA-TM-101369] p 126 N89-10215  
A comparison of reflector antenna designs for wide-angle scanning [NASA-TM-101459] p 127 N89-21138  
A segmented mirror antenna for radiometers [NASA-TM-102045] p 128 N89-23753
- LEE, SHUNG-WU**  
Shooting and bouncing rays - Calculating the RCS of an arbitrarily shaped cavity p 124 A89-34242  
High-frequency RCS of open cavities with rectangular and circular cross sections p 125 A89-39595  
A method for producing a shaped contour radiation pattern using a single shaped reflector and a single feed p 125 A89-42758  
Compensation of reflector antenna surface distortion using an array feed p 126 A89-53136
- LEE, W. E.**  
Crystallization and characterization of Y<sub>2</sub>O<sub>3</sub>-SiO<sub>2</sub> glasses p 80 A89-19486  
Microstructural evolution on crystallizing the glassy phase in a 6 weight percent Y<sub>2</sub>O<sub>3</sub>-Si<sub>3</sub>N<sub>4</sub> ceramic p 80 A89-19487
- LEE, YOUNG S.**  
Intersatellite link application to commercial communications satellites p 43 A89-39144
- LEI, J. F.**  
Elevated temperature strain gages p 173 N89-12886
- LEIB, S. J.**  
Nonlinear interaction between the sinuous and varicose instability modes in a plane wake p 147 A89-33779
- LEISSLER, GEORGE W.**  
T55-L-712 turbine engine compressor housing refurbishment-plasma spray project [NASA-TM-101310] p 100 N89-10156
- LEKAN, JACK**  
Microgravity research in NASA ground-based facilities [AIAA PAPER 89-0236] p 118 A89-25201

- Microgravity research in NASA ground-based facilities [NASA-TM-101397] p 240 N89-15047
- LEMKEY, F. D.**  
Iron-base superalloys - A phase analysis of the multicomponent system (Fe-Mn-Cr-Mo-Nb-Al-Si-C) p 95 A89-17379
- LENART, J.**  
Optoelectronic techniques for broadband switching p 131 A89-15825
- LENART, JOE**  
Study of optoelectronic switch for satellite-switched time-division multiple access [NASA-CR-179630] p 135 N89-13706
- LEONARD, B. P.**  
Simple high-accuracy resolution program for convective modelling of discontinuities p 143 A89-17459  
Universal limiter for high order explicit conservative advection schemes p 151 A89-45398  
Universal limiter for transient interpolation modeling of the advective transport equations: The ULTIMATE conservative difference scheme [NASA-TM-100916] p 222 N89-14794
- LEONARD, REGIS F.**  
GaAs MMIC elements in phased-array antennas p 131 A89-15827
- LEONIDA, A.**  
Hydrogen-oxygen proton-exchange membrane fuel cells and electrolyzers p 211 N89-22996
- LEPICOVSKY, J.**  
Effects of nozzle exit boundary-layer conditions on excitability of heated free jets p 149 A89-36908
- LERCH, BRADLEY A.**  
Optimum interface properties for metal matrix composites [NASA-TM-102295] p 205 N89-27223
- LEVY, R.**  
Bipolar coordinates for computation of transition duct flows p 148 A89-34912
- LEWICKI, D. G.**  
Transmission overhaul and replacement predictions using Weibull and renewal theory [AIAA PAPER 89-2919] p 180 A89-47173  
Computerized life and reliability modeling for turboprop transmissions p 181 A89-53364  
Tooth contact shift in loaded spiral bevel gears o, IL, 25-27 Apr. 1989; sponsored by ASME [NASA-TM-101438] p 183 N89-14453  
Transmission overhaul and replacement predictions using Weibull and renewal theory [NASA-TM-102022] p 186 N89-22925
- LEWICKI, DAVID G.**  
Effect of advanced component technology on helicopter transmissions [NASA-TM-101431] p 182 N89-13794
- LEWIS, J. W. L.**  
Recovery of excitation intensity dependence in pulsed, focused beams - Nonsaturated case p 177 A89-17507
- LI, X.**  
High-efficiency solar cells fabricated from direct-current magnetron sputtered n-indium tin oxide onto p-InP grown by atmospheric pressure metalorganic vapor phase epitaxy p 133 A89-44518  
High-efficiency indium tin oxide/indium phosphide solar cells p 208 A89-44883
- LIANG, BAISHEN**  
Laboratory studies of binary salt CVD in combustion gas environments p 89 A89-12335  
Laboratory studies of the deposition of alkali sulfate vapors from combustion gases using a flash-evaporation technique p 89 A89-12338
- LIAO, W. L.**  
Effects of operating parameters on PAFC stack performance p 207 A89-15250
- LIEBECK, R. H.**  
Multiple Application Propfan Study (MAPS): Advanced tactical transport [NASA-CR-175003] p 28 N89-19300
- LIEBERT, CURT H.**  
Heat flux measurements [NASA-TM-101428] p 173 N89-14418
- LIGRANI, P. M.**  
Spatial resolution and downwash velocity corrections for multiple-hole pressure probes in complex flows p 171 A89-45909
- LILLINGTON, D. R.**  
High efficiency GaAs-Ge tandem solar cells grown by MOVCD p 213 N89-24721
- LIM, H. S.**  
The effect of different alkali metal hydroxides on nickel electrode life p 207 A89-15280  
KOH concentration effect on cycle life of nickel-hydrogen cells. III - Cycle life test p 207 A89-23283
- LIM, TEIK C.**  
Modal analysis of gear housing and mounts [NASA-TM-101445] p 184 N89-21244

PERSONAL AUTHOR INDEX

- LIN, CHIN-SHUN**  
Axisymmetric confined turbulent jet directed towards the liquid surface from below  
[AIAA PAPER 89-0172] p 145 A89-25148  
Numerical studies of the effects of jet-induced mixing on liquid-vapor interface condensation  
[AIAA PAPER 89-1744] p 152 A89-48958  
Axisymmetric confined turbulent jet directed towards the liquid surface from below  
[NASA-TM-101409] p 158 N89-13749  
Numerical studies of the effects of jet-induced mixing on liquid-vapor interface condensation  
[NASA-CR-182285] p 163 N89-23818
- LIN, HSIANG HSI**  
Dynamic loading of spur gears with linear or parabolic tooth profile modification  
[NASA-TM-101444] p 183 N89-15413
- LIN, N. J.**  
New results concerning the use of kinematically redundant manipulators in microgravity environments  
[AIAA PAPER 89-3562] p 215 A89-52647
- LIN, R. R.**  
Piezoelectric pushers for active vibration control of rotating machinery p 171 A89-47717
- LIN, S. S.**  
Interdiffusional effects between TiBe12 and NiAl intermetallics p 95 A89-21395
- LINDHOLM, ULRIC S.**  
Constitutive modeling for isotropic materials p 195 N89-12904
- LINDSTROM, D. R.**  
Data report for the Siple Coast (Antarctica) project  
[NASA-TM-100708] p 206 N89-10403
- LING, H.**  
Ray-tube integration in shooting and bouncing ray method p 124 A89-15152
- LING, HAO**  
Shooting and bouncing rays - Calculating the RCS of an arbitrarily shaped cavity p 124 A89-34242  
High-frequency RCS of open cavities with rectangular and circular cross sections p 125 A89-39595
- LIU, M.-F.**  
Three dimensional viscous analysis of a hypersonic inlet  
[AIAA PAPER 89-0004] p 4 A89-29924  
Three dimensional viscous analysis of a hypersonic inlet  
[NASA-TM-101474] p 13 N89-16759
- LIU, MAY-FUN**  
PNS calculations for 3-D hypersonic corner flow with two turbulence models p 1 A89-14979  
[AIAA PAPER 88-2958] p 1 A89-14979  
Three dimensional PNS solutions of hypersonic internal flows with equilibrium chemistry  
[AIAA PAPER 89-0002] p 146 A89-28401
- LIU, MENG-SING**  
Flux splitting algorithms for two-dimensional viscous flows with finite-rate chemistry  
[AIAA PAPER 89-0388] p 146 A89-28409  
Conservative treatment of boundary interfaces for overlaid grids and multi-level grid adaptations  
[AIAA PAPER 89-1980] p 5 A89-41823  
A time accurate finite volume high resolution scheme for three dimensional Navier-Stokes equations  
[AIAA PAPER 89-1994] p 6 A89-41837  
A detailed analysis of inviscid flux splitting algorithms for real gases with equilibrium or finite-rate chemistry  
p 151 A89-45424  
A Newton/upwind method and numerical study of shock wave/boundary layer interactions p 6 A89-45468  
A numerical study of ENO and TVD schemes for shock capturing  
[NASA-TM-101355] p 222 N89-11469  
Conservative treatment of boundary interfaces for overlaid grids and multi-level grid adaptations  
[NASA-TM-102080] p 15 N89-24269
- LIU, S. H.**  
Highly oriented Ti2Ba2Ca2Cu3O10 thin films by pulsed laser evaporation p 236 A89-30421  
Preparation of high T(c) Ti-Ba-Ca-Cu-O thin films by pulsed laser evaporation and Ti2O3 vapor processing p 236 A89-38608
- LIPO, THOMAS A.**  
A versatile power converter for high-frequency link systems p 131 A89-21200  
Study of the generator/motor operation of induction machines in a high frequency link space power system  
[NASA-CR-179600] p 63 N89-11809
- LITT, JONATHAN**  
An expert system for restructurable control  
[NASA-TM-101378] p 220 N89-12309
- LITT, JONATHAN S.**  
A real-time simulator of a turbofan engine  
[NASA-TM-100869] p 31 N89-20995
- LITVIN, F. L.**  
Transmission errors and bearing contact of spur, helical and spiral bevel gears  
[SAE PAPER 881294] p 179 A89-21000  
Crowned spur gears - Methods for generation and tooth contact analysis. I - Basic concepts, generation of the pinion tooth surface by a plane p 179 A89-29306  
Crowned spur gears - Methods for generation and Tooth Contact Analysis. II - Generation of the pinion tooth surface by a surface of revolution p 180 A89-37665  
Generation of a crowned pinion tooth surface by a surface of revolution p 181 N89-10282  
[NASA-TM-100260] p 181 N89-10282  
Generation of a crowned pinion tooth surface by a plane  
[NASA-TM-100259] p 181 N89-10283  
Tooth contact shift in loaded spiral bevel gears o, IL, 25-27 Apr. 1989; sponsored by ASME  
[NASA-TM-101438] p 183 N89-14453  
Topology of modified helical gears  
[NASA-TM-102134] p 187 N89-28015
- LITVIN, FAYDOR L.**  
Topology of modified helical gears and Tooth Contact Analysis (TCA) program  
[NASA-CR-4224] p 186 N89-22920
- LIU, A.**  
Thermal barrier coating life prediction model development p 109 N89-12920  
Thermal barrier coating life-prediction model development p 200 N89-17331
- LIU, H. W.**  
Morphological study of near threshold fatigue crack growth in a coarse grain aluminum alloy p 94 A89-12326  
Resolved shear stress intensity coefficient and fatigue crack growth in large crystals p 96 A89-22048  
Grain boundary oxidation and its effects on high temperature fatigue life p 101 N89-12918
- LIU, J. T. C.**  
Coherent structures in transitional and turbulent free shear flows p 147 A89-28999  
Multiple coherent mode interaction in a developing round jet  
[AIAA PAPER 89-0967] p 147 A89-30483
- LIU, JONG-SHANG**  
Unsteady Euler cascade analysis  
[AIAA PAPER 89-0322] p 3 A89-28406  
Numerical investigation of chemically reacting flows in ramjet dump combustors  
[AIAA PAPER 89-0387] p 22 A89-28408
- LIU, W. K.**  
Kuhn-Tucker optimization based reliability analysis for probabilistic finite elements p 187 A89-25852
- LIU, WING-KAM**  
Probabilistic Finite Elements (PFEM) structural dynamics and fracture mechanics p 206 N89-29803
- LIVIO, MARIO**  
Nucleosynthesis, neutrino bursts and gamma-rays from coalescing neutron stars p 241 A89-46577
- LO, YUEN TZE**  
Rigorous analysis of a circular patch antenna excited by a microstrip transmission line p 125 A89-53134
- LOCCI, I. E.**  
Analysis of microalloy precipitate reversion in steels p 94 A89-15108  
The influence of annealing in the ferrite-plus-austenite phase field on the stability of vanadium carbide precipitates p 97 A89-32803
- LOCCI, IVAN E.**  
Microstructures in rapidly solidified niobium aluminides p 95 A89-18193  
Rapid solidification research at the NASA Lewis Research Center p 95 A89-18203  
The role of rapid solidification processing in the fabrication of fiber reinforced metal matrix composites  
[NASA-TM-101450] p 85 N89-15201
- LOCK, JAMES A.**  
An improved correction algorithm for number density measurements made with the forward scattering spectrometer probe p 170 A89-44122  
A correction algorithm for particle size distribution measurements made with the forward-scattering spectrometer probe p 170 A89-44123
- LOEFFLER, IRVIN J.**  
Cruise noise of an advanced counterrotation turboprop measured from an adjacent aircraft p 20 A89-15080  
Measured far-field flight noise of a counterrotation turboprop at cruise conditions p 228 N89-15686  
[NASA-TM-101383] p 228 N89-15686
- LOEWENTHAL, STUART H.**  
Tribology: The Story of Lubrication and Wear  
[NASA-TM-101430] p 203 N89-24635
- LOFERSKI, JOSEPH J.**  
Deposition and characterization of ZnS/Si heterojunctions produced by vacuum evaporation  
[NASA-TM-101359] p 135 N89-11129
- LOGRASSO, T. A.**  
A facility for precise temperature control applications in microgravity p 48 A89-36956  
Isothermal dendritic growth: A low gravity experiment p 121 N89-20299
- LONGLEY, J. P.**  
Calculations of inlet distortion induced compressor flow field instability p 8 A89-52498
- LORENZ, GARY V.**  
RE-1000 free-piston Stirling engine sensitivity test results  
[NASA-TM-88846] p 210 N89-19737
- LORENZO, CARL F.**  
A reusable rocket engine intelligent control  
[AIAA PAPER 88-3114] p 48 A89-14981
- LOVELACE, THOMAS B.**  
Fatigue crack growth model RANDOM2 user manual. Appendix 1: Development of advanced methodologies for probabilistic constitutive relationships of material strength models  
[NASA-CR-184775-APP-1] p 201 N89-19581  
Fatigue strength reduction model: RANDOM3 and RANDOM4 user manual. Appendix 2: Development of advanced methodologies for probabilistic constitutive relationships of material strength models  
[NASA-CR-184796-APP-2] p 201 N89-19582  
Fatigue crack growth model RANDOM2 user manual, appendix 1  
[NASA-CR-184939] p 203 N89-23890  
Fatigue strength reduction model: RANDOM3 and RANDOM4 user manual, appendix 2  
[NASA-CR-184940] p 203 N89-23891
- LOVELY, R.**  
Photovoltaic module on-orbit assembly for Space Station Freedom  
[NASA-TM-102297] p 47 N89-26887
- LOVELY, RONALD G.**  
Solar dynamic power for Space Station Freedom  
[IAF PAPER ICOSP89-4-1] p 55 A89-46517  
Solar dynamic power for space station freedom  
[NASA-TM-102016] p 67 N89-23516  
Solar dynamic power module design  
[NASA-TM-102055] p 70 N89-25269
- LOW, CHARLES A., JR.**  
Successful completion of a cyclic ground test of a mercury ion Auxiliary Propulsion System p 59 A89-47450
- LOWELL, C. E.**  
Computer simulation of cyclic oxidation p 91 A89-29295
- LOWELL, CARL E.**  
Light weight polymer matrix composite material  
[NASA-CASE-LEW-14734-1] p 87 N89-23623
- LU, C. Y.**  
Strain measurements in a rotary engine housing  
[SAE PAPER 890333] p 181 A89-51493
- LU, CHENG Y.**  
Estimated performance and future potential of solar dynamic and photovoltaic power systems for selected LEO and HEO missions  
[NASA-TM-102083] p 72 N89-25280
- LU, CHENG-YI**  
Mathematical modeling of solid oxide fuel cells  
[NASA-CR-182188] p 209 N89-12122  
Assessment and comparison of 100-MW coal gasification phosphoric acid fuel cell power plants  
[NASA-CR-182189] p 209 N89-13103
- LUCK, R.**  
Observer design for compensation of network-induced delays in integrated communication and control systems p 220 A89-35044
- LUCK, ROGELIO**  
Extended observability of linear time-invariant systems under recurrent loss of output data  
[AIAA PAPER 89-3510] p 220 A89-52603  
An observer-based compensator for distributed delays in integrated control systems  
[AIAA PAPER 89-3541] p 35 A89-52628
- LUIDENS, ROGER W.**  
Aeronautical applications of high-temperature superconductors  
[AIAA PAPER 89-2142] p 23 A89-53304  
Aeronautical applications of high-temperature superconductors  
[NASA-TM-102311] p 33 N89-26008
- LYONS, V. J.**  
Optical measurements of soot and temperature profiles in premixed propane-oxygen flames p 92 A89-35008
- LYONS, VALERIE J.**  
Determination of combustion gas temperatures by infrared radiometry in sooting and nonsooting flames  
[NASA-TP-2900] p 164 N89-25409

**LYTLE, JOHN K.**

A simple algebraic grid adaptation scheme with applications to two- and three-dimensional flow problems  
[AIAA PAPER 89-1984] p 5 A89-41827

**M**

**MACAYEAL, D. R.**

Data report for the Siple Coast (Antarctica) project  
[NASA-TM-100708] p 206 N89-10403

**MACIEJEWSKI, PAUL**

Heat transfer with very high free-stream turbulence and streamwise vortices p 157 N89-12900  
Heat transfer with very high free-stream turbulence and heat transfer with streamwise vortices p 160 N89-17309

**MACINNES, J. M.**

Mesh refinement in a two-dimensional large eddy simulation of a forced shear layer  
[NASA-TM-102129] p 166 N89-26180

**MACKAY, R. A.**

Influence of precipitate morphology on intermediate temperature creep properties of a nickel-base superalloy single crystal p 96 A89-26872

**MACKAY, REBECCA A.**

Materials technology assessment for a 1050 K Stirling space engine design  
[NASA-TM-101342] p 77 N89-11815

**MACKIN, MICHAEL A.**

Laboratory process control using natural language commands from a personal computer  
[NASA-TM-101988] p 218 N89-24055

**MACRAE, G.**

Structural and thermal response of 30 cm diameter ion thruster optics  
[AIAA PAPER 89-2719] p 58 A89-47042

**MACRAE, G. S.**

Structural and thermal response of 30 cm diameter ion thruster optics  
[NASA-TM-102124] p 75 N89-27703

**MACTAGGART, R.**

GaAs circuits for monolithic optical controller p 131 A89-15828

**MADABHUSHI, R. K.**

Bipolar coordinates for computation of transition duct flows p 148 A89-34912

**MAFFEO, R. J.**

Component specific modeling p 25 N89-12907

**MAHAJAN, APARAJIT J.**

On the role of artificial viscosity in Navier-Stokes solvers  
[AIAA PAPER 89-1947] p 5 A89-41794

**MAINS, R. K.**

Microwave and millimeter-wave power generation in silicon carbide (SiC) IMPATT devices  
[NASA-CR-185050] p 139 N89-26143

**MAISEL, JAMES E.**

Identification of high performance and component technology for space electrical power systems for use beyond the year 2000  
[NASA-CR-183003] p 62 N89-11807

**MAITLAND, D. J.**

Intensity-based fibre-optic sensing system using contrast modulation of subcarrier interference pattern p 170 A89-39302

**MAJUMDAR, B. C.**

Stability of a rigid rotor supported on oil-film journal bearings under dynamic load  
[NASA-TM-102309] p 166 N89-27114

**MALIK, S. N.**

Elevated temperature crack growth p 196 N89-12915

Elevated temperature crack growth p 200 N89-17335

**MALONEY, THOMAS M.**

Mathematical modeling of solid oxide fuel cells  
[NASA-CR-182188] p 209 N89-12122

**MANDELL, M. J.**

A model of electron collecting plasma contractors  
[AIAA PAPER 89-1560] p 232 A89-40190

**MANDERSCHIED, J. M.**

Simplified cyclic structural analysis of SSME turbine blades p 63 N89-12632

**MANDERSCHIED, JANE M.**

Noninteractive macroscopic reliability model for ceramic matrix composites with orthotropic material symmetry  
[NASA-TM-101414] p 198 N89-15437

**MANI, A.**

Probabilistic Finite Elements (PFEM) structural dynamics and fracture mechanics p 206 N89-29803

**MANI, R.**

High speed turboprop aeroacoustic study (single rotation). Volume 1: Model development  
[NASA-CR-182257-VOL-1] p 229 N89-24139

**MANKBADI, REDA R.**

Effects of core turbulence on jet excitability  
[AIAA PAPER 89-0966] p 147 A89-30482

Effects of core turbulence on jet excitability  
[NASA-TM-101405] p 159 N89-14403

On the conditions for resonance interactions of instability waves in the axisymmetric jet  
[NASA-TM-101477] p 162 N89-21196

Multiwave interactions in turbulent jets  
[NASA-TM-101985] p 168 N89-29714

**MANNAN, S. K.**

Elevated temperature slow plastic deformation of NiAl/TiB2 particulate composites p 81 A89-31689

1200 to 1400 K slow strain rate compressive behavior of small grain size NiAl/Ni2AlTi alloys and NiAl/Ni2AlTi-TiB2 composites p 99 A89-53497

**MANNING, S. L.**

Thermal barrier coating life prediction model development p 200 N89-17333

**MANSON, S. S.**

Exposure time considerations in high temperature low cycle fatigue p 192 A89-29600

**MANTENIEKS, M. A.**

Performance of a 100 kW class applied field MPD thruster  
[AIAA PAPER 89-2710] p 57 A89-47035

**MANTENIEKS, MARIS A.**

Performance and lifetime assessment of MPD arc thruster technology  
[AIAA PAPER 88-3211] p 53 A89-16485

Test facility and preliminary performance of a 100 kW class MPD thruster  
[NASA-TM-102021] p 68 N89-23520

Performance of a 100 kW class applied field MPD thruster  
[NASA-TM-102312] p 74 N89-27701

**MANZELLA, D. H.**

Effect of ambient pressure on the performance of a resistojet  
Investigation of a liquid-fed water resistojet plume  
[AIAA PAPER 89-2840] p 58 A89-47117

Investigation of a liquid-fed water resistojet plume  
[NASA-TM-102310] p 75 N89-27706

**MANZELLA, DAVID H.**

The effect of electrode configuration on arcjet performance  
[AIAA PAPER 89-2722] p 58 A89-47044

**MANZO, M. A.**

Alkaline fuel cell performance investigation p 207 A89-15258

**MANZO, MICHELLE A.**

The effect of compression on Individual Pressure Vessel Nickel/Hydrogen components p 50 A89-15281

Small scale bipolar nickel-hydrogen testing p 208 A89-44005

Nickel-hydrogen capacity loss on storage p 138 N89-23007

**MARABLE, R. W.**

Design, fabrication and test of the RL10 derivative II chamber/primary nozzle  
[NASA-CR-179595] p 68 N89-23519

**MARCUS, H. L.**

Interdiffusional effects between TiBe12 and NiAl intermetallics p 95 A89-21395

**MAREK, C. JOHN**

Transition limits for water-droplet crystallization with the NASA Lewis icing nozzle p 152 A89-50071

**MARGRAF, TRACEY**

Crystallization of BaF2-ZnF2-YbF3-ThF4 glass p 230 A89-12236

**MARK, HERMAN**

The effect of the near earth micrometeoroid environment on a highly reflective mirror surface  
[AIAA PAPER 88-0026] p 40 A89-17939

**MARK, W. D.**

Effects of bearing offset and flexibility on the mesh force distribution of spiral bevel gears p 178 A89-19834

An extremum principle for computation of the zone of tooth contact and generalized transmission error of spiral bevel gears p 178 A89-19835

**MARRA, JOHN E.**

Reactions of silicon-based ceramics in mixed oxidation chlorination environments p 105 A89-21442

The behavior of SiC and Si3N4 ceramics in mixed oxidation/chlorination environments p 106 A89-33616

**MARSH, D.**

Transport critical current and magnetization measurements of melt-processed YBa2Cu3O(7-x) p 234 A89-20037

**MARSHALL, MATTHEW F.**

Evolutionary growth for Space Station Freedom electrical power system  
[NASA-TM-102339] p 76 N89-28570

**MARTIN, M.**

High speed balancing applied to the T700 engine  
[NASA-CR-180899] p 184 N89-20472

**MARTIN, R. E.**

Alkaline fuel cell performance investigation p 207 A89-15258

**MARTINELL, JOHN**

Nuclear thermal rockets - Next step to space p 55 A89-40480

**MARTINEZ, A.**

Orbit transfer rocket engine technology program. Phase 2: Advanced engine study  
[NASA-CR-179602] p 61 N89-10119

**MARTZAKLIS, KONSTANTINOS S.**

Channelized coplanar waveguide: Discontinuities, junctions, and propagation characteristics  
[NASA-TM-101483] p 137 N89-21172

**MASER, J. G.**

Parametric studies of advanced turboprops  
[NASA-TM-101389] p 197 N89-14465

**MASULANIEC, KONSTANTY C.**

A numerical simulation of the full two-dimensional electrothermal de-icer pad  
[NASA-CR-4194] p 19 N89-14235

**MASTERS, PHILIP A.**

High-pressure calorimeter chamber tests for liquid oxygen/kerosene (LOX/RP-1) rocket combustion  
[NASA-TP-2862] p 65 N89-15979

**MASTERS, ROBERT M.**

Technique for temperature compensation of eddy-current proximity probes  
[NASA-TP-2880] p 173 N89-15380

**MATA, F.**

Engineering calculations for solving the orbital allotment problem  
[NASA-CR-184607] p 217 N89-13993

**MATERNA, DAVID M.**

Design of a GaAs travelling wave Mach-Zehnder electro-optic modulator p 130 A89-10342

**MATOSSIAN, J. N.**

Model for computing volume-averaged plasma properties in electron-bombardment ion thrusters p 54 A89-28339

Mercury ion thruster technology  
[NASA-CR-174974] p 66 N89-21834

**MATTERN, DUANE**

Integrated flight/propulsion control system design based on a decentralized, hierarchical approach  
[AIAA PAPER 89-3519] p 35 A89-53301

**MATTERN, DUANE L.**

Integrated flight/propulsion control system design based on a centralized approach  
[AIAA PAPER 89-3520] p 35 A89-52611

Integrated flight/propulsion control system design based on a centralized approach  
[NASA-TM-102137] p 35 N89-26009

**MATUS, LAWRENCE G.**

Crystal growth of SiC for electronic applications p 132 A89-33625

**MAUL, WILLIAM A.**

The development of power specific redlines for SSME safety monitoring  
[AIAA PAPER 89-2413] p 61 A89-53305

The development of power specific redlines for SSME safety monitoring  
[NASA-CR-185121] p 41 N89-26027

**MAURER, GERHARD**

Morphological study of near threshold fatigue crack growth in a coarse grain aluminum alloy p 94 A89-12326

**MAYRAND, C. H.**

Multiple-Purpose Subsonic Naval Aircraft (MPSNA) Multiple Application Propfan Study (MAPS)  
[NASA-CR-175096] p 18 N89-19289

**MAYS, J. C.**

Oxide-dispersion-strengthened turbine blades. Volume 2  
[NASA-CR-179561-VOL-2] p 28 N89-18487

**MAZELSKY, R.**

Evaluation of transport conditions during physical vapor transport growth of opto-electronic crystals  
[AIAA PAPER 89-0229] p 118 A89-25197

**MCBRIDE, BONNIE J.**

Experimental verification of the thermodynamic properties for a jet-A fuel  
[NASA-TM-101475] p 117 N89-17017

**MCCAULEY, L. A.**

Unique mission options available with a megawatt-class nuclear electric propulsion system  
[NASA-TM-101220] p 65 N89-17618

**MCCLUNG, R. C.**

An approximate methods approach to probabilistic structural analysis  
[AIAA PAPER 89-1369] p 193 A89-30844

**MCCLURE, DONALD J.**

Durable thin film coatings for reflectors used in low earth orbit p 77 A89-33150

- MCCONNAUGHEY, H. V.**  
Impact of ETO propellants on the aerothermodynamic analyses of propulsion components  
[AIAA PAPER 88-3091] p 53 A89-16486
- MCDANIELS, DAVID L.**  
Tungsten fiber reinforced copper matrix composites: A review  
[NASA-TP-2924] p 88 N89-27796
- MCDANIELS, DAVID L.**  
Materials technology assessment for a 1050 K Stirling space engine design  
[NASA-TM-101342] p 77 N89-11815
- MCDONALD, H.**  
Turbine stator flow field simulations p 157 N89-12902  
Two- and three-dimensional turbine blade row flow field simulations p 161 N89-17313
- MCDONELL, V. G.**  
Evolution of particle-laden jet flows - A theoretical and experimental study p 146 A89-27693  
A numerical and experimental study of confined swirling jets  
[AIAA PAPER 89-2898] p 151 A89-47161  
A numerical and experimental study of coaxial jets p 153 A89-52500
- MCDONNELL, V. G.**  
Aerothermal modeling program, phase 2. Element C: Fuel injector-air swirl characterization p 156 N89-12892
- MCLEROY, J.**  
Hydrogen-oxygen proton-exchange membrane fuel cells and electrolyzers p 211 N89-22996
- MCGAW, M. A.**  
The NASA Lewis Research Center High Temperature Fatigue and Structures Laboratory p 194 A89-43528
- MCGAW, MICHAEL A.**  
Automation software for a materials testing laboratory p 217 N89-12917
- MCKINZIE, D. J.**  
Control of laminar separation over airfoils by acoustic excitation  
[AIAA PAPER 89-0565] p 3 A89-25454  
A natural low-frequency oscillation of the flow over an airfoil near stalling conditions p 6 A89-45437  
Control of laminar separation over airfoils by acoustic excitation  
[NASA-TM-101379] p 9 N89-12552
- MCKISSOCK, B. I.**  
Extended SP-100 reactor power systems capability p 52 A89-15392
- MCKISSOCK, BARBARA I.**  
Space nuclear reactor shields for manned and unmanned applications  
[NASA-TM-102064] p 71 N89-25272
- MCKNIGHT, R. L.**  
On 3D inelastic analysis methods for hot section components p 196 N89-12906  
Component specific modeling p 25 N89-12907  
Thermal barrier coating life prediction model p 109 N89-12921  
Thermal barrier coating life prediction model development  
[NASA-CR-180807] p 110 N89-13621
- MCLALLIN, K. L.**  
The Solar Dynamic radiator with a historical perspective p 51 A89-15340  
The solar dynamic radiator with a historical perspective  
[NASA-TM-100972] p 45 N89-10117
- MCLALLIN, KERRY L.**  
Evolutionary growth for Space Station Freedom electrical power system  
[NASA-TM-102339] p 76 N89-28570
- MCURTTRY, P. A.**  
Effects of heat release on the large-scale structure in turbulent mixing layers p 147 A89-31844  
The use of direct numerical simulation in the study of turbulent, chemically-reacting flows p 152 A89-51873
- MENELIS, MARK E.**  
A modified VAPEPS method for predicting vibroacoustic response of unreinforced mass loaded honeycomb panels  
[NASA-TM-101467] p 46 N89-16905
- MCVEY, JOHN B.**  
Application of advanced diagnostics to airblast injector flows p 160 N89-17306
- MEADOR, MARY ANN B.**  
Addition polymers from 1,4,5,8-tetrahydro-1,4,5,8-diepoxyanthracene and Bis-dienes. 2: Evidence for thermal dehydration occurring in the cure process  
[NASA-TM-101385] p 112 N89-15235
- MEADOR, MICHAEL A.**  
Addition polymers from 1,4,5,8-tetrahydro-1,4,5,8-diepoxyanthracene and Bis-dienes. 2: Evidence for thermal dehydration occurring in the cure process  
[NASA-TM-101385] p 112 N89-15235
- MEHDI, I.**  
Microwave and millimeter-wave power generation in silicon carbide (SiC) IMPATT devices  
[NASA-CR-185050] p 139 N89-26143
- MEHMED, O.**  
Analytical flutter investigation of a composite propfan model p 195 A89-48663
- MEHMED, ORAL**  
Experimental investigation of propfan aeroelastic response in off-axis flow with mistuning  
[AIAA PAPER 88-3153] p 20 A89-17941  
Aeroelastic response of metallic and composite propfan models in yawed flow  
[AIAA PAPER 88-3154] p 20 A89-17942  
Aeroelastic analysis of prop fan blades with a semiempirical dynamic stall model  
[AIAA PAPER 89-2695] p 194 A89-47025
- MEISTER, JEFFREY P.**  
Mechanics of materials model p 199 N89-17319
- MEITNER, PETER L.**  
A generalized one dimensional computer code for turbomachinery cooling passage flow calculations  
[AIAA PAPER 89-2574] p 151 A89-46934  
A generalized one-dimensional computer code for turbomachinery cooling passage flow calculations  
[NASA-TM-102079] p 163 N89-22862
- MELIS, M. E.**  
A high heat flux experiment for verification of thermostructural analysis p 148 A89-35002
- MELIS, MATTHEW E.**  
A high heat flux experiment for verification of thermostructural analysis  
[NASA-TM-100931] p 155 N89-12026
- MENON, S.**  
Shock-wave-induced mixing enhancement in scramjet combustors  
[AIAA PAPER 89-0104] p 145 A89-25091
- MERCER, CAROLYN R.**  
Speckle interferometry using fiber optic phase stepping  
[NASA-TM-102331] p 176 N89-27999
- MERKEL, KENNETH G.**  
Characterization of multilayer GaAs/AlGaAs transistor structures by variable angle spectroscopic ellipsometry p 133 A89-49998
- MERRIGAN, M.**  
Transient performance evaluation of an integrated heat pipe-thermal storage system p 49 A89-15209
- MERRILL, WALTER C.**  
A reusable rocket engine intelligent control  
[AIAA PAPER 88-3114] p 48 A89-14981  
Advanced detection, isolation, and accommodation of sensor failures - Real-time evaluation p 34 A89-16156  
Identification of Space Shuttle Main Engine dynamics p 61 A89-54068  
Sensor failure detection for jet engines  
[NASA-TM-101396] p 25 N89-13432  
Identification of space shuttle main engine dynamics  
[NASA-TM-101982] p 66 N89-20199  
A real-time simulator of a turbofan engine  
[NASA-TM-100869] p 31 N89-20995  
Neuromorphic learning of continuous-valued mappings in the presence of noise: Application to real-time adaptive control  
[NASA-TM-101999] p 221 N89-24856  
A real time microcomputer implementation of sensor failure detection for turbofan engines  
[NASA-TM-102327] p 216 N89-29032
- MERROW, JAMES E.**  
Atomic oxygen effects on materials p 78 N89-23540
- MERTE, H., JR.**  
Combined roles of buoyancy and orientation in nucleate pool boiling p 119 A89-35015
- METCALFE, R. W.**  
Effects of heat release on the large-scale structure in turbulent mixing layers p 147 A89-31844
- METZGER, D. E.**  
Heat transfer in the tip region of a rotor blade simulator p 157 N89-12898  
Heat transfer in the tip region of a rotor blade simulator p 161 N89-17312
- METZGER, F. B.**  
Results of acoustic tests of a prop-fan model p 224 A89-10112
- MEYER, DUANE E.**  
Growth of diamond by RF plasma-assisted chemical vapor deposition p 90 A89-20474  
Radio-frequency plasma chemical vapor deposition growth of diamond p 236 A89-44552
- MEYER, T. G.**  
Life prediction and constitutive models for engine hot section p 188 N89-12916  
Fatigue life prediction modeling for turbine hot section materials p 30 N89-20142
- MEYER, THOMAS G.**  
High temperature constitutive and crack initiation modeling of coated single crystal superalloys p 112 N89-17334
- MEYERS, G. J.**  
Fracture mechanics applied to elevated temperature crack growth p 195 A89-47705
- MEYN, E. H.**  
Vibration testing of impact-damaged composite laminates  
[AIAA PAPER 89-1411] p 81 A89-30883
- MEYN, ERWIN H.**  
Vibration testing of impact-damaged composite laminates  
[NASA-TM-4115] p 87 N89-25290
- MICHAL, G. M.**  
Analysis of microalloy precipitate reversion in steels p 94 A89-15108  
The influence of annealing in the ferrite-plus-austenite phase field on the stability of vanadium carbide precipitates p 97 A89-32803
- MICKLE, MARLIN H.**  
Computer simulation of a pilot in V/STOL aircraft control loops  
[NASA-CR-184815] p 215 N89-21479
- MIESKOWSKI, DIANE M.**  
Hot isostatic pressing of silicon nitride with boron nitride, boron carbide, and carbon additions p 107 A89-41744  
Strength of hot isostatically pressed and sintered reaction bonded silicon nitrides containing Y2O3  
[NASA-TM-101443] p 112 N89-15257
- MIHALOEWSKI, JAMES R.**  
Integrated flight/propulsion control study for STOVL applications  
[AIAA PAPER 89-2908] p 34 A89-47166
- MIHELIC, M. S.**  
Measurements of heat transfer distribution over the surfaces of highly loaded turbine nozzle guide vanes p 141 A89-12752
- MIHELIC, JUDITH A.**  
Undercutting of defects in thin film protective coatings on polymer surfaces exposed to atomic oxygen  
[NASA-TM-101986] p 115 N89-23691
- MIKELLIDES, PAYLOS**  
Plasma flow processes within magnetic nozzle configurations  
[AIAA PAPER 89-2711] p 57 A89-47036
- MIKELSON, DANIEL C.**  
Aircraft engines. III p 21 A89-22927
- MILES, G. A.**  
Development of an analytical model to assess fuel property effects on combustor performance p 21 A89-20949
- MILLAN, P. P., JR.**  
Oxide-dispersion-strengthened turbine blades. Volume 2  
[NASA-CR-179561-VOL-2] p 28 N89-18487
- MILLER, BRENT A.**  
A perspective on future directions in aerospace propulsion system simulation  
[NASA-TM-102038] p 31 N89-21798
- MILLER, CHRISTOPHER J.**  
Euler analysis of a swirl recovery vane design for use with an advanced single-rotation propfan  
[AIAA PAPER 88-3152] p 2 A89-17940
- MILLER, D.**  
Flight hardware and tele-operations supporting the Isothermal Dendritic Growth Experiment aboard the Space Shuttle  
[AIAA PAPER 89-0863] p 118 A89-25627
- MILLER, DEAN R.**  
Development and refinement of test bed simulations  
[NASA-TM-102335] p 75 N89-27702
- MILLER, ERIC L.**  
Description of an oscillating flow pressure drop test rig p 142 A89-15188  
On the dynamic response of pressure transmission lines in the research of helium-charged free piston Stirling engines  
[NASA-TM-102121] p 175 N89-24593
- MILLER, G. R.**  
Analysis of interface crack branching  
[NASA-CR-182273] p 202 N89-21265
- MILLER, R. A.**  
Life modeling of thermal barrier coatings for aircraft gas turbine engines p 30 N89-20143
- MILLER, ROBERT A.**  
HOST surface protection R and T overview p 109 N89-12883

## MILLER, THOMAS L.

A study on thermal barrier coatings including thermal expansion mismatch and bond coat oxidation p 109 N89-12919

The effect of oxidation on the high heat flux behavior of a thermal barrier coating p 110 N89-13646

High resolution video monitoring of coating thickness during plasma spraying p 102 N89-15218

[NASA-TM-101423]

Thermal expansion mismatch and plasticity in thermal barrier coating p 200 N89-17330

## MILLER, THOMAS L.

Icing research tunnel test of a model helicopter rotor [NASA-TM-101878] p 29 N89-19305

## MILLIGAN, WALTER W.

Constitutive behavior of single crystal PWA 1480 and directionally solidified MAR-M 246 under monotonic and cyclic loads at high and low temperature p 100 N89-12634

Deformation modeling and constitutive modeling for anisotropic superalloys [NASA-CR-4215] p 202 N89-21258

## MILLS, MARC G.

Ion optics for high power 50-cm-dia ion thrusters [AIAA PAPER 89-2717] p 58 A89-47040

Ion optics for high power 50-cm-dia ion thrusters [NASA-TM-102143] p 76 N89-28571

## MILLWATER, H. R.

An approximate methods approach to probabilistic structural analysis [AIAA PAPER 89-1369] p 193 A89-30844

An advanced probabilistic structural analysis method for implicit performance functions [AIAA PAPER 89-1371] p 193 A89-30846

## MINER, R. V.

High temperature isothermal and cyclic oxidation behavior of a single crystal Ni base superalloy p 94 A89-12625

Effects of cobalt concentration on the relative resistance to octahedral and cube slip in nickel-base superalloys p 94 A89-17115

Influence of precipitate morphology on intermediate temperature creep properties of a nickel-base superalloy single crystal p 96 A89-26872

Isothermal and 'bithermal' thermomechanical fatigue behavior of a NiCoCrAlY-coated single crystal superalloy p 177 A89-36457

The low cycle fatigue deformation response of a single-crystal superalloy at 650 C p 99 A89-52204

An investigation of environmental influence on the creep behavior of a low pressure plasma sprayed NiCoCrAlY alloy p 110 N89-13648

## MINNETYAN, L.

Structural behavior of composites with progressive fracture [AIAA PAPER 89-1271] p 192 A89-30754

## MIRANDA, F. A.

Millimeter wave transmission studies of YBa<sub>2</sub>Cu<sub>3</sub>O<sub>7-δ</sub> thin films in the 26.5 to 40.0 GHz frequency range [NASA-TM-102345] p 237 N89-30088

## MIRANDA, FELIX A.

Measurements of complex permittivity of microwave substrates in the 20 to 300 K temperature range from 26.5 to 40.0 GHz [NASA-TM-102123] p 123 N89-27038

## MIRTICH, MICHAEL J.

The effect of the near earth micrometeoroid environment on a highly reflective mirror surface [AIAA PAPER 88-0026] p 40 A89-17939

Automated data acquisition and processing for a Hohlraum reflectometer [NASA-TM-101393] p 173 N89-14416

The emittance of space radiator materials measured at elevated temperatures p 66 N89-20193

[NASA-TM-101948]

Diamondlike carbon protective coatings for optical windows [NASA-TM-102111] p 231 N89-27506

Ion beam and plasma methods of producing diamondlike carbon films [NASA-TM-102301] p 116 N89-27836

## MISRA, AJAY K.

Densities of some molten fluoride salt mixtures suitable for heat storage in space power applications p 77 A89-41444

Thermodynamic analysis of compatibility of several reinforcement materials with FeAl alloys [NASA-CR-4172] p 83 N89-10128

Thermodynamic analysis of compatibility of several reinforcement materials with beta phase NiAl alloys [NASA-CR-4171] p 84 N89-10131

Thermodynamic analysis of chemical compatibility of several reinforcement materials with niobium aluminides [NASA-CR-182260] p 86 N89-21036

Theoretical analysis of compatibility of several reinforcement materials with NiAl and FeAl matrices [NASA-CR-182291] p 86 N89-23622

## MITCHELL, C. R.

Viscous analysis of high speed flows using an upwind finite volume technique [AIAA PAPER 89-0001] p 144 A89-25001

## MITCHELL, G. H.

Multiple Application Propfan Study (MAPS): Advanced tactical transport [NASA-CR-175003] p 28 N89-19300

## MITCHELL, GLENN A.

Experimental aerodynamic performance of advanced 40 deg-swept 10-blade propeller model at Mach 0.6 to 0.85 [NASA-TM-88969] p 9 N89-10865

## MITCHELL, T. E.

Transient oxidation of single-crystal beta-NiAl p 98 A89-37899

## MIYOSHI, K.

Adhesion, friction, and wear of plasma-deposited thin silicon nitride films at temperatures to 700 C p 107 A89-48250

Adhesion, friction, and wear of plasma-deposited thin silicon nitride films at temperatures to 700 C [NASA-TM-101377] p 109 N89-11913

## MIYOSHI, KAZUHIKA

Tribological properties of structural ceramics p 107 A89-51258

Adhesion, friction and micromechanical properties of ceramics p 107 A89-54277

Deformation and fracture of single-crystal and sintered polycrystalline silicon carbide produced by cavitation p 108 A89-54985

Adhesion in ceramics and magnetic media [NASA-TM-101476] p 113 N89-19435

Design, development and applications of novel techniques for studying surface mechanical properties [NASA-TM-101959] p 113 N89-20253

## MIZUTANI, HACHIRO

Effects of lubrication on the performance of high speed spur gears [NASA-TM-101969] p 186 N89-22919

## MLADSI, S. W.

Preliminary study of creep thresholds and thermomechanical response in Haynes 188 at temperatures in the range 649 to 871 C p 200 N89-17327

## MOAT, RICHARD

Baseband processor hardware for Advanced Communication Technology Satellite (ACTS) p 43 A89-38298

## MOFFAT, ROBERT J.

Heat transfer with very high free-stream turbulence and streamwise vortices p 157 N89-12900

Heat transfer with very high free-stream turbulence and heat transfer with streamwise vortices p 160 N89-17309

## MONGIA, H.

Solution of three-dimensional flow problems using a flux-spline method [AIAA PAPER 89-0687] p 146 A89-25543

## MONGIA, H. C.

Evolution of particle-laden jet flows - A theoretical and experimental study p 146 A89-27693

A numerical and experimental study of confined swirling jets [AIAA PAPER 89-2898] p 151 A89-47161

A numerical and experimental study of coaxial jets p 153 A89-52500

Improved numerical methods for turbulent viscous flows aerothermal modeling program, phase 2 [NASA-CR-182169] p 154 N89-12010

Aerothermal modeling program, phase 2. Element B: Flow interaction experiment p 156 N89-12890

Aerothermal modeling program, phase 2. Element C: Fuel injector-air swirl characterization p 156 N89-12892

Aerothermal modeling program, phase 2, element B: Flow interaction experiment p 160 N89-17304

Assessment, development, and application of combustor aerothermal models p 30 N89-20138

## MONHEISER, JEFF M.

Experimental validation of a phenomenological model of the plasma contacting process p 232 A89-43357

## MONTAGUE, J.

Piezoelectric pushers for active vibration control of rotating machinery p 171 A89-47717

## MOOIWEER, A.

Multiple Application Propfan Study (MAPS): Advanced tactical transport [NASA-CR-175003] p 28 N89-19300

## MOON, H. K.

Heat transfer in the tip region of a rotor blade simulator p 157 N89-12898

## MOON, YOUNG J.

Interaction of an oblique shock wave with turbulent hypersonic blunt body flows [AIAA PAPER 89-0272] p 3 A89-28405

Conservative treatment of boundary interfaces for overlaid grids and multi-level grid adaptations [AIAA PAPER 89-1980] p 5 A89-41823

Conservative treatment of boundary interfaces for overlaid grids and multi-level grid adaptations [NASA-TM-102080] p 15 N89-24269

## MOORE, G. C.

Turbofan forced mixer lobe flow modeling. Part 3: Application to augment engines [NASA-CR-4147-Pt-3] p 8 N89-10025

## MOORE, JOAN G.

A prediction of 3-D viscous flow and performance of the NASA low-speed centrifugal compressor [NASA-CR-184765] p 160 N89-16132

## MOORE, JOHN

A prediction of 3-D viscous flow and performance of the NASA low-speed centrifugal compressor [NASA-CR-184765] p 160 N89-16132

## MOORE, R. D.

Supersonic throughflow fans p 27 N89-16837

## MOORE, THOMAS G.

An application of the WKB technique to the on-surface radiation condition p 124 A89-21222

Theory and application of radiation boundary operators p 224 A89-24191

## MOORE, THOMAS J.

Failure analysis of a Stirling engine heat pipe [NASA-TM-101418] p 103 N89-20227

## MOORHEAD, PAUL E.

High temperature stress-strain analysis p 196 N89-12913

Structural response of an advanced combustor liner: Test and analysis p 200 N89-17329

## MORALES, WILFREDO

Degradation and crosslinking of perfluoroalkyl polyethers under X-ray irradiation in ultrahigh vacuum [NASA-TP-2910] p 114 N89-21103

Reaction of perfluoroalkylpolyethers (PFPE) with 440C steel in vacuum under sliding conditions at room temperature [NASA-TP-2883] p 115 N89-26091

## MOREL, THOMAS

Methods for heat transfer and temperature field analysis of the insulated diesel, phase 3 [NASA-CR-182237] p 239 N89-23382

## MOREY, DENNIS

Space reactor assessment and validation study p 230 N89-13227

## MORI, SHIGEYUKI

Degradation and crosslinking of perfluoroalkyl polyethers under X-ray irradiation in ultrahigh vacuum [NASA-TP-2910] p 114 N89-21103

Reaction of perfluoroalkylpolyethers (PFPE) with 440C steel in vacuum under sliding conditions at room temperature [NASA-TP-2883] p 115 N89-26091

## MORKOC, H.

Calculation of the electron wave function in a graded-channel double-heterojunction modulation-doped field-effect transistor p 134 A89-54417

## MORREN, W. EARL

Performance characterizations of an engineering model multipropellant resistojet p 54 A89-28340

## MOSES, R. L.

Analysis of modified SMI method for adaptive array weight control [NASA-CR-184904] p 127 N89-20364

## MOSTAFA, A. A.

Evolution of particle-laden jet flows - A theoretical and experimental study p 146 A89-27693

Aerothermal modeling program, phase 2. Element C: Fuel injector-air swirl characterization p 156 N89-12892

## MOUNT-CAMPBELL, C.

Engineering calculations for solving the orbital allotment problem [NASA-CR-184607] p 217 N89-13993

## MOUROU, G. A.

External electro-optic probing of millimeter-wave integrated circuits [NASA-TM-101990] p 128 N89-21142

## MUI, D. S. L.

Calculation of the electron wave function in a graded-channel double-heterojunction modulation-doped field-effect transistor p 134 A89-54417

## MUKAI, D. J.

Analysis of interface crack branching [NASA-CR-182273] p 202 N89-21265

## MULAC, RICHARD A.

Average-passage simulation of counter-rotating propfan propulsion systems as applied to cruise missiles [AIAA PAPER 89-2943] p 7 A89-47187



- Average-passage simulation of counter-rotating propfan propulsion systems as applied to cruise missiles  
[NASA-TM-102043] p 14 N89-23416
- MULARZ, E. J.**  
Assessment, development, and application of combustor aerothermal models p 30 N89-20138
- MULLER, WOLFGANG**  
Electronic structure of BaO/W cathode surfaces p 132 A89-26862
- MUNGUR, P.**  
High speed turboprop aeroacoustic study (single rotation). Volume 1: Model development  
[NASA-CR-182257-VOL-1] p 229 N89-24139
- MUNROE, PAUL**  
Room temperature tensile ductility in polycrystalline B2 Ni-30Al-20Fe p 98 A89-44568
- MUNTZ, E. P.**  
Liquid droplet generation  
[NASA-CR-182246] p 166 N89-26182
- MURMANIS, LIDIJA L.**  
Improving the fatigue resistance of adhesive joints in laminated wood structures  
[NASA-CR-182165] p 85 N89-12675
- MURPHY, G.**  
The POLAR code wake model - Comparison with in situ observations p 233 A89-45632
- MURPHY, G. B.**  
The plasma wake of the Shuttle Orbiter p 215 A89-43680
- Plasma density, temperature and turbulence in the wake of the Shuttle Orbiter p 233 A89-53209
- MURPHY, KENNETH S.**  
Evaluation of coated columbium test panels having application to a secondary nozzle extension for the RL10 rocket engine system, parts 1 and 2  
[NASA-CR-180809] p 64 N89-13493
- MURTHY, D. V.**  
Analytical flutter investigation of a composite propfan model p 195 A89-48663
- MURTHY, DURBHA V.**  
Experimental investigation of propfan aeroelastic response in off-axis flow with mistuning  
[AIAA PAPER 88-3153] p 20 A89-17941
- A computational procedure for automated flutter analysis p 191 A89-28070
- Solution and sensitivity analysis of a complex transcendental eigenproblem with pairs of real eigenvalues  
[NASA-CR-182241] p 197 N89-13819
- MURTHY, P. L. N.**  
Finite element substructuring methods for composite mechanics p 80 A89-26291
- Structural behavior of composites with progressive fracture  
[AIAA PAPER 89-1271] p 192 A89-30754
- A probabilistic approach to composite micromechanics  
[NASA-TM-101366] p 85 N89-12684
- Fracture toughness computational simulation of general delaminations in fiber composites  
[NASA-TM-101415] p 85 N89-13521
- Simplified procedures for designing adhesively bonded composite joints  
[NASA-TM-102120] p 87 N89-26048
- Metal matrix composite micromechanics: In-situ behavior influence on composite properties  
[NASA-TM-102302] p 88 N89-26924
- Computational simulation of high temperature metal matrix composites cyclic behavior  
[NASA-TM-102115] p 88 N89-27795
- MURTHY, PAPPU L. N.**  
Composite interlaminar fracture toughness - Three-dimensional finite-element modeling for mixed mode I, II, and fracture p 190 A89-16278
- Free-edge delamination - Laminate width and loading conditions effects p 193 A89-36294
- Design procedures for fiber composite box beams p 195 A89-48674
- MURTHY, POPPU L. N.**  
Fiber composite sandwich thermostructural behavior - Computational simulation p 190 A89-11246
- MURTHY, S. N. B.**  
Effect of heavy rain on aviation engines  
[AIAA PAPER 89-0799] p 22 A89-28462
- Aerothermal modeling program, phase 2. Element B: Flow interaction experiment p 156 N89-12891
- Analysis of supersonic plug nozzle flowfield and heat transfer  
[NASA-CR-179554] p 10 N89-13397
- Aerothermal modeling program, Phase 2, element B: Flow interaction experiment p 160 N89-17304
- MYERS, IRA T.**  
The application of high temperature superconductors to space electrical power distribution components p 50 A89-15287

- MYERS, R. M.**  
Performance of a 100 kW class applied field MPD thruster  
[AIAA PAPER 89-2710] p 57 A89-47035
- Plume characteristics of MPD thrusters - A preliminary examination  
[AIAA PAPER 89-2832] p 39 A89-47113
- MYERS, ROGER M.**  
Performance of a 100 kW class applied field MPD thruster  
[NASA-TM-102312] p 74 N89-27701
- Plume characteristics of MPD thrusters: A preliminary examination  
[NASA-CR-185130] p 76 N89-29483

## N

- NAGARAJAN, R.**  
Transport-induced shifts in condensate dew-point and composition in multicomponent systems with chemical reaction p 89 A89-12333
- Vapor deposition and condensate flow on combustion turbine blades - Theoretical model to predict/understand some corrosion rate consequences of molten alkali sulfate deposition in the field or laboratory p 21 A89-20950
- NAGEM, RAYMOND J.**  
Energy in elastic fiber embedded in elastic matrix containing incident SH wave  
[NASA-CR-4205] p 188 N89-18694
- NAGPAL, VINOD K.**  
Probabilistic structural analysis to quantify uncertainties associated with turbopump blades p 194 A89-36920
- NAHRA, H. K.**  
Low earth orbit environmental effects on the Space Station photovoltaic power generation systems p 55 A89-29123
- NAHRA, HENRY K.**  
Review of the environmental effects of the Space Station Freedom photovoltaic power module  
[NASA-TM-102076] p 46 N89-24418
- Effect of micrometeoroid and space debris impacts on the Space Station Freedom solar array surfaces  
[NASA-TM-102287] p 47 N89-26035
- NAKAZAWA, S.**  
An approach to probabilistic finite element analysis using a mixed-iterative formulation p 191 A89-25849
- NAKAZAWA, SHOHEI**  
MHOST version 4.2. Volume 1: Users' manual  
[NASA-CR-182235-VOL-1] p 217 N89-13996
- NALETTE, T.**  
Hydrogen-oxygen proton-exchange membrane fuel cells and electrolyzers p 211 N89-22996
- NALLASAMY, M.**  
High-speed propeller performance and noise predictions at takeoff/landing conditions p 226 A89-39195
- Prediction of unsteady blade surface pressures on an advanced propeller at an angle of attack  
[AIAA PAPER 89-1060] p 227 A89-40473
- Large scale advanced propeller blade pressure distributions - Prediction and data  
[AIAA PAPER 89-2696] p 7 A89-47026
- NAMKOONG, DAVID**  
Flight experiment of thermal energy storage  
[NASA-TM-102081] p 69 N89-24440
- NANDAPURKAR, P.**  
Heat of mixing and morphological stability p 143 A89-21296
- Enthalpies of a binary alloy during solidification p 96 A89-22559
- Thermosolutal convection during dendritic solidification  
[AIAA PAPER 89-0626] p 118 A89-25495
- NARAGHI, M. H. N.**  
Radiative heat transfer in rocket thrust chambers and nozzles  
[AIAA PAPER 89-1720] p 150 A89-43235
- Radiative transfer in rectangular enclosures - A discretized exchange factor solution p 153 A89-53262
- Three dimensional thermal analysis of rocket thrust chambers  
[NASA-TM-101973] p 66 N89-21025
- NARAYANAN, G. V.**  
Aeroelastic response of metallic and composite propfan models in yawed flow  
[AIAA PAPER 88-3154] p 20 A89-17942
- Analytical flutter investigation of a composite propfan model p 195 A89-48663
- NATHAL, M. V.**  
Influence of precipitate morphology on intermediate temperature creep properties of a nickel-base superalloy single crystal p 96 A89-26872
- NATHAL, MICHAEL V.**  
Status and prognosis for alternative engine materials p 97 A89-36419

- NAUJOKAS, GERALD J.**  
A program for advancing the technology of space concentrators  
[NASA-TM-102139] p 76 N89-29484
- NAZIHI-ANOUS, N.**  
Aerodynamically-driven condensate layer thickness distributions on isothermal cylindrical surfaces p 140 A89-12337
- NEALY, D. A.**  
Measurements of heat transfer distribution over the surfaces of highly loaded turbine nozzle guide vanes p 141 A89-12752
- NELSON, A. J.**  
Growth of diamond by RF plasma-assisted chemical vapor deposition p 90 A89-20474
- NELSON, C.**  
An entrance region friction factor model applied to annular seal analysis - Theory versus experiment for smooth and honeycomb seals  
[ASME PAPER 88-TRIB-41] p 179 A89-34798
- NELSON, E.**  
Comparison of 3D computation and experiment for non-axisymmetric nozzles  
[AIAA PAPER 89-0007] p 22 A89-28403
- Comparison of 3D computation and experiment for non-axisymmetric nozzles  
[NASA-CR-182245] p 14 N89-20921
- NELSON, R. S.**  
Fatigue life prediction modeling for turbine hot section materials p 30 N89-20142
- NELSON, RICHARD S.**  
Creep fatigue life prediction for engine hot section materials (isotropic): Fourth year progress review p 188 N89-12914
- Creep fatigue life prediction for engine hot section materials (ISOTROPIC) fifth year progress review p 201 N89-17336
- NELSON, ROBERT S.**  
OTVE combustor wall condition monitoring  
[NASA-CR-182275] p 73 N89-26899
- NESBITT, JAMES A.**  
Predicting minimum Al concentrations for protective scale formation on Ni-base alloys. I - Isothermal oxidation. II - Cyclic oxidation p 98 A89-40116
- NESMITH, B.**  
Nuclear reactor power as applied to a space-based radar mission  
[NASA-TM-101200] p 230 N89-14831
- NEUMANN, J.**  
Thermal barrier coating life-prediction model development  
[NASA-CR-175002] p 26 N89-13433
- NEUMANN, J. F.**  
Thermal barrier coating life prediction model development p 109 N89-12920
- Thermal barrier coating life-prediction model development p 200 N89-17331
- NEWMAN, F. A.**  
The design and development of transonic multistage compressors p 27 N89-16834
- NEWTON, F. C.**  
Multiple Application Propfan Study (MAPS): Advanced tactical transport  
[NASA-CR-175003] p 28 N89-19300
- NG, W. F.**  
Viscous analysis of high speed flows using an upwind finite volume technique  
[AIAA PAPER 89-0001] p 144 A89-25001
- Turbulence modeling in a hypersonic inlet p 8 A89-53931
- NGUYEN, HUNG LEE**  
Investigation of low NOx staged combustor concept in high-speed civil transport engines  
[AIAA PAPER 89-2942] p 23 A89-47186
- Investigation of low NOx staged combustor concept in high-speed civil transport engines p 32 N89-22606
- On the applications of algebraic grid generation methods based on transfinite interpolation  
[NASA-TM-102095] p 33 N89-26003
- NIEDRA, JANIS M.**  
Paralleling power MOSFETs in their active region: Extended range of passively forced current sharing  
[NASA-CR-180902] p 139 N89-26150
- NIEDZWIECKI, RICHARD W.**  
Investigation of low NOx staged combustor concept in high-speed civil transport engines  
[AIAA PAPER 89-2942] p 23 A89-47186
- Investigation of low NOx staged combustor concept in high-speed civil transport engines  
[NASA-TM-101977] p 32 N89-22606
- NIGHTINGALE, L.**  
Design and test of a propfan gear system p 179 A89-22290

**NIKJOOY, M.**

- On the modelling of scalar and mass transport in combustor flows p 92 A89-38658  
A numerical and experimental study of confined swirling jets [AIAA PAPER 89-2898] p 151 A89-47161  
A numerical and experimental study of coaxial jets p 153 A89-52500  
Aerothermal modeling program, phase 2. Element B: Flow interaction experiment p 156 N89-12891  
Aerothermal modeling program, phase 2, element B: Flow interaction experiment p 160 N89-17304

**NIKNAFS, H. S.**

- Universal limiter for high order explicit conservative advection schemes p 151 A89-45398

**NIRMALAN, V.**

- The effects of leading edge and downstream film cooling on turbine vane heat transfer [NASA-CR-182133] p 158 N89-13754  
Turbine airfoil film cooling p 161 N89-17315

**NISSLEY, D. M.**

- Life prediction and constitutive models for engine hot section p 188 N89-12916  
Fatigue life prediction modeling for turbine hot section materials p 30 N89-20142

**NISSLEY, DAVID M.**

- High temperature constitutive and crack initiation modeling of coated single crystal superalloys p 112 N89-17334

**NIX, W. D.**

- Mechanisms of elevated-temperature deformation in the B2 aluminides NiAl and CoAl p 94 A89-17378

**NOBLE, JACK**

- The 25 kW solar thermal Stirling hydraulic engine system: Conceptual design [NASA-CR-180889] p 239 N89-14182

**NOEBE, RONALD D.**

- The role of rapid solidification processing in the fabrication of fiber reinforced metal matrix composites [NASA-TM-101450] p 85 N89-15201

**NONAMI, KENZOU**

- Active vibration control for flexible rotor by optimal direct-output feedback control [NASA-TM-101972] p 31 N89-22605

**NORBY, W. P.**

- Isolated testing of highly maneuverable inlet concepts [NASA-CR-179544] p 26 N89-13437

**NOWAK, GREGORY**

- Thermo-oxidative stability studies of Celion 6000/PMR-15 unidirectional composites, PMR-15, and Celion 6000 fiber p 79 A89-14099

**NOWOTNY, H.**

- Iron-base superalloys - A phase analysis of the multicomponent system (Fe-Mn-Cr-Mo-Nb-Al-Si-C) p 95 A89-17379

**O**

**O'BRIEN, J. E.**

- Heat transfer in gas turbine engines and three-dimensional flows; Proceedings of the Symposium, ASME Winter Annual Meeting, Chicago, IL, Nov. 27-Dec. 2, 1988 p 148 A89-34926  
Effects of wake passing on stagnation region heat transfer p 148 A89-34928

**O'DONNELL, P. M.**

- Energy storage considerations for a robotic Mars surface sampler p 49 A89-15267

**O'MARA, T. M.**

- Determination of longitudinal aerodynamic derivatives using flight data from an icing research aircraft [AIAA PAPER 89-0754] p 34 A89-28454

**OBERLE, LAWRENCE G.**

- Comparison of the bidirectional reflectance distribution function of various surfaces p 230 A89-41530  
Laser anemometry: A status report p 177 N89-12885

**O'BRIEN, J. E.**

- Some characteristics of bypass transition in a heated boundary layer [NASA-TM-102126] p 164 N89-24577

**OEFTERING, R. C.**

- The modular combustion facility for the Space Station laboratory - A requirements and capabilities study [AIAA PAPER 89-0505] p 44 A89-28421

**OH, J. E.**

- Molecular beam epitaxial growth of high-quality InSb on InP and GaAs substrates [NASA-CR-185440] p 236 N89-26739  
Surface morphologies and electrical properties of molecular beam epitaxial InSb and InAs(x)Sb(1-x) grown on GaAs and InP substrates [NASA-CR-185439] p 237 N89-26740

**OHTANI, RYUICHI**

- Creep life prediction based on stochastic model of microstructurally short crack growth p 193 A89-36185  
Stochastic modeling of crack initiation and short-crack growth under creep and creep-fatigue conditions [NASA-TM-101358] p 199 N89-17286

**OKADA, TSUNENORI**

- Deformation and fracture of single-crystal and sintered polycrystalline silicon carbide produced by cavitation p 108 A89-54985

**OLSHAVSKY, MICHAEL A.**

- Addition of polymers from 1,4,5,8-tetrahydro-1,4,5,8-diepoxyanthracene and Bis-dienes. 2: Evidence for thermal dehydration occurring in the cure process [NASA-TM-101385] p 112 N89-15235

**OLSON, SANDRA L.**

- The effects of radiative heat loss on microgravity flame spread [AIAA PAPER 89-0504] p 91 A89-28420  
Fire safety applications for spacecraft [NASA-TM-101463] p 42 N89-24413

**OMARA, T. M.**

- Determination of longitudinal aerodynamic derivatives using flight data from an icing research aircraft [NASA-TM-101427] p 35 N89-15121

**ONEILL, MARK J.**

- Domed Fresnel lens concentrator technology for space application p 213 N89-24732

**ORAN, ELAINE S.**

- Time-dependent computational studies of flames in microgravity [NASA-CR-182298] p 122 N89-25353

**ORELL, M. K.**

- Improved high-temperature resistant matrix resins [NASA-CR-180826] p 114 N89-21105

**ORME, MELISSA**

- Liquid droplet generation [NASA-CR-182246] p 166 N89-26182

**ORTIZ, M.**

- Thermal barrier coating life prediction model development p 200 N89-17333

**ORZESKO, S.**

- Thin-film hermeticity - A quantitative analysis of diamondlike carbon using variable angle spectroscopic ellipsometry p 234 A89-13945

**OSHIDA, YOSHIKI**

- Grain boundary oxidation and its effects on high temperature fatigue life p 101 N89-12918

**OSWALD, FRED B.**

- Finite-element grid improvement by minimization of stiffness matrix trace p 194 A89-42339  
Improvement in finite element meshes: Heat transfer in an infinite cylinder [NASA-TM-101410] p 182 N89-14450  
Dynamic loading of spur gears with linear or parabolic tooth profile modification [NASA-TM-101444] p 183 N89-15413

**P**

**PADOVAN, JOE**

- Hierarchical Poly Tree computer architectures defined by computational multidisciplinary mechanics p 218 A89-50100  
Cyclic stress analysis of ceramic coated gas turbine seals p 111 N89-13662

**PAGE, R. A.**

- Inelastic deformation and dislocation structure of a nickel alloy - Effects of deformation and thermal histories p 99 A89-50313

**PAGE, RUSSELL J.**

- Preliminary design study of hydrogen and ammonia resistojets for prime and auxiliary thrusters [NASA-CR-182176] p 62 N89-10943

**PAGNI, P. J.**

- Optical measurements of soot and temperature profiles in premixed propane-oxygen flames p 92 A89-35008

**PAI, SHANTARAM S.**

- Calculation of Weibull strength parameters and Batdorf flow-density constants for volume- and surface-flaw-induced fracture in ceramics [NASA-TM-100890] p 196 N89-12930

**PALAZZOLO, A. B.**

- Piezoelectric pushers for active vibration control of rotating machinery p 171 A89-47717

**PALMQUIST, S.**

- GaAs circuits for monolithic optical controller p 131 A89-15828

**PAMIDI, P. R.**

- NASTRAN supplemental documentation for modal forced vibration analysis of aerodynamically excited turbosystems [NASA-CR-174967] p 201 N89-19583

**PANEK, MIROSLAW**

- The large-scale microwave background anisotropy in decaying particle cosmology p 240 A89-15426

**PANTHAKI, M. J.**

- Graphical postprocessing for 3-D mesh quality evaluation p 217 A89-38846

**PANTIC, D. M.**

- Adhesion, friction, and wear of plasma-deposited thin silicon nitride films at temperatures to 700 C p 107 A89-48250

- Adhesion, friction, and wear of plasma-deposited thin silicon nitride films at temperatures to 700 C [NASA-TM-101377] p 109 N89-11913

**PARANG, MASOOD**

- An experimental and analytical investigation of thermoacoustic convection heat transfer in gravity and zero-gravity environments [NASA-CR-179575] p 120 N89-11920

**PARK, A.**

- Measurement of the properties of lossy materials inside a finite conducting cylinder [NASA-CR-182500] p 126 N89-10223  
Material parameter determination from scattering measurements [NASA-CR-183312] p 126 N89-10225

**PARKES, J. E.**

- Performance of a 100 kW class applied field MPD thruster [AIAA PAPER 89-2710] p 57 A89-47035

**PARKES, JAMES E.**

- Test facility and preliminary performance of a 100 kW class MPD thruster [NASA-TM-102021] p 68 N89-23520  
Performance of a 100 kW class applied field MPD thruster [NASA-TM-102312] p 74 N89-27701

**PARKS, D. E.**

- A model of electron collecting plasma contractors [AIAA PAPER 89-1560] p 232 A89-40190

**PATAG, A. E.**

- Modeling of pulsed propellant reorientation [AIAA PAPER 89-2727] p 61 A89-53306  
Modeling of pulsed propellant reorientation [NASA-TM-102117] p 165 N89-26178

**PATAG, ALFREDO E.**

- Modeling of impulsive propellant reorientation [AIAA PAPER 89-0628] p 54 A89-25496  
Modeling of impulsive propellant reorientation [NASA-TM-101440] p 64 N89-13495

**PATANKAR, S.**

- Solution of three-dimensional flow problems using a flux-spline method [AIAA PAPER 89-0687] p 146 A89-25543

**PATANKAR, S. V.**

- A block-corrected subdomain solution procedure for recirculating flow calculations p 152 A89-50147  
Improved numerical methods for turbulent viscous flows aerothermal modeling program, phase 2 [NASA-TM-102169] p 154 N89-12010

**PATANKAR, SUHAS V.**

- Aerothermal modeling program, phase 2 p 156 N89-12890  
Efficient numerical techniques for complex fluid flows p 156 N89-12894  
Development of low Reynolds number two equation turbulence models for predicting external heat transfer on turbine blades p 157 N89-12901  
A low-Reynolds-number two-equation turbulence model for predicting heat transfer on turbine blades p 160 N89-17310

**PATERSON, R. W.**

- Turbofan forced mixer lobe flow modeling. 1: Experimental and analytical assessment [NASA-CR-4147-PT-1] p 11 N89-14221

**PATERSON, W. R.**

- Electron velocity distributions and plasma waves associated with the injection of an electron beam into the ionosphere p 215 A89-43698

**PATHAK, P. H.**

- Analysis of the EM scattering from arbitrary open-ended waveguide cavities using axial Gaussian Beam tracking [NASA-CR-185054] p 128 N89-24518  
A hybrid asymptotic-modal analysis of the EM scattering by an open-ended S-shaped rectangular waveguide cavity [NASA-CR-185053] p 129 N89-24519

**PATHAK, PRABHAKAR H.**

- Modal, ray, and beam techniques for analyzing the EM scattering by open-ended waveguide cavities p 125 A89-39594

**PATIL, M. B.**

- Calculation of the electron wave function in a graded-channel double-heterojunction modulation-doped field-effect transistor p 134 A89-54417

- PATRICK, W. P.**  
Near wakes of advanced turbopropellers  
[AIAA PAPER 89-1095] p 5 A89-33735
- PATTERSON, ALEX G.**  
Development and refinement of test bed simulations  
[NASA-TM-102335] p 75 N89-27702
- PATTERSON, ALEXANDER G.**  
Distortion and regulation characterization of a Mapham inverter  
[NASA-TM-102089] p 139 N89-26148
- PATTERSON, M. J.**  
Electric propulsion options for 10 kW class earth space missions  
[NASA-TM-102337] p 74 N89-26906
- PATTERSON, MICHAEL J.**  
Performance of 10-kW class xenon ion thrusters  
[AIAA PAPER 88-2914] p 48 A89-14978  
Ground-based plasma contactor characterization  
p 233 A89-43359  
Closed-drift thruster investigations  
[NASA-CR-179497] p 62 N89-11808
- PAULEY, WAYNE**  
Heat transfer with very high free-stream turbulence and streamwise vortices p 157 N89-12900  
Heat transfer with very high free-stream turbulence and heat transfer with streamwise vortices p 160 N89-17309
- PAULEY, WAYNE R.**  
Experimental study of the development of longitudinal vortex pairs embedded in a turbulent boundary layer p 140 A89-11107
- PAULSEN, PHILLIP E.**  
Oxidation and protection of fiberglass-epoxy composite masts for photovoltaic arrays in the low earth orbital environment p 44 A89-35316  
Evaluation of atomic oxygen resistant protective coatings for fiberglass-epoxy composites in LEO  
[NASA-TM-101955] p 114 N89-21100  
Simulation of the low earth orbital atomic oxygen interaction with materials by means of an oxygen ion beam  
[NASA-TM-101971] p 114 N89-21104
- PAYSON, J. SCOTT**  
Radiation resistance studies of amorphous silicon films p 213 N89-24738
- PEASE, D. M.**  
X-ray based extensometry  
[NASA-CR-185058] p 176 N89-25432
- PECK, TIMOTHY L.**  
Townsend coefficients for electron scattering over dielectric surfaces p 231 A89-16409
- PENKO, P. F.**  
Effect of ambient pressure on the performance of a resistojel p 55 A89-44111
- PENKO, PAUL F.**  
The effect of test-cell pressure on resistojel nozzle flow  
[AIAA PAPER 89-2838] p 58 A89-47116
- PEPPER, D. W.**  
Heat transfer in gas turbine engines and three-dimensional flows; Proceedings of the Symposium, ASME Winter Annual Meeting, Chicago, IL, Nov. 27-Dec. 2, 1988 p 148 A89-34926
- PEPPER, STEPHEN V.**  
Surface temperature determination in surface analytic systems by infrared optical pyrometry p 169 A89-17347  
Auger analysis of a fiber/matrix interface in a ceramic matrix composite p 82 A89-35311
- PEREZ-DAVIS, MARLA E.**  
The effect of compression on Individual Pressure Vessel Nickel/Hydrogen components p 50 A89-15281  
Mars manned transportation vehicle  
[NASA-TM-101487] p 210 N89-20545
- PERIDIER, VALLORIE**  
An algorithm for unsteady flows with strong convection  
[NASA-TM-100828] p 221 N89-10575
- PERINO, MARIA ANTONIETTA**  
Lunar production of solar cells  
[NASA-TM-102102] p 242 N89-27619
- PERRY, A. J.**  
Adhesion scratch testing - A round-robin experiment p 171 A89-54281
- PERRY, W. D.**  
Compatibility of molten salts with advanced solar dynamic receiver materials  
[AIAA PAPER 89-1756] p 83 A89-48957
- PETERS, CARROLL E.**  
Influence of bulk turbulence and entrance boundary layer thickness on the curved duct flow field p 156 N89-12896
- PETERS, L., JR.**  
Calculation of the effects of ice on the backscatter of a ground plane  
[NASA-CR-183303] p 126 N89-10213
- Material parameter determination from scattering measurements  
[NASA-CR-183312] p 126 N89-10225
- PETERSEN, R. A.**  
On the preferred mode of jet instability p 140 A89-11567
- Effects of excitation level on the stability of an axisymmetric mixing layer p 2 A89-16882
- PETRARCA, D. A.**  
Hardware development for the Surface Tension Driven Convection Experiment aboard the USML-1 Spacelab mission  
[AIAA PAPER 89-0406] p 47 A89-25341  
Hardware development for the surface tension driven convection experiment aboard the USML-1 spacelab mission  
[NASA-TM-101404] p 48 N89-11804
- PETRASEK, D. W.**  
The effect of Co alloying content on the kinetics of reaction zone growth in tungsten fiber reinforced superalloy composites p 79 A89-11324  
Reaction kinetics between fiber and matrix p 83 A89-36420
- PETRASEK, DONALD W.**  
Thermal-mechanical fatigue test apparatus for metal matrix composites and joint attachments p 79 A89-15727  
Materials technology assessment for a 1050 K Stirling space engine design  
[NASA-TM-101342] p 77 N89-11815  
Fiber reinforced superalloys for rocket engines  
[NASA-TM-100880] p 86 N89-15990  
Refractory metal alloys and composites for space nuclear power systems  
[NASA-TM-101364] p 102 N89-16986  
Fiber reinforced superalloys for rocket engines p 103 N89-22673
- PHAM, M.**  
Hydrogen-oxygen proton-exchange membrane fuel cells and electrolyzers p 211 N89-22996
- PHILIPP, W. H.**  
Improved synthesis of ceramic superconductors with alkaline earth peroxides - Synthesis and processing of Ba<sub>2</sub>YCu<sub>3</sub>O<sub>7-x</sub> p 235 A89-22887
- PHILLIPS, R. E.**  
Thermal effects on the mechanical properties of SiC fiber reinforced reaction bonded silicon nitride matrix (SiC/RBSN) composites p 84 N89-10134  
Laminate behavior for SiC fiber-reinforced reaction-bonded silicon nitride matrix composites  
[NASA-TM-101350] p 84 N89-10952
- PHUCHAROEN, WORAPHAT**  
A study on thermal barrier coatings including thermal expansion mismatch and bond coat oxidation p 109 N89-12919  
Thermal expansion mismatch and plasticity in thermal barrier coating p 200 N89-17330
- PIAN, THEODORE H. H.**  
A 20-DOF hybrid stress general shell element p 191 A89-21133
- PICKETT, J. S.**  
The plasma wake of the Shuttle Orbiter p 215 A89-43680  
Plasma density, temperature and turbulence in the wake of the Shuttle Orbiter p 233 A89-53209  
Plasma density fluctuations observed during Space Shuttle Orbiter water releases p 233 A89-54759
- PIERCE, VICKY G.**  
High-temperature LDV seed particle development  
[NASA-CR-182265] p 175 N89-23851
- PILSNER, B. H.**  
Thermal barrier coating life prediction model p 109 N89-12921  
Thermal barrier coating life prediction model development  
[NASA-CR-180807] p 110 N89-13621
- PILTCH, NANCY D.**  
Microgravity Combustion Diagnostics Workshop  
[NASA-CP-10017] p 120 N89-17682
- PIRAN, TSVI**  
Nucleosynthesis, neutrino bursts and gamma-rays from coalescing neutron stars p 241 A89-46577
- PIROUZ, P.**  
Transmission electron microscopy of composites p 79 A89-14560  
Indentation plasticity and fracture in silicon  
[NASA-TP-2863] p 100 N89-10996
- PISZCZOR, MICHAEL F., JR.**  
Domed Fresnel lens concentrator technology for space application p 213 N89-24732
- PISZCZOR, MICHAEL, JR.**  
NASA advanced space photovoltaic technology-status, potential and future mission applications  
[NASA-TM-102093] p 75 N89-27705
- PITARRESI, JAMES M.**  
Nonlinear analysis using temporal finite elements p 221 A89-28030
- PLA, FREDERIC G.**  
In-flight measurement of propeller noise on the fuselage of an airplane  
[NASA-TM-102285] p 229 N89-25675
- PLATTE, M. M.**  
Multiple Application Propfan Study (MAPS): Advanced tactical transport  
[NASA-CR-175003] p 28 N89-19300
- PLENCNER, ROBERT M.**  
Plotting component maps in the Navy/NASA Engine Program (NNEP): A method and its usage  
[NASA-TM-101433] p 26 N89-14239
- PLINE, A. D.**  
Hardware development for the Surface Tension Driven Convection Experiment aboard the USML-1 Spacelab mission  
[AIAA PAPER 89-0406] p 47 A89-25341  
Hardware development for the surface tension driven convection experiment aboard the USML-1 spacelab mission  
[NASA-TM-101404] p 48 N89-11804
- PLINE, ALEXANDER D.**  
Development of an infrared imaging system for the surface tension driven convection experiment  
[NASA-TM-101479] p 174 N89-17211  
Infrared surface temperature measurements for the surface tension driven convection experiment  
[NASA-TM-101353] p 175 N89-21224
- PLOGE, E.**  
User needs, benefits and integration of robotic systems in a space station laboratory  
[NASA-CR-182261] p 185 N89-22108
- PODANY, MARK**  
Study of optical output couplers for submillimeter wavelength backward-wave oscillators (BWO's) p 132 A89-32857  
Study of optical output couplers for submillimeter wavelength backward-wave oscillators (BWO's)  
[NASA-TM-101360] p 134 N89-11128
- PODBOY, GARY G.**  
Laser velocimeter measurements of the flowfield generated by an advanced counterrotating propeller  
[AIAA PAPER 89-0434] p 3 A89-26373  
Laser velocimeter measurements of the flowfield generated by an advanced counterrotating propeller  
[NASA-TM-101437] p 10 N89-13409
- POIRIER, D. R.**  
Heat of mixing and morphological stability p 143 A89-21296  
Enthalpies of a binary alloy during solidification p 96 A89-22559  
Thermosolutal convection during dendritic solidification  
[AIAA PAPER 89-0626] p 118 A89-25495  
Computer simulation of macrosegregation in directionally solidified circular ingots  
[NASA-CR-182838] p 122 N89-21134
- POLLACK, FRANK G.**  
Summary of laser speckle photogrammetry for HOST p 177 N89-12889
- POLLAK, TOM**  
An experimental analysis of a doped lithium fluoride direct absorption solar receiver p 49 A89-15245
- PONCHAK, DENISE S.**  
Intersatellite link application to commercial communications satellites p 43 A89-39144
- PONCHAK, GEORGE E.**  
Modeling of some coplanar waveguide discontinuities p 131 A89-24139  
Channelized coplanar waveguide: Discontinuities, junctions, and propagation characteristics  
[NASA-TM-101483] p 137 N89-21172  
Performance of five 30 GHz satellite receivers  
[NASA-TM-101960] p 129 N89-25365
- POPPEL, G. L.**  
Fiber optic control system integration  
[NASA-CR-179568] p 231 N89-13256
- POTAPCZUK, M.**  
Modeling of surface roughness effects on glaze ice accretion  
[AIAA PAPER 89-0734] p 16 A89-28451
- POTAPCZUK, M. G.**  
The low frequency oscillation in the flow over a NACA0012 airfoil with an iced leading edge  
[NASA-TM-102018] p 14 N89-23417
- POTAPCZUK, MARK G.**  
An overview of the current NASA program on aircraft icing research  
[SAE PAPER 881386] p 16 A89-28192  
An experimental investigation of multi-element airfoil ice accretion and resulting performance degradation  
[AIAA PAPER 89-0752] p 4 A89-28453

- An experimental investigation of multi-element airfoil ice accretion and resulting performance degradation  
[NASA-TM-101441] p 12 N89-15084
- POTAPCZUK, MARK G.**  
Predictions of airfoil aerodynamic performance degradation due to icing  
[NASA-TM-101434] p 10 N89-13412
- POUCH, J. J.**  
Characterization of GaAlAs optical waveguide heterostructures grown by molecular beam epitaxy  
p 130 A89-10343  
Structural chemistry of Au(III)-substituted Ba<sub>2</sub>YCu<sub>3</sub>O(7- $\delta$ )  
p 89 A89-12620  
Interaction of Au, Ag, and Bi ions with Ba<sub>2</sub>YCu<sub>3</sub>O(7-y)  
- Implications for superconductor applications  
p 235 A89-22886  
Improved synthesis of ceramic superconductors with alkaline earth peroxides - Synthesis and processing of Ba<sub>2</sub>YCu<sub>3</sub>O(7-x)  
p 235 A89-22887  
Adhesion, friction, and wear of plasma-deposited thin silicon nitride films at temperatures to 700 C  
p 107 A89-48250  
Adhesion, friction, and wear of plasma-deposited thin silicon nitride films at temperatures to 700 C  
[NASA-TM-101377] p 109 N89-11913
- POUCH, JOHN J.**  
Thin-film hermeticity - A quantitative analysis of diamondlike carbon using variable angle spectroscopic ellipsometry  
p 234 A89-13945  
Characterization of ZrO<sub>2</sub> buffer layers for sequentially evaporated Y-Ba-CuO on Si and Al<sub>2</sub>O<sub>3</sub> substrates  
[NASA-TM-101432] p 135 N89-13722
- POVINELLI, LOUIS A.**  
CFD validation experiments for internal flows  
p 161 N89-18635  
Advanced computational techniques for hypersonic propulsion  
[NASA-TM-102005] p 163 N89-23809  
Least-squares finite element method for fluid dynamics  
[NASA-TM-102352] p 223 N89-30008
- POWELL, J. A.**  
Raman determination of layer stresses and strains for heterostructures and its application to the cubic SiC/Si system  
p 234 A89-21871
- POWELL, J. ANTHONY**  
Crystal growth of SiC for electronic applications  
p 132 A89-33625
- POWELL, KENNETH G.**  
A genuinely multi-dimensional upwind cell-vertex scheme for the Euler equations  
[NASA-TM-102029] p 223 N89-24872
- POWER, G. D.**  
The effects of inlet turbulence and rotor/stator interactions on the aerodynamics and heat transfer of a large-scale rotating turbine model, volume 1  
[NASA-CR-4079] p 159 N89-13756
- POWER, JOHN L.**  
Successful completion of a cyclic ground test of a mercury ion Auxiliary Propulsion System  
p 59 A89-47450  
Development of a high power microwave thruster, with a magnetic nozzle, for space applications  
[NASA-TM-102321] p 74 N89-26904
- POWERS, ALBERT G.**  
COLD-SAT: An orbital cryogenic hydrogen technology experiment  
p 73 N89-26044
- POWERS, LYNN M.**  
Reliability-based failure analysis of brittle materials  
[NASA-CR-184799] p 189 N89-20489
- PRATT, TIMOTHY**  
Coded multiple chirp spread spectrum system and overlay service  
p 124 A89-26769  
Study of spread spectrum multiple access systems for satellite communications with overlay on current services: Executive summary  
[NASA-CR-180827-EXEC-SUMM] p 128 N89-23756  
Study of spread spectrum multiple access systems for satellite communications with overlay on current services  
[NASA-CR-180827] p 128 N89-23757
- PRICE, HAROLD G.**  
Liquid oxygen cooling of high pressure LOX/hydrocarbon rocket thrust chambers  
p 63 N89-12649  
High-pressure calorimeter chamber tests for liquid oxygen/kerosene (LOX/RP-1) rocket combustion  
[NASA-TP-2862] p 65 N89-15979
- PROBST, H. B.**  
Effects of crucible wetting during solidification of immiscible Pb-Zn alloys  
[AIAA PAPER 89-0304] p 118 A89-25261  
Computer simulation of cyclic oxidation  
p 91 A89-29295

- PROBST, HUBERT B.**  
Effects of crucible wetting during solidification of immiscible Pb-Zn  
[NASA-TM-101372] p 120 N89-14341
- PROCTOR, M.**  
Design and test of an oxygen turbopump for a dual expander cycle rocket engine  
[AIAA PAPER 89-2305] p 56 A89-46737
- PROCTOR, MARGARET P.**  
Leakage predictions for Rayleigh-step, helium-purge seals  
[NASA-TM-101352] p 64 N89-14255
- PROVENCHER, C.**  
A laser communication experiment utilizing the ACT satellite and an airborne laser transceiver  
p 43 A89-15811
- PRUSSING, JOHN E.**  
Optimal terminal maneuver for a cooperative impulsive rendezvous  
p 38 A89-36946
- PRYDZ, R. A.**  
Interior noise in the untreated Gulfstream II Propan Test Assessment (PTA) aircraft  
[AIAA PAPER 89-1119] p 17 A89-33754
- PRZYBYSEWSKI, JOHN S.**  
Development of a high temperature thin film static strain gage  
p 174 N89-17299
- PURVIS, C. K.**  
Overview of environmental factors  
p 240 N89-23529  
Surface phenomena in plasma environments  
p 234 N89-23555

## Q

- QUEALY, ANGELA**  
A message passing kernel for the hypercluster parallel processing test bed  
[NASA-TM-101952] p 218 N89-20684  
Initial operating capability for the hypercluster parallel-processing test bed  
[NASA-TM-101953] p 218 N89-20685
- QUENTMEYER, RICHARD J.**  
Thrust chamber thermal barrier coating techniques  
p 115 N89-22671
- QUINN, R. D.**  
Robots for manipulation in a micro-gravity environment  
p 215 A89-11682  
New results concerning the use of kinematically redundant manipulators in microgravity environments  
[AIAA PAPER 89-3562] p 215 A89-52647

## R

- RADENS, C. J.**  
Characterization of GaAlAs optical waveguide heterostructures grown by molecular beam epitaxy  
p 130 A89-10343
- RADHAKRISHNA, M. C.**  
Microlaminate composites as thermal barrier coatings  
p 83 A89-54261
- RADIL, K. C.**  
Computerized life and reliability modeling for turboprop transmissions  
p 181 A89-53364
- RAE, WILLIAM J.**  
Turbine-stage heat transfer - Comparison of short-duration measurements with state-of-the-art predictions  
p 142 A89-16458
- RAHMAT-SAMII, Y.**  
A comparison of reflector antenna designs for wide-angle scanning  
[NASA-TM-101459] p 127 N89-21138
- RAI, A. K.**  
Characterization of multilayer GaAs/AlGaAs transistor structures by variable angle spectroscopic ellipsometry  
p 133 A89-49998
- RAITANO, P.**  
Performance of a 100 kW class applied field MPD thruster  
[AIAA PAPER 89-2710] p 57 A89-47035
- RAITANO, PAUL**  
Test facility and preliminary performance of a 100 kW class MPD thruster  
[NASA-TM-102021] p 68 N89-23520  
Performance of a 100 kW class applied field MPD thruster  
[NASA-TM-102312] p 74 N89-27701
- RAITHBY, G. D.**  
Improved numerical methods for turbulent viscous recirculating flows  
p 156 N89-12895
- RAITT, W. JOHN**  
A numerical model of electrodynamics of plasma within the contaminant gas cloud of the Space Shuttle Orbiter at low earth orbit  
p 233 A89-45631

- RAJ, RISHI S.**  
An experimental study of near wall flow parameters in the blade end-wall corner region  
[NASA-CR-4211] p 12 N89-15898
- RAJAGOPAL, K. R.**  
Probabilistic structural analysis methods and applications  
p 190 A89-16939
- RAMAMURTI, R.**  
Simulation of 2-dimensional viscous flow through cascades using a semi-elliptic analysis and hybrid C-H grids  
[NASA-CR-4180] p 10 N89-12553
- RAMAN, GANESH**  
Effects of core turbulence on jet excitability  
[AIAA PAPER 89-0966] p 147 A89-30482  
Subharmonic and fundamental high amplitude excitation of an axisymmetric jet  
[AIAA PAPER 89-0993] p 149 A89-37825  
Effects of core turbulence on jet excitability  
[NASA-TM-101405] p 159 N89-14403  
On the conditions for resonance interactions of instability waves in the axisymmetric jet  
[NASA-TM-101477] p 162 N89-21196
- RAMASWAMY, V. G.**  
Constitutive modeling for isotropic materials  
[NASA-CR-174805] p 26 N89-13436
- RAMINS, PETER**  
Isotropic graphite multistage depressed collectors - A progress report  
p 132 A89-31988  
Performance of a multistage depressed collector with machined titanium electrodes  
[NASA-TP-2891] p 136 N89-15337  
Design, fabrication, and performance of brazed, graphite electrode, multistage depressed collectors with 500-W, continuous wave, 4.8- to 9.6-GHz traveling-wave tubes  
[NASA-TP-2904] p 136 N89-21171
- RAMSEY, JOHN K.**  
Influence of thickness and camber on the aeroelastic stability of supersonic throughflow fans: An engineering approach  
[NASA-TM-101949] p 15 N89-25957
- RAMSIE, R. D.**  
Alkoxysilane adsorption on metal oxide substrates  
p 92 A89-44536
- RAUAUDO, R. J.**  
Determination of longitudinal aerodynamic derivatives using flight data from an icing research aircraft  
[AIAA PAPER 89-0754] p 34 A89-28454  
Determination of longitudinal aerodynamic derivatives using flight data from an icing research aircraft  
[NASA-TM-101427] p 35 N89-15121
- RAUAUDO, RICHARD**  
In-flight measurement of propeller noise on the fuselage of an airplane  
[NASA-TM-102285] p 229 N89-25675
- RAUAUDO, RICHARD J.**  
An overview of the current NASA program on aircraft icing research  
[SAE PAPER 881386] p 16 A89-28192  
NASA's program on icing research and technology  
[NASA-TM-101989] p 1 N89-22569
- RAQUET, JOHN F.**  
Arcjet cathode phenomena  
[NASA-TM-102099] p 167 N89-27121
- RASHIDIN, NASSER**  
Numerical studies of convective heat transfer in an inclined semiannular enclosure  
[NASA-TM-102011] p 123 N89-28666
- RATAJCZAK, ANTHONY F.**  
The introduction of space technology power systems into developing countries  
[NASA-TM-102042] p 71 N89-25274
- RAWLIN, VINCENT K.**  
Performance of 10-kW class xenon ion thrusters  
[AIAA PAPER 88-2914] p 48 A89-14978  
Ion optics for high power 50-cm-dia ion thrusters  
[AIAA PAPER 89-2717] p 58 A89-47040  
Performance of large area xenon ion thrusters for orbit transfer missions  
[NASA-TM-102049] p 69 N89-24436  
Ion optics for high power 50-cm-dia ion thrusters  
[NASA-TM-102143] p 76 N89-28571
- RAY, A.**  
Observer design for compensation of network-induced delays in integrated communication and control systems  
p 220 A89-35044
- RAY, ASOK**  
Integrated communication and control systems. I - Analysis  
[ASME PAPER 88-WA/DSC-1] p 219 A89-22499  
Integrated communication and control systems. II - Design considerations  
[ASME PAPER 88-WA/DSC-2] p 219 A89-22500  
Extended observability of linear time-invariant systems under recurrent loss of output data  
[AIAA PAPER 89-3510] p 220 A89-52603

- An observer-based compensator for distributed delays in integrated control systems  
[AIAA PAPER 89-3541] p 35 A89-52628
- RAY, PRADOSH K.**  
Arc restrike in the rail accelerator p 39 A89-32065  
Arc-driven rail accelerator research  
[NASA-CR-179584] p 40 N89-13445
- RAY, R.**  
Dispersoids in rapidly solidified B2 nickel aluminides p 98 A89-43023
- REASONER, D. L.**  
The plasma wake of the Shuttle Orbiter p 215 A89-43680
- RECK, GREGORY M.**  
Aircraft engines. III p 21 A89-22927
- REDDY, D. R.**  
Three dimensional viscous analysis of a hypersonic inlet  
[AIAA PAPER 89-0004] p 4 A89-29924  
Mach 5 inlet CFD and experimental results  
[AIAA PAPER 89-2355] p 6 A89-46769  
Three dimensional viscous analysis of a hypersonic inlet  
[NASA-TM-101474] p 13 N89-16759  
Mach 5 inlet CFD and experimental results  
[NASA-TM-102317] p 33 N89-27670
- REDDY, K. T.**  
Degradation mechanisms of n-dodecane with sulfur and nitrogen dopants during thermal stressing p 116 A89-22277
- REDDY, N. N.**  
Installed propfan (SR-7L) far-field noise characteristics  
[AIAA PAPER 89-1056] p 225 A89-36216  
Lateral noise attenuation of the advanced propeller of the propfan test assessment aircraft  
[AIAA PAPER 89-1057] p 226 A89-36217
- REDDY, T. S. R.**  
Aeroelastic analysis of prop fan blades with a semiempirical dynamic stall model  
[AIAA PAPER 89-2695] p 194 A89-47025  
Numerical analysis of supersonic flow through oscillating cascade sections by using a deforming grid  
[AIAA PAPER 89-2805] p 8 A89-50810  
Analysis of an unswept propfan blade with a semiempirical dynamic stall model  
[NASA-TM-4083] p 27 N89-15112  
Numerical analysis of supersonic flow through oscillating cascade sections by using a deforming grid  
[NASA-TM-102053] p 15 N89-25119
- REED, BRIAN D.**  
Weight savings in aerospace vehicles through propellant scavenging  
[SAE PAPER 1818] p 40 A89-50814  
Advanced APS impacts on vehicle payloads  
[NASA-TM-102086] p 41 N89-25254
- REED, C. B.**  
Use of high temperature superconductors in magnetoplasmadynamic systems  
[NASA-TM-101219] p 236 N89-11553
- REED, JAMES**  
Hydrogen-bromine fuel cell advance component development  
[NASA-TM-101345] p 208 N89-10405
- REEHORST, A. L.**  
Determination of longitudinal aerodynamic derivatives using flight data from an icing research aircraft  
[AIAA PAPER 89-0754] p 34 A89-28454  
Determination of longitudinal aerodynamic derivatives using flight data from an icing research aircraft  
[NASA-TM-101427] p 35 N89-15121
- REEHORST, ANDREW L.**  
An overview of the current NASA program on aircraft icing research  
[SAE PAPER 881386] p 16 A89-28192
- REID, MARGARET A.**  
Impedance studies of Ni/Cd and Ni/H cells using the cell case as reference electrode p 137 N89-23002
- REILLY, C.**  
Engineering calculations for solving the orbital allotment problem  
[NASA-CR-184607] p 217 N89-13993
- REINMANN, JOHN J.**  
NASA's program on icing research and technology  
[NASA-TM-101989] p 1 N89-22569
- RENO, CHARLES**  
Interactive grid generation for turbomachinery flow field simulations  
[NASA-TM-101301] p 9 N89-11717
- RENZ, DAVID D.**  
Power components for the Space Station 20-kHz power distribution system p 130 A89-15387  
Multi-hundred kilowatt roll ring assembly evaluation results p 123 A89-15388
- RESHOTKO, E.**  
Some characteristics of bypass transition in a heated boundary layer  
[NASA-TM-102126] p 164 N89-24577
- RESLER, EDWIN L., JR.**  
Propulsion over a wide Mach number range  
[NASA-CR-182267] p 29 N89-20134
- RHATIGAN, JENNIFER L.**  
Numerical model of solar dynamic radiator for parametric analysis  
[NASA-TM-102054] p 67 N89-22653
- RHATT, R. T.**  
Laminate behavior for SiC fiber-reinforced reaction-bonded silicon nitride matrix composites  
[NASA-TM-101350] p 84 N89-10952
- RICE, E. J.**  
Large amplitude acoustic excitation of swirling turbulent jets  
[AIAA PAPER 89-0970] p 4 A89-29098  
Effect of initial swirl distribution on the evolution of a turbulent jet p 149 A89-36906  
Large amplitude acoustic excitation of swirling turbulent jets  
[NASA-TM-101950] p 13 N89-18417
- RICE, EDWARD J.**  
Effects of core turbulence on jet excitability  
[AIAA PAPER 89-0966] p 147 A89-30482  
Subharmonic and fundamental high amplitude excitation of an axisymmetric jet  
[AIAA PAPER 89-0993] p 149 A89-37825  
Effects of core turbulence on jet excitability  
[NASA-TM-101405] p 159 N89-14403  
On the conditions for resonance interactions of instability waves in the axisymmetric jet  
[NASA-TM-101477] p 162 N89-21196
- RICHARD, J. A.**  
User needs, benefits and integration of robotic systems in a space station laboratory  
[NASA-CR-182261] p 185 N89-22108
- RIDDLEBAUGH, S. M.**  
Development of an analytical model to assess fuel property effects on combustor performance p 21 A89-20949
- RIEKER, LORRA L.**  
Space Station Freedom electrical power system hardware commonality with the United States Polar Platform  
[NASA-TM-102074] p 69 N89-24439
- RIFF, R.**  
Nonisothermal elastoviscoplastic snap-through and creep buckling of shallow arches p 194 A89-47370  
Analysis of shell-type structures subjected to time-dependent mechanical and thermal loading  
[NASA-CR-183005] p 197 N89-14457
- RIFF, RICHARD**  
Non-isothermal buckling behavior of viscoplastic shell structures  
[NASA-CR-183013] p 197 N89-12931  
Considerations in development and implementation of elasto-viscoplastic constitutive model for high temperature applications  
[NASA-CR-183403] p 197 N89-12932
- RIGGLE, PETER**  
The 25 kW solar thermal Stirling hydraulic engine system: Conceptual design  
[NASA-CR-180889] p 239 N89-14182
- RILEY, J. J.**  
Effects of heat release on the large-scale structure in turbulent mixing layers p 147 A89-31844  
The use of direct numerical simulation in the study of turbulent, chemically-reacting flows p 152 A89-51873
- RILEY, JAMES T.**  
Analytical ice shape predictions for flight in natural icing conditions  
[NASA-CR-182234] p 18 N89-13428
- RIVER, BRYAN H.**  
Improving the fatigue resistance of adhesive joints in laminated wood structures  
[NASA-CR-182165] p 85 N89-12675
- RIVERA, JUAN C.**  
Protoflight photovoltaic power module system-level tests in the space power facility  
[NASA-TM-102066] p 46 N89-25267
- RIZK, MAGDI H.**  
Optimizing advanced propeller designs by simultaneously updating flow variables and design parameters p 5 A89-39189  
Aerodynamic optimization by simultaneously updating flow variables and design parameters with application to advanced propeller designs  
[NASA-CR-182181] p 24 N89-11750  
User's manual for an aerodynamic optimization scheme that updates flow variables and design parameters simultaneously  
[NASA-CR-182180] p 10 N89-13399
- ROBERTS, ALLEN F.**  
The introduction of space technology power systems into developing countries  
[NASA-TM-102042] p 71 N89-25274
- ROBERTS, E. P.**  
Data report for the Siple Coast (Antarctica) project  
[NASA-TM-100708] p 206 N89-10403
- ROBINSON, D. N.**  
A viscoplastic constitutive theory for metal matrix composites at high temperature p 80 A89-20725  
A multiaxial theory of viscoplasticity for isotropic materials p 196 N89-12908  
Thermomechanical characterization of Hastelloy-X under uniaxial cyclic loading p 196 N89-12909
- ROBINSON, RAYMOND S.**  
Closed-drift thruster investigations  
[NASA-CR-179497] p 62 N89-11808
- ROBINSON, W. W.**  
Further development of the dynamic gas temperature measurement system p 172 N89-12884
- ROCK, STEPHEN M.**  
Effect of model uncertainty on failure detection - The threshold selector p 219 A89-17965
- RODRIGUEZ, A.**  
The effect of Co alloying content on the kinetics of reaction zone growth in tungsten fiber reinforced superalloy composites p 79 A89-11324
- ROELKE, R. J.**  
Efficient numerical simulation of a one-dimensional electrothermal deicer pad p 144 A89-22811
- ROELKE, RICHARD J.**  
A generalized one dimensional computer code for turbomachinery cooling passage flow calculations  
[AIAA PAPER 89-2574] p 151 A89-46934  
A generalized one-dimensional computer code for turbomachinery cooling passage flow calculations  
[NASA-TM-102079] p 163 N89-22662
- ROESCH, J. F.**  
Advanced modulation technology development for earth station demodulator applications  
[NASA-CR-185126] p 43 N89-26880
- ROHN, DOUGLAS A.**  
The impact of an IVA robot on the Space Station microgravity environment  
[AIAA PAPER 89-0596] p 44 A89-28438
- ROHRER, N. J.**  
Sequentially evaporated thin Y-Ba-Co-O superconducting films on microwave substrates  
[NASA-TM-102068] p 138 N89-23791
- ROHRER, NORMAN J.**  
Sequentially evaporated thin Y-Ba-Cu-O superconductor films: Composition and processing effects  
[NASA-TM-101388] p 134 N89-10235  
Characterization of ZrO<sub>2</sub> buffer layers for sequentially evaporated Y-Ba-Cu-O on Si and Al<sub>2</sub>O<sub>3</sub> substrates  
[NASA-TM-101432] p 135 N89-13722
- ROLLBUHLER, R. JAMES**  
Gas turbine alternative fuels combustion characteristics  
[NASA-TM-101470] p 210 N89-21417
- ROMANOFISKY, R.**  
External electro-optic probing of millimeter-wave integrated circuits p 133 A89-45266
- ROMANOFISKY, ROBERT R.**  
Universal test fixture for monolithic mm-wave integrated circuits calibrated with an augmented TRD algorithm  
[NASA-TP-2875] p 127 N89-17767  
External electro-optic probing of millimeter-wave integrated circuits  
[NASA-TM-101990] p 128 N89-21142  
Analytical and experimental procedures for determining propagation characteristics of millimeter-wave gallium arsenide microstrip lines  
[NASA-TP-2899] p 136 N89-21169  
Channelized coplanar waveguide: Discontinuities, junctions, and propagation characteristics  
[NASA-TM-101483] p 137 N89-21172  
Performance of five 30 GHz satellite receivers  
[NASA-TM-101960] p 129 N89-25365
- ROSE, JAMES H.**  
Connection between energy relations of solids and molecules p 91 A89-26406  
Universal features of the equation of state of solids p 237 A89-48960
- ROSENTHAL, BRUCE N.**  
Ground-based simulation of telepresence for materials science experiments  
[AIAA PAPER 89-0597] p 119 A89-28439
- ROSNER, D. A.**  
Deposition of Na<sub>2</sub>SO<sub>4</sub> from salt-seeded combustion gases of a high velocity burner rig p 89 A89-12330
- ROSNER, D. E.**  
Rational engineering correlations of diffusional and inertial particle deposition behavior in non-isothermal forced convection environments p 140 A89-12327

- Transport-induced shifts in condensate dew-point and composition in multicomponent systems with chemical reaction p 89 A89-12333
- Optical methods and results of dew point and deposition rate measurements in salt/ash-containing combustion gases - B2O3(l) deposition rates by interference methods and comparisons with theory p 89 A89-12334
- Laboratory studies of binary salt CVD in combustion gas environments p 89 A89-12335
- Use of a generalized Stokes number to determine the aerodynamic capture efficiency of non-Stokesian particles from a compressible gas flow p 140 A89-12336
- Aerodynamically-driven condensate layer thickness distributions on isothermal cylindrical surfaces p 140 A89-12337
- Windward fraction of the total mass or heat transport for flow past a circular cylinder p 141 A89-12339
- Effect of particulate thermophoresis in reducing the fouling rate advantages of effusion-cooling p 141 A89-14599
- Viscous dissipation effects on thermophoretically augmented aerosol particle transport across laminar boundary layers p 141 A89-14600
- Boundary layer effects on particle impaction and capture p 143 A89-19123
- Mass transfer across combustion gas thermal boundary layers - Power production and materials processing implications p 143 A89-20425
- ROSNER, DANIEL E.**
- Laboratory studies of the deposition of alkali sulfate vapors from combustion gases using a flash-evaporation technique p 89 A89-12338
- Thermophoretically enhanced mass transport rates to solid and transpiration-cooled walls across turbulent (law-of-the-wall) boundary layers p 141 A89-12340
- Optical experiments on thermophoretically augmented submicron particle deposition from 'dusty' high temperature gas flows p 90 A89-14799
- Vapor deposition and condensate flow on combustion turbine blades - Theoretical model to predict/understand some corrosion rate consequences of molten alkali sulfate deposition in the field or laboratory p 21 A89-20950
- Theoretical studies in support of the 3M-vapor transport (PVTOS-) experiments [NASA-CR-185122] p 165 A89-26179
- ROSS, H.**
- Radiative structures of lycopodium-air flames in low gravity [AIAA PAPER 89-0500] p 91 A89-25406
- Particle cloud mixing in microgravity [NASA-TM-101484] p 121 A89-20321
- ROSS, H. D.**
- Behavior in normal and reduced gravity of an enclosed liquid/gas system with nonuniform heating from above [AIAA PAPER 89-0070] p 145 A89-25061
- Behavior in normal and reduced gravity of an enclosed liquid/gas system with nonuniform heating from above [NASA-TM-101471] p 120 A89-17046
- ROSS, HOWARD D.**
- Feasibility of reduced gravity experiments involving quiescent, uniform particle cloud combustion [NASA-TM-101371] p 122 A89-26114
- ROTH, DON J.**
- Ultrasonic imaging of porosity variations produced during sintering p 107 A89-48892
- Dynamic porosity variations in ceramics [NASA-TM-101340] p 112 A89-17668
- Interfacing laboratory instruments to multiuser, virtual memory computers [NASA-TM-4106] p 188 A89-19578
- Non-uniform transition conductivity of superconducting ceramic [NASA-TM-102133] p 189 A89-28851
- ROUSSEAU, A. L.**
- Development of a 75-watt 60-GHz traveling-wave tube for intersatellite communications [NASA-CR-182135] p 138 A89-24530
- ROYCE, LOLA**
- Probabilistic analysis for fatigue strength degradation of materials [NASA-CR-182844] p 198 A89-15434
- RUBINSTEIN, E. R.**
- Isothermal dendritic growth: A low gravity experiment p 121 A89-20299
- RUBINSTEIN, ROBERT**
- Probabilistic structural analysis to quantify uncertainties associated with turbopump blades p 194 A89-38920
- Structural tailoring of Space Shuttle Main Engine turbopump blades SSME/STAEBl p 55 A89-44106
- RUDNICK, STANLEY J.**
- High temperature superconducting magnetic energy storage for future NASA missions p 50 A89-15288
- RUHLE, M.**
- TEM studies of oxidized NiAl and Ni3Al cross sections p 99 A89-46506
- RUMSEY, C. L.**
- A natural low-frequency oscillation of the flow over an airfoil near stalling conditions p 6 A89-45437
- RUNCHAL, A. K.**
- Improved numerical methods for turbulent viscous flows aerothermal modeling program, phase 2 [NASA-CR-182169] p 154 A89-12010
- Aerothermal modeling program, phase 2 p 156 A89-12890
- RUPP, GEORGE D.**
- Mach 5 inlet CFD and experimental results [AIAA PAPER 89-2355] p 6 A89-46769
- Mach 5 inlet CFD and experimental results [NASA-TM-102317] p 33 A89-27670
- RUSSEL, W. B.**
- An asymptotic description of transient settling and ultrafiltration of colloidal dispersions p 144 A89-24603
- RUSSELL, J. C.**
- Fiber optic control system integration [NASA-CR-179568] p 231 A89-13256
- RUSSELL, LOUIS M.**
- Experimental determination of stator endwall heat transfer [NASA-TM-101419] p 159 A89-15366
- High-resolution liquid-crystal heat-transfer measurements on the end wall of a turbine passage with variations in Reynolds number [NASA-TM-100827] p 161 A89-18664
- RUSSELL, SID**
- Application of advanced diagnostics to airblast injector flows p 160 A89-17306
- RUTLEDGE, SHARON K.**
- Oxidation and protection of fiberglass-epoxy composite masts for photovoltaic arrays in the low earth orbital environment p 44 A89-35316
- Low earth orbital atomic oxygen simulation for materials durability evaluation p 45 A89-51123
- The NASA atomic oxygen effects test program p 93 A89-12589
- Evaluation of atomic oxygen resistant protective coatings for fiberglass-epoxy composites in LEO [NASA-TM-101955] p 114 A89-21100
- Simulation of the low earth orbital atomic oxygen interaction with materials by means of an oxygen ion beam [NASA-TM-101971] p 114 A89-21104
- Atomic oxygen effects on materials p 78 A89-23540
- Undercutting of defects in thin film protective coatings on polymer surfaces exposed to atomic oxygen [NASA-TM-101986] p 115 A89-23691
- RUYTEN, WILHELMUS M.**
- Recovery of excitation intensity dependence in pulsed, focused beams - Nonsaturated case p 177 A89-17507
- RYBICKI, GEORGE C.**
- Effect of the theta-alpha-Al2O3 transformation on the oxidation behavior of beta-NiAl+Zr p 98 A89-38600
- Indentation plasticity and fracture in silicon [NASA-TP-2863] p 100 A89-10996
- S**
- SACKSTEDER, K. R.**
- Facilities for microgravity combustion research [IAF PAPER 88-355] p 117 A89-17784
- The solid surface combustion Space Shuttle experiment hardware description and ground-based test results [AIAA PAPER 89-0503] p 119 A89-28419
- The modular combustion facility for the Space Station laboratory - A requirements and capabilities study [AIAA PAPER 89-0505] p 44 A89-28421
- The solid surface combustion space shuttle experiment hardware description and ground-based test results [NASA-TM-101963] p 123 A89-19446
- SACKSTEDER, KURT R.**
- Fire behavior and risk analysis in spacecraft [NASA-TM-100944] p 42 A89-10111
- SADLER, GERALD G.**
- Simulation test beds for the Space Station electrical power system p 39 A89-15352
- SALEEB, A. F.**
- On finite element implementation and computational techniques for constitutive modeling of high temperature composites [NASA-CR-185120] p 204 A89-26261
- SALEM, JONATHAN A.**
- Crack growth resistance of textured alumina p 105 A89-26452
- Fracture resistance of a TiB2 particle/SiC matrix composite at elevated temperature p 81 A89-31074
- Ultrasonic imaging of textured alumina [NASA-TM-101478] p 189 A89-28853
- SALIKUDDIN, M.**
- Installed propfan (SR-7L) far-field noise characteristics [AIAA PAPER 89-1056] p 225 A89-36216
- SALTSMAN, J. F.**
- Total strain version of strainrange partitioning for thermomechanical fatigue at low strains p 201 A89-17337
- SALTSMAN, JAMES F.**
- Procedures for characterizing an alloy and predicting cyclic life with the total strain version of Strainrange Partitioning [NASA-TM-4102] p 203 A89-25485
- SAMET, M. M.**
- On the preferred mode of jet instability p 140 A89-11567
- Effects of excitation level on the stability of an axisymmetric mixing layer p 2 A89-16882
- SAMIMY, M.**
- Performance of laser Doppler velocimeter with polydisperse seed particles in high-speed flows p 169 A89-22279
- Experimental study of isothermal swirling flows in a dump combustor p 21 A89-23182
- An experimental study of a reattaching supersonic shear layer [AIAA PAPER 89-1801] p 6 A89-42036
- Compressibility and shock wave interaction effects on free shear layers [AIAA PAPER 89-2460] p 7 A89-46847
- SAMUELSEN, G. S.**
- Evolution of particle-laden jet flows - A theoretical and experimental study p 146 A89-27693
- A numerical and experimental study of confined swirling jets [AIAA PAPER 89-2898] p 151 A89-47161
- A numerical and experimental study of coaxial jets p 153 A89-52500
- Aerothermal modeling program, phase 2. Element C: Fuel injector-air swirl characterization p 156 A89-12892
- SANDERS, W. A.**
- Crystallization and characterization of Y2O3-SiO2 glasses p 80 A89-19486
- Microstructural evolution on crystallizing the glassy phase in a 6 weight percent Y2O3-Si3N4 ceramic p 80 A89-19487
- SANDERS, WILLIAM A.**
- Hot isostatic pressing of silicon nitride with boron nitride, boron carbide, and carbon additions p 107 A89-41744
- A sintering model for SiC(sub)w/Si3N4 composites [NASA-TM-101336] p 108 A89-10166
- Slurry-pressing consolidation of silicon nitride [NASA-TM-101365] p 109 A89-12746
- Strength of hot isostatically pressed and sintered reaction bonded silicon nitrides containing Y2O3 [NASA-TM-101443] p 112 A89-15257
- SANKAR, L. N.**
- Evaluation of three turbulence models for the prediction of steady and unsteady airflows [AIAA PAPER 89-0609] p 3 A89-25485
- Technique for the prediction of airfoil flutter characteristics in separated flow p 191 A89-27744
- Evaluation of three turbulence models for the prediction of steady and unsteady airflows [NASA-TM-101413] p 10 A89-12555
- SANKOVIC, JOHN M.**
- The effects of arcjet thruster operating condition constriction geometry on the plasma plume [AIAA PAPER 89-2723] p 60 A89-50809
- The effects of arcjet operating condition and constriction geometry on the plasma plume [NASA-TM-102284] p 72 A89-25281
- SANTORO, G. J.**
- Deposition of Na2SO4 from salt-seeded combustion gases of a high velocity burner rig p 89 A89-12330
- Determination of convective diffusion heat/mass transfer rates to burner rig test targets comparable in size to cross-stream jet diameter p 141 A89-12753
- SANTORO, GILBERT J.**
- Microgravity Combustion Diagnostics Workshop [NASA-CP-10017] p 120 A89-17682
- SANZ, J. M.**
- Automated design of controlled-diffusion blades [ASME PAPER 88-GT-139] p 2 A89-15967
- SANZ, JOSE M.**
- A compendium of controlled diffusion blades generated by an automated inverse design procedure [NASA-TM-101968] p 31 A89-20996
- SARAVANOS, D. A.**
- Mechanics of damping for fiber composite laminates including hygro-thermal effects [AIAA PAPER 89-1191] p 192 A89-30681
- Tailoring of composite links for optimal damped elasto-dynamic performance [NASA-TM-102094] p 88 A89-26912



- Unified micromechanics of damping for unidirectional fiber reinforced composites  
[NASA-TM-102107] p 88 N89-26919
- SARIGUL, NESRIN**  
A novel approach in formulation of special transition elements: Mesh interface elements  
[NASA-CR-184768] p 199 N89-16193  
Specialty functions singularity mechanics problems p 206 N89-29805
- SARV, HAMID**  
NOx formation from the combustion of monodisperse n-heptane sprays doped with fuel-nitrogen additives p 116 A89-42695
- SAUNDERS, NEAL T.**  
Turbomachinery technology for high-speed civil flight [NASA-TM-102092] p 32 N89-24320
- SAUNDERS, ROGER**  
Advanced heat receiver conceptual design study [NASA-CR-182177] p 209 N89-16224
- SAVAGE, M.**  
Transmission overhaul and replacement predictions using Weibull and renewal theory [AIAA PAPER 89-2919] p 180 A89-47173  
Computerized life and reliability modeling for turboprop transmissions p 181 A89-53364  
Tooth contact shift in loaded spiral bevel gears o, IL, 25-27 Apr. 1989; sponsored by ASME [NASA-TM-101438] p 183 N89-14453  
Vibration signature analysis of multistage gear transmission [NASA-TM-101442] p 184 N89-18685  
Transmission overhaul and replacement predictions using Weibull and renewal theory [NASA-TM-102022] p 186 N89-22925
- SAVINELL, R. F.**  
Theoretical performance of hydrogen-bromine rechargeable SPE fuel cell p 207 A89-23290
- SAVINO, JOSEPH M.**  
A program for advancing the technology of space concentrators [NASA-TM-102139] p 76 N89-29484
- SCHEMME, TERRY D.**  
Closed-drift thruster investigations [NASA-CR-179497] p 62 N89-11808
- SCHEUERMANN, COULSON M.**  
Materials technology assessment for a 1050 K Stirling space engine design [NASA-TM-101342] p 77 N89-11815
- SCHILLER, D. N.**  
Behavior in normal and reduced gravity of an enclosed liquid/gas system with nonuniform heating from above [AIAA PAPER 89-0070] p 145 A89-25061  
Behavior in normal and reduced gravity of an enclosed liquid/gas system with nonuniform heating from above [NASA-TM-101471] p 120 N89-17046
- SCHILLER, DAVID N.**  
Experiment plans to study preignition processes of a pool fire in low gravity [NASA-CR-182256] p 121 N89-19442
- SCHLOSSER, HERBERT**  
Connection between energy relations of solids and molecules p 91 A89-26406
- SCHMIDT, DAVID K.**  
Model-based analysis of control/display interaction in the hover task p 215 A89-36933
- SCHMIDT, RODNEY C.**  
Development of low Reynolds number two equation turbulence models for predicting external heat transfer on turbine blades p 157 N89-12901  
A low-Reynolds-number two-equation turbulence model for predicting heat transfer on turbine blades p 160 N89-17310
- SCHNEIDER, J. A.**  
Advanced H2/O2 space engine parametrics [AIAA PAPER 89-2300] p 57 A89-46855
- SCHNEIDER, JON C.**  
Average-passage simulation of counter-rotating propfan propulsion systems as applied to cruise missiles [AIAA PAPER 89-2943] p 7 A89-47187  
Average-passage simulation of counter-rotating propfan propulsion systems as applied to cruise missiles [NASA-TM-102043] p 14 N89-23416
- SCHNEIDER, STEVEN J.**  
Weight savings in aerospace vehicles through propellant scavenging [SAWE PAPER 1818] p 40 A89-50814  
Advanced APS impacts on vehicle payloads [NASA-TM-102086] p 41 N89-25254
- SCHOCK, H.**  
Stratified charge rotary engine - Internal flow studies at the MSU engine research laboratory [SAE PAPER 890331] p 181 A89-51477
- SCHOCK, HAROLD J.**  
Regressed relations for forced convection heat transfer in a direct injection stratified charge rotary engine [SAE PAPER 880626] p 178 A89-12308
- SCHOCK, HAROLD J., JR.**  
Calculations of the unsteady, three-dimensional flow field inside a motored Wankel engine [SAE PAPER 880625] p 19 A89-12307
- SCHOENDORF, JOHN F.**  
Creep fatigue life prediction for engine hot section materials (isotropic): Fourth year progress review p 188 N89-12914
- SCHOENMAN, LEN**  
Friction-induced ignition of metals in high-pressure oxygen p 97 A89-32932
- SCHOENMAN, LEONARD**  
Orbit transfer rocket engine technology program: Oxygen materials compatibility testing [NASA-CR-182195] p 64 N89-14256
- SCHRAG, R. L.**  
Electroimpulse peicing - Electrodynamical solution by discrete elements p 17 A89-39193
- SCHRAMM, DAVID N.**  
Nucleosynthesis, neutrino bursts and gamma-rays from coalescing neutron stars p 241 A89-46577
- SCHREIBER, H. A.**  
Experimental investigation of the performance of a supersonic compressor cascade [NASA-TM-100879] p 9 N89-10858
- SCHREIBER, JEFFREY G.**  
The design and fabrication of a Stirling engine heat exchanger module with an integral heat pipe p 142 A89-15190  
RE-1000 free-piston Stirling engine sensitivity test results [NASA-TM-88846] p 210 N89-19737  
Initial characterization of a modular heat exchanger with an integral heat pipe [NASA-TM-102097] p 239 N89-25078  
Comparison of conceptual designs for 25 kWe advanced Stirling conversion systems for dish electric application [NASA-TM-102085] p 239 N89-26781
- SCHRIEVER, D.**  
Electron velocity distributions and plasma waves associated with the injection of an electron beam into the ionosphere p 215 A89-43698
- SCHULZE, NORMAN**  
NASA Aerospace Flight Battery Systems Program - Issues and actions p 49 A89-15224
- SCHUPP, DONALD A.**  
Stability of bulk Ba2YCu3O(7-x) in a variety of environments [NASA-TM-101401] p 111 N89-14310
- SCHUSTER, J. R.**  
COLD-SAT: An orbital cryogenic hydrogen technology experiment [NASA-TM-102303] p 73 N89-26044
- SCHWEIGER, F. A.**  
Revolutionary opportunities for materials and structures study, addendum no. 1 [NASA-CR-179642-ADD-1] p 47 N89-29478
- SCOTT, J. N.**  
Navier-Stokes solution to the flowfield over ice accretion shapes p 1 A89-12557  
A numerical investigation of the influence of surface roughness on heat transfer in ice accretion [AIAA PAPER 89-0737] p 146 A89-25554
- SCOTT, J. R.**  
Time domain numerical calculations of unsteady vortical flows about a flat plate airfoil [NASA-TM-102318] p 168 N89-29726
- SCOTT, JAMES R.**  
Numerical solution of periodic vortical flows about a thin airfoil [AIAA PAPER 89-1691] p 7 A89-48955  
Numerical solution of periodic vortical flows about a thin airfoil [NASA-TM-101998] p 14 N89-23413
- SEASHOLTZ, R. G.**  
Advanced high temperature instrument for hot section research applications p 29 N89-20137
- SEASHOLTZ, RICHARD G.**  
Comparison of the bidirectional reflectance distribution function of various surfaces p 230 A89-41530  
Three component laser anemometer measurements in an annular cascade of core turbine vanes with contoured end wall [NASA-TP-2846] p 9 N89-10844  
Laser anemometry: A status report p 177 N89-12885
- SECUNDE, RICHARD R.**  
Solar dynamic power for Space Station Freedom [IAF PAPER ICOSP89-4-1] p 55 A89-46517  
Solar dynamic power for space station freedom [NASA-TM-102016] p 67 N89-23516  
Solar dynamic power module design [NASA-TM-102055] p 70 N89-25269
- SEGALL, B.**  
Shubnikov-de Haas measurements of the 2-D electron gas in pseudomorphic In(0.1)Ga(0.9)As grown on GaAs p 235 A89-29299
- SEINER, JOHN M.**  
Supersonic jet noise and the high speed civil transport [AIAA PAPER 89-2358] p 227 A89-46772
- SEKLER, J.**  
The scratch test - Different critical load determination techniques p 171 A89-54278
- SELLECK, M. E.**  
Isothermal dendritic growth: A low gravity experiment p 121 N89-20299
- SENA, J. T.**  
Transient performance evaluation of an integrated heat pipe-thermal storage system p 49 A89-15209
- SENNEFF, J. M.**  
Space station auxiliary thrust chamber technology [NASA-CR-179650] p 46 N89-11803
- SESHADRI, K.**  
Optical methods and results of dew point and deposition rate measurements in salt/ash-containing combustion gases - B2O3(l) deposition rates by interference methods and comparisons with theory p 89 A89-12334
- SESHADRI, SRINIVASA G.**  
Fracture resistance of a TiB2 particle/SiC matrix composite at elevated temperature p 81 A89-31074
- SETTLES, G. S.**  
Skin-friction measurements by laser interferometry p 167 N89-28737
- SEUME, J. R.**  
Effect of transition on oscillation flow losses in Stirling engine coolers and heaters p 142 A89-15189
- SHAKER, FRANCIS J.**  
Free-vibration characteristics and correlation of a Space Station split-blanket solar array [AIAA PAPER 89-1252] p 44 A89-30737  
Free-vibration characteristics and correlation of a space station split-blanket solar array [NASA-TM-101452] p 198 N89-15438
- SHALKHAUSER, KURT A.**  
Universal test fixture for monolithic mm-wave integrated circuits calibrated with an augmented TRD algorithm [NASA-TP-2875] p 127 N89-17767
- SHALKHAUSER, MARY JO**  
Digital CODEC for real-time processing of broadcast quality video signals at 1.8 bits/pixel [NASA-TM-102325] p 129 N89-27927
- SHALKHAUSER, MARY JO W.**  
Design and implementation of a microcomputer-based user interface controller for burst data communications satellite ground terminals [NASA-TM-101375] p 43 N89-13457  
Digitally modulated bit error rate measurement system for microwave component evaluation [NASA-TP-2912] p 40 N89-28545
- SHALTENS, RICHARD K.**  
Comparison of conceptual designs for 25 kWe advanced Stirling conversion systems for dish electric application [NASA-TM-102085] p 239 N89-26781
- SHAMROTH, S. J.**  
Turbine stator flow field simulations p 157 N89-12902  
Two- and three-dimensional turbine blade row flow field simulations p 161 N89-17313
- SHANNON, JOHN L., JR.**  
Crack growth resistance of textured alumina p 105 A89-26452
- SHAPIRO, WILBUR**  
Advanced helium purge seals for Liquid Oxygen (LOX) turbopumps [NASA-CR-182105] p 184 N89-21239
- SHAW, B. D.**  
Interactions between gaseous electrical discharges and single liquid droplets p 90 A89-19298
- SHAW, ROBERT J.**  
Predictions of airfoil aerodynamic performance degradation due to icing [NASA-TM-101434] p 10 N89-13412  
NASA's program on icing research and technology [NASA-TM-101989] p 1 N89-22569
- SHEFFLER, K. D.**  
Thermal barrier coating life prediction model p 110 N89-12922  
Thermal barrier coating life prediction model development p 200 N89-17333
- SHEH, M.**  
Constitutive modeling for single crystal superalloys p 101 N89-12911
- SHEIBLEY, DEAN W.**  
Status of the Space Station power system p 54 A89-23281
- SHENG, Z. Z.**  
Transport critical current and magnetization measurements of melt-processed YBa2Cu3O(7-x) p 234 A89-20037

- SHEPHERD, KEVIN**  
Return of the turboprops p 20 A89-12953
- SHERER, T. N.**  
Intensity-based fibre-optic sensing system using contrast modulation of subcarrier interference pattern p 170 A89-39302
- SHERWOOD, L. T.**  
Sensors for ceramic components in advanced propulsion systems: Summary of literature survey and concept analysis, task 3 report [NASA-CR-180900] p 172 N89-11192
- SHETTY, DINESH K.**  
Fracture toughness of polycrystalline ceramics in combined mode I and mode II loading p 105 A89-26457
- SHEU, W. H.**  
Analysis of supersonic plug nozzle flowfield and heat transfer [NASA-CR-179554] p 10 N89-13397
- SHIEH, TSAY-JIU**  
Computer analysis of the negative differential resistance switching phenomenon of double-injection devices p 134 A89-54963
- SHIH, TOM I.-P.**  
Calculations of the unsteady, three-dimensional flow field inside a motored Wankel engine [SAE PAPER 880625] p 19 A89-12307
- SHIMP, N. R.**  
Design and test of an oxygen turbopump for a dual expander cycle rocket engine [AIAA PAPER 89-2305] p 56 A89-46737
- SHUEN, JIAN-SHUEN**  
A numerical study of chemically reacting flow in nozzles [NASA-TM-102135] p 70 N89-24444
- SHUEN, JIAN-SHUEN**  
Three dimensional simulation of an underexpanded jet interacting with a supersonic cross flow [AIAA PAPER 88-3181] p 2 A89-14982  
Numerical study of the interactions between droplets at intermediate Reynolds numbers p 142 A89-16451  
Flux splitting algorithms for two-dimensional viscous flows with finite-rate chemistry [AIAA PAPER 89-0388] p 146 A89-28409  
Three-dimensional calculation of supersonic reacting flows using an LU scheme [AIAA PAPER 89-0391] p 146 A89-28410  
A detailed analysis of inviscid flux splitting algorithms for real gases with equilibrium or finite-rate chemistry p 151 A89-45424  
A numerical study of chemically reacting flow in nozzles [AIAA PAPER 89-2793] p 60 A89-49687
- SHUO, HUNG CHANG**  
Computer-aided design of bevel gear tooth surfaces [NASA-TM-101449] p 183 N89-17248
- SHUSTER, J. R.**  
COLD-SAT orbital experiment configured for Atlas launch p 45 A89-53327
- SIDI, AVRAM**  
Recursive algorithms for vector extrapolation methods p 221 A89-14397
- SIEGEL, R.**  
Transient radiative cooling of an absorbing and scattering cylinder p 146 A89-28958
- SIEVERS, G. KEITH**  
Return of the turboprops p 20 A89-12953
- SILVESTRO, J. W.**  
Aperture impedance of flared horns p 125 A89-43543
- SILVESTRO, JOHN W.**  
Mutual coupling in a finite planar array with interelement holes present p 125 A89-42768
- SIMITSES, G. J.**  
Non-isothermal buckling behavior of viscoplastic shell structures [NASA-CR-183013] p 197 N89-12931  
Analysis of shell-type structures subjected to time-dependent mechanical and thermal loading [NASA-CR-183005] p 197 N89-14457  
Analysis of shell-type structures subjected to time-dependent mechanical and thermal loading [NASA-CR-184989] p 203 N89-24669
- SIMITSES, GEORGE J.**  
Solution methods for one-dimensional viscoelastic problems p 191 A89-19914
- SIMON, T. W.**  
Effect of transition on oscillation flow losses in Stirling engine coolers and heaters p 142 A89-15189  
Development of a special-purpose test surface guided by uncertainty analysis p 144 A89-22736
- SIMONEAU, R. J.**  
Heat transfer in aerospace propulsion p 153 A89-53282  
Review and assessment of the database and numerical modeling for turbine heat transfer p 30 N89-20139
- SIMONEAU, ROBERT J.**  
CFD in the context of IHPTET - The Integrated High Performance Turbine Engine Technology Program [AIAA PAPER 89-2904] p 154 A89-53307  
CFD in the context of IHPTET: The Integrated High Performance Turbine Technology Program [NASA-TM-102132] p 165 N89-26174
- SIMONS, RAINEE N.**  
Modeling of some coplanar waveguide discontinuities, junctions, and propagation characteristics [NASA-TM-101483] p 131 A89-24139  
Channelized coplanar waveguide: Discontinuities, junctions, and propagation characteristics [NASA-TM-101483] p 137 N89-21172
- SIMONS, STEPHEN N.**  
Energy storage and thermal control system design status [NASA-TM-102136] p 46 N89-24427
- SINGER, B. A.**  
Spatial resolution and downwash velocity corrections for multiple-hole pressure probes in complex flows p 171 A89-45909
- SINGER, JOSEPH**  
Oxygen electrode bifunctional electrocatalyst NiCo<sub>2</sub>O<sub>4</sub> spinel [NASA-TM-100947] p 208 N89-10409  
Corrosion testing of candidates for the alkaline fuel cell cathode p 212 N89-23000
- SINGER, S.**  
Starting characteristics of direct current motors powered by solar cells [NASA-TM-101981] p 136 N89-19493  
Magnification of starting torques of dc motors by maximum power point trackers in photovoltaic systems [NASA-TM-102040] p 138 N89-23792
- SINGH, DILEEP**  
Fracture toughness of polycrystalline ceramics in combined mode I and mode II loading p 105 A89-26457
- SINGH, N. B.**  
Dendritic solidification in binary alloys p 96 A89-22560  
Measurement of the diffusion coefficient of acetone in succinonitrile at its melting point p 237 A89-23488  
Evaluation of transport conditions during physical vapor transport growth of opto-electronic crystals [AIAA PAPER 89-0229] p 118 A89-25197
- SINGH, RAJ.**  
Modal analysis of gear housing and mounts [NASA-TM-101445] p 184 N89-21244
- SIRIGNANO, W. A.**  
Behavior in normal and reduced gravity of an enclosed liquid/gas system with nonuniform heating from above [AIAA PAPER 89-0070] p 145 A89-25061  
Behavior in normal and reduced gravity of an enclosed liquid/gas system with nonuniform heating from above [NASA-TM-101471] p 120 N89-17046
- SIROCKY, PAUL J.**  
High temperature flexible seal [NASA-CASE-LEW-14695-1] p 187 N89-28830
- SKEBE, S. A.**  
Turbobfan forced mixer lobe flow modeling. 1: Experimental and analytical assessment [NASA-CR-4147-PT-1] p 11 N89-14221
- SKUPINSKI, ROBERT C.**  
Results from baseline tests of the SPRE 1 and comparison with code model predictions [NASA-TM-102044] p 68 N89-23527
- SLABY, JACK G.**  
Free-piston Stirling technology for space power [IAF PAPER ICOSP89-5-7] p 56 A89-46520  
Free-piston Stirling technology for space power [NASA-TM-101956] p 66 N89-20194
- SLATER, HOWARD A.**  
Performance of multimirror quartzline lamps in a high-pressure, underwater environment [NASA-TM-101374] p 172 N89-10269
- SLINEY, HAROLD E.**  
Hot piston ring/cylinder liner materials - Selection and evaluation [SAE PAPER 880544] p 178 A89-12304  
Some composite bearing and seal materials for gas turbine applications: A review [NASA-TM-101451] p 111 N89-14338  
Tribology: The Story of Lubrication and Wear [NASA-TM-101430] p 203 N89-24635  
Solid lubricant materials for high temperatures: A review p 203 N89-24636
- SMIALEK, J. L.**  
Transient oxidation of single-crystal beta-NiAl p 98 A89-37899  
Influence of alloying elements on the oxidation behavior of NiAl<sub>3</sub> [NASA-TM-101398] p 100 N89-12717
- SMIALEK, JAMES L.**  
The effect of sulfur and zirconium co-doping on the oxidation of NiCrAl p 94 A89-13933
- Effect of the theta-alpha-Al<sub>2</sub>O<sub>3</sub> transformation on the oxidation behavior of beta-NiAl + Zr p 98 A89-38600  
Molten salt corrosion of SiC and Si<sub>3</sub>N<sub>4</sub> [NASA-TM-101346] p 108 N89-11912  
Oxidation behavior of FeAl + Hf, Zr, B [NASA-TM-101402] p 102 N89-14297  
The oxidation of Ni-rich Ni-Al intermetallics [NASA-TM-101455] p 102 N89-15233  
Hot corrosion of ceramic engine materials [NASA-TM-101439] p 112 N89-16065
- SMITH, BRIAN S.**  
InP homojunction solar cell performance on the LIPS 3 flight experiment [NASA-TM-101390] p 209 N89-12123
- SMITH, CHARLES C.**  
The effect of test-cell pressure on resistojel nozzle flow [AIAA PAPER 89-2838] p 58 A89-47116
- SMITH, G. E.**  
Three dimensional viscous analysis of a hypersonic inlet [AIAA PAPER 89-0004] p 4 A89-29924  
Three dimensional viscous analysis of a hypersonic inlet [NASA-TM-101474] p 13 N89-16759
- SMITH, GREGORY E.**  
PNS calculations for 3-D hypersonic corner flow with two turbulence models [AIAA PAPER 88-2958] p 1 A89-14979
- SMITH, J. M.**  
Summary and evaluation of the Strategic Defense Initiative Space Power Architecture Study [NASA-TM-102012] p 69 N89-24443
- SMITH, JOHN M.**  
SP-100 nuclear space power systems with application to space commercialization [NASA-TM-101403] p 63 N89-12665
- SMITH, JOHN R.**  
Connection between energy relations of solids and molecules p 91 A89-26406  
Universal features of the equation of state of solids p 237 A89-48960  
Avalanche in adhesion p 100 A89-54495
- SMITH, RICHARD L.**  
Expert systems applied to spacecraft fire safety [NASA-CR-182266] p 42 N89-23501
- SMITH, T. E.**  
Effect of design variables, temperature gradients, and speed on life and reliability of a rotating disk p 180 A89-47719
- SMITH, TODD E.**  
A review of turbomachinery blade-row interaction research [NASA-CR-182211] p 24 N89-12567
- SMITHRICK, JOHN J.**  
Effect of LEO cycling at shallow depths of discharge on MANTECH IPV nickel-hydrogen cells p 49 A89-15278
- SNYDER, CHRISTOPHER A.**  
Advanced core technology: Key to subsonic propulsion benefits [NASA-TM-101420] p 26 N89-14237
- SNYDER, PAUL G.**  
Characterization of multilayer GaAs/AlGaAs transistor structures by variable angle spectroscopic ellipsometry p 133 A89-49998
- SO, R. M. C.**  
On the modelling of scalar and mass transport in combustor flows p 92 A89-38658
- SOCKOL, PETER M.**  
Unsteady Euler cascade analysis [AIAA PAPER 89-0322] p 3 A89-28406
- SOH, W. Y.**  
Unsteady solution of incompressible Navier-Stokes equations p 141 A89-15143
- SOH, WOO-YUNG**  
Application of a lower-upper implicit scheme and an interactive grid generation for turbomachinery flow field simulations [NASA-TM-101412] p 11 N89-15077
- SOHN, K. H.**  
Some characteristics of bypass transition in a heated boundary layer [NASA-TM-102126] p 164 N89-24577
- SOKOLOWSKI, DANIEL E.**  
Turbine Engine Hot Section Technology (HOST) Project p 25 N89-12877  
Toward improved durability in advanced aircraft engine hot sections [NASA-TM-4087] p 29 N89-20135  
NASA HOST project overview p 29 N89-20136  
Views on the impact of HOST p 31 N89-20144
- SOLOMON, A. D.**  
Thermal analysis of heat storage canisters for a solar dynamic, space power system p 54 A89-29113

- SOLOMONOFF, A.**  
Global properties of pseudospectral methods  
p 221 A89-37746
- SOMERTON, C.**  
Stratified charge rotary engine - Internal flow studies at the MSU engine research laboratory  
[SAE PAPER 890331] p 181 A89-51477
- SOMERVILLE, W. A.**  
Issues and opportunities in space photovoltaics  
[NASA-TM-101425] p 65 N89-15171
- SONIN, A. A.**  
Vapor condensation at a turbulent liquid surface in systems with possible spaced-based applications  
[AIAA PAPER 89-2846] p 151 A89-47122
- SOOD, PRADEEP K.**  
A versatile power converter for high-frequency link systems  
p 131 A89-21200  
Study of the generator/motor operation of induction machines in a high frequency link space power system  
[NASA-CR-179600] p 63 N89-11809
- SORENSEN, TORVALD**  
The 25 kW solar thermal Stirling hydraulic engine system: Conceptual design  
[NASA-CR-180889] p 239 N89-14182
- SOTOMAYOR, J. L.**  
Compensation for effects of ambient temperature on rare-earth doped fiber optic thermometer  
[NASA-TM-102282] p 176 N89-27998
- SOULE, MATTHEW**  
Large-scale Advanced Prop-fan (LAP) hub/blade retention design report  
[NASA-CR-174786] p 28 N89-19299
- SOURS, THOMAS**  
Photovoltaic module on-orbit assembly for Space Station Freedom  
[NASA-TM-102297] p 47 N89-26887
- SOURS, THOMAS J.**  
A definition study of the on-orbit assembly operations for the outboard photovoltaic power modules for Space Station Freedom  
[NASA-TM-102006] p 41 N89-20171
- SOVEY, J. S.**  
Performance of a 100 kW class applied field MPD thruster  
[AIAA PAPER 89-2710] p 57 A89-47035  
Use of high temperature superconductors in magnetoplasmadynamic systems  
[NASA-TM-101219] p 236 N89-11553
- SOVEY, JAMES S.**  
Performance and lifetime assessment of MPD arc thruster technology  
[AIAA PAPER 88-3211] p 53 A89-16485  
Performance characterizations of an engineering model multipropellant resistojet  
p 54 A89-28340  
Electromagnetic emission experiences using electric propulsion systems  
p 61 A89-53354  
Test facility and preliminary performance of a 100 kW class MPD thruster  
[NASA-TM-102021] p 68 N89-23520  
Performance of a 100 kW class applied field MPD thruster  
[NASA-TM-102312] p 74 N89-27701
- SOVIE, AMY J.**  
Arcjet nozzle design impacts  
[NASA-TM-102050] p 68 N89-23522
- SOVIE, R. J.**  
Extended SP-100 reactor power systems capability  
p 52 A89-15392
- SOVIE, RONALD J.**  
Power systems for production, construction, life support, and operations in space  
p 37 A89-45803  
Space power technologies  
p 38 N89-11770
- SPENCE, ROD**  
A laser communication experiment utilizing the ACT satellite and an airborne laser transceiver  
p 43 A89-15811
- SPRISSLER, B.**  
Elevated temperature slow plastic deformation of NiAl/TiB<sub>2</sub> particulate composites  
p 81 A89-31689
- SROLOVITZ, D. J.**  
A Monte Carlo-finite element model for strain energy controlled microstructural evolution - 'Ratting' in superalloys  
p 96 A89-24358
- STAHL, MARK**  
Effect of length of chopped pristine and intercalated graphite fibers on the resistivity of fiber networks  
[NASA-TM-101395] p 84 N89-11826
- STANG, DAVID B.**  
Cruise noise of the 2/9 scale model SR-7A propeller  
p 224 A89-12561  
Ultrasonic imaging of porosity variations produced during sintering  
p 107 A89-48892  
Dynamic porosity variations in ceramics  
[NASA-TM-101340] p 112 N89-17668
- Interfacing laboratory instruments to multiuser, virtual memory computers  
[NASA-TM-4106] p 188 N89-19578  
Ultrasonic imaging of textured alumina  
[NASA-TM-101478] p 189 N89-28853
- STANKIEWICZ, NORBERT**  
Study of optical output couplers for submillimeter wavelength backward-wave oscillators (BWO's)  
p 132 A89-32857  
Study of optical output couplers for submillimeter wavelength backward-wave oscillators (BWO's)  
[NASA-TM-101360] p 134 N89-11128
- STARKEN, H.**  
Experimental investigation of the performance of a supersonic compressor cascade  
[NASA-TM-100879] p 9 N89-10858
- STEADMAN, KARL**  
Adaptive array for weak interfering signals: Geostationary satellite experiments  
[NASA-CR-185450] p 129 N89-26126
- STEARNS, C. A.**  
Deposition of Na<sub>2</sub>SO<sub>4</sub> from salt-seeded combustion gases of a high velocity burner rig  
p 89 A89-12330
- STEBBINS, ALBERT**  
Patterns of the cosmic microwave background from evolving string networks  
p 240 A89-14618  
Cosmic strings and the large-scale structure  
p 240 A89-19604  
Is the great attractor really a great wall?  
p 241 A89-36278
- STEFANI, FRANCIS**  
A heat-driven monochromatic light source  
p 224 A89-41722
- STEFKO, GEORGE L.**  
Wind-tunnel results of advanced high-speed propellers at takeoff, climb, and landing Mach numbers  
[NASA-TM-87030] p 13 N89-19265
- STEGEMAN, JAMES**  
Calculations of the unsteady, three-dimensional flow field inside a motored Wankel engine  
[SAE PAPER 880625] p 19 A89-12307
- STEINBRONN, OTTO**  
An analysis of possible advanced space strategies featuring the role of space resource utilization  
[IAF PAPER 88-587] p 37 A89-17861
- STEINETZ, BRUCE M.**  
High temperature flexible seal  
[NASA-CASE-LEW-14695-1] p 187 N89-28830
- STEINKE, R. J.**  
The design and development of transonic multistage compressors  
p 27 N89-16834
- STEINMANN, P. A.**  
The scratch test - Different critical load determination techniques  
p 171 A89-54278  
Adhesion scratch testing - A round-robin experiment  
p 171 A89-54281
- STEINTHORSSON, ERLENDUR**  
Calculations of the unsteady, three-dimensional flow field inside a motored Wankel engine  
[SAE PAPER 880625] p 19 A89-12307
- STELLA, PAUL M.**  
NASA advanced space photovoltaic technology-status, potential and future mission applications  
[NASA-TM-102093] p 75 N89-27705
- STEPHENS, J. R.**  
Influence of alloying elements on the oxidation behavior of NbAl<sub>3</sub>  
[NASA-TM-101398] p 100 N89-12717
- STEPHENS, JOSEPH R.**  
Space 2010  
p 77 A89-23028  
Status and prognosis for alternative engine materials  
p 97 A89-36419  
Fiber reinforced superalloys for rocket engines  
[NASA-TM-100880] p 86 N89-15990  
Refractory metal alloys and composites for space nuclear power systems  
[NASA-TM-101364] p 102 N89-16986  
Fiber reinforced superalloys for rocket engines  
p 103 N89-22673  
Intermetallic and ceramic matrix composites for 815 to 1370 C (1500 to 2500 F) gas turbine engine applications  
[NASA-TM-102326] p 88 N89-29490
- STEPHENSON, S. N.**  
Data report for the Siple Coast (Antarctica) project  
[NASA-TM-100708] p 206 N89-10403
- STEUBER, THOMAS J.**  
Simulation of the low earth orbital atomic oxygen interaction with materials by means of an oxygen ion beam  
[NASA-TM-101971] p 114 N89-21104
- STEVENS, N. JOHN**  
Large structure current collection in plasma environments  
[AIAA PAPER 89-0496] p 44 A89-25405
- STEVENSON, WARREN H.**  
The turbulence characteristics of a separated flow with combustion  
p 92 A89-33369  
Parametric study of statistical bias in laser Doppler velocimetry  
p 171 A89-47378
- STINESPRING, C. D.**  
Surface studies relevant to silicon carbide chemical vapor deposition  
p 91 A89-27966
- STOCK, T. A.**  
A probabilistic approach to composite micromechanics  
[NASA-TM-101366] p 85 N89-12684
- STOCKS, DANA R.**  
Further development of the dynamic gas temperature measurement system. Volume 2: Computer program user's manual  
[NASA-CR-179513-VOL-2] p 173 N89-13771
- STOLTZFUS, JOEL**  
Friction-induced ignition of metals in high-pressure oxygen  
p 97 A89-32932
- STONE, JAMES R.**  
The NASA Electric Propulsion Program  
p 59 A89-47428
- STONER, WILLIS A.**  
Preliminary design study of hydrogen and ammonia resistojets for prime and auxiliary thrusters  
[NASA-CR-182176] p 62 N89-10943
- STOUFFER, D. C.**  
Constitutive modeling for single crystal superalloys  
p 101 N89-12911
- STRANGMAN, T. E.**  
Thermal barrier coating life prediction model development  
p 109 N89-12920  
Thermal barrier coating life-prediction model development  
[NASA-CR-175002] p 26 N89-13433  
Thermal barrier coating life-prediction model development  
p 200 N89-17331
- STRAZISAR, A. J.**  
An LDA (Laser-Doppler Anemometry) investigation of three-dimensional normal shock wave boundary-layer interactions  
p 14 N89-20956
- STROCK, THOMAS W.**  
Hot gas ingestion testing of an advanced STOVL concept in the NASA Lewis 9- by 15-foot low speed wind tunnel with flow visualization  
[NASA-TM-100952] p 11 N89-15078
- STRUMPF, H. J.**  
Advanced solar receivers for space power  
p 54 A89-29116
- STRUMPF, HAL J.**  
Advanced space solar dynamic receivers  
p 52 A89-15343
- STUBBS, R. M.**  
Technology requirements for an orbiting fuel depot - A necessary element of a space infrastructure  
[IAF PAPER 88-035] p 37 A89-17641
- STUBSTAD, JOHN M.**  
Solution methods for one-dimensional viscoelastic problems  
p 191 A89-19914
- SU, S. F.**  
Optoelectronic techniques for broadband switching  
p 131 A89-15825
- SU, SHING-FONG**  
Study of optoelectronic switch for satellite-switched time-division multiple access  
[NASA-CR-179630] p 135 N89-13706
- SULLIVAN, J. P.**  
Aerothermal modeling program, phase 2. Element B: Flow interaction experiment  
p 156 N89-12891  
Aerothermal modeling program, Phase 2, element B: Flow interaction experiment  
p 160 N89-17304
- SULLIVAN, JOHN P.**  
Propeller/wing interaction  
[AIAA PAPER 89-0535] p 17 A89-25429  
Aerodynamic interaction between propellers and wings  
p 8 A89-50062
- SULLIVAN, TIMOTHY J.**  
NASA Lewis Stirling engine computer code evaluation  
[NASA-CR-182248] p 214 N89-24741
- SULTANIAN, B. K.**  
The effects of leading edge and downstream film cooling on turbine vane heat transfer  
[NASA-CR-182133] p 158 N89-13754  
Turbine airfoil film cooling  
p 161 N89-17315
- SUN, D. J.**  
Convective flows in enclosures with vertical temperature or concentration gradients  
[AIAA PAPER 89-0069] p 118 A89-25060  
Convective flows in enclosures with vertical temperature or concentration gradients  
[NASA-TM-101373] p 120 N89-12753
- SUNDBERG, GALE R.**  
Cooperating expert systems for Space Station - Power/thermal subsystem testbeds  
p 38 A89-15350

**SUNDBERG, RICHARD C.**

- Development and testing of a 20-kHz component test bed  
[NASA-TM-102141] p 139 N89-25403  
Distortion and regulation characterization of a Mapham inverter  
[NASA-TM-102089] p 139 N89-26148  
Frequency domain model for analysis of paralleled, series-output-connected Mapham inverters  
[NASA-TM-102140] p 139 N89-26149
- SUTTON, R. D.**  
Development of an analytical model to assess fuel property effects on combustor performance  
p 21 A89-20949
- SWANSON, G. A.**  
Life prediction and constitutive models for engine hot section  
p 188 N89-12916  
Fatigue life prediction modeling for turbine hot section materials  
p 30 N89-20142
- SWANSON, GUSTAV A.**  
High temperature constitutive and crack initiation modeling of coated single crystal superalloys  
p 112 N89-17334
- SWARTZ, C. K.**  
Radiation resistance and comparative performance of ITO/InP and n/p InP homojunction solar cells  
[NASA-TM-101387] p 135 N89-12819  
Indium phosphide solar cell research in the US: Comparison with nonphotovoltaic sources  
[NASA-TM-102103] p 124 N89-27868
- SWARTZ, CLIFFORD K.**  
Progress in indium phosphide solar cell research  
p 212 N89-24707  
Predicted performance of InP solar cells in Cassegrainian and slats space concentrator arrays at 20 to 100 AMO, 80 to 100 C  
p 212 N89-24711
- SWARTZLANDER, A. B.**  
Growth of diamond by RF plasma-assisted chemical vapor deposition  
p 90 A89-20474
- SWEC, DIANE M.**  
Diamondlike carbon protective coatings for optical windows  
[NASA-TM-102111] p 231 N89-27506  
Ion beam and plasma methods of producing diamondlike carbon films  
[NASA-TM-102301] p 116 N89-27836
- SWETTE, L.**  
Oxygen electrodes for rechargeable alkaline fuel cells  
p 211 N89-22998
- SWIFT, G.**  
Near-field acoustic characteristics of a single-rotor propfan  
[AIAA PAPER 89-1055] p 23 A89-36215  
Fluctuating pressures on wing surfaces in the slipstream of a single-rotor propfan  
[AIAA PAPER 89-1058] p 226 A89-36218
- SZEKELY, J.**  
Fluid flow phenomena in the generation of boron carbide suspensions in magnesium melts  
p 79 A89-19472
- SZEMENYEI, BRIAN**  
OTVE combustor wall condition monitoring  
[NASA-CR-182275] p 73 N89-26899
- SZUCH, JOHN R.**  
Application of advanced computational technology to propulsion CFD  
p 142 A89-16957  
A perspective on future directions in aerospace propulsion system simulation  
[NASA-TM-102038] p 31 N89-21798
- SZYDLIC, P. P.**  
Shubnikov-de Haas measurements of the 2-D electron gas in pseudomorphic In(0.1)Ga(0.9)As grown on GaAs  
p 235 A89-29299
- T**
- TABIB-AZAR, MASSOOD**  
Deep-level transient spectroscopy of Al(x)Ga(1-x)As/GaAs using nondestructive acousto-electric voltage measurement  
p 133 A89-42742
- TAFFLOVE, ALLEN**  
An application of the WKB technique to the on-surface radiation condition  
p 124 A89-21222  
Theory and application of radiation boundary operators  
p 224 A89-24191  
Review of FD-TD numerical modeling of electromagnetic wave scattering and radar cross section  
p 19 A89-45107
- TAGHAVI, K.**  
Effects of furnace temperature profile on the interface shape during Bridgman crystal growth  
p 119 A89-53278

**TAGHAVI, R.**

- Large amplitude acoustic excitation of swirling turbulent jets  
[AIAA PAPER 89-0970] p 4 A89-29098  
Effect of initial swirl distribution on the evolution of a turbulent jet  
p 149 A89-36906  
Large amplitude acoustic excitation of swirling turbulent jets  
[NASA-TM-101950] p 13 N89-18417
- TAGHAVI, RAHMAT**  
Turbulent swirling jets with excitation  
[NASA-CR-180895] p 16 N89-29329
- TAMMARU, I.**  
Development of a 75-watt 60-GHz traveling-wave tube for intersatellite communications  
[NASA-CR-182135] p 138 N89-24530
- TAN, C. S.**  
Calculations of inlet distortion induced compressor flow field instability  
p 8 A89-52498
- TAN, H. Q.**  
Symbolic generation of constitutive equations  
p 221 A89-34963  
Symbolic derivation of material property matrices in finite element analysis  
p 216 A89-34964
- TANGIRALA, V.**  
Radiative structures of lycopodium-air flames in low gravity  
[AIAA PAPER 89-0500] p 91 A89-25406  
Particle cloud mixing in microgravity  
[NASA-TM-101484] p 121 N89-20321
- TANGIRALA, VENKAT**  
Feasibility of reduced gravity experiments involving quiescent, uniform particle cloud combustion  
[NASA-TM-101371] p 122 N89-26114
- TATRO, C. A.**  
Photovoltaic power modules for NASA's manned Space Station  
p 55 A89-29122
- TAULBEE, DALE B.**  
Turbine-stage heat transfer - Comparison of short-duration measurements with state-of-the-art predictions  
p 142 A89-16458  
Prediction of unsteady rotor-surface heat transfer from wake passages  
[AIAA PAPER 89-1692] p 150 A89-43210
- TAYLOR, A. C., III**  
Viscous analysis of high speed flows using an upwind finite volume technique  
[AIAA PAPER 89-0001] p 144 A89-25001  
Turbulence modeling in a hypersonic inlet  
p 8 A89-53931
- TELESMAN, JACK**  
Influence of fatigue crack wake length and state of stress on crack closure  
p 191 A89-17432  
Accelerated fatigue crack growth behavior of PWA 1480  
p 97 A89-36461  
Fatigue crack growth behavior of a single crystal alloy as observed through an in situ fatigue loading stage  
p 99 A89-45946  
Fatigue crack growth study of SCS6/Ti-15-3 composite  
[NASA-TM-102332] p 104 N89-26989
- TEREN, FRED**  
Space Station Freedom power management and distribution system design  
[NASA-TM-102283] p 73 N89-26045
- TEW, ROY C.**  
Two-dimensional numerical simulation of a Stirling engine heat exchanger  
[NASA-TM-102057] p 164 N89-23823
- TEW, ROY C., JR.**  
Status of several Stirling loss characterization efforts and their significance for Stirling space power development  
p 49 A89-15187
- TEWARI, S. N.**  
Microsegregation in directionally solidified Pb-8.4 at. pct Au alloy  
p 94 A89-12758
- THACKER, B. H.**  
An approximate methods approach to probabilistic structural analysis  
[AIAA PAPER 89-1369] p 193 A89-30844
- THALLER, LAWRENCE H.**  
Space Electrochemical Research and Technology Conference, Cleveland, OH, Apr. 14-16, 1987, Proceedings  
p 207 A89-23280
- THANEDAR, P. B.**  
Structural tailoring of laminate properties  
[AIAA PAPER 89-1367] p 192 A89-30842
- THEIL, JEREMY A.**  
Effects of microstructure and nonstoichiometry on electrical properties of vanadium dioxide films  
p 236 A89-44527
- THESLING, WILLIAM**  
Predicted performance of InP solar cells in Cassegrainian and slats space concentrator arrays at 20 to 100 AMO, 80 to 100 C  
p 212 N89-24711

**THOMAS, R. D.**

- A V-grooved GaAs solar cell  
[NASA-TM-101970] p 211 N89-22177  
The GaAs solar cells with V-grooved emitters  
[NASA-TM-102104] p 214 N89-26291
- THOMPSON, D.**  
Highly oriented Ti2Ba2Ca2Cu3O10 thin films by pulsed laser evaporation  
p 236 A89-30421  
Preparation of high T(c) Ti-Ba-Ca-Cu-O thin films by pulsed laser evaporation and TiO3 vapor processing  
p 236 A89-38608
- THOMPSON, E. D.**  
Design and simulated performance of a CARS spectrometer for dynamic temperature measurements using electronic heterodyning  
p 170 A89-37298
- THOMPSON, H. DOYLE**  
The turbulence characteristics of a separated flow with combustion  
p 92 A89-33369  
Parametric study of statistical bias in laser Doppler velocimetry  
p 171 A89-47378
- THOMPSON, JOE F.**  
Transonic flow solutions on general 3D regions using composite-block grids  
p 6 A89-45428
- THOMPSON, R. L.**  
Structural analysis methods development for turbine hot section components  
p 30 N89-20140
- THOMPSON, ROBERT L.**  
HOST structural analysis program overview  
p 195 N89-12881  
High temperature stress-strain analysis  
p 196 N89-12913  
Structural response of an advanced combustor liner: Test and analysis  
p 200 N89-17329
- TIEN, J. K.**  
The effect of Co alloying content on the kinetics of reaction zone growth in tungsten fiber reinforced superalloy composites  
p 79 A89-11324  
Interdiffusional effects between TiB2 and NiAl intermetallics  
p 95 A89-21395  
Reaction kinetics between fiber and matrix  
p 83 A89-36420
- TINETTI, ANA F.**  
Generic icing effects on forward flight performance of a model helicopter rotor  
p 18 A89-41093
- TIPTON, M. T.**  
Component specific modeling  
p 25 N89-12907
- TIRMIZI, S. H.**  
A facility for precise temperature control applications in microgravity  
p 48 A89-36956
- TITRAN, ROBERT H.**  
Refractory metal alloys and composites for space nuclear power systems  
[NASA-TM-101364] p 102 N89-16986  
Tensile and creep rupture behavior of P/M processed Nb-base alloy, WC-3009  
[NASA-TM-101954] p 78 N89-19371
- TOBIN, S. P.**  
High efficiency GaAs-Ge tandem solar cells grown by MOCVD  
p 213 N89-24721
- TODD, E. S.**  
Three-dimensional inelastic analysis methods for hot section components  
p 199 N89-17316
- TONG, M.**  
Structural response of an advanced combustor liner: Test and analysis  
p 200 N89-17329
- TOOGOOD, T. L.**  
Multiple Application Propfan Study (MAPS): Advanced tactical transport  
[NASA-CR-175003] p 28 N89-19300
- TOWNE, CHARLES E.**  
Computational methods for inlet airframe integration  
p 13 N89-16752
- TOWNSEND, D. P.**  
The role of thermal and lubricant boundary layers in the transient thermal analysis of spur gears  
[NASA-TM-101435] p 182 N89-14452  
Vibration signature analysis of multistage gear transmission  
[NASA-TM-101442] p 184 N89-18685
- TOWNSEND, DENNIS P.**  
Surface fatigue life of carburized and hardened M50NiL and AISI 9310 spur gears and rolling-contact test bars  
[AIAA PAPER 89-2819] p 180 A89-47105  
Effect of advanced component technology on helicopter transmissions  
p 182 N89-13794  
Dynamic loading of spur gears with linear or parabolic tooth profile modification  
[NASA-TM-101444] p 183 N89-15413  
Wear consideration in gear design for space applications  
[NASA-TM-101457] p 183 N89-15414  
Lubricant jet flow phenomena in spur and helical gears with modified addendums; for radially directed individual jets  
[NASA-TM-101460] p 183 N89-15415

- Surface fatigue life of carburized and hardened M50NiL and AISI 9310 spur gears and rolling-contact test bars [NASA-TM-101979] p 185 N89-22111
- Effects of lubrication on the performance of high speed spur gears [NASA-TM-101969] p 186 N89-22919
- Tribology: The Story of Lubrication and Wear [NASA-TM-101430] p 203 N89-24635
- TRAN, LE**  
Prediction of unsteady rotor-surface heat transfer from wake passages [AIAA PAPER 89-1692] p 150 A89-43210
- TRELA, WALTER**  
Improved silicon carbide for advanced heat engines. I - Process development for injection molding p 106 A89-33619
- TRIBBLE, A.**  
The plasma wake of the Shuttle Orbiter p 215 A89-43680
- TRIBBLE, A. C.**  
Plasma density, temperature and turbulence in the wake of the Shuttle Orbiter p 233 A89-53209
- TRIPP, DAVID E.**  
A review of failure models for unidirectional ceramic matrix composites under monotonic loads [NASA-TM-101421] p 198 N89-14470
- TROTH, D. L.**  
Development of an analytical model to assess fuel property effects on combustor performance p 21 A89-20949
- TROUDET, TERRY**  
Neuromorphic learning of continuous-valued mappings in the presence of noise: Application to real-time adaptive control [NASA-TM-101999] p 221 N89-24856
- TROWBRIDGE, D.**  
Finite element applications to explore the effects of partial bonding on metal matrix composite properties [AIAA PAPER 89-1175] p 192 A89-30666
- Finite element applications to explore the effects of partial bonding on metal matrix composite properties [NASA-TM-101482] p 86 N89-20206
- TRUDELL, JEFFERY J.**  
Thermal distortion analysis of the Space Station solar dynamic concentrator p 51 A89-15341
- TSAI, C. T.**  
Influence of airfoil thickness on convected gust interaction noise [AIAA PAPER 89-1082] p 225 A89-33725
- TSAI, Y.-L. PETER**  
Three-dimensional calculation of supersonic reacting flows using an LU scheme [AIAA PAPER 89-0391] p 146 A89-28410
- TSAO, NAI-KUAN**  
On the accuracy of solving triangular systems in parallel [NASA-TM-101384] p 222 N89-12337
- On the equivalence of Gaussian elimination and Gauss-Jordan reduction in solving linear equations [NASA-TM-101466] p 222 N89-20710
- On the equivalence of a class of inverse decomposition algorithms for solving systems of linear equations [NASA-TM-102036] p 223 N89-24865
- TSENG, JESSE I. S.**  
Navier-Stokes calculation of solid-propellant rocket motor internal flowfields [AIAA PAPER 88-3182] p 48 A89-14983
- TSUI, P.**  
Convection and chemistry effects in CVD: A 3-D analysis for silicon deposition [NASA-TM-102001] p 78 N89-21032
- TSUKAMOTO, S.**  
Molecular beam epitaxial growth of high-quality InSb on InP and GaAs substrates [NASA-CR-185440] p 236 N89-26739
- Surface morphologies and electrical properties of molecular beam epitaxial InSb and InAs(x)Sb(1-x) grown on GaAs and InP substrates [NASA-CR-185439] p 237 N89-26740
- TU, Y. K.**  
Vibration signature analysis of multistage gear transmission [NASA-TM-101442] p 184 N89-16685
- TURAN, A.**  
Improved numerical methods for turbulent viscous recirculating flows p 156 N89-12895
- TURKEL, E.**  
Global properties of pseudospectral methods p 221 A89-37746
- TURNER, MICHAEL S.**  
Superheavy magnetic monopoles and main-sequence stars p 240 A89-20377
- Limits to the radiative decays of neutrinos and axions from gamma-ray observations of SN 1987A p 242 A89-26985
- Is the great attractor really a great wall? p 241 A89-36278
- TURNER, GEORGE E.**  
Aeronautical applications of high-temperature superconductors [AIAA PAPER 89-2142] p 23 A89-53304
- Aeronautical applications of high-temperature superconductors [NASA-TM-102311] p 33 N89-26008
- TURNOCK, STEPHEN R.**  
Investigation of surface water behavior during glaze ice accretion p 16 A89-27739
- TURNQUIST, SCOTT R.**  
Space station electrical power system availability study [NASA-CR-182198] p 45 N89-11802
- TWEED, D. L.**  
Experimental investigation of the performance of a supersonic compressor cascade [NASA-TM-100879] p 9 N89-10858
- TWOMBLY, MARK A.**  
Space station electrical power system availability study [NASA-CR-182198] p 45 N89-11802
- U**
- UEDA, K.**  
Improved high-temperature resistant matrix resins [NASA-CR-180826] p 114 N89-21105
- UHERKA, KENNETH**  
Aeronautical applications of high-temperature superconductors [AIAA PAPER 89-2142] p 23 A89-53304
- Aeronautical applications of high-temperature superconductors [NASA-TM-102311] p 33 N89-26008
- UMASHANKAR, KORADA R.**  
Review of FD-TD numerical modeling of electromagnetic wave scattering and radar cross section p 19 A89-45107
- V**
- VALCO, G. J.**  
Plasma deposited silicon nitride for indium phosphide encapsulation p 235 A89-27794
- Sequentially evaporated thin Y-Ba-Co-O superconducting films on microwave substrates [NASA-TM-102068] p 138 N89-23791
- Millimeter wave transmission studies of YBa<sub>2</sub>Cu<sub>3</sub>O<sub>7</sub>-delta thin films in the 26.5 to 40.0 GHz frequency range [NASA-TM-102345] p 237 N89-30088
- VALCO, GEORGE J.**  
Sequentially evaporated thin Y-Ba-Cu-O superconductor films: Composition and processing effects [NASA-TM-101388] p 134 N89-10235
- Characterization of ZrO<sub>2</sub> buffer layers for sequentially evaporated Y-Ba-Cu-O on Si and Al<sub>2</sub>O<sub>3</sub> substrates [NASA-TM-101432] p 135 N89-13722
- VALDMANIS, J. A.**  
External electro-optic probing of millimeter-wave integrated circuits p 133 A89-45266
- External electro-optic probing of millimeter-wave integrated circuits [NASA-TM-101990] p 128 N89-21142
- VALGORA, MARTIN E.**  
Power considerations for an early manned Mars mission utilizing the space station [NASA-TM-101436] p 63 N89-13492
- VALISETTY, RAO R.**  
Sublimate- or ply-level analysis of composites and strain energy release rates of end-notch and mixed-mode fracture specimens p 190 A89-16279
- VALLI, J.**  
Adhesion scratch testing - A round-robin experiment p 171 A89-54281
- VAN LEER, BRAM**  
A detailed analysis of inviscid flux splitting algorithms for real gases with equilibrium or finite-rate chemistry p 151 A89-45424
- VAN OMMERING, G.**  
Space Station battery system design and development p 52 A89-15378
- VANDERPLAATS, G. N.**  
Gear optimization [NASA-CR-4201] p 182 N89-13793
- VANDERSANDE, J. W.**  
High temperature thermal conductivity measurements on lanthanum sulfides using the flash method p 77 A89-16500
- VANDIEP, G. PHAM**  
Liquid droplet generation [NASA-CR-182246] p 166 N89-26182
- VANDOMMELEN, LEON L.**  
On the Lagrangian description of unsteady boundary layer separation. Part 2: The spinning sphere [NASA-TM-102027] p 163 N89-22861
- On the Lagrangian description of unsteady boundary layer separation. Part 1: General theory [NASA-TM-102026] p 164 N89-23821
- VANDOORMAAL, J. P.**  
Improved numerical methods for turbulent viscous recirculating flows p 156 N89-12895
- VANLEER, BRAM**  
A genuinely multi-dimensional upwind cell-vertex scheme for the Euler equations [NASA-TM-102029] p 223 N89-24872
- VANNUCCI, RAYMOND D.**  
Mechanical properties characterization of composite sandwich materials intended for space antenna applications p 81 A89-32885
- Materials technology assessment for a 1050 K Stirling space engine design [NASA-TM-101342] p 77 N89-11815
- VANOMMERING, GERT**  
Energy storage and thermal control system design status [NASA-TM-102136] p 46 N89-24427
- VANOVERBEKE, THOMAS J.**  
A numerical study of chemically reacting flow in nozzles [AIAA PAPER 89-2793] p 60 A89-49687
- A numerical study of chemically reacting flow in nozzles [NASA-TM-102135] p 70 N89-24444
- VANSTONE, R. H.**  
Elevated temperature crack growth p 196 N89-12915
- Constitutive modeling for isotropic materials [NASA-CR-174805] p 26 N89-13436
- Elevated temperature crack growth p 200 N89-17335
- VARY, A.**  
Concepts for interrelating ultrasonic attenuation, microstructure, and fracture toughness in polycrystalline solids p 95 A89-19852
- Nondestructive evaluation/characterization of composite materials and structures using the acousto-ultrasonic techniques p 188 A89-36571
- VARY, ALEX**  
The acousto-ultrasonic approach p 188 A89-32305
- Acousto-ultrasonics - An update p 188 A89-42864
- VASZARI, J. P.**  
Development of a 75-watt 60-GHz traveling-wave tube for intersatellite communications [NASA-CR-182135] p 138 N89-24530
- VENTO, D. M.**  
The solid surface combustion Space Shuttle experiment hardware description and ground-based test results [AIAA PAPER 89-0503] p 119 A89-28419
- The solid surface combustion space shuttle experiment hardware description and ground-based test results [NASA-TM-101963] p 123 N89-19446
- VERDON, J. M.**  
The effects of inlet turbulence and rotor/stator interactions on the aerodynamics and heat transfer of a large-scale rotating turbine model, volume 1 [NASA-CR-4079] p 159 N89-13756
- VERNON, S. M.**  
High efficiency GaAs-Ge tandem solar cells grown by MOCVD p 213 N89-24721
- VERRILLI, MICHAEL J.**  
Oxide scale stresses in polycrystalline Ni200 p 98 A89-38859
- Isothermal life prediction of composite lamina using a damage mechanics approach [NASA-TM-102032] p 87 N89-24460
- VERZWYVELT, S. A.**  
The effect of different alkali metal hydroxides on nickel electrode life p 207 A89-15280
- KOH concentration effect on cycle life of nickel-hydrogen cells. III - Cycle life test p 207 A89-23283
- VINET, PASCAL**  
Universal features of the equation of state of solids p 237 A89-48960
- VINYARD, SHANNON**  
The effect of insulated combustion chamber surfaces on direct-injected diesel engine performance, emissions, and combustion [NASA-CR-182204] p 239 N89-17548
- VISWANADHAM, R. K.**  
Elevated temperature slow plastic deformation of NiAl/TiB<sub>2</sub> particulate composites p 81 A89-31689
- 1200 to 1400 K slow strain rate compressive behavior of small grain size NiAl/Ni<sub>2</sub>AlTi alloys and NiAl/Ni<sub>2</sub>AlTi-TiB<sub>2</sub> composites p 99 A89-53497

## VITERI, F.

## VITERI, F.

Design and test of an oxygen turbopump for a dual expander cycle rocket engine  
[AIAA PAPER 89-2305] p 56 A89-46737

## VOGT, SCOTT T.

Launch packaging options for the photovoltaic power module cargo element  
[NASA-TM-102072] p 71 N89-25275

## VOGT, WILLIAM G.

Computer simulation of a pilot in V/STOL aircraft control loops  
[NASA-CR-184815] p 215 N89-21479

## VON GLAHN, U. H.

Rectangular nozzle plume velocity modeling for use in jet noise prediction  
[AIAA PAPER 89-2357] p 7 A89-46771

## VONGLAHN, U. H.

Rectangular nozzle plume velocity modeling for use in jet noise prediction  
[NASA-TM-102047] p 14 N89-22577

## VRABEL, DEBORAH

Advanced turboprop project  
[NASA-SP-495] p 24 N89-12565

## W

## WACHTER, J. P.

COLD-SAT orbital experiment configured for Atlas launch  
p 45 A89-53327

## WACHTER, JOSEPH P.

COLD-SAT: An orbital cryogenic hydrogen technology experiment  
[NASA-TM-102303] p 73 N89-26044

## WAGNER, D. A.

Design and test of a propfan gear system  
p 179 A89-22290

## WAGNER, J.

Coolant passage heat transfer with rotation  
p 157 N89-12899

## WAGNER, J. H.

Coolant passage heat transfer with rotation  
p 161 N89-17314

## WAHIDUZZAMAN, SYED

Methods for heat transfer and temperature field analysis of the insulated diesel, phase 3  
[NASA-CR-182237] p 239 N89-23382

## WALKER, J. D. A.

Asymptotic structure and similarity solutions for three-dimensional turbulent boundary layers  
[AIAA PAPER 89-1863] p 150 A89-42090

## WALKER, J. DAVID A.

An algorithm for unsteady flows with strong convection  
[NASA-TM-100828] p 221 N89-10575

## WALKER, K. P.

Constitutive modelling of single crystal and directionally solidified superalloys  
p 101 N89-12912

## WALKER, KEVIN P.

Constitutive modelling of single crystal and directionally solidified superalloys  
p 102 N89-17325

Nonlinear mesomechanics of composites with periodic microstructure  
[NASA-TM-102051] p 204 N89-26260

## WALLACE, J. F.

Gravitational macrosegregation in unidirectionally solidified lead-tin alloy  
p 117 A89-17112

## WALLACE, ROBERT L.

Programmable rate modem utilizing digital signal processing techniques  
[NASA-CR-185124] p 43 N89-26879

## WALTON, E.

Electromagnetic properties of ice coated surfaces  
[NASA-CR-184780] p 127 N89-20355

## WALTON, E. K.

Engineering calculations for solving the orbital allotment problem  
[NASA-CR-184607] p 217 N89-13993

## WALTON, ERIC K.

An experimental adaptive array to suppress weak interfering signals  
p 124 A89-22455

## WALTON, J.

High speed balancing applied to the T700 engine  
[NASA-CR-180899] p 184 N89-20472

## WANG, C. R.

Correlations of velocity and temperature fluctuations in the stagnation-point flow of circular cylinder in turbulent flow  
p 148 A89-34927

## WANG, J.

Induced emission of radiation from a large space-station-like structure in the ionosphere  
p 44 A89-31915

## WANG, L.

Gravitational macrosegregation in unidirectionally solidified lead-tin alloy  
p 117 A89-17112

## WANG, L. W.

Convective flows in enclosures with vertical temperature or concentration gradients  
[AIAA PAPER 89-0069] p 118 A89-25060

Thermosolutal convection in high-aspect-ratio enclosures  
p 153 A89-53288

Convective flows in enclosures with vertical temperature or concentration gradients  
[NASA-TM-101373] p 120 N89-12753

## WANG, LIN-WEN

Numerical studies of convective heat transfer in an inclined semiannular enclosure  
[NASA-TM-102011] p 123 N89-28666

## WANG, N.

Electromagnetic properties of ice coated surfaces  
[NASA-CR-184780] p 127 N89-20355

## WANG, T.

Development of a special-purpose test surface guided by uncertainty analysis  
p 144 A89-22736

## WANHAINE, J. S.

Hardware development for the Surface Tension Driven Convection Experiment aboard the USML-1 Spacelab mission  
[AIAA PAPER 89-0406] p 47 A89-25341

Hardware development for the surface tension driven convection experiment aboard the USML-1 spacelab mission  
[NASA-TM-101404] p 48 N89-11804

## WANLASS, M. W.

High-efficiency solar cells fabricated from direct-current magnetron sputtered n-indium tin oxide onto p-InP grown by atmospheric pressure metalorganic vapor phase epitaxy  
p 133 A89-44518

High-efficiency indium tin oxide/indium phosphide solar cells  
p 208 A89-44863

## WARD, JAMES

An experimental adaptive array to suppress weak interfering signals  
p 124 A89-22455

## WARK, CANDACE E.

Thermal measurements for jets in disturbed and undisturbed crosswind conditions  
p 20 A89-16102

## WARNER, J. D.

Improved synthesis of ceramic superconductors with alkaline earth peroxides - Synthesis and processing of Ba<sub>2</sub>YCu<sub>3</sub>O<sub>7-x</sub>  
p 235 A89-22887

Sequentially evaporated thin Y-Ba-Cu-O superconducting films on microwave substrates  
[NASA-TM-102068] p 138 N89-23791

Millimeter wave transmission studies of YBa<sub>2</sub>Cu<sub>3</sub>O<sub>7-delta</sub> thin films in the 26.5 to 40.0 GHz frequency range  
[NASA-TM-102345] p 237 N89-30088

## WARNER, JOSEPH D.

Sequentially evaporated thin Y-Ba-Cu-O superconductor films: Composition and processing effects  
[NASA-TM-101388] p 134 N89-10235

Characterization of ZrO<sub>2</sub> buffer layers for sequentially evaporated Y-Ba-Cu-O on Si and Al<sub>2</sub>O<sub>3</sub> substrates  
[NASA-TM-101432] p 135 N89-13722

## WARS, S.

Large scale advanced propeller blade pressure distributions - Prediction and data  
[AIAA PAPER 89-2696] p 7 A89-47026

## WASYNICZUK, O.

Dynamic characteristics of a 20 kHz resonant power system - Fault identification and fault recovery  
p 52 A89-15357

Simulation and control of a 20 kHz spacecraft power system  
p 130 A89-15391

## WATKINS, W. B.

Further development of the dynamic gas temperature measurement system  
p 172 N89-12884

## WATSON, GORDON K.

Materials technology assessment for a 1050 K Stirling space engine design  
[NASA-TM-101342] p 77 N89-11815

## WAWRZYNEK, P. A.

Graphical postprocessing for 3-D mesh quality evaluation  
p 217 A89-38846

## WEBER, G.

Component specific modeling  
p 25 N89-12907

## WEEKS, DAVID J.

Cooperating expert systems for Space Station - Power/thermal subsystem testbeds  
p 38 A89-15350

## WEIKLE, DONALD H.

Laser anemometry: A status report  
p 177 N89-12885

## Heat flux measurements

[NASA-TM-101428] p 173 N89-14418

## WEINBERG, B. C.

Two- and three-dimensional turbine blade row flow field simulations  
p 161 N89-17313

## WEINBERG, I.

Progress in InP solar cell research  
p 130 A89-15308

Radiation resistance and comparative performance of ITO/InP and n/p InP homojunction solar cells  
[NASA-TM-101387] p 135 N89-12819

Indium phosphide solar cell research in the US: Comparison with nonphotovoltaic sources  
[NASA-TM-102103] p 124 N89-27868

## WEINBERG, IRVING

InP homojunction solar cell performance on the LIPS 3 flight experiment  
[NASA-TM-101390] p 209 N89-12123

Progress in indium phosphide solar cell research  
p 212 N89-24707

Predicted performance of InP solar cells in Cassegrainian and slats space concentrator arrays at 20 to 100 AMO, 80 to 100 C  
p 212 N89-24711

## WEIR, LOIS J.

Mach 5 inlet CFD and experimental results  
[AIAA PAPER 89-2355] p 6 A89-46769

Mach 5 inlet CFD and experimental results  
[NASA-TM-102317] p 33 N89-27670

## WEISS, CARL

Integrated flight/propulsion control study for STOVL applications  
[AIAA PAPER 89-2908] p 34 A89-47166

## WEIZER, VICTOR G.

The interaction of gold with gallium arsenide  
p 90 A89-16416

The effect of metal surface passivation on the Au-InP interaction  
p 132 A89-30443

Metal-silicon reaction rates - The effects of capping  
p 93 A89-52202

## WELSCH, G.

The low cycle fatigue deformation response of a single-crystal superalloy at 650 C.  
p 99 A89-52204

## WERNET, MARK P.

Application of optical correlation techniques to particle imaging  
[AIAA PAPER 88-4661] p 169 A89-14985

Laser anemometry: A status report  
p 177 N89-12885

A vector scanning processing technique for pulsed laser velocimetry  
[NASA-TM-102048] p 175 N89-23850

## WERNLUND, J. V.

Advanced modulation technology development for earth station demodulator applications  
[NASA-CR-185126] p 43 N89-26880

## WESSBECHER, DOROTHY E.

Synthesis and stability of Br<sub>2</sub>, ICl and IBr intercalated pitch-based graphite fibers  
p 106 A89-37670

## WESTFALL, LEONARD J.

Thermal-mechanical fatigue test apparatus for metal matrix composites and joint attachments  
p 79 A89-15727

## WETCH, J. R.

Megawatt Class Nuclear Space Power Systems (MCNSPS) conceptual design and evaluation report. Volume 1: Objectives, summary results and introduction  
[NASA-CR-179614-VOL-1] p 209 N89-17941

Megawatt Class Nuclear Space Power Systems (MCNSPS) conceptual design and evaluation report. Volume 4: Concepts selection, conceptual designs, recommendations  
[NASA-CR-179614-VOL-4] p 210 N89-18967

Megawatt Class Nuclear Space Power Systems (MCNSPS) conceptual design and evaluation report. Volume 3, technologies 2: Power conversion  
[NASA-CR-179614-VOL-3] p 211 N89-22980

Megawatt Class Nuclear Space Power Systems (MCNSPS) conceptual design and evaluation report. Volume 2, technologies 1: Reactors, heat transport, integration issues  
[NASA-CR-179614-VOL-2] p 211 N89-22981

## WETHERHOLD, ROBERT C.

A probabilistic formulation for fracture energy of continuous fibre-matrix composites  
p 83 A89-39996

## WHALEN, T. J.

Improved silicon carbide for advanced heat engines  
[NASA-CR-179477] p 112 N89-15251

Improved silicon carbide for advanced heat engines. I - Process development for injection molding  
p 106 A89-33619

Improved silicon carbide for advanced heat engines. II - Pressureless sintering and mechanical properties of injection molded silicon carbide  
p 106 A89-33620

## WHEELER, DONALD R.

Surface temperature determination in surface analytic systems by infrared optical pyrometry  
p 169 A89-17347

## WHITAKER, J. F.

External electro-optic probing of millimeter-wave integrated circuits  
p 133 A89-45266



## PERSONAL AUTHOR INDEX

- External electro-optic probing of millimeter-wave integrated circuits  
[NASA-TM-101990] p 128 N89-21142
- WHITE, ALAN**  
Big savings from small holes p 45 A89-36724
- WHITE, K. ALAN, III**  
Moving Belt Radiator technology issues p 49 A89-15208
- WHITE, MAURICE**  
The 25 kW solar thermal Stirling hydraulic engine system: Conceptual design  
[NASA-CR-180889] p 239 N89-14182
- WHITEHAIR, STAN**  
Experiments and analysis of a compact electrothermal thruster p 59 A89-47494  
Experiments and analysis of a compact electrothermal thruster p 75 N89-27773
- WHITFIELD, C. E.**  
High speed turboprop aeroacoustic study (single rotation). Volume 1: Model development  
[NASA-CR-182257-VOL-1] p 229 N89-24139
- WHITFIELD, DAVID L.**  
A simple time-accurate turbomachinery algorithm with numerical solutions of an uneven blade count configuration  
[AIAA PAPER 89-0206] p 179 A89-25181  
Transonic flow solutions on general 3D regions using composite-block grids p 6 A89-45428
- WHITLOW, JOHN B., JR.**  
Return of the turboprops p 20 A89-12953  
NASA/industry advanced turboprop technology program p 20 A89-13504
- WHITMAN, PAMELA K.**  
Comparison of the surface charge behavior of commercial silicon nitride and silicon carbide powders p 105 A89-21444
- WHITTENBERGER, D.**  
High temperature thermal conductivity measurements on lanthanum sulfides using the flash method p 77 A89-16500
- WHITTENBERGER, J. D.**  
A preliminary report on the effects of long-term exposure of LiOH on pure nickel p 90 A89-12624  
Use of pure nickel and LiOH for thermal energy storage p 91 A89-23146
- WHITTENBERGER, J. DANIEL**  
Elevated temperature slow plastic deformation of NiAl/TiB<sub>2</sub> particulate composites p 81 A89-31689  
1200 to 1400 K slow strain rate compressive behavior of small grain size NiAl/Ni<sub>2</sub>AlTi alloys and NiAl/Ni<sub>2</sub>AlTi-TiB<sub>2</sub> composites p 99 A89-53497  
Effect of grain size on the high temperature properties of B<sub>2</sub> aluminides  
[NASA-TM-101382] p 101 N89-12720
- WHYTE, WAYNE A., JR.**  
Digital CODEC for real-time processing of broadcast quality video signals at 1.8 bits/pixel  
[NASA-TM-102325] p 129 N89-27927
- WICHNER, R. P.**  
Thermal analysis of heat storage canisters for a solar dynamic, space power system p 54 A89-29113
- WILBUR, PAUL J.**  
Plasma contacting - An enabling technology  
[AIAA PAPER 89-0677] p 231 A89-25537  
Ground-based tests of hollow cathode plasma contactors  
[AIAA PAPER 89-1558] p 232 A89-40188  
Experimental validation of a phenomenological model of the plasma contacting process p 232 A89-43357  
The divergence characteristics of constrained-sheath optics systems for use with 5-eV atomic oxygen sources  
[NASA-CR-182238] p 229 N89-19973  
Space plasma contractor research, 1988  
[NASA-CR-182283] p 233 N89-21658
- WILKINSON, R. ALLEN**  
Raman intensity as a probe of concentration near a crystal growing in solution  
[NASA-TP-2865] p 174 N89-16139
- WILL, HERBERT A.**  
Laboratory process control using natural language commands from a personal computer  
[NASA-TM-101988] p 218 N89-24055
- WILLHOITE, BRYAN C.**  
Energy storage and thermal control system design status  
[NASA-TM-102136] p 46 N89-24427
- WILLIAMS, ANTHONY D.**  
The development of an intelligent interface to a computational fluid dynamics flow-solver code p 216 A89-16963
- WILLIAMS, C. M.**  
Experimental evidence for a transverse magnetization of the Abrikosov lattice in anisotropic superconductors p 234 A89-21473
- WILLIAMS, F. A.**  
Interactions between gaseous electrical discharges and single liquid droplets p 90 A89-19298
- WILLIAMS, JAMES H., JR.**  
Energy in elastic fiber embedded in elastic matrix containing incident SH wave  
[NASA-CR-4205] p 188 N89-18694
- WILLIAMS, JOHN D.**  
Plasma contacting - An enabling technology  
[AIAA PAPER 89-0677] p 231 A89-25537  
Ground-based tests of hollow cathode plasma contactors  
[AIAA PAPER 89-1558] p 232 A89-40188  
Experimental validation of a phenomenological model of the plasma contacting process p 232 A89-43357  
Space plasma contractor research, 1988  
[NASA-CR-182283] p 233 N89-21658
- WILLIAMS, MARC H.**  
Aeroelastic response of metallic and composite propfan models in yawed flow  
[AIAA PAPER 88-3154] p 20 A89-17942
- WILLIAMS, P. T.**  
Thermal analysis of heat storage canisters for a solar dynamic, space power system p 54 A89-29113
- WILLIAMS, W. D.**  
Plasma deposited silicon nitride for indium phosphide encapsulation p 235 A89-27794
- WILLIS, EDWARD A.**  
Engineering study on the rotary-vee engine concept  
[SAE PAPER 890332] p 181 A89-51492  
Engineering study of the rotary-vee engine concept  
[NASA-TM-101995] p 33 N89-26007
- WILLOUGHBY, A. J.**  
Technology requirements for an orbiting fuel depot - A necessary element of a space infrastructure  
[IAF PAPER 88-035] p 37 A89-17641
- WILSON, D.**  
Development of a 39.5 GHz Karp traveling wave tube for use in space  
[NASA-CR-182182] p 136 N89-15336
- WILSON, D. G.**  
Modeling cyclic melting and refreezing in a hollow metal canister  
[NASA-CR-184630] p 217 N89-15623
- WILSON, JEFFREY D.**  
Computationally generated velocity taper for efficiency enhancement in a coupled-cavity traveling-wave tube p 132 A89-31987
- WILSON, RAYMOND B.**  
Three-dimensional inelastic analysis for hot section components, BEST 3D code p 199 N89-17317
- WILT, D. M.**  
A V-grooved GaAs solar cell  
[NASA-TM-101970] p 211 N89-22177  
The GaAs solar cells with V-grooved emitters  
[NASA-TM-102104] p 214 N89-26291
- WILT, DAVID M.**  
Chemical etching and organometallic chemical vapor deposition on varied geometries of GaAs p 213 N89-24728
- WILT, T.**  
On finite element implementation and computational techniques for constitutive modeling of high temperature composites  
[NASA-CR-185120] p 204 N89-26261
- WILT, T. E.**  
Fracture toughness computational simulation of general delaminations in fiber composites  
[NASA-TM-101415] p 85 N89-13521
- WINKELJOHN, D. M.**  
Multiple-Purpose Subsonic Naval Aircraft (MPSNA)  
Multiple Application Propfan Study (MAPS)  
[NASA-CR-175096] p 18 N89-19289
- WINSA, E.**  
Flight hardware and tele-operations supporting the Isothermal Dendritic Growth Experiment aboard the Space Shuttle  
[AIAA PAPER 89-0863] p 118 A89-25627  
A facility for precise temperature control applications in microgravity p 48 A89-36956  
Isothermal dendritic growth: A low gravity experiment p 121 N89-20299
- WINSLOW, CINDY**  
Space Station Freedom Solar Array design development  
[NASA-TM-102105] p 70 N89-24448
- WINTER, J. M.**  
Extended SP-100 reactor power systems capability p 52 A89-15392
- WINTER, JERRY M.**  
CSTI High Capacity Power  
[NASA-TM-102059] p 72 N89-25282
- WINTERBOTTOM, W. L.**  
Improved silicon carbide for advanced heat engines  
[NASA-CR-179477] p 112 N89-15251
- WITKOWSKI, DAVE P.**  
Aerodynamic interaction between propellers and wings p 8 A89-50062
- WITKOWSKI, DAVID P.**  
Propeller/wing interaction  
[AIAA PAPER 89-0535] p 17 A89-25429
- WLEZIEN, R. W.**  
Near-field acoustic environment of a supersonic plume adjacent to a wall  
[AIAA PAPER 89-1137] p 225 A89-33767
- WOLF, S. A.**  
Experimental evidence for a transverse magnetization of the Abrikosov lattice in anisotropic superconductors p 234 A89-21473
- WOLFF, STEVE**  
Mass flow meter using the triboelectric effect for measurement in cryogenics  
[NASA-CR-179572] p 155 N89-12836
- WONG, CARLA M.**  
Cooperating expert systems for Space Station - Power/thermal subsystem testbeds p 38 A89-15350
- WONG, W. A.**  
Unique mission options available with a megawatt-class nuclear electric propulsion system  
[NASA-TM-101220] p 65 N89-17618
- WONG, YAU SHU**  
Absorbing boundary conditions for second-order hyperbolic equations  
[NASA-TM-102009] p 223 N89-22397
- WOOD, C.**  
High temperature thermal conductivity measurements on lanthanum sulfides using the flash method p 77 A89-16500
- WOOD, J. GARY**  
Description of an oscillating flow pressure drop test rig p 142 A89-15188
- WOOD, JERRY R.**  
A perspective on future directions in aerospace propulsion system simulation  
[NASA-TM-102038] p 31 N89-21798
- WOODS, C. M.**  
The solution of the Elrod algorithm for a dynamically loaded journal bearing using multigrid techniques  
[ASME PAPER 88-TRIB-23] p 148 A89-34795
- WOODWARD, R. P.**  
High-speed propeller performance and noise predictions at takeoff/landing conditions p 226 A89-39195
- WOODWARD, RICHARD P.**  
Cruise noise of an advanced counterrotation turboprop measured from an adjacent aircraft p 20 A89-15080  
Unsteady blade pressure measurements on a model counterrotation propeller  
[AIAA PAPER 89-1144] p 226 A89-40175  
Noise of a model counterrotation propeller with simulated fuselage and support pylon at takeoff/approach conditions  
[AIAA PAPER 89-1143] p 227 A89-48953  
Measured far-field flight noise of a counterrotation turboprop at cruise conditions  
[NASA-TM-101383] p 228 N89-15686  
Unsteady blade pressure measurements on a model counterrotation propeller  
[NASA-TM-102002] p 228 N89-20779  
Noise of a model counterrotation propeller with simulated fuselage and support pylon at takeoff/approach conditions  
[NASA-TM-101996] p 228 N89-24138  
In-flight measurement of propeller noise on the fuselage of an airplane  
[NASA-TM-102285] p 229 N89-25675
- WOODYARD, JAMES R.**  
Radiation resistance studies of amorphous silicon films p 213 N89-24738
- WOOLLAM, JOHN A.**  
Thin-film hermeticity - A quantitative analysis of diamondlike carbon using variable angle spectroscopic ellipsometry p 234 A89-13945  
Growth of diamond by RF plasma-assisted chemical vapor deposition p 90 A89-20474  
Preparation of high T(c) Ti-Ba-Ca-Cu-O thin films by pulsed laser evaporation and TiO<sub>3</sub> vapor processing p 236 A89-38608  
Radio-frequency plasma chemical vapor deposition growth of diamond p 236 A89-44552  
Characterization of multilayer GaAs/AlGaAs transistor structures by variable angle spectroscopic ellipsometry p 133 A89-49998
- WORMHOUDT, J. C.**  
Surface studies relevant to silicon carbide chemical vapor deposition p 91 A89-27966
- WRIGHT, R. A.**  
Multiple Application Propfan Study (MAPS): Advanced tactical transport  
[NASA-CR-175003] p 28 N89-19300

## WRIGHT, T.

Advanced modulation technology development for earth station demodulator applications  
[NASA-CR-185126] p 43 N89-26880

## WRIGHT, W. B.

Efficient numerical simulation of a one-dimensional electrothermal deicer pad p 144 A89-22811  
Two-dimensional simulation of electrothermal deicing of aircraft components p 17 A89-39194

## WRIGHT, W. F.

Improved high-temperature resistant matrix resins  
[NASA-CR-180826] p 114 N89-21105

## WRIGHT, WILLIAM B.

A comparison of numerical methods for the prediction of two-dimensional heat transfer in an electrothermal deicer pad  
[NASA-CR-4202] p 19 N89-13429

## WU, JIUNN-CHI

Evaluation of three turbulence models for the prediction of steady and unsteady airloads  
[AIAA PAPER 89-0609] p 3 A89-25485  
Technique for the prediction of airfoil flutter characteristics in separated flow p 191 A89-27744  
Evaluation of three turbulence models for the prediction of steady and unsteady airloads  
[NASA-TM-101413] p 10 N89-12555

## WU, Y.-T.

Probabilistic structural analysis methods and applications p 190 A89-16939  
Probabilistic methods for structural response analysis p 223 A89-25843  
An approximate methods approach to probabilistic structural analysis  
[AIAA PAPER 89-1369] p 193 A89-30844  
An advanced probabilistic structural analysis method for implicit performance functions  
[AIAA PAPER 89-1371] p 193 A89-30846

## WU, YUE

A model for including thermal conduction in molecular dynamics simulations p 237 A89-41259

## Y

## YAMAGUCHI, KEIKO

Modeling of surface roughness effects on glaze ice accretion  
[AIAA PAPER 89-0734] p 16 A89-28451

## YAMAMOTO, O.

Large scale advanced propeller blade pressure distributions - Prediction and data  
[AIAA PAPER 89-2696] p 7 A89-47026

## YANEY, D. L.

Mechanisms of elevated-temperature deformation in the B2 aluminides NiAl and CoAl p 94 A89-17378

## YANG, VIGOR

Navier-Stokes calculation of solid-propellant rocket motor internal flowfields  
[AIAA PAPER 88-3182] p 48 A89-14983

## YEH, FREDERICK C.

Experience with advanced instrumentation in a hot section cascade  
[NASA-TM-102294] p 167 N89-27980

## YEH, HUN C.

Improved silicon nitride for advanced heat engines  
[NASA-CR-179525] p 113 N89-19421

## YEUM, K. S.

Computer simulation of macrosegregation in directionally solidified circular ingots  
[NASA-CR-182838] p 122 N89-21134

## YOKOTA, JEFFREY W.

LU implicit multigrid algorithm for the three-dimensional Euler equations p 143 A89-19906  
A diagonally inverted LU implicit multigrid scheme for the 3-D Navier-Stokes equations and a two equation model of turbulence  
[AIAA PAPER 89-0467] p 145 A89-25382  
A diagonally inverted LU implicit multigrid scheme for the 3-D Navier-Stokes equations and a two equation model of turbulence  
[NASA-CR-182209] p 9 N89-10863

## YOON, SEOKKWAN

Application of a lower-upper implicit scheme and an interactive grid generation for turbomachinery flow field simulations  
[NASA-TM-101412] p 11 N89-15077

## YORK, THOMAS M.

Plasma flow processes within magnetic nozzle configurations  
[AIAA PAPER 89-2711] p 57 A89-47036  
The effects of magnetic nozzle configurations on plasma thrusters  
[NASA-CR-184678] p 64 N89-15170

## YOUNG, G. W.

Steady-state thermal-solutal diffusion in a float zone p 119 A89-40897

## YOUNG, JEFFREY W.

Modal representations in control/structure interaction p 45 A89-54114

## YU, PING

Time domain numerical calculations of unsteady vortical flows about a flat plate airfoil  
[NASA-TM-102318] p 168 N89-29726

## YU, SHENG-TAO

Three dimensional simulation of an underexpanded jet interacting with a supersonic cross flow  
[AIAA PAPER 88-3181] p 2 A89-14982  
Three-dimensional calculation of supersonic reacting flows using an LU scheme  
[AIAA PAPER 89-0391] p 146 A89-28410

## YUAN, TONY

Effect of alcohol addition on shock-initiated formation of soot from benzene p 90 A89-12903

## YUHAS, JOHN S.

T55-L-712 turbine engine compressor housing refurbishment-plasma spray project  
[NASA-TM-101310] p 100 N89-10156

## YUNG, CHAIN-NAN

Numerical studies of convective heat transfer in an inclined semiannular enclosure  
[NASA-TM-102011] p 123 N89-28666

## Z

## ZAKRAJESEK, JAMES J.

Comparison study of gear dynamic computer programs at NASA Lewis Research Center  
[NASA-TP-2901] p 184 N89-21243

## ZAKRAJESEK, JAMES J.

Modal analysis of gear housing and mounts  
[NASA-TM-101445] p 184 N89-21244

## ZAMAN, A.

Adaptive feed array compensation system for reflector antenna surface distortion  
[NASA-TM-101458] p 127 N89-17756

## ZAMAN, K. B. M. Q.

Control of laminar separation over airfoils by acoustic excitation  
[AIAA PAPER 89-0565] p 3 A89-25454  
A natural low-frequency oscillation of the flow over an airfoil near stalling conditions p 6 A89-45437

Control of laminar separation over airfoils by acoustic excitation  
[NASA-TM-101379] p 9 N89-12552  
The low frequency oscillation in the flow over a NACA0012 airfoil with an iced leading edge  
[NASA-TM-102018] p 14 N89-23417

## ZAPLATYNSKY, ISIDOR

The effect of Al<sub>2</sub>O<sub>3</sub>, CaO, Cr<sub>2</sub>O<sub>3</sub> and MgO on devitrification of silica  
[NASA-TM-101335] p 77 N89-10124

## ZARETSKY, E. V.

Ceramic bearings for use in gas turbine engines  
[AIAA PAPER 89-0565] p 3 A89-25454  
Effect of design variables, temperature gradients, and speed on life and reliability of a rotating disk p 180 A89-47719

Effect of design variables, temperature gradients, and speed on life and reliability of a rotating disk p 180 A89-47719

## ZARETSKY, ERWIN V.

Selection of rolling-element bearing steels for long-life applications p 180 A89-47250  
Investigation of Weibull statistics in fracture analysis of cast aluminum  
[NASA-TM-102000] p 165 N89-21245

Tribology: The Story of Lubrication and Wear  
[NASA-TM-101430] p 203 N89-24635

## ZAVESKY, R.

Structural and thermal response of 30 cm diameter ion thruster optics  
[AIAA PAPER 89-2719] p 58 A89-47042

## ZAVESKY, R. J.

The solid surface combustion Space Shuttle experiment hardware description and ground-based test results  
[AIAA PAPER 89-0503] p 119 A89-28419

The solid surface combustion space shuttle experiment hardware description and ground-based test results  
[NASA-TM-101963] p 123 N89-19446

Structural and thermal response of 30 cm diameter ion thruster optics  
[NASA-TM-102124] p 75 N89-27703

## ZEHE, MICHAEL J.

Acidic attack of perfluorinated alkyl ether lubricant molecules by metal oxide surfaces  
[NASA-TM-101962] p 93 N89-19402

## ZERNIC, MICHAEL J.

Evolutionary growth for Space Station Freedom electrical power system  
[NASA-TM-102339] p 76 N89-28570

## ZHANG, J.

Transmission errors and bearing contact of spur, helical and spiral bevel gears  
[SAE PAPER 881294] p 179 A89-21000

Crowned spur gears - Methods for generation and tooth contact analysis. I - Basic concepts, generation of the pinion tooth surface by a plane p 179 A89-29306

Crowned spur gears - Methods for generation and Tooth Contact Analysis. II - Generation of the pinion tooth surface by a surface of revolution p 180 A89-37665

Generation of a crowned pinion tooth surface by a surface of revolution  
[NASA-TM-100260] p 181 N89-10282

Generation of a crowned pinion tooth surface by a plane  
[NASA-TM-100259] p 181 N89-10283

Topology of modified helical gears  
[NASA-TM-102134] p 187 N89-28015

## ZHANG, JIAO

Topology of modified helical gears and Tooth Contact Analysis (TCA) program  
[NASA-CR-4224] p 186 N89-22920

## ZHANG, NING-TIAN

Gear optimization  
[NASA-CR-4201] p 182 N89-13793

## ZHUANG, G. R.

Alkoxyisilane adsorption on metal oxide substrates p 92 A89-44536

## ZIEMIANSKI, JOSEPH A.

NASA/industry advanced turboprop technology program p 20 A89-13504

## ZIMMERMAN, M.

A comparison of reflector antenna designs for wide-angle scanning  
[NASA-TM-101459] p 127 N89-21138  
A segmented mirror antenna for radiometers  
[NASA-TM-102045] p 128 N89-23753

## ZIPP, MARK E.

Computer simulation of a pilot in V/STOL aircraft control loops  
[NASA-CR-184815] p 215 N89-21479

## ZOLTAN, A.

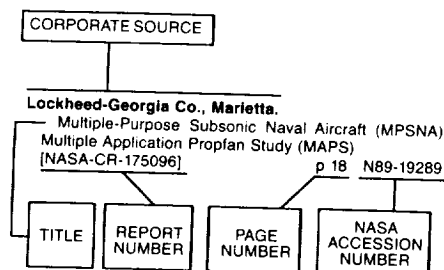
High temperature thermal conductivity measurements on lanthanum sulfides using the flash method p 77 A89-16500

## ZURAWSKI, ROBERT L.

NASA's Chemical Transfer Propulsion Program for Pathfinder  
[AIAA PAPER 89-2298] p 37 A89-46735

The Pathfinder Chemical Transfer Propulsion program  
[NASA-TM-102084] p 41 N89-24409  
NASA's Chemical Transfer Propulsion Program for Pathfinder  
[NASA-TM-102298] p 41 N89-26876

## Typical Corporate Source Index Listing



Listings in this index are arranged alphabetically by corporate source. The title of the document provides the user with a brief description of the subject matter. The report number helps to indicate the type of document cited (e.g., NASA report, translation, NASA contractor report). The NASA accession number denotes the number by which the citation is identified. The titles are arranged under each corporate source in ascending accession number order.

## A

- Adiabatics, Inc., Columbus, IN.**  
Adiabatic Wankel type rotary engine  
[NASA-CR-182233] p 28 N89-17599
- Aerodyne Research, Inc., Billerica, MA.**  
Surface studies relevant to silicon carbide chemical vapor deposition p 91 A89-27966
- Aerojet TechSystems Co., Sacramento, CA.**  
Friction-induced ignition of metals in high-pressure oxygen p 97 A89-32932  
Miniature multiple-function probe for OTV turbopump health monitoring  
[AIAA PAPER 89-2303] p 56 A89-46736  
Design and test of an oxygen turbopump for a dual expander cycle rocket engine  
[AIAA PAPER 89-2305] p 56 A89-46737  
Integrated control and health management. Orbit transfer rocket engine technology program  
[NASA-CR-182122] p 62 N89-11805  
Orbit transfer rocket engine technology program: Oxygen materials compatibility testing  
[NASA-CR-182195] p 64 N89-14256  
Integrated control and health monitoring capacitive displacement sensor development task. Orbit transfer rocket engine technology program  
[NASA-CR-182279] p 176 N89-26208
- Aerostructures, Inc., Arlington, VA.**  
Modal forced vibration analysis of aerodynamically excited turbosystems  
[NASA-CR-174966] p 201 N89-18696  
NASTRAN supplemental documentation for modal forced vibration analysis of aerodynamically excited turbosystems  
[NASA-CR-174967] p 201 N89-19583
- Air Force Wright Aeronautical Labs., Wright-Patterson AFB, OH.**  
Characterization of multilayer GaAs/AlGaAs transistor structures by variable angle spectroscopic ellipsometry p 133 A89-49998

- Air Research and Development Command, Wright-Patterson AFB, OH.**  
CFD in the context of IHPTET - The Integrated High Performance Turbine Engine Technology Program  
[AIAA PAPER 89-2904] p 154 A89-53307
- AirResearch Casting Co., Torrance, CA.**  
Improved silicon nitride for advanced heat engines  
[NASA-CR-179525] p 113 N89-19421
- Akron Univ., OH.**  
IECON '87: Industrial applications of control and simulation; Proceedings of the 1987 International Conference on Industrial Electronics, Control, and Instrumentation, Cambridge, MA, Nov. 3, 4, 1987  
[SPIE-853] p 219 A89-10798  
Simple high-accuracy resolution program for convective modelling of discontinuities p 143 A89-17459  
Accurate boundary conditions for exterior problems in gas dynamics p 143 A89-20223  
A viscoplastic constitutive theory for metal matrix composites at high temperature p 80 A89-20725  
Finite element applications to explore the effects of partial bonding on metal matrix composite properties  
[AIAA PAPER 89-1175] p 192 A89-30666  
Symbolic generation of constitutive equations p 221 A89-34963  
Symbolic derivation of material property matrices in finite element analysis p 216 A89-34964  
Steady-state thermal-solutal diffusion in a float zone p 119 A89-40897  
Alkoxysilane adsorption on metal oxide substrates p 92 A89-44536  
Universal limiter for high order explicit conservative advection schemes p 151 A89-45398  
Transmission overhaul and replacement predictions using Weibull and renewal theory  
[AIAA PAPER 89-2919] p 180 A89-47173  
Hierarchical Poly Tree computer architectures defined by computational multidisciplinary mechanics p 218 A89-50100  
The effects of arcjet thruster operating condition constrictor geometry on the plasma plume  
[AIAA PAPER 89-2723] p 60 A89-50809  
Computerized life and reliability modeling for turboprop transmissions p 181 A89-53364  
Computational fluid dynamic control p 220 A89-53984  
A multiaxial theory of viscoplasticity for isotropic materials p 196 N89-12908  
On finite element implementation and computational techniques for constitutive modeling of high temperature composites  
[NASA-CR-185120] p 204 N89-26261
- Alfred Univ., NY.**  
Preparation and evaluation of silicon nitride matrices for silicon nitride-SiC fiber composites  
[NASA-CR-184798] p 115 N89-23678
- Allied-Signal Aerospace Co., Torrance, CA.**  
Advanced space solar dynamic receivers p 52 A89-15343
- Ames Lab., IA.**  
Connection between energy relations of solids and molecules p 91 A89-26406  
Free energy surfaces in the superconducting mixed state p 236 A89-43928
- Analogom, Inc., Westlake, OH.**  
Electronic structure of BaO/W cathode surfaces p 132 A89-26862
- Analex Corp., Cleveland, OH.**  
Deposition of Na<sub>2</sub>SO<sub>4</sub> from salt-seeded combustion gases of a high velocity burner rig p 89 A89-12330  
Thermal distortion analysis of the Space Station solar dynamic concentrator p 51 A89-15341  
Technology requirements for an orbiting fuel depot - A necessary element of a space infrastructure  
[IAF PAPER 88-035] p 37 A89-17641  
Axisymmetric confined turbulent jet directed towards the liquid surface from below  
[AIAA PAPER 89-0172] p 145 A89-25148  
Study of optical output couplers for submillimeter wavelength backward-wave oscillators (BWO's) p 132 A89-32857

- Numerical studies of the effects of jet-induced mixing on liquid-vapor interface condensation  
[AIAA PAPER 89-1744] p 152 A89-48958  
Numerical studies of the effects of jet-induced mixing on liquid-vapor interface condensation  
[NASA-CR-182285] p 163 N89-23818  
Computed performance of the half-scale accurate antenna reflector  
[NASA-CR-182284] p 139 N89-24532
- Argonne National Lab., IL.**  
High temperature superconducting magnetic energy storage for future NASA missions p 50 A89-15288  
Aeronautical applications of high-temperature superconductors  
[AIAA PAPER 89-2142] p 23 A89-53304
- Arinc Research Corp., Annapolis, MD.**  
Space station electrical power system availability study  
[NASA-CR-182198] p 45 N89-11802
- Arizona State Univ., Tempe.**  
Calibration of single particle sizing velocimeters using photomask reticles p 170 A89-33379  
On the modelling of scalar and mass transport in combustor flows p 92 A89-38658  
Identification of high performance and component technology for space electrical power systems for use beyond the year 2000  
[NASA-CR-183003] p 62 N89-11807  
Heat transfer in the tip region of a rotor blade simulator p 157 N89-12898  
Heat transfer in the tip region of a rotor blade simulator p 161 N89-17312
- Arizona Univ., Tucson.**  
On the preferred mode of jet instability p 140 A89-11567  
Effects of excitation level on the stability of an axisymmetric mixing layer p 2 A89-16882  
Heat of mixing and morphological stability p 143 A89-21296  
Enthalpies of a binary alloy during solidification p 96 A89-22559  
Thermosolutal convection during dendritic solidification  
[AIAA PAPER 89-0626] p 118 A89-25495  
Influence of airfoil thickness on convected gust interaction noise  
[AIAA PAPER 89-1082] p 225 A89-33725  
Three-dimensional wave packets and instability waves in free shear layers and their receptivity p 149 A89-38619  
Computer simulation of macrosegregation in directionally solidified circular ingots  
[NASA-CR-182838] p 122 N89-21134
- Arkansas Univ., Fayetteville.**  
Transport critical current and magnetization measurements of melt-processed YBa<sub>2</sub>Cu<sub>3</sub>O<sub>7-x</sub> p 234 A89-20037
- Army Aviation Research and Development Command, Cleveland, OH.**  
Transmission errors and bearing contact of spur, helical and spiral bevel gears  
[SAE PAPER 881294] p 179 A89-21000  
Computerized life and reliability modeling for turboprop transmissions p 181 A89-53364  
An expert system for restructurable control  
[NASA-TM-101378] p 220 N89-12309  
Improvement in finite element meshes: Heat transfer in an infinite cylinder  
[NASA-TM-101410] p 182 N89-14450  
The role of thermal and lubricant boundary layers in the transient thermal analysis of spur gears  
[NASA-TM-101435] p 182 N89-14452  
Results of inphase axial-torsional fatigue experiments on 304 stainless steel  
[NASA-TM-101464] p 201 N89-20514  
Comparison study of gear dynamic computer programs at NASA Lewis Research Center  
[NASA-TP-2901] p 184 N89-21243
- Army Aviation Systems Command, Cleveland, OH.**  
Impact of ETO propellants on the aerothermodynamic analyses of propulsion components  
[AIAA PAPER 88-3091] p 53 A89-16486

## Army Propulsion Lab.

- A generalized one dimensional computer code for turbomachinery cooling passage flow calculations [AIAA PAPER 89-2574] p 151 A89-46934
- Transmission overhaul and replacement predictions using Weibull and renewal theory [AIAA PAPER 89-2919] p 180 A89-47173
- Piezoelectric pushers for active vibration control of rotating machinery p 171 A89-47717
- Fuel properties effect on the performance of a small high temperature rise combustor [AIAA PAPER 89-2901] p 23 A89-52025
- Effect of advanced component technology on helicopter transmissions [NASA-TM-101431] p 182 N89-13794
- Experimental verification of the thermodynamic properties for a jet-A fuel [NASA-TM-101475] p 117 N89-17017
- Computer-aided design of bevel gear tooth surfaces [NASA-TM-101449] p 183 N89-17248
- High speed balancing applied to the T700 engine [NASA-CR-180899] p 184 N89-20472
- Modal analysis of gear housing and mounts [NASA-TM-101445] p 184 N89-21244
- A data acquisition and control program for axial-torsional fatigue testing [NASA-TM-102041] p 205 N89-28029
- Army Propulsion Lab., Cleveland, OH.**
- Advanced transmission studies p 178 A89-18906
- Contingency power for small turboshaft engines p 21 A89-22291
- Performance of the forward scattering spectrometer probe in NASA's Icing Research Tunnel [AIAA PAPER 89-0769] p 169 A89-25570
- The solution of the Elrod algorithm for a dynamically loaded journal bearing using multigrid techniques [ASME PAPER 88-TRIB-23] p 148 A89-34795
- A review and forecast of engine system research at the Army Propulsion Directorate p 23 A89-36397
- Auburn International, Inc., Danvers, MA.**
- Mass flow measurement of liquid cryogenics using the triboelectric effect [NASA-CR-179519] p 155 N89-12837
- Auburn Univ., AL.**
- Compatibility of molten salts with advanced solar dynamic receiver materials [AIAA PAPER 89-1756] p 83 A89-48957
- Avco-Everett Research Lab., MA.**
- Improved numerical methods for turbulent viscous recirculating flows p 156 N89-12895
- Avco Lycoming Div., Stratford, CT.**
- Unsteady Euler cascade analysis [AIAA PAPER 89-0322] p 3 A89-28406
- Numerical investigation of chemically reacting flows in ramjet dump combustors [AIAA PAPER 89-0387] p 22 A89-28408
- B**
- Ben Gurion Univ. of the Negev, Beersheva (Israel).**
- Nucleosynthesis, neutrino bursts and gamma-rays from coalescing neutron stars p 241 A89-46577
- Bolt, Beranek, and Newman, Inc., Cambridge, MA.**
- Effects of bearing offset and flexibility on the mesh force distribution of spiral bevel gears p 178 A89-19834
- An extremum principle for computation of the zone of tooth contact and generalized transmission error of spiral bevel gears p 178 A89-19835
- Bradley Univ., Peoria, IL.**
- The effects of radiative heat loss on microgravity flame spread [AIAA PAPER 89-0504] p 91 A89-28420
- Brown Univ., Providence, RI.**
- A new Space Station power system p 53 A89-20016
- Coherent structures in transitional and turbulent free shear flows p 147 A89-28999
- Multiple coherent mode interaction in a developing round jet [AIAA PAPER 89-0967] p 147 A89-30483
- C**
- Cairo Univ. (Egypt).**
- Effects of core turbulence on jet excitability [NASA-TM-101405] p 159 N89-14403
- On the conditions for resonance interactions of instability waves in the axisymmetric jet [NASA-TM-101477] p 162 N89-21196
- Isothermal life prediction of composite lamina using a damage mechanics approach [NASA-TM-102032] p 87 N89-24460
- California State Univ., Long Beach.**
- Calculation of flow over iced airfoils p 5 A89-40905

- Effects of environmentally imposed roughness on airfoil performance [NASA-CR-179639] p 17 N89-11725
- California Univ., Berkeley.**
- Patterns of the cosmic microwave background from evolving string networks p 240 A89-14618
- Interaction of an oblique shock wave with turbulent hypersonic blunt body flows [AIAA PAPER 89-0272] p 3 A89-28405
- Optical measurements of soot and temperature profiles in premixed propane-oxygen flames p 92 A89-35008
- California Univ., Davis.**
- Pdf - Transport equations for chemically reacting flows p 152 A89-51880
- California Univ., Irvine.**
- Behavior in normal and reduced gravity of an enclosed liquid/gas system with nonuniform heating from above [AIAA PAPER 89-0070] p 145 A89-25061
- Evolution of particle-laden jet flows - A theoretical and experimental study p 146 A89-27693
- A numerical and experimental study of confined swirling jets [AIAA PAPER 89-2898] p 151 A89-47161
- A numerical and experimental study of coaxial jets p 153 A89-52500
- Behavior in normal and reduced gravity of an enclosed liquid/gas system with nonuniform heating from above [NASA-TM-101471] p 120 N89-17046
- Experiment plans to study preignition processes of a pool fire in low gravity [NASA-CR-182256] p 121 N89-19442
- California Univ., La Jolla.**
- Radiative structures of lycopodium-air flames in low gravity [AIAA PAPER 89-0500] p 91 A89-25406
- California Univ., Los Angeles.**
- Electron velocity distributions and plasma waves associated with the injection of an electron beam into the ionosphere p 215 A89-43698
- Micro laminate composites as thermal barrier coatings p 83 A89-54261
- California Univ., Santa Barbara.**
- Is the great attractor really a great wall? p 241 A89-36278
- TEM studies of oxidized NiAl and NiAl cross sections p 99 A89-46506
- Gear optimization [NASA-CR-4201] p 182 N89-13793
- Calspan-Buffalo Univ. Research Center, NY.**
- Turbine-stage heat transfer - Comparison of short-duration measurements with state-of-the-art predictions p 142 A89-16458
- Development of BEM for ceramic composites [NASA-CR-183313] p 111 N89-14311
- Development of an integrated BEM approach for hot fluid structure interaction [NASA-CR-184587] p 27 N89-15114
- Calspan Corp., Arnold AFS, TN.**
- Experimental evaluation of resistojet thruster plume shields p 59 A89-47487
- Cambridge Univ. (England).**
- Calculations of inlet distortion induced compressor flow field instability p 8 A89-52498
- Carnegie-Mellon Univ., Pittsburgh, PA.**
- A heat-driven monochromatic light source p 224 A89-41722
- Dynamics of face and annular seals with two-phase flow [NASA-CR-183352] p 182 N89-12870
- Thermal effects in two-phase flow through face seals [NASA-CR-185968] p 182 N89-13788
- Case Western Reserve Univ., Cleveland, OH.**
- Design of a GaAlAs travelling wave Mach-Zehnder electro-optic modulator p 130 A89-10342
- Robots for manipulation in a micro-gravity environment p 215 A89-11682
- Transmission electron microscopy of composites p 79 A89-14560
- Application of optical correlation techniques to particle imaging [AIAA PAPER 88-4661] p 169 A89-14985
- Analysis of microalloy precipitate reversion in steels p 94 A89-15108
- Microwave response of an HEMT photoconductor p 131 A89-15824
- Bulk undercooling, nucleation, and macrosegregation of Pb-Sn alloys p 117 A89-17106
- Gravitational macrosegregation in unidirectionally solidified lead-tin alloy p 117 A89-17112
- Macrosegregation in undercooled Pb-Sn eutectic alloys p 95 A89-19621
- Comparison of the surface charge behavior of commercial silicon nitride and silicon carbide powders p 105 A89-21444

- Experimental evidence for a transverse magnetization of the Abrikosov lattice in anisotropic superconductors p 234 A89-21473
- Theoretical performance of hydrogen-bromine rechargeable SPE fuel cell p 207 A89-23290
- Experimental and numerical investigation of an oblique shock wave/turbulent boundary layer interaction with continuous suction [AIAA PAPER 89-0357] p 4 A89-28407
- A parametric LQ approach to multiobjective control system design p 219 A89-28605
- Shubnikov-de Haas measurements of the 2-D electron gas in pseudomorphic In(0.1)Ga(0.9)As grown on GaAs p 235 A89-29299
- Exposure time considerations in high temperature low cycle fatigue p 192 A89-29600
- Critical currents of aligned grains of Ti-Ba-Ca-Cu-O compounds p 235 A89-30335
- On the orthorhombic phase in ZrO<sub>2</sub>-based alloys p 105 A89-30631
- The influence of annealing in the ferrite-plus-austenite phase field on the stability of vanadium carbide precipitates p 97 A89-32803
- Interfacial adhesion - Theory and experiment p 97 A89-35307
- Auger analysis of a fiber/matrix interface in a ceramic matrix composite p 82 A89-35311
- Identification of structural interface characteristics using component mode synthesis p 193 A89-36177
- Doping directed at the oxygen sites in Y1Ba2Cu3O(7-delta) - The effect of sulfur, fluorine, and chlorine p 133 A89-37824
- Comparison of the bidirectional reflectance distribution function of various surfaces p 230 A89-41530
- Deep-level transient spectroscopy of Al(x)Ga(1-x)As/GaAs using nondestructive acousto-electric voltage measurement p 133 A89-42742
- Aperture impedance of flared horns p 125 A89-43543
- Free energy surfaces in the superconducting mixed state p 236 A89-43928
- Pulsed ion beam investigation of the kinetics of surface reactions p 93 A89-44542
- Tribological properties of structural ceramics p 107 A89-51258
- The low cycle fatigue deformation response of a single-crystal superalloy at 650 C p 99 A89-52204
- New results concerning the use of kinematically redundant manipulators in microgravity environments [AIAA PAPER 89-3562] p 215 A89-52647
- Avalanche in adhesion p 100 A89-54495
- Deformation and fracture of single-crystal and sintered polycrystalline silicon carbide produced by cavitation p 108 A89-54985
- Thermodynamic analysis of compatibility of several reinforcement materials with FeAl alloys [NASA-CR-4172] p 83 N89-10128
- Thermodynamic analysis of compatibility of several reinforcement materials with beta phase NiAl alloys [NASA-CR-4171] p 84 N89-10131
- Microwave characteristics of interdigitated photoconductors on a HEMT structure [NASA-CR-182197] p 135 N89-12820
- Local-global analysis of crack growth in continuously reinforced ceramic matrix composites [NASA-CR-182231] p 197 N89-13820
- Analysis of interface crack branching [NASA-CR-182273] p 202 N89-21265
- Finite element modeling of frictionally restrained composite interfaces [NASA-CR-182281] p 203 N89-23918
- Chicago Univ., IL.**
- Patterns of the cosmic microwave background from evolving string networks p 240 A89-14618
- Cosmic strings - A problem or a solution? p 240 A89-19610
- Superheavy magnetic monopoles and main-sequence stars p 240 A89-20377
- Limits to the radiative decays of neutrinos and axions from gamma-ray observations of SN 1987A p 242 A89-26985
- Is the great attractor really a great wall? p 241 A89-36278
- The stability analysis of magnetohydrodynamic equilibria - Comparing the thermodynamic approach with the energy principle p 232 A89-39391
- Nucleosynthesis, neutrino bursts and gamma-rays from coalescing neutron stars p 241 A89-46577
- Cincinnati Univ., OH.**
- Characterization of GaAlAs optical waveguide heterostructures grown by molecular beam epitaxy p 130 A89-10343
- Behavior in normal and reduced gravity of an enclosed liquid/gas system with nonuniform heating from above [AIAA PAPER 89-0070] p 145 A89-25061

- Plasma deposited silicon nitride for indium phosphide encapsulation p 235 A89-27794
- Vision sensing techniques in aeronautics and astronautics p 219 A89-31087
- Oxide scale stresses in polycrystalline Ni200 p 98 A89-38859
- Finite-element grid improvement by minimization of stiffness matrix trace p 194 A89-42339
- Submicron nickel-oxide-gold tunnel diode detectors for rectennas p 133 A89-43469
- Adhesion, friction, and wear of plasma-deposited thin silicon nitride films at temperatures to 700 C p 107 A89-48250
- Adhesion, friction, and wear of plasma-deposited thin silicon nitride films at temperatures to 700 C [NASA-TM-101377] p 109 N89-11913
- Simulation of 2-dimensional viscous flow through cascades using a semi-elliptic analysis and hybrid C-H grids [NASA-CR-4180] p 10 N89-12553
- Constitutive modeling for single crystal superalloys p 101 N89-12911
- Behavior in normal and reduced gravity of an enclosed liquid/gas system with nonuniform heating from above [NASA-TM-101471] p 120 N89-17046
- City Coll. of the City Univ. of New York, NY.**
- An experimental study of near wall flow parameters in the blade end-wall corner region [NASA-CR-4211] p 12 N89-15898
- Clarkson Univ., Potsdam, NY.**
- Structural behavior of composites with progressive fracture [AIAA PAPER 89-1271] p 192 A89-30754
- Clemson Univ., SC.**
- Development of a special-purpose test surface guided by uncertainty analysis p 144 A89-22736
- Mutual coupling in a finite planar array with interelement holes present p 125 A89-42768
- Aperture impedance of flared horns p 125 A89-43543
- Cleveland State Univ., OH.**
- Fiber-optic temperature sensor using a spectrum-modulating semiconductor etalon p 168 A89-10366
- Fiber composite sandwich thermostructural behavior - Computational simulation p 190 A89-11246
- Structural chemistry of Au(III)-substituted Ba2YCu3O(7-delta) p 89 A89-12620
- Microsegregation in directionally solidified Pb-8.4 at. pct Au alloy p 94 A89-12758
- Radiographic and ultrasonic characterization of sintered silicon carbide p 187 A89-14700
- Composite interlaminar fracture toughness - Three-dimensional finite-element modeling for mixed mode I, II, and fracture p 190 A89-16278
- A viscoplastic constitutive theory for metal matrix composites at high temperature p 80 A89-20725
- Dendritic solidification in binary alloys p 96 A89-22560
- Interaction of Au, Ag, and Bi ions with Ba2YCu3O(7-y) - Implications for superconductor applications p 235 A89-22886
- Finite element substructuring methods for composite mechanics p 80 A89-26291
- Connection between energy relations of solids and molecules p 91 A89-26406
- Structural behavior of composites with progressive fracture [AIAA PAPER 89-1271] p 192 A89-30754
- Oxidation and protection of fiberglass-epoxy composite masts for photovoltaic arrays in the low earth orbital environment p 44 A89-35316
- Free-edge delamination - Laminar width and loading conditions effects p 193 A89-36294
- Intensity-based fibre-optic sensing system using contrast modulation of subcarrier interference pattern p 170 A89-39302
- An improved correction algorithm for number density measurements made with the forward scattering spectrometer probe p 170 A89-44122
- A correction algorithm for particle size distribution measurements made with the forward-scattering spectrometer probe p 170 A89-44123
- A self diagnostic system for piezoelectric sensors [AIAA PAPER 89-2638] p 171 A89-46980
- Design procedures for fiber composite box beams p 195 A89-48674
- Strain measurements in a rotary engine housing [SAE PAPER 890333] p 181 A89-51493
- Mathematical modeling of solid oxide fuel cells [NASA-CR-182188] p 209 N89-12122
- Assessment and comparison of 100-MW coal gasification phosphoric acid fuel cell power plants [NASA-CR-182189] p 209 N89-13103
- Examination of coating failure by acoustic emission p 110 N89-13654

- Stochastic modeling of crack initiation and short-crack growth under creep and creep-fatigue conditions [NASA-TM-101358] p 199 N89-17286
- Reliability-based failure analysis of brittle materials [NASA-CR-184799] p 189 N89-20489
- Colorado State Univ., Fort Collins.**
- Plasma contacting - An enabling technology [AIAA PAPER 89-0677] p 231 A89-25537
- Ground-based tests of hollow cathode plasma contactors [AIAA PAPER 89-1558] p 232 A89-40188
- Experimental validation of a phenomenological model of the plasma contacting process p 232 A89-43357
- Closed-drift thruster investigations [NASA-CR-179497] p 62 N89-11808
- The divergence characteristics of constrained-sheath optics systems for use with 5-eV atomic oxygen sources [NASA-CR-182238] p 229 N89-19973
- Space plasma contractor research, 1988 [NASA-CR-182283] p 233 N89-21658
- Columbia Univ., New York, NY.**
- The effect of Co alloying content on the kinetics of reaction zone growth in tungsten fiber reinforced superalloy composites p 79 A89-11324
- Interdiffusional effects between TiBe12 and NiAl intermetallics p 95 A89-21395
- Reaction kinetics between fiber and matrix p 83 A89-36420
- Communications Satellite Corp., Clarksburg, MD.**
- Intersatellite link application to commercial communications satellites p 43 A89-39144
- Assessment of satellite communications quality study. Addendum 1: Impact of propagation delay on data transmission [NASA-CR-182229] p 126 N89-14369
- Connecticut Univ., Storrs.**
- Iron-base superalloys - A phase analysis of the multicomponent system (Fe-Mn-Cr-Mo-Nb-Al-Si-C) p 95 A89-17379
- Biaxial thermo-mechanical fatigue p 194 A89-43527
- Fracture mechanics applied to elevated temperature crack growth p 195 A89-47705
- Constitutive modelling of single crystal and directionally solidified superalloys p 101 N89-12912
- X-ray based extensometry [NASA-CR-185058] p 176 N89-25432
- Cooper Union, New York, NY.**
- Kinetics of fracture in Fe-3Si steel under mode I loading p 99 A89-47320
- Cornell Univ., Ithaca, NY.**
- Diagonal implicit multigrid algorithm for the Euler equations p 1 A89-11110
- LU implicit multigrid algorithm for the three-dimensional Euler equations p 143 A89-19906
- Graphical postprocessing for 3-D mesh quality evaluation p 217 A89-38846
- Propulsion over a wide Mach number range [NASA-CR-182267] p 29 N89-20134
- Multigrid calculation of three-dimensional turbomachinery flows [NASA-CR-185332] p 165 N89-26172
- Cummings (Robert L.), Litchfield, OH.**
- Performance estimates for the Space Station power system Brayton Cycle compressor and turbine [NASA-CR-182263] p 73 N89-26903

## D

- Dartmouth Coll., Hanover, NH.**
- Room temperature tensile ductility in polycrystalline B2 Ni-30Al-20Fe p 98 A89-44568
- Dayton Univ., OH.**
- Navier-Stokes solution to the flowfield over ice accretion shapes p 1 A89-12557
- A numerical investigation of the influence of surface roughness on heat transfer in ice accretion [AIAA PAPER 89-0737] p 146 A89-25554
- Delaware Univ., Newark.**
- A new structure for comparing surface passivation materials of GaAs solar cells p 213 N89-24725
- Deskin Research Group, Santa Clara, CA.**
- Compensation of reflector antenna surface distortion using an array feed p 126 A89-53136
- Detroit Diesel Allison, Indianapolis, IN.**
- Measurements of heat transfer distribution over the surfaces of highly loaded turbine nozzle guide vanes p 141 A89-12752
- Improved numerical methods for turbulent viscous flows aerothermal modeling program, phase 2 [NASA-CR-182169] p 154 N89-12010
- AGT (Advanced Gas Turbine) technology project [NASA-CR-182127] p 186 N89-26246

- Douglas Aircraft Co., Inc., Long Beach, CA.**
- Multiple Application Propfan Study (MAPS): Advanced tactical transport [NASA-CR-175003] p 28 N89-19300
- Drexel Univ., Philadelphia, PA.**
- Degradation mechanisms of n-dodecane with sulfur and nitrogen dopants during thermal stressing p 116 A89-22277
- NOx formation from the combustion of monodisperse n-heptane sprays doped with fuel-nitrogen additives p 116 A89-42695
- Duke Univ., Durham, NC.**
- On the role of artificial viscosity in Navier-Stokes solvers [AIAA PAPER 89-1947] p 5 A89-41794

## E

- Ecole Centrale de Lyon (France).**
- Universal features of the equation of state of solids p 237 A89-48960
- Ecole Polytechnique, Palaiseau (France).**
- Patterns of the cosmic microwave background from evolving string networks p 240 A89-14618
- Electric Propulsion Lab., Inc., Lancaster, CA.**
- A detailed model of electrothermal propulsion systems [AIAA PAPER 89-2262] p 56 A89-46707
- A detailed model of ion propulsion systems [AIAA PAPER 89-2268] p 56 A89-46712
- User interactive electric propulsion software design [AIAA PAPER 89-2376] p 57 A89-46783
- A 50 cm diameter annular ion engine [AIAA PAPER 89-2716] p 57 A89-47039
- Thermal mechanical analyses of large diameter ion accelerator systems [AIAA PAPER 89-2718] p 58 A89-47041
- Emerson Electric Co., Saint Louis, MO.**
- A versatile power converter for high-frequency link systems p 131 A89-21200
- Engineering Science Software, Inc., Smithfield, RI.**
- Constitutive modelling of single crystal and directionally solidified superalloys p 102 N89-17325
- Exeter Univ. (England).**
- The upper-branch stability of compressible boundary layer flows [NASA-TM-102128] p 167 N89-28748
- Exfluor Research Corp., Austin, TX.**
- The preparation of new perfluoro ether fluids exhibiting excellent thermal-oxidative stabilities p 76 A89-12760

## F

- Fermi National Accelerator Lab., Batavia, IL.**
- The large-scale microwave background anisotropy in decaying particle cosmology p 240 A89-15426
- Cosmic strings and the large-scale structure p 240 A89-19604
- Cosmic strings - A problem or a solution? p 240 A89-19610
- Superheavy magnetic monopoles and main-sequence stars p 240 A89-20377
- Limits to the radiative decays of neutrinos and axions from gamma-ray observations of SN 1987A p 242 A89-26985
- Is the great attractor really a great wall? p 241 A89-36278
- The stability analysis of magnetohydrodynamic equilibria - Comparing the thermodynamic approach with the energy principle p 232 A89-39391
- Nucleosynthesis, neutrino bursts and gamma-rays from coalescing neutron stars p 241 A89-46577
- A coasting cosmology p 241 A89-53833
- Florida Univ., Gainesville.**
- Calculations of the unsteady, three-dimensional flow field inside a motored Wankel engine [SAE PAPER 880625] p 19 A89-12307
- Flow Research, Inc., Kent, WA.**
- Shock-wave-induced mixing enhancement in scramjet combustors [AIAA PAPER 89-0104] p 145 A89-25091
- Preliminary study of the interactions caused by crossing shock waves and a turbulent boundary layer [AIAA PAPER 89-0359] p 145 A89-25303
- Optimizing advanced propeller designs by simultaneously updating flow variables and design parameters p 5 A89-39189
- Aerodynamic optimization by simultaneously updating flow variables and design parameters with application to advanced propeller designs [NASA-CR-182181] p 24 N89-11750
- User's manual for an aerodynamic optimization scheme that updates flow variables and design parameters simultaneously [NASA-CR-182180] p 10 N89-13399

**H**

**Ford Aerospace and Communications Corp., Palo Alto, CA.**

- Space Station battery system design and development p 52 A89-15378
- COLD-SAT orbital experiment configured for Atlas launch p 45 A89-53327
- The potential impact of MMICs on future satellite communications p 126 N89-17078 [NASA-CR-182227]
- The potential impact of MMICs on future satellite communications: Executive summary [NASA-CR-182227-EXEC-SUMM] p 127 N89-17079

**Ford Motor Co., Dearborn, MI.**

- Improved silicon carbide for advanced heat engines. I - Process development for injection molding p 106 A89-33619
- Improved silicon carbide for advanced heat engines. II - Pressureless sintering and mechanical properties of injection molded silicon carbide p 106 A89-33620
- Improved silicon carbide for advanced heat engines [NASA-CR-179477] p 112 N89-15251

**Forest Products Lab., Madison, WI.**

- Improving the fatigue resistance of adhesive joints in laminated wood structures p 85 N89-12675 [NASA-CR-182165]

**Fukui Univ. (Japan).**

- Deformation and fracture of single-crystal and sintered polycrystalline silicon carbide produced by cavitation p 108 A89-54985

**G**

**Garrett Corp., Torrance, CA.**

- Advanced solar receivers for space power p 54 A89-29116

**Garrett Turbine Engine Co., Phoenix, AZ.**

- Thermal barrier coating life prediction model development p 109 N89-12920
- Thermal barrier coating life-prediction model development [NASA-CR-175002] p 26 N89-13433
- Thermal barrier coating life-prediction model development p 200 N89-17331
- Oxide-dispersion-strengthened turbine blades. Volume 2 [NASA-CR-179561-VOL-2] p 28 N89-18487

**Gedeon Associates, Athens, OH.**

- Description of an oscillating flow pressure drop test rig p 142 A89-15188

**General Dynamics Corp., San Diego, CA.**

- An analysis of possible advanced space strategies featuring the role of space resource utilization [IAF PAPER 88-587] p 37 A89-17861
- COLD-SAT orbital experiment configured for Atlas launch p 45 A89-53327

**General Electric Co., Cincinnati, OH.**

- Surface fatigue life of carburized and hardened M50NiL and AISI 9310 spur gears and rolling-contact test bars [AIAA PAPER 89-2819] p 180 A89-47105
- Sensors for ceramic components in advanced propulsion systems: Summary of literature survey and concept analysis, task 3 report p 172 N89-11192 [NASA-CR-180900]
- Fiber optic control system integration p 231 N89-13256 [NASA-CR-179568]
- Constitutive modeling for isotropic materials [NASA-CR-174805] p 26 N89-13436
- Thermal barrier coating life prediction model development p 110 N89-13621 [NASA-CR-180807]
- Elevated temperature crack growth p 200 N89-17335

- High speed turboprop aeroacoustic study (single rotation). Volume 1: Model development [NASA-CR-182257-VOL-1] p 229 N89-24139
- Revolutionary opportunities for materials and structures study, addendum p 34 N89-29351 [NASA-CR-179642-ADD]
- Revolutionary opportunities for materials and structures study, addendum no. 1 [NASA-CR-179642-ADD-1] p 47 N89-29478

**General Electric Co., Fairfield, CT.**

- Heat transfer in gas turbine engines and three-dimensional flows; Proceedings of the Symposium, ASME Winter Annual Meeting, Chicago, IL, Nov. 27-Dec. 2, 1988 p 148 A89-34926
- On 3D inelastic analysis methods for hot section components p 196 N89-12906
- Component specific modeling p 25 N89-12907
- Elevated temperature crack growth p 196 N89-12915
- Thermal barrier coating life prediction model p 109 N89-12921

**General Motors Corp., Detroit, MI.**

- Aerothermal modeling program, phase 2 p 156 N89-12890
- Aerothermal modeling program, phase 2. Element B: Flow interaction experiment p 156 N89-12891
- Aerothermal modeling program, phase 2. Element C: Fuel injector-air swirl characterization p 156 N89-12892
- Turbine airfoil film cooling p 158 N89-12903

**General Motors Corp., Indianapolis, IN.**

- Development of an analytical model to assess fuel property effects on combustor performance p 21 A89-20949
- Design and test of a propan gear system p 179 A89-22290
- Solution of three-dimensional flow problems using a flux-spline method [AIAA PAPER 89-0687] p 146 A89-25543
- Evolution of particle-laden jet flows - A theoretical and experimental study p 146 A89-27683
- A numerical and experimental study of confined swirling jets [AIAA PAPER 89-2898] p 151 A89-47161
- A numerical and experimental study of coaxial jets p 153 A89-52500

- The effects of leading edge and downstream film cooling on turbine vane heat transfer [NASA-CR-182133] p 158 N89-13754
- Aerothermal modeling program. Phase 2, element B: Flow interaction experiment p 160 N89-17304
- Two- and three-dimensional turbine blade row flow field simulations p 161 N89-17313
- Turbine airfoil film cooling p 161 N89-17315

**General Motors Research Labs., Warren, MI.**

- Connection between energy relations of solids and molecules p 91 A89-26406
- Universal features of the equation of state of solids p 237 A89-48960
- Avalanche in adhesion p 100 A89-54495

**George Washington Univ., Washington, DC.**

- Determination of longitudinal aerodynamic derivatives using flight data from an icing research aircraft [AIAA PAPER 89-0754] p 34 A89-28454

**Georgia Inst. of Tech., Atlanta.**

- Solution methods for one-dimensional viscoelastic problems p 191 A89-19914
- Evaluation of three turbulence models for the prediction of steady and unsteady airloads [AIAA PAPER 89-0609] p 3 A89-25485
- Technique for the prediction of airfoil flutter characteristics in separated flow p 191 A89-27744
- Nonisothermal elastoviscoplastic snap-through and creep buckling of shallow arches p 194 A89-47370
- Constitutive behavior of single crystal PWA 1480 and directionally solidified MAR-M 246 under monotonic and cyclic loads at high and low temperature p 100 N89-12634

- Non-isothermal buckling behavior of viscoplastic shell structures [NASA-CR-183013] p 197 N89-12931
- Considerations in development and implementation of elasto-viscoplastic constitutive model for high temperature applications [NASA-CR-183403] p 197 N89-12932
- Analysis of shell-type structures subjected to time-dependent mechanical and thermal loading [NASA-CR-183005] p 197 N89-14457
- Deformation modeling and constitutive modeling for anisotropic superalloys [NASA-CR-42115] p 202 N89-21258
- Analysis of shell-type structures subjected to time-dependent mechanical and thermal loading [NASA-CR-184989] p 203 N89-24669

**Giner, Inc., Waltham, MA.**

- Oxygen electrodes for rechargeable alkaline fuel cells p 211 N89-22998

**Gordon (Sanford), Cleveland, OH.**

- NNEPEQ - Chemical equilibrium version of the Navy/NASA Engine Program [ASME PAPER 88-GT-314] p 22 A89-24989

**Grumman Aerospace Corp., Bethpage, NY.**

- Solar dynamic heat rejection technology. Task 1: System concept development [NASA-CR-179618] p 158 N89-13731

**GTE Labs., Inc., Waltham, MA.**

- Optoelectronic techniques for broadband switching p 131 A89-15825
- Study of optoelectronic switch for satellite-switched time-division multiple access [NASA-CR-179630] p 135 N89-13706
- A comparative study of the influence of buoyancy driven fluid flow on GaAs crystal growth p 121 N89-20295

**GTE Valente Corp., Troy, MI.**

- Adhesion scratch testing - A round-robin experiment p 171 A89-54281

**Hamilton Standard Div., United Aircraft Corp., Windsor Locks, CT.**

- Large-scale Advanced Prop-fan (LAP) hub/blade retention design report [NASA-CR-174786] p 28 N89-19299

**Harris Corp., Melbourne, FL.**

- A 20 GHz low noise, low cost receiver for digital satellite communication system, ground terminal applications [NASA-CR-182243] p 127 N89-19449
- Advanced modulation technology development for earth station demodulator applications [NASA-CR-185126] p 43 N89-26880

**Harvard Univ., Cambridge, MA.**

- Connection between energy relations of solids and molecules p 91 A89-26406

**Hebrew Univ., Jerusalem (Israel).**

- Nucleosynthesis, neutrino bursts and gamma-rays from coalescing neutron stars p 241 A89-46577

**High Technology Corp., Hampton, VA.**

- Spatial resolution and downwash velocity corrections for multiple-hole pressure probes in complex flows p 171 A89-45909

**Honeywell, Inc., Bloomington, MN.**

- GaAs circuits for monolithic optical controller p 131 A89-15828
- Development of gallium arsenide high-speed, low-power serial parallel interface modules: Executive summary [NASA-CR-182272] p 137 N89-21173

**Houston Univ., TX.**

- Passive and active control of jet turbulence p 140 A89-10176
- Turbulence management in free shear flows by control of coherent structures p 147 A89-30908
- Effects of heat release on the large-scale structure in turbulent mixing layers p 147 A89-31844
- Huff (Ronald G.) and Associates, North Olmsted, OH. Noise generated by a flight weight, air flow control valve in a vertical takeoff and landing aircraft thrust vectoring system [NASA-CR-182232] p 228 N89-20776

**Huff and Associates, Cleveland, OH.**

- Unsteady heat transfer in turbine blade ducts - Focus on combustor sources p 153 A89-53286

**Hughes Aircraft Co., El Segundo, CA.**

- A method for producing a shaped contour radiation pattern using a single shaped reflector and a single feed p 125 A89-42758
- Compensation of reflector antenna surface distortion using an array feed p 126 A89-53136

**Hughes Aircraft Co., Malibu, CA.**

- The effect of different alkali metal hydroxides on nickel electrode life p 207 A89-15280

**Hughes Aircraft Co., Torrance, CA.**

- Development of a 75-watt 60-GHz traveling-wave tube for intersatellite communications [NASA-CR-182135] p 138 N89-24530

**Hughes Research Labs., Malibu, CA.**

- KOH concentration effect on cycle life of nickel-hydrogen cells. III - Cycle life test p 207 A89-23283
- Model for computing volume-averaged plasma properties in electron-bombardment ion thrusters p 54 A89-28339
- Mercury ion thruster technology [NASA-CR-174974] p 66 N89-21834

**I**

**Idaho National Engineering Lab., Idaho Falls.**

- Kinetic energy equations for the average-passage equation system p 237 A89-28347

**Idaho Univ., Moscow.**

- Effects of cobalt concentration on the relative resistance to octahedral and cube slip in nickel-base superalloys p 94 A89-17115

**Illinois Inst. of Tech., Chicago.**

- Rapid solidification research at the NASA Lewis Research Center p 95 A89-18203

**Illinois Univ., Champaign.**

- Townsend coefficients for electron scattering over dielectric surfaces p 231 A89-16409

**Illinois Univ., Chicago.**

- Transmission errors and bearing contact of spur, helical and spiral bevel gears [SAE PAPER 881294] p 179 A89-21000
- Crowned spur gears - Methods for generation and tooth contact analysis. I - Basic concepts, generation of the pinion tooth surface by a plane p 179 A89-29306
- Crowned spur gears - Methods for generation and Tooth Contact Analysis. II - Generation of the pinion tooth surface by a surface of revolution p 180 A89-37665
- Damage analysis of a crack layer p 194 A89-42984



- Review of FD-TD numerical modeling of electromagnetic wave scattering and radar cross section p 19 A89-45107
- Topology of modified helical gears and Tooth Contact Analysis (TCA) program [NASA-CR-4224] p 186 N89-22920
- Illinois Univ., Urbana.**
- Ray-tube integration in shooting and bouncing ray method p 124 A89-15152
- Shubnikov-de Haas measurements of the 2-D electron gas in pseudomorphic  $\text{In}(0.1)\text{Ga}(0.9)\text{As}$  grown on GaAs p 235 A89-29299
- Shooting and bouncing rays - Calculating the RCS of an arbitrarily shaped cavity p 124 A89-34242
- Nondestructive evaluation/characterization of composite materials and structures using the acousto-ultrasonic techniques p 188 A89-36571
- Optimal terminal maneuver for a cooperative impulsive rendezvous p 38 A89-36946
- High-frequency RCS of open cavities with rectangular and circular cross sections p 125 A89-39595
- A method for producing a shaped contour radiation pattern using a single shaped reflector and a single feed p 125 A89-42758
- High pressure multiaxial extensometry p 170 A89-43532
- Effects of microstructure and nonstoichiometry on electrical properties of vanadium dioxide films p 236 A89-44527
- Rigorous analysis of a circular patch antenna excited by a microstrip transmission line p 125 A89-53134
- Compensation of reflector antenna surface distortion using an array feed p 126 A89-53136
- Calculation of the electron wave function in a graded-channel double-heterojunction modulation-doped field-effect transistor p 134 A89-54417
- Illinois Univ., Urbana-Champaign.**
- A comparison of reflector antenna designs for wide-angle scanning [NASA-TM-101459] p 127 N89-21138
- Imperial Coll. of Science and Technology, London (England).**
- Coherent structures in transitional and turbulent free shear flows p 147 A89-28999
- Innovative Dynamics, Ithaca, NY.**
- Distributed ice accretion sensor for smart aircraft structures [AIAA PAPER 89-0772] p 17 A89-25571
- Insitec, Inc., San Ramon, Ca.**
- Calibration of single particle sizing velocimeters using photomask reticles p 170 A89-33379
- Institut d'Astrophysique, Paris (France).**
- Patterns of the cosmic microwave background from evolving string networks p 240 A89-14618
- International Business Machines Corp., Yorktown Heights, NY.**
- Experiments and analysis of a compact electrothermal thruster p 59 A89-47494
- International Fuel Cells Corp., South Windsor, CT.**
- Alkaline fuel cell performance investigation p 207 A89-15258
- Iowa State Univ. of Science and Technology, Ames.**
- Experimental evidence for a transverse magnetization of the Abrikosov lattice in anisotropic superconductors p 234 A89-21473
- Critical currents of aligned grains of Ti-Ba-Ca-Cu-O compounds p 235 A89-30335
- Universal features of the equation of state of solids p 237 A89-48960
- Iowa Univ., Iowa City.**
- Coherent Cerenkov radiation from the Spacelab 2 electron beam p 231 A89-24292
- The plasma wake of the Shuttle Orbiter p 215 A89-43680
- Electron velocity distributions and plasma waves associated with the injection of an electron beam into the ionosphere p 215 A89-43698
- Plasma density, temperature and turbulence in the wake of the Shuttle Orbiter p 233 A89-53209
- Plasma density fluctuations observed during Space Shuttle Orbiter water releases p 233 A89-54759
- Iwate Univ., Morioka (Japan).**
- Degradation and crosslinking of perfluoroalkyl polyethers under X-ray irradiation in ultrahigh vacuum [NASA-TP-2910] p 114 N89-21103
- Jet Propulsion Lab., California Inst. of Tech., Pasadena.**
- Nuclear reactor power as applied to a space-based radar mission p 51 A89-15317
- Systems aspects of a space nuclear reactor power system p 51 A89-15327

- High temperature thermal conductivity measurements on lanthanum sulfides using the flash method p 77 A89-16500
- The plasma wake of the Shuttle Orbiter p 215 A89-43680
- The POLAR code wake model - Comparison with in situ observations p 233 A89-45632
- The NASA Electric Propulsion Program p 59 A89-47428
- Plasma density, temperature and turbulence in the wake of the Shuttle Orbiter p 233 A89-53209
- Systems autonomy technology: Executive summary and program plan [NASA-TM-100999] p 216 N89-18045
- A comparison of reflector antenna designs for wide-angle scanning [NASA-TM-101459] p 127 N89-21138
- John Carroll Univ., Cleveland, OH.**
- Fiber-optic temperature sensor using a spectrum-modulating semiconductor etalon p 168 A89-10366

## K

- Kansas Univ., Lawrence.**
- Large amplitude acoustic excitation of swirling turbulent jets [AIAA PAPER 89-0970] p 4 A89-29098
- Effect of initial swirl distribution on the evolution of a turbulent jet p 149 A89-36906
- A model for including thermal conduction in molecular dynamics simulations p 237 A89-41259
- Kansas Univ. Center for Research, Inc., Lawrence.**
- Large amplitude acoustic excitation of swirling turbulent jets [AIAA PAPER 89-0970] p 4 A89-29098
- Turbulent swirling jets with excitation [NASA-CR-180895] p 16 N89-29329
- Karlsruhe Univ. (Germany, F.R.).**
- Morphological study of near threshold fatigue crack growth in a coarse grain aluminum alloy p 94 A89-12326
- Kent State Univ., OH.**
- Avalanche in adhesion p 100 A89-54495
- Kentucky Univ., Lexington.**
- Effects of furnace temperature profile on the interface shape during Bridgman crystal growth p 119 A89-53278
- Kyoto Univ. (Japan).**
- Creep life prediction based on stochastic model of microstructurally short crack growth p 193 A89-36185
- Stochastic modeling of crack initiation and short-crack growth under creep and creep-fatigue conditions [NASA-TM-101358] p 199 N89-17286

## L

- Lagos Univ. (Nigeria).**
- Application of multi-grid methods for solving the Navier-Stokes equations p 153 A89-53172
- Lawrence Livermore National Lab., CA.**
- Patterns of the cosmic microwave background from evolving string networks p 240 A89-14618
- Cosmic strings - A problem or a solution? p 240 A89-19610
- Plasma flow processes within magnetic nozzle configurations [AIAA PAPER 89-2711] p 57 A89-47036
- Lehigh Univ., Bethlehem, PA.**
- Design and simulated performance of a CARS spectrometer for dynamic temperature measurements using electronic heterodyning p 170 A89-37298
- Asymptotic structure and similarity solutions for three-dimensional turbulent boundary layers [AIAA PAPER 89-1863] p 150 A89-42090
- Lockheed Aeronautical Systems Co., Burbank, CA.**
- Interior noise in the untreated Gulfstream II Propfan Test Assessment (PTA) aircraft [AIAA PAPER 89-1119] p 17 A89-33754
- Lockheed Aeronautical Systems Co., Marietta, GA.**
- Near-field acoustic characteristics of a single-rotor propfan [AIAA PAPER 89-1055] p 23 A89-36215
- Installed propfan (SR-7L) far-field noise characteristics [AIAA PAPER 89-1056] p 225 A89-36216
- Lateral noise attenuation of the advanced propeller of the propfan test assessment aircraft [AIAA PAPER 89-1057] p 226 A89-36217
- Fluctuating pressures on wing surfaces in the slipstream of a single-rotor propfan [AIAA PAPER 89-1058] p 226 A89-36218
- Effects of nozzle exit boundary-layer conditions on excitability of heated free jets p 149 A89-36908

- Lockheed-Georgia Co., Marietta.**
- Multiple-Purpose Subsonic Naval Aircraft (MPSNA) Multiple Application Propfan Study (MAPS) [NASA-CR-175096] p 18 N89-19289
- Lockheed Missiles and Space Co., Palo Alto, CA.**
- Mechanisms of elevated-temperature deformation in the B2 aluminides NiAl and CoAl p 94 A89-17378
- A 20-DOF hybrid stress general shell element p 191 A89-21133
- Lockheed Missiles and Space Co., Sunnyvale, CA.**
- PV modules for ground testing [NASA-CR-179476] p 208 N89-11315
- Los Alamos National Lab., NM.**
- Transient performance evaluation of an integrated heat pipe-thermal storage system p 49 A89-15209
- Transient oxidation of single-crystal beta-NiAl p 98 A89-37899
- Nuclear reactor power as applied to a space-based radar mission [NASA-TM-101200] p 230 N89-14831
- Louisiana State Univ., Baton Rouge.**
- Engineering study on the rotary-vee engine concept [SAE PAPER 890332] p 161 A89-51492
- LTV Missiles and Electronics Group, Dallas, TX.**
- The Solar Dynamic radiator with a historical perspective p 51 A89-15340

## M

- Manhattan Coll., New York.**
- Radiative heat transfer in rocket thrust chambers and nozzles [AIAA PAPER 89-1720] p 150 A89-43235
- Radiative transfer in rectangular enclosures - A discretized exchange factor solution p 153 A89-53262
- MARC Analysis Research Corp., Palo Alto, CA.**
- An approach to probabilistic finite element analysis using a mixed-iterative formulation p 191 A89-25849
- MHOST version 4.2. Volume 1: Users' manual [NASA-CR-182235-VOL-1] p 217 N89-13996
- Marko Materials, Inc., North Billerica, MA.**
- Dispersoids in rapidly solidified B2 nickel aluminides p 98 A89-43023
- Marquardt Corp., Van Nuys, CA.**
- Heat transfer in gas turbine engines and three-dimensional flows; Proceedings of the Symposium, ASME Winter Annual Meeting, Chicago, IL, Nov. 27-Dec. 2, 1988 p 148 A89-34926
- Martin Marietta Energy Systems, Inc., Oak Ridge, TN.**
- Thermal analysis of heat storage canisters for a solar dynamic, space power system p 54 A89-29113
- Martin Marietta Labs., Baltimore, MD.**
- Elevated temperature slow plastic deformation of NiAl/TiB<sub>2</sub> particulate composites p 81 A89-31689
- 1200 to 1400 K slow strain rate compressive behavior of small grain size NiAl/Ni<sub>2</sub>AlTi alloys and NiAl/Ni<sub>2</sub>AlTi-TiB<sub>2</sub> composites p 99 A89-53497
- Maryland Univ., College Park.**
- Nucleosynthesis, neutrino bursts and gamma-rays from coalescing neutron stars p 241 A89-46577
- Critical fluid light scattering p 121 N89-20320
- Massachusetts Inst. of Tech., Cambridge.**
- Fluid flow phenomena in the generation of boron carbide suspensions in magnesium melts p 79 A89-19472
- A 20-DOF hybrid stress general shell element p 191 A89-21133
- Investigation of surface water behavior during glaze ice accretion p 16 A89-27739
- Active suppression of aerodynamic instabilities in turbomachines p 3 A89-28341
- Modeling of surface roughness effects on glaze ice accretion [AIAA PAPER 89-0734] p 16 A89-28451
- Induced emission of radiation from a large space-station-like structure in the ionosphere p 44 A89-31915
- Bounds on current collection from the far field by plasma clouds in the ionosphere p 214 A89-34791
- Calculation of unsteady flows in turbomachinery using the linearized Euler equations p 149 A89-36916
- The physics of positively biased conductors surrounded by dielectrics in contact with a plasma p 232 A89-39395
- Vapor condensation at a turbulent liquid surface in systems with possible spaced-based applications [AIAA PAPER 89-2846] p 151 A89-47122
- Calculations of inlet distortion induced compressor flow field instability p 8 A89-52498
- The influence of ice accretion physics on the forecasting of aircraft icing conditions p 16 A89-54803
- Energy in elastic fiber embedded in elastic matrix containing incident SH wave p 188 N89-18694
- [NASA-CR-4205]

- Massachusetts Inst. of Tech., Lexington.**  
Design of a GaAlAs travelling wave Mach-Zehnder electro-optic modulator p 130 A89-10342  
Theory and application of radiation boundary operators p 224 A89-24191
- Max-Planck-Institut für Extraterrestrische Physik, Garching (Germany, F.R.).**  
Electron velocity distributions and plasma waves associated with the injection of an electron beam into the ionosphere p 215 A89-43698
- Maxwell Labs., Inc., La Jolla, CA.**  
A model of electron collecting plasma contractors [AIAA PAPER 89-1560] p 232 A89-40190
- McDonnell-Douglas Astronautics Co., Saint Louis, MO.**  
Average-passage simulation of counter-rotating propfan propulsion systems as applied to cruise missiles [AIAA PAPER 89-2943] p 7 A89-47187
- McDonnell-Douglas Research Labs., Saint Louis, MO.**  
Near-field acoustic environment of a supersonic plume adjacent to a wall [AIAA PAPER 89-1137] p 225 A89-33767
- Mechanical Technology, Inc., Latham, NY.**  
Mod II Stirling engine overviews [SAE PAPER 880539] p 177 A89-12301  
Alternative fuel capabilities of the Mod II Stirling vehicle [SAE PAPER 880543] p 177 A89-12303  
Conceptual design of an advanced Stirling conversion system for terrestrial power generation [NASA-CR-180890] p 238 A89-12504  
High speed balancing applied to the T700 engine [NASA-CR-180899] p 184 A89-20472  
Advanced helium purge seals for Liquid Oxygen (LOX) turbopumps [NASA-CR-182105] p 184 A89-21239
- Michigan State Univ., East Lansing.**  
Calculations of the unsteady, three-dimensional flow field inside a motored Wankel engine [SAE PAPER 880625] p 19 A89-12307  
Regressed relations for forced convection heat transfer in a direct injection stratified charge rotary engine [SAE PAPER 880626] p 178 A89-12308  
Thermal measurements for jets in disturbed and undisturbed crosswind conditions p 20 A89-16102  
Investigations of microwave plasmas - Applications in electrothermal thruster systems [AIAA PAPER 89-2378] p 57 A89-46784  
Experiments and analysis of a compact electrothermal thruster p 59 A89-47494  
Stratified charge rotary engine - Internal flow studies at the MSU engine research laboratory [SAE PAPER 890331] p 181 A89-51477  
Experiments and analysis of a compact electrothermal thruster p 75 A89-27773
- Michigan Technological Univ., Houghton.**  
The surface morphology of crystals melting under solutions of different densities p 235 A89-23482
- Michigan Univ., Ann Arbor.**  
A Monte Carlo-finite element model for strain energy controlled microstructural evolution - 'Rafting' in superalloys p 96 A89-24358  
Combined roles of buoyancy and orientation in nucleate pool boiling p 119 A89-35015  
External electro-optic probing of millimeter-wave integrated circuits p 133 A89-45266  
A detailed analysis of inviscid flux splitting algorithms for real gases with equilibrium or finite-rate chemistry p 151 A89-45424  
Turbulent multiphase flows p 152 A89-51883  
A genuinely multi-dimensional upwind cell-vertex scheme for the Euler equations [NASA-TM-102029] p 223 A89-24872  
Microwave and millimeter-wave power generation in silicon carbide (SiC) IMPATT devices [NASA-CR-185050] p 139 A89-26143  
Molecular beam epitaxial growth of high-quality InSb on InP and GaAs substrates [NASA-CR-185440] p 236 A89-26739  
Surface morphologies and electrical properties of molecular beam epitaxial InSb and InAs(x)Sb(1-x) grown on GaAs and InP substrates [NASA-CR-185439] p 237 A89-26740
- Midwest Research Inst., Golden, CO.**  
Growth of diamond by RF plasma-assisted chemical vapor deposition p 90 A89-20474  
High-efficiency solar cells fabricated from direct-current magnetron sputtered n-indium tin oxide onto p-InP grown by atmospheric pressure metalorganic vapor phase epitaxy p 133 A89-44518  
High-efficiency indium tin oxide/indium phosphide solar cells p 208 A89-44883
- Milletus Associates, Inc., Albuquerque, NM.**  
Film annotation system for a space experiment [NASA-CR-185114] p 176 A89-27152
- Minnesota Mining and Mfg. Co., Saint Paul.**  
Durable thin film coatings for reflectors used in low earth orbit p 77 A89-33150
- Minnesota Univ., Minneapolis.**  
Effect of transition on oscillation flow losses in Stirling engine coolers and heaters p 142 A89-15189  
Development of a special-purpose test surface guided by uncertainty analysis p 144 A89-22736  
Solution of three-dimensional flow problems using a flux-spline method [AIAA PAPER 89-0687] p 146 A89-25543  
A block-corrected subdomain solution procedure for recirculating flow calculations p 152 A89-50147  
Rigorous analysis of a circular patch antenna excited by a microstrip transmission line p 125 A89-53134  
Efficient numerical techniques for complex fluid flows p 156 A89-12894  
Development of low Reynolds number two equation turbulence models for predicting external heat transfer on turbine blades p 157 A89-12901  
A low-Reynolds-number two-equation turbulence model for predicting heat transfer on turbine blades p 160 A89-17310
- Mississippi State Univ., Mississippi State.**  
A simple time-accurate turbomachinery algorithm with numerical solutions of an uneven blade count configuration [AIAA PAPER 89-0206] p 179 A89-25181  
The solid surface combustion Space Shuttle experiment hardware description and ground-based test results [AIAA PAPER 89-0503] p 119 A89-28419  
Transonic flow solutions on general 3D regions using composite-block grids p 6 A89-45428  
Extended observability of linear time-invariant systems under recurrent loss of output data [AIAA PAPER 89-3510] p 220 A89-52603  
An observer-based compensator for distributed delays in integrated control systems [AIAA PAPER 89-3541] p 35 A89-52628
- Missouri Univ., Rolla.**  
Effects of wind-tunnel wall absorption on acoustic radiation of propellers p 225 A89-22285
- Moog, Inc., East Aurora, NY.**  
Fracture mechanics applied to elevated temperature crack growth p 195 A89-47705
- Motorola, Inc., Chandler, AZ.**  
Baseband processor hardware for Advanced Communication Technology Satellite (ACTS) p 43 A89-38298
- Mutl-Metals, Louisville, KY.**  
Elevated temperature slow plastic deformation of NiAl/TiB<sub>2</sub> particulate composites p 81 A89-31689  
1200 to 1400 K slow strain rate compressive behavior of small grain size NiAl/Ni<sub>2</sub>AlTi alloys and NiAl/Ni<sub>2</sub>AlTi-TiB<sub>2</sub> composites p 99 A89-53497
- Multipoint Communications Corp., Sunnyvale, CA.**  
Programmable rate modem utilizing digital signal processing techniques [NASA-CR-185124] p 43 A89-26879

## N

## National Aeronautics and Space Administration, Washington, DC.

- Return of the turboprops p 20 A89-12953  
NASA Aerospace Flight Battery Systems Program - Issues and actions p 49 A89-15224  
Aircraft engines. III p 21 A89-22927  
Nuclear thermal rockets - Next step to space p 55 A89-40480  
NASA's Chemical Transfer Propulsion Program for Pathfinder [AIAA PAPER 89-2298] p 37 A89-46735  
The NASA Electric Propulsion Program p 59 A89-47428

## National Aeronautics and Space Administration, Ames Research Center, Moffett Field, CA.

- Cooperating expert systems for Space Station - Power/thermal subsystem testbeds p 38 A89-15350  
Systems autonomy technology: Executive summary and program plan [NASA-TM-100999] p 216 A89-18045

## National Aeronautics and Space Administration, Goddard Space Flight Center, Greenbelt, MD.

- Systems autonomy technology: Executive summary and program plan [NASA-TM-100999] p 216 A89-18045

## National Aeronautics and Space Administration, John F. Kennedy Space Center, Cocoa Beach, FL.

- Systems autonomy technology: Executive summary and program plan [NASA-TM-100999] p 216 A89-18045

## National Aeronautics and Space Administration.

- Lyndon B. Johnson Space Center, Houston, TX.**  
Cooperating expert systems for Space Station - Power/thermal subsystem testbeds p 38 A89-15350  
Systems autonomy technology: Executive summary and program plan [NASA-TM-100999] p 216 A89-18045

## National Aeronautics and Space Administration, Langley Research Center, Hampton, VA.

- Return of the turboprops p 20 A89-12953  
Determination of longitudinal aerodynamic derivatives using flight data from an icing research aircraft [AIAA PAPER 89-0754] p 34 A89-28454  
A natural low-frequency oscillation of the flow over an airfoil near stalling conditions p 6 A89-45437  
Supersonic jet noise and the high speed civil transport [AIAA PAPER 89-2358] p 227 A89-46772  
Systems autonomy technology: Executive summary and program plan [NASA-TM-100999] p 216 A89-18045

## National Aeronautics and Space Administration, Marshall Space Flight Center, Huntsville, AL.

- Cooperating expert systems for Space Station - Power/thermal subsystem testbeds p 38 A89-15350  
Impact of ETO propellants on the aerothermodynamic analyses of propulsion components [AIAA PAPER 88-3091] p 53 A89-16486  
The plasma wake of the Shuttle Orbiter p 215 A89-43680  
Systems autonomy technology: Executive summary and program plan [NASA-TM-100999] p 216 A89-18045

## National Aeronautics and Space Administration, White Sands Test Facility, NM.

- Friction-induced ignition of metals in high-pressure oxygen p 97 A89-32932

## National Central Univ., Chung-Li (Taiwan).

- Technique for the prediction of airfoil flutter characteristics in separated flow p 191 A89-27744

## National Cheng Kung Univ., Tainan (Taiwan).

- Convective flows in enclosures with vertical temperature or concentration gradients [AIAA PAPER 89-0069] p 118 A89-25060  
Thermosolutal convection in high-aspect-ratio enclosures p 153 A89-53288

## National Inst. of Standards and Technology, Gaithersburg, MD.

- Expert systems applied to spacecraft fire safety [NASA-CR-182266] p 42 A89-23501

## Naval Postgraduate School, Monterey, CA.

- Coded multiple chirp spread spectrum system and overlay service p 124 A89-26769  
Spatial resolution and downwash velocity corrections for multiple-hole pressure probes in complex flows p 171 A89-45909  
A numerical method for computing unsteady 2-D boundary layer flows [NASA-CR-4198] p 155 A89-12835

## Naval Research Lab., Washington, DC.

- Experimental evidence for a transverse magnetization of the Abrikosov lattice in anisotropic superconductors p 234 A89-21473  
Time-dependent computational studies of flames in microgravity [NASA-CR-182298] p 122 A89-25353

## Nebraska Univ., Lincoln.

- Thin-film hermeticity - A quantitative analysis of diamondlike carbon using variable angle spectroscopic ellipsometry p 234 A89-13945  
Growth of diamond by RF plasma-assisted chemical vapor deposition p 90 A89-20474  
Highly oriented Ti<sub>2</sub>Ba<sub>2</sub>Ca<sub>2</sub>Cu<sub>3</sub>O<sub>10</sub> thin films by pulsed laser evaporation p 236 A89-30421  
Preparation of high T<sub>c</sub> (Ti-Ba-Ca-Cu-O) thin films by pulsed laser evaporation and TiO<sub>3</sub> vapor processing p 236 A89-38608  
Radio-frequency plasma chemical vapor deposition growth of diamond p 236 A89-44552  
Characterization of multilayer GaAs/AlGaAs transistor structures by variable angle spectroscopic ellipsometry p 133 A89-49998

## North American Philips Co., Inc., Briarcliff Manor, NY.

- The effect of Co alloying content on the kinetics of reaction zone growth in tungsten fiber reinforced superalloy composites p 79 A89-11324

## North Carolina State Univ., Raleigh.

- The turbulence characteristics of a separated flow with combustion p 92 A89-33369  
Parametric study of statistical bias in laser Doppler velocimetry p 171 A89-47378

## Northwestern Univ., Evanston, IL.

- An application of the WKBJ technique to the on-surface radiation condition p 124 A89-21222  
Theory and application of radiation boundary operators p 224 A89-24191

- Kuhn-Tucker optimization based reliability analysis for probabilistic finite elements p 187 A89-25852  
Review of FD-TD numerical modeling of electromagnetic wave scattering and radar cross section p 19 A89-45107  
Elevated temperature strain gages p 173 N89-12886  
Probabilistic Finite Elements (PFEM) structural dynamics and fracture mechanics p 206 N89-29803  
**Notre Dame Univ., IN.**  
Numerical solution of periodic vortical flows about a thin airfoil [AIAA PAPER 89-1691] p 7 A89-48955
- O**
- Oak Ridge National Lab., TN.**  
Modeling cyclic melting and refreezing in a hollow metal canister [NASA-CR-184630] p 217 N89-15623  
**Ohio State Univ., Columbus.**  
Ray-tube integration in shooting and bouncing ray method p 124 A89-15152  
Crystallization and characterization of Y2O3-SiO2 glasses p 80 A89-19486  
Microstructural evolution on crystallizing the glassy phase in a 5 weight percent Y2O3-Si3N4 ceramic p 80 A89-19487  
Reactions of silicon-based ceramics in mixed oxidation chlorination environments p 105 A89-21442  
Performance of laser Doppler velocimeter with polydisperse seed particles in high-speed flows p 169 A89-22279  
An experimental adaptive array to suppress weak interfering signals p 124 A89-22455  
Experimental study of isothermal swirling flows in a dump combustor p 21 A89-23182  
Studies of transition in boundary layers [AIAA PAPER 89-0034] p 2 A89-25029  
The behavior of SiC and Si3N4 ceramics in mixed oxidation/chlorination environments p 106 A89-33616  
Shooting and bouncing rays - Calculating the RCS of an arbitrarily shaped cavity p 124 A89-34242  
The secondary flow and its stability for natural convection in a tall vertical enclosure p 149 A89-37931  
Modal, ray, and beam techniques for analyzing the EM scattering by open-ended waveguide cavities p 125 A89-39594  
High-frequency RCS of open cavities with rectangular and circular cross sections p 125 A89-39595  
An experimental study of a reattaching supersonic shear layer [AIAA PAPER 89-1801] p 6 A89-42036  
Compressibility and shock wave interaction effects on free shear layers [AIAA PAPER 89-2460] p 7 A89-46847  
Plasma flow processes within magnetic nozzle configurations [AIAA PAPER 89-2711] p 57 A89-47036  
Calculation of the effects of ice on the backscatter of a ground plane [NASA-CR-183303] p 126 N89-10213  
Measurement of the properties of lossy materials inside a finite conducting cylinder [NASA-CR-182500] p 126 N89-10223  
Material parameter determination from scattering measurements [NASA-CR-183312] p 126 N89-10225  
Engineering calculations for solving the orbital allotment problem [NASA-CR-184607] p 217 N89-13993  
The effects of magnetic nozzle configurations on plasma thrusters [NASA-CR-184678] p 64 N89-15170  
A novel approach in formulation of special transition elements: Mesh interface elements [NASA-CR-184768] p 199 N89-16193  
Electromagnetic properties of ice coated surfaces [NASA-CR-184780] p 127 N89-20355  
Analysis of modified SMI method for adaptive array weight control [NASA-CR-184904] p 127 N89-20364  
Analysis of the EM scattering from arbitrary open-ended waveguide cavities using axial Gaussian Beam tracking [NASA-CR-185054] p 128 N89-24518  
A hybrid asymptotic-modal analysis of the EM scattering by an open-ended S-shaped rectangular waveguide cavity [NASA-CR-185053] p 129 N89-24519  
Analysis of modified SMI method for adaptive array weight control [NASA-CR-185493] p 19 N89-25993  
Adaptive array for weak interfering signals: Geostationary satellite experiments [NASA-CR-185450] p 129 N89-26126

- Interaction between Tollmien-Schlichting waves and free-stream disturbances in boundary-layer flows [NASA-CR-185847] p 167 N89-27118  
Specialty functions singularity mechanics problems p 206 N89-29805  
**Oregon State Univ., Corvallis.**  
Space reactor assessment and validation study p 230 N89-13227

## P

- Page (R. J.) Co., Santa Ana, CA.**  
Preliminary design study of hydrogen and ammonia resistojets for prime and auxiliary thrusters [NASA-CR-182176] p 62 N89-10943  
**Pennsylvania State Univ., New Kensington.**  
Interfacial adhesion - Theory and experiment p 97 A89-35307  
**Pennsylvania State Univ., University Park.**  
Effect of alcohol addition on shock-initiated formation of soot from benzene p 90 A89-12903  
Navier-Stokes calculation of solid-propellant rocket motor internal flowfields [AIAA PAPER 88-3182] p 48 A89-14983  
Integrated communication and control systems. I - Analysis [ASME PAPER 88-WA/DSC-1] p 219 A89-22499  
Integrated communication and control systems. II - Design considerations [ASME PAPER 88-WA/DSC-2] p 219 A89-22500  
Observer design for compensation of network-induced delays in integrated communication and control systems p 220 A89-35044  
Formation of polycyclic aromatic hydrocarbons in circumstellar envelopes p 241 A89-14385  
Extended observability of linear time-invariant systems under recurrent loss of output data [AIAA PAPER 89-3510] p 220 A89-52603  
An observer-based compensator for distributed delays in integrated control systems [AIAA PAPER 89-3541] p 35 A89-52628  
Skin-friction measurements by laser interferometry p 167 N89-28737  
**Pennsylvania Univ., Philadelphia.**  
Synthesis and stability of Br2, ICl and IBr intercalated pitch-based graphite fibers p 106 A89-37670  
**Physical Sciences, Inc., Andover, MA.**  
High-temperature LDV seed particle development [NASA-CR-182265] p 175 N89-23851  
**Pioneer Engineering and Mfg. Co., Inc., Madison Heights, MI.**  
Conceptual design of an advanced Stirling conversion system for terrestrial power generation [NASA-CR-180890] p 238 N89-12504  
**Pittsburgh Univ., PA.**  
Raman determination of layer stresses and strains for heterostructures and its application to the cubic SiC/Si system p 234 A89-21871  
On the performance of finite journal bearings lubricated with micropolar fluids p 181 A89-54977  
Computer simulation of a pilot in V/STOL aircraft control loops [NASA-CR-184815] p 215 N89-21479  
**Pratt and Whitney Aircraft, East Hartford, CT.**  
Turbofan forced mixer lobe flow modeling. Part 3: Application to augment engines [NASA-CR-4147-PT-3] p 8 N89-10025  
Further development of the dynamic gas temperature measurement system p 172 N89-12884  
Coolant passage heat transfer with rotation p 157 N89-12899  
Creep fatigue life prediction for engine hot section materials (isotropic): Fourth year progress review p 188 N89-12914  
Life prediction and constitutive models for engine hot section p 188 N89-12916  
Thermal barrier coating life prediction model development p 110 N89-12922  
Turbofan forced mixer lobe flow modeling. 1: Experimental and analytical assessment [NASA-CR-4147-PT-1] p 11 N89-14221  
Turbofan forced mixer lobe flow modeling. 2: Three-dimensional inviscid mixer analysis (FLOMIX) [NASA-CR-4147-PT-2] p 11 N89-14222  
Coolant passage heat transfer with rotation p 161 N89-17314  
Three-dimensional inelastic analysis methods for hot section components p 199 N89-17316  
Three-dimensional inelastic analysis for hot section components, BEST 3D code p 199 N89-17317  
Thermal barrier coating life prediction model development p 200 N89-17333  
High temperature constitutive and crack initiation modeling of coated single crystal superalloys p 112 N89-17334

- Creep fatigue life prediction for engine hot section materials (ISOTROPIC) fifth year progress review p 201 N89-17336  
**MATE program: Erosion resistant compressor airfoil coating, volume 2** [NASA-CR-179645] p 113 N89-18550  
Structural Tailoring of Advanced Turboprops (STAT) programmer's manual [NASA-CR-182164] p 29 N89-20132  
Fatigue life prediction modeling for turbine hot section materials p 30 N89-20142  
**Pratt and Whitney Aircraft, West Palm Beach, FL.**  
Fuel properties effect on the performance of a small high temperature rise combustor [AIAA PAPER 89-2901] p 23 A89-52025  
Evaluation of coated columbium test panels having application to a secondary nozzle extension for the RL10 rocket engine system, parts 1 and 2 [NASA-CR-180809] p 64 N89-13493  
Further development of the dynamic gas temperature measurement system. Volume 2: Computer program user's manual [NASA-CR-179513-VOL-2] p 173 N89-13771  
Design and analysis report for the flight weight 20-inch Columbian secondary nozzle for the RL10 engine [NASA-CR-179612] p 65 N89-16918  
Design, fabrication and test of the RL10 derivative II chamber/primary nozzle [NASA-CR-179595] p 68 N89-23519  
**Pratt and Whitney Aircraft Group, West Palm Beach, FL.**  
Performance potential of air turbo-ramjet employing supersonic through-flow fan [AIAA PAPER 89-0010] p 22 A89-25006  
**Princeton Univ., NJ.**  
Interactions between gaseous electrical discharges and single liquid droplets p 90 A89-19298  
An asymptotic description of transient settling and ultrafiltration of colloidal dispersions p 144 A89-24603  
Preliminary study of the interactions caused by crossing shock waves and a turbulent boundary layer [AIAA PAPER 89-0359] p 145 A89-25303  
Droplet combustion drop tower tests using models of the space flight apparatus [AIAA PAPER 89-0501] p 119 A89-28418  
**Princeton Univ. Observatory, NJ.**  
Nucleosynthesis, neutrino bursts and gamma-rays from coalescing neutron stars p 241 A89-46577  
**Purdue Univ., West Lafayette, IN.**  
Investigation of oscillating cascade aerodynamics by an experimental influence coefficient technique [AIAA PAPER 88-2815] p 1 A89-14976  
Dynamic characteristics of a 20 kHz resonant power system - Fault identification and fault recovery p 52 A89-15357  
Simulation and control of a 20 kHz spacecraft power system p 130 A89-15391  
Aeroelastic response of metallic and composite propan models in yawed flow [AIAA PAPER 88-3154] p 20 A89-17942  
Propeller/wing interaction [AIAA PAPER 89-0535] p 17 A89-25429  
Experimental investigation of transonic oscillating cascade aerodynamics [AIAA PAPER 89-0321] p 3 A89-26369  
Effect of heavy rain on aviation engines [AIAA PAPER 89-0799] p 22 A89-28462  
The turbulence characteristics of a separated flow with combustion p 92 A89-33369  
Model-based analysis of control/display interaction in the hover task p 215 A89-36933  
Parametric study of statistical bias in laser Doppler velocimetry p 171 A89-47378  
Aerodynamic interaction between propellers and wings p 8 A89-50062  
Analysis of supersonic plug nozzle flowfield and heat transfer [NASA-CR-179554] p 10 N89-13397  
LDV measurements in an annular combustor model [NASA-CR-182207] p 159 N89-13755  
The effect of prewhirl on the internal aerodynamics and performance of a mixed flow research centrifugal compressor [NASA-CR-184756] p 161 N89-19503

## R

- RE/SPEC, Inc., Albuquerque, NM.**  
Graphical postprocessing for 3-D mesh quality evaluation p 217 A89-38846  
**Rensselaer Polytechnic Inst., Troy, NY.**  
Crystallization of BaF2-ZnF2-YbF3-ThF4 glass p 230 A89-12236  
Dendritic solidification in binary alloys p 96 A89-22560

## Ricardo-ITI

Measurement of the diffusion coefficient of acetone in succinonitrile at its melting point p 237 A89-23488  
Flight hardware and tele-operations supporting the Isothermal Dendritic Growth Experiment aboard the Space Shuttle

[AIAA PAPER 89-0863] p 118 A89-25627  
Development and applications of optical interferometric micrometry in the Angstrom and subangstrom range p 170 A89-27663

Ground-based simulation of telepresence for materials science experiments  
[AIAA PAPER 89-0597] p 119 A89-28439

A facility for precise temperature control applications in microgravity p 48 A89-36956

## Ricardo-ITI, Westmont, IL.

Methods for heat transfer and temperature field analysis of the insulated diesel, phase 3  
[NASA-CR-182237] p 239 N89-23382

## Rochester Univ., NY.

External electro-optic probing of millimeter-wave integrated circuits p 133 A89-45266

## Rocket Research Corp., Redmond, WA.

Electromagnetic emission experiences using electric propulsion systems p 61 A89-53354

## Rockwell International Corp., Canoga Park, CA.

An integrated and modular digital modeling approach for the Space Station electrical power system development p 50 A89-15298

The Solar Dynamic radiator with a historical perspective p 51 A89-15340

Probabilistic structural analysis methods and applications p 190 A89-16939

Experimental results for labyrinth gas seals with honeycomb stators - Comparisons to smooth-stator seals and theoretical predictions p 179 A89-24992

[ASME PAPER 88-TRIB-40] p 179 A89-24992  
Preliminary study of the interactions caused by crossing shock waves and a turbulent boundary layer  
[AIAA PAPER 89-0358] p 145 A89-25303

The influence of high thermal gradient casting, hot isostatic pressing and alternate heat treatment on the structure and properties of a single crystal nickel base superalloy p 97 A89-36427

Solar dynamic power for Space Station Freedom  
[IAF PAPER ICOSP89-4-1] p 55 A89-46517

Fiberoptics for liquid propellant rocket engine environments p 230 A89-46812  
[AIAA PAPER 89-2416] p 230 A89-46812

Orbit transfer rocket engine technology program. Phase 2: Advanced engine study p 61 N89-10119

[NASA-CR-179602] p 61 N89-10119  
Space station WP-04 power system preliminary analysis and design document, volume 3 p 64 N89-15164

[NASA-CR-179587-VOL-3] p 64 N89-15164  
Advanced single crystal for SSME turbopumps p 103 N89-21072

[NASA-CR-182244] p 103 N89-21072  
OTVE combustor wall condition monitoring p 73 N89-26899

[NASA-CR-182275] p 73 N89-26899  
Space station hydrogen/oxygen thruster technology p 74 N89-26905

[NASA-CR-182280] p 74 N89-26905  
OTVE turbopump condition monitoring, task E.5 p 189 N89-27204

[NASA-CR-182274] p 189 N89-27204

## Rome Air Development Center, Griffis AFB, NY.

Optoelectronic signal processing for phased-array antennas; Proceedings of the Meeting, Los Angeles, CA, Jan. 12, 13, 1988 p 124 A89-15819

[SPIE-886] p 124 A89-15819

## Ruhr Univ., Bochum (Germany, F.R.).

The stability analysis of magnetohydrodynamic equilibria - Comparing the thermodynamic approach with the energy principle p 232 A89-39391

## S

## Sanders Associates, Inc., Nashua, NH.

An experimental analysis of a doped lithium fluoride direct absorption solar receiver p 49 A89-15245

Conceptual design of an advanced Stirling conversion system for terrestrial power generation p 238 N89-12504

[NASA-CR-180890] p 238 N89-12504  
Advanced heat receiver conceptual design study p 209 N89-18224

[NASA-CR-182177] p 209 N89-18224

## Sandia National Labs., Albuquerque, NM.

The effect of different module configurations on the radiation tolerance of multijunction solar cells p 209 N89-17356

[NASA-TM-101251] p 209 N89-17356

## Sandia National Labs., Livermore, CA.

The use of direct numerical simulation in the study of turbulent, chemically-reacting flows p 152 A89-51873

## Science Applications International Corp., Sunnyvale, CA.

Mass flow meter using the triboelectric effect for measurement in cryogenics p 155 N89-12836

[NASA-CR-179572] p 155 N89-12836

## Scientific Research Associates, Inc., Glastonbury, CT.

Bipolar coordinates for computation of transition duct flows p 148 A89-34912

Two- and three-dimensional turbine blade row flow field simulations p 161 N89-17313

## SDRC, Inc., San Diego, CA.

Modal representations in control/structure interaction p 45 A89-54114

[AIAA PAPER 89-1369] p 193 A89-30844

An advanced probabilistic structural analysis method for implicit performance functions p 193 A89-30846

[AIAA PAPER 89-1371] p 193 A89-30846  
Inelastic deformation and dislocation structure of a nickel alloy - Effects of deformation and thermal histories p 99 A89-50313

Constitutive modeling for isotropic materials p 195 N89-12904

The effect of insulated combustion chamber surfaces on direct-injected diesel engine performance, emissions, and combustion p 239 N89-17548

[NASA-CR-182204] p 239 N89-17548

Space Power, Inc., San Jose, CA.  
A heat-driven monochromatic light source p 224 A89-41722

Megawatt Class Nuclear Space Power Systems (MCNSPS) conceptual design and evaluation report. Volume 1: Objectives, summary results and introduction p 209 N89-17941

[NASA-CR-179614-VOL-1] p 209 N89-17941  
Megawatt Class Nuclear Space Power Systems (MCNSPS) conceptual design and evaluation report. Volume 4: Concepts selection, conceptual designs, recommendations p 210 N89-18967

[NASA-CR-179614-VOL-4] p 210 N89-18967  
Megawatt Class Nuclear Space Power Systems (MCNSPS) conceptual design and evaluation report. Volume 3, technologies 2: Power conversion p 211 N89-22980

[NASA-CR-179614-VOL-3] p 211 N89-22980  
Megawatt Class Nuclear Space Power Systems (MCNSPS) conceptual design and evaluation report. Volume 2, technologies 1: Reactors, heat transport, integration issues p 211 N89-22981

[NASA-CR-179614-VOL-2] p 211 N89-22981

## Sperry Corp., Phoenix, AZ.

Multi-hundred kilowatt roll ring assembly p 135 N89-15335

[NASA-CR-174832] p 135 N89-15335

Standard Oil Engineered Materials Co., Niagara Falls, NY.

Fracture resistance of a TiB<sub>2</sub> particle/SiC matrix composite at elevated temperature p 81 A89-31074

[NASA-CR-174832] p 81 A89-31074

Stanford Univ., CA.  
Experimental study of the development of longitudinal vortex pairs embedded in a turbulent boundary layer p 140 A89-11107

Probabilistic structural analysis methods and applications p 190 A89-16939

Mechanisms of elevated-temperature deformation in the B2 aluminides NiAl and CoAl p 94 A89-17378

An approach to probabilistic finite element analysis using a mixed-iterative formulation p 191 A89-25849

A numerical model of electrodynamics of plasma within the contaminant gas cloud of the Space Shuttle Orbiter at low earth orbit p 233 A89-45631

Heat transfer with very high free-stream turbulence and streamwise vortices p 157 N89-12900

Heat transfer with very high free-stream turbulence and heat transfer with streamwise vortices p 160 N89-17309

State Univ. of New York, Binghamton.  
Nonlinear analysis using temporal finite elements p 221 A89-28030

State Univ. of New York, Buffalo.

A probabilistic formulation for fracture energy of continuous fibre-matrix composites p 83 A89-39996

Prediction of unsteady rotor-surface heat transfer from wake passages p 150 A89-43210

[AIAA PAPER 89-1692] p 150 A89-43210  
Advanced development of the boundary element method for steady-state heat conduction p 154 A89-54766

Development of BEM for ceramic composites p 111 N89-14311

[NASA-CR-183313] p 111 N89-14311

## State Univ. of New York, Plattsburgh.

Shubnikov-de Haas measurements of the 2-D electron gas in pseudomorphic In(0.1)Ga(0.9)As grown on GaAs p 235 A89-29299

## State Univ. of New York, Stony Brook.

Accurate boundary conditions for exterior problems in gas dynamics p 143 A89-20223

## Stirling Technology Co., Richland, WA.

The 25 kW solar thermal Stirling hydraulic engine system: Conceptual design p 239 N89-14182

[NASA-CR-180889] p 239 N89-14182

## Sundstrand Corp., Rockford, IL.

Transient performance evaluation of an integrated heat pipe-thermal storage system p 49 A89-15209

## Sunpower, Inc., Athens, OH.

Description of an oscillating flow pressure drop test rig p 142 A89-15188

Sverdrup Technology, Inc., Middleburg Heights, OH.  
The interaction of gold with gallium arsenide p 90 A89-16416

Microstructures in rapidly solidified niobium aluminides p 95 A89-18193

High angle-of-attack hypersonic aerodynamics p 2 A89-19918

Comparison of 3D computation and experiment for non-axisymmetric nozzles p 22 A89-28403

[AIAA PAPER 89-0007] p 22 A89-28403  
Modeling of surface roughness effects on glaze ice accretion p 16 A89-28451

[AIAA PAPER 89-0734] p 16 A89-28451  
Three dimensional viscous analysis of a hypersonic inlet p 4 A89-29924

[AIAA PAPER 89-0004] p 4 A89-29924  
Probabilistic structural analysis to quantify uncertainties associated with turbopump blades p 194 A89-36920

Transient oxidation of single-crystal beta-NiAl p 98 A89-37899

Structural tailoring of Space Shuttle Main Engine turbopump blades SSME/STAEBL p 55 A89-44106

Piezoelectric pushers for active vibration control of rotating machinery p 171 A89-47717

Metal-silicon reaction rates - The effects of capping p 93 A89-52202

## Sverdrup Technology, Inc., Cleveland, OH.

Cruise noise of the 2/9 scale model SR-7A propeller p 224 A89-12561

PNS calculations for 3-D hypersonic corner flow with two turbulence models p 1 A89-14979

[AIAA PAPER 88-2958] p 1 A89-14979  
High speed inlet calculations with real gas effects p 2 A89-14980

[AIAA PAPER 88-3076] p 2 A89-14980  
Three dimensional simulation of an underexpanded jet interacting with a supersonic cross flow p 2 A89-14982

[AIAA PAPER 88-3181] p 2 A89-14982  
Navier-Stokes calculation of solid-propellant rocket motor internal flowfields p 48 A89-14983

[AIAA PAPER 88-3182] p 48 A89-14983  
Unsteady solution of incompressible Navier-Stokes equations p 141 A89-15143

Description of an oscillating flow pressure drop test rig p 142 A89-15188

Advanced sensible heat solar receiver for space power p 52 A89-15415

Vibration, performance, flutter and forced response characteristics of a large-scale propfan and its aeroelastic model p 21 A89-17943

[AIAA PAPER 88-3155] p 21 A89-17943  
Rapid solidification research at the NASA Lewis Research Center p 95 A89-18203

A diagonally inverted LU implicit multigrid scheme for the 3-D Navier-Stokes equations and a two equation model of turbulence p 145 A89-25382

[AIAA PAPER 89-0467] p 145 A89-25382  
Performance of the forward scattering spectrometer probe in NASA's Icing Research Tunnel p 169 A89-25570

[AIAA PAPER 89-0769] p 169 A89-25570  
Flight hardware and tele-operations supporting the Isothermal Dendritic Growth Experiment aboard the Space Shuttle p 118 A89-25627

[AIAA PAPER 89-0863] p 118 A89-25627  
Three dimensional PNS solutions of hypersonic internal flows with equilibrium chemistry p 146 A89-28401

[AIAA PAPER 89-0002] p 146 A89-28401  
The effect of adaptive grid on hypersonic nozzle flow calculations p 54 A89-28402

[AIAA PAPER 89-0006] p 54 A89-28402  
Interaction of an oblique shock wave with turbulent hypersonic blunt body flows p 3 A89-28405

[AIAA PAPER 89-0272] p 3 A89-28405  
Numerical investigation of chemically reacting flows in ramjet dump combustors p 22 A89-28408

[AIAA PAPER 89-0387] p 22 A89-28408  
Flux splitting algorithms for two-dimensional viscous flows with finite-rate chemistry p 146 A89-28409

[AIAA PAPER 89-0388] p 146 A89-28409

- Three-dimensional calculation of supersonic reacting flows using an LU scheme  
[AIAA PAPER 89-0391] p 146 A89-28410
- An experimental investigation of multi-element airfoil ice accretion and resulting performance degradation  
[AIAA PAPER 89-0752] p 4 A89-28453
- The effect of metal surface passivation on the Au-In-P interaction  
p 132 A89-30443
- Effects of core turbulence on jet excitability  
[AIAA PAPER 89-0966] p 147 A89-30482
- Nonlinear interaction between the sinuous and varicose instability modes in a plane wake  
p 147 A89-33779
- Strength distribution of reinforcing fibers in a Nicalon fiber/chemically vapor infiltrated silicon carbide matrix composite  
p 82 A89-34844
- Model-based analysis of control/display interaction in the hover task  
p 215 A89-36933
- Subharmonic and fundamental high amplitude excitation of an axisymmetric jet  
[AIAA PAPER 89-0993] p 149 A89-37825
- High-speed propeller performance and noise predictions at takeoff/landing conditions  
p 226 A89-39195
- Prediction of unsteady blade surface pressures on an advanced propeller at an angle of attack  
[AIAA PAPER 89-1060] p 227 A89-40473
- Assessment of numerical techniques for unsteady flow calculations  
[AIAA PAPER 89-1956] p 150 A89-41803
- Conservative treatment of boundary interfaces for overlaid grids and multi-level grid adaptations  
[AIAA PAPER 89-1980] p 5 A89-41823
- A simple algebraic grid adaptation scheme with applications to two- and three-dimensional flow problems  
[AIAA PAPER 89-1984] p 5 A89-41827
- A time accurate finite volume high resolution scheme for three dimensional Navier-Stokes equations  
[AIAA PAPER 89-1994] p 6 A89-41837
- High temperature optical strain measurement system  
p 170 A89-43842
- Effect of ambient pressure on the performance of a resistojet  
p 55 A89-44111
- An improved correction algorithm for number density measurements made with the forward scattering spectrometer probe  
p 170 A89-44122
- A correction algorithm for particle size distribution measurements made with the forward-scattering spectrometer probe  
p 170 A89-44123
- A detailed analysis of inviscid flux splitting algorithms for real gases with equilibrium or finite-rate chemistry  
p 151 A89-45424
- TEM studies of oxidized NiAl and Ni3Al cross sections  
p 99 A89-46506
- Antiproton powered propulsion with magnetically confined plasma engines  
[AIAA PAPER 89-2334] p 57 A89-46758
- Mach 5 inlet CFD and experimental results  
[AIAA PAPER 89-2355] p 6 A89-46769
- A generalized one dimensional computer code for turbomachinery cooling passage flow calculations  
[AIAA PAPER 89-2574] p 151 A89-46934
- Large scale advanced propeller blade pressure distributions - Prediction and data  
[AIAA PAPER 89-2696] p 7 A89-47026
- Performance of a 100 kW class applied field MPD thruster  
[AIAA PAPER 89-2710] p 57 A89-47035
- The effect of electrode configuration on arcjet performance  
[AIAA PAPER 89-2722] p 58 A89-47044
- Plume characteristics of MPD thrusters - A preliminary examination  
[AIAA PAPER 89-2832] p 39 A89-47113
- Investigation of a liquid-fed water resistojet plume  
[AIAA PAPER 89-2840] p 58 A89-47117
- Average-passage simulation of counter-rotating propfan propulsion systems as applied to cruise missiles  
[AIAA PAPER 89-2943] p 7 A89-47187
- Effect of design variables, temperature gradients, and speed on life and reliability of a rotating disk  
p 180 A89-47719
- Fresnel diffraction by spherical obstacles  
p 231 A89-48249
- Analytical flutter investigation of a composite propfan model  
p 195 A89-48663
- Ultrasonic imaging of porosity variations produced during sintering  
p 107 A89-48892
- A premixed hydrogen/oxygen catalytic igniter  
[AIAA PAPER 89-2302] p 59 A89-49683
- A numerical study of chemically reacting flow in nozzles  
[AIAA PAPER 89-2793] p 60 A89-49687
- A supersonic through-flow fan engine airframe integration study  
[AIAA PAPER 89-2140] p 18 A89-50802
- Low-speed wind tunnel performance of high-speed counterrotating propellers at angle-of-attack  
[AIAA PAPER 89-2583] p 8 A89-50808
- Engineering study on the rotary-vee engine concept  
[SAE PAPER 890332] p 181 A89-51492
- Integrated flight/propulsion control system design based on a centralized approach  
[AIAA PAPER 89-3520] p 35 A89-52611
- Integrated flight/propulsion control system design based on a decentralized, hierarchical approach  
[AIAA PAPER 89-3519] p 35 A89-53301
- The development of power specific redlines for SSME safety monitoring  
[AIAA PAPER 89-2413] p 61 A89-53305
- Turbopfan engine control system design using the LQG/LTR methodology  
p 23 A89-53956
- Stability robustness improvement of direct eigenspace assignment based feedback systems using singular value sensitivities  
p 220 A89-53958
- A diagonally inverted LU implicit multigrid scheme for the 3-D Navier-Stokes equations and a two equation model of turbulence  
[NASA-CR-182209] p 9 A89-10863
- A preliminary design study of supersonic through-flow fan inlets  
[NASA-CR-182224] p 24 A89-11751
- A control-volume method for analysis of unsteady thrust augmenting ejector flows  
[NASA-CR-182203] p 24 A89-12566
- A review of turbomachinery blade-row interaction research  
[NASA-CR-182211] p 24 A89-12567
- Analytical ice shape predictions for flight in natural icing conditions  
[NASA-CR-182234] p 18 A89-13428
- HASA: Hypersonic Aerospace Sizing Analysis for the preliminary design of aerospace vehicles  
[NASA-CR-182226] p 18 A89-15107
- Three dimensional viscous analysis of a hypersonic inlet  
[NASA-TM-101474] p 13 A89-16759
- NASA powered lift facility internally generated noise and its transmission to the acoustic far field  
[NASA-CR-182217] p 36 A89-16882
- Experimental verification of the thermodynamic properties for a jet-A fuel  
[NASA-TM-101475] p 117 A89-17017
- Noise generated by a flight weight, air flow control valve in a vertical takeoff and landing aircraft thrust vectoring system  
[NASA-CR-182232] p 228 A89-20776
- Comparison of 3D computation and experiment for non-axisymmetric nozzles  
[NASA-CR-182245] p 14 A89-20921
- Thermodynamic analysis of chemical compatibility of several reinforcement materials with niobium aluminides  
[NASA-CR-182260] p 86 A89-21036
- Theoretical analysis of compatibility of several reinforcement materials with NiAl and FeAl matrices  
[NASA-CR-182291] p 86 A89-23622
- A premixed hydrogen/oxygen catalytic igniter  
[NASA-CR-185113] p 70 A89-24445
- NASA Lewis Stirling engine computer code evaluation  
[NASA-CR-182248] p 214 A89-24741
- Turbopfan engine control system design using the LQG/LTR methodology  
[NASA-CR-182303] p 33 A89-26004
- The development of power specific redlines for SSME safety monitoring  
[NASA-CR-185121] p 41 A89-26027
- Two-tiered design analysis of a radiator for a solar dynamic powered Stirling engine  
[NASA-CR-182301] p 46 A89-26031
- Paralleling power MOSFETs in their active region: Extended range of passively forced current sharing  
[NASA-CR-180902] p 139 A89-26150
- Two-dimensional high temperature optical strain measurement system, phase 2  
[NASA-CR-185116] p 176 A89-26218
- Stability robustness improvement of direct eigenspace assignment based feedback systems using singular value sensitivities  
[NASA-CR-182302] p 36 A89-27672
- Antiproton powered propulsion with magnetically confined plasma engines  
[NASA-CR-185131] p 74 A89-27700
- Plume characteristics of MPD thrusters: A preliminary examination  
[NASA-CR-185130] p 76 A89-29483
- Swiss Center for Electronics and Microtechnology, Inc., Neuchatel.**  
The scratch test - Different critical load determination techniques  
p 171 A89-54278
- Adhesion scratch testing - A round-robin experiment  
p 171 A89-54281
- Syracuse Univ., NY.**  
Morphological study of near threshold fatigue crack growth in a coarse grain aluminum alloy  
p 94 A89-12326
- Resolved shear stress intensity coefficient and fatigue crack growth in large crystals  
p 96 A89-22048
- Grain boundary oxidation and its effects on high temperature fatigue life  
p 101 A89-12918
- Systems Control Technology, Inc., Palo Alto, CA.**  
Effect of model uncertainty on failure detection - The threshold selector  
p 219 A89-17965
- Systems Science and Software, La Jolla, CA.**  
The POLAR code wake model - Comparison with in situ observations  
p 233 A89-45632
- Systems Science and Software, San Diego, CA.**  
On the need for space tests of plasma contactors as electron collectors  
p 232 A89-43356
- T**
- Tanksley (W. L.) and Associates, Inc., Cleveland, OH.**  
Thermal distortion analysis of the Space Station solar dynamic concentrator  
p 51 A89-15341
- Technical Research Centre of Finland, Espoo.**  
Adhesion scratch testing - A round-robin experiment  
p 171 A89-54281
- Technion - Israel Inst. of Tech., Haifa.**  
Recursive algorithms for vector extrapolation methods  
p 221 A89-14397
- Nucleosynthesis, neutrino bursts and gamma-rays from coalescing neutron stars  
p 241 A89-46577
- Extended observability of linear time-invariant systems under recurrent loss of output data  
[AIAA PAPER 89-3510] p 220 A89-52603
- Tel-Aviv Univ. (Israel).**  
Global properties of pseudospectral methods  
p 221 A89-37746
- Common source-multiple load vs. separate source-individual load photovoltaic system  
[NASA-TM-101465] p 136 A89-15338
- Starting characteristics of direct current motors powered by solar cells  
[NASA-TM-101981] p 136 A89-19493
- The Mars climate for a photovoltaic system operation  
[NASA-TM-101994] p 136 A89-20385
- Solar radiation on Mars  
[NASA-TM-102299] p 242 A89-27623
- Teledyne Brown Engineering, Huntsville, AL.**  
The impact of an IVA robot on the Space Station microgravity environment  
[AIAA PAPER 89-0596] p 44 A89-28438
- User needs, benefits and integration of robotic systems in a space station laboratory  
[NASA-CR-182261] p 185 A89-22108
- Temple Univ., Philadelphia, PA.**  
Degradation mechanisms of n-dodecane with sulfur and nitrogen dopants during thermal stressing  
p 116 A89-22277
- Tennessee Univ., Knoxville.**  
An experimental and analytical investigation of thermoacoustic convection heat transfer in gravity and zero-gravity environments  
[NASA-CR-179575] p 120 A89-11920
- Tennessee Univ., Tullahoma.**  
Recovery of excitation intensity dependence in pulsed, focused beams - Nonsaturated case  
p 177 A89-17507
- Tennessee Univ. Space Inst., Tullahoma.**  
Influence of bulk turbulence and entrance boundary layer thickness on the curved duct flow field  
[NASA-CR-4188] p 155 A89-12838
- Influence of bulk turbulence and entrance boundary layer thickness on the curved duct flow field  
p 156 A89-12896
- Texas A&M Univ., College Station.**  
Experimental results for labyrinth gas seals with honeycomb stators - Comparisons to smooth-stator seals and theoretical predictions  
[ASME PAPER 88-TRIB-40] p 179 A89-24992
- On ice shape prediction methodologies and comparison with experimental data  
[AIAA PAPER 89-0732] p 16 A89-30650
- Annular honeycomb seals: Test results for leakage and rotordynamic coefficients - Comparisons to labyrinth and smooth configurations  
[ASME PAPER 88-TRIB-35] p 179 A89-34794
- An entrance region friction factor model applied to annular seal analysis - Theory versus experiment for smooth and honeycomb seals  
[ASME PAPER 88-TRIB-41] p 179 A89-34798
- Determination of near and far field acoustics for advanced propeller configurations  
[AIAA PAPER 89-1040] p 226 A89-40469

## Texas Univ.

- An acoustic experimental and theoretical investigation of single disc propellers [AIAA PAPER 89-1146] p 227 A89-40478
- Generic icing effects on forward flight performance of a model helicopter rotor p 18 A89-41093
- Piezoelectric pushers for active vibration control of rotating machinery p 171 A89-47717
- Annular honeycomb seals: Test results for leakage and rotordynamic coefficients; comparisons to labyrinth and smooth configurations p 185 N89-22899
- Friction factor data for flat plate tests of smooth and honeycomb surfaces [NASA-CR-184977] p 186 N89-23876

## Texas Univ., Arlington.

- Computer analysis of the negative differential resistance switching phenomenon of double-injection devices p 134 A89-54963

## Texas Univ., Austin.

- Ray-tube integration in shooting and bouncing ray method p 124 A89-15152
- Interdiffusional effects between TiBe12 and NiAl intermetallics p 95 A89-21395
- Shooting and bouncing rays - Calculating the RCS of an arbitrarily shaped cavity p 124 A89-34242
- High-frequency RCS of open cavities with rectangular and circular cross sections p 125 A89-39595

## Texas Univ., San Antonio.

- Probabilistic constitutive relationships for material strength degradation models [AIAA PAPER 89-1368] p 192 A89-30843
- Probabilistic analysis for fatigue strength degradation of materials [NASA-CR-182844] p 198 N89-15434
- Fatigue crack growth model RANDOM2 user manual. Appendix 1: Development of advanced methodologies for probabilistic constitutive relationships of material strength models [NASA-CR-184775-APP-1] p 201 N89-19581
- Fatigue strength reduction model: RANDOM3 and RANDOM4 user manual. Appendix 2: Development of advanced methodologies for probabilistic constitutive relationships of material strength models [NASA-CR-184796-APP-2] p 201 N89-19582
- Fatigue crack growth model RANDOM2 user manual, appendix 1 [NASA-CR-184939] p 203 N89-23890
- Fatigue strength reduction model: RANDOM3 and RANDOM4 user manual, appendix 2 [NASA-CR-184940] p 203 N89-23891

## Textron Bell Aerospace Co., Buffalo, NY.

- Nonlinear analysis using temporal finite elements p 221 A89-28030
- Space station auxiliary thrust chamber technology [NASA-CR-179650] p 46 N89-11803

## Thermacore, Inc., Lancaster, PA.

- Conceptual design of an advanced Stirling conversion system for terrestrial power generation [NASA-CR-180890] p 238 N89-12504

## Tokyo Univ. (Japan).

- Fracture resistance of a TiB2 particle/SiC matrix composite at elevated temperature p 81 A89-31074

## Toledo Univ., OH.

- A Fourier analysis for a fast simulation algorithm p 130 A89-15367
- Experimental investigation of propfan aeroelastic response in off-axis flow with mistuning [AIAA PAPER 88-3153] p 20 A89-17941
- Efficient numerical simulation of a one-dimensional electrothermal deicer pad p 144 A89-22811
- Coded multiple chirp spread spectrum system and overlay service p 124 A89-26769
- A computational procedure for automated flutter analysis p 191 A89-28070
- Investigation of the flow in the diffuser section of the NASA Lewis Icing Research Tunnel [AIAA PAPER 89-0755] p 36 A89-28455
- Application of a full-potential solver to bending-torsion flutter in cascades [AIAA PAPER 89-1386] p 34 A89-30859
- Langmuir probe measurements of an arcjet exhaust p 55 A89-39031
- Two-dimensional simulation of electrothermal deicing of aircraft components p 17 A89-39194
- Flow of rarefied gases over two-dimensional bodies [AIAA PAPER 89-1970] p 5 A89-41814
- Effect of ambient pressure on the performance of a resistojet p 55 A89-44111
- Aeroelastic analysis of prop fan blades with a semiempirical dynamic stall model [AIAA PAPER 89-2695] p 194 A89-47025
- The effect of test-cell pressure on resistojet nozzle flow [AIAA PAPER 89-2838] p 58 A89-47116
- Rarefied gas flow through two-dimensional nozzles [AIAA PAPER 89-2893] p 7 A89-47156

- Analytical flutter investigation of a composite propfan model p 195 A89-48663
- A design procedure for the phase-controlled parallel-loaded resonant inverter p 134 A89-50472
- Numerical analysis of supersonic flow through oscillating cascade sections by using a deforming grid [AIAA PAPER 89-2805] p 8 A89-50810
- A comparison of numerical methods for the prediction of two-dimensional heat transfer in an electrothermal deicer pad [NASA-CR-4202] p 19 N89-13429
- Solution and sensitivity analysis of a complex transcendental eigenproblem with pairs of real eigenvalues [NASA-CR-182241] p 197 N89-13819
- A numerical simulation of the full two-dimensional electrothermal de-icer pad [NASA-CR-4194] p 19 N89-14235

## Toronto Univ. (Ontario).

- Is the great attractor really a great wall? p 241 A89-36278

## TRW, Inc., Redondo Beach, CA.

- Interactions between gaseous electrical discharges and single liquid droplets p 90 A89-19298
- Large structure current collection in plasma environments [AIAA PAPER 89-0496] p 44 A89-25405
- Droplet combustion drop tower tests using models of the space flight apparatus [AIAA PAPER 89-0501] p 119 A89-28418

## TRW Space Technology Labs., Redondo Beach, CA.

- Improved high-temperature resistant matrix resins [NASA-CR-180826] p 114 N89-21105

## Tuskegee Inst., AL.

- Arc strike in the rail accelerator p 39 A89-32065
- Arc-driven rail accelerator research [NASA-CR-179584] p 40 N89-13445

## U

## United Technologies Corp., East Hartford, CT.

- Fracture mechanics applied to elevated temperature crack growth p 195 A89-47705

## United Technologies Corp., West Palm Beach, FL.

- Integrated flight/propulsion control study for STOVL applications [AIAA PAPER 89-2908] p 34 A89-47166

## United Technologies Corp., Windsor Locks, CT.

- Results of acoustic tests of a prop-fan model p 224 A89-10112

- Sound power spectrum and wave drag of a propeller in flight [AIAA PAPER 89-1081] p 225 A89-33724

- Near wakes of advanced turbopropellers [AIAA PAPER 89-1095] p 5 A89-33735

## United Technologies Research Center, East Hartford, CT.

- Iron-base superalloys - A phase analysis of the multicomponent system (Fe-Mn-Cr-Mo-Nb-Al-Si-C) p 95 A89-17379

- Performance potential of air turbo-ramjet employing supersonic through-flow fan [AIAA PAPER 89-0010] p 22 A89-25006

- Near wakes of advanced turbopropellers [AIAA PAPER 89-1095] p 5 A89-33735

- Calculation of unsteady flows in turbomachinery using the linearized Euler equations p 149 A89-36916

- Measurement of airfoil heat transfer coefficients on a turbine stage p 157 N89-12897

- The effects of inlet turbulence and rotor/stator interactions on the aerodynamics and heat transfer of a large-scale rotating turbine model, volume 1 [NASA-CR-4079] p 159 N89-13756

- An analysis for high speed propeller-nacelle aerodynamic performance prediction. Volume 1: Theory and application [NASA-CR-4199-VOL-1] p 12 N89-15896

- An analysis for high speed propeller-nacelle aerodynamic performance prediction. Volume 2: User's manual [NASA-CR-4199-VOL-2] p 12 N89-15897

- Supersonic through-flow fan assessment [NASA-CR-182202] p 27 N89-16843

- Development of a high temperature thin film static strain gage p 174 N89-17299

- Application of advanced diagnostics to aircraft injector flows p 160 N89-17306

- Measurement of airfoil heat transfer coefficients on a turbine stage p 160 N89-17311

## Universal Energy Systems, Inc., Dayton, OH.

- Characterization of multilayer GaAs/AlGaAs transistor structures by variable angle spectroscopic ellipsometry p 133 A89-49998

## University of Eastern Kentucky, Richmond.

- Study of optical output couplers for submillimeter wavelength backward-wave oscillators (BWO's) p 132 A89-32857

## University of South Florida, Tampa.

- Evaluation of alternative phase change materials for energy storage in solar dynamic applications p 208 A89-29114

- Thermal evaluation of advanced solar dynamic heat receiver performance [NASA-CR-185117] p 214 N89-27256

## University of Southern California, Los Angeles.

- Liquid droplet generation [NASA-CR-182246] p 166 N89-26182

## Utah State Univ., Logan.

- A numerical model of electrodynamics of plasma within the contaminant gas cloud of the Space Shuttle Orbiter at low earth orbit p 233 A89-45631

## Utah Univ., Salt Lake City.

- Fracture toughness of polycrystalline ceramics in combined mode I and mode II loading p 105 A89-26457

- Effects of heat release on the large-scale structure in turbulent mixing layers p 147 A89-31844

## V

## Varian Associates, Palo Alto, CA.

- Development of a 39.5 GHz Karp traveling wave tube for use in space [NASA-CR-182182] p 136 N89-15336

## Virginia Polytechnic Inst. and State Univ., Blacksburg.

- Viscous analysis of high speed flows using an upwind finite volume technique [AIAA PAPER 89-0001] p 144 A89-25001

- Coded multiple chirp spread spectrum system and overlay service p 124 A89-26769

- Turbulence modeling in a hypersonic inlet p 8 A89-53931

- A prediction of 3-D viscous flow and performance of the NASA low-speed centrifugal compressor [NASA-CR-184765] p 160 N89-16132

- A study of the stress wave factor technique for evaluation of composite materials [NASA-CR-4195] p 189 N89-21256

- Study of spread spectrum multiple access systems for satellite communications with overlay on current services: Executive summary [NASA-CR-180827-EXEC-SUMM] p 128 N89-23756

- Study of spread spectrum multiple access systems for satellite communications with overlay on current services [NASA-CR-180827] p 128 N89-23757

## W

## Washington Univ., Saint Louis, MO.

- Modeling of impulsive propellant reorientation [AIAA PAPER 89-0628] p 54 A89-25496

- Modeling of pulsed propellant reorientation [AIAA PAPER 89-2727] p 61 A89-53306

## Washington Univ., Seattle.

- Crack growth resistance of textured alumina p 105 A89-26452

- Effects of heat release on the large-scale structure in turbulent mixing layers p 147 A89-31844

- Strength distribution of reinforcing fibers in a Nicalon fiber/chemically vapor infiltrated silicon carbide matrix composite p 82 A89-34844

- The use of direct numerical simulation in the study of turbulent, chemically-reacting flows p 152 A89-51873

## Wayne State Univ., Detroit, MI.

- On the equivalence of Gaussian elimination and Gauss-Jordan reduction in solving linear equations [NASA-TM-101466] p 222 N89-20710

- Radiation resistance studies of amorphous silicon films p 213 N89-24738

## Westinghouse Electric Corp., Pittsburgh, PA.

- Effects of operating parameters on PAFC stack performance p 207 A89-15250

- Measurement of the diffusion coefficient of acetone in succinonitrile at its melting point p 237 A89-23488

## Westinghouse Research and Development Center, Pittsburgh, PA.

- Raman determination of layer stresses and strains for heterostructures and its application to the cubic SiC/Si system p 234 A89-21871

- Dendritic solidification in binary alloys p 96 A89-22560

- Evaluation of transport conditions during physical vapor transport growth of opto-electronic crystals [AIAA PAPER 89-0229] p 118 A89-25197



**Wichita State Univ., KS.**

Electroimpulse deicing - Electrodynamical solution by discrete elements p 17 A89-39193

**Wisconsin Univ., Madison.**

A versatile power converter for high-frequency link systems p 131 A89-21200

Study of the generator/motor operation of induction machines in a high frequency link space power system [NASA-CR-179600] p 63 N89-11809

**Y****Yale Univ., New Haven, CT.**

Rational engineering correlations of diffusional and inertial particle deposition behavior in non-isothermal forced convection environments p 140 A89-12327

Deposition of Na<sub>2</sub>SO<sub>4</sub> from salt-seeded combustion gases of a high velocity burner rig p 89 A89-12330

Transport-induced shifts in condensate dew-point and composition in multicomponent systems with chemical reaction p 89 A89-12333

Optical methods and results of dew point and deposition rate measurements in salt/ash-containing combustion gases - B<sub>2</sub>O<sub>3</sub>(l) deposition rates by interference methods and comparisons with theory p 89 A89-12334

Laboratory studies of binary salt CVD in combustion gas environments p 89 A89-12335

Use of a generalized Stokes number to determine the aerodynamic capture efficiency of non-Stokesian particles from a compressible gas flow p 140 A89-12336

Aerodynamically-driven condensate layer thickness distributions on isothermal cylindrical surfaces p 140 A89-12337

Laboratory studies of the deposition of alkali sulfate vapors from combustion gases using a flash-evaporation technique p 89 A89-12338

Windward fraction of the total mass or heat transport for flow past a circular cylinder p 141 A89-12339

Thermophoretically enhanced mass transport rates to solid and transpiration-cooled walls across turbulent (law-of-the-wall) boundary layers p 141 A89-12340

Effect of particulate thermophoresis in reducing the fouling rate advantages of effusion-cooling p 141 A89-14599

Viscous dissipation effects on thermophoretically augmented aerosol particle transport across laminar boundary layers p 141 A89-14600

Optical experiments on thermophoretically augmented submicron particle deposition from 'dusty' high temperature gas flows p 90 A89-14799

Boundary layer effects on particle impaction and capture p 143 A89-19123

Mass transfer across combustion gas thermal boundary layers - Power production and materials processing implications p 143 A89-20425

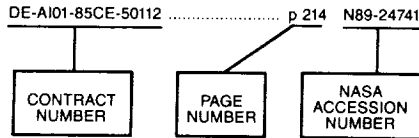
Vapor deposition and condensate flow on combustion turbine blades - Theoretical model to predict/understand some corrosion rate consequences of molten alkali sulfate deposition in the field or laboratory p 21 A89-20950

Theoretical studies in support of the 3M-vapor transport (PVTOS-) experiments [NASA-CR-185122] p 165 N89-26179



# CONTRACT NUMBER INDEX

## Typical Contract Number Index Listing



Listings in this index are arranged alphanumerically by contract number. Under each contract number the NASA accession numbers denoting documents that have been produced as a result of research done under that contract are arranged in ascending order. The NASA accession number denotes the number by which the citation is identified.

DE-AI01-85CE-50112	p 214	N89-24741	p 141	A89-14600
DE-AI01-86CE-50162	p 239	N89-23382	p 143	A89-19123
DE-AI03-86SF-16310	p 102	N89-16986	p 143	A89-20425
	p 103	N89-17649	p 21	A89-20950
	p 104	N89-28627	p 183	N89-15414
	p 104	N89-29522	p 183	N89-15415
DE-AI05-82OR-1005	p 210	N89-19737	p 99	A89-47320
DE-AI21-80ET-17088	p 209	N89-12122	p 120	N89-11920
	p 209	N89-13103	p 20	A89-16102
DE-AT04-85AL-33408	p 238	N89-12504	p 94	A89-17378
	p 239	N89-14182	p 92	A89-38658
	p 239	N89-26781	p 111	N89-13662
DE-FG02-84ER-45110	p 105	A89-30631	p 95	A89-17379
DE-FG02-85ER-45210	p 144	A89-24603	p 10	N89-13397
DE-FG03-86ER-13608	p 140	A89-11107	p 17	A89-39193
DEN3-168	p 186	N89-26246	p 144	A89-22736
DEN3-27	p 105	A89-17097	p 125	A89-42768
DEN3-290	p 207	A89-15250	p 125	A89-43543
DEN3-32	p 177	A89-12301	p 59	A89-47494
	p 177	A89-12303	p 75	N89-27773
DEN3-330	p 239	N89-17548	p 188	N89-18694
DEN3-342	p 239	N89-23382	p 48	A89-36956
DEN3-371	p 239	N89-14182	p 192	A89-29600
DEN3-372	p 238	N89-12504	p 191	A89-21133
DOT-FA03-83-A-00328	p 22	A89-28462	p 94	A89-12326
DTFA-03-81-A-00209	p 18	N89-13428	p 96	A89-22048
F04611-86-K-0082	p 48	A89-14983	p 101	N89-12918
F19628-82-C-0140	p 19	A89-45107	p 226	A89-40469
F19628-85-C-0052	p 125	A89-53134	p 227	A89-40478
F19628-86-C-0056	p 233	A89-45632	p 225	A89-33725
F19628-88-K-0011	p 215	A89-43698	p 131	A89-21200
F19628-88-K-0022	p 215	A89-43698	p 19	A89-12307
F30602-79-C-0039	p 19	A89-45107	p 80	A89-20725
F33615-84-K-1550	p 125	A89-39594	p 196	N89-12908
F49620-76-C-0020	p 89	A89-12334	p 116	A89-42695
F49620-82-K-0020	p 140	A89-12327	p 217	A89-38846
	p 140	A89-12336	p 140	A89-10176
	p 141	A89-12340	p 147	A89-30908
	p 141	A89-14599	p 79	A89-11324
	p 90	A89-14799	p 83	A89-36420
	p 143	A89-19123	p 117	A89-17112
F49620-82-K-0033	p 179	A89-24992	p 125	A89-53134
	p 179	A89-34794	p 125	A89-42758
	p 185	N89-22899	p 126	A89-53136
F49620-85-C-0013	p 21	A89-23182	p 126	N89-10215
F49620-85-C-0033	p 221	N89-10575	p 128	N89-23753
F49620-86-C-0094	p 145	A89-25303	p 213	N89-24725
F49620-87-C-0016	p 133	A89-45266	p 170	A89-37298
F49620-88-C-0082	p 2	A89-25029	p 224	A89-41722
NAGW-1340	p 241	A89-53833	p 231	A89-24292
NAGW-199	p 82	A89-34844	p 215	A89-43680
NAGW-235	p 231	A89-24292	p 215	A89-43698
	p 215	A89-43698	p 233	A89-45632
	p 233	A89-45631	p 233	A89-53209
NAG2-373	p 1	A89-11110	p 233	A89-54759
NAG3-1016	p 147	A89-30483	p 140	A89-11567
NAG3-122	p 12	N89-15898	p 2	A89-16882
NAG3-154	p 234	A89-13945	p 170	A89-43532
	p 133	A89-49998	p 105	A89-21444
NAG3-159	p 217	N89-13993	p 142	A89-16458
NAG3-164	p 178	A89-12751	p 124	A89-34242
NAG3-166	p 182	N89-12870	p 125	A89-39595
	p 182	N89-13788	p 125	A89-39594
NAG3-167	p 92	A89-38658	p 128	N89-24518
NAG3-168	p 139	N89-26143	p 129	N89-24519
NAG3-172	p 189	N89-21256	p 90	A89-12903
NAG3-181	p 179	A89-24992	p 22	A89-28462
	p 179	A89-34794	p 149	A89-38619
	p 179	A89-34798	p 98	A89-37899
	p 185	N89-22899	p 207	A89-23290
	p 186	N89-23876	p 173	N89-12886
NAG3-183	p 116	A89-22277	p 92	A89-33369
NAG3-188	p 183	N89-17248	p 171	A89-47378
NAG3-190	p 152	A89-51883	p 100	N89-12634
NAG3-194	p 10	N89-12553	p 202	N89-21258
NAG3-201	p 140	A89-12327	p 101	N89-12911
	p 89	A89-12333	p 184	A89-43527
	p 89	A89-12334	p 101	N89-12912
	p 140	A89-12336	p 102	N89-17325
	p 140	A89-12337	p 140	A89-11107
	p 141	A89-12339	p 157	N89-12900
	p 141	A89-12340	p 160	N89-17309
	p 141	A89-14599	p 167	N89-28737
NAG3-20				
NAG3-223				
NAG3-239				
NAG3-245				
NAG3-248				
NAG3-260				
NAG3-265				
NAG3-271				
NAG3-281				
NAG3-284				
NAG3-286				
NAG3-291				
NAG3-305				
NAG3-328				
NAG3-333				
NAG3-337				
NAG3-33				
NAG3-348				
NAG3-354				
NAG3-357				
NAG3-361				
NAG3-363				
NAG3-379				
NAG3-382				
NAG3-395				
NAG3-408				
NAG3-410				
NAG3-417				
NAG3-418				
NAG3-419				
NAG3-422				
NAG3-432				
NAG3-437				
NAG3-449				
NAG3-460				
NAG3-465				
NAG3-468				
NAG3-469				
NAG3-475				
NAG3-476				
NAG3-477				
NAG3-481				
NAG3-485				
NAG3-498				
NAG3-500				
NAG3-501				
NAG3-503				
NAG3-511				
NAG3-512				
NAG3-522				
NAG3-527				

## NAG3-534

## CONTRACT NUMBER INDEX

NAG3-534	p 191 A89-19914		p 19 N89-13429	NASA ORDER C-31003-J	p 45 N89-11802
	p 194 A89-47370		p 19 N89-14235	NASA ORDER C-32000-M	p 42 N89-23501
	p 197 N89-12931	NAG3-730	p 191 A89-27744	NASA ORDER C-80001-G	p 122 N89-25353
	p 197 N89-12932	NAG3-731	p 151 A89-47122	NASA ORDER C-80015-F	p 85 N89-12675
	p 197 N89-14457	NAG3-732	p 7 A89-48955	NASA ORDER C-80017-F	p 155 N89-12835
	p 203 N89-24669	NAG3-741	p 231 A89-16409	NASA ORDER C-80019-F	p 171 A89-45909
NAG3-535	p 206 N89-29803	NAG3-742	p 197 N89-13819	NASA ORDER C-99066-G	p 222 N89-12337
NAG3-536	p 124 A89-22455	NAG3-743	p 2 A89-25029		p 158 N89-13741
	p 127 N89-20364		p 167 N89-27118		p 222 N89-14794
	p 19 N89-25993	NAG3-745	p 124 A89-15152		p 222 N89-20710
	p 129 N89-26126	NAG3-752	p 230 N89-13227		p 162 N89-21192
NAG3-553	p 192 A89-29600	NAG3-754	p 194 A89-42984		p 162 N89-21196
NAG3-55	p 183 N89-14453	NAG3-758	p 79 A89-14580		p 162 N89-21197
NAG3-560	p 235 A89-23482	NAG3-761	p 215 A89-52647		p 222 N89-21595
NAG3-577	p 5 A89-41814	NAG3-763	p 171 A89-47717		p 222 N89-22392
	p 55 A89-44111	NAG3-764	p 169 A89-22279		p 223 N89-22397
	p 58 A89-47116		p 21 A89-23182		p 164 N89-24575
	p 7 A89-47156		p 6 A89-42036		p 223 N89-24865
NAG3-578	p 54 A89-25496		p 7 A89-46847		p 223 N89-24872
	p 64 N89-13495	NAG3-767	p 179 A89-25181		p 166 N89-27115
	p 165 N89-26178		p 6 A89-45428		p 168 N89-28749
NAG3-579	p 157 N89-12901	NAG3-768	p 3 A89-25485		p 168 N89-29714
	p 160 N89-17310	NAG3-76	p 39 A89-32065		p 223 N89-30008
NAG3-581	p 142 A89-16458		p 40 N89-13445	NASA-SAA-C-99066-G	p 164 N89-23821
	p 150 A89-43210	NAG3-771	p 150 A89-42090	NAS1-17070	p 221 A89-37746
NAG3-584	p 144 A89-24803	NAG3-775	p 98 A89-44568	NAS1-18107	p 221 A89-37746
NAG3-590	p 89 A89-12335	NAG3-776	p 231 A89-25537	NAS3-20072	p 113 N89-18550
	p 21 A89-20950		p 232 A89-40188	NAS3-20073	p 28 N89-18487
NAG3-591	p 236 A89-44527		p 232 A89-43357	NAS3-20961	p 12 N89-15896
NAG3-596	p 152 A89-50147		p 233 N89-21658		p 12 N89-15897
	p 156 N89-12894	NAG3-784	p 126 N89-10223	NAS3-22142	p 12 N89-15896
NAG3-598	p 142 A89-15189		p 126 N89-10225		p 12 N89-15897
NAG3-599	p 87 N89-25300	NAG3-789	p 105 A89-26457	NAS3-22234	p 207 A89-15258
NAG3-601	p 5 A89-40905	NAG3-790	p 199 N89-16193	NAS3-22238	p 207 A89-15280
	p 17 N89-11725		p 206 N89-29805		p 207 A89-23283
NAG3-603	p 234 A89-21871	NAG3-791	p 229 N89-19973	NAS3-22257	p 12 N89-15896
NAG3-613	p 235 A89-29299	NAG3-792	p 233 A89-45631		p 12 N89-15897
	p 134 A89-54417	NAG3-803	p 29 N89-20134	NAS3-22550	p 195 A89-47705
NAG3-617	p 155 N89-12838	NAG3-805	p 38 A89-36946	NAS3-22761	p 141 A89-12752
	p 158 N89-12896	NAG3-813	p 92 A89-44536	NAS3-23039	p 8 N89-10025
NAG3-61	p 4 A89-28407	NAG3-814	p 234 A89-21473		p 11 N89-14221
NAG3-623	p 157 N89-12898		p 133 A89-37824	NAS3-23051	p 28 N89-19299
	p 161 N89-17312	NAG3-816	p 133 A89-42742	NAS3-2317	p 157 N89-12897
NAG3-626	p 16 A89-30650	NAG3-822	p 187 A89-25852	NAS3-2317	p 136 N89-15336
	p 18 A89-41093	NAG3-823	p 219 A89-22499	NAS3-23259	p 221 A89-28030
NAG3-627	p 145 A89-25061		p 219 A89-22500	NAS3-23279	p 188 N89-12914
	p 121 N89-19442		p 220 A89-35044	NAS3-23288	p 201 N89-17336
NAG3-631	p 63 N89-11809		p 220 A89-52603		p 62 N89-10943
NAG3-635	p 124 A89-21222		p 35 A89-52628	NAS3-23337	p 138 N89-24530
	p 224 A89-24191	NAG3-824	p 80 A89-19486	NAS3-23351	p 110 N89-13621
	p 19 A89-45107	NAG3-833	p 213 N89-24738	NAS3-23493	p 90 A89-12903
NAG3-645	p 1 A89-11110	NAG3-843	p 57 A89-47036	NAS3-23542	p 25 N89-12907
	p 143 A89-19906		p 64 N89-15170	NAS3-23687	p 157 N89-12899
	p 165 N89-26172	NAG3-848	p 52 A89-15357	NAS3-23691	p 161 N89-17314
NAG3-655	p 181 N89-10282	NAG3-851	p 214 N89-27256		p 161 N89-17313
	p 181 N89-10283	NAG3-854	p 176 N89-25432	NAS3-23695	p 154 A89-54766
	p 186 N89-22920	NAG3-856	p 197 N89-13820	NAS3-23697	p 217 N89-13996
NAG3-656	p 29 N89-20133		p 202 N89-21265		p 199 N89-17316
NAG3-659	p 219 A89-28605		p 203 N89-23918		p 199 N89-17317
	p 220 N89-12283	NAG3-862	p 83 A89-39996		p 196 N89-12906
NAG3-663	p 119 A89-35015	NAG3-866	p 236 A89-30421	NAS3-23698	p 199 N89-17321
NAG3-664	p 218 A89-50100		p 236 A89-38608		p 178 A89-19834
NAG3-665	p 1 A89-12557	NAG3-867	p 198 N89-15434	NAS3-23703	p 178 A89-19835
	p 146 A89-25554		p 201 N89-19581		p 149 A89-36908
NAG3-666	p 16 A89-27739		p 201 N89-19582	NAS3-23708	p 159 N89-13756
	p 16 A89-28451		p 203 N89-23890	NAS3-23717	p 160 N89-17311
	p 16 A89-54803		p 203 N89-23891		p 225 A89-33724
NAG3-667	p 152 A89-51880	NAG3-869	p 179 A89-25181	NAS3-23720	p 5 A89-33735
NAG3-668	p 90 A89-12903	NAG3-870	p 144 A89-25001		p 229 N89-24139
	p 241 A89-41385	NAG3-872	p 221 A89-34963	NAS3-23721	p 173 N89-12887
NAG3-673	p 147 A89-28999		p 216 A89-34964	NAS3-23722	p 174 N89-17299
	p 147 A89-30483	NAG3-873	p 234 A89-20037		p 56 A89-46736
NAG3-676	p 8 A89-53931	NAG3-882	p 204 N89-26260	NAS3-23772	p 56 A89-46737
NAG3-681	p 214 A89-34791	NAG3-888	p 111 N89-14311		p 57 A89-46855
NAG3-682	p 177 A89-17507	NAG3-889	p 171 A89-46980		p 62 N89-11805
NAG3-683	p 182 N89-13793	NAG3-892	p 150 A89-43235		p 64 N89-14258
NAG3-695	p 44 A89-31915	NAG3-898	p 165 N89-26179		p 176 N89-26208
	p 232 A89-39395	NAG3-901	p 204 N89-26261		p 61 N89-10119
NAG3-696	p 93 A89-44542	NAG3-904	p 220 A89-53984	NAS3-23773	p 73 N89-26899
NAG3-701	p 83 A89-54261	NAG3-913	p 126 N89-10213		p 189 N89-27204
NAG3-708	p 130 A89-15387		p 127 N89-20355	NAS3-23775	p 54 A89-28339
	p 134 A89-50472	NAG3-919	p 160 N89-16132		p 66 N89-21834
NAG3-712	p 27 N89-15114	NAG3-926	p 145 A89-25303		p 43 A89-38298
NAG3-714	p 62 N89-11807	NAG3-95	p 90 A89-20474	NAS3-23790	p 126 N89-14369
NAG3-717	p 219 A89-31087		p 236 A89-44552		p 54 A89-28339
NAG3-720	p 95 A89-21395	NAG3-984	p 176 N89-27998	NAS3-23860	p 209 N89-17941
	p 83 A89-38420	NAG3-988	p 236 N89-26739	NAS3-23867	p 210 N89-18967
NAG3-723	p 143 A89-21296		p 237 N89-26740		p 211 N89-22980
	p 96 A89-22559	NAG4-1	p 215 A89-36933		p 211 N89-22981
	p 118 A89-25495	NAG9-120	p 232 A89-43357	NAS3-23881	p 232 A89-40190
	p 122 N89-21134	NASA ORDER C-22187-M	p 73 N89-26903		p 232 A89-43356
NAG3-724	p 5 A89-41794	NASA ORDER C-30001-J	p 54 A89-29113	NAS3-23891	p 91 A89-27966
NAG3-727	p 121 N89-20320		p 217 N89-15623	NAS3-23925	p 191 A89-17396
NAG3-729	p 215 N89-21479	NASA ORDER C-30004-J	p 59 A89-47487		p 99 A89-50313
NAG3-72	p 144 A89-22811	NASA ORDER C-30005-K	p 133 A89-44518		p 195 N89-12904
	p 17 A89-39194		p 208 A89-44883		

**474-12-10**

D-3

	p 46	N89-16905		p 32	N89-22607		p 182	N89-13793
	p 89	N89-24438		p 14	N89-23413		p 182	N89-13794
474-18-00	p 76	N89-28570		p 14	N89-23417		p 182	N89-14450
474-18-10	p 47	N89-26887		p 32	N89-23465		p 182	N89-14452
474-42-10	p 139	N89-25403		p 163	N89-23809		p 183	N89-14453
	p 73	N89-26045		p 164	N89-23821		p 183	N89-15413
	p 139	N89-26148		p 15	N89-24269		p 183	N89-15414
	p 139	N89-26149		p 164	N89-24575		p 183	N89-15415
	p 75	N89-27702		p 164	N89-24577		p 183	N89-17248
474-46-10	p 114	N89-21100		p 223	N89-24865		p 184	N89-18685
	p 115	N89-23691		p 223	N89-24872		p 184	N89-21243
	p 46	N89-24418		p 164	N89-25409		p 184	N89-21244
	p 69	N89-24439		p 224	N89-25670		p 185	N89-22111
	p 70	N89-24448		p 165	N89-26174		p 186	N89-22919
	p 46	N89-25267		p 165	N89-26175		p 186	N89-22920
	p 71	N89-25273		p 166	N89-26180		p 186	N89-22925
	p 71	N89-25275		p 129	N89-27823		p 186	N89-24607
	p 47	N89-26035		p 167	N89-27980		p 187	N89-28015
	p 165	N89-26177		p 167	N89-28748	505-63-81	p 84	N89-10134
474-52-10	p 45	N89-10117		p 168	N89-28749		p 84	N89-10952
	p 67	N89-22653		p 16	N89-29329		p 155	N89-12026
	p 67	N89-23516		p 168	N89-29714		p 197	N89-13820
	p 70	N89-25269		p 168	N89-29725		p 166	N89-27114
	p 72	N89-25283		p 168	N89-29726	505-66-11	p 203	N89-25485
	p 73	N89-26903		p 223	N89-30008	505-68-1A	p 172	N89-12845
474-74-10	p 40	N89-14247	505-62-27	p 162	N89-21197	505-68-11	p 17	N89-11725
481-01-02	p 74	N89-26905	505-62-3B	p 36	N89-22617		p 10	N89-13412
481-54-02	p 63	N89-11809	505-62-51	p 33	N89-26007		p 18	N89-13428
482-56-87	p 158	N89-13731	505-62-61	p 9	N89-10858		p 19	N89-13429
483-31-02	p 45	N89-11802		p 29	N89-20133		p 19	N89-14235
483-32-12	p 45	N89-11802		p 32	N89-22606		p 12	N89-15084
485-40-02	p 64	N89-15164	505-62-71	p 24	N89-12566		p 35	N89-15121
485-40-02	p 86	N89-21036		p 11	N89-15078		p 29	N89-19305
505-01-01	p 103	N89-20228		p 228	N89-20776		p 1	N89-22569
505-43-02	p 159	N89-14386		p 32	N89-24318		p 17	N89-25978
505-43-14	p 220	N89-12283		p 32	N89-24319	505-69-41	p 26	N89-14237
505-44-2C	p 128	N89-21142		p 15	N89-29323	505-69-61	p 24	N89-11751
505-45-48	p 13	N89-19265	505-62-91	p 10	N89-13397		p 18	N89-15107
505-60-01	p 101	N89-13566		p 14	N89-22577		p 32	N89-24320
505-62-OK	p 100	N89-10156	505-63-01	p 101	N89-12720		p 33	N89-26008
	p 184	N89-20472		p 109	N89-12746		p 34	N89-29351
505-62-OK	p 220	N89-12309		p 110	N89-13642	505-80-21	p 166	N89-27103
505-62-01	p 172	N89-11198		p 102	N89-15218		p 33	N89-27670
	p 25	N89-13432		p 112	N89-15257	505-90-01	p 10	N89-12555
	p 174	N89-18671		p 28	N89-18487		p 26	N89-14238
	p 31	N89-20995		p 113	N89-18550		p 189	N89-21256
	p 218	N89-24055	505-63-1A	p 77	N89-10124		p 14	N89-23416
	p 33	N89-26004		p 108	N89-10166		p 163	N89-23813
	p 35	N89-26009		p 100	N89-10996	505-90-11	p 78	N89-15981
	p 36	N89-27672		p 108	N89-11912	506-41-11	p 61	N89-10122
	p 176	N89-27998		p 111	N89-13666		p 135	N89-11129
	p 216	N89-29032		p 111	N89-14338		p 209	N89-12123
505-62-20	p 158	N89-13741		p 85	N89-15201		p 135	N89-12819
505-62-21	p 8	N89-10025		p 78	N89-21032		p 65	N89-15171
	p 154	N89-10242		p 114	N89-21103		p 136	N89-15338
	p 154	N89-10246		p 115	N89-21895		p 65	N89-16917
	p 221	N89-10575		p 86	N89-22684		p 136	N89-19493
	p 9	N89-10844		p 115	N89-26091		p 136	N89-20385
	p 9	N89-10863		p 116	N89-26095		p 137	N89-21174
	p 222	N89-11469	505-63-1B	p 24	N89-10043		p 211	N89-22177
	p 9	N89-11717		p 24	N89-12567		p 67	N89-22651
	p 155	N89-12028		p 196	N89-12930		p 212	N89-23025
	p 222	N89-12337		p 199	N89-17286		p 67	N89-23517
	p 9	N89-12552		p 29	N89-20135		p 138	N89-23792
	p 10	N89-12553		p 201	N89-20514		p 138	N89-24529
	p 158	N89-13754		p 202	N89-21258		p 212	N89-24704
	p 159	N89-13757		p 202	N89-21266		p 72	N89-25277
	p 11	N89-14221		p 31	N89-22605		p 73	N89-26041
	p 11	N89-14222		p 202	N89-22939		p 214	N89-26291
	p 159	N89-14403		p 86	N89-23621		p 214	N89-26292
	p 222	N89-14794		p 87	N89-24459		p 42	N89-26877
	p 11	N89-15077		p 15	N89-25957		p 242	N89-27619
	p 159	N89-15366		p 205	N89-28029		p 75	N89-27705
	p 117	N89-17017		p 205	N89-28036	506-41-21	p 124	N89-27868
	p 218	N89-17422	505-63-1D	p 185	N89-21245		p 208	N89-10405
	p 223	N89-17453	505-63-11	p 85	N89-12684		p 208	N89-10409
	p 13	N89-18417		p 85	N89-13521		p 93	N89-22710
	p 161	N89-18664		p 85	N89-13522		p 211	N89-22982
	p 224	N89-19965		p 197	N89-13819	506-41-3K	p 69	N89-24443
	p 161	N89-20407		p 197	N89-14465	506-41-31	p 69	N89-24440
	p 217	N89-20641		p 86	N89-20206		p 78	N89-24451
	p 218	N89-20684		p 87	N89-25290		p 214	N89-27256
	p 218	N89-20685		p 204	N89-25490		p 76	N89-29484
	p 222	N89-20710		p 87	N89-26048	506-41-41	p 111	N89-14310
	p 14	N89-20921		p 204	N89-26259		p 214	N89-25506
	p 31	N89-20996		p 88	N89-26912		p 231	N89-27506
	p 93	N89-21051		p 88	N89-26919		p 75	N89-27704
	p 162	N89-21192		p 88	N89-26924	506-41-42	p 116	N89-27836
	p 162	N89-21196		p 88	N89-27795	506-41-51	p 166	N89-26182
	p 222	N89-21595	505-63-31	p 198	N89-15437	506-42-11	p 70	N89-24445
	p 31	N89-21798		p 198	N89-16183	506-42-21	p 61	N89-10119
	p 31	N89-21799		p 202	N89-21265		p 62	N89-11805
	p 162	N89-22053		p 203	N89-23918		p 64	N89-14255
	p 222	N89-22392		p 204	N89-26261		p 173	N89-15380
	p 223	N89-22397	505-63-51	p 181	N89-10282		p 189	N89-27204
	p 14	N89-22573		p 181	N89-10283	506-42-31	p 68	N89-23520

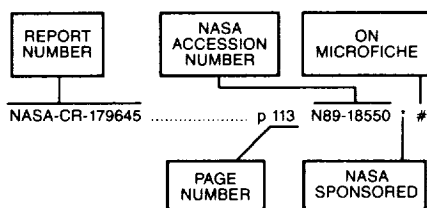


	p 69	N89-24436		p 84	N89-10131	778-35-13	p 214	N89-24741
	p 70	N89-24446		p 198	N89-14470	906-85-44	p 62	N89-10944
	p 72	N89-25281		p 112	N89-15235		p 238	N89-11637
	p 74	N89-26904		p 188	N89-19578	946-02-20	p 71	N89-25271
	p 74	N89-26906		p 189	N89-20490			
	p 167	N89-27121		p 189	N89-28853			
	p 74	N89-27701	553-13-00	p 41	N89-26027			
	p 75	N89-27703		p 204	N89-26260			
	p 75	N89-27706	553-13	p 185	N89-22891			
	p 76	N89-28571		p 205	N89-28030			
506-42-32	p 76	N89-29483	582-01-11	p 155	N89-12835			
506-42-41	p 68	N89-23522		p 173	N89-14418			
506-42-51	p 74	N89-27700		p 65	N89-15979			
	p 70	N89-24444		p 66	N89-20199			
506-43-11	p 41	N89-25254		p 66	N89-21025			
	p 109	N89-11913		p 175	N89-24591			
	p 112	N89-17668		p 221	N89-24856			
	p 188	N89-18694		p 176	N89-26218			
	p 93	N89-19402		p 176	N89-27999			
	p 113	N89-19435	582-01-21	p 70	N89-24447			
	p 113	N89-20253	584-01-21	p 134	N89-11128			
	p 114	N89-21104	586-01-01	p 77	N89-11815			
	p 189	N89-28851	586-01-11	p 173	N89-14416			
506-44-2A	p 139	N89-24532		p 102	N89-16986			
506-44-2C	p 136	N89-21169		p 103	N89-17649			
	p 137	N89-21172		p 209	N89-17941			
506-44-20	p 127	N89-17767		p 66	N89-20193			
	p 137	N89-22020		p 66	N89-20194			
	p 138	N89-23791		p 103	N89-20227			
	p 129	N89-24520		p 210	N89-21419			
	p 123	N89-27038		p 211	N89-22980			
	p 237	N89-30088		p 211	N89-22981			
506-44-21	p 134	N89-10235		p 68	N89-23518			
	p 135	N89-12820		p 68	N89-23527			
	p 136	N89-15337		p 164	N89-23823			
	p 103	N89-17650		p 46	N89-24427			
	p 136	N89-21171		p 175	N89-24593			
506-48-21	p 138	N89-24530		p 239	N89-25078			
	p 64	N89-13495		p 71	N89-25272			
	p 158	N89-13749		p 72	N89-25280			
	p 47	N89-26036		p 72	N89-25282			
	p 73	N89-26044		p 88	N89-27796			
	p 38	N89-28535		p 104	N89-28627			
506-48-91	p 218	N89-17424		p 104	N89-29522			
506-49-21	p 127	N89-17079	586-01-21	p 46	N89-26031			
	p 210	N89-20545	591-23-21	p 67	N89-22652			
506-49-3A	p 63	N89-13492		p 165	N89-26178			
506-55-22	p 40	N89-13445	591-41-11	p 41	N89-24409			
506-55-6E	p 210	N89-19737	591-41-21	p 41	N89-26876			
506-61-42	p 136	N89-15336	591-41-41	p 66	N89-20192			
506-62-21	p 166	N89-27115	595-41-11	p 242	N89-26799			
510-01-0A	p 113	N89-20252	643-10-01	p 128	N89-23756			
	p 87	N89-25300		p 128	N89-23757			
	p 204	N89-26260		p 129	N89-27927			
	p 205	N89-27223	650-60-20	p 126	N89-10215			
510-01-01	p 88	N89-29490		p 127	N89-17756			
	p 100	N89-12717		p 127	N89-21138			
	p 102	N89-14297		p 128	N89-23753			
	p 102	N89-15233	650-60-21	p 137	N89-21173			
	p 78	N89-19371		p 43	N89-26880			
	p 86	N89-23622	650-60-23	p 43	N89-13457			
533-04-1A	p 104	N89-26989		p 129	N89-25365			
533-04-11	p 217	N89-13996		p 40	N89-28545			
	p 195	N89-12876	650-60-26	p 135	N89-13706			
	p 159	N89-13756	674-03-03	p 42	N89-23501			
	p 199	N89-17298	674-22-05	p 120	N89-17046			
533-04-12	p 155	N89-12838		p 121	N89-19442			
533-05-01	p 112	N89-15251		p 122	N89-25353			
	p 113	N89-19421		p 122	N89-28665			
535-03-01	p 227	N89-10603	674-24-05	p 174	N89-16139			
	p 9	N89-10865	674-25-05-08	p 162	N89-22054			
	p 24	N89-11750		p 123	N89-28666			
	p 24	N89-12565	674-25-05	p 120	N89-12753			
	p 10	N89-13409		p 120	N89-14341			
	p 11	N89-14220		p 104	N89-23664			
	p 27	N89-15112	674-26-05	p 114	N89-21894			
	p 228	N89-15685		p 78	N89-25285			
	p 228	N89-15686	674-28-05	p 240	N89-15047			
	p 12	N89-15896	694-00-01	p 121	N89-20321			
	p 12	N89-15897		p 122	N89-26114			
	p 27	N89-15913	694-03-03	p 48	N89-11804			
	p 18	N89-19289		p 174	N89-17211			
	p 228	N89-20779		p 120	N89-17682			
	p 36	N89-21002		p 123	N89-19446			
	p 228	N89-21628		p 123	N89-20324			
	p 228	N89-24138		p 175	N89-21224			
	p 229	N89-24139		p 185	N89-22108			
	p 229	N89-24886	763-01-21	p 61	N89-10123			
	p 15	N89-25119		p 13	N89-16759			
	p 229	N89-25675	776-81-63	p 239	N89-26781			
535-05-01	p 24	N89-12568	778-17-01	p 209	N89-12122			
	p 29	N89-20134		p 209	N89-13103			
	p 33	N89-25238	778-32-11	p 112	N89-16065			
535-05-10	p 163	N89-22862		p 210	N89-21417			
535-07-01	p 83	N89-10128		p 115	N89-24487			
	p 84	N89-10130	778-34-22	p 239	N89-23382			



# REPORT/ACCESSION NUMBER INDEX

## Typical Report Number Index Listing



Listings in this index are arranged alphanumerically by report number. The NASA accession number denotes the number by which the citation is identified. An asterisk (\*) indicates that the item is a NASA report. A pound sign (#) indicates that the item is available on microfiche.

A-88174 ..... p 216 N89-18045 \* #

AAE-AARL-P-89-1 ..... p 64 N89-15170 \* #

AD-A201035 ..... p 84 N89-10952 \* #  
 AD-A201036 ..... p 181 N89-10283 \* #  
 AD-A201037 ..... p 181 N89-10282 \* #  
 AD-A201038 ..... p 220 N89-12309 \* #  
 AD-A201681 ..... p 84 N89-10130 \* #  
 AD-A205373 ..... p 164 N89-25409 \* #  
 AD-A205574 ..... p 182 N89-14452 \* #  
 AD-A205575 ..... p 183 N89-15414 \* #  
 AD-A205576 ..... p 183 N89-15415 \* #  
 AD-A205577 ..... p 172 N89-12845 \* #  
 AD-A206258 ..... p 183 N89-15413 \* #  
 AD-A206830 ..... p 31 N89-20995 \* #  
 AD-A206969 ..... p 184 N89-21244 \* #  
 AD-A207009 ..... p 93 N89-21051 \* #  
 AD-A212958 ..... p 166 N89-27114 \* #  
 AD-A213170 ..... p 186 N89-22920 \* #

AI-120 ..... p 28 N89-17599 \* #

AIAA PAPER 88-0026 ..... p 40 A89-17939 \* #  
 AIAA PAPER 88-2815 ..... p 1 A89-14976 \* #  
 AIAA PAPER 88-2901 ..... p 37 A89-14977 \* #  
 AIAA PAPER 88-2914 ..... p 48 A89-14978 \* #  
 AIAA PAPER 88-2958 ..... p 1 A89-14979 \* #  
 AIAA PAPER 88-3076 ..... p 2 A89-14980 \* #  
 AIAA PAPER 88-3091 ..... p 53 A89-16486 \* #  
 AIAA PAPER 88-3114 ..... p 48 A89-14981 \* #  
 AIAA PAPER 88-3152 ..... p 2 A89-17940 \* #  
 AIAA PAPER 88-3153 ..... p 20 A89-17941 \* #  
 AIAA PAPER 88-3154 ..... p 20 A89-17942 \* #  
 AIAA PAPER 88-3155 ..... p 21 A89-17943 \* #  
 AIAA PAPER 88-3181 ..... p 2 A89-14982 \* #  
 AIAA PAPER 88-3182 ..... p 48 A89-14983 \* #  
 AIAA PAPER 88-3211 ..... p 53 A89-16485 \* #  
 AIAA PAPER 88-4661 ..... p 169 A89-14985 \* #  
 AIAA PAPER 88-4664 ..... p 20 A89-13725 \* #  
 AIAA PAPER 89-0001 ..... p 144 A89-25001 \* #  
 AIAA PAPER 89-0002 ..... p 146 A89-28401 \* #  
 AIAA PAPER 89-0004 ..... p 4 A89-29924 \* #  
 AIAA PAPER 89-0006 ..... p 54 A89-28402 \* #  
 AIAA PAPER 89-0007 ..... p 22 A89-28403 \* #  
 AIAA PAPER 89-0010 ..... p 22 A89-25006 \* #  
 AIAA PAPER 89-0034 ..... p 2 A89-25029 \* #  
 AIAA PAPER 89-0053 ..... p 145 A89-25047 \* #  
 AIAA PAPER 89-0069 ..... p 118 A89-25060 \* #  
 AIAA PAPER 89-0070 ..... p 145 A89-25061 \* #  
 AIAA PAPER 89-0104 ..... p 145 A89-25091 \* #  
 AIAA PAPER 89-0172 ..... p 145 A89-25148 \* #  
 AIAA PAPER 89-0205 ..... p 2 A89-25180 \* #  
 AIAA PAPER 89-0206 ..... p 179 A89-25181 \* #  
 AIAA PAPER 89-0228 ..... p 119 A89-30450 \* #

AIAA PAPER 89-0229 ..... p 118 A89-25197 \* #  
 AIAA PAPER 89-0236 ..... p 118 A89-25201 \* #  
 AIAA PAPER 89-0272 ..... p 3 A89-28405 \* #  
 AIAA PAPER 89-0304 ..... p 118 A89-25261 \* #  
 AIAA PAPER 89-0321 ..... p 3 A89-26389 \* #  
 AIAA PAPER 89-0322 ..... p 3 A89-28406 \* #  
 AIAA PAPER 89-0357 ..... p 4 A89-28407 \* #  
 AIAA PAPER 89-0359 ..... p 145 A89-25303 \* #  
 AIAA PAPER 89-0387 ..... p 22 A89-28408 \* #  
 AIAA PAPER 89-0388 ..... p 146 A89-28409 \* #  
 AIAA PAPER 89-0391 ..... p 146 A89-28410 \* #  
 AIAA PAPER 89-0406 ..... p 47 A89-25341 \* #  
 AIAA PAPER 89-0434 ..... p 3 A89-26373 \* #  
 AIAA PAPER 89-0437 ..... p 4 A89-28413 \* #  
 AIAA PAPER 89-0467 ..... p 145 A89-25382 \* #  
 AIAA PAPER 89-0496 ..... p 44 A89-25405 \* #  
 AIAA PAPER 89-0500 ..... p 91 A89-25406 \* #  
 AIAA PAPER 89-0501 ..... p 119 A89-28418 \* #  
 AIAA PAPER 89-0503 ..... p 119 A89-28419 \* #  
 AIAA PAPER 89-0504 ..... p 91 A89-28420 \* #  
 AIAA PAPER 89-0505 ..... p 44 A89-28421 \* #  
 AIAA PAPER 89-0535 ..... p 17 A89-25429 \* #  
 AIAA PAPER 89-0565 ..... p 3 A89-25454 \* #  
 AIAA PAPER 89-0596 ..... p 44 A89-28438 \* #  
 AIAA PAPER 89-0597 ..... p 119 A89-28439 \* #  
 AIAA PAPER 89-0609 ..... p 3 A89-25485 \* #  
 AIAA PAPER 89-0626 ..... p 118 A89-25495 \* #  
 AIAA PAPER 89-0628 ..... p 54 A89-25496 \* #  
 AIAA PAPER 89-0677 ..... p 231 A89-25537 \* #  
 AIAA PAPER 89-0687 ..... p 146 A89-25543 \* #  
 AIAA PAPER 89-0732 ..... p 16 A89-30650 \* #  
 AIAA PAPER 89-0734 ..... p 16 A89-28451 \* #  
 AIAA PAPER 89-0737 ..... p 146 A89-25554 \* #  
 AIAA PAPER 89-0752 ..... p 4 A89-28453 \* #  
 AIAA PAPER 89-0754 ..... p 34 A89-28454 \* #  
 AIAA PAPER 89-0755 ..... p 36 A89-28455 \* #  
 AIAA PAPER 89-0769 ..... p 189 A89-25570 \* #  
 AIAA PAPER 89-0772 ..... p 17 A89-25571 \* #  
 AIAA PAPER 89-0799 ..... p 22 A89-28462 \* #  
 AIAA PAPER 89-0883 ..... p 118 A89-25627 \* #  
 AIAA PAPER 89-0966 ..... p 147 A89-30482 \* #  
 AIAA PAPER 89-0967 ..... p 147 A89-30483 \* #  
 AIAA PAPER 89-0970 ..... p 4 A89-29098 \* #  
 AIAA PAPER 89-0978 ..... p 150 A89-40400 \* #  
 AIAA PAPER 89-0993 ..... p 149 A89-37825 \* #  
 AIAA PAPER 89-1040 ..... p 226 A89-40469 \* #  
 AIAA PAPER 89-1044 ..... p 225 A89-36214 \* #  
 AIAA PAPER 89-1055 ..... p 23 A89-36215 \* #  
 AIAA PAPER 89-1056 ..... p 225 A89-36216 \* #  
 AIAA PAPER 89-1057 ..... p 226 A89-36217 \* #  
 AIAA PAPER 89-1058 ..... p 226 A89-36218 \* #  
 AIAA PAPER 89-1059 ..... p 226 A89-40472 \* #  
 AIAA PAPER 89-1060 ..... p 227 A89-40473 \* #  
 AIAA PAPER 89-1081 ..... p 225 A89-33724 \* #  
 AIAA PAPER 89-1082 ..... p 225 A89-33725 \* #  
 AIAA PAPER 89-1095 ..... p 5 A89-33735 \* #  
 AIAA PAPER 89-1119 ..... p 17 A89-33754 \* #  
 AIAA PAPER 89-1137 ..... p 225 A89-33767 \* #  
 AIAA PAPER 89-1143 ..... p 227 A89-48953 \* #  
 AIAA PAPER 89-1144 ..... p 226 A89-40175 \* #  
 AIAA PAPER 89-1146 ..... p 227 A89-40478 \* #  
 AIAA PAPER 89-1175 ..... p 192 A89-30666 \* #  
 AIAA PAPER 89-1191 ..... p 192 A89-30681 \* #  
 AIAA PAPER 89-1252 ..... p 44 A89-30737 \* #  
 AIAA PAPER 89-1260 ..... p 22 A89-30745 \* #  
 AIAA PAPER 89-1271 ..... p 192 A89-30754 \* #  
 AIAA PAPER 89-1367 ..... p 192 A89-30842 \* #  
 AIAA PAPER 89-1368 ..... p 192 A89-30843 \* #  
 AIAA PAPER 89-1369 ..... p 193 A89-30844 \* #  
 AIAA PAPER 89-1371 ..... p 193 A89-30846 \* #  
 AIAA PAPER 89-1386 ..... p 34 A89-30859 \* #  
 AIAA PAPER 89-1411 ..... p 81 A89-30883 \* #  
 AIAA PAPER 89-1547 ..... p 37 A89-40177 \* #  
 AIAA PAPER 89-1558 ..... p 232 A89-40188 \* #  
 AIAA PAPER 89-1560 ..... p 232 A89-40190 \* #  
 AIAA PAPER 89-1691 ..... p 7 A89-48955 \* #  
 AIAA PAPER 89-1692 ..... p 150 A89-43210 \* #  
 AIAA PAPER 89-1720 ..... p 150 A89-43235 \* #  
 AIAA PAPER 89-1744 ..... p 152 A89-48958 \* #  
 AIAA PAPER 89-1756 ..... p 83 A89-48957 \* #  
 AIAA PAPER 89-1801 ..... p 6 A89-42036 \* #  
 AIAA PAPER 89-1863 ..... p 150 A89-42090 \* #  
 AIAA PAPER 89-1947 ..... p 5 A89-41794 \* #

AIAA PAPER 89-1956 ..... p 150 A89-41803 \* #  
 AIAA PAPER 89-1970 ..... p 5 A89-41814 \* #  
 AIAA PAPER 89-1980 ..... p 5 A89-41823 \* #  
 AIAA PAPER 89-1984 ..... p 5 A89-41827 \* #  
 AIAA PAPER 89-1994 ..... p 6 A89-41837 \* #  
 AIAA PAPER 89-2140 ..... p 18 A89-50802 \* #  
 AIAA PAPER 89-2142 ..... p 23 A89-53304 \* #  
 AIAA PAPER 89-2262 ..... p 56 A89-46707 \* #  
 AIAA PAPER 89-2268 ..... p 56 A89-46712 \* #  
 AIAA PAPER 89-2298 ..... p 37 A89-46735 \* #  
 AIAA PAPER 89-2300 ..... p 57 A89-46855 \* #  
 AIAA PAPER 89-2302 ..... p 59 A89-49683 \* #  
 AIAA PAPER 89-2303 ..... p 56 A89-46736 \* #  
 AIAA PAPER 89-2305 ..... p 56 A89-46737 \* #  
 AIAA PAPER 89-2322 ..... p 151 A89-46749 \* #  
 AIAA PAPER 89-2334 ..... p 57 A89-46758 \* #  
 AIAA PAPER 89-2355 ..... p 6 A89-46769 \* #  
 AIAA PAPER 89-2357 ..... p 7 A89-46771 \* #  
 AIAA PAPER 89-2358 ..... p 227 A89-46772 \* #  
 AIAA PAPER 89-2376 ..... p 57 A89-46783 \* #  
 AIAA PAPER 89-2378 ..... p 57 A89-46784 \* #  
 AIAA PAPER 89-2413 ..... p 61 A89-53305 \* #  
 AIAA PAPER 89-2416 ..... p 230 A89-46812 \* #  
 AIAA PAPER 89-2460 ..... p 7 A89-46847 \* #  
 AIAA PAPER 89-2534 ..... p 36 A89-46905 \* #  
 AIAA PAPER 89-2574 ..... p 151 A89-46934 \* #  
 AIAA PAPER 89-2583 ..... p 8 A89-50808 \* #  
 AIAA PAPER 89-2638 ..... p 171 A89-46980 \* #  
 AIAA PAPER 89-2669 ..... p 154 A89-54424 \* #  
 AIAA PAPER 89-2695 ..... p 194 A89-47025 \* #  
 AIAA PAPER 89-2696 ..... p 7 A89-47026 \* #  
 AIAA PAPER 89-2710 ..... p 57 A89-47035 \* #  
 AIAA PAPER 89-2711 ..... p 57 A89-47036 \* #  
 AIAA PAPER 89-2716 ..... p 57 A89-47039 \* #  
 AIAA PAPER 89-2717 ..... p 58 A89-47040 \* #  
 AIAA PAPER 89-2718 ..... p 58 A89-47041 \* #  
 AIAA PAPER 89-2719 ..... p 58 A89-47042 \* #  
 AIAA PAPER 89-2722 ..... p 58 A89-47044 \* #  
 AIAA PAPER 89-2723 ..... p 60 A89-50809 \* #  
 AIAA PAPER 89-2725 ..... p 60 A89-49685 \* #  
 AIAA PAPER 89-2727 ..... p 61 A89-53306 \* #  
 AIAA PAPER 89-2739 ..... p 60 A89-49686 \* #  
 AIAA PAPER 89-2793 ..... p 60 A89-49687 \* #  
 AIAA PAPER 89-2805 ..... p 8 A89-50810 \* #  
 AIAA PAPER 89-2819 ..... p 180 A89-47105 \* #  
 AIAA PAPER 89-2829 ..... p 39 A89-47110 \* #  
 AIAA PAPER 89-2832 ..... p 39 A89-47113 \* #  
 AIAA PAPER 89-2837 ..... p 60 A89-50811 \* #  
 AIAA PAPER 89-2838 ..... p 58 A89-47116 \* #  
 AIAA PAPER 89-2840 ..... p 58 A89-47117 \* #  
 AIAA PAPER 89-2846 ..... p 151 A89-47122 \* #  
 AIAA PAPER 89-2883 ..... p 117 A89-47148 \* #  
 AIAA PAPER 89-2893 ..... p 7 A89-47156 \* #  
 AIAA PAPER 89-2898 ..... p 151 A89-47161 \* #  
 AIAA PAPER 89-2901 ..... p 23 A89-52025 \* #  
 AIAA PAPER 89-2904 ..... p 154 A89-53307 \* #  
 AIAA PAPER 89-2906 ..... p 23 A89-49688 \* #  
 AIAA PAPER 89-2908 ..... p 34 A89-47166 \* #  
 AIAA PAPER 89-2919 ..... p 180 A89-47173 \* #  
 AIAA PAPER 89-2942 ..... p 23 A89-47186 \* #  
 AIAA PAPER 89-2943 ..... p 7 A89-47187 \* #  
 AIAA PAPER 89-3510 ..... p 220 A89-52603 \* #  
 AIAA PAPER 89-3519 ..... p 35 A89-53301 \* #  
 AIAA PAPER 89-3520 ..... p 35 A89-52611 \* #  
 AIAA PAPER 89-3541 ..... p 35 A89-52628 \* #  
 AIAA PAPER 89-3562 ..... p 215 A89-52647 \* #  
 AIAA PAPER 89-5014 ..... p 117 A89-51339 \* #

AIAA-88-0453 ..... p 121 N89-20321 \* #  
 AIAA-88-0467 ..... p 9 N89-10863 \* #  
 AIAA-88-3025 ..... p 11 N89-15078 \* #  
 AIAA-88-3155 ..... p 24 N89-10043 \* #  
 AIAA-89-0004 ..... p 13 N89-16759 \* #  
 AIAA-89-0007 ..... p 14 N89-20921 \* #  
 AIAA-89-0053 ..... p 155 N89-12028 \* #  
 AIAA-89-0069 ..... p 120 N89-12753 \* #  
 AIAA-89-0095 ..... p 223 N89-24872 \* #  
 AIAA-89-0172 ..... p 158 N89-13749 \* #  
 AIAA-89-0236 ..... p 240 N89-15047 \* #  
 AIAA-89-0406 ..... p 48 N89-11804 \* #  
 AIAA-89-0434 ..... p 10 N89-13409 \* #  
 AIAA-89-0437 ..... p 11 N89-14220 \* #  
 AIAA-89-0565 ..... p 9 N89-12552 \* #

AIAA-89-0609	p 10	N89-12555 *	BELL-REPT-8911-950003	p 46	N89-11803 *	E-4332	p 108	N89-11038 *
AIAA-89-0628	p 64	N89-13495 *				E-4335	p 134	N89-11128 *
AIAA-89-0752	p 12	N89-15084 *	CONF-880466-5	p 236	N89-11553 *	E-4340	p 227	N89-10603 *
AIAA-89-0754	p 35	N89-15121 *	CONF-880702-23	p 230	N89-14831 *	E-4350	p 77	N89-10124 *
AIAA-89-0755	p 17	N89-25978 *	CONF-880784-5	p 65	N89-17618 *	E-4352	p 109	N89-12746 *
AIAA-89-0769	p 172	N89-12845 *	CONF-880965-2	p 209	N89-17356 *	E-4354	p 108	N89-10166 *
AIAA-89-0966	p 159	N89-14403 *				E-4357	p 162	N89-22054 *
AIAA-89-0970	p 13	N89-18417 *	DE88-011954	p 236	N89-11553 *	E-4358	p 112	N89-17668 *
AIAA-89-1059	p 228	N89-21628 *	DE89-000304	p 209	N89-17356 *	E-4360	p 61	N89-10122 *
AIAA-89-1143	p 228	N89-24138 *	DE89-000341	p 230	N89-14831 *	E-4361	p 136	N89-21171 *
AIAA-89-1144	p 228	N89-20779 *	DE89-001325	p 217	N89-15623 *	E-4362	p 77	N89-11815 *
AIAA-89-1744	p 163	N89-23818 *	DE89-001738	p 65	N89-17618 *	E-4366	p 101	N89-13566 *
AIAA-89-1980	p 15	N89-24269 *				E-4368	p 208	N89-10405 *
AIAA-89-2298	p 41	N89-26876 *	DOE/NASA/0015-1	p 85	N89-12675 *	E-4369	p 62	N89-10944 *
AIAA-89-2302	p 70	N89-24445 *	DOE/NASA/0017-5	p 209	N89-12122 *	E-4370	p 108	N89-11912 *
AIAA-89-2334	p 74	N89-27700 *	DOE/NASA/0017-7	p 209	N89-13103 *	E-4374	p 11	N89-15077 *
AIAA-89-2355	p 33	N89-27670 *	DOE/NASA/0168-11	p 186	N89-26246 *	E-4375	p 84	N89-10134 *
AIAA-89-2357	p 14	N89-22577 *	DOE/NASA/0330-3	p 239	N89-17548 *	E-4377	p 84	N89-10952 *
AIAA-89-2413	p 41	N89-26027 *	DOE/NASA/0342-3	p 239	N89-23382 *	E-4379	p 64	N89-14255 *
AIAA-89-2534	p 36	N89-22617 *	DOE/NASA/0371-1	p 239	N89-14182 *	E-4380	p 19	N89-13429 *
AIAA-89-2583	p 15	N89-25121 *	DOE/NASA/0372-1	p 238	N89-12504 *	E-4381	p 19	N89-14235 *
AIAA-89-2669	p 166	N89-27103 *	DOE/NASA/1005-11	p 210	N89-19737 *	E-4382	p 12	N89-15896 *
AIAA-89-2710	p 74	N89-27701 *	DOE/NASA/16310-10	p 104	N89-28627 *	E-4383	p 175	N89-21224 *
AIAA-89-2717	p 76	N89-28571 *	DOE/NASA/16310-11	p 104	N89-29522 *	E-4384	p 222	N89-11469 *
AIAA-89-2719	p 75	N89-27703 *	DOE/NASA/16310-7	p 103	N89-17649 *	E-4385	p 189	N89-12156 *
AIAA-89-2723	p 72	N89-25281 *	DOE/NASA/16310-8	p 102	N89-16986 *	E-4386	p 84	N89-10130 *
AIAA-89-2725	p 70	N89-24446 *	DOE/NASA/33408-3	p 239	N89-26781 *	E-4386	p 199	N89-17286 *
AIAA-89-2727	p 165	N89-26178 *	DOE/NASA/4105-4	p 214	N89-24741 *	E-4389	p 135	N89-11129 *
AIAA-89-2739	p 70	N89-24447 *	DOE/NASA/50111-2	p 112	N89-16065 *	E-4390	p 114	N89-21894 *
AIAA-89-2793	p 70	N89-24444 *	DOE/NASA/50111-3	p 210	N89-21417 *	E-4393	p 27	N89-15913 *
AIAA-89-2805	p 15	N89-25119 *				E-4394	p 155	N89-12835 *
AIAA-89-2832	p 76	N89-29483 *	DOT/FAA/CT-88/19	p 18	N89-13428 *	E-4395	p 238	N89-11637 *
AIAA-89-2837	p 72	N89-25283 *				E-4396	p 172	N89-11198 *
AIAA-89-2840	p 75	N89-27706 *	E-1737	p 159	N89-14386 *	E-4397	p 174	N89-16139 *
AIAA-89-2901	p 33	N89-25238 *	E-2417	p 13	N89-19265 *	E-4398	p 102	N89-16986 *
AIAA-89-2904	p 165	N89-26174 *	E-2645	p 65	N89-15979 *	E-4399	p 12	N89-15897 *
AIAA-89-2906	p 32	N89-24318 *	E-3205	p 195	N89-12876 *	E-4400	p 136	N89-15337 *
AIAA-89-2919	p 186	N89-22925 *	E-3269	p 154	N89-10246 *	E-4402	p 25	N89-13432 *
AIAA-89-2942	p 32	N89-22606 *	E-3277	p 210	N89-19737 *	E-4404-1	p 164	N89-24575 *
AIAA-89-2943	p 14	N89-23416 *	E-3437	p 9	N89-10865 *	E-4405	p 85	N89-12684 *
AIAA-89-3520	p 35	N89-26009 *	E-3536	p 159	N89-13756 *	E-4406	p 155	N89-12028 *
			E-3557	p 101	N89-12720 *	E-4408	p 126	N89-10215 *
AIRESEARCH-86-60365	p 113	N89-19421 *	E-3574	p 238	N89-18259 *	E-4412	p 9	N89-10863 *
			E-3714	p 174	N89-18671 *	E-4413	p 182	N89-14452 *
ALLISON-EDR-13481	p 158	N89-13754 *	E-3727	p 166	N89-27114 *	E-4417	p 122	N89-26114 *
			E-3745	p 199	N89-17298 *	E-4419	p 120	N89-14341 *
ARINC-RP-5149-11-01-4744	p 45	N89-11802 *	E-3887	p 181	N89-10283 *	E-4421	p 120	N89-12753 *
			E-3888	p 181	N89-10282 *	E-4422	p 24	N89-12567 *
ASME PAPER 88-GT-139	p 2	A89-15967 *	E-3983	p 127	N89-17767 *	E-4425	p 110	N89-13642 *
ASME PAPER 88-GT-314	p 22	A89-24989 *	E-4004	p 161	N89-18664 *	E-4426	p 217	N89-20641 *
ASME PAPER 88-TRIB-23	p 148	A89-34795 *	E-4016	p 221	N89-10575 *	E-4427	p 172	N89-10269 *
ASME PAPER 88-TRIB-35	p 179	A89-34794 *	E-4022	p 85	N89-13522 *	E-4428	p 43	N89-13457 *
ASME PAPER 88-TRIB-40	p 179	A89-24992 *	E-4054	p 187	N89-28015 *	E-4429	p 112	N89-15257 *
ASME PAPER 88-TRIB-41	p 179	A89-34798 *	E-4071	p 32	N89-22606 *	E-4430	p 26	N89-14238 *
ASME PAPER 88-WA/DSC-1	p 219	A89-22499 *	E-4083	p 11	N89-14221 *	E-4431	p 109	N89-11913 *
ASME PAPER 88-WA/DSC-2	p 219	A89-22500 *	E-4084	p 11	N89-14222 *	E-4433	p 220	N89-12309 *
			E-4085	p 8	N89-10025 *	E-4434	p 9	N89-12552 *
ASTM STP-1003	p 81	A89-32882 *	E-4094	p 154	N89-10242 *	E-4435	p 172	N89-12845 *
			E-4113	p 9	N89-10858 *	E-4437	p 228	N89-15686 *
ATC-2459-42-1	p 62	N89-11805 *	E-4114	p 86	N89-15990 *	E-4438	p 102	N89-15233 *
			E-4116	p 36	N89-21002 *	E-4439	p 222	N89-12337 *
AVSCOM-TM-88-C-005	p 183	N89-17248 *	E-4128	p 196	N89-12930 *	E-4442	p 112	N89-15235 *
			E-4144	p 184	N89-21243 *	E-4445	p 61	N89-10123 *
AVSCOM-TR-87-C-26	p 166	N89-27114 *	E-4147	p 228	N89-15685 *	E-4446	p 164	N89-25409 *
AVSCOM-TR-87-C-33	p 181	N89-10283 *	E-4169	p 222	N89-14794 *	E-4447	p 135	N89-12819 *
AVSCOM-TR-87-C-34	p 181	N89-10282 *	E-4183	p 9	N89-10844 *	E-4448	p 134	N89-10235 *
AVSCOM-TR-87-C-35	p 181	N89-19503 *	E-4184	p 100	N89-10996 *	E-4449	p 85	N89-15201 *
AVSCOM-TR-87-C-36	p 183	N89-14453 *	E-4196	p 27	N89-15112 *	E-4451	p 197	N89-14465 *
AVSCOM-TR-87-C-38	p 182	N89-13794 *	E-4199	p 218	N89-17422 *	E-4452	p 185	N89-21245 *
AVSCOM-TR-88-C-003	p 183	N89-15413 *	E-4202	p 155	N89-12026 *	E-4454	p 209	N89-12123 *
AVSCOM-TR-88-C-007	p 184	N89-20472 *	E-4209	p 115	N89-26091 *	E-4456	p 40	N89-28545 *
AVSCOM-TR-88-C-008	p 164	N89-25409 *	E-4213	p 120	N89-17682 *	E-4457	p 203	N89-25485 *
AVSCOM-TR-88-C-010	p 184	N89-21243 *	E-4225	p 183	N89-15413 *	E-4458	p 155	N89-12838 *
AVSCOM-TR-88-C-021	p 182	N89-14450 *	E-4226	p 182	N89-14450 *	E-4459	p 182	N89-13793 *
AVSCOM-TR-88-C-022	p 201	N89-20514 *	E-4227	p 185	N89-22891 *	E-4461	p 24	N89-12566 *
AVSCOM-TR-88-C-023	p 220	N89-12309 *	E-4232	p 42	N89-10111 *	E-4465	p 78	N89-15981 *
AVSCOM-TR-88-C-027	p 84	N89-10130 *	E-4238	p 208	N89-10409 *	E-4466	p 173	N89-14416 *
AVSCOM-TR-88-C-028	p 84	N89-10134 *	E-4250	p 11	N89-15078 *	E-4468	p 29	N89-20135 *
AVSCOM-TR-88-C-032	p 182	N89-14452 *	E-4254	p 233	N89-14842 *	E-4469	p 108	N89-11911 *
AVSCOM-TR-88-C-033	p 183	N89-15414 *	E-4260	p 24	N89-10043 *	E-4472	p 63	N89-13492 *
AVSCOM-TR-88-C-034	p 183	N89-15415 *	E-4265	p 45	N89-10117 *	E-4474	p 84	N89-11826 *
AVSCOM-TR-88-C-036	p 172	N89-12845 *	E-4273	p 136	N89-21169 *	E-4474	p 36	N89-16882 *
AVSCOM-TR-88-C-037	p 24	N89-12568 *	E-4275	p 100	N89-12717 *	E-4477	p 240	N89-15047 *
AVSCOM-TR-88-C-040	p 184	N89-18685 *	E-4280	p 198	N89-16183 *	E-4483	p 158	N89-13741 *
AVSCOM-TR-88-C-041	p 184	N89-21244 *	E-4282	p 9	N89-11717 *	E-4484	p 111	N89-13666 *
AVSCOM-TR-88-C-30	p 84	N89-10952 *	E-4286	p 10	N89-12553 *	E-4485	p 111	N89-14310 *
AVSCOM-TR-89-C-001	p 31	N89-20995 *	E-4290	p 223	N89-17453 *	E-4486	p 102	N89-14297 *
AVSCOM-TR-89-C-001	p 93	N89-21051 *	E-4298	p 222	N89-22392 *	E-4487	p 63	N89-12665 *
AVSCOM-TR-89-C-002	p 186	N89-22920 *	E-4299	p 84	N89-10131 *	E-4488	p 48	N89-11804 *
AVSCOM-TR-89-C-002	p 205	N89-28029 *	E-4301	p 100	N89-10156 *	E-4489	p 188	N89-18694 *
AVSCOM-TR-89-C-004	p 33	N89-25238 *	E-4311	p 78	N89-19371 *	E-4490	p 24	N89-11751 *
AVSCOM-TR-89-C-004	p 187	N89-28015 *	E-4312	p 220	N89-12283 *	E-4495	p 103	N89-17650 *
AVSCOM-TR-89-C-007	p 186	N89-22925 *	E-4316	p 173	N89-15380 *	E-4496	p 18	N89-15107 *
AVSCOM-TR-89-C-010	p 186	N89-24607 *	E-4318	p 88	N89-27796 *	E-4497	p 159	N89-14403 *
AVSCOM-TR-89-C-011	p 185	N89-22111 *	E-4319	p 209	N89-12122 *	E-4498	p 202	N89-22939 *
AVSCOM-TR-89-C-013	p 163	N89-22862 *	E-4320	p 209	N89-13103 *	E-4499	p 158	N89-13749 *

E-4500	p 114	N89-21103 * #	E-4652	p 218	N89-20684 * #	E-4809	p 175	N89-24591 * #
E-4503	p 159	N89-13757 * #	E-4653	p 66	N89-20194 * #	E-4812	p 42	N89-23501 * #
E-4506	p 12	N89-15898 * #	E-4654	p 113	N89-20253 * #	E-4815	p 164	N89-23823 * #
E-4507	p 10	N89-12555 * #	E-4655	p 222	N89-21595 * #	E-4816	p 212	N89-23025 * #
E-4509	p 11	N89-14220 * #	E-4657	p 73	N89-26903 * #	E-4817	p 72	N89-25282 * #
E-4510	p 188	N89-19578 * #	E-4660	p 93	N89-19402 * #	E-4818	p 71	N89-25271 * #
E-4511	p 42	N89-24413 * #	E-4661	p 123	N89-19446 * #	E-4819	p 165	N89-26177 * #
E-4512	p 198	N89-15437 * #	E-4662	p 113	N89-20252 * #	E-4820	p 214	N89-25506 * #
E-4513	p 85	N89-13521 * #	E-4663	p 162	N89-21197 * #	E-4821	p 71	N89-25272 * #
E-4515	p 24	N89-12568 * #	E-4665	p 31	N89-20996 * #	E-4823	p 46	N89-25267 * #
E-4516	p 103	N89-20227 * #	E-4666	p 186	N89-22919 * #	E-4825	p 138	N89-23791 * #
E-4517	p 159	N89-15366 * #	E-4668	p 211	N89-22177 * #	E-4831	p 71	N89-25275 * #
E-4518	p 87	N89-25290 * #	E-4670	p 204	N89-26260 * #	E-4832	p 71	N89-25273 * #
E-4519	p 26	N89-14237 * #	E-4671	p 114	N89-21104 * #	E-4833	p 69	N89-24439 * #
E-4520	p 198	N89-14470 * #	E-4672	p 31	N89-22605 * #	E-4835	p 72	N89-25277 * #
E-4521	p 136	N89-15338 * #	E-4673	p 66	N89-21025 * #	E-4836	p 46	N89-24418 * #
E-4522	p 65	N89-16917 * #	E-4675	p 93	N89-21051 * #	E-4838	p 32	N89-24318 * #
E-4523	p 102	N89-15218 * #	E-4676	p 228	N89-21628 * #	E-4839	p 163	N89-22862 * #
E-4524	p 122	N89-28665 * #	E-4677	p 29	N89-19305 * #	E-4841	p 167	N89-27121 * #
E-4525	p 10	N89-13409 * #	E-4678	p 185	N89-22111 * #	E-4842	p 15	N89-24269 * #
E-4526	p 65	N89-15171 * #	E-4679	p 210	N89-21419 * #	E-4843	p 69	N89-24440 * #
E-4528	p 35	N89-15121 * #	E-4680	p 66	N89-20199 * #	E-4844	p 166	N89-26180 * #
E-4530	p 173	N89-14418 * #	E-4682	p 163	N89-23813 * #	E-4846	p 72	N89-25280 * #
E-4531	p 182	N89-13794 * #	E-4683	p 86	N89-22684 * #	E-4847	p 41	N89-24409 * #
E-4532	p 183	N89-15414 * #	E-4684	p 228	N89-20779 * #	E-4849	p 17	N89-25978 * #
E-4533	p 183	N89-15415 * #	E-4685	p 168	N89-29714 * #	E-4851	p 46	N89-26031 * #
E-4534	p 184	N89-18685 * #	E-4686	p 115	N89-23691 * #	E-4853	p 36	N89-27672 * #
E-4535	p 203	N89-24635 * #	E-4689	p 32	N89-23465 * #	E-4854	p 139	N89-26148 * #
E-4536	p 135	N89-13722 * #	E-4690	p 218	N89-24055 * #	E-4855	p 205	N89-28030 * #
E-4537	p 187	N89-13820 * #	E-4692	p 1	N89-22569 * #	E-4856	p 75	N89-27705 * #
E-4539	p 26	N89-14239 * #	E-4693	p 128	N89-21142 * #	E-4857	p 33	N89-25238 * #
E-4541	p 10	N89-13412 * #	E-4695	p 202	N89-21266 * #	E-4859	p 239	N89-25078 * #
E-4542	p 183	N89-14453 * #	E-4696	p 42	N89-26877 * #	E-4860	p 35	N89-26009 * #
E-4543	p 202	N89-21258 * #	E-4697	p 29	N89-20133 * #	E-4861	p 32	N89-24319 * #
E-4544	p 112	N89-16065 * #	E-4698	p 33	N89-26007 * #	E-4864	p 32	N89-24319 * #
E-4545	p 64	N89-13495 * #	E-4700	p 228	N89-24138 * #	E-4865	p 15	N89-29323 * #
E-4546	p 12	N89-15084 * #	E-4701	p 93	N89-22710 * #	E-4866	p 242	N89-27623 * #
E-4547	p 18	N89-13428 * #	E-4702	p 78	N89-21032 * #	E-4868	p 242	N89-27619 * #
E-4550-1	p 136	N89-19493 * #	E-4703	p 14	N89-23413 * #	E-4869	p 165	N89-26174 * #
E-4551	p 184	N89-21244 * #	E-4706	p 221	N89-24856 * #	E-4870	p 124	N89-27868 * #
E-4552	p 103	N89-17649 * #	E-4707	p 68	N89-23518 * #	E-4871	p 214	N89-26291 * #
E-4553	p 40	N89-14247 * #	E-4708	p 211	N89-22982 * #	E-4873	p 70	N89-24448 * #
E-4556	p 228	N89-20776 * #	E-4710	p 78	N89-25285 * #	E-4874	p 204	N89-25490 * #
E-4557	p 123	N89-20324 * #	E-4711	p 163	N89-23809 * #	E-4875	p 88	N89-26919 * #
E-4558	p 183	N89-17248 * #	E-4712	p 41	N89-20171 * #	E-4876	p 88	N89-26912 * #
E-4560	p 197	N89-13819 * #	E-4719	p 223	N89-22397 * #	E-4877	p 70	N89-24446 * #
E-4561	p 111	N89-14338 * #	E-4721	p 14	N89-22573 * #	E-4880	p 72	N89-25281 * #
E-4563	p 198	N89-15438 * #	E-4723	p 123	N89-28666 * #	E-4881	p 224	N89-25670 * #
E-4565	p 115	N89-21895 * #	E-4724	p 69	N89-24443 * #	E-4882	p 231	N89-27506 * #
E-4568	p 127	N89-17756 * #	E-4725	p 162	N89-22053 * #	E-4883	p 165	N89-26175 * #
E-4569	p 127	N89-21138 * #	E-4727	p 14	N89-23417 * #	E-4886	p 15	N89-25121 * #
E-4570	p 86	N89-23621 * #	E-4729	p 242	N89-23397 * #	E-4888	p 70	N89-24447 * #
E-4572	p 87	N89-25300 * #	E-4730	p 67	N89-23516 * #	E-4891	p 88	N89-27795 * #
E-4574	p 14	N89-20921 * #	E-4731	p 41	N89-25254 * #	E-4892	p 116	N89-26095 * #
E-4576	p 201	N89-20514 * #	E-4734	p 73	N89-26041 * #	E-4897	p 165	N89-26178 * #
E-4577	p 222	N89-20710 * #	E-4735	p 87	N89-24459 * #	E-4898	p 72	N89-25283 * #
E-4578	p 31	N89-20995 * #	E-4739	p 14	N89-22577 * #	E-4899	p 204	N89-26259 * #
E-4579	p 46	N89-16905 * #	E-4740	p 138	N89-24529 * #	E-4900	p 87	N89-26048 * #
E-4580	p 214	N89-24741 * #	E-4741	p 138	N89-23792 * #	E-4902	p 76	N89-29484 * #
E-4583	p 218	N89-17424 * #	E-4742	p 68	N89-23520 * #	E-4903	p 175	N89-24593 * #
E-4584	p 210	N89-21417 * #	E-4744	p 67	N89-23517 * #	E-4904	p 123	N89-27038 * #
E-4585	p 120	N89-17046 * #	E-4746	p 32	N89-24320 * #	E-4910	p 75	N89-27703 * #
E-4587	p 212	N89-24704 * #	E-4747	p 67	N89-22651 * #	E-4912	p 139	N89-26150 * #
E-4588	p 186	N89-24607 * #	E-4748	p 139	N89-24532 * #	E-4913	p 164	N89-24577 * #
E-4589	p 162	N89-21192 * #	E-4749	p 163	N89-23818 * #	E-4916	p 242	N89-26799 * #
E-4592	p 13	N89-16759 * #	E-4750	p 67	N89-22652 * #	E-4921	p 167	N89-28748 * #
E-4593	p 117	N89-17017 * #	E-4754	p 104	N89-28627 * #	E-4923	p 214	N89-26292 * #
E-4594	p 137	N89-21174 * #	E-4756	p 186	N89-22925 * #	E-4928	p 176	N89-26218 * #
E-4596	p 113	N89-19435 * #	E-4759	p 104	N89-23664 * #	E-4932	p 189	N89-28851 * #
E-4598	p 162	N89-21196 * #	E-4760	p 36	N89-22617 * #	E-4933	p 70	N89-24444 * #
E-4600	p 189	N89-28853 * #	E-4761	p 129	N89-27923 * #	E-4936	p 46	N89-24427 * #
E-4605	p 174	N89-17211 * #	E-4764	p 78	N89-24451 * #	E-4938	p 166	N89-27103 * #
E-4606	p 229	N89-24886 * #	E-4765	p 33	N89-26004 * #	E-4939	p 76	N89-28571 * #
E-4608	p 31	N89-21798 * #	E-4767	p 137	N89-22020 * #	E-4940	p 139	N89-26149 * #
E-4609	p 103	N89-20228 * #	E-4770	p 164	N89-23821 * #	E-4941	p 139	N89-25403 * #
E-4610	p 86	N89-20206 * #	E-4771	p 163	N89-22861 * #	E-4946	p 166	N89-27115 * #
E-4616	p 137	N89-21172 * #	E-4772	p 223	N89-24872 * #	E-4949	p 176	N89-27998 * #
E-4618	p 121	N89-20321 * #	E-4775	p 87	N89-24480 * #	E-4950	p 41	N89-26027 * #
E-4620	p 129	N89-25365 * #	E-4778	p 33	N89-26003 * #	E-4951	p 73	N89-26045 * #
E-4621	p 129	N89-24520 * #	E-4785	p 223	N89-24865 * #	E-4952	p 33	N89-26008 * #
E-4622	p 224	N89-19965 * #	E-4787	p 70	N89-24445 * #	E-4953	p 229	N89-25675 * #
E-4626	p 186	N89-22920 * #	E-4790	p 205	N89-28029 * #	E-4955	p 47	N89-26036 * #
E-4627	p 210	N89-20545 * #	E-4791	p 14	N89-23416 * #	E-4962	p 47	N89-26035 * #
E-4629	p 161	N89-20407 * #	E-4792	p 68	N89-23527 * #	E-4964	p 167	N89-27980 * #
E-4632	p 189	N89-20490 * #	E-4793	p 128	N89-23753 * #	E-4965	p 205	N89-27223 * #
E-4634	p 32	N89-22607 * #	E-4794	p 115	N89-24487 * #	E-4973	p 168	N89-28749 * #
E-4635	p 31	N89-21799 * #	E-4796	p 86	N89-23622 * #	E-4976	p 47	N89-26887 * #
E-4636	p 42	N89-20179 * #	E-4798	p 175	N89-23850 * #	E-4976	p 41	N89-26876 * #
E-4641	p 66	N89-20193 * #	E-4799	p 71	N89-25274 * #	E-4980	p 116	N89-27836 * #
E-4642	p 15	N89-25957 * #	E-4801	p 69	N89-24436 * #	E-4982	p 88	N89-26924 * #
E-4643	p 13	N89-18417 * #	E-4802	p 68	N89-23522 * #	E-4984	p 73	N89-26044 * #
E-4645	p 136	N89-20385 * #	E-4804	p 69	N89-24438 * #	E-4988	p 205	N89-28036 * #
E-4646	p 66	N89-20192 * #	E-4805	p 15	N89-25119 * #	E-4995	p 104	N89-29522 * #
E-4647	p 218	N89-20685 * #	E-4806	p 239	N89-26781 * #	E-4997	p 38	N89-28535 * #
E-4648	p 86	N89-21036 * #	E-4807	p 67	N89-22653 * #	E-5005	p 75	N89-27706 * #
E-4649	p 114	N89-21100 * #	E-4808	p 70	N89-25269 * #	E-5006	p 74	N89-27701 * #
						E-5011	p 33	N89-27670 * #

E-5014	p 168	N89-29726 * #	NAS 1.15:100259	p 181	N89-10283 * #	NAS 1.15:101411	p 159	N89-13757 * #
E-5017	p 74	N89-26904 * #	NAS 1.15:100260	p 181	N89-10282 * #	NAS 1.15:101412	p 11	N89-15077 * #
E-5018	p 76	N89-29483 * #	NAS 1.15:100708	p 206	N89-10403 * #	NAS 1.15:101413	p 10	N89-12555 * #
E-5025	p 74	N89-27700 * #	NAS 1.15:100827	p 161	N89-18664 * #	NAS 1.15:101414	p 198	N89-15437 * #
E-5026	p 129	N89-27927 * #	NAS 1.15:100828	p 221	N89-10575 * #	NAS 1.15:101415	p 85	N89-13521 * #
E-5027	p 88	N89-29490 * #	NAS 1.15:100832	p 85	N89-13522 * #	NAS 1.15:101416	p 24	N89-12568 * #
E-5029	p 216	N89-29032 * #	NAS 1.15:100869	p 31	N89-20995 * #	NAS 1.15:101417	p 11	N89-14220 * #
E-5035	p 168	N89-29725 * #	NAS 1.15:100879	p 9	N89-10858 * #	NAS 1.15:101418	p 103	N89-20227 * #
E-5040	p 176	N89-27999 * #	NAS 1.15:100880	p 86	N89-15990 * #	NAS 1.15:101419	p 159	N89-15366 * #
E-5041	p 104	N89-26989 * #	NAS 1.15:100883	p 36	N89-21002 * #	NAS 1.15:101420	p 26	N89-14237 * #
E-5043	p 75	N89-27702 * #	NAS 1.15:100890	p 196	N89-12930 * #	NAS 1.15:101421	p 198	N89-14470 * #
E-5046	p 74	N89-26906 * #	NAS 1.15:100916	p 222	N89-14794 * #	NAS 1.15:101422	p 65	N89-16917 * #
E-5047	p 76	N89-28570 * #	NAS 1.15:100925	p 238	N89-24216 * #	NAS 1.15:101423	p 102	N89-15218 * #
E-5053	p 237	N89-30088 * #	NAS 1.15:100931	p 155	N89-12026 * #	NAS 1.15:101424	p 122	N89-28665 * #
E-5055	p 75	N89-27704 * #	NAS 1.15:100944	p 42	N89-10111 * #	NAS 1.15:101425	p 65	N89-15171 * #
E-5061	p 223	N89-30008 * #	NAS 1.15:100947	p 208	N89-10409 * #	NAS 1.15:101427	p 35	N89-15121 * #
EDR-13295	p 186	N89-26246 * #	NAS 1.15:100952	p 11	N89-15078 * #	NAS 1.15:101428	p 173	N89-14418 * #
EDR-13519	p 154	N89-12010 * #	NAS 1.15:100968	p 172	N89-11198 * #	NAS 1.15:101430	p 203	N89-24635 * #
ELS-TR-716111-6	p 127	N89-20364 * #	NAS 1.15:100972	p 45	N89-10117 * #	NAS 1.15:101431	p 182	N89-13794 * #
ESL-TR-719300-3	p 126	N89-10225 * #	NAS 1.15:100999	p 216	N89-18045 * #	NAS 1.15:101432	p 135	N89-13722 * #
ESL-TR-720964-1	p 126	N89-10213 * #	NAS 1.15:101009	p 230	N89-14831 * #	NAS 1.15:101433	p 26	N89-14239 * #
ESL-718688-7	p 217	N89-13993 * #	NAS 1.15:101200	p 236	N89-11553 * #	NAS 1.15:101434	p 10	N89-13412 * #
ESL-720964-2	p 127	N89-20355 * #	NAS 1.15:101219	p 65	N89-17618 * #	NAS 1.15:101435	p 182	N89-14452 * #
FDA-89-07	p 165	N89-26172 * #	NAS 1.15:101220	p 209	N89-17356 * #	NAS 1.15:101436	p 63	N89-13492 * #
FLOW-RR-447	p 24	N89-11750 * #	NAS 1.15:101251	p 154	N89-10242 * #	NAS 1.15:101437	p 10	N89-13409 * #
FR-19625	p 68	N89-23519 * #	NAS 1.15:101298	p 9	N89-11717 * #	NAS 1.15:101438	p 183	N89-14453 * #
FR-719300-4	p 126	N89-10223 * #	NAS 1.15:101301	p 222	N89-22392 * #	NAS 1.15:101439	p 112	N89-16065 * #
GARRETT-21-5278-2-VOL-2	p 28	N89-18487 * #	NAS 1.15:101308	p 100	N89-10156 * #	NAS 1.15:101440	p 64	N89-13495 * #
HSER-9247	p 28	N89-19299 * #	NAS 1.15:101310	p 220	N89-12283 * #	NAS 1.15:101441	p 12	N89-15084 * #
IAF PAPER ICOSP89-1-8	p 55	A89-46513 * #	NAS 1.15:101316	p 24	N89-10043 * #	NAS 1.15:101442	p 184	N89-18685 * #
IAF PAPER ICOSP89-4-1	p 55	A89-46517 * #	NAS 1.15:101322	p 227	N89-10603 * #	NAS 1.15:101443	p 112	N89-15257 * #
IAF PAPER ICOSP89-5-7	p 56	A89-46520 * #	NAS 1.15:101329	p 77	N89-10124 * #	NAS 1.15:101444	p 183	N89-15413 * #
IAF PAPER ICOSP89-9-5	p 241	A89-46529 * #	NAS 1.15:101335	p 108	N89-10166 * #	NAS 1.15:101445	p 184	N89-21244 * #
IAF PAPER ICOSP89-9-6	p 39	A89-46530 * #	NAS 1.15:101336	p 162	N89-22054 * #	NAS 1.15:101446	p 103	N89-17649 * #
IAF PAPER 88-035	p 37	A89-17641 * #	NAS 1.15:101338	p 112	N89-17668 * #	NAS 1.15:101447	p 40	N89-14247 * #
IAF PAPER 88-198	p 42	A89-17720 * #	NAS 1.15:101340	p 61	N89-10122 * #	NAS 1.15:101448	p 123	N89-20324 * #
IAF PAPER 88-221	p 53	A89-17730 * #	NAS 1.15:101341	p 77	N89-11815 * #	NAS 1.15:101449	p 183	N89-17248 * #
IAF PAPER 88-355	p 117	A89-17784 * #	NAS 1.15:101342	p 208	N89-10405 * #	NAS 1.15:101450	p 85	N89-15201 * #
IAF PAPER 88-587	p 37	A89-17861 * #	NAS 1.15:101345	p 108	N89-11912 * #	NAS 1.15:101451	p 111	N89-14338 * #
IAF-89-057	p 73	N89-26044 * #	NAS 1.15:101348	p 84	N89-10134 * #	NAS 1.15:101452	p 198	N89-15438 * #
ICOMP-88-11	p 222	N89-14794 * #	NAS 1.15:101349	p 108	N89-11038 * #	NAS 1.15:101455	p 102	N89-15233 * #
ICOMP-88-16	p 222	N89-22392 * #	NAS 1.15:101350	p 84	N89-10952 * #	NAS 1.15:101456	p 115	N89-21895 * #
ICOMP-88-18	p 222	N89-11469 * #	NAS 1.15:101355	p 64	N89-14255 * #	NAS 1.15:101457	p 183	N89-15414 * #
ICOMP-88-19	p 222	N89-12337 * #	NAS 1.15:101359	p 175	N89-21224 * #	NAS 1.15:101458	p 127	N89-17756 * #
ICOMP-88-20	p 158	N89-13741 * #	NAS 1.15:101360	p 62	N89-10944 * #	NAS 1.15:101459	p 127	N89-21138 * #
ICOMP-88-21	p 159	N89-14403 * #	NAS 1.15:101361	p 222	N89-11469 * #	NAS 1.15:101460	p 183	N89-15415 * #
ICOMP-88-22	p 159	N89-13757 * #	NAS 1.15:101362	p 84	N89-10130 * #	NAS 1.15:101461	p 86	N89-23621 * #
ICOMP-88-5	p 221	N89-10575 * #	NAS 1.15:101365	p 199	N89-17286 * #	NAS 1.15:101462	p 223	N89-17453 * #
ICOMP-89-10	p 164	N89-24575 * #	NAS 1.15:101366	p 135	N89-11129 * #	NAS 1.15:101463	p 42	N89-24413 * #
ICOMP-89-11	p 223	N89-24865 * #	NAS 1.15:101367	p 134	N89-11128 * #	NAS 1.15:101464	p 201	N89-20514 * #
ICOMP-89-12	p 168	N89-29714 * #	NAS 1.15:101369	p 27	N89-15913 * #	NAS 1.15:101465	p 136	N89-15338 * #
ICOMP-89-13	p 223	N89-24872 * #	NAS 1.15:101371	p 238	N89-11637 * #	NAS 1.15:101466	p 222	N89-20710 * #
ICOMP-89-14	p 165	N89-26175 * #	NAS 1.15:101372	p 102	N89-16986 * #	NAS 1.15:101467	p 46	N89-16905 * #
ICOMP-89-15	p 167	N89-28748 * #	NAS 1.15:101373	p 109	N89-12746 * #	NAS 1.15:101469	p 218	N89-17424 * #
ICOMP-89-16	p 166	N89-27115 * #	NAS 1.15:101374	p 85	N89-12684 * #	NAS 1.15:101470	p 210	N89-21417 * #
ICOMP-89-18	p 168	N89-28749 * #	NAS 1.15:101376	p 155	N89-12028 * #	NAS 1.15:101471	p 120	N89-17046 * #
ICOMP-89-19	p 168	N89-29726 * #	NAS 1.15:101377	p 126	N89-10215 * #	NAS 1.15:101473	p 162	N89-21192 * #
ICOMP-89-20	p 222	N89-26175 * #	NAS 1.15:101378	p 122	N89-26114 * #	NAS 1.15:101474	p 13	N89-16759 * #
ICOMP-89-21	p 167	N89-28748 * #	NAS 1.15:101379	p 120	N89-14341 * #	NAS 1.15:101475	p 117	N89-17017 * #
ICOMP-89-22	p 166	N89-27115 * #	NAS 1.15:101380	p 120	N89-12753 * #	NAS 1.15:101476	p 113	N89-19435 * #
ICOMP-89-23	p 168	N89-28749 * #	NAS 1.15:101381	p 172	N89-10269 * #	NAS 1.15:101477	p 162	N89-21196 * #
ICOMP-89-24	p 168	N89-29726 * #	NAS 1.15:101382	p 43	N89-13457 * #	NAS 1.15:101478	p 189	N89-28853 * #
ICOMP-89-25	p 222	N89-21595 * #	NAS 1.15:101383	p 26	N89-14238 * #	NAS 1.15:101479	p 174	N89-17211 * #
ICOMP-89-26	p 168	N89-29725 * #	NAS 1.15:101384	p 109	N89-11913 * #	NAS 1.15:101480	p 229	N89-24886 * #
ICOMP-89-27	p 223	N89-30008 * #	NAS 1.15:101385	p 220	N89-12309 * #	NAS 1.15:101481	p 103	N89-20228 * #
ICOMP-89-28	p 222	N89-20710 * #	NAS 1.15:101386	p 9	N89-12552 * #	NAS 1.15:101482	p 86	N89-20206 * #
ICOMP-89-29	p 162	N89-21192 * #	NAS 1.15:101387	p 114	N89-21894 * #	NAS 1.15:101483	p 137	N89-21172 * #
ICOMP-89-30	p 162	N89-21196 * #	NAS 1.15:101388	p 172	N89-12845 * #	NAS 1.15:101484	p 121	N89-20321 * #
ICOMP-89-31	p 161	N89-20407 * #	NAS 1.15:101389	p 101	N89-12720 * #	NAS 1.15:101485	p 129	N89-24520 * #
ICOMP-89-32	p 162	N89-21197 * #	NAS 1.15:101390	p 228	N89-15686 * #	NAS 1.15:101486	p 224	N89-19965 * #
ICOMP-89-33	p 223	N89-22397 * #	NAS 1.15:101392	p 222	N89-12337 * #	NAS 1.15:101487	p 210	N89-20545 * #
ICOMP-89-34	p 164	N89-23821 * #	NAS 1.15:101393	p 112	N89-15235 * #	NAS 1.15:101488	p 161	N89-20407 * #
ICOMP-89-35	p 164	N89-23821 * #	NAS 1.15:101394	p 61	N89-10123 * #	NAS 1.15:101489	p 189	N89-20490 * #
ICOMP-89-36	p 164	N89-23821 * #	NAS 1.15:101395	p 135	N89-12819 * #	NAS 1.15:101490	p 32	N89-22607 * #
ICOMP-89-37	p 164	N89-23821 * #	NAS 1.15:101396	p 134	N89-10235 * #	NAS 1.15:101491	p 31	N89-21799 * #
ICOMP-89-38	p 164	N89-23821 * #	NAS 1.15:101397	p 197	N89-14465 * #	NAS 1.15:101492	p 42	N89-20179 * #
ICOMP-89-39	p 164	N89-23821 * #	NAS 1.15:101398	p 209	N89-12123 * #	NAS 1.15:101493	p 66	N89-20193 * #
ICOMP-89-40	p 164	N89-23821 * #	NAS 1.15:101399	p 78	N89-15981 * #	NAS 1.15:101494	p 15	N89-25957 * #
ICOMP-89-41	p 164	N89-23821 * #	NAS 1.15:101400	p 173	N89-14416 * #	NAS 1.15:101495	p 13	N89-18417 * #
ICOMP-89-42	p 164	N89-23821 * #	NAS 1.15:101401	p 108	N89-11911 * #	NAS 1.15:101496	p 66	N89-20192 * #
ICOMP-89-43	p 164	N89-23821 * #	NAS 1.15:101402	p 84	N89-11826 * #	NAS 1.15:101497	p 218	N89-20684 * #
ICOMP-89-44	p 164	N89-23821 * #	NAS 1.15:101403	p 25	N89-13432 * #	NAS 1.15:101498	p 218	N89-20685 * #
ICOMP-89-45	p 164	N89-23821 * #	NAS 1.15:101404	p 240	N89-15047 * #	NAS 1.15:101499	p 78	N89-19371 * #
ICOMP-89-46	p 164	N89-23821 * #	NAS 1.15:101405	p 100	N89-12717 * #	NAS 1.15:101500	p 114	N89-21100 * #
ICOMP-89-47	p 164	N89-23821 * #	NAS 1.15:101406	p 158	N89-13741 * #	NAS 1.15:101501	p 66	N89-20194 * #
ICOMP-89-48	p 164	N89-23821 * #	NAS 1.15:101407	p 111	N89-13666 * #	NAS 1.15:101502	p 87	N89-24459 * #
ICOMP-89-49	p 164	N89-23821 * #	NAS 1.15:101408	p 111	N89-14310 * #	NAS 1.15:101503	p 113	N89-20253 * #
ICOMP-89-50	p 164	N89-23821 * #	NAS 1.15:101409	p 102	N89-14297 * #	NAS 1.15:101504	p 129	N89-25365 * #
ICOMP-89-51	p 164	N89-23821 * #	NAS 1.15:101410	p 63	N89-12665 * #	NAS 1.15:101505	p 222	N89-21595 * #
ICOMP-89-52	p 164	N89-23821 * #	NAS 1.15:101411	p 48	N89-11804 * #	NAS 1.15:101506	p 93	N89-19402 * #
ICOMP-89-53	p 164	N89-23821 * #	NAS 1.15:101412	p 159	N89-14403 * #	NAS 1.15:101507	p 123	N89-19446 * #
ICOMP-89-54	p 164	N89-23821 * #	NAS 1.15:101413	p 202	N89-22939 * #	NAS 1.15:101508	p 113	N89-20252 * #
ICOMP-89-55	p 164	N89-23821 * #	NAS 1.15:101414	p 228	N89-15685 * #	NAS 1.15:101509	p 162	N89-21197 * #
ICOMP-89-56	p 164	N89-23821 * #	NAS 1.15:101415	p 101	N89-13568 * #	NAS 1.15:101510	p 31	N89-20996 * #
ICOMP-89-57	p 164	N89-23821 * #	NAS 1.15:101416	p 158	N89-13749 * #	NAS 1.15:101511	p 186	N89-22919 * #
ICOMP-89-58	p 164	N89-23821 * #	NAS 1.15:101417	p 182	N89-14450 * #	NAS 1.15:101512	p 211	N89-22177 * #
ICOMP-89-59	p 164	N89-23821 * #	NAS 1.15:101418					
ICOMP-89-60	p 164	N89-23821 * #	NAS 1.15:101419					
ICOMP-89-61	p 164	N89-23821 * #	NAS 1.15:101420					
ICOMP-89-62	p 164	N89-23821 * #	NAS 1.15:101421					
ICOMP-89-63	p 164	N89-23821 * #	NAS 1.15:10					

NAS 1.15:101971	p 114	N89-21104 * #	NAS 1.15:102082	p 78	N89-24451 * #	NAS 1.15:4102	p 203	N89-25485 * #
NAS 1.15:101972	p 31	N89-22605 * #	NAS 1.15:102083	p 72	N89-25280 * #	NAS 1.15:4103	p 217	N89-20641 * #
NAS 1.15:101973	p 66	N89-21025 * #	NAS 1.15:102084	p 41	N89-24409 * #	NAS 1.15:4106	p 188	N89-19578 * #
NAS 1.15:101975	p 93	N89-21051 * #	NAS 1.15:102085	p 239	N89-26781 * #	NAS 1.15:4115	p 87	N89-25290 * #
NAS 1.15:101976	p 228	N89-21628 * #	NAS 1.15:102086	p 41	N89-25254 * #	NAS 1.15:4128	p 87	N89-25300 * #
NAS 1.15:101977	p 32	N89-22606 * #	NAS 1.15:102087	p 17	N89-25978 * #	NAS 1.15:83439	p 159	N89-14386 * #
NAS 1.15:101978	p 29	N89-19305 * #	NAS 1.15:102088	p 139	N89-26148 * #	NAS 1.15:87030	p 13	N89-19265 * #
NAS 1.15:101979	p 185	N89-22111 * #	NAS 1.15:102091	p 205	N89-28030 * #	NAS 1.15:88846	p 210	N89-19737 * #
NAS 1.15:101980	p 210	N89-21419 * #	NAS 1.15:102092	p 32	N89-24320 * #	NAS 1.15:88969	p 9	N89-10865 * #
NAS 1.15:101981	p 136	N89-19493 * #	NAS 1.15:102093	p 75	N89-27705 * #	NAS 1.15:89855	p 154	N89-10246 * #
NAS 1.15:101982	p 66	N89-20199 * #	NAS 1.15:102094	p 88	N89-26912 * #	NAS 1.15:89887	p 238	N89-18259 * #
NAS 1.15:101983	p 163	N89-23813 * #	NAS 1.15:102095	p 33	N89-26003 * #	NAS 1.16:182232	p 228	N89-20776 * #
NAS 1.15:101984	p 86	N89-22684 * #	NAS 1.15:102096	p 33	N89-25238 * #	NAS 1.21:495	p 24	N89-12565 * #
NAS 1.15:101985	p 168	N89-29714 * #	NAS 1.15:102097	p 239	N89-25078 * #	NAS 1.26:174786	p 28	N89-19299 * #
NAS 1.15:101986	p 115	N89-23691 * #	NAS 1.15:102098	p 32	N89-24319 * #	NAS 1.26:174805	p 26	N89-13436 * #
NAS 1.15:101987	p 32	N89-23465 * #	NAS 1.15:102099	p 167	N89-27121 * #	NAS 1.26:174832	p 135	N89-15335 * #
NAS 1.15:101988	p 218	N89-24055 * #	NAS 1.15:102100	p 72	N89-25277 * #	NAS 1.26:174966	p 201	N89-18696 * #
NAS 1.15:101989	p 1	N89-22569 * #	NAS 1.15:102101	p 15	N89-29323 * #	NAS 1.26:174967	p 201	N89-19583 * #
NAS 1.15:101990	p 128	N89-21142 * #	NAS 1.15:102102	p 242	N89-27619 * #	NAS 1.26:174974	p 66	N89-21834 * #
NAS 1.15:101991	p 202	N89-21266 * #	NAS 1.15:102103	p 124	N89-27868 * #	NAS 1.26:175002	p 26	N89-13433 * #
NAS 1.15:101992	p 42	N89-26877 * #	NAS 1.15:102104	p 214	N89-26291 * #	NAS 1.26:175003	p 28	N89-19300 * #
NAS 1.15:101993	p 29	N89-20133 * #	NAS 1.15:102105	p 70	N89-24448 * #	NAS 1.26:175096	p 18	N89-19289 * #
NAS 1.15:101994	p 136	N89-20385 * #	NAS 1.15:102106	p 204	N89-25490 * #	NAS 1.26:179476	p 208	N89-11315 * #
NAS 1.15:101995	p 33	N89-26007 * #	NAS 1.15:102107	p 88	N89-26919 * #	NAS 1.26:179477	p 112	N89-15251 * #
NAS 1.15:101996	p 228	N89-24138 * #	NAS 1.15:102108	p 70	N89-24446 * #	NAS 1.26:179497	p 62	N89-11808 * #
NAS 1.15:101997	p 93	N89-22710 * #	NAS 1.15:102110	p 224	N89-25670 * #	NAS 1.26:179513-VOL-2	p 173	N89-13771 * #
NAS 1.15:101998	p 14	N89-23413 * #	NAS 1.15:102111	p 231	N89-27506 * #	NAS 1.26:179519	p 155	N89-12837 * #
NAS 1.15:101999	p 221	N89-24856 * #	NAS 1.15:102112	p 165	N89-26175 * #	NAS 1.26:179525	p 113	N89-19421 * #
NAS 1.15:102000	p 185	N89-21245 * #	NAS 1.15:102113	p 70	N89-24447 * #	NAS 1.26:179544	p 26	N89-13437 * #
NAS 1.15:102001	p 78	N89-21032 * #	NAS 1.15:102115	p 88	N89-27795 * #	NAS 1.26:179554	p 10	N89-13397 * #
NAS 1.15:102002	p 228	N89-20779 * #	NAS 1.15:102116	p 116	N89-26095 * #	NAS 1.26:179561-VOL-2	p 28	N89-18487 * #
NAS 1.15:102003	p 68	N89-23518 * #	NAS 1.15:102117	p 165	N89-26178 * #	NAS 1.26:179568	p 231	N89-13256 * #
NAS 1.15:102004	p 78	N89-25285 * #	NAS 1.15:102118	p 72	N89-25283 * #	NAS 1.26:179572	p 155	N89-12636 * #
NAS 1.15:102005	p 163	N89-23809 * #	NAS 1.15:102119	p 204	N89-26259 * #	NAS 1.26:179575	p 120	N89-11920 * #
NAS 1.15:102006	p 41	N89-20171 * #	NAS 1.15:102120	p 87	N89-26048 * #	NAS 1.26:179584	p 40	N89-13445 * #
NAS 1.15:102008	p 137	N89-21174 * #	NAS 1.15:102121	p 175	N89-24593 * #	NAS 1.26:179587-VOL-3	p 64	N89-15164 * #
NAS 1.15:102009	p 223	N89-22397 * #	NAS 1.15:102122	p 104	N89-28627 * #	NAS 1.26:179595	p 68	N89-23519 * #
NAS 1.15:102010	p 14	N89-22573 * #	NAS 1.15:102123	p 123	N89-27038 * #	NAS 1.26:179600	p 63	N89-11809 * #
NAS 1.15:102011	p 123	N89-28666 * #	NAS 1.15:102124	p 75	N89-27703 * #	NAS 1.26:179602	p 61	N89-10119 * #
NAS 1.15:102012	p 69	N89-24443 * #	NAS 1.15:102126	p 164	N89-24577 * #	NAS 1.26:179612	p 65	N89-16918 * #
NAS 1.15:102013	p 162	N89-22053 * #	NAS 1.15:102127	p 242	N89-26799 * #	NAS 1.26:179614-VOL-1	p 209	N89-17941 * #
NAS 1.15:102015	p 242	N89-23397 * #	NAS 1.15:102128	p 167	N89-28748 * #	NAS 1.26:179614-VOL-2	p 211	N89-22981 * #
NAS 1.15:102016	p 67	N89-23516 * #	NAS 1.15:102129	p 168	N89-26180 * #	NAS 1.26:179614-VOL-3	p 211	N89-22980 * #
NAS 1.15:102017	p 73	N89-26041 * #	NAS 1.15:102131	p 214	N89-26292 * #	NAS 1.26:179618-VOL-4	p 210	N89-18967 * #
NAS 1.15:102018	p 14	N89-23417 * #	NAS 1.15:102132	p 165	N89-26174 * #	NAS 1.26:179618	p 158	N89-13731 * #
NAS 1.15:102019	p 67	N89-23517 * #	NAS 1.15:102133	p 189	N89-28851 * #	NAS 1.26:179630	p 135	N89-13706 * #
NAS 1.15:102020	p 67	N89-22651 * #	NAS 1.15:102134	p 187	N89-28015 * #	NAS 1.26:179639	p 17	N89-11725 * #
NAS 1.15:102021	p 68	N89-23520 * #	NAS 1.15:102135	p 70	N89-24444 * #	NAS 1.26:179642-ADD-1	p 47	N89-29478 * #
NAS 1.15:102022	p 186	N89-22925 * #	NAS 1.15:102136	p 46	N89-24427 * #	NAS 1.26:179642-ADD	p 34	N89-29351 * #
NAS 1.15:102023	p 104	N89-23664 * #	NAS 1.15:102137	p 35	N89-26009 * #	NAS 1.26:179645	p 113	N89-18550 * #
NAS 1.15:102024	p 129	N89-27923 * #	NAS 1.15:102138	p 166	N89-27103 * #	NAS 1.26:179650	p 46	N89-11803 * #
NAS 1.15:102025	p 137	N89-22020 * #	NAS 1.15:102139	p 76	N89-29484 * #	NAS 1.26:180807	p 110	N89-13621 * #
NAS 1.15:102026	p 164	N89-23821 * #	NAS 1.15:102140	p 139	N89-26149 * #	NAS 1.26:180809	p 64	N89-13493 * #
NAS 1.15:102027	p 163	N89-22861 * #	NAS 1.15:102141	p 139	N89-25403 * #	NAS 1.26:180826	p 114	N89-21105 * #
NAS 1.15:102028	p 36	N89-22617 * #	NAS 1.15:102142	p 166	N89-27115 * #	NAS 1.26:180827-EXEC-SUMM	p 128	N89-23756 * #
NAS 1.15:102029	p 223	N89-24872 * #	NAS 1.15:102143	p 76	N89-28571 * #	NAS 1.26:180827	p 128	N89-23757 * #
NAS 1.15:102030	p 164	N89-24575 * #	NAS 1.15:102144	p 168	N89-29725 * #	NAS 1.26:180889	p 239	N89-14182 * #
NAS 1.15:102032	p 87	N89-24460 * #	NAS 1.15:102282	p 176	N89-27998 * #	NAS 1.26:180890	p 238	N89-12504 * #
NAS 1.15:102036	p 223	N89-24865 * #	NAS 1.15:102283	p 73	N89-26045 * #	NAS 1.26:180895	p 16	N89-29329 * #
NAS 1.15:102038	p 31	N89-21798 * #	NAS 1.15:102284	p 72	N89-25281 * #	NAS 1.26:180899	p 184	N89-20472 * #
NAS 1.15:102039	p 67	N89-22652 * #	NAS 1.15:102285	p 229	N89-25675 * #	NAS 1.26:180900	p 172	N89-11192 * #
NAS 1.15:102040	p 138	N89-23792 * #	NAS 1.15:102286	p 47	N89-26036 * #	NAS 1.26:180902	p 139	N89-26150 * #
NAS 1.15:102041	p 205	N89-28029 * #	NAS 1.15:102287	p 47	N89-26035 * #	NAS 1.26:182105	p 184	N89-21239 * #
NAS 1.15:102042	p 71	N89-25274 * #	NAS 1.15:102292	p 15	N89-25121 * #	NAS 1.26:182122	p 62	N89-11805 * #
NAS 1.15:102043	p 14	N89-23416 * #	NAS 1.15:102293	p 168	N89-28749 * #	NAS 1.26:182127	p 186	N89-26246 * #
NAS 1.15:102044	p 68	N89-23527 * #	NAS 1.15:102294	p 167	N89-27980 * #	NAS 1.26:182133	p 158	N89-13754 * #
NAS 1.15:102045	p 128	N89-23753 * #	NAS 1.15:102295	p 205	N89-27223 * #	NAS 1.26:182135	p 138	N89-24530 * #
NAS 1.15:102046	p 115	N89-24487 * #	NAS 1.15:102297	p 47	N89-26887 * #	NAS 1.26:182164	p 29	N89-20132 * #
NAS 1.15:102047	p 14	N89-22577 * #	NAS 1.15:102298	p 41	N89-26876 * #	NAS 1.26:182165	p 85	N89-12675 * #
NAS 1.15:102048	p 175	N89-23850 * #	NAS 1.15:102299	p 242	N89-27623 * #	NAS 1.26:182169	p 154	N89-12010 * #
NAS 1.15:102049	p 69	N89-24436 * #	NAS 1.15:102301	p 116	N89-27836 * #	NAS 1.26:182176	p 62	N89-10943 * #
NAS 1.15:102050	p 68	N89-23522 * #	NAS 1.15:102302	p 88	N89-26924 * #	NAS 1.26:182177	p 209	N89-16224 * #
NAS 1.15:102051	p 204	N89-26260 * #	NAS 1.15:102303	p 73	N89-26044 * #	NAS 1.26:182180	p 10	N89-13399 * #
NAS 1.15:102052	p 69	N89-24438 * #	NAS 1.15:102307	p 104	N89-29522 * #	NAS 1.26:182181	p 24	N89-11750 * #
NAS 1.15:102053	p 15	N89-25119 * #	NAS 1.15:102308	p 38	N89-28535 * #	NAS 1.26:182182	p 136	N89-15336 * #
NAS 1.15:102054	p 67	N89-22653 * #	NAS 1.15:102309	p 166	N89-27114 * #	NAS 1.26:182188	p 209	N89-12122 * #
NAS 1.15:102055	p 70	N89-25269 * #	NAS 1.15:102310	p 75	N89-27706 * #	NAS 1.26:182189	p 209	N89-13103 * #
NAS 1.15:102056	p 175	N89-24591 * #	NAS 1.15:102311	p 33	N89-26008 * #	NAS 1.26:182195	p 64	N89-14256 * #
NAS 1.15:102057	p 164	N89-23823 * #	NAS 1.15:102312	p 74	N89-27701 * #	NAS 1.26:182197	p 135	N89-12620 * #
NAS 1.15:102058	p 212	N89-23025 * #	NAS 1.15:102317	p 33	N89-27670 * #	NAS 1.26:182198	p 45	N89-11802 * #
NAS 1.15:102059	p 72	N89-25282 * #	NAS 1.15:102318	p 168	N89-29726 * #	NAS 1.26:182202	p 27	N89-16843 * #
NAS 1.15:102061	p 71	N89-25271 * #	NAS 1.15:102321	p 74	N89-26904 * #	NAS 1.26:182203	p 24	N89-12566 * #
NAS 1.15:102063	p 165	N89-26177 * #	NAS 1.15:102325	p 129	N89-27827 * #	NAS 1.26:182204	p 239	N89-17548 * #
NAS 1.15:102064	p 214	N89-25506 * #	NAS 1.15:102326	p 88	N89-29490 * #	NAS 1.26:182207	p 159	N89-13755 * #
NAS 1.15:102064	p 71	N89-25272 * #	NAS 1.15:102327	p 216	N89-29032 * #	NAS 1.26:182209	p 9	N89-10863 * #
NAS 1.15:102066	p 46	N89-25267 * #	NAS 1.15:102331	p 176	N89-27999 * #	NAS 1.26:182211	p 24	N89-12567 * #
NAS 1.15:102068	p 138	N89-23791 * #	NAS 1.15:102332	p 104	N89-26989 * #	NAS 1.26:182217	p 36	N89-16882 * #
NAS 1.15:102072	p 71	N89-25275 * #	NAS 1.15:102335	p 75	N89-27702 * #	NAS 1.26:182224	p 24	N89-11751 * #
NAS 1.15:102073	p 71	N89-25273 * #	NAS 1.15:102337	p 74	N89-26906 * #	NAS 1.26:182226	p 18	N89-15107 * #
NAS 1.15:102074	p 69	N89-24439 * #	NAS 1.15:102338	p 205	N89-28036 * #	NAS 1.26:182227-EXEC-SUMM	p 127	N89-17079 * #
NAS 1.15:102075	p 138	N89-24529 * #	NAS 1.15:102339	p 76	N89-28570 * #	NAS 1.26:182227	p 126	N89-17078 * #
NAS 1.15:102076	p 46	N89-24418 * #	NAS 1.15:102347	p 237	N89-30088 * #	NAS 1.26:182229	p 126	N89-14369 * #
NAS 1.15:102078	p 32	N89-24318 * #	NAS 1.15:102352	p 75	N89-27704 * #	NAS 1.26:182231	p 197	N89-13820 * #
NAS 1.15:102079	p 163	N89-22862 * #	NAS 1.15:102352	p 223	N89-30008 * #	NAS 1.26:182233	p 28	N89-17599 * #
NAS 1.15:102080	p 15	N89-24269 * #	NAS 1.15:102352	p 27	N89-15112			



NAS 1.26:182237	p 239	N89-23382 *	NAS 1.26:4202	p 19	N89-13429 *	NASA-CR-179645	p 113	N89-18550 *
NAS 1.26:182238	p 229	N89-19973 *	NAS 1.26:4205	p 188	N89-18694 *	NASA-CR-179650	p 46	N89-11803 *
NAS 1.26:182241	p 197	N89-13819 *	NAS 1.26:4211	p 12	N89-15898 *	NASA-CR-180807	p 110	N89-13621 *
NAS 1.26:182243	p 127	N89-19449 *	NAS 1.26:4215	p 202	N89-21258 *	NASA-CR-180809	p 64	N89-13493 *
NAS 1.26:182244	p 103	N89-21072 *	NAS 1.26:4224	p 186	N89-22920 *	NASA-CR-180826	p 114	N89-21105 *
NAS 1.26:182245	p 14	N89-20921 *	NAS 1.55:10017	p 120	N89-17682 *	NASA-CR-180827-EXEC-SUMM	p 128	N89-23756 *
NAS 1.26:182246	p 166	N89-26182 *	NAS 1.55:10018	p 233	N89-14842 *	NASA-CR-180827	p 128	N89-23757 *
NAS 1.26:182248	p 214	N89-24741 *	NAS 1.55:10019	p 110	N89-13642 *	NASA-CR-180889	p 239	N89-14182 *
NAS 1.26:182256	p 121	N89-19442 *	NAS 1.55:10029	p 211	N89-22982 *	NASA-CR-180890	p 238	N89-12504 *
NAS 1.26:182257-VOL-1	p 229	N89-24139 *	NAS 1.55:2444	p 195	N89-12876 *	NASA-CR-180895	p 16	N89-29329 *
NAS 1.26:182260	p 86	N89-21036 *	NAS 1.55:2493	p 199	N89-17298 *	NASA-CR-180899	p 184	N89-20472 *
NAS 1.26:182261	p 185	N89-22108 *	NAS 1.55:3026	p 185	N89-22891 *	NASA-CR-180900	p 172	N89-11192 *
NAS 1.26:182263	p 73	N89-26903 *	NAS 1.55:3030	p 212	N89-24704 *	NASA-CR-180902	p 139	N89-26150 *
NAS 1.26:182265	p 175	N89-23851 *	NAS 1.60:2845	p 198	N89-10844 *	NASA-CR-182105	p 184	N89-21239 *
NAS 1.26:182266	p 42	N89-23501 *	NAS 1.60:2846	p 9	N89-10844 *	NASA-CR-182122	p 62	N89-11805 *
NAS 1.26:182267	p 29	N89-20134 *	NAS 1.60:2862	p 65	N89-15979 *	NASA-CR-182127	p 186	N89-26246 *
NAS 1.26:182272	p 137	N89-21173 *	NAS 1.60:2863	p 100	N89-10996 *	NASA-CR-182133	p 158	N89-13754 *
NAS 1.26:182273	p 202	N89-21265 *	NAS 1.60:2865	p 174	N89-16139 *	NASA-CR-182135	p 138	N89-24530 *
NAS 1.26:182274	p 189	N89-27204 *	NAS 1.60:2875	p 127	N89-17767 *	NASA-CR-182164	p 29	N89-20132 *
NAS 1.26:182275	p 73	N89-26899 *	NAS 1.60:2880	p 173	N89-15380 *	NASA-CR-182165	p 85	N89-12675 *
NAS 1.26:182279	p 176	N89-26208 *	NAS 1.60:2883	p 115	N89-26091 *	NASA-CR-182169	p 154	N89-12010 *
NAS 1.26:182280	p 74	N89-26905 *	NAS 1.60:2891	p 136	N89-15337 *	NASA-CR-182176	p 62	N89-10943 *
NAS 1.26:182281	p 203	N89-23918 *	NAS 1.60:2892	p 218	N89-17422 *	NASA-CR-182177	p 209	N89-16224 *
NAS 1.26:182283	p 233	N89-21658 *	NAS 1.60:2899	p 136	N89-21169 *	NASA-CR-182180	p 10	N89-13399 *
NAS 1.26:182284	p 139	N89-24532 *	NAS 1.60:2900	p 164	N89-25409 *	NASA-CR-182181	p 24	N89-11750 *
NAS 1.26:182285	p 163	N89-23818 *	NAS 1.60:2901	p 184	N89-21243 *	NASA-CR-182182	p 136	N89-15336 *
NAS 1.26:182291	p 86	N89-23622 *	NAS 1.60:2902	p 103	N89-17650 *	NASA-CR-182188	p 209	N89-12122 *
NAS 1.26:182298	p 122	N89-25353 *	NAS 1.60:2904	p 136	N89-21171 *	NASA-CR-182189	p 209	N89-13103 *
NAS 1.26:182301	p 46	N89-26031 *	NAS 1.60:2910	p 114	N89-21103 *	NASA-CR-182195	p 64	N89-14256 *
NAS 1.26:182302	p 36	N89-27672 *	NAS 1.60:2911	p 186	N89-24607 *	NASA-CR-182197	p 135	N89-12820 *
NAS 1.26:182303	p 33	N89-26004 *	NAS 1.60:2912	p 40	N89-28545 *	NASA-CR-182198	p 45	N89-11802 *
NAS 1.26:182500	p 126	N89-10223 *	NAS 1.60:2924	p 88	N89-27796 *	NASA-CR-182202	p 27	N89-16843 *
NAS 1.26:182838	p 122	N89-21134 *	NAS 1.71:LEW-14124-1	p 177	N89-28806 *	NASA-CR-182203	p 24	N89-12566 *
NAS 1.26:182844	p 198	N89-15434 *	NAS 1.71:LEW-14295-1	p 123	N89-14348 *	NASA-CR-182204	p 239	N89-17548 *
NAS 1.26:183003	p 62	N89-11807 *	NAS 1.71:LEW-14472-1	p 85	N89-14259 *	NASA-CR-182207	p 159	N89-13755 *
NAS 1.26:183005	p 197	N89-14457 *	NAS 1.71:LEW-14679-1	p 116	N89-28651 *	NASA-CR-182209	p 9	N89-10863 *
NAS 1.26:183013	p 197	N89-12931 *	NAS 1.71:LEW-14695-1	p 187	N89-28830 *	NASA-CR-182211	p 24	N89-12567 *
NAS 1.26:183303	p 126	N89-10213 *	NAS 1.71:LEW-14734-1	p 87	N89-23623 *	NASA-CR-182217	p 36	N89-16882 *
NAS 1.26:183312	p 126	N89-10225 *	NAS 1.71:LEW-14848-1	p 40	N89-28549 *	NASA-CR-182224	p 24	N89-11751 *
NAS 1.26:183313	p 111	N89-14311 *				NASA-CR-182226	p 18	N89-15107 *
NAS 1.26:183352	p 182	N89-12870 *	NASA-CASE-LEW-14124-1	p 177	N89-28806 *	NASA-CR-182227-EXEC-SUMM	p 127	N89-17079 *
NAS 1.26:183403	p 197	N89-12932 *	NASA-CASE-LEW-14134-2	p 102	N89-14303 *	NASA-CR-182227	p 126	N89-17078 *
NAS 1.26:184567	p 27	N89-15114 *	NASA-CASE-LEW-14295-1	p 123	N89-14348 *	NASA-CR-182229	p 126	N89-14369 *
NAS 1.26:184607	p 217	N89-13993 *	NASA-CASE-LEW-14297-1	p 172	N89-12048 *	NASA-CR-182231	p 197	N89-13820 *
NAS 1.26:184630	p 217	N89-15623 *	NASA-CASE-LEW-14392-2	p 116	N89-29538 *	NASA-CR-182232	p 228	N89-20776 *
NAS 1.26:184678	p 64	N89-15170 *	NASA-CASE-LEW-14472-1	p 85	N89-14259 *	NASA-CR-182233	p 28	N89-17599 *
NAS 1.26:184756	p 161	N89-19503 *	NASA-CASE-LEW-14679-1	p 116	N89-28651 *	NASA-CR-182234	p 18	N89-13428 *
NAS 1.26:184765	p 160	N89-16132 *	NASA-CASE-LEW-14695-1	p 187	N89-28830 *	NASA-CR-182235-VOL-1	p 217	N89-13996 *
NAS 1.26:184768	p 199	N89-16193 *	NASA-CASE-LEW-14734-1	p 87	N89-23623 *	NASA-CR-182237	p 239	N89-23382 *
NAS 1.26:184775-APP-1	p 201	N89-19581 *	NASA-CASE-LEW-14848-1	p 40	N89-28549 *	NASA-CR-182238	p 229	N89-19973 *
NAS 1.26:184780	p 127	N89-20355 *				NASA-CR-182241	p 197	N89-13819 *
NAS 1.26:184796-APP-2	p 201	N89-19582 *	NASA-CP-10017	p 120	N89-17682 *	NASA-CR-182243	p 127	N89-19449 *
NAS 1.26:184798	p 115	N89-23678 *	NASA-CP-10018	p 233	N89-14842 *	NASA-CR-182244	p 103	N89-21072 *
NAS 1.26:184799	p 189	N89-20489 *	NASA-CP-10019	p 110	N89-13642 *	NASA-CR-182245	p 14	N89-20921 *
NAS 1.26:184815	p 215	N89-21479 *	NASA-CP-10029	p 211	N89-22982 *	NASA-CR-182246	p 166	N89-26182 *
NAS 1.26:184904	p 127	N89-20364 *	NASA-CP-2444	p 195	N89-12876 *	NASA-CR-182248	p 214	N89-24741 *
NAS 1.26:184939	p 203	N89-23890 *	NASA-CP-2493	p 199	N89-17298 *	NASA-CR-182256	p 121	N89-19442 *
NAS 1.26:184940	p 203	N89-23891 *	NASA-CP-3026	p 185	N89-22891 *	NASA-CR-182257-VOL-1	p 229	N89-24139 *
NAS 1.26:184977	p 186	N89-23876 *	NASA-CP-3030	p 212	N89-24704 *	NASA-CR-182260	p 86	N89-21036 *
NAS 1.26:184989	p 203	N89-24669 *				NASA-CR-182261	p 185	N89-22108 *
NAS 1.26:185050	p 139	N89-26143 *	NASA-CR-174786	p 28	N89-19299 *	NASA-CR-182263	p 73	N89-26903 *
NAS 1.26:185053	p 129	N89-24519 *	NASA-CR-174805	p 26	N89-13436 *	NASA-CR-182265	p 175	N89-23851 *
NAS 1.26:185054	p 128	N89-24518 *	NASA-CR-174832	p 135	N89-15335 *	NASA-CR-182266	p 42	N89-23501 *
NAS 1.26:185058	p 176	N89-25432 *	NASA-CR-174966	p 201	N89-18696 *	NASA-CR-182267	p 29	N89-20134 *
NAS 1.26:185113	p 70	N89-24445 *	NASA-CR-174967	p 201	N89-19583 *	NASA-CR-182272	p 137	N89-21173 *
NAS 1.26:185114	p 176	N89-27152 *	NASA-CR-174974	p 66	N89-21834 *	NASA-CR-182273	p 202	N89-21265 *
NAS 1.26:185116	p 176	N89-26218 *	NASA-CR-175002	p 26	N89-13433 *	NASA-CR-182274	p 189	N89-27204 *
NAS 1.26:185117	p 214	N89-27256 *	NASA-CR-175003	p 28	N89-19300 *	NASA-CR-182275	p 73	N89-26899 *
NAS 1.26:185120	p 204	N89-26261 *	NASA-CR-175096	p 18	N89-19289 *	NASA-CR-182279	p 176	N89-26208 *
NAS 1.26:185121	p 41	N89-26027 *	NASA-CR-179476	p 208	N89-11315 *	NASA-CR-182280	p 74	N89-26905 *
NAS 1.26:185122	p 165	N89-26179 *	NASA-CR-179477	p 112	N89-15251 *	NASA-CR-182281	p 203	N89-23918 *
NAS 1.26:185124	p 43	N89-26879 *	NASA-CR-179497	p 62	N89-11808 *	NASA-CR-182283	p 233	N89-21658 *
NAS 1.26:185126	p 43	N89-26880 *	NASA-CR-179513-VOL-2	p 173	N89-13771 *	NASA-CR-182284	p 139	N89-24532 *
NAS 1.26:185130	p 76	N89-29483 *	NASA-CR-179519	p 155	N89-12837 *	NASA-CR-182285	p 163	N89-23818 *
NAS 1.26:185131	p 74	N89-27700 *	NASA-CR-179525	p 113	N89-19421 *	NASA-CR-182291	p 86	N89-23622 *
NAS 1.26:185332	p 165	N89-26172 *	NASA-CR-179544	p 26	N89-13437 *	NASA-CR-182298	p 122	N89-25353 *
NAS 1.26:185439	p 237	N89-26740 *	NASA-CR-179554	p 10	N89-13397 *	NASA-CR-182301	p 46	N89-26031 *
NAS 1.26:185440	p 236	N89-26739 *	NASA-CR-179561-VOL-2	p 28	N89-18487 *	NASA-CR-182302	p 36	N89-27672 *
NAS 1.26:185450	p 129	N89-26126 *	NASA-CR-179568	p 231	N89-13256 *	NASA-CR-182303	p 33	N89-26004 *
NAS 1.26:185493	p 19	N89-25993 *	NASA-CR-179572	p 155	N89-12836 *	NASA-CR-182500	p 122	N89-10223 *
NAS 1.26:185847	p 167	N89-27118 *	NASA-CR-179575	p 120	N89-11920 *	NASA-CR-182638	p 126	N89-21134 *
NAS 1.26:185968	p 182	N89-13788 *	NASA-CR-179584	p 40	N89-13445 *	NASA-CR-182644	p 198	N89-15434 *
NAS 1.26:4079	p 159	N89-13756 *	NASA-CR-179587-VOL-3	p 64	N89-15164 *	NASA-CR-183003	p 62	N89-11807 *
NAS 1.26:4147-PT-3	p 8	N89-10025 *	NASA-CR-179585	p 68	N89-23519 *	NASA-CR-183005	p 197	N89-14457 *
NAS 1.26:4147-PT-1	p 11	N89-14221 *	NASA-CR-179600	p 63	N89-11809 *	NASA-CR-183013	p 197	N89-12931 *
NAS 1.26:4147-PT-2	p 11	N89-14222 *	NASA-CR-179602	p 61	N89-10119 *	NASA-CR-183303	p 126	N89-10213 *
NAS 1.26:4171	p 84	N89-10131 *	NASA-CR-179612	p 65	N89-16918 *	NASA-CR-183312	p 126	N89-10225 *
NAS 1.26:4172	p 83	N89-10128 *	NASA-CR-179614-VOL-1	p 209	N89-17941 *	NASA-CR-183313	p 111	N89-14311 *
NAS 1.26:4180	p 10	N89-12553 *	NASA-CR-179614-VOL-2	p 211	N89-22981 *	NASA-CR-183352	p 182	N89-12870 *
NAS 1.26:4188	p 155	N89-12838 *	NASA-CR-179614-VOL-3	p 211	N89-22980 *	NASA-CR-183403	p 197	N89-12932 *
NAS 1.26:4194	p 19	N89-14235 *	NASA-CR-179614-VOL-4	p 210	N89-18967 *	NASA-CR-184587	p 27	N89-15114 *
NAS 1.26:4195	p 189	N89-21256 *	NASA-CR-179618	p 158	N89-13731 *	NASA-CR-184607	p 217	N89-13993 *
NAS 1.26:4198	p 155	N89-12835 *	NASA-CR-179630	p 135	N89-13706 *	NASA-CR-184630	p 217	N89-15623 *
NAS 1.26:4199-VOL-1	p 12	N89-15896 *	NASA-CR-179639	p 17	N89-11725 *	NASA-CR-184678	p 64	N89-15170 *
NAS 1.26:4199-VOL-2	p 12	N89-15897 *	NASA-CR-179642-ADD-1	p 47	N89-29478 *	NASA-CR-184756	p 161	N89-19503 *
NAS 1.26:4201	p 182	N89-13793 *	NASA-CR-179642-ADD	p 34	N89-29351 *	NASA-CR-184765	p 160	N89-16132 *

NASA-CR-184768	p 199	N89-16193 * #	NASA-TM-101348	p 84	N89-10134 * #	NASA-TM-101452	p 198	N89-15438 * #
NASA-CR-184775-APP-1	p 201	N89-19581 * #	NASA-TM-101349	p 108	N89-11038 * #	NASA-TM-101455	p 102	N89-15233 * #
NASA-CR-184780	p 127	N89-20355 * #	NASA-TM-101350	p 84	N89-10952 * #	NASA-TM-101456	p 115	N89-21895 * #
NASA-CR-184796-APP-2	p 201	N89-19582 * #	NASA-TM-101352	p 64	N89-14255 * #	NASA-TM-101457	p 183	N89-15414 * #
NASA-CR-184798	p 115	N89-23678 * #	NASA-TM-101353	p 175	N89-21224 * #	NASA-TM-101458	p 127	N89-17756 * #
NASA-CR-184799	p 189	N89-20489 * #	NASA-TM-101354	p 62	N89-10944 * #	NASA-TM-101459	p 127	N89-21138 * #
NASA-CR-184815	p 215	N89-21479 * #	NASA-TM-101355	p 222	N89-11469 * #	NASA-TM-101460	p 183	N89-15415 * #
NASA-CR-184904	p 127	N89-20364 * #	NASA-TM-101356	p 84	N89-10130 * #	NASA-TM-101461	p 86	N89-23621 * #
NASA-CR-184939	p 203	N89-23890 * #	NASA-TM-101358	p 199	N89-17286 * #	NASA-TM-101462	p 223	N89-17453 * #
NASA-CR-184940	p 203	N89-23891 * #	NASA-TM-101359	p 135	N89-11129 * #	NASA-TM-101463	p 42	N89-24413 * #
NASA-CR-184977	p 186	N89-23876 * #	NASA-TM-101360	p 134	N89-11128 * #	NASA-TM-101464	p 201	N89-20514 * #
NASA-CR-184989	p 203	N89-24669 * #	NASA-TM-101361	p 27	N89-15913 * #	NASA-TM-101465	p 136	N89-15338 * #
NASA-CR-185050	p 139	N89-26143 * #	NASA-TM-101362	p 238	N89-11637 * #	NASA-TM-101466	p 222	N89-20710 * #
NASA-CR-185053	p 129	N89-24519 * #	NASA-TM-101364	p 102	N89-16986 * #	NASA-TM-101467	p 46	N89-16905 * #
NASA-CR-185054	p 128	N89-24518 * #	NASA-TM-101365	p 109	N89-12746 * #	NASA-TM-101469	p 218	N89-17424 * #
NASA-CR-185058	p 176	N89-25432 * #	NASA-TM-101366	p 85	N89-12684 * #	NASA-TM-101470	p 210	N89-21417 * #
NASA-CR-185113	p 70	N89-24445 * #	NASA-TM-101367	p 155	N89-12028 * #	NASA-TM-101471	p 120	N89-17046 * #
NASA-CR-185114	p 176	N89-27152 * #	NASA-TM-101369	p 126	N89-10215 * #	NASA-TM-101473	p 162	N89-21192 * #
NASA-CR-185116	p 176	N89-26218 * #	NASA-TM-101371	p 122	N89-26114 * #	NASA-TM-101474	p 13	N89-16759 * #
NASA-CR-185117	p 214	N89-27256 * #	NASA-TM-101372	p 120	N89-14341 * #	NASA-TM-101475	p 117	N89-17017 * #
NASA-CR-185120	p 204	N89-26261 * #	NASA-TM-101373	p 120	N89-12753 * #	NASA-TM-101476	p 113	N89-19435 * #
NASA-CR-185121	p 41	N89-26027 * #	NASA-TM-101374	p 172	N89-10269 * #	NASA-TM-101477	p 162	N89-21196 * #
NASA-CR-185122	p 165	N89-26179 * #	NASA-TM-101375	p 43	N89-13457 * #	NASA-TM-101478	p 189	N89-28853 * #
NASA-CR-185124	p 43	N89-26879 * #	NASA-TM-101376	p 26	N89-14238 * #	NASA-TM-101479	p 174	N89-17211 * #
NASA-CR-185126	p 43	N89-26880 * #	NASA-TM-101377	p 109	N89-11913 * #	NASA-TM-101480	p 229	N89-24886 * #
NASA-CR-185130	p 76	N89-29483 * #	NASA-TM-101378	p 220	N89-12309 * #	NASA-TM-101481	p 103	N89-20228 * #
NASA-CR-185131	p 74	N89-27700 * #	NASA-TM-101379	p 9	N89-12552 * #	NASA-TM-101482	p 86	N89-20206 * #
NASA-CR-185332	p 165	N89-26172 * #	NASA-TM-101380	p 114	N89-21894 * #	NASA-TM-101483	p 137	N89-21172 * #
NASA-CR-185439	p 237	N89-26740 * #	NASA-TM-101381	p 172	N89-12845 * #	NASA-TM-101484	p 121	N89-20321 * #
NASA-CR-185440	p 236	N89-26739 * #	NASA-TM-101382	p 101	N89-12720 * #	NASA-TM-101485	p 129	N89-24520 * #
NASA-CR-185450	p 129	N89-26126 * #	NASA-TM-101383	p 228	N89-15686 * #	NASA-TM-101486	p 224	N89-19965 * #
NASA-CR-185493	p 19	N89-25993 * #	NASA-TM-101384	p 222	N89-12337 * #	NASA-TM-101487	p 210	N89-20545 * #
NASA-CR-185847	p 167	N89-27118 * #	NASA-TM-101385	p 112	N89-15235 * #	NASA-TM-101488	p 161	N89-20407 * #
NASA-CR-185968	p 182	N89-13788 * #	NASA-TM-101386	p 61	N89-10123 * #	NASA-TM-101489	p 189	N89-20490 * #
NASA-CR-4079	p 159	N89-13756 * #	NASA-TM-101387	p 135	N89-12819 * #	NASA-TM-101944	p 32	N89-22607 * #
NASA-CR-4147-PT-3	p 8	N89-10025 * #	NASA-TM-101388	p 134	N89-10235 * #	NASA-TM-101945	p 31	N89-21799 * #
NASA-CR-4147-PT-1	p 11	N89-14221 * #	NASA-TM-101389	p 197	N89-14465 * #	NASA-TM-101947	p 42	N89-20179 * #
NASA-CR-4147-PT-2	p 11	N89-14222 * #	NASA-TM-101390	p 209	N89-12123 * #	NASA-TM-101948	p 66	N89-20193 * #
NASA-CR-4171	p 84	N89-10131 * #	NASA-TM-101392	p 78	N89-15981 * #	NASA-TM-101949	p 15	N89-25957 * #
NASA-CR-4172	p 83	N89-10128 * #	NASA-TM-101393	p 173	N89-14416 * #	NASA-TM-101950	p 13	N89-18417 * #
NASA-CR-4180	p 10	N89-12553 * #	NASA-TM-101394	p 108	N89-11911 * #	NASA-TM-101951	p 66	N89-20192 * #
NASA-CR-4188	p 155	N89-12838 * #	NASA-TM-101395	p 84	N89-11826 * #	NASA-TM-101952	p 218	N89-20684 * #
NASA-CR-4194	p 19	N89-14235 * #	NASA-TM-101396	p 25	N89-13432 * #	NASA-TM-101953	p 218	N89-20685 * #
NASA-CR-4195	p 189	N89-21256 * #	NASA-TM-101397	p 240	N89-15047 * #	NASA-TM-101954	p 78	N89-19371 * #
NASA-CR-4198	p 155	N89-12835 * #	NASA-TM-101398	p 100	N89-12717 * #	NASA-TM-101955	p 114	N89-21100 * #
NASA-CR-4199-VOL-1	p 12	N89-15896 * #	NASA-TM-101399	p 158	N89-13741 * #	NASA-TM-101956	p 66	N89-20194 * #
NASA-CR-4199-VOL-2	p 12	N89-15897 * #	NASA-TM-101400	p 111	N89-13666 * #	NASA-TM-101957	p 87	N89-24459 * #
NASA-CR-4201	p 182	N89-13793 * #	NASA-TM-101401	p 111	N89-14310 * #	NASA-TM-101959	p 113	N89-20253 * #
NASA-CR-4202	p 19	N89-13429 * #	NASA-TM-101402	p 102	N89-14297 * #	NASA-TM-101960	p 129	N89-25365 * #
NASA-CR-4205	p 188	N89-18694 * #	NASA-TM-101403	p 63	N89-12665 * #	NASA-TM-101961	p 222	N89-21595 * #
NASA-CR-4211	p 12	N89-15898 * #	NASA-TM-101404	p 48	N89-11804 * #	NASA-TM-101962	p 93	N89-19402 * #
NASA-CR-4215	p 202	N89-21258 * #	NASA-TM-101405	p 159	N89-14403 * #	NASA-TM-101963	p 123	N89-19446 * #
NASA-CR-4224	p 186	N89-22920 * #	NASA-TM-101406	p 202	N89-22939 * #	NASA-TM-101964	p 113	N89-20252 * #
NASA-SP-495	p 24	N89-12565 * #	NASA-TM-101407	p 228	N89-15685 * #	NASA-TM-101965	p 162	N89-21197 * #
NASA-TM-100152	p 174	N89-18671 * #	NASA-TM-101408	p 101	N89-13566 * #	NASA-TM-101968	p 31	N89-20996 * #
NASA-TM-100259	p 181	N89-10283 * #	NASA-TM-101409	p 158	N89-13749 * #	NASA-TM-101969	p 186	N89-22919 * #
NASA-TM-100260	p 181	N89-10282 * #	NASA-TM-101410	p 182	N89-14450 * #	NASA-TM-101970	p 211	N89-22177 * #
NASA-TM-100708	p 206	N89-10403 * #	NASA-TM-101411	p 159	N89-13757 * #	NASA-TM-101971	p 114	N89-21104 * #
NASA-TM-100827	p 161	N89-18664 * #	NASA-TM-101412	p 11	N89-15077 * #	NASA-TM-101972	p 31	N89-22605 * #
NASA-TM-100828	p 221	N89-10575 * #	NASA-TM-101413	p 10	N89-12555 * #	NASA-TM-101973	p 66	N89-21025 * #
NASA-TM-100832	p 85	N89-13522 * #	NASA-TM-101414	p 198	N89-15437 * #	NASA-TM-101975	p 93	N89-21051 * #
NASA-TM-100869	p 31	N89-20995 * #	NASA-TM-101415	p 85	N89-13521 * #	NASA-TM-101976	p 228	N89-21628 * #
NASA-TM-100879	p 9	N89-10858 * #	NASA-TM-101416	p 24	N89-12568 * #	NASA-TM-101977	p 32	N89-22606 * #
NASA-TM-100880	p 86	N89-15990 * #	NASA-TM-101417	p 11	N89-14220 * #	NASA-TM-101978	p 29	N89-19305 * #
NASA-TM-100883	p 36	N89-21002 * #	NASA-TM-101418	p 103	N89-20227 * #	NASA-TM-101979	p 185	N89-22111 * #
NASA-TM-100890	p 196	N89-12930 * #	NASA-TM-101419	p 159	N89-15366 * #	NASA-TM-101980	p 210	N89-21419 * #
NASA-TM-100916	p 222	N89-14794 * #	NASA-TM-101420	p 26	N89-14237 * #	NASA-TM-101981	p 136	N89-19493 * #
NASA-TM-100925	p 238	N89-24216 * #	NASA-TM-101421	p 198	N89-14470 * #	NASA-TM-101982	p 66	N89-20199 * #
NASA-TM-100931	p 155	N89-12026 * #	NASA-TM-101422	p 65	N89-16917 * #	NASA-TM-101983	p 163	N89-23813 * #
NASA-TM-100944	p 42	N89-10111 * #	NASA-TM-101423	p 102	N89-15218 * #	NASA-TM-101984	p 86	N89-22684 * #
NASA-TM-100947	p 208	N89-10409 * #	NASA-TM-101424	p 122	N89-28665 * #	NASA-TM-101985	p 168	N89-29714 * #
NASA-TM-100952	p 11	N89-15078 * #	NASA-TM-101425	p 65	N89-15171 * #	NASA-TM-101986	p 115	N89-23691 * #
NASA-TM-100968	p 172	N89-11198 * #	NASA-TM-101426	p 35	N89-15121 * #	NASA-TM-101987	p 32	N89-23465 * #
NASA-TM-100972	p 45	N89-10117 * #	NASA-TM-101428	p 173	N89-14418 * #	NASA-TM-101988	p 218	N89-24055 * #
NASA-TM-100999	p 216	N89-18045 * #	NASA-TM-101430	p 203	N89-24635 * #	NASA-TM-101989	p 1	N89-22569 * #
NASA-TM-101200	p 230	N89-14831 * #	NASA-TM-101431	p 182	N89-13794 * #	NASA-TM-101990	p 128	N89-21142 * #
NASA-TM-101219	p 236	N89-11553 * #	NASA-TM-101432	p 135	N89-13722 * #	NASA-TM-101991	p 202	N89-21266 * #
NASA-TM-101220	p 65	N89-17618 * #	NASA-TM-101433	p 26	N89-14239 * #	NASA-TM-101992	p 42	N89-26877 * #
NASA-TM-101251	p 209	N89-17356 * #	NASA-TM-101434	p 10	N89-13412 * #	NASA-TM-101993	p 29	N89-20133 * #
NASA-TM-101298	p 154	N89-10242 * #	NASA-TM-101435	p 182	N89-14452 * #	NASA-TM-101994	p 136	N89-20385 * #
NASA-TM-101301	p 9	N89-11717 * #	NASA-TM-101436	p 63	N89-13492 * #	NASA-TM-101995	p 33	N89-26007 * #
NASA-TM-101308	p 222	N89-22392 * #	NASA-TM-101437	p 10	N89-13409 * #	NASA-TM-101996	p 228	N89-24138 * #
NASA-TM-101310	p 100	N89-10156 * #	NASA-TM-101438	p 183	N89-14453 * #	NASA-TM-101997	p 93	N89-22710 * #
NASA-TM-101316	p 220	N89-12283 * #	NASA-TM-101439	p 112	N89-16065 * #	NASA-TM-101998	p 14	N89-23413 * #
NASA-TM-101322	p 24	N89-10043 * #	NASA-TM-101440	p 64	N89-13495 * #	NASA-TM-101999	p 221	N89-24856 * #
NASA-TM-101329	p 227	N89-10603 * #	NASA-TM-101441	p 12	N89-15084 * #	NASA-TM-102000	p 185	N89-21245 * #
NASA-TM-101335	p 77	N89-10124 * #	NASA-TM-101442	p 184	N89-18685 * #	NASA-TM-102001	p 78	N89-21032 * #
NASA-TM-101336	p 108	N89-10166 * #	NASA-TM-101443	p 112	N89-15257 * #	NASA-TM-102002	p 228	N89-20779 * #
NASA-TM-101338	p 162	N89-22054 * #	NASA-TM-101444	p 183	N89-15413 * #	NASA-TM-102003	p 68	N89-23518 * #
NASA-TM-101340	p 112	N89-17668 * #	NASA-TM-101445	p 184	N89-21244 * #	NASA-TM-102004	p 78	N89-25285 * #
NASA-TM-101341	p 61	N89-10122 * #	NASA-TM-101446	p 103	N89-17649 * #	NASA-TM-102005	p 163	N89-23809 * #
NASA-TM-101342	p 77	N89-11815 * #	NASA-TM-101447	p 40	N89-14247 * #	NASA-TM-102006	p 41	N89-20171 * #
NASA-TM-101345	p 208	N89-10405 * #	NASA-TM-101448	p 123	N89-20324 * #	NASA-TM-102008	p 137	N89-21174 * #
NASA-TM-101346	p 108	N89-11912 * #	NASA-TM-101449	p 183	N89-17248 * #	NASA-TM-102009	p 223	N89-22397 * #
			NASA-TM-101450	p 85	N89-15201 * #	NASA-TM-102010	p 14	N89-22573 * #
			NASA-TM-101451	p 111	N89-14338 * #	NASA-TM-102011	p 123	N89-28666 * #

NASA-TM-102012	p 69	N89-24443 *	#	NASA-TM-102126	p 164	N89-24577 *	#	PURDUE-MS-34971	p 159	N89-13755 *	#
NASA-TM-102013	p 162	N89-22053 *	#	NASA-TM-102127	p 242	N89-26799 *	#	PW-5574-212-VOL-2	p 113	N89-18550 *	#
NASA-TM-102015	p 242	N89-23397 *	#	NASA-TM-102128	p 167	N89-28748 *	#	PWA-5967-51	p 29	N89-20132 *	#
NASA-TM-102016	p 67	N89-23516 *	#	NASA-TM-102129	p 166	N89-26180 *	#	REPT-CC0134	p 64	N89-14256 *	#
NASA-TM-102017	p 73	N89-26041 *	#	NASA-TM-102131	p 214	N89-26292 *	#	REPT-21-5477	p 26	N89-13433 *	#
NASA-TM-102018	p 14	N89-23417 *	#	NASA-TM-102132	p 165	N89-26174 *	#	REPT-719630-1	p 128	N89-24518 *	#
NASA-TM-102019	p 67	N89-23517 *	#	NASA-TM-102133	p 189	N89-28851 *	#	REPT-719630-2	p 129	N89-24519 *	#
NASA-TM-102020	p 67	N89-22851 *	#	NASA-TM-102134	p 187	N89-28015 *	#	REPT-86-9-71	p 10	N89-12553 *	#
NASA-TM-102021	p 68	N89-23520 *	#	NASA-TM-102135	p 70	N89-24444 *	#	REPT-80B-0214	p 206	N89-10403 *	#
NASA-TM-102022	p 186	N89-22925 *	#	NASA-TM-102136	p 46	N89-24427 *	#	REPT-8803	p 239	N89-14182 *	#
NASA-TM-102023	p 104	N89-23664 *	#	NASA-TM-102137	p 35	N89-26009 *	#	RI/RD-87-126	p 61	N89-10119 *	#
NASA-TM-102024	p 129	N89-27923 *	#	NASA-TM-102138	p 166	N89-27103 *	#	RI/RD-88-273	p 103	N89-21072 *	#
NASA-TM-102025	p 137	N89-22020 *	#	NASA-TM-102139	p 76	N89-29484 *	#	RI/RD85-320-2-VOL-3	p 64	N89-15164 *	#
NASA-TM-102026	p 164	N89-23821 *	#	NASA-TM-102140	p 139	N89-26149 *	#	RI/RD88-256	p 74	N89-26905 *	#
NASA-TM-102027	p 163	N89-22861 *	#	NASA-TM-102141	p 139	N89-25403 *	#	RI/RD89-212	p 73	N89-26899 *	#
NASA-TM-102028	p 36	N89-22617 *	#	NASA-TM-102142	p 166	N89-27115 *	#	RI/RD89-214-TASK-E.5	p 189	N89-27204 *	#
NASA-TM-102029	p 223	N89-24872 *	#	NASA-TM-102143	p 76	N89-28571 *	#	R87-AEB586	p 110	N89-13621 *	#
NASA-TM-102030	p 164	N89-24575 *	#	NASA-TM-102230	p 168	N89-29725 *	#	R87AEB111	p 231	N89-13256 *	#
NASA-TM-102032	p 87	N89-24460 *	#	NASA-TM-102282	p 176	N89-27998 *	#	SAE PAPER 880539	p 177	A89-12301 *	#
NASA-TM-102036	p 223	N89-24865 *	#	NASA-TM-102283	p 73	N89-26045 *	#	SAE PAPER 880543	p 177	A89-12303 *	#
NASA-TM-102038	p 31	N89-21798 *	#	NASA-TM-102284	p 72	N89-25281 *	#	SAE PAPER 880544	p 178	A89-12304 *	#
NASA-TM-102039	p 67	N89-22652 *	#	NASA-TM-102285	p 229	N89-25675 *	#	SAE PAPER 880545	p 48	A89-12305 *	#
NASA-TM-102040	p 138	N89-23792 *	#	NASA-TM-102286	p 47	N89-26036 *	#	SAE PAPER 880625	p 19	A89-12307 *	#
NASA-TM-102041	p 205	N89-28029 *	#	NASA-TM-102287	p 47	N89-26035 *	#	SAE PAPER 880626	p 178	A89-12308 *	#
NASA-TM-102042	p 71	N89-25274 *	#	NASA-TM-102292	p 15	N89-25121 *	#	SAE PAPER 881294	p 179	A89-21000 *	#
NASA-TM-102043	p 14	N89-23416 *	#	NASA-TM-102293	p 168	N89-28749 *	#	SAE PAPER 881386	p 16	A89-28192 *	#
NASA-TM-102044	p 68	N89-23527 *	#	NASA-TM-102294	p 167	N89-27980 *	#	SAE PAPER 890331	p 181	A89-51477 *	#
NASA-TM-102045	p 128	N89-23753 *	#	NASA-TM-102295	p 205	N89-27223 *	#	SAE PAPER 890332	p 181	A89-51492 *	#
NASA-TM-102046	p 115	N89-24487 *	#	NASA-TM-102297	p 47	N89-26887 *	#	SAE-89-0332	p 33	N89-26007 *	#
NASA-TM-102047	p 14	N89-22577 *	#	NASA-TM-102298	p 41	N89-26876 *	#	SAIC-87/1612	p 155	N89-12836 *	#
NASA-TM-102048	p 175	N89-23850 *	#	NASA-TM-102299	p 242	N89-27623 *	#	SAND-88-0628C	p 209	N89-17356 *	#
NASA-TM-102049	p 69	N89-24436 *	#	NASA-TM-102301	p 116	N89-27836 *	#	SAWE PAPER 1818	p 40	A89-50814 *	#
NASA-TM-102050	p 68	N89-23522 *	#	NASA-TM-102302	p 88	N89-26924 *	#	SPI-25-1-VOL-2	p 211	N89-22981 *	#
NASA-TM-102051	p 204	N89-26260 *	#	NASA-TM-102303	p 73	N89-26044 *	#	SPI-25-1-VOL-3	p 211	N89-22980 *	#
NASA-TM-102052	p 69	N89-24438 *	#	NASA-TM-102307	p 104	N89-29522 *	#	SPI-25-1-VOL-4	p 210	N89-18967 *	#
NASA-TM-102053	p 15	N89-25119 *	#	NASA-TM-102308	p 38	N89-28535 *	#	SPI-25-1	p 209	N89-17941 *	#
NASA-TM-102054	p 67	N89-22653 *	#	NASA-TM-102309	p 166	N89-27114 *	#	SPIE-853	p 219	A89-10798 *	#
NASA-TM-102055	p 70	N89-25269 *	#	NASA-TM-102310	p 75	N89-27706 *	#	SPIE-886	p 124	A89-15819 *	#
NASA-TM-102056	p 175	N89-24591 *	#	NASA-TM-102311	p 33	N89-26008 *	#	SWRI-8966	p 239	N89-17548 *	#
NASA-TM-102057	p 164	N89-23823 *	#	NASA-TM-102312	p 74	N89-27701 *	#	S71-5240-1/2-0	p 135	N89-15335 *	#
NASA-TM-102058	p 212	N89-23025 *	#	NASA-TM-102317	p 33	N89-27670 *	#	TBE-SSD-P601-89-40	p 185	N89-22108 *	#
NASA-TM-102059	p 72	N89-25282 *	#	NASA-TM-102318	p 168	N89-29726 *	#	TL-SEAL-1-89	p 186	N89-23876 *	#
NASA-TM-102061	p 71	N89-25271 *	#	NASA-TM-102321	p 74	N89-26904 *	#	TRG-JM/89-1	p 160	N89-16132 *	#
NASA-TM-102062	p 165	N89-26177 *	#	NASA-TM-102322	p 129	N89-27927 *	#	US-PATENT-APPL-SN-038560	p 116	N89-29538 *	#
NASA-TM-102063	p 214	N89-25506 *	#	NASA-TM-102326	p 88	N89-29490 *	#	US-PATENT-APPL-SN-108331	p 102	N89-14303 *	#
NASA-TM-102064	p 71	N89-25272 *	#	NASA-TM-102327	p 216	N89-29032 *	#	US-PATENT-APPL-SN-244377	p 123	N89-14348 *	#
NASA-TM-102066	p 46	N89-25267 *	#	NASA-TM-102331	p 176	N89-27999 *	#	US-PATENT-APPL-SN-251499	p 85	N89-14259 *	#
NASA-TM-102068	p 138	N89-23791 *	#	NASA-TM-102332	p 104	N89-26989 *	#	US-PATENT-APPL-SN-279624	p 87	N89-23623 *	#
NASA-TM-102072	p 71	N89-25275 *	#	NASA-TM-102335	p 75	N89-27702 *	#	US-PATENT-APPL-SN-292146	p 187	N89-28830 *	#
NASA-TM-102073	p 71	N89-25273 *	#	NASA-TM-102337	p 74	N89-26906 *	#	US-PATENT-APPL-SN-381240	p 116	N89-28651 *	#
NASA-TM-102074	p 69	N89-24439 *	#	NASA-TM-102338	p 205	N89-28036 *	#	US-PATENT-APPL-SN-382885	p 40	N89-28549 *	#
NASA-TM-102075	p 138	N89-24529 *	#	NASA-TM-102339	p 76	N89-28570 *	#	US-PATENT-APPL-SN-396263	p 177	N89-28806 *	#
NASA-TM-102076	p 46	N89-24418 *	#	NASA-TM-102345	p 237	N89-30088 *	#	US-PATENT-APPL-SN-886149	p 116	N89-29538 *	#
NASA-TM-102078	p 32	N89-24318 *	#	NASA-TM-102347	p 75	N89-27704 *	#	US-PATENT-APPL-SN-917125	p 172	N89-12048 *	#
NASA-TM-102079	p 163	N89-22862 *	#	NASA-TM-102352	p 223	N89-30008 *	#	US-PATENT-CLASS-126-443	p 172	N89-12048 *	#
NASA-TM-102080	p 15	N89-24269 *	#	NASA-TM-4083	p 27	N89-15112 *	#	US-PATENT-CLASS-126-901	p 172	N89-12048 *	#
NASA-TM-102081	p 69	N89-24440 *	#	NASA-TM-4087	p 29	N89-20135 *	#	US-PATENT-CLASS-165-41	p 172	N89-12048 *	#
NASA-TM-102082	p 78	N89-24451 *	#	NASA-TM-4102	p 203	N89-25485 *	#	US-PATENT-CLASS-165-904	p 172	N89-12048 *	#
NASA-TM-102083	p 72	N89-25280 *	#	NASA-TM-4103	p 217	N89-20641 *	#	US-PATENT-CLASS-420-54	p 102	N89-14303 *	#
NASA-TM-102084	p 41	N89-24409 *	#	NASA-TM-4106	p 188	N89-19578 *	#	US-PATENT-CLASS-420-62	p 102	N89-14303 *	#
NASA-TM-102085	p 239	N89-26781 *	#	NASA-TM-4115	p 87	N89-25290 *	#	US-PATENT-CLASS-420-79	p 102	N89-14303 *	#
NASA-TM-102086	p 41	N89-25254 *	#	NASA-TM-4128	p 87	N89-25300 *	#	US-PATENT-CLASS-420-80	p 102	N89-14303 *	#
NASA-TM-102087	p 17	N89-25978 *	#	NASA-TM-83439	p 159	N89-14386 *	#	US-PATENT-CLASS-420-81	p 102	N89-14303 *	#
NASA-TM-102089	p 139	N89-26148 *	#	NASA-TM-87030	p 13	N89-19265 *	#	US-PATENT-CLASS-428-288	p 116	N89-29538 *	#
NASA-TM-102091	p 205	N89-28030 *	#	NASA-TM-88846	p 210	N89-19737 *	#	US-PATENT-CLASS-428-367	p 116	N89-29538 *	#
NASA-TM-102092	p 32	N89-24320 *	#	NASA-TM-88969	p 9	N89-10865 *	#	US-PATENT-CLASS-428-375	p 116	N89-29538 *	#
NASA-TM-102093	p 75	N89-27705 *	#	NASA-TM-89855	p 154	N89-10246 *	#	US-PATENT-CLASS-428-390	p 116	N89-29538 *	#
NASA-TM-102094	p 88	N89-26912 *	#	NASA-TM-89887	p 238	N89-18259 *	#	US-PATENT-CLASS-428-408	p 116	N89-29538 *	#
NASA-TM-102095	p 33	N89-26003 *	#	NASA-TP-2845	p 198	N89-16183 *	#	US-PATENT-CLASS-428-698	p 116	N89-29538 *	#
NASA-TM-102096	p 33	N89-25238 *	#	NASA-TP-2846	p 9	N89-10844 *	#	US-PATENT-4,770,232	p 172	N89-12048 *	#
NASA-TM-102097	p 239	N89-25078 *	#	NASA-TP-2862	p 65	N89-15979 *	#	US-PATENT-4,780,276	p 102	N89-14303 *	#
NASA-TM-102098	p 32	N89-24319 *	#	NASA-TP-2863	p 100	N89-10996 *	#	US-PATENT-4,781,993	p 116	N89-29538 *	#
NASA-TM-102099	p 167	N89-27121 *	#	NASA-TP-2865	p 174	N89-16139 *	#				
NASA-TM-102100	p 72	N89-25277 *	#	NASA-TP-2875	p 127	N89-17767 *	#				
NASA-TM-102101	p 15	N89-29323 *	#	NASA-TP-2880	p 173	N89-15380 *	#				
NASA-TM-102102	p 242	N89-27619 *	#	NASA-TP-2883	p 115	N89-26091 *	#				
NASA-TM-102103	p 124	N89-27868 *	#	NASA-TP-2891	p 136	N89-15337 *	#				
NASA-TM-102104	p 214	N89-26291 *	#	NASA-TP-2892	p 218	N89-17422 *	#				
NASA-TM-102105	p 70	N89-24448 *	#	NASA-TP-2899	p 136	N89-21189 *	#				
NASA-TM-102106	p 204	N89-25490 *	#	NASA-TP-2900	p 164	N89-25409 *	#				
NASA-TM-102107	p 88	N89-26919 *	#	NASA-TP-2901	p 184	N89-21243 *	#				
NASA-TM-102108	p 70	N89-24446 *	#	NASA-TP-2902	p 103	N89-17650 *	#				
NASA-TM-102110	p 224	N89-25670 *	#	NASA-TP-2904	p 136	N89-21171 *	#				
NASA-TM-102111	p 231	N89-27506 *	#	NASA-TP-2910	p 114	N89-21103 *	#				
NASA-TM-102112	p 165	N89-26175 *	#	NASA-TP-2911	p 186	N89-24607 *	#				
NASA-TM-102113	p 70	N89-24447 *	#	NASA-TP-2912	p 40	N89-28545 *	#				
NASA-TM-102115	p 88	N89-27795 *	#	NASA-TP-2924	p 88	N89-27796 *	#				
NASA-TM-102116	p 116	N89-26095 *	#	ORNL-6497	p 217	N89-15623 *	#				
NASA-TM-102117	p 165	N89-26178 *	#	P/W/GPD-FR-19381-VOL-2	p 173	N89-13771 *	#				
NASA-TM-102118	p 72	N89-25283 *	#	PNL-SA-15519	p 65	N89-17618 *	#				
NASA-TM-102119	p 204	N89-26259 *	#	PSI-2062/TR-890	p 175	N89-23851 *	#				
NASA-TM-102120	p 87	N89-26048 *	#								
NASA-TM-102121	p 175	N89-24593 *	#								
NASA-TM-102122	p 104	N89-28627 *	#								
NASA-TM-102123	p 123	N89-27038 *	#								
NASA-TM-102124	p 75	N89-27703 *	#								

*REPORT NUMBER INDEX*

**W-10301**

UTRC-R86-956480-VOL-1 ..... p 159 N89-13756 \* #  
UTRC-R88-957367-31 ..... p 27 N89-16843 \* #  
UTSI/88-07 ..... p 155 N89-12838 \* #  
W-10301 ..... p 138 N89-24530 \* #

# Report Documentation Page

1. Report No. NASA TM-102542		2. Government Accession No.		3. Recipient's Catalog No.	
4. Title and Subtitle Bibliography of Lewis Research Center Technical Publications Announced in 1989				5. Report Date May 1990	
				6. Performing Organization Code	
7. Author(s)				8. Performing Organization Report No. E-5352	
				10. Work Unit No. None	
9. Performing Organization Name and Address National Aeronautics and Space Administration Lewis Research Center Cleveland, Ohio 44135-3191				11. Contract or Grant No.	
				13. Type of Report and Period Covered Technical Memorandum	
12. Sponsoring Agency Name and Address National Aeronautics and Space Administration Washington, D.C. 20546-0001				14. Sponsoring Agency Code	
15. Supplementary Notes Compiled by Technical Information Services Division, Lewis Research Center.					
16. Abstract This compilation of abstracts describes and indexes the technical reporting that resulted from the scientific and engineering work performed and managed by the Lewis Research Center in 1989. All the publications were announced in the 1989 issues of STAR (Scientific and Technical Aerospace Reports) and/or IAA (International Aerospace Abstracts). Included are research reports, journal articles, conference presentations, patents and patent applications, and theses.					
17. Key Words (Suggested by Author(s)) Bibliographies Abstracts Documentation Indexes (Documentation)				18. Distribution Statement Unclassified - Unlimited Subject Category 82	
19. Security Classif. (of this report) Unclassified		20. Security Classif. (of this page) Unclassified		21. No. of pages 393	
				22. Price* A17	